ORGANOMETALLICS

Volume 14, Number 2, February 1995

Communications

Transition-Metal-Substituted Acylphosphanes and Phosphaalkenes. 26.[1] Synthesis and Structure of the 2-Metallo-1,2,3-diazaphospholes $(\eta^5\text{-}C_5Me_5)(CO)_2Fe{-}N{-}P{=}C(NMe_2){-}C(CO_2R){=}N$ (R = Et, *t*Bu)

Lothar Weber,* Olaf Kaminski, H.-G. Stammler, and Beate Neumann

Fakultät für Chemie, Universität Bielefeld, Universitätsstrasse 25, D-33615 Bielefeld, Germany

Received November 15, 1994[⊗]

Summary: Treatment of the metallophosphaalkene $(\eta^5\text{-}C_5Me_5)(CO)_2Fe{-}P{=}C(NMe_2)_2$ with diazoacetates N_2CHCO_2R (R = Et, tBu) afforded the novel N-metalated 1,2,3-diazaphospholes $(\eta^5\text{-}C_5Me_5)(CO)_2Fe{-}N{-}P{=}C(NMe_2)C(CO_2R){=}N$ (R = Et, tBu) as the formal result of a dipolar [3 + 2] cycloaddition which is followed by the elimination of dimethylamine and a sigmatropic 1,2-shift of the metal fragment from phosphorus to nitrogen. The molecular structure of one representative (R = tBu) was established by a single-crystal X-ray analysis.

The combination of reactive sites in metallophosphaalkenes such as $(\eta^5\text{-}C_5Me_5)(CO)_2Fe{-}P{=}CR^1R^2$ ($R^1 = R^2 = SiMe_3$,[2] NMe_2[3]) renders them versatile as useful building blocks in organometallic synthesis. Thus, the compound $(\eta^5\text{-}C_5Me_5)(CO)_2Fe{-}P{=}C(NMe_2)_2$ (**1**) was conveniently converted into 1-metallo-1,2-dihydrophosphetes **I**[3] and **IV**[4] when reacted with fumarodinitrile and dimethyl fumarate or methyl butynoate, respectively.

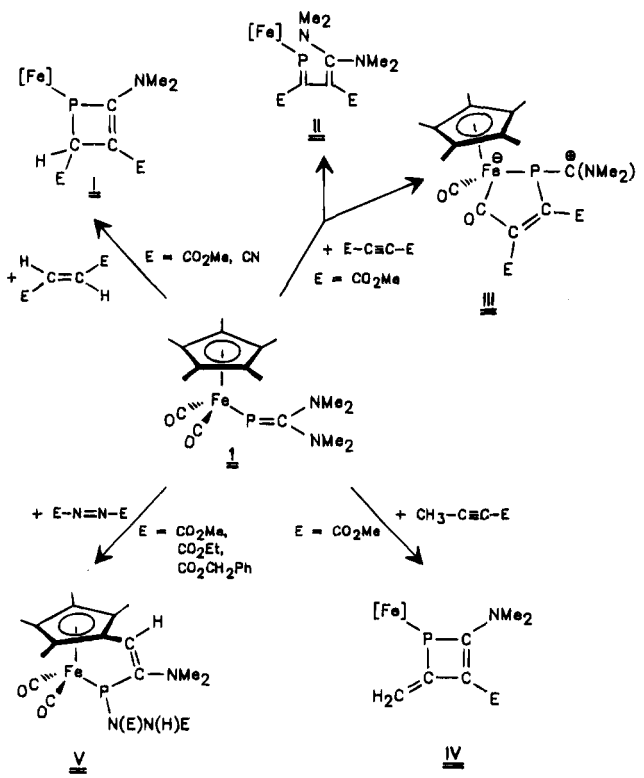

⊗ Abstract published in *Advance ACS Abstracts*, January 1, 1995.

(1) Part 25: Weber, L.; Kaminski, O.; Boese, R.; Bläser, D. *Organometallics*, in press.

(2) Niecke, E.; Metternich, H.-J.; Nieger, M.; Gudat, D.; Wenderoth, P.; Malisch, W.; Hahner, C.; Reich, W. *Chem. Ber.* **1993**, *126*, 1299.

(3) Weber, L.; Kaminski, O.; Stammler, H.-G.; Neumann, B.; Romanenko, V. D. *Z. Naturforsch.* **1993**, *48B*, 1784.

(4) Weber, L.; Kaminski, O.; Stammler, H.-G.; Neumann, B.; Boese, R. *Z. Naturforsch.* **1994**, *49B*, 1693.

0276-7333/95/2314-0581$09.00/0

Treatment of **1** with dimethyl acetylenedicarboxylate furnished a mixture of 1-metallo-1-phospha-1,3-butadiene **II** and the metallaheterocycle **III**,[4] whereas the synthesis of the condensation products **V** was achieved upon exposure of **1** to dialkyl azodicarboxylates.[1]

The step from electron-deficient azo compounds to diazocarboxylates was obvious. Here we report on the chemical behavior of **1** toward ethyl diazoacetate (**2a**) and *tert*-butyl diazoacetate (**2b**), both of which are known as potent 1,3-dipoles.

Treatment of a diethyl ether solution of **1** with a slight excess of the esters **2a,b** at −30 °C afforded the products as yellow (**3a**) or red (**3b**) crystalline solids, respectively. The structure of **3a,b** was assigned on the basis of spectral evidence[5] and confirmed by the single-crystal X-ray diffraction study of **3b**. The ^{31}P NMR spectra exhibit a singlet resonance at δ 229.1 (**3a**) and 228.8 ppm (**3b**). These shifts compare well with the $\delta(^{31}P)$ NMR shifts of the metal-free 2*H*-1,2,3-diazaphospholes **4** (R = Me, δ 228.9 ppm), **5** (R = Ph, δ 225 ppm), and **6** (R = 2-py, δ 228.1 ppm).[6]

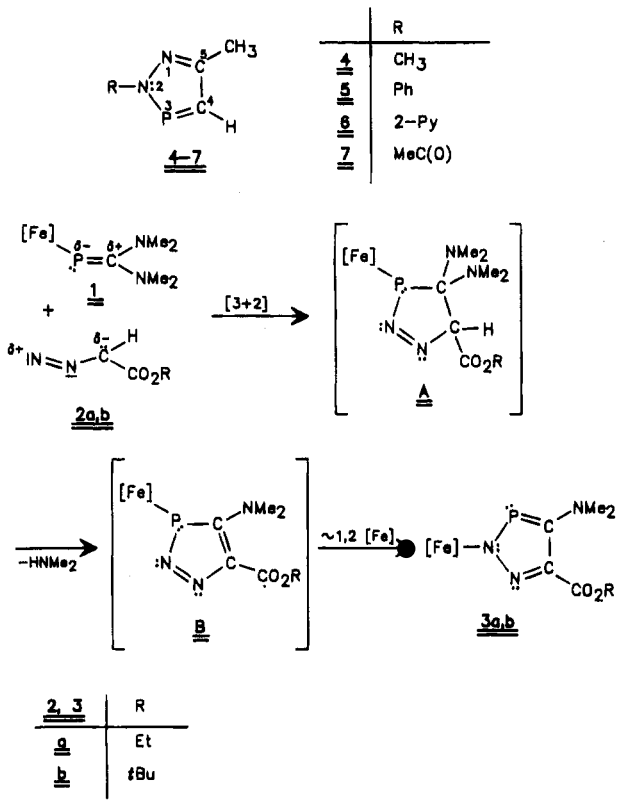

In the ^{1}H NMR spectrum two singlets at δ 2.86 and 2.87 ppm and a singlet at δ 1.27 (**3b**) or 1.28 ppm (**3a**) are readily assigned to the two chemically and magnetically different *N*-methyl groups and the C_5Me_5 protons in **3b** and **3a**, respectively. The ethyl group in **3a** and the *tert*-butyl group in **3b** gave rise to resonances at δ 1.18 (t, $^3J_{HH}$ = 7.1 Hz), 4.31 (q, $^3J_{HH}$ = 7.1 Hz), and 1.62 (s) ppm, respectively.

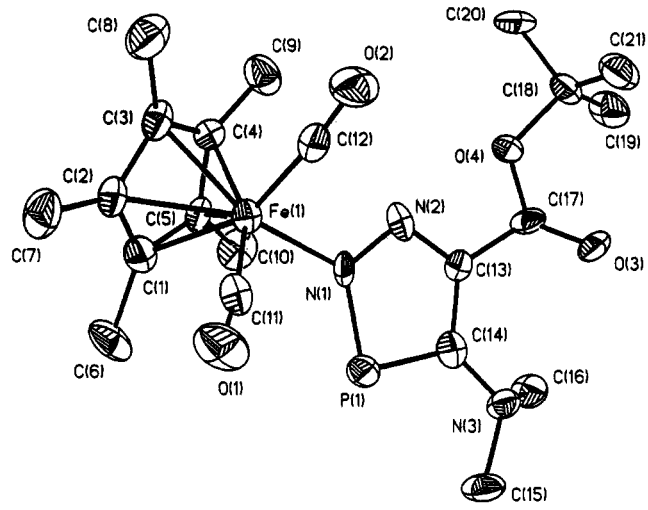

Figure 1. Molecular structure of **3b**. Important bond lengths (Å) and angles (deg) are as follows: Fe−C(cp*) = 2.120(3)−2.139(3), Fe−C(11) = 1.782(8), Fe−C(12) = 1.770(9), Fe−N(1) = 1.953(6), P−N(1) = 1.703(6), P−C(14) = 1.746(8), C(13)−C(14) = 1.425(10), N(2)−C(13) = 1.346(8), N(1)−N(2) = 1.342(7), C(13)−C(17) = 1.488(10), N(3)−C(14) = 1.390(9); Fe−N(1)−N(2) = 118.9(5), Fe−N(1)−P = 126.3(4), P−N(1)−N(2) = 114.7(5), N(1)−N(2)−C(13) = 111.1(7), N(2)−C(13)−C(14) = 116.2(7), N(1)−P−C(14) = 91.0(4).

In the $^{13}C\{^1H\}$ NMR spectrum of the products the amino-substituted ring carbon atom is observed as a doublet at δ 184.0 ($^1J_{PC}$ = 50.4 Hz) (**3a**) or 183.5 ppm ($^1J_{PC}$ = 50.2 Hz) (**3b**), respectively. A singlet at δ 146.2 ppm in **3a** and a doublet at δ 147.5 ($^2J_{PC}$ = 9.2 Hz) ppm in **3b** are attributed to the alkoxycarbonyl-functionalized ring carbons. The terminal carbonyl ligands cause a singlet at δ 214.0 ppm in **3a** and a doublet at δ 215.1 ($^3J_{PC}$ = 5.1 Hz) ppm in **3b**. The carbon atoms of the ester carbonyls are observed at δ 163.3 s (**3a**) and δ 162.8 (d, $^3J_{PC}$ = 2.9 Hz) in **3b**. In diazaphosphole **4** for comparison, doublets at δ 135.3 ($^1J_{PC}$ = 35.4 Hz) and 155.7 ($^2J_{PC}$ = 8.8 Hz) ppm are due to the ring carbons C(4) and C(5).[6]

Complex **3a** displays two intense ν(CO) bands for the $Fe(CO)_2$ groups at 2024 and 1972 cm^{-1}, whereas the carbonyl stretch of the ester function gives rise to a band of medium intensity at 1695 cm^{-1}.

The most interesting feature of the molecular structure of **3b** (Figure 1)[7] is the geometry of the heterocyclic ligand, which is attached to the iron center by an Fe−N single bond of 1.953(6) Å. In low-valent iron carbonyl

(5) **3a**: ^{1}H NMR (300 MHz, C_6D_6) δ 1.18 (t, $^3J_{HH}$ = 7.1 Hz, CH_2CH_3), 1.27 [s, 15H, $C_5(CH_3)_5$], 2.86 (s, 3H, NCH_3), 2.87 (s, 3H, NCH_3), 4.31 (q, $^3J_{HH}$ = 7.1 Hz, CH_2CH_3); $^{13}C\{^1H\}$ NMR (75 MHz, C_6D_6) δ 8.7 [s, $C_5(CH_3)_5$], 14.7 (s, CH_2CH_3), 47.3 (s, NCH_3), 47.45 (s, NCH_3), 59.5 (s, CH_2CH_3), 97.8 (s, $C_5(CH_3)_5$), 146.2 (s, P=C−*C*), 163.3 (s, *C*O$_2$Et), 184.0 (d, $^1J_{PC}$ = 50.4 Hz, P=C), 214.0 (s, FeCO); $^{31}P\{^1H\}$ NMR (40.5 MHz, C_6D_6) δ 229.1 s; MS (EI, 70 eV) *m/e* 447 (19%, M$^+$), 391 (100%, M$^+$ −2CO), 247 [37%, $(C_5Me_5)(CO)_2Fe^+$]. **3b**: ^{1}H NMR (300 MHz, C_6D_6) δ 1.28 [s, 15H, $C_5(CH_3)_5$], 1.62 (s, 9H, *t*Bu), 2.86 (s, 3H, NCH_3), 2.87 (s, 3H, NCH_3); $^{13}C\{^1H\}$ NMR (75 MHz, C_6D_6) δ 8.7 [d, $^4J_{PC}$ = 0.6 Hz, $C_5(CH_3)_5$], 26.7 [s, $C(CH_3)_3$], 47.4 (s, NCH_3), 47.6 (s, NCH_3), 78.7 [s, $C(CH_3)_3$], 97.8 [s, $C_5(CH_3)_5$], 147.5 (d, $^2J_{PC}$ = 9.2 Hz, P=C−*C*), 162.8 (d, $^3J_{PC}$ = 2.9 Hz, *C*O$_2$*t*Bu), 183.5 (d, $^1J_{PC}$ = 50.2 Hz, P=C), 215.1 (d, $^3J_{PC}$ = 5.1 Hz, FeCO); $^{31}P\{^1H\}$ NMR (40.5 MHz, C_6D_6) δ 228.8 s; MS (EI, 70 eV) *m/e* 475 (25%, M$^+$), 419 (45%, M$^+$ − 2CO), 363 (100%, M$^+$ − 2CO − CH_2=CMe_2), 247 [21%, $(C_5Me_5)(CO)_2Fe^+$].

(6) Weinmaier, J. H.; Brunnhuber, G.; Schmidpeter, A. *Chem. Ber.* **1980**, *113*, 2278.

(7) Crystal data for complex **3b**: space group $P2_1/c$, a = 11.335(3) Å, b = 17.273(5) Å, c = 12.316(3) Å, β = 90.87(2)°, V = 2411.1(11) Å^3, Z = 4, ϱ_{calc} = 1.309 g/cm^3, Mo Kα (graphite monochromator, λ = 0.710 73 Å), ω scan, data collection at 183 K (3° ≤ 2θ ≤ 50°); 4274 unique reflections Siemens P2(1) four-circle diffractometer, structure solved by direct methods and refinement by full-matrix least squares, using Siemens SHELXTL PLUS/SHEXL-93. All non-hydrogen atoms were refined anisotropically with 258 parameters and 226 restraints (hydrogen atoms in calculated positions riding on the corresponding C atoms). R_F = 0.089 and wR_{F^2} = 0.105 for 1771 reflections with $F_0 > 4\sigma(F_0)$ and maximum rest electron density 0.5 e/Å^3.

complexes with nitrogen-containing ligands Fe–N single bonds usually range from ca. 1.80 to 2.00 Å.[8]

The endocyclic ring distances N(1)–N(2) (1.342(7) Å), P–N(1) (1.703(6) Å), P–C(14) (1.746(8) Å), N(2)–C(13) (1.346(8) Å), and C(13)–C(14) (1.425(10) Å) compare well with the corresponding parameters in **7** (1.34, 1.68, 1.75, 1.34, and 1.44 Å, respectively).[9] The endocyclic angles at phosphorus in both compounds are determined to be 91.0(4)° (**3b**) and 89°. The Fe atom is located in the plane of the heterocycle, which encloses a dihedral angle with the plane defined by the atoms Fe, C(11), C(12), O(1), and O(2) of 85.4°.

The results reported here merit attention for several reasons.

(1) 1,3-Dipolar cycloadditions of acyldiazoalkanes with properly 1,2-functionalized phosphaalkenes such as $Me_3Si{-}P = C(R^1)(OSiMe_3)$ or $Cl{-}P{=}C(R^1)(SiMe_3)$ usually afford 1,2,4-diazaphospholes and not the 1,2,3-isomers described here.[10] Diazoalkanes also add to phosphaalkynes $R^2C{\equiv}P$ (R^2 = neopentyl, *i*Pr, *t*Bu, other tertiary alkyl groups) regiospecifically with the formation of a P–C bond. The regioisomeric 1,2,3-diazaphospholes, however, result as minor products from the cycloaddition of *tert*-butyl diazoacetate to $HC{\equiv}P$[12] or $CF_3CH{=}N_2$ and $N_2{=}CH{-}CO_2Me$ to $iPr_2N{-}C{\equiv}P$.[13]

(2) The coordination chemistry of 1,2,3-diazaphospholes has been scarcely developed and features a few P- and N-coordinated complexes where the ring invariantly donates two electrons via the respective lone pair.[14]

Compounds **3a,b** are the first transition-metal derivatives of 2*H*-1,2,3-diazaphospholes where a 17-valence-electron fragment is linked to the ring atom N(2) in place of an organic substituent. π Complexes of 1,2,3-diazaphospholes are still unknown.

The facile loss of two CO ligands in the mass spectra (EI and CI) of **3a,b** gives evidence for a facile σ/π rearrangement. Preliminary attempts, however, to reproduce this rearrangement on a preparative scale either in boiling xylene or by UV irradiation failed. Investigations on the chemistry of 2-metallo-1,2,3-diazaphospholes are underway.

Acknowledgment. Our work was generously supported by the Deutsche Forschungsgemeinschaft, Bonn, Germany, the Fonds der Chemischen Industrie, Frankfurt, Germany, and BASF AG, Ludwigshafen, Germany. This assistance is gratefully acknowledged.

Supplementary Material Available: Tables of crystal data and structure refinement details, positional and thermal parameters, and bond distances and angles for **3b** (7 pages). Ordering information is given on any current masthead page.

OM940866B

(8) (a) Baikie, P. E.; Mills, O. S. *J. Chem. Soc., Chem. Commun.* **1966**, 707. (b) Doedens, R. J. *Inorg. Chem.* **1969**, *8*, 570; **1970**, *9*, 429. (c) Frühauf, H.-W.; Landers, A.; Goddard, R.; Krüger, C. *Angew. Chem.* **1978**, *90*, 56; *Angew. Chem., Int. Ed. Engl.* **1978**, *17*, 64. (d) Berndt, A. F.; Barnett, K. W. *J. Organomet. Chem.* **1980**, *184*, 211.

(9) Vilkov, L. V.; Khaikin, L. S.; Vasilev, A. F.; Ignatova, N. P.; Melnikov, N. N.; Negrebetskii, V. V.; Shvetsov-Shilovskii, N. I.; *Dokl. Akad. Nauk SSSR* **1971**, *197*, 1081 (cited in ref 10, p 281).

(10) Schmidpeter, A.; Karaghiosoff, K. In *Multiple Bonds and Low Coordination on Phosphorus Chemistry*; Regitz, M., Scherer, O. J., Eds.; Thieme: Stuttgart, Germany, 1990; p 258 and literature cited therein.

(11) Regitz, M.; Binger, P. *Angew. Chem.* **1988**, *100*, 1541; *Angew. Chem., Int. Ed. Engl.* **1988**, *27*, 1484.

(12) Fuchs, E. P. O.; Hermesdorf, M.; Schnurr, W.; Rösch, W.; Heydt, H.; Regitz, M.; Binger, P. *J. Organomet. Chem.* **1988**, *338*, 329.

(13) Grobe, J.; Le Van, D.; Hegemann, M.; Krebs, B.; Läge, M. *Chem. Ber.* **1992**, *125*, 411.

(14) P-coordinated complexes 1,2,3-diazaphospholes have been described with $Cr(CO)_5$,[6,15] $W(CO)_5$,[15] $Fe(CO)_4$,[15] $Mn(Mecp)(CO)_2$,[15] $Pt(PPh_3)_n$ (n = 2, 3),[16] and *cis*-$PtCl_2(PEt_3)$.[17] In a *trans*-$PdCl_2(PEt_3)$ complex the heterocycle is N-coordinated, whereas the reaction of $[PtBr_2(PEt_3)]_2$ with 2,5-dimethyl-1,2,3-diazaphosphole afforded a 2:1 mixture of the cis-P isomer and the trans-N isomer of $PtBr_2(PEt_3)$.[17] In gold 1,2,3-diazaphosphole complexes N- or P-coordination is governed by the nature of the substituents at the heterocycle.[18]

(15) Weinmaier, J. H.; Tautz, H.; Schmidpeter, A. *J. Organomet. Chem.* **1980**, *185*, 53.

(16) Kraijkamp, J. G.; van Koten, G.; Vrieze, K.; Grove, D. M.; Klop, E. A.; Spek, A. L.; Schmidpeter, A. *J. Organomet. Chem.* **1983**, *256*, 375.

(17) Kraijkamp, J. G.; Grove, D. M.; van Koten, G.; Schmidpeter, A. *Inorg. Chem.* **1988**, *27*, 2612.

(18) Dash, K. C.; Schmidbaur, H.; Schmidpeter, A. *Inorg. Chim. Acta* **1980**, *41*, 167.

A Silica-Supported Magnesium–Anthracene Complex

Tania R. van den Ancker and Colin L. Raston*

Faculty of Science and Technology, Griffith University, Nathan, Brisbane, Queensland 4111, Australia

Received October 11, 1994®

Summary: Hydroxyl-depleted silica surfaces derived from treating chloropropylsilyl- (or chloropropylsilyl/trimethylsilyl-) functionalized silica with $H_3Al{\cdot}NMe_3$ afford the corresponding organolithium reagent when treated with Li^+(biphenyl)$^{\bullet-}$; successive treatment with 9-(chlorodimethylsilyl)anthracene and Mg(anthracene)(THF)$_3$ generates anthracene and silica-supported "magnesium–anthracene", which gives Grignard reagents of benzylic halides in tetrahydrofuran in excellent yield with the spent silica-supported anthracene being readily recycled.

The magnesium–anthracene complex [Mg(anthracene)(THF)$_3$] (**1**; THF = tetrahydrofuran) is an important source of magnesium *via* either reactions from activated magnesium arising from decomposition of **1** to its constituents or reactions involving the complex directly.[1–9] For the latter the formation of Grignard reagents of benzylic halides in almost quantitative yield is noteworthy; such reagents can be difficult to prepare using the classical method of Grignard reagent formation, and even using highly activated forms of magnesium.[4–9] Generating Grignard reagents using this method, however, yields solutions loaded with anthracene. Earlier work to overcome this potential inconvenience centered on developing a polystyrene-supported magnesium–anthracene complex. This approach suffers from relatively low loading of the active sites which are anthracene radical anion and dianion species, rather than exclusively dianion species as in the model compound [Mg(9-PhCH$_2$(Me)$_2$SiC$_{14}$H$_{10}$)(THF)$_2$] and also **1**. In addition, there is a *ca.* 10% reduction in the ability of the spent polymer to take up magnesium after successive uses.[8]

We now report the synthesis and characterization of silica-supported magnesium–anthracene materials and their utility in generating Grignard reagents of benzylic halides. Other highlights of this work are the use of the trimethylamine adduct of alane, $H_3Al{\cdot}NMe_3$,[10] to effectively deplete surface hydroxyl groups, and the use of a group 1 radical anion arene species to generate a surface-bound organolithium reagent, "$-O)_3Si(CH_2)_3Li$".

Silica powders were treated with $(MeO)_3Si(CH_2)_3Cl$, yielding **2**, and then $ClSiMe_3$ to "end cap" residual Si–OH groups (**2′**) using literature procedures, although with minor variation in the case of **2**, which featured anhydrous toluene as the solvent rather than moist xylene.[11] Treating both powders with alane gave materials further depleted of Si–OH groups and having residual Al–H moieties, **3** and **3′** respectively (Scheme 1).[12] These were readily converted to the corresponding lithium reagents **4** and **4′**, followed by the anthracene-supported species **5** and **5′**, and then the target supported "magnesium–anthracene" species **6** and **6′**. The last step involved metathetical exchange with compound **1**, which is favored by the ability of silicon to stabilize charge by polarization.[3,8] The powders were characterized using FTIR and ^{13}C CP/MAS NMR.

In the absence of treating **2** or **2′** with $H_3Al{\cdot}NMe_3$ a several-fold excess of Li^+(biphenyl)$^{\bullet-}$ was required to generate the supported lithium reagent; similar treatment was necessary for **1** to form supported magnesium–anthracene, presumably because of the reactivity of residual hydroxyl groups. Instead, the use of alane dispenses with the conventional trimethylsilyl end-capping step. Methyllithium in tetrahydrofuran (=THF) was also found to be effective in removing interfering

® Abstract published in *Advance ACS Abstracts,* January 1, 1995.

(1) (a) Bogdanovic, B.; Janke, N.; Kruger, C.; Mynott, R.; Schlichte, K.; Westeppe, U. *Angew. Chem., Int. Ed. Engl.* **1985**, *24*, 960. (b) Lehmkuhl, H.; Skakoor, A.; Mehler, K.; Kruger, C.; Angermund, K.; Tsav, Y.-H. *Chem. Ber.* **1985**, *118*, 4239. (c) Bogdanovic, B.; Liao, S.; Mynott, R.; Schlichte, K.; Westeppe, U. *Chem. Ber.* **1984**, *117*, 1378.
(2) Itsuno, S.; Darling, G. D.; Stover, H. D.; Frechet, J. M. J. *J. Org. Chem.* **1987**, *52*, 4644.
(3) (a) Oppolzer, W.; Schneider, P. *Tetrahedron Lett.* **1984**, *25*, 3305. (b) Bonnemann, H.; Bogdanovic, B.; Brinkmann, R.; Spliethoff, B.; He, D.-W. *J. Organomet. Chem.* **1993**, *451*, 31. (c) Benn, R.; Bogdanovic, B.; Bruning, M.; Grondey, H.; Herrmann, W.; Kinzelmann, H.-G.; Seevogel, K. *Chem. Ber.* **1993**, *126*, 225.
(4) Bogdanovic, B. *Acc. Chem. Res.* **1988**, *21*, 261.
(5) (a) Alonso, T.; Harvey, S.; Junk, P. C.; Raston, C. L.; Skelton, B. W.; White, A. H. *Organometallics* **1987**, *6*, 2110. (b) Brooks, W. M.; Lincoln, F. J.; McGinnity, J. J.; Raston, C. L.; Sue, R. S. *Organometallics* **1991**, *10*, 2098.
(6) (a) Harvey, S.; Junk, P. C.; Raston, C. L.; Salem, G. *J. Org. Chem.* **1988**, *53*, 3134. (b) Gallagher, M. J.; Harvey, S.; Raston, C. L.; Sue, R. E. *J. Chem. Soc., Chem. Commun.* **1988**, 289.
(7) Nicoletti, T. M.; Raston, C. L.; Sargent, M. V. *J. Chem. Soc., Chem. Commun.* **1988**, 1491; *J. Chem. Soc., Perkin Trans. 1*, **1990**, 133.
(8) Harvey, S.; Raston, C. L. *J. Chem. Soc., Chem. Commun.* **1988**, 652.
(9) (a) Bogdanovic, B.; Janke, N.; Kinzelmann, H.-G.; Westeppe, U. *Chem. Ber.* **1988**, *121*, 33. (b) Bartmann, E.; Bogdanovic, B.; Janke, N.; Liao, S.; Schlichte, K.; Spliethoff, B.; Treber, J.; Westeppe, U.; Wilczok, U. *Chem. Ber.* **1990**, *123*, 1517. (c) Bogdanovic, B.; Janke, N.; Kinzelmann, H.-G. *Chem. Ber.* **1990**, *123*, 1507. (d) Bogdanovic, B.; Janke, N.; Kinzelmann, H.-G.; Seevogel, K.; Treber, J. *Chem. Ber.* **1990**, *123*, 1529.
(10) Atwood, J. L.; Bennett, F. R.; Elms, F. M.; Jones, C.; Raston, C. L.; Robinson, K. D. *J. Am. Chem. Soc.* **1991**, *113*, 8183. (b) Jones, C.; Koutsantonis, G. A.; Raston, C. L. *Polyhedron* **1993**, *12*, 1829 and references therein.
(11) Dudler, V.; Lindoy, L. F.; Sallin, D.; Schlaepfer, C. W. *Aust. J. Chem.* **1987**, *40*, 1557.
(12) Powders **2** and **2′** were prepared from silica gel (Fluka, 200 mesh) in toluene.[11] To a suspension of **2** (13.5 g) in THF (75 mL) at 0 °C was slowly added $H_3Al{\cdot}NMe_3$ (6.4 g). After gas evolution ceased, the mixture was stirred overnight at *ca.* 20 °C, whereupon the solid was collected, washed with THF, and then dried *in vacuo* at 60 °C for 2 h as powder **3** (14.1 g): ν(Al–H) 1875 cm^{-1}; ^{13}C CP/MAS NMR (20.1 MHz) δ 11.8 (CH$_2$Si), 26.5 (CH$_2$CH$_2$CH$_2$), 47.8 (CH$_2$Cl) (**3′**: 2.3 (SiCH$_3$), 11.9, 27.7, 47.2). To a suspension of **3** (1.60 g) in THF (50 mL) was added Li(biphenyl) (*ca.* 30% excess) in THF (*ca.* 0.3 M), and the deep blue mixture was stirred overnight. 9-(Chlorodimethylsilyl)anthracene (0.47 g) was then added and the yellow mixture stirred overnight. The powder **5** was filtered, washed with THF, and then dried *in vacuo* at 60 °C for 6 h (1.96 g): ν(Al–H) 1880 cm^{-1}; ^{13}C CP/MAS NMR (20.1 MHz) δ 11.5 (CH$_2$Si), 18.0 (CH$_2$SiCH$_3$), 28.0 (CH$_2$CH$_2$CH$_2$), 48.0 (small peak, CH$_2$Cl), 128.8 (C_{arom}) (**5′**: 2.3 (SiCH$_3$) 11.8, 17.2, 26.0, 47.8 (small peak), 127.2). The powder **5** (2.0 g) was dispersed in THF (25 mL) and compound **1** (0.9 g) added slowly, yielding a deep green mixture. The powder **6** was collected, washed with THF, and then dried *in vacuo* as a green powder (2.0 g, ν(Al–H) 1880 cm^{-1}). Preparations of **3′–6′** are similar.

0276-7333/95/2314-0584$09.00/0

Scheme 1

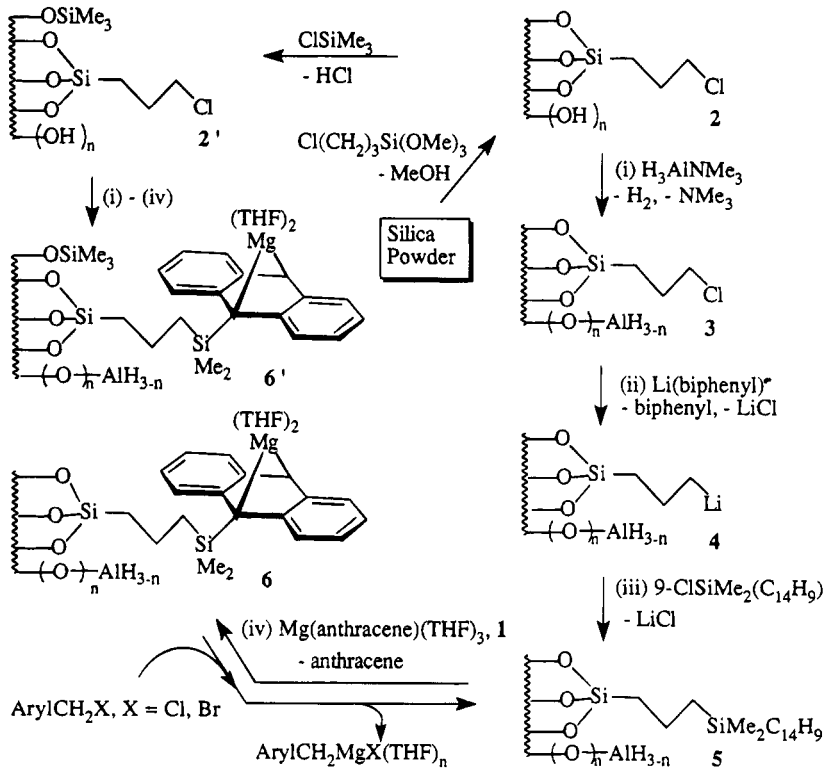

hydroxyl groups,[13] although $H_3Al{\cdot}NMe_3$ is preferable because of its ease of synthesis and good solubility in a variety of solvents. Moreover, the presence of three nucleophilic species per metal center may favor removal of more deeply embedded hydroxyl groups after initial formation of $-O-AlH_2$ (proximity effect). This aside, there are residual aluminum hydride species (IR) which are not reactive toward the chloropropyl groups. This is consistent with the formation of stable alane adducts of chloroalkyl-functionalized tertiary amine, 3-chloroquinuclidine.[14]

The supported lithium reagents **4** and **4′** were quenched with $ClSiMe_3$, affording the corresponding (trimethylsilyl)propyl derivatives.[13] Powders **6** and **6′** are diamagnetic, and given the amount of uptake of magnesium by **5** and **5′**, and the amount of magnesium delivered in forming Grignard reagents, the anthracene sites are based on dianions as in the parent compound **1**. The presence of both radical anion and dianion sites in a related polymer-supported reagent[8] presumably arises from space limitations and/or electrostatic restrictions with the polymer.

Powders **6** and **6′** were effective in generating Grignard reagents from benzylic halides in high yield.[15] Results for selected reactions for powder **6** are given in Table 1. The spent powders can be reloaded with magnesium, as demonstrated for cycles involving the formation of Grignard reagents of benzyl chloride and bromide, with less than 1% reduction in the uptake of magnesium after each cycle. More difficult to prepare poly Grignard reagents were also investigated, and in all cases the yields were high and comparable with those for the parent compound **1**, without the complication of having the solutions containing anthracene.

Table 1. Yields of Grignard Reagents[a] (%) Prepared from Selected Benzylic Chlorides using Silica-Supported 6 and Recycled Supported 6 and, for Comparison, Corresponding Yields using Mg(anthracene)(THF)$_3$ (1)[b]

		6			
benzylic halide	6	1st recycle	2nd recycle	3rd recycle	1
$PhCH_2Cl$	90	90	90	90	95
$PhCH_2Br$	90	85	85		85
$1,2\text{-}(ClCH_2)_2C_6H_4$[c]	85				90
$1,3,5\text{-}(BrCH_2)_3C_6H_3$[c]	85	90			

[a] Established by quenching an aliquot with 0.1 M HCl, back-titrating with 0.1 M NaOH, and isolating the $ClSiMe_3$/acid-quenched derivatives. [b] Benzylic chlorides in THF were added to a slurry of **6** or **1** in THF at *ca.* 20 °C for target concentrations of 0.1 M of the Grignard reagent. [c] Yield of di and tri Grignard reagents.

Acknowledgment. We thank the Australian Research Council for support of this work.

OM940779J

(13) van den Ancker, T. R.; Raston, C. L., unpublished results.
(14) Jones, C. Ph.D. Thesis, Griffith University, 1992.

(15) As a typical experiment, benzyl chloride (0.075 g, 0.6 mmol) in THF (10 mL) was slowly added to a suspension of **6** (0.63 g) in THF (5 mL), complete consumption of the supported magnesium–anthracene species being characterized by a change in color from deep green to pale yellow on the addition of 1 drop. The mixture was filtered to remove the magnesium-depleted silica, **5**, and the activity of the solution was determined by titration (see Table 1). $ClSiMe_3$ (0.11 g, 1.0 mmol) was then added, the volatiles were removed *in vacuo*, and hexane (10 mL) was added. Filtration followed by removal of the solvent *in vacuo* yielded ((trimethylsilyl)methyl)benzene (0.087 g, 88% yield, purity checked by GC/MS and $^1H/^{13}C$ NMR spectroscopy).

A Planar Skeleton Heterocyclyne, 1,1-Diphenyl-4,5:8,9-dibenzo-1-silacycloundeca-4,8-diene-2,6,10-triyne, and Its Nickel(0) Complex

Li Guo, John D. Bradshaw, Claire A. Tessier, and Wiley J. Youngs

Organometallics, **1995**, 14 (2), 586-588• DOI: 10.1021/om00002a003 • Publication Date (Web): 01 May 2002

A Planar Skeleton Heterocyclyne, 1,1-Diphenyl-4,5:8,9-dibenzo-1-silacycloundeca-4,8-diene-2,6,10-triyne, and Its Nickel(0) Complex

Li Guo, John D. Bradshaw, Claire A. Tessier,* and Wiley J. Youngs*

Department of Chemistry, The University of Akron, Akron, Ohio 44325-3601

Received September 28, 1994[⊗]

*Summary: A silicon-containing heterocyclyne (**2**) has been synthesized and characterized. Reaction of Ni(COD)$_2$ with **2** affords a planar complex (**3**) in very high yield. The X-ray crystal structure shows that Ni(0) resides in the pocket of **2** and coordinates with unusual "trans" geometry alkynes.*

During the study of the synthesis and reaction chemistry of nickel(0) cyclotriyne complexes, significant reactivity differences have been observed that appear to be primarily correlated with the sizes of the central pockets.[1] The Ni(0)–C(alkyne) distances in Ni(TBC) and Ni(TPC) average about 1.96 Å, whereas other

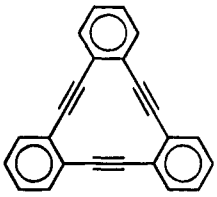

TBC

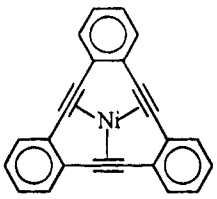

Ni(TBC)

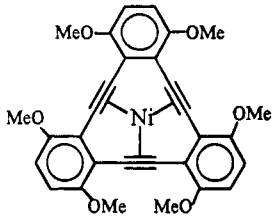

Ni(TPC)

Ni(0)–C(alkyne) distances as short as 1.88 Å have been reported.[2] This suggests that the pocket of TBC is slightly larger than the optimum size for maximizing the bond strength between the alkynes and a centrally bound nickel(0). The bonding interaction can affect the reactivities of the nickel(0) complexes toward small molecules such as CO and O_2, a crucial point in our exploration for CO sensors.[3] To decrease the size of the cyclotriyne pocket, an analog of TBC in which one of the benzo rings is replaced with an $SiPh_2$ moiety has been prepared and its nickel(0) complex has been investigated.

The reaction of 2,2′-diethynyltolane (**1**)[4] with *n*-butyllithium in THF at room temperature, followed by addition of dichlorodiphenylsilane, heating to 50 °C, and workup, results in the formation of the colorless heterocyclyne **2** in 53% isolated yield. The reaction of **2** with Ni(COD)$_2$ (COD = 1,5-cyclooctadiene) gives the red complex **3** in very high yield.[5] Complex **3** is air stable in the solid state.

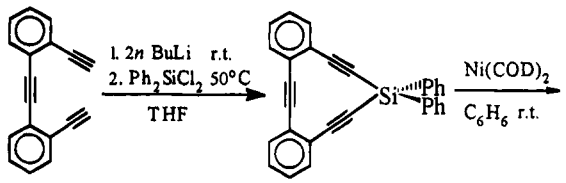

1 **2**

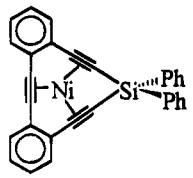

3

⊗ Abstract published in *Advance ACS Abstracts*, January 15, 1995.

(1) (a) Ferrara, J. D.; Tanaka, A. A.; Fierro, C.; Tessier-Youngs, C. A.; Youngs, W. J. *Organometallics* **1989**, *8*, 2089–2098. (b) Youngs, W. J.; Kinder, J. D.; Bradshaw, J. D.; Tessier, C. A. *Organometallics* **1993**, *12*, 2406–2407.

(2) (a) Dickson, R. S.; Ibers, J. A. *J. Organomet. Chem.* **1972**, *36*, 191–207. (b) Pöschke, K. R.; Mynott, R.; Angermund, K.; Krüger, C. *Z. Naturforsch., B* **1985**, *40*, 199–209. (c) Bonrath, W.; Pöschke, K. R.; Wilke, G.; Angermund, K.; Krüger, C. *Angew. Chem., Int. Ed. Engl.* **1988**, *6*, 833–835.

(3) Youngs, W. J.; Tessier, C. A.; Kinder, J. D. U.S. Patent 5 132 231, July 1992.

(4) Diercks, R.; Vollhardt, K. P. C. *Angew. Chem., Int. Ed. Engl.* **1986**, *3*, 266–267.

(5) All manipulations were carried out under an inert atmosphere using standard Schlenk techniques unless specified otherwise. **2**: To a solution of **1** (250 mg, 1.11 mmol) in 60 mL of THF was added 1.33 mL of freshly standardized *n*-BuLi (Kofron, W. G.; Baclawski, L. M. *J. Org. Chem.* **1976**, *41*, 1879–1880) in hexane (1.66 M, 2.21 mmol) at room temperature. After 4 h the resulting dilithio-2,2′-diethynyltolane was transferred via cannula to a solution of dichlorodiphenylsilane (0.23 mL, 1.11 mmol, HCl contaminate removed in vacuo prior to use) in 440 mL of THF. The mixture was stirred at 50 °C for 10 h. Water and methylene chloride were added in air to the mixture, and the organic phase was washed with water. The crude product was purified by chromatography on silica gel with 1:9 CH_2Cl_2–hexanes as the eluent to give 240 mg of colorless **2**. Crystallization of **2** from methylene chloride gave crystals suitable for X-ray structure determination. $C_{30}H_{18}Si$ (M_r 406.56): Anal. Calcd C, 88.63; H, 4.46. Found: C, 88.54; H, 4.82. ^{1}H NMR (300 MHz, C_6D_6) δ 7.98 (m, 4H), 7.48 (d, 2H), 7.33 (d, 2H), 7.13 (m, overlap with solvent), 6.81 (t, 2H), 6.75 (t, 2H); ^{13}C NMR (300 MHz, [D]$_8$-THF) δ 136.0, 133.5, 133.1, 131.7, 131.4, 130.0, 129.4, 129.3, 129.1, 125.7, 110.9, 96.9, 93.4; ^{1}H{^{29}Si}-HMBC NMR (600 MHz, [D]$_8$-THF) δ −45.00; EI MS *m/z* 406. **3**: To a colorless solution of **2** (90 mg, 0.22 mmol) in 10 mL of benzene was added Ni(COD)$_2$ (60.5 mg, 0.22 mmol). The solution immediately turned deep red. The reaction mixture was stirred at room temperature for 8 h. After removal of the solvent and COD in vacuo, a deep red powder was isolated (quantitative yield by NMR). Crystals suitable for X-ray structure analysis were obtained from benzene. $C_{30}H_{18}NiSi$ (M_r 465.24): ^{1}H NMR (300 MHz, C_6D_6) δ 8.05 (m, 4H), 7.85 (d, 2H), 7.72 (d, 2H), 7.15 (m, overlap with solvent), 6.93 (m, 4H); ^{13}C NMR (300 MHz, [D]$_8$-THF) δ 141.1, 138.0, 135.5, 135.3, 131.3, 131.1, 130.5, 129.2, 2 signals at 129.0, 128.2, 107.1, 73.8; ^{1}H{^{29}Si}-HMBC NMR (600 MHz, [D]$_8$-THF) δ −52.39; MS: *m/z* 464 (^{58}Ni).

0276-7333/95/2314-0586$09.00/0

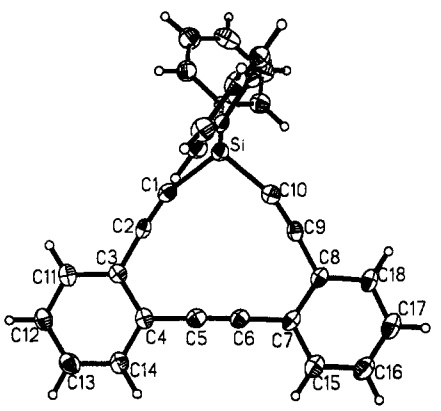

2

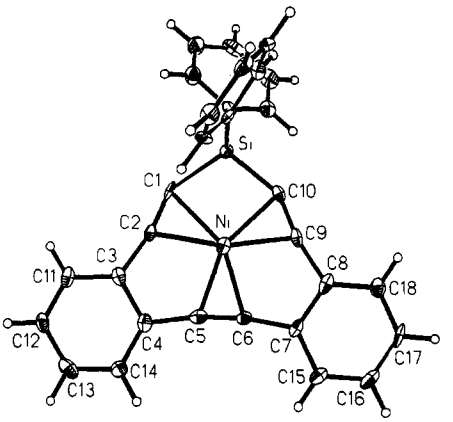

3

Figure 1. Molecular structures of compounds **2** and **3** with thermal ellipsoids drawn at 50% probability.

The ^{1}H NMR spectra of compounds **2** and **3** exhibit very similar patterns. Signals in the spectra of complex **3** are shifted downfield from the resonances in the spectra of the free ligand **2**. Similar results were observed for Ni(TBC) in the ^{1}H NMR spectra relative to that of TBC.[1] All signals in the ^{13}C NMR spectra of **3** shift down field except for the signal for C1/C10 (see the labeling diagram in Figure 1), assigned by using a ^{1}H coupled ^{13}C NMR experiment. Unexpectedly this resonance shifts upfield from 96.9 ppm in **2** to 73.8 ppm in **3**, indicating that the coordination of Ni(0) shields the alkyne carbons adjacent to the silicon exclusively. A ^{1}H{^{29}Si}-HMBC NMR experiment[6] showed that complexing **2** with nickel(0) also shifts the Si signal upfield from −45.0 ppm for **2** to −52.4 ppm for **3**. The IR spectrum of **2** exhibits one strong band at 2153 cm^{-1} for the $\nu_{C\equiv C}$ stretch. Complex **3** shows two strong $\nu_{C\equiv C}$ stretching bands at 1996 and 1922 cm^{-1}.

The X-ray structures of compounds **2** and **3** are shown in Figure 1,[7,8] and selected bond distances and angles are given in Table 1. Compounds **2** and **3** crystallize in the space group $P2_1/n$ with nearly equivalent unit cell dimensions. For **2** the average distance from each alkyne carbon to the centroid of the six alkyne carbons is 2.069 Å, 0.02 Å less than the comparable distance in TBC.[9] Contrary to our expectations, the average Ni to alkyne distance in **3** is longer than in Ni(TBC). The Ni to C(alkyne) distances average 1.958 Å in Ni(TBC) and 2.015 Å in complex **3**, where they range from 1.989(4) (Ni−C6) to 2.052(4) Å (Ni−C1). The nickel is bound to the three alkynes as in Ni(TBC) but also shows a short contact to the silicon in the ring.

Table 1. Selected Interatomic Distances (Å) (Standard Deviations in Parentheses) and Angles (deg) for 2 and 3

	2	3
Si−C1	1.818(3)	1.840(5)
Si−C10	1.826(3)	1.840(5)
C1−C2	1.208(4)	1.250(6)
C2−C3	1.430(4)	1.437(7)
C4−C5	1.435(4)	1.447(7)
C5−C6	1.194(4)	1.237(6)
C6−C7	1.429(4)	1.439(7)
C8−C9	1.434(4)	1.450(7)
C9−C10	1.205(3)	1.253(6)
C1−Si−C10	101.6(1)	107.1(2)
Si−C1−C2	162.5(2)	149.5(5)
Si−C10−C9	163.5(3)	150.3(4)
C1−C2−C3	174.7(3)	168.4(6)
C8−C9−C10	174.4(3)	170.0(5)
C4−C5−C6	177.5(3)	172.0(6)
C5−C6−C7	178.3(3)	171.1(5)
Ni−Si		2.509(2)
Ni−C1		2.052(4)
Ni−C2		1.999(5)
Ni−C5		1.990(5)
Ni−C6		1.989(4)
Ni−C9		2.005(5)
Ni−C10		2.047(5)
Ni−C1−C2		69.7(3)
Ni−C2−C1		74.4(3)
Ni−C10−C9		70.1(3)
Ni−C9−C10		73.8(3)

An unusual mode of alkyne bonding to a metal is observed in which the alkyne substituents have a trans geometry rather than the cis geometry expected from the Dewar−Chatt−Duncanson bonding model.[10] The trans geometry is all the more surprising if one considers that planarity of the central pocket is preserved in **3**. The silicon does not deviate any more from the principal plane of the ligand[11] (0.118 Å, mean deviation

(6) Bax, A.; Summers, M. F. *J. Am. Chem. Soc.* **1986**, *108*, 2093−2094.

(7) Crystal structure for **2**: colorless parallelepiped, crystal size 0.20 × 0.40 × 0.60 mm^3, monoclinic space group $P2_1/n$ (No. 14), a = 12.321(2) Å, b = 10.034(2) Å, c = 18.736(4) Å, β = 108.08(3)°, V = 2201.9(7) Å^3, Z = 4, ϱ_{calcd} = 1.226 g cm^{-3}, T = 130 K, graphite monochromator, Mo Kα radiation, θ range 1.76−22.50°, 3768 reflections collected, 2875 independent and 2133 observed with $I > 2.0\sigma(I)$, R1 = 0.0418 (based on F), R2w = 0.0744 (based on F^2) using 283 parameters. Crystal structure for **3**: red parallelepiped, 0.15 × 0.20 × 0.40 mm^3, monoclinic space group $P2_1/n$, a = 12.231(2) Å, b = 10.028(2) Å, c = 18.718(4) Å, β = 107.62(3)°, V = 2188.1(7) Å^3, Z = 4, ϱ_{calcd} = 1.412 g cm^{-3}, T = 130 K, Mo Kα radiation, θ range 1.77−22.50°, 3755 reflections collected, 2860 independent and 2148 observed with $I > 2.0\sigma(I)$, semiempirical absorption correction (min/max transmission 0.692/0.800), structure solution using direct methods, R1 = 0.0459 (based on F), R2w = 0.0869 (based on F^2) using 291 parameters.

(8) (a) SHELXTL-Plus; Siemens Analytical Instruments, Inc., Madison, WI, 1990. (b) Sheldrick, G. M. SHELXL-93 Program for the Refinement of Crystal Structures; University of Göttingen, Göttingen, Germany, 1993.

(9) Bradshaw, J. D.; Tessier, C. A.; Youngs, W. J. Unpublished results of low-temperature TBC crystal structure.

(10) (a) General references in: Ferrara, J. D.; Tessier-Youngs, C.; Youngs, W. J. *J. Am. Chem. Soc.* **1985**, *107*, 6719−6721. See also: (b) Sappa, E.; Tiripicchio, A.; Braunstein, P. *Chem. Rev.* **1983**, *83*, 203−239. (c) Gervasio, G.; Rossetti, R.; Stanghellini, P. L. *Organometallics* **1985**, *4*, 1612−1619. (d) Tatsumi, K.; Hoffmann, R.; Templeton, J. L. *Inorg. Chem.* **1982**, *21*, 466−468. (e) Ittel, S. D.; Ibers, J. A. *Adv. Organomet. Chem.* **1976**, *14*, 33.

(11) The principal plane of ligand **2** was calculated as the least-squares plane including Si and carbons C1−C18 inclusive.

0.055 Å) toward what would be a cis configuration than it does in the free ligand (0.120 Å, mean deviation 0.059 Å). In complex **3**, C1 and C10 are displaced away from the nickel(0); thus, the Si–C1–C2 and Si–C10–C9 angles are reduced by an average of 13.1° in comparison with those in ligand **2**. C2 and C9 are displaced toward the nickel atom, causing the C1–C2–C3 and C8–C9–C10 angles to change by an average of 16.3°. In complex **3**, the average C≡C bond distance of these two alkynes is 1.252 Å, which is 0.015 Å longer than that of the third alkyne C5–C6. A similar bonding geometry is found in the Co(CO) complex of $(\eta^5\text{-}C_5H_4SiMe_3)_2Ti(CCPh_2)_2$,[12] where the coordinated cobalt may interact with a nearly tetrahedral titanium and is bound to two unusual trans-geometry acetylides.

The coordination of the nickel into the trialkyne pocket expands the alkyne–silicon–alkyne angle from 101.6(1)° in **2** to 107.1(2)° in **3**. Other angles at silicon change by less than 1.5° in going from **2** to **3**. The nickel–silicon distance 2.509(2) Å can be compared with known Ni–Si distances of 2.283 and 2.182 Å in the compounds $Ni(SiCl_3)_2(CO)_3$ and $Ni(SiF_3)_2(PMe_3)_3$, respectively,[13] and the sum of the covalent radii of Ni and Si, which is about 2.34–2.41 Å.[14] The nickel–silicon distance in **3** may also be compared to those calculated for the theoretical compounds $Ni(SiH_2)_6$ and $Ni(SiH_2)_5$ (Ni–Si = 2.41 and 2.20 Å, respectively).[15] Though the Ni–Si distance might indicate a weak Ni–Si bond, we have no unambiguous evidence that this is so.

It is well-known that polycarbosilanes containing main-chain acetylenic units have electron delocalization through the Si atoms via σ^*-π hyperconjugation.[16] In σ^*–π hyperconjugation, it is generally accepted that Si can stabilize partial β-positive and α-negative charges provided the Si–C bond is coplanar with the vacant orbital on the β-carbon.[17] Asymmetrically substituted acetylenes show a significant increase in polarization on coordination to Ni(0).[18] Polarization of an acetylene bond should give rise to different bonding distances for each of the acetylenic carbons to the complexed metal as in $(Ph_3P)_2Ni[PhCCSiMe_3]$.[18] Consistent with this, the Ni–C1 and Ni–C10 distances are longer (ca. 0.05 Å) than the Ni–C2 and Ni–C9 distances. This may partially account for the expansion of the C1–Si–C10 angle and the novel trans geometry of the complexed acetylenes directly adjacent to the silicon.

Analogs of **2** and **3** with two electron-donating groups (diisopropyl) on silicon and germanium analogs of **2** and **3** have been synthesized. The reactivities of complex **3** with carbon monoxide and oxygen are under investigation. These will be discussed in a subsequent paper.

Acknowledgment. We thank the National Science Foundation (Grant No. 5-32129) for financial support, Dr. Dale Ray, Prof. Peter Rinaldi, and Richard Simons for assistance in acquiring the $^1H\{^{29}Si\}$-HMBC NMR spectra, Michael Polce and Prof. Chrys Wesdemiotis for providing the MS data, and James Howe (deceased) for library research.

Supplementary Material Available: Crystallographic data for **2** and **3**, including tables of data collection and structure determination details, atomic coordinates, bond distances and angles, and thermal parameters (19 pages). Ordering information is given on any current masthead page.

OM9407518

(12) Lang, H.; Imhof, W. *Chem. Ber.* **1992**, *125*, 1307–1311.
(13) (a) Janikowski, S. K.; Radonovich, L. J.; Groshens, T. J.; Klabunde, K. J. *Organometallics* **1985**, *4*, 396–398. (b) Bierschenk, T. R.; Guerra, M. A.; Juhlke, T. J.; Larson, S. B.; Lagow, R. J. *J. Am. Chem. Soc.* **1987**, *109*, 4855–4860.
(14) (a) The available values of covalent radii are for Ni(II) complexes. It would be expected that Ni(0) would be slightly larger than Ni(II). (b) Huheey, J. E.; Keiter, E. A.; Keiter, R. L. *Inorganic Chemistry*, 4th ed.; Harper Collins: New York, 1993; p 292.
(15) Tang, H.; Hoffman, D. M.; Albright, T. A.; Deng, H.; Hoffmann, R. *Angew. Chem., Int. Ed. Engl.* **1993**, *32*, 1616–1618.
(16) Corriu, R. J. P.; Douglas, W. E.; Yang, Z; Karakus, Y.; Cross, G. H.; Bloor, D. *J. Organomet. Chem.* **1993**, *455*, 69–76.
(17) Bassindale, A. R.; Taylor, P. G. In *The Chemistry of Organic Silicon Compounds*; Patai, S., Rappoport, Z., Eds.; Wiley: New York, 1989; Vol. 2, Chapter 14.
(18) Bartik, T.; Happ, B.; Iglewsky, M.; Bandmann, H.; Boese, R.; Heimbach, P.; Hoffmann, T.; Wenschuh, E. *Organometallics* **1992**, *11*, 1235–1241.

Partial Desulfurization of a Coordinated Xanthate and Concomitant Sulfur Insertion into a Molybdenum–Acetyl Bond

Leopoldo Contreras, Antonio Pizzano, Luis Sánchez,* and Ernesto Carmona*

Departamento de Química Inorgánica-Instituto de Ciencia de Materiales, Universidad de Sevilla-Consejo Superior de Investigaciones Científicas, Apdo 553, 41071 Sevilla, Spain

Angeles Monge and Caridad Ruiz

Instituto de Ciencia de Materiales, Sede D, Consejo Superior de Investigaciones Científicas, Serrano 113, 28006 Madrid, Spain, and Facultad de Ciencias Químicas, Universidad Complutense, 28040 Madrid, Spain

Received September 19, 1994®

Summary: The acetyls Mo(C(O)Me)(S_2COR)(CO)(PMe_3)$_2$ undergo partial desulfurization of the ligated xanthate and coupling of the resulting S atom with the acetyl group to furnish complexes containing coordinated alkoxythiocarbonyl and monothioacetate ligands, Mo(SOCMe)(η^2-C(S)OMe)(CO)(PMe_3)$_2$. Metathetical replacement of the MeCOS$^-$ ligand by ROCS$_2^-$ affords Mo(S_2COR)(η^2-C(S)OR)(CO)(PMe_3)$_2$, which can be prepared in a one-pot synthesis from Mo(η^2-C(O)Me)Cl(CO)(PMe_3)$_3$ and 2 equiv of KS_2COR. The structure of the t-Bu derivative has been determined by X-ray crystallography.

The acyl ligand is an important organometallic functionality.[1] While many investigations have focused on the synthetic and structural aspects of this entity, comparatively less attention has been devoted to its reaction chemistry. In recent years, however, the need to understand the intermediary role of transition-metal acyls in many stoichiometric and catalytic reactions[2] has motivated a number of reactivity studies. Of particular interest are those processes that involve the coupling of the acyl with other unsaturated groups, which, at least in a formal sense, can be considered as insertion reactions. Transformations of M–acyls that involve also olefins or alkynes,[3] CO,[4] alkylidenes,[5] and other groups[6] are presently known. In this contribution we wish to describe an unusual reaction that entails the coupling of a Mo-bound acetyl ligand, C(O)Me, with a sulfur atom derived from a coordinated xanthate, S_2COR. Apart from their inherent interest in M–acyl chemistry, reactions of this type that form or break C–S bonds are of academic and industrial relevance.[7]

Solutions of the acyl–xanthate complexes[8] Mo(C(O)Me)(S_2COR)(CO)(PMe_3)$_2$ (**1**; R = Me, *i*-Pr) rearrange readily to the alkoxythiocarbonyl derivatives **2** when stirred at room temperature over a period of 1–2 days. As shown in eq 1, the process involves partial desul-

$$\underset{\mathbf{1}}{\mathrm{Mo(C(O)Me)(S_2COR)(CO)(PMe_3)_2}} \xrightarrow{20\ ^\circ\mathrm{C}} \underset{\mathbf{2}}{\mathrm{Mo(\eta^2\text{-}SOCMe)(\eta^2\text{-}C(S)OR)(CO)(PMe_3)_2}} \quad (1)$$

furization of a coordinated xanthate ligand[9,10] to an alkoxythiocarbonyl fragment with subsequent incorporation of the S atom into the acyl group[11,12] to yield a

® Abstract published in *Advance ACS Abstracts*, December 1, 1994.

(1) (a) Durfee, L. D.; Rothwell, I. P. *Chem. Rev.* **1988**, *88*, 1059. (b) Cutler, A. R.; Hanna, P. K.; Vites, J. C. *Chem. Rev.* **1988**, *88*, 1363.

(2) (a) Cotton, F. A.; Wilkinson, G. *Advanced Inorganic Chemistry*; Wiley: New York, 1988. (b) Collman, J. P.; Hegedus, L. S.; Norton, J. R.; Finke, R. G. *Principles and Applications of Organotransition Metal Chemistry*; University Science Books: Mill Valley, CA, 1987. (c) Davies, S. *Organotransition Metal Chemistry: Applications to Organic Synthesis*. Pergamon Press: Oxford, U.K., 1982.

(3) See for example: (a) Brookhart, M.; Rix, F. C.; DeSimone, J. M.; Barborak, J. C. *J. Am. Chem. Soc.* **1992**, *114*, 5894. (b) van Asselt, R.; Gielens, E. E. C. G.; Rülke, R. E.; Vrieze, K.; Elsevier, C. J. *J. Am. Chem. Soc.* **1994**, *116*, 976. (c) van Asselt, R.; Gielens, E. E. C. G.; Rülke, R. E.; Elsevier, C. J. *J. Chem. Soc., Chem. Commun.* **1993**, 1203. (d) Brumbaugh, J. S.; Whittle, R. R.; Parvez, M.; Sen, A. *Organometallics* **1990**, *9*, 1735. (e) Carmona, E.; Gutiérrez-Puebla, E.; Monge, A.; Marín, J. M.; Paneque, M.; Poveda, M. L. *Organometallics* **1989**, *8*, 967. (f) Guram, A. S.; Guo, Z.; Jordan, R. F. *J. Am. Chem. Soc.* **1993**, *115*, 4902. (g) Curtis, M. D.; Real, J.; Hirpo, W.; Butler, W. M. *Organometallics* **1990**, *9*, 66.

(4) Sheridan, J. B.; Johnson, J. R.; Handwerker, B. M.; Geoffroy, G. L. *Organometallics* **1988**, *7*, 2404.

(5) Adams, H.; Bailey, N. A.; Tattershall, C. E.; Winter, M. J. *J. Chem. Soc., Chem. Commun.* **1991**, 912.

(6) (a) Han, S.-H.; Song, J.-S.; Macklin, P. D.; Nguyen, S. T.; Geoffroy, G. L.; Rheingold, G. L. *Organometallics* **1989**, *8*, 2127. (b) Yang, G.-M.; Lee, G.-H.; Peng, S.-M.; Liu, R.-S. *J. Chem. Soc., Chem. Commun.* **1991**, 478. (c) Hart, I. H.; Jeffery, J. C.; Lowry, R. M.; Stone, F. G. A. *Angew. Chem., Int. Ed. Engl.* **1988**, *27*, 1703.

(7) (a) Schuman, S. C.; Shalit, H. *Catal. Rev.* **1970**, *4*, 245. (b) Riaz, U.; Curnow, O. J.; Curtis, M. D. *J. Am. Chem. Soc.* **1994**, *116*, 4357. (c) Delgado, E.; Emo, A. T.; Jeffery, J. C.; Simmons, N. D.; Stone, F. G. A. *J. Chem. Soc., Dalton Trans.* **1985**, 1323.

(8) Contreras, L.; Monge, A.; Pizzano, A.; Ruiz, C.; Sánchez, L.; Carmona, E. *Organometallics* **1992**, *11*, 3971. These compounds have been shown to exist in solution as equilibrium mixtures that contain mainly the η^2-acyl (Mo(C(O)Me)) and the agostic (Mo(C(O)Me)) isomeric structures.

(9) Although the cleavage of one or both of the C–S bonds of a coordinated dithiocarbamate is a known process,[10] the analogus transformation of a coordinated xanthate is a much rarer reaction.

(10) (a) Herrick, R. S.; Nieter-Burgmayer, S. J.; Templeton, J. L. *J. Am. Chem. Soc.* **1983**, *105*, 2599. (b) Brower, D. C.; Tonker, T. L.; Morrow, J. R.; Rivers, D. S.; Templeton, J. L. *Organometallics* **1986**, *5*, 1093. (c) Gilleti, P. F.; Femec, D. A.; Keen, F. I.; Brown, T. M. *Inorg. Chem.* **1992**, *31*, 4008. (d) Hitchcock, P. B.; Lappert, M. F.; McGeary, M. J. *J. Am. Chem. Soc.* **1990**, *112*, 5658. (e) Hitchcock, P. B.; Lappert, M. F.; McGeary, M. J. *Organometallics* **1990**, *9*, 2645. (f) Coffey, T. A.; Forster, G. D.; Hogarth, G. *J. Chem. Soc., Chem. Commun.* **1993**, 1524. (g) Ricard, L.; Estienne, J.; Weiss, R. *Inorg. Chem.* **1973**, *12*, 2182. (h) Mayr, A.; McDermott, G. A.; Dorries, A. M.; Holder, A. K.; Fultz, W. C.; Rheingold, A. L. *J. Am. Chem. Soc.* **1986**, *108*, 310.

(11) The related insertion of a sulfur atom into a V(η^2-C(N-*t*-Bu)-Mes) linkage has been described recently by Floriani and co-workers. See: Vivanco, M.; Ruiz, J.; Floriani, C.; Chiesi-Villa, A.; Rizzoli, C. *Organometallics* **1993**, *12*, 1802.

(12) Some complexes of alkoxythiocarbonyl ligands are known, and two of them[12a,b] have been structurally characterized by X-ray methods. See: (a) Robert, P.; Le Bozec, H.; Dixneuf, P. H.; Hartsock, F.; Taylor, N. J.; Carty, A. J. *Organometallics* **1982**, *1*, 1148. (b) Samb, A.; Demerseman, B.; Dixneuf, P. H.; Mealli, C. *Organometallics* **1988**, *7*, 26. (c) Critchlow, P. B.; Robinson, S. D. *Inorg. Chem.* **1978**, *17*, 1903. (d) Esteruelas, M. A.; Oro, L. A.; Ruiz, N. *Inorg. Chem.* **1993**, *32*, 3793.

0276-7333/95/2314-0589$09.00/0

monothiocarboxylate ligand. The reactions are not, however, clean and produce in addition small amounts (less than 5% by ^{1}H and ^{31}P{^{1}H} NMR) of other unidentified species. This and the high solubility of compounds **2** in common organic solvents have precluded their isolation in a pure crystalline form.

Evidence for the proposed formulation for **2** comes from spectroscopic data. The alkoxythiocarbonyl ligand gives rise to a strong IR absorption at ca. 1270 cm^{-1}, close to the value of 1290 cm^{-1} found by Dixneuf and co-workers in the iron complex Fe(η^2-C(S)OMe)(CO)(P(OMe)$_3$)(Ph$_2$PCH=C(*t*-Bu)S).[12a] In addition, the Mo-bound alkoxythiocarbonyl carbon gives rise to a triplet ($^2J_{CP}$ = 20 Hz) at the very low-field chemical shift value of ca. 290 ppm. This suggests considerable carbenoid character (structure **C**, see below).

Reactivity studies provide supplementary, and moreover unequivocal, corroboration of the structure of compounds **2**. Interaction of these complexes with 1 equiv of a xanthate salt, KS$_2$COR, proceeds[13] with metathetical replacement of the monothiocarboxylate ligand by the xanthate, as depicted in eq 2 for the isopropyl derivative **2b**. The liberated KSOCMe salt has

$$\underset{\textbf{2b}}{\mathrm{Mo}(\eta^2\text{-OSCMe})(\eta^2\text{-C(S)O-}i\text{-Pr})(\mathrm{CO})(\mathrm{PMe_3})_2} \xrightarrow{\mathrm{KS_2CO}\text{-}i\text{-Pr}} \underset{\textbf{3b}}{\mathrm{Mo(S_2CO}\text{-}i\text{-Pr})(\eta^2\text{-C(S)O-}i\text{-Pr})(\mathrm{CO})(\mathrm{PMe_3})_2} + \mathrm{KSOCMe} \quad (2)$$

been isolated and identified by comparison of its IR and ^{1}H and ^{13}C{^{1}H} NMR spectra with those of an authentic sample. Complex **3b** is a red crystalline solid that exhibits ν(CS) at ca. 1270 cm^{-1} and δ(Mo−*C*(S)O-*i*-Pr) at 295 ppm (t,$^2J_{CP}$ = 19 Hz). The observation of virtually coupled triplets for the PMe$_3$ groups, in both the ^{1}H and ^{13}C{^{1}H} NMR spectra, and of a carbonyl resonance at ca. 245 ppm (t, $^2J_{CP}$ = 15 Hz) are in accord with structure **A** for these compounds.

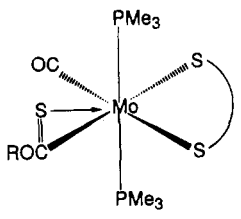

A

The reaction chemistry summarized in eqs 1 and 2 suggests compounds of type **3** may be prepared in a one-pot procedure by treatment of the starting acetyl Mo(η^2-C(O)Me)Cl(CO)(PMe$_3$)$_3$ with ca. 2.2 equiv of KS$_2$COR. Equation 3 exemplifies this synthetic methodology for

$$\mathrm{Mo}(\eta^2\text{-C(O)Me})\mathrm{Cl}(\mathrm{CO})(\mathrm{PMe_3})_3 \xrightarrow[-\mathrm{KSOCMe}]{2\mathrm{KS_2CO}\text{-}t\text{-Bu}} \underset{\textbf{3c}}{\mathrm{Mo(S_2CO}\text{-}t\text{-Bu})(\eta^2\text{-C(S)O-}t\text{-Bu})(\mathrm{CO})(\mathrm{PMe_3})_2} \quad (3)$$

the *t*-Bu derivative **3c**. Moderate yields of compounds **3** (30−40%) can be obtained in this way, small amounts

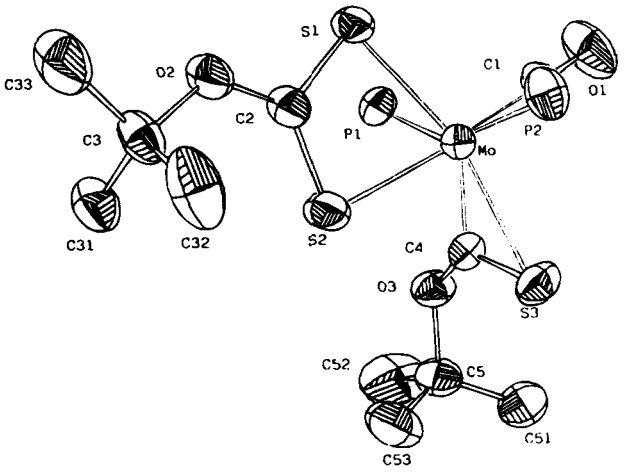

Figure 1. ORTEP diagram of Mo(S$_2$CO-*t*-Bu)(η^2-C(S)O-*t*-Bu)(CO)(PMe$_3$)$_2$ (**3c**).

of the corresponding bis(xanthate) Mo(S$_2$COR)$_2$(CO)(PMe$_3$)$_2$[13] also being formed.

Complex **3c** has been structurally characterized by X-ray crystallography,[14] and an ORTEP diagram is shown in Figure 1. The coordination polyhedron around molybdenum is a distorted octahedron, with the two PMe$_3$ ligands axial and the carbonyl, the bidentate xanthate, and the C(S)OR ligands all equatorial. While the S atom of the last group is on the equatorial plane, its carbon atom is slightly raised above this plane, making the coordination of the η^2-C(S)OR fragment in complexes of this type closely reminiscent of that of the related η^2-C(O)R ligand.[1,15] The Mo−C4 distance of 2.018(3) Å, while somewhat longer than the Mo−CO separation of 1.914(3) Å, is significantly shorter than the value of 2.3−2.4 Å typically found in Mo(II)−alkyl complexes.[16] This result denotes considerable π-bonding within the Mo−η^2-C(S)OR linkage and, hence, an important contribution of the carbene resonance structure **C**, which is also in accord with the very low-field chemical shift characteristic of this Mo-bound carbon

(13) In the presence of an excess of the xanthate (≥2 equiv) the bis(xanthate) Mo(S$_2$COR)$_2$(CO)(PMe$_3$)$_2$ and other unidentified species are also formed. See: Carmona, E.; Contreras, L.; Sánchez, L. J.; Gutiérrez-Puebla, E.; Monge, A. *J. Chem. Soc., Dalton Trans.* **1989**, 2003.

(14) Crystal data for **3c**: $C_{17}H_{36}MoO_3P_2S_3$, M_r = 542.5, triclinic, space group $P\bar{1}$, a = 9.619(3) Å, b = 10.794(2) Å, c = 14.736(2) Å, α = 75.64(1)°, β = 83.45(1)°, γ = 111.10(2)°, V = 1347(3) Å^3, Z = 2, D_c = 1.34 g cm^{-3}, μ(Mo Kα) = 8.281 cm^{-1} (graphite monochromated), λ = 0.710 69 Å, F(000) = 564. Data were collected on an Enraf-Nonius CAD-4 diffractometer at 295 K. The intensities were corrected for Lorentz and polarization effects. Scattering factors for neutral atoms and anomalous dispersion correction for Mo were taken from ref 22. Of the 7856 unique reflections, 5941 with $I \geq 2\sigma(I)$ were used in refinement. The structure was solved by Patterson and Fourier methods. An empirical absorption correction[23] was applied at the end of the isotropic refinement. Final refinement with fixed isotropic factors and coordinates for H atoms gave R_F = 0.032 and $R(w)_F$ = 0.034. Most of the calculations were carried out with the X-Ray 80 system.[24]

(15) (a) Carmona, E.; Marín, J. M.; Poveda, M. L.; Sánchez, L. J.; Rogers, R. D.; Atwood, J. L. *J. Chem. Soc., Dalton Trans.* **1983**, 1003. (b) Carmona, E.; Sánchez, L. J.; Marín, J. M.; Poveda, M. L.; Atwood, J. L.; Riester, R. D.; Rogers, R. D. *J. Am. Chem. Soc.* **1984**, *106*, 3214. (c) Desmond, T.; Lalor, F. J.; Ferguson, G.; Ruhl, B.; Parvez, M. J. *J. Chem. Soc., Chem. Commun.* **1983**, 55. (d) Curtis, M. D.; Shiu, K.-B.; Butler, W. M. *J. Am. Chem. Soc.* **1986**, *108*, 1550. (e) Carmona, E.; Muñoz, M. A.; Rogers, R. D. *Inorg. Chem.* **1988**, *27*, 1598. (f) Rusik, C. A.; Collins, M. A.; Gamble, A. S; Tonker, T. L.; Templeton, J. L. *J. Am. Chem. Soc.* **1989**, *111*, 2550.

(16) (a) Carmona, E.; Wilkinson, G.; Rogers, R. D.; Hunter, W. E.; Zaworotko, M. J.; Atwood, J. L. *J. Chem. Soc., Dalton Trans.* **1980**, 229. (b) Girolami, G. S.; Mainz, V. V.; Andersen, R. A.; Vollmer, S. H.; Day, V. W. *J. Am. Chem. Soc.* **1981**, *103*, 3953.

atom. The C4–S3 bond length of 1.670(4) Å is midway between expected values for related C=S (ca. 1.55 Å) and C–S bonds (1.79–1.86 Å).[17]

B **C**

As might be expected, the propensity of the above acyls to undergo insertion of a sulfur atom also manifests itself during the course of reactivity studies. Thus, when carbon monoxide is bubbled through solutions at −20 °C, complexes **1** add one molecule of CO and convert into the alkoxythiocarbonyl derivatives **4** (eq 4). The

$$\underset{\mathbf{1a,b}}{Mo(C(O)Me)(S_2COR)(CO)(PMe_3)_2} \xrightarrow[-20\ °C]{CO} \underset{\mathbf{4a,b}}{Mo(\eta^1\text{-}SOCMe)(\eta^2\text{-}C(S)OR)(CO)_2(PMe_3)_2} \quad (4)$$

Mo–η^2-C(S)OMe entity exhibits spectroscopic properties[18] analogous to those of the related complexes **2** and **3**. However, the monothioacetate ligand gives rise to an IR absorption at 1620 cm^{-1}, indicative of Mo–η^1-SC(O)Me coordination.[19] Compounds **4** exist in solution as a mixture of several isomeric species whose characteristics are presently under investigation.[20] When they stand at room temperature under nitrogen, compounds **4** slowly lose CO with concomitant change in the coordination mode of the SOCMe ligand from η^1 to η^2, thereby affording the already described monocarbonyl species **2**.

In summary, we have shown that the xanthate–acetyl complexes $Mo(C(O)Me)(S_2COR)(CO)(PMe_3)_2$ (**1**) undergo partial desulfurization of the coordinated xanthate and insertion of the sulfur atom into the Mo–acyl bond to yield complexes containing alkoxythiocarbonyl and monothioacetate ligands. Although compounds **1** exist in solution as equilibrium mixtures of the isomeric η^2 and agostic acyl formulations, the well-known electrophilicity of the M-bound η^2-acyl carbon[21] suggests the former is the active species in this transformation.

Acknowledgment. We thank the Dirección General de Investigación Científica y Técnica (Grant No. PB91-0612-C03-01) and Junta de Andalucía for the award of research fellowships. Thanks are also due to the University of Sevilla for free access to its analytical and NMR facilities.

Supplementary Material Available: Crystallographic tables giving details of the structure determination, crystal and refinement data, bond distances and angles, fractional coordinates, and thermal parameters for **3c** (7 pages). Ordering information is given on any current masthead page.

OM940729E

(17) Rickard, C. E. F.; Roper, W. R.; Salter, D. M.; Wright, L. J. *Organometallics* **1992**, *11*, 3931 and references therein.

(18) Spectroscopic data for selected compounds are as follows. **2b**: ^{1}H NMR (C_6D_6) δ 4.84 (heptet (h), CH *i*-Pr, 1H), 2.00 (t, SOCMe, J_{HP} = 2.8 Hz, 3H), 1.46 (t, PMe_3, J_{appHP} = 3.8 Hz, 18H), 1.05 (d, CH_3, *i*-Pr, 6H); $^{31}P\{^1H\}$ NMR (C_6D_6) δ 7.7 s; $^{13}C\{^1H\}$ NMR (C_6D_6) δ 295.0 (t, *C*(S)O-*i*-Pr, J_{CP} = 20 Hz), 247.4 (t, CO, J_{CP} = 14 Hz), 217.2 (t, SO*C*Me, J_{CP} = 5 Hz), 89.6 (s, CH), 34.8 (s, SOC*Me*), 21.6 (s, CH_3 *i*-Pr), 16.7 (t, PMe_3, J_{appCP} = 12 Hz); IR (Nujol mull) 1805 s (ν(CO)), 1624 w and 1518 m (SOCMe), 1271 s, 1155 s, and 1093 s (C(S)O-*i*-Pr) cm^{-1}. **3b**: ^{1}H NMR (C_6D_6) δ 5.37 (h, CH *i*-Pr xant, 1H), 4.90 (h, CH *i*-Pr, 1H), 1.51 (t, PMe_3, J_{appHP} = 3.8 Hz, 18H), 1.08 (d, CH_3 *i*-Pr, 6H), 1.07 (d, CH_3 *i*-Pr, 6H); $^{31}P\{^1H\}$ NMR (C_6D_6) δ 5.3 s; $^{13}C\{^1H\}$ NMR (C_6D_6) δ 297.0 (t, *C*(S)O-*i*-Pr, J_{CP} = 19 Hz), 241.3 (t, CO, J_{CP} = 15 Hz), 220.5 (t, S_2*C*O-*i*-Pr, J_{CP} = 7 Hz), 89.2 (s, CH), 74.2 (s, CH xant), 21.6 (s, CH_3 *i*-Pr), 21.4 (s, CH_3 *i*-Pr), 16.5 (t, PMe_3, J_{appCP} = 12 Hz); IR (Nujol mull) 1801 s (ν(CO)), 1271 s (C(S)O-*i*-Pr), 1221, 1093, and 1043 (S_2CO-*i*-Pr) cm^{-1}. Anal. Calcd for $C_{15}H_{32}MoO_3P_2S_3$: C, 35.0; H, 6.2. Found: C, 35.4; H, 6.2. **3c**: ^{1}H NMR (C_6D_6) δ 1.51 (t, PMe_3, J_{appHP} = 3.8 Hz, 18H), 1.47 (s, *t*-Bu, 9H), 1.44 (s, *t*-Bu, 9H); $^{31}P\{^1H\}$ NMR (C_6D_6) δ 6.2 s; $^{13}C\{^1H\}$ NMR (C_6D_6) δ 293.4 (t, *C*(S)O-*t*-Bu, J_{CP} = 19 Hz), 242.3 (t, CO, J_{CP} = 15 Hz), 220.2 (t, S_2*C*O-*t*-Bu, J_{CP} = 7 Hz), 91.4 (s, *C*Me$_3$), 86.9 (s, *C*Me$_3$), 28.1 (s, C*Me*$_3$), 27.3 (s, C*Me*$_3$), 16.6 (t, PMe_3, J_{appCP} = 12 Hz); IR (Nujol mull) 1790 s (ν(CO)), 1278 s (C(S)O-*t*-Bu), 1237, 1131, and 1048 (S_2CO-*t*-Bu) cm^{-1}. Anal. Calcd for $C_{17}H_{36}MoO_3P_2S_3$: C, 37.6; H, 6.6. Found: C, 37.2; H, 6.6 **4b**: ^{1}H NMR (C_7D_8, −30 °C) δ 5.05 (h, CH *i*-Pr, 1H), 2.63 (s, SOCMe, 3H), 1.17 (d, PMe_3, J_{HP} = 9.5 Hz, 9H), 1.08 (d, CH_3 *i*-Pr, 6H), 1.04 (d, PMe_3, J_{HP} = 7.4 Hz, 9H); $^{31}P\{^1H\}$ NMR (C_7D_8, −30 °C) δ −0.9 (d, J_{PP} = 15 Hz), −16.3 (d); $^{13}C\{^1H\}$ NMR (acetone-d_6, −90 °C; low field signals not observed) δ 90.1 (s, CH), 36.0 (s, SOC*Me*), 22.3 (s, CH_3 *i*-Pr), 18.6 (d, PMe_3, J_{CP} = 28 Hz), 13.9 (d, PMe_3, J_{CP} = 23 Hz); $^{13}C\{^1H\}$ NMR (C_6D_6) δ 284.4 (br t, *C*(S)O-*i*-Pr, J_{CP} = 10 Hz), 234.0 (dd, CO, J_{CP} = 25, 14 Hz), 216.8 (dd, CO, J_{CP} = 58, 18 Hz), 213.1 (s, SOCMe), 90.3 (s, CH), 35.5 (s, SOC*Me*), 21.6 (s, CH_3 *i*-Pr), 18.7 (d, PMe_3, J_{CP} = 27 Hz), 14.4 (d, PMe_3, J_{CP} = 21 Hz); IR (Nujol mull) 1966 and 1887 s (ν(CO)), 1286 s (SOCMe), 1142 s and 1088 s (C(S)O-*i*-Pr) cm^{-1}. Anal. Calcd for $C_{14}H_{28}MoO_4P_2S_2$: C, 34.8; H, 5.8. Found: C, 34.9; H, 5.7.

(19) (a) El-Hinnawi, M. A.; Al-Ajlouni, A. M.; AbuNasser, J. S.; Powell, A. K.; Vahrenkamp, H. *J. Organomet. Chem.* **1989**, *359*, 79. (b) El-Hinnawi, M. A.; Sumadi, M. L.; Esmadi, F. T.; Jibril, I.; Imhof, W.; Huttner, G. *J. Organomet. Chem.* **1989**, *377*, 373. (c) Hunter, J. A.; Lindsell, E.; McCullough, K. J.; Parr, R. A.; Scholes, M. L. *J. Chem. Soc., Dalton Trans.* **1990**, 2145.

(20) When solutions of **4a,b** are maintained below −20 °C, NMR studies show the presence of only one isomer with inequivalent *cis* PMe_3 groups. When they are warmed to 0 °C, these species are partially, although irreversibly, transformed into an equilibrium mixture of isomers whose precise nature is at present under investigation.

(21) (a) Arnold, J.; Tilley, T. D.; Rheingold, A. L. *J. Am. Chem. Soc.* **1986**, *108*, 5355. (b) Arnold, J.; Tilley, T. D.; Rheingold, A. L.; Geib, S. J.; Arif, A. M. *J. Am. Chem. Soc.* **1989**, *111*, 149. (c) Arnold, J.; Tilley, T. D.; Rheingold, A. L; Geib, S. J. *Inorg. Chem.* **1987**, *26*, 2556. (d) Bonnesen, P. V.; Yau, P. K. L.; Hersh, W. H. *Organometallics* **1987**, *6*, 1587. (e) Tikkanen, W.; Ziller, J. W. *Organometallics* **1991**, *10*, 2266. (f) Karsch, H. H.; Müller, G.; Krüger, C. *J. Organomet. Chem.* **1985**, *273*, 195. (g) Berg, F. J.; Petersen, J. L. *Organometallics* **1989**, *8*, 2461.

(22) *International Tables for X-Ray Crystallography*; Kynoch Press: Birmingham, U.K., 1974; Vol. IV.

(23) Walker, N.; Stuart, D. *Acta Crystallogr.* **1983**, *A39*, 158.

(24) Stewart, J. M. The X-Ray80 System; Computer Science Center, University of Maryland: College Park, MD, 1985.

Articles

Kinetics and Mechanisms of Halogen Abstraction Reactions of the 17-Electron, Metal-Centered Radical $CpCr(CO)_3$ with Organic Halides

Trisha A. Huber, Donal H. Macartney,* and Michael C. Baird*

Department of Chemistry, Queen's University, Kingston, Ontario, Canada K7L 3N6

Received October 7, 1994®

This paper describes detailed kinetics investigations of the reactions of the 17-electron compound $CpCr(CO)_3$, formed by thermal homolysis of the metal–metal-bonded dimer $[CpCr(CO)_3]_2$, with the non-β-hydrogen-containing organic halides $BrCH_2CN$, $BrCH_2CO_2Me$, CF_3CH_2I, and p-$NO_2C_6H_4CH_2Br$, in addition to less detailed kinetics investigations of the reactions of $CpCr(CO)_3$ with the homologous series of alkyl iodides MeI, EtI, *i*-PrI, and *t*-BuI, with the benzylic bromides p-$XC_6H_4CH_2Br$ (X = H, NO_2, CN, CF_3, OMe, Me, F, *t*-Bu), and with the β-hydrogen-containing substrate PhCHMeBr. In most cases, the rate law followed and the observed relative rates are consistent with rate-determining steps involving halogen atom transfer from carbon to chromium. The resulting organic radicals can then in most cases couple with a second molecule of $CpCr(CO)_3$ to form the corresponding 18-electron, unstable alkylchromium compounds $CpCr(CO)_3R$; in cases of organic radicals containing β-hydrogen atoms, however, $CpCr(CO)_3$ can abstract a hydrogen atom to form an olefin plus the metal hydride $CpCr(CO)_3H$. The latter in turn can transfer the hydridic hydrogen atom to the organic radicals to form the corresponding aliphatic products.

Most organometallic complexes satisfy the 18-electron rule, which would have the sum of the ligand and metal valence shell electrons equal to 18.[1] Recent years, however, have witnessed the emergence of an important subset of organotransition metal complexes, containing 17 valence electrons, which are most often prepared via photolysis reactions of the corresponding metal–metal-bonded, 18-electron dimers and redox reactions of 18-electron monomers and dimers.[2] Many 17-electron species are exceedingly reactive and may only be observed in low-temperature matrices. They take part in a variety of redox, atom abstraction, and coupling processes, reacting at near diffusion-controlled rates at ambient temperatures.

There are now known, however, several examples of 17-electron compounds which are stabilized significantly with respect to dimerization to the 18-electron, metal–metal-bonded analogues by substitution of small ligands by more sterically demanding ligands (*e.g.* CO by tertiary phosphines[3] and η^5-C_5H_5 by η^5-C_5Me_5[3h] and η^5-C_5Ph_5[4]). Other stable 17-electron complexes which are of interest in the present context are the isoelectronic series $M(CO)_{5-n}L_n$ (M = Mn, Re; L = tertiary phosphines),[3a–3] $[Co(CN)_5]^{3-}$,[5a,d,e] and $M(DH)_2L$ (M = Co, Rh; L = amine, phosphine; DH = dimethylglyoximate)[5b,c,f,6] all of which assume square pyramidal structures.

The development of synthetic methodologies for the preparation of a variety of 17-electron complexes has also resulted in several investigations of the mechanisms of the more important classes of reactions,

® Abstract published in *Advance ACS Abstracts*, December 1, 1994.

(1) Collman, J. P.; Hegedus, L. S.; Norton, J. R.; Finke, R. G. *Principles and Applications of Organotransition Metal Chemistry*; University Science Books: Mill Valley, CA, 1987; Chapter 2.

(2) For reviews, see (a) Baird, M. C. *Chem. Rev.* **1988**, *88*, 1217. (b) Trogler, W. C., Ed. *Organometallic Radical Processes*; Elsevier: Amsterdam, 1990. (c) Connelly, N. G.; Geiger, W. E. *Adv. Organomet. Chem.* **1984**, *23*, 1. (d) Tyler, D. R. *Prog. Inorg. Chem.* **1988**, *36*, 125. (e) Kochi, J. K. *Organometallic Mechanisms and Catalysis*; Academic Press: New York, 1978.

(3) (a) McCullen, S. B.; Brown, T. L. *J. Am. Chem. Soc.* **1982**, *104*, 7496. (b) Kidd, D. R.; Cheng, C. P.; Brown, T. L. *J. Am. Chem. Soc.* **1978**, *100*, 4103. (c) Walker, H. W.; Rattinger, G. B.; Belford, R. L.; Brown, T. L. *Organometallics* **1983**, *2*, 775. (d) Herrick, R. S.; Herrinton, T. R.; Walker, H. W.; Brown, T. L. *Organometallics* **1985**, *4*, 42. (e) Hanckel, J. M.; Lee, K.-W.; Rushman, P.; Brown, T. L. *Inorg. Chem.* **1986**, *25*, 1852. (f) Cooley, N. A.; Watson, K. A.; Fortier, S.; Baird, M. C. *Organometallics* **1986**, *5*, 2563. (g) Cooley, N. A.; MacConnachie, P. T. F.; Baird, M. C. *Polyhedron* **1988**, *7*, 1965. (h) Watkins, W. C.; Jaeger, T.; Kidd, C. E.; Fortier, S.; Baird, M. C.; Kiss, G.; Roper, G. C.; Hoff, C. D. *J. Am. Chem. Soc.* **1992**, *114*, 907.

(4) (a) Broadley, K.; Lane, G. A.; Connelly, N. G.; Geiger, W. E. *J. Am. Chem. Soc.* **1983**, *105*, 2486. (b) Connelly, N. G.; Geiger, W. E.; Lane, G. A.; Raven, S. J.; Rieger, P. H. *J. Am. Chem. Soc.* **1986**, *108*, 6219. (c) Connelly, N. G.; Raven, S. J. *J. Chem. Soc., Dalton Trans.* **1986**, 1613. (d) Connelly, N. G.; Raven, S. J.; Geiger, W. E. *J. Chem. Soc., Dalton Trans.* **1987**, 467. (e) Lane, G. A.; Geiger, W. E.; Connelly, N. G. *J. Am. Chem. Soc.* **1987**, *109*, 402. (f) DeGray, J. A.; Geiger, W. E.; Lane, G. A.; Rieger, P. H. *Inorg. Chem.* **1991**, *30*, 4100. (g) Fei, M.; Sur, S. K.; Tyler, D. R. *Organometallics* **1991**, *10*, 419. (h) Hoobler, R. J.; Hutton, M. A.; Dillard, M. M.; Castellani, M. P.; Rheingold, A. L.; Rieger, A. L.; Rieger, P. H.; Richards, T. C.; Geiger, W. E. *Organometallics* **1993**, *12*, 116.

(5) (a) Chock, P. B.; Halpern, J. *J. Am. Chem. Soc.* **1969**, *91*, 582. (b) Halpern, J.; Phelan, P. F. *J. Am. Chem. Soc.* **1972**, *94*, 1881. (c) Schneider, P. W.; Phelan, P. F.; Halpern, J. *J. Am. Chem. Soc.* **1969**, *91*, 77. (d) Halpern, J.; Maher, J. P. *J. Am. Chem. Soc.* **1964**, *86*, 2311. (e) Halpern, J.; Maher, J. P. *J. Am. Chem. Soc.* **1965**, *87*, 5361. (f) Marzilli, L. G.; Marzilli, P. A.; Halpern, J. *J. Am. Chem. Soc.* **1970**, *92*, 5752. This paper describes a system similar to the DH system.

(6) Howes, K. R.; Bakac, A.; Espenson, J. H. *Inorg. Chem.* **1988**, *27*, 3147.

0276-7333/95/2314-0592$09.00/0

including ligand substitution (eq 1) and atom abstraction (eq 2) processes.[2]

$$ML_n + L' \rightarrow MnL_{n-1}L' + L \quad (1)$$

$$ML_n + RX \rightarrow ML_nX + R \quad (2)$$

$$RX = \text{alkyl halide}$$

Ligand substitution reactions of 17-electron compounds generally proceed much more rapidly than do substitution reactions of 18-electron analogues and via associative rather than the dissociative mechanisms of most 18-electron compounds.[7] Reactions of 17-electron compounds with organic halides often result in halogen atom abstraction and formation of the corresponding organic radicals, which may undergo a variety of secondary reactions.[8] Mechanistic studies of several reactions have been reported, e.g.

$$M(CO)_4L + RX \rightarrow M(CO)_4LX \quad (3)^{3d,e}$$

$$M = Mn, Re; RX = CX_4, CHX_3, PhCH_2X, CH_2X_2; X = Br, Cl$$

$$2Co(CN)_5^{3-} + RX \rightarrow Co(CN)_5X^{3-} + Co(CN)_5R^{3-} \quad (4)^{5a,d,e}$$

$$RX = MeI, EtI, PrI, Me_2CHI, Me_3CI, PhCH_2I$$

$$2Co(CN)_5^{3-} + RX \rightarrow Co(CN)_5X^{3-} + Co(CN)_5R^{3-} + Co(CN)_5H^{3-} + \text{alkene} + \text{alkane} \quad (5)^{5a,d,e}$$

$$RX = EtI, PrI, Me_2CHI, Me_3CI$$

$$2Co(DH)_2B + RX \rightarrow XCo(DH)_2B + RCo(DH)_2B \quad (6)^{5b,c}$$

$$R = YC_6H_4CH_2X; Y = Me, CN, Br, NO_2; X = Cl, Br, I; B = N, P\text{-donors}$$

Two possible mechanistic extremes for these types of reactions have been considered, direct halogen atom abstraction (eq 7), in which the 17-electron complex behaves as a metal-centered radical, and outer-sphere electron transfer followed by halide transfer (eqs 8 and 9).[8,9]

$$L_nM + RX \rightarrow [L_nM\cdots X\cdots R]^{\ddagger} \rightarrow L_nMX + R \quad (7)$$

$$L_nM + RX \xrightarrow{e^- \text{ transfer}} L_nM^+ + RX^- \quad (8)$$

$$L_nM^+ + RX^- \rightarrow L_nMX + R \quad (9)$$

Direct halogen atom abstraction processes are generally characterized by both insensitivity to solvent polarity, since the reactions involve little charge transfer in the transition states, and significant dependence of the reaction rate on the C–X bond strengths. As C–X bond strengths increase in the order R–I < R–Br < R–Cl, rate constants for reactions proceeding as in eq 7 generally decrease in the order RI > RBr > RCl, ranging over several orders of magnitude. In contrast, rate constants for the outer-sphere electron-transfer process of eqs 8 and 9 generally exhibit a dependence on the reduction potentials of the organic halides, a large solvent effect (as anticipated for reactions involving electron transfer[10]), and a negligible dependence on the nature of the halogen.

Among the earliest studies of metal-centered radicals with organic halides were those of Halpern *et al.*,[5] who investigated reactions of alkyl halides with the anion $Co(CN)_5^{3-}$ and with bis(glyoximato)cobalt(II) complexes $Co(DH)_2B$ (eqs 4–6). In general, the results were consistent with rate-determining halogen abstraction processes (eq 7), although a polar transition state seemed to apply in the DH systems. In contrast, analogous reactions of Co(salen)L (salen = *N,N'*-bis(salicylidene)ethylenediamino; L = nitrogen donors) with substituted nitrobenzyl halides were found to proceed via outer-sphere electron transfer, as in eqs 8 and 9, since the rate constants exhibit little dependence on the halogen atom.[5f] Investigations by Espenson *et al.*[6] of the reactions of $Rh(DH)_2PPh_3$ with alkyl halides and by Brown *et al.* of the reactions of $M(CO)_4L$ and $M(CO)_3L_2$ (L = CO, PR_3; M = Mn, Re[3a–e,9]) with various alkyl halides also demonstrated the importance of electron transfer during halogen abstraction processes involving these reactants.

An extensive study of the reaction kinetics of $CpM(CO)_3$ (M = Mo, W; Cp = η^5-C_5H_5), produced by laser flash photolysis of the corresponding dimers, with a large number of organic halides (eq 10) has recently

$$CpM(CO)_3 + RX \rightarrow CpM(CO)_3X + R \quad (10)$$

been reported by Espenson *et al.*[11] The results indicated that reactions of these radicals follow the reactivity order (RI > RBr > RCl) expected for an atom abstraction process, while outer-sphere electron transfer was ruled out because the rates of reaction did not exhibit a significant solvent dependence and *p*-substituted benzyl bromides did not exhibit the range of reactivities expected for outer-sphere electron transfer. Unfortunately the fates of the organic radicals were not determined; coupling of photogenerated 17-electron species with organic radicals is not normally observed, apparently because of low steady-state concentrations of carbon- and metal-centered radicals.

We have in recent years demonstrated that the persistent metal-centered radical $CpCr(CO)_3$, formed via reversible, thermal homolysis of the corresponding dimer, reacts with a number of organic halides as follows:[3f,12]

$$[CpCr(CO)_3]_2 \rightleftharpoons 2CpCr(CO)_3 \quad (11)$$

$$2CpCr(CO)_3 + RX \rightarrow CpCr(CO)_3X + CpCr(CO)_3R \quad (12)$$

(7) Trogler, W. C. In ref 2b.
(8) Brown, T. L. In ref 2b.
(9) Lee, K.-W.; Brown, T. L. *J. Am. Chem. Soc.* **1987**, *109*, 3269.
(10) Kosower, E. M.; Mohammad, M. *J. Am. Chem. Soc.* **1968**, *90*, 3271.
(11) Scott, S. L.; Espenson, J. H.; Zhu, Z. *J. Am. Chem. Soc.* **1993**, *115*, 1789.
(12) MacConnachie, C. A.; Nelson, J. M.; Baird, M. C. *Organometallics* **1992**, *11*, 2521.

R = Me, $CH_2{=}CHCH_2$, $PhCH_2$, CH_2CO_2R' (R' = Me, Et), CH_2CN, $CH_2CH{=}CHCO_2CH_3$, $CH(CO_2Me)_2$; X = Br, I

However, with organic halides containing β-hydrogen atoms, $[CpCr(CO)_3]_2$ reacts in a rather more complicated fashion, as exemplified in eq 13 with ethyl iodide.

$$2CpCr(CO)_3 + CH_3CH_2I \rightarrow CpCr(CO)_3I + CpCr(CO)_3H + C_2H_6 + CH_2{=}CH_2 \quad (13)$$

Qualitatively, reactivities were found to vary in the orders RI > RBr > RCl and 3° > 2° > 1°, consistent with inner-sphere halogen abstraction as in eqs 7 and 14. The alkyl products of eq 12 were thought to be a result of rapid coupling of the alkyl with chromium radicals (eq 15), the hydride complex and organic products of eq 13 a result of secondary processes (eqs 16 and 17).

$$CpCr(CO)_3 + CH_3CH_2I \rightarrow CpCr(CO)_3X + CH_3CH_2 \quad (14)$$

$$CpCr(CO)_3 + CH_3CH_2 \rightarrow CpCr(CO)_3CH_2CH_3 \quad (15)$$

$$CpCr(CO)_3 + CH_3CH_2 \rightarrow CpCr(CO)_3H + CH_2{=}CH_2 \quad (16)$$

$$CpCr(CO)_3H + CH_3CH_2 \rightarrow CpCr(CO)_3 + C_2H_6 \quad (17)$$

A distinguishing feature of this chromium system is that, unlike photolytically generated organometallic radicals, for which the steady-state metal-centered radical concentration is minimal, the chromium-centered radical is present in sufficiently high concentrations[3h,13] that it readily couples with the organic radical and products containing the latter may be identified. For these reasons, a more detailed mechanistic investigation of this system was deemed desirable, has been carried out, and is reported here. Preliminary accounts of aspects of this work have appeared elsewhere.[14]

Experimental Section

All experiments were carried out under nitrogen using standard Schlenk line techniques, a Vacuum Atmospheres glovebox, and dried, thoroughly deoxygenated solvents. Infrared spectra were acquired using Bruker IFS 85 and IFS 25 FT-IR spectrometers, and ^1H NMR spectra using Bruker AM 400 and AM 200 spectrometers; IR and ^1H NMR data are presented in Tables 1 and 2, respectively. All ^2H, ^{13}C, and ^{19}F NMR spectra were acquired using a Bruker AM 400 spectrometer operating at 61.4, 100.6, and 376.5 MHz, respectively. GCMS data were obtained with a Fisons VG Quattro GCMS spectrometer. $[CpCr(CO)_3]_2$, $CpCr(CO)_3H$, $CpCr(CO)_3Br$ and $CpCr(CO)_3I$,[3f–h,12] 2,3-diphenylbutane,[15a] partially deuterated cyclopentadiene ($C_5H_xD_{6-x}$),[15b] and p-$CH_3OC_6H_4CH_2Br$[16] were prepared as described elsewhere.

Table 1. Infrared Data[a]

compd	ν(CO) (cm^{-1})
$[CpCr(CO)_3]_2 \rightleftharpoons 2CpCr(CO)_3$	2010 (m), 1946 (vs), 1920 (m), 1905 (m)
$Na[CpCr(CO)_3]$	1897 (s), 1795 (s), 1744 (vs, br)[b]
$CpCr(CO)_3H$	2012 (s), 1925 (s, br)
$CpCr(CO)_3I$	2030 (s), 1974 (vs), 1951 (m)
$CpCr(CO)_3Br$	2043 (s), 1989 (vs), 1960 (m)
$[CpCr(CO)_2]_2$	1902 (s), 1878 (s)
$CpCr(CO)_3Me$	2008 (s), 1930 (s, br)
$CpCr(CO)_3CH_2Ph$	2002 (s), 1927 (s, br)
$CpCr(CO)_3CH_2C_6H_4Me$	2001 (s), 1925 (s, br)
$CpCr(CO)_3CH_2C_6H_4NO_2$	2002 (s), 1922 (s, br)
$CpCr(CO)_3CH_2C_6H_4CN$	2005 (s), 1935 (s, br)
$CpCr(CO)_3CH_2C_6H_4CF_3$	2005 (s), 1930 (s, br)
$CpCr(CO)_3CH_2C_6H_4OMe$	1998 (s), 1921 (s, br)
$CpCr(CO)_3CH_2C_6H_4Me$-o	2002 (s), 1920 (s, br)
$CpCr(CO)_3CH_2CF_3$	≈2002 (s), ≈1930 (s, br)[c]
$CpCr(CO)_3CH_2CN$	2027 (s), 1946 (s, br)
$CpCr(CO)_3CH_2CO_2Me$	2019 (s), 1949 (s, br), 1747 (s)

[a] In toluene. [b] In THF. [c] Approximate, due to overlap with dimer–monomer absorbances.

General Procedures for Identification of Reaction Products and for Performing Kinetics Experiments. By ^1H NMR Spectroscopy. Solutions of $[CpCr(CO)_3]_2$ were prepared by dissolving 8–12 mg of dimer (0.010–0.015 M) in 2 mL of toluene-d_8. NMR samples normally utilized 0.50 mL of such a solution, each sample being sealed with a septum and parafilm prior to addition of organic halide. Dimer concentrations were determined by integration of the initial dimer–monomer Cp resonance relative to the area(s) of the resonance(s) of the organic halide immediately after addition of the latter. After the sample had equilibrated at the desired temperature, a 10- to 20-fold excess of organic halide (neat if a liquid; in toluene-d_8 if a solid) was added using a Hamilton gastight microliter syringe. The NMR tube was shaken vigorously, and monitoring of the reaction began.

By IR Spectroscopy. All samples for IR kinetic studies were prepared by the following general procedure. About 15–25 mg of $[CpCr(CO)_3]_2$ (0.037–0.062 mmol) was weighted into a Schlenk tube, which was sealed with a rubber septum. A measured volume of toluene (5–20 mL) was syringed into the flask, the dimer was stirred until dissolution was complete, and the flask was transferred to a water bath set at 25 °C. The desired volume of organic halide was injected into the solution using a Hamilton gastight microliter syringe, and the reaction was monitored while being maintained in total darkness. Reactions were monitored by observing the growth of the carbonyl stretching bands presented in Table 1.

Kinetic Simulations. The program GEAR[17] was utilized for kinetic simulations.

Results and Discussion

Reactions of $[CpCr(CO)_3]_2$ with organic halides may be separated into two categories, those involving organic halides without (eq 12) and those involving organic halides with (eq 13) β-hydrogen atoms. Our investigation has been further complicated (i) because reaction rates with various substrates were found to vary enormously, (ii) because of thermal and photochemical sensitivity of both reactants and products, and (iii) because overlap of resonances and/or exchange processes rendered variable-temperature ^1H NMR spectroscopy inoperative in some cases, necessitating the utilization of IR spectroscopy at ambient temperature

(13) (a) McLain, S. J. *J. Am. Chem. Soc.* **1988**, *110*, 643. (b) Yao, Q.; Bakac, A.; Espenson, J. H. *Organometallics* **1993**, *12*, 2010. (c) Madach, T.; Vahrenkamp, H. *Z. Naturforsch.* **1978**, *33b*, 1301.

(14) (a) Goulin, C. A.; Huber, T. A.; Nelson, J. M.; Macartney, D. H.; Baird, M. C. *J. Chem. Soc., Chem. Commun.* **1991**, 798. (b) Huber, T. A.; Macartney, D. H.; Baird, M. C. *Organometallics* **1993**, *12*, 4715.

(15) (a) Greene, F. D.; Berwick, M. A.; Stowell, J. C. *J. Am. Chem. Soc.* **1970**, *92*, 867. (b) Switzer, M. E.; Rettig, M. F. *Inorg. Chem.* **1974**, *13*, 1975.

(16) Waddling, C. Private communication.

(17) The kinetic simulation program GEAR was purchased from Project SERAPHIM, University of Wisconsin.

only. Thus, although we anticipated and eventually demonstrated a general, common rate-determining step, different procedures were necessary with different organic halides.

The approach to gaining a mechanistic understanding of these reactions described herein has involved (a) detailed kinetics studies of the reactions of $[CpCr(CO)_3]_2$ with the non-β-hydrogen-containing organic halides $BrCH_2CN$, $BrCH_2CO_2Me$, CF_3CH_2I, and p-$NO_2C_6H_4$-CH_2Br, chosen because their reactions were known or found to proceed cleanly as in eq 12 and because their rates of reactions are such that they could be readily monitored by ^1H NMR spectroscopy over a range of temperatures. These experiments were carried out to test a rate equation (see below) derived on the basis of the mechanism postulated previously and outlined in eqs 11, 14 and 15.

This investigation has also involved complementary, less detailed comparisons of the rates of reactions (b) of the aliphatic alkyl iodides MeI, EtI, i-PrI and t-BuI, in order to verify the previously reported[12] qualitative correlation of rates with nature of the alkyl group, (c) of the benzylic bromides p-$XC_6H_4CH_2Br$ (X = H, NO_2, CN, CF_3, OMe, Me, F, t-Bu), in order to identify relevant substituent effects, and (d) of PhCHMeBr, the only β-hydrogen-containing substrate for which the formation of organic products could be satisfactorily monitored by ^1H NMR spectroscopy.

(a) Reactions of $[CpCr(CO)_3]_2$ with $BrCH_2CN$, $BrCH_2CO_2Me$, CF_3CH_2I, and p-$NO_2C_6H_4CH_2Br$. Attempted kinetic studies with ICH_2CN and ICH_2CO_2Et revealed that reactions of these substrates[12] proceed far too quickly to be monitored effectively, even at very low temperatures (230 K). Therefore, in order to work with reaction rates sufficiently slow to permit effective monitoring, the analogous organic bromides, $BrCH_2CN$ and $BrCH_2CO_2Me$, were utilized. Spectroscopic experiments involving the previously reported[12] reactions of $[CpCr(CO)_3]_2$ with these organic halides were carried out, monitored by IR and ^1H NMR spectroscopy; in both cases the products were identified by their spectroscopic properties (Tables 1 and 2) and the stoichiometries were found to be as previously described.[12] Kinetics experiments, in toluene-d_8, involving $BrCH_2CO_2Me$ were carried out at 274, 280, 285, 291, and 296 K, and those involving $BrCH_2CN$ at 246, 252, and 257 K, the ^1H resonances of the alkyl products being monitored.

In order to assess possible solvent effects, the reaction of $[CpCr(CO)_3]_2$ with $BrCH_2CO_2Me$ was monitored by IR spectroscopy in THF, EtOH, CH_2Cl_2, and benzene, the spectra revealing in all cases the presence of the products, $CpCr(CO)_3Br$ and $CpCr(CO)_3CH_2CO_2Me$. Furthermore, a qualitative study of the reaction in THF, EtOH, CH_2Cl_2, and benzene at 298 K and monitored by IR spectroscopy showed that the polarity of the solvent has little effect on the rate of reaction. The reaction of $[CpCr(CO)_3]_2$ with $BrCH_2CN$ was similarly monitored by IR spectroscopy in THF, EtOH, and CH_2Cl_2, the spectra revealing in all cases the presence of the products, $CpCr(CO)_3Br$ and $CpCr(CO)_3CH_2CN$. A qualitative study of the reaction in toluene, THF, EtOH, CH_2Cl_2, and benzene at 298 K and monitored by IR spectroscopy showed that in this case also the polarity of the solvent has little effect on the rate of reaction.

In contrast to $BrCH_2CN$ and $BrCH_2CO_2Me$, the reactions of $[CpCrCO)_3]_2$ with CF_3CH_2I and p-$NO_2C_6H_4$-CH_2Br have not been investigated previously and the alkyl products in both cases had to be characterized. Although both were found to be too unstable, thermally and/or to light, to be isolated in an analytically pure form and had to be characterized spectroscopically, there are fortunately no ambiguities with respect to formulations.

Table 2. ^1H NMR Data[a]

compd	chem shift (δ)
$CpCr(CO)_3H$	3.95 (s, Cp), −5.65 (s, H)
$CpCr(CO)_3I$	3.98 (s, Cp)
$CpCr(CO)_3Br$	3.98 (s, Cp)
$[CpCr(CO)_2]_2$	4.24 (s, Cp)
$CpCr(CO)_3Me$	3.97 (s, Cp), 0.62 (s, Me)
$CpCr(CO)_3CH_2Ph$	3.97 (s, Cp), 2.11 (s, CH_2)
$CpCr(CO)_3CH(CH_3)_2$	4.44 (s, Cp), 2.86 (septet, CH), 1.16 (d, $(CH_3)_2$)
$CpCr(CO)_3CH_2C_6H_4Me$	4.25 (s, Cp), 3.97 (s, CH_2), 2.07 (s, CH_3)
$CpCr(CO)_3CH_2C_6H_4t$-Bu	3.96 (s, Cp), 3.00 (s, CH_2), 1.22 (s, t-Bu)
$CpCr(CO)_3CH_2C_6H_4NO_2$	3.79 (s, Cp), 2.43 (s, CH_2)
$CpCr(CO)_3CH_2C_6H_4CN$	3.85 (s, Cp), 2.49 (s, CH_2)
$CpCr(CO)_3CH_2C_6H_4CF_3$	3.92 (s, Cp), 2.66 (s, CH_2)
$CpCr(CO)_3CH_2C_6H_4OMe$	3.99 (s, Cp), 4.15 (s, CH_2), 3.22 (s, CH_3O)
$CpCr(CO)_3CH_2C_6H_4F$	3.91 (s, Cp), 2.79 (s, CH_2)
$CpCr(CO)_3CH_2CF_3$	4.12 (s, Cp), 1.65 (q, CH_2)
$CpCr(CO)_3CH_2CN$	4.00 (s, Cp), 0.92 (s, CH_2)
$CpCr(CO)_3CH_2CO_2Me$	4.19 (s, Cp), 1.75 (s, CH_2), 3.46 (s, CH_3)

[a] In toluene-d_8 at 295 K.

An IR study of the reaction of CF_3CH_2I with $[CpCr(CO)_3]_2$ in toluene revealed that $CpCr(CO)_3I$ and a product with carbonyl stretching absorptions at ~2012 and ~1925 cm^{-1} are formed; the latter was unstable, however, as its absorbances decreased significantly in intensity after ~3 h. Since alkylchromium complexes exhibit two absorbances in the carbonyl region at ~2000 and ~1925 cm^{-1} (Table 1), the unstable product is undoubtedly $CpCr(CO)_3CH_2CF_3$. NMR spectra of reaction mixtures in toluene-d_8 were also consistent with this conclusion, exhibiting ^1H resonances at δ 4.12 (s, 5H, Cp) and δ 1.65 (1:3:3:1 q, $^3J_{HF}$ = 14 Hz, 2H, CH_2) and a ^{19}F resonance at δ 49.3 relative to $CFCl_3$ (1:2:1 t, $^3J_{HF}$ = 14 Hz, CF_3). Thus it was concluded that the reaction of $[CpCr(CO)_3]_2$ and CF_3CH_2I proceeds cleanly to yield $CpCr(CO)_3I$ and $CpCr(CO)_3CH_2CF_3$, although attempts to isolate the alkyl complex were unsuccessful because of its low stability.

Kinetics experiments were carried out at 274, 280, 285, and 291 K in toluene-d_8, the ^1H resonances of the product, $CpCr(CO)_3CH_2CF_3$, being monitored. The reaction of $[CpCr(CO)_3]_2$ with CF_3CH_2I was also monitored by IR spectroscopy in ethyl ether and THF, the spectra revealing in both cases the presence of $CpCr(CO)_3CH_2$-CF_3 and $CpCr(CO)_3I$; a qualitative study of the reaction in THF, ethyl ether, and toluene at 298 K and monitored by IR spectroscopy showed that the polarity of the solvent has little effect on the rate of reaction.

An IR study of the reaction of $[CpCr(CO)_3]_2$ with p-$NO_2C_6H_4CH_2Br$ in toluene revealed that $CpCr(CO)_3Br$ and another product, presumably $CpCr(CO)_3CH_2C_6H_4$-NO_2 (2002 and 1922 cm^{-1}) (Table 1), had formed within 1 min. Within ~30 min, the latter had begun to decompose. In a complementary ^1H NMR experiment, product resonances appeared at δ 3.79 (s, 5H, Cp), δ 2.43 (s, 2H, CH_2), δ 6.47 (d, 2H, CH), and δ 7.57 (d, 2H, CH), consistent with the formulation $CpCr(CO)_3CH_2C_6H_4$-NO_2.

Since p-$NO_2C_6H_4CH_2Br$ is a solid of limited solubility in toluene-d_8, ^1H NMR experiments necessitated the use of less concentrated solutions of the dimer than was the case with other organic halides, resulting in less accurate integrating of the initial NMR spectra. The kinetics experiments for the reaction of $[CpCr(CO)_3]_2$ with p-$NO_2C_6H_4CH_2Br$ also span a smaller concentration range and were carried out as above utilizing solutions of dimer (0.010–0.015 M) and of p-$NO_2C_6H_4$-CH_2Br (0.29–1.1 M) at 263, 269, 274, and 280 K in toluene-d_8. The ^1H resonances of the product, $CpCr(CO)_3$-$CH_2C_6H_4NO_2$, at δ 3.79 and δ 2.43 were monitored.

The kinetics runs with $BrCH_2CO_2Me$, CF_3CH_2I, $BrCH_2CN$, and p-$NO_2C_6H_4CH_2Br$ were thus all carried out in toluene-d_8 under pseudo-first-order conditions with the organic halides in excess, and were monitored by ^1H NMR spectroscopy. Assuming that the reactions under consideration are not reversible, it was possible to utilize an integrated rate expression (eq 18, where

$$\frac{\sqrt{8K_{eq}([Cr]_0 - 2[CrR]) + K_{eq}^2} - K_{eq}}{K_{eq}} + \ln(\sqrt{8K_{eq}[[Cr]_0 - 2[CrR]] + K_{eq}^2} - K_{eq}) = -2k[RX]t + \text{constant} \quad (18)$$

$$\text{constant} = \frac{\sqrt{K_{eq}^2 + 8[Cr]_0K_{eq}} - K_{eq}}{K_{eq}} + \ln(\sqrt{K_{eq}^2 + 8[Cr]_0K_{eq}} - K_{eq})$$

K_{eq} is the equilibrium constant for eq 11; see also the supplementary material) which is a modification of the integrated rate expression utilized previously in a kinetics investigation of substitution reactions of $CpCr(CO)_3$.[18] This assumes that the rate-determining step proceeds as in eq 7 and involves irreversible transfer of the halogen atom to the chromium. Plots of the left-hand side of eq 18 vs time yielded straight lines of slope $-k_{obs}$, as illustrated by a representative example in Figure 1, and second-order rate constants were obtained by division of k_{obs} by 2[RX]. For each organic halide and temperature, k_{obs} versus [RX] was plotted to ensure linearity (see, for example, Figure 2). The actual rate constants were then obtained by taking the average of the calculated values, the errors associated with the actual rate constants being the standard deviations. The excellent fit of the data of the rate equation for all four organic halides confirms that the halogen-transfer steps are indeed rate-determining.

The rate constants for each organic halide were determined at various temperatures, and Eyring plots ($\ln(k/T)$ vs $1/T$) were used to determine the activation parameters. The second-order rate constants and the activation parameters for reactions of $[CpCr(CO)_3]_2$ with $BrCH_2CO_2Me$, CF_3CH_2I, $BrCH_2CN$, and p-$NO_2C_6H_4$-CH_2Br are given in Table 3. The negative entropies of activation and the applicability of the rate law support the proposed mechanism. Negative entropies of activation indicate that the rate-determining step is associative, and an associative mechanism is consistent with a transition state in which $CpCr(CO)_3$ and the organic moiety are bridged by the halogen atom (eq 7). Halpern and Phelan[5b] have reported variable-temperature studies of the reactions of $Co(DH)_2B$ (DH = dioximato; B = neutral amine or phosphine) with various benzyl and substituted benzyl halides (eq 6) and have proposed a mechanism analogous to that suggested here. Activation parameters determined for the reaction of $PhCH_2$-Br with two of the cobalt complexes are $\Delta H^\ddagger = 10.1 \pm 0.5$ kcal mol^{-1} and $\Delta S^\ddagger = -32 \pm 2$ eu, for $Co(DH)_2PPh_3$, and $\Delta H^\ddagger = 9.9 \pm 0.5$ kcal mol^{-1} and $\Delta S^\ddagger = -29 \pm 2$ eu, for $Co(DH)_2$(pyridine). The entropies of activation obtained for the reactions of $[CpCr(CO)_3]_2$ with organic halides are significantly lower (less negative) than those of the cobaloximes, for reasons which are not clear.

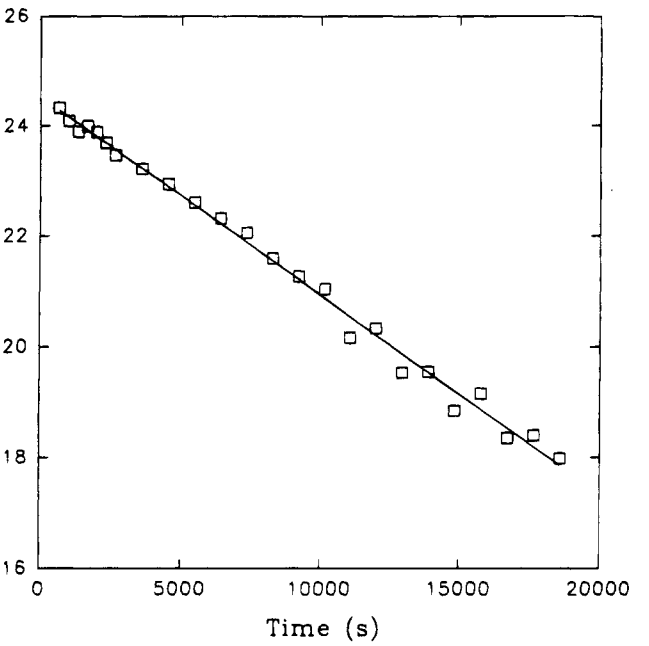

Figure 1. Plot of the left-hand side of eq 18 vs time for the reaction of $BrCH_2CO_2Me$ with $[CpCr(CO)_3]_2$.

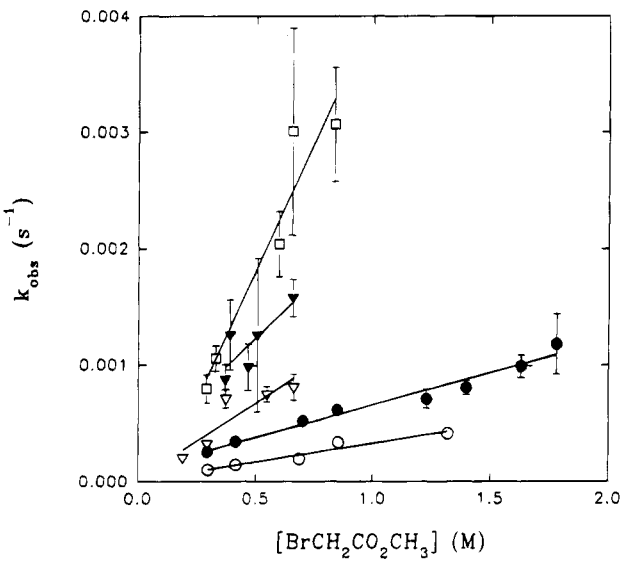

Figure 2. Plots of k_{obs} vs $[BrCH_2CO_2Me]$ at 274 K (○), 280 K (●), 285 K (▽), 291 K (▼), and 296 K (□).

(b) Reactions of $[CpCr(CO)_3]_2$ with MeI, EtI, *i*-PrI, and *t*-BuI. The reaction of $[CpCr(CO)_3]_2$ with MeI has been shown to proceed as in eq 12,[3f] and reactions with EtI, *i*-PrI, and *t*-BuI have been shown to proceed as in eq 13.[12] While NMR spectroscopy is a very

(18) Watkins, W. C.; Hensel, K.; Fortier, S.; Macartney, D. H.; Baird, M. C.; McLain, S. J. *Organometallics* **1992**, *11*, 2418.

Table 3. Rate Constants and Activation Parameters

RX	T (K)	k_2 (M^{-1} s^{-1})	$\Delta H^{\ddagger}$ (kcal mol^{-1})	$\Delta S^{\ddagger}$ (cal K^{-1} mol^{-1})
$BrCH_2CO_2Me$	274	1.71×10^{-4} (±0.22)	16.8(±1.8)	−14(±6)
	280	3.52×10^{-4} (±0.60)		
	285	6.74×10^{-4} (±1.69)		
	291	1.26×10^{-3} (±0.22)		
	296	1.77×10^{-3} (±0.34)		
CF_3CH_2I	274	4.03×10^{-4} (±1.14)	19.5(±2.6)	−3(±8)
	280	8.75×10^{-4} (±1.65)		
	285	1.34×10^{-3} (±0.16)		
	291	3.59×10^{-3} (±0.88)		
$BrCH_2CN$	246	1.56×10^{-3} (±0.36)	13.8(±2.1)	−15(±6)
	252	3.86×10^{-3} (±0.32)		
	257	7.80×10^{-3} (±0.90)		
	263	1.05×10^{-2} (±0.26)		
p-$O_2NC_6H_4CH_2Br$	263	2.20×10^{-2} (±0.41)	14.1(±3.4)	−13(±10)
	269	2.75×10^{-2} (±0.56)		
	274	6.45×10^{-2} (±2.00)		
	280	1.08×10^{-1} (±0.25)		
p-$O_2NC_6H_4CH_2Br$	278	0.11[a]		
p-$F_3CC_6H_4CH_2Br$	278	1.40×10^{-2} (±0.29)		
p-$NCC_6H_4CH_2Br$	278	2.99×10^{-2} (±0.91)		
p-$Bu^tC_6H_4CH_2Br$	278	9.16×10^{-3} (±0.62)		
MeI	298	8.75×10^{-5} (±2.13)		
EtI	298	4.42×10^{-4} (±0.36)		
i-PrI	298	1.54×10^{-2} (±0.70)		
t-BuI	298	5.04×10^{-2} (±0.26)		

[a] Estimated on the basis of the activtion parameters.

useful method for monitoring the reactions, not all of the organometallic products can be observed at room temperature in the cases of EtI, i-PrI, and t-BuI. Since the chemical shift and the line width of the dimer–monomer Cp resonance are not only concentration- and temperature-dependent but also, because of exchange processes,[12] subject to exchange braodening and averaging with the corresponding resonances of $CpCr(CO)_3H$, $CpCr(CO)_3Br$, and $CpCr(CO)_3I$, the position and appearance of the Cp resonance changed as the reactions proceeded. In each initial spectrum, the resonance appeared as a very broad band at ~δ 5. After addition of organic halide, the averaged Cp resonance first broadened and then narrowed and shifted upfield as the proportions of monomer, halo complex, and hydrido complex increased. For these reasons, progress of the reactions could not be monitored by appearance of $CpCr(CO)_3X$ but only by monitoring the growth of the methylchromium compound in the case of methyl iodide and by monitoring the growth of the organic products and $CpCr(CO)_3H$ (δ −5.65) in other cases.

Although the MeI reaction yields primary products which may readily be monitored by NMR spectroscopy, the temperature range over which the reaction proceeds at a useful rate was very small. Thermal decomposition of $[CpCr(CO)_3]_2$ and the volatility of MeI (bp 41 °C) precluded kinetic studies at temperatures above ambient, and the reaction proceeds at negligible rates at temperatures below. Therefore the kinetics experiments were carried out at 298 K (toluene-d_8), the ^1H resonances of the alkyl product being monitored. The second-order rate constant is given in Table 3.

Exploratory and kinetics experiments involving the previously reported[12] reactions of $[CpCrCO)_3]_2$ with EtI, i-PrI, and t-BuI were carried out similarly, in each case $CpCrCO)_3I$ and the anticipated organic products being observed. The kinetics experiments were carried out at 298 K (toluene), the carbonyl stretching bands of the $CpCrCO)_3I$ being monitored. It was found that the second-order rate constants decreased in the order t-BuI > i-PrI > EtI > MeI (Table 3).

A series of complementary NMR experiments were also carried out with the β-hydrogen-containing alkyl iodides. Thus the reaction of $[CpCr(CO)_3]_2$ with EtI was investigated by ^1H NMR spectroscopy at a lower temperature (288 K), and while the previously reported[12] organic and organometallic products were observed, the experiment also revealed previously unobserved complexities. Two singlets in the Cp region, at δ 3.99 and δ 4.42 and initially of comparable intensity, were observed; as the reaction proceeded, the singlet at δ 4.42 increased in intensity at a faster rate than that at δ 3.99. In addition to these resonances, a triplet at δ 1.07, a quartet at δ 1.90, and the hydride singlet of $CpCr(CO)_3H$ at δ −5.65 were observed to grow in. It was thought that perhaps one of the singlets in the Cp region could be attributed to the chromium ethyl complex, $CpCr(CO)_3Et$, and it seemed likely that the singlet at δ 3.99 would be the Cp resonance since the analogous methyl complex exhibits a Cp singlet at δ 3.97 (Table 2). However, the Cp resonances of what appear to be the corresponding isopropyl and *tert*-butyl complexes, $CpCr(CO)_3(i\text{-Pr})$ and $CpCr(CO)_3(t\text{-Bu})$, appear at δ 4.44 (see below), and the singlet at δ 4.42 may also be tentatively assigned to the Cp resonance of $CpCr(CO)_3Et$. Interestingly, the singlet at δ 3.99 may possibly also be attributed to the benzyl complex, $CpCr(CO)_3CD_2C_6D_5$, which would arise from attack of the ethyl radical on the solvent, resulting in a deuterated benzyl radical which could then couple with a chromium radical. While the abstraction product, C_2H_5D, was not observed, its resonance[19] would be obscured by resonances of the excess organic halide.

It was also initially thought that the quartet at δ 1.90 and the triplet at δ 1.07 could be assigned as the ethyl resonances of the presumed $CpCr(CO)_3Et$ and thus would be mutually coupled. However, decoupling experiments proved otherwise. Irradiation of the triplet did not result in collapse of the quartet at δ 1.90, but careful examination showed that the collapse occurred to a quartet, which was partially obscured, on the low-field side of the EtI quartet, at δ 2.67. Irradiation of the quartet at δ 1.90 did not result in any observable collapse. Presumably the triplet to which it is coupled was obscured by the resonances of the excess EtI. Integrations were also difficult, because of the close proximity of the more intense EtI resonances, and NOE experiments proved inconclusive.

It was not until the reaction had proceeded for over 1 h that evidence for the formation of ethylene (δ 5.25) and $CpCr(CO)_3H$ (δ −5.65) appeared; ethane (δ 0.89) was not observed for another 1 h. (At this point the presence of $[CpCrCO)_3]_2$, $CpCrCO)_3I$, and $CpCrCO)_3H$ was verified by observation of their Cp resonances on lowering the temperature of the reaction mixture of 243 K.) The temperature of the reaction mixture was then slowly raised. Although it was expected that the resonances attributed to $CpCrCO)_3Et$ would decrease, they were still growing at 323 K and this compound is reasonably thermally stable. Perhaps light sensitivity has hindered previous attempts to identify this reaction product,[12] where very broad ^1H NMR resonances of

(19) Hansen, P. E. In *Annual Reports on NMR Spectroscopy*; Webb, G. A., Ed.; Academic Press: London, 1983; Vol. 15, p 105.

reaction products were obtained over long periods of spectral accumulations, the sample having being occasionally exposed to light.

Attempts to obtain spectra in the absence of unreacted ethyl iodide failed because the reaction is very slow and a large excess of ethyl iodide is necessary to attain a useful rate. In an experiment in which only a slight excess was used, the reaction was allowed to proceed in the dark at room temperature overnight but significant decomposition occurred and only a severely broadened ^{1}H NMR spectrum was obtained the next day.

The reaction of $[CpCr(CO)_3]_2$ with *i*-PrI was similarly investigated by ^{1}H NMR spectroscopy at lower temperatures and was found to proceed at a useful rate at 283 K. Again the previously reported[12] organic and organometallic products were observed, but again the experiment provided a surprise since a singlet in the Cp region of the spectrum, at δ 4.44, was also observed. As the reaction proceeded, the latter became more intense and additional product peaks, a doublet at δ 1.16 and a septet at δ 2.86, became evident. The relative integrations of the resonances at δ 4.44, δ 2.86, and δ 1.16 were ~5:1:6, consistent with their assignment to the isopropyl complex, $CpCr(CO)_3CHMe_2$, and NOE and decoupling experiments were carried out. The results were as anticipated, with irradiation of the doublet and septet resulting in mutual decoupling. NOE experiments in which the Cp signal was irradiated resulted in enhancement of the doublet, while irradiation of the doublet similarly resulted in enhancements of both the Cp and the septet resonances. Thus all three resonances seem safely attributed to $CpCr(CO)_3CHMe_2$.

Subsequent to appearance of the resonances of $CpCr(CO)_3CHMe_2$, resonances of propylene (δ 5.70 (m), δ 5.03 (m), δ 4.95 (m), δ 1.52 (d)) and propane (δ 0.87 (t), δ 1.27 (m)) also appeared. All resonances for the alkyl complex, propane, and propylene continued to increase in intensity at 283 K, but after ~40 min, while the intensity of the hydride resonance remained essentially constant and those of the organic products continued to increase, the intensities of the resonances of the alkylchromium compound began to diminish.

In order to confirm the source of the hydridic hydrogen atom of $CpCr(CO)_3H$, a reaction of $[CpCr(CO)_3]_2$ with $(CD_3)_2CHI$, monitored by ^{2}H NMR spectroscopy, was carried out. The deuterium resonance of $CpCr(CO)_3D$ was indeed observed (δ −5.65), consistent with the source of the hydride hydrogen being the β-position of the organic moiety. There were also observed resonances at δ 0.85, δ 1.12, and δ 4.95, attributable to the CD_3 groups of $(CD_3)_2CHD$ and $CpCr(CO)_3CH(CD_3)_2$, and the CD_2 resonance of $CD_3CH{=}CD_2$, respectively. The CHD resonance of $(CD_3)_2CHD$ and the CD_3 resonance of $CD_3CH{=}CD_2$ were obscured by other resonances.

The reaction of $[CpCr(CO)_3]_2$ with Me_3CI was monitored, as described above for *i*-PrI, by ^{1}H NMR spectroscopy. Resonances of the hydride and of the organic products, isobutane (δ 1.62 (m), δ 0.85 (d)) and isobutene (δ 4.74 (m), δ 1.61 (m)) were observed, in addition to a singlet at δ 4.44! A complementary experiment, in which Me_3CI was treated with excess $[CpCr(CO)_3]_2$ and the products were analyzed by ^{1}H NMR spectroscopy and GC−MS, clearly revealed the absence of hexamethylethane among the products. An IR study of the reaction of $[CpCr(CO)_3]_2$ with Me_3CI was also undertaken in the presence of the radical scavenger TEMPO, following a preliminary experiment in which it was shown that TEMPO does not react with $CpCr(CO)_3$. It was found that addition of TEMPO has little effect on the rate of conversion of dimer to $CpCr(CO)_3I$ and $CpCr(CO)_3H$, indicating that any *t*-Bu radical formed was not scavenged by TEMPO.

The singlet observed at δ 4.44 may possibly be attributed to $CpCr(CO)_3(t\text{-Bu})$ although the expected methyl resonance was obscured. As noted above, the Cp chemical shifts of the compounds $CpCr(CO)_3H$, $CpCr(CO)_3Me$, and $CpCr(CO)_3CH_2C_6H_5$ are all δ 3.97 ± 0.02, while the Cp resonance of $CpCr(CO)_3CH_2CO_2Me$, containing an electron-withdrawing alkyl group, is observed at δ 4.19. Thus the Cp chemical shifts of the new compounds $CpCr(CO)_3CH_2CF_3$ (δ 4.12) and $CpCr(CO)_3CH_2C_6H_4NO_2$ (δ 3.79), seem reasonable, but those of the presumed $CpCr(CO)_3Et$, $CpCr(CO)_3CHMe_2$, and $CpCr(CO)_3CMe_3$ (δ 4.42, δ 4.44, and δ 4.44, respectively) are deshielded rather more than would be anticipated on the basis of $CpCr(CO)_3Me$ (δ 3.97). We cannot unambiguously rationalize these apparent anomalies but note that severe steric congestion weakens and lengthens the chromium−chromium bond of the dimer, $[CpCr(CO)_3]_2$.[3h] The chromium−carbon bonds of the ethyl-, isopropyl- and *tert*-butylchromium compounds may well be similarly weakened and lengthened, resulting in diminished electron density being released from the alkyl ligands to the chromium and in concomitant deshielding of the Cp resonances. On the other hand, one might well ask why these compounds would be stable with respect to β-elimination processes, and the answer may well lie, paradoxically, in the above-mentioned steric congestion! We note that the compounds $Cr(t\text{-Bu})_4$ and $CpFe(CO)_2(t\text{-Bu})$ both exhibit unusual thermal stability, apparently because these highly crowded *tert*-butyl compounds cannot readily increase their coordination numbers to accommodate formation of the presumed intermediate isobutene hydride complexes.[20] In the absence of Cp slippage, the same rationale may apply here.

Complementing the above experiments, solutions of $CpCr(CO)_3H$ in toluene-d_8 were treated with propylene and isobutene (1 atm) at 278 K, but no reactions occurred over 2 h. A mixture of $CpCr(CO)_3H$ and styrene in toluene-d_8 at 298 K did react, however, forming significant amounts of ethylbenzene (δ 2.43 (q), δ 1.10 (t)) within 2 h.

(c) Reactions of $[CpCr(CO)_3]_2$ with p-$XC_6H_4CH_2Br$ (X = H, NO_2, CN, CF_3, OMe, Me, F, *t*-Bu). Reactions of $[CpCr(CO)_3]_2$ with the benzyl bromides were investigated to ascertain the applicability of the rate law (eq 18) and to determine the effects of substituents on the rate contants for halogen transfer; activation parameters were not sought. While only the reaction of benzyl bromide has been previously reported, IR spectra of all of the reaction mixtures exhibited absorbances of $CpCr(CO)_3Br$ as well as absorbances in the regions 1998−2005 and 1921−1935 cm^{-1}, as anticipated for benzylchromium compounds (Table 1). Although the reactions in all cases proceeded cleanly in the early stages, exhibiting isosbestic points in the IR spectra (see Figure 3), the benzylchromium products

(20) (a) Kruse, W. *J. Organomet. Chem.* **1972**, *42*, C39. (b) Giering, W. P.; Rosenblum, M. *J. Organomet. Chem.* **1970**, *25*, C71.

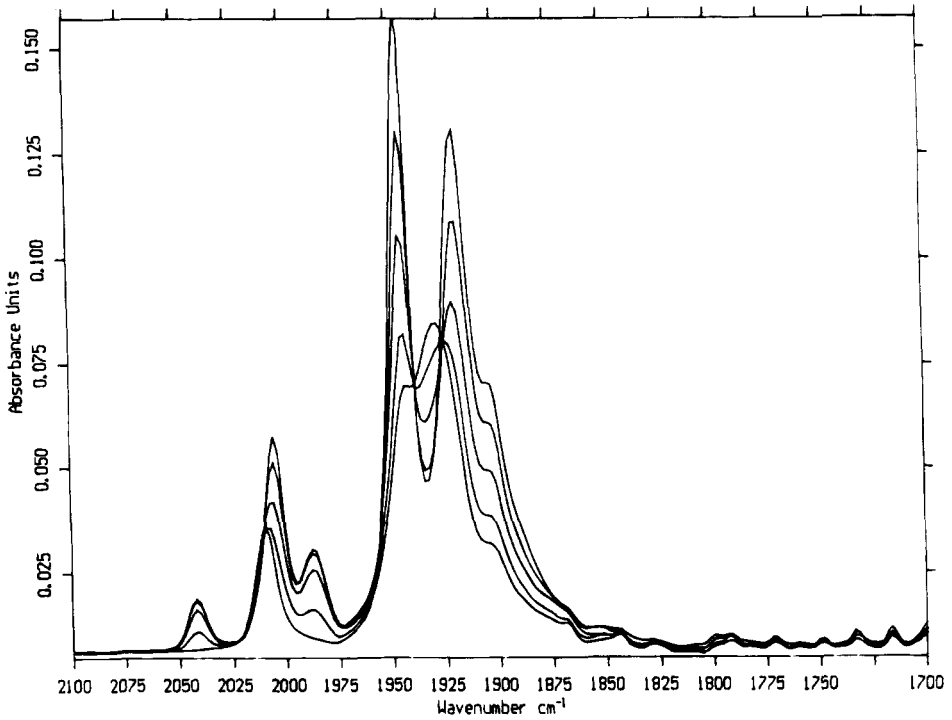

Figure 3. IR spectral changes during the reaction of p-$CF_3C_6H_4CH_2Br$ with $[CpCr(CO)_3]_2$.

were all found to be relatively unstable, their IR bands decreasing in intensity significantly within 1 h, and none could be isolated analytically pure. Reactions of the substituted benzyl bromides were also studied by ^1H NMR spectroscopy, and in all cases there appeared new resonances which were fully compatible with the anticipated formulations (Table 2) but no extraneous resonances. Since degradation appeared to be generally less significant during the NMR experiments than during the IR experiments, where brief exposure to light occurred, it would seem that the benzylchromium compounds are somewhat light sensitive.

Kinetics studies of the reactions of $[CpCr(CO)_3]_2$ with p-$XC_6H_4CH_2Br$ (X = H, MeO, F, CF_3, CN, Me, t-Bu) were attempted at 278 K in toluene-d_8, progress of the reactions being monitored by ^1H NMR spectroscopy. Unfortunately, because of overlapping resonances, sufficiently accurate integrations could not be obtained for X = H, Me, and MeO. The rate data for the other four substrates were successfully fitted to eq 18, and the second-order rate constants obtained are given in Table 3, where it is seen that the second-order rate constants at 278 K decrease in the order X = NO_2 > CN > CF_3 > t-Bu > F. Complementing these experiments, the rates of reactions of $[CpCr(CO)_3]_2$ with p-$XC_6H_4CH_2Br$ (X = H, Me, NO_2) were carried out in the dark at 298 K in toluene-d_8, progress of the reactions being monitored qualitatively by appearance of the high-frequency carbonyl stretching band of $CpCr(CO)_3Br$. Although of lower accuracy than the NMR experiments, the IR experiments showed clearly that the rates varied in the order $NO_2 \cong$ Me > H.

As noted previously,[12] both $CpCr(CO)_3CH_2Ph$ and bibenzyl are formed during reactions of $[CpCr(CO)_3]_2$ with benzyl bromide, the bibenzyl presumably via decomposition of the $CpCr(CO)_3CH_2Ph$. Indeed it was found, in the NMR experiments, that the concentration of $CpCr(CO)_3CH_2Ph$ had almost reached its maximum and the concentration of bibenzyl was already higher by the time that the first measurements could be made. Subsequent spectra showed an increase in bibenzyl formation, but the concentration of $CpCr(CO)_3CH_2Ph$ plateaued. For reasons which are not clear, formation of substituted bibenzyls is not a general feature of reactions of $[CpCr(CO)_3]_2$ with substituted benzyl bromides.

(d) Reaction of $[CpCr(CO)_3]_2$ with PhCHMeBr. The reaction of $[CpCr(CO)_3]_2$ with PhCHMeBr, monitored by IR and ^1H NMR spectroscopy, was shown to yield $CpCr(CO)_3Br$, $CpCr(CO)_3H$, styrene, and ethylbenzene, as previously reported.[12] In contrast to our unanticipated findings with the ethyl, isopropyl, and *tert*-butyl systems, however, there was no evidence (i.e. no new Cp resonance) for the formation of the alkylchromium compound $CpCr(CO)_3CHMePh$; this compound would presumably contain a much weaker chromium–carbon bond than does $CpCr(CO)_3CH_2Ph$.[21] Kinetics experiments were carried out at 268 K in toluene-d_8, the ^1H resonances of the styrene, ethylbenzene, and $CpCrCO)_3H$ being monitored. A representative plot of concentrations versus time is shown in Figure 4, where the solid lines show the best results of kinetic simulations (see below). As can be seen, and consistent with a previous report,[12] while styrene and the hydride appear initially to be produced at comparable rates, there is initially no evidence of ethylbenzene. After several minutes, however, formation of ethylbenzene is apparent, as is diminution of the hydride concentration. Thus ethylbenzene appears to be a secondary product. GC–MS and ^1H NMR spectroscopy were also employed to demonstrate that the organic coupling product, 2,3-diphenylbutane, had not formed.

(21) For comparative data, see: (a) Martinho Simões, J. A.; Beauchamp, J. L. *Chem. Rev.* **1990**, *90*, 629 and references therein. (b) Halpern, J. In *Bonding Energetics in Organometallic Compounds*; Marks, T. J., Ed.; ACS Symposium Series No. 428; American Chemical Society: Washington, DC, 1990; p 100.

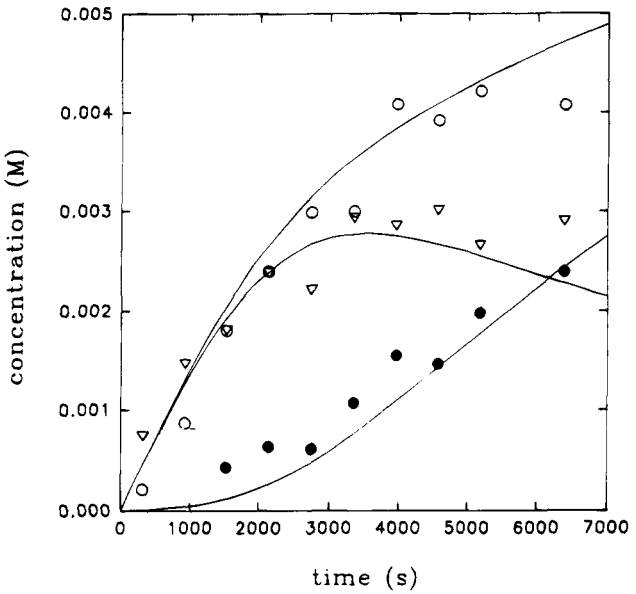

Figure 4. Simulated and experimental time dependence of products of the reaction of PhCHMeBr with $[CpCr(CO)_3]_2$: styrene (○); ethyl benzene (●); $CpCr(CO)_3H$ (▽).

Because of the complexities of this system, the variations in concentrations of the secondary products, $CpCr(CO)_3H$, styrene, and ethylbenzene, follow rate laws that are too complex to be derived in closed form. The kinetics of the system were therefore analyzed using kinetic simulations (GEAR),[17] in which the concentration time profiles (and hence the unknown rate constants) were calculated using the initial concentrations and known (or presumed) rate constants. In addition to the mechanistic scheme outlined in eqs 14–17, observations of apparent alkylchromium products in reactions of EtI, *i*-PrI, and *t*-BuI suggested that the alkyl complex $CpCr(CO)_3CHMePh$ may well form but be highly unstable with respect to decomposition, either by β-hydrogen elimination or by chromium–carbon bond homolysis, and the mechanistic scheme developed reflects these alternative possibilities. Regardless of the pathway, the rate-determining step is presumed to involve transfer of the bromine atom, and the subsequent steps are probably relatively rapid. Although the (bromoethyl)benzene system was experimentally simpler to study than the *tert*-butyl iodide system, in that the alkyl complex was not observed, it was complicated by a secondary reaction between styrene and $CpCr(CO)_3H$.

$$2CpCr(CO)_3H + PhCH{=}CH_2 \rightarrow [CpCr(CO)_3]_2 + PhCH_2CH_3 \quad (19)$$

For the kinetic simulations, the process shown in eqs 20–27 was used as a model with the known equilibrium constant K[3h,13] incorporated and the experimentally unknown rate constants k_{21}–k_{27} being varied. The simulated product concentrations were then compared to those determined experimentally.

$$[CpCr(CO)_3]_2 \rightleftharpoons 2CpCr(CO)_3 \qquad K = 1.9 \times 10^{-5}\ M \quad (20)$$

The simulated data fit the experimental reasonably well for up to approximately 60% of the reaction (Figure 4). Although the simulated data cannot be as reliable as those which were obtained more directly, variation of k_{22}–k_{27} by up to about 10% had negligible effect on the value found for k_{21}, and the results thus support the proposed mechanism. We note that the rate constant for bromine abstraction, k_{21}, is comparable to those of the other benzyl bromides (Table 3), presumably reflecting anticipated acceleration resulting from the weaker secondary carbon–bromine bond offset by increased steric hindrance to an associative reaction path in this case.

$$CpCr(CO)_3 + PhCHMeBr \rightarrow CpCr(CO)_3Br + PhCHMe \qquad k_{21} = 0.02\ M^{-1}\ s^{-1} \quad (21)$$

$$CpCr(CO)_3 + PhCHMe \rightarrow CpCr(CO)_3H + PhCH{=}CH_2 \qquad k_{22} = 10^9\ M^{-1}\ s^{-1} \quad (22)$$

$$CpCr(CO)_3 + PhCHMe \rightarrow CpCr(CO)_3CHMePh \qquad k_{23} = 10^9\ M^{-1}\ s^{-1} \quad (23)$$

$$CpCr(CO)_3CHMePh \rightarrow CpCr(CO)_3H + PhCH{=}CH_2 \qquad k_{24} = 10^3\ s^{-1} \quad (24)$$

$$CpCr(CO)_3H + PhCHMe \rightarrow CpCr(CO)_3 + PhCH_2CH_3 \qquad k_{25} = 10^7\ M^{-1}\ s^{-1} \quad (25)$$

$$CpCr(CO)_3H + PhCH{=}CH_2 \rightarrow CpCr(CO)_3 + PhCHMe \qquad k_{26} = 0.4\ M^{-1}\ s^{-1} \quad (26)$$

$$CpCr(CO)_3CHMePh \rightarrow CpCr(CO)_3 + PhCHMe \qquad k_{27} = 10^3\ s^{-1} \quad (27)$$

Concerning the Nature of the Rate-Determining Step. The results for all of the reactions investigated here are completely consistent with the halogen abstraction step (eq 14) generally being rate-limiting. As outlined above, the rate-determining step in reactions of metal-centered radicals with an organic halide involves, in the limit, cleavage of the carbon–halogen bond either via the inner-sphere mechanism of eq 7 or via direct electron transfer followed by halide transfer (eqs 8 and 9). If the former dominates, one would anticipate a correlation between the rate constants and the carbon–halogen bond strengths, D(C–X), with minimal solvent polarity effects. In contrast, if the latter dominates, one would antipate a correlation between the rate constants and the reduction potentials, $E_{1/2}$, of the organic halides, with significant solvent polarity effects but with little effect from the halogen. For instance, the ratio k_{Br}/k_{Cl} for the outer-sphere electron-transfer reaction of Co(salen)(MeIMD) with p-$NO_2C_6H_4CH_2X$ (X = Cl, Br) is approximately 2,[5f] while the rate constants for electron transfer of pyridinyl radicals with p-$NO_2C_6H_4CH_2Br$ in various solvents span 4 orders of magnitude.[10]

Although reduction potential and carbon–halogen bond strength data are not available for all of the four organic halides which were studied in detail, we note that there is no correlation between rate constants and the reduction potentials of *i*-PrI, EtI, and MeI (−1.58,

−1.54, and −1.33 V vs Hg/SCE in aqueous dioxane[22]). We have also confirmed previous qualitative reports[12] that alkyl iodides react much more rapidly than the corresponding alkyl bromides, that relative rates of reactions of alkyl iodides decrease in the order *t*-BuI (C−I bond energy 50.4 kcal mol^{-1})[23a] > *i*-PrI (C−I bond energy 53.1 kcal mol^{-1})[23a] > EtI (C−I bond energy 53.2 kcal mol^{-1})[23a] > MeI (C−I bond energy 56.1 kcal mol^{-1}),[23a] and that solvent effects are negligible for reactions of $BrCH_2CO_2Me$, $BrCH_2CN$, and CF_3CH_2I, at least. Similar correlations with bond strengths have many precedents in the literature and are found for both organic and organometallic radicals. For example, methyl, phenyl, and tributyltin radicals were found to exhibit similar reactivity toward organic iodides,[24] as do $Co(CN)_5^{3-}$,[5a] $CpW(CO)_3$,[11] and Cr(ethylenediamine)$_2^{2+}$,[24] and thus the present results are completely consistent with radical reactivity reported in the literature.

Possibly somewhat inconsistent with this picture, however, is the rate constant (7.1×10^{-3} M^{-1} s^{-1}) for halogen abstraction of CF_3CH_2I, which has a carbon−halogen bond strength of 56.3 kcal mol^{-1}.[23b] Despite having a carbon−halogen bond strength which is ~3 kcal mol^{-1} greater than that of EtI, the rate constant for CF_3CH_2I is 16 times greater than that of EtI. The apparently poor correlation of the rate constant with D(C−X) may indicate that the rate-determining step does not involve pure halogen abstraction and that a degree of inner-sphere electron transfer may also be important for this more electrophilic substrate. Brown *et al.*[9] have noted a reasonable correlation of rate constants with substituent constant (Hammett plot; $\varrho = 0.75$) for reactions of $Re(CO)_4L$ (L = PMe_3, P(O-*i*-Pr)$_3$) with various organic halides, the result indicating that electron density was being released to the halogen atoms during the rate-determining steps. In addition, Halpern and Phelan[5b] found that reactions of $Co(DH)_2$-PPh_3 with various *para*-substituted benzyl bromides resulted in a reasonable Hammett plot with $\varrho = 1.4$, the result again being consistent with inner-sphere electron transfer.

To assess such possible electronic effects, comparisons of the rates of reactions of $[CpCr(CO)_3]_2$ with *p*-XC_6H_4-CH_2Br (X = H, F, CF_3, CN, Me, *t*-Bu, NO_2) were carried out. Although most of these reactions were not amenable to as detailed studies as were possible with $BrCH_2CN$, $BrCH_2CO_2Me$, CF_3CH_2I, and *p*-$NO_2C_6H_4$-CH_2Br, it is clear that there is no correlation with the Hammett σ parameters; instead, both electron-donating and electron-attracting substituents accelerate the reactions relative to the reaction of benzyl bromide.

The ability of both electron-donating and electron-withdrawing *para* substituents to increase the rate of reactions forming benzylic radicals is well documented in the literature,[25] and Jackson *et al.*[25d−f] have shown that both electron-donating and electron-withdrawing *para* substituents serve to increase the rates of homolysis of benzylmercury compounds by stabilizing the benzylic radicals formed during the reactions. On this basis, the effects of *para* substituents on the rates of reactions of $[CpCr(CO)_3]_2$ with benzylic halides may also be understood.

Indeed, in a complementary investigation of the reactivities of various benzyl bromide derivatives, Clark and Wayner[25g] have shown that there is little correlation between carbon−bromine bond strengths and stabilities of the benzylic radicals. Thus stabilization of the product radicals may play an important role in driving halogen abstraction reactions of metal-centered radicals with organic iodides, thereby rationalizing both the relative rates of reactions of $[CpCr(CO)_3]_2$ with substituted benzyl bromides and the generally observed dramatic increases in reaction rates of many metal-centered radicals on going from EtI to *i*-PrI, which exhibit comparable C−I bond strengths.

Concerning Reactions of $[CpCr(CO)_3]_2$ with Organic Halides Containing β-Hydrogen Atoms. The product distributions and mechanism(s) for reactions of $[CpCr(CO)_3]_2$ with β-hydrogen-containing organic halides have undergone extensive experimental probing prior to this work,[12] but the reactions of these organic halides are now found to be more complicated than originally suggested. The mechanism originally proposed, as exemplified by eqs 11, 14, 16, and 17, involves rate-determining halogen atom abstraction, producing the halochromium complex and the organic radical, followed by reaction of the latter with $CpCr(CO)_3$ to yield $CpCr(CO)_3H$ and olefin. After formation of a significant amount of $CpCr(CO)_3H$, abstraction of the hydride hydrogen atom by the organic radical becomes competitive, a step which must apply generally as $CpCr(CO)_3H$ does not react directly with ethene, propene, or isobutene.

Our findings in this investigation, however, introduce the probability that coupling of organic radicals and chromium-centered radicals also generally occurs, although it is not clear whether the alkylchromium compounds formed are intermediates, via β-elimination processes, on the routes to some of the olefinic products. The chromium−carbon bond of the ethyl compound, $CpCr(CO)_3Et$, should be at least as strong as that of the isolable benzyl analogue, $CpCr(CO)_3CH_2Ph$,[21] and while homolysis of the chromium−carbon bond of $CpCr(CO)_3Et$ would give $CpCr(CO)_3$ and the ethyl radical, which might well react rapidly within the solvent cage to form $CpCr(CO)_3H$ and ethylene, it is not clear that this process would occur at a significant rate at temperatures as low as 288 K.

Another aspect of the overall reaction which should be addressed, however, is the possible involvement of

(22) Hawley, M. D. In *Encyclopedia of Electrochemistry of the Elements, Organic Section*; Bard, A. J., Lund, H., Eds.; M. Dekker: New York, 1980; Vol. XIV, p 8.

(23) (a) Egger, K. W.; Cocks, A. T. *Helv. Chim. Acta* **1973**, *56*, 1516. (b) Wu, E.-C.; Rodgers, A. S. *Int. J. Chem. Kinet.* **1973**, *5*, 1001.

(24) (a) Ingold, K. U. In *Free Radicals*; Kochi, J. K., Ed.; Wiley-Interscience: Toronto, 1973; Vol. I, p 37 and references therein. (b) Poutsma, M. L. In *Free Radicals*; Kochi, J. K., Ed.; Wiley-Interscience: Toronto, 1973; Vol. II, p 113 and references therein. (c) Castelhano, A. L.; Griller, D. *J. Am. Chem. Soc.* **1982**, *104*, 3655.

(25) (a) Arnold, D. R. In *Substituent Effects in Radical Chemistry*; Viehe, H. E., Janousek, Z., Mérenyi, R., Eds.; NATO ASI Series C; Reidel: Dordrecht, The Netherlands, 1986; Vol. 89, p 171. (b) Creary, X. In *Substituent Effects in Radical Chemistry*; Viehe, H. E., Janousek, Z., Mérenyi, R., Eds.; NATO ASI Series Reidel: Dordrecht, The Netherlands, 1986; Vol. 189, p 245. (c) Timberlake, J. W. In *Substituent Effects in Radical Chemistry*; Viehe, H. E., Janousek, Z., Mérenyi, R., Eds.; NATO ASI Series C; Reidel, Dordrecht, The Netherlands, 1986; Vol. 189, p 271. (d) Dinçtürk, S.; Jackson, R. A.; Townson, M.; Agirbas, H.; Billingham, N. C.; March, G. *J. Chem. Soc., Perkin Trans. 2* **1981**, 1121. (e) Dinçtürk, S.; Jackson, R. A. *J. Chem. Soc., Perkin Trans. 2* **1981**, 1127. (f) Agirbas, H.; Jackson, R. A. *J. Chem. Soc., Perkin Trans. 2* **1983**, 739. (g) Clark, K. B.; Wayner, D. D. M. *J. Am. Chem. Soc.* **1991**, *113*, 9363.

free organic radicals. Many organic radicals are known to undergo self-reactions in solution at diffusion-controlled rates ($\sim 10^9$ M^{-1} s^{-1}).[26] As illustrated for ethyl radicals, organic radicals may readily undergo coupling (eq 28) and disproportionation (eq 29) self-

$$2CH_3CH_2 \xrightarrow{k_c} CH_3CH_2CH_2CH_3 \quad (28)$$

$$2CH_3CH_2 \xrightarrow{k_d} CH_3CH_3 + CH_2CH_2 \quad (29)$$

reactions. The ratio k_d/k_c has been quantified for a large number of radicals and, for a given radical, exhibits very little dependence on temperature and solvent.[26] The ratio varies highly, however, with the nature of the radical, being 0.16–0.35 for the ethyl radical[26] and 0.09–0.11 for the $PhCHCH_3$ radical[27] (combination favored), in contrast to 5.4–7.3 for the *tert*-butyl radical (disproportionation favored). Failures in general to observe organic coupling products in this and earlier work[12] thus require that alkene formation does not involve self-reactions of free organic radicals, presumably because the steady state concentrations of these species are very low.

Radical reactions with the solvent, toluene, may well be significant, however. Consider the reaction of $CpCr(CO)_3$ with MeI, in which the first step is as in eq 14 (R = Me). The products, $CpCr(CO)_3I$ and the methyl radical, would diffuse from the solvent cage very rapidly,[28] and the latter would have the options of reacting with the available $CpCr(CO)_3$ radicals or with the solvent, i.e. as eqs 15 and 30, respectively. For the latter

$$Me + PhCH_3 \rightarrow CH_4 + PhCH_2 \quad (30)$$

reaction, activation parameters are known,[29] and the pseudo-first-order rate constant for disappearance of methyl radicals at 280 K can be estimated to be ~ 30 s^{-1}. Although this process would be in competition with the coupling reaction of eq 15, if one assumes that $[CpCr(CO)_3] \approx 10^{-3}$ M and that the second-order rate constant for coupling of carbon- and chromium-centered radicals is 10^4–10^7 M^{-1} s^{-1},[25b] then the pseudo-first-order rate constant for consumption of methyl radicals as in eq 15 is in fact several orders of magnitude higher than ~ 30 s^{-1}. On this basis, the putative reaction of ethyl radicals with the toluene solvent, resulting in the formation of $CpCr(CO)_3CH_2Ph$ during the reaction of ethyl iodide with $[CpCr(CO)_3]_2$, would be unlikely unless the rate constant for coupling of ethyl radical and $CpCr(CO)_3$ is much lower than the corresponding coupling rate constant of methyl radicals (for steric reasons, for instance).

Acknowledgment. Financial support from the Natural Sciences and Engineering Research Council (Research Grants to D.H.M. and M.C.B.) and the Government of Ontario (Graduate Scholarship to T.A.H.) made this research possible. We are also indebted to J. A. Stone and B. K. Hunter for experimental assistance and advice.

Supplementary Material Available: Text giving a derivation of kinetic rate equations (4 pages). Ordering information is given on any current masthead page.

OM940777Z

(26) Alfassi, Z. B. In *Chemical Kinetics of Small Organic Radicals*; Alfassi, Z. B., Ed.; CRC Press: Boca Raton, FL, 1988; Vol. 1, p 129.
(27) Gibian, M. J.; Corley, R. C. *J. Am. Chem. Soc.* **1972**, *94*, 4178.
(28) Koenig, T. W.; Hay, B. P.; Finke, R. G. *Polyhedron* **1988**, *7*, 1499.
(29) Tedder, J. M. *Tetrahedron* **1982**, *38*, 313.

Reaction of 1,3-Butadiene and Allene with a Diosmacyclobutane†

Nikolaos Spetseris, Jack R. Norton,* and Christopher D. Rithner

Department of Chemistry, Colorado State University, Fort Collins, Colorado 80523

Received July 14, 1994®

The reaction of the diosmacyclobutane **3** with butadiene gives as a kinetic product the 1,2 adduct $Os_2(CO)_8[\mu\text{-}CH_2CH(CH{=}CH_2)]$ (**4**); the thermodynamic product is an allyl acyl dinuclear complex $Os_2(CO)_8(\mu\text{-}C(O)CH_2\text{-}\eta^3\text{-}CH_2CHCH_2)$ (**6**), derived from **4** by CO insertion. Photolysis of $Os_3(CO)_{12}$ in the presence of butadiene gives **6**, $Os_2(CO)_7(\mu\text{-}CH_2\text{-}\eta^3\text{-}CH_2CHCH_2)$ (**7**), and (butadiene)$Os(CO)_3$ (**8**). The structure of **7** has been confirmed by X-ray crystallography: orthorhombic, space group $P2_12_12_1$, a = 6.928(2) Å, b = 9.473(2) Å, c = 20.683(4) Å, V = 1357.4(6) Å^3, and Z = 4. The reaction of $Na_2[Os_2(CO)_8]$ with 3,4-dichloro-1-butene or *cis*-1,4-dichloro-2-butene gave **7** as the principal product. Neither **4** nor **6** rearranged to **7** under thermal conditions, and attempts to carbonylate **7** to **4** or **6** failed at pressures of up to 120 psig. The reaction of **3** with allene gives as a kinetic product the 1,2 adduct $Os_2(CO)_8[\mu\text{-}CH_2C({=}CH_2)]$ (**9**); the thermodynamic product is $Os_2(CO)_8(\mu\text{-}\eta^3\text{-}CH_2CCH_2)$ (**10**). Photolysis of $Os_3(CO)_{12}$ in the presence of allene gives **9**, **10**, and (allene)$Os(CO)_4$ (**11**). Allene is bound more tightly than butadiene to the $Os_2(CO)_8$ unit. The exclusive formation of 1,2 adducts from both butadiene and allene is explained by the fact that substitution in the diosmacyclobutane system occurs via an intermediate **12** with the olefin coordinated to only one osmium atom.

Introduction

Matrix isolation[1,2] and transient[2] IR spectroscopy studies have shown that $Os_2(CO)_8$ is formed from the photolysis of the diosmacyclobutane **1** (eq 1). Further-

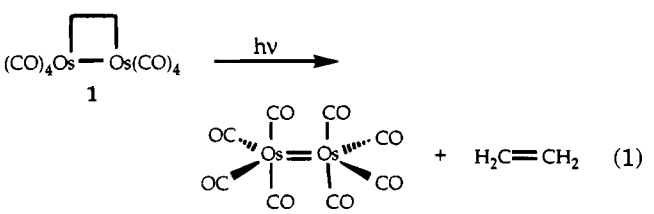

(1)

more, the matrix studies have proven that $Os_2(CO)_8$ does *not* have the threefold axis that would make it paramagnetic, suggesting that it instead has the Os/Os double bond shown.[1]

The ethylene is readily displaced from **1** by free olefins or acetylenes, particularly those with electron-withdrawing substituents (eqs 2 and 3).[3,4a] The extent to which stereochemistry is retained in these reactions (see eq 4)[4] is surprising when we consider that $Os(CO)_4$ is isolobal with CH_2: stereochemistry is lost—via a diradical mechanism—when two olefins are formed from cyclobutane.[5] The retention of stereochemistry in eq 4

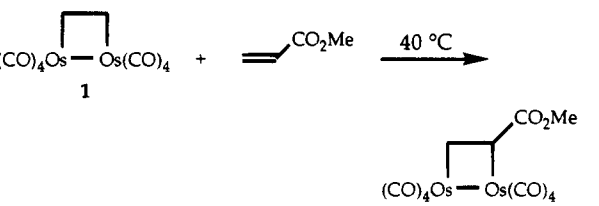

(2)

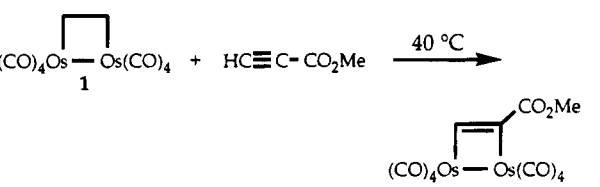

(3)

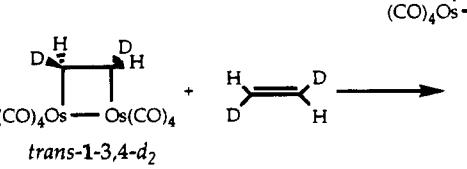

trans-**1**-3,4-d_2

Exchange with retention of stereochemistry (stereochemical excess > 99.1 %) (4)

is reminiscent of that found in concerted reactions such as Diels–Alder and 1,3-dipolar cycloadditions.[6,7]

Evidence for a dimetalla-Diels–Alder reaction involving a metal–metal double bond has been reported by Hersh and Bergman.[8] The benzodicobaltacyclohexene

† Dedicated to Professor Helmut Werner on the occasion of his 60th birthday.

® Abstract published in *Advance ACS Abstracts*, December 1, 1994.

(1) Haynes, A.; Poliakoff, M.; Turner, J. J.; Bender, B. R.; Norton, J. R. *J. Organomet. Chem.* **1990**, *383*, 497.
(2) Grevels, F.-W.; Klotzbücher, W. E.; Seils, F.; Schaffner, K.; Takats, J. *J. Am. Chem. Soc.* **1990**, *112*, 1995.
(3) (a) Burke, M. R.; Takats, J. *J. Organomet. Chem.* **1986**, *302*, C25. (b) Takats, J. *Polyhedron* **1988**, 931. (c) Burke, M. R.; Seils, F.; Takats, J. *Organometallics* **1994**, *13*, 1445. (d) Hembre, R. T. Ph.D. Dissertation, Colorado State University, Fort Collins, CO, 1987.
(4) (a) Hembre, R. T.; Scott, C. P.; Norton, J. R. *J. Am. Chem. Soc.* **1987**, *109*, 3468. (b) Hembre, R. T.; Ramage, D. L.; Scott, C. P.; Norton, J. R. *Organometallics* **1994**, *13*, 2995.
(5) (a) Chickos, J. S.; Annamalai, A.; Keiderling, T. A. *J. Am. Chem. Soc.* **1986**, *108*, 4398. (b) Chickos, J. S. *J. Org. Chem.* **1979**, *44*, 780.
(6) For Diels–Alder reactions, see: Houk, K. N.; Lin, Y.; Brown, F. K. *J. Am. Chem. Soc.* **1986**, *108*, 554.
(7) For 1,3 dipolar cycloaddition reactions, see: (a) Bihlmaier, W.; Geittner, J.; Huisgen, R.; Reissig, H. U. *Heterocycles* **1978**, *10*, 147. (b) Houk, K. N.; Firestone, R. A.; Munchausen, L. L.; Mueller, P. H.; Arison, B. H.; Garcia, L. A. *J. Am. Chem. Soc.* **1985**, *107*, 7227.
(8) (a) Theopold, K. H.; Hersh, W. H.; Bergman, R. G. *Isr. J. Chem.* **1982**, *22*, 27. (b) Hersh, W. H.; Hollander, F. J.; Bergman, R. G. *J. Am. Chem. Soc.* **1983**, *105*, 5834. (c) Hersh, W. H.; Bergman, R. G. *J. Am. Chem. Soc.* **1983**, *105*, 5846.

0276-7333/95/2314-0603$09.00/0

2 reversibly forms *o*-xylylene and a dinuclear complex that contains a cobalt/cobalt double bond (eq 5).

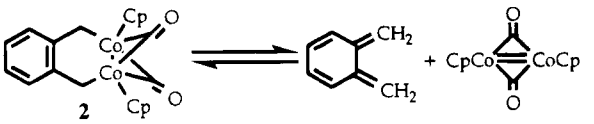

(5)

We have therefore examined the reaction of diosmacyclobutanes with various dienes. A convenient diosmacyclobutane has been the propylene adduct **3**,[1] known[9] to be more reactive than **1**. In particular, we wanted to see whether butadiene would give **4** (the formal product of [2 + 2] addition to the double bond of $Os_2(CO)_8$) or **5** (the formal product of [4 + 2] addition) (eq 6).

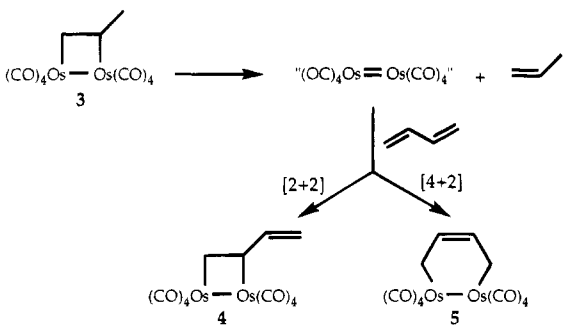

(6)

A 1,2 adduct has already been reported by Takats and co-workers from the reaction between **1** and an activated diene (eq 7).[3b,10]

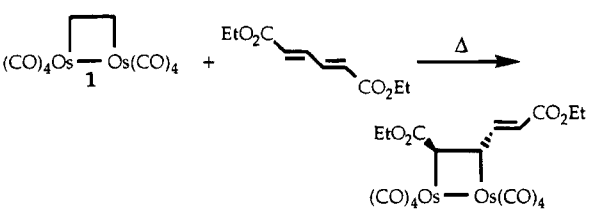

(7)

Experimental Section

Reactions and manipulations were performed using standard Schlenk techniques, under an atmosphere of nitrogen purified by passage through BTS catalyst (BASF) and molecular sieves (3 Å Linde). Chromatography was performed on a Chromatotron (Harrison Research Inc.) with silica gel as the adsorbent.

^{1}H NMR spectra were recorded at 300 MHz and ^{13}C spectra at 75.5 MHz on a Bruker AC-300P spectrometer. NMR simulations were performed with the Bruker-supplied program PANIC (Parameter Adjustment in NMR by Iterative Calculation) on an Aspect 3000 computer. Phase-sensitive homonuclear double quantum filtered COSY spectra were acquired (256 increments of 512 points each) with the standard Bruker software COSYPHDQ. The sweep widths were 1800 Hz in t_2 and 900 Hz in t_1. Cosine weighting and zero filling were applied to both domains prior to Fourier transformation. The final resolution was about 3.5 Hz/point in F_2 and 7 Hz/point in F_1.

Carbon–hydrogen correlated spectra were acquired (64 increments of 1024 points each) with the standard Bruker software XHDEPTW. The sweep widths were 10 416 Hz in t_2 and 900 Hz in t_1. Cosine weighting and zero filling were applied to both domains prior to Fourier transformation. The final resolution was about 10 Hz/point in F_2 (^{13}C) and 7 Hz/point in F_1 (^{1}H).

Phase-sensitive proton-detected ("inverse-mode") hydrogen–carbon correlated spectra were acquired (128 increments of 1024 points each) with the standard Bruker software BIRD-DP9. The sweep widths were 16 000 Hz in t_2 and 2000 Hz in t_1. A BIRD pulse was used to suppress ^{1}H–^{12}C magnetization. Garp-64 broad-band decoupling was applied to ^{13}C during ^{1}H detection. Cosine weighting and zero filling were applied to both domains prior to Fourier transformation. The final resolution was about 125 Hz/point in F_2 (^{13}C) and 2 Hz/point in F_1 (^{1}H).

Difference nuclear Overhauser enhancement (NOE) experiments were acquired by using the standard Bruker pulse program, NOEMULT. This experiment rapidly hops the irradiation frequency across the multiplet being saturated and thus requires less power and produces fewer anomalies.[11]

IR spectra were recorded on a Perkin-Elmer 983 spectrophotometer. Mass spectra were obtained on a VG 7070 EQ-HF mass spectrometer. Elemental analyses were performed by Midwest Microlab.

Pentane was purchased from Aldrich and was purified by stirring over concentrated H_2SO_4, passage through a 20 × 3 cm column of alumina, and distillation from Na/benzophenone/tetraglyme. Dichloromethane and THF were distilled from P_4O_{10} and Na/benzophenone, respectively. Dichloromethane-d_2 and ^{13}CO were purchased from Cambridge Isotopes. CD_2Cl_2 was dried by vacuum distillation from P_4O_{10}.

$Os_3(CO)_{12}$,[12] ^{13}C-enriched $Os_3(CO)_{12}$,[13] $(C_2H_4)Os_2(CO)_8$ (**1**),[14] $(CH_3CHCH_2)Os_2(CO)_8$ (**3**),[1] $Na_2Os(CO)_4$,[15] and $Na_2Os_2(CO)_8$[16] were prepared by literature procedures.

Photolyses were performed by a modification of the procedures used for the preparation of diosmacyclobutanes.[14b–d] The output of a high pressure 450-W Hanovia lamp was passed through a saturated aqueous solution of $NaNO_2$ so that only light with λ > 435 nm remained.

Preparation of $(C_4H_6)Os_2(CO)_8$ (4) and $(C(O)C_4H_6)Os_2(CO)_7$ (6) from $(CH_3CHCH_2)Os_2(CO)_8$ (3) and Butadiene. In a Fischer–Porter pressure vessel was dissolved 100 mg (0.15 mmol) of **3** in 20 mL of pentane. The vessel was initially charged with 30 psig butadiene, then vented, and charged three times with butadiene to displace the dissolved air; it was wrapped in aluminum foil to preclude photochemical reactions. The reaction mixture was stirred at room temperature under 30 psig of butadiene; every h it was vented and recharged with butadiene in order to remove the propylene released. IR showed the reaction to be complete after 8–10 h. The colorless homogeneous solution was transferred by cannula under pressure of butadiene into a Schlenk flask

(9) (a) Bender, B. R.; Ramage, D. L.; Norton, J. R.; Wiser, D. C.; Rappé, A. K., manuscript in preparation. (b) Ramage, D. L.; Wiser, D. C.; Norton, J. R., manuscript in preparation.

(10) X-ray crystallography has established a different structure (the result of nucleophilic attack on a carbonyl ligand) for the 1,2 adduct previously reported[3b] as the product of the reaction between **1** and a diazadiene: Takats, J., personal communication.

(11) Neuhaus, D. *J. Magn. Reson.* **1983**, *53*, 109.

(12) Johnson, B. F. G.; Lewis, J.; Kilty, P. A. *J. Chem. Soc. A* **1968**, 2859.

(13) Cetini, G.; Gambino, O.; Sappa, E.; Vaglio, E. G. A. *Atti Accad. Sci. Torino* **1967**, *101*, 855.

(14) (a) Motyl, K. M.; Norton, J. R.; Schauer, C. K.; Anderson, O. P. *J. Am. Chem. Soc.* **1982**, *104*, 7325. (b) Anderson, O. P.; Bender, B. R.; Norton, J. R.; Vergamini, P. J.; Larson, A. C. *Organometallics* **1991**, *10*, 3145. (c) Burke, M. R.; Takats, J.; Grevels, F.-W.; Reuvers, J. G. A. *J. Am. Chem. Soc.* **1983**, *105*, 4092. (d) Poë, A. J.; Sekhar, C. V. *J. Am. Chem. Soc.* **1986**, *108*, 3673.

(15) (a) Fischer, W.; Hembre, R. T.; Sidler, D. R.; Norton, J. R. *Inorg. Chim. Acta* **1992**, *198–200*, 57. (b) Carter, W. J.; Kelland, W. J.; Okrasinski, S. J.; Warner, K. E.; Norton, J. R. *Inorg. Chem.* **1982**, *21*, 3955, and references therein.

(16) (a) Hembre, R. T. Ph.D. Dissertation, Colorado State University, Fort Collins, CO, 1985. (b) Bhattacharyya, N. K.; Coffy, T. J.; Quintana, W.; Salupo, T. A.; Bricker, J. C.; Shay, T. B.; Payne, M.; Shore, S. *Organometallics* **1990**, *9*, 2368. (c) Bender, B. R. Ph.D. Dissertation, Colorado State University, Fort Collins, CO, 1990. (d) Anson, C. E.; Sheppard, N.; Powell, D. B.; Norton, J. R.; Fischer, W.; Keiter, R. L.; Johnson, B. F. G.; Lewis, J.; Bhattacharrya, A. K.; Knox, S. A. R.; Turner, M. L. *J. Am. Chem. Soc.* **1994**, *116*, 3058.

precooled to −80 °C. Solvent removal under vacuum at −80 °C gave a white-yellow solid. After vacuum transfer of CD_2Cl_2 and warming to −40 °C, the resulting solution was added to an NMR tube precooled to −40 °C; the tube was then sealed in vacuo.

Both ^1H and ^{13}C NMR suggested that two compounds were present in a 2:1 ratio. The ^1H and ^{13}C peaks due to each compound were identified by $^1H-^1H$ decoupling, COSY, and $^{13}C-^1H$ correlated spectra. The attribution of one set of peaks to **6** was confirmed after its independent photochemical synthesis (next section).

For $C_4H_6Os_2(CO)_8$ (**4**), ^1H NMR (CD_2Cl_2): δ 1.54 (dd, 1H, $^2J_{gem} = -10.4$ Hz, $^3J_{trans} = 12.8$ Hz), 1.83 (dd, 1H, $^2J_{gem} = 10.4$ Hz, $^3J_{cis} = 6.7$ Hz), 2.62 (m, 1H, $^3J_{trans} = 12.8$ Hz, $^3J_{cis} = 6.7$ Hz, $^3J = 6.8$ Hz, $^4J = 1.6$ Hz, $^4J = 1.6$ Hz), 4.23 (ddd, 1H, $^3J_{cis} = 10.2$ Hz, $^2J_{gem} = -1.6$ Hz, $^4J = 1.6$ Hz), 4.47 (ddd, 1H, $^3J_{trans} = 17.0$ Hz, $^2J_{gem} = -1.6$ Hz, $^4J = 1.6$ Hz), 5.87 (ddd, 1H, $^3J_{trans} = 17.0$ Hz, $^3J_{cis} = 10.2$ Hz, $^3J = 6.8$ Hz). ^{13}C NMR (CD_2Cl_2): δ −21.0 (CH_2, $J_{CH} = 134$ Hz, $^2J_{CH} = 5.5$ Hz), 1.0 (CH, $J_{CH} = 140$ Hz), 102.0 (CH_2, $J_{CH} = 155$ Hz, $^2J_{CH} = 5.7$ Hz), 155.0 (CH, $J_{CH} = 150$ Hz), 168.8 (CO), 169.4 (CO), 172.0 (CO), 172.5 (CO), 179.9 (2CO), 181.4 (CO), 181.5 (CO). IR (pentane): 2120.0 (w), 2080.0 (vs), 2040.0 (s), 2031.0 (s), 2010.0 (s), 1993.0 (m) cm^{-1}.

For $(C(O)C_4H_6)Os_2(CO)_7$ (**6**), ^1H NMR (CD_2Cl_2): δ 2.41 (m, 3H, COCH*H*, C*H*=CH*H*), 3.58 (ddd, 1H, CH=CH*H*, $J_{HH} = 7.7$ Hz, $J_{HH} = 6.9$ Hz, $J_{HH} = 3.5$ Hz), 4.18 (m, 2H, COCH*H*C*H*CH). ^{13}C NMR (CD_2Cl_2): δ 25.9 (CH_2, $J_{CH} = 161$ Hz), 49.0 (CH, $J_{CH} = 161$ Hz), 70.0 (CH_2, $J_{CH} = 128$ Hz), 93.0 (CH, $J_{CH} = 159$ Hz), 164.9 (CO), 172.4 (CO), 183.9 (CO), 186.2 (CO), 186.7 (CO), 187.2 (CO), 187.7 (CO), 218.0 (*C*OC$_4$H$_6$). IR (CH_2Cl_2): 2115.5 (m), 2097.5 (w), 2072.5 (w), 2068.0 (m), 2055.5 (s), 2025.0 (vs), 1980.0 (s), 1625.1 (w) cm^{-1}. Its mass spectrum showed a parent ion peak at *m/e* 662 (^{192}Os) with the appropriate isotopic distribution.

Preparation of $C_4H_6Os_2(CO)_8$ (4), $(C(O)C_4H_6)Os_2(CO)_7$ (6), $C_4H_6Os_2(CO)_7$ (7), and $(C_4H_6)Os(CO)_3$ (8) by the Photochemical Fragmentation of $Os_3(CO)_{12}$. $Os_3(CO)_{12}$ (300 mg, 0.33 mmol) was suspended in 300 mL of CH_2Cl_2 in a Fischer–Porter pressure vessel. The vessel was then charged and vented three times with 30 psig of butadiene in order to displace the dissolved air. The yellow heterogeneous solution became colorless and homogeneous after photolysis under 30 psig of butadiene for 10 h with visible light ($\lambda > 435$ nm). All but 1 mL of the solvent was removed under vacuum at 0 °C, and the mixture was applied to a Chromatotron plate. Elution with pentane, under a flow of N_2 cooled by passage through copper tubing immersed in liquid N_2, gave the new compound **7** (62 mg, 30% yield) and the known **8**[17] (65 mg, 60% yield); solvent was removed under vacuum at 0 °C to avoid decomposition. Further elution under the same conditions with a 1:1 mixture of diethyl ether and pentane gave **6** and a small quantity of **4** (combined R_f 0.20) in a combined yield of 25% (54 mg); again, solvent was removed under vacuum at 0 °C to avoid decomposition.

For $C_4H_6Os_2(CO)_7$ (**7**), ^1H NMR (CD_2Cl_2): δ 0.39 (dd, 1H, $^2J_{gem} = -7.9$ Hz, $^3J = 8.4$ Hz), 1.65 (dd, 1H, $^3J = 8.7$ Hz, $^2J_{gem} = -7.9$ Hz), 1.75 (dd, 1H, $^2J_{gem} = -4.1$ Hz, $^3J_{trans} = 10.3$ Hz), 2.52 (m, 1H, $^2J_{gem} = -4.1$ Hz, $^3J_{cis} = 6.6$ Hz), 4.37 (m, 1H, $^3J_{cis} = 6.6$ Hz, $^3J_{cis} = 7.0$ Hz, $^3J_{trans} = 10.3$ Hz), 5.43 (m, 1H, $^3J_{cis} = 7.0$ Hz, $^3J_{HH} = 8.7$ Hz, $^3J_{HH} = 8.4$ Hz). ^{13}C NMR (CD_2Cl_2): δ −11.5 (CH_2, $J_{CH} = 139$ Hz), 18.0 (CH_2, $J_{CH} = 155$ Hz), 73.6 (CH, $J_{CH} = 163$ Hz), 78.7 (CH, $J_{CH} = 171$ Hz). IR (pentane): 2106.0 (w), 2048.0 (vs), 2029.0 (s), 2020.0 (vs), 2003.0 (s), 1980.5 (m), 1973.0 (m) cm^{-1}. Its mass spectrum showed a parent ion peak at *m/e* 634 (^{192}Os) with the appropriate isotopic distribution. Anal. Calcd for $C_{11}H_6O_7Os_2$: C, 20.96; H, 0.96. Found: C, 21.03; H, 1.06.

^{13}C-Enriched 6 (6*) was synthesized from ^{13}C-enriched $Os_3(CO)_{12}$;[13] the ^{13}C content of the latter was 16.5% (analysis, by overdetermined-least-squares methods, of the observed parent ion multiplet vs the isotopic distribution calculated for Os_3—program MASSPEC). Photochemical fragmentation in the presence of butadiene according to the previous procedure gave **6***, with ^{13}C NMR (CD_2Cl_2) δ 69.9 (CH_2, $J_{CC} = 24.8$ Hz).

Preparation of $C_4H_6Os_2(CO)_7$ (7) from the Reaction of $Na_2Os_2(CO)_8$ with Dichlorobutenes. In a typical experiment, $Na_2Os_2(CO)_8$ was prepared in situ by titrating $(C_2H_4)Os_2(CO)_8$ (**1**; 200 mg, 0.32 mmol) with a standard solution of Na/Ph_2C=O in THF [2.0 g (87 mmol) of Na, and 1.0 g (5.6 mmol) of Ph_2C=O, in 40 mL of THF] until a purple color persisted.[16c,d] Subsequently *cis*-1,4-dichloro-2-butene (0.33 mL, 3.2 mmol, 10 equiv) was added dropwise. The solution turned orange, and a white precipitate formed. After filtration through silica, the homogeneous solution was chromatographed with pentane as the eluant. The most intense band (R_f 0.60) contained (after solvent removal at 0 °C) 50 mg (0.08 mmol, 25% yield) of **7**. Low yields of several other bands were observed but not identified. Treatment of $Na_2Os_2(CO)_8$ with 3,4-dichloro-1-butene in the same fashion gave **7** in 20% yield; *trans*-1,4-dichloro-2-butene gave **7** in 22% yield.

Preparation of $C_3H_4Os_2(CO)_8$ (9) and $C_3H_4Os_2(CO)_7$ (10) from $(CH_3CHCH_2)Os_2(CO)_8$ (3) and Allene. As in the butadiene reaction above, **3** (100 mg, 0.15 mmol) was dissolved in 20 mL of pentane. The vessel was initially charged with 40 psig of allene, then vented, and charged three times with allene to displace the dissolved air; it was wrapped in aluminum foil to preclude photochemical reactions. The reaction mixture was stirred at room temperature under 40 psig of allene; every h it was vented and recharged with allene in order to remove the propylene released. After 8–10 h the reaction contained a 9:1 mixture of **9** and **10**. **9** is thermally unstable and was characterized in solution. ^1H NMR (CD_2Cl_2): δ 2.09 (dd, 2H, $^4J_{HH} = 1.7$ Hz, $^4J_{HH} = 1.6$ Hz) 4.62 (dt, 1H, $^4J_{HH} = 1.6$ Hz, $^2J_{gem} = -2.4$ Hz), 5.73 (dt, 1H, $^4J_{HH} = 1.7$ Hz, $^2J_{gem} = -2.4$ Hz). ^{13}C NMR (CD_2Cl_2): δ −11.90 (CH_2, $J_{CH} = 136$ Hz, $^3J_{CH} = 8.5$ Hz, $^3J_{CH} = 14.5$ Hz), 115.6 (CH_2, $J_{CH} = 154$ Hz, $^3J_{CH} = 5.7$ Hz), 124.1 (=C=), 167.6 (CO), 168.9 (CO), 172.4 (CO), 173.6 (2CO), 180.4 (CO), 180.7 (2CO's). IR (pentane): 2126.5 (w), 2084.0 (s), 2044.0 (s), 2039.0 (s), 2027.5 (m), 2014.5 (m), 1999.0 (m), 1987.5 (w) cm^{-1}. Its mass spectrum showed a parent ion peak at *m/e* 648 (^{192}Os) with the appropriate isotopic distribution.

When the reaction was allowed to proceed for an additional 10 h, only **10**—a white crystalline material that is air and temperature stable—was isolated. **10** was first synthesized by Deeming and co-workers, and characterized by ^1H NMR, IR, and mass spectrometry.[18] ^{13}C NMR (CD_2Cl_2): δ 52.9 (CH_2, $J_{CH} = 157$ Hz, $^3J_{CH} = 7.2$ Hz, $^3J_{CH} = 12.8$ Hz), 146.4 (=C=), 167.3 (CO), 175.4 (CO), 176.7 (CO), 179.3 (2CO's), 180.8 (2CO).

Equilibrium Constant Measurements for 3 + Butadiene and 3 + Allene. A sample of **3** (20 mg, 0.031 mmol) was placed in an NMR tube, and 181 Torr (0.046 mmol) of butadiene and 0.5 mL of dry CD_2Cl_2 were condensed onto it. The mixture was warmed to 0 °C, and the reaction followed by ^1H NMR for 72 h. The reaction between **3** and allene was monitored in the same way.

Preparation of $C_3H_4Os_2(CO)_7$ (10) and η^2-$C_3H_4Os(CO)_4$ (11) by the Photochemical Fragmentation of $Os_3(CO)_{12}$ in the Presence of Allene. By the procedure described above for the butadiene case, $Os_3(CO)_{12}$ (300 mg, 0.33 mmol) was photolyzed under 40 psig of allene. Compounds **10** (R_f 0.6) and **11** (R_f 0.7) were separated by elution with pentane on a chromatotron. Solvent-free **10** (69 mg, 0.13 mmol, 40% yield) was obtained as a white solid by solvent removal at 0 °C.

Solvent-free **11** was obtained by high-vacuum fractionation. After freeze–pump–thaw degassing, the pentane solution (0 °C) containing **11** was fractionated under dynamic vacuum (10^{-4} mmHg) by slowly passing it through two U-traps in

(17) Zobl-Ruh, S.; von Philipsborn, W. *Helv. Chim. Acta* **1980**, *63*, 773.

(18) Bates, P. A.; Hursthouse, M. B.; Arce, A. J.; Sanctis, Y. D.; Deeming, A. J. *J. Chem. Soc., Dalton Trans.* **1987**, 2935.

Table 1. Summary of Crystal Data for 7

formula	$C_{11}H_6O_7Os_2$
temperature (°C)	−105
crystal size (mm)	0.40 × 0.30 × 0.15
space group	$P2_12_12_1$
a (Å)	6.928(2)
b (Å)	9.473(2)
c (Å)	20.683(4)
diffractometer	Siemens P3
radiation	Mo Kα, graphite monochromator
wavelength (Å)	0.710 73
index ranges	$0 \le h \le 10, 0 \le k \le 14, 0 \le l \le 31$
2θ range	4.0−65°
no. of reflcns collected	2819
no. of obsd reflcns	2274 ($F > 6.0\sigma(F)$)
no. of parameters	92
μ (mm^{-1})	18.7
absorption correction	semiempirical
R_F (%)	6.22
R_{wF} (%)	7.43

series, the first at −40 °C (CH_3CN/liquid N_2 slush) and the second at −196 °C. Pure **11** was obtained after 12 h as clear, colorless crystals (62 mg, 0.18 mmol, 55% yield) in the −40 °C trap. The colorless oily **11** yellows upon standing at room temperature, but is stable indefinitely when stored at −20 °C. ^{1}H NMR (CD_2CL_2): δ 1.79 (t, 2H, $^4J_{HH}$ = 3.00 Hz), 5.56 (t, 1H, $^4J_{HH}$ = 3.13 Hz), 6.76 (t, 1H, $^4J_{HH}$ = 2.91 Hz). ^{13}C NMR (CD_2Cl_2): δ −10.9 (CH_2, J_{CH} = 160 Hz, $^3J_{CH}$ = 3.1 Hz, $^3J_{CH}$ = 9.9 Hz), 109.5 (CH_2, J_{CH} = 160 Hz, $^3J_{CH}$ = 3.7 Hz), 143.2 (=C=). ^{13}C NMR (CD_2Cl_2, −40 °C): −11.6 (CH_2), 109.1 (CH_2), 142.9 (=C=), 175.8 (2CO), 176.7 (CO), 177.9 (CO). IR (pentane): 2119.5 (m), 2036.5 (vs), 2000.5 (s), 1697.0 (w) cm^{-1}. Its mass spectrum showed a parent ion peak at *m/e* 344 (^{192}Os) with the appropriate isotopic distribution.

X-ray Determination of the Structure of 7. Complex **7** crystallized from pentane by slow cooling to −80 °C. Single crystal X-ray data were collected at −105 °C using a pale yellow crystal of dimensions 0.40 × 0.30 × 0.15 mm on a Siemens R3m/V diffractometer equipped with a molybdenum tube [$\lambda(K\alpha_1)$ = 0.709 26 Å; $\lambda(K\alpha_2$ = 0.713 54 Å] and a graphite monochromator. The compound crystallized in the chiral orthorhombic space group $P2_12_12_1$ with four molecules in a cell of dimensions a = 6.928(2) Å, b = 9.473(2) Å, c = 20.683(4) Å, and V = 1357.4(6) Å^3. A total of 2819 independent reflections were gathered, the octants collected being $+h,+k,+l$, using the Wyckoff scan method. Three standard reflections were measured after every 100 reflections collected. The structure was solved by direct methods and refined by full-matrix least-squares techniques using structure solution programs from the SHELXTL system.[19] The two osmium atoms were refined anisotropically, while other nonhydrogen atoms were refined isotropically due to large residual electron densities near the heavy atoms. Hydrogen atoms were placed in fixed calculated positions (C−H = 0.96 Å). The structure has been refined to conventional R factor values of R = 0.0622 and R_w = 0.0743 on the basis of 2274 observed reflections with $I > 3\sigma(I)$ in the 2θ range 4−65° (R = 0.0761, R_w = 0.0782 for all data), giving a data to parameter ratio of 25:1. Despite the use of both semiempirical and empirical[20] absorption correction techniques, several large peaks in the Fourier remained near the osmium atoms, the maximum and minimum residual densities being 8.55 and −3.57 e Å^{-3}, respectively, with μ = 18.7 mm^{-1}. The results of absolute configuration tests were inconclusive. The details of the crystal data as well as the atomic coordinates for **7** are given in Tables 1 and 2.

Results and Discussion

Reaction of $(CH_3CHCH_2)Os_2(CO)_8$ (3) with 1,3-Butadiene. A solution of **3** was stirred under butadiene at room temperature, with repeated venting in order to remove the propylene released. Two products were formed in an initial ratio of 2:1 (eq 8). The major product

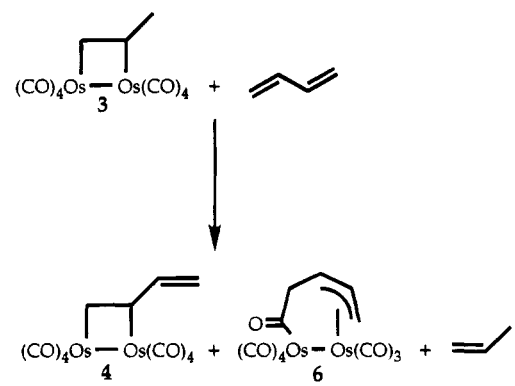

(8)

was the [2 + 2] adduct **4** (see below), with no evidence of the Diels−Alder product **5**; the minor product proved to be a dinuclear allyl acyl complex (**6**). IR and ^{1}H NMR showed no intermediates.

4 is unstable above −40 °C in the absence of butadiene but has been characterized by low-temperature NMR techniques as part of a mixture with **6**. The inverse detected (BIRDDP9) ^{13}C−^{1}H correlated 2D NMR spectra of **4** and **6** shown in Figure 1 permitted the assignment of ^{1}H and ^{13}C NMR resonances to both **4** and **6**.

The ^{1}H NMR spectrum of **4** displays the six different chemical shifts—three in the olefinic region—expected for its unsymmetrical structure. (The diosmacyclohexene **5**, with C_{2v} symmetry, would show only two proton chemical shifts.) The ^{13}C NMR spectrum of **4** shows four signals due to the butadiene ligand: two come from carbons σ-bonded to osmium and have J_{CH} values characteristic of sp^3 carbons in a diosmacyclobutane ring (J_{CH} in **1** is 135 Hz[13b]); two plainly arise from sp^2 carbons in an uncoordinated double bond. The number of ^{13}C NMR carbonyl signals (eight) and the IR of **4** plainly establish that it is dinuclear.

6 is unstable above 0 °C in the absence of butadiene but can be obtained pure from the photolysis of $Os_3(CO)_{12}$ and butadiene (see below). Its ^{13}C NMR spectrum shows evidence for an allyl ligand (three signals belong-

Table 2. Atomic Coordinates (×10^4) and Equivalent Isotropic Displacement Coefficients (Å × 10^3) for 7

	x	y	z	U(eq)
Os(1)	1115(1)	6437(1)	8779(1)	16(1)
Os(2)	2193(1)	3484(1)	8681(1)	14(1)
C(1)	3488(33)	7170(23)	8122(10)	20(4)
C(2)	4101(35)	7267(24)	8782(10)	25(4)
C(3)	4307(32)	6028(21)	9170(10)	17(4)
C(4)	4836(34)	4623(24)	8917(11)	24(4)
C(5)	−384(31)	5809(21)	9500(9)	17(4)
O(5)	−1312(27)	5413(20)	9927(8)	30(4)
C(6)	437(35)	8335(24)	8918(10)	24(4)
O(6)	−111(32)	9489(24)	9038(10)	47(5)
C(7)	−624(37)	6010(23)	8118(11)	23(4)
O(7)	−1724(25)	5782(18)	7699(8)	26(4)
C(8)	1979(35)	3271(26)	9625(11)	26(5)
O(8)	1935(30)	3204(22)	10164(9)	38(5)
C(9)	2489(31)	3957(20)	7758(9)	15(4)
O(9)	2608(29)	4180(18)	7225(8)	29(4)
C(10)	3531(33)	1724(22)	8613(10)	21(4)
O(10)	4323(26)	671(17)	8555(8)	26(3)
C(11)	−355(30)	2773(20)	8514(9)	15(3)
O(11)	−1843(25)	2342(18)	8381(8)	26(4)

(19) Sheldrick, G. M. *SHELXTL Crystallographic System*, Version 4.2/Iris; Siemens Analytical X-ray Insts. Inc., Madison, WI, 1991.
(20) Hope, H.; Moezzi, B. *XABS*; Chemistry Department, University of California, Davis, CA, 1987.

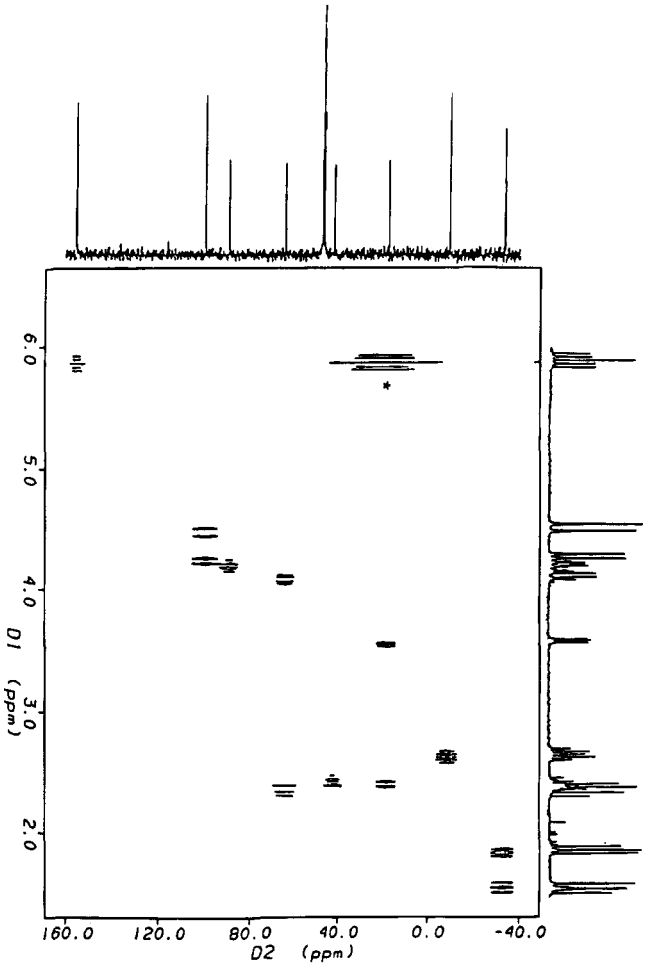

Figure 1. Inverse detected (BIRDDP9) $^{13}C-^{1}H$ correlated 2D NMR spectrum of **4** and **6**. $*t_1$ noise.

ing to sp^2 carbons),[21] as well as a signal belonging to an sp^3 methylene that, at δ 70, is too far downfield to be σ-bonded to an osmium. Another ^{13}C NMR peak, at δ 218, can be assigned to an acyl carbon; the IR shows a peak at 1628 cm^{-1}. (Carbonyl stretches at 1634 and 1648 cm^{-1} have been observed[22] in other diosmium acyl complexes.)

The possibility that **6** was an acyl isomer of **4** has been tested by determining $^1J_{CC}$ between the acyl and methylene carbons. When a sample of $Os_3(CO)_{12}$ with 16.5% ^{13}CO is converted into **6*** by photolysis with butadiene (see below), its ^{13}C NMR signal at δ 70.0 (C2) shows satellites with a J_{CC} of 24.8 Hz (Figure 2). The methylene must thus be bonded to the acyl carbon,[23] and **6** must have the structure shown.[24]

Interconversion of 4 and 6. When a 2:1 mixture of **4** and **6** (as initially formed from **3** and butadiene) was kept at 0 °C for 10 h in the presence of excess butadiene, much of **4** isomerized to **6**. The composition

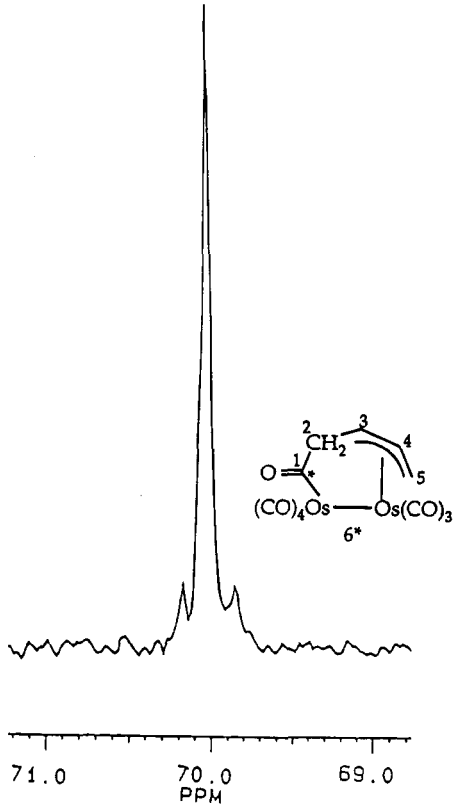

Figure 2. sp^3 methylene region of the ^{13}C NMR spectrum (75.5 MHz, CD_2Cl_2) of **6***. The singlet is due to the 83.5% of the molecules that are unlabeled, while the doublet (J_{CC} = 24.8 Hz) is due to the 16.5% of the molecules that are labeled.

of the equilibrium mixture implied K_{eq} = 8.9 at 0 °C (eq 9). The kinetic product of the reaction of **3** with butadiene is thus **4**, while the thermodynamic one is **6**.

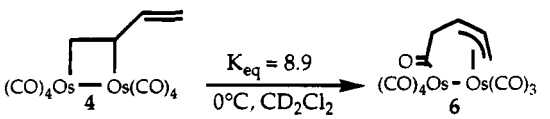

(9)

The facile conversion of **4** → **6** finds precedent in the recently reported rearrangement of $CpRe(CO)_2(\eta^1\text{-allyl})(CHMe_2)$ to $CpRe(CO)(\eta^3\text{-allyl})(C(O)CHMe_2)$.[25] The latter involves "isopropyl migration to CO concerted with η^1- to η^3-allyl rearrangement".

We know of no precedent for the structure of **4** or the structure of **6** in the dinuclear coordination chemistry

(21) Mann, B. E.; Taylor, B. F. *^{13}C NMR Data for Organometallic Compounds*; Academic: New York, 1981; pp 200–210.

(22) Bullock, R. M.; Hembre, R. T.; Norton, J. R. *J. Am. Chem. Soc.* **1988**, *110*, 7868.

(23) $^1J_{CC}$ between an organic carbonyl carbon and the carbon of an sp^3 substituent is about 40 Hz: Kalinowski, H. O.; Berger, S.; Braun, S. *^{13}C-NMR-Spectroskopie*; Georg Thieme Verlag: Stuttgart, Germany, 1984; p 501.

(24) The sp^3 CH_2 of **6** is shifted downfield (δ 70) by the carbonyl group. Compare the effect of CO and Os on sp^3 carbons in the following compounds: $(CH_3)_2C{=}O$ (δ 30), $(CH_3)_2Os_2(CO)_8$ (δ −42), $Os_2(CO)_7(\mu\text{-}CH_2\text{-}\eta^3\text{-}CH_2CHCH_2)$ (**7**; δ −11), and $Os_2(CO)_7(\mu\text{-}C(O)CH_2\text{-}\eta^3\text{-}CH_2\text{-}CHCH_2)$ (**6**; δ 70).

(25) Casey, C. P.; Vosejpka, P. C.; Underiner, T. L.; Slough, G. A.; Gavney, J. A., Jr. *J. Am. Chem. Soc.* **1993**, *115*, 6680.

(26) (a) Krüger, C.; Müller, G.; Erker, G. *Adv. Organomet. Chem.* **1985**, *24*, 1. (b) Kreiter, C. G. *Adv. Organomet. Chem.* **1986**, *25*, 297. (c) Ziegler, M. *Z. Anorg. Allg. Chem.* **1967**, *355*, 12. (d) Adams, V. C.; Jarvis, J. A. J.; Kilbourne, B. T.; Owston, P. G. *J. Chem. Soc. D* **1971**, 467. (e) Tachikawa, M.; Shapley, J. R.; Haltiwanger, R. C.; Pierpont, C. G. *J. Am. Chem. Soc.* **1976**, *98*, 4651. (f) Franzreb, K.-H.; Kreiter, C. G. *Z. Naturforsch.* **1982**, *37B*, 1058. (g) Kreiter, C. G.; Lipps, W. *Chem. Ber.* **1982**, *115*, 973. (h) Franzreb, K.-H.; Kreiter, C. G. *J. Organomet. Chem.* **1983**, *246*, 189. (i) Vollhardt, K. P.; King, J. A., Jr. *Organometallics* **1983**, *2*, 684. (j) Fryzuk, M. D.; Jones, T.; Einstein, F. W. B. *J. Chem. Soc., Chem. Commun.* **1984**, 1556. (k) Fryzuk, M. D.; Piers, W. E.; Rettig, S. J. *J. Am. Chem. Soc.* **1985**, *107*, 8259. (l) Lewandos, G. S.; Knox, S. A. R.; Orpen, G. A. *J. Chem. Soc., Dalton Trans.* **1987**, 2703. (m) Wedt, G.; Kaub, J.; Kreiter, C. G. *Chem. Ber.* **1989**, *122*, 215. (n) Meszaros, M. W.; Gohdes, M. A.; Casey, C. P. *Organometallics* **1988**, *7*, 2103. (o) Fryzuk, M. D.; Piers, W. E.; Rettig, S. J.; Einstein, F. W. B.; Jones, T.; Albright, T. A. *J. Am. Chem. Soc.* **1989**, *111*, 5709. (p) Erker, G.; Noe, R.; Krüger, C.; Werner, S. *Organometallics* **1992**, *11*, 4174.

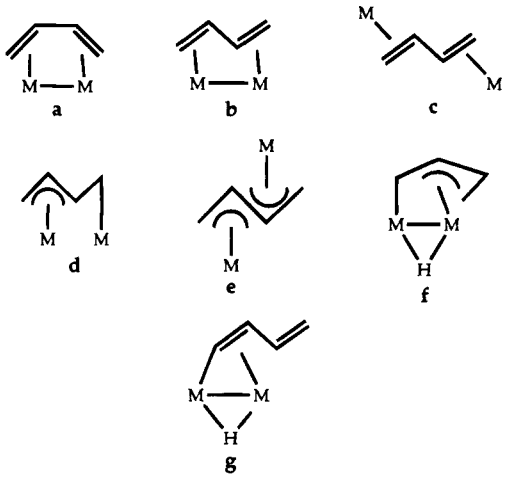

Figure 3. Most common bridging geometries for butadiene: **a**,[24a,b,i] **b**,[24a,b,e,f] **c**,[24a,b–d] **d**,[24a,b,g] **e**,[24a,b,k] **f**,[24a,b,j] and **g**.[24a,b,h,l,o]

of butadiene itself. (Earlier results from Takats and coworkers, eq 7, gave a [2 + 2] adduct, but involved an activated diene.[3b]) Figure 3 shows the most common bridging geometries for butadiene.[26] It can have either the *s-cis* or *s-trans* conformation while bridging a metal–metal bond (**a**, **b**); it can bridge two noninteracting metals (**c**–**e**); it can bridge after C–H activation (**f**, **g**).

Photochemical Reaction of $Os_3(CO)_{12}$ with Butadiene. The photolysis of $Os_3(CO)_{12}$ with long-wavelength light (λ > 370 nm) in the presence of olefins has proven to be an efficient way of making mono- and diosmium olefin complexes.[14b–d] We thus photolyzed $Os_3(CO)_{12}$ in the presence of butadiene in order to compare the resulting dinuclear complexes (eq 10) with those from the thermal reaction (eq 8).

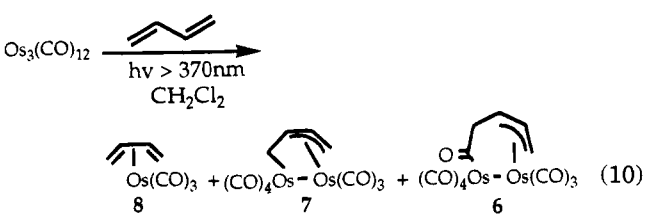

(10)

The principal product (60%) was the known[17] monoosmium butadiene complex **8**. However, substantial amounts of both **6** (20%) and a new dinuclear complex, **7** (30%), were also formed. **7** is not a secondary photoproduct: irradiation of an equilibrium mixture of **4** and **6** (from the thermal reaction) with butadiene gave no **7**.

The new butadiene adduct **7** is stable at room temperature even in the presence of air. Its ^1H and ^{13}C NMR spectra have been assigned with the help of ^1H–^1H homonuclear COSY (COSYPHDQ) and ^1H–^{13}C heteronuclear correlation (XHDEPTW). Its ^1H NMR spectrum displays six different resonances, implying an asymmetric binding mode for the butadiene ligand; its ^{13}C NMR spectrum shows evidence for an allyl ligand[21] and for an sp^3 carbon that is σ-bonded to an osmium. Its mass spectrum and analysis show that it has one carbonyl less than **4** and **6**.

The structure of **7** has been confirmed by X-ray diffraction. This bonding mode is rare for butadiene. We are aware of only one dinuclear butadiene complex

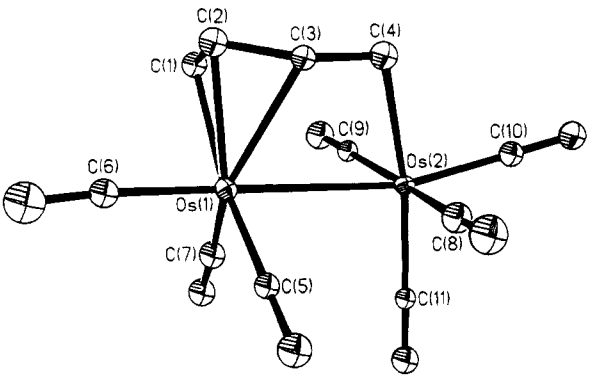

Figure 4. Molecular structure of $Os_2(CO)_7(\mu\text{-}CH_2\text{-}\eta^3\text{-}CH_2\text{-}CHCH_2)$ (**7**).

with a similar structure, $W_2(OCH_2\text{-}^tBu)_6(py)(C_4H_6)$ reported by Chisholm and co-workers.[27] The butadiene ligands in **7** and in the tungsten compound differ in only one way: C4 in **7** is σ-bonded to only one osmium, whereas the corresponding methylene carbon in the tungsten analog bridges both metals. Perhaps as a result, J_{CH} of C4 in **7** is 139 Hz to both protons, whereas J_{CH} is different for the two C–H bonds within the methylene in the tungsten compound (149 Hz to one proton and 124 to the other).

Reaction of $Na_2Os_2(CO)_8$ with Dichlorobutenes. In an attempt to independently synthesize **4** and perhaps **5** (eq 11), $Na_2Os_2(CO)_8$ was treated with 3,4-dichloro-1-butene and *cis*-1,4-dichloro-2-butene, respectively.

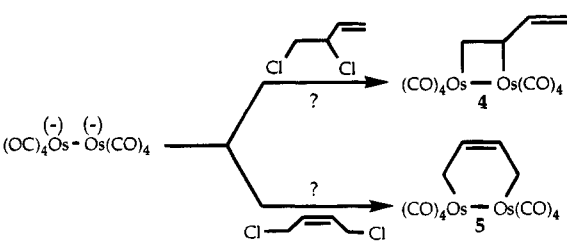

(11)

In both cases, and with *trans*-1,4-dichloro-2-butene, the product of the reaction was **7** (eq 12) in about 20–25% yield.

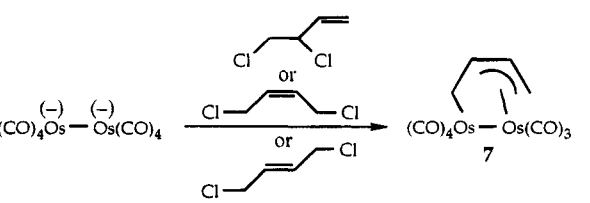

(12)

We have been unable to interconvert **7** and the **4**/**6** equilibrium mixture. Attempts to carbonylate **7** at pressures of up to 120 psig gave neither **4** nor **6** (eq 13).

(27) Chisholm, M. H.; Huffman, J. C.; Lucas, E. A.; Lubkovsky, E. B. *Organometallics* **1991**, *10*, 3424.

(28) As **7** is not formed from **4** or **6**, the formation of **7** in eq 12 probably occurs by an electron transfer mechanism. (Note the similar yields from *cis*- and *trans*-1,4-dichloro-2-butene.) Electron transfer to a 1,3-diiodide from a dinuclear radical *monoanion* has been suggested: Yang, G. K.; Bergman, R. G. *J. Am. Chem. Soc.* **1983**, *105*, 6045.

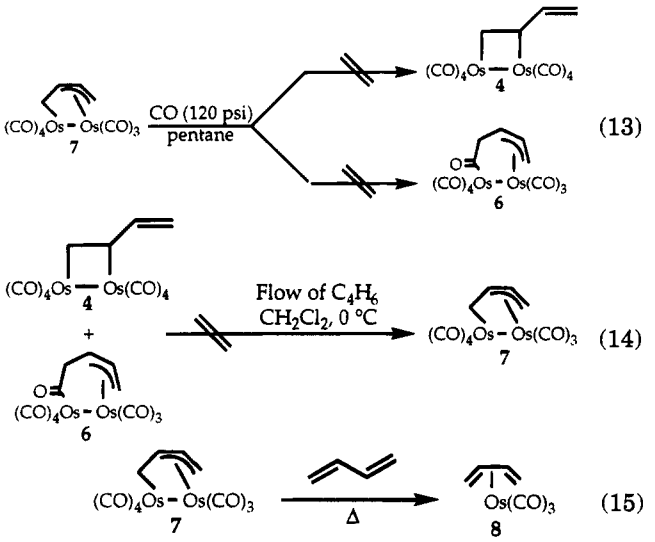

A **4**/**6** mixture gave no **7** in the presence of a flow of butadiene (eq 14), just as it had not given any **7** photochemically (recall the discussion after eq 10 above).[28] When **7** was heated under a pressure of butadiene it rearranged to the known[17] **8** (eq 15).

Reaction of $(CH_3CHCH_2)Os_2(CO)_8$ (3) with Allene. A solution of **3** was stirred under allene at room temperature, with repeated venting in order to remove the propylene released. After 10 h, IR showed that the reaction was complete; ^1H NMR showed that two products had been formed in a 9:1 ratio (eq 16).

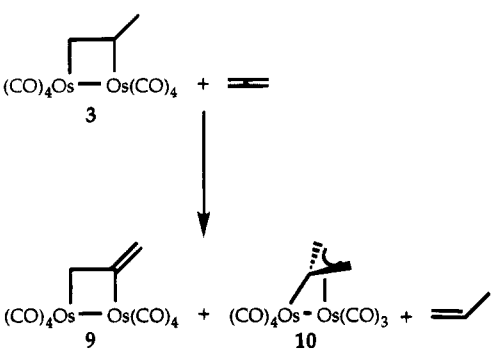

The minor product proved to be **10**, first synthesized by Deeming and co-workers.[18] The major product (**9**) was plainly that expected from a formal [2 + 2] addition reaction. Three signals in the ^{13}C NMR of **9** (one quaternary carbon and two methylenes) arise from allenic carbons. The six carbonyl peaks in its ^{13}C NMR, intensity ratio 2:2:1:1:1:1, require a plane of symmetry containing the allene ligand and the two osmiums. In the ^1H NMR of **9** there are three different resonances, two for the olefinic protons and one for the ring protons. Protons H_1 and H_2 couple to H_3 identically so they are indistinguishable by ^1H NMR (Figure 5).

In order to differentiate between H_1 and H_2 of **9**, a difference NOE experiment was performed (Figure 5). When H_3 was irradiated, H_1 showed a positive effect of 2%, while H_2 showed a negative effect of −1%. Molecular modeling studies[29−31] predict that $d(H_3-H_1)$ should be 2.84 Å, $d(H_1-H_2)$ should be 1.70 Å, and the $H_3-H_1-H_2$ angle should be 111°. The geometry of the molecule is such that the observed negative effect is in agreement

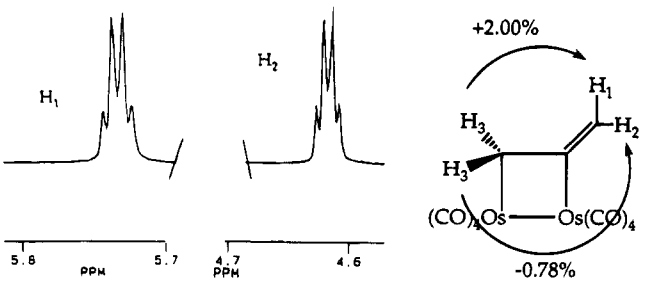

Figure 5. (Left) ^1H NMR of **9** in the region of H_1 and H_2. (Right) Observed NOE.

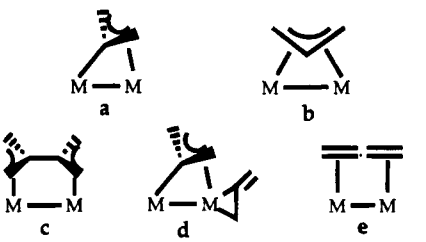

Figure 6. Most common bonding modes for allene as a bridging ligand: **a**,[33b,c,h,q,17] **b**,[33e,m,n,p,17] **c**,[33a−c] **d**,[33n,p] and **e**.[33fj−l]

with the "three-spin effect".[32] The allene complex **9** does not show any fluxional behavior up to 25 °C.[33]

The allene ligand in **9** is the first example of this bonding mode for allene in a homobimetallic system; a known heterobimetallic example is $[(CO)_3Fe(\mu\text{-dppm})\{\mu\text{-}C(CH_2)CH_2\}Pt(PPh_3)]$.[34] The coordination chemistry of allene with mono- and dinuclear centers has been reviewed,[35] the most common ways in which allene serves as a bridging ligand are shown in Figure 6.[36]

When a 9:1 mixture of **9** and **10** was kept under 2 atm of allene at 25 °C for 48 h, all of the **9** rearranged to **10** (eq 17). **9** is thus the kinetic product of reaction 16, while **10** is the thermodynamic one.

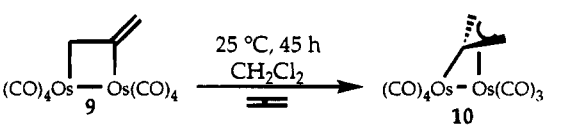

Photochemical Reaction of $Os_3(CO)_{12}$ with Allene. When $Os_3(CO)_{12}$ was photolyzed in the presence of allene (eq 18), **10** was obtained in 40% yield along with a 55% yield of the mononuclear osmium complex **11**.

(29) Coordinates for the parent diosmacyclobutane **1** were obtained from ab initio calculations by A. K. Rappé.[9a] Minimizations were done using the Dreiding force field[30] with the Biograf molecular simulation program, Version 2.2.[31] The structure was minimized by use of a conjugate gradient technique with the carbon, osmium, and oxygen atoms of the $Os_2(CO)_8$ fragment constrained to the ab initio geometry. The Os van der Waals parameters used were R = 3.00 Å and ϵ = 0.055 kcal/mol.

(30) Mayo, S. L.; Olafson, B. D.; Goddard, W. A. *J. Phys. Chem.* **1990**, *94*, 8897.

(31) Biograf was obtained from the BioDesign subsidiary of Molecular Simulations Inc., 199 S. Los Robles Ave., Suite 540, Pasadena, CA 91101.

(32) Derome, A. E. *Modern NMR Techniques for Chemistry Research*; Pergamon Press: New York, 1987; Chapter 5.

(33) Mononuclear allene complexes are frequently fluxional. See: Shoshan, R. B.; Pettit, R. *J. Am. Chem. Soc.* **1967**, *89*, 2231.

(34) (a) Fontaine, X. L. R.; Jacobsen, G. B.; Shaw, B. L.; Thornton-Pett, M. *J. Chem. Soc., Dalton Trans.* **1988**, 1185. (b) Fontaine, X. L. R.; Jacobsen, G. B.; Shaw, B. L.; Thornton-Pett, M. *J. Chem. Soc., Chem. Commun.* **1987**, 662.

(35) Bowden, F. L.; Giles, R. *Coord. Chem. Rev.* **1976**, *20*, 81.

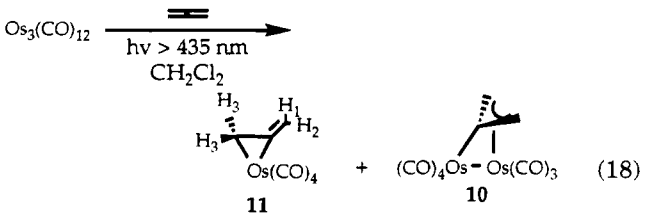

11 is an air- and temperature-stable liquid. Its ^{13}C NMR consists of the expected three signals from the allyl ligand and (below −40 °C) carbonyls in a 2:1:1 ratio. Another difference NOE experiment was performed to distinguish between the olefinic protons and showed a positive effect of 1% for H_1 and no effect for H_2. (The fact that the effect at H_2 is no longer negative for **11** implies that the geometry of H_1, H_2, and H_3 differs in detail from that of **9**.) As with **9**, the allene ligand of **11** showed no fluxional behavior up to 60 °C.

Relative Equilibrium Constants for the Binding of Butadiene vs Allene to the $Os_2(CO)_8$ Fragment. After 72 h at 0 °C, equilibrium was established among **3**, butadiene, **4**, **6**, and propene (eq 8). ^1H NMR measurement of the relative intensities of the peaks of **3**, butadiene, **4**, and propene implied an equilibrium constant of 1.4 for eq 19. Similarly, after 72 h at 0 °C,

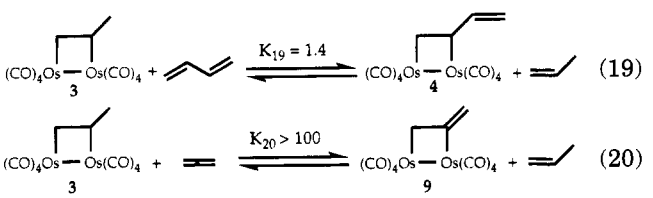

equilibrium was established among **3**, allene, **9** (without the formation of a significant amount of **10**), and propene (eq 20). The equilibrium constant was too large to measure, implying that allene is bound much more tightly than butadiene.

The heat of hydrogenation of one double bond of allene (ΔH for eq 21) is 41.2 kcal mol^{-1} at 82 °C, while that for one double bond of butadiene (ΔH for eq 22) is 27.0 kcal mol^{-1} at 82 °C.[37] The difference, 14.2 kcal mol^{-1},

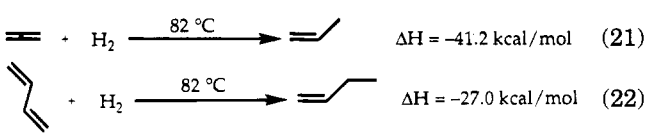

predicts a much larger binding constant for the coordination of one double bond of allene than of butadiene. This difference in double bond stability must be at least partly responsible for the fact that K_{20} is much larger than K_{19}.

Conclusion

It is becoming clear[9] that the exchange reactions of diosmacyclobutanes proceed via bridge-opened intermediates such as **12**. Detailed kinetic studies[9] of the reaction of **1** with olefins with electron-withdrawing substituents have established an associative mechanism (Scheme 1) for the exchange of **12** with incoming olefins; a dissociative mechanism, involving $Os_2(CO)_8$ after all, is possible with relatively unreactive olefins. Matrix isolation[1] and transient[2] IR studies have shown that

Scheme 1

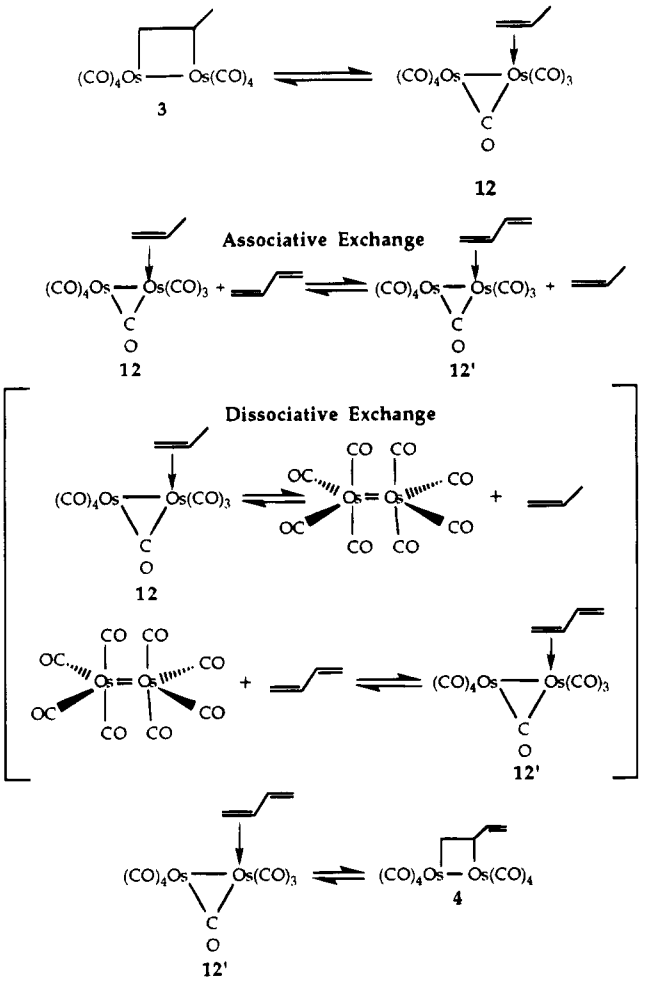

species like **12** are formed by the reaction of $Os_2(CO)_8$ with incoming olefins.

With either associative or dissociative exchange, Scheme 1 explains why we have obtained formal [2 + 2] addition products with butadiene and allene. Associative exchange gives **12′** with only one C−C double bond coordinated, and isomerization gives a product like **4** or **9**. Dissociative exchange would also lead to **12′** and thus to **4** or **9**.

As we have been unable to prepare the butadiene

(36) (a) Nakamura, A. *Bull. Chem. Soc. Jpn.* **1966**, *39*, 543. (b) Shoshan, R. B.; Pettit, R. *Chem. Commun.* **1968**, 247. (c) Davis, R. E. *Chem. Commun.* **1968**, 248. (d) Gervasio, G.; Osella, D.; Valle, M. *Inorg. Chem.* **1976**, *15*, 1221. (e) Bailey, W. I., Jr.; Chisholm, M. H.; Cotton, F. A.; Murillo, C. A.; Rankel, L. A. *J. Am. Chem. Soc.* **1978**, *100*, 802. (f) Lewis, L. N.; Huffmann, J. C.; Caulton, K. G. *J. Am. Chem. Soc.* **1980**, *102*, 403. (g) Al-Obaidi, Y. N.; Baker, P. K.; Green, M.; White, N. D.; Taylor, G. E. *J. Chem. Soc., Dalton Trans.* **1981**, 2321. (h) Johnson, B. F. G.; Lewis, J.; Raithby, P. R.; Sankey, S. W. *J. Organomet. Chem.* **1982**, *232*, C65. (i) Aime, S.; Gobetto, R.; Osella, D. *Organometallics* **1982**, *1*, 640. (j) Hoel, E. L.; Ansell, G. B.; Leta, S. *Organometallics* **1986**, *5*, 585. (k) Casey, C. P.; Austin, E. A. *Organometallics* **1986**, *5*, 584. (l) Casey, C. P.; Austin, E. A. *J. Am. Chem. Soc.* **1988**, *110*, 7106. (m) Cayton, R. H.; Chisholm, M. H.; Hampden-Smith, M. J. *J. Am. Chem. Soc.* **1988**, *110*, 4438. (n) Cayton, R. H.; Chacon, S. T.; Chisholm, M. H.; Hampden-Smith, M. J.; Huffman, J. C.; Folting, K.; Ellis, P. D.; Huggins, B. A. *Angew. Chem., Int. Ed. Engl.* **1989**, *28*, 1523. (o) Arce, A. J.; DeSantis, Y.; Deeming, A. J.; Hardcastle, K. I.; Lee, R. *J. Organomet. Chem.* **1991**, *406*, 209. (p) Chacon, S. T.; Chisholm, M. H.; Folting, K.; Huffman, J. C.; Hampden-Smith, M. J. *Organometallics* **1991**, *10*, 3722. (q) Seyferth, D.; Anderson, L. L.; Davis, W. B.; Cowie, M. *Organometallics* **1992**, *11*, 3736. (r) Wu, I. Y.; Tseng, T. W.; Chen, C. T.; Cheng, M. C.; Lin, Y. C.; Wang, Y. *Inorg. Chem.* **1993**, *32*, 1539.

(37) Jensen, J. L. *Prog. Phys. Org. Chem.* **1976**, *12*, 189.

Diels–Alder product **5**,[38] we remain uncertain of its energetics; we cannot be sure we would have seen it if it had been formed in any of the reactions in this paper. We have found no evidence that the diosmacyclobutane system is capable of the kind of cycloaddition reaction (reversible dissociation into *o*-xylylene and Co=Co, eq 5) that Hersh and Bergman have established for the benzodicobaltacyclohexene **2**. Of course the thermodynamic driving force for the formation of **5** from butadiene is surely far less than that for the formation of **2** from *o*-xylylene.

Acknowledgment. We thank the Department of Energy, Office of Basic Energy Research (DOE Award DE-FG02-84ER13299), for funding this project, and Colonial Metals and Degussa Chemical Co. for the generous loan of OsO_4. We also thank Dr. Robert Barkley (University of Colorado, Boulder, CO) for mass spectrometry, Dr. Patricia Goodson (University of Wyoming) for X-ray crystallography, and Dawn C. Wiser and Prof. Anthony K. Rappé for the modeling studies. We are grateful to Dr. Bruce Bender and Dr. Rick Sidler for valuable discussions, and to Karen Hennessey for preliminary work with **1**, **3**, and butadiene.

(38) The diosmacyclohexane analogous to **5**, (μ-$CH_2CH_2CH_2CH_2$)-$Os_2(CO)_8$, is stable. It has been prepared from $Na_2[Os_2(CO)_8]$ and $TfOCH_2CH_2CH_2CH_2OTf$: Birdwhistell, K. R.; Norton, J. R., unpublished work.

Supplementary Material Available: Crystal structure data for **7**, including tables of atomic parameters, anisotropic thermal parameters, bond distances, and bond angles (2 pages). Ordering information is given on any current masthead page.

OM940558D

Synthesis and Reactions of Stable 16-Electron Osmium(0) Complexes $[OsCl(NO)(PR_3)_2]$ Including the X-ray Crystal Structure of $[OsCl_2(NO)(\eta^1\text{-}CH{=}C{=}CPh_2)(P\text{-}i\text{-}Pr_3)_2]$†

Helmut Werner,* Ruth Flügel, Bettina Windmüller, Annette Michenfelder, and Justin Wolf

Institut für Anorganische Chemie der Universität Würzburg, Am Hubland, D-97074 Würzburg, Germany

Received August 29, 1994®

The reaction of $[OsCl(NO)(PPh_3)_3]$ (**1**) with P-*i*-Pr_3 and P-*i*-Pr_2Ph affords almost quantitatively the 16-electron square-planar osmium(0) complexes $[OsCl(NO)(PR_3)_2]$ (**2**, **3**). In toluene at room temperature or below, compounds **2** and **3** react spontaneously with CO, H_2, and CH_2N_2 to give the carbonylosmium(0), dihydridoosmium(II), and methyleneosmium(0) derivatives **4**–**9** in excellent yields. While **2** and **3** on treatment with HC≡CPh form the alkynyl(hydrido)osmium(II) complexes **10** and **11**, attempts to rearrange these compounds to the vinylideneosmium(0) isomers failed. Reaction of **2** and **3** with the alkynols $HC{\equiv}CCMe_2OH$ and $HC{\equiv}CCPh_2OH$ also produces six-coordinate alkynyl(hydrido) complexes **12**–**14**, which similar to **10** and **11**, are inert with regard to isomerization. Compounds **13** and **14** react, however, with chloride-containing acidic alumina to give the η^1-allenylosmium(II) derivatives $[OsCl_2(NO)(\eta^1\text{-}CH{=}C{=}CPh_2)(PR_3)_2]$ (**15**, **16**) in 40–50% yield. The X-ray crystal structure analysis of **15** (monoclinic space group $P2_1$ with a = 9.901(1) Å, b = 16.041(1) Å, c = 11.812(6) Å, β = 111.59(1)°, and Z = 2) reveals an octahedral geometry around osmium with *trans* disposed phosphine and *cis* disposed chlorine ligands. The C=C=C chain is nearly linear with C–C distances that are almost identical to those of allenes.

Introduction

Whereas an almost unlimited number of transition-metal compounds of the d^8-systems Rh(I), Ir(I), Ni(II), Pd(II), Pt(II), and Au(III) with a 16-electron configuration and of general composition $[ML_4]$ (L = monodentate ligand) are known,[1] only a very few examples of corresponding Fe(0), Ru(0), and Os(0) complexes that are stable under normal conditions have been described. Stiddard and Townsend[2] reported the generation of an extremely reactive ruthenium compound $[RuCl(NO)(PPh_3)_2]$ by reduction of $[RuCl_3(NO)(PPh_3)_2]$ with Zn or Zn/Cu which was subsequently used in reactivity studies[3] but only prepared in situ and not isolated.

When we attempted to extend the broad chemistry of the coordinatively unsaturated rhodium(I) complex $[RhCl(P\text{-}i\text{-}Pr_3)_2]$[4] to related bis(triisopropylphoshine)-ruthenium and -osmium species, we failed to prepare compounds of the type $[MCl_2(P\text{-}i\text{-}Pr_3)_2]$ (M = Ru, Os); instead we obtained the carbonyl(chloro)hydrido derivatives $[MHCl(CO)(P\text{-}i\text{-}Pr_3)_2]$.[5] Since the electron count of one hydrogen and one CO is equivalent to that of one NO, we speculated about the existence of four-coordinate chloro(nitrosyl) complexes which with sterically demanding phosphine ligands such as P-*i*-Pr_3 or PCy_3 should be more stable than the bis(triphenylphosphine) compound $[RuCl(NO)(PPh_3)_2]$.[2,3]

Here we report the synthesis of $[OsCl(NO)(P\text{-}i\text{-}Pr_3)_2]$ (**2**), which is the first structurally characterized $[OsL_4]$ complex, and of its P-*i*-Pr_2Ph counterpart **3**. We also describe studies on the reactivity of compounds **2** and **3** which were originally undertaken with the aim to prepare a series of carbene, vinylidene, and allenylidene complexes having $[OsCl(NO)(PR_3)_2]$ as a building block. Some preliminary results of this work were already communicated.[6]

Results and Discussion

Preparation of the Four-Coordinate Complexes *trans*-$[OsCl(NO)(PR_3)_2]$ (2, 3). The 18-electron compound $[OsCl(NO)(PPh_3)_3]$ (**1**), which was first synthesized by Roper et al. and used for the preparation of carbene, sulfur dioxide, and disulfoxide osmium(0) complexes,[7,8] reacts with P-*i*-Pr_3 and P-*i*-Pr_2Ph in toluene at room temperature with a complete removal of the triphenylphosphine ligands to give **2** and **3** in excellent yields (Scheme 1). Both compounds are dark-

† Dedicated to Professor F. Albert Cotton on the occasion of his 65th birthday.

® Abstract published in *Advance ACS Abstracts*, December 1, 1994.

(1) *Comprehensive Coordination Chemistry*; Wilkinson, G., Gillard, R. D., McCleverty, J. A., Eds.; Pergamon: New York, 1987; Vols. 4 and 5.

(2) Stiddard, M. H. B.; Townsend, R. E. *J. Chem. Soc., Chem. Commun.* **1969**, 1372.

(3) (a) Reed, J.; Pierpont, C. G.; Eisenberg, R. *Inorg. Synth.* **1976**, *16*, 21–24. (b) Jones, C. J.; McCleverty, J. A.; Rothin, A. S. *J. Chem. Soc., Dalton Trans.* **1985**, 401–403.

(4) Short reviews: (a) Werner, H. *Nachr. Chem. Tech. Lab.* **1992**, *40*, 435–444. (b) Werner, H. *J. Organomet. Chem.* **1994**, *475*, 45–55.

(5) Esteruelas, M. A.; Werner, H. *J. Organomet. Chem.* **1986**, *303*, 221–231.

(6) Werner, H.; Michenfelder, A.; Schulz, M. *Angew. Chem.* **1991**, *103*, 617–618. *Angew. Chem., Int. Ed. Engl.* **1991**, *30*, 596–598.

(7) (a) Hill, A. F.; Roper, W. R.; Waters, J. M.; Wright, A. H. *J. Am. Chem. Soc.* **1983**, *105*, 5939–5940. (b) Roper, W. R. *J. Organomet. Chem.* **1986**, *300*, 167–190. (c) Gallop, M. A.; Roper, W. R. *Adv. Organomet. Chem.* **1986**, *25*, 121–198.

(8) Herberhold, M.; Hill, A. F. *J. Organomet. Chem.* **1990**, *387*, 323–336.

0276-7333/95/2314-0612$09.00/0

Scheme 1

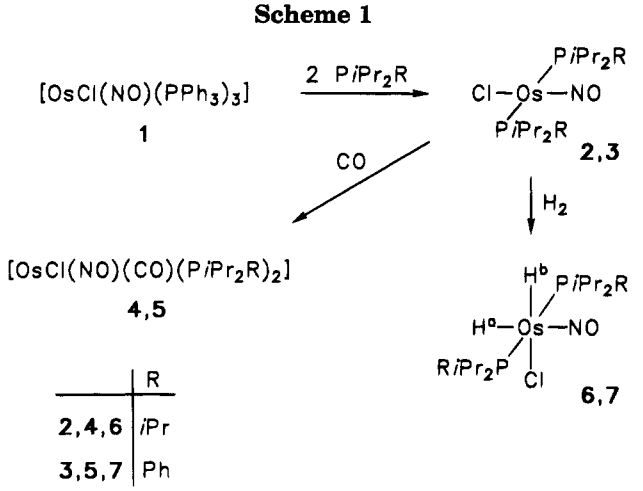

green crystalline solids which are quite air-sensitive and, with the exception of pentane and hexane, soluble in most common organic solvents. The ^{1}H NMR spectra, which for **2** show *one* and for **3** (due to the prochirality of the phosphorous atoms) *two* doublets of virtual triplets for the PCHCH_3 protons, indicate a square-planar configuration with *trans*-disposed phosphine ligands. This has been substantiated by the X-ray structure analysis of **2** which reveals that both the N–Os–Cl and P–Os–P units are nearly linear.[6] Since the osmium atom lies on the crystallographic center of symmetry, a 1:1 disorder of the Cl and NO ligands results,[9] which is also characteristic of other square-planar complexes *trans*-[MCl(L)(P-*i*-Pr$_3$)$_2$] (M = Rh or Ir).[10] Although both **2** and **3** decompose only at ca. 75 °C, they have to be stored at low temperature (below −10 °C) under an atmosphere of purified argon.

In contrast to the isoelectronic compound *trans*-[IrCl(CO)(P-*i*-Pr$_3$)$_2$],[11] the osmium complexes **2** and **3** react not only with Lewis acids such as CH_3I, HCl, CF_3CO_2H, etc.,[6,12] but also with Lewis bases. An almost instantaneous reaction occurs with CO which leads quantitatively to the formation of the five-coordinate carbonyl compounds **4** and **5**. They are bright yellow air-stable solids which have been characterized by elemental analysis and spectroscopic techniques. Since the position of the N–O stretching frequency in the IR spectra of **4** and **5** differs by ca. 200 cm^{-1}, we assume that the stereochemistry of the two complexes is not the same. As is shown in Figure 1, for the molecules of the general composition [OsCl(NO)(CO)L$_2$] four stereoisomers could exist provided that the two ligands L are equivalent. The latter has been confirmed by ^{1}H and ^{31}P NMR measurements (for details see Experimental Section). From the four stereoisomers, we consider **D** as being unlikely due to the *trans* disposition of the two strong π-acceptor ligands CO and NO. For five-coordinate osmium(0) compounds the trigonal-bipyramidal con-

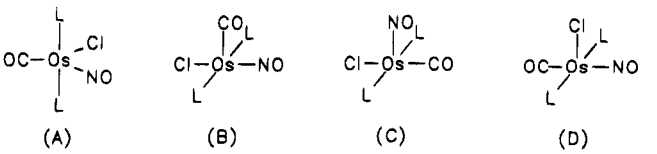

Figure 1. Possible stereoisomers of compounds **4** and **5** with *trans*-disposed phosphine ligands.

figuration in general seems to be favored and this has also been substantiated by X-ray structural analysis of the carbene complexes [OsCl(NO)(=CH$_2$)(PPh$_3$)$_2$][7a] and [OsCl(NO)(=CF$_2$)(PPh$_3$)$_2$].[13] We know, however, from our work on related 16-electron aryl(chloro) and vinyl(chloro) metal derivatives,[14,15] that the energy difference between the trigonal-bipyramidal and the square-pyramidal geometry is probably quite small and, therefore, predictions about which of the stereoisomers **A**, **B**, or **C** is preferred should be made with great caution.

The reactions of **2** and **3** with H_2 also proceed quite rapidly and give the expected dihydridoosmium(II) complexes **6** and **7** in 80–90% yield. Both are bright yellow solids for which, due to the appearance of *two* high-field signals in the ^{1}H NMR spectra, a *cis* arrangement of the hydride ligands can be proposed. If we take the strong *trans* influence of the NO ligand into consideration, we assign the resonance at δ −2.2 to H^a and that at δ −10.1 to H^b (see Scheme 1). According to the ^{1}H and ^{31}P NMR data of **6** and **7**, there is no doubt that the two phosphines are *trans* to each other. It should be mentioned that on treatment of Vaska's compound *trans*-[IrCl(CO)(PPh$_3$)$_2$] (which is structurally related to **2** and **3**) with H_2 also a dihydridometal derivative with *cis*-disposed hydrido and *trans*-disposed phosphine ligands is formed.[16]

Reactions of Compounds 2, 3 with Diazomethane and Terminal Alkynes. In attempting to build a series of osmium complexes of the type [Os]=CR$_2$, [Os]=C=CR$_2$, and [Os]=C=C=CR$_2$ where [Os] is [OsCl(NO)(P-*i*-Pr$_3$)$_2$] or [OsCl(NO)(P-*i*-Pr$_2$Ph)$_2$], we first studied the reactivity of **2** and **3** toward CH_2N_2 and other diazomethane derivatives. It was known from Roper's work that the 18-electron compound [OsCl(NO)(PPh$_3$)$_3$] reacts with CH_2N_2 by ligand substitution to give [OsCl(NO)(=CH$_2$)(PPh$_3$)$_2$] and PPh$_3$.[7a]

The reactions of the 16-electron species **2** and **3** with diazomethane proceed in benzene at room temperature virtually instantaneously and afford the carbene complexes **8** and **9** in 70–75% yield. In contrast to CH_2N_2, phenyl and diphenyldiazomethane are completely inert toward **2** and **3** and even on prolonged heating do not react with the starting materials. Compounds **8** and **9** (Scheme 2) are orange crystalline solids which are thermally remarkably stable (dec temp 197 °C and 189 °C, respectively) and can be handled in air. The most typical NMR spectroscopic features are the low-field signals for the CH$_2$ protons at δ 14.52 (**8**) and 14.36 (**9**) in the ^{1}H NMR and for the CH$_2$ carbon atom at δ 200.1 (**8**) and 210.4 (**9**) in the ^{13}C NMR spectra. Since in the IR spectra of **8** (1600 cm^{-1}) and **9** (1607 cm^{-1}) the ν-

(9) Schulz, M. Dissertation, Universität Würzburg, 1991.
(10) (a) Busetto, C.; D'Alfonso, A.; Maspero, F.; Perego, G.; Zazzetta, A. *J. Chem. Soc., Dalton Trans.* **1977**, 1828–1834. (b) Thorn, D. L.; Tulip, T. H.; Ibers, J. A. *J. Chem. Soc., Dalton Trans.* **1979**, 2022–2025. (c) Schenk, W. A.; Leissner, J.; Burschka, C. *Angew. Chem.* **1984**, *96*, 787–788; *Angew. Chem., Int. Ed. Engl.* **1984**, *23*, 806–807. (d) Dahlenburg, L.; Yardimcioglu, A. *J. Organomet. Chem.* **1985**, *291*, 371–386.
(11) (a) Strohmeier, W.; Onoda, T. *Z. Naturforsch., B: Anorg. Chem., Org. Chem.* **1968**, *23*, 1377–1379. (b) Werner, H.; Höhn, A. *Z. Naturforsch., B: Anorg. Chem., Org. Chem.* **1984**, *39*, 1505–1509.
(12) Flügel, R. Diplomarbeit, Universität Würzburg, 1993.
(13) Brothers, P. J.; Roper, W. R. *Chem. Rev.* **1988**, *88*, 1293–1326.
(14) Werner, H.; Höhn, A.; Dziallas, M. *Angew. Chem.* **1986**, *98*, 1112–1114. *Angew. Chem., Int. Ed. Engl.* **1986**, *25*, 1090–1092.
(15) Werner H.; Esteruelas, M. A.; Otto, H. *Organometallics* **1986**, *5*, 2295–2299.
(16) Vaska, L.; DiLuzio, J. W. *J. Am. Chem. Soc.* **1962**, *84*, 679–680.

Scheme 2

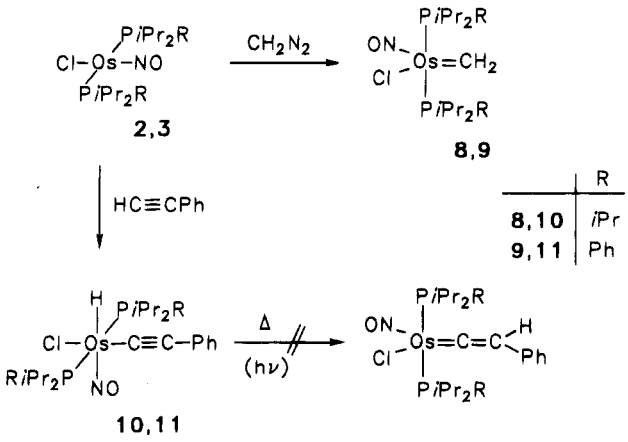

Scheme 3

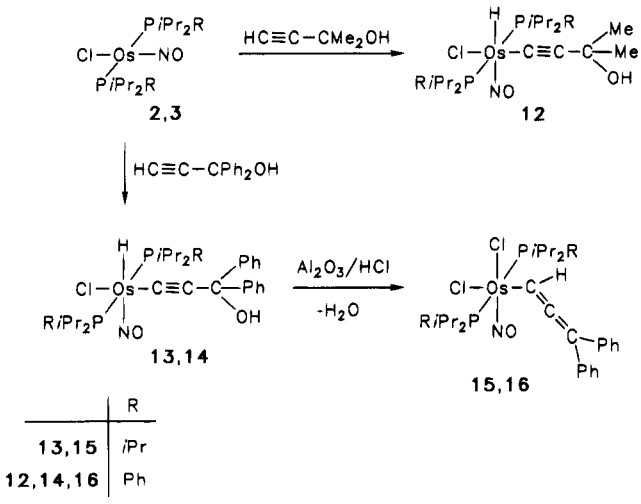

(NO) band appears at about the same wavenumber as that of $[OsCl(NO)(=CH_2)(PPh_3)_2]$,[7a] we assume that the new carbene osmium derivatives also have a trigonal-bipyramidal geometry.

The synthesis of the vinylidene complexes $[OsCl(NO)(=C=CHPh)(PR_3)_2]$ was attempted via thermal or photochemical rearrangement of the alkynyl(hydrido)osmium(II) isomers **10** and **11**. The latter are obtained (Scheme 2) in excellent yields by oxidative addition of phenylacetylene to **2** and **3** in toluene at room temperature. The ^1H NMR data of **10** and **11** (both are red air-stable solids) are noteworthy insofar as the signal of the Os*H* proton appears at unusually low fields (δ −0.72 for **10** and δ −0.85 for **11**) which is certainly due to the strong *trans* influence of the NO ligand. All attempts to rearrange the alkynyl(hydrido) compounds to the phenylvinylidene isomers failed; the structurally related octahedral iridium complex $[IrHCl(C{\equiv}CPh)(CO)(P\text{-}i\text{-}Pr_3)_2]$ is also surprisingly inert.[11b]

The terminal alkynols $HC{\equiv}CCMe_2OH$ and $HC{\equiv}CCPh_2OH$ behave similarly as phenylacetylene toward **2** and **3**. When suspensions of the 16-electron compounds are stirred for 12 h in toluene at room temperature, a change of color from green to red occurs and the functionalized alkynyl(hydrido)osmium(II) complexes **12**−**14** are formed in 70−80% yield (Scheme 3). According to the IR and NMR spectroscopic data there is no doubt that the ligand arrangement of **10**, **11** and of **12**−**14** is the same.

Since we knew that allenylidene metal complexes $L_nM{=}C{=}C{=}CRR'$ can be prepared from alkynols $HC{\equiv}C\text{-}CRR'OH$ via intermediately formed alkyne, alkynyl(hydrido), and vinylidene metal derivatives,[17,18] we attempted to use compounds **13** and **14** for the same purpose. On treatment with acidic alumina, which in the case of *trans*-$[RhCl(=C=CHCRR'OH)(P\text{-}i\text{-}Pr_3)_2]$ (R = Ph, R′ = H, Ph, Tol; R, R′ = $C_{12}H_8$) leads to the formation of *trans*-$[RhCl(C=C=CRR')(P\text{-}i\text{-}Pr_3)_2]$,[18a,b] the osmium complexes also react quite rapidly. However, instead of the expected products $[OsCl(NO)(=C=C=CPh_2)(PR_3)_2]$ the allenylosmium(II) compounds **15** and **16** are obtained (Scheme 3). Although we have no evidence, it nevertheless is conceivable that during the reactions of **13** and **14** with Al_2O_3 the complexes $[OsCl(NO)(=C=C=CPh_2)(PR_3)_2]$ are initially formed which with H^+ and Cl^- (both ions are present on commercial acidic alumina) give the allenyl derivatives. We note in this context that rhodium−carbon and osmium−carbon double bond systems such as $[C_5H_5Rh(=CPh_2)(PMe_3)]$,[19] $[C_5H_5Rh(=C=CHR)(P\text{-}i\text{-}Pr_3)]$,[20] and $[C_6H_6Os(=C=CHPh)(P\text{-}i\text{-}Pr_3)]$[21] also react with HX (X = Cl, CF_3CO_2) by attack to the M=C double bond. Characteristic spectroscopic features of **15** and **16** are the C=C=C stretching frequency in the IR spectra at about 1880 cm^{-1} and the three resonances in the ^{13}C NMR spectra at δ 76.2, 203.4, 104.4 (for **15**) and 79.1, 199.1, 101.0 (for **16**) for the α, β, and γ allenyl carbon atoms. In contrast to the related vinyl osmium compounds,[21] it is not unusual that the signal of the metal-bonded carbon appears at higher field than the signal of Cβ and Cγ.[22]

Molecular Structure of Compound 15. A single-crystal X-ray diffraction investigation of the allenyl complex **15** confirms the structural proposal shown in Scheme 3. The SCHAKAL drawing (Figure 2) reveals that the geometry about the osmium(II) center is nearly octahedral with the two chlorines *cis* and the two phosphines *trans* to each other. The largest corner-to-center-to-corner angles of the octahedron are found for Cl2−Os−N (96.8(1)°) and P1−Os−C1 (95.8(2)°) which is probably due to steric hindrance between the isopropyl substituents on P1 and one of the phenyl groups on C3. The Os−N−O unit is almost linear (174.4(5)°) as is the arrangement Cl1−Os−N (176.6(1)°). We note in particular that the distance Os−Cl1 is about 0.1 Å shorter than the distance Os−Cl2 which we attribute to the strong *trans* influence of the nitrosyl ligand. The bond length Os−C1 (2.110(5) Å) is what would be expected for a Os−C_{sp^2} single bond and comparable to that of the vinylosmium derivative $[C_6H_6OsI(CH{=}CHPh)(P\text{-}i\text{-}Pr_3)]$ (2.090(7) Å).[21] The carbon−carbon distances C1−C2 and C2−C3 in the Os−C=C=C chain (see Table 1) are nearly identical and quite similar to those found in $H_2C{=}C{=}CH_2$ and allene derivatives.[23] The

(17) Selegue, J. P. *Organometallics* **1982**, *1*, 217−218.
(18) (a) Werner, H.; Rappert, T. *Chem. Ber.* **1993**, *126*, 669−678. (b) Werner, H.; Rappert, T.; Wiedemann, R.; Wolf, J.; Mahr, N. *Organometallics* **1994**, *13*, 2721−2727. (c) Werner, H.; Stark, A.; Steinert, P.; Grünwald, C.; Wolf, J. *Chem. Ber.* **1994**, *127*, in press.
(19) Schwab, P. Dissertation, Universität Würzburg, 1994.
(20) Wolf, J.; Werner, H. *J. Organomet. Chem.* **1987**, *336*, 413−428.
(21) Werner, H.; Weinand, R.; Knaup, W.; Peters, K.; von Schnering, H. G. *Organometallics* **1991**, *10*, 3967−3977.
(22) Hesse, M.; Meier, H.; Zeeh, B. *Spektroskopische Methoden in der organischen Chemie*, 3rd ed., G. Thieme: Stuttgart, 1987; p 44.
(23) (a) Maki, A. G.; Toth, R. A. *J. Mol. Spectrosc.* **1965**, *17*, 136−155. (b) Groth, P. *Acta Chem. Scand.* **1973**, *27*, 3302−3307.

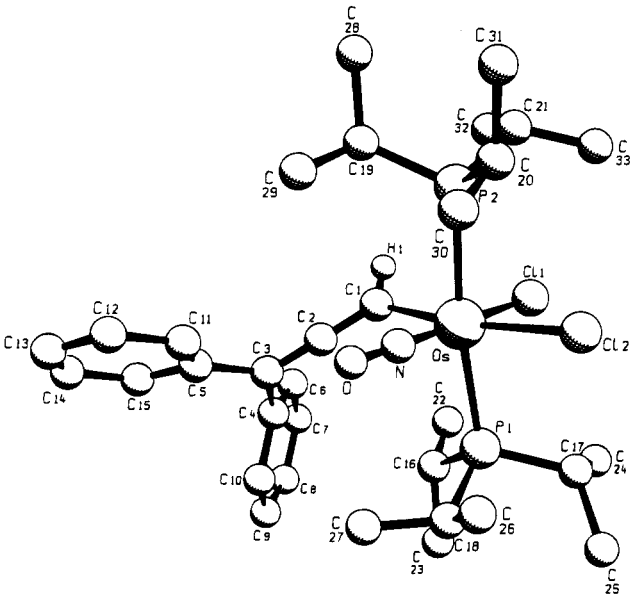

Figure 2. SCHAKAL diagram for the molecular structure of **15**.

Table 1. Selected Bond Distances and Angles with Esd's for 15

	Bond Distances (Å)		
Os−Cl1	2.396(2)	C1−C2	1.307(8)
Os−Cl2	2.489(1)	C2−C3	1.302(9)
Os−P1	2.449(2)	C3−C4	1.51(1)
Os−P2	2.523(2)	C3−C5	1.50(1)
Os−N	1.733(6)	C1−H1	0.95(7)
Os−C1	2.110(5)	N−O	1.106(8)
	Bond Angles (deg)		
Cl1−Os−Cl2	86.45(6)	P1−Os−C1	95.8(2)
Cl1−Os−P1	84.15(6)	P2−Os−N	91.0(2)
Cl1−Os−P2	90.24(6)	P2−Os−C1	89.1(2)
Cl1−Os−N	176.6(1)	N−Os−C1	91.3(2)
Cl1−Os−C1	85.5(1)	Os−N−O	174.4(5)
Cl2−Os−P1	88.40(5)	Os−C1−C2	129.6(4)
Cl2−Os−P2	85.96(5)	C1−C2−C3	175.4(6)
Cl2−Os−N	96.8(1)	C2−C3−C4	119.0(7)
Cl2−Os−C1	170.5(1)	C2−C3−C5	122.6(6)
P1−Os−P2	172.28(5)	C4−C3−C5	118.3(6)
P1−Os−N	94.9(2)	Os−C1−H1	115.(4)

bond angle Os−C1−C2 (129.6(4)°) deviates somewhat from the 120° value which is probably due to the considerable difference in size of the substituents at C1. It is presumably also for steric reasons that the two planes [Os,C1,C2,C3,H1] and [C1,C2,C3,C4,C5] are not really perpendicular to each other, the dihedral angle being 100.5(12)°.

Concluding Remarks

In this work we have described the preparation of the first stable and structurally characterized osmium(0) complexes in which the metal center only has a 16-electron configuration. We are convinced that it is the bulkiness of the phosphine ligands that allows the isolation of compounds **2** and **3** and which prevents the formation of electronically saturated species such as $[OsCl(NO)(PR_3)_3]$ or $[Os(\mu\text{-}Cl)(NO)(PR_3)_2]_2$. It should be emphasized that the yield of the isolated complexes $[OsCl(NO)(P\text{-}i\text{-}Pr_3)_2]$ (**2**) and $[OsCl(NO)(P\text{-}i\text{-}Pr_2Ph)_2]$ (**3**) is better than 90%!

As far as the reactivity of **2** and **3** is concerned, we note that on treatment with carbon monoxide or diazomethane addition of CO or CH_2 to the metal center occurs, leading to the five coordinate 18-electron osmium(0) compounds **4**, **5** and **8**, **9**, respectively. In contrast, with H_2 and terminal alkynes oxidative addition reactions take place which yield six-coordinate (equally 18-electron) osmium(II) complexes **6**, **7** and **10**–**14** with the incoming ligands H and C≡CR probably *cis* disposed. The most noteworthy facet of the chemistry of the alkynyl(hydrido)osmium derivatives **13** and **14**, which derive from the alkynol $HC{\equiv}CCPh_2OH$, is that they do not rearrange to give the isomeric osmium vinylidenes $[OsCl(NO)(=C=CHCPh_2OH)(PR_3)_2]$ like some related ruthenium(II) compounds[18c] but react with acidic alumina unexpectedly to afford the allenylosmium(II) complexes **15** and **16**. There is a variety of η^1-allenyl transition-metal compounds known but almost all of them were prepared by oxidative addition of propargyl or allenyl halides to nucleophilic metal precursors.[24] Although at present no conclusions regarding the mechanism of formation of **15**, **16** from **13**, **14** can be drawn, the possibility exists that allenylidene osmium species $[OsHCl(NO)(=C=C=CR_2)(PR_3)_2]^+$ are involved as intermediates which by a 1,2-H shift (promoted by Cl^-) of the metal-bound hydrogen to the α-carbon atom of the Os=C=C=C chain gives the final products.

It is finally worth mentioning that the molecular structure of **15** is one of the few reported of mononuclear η^1-allenyl metal complexes where the allenyl−metal bond is not supported by additional π-bonding of the Cβ−Cγ bond to the metal center.[24,25] The only other structurally characterized allenylosmium complex belongs to this class of π-complexes and has been prepared on a completely different route.[26] As far as the original aim of our present studies is concerned, the challenge remains! The future goal will be to find a method for transforming the alkynyl(hydrido)osmium compounds to the vinylidene isomers and to prepare the desired allenylideneosmium(0) complexes possibly by HCl elimination from the new η^1-allenylosmium(II) derivatives.

Experimental Section

All reactions were carried out under an atmosphere of argon by Schlenk tube techniques. The starting material **1**[7a] and the phosphine $P\text{-}i\text{-}Pr_2Ph$[27] were prepared as described in the literature. $P\text{-}i\text{-}Pr_3$ was a commercial product from Aldrich. NMR spectra were recorded on Bruker AC 200 and Bruker AMX 400 instruments, and IR spectra on a Perkin-Elmer 1420 infrared spectrophotometer. Melting points were determined by DTA.

Preparation of *trans*-$[OsCl(NO)(P\text{-}i\text{-}Pr_3)_2]$ (2). A suspension of **1** (150 mg, 0.18 mmol) in 15 mL of benzene was treated with an excess of $P\text{-}i\text{-}Pr_3$ (85 μL, 0.45 mmol) and then stirred for 30 min at room temperature. The solution was concentrated to ca. 3 mL in vacuo and 5 mL of hexane was

(24) (a) Jacobs, T. L. in *The Chemistry of the Allenes*; Landor, S. R., Ed.; Academic Press: London, 1982; Vol. 2, p 334. (b) Wojcicki, A.; Shuchart, C. E. *Coord. Chem. Rev.* **1990**, *105*, 35–60. (c) Elsevier, C. J.; Kleijn, H.; Boersma, J.; Vermeer, P. *Organometallics* **1986**, *5*, 716–720. (d) Keng, R.-S.; Lin, Y.-C. *Organometallics* **1990**, *9*, 289–291. (e) Shuchart, C. E.; Willis, R. R.; Wojcicki, A. *J. Organomet. Chem.* **1992**, *424*, 185–198.

(25) (a) Andrianov, B. G.; Zlotina, I. B.; Chomutov, M. A.; Kolobova, N. E.; Struchkov, Yu. T. *Koord. Khim.* **1978**, *4*, 298. (b) Wojcicki, A. *New J. Chem.* **1994**, *18*, 61. (c) Wouters, J. M. A.; Klein, R. A.; Elsevier, C. J.; Häming, L.; Stam, C. H. *Organometallics*, submitted for publication.

(26) Gotzig, J.; Otto, H.; Werner, H. *J. Organomet. Chem.* **1985**, *287*, 247–254.

(27) Kukla, F. Dissertation, Universität Würzburg, in preparation.

added. Dark green air-sensitive crystals precipitated which were filtered off, washed with 10 mL of pentane, and dried in vacuo: yield 84 mg (91%); mp 77 °C dec. Anal. Calcd for $C_{18}H_{42}ClNOOsP_2$: C, 37.35; H, 7.35; N, 2.43. Found: C, 36.87; H, 7.67; N, 2.11. IR (KBr): ν(NO) 1700 cm^{-1}. ^{1}H NMR (C_6D_6, 200 MHz): δ 2.62 (m, 6H, PC*H*CH$_3$), 1.37 (dvt, N = 13.5, J(HH) = 7.1 Hz, 36H, PCHC*H*$_3$). ^{31}P NMR (C_6D_6, 81.0 MHz): δ 37.82 (s).

Preparation of *trans*-[OsCl(NO)(P-*i*-Pr$_2$Ph)$_2$] (3). This compound was prepared analogously as described for **2**, using **1** (150 mg, 0.18 mmol) and P-*i*-Pr$_2$Ph (88 μL, 0.45 mmol). A dark green air-sensitive solid was isolated: yield 112 mg (97 %); mp 75 °C dec. Anal. Calcd for $C_{24}H_{38}ClNOOsP_2$: C, 44.75; H, 5.89; N, 2.17. Found: C, 45.10; H, 5.51; N, 1.74. IR (THF): ν(NO) 1710 cm^{-1}. ^{1}H NMR (C_6D_6, 200 MHz): 7.31–6.95 (m, 10H, C_6H_5), 2.90 (m, 4H, PC*H*CH$_3$), 1.43 (dvt, N = 14.5, J(HH) = 6.9 Hz, 12H, PCHC*H*$_3$), 1.14 (dvt, N = 14.1, J(HH) = 6.7 Hz, 12H, PCHC*H*$_3$). ^{31}P NMR (C_6D_6, 36.2 MHz): δ 39.61 (s).

Preparation of [OsCl(CO)(NO)(P-*i*-Pr$_3$)$_2$] (4). A slow stream of CO was passed for 1 min through a solution of **2** (101 mg, 0.16 mmol) in 10 mL of toluene. An immediate color change from dark green to yellow occured. After the solution was concentrated to ca. 2 mL in vacuo, 5 mL of pentane was added. A yellow air stable solid was formed which was filtered off, repeatedly washed with pentane, and dried in vacuo; yield 97 mg (92%); mp 101 °C dec. Anal. Calcd for $C_{19}H_{42}ClNO_2OsP_2$: C, 37.77; H, 7.01; N, 2.32. Found: C, 37.56; H, 6.89; N, 2.07. IR (KBr): ν(CO) 1895, ν(NO) 1755 cm^{-1}. ^{1}H NMR ($CDCl_3$, 200 MHz): δ 2.83 (m, 4H, PC*H*CH$_3$), 1.39 (dvt, N = 14.0, J(HH) = 6.8 Hz, 18H, PCHC*H*$_3$), 1.25 (dvt, N = 14.0, J(HH) = 6.8 Hz, 18H, PCHC*H*$_3$). ^{31}P NMR (C_6D_6, 81.0 MHz): δ 23.65 (s).

Preparation of [OsCl(CO)(NO)(P-*i*-Pr$_2$Ph)$_2$] (5). This compound was prepared analogously as described for **4**, using **3** (155 mg, 0.24 mmol) as starting material. A yellow microcrystalline solid was obtained: yield 155 mg (96%); mp 142 °C dec. Anal. Calcd for $C_{25}H_{38}ClNO_2OsP_2$: C, 44.67; H, 5.70; N, 2.08. Found: C, 44.48; H 5.88; N, 1.89. IR (KBr): ν(CO) 1896, ν(NO) 1560 cm^{-1}. ^{1}H NMR ($CDCl_3$, 200 MHz): δ 7.56–7.22 (m, 10H, C_6H_5), 3.31 (m, 2H, PC*H*CH$_3$), 3.00 (m, 2H, PC*H*CH$_3$), 1.40 (dvt, N = 14.4, J(HH) = 6.9 Hz, 6H, PCHC*H*$_3$), 1.13 (dvt, N = 14.8, J(HH) = 7.0 Hz, 6H, PCHC*H*$_3$), 1.01 (dvt, N = 14.0, J(HH) = 6.8 Hz, 6H, PCHC*H*$_3$), 0.85 (dvt, N = 14.6, J(HH) = 7.2 Hz, 6H, PCHC*H*$_3$). ^{31}P NMR ($CDCl_3$, 81.0 MHz): δ 24.02 (s).

Preparation of [OsH$_2$Cl(NO)(P-*i*-Pr$_3$)$_2$] (6). A stream of H_2 was passed for 3 min through a solution of **2** (134 mg, 0.23 mmol) in 10 mL of toluene. An immediate color change from dark green to yellow occured. After the reaction mixture was concentrated to ca. 2 mL in vacuo, 10 mL of pentane was added. On cooling to −78 °C a yellow crystalline solid separated which was filtered off, washed with small quantities of pentane, and dried in vacuo: yield 123 mg (92%); mp 102 °C dec. Anal. Calcd for $C_{18}H_{44}ClNOOsP_2$: C, 37.39; H, 7.67; N, 2.42. Found: C, 36.89; H, 7.66; N, 2.11. IR (KBr): ν(OsH) 2130, 2050, ν(NO) 1713 cm^{-1}. ^{1}H NMR ($CDCl_3$, 200 MHz): δ 3.08 (m, 6H, PC*H*CH$_3$), 1.23 (dvt, N = 15.2, J(HH) = 7.7 Hz, 18H, PCHC*H*$_3$), 1.13 (dvt, N = 14.9, J(HH) = 6.9 Hz, 18H, PCHC*H*$_3$), −2.16 (dt, J(PH) = 23.4, J(HH) = 7.3 Hz, 1H, OsH), −10.03 (dt, J(PH) = 14.3, J(HH) = 7.3 Hz, 1H, OsH). ^{31}P NMR (C_6D_6, 81.0 MHz): δ 30.68 (s).

Preparation of [OsH$_2$Cl(NO)(P-*i*-Pr$_2$Ph)$_2$] (7). This compound was prepared analogously as described for **6**, starting with **3** (145 mg, 0.23 mmol) in 15 mL of toluene. A yellow microcrystalline solid was isolated: yield 119 mg (82%); mp 99 °C dec. Anal. Calcd for $C_{24}H_{40}ClNOOsP_2$: C, 44.61; H, 6.24; N, 2.16. Found: C, 45.02, H, 5.96; N, 1.78. IR (KBr): ν(OsH) 2140, 2059, ν(NO) 1706 cm^{-1}. ^{1}H NMR ($CDCl_3$, 200 MHz): δ 7.71–7.09 (m, 10H, C_6H_5), 3.01 (m, 2H, PC*H*CH$_3$), 2.80 (m, 2H, PC*H*CH$_3$), 1.20 (dvt, N = 15.7, J(HH) = 7.9 Hz, 6H, PCHC*H*$_3$), 1.16 (dvt, N = 14.8, J(HH) = 6.7 Hz, 6H, PCHC*H*$_3$), 1.12 (dvt, N = 14.9, J(HH) = 6.7 Hz, 6H, PCHC*H*$_3$), 1.07 (dvt, N = 14.7, J(HH) = 6.7 Hz, 6H, PCHC*H*$_3$), −2.25 (dt, J(PH) = 25.1, J(HH) = 7.9 Hz, 1H, OsH), −10.15 (dt, J(PH) = 15.3, J(HH) = 6.9 Hz, 1H, OsH). ^{31}P NMR ($CDCl_3$, 81.0 MHz): δ 29.08 (s).

Preparation of [OsCl(NO)(=CH$_2$)(P-*i*-Pr$_3$)$_2$] (8). A suspension of **2** (203 mg, 0.35 mmol) in 15 mL of toluene was treated at 0 °C dropwise with a solution of CH_2N_2 in ether. A slow color change from dark green to orange accompanied by a gas evolution occurred. After the solvent was removed in vacuo, the oily residue was dissolved in 2 mL of benzene, and the solution was chromatographed on Al_2O_3 (neutral, activity grade V, height of column 4 cm). With benzene, an orange fraction was eluted which was brought to dryness in vacuo. The residue was dissolved in 3 mL of ethanol/CH_2Cl_2 (1:1). The solution was slowly evaporated in vacuo until the formation of a crystalline orange solid was observed. This was filtered off and dried in vacuo; yield 156 mg (75%); mp 197 °C dec. Anal. Calcd for $C_{19}H_{44}ClNOOsP_2$: C, 38.67; H, 7.52; N, 2.37. Found: C, 38.46; H, 7.81; N, 2.59. IR (KBr): ν(NO) 1600 cm^{-1}. ^{1}H NMR (C_6D_6, 400 MHz): δ 14.52 (t, J(PH) = 18.2 Hz, 2H, Os=CH$_2$), 3.32 (m, 6H, PC*H*CH$_3$), 1.65 (dvt, N = 13.7, J(HH) = 6.9 Hz, 18H, PCHC*H*$_3$), 1.34 (dvt, N = 14.2, J(HH) = 7.0 Hz, 18H, PCHC*H*$_3$). ^{13}C NMR ($CDCl_3$, 50.3 MHz): δ 200.08 (t, J(PC) = 14.2 Hz, Os=CH$_2$), 23.03 (vt, N = 25.4 Hz, P*C*HCH$_3$), 19.44, 18.83 (both s, PCH*C*H$_3$). ^{31}P NMR ($CDCl_3$, 81.0 MHz): δ 10.77 (s).

Preparation of [OsCl(NO)(=CH$_2$)(P-*i*-Pr$_2$Ph)$_2$] (9). This compound was prepared analogously as described for **8**, using **3** (230 mg, 0.36 mmol) in 15 mL of toluene as starting material. An orange air-stable solid was obtained: yield 167 mg (71%); mp 189 °C dec. Anal. Calcd for $C_{25}H_{40}ClNOOsP_2$: C, 45.62; H, 6.13; N, 2.13. Found: C, 46.12; H, 5.62; N, 1.65. IR (KBr): ν(NO) 1607 cm^{-1}. ^{1}H NMR (C_6D_6, 400 MHz): δ 14.36 (t, J(PH) = 17.7 Hz, Os=CH$_2$), 7.62–7.02 (m, 10H, C_6H_5), 3.44 (m, 2H, PC*H*CH$_3$), 2.75 (m, 2H, PC*H*CH$_3$), 1.32 (dvt, N = 14.6, J(HH) = 6.7 Hz, 6H, PCHC*H*$_3$), 1.23 (dvt, N = 15.3, J(HH) = 6.7 Hz, 6H, PCHC*H*$_3$), 1.05 (dvt, N = 14.3, J(HH) = 6.8 Hz, 6H, PCHC*H*$_3$), 0.94 (dvt, N = 13.9, J(HH) = 6.7 Hz, 6H, PCHC*H*$_3$). ^{13}C NMR (C_6D_6, 100.6 MHz): δ 210.44 (t, J(PC) = 13.0 Hz, Os=CH$_2$), 135.53, 128.79 (both vt, N = 8.6 and 9.7 Hz, ortho-C and meta-C of PC$_6$H$_5$), 131.95 (s, para-C of PC$_6$H$_5$), 128.34 (vt, N = 40.6 Hz, ipso-C of PC$_6$H$_5$), 25.60 (vt, N = 29.7 Hz, P*C*HCH$_3$), 24.62 (vt, N = 27.2 Hz, P*C*HCH$_3$), 20.44, 19.50, 19.33, 17.60 (all s, PCH*C*H$_3$). ^{31}P NMR (C_6D_6, 162.0 MHz): δ 21.79 (s).

Preparation of [OsHCl(C≡CPh)(NO)(P-*i*-Pr$_3$)$_2$] (10). A suspension of **2** (182 mg, 0.32 mmol) in 10 mL of toluene was treated at room temperature dropwise with phenylacetylene (35 μL, 33 mg, 0.32 mmol). A spontaneous color change from dark green to red occurred. After the solution was stirred for 4 h, the solvent was removed in vacuo. The residue was dissolved in 2 mL of benzene, and the solution was chromatographed on Al_2O_3 (neutral, activity grade V, height of column 4 cm). With benzene a red fraction was eluted which was concentrated to 2 mL in vacuo. After addition of 10 mL of pentane a red solid precipitated which was filtered off and dried in vacuo: yield 197 mg (92%); mp 162 °C dec. Anal. Calcd for $C_{26}H_{48}ClNOOsP_2$: C, 46.04; H, 7.13; N, 2.06. Found: C, 46.18; H, 7.36; N, 2.11. IR (KBr): ν(OsH) 2205, ν(C≡C) 2115, ν(NO) 1795 cm^{-1}. ^{1}H NMR ($CDCl_3$, 200 MHz): δ 7.65–7.42 (m, 5H, C_6H_5), 3.03 (m, 6H, PC*H*CH$_3$), 1.28 (dvt, N = 14.2, J(HH) = 6.9 Hz, 18H, PCHC*H*$_3$), 1.15 (dvt, N = 14.5, J(HH) = 7.1 Hz, 18H, PCHC*H*$_3$), −0.72 (t, J(PH) = 25.5 Hz, 1H, OsH). ^{31}P NMR ($CDCl_3$, 81.0 MHz): δ 18.21 (s).

Preparation of [OsHCl(C≡CPh)(NO)(P-*i*-Pr$_2$Ph)$_2$] (11). This compound was prepared analogously as described for **10** by using **3** (210 mg, 0.33 mmol) in 15 mL of toluene as starting material. Red air-stable crystals were obtained: yield 182 mg (75%); mp 127 °C dec. Anal. Calcd for $C_{32}H_{44}ClNOOsP_2$: C, 51.45; H, 5.90; N, 1.87. Found: C, 50.98; H, 5.39; N, 1.66. IR (THF): ν(OsH) 2200, ν(C≡C) 2099, ν(NO) 1780 cm^{-1}. ^{1}H NMR

(C_6D_6, 400 MHz): δ 7.59–7.28 (m, 15H, C_6H_5), 3.15 (m, 2H, PC*H*CH$_3$), 3.07 (m, 2H, PC*H*CH$_3$), 1.16 (dvt, *N* = 13.4, *J*(HH) = 6.9 Hz, 6H, PCHC*H*$_3$), 1.10 (dvt, *N* = 13.4, *J*(HH) = 7.2 Hz, 6H, PCHC*H*$_3$), 1.09 (dvt, *N* = 15.0, *J*(HH) = 7.5 Hz, 6H, PCHC*H*$_3$), 1.07 (dvt, *N* = 13.2, *J*(HH) = 6.4 Hz, 6H, PCHC*H*$_3$), −0.85 (t, *J*(PH) = 24.8 Hz, 1H, OsH). ^{13}C NMR ($CDCl_3$, 100.6 MHz): δ 133.74, 126.27 (both vt, *N* = 8.3 and 9.2 Hz, ortho-C and meta-C of PC$_6$H$_5$), 130.06, 129.25, 126.37, 123.95 (all s, ortho-C, meta-C, and para-C of C_6H_5, para-C of PC$_6$H$_5$), 127.38 (s, ipso-C of C_6H_5), 123.80 (vt, *N* = 46.8 Hz, ipso-C of PC$_6$H$_5$), 101.25 (s, OsC≡*C*Ph), 80.04 (t, *J*(PC) = 11.1 Hz, Os*C*≡CPh), 22.82 (vt, *N* = 32.2 Hz, P*C*HCH$_3$), 21.88 (vt, *N* = 30.2 Hz, P*C*HCH$_3$), 16.72, 16.53, 16.37, 15.72 (all s, PCH*C*H$_3$). ^{31}P NMR ($CDCl_3$, 81.0 MHz): δ 22.14 (s).

Preparation of [OsHCl(C≡CCMe$_2$OH)(NO)(P-*i*-Pr$_2$Ph)$_2$] (12). A suspension of **3** (172 mg, 0.27 mmol) in 10 mL of toluene was treated dropwise with HC≡CCMe$_2$OH (29 μL, 0.30 mmol) at room temperature. After the reaction mixture was stirred for 12 h, a color change from green to red had occurred. The solvent was removed in vacuo, and the oily residue was dissolved in 2 mL of benzene. The solution was chromatographed on Al_2O_3 (neutral, activity grade III, height of column 4 cm). With benzene a red fraction was eluted which was brought to dryness in vacuo. The residue was suspended in 15 mL of pentane and stirred for 30 min in an ultrasonic bath. A pale red solid was formed which was filtered off and dried in vacuo: yield 133 mg (69%); mp 103 °C dec. Anal. Calcd for $C_{23}H_{50}ClNOOsP_2$: C, 42.88; H, 7.70; N, 2.17. Found: C, 42.71; H, 7.63; N, 2.01. IR (THF): ν(OH) 3450, ν(OsH) 2110, ν(C≡C) 2078, ν(NO) 1720 cm^{-1}. ^{1}H NMR (C_6D_6, 200 MHz): δ 7.78–7.19 (m, 10H, C_6H_5), 3.53 (m, 2H, P*C*HCH$_3$), 3.07 (m, 2H, P*C*HCH$_3$), 2.37 (s, 1H, OH), 1.80 (s, 6H, C(C*H*$_3$)$_2$OH), 1.75 (dvt, *N* = 14.8, *J*(HH) = 7.5 Hz, 6H, PCHC*H*$_3$), 1.58 (dvt, *N* = 14.7, *J*(HH) = 7.4 Hz, 6H, PCHC*H*$_3$), 1.31 (dvt, *N* = 15.1, *J*(HH) = 7.7 Hz, 6H, PCHC*H*$_3$), 1.19 (dvt, *N* = 14.9, *J*(HH) = 6.8 Hz, 6H, PCHC*H*$_3$), −0.74 (t, *J*(PH) = 25.6 Hz, 1H, OsH). ^{31}P NMR ($CDCl_3$, 81.0 MHz): δ 22.46 (s).

Preparation of [OsHCl(C≡CCPh$_2$OH)(NO)(P-*i*-Pr$_3$)$_2$] (13). A suspension of **2** (230 mg, 0.39 mmol) in 20 mL of toluene was treated at room temperature with a 0.4 M solution of HC≡CCPh$_2$OH in toluene (0.9 mL, 0.39 mmol). After the reaction mixture was stirred for 24 h, a color change from green to red had occurred. The solvent was removed in vacuo, the oily residue was dissolved in 2 mL of benzene, and the solution was chromatographed on Al_2O_3 (neutral, activity grade V, height of column 5 cm). With benzene, a red fraction was eluted which was brought to dryness in vacuo. The residue was suspended in 15 mL of pentane, and the suspension was treated for 1 h in an ultrasonic bath. After the solvent was removed, a red air-stable solid was isolated which was dried in vacuo: yield 251 mg (81%); mp 101 °C dec. Anal. Calcd for $C_{33}H_{54}ClNO_2OsP_2$: C, 50.53; H, 6.93; N, 1.78. Found: C, 50.69; H, 6.72; N, 1.42. IR (THF): ν(OH) 3560, ν(OsH) = 2114, ν(C≡C) 2075, ν (NO) 1753 cm^{-1}. ^{1}H NMR (C_6D_6, 200 MHz): 7.87–7.02 (m, 10H, C_6H_5), 2.87 (m, 6H, P*C*HCH$_3$), 2.43 (m, 1H, OH), 1.16 (dvt, *N* = 14.3, *J*(HH) = 7.3 Hz, 18H, PCHC*H*$_3$), 1.15 (dvt, *N* = 13.9, *J*(HH) = 7.3 Hz, 18H, PCHC*H*$_3$), −0.87 (t, *J*(PH) = 23.9 Hz, 1H, OsH). ^{13}C NMR (C_6D_6, 50.3 MHz): δ 135.05 (s, ipso-C of C_6H_5), 132.49, 132.29, 131.65 (all s, ortho-C, meta-C, and para-C of C_6H_5), 102.1 (s, OsC≡*C*R), 77.54 (t, *J*(PC) =10.5 Hz, Os*C*≡CR), 75.38 (s, *C*Ph$_2$-OH), 24.34 (vt, *N* = 28.1 Hz, P*C*HCH$_3$), 18.78, 18.61 (both s, PCH*C*H$_3$). ^{31}P NMR (C_6D_6, 81.0 MHz): δ 19.71 (s).

Preparation of [OsHCl(C≡CCPh$_2$OH)(NO)(P-*i*-Pr$_2$Ph)$_2$] (14). This compound was prepared analogously as described for **13**, using **3** (298 mg, 0.46 mmol) in 20 mL of toluene as starting material. A red air-stable solid was obtained: yield 323 mg (82%); mp 88 °C dec. Anal. Calcd for $C_{39}H_{50}ClNO_2OsP_2$: C, 54.94; H, 5.91; N, 1.64. Found: C, 54.95; H, 5.76; N, 1.38. IR (THF): ν(OH) 3570, ν(OsH) 2112, ν(C≡C) 2080, ν(NO) 1736 cm^{-1}. ^{1}H NMR (C_6D_6, 400 MHz): δ 7.46–6.92 (m, 20H, C_6H_5), 3.09 (m, 2H, P*C*HCH$_3$), 2.89 (m, 2H, P*C*HCH$_3$), 2.42 (s, 1H, OH), 1.05 (dvt, *N* = 14.3, *J*(HH) = 6.9 Hz, 6H, PCHC*H*$_3$), 1.02 (dvt, *N* = 13.9, *J*(HH) = 6.8 Hz, 6H, PCHC*H*$_3$), 0.98 (dvt, *N* = 13.8, *J*(HH) = 6.8 Hz, 6H, PCHC*H*$_3$), 0.91 (dvt, *N* = 14.5, *J*(HH) = 6.6 Hz, 6H, P*C*HCH$_3$), −0.98 (t, *J*(PH) = 24.8 Hz, 1H, OsH). ^{13}C NMR (C_6D_6, 100 MHz): δ 134.70, 127.83 (both vt, *N* = 8.6 and 9.5 Hz, ortho-C and meta-C of PC$_6$H$_5$), 132.14 (s, ipso-C of C_6H_5), 130.56, 127.34, 126.46, 126.13 (all s, ortho-C, meta-C, and para-C of C_6H_5, para-C of PC$_6$H$_5$), 125.35 (vt, *N* = 45.6 Hz, ipso-C of PC$_6$H$_5$), 104.62 (s, OsC≡*C*R), 75.47 (s, *C*Ph$_2$OH), 74.41 (t, *J*(PC) = 12.2 Hz, Os*C*≡CR), 23.50 (vt, *N* = 34.5 Hz, P*C*HCH$_3$), 22.57 (vt, *N* = 29.3 Hz, P*C*HCH$_3$), 17.96, 17.75, 17.61, 16.64 (all s, PCH*C*H$_3$). ^{31}P NMR (C_6D_6, 162.0 MHz): δ 22.46 (s).

Preparation of [OsCl$_2$(CH=C=CPh$_2$)(NO)(P-*i*-Pr$_3$)$_2$] (15). A solution of **13** (251 mg, 0.32 mmol) in 1 mL of benzene was passed through a column with Al_2O_3 (acidic, activity grade I, height of column 5 cm). During the elution with benzene, a color change from red to yellow occurred. The yellow fraction was separated and brought to dryness in vacuo. The residue was suspended in 10 mL of pentane, and the suspension was treated for 10 min in an ultrasonic bath. After the solvent was removed in vacuo, a yellow air-stable solid was obtained which was filtered off and dried in vacuo: yield 123 mg (48%); mp 175 °C dec. Anal. Calcd for $C_{33}H_{53}Cl_2NOOsP_2$: C, 49.37; H, 6.65; N, 1.74. Found: C, 49.61; H, 6.76; N, 1.72. IR (KBr): ν(C=C=C) 1881, (NO) 1780 cm^{-1}. ^{1}H NMR ($CDCl_3$, 400 MHz): δ 8.08 (t, *J*(PH) = 2.0 Hz, 1H, OsC*H*=C=CPh$_2$), 7.37–7.06 (m, 10H, C_6H_5), 2.94 (m, 6H, P*C*HCH$_3$), 1.33 (dvt, *N* = 13.8, *J*(HH) = 7.1 Hz, 18H, PCHC*H*$_3$), 1.19 (dvt, *N* = 13.3, *J*(HH) = 7.2 Hz, 18H, PCHC*H*$_3$). ^{13}C NMR ($CDCl_3$, 100.6 MHz): δ 203.40 (s, OsCH=*C*=CPh$_2$), 141.00 (s, ipso-C of C_6H_5), 129.20 (s, para-C of C_6H_5), 128.18, 126.44 (both s, ortho-C and meta-C of C_6H_5), 104.37 (s, OsCH=C=*C*Ph$_2$), 76.20 (t, *J*(PC) = 6.8 Hz, Os*C*H=C=CPh$_2$), 25.74 (vt, *N* = 23.5 Hz, P*C*HCH$_3$), 20.97, 20.54 (both s, PCH*C*H$_3$). ^{31}P NMR ($CDCl_3$, 162.0 MHz): δ −4.37 (s, J(^{187}Os^{31}P) = 156.2 Hz).

Preparation of [OsCl$_2$(CH=C=CPh$_2$)(NO)(P-*i*-Pr$_2$Ph)$_2$] (16). This compound was prepared analogously as described for **15**, using **14** (240 mg, 0.28 mmol) in 1 mL of benzene as starting material. A red air-stable solid was isolated: yield 103 mg (42%); mp 195 °C dec. Anal. Calcd for $C_{39}H_{49}Cl_2NOOsP_2$: C, 53.78; H, 5.67; N, 1.60. Found: C, 53.40; H, 5.60; N, 1.55. IR (KBr): ν(C=C=C) 1884, ν(NO) 1808 cm^{-1}. ^{1}H NMR ($CDCl_3$, 400 MHz): δ 7.35 (t, *J*(PH) = 2.0 Hz, 1H, OsC*H*=C=CPh$_2$), 7.28–6.97 (m, 20H, C_6H_5), 3.41 (m, 2H, P*C*HCH$_3$), 3.22 (m, 2H, P*C*HCH$_3$), 1.42 (dvt, *N* = 14.9, *J*(HH) = 7.5 Hz, 6H, PCHC*H*$_3$), 1.33 (dvt, *N* = 15.1, *J*(HH) = 7.7 Hz, 6H, PCHC*H*$_3$), 1.17 (dvt, *N* = 14.3, *J*(HH) = 7.2 Hz, 6H, PCHC*H*$_3$), 1.12 (dvt, *N* = 14.2, *J*(HH) = 7.1 Hz, 6H, PCHC*H*$_3$). ^{13}C NMR ($CDCl_3$, 100.6 MHz): δ 199.06 (s, OsCH=*C*=CPh$_2$), 138.27 (s, ipso-C of C_6H_5), 131.42, 126.43 (both vt, *N* = 6.6 and 8.4 Hz, ortho-C, and meta-C of PC$_6$H$_5$), 128.34, 127.39, 126.96, 126.58 (all s, ortho-C, meta-C, and para-C of C_6H_5, para-C of PC$_6$H$_5$), 101.01 (s, OsCH=C=*C*Ph$_2$), 79.06 (t, *J*(PC) = 6.5 Hz, OsCH=C=CPh$_2$), 23.30 (vt, *N* = 25.0 Hz, P*C*HCH$_3$), 22.84 (vt, *N* = 26.1 Hz, P*C*HCH$_3$), 18.92, 18.58, 17.56, 17.07 (all s, PCH*C*H$_3$). ^{31}P NMR ($CDCl_3$, 162.0 MHz): δ −9.12 (s, J(^{187}Os^{31}P) = 161.2 Hz).

Crystal Structure Analysis of 15. Single crystals were grown from THF. Crystal data (from 23 reflections, 10° < θ < 15°): monoclinic, space group $P2_1$ (No. 4); *a* = 9.901(1) Å, *b* = 16.041(1) Å, *c* = 11.812(6) Å, β = 111.59(1)°, *V* = 1744(1) Å^3, *Z* = 2, d_{calcd} = 1.529 g cm^{-3}, μ(Mo Kα) = 39.3 cm^{-1}; crystal size 0.13 × 0.3 × 0.35 mm; Enraf-Nonius CAD4 diffractometer, Mo Kα radiation (0.70930 Å, graphite monochromator, zirconium filter (factor 15.41); *T* = 293 K; ω/θ scan, max 2θ = 56°; 4585 reflections measured, 4338 independent reflections, 4100 regarded as being observed ($F_0 > 3\sigma(F_0)$). Intensity data were corrected for Lorentz and polarization effects, and an empirical absorption correction (ψ-scan method) was applied (minimum transmission 64.01%). The structure was solved by the Patterson method (SHELXS-86). Atomic coordinates and

anisotropic thermal parameters of the non-hydrogen atoms were refined by full-matrix least squares (363 parameters, unit weights, Enraf-Nonius SDP). The hydrogen atom H1 could be located by a difference Fourier analysis and was isotropically refined. The positions of all other hydrogen atoms were calculated according to an ideal geometry (C−H distance 0.95 Å) and were included in the structure factor calculation in the last refinement cycle. The isopropyl methyl groups at C17 are disordered; the corresponding disordered positions were taken with a weighting scheme of 0.7 to 0.3 and refined isotropically. $R = 0.022$, $R_w = 0.025$; reflex/parameter ratio 11.3; residual electron density +0.734/−0.707 e $Å^{-3}$.

Acknowledgment. We thank the Deutsche Forschungsgemeinschaft (SFB 347) and the Fonds der Chemischen Industrie for financial support, and in particular Degussa AG for various gifts of chemicals. We also gratefully acknowledge support by Mrs. M.-L. Schäfer, B. Stempfle, and Dr. W. Buchner (NMR spectra), Mrs. A. Burger, Mrs. U. Neumann, and C. P. Kneis (elemental analyses), and Mrs. R. Schedl for DTA measurements.

Supplementary Material Available: Tables giving crystal data and data collection and refinement parameters, all bond distances and angles, least-squares planes and deviations therefrom, anisotropic thermal parameters, and positional parameters for **15** (10 pages). Ordering information is given on any current masthead page.

OM940690D

Synthetic, Structural, and Theoretical Studies on a Novel Rhodium(I) Complex Containing a π-Allyl-Type Ylide Ligand

Helmut Werner,*,† Norbert Mahr,† Gernot Frenking,*,‡ and Volker Jonas‡

Institut für Anorganische Chemie der Universität Würzburg, Am Hubland, D-97074 Würzburg, Germany, and Fachbereich Chemie der Philipps-Universität Marburg, Hans-Meerwein-Strasse, D-35043 Marburg, Germany

Received September 12, 1994®

Whereas the reaction of $[RhCl(P\text{-}i\text{-}Pr_3)_2]_n$ (**1**) with $[CPh(Me)OH](CO_2Et)CN_2$ and $PhCHN_2$ gives the diazoalkane and dinitrogen complexes *trans*-$[RhCl\{N_2C(CO_2Et)(CPh(Me)OH)\}(P\text{-}i\text{-}Pr_3)_2]$ (**2**) and *trans*-$[RhCl(N_2)(P\text{-}i\text{-}Pr_3)_2]$ (**3**), respectively, the mononuclear yliderhodium(I) compound $[RhCl(P\text{-}i\text{-}Pr_3)(i\text{-}Pr_3P{=}CHC(O)Ph)]$ (**4**) is obtained on treatment of **1** with $PhC(=O)CHN_2$. It reacts with CO or CN-*t*-Bu to generate the formerly unknown acyl ylide $i\text{-}Pr_3PCHC(O)Ph$ (**5**). The X-ray structure analysis of **4** (monoclinic, space group $P2_1/c$ (No. 14), with a = 11.280(3) Å, b = 15.201(2) Å, c = 17.041(5) Å, β = 92.36(1)°, and Z = 4) reveals the presence of a η^3-allyl-type unit which is coordinated via oxygen and two carbon atoms to the metal center. The nature of the bonding between the modified acyl ylide ligand $H_3PCHC(=O)CH_3$ and rhodium(I) has been investigated by ab initio methods at the MP2 level. The calculated structure of the hypothetical molecule $[RhCl(PH_3)\{H_3PCHC(O)CH_3\}]$ (**4′**) is very similar to the geometry of **4** obtained by X-ray analysis. In contrast to **1**, the alkynylrhodium(I) compounds *trans*-$[Rh(C{\equiv}CR)(C_2H_4)(P\text{-}i\text{-}Pr_3)_2]$ (**6**, **7**) react with $PhC(=O)CHN_2$ to give the diazoalkane complexes *trans*-$[Rh(C{\equiv}CR)\{N_2C(H)(COPh)\}(P\text{-}i\text{-}Pr_3)_2]$ (**11**, **15**). The preparation of other derivatives of composition *trans*-$[Rh(C{\equiv}CR)(N_2CR'R'')(P\text{-}i\text{-}Pr_3)_2]$ (**8–10**, **12–14**) will also be described.

Introduction

During attempts to extend the series of rhodium–carbon double bond systems *trans*-$[RhCl(=C{=}CRR')L_2]$[1] and *trans*-$[RhCl(=C{=}C{=}CRR')L_2]$[2] to include the corresponding carbene rhodium complexes *trans*-$[RhCl(=CRR')L_2]$ (L = P-*i*-Pr_3, PR-*i*-Pr_2, PMe-*t*-Bu_2 etc.), we recently found[3] that with $[RhCl(P\text{-}i\text{-}Pr_3)_2]_n$ (**1**) as starting material neither CH_2N_2 nor CPh_2N_2 forms the expected product containing a $Rh{=}CR_2$ bond. Instead, with CH_2N_2 the ethene derivative *trans*-$[RhCl(C_2H_4)(P\text{-}i\text{-}Pr_3)_2]$ and with CPh_2N_2 the diphenyldiazomethane rhodium complex *trans*-$[RhCl(N_2CPh_2)(P\text{-}i\text{-}Pr_3)_2]$ were obtained. Whereas the latter is stable at room temperature under argon, it smoothly reacts with ethene to give *trans*-$[RhCl(C_2H_4)(P\text{-}i\text{-}Pr_3)_2]$ and, surprisingly, 1.1-diphenylpropene. This olefin, which formally is built up by the linking of the $:CPh_2$ fragment of the diazoalkane with the ethene isomer $:CHCH_3$, can be prepared catalytically from C_2H_4 and CPh_2N_2 in the presence of various mono- or dimeric rhodium(I) complexes.[3,4] With $[RhCl(C_2H_4)_2]_2$ as the catalyst, turnover numbers of about 500 have been achieved.[5] Although for other substrates, which may contain a functional group in either the starting olefin or the diazo derivative, the turnover numbers are much less (usually 5–30), the important point is that in most of these catalytic processes a high degree of regio- and stereoselectivity is observed.[5,6]

In order to gain more insight into the mechanism of the novel C–C coupling reaction, we decided inter alia to prepare rhodium(I) compounds with other diazoalkanes than CPh_2N_2 and to vary the anionic ligand X^- which in most of the previous work was chloride. In the course of these studies we discovered the formation of a new phosphorus ylide which is generated in the coordination sphere of the metal but can easily be displaced by CO. The π-allyl type bonding of the ylide, for which there is no precedence, has been confirmed by X-ray crystallography and investigated in detail by ab initio calculations. This work will also be described.

Results and Discussion

Reactions of Functionalized Diazoalkanes with $[RhCl(P\text{-}i\text{-}Pr_3)_2]$. In analogy to CPh_2N_2 and other diaryldiazomethane derivatives,[5,6] the chiral compound $[CPh(Me)OH](CO_2Et)CN_2$ reacts with **1** to give a diazoalkane rhodium complex instead of a carbene rhodium compound (Scheme 1). Compound **2** which has

† Universität Würzburg.
‡ Universität Marburg.
® Abstract published in *Advance ACS Abstracts*, December 1, 1994.

(1) (a) Garcia Alonso, F. J.; Höhn, A.; Wolf, J.; Otto, H.; Werner, H. *Angew. Chem.* **1985**, *97*, 401–402. *Angew. Chem. Int. Ed. Engl.* **1985**, *24*, 406–407. (b) Werner, H.; Garcia Alonso, F. J.; Otto, H.; Wolf, J. *Z. Naturforsch., B: Anorg. Chem., Org. Chem.* **1988**, *43*, 722–726. (c) Werner, H.; Brekau, U. *Z. Naturforsch., B: Anorg. Chem., Org. Chem.* **1989**, *44*, 1438–1446. (d) Rappert, T.; Nürnberg, O.; Mahr, N.; Wolf, J.; Werner, H. *Organometallics* **1992**, *11*, 4156–4164.

(2) (a) Werner, H.; Rappert, T. *Chem. Ber.* **1993**, *126*, 669–678. (b) Werner, H.; Rappert, T.; Wiedemann, R.; Wolf, J.; Mahr, N. *Organometallics* **1994**, *13*, 2721–2727.

(3) Wolf, J.; Brandt, L.; Fries, A.; Werner, H. *Angew. Chem.* **1990**, *102*, 584–586. *Angew. Chem. Int. Ed. Engl.* **1990**, *29*, 510–512.

(4) Short reviews: (a) Werner, H. Ninth Synthetic Organic Chemistry Symposium (SOCS-9), Kyoto, 1992, Abstr. pp 29–33. (b) Werner, H. *J. Organomet. Chem.* **1994**, *475*, 45–55.

(5) Mahr, N. Dissertation, Universität Würzburg, 1994.

(6) (a) Brandt, L. Dissertation, Universität Würzburg, 1991. (b) Fries, A. Dissertation, Universität Würzburg, 1993.

0276-7333/95/2314-0619$09.00/0

Scheme 1

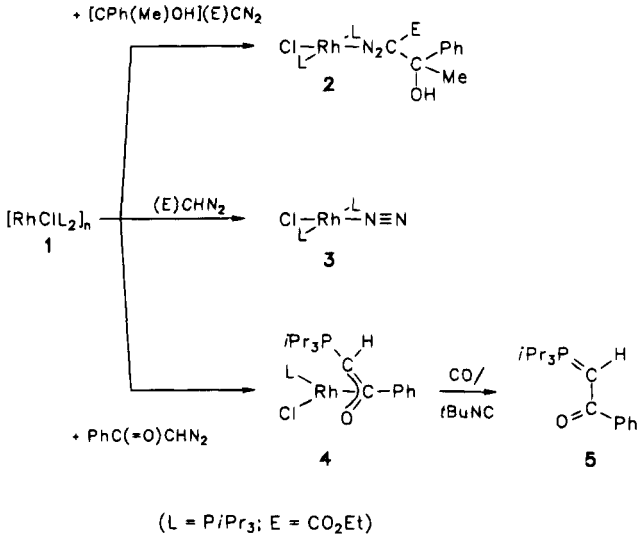

been isolated as a red air-sensitive solid is both thermally stable and chemically rather inert. In presence of ethylene it does not undergo a ligand exchange like *trans*-[RhCl(N_2CPh_2)(P-*i*-Pr_3)$_2$] and on heating it does not eliminate a carbene fragment. The "end-on" coordination of the diazoalkane ligand in **2** is indicated by the N−N stretching frequency in the IR spectrum (1955 cm^{-1}) which appears in the same region as for similar square-planar diazoalkane rhodium[3,5] and iridium compounds.[7] The position of the ν(C=O) band in the spectrum of **2** and in that of the free ligand is almost identical and thus an additional interaction between the carbonyl group and the metal center can be excluded.

Surprisingly, on treatment of **1** with the diazoacetic ester (CO_2Et)CHN_2 the dinitrogen complex **3** is formed instead of a diazoalkane rhodium compound related to **2**. This compound has originally been prepared by Busetto and co-workers from [RhCl(C_8H_{14})$_2$]$_2$ and P-*i*-Pr_3 in the presence of N_2[8] and has been crystallographically characterized by Ibers at al.[9] Compound **3** is also obtained from **1** and CH_3CHN_2, $PhCHN_2$ or other highly reactive diazoalkanes which cannot be used together with ethene as substrates in the new olefin synthesis.

An unexpected product is formed in the reaction of **1** with 1-diazo-2-phenylethanone. If the two starting materials are combined in ether solution at room temperature, a spontaneous gas evolution (N_2) occurs and after a short time a red solid precipitates. With the exception of pentane, hexane, and ether, this new compound **4** (Scheme 1) is easily soluble in most common organic solvents but is not exceedingly stable in solution. The rhodium-mediated formation of an acyl ylide ligand of composition *i*-Pr_3PCHC(=O)Ph is indicated by a signal for the C*H* proton at δ 2.19 in the ^{1}H NMR, by a doublet-of-doublets for the *C*H carbon at δ 9.04 in the ^{13}C NMR, and by the appearance of another doublet-of-doublets at δ 39.14 in the ^{31}P-NMR spectrum having a Rh−P coupling constant of 7.4 Hz. This value is much smaller than that of the second ^{31}P signal at δ 67.60 [J(RhP) = 214 Hz] which belongs to the phosphorus atom of the P-*i*-Pr_3 ligand. Characteristic features, which support the assumption that the ylide is coordinated via carbon *and* oxygen to the metal, are the ^{13}C NMR resonance of the carbonyl carbon atom at δ 191.68 that is shifted to higher field compared with an uncoordinated PhC=O group and the position of the ν(C=O) band in the IR spectrum which appears at significantly lower wave numbers (1572 cm^{-1}) than for intact acetophenone derivatives.[10] We note that a similar low-frequency shift of the C=O stretch has been observed for rhodium[11] and iridium complexes[12] in which a substituted vinyl ligand such as CH=CH-C(R)=O or CH=CMe-C(R)=O (R = Me, OMe) is linked via the α-carbon and the carbonyl oxygen atom to the metal.

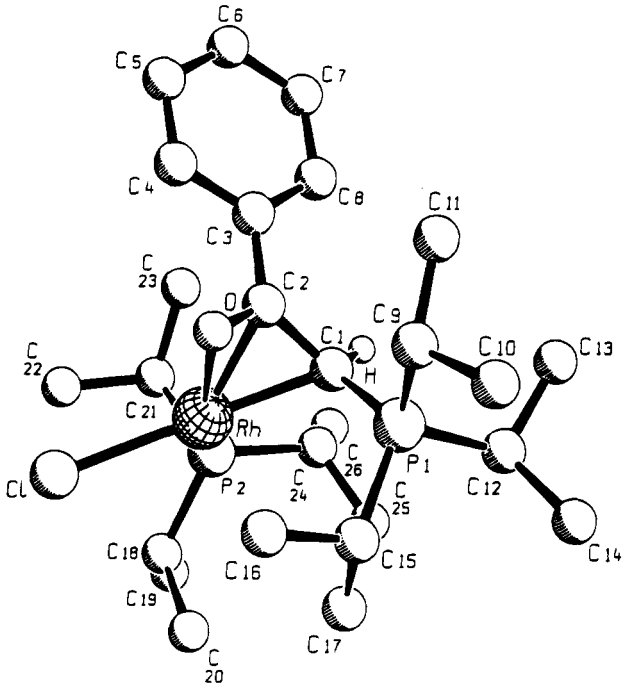

Figure 1. Molecular structure of **4**.

Molecular Structure of 4. Since on the basis of the spectroscopic data the exact arrangement of the ylide ligand to the Rh(PR_3)X fragment could not be established unambigously, a single-crystal X-ray analysis of compound **4** was carried out. The SCHAKAL drawing (Figure 1) reveals that the four atoms Cl, P2, O, and C1 form a distorted square around the metal with the carbon atom C2 above the respective plane. The bond length Rh−C1 [2.101(4) Å] is comparable to that in other ylide-rhodium complexes,[13] and this is equally true for the Rh−C1−P1 bond angle (Table 1). The P−C1 distance [1.799(4) Å] is shorter than would be expected for a phosphorus−carbon single bond but is in good agreement with data for related metal ylides.[14]

The most interesting aspect of the structure, however, is the coordination of the acyl group which together with

(7) Brandt, L.; Wolf, J.; Werner, H. *J. Organomet. Chem.* **1993**, *444*, 235−244.
(8) Busetto, C.; D'Alfonso, A.; Maspero, F.; Perego, G.; Zazzetta, A. *J. Chem. Soc., Dalton Trans.* **1977**, 1828−1834.
(9) Thorn, D. L.; Tulip, T. H.; Ibers, J. A. *J. Chem. Soc., Dalton Trans.* **1979**, 2022−2025.
(10) Hesse, M.; Meier, H.; Zeeh, B. *Spektroskopische Methoden in der organischen Chemie*, 3rd ed.; Verlag Thieme: Stuttgart-New York, 1987; Chapter 2.
(11) Dirnberger, T.; Werner, H. *Chem. Ber.* **1992**, *125*, 2007−2014.
(12) (a) Werner, H.; Dirnberger, T.; Schulz, M. *Angew. Chem.* **1988**, *100*, 993−994. *Angew. Chem. Int. Ed. Engl.* **1988**, *27*, 948−950. (b) Dirnberger, T. Dissertation, Universität Würzburg, 1991. (c) Papenfuhs, B. Diplomarbeit, Universität Würzburg, 1990.
(13) (a) Werner, H.; Hofmann, L.; Paul, W.; Schubert, U. *Organometallics* **1988**, *7*, 1106−1111. (b) Werner, H.; Schippel, O.; Wolf, J.; Schulz, M. *J. Organomet. Chem.* **1991**, *417*, 149−162.

Table 1. Selected Experimental Bond Distances and Angles with ESD's for 4[a]

	Bond Distances (Å)		
Rh−C1	2.369 (1); (2.311)	P1−C15	1.839 (4)
Rh−P2	2.213 (1); (2.182)	P2−C18	1.859 (5)
Rh−O	2.177 (3); (2.126)	P2−C21	1.866 (5)
Rh−C1	2.101 (4); (2.032)	P2−C24	1.870 (5)
Rh−C2	2.041 (4); (1.983)	O−C2	1.305 (5); (1.333)
P1−C1	1.799 (4); (1.763)	C1−C2	1.438 (6); (1.487)
P1−C9	1.821 (4)	C1−H	1.07 (4); (1.092)
P1−C12	1.830 (4)	C2−C3	1.489 (6); (1.502)
	Bond Angles (deg)		
C1−Rh−P2	93.11 (4); (89.3)	Rh−O−C2	66.4 (2); (65.3)
C1−Rh−O	101.19 (8); (104.6)	Rh−C1−P1	117.9 (2); (101.4)
C1−Rh−C1	163.6 (1); (166.6)	Rh−C1−C2	67.5 (2); (66.5)
C1−Rh−C2	131.6 (1); (136.9)	P1−C1−C2	116.7 (3); (115.2)
P2−Rh−O	158.57 (9); (162.4)	Rh−C2−O	77.8 (2); (77.0)
P2−Rh−C1	102.6 (1); (99.2)	Rh−C2−C1	72.0 (2); (70.0)
P2−Rh−C2	123.7 (1); (125.1)	Rh−C2−C3	124.0 (3); (131.7)
O−Rh−C1	65.2 (1); (69.4)	O−C2−C1	114.4 (4); (114.1)
O−Rh−C2	35.9 (1); (37.6)	O−C2−C3	120.0 (4); (121.4)
C1−Rh−C2	40.6 (2); (43.5)	C1−C2−C3	125.2 (4); (123.3)

[a] Calculated values for 4′ are given in parentheses.

the carbon atom C1 forms a η^3-allyl-type unit. Evidence for this is provided by (i) the almost perpendicular arrangement of the [Cl, Rh, P2] and the [C1, C2, O] planes [dihedral angle 91.2(9)°], (ii) the C1−C2−O angle of 114.4(4)° which is significantly shorter than for a free sp^2 ylide carbon center,[14] but quite similar to that in η^3-allyl or η^3-benzyl rhodium compounds,[15] and (iii) the shortening of the C1−C2 and the lengthening of the C2−O distances if compared with those of corresponding η^1-bonded ylide complexes.[14] It should be mentioned that an analogous elongation of the C−O bond has been found in several aldehyde and ketone transition-metal compounds in which the carbonyl moiety is linked via carbon and oxygen to the metal center,[16] as well as in oxoallyl-type metal complexes.[17] We also note that Alt et al.[18] have prepared cyclopentadienyl molybdenum and tungsten compounds of composition $[C_5H_5M\{\kappa^2\text{-}(O,C)\text{-}OC(CH_3){=}CHCHPMe_3\}(CO)_2]$ (M = Mo, W) in which the acyl ylide unit is generated from an acylvinyl ligand and PMe_3 and where a similar bonding situation as in **4** exists. Other relevant structural data for **4** are the Rh−O bond length of 2.177(3) Å which is almost identical to that in $[Rh(\eta^2\text{-}O_2CCH_3)(P\text{-}i\text{-}Pr_3)_2]$,[15a] the Rh−P2 distance of 2.213(1)Å which is shorter than in

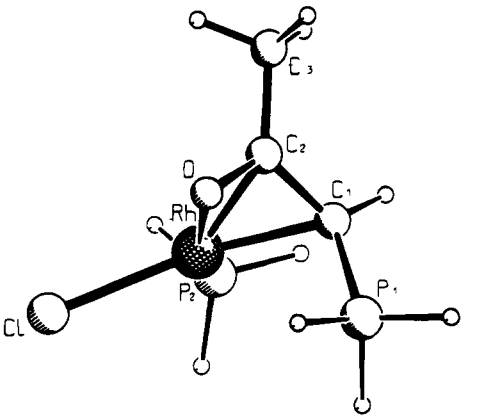

Figure 2. Optimized geometry of 4′.

$[Rh(\eta^3\text{-}CH_2C_6H_4\text{-}4\text{-}CH_3)(P\text{-}i\text{-}Pr_3)_2]$ [2.343(3) and 2.253(3) Å][15a] or $[C_5H_5Rh({=}C{=}CHPh)(P\text{-}i\text{-}Pr_3)]$ [2.263(6) Å],[19] and the small dihedral angle [14.9(13)°] between the [C1, C2, O] plane and the plane of the phenyl group. This indicates a substantial degree of π−π interaction between the six-membered ring and the η^3-allyl-type ligand.

Theoretical Studies. In order to investigate the bonding situation between the rhodium atom and the η^3-allyl-type unit of **4**, we optimized the geometry of the complex **4′** at the MP2 level using quantum mechanical ab initio methods. The P-*i*-Pr_3 groups of **4** are replaced in **4′** by PH_3 groups and the phenyl substituent is replaced by a methyl group. Details of the theoretical calculations are given in the method section. Previous studies have shown that the geometries of low-valent transition metal complexes are predicted at this level of theory in good agreement with experiment.[20]

The optimized geometry of **4′** is shown in Figure 2. The calculated structure of the η^3-allylrhodium unit of **4′** is very similar to the geometry of **4** obtained by X-ray structure analysis (Figure 1). The optimized geometry of **4′** has a bicyclic central moiety with a calculated folding angle of 122° between the Rh−C1−C2 plane and the Rh−C2−O plane. The X-ray structure analysis of **4** gives a folding angle of 121.0(3)° between the Rh−C1-C2 and the Rh−C2−O planes. The theoretically predicted bond lengths of **4′** are in good agreement with the experimental values of **4** (Table 1), if the different substituents of the two complexes are taken into account. The theoretical bond lengths between Rh and the η^3-allyl-type unit are slightly shorter (Rh−C1 = 2.032 Å; Rh−C2 = 1.983 Å; Rh−O = 2.126 Å) than the observed interatomic distances (Rh−C1 = 2.101 Å; Rh−C2 = 2.041 Å; Rh−O = 2.177 Å).

The nature of the bonding of the η^3-allylrhodium unit is revealed by the topological analysis of the electron density distribution and the associated gradients and Laplacian.[21] Figure 3 shows the contour line diagrams of the Laplacian of **4′** in the Rh−C1−C2 plane (Figure 3a) and in the Rh−C2−O plane (Figure 3b). The electronic structure of the Rh−C1−C2 unit is characterized by three bond paths and three bond critical points between the three atoms and one ring critical point.

(14) Inter alia: (a) Facchin, G.; Bertani, R.; Calligaris, M.; Nardin, G.; Mari, M. *J. Chem. Soc., Dalton Trans.* **1987**, 1381−1387. (b) Facchin, G.; Bertani, R.; Zanotto, L.; Calligaris, M.; Nardin, G. *J. Organomet. Chem.* **1989**, *366*, 409−420. (c) Vicente, J.; Chicote, M. T.; Fernandez-Baeza, J.; Martin, J.; Saura-Clamas, I.; Turpin, J.; Jones, R. G. *J. Organomet. Chem.* **1987**, *331*, 409−421.

(15) (a) Werner, H.; Schäfer, M.; Nürnberg, O.; Wolf, J. *Chem. Ber.* **1994**, *127*, 27−38. (b) Chappel, S. D.; Cole-Hamilton, D. J.; Galas, A. M. R.; Hursthouse, M. B.; Walker, N. P. C. *Polyhedron* **1985**, *4*, 121−125. (c) Burch, R. R.; Muetterties, E. L.; Day, V. W. *Organometallics* **1982**, *1*, 188−197.

(16) (a) Martin, B. D.; Matchett, S. A.; Norton, J. R.; Anderson, O. P. *J. Am. Chem. Soc.* **1985**, *107*, 7952−7959. (b) Huang, Y. H.; Gladysz, J. A. *J. Chem. Educ.* **1988**, *65*, 298−303. (c) Klein, D. P.; Mendez, N. Q.; Seyler, J. W.; Arif, A. M.; Gladysz, J. A. *J. Organomet. Chem.* **1993**, *450*, 157−164. (d) Mendez, N. Q.; Arif, A. M.; Gladysz, J. A. *Angew. Chem.* **1990**, *102*, 1507−1509. *Angew. Chem. Int. Ed. Engl.* **1990**, *29*, 1473−1475. (e) Mendez, N. Q.; Mayne, C. L.; Gladysz, J. A. *Angew. Chem.* **1990**, *102*, 1509−1511. *Angew. Chem. Int. Ed. Engl.* **1990**, *29*, 1475−1477.

(17) (a) Guggolz, E.; Ziegler, M. L.; Biersack, H.; Herrmann, W. A. *J. Organomet. Chem.* **1980**, *194*, 317−324. (b) Hart, I. J.; Jeffery, J. C.; Lowry, R. M.; Stone, F. G. A. *Angew. Chem.* **1988**, *100*, 1769−1770. *Angew. Chem. Int. Ed. Engl.* **1988**, *27*, 1703−1704. (c) Dossett, S. J.; Pilotti, M. U.; Stone, F. G. A. *Polyhedron* **1990**, *9*, 2953−2958.

(18) Alt, H. J.; Schwärzle, J. A.; Kreissl, F. R. *J. Organomet. Chem.* **1978**, *152*, C57−C59.

(19) Werner, H.; Wolf, J.; Garcia Alonso, F. J.; Ziegler, M. L.; Serhadli, O. *J. Organomet. Chem.* **1987**, *336*, 397−411.

(20) (a) Ehlers, A. W.; Frenking, G. *J. Am. Chem. Soc.* **1994**, *116*, 1514−1520. (b) Ehlers, A. W.; Frenking, G. *Organometallics*, submitted.

Thus, the topology of the electronic structure indicates the cyclic nature of the Rh−C1−C2 moiety, which should be considered as a rhodium−cyclopropane unit.[21] The C1 and C2 carbon atoms possess droplet-shaped areas of electron concentration ($\nabla^2\varrho(r) < 0$, solid lines) pointing toward the rhodium atom, which illustrates the electron donation toward the metal atom.

The Laplacian distribution of the Rh−C2−O unit (Figure 3b) shows a different type of structure. There are bond paths between Rh and C2 and between C2 and the oxygen atom, but there is *no* bond path between Rh and O. This means that the Rh−C2−O unit should *not* be considered as a cyclic structure. Although the interatomic distance between Rh and O is rather short (Rh−O = 2.126 Å in **4′**, 2.177 Å in **4**), the gradient field indicates that there is no bond between these atoms. The attractive Coulomb interactions between Rh and O in **4′** are not sufficient to form a bond as defined by the topological analysis of the electronic structure.[21]

Generation of the Free Ylide. Since in contrast to ordinary π-allyl transition metal complexes the allyl-type ligand in **4** is nonionic, it can easily be displaced from the coordination sphere by CO. If carbon monoxide is passed through a solution of **4** in toluene, a change of color from orange-red to bright yellow occurs. After removal of the solvent and extraction of the residue with pentane, a mixture of products is obtained which consists of the free ylide **5** (Scheme 1) as well as equal quantities of $[RhCl(CO)_2]_2$[22] and *trans*-$[RhCl(CO)(P\text{-}i\text{-}Pr_3)_2]$.[8] If *tert*-butyl isocyanide is used instead of CO, the ylide **5** is isolated as a light-yellow oil. Typical features of the ^{1}H-NMR spectrum of **5** are (i) the doublet of the i-$Pr_3PC\mathit{H}$ proton at δ 3.59 which is shifted by ca. 4 ppm to lower field compared with i-Pr_3PCH_2,[23] and (ii) the large P−H coupling constant of this signal of 19.5 Hz which reveals a considerable contribution of the zwitterionic resonance form i-Pr_3P^+−CH=C(Ph)O$^-$.[24] The ^{13}C NMR spectrum of **5** displays besides the signals for the isopropylphosphine and phenyl carbons a resonance for the ylide carbon atom at δ 42.04, significantly deshielded compared with **4**, and a characteristic doublet for the carbonyl carbon atom at δ 184.68. In the ^{31}P NMR spectrum of **5** the signal is observed at about the same chemical shift as that of the unsubstituted ylide i-Pr_3PCH_2.[23]

Reaction of the Alkynyl Complexes *trans*-[Rh(C≡CR)(C_2H_4)(P-*i*-Pr_3)$_2$]. In view of the fact that in square-planar iridium complexes *trans*-$[IrX(C_2H_4)(P\text{-}i\text{-}Pr_3)_2]$ the replacement of X = Cl for X = CH_3 favors the coordination of a N_2CRR' ligand,[7] we were interested to find out whether a similar effect is also observed in rhodium chemistry. Since alkyl rhodium compounds such as *trans*-$[RhCH_3(C_2H_4)(P\text{-}i\text{-}Pr_3)_2]$ or *trans*-$[RhCH_2Ph(C_2H_4)(P\text{-}i\text{-}Pr_3)_2]$ are still unknown,[25] we decided to use the alkynyl(ethene) complexes **6** and **7** as related starting materials.[26] They both react with Ph_2CN_2, $C_{12}H_8CN_2$, PhC(=O)CPhN_2, and PhC(=O)CHN_2 by elimination of ethene to give the expected products (Scheme 2). Compounds **8-15** are deeply colored microcrystalline solids which are only moderately air-sensitive and considerably more stable in solution than their chlororhodium counterparts *trans*-$[RhCl(N_2CRR')(P\text{-}i\text{-}Pr_3)_2]$. The yield of **8-15** in the straightforward synthesis is 80−95%. The proposed structure with an end-on bonded diazoalkane ligand is supported in particular by the IR spectra in which the ν(N≡N) stretch (~1920 cm^{-1}) is shifted by ca. 100−150 cm^{-1} to lower wavenumbers compared with the parent N_2CRR' molecules. The chemical shift and the splitting pattern of the signals for the phosphines in the ^{1}H, ^{13}C, and ^{31}P NMR spectra are very similar to those of **6** and **7** and therefore we assume that the stereochemistry of the starting materials and the products is the same. It should be emphasized that in contrast to **1** (see Scheme 1) compounds **6**

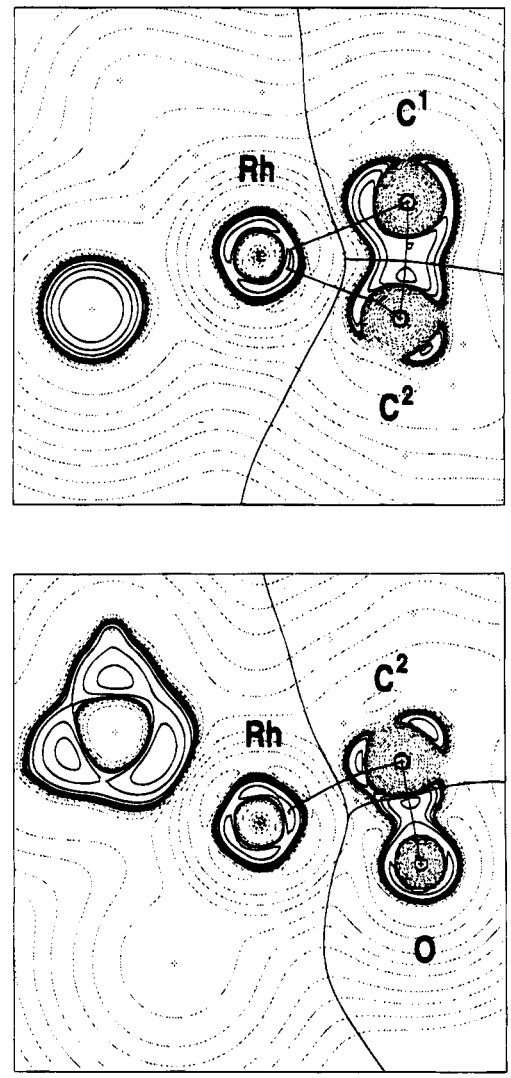

Figure 3. Contour line diagrams of the Laplacian distribution $\nabla^2\varrho(\mathbf{r})$ for **4′**. Dashed lines indicate charge depletion ($\nabla^2\varrho(\mathbf{r}) > 0$), solid lines indicate charge concentration ($\nabla^2\varrho(\mathbf{r}) < 0$). The solid lines connecting the atomic nuclei are the bond paths; the solid lines separating the atomic nuclei indicate the zero-flux surfaces in the plane. The crossing points of the bond paths and zero-flux surfaces are the bond critical points $\mathbf{r}_b$.

(21) Bader, R. F. W. *Atoms in Molecules. A Quantum Theory*; Oxford Univ. Press: Fair Lawn, NJ, 1990.
(22) McCleverty, J. A.; Wilkinson, G. *Inorg. Synth.* **1968**, *8*, 211−214.
(23) Köster, R.; Simic, D.; Grassberger, M. A. *Liebigs. Ann. Chem.* **1970**, *739*, 211−219.
(24) (a) Malisch, W.; Rankin, D.; Schmidbaur, H. *Chem. Ber.* **1971**, *104*, 145−149. (b) Ostoja-Starzewski, K. A.; tom Dieck, H. *Phosphorus* **1976**, *6*, 177−189.
(25) Schäfer, M. Dissertation, Universität Würzburg, 1994.
(26) (a) Schäfer, M.; Wolf, J.; Werner, H. *J. Chem. Soc., Chem. Commun.* **1991**, 1341−1343. (b) Schäfer, M.; Wolf, J.; Werner, H. *J. Organomet. Chem.* **1994**, in press.

Scheme 2

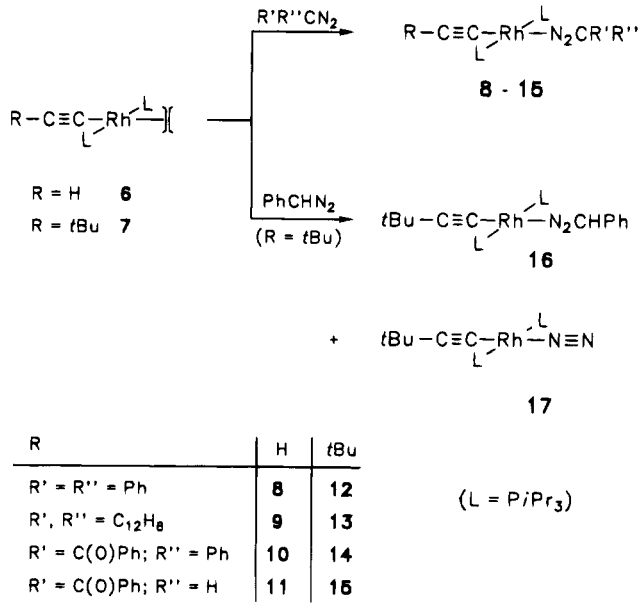

R	H	*t*Bu
R' = R'' = Ph	**8**	**12**
R', R'' = $C_{12}H_8$	**9**	**13**
R' = C(O)Ph; R'' = Ph	**10**	**14**
R' = C(O)Ph; R'' = H	**11**	**15**

and **7** react with $PhC(=O)CHN_2$ to give a stable diazoalkane complex and not an ylide rhodium(I) derivative.

In contrast to compound **1**, which reacts with $PhCHN_2$ by decomposition of the diazoalkane, the alkynyl complex **7** on treatment with phenyldiazomethane affords two products. It is quite obvious from NMR measurements at variable temperatures that the expected diazoalkane rhodium complex **16** (see Scheme 2) is formed initially. However, it then is converted with a comparable reaction rate to the dinitrogen derivative **17**. Several attempts to separate the two compounds by fractional crystallization or column chromatography failed. The IR spectrum of the product mixture displays a N–N stretching frequency for **16** at 1935 cm^{-1} and for **17** at 2120 cm^{-1}, the latter of which is quite similar to that of *trans*-[RhCl(N_2)(P-*i*-Pr_3)$_2$].[8,9]

Concluding Remarks

The present investigations have shown that the reaction of **1** with substituted diazoalkanes can lead to products of different structural types. The most unusual of these products certainly is the acyl ylide complex **4** in which a η^3-allyl-type unit is coordinated to the metal center. Although the X-ray structural data of **4** reveal a rather short interatomic distance between rhodium and oxygen, ab initio calculations indicate that there is no bond between these atoms. Despite this result, we nevertheless consider the novel acyl ylide *i*-$Pr_3PCHC(=O)Ph$ as a 4-electron donor ligand which provides a 16-electron configuration for the rhodium(I) atom in compound **4**. A similar bonding situation probably exists in some oxoallyl or aldehyde and ketone transition-metal complexes in which a M–O interaction is also indicated by the structural data.[16,17]

Experimental Section

All reactions were carried out under an atmosphere of argon by Schlenk tube techniques. The starting materials [RhCl(P-*i*-Pr_3)$_2$]$_n$ (**1**),[27] *trans*-[Rh(C≡CH)(C_2H_4)(P-*i*-Pr_3)$_2$] (**6**),[26] *trans*-[Rh(C≡C-*t*-Bu)(C_2H_4)(P-*i*-Pr_3)$_2$] (**7**),[26] [CPh(Me)OH](CO_2Et)CN_2,[28] PhC(=O)CHN_2,[29] Ph_2CN_2,[30] $C_{12}H_8CN_2$,[31] PhC(=O)$PhCN_2$,[32] and $PhCHN_2$[33] were prepared by published procedures. Other substrates were commercial products from Aldrich and Fluka. NMR spectra were recorded on JEOL FX 90 Q, Bruker AC 200, and Bruker AMX 400 instruments, and IR spectra on a Perkin-Elmer 1420 infrared spectrometer. Melting points were measured by DTA.

Preparation of *trans*-[RhCl{$N_2C(CO_2Et)(CPh(Me)OH)$}(P-*i*-Pr_3)$_2$] (2). A solution of **1** (76 mg, 0.166 mmol for $n = 1$) in 10 mL of ether was treated at −50 °C with a solution of [CPh(Me)OH](CO_2Et)CN_2 (78 mg, 0.16 mmol) in 5 mL of ether and with continuous stirring slowly warmed up to room temperature. A color change from violet to red occurred. The reaction mixture was concentrated to ca. 1 mL in vacou and 5 mL of pentane was added. After the solution was stored at −78 °C, red crystals precipitated, which were filtered off, washed with pentane (−30 °C), and dried in vacuo: yield 92 mg (80%); mp 98 °C dec. Anal. Calcd for $C_{29}H_{56}N_2ClO_3P_2Rh$: C, 51.99; H, 8.14; N, 4.04. Found: C, 52.05; H, 8.97; N, 3.88. IR (KBr): ν(OH) 3400, ν(N=N) 1955, ν(C=O) 1615 cm^{-1}. ^1H NMR (C_6D_6, 200 MHz): δ 7.68 (d, ^3J(HH) = 6.1 Hz, 2H, ortho-H of C_6H_5), 7.25–7.04 (m, 3H, C_6H_5), 5.20 (br, s, 1H, O*H*), 4.01 (q, ^3J(HH) = 7.1 Hz, 2H, CH_2CH_3), 2.39 (m, 6H, PC*H*CH_3), 1.78 (s, 3H, CCH_3), 1.30 (dvt, *J*(HH) = 7.0, *N* = 13.5 Hz, 18H, PCHCH_3), 1.27 (dvt, *J*(HH) = 7.0, *N* = 13.5 Hz, 18H, PCHCH_3), 0.95 (t, ^3J(HH) = 7.1 Hz, 3H, CH_2CH_3). ^{13}C NMR (C_6D_6, 50.3 MHz): δ 162.47 (s, *C*=O), 149.55 (s, ipso-C of C_6H_5), 128.33, 127.06, 125.42 (all s, C_6H_5), 77.95 (br, s, *C*N_2), 70.95 (s, *C*(CH_3)OH), 59.79 (s, O*C*H_2CH_3), 30.40 (s, C(*C*H_3)OH), 23.66 (vt, *N* = 18.3 Hz, P*C*HCH_3), 19.95 (s, PCH*C*H_3), 14.67 (s, O*C*H_2CH_3). ^{31}P NMR (C_6D_6, 81.0 MHz): δ 42.39 (d, ^1J(RhP) = 117.7 Hz).

Reaction of 1 with (CO_2Et)CHN_2. A solution of **1** (61 mg, 0.13 mmol) in 5 mL of pentane was treated as described for **2** with a solution of (CO_2Et)CHN_2 (15mg, 0.13 mmol) in 2 mL of pentane. A light-brown solid was obtained which spectroscopically was identified as *trans*-[RhCl(N_2)(P-*i*-Pr_3)$_2$] (**3**).[2a]

Preparation of [RhCl(P-*i*-Pr_3)(*i*-Pr_3P=CHC(O)Ph)] (4). A solution of **1** (90 mg, 0.22 mmol) in 5 mL of ether was treated with a solution of PhC(=O)CHN_2 (32 mg, 0.22 mmol) in 2 mL of ether. A spontaneous color change from violet to red-brown occurred and a gas evolution took place. After the solution had been stirred for 1 min at room temperature, an orange-red air-sensitive solid precipitated which was separated from the mother liquor at −30 °C, washed with 5 mL of pentane (−30 °C), and dried in vacuo: yield 97 mg (77%); mp 90 °C dec. Anal. Calcd for $C_{26}H_{48}ClOP_2Rh$: C, 54.13; H, 8.38. Found: C, 54.41; H, 8.41. MS (70 eV): *m/z* = 278 (0.35) (*i*-Pr_3P=CHC(O)$C_6H_5^+$), 201 (0.13) (*i*-Pr_3P=$CHCO^+$), 105 (0.90) ($C_6H_5CO^+$). IR (KBr): ν(C=O) 1520, ν(P=C) 885 cm^{-1}. ^1H NMR (C_6D_6, 400 MHz): δ 8.41 (d, ^3J(HH) = 7.3 Hz, 2H, ortho-H of C_6H_5), 7.36–7.04 (m, 3H, C_6H_5), 2.47 (m, 3H, RhPC*H*CH_3), 2.17 (m, 3H, C=PC*H*CH_3), 2.19 (d, ^2J(PH) = 14.7 Hz, 1H, P=C*H*), 1.26 (dd, ^3J(HH) = 7.4, ^3J(PH) = 14.8 Hz, 9H, RhPCHCH_3), 1.21 (dd, ^3J(HH) = 7.4, ^3J(PH) = 13.2 Hz, 9H, RhPCHCH_3), 1.12 (dd, ^3J(HH) = 7.2, ^3J(PH) = 13.1 Hz, 9H, C=PCHCH_3), 1.07 (dd, ^3J(HH) = 7.5, ^3J(PH) = 15.5 Hz, 9H, C=PCHCH_3). ^{13}C NMR (C_6D_6, 50.3 MHz): δ 191.68 (d, ^1J(RhC) = 45.8 Hz, *C*=O), 128.83, 128.30, 127.78, 126.49 (all s, C_6H_5), 26.38 (d, ^1J(PC) = 21.6 Hz, C=P*C*HCH_3), 22.83 (d, ^1J(PC) = 43.4 Hz, RhP*C*HCH_3), 20.33, 20.15 (both s,

(27) Werner, H.; Wolf, J.; Höhn, A. *J. Organomet. Chem.* **1985**, *287*, 395–407.

(28) Schöllkopf, U.; Bánhidai, B.; Frasnelli, H.; Meyer, R.; Beckhaus, H. *Liebigs Ann. Chem.* **1974**, 1767–1783.

(29) Regitz, M.; Menz, F. *Chem. Ber.* **1968**, *101*, 2622–2632.

(30) (a) Smith, L. I.; Howard, K. L. *Organic Synthesis*; Wiley: New York, 1955; Collect. Vol. 3, pp 351–352. (b) Miller, J. B. *J. Org. Chem.* **1959**, *24*, 560–561.

(31) Baltzly, R.; Metha, N. B.; Russel, P. B.; Brooks, R. E.; Grivsky, E. M.; Steinberg, A. M. *J. Org. Chem.* **1961**, *26*, 3669–3676.

(32) Nenitzescu, C. D.; Solomonica, E. *Organic Synthesis*; Wiley: New York, 1993; Collect. Vol. 2, pp 496–497.

(33) Yates, P.; Shapiro, B. L. *J. Org. Chem.* **1958**, *23*, 759–760.

C=PCH*C*H$_3$), 18.20, 18.02 (both d, ^2J(PC) = 2.6 Hz, RhPCH*C*H$_3$), 9.07 (dd, ^1J(RhC) = 42.5, ^2J(PC) = 22.2 Hz, P=*C*). ^{31}P NMR (C$_6$D$_6$, 36.2 MHz): δ 67.60 (dd, ^1J(RhP) = 213.5, ^3J(PP) = 4.4 Hz, Rh*P*), 39.14 (dd, ^2J(RhP) = 7.4, ^3J(PP) = 4.4 Hz, C=*P*).

Preparation of *i*-Pr$_3$P=CHC(O)Ph (5). (a) A slow stream of CO was passed for ca. 30 s through a solution of **4** (60 mg, 0.10 mmol) in 7 mL of toluene at room temperature. After the solution had been stirred for 20 min, the solvent was removed and the residue was extracted with 30 mL of hexane. The extract contained a mixture of *trans*-[RhCl(CO)(P-*i*-Pr$_3$)$_2$] and **5**. (b) A solution of **4** (121 mg, 0.21 mmol) in 10 mL of toluene was treated with *t*-BuNC (25 μl, 0.21 mmol) at room temperature. A gradual color change from red-orange to orange-yellow occurred. After the solution was stirred for 20 min, it was worked up as described for a. Removal of the solvent from the extract gave a yellow oil: yield 39 mg (67%). ^{1}H NMR (C$_6$D$_6$, 200 MHz): δ 8.35 (d, ^3J(HH) = 7.9, ^4J(HH) = 1.8 Hz, 2H, ortho-H of C$_6$*H*$_5$), 7.33−7.15 (m, 3H, C$_6$*H*$_5$), 3.59 (d, ^2J(PH) = 19.5 Hz, 1H, P=C*H*C(O)Ph), 2.35 (m, 3H, PC*H*CH$_3$), 0.96 (dd, ^3J(HH) = 7.3, ^3J(PH) = 14.8 Hz, 18H, PCHC*H*$_3$). ^{13}C NMR (C$_6$D$_6$, 50.3 MHz): δ 184.68 (d, ^2J(PC) = 4.2 Hz, *C*=O), 143.51 (d, ^3J(PC) = 14.8 Hz, ipso-C of C$_6$H$_5$), 128.80, 127.85, 127.38 (all s, *C*$_6$H$_5$), 42.04 (d, ^1J(PC) = 98.9 Hz, P=*C*HC(O)Ph), 22.36 (d, ^1J(PC) = 50.4 Hz, P*C*HCH$_3$), 17.67 (d, ^2J(PC) = 18.5 Hz, PCH*C*H$_3$). ^{31}P NMR (C$_6$D$_6$, 81.0 MHz): δ 38.92 (s).

Preparation of *trans*-[Rh(C≡CH)(N$_2$CPh$_2$)(P-*i*-Pr$_3$)$_2$] (8). A solution of **6** (65 mg, 0.13 mmol) in 5 mL of pentane was treated under stirring at −30 °C with a solution of Ph$_2$CN$_2$ (34 mg, 0.13 mmol) in 2 mL of pentane. While the reaction mixture was warmed up to room temperature, a color change from red to green occurred and a green solid precipitated. After the solution had been further stirred for 10 min, the solvent was removed in vacuo. The residue was dissolved in 10 mL of pentane and the solution was stored at −78 °C. Green crystals precipitated which were filtered off, washed with pentane (−30 °C), and dried in vacuo: yield 70 mg (80%); mp 35 °C dec. Anal. Calcd for C$_{33}$H$_{53}$N$_2$P$_2$Rh: C, 61.68; H, 8.31; N, 4.36. Found: C, 61.42; H, 8.30; N, 4.01. MS (70 eV): *m/z* 642 (0.05) (M$^+$), 448 (0.52) (M$^+$ − Ph$_2$CN$_2$), 166 (0.23) (CPh$_2^+$). IR (hexane): ν(≡CH) 3280, ν(C≡C) 1935, ν(N=N) 1920 cm^{-1}. ^{1}H NMR (C$_6$D$_6$, 200 MHz): δ 7.42−6.90 (m, 10H, C$_6$*H*$_5$), 3.02 (d, ^3J(RhH) = 2.0 Hz, 1H, C≡C*H*, ^4J(PH) not resolved), 2.43 (m, 6H, PC*H*CH$_3$), 1.29 (dvt, J(HH) = 7.1, N = 13.3 Hz, 36H, PCHC*H*$_3$). ^{13}C NMR (C$_6$D$_6$, 50.3 MHz): δ 129.90, 129.04, 124.89, 124.41 (all s, *C*$_6$H$_5$), 113.83 (dt, ^2J(RhC) = 15.3, ^3J(PC) = 3.2 Hz, C≡*C*H), 109.18 (dt, ^1J(RhC) = 51.3, ^2J(PC) = 20.8 Hz, *C*≡CH), 75.46 (br, s, *C*N$_2$), 24.86 (vt, N = 18.5 Hz, P*C*HCH$_3$), 20.45 (s, PCH*C*H$_3$). ^{31}P NMR (C$_6$D$_6$, 81.0 MHz): δ 46.42 (d, ^1J(RhP) = 132.2 Hz).

Preparation of *trans*-[Rh(C≡CH){N$_2$C(C$_{12}$H$_8$)}(P-*i*-Pr$_3$)$_2$] (9). A solution of **6** (86 mg, 0.18 mmol) in 8 mL of pentane was treated as described for **8** with a solution of (C$_{12}$H$_8$)CN$_2$ (35 mg, 0.18 mmol) in 4 mL of pentane. After the solvent was removed in vacuo, the residue was dissolved in 5 mL of acetone and the solution was stored at −78 °C. Olive-green crystals precipitated which were filtered off and dried in vacuo: yield 91 mg (79%); mp 89 °C dec. Anal. Calcd for C$_{33}$H$_{51}$N$_2$P$_2$Rh: C, 61.87; H, 8.03; N, 4.37. Found: C, 61.74; H, 8.23; N, 3.91. IR (KBr): ν(≡CH) 3240, ν(C≡C) 1935, ν(N=N) 1920 cm^{-1}. ^{1}H NMR (C$_6$D$_6$, 200 MHz): δ = 7.86−7.10 (m, 8H, C$_{12}$*H*$_8$), 3.12 (dt, ^3J(RhH) = 2.0, ^4J(PH) = 1.8 Hz, 1H, C≡C*H*), 2.41 (m, 6H, PC*H*CH$_3$), 1.25 (dvt, J(HH) = 7.1, N = 13.5 Hz, 36H, PCHC*H*$_3$). ^{13}C NMR (C$_6$D$_6$, 50.3 MHz): δ 131.54, 130.46, 125.70, 122.65, 121.05, 118.55 (all s, *C*$_{12}$H$_8$), 116.26 (dt, ^2J(RhC) = 14.3, ^3J(PC) = 3.7 Hz, C≡*C*H), 71.20 (br, s, *C*N$_2$), 24.92 (vt, N = 18.5 Hz, P*C*HCH$_3$), 20.31 (s, PCH*C*H$_3$), signal of *C*≡CH obscured by signals of *C*$_6$D$_6$. ^{31}P NMR (C$_6$D$_6$, 81.0 MHz): δ 48.08 (d, ^1J(RhP) = 129.3 Hz).

Preparation of *trans*-[Rh(C≡CH){N$_2$C(Ph)(COPh)}(P-*i*-Pr$_3$)$_2$] (10). A solution of **6** (73 mg, 0.15 mmol) in 8 mL of pentane was treated as described for **8** with a solution of PhC(O)PhCN$_2$ (34 mg, 0.15 mmol) in 2 mL of pentane. Red crystals were obtained; yield 92 mg (91%); mp 64 °C dec. Anal. Calcd for C$_{34}$H$_{53}$N$_2$OP$_2$Rh: C, 60.89; H, 7.96; N, 4.17. Found: C, 60.80; H, 8.02; N, 4.25. IR (hexane): ν(≡CH) 3262, ν(C≡C) 1940, ν(N=N) 1915 cm^{-1}. ^{1}H NMR (C$_6$D$_6$, 200 MHz): δ 7.58−6.89 (m, 10H, C$_6$*H*$_5$), 2.66 (m, 6H, PC*H*CH$_3$), 2.48 (dt, ^3J(RhH) = 2.4, ^4J(PH) = 1.3 Hz, 1H, C≡C*H*), 1.26 (dvt, J(HH) = 7.1, N = 13.5 Hz, 18H, PCHC*H*$_3$), 1.20 (dvt, J(HH) = 6.9, N = 13.0 Hz, 18H, PCHC*H*$_3$). ^{13}C NMR (C$_6$D$_6$, 50.3 MHz): δ 155.03 (s, *C*=O), 140.09, 139.56, 130.02, 129.36, 128.28, 125.02 (all s, *C*$_6$H$_5$), 99.80 (br, s, *C*N$_2$), 99.67 (dt, ^2J(RhC) = 12.9, ^3J(PC) = 3.0 Hz, C≡*C*H), 97.61 (dt, ^1J(RhC) = 54.5, ^2J(PC) = 15.5 Hz, *C*≡CH), 24.07 (vt, N = 17.6 Hz, P*C*HCH$_3$), 19.95, 19.80 (both s, PCH*C*H$_3$). ^{31}P NMR (C$_6$D$_6$, 81.0 MHz): δ 37.86 (d, ^1J(RhP) = 126.4 Hz).

Preparation of *trans*-[Rh(C≡CH){N$_2$C(H)(COPh)}(P-*i*-Pr$_3$)$_2$] (11). A solution of **6** (52 mg, 0.11 mmol) in 8 mL of pentane was treated as described for **8** with a solution of PhC(=O)CHCN$_2$ (16 mg, 0.11 mmol) in 2 mL of pentane. Red crystals were obtained: yield 51 mg (78%); mp 118 °C dec. Anal. Calcd for C$_{28}$H$_{49}$N$_2$OP$_2$Rh: C, 56.56; H, 8.31; N, 4.71. Found: C, 56.63; H, 8.31; N, 4.40. IR (KBr): ν(≡CH) 3270, ν(C≡C) 1938, ν(N=N) 1910, ν(C=O) 1600, 1577 cm^{-1}. ^{1}H NMR (C$_6$D$_6$, 200 MHz): δ 7.91 (d, ^3J(HH) = 7.2 Hz, 2H, ortho-H of C$_6$*H*$_5$), 7.24−7.11 (m, 3H, C$_6$*H*$_5$), 2.64 (m, 6H, PC*H*CH$_3$), 2.45 (dt, ^3J(RhH) = 2.4, ^4J(PH) = 1.4 Hz, 1H, C≡C*H*), 1.53 (s, 1H, N$_2$C*H*), 1.27 (dvt, J(HH) = 7.1, N = 13.5 Hz, 18H, PCHC*H*$_3$), 1.18 (dvt, J(HH) = 6.9, N = 13.5 Hz, 18H, PCHC*H*$_3$). ^{13}C NMR (C$_6$D$_6$, 50.3 MHz): δ 152.57 (s, *C*=O), 136.32, 129.48, 128.29, 126.67 (all s, *C*$_6$H$_5$), 98.76 (dt, ^2J(RhC) = 12.9, ^3J(PC) = 3.6 Hz, C≡*C*H), 81.13 (br, s, *C*N$_2$), 24.06 (vt, N = 18.5 Hz, P*C*HCH$_3$), 19.93, 19.78 (both s, PCH*C*H$_3$), signal of *C*≡CH obscured by signals of *C*$_6$D$_6$. ^{31}P NMR (C$_6$D$_6$, 81.0 MHz): δ 37.74 (d, ^1J(RhP) = 124.8 Hz).

Preparation of *trans*-[Rh(C≡C*t*-Bu)(N$_2$CPh$_2$)(P-*i*-Pr$_3$)$_2$] (12). A solution of **7** (102 mg, 0.19 mmol) in 5 mL of pentane was treated as described for **8** with a solution of Ph$_2$CN$_2$ (37 mg, 0.19 mmol) in 2 mL of pentane. Green crystals were obtained; yield 127 mg (95%); mp 94 °C dec. Anal. Calcd C$_{37}$H$_{61}$N$_2$P$_2$Rh: C, 63.60; H, 8.80; N, 4.04. Found: C, 63.37; H, 8.96; N, 3.64. IR (hexane): ν(C≡C) 2070, ν(N=N) 1930 cm^{-1}. ^{1}H NMR (C$_6$D$_6$, 200 MHz): δ 7.44-6.81 (m, 10H, C$_6$*H*$_5$), 2.42 (m, 6H, PC*H*CH$_3$), 1.28 (dvt, J(HH) = 6.9, N = 15.2 Hz, 36H, PCHC*H*$_3$), 1.26 (s, 9H, C(C*H*$_3$)$_3$). ^{13}C NMR (C$_6$D$_6$, 50.3 MHz): δ 136.81 (dt, ^2J(RhC) = 14.4, ^3J(PC) = 3.2 Hz, C≡*C*R), 130.25, 128.98, 124.71, 124.03 (all s, *C*$_6$H$_5$), 98.46 (dt, ^1J(RhC) = 51.3, ^2J(PC) = 20.8 Hz, *C*≡CR), 75.24 (br, s, *C*N$_2$), 32.57 (s, *C*CH$_3$), 29.80 (s, C*C*H$_3$), 24.70 (vt, N = 18.5 Hz, P*C*HCH$_3$), 20.41 (s, PCH*C*H$_3$). ^{31}P NMR (C$_6$D$_6$, 81.0 MHz): δ 46.92 (d, ^1J(RhP) = 132.2 Hz).

Preparation of *trans*-[Rh(C≡C*t*-Bu){N$_2$C(C$_{12}$H$_8$)}(P-*i*-Pr$_3$)$_2$] (13). A solution of **7** (97 mg, 0.18 mmol) in 8 mL of pentane was treated as described for **8** with a solution of (C$_{12}$H$_8$)CN$_2$ (35 mg, 0.18 mmol) in 2 mL of pentane. Green crystals were obtained: yield 104 mg (82%); mp 109 °C dec. Anal. Calcd for C$_{37}$H$_{59}$N$_2$P$_2$Rh: C, 63.78; H, 8.89; N, 4.02. Found: C, 63.92; H, 8.80; N, 3.97. MS (70 eV): *m/z* 696 (0.04) (M$^+$). IR (C$_6$H$_6$): ν(C≡C) 2050, ν(N=N) 1930 cm^{-1}. ^{1}H NMR (C$_6$D$_6$, 200 MHz): δ 7.88−7.10 (m, 8H, C$_{12}$*H*$_8$), 2.42 (m, 6H, PC*H*CH$_3$), 1.25 (dvt, J(HH) = 7.1, N = 13.5 Hz, 36H, PCHC*H*$_3$), 1.22 (s, 9H, C(CH$_3$)$_3$). ^{13}C NMR (C$_6$D$_6$, 50.3 MHz): δ 139.89 (dt, ^2J(RhC) = 13.9, ^3J(PC) = 3.2 Hz, C≡*C*R), 130.31, 129.35, 125.52, 122.23, 120.95, 118.51 (all s, *C*$_{12}$H$_8$), 97.99 (dt, ^1J(RhC) = 51.8, ^2J(PC) = 21.3 Hz, *C*≡CR), 74.42 (br, s, *C*N$_2$), 32.38 (s, *C*CH$_3$), 29.73 (s, CCH3), 24.77 (vt, N = 19.4 Hz, P*C*HCH$_3$), 20.25 (s, PCH*C*H$_3$). ^{31}P NMR (C$_6$D$_6$, 81.0 MHz): δ 48.15 (d, ^1J(RhP) = 129.3 Hz).

Preparation of *trans*-[Rh(C≡C-*t*-Bu){N$_2$C(Ph)(COPh)}(P-*i*-Pr$_3$)$_2$] (14). A solution of **7** (100 mg, 0.19 mmol) in 5 mL of pentane was treated as described for **8** with a solution of PhC(O)PhCN$_2$ (42 mg, 0.19 mmol) in 2 mL of pentane. Red

crystals were obtained: yield 120 mg (87%); mp 86 °C dec. Anal. Calcd for $C_{38}H_{61}N_2OP_2Rh$: C, 62.80; H, 8.46; N, 3.85. Found: C, 63.69; H, 8.73; N, 3.42. IR (KBr): ν(C≡C) 2080, ν(N=N) 1930, ν(C=bbO) 1610 cm^{-1}. ^{1}H NMR (C_6D_6, 200 MHz): δ 7.63–6.87 (m, 10H, C_6H_5), 2.67 (m, 6H, PC*H*CH$_3$), 1.39 (s, 9H, C(C*H*$_3$)$_3$), 1.25 (dvt, *J*(HH) = 7.1, *N* = 13.5 Hz, 18H, PCHC*H*$_3$), 1.20 (dvt, *J*(HH) = 6.9, *N* = 12.8 Hz, 18H, PCHC*H*$_3$). ^{13}C NMR (C_6D_6, 50.3 MHz): δ 154.42 (s, *C*=O), 140.22, 139.55, 129.94, 129.32, 128.27, 127.50 (all s, *C*$_6$H$_5$), 120.80 (dt, ^2J(RhC) = 12.5, ^3J(PC) = 2.4 Hz, C≡*C*R), 99.90 (br, s, *C*N$_2$), 84.72 (dt, ^1J(RhC) = 55.0, ^2J(PC) = 16.2 Hz, *C*≡CR), 32.62 (s, *C*CH$_3$), 29.99 (s, C*C*H$_3$), 23.95 (vt, *N* = 18.6 Hz, PC*H*CH$_3$), 19.94, 19.74 (both s, PCH*C*H$_3$). ^{31}P NMR (C_6D_6, 81.0 MHz): δ 38.11 (d, ^1J(RhP) = 127.9 Hz).

Preparation of *trans*-[Rh(C≡C-*t*-Bu){N$_2$C(H)(COPh)}(P-*i*-Pr$_3$)$_2$] (15). A solution of **7** (100 mg, 0.19 mmol) in 5 mL of pentane was treated as described for **8** with a solution of PhC(=O)CHN$_2$ (30 mg, 0.20 mmol) in 2 mL of pentane. Orange-red crystals were obtained; yield 114 mg (93%); mp 126 °C dec. Anal. Calcd for $C_{32}H_{57}N_2OP_2Rh$: C, 59.07; H, 8.83; N, 4.31. Found: C, 59.90; H, 9.40; N, 4.22. IR (KBr): ν(C≡C) 2105, ν(N=N) 1935 cm^{-1}. ^{1}H NMR (C_6D_6, 200 MHz): δ 7.96–6.95 (m, 5H, C_6H_5), 2.52 (m, 6H, PC*H*CH$_3$), 1.43 (s, 1H, N$_2$C*H*), 1.39 (s, 9H, C(C*H*$_3$)$_3$), 1.25 (dvt, *J*(HH) = 6.5, *N* = 13.7 Hz, 18H, PCHC*H*$_3$), 1.17 (dvt, *J*(HH) = 6.6, *N* = 12.8 Hz, 18H, PCHC*H*$_3$). ^{13}C NMR (C_6D_6, 50.3 MHz): δ 151.83 (s, *C*=O), 138.51, 129.37, 128.20, 126.64 (all s, *C*$_6$H$_5$), 119.66 (dt, ^2J(RhC) = 12.0, ^3J(PC) = 2.0 Hz, C≡*C*R), 85.04 (dt, ^1J(RhC) = 54.6, ^2J(PC) = 15.7 Hz, *C*≡CR), 81.39 (br, s, *C*N$_2$), 32.63 (s, *C*CH$_3$), 30.07 (s, C*C*H$_3$), 23.95 (vt, *N* = 17.3 Hz, P*C*HCH$_3$), 19.87, 19.71 (both s, PCH*C*H$_3$). ^{31}P NMR (C_6D_6, 81.0 MHz): δ 37.39 (d, ^1J(RhP) = 126.4 Hz).

Reaction of 7 with PhCHN$_2$. A solution of **7** (71 mg, 0.13 mmol) in 5 mL of pentane was treated at −78 °C with a solution of PhCHN$_2$ (16 mg, 0.13 mmol) in 3 mL of pentane and with continuous stirring slowly warmed up to room temperature. At ca. −30 °C the color changed from violet to green. The solution was concentrated to 2 mL in vacuo and then stored at −78 °C. A brown solid precipitated which was filtered off, washed with pentane (−30 °C), and dried in vacuo. The solid was identified by ^{1}H- and ^{31}P-NMR spectroscopy as a 1:3 mixture of *trans*-[Rh(C≡C-*t*-Bu)(N$_2$CHPh)(P-*i*-Pr$_3$)$_2$] (**16**) and *trans*-[Rh(C≡C*t*-Bu)(N$_2$)(P-*i*-Pr$_3$)$_2$] (**17**). Further attempts to separate the two products failed. ^{1}H NMR spectra at variable temperature indicated that at −40 °C primarily the complex **16** was formed, which at 0 °C decomposed to give **17**. Data for **16**: IR (C_6H_6): ν(C≡C) 2060, ν(N=N) 1935 cm^{-1}. ^{1}H NMR (C_6D_6, 200 MHz): δ 4.14 (s, 1H, N$_2$C*H*), 2.46 (m, 6H, PC*H*CH$_3$), 1.33 (dvt, *J*(HH) = 6.0, *N* = 12.8 Hz, 36H, PCHC*H*$_3$), 1.27 (s, 9H, C(C*H*$_3$)$_3$), signal of C_6H_5 not exactly located. ^{31}P NMR (C_6D_6, 81.0 MHz): δ 46.96 (d, ^1J(RhP) = 136.6 Hz). Data for **17**: IR (C_6H_6): ν(N≡N) 2120 cm^{-1}. ^{1}H NMR (C_6D_6, 200 MHz): δ 2.42 (m, 6H, PC*H*CH$_3$), 1.31 (dvt, *J*(HH) = 5.8, *N* = 13.1 Hz, 36H, PCHC*H*$_3$), 1.29 (s, 9H, C(C*H*$_3$)$_3$). ^{31}P NMR (C_6D_6, 81.0 MHz): δ 39.73 (d, ^1J(RhP) = 127.9 Hz).

X-ray Structural Analysis of 4. Single crystals were grown from hexane/benzene. Crystal data (from 23 reflections, 10° < θ < 14°): monoclinic, space group $P2_1/c$ (No. 14), a = 11.280(3) Å, b = 15.201(2) Å, c = 17.041(5) Å, β = 92.36(1)°, V = 2919(1) Å^3, Z = 4, d_{calcd} = 1.312 g cm^{-3}, μ(Mo K$_\alpha$) = 7.9 cm^{-1}; crystal size 0.25 × 0.15 × 0.15 mm; Enraf-Nonius CAD4 diffractometer, Mo K$_\alpha$ radiation (0.709 30 Å), graphite monochromator, zirkon filter (factor 16.4); T = 223 K; ω/2θ-scan, max 2θ = 46°; 4243 independent reflections measured, 2618 regarded as beeing observed [$F_o > 3\sigma(F_o)$]. Intensity data were corrected for Lorentz and polarization effects, and an empirical absorption correction (ψ-scan method) was applied. The minimum transmission was 97.56%. The structure was solved by direct methods (SHELXS-86). Atomic coordinates and anisotropic thermal parameters of the non-hydrogen atoms were refined by full-matrix least squares (329 parameters, unit weights, Enraf-Nonius SDP).[34] The positions of the ylide-hydrogen atom H was located in the difference-Fourier-synthesis and isotropically refined. The position of the other hydrogen atoms were calculated according to ideal geometry (distance C−H 0.95 Å) and refined using the riding method. R = 0.032, R_w = 0.035; reflex/parameter ratio 7.96; residual electron density +0.530/−0.475 eV Å^{-3}.

Computational Methods. The calculations have been carried out using effective core potentials (ECP) for Rh, P, and Cl. The quasirelativistic ECP for Rh has a large valence-shell basis set (311111/22111/411).[35a] The valence-shell basis sets for P and Cl have DZ+P quality (31/31/1).[35b] For C and O a standard DZ+P basis set has been used, and for H a DZ basis set has been used.[36] The geometry optimization was performed at the MP2 level (Møller–Plesset perturbation theory terminated at second order)[37] using the program TURBOMOLE.[38]

Acknowledgment. We thank the Deutsche Forschungsgemeinschaft (SFB 347) and the Fonds der Chemischen Industrie for financial support, and in particular Degussa AG for various gifts of chemicals. We also gratefully acknowledge support by Mrs. M.-L. Schäfer and Dr. W. Buchner (NMR spectra), Mrs. A. Burger, Mrs. R. Schedl, and C. P. Kneis (elemental analyses and DTA), and Dr. J. Wolf for helpful discussions.

Supplementary Material Available: Tables giving crystal data and data collection and refinement parameters, all bond distances and angles, least-square planes and deviations therefrom, anisotropic thermal parameters, and positional parameters for **4** (13 pages). Ordering information is given on any current masthead page.

OM940714G

(34) Frenz, B. A. The Enraf-Nonius CAD4 SDP—a real time system for concurrent X-ray data collection and structure determination. In *Computing in Crystallography*; Delft University Press: Delft, Holland, 1978; pp 64–71.

(35) (a) Dolg, M.; Wedig, U.; Stoll, H.; Preuss, H. *J. Chem. Phys.* **1987**, *86*, 866–872. (b) Bergner, A.; Dolg, M.; Küchle, W.; Stoll, H.; Preuss, H. *Mol. Phys.* **1993**, *80*, 1431–1441. The exponents of the d-type polarization functions are 0.55 for P and 0.75 for Cl.

(36) (a) Huzinaga, S., Ed. *Gaussian Basis Sets for Molecular Calculations*; Elsevier: Amsterdam, 1984. (b) Dunning, T. H., Jr. *J. Chem. Phys.* **1970**, *53*, 2823–2833.

(37) (a) Møller, C.; Plesset, M. S. *Phys. Rev.* **1943**, *46*, 618–622. (b) Binkley, J. S.; Pople, J. A. *Int. J. Quantum Chem.* **1975**, *9*, 229–236.

(38) (a) Häser, M.; Ahlrichs, R. *J. Comput. Chem.* **1989**, *10*, 104–111. (b) Ahlrichs, R.; Bär, M.; Häser, M.; Horn, H.; Kölmel, C. *Chem. Phys. Lett.* **1989**, *162*, 165–169. (c) Horn, H.; Weiss, H.; Häser, M.; Ehrig, M.; Ahlrichs, R. *J. Comput. Chem.* **1991**, *12*, 1058–1064. (d) Häser, M.; Almlöf, J.; Feyereisen, M. W. *Theor. Chim. Acta* **1991**, *79*, 115–122. (e) Haase, F.; Ahlrichs, R. *J. Comput. Chem.* **1993**, *14*, 907–912.

Reactions of Acetylide Clusters $Cp^*WRe_2(CO)_9(CCR)$, R = Ph, $C(Me)=CH_2$, and Cyclohexenyl, with Thiophenol. Formation of WRe_2 Thiolate Alkyne and Vinylalkylidyne Derivatives

Jiunn-Jang Peng,[†] Shie-Ming Peng,*[,‡] Gene-Hsiang Lee,[‡] and Yun Chi*[,†]

Departments of Chemistry, National Tsing Hua University, Hsinchu 300, Taiwan, Republic of China, and National Taiwan University, Taipei 107, Taiwan, Republic of China

Received August 22, 1994[⊗]

Heterometallic acetylide cluster $Cp^*WRe_2(CO)_9(CCPh)$ (**1a**) reacted with thiophenol in refluxing toluene to afford two acetylene clusters $Cp^*WRe_2(CO)_8(\mu_3\text{-SPh})(CH{=}CPh)$ (**2a**) and $Cp^*WRe_2(CO)_7(\mu\text{-SPh})(CH{=}CPh)$ (**3a**). Their structures were determined by X-ray diffraction studies. Crystal data of **2a**: space group $I2/c$; a = 20.017(4) Å, b = 11.869(6) Å, c = 29.622(5) Å, β = 98.50(2)°, Z = 8, R = 0.039, and R_w = 0.032 for 3279 observed reflections with $I > 2\,\sigma(I)$. Crystal data of **3a**: space group $P2_1/n$; a = 10.839(5) Å, b = 17.112(4) Å, c = 16.581(7) Å, β = 94.16(3)°, Z = 4, R = 0.042, and R_w = 0.042 for 3323 observed reflections with $I > 2\sigma(I)$. The structure of **2a** possesses a V-shaped core geometry with a face-bridging thiolate ligand and a phenylacetylene adopting a $\mu_3\text{-}\eta^2$ (∥) mode, whereas cluster **3a** contains a triangular skeleton with an edge-bridging thiolate fragment and a unique $\mu_3\text{-}\eta^2(\perp)$ phenylacetylene ligand. Heating of **2a** afforded **3a** via elimination of a CO; the latter process could be partially reversed by addition of a CO atmosphere. Upon switching to vinylacetylide clusters $Cp^*WRe_2(CO)_9$ ($CCC{=}CH(CH_2)_4$) (**1c**) and $Cp^*WRe_2(CO)_9(CCCMe{=}CH_2)$ (**1d**), only the alkylidyne clusters $Cp^*WRe_2(CO)_7(\mu\text{-SPh})_2$ ($CCH{=}C(CH_2)_5$) (**4a**) and $Cp^*WRe_2(CO)_7(\mu\text{-SPh})_2(CCH{=}CMe_2)$ (**4b**) were obtained. Crystals of **4a** are triclinic, space group $P\bar{1}$; a = 10.149(1) Å, b = 12.151(4) Å, c = 17.442(2) Å, α = 84.79(2)°, β = 76.40(1)°, γ = 70.39(2)°, Z = 2, R = 0.023, and R_w = 0.022 for 4557 reflections with $I > 2\,\sigma(I)$. Clusters **4**, exhibiting an open triangular arrangement, possess two thiolate ligands and an asymmetric vinylalkylidyne weakly bridging a W–Re edge (μ-W–C = 1.858(7) Å, μ-Re–C = 2.339(6) Å).

Transition-metal cluster compounds containing alkyne ligands have recently been the focus of considerable attention.[1] The ability of alkynes to adopt various coordination modes[2] and their promising potential in serving as precursors for organic synthesis have promoted extensive investigation of alkyne clusters.[3] Our discovery of a feasible and high-yield method of preparing heterometallic acetylide clusters $LWOs_2(CO)_8(CCR)$, $LWRu_2(CO)_8(CCR)$, and $LWRe_2(CO)_9(CCR)$, L = Cp, Cp*; R = Ph, Bu^t, $CMe{=}CH_2$, etc.,[4] has given us an excellent opportunity to probe the reactivity of these trinuclear acetylide complexes. As a result, we have carried out the reactivity studies of $CpWOs_2(CO)_8(CCPh)$ with disubstituted alkynes and tungsten hydride complexes[5] and have examined the C–C bond coupling reaction between $CpWRu_2(CO)_8(CCPh)$ and metal acetylide complexes.[6] Moreover, for the WRe_2 clusters $Cp^*WRe_2(CO)_9(CCCMe{=}CH_2)$, which contain a highly unsaturated vinylacetylide, we also explored the reactions with hydrogen and alcohols.[7]

In the present paper, we report the direct reaction of the acetylide cluster $Cp^*WRe_2(CO)_9(CCPh)$ with thiophenol; the latter has been shown to be an effective reagent for the preparation of sulfur-containing clusters.[8] Interestingly, such a trimetallic system has provided two novel phenylacetylene clusters via oxidative addition of thiophenol and hydrogen transfer to the α-carbon of the

† National Tsing Hua University.
‡ National Taiwan University.
⊗ Abstract published in *Advance ACS Abstracts*, December 1, 1994.

(1) (a) Carty, A. J. *Pure Appl. Chem.* **1982**, *54*, 113. (b) Sappa, E.; Tiripicchio, A.; Braunstein, P. *Chem. Rev.* **1983**, *83*, 203. (c) Raithby, P. R.; Rosales, M. J. *Adv. Inorg. Chem. Radiochem.* **1985**, *29*, 169.

(2) (a) Adams, R. D.; Chen, G.; Qu, X.; Wu, W.; Yamamoto, J. H. *Organometallics* **1993**, *12*, 3029. (b) Adams, R. D.; Chen, G.; Qu, X.; Wu, W. *Organometallics* **1993**, *12*, 3426. (c) Adams, R. D.; Chen, G.; Chi, Y.; Wu, W.; Yin, J. *Organometallics* **1992**, *11*, 1480. (d) Dickson, R. S. *Polyhedron* **1991**, *10*, 1995. (e) Dickson, R. S.; Paravagna, O. M. *Organometallics* **1991**, *10*, 721. (f) Corrigan, J. F.; Doherty, S.; Taylor, N. J.; Carty, A. J. *Organometallics* **1993**, *12*, 1365. (g) Hirpo, W.; Curtis, M. D. *Organometallics* **1994**, *13*, 2706. (h) Rosenberg, E.; Bracker-Novak, J.; Gellert, R. W.; Aime, S.; Gobetto, R.; Osella, D. *J. Organomet. Chem.* **1989**, *365*, 163. (i) Rosenberg, E.; Wang, J.; Gellert, R. W. *Organometallics* **1988**, *7*, 1093. (j) Farrugia, L. J.; Shirley, E. R. *Organometallics* **1992**, *11*, 196.

(3) (a) Jeannin, Y. *Transition Met. Chem.* **1993**, *18*, 122. (b) Ojima, I.; Donovan, R. J.; Ingallina, P.; Clos, N.; Shay, W. R.; Eguchi, M.; Zeng, Q.; Korda, A. *J. Cluster Sci.* **1992**, *3*, 423. (c) Rudler, H.; Audouin, M.; Chelain, E.; Denise, B.; Goumont, R.; Massoud, A.; Parlier, A.; Pacreau, A.; Rudler, M. *Chem. Soc. Rev.* **1991**, *20*, 503. (d) Shore, N. E. *Chem. Rev.* **1988**, *88*, 1081. (e) Adams, R. D.; Cortopassi, J. E.; Pompeo, M. P. *Organometallics* **1992**, *11*, 1. (f) Johnson, D. K.; Rukachaisirikul, T.; Sun, Y.; Taylor, N. J.; Canty, A. J.; Carty, A. J. *Inorg. Chem.* **1993**, *32*, 5544. (g) Adams, R. D.; Chen, G.; Chen, L.; Wu, W.; Yin, J. *Organometallics* **1993**, *12*, 3431. (h) Adams, R. D.; Chen, L.; Huang, M. *Organometallics* **1994**, *13*, 2696.

(4) (a) Chi, Y.; Lee, G.-H.; Peng, S.-M.; Liu, B.-J. *Polyhedron* **1989**, *8*, 2003. (b) Chi, Y.; Lee, G.-H.; Peng, S.-M.; Wu, C.-H. *Organometallics* **1989**, *8*, 1574. (c) Hwang, D.-K.; Chi, Y.; Peng, S.-M.; Lee, G.-H. *Organometallics* **1990**, *9*, 2709.

(5) (a) Chi, Y.; Huttner, G.; Imhof, W. *J. Organomet. Chem.* **1990**, *384*, 93. (b) Chi, Y.; Wu, C.-H.; Peng, S.-M.; Lee, G.-H. *Organometallics* **1991**, *10*, 1676.

(6) Hwang, D.-K.; Lin, P.-J.; Chi, Y.; Peng, S.-H.; Lee, G.-H. *J. Chem. Soc., Dalton Trans.* **1991**, 2161.

(7) Cheng, P.-S.; Chi, Y.; Peng, S.-H.; Lee, G.-H. *Organometallics* **1993**, *12*, 250.

0276-7333/95/2314-0626$09.00/0

coordinated acetylide ligand. In these alkyne clusters, the bonding mode of the alkyne is of particular interest. One complex is a 50-electron cluster exhibiting a μ_3-η^2 parallel orientation with respect to two nonbonded metal atoms, while the second belong to an unsaturated 46-electron alkyne cluster bearing an unusual μ_3-η^2 perpendicular mode. Additionally, clusters containing an alkylidyne ligand, as formed by addition of two thiophenol molecules, are indicated here by selecting of a vinylacetylide to replace the acetylide ligand. The full spectroscopic and structural characterizations of these new clusters are also given.

Experimental Procedures

General Information and Materials. Infrared spectra were recorded on a Perkin-Elmer 2000 FT-IR spectrometer. ^{1}H and ^{13}C NMR spectra were recorded on a Bruker AM-400 or a Varian Unity-400 instrument; the chemical shifts are quoted with respect to internal standard tetramethylsilane. Mass spectra were obtained on a JEOL SX-102A or a HX110 instrument operating in fast atom bombardment (FAB) mode. The acetylide clusters Cp*$WRe_2(CO)_9$(CCR), R = Ph, C(Me)=CH_2-, and cyclohexenyl, were prepared from the reactions of the acetylide complexes Cp*$W(CO)_3$(CCR) and the rhenium acetonitrile complex $Re_2(CO)_8(CH_3CN)_2$ according to literature procedures.[9] All reactions were performed under a nitrogen atmosphere using deoxygenated solvents dried with an appropriate reagent. The progress of reactions was monitored by analytical thin-layer chromatography (5735 Kiesel gel 60 F_{254}, E. Merck) and the products were separated on commercially available preparative thin-layer chromatographic plates (Kiesel gel 60 F_{254}, E. Merck). Elemental analyses were performed at the NSC Regional Instrumentation Center at National Cheng Kung University, Tainan, Taiwan.

Reaction of Cp*$WRe_2(CO)_9$(CCPh) with Thiophenol. A toluene solution (30 mL) of Cp*$WRe_2(CO)_9$(CCPh) (**1a**, 86 mg, 0.082 mmol) and thiophenol (33 μL, 0.324 mmol) was heated at reflux under nitrogen for 10 min, during which period the color changed from orange-red to dark-brown. After allowing the solution to cool to room temperature, the solvent was evaporated and the residue was separated by thin-layer chromatography. Development with a 1:1 mixture of dichloromethane and hexane afforded two major bands, which were then removed from the silica gel TLC plates by extraction with dichloromethane and concentration, thereby producing 30 mg of red Cp*$WRe_2(CO)_8$(μ_3-SPh)(CH=CPh), (**2a**, 0.026 mmol, 32%) and 28 mg of black Cp*$WRe_2(CO)_7$(μ-SPh)(CH=CPh), (**3a**, 0.025 mmol, 31%). Crystals of both **2a** and **3a** suitable for X-ray analysis were obtained from a layered solution of dichloromethane–heptane at room temperature.

Spectral data for **2a**. MS (FAB, ^{184}W, ^{187}Re): *m/z* 1128 (M^+). IR (C_6H_{12}): ν(CO), 2036 (s), 2009 (vs), 1985 (w), 1955 (m), 1937 (w), 1897 (w) cm^{-1}; ^{1}H NMR (400 MHz, $CDCl_3$, 294 K): δ 8.06 (s, 1 H, C*H*=CPh), 7.32–6.86 (m, 10H, Ph), 2.06 (s, 15H, C_5Me_5). ^{13}C NMR (100 MHz, $CDCl_3$, 294 K): δ 219.2 (J_{W-C} = 165 Hz), 216.7 (J_{W-C} = 170 Hz), 197.8 (3C), 191.3 (3C, br); 200.7 (1C, CH=*C*Ph), 168.0 (1C, *C*H=CPh, J_{W-C} = 62 Hz), 160.2 (*i*-C_6H_5), 135.8 (*i*-C_6H_5), 131.6 (*m*-C_6H_5), 130.4 (*p*-C_6H_5), 129.1 (*m*-C_6H_5), 127.6 (*o*-C_6H_5), 126.2 (*o*-C_6H_5), 124.2 (*p*-C_6H_5), 106.2 (C_5Me_5), 10.8 (C_5*Me*$_5$). Anal. Calcd for $C_{32}H_{26}O_8SRe_2W\cdot{}^1/_2CH_2Cl_2$: C, 33.38, H, 2.33. Found: C, 33.40; H, 2.30.

Spectral data for **3a**. MS (FAB, ^{184}W, ^{187}Re): *m/z* 1100 (M^+). IR (C_6H_{12}): ν(CO), 2045 (s), 2015 (vs), 1965 (s, br), 1953 (w), 1926 (m), 1907 (w), 1772 (vw) cm^{-1}. ^{1}H NMR (400 MHz, $CDCl_3$, 294 K): δ 12.03 (s, 1H, C*H*=CPh), 7.15–6.81 (m, 10H, Ph), 2.07 (s, 15H, C_5Me_5). ^{13}C NMR (100 MHz, $CDCl_3$, 294 K): δ 219.7 (J_{W-C} = 185 Hz), 197.1 (3C, br), 194.5 (1C), 193.6 (1C), 186.9 (1C); 184.3 (*C*H=CPh, J_{W-C} = 56 Hz), 143.1 (CH=*C*Ph), 138.8 (*i*-C_6H_5), 132.5 (*m*-C_6H_5), 131.1 (*m*-C_6H_5), 128.4 (*p*-C_6H_5), 128.3 (*o*-C_6H_5), 128.1 (*i*-C_6H_5), 128.0 (*p*-C_6H_5), 127.5 (*o*-C_6H_5), 106.2 (C_5Me_5), 10.7 (C_5*Me*$_5$). Anal. Calcd for $C_{31}H_{26}O_7S_2Re_2W$: C, 33.88, H, 2.38. Found: C, 33.71; H, 2.37.

Thermolysis of Cp*$WRe_2(CO)_8$(μ_3-SPh)(CH=CPh). A toluene solution (30 mL) of **2a** (22 mg) was heated at reflux for 1 h. Following removal of the solvent under vacuum, the residue was separated by thin-layer chromatography (dichloromethane–hexane 1:1) and recrystallization, producing 10 mg of black Cp*$WRe_2(CO)_7$(μ-SPh)(CH=CPh) (**3a**, 0.025 mmol, 47%).

Reaction of Cp*$WRe_2(CO)_7$(μ-SPh)(CH=CPh) with CO. A toluene solution (30 mL) of **3a** (17 mg) was heated at reflux for 1 h under 1 atm of carbon monoxide. Following removal of the solvent in vacuo, the residue was separated by thin-layer chromatography (dichloromethane–hexane 1:1), producing 6 mg of a mixture of **2a** and **3a** in an equal proportion.

Reaction of Cp*$WRe_2(CO)_9$(CCCH=CHOMe) with Thiophenol. A toluene solution (30 mL) of Cp*$WRe_2(CO)_9$-(CCCH=CHOMe) (**1b**, 60 mg, 0.058 mmol) and thiophenol (24 μL, 0.235 mmol) was heated at reflux under nitrogen for 10 min. During which period, the color changed from orange-red to dark-brown. After allowing the solution to cool to room temperature, the solvent was evaporated and the residue was subjected to thin-layer chromatography (dichloromethane–hexane 1:1) and recrystallization (dichloromethane–heptane), giving 11 mg of red-brown Cp*$WRe_2(CO)_7$(μ-SPh)-(CH=CCH=CHOMe) (**3b**, 0.0102 mmol, 17%).

Spectral data for **3b**. MS (FAB, ^{184}W, ^{187}Re): *m/z* 1080 (M^+). IR (C_6H_{12}): ν(CO), 2042 (s), 2011 (s), 1960 (vs), 1949 (m), 1924 (s), 1907 (w), 1769 (vw) cm^{-1}. ^{1}H NMR (400 MHz, $CDCl_3$, 294 K): δ 12.32 (s, 1H, C*H*=CCH=CHOMe), 7.26–7.10 (m, 3H, Ph), 6.88 (d, 2H, Ph), 5.37 (d, 1H, CH=C*H*OMe, J_{H-H} = 6 Hz), 4.95 (d, 1H, C*H*=CHOMe, J_{H-H} = 6 Hz), 3.80 (s, 3H, OMe), 2.04 (s, 15H, C_5Me_5).

Reaction of Cp*$WRe_2(CO)_9$(CCC_6H_9) with Thiophenol. A toluene solution (30 mL) of Cp*$WRe_2(CO)_9$ (CCC=CH(CH_2)$_4$) (**1c**, 113 mg, 0.108 mmol) and thiophenol (44 μL, 0.432 mmol) was refluxed under nitrogen for 5 min, during which period the color changed from orange-red to dark-brown. After the solution reached room temperature, the solvent was evaporated and the residue was subjected to thin-layer chromatography. Development with a 1:1 mixture of dichloromethane and hexane afforded one brown band, which was then removed from the silica gel TLC plates by extraction with dichloromethane and concentration. Further purification by recrystallization from a dichloromethane–heptane mixture produced 40 mg of Cp*$WRe_2(CO)_7$(μ-SPh)$_2$ (CCH=C(CH_2)$_5$) (**4a**, 0.033 mmol, 31%) as orange crystalline material. The analogous alkylidyne cluster Cp*$WRe_2(CO)_7$(μ-SPh)$_2$(CCH=CMe_2) (**4b**) was obtained in 36% yield from reaction of Cp*$WRe_2(CO)_9$-(CCCMe=CH_2) with thiophenol under similar conditions.

Spectral data for **4a**. MS (FAB, ^{184}W, ^{187}Re): *m/z* 1214 (M^+). IR (CH_2Cl_2): ν(CO), 2032 (m), 2017 (vs), 1948 (br, s), 1910 (br, s), 1802 (br, w) cm^{-1}. ^{1}H NMR (400 MHz, $CDCl_3$, 294 K): δ 7.54–7.46 (m, 7H), 7.21–7.25 (m, 2H), 7.07 (t, 1H, J_{H-H} = 7.4 Hz), 6.18 (s, 1H, C*H*=C), 2.24–2.03 (m, 4H, CH_2), 1.87 (s, 15H, C_5Me_5), 1.71–1.40 (m, 6H, CH_2). ^{13}C NMR (100 MHz, $CDCl_3$, 294 K): δ 243.8 (J_{W-C} = 151 Hz), 196.7, 196.5, 192.3, 190.7, 190.6, 190.4; 302.7 (*C*CH=CR_2, J_{W-C} = 215 Hz), 142.3 (*i*-C_6H_5), 141.2 (*C*CH=CR_2, J_{W-C} = 30 Hz), 137.8 (*i*-C_6H_5), 132.0 (*o*–

(8) (a) Johnson, B. F. G.; Lewis, J.; Nelson, W. J. H.; Nicholls, J. N.; Vargas, *J. Organomet. Chem.* **1983**, *249*, 255. (b) Cowie, A. G.; Johnson, B. F. G.; Lewis, J.; Nicholls, J. N.; Raithby, P. R.; Rosales, M. J. *J. Chem. Soc., Dalton Trans.* **1983**, 2311. (c) Boyar, E.; Deeming, A. J.; Henrick, K.; MacPartlin, M.; Scott, A. *J. Chem. Soc., Dalton Trans.* **1986**, 1431. (d) Adams, R. D. *Polyhedron* **1986**, *4*, 2003. (e) Chi, Y.; Shapley, J. R.; Ziller, J. W.; Churchill, M. R. *Organometallics* **1987**, *6*, 301. (f) Adams, R. D.; Babin, J. E.; Kim, H.-S. *Organometallics* **1987**, *6*, 749.

(9) Peng, J.-J.; Horng, K.-M.; Cheng, P.-S.; Chi, Y.; Peng, S.-H.; Lee, G.-H. *Organometallics* **1994**, *13*, 2365.

Table 1. Experimental Data for the X-ray Diffraction Studies[a]

compound	**2a**	**3a**	**4a**
formula	$C_{32}H_{26}O_8SRe_2W\cdot{}^1/_2CH_2Cl_2$	$C_{31}H_{26}O_7SRe_2W$	$C_{37}H_{36}O_7S_2Re_2W\cdot{}^1/_2CH_2Cl_2$
mol wt	1169.32	1098.87	1256.52
crystal system	monoclinic	monoclinic	triclinic
space group	*I*2/*c*	$P2_1/n$	$P\bar{1}$
a (Å)	20.017(4)	10.839(5)	10.149(1)
b (Å)	11.869(6)	17.112(4)	12.151(4)
c (Å)	29.622(5)	16.581(7)	17.442(2)
α (deg)			84.79(2)
β (deg)	98.50(2)	94.16(3)	76.40(1)
γ (deg)			70.39(2)
V (Å^3)	6960(4)	3067(2)	1969.2(7)
Z	8	4	2
D_{calcd} (g/cm^3)	2.230	2.380	2.116
F(000)	4310	2031	1180
h,k,l ranges	−21 to 21,0−12,0−31	−11 to 11,0−18,0−17	−9 to 10,0−13,−18 to 18
crystal size (mm)	0.05 × 0.25 × 0.40	0.25 × 0.35 × 0.50	0.25 × 0.25 × 0.30
μ(Mo Kα) (cm^{-1})	105.9	119.2	94.09
transmission factors (min, max)	0.309, 1.000	0.368, 1.000	0.834, 1.000
no. of std reflctns, variation	3, ≤4%	3, ≤4%	3, ≤2%
no. of data, data with $I > 2\sigma(I)$	4531, 3279	4009, 3323	5116, 4557
no. of atoms, parameters	72, 416	68, 360	87, 456
maximum Δ/σ ratio	0.011	0.023	0.007
R_F; R_w	0.039; 0.032	0.042; 0.042	0.023; 0.020
GOF	1.65	2.55	1.97

[a] Common features: λ(Mo Kα) = 0.709 30 Å; Nonius CAD-4 diffractometer, 298 K; $R_F = \Sigma(F_o - F_c)/\Sigma(F_o)$, $R_w = \{\Sigma[w(F_o - F_c)^2]/\Sigma w(F_o)^2\}^{1/2}$, $w = 1/\sigma^2(F_o)$; GOF = $[\Sigma w|F_o - F_c|^2/(N_o - N_v)]^{1/2}$ (N_o, number of observations; N_v, number of variables).

C_6H_5), 129.7 (*o*-C_6H_5), 129.6 (*m*-C_6H_5), 127.9 (*m*-C_6H_5), 126.4 (*p*-C_6H_5), 126.2 (*p*-C_6H_5), 106.9 (C_5Me_5), 53.3 (CCH=CR_2), 35.8 (CH_2), 30.9 (CH_2), 29.2 (CH_2), 27.3 (CH_2), 26.3 (CH_2), 9.5 (C_5Me_5). Anal. Calcd for $C_{37}H_{36}O_7S_2Re_2W\cdot{}^1/_2CH_2Cl_2$: C, 35.87, H, 2.97. Found: C, 35.85; H, 2.99.

Spectral data for **4b**. MS (FAB, ^{184}W, ^{187}Re): *m/z* 1174 (M$^+$). IR (C_6H_{12}): ν(CO), 2037 (m), 2022 (vs), 1959 (s), 1934 (vw), 1912 (s), 1810 (w) cm^{-1}. ^{1}H NMR (300 MHz, $CDCl_3$, 294 K): δ 7.54−7.46 (m, 7H), 7.21−7.25 (t, 2H, J_{H-H} = 7.6 Hz), 7.07 (t, 1H, J_{H-H} = 7.4 Hz), 6.30 (s, 1H, CC*H*=CMe_2), 1.88 (s, 3H, Me), 1.88 (s, 15H, C_5Me_5), 1.70 (s, 3H, Me). Anal. Calcd for $C_{34}H_{32}O_7S_2Re_2W$: C, 34.81, H, 2.75. Found: C, 34.74; H, 2.76.

X-ray Crystallography. Diffraction measurements of complexes **2a**, **3a**, and **4a** were carried out on a Nonius CAD-4 diffractometer. All reflections were corrected for Lorentz, polarization, and absorption effects. Data deduction and refinement were performed using the NRCC-SDP-VAX packages. Lattice parameters of **2a** were determined from 25 randomly selected high-angle reflections with 2θ angles in the range 16.72−20.94°. The space group *I*2/*c* was identified on the basis of systematic absences and confirmed by successfully solving the crystal structure. Absorption corrections were made by the θ scan method; in addition, the minimum and maximum transmission factors were 0.31 and 1.00, respectively. The unit cell contains four disordered dichloromethane solvent molecules. Anisotropic thermal parameters were introduced for all non-hydrogen atoms. Full-matrix least-squares refinement with 72 atoms and 416 parameters gave $R = 0.039$ and $R_w = 0.032$, for 3279 reflections with $I > 2\sigma(I)$. The residual electron density on the difference Fourier map is ~1.40 e/Å^3.

For complex **3a**, the lattice parameters were determined from 25 randomly selected high-angle reflections with 2θ angles in the range 15.10−29.82°. The minimum and maximum transmission factors were 0.37 and 1.00, respectively. Anisotropic temperature factors were assigned to all other non-hydrogen atoms. Full-matrix least-squares refinement with 68 atoms and 320 parameters gave $R = 0.042$ and $R_w = 0.032$ for 3323 reflections with $I > 2\sigma(I)$.

Lattice parameters of **4a** were determined from 25 selected reflections with 2θ angles in the range 19.22−28.72°. Empirical absorption corrections were performed, and the minimum and maximum transmission factors were 0.83 and 1.00, respectively. The structures were solved by a direct method and refined by least-squares cycles. Additionally, hydrogen

Table 2. Atomic Coordinates and Equivalent Isotropic Displacement Coefficients for 2a

	x	*y*	*z*	B_{eq}, Å^2
W	0.15415(4)	0.70321(5)	0.137588(20)	3.11(3)
Re1	0.17558(3)	0.37960(5)	0.079236(20)	2.80(3)
Re2	0.22198(3)	0.49234(5)	0.168090(19)	2.77(3)
S	0.11303(19)	0.5132(3)	0.11761(12)	2.93(18)
C1	0.1102(9)	0.6891(15)	0.1942(5)	5.0(10)
C2	0.2327(9)	0.7639(13)	0.1831(5)	4.9(9)
C3	0.1496(11)	0.3882(16)	0.0151(5)	6.8(12)
C4	0.1148(8)	0.2559(13)	0.0851(5)	3.9(8)
C5	0.2370(7)	0.2704(12)	0.0671(4)	3.0(7)
C6	0.2427(8)	0.3331(14)	0.1751(4)	4.4(8)
C7	0.1910(7)	0.4807(12)	0.2272(4)	3.4(7)
C8	0.3127(9)	0.5295(15)	0.1972(5)	5.3(10)
C9	0.0339(8)	0.4673(12)	0.1318(5)	3.5(8)
C10	0.0199(9)	0.4622(20)	0.1747(5)	7.9(13)
C11	−0.0429(11)	0.4305(23)	0.1832(6)	11.1(18)
C12	−0.0923(10)	0.4047(18)	0.1492(6)	7.2(12)
C13	−0.0781(9)	0.4105(17)	0.1049(6)	6.8(11)
C14	−0.0153(9)	0.4416(15)	0.0964(5)	5.1(9)
C15	0.2380(8)	0.6207(12)	0.1120(4)	3.2(7)
C16	0.2462(7)	0.5151(12)	0.0909(4)	2.7(6)
C17	0.3141(7)	0.5023(12)	0.0759(4)	3.2(7)
C18	0.3313(8)	0.5593(13)	0.0389(5)	4.2(8)
C19	0.3928(8)	0.5462(14)	0.0237(5)	4.7(9)
C20	0.4393(8)	0.4718(14)	0.0451(6)	5.2(10)
C21	0.4255(8)	0.4116(13)	0.0821(5)	4.2(9)
C22	0.3639(8)	0.4257(12)	0.0971(5)	3.6(8)
C23	0.1089(10)	0.8803(14)	0.1320(5)	6.1(12)
C24	0.0602(9)	0.8089(16)	0.1104(6)	6.6(11)
C25	0.0824(10)	0.7697(14)	0.0714(5)	5.9(10)
C26	0.1474(9)	0.8073(15)	0.0701(5)	5.6(10)
C27	0.1647(9)	0.8813(15)	0.1076(5)	5.8(10)
C28	0.0986(18)	0.9573(20)	0.1702(7)	15.7(25)
C29	−0.0090(13)	0.789(3)	0.1202(10)	16.2(22)
C30	0.0418(15)	0.6968(20)	0.0336(7)	13.3(19)
C31	0.1870(14)	0.7878(21)	0.0320(7)	13.2(19)
C32	0.2257(14)	0.9484(22)	0.1112(10)	16.6(21)
O1	0.0841(6)	0.6898(11)	0.2261(3)	6.7(7)
O2	0.2748(7)	0.7972(11)	0.2076(4)	8.4(8)
O3	0.1305(8)	0.3990(13)	−0.0229(3)	8.9(10)
O4	0.0777(6)	0.1819(10)	0.0885(4)	7.2(8)
O5	0.2740(5)	0.1965(9)	0.0620(3)	4.8(6)
O6	0.2562(7)	0.2389(9)	0.1824(3)	6.7(7)
O7	0.1740(6)	0.4687(10)	0.2619(3)	5.8(7)
O8	0.3666(6)	0.5542(13)	0.2134(4)	8.3(9)
C33	0.4769(21)	0.382(4)	0.2228(19)	15.1(46)
CL	0.5692(8)	0.3034(9)	0.2381(4)	27.2(14)

Table 3. Atomic Coordinates and Equivalent Isotropic Displacement Coefficients for 3a

	x	y	z	B_{eq}, Å^2
W	0.35480(6)	0.78772(4)	0.08229(4)	1.80(3)
Re1	0.11712(6)	0.82330(4)	0.01759(4)	1.92(3)
Re2	0.18841(6)	0.89505(4)	0.16667(4)	2.26(3)
S	0.2657(4)	0.74167(23)	−0.04539(24)	2.31(17)
C1	0.3390(14)	0.8948(8)	0.0422(9)	2.0(3)
C2	−0.0221(15)	0.7583(9)	−0.0150(10)	2.7(8)
C3	−0.0036(15)	0.8998(9)	0.0474(9)	2.7(7)
C4	0.1156(14)	0.8809(8)	−0.0828(10)	2.7(8)
C5	0.0494(16)	0.9110(8)	0.2233(10)	3.3(8)
C6	0.1842(15)	1.0029(9)	0.1375(10)	2.8(3)
C7	0.2887(19)	0.9197(10)	0.2601(11)	4.2(10)
C8	0.2299(14)	0.6393(9)	−0.0473(10)	2.4(8)
C9	0.1796(16)	0.5984(9)	0.0152(10)	3.2(8)
C10	0.1551(19)	0.5201(10)	0.0065(12)	4.5(10)
C11	0.1825(20)	0.4813(10)	−0.0630(12)	4.6(11)
C12	0.2239(19)	0.5235(10)	−0.1261(11)	4.3(10)
C13	0.2505(16)	0.6013(9)	−0.1186(10)	2.9(8)
C14	0.2547(16)	0.7778(9)	0.1864(10)	2.9(8)
C15	0.1531914)	0.7659(8)	0.1415(9)	1.7(3)
C16	0.0530(14)	0.7157(8)	0.1781(9)	2.3(7)
C17	−0.0693(16)	0.7346(10)	0.1744(11)	3.6(9)
C18	−0.1504(17)	0.6918(11)	0.2157(13)	4.6(10)
C19	−0.1108(17)	0.6277(10)	0.2592(11)	4.1(9)
C20	0.0088(19)	0.6064(10)	0.2623(12)	4.5(10)
C21	0.0917(15)	0.6483(9)	0.2218(10)	2.8(8)
C22	0.5322(14)	0.7131(10)	0.0511(10)	2.9(8)
C23	0.5034(14)	0.6933(8)	0.1318(9)	2.3(7)
C24	0.5209(14)	0.7621(9)	0.1798(10)	2.8(8)
C25	0.5527(16)	0.8244(9)	0.1266(10)	3.2(4)
C26	0.5562(15)	0.7932(9)	0.0475(10)	3.0(8)
C27	0.5435(18)	0.6556(11)	−0.0171(12)	4.8(10)
C28	0.4759(18)	0.6151(10)	0.1629(11)	4.1(10)
C29	0.5239(17)	0.7650(10)	0.2690(11)	3.9(9)
C30	0.5955(18)	0.9057(11)	0.1529(12)	4.5(10)
C31	0.5999(18)	0.8347(11)	−0.0228(12)	4.4(9)
O1	0.3610(11)	0.9537(6)	0.0118(7)	3.5(6)
02	−0.1025(12)	0.7168(8)	−0.0320(8)	5.5(7)
O3	−0.0861(11)	0.9409(7)	0.0526(8)	4.6(6)
O4	0.1181(12)	0.9153(6)	−0.1437(7)	3.9(6)
O5	−0.0376(13)	0.9226(8)	0.2619(9)	6.4(8)
O6	0.1850(12)	1.0697(7)	0.1240(8)	4.8(7)
07	0.3525(17)	0.9305(9)	0.3202(9)	7.8(10)

atoms of the pentamethylcyclopentadienyl, the phenyl, and the methylene groups were calculated at idealized positions with fixed temperature coefficients and were also included in the structure factor calculation. The presence of 1/2 equiv of CH_2Cl_2 solvent molecule was unambiguously identified on the difference Fourier map. Full-matrix least-squares refinement with 87 atoms and 456 parameters gave $R = 0.023$ and $R_w = 0.020$ for 4557 reflections with $I > 2\sigma(I)$. The combined data collection and refinement parameters are summarized in Table 1. Atomic positional parameters for **2a**, **3a**, and **4a** are presented in Tables 2–4, whereas selected bond angles and lengths are listed in Tables 5–7, respectively.

Results

Reaction of $Cp^*WRe_2(CO)_9(CCPh)$ (**1a**) with thiophenol proceeds rapidly in refluxing toluene solution, producing two novel phenylacetylene clusters $Cp^*WRe_2(CO)_8(\mu_3\text{-SPh})(CH{=}CPh)$ (**2a**) and $Cp^*WRe_2(CO)_7(\mu\text{-SPh})(CH{=}CPh)$ (**3a**) in moderate yields. Both compounds were generated by 1:1 combination of the starting materials, as revealed by FAB mass spectrometry, microanalysis, and IR, ^1H, and ^{13}C NMR determinations.

Characterization of 2. Complex **2a** exhibited a signal at δ 8.06 in addition to the expected signals for Cp* ligand and two phenyl fragments in the ^1H NMR spectrum. This information suggests that the hydrogen

Table 4. Atomic Coordinates and Equivalent Isotropic Displacement Coefficients for 4a

	x	y	z	B_{eq}, Å^2
W	0.13815(3)	0.125870(24)	0.184302(16)	2.301(13)
Re1	0.00037(3)	0.229107(25)	0.344407(16)	2.516(14)
Re2	−0.11480(3)	0.32825(3)	0.149845(16)	2.477(14)
S1	0.06435(18)	0.32753(14)	0.21995(10)	2.34(8)
S2	−0.21921(18)	0.27337(15)	0.28777(10)	2.72(8)
C1	−0.0155(7)	0.1115(6)	0.1369(4)	3.6(4)
C2	−0.0831(8)	0.1479(6)	0.4315(4)	3.8(4)
C3	0.1738(8)	0.1830(6)	0.3792(4)	3.8(4)
C4	−0.0631(7)	0.3659(6)	0.4083(4)	3.4(4)
C5	−0.0155(7)	0.3459(6)	0.0455(4)	2.8(4)
C6	−0.2254(7)	0.4889(6)	0.1495(4)	3.5(4)
C7	−0.2517(7)	0.2948(7)	0.1067(4)	4.0(4)
C8	0.0700(7)	0.0542(5)	0.2765(4)	2.9(4)
C9	0.0603(8)	−0.0483(6)	0.3241(4)	3.5(4)
C10	−0.0279(8)	−0.1116(6)	0.3266(4)	4.3(4)
C11	−0.0147(10)	−0.2188(7)	0.3784(5)	6.3(6)
C12	−0.0001(12)	−0.3218(8)	0.3307(7)	9.3(8)
C13	−0.1239(12)	−0.2936(9)	0.2886(7)	10.2(8)
C14	−0.1318(11)	−0.1857(10)	0.2361(6)	8.9(8)
C15	−0.1428(10)	−0.0817(8)	0.2807(5)	6.4(6)
C16	0.1836(7)	0.4128(5)	0.1942(4)	2.5(3)
C17	0.2795(8)	0.4078(6)	0.2399(4)	3.6(4)
C18	0.3708(8)	0.4726(6)	0.2163(5)	4.5(5)
C19	0.3678(8)	0.5394(6)	0.1491(5)	4.6(5)
C20	0.2693(9)	0.5451(7)	0.1053(5)	5.0(5)
C21	0.1767(8)	0.4824(6)	0.1278(4)	3.7(4)
C22	−0.3622(7)	0.3887(6)	0.3402(4)	3.0(4)
C23	−0.4816(8)	0.3632(7)	0.3838(4)	4.3(4)
C24	−0.5987(8)	0.4511(8)	0.4242(5)	6.0(5)
C25	−0.5958(9)	0.5619(8)	0.4214(5)	6.2(5)
C26	−0.4779(9)	0.5890(7)	0.3794(5)	5.4(5)
C27	−0.3624(8)	0.5035(7)	0.3402(4)	4.2(4)
C28	0.3905(7)	0.0725(6)	0.1598(4)	3.0(3)
C29	0.3522(7)	0.1179(6)	0.0865(4)	3.0(3)
C30	0.2882(7)	0.0449(6)	0.0630(4)	3.4(4)
C31	0.2859(7)	−0.0447(6)	0.1199(4)	3.6(4)
C32	0.3526(8)	−0.0295(6)	0.1779(4)	3.8(4)
C33	0.4798(7)	0.1120(7)	0.2014(4)	4.4(4)
C34	0.3872(8)	0.2205(6)	0.0395(4)	3.9(4)
C35	0.2439(9)	0.0562(7)	−0.0162(4)	5.1(5)
C36	0.2384(9)	−0.1469(7)	0.1119(5)	5.5(5)
C37	0.4005(9)	0.1194(7)	0.2411(5)	6.3(5)
O1	−0.0701(5)	0.0600(4)	0.1063(3)	4.8(3)
O2	−0.1389(6)	0.1022(5)	0.4831(3)	5.8(3)
O3	0.2808(6)	0.1554(5)	0.4010(3)	6.6(4)
O4	−0.0949(6)	0.4462(5)	0.4467(3)	5.7(3)
O5	0.0450(5)	0.3556(4)	−0.0192(3)	4.7(3)
O6	−0.2927(6)	0.5872(5)	0.1468(3)	5.7(3)
O7	−0.3325(6)	0.2725(5)	0.0783(3)	5.7(4)
C38	0.5752(17)	1.0233(14)	0.4670(9)	5.1(4)
CL	0.5133(4)	0.8974(3)	0.45931(24)	13.3(3)

Table 5. Selected Interatomic Distances (Å) and Angles (deg) of 2a

W−Re(2)	2.926(1)	Re(1)−Re(2)	2.976(1)
W···Re(1)	4.260(2)	W−S	2.443(4)
Re(1)−S	2.408(4)	Re(2)−S	2.468(4)
W−C(15)	2.17(2)	Re(2)−C(15)	2.31(1)
Re(1)−C(16)	2.14(1)	Re(2)−C(16)	2.42(1)
C(15)−C(16)	1.42(2)	∠W−Re(2)−Re(1)	92.38(3)

Table 6. Selected Interatomic Distances (Å) and Angles (deg) of 3a

W−Re(2)	2.992(1)	Re(1)−Re(2)	2.817(1)
W−Re(1)	2.785(2)	W−S	2.396(4)
Re(1)−S	2.424(4)	W−C(14)	2.11(2)
Re(2)−C(14)	2.15(2)	W−C(15)	2.49(2)
Re(1)−C(15)	2.29(1)	Re(2)−C(15)	2.28(1)
C(14)−C(15)	1.30(2)	∠W−Re(1)−Re(2)	64.54(3)
∠W−Re(2)−Re(1)	57.21(3)	∠Re(1)−W−Re(2)	58.25(3)

of the thiophenol molecule is now transferred to a carbon atom of the acetylide ligand. Consistent with this assignment, two ^{13}C NMR signals were observed at δ 200.7 and 168.0 (J_{W-C} = 62 Hz), which were

Table 7. Selected Interatomic Distances (Å) and Angles (deg) of 4a

W−Re(1)	2.9916(6)	W−Re(2)	3.0363(6)
Re(1)···Re(2)	3.8094(6)	W−S(1)	2.404(2)
Re(1)−S(1)	2.440(2)	Re(2)−S(1)	2.415(2)
Re(1)−S(2)	2.523(2)	Re(2)−S(2)	2.518(2)
W−C(8)	1.858(7)	Re(1)−C(8)	2.339(6)
C(8)−C(9)	1.452(9)	C(9)−C(10)	1.35(1)
W−C(1)	1.991(7)	Re(2)−C(1)	2.494(7)
∠Re(1)−W−Re(2)	78.39(2)	∠W−C(8)−Re(1)	90.2(3)
∠W−C(8)−C(9)	152.5(2)	∠Re(1)−C(8)−C(9)	116.4(4)
∠W−C(1)−O(1)	154.2(6)	∠Re(2)−C(1)−O(1)	121.1(5)
∠C(8)−C(9)−C(10)	129.3(7)	∠C(11)−C(10)−C(15)	115.7(7)

assigned to the CPh and CH carbons of the ligated phenylacetylene, respectively. In addition, two sharp W−CO resonances appeared at δ 219.2 (J_{W-C} = 165 Hz) and 216.7 (J_{W-C} = 170 Hz) and one sharp Re−CO signal appeared at δ 197.8 (3C) and a broad Re−CO signal at δ 191.3 (3C), implying that the molecule possesses one $Cp^*W(CO)_2$ subunit and two $Re(CO)_3$ metal fragments with fast threefold CO scrambling.

The molecular structure of **2a** has been confirmed by X-ray diffraction analysis. The bond distances and angles are presented in Table 5. As shown in Figure 1, the molecule consists of a V-shaped WRe_2 arrangement. Each rhenium is bonded to three terminal CO ligands. The tungsten atom is coordinated by two terminal CO and a Cp* ligand. The angle ∠W−Re(2)−Re(1) is fairly acute, 92.38(3)°. The W−Re(1) distance (4.260(2) Å) is too long to permit the occurrence of any significant metal−metal interaction, while the W−Re(2) distance (2.926(1) Å) is in the range expected for W−Re single-bond interaction. The thiolate grouping caps all three metal atoms with slight variation of M−S distances, i.e., W−S = 2.443(4) Å, Re(1)−S = 2.408(4) Å, and Re(2)−S = 2.468(4) Å. The phenylacetylene group is coordinated to the metal core via the typical $2\sigma + \pi$ bonding mode with the C(15)−C(16) backbone parallel to the nonbonding W−Re(2) vector. An alternative description would be to consider that phenylacetylene adopts the classical μ_3-η^2 mode, which is similar to that observed for the alkyne in the complex $Os_3(CO)_9(\mu\text{-Br})(C_2CH_2CH_2)(\mu\text{-H})$.[10] Assuming that the phenyl thiolate ligand serves as a five-electron donor, this molecule contains 50 valence electrons, which agrees with the electron counting of trinuclear clusters with only two metal−metal bonds.

Characterization of 3. For the second phenylacetylene cluster **3a**, the molecule contains one CO less than those of **2a**. This is identified by mass spectrometry and the observation of five CO signals at δ 219.7 (J_{W-C} = 185 Hz), 197.1 (3C, br), 194.5 (1C), 193.6 (1C), and 186.9 (1C) in its ^{13}C NMR spectrum. The IR spectrum showed the appearance of a low-frequency CO stretching band at 1772 cm^{-1} and six terminal CO bands in the region 2045−1907 cm^{-1}, revealing the presence of one bridging CO ligand. The hydrogen of the phenylacetylene appeared at δ 12.03. This observed chemical shift is downfield to that of **2a**, suggesting that the CH fragment is located near the Cp* ligand and, thus, is strongly deshielded by its ring current. This argument is in agreement with the result of X-ray crystal structure.

The structure of **3a** is depicted in Figure 2 and the metric parameters are presented in Table 6. It can be

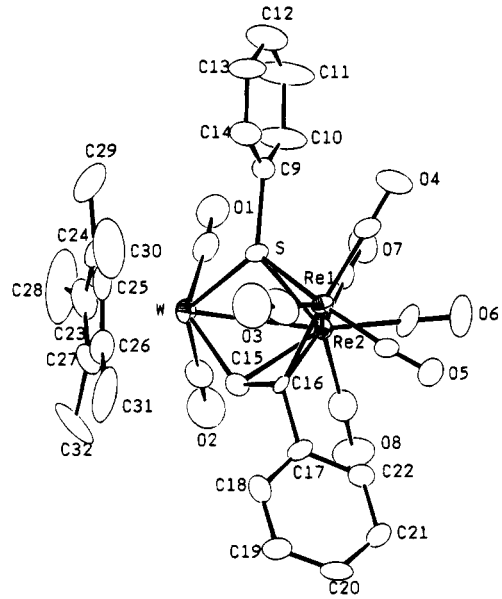

Figure 1. Molecular structure of **2a** and the atomic numbering scheme.

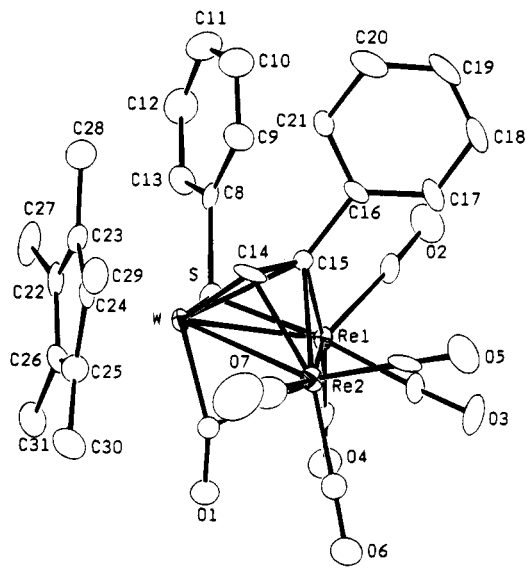

Figure 2. Molecular structure of **3a** and the atomic numbering scheme.

seen that the molecule contains a triangular geometry with two $Re(CO)_3$ units, and a semibridging CO spans the W−Re(2) edge. The length of the W−Re(1) bond (2.785(2) Å) is markedly shorter than the other two metal−metal bonds (vs W−Re(2) = 2.992(1) Å and Re(1)−Re(2) = 2.817(1) Å). The thiolate group bridged the W−Re(1) bond. The resulting S−W−Re(1) face is parallel to the WRe_2 plane. Furthermore, the metal−sulfur distances (W−S = 2.396(4) Å and Re(1)−S = 2.424(4) Å) are comparable with those found in **2a**, suggesting that it donates only three electrons to the cluster. For the ligated phenylacetylene fragment, the C(14)−C(15) vector is perpendicular to the W−Re(2) bond. The atom C(15) is coordinated to all three metal atoms (W−C(15) = 2.49(2) Å, Re(1)−C(15) = 2.29(1) Å, and Re(2)−C(15) = 2.28(1) Å), while the atom C(14) has even closer M−C contacts (W−C(14) = 2.11(2) Å and Re(2)−C(14) = 2.15(2) Å). Thus, this phenylacetylene ligand possesses the novel perpendicular μ_3-η^2 (⊥) mode, as observed in the unsaturated, 46-electron trinuclear

(10) Adams, R. D.; Chen, L.; Qu, X. *Organometallics* **1994**, *13*, 1992.

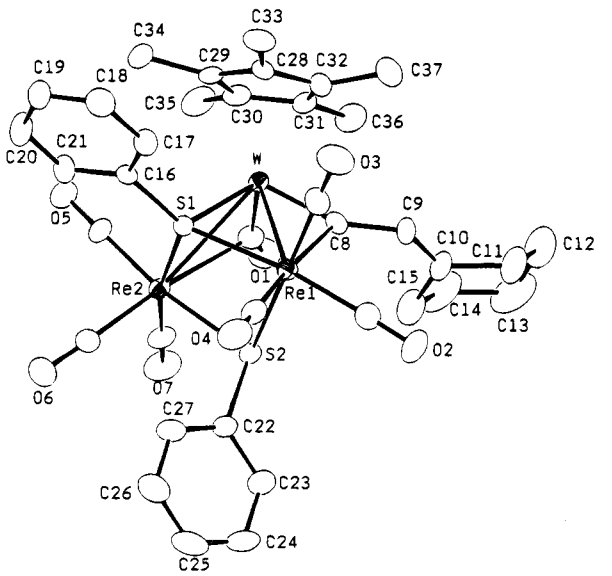

Figure 3. Molecular structure of **4a** and the atomic numbering scheme.

clusters containing alkyne ligand.[11] A few examples of alkyne clusters adopting the μ_3-η^2 ($\perp$) mode have been documented in literature,[12] and an even more recently, an example of the alkyne ligand sitting on triruthenium and triosmium frameworks, as modified by the coordination of dppm ligand, has been discussed.[13]

Furthermore, the phenyl group is located on the carbon atom that is farther away from the W atom, while the CH terminal of the phenylacetylene ligand is pointed directly toward the W atom. This geometry is obviously the result of the minimization of the unfavorable steric interaction between the bulky phenyl substituent and Cp* ligand. Similar conformation has been observed by Shriver et al. in the unstable terminal alkyne complexes $Fe_3(CO)_9(REC_2H)$, R = Me, Et, Pr; E = O, S, generated by protonation of the anionic acetylide clusters $[Fe_3(CO)_9(CCER)]^-$.[14]

Synthesis of Vinylalkylidyne Clusters 4. The reaction of vinylacetylide $Cp^*WRe_2(CO)_9(CCCH{=}CHOMe)$ (**1b**) with excess thiophenol follows a similar route and produces the unsaturated 46-electron complex $Cp^*WRe_2(CO)_7(\mu\text{-SPh})(CH{=}CCH{=}CHOMe)$ (**3b**) as the exclusive product. However, the reactions take a different course when vinylacetylide clusters $Cp^*WRe_2(CO)_9(CCC{=}CH(CH_2)_4)$ (**1c**) and $Cp^*WRe_2(CO)_9(CCCMe{=}CH_2)$ (**1d**) were employed. The former reaction afforded $Cp^*WRe_2(CO)_7(\mu\text{-SPh})_2(CCH{=}C(CH_2)_5)$ (**4a**) in 31% yield, while the reaction of **1d** produced the derivative $Cp^*WRe_2(CO)_7(\mu\text{-SPh})_2(CCH{=}CMe_2)$ (**4b**) in a slightly higher yield under similar conditions. These two new clusters are produced through the introduction of two thiophenol molecules and elimination of two CO ligands. Meanwhile, one SH proton of the thiophenol molecules has been transferred to the ω-carbon of the vinylacetylide group to generate a methylene group in **4a** and a methyl group in **4b**, respectively. The second hydrogen is added to the β-carbon to produce the observed olefinic CH fragment. For a control experiment by addition of an equimolar amount of thiophenol to the solution, we obtained only a trace amount of **4** and a black, unknown cluster compound, which decomposed rapidly during workup.

The ^1H NMR spectra of these two clusters exhibit the expected signals for two phenyl fragments in the region δ 7.54–7.07. The aliphatic methylene groups of **4a** appear within the region δ 2.24–1.40, while the two methyl groups of **4b** resonate at δ 1.88 and 1.70. The proton of the second thiophenol molecule is coordinated to an acetylide carbon, as indicated by a downfield signal at δ 6.18 (**4a**) and 6.30 (**4b**). The chemical shifts of these resonances are in the region for olefinic protons. Consistent with the ^1H NMR data, the ^{13}C NMR spectrum of **4a** exhibits, in addition to seven CO signals and five CH_2 resonances, three unique signals at δ 302.7 (J_{W-C} = 215 Hz), 141.2 (J_{W-C} = 30 Hz), and 53.3. On the basis of their chemical shifts, the first two signals can be assigned to an alkylidyne and an olefinic CH carbon, respectively. Thus, this spectral information implies that the vinylacetylide fragments ($CCC{=}CH(CH_2)_4$, $CCCMe{=}CH_2$) in the starting materials have now been transformed into vinylalkylidyne ligands (μ-$CCH{=}C(CH_2)_5$, μ-$CCH{=}CMe_2$).

Crystal Structure of 4a. As shown in Figure 1, the molecule consists of an open triangular WRe_2 core bridged by two thiolate ligands and a vinylalkylidyne fragment. Each rhenium atom is coordinated with three terminal CO ligands, and the tungsten atom is capped by a Cp* ligand and bonded to a bridging CO group. The W–Re(1) and W–Re(2) distances are 2.9916(6) and 3.0363(6) Å, respectively. (see Table 7). The Re(1)–Re(2) distance (3.8094(6) Å) is substantially longer than the Re–Re distance (3.041(1) Å) observed for $Re_2(CO)_{10}$,[15] indicating that no Re–Re interaction occurs within the cluster. One thiolate group lies on the WRe_2 surface with three short M–S distances, W–S(1) = 2.404(2), Re(1)–S(1) = 2.440(2), and Re(1)–S(2) = 2.415(2) Å. These M–S distances are about 0.1 Å shorter than those associated with the second thiolate group, which bridges the Re(1) and Re(2) atoms, with Re–S distances being 2.523(2) and 2.518(2) Å. The latter is typical for thiolate groupings bridging two nonbonded rhenium atoms (2.519–2.533 Å).[16]

The vinylalkylidyne group, generated by hydrogen atom migration, bridges the W–Re(1) edge. The C(8)–C(9) and C(9)–C(10) distances, 1.452(9) and 1.35(1) Å, are comparable to those of the C–C single and double bonds, which confirm the identification of vinyl sub-

(11) Deeming, A. J.; Arce, A. J.; De Sanctis, Y. *Mater. Chem. Phys.* **1991**, *29*, 323.
(12) (a) Blount, J. F.; Dahl, L. F.; Hoogzand, C.; Hübel, W. *J. Am. Chem. Soc.* **1966**, *88*, 292. (b) Busetto, L.; Green, M.; Howard, J. A. K.; Hessner, B.; Jeffrey, J. C.; Mills, R. M.; Stone, F. G. A.; Woodward, P. *J. Chem. Soc., Chem. Commun.* **1981**, 1101. (c) Busetti, V.; Granozzi, G.; Aime, S.; Gobetto, R.; Osella, D. *Organometallics* **1984**, *3*, 1510. (d) Carty, A. J.; Taylor, N. J.; Sappa, E. *Organometallics* **1988**, *7*, 292.
(13) (a) Rivomanana, S.; Lavigne, G.; Lugan, N.; Bonnet, J.-J. *Inorg. Chem.* **1991**, *30*, 4110. (b) Clucas, J. A.; Dolby, P. A.; Harding, M. M.; Smith, A. K. *J. Chem. Soc., Chem. Commun.* **1987**, 1829. (c) Brown, M. P.; Dolby, P. A.; Harding, M. M.; Mathews, A. J.; Smith, A. K.; Osella, D.; Arbrun, M.; Gobetto, R.; Raithby, P. R.; Zanello, P. *J. Chem. Soc., Dalton Trans.* **1993**, 827.
(14) Jensen, M. P.; Shriver, D. F. *Organometallics* **1992**, *11*, 3385. (b) Hriljac, J. A.; Shriver, D. F. *J. Am. Chem. Soc.* **1987**, *109*, 6010.
(15) Churchill, M. R.; Amoh, K. N.; Wasserman, H. J. *Inorg. Chem.* **1981**, *20*, 1609.
(16) (a) Adams, R. D.; Cortopassi, J. E.; Falloon, S. B. *Organometallics* **1992**, *11*, 2420. (b) Adams, R. D.; Chen, L.; Wu, W. *Organometallics* **1993**, *12*, 4962.

Scheme 1

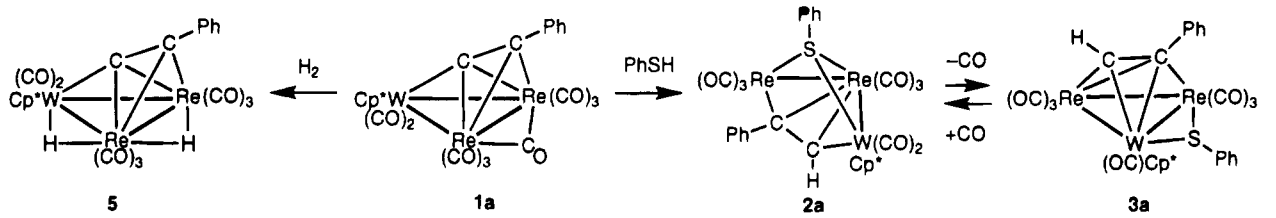

Scheme 2

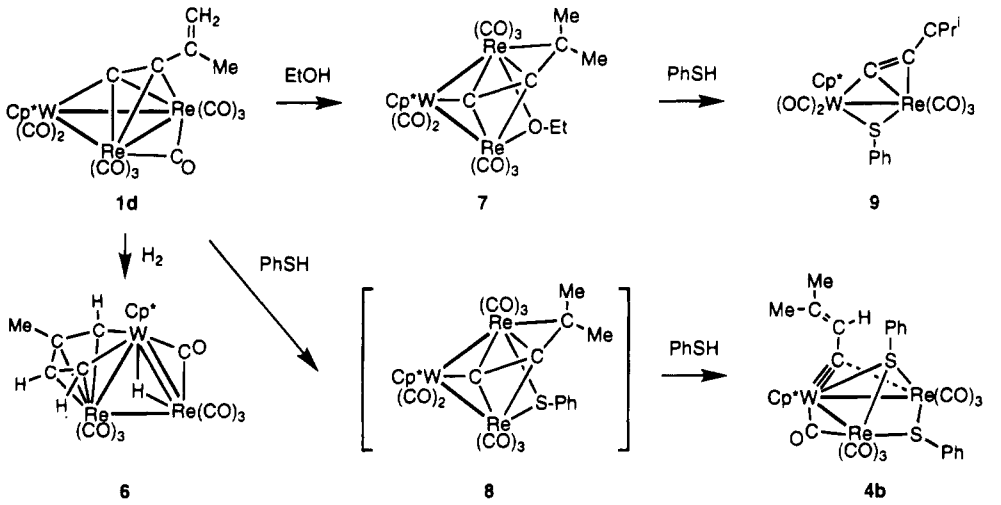

stituent. Most interesting, the W−C(8) distance (1.858(7) Å) is shorter than the Re(1)−C(8) distance (2.339(6) Å). Whereas the W−C(8)−C(9) angle (152.5(2)°) is also much larger than the respective Re(1)−C(8)−C(9) angle (116.4(4)°). This W−C distance observed is evidently shorter than the W−C distances (2.01 Å) of the doubly bridging alkylidyne ligand in the ditungsten complexes $Cp_2W_2(CO)_3Me(\mu\text{-}CR)$, R = C_6H_4Me or C_6H_4OMe,[17] and the W−C double bonds in W_2Re alkylidyne complexes (1.99−2.07 Å).[18] However, this unusually short W−C separation compares well with that in the neutral complex $CpW(CO)_2(\equiv CTol)$ (1.82(2) Å)[19] and the ionic carborane complex $[(C_2B_9H_9Me_2)W(CO)_2(\equiv CPh)][PPh_4]$ (1.82(3)−1.84(3) Å).[20] This indicates that this vinylalkylidyne retains substantial W≡C triple-bond character and that the α-carbon interacts only weakly with the rhenium atom. Indeed, the observed deshielded ^{13}C chemical shift and the large J_{W-C} coupling for this alkylidyne carbon (302.7, J_{W-C} = 215 Hz) are in accord with this assignment.[21] Dinuclear complexes containing a tungsten−alkylidyne ligand weakly bridged to the W−Pt and W−Rh edges have also been reported by Stone and co-workers.[22]

Discussion

A summary of the reactions of the WRe_2 acetylide cluster is shown in Scheme 1. According to our previous report, this cluster is stable and does not react with alcohols, but forms a dihydride cluster $Cp^*WRe(CO)_8(\mu\text{-}H)_2(CCPh)$ (**5**) upon treatment with H_2.[9] No hydrogen migration to the acetylide was observed even under the extensive heating. In contrast, the introduction of thiophenol induces the hydrogen transfer to the ligated acetylide, thereby producing two phenylacetylene clusters **2a** and **3a**. The first compound is a 50-electron cluster with a face-bridging thiolate ligand and an alkyne adopting $\mu_3\text{-}\eta^2$ (∥) mode, while the second cluster **3a** is best considered as a 46-electron cluster possessing edge-bridging thiolate and $\mu_3\text{-}\eta^2$ (⊥) alkyne ligand. Heating of **2a** in refluxing toluene solution leads to decarbonylation and the formation of **3a** in moderate yield. In contrast, cluster **3a** reacts with CO to form an approximate 1:1 mixture of **2a** and **3a** in refluxing toluene. Bruce and co-workers have reported a similar example of hydrogen transfer to the coordinated acetylide fragment for the reaction of $Ru_5(\mu_5\text{-}C_2PPh_2)(\mu\text{-}PPh_2)(CO)_{13}$ with RSH (R = Me, Ph).[23]

The corresponding reactions of WRe_2 vinylacetylide clusters are depicted in Scheme 2, using the vinylacetylide cluster **1d** as an illustrative example. In contrast to the formation of metallacyclopentadienyl and allenylidene clusters **6** and **7**,[7] the reaction of **1d** with thiophenol produced the vinylalkylidyne cluster established. Based on the chemistry observed between vinylacetylide with alcohols, it is reasonable to propose that this reaction may proceeded via the formation of a thiolate−allenylidene cluster **8** as an intermediate. This would be followed by addition of a second thiophenol and transfer of hydrogen to the β-carbon of the ligated allenylidene to yield the vinylalkylidyne clusters, as indicated below:

(17) Hart, I. J.; Howard, J. A. K.; Lowry, R. M.; Spaniol, T. P.; Stone, F. G. A. *Polyhedron* **1989**, *8*, 2035.
(18) Carriedo, G. A.; Jeffery, J. C.; Stone, F. G. A. *J. Chem. Soc., Dalton Trans.* **1984**, 1594.
(19) Fischer, E. O.; Lindner, T. L.; Huttner, G.; Friedrich, P.; Kreissl, F. R.; Besenhard, J. O. *Chem. Ber.* **1977**, *110*, 3397.
(20) Baumann, F. E.; Howard, J. A. K.; Musgrove, R. J.; Sherwood, P.; Stone, F. G. A. *J. Chem. Soc., Dalton Trans.* **1988**, 1879.
(21) Green, M.; Howard, J. A. K.; de M. Jelfs, A. N.; Nunn, C. M.; Stone, F. G. A. *J. Chem. Soc., Dalton Trans.* **1987**, 2219.
(22) Byers, P. K.; Carr, N.; Stone, F. G. A. *J. Organomet. Chem.* **1990**, *384*, 315. (b) Devore, D. D.; Howard, J. A. K.; Jeffery, J. C.; Pilotti, M. U.; Stone, F. G. A. *J. Chem. Soc., Dalton Trans.* **1989**, 303.
(23) Adams, C. J.; Bruce, M. I.; Skelton, B. W.; White, A. H. *J. Organomet. Chem.* **1993**, *452*, 121.

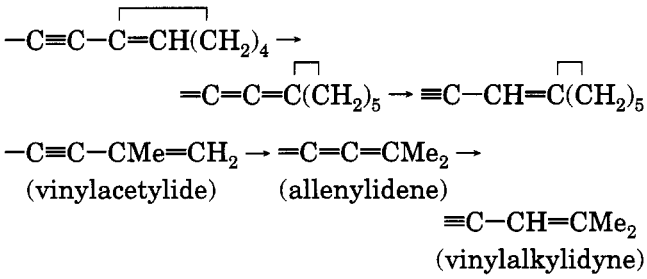

However, many factors have affected the reaction pattern. When the solution of **1b** is treated with thiophenol, only the unsaturated acetylene cluster **3b** is formed. This indicates that the vinyl substitutent also plays a crucial role in determining the reaction pathway. Furthermore, heating of the analogous alkoxyallenylidene **7** in the presence of thiophenol affords not the expected vinylalkylidyne cluster, but has generated an acetylide complex $Cp^*WRe(CO)_5(\mu\text{-SPh})(CCPr^i)$ (**9**) as the only isolable compound. In this dinuclear complex, the observed isopropylacetylene is apparently generated by hydrogen migration to the γ-carbon of the allenylidene, indicating an example for the influence of the bridging alkoxyl group.

Acknowledgment. We thank the National Science Council of the Republic of China for financial support (Grant NSC 83-0208-M007-43).

Supplementary Material Available: Tables of complete crystal data, bond distances, and hydrogen atom coordinates of **2a**, **3a**, and **4a** (6 pages). Ordering information is given on any current masthead page.

OM940670B

1,4-Diethynylbenzene Bridged Fe(Cp*)(dppe) Units: Mixed-Valence 35-Electron and Bisiron(III) 34-Electron Complexes

Nathalie Le Narvor and Claude Lapinte*

Laboratoire de Chimie des Complexes de Métaux de Transition et Synthèse Organique, URA CNRS 415, Université de Rennes I, Campus de Beaulieu, 35042 Rennes Cedex, France

Received July 20, 1994[⊗]

Reaction of the bis(alkyne) $HC{\equiv}CC_6H_4C{\equiv}CH$ with 2 equiv of $[Fe(\eta^5C_5Me_5)(\eta^2dppe)Cl]$ (**1**) [dppe = ethylenebis(diphenylphosphine)] and NH_4PF_6 in methanol produces the vinylidene complex $[\{Fe(\eta^5C_5Me_5)(\eta^2dppe)\}_2\text{-}\mu\text{-}(C{=}CHC_6H_4CH{=}C)][PF_6]_2$ (**2**), isolated as a brown powder in 83% yield. This complex is readily deprotonated by 2 equiv of $KOBu^t$ in THF and yields the alkynyl derivative $[\{Fe(\eta^5C_5Me_5)(\eta^2dppe)\}_2\text{-}\mu\text{-}(C{\equiv}CC_6H_4C{\equiv}C)]$ (**3**) as a thermally stable orange solid in 96% yield. The addition of 2 equiv of $[\{Fe(\eta^5C_5Me_5)_2][PF_6]$ to a CH_2Cl_2 solution of **3** gave the Fe(III)–Fe(III) complex **5**, isolated as a dark green microcrystalline solid in 90% yield that is air and thermally stable. The paramagnetic salt 5 was characterized by IR in the solid state, and in solution, by Mössbauer and ESR spectroscopies, and magnetic susceptibility measurements. The CV shows two reversible redox systems with quite a large wave separation ($|\Delta E_0| = 0.26$ V) corresponding to a large comproportionation constant ($K_c = 2.6 \times 10^4$). The mixed-valence complex $[\{Fe(\eta^5C_5Me_5)(\eta^2dppe)\}_2\text{-}\mu\text{-}(C{\equiv}CC_6H_4C{\equiv}C)][PF_6]$ (**4**) was prepared and isolated in 95% yield by addition of a stoichiometric amount of $[Fe(C_5H_5)_2][PF_6]$ to a suspension of **3** in CH_2Cl_2. As shown in Mössbauer, ESR, and IR spectroscopies, the rigid binuclear assembly allows the odd-electron delocalization on the two metal centers over an 11.89-Å span.

The experimental and theoretical study of intramolecular long-distance electron transfer is a very active research area.[1] The consequences of this process are of crucial importance in domains such as biology, solid state chemistry, inorganic reaction mechanisms, and finally the emerging field of molecular electronics.[2] Therefore, there is a rapidly growing interest in the chemical, physical, and material properties of compounds in which a conjugated pathway spans two transition metal centers.[3] Although considerable literature has appeared on the Fe(II)–Fe(II) biferrocene and related sandwich systems,[4] the half-sandwich compounds did not receive similar attention as potential mixed-valence polymetallic derivatives. Recently, we reported the first FeC_4Fe bridged mixed-valence complex which was delocalized on the infrared time scale,[5] and in the same time, the similar ReC_4Re system was described by Gladysz's group.[6] We have also used 1,4-bis(ethynyl)benzene, as a more easily accessible rigid-rod bridging ligand[3e–h] to connect two electron-rich organo iron units, and we report here the synthesis, characterization, and basic physical properties of the 35-electron mixed-valence acetylide diiron complex $[\{Fe(\eta^5\text{-}C_5Me_5)(dppe)\}_2\text{-}(\mu C_2C_6H_4C_2)][PF_6]$ [dppe = ethylenebis(diphenylphosphine)] and those of its 36- and 34-electron derivatives.

Results and Discussion

1. Synthesis of the Binuclear Complex $[\{Fe(\eta5\text{-}C_5Me_5)(\eta^2\text{-}dppe)\}_2\text{-}\mu\text{-}(C{\equiv}CC_6H_4C{\equiv}C)]$ (3). Complex **3** was prepared in a two-step procedure involving formation of the corresponding vinylidene followed by deprotonation. The same route was previously used to

⊗ Abstract published in *Advance ACS Abstracts*, December 1, 1994.

(1) Evenson, J. W.; Karplus, M. *Science* **1993**, *262*, 1247–1249.

(2) (a) *Metal-Containing polymeric systems*; Sheats, J. E., Carraher, C. E., Jr., Eds.; Plenum: New York, 1985. (b) *Electrical Properties of Polymers*; Seanor, D. A., Ed.; Academic: New York, 1982; Vols. 1–3.

(3) (a) Beck, W.; Niemer, B.; Wieser, M. *Angew. Chem., Int. Ed. Engl.* **1993**, *32*, 923. (b) Hunter, A. D. *Organometallics* **1989**, *8*, 118. (c) Maatta, E. A.; Devore, D. D. *Angew. Chem., Int. Ed. Engl.* **1988**, *27*, 569. (d) Collman, J. P.; McDevitt, J. T.; Leidner, C. R.; Yee, G. T.; Torrance, J. B.; Little, W. A. *J. Am. Chem. Soc.* **1987**, *109*, 4606. (e) Davies, S. J.; Johnson, B. F. G.; Fhan, M. S.; Lewis, J. *J. Chem. Soc., Chem. Commun.* **1991**, 187. (f) Khan, M. S.; Davies, S. J.; Kakar, A. K.; Schwartz, D.; Lin, B.; Johnson, B. F. G.; Lewis, J. *J. Organomet. Chem.* **1992**, *424*, 87. (g) Fyfe, H. B.; Mlekuz, M.; Zargarian, D.; Taylor, N. J.; Marder, T. B. *J. Chem. Soc., Chem. Commun.* **1991**, 188. (h) Stang, P. J.; Tykwinski, R. *J. Am. Chem. Soc.* **1992**, *114*, 4411.

(4) (a) Le Vanda, C.; Cowan, D. O.; Leitch, C.; Bechgaard, K. *J. Am. Chem. Soc.* **1974**, *96*, 6788. (b) Kramer, J. A.; Hendrickson, D. N. *Inorg. Chem.* **1980**, *19*, 3330. (c) Le Vanda, C.; Bechgaard, K.; Cowan, D. O.; Mueller-Westerhoff, U. T.; Eilbracht, P.; Candela, G. A.; Collins, R. *J. Am. Chem. Soc.* **1976**, *98*, 3181. (d) Le Vanda, C.; Bechgaard, K.; Cowan, D. O. *J. Org. Chem.* **1976**, *41*, 2700. (e) Dong, T.-Y.; Cohn, M. J.; Hendrickson, D. N.; Pierpont, C. G. *J. Am. Chem. Soc.* **1985**, *107*, 4777. (f) Dong, T.-Y.; Hendrickson, D. N.; Pierpont, C. G.; Moore, M. F. *J. Am. Chem. Soc.* **1986**, *108*, 963. (g) Talham, D. R., Cowan, D. O. *Organometallics* **1984**, *3*, 1712. (h) Moore, M. F.; Wilson, S. R.; Cohn, M. J.; Dong, T.-Y.; Mueller-Westerhoff, U. T.; Hendrickson, D. N. *Inorg. Chem.* **1985**, *24*, 4559. (i) Dong, T.-Y.; Kamba, T.; Hendrickson, D. N. *J. Am. Chem. Soc.* **1986**, *108*, 4423. (j) Lowery, M. D.; Hammack, W. S.; Drickamer, H. G.; Hendrickson, D. N. *J. Am. Chem. Soc.* **1987**, *109*, 8019. (k) Webb, R. J.; Rheingold, A. L.; Geib, S. J.; Taley, D. L.; Hendrickson, D. N. *Angew. Chem. Int. Ed. Engl.* **1989**, *28*, 1388. (l) Webb, R. J.; Geib, S. J.; Staley, D. L.; Rheingold, A. L.; Hendrickson, D. N. *J. Am. Chem. Soc.* **1990**, *112*, 5031. (m) Webb, R. J.; Dong, T.-Y.; Pierpont, C. G.; Boone, S. R.; Chadha, R. K.; Hendrickson, D. N. *J. Am. Chem. Soc.* **1991**, *113*, 4806. (n) Dong, T.-Y.; Sohel, C.-C.; Hwang, M. Y.; Lee, T.-Y.; Yeh, S.-K.; Wen, Y.-S. *Organometallics*, **1992**, *11*, 573.

(5) Le Narvor, N.; Lapinte, C. *J. Chem. Soc., Chem. Commun.* **1993**, 357.

(6) (a) Zhou, Y.; Seyler, J. W.; Weng, W.; Arif, A. M.; Gladysz, J. A. *J. Am. Chem. Soc.* **1993**, *115*, 8509. (b) Seyler, J. W.; Weng, W.; Zhou, Y.; Gladysz, J. A. *Organometallics*, **1993**, *12*, 3802.

0276-7333/95/2314-0634$09.00/0

prepare the related mononuclear alkynyl complexes.[7] The main synthetic access described for the preparation of vinylidene complexes $[M]^{+}{=}C{=}C(H)(R)$ uses the reaction of terminal alkynes with [M]–X complexes in the presence of a halide anion abstractor.[8] Treatment of the terminal bis(alkyne) $HC{\equiv}CC_6H_4C{\equiv}CH$ with 2 equiv of $[\{Fe(\eta^5C_5Me_5)(\eta^2dppe)Cl)]$ (**1**) and NH_4PF_6 in methanol produced, after 16 h, a brown-orange solution from which the expected vinylidene complex $[\{Fe(\eta^5C_5Me_5)(\eta^2dppe)\}_2\text{-}\mu\text{-}(CHC_6H_4CH{=}C)][PF_6]_2$ (**2**) was isolated as a brown powder in 83% yield (eq 1).

$$\underset{\mathbf{1}}{(\eta^5\text{-}C_5Me_5)(dppe)FeCl} + HC{\equiv}CC_6H_4C{\equiv}CH + NH_4PF_6 \rightarrow \underset{\mathbf{2}}{(\eta^5\text{-}C_5Me_5)(dppe)Fe(C{=}CHC_6H_4CH{=}C)Fe(dppe)\text{-}(\eta^5\text{-}C_5Me_5)][PF_6]_2} + NH_4Cl \quad (1)$$

This reaction is interesting in that the binuclear bis(vinylidene) product is the exclusive product. There is evidence neither for a mononuclear vinylidene complex, $[\{Fe(\eta^5C_5Me_5)(\eta^2dppe)\}(C{=}CHC_6H_4C{\equiv}CH)][PF_6]$, nor for alkoxycarbene derivatives resulting from methanol addition.[9] The ^1H NMR spectrum of $[\{Fe(\eta^5C_5Me_5)(\eta^2\text{-}dppe)\}_2(C{=}CHC_6H_4CH{=}C)][PF_6]_2$ (**2**) shows a characteristic triplet for the H atoms bound to the β-carbon atoms of the bis(vinylidene) ligand (δ 4.94, $^4J_{PH}$ = 4 Hz). Similarly, the ^{13}C NMR spectrum shows a triplet (δ 363.0, $^2J_{PC}$ = 33 Hz) and a doublet of triplets (δ 125.9, $^1J_{CH}$ = 153 Hz, $^3J_{PC}$ = 4.8 Hz) for the Cα and Cβ vinylidene carbon atoms. The IR spectrum (Nujol) also provides evidence for the presence of the vinylidene ligand with $\nu_{(C=C)}$ at 1617 cm^{-1}.

The complex $[\{Fe(\eta^5C_5Me_5)(\eta^2dppe)\}_2\text{-}\mu\text{-}(C{=}CHC_6H_4\text{-}CH{=}C)][PF_6]_2$ (**2**) is readily deprotonated by 2 equiv of $KOBu^t$ in THF, giving the corresponding alkynyl complex $[\{Fe(\eta^5C_5Me_5)(\eta^2dppe)\}_2\text{-}\mu\text{-}(C{\equiv}CC_6H_4C{\equiv}C)]$ (**3**) as a thermally stable orange solid in 96% yield (eq 2). This

$$[\underset{\mathbf{2}}{\eta^5\text{-}(C_5Me_5)(dppe)Fe(C{=}CHC_6H_4CH{=}C)Fe(dppe)\text{-}(\eta^5\text{-}C_5Me_5)}] + 2KOBu^t \rightarrow \underset{\mathbf{3}}{(\eta^5\text{-}C_5Me_5)(dppe)Fe(C{\equiv}CC_6H_4C{\equiv}C)Fe(dppe)\text{-}(\eta^5\text{-}C_5Me_5)} + 2KPF_6 \quad (2)$$

compound is insoluble in many solvents. Its extraction with a soxlet apparatus with toluene gave **3** as an analytically pure powder of (89%), which was characterized by IR, Mössbauer, and ^1H NMR spectroscopy and cyclic voltammetry.

Scheme 1

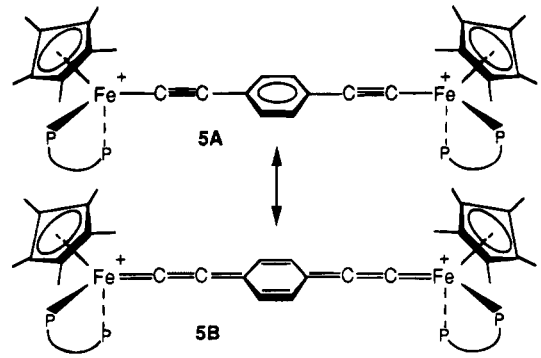

The FT-IR spectrum of **3**, which exhibits a cyclic voltammogram identical to that of **5** (*vide infra*), shows the presence of the alkynyl ligand $\nu_{(C\equiv C)}$ at 2051 (Nujol, cm^{-1}). A Mössbauer spectrum, in the solid state, was run at 78 K and least-squares fitted with Lorentzian line shapes (Table 1). It consists of a Fe(II) characteristic doublet (ΔE_Q = 2.020 mm·s^{-1}). Moreover, from computer modeling measurements, the iron to iron separation in **3** can be estimated to be 11.89 Å.[10] The nanoscale-long distances between the metal centers, the electron transfer, and the electronic coupling between the two redox sites are of interest for further studies.

2. Synthesis of the 34-Electron Binuclear Complex $[\{Fe(\eta^5C_5Me_5)(\eta^2dppe)\}_2\text{-}\mu\text{-}(C{\equiv}CC_6H_4C{\equiv}C)][PF_6]_2$ (5). The addition of 2 equiv of $[Fe(\eta^5C_5\text{-}Me_5)_2][PF_6]$ to a CH_2Cl_2 suspension of $[\{Fe(\eta^5C_5Me_5)\text{-}(\eta^2dppe)\}_2\text{-}\mu\text{-}(C{\equiv}CC_6H_4C{\equiv}C)]$ (**3**) resulted in a rapid color change from orange to deep green. Addition of pentane to the reaction mixture then gave the Fe(III)–Fe(III) complex **5** isolated as a green microcrystalline solid in 90% yield which is air and thermally stable (eq 3). The analytically pure salt **5** was characterized by

$$\underset{\mathbf{3}}{(\eta^5\text{-}C_5Me_5)(dppe)Fe(C{\equiv}CC_6H_4C{\equiv}C)Fe(dppe)\text{-}(\eta^5\text{-}C_5Me_5)} + 2[Cp_2Fe][PF_6] \rightarrow \underset{\mathbf{5}}{[(\eta^5\text{-}C_5Me_5)(dppe)Fe(C{\equiv}CC_6H_4C{\equiv}C)Fe(dppe)\text{-}(\eta^5\text{-}C_5Me_5)][PF_6]_2} + 2Cp_2Fe \quad (3)$$

IR in the solid state and in solution (cm^{-1}, CH_2Cl_2/Nujol, $\nu_{C\equiv C}$ = 1991/1983). Of particular interest is the comparison of the IR spectra of **3** and **5** with those of the mononuclear, related species $Fe(\eta^5C_5Me_5)(\eta^2dppe)(C{\equiv}C\text{-}C_6H_5)$ (**6**) and $[Fe(\eta^5C_5Me_5)(\eta^2dppe)\ (C{\equiv}CC_6H_5)]PF_6$ (**7**).[7] Upon one-electron oxidation of **6**, $\nu_{(C\equiv C)}$ was reduced by 27 cm^{-1} (cm^{-1}, $\nu_{(C\equiv C)}$, **6/7**, 2049/2022), whereas the two-electron oxidation of **3** produces a decrease of $\nu_{(C\equiv C)}$ by 70 cm^{-1}. The low stretching frequency for the C≡C triple bond in complex **5** indicates a diminution of the bond order and a contribution of the cumulenic resonance structure, as shown by the canonical forms A and B in Scheme 1.

(7) Connelly, N. G.; Gamasa, M. P.; Gimeno, J.; Lapinte, C.; Lastra, E.; Maher, J. P.; Le Narvor, N.; Rieger, A. L.; Rieger, P. H. *J. Chem. Soc., Dalton Trans.* **1993**, 2575.

(8) For general reviews, see: (a) Bruce, M. I.; Swincer, A. G. *Adv. Organomet. Chem.* **1987**, *52*, 3940. (b) Bruce, M. I. *Chem. Rev.* **1991**, *91*, 197.

(9) (a) Davison, A.; Selegue, J. P. *J. Am. Chem. Soc.* **1978**, *100*, 7763. (b) Adams, R. D.; Davison, A.; Selegue, J. P. *J. Am. Chem. Soc.* **1979**, *101*, 7232. (c) Bruce, M. I.; Humphrey, M. G. Koutsantonis, G. A.; Liddell, M. J. *J. Organomet. Chem.* **1987**, *326*, 247. (d) Boland-Lussier, B. E.; Hughes, R. P. *Organometallics*, **1982**, *1*, 635. (e) Knors, C.; Kuo, G. H.; Lauher, J. W.; Eigenbrot, C.; Helquist, P. *Organometallics* **1987**, *6*, 988. (f) Boland-Lussier, B. E.; Churchill, M. R.; Hughes, R. P.; Rheingold, A. L. *Organometallics* **1982**, *1*, 628. (g) Davison, A.; Selegue, J. P. *J. Am. Chem. Soc.* **1980**, *102*, 2455. (h) Davies, S. G.; Smallridge, A. J. *J. Organomet. Chem.* **1990**, *395*, C39.

(10) Molecular modeling system Chem3D from Cambridge Scientific Computing, Cambridge, MA.

(11) In agreement with preliminary results of MO calculations: Halley, J.-F.; Frapper, G., work in progress.

Table 1. ^{57}Fe Mössbauer spectral fitting parameters at 78 K for [{Fe(η^5C$_5$Me$_5$)(η^2dppe)}$_2$-μ-(C≡CC$_6$H$_4$C≡C)] (3) [{Fe(η^5C$_5$Me$_5$)(η^2dppe)}$_2$-μ-(C≡CC$_6$H$_4$C≡C)][PF$_6$] (4), and [{Fe(η^5C$_5$Me$_5$)(η^2dppe)}$_2$-μ-(C≡CC$_6$H$_4$C≡C)][PF$_6$]$_2$ (5)

Compounds	ΔE_Q (I S)[a] (mm·s^{-1})		
3 (77 K)	2.020 (0.265)		
4 (5 K)	1.963 (0.260)	1.250 (0.209)	0.790 (0.235)
4 (77 K)	1.961 (0.248)	1.111 (0.203)	0.710 (0.246)
4 (220 K)	1.977 (0.221)	1. 160 (0.165)	0.715 (0.200)
5 (77 K)			0.911 (0.239)

[a] Isomer shift relative to iron foil at room temperature.

Magnetic susceptibility measurements of complex **5** were performed on a SQUID magnetometer over the temperature range 5–300 K. The molar paramagnetic susceptibility (χ_M) vs temperature can be fitted with the Curie–Weiss law, $\chi_M = \chi_0 + C/(T - \theta)$ with $\theta = -2.9$ K, $\chi_0 = 6.0172 \times 10^{-4}$ emu/mol. There is a gradual decrease of the χ_M with an increase of the temperature. In the range 20–300 K, the magnetic moment is found to be rather weak ($\mu_{eff} = 1.23\ \mu_B$) and its determination in solution by the Evans method (1.10 μ_B) probes the measurements in the solid state and indicates the molecular origin of the magnetic behavior. This value, significantly lower than that determined for the mononuclear compound **7** (1.60 μ_B), is evidence of the paramagnetic character of **5** and indicates an antiferromagnetic coupling between the two 17-electron metal centers. The d orbitals on the two iron ions would become admixed with the π orbitals from the bridging 1,4-diethynylbenzene ligand (canonical form B in Scheme 1).[11] This finding, which corroborates the IR data, is in agreement with the ESR spectrum of **5** (in a CH$_2$Cl$_2$/C$_2$H$_4$Cl$_2$ (1:1) glass) run at 77 K, which exhibits three broad **g** tensor components without hyperfine structure characteristic of metal centered radicals. The intensity of the signals is very weak and corresponds to about ~1% of those observed in the case of the mononuclear complex **7**. On the other hand, the **g** values (g_1 = 1.9669, g_2 = 2.0356, g_3 = 2.1142) determined for **5** are different from those measured under the same conditions for the 17-electron phenylalkynyl complex **7** (g_1 = 1.975, g_2 = 2.033, g_3 = 2.464) and related species.[12] The three well-separated features for the latter correspond to the three components of the **g** tensor expected for species having pseudooctahedral symmetry. The g_1 and g_2 values are closed to the free electron **g** value (**g** = 2.0023) whereas the g_3 value is much higher, as usually observed for 17-electron iron(III) compounds having a singly occupied HOMO with a predominant metallic character.[12] The ^{57}Fe Mössbauer spectrum of a crystallized sample of **5** recorded at zero field (78 K) is in accord with the presence of iron(III) centers (Table 1). Note that the Mössbauer parameters of the alkynyl iron(III) complexes are slightly different from those of the related alkyl compounds, suggesting a change in the ligand-field symmetry induced by the alkynyl ligand bound to the iron centers.[12,13]

The initial scan in the cyclic voltammogram of complex **5** from +0.5 to −1.5 V [*vs* standard calomel electrode (SCE)] is characterized by two reversible one-

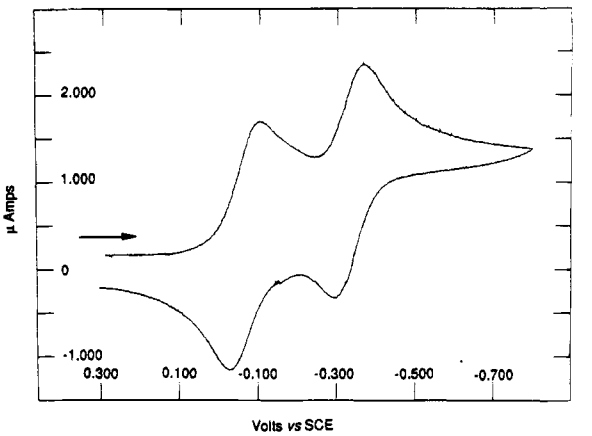

Figure 1. Cyclic voltammogram at 20 °C of [{Fe(η^5C$_5$Me$_5$)(η^2dppe)}$_2$-μ-(C≡CC$_6$H$_4$C≡C)][PF$_6$]$_2$ (**5**) in 0.1 M [*n*-Bu$_4$N][PF$_6$]/CH$_2$Cl$_2$: Pt electrode; V vs SCE; scan rate, 100 mV·s^{-1}.

electron waves in dichloromethane with the (i_p^a/i_p^c) current ratio of unity (Figure 1). At the Pt anode, the two reduction waves are observed at E_0 −0.055 V and −0.315 V *vs* SCE (*cf.* ferrocene +0.420 V vs SCE). For the two redox systems, the anodic and cathodic peak separation ($E_p^a - E_p^c$) is 0.060 V with a 0.100 V·s^{-1} scan rate.

The low values of the oxidation potentials show these half-sandwich complexes to be electron-rich compounds. The quite large wave separation ($|\Delta E_0|$ = 0.26 V) leads to an large comproportionation constant (eq 4; K_c = 2.6

$$\text{Fe(II)–Fe(II)} + \text{Fe(III)–Fe(III)} \rightleftharpoons 2(\text{Fe(II)–Fe(III)}) \quad (4)$$

× 10^4) and establishes that the delocalization of the odd-electron density is larger than in the biferrocenium series when the two metallic units are linked by one ethynyl group between two cyclopentadienyl rings.[4c,d]

Nevertheless, the separation between the two waves is smaller than in the voltammogram of the biferrocenium complexes with two ethynyl bridges between the sandwich units[4d] and the isostructural compound {Fe(η^5C$_5$Me$_5$)(η^2dppe)}$_2$-μ-(C≡CC≡C) (K_c = 1 × 10^{12}).[5] The comproportionation constant K_c obtained for the equilibrium represented by eq 4 led us to believe that the mixed-valence Fe(II)–Fe(III) complex **4** is an accessible synthetic target.

3. Synthesis of the 35-Electron Binuclear Complex [{Fe(η^5C$_5$Me$_5$)(η^2dppe)}$_2$-μ-(C≡CC$_6$H$_4$C≡C)][PF$_6$] (4). The addition of a stoichiometric amount of [Fe(C$_5$H$_5$)$_2$][PF$_6$] to a suspension of **3** in CH$_2$Cl$_2$ resulted in a slow dissolution of the starting material and appearance of a pink color. After precipitation by pentane, the mixed-valence complex **4** was recovered as analytically pure, pink microcrystals in 95% yield and characterized by CV and IR, Mössbauer, and ESR spectroscopies. It is a thermally and air-stable compound with CV waves identical to those of its Fe(III)–Fe(III) parent complexes **3** and **5**. Oxidation of **4** with 1 equiv of [Fe(C$_5$H$_5$)$_2$][PF$_6$] in CH$_2$Cl$_2$ produces the deep green compound **5**, whereas the reduction of **5** with 1 or 2 equiv of cobaltocene, respectively, affords the pink complex **4** or the orange neutral derivative **3**, establish-

(12) Roger, C.; Hamon, P.; Toupet, L.; Rabaa, H.; Saillard, J.-Y.; Hamon, J.-R.; Lapinte, C. *Organometallics*, **1991**, *10*, 1045.
(13) Greenwood, N. N.; Gibb, T. C. *Mössbauer Spectroscopy;* Chapman and Hall: London, 1971.

Scheme 2

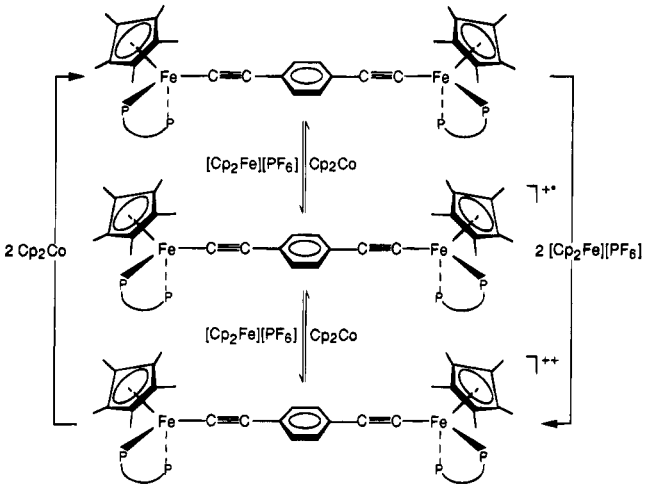

ing the reversible character of the two redox systems (Scheme 2).

^{57}Fe Mössbauer spectroscopy is suitable for the identification of the oxidation states of iron in these compounds because the quadrupole splittings and isomer shifts are well differentiated for the Fe(II) and Fe(III) in sandwich and piano-stool complexes. Therefore, the Mössbauer spectrum of **4** was run at 78 K and least-squares fitted with Lorentzian line shapes (Figure 2a). Surprisingly, it consists of a three-doublet signal corresponding to the presence of Fe(II), Fe(III), and an intermediate valence (see Table 1).

It is clear from the values of the quadrupole splittings that the presence of three doublets is not due to the dismutation of the mixed-valence complex **4** into the binuclear Fe(II)−Fe(II) and Fe(III)−Fe(III) derivatives **3** and **5**. Moreover, such an explanation is not consistent with the large comproporpionation constant value. The valence-trapped and -detrapped signal ratio depends on the solid sample. Successive recrystallizations of the same sample from a CH_2Cl_2/pentane mixture led to the observation of random variations of the percentage of the valence-detrapped from 44 to 72% at 77 K. Simultaneous observation of an iron-localized and -delocalized mixed valence is rare but not unprecedented. Similar behavior has already been observed by Hendrickson and co-workers for the 1′,1‴-dibenzylbiferrocenium triiodide monocation **8**.[4m] The rate of intramolecular electron transfer in this mixed-valence complex is extremely sensitive to the perturbation of the environment caused by differences in crystal-packing arrangements. Two polymorphs of the monocation **8** have been found in the solid; one is valence-trapped while the other is detrapped.[4m] Mössbauer spectroscopy of solid samples of the mixed-valence compound **4** cannot distinguish between the crystal packing or the molecular origin of the factors controlling the intramolecular electron-transfer rate. However, it can be used to monitor the intramolecular electron-transfer rate in mixed-valence complexes. When the intracation electron-transfer rate is slower than $\sim 10^6$ s^{-1}, discrete iron valences are sensed by the Mössbauer technique; the spectrum consists of a superposition of two quadrupole-split doublets typical of Fe(II) and Fe(III) compounds. When the rate of intramolecular electron transfer exceeds $\sim 10^9$ s^{-1}, a single average valence quadrupole-

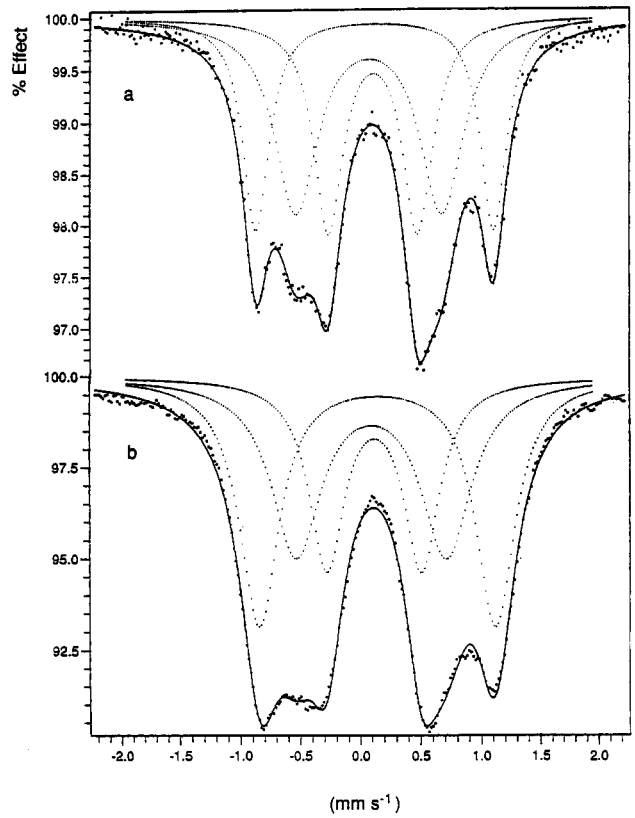

Figure 2. ^{57}Fe Mössbauer spectrum for [{Fe(η^5C$_5$Me$_5$)(η^2-dppe)}$_2$-μ-(C≡CC$_6$H$_4$C≡C)] [PF$_6$] (**4**) at 78 (a) and 5 K (b). The velocity scale is referenced to iron metal.

split doublet is observed, indicating that, on the Mössbauer time scale, both iron centers are equivalent.[41]

The spectrum of the sample, the trapped to detrapped 60:40 ratio of which was observed at 77 K, was also run at 220 and 5 K. No significative change in the spectrum was observed at 220 K, and the ratio of the Fe(II) and Fe(III) contribution of the trapped valence remained ~1. There are two interesting reversible changes between the spectra recorded at 5 and 77 K (Figure 2). As the calculated percentage of the Fe(III) contribution remains constant, we observed in the spectrum run at 5 K an increase in the contribution of Fe(II) and a decrease of the detrapped valence. The result is the observation of three doublets corresponding to Fe(II)/Fe(intermediate)/Fe(III) in the ratio 39:31:30. The excess of the Fe(II) form with respect of the Fe(III) component in the valence-trapped system could be the consequence of the delocalization of the odd electron in a π orbital of the diethynylbenzene bridging ligand (Scheme 3).

The 77 K ESR spectrum of the binuclear complex [{Fe(η^5C$_5$Me$_5$)(η^2dppe)}$_2$-μ-(C≡CC$_6$H$_4$C≡C)][PF$_6$] (**4**) in CH_2Cl_2/$C_2H_4Cl_2$ (1:1) glass shows three well-separated features without hyperfine structure corresponding to the three components of the g tensor. The **g** tensors (g_1 = 2.031; g_2 = 2.043; g_3 = 2.199) are quite different from those of the mononuclear 17-electron complex [{Fe(η^5C$_5$Me$_5$)(η^2dppe)}(η^1C≡CC$_6$H$_5$)][PF$_6$] (**7**) (*vide supra*). The **g**-tensor anisotropy is significantly smaller in the mixed-valence complex **4** than in the Fe(III) mononuclear compound **7**. It has been reported for the biferrocenium series that mixed-valence compounds with an intramolecular electron-transfer rate in excess of the ESR time scale have a weak angular momentum.[41] These considerations support the fact that the odd

Scheme 3

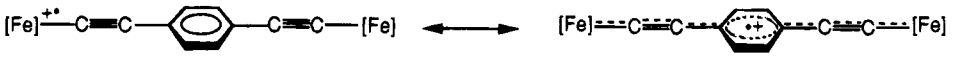

4A 4B

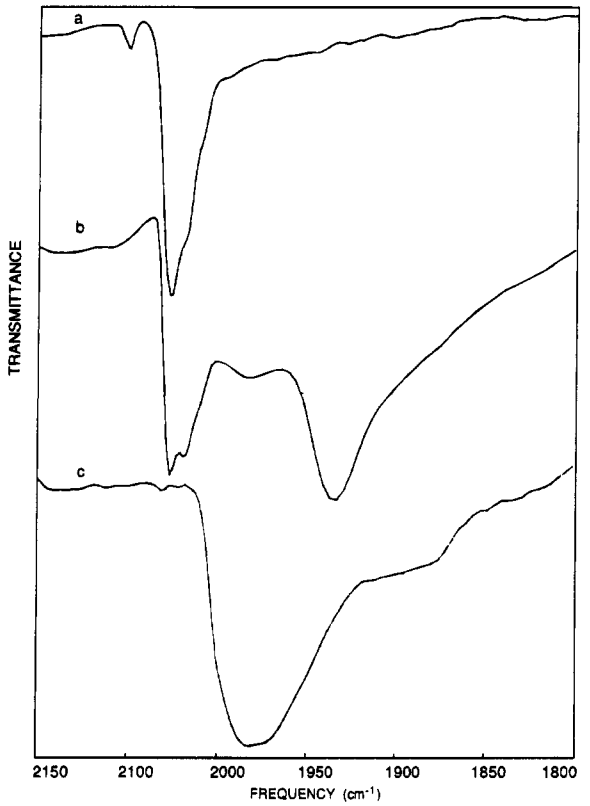

Figure 3. Infrared spectra of 20 °C Nujol dispersion of (a) $[\{Fe(\eta^5C_5Me_5)(\eta^2dppe)\}_2\text{-}\mu\text{-}(C{\equiv}CC_6H_4C{\equiv}C)]$ (**3**), (b), $[\{Fe(\eta^5C_5Me_5)(\eta^2dppe)\}_2\text{-}\mu\text{-}(C{\equiv}CC_6H_4C{\equiv}C)][PF_6]$ (**4**), and (c) $[\{Fe(\eta^5C_5Me_5)(\eta^2dppe)\}_2\text{-}\mu\text{-}(C{\equiv}CC_6H_4C{\equiv}C)]\,[PF_6]_2$ **5** in the 1800−2100-cm^{-1} region.

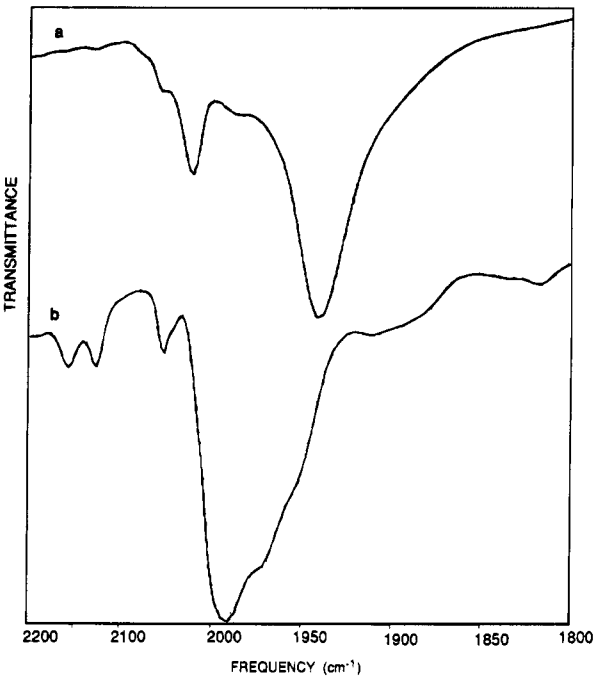

Figure 4. Infrared spectra of 20 °C CH_2Cl_2 solution of (a) $[\{Fe(\eta^5C_5Me_5)(\eta^2dppe)\}_2\text{-}\mu\text{-}(C{\equiv}CC_6H_4C{\equiv}C)][PF_6]$ (**4**) and (b) $[\{Fe(\eta^5C_5Me_5)(\eta^2dppe)\}_2\text{-}\mu\text{-}(C{\equiv}CC_6H_4C{\equiv}C)][PF_6]_2$ (**5**) in the 1800−2100-cm^{-1} region.

electron in **4** would be delocalized on the ESR time scale (10^{-9} s), on both the two metal centers and the π system of the bridging ligand.

Comparison of the infrared spectra of the mixed-valence complex **4** with those of the neutral **3** and the dication **5** iron complexes should provide the most direct indication of electronic delocalization on a short time scale. If the IR bands for a given mixed-valence compound occur at a frequency intermediate between those for the corresponding unoxidized and dioxidized species, then it can be concluded that the intramolecular electron-transfer rate is fast in the IR time scale (10^{-13} s). The equivalence of the two metal sites is indicated by the terminal ligand vibrations, but to the best of our knowledge, the IR stretching band of the bridge was not taken as diagnostic of the mixed-valence delocalization.[4,6,14] The solid state and CH_2Cl_2 solution infrared spectra of the three complexes are shown in Figures 3 and 4.

The neutral complex **3** was not sufficiently soluble to allow an infrared spectrum to be measured in solution. The major stretching bands in the IR spectrum (cm^{-1}, Nujol/CH_2Cl_2) of the mixed-valence complex **4** are found at 2052/2019, 1983/1991 and 1934/1939 and correspond to the $\nu_{(C\equiv C)}$ of the 1,4-diethynylbenzene bridge. The bands at 2052 and 1983 cm^{-1} are mere superpositions of those found for the isolated Fe(II) and Fe(III) sites. The new $\nu_{(C\equiv C)}$ band located at 1934/1939 cm^{-1}, a lower frequency than those of the Fe(III) sites, constitutes the feature of the IR spectrum. For a given solid sample of **4**, comparison of the Mössbauer and IR spectra allows us to observe a relationship between the intensity of the 1934-cm^{-1} IR band and that of the Mössbauer doublet corresponding to the valence-detrapped contribution. Our data do not afford an unambiguous conclusion that **4** is valence trapped or -detrapped on the IR spectroscopy time scale. However, these results, taken as a whole with the Mössbauer data, reveal a nonclassical behavior for **4** which shows both the characteristics of a delocalized and localized mixed-valence complex. In terms of the Robin and Day classification, the 35-electron mixed-valence complex **4** can be considered as a borderline compound between the classes II and III.[15]

In conclusion, we have synthesized a rigid binuclear assembly that allows electron delocalization on two metal centers, over an ~11.89-Å span. This wirelike molecular system is easily accessible in the form of the three stable 36-, 35-, and 34-electron complexes. The unusual behavior of the 35-electron mixed-valence complex **4** could not be regarded as a consequence of a polymorphism as previously observed in the biferroce-

(14) (a) Geiger, W. E.; Van Order, N.; Pierce, D. T.; Bitterwolf, T. E.; Rheingold, A. L.; Chasteen N. D. *J. Am. Chem. Soc.* **1991**, *10*, 2403. (b) Atwood, C. G.; Geiger, W. E.; Rheingold, A. L. *J. Am. Chem. Soc.* **1993**, *115*, 5310.

(15) Robin, M. B.; Day, P. *Adv. Inorg. Chem. Radiochem.* **1967**, *10*, 247.

nium series, since the solution and solid state infrared spectra are quite similar. It seems that the intramolecular electron-transfer rate could be controlled by molecular properties such as conformational changes.[16] This will be the subject of future research in our group.

Experimental Section

General Data. Reagent grade tetrahydrofuran (THF), diethyl ether, and pentane were dried and distilled from sodium benzophenone ketyl prior to use. Pentamethylcyclopentadiene was prepared according to the published procedure[17] and other chemicals were used as received. All the manipulations were carried out under an argon atmosphere using Schlenk techniques or in a Jacomex 532 drybox filled with nitrogen. Routine NMR spectra were recorded using a Bruker AW 80-MHz. High-field NMR spectra experiments were performed on a multinuclear Bruker 300-MHz instrument. Chemical shifts are given in part per million relative to tetramethylsilane (TMS) for ^{1}H and ^{13}C NMR spectra and H_3PO_4 for ^{31}P NMR spectra. Cyclic voltammograms were recorded by using a PAR 263 instrument. X-Band ESR spectra were recorded on a Bruker ESP-300E spectrometer at 77 K in liquid nitrogen. Mössbauer spectra were recorded with a 2.5×10^{-2} C (9.25×10^8 Bq) ^{57}Co source using a symmetric triangular sweep mode.[18] Magnetic susceptibility were performed with a susceptometer quantum interface device (SQUID) instrument. The interatomic distances have been measured with the molecular modeling system Chem3D from Cambridge Scientific Computing. Elemental analyses were performed at the Center for Microanalyses of the CNRS at Lyon-Solaise, France.

1. Binuclear Bis(vinylidene) Complex [{Fe(η^5C$_5$Me$_5$) (η^2dppe)}$_2$-μ-(=C=CHC$_6$H$_4$HC=C=)][PF$_6$]$_2$. To Fe(η^5C$_5$Me$_5$)(η^2dppe)Cl[12] (0.37 g, 0.59 mmol) in MeOH (30 mL) at 20 °C was added HC≡CC$_6$H$_4$C≡CH (0.03 g, 0.28 mmol) and NH_4PF_6 (0.098 g, 0.60 mmol). The solution was stirred for 16 h, and then the solvent was removed *in vacuo*. The residue was extracted with CH_2Cl_2, the extract was concentrated *in vacuo*, and diethyl ether was added to precipitate the product as a pale brown powder which was washed with diethyl ether and dried *in vacuo* to give 0.30 g of **6** (83%). Anal. Calcd for $C_{82}H_{84}F_{12}Fe_2PF_6$: C, 61.75; H, 5.31. Found: C, 61.76; H, 5.31. IR (Nujol, cm^{-1}): 1671 (m, C=C). ^{1}H NMR (300 MHz, CD_2Cl_2) δ_H 1.57 (s, 30H, C$_5$Me$_5$), 2.50, 3.05 (2 m, 8H, PCH$_2$), 4.94 (t, 2H, $^4J_{PH}$ = 4 Hz, CH), 5.92 (s, 4H, C$_6$H$_4$), 7.14−7.53 (m, 40H, Ph). ^{13}C NMR {^{1}H} (300 MHz, CD_2Cl_2) δ_C 363.0 (t, $^2J_{PC}$ = 34 Hz, C=CH), 133.5−123.8 (m, Ph), 125.9 (s, C=CH), 100.4 (s, C$_5$Me$_5$), 29.5 (t, $^1J_{PC}$ = 22 Hz, PCH$_2$), 10.4 (s, C$_5$Me$_5$). ^{31}P NMR (300 MHz, CD_2Cl_2) δ_P 87.7 (s).

2. Binuclear Bis(alkynyl) Complex [{Fe(η^5C$_5$Me$_5$) (η^2dppe)}$_2$-μ-(C≡CC$_6$H$_4$C≡C)] (3). KO^{t}Bu (0.255 g, 2.37 mmol) was added to a solution of [{Fe(η^5C$_5$Me$_5$)(η^2-dppe)}$_2$-μ-(C=XHC$_6$H$_4$CH=C)][PF$_6$] (1.45 g, 0.92 mmol) in THF (40 mL) under argon. The resulting brown solution was stirred for 15 min and evaporated to dryness *in vacuo*. The toluene extraction of the crude residue with a soxlet apparatus requires 4 days. After removal of the solvent, the solid is washed with 10 mL of pentane and dried *in vacuo* to give **7** (1.14 g, 96%). Anal. Calcd for $C_{82}H_{82}Fe_2P_4$: C, 75.58 ; H, 6.34. Found: C, 75.86 ; H, 6.07. FT-IR (Nujol, cm^{-1}): 2051 (w, C≡C). ^{1}H NMR (300 MHz, CD_2Cl_2) δ_H 1.30 (s, 30H, C$_5$Me$_5$), 2.11 (m, 8H, PCH$_2$), 8.79 (m, 4H, C$_6$H$_4$), 8.31 (m, 40H, Ph).

3. Binuclear Bis(alkynyl) Complex [{Fe(η^5C$_5$Me$_5$) (η^2dppe)}$_2$-μ-(C≡CC$_6$H$_4$C≡C)][PF$_6$] (4). (A) To [{Fe(η^5C$_5$Me$_5$)(η^2dppe)}$_2$(-μ-C≡CC$_6$H$_4$C≡C)] (**3**) (0.190 g, 0.15 mmol) in CH_2Cl_2 (10 cm^3) at 20 °C was added [Fe(η-C$_5$Me$_5$)][PF$_6$] (0.046 g, 0.142 mmol). The solution was stirred at 20 °C and then reduced to very low volume *in vacuo*. Addtion of pentane gave a precipitate which was recrystallized from CH_2Cl_2/diethyl ether to give pink microcrystals, yield 0.190 g (95%).

(B) To [{Fe(η^5C$_5$Me$_5$)(η^2dppe)}$_2$-μ-(C≡CC$_6$H$_4$C≡C)]-[PF$_6$]$_2$ (**5**) (0.190 g, 0.15 mmol) in CH_2Cl_2 (10 cm^3) at 20°C was added [Co(η-C$_5$H$_5$)$_2$] (0.026 g, 0.142 mmol). The solution turned from deep green to pink and the volume was reduced *in vacuo*. Addition of pentane gave a precipitate which was recrystallized from CH_2Cl_2/iethyl ether to give pink microcrystals, yield 0.152 g (74%). The ^{1}H NMR spectrum showed **4** was isolated as a solvate containing 1.5 mol of CH_2Cl_2 per mole. Anal. Calcd for $C_{82}H_{82}F_6Fe_2P_5$·1.5 CH_2Cl_2: C, 63.66; H, 5.44. Found: C, 63.85; H, 5.14. FT−IR ($\nu_{C\equiv C}$, CH_2Cl_2/Nujol, cm^{-1}): 2019/2052, 1991/1983, 1939/1934.

4. Synthesis of the Binuclear Bis(alkenyl) Complex [{Fe(η^5C$_5$Me$_5$)(η^2dppe)}$_2$-μ-(C≡CC$_6$H$_4$C≡C)]-[PF$_6$]$_2$ (5). To [{Fe(η^5C$_5$Me$_5$) (η^2dppe)}$_2$-μ-(C≡C-C$_6$H$_4$C≡C)] (0.20 g, 0.15 mmol) in CH_2Cl_2 (20 mL) at 20 °C was added [{Fe(η^5C$_5$Me$_5$)[PF$_6$] (0.099 g, 0.29 mmol). The solution was stirred at 20 °C for 5 h and then reduced to very low volume *in vacuo*. After filtration of the solution, addition of pentane gave a deep green precipitate which was washed with pentane (3 × 10 mL) and dried *in vacuo* to give **5** (0.220 g, 90%). The ^{1}H NMR spectrum showed **5** was isolated as a solvate containing 1.5 mol of CH_2Cl_2 per mole. Anal. Calcd for $C_{82}H_{82}F_{12}Fe_2P_6$; 1.5 CH_2Cl_2: C, 58.29; H, 4.98. Found: C, 58.63; H, 5.03. FT-IR (CH_2Cl_2/Nujol, cm^{-1}): 1991/1984 (w, $\nu_{C\equiv C}$).

Acknowledgment. We are grateful to Dr. S. Sinbandhit (CRMPO, Rennes) for NMR assistance, to Dr. G. Linares and Pr. F. Varret (Paris) for Mössbauer facilities, and to Dr. J.-F. Halley and G. Frapper for helpful discussions; we are also indebted to the Laboratoires Standa (Caen, France) for financial support to N.L.N.

OM9406299

(16) Woitellier, S.; Launay, J. P.; Spangler, C. W. *Inorg. Chem.* **1989**, *28*, 758. (b) Launay, J. P.; Tourrel-Pagis, M.; Lipskier, J.-F.; Marvaud, C. J. *Inorg. Chem.* **1991**, *30*, 1033.
(17) Kohl, F. X.; Jutzi, P. *J. Organomet. Chem.* **1983**, *243*, 119.
(18) Varret, F.; Mariot, J.-P; Hamon, J.-R.; Astruc, D. *Hyperfine Interact.* **1988**, *39*, 67.

Rate and Mechanism of the Reductions of Iron Pentacarbonyl and Chromium Hexacarbonyl to Their Metalate Complexes

Christian Amatore,*,† Paul J. Krusic,‡ Steen U. Pedersen,§ and Jean-Noël Verpeaux†

Département de Chimie de l'Ecole Normale Supérieure, URA CNRS 1679, 24 rue Lhomond, F-75231 Paris Cedex 05, France, Central Research and Development Department, E. I. du Pont de Nemours and Company, Experimental Station, E328 Wilmington, Delaware 19898, and Department of Chemistry, Aarhus University, DK-8000 Aarhus, Denmark

Received April 11, 1994®

The electrochemical reductions of $Fe(CO)_5$ and $Cr(CO)_6$ in THF were shown to proceed by an ECE mechanism leading to the electrogenerated dianions $Fe(CO)_4^{2-}$ and $Cr(CO)_5^{2-}$, respectively. The initial 19-electron anion radical $Fe(CO)_5^-$ could not be observed by the fastest direct electrochemical methods but was shown to have an approximate lifetime of 10 ns. $Cr(CO)_6^-$ also could not be observed by fast scan cyclic voltammetry, and its lifetime was estimated to lie in the range 50 μs to 10 ns. In the absence of an electrophile, the electrogenerated dianions further react slowly via a nucleophilic substitution reaction with the parent $Fe(CO)_5$ and $Cr(CO)_6$ to yield the dimers $Fe_2(CO)_8^{2-}$ and $Cr_2(CO)_{10}^{2-}$, respectively. The corresponding rate constants were estimated at 120 ($Fe(CO)_4^{2-}$ + $Fe(CO)_5$) and 0.95 M^{-1} s^{-1} ($Cr(CO)_5^{2-}$ + $Cr(CO)_6$). Although these rate constants are rather modest, their magnitudes are sufficient to explain why $Fe_2(CO)_8^{2-}$ and $Cr_2(CO)_{10}^{2-}$ are the major products of the electroreductions of $Fe(CO)_5$ and $Cr(CO)_6$ when the electrolyses are performed under classical conditions (*viz.*, batch electrolyses; $t_{elec} \geq 0.5$ h). Conversely, when generated by fast exhaustive electrolysis in a percolating flow cell (t_{elec} less than a few seconds), $Fe(CO)_4^{2-}$ is the single electrolysis product that remains stable for minutes in the dry electrochemical medium in the absence of $Fe(CO)_5$.

Introduction

Two-electron reduction via single electron transfer steps of simple metal carbonyls $M(CO)_n$ is the preferred route to anionic $M(CO)_{n-1}^{2-}$ "ate" complexes, which are powerful nucleophiles and reducing reagents widely used in organic and organometallic chemistry.[1,2] The electrochemical reduction of metal carbonyls has therefore received particular attention from the early days of organometallic electrochemistry.[3] The first reports concerning iron pentacarbonyl led to the conclusion that the anion radical $Fe(CO)_4^-$, formed upon one-electron reduction and CO cleavage, underwent a fast dimerization to yield the binuclear dianion $Fe_2(CO)_8^{2-}$ in a one-electron process.[4] Such a scheme implied two consequences: (i) the mononuclear dianion $Fe(CO)_4^{2-}$ could only be formed upon further reduction of $Fe_2(CO)_8^{2-}$, *i.e.*, by using a second equivalent of powerful reductant such as sodium amalgam or sodium naphthalene,[5] and (ii) an electrochemical preparation of this mononuclear dianion would then prove impossible since $Fe_2(CO)_8^{2-}$ is generally not reducible at an electrode before the reduction of the supporting electrolyte or the medium.

In a more recent study,[6] the use of microelectrodes allowed us to determine the standard potential for the couple $Fe(CO)_4^{2-}/Fe(CO)_4^-$. Its value proved unambiguously that dimerization of the anion radical $Fe(CO)_4^-$ could not compete with its reduction to $Fe(CO)_4^{2-}$ when the potential was set on the reduction wave of iron pentacarbonyl. In other words, reduction of $Fe(CO)_5$ had to follow an ECE mechanism (reactions 1–3, Scheme 1), leading directly to tetracarbonyl ferrate $Fe(CO)_4^{2-}$.

Scheme 1

$$Fe(CO)_5 + e \rightleftharpoons Fe(CO)_5^- \quad (1)$$

$$Fe(CO)_5^- \rightarrow Fe(CO)_4^- + CO \quad (2)$$

$$Fe(CO)_4^- + e \rightleftharpoons Fe(CO)_4^{2-} \quad (3)$$

$$Fe(CO)_4^{2-} + Fe(CO)_5 \rightarrow Fe_2(CO)_8^{2-} + CO \quad (4)$$

This result was very recently confirmed by infrared spectroelectrochemistry.[7] However, this scheme implies

† Ecole Normale Supérieure.
‡ E. I. du Pont de Nemours and Co.
§ Aarhus University.
® Abstract published in *Advance ACS Abstracts*, December 15, 1994.

(1) (a) See: *Comprehensive Organometallic Chemistry*; Wilkinson, G., Stone, F. G. A., Eds.; Pergamon Press: Oxford, 1982. (b) Connelly, J. P.; Geiger, W. E. The electron transfer reactions of mononuclear organotransition metal complexes. In *Advances in Organometallic Chemistry*; Stone, F. G. A., West, R., Eds.; Academic Press: Orlando, FL, 1984; Vol. 23.
(2) Collman, J. P. *Acc. Chem. Res.* **1975**, *8*, 342.
(3) (a) Vlcek, A. A. *Nature (London)* **1956**, 1043. (b) Dessy, R. E.; Stary, F. E.; King, R. B.; Waldrop, H. *J. Am. Chem. Soc.* **1966**, *88*, 471.
(4) (a) Pickett, C. J.; Pletcher, D. *J. Chem. Soc., Dalton Trans.* **1975**, 879. (b) Bond, A. M.; Dawson, P. A.; Peake, B. M.; Robinson, B. H.; Simpson, J. *Inorg. Chem.* **1977**, *16*, 2199. (c) Bezems, G. J.; Rieger, P. H.; Visco, S. *J. Chem. Soc., Chem. Commun.* **1981**, 265. (d) El Murr, N.; Chaloyard, A. *Inorg. Chem.* **1982**, *21*, 2206.
(5) (a) Strong, H.; Krusic, P. J.; San Filippo, J., Jr. *Inorg. Synth.* **1986**, *24*, 157. (b) Heck, R. F.; Breslow, D. S. *J. Am. Chem. Soc.* **1963**, *85*, 2779.
(6) Amatore, C.; Verpeaux, J.-N.; Krusic, P. J. *Organometallics* **1988**, *7*, 2426.

0276-7333/95/2314-0640$09.00/0

a two-electron consumption, in apparent disagreement with the actual overall one-electron consumption and with the formation of $Fe_2(CO)_8^{2-}$ as the major product observed on the longer time scale of preparative electrolysis.[4] To reconcile these results, a coupling reaction between $Fe(CO)_4^{2-}$ and unreacted iron pentacarbonyl had to be considered (reaction 4, Scheme 1).

The reaction of $Fe(CO)_4^{2-}$ with $Fe(CO)_5$ (eq 4) is well-known with sodium as countercation (Collman's reagent) and provides a convenient chemical route to $Na_2Fe_2(CO)_8$.[8] Its rate constant (sodium salt in acetonitrile at 27 °C) was recently measured by infrared stopped-flow techniques[9] and was found to be 4.6 M^{-1} s^{-1}.

A major consequence of the direct generation of $Fe(CO)_4^{2-}$ upon ECE reduction of iron pencarbonyl is the possibility of *in situ* electrogeneration and alkylation of this highly sensitive reagent by electrolysis of $Fe(CO)_5$ in the presence of an electrophile, such as an organic halide. Such a scheme appears possible if the alkylation is fast enough to compete with the coupling reaction (4) leading to $Fe_2(CO)_8^{2-}$. While investigating the practical feasibility of the electrogeneration of alkylferrates, we found that alkyl halides that should not have been able to compete with $Fe(CO)_5$, according to the second-order rate constant of the $Fe(CO)_5$ + $Fe(CO)_4^{2-}$ coupling reaction (in the 10^6 M^{-1} s^{-1} range) that we reported in our preliminary communication,[6] actually led to substantial amounts of alkylation.[10] We therefore questioned our previous determination and found that the true value (tetrabutylammonium countercation in THF at 20 °C) is much smaller and more compatible with the value reported by Atwood *et al.*[9]

In this paper, we wish to describe in detail the electrochemical reductions of iron pentacarbonyl and chromium hexacarbonyl using modern electrochemical techniques. We also wish to rectify the erroneous rate constant given in our preliminary communication[6] for the $Fe(CO)_5$ + $Fe(CO)_4^{2-}$ reaction. This error illustrates the difficulties encountered in the determination of the absolute number of electrons involved in transient electrochemical experiments in the absence of independent knowledge of the pertinent diffusion coefficients (for a discussion of such aspects, see ref 11).

Results and Discussion

Electrochemical Reduction of $Fe(CO)_5$ and Electrogeneration of $Fe(CO)_4^{2-}$. Some of the following results on the cyclic voltammetry of $Fe(CO)_5$ in THF have already been presented in a preliminary communication.[6] Two cyclic voltammograms are shown in Figure 1. At a potential scan rate of 1 V s^{-1}, the results are essentially the same as those reported by previous authors:[4] an irreversible reduction wave R_1 (peak potential, $E^p = -2.67$ V *vs* Ag/Ag^+) is followed by two associated anodic peaks O_2 and O_3 (Figure 1, left). A

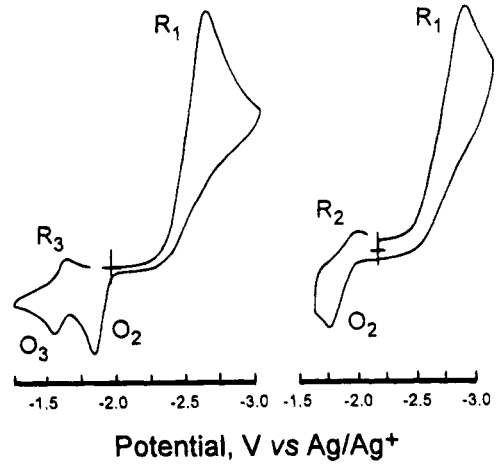

Figure 1. Cyclic voltammetry of 2 mM $Fe(CO)_5$ in THF (containing 0.3 M NBu_4BF_4) at a gold disk electrode (0.5 mm diameter); scan rates of 1 (left) or 20 (right) V s^{-1} at 20 °C.

third oxidation wave O_4 can also be seen at a much more positive potential (−0.09 V). Wave O_3 is chemically reversible, as shown by the reduction wave R_3 observed upon inversion of the potential scan after wave O_3. At faster scan rates (*i.e.*, 20 V s^{-1} and above), wave O_2 starts showing chemical reversibility (Figure 1, right), while waves O_3 and O_4 become less prominent.

Existence and Lifetime of the 19-Electron $Fe(CO)_5^-$. The very first step of the reduction process is the electron transfer to $Fe(CO)_5$ and cleavage. Since no chemical reversibility of wave R_1 could be observed even at potential scan rates as high as 300 000 V s^{-1}, the initial 19-electron anion radical $Fe(CO)_5^-$ must have a lifetime of less than 5 μs.[12] Despite its very short lifetime, this intermediate could be trapped by an efficient hydrogen atom donor such as tributyltin hydride to yield the corresponding formyl complex:[13]

$$Fe(CO)_5^- + R_3SnH \rightarrow [Fe(CO)_4(CHO)]^- + R_3Sn^\bullet$$

To allow an almost quantitative interception of $Fe(CO)_5^-$ under these conditions, the lifetime of this intermediate must be longer than 10 ns.[14] It can be concluded that carbon monoxide loss from $Fe(CO)_5^-$ occurs with a rate constant in the range of 2×10^5 to 1×10^8 s^{-1} (*vide infra*).

Redox catalysis experiments were undertaken in order to improve this rough estimate. Accordingly, several aromatic hydrocarbons giving rise to reversible

(7) Curran, D. J.; Graham, P. B.; Rausch, M. D. *Organometallics* **1993**, *12*, 2380.

(8) (a) Collman, J. P.; Finke, R. G.; Matlock, P. L.; Wahren, R.; Brauman, J. I. *J. Am. Chem. Soc.* **1976**, *98*, 4685. (b) Collman, J. P.; Finke, R. G.; Matlock, P. L.; Wahren, R.; Komoto, R. G.; Brauman, J. I. *J. Am. Chem. Soc.* **1978**, *100*, 1119.

(9) Zhen, Y.; Atwood, J. D. *Organometallics* **1991**, *10*, 2778.

(10) Amatore, C.; Pedersen, S. U.; Verpeaux, J. N., unpublished results (1993–1994).

(11) Amatore, C.; Azzabi, M.; Calas, P.; Jutand, A.; Lefrou, C.; Rollin, Y. *J. Electroanal. Chem.* **1990**, *288*, 45.

(12) (a) For an EC system in cyclic voltammetry, a chemically irreversible voltammogram is observed for a scan rate v provided that the follow-up rate constant k is such that $k \gg v/\Delta E$, with $\Delta E = E^p_c + E^p_a - 2E_{inv}$ (see Nicholson, R. S.; Shain, I. *Anal. Chem.* **1964**, *36*, 704). Since no reversibility was observed at room temperature (or even at −40 °C) for v greater than 10^5 V s^{-1}, the above inequality implies that $k > 2 \times 10^5$ s^{-1}. (b) For an EC bimolecular process, the same limit is valid, provided that k is replaced by kC^0 (*viz.*, $kC^0 \gg v/\Delta E$), where C^0 is the initial concentration of the electroactive species.

(13) (a) Narayanan, B. A.; Kochi, J. K. *J. Organomet. Chem.* **1984**, *272*, C49. (b) Narayanan, B. A.; Kochi, J. K.; Amatore, C. *Organometallics* **1986**, *5*, 926.

(14) Under the conditions where the cleavage of CO (first-order rate constant, k_1) competes with H atom transfer from Bu_3SnH (second-order rate constant, k_2), the yield of the formyl derivative is given by $k_2[Bu_3SnH]/(k_2[Bu_3SnH] + k_1)$. Since no decarbonylation product (*e.g.*, <10%) could be observed,[13] one obtains $10k_1 < k_2[Bu_3SnH]$. In the experiment described in ref 13, $[Bu_3SnH] = 0.25$ M, and k_2 must be smaller than the diffusion limit; therefore, $k_2[Bu_3SnH] < 10^9$ s^{-1}, which implies $k_1 < 10^8$ s^{-1}.

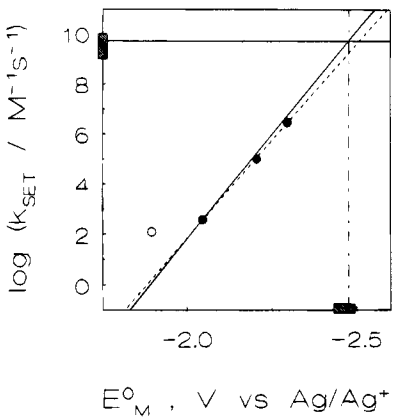

Figure 2. Rate constants k_{SET} of the homogeneous reduction of 2 mM $Fe(CO)_5$ in THF (containing 0.3 M NBu_4BF_4) by a series of aromatic anion radicals $M^{\bullet-}$ (solid circles, from left to right, M = azobenzene, 1,4 diacetylbenzene, and 1,4 dicyanobenzene) determined by redox catalysis (see text and eq 5) at 20 °C. The best regression line for the correlation of log (k_{SET}) *vs* E^0_M (*viz.*, *vs* the standard potential of the reversible $M/M^{\bullet-}$ couple) has a slope of 1/65 mV^{-1} and is shown as a dotted line. The theoretical limit expected for a diffusion-controlled electron transfer limited by diffusion of the products (slope 1/60 mV^{-1})[16,17] is shown by the solid line. The horizontal solid line corresponds to log k_{SET} = log k_{dif} (see text). Both solid lines intersect at $E^0_M = E^0_{Fe(CO)_5}$.[16] The hatched rectangle on the vertical axis figures the imprecision on the value of k_{dif}; the hatched rectangle on the horizontal axis shows the resulting uncertainty on $E^0_{Fe(CO)_5}$. The circle in the lower left part of the diagram features reaction 4, *i.e.*, when $M^{\bullet-}$ = $Fe(CO)_4^{2-}$, and was determined by stopped-flow techniques under the same conditions (see text).

redox systems ($M/M^{\bullet-}$) were selected as redox mediators. For each of them, k_{SET}, the rate constant of the forward electron transfer from the reduced form ($M^{\bullet-}$) of the mediator to iron pentacarbonyl, was determined using a now classical method:[15]

$$M^{\bullet-} + Fe(CO)_5 \overset{k_{SET}}{\rightleftharpoons} M + \{Fe(CO)_5^- \xrightarrow{k_1} \text{cleavage}\} \quad (5)$$

A plot of log k_{SET} *vs* the standard potentials of the corresponding redox mediators gave a straight line (Figure 2) whose slope was 1/65 mV^{-1} $decade^{-1}$, *i.e.*, close to the theoretical value of 1/60 mV^{-1} $decade^{-1}$, indicative of a diffusion-controlled process (with perhaps a slight contribution of mixed activation–diffusion control for the more reducing anion radicals).[16,17] The intersection of this experimental regression line with the horizontal line at log k_{dif} provided a determination of the standard potential of $Fe(CO)_5$ as shown in Figure 2.[16] Using $k_{dif} \approx 5 \times 10^9$ M^{-1} s^{-1} in THF at 20 °C, we obtained $E^0 \approx -2.47$ V *vs* Ag/Ag^+. Since k_{dif} is not known with precision ($10^9 \leq k_{dif} \leq 10^{10}$ M^{-1} s^{-1}) under our conditions an error of ±30 mV is associated to the value of the standard potential, E^0, see Figure 2; hence, -2.43 V $\leq E^0 \leq -2.49$ V.

The fact that the standard potential E^0 is less negative than the voltammetric peak potential indicates that upon direct electrochemical reduction the overall kinetic process is controlled by the heterogeneous electron transfer step.[18] This was further demonstrated by plotting the CV peak potential *vs* the logarithm of the potential scan rate, leading to a 69 mV/decade slope, corresponding to $\alpha = 0.43$.[18] Therefore, variations of E^p with the potential scan rate cannot be used to get any information on the rate of the chemical (cleavage) step.[19] However, since the indirect reduction of $Fe(CO)_5$ by various anion radicals is controlled by the electron transfer step (see above), that cleavage must be fast compared to the backward SET, whose rate constant is close to the diffusion limit.

This provides a minimum value for the cleavage rate constant, k_1, under discussion. Indeed, k_1 must be at least 10 times higher than the backward homogeneous electron transfer:

$$k_1 \geq 10k_{dif}[M] \approx 10k_{dif}(\epsilon C^0_M)$$

where C^0_M is the concentration of the mediator and ϵ is a constant whose value has been determined to be 0.63.[19] It follows that k_1 is higher than *ca.* $3 \times 10^{10} C^0_M$. The experimental value for the concentration of the mediator being 2 mM, this condition shows that k_1 is larger than or equal to *ca.* 5×10^7 s^{-1}. Therefore, complete quenching of the intermediate $Fe(CO)_5^-$ by tributyltin hydride leads to a maximum value of this cleavage rate constant of 10^8 s^{-1}, whereas redox catalysis shows that the same rate constant is at least 5×10^7 s^{-1}. It can then be safely concluded that the cleavage rate constant is in the range of 0.5×10^8 to 1×10^8 s^{-1}, although it could not be determined precisely.

Assignment of Waves O_2 and O_3. The independent cyclic voltammograms of $Na_2Fe(CO)_4$[20] and $Na_2Fe_2(CO)_8$

(15) Andrieux, C. P.; Blocman, C.; Dumas-Bouchiat, J. M.; Savéant, J. M. *J. Am. Chem. Soc.* **1979**, *101*, 3431.

(16) The correlation line in Figure 2 corresponds to a kinetic regime in which the overall rate constant of the electron transfer is controlled by the diffusion of the products to form the postcomplex cage (*viz.*, that constituted by the pair $[Fe(CO)_5^-,M]$).[17] Under such circumstances, the overall rate constant is given by $k_{SET} = k_{dif} \exp(-\Delta G^0/RT)$, where $\Delta G^0 = F(E^0_M - E^0_{Fe(CO)_5}) \gg 0$ is the overall free enthalpy of the electron transfer between $M^{\bullet-}$ and $Fe(CO)_5$, *viz.*, corresponding to the left-hand side equilibrium in eq 5. Since $F/(RT \ln 10) \approx (1/60)$ mV^{-1} at 20 °C, such a formulation predicts (i) that log k_{SET} must depend on E^0_M with a slope of 1/60 mV^{-1} at 20 °C and (ii) that extrapolation of the corresponding plot at log k_{SET} = log k_{dif} corresponds to $E^0_M = E^0_{Fe(CO)_5}$.[17] These properties were used to evaluate $E^0_{Fe(CO)_5}$ on the basis of the construction in Figure 2 (solid lines). It is noteworthy that when $k_{SET} \approx k_{dif} \exp(-\Delta G^0/RT)$, the overall rate constant k_{SET} of the electron transfer is much smaller than the activation rate constant k_{act} that features the activation-controlled step of the sequence of events leading to electron transfer, *viz.*, that corresponding to the "true chemical" transformation of the reactant cage, $[Fe(CO)_5,M^{\bullet-}]$, into that of the products, $[Fe(CO)_5^-,M]$:[17]

$$1/k_{SET} = 1/k_{act} + 1/k_{dif}^{react} + [\exp(\Delta G^0/RT)]/k_{dif}^{prod}$$

where k_{dif}^{react} and k_{dif}^{prod} are the diffusion rate constants of formation of the reactant and product cages, respectively. Since the work terms corresponding to the formation of both cages from their free components are expected to be identical, one may safely consider that $k_{dif}^{react} \approx k_{dif}^{prod} = k_{dif}$.[17] Therefore, for $\Delta G^0 \gg 0$ and $k_{act} \gg k_{dif} \exp(-\Delta G^0/RT)$, one has

$$1/k_{SET} \approx \exp(\Delta G^0/RT)/k_{dif}$$

(17) For a detailed discussion of these aspects, see, *e.g.*: (a) Schlesener, C. J.; Amatore, C.; Kochi, J. K. *J. Am. Chem. Soc.* **1984**, *106*, 3567. (b) Amatore, C. In *Organic Electrochemistry*, 3rd ed.; Lund, H., Baizer, M. M., Eds.; Dekker: New York, 1991; pp 11–119. (c) Amatore, C.; Kochi, J. K. In *Advances in Electron Transfer Chemistry*; Mariano, P. S., Ed.; Jai Press Inc.: Greenwich, CT, 1991; Vol. 1, Chapter 3, pp 55–148.

(18) Bard, A. J.; Faulkner, R. L. *Electrochemical Methods*; J. Wiley and Sons: New York, 1980. For an irreversible electron transfer kinetics (transfer coefficient α), a slope of $30/\alpha$ mV/decade of log v is expected for peak potentials. From the experimental slope of 69 mV/decade, $\alpha = 30/69 = 0.43$.

(19) Alam, N.; Amatore, C.; Combellas, C.; Thiébault, A.; Verpeaux, J. N. *J. Org. Chem.* **1990**, *55*, 6347.

allowed us to assign the oxidation peaks O_2, O_3, and O_4 to the following processes:

wave O_2/R_2

$$Fe(CO)_4^{2-} - e \rightleftharpoons Fe(CO)_4^- \qquad E^0 = -1.89 \text{ V } vs \text{ Ag/Ag}^+$$

$$2Fe(CO)_4^- \rightarrow Fe_2(CO)_8^{2-} \qquad k \approx 5 \times 10^5 \text{ M}^{-1} \text{ s}^{-1}$$

wave O_3/R_3

$$Fe_2(CO)_8^{2-} - e \rightleftharpoons Fe_2(CO)_8^- \qquad E^0 = -1.62 \text{ V } vs \text{ Ag/Ag}^+$$

wave O_4

$$Fe_2(CO)_8^- - e \rightarrow Fe_2(CO)_8 \qquad E^p = -0.09 \text{ V } vs \text{ Ag/Ag}^+$$

$$Fe_2(CO)_8 \rightarrow etc.$$

Rate Constant for the Dimerization of Fe(CO)$_4^-$. Partial reversibility of wave O_2 is indicative of the stability of $Fe(CO)_4^-$ *vs* dimerization in this range of potential. Comparison of experimental cyclic voltammograms such as that of Figure 1, right, with simulated ones[21] at various concentrations and scan rates allowed an estimation of the rate constant for the dimerization of $Fe(CO)_4^-$: $k \approx 5 \times 10^5$ M^{-1} s^{-1}. This implies a lifetime of a few milliseconds for this intermediate in the millimolar concentration range at ambient temperature.

Formation of Fe(CO)$_4^{2-}$. The reduction potential of $Fe(CO)_5$ is much more negative ($E^p = -2.67$ V at 1 V s^{-1}) than the standard potential for the couple $Fe(CO)_4^-$/$Fe(CO)_4^{2-}$ ($E^0 = -1.89$ V). Due to such a driving force for reduction, dimerization of $Fe(CO)_4^-$ radicals generated at the reduction potential of $Fe(CO)_5$ cannot compete with further reduction to the dianion.[22] Therefore, the $Fe(CO)_4^{2-}$, which is oxidized at wave O_2, is necessarily produced at R_1 by an ECE process according to the sequence of eqs 1−3 in Scheme 1. This conclusion is further confirmed by the observation that wave R_1 involves an overall two-electron process (*vide infra*).

Formation of Fe$_2$(CO)$_8^{2-}$ under Reducing Conditions. Exhaustive electrolysis of iron pentacarbonyl in THF on the plateau of wave R_1 results in an overall one-electron consumption and a nearly quantitative formation of $Fe_2(CO)_8^{2-}$.[4] The considerations made so far, however, imply a two-electron process (ECE mechanism) and no formation of $Fe_2(CO)_8^{2-}$ at R_1.

To resolve this apparent contradiction, it was crucial to determine the absolute number of electrons, n, exchanged at wave R_1 to make sure that the reduction of $Fe(CO)_5$ is actually a two-electron process on the time scale of cyclic voltammetry. Slow follow-up reactions, inoperative during the short time scale of cyclic voltammetry ($t < 1$ s, $n = 2$ e), may well take place on the much longer time scale ($t > 0.5$ h) of preparative electrolysis and may lead to a different overall electron consumption ($n = 1$) because of the formation of a different reaction product, $Fe_2(CO)_8^{2-}$.

Another way to resolve the contradiction consists in establishing the origin of $Fe_2(CO)_8^{2-}$ oxidized at wave O_3. Since $Fe_2(CO)_8^{2-}$ cannot be formed by dimerization of $Fe(CO)_4^-$ while the electrode potential is located at wave R_1 (see above), it must originate *either* by dimerization of $Fe(CO)_4^-$ formed at wave O_2 *or* by the reaction that takes place during preparative electrolysis and consumes $Fe(CO)_4^{2-}$. Double-step chronoamperometry would allow us to make this distinction by establishing the relative amount of $Fe(CO)_4^{2-}$ and $Fe_2(CO)_8^{2-}$ produced in the diffusion layer when the electrode is polarized at wave R_1 during a short reaction time ($t < 1$ s).

Both approaches led to the conclusion that $Fe(CO)_4^{2-}$ is the reaction product at short reaction times (*vide infra*). Since the electrochemistry of $Cr(CO)_6$ presents the very same dichotomy (*vide infra*), we shall illustrate here the first approach based on the absolute determination of the number, n, of electrons consumed at R_1, reserving the second approach, based on double-step chronoamperometry, for the section devoted to $Cr(CO)_6$.

(a) Absolute Determination of the Number of Electrons, *n*, Exchanged at Wave R$_1$. It is an amazing fact that the absolute determination of the number of electrons exchanged at a voltammetric wave has remained until recently an open question. The fundamental reason for this difficulty is that in any transient or steady state microelectrolysis techniques, the current measured depends on two unknown parameters, n and the diffusion coefficient D. Comparison of the size of a wave with that of another compound (used as a standard) is of poor value since the two diffusion coefficients may be quite different.[11]

Recently, a technique for the absolute determination of n has been developed that relies on the comparison of the responses in chronoamperometry with those obtained under steady state conditions at an ultramicroelectrode[11] in the presence of a reference compound. Accordingly, we applied a series of potential steps of duration θ on the reduction wave R_1 and on the oxidation wave of ferrocene in the same solution and at the same electrode. After normalization to the same concentration

$$(i_{R_1}/i_{Fc})_{chrono} = n(D/D_{Fc})^{1/2} = 2.00 \pm 0.03$$

where n is the number of electrons consumed at R_1 and

(20) Direct electrochemical oxidation of $Fe(CO)_4^{2-}$ was performed in THF/HMPA (95/5 v/v) without supporting electrolyte[6] to avoid the rapid protonation of Collman's reagent by tetrabutylammonium cations (Hoffmann reaction).

(21) Simulations were performed using a multipurpose general program (explicit finite differences with exponentially expanding grids) developed by Gosser and kindly given to us by the author. For more details, see: Gosser, D. K., Jr.; Zhang, F. *Talanta* **1991**, *38*, 715. This program cannot incorporate rate constants of the order of magnitude of those corresponding to carbon monoxide expulsion from the 19-electron intermediates $Fe(CO)_5^-$ and $Cr(CO)_6^-$. Therefore, in the simulations, we took advantage of the fact that the reduction waves of $Fe(CO)_5$ and $Cr(CO)_6$ are controlled by the kinetics of the first electron transfer (reaction 1 or 1′)[18] and not by the follow-up chemical step (reaction 2 or 2′). Therefore, the rate constants corresponding to reactions 2 and 2′ were introduced in the simulations with sufficiently large values with respect to the scan rate (*viz.*, such that $k = 100RT/Fv$)[17b] but not at the true values that should correspond to estimated lifetimes of *ca.* 10 ns for $Fe(CO)_5^-$ or between 10 ns and 50 μs for $Cr(CO)_6^-$ 19-electron intermediates. We verified that the simulations of the R_1 and O_2/R_2 waves were not affected by the values of these rate constants, as expected,[17b,18] by varying them between $50RT/Fv$ and $500RT/Fv$.

(22) Dimerization of a reducible species cannot compete significantly with its reduction. This would be true even if the dimerization rate constant were diffusion controlled (see: Amatore, C.; Savéant, J. M. *J. Electroanal. Chem.* **1981**, *125*, 1). A value of 5×10^5 M^{-1} s^{-1} determined here makes a dimerization even less possible at such a negative potential.

the D's are the respective diffusion coefficients. A similar series of experiments at a gold microdisc electrode (10 μm diameter), where steady state conditions prevailed, gave

$$(i_{R_1}/i_{Fc})_{stst} = nD/D_{Fc} = 2.05$$

The determination of n and D can then be made by solving the two equations. This gives $n = 1.95 \pm 0.06$ and $D/D_{Fc} = 1.05 \pm 0.05$. Since $D_{Fc} = 8.0 \times 10^{-6}$ cm^2 s^{-1} under these experimental conditions,[11] $D = 8.4 \times 10^{-6}$ cm^2 s^{-1}.

The foregoing shows that the reduction of $Fe(CO)_5$ is indeed a two-electron process on the time scale of cyclic voltammetry, *i.e.*, for characteristic times from 5 to 500 ms, yielding $Fe(CO)_4^{2-}$ whatever the potential scan rate.[23] We conclude that the follow-up reaction transforming $Fe(CO)_4^{2-}$ into $Fe_2(CO)_8^{2-}$ on the time scale of preparative electrolysis, leading to a decrease from 2 to 1 electron/mol of iron pentacarbonyl, does not take place on the time scale of cyclic voltammetry. The observation of an oxidation wave O_3 for $Fe_2(CO)_8^{2-}$ under CV conditions (Figure 1) is then the result of the rapid dimerization of $Fe(CO)_4^-$ formed at wave O_2 by oxidation of $Fe(CO)_4^{2-}$ when the anodic scan is performed.

(b) Coupling Reaction between $Fe(CO)_4^{2-}$ and $Fe(CO)_5$. From the foregoing it is clear that the $Fe_2(CO)_8^{2-}$ observed in CV and in preparative scale electrolysis results from two different mechanisms. That observed in CV (wave O_3) is formed entirely by dimerization of $Fe(CO)_4^-$ generated at wave O_2 when the diffusion layer content is examined during the anodic scan, whereas the $Fe_2(CO)_8^{2-}$ produced under electrolysis conditions with the potential kept constant at the plateau value of wave R_1 must be formed by another mechanism. The most likely process is a slow reaction (compared to the time scale of CV) involving $Fe(CO)_4^{2-}$ and unreacted $Fe(CO)_5$. This reaction, which is indeed used as a convenient chemical route to $Na_2Fe_2(CO)_8$,[8] explains the overall consumption of 1 F in the exhaustive electrolysis, since one half of the starting $Fe(CO)_5$ is reduced using 2 electrons/mol, and the other half is consumed in a zero-electron chemical reaction.

$$Fe(CO)_4^{2-} + Fe(CO)_5 \rightarrow Fe_2(CO)_8^{2-} + CO$$

The fact that this reaction does not occur on the time scale of slow cyclic voltammetry ($t \leq 1$s) for a 2 mM solution of $Fe(CO)_5$ implies that its rate constant must be less than a few hundred M^{-1} s^{-1}.[12]

The kinetics of reaction 4 can be monitored by infrared stopped-flow techniques (see Experimental Section). A fresh solution of $[Fe(CO)_4^{2-}][NBu_4^+]_2$, obtained by rapid exhaustive electrolysis of a $Fe(CO)_5$ solution through a flow cell, was reacted with an excess of $Fe(CO)_5$. The reaction kinetics was followed by the decay of the characteristic IR band at 1740 cm^{-1} of $[Fe(CO)_4^{2-}][NBu_4^+]_2$ and by the growth of the bands at 1860 and 1910 cm^{-1} of $[Fe_2(CO)_8^{2-}][NBu_4^+]_2$ (see Experimental Section and Figure 3). The rate constant obtained by infrared stopped flow is 120 ± 20 M^{-1} s^{-1} in THF. This rate is significantly faster than the rate determined by Atwood[9] for the related sodium derivative in acetonitrile but much slower than the erroneous one we reported previously.[6,23] The non-ion-paired $Fe(CO)_4^{2-}$ formed here is expected to be a stronger nucleophile than the sodium ion-paired species; the solvent may also play a crucial role in the course of the reaction.

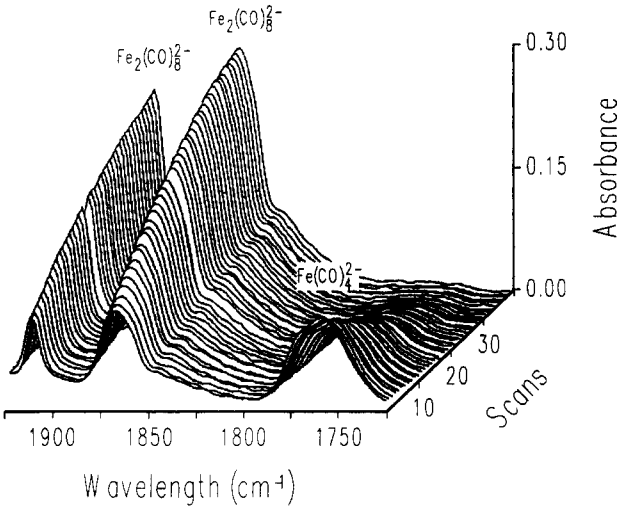

Figure 3. IR spectra recorded in rapid scanning mode during a stopped-flow experiment when a 0.5 mM solution of $Fe(CO)_4^{2-}$ in THF containing 0.1 M NBu_4BF_4, was mixed with a 5 mM solution of $Fe(CO)_5$ in the same solvent at 20 °C (see text and Experimental Section). Consumption of $Fe(CO)_4^{2-}$ and concomitant formation of $Fe_2(CO)_8^{2-}$ are monitored as a function of time.

The experimental value of 120 M^{-1} s^{-1}, determined above, can be compared with the predicted value for the rate constant of a pure electron transfer to $Fe(CO)_5$ from an outer-sphere reductant with a standard potential of $E^0 = -1.89$ V (*i.e.*, identical to that of $Fe(CO)_4^{2-}$). Such a comparison should allow a choice between a SET mechanism or an inner-sphere nucleophilic process for the coupling reaction under discussion. It can be seen in Figure 2 that the experimental point corresponding to the rate of the coupling between $Fe(CO)_4^{2-}$ (tetraalkylammonium countercation) and $Fe(CO)_5$ lies well above the straight line representing the correlation between E^0 of various aromatic anion radicals and log k_{SET}. In other words, the observed reaction is about 100 times faster than that expected for a diffusion-controlled electron transfer between these two species, indicating that an outer-sphere SET mechanism must be ruled out for our non-ion-paired dianion. Therefore, reaction 4 involves important innersphere contributions as appropriate for a nucleophilic substitution.[24]

Finally, it was important, from a synthetic point of view, to measure the rate of the reaction between $[Fe(CO)_4^{2-}][n\text{-}Bu_4N^+]_2$ and the medium, namely THF containing 0.1 M $[n\text{-}Bu_4N^+][BF_4^-]$. It was found by infrared stopped-flow techniques that the product of this reaction is $HFe(CO)_4^-$ (identified by its absorption at 1881 cm^{-1}, see Experimental Section) and that the half-life of the reaction is 130 s. This means that protonation of $Fe(CO)_4^{2-}$ by this medium can be neglected if the Fe-

(23) In our preliminary communication,[6] we used a classical calibration method to evaluate n, which led us to conclude that the number of electrons exchanged at R_1 was dependent on the potential scan rate. From this dependence, we then derived an erroneous value for the rate constant of the coupling reaction between $Fe(CO)_4^{2-}$ and $Fe(CO)_5$. We know now that this erroneous result was due to undetected fouling of the electrode surface, probably due to adsorption of CO generated upon cleavage of $Fe(CO)_5^-$ (eq 2). For this reason, the greatest care has been taken in this study to check the absence of any electrode fouling, and the electrode was repolished between each CV or each chronoamperometric experiment.

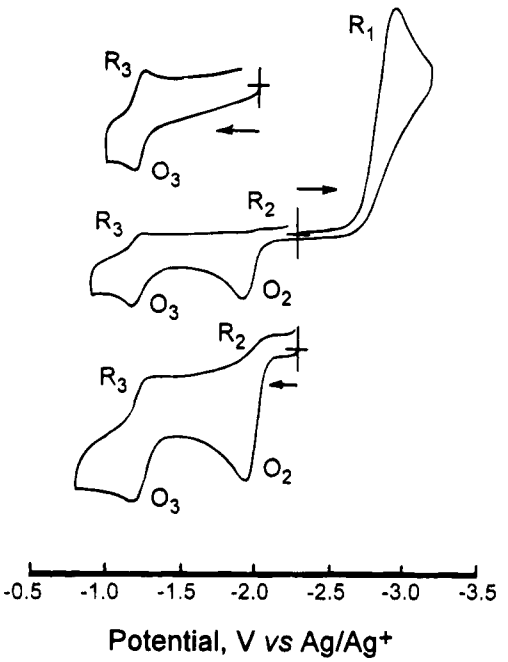

Figure 4. (Middle) Cyclic voltammetry of 2 mM $Cr(CO)_6$ at 10 V s^{-1}. (Bottom) Cyclic voltammetry of 2 mM $K_2Cr(CO)_5$, at 10 V s^{-1}. (Top) Cyclic voltammetry of 1 mM $Na_2Cr_2(CO)_{10}$ at 1 V s^{-1} [26] in THF (containing 0.3 M NBu_4BF_4) at 20 °C. Gold disk electrode, 0.5 mm diameter.

$(CO)_5$ concentration is in the millimolar range or greater, as it is much slower than the coupling with iron pentacarbonyl in reaction 4. The protonation reaction is sufficiently fast, however, to prevent the direct electrochemical investigation of the redox behavior of $Fe(CO)_4^{2-}$ in this medium[20] since the preparative of an electrochemical experiment obviously requires more than 2 min.

Electrochemical Reduction of Cr(CO)$_6$ and Electrogeneration of Cr(CO)$_5^{2-}$. The electrochemical reduction of chromium hexacarbonyl has been the subject of previous investigations.[25] It was concluded that the chemically irreversible reduction produces the 17-electron $Cr(CO)_5^-$ radical anion via rapid loss of CO from the initially formed 19-electron $Cr(CO)_6^-$ and that this radical is sufficiently stable ($t_{1/2}$ > 1s) to be detected by its oxidation wave upon scan reversal in cyclic voltammetry. On the longer time scale of exhaustive electrolysis, it was found that the final product was $Cr_2(CO)_{10}^{2-}$, thought to arise by dimerization of the $Cr(CO)_5^-$ radical anions. Because of the apparent similarity of this case with the preceding one, we decided to reinvestigate the cyclic voltammetry of $Cr(CO)_6$ in THF.

The cyclic voltammogram of $Cr(CO)_6$ at 10 V s^{-1} in THF is very reminiscent of that of $Fe(CO)_5$ (Figure 4, middle). The chemically irreversible reduction at R_1 is followed, on scan reversal, by two oxidation waves O_2 and O_3. Associated reduction peaks R_2 and R_3 are visible on the second cathodic scan, indicating that both waves O_2 and O_3 are chemically partially reversible. Assignments of the couples O_2/R_2 and O_3/R_3 were made by independent cyclic voltammetry of authentic samples of $M_2Cr(CO)_5$ (M = Na, K) and $Na_2Cr_2(CO)_{10}$ (*cf.* Figure 4 bottom and top):

wave O_2/R_2

$$Cr(CO)_5^{2-} - e \rightleftharpoons Cr(CO)_5^- \qquad E^0 = -2.00 \text{ V } vs \text{ Ag/Ag}^+$$

$$2Cr(CO)_5^- \rightarrow Cr_2(CO)_{10}^{2-} \qquad k \approx 5 \times 10^5 \text{ M}^{-1} \text{ s}^{-1}$$

wave O_3/R_3

$$Cr_2(CO)_{10}^{2-} - e \rightleftharpoons Cr_2(CO)_{10}^- \qquad E^0 = -1.22 \text{ V } vs \text{ Ag/Ag}^+$$

The $Cr(CO)_5^-$ radical anion generated upon oxidation of $Cr(CO)_5^{2-}$ at O_2 undergoes a fast dimerization to yield $Cr_2(CO)_{10}^{2-}$, which is then observed at O_3. As in the case of iron pentacarbonyl, simulation[21] of the pertinent series of voltammograms as a function of potential scan rate and concentration allowed us to estimate a rate of dimerization of about 5×10^5 M^{-1} s^{-1}, identical within experimental error to the corresponding rate for $Fe(CO)_4^-$. No special attempts have been made to characterize kinetically the O_3/R_3 wave reversibility.[26]

No reversibility could be observed for wave R_1 even at scan rates in the 10^3–10^4 V s^{-1} range. The initially

(24) In the formulation used in footnote 16, $\Delta G^0 = F(E^0_M - E^0_{Fe(CO)_5})$. The fact that for reaction 4, the rate constant is about 100 times larger than expected for an endoergonic diffusion-controlled electron transfer implies that ΔG^0_4 for reaction 4 is less than it would be for an electron transfer. Assuming that k_{dif} values are comparable for both reactions, a rather reasonable hypothesis, and that reaction 4 is still under diffusion control, one has

$$\Delta G^0_4 \approx F(E^0_{Fe(CO)_4^{2-}} - E^0_{Fe(CO)_5}) - RT \ln 100$$

ΔG^0_4 would be even smaller if reaction 4 is under activation control or mixed diffusion/activation control.[17] Therefore, the product(s) of reaction 4 correspond to a system that is at least $RT \ln 100 \approx 2.7$ kcal/mol (11.4 kJ/mol) more stable than that which would result from an electron transfer, *viz.*, $Fe(CO)_4^- + Fe(CO)_5^-$. However, one cannot decide if this reaction corresponds to a "true" nucleophilic substitution, *viz.*, where the carbon monoxide ligand has already been expelled, or simply to a chemical interaction between the two paramagnetic iron centers, yet without carbon monoxide expulsion.

(25) (a) Pickett, C. J.; Pletcher, D. *J. Chem. Soc., Dalton Trans.* **1976**, 749. (b) Seurat, A.; Lemoine, P.; Gross, M. *Electrochim. Acta* **1978**, *23*, 1219.

(26) The O_3/R_3 wave shown in Figure 4, top (obtained using an authentic sample of $[Na^+]_2[Cr_2(CO)_{10}^{2-}]$) is nearly completely reversible, even at the slowest scan rates (1 V s^{-1} or less), while waves O_3/R_3 appear much less reversible (even at a higher scan rate of 10 V s^{-1}!) in Figure 4, middle and bottom, suggesting at first glance a considerable stability for the $[Na^+][Cr_2(CO)_{10}^-]$ anion radical *vis à vis* its tetrabutylammonium analogue. However, this cannot be rationalized so easily, since it should be kept in mind that the electrochemistry of $[Na^+]_2[Cr_2(CO)_{10}^{2-}]$ (Figure 4, top) was performed in the presence of a large excess of $[NBu_4^+][BF_4^-]$ supporting electrolyte. Tentative interpretations including countercation effect (effect of Na^+ under the conditions of Figure 4, top) may be considered but would require additional investigations (under our electrochemical conditions). Conceivably, the stability of $Cr_2(CO)_{10}^-$ anion radicals may depend critically on the presence in the diffusion layer of "remnants" of other oxidation processes that occur simultaneously (*e.g.*, $Cr(CO)_5^-$ that is still formed on the plateau of wave O_2 while wave O_3/R_3 is scanned). Obviously, such complications are absent when one starts from an authentic solution of $Cr_2(CO)_{10}^{2-}$ as in Figure 4, top. In agreement with this second interpretation, the extents of chemical reversibility of the O_3/R_3 wave in Figure 4, middle and bottom, are comparable. Finally, it is noteworthy that diffusional effects may also be partly responsible for an apparent decrease in the reversibility of O_3/R_3 in Figure 4, middle and bottom. Indeed, diffusional removal from the electrode vicinity is expected to be less when starting from a solution of $Cr_2(CO)_{10}^{2-}$ than when starting from $Cr(CO)_6$ or $Cr(CO)_5^{2-}$. For a discussion on the effect of diffusion on removal–replenishment of the diffusion layer and therefore on the size of voltammetric waves, see: Guedes Da Silva, M. F. C.; Frausto Da Silva, J. J. R.; Pombeiro, A. J. L.; Amatore, C.; Verpeaux, J. N. *Organometallics* **1994**, *13*, 3943. Based on these considerations and on the fact that such a study would not be strictly relevant to the present work, we did not undertake a quantitative investigation of the kinetics involved at wave O_3/R_3.

formed 19-electron $Cr(CO)_6^-$ anion radical has therefore a lifetime of less than 50 μs. In spite of its short life, this intermediate can also be intercepted in the presence of tributyltin hydride to give the corresponding formyl derivative.[13] As indicated above for $Fe(CO)_5^-$,[14] this implies that the lifetime of $Cr(CO)_6^-$ must also be more than a few tens of nanoseconds. On the much longer time scale of cyclic voltammetry, this anion radical loses CO. Here also an ECE process (reactions 1′–3′ in Scheme 2) takes place because the potential at which the 17-electron $Cr(CO)_5^-$ anion radical is formed is much more negative than its standard reduction potential.

Scheme 2

$$Cr(CO)_6 + e \rightleftharpoons Cr(CO)_6^- \quad (1')$$

$$Cr(CO)_6^- \rightarrow Cr(CO)_5^- + CO \quad (2')$$

$$Cr(CO)_5^- + e \rightleftharpoons Cr(CO)_5^{2-} \quad (3')$$

$$Cr(CO)_6 + Cr(CO)_5^{2-} \rightarrow Cr_2(CO)_{10}^{2-} + CO \quad (4')$$

As in the electrochemistry of iron pentacarbonyl, we are faced with a dichotomy regarding the formation of $Cr_2(CO)_{10}^{2-}$, which is observed at O_3: it may be produced exclusively by dimerization of $Cr(CO)_5^-$ anion radicals formed at O_2 only,[22] or there may be also a contribution of a coupling reaction between $Cr(CO)_5^{2-}$ and $Cr(CO)_6$ (reaction 4′ in Scheme 2).

This question can be settled by determining the absolute number of electrons, n, exchanged at wave R_1 as described in the previous section. Observation of a bielectronic reduction wave would rule out any significant interference by reaction 4′ at wave R_1 during CV or chronoamperometric experiments. We wish to show in the following that double-step chronoamperometry can also provide the answer by the quantitative determination of (i) the current associated with wave O_2 and (ii) the cumulative current associated with O_2 and O_3.

In a first series of experiments, the initial potential step of duration θ is set on the plateau of wave R_1, while the second step of identical duration θ, which follows immediately after the first one, is set at a potential between waves O_2 and O_3. A series of anodic currents $i_{1a}(\theta)$ is then determined as a function of the pulse duration θ. In a second series of experiments, the first step is as before, but the second potential step is now set on the plateau of wave O_3. A second series of anodic currents $i_{2a}(\theta)$ is then measured so that the ratio $R_e(\theta) = i_{2a}(\theta)/i_{1a}(\theta)$ can be evaluated for each value of θ. Since the two oxidation processes at O_2 and O_3 are monoelectronic, $R_e(\theta)$ is given by

$$R_e(\theta) = 1.5 + 0.5[y_\theta/(1 - y_\theta)]$$

where y_θ is the yield of $Cr_2(CO)_{10}^{2-}$ that may be formed during the cathodic pulse of duration θ at wave R_1 according to the following balanced equation:

$$Cr(CO)_6 + (2 - y_\theta)e \rightarrow (1 - y_\theta)Cr(CO)_5^{2-} + (y_\theta/2)Cr_2(CO)_{10}^{2-} + CO$$

The experimental value of $R_e(\theta)$ was found to be constant within the accuracy of the measurements (1 ms $\leq \theta \leq$ 500 ms) and equal to 1.5, indicating that the yield of $Cr_2(CO)_{10}^{2-}$ is negligible at wave R_1 (*viz.*, $y_\theta \ll 1$). We conclude that all the $Cr_2(CO)_{10}^{2-}$ observed at wave O_3 on this time scale originates from the dimerization of $Cr(CO)_5^-$ formed at O_2.

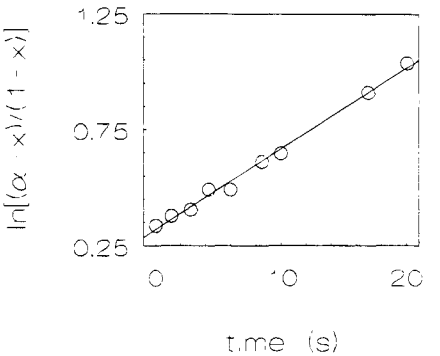

Figure 5. Variations of the concentration of (2/α) mM $Cr(CO)_5^{2-}$ in THF (containing 0.3 M NBu_4BF_4), monitored by cyclic voltammetry in the presence of 2 mM $Cr(CO)_6$ (see text and Experimental Section) at 20 °C. $x = [Cr(CO)_5^{2-}]/[Cr(CO)_5^{2-}]_0$. The time in seconds on the horizontal axis refers to an arbitrary origin. Regression line: correlation coefficient, 0.9965; k = 0.95 M^{-1} s^{-1}; α = 1.4.

According to the foregoing, the final product of electrolysis of $Cr(CO)_6$ should be $Cr(CO)_5^{2-}$, with a net consumption of 2 F/mol. Since the final product in exhaustive electrolysis is in fact $Cr_2(CO)_{10}^{2-}$,[25] a coupling reaction between chromium hexacarbonyl and pentacarbonylchromate dianion must be operative on the longer time scale of preparative electrolysis (reaction 4′).

The rate of this bimolecular reaction (reaction 4′) was found to be significantly smaller than that of its analogue involving iron pentacarbonyl and tetracarbonylferrate dianion (reaction 4). The corresponding kinetics could then be investigated by monitoring the decay of the peak currents at O_2 in the cyclic voltammogram of a solution of $Na_2Cr(CO)_5$ (*cf.* Figure 4, bottom) as a function of time after the addition of $Cr(CO)_6$. The required amount of sodium pentacarbonylchromate ($Na_2Cr(CO)_5$) to form a 2 mM solution was dissolved in THF containing an excess (0.3 M) of tetrabutylammonium tetrafluoroborate. An equimolar amount of chromium hexacarbonyl was added to this solution at time zero, and cyclic voltammograms were recorded every few minutes. Measurement of the peak current of wave O_2, which is proportional to the concentration of $Cr(CO)_5^{2-}$, allowed us to plot the ratio $[Cr(CO)_5^{2-}]/[Cr(CO)_5^{2-}]_0$ as a function of time. Kinetic treatment of the data (see Figure 5) was complicated by the fact that some of the initial $Cr(CO)_5^{2-}$ very rapidly reacted with traces of acidic or electrophilic impurities. This reaction occurred only during the initial stages of the experiment, due to a rapid titration of the acidic impurities. To avoid kinetic interferences between reaction 4 and the rapid protonation of $Cr(CO)_5^{2-}$, $Cr(CO)_6$ (1 equiv) was added after completion of this reaction, indicated by the observation of a constant oxidation peak current for $Cr(CO)_5^{2-}$. However, this led to an underestimation (a few tens percent) of the concentration, $[Cr(CO)_5^{2-}]_0$, of the chromate dianion at time zero (that is, at the time when $Cr(CO)_6$ was added) and therefore to an underestimation of the real ratio $[Cr(CO)_6]_0/[Cr(CO)_5^{2-}]_0$. Taking these com-

plications into account and using a double regression procedure, the rate constant of reaction 4′ was found to be $k = 0.95 \pm 0.05\ M^{-1}\ s^{-1}$ (see Experimental Section).

Electron Spin Resonance of Radical Intermediates. In this section we summarize briefly the ESR properties of the radical intermediates in the electrochemical reduction of iron and chromium carbonyls.

The anisotropic ESR spectrum of the 19-electron $Fe(CO)_5^-$ radical anion has been observed at 20 K in γ-irradiated single crystals of $Cr(CO)_6$ doped with $Fe(CO)_5$.[27] A careful analysis of the g-, ^{57}Fe-, and ^{13}C-tensors and of the orientations of their principal axes showed that this radical is essentially an organic acyl radical (principal g values, 1.9894, 2.0026, and 2.0103; $g_{av} = 2.0008$), with the unpaired electron residing mostly in an sp^2 hybrid orbital of the apical carbon in a square pyramidal structure. The apical Fe−C−O bond is strongly bent (≈120°). Isotopic labeling with ^{13}C revealed that only one of the five carbons has a large ^{13}C hyperfine interaction (principal values, 94.2, 70.3, 75.5 G; average, 80.0 G), appropriate for the acyl carbon with the unpaired electron in an orbital of large s character. The rapid loss of CO in solution by this radical intermediate is therefore analogous to the decarbonylation of an organic acyl radical. Like organic acyl radicals, it is capable of abstracting weakly bonded hydrogen atoms to form a formyl derivative. As in many other 19-electron species, the 19th electron in $Fe(CO)_5^-$ resides mostly on a ligand. MO calculations are in accord with the bent acyl radical structure for $Fe(CO)_5^-$.[28] No ESR information is available for the analogous 19-electron $Cr(CO)_6^-$ radical anion. A similar bent acyl radical structure with the 19th electron on a CO ligand appears inevitable, however, since this radical can also be intercepted by tri-*n*-butyltin hydride to give $Cr(CO)_5CHO^-$.[13]

The isotropic solution ESR spectrum of the $Fe(CO)_4^-$ radical anion, isoelectronic with the $Co(CO)_4$ radical, was observed by UV photolysis of dilute THF/2-MeTHF solutions of $Na_2Fe_2(CO)_8$ (0.005 M) below −80 °C as a single absorption with a g value of 2.0486 and a temperature-dependent line width (4.7 G at −110 °C and 8.7 G at −90 °C).[29] The spectrum decays on shuttering the light with a half-life that is temperature dependent: 2 s at −80 °C and 16 s at −120 °C. If the solution is frozen to a glass by lowering the temperature to −170 °C without interruption of the irradiation, the powder spectrum of $Fe(CO)_4^-$ is obtained corresponding to an axial g tensor ($g_\perp = 2.0707$, $g_\parallel = 2.0039$, $g_{av} = 2.0484$). ^{13}C labeling of the starting $Fe_2(CO)_8^{2-}$ dianion provided no additional information since it led to very broad solution and solid state spectra.

An axial g tensor with $g_\parallel$ very close to the free spin value ($g_e = 2.002\ 32$), and $g_\perp$ shifted to a higher value is expected by first-order spin−orbit interaction treatment in the case of axial symmetry for an electron residing in a d_{z^2} orbital.[30] This is consistent with a trigonal pyramidal geometry of C_{3v} symmetry for the $Fe(CO)_4^-$ radical which has also been established by an IR analysis for $Fe(CO)_4^-$ isolated in an inert gas matrix at 10 K.[31] MO considerations show that for an $M(CO)_4$ fragment of C_{3v} symmetry and a d^9 electron count, the odd electron occupies a highly directional a_1 (d_{z^2}) orbital pointing in the opposite direction of the apical CO ligand.[32] The radical is thus prepared for easy dimerization, yielding the $Fe_2(CO)_8^{2-}$ dimer, whose structure (with a single Fe−Fe bond) is indeed made up of the union of two trigonal pyramidal fragments.[33] The ESR data for $Fe(CO)_4^-$ are in agreement with a recent theoretical study of this radical.[34]

Because of its stability and ease of formation, the $Fe_2(CO)_8^-$ radical anion is ubiquitous as an impurity in solutions of many iron carbonylate anions and can be recognized by its single ESR absorption in solution with $g_{iso} = 2.0385$.[35] It is best formed by oxidation of the $Fe_2(CO)_8^{2-}$ dianion with ferrocenium tetrafluoroborate. In a 2-MeTHF glass at −170 °C, it displays a nearly axial g-tensor (2.0557, 2.0501, 2.0094).[36] Two single-crystal ESR studies led to the conclusion that the radical in its most stable form has two bridging CO ligands.[36,37] The presence of bridging ligands in $Fe_2(CO)_8^-$ in solution is also confirmed by the infrared spectrum, which shows a characteristic vibration at 1730 cm^{-1}.[36]

The solution ESR spectrum of the $Cr(CO)_5^-$ radical anion, isoelectronic with the $Mn(CO)_5$ radical, was obtained by *in situ* UV irradiation of THF solutions of $K_2Cr_2(CO)_{10}$ as a single absorption with $g = 2.0143$ and a peak-to-peak line width of only 0.8 G at −95 °C.[29] When the light is shut off, the absorption decays with a half-life of 5 s following second-order kinetics. At higher temperatures, the intensity decreases rapidly, as does the decay time. At −45 °C, the half-life is only 0.7 s. Enrichment of $Cr_2(CO)_{10}^{2-}$ with ^{13}C afforded under the same conditions a multiplet of 11 lines attributed to the superposition of the spectra of six $Cr(^{13}CO)_n(CO)_{5-n}$ radicals with $n = 0-5$ in statistically determined abundances having a ^{13}C splitting of 6.86 G for five equivalent CO ligands. The equivalence of five CO ligands was attributed to the high fluxional nature of the radical in solution characteristic of five-coordinate structures that can interchange rapidly between square pyramidal and trigonal pyramidal structures.

The powder spectrum of the $Cr(CO)_5^-$ radical anion was obtained by freezing a 2-MeTHF solution of the $Cr_2(CO)_{10}^{2-}$ dianion to a glass while it was irradiated with UV light.[29] The resulting spectrum was appropriate for an axially symmetric g-tensor with principal components $g_\perp = 2.0205$ and $g_\parallel = 2.001\ 95$ ($g_{av} = 2.0143$). These values are in excellent agreement with the g-tensor established for the $Cr(CO)_5^-$ radical in γ-irradiated single crystals of $PPN^+HCr(CO)_5^-$.[38] A g-tensor with $g_\parallel \approx g_e$ and $g_\perp$ shifted to higher values is

(27) Fairhurst, S. A.; Morton, J. R.; Preston, K. F. *J. Chem. Phys.* **1982**, *77*, 5872.
(28) Anderson, A. B.; Kang, D. B. *Inorg. Chem.* **1984**, *23*, 1170.
(29) Krusic, P. J.; Subra, R., to be published.
(30) Reuveni, A.; Malatesta, V.; McGarvey, B. R. *Can. J. Chem.* **1977**, *55*, 70.
(31) Breeze, P. A.; Burdett, J. K.; Turner, J. J. *Inorg. Chem.* **1981**, *20*, 3369.
(32) Elian, M.; Hoffmann, R. *Inorg. Chem.* **1975**, *14*, 1058.
(33) Chin, H. B.; Smith, M. B.; Wilson, R. D.; Bau, R. *J. Am. Chem. Soc.* **1974**, *96*, 5282.
(34) Grand, A.; Krusic, P. J.; Noodleman, L.; Subra, R. *Mol. Struct.* **1991**, *226*, 251.
(35) Krusic, P. J.; San Filippo, J., Jr.; Hutchinson, B.; Hance, R. L.; Daniels, L. M. *J. Am. Chem. Soc.* **1981**, *103*, 2129.
(36) Morton, J. R.; Preston, K. F.; Le Page, Y.; Krusic, P. J. *J. Chem. Soc., Faraday Trans. 1* **1989**, *85*, 4019.
(37) Krusic, P. J.; Morton, J. R.; Preston, K. F.; Williams, A. J.; Lee, F. L. *Organometallics* **1990**, *9*, 697.
(38) Hynes, R. C.; Preston, K. F.; Springs, J. J.; Williams, A. J. *Organometallics* **1990**, *9*, 2298.

expected for an odd electron in a d_{z^2} orbital (see above). This is the orbital that is singly occupied according to the d orbital scheme predicted for a square pyramidal $M(CO)_5$ fragment of C_{4v} symmetry with a d^7 electron count.[32] By admixture of s and p character, as in the isoelectronic and isostructural $Mn(CO)_5$ radical,[32] the unpaired electron is in a highly directional orbital (a_1), pointing in the opposite direction of the apical CO ligand of the square pyramidal structure. The radical is thus ready for dimerization to yield $Cr_2(CO)_{10}^{2-}$, whose structure is indeed the result of the union of two square pyramidal fragments.[39]

Conclusion

We have shown that the reduction of iron and chromium carbonyls involves 2 electrons/mol via ECE-type mechanisms, leading to the electrogenerated metalate complexes $Fe(CO)_4^{2-}$ and $Cr(CO)_5^{2-}$. These dianionic species react with the parent compounds $Fe(CO)_5$ and $Cr(CO)_6$ to yield the corresponding binuclear dianions $Fe_2(CO)_8^{2-}$ and $Cr_2(CO)_{10}^{2-}$ upon nucleophilic displacement of one CO ligand. The latter reactions are sufficiently slow not to interfere with the course of several more useful chemical sequences.[1,2] Among these is the alkylation of the metalate complexes that is expected to take place when the electrolysis is carried out in the presence of an added electrophile, *e.g.*, an organic halide. An important consequence is therefore the possibility of an *in situ* electrogeneration of Collman-type anions from easily available iron and chromium carbonyls and their subsequent use as carbonylation reagents. The scope and limits of this approach are presently under investigation.

Experimental Section

Chemicals. All reactants were of commercial origin. Products were identified by their reported IR spectra (see text). THF and acetonitrile (ACN) were distilled and stored under argon prior to use. Supporting electrolyte was prepared by precipitation from a solution of tetrabutylammonium hydrogen sulfate and sodium tetrafluoroborate. It was washed, recrystallized, and dried under vacuum. It was stored under argon prior use.

General Experimental Setup. Cyclic voltammetric and chronoamperometric experiments were carried out in a glovebox (continuously regenerated nitrogen atmosphere, Jacomex), using a home-built potentiostat allowing IR compensation through positive feedback at faster potential scan rates.[40] The potential wave forms were provided by a EGG-PAR Model 175 signal generator, except for ultrafast cyclic voltammetry,[41] where a HP 3314A was used. A digital oscilloscope (Nicolet 3091 or 4094C/4180 for ultrafast cyclic voltammetry) was used to store digitally the voltammograms or chronoamperograms and to measure their current and/or potential characteristics. The working electrodes were circular cross sections of gold wires of either 0.125 mm diameter (for fast scan rates or short times) or 0.50 mm diameter (for slower scan rates or long times) sealed in Pyrex, polished with alumina. For steady state experiments or ultrafast cyclic voltammetry, 10 and 50 μm diameter gold disc electrodes were used to minimize ohmic drop and time constants, respectively.[41] The counter electrode was a platinum wire spiral of approximately 1 cm^2 effective area. The reference electrode was a $Ag/AgBF_4$ (0.02 M) electrode (Tacussel) in THF containing $[nBu_4N^+][BF_4^-]$ (0.3 M). Using such a reference electrode, the standard potential, E^0_{Fc/Fc^+}, for the ferrocene/ferrocenium couple was −0.225 V. We determined $E^0_{Fc/Fc^+} = +0.565$ V *vs* SCE (Tacussel SCE reference electrode) in this same medium; hence, one can infer potentials *vs* SCE by adding +0.79 V to the values given here. The cell required 10 mL of test solution and 2 mL of supporting electrolyte solution for the side arm bridge compartment segregating the reference electrode from the test solution by means of two fine frits. $[nBu_4N^+][BF_4^-]$ was used as supporting electrolyte, and the concentration of the active substrate was 2 mM, except when stated otherwise.

Redox Catalysis Experiments. Determination of Standard Potential of $Fe(CO)_5$ and Estimation of the Lifetime of $Fe(CO)_5^-$. The voltammetric cell was filled with 10 mL of THF containing 0.3 M $[nBu_4N^+][BF_4^-]$. The mediator, an aromatic compound (see text and Figure 2), was added, leading to a 2.0 mM solution. The working electrode was a 0.3 mm diameter gold disc electrode. The normalized peak currents $I_{p,r}/v^{1/2}$, where $I_{p,r}$ is the measured peak reduction current for the chemically reversible redox system of the aromatic compound and its anion radical, and v is the scan rate, were determined for scan rates in the interval 0.1−10 V s^{-1}. The normalized currents for each mediator were found to be constant within the accuracy (a few percent) of their measurements. $Fe(CO)_5$ was then added in 2.5−5-fold excess relative to the mediator, and the catalytic peak current of the mediator was measured from scan rates equal to 0.02 up to 100 V s^{-1} or up to the smallest scan rate, regenerating a reversible voltammogram for the mediator. The rate constant, k_{SET}, of the single electron transfer reaction between the aromatic anion radical and $Fe(CO)_5$ could then be determined by plotting the logarithm of the normalized catalytic peak current of the mediator ($\log I_{p,c}/I_{p,r}$) against the logarithm of the scan rate and by comparison with simulated working curves.[15] Working curves were generated by explicit finite difference methods and corresponded to a classical redox catalysis situation.[15]

Determination of the Absolute Number of Electrons[11] Involved in the Initial Reduction of $Fe(CO)_5$. (a) Chronoamperometric Measurements. The voltammetric cell was filled with 10 mL of THF containing 0.3 M $[nBu_4N^+][BF_4^-]$; $Fe(CO)_5$ (3.92 mg, leading to a 2.0 mM solution) and ferrocene (7.72 mg, leading to a 4.15 mM solution) were added. The working electrode was a 0.125 mm diameter gold disc. The rest electrode potential was −2.1 V. At time zero, the electrode potential was set at −3.0 V (*i.e.*, on the plateau of wave R_1), and the current was measured after a duration time θ. The potential was then stepped back to −2.1 V. After the solution was stirred, the electrode potential was stepped to 0.05 V (*i.e.*, on the plateau of the ferrocene wave), again for the same duration θ. Current was then determined and the electrode potential stepped back to −2.1 V. To ensure that no fouling[23] of the electrode occurred, a second cathodic (−3.0 V) step of duration θ was performed. The electrode was then polished, and a new series of experiments was performed for a different value of θ. For each series of experiments, the ratio of the current at time θ for $Fe(CO)_5$ and ferrocene was determined and corrected for the ratio of concentrations. Note that the ratio $[Cp_2Fe]/[Fe(CO)_5] \approx 2.07$ was selected so that the magnitudes of the experimental currents were similar for both species so that any residual ohmic drop was comparable for both waves. For characteristic time, $T_c = \theta$, varying from 3 to 100 ms, the normalized current intensity ratio was found equal to 2.00 ± 0.03, giving[11]

$$(i_{R_1}/i_{Fc})_{chrono} = n(D/D_{Fc})^{1/2} = 2.00 \pm 0.03$$

(b) Steady State Voltammetry at Ultramicroelectrodes. The same solution containing $Fe(CO)_5$ and Cp_2Fe was

(39) Handy, L. B.; Ruff, J. K.; Dahl, L. F. *J. Am. Chem. Soc.* **1970**, *92*, 7312.
(40) Amatore, C.; Lefrou, C.; Pflüger, F. *J. Electroanal. Chem.* **1989**, *270*, 43−59.
(41) Amatore, C.; Lefrou, C. *J. Electroanal. Chem.* **1992**, *324*, 33−58.

used. Two working ultramicroelectrodes (gold discs, diameters 10 and 50 μm) were used. The potential scan rate was set to a low value (*viz.*, 10−20 mV s^{-1}) so that the voltammograms exhibited steady state behavior. The current plateau intensities were measured for both reduction of Fe(CO)$_5$ and oxidation of Cp$_2$Fe, and their ratios were normalized to take into account the difference in concentrations. For both electrodes, $(i_{R_1}/i_{Fc})_{stst}$ was found equal to 2.05, giving[11]

$$(i_{R_1}/i_{Fc})_{stst} = nD/D_{Fc} = 2.05$$

Extraction of n and D/D_{Fc} from the above equations[11] gave the following values: $n = 1.95 \pm 0.06$ and $D/D_{Fc} = 1.05 \pm 0.05$. D_{Fc} has been determined[11] to be 8.0×10^{-6} cm^2 s^{-1} in this medium, thus leading to 8.4×10^{-6} cm^2 s^{-1} for D. The characteristic time for these two determinations[11] can then be calculated: $T_c = r_0^2/D = 31$ ms for the 10 μm diameter electrode and 781 ms for the 50 μm diameter electrode. The first value is in the range of the characteristic time of the chronoamperometry experiments, thus validating the determination of $n = 2$. The fact that the reduction remains a two-electron process at a much longer characteristic time (781 ms, same value for nD/D_{Fc}) shows that even on this rather large time scale, the reaction between Fe(CO)$_4^{2-}$ and Fe(CO)$_5$ is still negligible. Indeed, interference by this reaction would be expected to lead to a decrease in the apparent electron consumption from 2 to 1 electron/Fe(CO)$_5$. That was our interpretation[6] before we realized that the effect was actually caused by fouling of the electrode surface.

Double-Step Chronoamperometry in the Reduction of Cr(CO)$_6$. A 2.36 mM solution of Cr(CO)$_6$ in THF containing 0.15 M [n-Bu$_4$N$^+$][BF$_4^-$], was used. The working electrode was a gold disc, 0.125 mm diameter. The rest potential was set at −2.5 V (no electrochemical reaction). In a first series of experiments, a potential step of duration θ was performed at −3.26 V (reduction of Cr(CO)$_6$), immediately followed by a second step of identical duration θ at −1.76 V (oxidation of Cr(CO)$_5^{2-}$, wave O$_2$). In a second series of experiments, the second step was performed at −0.96 V to include also the oxidation of Cr$_2$(CO)$_{10}^{2-}$ (wave O$_3$). The characteristic time θ was varied from 1 to 100 ms. Comparison of the currents at the end of the second steps for a given value of θ in each series showed that $i_{O_2+O_3} = 1.5 i_{O_2}$ independently of θ, thus establishing that $i_{O_3} = 0.5 i_{O_2}$ over the whole time range investigated.

Determination of the Rate Constant for the Reaction between Cr(CO)$_5^{2-}$ and Cr(CO)$_6$. The voltammetry cell was filled with 10 mL of THF containing 0.15 M [nBu$_4$N$^+$][BF$_4^-$] and 100 μL of a 0.2 M solution of Na$_2$Cr(CO)$_5$ in HMPA. Using a 0.5 mm diameter gold disc electrode, the concentration of Cr(CO)$_5^{2-}$ was monitored by measuring its oxidation peak current intensity in cyclic voltammetry at 1 V s^{-1}. It was observed that, before addition of Cr(CO)$_6$, the concentration of Cr(CO)$_5^{2-}$ slowly decayed with time to reach a plateau. Cr(CO)$_6$ was introduced into the solution after this plateau was achieved, and the decay of Cr(CO)$_5^{2-}$ was monitored *vs* time. The loss of Cr(CO)$_5^{2-}$ before Cr(CO)$_6$ was added resulted in an underestimation of the Cr(CO)$_5^{2-}$ initial concentration at the moment when Cr(CO)$_6$ was introduced into the cell. A double regression analysis of the experimental kinetic data was then performed based on the following rate law:

$$\ln[(\alpha - x)/(1 - x)] = k[\mathrm{Cr(CO)_6}]_0[(\alpha - 1)/\alpha]t + \ln \alpha$$

where $\alpha = [\mathrm{Cr(CO)_6}]_0/[\mathrm{Cr(CO)_5^{2-}}]_0$ and $x = [\mathrm{Cr(CO)_5^{2-}}]/[\mathrm{Cr(CO)_5^{2-}}]_0$; $[\mathrm{Cr(CO)_5^{2-}}]_0$ is the unknown concentration of Cr(CO)$_5^{2-}$ at the time ($t = 0$) when Cr(CO)$_6$ was introduced into the cell. A double regression analysis based on α and k afforded $k = 0.95 \pm 0.05$ M^{-1} s^{-1}, with a correlation coefficient $r = 0.9965$. It is noteworthy that the values of k and r were not very sensitive to changes in the value of α around its best determined value ($\alpha = 1.4$). Therefore, the best value for α was determined on the basis that the intercept of the regression line must be equal to that (*viz.*, ln α) deduced from the selected α value.

Determination of the Rate Constant for the Reaction between Fe(CO)$_4^{2-}$ and Fe(CO)$_5$. An infrared stopped-flow kinetic system was used to determine the rate constant for the reaction between [n-Bu$_4$N$^+$]$_2$[Fe(CO)$_4^{2-}$] and Fe(CO)$_5$ in both THF and acetonitrile containing 0.1 M [n-Bu$_4$N$^+$][BF$_4^-$]. A homemade plunger unit for stop-flow was used containing three syringes, two of which were driven synchronously (A and B), and the third (C) was the stop syringe. Solution A was 1.0 mM in Fe(CO)$_5$ and passed through an electrochemical flow cell equipped with a carbon fibers mesh cathode operated at a potential of −3.0 V *vs* Ag/Ag$^+$. Solution B was either THF (or acetonitrile) containing 0.1 M [n-Bu$_4$N$^+$][BF$_4^-$] or a solution of Fe(CO)$_5$ (*e.g.*, [Fe(CO)$_5$]$_B$ = 10 mM) in the same medium. Solutions A and B were mixed in a T-piece just *prior* to entering the IR cell (Perkin-Elmer). This resulted in dilution by a factor of 2 of the initial concentrations. The outlet from the IR cell was connected to the stop syringe of the plunger unit. All tubings, connectors, and T-piece were made of Teflon or Tefzel obtained from Omnifit. The concentrations were kept low in order to decrease the rate of the coupling reaction. A Nicolet system 800 FT-IR apparatus was used in the rapid scanning mode to record up to 11 spectra/s with a wavenumber resolution of 8 cm^{-1}.

The efficiency of the electrolysis (solution A) and the reaction between electrogenerated [Fe(CO)$_4^{2-}$][n-Bu$_4$N$^+$]$_2$ and the medium (THF containing 0.1 M [n-Bu$_4$N$^+$][BF$_4^-$]) was examined when syringe B was filled with the medium only. Under such conditions, no IR absorption of significant magnitude was observed for Fe(CO)$_5$ (1994 cm^{-1}) or Fe$_2$(CO)$_8^{2-}$ (1860 and 1910 cm^{-1}), indicating that electrolysis was complete and that a negligible amount of Fe(CO)$_4^{2-}$ had reacted with the parent Fe(CO)$_5$ during the short electrolysis time. With time, however, the IR band (1740 cm^{-1}) due to [Fe(CO)$_4^{2-}$][n-Bu$_4$N$^+$]$_2$ slowly decayed ($t_{1/2}$ = 130 s) to afford [HFe(CO)$_4^-$][n-Bu$_4$N$^+$] (observed at 1881 cm^{-1}). The data obtained for the decay of [Fe(CO)$_4^{2-}$][n-Bu$_4$N$^+$]$_2$ at 1740 cm^{-1} were then treated under pseudo-first-order conditions.

The kinetics of the reaction between [Fe(CO)$_4^{2-}$][n-Bu$_4$N$^+$]$_2$ and Fe(Co)$_5$ were obtained by the same procedure, except that syringe B was now filled with a solution of Fe(CO)$_5$ (whose concentration, [Fe(CO)$_5$]$_B$, was in excess *vis à vis* that [Fe(CO)$_5$]$_A$ used in syringe A). Under these conditions, the decay of [Fe(CO)$_4^{2-}$][n-Bu$_4$N$^+$]$_2$ (1740 cm^{-1}) was associated with a growth of Fe$_2$(CO)$_8^{2-}$ (1860 and 1910 cm^{-1}) concentration and no significant formation of [HFe(CO)$_4^-$][n-Bu$_4$N$^+$] (1881 cm^{-1}). The data obtained for the decay of [Fe(CO)$_4^{2-}$]2[n-Bu$_4$N$^+$] were treated kinetically under pseudo-first-order conditions since [Fe(CO)$_5$]$_B$ ≫ [Fe(CO)$_5$]$_A$ ≈ [Fe(CO)$_4^{2-}$]$_A$. By varying the Fe(CO)$_5$ concentration (within the 10 mM range) in syringe B, it was verified that the pseudo-first-order rate constant was proportional to [Fe(CO)$_5$]$_B$, as it must be for reaction 4 (see text).

Acknowledgment. Part of this work has been funded by CNRS and ENS (Paris) and the University of Aarhus (Denmark). Cooperation between the Paris and Aarhus groups was made possible through support of European Community (HCM Network No. CHRXCT 920073). We are also grateful that Brian Bech Nielsen, Physical Department, University of Aarhus, Denmark, gave us the possibility and assistance to use his Nicolet FT-IR instrument for the stopped-flow measurements.

OM940276D

Insertion Chemistry of $HTc(CO)_3(PPh_3)_2$

Jessica Cook,[†] Alan Davison,*[,†] William M. Davis,[†] and Alun G. Jones[‡]

Department of Chemistry, Massachusetts Institute of Technology, Cambridge, Massachusetts 02139, and Department of Radiology, Harvard Medical School and Brigham and Women's Hospital, Boston, Massachusetts 02115

Received August 17, 1994[⊗]

The technetium(I) monohydride complex $HTc(CO)_3(PPh_3)_2$ (**1**) has been prepared by treatment of the trihydride $H_3Tc(PPh_3)_4$ with CO(g) in benzene. Reaction of **1** with [*p*-^{t}Bu-(C_6H_4)N_2]PF_6 affords [$Tc(CO)_3$(NHN(*p*-^{t}Bu(C_6H_4))$(PPh_3)_2$]PF_6 (**2a**) in 67% yield. The molecular structure for **2a** was determined by X-ray diffraction to have the following parameters: space group $P2_1/n$, a = 14.030(3) Å, b = 14.123(3) Å, c = 25.227(5) Å, β = 96.09-(2)°, monoclinic, and Z = 4. Addition of 1 equiv of 1,8-diazabicyclo[5.4.0]undecene to MeCN solutions of **2a** gives the neutral diazene complex, $Tc(CO)_3$(NN(*p*-^{t}Bu(C_6H_4))$(PPh_3)_2$ (**2b**). Treatment of **1** with the heterocumulenes CS_2 and $N(CH_3)CS$, yields $Tc(CO)_2(\eta^2$-$S_2CH)(PPh_3)_2$ (**3**) and $Tc(CO)_2(\eta^2$-$N(CH_3)$,SCH)$(PPh_3)_2$ (**4**). Complex **1** also reacts with electron-deficient acetylenes. When **1** is treated with 1 equiv of dimethylacetylenedicarboxylate, $Tc(CO)_2$[−C(CO_2Me)=CH(C(O)OMe)]$(PPh_3)_2$ (**5**) is obtained. In **5**, the acetylene ligand is coordinated through both a vinylic carbon atom and a carbonyl oxygen atom forming a five-membered chelate ring. Treatment with the less electrophilic acetylene methyl propiolate affords $Tc(CO)_3$[−C(CO_2Me)=CH_2]$(PPh_3)_2$ (**6**) in 57% yield.

Introduction

Some of the more significant reactions displayed by terminal transition metal hydride complexes include intra- and intermolecular hydride transfers, reductive elimination reactions, exchange reactions with H_2, H_2O, and ROH, and hydrogen migration reactions.[1] This latter reaction, involving the insertion of an electrophilic substrate into a metal hydride bond, has many industrial applications.[2] For example such insertions are believed to be important steps in hydrogenation reactions,[3] olefin isomerization,[4] Fischer–Tropsch chemistry,[5] and hydrosilation reactions.[6]

Although the Re analog[7] of the monohydride complex $HTc(CO)_3(PPh_3)_2$ (**1**) has been known for some time, few reports regarding its insertion chemistry have appeared.[8,9] This is surprising since the insertion chemistry of $HW(CO)_2(NO)(PR_3)_2$ (where R = Ph, Me, Et) has received a great deal of attention.[10,11] As part of our interest in the chemistry of technetium hydride complexes, we have developed a simple synthetic route for **1** and explored its reactivity with heterocumulenes, electron-deficient acetylenes, and diazonium salts.

Results and Discussion

The technetium(I) monohydride complex $HTc(CO)_3(PPh_3)_2$ (**1**) was prepared in 71% yield by the reductive carbonylation of the polyhydride $H_3Tc(PPh_3)_4$[12] with CO(g) in benzene. The FAB(+) mass spectrum of **1** shows two major peaks at 707 and 679 amu which correspond to the fragments $Tc(CO)_3(PPh_3)_2$ and $Tc(CO)_2(PPh_3)_2$. The hydride ligand was observed in the ^{1}H NMR spectrum as a triplet at δ −4.8 (J_{P-H} = 19.5 Hz).

The carbonyl resonances for **1** could only be observed by $^{13}C\{H\}$ NMR spectroscopy for the ^{13}C-labeled complex $HTc(^{13}CO)_3(PPh_3)_2$. The carbonyl region of the $^{13}C\{H\}$ NMR spectrum shows one broad resonance at δ 209.5 which has a shoulder centered at δ ~208. The $^{31}P\{H\}$ NMR spectrum of **1** also shows an extremely broad peak at δ ~57. The broadening of peaks in $^{31}P\{H\}$ NMR and $^{13}C\{H\}$ NMR spectra of Tc complexes is believed to be caused by coupling between the quadrapolar ^{99}Tc nucleus (I = $^9/_2$) and the bound carbon or phosphorus nuclei. This effect has been reported for a number of Tc complexes.[13,14]

Complex **1** undergoes a number of interesting insertion reactions when treated with unsaturated substrates. Arene diazonium salts react rapidly with **1** to

[†] Massachusetts Institute of Technology.
[‡] Harvard Medical School and Brigham and Women's Hospital.
[⊗] Abstract published in *Advance ACS Abstracts*, December 1, 1994.

(1) Moore, D. S.; Robinson, S. D. *Chem. Soc. Rev.* **1983**, *12*, 415.
(2) Collman, J. P.; Hegedus, L. S.; Norton, J. R.; Finke, R. G. In *Principles and Applications of Organotransition Metal Chemistry*; 2nd ed.; University Science Books: Mill Valley, CA, 1987; pp 524–679.
(3) James, B. R. *Adv. Organomet. Chem.* **1979**, *17*, 319.
(4) Evans, D.; Osborn, J. A.; Wilkinson, G. *J. Chem. Soc. A* **1968**, 3133.
(5) Masters, C. M. *Adv. Organomet. Chem.* **1979**, *17*, 61.
(6) Randolf, C. L.; Wrighton, M. S. *J. Am. Chem. Soc.* **1986**, *108*, 3366.
(7) Freni, M.; Giusto, D.; Romiti, P. *J. Inorg. Nucl. Chem.* **1971**, *55*, 4093.
(8) Albano, V. G.; Bellon, P. L.; Ciani, G. *J. Organomet. Chem.* **1971**, *31*, 75–87.
(9) Several papers dealing with the insertion chemistry of the complex $HRe(CO)_2(PPh_3)_3$ have been published. This complex dissociates a phosphine ligand in solution. For example, see: Hillhouse, G. L. *J. Am. Chem. Soc.* **1985**, *107*, 7772–7773.
(10) Hillhouse, G. L.; Haymore, B. L. *Inorg. Chem.* **1987**, *26*, 1876–1885.
(11) van der Zeijden, A. A. H.; Bosch, H. W.; Berke, H. *Organometallics* **1992**, *11*, 563–573.
(12) The synthesis of $H_3Tc(PPh_3)_4$ was reported at the Chicago, IL ACS Meeting (August 22–27, 1993). A manuscript containing further details regarding $H_3Tc(PPh_3)_4$ is in preparation.
(13) O'Connell, L. A.; Pearlstein, R. M.; Davison, A.; Kronague, J. F.; Jones, A. G. *Inorg. Chim. Acta* **1989**, *161*, 39–43.
(14) Watson, P. L.; Albanese, J. A.; Calabrese, J. C.; Ovenall, D. W.; Smith, R. G. *Inorg. Chem.* **1991**, *30*, 4638–4643.

0276-7333/95/2314-0650$09.00/0

Table 1. Crystal and Date Collection Parameters for 2a

empirical formula	$C_{50}H_{46}N_2O_3F_6P_3Cl_2Tc$
crystal parameters	
a (Å)	14.030(3)
b (Å)	14.123(3)
c (Å)	25.227(5)
β (deg)	96.09(2)
V (Å^3)	4971(3)
T (°C)	-72 ± 1
space group	$P2_1/n$
formula wt (amu)	1097.74
Z	4
D_{calc} (g/cm^3)	1.467
μ_{calc} (cm^{-1})	5.44
size (mm)	0.25 × 0.30 × 0.43
data measurement parameters	
diffractometer	Enraf-Nonius CAD-4
radiation	Mo Kα (λ) = 0.710 69 Å)
scan type	$\omega-2\Theta$
scan rate (deg/min (in Ω))	1.9−16.5
scan width (deg)	0.80 + 0.35 tan Θ
$2\Theta_{max}$ (deg)	45.0
no. of reflections	
total	7139
unique	6814 (R_{int} = 0.032)
corrections	Lorentz polarization absorption (trans factors 0.94−1.13)
secondary ext	coeff 0.80004 × 10^{-7}
structure solution and refinement	
structure solution	direct methods
refinement	full-matrix least squares
function minimized	$\sum_w(\|F_o\| - \|F_c\|)^2$
least-squares wt	$4F_o^2/\sigma^2(F_o^2)$
p-factor	0.01
no. of observations ($I > 3.00\ \sigma(I)$)	4404
no. of variables	375
residuals	R = 0.059; R_w = 0.055
goodness of fit	2.02
max peak in diff map (e$^-$/Å^3)	0.98
min peak in diff map (e$^-$/Å^3)	−0.80

produce the phenyldiazene cation **2a** in 67% yield. The formation of an α-insertion product is consistent with the terminal N atom in R−N=N$^+$ being electrophilic. In the ^{1}H NMR spectrum of **2a**, the N−H proton is observed as a singlet at δ 12.3. The ν(N=N) stretches are tentatively assigned to weak peaks at 1487 and 1445 cm^{-1} in the IR spectrum.

A single crystal X-ray diffraction study of **2a** was undertaken. Diffusion of pentane into a CH_2Cl_2 solution at −40 °C results in the formation of yellow parallelepiped crystals. The complex crystallizes with one CH_2Cl_2 solvate molecule. Data and collection parameters are given in Table 1 and the Experimental Section. An ORTEP diagram is given in Figure 1. Bond lengths and angles and positional parameters are given in Tables 2−4, respectively. One of the phenyl groups of the triphenylphosphine ligands is disordered; this is described in the Experimental Section.

Complex **2a** has a slightly distorted octahedral geometry with two axial PPh_3 ligands, three meridionally arranged CO ligands, and a bent organohydrazide ligand with a Tc−N(1)−N(2) angle of 124.2(5)°. The long Tc−N(1) distance of 2.157(6) Å indicates that there is very little multiple bond character between Tc and N(1). Typically, M=N(1) bond lengths for M=N(1)=NHR species are ~1.7 Å.[15,16] Also there is a short N(1)−N(2) distance of 1.243(8) Å which is consistent

(15) Nicholson, T.; deVries, N.; Davison, A.; Jones, A. G. *Inorg. Chem.* **1989**, *28*, 3813−3819.
(16) Abrams, M. J.; Larsen, S. K.; Shaikh, S. N.; Zubieta, J. *Inorg. Chim. Acta* **1991**, *185*, 7−15.

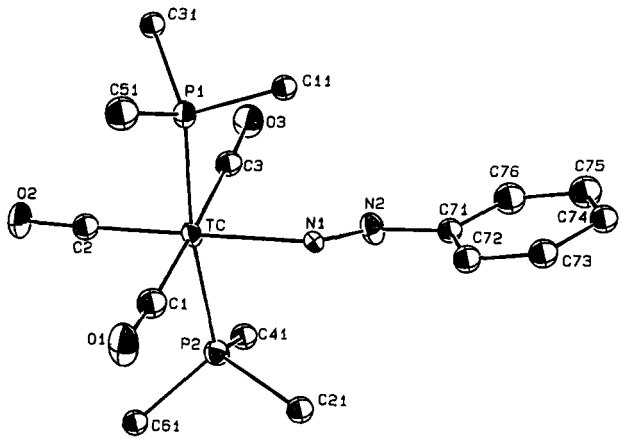

Figure 1. ORTEP drawing of **2a** (30% probability ellipsoids). The phenyl groups of the phosphines, the ^{t}Bu group on the hydrazido phenyl ring, and the CH_2Cl_2 solvate molecule were omitted for the sake of clarity.

Table 2. Selected Intramolecular Distances for 2a

atom 1	atom 2	distance (Å)	atom 1	atom 2	distance (Å)
Tc	P(1)	2.453(2)	Tc	C(3)	1.985(8)
Tc	P(2)	2.461(2)	C(1)	O(1)	1.127(9)
Tc	N(1)	2.157(6)	C(2)	O(2)	1.156(9)
Tc	C(1)	1.999(9)	C(3)	O(3)	1.131(8)
Tc	C(2)	1.910(8)	N(1)	N(2)	1.243(8)

Table 3. Selected Intramolecular Bond Angles for 2a

atom 1	atom 2	atom 3	angles (deg)	atom 1	atom 2	atom 3	angles (deg)
Tc	N(1)	N(2)	124.2(5)	P(2)	Tc	C(2)	94.5(2)
P(1)	Tc	P(2)	173.37(8)	P(2)	Tc	C(3)	92.8(2)
P(1)	Tc	N(1)	86.9(2)	N(1)	Tc	C(1)	92.6(3)
P(1)	Tc	C(1)	94.2(2)	N(1)	Tc	C(2)	178.0(3)
P(1)	Tc	C(2)	91.7(2)	N(1)	Tc	C(3)	89.7(3)
P(1)	Tc	C(3)	84.9(2)	C(1)	Tc	C(2)	86.1(3)
P(2)	Tc	N(1)	86.8(2)	C(1)	Tc	C(3)	177.5(3)
P(2)	Tc	C(1)	88.3(2)	C(2)	Tc	C(3)	91.6(3)

with a double bond between the nitrogen atoms. On the basis of the bond lengths and angles and spectroscopic data, the organohydrazide moiety in **2a** is best described as a (1−) aryldiazene ligand.[15] The aryldiazene ligand exerts a structural *trans* influence that is manifested in the slight lengthening of the C(2)−O(2) distance to 1.156(9) Å as compared with an average C−O distance for the *cis* carbonyls of 1.129 Å.

Addition of excess 1,8-diazabicyclo[5.4.0]undecene (DBU) to MeCN solutions of **2a** results in the rapid precipitation of the yellow complex **2b**. In the IR spectrum of **2b** ν(N=N) is tentatively assigned to peaks at 1481 and 1434 cm^{-1}. There were no peaks visible that could be assigned to a ν(Tc=N) stretch. Also, the N−H peak at δ 12.3 is no longer observed in the ^{1}H NMR spectrum of **2b**. The deprotonation of **2b** is not reversible, and the reaction of **2b** with proton sources does not afford **2a**. Further details regarding the reactivity of **2b** will be published separately.

The heterocumulenes, CS_2 and $N(CH_3)CS$, react with **1** to give the yellow complexes $Tc(CO)_2(\eta^2\text{-}S_2CH)(PPh_3)_2$ (**3**) and $Tc(CO)_2(\eta^2\text{-}N(CH_3),SCH)(PPh_3)_2$ (**4**) in 72% and 45% yield, respectively. These reactions occur with the hydride ligand being transferred to the electronically deficient carbon atom of X=C=Y (where X = S; Y = S, $N(CH_3)$). The hydrogen atom is observed in the ^{1}H NMR spectra at δ 10.13 for **3** and δ 7.38 for **4**. As was seen with **1**, the carbonyl resonances could only be

Table 4. Postional Parameters and Estimated Standard Deviations (Å^2) for $[Tc(CO)_3(NHN(p\text{-}^tBu(C_6H_4))(PPh_3)_2]PF_6$ 2a

atom	x	y	z	B(eq)	atom	x	y	z	B(eq)
Tc	0.26762(5)	0.18858(5)	0.15795(2)	1.91(3)	C(52A)	0.498(1)	0.037(1)	0.1261(6)	2.1(3)
P(1)	0.4426(1)	0.2045(1)	0.17139(8)	2.2(1)	C(52B)	0.580(1)	0.069(1)	0.1500(7)	3.7(4)
P(2)	0.0915(2)	0.1927(2)	0.14322(8)	2.3(1)	C(53A)	0.567(1)	−0.023(1)	0.1082(6)	2.2(3)
O(1)	0.2628(5)	0.0754(4)	0.0515(2)	5.7(4)	C(54C)	0.6455(8)	0.0044(8)	0.1087(4)	6.1(3)
O(2)	0.2784(4)	−0.0081(4)	0.2096(2)	4.2(3)	C(53B)	0.597(1)	−0.001(1)	0.0648(8)	4.7(4)
O(3)	0.2759(4)	0.2861(4)	0.2691(2)	3.5(3)	C(55A)	0.687(1)	0.094(1)	0.1165(6)	2.3(3)
N(1)	0.2654(4)	0.3256(4)	0.1201(2)	2.0(3)	C(55B)	0.522(1)	0.054(1)	0.0411(7)	3.7(4)
N(2)	0.2384(5)	0.3996(5)	0.1405(2)	2.8(3)	C(56A)	0.623(1)	0.157(1)	0.1360(6)	2.1(3)
C(1)	0.2673(6)	0.1205(6)	0.0885(3)	3.2(2)	C(56B)	0.473(1)	0.116(1)	0.0741(7)	3.2(4)
C(2)	0.2730(5)	0.0660(6)	0.1901(3)	2.4(2)	C(61)	0.0334(5)	0.0803(5)	0.1239(3)	2.3(2)
C(3)	0.2703(6)	0.2513(5)	0.2285(3)	2.3(2)	C(62)	0.0515(6)	0.0018(6)	0.1567(3)	3.3(2)
C(11)	0.4745(5)	0.3238(5)	0.1540(3)	2.1(1)	C(63)	0.0083(6)	−0.0850(6)	0.1447(3)	3.7(2)
C(12)	0.4990(5)	0.3479(5)	0.1044(3)	2.5(2)	C(64)	−0.0553(7)	−0.0929(7)	0.0995(4)	4.7(2)
C(13)	0.5118(6)	0.4423(6)	0.0901(3)	3.6(2)	C(65)	−0.0732(7)	−0.0161(8)	0.0665(4)	5.3(2)
C(14)	0.5016(6)	0.5122(6)	0.1265(3)	4.0(2)	C(66)	−0.0292(7)	0.0711(7)	0.0786(4)	4.5(2)
C(15)	0.4775(6)	0.4911(6)	0.1767(3)	3.5(2)	C(71)	0.2458(5)	0.4873(5)	0.1131(3)	2.1(2)
C(16)	0.4636(6)	0.3970(6)	0.1905(3)	2.9(2)	C(72)	0.2663(6)	0.4970(6)	0.0610(3)	2.7(2)
C(21)	0.0458(5)	0.2732(5)	0.0893(3)	2.5(2)	C(73)	0.2776(6)	0.5865(6)	0.0405(3)	2.9(2)
C(22)	−0.0294(6)	0.3347(6)	0.0952(3)	3.7(2)	C(74)	0.2701(6)	0.6678(6)	0.0701(3)	2.7(2)
C(23)	−0.0648(7)	0.3914(7)	0.0524(4)	4.3(2)	C(75)	0.2483(6)	0.6562(6)	0.1221(3)	3.6(2)
C(24)	−0.0280(6)	0.3853(6)	0.0051(3)	3.8(2)	C(76)	0.2358(6)	0.5676(6)	0.1431(3)	3.5(2)
C(25)	0.0449(6)	0.3260(6)	−0.0014(3)	3.6(2)	C(741)	0.2841(7)	0.7669(6)	0.0478(4)	3.8(2)
C(26)	0.0829(6)	0.2693(6)	0.0406(3)	3.0(2)	C(742)	0.1934(8)	0.8213(8)	0.0468(4)	6.4(3)
C(31)	0.5005(5)	0.1901(6)	0.2396(3)	2.3(1)	C(743)	0.318(1)	0.765(1)	−0.0059(6)	10.0(4)
C(32)	0.4618(6)	0.1301(6)	0.2746(3)	3.3(2)	C(744)	0.3596(8)	0.8198(8)	0.0844(4)	6.4(3)
C(33)	0.5102(7)	0.1135(7)	0.3258(4)	4.3(2)	Cl(1)	0.7574(2)	0.3782(3)	0.1620(1)	9.5(2)
C(34)	0.5955(6)	0.1591(6)	0.3407(3)	3.9(2)	Cl(2)	0.7193(3)	0.4726(2)	0.2584(2)	10.6(3)
C(35)	0.6337(6)	0.2188(6)	0.3063(3)	3.8(2)	C(1S)	0.750(1)	0.481(1)	0.1959(6)	11.4(5)
C(36)	0.5877(6)	0.2344(6)	0.2556(3)	3.4(2)	H(1)	0.8061	0.5194	0.1935	12.0
C(41)	0.0305(5)	0.2326(5)	0.1933(3)	2.3(2)	H(2)	0.6977	0.5223	0.1735	12.0
C(42)	−0.0442(6)	0.1821(6)	0.2187(3)	3.4(2)	P(3)	0.8307(2)	0.2057(2)	0.45121(8)	2.8(1)
C(43)	−0.0885(6)	0.2151(6)	0.2618(3)	4.0(2)	F(1)	0.7444(4)	0.2755(4)	0.4349(2)	5.8(3)
C(44)	−0.0598(6)	0.2993(7)	0.2853(3)	4.0(2)	F(2)	0.7573(4)	0.1194(4)	0.4475(2)	5.7(3)
C(45)	0.0112(6)	0.3513(6)	0.2660(3)	3.6(2)	F(3)	0.8149(3)	0.2183(3)	0.5130(2)	3.9(2)
C(46)	0.0562(5)	0.3190(6)	0.2238(3)	2.8(2)	F(4)	0.9147(4)	0.1349(4)	0.4686(2)	5.5(3)
C(51A)	0.531(1)	0.130(1)	0.1413(7)	1.7(4)	F(5)	0.9018(4)	0.2907(4)	0.4563(2)	6.9(4)
C(51B)	0.503(1)	0.122(1)	0.1289(7)	1.7(4)	F(6)	0.8440(4)	0.1920(4)	0.3902(2)	6.1(3)

observed for the ^{13}CO-enriched complexes. The $^{13}C\{H\}$ NMR spectrum of **3** shows the β-carbon atom at δ 236.12 and the carbonyl resonance as a broad peak at δ 202. For **4** the β-carbon atom occurs δ 180.61 and the two nonequivalent carbonyl ligands occur in a 1:1 ratio of δ 219 and 211. Mass spectrometry also supports the η^2-coordination of the CS_2 and $N(CH_3)CS$ ligands showing parent ion peaks at 756 amu for **3** and 753 amu for **4**. The bidentate nature of these ligands is preserved even when complexes **3** and **4** are heated in the presence of a potential ligand like CO. When **1** is treated with other heterocumulenes such as CO_2 and COS, only starting material is isolated from the reaction mixture. This lack of reactivity may result from the low pressures (1 atm) under which the reactions were attempted.[17]

Activated acetylenes also insert into the Tc−H bond of $HTc(CO)_3(PPh_3)_2$. Treatment of **1** with 1 equiv of $MeO_2CC{\equiv}CCO_2Me$ affords the bright yellow complex **5**. The two unique methoxy resonances appear in the ^{1}H NMR spectrum of **5** as singlets at δ 2.78 and 3.32. The vinylic H atom is clearly observed as a sharp triplet at 6.71 ppm with J_{P-H} = 2.65 Hz. The presence of both a noncoordinating and a coordinating organic carbonyl group is confirmed by IR spectroscopy where ν(C=O) occurs at 1702 and 1593 cm^{-1}, respectively.

In the ^{1}H-coupled−^{13}C NMR spectrum of **5**, the β-vinylic carbon atom appears at δ 178 as a doublet with J_{C-H} = 166 Hz, confirming the presence of the vinylic H atom. The α-vinylic carbon occurs as a slightly broadened singlet at δ 229. The absence of any resolved phosphorus−carbon coupling is attributed to the influence of the quadrapolar ^{99}Tc ($I = 9/2$) nucleus, which is also responsible for the severe broadening of the carbonyl resonances.

The high chemical shift values of the α-vinylic carbon atom is attributed to contributions from the resonance structure $\overline{M{=}C{-}C{=}C{-}O}$. This imparts more carbenoid character to the α-vinyl carbon and results in a low field shift of the resonance. A similar effect has been observed in other complexes containing five-membered rings of the type $\overline{M{-}C{=}C{-}C{=}O}$.[11,18,19]

1 reacts much slower with less electrophilic acetylenes. The addition of excess $HC{\equiv}CCO_2Me$ to toluene solutions of **1** followed by stirring for 4.5 h affords **6** in 57% yield. The length of the reaction time is critical; longer times result in a significantly lower yield. This is in contrast to the reaction of **1** with DMAD, which occurs rapidly and shows no decomposition with time. In agreement with the proposed η^1-coordination of the acetylene ligand, ν(C=O) occurs at 1675 cm^{-1} in the IR spectrum. If the carboxylate oxygen atom was coordinated to the technetium center, ν(C=O) would be expected to occur at a much lower wavenumber than that observed for free methyl propiolate (1724 cm^{-1}). Also, the observed ν(C≡O) stretches at 2042 (m), 1956 (s), and 1905 (s) cm^{-1} are typical of three meridionally

(17) Higher pressures of CO_2 could not be used due to regulations regarding the handling of radioactive ^{99}Tc.

(18) Vessey, J. D.; Mawby, R. J. *J. Chem. Soc., Dalton Trans.* **1993**, 51−58.

(19) Werner, H.; Weinand, R.; Otto, H. *J. Organomet. Chem.* **1986**, *307*, 49.

Scheme 1

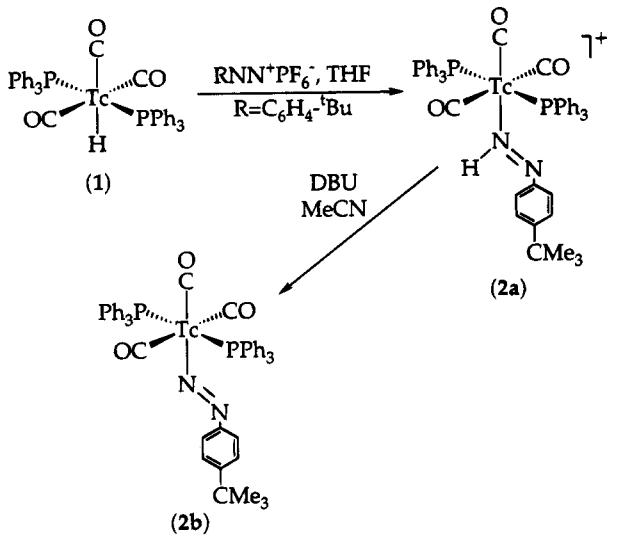

Scheme 2

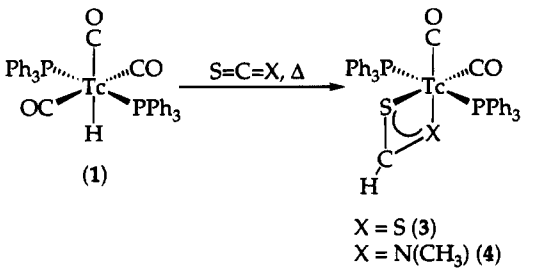

Scheme 3

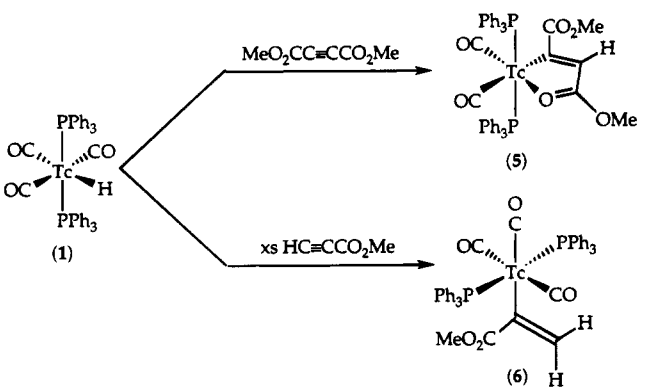

arranged CO ligands.[20] The mass spectrum which shows a parent peak at 791 amu also supports η^1-coordination of the acetylene ligand.

In the ^1H NMR spectrum of **6**, two unique doublets for the β-vinylic protons are observed at δ 6.70 and 5.51 with J_{H-H} = 4.2 Hz. These doublets are not sharp as the phosphorus coupling is not resolved. This value is characteristic of a geminal rather than *cis* or *trans* coupling constant.[21] The methoxy resonance is observed as a singlet at δ 3.13. The α-vinylic carbon is observed as a broadened singlet at δ 166 in both the ^1H-coupled and ^1H-decoupled ^{13}C NMR spectra. As was seen for **5**, phosphorus coupling to the α-carbon atom is not resolved. The β-vinylic carbon atom was obscured by resonances corresponding to the phenyl rings of the phosphine ligands.

In the ^1H NMR spectrum of the product resulting from the insertion of methyl propiolate into the Tc–D bond of $DTc(CO)_3(PPh_3)_2$,[22] the signal at δ 6.79 is absent. Cleavage of the vinyl ligand with CH_3CO_2H resulted in the formation of $Tc(CO)_2(\eta^2\text{-}O_2CCH_3)(PPh_3)_2$[23] and deuterated methyl acrylate. This reaction is believed to proceed stereospecifically with only one isomer of methyl acrylate being observed by ^1H NMR. The location of the deuterium atom as being *cis* to the CO_2Me group is confirmed in the ^1H NMR spectrum by the appearance of two sharp doublets at δ 5.93 and 6.45 for the *cis*-coupled olefin protons (J_{H-H} = 10.9 Hz). This value is consistent with *cis*-coupled olefinic protons.[21] No reactivity of **1** with bulkier acetylenes such as $PhC{\equiv}CCO_2Me$ was observed.

Conclusions

The complex *trans*-$HTc(CO)_3(PPh_3)_2$ (**1**) shows a wide range of reactivity with a variety of unsaturated substrates including heterocumulenes, electron-deficient acetylenes, and diazonium salts. These reactions proceed via transfer of the hydride ligand to the most electrophilic atom of the substrate. This behavior is consistent with the hydride ligand of **1** being hydridic rather than acidic.

Experimental Section

Caution! Technetium-99 is a weak β^--emitter (E = 0.292 MeV, $t_{1/2}$ = 2.12 × 10^5 years). All work has been done in laboratories approved for the use of low levels of radioactive materials. Precautions have been detailed elsewhere.[24]

Reagents and solvents were used as received unless otherwise stated. Drybox solvents (toluene, THF, pentane, Et_2O) were distilled from sodium/benzophenone. A "bomb" refers to a cylindrical glass vessel sealed to a Kontes high-vacuum stopcock. A Mattson Cynus 100 FTIR instrument was used to record all infrared spectra. Only representative IR data are given. Fast atom bombardment mass spectra (FABMS(+)) were obtained using a MAT 731 mass spectrometer operating at an accelerating voltage of 8 kV and equipped with a Ion Tech B11N FAB gun. The FAB gun produces a beam of 6–8 keV xenon neutrals. All compounds were run in a matrix of neat 3-nitrobenzyl alcohol. ^1H, ^{13}C, and ^{31}P NMR were recorded at 300.0, 75.429, and 121.421 MHz, respectively, on a Unity Varian spectrometer, unless otherwise noted. All $^{31}P\{H\}$ NMR are referenced to an external standard of 85% phosphoric acid in $CDCl_3$. The elemental analyses were performed by Atlantic Microlab, Norcross, GA.

$HTc(CO)_3(PPh_3)_2$ (1). $H_3Tc(PPh_3)_4$[12] (100.9 mg, 0.088 mmol) was dissolved in 20 mL of C_6H_6 under a CO(g) atmosphere. After being stirred for ~1.5 h, the faint yellow solution was layered with 100 mL of EtOH and allowed to stand overnight in a freezer (−20 °C). The colorless microcrystalline material that precipitated was collected by filtration, washed with EtOH and Et_2O, and dried *in vacuo*. The

(20) Abel, E. W.; Tyfield, S. P. *Can. J. Chem.* **1969**, *47*, 4627–4633.
(21) Pretsch, E.; Seibl, J.; Simon, W. *Tables of Spectral Data for Structure Determination of Organic Compounds*; Springer-Verlag: New York, 1983.
(22) Cook, J.; Davison, A.; Jones, A. G. Manucript in preparation. The complex $DTc(CO)_3(PPh_3)_2$ was not prepared directly from the trihydride $H_3Tc(PPh_3)_4$.
(23) Cook, J.; Davison, A.; Jones, A. G. A manuscript describing the synthesis and characterization of $Tc(CO)_2(O_2CCH_3)(PPh_3)_2$ and other reactions of **1** with protic acids has been submitted for publication.
(24) Davison, A.; Orvig, C.; Trop, H. S.; DePamphilis, B.; Jones, A. G. *Inorg. Chem.* **1980**, *19*, 1988.
(25) It has been found by workers in our laboratory that analytical analyses of Tc complexes can be up to one carbon low. This may be due to incomplete combustion, which leads to the formation of TcC. The best analytical data obtained for the reported complexes are presented. deVries, N.; Jones, A. G.; Davison, A. *Inorg. Chem.* **1989**, *19*, 3728.

material can be recrystallized from CH_2Cl_2/pentane at −20 °C. Yield: 44.1 mg, 71%.

Anal. Calcd for $C_{39}H_{31}O_3P_2Tc$: C, 66.11; H, 4.41. Found: C, 65.70;[25] H, 4.49. IR(KBr): ν 2023 (m, C≡O); 1962 (sh); 1923 (br s, C≡O); 1859 (m, C≡O). ^{1}H NMR (CD_2Cl_2) δ (ppm): −4.8 (t, J_{P-H} = 19.5 Hz, Tc*H*); 7.0 (m, 18 H, P(C_6H_5)); 7.8 (m, 12H, P(C_6H_5)). ^{13}C{H} NMR (CD_2Cl_2, HTc(^{13}CO)$_3$(PPh$_3$)$_2$) δ (ppm): 128.39 (t, J_{P-C} = 4.5 Hz, P(C_6H_5)$_3$ ortho or meta); 129.89 (s, P(C_6H_5)$_3$ para); 133.82 (t, J_{P-C} = 6.2 Hz, P(C_6H_5)$_3$ ortho or meta); 137.57 (t, J_{P-C} = 20.4 Hz, P(C_6H_5)$_3$ ipso); 209.5 (br, s, *cis*-CO); 207 (sh, *trans*-CO). ^{31}P{H} NMR ($CDCl_3$) δ (ppm): ~57 (br, line width ~5000 Hz). FABMS(+) *m/z*: 707 [Tc(CO)$_3$(PPh$_3$)$_2$]$^+$; 679 [Tc(CO)$_2$(PPh$_3$)$_2$]$^+$.

[Tc(CO)$_3$(NHN(*p*-^{t}Bu(C$_6$H$_4$))(PPh$_3$)$_2$]PF$_6$ (2a). In the drybox, a solution containing [*p*-^{t}Bu(C$_6$H$_4$)N$_2$]PF$_6$ (49.5 mg, 0.16 mmol) in 5 mL of THF was added to a solution containing HTc(CO)$_3$(PPh$_3$)$_2$ (**1**; 104.12 mg, 0.15 mmol) in 15 mL of THF. After being stirred for 6 h, the yellow-brown reaction mixture was filtered through Celite. The volume of the reaction mixture was reduced to ~3 mL under vacuum. The addition of 3 mL of heptane followed by storage overnight at −40 °C yielded bright yellow crystals. The crystals were collected by filtration, washed with 10 mL heptane, and dried *in vacuo*. Yield: 142 mg, 67%.

Anal. Calcd for $C_{49}H_{44}F_6N_2O_3P_3Tc$: C, 58.00; H, 4.43; N, 2.76. Found: C, 57.52; H, 4.29; N, 2.70. IR(KBr): ν 2071 (w, C≡O); 1987 (s, C≡O); 1929 (s, C≡O); 1487, 1445 (N=N). ^{1}H NMR (CD_2Cl_2) δ (ppm): 1.32 (s, 9H, ^{t}Bu); 6.77 (AA′BB′, 2H, J = 8.8 Hz, N(C_6H_4)); 7.37 (m, 12H, P(C_6H_5)); 7.49 (m, 18H, P(C_6H_5)); 12.30 (s, 1H, N*H*NR). ^{13}C{H} NMR (CD_2Cl_2) δ (ppm): 31.11 (s, C(CH_3)$_3$); 35.76 (s, *C*(CH_3)$_3$); 121.22 (s, C_6H_4-Bu); 126.52 (s, C_6H_4-Bu); 129.63 (t, J_{P-C} = 6.0 Hz, P(C_6H_5)$_3$ ortho or meta); 131.29 (s, P(C_6H_5)$_3$ para); 132.58 (t, J_{P-C} = 21.3 Hz, P(C_6H_5)$_3$ ipso); 132.95 (s, C_6H_4-Bu); 133.35 (t, J_{P-C} = 6.1 Hz, P(C_6H_5)$_3$ ortho or meta); 150.10 (s, C_6H_4-Bu). ^{31}P{H} NMR(CD_2Cl_2) δ (ppm): 44 (br). FABMS(+) *m/z*: 869 [Tc(CO)$_3$(NHN(*p*-^{t}Bu(C$_6$H$_4$)(PPh$_3$)$_2$]; 841 [Tc(CO)$_2$(NHN(*p*-^{t}Bu(C$_6$H$_4$))(PPh$_3$)$_2$]; 679 [Tc(CO)$_2$(PPh$_3$)$_2$].

X-ray Crystal Structure Determination of 2a. Yellow parallelepiped crystals were grown by slow vapor diffusion of pentane into a CH_2Cl_2 solution of [Tc(CO)$_3$(NHN(*p*-^{t}Bu(C$_6$H$_4$))(PPh$_3$)$_2$]PF$_6$ at −40 °C. A suitable crystal was selected and mounted on a glass fiber under a stream of N_2. The mounted crystal was then transferred to an Enraf-Nonius CAD-4 diffractometer with graphite monochromated Mo Kα radiation. Cell constants and an orientation matrix for data collection, obtained from a least-squares refinement using the setting angles of 25 carefully centered reflections in the range 14.00 < 2θ < 27.00°, corresponded to a monoclinic cell. Based on the systematic absences, the space group was determined to be $P2_1/n$. The final cell parameters are given in Table 1.

The data were collected at a temperature of −72 ± 1 °C using the $\omega-2\theta$ scan technique to a maximum 2θ value of 45.0°. Ω scans of several intense reflections, made prior to data collection, had an average width at half-height of 0.29° with a take-off angle of 2.8°. Of the 7139 reflections that were collected, 6814 were unique (R_{int} = 0.032); equivalent reflections were merged. The intensities of three representative reflections that were measured after every 60 min of X-ray exposure time remained constant throughout data collection, indicating crystal and electronic stability (no decay correction was applied). The linear absorption absorption coefficient for Mo Kα is 5.4 cm^{-1}. An empirical absorption correction, using the program DIFABS, was applied that resulted in transmission factors ranging from 0.94 to 1.13. The data corrections for secondary extinction were applied (coefficient 0.80004 × 10^{-7}).

The structure was solved by direct methods. The nonhydrogen atoms were refined either anisotropically or isotropically. The final cycle of full-matrix least-squares refinement was based on 4404 observed reflections ($I > 3.00\sigma(I)$) and 375 variable parameters and converged with R = 0.059; R_w = 0.055. The standard deviation of an observation of unit weight was 2.02. The weighing scheme was based on counting statistics and included a factor (p = 0.01) to downweight the intense reflections. The maximum and minimum peaks on the final difference Fourier map corresponded to 0.98 and −0.80 e$^-$/Å^3, respectively.

Neutral atom scattering factors were taken from Cromer and Waber.[26] Anomalous dispersion effects were included in F_{calc}; the values of Df′ and Df″ were those of Cromer. All calculations were performed using the TEXSAN crystallographic software package of Molecular Structure Corp.

This structure was troublesome in that disorder was discovered in one of the phenyl groups of the triphenylphosphine ligands. The problem was modeled as an 11-carbon moiety where both phenyls share a common atom. This atom is meta to the phosphorus atoms of one of the groups and para to the same atom in the other ring. A figure of the observed disorder is included in the supplementary material. As a result of the disorder and the sharp cutoff of observed data, only those atoms with atomic number seven or greater were refined anisotropically.

Tc(CO)$_3$(NN(*p*-^{t}Bu(C$_6$H$_4$))(PPh$_3$)$_2$ (2b). In the drybox, DBU (0.17 mL) was added to a solution of [Tc(CO)$_3$(NHN(*p*-^{t}Bu(C$_6$H$_4$))(PPh$_3$)$_2$]PF$_6$ (**2a**; 83.1 mg, 0.082 mmol) dissolved in 5 mL of MeCN. The yellow reaction mixture was stirred for 2 h, during which time an orange-yellow solid precipitated. The solid was filtered onto a fritted disk, washed with 10 mL of Et_2O, and dried *in vacuo*. Yield: 52.4 mg, 85%.

Anal. Calcd for $C_{49}H_{43}N_2O_3P_2Tc$: C, 67.75; H, 4.99; N, 3.22. Found: C, 67.25; H, 4.79; N, 3.01. IR(KBr): ν 1925 (C≡O); 1850 (C≡O); 1481, 1434 (N=N). ^{1}H NMR(CD_2Cl_2) δ (ppm): 1.25 (s, 9H, ^{t}Bu); 6.45 (AA′BB′, 2H, J = 8.8Hz, N(C_6H_4)); 6.96 (AA′BB′, 2H, J = 8.4Hz, N(C_6H_4)); 7.32 (m, 12H, P(C_6H_5)); 7.48 (m, 18H, P(C_6H_5)). ^{13}C{H} NMR (CD_2Cl_2) δ (ppm): 31.52 (s, C(CH_3)$_3$); 51.24 (s, *C*(CH_3)$_3$); 119.86 (s, C_6H_4-Bu); 125.38 (s, C_6H_4-Bu); 128.58 (t, J_{P-C} = 6.2 Hz, P(C_6H_5)$_3$ ortho or meta); 130.11 (s, P(C_6H_5)$_3$ para); 130.56 (s, C_6H_4-Bu); 134.16 (t, J_{P-C} = 6.0 Hz, P(C_6H_5)$_3$ ortho or meta); 135.49 (t, J_{P-C} = 21.3 Hz, P(C_6H_5)$_3$ ipso); 150.99 (s, C_6H_4-Bu). ^{31}P{H} NMR(CD_2Cl_2) δ (ppm): ~54 (br). FABMS(+) *m/z*: 868 [Tc(CO)$_3$(NN(*p*-^{t}Bu(C$_6$H$_4$))(PPh$_3$)$_2$]; 841 [Tc(CO)$_2$(NN(*p*-^{t}Bu(C$_6$H$_4$))(PPh$_3$)$_2$]; 679 [Tc(CO)$_2$(PPh$_3$)$_2$].

Tc(CO)$_2$(η^2-S$_2$CH)(PPh$_3$)$_2$ (3). A solution containing 10 mL of CS_2 and HTc(CO)$_3$(PPh$_3$)$_2$ (**1**; 58.4 mg, 0.082 mmol) was allowed to reflux for 1.5 h. The volume of the reaction mixture was reduced to 3 mL of CS_2 under a stream of N_2 and combined with 50 mL of EtOH. A bright yellow precipitate was isolated on a fritted disk, washed with 10 mL of EtOH, and allowed to dry *in vacuo*. Recrystallization was effected by the slow evaporation of a benzene/EtOH mixture at room temperature. Yield: 45.1 mg, 72%.

Anal. Calcd for $C_{39}H_{31}O_2P_2S_2Tc$: C, 61.91; H, 4.13; S, 8.47. Found: C, 61.50; H, 4.19; S, 8.03. IR(KBr): ν 1934 (s, C≡O); 1865 (s, C≡O). ^{1}H NMR (CD_2Cl_2) δ (ppm): 7.39 (m, 18H, P(C_6H_5)); 7.62 (m, 12H, P(C_6H_5)); 10.13 (br, 1H, S$_2$C*H*). ^{13}C{H} NMR (CD_2Cl_2, Tc(^{13}CO)$_2$(η^2-S,SCH)(PPh$_3$)$_2$, 125.697 MHz) δ (ppm): 128.18 (t, J_{P-C} = 4.0 Hz, P(C_6H_5)$_3$ ortho or meta); 129.92 (s, P(C_6H_5)$_3$ para); 134.42 (t, J_{P-C} = 6.0 Hz, P(C_6H_5)$_3$ ortho or meta); 135.23 (t, J_{P-C} = 19.8 Hz, P(C_6H_5)$_3$ ipso); 202 (br, ~500 Hz wide, CO); 236.12 (s, η^2-S,SCH). ^{13}C NMR(CD_2Cl_2) δ (ppm): 236.12 (d, J_{C-H} = 181 Hz, η^2-S,SCH). ^{31}P{H} NMR (CD_2Cl_2) δ (ppm): ~48 (br). FABMS(+) *m/z*: 756 [Tc(CO)$_2$(η^2-S,SCH)(PPh$_3$)$_2$]; 728 [Tc(CO)(η^2-S,SCH)(PPh$_3$)$_2$]; 700 [Tc(η^2-S,SCH)(PPh$_3$)$_2$].

Tc(CO)$_2$(η^2-N(CH$_3$),SCH)(PPh$_3$)$_2$ (4). In the drybox, a bomb was charged with HTc(CO)$_3$(PPh$_3$)$_2$ (**1**; 142.3 mg, 0.21 mmol), 1 mL of CH_3NCS, and 10 mL of toluene. It was removed from the drybox and heated at 40 °C for 24 h. As the reaction proceeded, the initially colorless solution turned

(26) Cromer, D. T.; Waber, J. T. *International Tables for X-ray Crystallography*; Kynoch Press: Birmingham, U.K., 1974; Table 2. 3. 1.

a pale yellow. After this period, the reaction mixture was filtered through Celite to remove a small amount of black insoluble material. All volatiles were removed using a vacuum pump, leaving a bright yellow solid. The residue was dissolved in 20 mL of CH_2Cl_2 and layered with 20 mL of MeOH. Slow evaporation at room temperature yielded pale yellowish crystals, which were filtered on a fritted disk, washed with Et_2O and MeOH, and dried *in vacuo*. Yield: 68.3 mg, 45%.

Anal. Calcd for $C_{40}H_{34}NO_2P_2STc$: C, 63.75; H, 4.55; N, 1.86; S, 4.25. Found: C, 62.42; H, 4.53; N, 1.95; S, 4.29. IR(KBr): ν 1927 (s, C≡O); 1839 (s, C≡O). ^1H NMR(CD_2Cl_2) δ (ppm): 0.40 (s, 3H, NCH_3); 7.05 (m, 18H, $P(C_6H_5)$); 7.38 (s, 1H, CH_3-NC*H*S); 7.99 (m, 12H, $P(C_6H_5)$). $^{13}C\{H\}$ NMR (CD_2Cl_2, Tc-($^{13}CO)_2(\eta^2$-N(CH_3),SCHP)($PPh_3)_2$, 125.697 MHz) δ (ppm): 45.41 (s, NCH_3); 128.13 (t, J_{P-C} = 4.5 Hz, $P(C_6H_5)_3$ ortho or meta); 129.82 (s, $P(C_6H_5)_3$ para); 134.26 (t, J_{P-C} = 6.2 Hz, $P(C_6H_5)_3$ ortho or meta); 135.36 (t, J_{P-C} = 19.9 Hz, $P(C_6H_5)_3$ ipso); 180.61 (s, CH_3NCHS); 211 (br, ~600 Hz, CO); 219 (br, ~600 Hz, CO). $^{31}P\{H\}$ NMR(CD_2Cl_2) δ (ppm): ~45 (br). FABMS(+) *m/z*: 753 [$Tc(CO)_2(\eta^2$-S,N(CH_3)CH)($PPh_3)_2$]; 725 [$Tc(CO)_2$(SCH)($PPh_3)_2$]; 679 [$Tc(CO)_2(PPh_3)_2$].

$Tc(CO)_2$[−C(CO_2Me)=CH(C(O)OMe)]($PPh_3)_2$ (5). In the drybox, a flask was charged with $HTc(CO)_3(PPh_3)_2$ (**1**; 149.3 mg, 0.21 mmol); $MeO_2CC{\equiv}CCO_2Me$ (26 μL, 0.21 mmol), and 10 mL of toluene. The reaction mixture was stirred for 1.5 h, filtered through Celite, and evaporated to dryness under vacuum. The bright yellow viscous residue was combined with 10 mL of MeCN and stirred overnight. The resulting yellow solid was collected by filtration, washed with Et_2O and MeCN, and dried *in vacuo*. Yield: 81.6 mg, 41%.

Anal. Calcd for $C_{44}H_{37}O_6P_2Tc$: C, 64.24; H, 4.53. Found: C, 63.87; H, 4.52. IR(KBr): ν 1930 (s, C≡O); 1848 (s, C≡O); 1702 (C=O, noncoord); 1593 (C=O, coord). ^1H NMR (C_6D_6) δ (ppm): 2.78 (s, 3H, CO_2*Me*); 3.32 (s, 3H, CO_2*Me*); 6.71 (t, 1H, vinylic H, J_{P-H} = 2.65 Hz); 7.0 (m, 18 H, $P(C_6H_5)$); 7.9 (m, 12 H, $P(C_6H_5)$). ^{13}C NMR (CD_2Cl_2) δ (ppm): 127.8 (d, β-vinylic C, J_{C-H} = 166 Hz). $^{13}C\{H\}$ NMR (CD_2Cl_2) δ (ppm): 50.4 (s, CO_2*Me*); 52.0 (s, CO_2*Me*); 127.8 (s, β-vinylic C); 128.75 (t, J_{P-C} = 4.2 Hz, $P(C_6H_5)_3$ ortho or meta); 130.60 (s, $P(C_6H_5)_3$ para); 132.45 (t, J_{P-C} = 20.0 Hz, $P(C_6H_5)_3$ ipso); 134.03 (t, J_{P-C} 5.4 Hz, $P(C_6H_5)_3$ ortho or meta); 174.5 (s, *C*O_2Me); 180.8 (s, *C*O_2-Me); 214 (br, CO); 220 (br, CO); 229 (s, α-vinylic C). $^{31}P\{H\}$ NMR (CD_2Cl_2) δ (ppm): 53 (br). FABMS(+) *m/z*: 823 [Tc-$(CO)_2$[−C(CO_2Me)=CH(C(O)OMe)]($PPh_3)_2$]; 795 [Tc(CO)[−C-(CO_2Me)=CH(C(O)OMe)]($PPh_3)_2$].

$Tc(CO)_3$(−C(CO_2Me)=CH_2)($PPh_3)_2$ (6). In the drybox, a flask was charged with $HTc(CO)_3(PPh_3)_2$ (**1**; 112 mg, 0.16 mmol), $HC{\equiv}CCO_2Me$ (0.70 mL, 7.9 mmol), and 10 mL of toluene. The reaction mixture was stirred for 5 h, filtered through Celite, and evaporated to dryness under vacuum. The pale pink material was suspended in 15 mL of Et_2O, collected by filtration, washed with Et_2O, and dried *in vacuo*. Yield: 79.2 mg, 57%.

Repeated attempts failed to give a satisfactory analysis of this complex; results were consistently ≥2% low for carbon. IR(KBr): ν 2042 (m, C≡O); 1956 (s, C≡O); 1905 (s, C≡O); 1675 (C=O, noncoord). ^1H NMR (C_6D_6) δ (ppm): 3.13 (s, 3H, CO_2*Me*); 5.51 (1H, vinylic H, J_{H-H} = 4.2 Hz); 6.70 (1H, vinylic H, J_{H-H} = 4.2 Hz); 6.95 (m, 18 H, $P(C_6H_5)$); 7.5 (m, 12 H, $P(C_6H_5)$). $^{13}C\{H\}$ NMR (CD_2Cl_2) δ (ppm): 49.8 (s, CO_2*Me*); 128.45 (t, J_{P-C} = 4.5 Hz, $P(C_6H_5)_3$ ortho or meta); 129.99 (s, $P(C_6H_5)_3$ para); 133.61 (t, J_{P-C} = 19.4 Hz, $P(C_6H_5)_3$ ipso); 134.53 (t, J_{P-C} = 6.0 Hz, $P(C_6H_5)_3$ ortho or meta); 166 (br s, α-vinylic C); 173.4 (s, *C*O_2Me). $^{31}P\{H\}$ NMR (CD_2Cl_2) δ (ppm): 45 (br). FABMS(+) *m/z*: 791 [$Tc(CO)_3$[−C(CO_2Me)=CH_2]($PPh_3)_2$]; 763 [$Tc(CO)_2$[−C(CO_2Me)=CH_2]($PPh_3)_2$]; 707 [$Tc(CO)_3(PPh_3)_2$].

Reaction of $DTc(CO)_3(PPh_3)_2$[22] with HC≡CCO_2Me. This reaction was carried out as described for **6** with the substitution of $DTc(CO)_3(PPh_3)_2$ for **1**.

^1H NMR (C_6D_6) δ (ppm): 3.18 (s, 3H, CO_2*Me*); 5.54 (t, vinylic H, J_{P-H} = 2.8 Hz); 6.95 (m, 18 H, $P(C_6H_5)$); 7.5 (m, 12 H, $P(C_6H_5)$).

Reaction of $Tc(CO)_3$(−C(CO_2Me)=CHD)($PPh_3)_2$ with CH_3CO_2H. To $Tc(CO)_3$(−C(CO_2Me)=CHD)($PPh_3)_2$ (45.9 mg, 0.058 mmol) dissolved in C_6D_6 (~3 mL) was added 1.0 equiv of CH_3CO_2H (0.058 mmol, 3.3 μL). Approximately 1 mL of this solution was withdrawn and added to an NMR tube containing 3 mL of C_6D_6.

^1H NMR (C_6D_6) δ (ppm): $Tc(CO)_2(\eta^2$-$O_2CCH_3)(PPh_3)_2$[23] and $H_1DC{=}C(CO_2Me)H_2$: 0.59 (s, η^2-O_2CC*H*$_3$); 3.35 (s, CO_2*Me*); 5.93 (d, J_{H1H2} = 10.9 Hz); 6.45 (d, J_{H1H2} = 10.9 Hz); 7.38 (m, 30 H, $P(C_6H_5)$).

Acknowledgment. This research was sponsored by U.S. Public Health Service Grant 5 R37 CA34970. Ammonium pertechnetate was supplied as a gift by Du Pont/Biomedical Products. The authors thank Dr. Catherine Costello and Cheng-hui Zeng of the NIH Northeastern Regional Mass Spectrometry Facility for the FAB(+) mass spectra.

Supplementary Material Available: A diagram depicting the disorder problem in the phenyl rings of the PPh_3 ligands and tables of bond lengths and angles and of anisotropic thermal parameters for **2a** (19 pages). Ordering information is given on any current masthead page.

OM9406613

Selective Cross-Coupling of 2,3-Dimethylbutadiene and Isoprene with α-Olefins Catalyzed by Titanium Aryloxide Compounds

Gary J. Balaich, John E. Hill, Steve A. Waratuke, Phillip E. Fanwick, and Ian P. Rothwell*

Department of Chemistry, Purdue University, West Lafayette, Indiana 47907

Received September 29, 1994[⊗]

The titanacyclopentane complex $[(Ar'O)_2Ti(CH_2)_4]$ (Ar'O = 2,6-diphenylphenoxide) **(1)** reacts with butadiene or isoprene to form the π-allyl complexes $[(Ar'O)_2Ti(CH_2CH{=}CHCH_2CH_2CH_2)]$ **(2)** and $[(Ar'O)_2Ti(CH_2CMe{=}CHCH_2CH_2CH_2)]$ **(3)**. In contrast, **1** reacts with 2,3-dimethylbutadiene to initially form the titanacyclopent-3-ene complex $[(Ar'O)_2Ti(CMe{=}CMeCH_2)]$ **(4)** and free ethylene. The solid state structure of **4** shows a bent titanacyclic ring with a fold angle of 75°. The ^1H NMR spectrum of **4** shows nonequivalent α-CH_2 protons, indicating that the bent structure is maintained in solution and that flipping of the metallacycle ring is slow on the NMR time scale. Sodium amalgam reduction of the dichloride complex $[(Ar''O)_2TiCl_2]$ (Ar''O = 2,6-diisopropylphenoxide) in the presence of 2,3-dimethylbutadiene has been shown to produce the titanacyclopent-3-ene complex $[(Ar''O)_2Ti(CHCMe{=}CHMe)]$ **(7)** which has similar spectroscopic (^1H, ^{13}C NMR) properties to those of **4**. Complex **4** reacts with ethylene to produce the titanacyclohept-3-ene complex $[(Ar'O)_2Ti(CH_2CMe{=}CMeCH_2CH_2CH_2)]$ **(5)**. It has been shown that **5** consists of a mixture of *cis*- and *trans*-titanacyclohept-3-ene complexes in solution, **5a** and **5b**, with **5b** as the major (80%) isomer. In the absence of ethylene or 2,3-dimethylbutadiene, the isomeric mixture of **5a** and **5b** slowly converts to the titanacyclopent-3-ene complex $[(Ar'O)_2Ti(CH_2CMe{=}CMeCHEt)]$ **(6)**. In the presence of an excess of 2,3-dimethylbutadiene and 1 atm of ethylene at 70 °C, **5** produces the cross-coupled product 4,5-dimethylhexa-1,4-diene catalytically with a turnover rate of ~8 Ti^{-1} h^{-1}. The titanacyclopentadiene complexes $[(Ar'O)_2Ti(C_4Et_4)]$ **(8)** and $[(Ar''O)_2Ti\{C_2(SiMe_3)_2C_6H_8\}]$ **(9)** as well as **7** have been shown to be catalyst precursors in the cross-coupling of 2,3-dimethylbutadiene with α-olefins ($CH_2{=}CHR$, R = Me, ET, Ph, Bu^n, $SiMe_3$). These reactions catalytically produce mixtures of substituted acyclic 1,4-diene products, which have been identified by ^1H and ^{13}C NMR, GC, and MS. The cross-coupling of isoprene and styrene to form 1,4-diene products has also been carried out using complexes **8** and **9** as precursors. In the isoprene/styrene cross-coupling reaction, isoprene dimerization was also observed to form vinylcyclohexenes and the linear dimer, 2,7-dimethyl-1,3,6-octatriene. Kinetic studies of the cross-coupling reaction have been carried out. Plots of concentration of substrates vs time show that there is an approximate zero-order dependence on diene or α-olefin concentration and a first-order dependence on [Ti]. Comparison of the observed product distributions from the cross-coupling reactions of 2,3-dimethylbutadiene with proteo and perdeuterated styrene provides evidence that isomerization of an initially formed β-phenyl titanacyclohept-3-ene to an α-phenyl titanacyclohept-3-ene occurs prior to elimination of the organic products. Further evidence for the isomerization was obtained from the results of a crossover experiment, in which a 50/50 mixture of proteo and perdeuterated styrene was reacted with 2,3-dimethylbutadiene in the presence of a catalytic amount of **8**. The observed products from isoprene dimerization can be accounted for by invoking β-hydrogen abstraction and ring closure reactions of titanacyclohept-3-ene intermediates. Crystal data: at −60 °C for $TiC_{42}H_{36}O_2$ **(4)** a = 35.351(3) Å, b = 37.927(3) Å, c = 9.755(1) Å, Z = 16, d_{calcd} = 1.261 g cm^{-3} in space group *Fdd*2.

Introduction

Compounds of the Group 4 transition metals supported by cyclopentadiene ligands continue to dominate the homogeneous organometallic chemistry of these metals.[1–5] Current research efforts in our group are focused on evaluating the use of aryloxide ancillary ligation for supporting both stoichiometric and catalytic organic transformations at Group 4 metal centers. Recent work has produced a series of stable titanacyclopentadiene complexes containing 2,6-diphenylphenoxide (Ar'O) and 2,6-diisopropylphenoxide (Ar''O) as supporting ligands.[6] These complexes prove to be an excellent entry into the organometallic chemistry of

⊗ Abstract published in *Advance ACS Abstracts*, December 1, 1994.

(1) (a) Buchwald, S. L.; Nielsen, R. B. *Chem. Rev.* **1988**, *88*, 1047. (b) Buchwald, S. L.; Watson, B. T.; Lum, R. T.; Nugent, W. A. *J. Am. Chem. Soc.* **1987**, *109*, 7173. (c) Buchwald, S. L.; Nielsen, R. B. *J. Am. Chem. Soc.* **1989**, *111*, 2870. (d) Buchwald, S. L.; Watson, B. T.; Wannamaker, M. W.; Dewan, J. C. *J. Am. Chem. Soc.* **1989**, *111*, 4486. (e) Buchwald, S. L.; King, S. M. *J. Am. Chem. Soc.* **1991**, *113*, 258. (f) Buchwald, S. L.; Wannamaker, M. W.; Watson, B. *J. Am. Chem. Soc.* **1989**, *111*, 776. (g) Buchwald, S. L.; Nielsen, R. B. *J. Am. Chem. Soc.* **1988**, *110*, 3171.

0276-7333/95/2314-0656$09.00/0

titanium and have been demonstrated to participate in a wide range of stoichiometric as well as catalytic reactivity.[6]

In a recent communication, we reported the titanium aryloxide catalyzed cross-coupling of ethylene and 2,3-dimethylbutadiene to form 4,5-dimethylhexa-1,4-diene.[7] More recent work has shown that the scope of this reaction can be extended to α-olefins and the use of isoprene as the diene component. In this paper we wish to report our observations on the regio- and stereochemistry of this reactivity in addition to mechanistic results which give insight into the reaction pathways that are present in the catalytic cycle.

Results and Discussion

Synthesis and Characterization of Organotitanium Compounds. Reaction of hydrocarbon solutions of the red titanacyclopentane complex $[(Ar'O)_2Ti(CH_2)_4]$ (**1**)[8] with butadiene or isoprene results in the formation of the complexes **2** and **3** (Scheme 1). The ^1H and ^{13}C NMR spectra of **2** and **3** are consistent with their formulation as π-allyl forms of *trans*-titanacyclohept-3-ene complexes in solution, and an incomplete X-ray diffraction study on **3** confirms the regiochemistry shown. Compounds **2** and **3** are stable in benzene solution for days at 25 °C with almost no detectable (^1H NMR) decomposition or rearrangements. Furthermore, neither **2** or **3** will react with excess ethylene and/or added butadiene (for **2**) or isoprene (for **3**). An analogous regioselectivity in the formation of a metallacyclohept-3-ene ring has been observed in the reaction of the s-*cis* isoprene complex $[Cp_2Zr(CH_2CMe{=}CHCH_2)]$ with various olefins.[9a,b]

Hydrocarbon solutions of the red complex **1** react with 2,3-dimethylbutadiene to initially form the titanacyclopent-3-ene complex $[(Ar'O)_2Ti(CH_2CMe{=}CMeCH_2)]$ (**4**) along with ethylene (Scheme 1). Purple crystals of **4** were obtained from hexane solution and subjected to a single-crystal X-ray diffraction analysis.[7] The solid

Scheme 1[a]

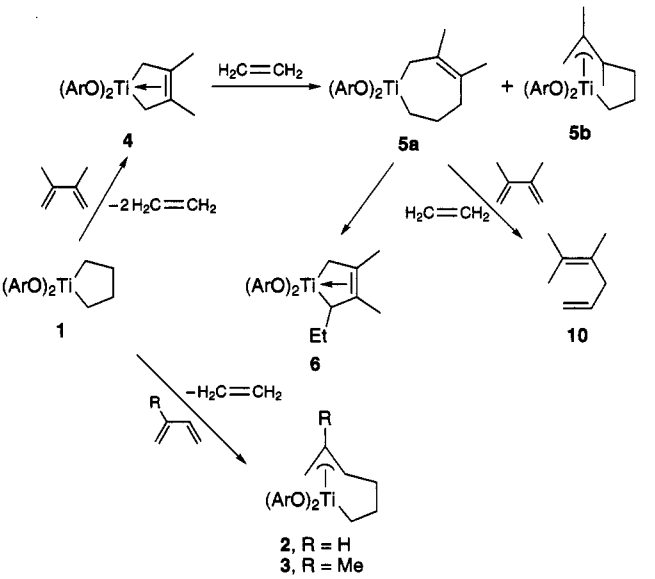

[a] ArO = 2,6-diphenylphenoxide.

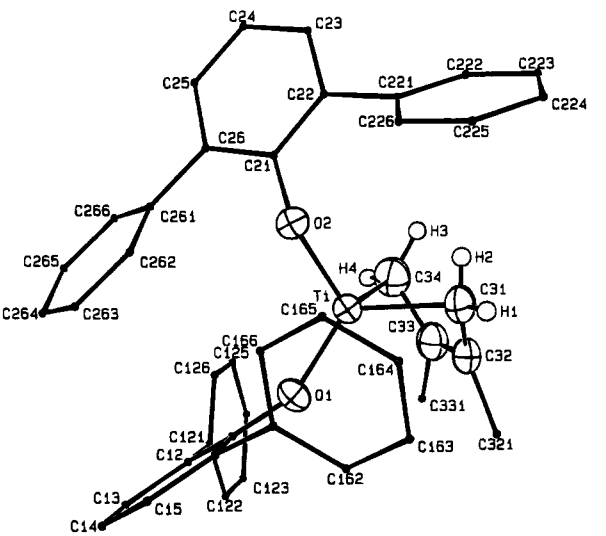

Figure 1. ORTEP view of the titanacyclopent-3-ene complex **4**.

Table 1. Selected Bond Distances (Å) and Angles (deg) for $[(ArO)_2Ti(CHCMe{=}CHMe)]$ (ArO = 2,6-Diphenylphenoxide) (4)

Ti−O(1)	1.804(2)	Ti−C(34)	2.109(5)
Ti−O(2)	1.843(2)	C(31)−C(32)	1.436(5)
Ti−C(31)	2.096(4)	C(32)−C(33)	1.384(6)
Ti−C(32)	2.299(3)	C(33)−C(34)	1.442(6)
Ti−C(33)	2.290(4)		
O(1)−Ti−O(2)	115.2(1)	C(31)−C(32)−C(33)	121.9(4)
C(31)−Ti−C(34)	87.0(1)	C(32)−C(33)−C(34)	121.4(4)
Ti−C(31)−C(32)	78.8(2)	Ti−O(1)−C(11)	151.2(1)
Ti−C(34)−C(33)	77.8(3)	Ti−O(2)−C(21)	143.6(2)

state structure of **4** shows a pseudotetrahedral coordination sphere about the metal center with a bent titanacyclic ring with a fold angle of 75° (Figure 1, Table 1). Within the titanacyclic ring of **4**, the shorter carbon−carbon bond distance, C(32)−C(33) = 1.384(6) Å, compared to the longer carbon−carbon bond distances, C(31)−C(32) = 1.436(5) and C(33)−C(34) = 1.442(6) Å, is consistent with a titanacyclopent-3-ene structure. Coordination of the butadiene unit to the $[Ti(OAr)_2]$ fragment in **4** is very similar to that reported

(2) (a) Walsh, P. J.; Baranger, A. M.; Bergman, R. G. *J. Am. Chem. Soc.* **1992**, *114*, 1708. (b) Walsh, P. J.; Hollander, F. J.; Bergman, R. G. *J. Am. Chem. Soc.* **1988**, *110*, 8729. (c) Woo, H.; Freeman, W. P.; Tilley, T. D. *Organometallics* **1992**, *11*, 2198.

(3) (a) Erker, G.; Aulbach, M.; Mena, M.; Pfaff, R.; Sosna, F. *Chem. Scr.* **1989**, *29*, 451. (b) Coles, N.; Whitby, R. J.; Blagg, J. *Synlett* **1992**, 143. (c) Coles, N.; Whitby, R. J.; Blagg, J. *Synlett* **1990**, 271. (d) Erker, G.; Sosna, F.; Hoffman, U. *J. Organomet. Chem.* **1989**, *372*, 41. (e) Erker, G. *Angew. Chem., Int. Ed. Engl.* **1989**, *28*, 397. (f) Erker, G.; Czisch, P.; Kruger, C.; Wallis, J. M. *Organometallics* **1985**, *4*, 2059.

(4) (a) RajanBabu, T. V.; Nugent, W. A.; Taber, D. F.; Fagan, P. J. *J. Am. Chem. Soc.* **1988**, **110**, 7128. (b) Nugent, W. A.; Calabrese, J. C. *J. Am. Chem. Soc.* **1984**, *106*, 6422. (c) Parshall, G. W.; Nugent, W. A.; Chan, D. M.-T.; Tam, W. *Pure Appl. Chem.* **1985**, *57*, 1809. (d) Nugent, W. A.; Thorn, B. L.; Harlow, R. L. *J. Am. Chem. Soc.* **1987**, *109*, 2788.

(5) (a) Negishi, E.; Holmes, S. J.; Tour, J. M.; Miller, J. A.; Cederbaum, F. E.; Swanson, D. R.; Takahashi, T. *J. Am. Chem. Soc.* **1989**, *111*, 3336. (b) Swanson, D. R.; Rousset, C. J.; Negishi, E.; Takahashi, T.; Takashi, S.; Masahiro, S.; Yaseyo, U. *J. Org. Chem.* **1989**, *34*, 3521. (c) Takahashi, T.; Minouru, T.; Masahiko, S.; Yaseyo, U.; Negishi, E. *J. Chem. Soc., Chem. Commun.* **1989**, 852.

(6) Hill, J. E.; Balaich, G. J.; Fanwick, P. E.; Rothwell, I. P. *Organometallics* **1993**, *12*, 2911.

(7) Hill, J. E.; Balaich, G. J., Fanwick, P. E.; Rothwell, I. P. *Organometallics* **1991**, *10*, 3428.

(8) Hill, J. E.; Fanwick, P. E.; Rothwell, I. P. *Organometallics* **1991**, *10*, 15.

(9) (a) Yasuda, H.; Nakamura, A. *Angew. Chem., Int. Ed. Engl.* **1987**, *26*, 723. (b) Yasuda, H.; Kajihara, Y.; Nagasuna, K.; Mashima, K.; Nakamura, A. *Chem. Lett.* **1981**, 719. (c) Yamamoto, H.; Yasuda, H.; Tatsumi, K.; Lee, K.; Nakamura, A.; Chen, J.; Kai, Y.; Kasai, N. *Organometallics* **1989**, *8*, 105. (d) Erker, G.; Sosna, F.; Zwettler, R.; Kruger, C. *Organometallics* **1989**, *8*, 450.

Scheme 2[a]

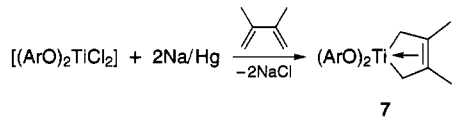

[a] ArO = 2,6-diisopropylphenoxide.

for related Group 4 metal diene complexes, e.g. [Cp_2M-(diene)] and [CpMX(diene)] (M = Ti, Zr, Hf).[9c,d] The Ti−O bond distances and the large Ti−O−C bond angles (Figure 1, Table 1) are typical of aryloxide compounds of Ti(IV).[6]

The ^{1}H NMR spectrum of a C_6D_6 solution of **4** shows two doublet resonances at δ 3.02 and 1.35 for the nonequivalent α-CH_2 protons, indicating that the bent structure is maintained in solution and that flipping of the metallacycle ring is slow on the NMR time scale. A single resonance at δ 87.9 in the ^{13}C NMR spectrum of **4** can be assigned to the equivalent α-carbons of the titanacyclopent-3-ene ring. These α-carbons couple to the two nonequivalent α-CH_2 protons, giving rise to $^1J(^{13}C-^1H)$ coupling constants of 138.2 and 160.8 Hz in the proton-coupled ^{13}C NMR spectrum of **4**.

The synthesis of a titanacyclopent-3-ene complex supported by 2,6-diisopropyl phenoxide ligands has also been achieved. The complex [(Ar″O)$_2$Ti(CH_2C-Me=CMeCH_2)] (**7**) can be obtained as a purple liquid by the room temperature sodium amalgam reduction of hydrocarbon solutions of the dichloride complex [(Ar″O)$_2$-$TiCl_2$] in the presence of an excess of 2,3-dimethylbutadiene (Scheme 2). Although the high solubility of **7** in hydrocarbon solvents prevented its isolation and purification as a crystalline material, the similarity of its spectroscopic data to those of **4** is consistent with its formulation.

In the reaction of **1** with 2,3-dimethylbutadiene, failure to separate **4** from generated free ethylene leads to a slow color change from purple to orange with the formation of a new organometallic compound [(Ar′O)$_2$Ti-(CH_2CMe=CMe$CH_2CH_2CH_2$)] (**5**). Compound **5** can also be obtained by reaction of ethylene (1 atm) with **4** (Scheme 1). The ^{1}H and ^{13}C NMR spectra of **5** show that it exists in solution as a mixture of two isomeric forms, **5a** and **5b**, which do not exchange rapidly on the NMR time scale. The major (80%) isomer **5b** has spectroscopic properties very similar to those of **2** and **3** and is hence formulated as containing a *trans*-titanacyclohept-3-ene ring. We formulate the minor isomer **5a** as containing a *cis*-titanacyclohept-3-ene ring. It is not possible on the basis of spectroscopic data to determine whether the ground-state structure of this molecule contains a σ- (not sterically viable for the *trans* isomer) or π-allyl bond.

Monitoring the ^{1}H NMR spectra of a solution of **5a** and **5b** in C_6D_6 over hours showed the clean conversion of the isomeric mixture into a new titanacyclopent-3-ene complex [(Ar′O)$_2$Ti(CHEtCMe=CMeCH_2) (**6**) (Scheme 1). A series of β-hydrogen abstraction and reinsertion reactions can account for the formation of **6** from **5a**. Addition of 2,3-dimethylbutadiene to **6** leads to the regeneration of **4** and free 1-ethyl-2,3-dimethylbutadiene.[7]

The titanacyclopentadiene complex [(Ar′O)$_2$Ti(C_4Et_4)] (**8**) can function as a precursor in the formation of **5**. This complex has been shown to react with ethylene to produce **1** (Scheme 3) along with 1 equiv of a substituted 1,3-cyclohexadiene.[8]

Scheme 3[a]

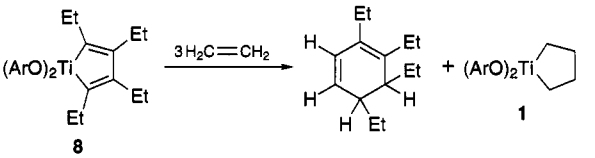

[a] ArO = 2,6-diphenylphenoxide.

Table 2[a]

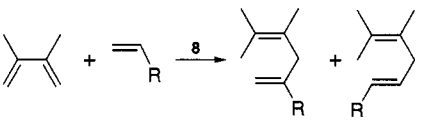

R	yield, % 11	*trans*-12
a, Ph	78	22
b, $SiMe_3$	90	10
c, *n*-Bu	84	16
d, Et	>90	<10
e, Me	>90	<10

[a] All reactions were carried out using 2 M concentrations of α-olefin and 2,3-dimethylbutadiene in C_6H_6 as solvent at 65 °C.

Formation and Characterization of Cross-Coupled Products. In the presence of excess 2,3-dimethylbutadiene, a solution of **5** readily absorbs ethylene, leading to the formation of 4,5-dimethylhexa-1,4-diene (**10**) (Scheme 1). At 70 °C a mixture of **5** (25 mg, 0.039 mmol) and 2,3-dimethylbutadiene (0.150 mL, 1.33 mmol) in C_6D_6 was found to produce 13.7 equiv of **10** in 100 min when exposed to 1 atm of ethylene, with greater than 95% of **5a** and **5b** still being present in solution. The acyclic 1,4-diene product of this reaction is the result of the coupling of 2,3-dimethylbutadiene with ethylene (1,4-hydro-vinylation) in a highly regioselective fashion. No Diels−Alder or 1,2-addition products or compounds derived from dimerization of ethylene or 2,3-dimethylbutadiene were observed.

The scope of this catalytic cross-coupling reaction has been extended. Reaction of 2,3-dimethylbutadiene with the α-olefins (CH_2=CHR, R = Ph, Bu^n, $SiMe_3$, Et, Me) in the presence of a catalytic amount of precursor **8** results in the formation of two, acyclic 1,4-addition products (Table 2) identified as the 2-substituted-4,5-dimethylhexa-1,4-diene compound **11** and the *trans*-1-substituted isomer *trans*-**12**. The tabulated results for the cross-coupling reactions catalyzed by **8** shows that the isomer distribution favors formation of **11** and that no *cis*-**12** isomers are observed either by NMR or GC analytical methods.

Selective catalytic cross-coupling of α-olefins and 2,3-dimethylbutadiene can also be achieved by using titanacyclic precursors supported by 2,6-diisopropylphenoxide ligands. We have reported the synthesis and characterization of the titanacyclopentadiene complex [(Ar″O)$_2$Ti{$C_2(SiMe_3)_2C_6H_8$}] (**9**).[10] Reaction of 2,3-dimethylbutadiene with styrene or vinyltrimethylsilane in the presence of a catalytic amount of **9** results in the formation of the same 1,4-addition product isomers **11** and *trans*-**12** observed using **8** as a catalyst precursor

(10) Balaich, G. J.; Fanwick, P. E.; Rothwell, I. P. *Organometallics* **1994**, *13*, 4117.

Table 3[a]

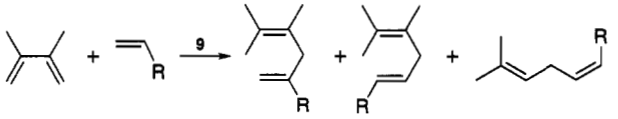

R	yield, % 11	*trans*-12	*cis*-12
a, Ph	57	43	
b, $SiMe_3$	53	42	5

[a] All reactions were carried out using 2 M concentrations of α-olefin and 2,3-dimethylbutadiene in C_6H_6 as solvent at 65 °C.

Table 4[a]

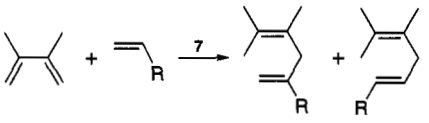

R	yield, % 11	*trans*-12
a, Ph	53	47
b, $SiMe_3$	76	24

[a] All reactions were carried out using 2 M concentrations of α-olefin and 2,3-dimethylbutadiene in C_6H_6 as solvent at 65 °C.

(Table 3). However, the ratio [**11**/*trans*-**12**] decreases, and in the case in which R = $SiMe_3$, 5% of the product distribution is accounted for by the *cis*-1-substituted stereoisomer *cis*-**12b**. This *cis*-**12** isomer was not observed in the cross-coupling reactions using **8** as a catalyst precursor. The reactivity of the titanacyclopent-3-ene complex **7** has also been investigated in the cross-coupling reactions (Table 4) and the [**11**/*trans*-**12**] ratios are similar to those obtained when **9** was used as the catalyst precursor.

We have also briefly investigated the ability of a combination of either of the dichlorides [$(Ar'O)_2TiCl_2$] or [$(Ar''O)_2TiCl_2$] "activated" with 2 equiv of *n*-BuLi to carry out the catalytic cross-coupling of styrene and 1,3-dimethylbutadiene. The solution generated from the 2,6-diphenylphenoxide precursor was found to catalytically produce a mixture of cross-coupled products **11** and *trans*-**12** at 65 °C that was identical (GC) to that produced using catalyst precursor **8**. However, the solutions formed by mixing the 2,6-diisopropylphenoxide [$(Ar''O)_2TiCl_2$] with 2 equiv of *n*-BuLi at room temperature failed to produce significant amounts of product. We have as yet not attempted to optimize conditions for the use of these binary catalysts.

In cross-coupling reactions in which isoprene is utilized as the diene component, a higher temperature (90 °C) is required, and the number of detected products increases dramatically (Schemes 4 and 5). In the reaction of isoprene and styrene catalyzed by the diphenylphenoxide complex **8** (Scheme 4), isomeric acyclic, cross-coupled products **13** (major component), **14**, and **15** can be detected in the ^1H NMR and **16** is detected in the gas chromatogram. In addition three, more volatile organic products were also formed. The ^1H NMR spectra are consistent with the formulation of these products as the cyclic, isoprene dimers 1,4-dimethyl-4-vinyl-1-cyclohexene (**17**) and 2,4-dimethyl-4-vinyl-1-cyclohexene (**18**) and the linear 2,7-dimethyl-1,3,6-octatriene (**19**). Reaction of isoprene with styrene

Scheme 4

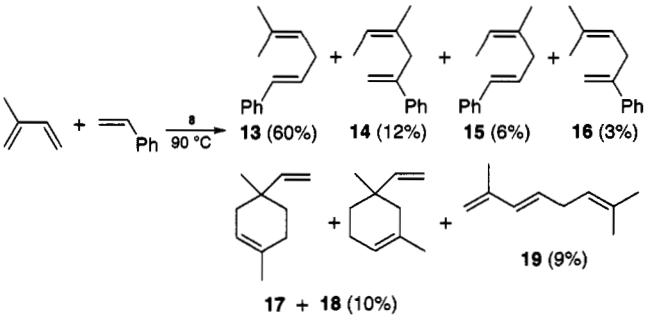

Scheme 5

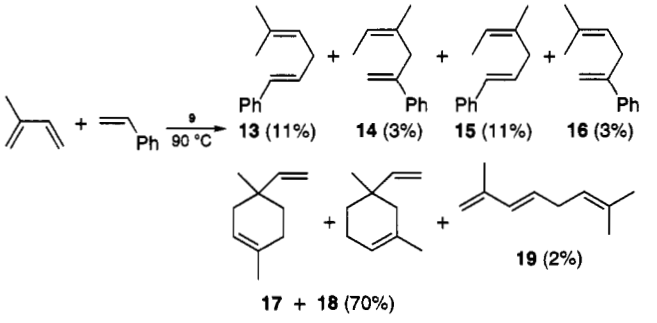

catalyzed by the complex **9** also gives rise to the same products (Scheme 5) although it can be seen that dimerization of isoprene is favored over cross-coupling by the use of 2,6-diisopropylphenoxide ancillary ligation. The catalytic tail-to-tail dimerization of isoprene by the zirconium complex [$Cp_2Zr(CH_2CMe{=}CHCH_2)$] to form 2,7-dimethyl-1,3,6-octatriene (**19**) has been reported,[9a,b] and the spectroscopic assignments for this and the cyclic dimers are found in the literature.[11]

Kinetic Studies. The kinetics of a number of these reactions has been monitored by both ^1H NMR and GC methods. In Figure 2 is shown the ^1H NMR spectrum of the final product mixture obtained from the reaction of styrene with 2,3-dimethylbutadiene (slight excess) catalyzed by **7** at 65 °C. An easily monitored ^1H NMR feature of the products is the resonances observed for the CH_2 group in **11** and *trans*-**12**, respectively. In the reaction employing styrene as α-olefin, these groups give rise to a singlet resonance at δ 3.16 (**11a**) and a doublet resonance at δ 2.87 *trans*-**12a**. Both isomers also give significantly different retention times upon gas chromatographic analysis, allowing accurate isomer ratios to be obtained.

Monitoring the ratio of the products [**11**/*trans*-**12**] during the course of the reaction of styrene with 2,3-dimethylbutadiene catalyzed by titanacyclopentadiene precursor **8** (Figure 3) shows that the observed isomer ratios are kinetically controlled. This plot indicates that, within experimental error, the isomer ratio remains constant as the concentrations of **11** and *trans*-**12** build up with time.

The concentration of substrates with time has also been monitored (^1H NMR) for the reactions of styrene, 1-hexene, and vinyltrimethylsilane with 2,3-dimethylbutadiene catalyzed by precursor **8**. These reactions

(11) (a) Moisenkov, A. M.; Veselovskii, V. V.; Dragan, V. A.; Ignatenko, A. V.; Strelenko, Yu. A. *Izvest. Akademii Nauk SSSR, Ser. Khim.* **1990**, 1368. (b) Hammond, G. S.; Turro, N. J.; Liu, K. S. H. *J. Org. Chem.* **1963**, *28*, 3297. (c) Goliaszewski, A.; Schwartz, J. *Tetrahedron* **1985**, *41*, 5779.

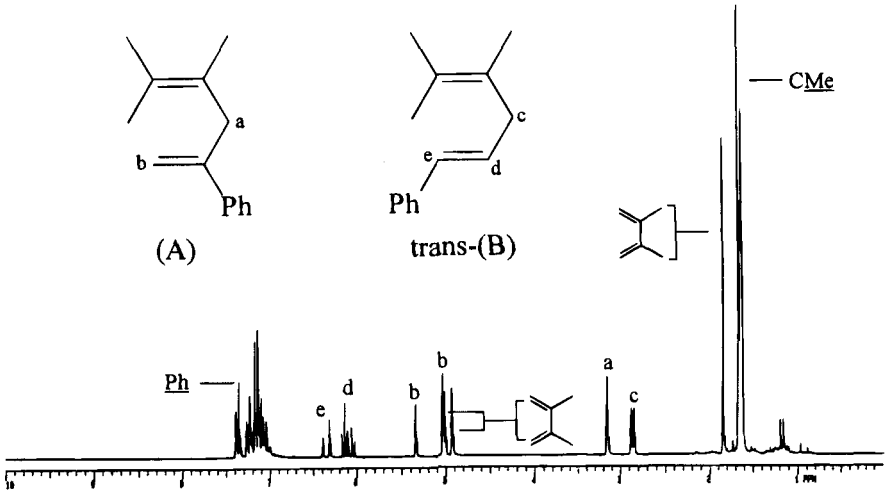

Figure 2. Cross-coupling of 2,3-dimethylbutadiene and styrene catalyzed by **7**, 200 MHz ^{1}H NMR spectrum of the reaction mixture.

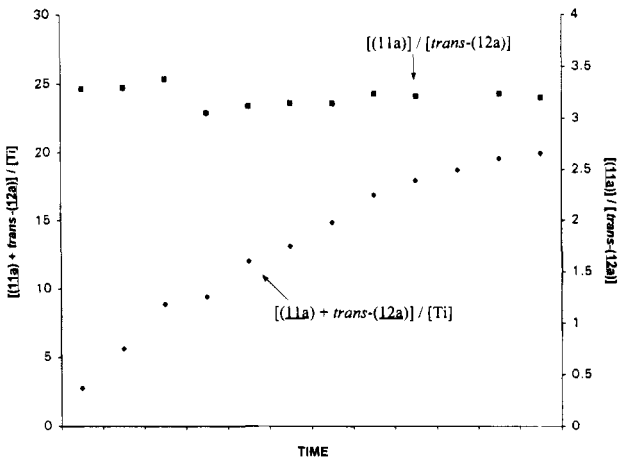

Figure 3. Plot of isomer ratio [**11a**]/[***trans*-12a**] and product concentration [**11a** + **12a**]/[Ti] vs time.

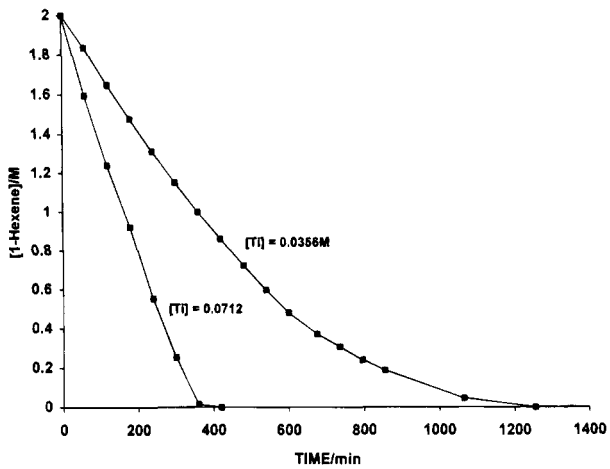

Figure 4. Plot of [1-hexene] = [2,3-dimethylbutadiene] vs time in the cross-coupling of 2,3-dimethylbutadiene and 1-hexene catalyzed by **8**.

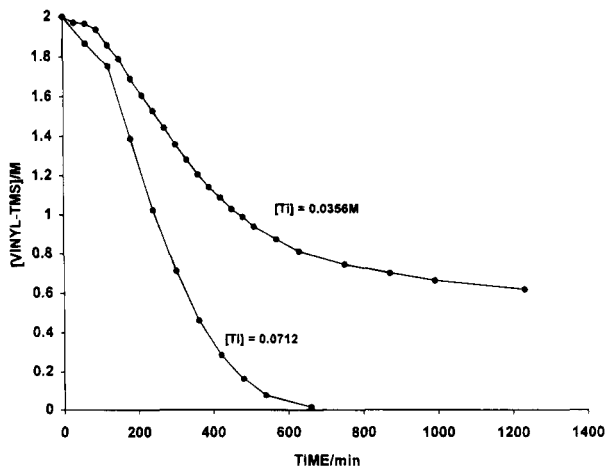

Figure 5. Plot of [vinyltrimethylsilane] = [2,3-dimethylbutadiene] vs time in the cross-coupling of 2,3-dimethylbutadiene and vinyltrimethylsilane catalyzed by **8**.

were carried out at 65 °C using 2 M concentrations of α-olefin and 2,3-dimethylbutadiene in C_6D_6 solvent. For each of the α-olefins, two reactions employing different total [Ti] were used to obtain plots of concentration of substrates (α-olefin or 2,3-dimethylbutadiene) vs time. An approximate zero-order dependence in substrate concentration is observed in the reaction of 1-hexene with 2,3-dimethylbutadiene for [Ti] = 0.0712 and 0.0356 M (Figure 4) but with definite curvature to the plots. The plot of concentration of substrates vs time in the reaction using vinyltrimethylsilane (Figure 5) shows that an induction period is present. We ascribe this induction period to a slow initial reaction of vinyltrimethylsilane with the catalyst precursor **8** to generate 1 equiv of a 1,3-cyclohexadiene and the active titanium catalyst.[12] It can also be seen that complete catalyst deactivation occurs prior to completion of the reaction when [Ti] = 0.0356 M (Figures 4 and 5).

The plots of concentration of substrates vs time show that there is a definite rate dependence in total [Ti]. We have found that it is informative to plot [product]/[Ti] ([product] = [**11**] + [*trans*-**12**]) vs time (Figure 6). These plots show the number of equivalents per titanium of product produced over time for each of the α-olefins. A decrease in catalyst activity with time is apparent for all of the reactions. However, the parallel behavior of these plots for different initial [Ti] confirms

(12) Rothwell, I. P. *Acc. Chem. Res.* **1988**, *21*, 153.
(13) (a) Kerschner, J. L.; Torres, E. M.; Fanwick, P. E.; Rothwell, I. P.; Huffman, J. C. *Organometallics* **1989**, *8*, 1424. (b) Kerschner, J. L.; Fanwick, P. E.; Rothwell, I. P.; Huffman, J. C. *Organometallics* **1989**, *8*, 1431.
(14) Kalinowski, H. O.; Berger, S.; Braun, S. *^{13}C-NMR-Spektroskopie*; Georg Thieme Verlag: Stuttgart, New York, 1984; p 115.

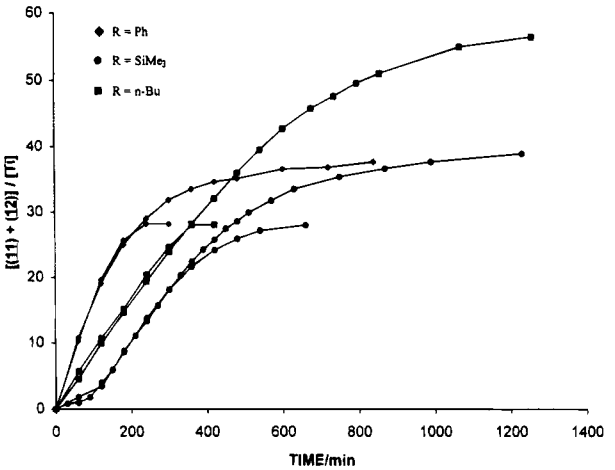

Figure 6. Cross-coupling of 2,3-dimethylbutadiene and styrene, vinyltrimethylstyrene, and 1-hexene catalyzed by **8**, [product]/[Ti] vs time.

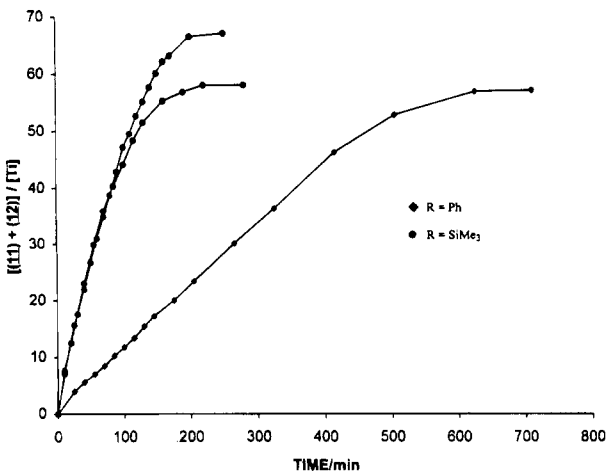

Figure 7. Cross-coupling of 2,3-dimethylbutadiene and α-olefins, styrene, and vinyltrimethylsilane catalyzed by **7**, [product]/[Ti] vs time.

that there is a first-order dependence in [Ti] (Figure 6). These plots also show that the rate of the reaction using styrene is slightly faster than the reactions using 1-hexene while the induction period complicates a kinetic assessment of vinyltrimethylsilane.

Plots of [product]/[Ti] with time for the reaction of vinyltrimethylsilane with 2,3-dimethylbutadiene catalyzed by butadiene complex **7** (Figure 7) show no induction period. Furthermore these plots and ones using styrene show very little catalyst deactivation with time when using the 2,6-diisopropylphenoxide precursor **7** compared to 2,6-diphenylphenoxide precursor **8**. This is highlighted by the spectrum in Figure 2 where titanacyclopent-3-ene complex **7** can still be detected after ~50 catalyst turnovers. One other piece of information that can be obtained from Figure 7 is that the cross-coupling reaction is faster when vinyltrimethylsilane is the α-olefin (30 equiv Ti^{-1} h^{-}) compared to styrene (8 equiv Ti^{-1} h^{-1}).

Labeling Studies. The effects of deuterium incorporation into the olefin were examined by carrying out the cross-coupling of styrene-d_8 with 2,3-dimethylbutadiene using titanacyclopentadiene (**8**) as catalyst precursor at 65 °C. This reaction was found to produce, at a slower rate than for protio styrene (*vide infra*), products **11*** and *trans*-**12*** analyzed by mass spectrometric analysis to both be d_8. A particularly striking observation is that incorporation of deuterium also leads to a change in the isomer ratio **11**/*trans*-**12** (Table 5, entries 1 and 2). In a subsequent crossover experiment, a 50/50 mixture of proteo and perdeuterated styrene was reacted with 2,3-dimethylbutadiene in the presence of a catalytic amount of **8** (Table 5, entry 3). Gas chromatographic and GC/MS analysis of the reaction mixture showed the presence of four major products: **11**-d_8, **11**-d_0, *trans*-**12**-d_8, and *trans*-**12**-d_0 with the deuterated molecules having shorter retention times.

Table 5[a]

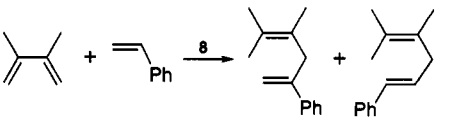

		yield, %	
		11a	*trans*-**12a**
1.	$PhCH{=}CH_2$	78	22
2.	$PhCD{=}CD_2$	57*	43*
3.	$PhCH{=}CH_2$	48	14
	$PhCD{=}CD_2$	20*	18*

[a] Solvent is C_6D_6; product percentages obtained by GC analysis. All reactions were performed with 2 M styrene and 2 M 2,3-dimethylbutadiene at 65 °C; * = deuterated products. Crossover experiment 3 used 2 M proteo styrene, 2 M perdeuterated styrene, and 2 M 2,3-dimethylbutadiene.

Table 6[a]

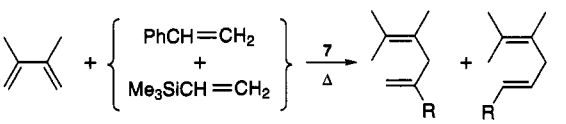

	yield, %	
R	A	*trans*-B
Ph	30	30
$SiMe_3$	30	10

[a] Solvent is C_6D_6; product percentages obtained by GC. Reaction performed at 65 °C.

Scheme 6

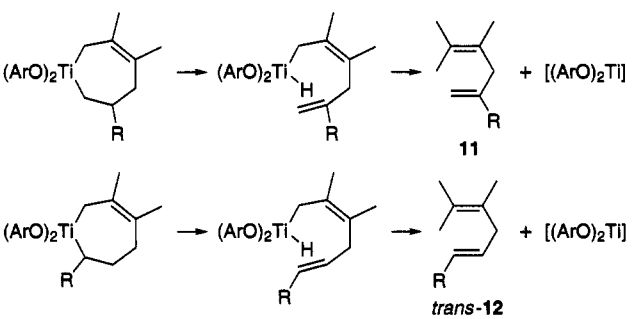

Mechanistic Considerations. Elimination from two intermediate titanacyclohept-3-ene complexes can account for the formation of **11** and *trans*-**12** (Scheme 6), while four possible metallacyclic intermediates are generated by differing regiochemical coupling of styrene and isoprene (Scheme 7). There has been extensive mechanistic work by Erker et al and Nakamura et al. on the reactivity of Group 4 metallocene derivatives of 1,3-butadienes. This work implies that direct ring expansion of the titanacyclopent-3-ene ring in complexes such as **7** and **8** by insertion of olefin is unlikely. Instead a pathway involving coupling of the olefin with

Scheme 7

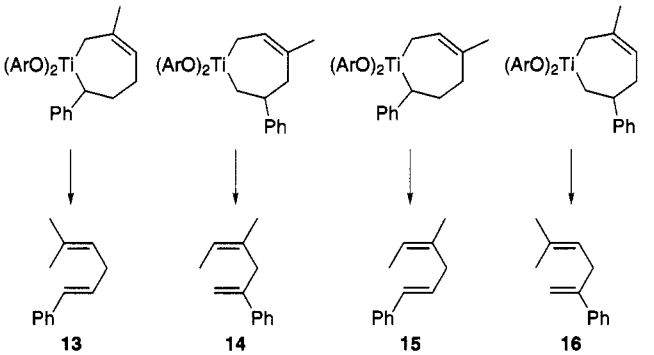

Scheme 8

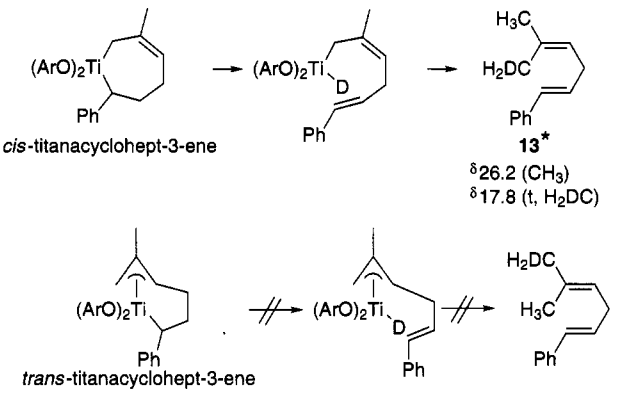

one of the diene double bonds is implicated to produce a 2-vinyltitanacyclopentane ring. This intermediate can then rearrange to form either *cis*- or *trans*-titanacyclohept-3-ene complexes such as **5a** and **5b**.

An important mechanistic question is whether elimination of the product occurs from either the *cis*- or *trans*-titanacyclohept-3-ene complexes or both. In the cross-coupling of styrene-d_8 with 2,3-dimethylbutadiene, the spectra of the products clearly show that deuterium incorporation occurs selectively into only one of the two methyl groups. However, the similarity of the chemical shifts of these methyl carbon atoms makes it impossible to unequivocally assign the deuterated methyl group as being *cis* or *trans* to the allylic function. This is not the case in the cross-coupling of styrene-d_8 with isoprene, where it is possible to conclusively show that deuterium incorporation occurs in the *cis*-methyl group of **13**, i.e., elimination takes place from the *cis*-titanacyclohept-3-ene ring (Scheme 8).

Although we have no direct evidence against it, we believe the fragment [(ArO)$_2$Ti] is not likely to form as a free species in solution during catalysis. Instead, displacement of the product 1,4-diene by either substrate olefin or 1,3-diene allows continuation of the catalytic cycle without release of this highly unsaturated species. It is particularly informative that the titanacyclohept-3-ene complex **5** does not eliminate 1,4-diene in the absence of added olefin/1,3-diene but instead undergoes ring contraction (Scheme 1).

The kinetic results indicate that the catalysis has a first-order dependence of [Ti] and a zero-order dependence on the olefin and 1,3-diene concentrations. Product distributions are kinetic in origin. Catalyst deactivation with time occurs in the case of the 2,6-diphenylphenoxide reagents. A reasonable explanation of this deactivation is the demonstrated tendency of

Scheme 9

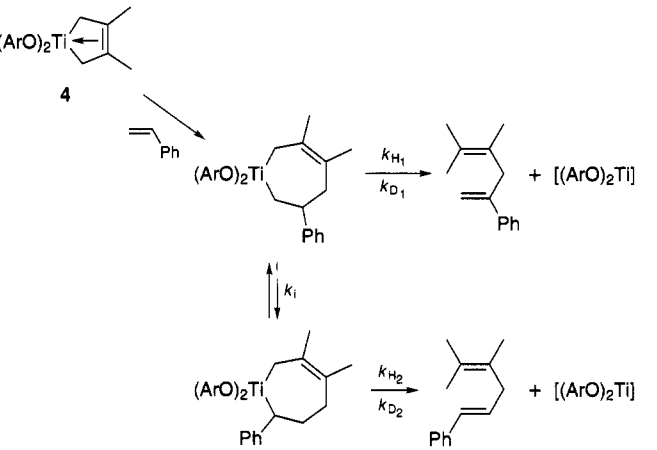

early d-block organometallic derivatives of 2,6-diphenylphenoxide to undergo cyclometalation.[12] The kinetic studies can be accommodated into a mechanistic pathway in which rate-determining β-hydrogen abstraction from intermediate titanacyclohept-3-ene ring takes place. This mechanism would also explain the decrease in the overall reaction rate upon deuteration of the olefin. In the case of the cross-coupling of styrene with 2,3-dimethylbutadiene, it was found that the product distribution also changed significantly upon deuteration of the olefin (Table 5). It is possible to rationalize this result using various mechanistic scenarios. We propose a reaction pathway in which coupling of styrene and 2,3-dimethylbutadiene products a β-phenyl titanacyclohept-3-ene complex as the initial kinetic product. This complex can then lead to elimination of 1,4-diene **11** or undergo isomerization (presumably by fragmentation back to coordinated styrene/diene) to the α-phenyl titanacyclohept-3-ene complex which can eliminate *trans*-**12** (Scheme 9). The isomerization of a kinetically formed β-phenyl titanacyclobutane ring into the α-phenyl regiosomer has been observed by Grubbs et al.[15] The introduction of deuterium into the styrene should have the effect of retarding (primary kinetic isotope effect k_{H1}/k_{D1}) the elimination of **11** but have little impact on the rate of isomerization (k_i) of the metallacycle ring hence leading to the observed increased proportion of *trans*-**12** in the product mixture.

The isoprene dimerization reactions can be viewed as taking place from the same type of titanacyclohept-3-ene intermediates as implicated in the cross-coupling reactions (vide supra). Three possible titanacyclohept-3-ene complexes can give rise to the observed vinylcyclohexenes and the linear dimer product (Scheme 10).

Experimental Section

All reactions were carried out under N_2 or vacuum using standard Schlenk techniques. Solvents were dried by distillation over Na/benzophenone under N_2. The synthesis of complexes **1**,[8] **8**,[6] and **9**[10] have been previously reported. Perdeuterated styrene was purchased from Aldrich Chemical Co. and used directly from the vial. Proton and ^{13}C NMR spectra were recorded using a Varian Gemini 200-MHz instrument. Gas chromatographic analyses were performed with a Hewlett Packard model 5890 Series II gas chromatograph using a capillary column (HP-1, cross-linked methyl silicone

(15) Ikariya, T.; Ho, S. C. H.; Grubbs, R. H. *Organometallics* **1985**, *4*, 199.

Scheme 10

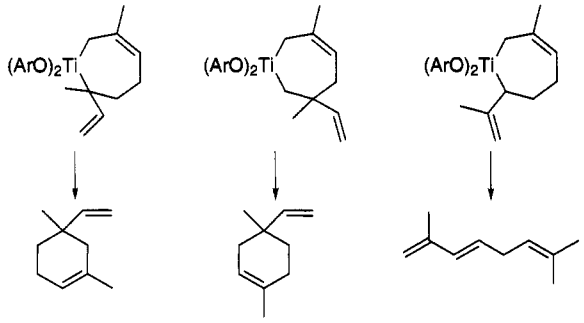

Table 7. Crystal Data and Data Collection Parameters

formula	$TiO_2C_{42}H_{36}$
formula weight	620.65
space group	*Fdd*2 (No. 43)
a, Å	35.351(3)
b, Å	37.927(3)
c, Å	9.755(1)
V, Å^3	13079(3)
Z	16
d_{calc}, g cm^{-3}	1.261
crystal dimensions, mm	0.63 × 0.35 × 0.25
temperature, °C	−60
radiation (wavelength)	Mo Kα (0.71073 Å)
monochromator	graphite
linear abs coef, cm^{-1}	2.91
absorption correction applied	none
diffractometer	Enraf-nonius CAD4
scan method	ω
h, *k*, *l* limits:	0 to 11, 0 to 41, 0 to 44
2θ range, deg	4.00−50.00
scan width, deg	0.66 + 0.35 tan θ
take-off angle, deg	2.95
programs used	Enraf-Nonius MolEN
F_{000}	5216.0
p-factor used in weighting	0.040
data collected	3167
unique data	3167
data with $I > 3.0\sigma(I)$	2559
no. of variables	421
largest shift/esd in final cycle	0.10
R	0.032
R_w	0.039
goodness of fit	1.147

gum; 25 m × 0.2 mm × 0.33 μm film thickness) with a flame ionization detector. Mass spectral and X-ray crystallographic data were acquired through Purdue in-house facilities. Crystal data and data collection parameters of the X-ray crystallographic analysis of **4** are given in Table 7.

Preparation of [(Ar′O)$_2$Ti(CH$_2$CH=CHCH$_2$CH$_2$CH$_2$)] (2). Solid **1** (0.25 g, 0.42 mmol) was dissolved in C_6H_6 (5 mL), and an excess of 1,3-butadiene was quickly added to the solution with a calibrated gas manifold. Vigorous stirring was continued for 5 min; then hexane was added to the benzene solution to induce the formation of light orange crystals of **2**. The crystals were washed with hexane and dried under vacuum. Anal. Calcd for $TiC_{42}H_{36}O_2$ (**2**): C, 81.28; H, 5.85. Found: C, 81.37; H, 5.92. ^{1}H NMR (C_6D_6, 30 °C): δ 6.8−7.4 (aromatics); 4.36 (td, *trans*, ^1J = 16 Hz, *cis*, ^1J = 8.5 Hz, TiCH$_2$C*H*); 3.21 (ddd, TiCH$_2$CHC*H*); 2.25 (m), 2.20 (m, TiCH$_2$C*H*$_2$); 1.90 (dd), 0.84 (dd, TiC*H*$_2$CH); 1.77 (dtd), 1.57 (ddt, TiCH$_2$CH$_2$C*H*$_2$); 1.69 (br d), −0.24 (dt, TiC*H*$_2$CH$_2$). Selected ^{13}C NMR (C_6D_6, 30 °C): δ 160.4, 160.3 (Ti−O−*C*); 140.7, 140.4 (ortho carbons on phenoxides); 133.5, 133.4 (ipso carbons on phenyls of phenoxides); 136.3, 135.6 (TiCH$_2$*C*HCH); 77.7, 77.2 (Ti*C*H$_2$); 45.3, 35.8 (TiCH$_2$*C*H$_2$*C*H$_2$).

Preparation of [(Ar′O)$_2$Ti(CH$_2$CMe=CHCH$_2$CH$_2$CH$_2$)] (3). A solution of **1** (0.25 g, 0.42 mmol) dissolved in C_6H_6 (5 mL) was quickly mixed with an excess of isoprene (0.084 mL, 0.84 mmol). The reaction mixture was stirred for 5 min; then the solvent was removed under vacuum. The resulting residue was redissolved in a minimum of hexane, from which bright orange crystals of **3** were isolated after 6 h. The crystals were washed with hexane and dried under vacuum. Anal. Calcd for $TiC_{43}H_{38}O_2$ (**3**): C, 81.38; H, 6.03. Found: C, 81.27; H, 6.00. ^{1}H NMR (C_6D_6, 30 °C): δ 6.8−7.6 (aromatics); 2.89 (dd, CMeC*H*); 2.18 (d), 0.87 (d, TiC*H*$_2$CMe); 2.12 (m), 1.9 (m, TiCH$_2$CH$_2$C*H*$_2$); 1.9 (m), 1.26 (m, TiCH$_2$C*H*$_2$CH$_2$); 1.62 (m), −0.06 (m, TiC*H*$_2$CH$_2$CH$_2$); 0.70 (s, C*Me*). Selected ^{13}C NMR (C_6D_6, 30 °C): δ 160.1 (Ti−O−*C*); 140.7 (ortho carbons on phenyls of phenoxides); 143.6 (*C*MeCH); 131.8 (CMe*C*H); 82.3, 72.0 (Ti*C*H$_2$); 43.9, 31.3 (TiCH$_2$*C*H$_2$*C*H$_2$); 18.6 (C*Me*).

Preparation of [(Ar′O)$_2$Ti(CH$_2$CMe=CMeCH$_2$)] (4). Solid [(OAr)$_2$Ti(CH$_2$)$_4$] (**1**) (0.5 g, 0.84 mmol) was placed in a solvent seal flask fitted with an addition funnel containing 3 equiv of 2,3-dimethylbutadiene (0.143 mL, 2.52 mmol) and C_6H_6 (10 mL). The diene/C_6H_6 solution was aded to the solid all at once, and the reaction mixture was immediately placed under vacuum to remove volatile ethylene and excess solvent. The resulting residue was redissolved in a minimum of benzene and layered with hexane to induce the formation of dark purple crystals of **4**. The crystals were washed with hexane and dried under vacuum. Hydrocarbon solutions of the crystalline product are green. Anal. Calcd for $TiC_{42}H_{36}O_2$ (**4**): C, 81.28; H, 5.85. Found: C, 80.87; H, 5.79. ^{1}H NMR (C_6D_6, 30 °C): δ 6.9 − 7.6 (aromatics); 3.02 (d), 1.35 (d, C*H*$_2$); 0.77 (s, C*Me*). Selected ^{13}C NMR (C_6D_6, 30 °C): δ 129.6 (*C*Me); 87.9 (Ti*C*H$_2$, $^1J(^{13}C-^1H)$ = 138.2, 160.8 Hz); 22.4 (C*Me*). Hydrolysis product 2,3-dimethyl-1-butene, ^{1}H NMR (C_6D_6, 30 °C): δ 4.76 (m, C*H*$_2$CMe); 2.13 (septet, C*H*Me$_2$); 1.61 (br, CH$_2$C*Me*); 0.94 (d, CH*Me*$_2$).

Preparation of [(Ar′O)$_2$Ti(CH$_2$CMe=CMeCH$_2$CH$_2$CH$_2$)] (5). Solid **1** (0.50 g, 0.84 mmol) was dissolved in C_6H_6 (10 mL), and the resulting solution was saturated with ethylene. One equivalent of 2,3-dimethylbutadiene (0.095 mL, 0.84 mmol) was added to the solution, and this was stirred for 10 min. The solvent was then removed under vacuum, and the resulting residue was redissolved in a minimum of benzene. The benzene solution was layered with hexane to induce the formation of dark orange crystals of **5**. The crystals were washed with hexane and dried under vacuum. Anal. Calcd for $TiC_{44}H_{40}O_2$ (**5**): C, 81.47; H, 6.22. Found: C, 81.28; H, 6.41. Selected ^{1}H NMR (C_6D_6, 30 °C); δ 6.8−7.5 (aromatics); 2.13 (d), 1.10 (d, TiC*H*$_2$CMe major isomer); 0.63 (s), 0.23 (s, C*Me*C*Me* major isomer); 1.33 (s), 0.94 (s, C*Me*C*Me* minor isomer). Selected ^{13}C NMR (C_6D_6, 30 °C): major isomer, δ 160.6, 160.5 (Ti−O−*C*), 143.8, 139.4 (*C*MeCMe), 140.8, 140.7 (ortho carbons on phenoxides), 133.5, 133.4 (ipso carbons on phenyls of phenoxides), 80.8, 70.6 (Ti*C*H$_2$), 45.2, 36.4 (TiCH$_2$*C*H$_2$*C*H$_2$), 21.2, 21.1 (C*Me*C*Me*); minor isomer, δ 92.1, 75.6 (Ti*C*H$_2$); 36.2, 36.0 (TiCH$_2$*C*H$_2$*C*H$_2$); 16.1, 15.5 (C*Me*C*Me*).

Preparation of [(Ar′O)$_2$Ti(CH$_2$CMe=CMeCHEt)] (6). Crystalline **5** (0.50 g, 0.77 mmol) was dissolved in C_6H_6 and allowed to stand at room temperature for 20 h. The solvent was then removed under vacuum and the resulting residue redissolved in a minimum of hexane. Dark purple crystals of compound **6** formed from the solution, and these were isolated, washed with hexane, and dried under vacuum. Hydrocarbon solutions of the purple crystals are green. Anal. Calcd for $TiC_{44}H_{40}O_2$ (**6**): C, 81.47; H, 6.13. Found: C, 78.18, H, 5.88. ^{1}H NMR (C_6D_6, 30 °C): δ 6.8−7.7 (aromatics); 2.80 (d), 1.18 (d, TiC*H*$_2$); 1.82 (t, TiC*H*Et); 1.70 (dp); 1.42 (p, CHC*H*$_2$CH$_3$); 0.68 (t, CH$_2$*Me*); 0.81 (s), 0.62 (s, C*Me*C*Me*). Selected ^{13}C NMR (C_6D_6, 30 °C): δ 160.7 (Ti−O−*C*); 127.8, 127.2 (*C*MeCMe); 108.4 (Ti*C*HEt, $^1J(^{13}C-^1H)$ = 127 Hz); 88.3 (Ti*C*H$_2$); 24.5 (*C*H$_2$Me); 23.1 (CH$_2$*Me*); 16.1, 15.5 (C*Me*C*Me*). Hydrolysis product 2,3-dimethyl-1-hexene, ^{1}H NMR (C_6D_6, 30 °C): δ 4.77 (t, C*H*$_2$CMe); 2.10 (m, C*H*Me); 1.58 (t, CH$_2$C*Me*); 1.2 (m, C*H*$_2$C*H*$_2$Me); 0.94 (d, CH*Me*); 0.82 (t, CH$_2$*Me*).

Preparation of [(Ar″O)$_2$Ti(CH$_2$CMe=CMeCH$_2$)] (7). A mixture of [(Ar″O)$_2$TiCl$_2$] (5.0 g, 10.6 mmol) and 2,3-dimethylbutadiene (1.8 mL, 1.3 g, 16.0 mmol) in Et$_2$O (100 mL) was stirred over a sodium amalgam (0.74 g, 31.8 mmol) for 18 h.

The initially deep red solution became intensely green colored within 5 min and finally turned a dark purple/brown color. The suspension was decanted from the mercury pool, filtered, and evaporated in vacuo to yield the product **7** as a viscous, purple liquid. ^{1}H NMR (C_6D_6, 30 °C): δ 6.8–7.3 (aromatics); 4.06 (d), 2.06 (d, ^2J = 8.7 Hz, TiCH_2); 1.73 (s, C*Me*=C*Me*); 1.21 (d, CH(CH_3)$_2$); 3.53 (septet, C*H*(CH_3)$_2$). Selected ^{13}C NMR (C_6D_6, 30 °C): δ 137.9 (*C*Me); 83.2 (Ti*C*H$_2$, ^1J(^{13}C–^{1}H) = 160.3 Hz, 134.3 Hz); 162.2 (Ti–O–*C*); 23.9 (CH(*C*H$_3$)$_2$); 27.9 (*C*H-(CH_3)$_2$).

Cross-Coupling Reaction of 2,3-Dimethylbutadiene with Ethylene Catalyzed by 5. In a J. Young Valve NMR tube, an excess of 2,3-dimethylbutadiene was added to a C_6D_6 solution of **5**. The solution was saturated with ethylene, and the ethylene was replenished as needed. The product, 4,5-dimethylhexa-1,4-diene (**10**) was formed catalytically over days at room temperature. A turnover rate of ~8 Ti^{-1} h^{-1} was calculated at 70 °C. ^{1}H NMR (C_6D_6, 30 °C), 4,5-dimethylhexa-1,4-diene: δ 5.74 (m, CH$_2$=C*H*); 5.00 (m, C*H*$_2$=CH); 2.72 (br d, CH$_2$); 1.58 (br s, *Me*$_2$C=C*Me*). ^{13}C NMR (C_6D_6, 30 °C), 4,5-dimethylhexa-1,4-diene: δ 137.1 (CH2=*C*H); 125.9, 125.7 (Me$_2$*C*=*C*Me); 115.0 (*C*H$_2$=CH); 39.4 (*C*H$_2$); 20.7, 20.3, 18.6 (*Me*$_2$C=C*Me*).

Cross-Coupling Reactions of 2,3-Dimethylbutadiene with α-Olefins (H$_2$C=CR, R = Ph, SiMe$_3$, Bu^n) Catalyzed by 7, 8, and 9. A predetermined amount of catalyst precursor **7**, **8**, or **9** was dissolved in C_6D_6 in a J. Young Valve NMR tube. To the catalyst precursor/C_6D_6 mixture were added predetermined amounts of the α-olefins and 2,3-dimethylbutadiene to make a total volume of 1 mL. A temperature-controlled bath was used to maintain the reaction mixture at 65 °C. The concentrations of 2,3-dimethylbutadiene, α-olefins, and 1,4-diene products **11** and **12** were determined as a function of time by ^{1}H NMR integration. Isomer distributions of the 1,4-diene products **11** and **12** were determined by gas chromatographic analysis. ^{1}H NMR (C_6D_6, 30 °C) R = Ph (**11a**): δ 6.9–7.5 (aromatics); 5.35 (d), 5.02 (d, C*H*$_2$=CPh, *gem* ^2J = 1.8 Hz); 3.16 (s, C*H*$_2$); 1.63 (s), 1.65 (s), 1.67 (s, *Me*$_2$C=C*Me*). ***trans*-12a**: δ 6.9–7.5 (aromatics); 6.39 (d, PhC*H*=CH, *trans* ^3J = 15.8 Hz); 6.13 (dt, PhCH=C*H*); 2.87 (d, C*H*$_2$, ^3J = 6.5 Hz); 1.63 (s), 1.65 (s), 1.67 (s, *Me*$_2$C=C*Me*). R = SiMe$_3$ (**11b**): δ 5.44 (m), 5.61 (m, C*H*$_2$=CSiMe$_3$); 0.12 (s, Si*Me*$_3$); 2.92 (s, C*H*$_2$); 1.64 (s), 1.67 (s, *Me*$_2$C=C*Me*). ***trans*-12b**: δ 5.73 (dt, Me$_3$-SiC*H*=CH, *trans* ^3J = 18.4 Hz); 6.06 (dt, Me$_3$SiCH=C*H*, ^3J = 5.9 Hz); 2.87 (d, C*H*$_2$); 0.11 (s, Si*Me*$_3$); 1.64 (s), 1.67 (s, *Me*$_2$C=C*Me*). ***cis*-12b**: δ 5.67 (d, Me$_3$SiC*H*=CH, *cis* ^3J = 14.3 Hz); 6.25 (dt, Me$_3$SiCH=C*H*, vinyl ^3J = 7.0 Hz); 1.64 (s), 1.67 (s, *Me*$_2$C=C*Me*). R = Bu^n (**11c**): δ 4.82 (s), 4.97 (s, C*H*$_2$=CBu^n); 2.72 (s, C*H*$_2$); 1.93 (t, C*H*$_2$Pr^n); 1.38 (p, CH$_2$C*H*$_2$Et); 1.25 (sextet, CH$_2$CH$_2$C*H*$_2$Me); 0.84 (t, CH$_2$*Me*, ^3J = 7.8 Hz); 1.61 (s, *Me*$_2$C=C*Me*). ***trans*-12c**: δ 5.38 (m, Bu^{n}C*H*=C*H*); 2.72 (d, C*H*$_2$); 1.93 (t, C*H*$_2$Pr^n); 1.38 (p, CH$_2$C*H*$_2$Et); 1.25 (sextet, CH$_2$-CH$_2$C*H*$_2$Me); 0.84 (t, CH$_2$*Me*, ^3J = 7.8 Hz). Selected ^{13}C NMR (C_6D_6, 30 °C) R = Ph (**11a**): δ 19.1, 20.9, 21.1 (*Me*$_2$C=C*Me*); 40.8 (*C*H$_2$); 113.0 (*C*H$_2$=CPh); 125.8, 142.9, 146.8 (CH$_2$=*C*Ph, Me$_2$*C*=CMe). ***trans*-12a**: δ 19.0, 20.7, 21.1 (*Me*$_2$C=C*Me*); 38.8 (*C*H$_2$); 131.0, 129.2 (Ph*C*=CH, PhC=*C*H). R = SiMe$_3$ (**11b**): δ 19.1, 20.9 (*Me*$_2$C=C*Me*); 41.0 (*C*H$_2$); 126.0, 131.5 (*C*H$_2$=*C*-HSiMe$_3$); 124.5, 149.5 (Me$_2$*C*=CMe); −0.1 (Si*Me*$_3$). ***trans*-12b**: δ 20.7, 21.0 (*Me*$_2$C=C*Me*); 42.7 (*C*H$_2$); 124.1, 130.3 (*C*H$_2$=*C*HSiMe$_3$); 124.5, 149.7 (Me$_2$*C*=CMe); −0.6 (Si*Me*$_3$). R = Bu^n (**11c**): δ 14.5 (CH$_2$*Me*); 18.8, 20.8, 20.9 (*Me*$_2$C=C*Me*); 23.2, 30.9, 36.5 (*C*H$_2$Pr^n, CH$_2$*C*H$_2$Et, CH$_2$CH$_2$*C*H$_2$Me); 41.8 (*C*H$_2$); 109.9 (*C*H$_2$=CBu^n); 113.4 (CH$_2$=*C*Bu^n); 126.0, 147.9 (Me$_2$*C*=CMe). ***trans*-12c**: δ 14.5 (CH$_2$CH$_2$*C*H$_2$Me); 23.0, 32.6, 33.0 (*C*H$_2$Pr^n, CH$_2$*C*H$_2$Et, CH$_2$CH$_2$*C*H$_2$Me); 38.4 (*C*H$_2$); 128.5, 131.1 (Bu^{n}CH=CH, Bu^{n}CH=*C*H); 126.0, 147.9 (Me$_2$*C*=CMe). MS(EI) R = Ph (**11a**): 186 (M$^+$, 27.1), 172 (11.1), 171 (100.0), 157 (10.3), 156 (18.8), 143 (40.4), 142 (10.8), 129 (28.5), 128 (22.2), 118 (10.7), 115 (18.7), 103 (36.0), 91 (25.9), 77 (27.1), 55 (23.2), 51 (10.4). ***trans*-12a**: 186 (M$^+$, 84.7), 172 (11.1), 171 (84.2), 156 (15.8), 143 (100.0), 141 (12.9), 129 (44.3), 128 (35.4), 117 (15.8), 116 (10.6), 115 (42.6), 104 (16.1), 95 (15.6), 93 (15.6), 91 (66.6), 77 (13.4), 67 (16.6), 65 (10.2), 55 (10.9). R = SiMe$_3$ (**11b**): 182 (M$^+$, 6.8), 73 (100.0). ***trans*-12b**: 182 (M$^+$, 9.4), 73 (100.0), 59 (11.9).

Cross-Coupling Reactions of 2,3-Dimethylbutadiene with α-Olefins (H$_2$C=)Cr, R = H, Me, Et) Catalyzed by 8. A predetermined amount of catalyst precursor **8** was dissolved in C_6D_6 in a J. Young Valve NMR tube. The α-olefins were added to the **8**/C_6D_6 mixture using a calibrated gas manifold. The reaction with ethylene as olefin was performed at 25 °C while a temperature controlled bath was used to maintain the temperature at 80 °C for the reactions using propylene and 1-butene. Isomer ratios of the 1,4-diene products **11** and **12** were determined from the ^{1}H NMR spectra. ^{1}H NMR (C_6D_6, 30 °C) R = Me (**11d**): δ 4.79 (m), 4.82 (m, C*H*$_2$=CMe); 1.62 (br s, *Me*$_2$C=C*Me*); 2.72 (s, C*H*$_2$). R = Pr^n (**11e**): δ 4.80 (m), 4.84 (m, C*H*$_2$=CPr^n); 2.74 (br s, C*H*$_2$); 0.89 (t, CH$_2$*Me*, ^3J = 7.5 Hz); 1.63 (br s, *Me*$_2$C=C*Me*). ***trans*-12e**: δ 1.00 (t, *Me*CH$_2$=CH, ^3J = 7.4 Hz); 1.92 (m, C*H*$_2$Me); 1.63 (br s, *Me*$_2$C=C*Me*). Selected ^{13}C NMR (C_6D_6, 30 °C) R = Me (**11d**): δ 43.3 (*C*H$_2$); 111.2 (*C*H$_2$=CMe). R = Et (**11e**): δ 12.7 (CH$_2$*Me*); 29.2 (*C*H$_2$-Me); 41.9 (*C*H$_2$); 108.9 (*C*H$_2$=CEt). MS(EI) R = Me (**11d**): (M$^+$, 9.5), 109 (81.7), 84 (22.0), 81 (22.3), 67 (100.0), 55 (45.3), 53 (16.4). ***trans*-12d**: (M$^+$, 30.3), 109 (49.8), 84 (69.6), 82 (10.1), 81 (29.2), 67 (100.0), 56 (22.4), 55 (45.1), 54 (23.0), 53 (17.6), 52 (21.5). R = Et (**11e**): 138 (M$^+$, 18.8), 123 (29.0), 109 (75.7), 95 (15.7), 81 (70.1), 79 (12.0), 69 (23.7), 68 (10.3), 67 (100.0), 55 (74.4), 53 (28.9). ***trans*-12e**: 138 (M$^+$, 52.5), 123 (28.8), 109 (40.6), 95 (37.2), 93 (10.6), 91 (12.7), 82 (11.2), 81 (100.0), 79 (20.6), 77 (14.5), 69 (18.4), 68 (14.4), 67 (95.2), 65 (12.4), 57 (12.8), 55 (75.7), 53 (30.9), 51 (13.2).

Cross-Coupling Reaction of 2,3-Dimethylbutadiene with Styrene Catalyzed by a Mixture of [(Ar′O)$_2$TiCl$_2$] with 2 equiv of *n*-BuLi. To a mixture of [(Ar″O)$_2$TiCl$_2$] (0.10 g, 0.16 mmol), 2,3-dimethylbutadiene (0.50 mL, 4.4 mmol), and styrene (0.50 mL, 4.4 mmol) in benzene (5 mL) was slowly added a solution of *n*-BuLi (0.13 mL of a 2.5 M solution, 0.32 mmol). The resulting mixture was heated at 65 °C and analyzed by GC to show the build up of **11a** and *trans*-**12a**.

Cross-Coupling Reaction of Isoprene with Styrene Catalyzed by 8. Catalyst precursor **8** (25 mg, 0.036 mmol) was dissolved in C_6D_6 (0.5 mL) in a J. Young Valve NMR tube. Styrene (0.2 mL, 0.18 g, 1.7 mmol) and isoprene (0.2 mL, 0.14 g, 2.1 mmol) were added to the **8**/C_6D_6 mixture. A temperature-controlled bath was used to maintain the reaction temperature at 90 °C. The build up of 1.4-addition and isoprene dimer products was monitored by GC and ^{1}H NMR. Additional 0.1 mL (0.07 g, 1.0 mmol) aliquots of isoprene were added after 23 and 42 h reaction time. After 63 h at 90 °C, the reaction mixture was eluted through a silica gel column, and the 1,4-addition products were analyzed by GC and ^{1}H and ^{13}C NMR. Selected ^{1}H NMR (C_6D_6, 30 °C) **13**: δ 6.8–7.7 (aromatics); 6.38 (d, PhC*H*=CH, *trans* ^3J = 15.8 Hz); 6.12 (dt, PhCH=C*H*, vinyl ^3J = 6.4 Hz); 2.83 (t, C*H*$_2$, vinyl ^3J = 6.9 Hz); 5.26 (t of septets, Me$_2$C=C*H*); 1.55 (s), 1.68 (s, *Me*). **14**: δ 6.9–7.8 (aromatics); 5.34 (m, C*H*$_2$=CPh); 3.13 (s, C*H*$_2$); 5.06 (q, MeC*H*=CMe); 1.58 (br s), 1.66 (br s, *Me*). **15**: δ 5.12 (q, MeC*H*=CMe); 3.14 (d, superimposed on singlet of **14**). Selected ^{13}C NMR (C_6D_6, 30 °C) **13**: δ 18.1 (*trans*-*Me*CMe=CH); 26.3 (*cis*-MeC*Me*=CH); 32.4 (*C*H$_2$); 133.1 (Me*C*Me=CH); 122.7 (MeCMe=*C*H).

Cross-Coupling Reaction of 2,3-Dimethylbutadiene with Perdeuterated Styrene Catalyzed by 8. Catalyst precursor **8** (25 mg, 0.036 mmol) was dissolved in C_6D_6 (0.52 mL) in a J. Young Valve NMR tube. Perdeuterated styrene (0.230 mL, 0.21 g, 1.9 mmol) and 2,3-dimethylbutadiene (0.25 mL, 0.18 g, 2.2 mmol) were added to the **8**/C_6D_6 mixture. A temperature-controlled bath was used to maintain the reaction temperature at 65 °C. The build up of the deuterated 1,4-diene isomers **11a*** and *trans*-**12a*** was followed by ^{1}H NMR, and the final isomer distribution was obtained by gas chromatographic analysis. ^{1}H NMR (C_6D_6, 30 °C) mixture, **11a*** and ***trans*-12a***: δ 1.62 (s), 1.64 (s), 1.66 (s, *Me*, C*H*$_2$D) 3.15

(s, CH_2, **11a***); 2.85 (s, CH_2, *trans*-**12a***). Selected ^{13}C NMR (C_6D_6, 30 °C) mixture, 11a* and *trans*-**12a***: δ 19.0, 19.1, 21.0, 21.1 ($H_2DCMe{=}CMe$); 20.3, 20.7 (t, $H_2DCMe{=}CMe$, $^1J(^{13}C-D)$ = 10.2 Hz); 38.7 (CH_2, *trans*-**12a***); 40.6 (CH_2, **11a***). MS (EI) **11a***: 194 (M^+, 51.5), 180 (12.6), 179 (100.0), 178 (55.8), 177 (34.5), 176 (10.8), 164 (13.0), 163 (16.5), 162 (13.6), 150 (23.5), 149 (30.1), 148 (18.0), 147 (12.2), 136 (11.0), 135 (17.7), 134 (25.8), 133 (19.2), 132 (10.2), 125 (16.7), 121 (11.4), 120 (12.2), 111 (10.9), 110 (43.7), 108 (11.8), 97 (12.7), 96 (20.2), 95 (10.8), 84 (10.7), 82 (32.0), 56 (17.9), 55 (12.1), 54 (16.8). ***trans*-12a***: 194 (M^+, 100.0), 179 (66.0), 178 (44.5), 163 (10.5), 151 (11.5), 150 (34.5), 149 (38.9), 148 (19.6), 147 (11.0), 136 (15.2), 135 (24.2), 134 (24.8), 133 (14.9), 124 (11.9), 121 (21.4), 120 (17.5), 111 (13.0), 110 (10.7), 98 (14.8), 97 (44.4), 96 (33.7), 95 (14.9), 68 (12.7), 54 (11.9).

Cross-Coupling Reaction of Isoprene with Perdeuterated Styrene Catalyzed by 8. Catalyst precursor **8** (25 mg, 0.036 mmol) was dissolved in C_6D_6 (0.5 mL) in a J. Young Valve NMR tube. Perdeuterated styrene (0.2 mL, 0.18 g, 1.6 mmol) and isoprene (0.2 mL, 0.14 g, 2.1 mmol) were added to the **8**/C_6D_6 mixture. A temperature-controlled bath was used to maintain the reaction temperature at 90 °C. The build up of 1,4-addition and isoprene dimer products was monitored by GC and ^1H NMR. After 58 h at 90 °C, the reaction mixture was eluted on a preparatory TLC plate, and ^1H and ^{13}C NMR spectra were taken on **13***. Selected ^1H NMR (C_6D_6, 30 °C) C*: δ 2,83 (d, CH_2, vinyl ^3J = 5.8 Hz); 5.2–5.4 (m, $CH_2DCMe{=}CH$); 1.54 (br s, $CH_2DCMe{=}CH$), 1.69 (br s, $CH_2DCMe{=}CH$). Selected ^{13}C NMR (C_6D_6, 30 °C) **13***: δ 17.8 ($CH_2DCMe{=}CH$, $^1J(^{13}C-D)$ = 19.2 Hz); 26.2 ($CH_2DCMe{=}CH$); 32.3 (CH_2); 133.1 ($CH_2DCMe{=}CH$); 122.7 ($CH_2DCMe{=}CH$).

Cross-Coupling Reaction of Isoprene with Styrene Catalyzed by 9. A similar procedure to that used in the cross-coupling reaction of isoprene with styrene catalyzed by **8** except using a catalytic amount of catalyst precursor **9** resulted in a product distribution consisting of isoprene dimer products and the four 1,4-addition products C–F. The ^1H and ^{13}C NMR data for the isoprene dimer products are given below.

Isoprene Dimerization Reactions Catalyzed by 8 and 9. Isoprene (0.2 mL, 0.18 g. 0.17 mmol) was combined with a catalytic amount of **8** or **9** in C_6D_6 (0.6 mL) in separate J. Young Valve NMR tubes. The build up of the isoprene dimer products was monitored by GC and ^1H NMR. The reaction mixtures were eluted through silica gel columns after 43 h (**8**) and 34 h (**9**), and the products were analyzed by GC and ^1H and ^{13}C NMR. Selected ^1H NMR (C_6D_6, 30 °C) 2,7-dimethyl-1,3,6-octatriene: δ 1.53 (s), 1.66 (s), 1.78 (s, *Me*); 2.77 (t, CH_2, vinyl ^3J = 6.9 Hz); 6.21 (dt), 5.58 (dt, $CH{=}CHCH_2$, *trans* ^3J = 15.3 Hz). Isomeric mixture of 1,4-dimethyl-4-vinyl-1-cyclohexene and 2,4-dimethyl-4-vinyl-1-cyclohexene: δ 0.99 (s, tertiary *Me*); 1.61 (br s, vinyl *Me* overlapping with CH_2 protons); 1.3–2.2 (m, ring CH_2); 4.8–5.4 (m, $CH{=}CH_2$ and ring $C{=}CH$); 5.82 (dd), 5.80 (dd, $CH{=}CH_2$, *trans* ^3J = 17.5 hz, *cis* ^3J = 10.7 Hz). Selected ^{13}C NMR (C_6D_6, 30 °C) isomeric mixture of 1,4-dimethyl-4-vinyl-1-cyclohexene and 2,4-dimethyl-4-vinyl-1-cyclohexene: δ 111.0 ($CH{=}CH_2$); 148.1, 148.2 ($CH{=}CH_2$); 124.2 (ring $C{=}CH$).

Acknowledgment. We would like to thank the National Science Foundation for financial support of this research.

Supplementary Material Available: Text describing the data collection, structure solution, and refinement and listings of crystal data, fractional coordinates, anisotropic thermal parameters, and full bond distances and angles for the X-ray diffraction study of **4** (23 pages). Ordering information is given on any current masthead page.

OM9407565

Nickel(IV) Bis((3)-1,2-dicarbollide) as an Acceptor Molecule in the Synthesis of Electrically Conducting Charge Transfer Complexes

Peter A. Chetcuti,* Walther Hofherr, André Liégard, Grety Rihs, and Günther Rist*

Material Science and Physics Department, Ciba-Geigy Ltd., CH-4002 Basel, Switzerland

Hugo Keller and Damian Zech

Physics Institute, University of Zürich, CH-8001 Zürich, Switzerland

Received February 22, 1994®

The reaction of {*closo*-(3)-1,2-$C_2B_9H_{11}$}$_2Ni^{IV}$ (**1**) with tetrathiotetracene (TTT) and tetraselenotetracene (TSeT) leads to novel electrically conducting charge transfer complexes. The ESR and magnetic susceptibility of the complexes $[TTT_2]^{\bullet+}$[{*closo*-(3)-1,2-$C_2B_9H_{11}$}$_2Ni^{III}]^{\bullet-}$ (**2**) and $[TSeT]^{\bullet+}$[{*closo*-(3)-1,2-$C_2B_9H_{11}$}$_2Ni^{III}]^{\bullet-}$ (**3**) were studied. The susceptibilities of both complexes exhibit approximately Curie–Weiss behavior. Complex **2** shows a slight deviation from the Curie–Weiss law in the temperature region where the crystals show a significant electrical conductivity. An electron transfer mechanism exists between the TTT radical cations and the [{*closo*-(3)-1,2-$C_2B_9H_{11}$}$_2Ni^{III}]^{\bullet-}$ anions, which is slowed with decreasing temperature. The single-crystal room-temperature electrical conductivities of **2** and **3** are 23.3 and 17.3 S·cm^{-1}, respectively. Single-crystal X-ray structures of **2** and **3** are reported and consist of segregated stacks of conducting TTT or TSeT cations and nickel dicarbollide anions. Crystal data for **2**: $C_{40}H_{38}B_{18}NiS_8$ + $C_6H_3Cl_3$, triclinic, $P\bar{1}$, a = 6.834(1) Å, b = 12.368(1) Å, c = 16.077(2) Å, α = 86.75(1)°, β = 101.54(1)°, γ = 102.54(1)°, V = 1299.5(5) Å^3, Z = 1, D(calcd) = 1,546 g·cm^{-3}, T = 295 K, λ = 0.7107 Å, crystal size 0.50 × 0.32 × 0.05 mm, and μ = 8.76 cm^{-1}. Of the 4252 reflections measured, in the range 6° < 2θ > 48°, 2937 were considered observed ($I > 3\sigma(I)$). The final R factor was R = 0.038, R_w = 0.043. Crystal data for **3**: $C_{22}H_{30}B_{18}NiSe_4$, triclinic, $P\bar{1}$, a = 7.010 (1) Å, b = 14.567 (1) Å, c = 15.589 (3) Å, α = 94.60 (1)°, β = 89.92 (2)°, γ = 99.03 (2)°, V = 1567.0(8) Å^3, Z = 1, D(calcd) = 1.830 g·cm^{-3}, T = 295 K, λ = 1.5418 Å, crystal size 0.50 × 0.11 × 0.01 mm, and μ = 64.85 cm^{-1}. Of the 5812 reflections measured, in the range 6° < 2θ > 134°, 4689 were considered observed ($I > 3\sigma(I)$). The final R factor was R = 0.071, R_w = 0.074.

Introduction

The design and synthesis of novel charge transfer complexes and the investigation of their electrical[1] and magnetic[2] properties is currently an area of considerable research interest. Although there are a number of examples of organometallic metallacene and arene donor complexes that form charge transfer complexes with organic acceptors,[3] there are only a few examples of inorganic and organometallic anions that constitute the acceptor moiety of charge transfer complexes.[4] With exception of the bis(dithioline) metal complexes,[5] there is no class of inorganic or organometallic acceptors that can be used for the synthesis of new charge transfer complexes. For this reason, the known ability of the dicarbollide dianion $[C_2B_9H_{11}]^{2-}$ [6] to stabilize metals in

® Abstract published in *Advance ACS Abstracts,* December 1, 1994.

(1) (a) Marks, T. J. *Angew. Chem., Int. Ed. Engl.* **1990**, *29*, 857–859. (b) Williams, J. M.; Beno, M. A.; Wang, H. H.; Leung, P. C. W.; Emge, T. J.; Geiser, U.; Carlson, K. D. *Acc. Chem. Res.* **1985**, *18*, 261–267. (c) Saito, G.; Ferraris, J. P. *Bull. Chem. Soc. Jpn.* **1980**, *53*, 2141–2145. (d) Torrance, J. B. *Acc. Chem. Res.* **1979**, *12*, 79–86. (e) Garito, A. F.; Heeger, A. J. *Acc. Chem. Res.* **1974**, *7*, 232–240.

(2) (a) Miller, J. S.; Epstein, A. J.; Reiff, W. M. *Chem. Rev.* **1988**, *88*, 201–220. (b) Miller, J. S. *Adv. Mater.* **1992**, *4*, 298–300.

(3) (a) Yee, G. T.; Manriquez, J. M.; Dixon, D. A.; McLean, R. S.; Groski, D. M.; Flippen, R. B.; Narayan, K. S.; Epstein, A. J.; Miller, J. S. *Adv. Mater.* **1991**, *3*, 309–311. (b) Broderick, W. E.; Hoffman, B. M. *J. Am. Chem. Soc.* **1991**, *113*, 6334–6335. (c) Ward, M. D.; Fagan, P. J.; Calabrese, J. C.; Johnson, D. C. *J. Am. Chem. Soc.* **1989**, *111*, 1719–1732. (d) Ward, M. D.; Calabrese, J. C. *Organometallics* **1989**, *8*, 593–602. (e) Miller, J. S.; Calabrese, J. C.; Rommelmann, H.; Chittipeddi, S. R.; Zhang, J. H.; Reiff, W. M.; Epstein, A. J. *J. Am. Chem. Soc.* **1987**, *109*, 769–781. (f) Lequan, R. M.; Lequan, M.; Jaouen, G.; Ouahab, L.; Batail, P.; Padiou, J.; Sutherland, R. G. *J. Chem. Soc., Chem. Commun.* **1985**, 116–118. (g) Shibaeva, R. P.; Atovmyan, L. O.; Orfanova, M. N. *Chem. Commun.* **1969**, 1494. (h) Goldberg, S. Z.; Spivack, B.; Stanley, G.; Eisenberg, R.; Braitsch, D. M.; Miller, J. S.; Abkowitz, M. *J. Am. Chem. Soc.* **1977**, *99*, 110–117. (i) Green, M. L. H.; Qin, J.; O'Hare, D.; Bunting, H. E.; Thompson, M. E.; Marder, S. R.; Chatakondu, K. *Pure Appl. Chem.* **1989**, *61*, 817–822.

(4) (a) Pénicaud, A.; Batail, P.; Davidson, P.; Levelut, A. M.; Coulon, C.; Perrin, C. *Chem. Mater.* **1990**, *2*, 117–123. (b) Pénicaud, A.; Batail, P.; Coulon, C.; Canadell, E.; Perrin, C. *Chem. Mater.* **1990**, *2*, 123–132. (c) Morse, D. B. *Chem. Mater.* **1990**, *2*, 33–38. (d) Morse, D. B.; Rauchfuss, T. B.; Wilson, S. R. *J. Am. Chem. Soc.* **1988**, *110*, 2646–2648.

(5) (a) Gama, V.; Henriques, R. T.; Bonfait, G.; Almeida, M.; Meetsma, A.; van Smaalen, S.; de Boer, J. L. *J. Am. Chem. Soc.* **1992**, *114*, 1986–1989. (b) Heuer, W. B.; Mountford, P.; Green, M. L. H.; Bott, S. G.; O'Hare, D.; Miller, J. S. *Chem. Mater.* **1990**, *2*, 764–772. (c) Miller, J. S.; Calabrese, J. C.; Epstein, A. J. *Inorg. Chem.* **1989**, *28*, 4230–4238. (d) Broderick, W. E.; Thompson, J. A.; Godfrey, M. R.; Sabat, M.; Hoffman, B. M. *J. Am. Chem. Soc.* **1989**, *111*, 7656–7657. (e) Interrante, L. V.; Bray, J. W.; Hart, H. R., Jr.; Kasper, J. S.; Piacente, P. A.; Watkins, G. D. *J. Am. Chem. Soc.* **1977**, *99*, 3523–3524. (f) Interrante, L. V.; Browall, K. W.; Hart, H. R., Jr.; Jacobs, I. S.; Watkins, G. D.; Wee, S. H. *J. Am. Chem. Soc.* **1975**, *97*, 889–890. (g) Kasper, J. S.; Interrante, L. V.; Secaur, C. A. *J. Am. Chem. Soc.* **1975**, *97*, 890–891. (h) Browall, K. W.; Interrante, L. V. *J. Coord. Chem.* **1973**, *3*, 27–38.

0276-7333/95/2314-0666$09.00/0

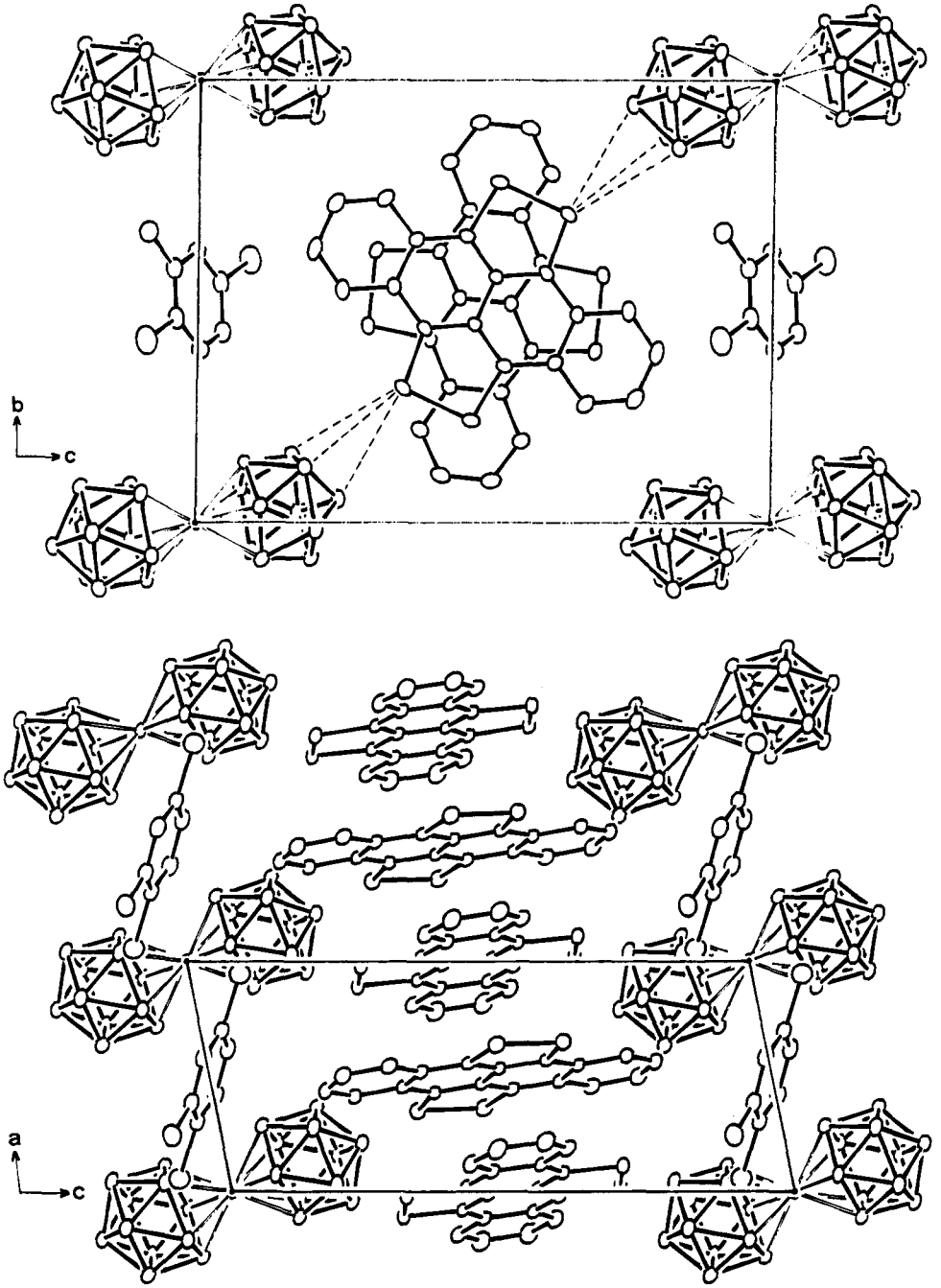

Figure 1. (a, top) Molecular packing of $[TTT_2]^{\cdot+}[\{closo\text{-}(3)\text{-}1,2\text{-}C_2B_9H_{11}\}_2Ni^{III}]^{\cdot-}$ **(2)** viewed down the *a*-axis. Hydrogen atoms have been omitted for clarity. (b, bottom) Molecular packing of $[TTT_2]^{\cdot+}[\{closo\text{-}(3)\text{-}1,2\text{-}C_2B_9H_{11}\}_2Ni^{III}]^{\cdot-}$ **(2)** viewed down the *b*-axis. Hydrogen atoms have been omitted for clarity.

high oxidation states[7] suggested that metallacarboranes containing the dicarbollide ligand of formula $M(C_2B_9H_{11})_2^{n-}$ (n = 0, 1, 2)[8] may provide a new class of compounds capable of acting as electron acceptors in the synthesis of charge transfer complexes. The polarizability of these molecules[9] would be expected to enhance intermolecular interactions between donor and acceptor moieties and the symmetric structures of the bisdicarbollide metal complexes would facilitate the molecular packing. The use of metallacarborane acceptors allows for a systematic variation of the spin system on the acceptor moiety of the charge transfer complex and should give rise to interesting magnetic properties with the appropriate donors. Another important feature of metallacarborane acceptor anions is their hydrolytic and oxygen stabilities,[8] which facilitates synthetic procedures and results in stable charge transfer salts.

We report the synthesis and properties of electrically conducting charge transfer complexes using the nickel

(6) (a) Hawthorne, M. F.; Young, D. C.; Wegner, P. A. *J. Am. Chem. Soc.* **1967**, *87*, 1818. (b) Warren, L. F.; Hawthorne, M. F. *J. Am. Chem. Soc.* **1967**, *89*, 470–471.

(7) (a) Zakharkin, L. I.; Kobak, V. V. *Izv. Akad. Nauk SSSR, Ser. Khim.* **1985**, *6*, 1449–1451. (b) Brown, D. A.; Fanning, M. O.; Fitzpatrick, N. J. *Inorg. Chem.* **1980**, *19*, 1823–1824. (c) Brown, D. A.; Fanning, M. O.; Fitzpatrick, N. J. *Inorg. Chem.* **1978**, *17*, 1620–1623. (d) Harris, C. B. *Inorg. Chem.* **1968**, *7*, 1517–1521.

(8) Hawthorne, M. F.; Young, D. C.; Andrews, T. D.; Howe, D. V.; Pilling, R. L.; Pitts, A. D.; Reintjes, M.; Warren, L. F., Jr.; Wegner, P. A. *J. Am. Chem. Soc.* **1968**, *90*, 879–896.

(9) Adler, R. G.; Hawthorne, M. F. *J. Am. Chem. Soc.* **1970**, *92*, 6174–6182.

Table 1. Atomic Coordinates and Equivalent Isotropic Displacement Parameters for 2[a]

atom	x	y	z	B (Å^2)
NI1	1.000	0.000	1.000	2.48(2)
CL2	0.7572(5)	0.3445(3)	1.0882(2)	5.61(8)
CL3	0.9447(3)	0.5912(2)	1.0896(1)	8.07(6)
S4	0.3631(2)	0.2295(1)	0.47751(8)	3.47(3)
S5	0.6500(2)	0.6978(1)	0.64212(8)	3.40(3)
S6	0.8910(2)	0.4426(1)	1.29567(7)	3.17(3)
S7	0.9774(2)	0.6139(1)	1.30848(7)	3.14(3)
C1	0.8917(7)	0.0370(4)	1.1116(3)	3.0(1)
C2	0.9605(8)	−0.0827(4)	1.1164(3)	3.7(1)
C19	0.5716(6)	0.5626(4)	0.6060(3)	2.58(9)
C20	0.5475(6)	0.4686(4)	0.6600(3)	2.70(9)
C21	0.5885(7)	0.4761(4)	0.7495(3)	3.5(1)
C22	0.5636(8)	0.3824(5)	0.7988(3)	4.4(1)
C23	0.4983(8)	0.2777(5)	0.7627(3)	4.3(1)
C24	0.4569(7)	0.2666(4)	0.6767(3)	3.6(1)
C25	0.4810(6)	0.3605(4)	0.6222(3)	2.8(1)
C26	0.4429(6)	0.3526(4)	0.5338(3)	2.59(9)
C27	0.4675(6)	0.4466(3)	0.4815(3)	2.26(9)
C28	0.9847(6)	0.5066(4)	1.4553(3)	2.38(9)
C29	1.0215(6)	0.6124(4)	1.4191(3)	2.51(9)
C30	0.9150(6)	0.2929(4)	1.5301(3)	2.67(9)
C31	0.8810(7)	0.1833(4)	1.5650(3)	3.7(1)
C32	0.8184(9)	0.0941(4)	1.5133(4)	4.6(1)
C33	0.7833(8)	0.1071(4)	1.4251(4)	4.4(1)
C34	0.8141(7)	0.2094(4)	1.3881(3)	3.5(1)
C35	0.8819(6)	0.3057(4)	1.4392(3)	2.71(9)
C36	0.9193(6)	0.4132(4)	1.4040(3)	2.47(9)
C37	0.6171(9)	0.4277(5)	1.0425(3)	4.9(1)
C38	0.6979(8)	0.5400(5)	1.0382(3)	4.7(1)
C39	0.5821(9)	0.6110(5)	0.9962(4)	5.0(1)
B4	1.0731(8)	0.1338(4)	1.0837(3)	2.8(1)
B5	1.0293(9)	0.1249(5)	1.1881(4)	3.6(1)
B6	0.9569(9)	−0.0167(5)	1.2101(3)	3.4(1)
B7	1.2108(8)	−0.0638(5)	1.0965(3)	3.3(1)
B8	1.2834(9)	0.0773(5)	1.0755(3)	3.4(1)
B9	1.279(1)	0.1510(5)	1.1664(4)	4.0(1)
B10	1.2076(9)	0.0539(5)	1.2467(4)	3.4(1)
B11	1.1599(9)	−0.0796(5)	1.2014(4)	3.5(1)
B12	1.3641(9)	0.0244(6)	1.1786(4)	3.9(1)

[a] Anisotropically refined atoms are given in the form of the isotropic equivalent displacement parameter defined as $(4/3)[a^2B(1,1) + b^2B(2,2) + c^2B(3,3) + ab(\cos\gamma)B(1,2) + ac(\cos\beta)B(1,3) + bc(\cos\alpha)B(2,3)]$.

complex {*closo*-(3)-1,2-$C_2B_9H_{11}$}$_2Ni^{IV}$ (**1**)[8,10] as an acceptor molecule[11] with tetrathiotetracene (TTT) and tetraselenotetracene (TSeT) as donor molecules. The X-ray crystal structure of the complex $[TTT_2]^{\bullet+}$[{*closo*-(3)-1,2-$C_2B_9H_{11}$}$_2Ni^{III}]^{\bullet-}$ (**2**) and $[TSeT]^{\bullet+}$[{*closo*-(3)-1,2-$C_2B_9H_{11}$}$_2Ni^{III}]^{\bullet-}$ (**3**) are reported together with a study of their ESR and magnetic properties.[12]

Results and Discussion

Complex **1** has two reversible one-electron reductions at +0.25 and −0.59 V[8] (*vs* SCE) forming the monoanion and dianion, respectively; both the neutral complex and its monoanion are moisture and oxygen stable. The strong reduction potential of **1** and its high stability and solubility properties make it a very versatile acceptor molecule for a wide range of donor molecules.[11] Reaction of **1** with equivalent amounts of TTT or TSeT dissolved in 1,2,4-trichlorobenzene (TCB) at 150 °C yielded on cooling black needle-shaped crystals of the complexes $[TTT_2]^{\bullet+}$[{*closo*-(3)-1,2-$C_2B_9H_{11}$}$_2Ni^{III}]^{\bullet-}$·TCB (**2**) and $[TSeT]^{\bullet+}$[{*closo*-(3)-1,2-$C_2B_9H_{11}$}$_2Ni^{III}]^{\bullet-}$ (**3**), respectively. When a 2:1 ratio of donor to **1** was used, the same product was obtained when TTT was the donor; however, in the case of TSeT, a mixture of **3** and TSeT was obtained.

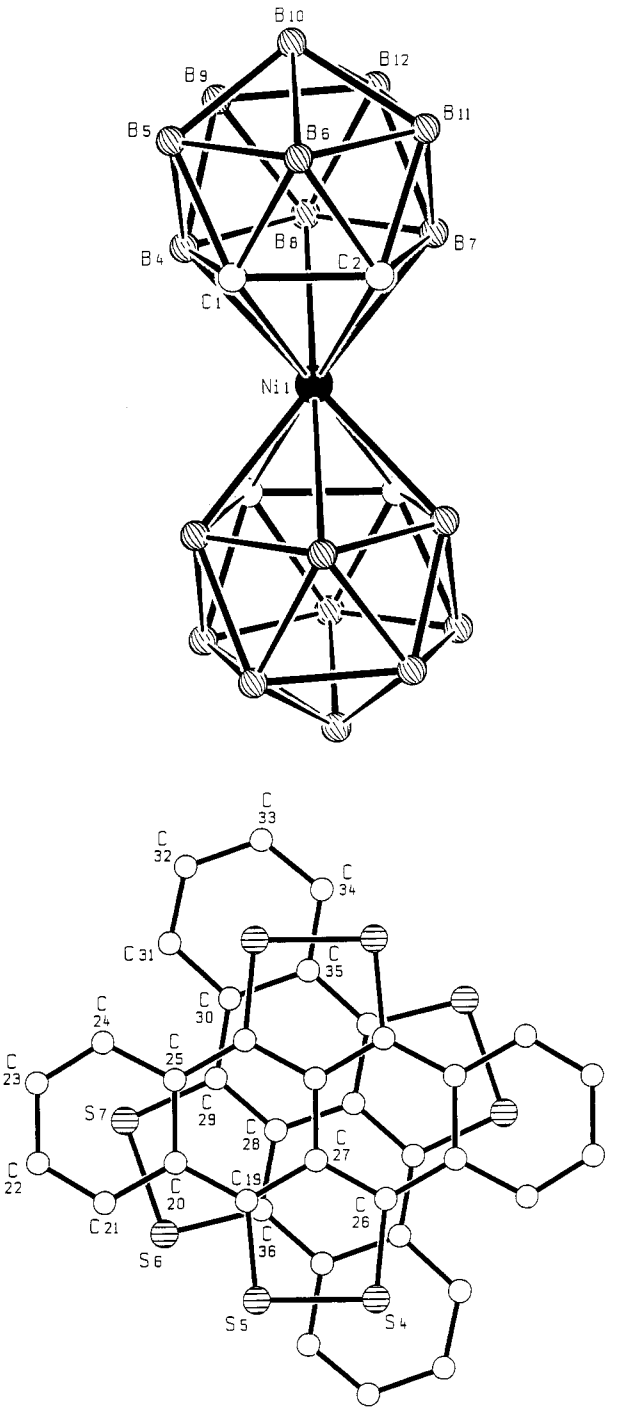

Figure 2. (a, top) Numbering scheme for [{*closo*-(3)-1,2-$C_2B_9H_{11}$}$_2Ni^{III}]^{\bullet-}$ anions of complex **2**. (b, bottom) Numbering scheme for $[TTT_2]^{\bullet+}$ cations of complex **2**.

X-ray Crystal Structure of $[TTT]_2^{\bullet+}$[{*closo*-(3)-1,2-$C_2B_9H_{11}$}$_2Ni^{III}]^{\bullet-}$·TCB (2). Slow cooling of the reaction

(10) (a) Warren, L. F., Jr.; Hawthorne, M. F. *J. Am. Chem. Soc.* **1970**, *92*, 1157–1173. (b) St. Clair, D.; Zalkin, A.; Templeton, D. H. *J. Am. Chem. Soc.* **1970**, *92*, 1173–1179.

(11) Complex **1** has been shown to form adducts involving partial charge transfer with Lewis bases and electron-rich aromatic systems (see ref 10a). While this paper was in preparation, we learned that another group was active in the area and will be publishing a paper on charge transfer complexes resulting from reaction between metallocene donors and metallacarborane acceptors. See: Forward, J. M.; Mingos, D. M. P.; Powell, A. V. *J. Organomet. Chem.*, in press. See also: Klikorka, J.; Pavlík, I.; Vecerníková, E.; Fojtková, M. *Proc. Conf. Coord. Chem.* **1971**, *3* (5), 171–178.

(12) Tetramethyltetrathiofulvalene and tetrathiofulvalene charge transfer complexes of metallacarboranes have also been isolated. Mingos, D. M. P.; *et al.* Manuscript in preparation. Personal communication.

solution between TTT and **1** yielded crystals suitable for an X-ray diffraction study. The crystal structure of **2** is best described as a centrosymmetric structure with disorder both at the nickel dicarbollide anion and at the solvent trichlorobenzene. It consists of separate stacks of formally $TTT^{0.5+}$ cations and $[\{closo\text{-}(3)\text{-}1,2\text{-}C_2B_9H_{11}\}_2\text{-}Ni^{III}]^{\bullet-}$ anions shown in Figure 1a,b. Each planar TTT cation is rotated by 72° relative to its adjacent neighbor and tilted at an angle of 3° to the stack direction with an interplanar spacing of 3.40 Å. This spacing is shorter than that observed for the TTT complexes of tetracyanoquinodimethane, $TTT(TCNQ)_2$, and bis(ethylene-1,2-ditholene)nickel, $TTT_{1.2}Ni(C_2H_2S_2)$, which have interplanar spacings at 3.52 [13] and 3.63 Å[5e], respectively. These complexes, however, have different overlap modes since the TTT cations are not rotated relative to one another in the stacks as in the case of **2**. Positional and thermal parameters for **2** are listed in Table 1, and the numbering scheme for the $TTT^{0.5+}$ cations and the nickel dicarbollide anions are given in Figure 2. The bisdicarbollide nickel anions stack with a nickel–nickel separation along the stacking axis of 6.834 Å and are arranged such that the molecular axis passing through the nickel and the apical boron atoms of each cage lies at an angle of 83° to the TTT stacking axis. There are three short interstack S–B interactions of 3.494, 3.588, and 3.641 Å between a sulfur atom on alternating TTT cations and a triangle of boron atoms (Figure 1) of the dicarbollide ligand. As evidenced from electron spin resonance (ESR) and magnetic susceptibility studies discussed below, electron transfer between the TTT stacks and the Ni(III) complex correlates with the electrical conductivity of the complex. It is possible that the short S–B interactions are important in the electron transfer process despite the fact that the delocalizations of the unpaired electron from the nickel center to the boron atoms of the dicarbollide cage not directly coordinated to the metal are small.[14] The S(4)–S(5) and S(6)–S(7) bond lengths are 2.070(2) and 2.082(2) Å, respectively, shorter than the S–S bond length in neutral TTT[15] and similar to other complexes in which the TTT has a formal charge of +0.5[16] as $(TTT_2)^+I_3^-$ (2.078(2) Å) or a charge of +1 as TTT(tetracyanoquinodimethane), 2.083 Å.[13,17]

Single X-ray Crystal Structure of $[TSeT]^{\bullet+}[\{closo\text{-}(3)\text{-}1,2\text{-}C_2B_9H_{11}\}_2Ni^{III}]^{\bullet-}$ (3). Fine black needles of **3** suitable for a single-crystal X-ray diffraction study were obtained by slow cooling of the reaction mixture between TSeT and **1**. The structure of **3** is shown in Figure 3, and positional and thermal parameters are listed in Table 2. The numbering scheme for **3** is shown in Figure 4. Complex **3** is a 1:1 charge transfer complex consisting of stacks of formally $TSeT^+$ cations and nickel dicarbollide anions lying with their molecular axes (passing through the nickel and apical borons) inclined at an angle of 62° to the stacking axis. The stacking arrangement of **3** is very similar to that of complex **2**. Each $TSeT^+$ cation is rotated relative to its adjacent neighbor in the stack by 72°, which is the same degree of rotation observed between adjacent TTT cations in the structure of complex **2**. The interplanar separation of 3.49 Å is a particularly short spacing when compared to other structurally characterized TSeT complexes in which the TSeT cations are not rotated relative to one another in the stacks.[18] The Se–Se bond distances for the TSeT cations (2.315(2) and 2.328(2) Å) are shorter

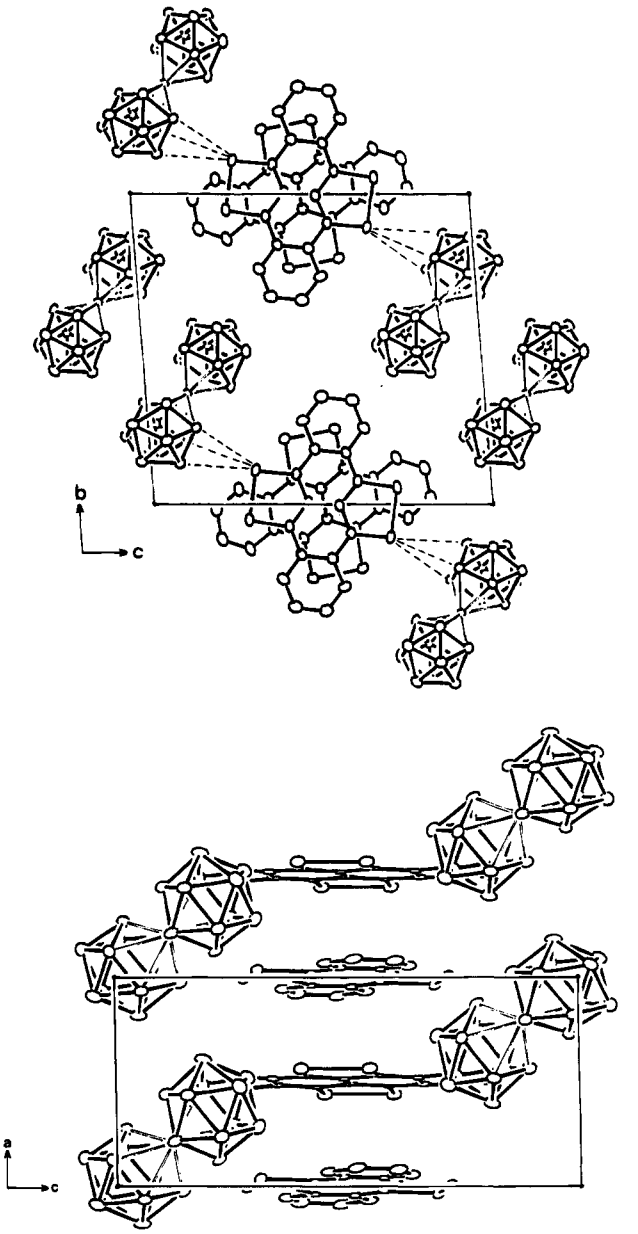

Figure 3. (a, top) Molecular packing of $[TSeT]^{\bullet+}[\{closo\text{-}(3)\text{-}1,2\text{-}C_2B_9H_{11}\}_2Ni^{III}]^{\bullet-}$ (**3**) viewed down the *a*-axis. Hydrogen atoms have been omitted for clarity. (b, bottom) Molecular packing of $[TSeT]^{\bullet+}[\{closo\text{-}(3)\text{-}1,2\text{-}C_2B_9H_{11}\}_2\text{-}Ni^{III}]^{\bullet-}$ (**3**) viewed down the *b*-axis. Hydrogen atoms have been ommited for clarity.

(13) Shibaeva, R. P.; Rozenberg, L. P. *Sov. Phys. Crystallogr.* **1976**, *20*, 581–583.
(14) Wiersema, R. J.; Hawthorne, M. F. *J. Am. Chem. Soc.* **1974**, *96*, 761–770.
(15) Dideberg, O.; Toussaint, J. *Acta Crystallogr.* **1974**, *B30*, 2481–2485.
(16) (a) Smith, D. L.; Luss, H. R. *Acta Crystallogr. Sect. B* **1977**, *33*, 1744. (b) Inabe, T.; Mitsuhahsi, T.; Maruyama, Y. *Chem. Lett.* **1988**, 429–432.
(17) (a) Shibaeva, R. P.; Kaminskii, V. F. *Sov. Phys. Crystallogr.* **1981**, *26*, 188–190. (b) Shibaeva, R. P.; Kaminskii, V. F.; Eremenko, O. N.; Yagubskii, É. B.; Khidekel, M. L. *Sov. Phys. Crystallogr.* **1980**, *25*, 31–33.
(18) (a) Hilti, B.; Mayer, C. W.; Rihs, G. *Solid State Commun.* **1982**, *41*, 787–791. (b) Zolotukhin, S. P.; Kaminskii, V. F.; Kotov, A. I.; Khidekel, M. L.; Shibaeva, R. P.; Yagubskii, É. B. *Izv. Akad. Nauk SSSR, Ser. Khim.* **1978**, *8*, 1816–1821. (c) Hilti, B.; Mayer, C. W.; Rihs, G. *Helv. Chim. Acta* **1978**, *61*, 1462–1469. (d) Schlueter, J. A.; Orihashi, Y.; Kanatzidis, M. G.; Liang, W.; Marks, T. J.; DeGroot, D. C.; Marcy, H. O.; McCarthy, W. J.; Kannewurf, C. R.; Inabe, T. *Chem. Mater.* **1991**, *3*, 1013–1015.

Table 2. Atomic Coordinates and Equivalent Isotropic Displacement Parameters for 3[a]

atom	*x*	*y*	*z*	*B* (Å^2)
SE1	−0.0349(2)	−0.1078(1)	0.69139(9)	3.25(3)
SE2	0.0061(2)	0.0524(1)	0.72163(9)	3.20(3)
SE3	0.4381(2)	−0.2403(1)	0.4511(1)	3.30(3)
SE4	0.4393(2)	−0.2081(1)	0.5998(1)	3.36(3)
NI1	0.2078(3)	0.3534(2)	1.1211(1)	2.67(4)
C1	0.438(2)	0.465(1)	1.108(1)	3.5(3)
C2	0.485(2)	0.397(1)	1.185(1)	3.6(3)
C3	0.273(2)	0.2572(9)	1.0217(9)	2.9(3)
C4	0.124(2)	0.321(1)	0.9895(9)	3.1(3)
C5	−0.026(1)	−0.0953(9)	0.5737(8)	2.4(2)
C6	−0.003(1)	−0.0062(9)	0.5455(8)	2.3(2)
C7	0.015(1)	0.0734(9)	0.6047(8)	2.5(2)
C8	0.039(1)	0.1647(9)	0.5770(8)	2.5(2)
C9	0.056(2)	0.244(1)	0.636(1)	3.7(3)
C10	0.079(2)	0.333(1)	0.607(1)	4.4(4)
C11	0.088(2)	0.344(1)	0.517(1)	4.3(3)
C12	0.069(2)	0.267(1)	0.458(1)	3.5(3)
C13	−0.045(2)	−0.176(1)	0.5134(9)	2.9(3)
C14	0.472(1)	−0.1129(9)	0.4332(8)	2.5(2)
C15	0.488(1)	−0.0490(9)	0.5055(9)	2.6(2)
C16	0.475(1)	−0.0788(9)	0.5885(8)	2.5(2)
C17	0.488(1)	−0.0152(9)	0.6625(9)	2.7(2)
C18	0.476(2)	−0.046(1)	0.7468(9)	3.4(3)
C19	0.494(2)	0.017(1)	0.818(1)	4.2(3)
C20	0.526(2)	0.115(1)	0.807(1)	4.0(3)
C21	0.538(2)	0.147(1)	0.7258(9)	3.6(3)
C22	0.482(1)	−0.084(1)	0.3478(8)	2.6(2)
B4	0.215(2)	0.499(1)	1.125(1)	3.1(3)
B5	0.434(2)	0.577(1)	1.154(1)	3.6(4)
B6	0.604(2)	0.510(1)	1.190(1)	3.9(4)
B7	0.294(2)	0.379(1)	1.253(1)	3.7(3)
B8	0.127(2)	0.448(1)	1.220(1)	3.1(3)
B9	0.236(2)	0.566(1)	1.226(1)	3.8(4)
B10	0.475(3)	0.573(1)	1.266(1)	4.5(4)
B11	0.517(3)	0.458(1)	1.283(1)	4.4(4)
B12	0.283(3)	0.491(2)	1.306(1)	4.5(4)
B13	−0.066(2)	0.321(1)	1.058(1)	3.2(3)
B14	−0.092(2)	0.254(1)	0.956(1)	3.9(4)
B15	0.133(3)	0.215(1)	0.931(1)	3.6(3)
B16	0.205(2)	0.207(1)	1.114(1)	2.8(3)
B17	−0.026(2)	0.243(1)	1.140(1)	3.3(3)
B18	−0.184(2)	0.203(1)	1.051(1)	3.8(4)
B19	−0.061(2)	0.136(1)	0.972(1)	3.7(3)
B20	0.182(2)	0.141(1)	1.011(1)	3.2(3)
B21	−0.017(2)	0.131(1)	1.085(1)	3.4(3)

[a] Anisotropically refined atoms are given in the form of the isotropic equivalent displacement parameter defined as $(^4/_3)[a^2B(1,1) + b^2B(2,2) + c^2B(3,3) + ab(\cos\gamma)B(1,2) + ac(\cos\beta)B(1,3) + bc(\cos\alpha)B(2,3)]$.

than those observed for neutral TSeT derivatives[19] as bis(diseleno)naphthalene (2.364 Å) and are about the as same observed for TSeT cations having a +0.5 charge[20] as $(TSeT_2)^+(SCN)^-$ (2.320(7) Å) or having a charge of +1[21] as $(TSeT)^+(CuBr_2)^-$ (2.317(3) Å). There are three short Se−B interactions at distances of 3.478(6), 3.551(6), and 3.590(6) Å (Figure 3) between a triangle of boron atoms of a dicarbollide cage and alternating $TSeT^+$ cations on the stack. The structure represents one of the few examples of a charge transfer complex of TSeT having a 1:1 stoichiometry.

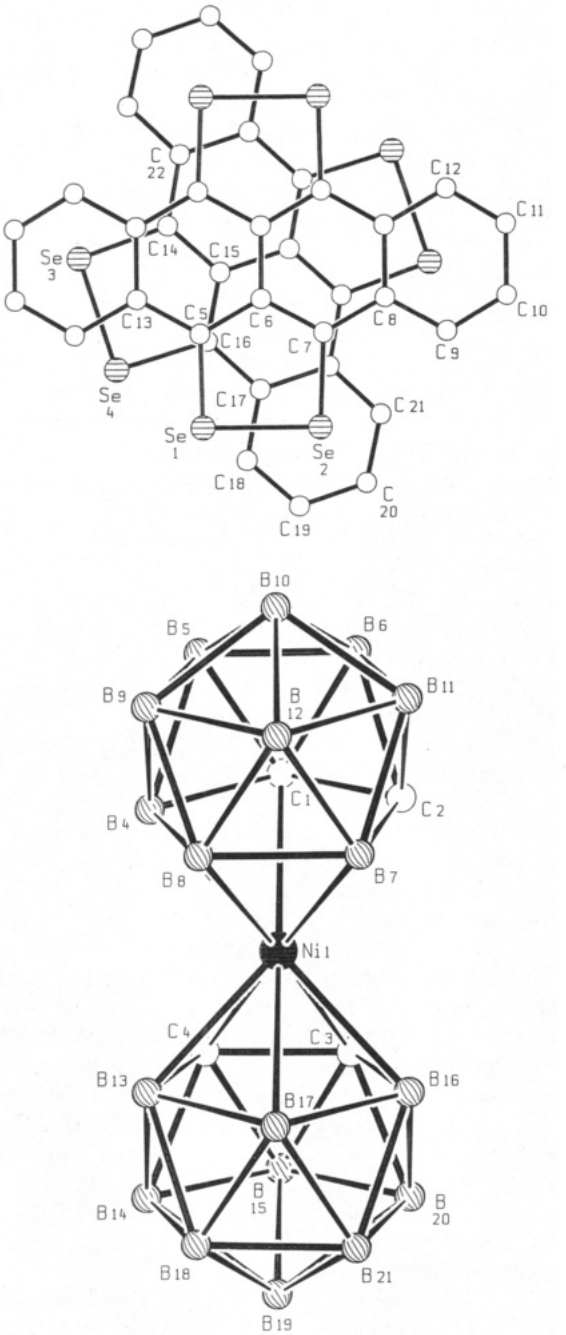

Figure 4. (a, top) Numbering scheme for $[\{closo\text{-}(3)\text{-}1,2\text{-}C_2B_9H_{11}\}_2Ni^{III}]^{\bullet-}$ anions of complex **3**. (b, bottom) Numbering scheme for $[TSeT]^{\bullet+}$ cations of complex **3**.

Electronic Studies. Single-crystal conductivity measurements of complexes **2** and **3** both show significant room-temperature electrical conductivities along the chain axes which decrease with temperature as is typical for semiconductors (Figure 5). Discontinuities in the curves are probably due to microcracks caused by thermal stress in the sample. Single crystals of **2** had an average room-temperature conductivity of 23.3 S·cm^{-1} (compact powder σ = 0.21 S·cm^{-1}). Complex **3** shows a higher compact powder conductivity of 2.02 S·cm^{-1}, two separate samples of single crystals had room-temperature conductivities of 17.3 and 7.7 S·cm^{-1}, respectively. The relatively high conductivity of **3** is unusual for a simple salt having a formal $TSeT^+$ stack of cations and must be a consequence of electron transfer between the nickel dicarbollide anions and the

(19) (a) Endres, H.; Keller, H. J.; Schweitzer, J. Q. D.; Veigel, J. *Acta Crystallogr. Sect. B* **1982**, *38*, 2855−2860. (b) Stark, J. C.; Reed, R.; Acampora, L. A.; Sandaman, D. J.; Jansen, S.; Jones, M. T.; Foxman, B. M. *Organometallics* **1984**, *3*, 732−735.

(20) (a) Shibaeva, R. P.; Kaminskii, V. F. *Sov. Phys. Crystallogr.* **1978**, *23*, 669−672. (b) Shibaeva, R. P.; Kaminskii, V. F.; Kotov, A. I.; Yagubskii, E. B.; Khidekel, M. L. *Sov. Phys. Crystallogr.* **1979**, *24*, 154−157.

(21) (a) Shibaeva, R. P.; Kaminskii, V. F.; Yagubskii, É. B.; Kushch, L. A. *Sov. Phys. Crystallogr.* **1983**, *28*, 48−50. (b) Shibaeva, R. P.; Kaminskii, V. F. *Sov. Phys. Crystallogr.* **1983**, *28*, 173−176. (c) Shibaeva, R. P.; Kaminskii, V. F. *Sov. Phys. Crystallogr.* **1984**, *29*, 361−363.

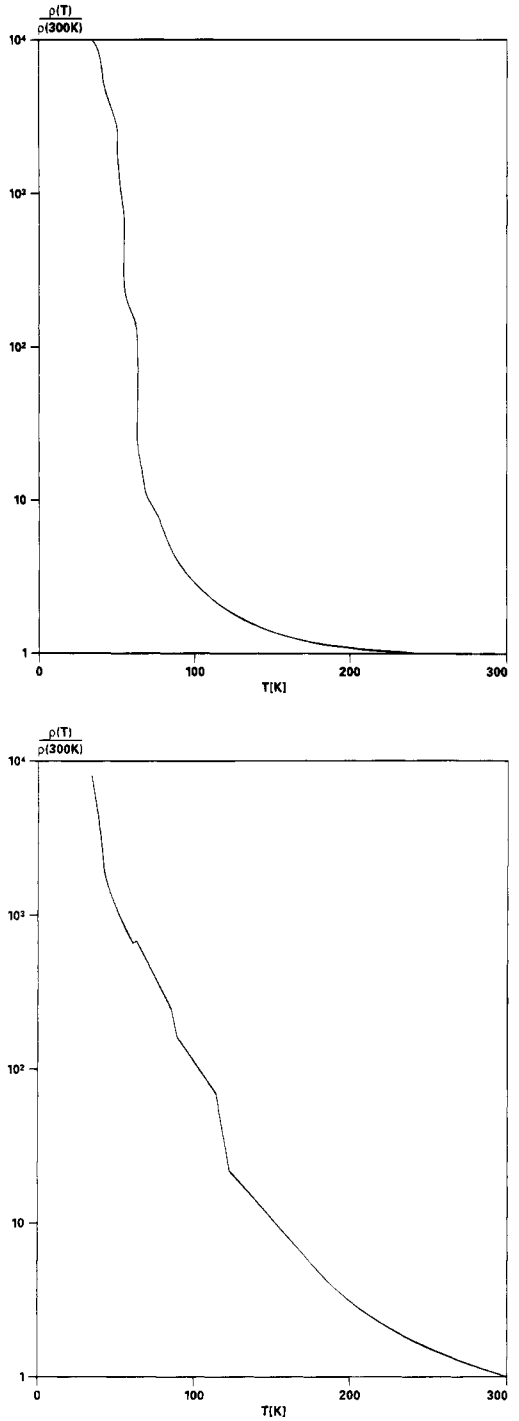

Figure 5. (a, top) Electrical conductivity of complex **2** as a function of temperature. (b, bottom) Electrical conductivity of complex **3** as a function of temperature.

TSeT cations, thereby creating a partially oxidized conducting stack. The high room-temperature conductivity of these complexes demonstrates that the structure of the nickel dicarbollide acceptor does not prevent the formation of electrically conducting stacks of donor cations in spite of the large size and nonplanar geometry of the anion.

ESR and Magnetic Studies. Complex 2. Transfer of a single electron from the TTT stacks to the nickel dicarbollide acceptor should in theory lead to two species with an unpaired spin. The two systems are the electron hole on the TTT stack (one hole for each TTT cation pair) and the spin of the unpaired electron on

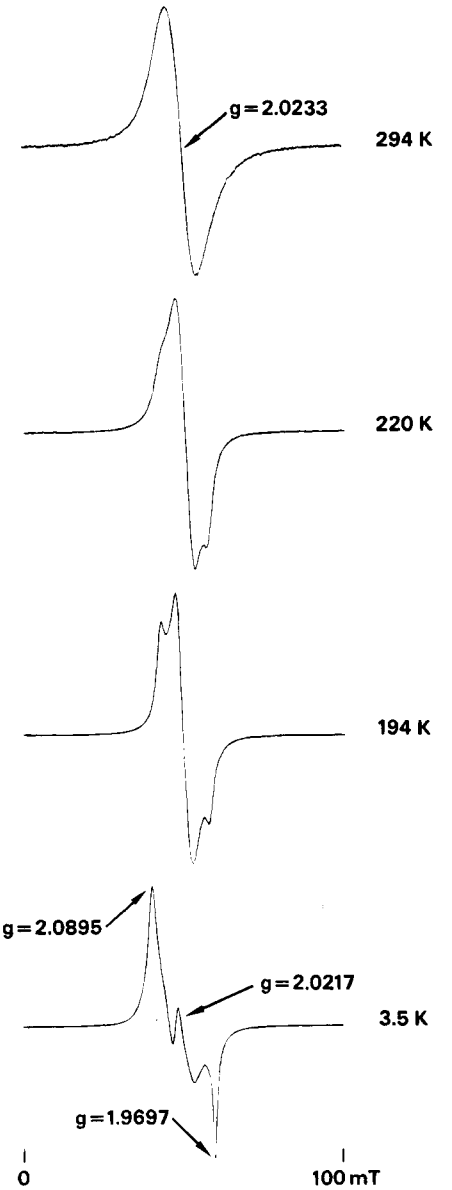

Figure 6. Line shape variation with temperature of the ESR spectrum of complex **2**.

the $[\{closo\text{-}(3)\text{-}1,2\text{-}C_2B_9H_{11}\}_2Ni^{III}]^{\bullet-}$ ion. The electron holes on the TTT stacks may be paired or unpaired. The nickel(III) ion is a d^7 spin system, and in a strong ligand field six electrons are paired resulting in a net spin of $S = {}^1/_2$.[22] The ESR powder spectrum at room temperature of complex **2** consists of a single broad resonance at $g = 2.0233$ (Figure 6). On cooling the polycrystalline sample to 3.5 K, the resonance at room temperature resolves itself to a powder spectrum typical of a **g**-tensor slightly distorted from axial symmetry with components of either rhombic or lower symmetry. The g-parameters along the three main axes (Figure 6) assume values $g_3 = 2.0895$, $g_2 = 2.0217$, and $g_1 = 1.9697$ with an isotropic value of $g_{iso} = 2.0270$. These values are typical for a nickel(III) ion[23] and are also in good agreement with the low symmetry of the nickel dicarbollide anion

(22) Schläler, H. L.; Gliemann, G. *Einführung in die Ligandfeldtheorie*; Akademische Verlagsgesellschaft: Frankfurt am Main, 1967; p 137.

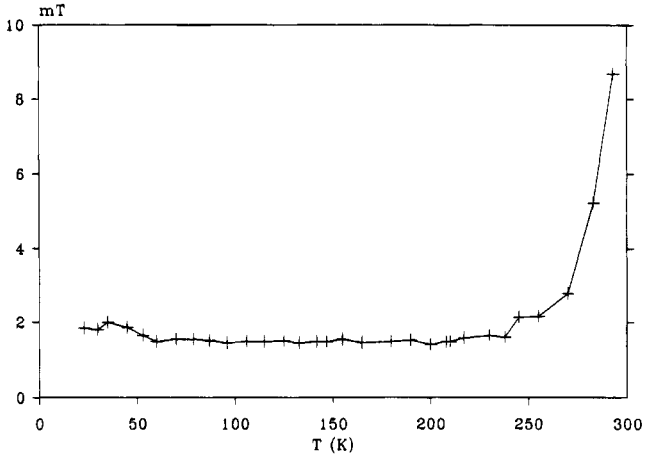

Figure 7. ESR line width of complex **2** as a function of temperature (single crystal, arbitrary orientation of the magnetic field in the crystal *bc* plane).

resulting from distinguishable boron and carbon atoms on the dicarbollide cages. In frozen solution the **g**-tensor of $[\{closo\text{-}(3)\text{-}1,2\text{-}C_2B_9H_{11}\}_2Ni^{III}]^{\bullet-}$ is axial ($g_{\parallel} = 2.06$ and $g_{\perp} = 2.01$).[14] For symmetry reasons the unique g-value at 2.06 of this axial system has to be the one corresponding to the axis passing through the nickel–apical borons of the nickel dicarbollide anion. For planar nickel(III) complexes,[23] $g_{\parallel} < g_{\perp}$ holds, with the unpaired electron residing mainly in the d_{z^2} orbital. The relationship $g_{\parallel} > g_{\perp}$ is indicative of an unpaired electron in a d_{xy} or $d_{x^2-y^2}$ orbital ($g_{\parallel} = g_z$) and a compressed arrangement of the ligand atoms.[23d]

The observed variation of the ESR spectrum of **2** with temperature can be explained by an electron transfer occurring at room temperature between the $TTT^{0.5+}$ and the nickel dicarbollide anions leading to a single broad signal. As the temperature is decreased the electron transfer is slowed down and the spectrum increasingly reflects that of a low-spin nickel(III) complex.[23] The electron transfer process between the nickel dicarbollide anions and the TTT stacks is also reflected in the temperature dependence of the ESR line width of a single crystal of **2**, which decreases drastically with the slowing down of the electron transfer process (Figure 7). The magnetic susceptibility (χ) of **2** was measured and corrections were made for the background signal originating from the quartz sample holder. A plot of χT (where T is the absolute temperature) against T is shown in Figure 8a. In the temperature region where the complex shows a significant electrical conductivity, χT shows a slight deviation from the Curie–Weiss law. The temperature dependence of $1/\chi$ is shown in Figure 8b. Neglecting spin exchange, an estimate of the number of unpaired electron spins can be obtained from Figure 8 by use of the Curie–Weiss law.[24] The magnetic susceptibility χ is given by

$$\chi = C/(T - \Theta)$$

where

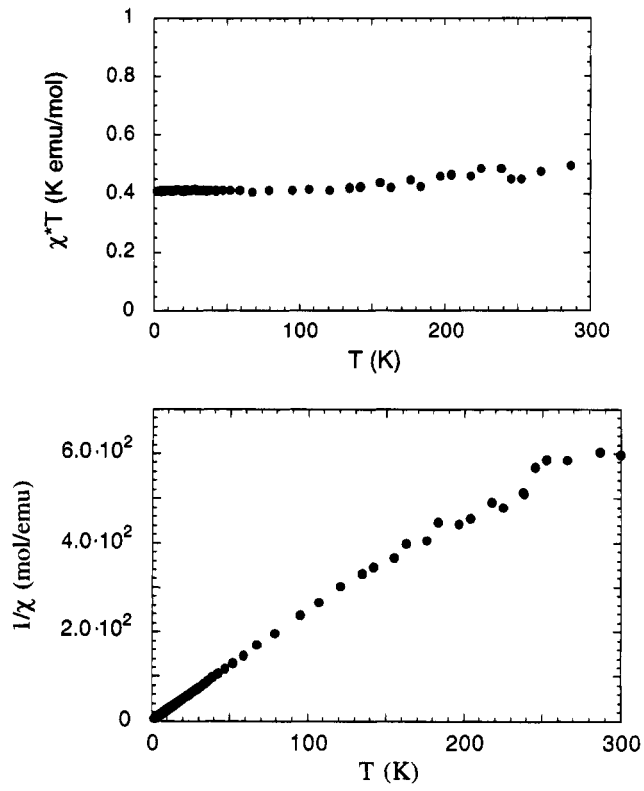

Figure 8. (a, top) Plot of χT versus temperature for complex **2** at 50 mT. (b, bottom) Plot of inverse susceptibility versus temperature for complex **2** at 50 mT.

$$C = N\beta^2 g^2 S(S+1)3k = 0.125 g^2 S(S+1) \quad \text{(K·emu/mol)}$$

where β is the Bohr magneton, k the Boltzmann constant, S the electron spin, Θ the Curie–Weiss constant, and N the number of spins per mole. At room temperature, electron transfer between the spins on the TTT stacks and the nickel(III) ions precludes the application of the Curie–Weiss law. At low temperatures, however, in the temperature region below 100 K where only the spins localized on the nickel(III) ion are observed in the ESR spectrum, the susceptibility exhibits Curie behavior with a small Θ value so that one obtains

$$\mu_{Ni}^{eff} = [(3k/N\beta^2)\chi T]^{1/2} = [g_{Ni}^2 S_{Ni}(S_{Ni}+1)]^{1/2} = 1.79$$

where μ_{Ni}^{eff} is the effective magnetic moment in units of Bohr magnetons β. The experimental value for μ_{Ni}^{eff} is in agreement with $S = 1/2$ and $g \approx 2$ characteristic of nickel(III) complexes. To evaluate the susceptibility at room temperature, a model including electron transfer and spin exchange is needed.

The angular dependence of the g-values for a single crystal was measured at five different temperatures (Figure 9). The a-axis of the crystal was used as the rotation axis and the magnetic field was oriented perpendicular to this crystal axis in the *bc* plane. The temperature dependence of the g-value for a given angle reflects the temperature-dependent electron transfer process as observed in the ESR powder spectra of **2** (Figure 6). The maximum and minimum g-values at 5 K from Figure 9 very closely match two of the **g**-tensor main values observed in the powder spectrum at 3.5 K (Figure 6) ($g_3 = 2.0895$ and $g_1 = 1.9697$). This implies

(23) (a) Bemtgen, J. M.; Gimpert, H. R.; von Zelewsky, A. *Inorg. Chem.* **1983**, *22*, 3576–3580. (b) Wieghardt, K.; Walz, W.; Nuber, B.; Weiss, J.; Ozarowski, A.; Stratemeier, H.; Reinen, D. *Inorg. Chem.* **1986**, *25*, 1650–1654. (c) de Castro, B.; Freire, C. *Inorg. Chem.* **1990**, *29*, 5113–5119. (d) Huang, V.-H.; Park, J.-B.; Adams, M. W. W.; Johnson, M. K. *Inorg. Chem.* **1993**, *32*, 375–376.

(24) Carlin, R. L. *Magnetochemistry*; Springler-Verlag: Berlin, Heidelberg, 1986; pp 10–12.

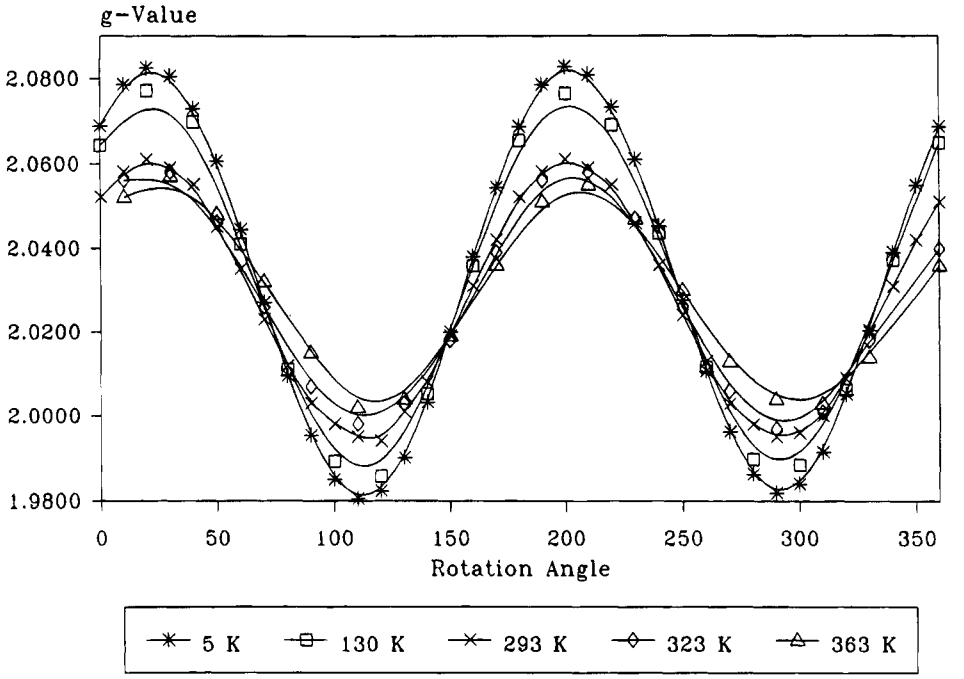

Figure 9. Variation of the g-values of complex **2** with temperature for a single crystal rotated around the a-axis.

Table 3. Details of Crystallographic Data Collection for 2 and 3

	2	3
formula	$2(C_{18}H_8S_4)Ni(B_9C_2H_{11})C_6H_3Cl_3$	$C_{18}H_8Se_4Ni(B_9C_2H_{11})$
MW	1209.96	863.61
crystal system	triclinic	triclinic
space group	$P\bar{1}$	$P\bar{1}$
a (Å)	6.834(1)	7.010(1)
b (Å)	12.368(1)	14.567(1)
c (Å)	16.077(2)	15.589(3)
α (°)	86.75(1)	94.60(1)
β (°)	101.54(1)	89.92(2)
γ (°)	102.54(1)	99.03(2)
V (Å^3)	1299.3(5)	1567.0(8)
Z	1	2
D_{calc} (g·cm^{-3})	1.546	1.830
crystal size (mm)	0.50 × 0.32 × 0.05	0.50 × 0118 × 0.01
diffractometer	Philips PW1100	Enraf-Nonius CAD4
radiation (graphite monochromated)	Mo Kα	Cu Kα
wavelength (Å)	0.7107	1.5118
scan mode	$\theta/2\theta$	$\theta/2\theta$
μ (cm^{-1})	8.76	64.85
F(000)	614	832
scan range (2θ)	6−48	6−134
transmission factors		1.00/0.71
no. of unique reflctns	4252	5812
no. of observed reflctns (I>3σ(I))	2937	4689
refinement method	full matrix	full matrix
no. of params	429	406
R	0.038	0.071
R_w	0.043	0.074
max/min density in final difference map (eÅ^{-3})	0.622/−0.558	1.232/−09833

that the corresponding **g**-tensor axes must nearly lie in the bc crystal plane. In frozen solution as mentioned earlier, the **g**-tensor of the nickel complex is axial[14] the main axis with the largest g-value ($g_{\parallel}$ = 2.06) being oriented parallel to the nickel−apical boron molecular axis. It follows that the g_3 value of 2.0895 corresponds to $g_{\parallel}$, indicating that the nickel−apical boron axis lies in the bc plane. This is in agreement with the X-ray analysis, which locates this axis approximately in the bc crystal plane. The orientation of the g_1 = 1.9697 axis in the molecular frame may then approximately be deduced from the X-ray analysis. If one makes the assumption that the **g**-tensor reflects the symmetry and strength of the crystal field exerted by the dicarbollide ligand, the orientation of the g-axes should be related to the local symmetry of the nickel dicarbollide complex. The crystal structure of **2** is described as a centrosymmetric structure with disorder at the nickel dicarbollide anion. ESR experiments do not reveal any disorder among the nickel complexes; the disorder must therefore arise within each nickel complex. As illustrated in Figure 10 (lower part), a model of the disorder is possible such that each nickel complex has a local twofold symmetry axis approximately perpendicular to the crystal a-axis. With this assumption, the g_3 and g_1 axes would be approximately oriented along the symmetry

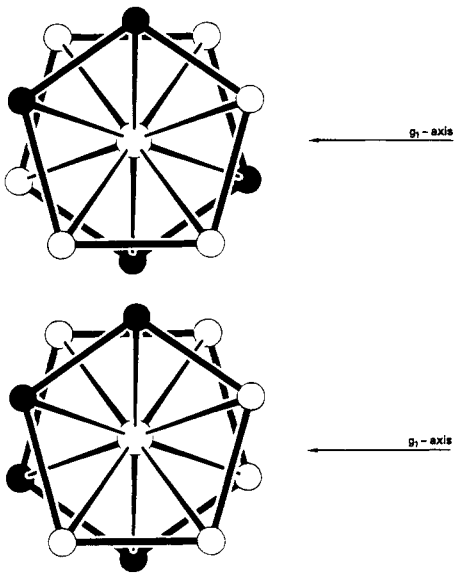

Figure 10. Orientation of g_1-axis with respect to the dicarbollide ligand: (upper) assumes a center of symmetry at the nickel site; (lower) assumes a local twofold axis at the nickel site.

axis of the complex. In the case of a local center of inversion, no relation would be present between the symmetry elements of the ligand arrangement and the g_1 and g_3 axes (Figure 10, upper part).

The observed temperature dependence of the g-value for the single-crystal ESR measurements (Figure 6) of **2** distinguishes it from the bis(ethylene-1,2-ditholene)-nickel complex of tetrathiotetracene, $TTT_{1.2}(NiS_4C_4H_4)$.[5e] The single-crystal ESR spectrum of $TTT_{1.2}(NiS_4C_4H_4)$ shows a single line in the temperature range 1.7–300 K attributed to the spin on the anion. The g-value was temperature independent, indicating that no interaction existed between the unpaired spins of the TTT cations with the nickel dithiolene anions.

Complex 3. The ESR spectra of a powder of **3** exhibited a temperature dependence similar to that observed for complex **2** (Figure 6), once again suggesting an electron transfer between electron holes on the conduction stacks and the nickel dicarbollide anions. At very low temperatures, the powder pattern was again typical for an $S = 1/2$ nickel(III) complex. The three canonical values of the low symmetry **g**-tensor were $g_3 = 2.0688$, $g_2 = 2.0332$, and $g_1 = 1.9707$. While the values g_2 and g_1 were very similar to those measured for complex **2**, the value for g_3 deviated substantially from the corresponding value for complex **2** ($g_1 = 2.0895$) but was close to the parameter measured in frozen solution.[22] The magnetic susceptibility of **3** was measured and corrected for the background signal of the quartz sample holder. A plot of χT and $1/\chi$ against T is shown in Figure 11. At low temperature (<10 K) a least-squares fit of the experimental susceptibility leads to a value of $\Theta = -1.42$ K, and below 100 K, $\mu_{Ni}^{eff} = 1.65$. The experimental susceptibility again agrees well with a spin $S_{Ni} = 1/2$ at most nickel sites. Over the whole temperature range the susceptibilities for complexes **2** an **3** follow approximately the Curie–Weiss law. Apparently the main contribution to the susceptibilities stems from the unpaired spins on the nickel ions and not from the electron spins on the conducting stacks. One of the TSeT molecules in each unit cell

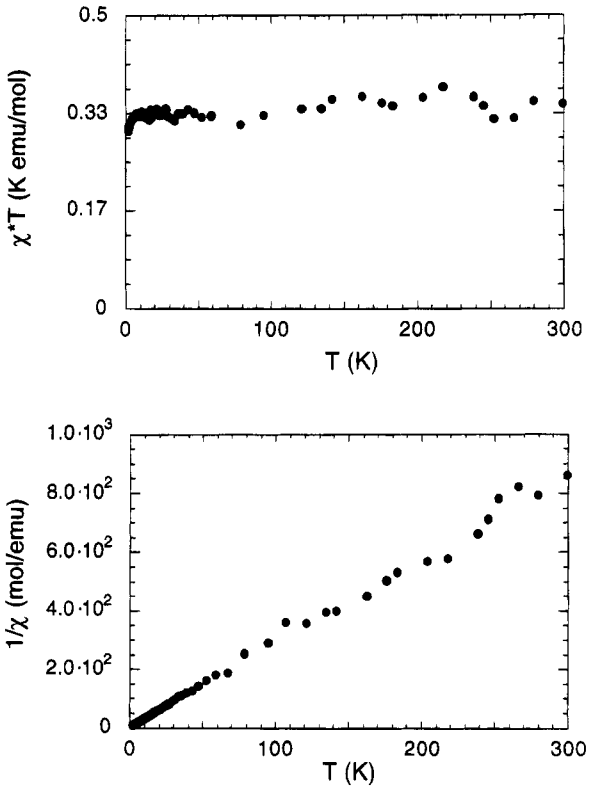

Figure 11. (a, top) Plot of χT versus temperature for complex **3** at 50 mT. (b, bottom) Plot of inverse susceptibility versus temperature for complex **3** at 50 mT.

exhibits very short Se–B distances to two adjacent Ni(III) complexes, the other TSeT cation was more isolated. The short Se–B distances are much shorter than the sum of the van der Waals radii. Two of the interactions involve boron atoms directly bonded to the nickel center, and these interactions might be responsible for the observed spin and electron transfer interactions.

In order to account for the susceptibility observed at high temperatures, a model needs to be invoked that includes electron transfer and coupling between electron spins. Single-crystal ESR measurements would be necessary in order adequately investigate the coupling mechanism; however, adequate crystals of **3** could not be grown.

Conclusion

The first electrically conducting charge transfer complexes have been synthesized using the metallacarborane complex $\{closo\text{-}(3)\text{-}1,2\text{-}C_2B_9H_{11}\}_2Ni^{IV}$ as an acceptor molecule with the donors TTT and TSeT. The X-ray crystals structures of **2** and **3** demonstrate that the nickel dicarbollide anion does not hinder the formation of electrically conducting stacks of donor cations and allows for interstack interactions which in the case of complexes **2** and **3** are essential in maintaining electrical conductivity. The further use of metallacarborane complexes as electron acceptors in combination with donor molecules should lead to a new family of charge transfer complexes with interesting electrical and magnetic properties.

Experimental Section

The preparation of complex **3** was carried out under an argon athmosphere using oxygen-degassed solvents; all other

reactions were carried out without any precautions to exclude oxygen or moisture. Solvents were reagent grade and used without any further purification. TTT[25] and TSeT[26] were prepared according to literature procedures as was the acceptor molecule nickel bisdicarbollide.[8]

Magnetic Measurements. The magnetic susceptibility χ of complexes **2** and **3** was measured in the temperature range of 2–300 K in an external magnetic field of 50 mT by means of Quantum Design superconducting quantum interference device (SQUID) magnetometer. The polycrystalline samples were mounted in a sample holder tube made of quartz glass in order to keep the magnetic background as low as possible.

Electrical Conductivity Measurements. dc conductivity measurements were carried out using the four-probe method. The crystals were mounted on gold wires of 10 μm thickness and placed in contact with Degussa platinum paste. The homemade sample holders were then placed in a Cryogenerator with two-stage cold head (Leybold), and the electrical conductivity was measured along the chain axis at temperature intervals of 2 K.

ESR Measurements. ESR experiments were performed on a Varian E9 ESR spectrometer equipped with an Oxford Instruments continuous-flow cryostat ESR 910 and a temperature controller ITC4.

Crystal Structure Analyses of Complexes 2 and 3. Crystal data for complexes **2** and **3** are given in Table 3. A suitable crystal of each complex was glued on top of glass fibers for data collection. No significant intensity variation was observed for three standard reflections during data collection. The measured intensities were corrected for Lorentz and polarization effects. For complex **3**, absorption corrections were applied, based on azimuthal scans of seven reflections with a diffractometer angle κ near 90°. The two structures were solved by direct methods. There were some problems encountered in distinguishing between boron and carbon atoms in the dicarbollide cages. The structure of **2** was first solved in space group $P\bar{1}$ with the nickel complex having C_i symmetry. Refinements with anisotropic temperature factors and all cage atoms taken as boron revealed two similar short (1.64 Å) bond lengths of adjacent bonds in the pentagon coordinated to the nickel atom, indicating a disorder. As ESR results indicated that the disorder must arise within each nickel complex, the structure was therefore transformed into the noncentrosymmetric space group $P1$. With this space group, however, the structure could not be properly refined. The best R-factor obtained was 0.076 having bond lengths between 1.52 and 1.92 Å with estimated standard deviations of 0.05 Å. It seems that structure **3** is best described having the centrosymmetric space group $P\bar{1}$ with disorder both in the nickel anion and in the solvent molecule trichlorobenzene. The two crystallographically independent TTT molecules lie on inversion centers. After refinements had converged to the R-factor of 0.044, a Fourier map was calculated. All hydrogen atoms could be located, and after including their positional parameters in the final refinements, the R-factor was lowered to 0.039. The nickel dicarbollide anion of structure **3** exhibits C_1 symmetry. Refinements of all cage atoms taken as boron gave in both pentagons coordinated to the nickel atom one short bond length. The corresponding atoms were taken to be carbon atoms. Further refinements resulted in physically reasonable anisotropic thermal vibration factors for all atoms. The hydrogen atoms could not be located.

Synthesis of $[TTT_2]^{\bullet+}[\{closo\text{-}(3)\text{-}1,2\text{-}C_2B_9H_{11}\}_2Ni^{III}]^{\bullet-}\cdot TCB$ (2). To a solution of 100 mg (0.284 mmol) of TTT in 100 mL of 1,2,4-trichlorobenzene at 120 °C was added a solution of $\{closo\text{-}(3)\text{-}1,2\text{-}C_2B_9H_{11}\}_2Ni^{IV}$ (**1**), 0.047 g (0.142 mmol) in 30 mL of 1,2,4-trichlorobenzene, at the same temperature. After being stirred for a few minutes, the solution was filtered and allowed to cool slowly to room temperature over 48 h. Black needles formed at about 40 °C which were filtered rinsed with hexane and dried under vacuum to yield 0.114 g (0.105 mmol) (74%) of **2**. Anal. Calcd for $C_{40}H_{38}B_{18}NiS_8.0.33C_6H_3Cl_3$: C, 46.31; H, 3.52; B, 17.86; Ni, 5.39; S, 23.55. Found: C, 46.52; H, 3.65; B, 16.8; Ni, 5.5, S, 23.68.

Synthesis of $[TSeT]^{\bullet+}[\{closo\text{-}(3)\text{-}1,2\text{-}C_2B_9H_{11}\}_2Ni^{III}]^{\bullet-}$ (3). To a solution 0.100 g (0.185 mmol of TSeT in 130 mL of 1,2,4-trichlorobenzene at 150 °C was added a solution of $\{closo\text{-}(3)\text{-}1,2\text{-}C_2B_9H_{11}\}_2Ni^{IV}$ (**1**), 0.060 g (0.185 mmol) in 30 mL of 1,2,4-trichlorobenzene, at the same temperature. The solution was stirred for a few minutes and then filtered hot and allowed to cool slowly over 48 h. Black needles formed at about 60 °C which were filtered, washed with hexane, and dried to yield 0.141 g (88%) of complex **3**. Anal. Calcd for $C_{22}H_{30}B_{18}NiSe_4$: C, 30.60; H, 3.50; B, 22.53; Ni, 6.80; Se, 35.67. Found: C, 31.12; H, 3.40; B, 21.3; Ni, 6.8; Se, 36.6.

Acknowledgment. We acknowledge Professor D. M. P. Mingos of the Imperial College of Science, London, for disclosing his results prior to publication. The technical assistance of T. Lochmann, J. Pfeiffer, and H. R. Walter are also gratefully acknowledged.

Supplementary Material Available: Listings of bond distances and bond angles for **2** and **3**, listings of general displacement parameters for **2** and **3**, and listings of atomic coordinates for **2** (15 pages). Ordering information is given on any current masthead page.

OM9401317

(25) Marschalk, C. *Bull. Soc. Chim. Fr.* **1948**, *15*, 418–428.
(26) Marschalk, C. *Bull. Soc. Chim. Fr.* **1952**, *46*, 1462–1469.

Ring-Methyl Activation in Pentamethylcyclopentadienyl Complexes. 4.[1] Syntheses, Structures, and Reactions of $[(C_5Me_4CH_2Cl)RuCl(CO)_2]$ and Related Compounds: X-ray Structures of $[(C_5Me_4CH_2Cl)RuCl(CO)_2]$ and $[(C_5Me_4CH_2OEt)Ru(PPh_3)(CO)_2](OTf)$

Li Fan, Michael L. Turner, Harry Adams, Neil A. Bailey, and Peter M. Maitlis*

Department of Chemistry, The University of Sheffield, Sheffield S3 7HF, England

Received August 24, 1994[⊗]

The dicarbonyl chloro complex $[(C_5Me_4CH_2Cl)RuCl(CO)_2]$ (**4**) is formed by carbonylation (1 atm, 20 °C, 5 min) of the dimeric tetramethylfulvene complex $[\{(C_5Me_4CH_2)RuCl_2\}_2]$ (**3**), which is in turn made by oxygenation (1 atm, 20 °C, 30 min) of $[\{(C_5Me_5)RuCl_2\}_2]$ (**1**); since both reactions proceed in high yield, **4** is a readily accessible starting material for a range of Cp*-substituted ruthenium complexes. The C–Cl in **4** is readily substituted by nucleophiles to give $[(C_5Me_4CH_2X)Ru(CO)_2Cl]$ (X = OH, OMe, OEt, O-*i*-Pr, OPh, OCH_2Ph, NEt_2, H), and by PPh_3 (in the presence of NH_4PF_6) to give $[(C_5Me_4CH_2PPh_3)Ru(CO)_2Cl]PF_6$. The Ru–Cl in the alkoxy complexes $[(C_5Me_4CH_2OR)Ru(CO)_2Cl]$ is replaced by reaction with KX to give $[(C_5Me_4CH_2OR)Ru(CO)_2X]$ (R = Me, X = Br, I, CN, SCN; R = Et, X = Br, I) and by PPh_3 in the presence of Ag^+ to give $[(C_5Me_4CH_2OEt)Ru(CO)_2(PPh_3)]^+$. Reaction of **4** with KCN or KSCN in MeOH gave a mixture of $[(C_5Me_4CH_2OMe)Ru(CO)_2X]$, $[(C_5Me_5)Ru(CO)_2X]$, and $[(C_5Me_4CH_2X)Ru(CO)_2X]$ (X = CN, SCN). The amines are quaternized; e.g., $[(C_5Me_4CH_2NEt_2)Ru(CO)_2Cl]$ reacted with MeI to give $[(C_5Me_4CH_2NEt_2Me)Ru(CO)_2I]I$. X-ray crystal structure determinations were carried out for $[(C_5Me_4CH_2Cl)Ru(CO)_2Cl]$ (orthorhombic, a = 18.291(3) Å, b = 11.087(17) Å, c = 6.877(12) Å, V = 1394.6(4) Å^3, Z = 4, D_c = 1.725 g cm^{-3}, space group *Pnma* (D_{2h}^{16}, No. 62)) and $[(C_5Me_4CH_2OEt)Ru(CO)_2(PPh_3)]^+(OTf)^-$ (triclinic, a = 10.496(12) Å, b = 12.509(9) Å, c = 12.738(7) Å, α = 90.25(5)°, β = 93.56(7)°, γ = 93.85(7)°, V = 1666(2) Å^3, Z = 2, D_c = 1.491 g cm^{-3}, space group $P\bar{1}$ (C_i^1 No. 2)).

Introduction

The functionalization of unsubstituted cyclopentadienyls is relatively straightforward. However, highly substituted cyclopentadienyls generally form more inert bonds to metals and hence are more interesting as potential catalysts, since ring loss during the catalytic cycles is less of a problem. We[2] and others,[3–5] have for some time been seeking ways to synthesize complexes bearing *permethyl*cyclopentadienyl ligands, e.g. η^5-C_5Me_4R, where R is a pendant arm. Our chief aim in this work is to put a functionality onto the arm which will act as a *hand* to grasp, orient, and rigidly hold potential reactants to the metal in such a way that highly stereospecific reactions can ensue. It is also of interest to examine the reactivity of such hand substituents when complexed to the metal.

Metal complexes with rings bearing handed arms can basically be made in two ways: (i) by reaction of the permethylcyclopentadiene or permethylcyclopentadienyl already bearing the substituent with a suitable metal salt[4,5] or (ii) by the functionalization of a metal permethylcyclopentadienyl complex.[2,3] The first route has the disadvantages that suitably substituted and functionalized permethylcyclopentadienyls are often hard to make and that, when they are attached to the metal, reagents (e.g. *n*-BuLi) often need to be used which do not tolerate some functionalities which one would like to use as a hand.

The second approach requires a facile method of activating the ring methyl without destroying the bond

⊗ Abstract published in *Advance ACS Abstracts*, December 1, 1994.

(1) Part 3: Gusev, O. V.; Sergeev, S.; Saez, I.; Maitlis, P. M. *Organometallics* **1994**, *13*, 2059.

(2) Miguel-Garcia, J. A.; Maitlis, P. M. *J. Chem. Soc., Chem. Commun.* **1990**, 1472. Gusev, O. V.; Rubezhov, A. Z.; Miguel-Garcia, J. A.; Maitlis, P. M. *Mendeleev Commun.* **1991**, 21. Miguel-Garcia, J. A.; Adams, H.; Bailey, N. A.; Maitlis, P. M. *J. Organomet. Chem.* **1991**, *413*, 427. Miguel-Garcia, J. A.; Adams, H.; Bailey, N. A.; Maitlis, P. M. *J. Chem. Soc., Dalton Trans.* **1992**, 131. See also: Kang, J. W.; Maitlis, P. M. *J. Organomet. Chem.* **1971**, *30*, 127. Hirai, K.; Nutton, A.; Maitlis, P. M. *J. Mol. Catal.* **1981**, *10*, 203.

(3) Hamon, J.-R.; Astruc, D. *Organometallics* **1988**, *7*, 1036. Astruc, D.; Roman, E.; Hamon, J. R.; Batail, P. *J. Am. Chem. Soc.* **1979**, *101*, 2240. Astruc, D. *Acc. Chem. Res.* **1986**, *19*, 377.

(4) Okuda, J. *Chem. Ber.* **1990**, *123*, 1649. Okuda, J.; Zimmermann, K.-H. *J. Organomet. Chem.* **1988**, *344*, C1. Okuda, J.; Zimmermann, K.-H. *Chem. Ber.* **1989**, *122*, 1645. Okuda, J.; Zimmermann, K. H. *Chem. Ber.* **1990**, *123*, 1641. Okuda, J.; Zimmermann, K.-H.; Herdtweck, E. *Angew. Chem.* **1991**, *103*, 446; *Angew. Chem., Int. Ed. Engl.* **1991**, *30*, 430. Okuda, J.; Zimmermann, K.-H. *Chem. Ber.* **1992**, *125*, 637. Okuda, J.; Herdtweck, E.; Zimmermann, K.-H. In *Organic Synthesis via Organometallics*; Dötz, K. H., Hoffmann, R. W., Eds.; Vieweg: Braunschweig, Germany, 1991; p 207. Zimmermann, K.-H.; Pilato, R. S.; Horváth, I. T.; Okuda, J. *Organometallics* **1992**, *11*, 3935.

(5) Jutzi, P.; Kristen, M. O.; Dahlhaus, J.; Neumann, B.; Stammler, H.-G. *Organometallics* **1993**, *12*, 2980. Jutzi, P.; Dahlhaus, J. *Synthesis* **1993**, 684. See also: Adams, H.; Bailey, N. A.; Colley, M.; Schofield, P. A.; White, C. *J. Chem. Soc., Dalton Trans.* **1994**, 1445. Dahlhaus, J.; Bangel, M.; Jutzi, P. *J. Organomet. Chem.* **1994**, *474*, 55.

(6) Werner, H.; Crisp, G. T.; Jolly, P. W.; Kraus, H.-J.; Krueger, C. *Organometallics* **1983**, *2*, 1370. Pattiasina, J. W.; Hissink, C. E.; de Boer, J. L.; Meetsma, A.; Teuben, J. H. *J. Am. Chem. Soc.* **1985**, *107*, 7758. Miller, F. D.; Sanner, R. D. *Organometallics* **1988**, *7*, 818. Glueck, D. S.; Bergman, R. G. *Organometallics* **1990**, *9*, 2862. Booij, M.; Meetsma, A.; Teuben, J. H. *Organometallics* **1991**, *10*, 3246. Luinstra, G. A.; Teuben, J. H. *J. Am. Chem. Soc.* **1992**, *114*, 3361. Horton, A. D. *Organometallics* **1992**, *11*, 3271.

(7) Schock, L. E.; Brock, C. P.; Marks, T. J. *Organometallics* **1987**, *6*, 232. McDade, C.; Brock, C. P.; Bercaw, J. E. *Organometallics* **1982**, *1*, 1629.

0276-7333/95/2314-0676$09.00/0

Scheme 1

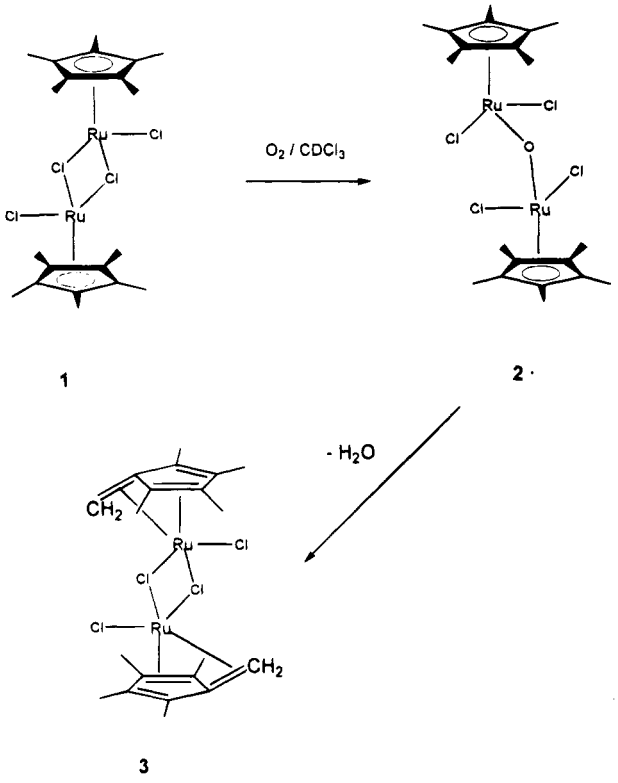

to the metal. C–H activation of ring methyls has been reported to occur under the influence of strong bases[6] or by thermal means.[7] We have recently found that the oxygen-promoted cleavage of a C–H bond takes place with conspicuous facility in $(\eta^5\text{-}C_5Me_5)Ru^{III}$ complexes under ambient conditions.[8,9] The C–H cleavage in $[\{(\eta^5\text{-}C_5Me_5)RuCl_2\}_2]$ (**1**)[10] leads to the η^6-tetramethylfulvene (TMF) complex **3**. When the reaction is carried out carefully, an intermediate μ-oxo complex, $[\{(\eta^5\text{-}C_5Me_5)\text{-}RuCl_2\}_2O]$ (**2**), can be trapped,[11] which spontaneously transforms into $[\{(\eta^6\text{-}C_5Me_4CH_2)RuCl_2\}_2]$ (**3**) with loss of water (Scheme 1).[12] The Ru(II) complexes of tetramethylfulvene exhibit interesting reactivity patterns leading to new chemistry, aspects of which are reported in this paper.

Results and Discussion

(i) Synthesis and Structure of $[(\eta^5\text{-}C_5Me_4CH_2Cl)\text{-}Ru(CO)_2Cl]$ (4). Reaction of the TMF complex **3** with carbon monoxide (1 atm, 20 °C, 5 min) gave the dicarbonyl chloride complex $[(\eta^5\text{-}C_5Me_4CH_2Cl)Ru(CO)_2Cl]$ (**4**) in high yield (Scheme 2). Since the conversion of **1** into **3** is essentially quantitative, this gives **4** in ca. 85% overall yield from **1**. The structure of **4** was deduced from its elemental analyses and spectroscopy (Table 1),

(8) Fan, L.; Turner, M. L.; Hursthouse, M. B.; Malik, K. M. A.; Gusev, O. V.; Maitlis, P. M. *J. Am. Chem. Soc.* **1994**, *116*, 385.
(9) Wei, C.; Aigbirhio, F.; Adams, H.; Bailey, N. A.; Hempstead, P. D.; Maitlis, P. M. *J. Chem. Soc., Chem. Commun.* **1991**, 883.
(10) Tilley, T. D.; Grubbs, R. H.; Bercaw, J. E. *Organometallics* **1984**, *3*, 274. Oshima, N.; Suzuki, H.; Moro-Oka, Y. *Chem. Lett.* **1984**, 1161. Koelle, U.; Kang, B.-S.; Thewalt, U. *J. Organomet. Chem.* **1990**, *386*, 267. Koelle, U.; Kossakowski, J.; Klaff, N.; Wesemann, L.; Englert, U.; Herberich, G. E. *Angew. Chem., Int. Ed. Engl.* **1991**, *30*, 690.
(11) Rao, K. M.; Day, C. L.; Jacobson, R. A.; Angelici, R. J. *Organometallics* **1992**, *11*, 2303.
(12) Fan, L. Ph.D. Thesis, University of Sheffield, 1993. Fan, L.; Wei, C. H.; Aigbirhio, F.; Turner, M. L.; Gusev, O. V.; Hursthouse, M. B.; Malik, K. M. A.; Maitlis, P. M. Manuscript in preparation.

Scheme 2

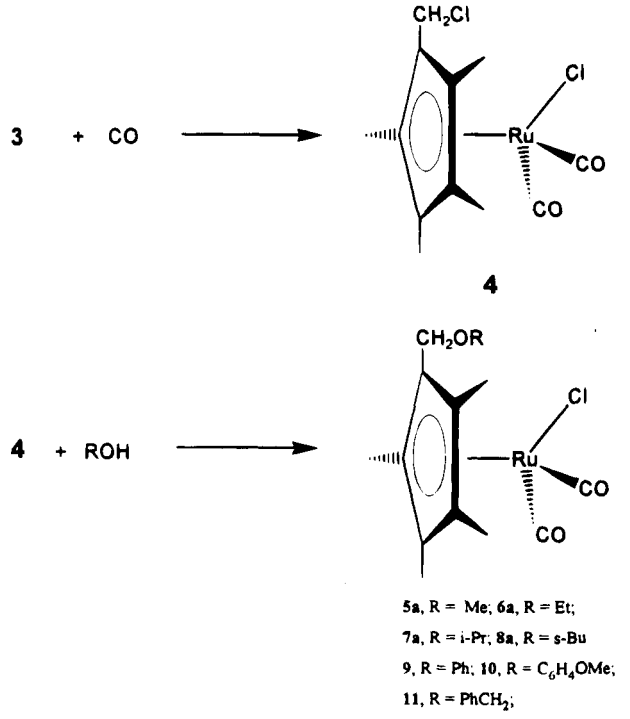

in particular two terminal metal carbonyls in the IR (ν-(CO) 1988, 2040 cm^{-1} (CH_2Cl_2)) and the ^1H and ^{13}C NMR spectra (Tables 2 and 3), which showed a η^5-$C_5Me_4CH_2$ ligand (^1H, δ 1.92, 1.98, (s, s, 2 × 2Me), 4.25 (CH_2); ^{13}C, δ 9.7, 9.9 (2 × 2Me), 36.7 (CH_2), 91.2, 99.9, and 106.1 (C_5 ring), and 197.4 (CO)).

An X-ray determination, which showed that the molecule comprises a ruthenium atom which is bonded to a chloride, two linear carbonyls, and a (η^5-chloromethyl)tetramethylcyclopentadienyl ligand, confirmed the structure of **4**. The molecule possesses crystallographically imposed mirror symmetry (through the Ru–Cl bond and the unique cyclopentadienyl carbon and its substituent). The conformation is such that the chloromethyl substituent is *trans* to the chloro ligand, i.e. it lies above the gap between the two symmetry-related carbonyls, an arrangement similar to that found in $[(\eta^5\text{-}C_5Me_4Et)Ru(CO)_2Br]$.[13] The closest lying cyclopentadienyl carbon is that which carries the chloromethyl substituent. The Ru–Cl bond length 2.422(3) Å is close to that found for the terminal chlorine in **3** (2.4037(11) Å), while the C–Cl bond (C(7)–Cl(2) = 1.787(12) Å) is that expected for a normal organic C(sp^3)–Cl bond. There are no noteworthy intermolecular contacts in **4**. The molecular structure, with atom labeling, is illustrated in Figure 1. Selected bond lengths and angles are given in Table 4.

(ii) Reactions of $[(\eta^5\text{-}C_5Me_4CH_2Cl)Ru(CO)_2Cl]$ (4). (a) With Alcohols and Phenols. Complex **4** underwent facile reactions with nucleophiles at the C–Cl, but the Ru–Cl was attacked only under more forcing conditions. Thus, heating **4** with methanol, ethanol, 2-propanol, or 2-butanol in the neat alcohol as solvent (no base present) gave the appropriate alkoxy complexes $[(\eta^5\text{-}C_5Me_4CH_2OR)Ru(CO)_2Cl]$ (**5a**, R = Me; **6a**, R = Et; **7a**, R = *i*-Pr; **8a**, R = *s*-Bu) (Scheme 2). The reactions were carried out under reflux in order to expel the HCl and to drive them to completion.

(13) Adams, H.; Bailey, N. A.; White, C. *Inorg. Chem.* **1983**, *22*, 1155.

Table 1. Microanalyses, IR Spectra, and Yields of New Complexes

complex no.	ν(CO)[a] (cm^{-1})	microanal.[b] (%) C	H	X	N	S	yield (%)
4	1988	40.2	3.9	19.0			85
	2040	(39.8)	(3.9)	(19.6)			
5a	1985	43.6	4.7	10.0			89
	2038	(43.6)	(4.7)	(9.9)			
5b	1983	38.3	4.1	20.2			92
	2036	(38.8)	(4.2)	(19.9)			
5c	1983	34.9	3.8	28.5			96
	2033	(34.8)	(3.8)	(28.3)			
5d[d]	1998	48.0	4.7		4.0		80
	2047	(48.3)	(4.9)		(4.0)		
5e[e]	1991	44.7	4.4		3.8	8.6	89
	2042	(44.2)	(4.5)		(3.7)	(8.4)	
6a	1984	45.4	5.1	9.4			92
	2037	(45.2)	(5.1)	(9.5)			
6b	1984	40.6	4.6	19.0			90
	2036	(40.4)	(4.6)	(19.2)			
6c	1982	36.3	4.2	27.7			94
	2033	(36.3)	(4.1)	(27.4)			
7a	1984	47.1	5.6	9.3			87
	2037	(46.7)	(5.6)	(9.2)			
8a	1984	48.1	5.8	8.8			91
	2037	(48.0)	(5.8)	(8.9)			
9	1985	51.75	4.7	8.5			69
	2035	(51.5)	(4.6)	(8.4)			
10	1986	51.1	4.8	7.4			63
	2039	(50.7)	(4.7)	(7.9)			
11	1984	52.2	4.9	8.1			75
	2037	(52.6)	(4.9)	(8.2)			
12d	2004	48.7	4.1		7.8		9
	2051	(48.9)	(4.1)		(8.1)		
12e	1998	41.7	3.6		6.4	15.5	75
	2046	(41.3)	(3.5)		(6.8)	(15.7)	
13[f]	1986	42.3	4.3	10.2			42
	2038	(41.9)	(4.4)	(10.3)			
14	1982	49.6	6.0	8.7	3.2		90
	2035	(49.6)	(5.9)	(8.6)	(3.4)		
15	1981	48.3	6.1	8.9	3.2		78
	2034	(48.1)	(6.0)	(8.9)	(3.5)		
16	1984	58.1	5.0	7.2	2.6		77
	2036	(58.2)	(4.9)	(7.2)	(2.8)		
17	1996	31.2	4.3	40.2	2.1		63
	2043	(32.3)	(4.3)	(40.2)	(2.2)		
18a	1978	43.9	4.5	10.7			80
	2032	(44.0)	(4.6)	(10.8)			
18d[d]	1992	49.0	4.8		4.4		77
	2042	(49.1)	(4.7)		(4.4)		
19	1998	48.9	4.0	5.1			82
	2047	(49.0)	(4.0)	(4.9)			
20	2007	52.6	4.2				73
	2055	(53.0)	(4.6)				

[a] In CH_2Cl_2 solution. [b] Found and calculated (in parentheses). [c] X = Cl, Br, I. [d] ν(CN) (cm^{-1}): 2122 (**18d**); 2096, 2122 (**12d**); 2122 (**5d**). [e] ν(SCN) (cm^{-1}): 2112 (**18e**); 2113, 2157 (**12e**); 2112 (**5e**). [f] ν(OH) (cm^{-1}): 3410 (br).

When the alcohol was a solid, or for other systems where it was not possible to use the reactant alcohol as solvent, a solution of the alcohol in tetrahydrofuran gave the best results; these reactions were accelerated by addition of triethylamine as a base to remove HCl. The complexes [(η^5-$C_5Me_4CH_2OR$)Ru(CO)$_2$(Cl)] (**9**, R = Ph; **10**, R = C_6H_4OMe; **11**, R = $PhCH_2$) were obtained in this way by reaction of **4** with phenol, 4-methoxyphenol, and benzyl alcohol, respectively.

When complex **4** was reacted with KX (X = Br, I) in acetone, a mixture was obtained that was shown by ^{1}H NMR spectroscopy to consist of several products, including [(η^5-$C_5Me_4CH_2X$)Ru(CO)$_2$Cl] and [(η^5-$C_5Me_4CH_2X$)-Ru(CO)$_2$X]. The closely similar solubilities prevented separation. However, when the reactions of **4** with KX were carried out in methanol or ethanol, the $C_5Me_4CH_2$-Cl ring chlorine was replaced by the alkoxy group, and halide exchange occurred at ruthenium to give [(η^5-$C_5Me_4CH_2OR$)Ru(CO)$_2$X] (**5b**, **6b**, X = Br; **5c**, **6c**, X = I) in excellent yields (Scheme 3). These reactions presumably occur via the primary formation of the alkoxy chloro complex **5a** or **6a**.

Table 2. ^{1}H NMR Spectra (δ, ppm) of New Complexes

complex no.	C_5Me_4	CH_2E	E
4	1.92 (6H), 1.98 (6H)	4.25	
5a	1.90 (6H), 1.94 (6H)	4.00	OMe, 3.40 (3H)
5b	1.96 (6H), 2.01 (6H)	4.05	OMe, 3.40 (3H)
5c	2.05 (6H), 2.15 (6H)	4.11	OMe, 3.41 (3H)
5d	1.98 (6H), 2.03 (6H)	4.07	OMe, 3.36 (3H)
5e	1.95 (6H), 2.03 (6H)	4.06	OMe, 3.40 (3H)
6a	1.90 (6H), 1.96 (6H)	4.06	OEt, 1.18 (t, 3H), 3.51 (q, 4H)
6b	1.94 (6H), 2.01 (6H)	4.08	OEt, 1.21 (t, 3H), 3.56 (q, 4H)
6c	2.05 (6H), 2.14 (6H)	4.13	OEt, 1.20 (t, 3H), 3.55 (q, 4H)
7a	1.85 (6H), 1.91 (6H)	4.00	O^{i}Pr, 1.15 (d, 6H), 3.64 (m, 1H)
8a	1.85 (3H), 1.86 (3H), 1.91 (3H), 1.92 (3H)	4.00 (dd)	O^{s}Bu, 0.86 (t, 3H), 1.12 (d, 3H), 1.48 (m, 2H), 3.38 (m, 1H)
9	1.95 (6H), 1.98 (6H)	4.62	OPh, 7.25 (m, 5H)
10	1.78 (6H), 1.84 (6H)	4.44	OC_6H_4OMe, 3.68 (3H), 6.87 (br, 4H)
11	1.90 (6H), 1.92 (6H)	4.10	$OPhCH_2$, 4.58 (2H), 7.35 (m, 5H)
12d	2.07 (6H), 2.15 (6H)	3.50	
12e	2.07 (6H), 2.10 (6H)	3.95	
13	1.88 (6H), 1.98 (6H)	4.28 (d)	OH, 2.52 (t, 1H)
14	1.89 (6H), 1.91 (6H)	3.06	$N(CH_2)_5$, 1.40 (m, 2H), 1.50 (m, 4H), 2.32 (m, 4H)
15	1.88 (6H), 1.90 (6H)	3.15	NEt_2, 0.98 (t, 6H), 2.45 (q, 4H)
16	1.64 (6H), 1.86 (6H)	4.35	NPh_2, 6.86−7.30 (m, 10H)
17[a]	2.16 (6H), 2.45 (6H)	4.62	NEt_2Me, 1.46 (t, 6H), 3.28 (s, 3H), 3.80 (q, 4H)
18a	1.90 (15H, Cp*)		
18d	2.03 (15H, Cp*)		
18e	1.92 (15H, Cp*)		
19[b]	1.34 (6H), 1.92 (6H)	4.68 (d), (J = 10 Hz)	PPh_3, 7.50−8.10 (m, 15H)
20[c]	1.80 (6H), 1.82 (6H)	4.06	OEt, 1.28 (t, 3H), 3.71 (q, 4H), PPh_3, 7.30−7.65 (m, 15H)

[a] In $(CD_3)_2CO$ solution. [b] In $(CD_3)_2CO$ solution. ^{31}P {^{1}H} NMR δ 18.5 ppm. [c] ^{31}P {^{1}H} NMR: δ 44.4 ppm.

Reaction of **5a** with KCN in methanol gave the cyano complex **5d** (80%), while reaction of **5a** with KSCN gave [(η^5-$C_5Me_4CH_2OMe$)Ru(CO)$_2$SCN] (**5e**; 89%). In contrast, direct reaction of the chloro complex **4** with KCN in MeOH gave a mixture shown by NMR spectroscopy to comprise three complexes: [(η^5-C_5Me_5)Ru(CO)$_2$CN] (**18d**; ca. 77%, see below), [(η^5-$C_5Me_4CH_2CN$)Ru(CO)$_2$CN] (**12d**; 9%), and [(η^5-$C_5Me_4CH_2OMe$)Ru(CO)$_2$CN] (**5d**; 14%) (Scheme 3); the first two were separated and isolated by column chromatography. Complex **4** also reacted with KSCN in methanol to give similar products, but in different ratios, as shown by ^{1}H NMR spectroscopy: [(η^5-C_5Me_5)Ru(CO)$_2$SCN] (**18e**; 15%), [(η^5-$C_5Me_4CH_2SCN$)Ru(CO)$_2$SCN] (**12e**; 75%), and [(η^5-$C_5Me_4CH_2OMe$)Ru(CO)$_2$SCN] (**5e**; 10%); again the last two could be separated and isolated by column chromatography.

Table 3. ^{13}C NMR Spectra (δ, ppm) of New Complexes

complex no.	C_5Me_4	CO	CH_2E	E
4	9.7, 9.9, 91.2, 99.9, 106.1	198.4	36.7	
5a	9.8, 10.0, 92.2, 100.5, 105.7	198.4	64.8	OMe, 59.0
5b	10.0, 10.2, 92.3, 100.4, 105.6	197.6	65.0	OMe, 59.0
5c	10.7, 10.8, 93.0, 100.3, 104.7	197.6	65.5	OMe, 59.0
5d	10.3, 10.4, 95.0, 101.4, 104.1	196.6	64.5	OMe, 59; CN, 126.1
5e	9.7, 9.9, 93.1, 100.2, 106.0	197.2	64.4	OMe, 59.1; SCN, 117.0
6a	9.7, 9.9, 92.6, 100.4, 105.6	198.0	62.8	OEt, 15.2, 66.8
6b	10.0, 10.2, 92.8, 100.3, 105.1	197.6	63.0	OEt, 15.2, 66.8
6c	10.7, 10.8, 92.4, 100.2, 104.6	197.6	63.6	OEt, 15.2, 66.7
7a	9.7, 9.8, 92.9, 100.4, 105.5	198.0	60.4	O^iPr, 22.2 ($(CH_3)_2$), 72.3 (CH)
8a	9.7, 9.8, 9.9, 92.7, 100.4, 105.5, 100.6	198.1	60.7	O^sBu, 9.6 (CH_3), 19.1 ($CH_2\mathit{CH_3}$), 29.0, ($\mathit{CH_2}CH_3$), 77.5 (CH)
9	9.8, 10.0, 90.5, 100.0, 107.1	197.4	60.7	114.8, 121.9, 129.7, 158.3
10	9.7, 9.9, 90.8, 100.2, 106.9	197.5	61.7	OC_6H_4OMe, 3.68 (Me), 114.7, 116.0, 152.5, 154.5
11	9.7, 9.9, 92.1, 100.4, 105.9	197.9	62.2	OCH_2Ph, 127.9, 128.1, 128.6, 137.4
12d	10.3, 10.4, 90.3, 101.4, 105.6	195.8	14.2	CN, 115.9
12e	10.1, 10.2, 91.7, 100.5, 106.2	196.4	28.4	SCN, 111.2
13	9.9, 10.1, 98.2, 100.1, 105.7	197.8	55.3	
14	9.8, 10.4, 96.0, 100.1, 104.7	198.5	54.4	$N(CH_2)_5$, 24.1, 26.0, 52.8
15	9.9, 10.4, 96.0, 100.1, 104.4	198.5	47.5	NEt_2, 11.6, 46.2
16	9.8, 9.9, 94.9, 99.5, 105.6	198.1	45.7	NPh_2, 122.6, 122.9, 129.4, 148.1
17[a]	8.4, 13.8, 86.2, 103.2, 107.8	197.8	59.6	NEt_2, 10.9, 56.9; NMe, 47.1
18d	10.4 (Cp*), 101.1 (Cp*)	197.5		CN, 128.7
18e	9.7 (Cp*), 101.1 (Cp*)	198.0		SCN, 117.8
19[a]	10.0, 10.4, 90.0, 102.4, 105.8	206.2	23.7 (d), (J = 49 Hz)	PPh_3, 117.0, 118.4, 127.3–138.6
20	9.8, 9.9, 100.5, 102.4, 107.6	198.0	61.9	OEt, 15.1, 67.2; PPh_3, 127.3–133.1

[a] In $(CD_3)_2CO$ solution.

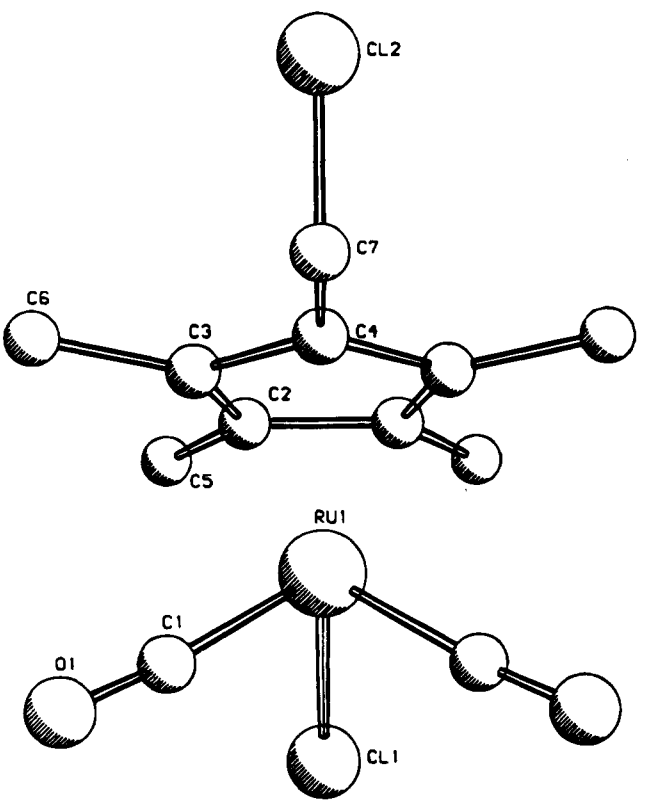

Figure 1. View of the structure of $[(\eta^5\text{-}C_5Mc_4CH_2Cl)Ru(CO)_2Cl]$ (**4**) from the X-ray determination, with hydrogens omitted.

The complexes **5–11** were air-stable as solids and could readily be purified by crystallization or chromatography; they were identified by their microanalyses and IR spectra (Table 1) and their NMR spectra. The ^1H and ^{13}C NMR spectra of the complexes **5–7** and **9–11** (Tables 2 and 3) showed the expected resonances: for example, two signals for the two different types of methyl groups and one signal for the substituted methylene. This showed the $C_5Me_4CH_2OR$ ligand to have a symmetric structure. In contrast, the ^1H NMR spectrum of complex **8a** showed four signals for the ring methyl groups and four signals for the ring CH_2O methylene, indicating the presence of a diastereotopic center (O–C(Me)(Et)(H)) on the $C_5Me_4CH_2O$-*s*-Bu ligand.

Table 4. Selected Bond Lengths (Å) and Angles (deg) for $[(\eta^5\text{-}C_5Me_4CH_2Cl)Ru(CO)_2Cl]$ (4) with Esd's

Ru(1)–Cl(1)	2.422(3)	Ru(1)–C(1)	1.882(8)
Ru(1)–C(2)	2.265(7)	Ru(1)–C(3)	2.238(7)
Ru(1)–C(4)	2.170(10)	O(1)–C(1)	1.132(10)
Cl(2)–C(7)	1.787(12)	C(3)–C(4)	1.432(9)
C(2)–C(3)	1.414(10)	C(4)–C(7)	1.479(13)
C(2)–C(2A)	1.455(13)		
Cl(1)–Ru(1)–C(1)	92.6(2)	Ru(1)–C(1)–O(1)	175.2(7)
Cl(2)–C(7)–C(4)	109.7(8)	C(1)–Ru(1)–C(1A)	90.6(5)

Scheme 3

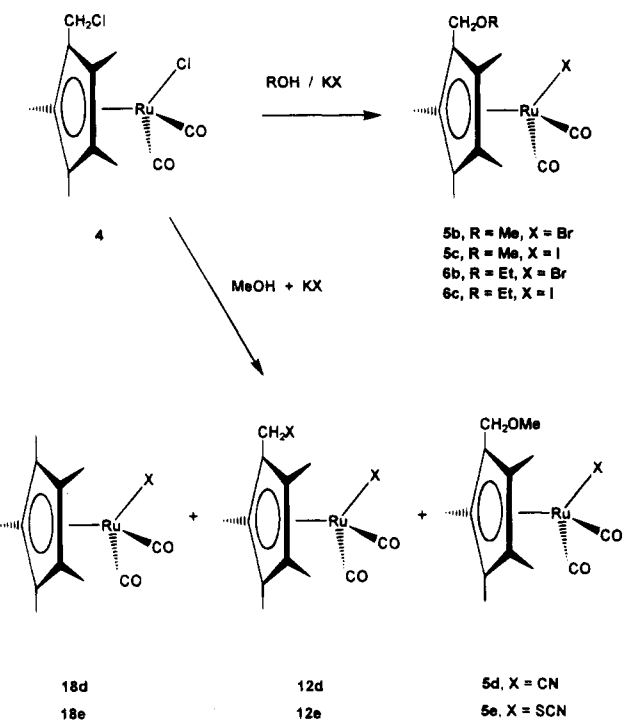

Scheme 4

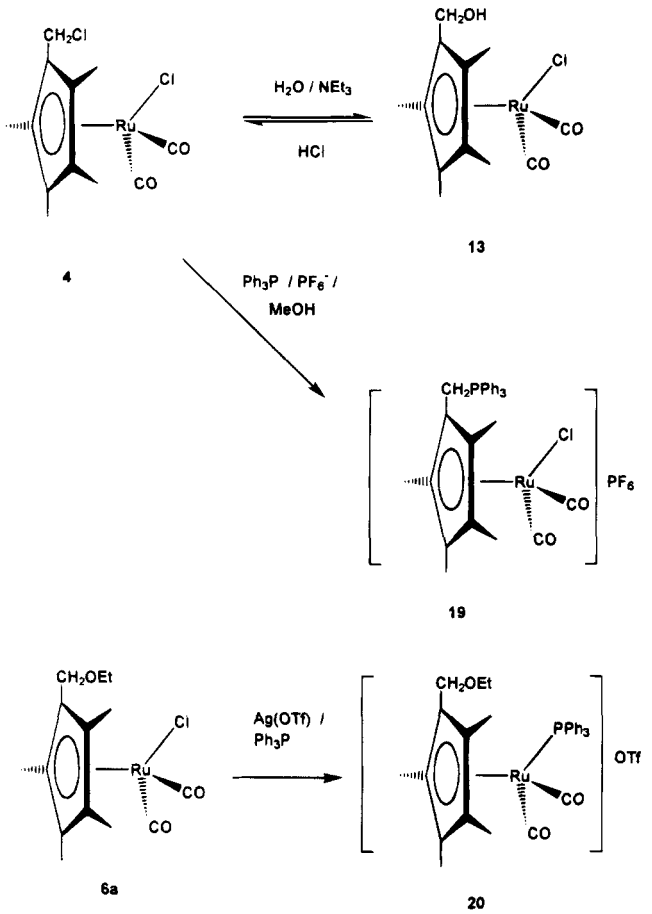

The spectrum also confirmed that it was the C–Cl which had been replaced by the O-*s*-Bu group.

The IR spectra of the alkoxy complexes showed two ν(CO) bands (ca. 1984 and 2037 cm^{-1}), slightly lower than those of the chloro complex **4** (ν(CO) 1988 and 2040 cm^{-1}), indicating that the alkoxy-substituted Cp* group $C_5Me_4CH_2OR$ is a slightly stronger electron donor to the metal than is $C_5Me_4CH_2Cl$.

(b) With Water. Complex **4** reacted only slowly with water; when the reaction was carried out in tetrahydrofuran in the presence of triethylamine, the hydroxy complex **13** was obtained in moderate yield (42%), together with some starting material and other products. The reaction was reversible; treatment of **13** and HCl quantitatively converted it back into **4**, as shown by ^{1}H NMR spectroscopy (Scheme 4). The ^{1}H NMR spectrum of complex **13** showed a doublet at δ 4.28 (J = 7 Hz) due to the substituted CH_2 and a triplet at δ 2.52 due to the hydroxy group, indicating coupling between them; ν(OH) was observed in the IR at 3410 cm^{-1}.

(c) With Amines. Reaction of the chloro complex **4** with secondary amines (R'_2NH) in ethanol gave two complexes, the amino complex [(η^5-$C_5Me_4CH_2NR'_2$)-$Ru(CO)_2Cl$] and the ethoxy complex [(η^5-$C_5Me_4CH_2OEt$)-$Ru(CO)_2Cl$] (**6a**) as well as the salt R'_2NH_2Cl.

$$[(\eta^5\text{-}C_5Me_4CH_2Cl)Ru(CO)_2Cl] + NR'_2H + EtOH \rightarrow [(\eta^5\text{-}C_5Me_4CH_2NR'_2)Ru(CO)_2Cl] + [(\eta^5\text{-}C_5Me_4CH_2OEt)Ru(CO)_2Cl]$$

This is a competitive reaction, where the ratio of the two complexes depends on the basicity of the amine. Thus, complex **4** reacted with piperidine and diethylamine to give [{η^5-$C_5Me_4CH_2N(CH_2)_5$}$Ru(CO)_2Cl$] (**14**) and [(η^5-$C_5Me_4CH_2NEt_2$)$Ru(CO)_2Cl$] (**15**) in 74 and 64% yields, respectively. In contrast, no [(η^5-$C_5Me_4CH_2$-NPh_2)$Ru(CO)_2Cl$] (**16**) was formed with the weaker base diphenylamine: the only product under these conditions was [(η^5-$C_5Me_4CH_2OEt$)$Ru(CO)_2Cl$] (**6a**). Improved yields were obtained when the reaction was carried out in diethyl ether, as the products **14** and **15** were obtained, essentially pure, after removal of the salt R'_2NH_2Cl by filtration.

$$[(\eta^5\text{-}C_5Me_4CH_2Cl)Ru(CO)_2Cl] + 2NR'_2H \rightarrow [(\eta^5\text{-}C_5Me_4CH_2NR'_2)Ru(CO)_2Cl] + NR'_2H_2{}^+Cl^-$$

14, R'_2N = piperindyl
15, R′ = Et

Even this last route did not yield **16**, which could, however, be obtained in good yield (77%) by the reaction of **4** with $HNPh_2$ in THF in the presence of triethylamine.

The amine complexes **14**–**16** were only slightly air-sensitive in the solid but quickly decomposed in solution. The ^{1}H and ^{13}C NMR spectra showed two signals for the methyl groups and one for the substituted CH_2 of the $C_5Me_4CH_2NR'_2$ ligand, indicating that the ligands have symmetric structures.

The reaction of [(η^5-$C_5Me_4CH_2NEt_2$)$Ru(CO)_2Cl$] with MeI gave the quaternary ammonium salt [(η^5-C_5Me_4-CH_2NEt_2Me)$Ru(CO)_2I$]I (**17**) in 63% yield; the ruthenium-bonded chloride was also exchanged for iodide. The

$$\underset{\mathbf{15}}{[(\eta^5\text{-}C_5Me_4CH_2NEt_2)Ru(CO)_2Cl]} + MeI \rightarrow \underset{\mathbf{17}}{[(\eta^5\text{-}C_5Me_4CH_2NEt_2Me)Ru(CO)_2I]I}$$

positive charge on the nitrogen of complex **17** raised the frequency of the ν(CO) bands (1996, 2043 cm^{-1}) by comparison with those in the uncharged complexes **4**–**16**; it also had the effect of separating the two signals of the ring methyl groups in the ^{1}H NMR spectrum more than in **15**.

(d) With Borohydride. The reaction of complex **4** with excess $NaBH_4$ in methanol gave two complexes: the methoxy-substituted complex **5a** (38%) and the C_5-Me_5 complex [(η^5-C_5Me_5)$Ru(CO)_2Cl$] (**18a**; 44%). When the reaction was carried out in THF, only **18a** (80%) was obtained.

$$\underset{\mathbf{4}}{[(\eta^5\text{-}C_5Me_4CH_2Cl)Ru(CO)_2Cl]} + NaBH_4 + MeOH \rightarrow \underset{\mathbf{18a}}{[(\eta^5\text{-}C_5Me_5)Ru(CO)_2Cl]} + \underset{\mathbf{5a}}{[(\eta^5\text{-}C_5Me_4CH_2OMe)Ru(CO)_2Cl]}$$

In contrast to these reactions of **4** with $NaBH_4$, studies on related systems found that $NaBH_4$ reacted with [$CpRu(PPh_3)_2Cl$] in THF with attack at the Ru-

bound Cl to afford $[CpRu(PPh_3)_2BH_4]$[14] and with $[CpRu(CO)_2Cl]$ to give the hydride $[CpRu(CO)_2H]$.[15]

(e) With Triphenylphosphine. Complex **4** reacted with triphenylphosphine in methanol in the presence of ammonium hexafluorophosphate to give $[(\eta^5\text{-}C_5Me_4CH_2PPh_3)Ru(CO)_2Cl][PF_6]$ (**19**) as yellow crystals (Scheme 4). The chlorine on the ring CH_2 was again replaced, this time by triphenylphosphine, but no substitution occurred at the metal.

The structure was deduced from the ^1H NMR and ^{13}C NMR spectra, which showed two singlets for the ring methyl groups (no coupling to phosphorus) and one doublet (J(P−H) = 10 Hz and J(P−C) = 49 Hz) for the ligand ring methylene. The coupling of the methylene to phosphorus and the absence of coupling to the ring methyls confirmed that PPh_3 is attached to the ring CH_2 and not to the ruthenium. The IR spectrum showed two ν(CO) bands at 1998 and 2047 cm^{-1}, close to those for the quaternary ammonium salt **17**, in agreement with a positive charge on the complex.

Further support for the structure of **19** came from the far-infrared spectra, which showed ν(Ru−Cl) at 313 cm^{-1}, close to ν(Ru−Cl) for complexes **4** (310 cm^{-1}), **6a** (300 cm^{-1}), and **14** (302 cm^{-1}), each of which bears a terminal Ru−Cl bond. There was no band in this region for $[(\eta^5\text{-}C_5Me_4CH_2OEt)Ru(CO)_2Br]$ but it did show ν(Ru−Br) at 240 cm^{-1}.

The reaction of **4** with PPh_3 in an alcohol in the presence of NH_4PF_6 did not give $[(\eta^5\text{-}C_5Me_4CH_2OR)Ru(CO)_2(PPh_3)][PF_6]$, but this complex was formed in the presence of a silver salt. Thus, the ethoxy complex $[(\eta^5\text{-}C_5Me_4CH_2OEt)Ru(CO)_2Cl]$ (**6a**) reacted with PPh_3 in the presence of silver trifluoromethanesulfonate (AgOTf) to give $[(\eta^5\text{-}C_5Me_4CH_2OEt)Ru(CO)_2(PPh_3)][OTf]$ (**20**).

The ^1H and ^{13}C NMR spectra showed two signals for the methyl groups and one for the substituted methylene of the $C_5Me_4CH_2OEt$ ligand, indicating a symmetric plane in the cation **20**. The IR spectrum showed ν(CO) bands at 2005 and 2054 cm^{-1}, again consistent with a formal positive charge on the complex.

The structure of **20** was confirmed by an X-ray determination. The cation comprises a ruthenium which is fairly symmetrically bonded to a $\eta^5\text{-}C_5Me_4CH_2OEt$ ligand, the ruthenium being 1.898 Å from the mean plane of the ring. Two carbonyls and a triphenylphosphine ligand are also bonded to the ruthenium. The counteranion is trifluoromethanesulfonate, which shows a rather irregular geometry and is probably disordered. The plane of the antiperiplanar $CH_2OCH_2CH_3$ chain is inclined at 54° to the mean plane of the five-membered ring, and the chain lies predominantly "below" the plane of the five-membered ring (i.e. on the same side as the ruthenium). The structure is illustrated in Figure 2. Selected bond lengths and angles are given in Table 5.

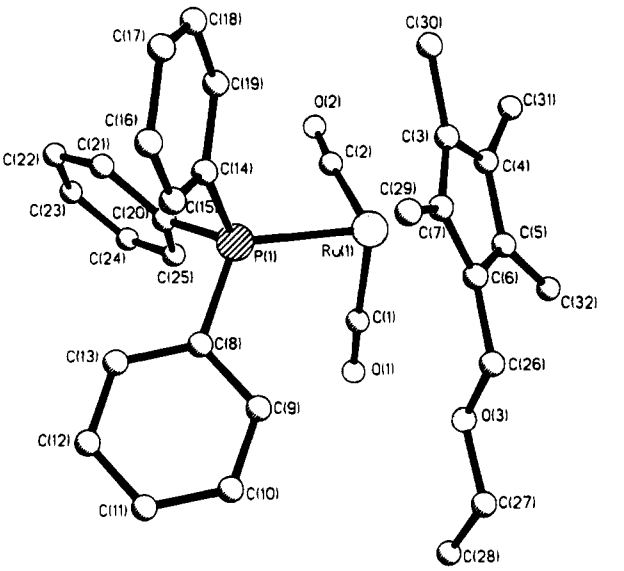

Figure 2. View of the structure of the cation of $[(\eta^5\text{-}C_5Me_4CH_2OEt)Ru(CO)_2(PPh_3)](OTf)$ (**20**) from the X-ray determination.

Table 5. Selected Bond Lengths (Å) and Angles (deg) for the Cation of $[(\eta^5\text{-}C_5Me_4CH_2OEt)Ru(CO)_2(PPh_3)](OTf)$ (20)

Ru(1)−P(1)	2.349(3)	Ru(1)−C(1)	1.892(10)
Ru(1)−C(2)	1.904(10)	Ru(1)−C(3)	2.258(9)
Ru(1)−C(4)	2.229(8)	Ru(1)−C(5)	2.227(9)
Ru(1)−C(6)	2.232(9)	Ru(1)−C(7)	2.290(9)
O(2)−C(2)	1.121(13)	O(1)−C(1)	1.127(12)
O(3)−C(27)	1.417(18)	O(3)−C(26)	1.416(13)
C(3)−C(7)	1.394(12)	C(3)−C(4)	1.423(12)
C(4)−C(5)	1.413(13)	C(6)−C(26)	1.501(14)
C(5)−C(6)	1.414(12)	C(27)−C(28)	1.428(24)
C(6)−C(7)	1.426(12)		
P(1)−Ru(1)−C(1)	90.3(3)	P(1)−Ru(1)−C(2)	88.6(3)
C(1)−Ru(1)−C(2)	94.2(4)	O(3)−C(26)−C(6)	109.2(8)
C(26)−O(3)−C(27)	111.4(10)		

Conclusion

Several novel and unexpected reactions occur in these ruthenium complexes. First and foremost is the facile transformation of the tetramethylfulvene **3** into the $\eta^5\text{-}C_5Me_4CH_2Cl$ complex **4** by reaction with CO. The simplest explanation is that it proceeds in three stages: first, breakage of the Cl bridge in **3**, then formation of a cationic tetramethylfulvene complex, and finally attack by the ionic chloride at the ring CH_2.

$$[\{(\eta^6\text{-}C_5Me_4CH_2)RuCl_2\}_2] + CO \rightarrow [(\eta^6\text{-}C_5Me_4CH_2)Ru(CO)Cl_2]$$

$$[(\eta^6\text{-}C_5Me_4CH_2)Ru(CO)Cl_2] + CO \rightarrow [(\eta^6\text{-}C_5Me_4CH_2)Ru(CO)_2Cl]Cl$$

$$[(\eta^6\text{-}C_5Me_4CH_2)Ru(CO)_2Cl]Cl \rightarrow [(\eta^5\text{-}C_5Me_4CH_2Cl)Ru(CO)_2Cl]$$

In favor of this suggestion is the readiness with which complex **4** itself undergoes nucleophilic substitution at the CH_2−Cl. However, more detailed discussion will need to await a full kinetic study.

Another interesting and useful feature of the chemistry of complex **4** is the ease with which it undergoes nucleophilic substitution at the CH_2−Cl, by reagents such as alcohols, amines, etc. This allows the attachment of functionalities which can act as arms and hands. Such reactions are in contrast with those of tetramethylfulvene complexes of other metals (Rh, Ir) we have made,[1,2] where $C_5Me_4CH_2$ reacts most readily with electrophiles (e.g. MeI, Me_3SiCl, etc.). In complex **2** $C_5Me_4CH_2$ is η^6 bonded (probably η^5:η^1 [12]) and a

(14) Blackmore, T.; Bruce, M. I.; Stone, F. G. A. *J. Chem. Soc. A* **1971**, 2376.
(15) Davison, A.; McCleverty, J. A.; Wilkinson, G. *J. Chem. Soc.* **1963**, 1133.

similar bonding situation involving the CH_2 may also be present in the transition state for substitution in **4** and related complexes. By comparison, in $[(\eta^5\text{-}C_5H_5)\text{-}M(\eta^4\text{-}C_5Me_4CH_2)]$ (M = Rh, Ir) the binding is only η^4. Thus, the ruthenium complexes are rather electrophilic (and hence reactive to Y^-) at the CH_2 while the rhodium and iridium complexes are more nucleophilic at the CH_2 and hence more susceptible to attack by Y^+.

Tetramethylfulvene sandwich complexes of the type $[(\eta^5\text{-}C_5R_5)(\eta^6\text{-}C_5Me_4CH_2)Ru]^+$ (R = H, Me) have also been made and have been found to react with nucleophiles in a manner similar to that for complex **4**;[16] this reinforces the idea that the CH_2 in a $\eta^6\text{-}C_5Me_4CH_2$ complex is probably inherently electrophilic.

Although many of the reactions we have studied involve attack at the Cp* CH_2, nucleophiles such as halide do react at the metal center, allowing access to a range of derivatives, $[(\eta^5\text{-}C_5Me_4CH_2OR)Ru(CO)_2X]$ (X = Cl, Br, I). Pseudohalides (CN or SCN) can react both ways, giving a number of products. However, the boundaries of reactivity are not yet clear; for example, triphenylphosphine only displaces the carbon-bonded Cl in complex **4**, to give **19**, and Ag^+ is needed to remove the Ru-bonded Cl in **6a** to give **20**. These are likely to be kinetic effects, reflecting the relative ease of different reaction paths, rather than thermodynamic. Thus, with suitable reagents, replacement either at the metal or at the ring CH_2 can be effected. This makes **4** and its congeners very valuable synthetic intermediates. Further work on these systems is in progress.

The ring functionality can be completely removed with borohydride, but unexpectedly, a number of other reagents also remove it and give the $\eta^5\text{-}C_5Me_5$ complex: for example, the formation of **18d** by reaction of the chloro complex **4** with KCN. Reaction of $[(\eta^5\text{-}C_5Me_4CH_2\text{-}OMe)Ru(CO)_2Cl]$ with KCN in methanol gave $[(\eta^5\text{-}C_5\text{-}Me_4CH_2OMe)Ru(CO)_2CN]$ quite cleanly, showing that the *C*-methoxy complex was not intermediate in the formation of **18d**. In addition complex **4** reacted with NaOH plus NaCl in refluxing methanol to give two completely dehalogenated products, $[\{(\eta^5\text{-}C_5Me_5)Ru\text{-}(CO)_2\}_2]$ (70%) and $[\{(\eta^5\text{-}C_5Me_4CH_2OMe)Ru(CO)_2\}_2]$ (30%), identified spectroscopically. Since small variations in the precise conditions give very different reactions, the routes by which the various types of $(\eta^5\text{-}C_5Me_5)Ru(CO)_2$ complexes are formed require further investigation, but we presume that hydride species, formed in situ, must be responsible.

Experimental Section

Reactions were carried out under nitrogen using standard Schlenk-line techniques; those involving silver salts were protected from light. Solvents and reagents were purified and dried by standard methods and were distilled under nitrogen immediately prior to use. Microanalyses were performed by the Sheffield University Microanalysis Service and are listed, together with yields and IR spectra, in Table 1. IR spectra were recorded as KBr disks on a Perkin-Elmer PE1710 Fourier transform spectrometer or as solutions in a CaF_2 solution cell with computerized subtraction of the solvent. ^1H and ^{13}C NMR spectra (Tables 2 and 3) were recorded on Bruker AM250, AC250, and WH400 instruments using the solvent or tetramethylsilane as internal standard.

(16) Koelle, U.; Grub, J. *J. Organomet. Chem.* **1985**, *289*, 133. Kirchner, K.; Dasgupta, S.; Schmid, R. *J. Chem. Res., Synop.* **1993**, 340.

Table 6. Atomic Coordinates ($\times 10^4$) and Temperature Factors ($Å^2 \times 10^3$) for $[(\eta^5\text{-}C_5Me_4CH_2Cl)Ru(CO)_2Cl]$ (4)

atom	*x*	*y*	*z*	U_{eq}[a]
Ru(1)	981(1)	2500	1139(1)	30(1)
Cl(1)	−278(2)	2500	2226(4)	46(1)
Cl(2)	3081(2)	2500	−3089(6)	70(1)
O(1)	1438(4)	4469(6)	3902(9)	70(2)
C(1)	1250(4)	3707(7)	2927(11)	44(3)
C(2)	683(4)	3156(6)	−1876(9)	29(2)
C(3)	1398(4)	3548(6)	−1411(9)	33(2)
C(4)	1834(5)	2500	−1054(14)	32(3)
C(5)	40(4)	3901(6)	−2404(11)	40(2)
C(6)	1669(4)	4836(6)	−1411(12)	46(2)
C(7)	2636(5)	2500	−776(18)	45(4)

[a] Equivalent isotropic *U*, defined as one-third of the trace of the orthogonalized U_{ij} tensor.

Preparation of $[(\eta^5\text{-}C_5Me_4CH_2Cl)Ru(CO)_2Cl]$ (4). The freshly prepared complex $[\{(C_5Me_5)RuCl_2\}_2]$[10] (**1**; 0.49 g) was dissolved in dichloromethane (100 mL) and briefly exposed to air (5 min). A slow stream of carbon monoxide (1 atm/20 °C) was then passed through the solution for 0.5 h. The solution was set aside for 2 h; then the solvent was removed in vacuo. The residue was extracted with diethyl ether (3 × 50 mL). This extract was chromatographed on a Florisil column (10 × 4 cm) using diethyl ether to elute a yellow band which gave yellow crystals of $[(C_5Me_4CH_2Cl)Ru(CO)_2Cl]$ (**4**; yield 0.48 g, 82%).

(ii) A similar reaction on $[(\eta^6\text{-}C_5Me_4CH_2)RuCl_2(Me_2SO)]$[9] (0.10 g, 0.26 mmol) gave yellow crystals of $[(\eta^5\text{-}C_5Me_4CH_2Cl)\text{-}Ru(CO)_2Cl]$ (**4**; 0.066 g, 70%).

X-ray Structure Determination of $[(\eta^5\text{-}C_5Me_4CH_2Cl)\text{-}Ru(CO)_2Cl]$ (4). Crystal data for $C_{12}H_{14}Cl_2O_2Ru$: M_r = 362.22; crystallized from ether as yellow oblongs; crystal dimensions 0.35 × 0.2 × 0.16 mm; orthorhombic, a = 18.291(3) Å, b = 11.087(17) Å, c = 6.877(12) Å, V = 1394.6(4) Å^3, Z = 4, D_c = 1.725 g cm^{-3}, space group *Pnma* (D_{2h}^{16}, No. 62), Mo Kα radiation ($\bar{\lambda}$ = 0.710 69 Å), μ(Mo Kα) = 14.77 cm^{-1}, $F(000)$ = 719.94.

Three-dimensional, room-temperature X-ray data were collected in the range $3.5 < 2\theta < 50°$ on a Nicolet R3 diffractometer by the ω-scan method. The 1008 independent reflections (of 1486 measured) for which $|F|/\sigma(|F|) > 3.0$ were corrected for Lorentz and polarization effects and for absorption by analysis of 10 azimuthal scans (minimum and maximum transmission coefficients 0.377 and 0.527). The structure was solved by direct methods and refined by blocked-cascade least-squares methods. The molecule possessed crystallographically imposed mirror symmetry. Hydrogen atoms were included in calculated positions and refined in the riding mode. Refinement converged at a final R = 0.0537 (R_w = 0.0541, 85 parameters, mean and maximum δ/σ 0.002, 0.012), with allowance for the thermal anisotropy of all non-hydrogen atoms. The minimum and maximum final electron densities were −1.16 and 0.73 e Å^{-3}. The weighting scheme $w^{-1} = \sigma^2(F) + 0.00154(F)^2$ was used in the latter stages of refinement. Complex scattering factors were taken from the program package SHELXTL[17] as implemented on the Data General DG30 computer. Table 4 lists selected bond lengths and angles, and atomic coordinates and temperature factors are contained in Table 6.

Preparation of $[(\eta^5\text{-}C_5Me_4CH_2OMe)Ru(CO)_2Cl]$ (5a). A solution of $[(C_5Me_4CH_2Cl)Ru(CO)_2Cl]$ (**4**; 0.1 g, 0.28 mmol) in methanol (30 mL) was refluxed for 6 h. After it was cooled, the solution was evaporated in vacuo to dryness and the residue crystallized from diethyl ether−pentane, to give yellow crystals of $[(C_5Me_4CH_2OMe)Ru(CO)_2Cl]$ (**5a**; 0.088 g, 89%). $[(\eta^5\text{-}C_5Me_4CH_2OEt)Ru(CO)_2Cl]$ (**6a**; yield 92%), $[(\eta^5\text{-}C_5Me_4CH_2O\text{-}i\text{-}Pr)Ru(CO)_2Cl]$ (**7a**; yield 87%), and $[(\eta^5\text{-}C_5Me_4CH_2O\text{-}s\text{-}Bu)Ru(CO)_2Cl]$ (**8a**; yield 91%) were made similarly.

(17) Sheldrick, G. M. SHELXTL, an integrated system for solving, refining and displaying crystal structures from diffraction data (Revision 5.1); University of Gottingen, Gottingen, Germany, 1985.

Preparation of [(η^5-$C_5Me_4CH_2OMe$)Ru(CO)$_2$I] (5c). [(η^5-$C_5Me_4CH_2OMe$)Ru(CO)$_2$I] (**5c**) was made (96% yield) by refluxing [(η^5-$C_5Me_4CH_2Cl$)Ru(CO)$_2$Cl] (**4**) in methanol containing NaI. [(η^5-$C_5Me_4CH_2OMe$)Ru(CO)$_2$Br] (**5b**; yield 92%), [(η^5-$C_5Me_4CH_2OEt$)Ru(CO)$_2$Br] (**6b**; yield 90%) [(η^5-$C_5Me_4CH_2OEt$)-Ru(CO)$_2$I] (**6c**; yield 0.12 g, 94%), [(η^5-C_5Me_4OMe)Ru(CO)$_2$CN] (**5d**; yield 80%), and [(η^5-$C_5Me_4CH_2OMe$)Ru(CO)$_2$SCN] (**5e**; yield 89%) were made similarly from **5a**. Reactions with ROH or R'$_2$NH and Et$_3$N in THF gave [(η^5-$C_5Me_4CH_2OC_6H_5$)Ru(CO)$_2$-Cl] (**9**; yield 69%), [(η^5-$C_5Me_4CH_2OC_6H_4OMe$)Ru(CO)$_2$Cl] (**10**; yield 63%), [(η^5-$C_5Me_4CH_2OBz$)Ru(CO)$_2$Cl] (**11**; yield 75%), and [{η^5-$C_5Me_4CH_2NPh_2$}Ru(CO)$_2$Cl] (**16**; yield 77%).

Preparation of [(η^5-$C_5Me_4CH_2OH$)Ru(CO)$_2$Cl] (13). Water (0.20 mL) and Et$_3$N (0.1 mL) were added to a solution of [(η^5-$C_5Me_4CH_2Cl$)Ru(CO)$_2$Cl] (**4**; 0.10 g, 0.28 mmol) in THF (15 mL). The solution was refluxed for 2 h. During this time, the solution turned orange. After the solution was cooled, the solvent was removed in vacuo, the residue extracted with diethyl ether, and the extract filtered. The concentrated filtrate was chromatographed on a silica column (10 × 2.5 cm), using diethyl ether as eluent, and gave yellow crystals of [(η^5-$C_5Me_4CH_2OH$)Ru(CO)$_2$Cl] (**13**; 0.04 g, 42%).

Preparation of [(η^5-C_5Me_5)Ru(CO)$_2$Cl] (18a). Sodium borohydride (0.05 g) and [(η^5-$C_5Me_4CH_2Cl$)Ru(CO)$_2$Cl] (**4**; 0.045 g) in THF (10 mL) were stirred (6 h/20 °C). The solvent was removed in vacuo and the residue extracted with diethyl ether and chromatographed on silica gel to give yellow crystals of [(η^5-C_5Me_5)Ru(CO)$_2$Cl] (**18a**; 0.036 g, 80%).

Preparation of [{η^5-$C_5Me_4CH_2N(CH_2)_5$}Ru(CO)$_2$Cl] (14). Complex **4** (0.12 g, 0.33 mmol) was dissolved in diethyl ether (20 mL), and piperidine (0.27 mL, 2.7 mmol) was added. The solution was refluxed (10 h, 20 °C); during this time, a white solid precipitated. After it was cooled, the solution was filtered. The concentrated filtrate was chromatographed on a silica column to give yellow crystals of [{η^5-$C_5Me_4CH_2N$-$(CH_2)_5$}Ru(CO)$_2$Cl] (**14**; 0.11 g, 90%). [{η^5-$C_5Me_4CH_2NEt_2$}-Ru(CO)$_2$Cl] (**15**; 78%) was made similarly.

Preparation of [(η^5-$C_5Me_4CH_2PPh_3$)Ru(CO)$_2$Cl][PF$_6$] (19). Complex **4** (0.16 g, 0.44 mmol), NH$_4$PF$_6$ (0.23 g, 1.4 mmol), and PPh$_3$ (0.15 g, 0.57 mmol) were reacted (5 h, 20 °C) in methanol (5 mL). After removal of the solvent yellow crystals of [(η^5-$C_5Me_4CH_2PPh_3$)Ru(CO)$_2$Cl][PF$_6$] (**19**; 0.26 g, 82%) were obtained from CH$_2$Cl$_2$−Et$_2$O.

Preparation of [(η^5-$C_5Me_4CH_2OEt$)Ru(CO)$_2$PPh$_3$][OTf] (20). A solution of AgOTf (0.07 g, 0.27 mmol) and PPh$_3$ (0.07 g, 0.27 mmol) in CH$_2$Cl$_2$ (5 mL) was added to complex **6a** (0.05 g, 0.135 mmol) dissolved in CH$_2$Cl$_2$ (20 mL). After the mixture was stirred (5 h, 20 °C), the solvent was removed and the residue crystallized from CH$_2$Cl$_2$−Et$_2$O to give pale yellow crystals of [(η^5-$C_5Me_4CH_2OEt$)Ru(CO)$_2$PPh$_3$][PF$_6$] (**20**; 0.06 g, 73%).

X-ray Structure Determination of [(η^5-$C_5Me_4CH_2OEt$)-Ru(CO)$_2$(PPh$_3$)][OTf] (20). Crystal data for $C_{33}H_{34}F_3O_6$-PRuS: M_r = 747.73, crystallized from dichloromethane−ether as pale yellow blocks; crystal dimensions 0.55 × 0.25 × 0.175 mm; triclinic, a = 10.496(12) Å, b = 12.509(9) Å, c = 12.738(7) Å, α = 90.25(5)°, β = 93.56(7)°, γ = 93.85(7)°, V = 1666(2) Å^3, Z = 2, D_c = 1.491 g cm^{-3}, space group $P\bar{1}$ (C_i^1 No. 2), Mo Kα radiation ($\bar{\lambda}$ = 0.710 69 Å), μ(Mo Kα) = 6.25 cm^{-1}, F(000) = 763.92.

Three-dimensional, room-temperature X-ray data were collected in the range 3.5 < 2θ < 45° on a Nicolet R3 diffractometer by the ω-scan method. The 3732 independent reflections (of 4667 measured) for which $|F|/\sigma(|F|)$ > 3.0 were corrected for Lorentz and polarization effects and for absorption by analysis of 4 azimuthal scans (minimum and maximum transmission coefficients 0.546 and 0.593). The structure was solved by direct methods and refined by blocked-cascade least-squares methods. Hydrogen atoms were included in calculated positions and refined in the riding mode. Refinement converged at a final R = 0.0813 (R_w = 0.0827, 406 parameters, mean and maximum δ/σ 0.006, 0.039), with allowance for the thermal anisotropy of all non-hydrogen atoms. Minimum and maximum final electron densities were −1.86 and 2.57 e Å^{-3}. The weighting scheme $w^{-1} = \sigma^2(F) + 0.00200(F)^2$ was used in the latter stages of refinement. Complex scattering factors were taken from the program package SHELXTL[17] as implemented on the Data General DG30 computer. Table 5 lists selected bond lengths and angles, and atomic coordinates and temperature factors are contained in Table 7.

Table 7. Atomic Coordinates (×10^4) and Temperature Factors (Å^2 × 10^3) for [(η^5-$C_5Me_4CH_2OEt$)Ru(CO)$_2$(PPh$_3$)](OTf) (20)

atom	x	y	z	U_{eq}[a]
Ru(1)	1609(1)	3177(1)	3238(1)	37(1)
P(1)	−270(2)	2751(2)	2181(2)	40(1)
O(1)	2899(7)	4224(6)	1416(6)	69(3)
O(2)	536(7)	5218(6)	3965(6)	80(3)
O(3)	3997(7)	1956(6)	1865(6)	75(3)
C(1)	2389(8)	3820(7)	2076(7)	48(3)
C(2)	889(8)	4455(8)	3663(7)	51(3)
C(3)	1644(8)	2267(7)	4766(7)	46(3)
C(4)	2663(8)	3078(7)	4803(7)	49(3)
C(5)	3501(8)	2854(7)	4015(7)	52(3)
C(6)	2991(8)	1909(7)	3490(7)	49(3)
C(7)	1861(8)	1534(7)	3980(7)	50(3)
C(8)	−92(8)	2182(7)	888(7)	47(3)
C(9)	1052(9)	1766(7)	638(7)	53(3)
C(10)	1171(11)	1356(9)	−345(8)	71(4)
C(11)	161(11)	1288(8)	−1078(9)	71(4)
C(12)	−971(12)	1657(10)	−822(9)	83(5)
C(13)	−1095(9)	2129(9)	142(8)	66(4)
C(14)	−1397(8)	1820(7)	2779(7)	48(3)
C(15)	−1789(8)	846(7)	2344(8)	58(4)
C(16)	−2602(10)	114(9)	2810(11)	76(5)
C(17)	−3029(10)	406(11)	3774(11)	79(5)
C(18)	−2678(10)	1365(11)	4237(9)	74(5)
C(19)	−1841(8)	2091(8)	3752(8)	56(3)
C(20)	−1167(8)	3917(7)	1845(7)	45(3)
C(21)	−2451(9)	3938(8)	2003(8)	64(4)
C(22)	−3096(11)	4837(10)	1719(10)	83(5)
C(23)	−2448(12)	5696(10)	1318(9)	82(5)
C(24)	−1217(12)	5687(9)	1172(10)	88(5)
C(25)	−570(10)	4796(8)	1420(9)	69(4)
C(26)	3647(10)	1277(9)	2702(8)	69(4)
C(27)	4711(15)	1420(15)	1140(11)	124(8)
C(28)	4941(15)	2109(18)	271(12)	163(11)
C(29)	1134(10)	506(7)	3732(9)	73(4)
C(30)	679(10)	2128(9)	5582(8)	72(4)
C(31)	2869(11)	3958(9)	5613(9)	80(5)
C(32)	4750(9)	3456(9)	3843(10)	71(4)
C(33)	6392(19)	3154(14)	7237(21)	146(10)
F(1)	6970(17)	3418(8)	8112(13)	235(9)
F(2)	6097(17)	3941(10)	6726(15)	290(10)
F(3)	7503(18)	2964(21)	6763(18)	314(14)
S(1)	5529(4)	1988(3)	7080(3)	97(1)
O(4)	4435(16)	2423(18)	7624(13)	261(12)
O(5)	5140(9)	1876(8)	6036(7)	110(4)
O(6)	6102(15)	1283(8)	7645(12)	202(8)

[a] Equivalent isotropic U, defined as one-third of the trace of the orthogonalized U_{ij} tensor.

Preparation of [(η^5-C_5Me_5)Ru(CO)$_2$CN] (18d) and [(η^5-$C_5Me_4CH_2CN$)Ru(CO)$_2$CN] (12d). Complex **4** (0.2 g, 0.55 mmol) and KCN (0.2 g, 3.08 mmol) were refluxed in methanol (20 mL; 5 h, 20 °C). The solvent was removed in vacuo and the residue chromatographed on a silica column with MeOH−Et$_2$O (1:10) as eluent to give a colorless band which yielded white crystals of [(η^5-C_5Me_5)Ru(CO)$_2$CN] (0.14 g, 77%) and a pale yellow band which gave yellow crystals of [(η^5-$C_5Me_4CH_2$-CN)Ru(CO)$_2$CN] (0.017 g, 9%).

Preparation of [(η^5-$C_5Me_4CH_2SCN$)Ru(CO)$_2$SCN] (12e) and [(η^5-$C_5Me_4CH_2OMe$)Ru(CO)$_2$SCN] (5e). [(η^5-C_5Me_4-CH_2Cl)Ru(CO)$_2$Cl] (**4**; 0.15 g) and KSCN (0.18 g) were refluxed in methanol (20 mL, 5 h). After the mixture was cooled, the solvent was removed in vacuo and the residue was crystallized from MeOH−Et$_2$O to give orange crystals of [(η^5-C_5Me_4-CH_2SCN)Ru(CO)$_2$SCN] (**12e**; 0.126 g, 75%). The mother liquor

was chromatographed on a silica column; elution with Et_2O gave a yellow band which gave yellow crystals of [(η^5-C_5Me_4-CH_2OMe)Ru$(CO)_2$SCN] (**5e**; 0.016 g, 10%). The complex [(η^5-C_5Me_5)Ru$(CO)_2$SCN], identified spectroscopically, was also detected.

Acknowledgment. We thank the ORS for some support, Dr. B. F. Taylor for NMR spectra, and Professor M. Vargaftik for helpful discussion.

Supplementary Material Available: Tables of bond distances and angles, anisotropic thermal parameters, and H atom positional parameters for **4** and **20** (3 pages). Ordering information is given on any current masthead page.

OM9406815

General Routes to Functional Organotin Trichlorides and Trialkoxides Involving the Tricyclohexylstannyl Group

Bernard Jousseaume,* Mohammed Lahcini, and Marie-Claude Rascle

Laboratoire de Chimie Organique et Organométallique, URA 35 CNRS, Université Bordeaux I, 351, cours de la Libération, 33405 Talence Cedex, France

François Ribot and Clément Sanchez

Laboratoire de Chimie de la Matière Condensée, URA 1466 CNRS, Tour 54, 4, place Jussieu, 75252 Paris Cedex 05, France

Received July 12, 1994[⊗]

New functional organotin trialkoxides have been prepared in two steps from the corresponding organotricyclohexyltins, which were obtained by coupling an organometal species with tricyclohexyltin chloride, by reaction of (tricyclohexylstannyl)lithium with an organic halide, or by hydrostannation of alkenes. Treatment of organotricyclohexyltins with tin tetrachloride gave the corresponding organotin trichlorides which were further transformed into functional organotin trialkoxides.

Introduction

The sol-gel process can be applied for the preparation of oxides of almost every metal, even if most of the studies have been devoted to silica, alumina, and titania.[1] However, the materials prepared in this way are subject to extensive shrinking, cracking, and shattering. Their mechanical properties can be improved by the incorporation of an organic phase linked to the metal atoms, to form organic–inorganic composite materials with covalent bonding between the two phases.[2] Most of the research on these hybrid organic–inorganic materials has been based on silicon derivatives,[3] since with transition metals the much more ionic metal–carbon bonds are not stable enough toward hydrolysis. Tin shows a behavior intermediate between those of silicon and transition metals. It forms strong bonds with carbon[4] and can easily expand its coordination sphere up to 8, which makes hydrolysis reactions of tin alkoxides very fast.[5] Tin oxide is an n-type semiconductor with applications for sensors, nonlinear optical devices, catalysts, etc.[6] For these reasons, tin was selected for the design and preparation of new hybrid organic–inorganic materials based on the combination of organic and inorganic networks homogeneously distributed in the material.[7] The aim of this work was thus to prepare functional organotin trialkoxides in which the three alkoxide groups would provide the inorganic network after hydrolysis and the organic moiety with a polymerizable function would be the precursor of the organic network.

Results and Discussion

Triorganotin alkoxides and diorganotin dialkoxides have been the subject of numerous studies,[8] and many different preparations of these compounds have been proposed in the literature. Only a few simple organotin trialkoxides are known, however, and their preparations are more limited.[9] One method involves the alcoholysis of organotin triamides by alcohols.[10] In a second method, the reaction between an organotin trihalide and an alkoxide is used.[11] Transalkoxylations, which are possible with triorganotin alkoxides and diorganotin dialkoxides,[8] are also of interest with organotin trialkoxides. They can lead to symmetrical or mixed alkoxides.[12] As the second method is a one-step procedure, it was preferred as an entry to functional organotin trialkoxides.

Organotin trihalides can only be prepared by a few methods,[13] the main one involving the cleavage of tetraorganotins by hydrogen halides, halogens, or tin tetrahalides.[14] As other methods are less general,[15–21]

⊗ Abstract published in *Advance ACS Abstracts,* December 1, 1994.

(1) Brinker, C. J.; Scherer, G. W. *Sol-Gel Science*; Academic Press: London, 1990.

(2) Ning, Y. P.; Mark, J. E. *Polym. Bull.* **1984**, *12*, 137. Schmidt, M. *J. Non-Cryst. Solids* **1988**, *100*, 51.

(3) Schmidt, H.; Scholze, H.; Kaiser, A. *J. Non-Cryst. Solids* **1984**, *63*, 1. Schmidt, H.; Seiferling, B. *Mater. Res. Soc. Symp. Proc.* **1986**, *73*, 739. Wilkes, G. L.; Orler, B.; Huang, H. *Polym. Prepr. (Am. Chem. Soc., Div. Polym. Chem.)* **1985**, *26*, 300.

(4) Neumann, W. P. *The Organic Chemistry of Tin*; Wiley: London, 1967; p 155. Poller, R. C. *The Chemistry of Organotin Compounds*; Logos: London, 1970; p 69.

(5) Bradley, D. C. *Coord. Chem. Rev.* **1967**, *2*, 299. Sanchez, C.; Ribot, F.; Doeuff, S. In *Inorganic and Organometallic Polymers with Special Properties*; Laine, R. M., Ed.; NATO ASI Series 206; Kluwer Academic: Dordrecht, The Netherlands, **1992**; p 267. Ribot, F.; Banse, F.; Sanchez, C. *Mater. Res. Soc. Symp. Proc.* **1992**, *271*, 45.

(6) Harrison, P. G. In *Chemistry of Tin*; Harrison, P. G., Ed.; Blackie: Glasgow, Scotland, 1989; p 421.

(7) Sanchez, C.; Ribot, F. *New J. Chem.*, in press.

(8) Bloodworth, A. J.; Davies, A. G. In *Organotin Compounds*; Sawyer, A. K., Ed.; Dekker: New York, 1972; Vol. 1, p 153. Wardell, J. L. In *Chemistry of Tin*; Harrison, P. G., Ed.; Blackie: Glasgow, Scotland, 1989; p 145.

(9) Schumann, H.; Schumann, I. In *Gmelin Handbook of Inorganic Chemistry*; Krüerke, U., Ed.; Springer-Verlag: Berlin, 1989; Organotin Compounds, Vol. 17, p 12.

(10) Lorberth, J.; Kula, M. R. *Chem. Ber.* **1964**, *97*, 3444. Thomas, M. *Can. J. Chem.* **1961**, *39*, 1386.

(11) Davies, A. G.; Smith, L.; Smith, P. J. *J. Organomet. Chem.* **1972**, *39*, 279. Gaur, D. P.; Srivastrava, G.; Mehrotra, R. C. *J. Organomet. Chem.* **1973**, *63*, 221. Reuter, H.; Schroder, D. *J. Organomet. Chem.* **1981**, *455*, 83.

(12) Gupta, V. D.; Narula, C. K. *Synth. React. Inorg. Met.-Org. Chem.* **1981**, *11*, 133.

(13) Schumann, H.; Schumann, I. In *Gmelin Handbook of Inorganic Chemistry*; Bitterer, H., Ed.; Springer-Verlag: Berlin, 1979; Organotin Compounds, Vol. 6, p 210.

0276-7333/95/2314-0685$09.00/0

this one was chosen to prepare the desired functional organotin trihalides. Treatment of tetrakis(4-vinylphenyl)tin[22] or tetrakis(3-butenyl)tin with 3 equiv of tin tetrachloride or hydrogen chloride was initially attempted, but it did not lead to the corresponding organotin trichlorides. Next, (4-vinylphenyl)tricyclohexyltin was chosen as the starting material. After reaction with tin tetrachloride, repeated crystallizations only gave impure product. However, (4-vinylphenyl)tin trichloride and tricyclohexyltin chloride could finally be separated by liquid–liquid extraction, as their solubilities are very different in polar and nonpolar solvents. When a mixture of (4-vinylphenyl)tin trichloride and tricyclohexyltin chloride, obtained after treatment of (4-vinylphenyl)tricyclohexyltin with 1 equiv of tin tetrachloride in pentane, was extracted with acetonitrile, the trichloride migrated into the acetonitrile phase, along with only a small amount of tricyclohexyltin chloride. (4-Vinylphenyl)tricyclohexyltin was purified by distillation and obtained in 77% yield. The cleavage of organotricyclohexyltins by tin tetrachloride had already been mentioned in the preparation of tricyclohexyltin chloride.[23] The reaction was extended to (3-butenyl)- and (4-pentenyl)tricyclohexyltin. Starting materials were prepared by the coupling of (3-butenyl)- or (4-pentenyl)magnesium bromide with tricyclohexyltin chloride. (4-Chloropent-4-enyl)tricyclohexyltin, $CH_2{=}CHCl(CH_2)_3SnCy_3$, could also be prepared in this way.

$$Cy_3SnR + SnCl_4 \rightarrow RSnCl_3 + Cy_3SnCl$$

$$R = 4\text{-}(CH_2{=}CH)C_6H_4,\ \text{yield } 73\%$$

$$R = CH_2{=}CH(CH_2)_2,\ \text{yield } 92\%$$

$$R = CH_2{=}CH(CH_2)_3,\ \text{yield } 87\%$$

In these procedures, the coupling of Grignard or lithium reagents was successfully used to prepare organotricyclohexyltins. However, two other routes to tetraorganotins, the coupling of stannylmetals with organic halides or tosylates[24] and the addition of organotin hydrides to unsaturated compounds,[25] are, in principle, applicable. To our knowledge, neither a (tricyclohexylstannyl)metal nor the addition of tricyclohexyltin hydride to an alkene has been reported. Tricyclohexyltin hydride adds to alkynes[26,27] but not to alkenes, even under high pressure.[28] The first of these routes has been tested with (tricyclohexylstannyl)lithium, prepared from the corresponding tin hydride using the procedure of Still.[29] The required tricyclohexyltin hydride was obtained by reduction of tricyclohexyltin hydroxide, a commercial starting material, with an excess of lithium aluminum hydride, thus avoiding the use[30] of tricyclohexyltin chloride. Reaction of (tricyclohexylstannyl)lithium with 1-chloropropane gave the coupling compound in only low yield, but with 1-bromopropane and methyl iodide, the reaction was preparatively useful. The coupling was successfully extended to 6-bromo-1,3-hexadiene, to give (3,5-hexadienyl)tricyclohexyltin in 67% yield.

$$Cy_3SnH \xrightarrow[-i\text{-}Pr_2NH]{i\text{-}Pr_2NLi} Cy_3SnLi \xrightarrow[-LiX]{RX} Cy_3SnR$$

$$RX = MeI,\ \text{yield } 63\%$$

$$RX = n\text{-}PrBr,\ \text{yield } 72\%$$

$$RX = CH_2{=}CHCH{=}CH(CH_2)_2Br,\ \text{yield } 67\%$$

$$RX = n\text{-}PrCl,\ \text{yield } 20\%$$

In the second approach, hydrostannation of unactivated alkenes such as allyl alcohol, 5-(benzyloxy)-1-pentene, and 3-butenyl acetate with tricyclohexyltin hydride in benzene under UV irradiation, or at reflux with azobis(isobutyronitrile) (AIBN) as initiator, failed. However, under more drastic conditions, without solvent at 110 °C and with portionwise addition of AIBN, using a small excess of alkene to avoid extensive formation of hexacyclohexyltin, addition products were recovered in good yield. The reaction was successfully extended to other alcohols (3-butenol, 4-pentenol, and 5-hexenol) and esters (2-propenyl and 4-pentenyl acetates). It was regiospecific, and the adducts were easily purified by column chromatography.

$$Cy_3SnH + H_2C{=}CHR \xrightarrow{AIBN} Cy_3SnCH_2CH_2R$$

R (% yield): CH_2OH (88), $(CH_2)_2OH$ (60), $(CH)_3OH$ (79), $(CH_2)_4OH$ (65), $(CH_2)_3OCH_2Ph$ (68), CH_2OCOCH_3 (78), $(CH_2)_2OCOCH_3$ (72), $(CH_2)_3OCOCH_3$ (71)

As in the previous case, these organotricyclohexyltins

(14) Davies, A. G.; Smith, P. J. In *Comprehensive Organometallic Chemistry*; Wilkinson, G., Stone, F. G. A., Abel, E. W., Eds.; Pergamon Press: Oxford, U.K., 1982; Vol. 2, p 591.
(15) Bulten, E. J. *J. Organomet. Chem.* **1975**, *97*, 167. Bulten, E. J.; Gruter, H. F. M.; Martens, H. F. *J. Organomet. Chem.* **1976**, *117*, 329. Murphy, J.; Poller, R. C. *J. Organomet. Chem. Libr.* **1979**, *9*, 189.
(16) Meyer, A. *Ber. Dtsch. Chem. Ges.* **1885**, *16*, 1442. Tchakirian, A.; Lesbre, M.; Lewinsohn, M. *Bull. Soc. Chim. Fr.* **1936**, 138. Druce, J. G. F. *J. Chem. Soc.* **1922**, 1859. Pope, W. J.; Peachy, S. *J. Chem. Soc.* **1903**, 7.
(17) Corey, E. J.; Eckrich, T. M. *Tetrahedron Lett.* **1983**, *24*, 163.
(18) Burley, J. W.; Hutton, R. E.; Oake, V. *J. Chem. Soc., Chem. Commun.* **1976**, 803. Hutton, R. E.; Burley, J. W. *J. Organomet. Chem.* **1978**, *156*, 369. Burley, J. W.; Hope, P.; Mack, A. G. *J. Organomet. Chem.* **1984**, *277*, 737. Harrison, P. G.; King, T. J.; Healy, M. A. *J. Organomet. Chem.* **1979**, *182*, 17. Bulten, E. J.; van den Hurk, J. W. G. *J. Organomet. Chem.* **1978**, *162*, 161. Howie, R. A.; Paterson, E. S.; Wardell, J. L.; Burley, J. W. *J. Organomet. Chem.* **1983**, *259*, 71.
(19) Ryu, I.; Suzuki, H.; Murai, S.; Sonoda, N. *Organometallics* **1987**, *6*, 212.
(20) Nakahira, H.; Ryu, I.; Ikebe, M.; Oku, Y.; Ogawa, A.; Kambe, N.; Sonoda, N.; Murai, S. *J. Org. Chem.* **1992**, *57*, 17. Ryu, I.; Murai, S.; Sonoda, N. *J. Org. Chem.* **1986**, *51*, 2389.
(21) Nakahira, H.; Ryu, I.; Ogawa, A.; Kambe, N.; Sonoda, N. *Organometallics* **1990**, *9*, 277. Nakamura, E.; Shimada, J. I.; Kuwajima, I. *Organometallics* **1985**, *4*, 641. Nakamura, E.; Kawajima, I. *Chem. Lett.* **1983**, 59.
(22) Schuman, H.; Rodewald, G.; Rodewald, U. *J. Organomet. Chem.* **1978**, *187*, 305.
(23) Kushlefsky, B. G.; Reifenberg, G. H.; Hirshman, J. L.; Considine, W. J. Ger. Offen. 1955463; *Chem. Abstr.* **1970**, *73*, 15000. Reifenberg, G. H.; Gitlitz, M. H. S. African Patent 7202018; *Chem. Abstr.* **1973**, *79*, 18853. We are indebted to Professor D. Seyferth for bringing these patents to our attention.
(24) See, for example: Lee, K.-W.; San Filippo, J. *Organometallics* **1982**, *1*, 1496. San Filippo, J.; Silbermann, J. *J. Am. Chem. Soc.* **1982**, *104*, 2831. Smith, G. F.; Kuivila, H. G.; Simon, R.; Sultan, L. *J. Am. Chem. Soc.* **1981**, *103*, 833. Kuivila, H. G. *Adv. Chem. Ser.* **1976**, *No. 157*, 41.
(25) van der Kerk, G. J. M.; Luijten, J. G. A.; Noltes, J. G. *Chem. Ind.* **1956**, 352. van der Kerk, G. J. M.; Noltes, J. G. *J. Appl. Chem.* **1959**, *9*, 106. Neumann, W. P. *Angew. Chem.* **1964**, *76*, 849.
(26) Corey, E. J.; Ulrich, P.; Fitzpatrick, J. M. *J. Am. Chem. Soc.* **1976**, *98*, 222.
(27) Rahm, A.; Grimau, J. *J. Organomet. Chem.* **1985**, *286*, 297.
(28) Rahm, A.; Ferkous, F.; Degueil-Castaing, M.; Jurczak, J.; Golebiowski. A. *Synth. Inorg. Met.-Org. Chem.* **1987**, *17*, 937.
(29) Still, W. C. *J. Am. Chem. Soc.* **1978**, *100*, 1481.
(30) Neumann, W. P.; Schneider, B.; Sommer, R. *Justus Liebigs Ann. Chem.* **1966**, *692*, 1.

Table 1. Yields and Selected ^{119}Sn NMR Data for Functional Organotin Trichlorides

compd	yield (%)	^{119}Sn chem shift (ppm)	$^{1}J_{Sn-C}$ (Hz)
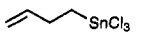	92	−5	672
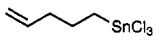	87	−1	664
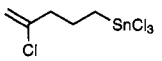	83	0	663
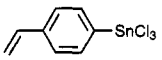	73	−68	1140
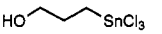	85	−112	845
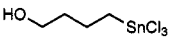	74	−147	848
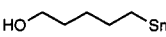	63	−80	894
	90	−95	807
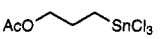	90	−38	746
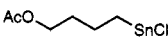	89	−47	724
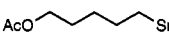	67	−67	735
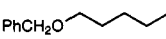	75	−1	665

Chart 1

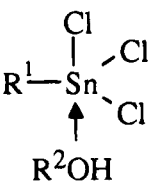

were treated by tin tetrachloride in order to prepare the corresponding functional organotin trichlorides. With (3,5-hexadienyl)tricyclohexyltin, the reaction failed. Only intractable mixtures were obtained, extensive polymerization occurring during the cleavage. With functional propyl-, butyl-, pentyl-, and hexyltricyclohexyltins, the reactions worked well, leading to the corresponding trichlorides in good yield (see Table 1). ^{119}Sn NMR spectroscopy resonances showed an upfield shift, with respect to nonfunctional alkyltin trichlorides, in trihalostannyl alcohols and esters; the effect was stronger with alcohols. In the alcohols, this could be indicative of pentacoordination of the metal (Chart 1), as has been established by X-ray and ^{119}Sn NMR spectroscopy for β- and γ-trichlorostannyl carbonyl compounds.[18,31] To check this hypothesis, trichlorobutyltin was mixed with 1 equiv of methanol. The chemical shift of the metal was at −181 ppm, in the same range as in the prepared trichlorostannyl alcohols, which confirmed the proposed pentacoordination. In esters, intermediate values may suggest an equilibrium between tetra- and pentacoordinated species, or a weak coordination. The variations of tin−carbon coupling constants, $^{1}J_{Sn-C}$, are indicative of changes in coordination at tin, within the same class of organotins.[32] β-Trichlorostannyl ketones, where the metal is pentacoordinated, show $^{1}J_{Sn-C}$ higher than 810 Hz,[33] whereas $^{1}J_{Sn-C}$ for butyltin trichloride, where the metal is tetracoordinated, was 648 Hz in deuteriochloroform and 939 Hz with 1 equiv of methanol. In trichlorostannyl alcohols, these values were in the range of 850−900 Hz, thus indicative of pentacoordination of the tin. In trichlorostannyl esters and ethers, they were intermediate between the values for tetracoordinated and pentacoordinated species. That confirmed the deductions based on ^{119}Sn NMR chemical shift studies.

Three organotin trialkoxides were prepared from functional organotin trichlorides, (3-butenyl)-, (4-pentenyl)- and (4-vinylphenyl)tin tri-*t*-amyloxide. The *t*-amyloxy group was chosen because $RSn(OCMe_2Et)_3$ compounds are liquids which can be purified by distillation. (3-Butenyl)- and (4-pentenyl)tin tri-*t*-amyloxides were prepared by the reaction of the corresponding trichloride with *t*-amyl alcohol, in the presence of diethylamine and 1 equiv of sodium *t*-amyloxide to complete the reaction.[34] With (4-vinylphenyl)tin trichloride, this method failed, the presence of a strong base leading to extensive polymerization. A procedure described for the preparation of tin tetraalkoxides,[35] using only diethylamine and *t*-amyl alcohol, was then successfully applied and gave the desired products in high yield.

$$RSnCl_3 + 3(t\text{-amyl})OH \xrightarrow[-HCl]{Et_2NH} RSn(O\text{-}t\text{-amyl})_3$$

R (% yield): $CH_2{=}CH(CH_2)_2$ (70), $CH_2{=}CH(CH_2)_3$ (75), 4-$(CH_2{=}CH)C_6H_4$ (72)

The synthesis and the properties of the new hybrid organic−inorganic materials, obtained after hydrolysis and polymerization of the organic function, will be published elsewhere.

Experimental Section

All reactions were carried out under a nitrogen atmosphere. Pentane, THF, and diethyl ether were distilled from sodium benzophenone ketyl prior use. Pyridine and diisopropylamine were distilled on KOH. Acetonitrile was distilled on CaH_2. Methanol, ethanol, and *t*-amyl alcohol were distilled from magnesium. Acetyl chloride and tin tetrachloride were distilled before use. ^{1}H NMR spectra were recorded on a Perkin-Elmer-Hitachi R 24A or a Bruker AC-250 spectrometer (solvent $CDCl_3$, internal reference Me_4Si), ^{13}C NMR spectra were taken on a Bruker AC-250 spectrometer (solvent $CDCl_3$, internal reference Me_4Si), ^{119}Sn NMR spectra were recorded on a Bruker AC-200 spectrometer (solvent C_6D_6, internal reference Me_4Sn). For NMR data, the multiplicity, coupling constants in Hz, and integration are given in parentheses. Tin−hydrogen and tin−carbon coupling constants (Hz) are given in brackets.

Preparation of 5-bromo-2-chloro-1-pentene.[36] In a three-necked flask was placed anhydrous potassium carbonate (34.3 g, 250 mmol), ethyl 3-oxobutanoate (28.3 g, 240 mmol), 2,3-dichloropropene (25 g, 220 mmol), and 132 mL of absolute ethanol. The mixture was heated at reflux for 16 h, and

(31) Omae, I. *J. Organomet. Chem. Libr.* **1986**, *18*. Wrackmeyer, B. *Annu. Rep. NMR Spectrosc.* **1985**, *16*, 73.

(32) Mitchell, T. *J. Organomet. Chem.* **1973**, *59*, 189. Harris, R. K.; Kennedy, J. D.; McFarlane, W. In *NMR and the Periodic Table*; Harris, R. K., Mann, B. E., Eds.; Academic Press: London, 1978; p 342. Jousseaume, B.; Noiret, N.; Pereyre, M.; Frances, J. M.; Petraud, M. *Organometallics* **1992**, *11*, 3910. Jousseaume, B.; Gouron, V.; Noiret, N.; Pereyre, M.; Frances, J. M. *J. Organomet. Chem.* **1993**, *450*, 97.

(33) Nakahira, H.; Ryu, I.; Ikebe, M.; Oku, Y.; Ogawa, A.; Kambe, N.; Sonoda, N.; Murai, S. *J. Org. Chem.* **1992**, *57*, 17.

(34) Greco, C. C. Eur. Pat. Appl. EP0252543.

(35) Thomas, I. M.; U.S. Patent 3,946,056. Chandler, C. D.; Fallon, G. D.; Koplick, A. J.; West, B. O. *Aust. J. Chem.* **1987**, *40*, 1427. Hampden-Smith, M. J.; Wark, T. A.; Rheingold, A.; Hoffmann, J. C. *Can. J. Chem.* **1991**, *69*, 121.

(36) Drouin, J. Ph.D. Thesis, Universite de Paris Sud, 1976.

ethanol was distilled off. A 300 mL amount of water was added at 0 °C, and the mixture was extracted with diethyl ether (3 × 80 mL). After drying and removal of the solvent, a mixture of ethyl and methyl 4-chloro-4-pentenoates and 5-chloro-5-hexen-2-one was distilled (bp 72 (0.1 mm), 15 g). Ethyl 4-chloro-4-pentenoate: ^{1}H NMR δ 1.24 (t, 8, 3H), 2.42–2.58 (m, 4H), 4.04 (q, 8, 2H), 5.10 (t, 2, 2H). To a solution of the mixture (40 g) in 360 mL of THF at 0 °C was added 620 mL of aqueous NaOH (1 N). The solution was stirred for 4 h at room temperature. It was then extracted three times with diethyl ether (120, 50, and 30 mL). Diethyl ether (120 mL) and a solution of 18 mL of 36 N H_2SO_4 in 120 mL of water were successively added to the aqueous phase, which was subsequently extracted with diethyl ether (2 × 100 mL). After drying, evaporation, and recrystallization in petroleum ether, 20 g of 4-chloro-4-pentenoic acid was recovered (mp 41 °C): ^{1}H NMR δ 2.6 (bs, 4H), 5.15 (bs, 2H), 12 (bs, 1H); ^{13}C NMR δ 32, 34, 113.3, 140.5, 178.7. To a mixture of lithium aluminum hydride (25 g, 400 mmol) in 500 mL of diethyl ether was added 4-chloro-4-pentenoic acid (28 g, 210 mmol) in 100 mL of ether. After 3 h, the mixture was hydrolyzed at 0 °C. The usual workup gave 4-chloro-1-pentenol (22 g, 86%; bp 100°C (40 mm)): ^{1}H NMR δ 1.72–1.78 (m, 2H), 2.35 (t, 6, 2H), 3.25 (bs, 1 H), 3.55 (t, 6, 2H), 5.11 (bs, 2H); ^{13}C NMR δ 30, 35.5, 61.1, 112.4, 142.3. To a solution of 4-chloro-1-pentenol (2 g, 16 mmol) and 0.5 mL of pyridine in 10 mL of diethyl ether was added a solution of phosphorus tribromide (2 g, 7 mmol) in 5 mL of diethyl ether, at −30 °C under nitrogen. The mixture was stirred at −30 °C for 1.5 h and warmed to room temperature for 1 h. The solution was then washed with a saturated NaCl solution and dried, and the solvent was evaporated. Purification by chromatography on silica gel gave 5-bromo-2-chloro-1-pentene (1 g, 35%): ^{1}H NMR δ 2.09 (tt, 7, 7, 2H), 2.43 (t, 7, 2H), 3.36 (t, 7, 2H), 5.19 (bs, 2H); ^{13}C NMR δ 29.8, 32.2, 37.3, 113.6, 140.8.

Coupling of Grignard Reagents with Tricyclohexyltin Chloride. In a three-necked flask under nitrogen was prepared a Grignard reagent from 250 mmol of the organic halide and 6.3 g of magnesium (260 mmol) in 150 mL of diethyl ether (THF with 4-chlorostyrene). The mixture was heated at reflux for 30 min and then was added slowly via cannula to a solution of tricyclohexyltin chloride[37] (60 g, 150 mmol) in 250 mL of diethyl ether. The resulting mixture was heated at reflux for 4 h. After hydrolysis with a saturated solution of NH_4Cl, the usual workup followed by recrystallization from absolute ethanol gave the tetraorganotin species. (4-Vinylphenyl)tricyclohexyltin: yield 75%; mp 109°C. Anal. Calcd for $C_{26}H_{40}Sn$: C, 66.26; H, 8.55. Found: C, 66.61; H, 8.74. ^{1}H NMR: δ 1.21–1.77 (m, 33H), 5.32 (d, 10, 1H), 5.83 (d, 18, 1H), 6.71 (dd, 10, 18, 1H), 7.38–7.50 (m, 4H). ^{13}C NMR: δ 27.1 [343], 27.2, 29.4 [56], 32.4 [16], 113.5, 125.7 [37], 137.1, 137.2, 137.7 [25], 141.1 [302]. ^{119}Sn NMR: δ −100. (3-Butenyl)tricyclohexyltin: yield 78%; mp 110 °C. Anal. Calcd for $C_{22}H_{40}Sn$: C, 62.43; H, 9.53. Found: C, 62.11; H, 9.28. ^{1}H NMR: δ 0.75–0.82 (m, [61], 2H), 1.2–1.77 (m, 33 H), 2.22 (m, [57], 2H), 4.80 (dd, 11, 1.7, 1H), 4.91 (dd, 17, 1.7, 1H), 5.85 (ddt, 11, 17, 6, 1H). ^{13}C NMR: δ 5.8 [256], 26.1 [324], 27.3, 29.3 [53], 29.8 [16], 32.5 [23], 112.4, 142.7 [53]. ^{119}Sn NMR δ −64. (4-Pentenyl)tricyclohexyltin: yield 81%; mp 108 °C. Anal. Calcd for $C_{23}H_{42}Sn$: C, 63.18; H, 9.68. Found: C, 62.85; H, 9.38. ^{1}H NMR: δ 0.67–0.75 (m, [60], 2H), 1.20–1.80 (m, 35 H), 2.05–2.15 (m, 2H), 4.77 (d, 10, 1H), 4.94 (d, 17, 1H), 5.81 (ddt, 17, 10, 6, 1H). ^{13}C NMR δ 6.4 [254], 25.9 [313], 26.9 [17], 27.3, 29.3 [54], 32.5 [23], 39.2 [53], 114.4, 139.1. ^{119}Sn NMR δ −65. (4-Chloropent-4-enyl)tricyclohexyltin: yield 74%; mp 78 °C. Anal. Calcd for $C_{23}H_{41}ClSn$: C, 58.56; H, 8.76. Found: C, 58.42; H, 8.94. ^{1}H NMR: δ 0.85–0.95 (m, 2H), 1.23–2.21 (m, 35H), 2.37 (t, 7, 2H), 5.01 (bs, 1H), 5.17 (bs, 1H). ^{13}C NMR: δ 5.4 [259], 25.1 [19], 25.9 [324], 26.5, 29.2 [53], 32.5 [16], 44.1 [54], 119.0, 142.7; ^{119}Sn NMR: δ −65.4.

(37) Pommier, J. C.; Pereyre, M.; Valade, J. *C. R. Acad. Sci.* **1965**, *260*, 6397.

Preparation of Tricyclohexyltin Hydride. To a suspension of tricyclohexyltin hydroxide (30 g, 78 mmol) in 100 mL of diethyl ether was slowly added 7.6 g (200 mmol) of lithium aluminum hydride under nitrogen. The mixture was refluxed for 3 h. After hydrolysis and the usual workup, the pure tin hydride was isolated by distillation in a Kugelrohr apparatus: yield 92%; bp 140 °C (10^{-3} mm) (lit.[30] bp 147 °C (10^{-3} mm)).

Preparation of (*E*)-6-Bromo-1,3-hexadiene. 3,5-Hexadienol[38] (10 g, 100 mmol) in 10 mL of diethyl ether was slowly added to a solution of tetrabromomethane (60 g, 180 mmol) and triphenylphosphine (47 g, 180 mmol) in 120 mL of diethyl ether. The mixture was heated at reflux for 1 h. After addition of 300 mL of pentane, the mixture was filtered. After evaporation of the solvents, the bromide was recovered by distillation: yield 75%; bp 52 °C (2 mm); ^{1}H NMR δ 2.62 (dt, 8, 7, 2H), 3.37 (t, 7, 2H), 4.98 (d, 10, 1H), 5.11 (d, 16, 1H), 5.75 (dt, 15, 8, 1H), 6.12 (dd, 15, 10, 1H), 6.31 (dt, 16, 10 1H); ^{13}C NMR δ 32.2, 35.9, 116.7, 130.9, 133.6, 136.7.

Coupling of (Tricyclohexylstannyl)lithium with Organic Halides. In a Schlenk tube at 0 °C, 20 mL of *n*-butyllithium (2.5 M) in hexane was added to diisopropylamine (4.8 g, 50 mmol) in 40 mL of THF. After 15 min at this temperature, tricyclohexyltin hydride (17 g, 46 mmol) was added slowly and the mixture was stirred for 15 min. At −40 °C, 55 mmol of the organic halide in 50 mL of THF was added. The mixture was warmed to room temperature and stirred for 16 h. After hydrolysis with a saturated solution of NH_4Cl at 0 °C and the usual workup, the tetraorganotins were recovered by column chromatography on silica gel (eluent petroleum ether). Methyltricyclohexyltin:[39] yield 63%. Propyltricyclohexyltin:[39] yield 72%. (*E*)-(3,5-Hexadienyl)tricyclohexyltin: yield 67%. Anal. Calcd for $C_{24}H_{42}Sn$: C, 64.16; H, 9.42. Found: C, 64.55; H, 9.86. ^{1}H NMR: δ 0.68–0.77 (m, [57], 2H), 1.2–2.2 (m, 33H), 2.24–2.36 (m, [53], 2H), 5.05 (d, 10, 1H), 5.15 (d, 17, 1H), 5.75 (dt, 16, 10, 1H), 6.08 (dd, 16, 10, 1H), 6.55 (dt, 17, 10, 1H). ^{119}Sn NMR: δ −65.

Hydrostannation Reactions. In a Schlenk tube under nitrogen, a mixture of the alkene (75 mmol), tricyclohexyltin hydride (22.5 g, 60 mmol), and AIBN (200 mg) was heated to 110 °C under nitrogen for 8 h. AIBN (200 mg) was added and the mixture heated for 8 h. The product was purified by chromatography on silica gel (petroleum ether/ethyl acetate 90/10). (3-Hydroxypropyl)tricyclohexyltin: yield 88%; mp 129 °C. Anal. Calcd for $C_{21}H_{40}SnO$: C, 59.04; H, 9.44. Found: C, 58.63; H, 9.17. ^{1}H NMR: δ 0.60–0.68 (m, [64], 2H), 1.19–1.79 (m, 35H), 3.50 (t, 6, 2H), 4.2 (bs, 1H). ^{13}C NMR: δ 1.8 [241], 27.2 [314], 28.9, 29.7 [54], 32.3 [16], 32.5 [16], 66.8 [60]. ^{119}Sn NMR: δ −63.2. (4-Hydroxybutyl)tricyclohexyltin: yield 60%; mp 131 °C. Anal. Calcd for $C_{22}H_{42}OSn$: C, 59.88; H, 9.59. Found: C, 60.14; H, 9.48. ^{1}H NMR: δ 0.70–0.78 (m, [61], 2H), 1.19–1.78 (m, 37H), 3.59 (t, 6, 2H), 5.14 (bs, 1H). ^{13}C NMR: δ 6.6 [255], 23.5 [16], 25.9 [333], 27.3, 29.3 [58], 32.4 [18], 38.1 [56], 62.6. ^{119}Sn NMR δ −65. (5-Hydroxypentyl)tricyclohexyltin: yield 79%; mp 110 °C. Anal. Calcd for $C_{23}H_{44}OSn$: C, 60.68; H, 9.74. Found: C, 60.92; H, 9.54. ^{1}H NMR: δ 0.64–0.73 (m [61], 2H), 1.10–1.78 (m, 39H), 2.36 (s, 1H), 3.54 (t, 7, 2H). ^{13}C NMR: δ 6.7 [267], 25.9 [333], 26.7 [18], 27.1, 29.8 [52], 32.3 [53], 32.4, 32.5 [16], 62.8. ^{119}Sn NMR δ −65. (6-Hydroxyhexyl)tricyclohexyltin: yield 65%. Anal. Calcd for $C_{24}H_{46}OSn$: C, 61.42; H, 9.88. Found: C, 61.89; H, 10.15. ^{1}H NMR: δ 0.72–0.81 (m [62], 2H), 1.11–1.84 (m, 41H), 3.63 (t, 7, 2H), 4.25 (bs, 1H). ^{13}C NMR: δ 6.7 [266], 25.3 [16], 25.3 [317], 27.3, 27.4, 28.9 [52], 32.5 [16], 32.6, 34.7 [51], 63.1. ^{119}Sn NMR: δ −64.8. (5-(Benzyloxy)pentyl)tricyclohexyltin: yield 68%. Anal. Calcd for $C_{30}H_{50}OSn$: C, 66.06; H, 9.24. Found: C, 66.28; H, 9.42. ^{1}H NMR δ 0.77–0.87 (m, 2H), 1.01–1.94 (m, 39H), 4.57 (t, 7, 2H), 6.43 (s, 2H), 7.39 (s, 5H). ^{13}C

(38) Martin, S. F.; Tu, C.; Chou, T. *J. Am. Chem. Soc.* **1980**, *102*, 5274.

(39) Gielen, M.; De Clercq, M.; De Poorter, B. *J. Organomet. Chem.* **1972**, *34*, 305.

NMR: δ 9.0 [251], 26.1 [302], 27.3, 27.4, 29.1, [57], 32.3, 32.5, 32.6, 70.6, 72.9, 127.5, 128.3. ^{119}Sn NMR: δ −64.4. (3-(Acetyloxy)propyl)tricyclohexyltin: yield 78%; mp 47 °C. Anal. Calcd for $C_{23}H_{42}O_2Sn$: C, 58.87; H, 9.02. Found: C, 58.95; H, 8.89. ^{1}H NMR: δ 0.67−0.78 (m [65], 2H), 1.12−1.84 (m, 35H), 2.04 (s, 3H), 3.96 (t, 7, 2H). ^{13}C NMR: δ 2.1 [247], 21.1, 26.1 [312], 26.4 [16], 27.3, 29.4 [53], 32.5 [16], 68.1 [54], 171.3. ^{119}Sn NMR: δ −64.0. (4-(Acetyloxy)butyl)tricyclohexyltin: yield 72%. Anal. Calcd for $C_{24}H_{44}O_2Sn$: C, 59.64; H, 9.18. Found: C, 59.97; H, 9.41. ^{1}H NMR: δ 0.58−0.67 (m [65], 2H), 1.12−1.80 (m, 37H), 2.02 (s, 3H), 3.93 (t, 7, 2H). ^{13}C NMR: δ 6.6 [247], 21.1, 25.5 [312], 26.8 [16], 27.3, 29.3 [53], 32.5 [16], 38.2 [54], 67.9, 171.3. ^{119}Sn NMR: δ −64.3. (5-(Acetyloxy)pentyl)tricyclohexyltin: yield 71%. Anal. Calcd for $C_{25}H_{46}O_2Sn$: C, 60.38; H, 9.32. Found: C, 60.12; H, 9.57. ^{1}H NMR: δ 0.64−0.73 (m [60], 2H), 1.12−1.84 (m, 39H), 2.08 (s, 3H), 4.02 (t, 7, 2H). ^{13}C NMR: δ 6.6 [258], 20.1, 25.9 [312], 27.0 [16], 27.2, 29.3 [55], 31.2 [58], 32.2, 32.3 [16], 64.7, 171.1. ^{119}Sn NMR: δ −65.0.

Preparation of Functional Organotin Trichlorides. To a solution of organotricyclohexyltin (50 mmol) in 100 mL of pentane was added slowly tin tetrachloride (50 mmol, 13.1 g) under nitrogen. After 3 h, 200 mL of acetonitrile and 200 mL of pentane were added and the mixture was stirred for 18 h. The mixture was decanted, and the acetonitrile solution was extracted with pentane (3 × 50 mL). Evaporation of acetonitrile gave the trichlorides, which were distilled in a Kugelrohr apparatus. Hydroxy-substituted organotrichlorotin decomposed during the distillation. Trichloro(4-vinylphenyl)tin was diluted with dry mineral oil (10% solution), and a few crystals of di-*tert*-butylcatechol were added before distillation: yield 73%; bp 100 °C (10^{-3} mm). Anal. Calcd for $C_8H_7Cl_3Sn$: C, 29.28; H, 2.15. Found: C, 28.96; H, 2.07. ^{1}H NMR: δ 5.29 (d, 10, 1H), 5.68 (d, 20, 1H), 6.70 (dd, 10, 20, 1H), 7.47 (s, 4H). ^{13}C NMR: δ 117.8, 127.9 [129], 134.2 [80], 134.9 [1140], 135.5 [19], 142.3 [26]. (3-Butenyl)tin trichloride: yield 92%; bp 85 °C (10^{-3} mm). Anal. Calcd for $C_4H_7SnCl_3$: C, 17.15; H, 2.52. Found: C, 17.34; H, 2.79. ^{1}H NMR: δ 2.61 (t, 8 [89], 2H), 2.78 (dt, 7, 8 [236], 2H), 5.17 (dd, 10, 1, 1H), 5.27 (dd, 17, 1, 1H), 5.95 (ddt, 10, 17, 7, 1H). ^{13}C NMR: δ 28.6 [58], 33.6 [672], 118.4, 136.0 [98]. (4-Pentenyl)tin trichloride: yield 87%; bp 90 °C (10^{-3} mm). Anal. Calcd for $C_5H_9Cl_3Sn$: C, 20.41; H, 3.08. Found: C, 20.87; H, 3.35. ^{1}H NMR (60 MHz): δ 2.2−2.6 (m, 6H), 5.0−5.15 (m, 2H), 5.6−6.3 (m, 1H). ^{13}C NMR: δ 23.9 [60], 33.4 [664], 34.9 [228], 118.3, 135.9. (4-Chloro-4-pentenyl)tin trichloride: yield 83%; bp 95 °C (10^{-3} mm). Anal. Calcd for $C_5H_8Cl_4Sn$: C, 18.27; H, 2.45. Found: C, 18.65; H, 2.62. ^{1}H NMR (C_3D_6O): δ 1.24 (t, 8 [85], 2H), 2.48 (m, [166], 2H), 2.91 (t, 8, 2H), 4.81 (s, 1H), 5.02 (s, 1H). ^{13}C NMR (C_3D_6O): δ 22.2 [60], 30.4 [664], 40.4 [228], 114.5, 140.2. (3-Hydroxypropyl)tin trichloride: yield 85%. Anal. Calcd for $C_3H_7OCl_3Sn$: C, 12.68; H, 2.48. Found: C, 13.11; H, 2.62. ^{1}H NMR: δ 2.02 (t, 5 [99], 2H), 2.32 (m [259], 2H), 3.71 (t, 5, 2H), 5.03 (bs, 1H). ^{13}C NMR: δ 25.2 [66], 26.7 [845], 61.1 [93]. (4-Hydroxybutyl)tin trichloride: yield 74%. Anal. Calcd for $C_4H_9OCl_3Sn$: C, 16.11; H, 3.04. Found: C, 15.84; H, 2.79. ^{1}H NMR: δ 1.75−1.83 (m, 2H), 2.14−2.27 (m, 2H), 2.41−2.49 (m, 2H), 4.05 (t, 6, 2H), 4.49 (bs, 1H). ^{13}C NMR: δ 25.5 [77], 30.4 [32], 39.3 [848]. (5-Hydroxypentyl)tin trichloride: yield 63%. Anal. Calcd for $C_5H_{11}OCl_3Sn$: C, 19.24; H, 3.55. Found: C, 19.04; H, 3.41. ^{1}H NMR: δ 1.45−1.55 (m [336], 2H), 1.57−1.63 (m, 2H), 1.80−1.88 (m, 2H), 2.14−2.18 (m [109], 2H), 3.94 (t, 6, 2H), 5.82 (bs, 1H). ^{13}C NMR: δ 25.8 [65], 29.7 [36], 31.1, 38.9 [894], 63.9. (6-Hydroxyhexyl)tin trichloride: yield 90%. Anal. Calcd for $C_6H_{13}OCl_3Sn$: C, 22.09; H, 4.02. Found: C, 22.42; H, 3.85. ^{1}H NMR: δ 1.40 (t, 5 [96], 2H), 1.62−1.64 (m, 2H), 1.78−1.83 (m, 2H), 2.27−2.34 (m, 2H), 3.79 (t, 6, 2H), 5.18 (bs, 1H). ^{13}C NMR: δ 24.6 [60], 30.9, 31.0, 31.7, 33.1 [807], 63.5. (3-(Acetyloxy)propyl)tin trichloride: yield 90%; mp 78 °C. Anal. Calcd for $C_5H_9O_2Cl_3Sn$: C, 18.41; H, 2.78. Found: C, 18.84; H, 3.15. ^{1}H NMR: δ 2.08 (s, 3H), 2.24−2.28 (m [96, 256], 4H), 4.13 (t, 7, 2H). ^{13}C NMR: δ 21.4, 23.9 [63], 29.9 [746], 64.9 [63], 171.9 (4-(Acetyloxy)butyl)tin trichloride: yield 89%; mp 86 °C. Anal. Calcd for $C_6H_{11}O_2Cl_3Sn$: C, 21.18; H, 3.25. Found: C, 21.42; H, 3.53. ^{1}H NMR: δ 1.67−1.73 (m, 2H), 1.92−1.96 (m, 2H), 2.02 (s, 3H), 2.29 (t, 6 [92], 2H), 4.09 (t, 6, 2H). ^{13}C NMR: δ 21.1, 21.6 [57], 30.9 [120], 32.9 [843], 63.5, 171.1. (5-(Acetyloxy)pentyl)tin trichloride: yield 67%. Anal. Calcd for $C_7H_{13}O_2Cl_3Sn$: C, 23.74; H, 3.70. Found: C, 23.96; H, 3.44. ^{1}H NMR: δ 1.41−1.59 (m, 2H), 1.68−1.74 (m, 2H), 1.82−1.88 (m, 2H), 2.15 (s, 3H), 2.38 (t [96], 2H), 4.10 (t, 2H). ^{13}C NMR: δ 21.3, 24.6 [61], 27.7, 28.5 [128], 35.5 [735], 65.1, 173.7. (5-(Benzyloxy)pentyl)tin trichloride: yield 75%. Anal. Calcd for $C_{12}H_{17}OCl_3Sn$: C, 35.83; H, 4.26. Found: C, 35.47; H, 4.51. ^{1}H NMR: δ 1.32−1.37 (m, 2H), 1.60−1.64 (m, 2H), 1.79−1.91 (m, 2H), 2.33 (t, 7 [87], 2H), 3.52 (t, 7, 2H), 4.53 (s, 2H), 7.31 (s, 5H). ^{13}C NMR: δ 24.7 [69], 28.1, 28.5 [116], 34.2 [665], 70.0, 73.0, 128.3, 128.6, 128.9, 137.1.

Preparation of Functional Organotin Tri-*tert*-amyloxides). In a three-necked flask, equipped with a mechanical stirrer, dropping funnel, and condenser, was placed the organotin trichloride (20 mmol) and 44 mL of dry pentane, under nitrogen. Diethylamine (4.5 g, 61 mmol) in 25 mL of pentane was added slowly at 0 °C. After the mixture was stirred for 3 h at room temperature, *tert*-amyl alcohol (6 g, 69 mmol) was added dropwise at 0 °C. The mixture was then stirred for 18 h at room temperature. It was filtered, and the solvents were evaporated. The products (diluted in dry mineral oil in the case of (4-vinylphenyl)tin tri-*tert*-amyloxide) were distilled in a Kugelrohr apparatus. (4-vinylphenyl)tin tri-*tert*-amyloxide: yield 70%; bp 110 °C (0.001 mm). Anal. Calcd for $C_{23}H_{40}O_3Sn$: C, 57.16; H, 8.34. Found: C, 56.84; H, 8.62. ^{1}H NMR: δ 0.95 (t, 7, 9H), 1.32 (s, 18H), 1.63 (q, 7, 6H), 5.36 (dd, 11, 0.7, 1H), 5.85 (dd, 18, 0.7, 1H), 6.65 (dd, 18, 11, 1H), 7.42−7.69 (m, 4H). ^{13}C NMR: δ 9.3, 31.2 [18], 38.5 [28], 75.3 [39], 115.5, 126.8 [96], 135.7 [57], 136.4 [11], 139.6, 139.9 [19]. ^{119}Sn NMR: δ −257. (3-Butenyl)tin tri-*tert*-amyloxide: yield 70%; bp 87 °C (0.001 mm). Anal. Calcd for $C_{19}H_{40}O_3Sn$: C, 52.44; H, 9.26. Found: C, 52.89; H, 9.51. ^{1}H NMR: δ 0.95 (t, 7, 9H), 1.27 (s, 18H), 1.43 (t, 7 [156], 2H), 1.59 (q, 7, 6H), 2.54 (dt, 7, 7 [105], 2H), 5.03 (d, 10, 1H), 5.24 (d, 17, 1H), 5.91 (ddt, 17, 10, 7, 1H). ^{13}C NMR: δ 9.1, 23.5 [761], 28.7 [40], 31.1 [16], 38.3 [126], 74.6 [38], 114.9, 139.3 [112]. ^{119}Sn NMR: δ −194. (4-Pentenyl)tin tri-*tert*-amyloxide: yield 75%; bp 90 °C (0.001 mm). Anal. Calcd for $C_{20}H_{42}O_3Sn$: C, 53.47; H, 9.42. Found: C, 53.12; H, 9.29. ^{1}H NMR: δ 0.93 (t, 7, 9 H), 1.19 (s, 18 H), 1.42 (t, 6, 2H), 1.45 (q, 7, 6H), 1.74−1.78 (m, 2 H), 2.14 (dt, 7, 7, 2H), 4.97 (d, 10, 1H), 5.65 (d, 17, 1H), 5.75 (ddt, 17, 10, 7, 1H). ^{13}C NMR: δ 9.2, 23.9 [758], 24.1 [40], 31.0, 36.9 [120], 38.5 [30], 74.7 [40], 115.5, 137.5. ^{119}Sn NMR: δ −193.

Acknowledgment. We are indebted to Sipcam-Phyteurop and to Schering-France for generous gifts of chemicals.

OM940551W

Vapor Phase Laser Photochemistry and Determination by Electron Diffraction of the Molecular Structure of $[(^tBu)GaS]_4$: Evidence for the Retention of the Ga_4S_4 Cubane Core during the MOCVD Growth of Cubic GaS

William M. Cleaver,[1a] Michael Späth,[1b] Dráhomír Hnyk,[1c,d] Graeme McMurdo,[1c] Michael B. Power,[1a] Michael Stuke,*[,1b] David W. H. Rankin,*[,1c] and Andrew R. Barron*[,1a]

Department of Chemistry, Harvard University, Cambridge, Massachusetts 02138, Max-Planck-Institut für biophysikalische Chemie, Postfach 2841, D-37018 Göttingen, Germany, and Department of Chemistry, University of Edinburgh, West Mains Road, Edinburgh EH9 3JJ, Scotland

Received September 2, 1994®

The vapor phase structure and decomposition of $[(^tBu)GaS]_4$ have been investigated by gas phase electron diffraction and UV-laser photolysis/time-of-flight mass spectrometry, respectively. The vapor phase structure of $[(^tBu)GaS]_4$, as determined by electron diffraction, consists of a distorted cubane Ga_4S_4 core. Salient structural parameters (r_a) include Ga–S = 2.365(2) Å and Ga–C = 1.976(4) Å. The electron diffraction structure is compared to that determined in the solid state by X-ray diffraction. The gas phase ultraviolet excimer laser-induced photolysis of $[(^tBu)GaS]_4$ has been studied using a photolysis wavelength of 248 nm. The photofragments were detected by laser ionization time-of-flight mass spectroscopy. The formation of photofragments $(^tBu)_xGa_4S_4$ (x = 0–3) is interpreted to indicate the stability of the Ga_4S_4 core. Solid state ablation studies additionally indicate the coupling of two cubane cores. These results are discussed with respect to the metal–organic chemical vapor deposition of the cubic phase of GaS, using $[(^tBu)GaS]_4$ as a single-source precursor.

Introduction

We have recently reported the metal–organic chemical vapor deposition (MOCVD) growth of a new phase of gallium sulfide (GaS) from the single-source precursor compound $[(^tBu)GaS]_4$ (**I**).[2,3] On the basis of electron

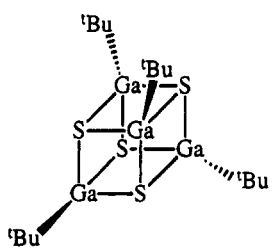

(I)

and X-ray diffraction studies, the new phase was proposed to have a face-centered cubic (*fcc*) structure. This previously unknown cubic phase of GaS has been found to be a suitable material for the electronic passivation[4] of GaAs surfaces.[5,6] In fact, independent theoretical studies have shown it to be the ideal passivation material for GaAs.[7] In addition, the materials large band gap (>3.5 eV) makes it suitable as the insulating "gate" layer in metal–insulator–semiconductor field effect transistor (MISFET)-type devices.[8] Given these fundamental technological developments associated with the new phase of GaS, it is of the utmost importance to understand the growth pathway from a single-source precursor, $[(^tBu)GaS]_4$, to this new solid state phase.

The formation of a meta-stable cubic phase, rather than the thermodynamic hexagonal phase,[9] was shown to be dependent only on the precursor's structure[3] and was rationalized by assuming that the Ga_4S_4 core of the precursor molecule remained intact during deposition and acted as a *predesigned molecular motif* to the solid state phase.[10] As such this system appears to be a rare example of a new solid state material being synthesized by molecular control and represents a unique opportunity for the study of the concept of "molecules to materials".

Evidence for the proposal of molecular control was initially based on electron impact and chemical ionization mass spectral data of the precursor compound,

* Authors to whom correspondence should be addressed.
® Abstract published in *Advance ACS Abstracts*, December 1, 1994.
(1) (a) Harvard University. (b) Max-Planck-Institut für biophysikalische Chemie. (c) University of Edinburgh. (d) On leave from the Institute of Inorganic Chemistry of the Academy of Science of the Czech Republic, 250 68 Řež near Prague, Czech Republic.
(2) MacInnes, A. N.; Power, M. B.; Barron, A. R. *Chem. Mater.* **1992**, *4*, 11.
(3) MacInnes, A. N.; Power, M. B.; Barron, A. R. *Chem. Mater.* **1993**, *5*, 1344.
(4) Passivation is defined as a process that reduces the density of available electronic states present at the surface of a semiconductor, thereby limiting hole and electron recombination possibilities.
(5) MacInnes, A. N.; Power, M. B.; Barron, A. R.; Jenkins, P. P., Hepp, A. F. *Appl. Phys. Lett.* **1993**, *62*, 771.
(6) Tabib-Azar, M.; Kang, S.; MacInnes, A. N.; Power, M. B.; Barron, A. R.; Jenkins, P. P., Hepp, A. F. *Appl. Phys. Lett.* **1993**, *63*, 625.
(7) Medvedev, Yu. V. *Appl. Phys. Lett.* **1994**, *64*, 3458.
(8) Jenkins, P. P.; MacInnes, A. N.; Tabib-Azar, M.; Barron, A. R. *Science* **1994**, *263*, 1751.
(9) (a) Hahn, H. *Angew. Chem.* **1958**, *65*, 538. (b) Kuhn, A.; Chevey, A. *Acta Crystallogr.* **1976**, *B32*, 983.
(10) Barron, A. R. *Comments Inorg. Chem.* **1993**, *14*, 123.

0276-7333/95/2314-0690$09.00/0

Scheme 1. EI Mass Spectral Fragmentation of [(ᵗBu)GaS]₄

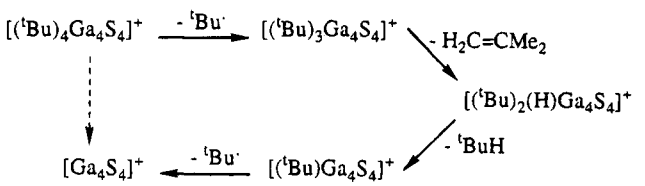

[(ᵗBu)GaS]$_4$, in which no fragmentation of the Ga_4S_4 core occurs (Scheme 1). However, no direct evidence was available to confirm that the cubane precursor's Ga_4S_4 core was retained through the CVD process, i.e., in the vapor phase during mass transport, during vapor phase decomposition, and on the growth surface. While we cannot, as yet, probe the MOCVD growth surface directly, we have embarked on a program attempting to determine the structure of [(ᵗBu)GaS]$_4$ under conditions of vapor transport and better understand its decomposition in the vapor phase.

Electron diffraction represents a powerful tool for nondestructive structural determination at high temperatures in the gas phase,[11] allowing for the direct confirmation of the vapor phase structure of [(ᵗBu)GaS]$_4$. Furthermore, we have previously reported that the UV-excimer laser photolysis of gallium alkyls is an excellent probe of their vapor phase decomposition pathways.[12] The results of our studies in both of these areas are presented herein.

Results and Discussion

Electron Diffraction Studies. While [(ᵗBu)GaS]$_4$ exhibits volatility at *ca.* 180 °C, during the MOCVD of GaS the vapor transfer lines are held at 220–240 °C to provide saturation of the carrier gas.[13] In order to confirm that [(ᵗBu)GaS]$_4$ remains intact during vapor phase transport, we determined its structure under analogous temperature conditions.

Using a stainless steel nozzle heated by flowing hot air, we have succeeded in measuring the electron diffraction pattern of [(ᵗBu)GaS]$_4$ in the vapor phase at 218 °C. The measurements were made at two camera distances, *viz.* 258.6 and 96.6 mm, with an electron wavelength of 0.0569 Å, giving a range of 2–26 Å^{-1} in the scattering variable, s. Three plates were exposed at each camera length.

Given the precedent of the solid state structure,[14] the molecular model of the heavy-atom skeleton of [(ᵗBu)GaS]$_4$ was based on two penetrating tetrahedra, Ga_4 and S_4, the center of each coinciding with the origin of the coordinate system. C_2 and C_3 symmetry operations were used to generate the appropriate geometry including the position of the *tert*-butyl groups. The structure was thus defined by four bonded distances, r(Ga–S), r(Ga–C), r(C–C), and r(C–H), and by one nonbonded distance, r(Ga···Ga). The Ga–C–C and C–C–H bond angles, as well as the twist angles (τ) of the methyl and *tert*-butyl groups around C–C and Ga–C bonds, were selected to complete the set of nine independent geometrical parameters, as listed in Table 1. The twist angles τ_1 and τ_2 were defined to be zero when the Ga(1)–C(1)–C(11)–H (τ_1) and S(2)–Ga(1)–C(1)–C(11) (τ_2) sets of atoms were coplanar. Values of τ_1 and $\tau_2 < 0$ indicate counterclockwise rotation around the C(1)–C(11) and Ga(1)–C(1) bonds, respectively, viewed from C(1) to C(11) and from Ga(1) to C(1). Overall the molecule had T symmetry. The molecular model for [(ᵗBu)GaS]$_4$ in its refined form, together with the atomic numbering, is presented in Figure 1.

Table 1. Selected Geometrical Parameters of [(ᵗBu)GaS]$_4$[a]

p_1	r(Ga···Ga)	3.111(3)	p_6	θ(Ga–C–C)	109.6(4)
p_2	r(Ga–S)	2.365(2)	p_7	θ(C–C–H)	108.0[b]
p_3	r(Ga–C)	1.976(4)	p_8	τ_1(CH$_3$ twist)	−3.3(2)
p_4	r(C–C)	1.534(3)	p_9	τ_2(CMe$_3$ twist)	−39.6(1)
p_5	r(C–H)	1.136(7)			

[a] Distances in angstroms and angles in degrees. Figures in parentheses are the estimated standard deviations of the last digits. [b] C–C–H angle fixed for refinement.

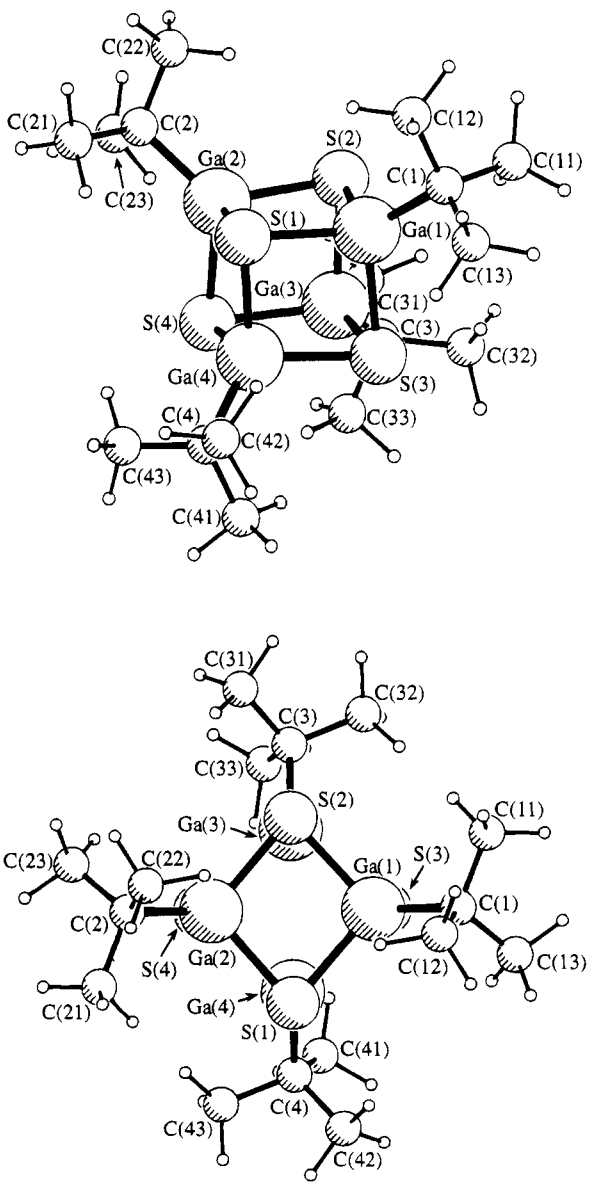

Figure 1. Two perspective views of [(ᵗBu)GaS]$_4$, together with the atomic numbering, in the optimum refinement of the electron diffraction analysis.

(11) Hargittai, I.; Hargittai, M. *Stereochemical Applications of Gas-Phase Electron Diffraction*; VCH Publishers: New York, 1988.

(12) (a) Cleaver, W. M.; Barron, A. R.; Zhang, Y.; Stuke, M. *Appl. Surf. Sci.* **1992**, *54*, 8. (b) Zhang, Y.; Cleaver, W. M.; Stuke, M.; Barron, A. R. *Appl. Phys. A* **1992**, *55*, 261.

(13) We have previously shown that [(ᵗBu)GaS]$_4$ shows no decomposition over this temperature range.

(14) Power, M. B.; Barron, A. R. *J. Chem. Soc., Chem. Commun.* **1991**, 1315.

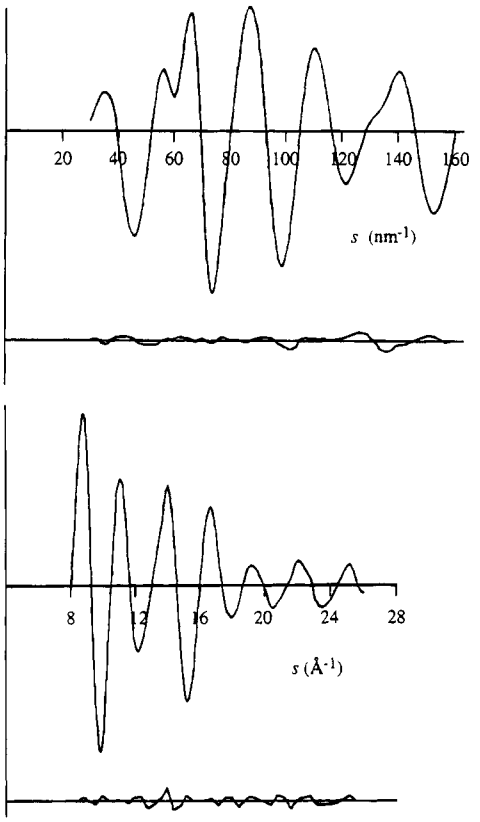

Figure 2. Experimental molecular scattering curves for [(ᵗBu)GaS]$_4$: nozzle-to-plate distances 258.56 (top) and 96.61 mm (bottom).

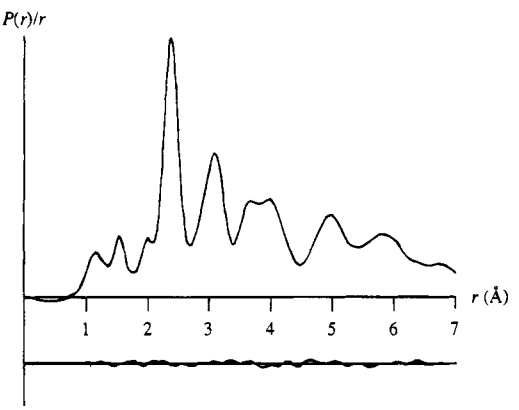

Figure 3. Observed and difference radial distribution curves, $P(r)/r$ against r, for [(ᵗBu)GaS]$_4$. Before Fourier inversion, the data were multiplied by $s\ \exp(0.002\ s^2)/(Z_{Ga} - f_{Ga})(Z_S - f_S)$.

The experimental molecular scattering curves are shown in Figure 2. The maximum of the short camera distance data had to be limited to $s = 26$ Å^{-1} because it proved to be impossible to obtain high-quality data at high values of the scattering variable, s. Combination of the scaled experimental data sets yielded the radial distribution curve reproduced in Figure 3, which is extraordinarily rich in structural information. The refinement of the geometrical parameters proceeded smoothly; it was possible to refine all the parameters defining the positions of the heavy atoms simultaneously, together with some parameters relating to the positions of the hydrogen atoms. The C−C−H bond angle could not be refined satisfactorily, all such attempts leading to an unreasonably small value (<106°). Both twist angles, τ_1 and τ_2, were also refined, although their values must be considered as "fitting factors" rather than real torsions. This is especially true for τ_1, since the *tert*-butyl methyl groups are undoubtedly mobile due to rotation about the C−C bonds. Table 1 shows the final refined geometrical parameters, while in Table 2 the interatomic distances are listed, along with the values of the corresponding amplitudes of vibration, some of which were coupled and varied in five blocks. The elements of the least-squares correlation matrix exceeding 50% are given in Table 3. Considering the magnitude of the molecule (60 atoms), an excellent agreement between the experimental and computed molecular intensities has been achieved. This optimum refinement corresponds to the value of $R_G = 0.073$ ($R_D = 0.064$).

The cubanelike structure of [(ᵗBu)GaS]$_4$ was found to be distorted from a regular cubic geometry; the Ga−S−Ga angle is decreased to 82.3(1)° and the S−Ga−S angle is increased to 97.3(1)° (see Table 4). Moreover, these rhombohedrally distorted faces are nonplanar with a fold on the diagonal Ga···Ga, of 10.0°. This is clearly significant given that the majority of dimeric gallium compounds are planar. However, it may be compared to the situation of the sulfur atoms in the dimeric thiolate compound [$I_2Ga(\mu$-S^{i}Pr)]$_2$,[15] in which the Ga_2S_2 ring is in a butterfly geometry with a deviation from planarity of 36.7(2)°.[16] These distortions may be accounted for as follows. First, according to VSEPR theory,[17] the repulsion between the nonbonded electron pair on the sulfide and the Ga−S bonded pairs should be greater than that between the Ga−S bonded pairs themselves. Second, if the geometries of the polyhedra are controlled by packing of the gallium and sulfide ions,[18] then from a consideration of the relative ionic radii for Ga^{3+} (0.62 Å) and the sulfide anion, 1.85 Å, the S···S distance should be longer than the Ga···Ga distance. Both of these explanations would result in a decrease in the Ga−S−Ga bond angle with a concomitant opening of the S−Ga−S bond angle, as is observed experimentally. Similar deformations from the regular cubic structure were observed in the X-ray diffraction studies of the first crystallographically characterized group 13−16 cubane compound, [MeIn(OH)(O_2PPh_2)]$_4$,[19] as well as the isostructural phosphorus−carbon, [(ᵗBu)CP]$_4$,[20] and arsenic−carbon, [(ᵗBu)CAs]$_4$,[21] cages. As is found for [(ᵗBu)$_2$Ga(μ-SH)]$_2$,[11] [(Ph)$_2$Ga(μ-SEt)]$_2$,[22] and halide-bridged dimers, [R(X)Ga(μ-Cl)]$_2$ (e.g., R = X = Me;[23] R = ᵗBu, X = Cl[24]), the spatial requirements

(15) Hoffmann, G. G.; Burschka, C. *Angew. Chem.* **1985**, *97*, 965; *Angew. Chem., Int. Ed. Engl.* **1985**, *24*, 970.
(16) This distortion has also been observed, in a pentagonal ring, in the thiacarborane, *nido*-7,8,10-$C_2SB_8H_{10}$, where the B−S−B angle is found to be *ca.* 94°, some 14° less than that for regular C_{5v} symmetry: Hnyk, D.; Hofmann, M.; Schleyer, P. v. R., to be published.
(17) Gillespie, R. J. *Molecular Geometry*, van Nostrand Reinhold: London, 1972.
(18) Mulliken atomic charges from Fenske−Hall calculations revealed the [(ᵗBu)GaS]$_4$ clusters to be fairly ionic. The charges on each S and Ga atom are −0.75 and +1.20, respectively: Subramanian, L.; Lichtenberger, D. L.; Power, M. B.; Barron, A. R., unpublished results.
(19) Arif, A. M.; Barron, A. R. *Polyhedron* **1988**, *7*, 2091.
(20) Wettling, T.; Schneider, J.; Wagner, O.; Kreiter, C. G., Regitz, M. *Angew. Chem., Int. Ed. Engl.* **1989**, *32*, 1013.
(21) Hitchcock, P. B.; Johnson, J. A.; Nixon, J. F. *Angew. Chem., Int. Ed. Engl.* **1993**, *27*, 103.
(22) Hoffman, G. G.; Burschlea, C. *J. Organomet. Chem.* **1984**, *267*, 229.

Table 2. Interatomic Distances (r_a, Å)[a] and Mean Amplitudes of VIbration (u, Å) for [(ᵗBu)GaS]₄

atomic pair	r_a[b]		u[b]	key to coupling scheme
Ga−S	2.365(2)	u_1	0.085(3)	
Ga−C	1.976(4)	u_2	0.047(6)	
C−C	1.534(3)	u_3	0.049(5)	
C−H	1.136(7)	u_4	0.085(7)	
Ga···Ga	3.111(3)	u_5	0.123(4)	
S···S	3.550(6)	u_6	0.110(7)	
Ga···S	4.079(4)	u_7	0.097(6)	
Ga(1)···C(11)	2.880(5)	u_8	0.114(8)	
Ga(1)···C(2)	4.861(5)	u_9	0.150(10)	
Ga(1)···C(21)	5.613(10)[c]	u_{10}	0.225(18)	i
Ga(1)···C(22)	5.076(9)[c]	u_{11}	0.236(8)	ii
Ga(1)···C(23)	5.885(9)[c]		0.225	i
S(1)···C(1)	3.764(4)	u_{12}	0.140(22)	
S(4)···C(1)	6.055(5)	u_{13}	0.155(3)	iii
S(1)···C(11)	5.032(6)[c]		0.189	ii
S(2)···C(11)	3.900(11)[c]		0.104[d]	
S(3)···C(11)	4.334(15)[c]	U_{14}	0.190(19)	
S(4)···C(11)	6.727(8)	u_{15}	0.229(18)	iv
C(1)···C(2)	6.338(8)		0.194	iii
C(1)···C(21)	7.045(15)[c]		0.160[d]	
C(1)···C(22)	6.160(11)[c]		0.194	iii
C(1)···C(23)	7.483(12)[c]		0.230[d]	
C(11)···C(12)	2.502(8)	u_{16}	0.086(26)	
C(11)···C(21)	7.984(27)[c]	u_{17}	0.263(38)	v
C(11)···C(22)	6.730(22)[c]		0.229	iv
C(11)···C(23)	8.009(12)[c]		0.263	v
C(12)···C(23)	7.460(21)[c]		0.230[d]	
C(12)···C(22)	5.705(26)[c]		0.225	i
C(13)···C(23)	8.662(16)[c]		0.190[d]	

[a] The Ga···H, S···H, C···H, and H···H nonbonded distances were included in the refinement, but they are not listed here. Their vibrational amplitudes were within the range 0.104−0.35 Å. [b] Least-squares standard deviations in the last digit are given in parentheses. [c] Dependent on the $C(CH_3)_3$ twist angle (τ_2). [d] Fixed.

Table 3. Analysis of the Electron Diffraction Pattern of [(ᵗBu)GaS]₄: Portion of the Least-Squares Correlation Matrix Listing Off-Diagonal Elements (×100) with Absolute Values ≥50%[a]

u_1	u_8	u_{10}	u_{12}	u_{13}	u_{15}	u_{16}	k_1	k_2	
79			65			93	58	65	p_2
		65		57					p_8
					52				p_9
			57			86	85	79	u_1
	75								u_5
			74						u_6
						63	51	59	u_{12}
		75							u_{13}
							65	71	u_{16}
								79	k_1

[a] k_1 and k_2 are scale factors.

of the sulfide anion results in a large Ga···Ga nonbonded distance across the Ga_2S_2 face (Table 4). This is in contrast to the values observed for hydride-bridged species (2.58−2.61 Å).[25]

It has been previously reported[26] that the solid state structures of several transition metal−chalcogenide cubane clusters, e.g., $[(X)FeS]_4^{n-}$, show distortion due to crystal packing forces. However, no direct comparison with a vapor phase system has been available. It is useful, therefore, to compare the electron diffraction structure obtained in the present work with that obtained previously by single-crystal X-ray diffraction techniques (see Table 4).[14] It is clear from Table 4 that all the chemically equivalent parameters are within experimental error the same. This suggests that the Ga_4S_4 core structure is sufficiently robust to be unaffected by any crystal-packing forces. Furthermore, the cores appear to be invariant over a significant temperature range, −90 to 220 °C.

Table 4. Comparison of Bond Lengths (Å) and Angles (deg) in [(ᵗBu)GaS]₄ As Determined by Electron Diffraction (ED) and X-Ray Diffraction (XRD)

parameter	ED	XRD[a]
Ga−S	2.365(2)	2.359(3)
Ga−C	1.976(4)	1.978(6)
Ga···Ga	3.111(3)	3.100(6)
S···S	3.550(6)	3.544(6)
S−Ga−S	97.3(1)	97.3(1)
Ga−S−Ga	82.3(1)	82.1(1)

[a] Power, M. B.; Barron, A. R. *J. Chem. Soc., Chem. Commun.* **1991**, 1315.

Vapor Phase Photolysis of [(ᵗBu)GaS]₄. It has been previously demonstrated that the gas phase infrared laser powered homogeneous pyrolysis (IR-LPHP) of group 13 organometallics closely mimics the decomposition that occurs under MOCVD conditions.[27] Attempts to study the gas phase decomposition of [(ᵗBu)GaS]₄ using IR-LPHP was precluded by the compound's limited volatility.[28] However, we have shown that under certain conditions the UV photochemical decomposition pathways for gallium alkyls follows that of their thermolysis.[12]

For any organometallic to be suitable for photolytic decomposition, it must absorb in the UV (or visible) at a wavelength corresponding to common laser or arc lamp emissions; for example, 193 (ArF excimer laser), 248 (KrF excimer laser), or 308 nm (XeCl excimer laser) would be desirable. Due to experimental difficulties in determining the vapor phase UV absorption spectrum of [(ᵗBu)GaS]₄, and since we have previously shown that the UV−visible spectrum of gallium alkyls in hydrocarbon solution is identical to that observed in the vapor phase,[12,29] the solution spectrum of [(ᵗBu)GaS]₄ was determined and is shown in Figure 4. The molar absorption coefficient (ϵ = 300 L.mol^{-1}cm^{-1}) of the major absorption at 220 nm is comparable to those previously measured for $GaMe_3$, Ga(ᵗBu)Me_2, and Ga(ᵗBu)$_2$Me.[29] Based on the UV spectrum of [(ᵗBu)GaS]₄ and our previous studies[12] a UV-excimer laser (248 nm) was chosen for photolysis.

To create and detect the various gallium containing photo products a TOF mass spectrometer[30] was equipped with a sample holder and quartz windows for two opposing collinear laser beams for photolysis and ionization. A schematic of the experimental apparatus is given in Figure 5.[31] The first UV-excimer laser (248 nm) photolyzes the precursor into neutral fragments. The second UV-excimer laser (248 nm), delayed by 0.4−0.5 μs, ionizes the photofragments. The ions are then accelerated in the mass spectrometer, and depending on the time of flight (TOF) of the accelerated ion, the

(23) Baxter, P. L; Downs, A. J.; Goode, M. J.; Rankin, D. W. H.; Robertson, H. E. *J. Chem. Soc., Dalton Trans.* **1990**, 2873.
(24) Power, M. B.; Cleaver, W. M.; Apblett, A. W.; Barron, A. R.; Ziller, J. W. *Polyhedron* **1992**, *11*, 477.
(25) Pulham, C. R.; Downs, A. J.; Goode, M. J.; Rankin, D. W. H.; Robertson, H. E. *J. Am. Chem. Soc.* **1991**, *113*, 5149.
(26) Snyder, B. S.; Holm, R. H. *Inorg. Chem.* **1988**, *27*, 2339, and references therein.
(27) Russel, D. K. *Coord. Chem. Rev.* **1992**, *112*, 131.
(28) Russell, D. K.; Barron, A. R., unpublished results.
(29) Cleaver, W. M.; Barron, A. R. Chemtronics **1989**, *4*, 146.
(30) Stuke, M. *Appl. Phys. Lett.* **1984**, *45*, 1175.
(31) Larciprete, R.; Stuke, M. *J. Phys. Chem.* **1986**, *90*, 4568.

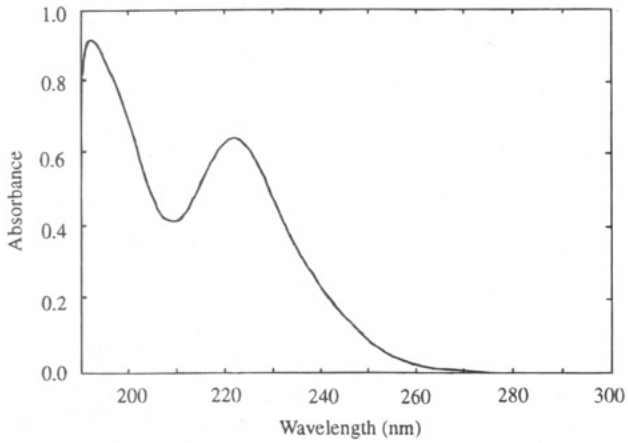

Figure 4. Solution UV–visible spectrum of $[(^tBu)GaS]_4$ (λ_{max} = 222 nm, ϵ = 300 L mol^{-1}cm^{-1}).

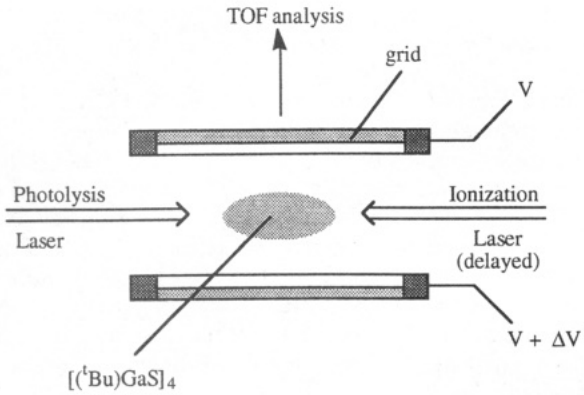

Figure 5. Schematic view of the collinear photolysis/ionization laser arrangement used to study the vapor phase photolysis of $[(^tBu)GaS]_4$.

mass can be determined (see Experimental Section). Variation of the source temperature was used to control the pressure of the vapor in the photolysis/ionization chamber. TOF mass spectra were as expected found to be essentially independent of pressure over the range 5.5×10^{-7}–1.7×10^{-6} mbar.

In order to separate the effects of the fragmentation and ionization laser sources, the laser fluence of the fragmentation laser was reduced. In a similar manner, the focus of the ionization source was systematically varied until ion fragmentation was minimized. Thus, the photochemical fragmentation was determined by collection of the TOF mass spectra obtained by photolysis only, ionization only, and both photolysis and ionization (see Figure 6).

The TOF mass spectrum obtained upon UV-excimer laser photolysis (in the absence of ionization laser irradiation) of $[(^tBu)GaS]_4$ vapor only shows peaks due to the dimethylcarbene ion $[C(CH_3)_2]^+$ (m/z = 42) and the methylcarbyne ion $[C(CH_3)]^+$ (m/z = 27); see Figure 6 (lower trace). However, their low intensity precludes any definitive discussion of their source. The major peak in the TOF mass spectrum of $[(^tBu)GaS]_4$ vapor, without prior photolysis, is that of the parent ion, $[(^tBu)_4Ga_4S_4]^+$ (m/z = 636, 100%). Subsequent peaks due to $[(^tBu)_3Ga_4S_4]^+$ (m/z = 579, 14%), $[(^tBu)_2Ga_4S_4]^+$ (m/z = 522, 5%), and $[C(CH_3)_3]^+$ (m/z = 57) are seen (see Figure 6, middle trace) in agreement with our previous 70 eV EI mass spectral data. From the upper trace in Figure 6 it can be seen that a combination of

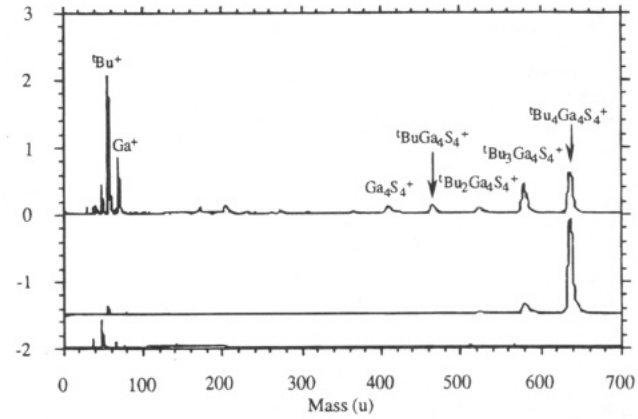

Figure 6. Traces for the time-of-flight mass spectra obtained for $[(^tBu)GaS]_4$, using the photolysis laser only (lower trace), the ionization laser only (middle trace) and both photolysis and ionization lasers (upper trace).

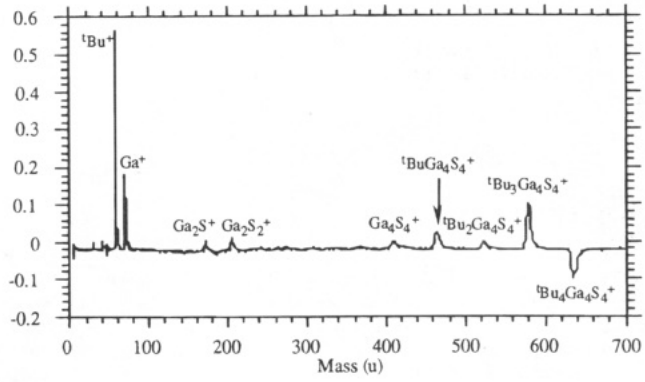

Figure 7. Difference trace for the TOF mass spectra of the photolysis laser only and the ionization laser only subtracted from the spectrum of $[(^tBu)GaS]_4$, obtained by use of both the photolysis and ionization lasers.

photolysis and ionization results in the significant enhancement of the $[(^tBu)_3Ga_4S_4]^+$, $[(^tBu)_2Ga_4S_4]^+$, and $[C(CH_3)_3]^+$ peaks. However, additional major peaks due to $[(^tBu)Ga_4S_4]^+$ (m/z = 465) and $[Ga_4S_4]^+$ (m/z = 419), as well as $^{69}Ga^+$ and $^{71}Ga^+$ ions, are also observed. The only other peaks that can be readily assigned are due to $[Ga_2S]^+$ (m/z = 170) and $[Ga_2S_2]^+$ (m/z = 202).

Subtraction of the photolysis-only and ionization-only spectra from the combination spectrum in Figure 6 results in a difference spectrum, Figure 7, in which positive (upward) peaks indicate an increase in the fragment upon photolysis, while negative (downward) peaks indicate a decrease in the abundance of a fragmentation product.

Based upon Figure 7, several observations may be made. First, the most obvious result of UV photolysis on $[(^tBu)GaS]_4$ vapor is the decrease in intensity of the parent ion and a concomitant increase in the intensity of the trialkyl fragment, $[(^tBu)_3Ga_4S_4]^+$, consistent with the photochemical bond homolysis of one Ga–C bond, eq 1, as the major photochemical reaction. Second, the

$$[(^tBu)GaS]_4 \xrightarrow{h\nu\ (248\ \mathrm{nm})} [(^tBu)_3Ga_4S_4] + {}^tBu^{\bullet} \quad (1)$$

relative intensity of the subsequent products due to loss of two, three, and four *tert*-butyl groups is independent of parent ion fragmentation, i.e., that of decreasing intensity with decreasing mass. The $[(^tBu)Ga_4S_4]^+$ ion is more abundant than the $[(^tBu)_2Ga_4S_4]^+$ ion. This

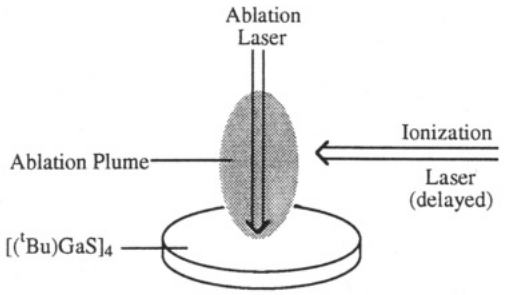

Figure 8. Schematic view of the setup used for the laser ablation of $[(^tBu)GaS]_4$.

suggests that $[(^tBu)_3Ga_4S_4]^+$ may undergo a second photochemical fragmentation, eq 2, since a similar two-

$$[(^tBu)_3Ga_4S_4] \xrightarrow{h\nu\ (248\ \mathrm{nm})} [(^tBu)Ga_4S_4] + 2^tBu^\bullet \quad (2)$$

$$GaMe_3 \xrightarrow{h\nu\ (\lambda < 250\ \mathrm{nm})} GaMe + 2Me^\bullet \quad (3)$$

alkyl elimination reaction has been shown to occur for $GaMe_3$ upon photolysis at wavelengths below 250 nm, eq 3.[32] N. B. the absence of $[(CH_3)_3CC(CH_3)_3]^+$ as a photo-fragment precludes reductive elimination of the two *tert*-butyl groups as a pathway, assuming that all alkane fragments are ionized. Third, the presence of core fragmentation peaks, $[Ga_2S]^+$ and $[Ga_2S_2]^+$, as well as Ga atoms, suggests that under the conditions of the present experiment the Ga_4S_4 core undergoes some fission (see below). Besides which the Ga_4S_4 core is clearly retained as the major fragment.

Laser Ablation of $[(^tBu)GaS]_4$. Considering that under thermal MOCVD conditions the precursor may initiate decomposition either in the gas phase or on the substrate surface, we investigated the photolysis of $[(^tBu)GaS]_4$ in the solid state as a simple model for surface decomposition.

A pellet (0.5 cm diameter) of $[(^tBu)GaS]_4$ was prepared in a 2 ton press and mounted on a platform within the TOF mass spectrometer. A 248 nm UV-excimer laser oriented perpendicular to the surface of the sample and another pulsed UV laser parallel to and above the surface were used as the ablation and ionization lasers, respectively. A schematic of the experimental arrangement is shown in Figure 8.

As with the vapor phase photolysis experiments described above, a background TOF mass spectrum was collected using the ionization laser only. As can be seen from the lower trace in Figure 10, the only significant peaks observed were that of the parent ion, and the major ionization fragmentation product, $M^+ - {}^tBu$ (see above). The presence of this signal suggests that $[(^tBu)GaS]_4$ is sufficiently volatile (at 25 °C, 1.7×10^{-6} mbar) to provide a significant vapor phase concentration above the solid sample.

The TOF mass spectrum obtained upon UV-excimer laser ablation of $[(^tBu)GaS]_4$ is shown in the upper traces in Figures 9 and 10. While, from Figure 10, it is clear that the parent ion peak is significantly increased in intensity it is worth noting the presence of fragments due to successive loss of *tert*-butyl, i.e., $[(^tBu)_xGa_4S_4]^+$ (x = 1−3). Related to this observation, the major

(32) Zhang, Y.; Beuermann, Th.; Stuke, M. *Appl. Phys. B* **1989**, *48*, 97.

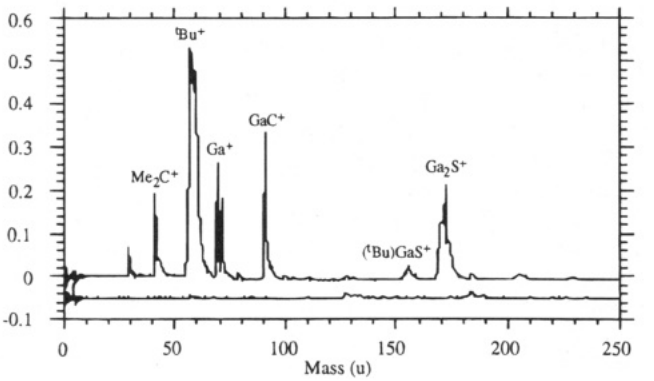

Figure 9. TOF mass spectra (0−250 amu) obtained for the laser ablation of $[(^tBu)GaS]_4$, using the ionization laser only (lower trace) and both the ablation and ionization lasers (upper trace).

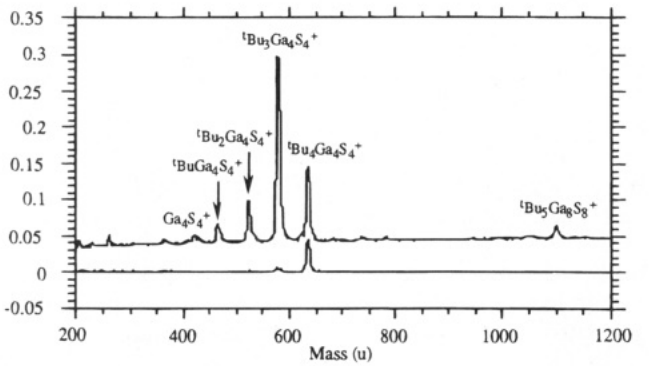

Figure 10. TOF mass spectra (200−1200 amu) obtained for the laser ablation of $[(^tBu)GaS]_4$, using the ionization laser only (lower trace) and both the ablation and ionization lasers (upper trace).

fragmentation peak upon ablation is that of the *tert*-butyl radical, consistent with Ga−C bond cleavage, a process obviously related to the MOCVD process (see Scheme 1). Additional peaks are seen due to the dimethyl-carbene ion $[C(CH_3)_2]^+$ and the methylcarbyne ion $[C(CH_3)]^+$, possibly as fragmentation products of *tert*-butyl groups. The peaks at masses 56 and 91 were determined to be background. These results are supportive of the vapor phase experiments (see above). However, two features are different in the TOF mass spectrum of laser-ablated $[(^tBu)GaS]_4$ as compared to the analogous vapor phase photolysis.

Whereas the vapor phase photolysis of $[(^tBu)GaS]_4$ shows some fragmentation of the cubane core as indicated from the presence of $[Ga_2S]^+$ (*ca.* 3%) and $[Ga_2S_2]^+$ (*ca.* 5%), the intensity of the former is greatly enhanced (40%) during laser ablation. In fact, the peak is comparable in intensity to that of $[(^tBu)_3Ga_4S_4]^+$. The source of $[Ga_2S]^+$ may be twofold. First, under ablation conditions the solid state photolysis of $[(^tBu)GaS]_4$ may yield more Ga_4S_4 core fragmentation. Alternatively, laser ablation may involve significant decomposition of $[(^tBu)GaS]_4$ to GaS. Supporting evidence for this process may be obtained from the TOF mass spectrum obtained from laser ablation of a sample of MOCVD grown cubic GaS, in which $[Ga_2S]^+$ and $[Ga_2S_2]^+$ are the major sulfur-containing fragments observed.

In the vapor phase photolysis mass spectrum the largest peak observed was that of the parent ion $[(^tBu)_4Ga_4S_4]^+$. In contrast, ablation of $[(^tBu)GaS]_4$ in the solid state allows for the observation of an octameric

fragment, $[(^tBu)_5Ga_8S_8]^+$ (m/z = 1093, 3%). We have previously observed that the solution thermolysis of $[(^tBu)GaS]_4$ in pentane yields the octameric cage compound $[(^tBu)GaS]_8$ in low yield.[33,34] However, the mass spectrum of $[(^tBu)GaS]_8$, like that of all the gallium sulfide clusters $[(^tBu)GaS]_n$, shows the parent ion with the only significant fragmentation being loss of a single *tert*-butyl group. Thus, it is unlikely that the peak at m/z = 1093 is due to the formation of $[(^tBu)GaS]_8$. Instead we tentatively propose that the $[(^tBu)_5Ga_8S_8]^+$ fragment is the $M^+ - {}^tBu$ fragment of $[(^tBu)_6Ga_8S_8]$ (**II**)

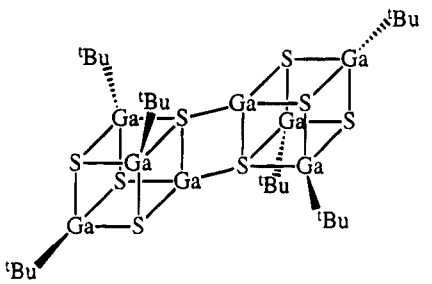

(**II**)

formed as a result of the coupling of two $[(^tBu)_3Ga_4S_4]$ units, clearly a process related to the growth of GaS thin films. We note, however, that without more in-depth studies it is not possible to establish where the dimerization event occurs: in the gas phase, in the plume, or in a subsequent cooled region of the expanded gas.

Conclusions

The vapor phase structure and decomposition of $[(^tBu)GaS]_4$ have been investigated by gas phase electron diffraction and UV-laser photolysis/time-of-flight mass spectrometry, respectively. By the use of gas phase electron diffraction we have determined that the Ga_4S_4 core of the cubane single-source precursor compound, $[(^tBu)GaS]_4$, remains intact under the conditions employed for vapor transport during the MOCVD growth of cubic GaS. In addition, the similarity of the core structures between the solid state (at −90 °C) and the gas phase (at 220 °C) attests to the high stability of the gallium−sulfide cubane core. Further evidence for the retention of the Ga_4S_4 core during the MOCVD growth of GaS films is obtained from vapor phase UV-laser photolysis/time-of-flight mass spectrometry, where the major photofragmentation is due to loss of the organic substituents *without core cleavage*, i.e., $[(^tBu)_x$-$Ga_4S_4]^+$ (x = 1−3). The coupling of two cubane cores is observed to occur during the laser ablation of a solid sample of $[(^tBu)GaS]_4$, suggestive of the growth of GaS films via the oligomerization of Ga_4S_4 subunits. We are at present attempting to study the surface decomposition of $[(^tBu)GaS]_4$ under UHV conditions, thus completing the cycle of molecular precursor to solid state material.

Experimental Section

General Procedures. $[(^tBu)GaS]_4$ was prepared according to previously published procedures,[35] and was purified by sublimation (170 ° C, at 10^{-2} mmHg). Measurement of the parent molecular ion by ultrashort laser mass spectroscopy[36] confirmed the purity. The solution UV spectrum was measured with a Perkin Elmer Lambda 4C UV/Vis spectrometer in hexane solution.

Table 5. Selected Electron Diffraction Data Collection Parameters for $[(^tBu)GaS]_4$

	nozzle-to-plate distance (mm)	
	258.56	96.61
weighting functions (Å^{-1})		
Δs	0.2	0.4
s_{min}	3.0	8.0
sw_1	5.0	10.0
sw_2	13.6	22.0
s_{max}	16.0	26.0
correlation parameter, p/h	0.4858	−0.1501
scale factor,[a] k	0.700(21)	0.559(20)
electron wavelength[b] (Å)	0.05690	0.05692

[a] Figures in parentheses are the estimated standard deviations of the last digits. [b] Determined by reference to the scattering pattern of benzene vapor.

Electron Diffraction. The electron diffraction patterns for $[(^tBu)GaS]_4$ were recorded photographically on Kodak Electron Image plates using the Edinburgh gas diffraction apparatus.[37] The sample was held at 216 °C during the experiments, and the stainless steel nozzle was held at 218 °C. Three plates at the long camera distance and three at the short distance were used, and plates were also obtained for benzene, under the same experimental conditions, to provide calibration of the electron wavelength. Plates were traced using a Joyce-Loebl Microdensitometer 6[38] at the Daresbury laboratory of the Science and Engineering Research Council.

The scattering data were analyzed using the data reduction[39] and least-squares refinement[39] programs described previously, with the electron scattering factors taken from ref 40. The weighting points needed to set up the off-diagonal weight matrices used in the least-squares refinements are listed in Table 5, together with other experimental parameters. The molecular scattering intensity curves are shown in Figure 2, and the radial distribution curve is given in Figure 3. Refined geometrical parameters are listed in Table 1, interatomic distances and amplitudes of vibration in Table 2, and the most significant elements of the least-squares correlation matrix in Table 3.

Time-of-Flight Mass Spectroscopy. A schematic of the experimental setup to measure the photoproducts is shown in Figure 11. The vacuum system (capable of UHV) consists of a main chamber, into which the sample is introduced by a molecular leak valve. The laser beam enters through a Suprasil quartz window after passing a variable attenuator and a spherical focusing lens with f = 250−500 mm. The focal intensity is in the range of megawatts to several gigawatts per square centimeter. Ions generated in the focus of the laser beam(s) are slightly pushed (*ca.* 100 V cm^{-1}) and accelerated (*ca.* 2000 V) before they drift through the field-free section in the differentially pumped (*ca.* 10^{-8} Torr) side arm, serving as the TOF mass analyzer. The ions are detected by a tandem channel plate detector, and the resulting signal is preamplified and transferred to a transient recorder (Tektronix 7612 D), which can store the complete mass spectrum

(33) Power, M. B.; Ziller, J. W.; Barron, A, R. *Organometallics* **1992**, *11*, 2783.

(34) Similar coupling of clusters has been observed for fullerenes; see: Whetten, R. L.; Jeretzian, C. *Clusters and Fullerenes*; World Scientific Publishing: London, 1993; p 226.

(35) Power, M. B.; Ziller, J. W.; Tyler, A. N.; Barron, A. R. *Organometallics* **1992**, *11*, 1055.

(36) Larciprete, R.; Stuke, M. *J. Cryst. Growth*, **1986**, *77*, 235.

(37) Huntley, C. M.; Laurenson, G. S.; Rankin, D. W. H. *J. Chem. Soc., Dalton Trans.* **1980**, 954.

(38) Cradock, S.; Koprowski, J.; Rankin, D. W. H. *J. Mol. Struct.* **1981**, *71*, 113.

(39) Boyd, A. S. F.; Laurenson, G. S.; Rankin, D. W. H. *J. Mol. Struct.* **1981**, *71*, 217.

(40) Ross, A. W.; Fink, M.; Hilderbrandt, R. In *International Tables for X-ray Crystallography*; Volume C, Wilson, A. J. C., Ed.; Kluwer Academic Publishers: Boston, 1992; p 245.

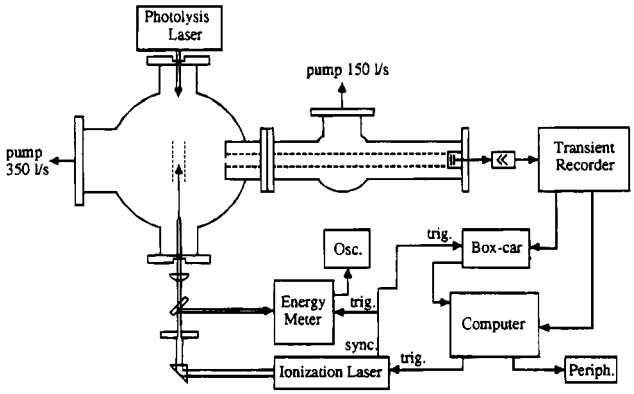

Figure 11. Schematic of the experimental setup[26] with UV-excimer lasers for photolysis and ionization for detection on perpendicular axes; *cf.* Figure 5.

for each laser shot. Data are transferred to a Macintosh computer, which also triggers the ionization laser.

The pulsed UV-excimer laser used as the photolysis/ablation source was a Lambda Physik EMG 103 MSC (248 nm). The excimer laser had a pulse duration of 15–20 ns (fwhm), and the cross section of the beam was varied with an iris of diameter of 2–4 mm, to give a homogeneous beam profile with suitable dimensions. A 0.5 ps UV-excimer laser was used as the ionization/detection laser at 248 nm. As was shown previously,[30,31] short UV-laser pulses considerably reduce the fragmentation in the mass spectra and sometimes avoid it completely.[36]

The laser ionization time-of-flight mass spectrometer, and its use for the detection of photoproducts under collision-free conditions, have previously been described in detail.[31,41,42] For vapor phase experiments, the photolysis laser and ionization laser were aligned collinear and opposing counterpropagating. The delay between photolysis and ionization was set at 4.2 μs. Spectra were taken as the average of 250 laser shots and data were taken at two pressures of the cube. For ablation experiments, the ablation laser was oriented first at a 45° angle and then perpendicular to the sample surface. The sample was placed 2–3 cm below the ionization laser aligned parallel to the surface. The delay between the ablation and the ionization was 200 μs. Spectra were taken as the average of 50 laser shots, exposing the same spot on the sample surface.

Acknowledgment. Financial support for this work was provided by the Office of Naval Research and the National Science Foundation (A.R.B.), the Bundesministerium für Forschung und Technologie BMFT 13N6159 (M.S.), and the Science and Engineering Research Council (SERC) (D.W.H.R.).

Registry Number supplied by authors. [(ᵗBu)-GaS]₄, 135283-83-9.

OM940695A

(41) Zhang, Y.; Stuke, M. *Chemtronics* **1988**, *3*, 230.
(42) Grady, A. S.; Mapplebeck, A. L.; Russell, D. K.; Taylorson, M. G. *J. Chem. Soc., Chem. Commun.* **1990**, 929.

Reaction of $Os_2(CO)_8(\mu\text{-}\eta^1,\eta^1\text{-}C_2H_4)$ with $(\eta^5\text{-}C_5H_5)Rh(CO)PR_3$ (R = Me, Ph): Characterization and Dynamic Processes in Isomeric $Os_2Rh(CO)_8(\eta^5\text{-}C_5H_5)PMe_3$

Jason Cooke† and Josef Takats*

Department of Chemistry, University of Alberta, Edmonton, Alberta, Canada T6G 2G2

Received August 12, 1994®

Thermal reaction of $Os_2(CO)_8(\mu\text{-}\eta^1,\eta^1\text{-}C_2H_4)$ with $(\eta^5\text{-}C_5H_5)Rh(CO)PR_3$ (R = Me, Ph) yields an array of trimetallic products. The known clusters, $Os_2Rh(CO)_9(\eta^5\text{-}C_5H_5)$ and $Os_3(CO)_{11}PR_3$, are recovered in each case while, for R = Me, a third product formulated as $Os_2Rh(CO)_8(\eta^5\text{-}C_5H_5)PMe_3$ (**1**) is also isolated. Compound **1** exists in solution as two interconvertible isomers **1a** and **1b**, each of which exhibits distinctly different modes of carbonyl scrambling processes due to the position of the PMe_3 ligand on one of the Os centers. Global carbonyl scrambling and isomer interconversion occur at high temperature via a restricted trigonal twist mechanism at the phosphine-substituted osmium center. Line shape analysis of the ^{13}C NMR spectra yields activation energies of $\Delta G^{\ddagger}_{239} = 11.5 \pm 0.4$ kcal·mol^{-1} for pairwise exchange in the $(OC)_4Os-Rh$ plane of **1a** and $\Delta G^{\ddagger}_{253} = 13.0 \pm 0.4$ kcal·mol^{-1} for merry-go-round CO migration in the Os–Os plane of **1b**. Line shape simulation of the ^1H NMR spectra provides an activation energy of $\Delta G^{\ddagger}_{303} = 15.1 \pm 0.4$ kcal·mol^{-1} for the isomer interconversion process.

Introduction

One of the remarkable features of transition metal carbonyl clusters and their derivatives is the wide range of carbonyl and other ligand migration processes exhibited by these molecules.[1] In a recent report from our laboratory, Washington and Takats described pairwise carbonyl exchange in the heterotrinuclear clusters $Os_2Rh(CO)_9(\eta^5\text{-}C_5R'_5)$ (R′ = H, Me).[2] For $Os_2Rh(CO)_9(\eta^5\text{-}C_5H_5)$, carbonyl scrambling was observed only across the Os–Rh centers, while in $Os_2Rh(CO)_9(\eta^5\text{-}C_5Me_5)$, global carbonyl migration was observed at high temperature. Subsequently, Riesen *et al.* have reported a similar study for the analogous $Os_2Ir(CO)_9(\eta^5\text{-}C_5R'_5)$ (R′ = H, Me) complexes,[3] the results of which essentially confirmed those established by Washington and Takats.

A fashionable method of providing support for the mechanism of carbonyl ligand migration in transition metal clusters has been the introduction of some form of built-in restriction to the system which physically makes it impossible for scrambling to occur via the proposed mechanism. Lack of carbonyl migration in the hindered system is then taken as evidence for the validity of the proposed mechanism in the unencumbered complex.[4] It is well-known that one method of preventing pairwise exchange of carbonyl ligands between metal centers is to introduce a ligand that is incapable of bridging the two metals. Phosphines and phosphites have been used extensively in such studies of trinuclear clusters of osmium.[5] With this in mind, and following the methodology established by Washington and Takats,[2] the reaction between $Os_2(CO)_8(\mu\text{-}\eta^1,\eta^1\text{-}C_2H_4)$ and $(\eta^5\text{-}C_5H_5)Rh(CO)PR_3$ (R = Me, Ph) was investigated with a view to introducing a phosphine ligand into the $Os_2Rh(CO)_9(\eta^5\text{-}C_5H_5)$ framework. The successful incorporation of a phosphine ligand at the group nine metal would effectively block carbonyl migration in the Os–Rh planes, and the absence of fluxionality would thus lend further credence to the pairwise exchange mechanisms proposed to explain the dynamic NMR features of the parent nonacarbonyl clusters. Conversely, phosphine substitution at an osmium center would open possibilities for isomer formation and diverse carbonyl scrambling processes.

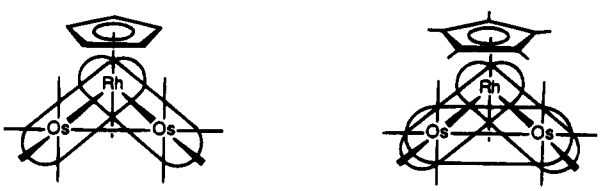

Figure 1. Carbonyl scrambling in $Os_2Rh(CO)_9(\eta^5\text{-}C_5R'_5)$ (R′ = H, Me).[2]

Experimental Section

General Procedures. All manipulations were performed under a static atmosphere of purified nitrogen or argon using standard Schlenk techniques. Solvents were dried by refluxing under nitrogen with the appropriate drying agent and were distilled just prior to use.

$Os_2(CO)_8(\mu\text{-}\eta^1,\eta^1\text{-}C_2H_4)$,[6] ^{13}CO-enriched $Os_2(CO)_8(\mu\text{-}\eta^1,\eta^1\text{-}C_2H_4)$,[2] and $(\eta^5\text{-}C_5H_5)Rh(CO)PR_3$ (R = Me,[7a] Ph[7b]) were prepared by published procedures.

† NSERC Undergraduate Research Awardee.

® Abstract published in *Advance ACS Abstracts*, December 1, 1994.

(1) (a) Evans, J. *Adv. Organomet. Chem.* **1977**, *16*, 319. (b) Band, E.; Muetterties, E. L. *Chem. Rev.* **1978**, *78*, 639. (c) Johnson, B. F. G.; Benfield, R. E. In *Transition Metal Clusters*; Johnson, B. F. G., Ed.; Wiley: Chichester, England, 1980; p 471. (d) Mann, B. E. *Comprehensive Organometallic Chemistry*; Wilkinson, G., Stone, F. G. A., Abel, E. W., Eds.; Pergamon: Oxford, U.K., 1982; Vol. 3, p 89.

(2) Washington, J.; Takats, J. *Organometallics* **1990**, *9*, 925.

(3) Riesen, A.; Einstein, F. W. B.; Ma, A. K.; Pomeroy, R. K.; Shipley, J. A. *Organometallics* **1991**, *10*, 3629.

(4) (a) Cotton, F. A.; Hunter, D. L.; Lahuerta, P.; White, A. J. *Inorg. Chem.* **1976**, *15*, 557. (b) Cotton, F. A.; Kruczynski, L.; White, A. J. *Inorg. Chem.* **1974**, *13*, 1402.

(5) (a) Alex, A. F.; Pomeroy, R. K. *Organometallics* **1987**, *6*, 2437. (b) Deeming, A. J. *Adv. Organomet. Chem.* **1986**, *26*, 1, and references therein.

0276-7333/95/2314-0698$09.00/0

Infrared spectra were recorded on a Bomem MB-100 FT-IR spectrometer. NMR spectra were obtained on Bruker WM-360 (^{1}H) and WP-400 (^{13}C, ^{31}P) spectrometers. ^{1}H and ^{13}C NMR chemical shifts (δ) were internally referenced to solvent and are reported in ppm relative to tetamethylsilane (TMS) while ^{31}P NMR chemical shifts were externally referenced to 85% H_3PO_4. Chemical shifts and isomer ratios (for **1**) were found to be both temperature and solvent dependent. NMR samples were prepared under nitrogen. The sample tubes were either sealed with a serum stopper or flame sealed under vacuum. Electron impact mass spectra were recorded on an AEI MS-12 spectrometer operating at 70 eV. Elemental analyses were performed by the Microanalytical Laboratory of this department.

Reaction of $Os_2(CO)_8(\mu\text{-}C_2H_4)$ with $(C_5H_5)Rh(CO)PMe_3$. $Os_2(CO)_8(\mu\text{-}C_2H_4)$ (53.7 mg, 0.0849 mmol) and $(C_5H_5)Rh(CO)PMe_3$ (23.0 mg, 0.0845 mmol) were placed in a three-necked 100 mL flask equipped with a reflux condenser. Degassed hexane (25 mL) was added, and the stirred solution was heated to *ca.* 50 °C in a silicon oil bath overnight (*ca.* 16 h). The solvent was removed *in vacuo*, leaving a deep red-brown residue. The residue was extracted with 2 × 1 mL CH_2Cl_2 and loaded, under argon, onto a 20 cm × 4 cm silica gel column packed in hexane. The column was eluted with 3:1 hexane/CH_2Cl_2. Three mobile bands (red, yellow, deep red) separated cleanly; an immobile yellow-brown band remained at the top of the column. The solvent was removed *in vacuo* from each fraction, and the respective residues were recrystallized from pentane at −80 °C. In order of recovery from the column, the air-stable solids were as follows: red-brown crystals of $Os_2Rh(CO)_9(C_5H_5)$[2] (11.6 mg, 17%), yellow crystals of $Os_3(CO)_{11}PMe_3$[8] (19.2 mg, 36%), and deep red crystals of $Os_2Rh(CO)_8(C_5H_5)PMe_3$ (**1**) (29.8 mg, 41%). Anal. Calcd for $C_{16}H_{14}O_8PRhOs_2$: C, 22.65; H, 1.66. Found: C, 22.89; H, 1.58. IR (pentane, ν_{CO}): 2083 m, 2079 sh, 2024 s, 2007 s, 1995 vs, 1977 m, 1964 m, 1953 mw, 1938 vw cm^{-1}. ^{1}H NMR (360 MHz): ($CDCl_3$; −20 °C) δ 5.48 (s, C_5H_5, **1b**), 5.40 (s, C_5H_5, **1a**), 1.90 (d, $^2J_{P-H}$ = 10.2 Hz, $P(CH_3)_3$, **1a**), 1.84 (d, $^2J_{P-H}$ = 10.2 Hz, $P(CH_3)_3$, **1b**), **1a**:**1b** = 3.0:1.0; (toluene-d_8; +80 °C) δ 5.18 (s, C_5H_5), 1.26 (d, $^2J_{P-H}$ = 10.2 Hz, $P(CH_3)_3$); (toluene-d_8; −20 °C) δ 5.16 (s, C_5H_5, **1b**), 5.00 (s, C_5H_5, **1a**), 1.03 (d, $^2J_{P-H}$ = 10.2 Hz, $P(CH_3)_3$, **1a**), 1.02 (d, $^2J_{P-H}$ = 10.2 Hz, $P(CH_3)_3$, **1b**), **1a**:**1b** = 2.1:1.0. ^{31}P{H} NMR (162 MHz): ($CDCl_3$; +50 °C) δ −49 (br); ($CDCl_3$; −20 °C) δ −46.43 (d, $^2J_{Rh-P}$ = 5.5 Hz, **1b**), −48.16 (s, **1a**), **1a**:**1b** = 3.0:1.0; (toluene-d_8; −20 °C) δ −48.28 (d, $^2J_{Rh-P}$ = 5.3 Hz, **1b**), −49.98 (s, **1a**), **1a**:**1b** = 2.1:1.0. ^{13}C NMR (100.6 MHz, toluene-d_8, CO region only): (+80 °C) δ 188.2 (br); (−53 °C) 198.8 (br d, $^1J_{Rh-C}$ = 37 Hz, 2C, **1a**), 198.6 (s, 2C, **1b**), 194.1 (br d, $^1J_{Rh-C}$ = 37 Hz, 2C, **1b**), 189.6 (s, 2C, **1a**), 188.3 (br, 2C, **1a**), 184.5 (br, 2C, **1b**), 178.5 (s, 1C, **1b**), 175.3 (s, 1C, **1a**), 175.1 (s, 1C, **1a**), 174.2 (s, 1C, **1b**). MS (70 eV, 180 °C, *m/e*): $M^+ - nCO$, $n = 0-8$.

Reaction of $Os_2(CO)_8(\mu\text{-}C_2H_4)$ with $(C_5H_5)Rh(CO)PPh_3$. $Os_2(CO)_8(\mu\text{-}C_2H_4)$ (32.0 mg, 0.0506 mmol) and $(C_5H_5)Rh(CO)PPh_3$ (23.5 mg, 0.0513 mmol) were dissolved in 25 mL benzene in a three-necked 100 mL flask equipped with a reflux condenser. Reaction conditions and workup procedures were analogous to that for the reaction with $(C_5H_5)Rh(CO)PMe_3$ except that the column was eluted with 4:1 hexane/CH_2Cl_2. In order of recovery from the column, the air-stable solids were red-brown crystals of $Os_2Rh(CO)_9(C_5H_5)$[2] (21.0 mg, 52%) and yellow crystals of $Os_3(CO)_{11}PPh_3$[9] (10.6 mg, 28%).

Variable-Temperature NMR Studies of Complex 1. Temperature measurements were made with a Bruker B-VT1000 temperature control unit using a Cu−constantan thermocouple; the temperature at the NMR spectrometer probe is believed to be accurate to ±1 K. Rate constants for the exchange processes were determined by visual comparison of computer-simulated and observed spectra (Carbonyl migration (^{13}C NMR) in **1a**: $k = 2.0 \pm 0.2$ s^{-1}, 203 K; 8.0 ± 0.5 s^{-1}, 213 K; 18 ± 1 s^{-1}, 220 K; 46 ± 2 s^{-1}, 227 K; 80 ± 5 s^{-1}, 233 K; 150 ± 10 s^{-1}, 239 K; 310 ± 20 s^{-1}, 246 K. Carbonyl migration (^{13}C NMR) in **1b**: $k = 1.2 \pm 0.2$ s^{-1}, 227 K; 2.6 ± 0.2 s^{-1}, 233 K; 6.0 ± 0.5 s^{-1}, 239 K; 14 ± 1 s^{-1}, 246 K; 30 ± 2 s^{-1}, 253 K. Isomer interconversion (^{1}H NMR): $k = 1.0 \pm 0.1$ s^{-1}, 253 K; 2.0 ± 0.2 s^{-1}, 263 K; 6.5 ± 0.5 s^{-1}, 273 K; 18 ± 1 s^{-1}, 283 K; 42 ± 2 s^{-1}, 293 K; 80 ± 5 s^{-1}, 303 K; 180 ± 10 s^{-1}, 313 K; 375 ± 25 s^{-1}, 323 K; 800 ± 50 s^{-1}, 333 K; 1500 ± 100 s^{-1}, 343 K; 2500 ± 200 s^{-1}, 353 K). The activation parameters for the dynamic processes were obtained by a least-squares linear regression fit to the Eyring equation (Carbonyl migration in **1a**: $\Delta H^\ddagger = 11.1 \pm 0.2$ kcal·mol^{-1}, $\Delta S^\ddagger = -1.5 \pm 0.8$ eu. Carbonyl migration in **1b**: $\Delta H^\ddagger = 13.8 \pm 0.2$ kcal·mol^{-1}, $\Delta S^\ddagger = 3.1 \pm 0.9$ eu. Isomer interconversion: $\Delta H^\ddagger = 13.7 \pm 0.2$ kcal·mol^{-1}, $\Delta S^\ddagger = -4.5 \pm 0.6$ eu). The free energies of activation were calculated from $\Delta G^\ddagger = \Delta H^\ddagger - T\Delta S^\ddagger$ and are reported at the coalescence temperatures (Carbonyl migration in **1a**: $\Delta G^\ddagger_{239} = 11.5 \pm 0.4$ kcal·mol^{-1}. Carbonyl migration in **1b**: $\Delta G^\ddagger_{253} = 13.0 \pm 0.4$ kcal·mol^{-1}. Isomer interconversion: $\Delta G^\ddagger_{303} = 15.1 \pm 0.4$ kcal·mol^{-1}). Alternatively, the free energies of activation can be calculated from $\Delta G^\ddagger = -RT_c \ln[(hk)(k_BT_c)^{-1}]$ (Carbonyl migration in **1a** at 239 K, $k = 150 \pm 10$ s^{-1}; $\Delta G^\ddagger_{239} = 11.5 \pm 0.3$ kcal·mol^{-1}. Carbonyl migration in **1b** at 253 K, $k = 30 \pm 2$ s^{-1}; $\Delta G^\ddagger_{253} = 13.0 \pm 0.3$ kcal·mol^{-1}. Isomer interconversion at 303 K, $k = 80 \pm 5$ s^{-1}; $\Delta G^\ddagger_{303} = 15.1 \pm 0.3$ kcal·mol^{-1}).[10] Computer simulation and calculation of activation parameters were carried out with programs written by Professor R. E. D. McClung of this department. A progressive change in the equilibrium composition of the isomerization process was taken into account while the variable-temperature ^{1}H NMR spectra were being simulated. Line shapes were matched to the rate of exchange, and the isomer ratio was adjusted to fit the peak heights. A roughly linear correlation of isomer ratio to temperature was found. For the carbonyl migration processes in **1a** and **1b**, the simulation was based on a model that assumed that the fast process in each isomer was in essence proceeding at an infinitely rapid rate; *i.e.*, the limiting spectrum exhibited signals characteristic of the averaged state for the fast process. The simulation was then focused upon the signals of **1a** and **1b** which were only affected by the slow carbonyl exchange process in each case (**1a**: δ 175.3, 175.1. **1b**: δ 178.5, 174.2).

Results and Discussion

Thermal reaction of $Os_2(CO)_8(\mu\text{-}\eta^1,\eta^1\text{-}C_2H_4)$ with $(\eta^5\text{-}C_5H_5)Rh(CO)PMe_3$ affords three trimetallic products. In

$$Os_2(CO)_8(\mu\text{-}\eta^1,\eta^1\text{-}C_2H_4) + (\eta^5\text{-}C_5H_5)Rh(CO)PMe_3 \xrightarrow[50\ °C,\ 16\ h]{hexane} Os_2Rh(CO)_9(\eta^5\text{-}C_5H_5)\ (17\%) + Os_3(CO)_{11}PMe_3\ (36\%) + Os_2Rh(CO)_8(C_5H_5)PMe_3\ (\mathbf{1})\ (41\%)$$

the analogous reaction with $(\eta^5\text{-}C_5H_5)Rh(CO)PPh_3$, only the known clusters $Os_2Rh(CO)_9(\eta^5\text{-}C_5H_5)$ and $Os_3(CO)_{11}PPh_3$ are formed. The $Os_2Rh(CO)_9(\eta^5\text{-}C_5H_5)$ and $Os_3(CO)_{11}PR_3$ complexes are readily identified by comparison of their characteristic IR spectra with those previously reported in the literature.[2,8,9] The product dis-

(6) Burke, M. R.; Seils, F.; Takats, J. *Organometallics* **1994**, *13*, 1445.
(7) (a) Feser, R.; Werner, H. *J. Organomet. Chem.* **1982**, *233*, 193. (b) Hart-Davis, A. J.; Graham, W. A. G. *Inorg. Chem.* **1970**, *9*, 2658.
(8) Deeming, A. J.; Underhill, M. *J. Chem. Soc., Dalton Trans.* **1973**, 2727.
(9) Bradford, C. W.; van Bronswijk, W.; Clark, R. J. H.; Nyholm, R. S. *J. Chem. Soc. A* **1970**, *17*, 2889.
(10) Sandström, J. *Dynamic NMR Spectroscopy*; Academic Press: London, 1982; p 96.

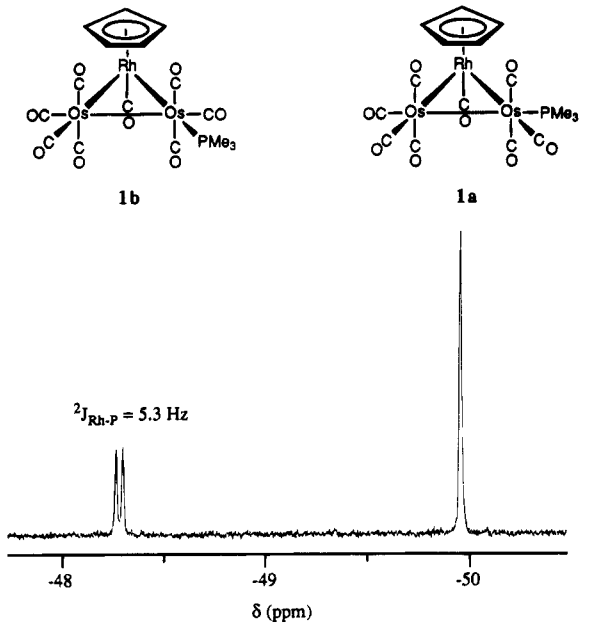

Figure 2. 162 MHz ^{31}P NMR spectrum of **1** at −20 °C in toluene-d_8 and schematic diagrams of the corresponding instantaneous solution structures of the isomeric forms **1a** and **1b**.

tribution, coupled with the known greater lability of the triphenylphosphine ligand,[11] suggests that the formation of the Os_2Rh clusters proceeds by phosphine, rather than carbonyl loss from $(\eta^5\text{-}C_5H_5)Rh(CO)PR_3$.[12]

Characterization of 1. The mass spectrum of **1** shows the molecular ion followed by sequential loss of eight carbonyl ligands; this, together with elemental analysis, suggests the formulation of **1** as $Os_2Rh(CO)_8(C_5H_5)PMe_3$. The NMR spectra are temperature dependent; full discussion of the rearrangement processes responsible for this are deferred for later discussion.

The ^{1}H NMR spectrum at −20 °C in toluene-d_8 shows two sets of signals for C_5H_5 and PMe_3 in a 2.1:1.0 (**1a**: **1b**) ratio, establishing the presence of two isomers in solution. The ^{31}P{H} NMR spectrum (Figure 2) also shows two signals at δ −49.98 (s, **1a**) and −48.28 (d, $^2J_{Rh-P}$ = 5.3 Hz, **1b**) in the same 2.1:1 ratio. The absence of large one-bond ^{103}Rh−^{31}P coupling constants immediately suggests that the PMe_3 ligand is bonded to osmium and not to rhodium in both isomers. Typically, $^1J_{Rh-P}$ exceeds 100 Hz (*cf.* $^1J_{Rh-P}$ = 186.0 Hz in $(C_5H_5)Rh(CO)PMe_3$).[13] The two-bond Rh−P splitting of 5.3 Hz in the minor isomer **1b** indicates a *trans* relationship between rhodium and phosphorus, while in the major isomer **1a**, the lack of observable Rh−P splitting suggests that the coupled nuclei are related by a nonlinear P−Os−Rh angle.[14] Equatorial phosphine substitution at osmium is clearly the only possible geometry that satisfies the *trans* relationship required for **1b** and is suggested for **1a** also. This is in accord

(11) Janowicz, A. H.; Bryndza, H. E.; Bergman, R. G. *J. Am. Chem. Soc.* **1981**, *103*, 1516.
(12) Substitution via phosphine dissociation has been documented in $(C_5H_5)Co(PPh_3)_2$[11] and accounts for the reactivity of $(C_5H_5)Co(PMe_3)_2$ (Leonard, K.; Werner, H. *Angew. Chem., Int. Ed. Engl.* **1977**, *16*, 649) and formation of $(C_5H_5)Rh(CO)PMe_3$ from $(C_5H_5)Rh(PMe_3)_2$.[7a] At present, we are unaware of any similar results for $(C_5H_5)Rh(CO)PR_3$ complexes.
(13) Bitterwolf, T. E. *Inorg. Chim. Acta* **1986**, *122*, 175.
(14) Verkade, J. G.; Quin, L. D. *^{31}P NMR in Stereochemical Analysis*; VCH: Deerfield Beach, FL, 1987; p 226.

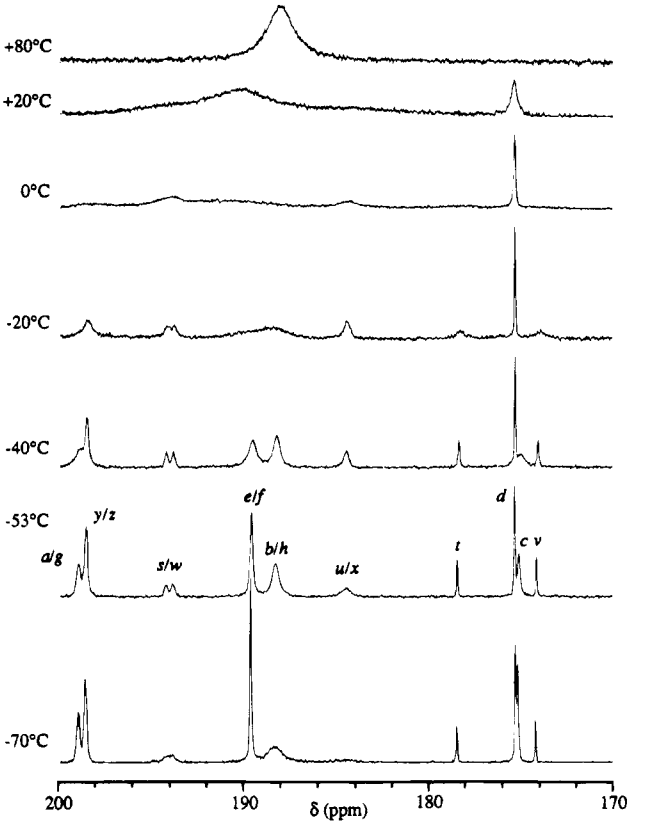

Figure 3. Variable−temperature ^{13}C NMR spectra of **1** at 100.6 MHz in toluene-d_8. For designation of the carbonyl ligands, see Scheme 1.

with the observation that phosphine ligands tend to occupy equatorial sites in trinuclear clusters of osmium[5] and is corroborated by the ^{13}C NMR spectra as none of the signals shows *trans* P−C coupling, which would be expected if an axial phosphine were present (*vide infra*).

Carbonyl Migration in 1a and 1b. The variable-temperature ^{13}C NMR spectra of **1** are shown in Figure 3. The line shape changes are reversible and are consistent with the intramolecular nature of carbonyl exchange processes. It is also clear from the figure that the low-temperature limiting spectrum has not been achieved. Indeed, the instantaneous structure of each isomer has C_1 symmetry and should give rise to eight distinct carbonyl signals (*i.e.*, 16 signals in total). Focusing at the −53 °C spectrum, one observes two similar signal patterns which can be reliably assigned to isomers **1a** and **1b** by integration. Each isomer exhibits three signals of intensity two (**1a** at δ 198.8 (d, $^1J_{Rh-C}$ = 37 Hz), 189.6, 188.3; **1b** at δ 198.6 (d, $^1J_{Rh-C}$ = 37 Hz), 194.1, 184.5) and two signals of intensity one (**1a** at δ 175.3, 175.1; **1b** at δ 178.5, 174.2), accounting for eight carbonyls per isomer.

The line shape changes observed below −20 °C can be rationalized by invoking the familiar pairwise carbonyl exchange mechanism,[15] which accounts for the fluxional nature of the parent $Os_2Rh(CO)_9(C_5H_5)$ cluster.[2] In transition metal clusters, this process requires that the carbonyls involved be roughly coplanar and that the coplanar ligands must all be mobile. In the case of $Os_2Rh(CO)_8(C_5H_5)PMe_3$, the phosphine ligands serve to block certain routes to exchange below −20 °C as they

(15) (a) Adams, R. D.; Cotton, F. A. *J. Am. Chem. Soc.* **1973**, *95*, 6589. (b) Cotton, F. A.; Hunter, D. L. *Inorg. Chim. Acta* **1974**, *11*, L9.

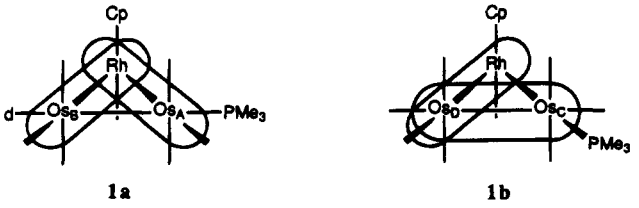

Figure 4. Allowed planes for pairwise CO exchange in **1a** and **1b** (Cp = η^5-C_5H_5).

Scheme 1. Pairwise CO Exchange Mechanism and Assignment of Signals as They Appear in the ^{13}C NMR Spectrum at −53 °C

(a) Isomer **1a**.

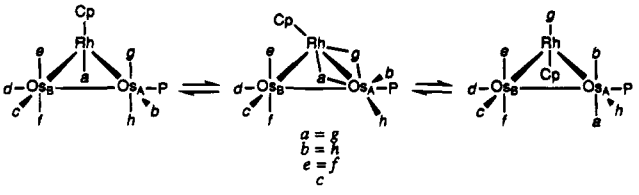

(b) Isomer **1b**.

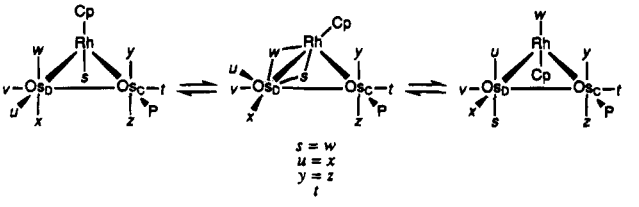

remain fixed in their respective equatorial sites. Figure 4 details the available planes for carbonyl migration in each isomer by assuming that the phosphine ligands remain static. Note that in isomer **1b** all carbonyls are allowed to scramble while in **1a** the carbonyl labeled *d* cannot be involved in a pairwise exchange process. This is significant because a single carbonyl signal at δ 175.3 remains sharp at and below −20 °C while the other signals broaden. This sharp signal is thus assigned to the unique, nonparticipating carbonyl *d* of **1a**.

Beginning with the major isomer **1a**, the assignment of the signals at −53 °C is based on a model where rapid exchange is occurring in the Os_A − Rh plane with no exchange in the Os_B−Rh plane (see Scheme 1a). This proposal is consistent with previous observations that substitution by a σ-donor group in trinuclear clusters of osmium facilitates the carbonyl scrambling process in the plane adjacent to, but not blocked by, the electron-donating ligand.[5] The signal at δ 175.1 is assigned to *c*, the other nonfluxional equatorial carbonyl under the exchange model proposed in Scheme 1a. Unlike *d*, signal *c* broadens with increasing temperature, indicating that its carbonyl lies within an exchange plane that is accessible at higher temperature. The sharp singlet of intensity two at δ 189.6 is attributed to the axial carbonyls *e* and *f*, which are rendered equivalent by rapid exchange in the Os_A−Rh plane. As was the case for *c*, this signal also broadens with increasing temperature. The two-carbonyl doublet at δ 198.8 ($^1J_{Rh-C}$ = 37 Hz) is assigned to carbonyls *a* and *g* because they exchange between Rh and an axial position on Os_A, time-averaging the expected one-bond rhodium-terminal carbonyl coupling of 77 Hz[2] to 37 Hz. The broad two-carbonyl singlet at δ 188.3 is assigned to carbonyls *b* and *h* as these ligands alternate between an axial and an equatorial position on Os_A. The presence of the cyclopentadienyl ligand at rhodium restricts the exchange to a back-and-forth movement that averages *a* and *g* and *b* and *h* but does not involve exchange between the two pairs. Between −53 and −20 °C, all signals of **1a** except *d* broaden and coalesce into the baseline. This is consistent with the onset of rapid exchange in the Os_B−Rh plane as this ultimately leads to the averaging of all signals except *d*. Below −53 °C, the *a/g* and *b/h* signals also broaden, indicating a decrease in the rate of exchange across the Os_A and Rh centers.

For the minor isomer **1b**, assignment of the signals at −53 °C is based on the exchange model given in Scheme 1b, which also shows the averaged signals. At this temperature, carbonyl migration is already fast in the Os_D−Rh plane with no exchange taking place in the Os_C−Os_D plane.[2] The two nonfluxional equatorial CO signals *v* and *t* are separated by 4.3 ppm. This is attributed to the fact that the carbonyls are bonded to two different osmium centers, one of which is phosphine substituted. In view of the generally observed downfield shift upon phosphine substitution, the signal at δ 178.5 is assigned to carbonyl *t*. Assignment of the remaining signals follows the discussion presented for **1a**. The signals corresponding to *s/w* and to *u/x* are not visible at −70 °C but rise from the baseline at −53 °C and sharpen further by −40 °C. This is clearly consistent with a slower rate of exchange in the Os_D−Rh plane at −70 °C followed by a progressively faster exchange rate as the temperature is raised. Above −53 °C, the signals assigned to *t*, *v*, and *y/z* all broaden and this heralds the onset of exchange in the Os_C−Os_D plane. In this case, eventually all the carbonyls of **1b** can exchange with one another as the two allowed exchange planes intersect at Os_D. Note that the exchange in the Os_C−Os_D plane is a full merry-go-round process.

The line shape changes in the ^{13}C NMR spectra reflect the normally observed effect that phosphine substitution at an osmium center has on the energetics of pairwise carbonyl exchange, namely, that pairwise exchange is more facile in a plane that includes a phosphine-substituted metal.[5] Thus, exchange in the Os_A−Rh plane of **1a** is more facile than that of the Os_B−Rh plane because Os_A is phosphine substituted while Os_B is not. Similarly, exchange in the Os_A−Rh plane of **1a** is more facile than that of the Os_D−Rh plane in **1b**. This is evident because, at −70 and −53 °C, the signals corresponding to exchanging carbonyls in **1b** are much broader than those of **1a**. The onset of carbonyl migration in the Os_C−Os_D plane of **1b**, which occurs above *ca.* −53 °C, can be compared to the parent $Os_2Rh(CO)_9(C_5H_5)$ cluster, which showed no evidence of carbonyl exchange between the two osmium centers at 0 °C.[2] Again, phosphine substitution at Os_C greatly facilitates this process in **1b**.

This enhanced trend in fluxionality also explains why the low-temperature limiting spectrum could not be achieved for **1**. The near-limiting temperature for $Os_2Rh(CO)_9(C_5H_5)$ was −115 °C and is expected to be lower for either isomer of **1**. Indeed, at the lowest recorded temperature (−100 °C, not shown in Figure 3), the only differences when compared to the −70 °C spectrum were the complete coalescence of signals *b/h* and *s/w* and some renewed broadening of the *a/g* and *y/z* resonances.

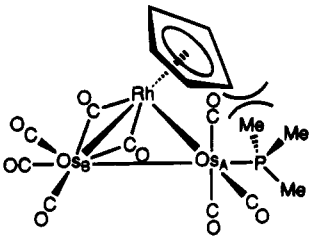

Figure 5. Steric influence of PMe_3 on the migration of the C_5H_5 group that accompanies pairwise carbonyl exchange in the Os_B–Rh plane of isomer **1a**.

A quantitative study of the slower carbonyl exchange processes in each isomer by line shape simulation yielded interesting results. The free energy of activation for pairwise CO exchange in the Os_C–Os_D plane of **1b** (13.0 ± 0.4 kcal·mol^{-1}) is similar to that for the analogous process in $Os_2Rh(CO)_9(C_5Me_5)$ (12.7 ± 0.3 kcal·mol^{-1}).[2] This is not unexpected as the function of both the PMe_3 and C_5Me_5 moieties is electron donation, which decreases the barrier to exchange in the Os–Os plane in each case relative to the *ca.* 17 kcal·mol^{-1} value for $Os_3(CO)_{12}$.[16]

A more interesting result is that the activation energy for pairwise exchange in the Os_B–Rh plane of **1a** (11.5 ± 0.4 kcal·mol^{-1}) is 3 kcal·mol^{-1} higher than for the similar process in the parent cluster, $Os_2Rh(CO)_9(C_5H_5)$ (8.4 ± 0.4 kcal·mol^{-1}).[2] Qualitatively, signal broadening is already observed at −115 °C (k = 20 s^{-1}) in $Os_2Rh(CO)_9(C_5H_5)$[2] while comparable broadening (k = 18 ± 1 s^{-1}) in **1a** is only seen at −53 °C. This finding was certainly unexpected, as one would predict a decrease in activation energy for the exchange because of electron donation by PMe_3 to Os_B. The absence of electronic rational made us search for possible steric arguments. As shown in Figure 5, the bridged intermediate required for the pairwise CO exchange brings the cyclopentadienyl ring through the plane of the metals such that the ring centroid is found approximately along an extension of the Os_B–Rh bond vector. The phosphine ligand is directly adjacent to the ring as it passes through this position, and it is possible that the steric interference exerted upon the cyclopentadienyl ring by the methyl groups of the phosphine ligand is sufficient to hinder its passage through the plane of the metals. Such a situation would clearly result in an increased barrier to carbonyl migration when compared with the unsubstituted analog.

Isomer Interconversion between 1a and 1b. The reversible temperature-dependent line shape changes in the ^1H and $^{31}P\{H\}$ NMR spectra clearly indicate that isomers **1a** and **1b** interconvert above −20 °C. The most likely mechanism for the isomer interconversion is a restricted trigonal twist (turnstile process) at the substituted osmium center, which brings about the desired transformation in a nondissociative manner.[5a] Line shape simulation of the variable-temperature ^1H NMR spectra provides a free energy of activation of 15.1 ± 0.4 kcal·mol^{-1} for the isomer interconversion, which is similar to the activation energies determined for the analogous turnstile processes in $Os_3(CO)_{10}[P(OMe)_3]_2$ (15.0 ± 0.4 kcal·mol^{-1}) and $Os_3(CO)_9[P(OMe)_3]_3$ (13.8 ± 0.4 kcal·mol^{-1}).[5a]

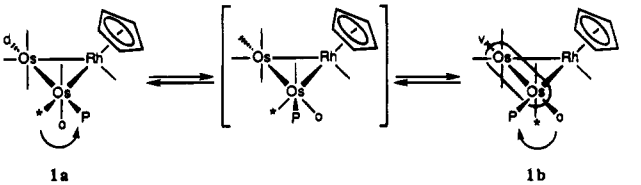

Figure 6. Restricted trigonal twist at the PMe_3-substituted Os center, which initiates participation of CO d in the carbonyl scrambling process.

The effect of the turnstile at the substituted osmium centers is to exchange the previously invariant carbonyl *d* of **1a** with an equatorial site (*v*) in **1b** (Figure 6). Consequently, signal *d* broadens above −20 °C in the ^{13}C NMR spectra (Figure 3). Although a high-temperature limiting ^{13}C NMR spectrum is not achieved, the broad signal observed in the +80 °C spectrum is an indication of averaging of all the carbonyl signals in accord with global carbonyl scrambling and rapid isomer interconversion.

Conclusions

Thermal reaction of $Os_2(CO)_8(\mu\text{-}\eta^1,\eta^1\text{-}C_2H_4)$ with $(\eta^5\text{-}C_5H_5)Rh(CO)PMe_3$ gave cluster **1**, which exists as a mixture of two interconverting isomers. Isomer interconversion at ambient temperature occurs via a restricted turnstile mechanism at the phosphine-substituted osmium center. In addition, each of the isomers exhibit carbonyl fluxionality at low temperature, which can be accounted for by the familiar pairwise carbonyl exchange mechanism. The ^{13}C NMR spectra additionally provide a clear illustration of the downfield shift of carbonyl resonances with phosphine substitution.[5] In particular, the signals attributed to the exchanging carbonyls in **1a** are downfield of their corresponding signals in **1b** because the exchange plane in the former includes a phosphine-substituted osmium center.

Acknowledgment. We thank the Natural Sciences and Engineering Research Council of Canada for funding and for an Undergraduate Summer Research Award to J.C. Financial support from University of Alberta is also gratefully acknowledged. The expert assistance of Dr. John Washington and Dr. Wenyi Fu in recording the variable-temperature NMR spectra presented in this study is sincerely appreciated. We thank Professor R. E. D. McClung for useful discussion and help with the simulation of the ^1H and ^{13}C NMR spectra.

OM940647Q

(16) (a) Foster, A.; Johnson, B. F. G.; Lewis, J.; Matheson, T. W.; Robinson, B. H.; Jackson, W. G. *J. Chem. Soc., Chem. Commun.* **1974**, 1042. (b) Aime, S.; Gambino, O.; Milone, L.; Sappa, E.; Rosenberg, E. *Inorg. Chim. Acta* **1975**, *15*, 53.

Alkyne Adducts of [Cp*Ru(SR)]$_2$ and Intermediates of the Ruthenium-Catalyzed Formation of Vinyl Thioethers (*Z*/*E*)-RSCR′=CHR″ from RSH and R′C≡CR″

U. Koelle,* Chr. Rietmann, J. Tjoe, T. Wagner, and U. Englert

Institute of Inorganic Chemistry, RWTH-Technical University at Aachen, Prof.-Pirlet-Strasse 1, D-52056 Aachen, Germany

Received July 5, 1994[⊗]

Binuclear Ru complexes Cp*Ru(μ–SR)$_2$RuCp* (**2**; R = Et, ^{i}Pr, ^{t}Bu) and the related complex Cp*Ru(η^1-C$_6$F$_5$)(μ-S)(μ-SC$_6$F$_5$)RuCp* (**3**) are active catalysts for the addition of thiols to polar alkynes at room temperature. The addition of alkynes to one Ru of **2** and **3**, respectively, is shown by NMR as the first step in the catalytic cycle. Four additional complexes, **7**–**10**, all characterized by single-crystal X-ray structures (Table 2), were isolated from the catalytic mixture. These are the insertion product of HC≡CCOOMe into the Ru–S bond of **2**, Cp*Ru(μ-SR)(μ_2-η^4-MeOOC≡CCHSR)RuCp* (**7a**), the double-vinylidene complex Cp*Ru{η^1-=C=C(COOMe)}(μ-S^{t}Bu)$_2$RuCp*{η^1-=C=C(COOMe)·CH=CH(COOMe)} (**8**), the double-insertion product of alkyne into **2c**, Cp*Ru(μ-S^{t}Bu){μ-η^4-(S^{t}Bu)C=C(COOMe)CH=CHCOOMe}-RuCp* (**9**), and a complex formed from linkage of five HC≡CCOOMe molecules with two RuCp* and one S^{t}Bu unit, (CpRu)$_2$ {η^4:η^4-C$_6$H-1-S^{t}Bu-2,3,5-(COOMe)$_3$-6-(C=C(COOMe)-CH=CHCOOMe)} (**10**). **7** and **8** are active catalysts; **9** and **10** are stop complexes of the catalytic cycle. On the basis of these isolated and characterized intermediates a mechanism for the catalytic cycle is suggested.

Introduction

A variety of mono- and polynuclear Cp*Ru–sulfur complexes have been the subject of increased recent interest due to the diversity of reactions they can undergo and the host of structures encountered. Apart from mononulcear Cp*RuL$_2$SR and cations [Cp*RuL$_2$-SR]$^+$ derived therefrom,[1] the main structural types comprise binuclear complexes such as Cp*Ru^{III}X(μ-SR)$_2$-Ru^{III}XCp*,[2] [Cp*Ru^{III}(μ-SR)$_3$Ru^{III}Cp*]X,[2,3] [Cp*Ru^{II}(μ-SR)$_3$Ru^{III}Cp*],[2] and [Cp*Ru^{II}L(μ-SR)$_2$LRu^{II}Cp*].[4] More recent additions are the sulfur analogues to the much investigated bridged alkoxo dimer [Cp*Ru(OMe)]$_2$ (**1**), i.e. [Cp*Ru(SR)]$_2$ (**2**),[5,6] with two 16-valence-electron (VE) coordinatively unsaturated Ru atoms and an upwards folded butterfly geometry similar to that of **1**.[5–7] Reaction of these dimers **2** as well as the mixed-valence complexes [Cp*Ru^{II}(μ-SR)$_3$Ru^{III}Cp*] with various alkynes is observed frequently at or slightly above ambient temperature, resulting in the coupling of two or three alkyne molecules in the Ru–Ru coordination sphere to give a great variability of products.[6–8] Thus, from [Cp*Ru(SR)]$_2$ (R = ^{i}Pr) and HC≡CSiMe$_3$ a complex was isolated containing an η^2-bound (Me$_3$Si)(Me$_3$-SiCH=C)CCSiMe$_3$ group[7] and *p*-TolC≡CH with the same bridging thiolate substrate has given a similar three-alkyne ligand chain complexing in an η^4 fashion over a (Cp*Ru)$_2$SR unit.[6] The reaction of the mixed-valence dimer [Cp*Ru^{II}((μ-SR)$_3$Ru^{III}Cp*] (R = ^{i}Pr) with ArC≡CH formed the product of oxidative addition and HSR elimination, i.e. [Cp*Ru(μ-SR)CAr]$_2$ which on protonation gave a complex where the two ArC≡C– moieties are coupled together.[8]

We have recently systematically studied exchange reactions and addition of two- and four-electron ligands to complexes **2**.[9] Exchange of the OMe groups in **1** with HSC$_6$F$_5$ has provided a new complex **3**, where oxidative addition of a C$_6$F$_5$S group leaves one coordinatively saturated and one unsaturated Ru. It was found that, with donor/acceptor ligands, depending on the ligand and on the bridging RS group, mono- as well as bis-addition products are formed.

We have now extended these investigations to incorporate alkynes as potential two- or four-electron ligands with the aim of studying addition of polar substrates to the alkyne in the Ru coordination sphere. It is shown in the following that complexes **2** catalyze the addition of thiols RSH to polar alkynes such as methyl propiolate (MP) or dimethyl acetylenedicarboxylate (DMAD) to give vinylthioethers (eq 1)at ambient temperature with moderate turnover frequencies and good turnover numbers. In some instances the reaction can be conducted with good stereochemical control. Most importantly, the isolation and characterization of various intermediates, including those which were shown to be active catalysts as well as complexes derived thereof but which are no

⊗ Abstract published in *Advance ACS Abstracts*, December 1, 1994.

(1) Amarasekera, J.; Rauchfuss, T. B. *Inorg. Chem.* **1989**, *28*, 3875.
(2) Dev, S.; Mizobe, Y.; Hidai, M. *Inorg. Chem.* **1990**, *29*, 4797–4801.
(3) (a) Dev, S.; Imagawa, K.; Mizobe, Y.; Cheng, G.; Wakatsuki, Y.; Yamazaki, H.; Hidai, M. *Organometallics* **1989**, *8*, 1232. (b) Hidai, M.; Imagawa, K.; Cheng, G.; Mizobe, Y.; Wakatsuki, Y.; Yamazaki, H. *Chem. Lett.* **1986**, 1299.
(4) (a) Knox, G. R.; Pryde, A. *J. Organomet. Chem.* **1974**, *74*, 105. (b) Killops, S. D.; Knox, S. A. R. *J. Chem. Soc., Dalton Trans.* **1978**, 1260.
(5) Koelle, U.; Rietmann, C.; Englert, U. *J. Organomet. Chem.* **1992**, *423*, C20.
(6) Nishio, M.; Matsuzaka, H.; Mizobe, Y.; Hidai, M. *J. Chem. Soc., Chem. Commun.* **1993**, 375.
(7) Matsuzaka, H.; Mizobe, Y.; Nishio, M.; Hidai, M. *J. Chem. Soc., Chem. Commun.* **1991**, 1011.
(8) Matsuzaka, H.; Hirayama, Y.; Nishio, M.; Mizobe, Y.; Hidai, M. *Organometallics* **1993**, *12*, 36.
(9) Hörnig, A.; Rietmann, C.; Englert, U.; Wagner, T.; Koelle, U. *Chem. Ber.* **1993**, *126*, 2609.

0276-7333/95/2314-0703$09.00/0

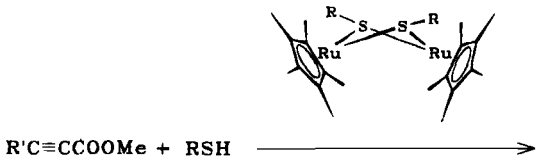

longer capable of catalyzing the reaction (defined as stop complexes), have yielded valuable information on the mechanistic steps in the catalysis.

Results

1. Addition of Alkynes to Thiol Complexes 2 and 3. Thiol complexes used in this study were $[Cp^*Ru(SR)]_2$ with R = Et (**2a**), ^{i}Pr (**2b**), ^{t}Bu (**2c**), and Bz (**2d**) (eq 2), the preparation and properties of which were described recently.[5,9] Due to the instantaneous and clean course of reaction 2 these thiol complexes can be produced conveniently in situ if examined in a catalytic reaction.

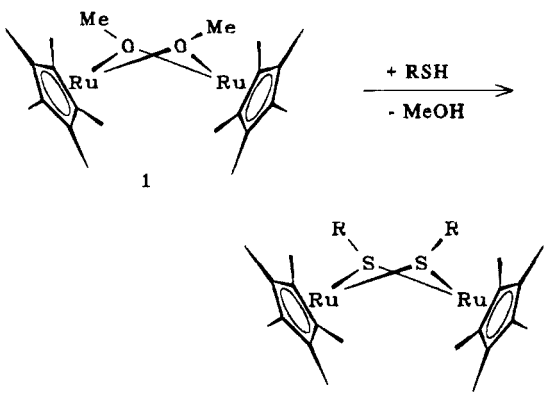

R	Et	^{i}Pr	^{t}Bu	Bz
2	a	b	c	d

Ligand addition reactions to **2** are easily followed through a characteristic color change from blue to green or orange, depending on the acceptor properties of the ligand. Thus, no reaction occurred on mixing **2c** with MeC≡CMe, PhC≡CPh, or Me_3SiC≡CH. A green addition product was formed when 2-butyne was added to a solution of **2a** in slight excess (eq 3). The ^{1}H NMR

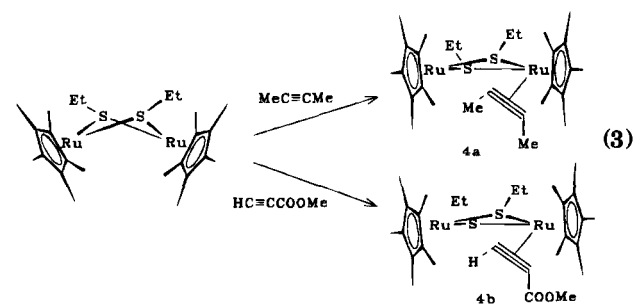

spectrum shows a singlet for two coincident Cp* groups at δ 1.52, one triplet for SCH_2CH_3 protons, and nonequivalent SCH_2CH_3 protons as well as singlets for coordinated (δ 1.83) and free (δ 1.65) 2-butyne which, together with the integration ratio, indicated the monoadduct **4a** where the alkyne is bound to one Ru, similar to what has been observed for e.g. ethylene and other two-electron ligands.[9] An analogous spectrum is shown by a mixture of **2a** and MP in slight excess. In this case $\Delta\delta$ of the two Cp* signals is larger, giving rise to well-separated peaks of equal intensity, whereas the SCH_2CH_3 group consists again of a triplet and a complicated pattern for inequivalent ethylenic protons. A further addition product **5** was isolated from **3** and MP (eq 4).

Table 1. *Z/E* Ratio of Vinyl Thioethers $R^1SC(R^2)$=C(H)COOMe (6) from Reaction 1 as Determined by GC (1/250 Catalyst/Substrate)

compd	R^1	R^2	*Z/E*
6a	^{t}Bu	H	2.15[a]
6a			5.53
6b	^{t}Bu	COOMe	1.07
6c	^{i}Pr	COOMe	1.01
6d	Et	H	0.84
6e	Et	COOMe	1.00
6f	C_6F_5	H	6.93
6g	C_6F_5	COOMe	5.71
6h	$PhCH_2$	H	2.01
6i	Ph	H	3.72

[a] Catalyst/substrate ratio 1/25.

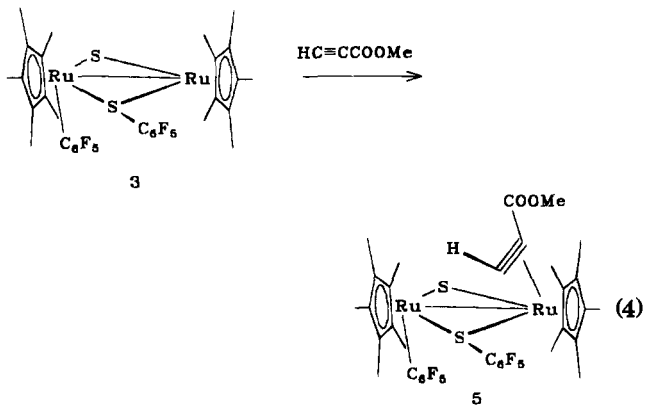

Since **3** has only one coordination site at Ru, monoaddition is the only possibility in this case. With excess MP the reaction did not proceed beyond the monoadduct, which was the only isolable product. Indicative of alkyne coordination as a perpendicular two-electron ligand is the chemical shift of the acetylenic proton at δ 9.0 in **5**. In **4b** the analogous proton resonates at δ 8.32. Whereas addition products **4a,b** can only be observed in the NMR, **5** has been isolated and fully characterized by analytical data. In other cases, e.g. **2c** and PhC≡CH, the addition product could not be observed simply because the reaction proceeded too fast to the insertion product **7** (*vide infra*).

2. Catalyzed Addition of Thiols to Polar Alkynes. Ru thiol complexes **2**, generated in situ from **1** and the respective thiol (eq 2), smoothly catalyze the addition of RSH to polar alkynes ROOCC≡CH (MP) and MeOOCC≡CCOOMe (DMAD), yielding vinyl thioethers **6**. Reactions were conducted in pentane solution at ambient temperature, where about 0.04 mmol of **1** was mixed with a 100–500-fold excess of alkyne and thiol in 1:1 molar ratio. After completion of the reaction the mixture was filtered over alumina to remove Ru complexes; the vinyl thioethers were eluted and characterized by ^{1}H and ^{13}C NMR, GC, and GC/MS (see Experimental Section). Table 1 lists results of experiments conducted with various thiols and alkynes.

From these examples it can be concluded that there is no obvious restriction in the thiol, whereas alkynes

reacted only if at least one carboxylate group was present. A mixture of *E* and *Z* isomers was produced in all reactions; however, the thermodynamically less favorable *Z* isomer prevailed. Isomers can be clearly identified in the NMR, where the vinyl proton of the *E* isomer close to sulfur resonates at lower field.

When reaction 1 using **1**, HS^{t}Bu, and MP was followed with time, by taking samples for GC analysis in intervals over 24 h, a change in the ratio of *Z*/*E* isomers as displayed in Figure 1 was detected. In an early stage of the reaction, i.e. after 0.5 h, the *Z*/*E* ratio was about 1 but changed with time to 5.5/1, which seems to be the final value. After about 20 h, GC control showed the reaction to be complete at ambient temperature. Adding fresh amounts of thiol and alkyne makes the catalysis start over again at a rate similar to the initial one with a nearly constant isomer ratio of 5/1. The turnover number reached after two additions of substrate was 890, but the catalyst could not be exhausted under these conditions.

The catalytically active mixture after some time shows an orange to brown color, different from that of either **1** or **2** and also different from the green color of the alkyne addition products. Thus, the species present in higher concentration in the catalytic mixture must be a different complex. Because the isomer ratio changed with time, it must be concluded that more than one catalytically active species is formed during the reaction. We therefore aimed at isolating intermediates of the catalysis.

3. Complexes Isolated from 2 and Alkynes. In addition to the alkyne adducts described above, products of insertion of one or two alkynes into one of the bridging Ru−S bonds could be isolated and characterized. Reacting **2c** with a stoichiometric quantity of MP (eq 5)

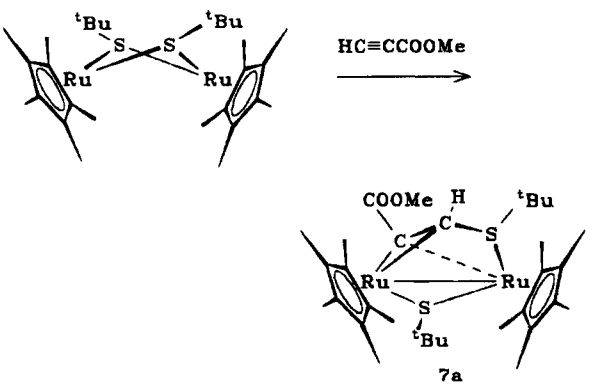

(5)

yielded the green compound **7a**, which could be crystallized from pentane at low temperature. Two separate Cp* and two S^{t}Bu signals (where one is found at δ 1.17, 0.5 ppm to high field from the bridging S^{t}Bu signal in the starting complex, and is assigned to a monodentate S^{t}Bu group), one COOMe signal, and a one-proton singlet at δ 4.55 in the ^{1}H NMR spectrum indicate a low-symmetry dinuclear complex composed of **2c** and the alkyne in a 1/1 ratio.

X-ray structure determination of a crystal grown from pentane confirmed this composition and gave structural details. An ORTEP view together with pertinent distances and angles is given in Figure 2. The molecule **7a** can be conceived as being formed through insertion of an alkyne into one Ru−S bond in the same anti-Markownikoff regiofashion as the final vinyl thioether,

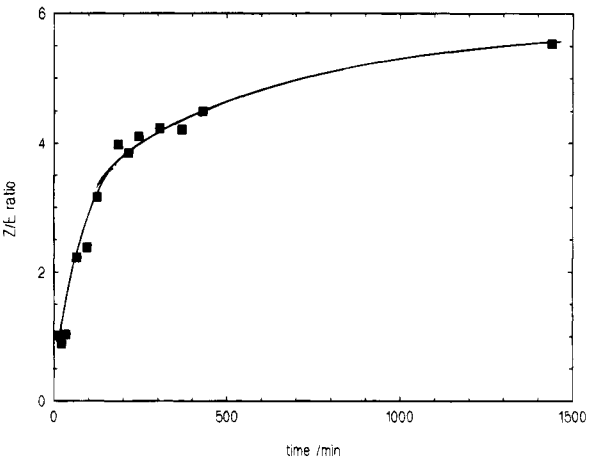

Figure 1. Change of *E*/*Z* isomer ratio in the course of vinyl thioether formation from MP and **2c**.

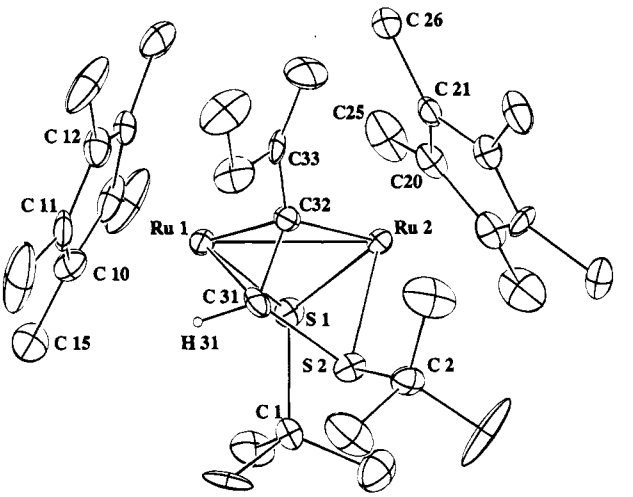

Figure 2. ORTEP view of the molecule **7a**, showing atom numbering.

Table 2. Parameters for X-ray Structure Determination of 7a and 8−10

	7a	8	9	10
space group (No.)	$P2_1/n$ (14)	$P\bar{1}$ (2)	$C2/c$	$P2_1/c$ (14)
temp (K)	293	258	293	253
molecules per unit cell	4	2	8	4
a (Å)	10.845(1)	9.527(3)	37.49(2)	20.670(3)
b (Å)	16.056(2)	13.497(4)	11.659(8)	12.27(4)
c (Å)	19.812(2)	17.306(6)	18.091(9)	19.48(3)
α (deg)	90.00	68.67(3)	90.00	90.00
β (deg)	104.560(8)	86.09(3)	108.14(5)	114.80(9)
γ (deg)	90.00	88.06(2)	90.00	90.00
V (Å^3)	3339(1)	2068(1)	7514(15)	4494(17)
scan range (deg)	$3 < \theta < 25$	$3 < \theta < 22$	$3 < \theta < 25$	$3 < \theta < 20$
abs coeff (cm^{-1})	10.33	8.54	9.29	7.56
empirical abs cor	PSI[20]	DIFABS[21]	PSI[20]	DIFABS[21]
no. of reflns	6316	5418	6037	4313
no. of observns	3169	2152	5091	1727
no. of params refined	344	221	398	245
R	0.073	0.126	0.022	0.137
R_w	0.041	0.089	0.032	0.118

i.e. SR bound to the hydrogen end of the unsymmetrical acetylene. Ru−S distances in the remaining bridging thiol unit are comparable to those in the coordinatively unsaturated starting material,[5] whereas the distance of the carbon-bound ^{t}BuS group to Ru2 is lengthened by about 0.1 Å. In addition the newly formed olefinic bond bridges the Ru−Ru unit unsymmetrically. One of the former Ru−S σ-bonds in the starting molecule is

Table 3. Selected Bond Lengths (Å) and Bond Angles (deg) in 7a[a]

Ru1–Ru2	2.746(2)	Ru2–C20	2.19(1)
Ru1–S1	2.292(4)	Ru2–C21	2.20(1)
Ru2–S1	2.339(3)	Ru2–C22	2.23(1)
Ru2–S2	2.422(4)	Ru2–C23	2.23(1)
Ru1–C10	2.23(2)	Ru2–C24	2.27(2)
Ru1–C11	2.20(2)	Ru2–C32	2.11(1)
Ru1–C12	2.24(2)	S1–C1	1.89(1)
Ru1–C13	2.26(2)	S2–C2	1.86(1)
Ru1–C14	2.22(2)	S2–C31	1.79(1)
Ru1–C31	2.14(1)	C31–C32	1.40(2)
Ru1–C32	2.03(1)	C32–C33	1.52(2)
Ru1–S1–Ru2	72.7(1)	S2–C31–C32	103(1)
C31–C32–C33	122(1)	C31–Ru1–C32	39.1(4)

[a] Numbers in parentheses in this and all following tables are estimated standard deviations in the last digit.

replaced by a very short (2.03 Å) C32–Ru2 σ-bond. However, the Ru1–C31 bond is rather short as well; thus, it seems justified to consider the Ru1–C31–C32 triangle as a metallacyclopropane, assigning a +III oxidation state to either Ru. Diamagnetism is then established by a Ru–Ru single bond of 2.75 Å. If we focus on the dihedral angles S2–C31–C32–C33 (132°) and H31–C31–C32–C33 (53°), it is obvious that the geometry of the complexed RSCH=C(COOMe) unit is closer to that of the *E* vinyl thioether, in accord with the *cis* disposition of H and COOMe in the alkyne adduct, the most probable precursor to **7a**.

Note that the product of catalysis (**6**) can form from **7** by solvolytic opening of one of the Ru–C(32) bonds by a thiol molecule substituting C(32) for the newly entered SR group (see below). Accordingly, it has been found that e.g. **7a** is catalytically active when treated with excess RSH/alkyne. Moreover, it could be verified by NMR that with excess thiol added to the isolated complex **7a**, the starting bis-thiol complex **2** was regenerated along with 1 mol of vinyl thioether **6**.

A similar insertion product, **7b**, was found from reaction of **2c** with PhC≡CH (eq 6). In this case the

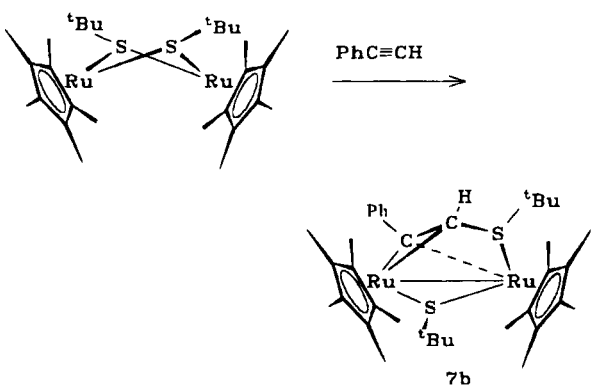

(6)

reaction stops at the stage of **7b** and does not proceed toward a vinyl thioether in the presence of excess thiol. From NMR integration a **2c**/PhC≡CH ratio of 1/1 is obvious; ^{t}Bu signals are found at δ 1.11 and 1.78, comparable to the ones in **7a**, as well as the vinylic proton signal at δ 4.58, also very close to the analogous proton in **7a**. It is mainly this latter proton shift which is diagnostic for the structure of **7b**, since the alternative, a π-complexed alkyne, would give a single proton resonance around 8–9 ppm as shown by **4b** and **5** above. The very close similarity of the vinylic protons in **7a**

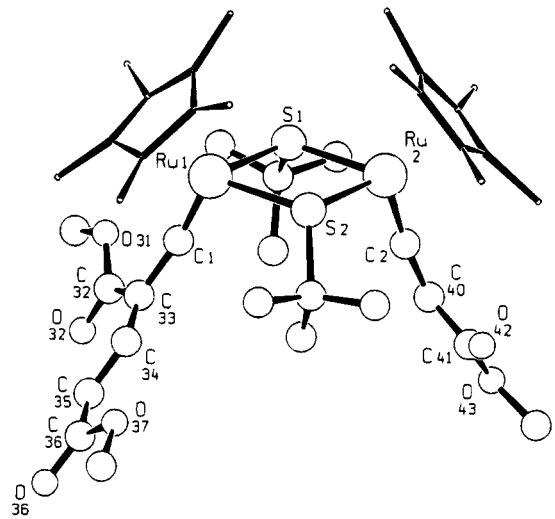

Figure 3. Schakal representation of the molecule **8**, showing atom numbering.

and **7b** also demonstrates the same regioaddition, i.e. Ph as the terminal group and hydrogen at the sulfur-bearing C atom in **7b**.

A second complex could be isolated from the reaction mixture if, for example, excess ^{t}BuSH and MP were added to **2c** and the reaction was quenched after some hours. As much as 80% of the Ru present in the mixture was isolated after chromatography in the form of the orange complex **8** of composition $(Cp^*RuS^tBu)_2(HC_2COOMe)_3$ established by ^{1}H and ^{13}C spectroscopy. The compound is air stable and does not react with phosphine; it should thus be coordinatively saturated. The ^{1}H NMR spectrum showed two nonequivalent Cp* and two equivalent ^{t}BuS groups, their chemical shift indicating a bridging position. The three remaining protons appear as an AB system in the same position with the coupling constant for an (*E*)-HC=CHCOOMe group and as one singlet in a vinylic position. The most noteworthy features in the ^{13}C NMR spectrum are two quaternary carbon resonances at the extreme position of δ 320 assignable to vinylidene type carbon atoms.

Key features of the structure of **8** were ultimately established by X-ray analysis of an orange crystal grown by slowly evaporating a xylene solution. The crystal quality allowed anisotropic refinement of only Ru and S atoms. All other atoms were refined isotropically. Hydrogen positions were calculated. The complex is of the type $Cp^*RuL(\mu\text{-}SR)_2RuL'Cp^*$, where L and L′ are two-electron ligands similar to the addition products of e.g. phosphine, isonitrile, or CO to compounds **2**.[9] Consequently, the Ru–Ru distance in **8** is in the nonbonding range. Ru–S distances are lengthened from about 2.32 Å in the Cp̂ analogue of **2a**[5] to 2.42/2.38 Å, and Ru–S–Ru angles have widened up from 83° (**2a**) to 103/104° in **8** as a consequence of lifted S–Ru back-bonding. As anticipated by the ^{13}C NMR chemical shifts, a double-vinylidene complex was revealed with one =C=CHCOOMe and one =C=C(COOMe)CH=CH-(COOMe) unit terminally bound to the Ru atoms of a symmetrical $(Cp^*RuS^tBu)_2$ core with Ru–C distances of 1.72(3) and 1.74(3) Å and Ru–C–C angles of 164 and 173°, respectively (Table 4). In the solid structure the =C(COOMe)(CH=CHCOOMe) and CH(COOMe) planes are oriented roughly perpendicular to the Ru–Ru vector but seem to rotate in solution to some extent, since

Table 4. Selected Bond Lengths (Å) and Bond Angles (deg) in 8

Ru1−Ru2	3.767(4)	S2−C60	1.88(3)
Ru1−S1	2.40(1)	C1−C33	1.48(4)
Ru1−S2	2.43(1)	C32−C33	1.44(4)
Ru1−C1	1.72(3)	C33−C34	1.38(3)
Ru2−S1	2.38(1)	C34−C35	1.37(4)
Ru2−S2	2.383(9)	C35−C36	1.39(5)
Ru2−C2	1.74(3)	C2−C40	1.40(5)
S1−C50	1.91(3)	C40−C41	1.46(4)
S1−Ru1−S2	75.8(3)	Ru1−C1−C33	164(3)
S1−Ru2−S2	77.0(3)	Ru2−C2−C40	173(3)
S1−Ru1−C1	103(1)	C1−C33−C34	121(2)
S1−Ru2−C2	105(1)	C32−C33−C34	126(3)
S2−Ru1−C1	107(1)	C33−C34−C35	125(2)
S2−Ru2−C2	103(1)	C34−C35−C36	118(3)
Ru1−S1−Ru2	104.1(2)	C2−C40−C41	125(2)
Ru1−S2−Ru2	103.1(2)		

inequivalent ^{t}Bu groups would result from the rigid arrangement. Conjugation of two carbomethoxy groups in the residue attached to Ru1 (obvious but less pronounced in the shorter chain at Ru2) has the effect of far-reaching bond length equalization within the carbon chain with particularly long $C_\alpha-C_\beta$ bonds (1.48 and 1.40 Å; Table 4), an observation that gives an explanation for the pseudo-C_{2v} solution structure.

Complex **8**, when treated with an RSH/R′C≡CR″ mixture, likewise turned out to be an active catalyst for the formation of vinyl thioethers. In contrast to the foregoing, the *Z/E* ratio obtained with **8** was much higher than if the catalysis was started with either **1** or **2**. Since *Z/E* ratios increased during catalysis, it is tempting to conclude that at the later stages of the reaction the catalytic cycle is driven more and more by **8**. Because this complex as the catalytically active species produces >80% *Z* vinyl thioether, it is evident that the (*E*)-HC=CHCOOMe unit present in the molecule cannot be transferred with the catalysis, only the =C=CH(COOMe) part, where the stereochemistry with respect to the vinyl thioether due to a further hydrogen shift has not yet been determined.

Two further complexes, **9** and **10**, both of them featuring an array of linked alkynes, were isolated from **2c** and excess MP (Scheme 1). Reaction over 15 h at ambient temperature gave after chromatographic workup about 40% **9** as dark brown plates. ^{1}H NMR showed two nonequivalent Cp* singlets and two isochronous ^{t}Bu groups as one signal, two COOMe groups (δ 3.41 and 3.46), and two one-proton singlets of coordinated vinylic protons at δ 4.55 and 4.66.

X-ray structure analysis performed with a dark brown crystal of **9** grown from pentane revealed the product of head-to-tail double-alkyne insertion into a Ru−S bond of **2c**, as shown in Figure 4. The (Cp*Ru)$_2$ unit in **9** is again bridged by one ^{t}BuS group and by a *cisoid* μ_2-η^4-dienyl unit. This latter moiety acts through a −C(COOMe)=C(^{t}BuS) group as a three-electron donor toward Ru1. As a consequence, the distances Ru−S are unequal but now Ru(1), showing an extremely short Ru1−C1 separation, shows a longer Ru−S distance in comparison to Ru2−S, whereas in **7** (*vide supra*) the shorter Ru−C corresponded to the shorter Ru−S_{bridge} distance. The very short distance Ru1−C1 of 1.889 Å is due an η^3 (σ,π) binding mode of the −(^{t}BuS)-*C*=*C*(COOMe)− vinyl group with no hydrogen at C1. Note that the Ru···Ru distance in **9** is closer to the one in **2** (nearly identical with Ru···Ru in **1**) and signifying only a weak interaction of the Ru atoms. The (^{t}BuS)C=C(COOMe)CH=CH(COOMe) bridging unit in **9** is related to the more extended of the vinylidene chains in **8** and can be thought of as being formed by transference of one bridging ^{t}BuS in **8** onto a vinylidene carbon as indicated in Scheme 1.

Complex **9** is inactive as a catalyst in thiol addition to alkynes and may thus be considered as a stop complex in the cycle. It forms, however, only if the alkyne is present in excess. With sufficient thiol in the reaction mixture, as is provided by the 1/1 thiol/alkyne mixture, the catalyst has not been found to be exhaustible.

Finally, complex **10** was isolated in about 10% yield from a reaction mixture containing **2c**, thiol, and MP after chromatography and crystallization from pentane. The ^{1}H NMR spectrum shows two Cp* singlets, five different carbomethoxy signals, and an AB system for an uncomplexed *trans*-CH=CHCOOMe group, along with a one-proton singlet at δ 6.38 assigned to an aromatic proton.

An X-ray structure determination, due to isotropic refinement imposed by moderate crystal quality, only converged to $R_w \approx 12\%$ but clearly shows the molecular backbone (Table 6). In **10** five molecules of MP have combined together with one ^{t}BuS group to form a 1,2,4-dienylide substituted benzene η^4 complexed to one Cp*Ru moiety and complexed through the sulfur atom, one double bond, and the terminal dienylic carbon to another Cp*Ru. The last two are completely ruptured. Note the two vicinal COOMe groups at C31 and C32 and the tail-to-tail-to-tail linkage of three C−C−COOMe units at C34. Despite the large errors due to the moderate quality of the structure it appears reasonable that the longest inner ring C−C distances are C30−C31 and C34−C35, i.e. the linkage of the two separately complexed parts of the six-membered ring. Furthermore, the short distance of Ru(1) to the highly unsaturated carbon C36 (2.05(4) Å) and the two formal C=C double bonds C36=C37 (1.33(4) Å) and C38=C39 (1.28(4) Å) appear very reasonable. Isolation of complex **10** provides the first example of a Ru_2S_n unit that has been cleaved completely by alkyne but otherwise adds yet another fabulous alkyne oligomerization product in the coordination sphere of a Ru_2S_n or a Ru_2O_n unit to the large number of known examples.[7,8,18] Complex **10** does not catalyze vinyl thioether formation.

4. Catalysis Performed with Cp*Ru(C_6F_5)(μ-SC_6F_5)(μ-S)RuCp* (3). Complex **3**, which is formed from **1** and HSC_6F_5 with oxidative addition of one C_6F_5−S bond,[9] likewise was active as a catalyst. The molecule has two different bridging ligands, i.e. μ-SC_6F_5 and μ-S, and one Ru is σ-coordinated in addition to a C_6F_5 group; thus there is only one coordinatively unsaturated center in the dimer.

In alkyne adduct formation **3** was less reactive than **2**. No reaction could be observed with substrates such as 2-butyne and phenylacetylene. An obvious reaction with DMAD over 6 h at ambient temperature did not lead to an isolable adduct but the vinyl thioether could be isolated in roughly stoichiometric amount.

Addition of HSC_6F_5 and MP to a catalytic quantity of **3** similarly led to the corresponding *Z/E* mixture of vinyl thioethers C_6F_5SCH=CHCOOMe in high yield. Note that in this case the *Z/E* ratio is as high as 9/1; thus, the reaction is more stereospecific than in the cases

Scheme 1

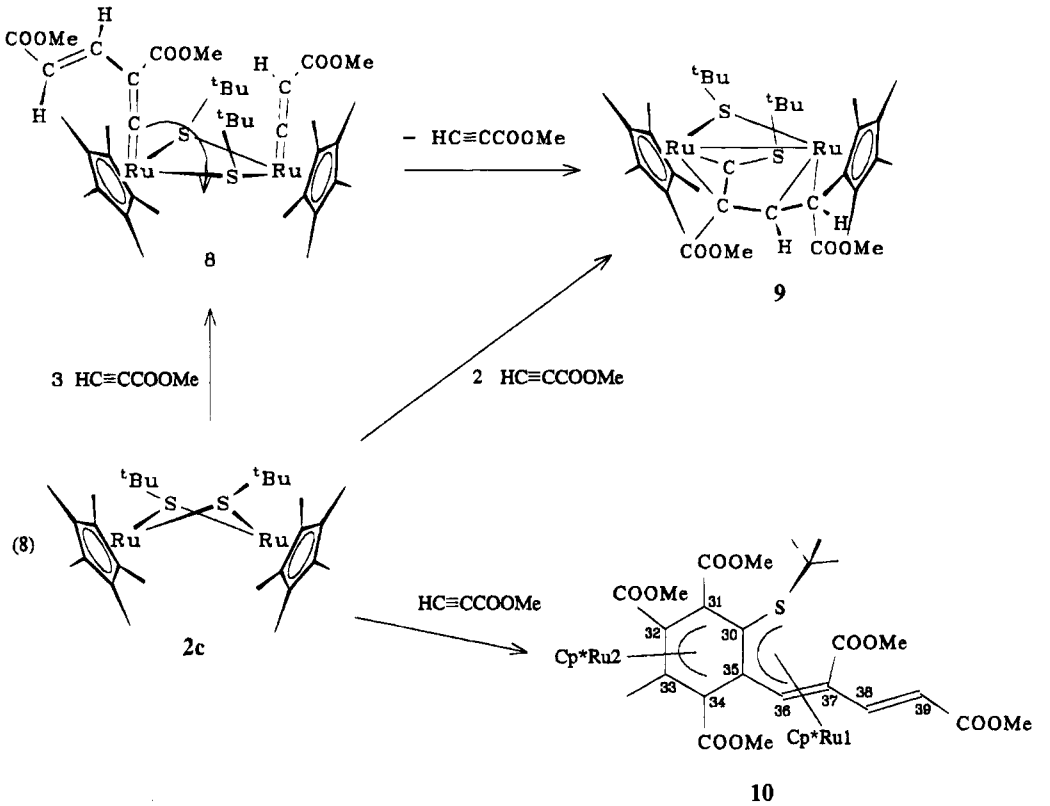

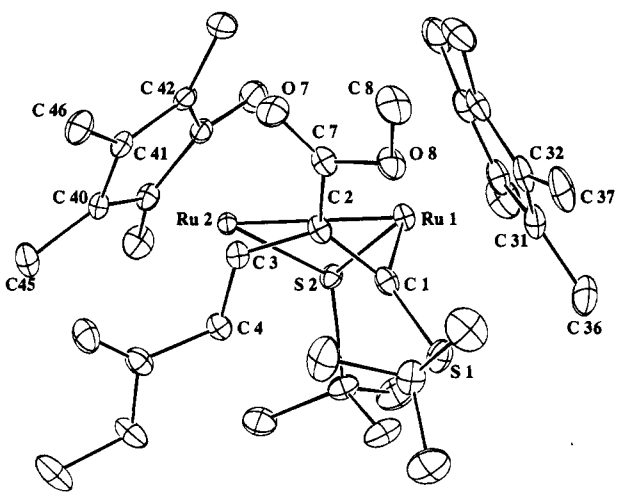

Figure 4. ORTEP view of the molecule **9**, showing atom numbering.

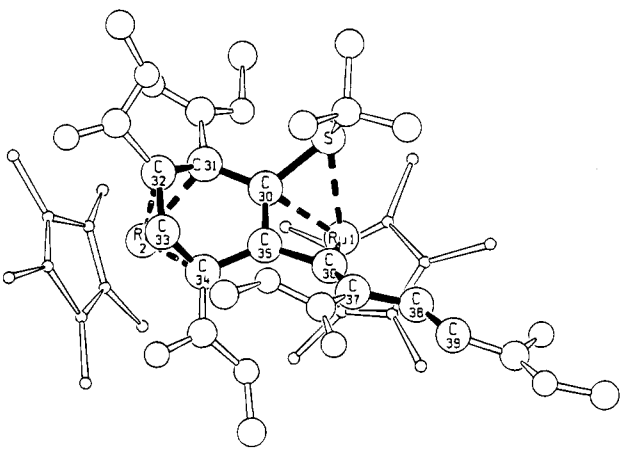

Figure 5. Schakal representation of the molecule **10**, showing atom numbering.

Table 5. Selected Bond Lengths (Å) and Bond Angles (deg) in 9

Ru1−Ru2	2.9956(2)	Ru2−C4	2.202(2)
Ru2−S2	2.2903(4)	Ru1−S2	2.3445(5)
S1−C1	1.683(2)	Ru1−C1	1.889(2)
C1−C2	1.442(3)	S2−C20	1.884(2)
C2−C7	1.482(3)	C2−C3	1.459(3)
C4−C5	1.466(3)	C3−C4	1.412(3)
Ru1−C2	2.292(2)	Ru2−C3	2.129(2)
Ru1−S2−Ru2	80.52(1)	Ru1−C1−S1	133.4(1)
Ru1−C1−C2	85.8(1)	S1−C1−C2	140.4(1)
C1−C2−C3	121.7(2)	C1−C2−C7	122.5(2)
C3−C2−C7	122.5(2)	C2−C3−C4	122.6(2)
C3−C4−C5	117.4(2)		

discussed above. No catalytic reaction was found with aliphatic thiols in the presence of **3**.

5. Reaction of 1 and 2 with MeOH/HC≡CCOOMe. The catalytic addition of thiols to polar alkynes has not been found to be transferable to the oxo system. The methoxo complex **1** evidently reacts with alkynes; thus, a dark violet color developed when **1** was treated with an excess of PhC≡CPh or PhC≡CH at low temperature, but no definitive products could be isolated. A pentane solution of **1** treated with excess MP or DMAD and either MeOH or EtOH turns brown, indicating a reaction, but no signs of vinyl ether were detected after chromatographic workup. However, if the SEt complex **2a** was treated with excess MP and MeOH (molar ratio 1/30) a 5/1 mixture of vinyl thioethers and vinyl ethers was found after chromatography. Assignment of vinyl signals to stereoisomers gave a *Z/E* ratio of about 5/1 for vinyl thioethers and about 1/1 for vinyl ethers. Product identification was by comparison of ^{1}H NMR shifts and coupling constants (of olefinic protons) with those of (*Z/E*)-EtSCH=CHCOOMe prepared in this

Table 6. Selected Bond Lengths (Å) and Bond Angles (deg) in 10

Ru1−S	2.354(9)	C30−C31	1.47(4)
Ru1−C30	2.14(3)	C31−C32	1.42(4)
Ru1−C35	2.23(3)	C32−C33	1.44(4)
Ru1−C36	2.05(3)	C33−C34	1.34(3)
Ru2−C31	2.22(4)	C34−C35	1.50(4)
Ru2−C32	2.10(3)	C30−C35	1.42(4)
Ru2−C33	2.09(3)	C35−C36	1.58(4)
Ru2−C34	2.17(3)	C36−C37	1.33(4)
S−C30	1.78(3)	C37−C38	1.44(4)
S−C42	1.85(4)	C38−C39	1.28(4)
		C39−C40	1.46(4)
S−Ru1−C30	46.5(8)	C30−C35−C34	115(3)
S−Ru1−C36	88(1)	C30−C31−C32	119(3)
S−C30−C35	124(3)	C31−C30−C35	113(3)
Ru1−S−C30	60.5(9)	C31−C32−C33	112(3)
Ru1−C30−S	73(1)	C33−C34−C35	113(3)
C30−S−C42	111(2)	C30−C35−C36	113(3)
C31−Ru2−C32	38(1)	C32−C33−C34	120(3)
C31−Ru2−C33	66(1)	C34−C35−C36	132(3)
C31−Ru2−C34	74(1)	C35−C36−C37	137(3)
C32−Ru2−C33	40(1)	C36−C37−C38	110(3)
C32−Ru2−C34	68(1)	C37−C38−C39	129(3)

work and of additional vinylic patterns present in the spectrum with literature data for ROCH=CHCOOMe. Separation was achieved by GC and confirmation as MeOCH=CHCOOMe was obtained through GC/MS. The reaction under these conditions appears to be still catalytic, though turnover numbers are only about 7, considerably lower than in the pure sulfur system.

Discussion

Classically the addition of OH functional molecules to alkynes is conducted under Brønsted or Lewis acid catalysis, though strongly basic conditions (KOR/crown ether in hydrocarbon[10]) have been shown to function as well. In transition-metal-catalyzed variants, alkyne coordination to the metal followed by addition of the OH functional component, alcohol or carboxylic acid, has been speculated on[11] or invoked from kinetic results,[12] the same as is suggested in the $RuH_2(PPh_3)_4$-catalyzed addition of alcohols to nitriles.[13] $Ru_3(CO)_{12}$ seems to be the first Ru complex that has been used to catalyze the reaction of polar alkynes.[14] This was later modified to include organometallic systems such as $Ru(C_8H_{11})_2/PR_3$/maleic anhydride[12] or $Ru_2(CO)_4(\mu\text{-OOCCR})_2L_2$, with L being either a carboxylic acid[15] or PPh_3.[16] A catalyzed addition of thiols to alkynes has not been reported. The Ru-catalyzed addition of OH-functional molecules to propiolic acids, however, to give vinyl esters[15] or of α-hydroxy carboxylic acids to give 1,3-dioxolan-5-ones,[15] has some bearing on the present investigations. In both cases the catalyst employed was a binuclear, doubly carboxylate bridged tetracarbonyl, $Ru_2(CO)_4(\mu\text{-OOCCR})_2L_2$, with L being either carboxylic acid or PPh_3. Whereas in the first case the addition to a terminal alkyne is purely Markownikoff, the regioselectivity in the second case was less stringent, giving Markownikoff as well as anti-Markownikoff products. Both reactions proceeded under much more drastic conditions, 100 and 145 °C, respectively. In the study of Rotem and Shvo[15] mononuclear complexes $Ru(CO)_2(OOCCR)_2(PPh_3)_2$ were isolated after quenching the reaction mixture with PPh_3, and from observations made when the reaction was conducted stepwise, it was concluded that the dinuclear precursor is cleaved by the alkyne and that stepwise addition of alkyne and carboxylic acid takes place in the coordination sphere of one Ru through an η^1-vinyl complex which is finally detached by hydrogen transfer from incoming acid.

Mild reaction conditions, i.e. pentane solution at room temperature (20−22 °C), characteristic for the catalysis under study, and a moderate turnover frequency as well as variation of the alkyne has allowed isolation of individual intermediates of the catalytic cycle. Addition of alkynes to coordinatively unsaturated Cp*Ru thiol complexes **2** as the first step has been found to proceed with polar and nonpolar alkynes leading to unsymmetrical monoadducts; in the case of **2** only one Ru becomes coordinatively saturated. The NMR spectrum of the addition product of the symmetrical alkyne 2-butyne to **2a** shows inequivalent CH_2 protons of the bridging SEt groups, denoting η^1-perpendicular rather than parallel addition, as was suggested for e.g. $Ru_2(CO)_4(\mu\text{-OOCCR})_2L_2$. A further possibility, i.e. perpendicular orientation of the alkyne acting as a symmetrical four-electron ligand, as is often found in alkyne addition products to various L_nM-ML_n moieties,[17] is likewise ruled out by the NMR spectra. Moreover, such a coordination mode in general gives rather stable compounds where the alkyne is not particularly activated toward addition of a nucleophile and thus should not appear as an intermediate in a catalytic cycle.

The insertion product **7**, or **13** with reference to Scheme 2, can be formed from **4** (**11**) simply by opening of a Ru−S bond and closing of an S−C bond without hydrogen shift.

A key compound identified as a catalytic intermediate is complex **8**. Condensation and oligomerization of various alkynes at a $Cp^*Ru(\mu\text{-SR})_2RuCp^*$ or $Cp^*Ru(\mu\text{-SR})_3RuCp^*$ unit are well documented,[6−8,18] examples among them showing a six-carbon chain (formed from $Me_3SiC{\equiv}CH$[7]) similar to that found in **8** but with a bridging rather than a terminal vinylidene group. However, the intermediacy of terminal vinylidene complexes, such as those isolated in the formation of **8**, has been frequently invoked to explain the observed reaction products.[8,18] A Cp*Ru(SR) moiety features a rather electron rich metal center prone to stabilize the vinylidene toward the acetylide. As shown in Scheme 2, an alternative to direct insertion of the alkyne leading to **7**/**13** is prior formation of a vinylidene, most probably via two metal oxidative addition to an acetylide as has been found for complexes **2** and $Cp^*Ru(\mu\text{-SR})_3RuCp^*$ in several cases,[2,8] and reprotonation at the β-carbon atom leading to an intermediate of type **12**. Rearrangement of **12** as detailed similarly for **4** would lead to the

(10) Steinborn, D.; Mosinski, H.; Rosenstock, T. *J. Organomet. Chem.* **1991**, *414*, C45.
(11) Steinborn, D.; Nünthel, R.; Krause, K. *J. Organomet. Chem.* **1991**, *414*, C54.
(12) Mitsudo, T.; Hori, Y.; Yamakawa, Y.; Watanabe, Y. *J. Org. Chem.* **1987**, *52*, 2230.
(13) (a) Murahashi, S.-I.; Sasao, S.; Saito, E.; Naota, T. *J. Org. Chem.* **1992**, *57*, 2521. (b) Murahashi, S.-I.; Sasao, S.; Saito, E.; Naota, T. *Tetrahedron* **1993**, *49*, 8805. (c) Naota, T.; Shichijo, Y.; Murahashi, S.-I. *J. Chem. Soc., Chem. Commun.* **1994**, 1359.
(14) Rotem, M.; Shvo, Y. *Organometallics* **1983**, *2*, 1689.
(15) Rotem, M.; Shvo, Y. *J. Organomet. Chem.* **1993**, *448*, 189.
(16) Neveux, M.; Seiller, B.; Hagedorn, F.; Bruneau, C.; Dixneuf, P. H. *J. Organomet. Chem.* **1993**, *451*, 133.
(17) Hoffman, D. M.; Hoffmann, R.; Fiesel, C. R. *J. Am. Chem. Soc.* **1982**, *104*, 3858.
(18) Matsuzaka, H.; Koizumi, H.; Takagi, Y.; Nishio, M.; Hidai, M. *J. Am. Chem. Soc.* **1993**, *115*, 10396.

Scheme 2

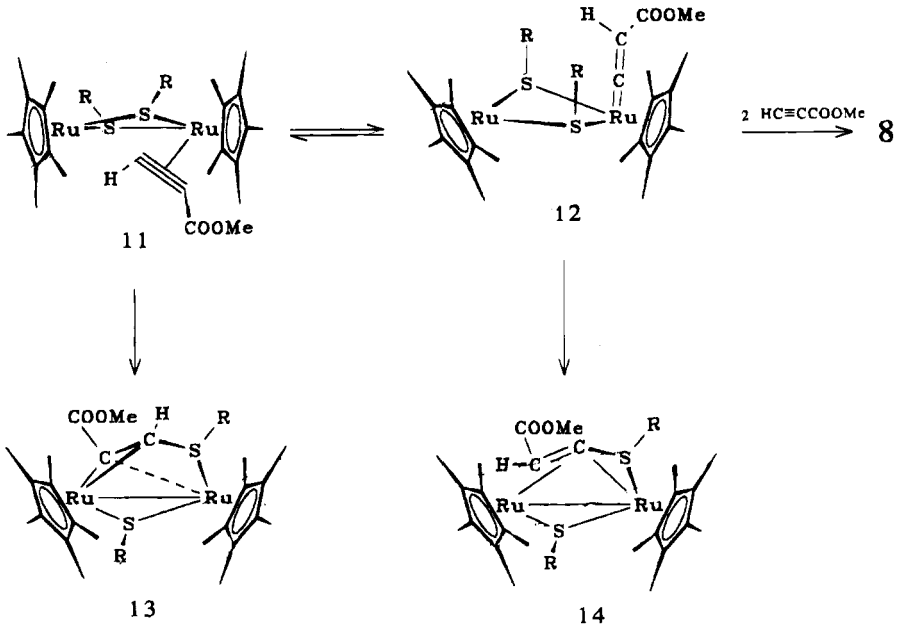

Scheme 3

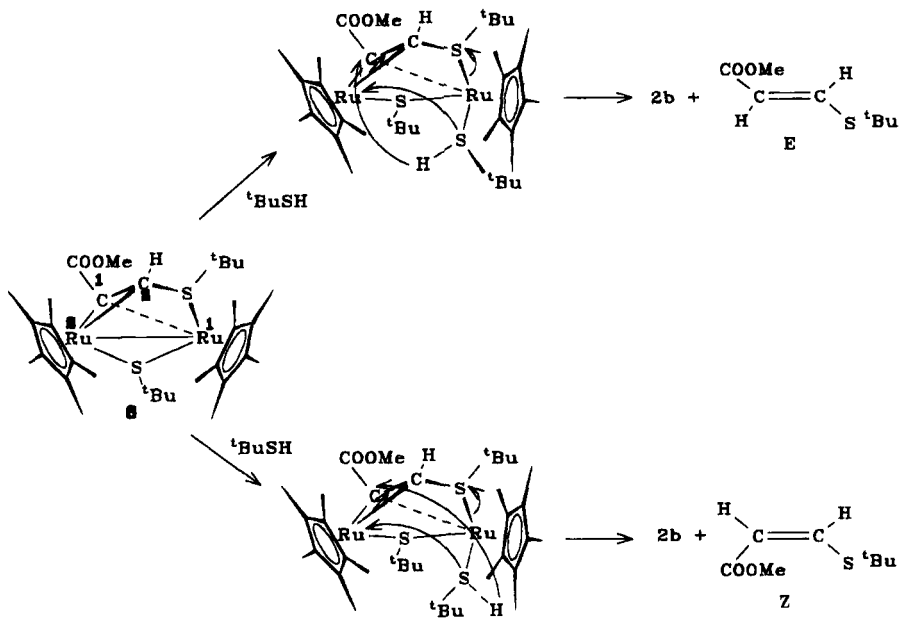

different insertion product **14**, not isolated, which can give vinyl thioether in the same way as explained for **7** below. Complex **12** with two more molecules of alkyne can convert to **8** (Scheme 1).

The isolated stop complex **9** can be thought of as being formed from **8** in a way completely analogous to the transformation **12** → **14** by insertion of the C_4H_2-$(COOMe)_2$ moiety into a Ru–S bond, as was indicated in Scheme 1. Note that in **9** the bridging C_4H_2-$(COOMe)_2$ unit has the same atom arrangement as the C_4 vinylidene chain in **8**. The reason **9** is no longer active as a catalyst is probably due to irreversible blocking of both Ru centers through coordination of one additional C=C bond of the double-alkyne unit.

Formation of vinyl thioethers from **7** (or **13** respectively) can be thought of as coordination of thiol followed by substitution of the terminal RS group with or without rupture of the Ru–Ru bond (Scheme 3). Transfer of hydrogen to the unsaturated carbon closes the cycle. Stereochemical alternatives leading to *Z* or *E* vinyl thioether, respectively, are given by addition of incoming thiol in two possible orientations and hydrogen transfer from either the front or the rear side as depicted for **7a** in Scheme 3. Alternatively, the same reaction sequence starting from **13** or **14**, respectively, could be responsible for the *Z*/*E* stereochemistry of the vinyl thioether.

As evidenced by the shifting *Z*/*E* ratio in the course of the catalysis (Figure 1) as well as the observation that the catalyst/substrate ratio has a large impact on the *Z*/*E* ratio (cf. first two entries in Table 1), catalysis must be driven by at least two different active species. Besides the insertion product **7** we assign to the vinylidene complex **8** the role of the second catalytically active species. Since complexes **7** are green whereas **8** is brown-orange, a slow color change of the reaction mixture from green to orange in the course of the catalysis is a visual indication of the formation of **7** and **8** in succession. Interestingly, this color change was

Scheme 4

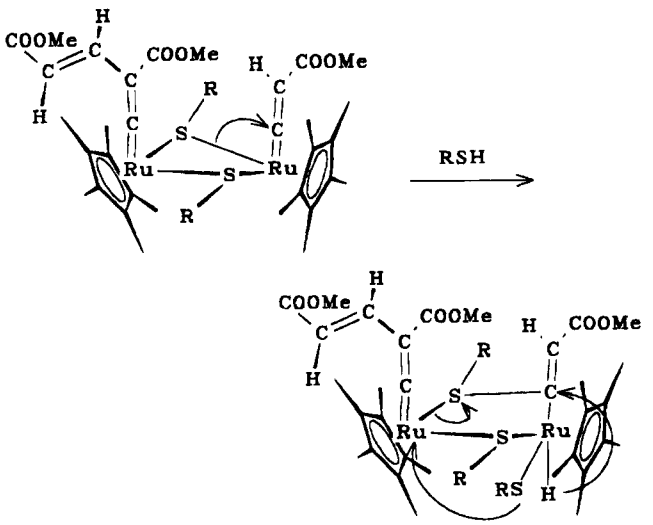

found to proceed slower if a $\hat{Cp}$ Ru ($\hat{Cp}$ = η^5-C_5Me_4Et) complex, **2**, was the catalyst precursor, which shows the sensitive response of the system to steric alterations. Note the high steric crowding around Ru in the structure of **8** where Cp* rings are located on one side and all other ligands are directed to the opposite direction.

A reaction sequence leading to vinyl thioethers analogous to the one detailed for **7**/**13** above can be envisaged by starting from **8** (Scheme 4). Since in **8** both metal centers are coordinatively saturated with no Ru–Ru bond, a Ru–S bond has to be opened in order to provide the additional coordination site for the attachment of entering thiol. Hydrogen transfer to the α-carbon of the C_2 vinylidene group and formation of the S–C_α bond gives the vinyl thioether. Note that the C_4 vinylidene gorup in **8** should remain bound to the metal throughout, since the *E* stereochemistry found for the CCH=CHCOOMe part is opposite to that of the product vinyl thioether generated with high preference from **8**.

In summary, there are a number of conceivable reaction paths leading from the starting complex **2** through characterized intermediates **7** and **8** to the products. Key steps of the catalytic cycle emerge: (i) addition of alkyne to coordinatively unsaturated Ru, (ii) insertion of coordinated alkyne into a Ru–S bond, and (iii) transfer of hydrogen from newly coordinated thiol to the unsaturated carbon and detachment of the vinyl thioether. Alkynyl → vinylidene rearrangement may precede insertion.

A second reaction branch appears in the linkage of alkyne units to form polyenyl chains attached in various ways to Cp*Ru or Cp*RuSR units, respectively, as in **8**–**10**. Such reactions have been widely observed with different alkynes and have yielded a plethora of complicated di- and multinuclear Cp*Ru complexes.[8,17,18] Whether this reaction mode ends up in a saturated, catalytically inactive stop complex or stops at a stage where the complex is still active in catalysis depends critically on thiol concentration in the reaction mixture. With sufficient thiol present, intermediate free coordination sites will be occupied by thiol rather than by internally coordinated double bonds, a condition for catalytic activity in this particular case.

It may be noted that the above cycle is one of the few cases of a truly bimetallic (although homometallic!) catalysis. In nucleophilic addition reactions to carbon–carbon multiple bonds a high-energy intermediate is inherently given by the vinyl (or alkyl) fragment generated after addition of the RE unit to one carbon atom. Whereas only one vacant coordination site at a metal is necessary to hold the alkyne, two are involved in stabilizing the vinylic intermediate, which is complexed as a three-electron ligand in **7**.

An intermediate corresponding to **7** is not possible in the case of **3**, where the starting complex has only one coordinatively unsaturated metal. However, migration of the Ru-bound C_6F_5 group to the bridging sulfur can occur in the course of the catalysis, yielding an intermediate analogous to **2**. NMR evidence for such a C_6F_5 migration has been found on treatment of **3** with CO.[9]

A final problem involves the catalytic action encountered with **2** and MeOH/HC≡CCOOMe. Although turnover is rather limited in this case, it should be contrasted with the reaction of **1** with the same substrates, where no vinyl ether formation could be detected. The observed turnover number of about 7 for the formation of vinyl ethers suggests that one RS bridge in the dimer is sufficient to drive the catalysis for a limited number of cycles and that it stops when all SR groups are eliminated from the starting complex **2** in the form of vinyl thioether. This in turn would mean that if the mechanism is analogous to the one outlined above, insertion of the alkyne into a Ru–O bond is feasible in some mixed Ru(μ-SR)(μ-OR′)Ru complex, but not in the neat oxo-bridged dimer **1**. This insertion to some extent has to compete successfully with insertion into the Ru–S bond in order to achieve the observed cycle number. Therefore, the insertion itself does not seem to be the most critical step in the oxo system. In contrast we have observed with quite different substrates, alkynes, amino alcohols, and amines among others, that these potential two-electron ligands, capable of coordinating to **1** in a loose manner but insufficient to form a stable addition product, induce CH activative degradation of a OMe group, leading finally to the stable, catalytically inactive hydride Cp*Ru(μ-H)$_2$(μ-CO)RuCp*.[19]

Experimental Section

All manipulations were performed under nitrogen with dry, nitrogen-saturated solvents. NMR spectra were run on Bruker SY 80 FT and Varian UNITY 300 and 500 spectrometers. GC was performed on a Siemens Sichromat 3 with an OV17 capillary column and GC/MS on a Hewlett-Packard 5995A instrument. Elemental analyses were performed by the microanalytical laboratory of our institute and by Analytische Laboratorien, Engelskirchen, Germany. Complexes **1**–**4** are all more or less air sensitive; the other compounds are less sensitive.

1. Formation of Vinyl Thioethers from Alkynes and Thiols Catalyzed by [Cp*Ru(μ-SR)]$_2$. (*Z*/*E*)-(MeOOC)(H)C=C(H)(S^{t}Bu). To a pentane solution containing 10 mg (0.037 mmol) (Cp*RuOMe)$_2$ was added successively 0.4 mL (3.1 mmol) of ^{t}BuSH, whence the solution turns blue, indicating the formation of [Cp*Ru(μ-S^{t}Bu)]$_2$. On addition of 0.28 mL (3.1 mmol) of HC≡CCOOMe the color slowly changes to orange-brown. After 3 h at ambient temperature the mixture was filtered over alumina to remove Ru complexes and the organic products were eluted with pentane/ether (9/1). After

(19) Koelle, U.; Kang, B.-S.; Thewalt, U. *Organometallics* **1992**, *11*, 2893.

the solvent was removed, 422 mg (78%) of 2/1 (*Z/E*)-^{t}BuSHC=CHCOOMe remained. ^{1}H NMR (acetone-d_6, *Z/E* isomers; δ): olefinic H, AB quartet δ_A 7.50/7.85, δ_B 5.83/5.88, J_{AB} = 10.5/15.5 Hz; *Me*OOC, 3.64/3.66; ^{t}Bu, 1.43. The isomer ratio from NMR integration was confirmed by GC (OV1, 180 °C), where *Z/E* was 68.3/31.7. MS on GC/MS was the same for both isomers (*m/z*; I_{rel}, %): 174 (10.6) M$^+$, 118 (46) M − C_4H_8, 87 (12.5) OCHC=CHSH, 59 (11.3) HC=CHSH/COOMe, 58 (13.6) HC=CSH, 57 (100) C_4H_9.

(*Z/E*)-(MeOOC)(H)C=C(COOMe)(S^{t}Bu). The same procedure was followed as described above using 0.037 mmol of Ru, 5.9 mmol of ^{t}BuSH, and 5.9 mmol of DMAD, yielding 1.22 g (89%) of 1/1 *Z/E* product by GC (t_r 51.8/48.2 min). ^{1}H NMR (acetone-d_6, *Z/E* isomers; δ): vinylic H 6.30/6.97; *Me*OOC, 3.82, 3.79/3.74, 3.68; ^{t}Bu, 1.32/1.42.

(*Z/E*)-(MeOOC)(H)C=C(COOMe)(S^{i}Pr) was prepared as described above with 0.037 mmol of Ru, 5.3 mmol of 2-propanethiol and 5.3 mmol of DMAD: yield 0.91 g (78.4%), *Z/E* 1/1 (GC). ^{1}H NMR (acetone-d_6 *Z/E* isomers; δ): vinylic H, 5.84/6.30; *Me*OOC, 3.85, 3.80/3.71, 3.66; ^{i}Pr, 1.23 (d)/1.34 (d), ^3J = 6.7 Hz.

(*Z/E*)-(MeOOC)(H)C=C(H)(SEt) was prepared as described above with 0.037 mmol of Ru, 4.1 mmol of ethanethiol, and 4.1 mmol of MP: yield 0.47 g (79.3%); *Z/E* 5/6 (GC). ^{1}H NMR (acetone-d_6, *Z/E* isomers; δ): AB quartet δ_A 6.58/7.69, δ_B 5.77/5.72, J_{AB} = 10.2/15.2 Hz; MeOOC, 3.42/3.45; C*H*$_2$CH$_3$, 2.16 (q), J = 7.5 Hz; CH$_2$C*H*$_3$, 0.89/0.83 (t).

(*Z/E*)-(MeOOC)(H)C=C(COOMe)(SEt) was prepared as described above with 0.037 mmol of Ru, 4.1 mmol of ethanethiol, and 4.1 mmol of DMAD: yield 0.83 g (82.8%); *Z/E* 1/1 (GC). ^{1}H NMR (acetone-d_6, *Z/E* isomers; δ): vinylic H, 5.76/6.26; *Me*OOC, 3.84, 3.80/3.70, 3.65; C*H*$_2$CH$_3$, 2.83/2.90 (q), J = 7.4 Hz; CH$_2$C*H*$_3$, 1.21/1.32 (t).

(*Z/E*)-(MeOOC)(H)C=C(H)(SC$_6$F$_5$) was prepared as described above with 0.037 mmol of Ru, 2.3 mmol of pentafluorothiophenol, and 2.3 mmol of MP: yield 0.5 g (78.2%); *Z/E* 7/1 (GC). ^{1}H NMR (acetone-d_6, *Z/E* isomers; δ): AB quartet δ_A 7.27/7.56, $^5J_{HF}$ = 0.8 Hz, δ_B 6.10/5.73, $^6J_{HF}$ = 0.7 Hz, J_{AB} = 10.2/15.1 Hz; *Me*OOC, 5.84/6.30, 3.76/3.65. ^{19}F NMR (acetone-d_6, *Z/E* isomers; δ): *o*-F, −130.0/−129.2 (d/d, ^3J_m = 16.0, ^5J_p = 2.8/^3J_m = 15.8, ^5J_p = 3.9 Hz); *p*-F, −149.4/−147.3 (t/t, ^3J_m = 20.4, ^5J_o = 2.8/^3J_m = 20.3, ^5J_o = 3.9 Hz); *m*-F, −156.6/−157.5 (d/d, ^3J_o = 15.9, ^3J_p = 20.4/$^3J_0$ = 15.7, ^3J_p = 20.4 Hz). IR (KBr, ν/cm^{-1}): 3042, 3006 (m, C=C*H*); 1689 (vs, C=O ester); 1640 (s, α,β-conjug C=C); 1242 (vs, C−O−C ester); 1173, 1093 (vs, C−F arom); 984 (vs, δ_{trans}-HC=CH); 692, 682 (m, δ_{cis}-HC=CH). Anal. Calcd for $C_{10}F_5H_5O_2S$ (M_r 284): C, 42.26; H, 1.77. Found: C, 42.11; H, 1.86.

(*Z/E*)-(MeOOC)(H)C=C(COOMe)(SC$_6$F$_5$) was prepared as described above with 0.037 mmol of Ru, 2.3 mmol of pentafluorothiophenol, and 2.3 mmol of DMAD: yield 0.715 g (93%); *Z/E* 6/1 (GC). ^{1}H NMR (acetone−d_6, *Z/E* isomers; δ): vinylic H, 6.69/6.03; *Me*OOC, 3.81, 3.62/3.72, 3.67. IR (KBr, ν/cm^{-1}): 1734 (vs, C=O ester); 1642 (vs, α,β-conjug C=C); 1262 (vs, C−O−C ester); 1191, 1094, (vs, C−F arom). Anal. Calcd for $C_{12}F_5H_7O_4S$ (M_r 342.2): C, 42.11; H, 2.06. Found: C, 41.57; H, 1.57.

(*Z/E*)-(MeOOC)(H)C=C(H)(SCH$_2$Ph) was prepared as described above with 0.037 mmol of Ru, 4.2 mmol of PhCH$_2$-SH, and 4.2 mmol of MP: yield 0.8 g (95%); *Z/E* 2/1 (GC). ^{1}H NMR (acetone-d_6; *Z/E* isomers; δ): CH$_2$*Ph*, 7.35/7.39; C*H*$_2$Ph, 4.05/4.16; vinylic H AB quartet, δ_A 7.33/7.74, δ_B 5.85/5.86, J_{AB} = 10.2/15.3 Hz; *Me*OOC, 3.64. ^{13}C NMR (CDCl$_3$, *Z/E* isomers; δ): MeOO*C*, 165.94/164.62; C=*C*SCH$_2$Ph, 147.81/145.28; ipso-C, 136.11/134.44; *m*-C, 127.99/127.84; *p*-C, 127.80/127.76; *o*-C, 126.51/126.75; C=*C*COOMe, 112.16/113.01; COO*Me*, 50.27/50.46; *C*H$_2$Ph, 38.38/35.57. Anal. Calcd for $C_{11}H_{12}O_2S$ (M_r 208): C, 63.44; H, 5.81. Found: C, 63.37; H, 5.86.

(*Z/E*)-(MeOOC)(H)C=C(H)(SPh) was prepared as described above with 0.037 mmol of Ru, 2.9 mmol of PhSH, and 2.9 mmol of MP: yield 0.5 g (87.5%); *Z/E* 3.71 (GC). ^{1}H NMR (acetone-d_6, *Z/E* isomers; δ): Ph and H$_A$ of the *Z* isomer, 7.60−7.26; AB quartet, δ_A 7.79, δ_B 5.95/5.63, J_{AB} = 10.1/15.1 Hz; *Me*OOC, 3.71/3.63.

2. Complexes Isolated. Cp*Ru{η^1-HC≡C(COOMe)}(μ-SC$_6$F$_5$)(μ-S)Ru(C$_6$F$_5$)Cp* (5a). To a pentane solution (20 mL) containing 0.14 g (0.16 mmol) of Cp*Ru(μ-SC$_6$F$_5$)(μ-S)Ru(C$_6$F$_5$)-Cp* (**3**) was added 0.015 mL (0.16 mmol) of MP. After 2 h without any noticeable color change the solution was concentrated to about 10 mL under reduced pressure. After the temperature was lowered for 24 h to −35 °C, 150 mg (97%) of **5a** crystallized as dark green cubes. ^{1}H NMR (C$_6$D$_6$; δ): *H*C≡C(COOMe), 9.00 (s, 1H); HC≡C(COO*Me*), 3.41 (s, 3H); Cp*, 1.40, 1.22 (s, 15H each). ^{19}F NMR (C$_6$D$_6$; δ): *o*-F, −100.04 (d/t, $^3J_{o,m}$ = 27.7, $^4J_{o,o}$ = 8.8 Hz), −114.48 (d/t, $^3J_{o,m}$ = 30.2, $^{4/5}J_{o,o/m}$ = 7.8 Hz), −129.64 (d/d $^3J_{o,m}$ = 27.7, $^4J_{o,o}$ = 8.8 Hz), −133.68 (d/d, $^3J_{o,m}$ = 26.0, $^4J_{o,o}$ = 7.1 Hz); *p*-F, −155.62 (t, $^3J_{p,m}$ = 21.2 Hz), −163.24 (t, $^3J_{p,m}$ = 20.3 Hz); *m*-F, −163.08 to −166.54 (m, 4F). Anal. Calcd for $C_{36}H_{34}F_{10}O_2Ru_2S_2$ (M_r 954.9): C, 45.28; H, 3.59; F, 19.90. Found: C, 45.11; H, 3.65; F, 20.08.

Cp^Ru{η^1-HC≡C(COOMe)}(μ-SC$_6$F$_5$)(μ-S)Ru(C$_6$F$_5$)-Cp^ (5b). The same procedure as for **5a** was followed. The yield was nearly quantitative. ^{1}H NMR C$_6$D$_6$; δ): *H*C≡C-(COOMe), 8.96 (s, 1H); HC≡C(COO*Me*), 3.44 (s, 3H); Cp^ 1.53, 1.46, 1.44, 1.36, 1.33, 1.30, 1.27, 1.25 (s, 3H each). ^{19}F NMR (C$_6$D$_6$, δ): *o*-F, −98.98(d/t, $^3J_{o,m}$ = 33.4 Hz), −113.91 (d/t, $^3J_{o,m}$ = 30.3, $^{4/5}J_{o,o/m}$ = 7.6 Hz), −129.13 (d/d, $^3J_{o,m}$ = 28.0, $^4J_{o,o}$ = 8.6 Hz), −133.51 (d/d, $^3J_{o,m}$ = 25.8, $^4J_{o,o}$ = 7.1 Hz); *p*-F, −155.27 (t, $^3J_{p,m}$ = 21.3 Hz), −162.87 (t, $^3J_{p,m}$ = 20.1 Hz); *m*-F, −163.24 to −166.28 (m, 4F). Anal. Calcd for $C_{38}H_{38}F_{10}O_2Ru_2S_2$ (M_r 983.9): C, 46.43; H, 3.90. Found: C, 46.07; H, 3.73.

Cp*Ru(μ-S^{t}Bu){μ:η^2:η^1:η^1-C(COOMe)=CHS^{t}Bu}-RuCp* (7a). To a pentane solution (20 mL) containing 0.12 g (0.2 mmol) of [Cp*Ru(μ-S^{t}Bu)]$_2$ was added at room temperature 0.02 mL (0.22 mmol) of MP. Over a period of 50 min the color changed from blue through dark green (after 30 min) to brown. After the solution was concentrated under reduced pressure to 10 mL, it was chromatographed over alumina (5% H$_2$O). The first dark green zone was eluted with pentane. The dark green solution was concentrated to about 10 mL and cooled to −35 °C, whence after 1 day 103 mg (75.2%) had crystallized as dark green cubes. ^{1}H NMR (C$_6$D$_6$, δ): C*H*S^{t}Bu, 4.55 (s, 1H); COO*Me*, 3.65 (s, 3H); Cp*, 1.81, 1.70 (s, 15H each); =CHS^t*Bu*, 1.17 (s, 9H); μ-S^t*Bu*, 1.73 (s, 9H). IR (KBr, ν/cm^{-1}): 1678, 1153 (vs, ν(C=O ester)). Anal. Calcd for $C_{32}H_{52}O_2$-Ru_2S_2 (M_r 735.0): C, 52.32; H, 7.08. Found: C, 52.16; H, 7.05.

A second brown compound was eluted with pentane/ether (2/1). After the solvent was removed, 33 mg (20% based on Ru) of **Cp*Ru(μ-S^{t}Bu){η^2:η^2-(S^{t}Bu)C=C(COOMe)-CH=CHCOOMe}RuCp* (9)** remained as brown microcrystals. Spectroscopic data are given below. The ratio **7/9** depends on the amount of MP used.

Cp*Ru(μ-S^{t}Bu){μ:η^2:η^1:η^1-C(Ph)=CHS^{t}Bu}RuCp* (7b). The same procedure was followed as described for **7a** using 150 mg (0.23 mmol) of **2c** and 25 μL (0.23 mmol) of PhC≡CH in 20 mL of pentane. The color change took 90 min; the reaction time was 17 h. The yield after chromatography was 140 mg (80%). ^{1}H NMR (C$_6$D$_6$; δ): C*H*S^{t}Bu, 4.48 (s, 1H); Ph, ~7.3 (m, 5H); Cp*, 1.59 (s, 30H); =CHS^t*Bu*, 1.11 (s, 9H); μ-S^t*Bu*, 1.77 (s, 9H).

Cp*Ru{η^1-=C=CH(COOMe)}(μ-S^{t}Bu)$_2$Ru{η^1-=C=C-(COOMe)CH=C(H)COOMe}Cp* (8a). To 20 mL of pentane containing 0.1 g (0.19 mmol) of **1** was added 0.5 mL (4.44 mmol) of HS^{t}Bu when the color changed rapidly from red to blue. Addition of 0.38 mL (4.27 mmol) of MP caused the solution to slowly turn orange-brown. After 15 h a small amount of solid was filtered off and the filtrate purified by chromatography over alumina (5% H$_2$O). With pentane (*Z/E*)-(MeOOC)CH=CH(S^{t}Bu) was eluted, and subsequently with ether/pentane (9/1) an orange band of the product was obtained. Removing the solvent left 110 mg (67%) of orange microcrystals. Crystals for X-ray determination were obtained by slow evaporation of a xylene solution. ^{1}H NMR (acetone-

d_6; δ): =C=C*H*, 4.48 (s, 1H); −C*H*=C*H*(COOMe), 7.92, 6.46 (AB quartet, ^3J = 15.2 Hz); COO*Me*, 3.67, 3.63, 3.56 (s, 3H each); Cp*, 1.66, 1.64 (s, 15H each); ^{t}Bu, 1.29 (s, 18H). ^{13}C NMR (C_6D_6; δ): =*C*=, 333.49, 332.13; *C*OOMe, 168.46, 166.50, 165.94; R*C*=, 138.93, 122.62, 111.27, 109.62; *C*$_5$(CH$_3$)$_5$, 102.29, 100.99; COO*C*H$_3$, 50.66, 50.51; *C*(CH$_3$)$_3$, 50.20; C(*C*H$_3$)$_3$, 32.07; C$_5$(*C*H$_3$)$_5$, 10.00, 9.98. IR (KBr ν/cm^{-1}): 1688 (vs, C=O ester); 1592 (m, C=C); 1158 (C−O−C ester).

The compound is also isolable in the catalytic reaction of **2c** with HS^{t}Bu and MP. The yield depends on the excess of HS^{t}Bu.

Cp^Ru{η^1-=C=CH(COOMe)}(μ-S^{t}Bu)$_2$Ru{η^1-=C=C-(COOMe)CH=C(H)COOMe}Cp^ (8b). The same procedure was followed as described for **8a**. ^{1}H NMR (C_6D_6; δ): =C=C*H*, 4.95 (s, 1H); −C*H*=C*H*(COOMe), 8.44, 7.36 (AB quartet, ^3J = 15.4 Hz); COO*Me*, 3.59, 3.53, 3.51 (s, 3H each); C*H*$_2$CH$_3$ (Cp^), 1.96, 1.86 (q, 2H each, ^3J = 7.5 Hz); CH$_2$C*H*$_3$(Cp^), 0.87, 0.80 (t, 3H each); C*H*$_3$(Cp^), 1.53, 1.46, 1.45, 1.40; ^{t}Bu, 0.87. ^{13}C NMR (C_6D_6; δ): *C*OOMe, 167.13, 165.17, 164.60; R*C*=, 137.57, 126.94, 126.55, 121.66, 109.97, 108.62; CH$_3$CH$_2$*C*(Cp^), 102.85, 101.97; CH$_3$*C*(Cp^), 102.77, 101.12, 100.4, 99.3; *C*H$_3$(Cp^), 8.78, 8.77, 8.43, 8.39; CH$_3$*C*H$_2$(Cp^), 17.52, 17.50; *C*H$_3$CH$_2$(Cp^), 12.58, 12.39; *C*(CH$_3$)$_3$, 48.29; C(*C*H$_3$)$_3$, 30.78.

Cp*Ru(μ-S^{t}Bu){μ-η^2:η^2-(S^{t}Bu)C=C(COOMe)CH=CH-(COOMe)}RuCp* (9). To 20 mL of a pentane solution containing 0.15 g (0.23 mmol) of **2c** was added 0.09 mL (1.02 mmol) of MP. Within 30 min at ambient temperature the color had changed from blue to reddish brown. After 15 h the solution was chromatographed over alumina (5% H_2O). A brown-red band was eluted with pentane/ether (8/2). After the solution was concentrated to about 10 mL, it was cooled to −35 °C. The complex separated within 1 day as dark brown flakes. The yield was 155 mg (82%). ^{1}H NMR (C_6D_6; δ): C*H*=C*H*(COOMe), 4.66, 4.55 (s, 1H each); COO*Me*, 3.46, 3.41 (s, 3H each); Cp*, 1.76, 1.72 (s, 15H each); 2, ^{t}Bu, 1.41 (6s, 18H). Anal. Calcd for $C_{36}H_{56}O_4Ru_2S_2$ (M_r 819.1): C, 52.79; H, 6.89; S, 7.83. Found: C, 52.66; H, 7.02; S, 8.00.

(Cp^Ru)$_2${(2,3,4,5-η):(1,1′,6,*S*-η)-C$_6$H-1-S^{t}Bu-2,3,5-(COOMe)$_3$-6-(C=C(COOMe)CH=CHCOOMe)} (10). The complex crystallized in about 10% yield from the first fraction of the chromatography in the course of the isolation of **8a** (see above). From the pentane solution containing mainly vinylthioethers brown orange crystals of **10** separated on standing for 3 weeks at ambient temperature. ^{1}H NMR (C_6D_6; δ): C*H*=C*H*COO*Me*, 8.71, 7.50 (AB quartet, $^3J_{AB}$ = 15.9 Hz), −C*H*=(arene), 6.38 (s, 1H); COO*Me*, 3.60, 3.58, 3.55, 3.47, 3.30 (s, 3H each); Cp*, 2.13, 1.54 (s, 15H each); ^{t}Bu, 0.79.

X-ray structure determinations were carried out on an Enraf-Nonius diffractometer, using graphite-monochromated Mo K$_\alpha$ radiation. Empirical absorption corrections were applied before averaging symmetry-equivalent reflections. Crystal data, data collection parameters, and refinement results are compiled in Table 2. The convergence results and the ratio between measured and observed reflections show that only the structure determination of **7** corresponds to good standards. In this structure all hydrogen atoms were located from difference Fourier syntheses. Therefore, an ORTEP representation of anisotropic thermal parameters is given only for this molecule. The remaining structures were mostly considered to contain connectivity information. In these cases hydrogen atoms in calculated positions (C−H = 0.98 Å) were included in structure factor calculations. Characteristic bond distances and angles are collected in Tables 3−6.

Acknowledgment. This work was supported by the Deutsche Forschungsgemeinschaft and by the Fonds der Chemischen Industrie, Frankfurt/M., Germany. A loan of RuCl$_3$ from Johnson-Matthey, Reading, U.K., is gratefully acknowledged.

Supplementary Material Available: Tables of crystal data, crystallographic procedures, atomic positional and thermal displacement parameters, and bond lengths for **7a**, **8**, **9**, and **10** (43 pages). Ordering information is given on any current masthead page.

OM940521T

(20) North, A. C. T.; Phillips, D. C.; Mathews, F. S. *Acta Crystallogr.* **1968**, *A24*, 351.
(21) Walker, N.; Stuart, D. *Acta Crystallogr.* **1983**, *A39*, 159.

Polymeric Organosilicon Systems. 21. Synthesis and Photochemical, Conducting, and Thermal Properties of (2,6- and 2,5-Diethynylenepyridylene)disilanylene Polymers

Atsutaka Kunai, Eiji Toyoda, Katsuhiro Horata, and Mitsuo Ishikawa*

Department of Applied Chemistry, Faculty of Engineering, Hiroshima University, Kagamiyama, Higashi-Hiroshima 724, Japan

Received June 3, 1994[⊗]

The reactions of 1,2-diethyl-1,2-dimethyl-, 1,1,2,2-tetraethyl-, 1,2-dibutyl-1,2-dimethyl-, and 1,2-dihexyl-1,2-dimethyl-1,2-diethynyldisilane (**1a–d**) with 2,6-dibromopyridine were carried out in the presence of a $Pd(PPh_3)_4$–CuI catalyst in refluxing triethylamine to give poly[(2,6-diethynylenepyridylene)disilanylenes] (**2a–d**) with molecular weights of 15 000–28 000. Similar treatments of **1a–d** with 2,5-dibromopyridine under the same conditions afforded poly[(2,5-diethynylenepyridylene)disilanylenes] (**3a–d**) with molecular weights of 19 000–39 000. Irradiation of **2a–d** and **3a–d** with a low-pressure mercury lamp resulted in cleavage of the silicon–silicon bonds. When **3a–d** were doped with iodine or ferric chloride vapor, polymers with conductivities of 10^{-4}–10^{-7} S·cm^{-1} level were obtained. Thermal properties of these polymers were also examined.

Introduction

There has been a considerable interest in the chemistry of silicon-containing polymers that can be used as functional materials. To date, many types of silicon-containing polymers have been synthesized by alkali metal condensation of dichlorosilyl derivatives[1] or bis(chlorosilyl)-substituted compounds.[2] The polymers obtained by this method always involve some siloxy units in the polymer backbone, which interrupt electron delocalization.

Recently, we have found two types of synthetic methods that involve no alkali metal condensation. One involves the thermal and catalytic ring-opening polymerization of 1,2,5,6-tetrasilacycloocta-3,7-diynes[3] and the other comprises the rhodium(I)-catalyzed reaction of 1,2-diethynyldisilanes.[4] The polymers obtained by these methods show no siloxy unit in the polymer backbone.

As a part of our investigation concerning the synthesis of the polymers that have a regular alternating arrangement of a disilanylene unit and π-electron system in the polymer backbone, we carried out the preparation of the polymers containing a diethynylenepyridylene unit as the π-electron system and examined their photolytic, conducting, and thermal properties. To our knowledge, this type of polymer is the first example for the alternating polymers involving a diethynylenepyridylene unit and silicon–silicon bond in the polymer backbone.[5]

Results and Discussion

In 1975, Sonogashira et al.[6] reported that the reaction of monosubstituted acetylenes with aromatic and heteroaromatic halides in the presence of a catalytic amount of a palladium complex and copper(I) iodide in diethylamine or triethylamine affords ethynyl-substituted aromatic compounds. Recently, Corriu and coworkers[7] have reported the preparation of (diethynylenearylene)silylene polymers by this method.

We are interested in the synthesis and application to the functionality materials of alternating polymers that involve the nitrogen-containing heteroaromatic ring in the polymer backbone and investigated the coupling reaction of 1,2-diethynyldisilanes and 2,5- and 2,6-dibromopyridine in the presence of a catalytic amount of tetrakis(triphenylphosphine)palladium(0) and copper(I) iodide. 1,2-Diethynyldisilanes used as starting compounds were prepared by the method reported previously.[3c]

When a mixture of 1 equiv of 1,2-diethyl-1,2-diethynyldimethyldisilane (**1a**) and 2,6-dibromopyridine in the

⊗ Abstract published in *Advance ACS Abstracts*, December 1, 1994.

(1) (a) West, R.; Maxka, J. *Inorganic and Organometallic Polymers*; ACS Symposium Series 360; American Chemical Society: Washington, DC, 1988; Chapter 2. (b) Matyjaszewsky, K.; Chen, L.; Kim, H. *Inorganic and Organometallic Polymers*; ACS Symposium Series 360; American Chemical Society: Washington, DC, 1988; Chapter 6.

(2) (a) Ishikawa, M.; Ni, H.; Matsuzaki, K.; Nate, K.; Inoue, T.; Yokono, H. *J. Polymer Sci., Polymer Lett. Ed.* **1984**, *22*, 669. (b) Nate, K.; Ishikawa, M.; Ni, H.; Watanabe, H.; Saheki, Y. *Organometallics* **1987**, *6*, 1673. (c) Ishikawa, M.; Nate, K. *Inorganic and Organometallic Polymers*; ACS Symposium Series 360; American Chemical Society: Washington, DC, 1988; p 209. (d) Ohshita, J.; Kanaya, D.; Ishikawa, M.; Yamanaka, T. *J. Organomet. Chem.* **1989**, *369*, C18. (e) Hong, H. H.; Weber, W. P. *Polymer Bull.* **1989**, *22*, 363. (f) Hu, S.; Weber, W. P. *Polymer Bull.* **1989**, *21*, 133. (g) Ohshita, J.; Kanaya, D.; Ishikawa, M.; Koike, T.; Yamanaka, T. *Macromolecules* **1991**, *24*, 2106.

(3) (a) Ishikawa, M.; Hasegawa, Y.; Hatano, T.; Kunai, A.; Yamanaka, T. *Organometallics* **1989**, *8*, 2741. (b) Ishikawa, M.; Hatano, T.; Horio, T.; Kunai, A. *J. Organomet. Chem.* **1991**, *412*, C31. (c) Ishikawa, M.; Hatano, T.; Hasegawa, Y.; Horio, T.; Kunai, A.; Miyai, A.; Ishida, T.; Tsukihara, T.; Yamanaka, T.; Koike, T.; Shioya, J. *Organometallics* **1992**, *11*, 1604.

(4) (a) Ohshita, J.; Furumori, K.; Ishikawa, M.; Yamanaka, T. *Organometallics* **1989**, *8*, 2084. (b) Ohshita, J.; Matsuguchi, A.; Furumori, K.; Hong, R.-F.; Ishikawa, M.; Yamanaka, T.; Koike, T.; Shioya, J. *Macromolecules* **1992**, *25*, 2134.

(5) Alternating polymers involving a diethynylenepyridylene group and silylene unit have been reported by Corriu et al.; see ref 7a–d.

(6) Sonogashira, K.; Tohda, Y.; Hagihara, N. *Tetrahedron Lett.* **1975**, 4467.

(7) (a) Corriu, R. J.-P.; Douglas, W. E.; Yang, Z.-X. *J. Polymer Sci. C, Polymer Lett.* **1990**, *28*, 431. (b) Corriu, R. J.-P.; Douglas, W. E.; Yang, Z.-X. *Eur. Polym. J.* **1993**, *29*, 1563. (c) Corriu, R. J.-P.; Douglas, W. E.; Yang, Z.-X. Karakus, Y.; Cross, G. H.; Bloor, D. *J. Organomet. Chem.* **1993**, *455*, 69. (d) Corriu, R. J.-P.; Douglas, W. E.; Yang, Z.-X. *J. Organomet. Chem.* **1993**, *456*, 35.

0276-7333/95/2314-0714$09.00/0

Scheme 1

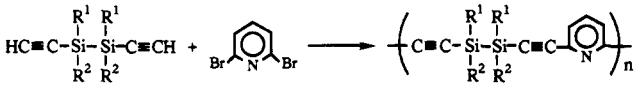

1a, R^1=Me, R^2=Et
1b, R^1=Et, R^2=Et
1c, R^1=Me, R^2=Bu
1d, R^1=Me, R^2=Hexyl

2a, R^1=Me, R^2=Et 39%
2b, R^1=Et, R^2=Et 70%
2c, R^1=Me, R^2=Bu 61%
2d, R^1=Me, R^2=Hexyl 81%

Scheme 2

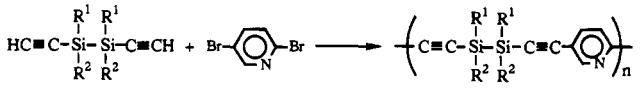

1a, R^1=Me, R^2=Et
1b, R^1=Et, R^2=Et
1c, R^1=Me, R^2=Bu
1d, R^1=Me, R^2=Hexyl

3a, R^1=Me, R^2=Et 53%
3b, R^1=Et, R^2=Et 90%
3c, R^1=Me, R^2=Bu 90%
3d, R^1=Me, R^2=Hexyl 83%

presence of a $Pd(PPh_3)_4$–CuI catalyst was heated to reflux in triethylamine, poly[(2,6-diethynylenepyridylene)-(1,2-diethyl-1,2-dimethyldisilanylene)] (**2a**) with a molecular weight of 15 000 was obtained after twice reprecipitation from methanol (Scheme 1). Similar reactions of 1,1,2,2-tetraethyl-, 1,2-dibutyl-1,2-dimethyl-, and 1,2-dihexyl-1,2-dimethyl-1,2-diethynyldisilane (**1b–d**) with 2,6-dibromopyridine under the same conditions afforded corresponding poly[(2,6-diethynylenepyridylene)disilanylenes] (**2b–d**) with molecular weights of 19 000–28 000 in high yields. Polymers **2a–d** are dark brown greaselike liquids and are soluble in common organic solvents such as aromatic solvents, ethers, and halocarbons.

2,5-Dibromopyridine also reacted with 1,2-diethynyldisilanes in the presence of the palladium catalyst to give poly[(2,5-diethynylenepyridylene)disilanylenes] (**3a–d**). Thus, the reaction of 1,2-diethynyldisilanes **1a–d** with 1 equiv of 2,5-dibromopyridine in the presence of a catalytic amount of $Pd(PPh_3)_4$–CuI in a refluxing triethylamine solution produced polymers **3a–d** with molecular weights of 19 000–39 000 in high yields (Scheme 2). Like polymers **2a–d**, polymers **3a–d** are dark brown greaselike liquids and are soluble in common organic solvents. Some of the properties of polymers **2a–d** and **3a–d** are shown in Table 1.

On the other hand, the similar reactions of 1,1,2,2-tetramethyl- and 1,2-dimethyl-1,2-diphenyl-1,2-diethynyldisilane with 2,5- and 2,6-dibromopyridine mainly afforded insoluble polymers, together with small amounts of oligomers (M_w = ca. 2500) which are soluble in methanol.

The structures of **2a–d** and **3a–d** were verified by spectroscopic analysis. IR spectra of these polymers show strong absorption bands at 2152–2156 cm^{-1}, due to stretching frequencies of a carbon–carbon triple bond. For **2b**, the ^{13}C NMR spectrum shows two resonances at δ 92.3 and 106.9 ppm, assigned to ethynyl carbons, and resonances at δ 4.6 and 8.3 ppm, attributed to methylene and methyl carbons in a diethylsilyl group, together with resonances due to pyridyl carbons (δ 127.0, 136.1, and 143.3), while the ^{29}Si NMR spectrum reveals a single resonance at δ −28.2 ppm, as expected for the symmetric and regular alternating structure of the polymer. In contrast to **2b**, polymers **2a,c,d** exhibit two signals due to a methylsilyl carbon in the ^{13}C NMR spectra and two signals due to the methylsilyl protons in the ^1H NMR spectra, arising from meso and *dl* isomers for a disilanylene unit in the polymer chain (see below). As a typical example, the ^1H and ^{13}C NMR spectra of **2a** are shown in Figures 1 and 2.

In contrast to the 2,6-pyridylene isomer **2b**, the ^{13}C NMR spectrum of a 2,5- isomer **3b** shows two resonances at δ 4.62 and 4.66 ppm, due to methylene carbons in a diethylsilyl group, and multiple resonances around δ 93.9 (three peaks), 97.0 (three peaks), 104.8, and 107.0 ppm, assigned to ethynyl carbons. The ^{29}Si NMR spectrum of **3b** also reveals two resonances at δ −28.49 and −28.38 ppm. These multiple signals may be caused by micro structures of 2,5-pyridylenedisilanylene units in the polymer backbone, as discussed below. For polymers **3a,c,d** which bear two chiral centers in a disilanylene unit, ^{13}C NMR spectra show three resonances due to a methylsilyl carbon, while ^{29}Si NMR spectra reveal multiple resonances in a region of δ −34.5 to −32.1 ppm.

In order to learn more about the chemical shifts of meso and *dl* isomers for disilanylene compounds, we examined NMR spectra of 1,2-bis(2-pyridylethynyl)- and 1,2-bis(3-pyridylethynyl)-1,2-dihexyl-1,2-dimethyldisilane (**4** and **5**) as model compounds. These compounds were synthesized by the reaction of **1d** with 2-bromo- or 3-bromopyridine under similar conditions as described for the synthesis of the polymers (Scheme 3).

As expected, 2-pyridyl compound **4** reveals two resonances due to a methylsilyl group in ^{13}C (δ −4.62 and −4.53), ^1H (δ 0.35 and 0.36), and ^{29}Si (δ −34.11 and −34.05) NMR spectra (see Table 1). For 3-pyridyl isomer **5**, two signals due to the methylsilyl group are also observed in the ^{13}C (δ −4.53 and −4.45) and ^1H (δ 0.34 and 0.35) NMR spectra, whereas, in its ^{29}Si NMR spectrum, a single resonance was observed at δ 34.39 ppm. On the other hand, signals due to ethynyl carbons in ^{13}C NMR spectrum appear as a singlet at δ 92.5 (SiC≡) and 106.7 (PyC≡) ppm for **4** and at δ 95.9 (SiC≡) and 104.4 (PyC≡) ppm for **5**, respectively.

These results clearly indicate that the double signals due to the methylsilyl group in the ^1H, ^{13}C, and ^{29}Si NMR spectra of 2,6-pyridylene isomer **2d**, as well as **2a** and **2c**, arise from *dl* and meso isomers. In the case of the 2,5-pyridylene isomers, the existence of three kinds of micro structures A–C (Chart 1) in the polymer backbone would be possible. If the resonances due to ethynyl carbons in polymer **3d** are compared with those in the model compounds, the resonances attributed to silyl-substituted ethynyl carbons appear as a multiplet in a slightly lower field (ca. 2 ppm) than that in **4** and **5**, while two signals due to pyridylene-substituted carbons show the same chemical shift as that in **4** and **5**, respectively. These results indicate that accumulation of the isomeric micro structures in the polymer affects the chemical shifts of silyl-substituted ethynyl carbons and, therefore, results in the multiple signals for those carbons. Polymers **3a–c** also reveal multiplet resonances for these carbons in their ^{13}C NMR spectra by the same reason. The multiple lines due to a methylsilyl group in the ^1H and ^{29}Si NMR spectra for the 2,5-pyridylene polymers can be explained by the existence of *dl* and meso isomers and the effect of the micro structures.

The polymers obtained by reprecipitation from benzene–methanol are still deeply colored, even after treatment with chromatography on alumina or silica or

Table 1. Properties of Polymers 2a–d and 3a–d and Model Compounds 4 and 5

			NMR chem shift, δ (no. of peaks)							
			^{13}C					^{1}H	^{29}Si	
compd	M_w (M_w/M_n)	UV: λ_{max}, nm (ε/C≡CSiSiC≡CPy)	SiC≡[a]	SiC≡[b]	PyC≡[a]	PyC≡[b]	SiMe	SiMe		
2a	15 000 (2.5)	304.4 (11 100)	92.8		106.3		−5.1 (2)	0.38 (2)	−32.1 (2)	
2b	19 000 (1.9)	304.2 (11 900)	92.3		106.9		4.6[c]		−28.2	
2c	28 000 (2.3)	312.2 (28 100)	93.3		106.4		−4.6 (2)	0.36 (2)	−33.8	
2d	20 000 (2.4)	306.2 (23 800)	93.1		106.3		−4.7 (2)	0.33 (2)	−33.8	
3a	19 000 (2.8)	311.6 (45 800)	94.5 (3)	97.5 (3)	106.5	104.3	−5.1 (3)	0.42 (2)	−32.4 (2)	−32.1 (3)
3b	19 000 (2.6)	318.0 (32 900)	93.9 (3)	97.0 (3)	107.0	104.8	4.6 (2)[c]		−28.5	−28.4
3c	24 000 (2.4)	314.0 (34 800)	94.8 (4)	97.9 (3)	106.4	104.3	−4.6 (3)	0.36 (2)	−34.2 (2)	−33.8 (3)
3d	39 000 (2.6)	313.4 (38 200)	94.9 (3)	97.9 (3)	106.5	104.3	−4.6 (3)	0.35	−34.2 (3)	−33.9 (3)
4	460.3	282.2 (22 400)	92.5		106.7		−4.6 (2)	0.36 (2)	−34.1 (2)	
5	460.3	280.0 (14 300)		95.9		104.4	−4.5 (2)	0.34 (2)	−34.4	

[a] In 2-PyC≡CSi. [b] In 3-PyC≡CSi. [c] Resonance due to $SiCH_2^-$.

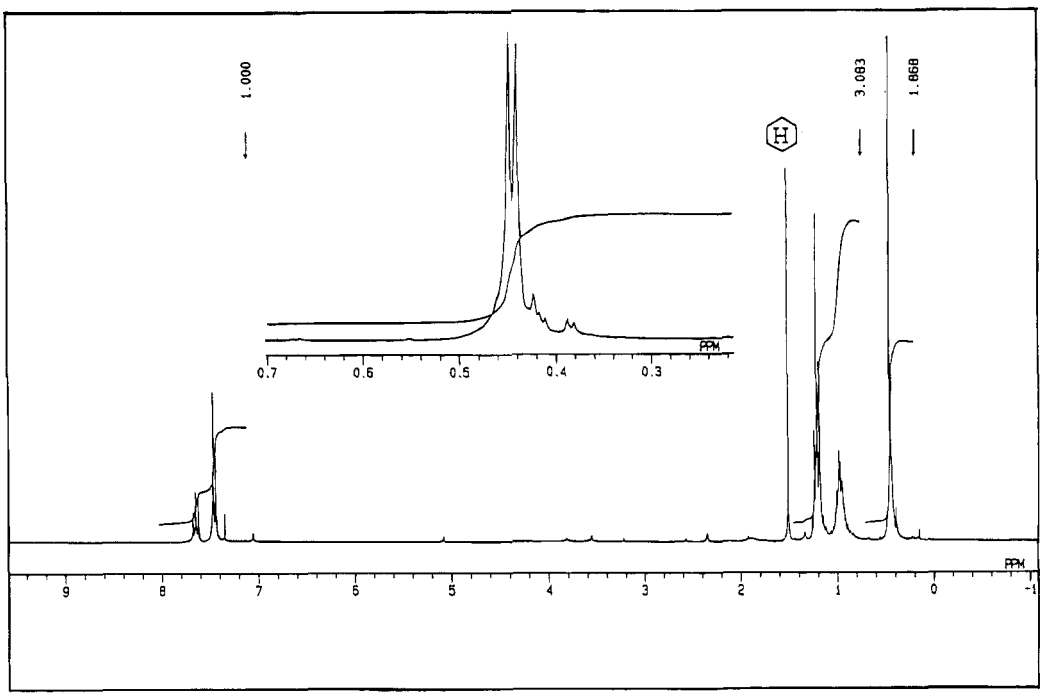

Figure 1. ^{1}H NMR spectrum for **2a**.

treatment with activated carbon. However, we have found that the dark brown color can be removed by treating the polymers with zinc powder and aqueous acetic acid in a short time under an inert atmosphere. For example, when a dark brown solution of polymer **3c** in benzene was stirred with zinc powder and 40% aqueous acetic acid under a nitrogen atmosphere for 5 min, a rapid decolorization of the solution was observed.[8] After immediate separation of the organic layer and neutralization with aqueous sodium bicarbonate, polymer **3c** was recovered in more than 90% yield as a light brown oil. No changes were observed for the molecular weight of the recovered **3c**.

Another point to be stressed is that the silicon–silicon bonds in the polymer backbone are not cleaved under the conditions used for the synthesis of the present polymers. Tanaka and his co-workers reported that some acetylenic compounds insert into the silicon–silicon bonds of octamethyltrisilane and the related polymers in the presence of a Pd complex catalyst in benzene at 120 °C.[9] If such insertion reaction of the acetylenic bonds of the polymers into the silicon–silicon bonds in the polymer backbone took place, branched or cross-linked structure would be formed. In order to check this possibility, we synthesized 1,2-bis(2-pyridylethynyl)tetramethyldisilane (**6**) as a model compound and examined the behavior toward the Pd catalyst. Thus, when a mixture of 1 equiv of 1,2-diethynyltetramethyldisilane and 2 equiv of 2-bromopyridine in the presence of the $Pd(PPh_3)_4$–CuI catalyst in triethylamine was heated to reflux for 8 h, compound **6** was obtained in 92% yield (GLC), as the sole product. No products arising from insertion of an ethynyl group into a silicon–silicon bond in the starting disilane were detected in the reaction mixture by GC-mass spectrometric analysis. Even in the prolonged reaction for 30 h under the same conditions, no change was observed for the yield of product **6**. A similar result was obtained in the synthesis of disilane **4**, indicating that insertion of the

(8) Similar treatment of **3c** with zinc–acetic acid under aerobic conditions for 1 h resulted in decrease of the molecular weight and also contamination of some siloxy bonds in the polymer backbone.

(9) They have reported that the $Pd(dba)_2$–$2P(OCH_2)_3CEt$ catalyst system is highly effective for the insertion of acetylenes to the Si–Si bonds, but $PdCl_2(PPh_3)_2$ and $Pd(PPh_3)_4$ show only low catalytic activity for this reaction: Yamashita, H.; Catellani, M.; Tanaka, M. *Chem. Lett.* **1991**, 241. See also: Horn, K. A.; Grossman, R. B.; Whitenack, A. A. *J. Organomet. Chem.* **1987**, *332*, 271.

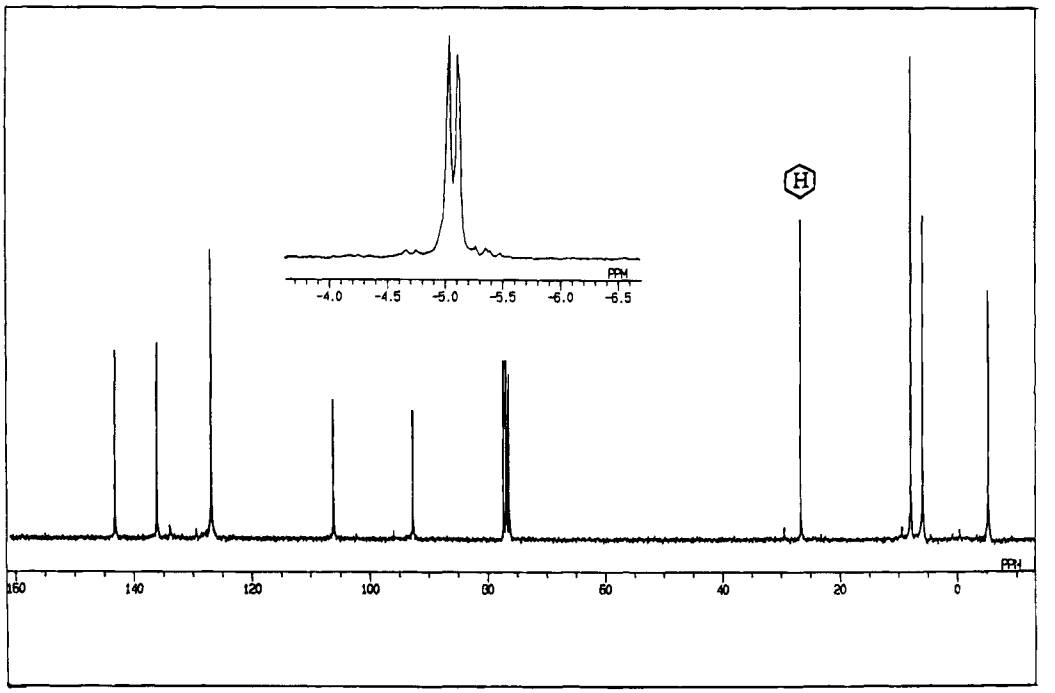

Figure 2. ^{13}C NMR spectrum for **2a**.

Scheme 3

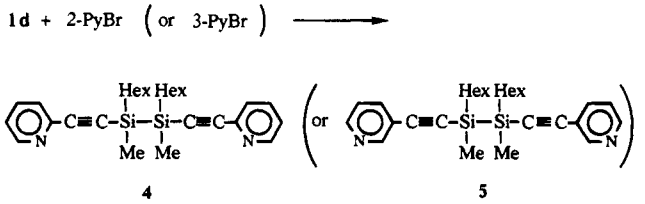

Chart 1

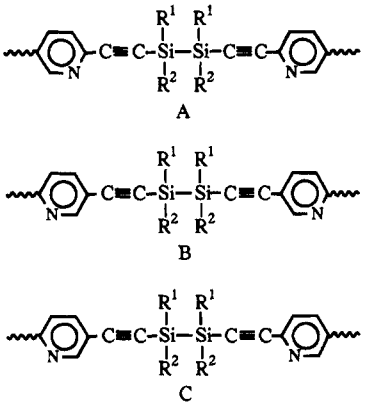

ethynyl group into the silicon–silicon bonds does not occur during the synthesis of the present polymers.

Although all of the spectrometric analyses undoubtedly support the structure of the polymers (see Figures 1 and 2), combustion analysis for some polymers shows lower carbon values than theoretical ones. For example, the carbon content for **3c** was determined to be 63% (calcd 70.04%). In such cases, the color of the ash obtained after combustion analysis is always gray, suggesting that a small amount of silicon carbide is produced. In order to clarify this, we carried out an ignition experiment for **3c** under the same conditions as those of elemental analysis, i.e., at 830 °C in an oxygen stream for 5 min. Although an ESCA spectrum of the resulting ash revealed a peak corresponding to carbon, no crystalline materials were detected by XRD analysis. However, after the ash was treated at 1500 °C under argon for 30 min, X-ray diffraction peaks due to β-silicon carbide were clearly observed. These results unambiguously show that the low carbon content observed for **3c** in elemental analysis is caused by the formation of silicon carbide.

We carried out the pyrolysis of the polymer **3c** under an argon atmosphere. Heating **3c** at 1500 °C for 30 min under argon afforded a hard black solid consisting of β-SiC, which was verified by XRD analysis. Peaks due to silicon nitride were not detected. The thermal behavior of the polymers was also examined by thermogravimetry under a nitrogen atmosphere. The TGA curves for all polymers display that the weight percent decreases rapidly in a range of 400–700 °C and becomes almost constant over 800 °C. The weight remaining at 1200 °C was found to be 33% for **2a**, 37% for **2b**, 32% for **2c**, and 31% for **2d**, in accordance with the formation of silicon carbide. Similar results were obtained for **3a–d**.

The (diethynylenepyridylene)disilanylene polymers exhibit strong UV absorption bands at 304–318 nm in a THF solution, which are lower in energy than 1,2-bis(pyridylethynyl)disilanes (282 nm for **4** and 280 nm for **5**). The absorption maxima and the extinction coefficients per (diethynylenepyridylene)disilanylene unit are given in Table 1. In general, polymers containing a disilanylene unit and π-electron system in the polymer backbone are photoactive. As expected, on irradiation of thin films of polymers **2a–d** and **3a–d** with UV light in air, absorption bands near 310 nm decrease rapidly (within 10 min), indicating that homolytic scission of silicon–silicon bonds in the polymer backbone readily occurs. Profiles of UV spectra obtained from irradiation of the film prepared from **3d** are shown in Figure 3, as a typical example. IR spectra of all of the resulting films show strong absorptions due to Si–OH and Si–O–Si bonds. The formation of the Si–OH and Si–O–Si bonds can best be explained by

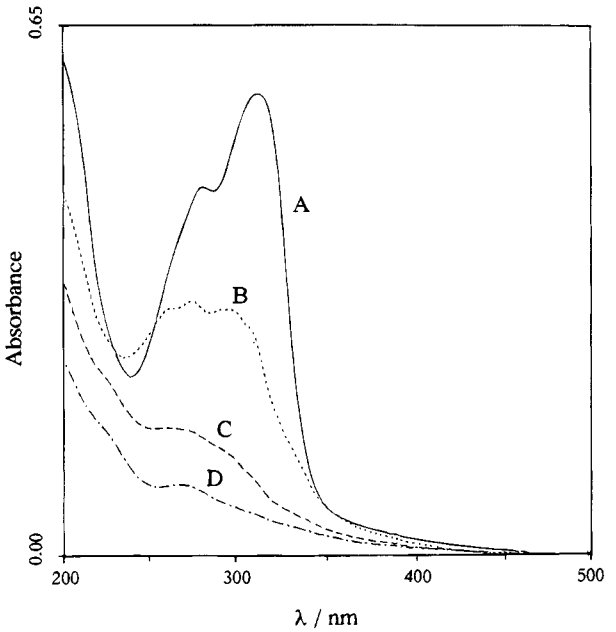

Figure 3. Changes in UV spectra of a thin film of **3d** on irradiation with UV light: (A) before irradiation; (B) after irradiation for 5 min; (C) after irradiation for 10 min; (D) after irradiation for 30 min.

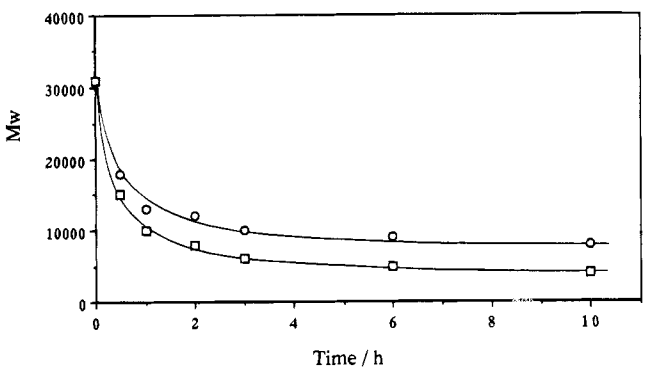

Figure 4. Plot of molecular weights of products vs irradiation time for **3d**: (○) irradiation in benzene; (□) irradiation in the presence of methanol in benzene.

the reaction of silyl radicals generated by photolytic scission of the silicon–silicon bonds in the polymer backbone with oxygen in air, as observed for poly[(*p*-disilanylene)phenylenes].[2b]

When benzene solutions of polymers **2a–d** and **3a–d** were photolyzed with a low-pressure mercury lamp bearing a Vycol filter, photodegradation products with low molecular weights were obtained in all cases. As can be seen in the photolysis of **3d** shown in Figure 4 as a typical example, the molecular weight of the product decreased rapidly with increasing irradiation time and remained unchanged after 3 h irradiation. Similar photolysis of **3d** in the presence of methanol afforded the product whose molecular weight was determined to be lower than that of the photoproduct obtained in the absence of methanol. The ^{1}H NMR spectrum of the resulting photoproduct displays signals due to methoxy protons. The photochemical behavior of the other polymers was also found to be similar to that of **3d**. These results clearly indicate that, upon irradiation, homolytic scission of a silicon-silicon bond takes place readily to generate silyl radicals, as reported previously.[2b]

Table 2. Conductivities of Polymers 3a–d Doped with I_2 and $FeCl_3$ Vapors

	conductivity, S·cm^{-1}			
polymer	with I_2 (thickness)[a]	(period)	with $FeCl_3$ (thickness)[b]	(period)
3a	7.9×10^{-7} (0.5 mm)	(5 days)	9.5×10^{-6} (1.3 mm)	(30 min)
3b	3.7×10^{-6} (0.3 mm)	(5 days)	3.2×10^{-5} (1.0 mm)	(40 min)
3c	1.9×10^{-6} (0.2 mm)	(5 days)	1.4×10^{-4} (1.3 mm)	(30 min)
3d	2.0×10^{-6} (0.1 mm)	(5 days)	1.9×10^{-5} (1.6 mm)	(40 min)

[a] Film. [b] Pellet.

In general, polymers composed of an alternating disilanylene unit and π-electron system are insulators. However, on treatment of the polymers with an oxidizing agent, they become conducting. Thus, cast films of **3a–d** were exposed to iodine vapor under atmospheric pressure for 5 days, and then an excess of I_2 vapor was evacuated under a reduced pressure (1 mmHg) for 30 min to give solid films (Table 2). The conductivity of the films was determined to be 7.9×10^{-7} (**3a**), 3.7×10^{-6} (**3b**), 1.9×10^{-6} (**3c**), and 2.0×10^{-7} (**3d**) S·cm^{-1} by the two-probe method under aerobic conditions. We also carried out doping of the polymers with ferric chloride. Thus, a film of the polymer was exposed to a $FeCl_3$ vapor supplied by heating the salt at 150 °C under reduced pressure (1 mmHg) for 30–40 min. The resulting black polymer was compressed into a pellet. The conductivity was found to be 9.5×10^{-6} (**3a**), 3.2×10^{-5} (**3b**), 1.4×10^{-4} (**3c**), and 1.9×10^{-5} (**3d**) S·cm^{-1}.

Experimental Section

General Methods. All reactions were carried out under an atmosphere of dry nitrogen. ^{1}H, ^{13}C, and ^{29}Si NMR spectra were recorded on a JEOL Model JNM-EX 270 and Bruker AM-X-400 spectrometers. Mass spectra were measured with Shimadzu Model QP 1000 and Hitachi M-80-B spectrometers. UV and IR spectra were recorded on Hitachi U-3210 and Perkin-Elmer 1600-FTIR spectrophotometers. ESCA spectra were measured with a Perkin-Elmer PHI 5400 instrument. XRD patterns were determined with a Rigaku RAD-1B instrument using a Ni-filtered Cu Kα radiation. Thermogravimetric analysis was performed using a Seiko TG/DTA 320 equipment. Molecular weights of polymers were determined by gel-permeation chromatography using Shodex 806 and 804 as the column and using THF as the eluent, relative to polystyrene standards.

Materials. Triethylamine used as the solvent for polymerization was dried over KOH and distilled just before use. Diethynyldisilanes **1a–d** were prepared by the method reported previously.[3c] 2,5-Dibromopyridine, 2,6-dibromopyridine, and the Pd catalyst were used as received.

Polymerization of 1a with 2,6-Dibromopyridine. A mixture of 0.205 g (1.05 mmol) of **1a**, 0.240 g (1.02 mmol) of 2,6-dibromopyridine, 26 mg (0.02 mmol) of tetrakis(triphenylphosphine)palladium, and 4 mg (0.02 mmol) of copper(I) iodide in 10 mL of triethylamine was stirred at 89 °C for 24 h. The solution was filtered, and after evaporation of the solvent, the residue was reprecipitated from benzene–methanol and dried under reduced pressure to give 0.103 g (39% yield) of **2a**: dark brown viscous liquid; M_w = 15 000, M_n = 5800 (M_w/M_n = 2.5); IR 2153 (C≡C) cm^{-1}; UV λ_{max} (THF) 304.4 nm (ϵ 11 100); ^{1}H NMR (δ, in $CDCl_3$) 0.37, 0.38 (two s, 6H, MeSi), 0.90 (m, 4H, $SiCH_2$), 1.14 (t, 6H, CH_3, J = 7.8 Hz), 7.38 (d, 2H, pyridyl C(3)H and C(5)H, J = 7.8 Hz), 7.58 (t, 1H, C(4)H, J = 7.8 Hz); ^{13}C NMR (δ, in $CDCl_3$) −5.14, −5.05 (MeSi), 6.06, 6.09 ($SiCH_2$), 8.12 (CH_3), 92.83 (SiC≡), 106.31 (C≡), 126.95 (pyridyl C(3) and C(5)), 136.14 (C(4)), 143.25 (C(2) and C(6)); ^{29}Si NMR (δ, in $CDCl_3$) −32.11, −32.16. Anal. Calcd for $(C_{15}H_{19}NSi_2)_n$: C, 66.85; H, 7.10; N, 5.19. Found: C, 66.34; H, 7.01; N, 5.07.

Polymerization of 1b with 2,6-Dibromopyridine. A mixture of 0.225 g (1.00 mmol) of **1b**, 0.236 g (1.00 mmol) of 2,6-dibromopyridine, 23 mg (0.02 mmol) of tetrakis(triphenylphosphine)palladium, and 6 mg (0.03 mmol) of copper(I) iodide in 10 mL of triethylamine was stirred at 89 °C for 60 h. The solution was filtered, and after evaporation of the solvent, the residue was reprecipitated from benzene–methanol and dried under reduced pressure to give 0.209 g (70% yield) of **2b**: dark brown viscous liquid; M_w = 19 000, M_n = 9700 (M_w/M_n = 1.9); IR 2152 (C≡C) cm^{-1}; UV λ_{max} (THF) 304.2 nm (ϵ 11 900); ^{1}H NMR (δ, in $CDCl_3$) 0.90 (q, 8H, $SiCH_2$, J = 7.6 Hz), 1.13 (t, 12H, CH_3, J = 7.6 Hz), 7.36 (d, 2H, pyridyl C(3)H and C(5)H, J = 7.8 Hz), 7.57 (t, 1H, C(4)H, J = 7.8 Hz); ^{13}C NMR (δ, in $CDCl_3$) 4.62 ($SiCH_2$), 8.32 (CH_3), 92.33 (SiC≡), 106.87 (C≡), 127.03 (pyridyl C(3) and C(5)), 136.08 (C(4)), 143.34 (C(2) and C(6)); ^{29}Si NMR (δ, in $CDCl_3$) −28.22. Anal. Calcd for $(C_{17}H_{23}NSi_2)_n$: C, 68.62; H, 7.79; N, 4.71. Found: C, 67.65; H, 7.69; N, 3.95.

Polymerization of 1c with 2,6-Dibromopyridine. A mixture of 0.260 g (1.04 mmol) of **1c**, 0.245 g (1.03 mmol) of 2,6-dibromopyridine, 23 mg (0.02 mmol) of tetrakis(triphenylphosphine)palladium, and 4 mg (0.02 mmol) of copper(I) iodide in 10 mL of triethylamine was stirred at 89 °C for 44 h. The solution was filtered, and after evaporation of the solvent, the residue was reprecipitated from benzene–methanol and dried under reduced pressure to give 0.198 g (61% yield) of **2c**: dark brown viscous liquid; M_w = 28 000, M_n = 12 000 (M_w/M_n = 2.3); IR 2152 (C≡C) cm^{-1}; UV λ_{max} (THF) 312.2 nm (ϵ 28 100); ^{1}H NMR (δ, in $CDCl_3$) 0.35, 0.36 (two s, 6H, MeSi), 0.88 (t, 10H, $SiCH_2$ and CH_3), 1.31–1.51 (m, 8H, CH_2), 7.35 (d, 2H, pyridyl C(3)H and C(5)H, J = 7.9 Hz), 7.55 (t, 1H, C(4)H, J = 7.9 Hz); ^{13}C NMR (δ, in $CDCl_3$) −4.60, −4.51 (MeSi), 13.73 ($SiCH_2$ and CH_3), 26.36, 26.72 (CH_2), 93.28 (SiC≡), 106.36 (C≡), 126.97 (pyridyl C(3) and C(5)), 136.15 (C(4)), 143.41 (C(2) and C(6)); ^{29}Si NMR (δ, in $CDCl_3$) −33.82. Anal. Calcd for $(C_{19}H_{27}NSi_2)_n$: C, 70.09; H, 8.36; N, 4.30. Found: C, 69.45; H, 8.56; N, 3.52.

Polymerization of 1d with 2,6-Dibromopyridine. A mixture of 0.318 g (1.04 mmol) of **1d**, 0.246 g (1.04 mmol) of 2,6-dibromopyridine, 26 mg (0.02 mmol) of tetrakis(triphenylphosphine)palladium, and 4 mg (0.02 mmol) of copper(I) iodide in 10 mL of triethylamine was stirred at 89 °C for 44 h. The solution was filtered, and after evaporation of the solvent, the residue was reprecipitated from benzene–methanol and dried under reduced pressure to give 0.307 g (81% yield) of **2d**: dark brown viscous liquid; M_w = 20 000, M_n = 8300 (M_w/M_n = 2.4); IR 2154 (C≡C) cm^{-1}; UV λ_{max} (THF) 306.2 nm (ϵ 23 800); ^{1}H NMR (δ, in $CDCl_3$) 0.32_6, 0.33_2 (two s, 6H, MeSi), 0.81 (m, 10H, $SiCH_2$ and CH_3), 1.15–1.53 (m, 16H, CH_2), 7.32 (d, 2H, pyridyl C(3)H and C(5)H, J = 7.9 Hz), 7.52 (t, 1H, C(4)H, J = 7.9 Hz); ^{13}C NMR (δ, in $CDCl_3$) −4.71, −4.62 (MeSi), 13.88, 13.91 ($SiCH_2$), 14.00 (CH_3), 22.45, 24.39, 31.36, 32.92 (CH_2), 93.14 (SiC≡), 106.25 (C≡), 126.83 (pyridyl C(3) and C(5)), 135.99 (C(4)), 143.27 (C(2) and C(6)); ^{29}Si NMR (δ, in $CDCl_3$) −33.82. Anal. Calcd for $(C_{23}H_{35}NSi_2)_n$: C, 72.37; H, 9.24; N, 3.67. Found: C, 70.41; H, 9.22; N, 2.96.

Polymerization of 1a with 2,5-Dibromopyridine. A mixture of 0.188 g (0.96 mmol) of **1a**, 0.223 g (0.94 mmol) of 2,5-dibromopyridine, 25 mg (0.02 mmol) of tetrakis(triphenylphosphine)palladium, and 4 mg (0.02 mmol) of copper(I) iodide in 10 mL of triethylamine was stirred at 89 °C for 24 h. The solution was filtered, and after evaporation of the solvent, the residue was reprecipitated from benzene–methanol and dried under reduced pressure to give 0.142 g (53% yield) of **3a**: dark brown viscous liquid; M_w = 19 000, M_n = 6700 (M_w/M_n = 2.8); IR 2155 (C≡C) cm^{-1}; UV λ_{max} (THF) 311.6 nm (ϵ 45 800); ^{1}H NMR (δ, in $CDCl_3$) 0.34, 0.35 (two s, 6H, SiMe), 0.85 (m, 4H, $SiCH_2$), 1.10 (t, 6H, CH_3, J = 7.8 Hz), 7.33 (m, 1H, pyridyl C(3)H), 7.61 (m, 1H, C(4)H), 8.58 (s, 1H, C(6)H); ^{13}C NMR (δ, in $CDCl_3$) −5.14, −5.07, −4.99 (SiMe), 6.07, 8.12 (SiEt), 94.39, 94.47, 94.54, 97.47, 97.52, 97.58 (SiC≡), 104.30, 106.45 (C≡), 119.41, 119.44 (pyridyl C(5)), 126.52, 126.60 (C(3)), 138.58, 138.63 (C(4)), 141.60(C(2)), 152.54 (C(6)); ^{29}Si NMR (δ, in $CDCl_3$) −32.45, −32.35, −32.18, −32.11, −32.09. Anal. Calcd for $(C_{15}H_{19}NSi_2)_n$: C, 66.85; H, 7.10; N, 5.19. Found: C, 65.09; H, 7.15; N, 5.23.

Polymerization of 1b with 2,5-Dibromopyridine. A mixture of 0.239 g (1.08 mmol) of **1b**, 0.239 g (1.01 mmol) of 2,5-dibromopyridine, 24 mg (0.02 mmol) of tetrakis(triphenylphosphine)palladium, and 4 mg (0.02 mmol) of copper(I) iodide in 10 mL of triethylamine was stirred at 89 °C for 17 h. The solution was filtered, and after evaporation of the solvent, the residue was reprecipitated from benzene–methanol and dried under reduced pressure to give 0.270 g (90% yield) of **3b**: dark brown viscous liquid; M_w = 19 000, M_n = 7300 (M_w/M_n = 2.6); IR 2155 (C≡C) cm^{-1}; UV λ_{max} (THF) 318.0 nm (ϵ 32 900); ^{1}H NMR (δ, in $CDCl_3$) 0.89 (m, 8H, $SiCH_2$), 1.13 (t, 12H, CH_3, J = 7.6 Hz), 7.34, 7.63 (two m, 2H, pyridyl C(3)H and C(4)H), 8.59 (s, 1H, C(6)H); ^{13}C NMR (δ, in $CDCl_3$) 4.62, 4.66 ($SiCH_2$), 8.29 (CH_3), 93.84, 93.91, 93.98, 96.89, 96.95, 97.00 (SiC≡), 104.80, 106.99 (C≡), 119.48 (pyridyl C(5)), 126.56, 126.63 (C(3)), 138.49, 138.54 (C(4)), 141.65 (C(2)), 152.54 (C(6)); ^{29}Si NMR (δ, in $CDCl_3$) −28.38, −28.49. Anal. Calcd for $(C_{17}H_{23}NSi_2)_n$: C, 68.62; H, 7.79; N, 4.71. Found: C, 67.22; H, 7.88; N, 4.18.

Polymerization of 1c with 2,5-Dibromopyridine. A mixture of 0.263 g (1.05 mmol) of **1c**, 0.239 g (1.01 mmol) of 2,5-dibromopyridine, 25 mg (0.02 mmol) of tetrakis(triphenylphosphine)palladium, and 4 mg (0.02 mmol) of copper(I) iodide in 10 mL of triethylamine was stirred at 89 °C for 17 h. The solution was filtered, and after evaporation of the solvent, the residue was reprecipitated from benzene–methanol and dried under reduced pressure to give 0.270 g (90% yield) of **3c**: dark brown viscous liquid; M_w = 24,000, M_n = 10 000 (M_w/M_n = 2.4); IR 2155 (C≡C) cm^{-1}; UV λ_{max} (THF) 314 nm (ϵ 34 000); ^{1}H NMR (δ, in $CDCl_3$) 0.35, 0.36 (two s, 6H, SiMe), 0.87 (m, 10H, $SiCH_2$ and CH_3), 1.37 (m, 4H, CH_2), 1.47 (m, 4H, CH_2), 7.33, 7.63 (two m, 2H, pyridyl C(3)H and C(4)H), 8.58 (s, 1H, C(6)H); ^{13}C NMR (δ, in $CDCl_3$) −4.68, −4.61, −4.52 (SiMe), 13.69, 26.24, 26.27, 26.66 (n-BuSi), 94.76, 94.82, 94.84, 94.90, 97.83, 97.89, 97.95 (SiC≡), 104.26, 106.42 (C≡), 119.43, 119.47, 119.51 (pyridyl C(5)), 126.50, 126.57 (C(3)), 138.55, 138.60 (C(4)), 141.58, 141.61, 141.65 (C(2)), 152.53 (C(6)); ^{29}Si NMR (δ, in $CDCl_3$) −34.25, −34.16, −33.93, −33.83, −33.73.

Polymerization of 1d with 2,5-Dibromopyridine. A mixture of 0.316 g (1.03 mmol) of **1d**, 0.244 g (1.03 mmol) of 2,5-dibromopyridine, 25 mg (0.02 mmol) of tetrakis(triphenylphosphine)palladium, and 5 mg (0.03 mmol) of copper(I) iodide in 10 mL of triethylamine was stirred at 89 °C for 20 h. The solution was filtered, and after evaporation of the solvent, the residue was reprecipitated from benzene–methanol twice and dried under reduced pressure to give 0.316 g (83% yield) of **3d**: dark brown viscous liquid; M_w = 39 000, M_n = 15 000 (M_w/M_n = 2.6); IR 2156 (C≡C) cm^{-1}; UV λ_{max} (THF) 313.4 nm (ϵ 38 200); ^{1}H NMR (δ, in $CDCl_3$) 0.35 (s, 6H, MeSi), 0.83 (br s, 10H, $SiCH_2$ and CH_3), 1.10–1.57 (m, 16H, CH_2), 7.33, 7.62 (two m, 2H, pyridyl C(3)H and C(4)H), 8.58 (s, 1H, C(6)H); ^{13}C NMR (δ, in $CDCl_3$) −4.65, −4.58, −4.51 (MeSi), 14.00, 22.48, 24.44, 31.39, 32.87, 32.94 (n-HexSi), 94.77, 97.86, 94.93, 97.84, 97.92, 97.99 (SiC≡), 104.30, 106.48 (C≡), 119.43, 126.48 (pyridyl C(5)), 126.45, 126.51 (C(3)), 138.47, 138.51 (C(4)), 141.67, 141.71 (C(2)), 152.52 (C(6)); ^{29}Si NMR (δ, in $CDCl_3$) −34.31, −34.25, −34.18, −34.00, −33.93, −33.88. Anal. Calcd for $(C_{23}H_{35}NSi_2)_n$: C, 72.37; H, 9.24; N, 3.67. Found: C, 71.96; H, 9.29; N, 3.18.

Synthesis of 4. A mixture of 0.318 g (1.03 mmol) of **1d**, 0.384 g (2.40 mmol) of 2-bromopyridine, 63 mg (0.05 mmol) of tetrakis(triphenylphosphine)palladium, and 10 mg (0.05 mmol) of copper(I) iodide in 10 mL of triethylamine was refluxed for 26 h. The solution was filtered, and the solvent was evaporated. Products were separated by preparative GPC eluting with chloroform to give **4** (78% yield by GLC) as a liquid: IR 2158 (C≡C) cm^{-1}; UV λ_{max} (THF) 249.2 (ϵ 23,600), 282.2 nm (ϵ 22,400); ^{1}H NMR (δ, in $CDCl_3$) 0.35, 0.36 (s, 6H, MeSi), 0.80

(mc, 10H, $SiCH_2$ and CH_3), 1.23 (mc, 8H, CH_2), 1.32 (mc, 4H, CH_2), 1.48 (mc, 4H, CH_2), 7.16 (dd, 2H, pyridyl C(5)H, J = 7.6 Hz, J = 5.0 Hz), 7.39 (d, 2H, pyridyl C(3)H, J = 7.9 Hz), 7.57 (td, 2H, pyridyl C(4)H, J = 7.9 Hz, J = 7.6 Hz), 8.52 (d, 2H, C(6)H, J = 5.0 Hz); ^{13}C NMR (δ, in $CDCl_3$) −4.62, −4.53 (MeSi), 13.95, 14.02, 22.48, 24.42, 31.41, 32.98 (CH_2), 92.53 (SiC≡), 106.72 (C≡), 122.82, 127.40 (pyridyl C(3) and C(5)), 135.89 (C(4)), 143.13 (C(2)), 149.79 (C(6)); ^{29}Si NMR (δ, in $CDCl_3$) −34.11, −34.05; MS m/z 460 (M^+). HRMS: calcd for $C_{28}H_{40}N_2Si_2$, m/z 460.2728; found, m/z 460.2701. Anal. Calcd for $C_{28}H_{40}N_2Si_2$: C, 72.98; H, 8.75, N, 6.08. Found: C, 72.82; H, 8.61; N, 6.06.

Synthesis of 5. A mixture of 0.326 g (1.06 mmol) of **1d**, 0.369 g (2.34 mmol) of 3-bromopyridine, 59 mg (0.05 mmol) of tetrakis(triphenylphosphine)palladium, and 11 mg (0.06 mmol) of copper(I) iodide in 10 mL of triethylamine was refluxed for 23 h. The solution was filtered, and the solvent was evaporated. Products were separated by preparative GPC eluting with chloroform to give **5** (66% yield by GLC) as a liquid: IR 2154 (C≡C) cm^{-1}; UV λ_{max} (THF) 249.0 (ϵ 26 200), 280.0 nm (ϵ 14 300); ^1H NMR (δ, in $CDCl_3$) 0.341, 0.347 (s, 6H, MeSi), 0.83 (mc, 10H, $SiCH_2$ and CH_3), 1.26 (mc, 8H, CH_2), 1.36 (mc, 4H, CH_2), 1.48 (mc, 4H, CH_2), 7.19 (dd, 2H, pyridyl C(5)H, J = 7.9 Hz, J = 5.0 Hz), 7.67 (dt, 2H, pyridyl C(4)H, J = 7.9 Hz, J = 1.7 Hz), 8.48 (dd, 2H, pyridyl C(6)H, J = 5.0 Hz, J = 1.7 Hz), 8.63 (d, 2H, C(2)H, J = 1.7 Hz); ^{13}C NMR (δ, in $CDCl_3$) −4.53, −4.45 (MeSi), 14.04, 22.52, 24.49, 31.45, 32.94 (CH_2), 95.90 (SiC≡), 104.44 (C≡), 120.41 (pyridyl C(3)), 122.84 (C(5)), 138.67 (C(4)), 148.55 (C(6)), 152.45 (C(2)); ^{29}Si NMR (δ, in $CDCl_3$) −34.39; MS m/z 460 (M^+). HRMS: calcd for $C_{28}H_{40}N_2Si_2$, m/z 460.2728; found, m/z 460.2668. Anal. Calcd for $C_{28}H_{40}N_2Si_2$: C, 72.98; H, 8.75, N, 6.08. Found: C, 72.71; H, 8.54; N, 5.87.

Synthesis of 6. A mixture of 0.171 g (1.03 mmol) of 1,2-diethynyltetramethyldisilane, 0.330 g (2.09 mmol) of 2-bromopyridine, 23 mg (0.02 mmol) of tetrakis(triphenylphosphine)-palladium, and 4 mg (0.02 mmol) of copper(I) iodide in 10 mL of triethylamine was heated to reflux for 8 h. After workup as usual, compound **6** was obtained in 92% yield (GLC). No products arising from Si−Si bond scission were detected in the reaction mixture by GC-mass spectrometric analysis. After the mixture was heated for 30 h under the same conditions, no change was observed in product distribution. Data for **6**: Mp 88.5−89 °C; UV λ_{max} (THF) 248.2 (ϵ 21 600), 281.6 nm (ϵ 19 100); IR 2156 (C≡C) cm^{-1}; ^1H NMR (δ, in $CDCl_3$) 0.44 (s, 12H, MeSi), 7.23 (dd, 2H, pyridyl C(5)H, J = 7.5 Hz, J = 5.0 Hz), 7.46 (d, 2H, pyridyl C(3)H, J = 7.5 Hz), 7.65 (t, 2H, pyridyl C(4)H, J = 7.5 Hz), 8.58 (d, 2H, C(6)H, J = 5.0 Hz); ^{13}C NMR (δ, in $CDCl_3$) −3.14 (MeSi), 92.80 (SiC≡), 106.43 (C≡), 122.97, 127.44 (pyridyl C(3) and C(5)), 136.01 (C(4)), 143.12 (C(2)), 149.92 (C(6)); ^{29}Si NMR (δ, in $CDCl_3$) −36.0; MS m/z 320 (M^+). Anal. Calcd for $C_{18}H_{20}N_2Si_2$: C, 67.45; H, 6.29, N, 8.74. Found: C, 67.53; H, 6.18; N, 8.61.

Decolorization of 3c. To a solution of **3c** (0.113 g, M_w = 14 200, M_w/M_n = 3.0) in 20 mL of benzene were added zinc powder (2.0 g) and 20 mL of 40% aqueous acetic acid. The mixture was stirred for 5 min under a nitrogen atmosphere, and then excess of zinc was filtered off. The organic layer was separated, washed with 5% aqueous sodium bicarbonate three times, and dried over magnesium sulfate. After evaporation of the solvent, **3c** was recovered in 90% yield as a light brown oil: M_w = 14 800, M_w/M_n = 2.7. IR and ^1H and ^{13}C NMR spectra were identical with those of the starting polymer.

Photolysis of Polymer Films. A polymer was dissolved in THF and cast onto a quartz or NaCl plate. The film was irradiated with a 6-W low-pressure mercury lamp in air for 30 min, and the progress of the reaction was monitored periodically by IR and UV spectroscopy. In all cases, absorption bands near 310 nm decreased rapidly within 10 min, and IR spectra of the resulting films showed strong absorptions at 3100 (Si−OH) and 1060 (Si−O−Si) cm^{-1}. As a typical example, changes in UV spectra for **3d** during the photolysis are shown in Figure 3.

Photolysis of Polymers in Solution. A solution of a polymer (15 mg) in benzene (25 mL) was irradiated with a 6-W low-pressure mercury lamp bearing a Vycol filter in the presence or absence of methanol (10 mL) under dry nitrogen. Changes in molecular weight were monitored by GPC. In all cases, the molecular weights of the product decreased rapidly with increasing irradiation time and remained unchanged after 3-h irradiation. As a typical example, changes in molecular weight for **3d** (M_w = 31 000, M_w/M_n = 1.7) in the presence or absence of methanol are shown in Figure 4.

Conductivity Measurement for Polymers Doped with I_2. A benzene solution of a polymer was cast into a thin film on a glass plate by evaporating the solvent. The film was dried in vacuo overnight and then exposed to saturated I_2 vapor for 5 days under atmospheric pressure. An excess of I_2 vapor was removed under reduced pressure (1 mmHg) for 30 min. The resulting solid film was cut into a small piece, and the conductivity was measured by the two-probe method. The results obtained for **3a−d** are shown in Table 2.

Conductivity Measurement for Polymers Doped with $FeCl_3$ Vapor. A thin film of a polymer was prepared in the same manner as described above. The film was held over ferric chloride powder which was placed in a glass vessel. Doping was performed under reduced pressure (1 mmHg) by heating the bottom of the glass vessel at 150 °C for 30−40 min. The resulting solid polymer was pressed into a pellet, and the conductivity was determined by the two-probe method. The results obtained for **3a−d** are shown in Table 2.

Pyrolysis of 3c. Polymer **3c** was solidified by preheating for 30 s. The sample was powdered finely and taken in an alumina crucible. Pyrolysis was carried out at 1500 °C in a quartz tube under an argon atmosphere for 30 min. The resulting material was examined by X-ray powder diffraction analysis. Diffraction peaks due to β-silicon carbide were observed clearly at 2θ = 35.50, 58.86, and 71.60°, corresponding to the distances of d = 2.53, 1.54, and 1.32 Å, respectively.

Thermogravimetric Analysis for Polymers. Thermal behavior of the polymers was examined by thermogravimetry under nitrogen. In all cases, a rapid weight loss of the polymer was found in a range 400−800 °C and then the weight became almost constant over 800 °C. The weight remaining at 1200 °C was found to be 33%, 37%, 32%, and 31% for **2a−d** and 34%, 24%, 30%, and 22% for **3a−d**, respectively.

Acknowledgment. This research was supported in part by a Grant-in-Aid for Developmental Scientific Research (No. 06555274) from the Ministry of Education, Science, and Culture, to which our thanks are due. We also express our appreciation to Shin-Etsu Chemical Co. Ltd., Nitto Electric Industrial Co. Ltd., Dow Corning Asia Ltd., Toshiba Silicone Co. Ltd., Sumitomo Electric Co. Ltd., Kaneka Corp., and the Japan High Polymer center for financial support. We are also indebted to Dr. Hitoshi Kawaji, Mr. Kazunari Ando, and Mr. Hiroomi Horie of our university for measurements of XRD and ESCA spectra.

OM940429X

Chemistry of Nitrogen Donors with μ_3-Imidoyl Triosmium Clusters: Dynamics of a Monometallic Site in a Trimetallic Cluster

Shariff E. Kabir and Edward Rosenberg*

Department of Chemistry, The University of Montana, Missoula, Montana 59812

Mike Day, Kenneth Hardcastle,* Erich Wolf, and Tim McPhillips

Department of Chemistry, California State University, Northridge, California 91330

Received July 25, 1994®

A detailed view of the ligand dynamics and coordination chemistry of a monometallic site is afforded by the study of the reactions of the trimetallic species (μ-H)(μ_3-η^2-C=N(CH$_2$)$_3$)-Os$_3$(CO)$_9$ (**2**) with nitrogen donor ligands. The kinetic site of attack is the axial position on the unbridged osmium atom, *syn* to the μ-imidoyl ligand in the products (μ-H)(μ-η^2-C=N-(CH$_2$)$_3$)Os$_3$(CO)$_9$(L) (**3a**, L = NH$_3$, **3b–e**, L = RNH$_2$, R = n-Bu, i-Bu, s-Bu, t-Bu; **3f**, L = pyrrolidine; **3g**, L = BzNH$_2$; **3h**, L = pyridine; **4a,b**, L = RCN, R = Me, Ph; **4c**, isomer of **4a**; **5a–c**, L = PR$_3$, R = Ph, Me, OMe). The initially formed *syn*-adducts isomerize to *anti/syn* mixtures. This isomerization is shown to be a first order process whose rate as well as the final *anti/syn* ratio is sensitive to the stereoelectronic properties of L. The mechanism of this isomerization process is shown to be a dissociative process for the amine and nitrile ligands. The formation constants for the complexes have been measured; they show a clear dependence on ligand cone angle and are much larger for the pure σ donor amines than the nitriles. The ^{13}C-NMR of **3a**, **3b**, **4a**, and **4c** proved to be a valuable tool for relating solution and solid state structures. Oxidation of (μ-H)(μ-η^2-C=N(CH$_2$)$_3$)Os$_3$(CO)$_{10}$ (**1**) with trimethylamine *N*-oxide in acetonitrile leads to formation of the regioisomer of **4a**, **4c** which allows for subsequent regiospecific phosphine substitution. The primary products of the thermolysis of **3a–h**, are **2** and free amine; however, in the case of **3f**, activation of the pyrrolidine ring leads to a bis-μ-imidoyl complex, (μ-H)$_2$(μ-η^2-C=N(CH$_2$)$_3$)$_2$Os$_3$(CO)$_8$ (**6**) as the major product. Solid state studies of **3a**, **3f**, **4a**, and **6** are reported and discussed in light of the dynamics studies. Compound **3a** crystallizes in the triclinic space group *P*1 with unit cell parameters a = 17.472 (6), b = 20.915 (5), c = 8.543 (2) Å, α = 80.16 (2), β = 78.24 (2), γ = 75.96 (2)°, V = 29.40 (2) Å^3 and Z = 6. Least squares refinement of 6345 observed reflections gave a final agreement factor of R = 0.080 (R_w = 0.087). Compound **3f** crystallizes in the orthorhombic space group $Pca2_1$ with unit cell parameters a = 16.530 (4), b = 17.249 (3), c = 15.955 (5) Å, V = 4549 (3) Å^3 and Z = 8. Least squares refinement of 4972 observed reflections gave a final agreement factor R = 0.061 (R_w = 0.057). Compound **4a** crystallizes in the triclinic space group *P*1 with unit cell parameters a = 9.586 (2), b = 13.510 (3), c = 9.504 (2) Å, α = 70.26 (2), β = 62.30 (1), γ = 77.66 (2)°, V = 1023 (1) Å^3, and Z = 2. Least squares refinement of 4872 observed reflections gave a final agreement factor of R = 0.058 (R_w = 0.061). Compound **6** crystallizes in the monoclinic space group $P2_1/c$ with unit cell parameters a = 16.634 (2), b = 8.872 (2), c = 16.201 (2) Å, β = 119.03 (2)°, V = 2091 (1) and Z = 4. Least squares refinement of 4714 observed reflections gave a final agreement factor R = 0.040 (R_w = 0.041).

Introduction

There has been considerable study of the factors controlling the rates of the associative components of ligand substitution at transition metal centers.[1] For the lower oxidation state carbonyl complexes, most studies have focused on traditional geometries in mononuclear complexes and on softer, kinetically stable ligands such as phosphines in the case of polymetallic species.[2,3]

In recent years it has become increasingly obvious that nitrogen donor ligands can form relatively stable

® Abstract published in *Advance ACS Abstracts*, December 15, 1994.

(1) (a) Twigg, M. V., Ed. *Mechanisms of Inorganic and Organometallic Reactions*, Plenum Press: New York, 1983–9; Vols. 1–6. (b) Jorden, R. B. *Reaction Mechanisms of Inorganic and Organometallic Systems*; Oxford University Press: New York, 1991. (c) Langford, C. H., Gray, H. B. *Ligand Substitution Processes*; W. A. Benjamin: New York, 1966. (d) Atwood, J. D. *Inorganic and Organometallic Reaction Mechanisms*; Brooks-Cole: Monterey, CA, 1985.

(2) (a) Darensbourg, D. J. *Adv. Organometal Chem.* **1982**, *21*, 113. (b) Darensbourg, D. J. In *The Chemistry of Metal Cluster Complexes*; Shriver, D. F., Kaesz, H. D., Adams, R. D.; VCH: New York, 1990; Ch. 4. (c) Johnson, B. F. G.; Roberts, Y. V.; Parsini, E. *J. Chem. Soc. Dalton Trans.* **1992**, 2573.

0276-7333/95/2314-0721$09.00/0

complexes with low oxidation state late transition metal centers. In this same period their importance as ancillary ligands in catalysis has grown.[4] Cone angles for amine ligands have been established for square planar palladium complexes.[5] In the case of polymetallic complexes, little information is available on the reactivity trends for nitrogen-based ligand additions to polymetallic species. This is surprising in light of the fact that the relatively labile species produced in these additions have proved to be valuable synthetic intermediates such as the "lightly stabilized" cluster $Os_3(CO)_{10}(CH_3CN)_2$.[6] We have recently been investigating a variation on the theme of "lightly stabilized clusters" in the chemistry of μ_3-imidoyl clusters.[7] This cluster bonding mode has been known for some time, but we have found that the reaction of certain secondary amines with the lightly stabilized cluster, $Os_3(CO)_{10}(CH_3CN)_2$, provides a convenient entry to μ-imidoyls (eq 1).[7]

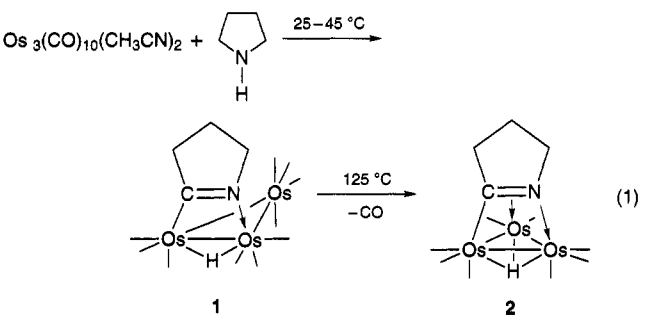

(1)

The μ-imidoyl (μ-H)(μ-η^2-C=N(CH$_2$)$_3$)Os$_3$(CO)$_{10}$ (**1**) decarbonylates quantitatively to yield (μ-H)(μ_3-η^2-C=N(CH$_2$)$_3$)Os$_3$(CO)$_9$ (**2**) which reacts at room temperature with a variety of two-electron donors (eq 2).[7] The

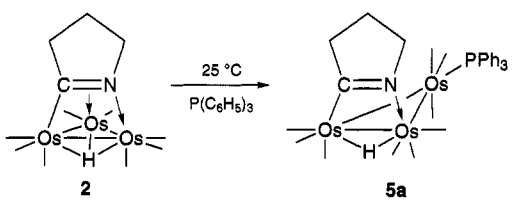

(2)

reactions result in apparent displacement of the C=N π-bond by the two electron donor, but our experiments on related ruthenium systems indicate that in some cases initial attack may in fact be at the metal atom coordinated to the nitrogen lone pair.[7c] Regardless of the kinetic site of attack, this class of compounds provides the opportunity to study the stereochemical and kinetic aspects of a single "lightly stabilized" osmium coordination site in a trimetallic species. In previous studies, we reported the reactions of μ_3-imidoyl clusters with various phosphines[7d] and isocyanides.[7a] We subsequently found that phosphine addition follows second order kinetics with the magnitude of the rate constants following the order expected for associative processes controlled by incoming ligand cone angle and donor ability (i.e., $P(CH_3)_3 > P(OCH_3)_3 > P(C_6H_5)_5$).[7c] We also found that the structure and the number of isomers present was quite sensitive to the structure of the imidoyl ligand as well as the bulkiness of the donor ligand.[7d] We report here the results of our studies of the reactions of μ_3-imidoyl clusters with ammonia, RNH_2 (R = n-Bu, i-Bu, s-Bu, t-Bu, benzyl, phenyl), R_2NH (R = Et, -(CH$_2$)$_4$-), R_3N (R = Et), pyridine, and RCN (R = Me, phenyl). The thermal behavior of the pyrrolidine adduct is reported and a detailed examination of the dynamics at the initial site of coordination has been completed. These results in turn prompted us to examine the mechanism of tripodal motion in the initially formed phosphine derivatives of **2** as well as the regiochemistry of ligand addition to the lightly stabilized cluster (μ-H)(μ-C=N(CH$_2$)$_3$)Os$_3$(CO)$_9$(CH$_3$CN) formed by amino oxide oxidation of **1** in acetonitrile.

Results

A. Complexes with Ammonia and Amines. Solutions of **2** in dichloromethane-d_2 which are saturated with 10% ^{15}N-enriched ammonia immediately show evidence of complex formation as seen from their ^{1}H-NMR. A new hydride resonance appears at −13.71 ppm along with the appearance of a new broad resonance at 2.99 ppm and the appearance of three relatively sharp methylene ring resonances at 3.40, 2.27, and 1.75 ppm which each integrate 2:3 with the new broad resonance at 2.99 ppm. A resonance observed at 0.5 ppm is due to free ammonia. Interestingly, the resonance assigned to the complexed NH_3 shows two sharp satellites ($^1J_{^{15}N-^1H}$ = 69.5 Hz), while the resonance for free ammonia shows no such satellites. This is undoubtedly due to exchange moduation of the coupling in the free ammonia (aided by trace moisture). Slow proton exchange for the complexed ammonia is consistent with a relatively slow on/off rate for this ligand. The observed magnitude of $^1J_{^{15}N-^1H}$ is slightly larger than for free ammonia under conditions of slow hydrogen exchange (61.5 Hz) as is the case for more conventional ammonia complexes.[8] Over a 20 h period we observed a slight decrease in the relative intensity of the hydride resonance of **2** at −18.0 ppm relative to that of the complex (μ-H)(μ-η^2-C=N(CH$_2$)$_3$)Os$_3$(CO)$_9$NH$_3$ (**3a**) but more importantly a new hydride resonance at −14.03 ppm grows in while the original peak at −13.71 ppm decreases in intensity. Monitoring this conversion in 1-h intervals for 20 h by ^{1}H-NMR affords a first order rate constant for this isomerization of $1.16 \pm 0.1 \times 10^{-3}$ m^{-1}. After more than 20 h, the ratio of these isomeric forms of **3a** continues to change until a final value of 6:1 is reached after ~40 h. The ratio of **3a** to **2** does not change further after 20 h in a sealed NMR tube and the formation constant for **3a** is calculated to be 15 (Table 1).

(3) (a) Brodie, M. M. J.; Chen, L.; Poe, A. J. *Int. J. Chem. Kinet.* **1988**, *20*, 467. (b) Johnson, B. F. G.; Roberts, Y. V. *J. Cluster Sci.* **1993**, *4*, 231.
(4) Togni, A.; Venanzi, L. M. *Angew. Chem., Int. Ed. Engl.* **1944**, *33*, 497.
(5) Trogler, W. C.; Seligson, A. L. *J. Am. Chem. Soc.* **1991**, *113*, 2520.
(6) (a) Tachikawa, M.; Shapley, J. R. *J. Organometal Chem.* **1977**, *124*, C19. (b) Shriver, D. F.; Kaesz, H. D.; Adams, R. D. *The Chemistry of Metal Cluster Complexes*; VCH: New York, 1990; Chapter 1, 5.
(7) (a) Day, M.; Espitia, D.; Hardcastle, K. I.; Kabir, S. E.; McPhillips, T.; Rosenberg, E.; Gobetto, R.; Milone, L.; Osella, D. *Organometallics* **1993**, *12*, 2309. (b) Rosenberg, E.; Kabir, S. E.; Hardcastle, K. I.; Day, M.; Wolf, E. *Organometallics* **1990**, *9*, 2214. (c) Rosenberg, E.; Freeman, W.; Carlos, Z.; Hardcastle, K.; Yoo, Y. J.; Milone, L.; Gobetto, R. *J. Cluster Sci.* **1992**, *3*, 439. (d) Day, M.; Espitia, D.; Hardcastle, K.; Kabir, S. E.; Rosenberg, E.; Gobetto, R.; Milone, L.; Osella, D. *Organometallics* **1991**, *10*, 3550. (e) Rosenberg, E.; Kabir, S. E.; Irving, M.; Hardcastle, K.; Day, M. *J. Cluster Sci.* **1994**, *5*, 481.
(8) Webb, G.; Witanouski, M. In *Nitrogen NMR*, Plenum Press: London, 1973.

Table 1. Formation Constants and Isomer Ratios for Amine Complexes of 2

ligand	compd	δ A[a] (ppm)	δ B[a] (ppm)	A/B	K_{eq}[b]	cone angle,[c] deg
NH_3	**3a**	−13.70	−14.03	6.0	15.0	94
n-$BuNH_2$	**3b**	−13.80	−14.03	3.2	1.25	106
i-$BuNH_2$	**3c**	−13.80	−14.03	3.0	1.25	106
s-$BuNH_2$	**3d**	−13.80	−14.04	2.1	0.37	113
t-$BuNH_2$	**3e**	−13.72	−13.83	0.50	0.005	123
pyrrolidine[d]	**3f**	−13.79	−14.33	0.21	0.18	120
$BzNH_2$	**3g**	−13.79	−14.03	1.41	0.11	106
pyridine[e]	**3h**	−13.62	–	–	0.04	–

[a] Chemical shifts rel to TMS. [b] ±15%, mol/dm^3. [c] Taken from ref 5. [d] A third very minor isomer is detected at −13.35 ppm (<5% of A). [e] Measured after only 4 h after which decomposition was significant.

Scheme 1

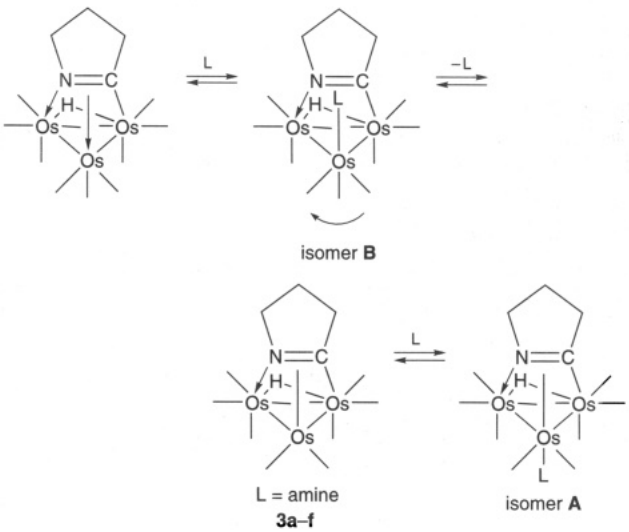

The structure of the initially formed adduct **B** and the slightly more thermodynamically stable **A** (Scheme 1) for **3a** can be inferred from the ^{13}CO-NMR of solutions of **3a** at 1 and 20 h after admixture of the reactants. The initially formed isomer **B** shows the expected nine ^{13}CO resonances (Table 2). The key features are the lack of observable *trans*-diaxial ^{13}CO−^{13}CO coupling on the carbonyl groups which do not exhibit any $^2J_{^{13}C-^1H}$ (i.e., the unbridged osmium atom). The presence of such coupling ($^2J_{^{13}C-^{13}C}$ = 30−40 Hz) is diagnostic for two mutually *trans*-carbonyls on the same osmium atom (*vide infra*).[7a,9] With the aid of the proton coupled spectra, we can make partial assignments (Table 2) and can tentatively assign the initially formed **B** to a structure where the ammonia resides in an axial position *syn* to the imidoyl ligand (Scheme 1). After 20 h the ^{13}C-NMR has changed with a new set of nine resonances (at this point the **A/B** is 3.0) which again show no evidence for *trans*-diaxial coupling between carbonyls and for which we can make the partial assignments in Table 2. We are thus left with a picture of an initially formed isomer **B** which undergoes a rearrangement to give a second axial conformer, **A**, in which the ammonia has an *anti* relationship to the μ-imidoyl ligand (Scheme 1).

To our knowledge this ammonia complex is only the third example of an ammonia osmium cluster complex, the first two being $Os_3(CO)_{11}NH_3$ and $H_2Os_3(CO)_{10}NH_3$

(9) Aime, S.; Gobetto, R.; Osella, D.; Milone, L.; Rosenberg, E.; Anslyn, E. *Inorg. Chem. Acta.* **1986**, *111*, 95.

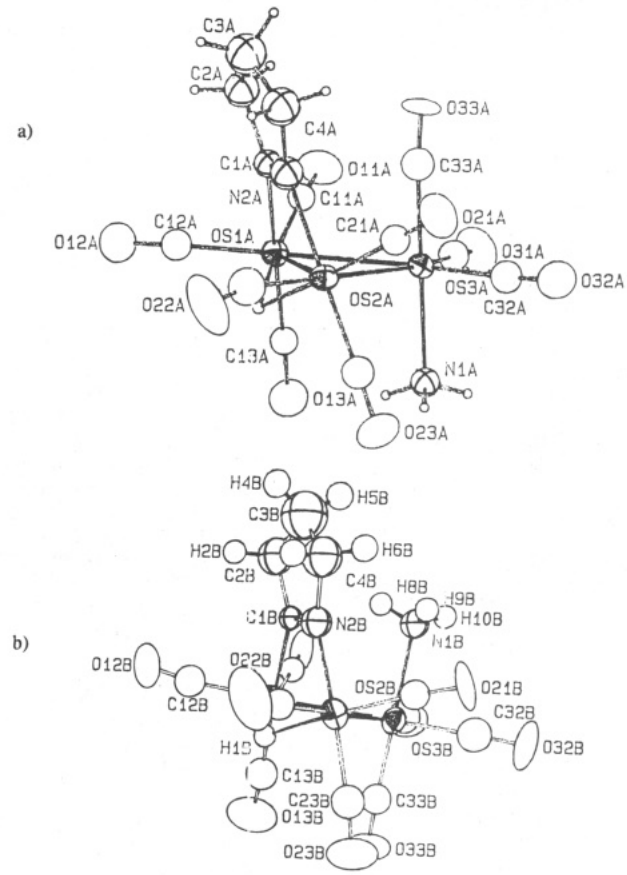

Figure 1. Solid state structures of molecule A and molecule B of **3a** showing the calculated position of the hydride and the ammonia hydrogens.

which were not structurally characterized.[10] We therefore undertook a solid state characterization of crystalline **3a** isolated from ammoniacal solutions of **2** in methylene chloride−hexane at −20 °C. The solid state structure of **3a** is shown in Figure 1, crystal data in Table 3, atomic coordinates in Table 4 and selected distances and bond angles in Table 5. There are three molecules in the asymmetric unit. Molecule A (Figure 1a) has the ammonia molecule in an axial coordination site on the opposite face of the cluster as the imidoyl ligand. Molecule B (Figure 1b) has the ammonia molecule in axial position on the same face as the imidoyl ligand and molecule C is an enantiomer of A with slightly different bond lengths and angles. The overall geometry of molecule B is the same as that proposed for first formed isomer, **B**, from the ^{1}H- and ^{13}C-NMR with the amine ligand *trans* to the other axial carbonyl on Os3. The Os3−N1 bond lengths are 2.24 (2) Å in all three molecules of the asymmetric unit. The angles made by the ammonia ligand with the Os_3 triangle bond vectors do not differ very much for the three molecules, varying from 89.7 (6) to 94.4 (6)°. Molecule **A** has the ammonia molecule on Os(3) on the opposite face of the cluster to the imidoyl ligand as proposed for isomer **A** in solution. It appears that the small difference in thermodynamic stability seen in solution is reflected in the solid state structure (2:1 isomer A:B ratio) where packing effects for the small NH_3 ligand should be minimal.

(10) (a) Süss-Fink, G. *Z. Naturforsch.* **1980**, *35B*, 454. (b) Aime, S.; Dastru, W.; Gobetto, R. *Organometallics*, 1994, submitted.

Table 2. ^{13}C-NMR Data for (μ-H)(μ-η^2-C=N(CH$_2$)$_3$)Os$_3$(CO)$_9$L[a]

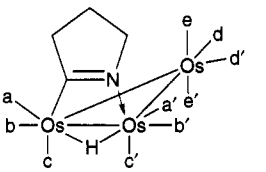

compd no.	L	isomer	a	a′	b	b′	c	c′	d	d′	e	e′
1[b]	CO	–	174.20 (10.7)	173.87 (12.7)	175.0 2.7	174.71 2.9	179.19 (1.0)	177.54 (1.0)	174.8	174.35	186.0 ($^2J_{CC}$ = 35.2)	183.50
3a	NH$_3$	**B**	180.60 (10.0)	180.75 (12.2)	181.37 (2.9)	181.47 (2.5)	180.37 (<1)	183.62 (<1)	183.63	184.25	L	184.87
3a	NH$_3$	**A**	177.71 (10.0)	178.00 (12.1)	181.01 (2.4)	181.24 (2.3)	184.40 (<1)	186.14 (<1)	184.32	184.91	185.56	L
3b	n-BuNH$_2$	**B**	180.04 (9.5)	180.21 (11.7)	180.56 (3.5)	180.69 (3.5)	178.93 (2.0)	180.88 (<1)	182.19	184.43	L	184.89
3b	n-BuNH$_2$	**A**	176.97 (9.5)	177.34 (11.6)	180.14 (3.0)	180.37 (3.5)	184.20 (<1)	186.03 (3.0)	184.03	184.33	184.70	L
4a	MeCN	**A**	178.97 (10.2)	179.02 (11.2)	181.01 (2.4)	181.10 (2.3)	182.95 (<1)	184.85 (<1)	182.35	183.0	186.84	L
4c	MeCN	–	176.55 (11.0)	177.38 (12.8)	174.70 (<1)	L	180.00 (<1)	185.14 (<1)	174.42	174.73	183.11 ($^2J_{CC}$ = 33.2)	185.84
5c[c]	P(OMe)$_3$	**C**	177.32 (9.0)	177.32 (9.9)	174.54 (2.1)	175.90 (<1)	179.29 (<1)	181.67 (<1)	L	178.99	191.12 ($^2J_{CC}$ = 40)	193.15
5c[c]	P(OMe)$_3$	**D**	176.37 (9.2)	176.74 (11.8)	175.00 (2.0)	175.90 (<1)	178.99 (<1)	180.47 (<1)	178.69	L	190.99 ($^2J_{CC}$ = 32.6)	192.82

[a] Assignments are based on the relative size of $^2J_{CH}$ (numbers in parentheses) between the carbonyls and the hydride (see ref 7a) the size of $^2J_{PC}$ (ref 7d) for **5c**. Primed and unprimed letters are interchangeably assigned, except e and e′ in **3** and **4**. [b] See ref 7a. [c] The assignments of each set of resonances to **C** and **D** (Scheme 1) are interchangeable.

Table 3. Crystal Data for 3a, 3f, 4a, and 6

compound	**3a**	**3f**	**4a**	**6**
formula	$C_{13}H_{10}Os_3N_2O_9$	$C_{17}H_{15}Os_3N_2O_9$	$C_{15}H_{10}Os_3N_2O_9$	$C_{16}H_{14}Os_3N_2O_9$
formula weight	908.83	961.92	932.6	932.90
crystal dimensions, mm^3	0.47 × 0.35 × 0.15	0.50 × 0.45 × 0.26	0.14 × 0.19 × 0.23	0.10 × 0.19 × 0.43
radiation, wavelength, A	Mo, 0.71073	Mo, 0.71073	Mo, 0.71073	Mo, 0.71073
temperature, °C	25 ± 1	25 ± 1	25 ± 1	25 ± 1
crystal system	triclinic	orthorhombic	triclinic	monoclinic
space group	$P1$	$Pca2_1$	$P1$	$P2_1/c$
a, Å	17.472 (6)	16.530 (4)	9.586 (2)	16.634 (2)
b, Å	20.915 (5)	17.249 (3)	13.510 (3)	8.872 (2)
c, Å	8.543 (2)	15.955 (5)	9.504 (3)	16.201 (2)
α, deg	80.16	–	70.26 (2)	–
β, deg	78.24 (2)	–	62.30 (1)	119.03 (1)
γ, deg	75.91 (2)	–	77.66 (2)	–
V, Å^3	2940 (2)	4549 (3)	1023 (1)	2091 (1)
Z	6	8	2	4
density, g/cm^3	3.08	2.81	2.60	2.96
absorption coeff μ, cm^{-1}	194.8	335.8	186.3	182.6
rel transmission coeff	0.135–1.000	0.512–1.000	0.462–0.998	0.314–0.999
scan type	ω–2θ	ω–2θ	ω–2θ	ω–2θ
scan rate, deg/min	5.49	8.23	8.23	8.23
scan width, deg	0.8 + 0.350 tan θ	0.9 + 0.350 tan θ	0.9 + 0.350 tan θ	0.8 + 0.350 tan θ
h,k,l ranges	h: −19 to 18 k: −22 to 22 l: 0 to 9	h: 0 to 22 k: 0 to 23 l: −24 to 24	h: −11 to 13 k: −17 to 18 l: 0 to 13	h: −22 to 22 k: −12 to 12 l: −23 to 23
2θ range, deg	4.0–46.0	4.0–60.0	4.0–60.0	4.0–60.0
structure solution	Patterson method	Patterson method	Patterson method	Patterson method
no. of unique data	7070	7274	5951	6455
no. of data used in L.S. refinement with $F_o > 3.0\sigma(F_o)$	6345	4972	4872	4714
weighting scheme, w	$4F_o^2/[\sigma(F_o)^2]^2$	$4F_o^2/[\sigma(F_o)^2]^2$	$4F_o^2/[\sigma(F_o)^2]^2$	$4F_o^2/[\sigma(F_o)^2]^2$
no. of parameters refined	505	558	262	268
R[a]	0.0805	0.0616	0.0579	0.0402
R_w[b]	0.0868	0.0574	0.0610	0.0406
ESD of obs of unit weight (GOF)	2.59	0.97	1.53	0.94

[a] $R = \Sigma[|F_o| - |F_c|]/\Sigma|F_o|$. [b] $R_w = [\Sigma w(|F_o| - |F_c|)^2/\Sigma w|F_o|^2]^{1/2}$.

The reactions of **2** with the amines listed in Table 1 were examined by ^{1}H-NMR. The exchange of the complexed and free amine were slow on the NMR time scale in all cases where coordination of the amines could be detected. The isolation of the crystalline amine complex could only be realized in the presence of large excesses of the amines, and the crystalline compound dissociates when redissolved in polar organic solvents. Table 1 lists values for the formation constants measured by ^{1}H-NMR methods. A 4- and 10-fold molar excess of amine was used in separate experiments and the solutions were monitored for at least 72 h. Equilibrium was reached in about 24 h and with the notable exception of pyridine, no appreciable decomposition was noted over this time period. In all cases, except *tert*-butylamine, a single new hydride resonance appeared at about −13.70 to −13.80 ppm (isomer **B**). As equilibrium is approached, a second hydride resonance appears at −14.0 ppm (isomer **A**) exactly as for **3a**. In the case of pyrrolidine, the initial hydride resonance remains the major component while for the n-, s- and i-butyl cases the resonance at −14.0 ppm becomes the

Table 4. Positional Parameters and Their Estimated Standard Deviations for 3a

atom	x	y	z	B (Å²)[a]	atom	x	y	z	B (Å²)[a]
Os1A	0.42561(7)	0.33110(6)	0.0355(1)	2.48(3)	C12B	0.126(2)	−0.075(2)	0.406(4)	4.5(8)*
Os2A	0.33189(8)	0.31084(6)	−0.1951(1)	2.50(3)	C13B	0.160(2)	0.033(2)	0.157(4)	4.8(8)*
Os3A	0.27548(8)	0.41777(6)	−0.0053(1)	2.50(3)	C21B	0.465(2)	−0.045(1)	0.348(3)	3.1(6)*
O11A	0.466(2)	0.447(1)	0.147(3)	5.2(7)	C22B	0.397(2)	−0.153(1)	0.306(3)	3.3(6)*
O12A	0.586(2)	0.234(1)	0.071(4)	7.5(9)	C23B	0.403(2)	−0.038(2)	0.077(4)	4.3(7)*
O13A	0.341(2)	0.278(1)	0.362(2)	5.1(7)	C31B	0.226(2)	0.161(2)	0.343(4)	5.1(8)*
O21A	0.243(2)	0.399(1)	−0.450(3)	5.9(7)	C32B	0.398(2)	0.113(2)	0.276(4)	4.9(8)*
O22A	0.397(2)	0.183(1)	−0.356(3)	8.4(9)	C33B	0.299(2)	0.090(2)	0.095(4)	4.1(7)*
O23A	0.186(1)	0.258(1)	−0.008(3)	5.1(6)	H1B	0.272	−0.064	0.247	4.0
O31A	0.268(2)	0.508(1)	0.243(2)	5.7(7)	H2B	0.170	−0.094	0.753	7.3
O32A	0.121(1)	0.482(1)	−0.139(3)	5.4(7)	H3B	0.173	−0.024	0.787	7.3
O33A	0.366(2)	0.501(1)	−0.273(3)	5.9(7)	H4B	0.269	−0.136	0.893	10.9
N1A	0.206(1)	0.360(1)	0.195(3)	3.1(5)*	H5B	0.287	−0.066	0.882	10.9
N2A	0.435(2)	0.349(1)	−0.301(3)	3.9(6)*	H6B	0.390	−0.098	0.712	7.6
C1A	0.473(2)	0.359(1)	−0.201(3)	2.7(6)*	H7B	0.357	−0.157	0.687	7.6
C2A	0.544(2)	0.385(2)	−0.287(4)	4.5(8)*	H8B	0.258	0.053	0.637	4.3
C3A	0.546(2)	0.388(2)	−0.463(4)	5.9(9)*	H9B	0.351	0.039	0.602	4.3
C4A	0.469(2)	0.369(2)	−0.482(4)	5.2(9)*	H10B	0.301	0.112	0.611	4.3
C11A	0.454(2)	0.404(1)	0.104(3)	2.6(6)*	Os1C	−0.04237(7)	0.36812(6)	−0.1903(1)	2.74(3)
C12A	0.527(2)	0.271(1)	0.054(3)	3.5(6)*	Os2C	−0.17857(8)	0.30163(6)	−0.0811(1)	2.86(3)
C13A	0.374(2)	0.301(1)	0.238(3)	2.8(6)*	Os3C	−0.01812(8)	0.22683(6)	−0.1624(1)	2.93(3)
C21A	0.276(2)	0.366(1)	−0.352(3)	3.2(6)*	O11C	0.111(2)	0.338(1)	−0.433(3)	6.3(7)
C22A	0.382(2)	0.233(2)	−0.303(4)	5.0(8)*	O12C	−0.063(1)	0.516(1)	−0.260(3)	5.6(7)
C23A	0.241(2)	0.278(2)	−0.080(4)	3.8(7)*	O13C	0.031(2)	0.361(1)	0.108(3)	6.5(8)
C31A	0.274(2)	0.474(1)	0.156(3)	3.4(6)*	O21C	−0.233(2)	0.193(1)	−0.190(3)	7.2(8)
C32A	0.177(2)	0.457(2)	−0.087(4)	3.7(7)*	O22C	−0.344(2)	0.387(1)	0.026(3)	7.5(8)
C33A	0.337(2)	0.469(2)	−0.172(4)	3.9(7)*	O23C	−0.178(2)	0.239(1)	0.270(3)	8(1)
H1A	0.389	0.266	−0.034	4.0	O31C	0.161(1)	0.179(1)	−0.267(3)	7.3(8)
H2A	0.592	0.356	−0.257	5.6	O32C	−0.058(2)	0.090(1)	−0.075(3)	7.3(9)
H3A	0.541	0.428	−0.261	5.6	O33C	0.007(2)	0.220(1)	0.182(3)	6.9(8)
H4A	0.592	0.359	−0.510	7.6	N1C	−0.037(2)	0.234(1)	−0.419(3)	3.7(5)*
H5A	0.546	0.432	−0.516	7.6	N2C	−0.173(2)	0.348(1)	−0.319(3)	3.4(5)*
H6A	0.434	0.405	−0.533	6.9	C1C	−0.111(2)	0.377(1)	−0.369(3)	1.8(5)*
H7A	0.481	0.332	−0.541	6.9	C2C	−0.115(2)	0.412(2)	−0.531(4)	5.6(9)*
H8A	0.241	0.333	0.263	4.0	C3C	−0.228(2)	0.361(2)	−0.438(4)	4.2(7)*
H9A	0.166	0.390	0.255	4.0	C4C	−0.180(3)	0.402(2)	−0.593(5)	7(1)*
H10A	0.181	0.333	0.151	4.0	C11C	0.058(2)	0.350(2)	−0.344(4)	4.4(7)*
Os1B	0.19253(8)	−0.00484(6)	0.3615(1)	2.79(3)	C12C	−0.060(2)	0.462(2)	−0.226(4)	3.6(7)*
Os2B	0.36677(8)	−0.05752(6)	0.3020(1)	2.92(3)	C13C	0.005(2)	0.363(2)	−0.010(4)	3.8(7)*
Os3B	0.30121(8)	0.08138(6)	0.3141(1)	2.94(3)	C21C	−0.213(2)	0.232(1)	−0.141(3)	3.0(6)*
O11B	0.079(1)	0.103(1)	0.538(3)	5.7(7)	C22C	−0.284(2)	0.358(1)	−0.027(3)	3.5(7)*
O12B	0.090(2)	−0.112(1)	0.446(3)	7.1(8)	C23C	−0.175(2)	0.263(2)	0.144(4)	4.6(8)*
O13B	0.139(2)	0.051(2)	0.039(3)	9 (1)	C31C	0.096(2)	0.199(1)	−0.227(3)	3.5(7)*
O21B	0.523(1)	−0.036(1)	0.366(3)	5.1(6)	C32C	−0.042(2)	0.141(2)	−0.118(4)	4.3(7)*
O22B	0.421(2)	−0.207(1)	0.308(4)	8.1(9)	C33C	−0.003(2)	0.223(2)	0.054(4)	4.0(7)*
O23B	0.425(2)	−0.033(2)	−0.058(3)	9 (1)	H1C	−0.136	0.369	−0.043	4.0
O31B	0.175(2)	0.211(1)	0.347(3)	6.6(8)	H2C	−0.067	0.396	−0.601	7.4
O32B	0.455(1)	0.136(1)	0.249(3)	6.6(8)	H3C	−0.122	0.458	−0.529	7.4
O33B	0.298(2)	0.097(1)	−0.041(3)	7.3(9)	H4C	−0.214	0.443	−0.628	8.6
N1B	0.303(2)	0.070(1)	0.579(3)	3.4(5)*	H5C	−0.162	0.376	−0.679	8.6
N2B	0.314(2)	−0.072(1)	0.543(3)	3.6(5)*	H6C	−0.278	0.388	−0.399	5.5
C1B	0.240(2)	−0.049(1)	0.572(3)	2.3(5)*	H7C	−0.235	0.321	−0.464	5.5
C2B	0.203(2)	−0.064(2)	0.743(4)	5.6(9)*	H8C	−0.092	0.248	−0.424	4.7
C3B	0.278(3)	−0.097(2)	0.823(5)	9(1)*	H9C	−0.009	0.265	−0.485	4.7
C4B	0.344(2)	−0.111(2)	0.695(4)	5.9(9)*	H10C	−0.016	0.192	−0.456	4.7
C11B	0.123(2)	0.063(1)	0.468(3)	3.0(6)*					

[a] Starred atoms were refined isotropically. Anisotropically refined atoms are given in the form of the isotropic equivalent displacement parameter defined as: $(4/3)[a^2B(1,1) + b^2B(2,2) + c^2B(3,3) + ab(\cos\gamma)B(1,2) + ac(\cos\beta)B(1,3) + bc(\cos\alpha)B(2,3)]$.

dominant component, as equilibrium is approached, as for **3a**. No complex formation could be detected under these conditions for Et_3N, Et_2NH, and $PhNH_2$ (i.e., $K_{eq} < 10^{-3}$).

Crystals of X-ray quality of $(\mu\text{-H})(\mu\text{-}\eta^2\text{-}\overline{C{=}N(CH_2)_3})\text{-}Os_3(CO)_9\overline{NH(CH_2)_4}$ (**3f**) were grown from methylene chloride–hexane solutions containing a 10-fold excess of pyrrolidine. The solid state structure of **3f** is shown in Figure 2, and crystal data are listed in Table 3, atomic coordinates in Table 6, and selected distances and bond angles in Table 7. This complex crystallizes with two unique molecules in the asymmetric unit which differ from each other slightly in the metal–metal and metal–ligand bond distances and angles. The C(1) and N atoms of the pyrrolidine ring were treated as completely disordered and appear as DN1 and DN2 for both molecules in the asymmetric unit (Table 7). The molecule consists of an isosceles triangle of osmium atoms with a longer metal–metal bond along the edge bridged by the hydride and the μ-η^2 imidoyl ligands. The pyrrolidine ligand is coordinated to the unbridged osmium atom (Os2) and is on the same face of the triangle as the imidoyl ligand as proposed for isomer **B**. The Os2–N2 bond is significantly longer than the Os1–DN bond (average values of 2.25 (2) and 2.12 (2) Å, respectively) but about the same as the analogous bond in **3a**. The overall geometry closely resembles that of **1** and **3a** with regard to the disposition of the carbonyl groups and the imidoyl ligand.[7a]

Table 5. Selected Bond Distances (Å) and Angles (deg) for 3a[a]

	A	B	C
	Bond Distance		
Os1−Os2	2.946(2)	2.944(2)	2.955(2)
Os1−Os3	2.851(2)	2.850(2)	2.857(2)
Os2−Os3	2.849(2)	2.863(2)	2.869(2)
Os3−N1	2.24(2)	2.24(2)	2.25(2)
Os2−N2	2.11(3)	2.08(2)	2.09(2)
Os1−C1	2.06(3)	2.11(3)	2.08(2)
Os−C(CO)[b]	1.92(3)	1.91(3)	1.92(3)
C−O[b]	1.14(4)	1.13(4)	1.12(4)
C1−N2	1.25(5)	1.26(4)	1.33(4)
C1−C2	1.49(5)	1.48(4)	1.46(4)
C2−C3	1.49(5)	1.55(6)	1.42(7)
C3−C4	1.54(6)	1.43(6)	1.63(5)
	A	**B**	**C**
	Angles		
Os1−Os2−Os3	58.92(4)	58.77(4)	58.23(4)
Os2−Os3−Os1	62.25(4)	62.03(4)	62.13(4)
Os2−Os1−Os3	58.83(4)	59.19(4)	59.14(4)
Os−C−O[b]	175.(3)	175.(3)	174.(3)
Os2−Os3−N1	94.4(6)	91.5(6)	89.7(6)
Os1−Os3−N1	93.8(6)	91.8(7)	90.4(6)

[a] Numbers in parenthesis are estimated standard deviations. [b] Average values.

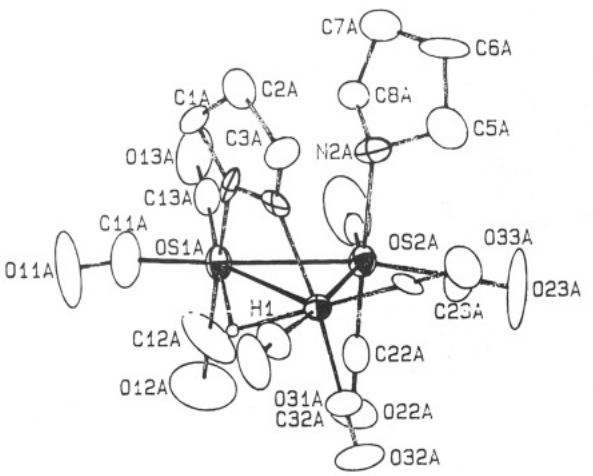

Figure 2. Solid state structure of **3f** showing the calculated position of the hydride.

Given the very similar values for the chemical shifts for the initially formed amine adducts of **2** (Table 1) and the fact that **3f** crystallizes in isomeric form **B** (crystals obtained show only one hydride resonance at −13.79 ppm initially on redissolution), we propose that coordination of these amines on the same face of the cluster as the imidoyl ligand is the kinetic product in all cases. We have observed similar behavior for the reactions of **2** with isocyanides and HX (X = Cl, Br, CF_3CO_2).[7a,11] The structure of the second isomer formed which shows a chemical shift of −14.00 ppm and is the major isomer for (μ-H)(μ-C=N(CH_2)$_3$Os$_3$(CO)$_9$L (L = n-BuNH$_2$, **3b**, i-BuNH$_2$, **3c**, s-BuNH$_2$, **3d**) (Table 1) can be deduced by an examination of the ^{13}C-NMR for **3b**. The ^{13}C-NMR (in the carbonyl region) of **3b** shows the expected nine resonances and with the aid of the proton coupled spectrum we can make the partial assignments shown in Table 2. The spectrum of **3b** after 1 h closely resembles that of the initial spectrum of **3a** and we can therefore assign its structure to isomer **B** (Scheme 1). After 48 h the ^{13}C-NMR of **3b** in the carbonyl region

(11) (a) Rosenberg, E.; Kabir, S. E.; Yin, M.; Nabuko, N.; Milone, L.; Gobetto, R.; Osella, D. Manuscript in preparation. (b) Hardcastle, K.; Irving, M. *J. Cluster Sci.* **1993**, *4*, 77.

Table 6. Positional Parameters and Their Estimated Standard Deviations for 3f

atom	*x*	*y*	*z*	*B* (Å^2)[a]
Os1A	0.13885(7)	−0.32843(7)	−0.10725(7)	3.25(2)
Os2A	0.06054(7)	−0.46336(6)	−0.040	3.20(2)
Os3A	0.02187(6)	−0.31482(6)	0.03040(7)	2.79(2)
O11A	0.214(2)	−0.179(1)	−0.172(2)	10.5(9)
O12A	0.038(2)	−0.342(2)	−0.267(1)	13(1)
O13A	0.279(1)	−0.425(2)	−0.169(2)	8.1(7)
O21A	0.143(2)	−0.581(2)	−0.163(2)	10.1(9)
O22A	−0.078(1)	−0.444(2)	−0.169(2)	8.3(7)
O23A	−0.057(2)	−0.572(2)	0.048(2)	11.7(8)
O31A	−0.013(2)	−0.152(1)	0.087(2)	6.7(6)
O32A	−0.146(1)	−0.320(2)	−0.043(2)	8.8(8)
O33A	−0.028(1)	−0.404(1)	0.183(1)	6.3(6)
N2A	0.159(1)	−0.483(1)	0.054(2)	4.1(5)
DN1A	0.197(1)	−0.309(1)	0.009(2)	2.9(5)
DN2A	0.144(1)	−0.304(1)	0.072(1)	2.9(5)
C1A	0.278(1)	−0.290(2)	0.034(2)	3.6(6)
C2A	0.271(2)	−0.290(2)	0.134(2)	4.5(7)
C3A	0.180(2)	−0.284(2)	0.151(2)	3.7(6)
C5A	0.134(2)	−0.524(2)	0.139(2)	5.9(9)
C6A	0.215(2)	−0.551(2)	0.175(2)	6.3(9)
C7A	0.280(2)	−0.536(2)	0.115(3)	7(1)
O33B	−0.096(1)	0.119(1)	−0.241(1)	6.3(5)
N2B	0.138(1)	0.188(1)	−0.163(1)	3.6(5)
DN1B	0.163(1)	0.020(1)	−0.129(1)	2.7(5)
DN2B	0.097(1)	0.015(1)	−0.174(1)	2.0(4)
C1B	0.239(2)	0.003(2)	−0.179(1)	3.1(6)
C2B	0.208(2)	−0.011(2)	−0.268(2)	4.1(7)
C3B	0.109(2)	−0.006(2)	−0.263(2)	3.5(6)
C5B	0.103(2)	0.227(2)	−0.236(2)	4.7(7)
C6B	0.175(2)	0.238(2)	−0.290(2)	5.1(8)
C7B	0.248(2)	0.229(2)	−0.241(2)	5.4(6)
C8B	0.220(2)	0.223(2)	−0.152(2)	4.6(7)
C11B	0.177(2)	−0.063(2)	0.024(2)	3.4(6)
C12B	0.105(2)	0.056(2)	0.115(2)	4.2(7)
C13B	0.235(1)	0.093(1)	0.016(1)	2.4(5)
C21B	0.132(2)	0.249(2)	0.015(2)	5.4(8)
C22B	−0.001(2)	0.169(2)	0.050(2)	5.0(8)
C23B	−0.017(2)	0.250(2)	−0.091(2)	4.5(7)
C31B	−0.043(2)	−0.074(2)	−0.128(2)	3.6(6)
C32B	−0.094(1)	0.048(2)	−0.026(2)	4.5(7)
C33B	−0.061(1)	0.091(2)	−0.192(2)	5.1(8)

[a] Anisotropically refined atoms are given in the form of the isotropic equivalent displacement parameter defined as: $(4/3)[a^2B(1,1) + b^2B(2,2) + c^2B(3,3) + ab(\cos\gamma)B(1,2) + ac(\cos\beta)B(1,3) + bc(\cos\alpha)B(2,3)]$.

Table 7. Selected Distances (Å) and Angles (deg) for 3f

	A	B
	Distances	
Os1−Os2	2.872(2)	2.856(1)
Os1−Os3	2.936(2)	2.929(1)
Os2−Os3	2.869(1)	2.881(1)
Os1−DN1[b]	2.11(2)	2.12(2)
Os3−DN2[b]	2.14(2)	2.12(2)
Os2−N2	2.24(2)	2.27(2)
DN1−DN2[b]	1.33(3)	1.31(3)
DN1−C1[b]	1.44(3)	1.51(3)
DN2−C3[b]	1.44(4)	1.48(3)
C1−C2	1.60(4)	1.52(4)
C2−C3	1.52(4)	1.64(4)
C5−C6	1.52(5)	1.49(4)
C6−C7	1.46(5)	1.46(4)
C7−C8	1.59(5)	1.50(4)
Os−C(CO)[c]	1.91(3)	1.90(3)
C−O[c]	1.14(4)	1.14(4)
	A	**B**
	Angles	
Os3−Os2−N2	90.0(7)	86.6(7)
Os3−Os1−C1	90.5(8)	86.0(8)
Os−C−O[c]	175.(3)	175(3)

[a] Numbers in parenthesis are estimated standard deviations. [b] Denotes disordering of C and N. [c] Average values.

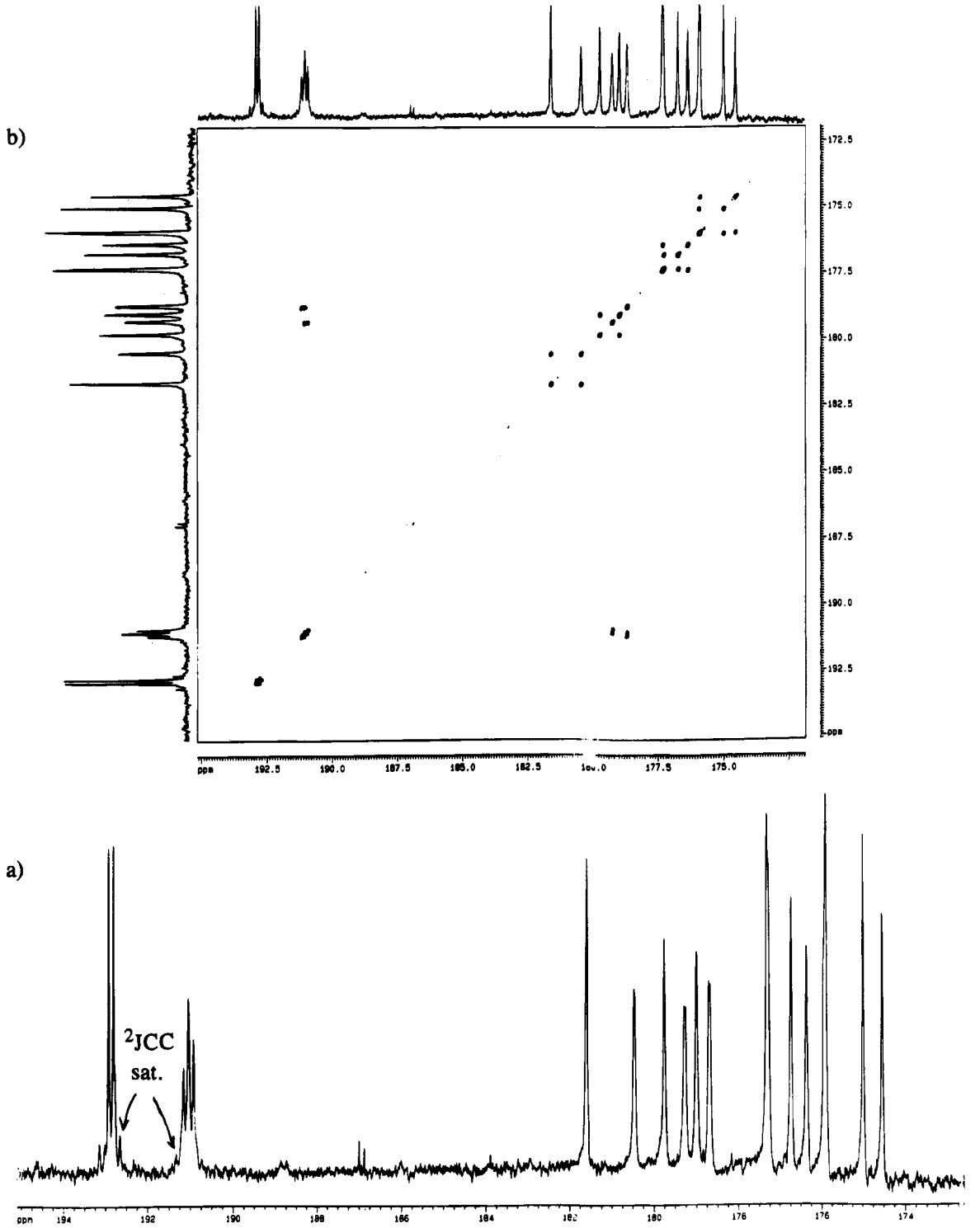

Figure 3. (a) ^{13}C-NMR spectrum in the carbonyl region of **5c** at 90 MHz in $CDCl_3$ at +23 °C. (b) 2D-^{13}C-EXSY spectrum of **5c** in the carbonyl region at 90 MHz in $CDCl_3$ at +23 °C; mixing time = 0.5 s.

has changed to a spectrum which closely resembles isomer **A** of **3a** (Table 2). Most importantly, we observe no *trans*-diaxial coupling in either isomer of **3b**. Thus it appears from both the solid state structural and solution NMR evidence that both **3a** and **3b** have similar structures in solution but that **3f** slightly prefers the *syn*-isomer **B**. In order to further corroborate our conclusions from the solution NMR work, we measured the ^{13}C-NMR of (μ-H)(μ-η^2-C=N(CH$_2$)$_3$)Os$_3$(CO)$_9$(P(OMe)$_3$) (**5c**) at +23 °C where we know the phosphine ligand is in an equatorial position and exists as two radial isomers **C** and **D** (Scheme 2).[7d] The ^{13}C-NMR of the mutually *trans*-diaxial carbonyls shows the expected satellites (Figure 3a). Furthermore, a ^{13}C-2D-EXSY experiment shows exchange cross peaks for only one of the two axial carbonyls on the phosphine-substituted osmium atom for each isomer (**C** and **D**) consistent with a tripodal motion of the phosphine, involving one radial and one axial carbonyl as previously shown for the related carbonyl exchange in **1** (Figure 3b).[3a] We recently showed that the interconversion of **C** and **D** is an intramolecular process and that phosphine dissocia-

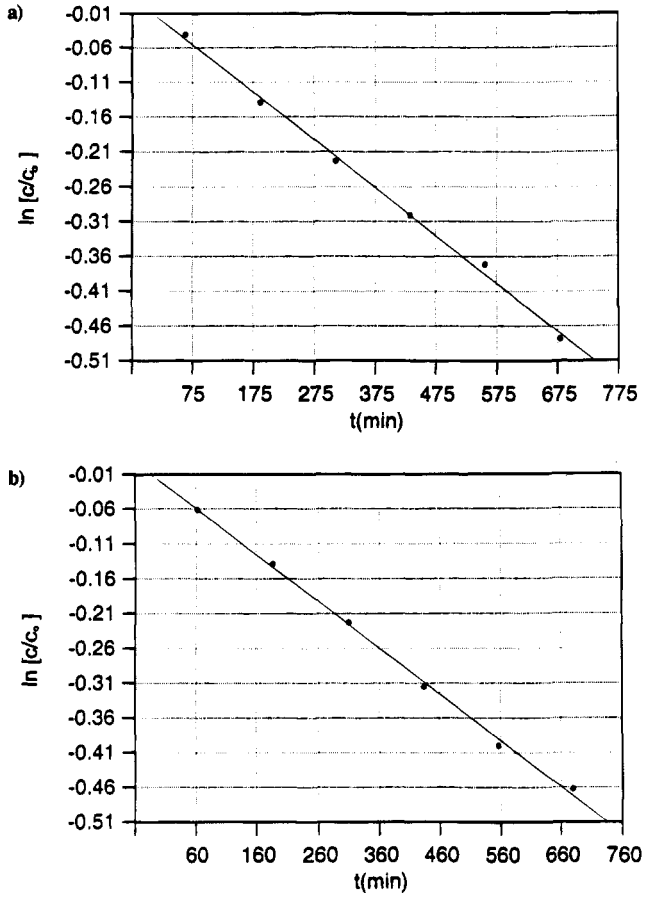

Figure 4. (a) Kinetic plot **B** to **A** isomerization for **3b** in the presence of a 10-fold excess of n-butylamine. (b) Kinetic plot of **B** to **A** isomerization for **3b** in the presence of a 20-fold excess of n-butylamine.

Scheme 2

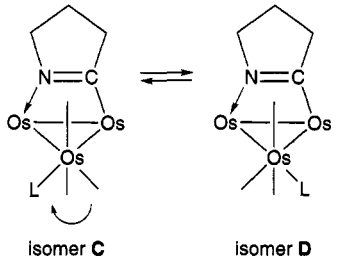

tion takes place at appreciable rates only at elevated temperatures.[7d,e] We have examined the rate of conversion of **B** to **A** in the presence of a 10- and 20-fold excess of n-butylamine directly after formation **3b** from **2**. In both experiments, conversion of **B** to **A** follows first order kinetics and gives first order rate constants of 6.87 $\pm$ 0.6 $\times$ 10^{-4} m^{-1} and 6.67 $\pm$ 0.6 $\times$ 10^{-4} m^{-1} (Figure 4). These results are consistent with either an intramolecular or a dissociative process for the conversion of **B** to **A**. In order to resolve this point, we examined the relationship between exchange with free amine and the conversion of **B** to **A**. A 20-fold excess of n-butylamine was added to a solution of **2** in $CDCl_3$. After 1 h, ^{1}H-NMR indicated ~90% conversion to **3b** and ~95% of **3b** was in isomeric form **B**. At this time, a 24-fold excess of pyrrolidine was added and the ^{1}H-NMR was monitored every hour for 15 h. After 1 h, hydride resonances assignable to **3f** began to appear. This continued over the course of the monitoring period until at the end of 15 h, isomers **B** and **A** of **3f** were present

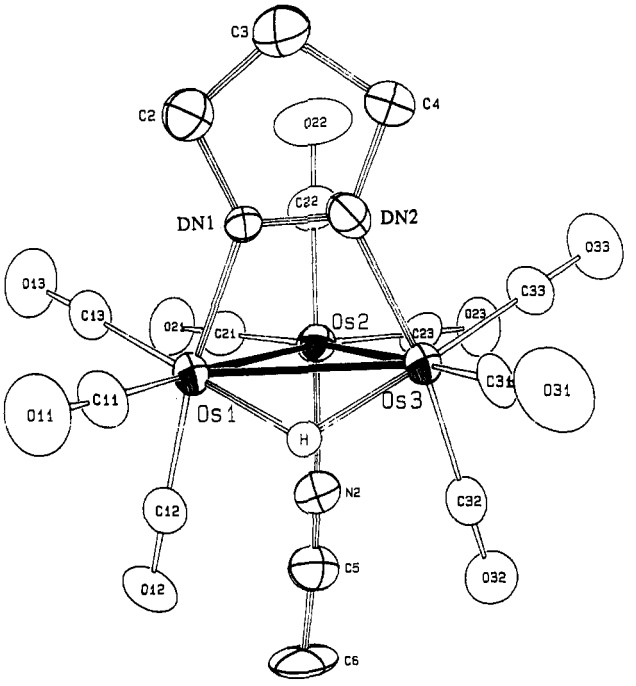

Figure 5. Solid state structure of **4a** showing the calculated position of the hydride.

in comparable amounts to those of **3b**. In addition, the conversion of **B** to **A** for **3b** during the 15 h period was noticeably repressed (~25%) compared to the experiments done in the absence of pyrrolidine (~50%). These results conclusively show that the isomerization of **B** to **A** is a dissociative first order process independent of amine concentration. The initial formation of isomer **B** of **3b** is sensitive to amine concentration since the k_{obs} values under these pseudo first order conditions are 5.6 $\times$ 10^{-2} m^{-1} (20-fold excess) and 3.1 $\times$ 10^{-2} m^{-1} (10-fold excess), giving second order rate constants of 8.0 and 7.8 $\pm$ 0.2 $\times$ 10^{-2} M^{-1} m^{-1}. This value is between the values of 1.2 $\times$ 10^{-2} and 5.0 $\times$ 10^{-1} M^{-1} m^{-1} obtained for PPh_3 and PMe_3 reacting with **2**.[3c] Taken together, these data point to a reaction pathway in which the μ_3-imidoyl undergoes coordination in a second order reaction forming isomer **B**. This is followed by a slower ligand dissociation to give a μ-imidoyl species which undergoes carbonyl group rearrangement and a relatively rapid ligand recapture (Scheme 1). We cannot exclude a rapid preequilibrium between μ- and μ_3-imidoyl species in the first step which would show a first order dependence on L until the rate of L association is fast with respect to imidoyl reassociation. Proving this would require examination over a much wider range of concentrations where secondary reactions lead to cluster degradation.

B. Complexes of 2 with Nitriles. The coordination of RCN (R = Me, Ph) with **2** proceeds analogously as with amines. The formation constants for (μ-H)(μ-η^2-C=N(CH$_2$)$_3$)Os$_3$(CO)$_9$(RCN) (R = CH_3, **4a**; R = C_6H_5, **4b**) are considerably smaller being 0.035 and 0.070 for acetonitrile and benzonitrile, respectively, and these values do not reflect the steric sensitivity seen with the amines. In contrast to the amines as well is the fact that only one isomer is observed at room temperature form 1 h to 4 days after addition of the nitrile to solutions of **2**.

The solid state structure of **4a** is shown in Figure 5,

Table 8. Positional Parameters and Their Estimated Standard Deviations for 4a

atom	x	y	z	B (Å²)[a]
Os1	0.43165(5)	0.18450(4)	0.20444(5)	2.43(1)
Os2	0.18254(5)	0.22113(4)	0.10473(5)	2.42(1)
Os3	0.23123(5)	0.38198(4)	0.20599(5)	2.30(1)
O11	0.696(1)	0.155(1)	0.308(1)	6.1(3)
O12	0.672(1)	0.2141(9)	−0.153(1)	5.3(3)
O13	0.416(1)	−0.0463(8)	0.265(1)	5.8(3)
O21	0.209(1)	0.0128(7)	0.032(1)	4.9(3)
O22	−0.048(1)	0.132(1)	0.457(1)	5.9(3)
O23	−0.087(1)	0.3285(8)	0.010(1)	4.9(3)
O31	0.294(1)	0.546(1)	0.320(1)	6.1(3)
O32	0.358(1)	0.5115(8)	−0.154(1)	4.8(3)
O33	−0.111(1)	0.4582(9)	0.284(1)	5.0(3)
N2	0.341(1)	0.2821(8)	−0.143(1)	3.0(2)
N1/C1*	0.262(1)	0.1898(8)	0.440(1)	2.6(3)
C1/N1*	0.169(1)	0.2754(9)	0.443(1)	2.9(3)
C2	0.219(2)	0.115(1)	0.611(2)	4.1(4)
C3	0.082(2)	0.173(1)	0.727(2)	4.4(4)
C4	0.053(2)	0.280(1)	0.609(1)	3.5(3)
C5	0.423(2)	0.305(1)	−0.280(1)	3.8(3)
C6	0.531(2)	0.331(1)	−0.453(2)	5.9(5)
C11	0.594(1)	0.170(1)	0.269(1)	3.4(3)
C12	0.582(2)	0.203(1)	−0.019(2)	3.9(4)
C13	0.418(1)	0.040(1)	0.242(1)	3.2(3)
C21	0.201(2)	0.091(1)	0.060(2)	3.9(4)
C22	0.044(1)	0.167(1)	0.323(2)	3.5(3)
C23	0.016(1)	0.290(1)	0.046(1)	3.0(3)
C31	0.275(1)	0.4819(9)	0.277(1)	2.7(3)
C32	0.310(1)	0.463(1)	−0.024(1)	3.3(3)
C33	0.017(1)	0.428(1)	0.252(1)	3.3(3)
H	0.438	0.329	0.156	4.0

[a] Anisotropically refined atoms are given in the form of the isotropic equivalent displacement parameter defined as: $(4/3)[a^2B(1,1) + b^2B(2,2) + c^2B(3,3) + ab(\cos\gamma)B(1,2) + ac(\cos\beta)B(1,3) + bc(\cos\alpha)B(2,3)]$.

Table 9. Selected Distances (Å) and Bond Angles (deg) for 4c[a]

Distances	
Os1−Os2	2.8507(7)
Os1−Os3	2.9357(6)
Os2−Os3	2.8512(7)
Os1−DN1[b]	2.08(1)
Os3−DN2[b]	2.10(1)
Os2−N2	2.10(1)
DN1−DN2[b]	1.30(1)
DN1−C2[b]	1.51(2)
DN2−C4[b]	1.46(2)
C2−C3	1.53(2)
C3−C4	1.56(2)
C5−C6	1.44(2)
Os−C(CO)[c]	1.89(1)
C−O[c]	1.14(2)
Angles	
Os1−Os2−Os3	61.98(2)
Os1−Os3−Os2	59.00(2)
Os2−Os1−Os3	59.02(2)
Os1−Os2−N2	90.3(3)
Os3−Os2−N2	92.5(3)
Os2−Os1−DN1[b]	88.3(3)
Os2−Os3−DN2[b]	87.5(3)
DN1−DN2−C4[b]	114(1)
DN2−DN1−C2[b]	112(1)
DN1−C2−C3[b]	105(1)
C2−C3−C4	104(1)
Os−C−O[c]	177(2)

[a] Numbers in parenthesis are estimated standard deviations. [b] Denotes disordering of C and N. [c] Average values.

crystal data are given in Table 3, atomic coordinates in Table 8, and selected distances and angles in Table 9. In the case of **4a**, there is only one molecule in the asymmetric unit but like **3f**, the C(1) and N(1) positions are disordered and are labeled DN1 and DN2 in the tables. In sharp contrast to **3f**, the nitrile ligand occupies an axial position on the opposite face of the cluster as the imidoyl ligand (isomer **A**, scheme 1). The overall geometry of the cluster is again very similar to **1**. The Os2−N2 bond length of 2.10 (1) Å is considerably shorter than the related metal−nitrogen bond lengths in **3a** and **3f** but is very similar to those found in the osmium cluster nitrile derivatives $Os_3(CO)_{10}(CH_3CN)_2$ and $Os_3(CO)_{11}(CH_3CN)$.[12]

It was very puzzling at first that only one isomer of **4a** is observed in solution until it was considered that a rearrangement of **B** to **A** (Scheme 1) could be much faster for the nitrile ligand than for the amine ligands. Indeed, when a 20-fold excess of acetonitrile is added to a solution of **2** in $CDCl_3$ at −50 °C, a hydride resonance at −14.30 ppm is initially observed. After the solution is warmed to room temperature over the course of 1 h, we observe a new hydride resonance at −14.36 ppm in a relative intensity of 8:1 with the initially observed peak at −14.30 ppm. Over the course of several hours at room temperature the peak at −14.30 gradually decreases. Thus the overall behavior of **4a** in solution conforms to the amine complexes but the **B** to **A** conversion is markedly faster.

C. The Reaction of 1 with Trimethylamine *N*-Oxide in Acetonitrile. The results presented so far show that for a range of nitrogen donor ligands the kinetic product results from apparent displacement of the C=N bond from the unbridged osmium atom in **2**. The reaction of **1**, however, with trimethylamine *N*-oxide in acetonitrile leads to the formation of the isomeric $(\mu\text{-H})(\mu\text{-}\eta^2\text{-}\overline{C{=}N(CH_2)_3})Os_3(CO)_9(CH_3CN)$ (**4c**) (eq 3), where the nitrile ligand is coordinated to the osmium

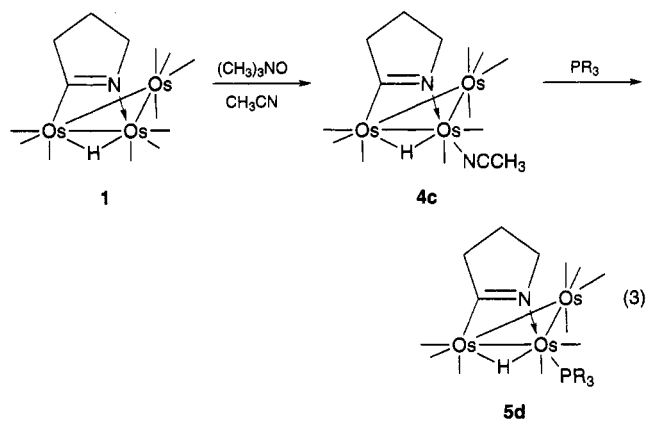

atom bound to the nitrogen of the imidoyl ligand. This is evident from the ^{13}C-NMR of **4c** which shows the expected nine resonances, the presence of a pair of *trans*-axial resonances with the expected $^{13}C-^{13}C$ satellites ($^2J_{C-C}$ = 33.2 Hz). The proton-coupled spectrum allows a partial assignment of resonances as for **3a** and **3b** but chemical evidence for the proposed structure comes from the reaction of **4c** with triphenylphosphine which yields $(\mu\text{-H})(\mu\text{-}\eta^2\text{-}\overline{C{=}N(CH_2)_3})Os_3(CO)_9(PPh_3)$ (**5d**) (eq 3), for which a solid state structure has been done.[7d]

The ^{13}C-NMR of **4a** is distinctly different and shows no *trans*-diaxial satellites. Reaction of **4a** with triphenylphosphine on the other hand gives only **5a**, which has also been structurally characterized (eq 4).[7d] Thus,

(12) Johnson, B. F. G.; Lewis, J.; Dawson, P. A.; Puga, J.; Ruthby, P. R.; Rosales, M. *J. Chem. Soc., Dalton Trans.* **1982**, 235.

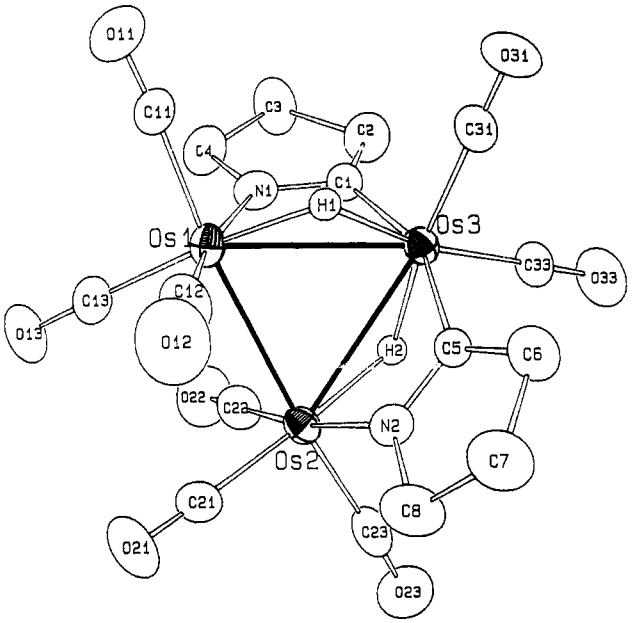

Figure 6. Solid state structure of **6** showing the calculated position of the hydrides.

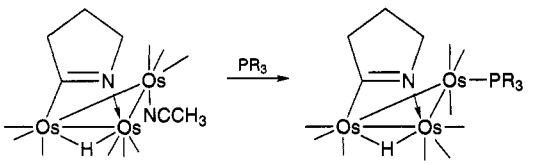

4a **5a**

by starting with **1**, converting to **4c** or by starting with **2** or **4a** we can control the regiochemistry of substitution in this class of molecules.

D. Thermolysis of 3f. Thermolysis of the amine adducts **3a–f** at temperatures of 60–100 °C results primarily in reversion to **2** along with minor, nonspecific decomposition. In the specific case of **3f**, however, reflux in cyclohexane in the presence of a 5-fold excess of pyrrolidine yields ~13% conversion to $(\mu\text{-H})_2(\mu\text{-}\eta^2\text{-}\overline{C{=}N(CH_2)_3})_2Os_3(CO)_8$ (**6**) (eq 5) which we have characterized by ^{1}H-NMR, infrared, and X-ray diffraction techniques. Lower yields of **6** are realized by thermolysis of **3f**. The structure of **6** is shown is in Figure 6, crystal data in Table 3, atomic coordinates in Table 10, and selected distances and angles in Table 11. The structure consists of an Os_3 triangle with two longer and one shorter metal–metal bonds. The longer edges are each bridged by a μ-hydride and μ-imidoyl ligand. The imidoyl ligands are disposed toward opposite faces of the triangle with both carbon atoms bound to Os3. The molecule possesses a two-fold axis which passes through Os3 and bisects the Os1–Os2 edge. The metal–ligand and intraligand bond distances are fairly typical for the imidoyl ligand.[3] This general type of structure has been observed in reactions of other heterocycles with triosmium clusters but the direct precursor (i.e., 3f) to these 2:1 heterocycle cluster structures was not previously known.[13]

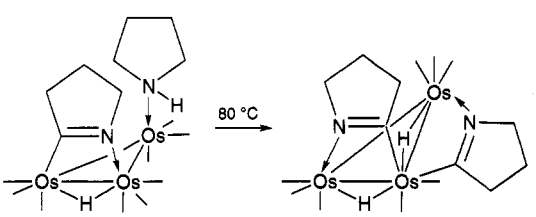

3f **6**

Table 10. Positional Parameters and Their Estimated Standard Deviations for 6

atom	*x*	*y*	*z*	*B* (Å^2)[a]
Os1	0.21908(2)	0.05069(4)	0.01525(2)	2.216(6)
Os2	0.27399(2)	0.27363(4)	−0.07413(2)	2.161(6)
Os3	0.25894(2)	−0.04442(4)	−0.13689(2)	2.084(6)
O11	0.1586(5)	−0.2076(9)	0.0982(5)	5.3(2)
O12	0.0316(5)	0.196(1)	−0.0919(6)	6.4(2)
O13	0.2801(5)	0.2619(8)	0.1838(4)	4.4(2)
O21	0.1808(5)	0.5142(9)	−0.0171(5)	6.0(2)
O22	0.4486(5)	0.290(1)	0.1168(5)	5.1(2)
O23	0.3562(5)	0.490(1)	−0.1598(5)	5.6(2)
O31	0.1644(5)	−0.3415(7)	−0.2097(5)	4.7(2)
O33	0.3601(5)	−0.0889(9)	−0.2456(5)	5.1(2)
N1	0.3460(4)	−0.0606(8)	0.0635(5)	2.6(2)
N2	0.1567(4)	0.2258(8)	−0.2063(4)	2.4(1)
C4	0.4177(6)	−0.106(1)	0.1616(6)	3.4(2)
C3	0.4789(7)	−0.219(1)	0.1460(6)	4.4(3)
C2	0.4487(6)	−0.207(1)	0.0382(6)	3.8(2)
C1	0.3607(6)	−0.1152(9)	−0.0024(5)	2.5(2)
C8	0.0848(7)	0.327(1)	−0.2765(7)	4.0(3)
C7	0.0251(8)	0.220(1)	−0.3576(7)	4.6(3)
C6	0.0778(7)	0.067(1)	−0.3348(6)	3.6(2)
C5	0.1561(5)	0.0914(9)	−0.2358(5)	2.1(2)
C11	0.1809(6)	−0.116(1)	0.0656(5)	3.1(2)
C12	0.1016(7)	0.143(1)	−0.0514(6)	4.0(2)
C13	0.2587(6)	0.181(1)	0.1221(6)	3.0(2)
C21	0.2168(7)	0.426(1)	−0.0389(6)	3.4(2)
C22	0.3839(6)	0.285(1)	0.0454(6)	3.1(2)
C23	0.3231(7)	0.408(1)	−0.1325(6)	3.6(2)
C31	0.1998(6)	−0.230(1)	−0.1814(5)	3.0(2)
C33	0.3221(6)	−0.074(1)	−0.2030(5)	3.0(2)
H1	0.1712	−0.0548	−0.0967	4.0
H2	0.3363	0.1217	−0.0975	4.0

[a] Anisotropically refined atoms are given in the form of the isotropic equivalent displacement parameter defined as: $(4/3)[a^2B(1,1) + b^2B(2,2) + c^2B(3,3) + ab(\cos\gamma)B(1,2) + ac(\cos\beta)B(1,3) + bc(\cos\alpha)B(2,3)]$.

Table 11. Selected Bond Distances (Å) and Angles (deg) for 6[a]

atom 1	atom 2	distance	atom 1	atom 2	distance
Os1	Os2	2.8509(5)	N1	C1	1.30(1)
Os1	Os3	2.9536(5)	C1	C2	1.52(1)
Os2	Os3	2.9636(5)	C2	C3	1.57(1)
Os1	N1	2.107(7)	C3	C4	1.54(2)
Os2	N2	2.125(5)	C4	N1	1.506(9)
Os3	C1	2.093(6)	N2	C5	1.28(1)
Os3	C5	2.077(7)	C5	C6	1.51(1)
Os1	H1	1.8440(3)	C6	C7	1.56(1)
Os2	H2	1.8485(4)	C7	C8	1.54(1)
Os3	H1	1.8545(4)	C8	N2	1.49(1)
Os3	H2	1.8544(3)	C	O(CO)	1.13(1)[b]
Os	C(CO)	1.90(3)[b]			

atom 1	atom 2	atom 3	angle	atom 1	atom 2	atom 3	angle
C4	N1	C1	113.6(7)	C8	N2	C5	114.8(6)
N1	C1	C2	111.7(6)	N2	C5	C6	112.1(6)
C1	C2	C3	103.8(9)	C5	C6	C7	102.7(7)
C2	C3	C4	105.1(7)	C6	C7	C8	106.4(7)
C3	C4	N1	104.4(8)	C7	C8	N2	102.9(8)
Os1	Os2	Os3	61.02(1)	Os1	Os3	Os2	57.60(1)
Os2	Os1	Os3	61.37(1)	Os	C	O(CO)[b]	178.(2)

[a] Numbers in parentheses are estimated standard deviations in the least significant digits. [b] Average values.

(13) Eisenstadt, A.; Giandomenico, C. M.; Frederick, M. F.; Laine, R. M. *Organometallics* **1985**, *4*, 2033.

Discussion

There are two important trends in the data (Table 1). First, there is a clear dependence of the formation constant on the cone angle of the amine, with angles >120° leading to little or no complex formation (t-$BuNH_2$, Et_2NH, Et_3N). Secondly, the bulkier ligands slightly favor the initially formed isomer **B** (molecule B of **3a**) which, based on the solid state structures of **3a** and **3f**, has the amine and the μ-imidoyl on the same face of the cluster. This suggests that the axial carbonyls *trans* to the μ-imidoyl ligand provide a slightly more crowded environment to the axial ligand on the unbridged osmium atom. The more diffuse π-electron density of the carbonyls may exert more repulsion than the tighter σ bond framework of the μ-imidoyl ligand, but this difference is apparently small. As might be expected, the pure donor amine ligands are found only in axial positions, directly *trans* to a π-acid carbonyl ligand.

The rate of the dissociative isomerization (Scheme 1) is much slower for all the ligands reported here compared to the intramolecular process associated with the more bulky phosphine ligands which occupy radial positions only on the unbridged osmium atom in **5a** and **5c**. Since less bulky ligands (e.g., CO, CNR) have relatively high barriers to tripodal motion, steric distortion of the geometry around the unbridged osmium must be responsible for the lower barriers observed with phosphines. Thus, the barriers calculated for intramolecular tripodal motion in the PR_3 complexes such as **5a** and **5c**, are 59.6, 69.5, and 67.5 ± 2 kJ/mol for R = Ph, Me, OMe, respectively, illustrating the inverse dependence on steric bulk.[14] In sharp contrast, the more labile nitrogen donors undergo isomerization by a dissociative pathway and it is reasonable that the order for the rates of the rearrangement, **B** to **A**, in the axially substituted series is **4a** ≫ **3a**,**b**. This order follows the expected bond strengths along the series and the magnitude of the formation constants reported here (**4a** ≪ **3a**,**b**). However, K_f for **3a** > **3b** while isomerization rates are almost the same. This may result from entropic effects on the rate arising from the alkyl group. Overall, these results imply that the depth of the potential well for L in the series controls the rate of the dissociative isomerization (Scheme 1). Most of the synthetic studies of osmium clusters with nitrogen containing ligands have focused on aromatic nitrogen heterocycles[16] and amine-substituted unsaturated hydrocarbons[17] with the goal of activating C−H, C−C, or C−N bonds. As a result, there is a relative paucity of structural information on simple amine adducts of osmium clusters. The osmium nitrogen bond lengths in **3a** and **3f** (2.24 (2) Å) are very similar to those reported for the trimethyl amine adduct, $(\mu\text{-H})(\mu_3\text{-}\eta^2\text{-MeNC}_4H_3)Os_3(CO)_8(NMe_3)$(2.25 (1) Å)[18] and a pyridine adduct $(\mu\text{-H})_2Os_5(CO)_{14}(NC_5H_5)$(2.21 (2) Å).[19]

It thus appears that the Os-N bonds in donor complexes of amines are relatively insensitive to the steric and electronic properties of the amine. On the other hand, the imidoyl Os-N bonds and Os-N bonds in η^2-amine complexes are considerably shorter and vary considerably from 2.10 to 2.17 (2) Å.[20]

The lower formation constants observed for the nitrile complexes **4a** and **4b** compared with amine complexes **3a**−**f** (~10^{-2}, Table 1) are consistent with the slightly greater ligand field strength ascribed to amines over nitriles.[21] It is interesting to note, however, that the higher formation constants for amines are not reflected in Os−N bond lengths observed in **3a** and **3f** (2.24 (2) Å) *versus* **4a** (2.10 (2) Å). The latter compares favorably with the Os−N bond lengths in the well known $Os_3(CO)_{11}(CH_3CN)$ and $Os_3(CO)_{10}(CH_3CN)_2$ (2.07 (2) and 2.12 (2) Å, respectively).[12] These bond lengths and the formation constants in Table 1 raise the important point, often noted in organometallic chemistry, that metal−ligand bond lengths very often do not correlate with bond strength and thermodynamic stability.

The regiospecific attack of trimethylamine *N*-oxide on **1** suggests that the nitrogen to osmium σ-donor bond may polarize carbonyls on the osmium atom to which they are bound making them more susceptible to nucleophilic attack by the amine oxide. Mechanistic studies on amine oxide oxidations of metal bound carbonyls indicate that nucleophilic attack by amine oxide at carbon is rate determining.[22]

The thermal behavior of the amine complexes is unremarkable, in that coordination is reversible below the temperature for further activation of the ligand except in the case of **3f**, where C−H activation of the coordinated amine occurs. This undoubtedly reflects the favorable geometry of the pyrrolidine ring for activation on the carbon adjacent to the coordinated nitrogen.[7]

Overall, the coordination site available on **2** offers a high selectivity for primary aliphatic amines and a relatively high conformational stability. Thus the rates of addition compare with smaller fairly basic phosphines.[7c] A much narrower range of ligand cone angles give stable complexes than for coordination sites on four-coordinate ground state geometries[5] and on the five-coordinate intermediates associated with ligand substitutions in octahedral complexes. This high degree of selectivity and the slowly dissociative and reversible nature of the complexation could prove useful for binding clusters to molecules of biological interest (if it can be transposed to aqueous media) and for stereoselective reactions of functionalized amines and nitriles.

Experimental Section

Materials. Complexes **1**, **2**, and **5a**−**d** were synthesized by known literature procedures.[7a,d] Amines were purchased from Aldrich, stored over potassium hydroxide, or used as received. Ammonia (10% ^{15}N-enriched) was purchased from Matheson and used as received. Acetonitrile (Baker) was distilled from CaH_2 and benzonitrile (Aldrich) was used as received.

(14) These values are estimated from the coalescence temperatures of the hydride signals for the two populated radial isomers (ref 7d) using the equation $\Delta G_c^{\ddagger}$ (kJ mol^{-1}) = (4.18) (4.57)(T_c)(9.97 + log(T_c/$\Delta\nu$)). See Kost, D.; Carlson, E. H.; Raban, M. *J. Chem. Soc., Chem. Commun.* **1971**, 656.

(15) Connor, J. A. *Transition Metal Clusters*, Johnson, B. F. G., Ed.; Wiley: Chichester, 1980; Chap. V.

(16) Deeming, A. J. *Adv. Organometal Chem.* **1986**, *26*, 1.

(17) Adams, R. D.; Danan, J. D.; Yves, J. *J. Cluster Sci.* **1992**, *3*, 1.

(18) Minassian, H. Masters Theis, California State University, Northridge, 1990.

(19) Johnson, B. F. G.; Lewis, J.; Nelson, W. J. H.; Pearsall, M. A.; Raithby, P. R.; Rosales, M. J.; McPartlin, M.; Sironi, A. *J. Chem. Soc., Dalton Trans.* **1987**, 327.

(20) Kabir, S. E.; Day, M.; Irving, M.; McPhillips, T.; Minassian, H.; rosenberg, E.; Hardcastle, K. I. *Organometallics* **1991**, *10*, 3997.

(21) Shriver, D. F.; Atkins, P.; Langford, C. H. *Inorganic Chemistry*; Freeman: New York, 1994; p 247.

(22) Shen, J.; Gao, Y.; Shi, Q.; Basolo, F. *Organometallics* **1989**, *8*, 2144.

Spectra. ^{1}H and ^{13}C-NMR spectra were obtained on a Bruker 360 MHz-AMX or Varian 400 MHz Unity Plus spectrometer. Chemical shifts are reported relative to TMS measured from the residual protons or the ^{13}C resonance of the solvent ($CDCl_3$). Infrared spectra were measured on a Perkin-Elmer 1420 dispersive spectrometer.

Formation Constant Measurements by ^{1}H-NMR. The amine or nitrile ligand was syringed into a solution of ~0.04 mmol of **2** in 0.6 mL of $CDCl_3$ in an NMR tube. A 4- or 10-fold excess of the ligand was used, since at these excesses measurable amounts of free and complexed clusters were present at equilibrium. The solutions were monitored, first at 1 h intervals and eventually at 8−10 h intervals for periods up to 72 h until no further change in the relative intensities of the free and complexed **2** were observed. The values reported in Table 1 are averages of at least two determinations and were within the expected precision limits of the experiment assuming each integrated intensity measurement (three) is accurate to ±5%. In the case of ammonia, a solution of **2** in CD_2Cl_2 was saturated with the gas by bubbling for ~3 min.

Kinetic Measurements. Solutions of **2** (0.04 mmol) in 0.6 mL of $CDCl_3$ were injected with a 10 or 20-fold excess of n-butylamine or saturated with NH_3 gas in an NMR tube. The tube was shaken once and inserted into the thermostated (+23 °C) probe; a spectrum was taken every hour for 15 h. Approximately 90 s elapsed between the amine addition and the first accumulation. Each accumulation took 96 s (32 transients, acquisition time = 2 s, relaxation delay = 1 s). The rate constants for the conversion of isomer **B** to isomer **A** (Scheme 1) for **3a** and **3b** were evaluated by measuring the integrated relative intensities of each isomer after 90% conversion of **2** to **3a** or **3b** (~1 h) at which point only isomer **B** was detected. Six points were chosen at 2 h intervals and fit to the integrated first order rate law $\ln c/c_o = -kt$ where c = rel int **A**/rel int **A** + rel int **B**. The square of the correlation coefficient for the **B** to **A** conversion for **3a** was 0.980, 0.996, and 0.997 for **3b** in the presence of a 10- and 20-fold excess of n-butylamine respectively. The k_{obs} for the conversion of **2** to **3b** was calculated using the Varian analysis program "kind" which fits the measured intensities to the equation $I_o = Ie^{-t/\tau} + I_\infty$. The calculated value of τ is the inverse of the pseudo first order rate constant in seconds. The errors reported are ±10% based on the expected error in relative integrated intensities for the NMR technique (±5%).

Amine Competition Experiment. A solution of **2** (10 mg, 0.011 mmol) in $CDCl_3$ (0.6 mL) was injected with 20 μL (0.20 mmole) of n-butylamine. The ^{1}H-NMR of this solution showed 90% conversion to a 9:1 mixture of isomers **B**:**A** of **3b** after 1 h. At this time, 20 μL (0.24 mmole) of pyrrolidine was injected into the solution and the ^{1}H-NMR was monitored at 1 h intervals for 15 h at +23 °C. At the end of this period, hydride resonances assignable to isomers **B** and **A** of **3f** were present in significant amounts. The relative intensities were 1.0:0.9:0.3:0.3 for **3b**(**B**), **3f**(**B**), **3f**(**A**), and **3b**(**A**), respectively (see Table 1 for chemical shifts).

Reaction of 2 with Pyrrolidine. Pyrrolidine (56 μL, 0.669 mmol) was added to a cyclohexane solution (80 mL) of **2** (0.121 g, 0.136 mmol). After it was stirred at room temperature for 5 h, the reaction mixture was heated to reflux for 2 h. The solvent was removed under vacuum and the residue was chromatographed by TLC on silica. Elution with hexane/CH_2Cl_2 (5:1, v/v) gave three bands from which the following compounds were isolated (in order of elution): $(\mu\text{-H})_2(\mu\text{-}\eta^2\text{-}\overline{C{=}N(CH_2)_3})_2Os_3(CO)_8$ (**6**) as orange crystals from hexane/CH_2Cl_2 at −20 °C (0.041 g, 31%) **2** (0.060 g, 50%) and $(\mu\text{-H})(\mu\text{-}\eta^2\text{-}\overline{C{=}N(CH_2)_3}(\eta^1\text{-}\overline{HN(CH_2)_4})Os_3(CO)_9$ (**3f**) as yellow crystals from hexane/CH_2Cl_2 at −20 °C (0.017 g, 13%) in the presence of excess pyrrolidine.

Spectral and Analytical Data for 6 and 3f. For **6**, IR (ν(CO) in hexane): 2080w, 2044s, 2023s, 1962s br, 1934w, br cm^{-1}; 360-MHz ^{1}H-NMR (in $CDCl_3$): 3.51 (m, 4H), 2.33 (m, 4H), 1.73 (m, 4H), −11.64 (s, 1H), −13.42 (s, 1H) ppm. Anal. Calcd for $C_{16}H_{14}N_2O_8Os_3$: C, 20.60; H, 1.52; N, 3.0. Found: C, 20.72; H, 1.38; N, 2.94. For **3f**, IR (ν(CO) in CH_2Cl_2): 2041s, 2016s, 1988s, 1962br, 1934br cm^{-1}. 400-MHz ^{1}H-NMR (in $CDCl_3$): 3.37 (m, 2H), 3.16 (br, 1H), 2.92 (m, 4H), 2.36 (m, 2H), 1.80 (m, 3H), 1.42 (m, 3H), −13.79 (s, 1H) ppm. Anal. Calcd for $C_{17}H_{16}N_2O_9Os_3$: C, 21.20; H, 1.68; N, 2.91. Found: C, 21.84; H, 1.64; N, 3.06.

Reaction of 2 with Acetonitrile. Compound **2** (0.020 g, 0.022 mmol) was slowly dissolved in acetonitrile (8 mL) by stirring at room temperature and allowed to stand in the freezer at −20 °C to give **4a** as orange crystals (0.018 g, 86%). IR (ν(CO) in CH_2Cl_2): 2040s, 2021s, 1972s, br, 1942m, br cm^{-1}. 400 MHz ^{1}H-NMR (in $CDCl_3$): 3.47 (m, 1H), 3.38 (m, 1H), 2.58 (s, 3H), 2.34 (m, 2H), 1.69 (m, 2H), −14.27 (s, 1H) ppm. Anal. Calcd for $C_{15}H_{10}N_2O_9$: C, 19.31; H, 1.08; N, 3.00. Found: C, 19.43; H, 0.90; N, 2.85.

Reaction of 2 with Ammonia. Ammonia gas was bubbled through a diethyl ether solution (20 mL) of **2** (0.065 g, 0.073 mmol) for 2 min. The color changed from pale yellow to orange. After the solvent was removed, the residue was dissolved in CH_2Cl_2, hexane added, and ammonia bubbled through the solution for 15 s. The flask was allowed to stand in the freezer at −20 °C to give $(\mu\text{-H})(\mu\text{-}\eta^2\text{-}\overline{C{=}N(CH_2)_3})Os_3(CO)_9(NH_3)$ (**3a**) as orange crystals (0.055 g, 83%). IR (ν(CO) in CH_2Cl_2): 2035s, 2015s, 1961s, br, 1934w, br, cm^{-1}. 400 MHz ^{1}H-NMR (in CD_2Cl_2): Isomer B, 3.40 (m, 2H), 2.99 (s, br, 3H), 2.27 (m, 2H), 1.75 (m, 1H), 1.62 (m, 1H), −13.70 (s, 1H) ppm: Isomer A, 3.45 (m, 2H), 3.41 (s, br, 3H), 2.35 (m, 2H), 1.66 (m, 2H), −13.97 (s, 1H) ppm. Anal. Calcd for $C_{13}H_{10}N_2O_9Os_3$: C, 17.18; H, 1.11; N, 3.08. Found: C, 17.25; H, 1.15; N, 2.98.

Reaction of 4a with $P(C_6H_5)_3$. A CH_2Cl_2 solution (20 mL) of $P(C_6H_5)_3$ (0.008 g, 0.031 mmol) was added to **4a** (0.023 g, 0.026 mmol). The reaction mixture was allowed to stir at room temperature for 30 min. The solvent was removed *in vacuo* and the residue was chromatographed by TLC on silica. Elution with hexane/CH_2Cl_2 (10:3, v/v) gave a single band which afforded $(\mu\text{-H})(\mu\text{-}\eta^2\text{-C{=}N(CH_2)_3})Os_3(CO)_9P(C_6H_5)_3$ (**5d**) as orange crystals (0.025 g, 89%). Identified by ^{1}H-NMR and infrared spectroscopy.[7d]

Synthesis of $(\mu\text{-H})(\mu\text{-}\eta^2\text{-}\overline{C{=}N(CH_2)_3})Os_3(CO)_9(CH_3CN)$ (4c). An acetonitrile solution of Me_3NO (0.007 g, 0.093 mmol) was added dropwise to a CH_2Cl_2 solution (10 mL) of $(\mu\text{-H})(\mu\text{-}\eta^2\text{-}\overline{C{=}N(CH_2)_3})Os_3(CO)_{10}$ (0.061 g, 0.066 mmol) containing 5 mL of acetonitrile. After 30 min of stirring at room temperature, the solution was filtered through a short florisil column. Removal of the solvent *in vacuo* afforded **4c** (0.049 g, 79%) as a yellow solid. IR (ν(CO) in CH_3CN): 2044s, 2004s, 1990sh, 1974sh, 1958w, 1926w cm^{-1}. 360 MHz ^{1}H-NMR (in CD_3CN/CD_2Cl_2): 3.79 (m, 1H), 3.54 (m, 1H), 2.52 (m, 2H), 2.16 (s, 3H), 1.74 (m, 2H), −14.75 (s, 1H) ppm.

Reaction of 4c with $P(C_6H_5)_3$. To an acetonitrile solution (15 mL) of **4c** (0.060 g, 0.064 mmol) was added $P(C_6H_5)_3$ (0.033 g, 0.126 mmol). The reaction mixture was stirred at room temperature for 10 min. The solvent was removed by rotary evaporation and the residue was chromatographed by TLC on silica gel. Elution with hexane/CH_2Cl_2 (3:1, v/v) gave a single band which yielded $(\mu\text{-H})(\mu\text{-}\eta^2\text{-}\overline{C{=}N(CH_2)_3})Os_3(CO)_9P(C_6H_5)_3$ (**5a**) as orange crystals from hexane/CH_2Cl_2 at −20 °C (0.063 g, 85%). Identified by ^{1}H-NMR and infrared spectroscopy.[7d]

Formation of 4c Followed by ^{1}H- and ^{13}C-NMR. Compound **2** (30% enriched in ^{13}CO, 37 mg, 0.041 mmol) was dissolved in 0.3 mL of CD_2Cl_2 and 0.1 mL of CD_3CN in a flame dried 5 mm NMR tube. The solution was degassed with nitrogen and then a solution containing 4 mg (0.053 mmol) in 0.2 mL of CD_3CN was added dropwise by syringe while the tube was held in a salt/ice bath at −20 °C. The solution is warmed to room temperature. At this point the ^{1}H-NMR shows at resonance at −14.0 ppm attributable to the trimethylamine adduct of **2** as the major species. Nitrogen gas

is then bubbled through the solution for a total of about 2 h during which time the resonance at −14.0 ppm gradually diminishes and is replaced by a resonance at −14.75 ppm attributable to **4c** as the dominant species. The ^{13}C-NMR was then measured at ambient temperature.

X-ray Structure Determination of 2, 5, and 7a. Crystals of **3a**, **3f**, **4a**, and **6** for X-ray examination were obtained from saturated solutions of each in hexane/dichloromethane solvent systems at −20 °C (**3a** and **3f** solutions contained excess ligand). Suitable crystals of each were mounted on glass fibers, placed in a goniometer head on an Enraf-Nonius CAD4 diffractometer, and centered optically. Unit cell parameters and an orientation matrix for data collection were obtained by using the centering program in the CAD4 system. Details of the crystal data are given in Table 1. For each crystal, the actual scan range was calculated by scan width − scan range ± 0.35 tan θ and backgrounds were measured by using the moving crystal-moving counter technique at the beginning and end of each scan. Two or three representative reflections were monitored every 2 h as a check on instrument and crystal stability and an additional two reflections were monitored for crystal orientation control. Lorentz, polarization and decay corrections were applied as was an empirical absorption correction based on a series of ψ scans.

Each of the structures was solved by the Patterson method using SHELXS-86, which revealed the positions of the metal atoms. All other non-hydrogen atoms were found by successive difference Fourier syntheses. The expected hydride positions were calculated by using the program HYDEX,[12] and all other hydrogens were positioned using the program HYDRO.[23] Hydrogen atom positions were included in the structure factor calculations but not refined in the final least squares cycles. All non-hydrogen atoms were refined anisotropically except in the case of **3a** where only the metal atoms and the oxygen atoms were refined anisotropically.

The rather subtle difference in the otherwise symmetrical pyrrolidine ring (N *vs* C, 7 electrons *vs* 6) resulted in positional isomerism or disorder in the metal clusters **3f** and **4a**. This was dealt with by treating the Cl and N atoms of the ring as having an average electron density of 6.5 and these atoms are referred to as DN1 and DN2 in the tables. Final refinement parameters for each crystal are listed in Table 1.

Scattering factors were taken from Cromer and Waber.[24] Anomalous dispersion corrections were those of Cromer.[25] All calculations were carried out on a DEC MicroVAX II computer using the MOLEN system of programs.

Acknowledgment. We gratefully acknowledge the National Science Foundation (E.R. CHE9319062) for research support and for an instrument grant (CHE-9302468) for purchase of a 400 MHz NMR. We thank one of the referees for helpful comments on the kinetic measurements.

Supplementary Material Available: Tables 12−15 listing anisotropic displacement parameters and Tables 16−19 listing complete bond distances and angles for **3a**, **3f**, **4a**, and **6** (32 pages). Ordering information is given on any masthead page.

OM940584B

(23) Schenk, H.; Ollthof-Hazelkamp, R.; von Konigsveld, H.; Bassi, G. C. *Computing in Crystallography*; Delft University Press: Holland, 1978, pp 64−74.

(24) Cromer, D. T.; Waber, J. T. *International Tables for X-ray Crystallography*; Kynoch Press: Birmingham, England, 1974; Vol. IV, Table 2.2B.

(25) Cromer, D. T. *International Tables for X-ray Crystallography*; Kynoch Press: Birmingham, England, 1974; Vol. IV, Table 2.3.1.

Method for the Benzotriazole-Mediated Synthesis of α-Silylalkylated Heterocycles and *N,N*-Dialkylanilines

Alan R. Katritzky,* Qingmei Hong, and Zhijun Yang

Center for Heterocyclic Compounds, Department of Chemistry, University of Florida, Gainesville, Florida 32611-7200

Received September 20, 1994[⊗]

N-(Benzotriazol-1-ylmethyl)carbazole and -indole undergo lithiation with butyllithium. The resulting anions react with a variety of silyl chlorides to give silylated intermediates which are transformed by displacement of the benzotriazolyl group with Grignard reagents into the corresponding α-silylalkylated heterocycles in excellent overall yields. Applying the same method to *N,N*-dimethylaniline leads to a novel approach for the synthesis of its 4-α-silylalkylated analogs.

Introduction

N-Alkylation of heterocycles, such as carbazoles and indoles, has been well documented.[1–6] The method most commonly employed involves treatment of the anions of N-heterocycles with alkylating reagents such as alkyl halides, alkyl esters of toluenesulfonic acid, and occasionally alcohols. Although N-alkylation is usually dominant, C-alkylation occurs to varying extents, depending on the solvent, the nature of the cation, and the alkylating agent.[7,8] In most of the alkylations described above, only primary alkyl groups can be introduced efficiently. Low yields are generally obtained with sterically hindered alkyl halides, and no reaction was observed with branched chain alkyl halides in the alkylation of carbazole.[9]

Despite the presumed resemblance of silylalkylation to normal alkylation and the tremendous industrial utility of organosilicon compounds,[10,11] few examples of α-silylalkylated heterocycles have been reported.[12] This might well be attributed to the relatively low reactivity of halogenoalkylsilanes (as α-silylalkylating reagents) and their limited availability. Trialkylsilyl substituents behave in a dichotomous manner, showing the properties of both electron donor and acceptor groups. Reactions which involve carbonium ion formation or development α to silicon are disfavored, as indicated by the fact that neither (chloromethyl)- nor (iodomethyl)trimethylsilane reacts with silver(I) ions.[13,14] Conversely, carbonium ion formation or development β to silicon is favored.

Previous work in our laboratory has demonstrated the use of benzotriazole as a synthetic auxiliary in the elaboration of many classes of compounds,[15] and in the synthesis of various types of N-substituted heterocycles and electron-rich aromatics.[16,17] We recently prepared a series of silylated (benzotriazolylmethyl)carbazole intermediates (**2a–e**) for the preparation of formylsilanes.[18] We now report that these and similar derivatives such as **2f** and **7** can be used for the synthesis of highly branched and sterically hindered *N*-α-silylalkylated carbazoles and indoles, and of 4-α-silylalkylated *N,N*-dialkylanilines.

Results and Discussion

As previously reported,[19] *N*-(benzotriazol-1-ylmethyl)carbazole (**1a**) and *N*-(benzotriazol-1-ylmethyl)indole (**1b**) were readily prepared by reaction of (chloromethyl)benzotriazole with carbazole and indole, respectively, in the presence of sodium hydroxide. Deprotonation of **1a** and **1b** with butyllithium occurred smoothly to give the corresponding carbanions which were quenched with silyl chlorides to afford the corresponding silylated intermediate products **2a–f** in good to excellent yields (Scheme 1 and Table 1). The generality of the reaction was reflected by its insensitivity to the steric and electronic nature (alkyl or aryl) of the substituents in the silyl chlorides. The structures of compounds **2a–f** were confirmed by ^{1}H and ^{13}C NMR spectroscopy and elemental analyses. Compared with the chemical shifts of α-alkylated *N*-(carbazol-9-ylmethyl)- and *N*-(indol-1-ylmethyl)benzotriazoles,[19,20] those of the methine carbons of the α-silylated derivatives **2a–f** were shifted upfield, indicating the shielding effect of silicon.

Heating (benzotriazol-1-yl)(carbazol-9-yl)(triisopropylsilyl)methane (**2a**) with an excess of phenylmagnesium

⊗ Abstract published in *Advance ACS Abstracts*, December 15, 1994.

(1) Papadopoulos, E. P.; Tabello, K. I. Y. *J. Org. Chem.* **1968**, *33*, 1299.
(2) Wang, N.-C.; Teo, K.-E.; Anderson, H. J. *Can. J. Chem.* **1977**, *55*, 4112.
(3) Santaniello, E.; Farachi, C.; Ponti, F. *Synthesis* **1979**, 617.
(4) Guida, W. C.; Mathre, D. J. *J. Org. Chem.* **1980**, *45*, 3172.
(5) Nishi, H.; Kohno, H.; Kano, T. *Bull. Chem. Soc. Jpn.* **1981**, *54*, 1897.
(6) Schmolka, S. J.; Zimmer, H. *Synthesis* **1984**, 29.
(7) Barco, A.; Benetti, S.; Pollini, G. P. *Synthesis* **1976**, 124.
(8) Nunomoto, S.; Kawakami, Y.; Yamashita, Y.; Takeuchi, H.; Eguchi, S. *J. Chem. Soc., Perkin Trans. 1* **1990**, 111.
(9) Kricha, L. J.; Ledwith, A. *J. Chem. Soc. Perkin Trans. 1* **1972**, 2292.
(10) Chvalovsky, V.; Bellama, J. M., Eds. *Carbon-Functional Organosilicon Compounds*; Plenum Press: New York, 1984.
(11) Ricci, A.; Degl'Innocenti, A. *Synthesis* **1989**, 647.
(12) Katritzky, A. R.; Lam, J. N. *Heteroatom Chem.* **1990**, *1*, 21.
(13) Eaborn, C. *Organosilicon Compounds*; Academic Press: New York, 1960.
(14) Ambasht, S.; Chiu, S. K.; Peterson, P. E.; Queen, J. *Synthesis* **1980**, 318.
(15) Katritzky, A. R.; Rachwal, S.; Hitchings, G. J. *Tetrahedron* **1991**, *47*, 2683.
(16) Katritzky, A. R.; Lang, H.; Lan, X. *Tetrahedron* **1993**, *49*, 2829.
(17) Katritzky, A. R.; Lang, H.; Lan, X. *Tetrahedron* **1993**, *49*, 7445.
(18) Katritzky, A. R.; Yang, Z.; Hong, Q. *J. Org. Chem.* **1994**, *59*, 5097.
(19) Katritzky, A. R.; Drewniak-Deyrup, M.; Lan, X.; Brunner, F. *J. Heterocycl. Chem.* **1989**, *26*, 829.
(20) Katritzky, A. R.; Yang, Z.; Lam, J. N. *J. Org. Chem.* **1991**, *56*, 2143.

0276-7333/95/2314-0734$09.00/0

Scheme 1

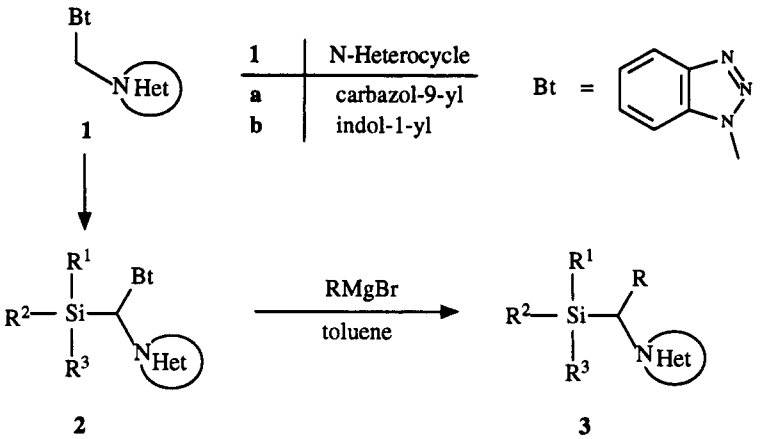

2	N-Het	R^1	R^2	R^3
a	carbazol-9-yl	Pr^i	Pr^i	Pr^i
b	carbazol-9-yl	Me	Me	Me
c	carbazol-9-yl	Ph	Ph	Ph
d	carbazol-9-yl	Me	Me	Bu^t
e	carbazol-9-yl	Bu^i	Bu^i	Bu^i
f	indol-1-yl	Me	Me	Bu^t

3	N-Het	R^1	R^2	R^3	R
a	carbazol-9-yl	Pr^i	Pr^i	Pr^i	Ph
b	carbazol-9-yl	Pr^i	Pr^i	Pr^i	Bu^n
c	carbazol-9-yl	Me	Me	Me	Ph
d	carbazol-9-yl	Ph	Ph	Ph	Bu^n
e	carbazol-9-yl	Ph	Ph	Ph	$PhCH_2$
f	carbazol-9-yl	Me	Me	Bu^t	$PhCH_2$
g	carbazol-9-yl	Bu^i	Bu^i	Bu^i	$PhCH_2$
h	indol-1-yl	Me	Me	Bu^t	Ph
i	indol-1-yl	Me	Me	Bu^t	Bu^n

Table 1. Preparation of N-α-Silylated (Benzotriazol-1-ylmethyl) Heterocycles 2a–f and 4-α-Silylated (Benzotriazol-1-ylmethyl)-*N,N*-dimethylanilines 7a,b

compd	yield (%)	mp (°C)	recryst solvent	molecular formula	found (calcd) C	H	N
2a	92	130–131	hexane	$C_{28}H_{34}N_4Si$	74.09	7.53	12.32
					(73.97	7.54	12.3)
2b	91	185–186	MeOH	$C_{22}H_{22}N_4Si$	71.22	5.99	15.08
					(71.32	5.99	15.13)
2c	95	237–238	MeOH	$C_{38}H_{28}N_4Si$	79.98	5.07	10.07
					(79.83	5.07	10.07)
2d	89	166–168	hexane	$C_{25}H_{28}N_4Si$	72.63	6.86	13.36
					(72.77	6.84	13.58)
2e	90	117–118	MeOH	$C_{31}H_{40}N_4Si$	75.14	8.20	11.33
					(74.95	8.12	11.28)
2f	66	138–140	hexane/AcOEt	$C_{24}H_{26}N_4Si$	69.32	7.25	15.53
					(69.59	7.23	15.45)
7a	51	195–196	MeOH/AcOEt	$C_{21}H_{30}N_4Si$	68.95	8.33	15.31
					(68.81	8.25	15.28)
7b	67	170–172	MeOH	$C_{18}H_{24}N_4Si$	66.66	7.55	17.42
					(66.62	7.45	17.27)

bromide in toluene under reflux for 20 h gave 9-(α-triisopropylsilylbenzyl)carbazole (**3a**) in almost quantitative yield (Scheme 1 and Table 2). The benzotriazole generated was readily removed during workup by washing the organic extracts with dilute aqueous sodium hydroxide. Under similar conditions, compounds **2a–f** reacted with a variety of alkyl and aryl Grignard reagents to afford the corresponding *N*-silylalkylated carbazoles and indoles in good to excellent yields. The substitution products **3a–i** were characterized by ^1H and ^{13}C NMR spectroscopy and elemental analyses. Displacement of benzotriazole in compounds of type **2** is proposed[15] to proceed via nucleophilic attack of a Grignard reagent on the iminium ions **4** and **5** (Scheme 2).

This method has been successfully extended to include *p*-silylalkylation of *N,N*-dimethylaniline. Previous methods for the ring alkylation of *N,N*-dialkylanilines have included reactions with alkenes in the presence of

Table 2. Preparation of N-α-Silylalkylated Heterocycles 3a–i and 4-α-Silylalkylated *N,N*-Dimethylanilines 8a–c

compd	yield (%)	mp (°C)	purification solvent	molecular formula	found (calcd) C	H	N
3a	94	99–101	hexane/AcOEt[a]	$C_{28}H_{35}NSi$	81.35	8.64	3.34
					(81.30	8.53	3.39)
3b	87	oil	hexane[b]	$C_{26}H_{39}NSi$	79.51	10.18	3.50
					(79.32	9.98	3.56)
3c	85	77–78	hexane[b]	$C_{22}H_{23}NSi$	80.28	7.17	4.08
					(80.19	7.04	4.25)
3d	81	142–143	hexane[b]	$C_{35}H_{33}NSi$	84.81	6.77	2.78
					(84.80	6.71	2.83)
3e	84	159–160	hexane[a]	$C_{38}H_{31}NSi$	86.16	5.90	2.64
					(86.20	5.87	2.57)
3f	77	59–60	hexane[b]	$C_{26}H_{31}NSi$	81.22	8.10	3.57
					(80.98	8.10	3.63)
3g	75	oil	hexane/AcOEt[b]	$C_{32}H_{43}NSi$	82.07	9.15	2.70
					(81.81	9.23	2.98)
3h	81	77–78	hexane[b]	$C_{21}H_{27}NSi$	78.17	8.51	4.33
					(78.45	8.46	4.36)
3i	77	oil	hexane[b]	$C_{19}H_{31}NSi$	76.04	10.59	4.53
					(75.68	10.36	4.64)
8a	85	108–109	MeOH[a]	$C_{21}H_{31}NSi$	77.42	9.72	4.31
					(77.49	9.61	4.31)
8b	81	oil	hexane[b]	$C_{18}H_{25}NSi$	75.92	9.01	5.08
					(76.26	8.89	4.94)
8c	88	oil	c	$C_{13}H_{23}NSi$	70.24	10.66	6.26
					(70.52	10.47	6.26)

[a] Recrystallization. [b] Column chromatography. [c] Further purification unnecessary.

aluminum powder or aluminum chloride.[21] High temperatures and high pressures are generally required and mixed ortho- and para-alkylations often resulted. Classical Friedel–Crafts methods have rarely been successfully applied to the alkylation of aniline derivatives due to the formation of complexes at the nitrogen atom which deactivates the ring.[22] There have been no

(21) Stroh, R.; Ebersberger, J.; Haberland, H.; Hahn, W. *Ring Alkylation of Aromatic Amines.* In *Newer Methods of Preparative Organic Chemistry*; Foerst, W., Ed.; Academic Press: New York, 1963; Vol 2, p 227.

Scheme 2

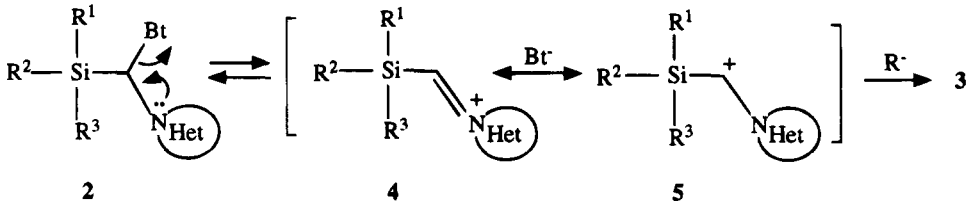

Scheme 3

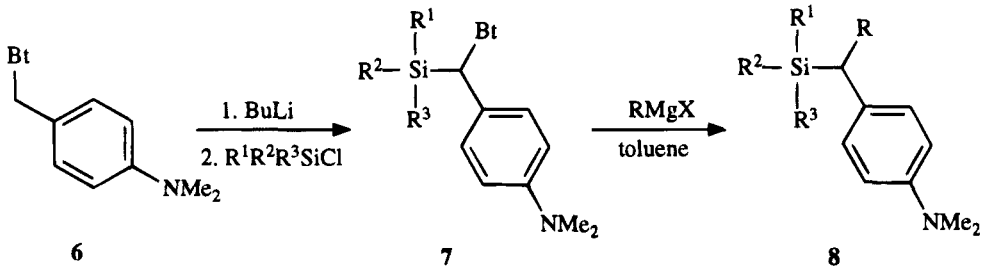

7	R^1	R^2	R^3
a	Me	Me	Bu^t
b	Me	Me	Me

8	R^1	R^2	R^3	R
a	Me	Me	Bu^t	Ph
b	Me	Me	Me	Ph
c	Me	Me	Me	Me

reports of the direct silylalkylation of *N,N*-dialkylanilines in the literature.

We have previously reported[23] that heating *N,N*-dimethylaniline and 1-(hydroxymethyl)benzotriazole in a solution of acetic acid and concd sulfuric acid gave 4-(benzotriazol-1-ylmethyl)-*N,N*-dimethylaniline (**6**) in 70% yield. Deprotonation of **6** with butyllithium followed by quenching with silyl chlorides provided the intermediate products **7** (Scheme 3 and Table 1). Subsequent displacement of benzotriazole with Grignard reagents under the same conditions described above afforded the corresponding 4-silylalkylated-*N,N*-dimethylanilines **8** in moderate yields (Table 2).

Experimental Section

General Comments. Melting points were determined on a bristoline hot-stage microscope and are uncorrected. ^{1}H (300 MHz) NMR spectra were recorded on a Varian VXR-300 (FT mode) spectrometer with Me_4Si as internal standard. ^{13}C NMR spectra were recorded at 75 MHz on the same instrument using solvent peaks ($CDCl_3$, δ 77.0 or DMSO-d_6, δ 39.5) as references. Elemental analyses (CHN) were carried out using a Carlo Erba 1106 elemental analyzer under the supervision of Dr. D. Powell, University of Florida. Tetrahydrofuran (THF) was freshly distilled from sodium–benzophenone. All moisture sensitive reactions were carried out in a dry argon atmosphere.

The following compounds were prepared using the literature procedures quoted: N-(benzotriazol-1-ylmethyl)carbazole (**1a**), mp 193–195 °C (lit.[20] mp 193–195 °C), *N*-(benzotriazol-1-ylmethyl)indole (**1b**), mp 175–176 °C (lit.[19] mp 176–178 °C), and 4-(benzotriazol-1-ylmethyl)-*N,N*-dimethylaniline (**6**), mp 167–169 °C (lit.[23] mp 167–168.5 °C). The preparation of compounds **2a–e** has already been reported.[18]

Lithiation of *N*-(Benzotriazol-1-ylmethyl) heterocycles 1 and 4-(Benzotriazol-1-ylmethyl)-*N,N*-dimethylaniline (6) and Subsequent Reaction with Silyl Chlorides. General Procedure for the Preparation of 2a–f and 7a,b. *n*-BuLi (2.5M in hexane; 4.4 mL, 11 mmol) was added to a solution of the appropriate N-(benzotriazol-1-ylmethyl) heterocycle **1** or 4-(benzotriazol-1-ylmethyl)-*N,N*-dimethylaniline (**6**) (10 mmol) in dry THF (80 mL) at −78 °C. The solution was stirred at −78 °C for 2 h, and then the appropriate electrophile (11 mmol) in THF (10 mL) was added. The mixture was stirred at −78 °C for a further 4 h and then at room temperature for 12 h. The reaction mixture was poured into saturated aqueous NH_4Cl (40 mL), and the aqueous layer was extracted with diethyl ether (3 × 30 mL). The combined organic layers were washed with water (1 × 25 mL) and dried ($MgSO_4$), and the solvent was evaporated under reduced pressure to afford the crude products which were then recrystallized to give analytically pure products (Table 1).

(Benzotriazol-1-yl)(*tert*-butyldimethylsilyl)(indol-1-yl)methane (2f). ^{1}H NMR ($CDCl_3$): δ 8.00 (d, 1 H, J = 7.3 Hz), 7.67 (d, 1 H, J = 8.3 Hz), 7.58 (d, 1 H, J = 7.9 Hz), 7.50 (d, 1 H, J = 8.2 Hz), 7.44–7.22 (m, 4 H), 7.13 (t, 1 H, J = 7.1 Hz), 6.74 (s, 1 H), 6.52 (d, 1 H, J = 3.4 Hz), 0.82 (s, 9 H), 0.39 (s, 3 H), 0.37 (s, 3 H). ^{13}C NMR ($CDCl_3$): δ 145.7, 136.0, 132.5, 128.4, 127.8, 126.9, 124.1, 122.3, 121.4, 120.10, 120.06, 109.4, 108.7, 103.8, 58.2, 26.6, 17.2, −5.4, −5.5.

(Benzotriazol-1-yl)(*tert*,butyldimethylsilyl)[4-(dimethylamino)phenyl]methane (7a). ^{1}H NMR ($CDCl_3$): δ 8.01 (d, 1 H, J = 8.3 Hz), 7.50–7.20 (m, 3 H), 7.18 (d, 2 H, J = 8.5 Hz), 6.61 (d, 2 H, J = 8.5 Hz), 5.24 (s, 1 H), 2.88 (s, 6 H), 0.79 (s, 9 H), 0.32 (s, 3 H), 0.18 (s, 3 H). ^{13}C NMR ($CDCl_3$): 149.1, 145.7, 133.5, 128.4, 127.0, 126.7, 123.5, 119.7, 112.4, 109.9, 53.3, 40.4, 27.2, 17.4, −5.4, −6.2.

(Benzotriazol-1-yl)[4-(dimethylamino)phenyl](trimethylsilyl)methane (7b). ^{1}H NMR ($CDCl_3$): δ 8.10–7.90 (m, 1 H), 7.28 (s, 3 H), 6.92 (d, 2 H, J = 8.5 Hz), 6.60 (d, 2 H, J = 8.5 Hz), 5.08 (s, 1 H), 2.87 (s, 6 H), 0.25 (s, 9 H). ^{13}C NMR ($CDCl_3$): δ 149.2, 145.9, 133.7, 127.3, 126.6, 125.9, 123.5, 119.5, 112.4, 110.5, 56.0, 40.4, −2.1.

Reaction of Compounds 2a–f and 7a,b with Grignard Reagents. General Procedure for the Preparation of 3a–i and 8a–c. The appropriate Grignard reagent (1 M in diethyl ether, 6 mL, 6 mmol) was added to a solution of the appropriate intermediate **2** or **7** (2 mmol) in dry toluene (30 mL). The ether was distilled off and the mixture refluxed for 20 h. The reaction mixture was poured into ice–water (30

(22) Olah, G. A. *Friedel–Crafts Chemistry*; John Wiley & Sons: New York, 1973; p 34.
(23) Katritzky, A. R.; Lan, X.; Lam, J. N. *Synthesis* **1990**, 341.

mL), stirred for 30 min, and extracted with diethyl ether (3 × 60 mL). The combined organic layers were washed with 2 N NaOH (2 × 20 mL) and water (2 × 30 mL) and dried over $MgSO_4$. The solvent was evaporated at reduced pressure to give the crude product which was purified as described in Table 2.

(Carbazol-9-yl)(triisopropylsilyl)phenylmethane (3a). ^{1}H NMR ($CDCl_3$): δ 8.09 (d, 2 H, J = 7.8 Hz), 7.60–7.44 (m, 2 H), 7.40 (t, 2 H, J = 7.1 Hz), 7.25 (m, 7 H), 5.84 (s, 1 H), 1.45 (heptet, 3 H, J = 7.5 Hz), 1.05 (d, 9 H, J = 7.5 Hz), 0.88 (d, 9 H, J = 7.5 Hz). ^{13}C NMR ($CDCl_3$): δ 141.0, 128.4, 126.6, 126.1, 125.3, 123.0, 120.2, 118.8, 111.8, 109.1, 48.2, 19.4, 19.2, 13.4.

1-(Carbazol-9-yl)-1-(triisopropylsilyl)pentane (3b). ^{1}H NMR ($CDCl_3$): δ 8.13–8.07 (m, 2 H), 7.59 (d, 1 H, J = 8.3 Hz), 7.49–7.38 (m, 3 H), 7.24–7.16 (m, 2 H), 4.47 (dd, 1 H, J_1 = 13.0 and J_2 = 2.7 Hz), 2.70–2.54 (m, 1 H), 1.96–1.83 (m, 1 H), 1.29 (heptet, 3 H, J = 7.3 Hz), 1.28–1.09 (m, 2 H), 1.05 (d, 9 H, J = 7.3 Hz), 1.02–0.83 (m, 2 H), 0.90 (d, 9 H, J = 7.3 Hz), 0.67 (t, 3 H, J = 7.3 Hz). ^{13}C NMR ($CDCl_3$): 142.0, 139.8, 125.3, 124.8, 123.3, 122.3, 120.2, 120.0, 118.23, 118.19, 110.8, 109.1, 44.4, 30.2, 22.3, 19.0, 13.8, 12.0.

(Carbazol-9-yl)(trimethylsilyl)phenylmethane (3c). ^{1}H NMR ($CDCl_3$): δ 8.12 (d, 2 H, J = 7.7 Hz), 7.45–7.27 (m, 4 H), 7.27–7.10 (m, 7 H), 5.56 (s, 1 H), 0.15 (s, 9 H). ^{13}C NMR ($CDCl_3$): δ 141.1, 139.8, 128.5, 126.3, 126.1, 125.3, 123.0, 120.2, 118.8, 110.2, 51.4, −0.08.

1-(Carbazol-9-yl)-1-(triphenylsilyl)pentane (3d). ^{1}H NMR ($CDCl_3$): δ 8.05 (t, 2 H, J = 8.0 Hz), 7.41–7.01 (m, 19 H), 6.89 (t, 1 H, J = 8.3 Hz), 6.50 (d, 1 H, J = 8.4 Hz), 4.87 (dd, 1 H, J_1 = 12.9 and J_2 = 3.4 Hz), 2.65–2.40 (m, 1 H), 2.01–1.87 (m, 1 H), 1.16–0.65 (m, 4 H), 0.46 (t, 3 H, J = 7.0 Hz). ^{13}C NMR ($CDCl_3$): δ 142.2, 139.5, 136.1, 133.0, 129.9, 128.0, 125.3, 124.6, 123.4, 122.3, 119.9, 119.8, 118.3, 118.2, 112.1, 108.7, 46.2, 29.6, 28.6, 22.0, 13.8.

1-(Carbazol-9-yl)-1-(triphenylsilyl)-2-phenylethane (3e). ^{1}H NMR ($CDCl_3$): δ 8.04 (d, 1 H, J = 7.8 Hz), 7.91 (d, 1 H, J = 6.7 Hz), 7.50–7.32 (m, 10 H), 7.32–7.20 (m, 6 H), 7.20–6.90 (m, 4 H), 6.90–6.73 (m, 4 H), 6.62–6.55 (m, 2 H), 5.21 (dd, 1 H, J_1 = 13.0 and J_2 = 2.7 Hz), 3.82 (t, 1 H, J = 13.0 Hz), 3.40 (dd, 1 H, J_1 = 13.0 and J_2 = 2.7 Hz). ^{13}C NMR ($CDCl_3$): δ 142.0, 140.0, 139.5, 136.1, 135.9, 132.8, 130.1, 128.1, 128.0, 126.0, 125.1, 124.6, 123.7, 122.0, 120.0, 119.4, 118.3, 118.0, 112.2, 108.5, 49.2, 34.9.

1-(*tert*-Butyldimethylsilyl)-1(carbazol-9-yl)-2-phenylethane (3f). ^{1}H NMR ($CDCl_3$): δ 7.62 (d, 1 H, J = 7.4 Hz), 7.50 (d, 1 H, J = 7.8 Hz), 7.13 (d, 1 H, J = 8.4 Hz), 7.00 (t, 1 H, J = 8.4 Hz), 6.85–6.65 (m, 2 H), 6.65–6.35 (m, 5 H), 6.30–6.15 (m, 2 H), 4.04 (dd, 1 H, J_1 = 12.6 and J_2 = 3.2 Hz), 3.18 (t, 1 H, J = 12.6 Hz), 2.63 (dd, 1 H, J_1 = 12.6 and J_2 = 3.2 Hz), 0.47 (s, 9 H), −0.47 (s, 6 H). ^{13}C NMR ($CDCl_3$): δ 141.5, 140.3, 139.8, 128.04, 128.00, 126.0, 125.2, 124.9, 123.4, 122.0, 120.4, 119.7, 118.3, 118.0, 110.0, 108.4, 45.8, 36.2, 26.7, 17.2, −5.0, −6.7.

1-(Carbazol-9-yl)-1-(triisobutylsilyl)-2-phenylethane (3g). ^{1}H NMR ($CDCl_3$): δ 8.08 (d, 1 H, J = 7.8 hz), 7.95 (d, 1 H, J = 7.6 Hz), 7.61 (d, 1 H, J = 8.3 Hz), 7.47 (t, 1 H, J = 8.1 Hz), 7.32–7.10 (m, 4 H), 7.22 (t, 1 H, J = 7.8 Hz), 6.95–6.80 (m, 3 H), 6.79–6.65 (m, 1 H), 4.52 (dd, 1 H, J_1 = 12.6 and J_2 = 3.0 Hz), 3.62 (t, 1 H, J = 12.6 Hz), 3.14 (dd, 1 H, J_1 = 12.6 Hz and J_2 = 3.0 Hz), 1.80–1.60 (m, 3 H), 1.00–0.60 (m, 24 H). ^{13}C NMR ($CDCl_3$): δ 141.9, 140.3, 139.7, 128.1, 128.0, 126.0, 125.1, 124.8, 123.5, 122.1, 120.3, 119.6, 118.2, 118.0, 110.9, 108.4, 48.0, 35.5, 26.9, 26.6, 24.6, 24.0.

(*tert*-Butyldimethylsilyl)(indol-1-yl)phenylmethane (3h). ^{1}H NMR ($CDCl_3$): δ 7.59 (d, 1 H, J = 7.7 Hz), 7.51 (d, 1 H, J = 3.2 Hz), 7.36 (d, 1 H, J = 8.3 Hz), 7.21 (d, 4 H, J = 4.3 Hz), 7.18–7.04 (m, 3 H), 6.54 (d, 1 H, J = 3.2 Hz), 5.23 (s, 1 H), 0.82 (s, 9 H), 0.27 (s, 3 H), 0.06 (s, 3 H). ^{13}C NMR ($CDCl_3$): δ 140.5, 137.0, 128.4, 128.3, 128.2, 127.2, 126.3, 121.4, 120.7, 119.3, 109.7, 100.9, 51.0, 27.1, 17.3, −5.0, −6.1.

1-(*tert*-Butyldimethylsilyl)-1-(indol-1-yl)pentane (3i). ^{1}H NMR ($CDCl_3$): δ 7.64 (d, 1 H, J = 7.8 Hz), 7.34 (d, 1 H, J = 8.5 Hz), 7.20 (t, 1 H, J = 6.0 Hz), 7.12–7.01 (m, 2 H), 6.55 (d, 1 H, J = 2.4 Hz), 4.03 (dd, 1 H, J_1 = 12.6 and J_2 = 2.5 Hz), 2.10–1.90 (m, 1 H), 1.90–1.75 (m, 1 H), 1.40–1.15 (m, 2 H), 1.15–1.00 (m, 2 H), 0.84 (s, 9 H), 0.78 (t, 3 H, J = 7.3 Hz), 0.18 (s, 3 H), −0.18 (s, 3 H). ^{13}C NMR ($CDCl_3$): δ 137.1, 127.8, 125.4, 120.9, 120.7, 118.7, 109.5, 101.3, 44.2, 32.2, 29.5, 26.7, 22.3, 16.8, 13.9, −6.6, −7.4.

(*tert*-Butyldimethylsilyl)[4-(dimethylamino)phenyl]phenylmethane (8a). ^{1}H NMR ($CDCl_3$): δ 7.58 (d, 2 H, J = 8.5 Hz), 7.56–7.49 (m, 4 H), 7.48–7.30 (m, 1 H), 6.97 (d, 2 H, J = 8.5 Hz), 3.78 (s, 1 H), 3.16 (s, 6 H), 1.04 (s, 9 H), 0.33 (s, 3 H), 0.30 (s, 3 H). ^{13}C NMR ($CDCl_3$): δ 148.3, 144.3, 129.6, 128.7, 128.1, 127.0, 124.8, 113.1, 42.4, 40.9, 27.1, 17.8, −5.7, −5.9.

[4-(Dimethylamino)phenyl](trimethylsilyl)phenylmethane (8b). ^{1}H NMR ($CDCl_3$): δ 7.30–7.15 (m, 4 H), 7.15–7.05 (m, 3 H), 6.67 (d, 2 H, J = 8.7 Hz), 3.41 (s, 1 H), 2.89 (s, 6 H), 0.03 (s, 9 H). ^{13}C NMR ($CDCl_3$): δ 148.3, 143.8, 131.0, 129.6, 128.4, 128.1, 124.6, 112.9, 44.6, 40.8, −1.6.

1-[4-(Dimethylamino)phenyl]-1-(trimethylsilyl)ethane (8c). ^{1}H NMR ($CDCl_3$): δ 6.92 (d, 2 H, J = 8.8 Hz), 6.68 (d, 2 H, J = 8.8 Hz), 2.87 (s, 6 H), 2.04 (q, 1 H, J = 7.7 Hz), 1.31 (d, 3 H, J = 7.7 Hz), −0.07 (s, 9 H). ^{13}C NMR ($CDCl_3$): δ 147.9, 134.1, 127.5, 113.0, 40.9, 28.2, 15.0, −3.3.

OM940730D

Paramagnetic (Benzyl)chromium Complexes as Homogeneous Ethylene Polymerization Catalysts

Gautam Bhandari, Youhyuk Kim, Jeffrey M. McFarland, Arnold L. Rheingold, and Klaus H. Theopold*

Department of Chemistry and Biochemistry, Center for Catalytic Science and Technology, University of Delaware, Newark, Delaware 19716

Received September 16, 1994[⊗]

The (benzyl)chromium(III) complexes $[Cp^*Cr(Bz)(\mu\text{-}Cl)]_2$ (**1**), $Cp^*Cr(py)(Bz)_2$ (**2**), $Cp^*Cr(THF)(Bz)_2$ (**3**), $[Cp^*Cr(THF)_2Bz]BPh_4$ (**4**), $[Cp^*Cr(bpy)Bz]BPh_4$ (**5**), $Li[Cp^*Cr(Bz)_3]$ (**6**), and $[Li(TMEDA)_2][Cp^*Cr(Bz)_3]$ (**7**) have been prepared. Reaction of **5** with strong bases (^{t}BuLi or $LiN(TMS)_2$) yielded Cp*Cr(bpy)Bz (**8**), the product of a reduction. The same complex was also produced by treatment of **2** or **3** with 2,2′-bipyridyl (bpy). The crystal structures of **1** (monoclinic, $C2/c$, a = 14.960(4) Å, b = 16.803(5) Å, c = 13.662(6) Å, β = 110.4(3)°, Z = 4), **2** (monoclinic, $P2_1/n$, a = 9.345(3) Å, b = 16.923(5) Å, c = 16.161(5) Å, β = 104.36(2)°, Z = 4), **6** (monoclinic, $P2_1/n$, a = 11.125(2) Å, b = 15.287(3) Å, c = 15.410(4) Å, β = 94.11(2)°, Z = 4), and **8** (triclinic, $P\bar{1}$, a = 9.056(3)Å, b = 11.568(6) Å, c = 11.602(4) Å, α = 73.56(3)°, β = 88.47(5)°, γ = 79.35(3)°, Z = 4) have been determined by X-ray diffraction. ^{2}H NMR spectroscopy was used to characterize complexes with perdeuteriated benzyl ligands; signal narrowing factors ($W(^1H)/W(^2H)$) ranged from 12 to 36. Neutral **3**, cationic **4**, and anionic **6** catalyzed the polymerization of ethylene.

Introduction

As part of our wide-ranging investigation of paramagnetic organometallic derivatives containing the Cp*Cr moiety,[1] we have prepared a number of complexes with benzyl ligands. Our studies are motivated—inter alia—by the prominent role of chromium catalysts in the coordination polymerization of ethylene,[2] and it was our hope that the relatively bulky benzyl substituent might stabilize coordinatively unsaturated chromium complexes, which could serve as homogeneous models for the commercially employed heterogeneous catalysts (i.e. Phillips and Union Carbide catalysts).[3] Herein we describe the syntheses and characterization of several new (benzyl)chromium complexes, including cationic, neutral, and anionic examples, as well as their activity as ethylene polymerization catalysts.

Results and Discussion

Syntheses. As described earlier, addition of 1 equiv of Cp*Li to a suspension of $CrCl_3(THF)_3$ in THF resulted in the formation of a blue solution of $[Cp^*Cr(\mu\text{-}Cl)Cl]_2$.[4] Addition of 1 equiv (per Cr) of (benzyl)magnesium chloride (BzMgCl) to this solution induced an immediate color change to purple. Standard workup of the reaction mixture and recrystallization from pentane yielded purple crystals of $[Cp^*Cr(Bz)(\mu\text{-}Cl)]_2$ (**1**) in 72% yield (see Scheme 1). This complex is a representative of a class of dimeric chromium(III) alkyls, which were prepared in this laboratory some time ago and all found to be purple.[4b] The molecular structure of **1** was determined by X-ray diffraction; the result of this determination is shown in Figure 1, and Table 1 lists selected interatomic distances and angles. The molecule exhibits crystallographic inversion symmetry; the pseudooctahedral coordination of the individual Cr^{III} ions in the three-legged piano-stool motif is characteristic of this class of alkyl complexes.[1] At 2.104(6) Å the Cr–C bond lengths are not significantly longer than the 2.09 Å average found in a series of related compounds, and the Cr–Cr distance of 3.343(1) Å rules out significant metal–metal bonding in this edge-sharing bioctahedron.

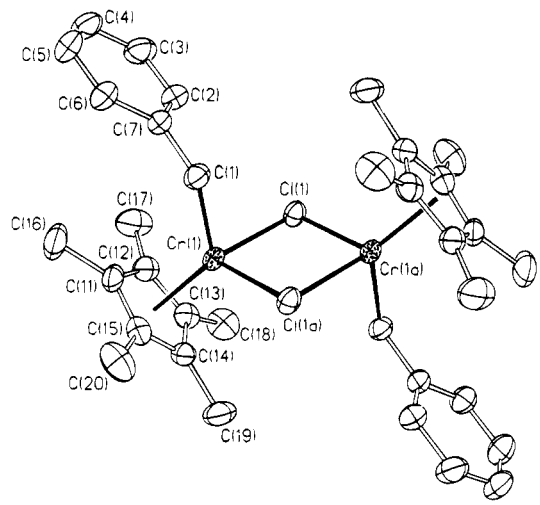

Figure 1. Molecular structure of $[Cp^*Cr(Bz)(\mu\text{-}Cl)]_2$ (**1**). Selected interatomic distances and angles are listed in Table 1.

⊗ Abstract published in *Advance ACS Abstracts,* December 15, 1994.

(1) Theopold, K. H. *Acc. Chem. Res.* **1990**, *23*, 263.

(2) (a) Thomas, B. J.; Theopold, K. H. *J. Am. Chem. Soc.* **1988**, *110*, 5902. (b) Thomas, B. J.; Noh, S.-K.; Schulte, G. K.; Sendlinger, S. C.; Theopold, K. H. *J. Am. Chem. Soc.* **1991**, *113*, 893. (c) Theopold, K. H.; Heintz, R. A.; Noh, S.-K.; Thomas, B. J. Homogeneous Chromium Catalysts for Olefin Polymerization. In *Homogeneous Transition Metal Catalyzed Reactions*; Moser, W. R., Slocum, D. W., Eds.; American Chemical Society: Washington, DC, 1992; p 591.

(3) (a) Clark, A. *Catal. Rev.* **1969**, *3*, 145. (b) Karol, F. J.; Karapinka, G. L.; Wu, C.; Dow, A. W.; Johnson, R. N.; Carrick, W. L. *J. Polym. Sci., Part A-1* **1972**, *10*, 2621. (c) Karol, F. J.; Brown, G. L.; Davison, J. M. *J. Polym. Sci., Polym. Chem. Ed.* **1973**, *11*, 413.

(4) (a) Benn, H.; Wilke, G.; Henneberg, D. *Angew. Chem., Int. Ed. Engl.* **1973**, *12*, 1001. (b) Richeson, D. S.; Mitchell, J. F.; Theopold, K. H. *Organometallics* **1989**, *8*, 2570.

0276-7333/95/2314-0738$09.00/0

Scheme 1

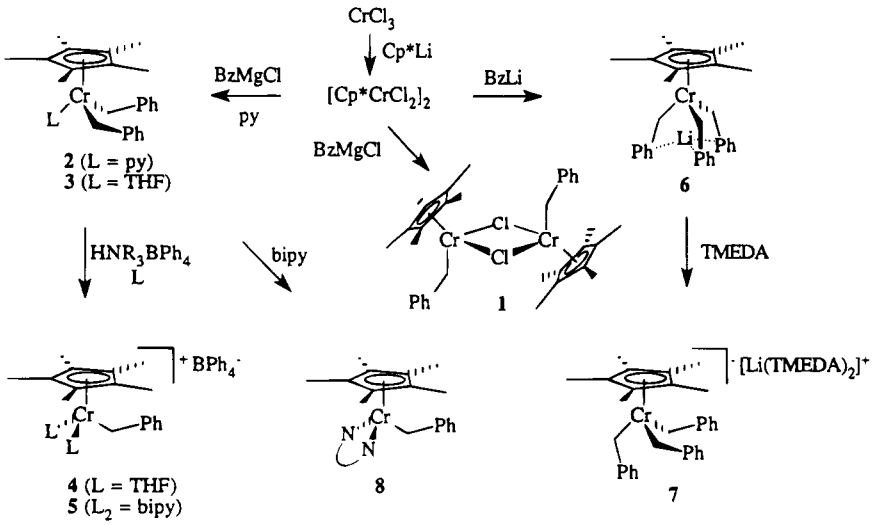

Table 1. Selected Interatomic Distances and Angles for $[Cp^*Cr(Bz)(\mu\text{-}Cl)]_2$ (1)

Distances (Å)			
Cr(1)−Cr(1a)	3.343(1)	Cr(1)−Cl(1)	2.380(5)
Cr(1)−Cl(1a)	2.386(5)	Cr(1)−C(1)	2.104(6)
Cr(1)−C_{Cp^*} (av)	2.237	C(1)−C(7)	1.465(6)
Angles (deg)			
Cl(1)−Cr(1)−C(1)	94.6(2)	Cl(1)−Cr(1)−Cl(1a)	90.9(1)
C(1)−Cr(1)−Cl(1a)	90.2(2)	Cr(1)−Cl(1)−Cr(1a)	89.1(1)
Cr(1)−C(1)−C(7)	121.4(3)		

Table 2. Selected Interatomic Distances and Angles for $Cp^*Cr(py)(Bz)_2$ (2)

Distances (Å)			
Cr−N	2.085(7)	Cr−C(11)	2.125(9)
Cr−C(12)	2.139(9)	Cr−C_{Cp^*} (av)	2.288
C(11)−C(26)	1.483(13)	C(12)−C(36)	1.485(14)
Angles (deg)			
N−Cr−C(11)	100.9(3)	N−Cr−C(12)	99.1(3)
C(11)−Cr−C(12)	93.5(4)	Cr−C(11)−C(26)	119.5(5)
Cr−C(12)−C(36)	124.0(6)		

Gradual addition of 2 equiv (per Cr) of BzMgCl to the $[Cp^*CrCl_2]_2$ solution resulted in a series of color changes, first to purple and finally to brown. Upon addition of an excess of pyridine (py) to the brown solution, its color rapidly changed to green. Normal workup of the reaction mixture and recrystallization from pentane afforded green crystals of $Cp^*Cr(py)(Bz)_2$ (**2**) in 67% yield (see Scheme 1). The molecular structure of **2** was determined by X-ray diffraction; the result of this determination is shown in Figure 2, and Table 2 lists selected interatomic distances and angles. The molecule exhibits no crystallographically imposed symmetry, and the Cr−C bond lengths are slightly longer than the aforementioned 2.09 Å average, probably reflecting a slightly weaker Cr−C_{Bz} bond.

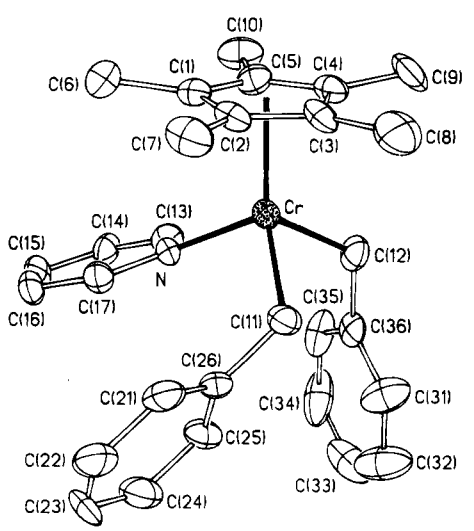

Figure 2. Molecular structure of $Cp^*Cr(py)Bz_2$ (**2**). Selected interatomic distances and angles are listed in Table 2.

Addition of donor molecules other than pyridine yielded analogous adducts. For example, addition of dioxane gave $Cp^*Cr(dioxane)(Bz)_2$, deemed worthy of spectroscopic characterization only. Surprisingly, even THF formed a stable complex, i.e. brown $Cp^*Cr(THF)(Bz)_2$ (**3**), which was isolated and fully characterized. Clean loss of 1 equiv of THF and the formation of $Cp^*Cr(py)(Bz)_2$ were observed by ^1H NMR upon addition of pyridine to a solution of **3** in C_6D_6. The marked stability of neutral **3** is somewhat surprising. For comparison, both $Cp^*Cr(THF)(Me)_2$ and $Cp^*Cr(THF)(CH_2SiMe_3)_2$ are stable only in THF solution. Upon removal of the solvent both lose THF rapidly to form $[Cp^*Cr(\mu\text{-}Me)(Me)]_2$[5] and $Cp^*Cr(CH_2SiMe_3)_2$, respectively. In contrast, **3** loses THF only upon heating (45 °C) under high vacuum, leaving behind a dark viscous oil. The ^1H NMR spectrum of this residue showed resonances consistent with an unligated benzyl complex, tentatively identified as $[Cp^*Cr(Bz)_2]_n$ (n = 1, 2). Addition of THF to this material restored the resonances of **3**. As we have not been able to crystallize the presumed $[Cp^*Cr(Bz)_2]_n$, its structure remains uncertain. We note, however, that its effective magnetic moment (determined by the Evans method)[6] measured μ_{eff} = 3.0 μ_B per Cr at room temperature, significantly reduced from the expected value for a mononuclear Cr^{III} complex ($S = {}^3/_2$, 3.87 μ_B). One possible explanation for this lowered moment is antiferromagnetic coupling of the chromium ion atoms in a binuclear structure, e.g.

(5) Noh, S.-K.; Sendlinger, S. C.; Janiak, C.; Theopold, K. H. *J. Am. Chem. Soc.* **1989**, *111*, 9127.
(6) Evans, D. F. *J. Chem. Soc.* **1959**, 2003.
(7) Busch, D. H. *Coord. Chem. Rev.* **1986**, *69*, 1.

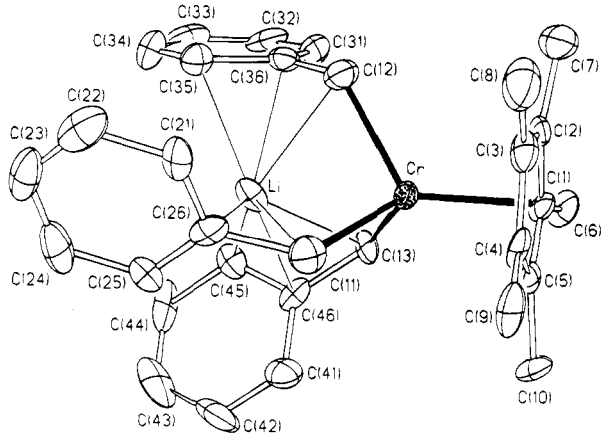

Figure 3. Molecular structure of Li[Cp*CrBz$_3$] (**6**). Selected interatomic distances and angles are listed in Table 3.

[Cp*Cr(μ-Bz)(Bz)]$_2$.[7] The reason for the unusually strong coordination of THF to the Cp*Cr(Bz)$_2$ fragment is presently unclear.

Cationic benzyl complexes were readily prepared. Thus, protonation of **2** in THF with [HNEt$_3$]BPh$_4$ gave [Cp*Cr(THF)$_2$Bz]BPh$_4$ (**4**), directly analogous to the structurally characterized [Cp*Cr(THF)$_2$Me]BPh$_4$.[2b] Purple crystals of **4** were quite soluble in THF and could be crystallized from THF/Et$_2$O. The labile THF ligands in **4** were readily replaced by 2,2′-bipyridine, for example. Thus, addition of 1 equiv of the latter to a THF solution of **4** caused an immediate color change to red-brown. Crystals of [Cp*Cr(bpy)Bz]BPh$_4$ (**5**) were obtained in nearly quantitative yield (93%). On the basis of our earlier work,[2a,b] there can be little doubt that these cationic complexes structurally feature pseudooctahedral coordination (η^5-Cp* and three 2-electron ligands) of chromium in a 15-valence-electron configuration.

Addition of 6 equiv of (benzyl)lithium to a blue solution of [Cp*CrCl$_2$]$_2$ in THF (prepared in situ) resulted in a series of color changes from blue to purple to brown to bright purple again. The use of Grignard reagent in this preparation produced the same sequence of color changes but proved unsuitable for product isolation, due to the formation of intractable, tarry residues. Standard workup and recrystallization from toluene/pentane yielded bright purple crystals of Li[Cp*Cr(Bz)$_3$] (**6**). The result of a crystal structure determination of **6** by X-ray diffraction is shown in Figure 3, and Table 3 contains selected structural parameters. **6** is closely related to **2** in its coordination geometry about Cr. The Cr−C$_{Bz}$ distances (average 2.17 Å) are slightly longer, probably reflecting steric crowding as well as some negative charge on chromium. The most unusual feature of the structure is the position of the lithium atom, which is sequestered by the benzyl groups—much like a baseball caught in a glove—and thereby forced into close proximity to the transition metal (Cr−Li = 2.54 Å). The lithium atom is bonded equally to all three benzyl groups in an allylic fashion. Indeed, the strutural motif bears close resemblance to that found in the triethylenediamine adduct of (benzyl)lithium.[8] All three benzyl groups are tilted such that

Table 3. Selected Interatomic Distances and Angles for Li[Cp*Cr(Bz)$_3$] (6)

Distances (Å)			
Cr−C(11)	2.171(13)	Cr−C(12)	2.178(12)
Cr−C(13)	2.157(13)	Cr−Li	2.540(20)
C(11)−Li	2.402(24)	C(12)−Li	2.419(25)
C(13)−Li	2.363(24)	C(11)−C(26)	1.479(19)
C(12)−C(36)	1.482(13)	C(13)−C(46)	1.481(18)
C(25)−Li	2.411(25)	C(26)−Li	2.252(24)
C(35)−Li	2.432(25)	C(36)−Li	2.348(25)
C(45)−Li	2.492(26)	C(46)−Li	2.311(26)
Cr−C$_{Cp*}$ (av)	2.300		
Angles (deg)			
C(11)−Cr−C(12)	95.2(5)	C(11)−Cr−C(13)	100.4(5)
C(12)−Cr−C(13)	97.9(5)	Cr−C(11)−C(26)	127.9(9)
Cr−C(12)−C(36)	124.3(9)	Cr−C(13)−C(46)	126.8(8)

Li−C(21), Li−C(31), and Li−C(41) are considerably longer than Li−C(25), Li−C(35), and Li−C(45) (0.75 Å on average). Because of this 3-fold asymmetry the molecules found in the crystal are chiral, although both enantiomers are present in equal proportions. The ^{1}H NMR spectrum of **6** is consistent with the molecular structure being the same in solution yet allowing for rapid interconversion of the enantiomers by a rearrangement of the benzyl ligands. In a static structure, the five phenyl protons would be inequivalent; however, only three resonances were observed (see Table 5).

In order to gauge the strength of the interaction of the lithium ion with the organometallic complex ion, an attempt was made to extract the former from its "pocket". Addition of TMEDA to a toluene solution of **6** resulted in immediate precipitation of a purple powder. Crystals of this compound could be grown by slow addition of ether to a saturated solution in CH$_2$Cl$_2$. Its spectroscopic and analytical data were consistent with the formulation [Li(TMEDA)$_2$][Cp*Cr(Bz)$_3$] (**7**). **7** could also be prepared in high yield via the Grignard route (see Experimental Section). The solubility characteristics of **7** are in keeping with its saltlike nature.

Another motivation for the investigation of chromium benzyl derivatives had been our hope to stabilize a Cr^{III}−C double bond, i.e. in a benzylidene complex. Among the proven methods for the formation of alkylidenes are deprotonation of cationic alkyls or sterically induced α-elimination from dialkyl precursors.[9] In this vein, treatment of cationic **5** with strong bases—such as LiN(SiMe$_3$)$_2$ and ^{t}BuLi—afforded a neutral chromium complex. Much to our satisfaction, the reaction of **2** or **3** with 2,2′-bipyridine (an embodiment of the second strategy) also produced the same complex. However, on the basis of the available evidence, we assign the formula Cp*Cr^{II}(bpy)Bz (**8**) to this new complex. Figure 4 shows the molecular structure of **8**, as determined by X-ray diffraction. Interatomic distances and angles are listed in Table 4. Most importantly, the Cr−C$_{Bz}$ bond distance of 2.111(6) Å is not significantly shorter than the corresponding distances in **1**, **2**, and **6**, which contain authentic benzyl ligands. While one might have expected a Cr^{II}−C bond to be slightly longer than the corresponding Cr^{III}−C bond, the observed value does not appear to be consistent with a chromium−carbon double bond. Furthermore, the Cr−C−C$_{ring}$ angle of 114.3(4)°

(8) Patterman, S. P.; Karle, J. L.; Stucky, G. D. *J. Am. Chem. Soc.* **1970**, *92*, 1150.

(9) Collman, J. P.; Hegedus, L. S.; Norton, J. R.; Finke, R. G. *Principles and Applications of Organotransition Metal Chemistry*; University Science Books: Mill Valley, CA, 1987; p 131.

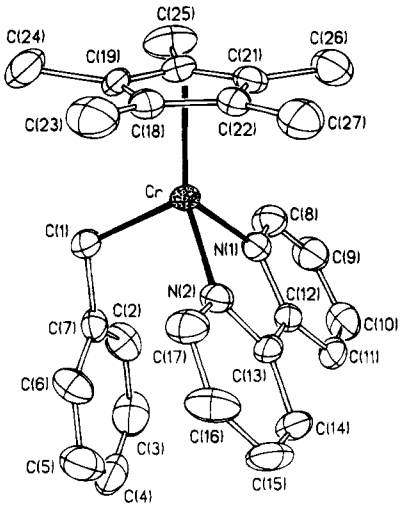

Figure 4. Molecular structure of Cp*Cr(bpy)Bz (**8**). Selected interatomic distances and angles are listed in Table 4.

Table 4. Selected Interatomic Distances and Angles for Cp*Cr(bpy)Bz (8)

	Distances (Å)		
Cr–N(1)	1.986(5)	Cr–N(2)	1.974(6)
Cr–C(1)	2.111(6)	C(1)–C(7)	1.490(10)
Cr–C_{Cp^*} (av)	2.250		
	Angles (deg)		
N(1)–Cr–N(2)	79.3(2)	N(1)–Cr–C(1)	93.9(2)
N(2)–Cr–C(1)	95.9(3)	Cr–C(1)–C(7)	114.3(4)

is closer to the expected value for tetrahedral hybridization than those in **1** (121.4°), **2** (119.5, 124.0°), and **6** (124.3, 126.8, 127.9°), arguing against a benzylidene moiety as well. The magnetic behavior of **8** was that expected of a Cr^{II} complex; i.e., its effective magnetic moment at room temperature measured $\mu_{eff} = 3.0(1)\ \mu_B$, consistent with a d^4 (Cr^{II}) configuration with two unpaired electrons, wholly incompatible with a d^3 (Cr^{III}) configuration. Curiously enough, reaction of **8** with the mild acid $[HNEt_3]BPh_4$ cleanly regenerated **5**, but this reaction must be an oxidation (yielding H_2), rather than a simple protonation. Consistent with this interpretation, i.e. the interconversion of **5** and **8** by redox chemistry rather than proton transfer, was their electrochemistry. Independent cyclic voltammetry measurements on THF solutions of **5** and **8** revealed the same reversible redox wave at −1.41 V (vs Fc^+/Fc) for both compounds.

Reduction of a cationic Cr^{III} complex by electron-rich reagents is not surprising; however, the formation of **8** by the reaction with bipyridine is unusual. Ligand substitution of pyridine (or THF) with the bidentate bipyridine would form a seven-coordinate complex, namely $Cp^*Cr(bpy)(Bz)_2$. As indicated by the lack of precedent for any such molecules in our previous work, this may well be an unstable coordination environment for Cr^{III}, which strongly prefers octahedral coordination. One possible pathway toward regaining the latter would be homolytic scission of a Cr–benzyl bond of the seven-coordinate intermediate, thereby leaving **8** (eq 1). On

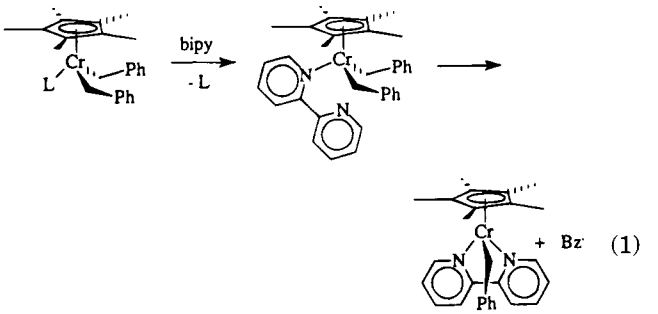

(1)

the basis of this working hypothesis, we have searched the reaction mixtures for products derived from benzyl radicals (toluene, 1,2-diphenylethane). None were found. However, monitoring the reaction by ^1H NMR revealed the presence of several small resonances attributable to paramagnetic reaction products other than **8**. Unfortunately, we have been unable—despite many attempts—to isolate or identify these species. It is possible that benzyl radicals formed in the way described above might attack the starting material or product, to form other organometallic compounds. Indeed, the early literature on organochromium chemistry provides evidence for such reactions.[10] However, under the present circumstances, our mechanistic proposal is but one possible explanation for the formation of **8**.

^2H NMR. ^1H NMR spectra of Cr^{III} complexes suffer from severe line broadening, leading—inter alia—to overlapping signals, uncertain integrals, and failure to detect some resonances altogether.[11] ^2H NMR spectroscopy of suitably labeled compounds has been advanced as a solution to these problems.[12] Owing to the ready availability of deuteriated benzyl groups from toluene-d_8, we decided to test the benefits of this technique. Using C_7D_7K and C_7D_7Li as reagents,[13] we have prepared $Cp^*Cr(THF)(Bz\text{-}d_7)_2$ (**3**-d_{14}), $[Cp^*Cr(THF)_2(Bz\text{-}d_7)]BPh4$ (**4**-d_7), $Li[Cp^*Cr(Bz\text{-}d_7)_3]$ (**6**-d_{21}), and $[Li(TMEDA)_2][Cp^*Cr(Bz\text{-}d_7)_3]$ (**7**-d_{21}) and recorded their ^1H and ^2H NMR spectra. The results are listed in Table 5. Several observations are worth commenting on. There occurred indeed a significant sharpening of the benzyl resonances, leading to better resolution of signals and more reliable integrals. The individual effects did not quite approach the theoretical value (i.e. $W(^2H)/W(^1H) = 42.4$),[12d] but in at least one case the effect was sufficient to resolve an asymmetrically shaped ^1H NMR peak of **6** into two separate ^2H resonances in the spectrum of **6**-d_{21}. Comparison of the ^2H and ^1H spectra also showed that one set of phenyl protons (presumably ortho H) had consistently been missed in the ^1H NMR (see question marks in Table 5), due to extreme broadening and/or overlap. In contrast to Köhler's findings,[12c] and despite searching the shift range ±3500 ppm, we have been unable to detect a ^2H NMR resonance for the benzylic position of, for example, **6**-d_{21}. While we have never detected a ^1H NMR resonance for protons in a position α to chromium in a

(10) Zeiss, H. H.; Sneeden, R. P. A. *Angew. Chem., Int. Ed. Engl.* **1967**, *6*, 435.

(11) (a) La Mar, G. N.; Horrocks, W. D.; Holm, R. H. *NMR of Paramagnetic Molecules*; Academic Press: New York, 1973. (b) Bertini, I.; Luchinat, C. *NMR of Paramagnetic Molecules in Biological Systems*; Benjamin/Cummings: Menlo Park, CA, 1986.

(12) (a) Wheeler, W. D.; Kaizaki, S.; Legg, J. I. *Inorg. Chem.* **1982**, *21*, 3248. (b) Wheeler, W. D.; Legg, J. I. *Inorg. Chem.* **1984**, *23*, 3798. (c) Grohmann, A.; Köhler, F. H.; Müller, G.; Zeh, H. *Chem. Ber.* **1989**, *122*, 897. (d) Hebendanz, N.; Köhler, F. H.; Scherbaum, F.; Schlesinger, B. *Magn. Reson. Chem.* **1989**, *27*, 798. (e) Blümel, J.; Hofmann, P.; Köhler, F. H. *Magn. Reson. Chem.* **1993**, *31*, 2.

(13) Schlosser, M.; Hartmann, J. *Angew. Chem., Int. Ed. Engl.* **1973**, *12*, 508.

Table 5. ^{1}H and ^{2}H Chemical Shifts of Selected Benzyl Complexes and Signal Narrowing Factors

compd	$\delta(^1H)$	$\delta(^2H)$	$\delta(^1H, d_n)^a$	$W(^1H)/W(^2H)$
3 (benzene)	−2.08 (19H)		−1.58 (15H)	
	?	−0.64 (4H)		
	5.90 (4H)		6.50 (4H)	
	ca. 23 (4H)		ca. 24 (4H)	
	28.71 (2H)	30.74 (2H)		21.3
	?	43.68 (4H)		
4 (THF)	−41.79 (15H)		−41.93 (15H)	
	−0.12 (2H)	−0.48 (2H)		13.8
	6.9−7.3 (20H)		6.8−7.3 (20H)	
	32.96 (1H)	32.97 (1H)		11.7
	?	34.43 (2H)		
6 (benzene)	−0.64 (6H)	−0.51 (6H)		13.0
	2.73 (15H)		3.57 (15H)	
	36.34 (9H)	36.12 (3H)		17.8
	?	37.72 (6H)		
7 (THF)	−0.69 (6H)	−1.98 (6H)		22.1
	2.15, 2.3 (32H)		2.15, 2.3 (32H)	
	20.31 (15H)		20.75 (15H)	35.5
	32.26 (3H)	33.81 (3H)		
	?	36.16 (6H)		

^{a} ^{1}H NMR shifts of deuteriated complexes.

Table 6. Ethylene Polymerization Activity of (Benzyl)chromium Complexes and Polymer Characterization

compd^a	solvent	time (min)	yield (mg)	M_w	M_n	M_w/M_n
1	benzene	480				
2	pentane	120				
3	pentane	45	224	7 044	4 996	1.41
3	THF	45				
4	CH_2Cl_2	45	556	29 940	14 896	2.01
6	toluene	120	515	12 520	5 140	2.44
6^b	toluene	200	335	27 320	12 320	2.22
6 + 1 BzLi^b	toluene	200	207	26 480	12 140	2.18
6 + 2 BzLi^b	toluene	200	143	20 640	9 039	2.22
7	CH_2Cl_2	120				
8	pentane	120				

^{a} Conditions: 50 mL of solution, [cat] = 2.2 mM, $P_i(C_2H_4)$ = 1.2 atm, room temperature. ^{b} Conditions: 51 mL of solution, [cat] = 0.84 mM, $P_i(C_2H_4)$ = 1.3 atm, room temperature.

mononuclear Cr^{III} complex, the failure of ^{2}H NMR spectroscopy in this particular instance was unexpected and somewhat disappointing. The routine identification of all hydrogen atoms (except hydrides) in paramagnetic complexes was one of the attractive features of the technique, and it is cast into doubt by our results. Finally, Table 5 reveals several examples of PIECS (i.e. *P*aramagnetic *I*sotope *E*ffects on *C*hemical *S*hifts).[14] For example, the ^{1}H chemical shifts associated with the Cp* ligands of the unlabeled compounds differ significantly from those of their deuteriated analogs. This kind of unusually large and long-range isotope effect is common in NMR spectra of paramagnetic compounds.[15]

Polymerization. In order to further our understanding of the structural requirements of chromium catalysts for ethylene polymerization, a selection of the complexes described above (i.e. **1**, **2**, **3**, **4**, **6**, **7**, and **8**) was tested for catalytic activity. In a typical experiment 0.111 mmol of catalyst was dissolved in 50 mL of solvent and exposed to 1.2 atm of ethylene at room temperature for up to 2 h. Precipitation of a white powder and a pressure decrease signaled formation of polyethylene. The polymer was isolated by filtration, washed with acetone, and dried in vacuo prior to molecular weight determination. Under these mild reaction conditions, only $[Cp^*Cr(THF)_2Bz]BPh_4$, $Cp^*Cr(THF)(Bz)_2$, and $Li[Cp^*Cr(Bz)_3]$ afforded significant amounts of polyethylene (see Table 6 for details). It is remarkable that the charge of the chromium complexes does not appear to be an important variable, as the catalysts include a cation, a neutral complex, and an anion. We have previously shown that the ethylene polymerization catalyst $[Cp^*Cr(THF)_2Me]BPh_4$ loses THF in solution and that the polymerization is inhibited by added THF.[2b] Presumably, the six-coordinate chromium must lose a ligand and open a coordination site for binding of ethylene, for polymerization to commence. By analogy, we suggest that polymerizations with the benzyl derivative $[Cp^*Cr(THF)_2Bz]BPh_4$ as well as $Cp^*Cr(THF)(Bz)_2$ proceed by a similar mechanism, involving substitution of the relatively weakly bound THF by ethylene. The observation that $Cp^*Cr(THF)(Bz)_2$ does not exhibit catalytic activity in THF solution is consistent with this proposal. The catalytic activity of $Li[Cp^*Cr(Bz)_3]$ was therefore a surprise, as dissociation of a benzyl ligand in toluene seemed unlikely to us. However, as the presence of small concentrations of (benzyl)lithium in toluene solutions of **6** could not be rigorously confirmed by ^{1}H NMR, we have probed the effect of added (benzyl)lithium on the catalytic activity. The results of these experiments are shown in Table 6 and Figure 5. While **6** is stable in the presence of the lithium reagent, there emerges a clear inhibitory effect of (benzyl)lithium on the rate of polymerization. We are thus forced to suggest that in toluene solution **6** exists in equilibrium with (benzyl)lithium and a coordinatively unsaturated chromium complex, probably $Cp^*Cr(Bz)_2$. The last species, or a dimer thereof, may also be formed by dissociation of THF from **3**, as outlined above. This formulation is also supported by the observation of the corresponding mass as the largest fragment in the mass spectra of both **2** and **3**.

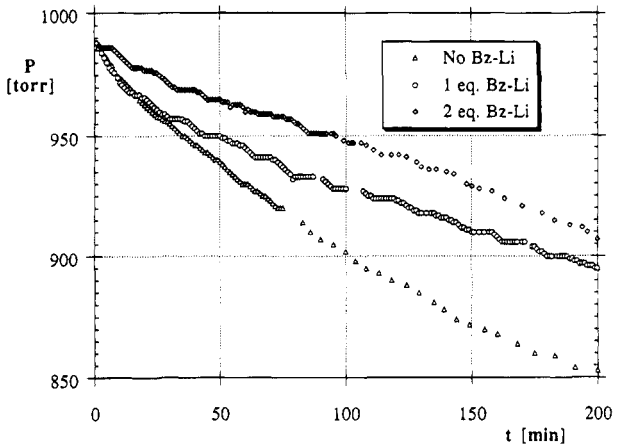

Figure 5. Ethylene uptake (pressure drop) due to polymerization by $Li[Cp^*CrBz_3]$ and various amounts of BzLi.

Conclusions

A variety of new (benzyl)chromium complexes has been prepared and structurally characterized. These

(14) Heintz, R. A.; Neiss, T. G.; Theopold, K. H. *Angew. Chem.* **1994**, *106*, 2389; *Angew. Chem., Int. Ed. Engl.*, in press.

(15) (a) Horn, R. R.; Everett, G. W., Jr. *J. Am. Chem. Soc.* **1971**, *93*, 7173. (b) Evans, B.; Smith, K. M.; La Mar, G. N.; Viscio, D. B. *J. Am. Chem. Soc.* **1977**, *99*, 7070. (c) Theopold, K. H.; Silvestre, J.; Byrne, E. K.; Richeson, D. S. *Organometallics*, **1989**, *8*, 2001. (d) Hebendanz, N.; Köhler, F. H.; Scherbaum, F.; Schlesinger, B. *Magn. Reson. Chem.* **1989**, *27*, 798. (e) Medforth, C. J.; Shiau, F.-Y.; La Mar, G. N.; Smith, K. M. *J. Chem. Soc., Chem. Commun.* **1991**, 590.

compounds reinforce our notion of the preference of Cr(III) for the pseudooctahedral coordination geometry of the Cp^*CrX_3 fragment with a 15-valence-electron configuration. Expansion of the coordination sphere to Cp^*CrX_4 is avoided strongly—i.e. even at the cost of loss of a benzyl ligand and reduction to Cr(II). On the other hand, dissociation of weakly bound ligands, to form Cp^*CrX_2, seems energetically feasible. Such coordinatively unsaturated 13-electron complexes appear to be intermediates in the catalysis of ethylene polymerization by Cr(III) alkyls.

Experimental Section

General Techniques. All manipulations of compounds were carried out by standard Schlenk, vacuum, and glovebox techniques. Pentane, diethyl ether, tetrahydrofuran, and toluene were distilled from purple sodium benzophenone/ketyl solutions. C_6H_6, C_6D_6 and THF-d_8 were all predried with Na and stored under vacuum over Na/K alloy. Pyridine was dried with CaH_2 and vacuum-distilled onto 4 Å molecular sieves. CD_2Cl_2 was dried with CaH_2 and stored under vacuum over 4 Å molecular sieves. $CrCl_3$ (anhydrous) was purchased from Strem Chemical Co. $C_6H_5CH_2MgCl$ was purchased from Aldrich Chemical Co. as a 2 M solution in ether or THF. $C_6H_5CH_2K$ and $C_6H_5CH_2Li$ were prepared by literature procedures;[13] substitution of toluene-d_8, and use of pentane as reaction solvent (instead of toluene), yielded their deuteriated analogs $C_6D_5CD_2K$ and $C_6D_5CD_2Li$. Organometallic reagents were titrated with diphenylacetic acid prior to use. CP grade ethylene was purified with a column of MnO and 4 Å molecular sieves. $CrCl_3(THF)_3$ and LiCp* were synthesized by literature procedures. ^1H NMR spectra were taken on Bruker AM-250 or WM-250 spectrometers. ^2H NMR spectra were recorded on the Bruker WM 250 spectrometer, using a 10 mm broad-band probe tuned to the ^2H resonance frequency. FTIR spectra were recorded on a Mattson Alpha Centauri spectrometer with a resolution of 4 cm^{-1}. Mass spectra were obtained by the University of Delaware Mass Spectrometry Facility. Elemental analyses were performed by Oneida Research Services, Whitesboro, NY 13492. Characterization of polyethylene samples was conducted at Chevron Chemical Company, Kingwood, TX. Room-temperature magnetic susceptibilities were determined using a Johnson Matthey magnetic susceptibility balance which utilizes a modification of the Gouy method. Molar magnetic susceptibilities were corrected for diamagnetism using Pascal's constants.

Bis((η^5-pentamethylcyclopentadienyl)(benzyl)(μ-chloro)chromium(III)), $[Cp^*(Bz)Cr(\mu\text{-}Cl)]_2$, (1). A THF solution (50 mL) of $[Cp^*CrCl_2]_2$ was formed by stirring $CrCl_3(THF)_3$ (0.791 g, 2.11 mmol) and Cp*Li (0.300 g, 2.11 mmol) together overnight. A 2.11 mL (1.00 equiv) amount of BzMgCl (1.0 M in Et_2O, 2.11 mmol) was added dropwise to this blue solution. The color of the solution rapidly changed to purple. The solution was stirred for 1.5 h, after which time 4−5 drops of 1,4-dioxane were added to aid the precipitation of $MgCl_2$. The volatiles were removed in vacuo, and the solid was extracted with toluene and crystallized from a mixture of toluene and pentane at −40 °C. Yield: 0.475 g (72%). ^1H NMR (C_6D_6): −21.45 (br, 15H), 1.78 (br, 2H), 22.05 and 23.19 (sh) (br, 3H) ppm. IR (KBr): 3055 (w), 3018 (w), 2953 (m), 2912 (s), 2854 (m), 1592 (m), 1484 (s), 1447 (m), 1377 (m), 1206 (m), 1027 (m), 746 (s), 698 (s), 531 (w), 442 (w) cm^{-1}. UV/vis (Et_2O): 543 (ϵ = 1470 M^{-1} cm^{-1}), 654 (sh, ϵ = 460 M^{-1} cm^{-1}) nm. Mp: 166 °C. μ_{eff} = 3.0(1) μ_B/Cr (295 K). Anal. Calcd for $C_{34}H_{44}Cl_2Cr_2$: C, 65.07; H, 7.07; N, 0.0. Found: C, 64.01; H, 6.48; N, <0.02. Mass spectrum (m/e): 536 ($Cp^*_2Cr_2Cl_2Bz^+$).

(η^5-Pentamethylcyclopentadienyl)bis(benzyl)(pyridine)chromium(III), $Cp^*Cr(py)(Bz)_2$ (2). A THF solution (50 mL) of $[Cp^*CrCl_2]_2$ was formed by stirring $CrCl_3(THF)_3$ (1.003 g, 2.67 mmol) and Cp*Li (0.382 g, 2.69 mmol) together for 1 h. A 2.67 mL (2.00 equiv) amount of BzMgCl (2.0 M in THF, 5.3 mmol) was added dropwise to this blue solution. Pyridine (2 mL) was added after another 1 h, and the solution was stirred for an additional 20 min. 1,4-Dioxane (3 mL) was then added to aid the precipitation of $MgCl_2$. After all volatiles were removed, the solid was extracted with Et_2O and crystallized from the same solvent at -40 °C. Total yield: 0.801 g (67%). Higher yields (80%) may be obtained by starting with isolated $[Cp^*CrCl_2]_2$. ^1H NMR (C_6D_6): −53.51 (br, 1H), 0.52 (br, 4H), 4.08 (br, 15H), 20.37 (br, 2H), 31.86 (br, 2H), 35.38 (br, 4H) ppm. IR (KBr): 3063 (s), 3013 (s), 2904 (s), 2866 (s), 1591 (s), 1483 (s), 1442 (s), 1377 (m), 1209 (s), 1026 (s), 976 (m), 800 (w), 748 (s), 698 (s), 530 (m) cm^{-1}. UV/vis (pentane): 428 (ϵ = 2340 M^{-1} cm^{-1}), 565 (sh, ϵ = 1100 M^{-1} cm^{-1}) nm. Mp: 135 °C. μ_{eff} = 4.2(1) μ_B (294 K). Anal. Calcd for $C_{29}H_{34}NCr$: C, 77.65; H, 7.64; N, 3.12. Found; C, 77.78; H, 7.85; N, 3.17. Mass spectrum (m/e): 369 ($Cp^*Cr(Bz)_2^+$).

(η^5-Pentamethylcyclopentadienyl)bis(benzyl)(tetrahydrofuran)chromium(III), $Cp^*Cr(THF)(Bz)_2$ (3). A THF solution (50 mL) of $[Cp^*CrCl_2]_2$ was formed by stirring $CrCl_3(THF)_3$ (1.009 g, 2.69 mmol) and Cp*Li (0.384 g, 2.70 mmol) together for 1 h. A 2.65 mL (2.00 equiv) amount of BzMgCl (2.0 M in THF, 5.3 mmol) was added dropwise to this blue solution. 1,4-Dioxane (3 mL) was added after 1 h, and the solution was stirred for an additional 1 h. After all volatiles were removed, the residue was extracted with pentane and dried. Crystallization from pentane gave 0.456 g (48%) of **3**. ^1H NMR (C_6D_6): −2.02 (br, 15H), −1.75 (sh), 5.90 (br, 4H), 23 (v br, 4H), 28.71 (br, 2H) ppm. IR (KBr): 3057 (s), 3005 (s), 2903 (s), 2869 (s), 1589 (s), 1483 (s), 1448 (s), 1377 (m), 1209 (s), 1020 (s), 977 (s), 860 (s), 800 (w), 748 (s), 698 (s), 530 (m), 416 (w) cm^{-1}. UV/vis (pentane): 456 (sh, ϵ = 1330 M^{-1} cm^{-1}), 721 (ϵ = 380 M^{-1} cm^{-1}) nm. Mp: 78 °C. μ_{eff} = 4.2(1) μ_B (295 K). Anal. Calcd for $C_{28}H_{37}OCr$: C, 76.16; H, 8.45. Found: C, 76.04: H, 8.23. MS (*m/e*): 369 ($Cp^*Cr(Bz)_2^+$).

(η^5-Pentamethylcyclopentadienyl)bis(benzyl)chromium(III), $[Cp^*Cr(Bz)_2]_n$. A small sample of **3** was heated to 45 °C under high vacuum for ca. 1 h. After this time the solid had been transformed into a brown viscous oil. ^1H NMR (C_6D_6): −6.25 (br, 4H), −1.19 (br, 15H), 22.76 (br, 2H) ppm. IR (Nujol): 3051 (m), 3012 (m), 1592 (s), 1482 (s), 1426 (m), 1383 (m), 1259 (w), 1211 (m), 1175 (m), 1087 (m), 1026 (s), 978 (m), 882 (w), 824 (w), 800 (m), 745 (s), 698 (s), 645 (w) cm^{-1}. UV/vis (pentane): 453, 726 nm. μ_{eff} = 3.0 μ_B (296 K), determined by the Evans method.

(η^5-Pentamethylcyclopentadienyl)bis(perdeuteriobenzyl)(tetrahydrofuran) chromium(III), $Cp^*Cr(THF)(Bz\text{-}d_7)_2$ (3-d_{14}). (Bz-d_7)K was used instead of BzMgCl in the procedure described above. Recrystallized yield: 38%. NMR: see Table 5. IR (KBr): 2961 (m), 2905 (s), 2855 (m), 2267 (m), 2114 (w), 1555 (s), 1446 (m), 1369 (s), 1170 (m), 1031 (m), 1019 (m), 858 (m), 832 (w), 795 (w), 743 (w), 550 (s), 455 (m) cm^{-1}. MS (*m/e*): 383 ($Cp^*Cr(Bz\text{-}d_7)_2^+$).

(η^5-Pentamethylcyclopentadienyl)(benzyl)bis(tetrahydrofuran)chromium(III) Tetraphenylborate, $[Cp^*Cr(THF)_2(Bz)]BPh_4$ (4). A 0.650 g (1.47 mmol) amount of $Cp^*Cr(Bz)_2THF$ was dissolved in 40 mL of THF. A 0.620 g (1.00 equiv, 1.47 mmol) amount of $HNEt_3BPh_4$ was slowly added to this solution while stirring. The color of the solution changed to purple over 30 min. The solution was stirred for an additional 1 h. All volatiles were then removed by evaporation. The purple residue was redissolved in THF and crystallized from THF/Et_2O at −40 °C. Yield: 0.970 g (89%). ^1H NMR (CD_2Cl_2): −43.85 (br, 15H), 7.38 and 7.06 (br, 36H), 32.98 (br, 2H), 45.15 (v br, 3H) ppm. IR (Nujol): 3053 (s), 2924 (s), 2854 (s), 1942 (w), 1878 (w), 1818 (w), 1579 (m), 1481 (s), 1458 (s), 1425 (m), 1377 (m), 1253 (w), 1205 (w), 1178 (w), 1130 (w), 1016 (m), 862 (s), 750 (s), 736 (s), 705 (s), 613 (m) cm^{-1}. UV/vis (THF): 356 (ϵ = 33 720 M^{-1} cm^{-1}), 526 (ϵ = 1450 M^{-1} cm^{-1}) nm. Mp: 119 °C. μ_{eff} = 4.1(1) μ_B (294 K). Anal. Calcd for $C_{49}H_{58}O_2BCr$: C, 79.34; H, 7.88. Found: C, 79.11; H, 7.73.

Table 7. Crystallographic Data for $[Cp^*Cr(Bz)(\mu\text{-}Cl)]_2$ (1), $Cp^*Cr(py)Bz_2$ (2), $Li[Cp^*CrBz_3]$ (6), and $Cp^*Cr(bpy)Bz$ (8)

	1	2	6	8
		(a) Crystal Parameters		
formula	$C_{34}H_{44}Cl_2Cr_2$	$C_{29}H_{34}CrN$	$C_{31}H_{36}CrLi$	$C_{27}H_{29}CrN_2$
fw	503.50	448.59	467.56	433.54
cryst syst	monoclinic	monoclinic	monoclinic	triclinic
space group	$C2/c$	$P2_1/n$	$P2_1/n$	$P\bar{1}$
a, Å	14.960(4)	9.345(3)	11.125(2)	9.056(3)
b, Å	16.803(5)	16.923(5)	15.287(3)	11.568(6)
c, Å	13.662(6)	16.161(5)	15.410(4)	11.602(4)
α, deg	73.56(3)			
β, deg	110.4(3)	104.36(2)	94.11(2)	88.47(5)
γ, deg	79.35(3)			
Z	4	4	4	4
cryst dimens, mm	0.30 × 0.40 × 0.90	0.36 × 0.36 × 0.40	0.28 × 0.30 × 0.36	0.20 × 0.20 × 0.36
cryst color	red	dark red	black	black
D(calc), g cm^{-3}	1.296	1.203	1.188	1.257
μ(Mo K$_\alpha$), cm^{-1}	8.60	4.64	4.30	5.01
T, K	293	293	293	293
		(b) Data Collection		
diffractometer	Siemens R3	Siemens R3	Siemens P4	Siemens R3
monochromator	graphite	graphite	graphite	graphite
radiation	Mo Kα	Mo Kα	Mo Kα	Mo Kα
2θ scan range, deg	4−48	4−47	4−45	4−45
data collected (hkl)	±17,+19,+15	±11,+19,+19	±12,+17,+17	±10,±13,+13
no. of rflns collected	2646	3962	3562	2604
no. of indep rflns	2527	3663	3417	2500
no. of obsd rflns ($F_o > n\sigma(F_o)$)	1843 (n = 5)	1393 (n = 5)	1422 (n = 3)	1820 (n = 4)
std rflns	3 std/197 rflns	3 std/197 rflns	3 std/197 rflns	3 std/197 rflns
var in stds, %	<1	<1	4	<1
		(c) Refinement		
R(F), %	4.04	6.56	8.97	5.87
R(wF), %	5.56	7.07	7.73	6.01
Δ/σ(max)	0.07	0.01	0.07	0.02
$\Delta(\varrho)$, e Å^{-3}	0.28	0.37	0.54	0.37
N_o/N_v	10.7	5.4	5.0	7.0
GOF	1.12	1.24	1.16	1.37

(η^5-Pentamethylcyclopentadienyl)(perdeuteriobenzyl)-bis(tetrahydrofuran)chromium(III) Tetraphenylborate, $[Cp^*Cr(THF)_2(Bz\text{-}d_7)]BPh_4$, (4-$d_7$). The same procedure as above was followed, using **3**-d_{14} as starting material. Yield: 67%. NMR: see Table 5. IR (KBr): 3054 (m), 3037 (m), 2998 (m), 2982 (m), 2917 (m), 2879 (m), 2270 (w), 1579 (w), 1558 (w), 1479 (m), 1458 (w), 1428 (m), 1377 (w), 1261 (w), 1183 (w), 1153 (w), 1067 (w), 1042 (m), 1032 (m), 846 (m), 743 (s), 707 (s), 612 (m), 602 (m), 549 (m) cm^{-1}.

(η^5-Pentamethylcyclopentadienyl)(benzyl)(2,2′-bipyridine)chromium(III) Tetraphenylborate, $[Cp^*Cr(bpy)(Bz)]BPh_4$ (5). 0.80 g of $[Cp^*Cr(Bz)(THF)_2]BPh_4$ (1.08 mmol) was dissolved in 40 mL of THF. A 0.169 g amount of 2,2′-bipyridine was added to this solution while stirring. The color changed from purple to red-brown. After 30 min the volatiles were removed by evaporation. The residue was crystallized from THF/Et_2O at −40 °C. Yield: 0.76 g (93%). ^{1}H NMR (CD_2Cl_2): −79.12 (br, 2H), −59.72 (br, 2H), −14.25 (br, 15H), 0.11 (br, 2H), 7.09 and 7.43 (br, 20H), 22.91 (br, 2H), 28.95 (br, 1H), 37.46 (br, 2H) ppm. IR (KBr): 3049 (s), 2995 (s), 2916 (m), 2877 (m), 1942 (w), 1880 (w), 1815 (w), 1697 (w), 1601 (s), 1477 (s), 1440 (s), 1379 (m), 1311 (w), 1263 (w), 1207 (w), 1176 (w), 1155 (w), 1064 (w), 1026 (m), 842 (w), 734 (s), 704 (s), 609 (m), 447 (w), 428 (w) cm^{-1}. UV/vis (THF): 380 (sh, ϵ = 4520 M^{-1} cm^{-1}), 480 (ϵ = 4110 M^{-1} cm^{-1}), 629 (ϵ = 650 M^{-1} cm^{-1}) nm. Mp: 164 °C dec. μ_{eff} = 4.3(1) μ_B (297 K). Anal. Calcd for $C_{51}H_{50}N_2BCr$: C, 81.27; H, 6.69; N, 3.72. Found: C, 81.23; H, 6.59; N, 3.59.

Lithium (η^5-Pentamethylcyclopentadienyl)tris(benzyl)-chromate(III), $Li[Cp^*Cr(Bz)_3]$ (6). $[Cp^*CrCl_2]_2$ was formed by reacting $CrCl_3(THF)_3$ (1.845 g, 4.92 mmol) with Cp*Li (0.700 g, 4.92 mmol) in THF overnight. The THF was then removed in vacuo and the solid residue redissolved in 40 mL of toluene. To this solution was added dropwise 28.4 mL (3.00 equiv) of BzLi (0.52 M in Et_2O). Within minutes the color of the solution changed to bright purple. After the mixture was stirred for 45 min, the solvent was evaporated under vacuum. The residual solid was extracted with toluene. Crystallization from a mixture of pentane and toluene at −40 °C gave purple crystals of $Li[Cp^*Cr(Bz)_3]$ in 63% yield. ^{1}H NMR (C_6D_6): −0.64 (br, 6H), 2.73 (br, 15H), 36.34 (br, 9H) ppm. IR (KBr): 3057 (m), 3013 (m), 2903 (s), 2856 (m), 1589 (s), 1477 (s), 1446 (m), 1375 (w), 1205 (s), 1174 (w), 1026 (w), 966 (s), 796 (m), 750 (s), 702 (s), 578 (w), 530 (s) cm^{-1}. UV/vis (Et_2O): 536 (ϵ = 1330 M^{-1} cm^{-1}), 603 (sh, ϵ = 890 M^{-1} cm^{-1}) nm. Mp: 175 °C. μ_{eff} = 4.0(1) μ_B (296 K). Anal. Calcd for $C_{31}H_{36}CrLi$: C, 79.63; H, 7.76. Found: C, 79.60; H, 7.65. MS (m/e): 459, 369 ($Cp^*Cr(Bz)_2^+$).

Lithium (η^5-Pentamethylcyclopentadienyl)tris(perdeuteriobenzyl) chromate(III), $Li[Cp^*Cr(Bz\text{-}d_7)_3]$ (6-d_{21}). The whole preparation (see above) was carried out in THF. Yield: 40%. NMR see table 5. IR (KBr): 2961 (m), 2903 (m), 2854 (m), 2266 (m), 2123 (w), 1555 (s), 1362 (s), 1274 (w), 1165 (m), 1031 (m), 832 (m), 795 (m), 740 (m), 554 (m), 522 (w), 456 (m) cm^{-1}. MS (m/e): 479, 383 ($Cp^*Cr(Bz\text{-}d_7)_2^+$).

Bis(tetramethylethylenediamine)lithium (η^5-Pentamethylcyclopentadienyl)tris(benzyl)chromate(III), $Li(TMEDA)_2[Cp^*Cr(Bz)_3]$ (7). A THF solution (50 mL) of $[Cp^*CrCl_2]_2$ was formed by stirring $CrCl_3(THF)_3$ (1.501 g, 3.98 mmol) and Cp*Li (0.568 g, 4.00 mmol) together for 1 h. A 6.0 mL (3.00 equiv) amount of BzMgCl (2.05 M in THF, 12.30 mmol) was added dropwise to this blue solution. 1,4-Dioxane (3 mL) was added after 1 h, and the solution was stirred for an additional 1 h. The purple solution was filtered and 3 mL of TMEDA added to it. This solution was stirred for an additional 1 h. After all volatiles were removed, the residue was extracted with ether and dried. Crude yield: 2.39 g (85%). By NMR this crude solid was found to be pure. ^{1}H NMR (CD_2Cl_2): −28.84 (br, 15H), −0.80 (br, 2H), 2.11, 2.34 (br, 32H), 7.2 (br, 10H), 34.2 (br, 1H), 38.23 (v br, 2H) ppm. IR (KBr): 3058 (m), 3048 (m), 3000 (sh), 2979 (sh), 2952 (s), 2905 (sh), 2885 (vs), 2848 (s), 2795 (m), 1587 (vs), 1478 (vs), 1456 (s),

1288 (m), 1211 (s), 1028 (s), 945 (s), 798 (m), 789 (m), 745 (s), 687 (s) cm^{-1}. UV/vis (THF): 554 (ϵ = 680 M^{-1} cm^{-1}), 633 (sh, ϵ = 360 M^{-1} cm^{-1}). Mp: 141 °C dec. μ_{eff} = 4.2(1) μ_B (295 K). Anal. Calcd for $C_{43}H_{68}N_4CrLi$: C, 73.78; H, 9.79; N, 8.00. Found: C, 73.83; H, 9.59; N, 7.68. MS (*m/e*): 459, 369 ($Cp^*Cr(Bz)_2^+$).

Bis(tetramethylethylenediamine)lithium (η^5-Pentamethylcyclopentadienyl)tris(perdeuteriobenzyl)chromate(III), Li(TMEDA)$_2$[Cp*Cr(Bz-*d*$_7$)$_3$] (7-*d*$_{21}$). An excess of TMEDA (0.5 mL) was added to a solution of **6**-*d*$_{21}$ (100 mg, 0.2 mmol) in toluene/pentane (1:4). The mixture was stirred for 30 min at room temperature and then cooled to −40 °C to induce crystallization; yield 72%. NMR: see Table 5. IR (KBr): 2969 (m), 2954 (s), 2889 (s), 2845 (s), 2795 (m), 2263 (m), 2197 (w), 2109 (w), 1550 (s), 1469 (s), 1457 (s), 1366 (s), 1287 (m), 1245 (w), 1177 (m), 1159 (m), 1127 (w), 1069 (w), 1031 (m), 1014 (w), 947 (m), 821 (m), 782 (m), 741 (m), 550 (m), 519 (w), 497 (w) cm^{-1}. MS (*m/e*): 479, 383 ($Cp^*Cr(Bz_{(d)})_2^+$).

(η^5-Pentamethylcyclopentadienyl)(benzyl)(2,2′-bipyridine)chromium(II), Cp*Cr(bpy)(Bz) (8). Method A. A 0.200 g (0.453 mmol) amount of $Cp^*Cr(Bz)_2(THF)$ was dissolved in 30 mL of THF. To this solution was added 0.071 g (0.46 mmol) of 2,2′-bipyridine. After 3 h the solvent was removed by evaporation. The remaining residue was dissolved in Et_2O and crystallized at −40 °C. Yield: 0.062 g (32%). ^1H NMR (C_6D_6): 2.87 (br, 2H), 10.59 (br, 15H), 20.96 (br, 2H), 21.68 (br, 1H), 24.78 (br, 1H), 87.95 (br, 2H), 91.74 (br, 2H) ppm. IR (KBr): 3005 (m), 2956 (m), 2904 (s), 1574 (s), 1492 (s), 1446 (s), 1373 (m), 960 (s), 731 (s), 694 (m) cm^{-1}. UV/vis (pentane): 486 (sh, ϵ = 1200 M^{-1} cm^{-1}), 506 (ϵ = 1300 M^{-1} cm^{-1}), 663 (ϵ = 790 M^{-1} cm^{-1}), 1004 (ϵ = 380 M^{-1} cm^{-1}), 1079 (ϵ = 390 M^{-1} cm^{-1}). Mp: 150 °C. μ_{eff} = 3.0(1) μ_B (295 K). Anal. Calcd for $C_{27}H_{30}N_2Cr$: C, 74.63; H, 6.96; N, 6.45. Found: C, 74.76; H, 7.04; N, 6.09. Mass spectrum (*m/e*): 434 (M^+), 343 ($Cp^*Cr(bpy)^+$).

Method B. A 0.222 g (0.29 mmol) amount of **5** was dissolved in 40 mL of THF. This solution was then cooled to −78 °C. A 0.17 mL (1.7 M in hexanes) amount of ^tBuLi was syringed into the purple solution. The color of the solution immediately changed to brown. The reaction mixture was stirred at −78 °C for 15 min and then warmed to room temperature. The THF was evaporated under vacuum and the residue extracted with pentane and dried. This solid was found to be pure by ^1H NMR. Yield: 90 mg (70%).

X-ray Crystallographic Structure Determinations for 1, 2, 6, and 8. Crystallographic data are collected in Table 7. The specimens were all mounted in Lindemann capillary tubes and photographically characterized. Crystals of **1**, **2**, and **7** were found to possess 2/*m* Laue symmetry. **1** possessed systematic absences in the data indicating either *C*2/*c* or *Cc*, with *Z* = 4; the presence of inversional molecular symmetry strongly indicated the former centrosymmetric alternative, which was verified by the results of refinement. Both **2** and **7** were found to belong to the $P2_1/n$ space group, while **8** showed $\bar{1}$ Laue symmetry and the preferred space group, based on the results of the refinement, was $P\bar{1}$. Ψ-Scan data showed negligible variation for all samples, and no corrections for absorption were needed. For **1** a correction for a portion of the crystal out of the beam was applied. The Cr atoms in each structure were located from Patterson maps. All non-hydrogen atoms were anisotropically refined, except for C(11) in **6**, which persistently produced non-positive-definite thermal parameters. For **2** and **6**, phenyl rings were constrained to be rigid, planar hexagons. Hydrogen atoms were treated as idealized contributions. All computations used SHELXTL software (various versions) (G. Sheldrick, Siemens XRD, Madison, WI).

Electrochemical Measurements. CV measurements were carried out using a Princeton Applied Research (PAR) Model 273 potentiostat/galvanostat. All measurements were made under a nitrogen atmosphere in a drybox. The working electrode was a platinum-disk electrode (1.66 mm diameter, scan rate 0.1−0.2 V s^{-1}) and a platinum wire served as an auxiliary electrode. The reference electrode was composed of a silver wire in contact with 0.01 M $AgNO_3$ and 0.1 M $[NBu_4]PF_6$ in MeCN. The reference electrode was separated from the cell by a compartment having a porous Vycor tip. This was filled with the supporting electrolyte and solvent. All measurements were carried out in THF (distilled from Na/K), with 0.5 M $[NBu_4]ClO_4$ as electrolyte. Concentrations of **4** and **7** were in the range 1−3 mM. Potentials were referenced to the ferrocenium/ferrocene (Fc^+/Fc) couple at the end of each run. *iR* compensation was applied.

Acknowledgment. We thank Drs. M. Carney and D. L. Beach of Chevron Chemical Co. for helpful discussions and polymer characterization data. This research was supported by grants from Chevron Chemical Co. and the National Science Foundation (Grant No. CHE-91225580). K.H.T. was the recipient of an Alfred P. Sloan Research fellowship (1992−1994).

Supplementary Material Available: Tables of positional and thermal parameters from the X-ray structure determinations of **1**, **2**, **6**, and **8** (13 pages). Ordering information is given on any current masthead page.

OM940724H

Ab Initio Theoretical Study on Ethylene Polymerization with Homogeneous Silylene-Bridged Group 4 Metallocene Catalysts. Ethylene Insertion and β-Elimination

Tohru Yoshida,[†,‡,§] Nobuaki Koga,[†,§] and Keiji Morokuma*[,†,∥]

Institute for Molecular Science, Okazaki 444, Japan, Polymer Synthesis, Yokkaichi Research Laboratory, Tosoh Corporation, 1-8, Kasumi, Yokkaichi 510, Japan, School of Informatics and Sciences, Nagoya University, Nagoya 464-01, Japan, and Cherry L. Emerson Center for Scientific Computation and Department of Chemistry, Emory University, Atlanta, Georgia 30322

Received October 17, 1994[⊗]

The mechanism of homogeneous polymerization of ethylene with silylene-bridged group 4 cationic metallocene model catalysts ($H_2SiCp_2M-Me^+$; M = Ti, Zr, Hf) has been studied by the *ab initio* MO method, with focus on two important reactions: the repetitive insertion of ethylene into the metal–alkyl bond along Cossee's direct insertion mechanism and the β-elimination, considered to be a termination or chain-transfer step. All stationary point structures are optimized at the RHF level (some for Zr at the RMP2 level as well), and the energetics is calculated at the RQCISD level. The insertion of ethylene into the M–Me bond proceeds through a four-centered transition state with a small activation energy of 7–10 kcal/mol, leading to the kinetic product having the γ-agostic propyl ligand with an exothermicity of about 30 kcal/mol. There is a clear difference in energy of reaction between Ti and the other metals, Ti being the least exothermic, consistent with the experimental relative order of insertion activity: Zr ≥ Hf > Ti. The peculiarity of Ti has been attributed to the size effect; the small radius of Ti makes its Ti transition states and intermediates more compact and crowded than those of the other metals. Isomerization of the γ-agostic product to the more stable β-agostic propyl complex requires a high activation energy, especially for Hf, a factor related to the ability to produce polymer with higher molecular weight. β-Elimination from the β-agostic propyl complex is endothermic by about 50 kcal/mol and takes place with difficulty. In addition, comparison has been made with recent theoretical calculations which gave no barrier.

I. Introduction

Transition-metal catalysts are used extensively in the chemical industry for the polymerization of ethylene, propylene, and other olefins.[1] Two types of important catalysts have been adopted widely for practical use: Ziegler–Natta catalysts, $TiCl_4/AlEt_3$, $TiCl_3/AlEt_3$, etc., and Phillips catalysts, CrO_3/SiO_2.[2] Olefin polymerization with these heterogeneous catalysts might involve several key reactions, including (1) generation of an active metal–alkyl site, (2) repetitive insertion of olefin into the metal–alkyl bond for chain propagation, and (3) chain termination/chain transfer by β-hydride elimination or by hydrogenolysis controlling the molecular weight of the polymer.

Since the controlled study of these catalyst systems is still hindered by the inherent complexities of heterogeneous colloidal and/or surface environments,[3] soluble titanium and zirconium complexes have been used as model systems for studies on the key reactions in catalytic olefin polymerization and are being developed for practical use. The most intensely studied catalysts are Cp_2MCl_2 ($Cp^- = \eta^5\text{-}C_5H_5^-$; M = Ti, Zr) in the presence of aluminum alkyl cocatalysts. In the 1960s, Shilov, on the basis of conductivity and electrodialysis studies, and Breslow, by UV–visible spectroscopic and chemical studies, proposed that the active species in the Cp_2TiCl_2/AlR_nCl_{3-n} (R = alkyl) model system is the cationic alkylated titanium complex.[4]

Several key advances with respect to the tacticity control of α-olefin polymerization in the 1980s generated renewed interest in the proposal that d^0 alkyl complexes Cp_2MR^+ are active species in the soluble catalytic systems. It is postulated that such cationic species are

† Institute for Molecular Science.
‡ Tosoh Corp.
§ Nagoya University.
∥ Emory University.
⊗ Abstract published in *Advance ACS Abstracts*, December 15, 1994.

(1) (a) Reich, L., Shindler, A., Eds. *Polymerization by Organometallic Compounds*; Wiley-Interscience: New York, 1966. (b) Lenz, R. W., Ed. *Organic Chemistry of Synthetic High Polymers*; Wiley-Interscience: New York, 1967. (c) Sinn, H.; Kaminsky, W. *Adv. Organomet. Chem.* **1980**, *18*, 99. (d) Quirk, R. P., Hsieh, H. L., Klingensmith, G. C., Tait, P. J., Eds. *Transition Metal Catalyzed Polymerization: Alkenes and Dienes*; Harwood Publishers for MMI Press: New York, 1983.

(2) (a) Clak, A. *Catal. Rev.* **1969**, *3*, 145. (b) Quirk, R. P., Ed. *Transition Metal Catalyzed Polymerizations*; Cambridge University Press: Cambridge, U.K., 1988.

(3) (a) Keii, T., Ed. *Kinetics of Ziegler-Natta Polymerization*; Kodansya: Tokyo, 1972. (b) Jenkins, A. D., Ledwith, A., Eds. *Reactivity, Mechanism, and Structure in Polymer Chemistry*; Wiley-Interscience: New York, 1974. (c) Elias, H.-G., Ed. *Macromolecules*; Plenum: New York, 1977. (d) Boor, J., Jr., Ed. *Ziegler-Natta Catalysts and Polymerization*; Academic Press: New York, 1979.

(4) (a) Breslow, D. S.; Newberg, N. R. *J. Am. Chem. Soc.* **1959**, *81*, 81. (b) Long, W. P.; Breslow, D. S. *J. Am. Chem. Soc.* **1960**, *82*, 1953. (c) Dyachkovskii, F. S.; Shilova, A. K.; Shilov, A. V. *J. Polym. Sci., Part C* **1967**, *16*, 2333.

0276-7333/95/2314-0746$09.00/0

formed by alkylation of Cp_2MCl_2 with aluminum alkyl, followed by halide abstraction.[5] The 14-electron, d^0 Cp_2MR^+ ion is coordinatively and electronically highly unsaturated. Thus, an olefin can smoothly coordinate and insert into the M−R bond. Other indirect supports for this mechanistic feature have been provided by a number of experimental results, including the isolation of the cationic titanium alkenyl complex ($Cp_2Ti[C(SiMe_3)=C(Me)Ph]^+$) by Eisch[6] and of $Cp_2Zr(Me)^+$ by Jordan.[7]

Furthermore, Watson, Bercaw, and Marks demonstrated that the neutral compounds $Cp^*_2M(R)$ (M = Lu, Sc) and $[Cp^*_2M(H)]_2$ (M = Lu, La, Nd), which in monomeric form are isoelectronic with Cp_2MR^+ (M = Ti, Zr), are active ethylene polymerization catalysts.[8] Watson directly observed propylene insertion into the Lu−Me bond of Cp^*_2LuMe.[9] These results that 3-coordinate, 14-electron, d^0 $Cp_2M(R)^{n+}$ complexes are the active species in the metallocene-based olefin polymerization strongly suggest that 4-coordinate alkyl complexes $Cp_2M(R)(X)$ (M = Ti, Zr; X = alkyl, aryl, halide, etc.) and 3-coordinate, d^1 $Cp_2Ti(R)$ complexes are invariably unreactive with olefins. Subsequently, Bochman and Theopold have given evidence which strongly corroborates the above conditions and have extended the applicability of this system as well.[10]

However, the factors affecting the polymerization rate have not been made clear as yet. β-Hydride elimination should be a termination path for olefin polymerization as well as a common decomposition route of metal alkyls.[11] It is not well established whether β-elimination is also a key step of chain transfer. Unlike the olefin insertion reaction, the β-hydride elimination reaction, generally not a rate-limiting step, is difficult to study, since other side reactions complicate the reaction profile.[12]

Under these circumstances, several theoretical studies including ours have been carried out to study the olefin insertion mechanism in polymerization with L_2M-Me^+ (L = Cl, Cp or L_2 = SiH_2Cp_2; M = Ti, Zr) according to the Cossee mechanism.[13−15] These studies have shown that olefins coordinate strongly to the cationic active intermediates and that the activation

Scheme 1[a]

Ethylene Insertion Reaction into Metal-Alkyl Bond

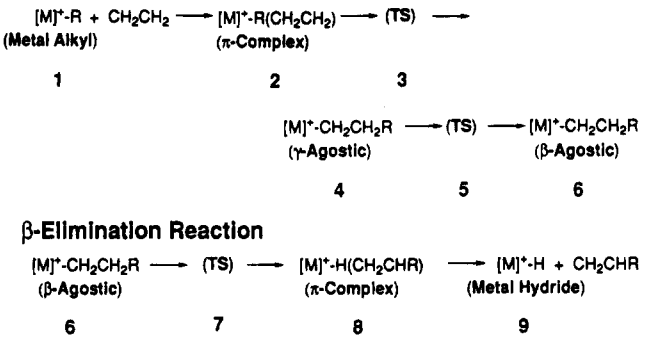

[a] Legend: $[M]^+ = H_2SiCp_2M^+$; M = Ti, Zr, Hf; R = CH_3.

barriers from the olefin complexes are low. According to our study on ethylene insertion with the active catalyst $SiH_2Cp_2ZrMe^+$ with restricted second-order Møller−Plesset (RMP2) energetics based on the restricted Hartree−Fock (RHF) optimized structures, (1) the binding energy of the ethylene π-complex is about 33 kcal/mol, (2) the activation energy from the π-complex is about 6 kcal/mol, (3) insertion gives a product with a γ-agostic interaction, which rearranges to the final product with a stronger β-agostic interaction, and (4) the β-agostic product is exothermic relative to the reactant by about 41 kcal/mol.[15b] On the basis of the structures thus determined, bulky substituents were introduced by the molecular mechanics (MM) method to demonstrate that tacticity control in propylene polymerization by the chiral zirconocene complex takes place via an indirect mechanism i.e., the mechanism in which the chiral catalyst controls the conformation of the growing polymer chain, which in turn controls the sense of approach of the inserting propylene monomer.[15b]

In the present paper, we extend our previous theoretical study and compare, among group 4 metals, the catalytic activities of the silylene-bridged metallocene catalysts in ethylene insertion and in β-elimination, as illustrated in Scheme 1. After a brief explanation of computational methods in section II, we will discuss in section III-A RHF structures for ethylene insertions, in which those of Zr reported before[15b] will be shown again for convenience. In section III-B the higher level RMP2 structures for M = Zr will be compared with the corresponding RHF structures. In section III-C the structures for β-elimination will be presented. In section IV the potential energy profiles of ethylene insertion as well as β-elimination will be compared among the three metals. In section V we compared the present results with other recent calculations. Concluding remarks will be given in section VI.

(5) (a) Watson, P. L.; Roe, D. C. *J. Am. Chem. Soc.* **1982**, *107*, 6471. (b) Keii, T., Soga, K., Eds. *Catalytic Polymerization of Olefin*; Elsevier: Amsterdam, 1986. (c) Kaminsky, W., Sinn, H., Eds. *Transition Metals and Organometallics as Catalysts for Olefin Polymerization*; Springer: New York, 1988.

(6) Eisch, J. J.; Piotrowski, A. M.; Brownstein, S. K.; Gabe, E. J.; Lee, F. L. *J. Am. Chem. Soc.* **1985**, *107*, 7219.

(7) Jordan, R. F.; Echols, S. F. *Inorg. Chem.* **1987**, *26*, 383.

(8) (a) Watson, P. L.; Parshall, G. W. *Acc. Chem. Res.* **1985**, *18*, 51. (b) Thompson, M. E.; Bercaw, J. E. *Pure Appl. Chem.* **1985**, *56*, 1. (c) Jeske, G.; Lauke, H.; Mauermann, H.; Sweptson, P. N.; Schumann, H.; Marks, T. *J. Am. Chem. Soc.* **1985**, *107*, 8091.

(9) Watson, P. L. *J. Am. Chem. Soc.* **1982**, *104*, 337.

(10) (a) Bochmann, M.; Jaggar, A. J.; Nicholls, J. C. *Angew. Chem., Int. Ed. Engl.* **1990**, *29*, 780. (b) Thomas, B. J.; Noh, S. K.; Schulte, G. K.; Sendlinger, S. C.; Theopold, K. H. *J. Am. Chem. Soc.* **1991**, *113*, 893.

(11) (a) Doherty, N. M.; Bercaw, J. E. *J. Am. Chem. Soc.* **1985**, *107*, 2670. (b) Burger, B. J.; Santarsiero, B. D.; Trimmer, M. S.; Bercaw, J. E. *J. Am. Chem. Soc.* **1988**, *110*, 3134.

(12) Resconi, L.; Piemontesi, F.; Franciscono, G.; Abis, L.; Fiorani, T. *J. Am. Chem. Soc.* **1992**, *114*, 1025.

(13) Cossee, P. *J. Catal.* **1964**, *3*, 80.

(14) (a) Fujimoto, H.; Yamasaki, T.; Mizutani, H.; Koga, N. *J. Am. Chem. Soc.* **1985**, *107*, 6157. (b) Jolly, C. A.; Marynick, D. S. *J. Am. Chem. Soc.* **1989**, *111*, 7968. (c) Meier, R. J.; Doremaele, G. H. J. v.; Iarlori, S.; Buda, F. *J. Am. Chem. Soc.* **1994**, *116*, 7274.

(15) (a) Kawamura-Kuribayashi, H.; Koga, N.; Morokuma, K. *J. Am. Chem. Soc.* **1992**, *114*, 2359. (b) Kawamura-Kuribayashi, H.; Koga, N.; Morokuma, K. *J. Am. Chem. Soc.* **1992**, *114*, 8687. (c) Rappé, A. K.; Castonguay, L. A. *J. Am. Chem. Soc.* **1992**, *114*, 5832.

(16) All the calculations were carried out with the following programs: GAUSSIAN 90 (Frisch, M. J.; Head-Gordon, M.; Trucks, G. W.; Foresman, J. B.; Schlegel, H. B.; Raghavachari, K.; Robb, M. A.; Binkley, J. S.; Gonzales, C.; DeFrees, J. S.; Fox, J. S.; Whiteside, R. A.; Seeger, R.; Melius, C. F.; Baker, J.; Martin, R. L.; Kahn, L. R.; Stewart, J. J. P.; Topiol, S.; Pople, J. A. Gaussian, Inc., Pittsburgh, PA, 1990), GAUSSIAN 92 (Frisch, M. J.; Trucks, G. W.; Head-Gordon, M.; Gill, P. M. W.; Wong, M. W.; Foresman, J. B.; Johnson, B. G.; Schlegel, H. B.; Robb, M. A.; Replogle, E. S.; Gomperts, R.; Andres, J. L.; Raghavachari, K.; Binkley, J. S.; Gonzalez, C.; Martin, R. L.; Fox, D. J.; Defrees, D. J.; Baker, J.; Stewart, J. J. P.; Pople, J. A. Gaussian, Inc., Pittsburgh PA, 1992), and GAUSSIAN 92/DFT (Frisch, M. J.; Trucks, G. W.; Schlegel, H. B.; Gill, P. M. W.; Johnson, B. G.; Wong, M. W.; Foresman, J. B.; Robb, M. A.; Head-Gordon, M.; Replogle, E. S.; Gomperts, R.; Andres, J. L.; Raghavachari, K.; Binkley, J. S.; Gonzalez, C.; Martin, R. L.; Fox, D. J.; Defrees, D. J.; Baker, J.; Stewart, J. J. P.; Pople, J. A. Gaussian, Inc., Pittsburgh PA, 1993).

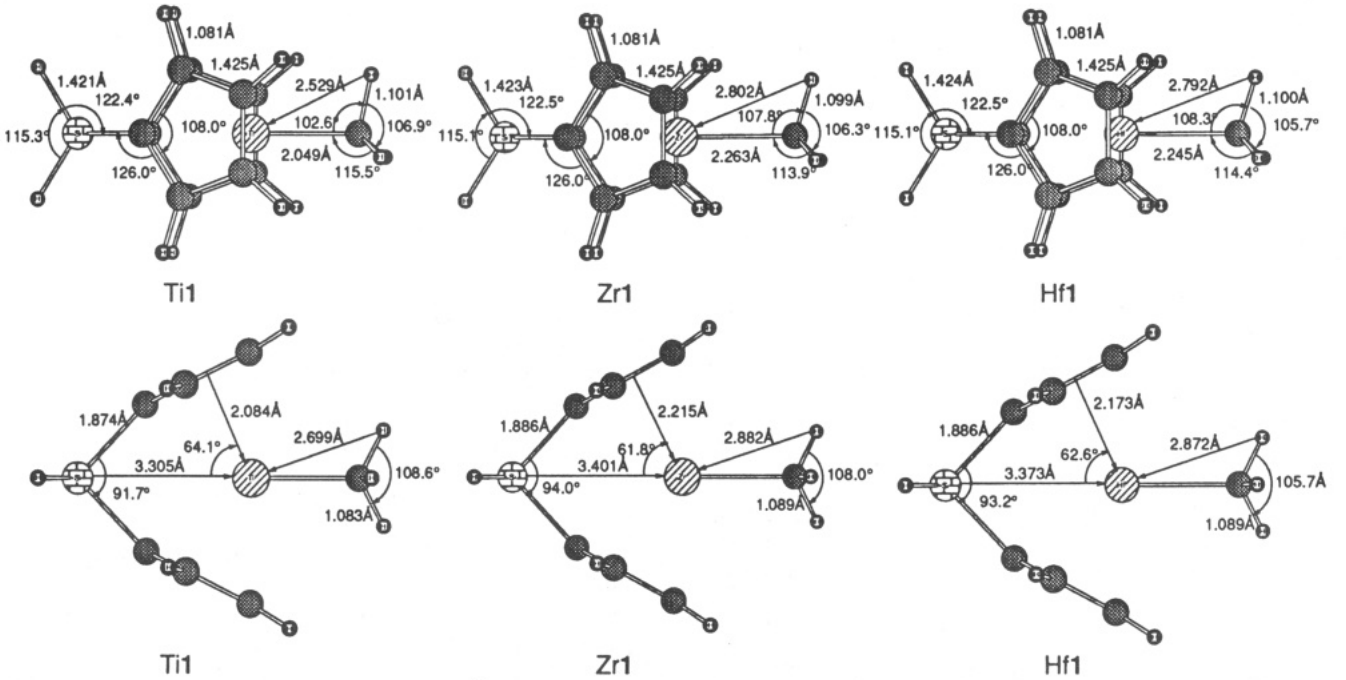

Figure 1. RHF optimized structures (in Å and deg) of reactants **1**. The top and side views are shown in the top and bottom rows, respectively.

II. Method of Calculation

The geometry optimization was carried out with the *ab initio* RHF energy gradient method.[16] For M = Zr, the geometries of reactant Zr**1a**, π-complex Zr**2a**, transition state Zr**3a**, and product with γ-agostic interaction Zr**4a** were optimized at the correlated RMP2 level as well.[17]

For each group 4 metal, the split valence basis functions (Ti, 311/311/41 for 3s4s/3p4p/3d; Zr, 311/311/31 for 4s5s/4p5p/4d; Hf, 311/311/21 for 5s6s/5p6p/5d) were used with the Hay and Wadt effective core potentials (ECPs).[18] Note that the outermost core *n*sp orbitals and electrons as well as the valence $nd(n+1)$sp orbitals and electrons of the metal are explicitly considered in the calculation. For atoms of the silylene-bridged bis(cyclopentadienyl) ligand, which is a spectator and does not participate directly in the present reaction, we used the small STO-3G[19a] basis functions and, for CH_3 and C_2H_4, the split-valence 3-21G[19b] basis functions. During all optimizations, the $H_2SiCp_2M^+$ fragment was assumed to maintain local C_s symmetry and the Cp moiety a local C_{5v} symmetry.[20] The structures of **1**, **2**, and **9** were determined with overall C_s symmetry constraint and those of **3**–**8** without any symmetry constraint.

For better energetics, the electron correlation effect was taken into account with the RMP2 level, the third-order restricted MP level (RMP3),[21] the fourth-order restricted MP level including single, double, and quadruple excitations (RMP4SDQ),[22] and the restricted quadratic configuration interaction including single and double excitations (RQCISD),[23] at the RHF optimized structures. In all electron correlation calculations, all valence electrons including 3s and 3p electrons for Ti, 4s and 4p electrons for Zr, and 5s and 5p electrons for Hf were correlated. It is known that the RHF wave functions of some Ti complexes suffer from triplet instability.[24] We checked the stabilities of the RHF wave functions of all stationary points, to find that those of only some Ti complexes are unstable with respect to becoming unrestricted Hartree–Fock (UHF) wave functions. In these unstable cases, we carried out the UHF and the second- and third-order unrestricted MP calculations (UMP2 and UMP3) with annihilation of the spin contaminants (PUHF, PUMP2, and PUMP3).

At the RMP2 optimized structures for Zr, we also carried out RMP2 energy calculations with the larger basis set: (8s5p) and (11s8p) basis functions for carbons and silicon with the split valence contraction[19c] and (4s) basis functions for hydrogens with [31] contraction.[19d] The d polarization functions were augmented on carbons of CH_3 and C_2H_4. The same ECP and valence basis functions as above were used for Zr.

In addition, we carried out some density functional calculations with Gaussian92/DFT.[17] In these calculations we used the same smaller basis functions and ECP mentioned above.

III. Geometries of Intermediates and Transition States

The optimized structures at the RHF level of **1**–**6** for ethylene insertion and of **7**–**9** for β-elimination are

(17) Møller, C.; Plesset, M. S. *Phys. Rev.* **1934**, *46*, 618.
(18) Hay, P. J.; Wadt, W. R. *J. Chem. Phys.* **1985**, *82*, 299.
(19) (a) Collins, J. B.; Schleyer, P. v. R.; Binkley, J. S.; Pople, J. A. *J. Chem. Phys.* **1976**, *64*, 5142. (b) Gordon, M. S.; Binkley, J. S.; Pople, J. A.; Pietro, J. A.; Hehre, W. J. *J. Am. Chem. Soc.* **1982**, *104*, 2797. (c) Huzinaga, S.; Andzelm, J.; Klbukowski, M.; Radzio-Andzelm, E.; Sakai, Y.; Tatewaki, H. *Gaussian Basis Sets for Molecular Calculations*; Elsevier: Amsterdam, 1984. (d) Dunning, T. H. *J. Chem. Phys.* **1970**, *53*, 2823.
(20) (a) The optimization with no symmetry constraint for Zr**1** gives quite a similar result: $Zr-C_{methyl}$ 2.262 Å; Zr–Si, 3.382 Å; C–C(average) in Cp ring, 1.442 Å; $Si-C_{Cp}$, 1.883 Å; $\angle Cp_{centroid}-Zr-Cp_{centroid}$, 63.0°; $\angle C_{Cp}-Si-C_{Cp}$, 94.0°; ∠C–C–C(average) in Cp, 108.6°. Relxation of constraint leads to an extra stabilization of only 3.6 kcal/mol, and the errors in the activation energy and the energy of reaction, the energy differences between two structures, are expected to be much smaller than this value. Even in the ethane oxidative addition to $CpRh(PH_3)$, where the oxidation number of the central metal increases by 2 and accordingly the Cp coordination mode drastically changes, the constraint of the Cp structure gave an error of 2 kcal/mol. During the present insertion reaction, the oxidation number is unchanged. Therefore, the error due to the constraint is negligible. (b) Koga, N.; Morokuma, K. *Organometallics* **1991**, *10*, 946.
(21) Pople, J. A.; Seeger, R.; Krishnan, R. *Int. J. Quantum Chem., Symp.* **1977**, *11*, 149.
(22) (a) Krishnan, R.; Pople, J. A. *Int. J. Quantum Chem.* **1978**, *14*, 91. (b) Krishnan, R.; Frisch, M. J.; Pople, J. A. *J. Chem. Phys.* **1980**, *72*, 4244.
(23) Pople, J. A.; Head-Gordon, M.; Raghavachari, K. *J. Chem. Phys.* **1987**, *87*, 5968.
(24) For PUHF, PUMP2, and PUMP3 in Tables 2 and 5, the values used come from the single annihilation up to the nonet state ($S+4$). The single annihilation of only two spin states, $S+1$ and $S+2$, can give a correct estimate. See: (a) Koga, N.; Yamashita, K.; Morokuma, K. *Chem. Phys. Lett.* **1991**, *184*, 359. (b) Koga, N.; Kawamura-Kuribayashi, H.; Morokuma, K. Unpublished results.

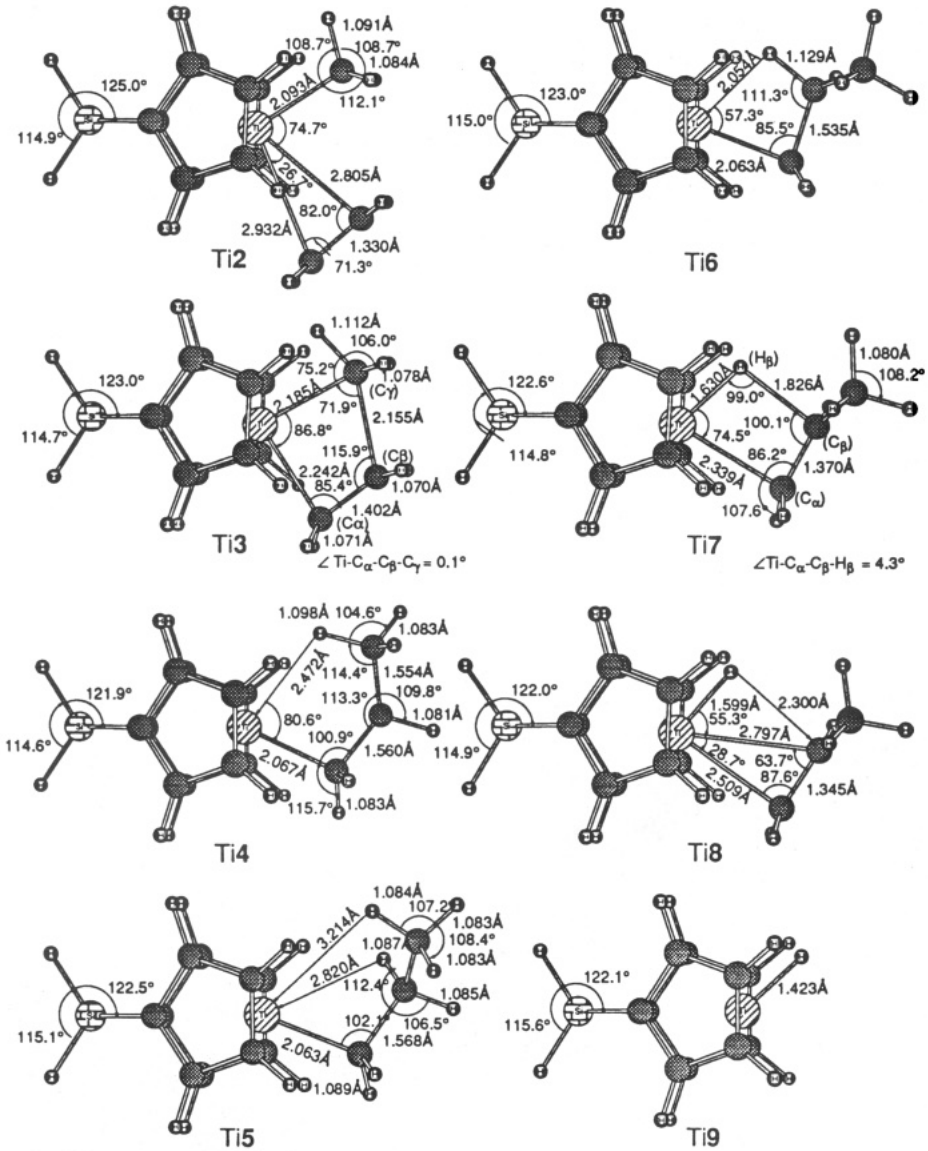

Figure 2. RHF optimized structures (in Å and deg) of π-complex Ti**2**, transition state Ti**3**, γ-agostic product Ti**4**, transition state Ti**5**, β-agostic product Ti**6**, transition state Ti**7**, π-complex Ti**8**, and metal hydride Ti**9**.

shown in Figure 1 for Ti**1**, Zr**1**, and Hf**1**, in Figure 2 for Ti**2**–Ti**9**, in Figure 3 for Zr**2**–Zr**9**, and in Figure 4 for Hf**2**–Hf**9**. Though the structures are generally similar among three metals, there are subtle differences to be noticed and discussed in detail.

A. RHF Structures in Ethylene Insertion. Reactant 1: $SiH_2Cp_2M-Me^+$. This structure was optimized under the C_s symmetry constraint. In Ti**1**, one of the $C_{methyl}-H$ bond lengths of 1.101 Å is 0.02 Å longer than the normal $C_{methyl}-H$ bond[25] and the corresponding $Ti-C_{methyl}-H$ angle of 102.6° is 7° smaller than the tetrahedral angle and 13° smaller than the other $Ti-C_{methyl}-H$ angle in the same methyl group, indicating an α-agostic interaction.[26] The interaction is much weaker in Zr**1** and Hf**1** with the shorter $C_{methyl}-H$ bond and the larger $M-C_{methyl}-H$ angle.

The electron deficiency of the central metal surely should create a driving force for this type of distortion. To compare briefly the stabilization effect of the α-agostic interaction among the three metals, the following calculations using assumed structures were carried out. Ti**1** with a $Ti-C_{methyl}-H$ angle of 107.8°, corresponding to the $Zr-C_{methyl}-H$ angle of Zr**1**, is 0.40 kcal/mol less stable than the optimized structure at the RMP2 level. When the $Zr-C_{methyl}-H$ angle of Zr**1** is 102.6°, corresponding to the $Ti-C_{methyl}-H$ angle of Ti**1**, Zr**1** is destabilized by 0.05 kcal/mol. For Hf**1**, the energy change is close to zero, showing that the potential surface for the methyl tilting is very soft. These results show that the α-agostic interaction in Ti**1** is the strongest among the reactants **1**. However, even with Ti**1**, the energy of the α-agostic interaction in the free catalyst **1** is small and is not likely to contribute significantly to the catalytic activity. Although it is difficult to find the origin of such a small energy difference, the above trend is in line with the order of the M–C distances. In Ti**1**, the M···HC interaction could be stronger because of the shorter Ti–C distance.

In **1**, the metal, Si, and C_{methyl} are nearly collinear, irrespective of the metal. Experimentally, it was found that with the counteranion nearby the $M-Si-C_{methyl}$ angle bends to give a *bent-sandwich* fragment.[27] The

(25) At the RHF/3-21G level, the $C-C_{methyl}-H$ angle of propylene is 110.8° and the $C_{methyl}-H$ length is 1.085 Å.

(26) (a) Koga, N.; Obara, S.; Morokuma, K. *J. Am. Chem. Soc.* **1984**, *106*, 4625. (b) Obara, S.; Koga, N.; Morokuma, K. *J. Organomet. Chem.* **1984**, *270*, C33.

(27) Yang, X.; Stern, C. L.; Marks, T. *J. Am. Chem. Soc.* **1991**, *113*, 3623.

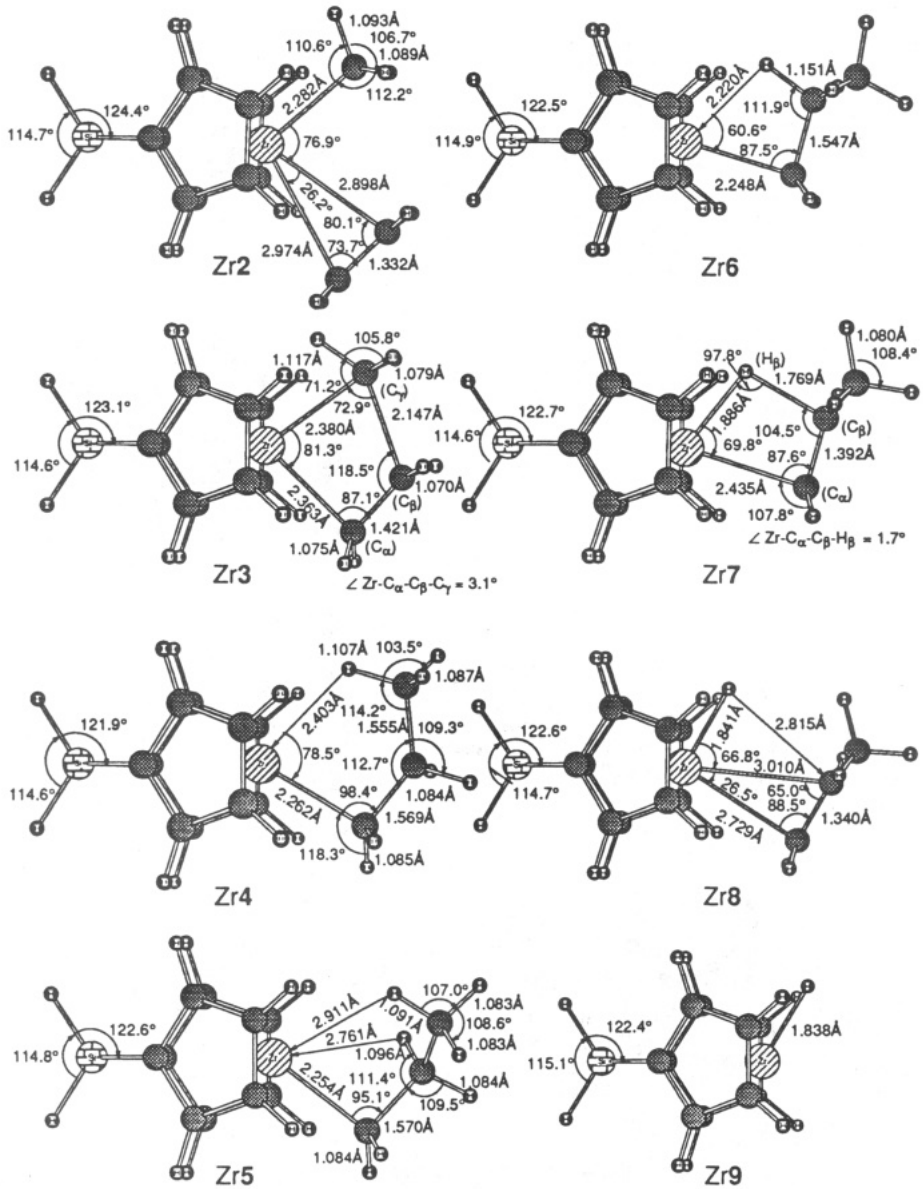

Figure 3. RHF optimized structures (in Å and deg) of π-complex Zr**2**, transition state Zr**3**, γ-agostic product Zr**4**, transition state Zr**5**, β-agostic product Zr**6**, transition state Zr**7**, π-complex Zr**8**, and metal hydride Zr**9**.

energy required to change the M−Si−C_{methyl} angle from 180° to 120° is less than 3 kcal/mol for all the metals, and this bending motion is very soft;[15b] a strong influence of the counteranion can easily change this angle. Bierwagen et al. have recently reported with the perfect pairing general valence bond (GVB-PP) method that Cp_2Ti-Me^+ prefers a pyramidal geometry with a 6 kcal/mol barrier separating it from a collinear geometry,[28] but their large barrier could be an artifact of very limited geometry optimization.

One can note that the Ti−C_{methyl} bond is about 0.2 Å shorter than the Zr−C_{methyl} and Hf−C_{methyl} bonds and that the Ti−$Cp_{centroid}$ distance (2.084 Å) is also shorter than the Zr−$Cp_{centroid}$ (2.215 Å) and Hf−$Cp_{centroid}$ (2.173 Å) distances by about 0.1 Å, reflecting the difference in the atomic radii of the central metals. The M−Cp centroid distances and the M−Me bond distances agree well with the available experimental results for the nonbridged metallocenes.[29] The representative experimental geometrical parameters are compared with the calculated ones in Table 1.

In the present study, we encounter a variety of differences in the M−C and M−Cp distances between the unique Ti metal and the (Zr, Hf) group, which are due to the smaller size of the Ti atom. We call this the size effect of Ti. The magnitude of the differences reflects the electronic and steric environments of the species in question (intermediate, transition states, or product complexes), affects the energetics, and plays an important role in differentiating the catalytic activity among the three metals.

π-Complex 2: $SiH_2Cp_2M-Me(C_2H_4)^+$. The structure was optimized under the C_s symmetry constraint. Ethylene coordinates nearly symmetrically to the metal. One can notice that the M−$C_{ethylene}$ distances are not sensitive to the metal and are quite similar: 2.932 and 2.805 Å (Ti), 2.974 and 2.898 Å (Zr), and 2.950 and 2.891

(28) Bierwagen, E. P.; Bercaw, J. E.; Goddard, W. A., III. *J. Am. Chem. Soc.* **1994**, *116*, 1481.

(29) (a) For Ti: Eisch, J. J.; Caldwell, K. R.; Werner, S.; Krüger, C. *Organometallics* **1991**, *10*, 3417. (b) For Zr: Jordan, R. F.; Bajgur, C. S.; Willet, R.; Scott, B. *J. Am. Chem. Soc.* **1986**, *108*, 7410. (c) For Hf: Johnson, P. L.; Cohen, S. A.; Marks, T. J.; Williams, J. M. *J. Am. Chem. Soc.* **1978**, *100*, 2709.

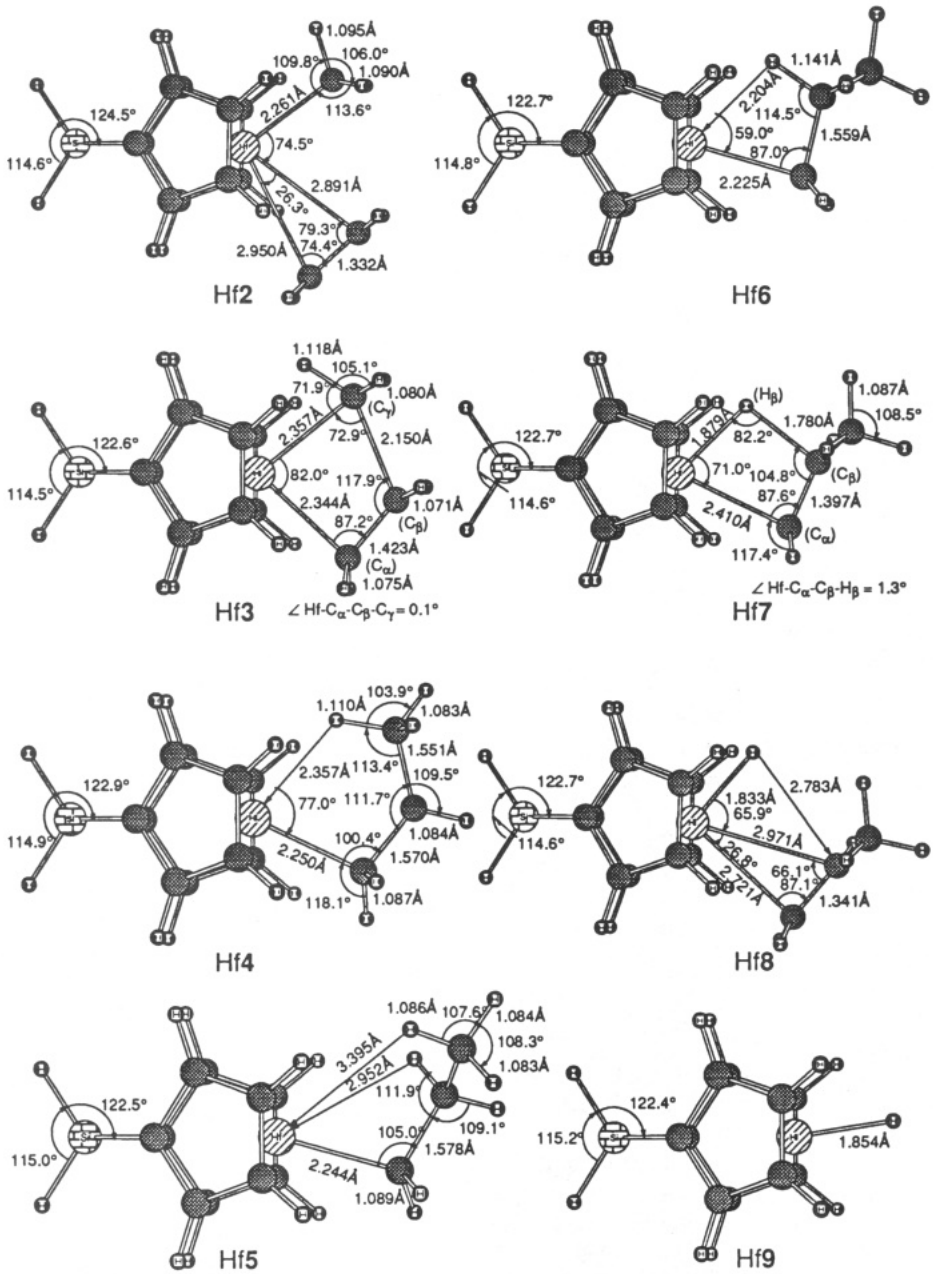

Figure 4. RHF optimized structures (in Å and deg) of π-complex Hf**2**, transition state Hf**3**, γ-agostic product Hf**4**, transition state Hf**5**, β-agostic product Hf**6**, transition state Hf**7**, π-complex Hf**8**, and metal hydride Hf**9**.

Table 1. Representative Structural Parameters for Reactant 1

param	exptl value[a] $[(RCp)_2M]L_2$	calcd value $[H_2SiCp_2MCH_3]^+$ (**1**)
Ti−methyl C (Å)	2.162	2.049
Ti−ring centroid (Å)	2.072, 2.082	2.084
∠ring centroid−Ti−ring centroid (deg)	131.4	128.2
Zr−methyl C (Å)	2.256	2.263
Zr−ring centroid (Å)	2.174 (av)	2.215
∠ring centroid−Zr−ring centroid (deg)	129.6	123.6
Hf−ring centroid (Å)	2.188	2.173
∠ring centroid−Hf−ring centroid (deg)	128.5	125.1

[a] See ref 29: for Ti, $Cp_2Ti(CH_2SiMe_3)(Cl)$; for Zr, $Cp_2Zr(Me)(THF)^+$; for Hf, $(MeCp)_2Hf(BH_4)_2$.

Å (Hf). Though the M−$C_{ethylene}$ distance is the shortest in Ti**2**, the difference in the M−$C_{ethylene}$ distance between Ti and the two other metals is much smaller than that in the M−C_{methyl} distance in **1**. Possibly the steric hindrance due to the shortest Ti−Cp distances weakens ethylene coordination in Ti**2**. Compared with Zr**2** and Hf**2**, Ti**2** suffers from a closer H···H contact between Cp_2 and the reaction sites, Me and C_2H_4 moieties.

The methyl groups of **2** are bent from the collinear M−Si−C_{methyl} structure by 53.6° (Ti), 46.8° (Zr), and 50.6° (Hf). This large bend does not cost much energy, as mentioned above, and provides an empty and easy coordination site for ethylene. The M−C_{methyl} bonds in **2** are longer than those in **1** by 0.044 Å (Ti), 0.019 Å (Zr), and 0.016 Å (Hf), presumably due to the electronic and steric effects of ethylene coordination. The Ti−C_{methyl} distance, which is shorter than the Zr−C_{methyl} and Hf−C_{methyl} distances, is influenced more by ethylene coordination. Due to electron donation from the coordinated ethylene to highly electron-deficient Ti**1**, the α-agostic interaction is less visible in Ti**2** than in Ti**1**; the methyl group is closer to tetrahedral.[24] The already weaker α-agostic interaction in Zr**1** and Hf**1** has almost

completely disappeared due to ethylene coordination in Zr**2** and Hf**2**.

The M−Cp centroid distances of **2** are slightly stretched by 0.031 Å (Ti), 0.017 Å (Zr), and 0.021 Å (Hf), to avoid steric contact between Cp and incoming ethylene. Ti**2** is the most crowded because of its shortest Ti−$Cp_{centroid}$ distance, and the geometrical changes are the largest. Such geometrical changes will be seen in various insertion as well as β-elimination reactions for silylene-bridged metallocenes. Even in such cases, the geometry change in the $H_2SiCp_2M^+$ moiety is small. While the $Cp_{centroid}$−M−$Cp_{centroid}$ plane is coplanar with the $Cp_{centroid}$−Si−$Cp_{centroid}$ plane in **1**, it deviates from the coplanarity by only 1.3−2° in **2**. The Cp−M−Si angle changes little during the reaction. These small changes are in contrast with large distortions, several degrees in the Cp−Zr−Cp angle, seen in hydrozirconation with $Cp_2Zr(Cl)(H)$.[30] The tightness of the present catalyst system may be attributed to its silylene-bridged structure.

Transition State 3. The four atoms forming the four-centered transition structure in transition state **3** are nearly coplanar with a small M−C_α−C_β−C_γ torsional angle (Ti, 0.1°; Zr, 3.1°; Hf, 0.1°), although a larger torsional angle would decrease the steric repulsion due to eclipsing between the methyl and ethylene moieties. The transition state for ethylene insertion into Cl_2TiMe^+ has a larger torsional angle of 10.7°.[15a] The planarity in **3** may be considered to minimize the steric repulsion due to the silylene-bridged bis(cyclopentadienyl) ligand.

The M−C_α distance, which was very long in **2**, is much shortened (Ti, 2.242 Å; Zr, 2.363 Å; Hf, 2.344 Å) in **3**, and this bond formation is nearly completed at this TS. The M−C_γ bond (Ti, 2.185 Å; Zr, 2.380 Å; Hf, 2.357 Å) is stretched slightly from that in **2** but still is not far from a normal single bond. Consequently, in **3** two bond distances, M−C_α to be formed and M−C_γ to be broken, are only 0.1−0.15 Å longer than the normal M−C_{methyl} bond distance in **2**, indicating a very tight transition state with asynchronous bond exchange. The Ti−C_α bond distance in Ti**3** is only 0.1 Å shorter than the M−C_α bond distances in Zr**3** and Hf**3**, whereas that in Ti**1** is 0.2 Å shorter than in Zr**1** and Hf**1**. Since the Ti−C_α bond in Ti**3** is partially formed and weak, it is easily stretched by the size effect, resulting in the smaller difference in **3** than in **1**.

One of the C−H bonds of the migrating methyl group in **3** is stretched by 0.034 Å (Ti), 0.038 Å (Zr), and 0.038 Å (Hf), indicating a strong α-agostic interaction.[31] One of the angles M−C_γ−H is distorted to 75.2° (Ti), 71.2° (Zr), and 71.9° (Hf). We have previously found that no agostic interaction takes place at the transition state of the reaction of ethylene with $Cp_2Zr(Cl)Me$, where the C−H distance is 1.08 Å and the Zr−C_{methyl}−H angle is 77°.[30] Thus, the smaller angle of 71−72° in Zr**3** and Hf**3** may be ascribed to the agostic interaction. By comparing the results for **Zr3** with those of the reaction of $Cp_2Zr(Cl)CH_3$, which requires a much higher activation energy, we have suggested that this agostic interaction plays a role in lowering the barrier[15b] and assists

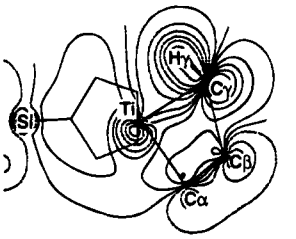

Figure 5. Contour map of the occupied molecular orbital 44 of Ti**3** in the Si−Ti−C_α plane. The contours are for ±0.01, ±0.03, ±0.05, ±0.07, ±0.09, ±0.11, ±0.13, and ±0.15 au, and the solid and dotted lines denote the positive and the negative values, respectively.

the formation of a polymer having high molecular weight. The driving force of this specific α-agostic interaction may be traced to the standard origin,[26] the donative interaction from the C−H σ bond to a vacant metal d orbital. The contour map of MO 44 of Ti**3**, shown in Figure 5 as an example, clearly represents a very favorable overlap between the C_γ−H σ bond and a Ti d orbital.

Product with γ-Agostic Interaction 4: SiH_2Cp_2M−$C_3H_7^+$. The reaction path from TS **3** leads to a local minimum on the potential surface, the insertion product **4** with a C_γ−H agostic interaction. In **4**, the agostic C_γ−H bond is stretched by 0.015 Å (Ti), 0.024 Å (Zr), and 0.027 Å (Hf) compared with the normal C−H bond.[25] These stretches suggest that this agostic interaction is weaker than that in TS **3** but stronger than that in the reactant **1**. Note that the agostic interaction in Ti**4** is weaker than that in Zr**4** and Hf**4**; the agostic C−H bond distance in Ti**1** is the shortest, and the Ti···H distance (2.472 Å) is even longer than the Zr···H and Hf···H distances (2.403 and 2.357 Å), despite the small size of Ti.

The M−C_α−C_β angle is about 100°: 100.9° (Ti), 98.4° (Zr), and 100.4° (Hf). The length of the M−C_α bond is close to that of **1**: 2.067 Å (Ti), 2.262 Å (Zr), 2.250 Å (Hf). The propyl moiety twists away from the nearly eclipsed conformation in TS **3** to reach an approximately staggered conformation, releasing the steric repulsion among the propyl CH_2 and CH_3 groups.

Transition State 5 for Isomerization of the Product. The transition state **5** for the isomerization of the γ-agostic product **4** to the more stable β-agostic product **6** has been located. During this isomerization the agostic interaction migrates from the C_γ−H to the C_β−H bond, and these two agostic interactions might take place simultaneously in **5**. However, the process turns out to depend on the central metal.

In Ti**5**, the agostic interaction has nearly disappeared, presumably because of the large steric hindrance around the small Ti; the C_γ−H and C_β−H bond lengths of 1.084 and 1.087 Å are normal, and the Ti···H_γ and the Ti···H_β distances of 3.214 and 2.820 Å are much longer than the Ti···H distances in Ti**4** and Ti**6**. In Zr**5**, both γ- and β-agostic interactions still exist; the C−H bond lengths of 1.096 and 1.091 Å are longer, and the Zr···H_γ and Zr···H_β distances of 2.911 and 2.761 Å are shorter than those in Ti**5**. In Hf**5**, the γ-agostic interaction disappears and β-agostic interaction remains; the C_β−H bond length is 1.094 Å and the C_γ−H bond is 1.086 Å, and the Hf···H_γ and the Hf···H_β distances are 3.395 and 2.952 Å, respectively. The Zr−C_α−C_β angle of Zr**5** is smaller, consistent with the strongest interactions, than the corresponding angle of Zr**4** by 3.3°. In contrast, in

(30) Endo, J.; Koga, N.; Morokuma, K. *Organometallics* **1993**, *12*, 2777.

(31) (a) Clawson, L.; Soto, J.; Buchwald, S. L.; Steigerwald, M. L.; Grubbs, R. H. *J. Am. Chem. Soc.* **1985**, *107*, 3377. (b) Piers, W. E.; Bercaw, J. E. *J. Am. Chem. Soc.* **1990**, *112*, 9406. (c) Klauledat, H.; Brintzinger, H.-H. *Angew. Chem., Int. Ed. Engl.* **1990**, *29*, 1412.

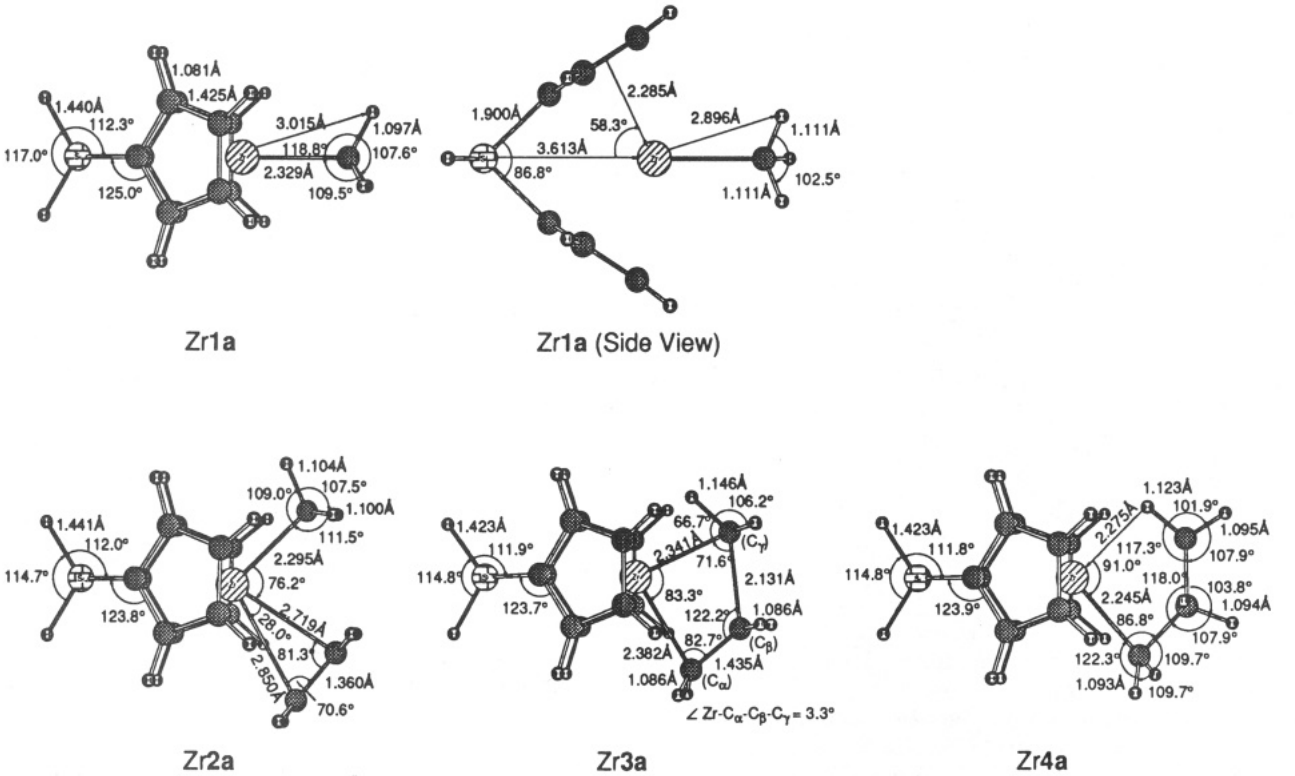

Figure 6. RMP2 optimized structures (in Å and deg) of reactant Zr**1a**, π-complex Zr**2a**, transition state Zr**3a**, and γ-agostic product Zr**4a**. The top and side views of Zr**1a** are shown in the top row.

Ti**5** and Hf**5**, the angle opens by 1.2° and by 4.6°, respectively. The shortest $H_{Cp}\cdots H_{agostic}$ distances in **5** are 2.341 and 2.375 Å (Ti), 2.704 and 2.567 Å (Zr), and 2.538 and 2.430 Å (Hf) for the $H_{Cp}\cdots H_{\gamma}$ and the $H_{Cp}\cdots H_{\beta}$ distances, respectively, showing that Zr**5** is the least crowded. The $H_{Cp}\cdots H_{agostic}$ distances in Hf**5** are shorter than those expected from the $H_{Cp}\cdots H_{agostic}$ distances in Zr**5** and the small difference between the Hf−Cp and the Zr−Cp distances. The reaction with the Hf complex seems to be the most difficult to reach the β-agostic product **6**, which will be substantiated by energetics in section IV.

Judging from the difference between the $M\cdots H_{\gamma}$ and the $M\cdots H_{\beta}$ distances, Zr**5** is the earliest, Ti**5** is next, and Hf**5** is the latest transition state. This point will be discussed in detail in connection with the energetics in section IV.

Product with β-Agostic Interaction 6: $SiH_2Cp_2M-C_3H_7^+$. The reaction reaches the more stable isomer **6** through TS **5** from the direct product **4** by the rotation around the $C_\alpha-C_\beta$ bond. In **6** a strong β-agostic interaction takes place; one of the C_β−H bonds in **6** is longer than the normal C−H bond length by 0.046 Å (Ti), 0.058 Å (Zr), and 0.058 Å (Hf), the stretching being greater than in **4**, which shows that the β-agostic interaction is stronger than the γ-agostic interaction.

The $C_\alpha-C_\beta-C_\gamma$ angle changes a little during the isomerization from **4** to **6**. However, the $M-C_\alpha-C_\beta$ angles in **6** become smaller than those of the γ-agostic product **4**, by 15.4° (Ti), 10.9° (Zr), and 13.4° (Hf), aiding a closer contact between M and H_β. The propyl $C_\alpha-C_\beta$ moiety of **6** is eclipsed, whereas that of **4** is staggered; the gain due to this strong agostic interaction is more than to upset the loss due to the eclipsed conformation. The structures of the **6** species are very similar to each other, with the exceptions of the about 0.2 Å shorter $Ti-C_\alpha$ (2.063 Å) and $Ti\cdots H$ (2.054 Å) distances.

The comparison of the structures of **4** and **6** with those[15a,b] of $Cl_2TiC_3H_7^+$ and $Cl_2ZrC_3H_7^+$ would give further support of the size effect, which destabilizes the intermediates and the transition states for Ti. The most stable isomers of these chloride complexes are those with γ-agostic interactions. Even in $Cl_2TiC_3H_7^+$ a strong γ-agostic interaction takes place, a different situation from that in the present Cp complexes. While the $Zr\cdots H_{\gamma}$ distance of 2.42 Å in γ-agostic $Cl_2ZrC_3H_7^+$ is similar to that of 2.403 Å in Zr**4**, the $Ti\cdots H_{\gamma}$ distance of 2.25 Å in γ-agostic $Cl_2TiC_3H_7^+$ is much shorter than 2.47 Å in Ti**4**. Since the results of Ti**6** suggest that the Ti atom is capable of making an agostic interaction, the absence of the agostic interaction in Ti**4** is definitely ascribed to the size effect of Ti.

B. RMP2 Structures for Ethylene Insertion into the Zirconocene Complex. For the present catalytic system where the group 4 metal has a M(IV) d^0 electronic configuration, one would not usually expect a major effect of electron correlation on molecular geometries, especially for the second- and third-row transition metals. Nevertheless, in order to assess the electron correlation effect, we have carried out RMP2 optimization for the structures of the reactant, π-complex, transition state, and γ-agostic product. This has also been prompted in part by recent results for Zr**1**−Zr**4** using the density functional theory (DFT) by Ziegler et al.,[32] which are very different from our previous RHF results. Since the DFT takes into account the electron correlation effect in an approximate way,[33] it would be interesting to compare the RMP2 structures with the DFT as well as the RHF structures. The RMP2 opti-

(32) (a) Woo, T. K.; Fan, L.; Ziegler, T. *Organometallics* **1994**, *13*, 432. (b) Woo, T. K.; Fan, L.; Ziegler, T. *Organometallics* **1994**, *13*, 2252.
(33) Vosko, S. H.; Wilk, J.; Nusair, M. *Can. J. Phys.* **1990**, *58*, 1200.

Table 2. Relative Energies of Stationary Structures in Ethylene Insertion and β-Elimination with $[H_2SiCp_2TiCH_3]^+$ (kcal/mol)[a,b]

method	π-complex **2**	TS **3**	γ-agostic **4**	TS **5**	β-agostic **6**	TS **7**	π-complex **8**	metal hydride (+propene) **9**
RHF	−13.0	1.3	−22.8	−19.9	−29.2	−10.3	−11.0	13.1
RMP2	−28.6	−27.3	−34.7	−27.9	−43.1	−24.5	−22.2	18.5
RMP3	−20.9	−10.0	−30.8	−25.6	−37.4	−17.7	−17.5	15.2
RMP4SDQ	−27.6	−24.5	−32.6	−26.3	−39.7	−21.7	−20.9	18.0
UHF		−0.4	−27.7	−25.9	−31.5	−10.4		
PUHF[c]		−19.2	−53.7	−52.1	−49.7	−15.7		
UMP2		2.5	17.6	26.3	−14.7	−17.4		
PUMP2[c]		−14.8	−7.2	1.2	−31.4	−22.2		
PUMP3[c]		−14.7	−29.3	−23.0	−41.0	−18.8		
RQCISD	−21.9	−14.8	−29.3	−23.8	−35.4	−17.0	−17.0	17.4

[a] Energy relative to the free complex **1** + ethylene at the RHF optimized geometries. [b] Total energies of reactant Ti**1** (au): RHF, −762.267 403; RMP2, −763.288 118; RMP3, −763.327 109; RMP4SDQ, −763.381 195; RQCISD, −763.379 648. Total energies of ethylene (au): RHF, −77.600 988; RMP2, −77.780 123; RMP3, −77.797 018; RMP4SDQ, −77.803 615; RQCISD, −77.806 826. Total energies of propylene (au): RHF, −116.424 009; RMP2, −116.693 399; RMP3, −116.718 224; RMP4SDQ, −117.727 142; RQCISD, −116.731 0.32. [c] Spin contaminants annihilated up to nonet.

mized structures, denoted as Zr**1a**–Zr**4a**, are shown in Figure 6. A detailed comparison will be made in section V.

All RMP2 optimized structures are similar to the RHF optimized structures in Figures 1 and 3. Ethylene coordinates to Zr symmetrically, from which the transition state **3** with a strong agostic interaction is reached, and the direct product is the γ-agostic propyl complex **4**. However, subtle differences can be seen. The covalent bonds such as the C–H and the Zr–C bonds have longer distances, as expected in correlated calculations.[34a] For instance, the Zr–C_{methyl} and Zr–Cp distances of Zr**1a** are 0.066 and 0.070 Å longer than those of Zr**1**. In addition, the electron correlation effects could enhance the electron donative interaction such as olefin coordination and agostic interaction. Consequently, in π-complex Zr**2a**, the two M–$C_{ethylene}$ distances are shortened by 0.124 and 0.179 Å in comparison with Zr**2**. The C–H stretch due to an agostic interaction in RMP2, 1.146 Å in Zr**3a** from 1.104 Å in Zr**2a**, is substantially larger than in RHF, 1.117 Å in Zr**3** from 1.093 Å in Zr**2**. In the γ-agostic Zr**4a**, the Zr···H_γ distance of 2.275 Å is shorter and the Zr–C_α–C_β angle of 86.8° is smaller than in Zr**4**.

C. RHF Structures in β-Elimination. Transition State 7. The β-elimination starts with the β-agostic insertion product **6** and goes over the transition state **7** to reach the propylene π-complex **8**, which can dissociate to give the free hydride **9**, as was shown in Scheme 1. In TS **7** the C_α–C_β–H_β angle becomes smaller by 11.2° (Ti), 7.4° (Zr), and 9.7° (Hf) relative to **6** to facilitate new bond formation. The metal, C_α, C_β, and H_β are more or less coplanar, the M–C_α–C_β–C_γ torsional angles being 4.3° (Ti), 1.7° (Zr), and 1.3° (Hf).

Comparison of the geometrical parameters among **6**, **7**, and **8** shows that the transition state **7** is closer to the product than to the reactant, with formation of new bonds nearly complete. Ti**7** is the latest among the three metals, which is further supported by looking at the distances of the breaking C_β–H_β bonds. The C–H bond is almost broken, while the M–C_α bond breakage has not progressed much, indicating a very asynchronous and tight nature of this transition state.

It is also interesting to compare this TS **7**, which can be viewed as the TS for insertion of propylene into an M–H bond starting from **8** and ending at **6**, with TS **3** for insertion of ethylene into an M–C bond starting from **2** and ending at **4**. It is clearly seen that the structure of TS **7** is closer to that of the olefin complex than TS **3** is; this difference is closely related to the energetics of the process, as will be discussed in section IV. Asynchronicity is more enhanced in TS **7** than in TS **3**, due to the small radius of a hydrogen atom, whose bond has to be broken earlier to allow a four-centered transition structure to be formed.

π-Complex 8: SiH_2Cp_2M–$H(C_3H_6)^+$). In **8**, propylene coordinates asymmetrically to avoid steric contact between its methyl group and Cp rings, which was not the case for the ethylene π-complex **2**. As discussed previously,[15a] in an asymmetrically coordinating olefin complex the carbon atom further away from the central metal develops a positive charge. The methyl substitution on this carbon delocalizes the charge and stabilizes the complex.

Zr**8** and Hf**8** are similar to each other in structure, just as in the case of the transition state Zr**7** and Hf**7**. However, Ti**8** is different in the H–M–C angle; the angle of 55.3° is about 10° smaller than 66.8° for Zr and 65.9° for Hf, presumably reflecting the crowdedness coming from the small size of the Ti complex. Compared with the M–H bond distances in **9** (Ti, 1.423 Å; Zr, 1.838 Å; Hf, 1.854 Å), the Ti–H bond in Ti**8** is greatly stretched (Ti, 1.599 Å; Zr, 1.841 Å (Zr); Hf, 1.833 Å). The C_β···H_β distance in Ti**8** is not very long (2.300 Å). These structural features suggest that there is a bonding interaction between hydride and propylene in Ti**8**.

Metal Hydride 9: SiH_2Cp_2M–H^+. Optimized under the C_s constraint, the Si–M–H angle is found to be bent by various degrees (Ti, 137.3°; Zr, 121.2°; Hf, 171.0°). This is in contrast with **1**, which is found to be linear. However, these tilts change the energy very little. For example, when **9** is optimized under C_{2v} symmetry, **9** is destabilized by 1.68 kcal/mol (Ti), 2.19 kcal/mol (Zr), and 0.02 kcal/mol (Hf) at the RHF level.

IV. Energetics

In this section we discuss the energetics of the ethylene insertion and β-elimination in detail with electron correlation taken into account. The results for Ti, Zr, and Hf complexes are shown in Table 2–4, respectively. At first we performed a series of MP calculations at the RHF optimized structures. These calculations for Ti, however, seem to be far from convergence in the perturbation series. Thus, in subsection A we will discuss the energetics for ethylene

(34) (a) Weiss, H.; Haase, F.; Ahlrichs, R. *Chem. Phys. Lett.* **1992**, *194*, 492. (b) Weiss, H.; Ehrig, M.; Ahlrichs, R. *J. Am. Chem. Soc.* **1994**, *116*, 4919.

Table 3. Relative Energies of Stationary Structures in Ethylene Insertion and β-Elimination with $[H_2SiCp_2ZrCH_3]^+$ (kcal/mol)[a,b]

method	π-complex **2**	TS **3**	γ-agostic **4**	TS **5**	β-agostic **6**	TS **7**	π-complex **8**	metal hydride (+propene) **9**
RHF	−19.0	−2.4	−23.8	−21.1	−26.8	−10.5	−16.3	9.2
RMP2	−33.4	−27.4	−38.4	−33.5	−40.9	−27.2	−28.2	10.7
RMP3	−29.4	−19.5	−34.6	−30.2	−36.9	−22.1	−24.9	10.5
RMP4SDQ	−30.1	−20.9	−34.6	−30.1	−36.6	−22.5	−25.5	10.1
RQCISD	−29.1	−19.7	−33.4	−29.0	−35.4	−21.5	−24.5	10.2

[a] Energy relative to the free complex **1** + ethylene at the RHF optimized geometries. [b] Total energies of reactant Zr**1** (au): RHF, −750.919 904; RMP2, −751.840 954; RMP3, −751.912 141; RMP4SDQ, −751.935 360; RQCISD, −751.945 326 8.

Table 4. Relative Eneriges of Stationary Structures in Ethylene Insertion and β-Elimination with $[H_2SiCp_2HfCH_3]^+$ (kcal/mol)[a,b]

method	π-complex **2**	TS **3**	γ-agostic **4**	TS **5**	β-agostic **6**	TS **7**	π-complex **8**	metal hydride (+propene) **9**
RHF	−17.6	0.6	−22.0	−19.0	−25.3	−8.3	−14.4	11.5
RMP2	−31.7	−24.6	−36.6	−27.0	−39.2	−24.2	−26.0	15.5
RMP3	−28.5	−17.8	−33.7	−25.3	−35.8	−20.1	−23.5	14.2
RMP4SDQ	−28.4	−18.5	−33.1	−24.4	−35.1	−19.9	−23.2	14.5
RQCISD	−27.6	−17.5	−32.1	−23.5	−34.0	−19.0	−22.4	14.5

[a] Energy relative to the free complex **1** + ethylene at the RHF optimized geometries. [b] Total energies of reactant Hf**1** (au): RHF, −753.251 937; RMP2, −754.144 828; RMP3, −754.218 922; RMP4SDQ, −754.241 401; RQCISD, −754.251 477.

insertion at the RQCISD level, the highest level of electron correlation. In subsection B the energetics for β-elimination will be discussed at the RQCISD level. In subsection C the HF wave functions for Ti and the results of MP calculations will be discussed. This last subsection can be skipped, unless one is interested in some details of theory and computation.

A. RQCISD Potential Energy Profile for Ethylene Insertion. As can be seen in the last two rows of Tables 2−4, ethylene coordination is exothermic with ethylene binding energies of 21.9 kcal/mol (Ti), 29.1 kcal/mol (Zr), and 27.6 kcal/mol (Hf). The weak ethylene coordination to Ti is consistent with the structural abnormality of Ti**2** discussed in section III-A and is ascribable to the short Ti−Cp distance, due to the small size of the Ti atom.

Ethylene insertion, from π-complex **2** through TS **3** to γ-agostic **4**, is exothermic by 7.4 kcal/mol (Ti), 4.3 kcal/mol (Zr), and 4.5 kcal/mol (Hf) with a low activation energy of 7.1 kcal/mol (Ti), 9.4 kcal/mol (Zr), and 10.1 kcal/mol (Hf) from the π-complex, showing that the elementary insertion reaction takes place easily. Because of the limited basis functions and the instability of the RHF wave functions of the Ti complexes, it would be hard to conclude at the present level of calculation which metal gives the lowest activation barrier for ethylene insertion. It is safe to say, however, that the activation energies are close to each other.

On the other hand, a clear difference can be seen in the energies relative to the reactants. The relative energies of Ti**2**, Ti**3**, and Ti**4** are higher than those of the Zr and Hf analogs, indicating that the Ti reaction is less favorable, if the reaction is started with the free active species **1**. As discussed in section III-A, the size effect operates and thus destabilizes Ti**3** and Ti**4** as well as Ti**2**. Zr**2**, Zr**3**, and Zr**4** were calculated to be slightly more stable than Hf**2**, Hf**3**, and Hf**4**, respectively. These results are, at least qualitatively, in agreement with the order of insertion activity reported experimentally: Ti < Hf ≤ Zr.[35] This point will be discussed again later.

Propyl complex **6** with a β-agostic interaction is more stable than the γ-agostic direct product **4** by 6.1 kcal/mol (Ti), 2.0 kcal/mol (Zr), and 1.9 kcal/mol (Hf). In Ti**6** the methyl group of the propyl ligand is located very far away from the H_2SiCp_2 fragment. Thus, the size effect in Ti**6** could be small and accordingly the β-agostic interaction in Ti**6** takes place as favorably as in Zr**6** and Hf**6**, as discussed structurally in the last section. The larger exothermicity of the Ti reaction from **4** to **6** is ascribed to the agostic interaction, which can take place in Ti**6** but only weakly in Ti**4**.

Isomerization of **4** to **6**, a change in the conformation, passes through transition state **5** with an activation energy of 5.5 kcal/mol (Ti), 4.4 kcal/mol (Zr), and 8.6 kcal/mol (Hf), which is consistent with the following structural features discussed in the previous section. Though Zr**5** makes an agostic interaction with both H_γ and H_β, Hf**5** makes an agostic interaction with H_β but not with H_γ, and in Ti**5** only a weak agostic interaction takes place. Judging from the difference between the $M\cdots H_\gamma$ and the $M\cdots H_\beta$ distances, Zr**5** is the earliest, Ti**5** is next, and Hf**5** is the latest transition state.

In order for further repetitive insertion to take place, it has been suggested that **6** need not participate in the propagation step. The less stable product **4** would easily undergo the coordination of the next ethylene more exothermically,[36] if nothing would intervene. It should be noted that the estimation of the experimental activation barrier for the polymer propagation step with the Zr complex[37] includes such a factor. In general, it has been experimentally found that the polymer with the highest molecular weight is obtained with the silylene-bridged hafnocene catalyst than with the zirconocene and the titanocene species.[38] This is in good agreement with the order of the activation barrier to this isomerization. The higher activation barrier for Hf**5** would afford the high polymer by preventing the formation of the β-agostic product Hf**6**, from which the termination step could start.

The overall energy of reaction from **1** + C_2H_4 to **6** does not depend much on the central metal: 35.4 kcal/mol

(35) Bochmann, M.; Lancaster, S. J. *J. Organomet. Chem.* **1992**, *434*, C1.

(36) Further olefin coordination to Zr**6** is downhill and proceeds without barrier. Kawamura-Kuribayashi, H.; Koga, N.; K. Morokuma, K. Unpublished results.

(37) Chien, J. C. W.; Razavi, A. J. *Polym. Sci., Part A: Polym. Chem.* **1988**, *26*, 2369.

(38) (a) Mise, T.; Kagayama, A.; Miya, S.; Yamazaki, H. *Chem. Lett.* **1991**, 1525. (b) Yano, A.; Yamada, S.; Sone, M.; Akimoto, A. Third Workshop on Polymerization and Application between Japan and Korea, Seoul, Korea, 1991.

(Ti), 35.4 kcal/mol (Zr), and 34.0 kcal/mol (Hf). The difference among them reflects the change in the M−C bond strength caused by shifting the agostic interaction from H_α to H_γ, since the other changes are formally the same. As discussed before, in **6** a strong β-agostic interaction takes place and the $M-C_\alpha-C_\beta$ angle is within the range of 85.5−87.5° for all the metals. Consequently, the energy of the overall reaction is not sensitive to the central metal.

Ti**4**, with a weak γ-agostic interaction, is 6.1 kcal/mol less stable than Ti**6**, with a strong β-agostic interaction. This may be compared with Zr**4** and Hf**4**, both having a strong γ-agostic interaction and only being 2 kcal/mol less stable than Zr**6** and Hf**6**, respectively.

B. Potential Energy Profile for β-Elimination. Irrespective of the metal, the β-elimination is very endothermic (Ti, 52.8 kcal/mol; Zr, 45.6 kcal/mol; Hf, 48.5 kcal/mol) and thermodynamically very unfavorable. Reflecting this endothermicity, the energy barrier at transition state **7** for β-elimination is 18.4 kcal/mol (Ti), 13.9 kcal/mol (Zr), and 15.0 kcal/mol (Hf). Compared with the propagation steps already discussed, this barrier is very high and the reaction is not favorable. The reverse barrier is very low, suggesting that reinsertion of olefin into the M−H bond of the newly formed metal hydride **9** will take place easily. This high barrier is consistent with the favorable polymer propagation found with these catalysts. Some investigations also suggest that the β-elimination might not be the chain termination step.[39]

Concerning the chain termination step, the question as to whether β-hydride or β-methyl elimination takes place has attracted recent attention.[40] The present calculations show that β-methyl elimination is more favorable kinetically as well as thermodynamically. Recent calculations by Sini et al. for the elimination reaction from $Cl_2ZrCH_3^+$ have shown that β-methyl elimination is more favorable,[41] in agreement with the present results. As shown by Sini et al., the $C-CH_3$ bond in propylene, the product of β-hydride elimination, is about 10 kcal/mol weaker than the C−H bond in ethylene, the dominant factor favoring β-methyl migration. Sini et al. have also discussed that the $M-CH_3$ hyperconjugation plays a role in favor of β-methyl migration, which makes the $M-CH_3$ bond stronger and thus β-methyl elimination more exothermic.

C. MP Potential Energy Profile for Insertion and β-Elimination. As mentioned above, this subsection is mainly for theoreticians interested in theoretical details and analysis of the wave functions and energies and can be skipped. The RHF wave functions of Ti alkyl complexes were often found to suffer from triplet instability. This is caused by a longer Ti−C bond distance than expected from the size of Ti 3d orbital and is ascribed to the small difference in size between 3d and closed 3sp shells.[23b] In the present case, the RHF wave functions of Ti**3**−Ti**7** were actually unstable, whereas those of all the Zr and Hf structures were stable. Accordingly, we carried out the PUMP calculations up to the third order (PUMP3) for Ti, in addition to RMP calculations up to the fourth order with single, double, and quadruple excitations (RMP4SDQ). In the PUMP calculations the spin contaminants up to nonet were projected out.

Table 5. Expectation Values $\langle S^2 \rangle$ of Unrestricted Wave Functions for Stationary Structures in Ethylene Insertion with $[H_2SiCp_2TiCH_3]^+$

method	TS **3**	γ-agostic **4**	TS **5**	β-agostic **6**	TS **7**
UHF	0.518	0.955	1.044	0.519	0.121
PUHF[a]	0.000	0.000	0.000	0.000	0.000
UMP2	0.424	0.818	0.903	0.424	0.093
PUMP2[a]	0.000	0.000	0.000	0.000	0.000

[a] Spin contanimants annihilated up to nonet.

Table 6. Relative Eneriges for Stationary Structures in Ethylene Insertion with $[H_2SiCp_2ZrCH_3]^+$ (kcal/mol)[a,b]

method	π-complex **2a**	TS **3a**	γ-agostic **4a**
RMP2	−34.7	−28.9	−40.9

[a] Energy relative to the free complex **1** + ethylene at the RMP2 optimized geometries. [b] Total energy of reactant Zr**1a** (au): −751.842 855. Total energy of ethylene (au): −77.781 314.

As shown in Table 5, UHF and UMP2 wave functions have large S^2 expectation values, up to 1.044, a clear sign of large higher spin contamination. At the transition states weakening of bonds may invite contamination by higher spin states. In the β- and γ-agostic structures the deformation of the propyl ligand may cause weakening of the Ti−C bond and large spin contamination.

The results of the MP calculations for Ti are shown in Table 2. The RMP calculations up to the fourth order, especially those for Ti**2** and Ti**3**, show that the perturbation series has not converged. This may be due to the large electron correlation which causes the instability of RHF wave functions. The PUMP calculations are also far from convergence. While in Ti**3** and Ti**7** the spin distribution (not shown) representing spin flip in the UHF calculation is seen only at the four-centered reaction site, in Ti**4**−Ti**6** the spin distribution spreads over the π-system of the Cp ligands as well as the reaction center. This indicates that for Ti**4**−Ti**6** the substantial electron correlation effect is already included at the UHF level. Therefore, at lower order perturbation levels the relative energies of Ti**4**−Ti**6** would behave differently from those of Ti**3** and Ti**7**.

The results for Zr and Hf in Tables 3 and 4 show that the perturbation series converges quickly and that even MP2 results are not very different from the RQCISD results. For Zr, as shown in Table 6, the RMP2 relative energies calculated at the RHF optimized structures are similar to those at the RMP2 optimized structures. These results, as well as the similarity of RHF and RMP2 structures, indicate that the HF wave function is a good approximation and that the single reference computational method with dynamic correlation taken into account is reliable. The energetics at the RMP3 level are very similar to those at the RQCISD level in the insertion as well as in the β-elimination for each metal. The RMP2 activation barriers are substantially underestimated.

Furthermore, in order to investigate the basis set effect, we calculated the energies for the Zr system with the larger basis set, defined in section II, at the RMP2

(39) It is proposed using the DFT that σ-metathesis is the most favorable chain termination in ethylene polymerization with Cp_2Sc-Me, giving the thermodynamically stable alkenyl complex: Woo, T. K.; Fan, L.; Ziegler, T. Symposium on 40 Years of Ziegler Catalysts, Freiburg, Germany, 1993. J. E. Bercaw, H.-H. Brintzinger, P. Corradini, also suggest this possibility in private communications.

(40) For instance: (a) Hajela, S.; Bercaw, J. E. *Organometallics* **1994**, *13*, 1147. (b) Eshuis, J. J. W.; Tan, Y. Y.; Meetsma, A.; Teuben, J. H. *Organometallics* **1992**, *11*, 362.

(41) Sini, G.; Macgregor, S. A.; Eisenstein, O.; Tueben, J. H. *Organometallics* **1994**, *13*, 1049.

Table 7. MP2 Energies (in kcal/mol) for Ethylene Insertion with $[H_2SiCp_2ZrCH_3]^+$ Calculated with a Larger Basis Set[a,b]

π-complex **2a**	TS **3a**	γ-agostic **4a**
−44.7	−41.5	−54.9

[a] Energy relative to the free complex **1** + ethylene at the RMP2 optimized geometries of Figure 3. [b] The larger basis set is defined in section II. Total energies (au): reactant Zr**1a**, −759.769 85; ethylene, −78.270 192.

level at the RMP2 structures determined with the smaller basis set. The results are shown in Table 7. This basis set lowers the activation barrier by 2.6 kcal/mol. Since the RMP2 barrier is underestimated, as mentioned above, this activation barrier of 3.2 kcal/mol is considered to be the lower limit and consequently the insertion reaction requires the nonnegligible activation energy.

If additivity is assumed, the best estimate of an activation barrier for Zr is 6.6−6.8 kcal/mol. The former was calculated as 3.2 (MP2 in Table 7) + {9.4 (RQCISD in Table 3) − 6.0 (MP2 in Table 3)} and the latter as 9.4 (RQCISD in Table 3) − {5.8 (MP2 in Table 6) − 3.2 (MP2 in Table 7)}.

V. Comparison with Previous Theoretical Studies

Most of the recent theoretical studies have shown that the activation energies in the model insertion reactions are negligible, which is different from our conclusions.[14c,32,34] In this section, we discuss the reasons for their much lower activation barriers, compared with our results.

Woo, Fan, and Ziegler have studied the reactions $H_2SiCp_2Zr{-}Me^+ + C_2H_4$ and other related reactions with DFT. They have obtained the potential energy profile along the assumed reaction path, the distance of the newly formed C−C bond, by optimizing the structure with the local density approximation (LDA) method and recalculating the energies with nonlocal exchange and correlation correction.[32] They have shown that the activation energy relative to the ethylene complex is quite small, about 1 kcal/mol, and that in the ethylene complex the pseudo-C_{3v} axis of the methyl group directs toward the midpoint between the metal and ethylene carbon, the ethylene complex being close to the transition state in structure. These results seem to suggest that their ethylene complex is located between the ethylene complex and the transition state on our reaction profile.

Meier and van Doremaele have studied the same reaction with the Car-Parinello method, the molecular dynamics simulation with energy calculations.[14c] They also used the LDA method.

It is known that the LDA method overestimates the correlation energy.[42] As shown in Table 3, the correlation energy at the transition state is larger than at the ethylene complex and the product. Accordingly, overestimation of the correlation energy at the transition state would stabilize the transition state artificially.[43] In the calculations by Ziegler et al., it is possible that the LDA geometry optimization misses the stable structure of the ethylene complex, because of the unrealistically stable transition state structure. Similarly, the LDA Car-Parinello calculations[14c] missed the activation barrier.

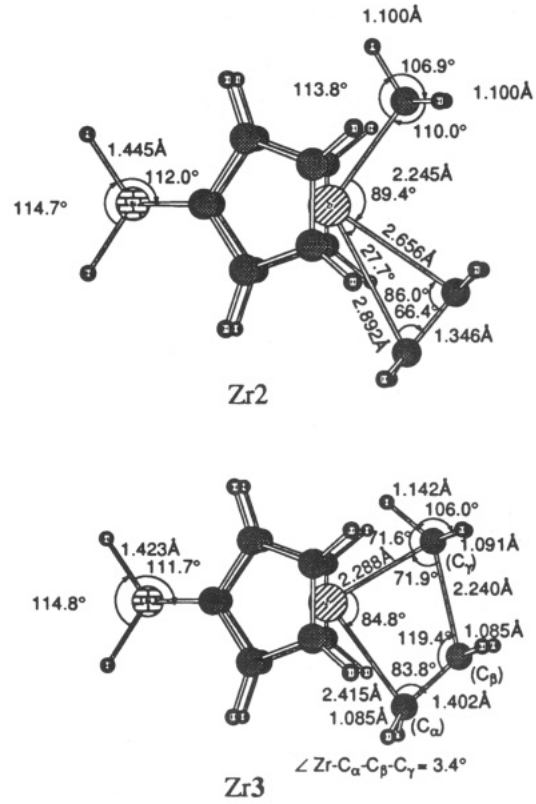

Figure 7. Optimized structures (in Å and deg) with density functional theory with nonlocal correction for π-complex Zr**2** and transition state Zr**3**.

In order to obtain additional evidence, we carried out DFT calculations for π-complex **2** and transition state **3** with M = Zr. The nonlocal density functional used is the Becke three-parameter exchange functional with the Perdew correlation functional.[44] The DFT optimized structures with the same basis set used in the rest of the paper are shown in Figure 7. The activation energy, the energy difference between these two structures, was calculated to be 1.7 kcal/mol. Compared with the RMP2 optimized structure of **2**, the DFT results show the larger $C_2H_4{-}Zr{-}CH_3$ angle and the more unsymmetrical coordination of ethylene. The shorter Zr−C bond distance of 2.66 Å is 0.07 Å shorter than the RMP2 bond distance. Upon coordination, the C−C bond is stretched by 0.02 Å from 1.328 Å in free ethylene, similar to the RHF and RMP2 structures; at the RHF level the C−C bond becomes longer, from 1.315 Å in free ethylene to 1.332 Å in **2** and at the MP2 level from 1.341 Å to 1.360 Å. This transition state determined with nonlocal correction is closer to the RMP2 as well as the RHF transition state than that at the LDA level.[32] This

(42) Ziegler, T. *Chem. Rev.* **1991**, *91*, 651.

(43) (a) Sakaki, Koga, and Kobayashi compared the energetics of ethylene insertion into the $[M]{-}CH_3$ bond with $[M] = Cl_2Zr^+$, $Pd(PH_3)(CH_3)$, and $(H_3P)Cu$ among the levels MP2, MP3, MP4, SDCI with size-consistent corrections, QCISD with triple excitation (QCISD(T)), and density functional with and without nonlocal correction.[43b] All the calculations were carried out for the RHF optimized structures, to show that without nonlocal correction the density functional calculations underestimate the activation energy by 7−13 kcal/mol. For instance, with $[M] = Cl_2Zr^+$ the density functional calculations gave an activation energy of 0.4 kcal/mol, and nonlocal correction increases it by 7.3 kcal/mol. The activation energies at the MP2, MP4, and QCISD(T) levels are 5.6, 7.2, and 7.6 kcal/mol, respectively. (b) Sakaki, S.; Koga, N.; Kobayashi, H. Unpublished data.

(44) (a) Becke, A. D. *J. Chem. Phys.* **1993**, *98*, 5648. (b) Perdew, J. P. *Phys. Rev.* **1986**, *B33*, 8822; **1986**, *B34*, 7406.

transition state is located slightly earlier, judging from the distance of the newly formed C−C bond and the C−C bond in the ethylene fragment. The activation energy of 1.7 kcal/mol is slightly larger than that by Ziegler et al. based on the LDA optimization and energy improvement by nonlocal correction. The barrier is still too low, compared to the QCISD result. Consequently, the previous theoretical studies with DFT should be treated with care.

Ahlrichs and his co-workers have studied the reaction of Cp_2Ti-Me^+ with C_2H_4 at the MP2 level with a large basis set.[34b] Their MP2 geometry optimization has shown that the reaction is downhill, leading to $Cp_2Ti-C_3H_7^+$ without any barrier. Our calculations, discussed in detail in section III, suggest that their calculations would be an artifact; our MP2 calculations for Ti gave the quite small activation barrier of 1.3 kcal/mol, while the RQCISD calculations gave the substantial barrier of 7 kcal/mol. To evaluate the activation barrier even semiquantitatively, a more sophisticated method is necessary, especially for M = Ti.

VI. Concluding Remarks

The mechanism of the homogeneous polymerization of ethylene with a silylene-bridged group 4 metallocene model catalyst has been studied by the *ab initio* MO method, with emphasis on the ethylene insertion and the β-elimination.

We have found three transition states: (1) the first transition state **3**, for the insertion leading to the direct product **4** with γ-agostic interaction, (2) the second transition state **5**, for isomerization from γ- to β-agostic product **6**, and (3) the transition state **7** for the β-elimination. In the insertion the transition state **3** is located midway between the π-complex **2** and the direct product **4** and has a nearly planar tight four-centered structure for each metal. Hf**5** is a substantially later transition state in comparison with Ti**5** and Zr**5**. The transition state **7** in the β-elimination resembles more the product, π-complex **8**, than the reactant **6** for each metal.

The energetics at the MP level can provide reliable potential energy surfaces for Zr and Hf. For Ti, the perturbation series is slow in convergence, and accordingly we described potential energy profiles at the high correlation RQCISD level to compare the catalytic reactivities among the group 4 metals. In the ethylene insertion reaction, ethylene coordination is quite exothermic. The activation barrier from the π-complex **2** to the transition state **3** is less than 10 kcal/mol, with an exothermicity of about 30 kcal/mol. Ti has been found to be the least exothermic from the free reactant **1** through the π-complex **2** and the transition state **3** to the γ-agostic product **4**, followed by Hf and then closely by Zr. This trend is qualitatively in agreement with the order of insertion activity reported experimentally: Ti < Hf ≤ Zr.[36] Since the experiment is carried out in solution, the reaction probably starts from a partially desolvated reactant which may be approximated by **1**, and the energy difference between **4** and **1** may be proportional to the exothermicity of reaction in solution.

We have found that Ti is unique among the three group 4 metals we compared. Structures of Ti complexes are in general more compact than those of Zr and Hf. This compactness is due to the small atomic radius of Ti. Because of this compactness, some structures of Ti complexes are unusually destabilized by steric repulsion, giving rise to unique structural features and energetics. We have called this the size effect, and it plays an important role in differentiating the catalytic activity of different metals. When bulkier substituents are introduced, Ti is likely to be affected most. When the steric effect of the growing polymer chain is taken into account, Ti again will be the most affected. These substituent and growing polymer chain effects will be discussed with a combination of molecular orbital and molecular mechanics methods in a separate paper.

The β-elimination, a side reaction leading to the chain transfer, has a quite high endothermicity of about 50 kcal/mol for each metal and is an unfavorable path. The reverse reaction of olefin insertion into an M−H bond has a very low barrier, and if an M−H bond is formed, it will be consumed by olefin immediately.

The ethylene insertion starts using a vacant metal d orbital of the cationic alkyl **1**, and the next olefins come repetitively into the metal−alkyl bond at the site where the agostic intearctions take place in **4** and **6**. The high endothermicity of β-elimination as well as the low barrier to insertion shows that the ethylene polymerization with the cationic alkyls can occur rapidly, resulting in the high-molecular-weight polymer. Especially, in the reaction with Hf, Hf**6** from which β-elimination could take place is difficult to access because of the high barrier at Hf**5**; this would provide Hf the potential of giving a longer polymer with narrower polydispersity.

Also, the reason the substantial energy barriers were missed in the recennt DFT calculations for Zr and in MP2 calculations for Ti was analyzed. For Ti, the MP2 level is not appropriate. Without a more sophisticated method, the TS would disappear.

Acknowledgment. A part of these calculations was carried out at the Computer Center of the Institute for Molecular Science. T.Y. was a visiting research fellow at IMS until this work was completed. Acknowledgment is also made to Mr. S. Maehama for his assistance in making the figures. This research was supported in part by grants-in-aid to N.K. and K.M. from the Ministry of Education, Science and Culture in Japan.

Supplementary Material Available: Figures giving side views with geometrical parameters for all optimized structures Ti**2**−Ti**9**, Zr**2**−Zr**9**, and Hf**2**−Hf**9** at the RHF level and for Zr**2a**−Zr**4a** at the RMP2 level (14 pages). Ordering information is given on any current masthead page.

OM9407971

Successful Application of a "Forgotten" Phosphine in Asymmetric Catalysis: A 9-Phosphabicyclo[3.3.1]non-9-yl Ferrocene Derivative as Chiral Ligand

Hendrikus C. L. Abbenhuis,[†,‡] Urs Burckhardt,[†] Volker Gramlich,[§] Christoph Köllner,[†] Paul S. Pregosin,*[,†] Renzo Salzmann,[†] and Antonio Togni*[,†]

Laboratory of Inorganic Chemistry and Institute of Crystallography and Petrography, Swiss Federal Institute of Technology, ETH-Zentrum, CH-8092 Zürich, Switzerland

Received October 3, 1994[⊗]

The technical mixture "phobane", containing the two isomers 9-phospha-9*H*-bicyclo[3.3.1]-nonane (**3a**) and 9-phospha-9*H*-bicyclo[4.2.1]nonane (**3b**) in a ~2:1 ratio was reacted with *N,N*-dimethyl-(*S*)-1–[(*R*)-2-(diphenylphosphino)ferrocenyl]ethylamine (**4**) in acetic acid. The clean amine substitution product is the new chiral biphosphine **5**. When only 2 equiv of **3** were reacted with **4**, a 4:1 mixture of the two isomeric products **5a** and **5b** were obtained. However, the use of a 10-fold excess of **3** afforded the pure [3.3.1]-isomer **5a**, 9-phospha-9-[(*S*)-1-{(*R*)-2-(diphenylphosphino)ferrocenyl}ethyl][3.3.1]bicyclononane, in 68% isolated yield. (*S*)-(*R*)-**5a** crystallizes in the orthorhombic space group $P2_12_12_1$, $Z = 4$, $a = 7.393(3)$ Å, $b = 19.261(5)$ Å, and $c = 19.546(8)$ Å. **5a** was used in the asymmetric Pd-catalyzed alkylation of 1,3-diphenyl-3-acetoxypropene with dimethyl malonate. Enantioselectivities up to 85% ee were obtained. The cationic Pd–allyl complexes $[Pd(\eta^3\text{-}C_3H_5)(\mathbf{5a})]O_3SCF_3$ (**6**) and $[Pd(\eta^3\text{-}PhCHCHCHPh)(\mathbf{5a})]O_3SCF_3$ (**7**) were prepared and characterized by X-ray diffraction. Complex **6** crystallizes in the monoclinic space group $P2_1$, $Z = 2$, $a = 9.162(4)$ Å, $b = 16.069(5)$ Å, $c = 11.816(5)$ Å, and $\beta = 96.86(3)°$. Crystalline **7** was obtained as a CH_2Cl_2 monosolvate and belongs to the triclinic system: space group $P1$, $Z = 1$, $a = 11.07(2)$ Å, $b = 11.216(14)$ Å, $c = 11.888(16)$ Å, $\alpha = 62.37(9)°$, $\beta = 65.96(11)°$, and $\gamma = 70.29(11)°$. The ligand assumes very different conformations in its complexes, as compared to the free state. Multidimensional ^{31}P, ^{13}C, and ^1H NMR studies reveal that **7** exists in solution as a mixture of four isomers. Aspects of the selective equilibria were elucidated using ^{31}P- and ^1H-exchange spectroscopy.

Introduction

We have recently shown that ferrocenyl derivatives containing two sterically and electronically different ligating phosphine units can impart high to very high degrees of enantioselection to several transition-metal-catalyzed reactions.[1] Thus, ligand **1** represents the

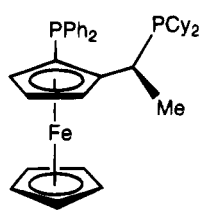

(*S*)-(*R*)-**1**

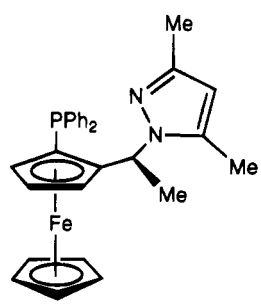

(*S*)-(*R*)-**2**

prototype of a class of chiral auxiliaries that are ideally suited for studying steric and electronic effects on stereoselectivity in asymmetric catalysis. The simple synthetic approach to such species also allows the incorporation of ligating fragments other than phosphines, with the recently reported pyrazole derivative **2** being an example.[2] We also showed that an important feature of ligand **1** is its virtually constant conformation in its complexes with transition-metal ions, as found in the solid state.[3] The same conformation, along with a site selective π-allyl isomerization of the corresponding cationic $Pd(\eta^3\text{-allyl})$ complex, has been found in solution by 2D NMR studies.[4]

With a view to understanding the factors governing the steric and electronic properties of these ligands, we were interested in the use of a conformationally rigid, compact, and electron-rich dialklyphosphine for the synthesis of new ferrocenyl derivatives. "Phobane", 9-phospha-9*H*-bicyclo[3.3.1]nonane (**3a**),[5] seemed a suitable starting material for further work in this field and could possibly be regarded as a sterically less bulky electronic equivalent of dicyclohexylphosphine. Furthermore it offers the advantage of being much less air-sensitive and, as a solid, more convenient to work with than simple dialkylphosphines. From a steric point of

[†] Laboratory of Inorganic Chemistry.
[‡] Present address: Eindhoven University of Technology, Laboratory of Inorganic Chemistry and Catalysis, Department of Chemistry, P.O. Box 513, 5600 MB Eindhoven, The Netherlands.
[§] Institute of Crystallography and Petrography.
[⊗] Abstract published in *Advance ACS Abstracts*, December 15, 1994.

(1) Togni, A.; Breutel, C.; Schnyder, A.; Spindler, F.; Landert, H.; Tijani, A. *J. Am. Chem. Soc.* **1994**, *116*, 4062–4066, and references cited therein.
(2) Schnyder, A.; Hintermann, L.; Togni, A. *Angew. Chem.*, in press.
(3) Togni, A.; Breutel, C.; Soares, M. C.; Zanetti, N.; Gerfin, T.; Gramlich, V.; Spindler, F.; Rihs, G. *Inorg. Chim. Acta* **1994**, *222*, 213–224.
(4) Breutel, C.; Pregosin, P. S.; Salzmann, R.; Togni, A. *J. Am. Chem. Soc.* **1994**, *116*, 4067–4068.

0276-7333/95/2314-0759$09.00/0

Scheme 1

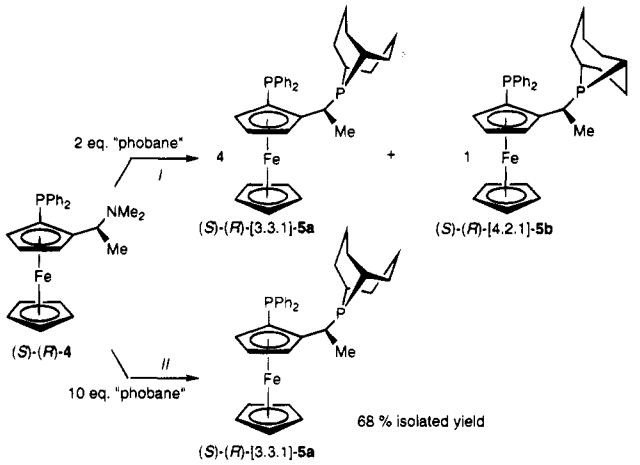

view, although there are no data available,[6] the "phobyl" fragment is probably less bulky than a diisopropylphosphine group. Compound **3a** is inexpensively produced on a large scale from 1,5-cyclooctadiene and phosphine (PH_3), a reaction that leads to a product mixture that contains phobane together with its [4.2.1]-isomer **3b** in a ~2:1 ratio (see eq 1).[5] Since no convenient method

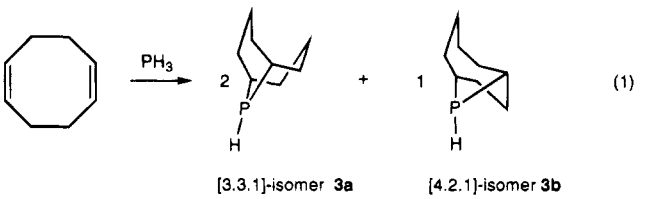

(1)

exists for the purification of the technical phobane mixture, its synthetic applications in organometallic chemistry and homogeneous catalysis are still very limited.[7] We report herein the successful incorporation of stereochemically uniform phobane (**3a**) into the corresponding ferrocenyl ligand of type **1**, as well as structural and catalytic studies on the new compound.

Results and Discussion

Synthesis. The reaction of the (diphenylphosphino)-ferrocenylethylamine (*S*)-(*R*)-**4** with ~2 equiv of the technical phobane mixture in acetic acid at 80 °C leads to clean substitution of the dimethylamino functionality by *both* bicyclic aliphatic phosphines **3a** and **3b** (Scheme 1, route i). An interesting observation, however, is that starting with the conventional 2:1 mixture of [3.3.1]- and [4.2.1]-isomers, the ferrocenyl diphosphines **5a,b** that

Table 1. Pd-Catalyzed Alkylation of 1,3-Diphenyl-3-acetoxypropene with Dimethyl Malonate[a]

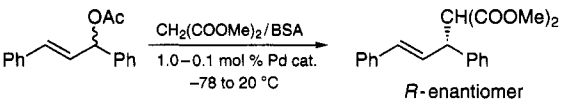

entry	mol % of cat.	T (°C)	time (h)	conversion (%)	ee (%)
1	1.0	20	0.2	51	74
			0.3	98	72
2	1.0	0	0.4	81	81
			1	100	80
3	1.0	−20	3	62	85
4	1.0	−78	29	20	76
			52	34	74
			192	100	66
5	0.1	20	3.3	5	80
			23	31	74
			70	39	71

[a] Catalytic experiments were carried out as described in ref 1.

are obtained show incorporation of the [3.3.1]- and [4.2.1]-fragments in a 4:1 ratio; i.e., the final product is enriched in the [3.3.1]-isomer. The two isomers **5a** and **5b** can best be distinguished from one another by ^{31}P NMR (**5a**, δ −26.8, −10.5; **5b**, −27.3, 26.2 for the aromatic and aliphatic phosphines, respectively). Although the product mixture can be very easily crystallized from ethanol, separation of the ferrocenyl diphosphines **5a** and **5b**, by either repeated crystallization or column chromatography over Al_2O_3, was not feasible. Fortunately, this problem can be easily overcome when the conversion of the ferrocenyl amine **4** is performed with a greater excess of phobane. Thus reaction of **4** with a ~10-fold excess of the phobane mixture leads to clean, kinetically controlled, formation of ferrocene **5a** in 68% isolated yield, containing the [3.3.1]-isomeric form of **3** exclusively (Scheme 1, route ii). The underlying reactivity differences between the two isomers **3a** and **3b** in the formation of **5** is very pronounced and has either not been observed in other reactions of phobane or not been put to use for the synthesis of isomerically pure phosphine derivatives. No obvious reason for such a drastically divergent reactivity can be put forward, however, in the less reactive [4.2.1]-isomer; the phosphorus atom is imbedded in a five-membered/seven-membered bicyclic system that will adopt a completely different conformation from that of the symmetric [3.3.1]-isomer. Because of this, the secondary phosphine functionality is possibly less accessible.

Asymmetric Palladium-Catalyzed Allylic Alkylation. With the new ligand (*S*)-(*R*)-**5a**, containing the rare phobyl fragment in hand, selected applications in asymmetric catalysis have been addressed. Since the parent compound of this class of ligands, derivative **1**, was previously shown to give high enantioselectivities in the Pd-catalyzed alkylation of 1,3-diphenyl-3-acetoxypropene with dimethyl malonate,[1] this same reaction was chosen in order to test the effectiveness of ligand **5a**. Experiments have been carried out at different temperatures and different catalyst concentrations in CH_2Cl_2, as reported previously.[1] The results are collected in Table 1. As can be seen there, the selectivity reaches a maximum of 85% ee, when the reaction is carried out utilizing 1 mol % of catalyst and at −20 °C. Although the ee is significantly lower than that obtained with **1** (93%), the activity of the catalyst is quite high,

(5) (a) Mason, R. G.; Van Winkle, J. L. U.S. Patent 3 400 163, Sept 3, 1968 (assigned to Shell Oil Co.). (b) For a laboratory procedure for phobane, see: Harris, T. V.; Pretzer, W. R. *Inorg. Chem.* **1985**, *24*, 4437–4439. See also: (c) Weferling, N. *Phosphorus Sulfur* **1987**, *30*, 641–644. For similar additions of phosphine(s) to olefins, see, e.g.: (d) Vedejs, E.; Peterson, M. J. *J. Org. Chem.* **1993**, *58*, 1985–1986. (e) Wiseman, J. R.; Krabbenhoft, H. O. *J. Org. Chem.* **1976**, *41*, 589–593. (f) Turnblom, E. W.; Katz, T. J. *J. Am. Chem. Soc.* **1973**, *95*, 4292–4311.

(6) For a review, see, e.g.: White, D.; Coville, N. J. *Adv. Organomet. Chem.* **1994**, *36*, 95–158, and references cited therein.

(7) For recent uses of phobane, see: (a) Weferling, N. Z. *Anorg. Allg. Chem.* **1987**, *548*, 55–62. (b) Kläui, W.; Song, C.-E. *Inorg. Chem.* **1989**, *28*, 3845–3849. No isomerically pure phobane derivatives were reported here. For a first observation of the incorporation of the [3.3.1]-isomer into ferrocenyl derivatives, see: (c) Abbenhuis, H. C. L.; Burckhardt, U.; Gramlich, V.; Togni, A.; Albinati, A.; Müller, B. *Organometallics* **1994**, *13*, 4481–4493.

Table 2. Experimental Data for the X-ray Diffraction Study of 5a, 6, and 7

	(S)-(R)-5a	6	7
formula	$C_{32}H_{36}FeP_2$	$C_{36}H_{41}F_3FeO_3P_2PdS$	$C_{48}H_{49}F_3FeO_3P_2PdS{\cdot}CH_2Cl_2$
mol wt	538.4	834.9	1072.0
crystal dimens, mm	0.15 × 0.15 × 0.25	0.2 × 0.2 × 0.3	0.08 × 0.15 × 0.16
data cool. T, °C	20	20	20
cryst syst	orthorhombic	monoclinic	triclinic
space group	$P2_12_12_1$	$P2_1$	$P1$
a (Å)	7.393(3)	9.162(4)	11.07(2)
b (Å)	19.261(5)	16.069(5)	11.216(14)
c (Å)	19.546(8)	11.816(5)	11.888(16)
α (deg)			62.37(9)
β (deg)		96.86(3)	65.96(11)
γ (deg)			70.29(11)
V (Å^3)	2783(2)	1727.1(12)	1174(3)
Z	4	2	1
ϱ(calcd) (g·cm^{-3})	1.285	1.605	1.516
μ (cm^{-1})	6.76	11.46	9.71
F(000)	1136	852	548
diffractometer	Syntex P21	Syntex P21	Simens R3m/V
radiation		Mo Kα (graphite monochrom), λ = 0.710 73 Å	
measured reflcns	$0 \le h \le 7, 0 \le k \le 20, 0 \le l \le 20$	$0 \le h \le 9, 0 \le k \le 17, -12 \le l \le 12$	$-9 \le h \le 10, -9 \le k \le 10, 0 \le l \le 11$
2θ range (deg)	3.0−44.0	3.0−45.0	3.0−40.0
scan type	ω	ω	ω
scan width (deg)	1.10	1.00	1.05
bkgd time (s)	0.3 × scan time	0.3 × scan time	0.25 × scan time
max scan speed (deg·min^{-1})	1.0−14.0 in ω	2.0−6.0 in ω	2.0−15.0 in ω
no. of indepnt data coll	1993	2360	2178
no. of obsd reflcns (n_o)	1764	2268	2139
	$\lvert F_o^2\rvert > 4.0\sigma(\lvert F\rvert^2)$	$\lvert F_o^2\rvert > 4.0\sigma(\lvert F\rvert^2)$	$\lvert F_o^2\rvert > 4.0\sigma(\lvert F\rvert^2)$
absorp correction	N/A	face-indexed numerical	
transm coeff		0.7123−0.7891	0.7858−0.8662
no. of params refined (n_v)	316	423	551
quantity minimized	$\sum w(F_o - F_c)^2$	$\sum w(F_o - F_c)^2$	$\sum w(F_o - F_c)^2$
weighting scheme	$w^{-1} = \sigma^2(F) + 0.0000F^2$	unit weights	$w^{-1} = \sigma^2(F) + 0.0015F^2$
R^a	0.0334	0.0243	0.0708
$R_w{}^b$	0.0335	0.025	0.071
GOF^c	3.07	1.04	1.92

$^a R = \sum(\lvert\lvert F_o\rvert - (1/k)\lvert F_c\rvert\rvert)/\sum\lvert F_o\rvert$. $^b R_w = \sum w(\lvert\lvert F_o\rvert - (1/k)\lvert F_c\rvert\rvert)^2/[\sum w\lvert F_o\rvert^2]^{1/2}$. ^{c} GOF $= [\sum w(\lvert F_o\rvert - (1/k)\lvert F_c\rvert)^2/(n_o - n_v)]^{1/2}$.

considering that complete conversion is attained even at −78 °C in less than 200 h with 1 mol % palladium catalyst. The selectivity shows a smooth dependence on the temperature, being at 20 °C and at −78 °C slightly, but significantly lower than at −20 °C. An important conversion dependence is also observed. This effect turns out to be more pronounced at −78 °C than at higher temperatures. Thus on going from 20 to 100% conversion, the enantioselectivity drops from 76 to 66% ee. The concentration of the catalyst does not seem to significantly influence the enantioface discrimination (compare entries 1 and 5 in Table 1).

X-Ray Structures of Ligand 5a and Its Palladium(η^3-allyl) Complexes 6 and 7. In order to confirm the incorporation of the 9-phosphabicyclo[3.3.1]-non-9-yl (phobyl) fragment into the new ligand **5a**, as well as to define conformational aspects in the solid state, an X-ray crystallographic study was carried out. Crystal and data collection parameters are given in Table 2, and a selection of bond distances and angles are provided by Table 3. A view of the molecule is shown in Figure 1. The structure turns out to be rather routine and all bonding parameters fall in the expected range.[8] The conformation adopted by **5a** in the solid state is comparable to the one previously found for ligand **1**;[3] however, both similarities and differences can be identified. The importance of the differences will become apparent later, when the conformational aspects of the Pd(allyl) complexes are discussed. Thus, as in **1**, the diphenylphosphino group in **5a** is arranged in such a way that the "upper" phenyl is in a pseudoaxial and the "lower" in a pseudoequatorial position with respect to the upper Cp ring (torsion angles C(5)−C(1)−P(1)−C(16) = 86° and C(5)−C(1)−P(1)−C(22) = −17°). In contrast to the situation found in **1**, the substituents at the stereogenic carbon C(6) cannot be clearly classified in terms of axial/equatorial, since the plane of the upper

Table 3. Selected Bond Distances (Å),[a] Angles (deg),[a] and Torsion Angles (deg) for (S)-(R)-5a

Bond Distances			
P(1)−C(1)	1.823(6)	P(1)−C(16)	1.837(6)
P(1)−C(22)	1.839(6)	P(2)−C(6)	1.875(7)
P(2)−C(8)	1.728(11)	P(2)−C(12)	1.896(8)
C(2)−C(6)	1.505(8)	C(6)−C(7)	1.535(9)
Fe−Cp(1)[b]	1.643	Fe−Cp(2)[b]	1.657
Bond Angles			
C(1)−P(1)−C(16)	103.1(3)	C(1)−P(1)−C(22)	103.1(3)
C(16)−P(1)−C(22)	103.1(3)	P(1)−C(1)−C(2)	123.9(4)
P(1)−C(1)−C(5)	128.5(4)	C(1)−C(2)−C(6)	127.5(5)
C(3)−C(2)−C(6)	124.9(5)	C(2)−C(6)−P(2)	108.0(4)
C(2)−C(6)−C(7)	113.8(5)	P(2)−C(6)−C(7)	107.5(4)
C(6)−P(2)−C(8)	111.0(4)	C(6)−P(2)−C(12)	103.5(3)
C(8)−P(2)−C(12)	94.6(4)	Cp(1)−Cp(2)[b]	5.6
Torsion Angles			
C(2)−C(6)−P(2)−C(8)	174	C(5)−C(1)−P(1)−C(16)	86
C(3)−C(2)−C(6)−C(7)	−69	C(2)−C(6)−P(1)−C(12)	73
C(5)−C(1)−P(1)−C(22)	−17		

[a] Number in parentheses are ESDs in the least significant digits. [b] Cp(1) and Cp(2) are the planes of the "upper" (C(1−5)) and "lower" (C(1′−5′) cyclopentadienyl rings, respectively.

(8) (a) Orpen, A. G.; Brammer, L.; Allen, F. H.; Kennard, O.; Watson, D. G.; Taylor, R. *J. Chem. Soc., Dalton Trans.* **1989**, Suppl. S1−S83. (b) Allen, F. H.; Kennard, O.; Watson, D. G.; Brammer, L.; Orpen, A. G.; Taylor, R. *J. Chem. Soc., Perkin Trans 2* **1987**, Suppl. S1−S19.

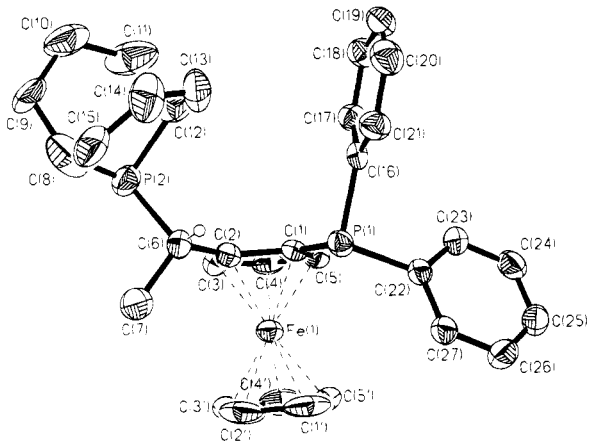

Figure 1. ORTEP view and atom numbering scheme of ligand (*S*)-(*R*)-**5a**. Thermal ellipsoids at the 50% probability level.

Table 4. Selected Bond Distances (Å),[a] Angles (deg),[a] and Torsion Angles (deg) for Complexes 6 and 7

	6	7
Bond Distances		
Pd−P(1)	2.283(2)	2.285(7)
Pd−P(2)	2.328(2)	2.301(5)
Pd−C(28), [C(34)][b]	2.166(9)	2.258(15)
Pd−C(29), [C(35)][b]	2.165(9)	2.242(21)
Pd−C(30), [C(36)][b]	2.235(8)	2.225(26)
Fe−Cp(1)[c]	1.673	1.649
Fe−Cp(2)[c]	1.653	1.659
Bond Angles		
P(1)−Pd−P(2)	97.8(1)	92.8(2)
P(1)−Pd−C(28)[C(34)][b]	93.0(2)	99.4(6)
P(2)−Pd−C(28)[C(34)][b]	169.1(2)	164.3(5)
P(2)−Pd−C(30)[C(36)][b]	102.9(2)	103.4(5)
P(1)−Pd−C(30)[C(36)][b]	159.1(2)	161.6(4)
C(28)−C(29)−C(30) [C(34)−C(35)−C(36)][b]	124.7(8)	118.5(16)
C(8)−P(2)−C(12)	95.5(3)	94.0(9)
Cp(1)−Cp(2)	6.5	7.1
Torsion Angles		
C(2)−C(6)−P(2)−C(8)	−82	−75
C(2)−C(6)−P(2)−C(12)	−177	−175
C(5)−C(1)−P(1)−C(16)	66	39
C(5)−C(1)−P(1)−C(22)	−42	−74
C(3)−C(2)−C(6)−C(7)	−84	−70
P(2)−Pd−P(1)−C(1)	4	33
P(1)−Pd−P(2)−C(6)	19	−54
Pd−P(1)−C(1)−C(2)	−12	−9
Pd−P(2)−C(6)−C(2)	−42	54

[a] Number in parentheses are ESDs in the least significant digits. [b] Numbering in brackets applies to **7** for corresponding atoms. [c] Cp(1) and Cp(2) are the planes of the "upper" (C(1−5)) and "lower" (C(1′−5′)) cyclopentadienyl rings, respectively.

Cp ring roughly bisects the angle P(2)−C(6)−C(7). This is also illustrated by the two torsion angles C(3)−C(2)−C(6)−P(2) and C(3)−C(2)−C(6)−C(7) of −50° and 69°, respectively. The two six-membered rings of the phobyl moiety assume a nearly perfect chair conformation. This is also the case for **6** and **7**, discussed below.

The two cationic complexes [Pd(η^3-C_3H_5)(**5a**)]O_3SCF_3 (**6**) and [Pd(η^3-PhCHCHCHPh)(**5a**)]O_3SCF_3 (**7**) were also studied by X-ray diffraction. Crystallographic parameters for both complexes are presented in Table 2, and a selection of bond distances and angles and torsion angles is provided in Table 4. The overall geometries of the cations **6** and **7** are depicted in Figures 2 and 3, respectively. The most interesting aspects of these two structures relate to the conformation of the chelate ring

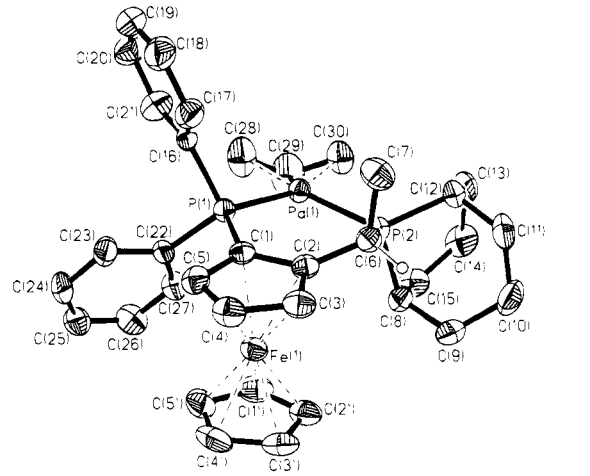

Figure 2. ORTEP view and atom numbering scheme of the cationic complex [Pd(η^3-C_3H_5)((*S*)-(*R*)-**5a**)]$^+$ (triflate salt, **6**). Thermal ellipsoids at the 50% probability level.

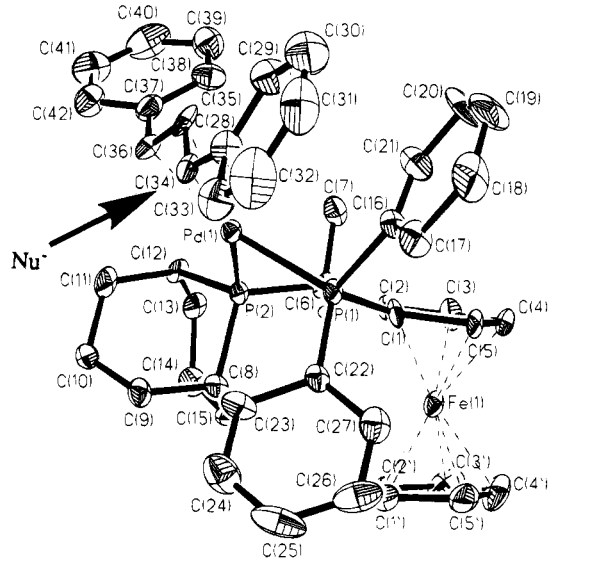

Figure 3. ORTEP view and atom numbering scheme of the cationic complex [Pd(η^3-PhCHCHCHPh)((*S*)-(*R*)-**5a**)]$^+$ (triflate salt, **7**). Thermal ellipsoids at the 50% probability level. The arrow shows the most probable site of preferred nucleophilic attack (see text).

and the relative position of the palladium center with respect to the upper Cp ring, other bonding parameters falling in the expected range. In both complexes, the Pd atoms show a pseudo-square-planar coordination geometry. However, due to the presence of the 1,3-phenyl substituents, a significant deviation from the ideal geometry is observed in derivative **7**. Thus, the plane Pd/P(1)/P(2) forms an angle of 16.6° with the plane defined by the metal center and the two terminal allylic carbon atoms (Pd/C(34)/C(36)), such that there is a clockwise rotation of the allyl fragment around the Pd−allyl axis, when looking from the ligand toward the metal center. The corresponding angle in complex **6** is 4.5°. Furthermore, the allylic fragment C(34)−C(35)−C(36) is bent away from the PdP_2 plane, as illustrated by the angle of 111° between these two planes. One of the allylic phenyl groups shows an important stacking interaction with one of the phenyl substituents on P(1). The two rings are almost ideally parallel, the angle and the distance between the corresponding planes being only 1.9° and ~3.3 Å, respectively. This stacking

Scheme 2. Four Observable Isomers of 7

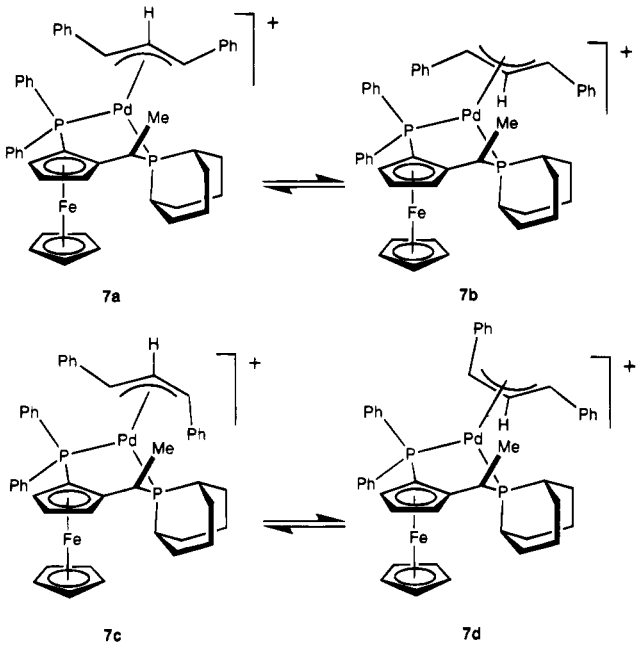

[a] The configuration of **7c,d** has been chosen arbitrarily.

interaction may be interpreted as a driving force for the rotation discussed above.

The most apparent difference between the two complexes is the relative position of the palladium atom. Whereas in the π-allyl derivative **6** the metal center is located slightly *below* (0.29 Å) the upper Cp ring, in complex **7** it is clearly *above* (1.16 Å). The conformation of the chelate ring in the latter compound is best described as a typical twisted chair. On the other hand, in **6**, five of the six atoms belonging to the metallacycle are coplanar within 0.07 Å. Carbon atom C(6) is thereby the only center clearly out of this plane (distance 0.54 Å). The observed differences between **6** and **7** are mainly a consequence of the conformational flexibility of the phobyl-containing side chain of the ligand. Because the 9-phosphabicyclononyl fragment is relatively small and very compact, it does not contribute in determining a particular, rigid conformation of that part of the molecule. Thus, its position with respect to the plane of the upper Cp ring varies from "all-above" in the free ligand to "all-below" in the Pd(allyl) complexes under study, as illustrated in the superimposition of the three structures in Figure 4. This is not the case for ligand **1**, which contains the more bulky dicyclohexylphosphino group and which is able to maintain a virtually constant conformation.[3]

NMR Studies of 7. ^{31}P NMR. Complex **7** shows interesting solution characteristics. The room-temperature ^{31}P NMR spectrum reveals several sharp and several broad components. A series of variable-temperature measurements in $CDCl_3$ between 223 K and ambient temperature showed that two components, **7a** and **7b**, were sharp throughout, a third complex became and stayed fairly sharp, **7c**, and the fourth, **7d** (see Scheme 2), became reasonably sharp with the optimum overall spectrum reached at 273 K, as shown in Figure 5. Each of the complexes shows an AX (or AB) spin system. The observed populations of these compounds are temperature dependent, and a summary of the pertinent ^{31}P NMR data is given in Table 5.

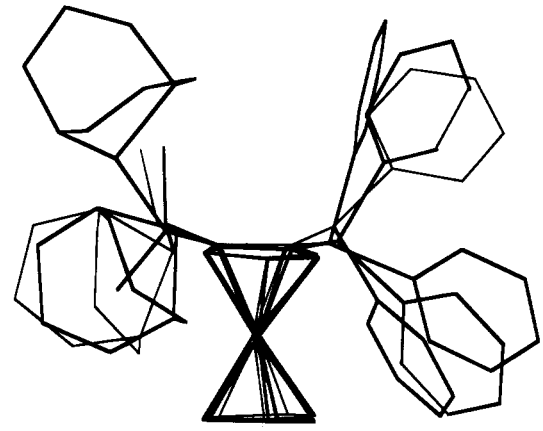

Figure 4. Superimposition of the structures of **5a**, **6**, and **7**, showing the complete lack of correspondence of the conformations of free and coordinated ligand (Pd(allyl) fragments of **6** and **7** are omitted for clarity).

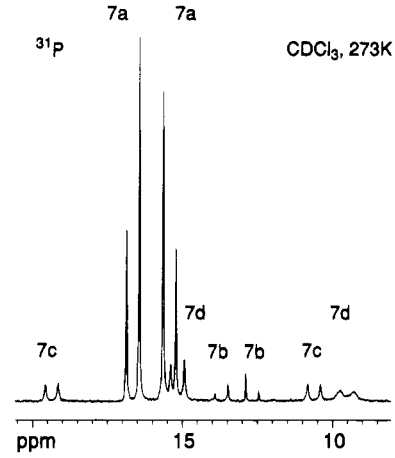

Figure 5. ^{31}P NMR spectrum of **7** (200 MHz, $CDCl_3$, 273 K). The four isomers are clearly visible.

Table 5. ^{31}P NMR Data for 7a–d ($CDCl_3$, 200 MHz)

			% isomer at given T		
nucleus	δ (ppm)	$2J$(P,P) (Hz)	297 K	273 K	223 K
		7a			
$P(Ph)_2$	15.4	86.3	70	69	67
P(phobyl)	16.6				
		7b			
$P(Ph)_2$	12.7	87.4	6	4	1
P(phobyl)	13.7				
		7c			
$P(Ph)_2$	10.6	85.9	7	9	13
P(phobyl)	19.4				
		7d			
$P(Ph)_2$	9.5	92.7	17	18	19
P(phobyl)	15.2				

For each of these complexes we assign the high-frequency resonance signal to the phobyl P atom and the low-frequency absorption to the PPh_2 moiety. For **7a** and **7b**, this assignment is supported by a ^{31}P, ^{1}H correlation; i.e., individual aromatic and aliphatic resonances correlate to these spins. Given the assignment, it is interesting to note that the PPh_2 ^{31}P spin in **7d** is that which remains dynamic at 273 K (and still so even at 223 K). A ^{31}P 2D exchange spectrum at ambient temperature reveals selective exchange processes, with **7a** and **7b** in exchange, and **7c** and **7d** in exchange, with the former pair illustrated in Figure 6. **7a** is not in observable equilibrium with either **7c** or **7d**; at this

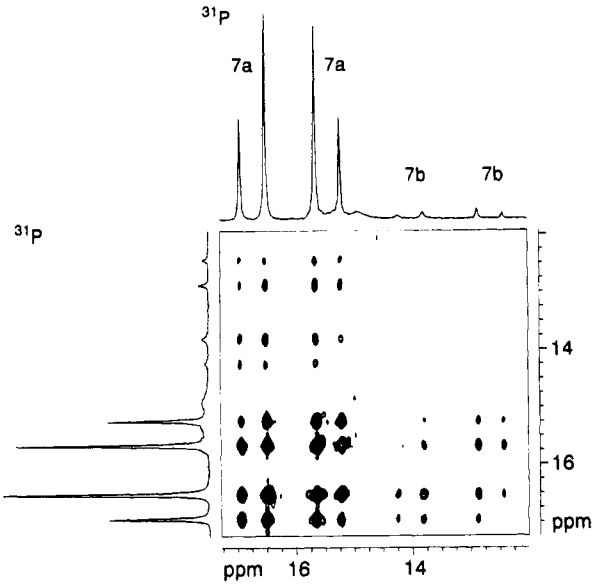

Figure 6. Section of the ^{31}P 2D exchange NMR spectrum at ambient temperature. The strong cross-peaks between **7a** and **7b** are readily observed, even though the on-diagonal signals for **7b** are too weak to be seen in this presentation.

Table 6. ^1H NMR Data for 7a ($CDCl_3$, 500 MHz, 297 K)

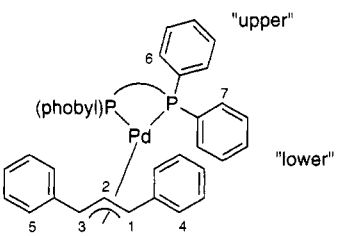

H	δ (ppm)	H	δ (ppm)
1	5.81	6	6.21
2	5.89	7	8.00
3	5.31	*C*HCH$_3$	3.37
4	6.65	CH*CH*$_3$	1.09
5	7.39	Cp	3.67

temperature, we see no exchange with mixing times of 0.5−1.0 s. Presumably, there is slow exchange, at least between **7b** and **7c**, as these two isomers show the most marked population change between 223 and 297 K. For the major isomer, the ^{31}P, ^1H correlation mentioned above also allows us to (a) assign the two terminal allyl protons and (b) assign the two sets of *ortho* PPh_2 protons, and both of these are important for the NOESY discussion that follows.

^1H NMR and NOESY for 7a. The ^1H spectrum for **7** at ambient temperature is dominated by **7a** (see Table 6). Using simple inspection, the ^{31}P, ^1H correlation, and a ^1H NOESY we could make the necessary assignments such that the major isomer, **7a**, could be recognized. *Complex **7a** has the structure found in the solid state.* Specifically, from the NOESY cross-peaks we note: (a) that NOE from the η^5-Cp to the lower set of ortho PPh_2 protons differentiates these two phenyl rings. (b) an NOE from the methyl group to the upper PPh_2 ortho protons supporting the assignment in (a). This latter NOE also shows the conformation of the chelate ring, i.e., the methyl group lies above the substituted Cp plane. (c) an NOE from one terminal allyl proton to the ortho protons of the lower PPh_2 phenyl, suggesting these anti protons are "down" and thus that the central allyl proton is "up". This is the key observation for the selection of **7a** as the correct structure. (d) there is an interaction from the CH_3 to one set of ortho phenyl protons from the 1,3-diphenyl allyl. (e) intra-allyl NOEs, which allow us to assign the second set of ortho phenyl protons from the 1,3-diphenyl allyl.

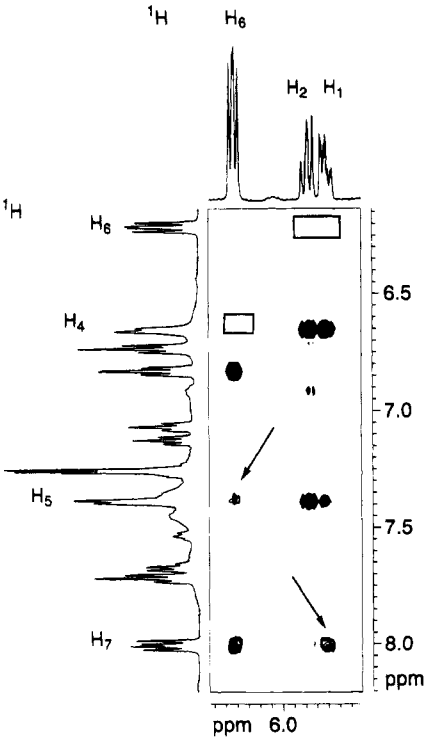

Figure 7. Section of the ^1H NOESY for **7a**. The arrows indicate the cross-peaks due to (a) NOE from one terminal allyl proton to the ortho protons of the lower PPh_2 phenyl, suggesting these anti protons are down and thus that the central allyl proton is up (lower right arrow), and (b) NOE from the ortho allyl phenyl protons near to the phobyl interacting with the upper PPh_2 ortho resonances, thus indicating some allyl rotation (middle left arrow). The empty spaces, indicated by the rectangles, are where one should find cross-peaks if there were no stacking of the allyl and upper PPh group.

Given all of these interactions (and of course the assignments), we can suggest further subtle solution−structural aspects: (f) there must be π-stacking of the upper PPh_2 phenyl and the immediately adjacent allyl phenyl. We note that the appropriate PPh_2 ortho resonances are at relatively low frequency (an anisotropic effect of the allyl phenyl group) and that there is *no NOE* between these two phenyl groups. This latter is more or less impossible unless the rings are stacked, in which case they are >3.3 Å apart. Interestingly, the rings must be rotating synchronously, as there is no restricted rotation, at ambient temperature, about either of the appropriate P−C or C−C bonds. (g) there is probably some clockwise rotation of the allyl group (seen from behind the allyl toward the Pd atom), as the ortho allyl phenyl protons near to the phobyl fragment show a weak NOE to the upper PPh_2 ortho resonances.

Figure 7 shows a section of the NOESY for **7a** in which points b, f, and g are emphasized; all three of these are supported by the solid-state structure of **7a**. The ^1H NOESY spectrum was measured in phase-sensitive mode so that both NOE and exchange can be

observed. We do find exchange between **7a** and **7b**, and this allows us to find the central allyl proton of **7b**. From the form of its signal (two relatively large spin–spin interactions), and the observation of two NOEs to the two different sets of ortho allyl phenyl protons, we can assign **7b** a syn/syn arrangement for the allyl phenyl groups. Unfortunately, the signals of **7c** and **7d** are too broad, and frequently under the signals of **7a**, for us to say anything definite with respect to structure. We assume that the two remaining isomers have the syn/anti arrangements, as indicated in Scheme 2; however, we cannot distinguish between the various syn/anti possibilities (or even exclude anti/anti isomers). Nevertheless, it is important to recognize the presence of these isomers, since they will possibly contribute to the overall enantioselectivity of the catalytic reaction.

The allyl ^{13}C chemical shifts for **7a** are interesting: δ 110.8 (central), 100.7 (trans to phobyl-P), and 80.8 (trans to PPh_2-P). Discounting steric effects, the 19.9 ppm difference between the two terminal carbons is a hint as to the electronic structure of **7a** and specifically, as to which terminal allylic center has more double character (that trans to the phobyl P).

The cationic complex **7** will be formed as an intermediate in the course of the catalytic alkylation of 1,3-diphenyl-3-acetoxypropene. Having shown that the *configuration* of this Pd(allyl) complex observed in the solid state corresponds to the preferred one existing in solution (**7a**), and because the absolute configuration of the product is known (*R*), one can determine the preferred site of nucleophilic attack. As indicated in Figure 3, this corresponds to the allylic carbon atom in pseudotrans position with respect to the phobyl group (attack on the other allyl terminus would lead to the other enantiomer). A tentative explanation for this observation is as follows. Since the aliphatic phosphine (the phobyl fragment) exerts a higher trans influence[9] than the diphenylphosphino group, the Pd–carbon bond trans to it should be weaker than the cis one. Such a weakening will increase the olefinic character and hence the electrophilicity of that carbon atom. This is also supported by the ^{13}C NMR data discussed above. However, care must be exercised in applying such ground-state criteria to a problem that is eminently kinetic in nature, i.e., enantioselectivity. Whether or not an enhanced ground-state electrophilicity will be paralleled by a low-energy path for nucleophilic attack cannot be decided on the basis of our data.

Conclusions

We have shown that an important reactivity difference between the two isomers of 9-phospha-9*H*-bicyclononane exists, when the technical 2:1 mixture is used as nucleophile. Thus, the new ferrocenyl phosphine **5a**, containing the [3.3.1]-fragment exclusively, could be prepared. It is to hope that, by exploiting such reactivity difference, the symmetric phobyl group will be incorporated in other chelating phosphine systems when a nonbulky aliphatic PR_2 group is needed. This will allow avoidance of the use of the air-sensitive and more expensive PMe_2 and PEt_2 synthons.

The application of ligand **5a** in the asymmetric allylic alkylation has shown it to be inferior to other chiral ligands for that particular reaction.[1] This may be attributed to the existence of at least four configurational isomers of the intermediate Pd(allyl) complex, as shown by our NMR studies of **7**. In a broader sense, the relatively low enantioselectivities observed may also be correlated to the high conformational freedom ligand **5a** displays. In other words, because **5a** can assume significantly different conformations, it is not able to create a well-defined chiral environment around the Pd center during catalysis.

Experimental Section

General Considerations. All reactions with air- or moisture-sensitive materials were carried out under Ar using standard Schlenk techniques. Freshly distilled, dry, and oxygen-free solvents were used throughout. Technical grade phobane (2:1 mixture of [3.3.1]- and [4.2.1]-isomers together with ~30% oxides) was obtained by courtesy of Prof. A. Salzer, RWTH Aachen, and was used as received. Routine ^1H (250.133 MHz), ^{13}C (62.90 MHz), and ^{31}P NMR (101.26 MHz) spectra were recorded with a Bruker AC 250 spectrometer. Chemical shifts are given in ppm and coupling constants (*J*) are given in hertz. The detailed NMR study of **7** has been carried out using $CDCl_3$ solutions and a Bruker AMX 500 spectrometer. Standard pulse sequences[10–12] were used for the NOESY, ^{31}P, ^{31}P exchange, ^{13}C, ^1H, and ^{31}P, ^1H spectra. NOESY spectra were measured using a 0.8 s mixing time, while two measurements for the ^{31}P, ^{31}P exchange were done using a 0.5 and 1 s mixing time. Merck silica gel 60 (70–230 mesh) was used for column chromatography. Optical rotations were measured with a Perkin-Elmer 241 polarimeter using 10 cm cells. Elemental anslyses were performed by the Mikroelementar-analytisches Laboratorium der ETH. Catalytic experiments and analyses of reaction products were carried out as previously described.[1]

9-Phospha-9-[(*S*)-1-{(*R*)-2-(diphenylphosphino)ferrocenyl}ethyl]bicyclo[3.3.1]nonane ((*S*)-(*R*)-5a). A yellow solution of *N,N*-dimethyl-(*S*)-1-[(*R*)-2-(diphenylphosphino)ferrocenyl]ethylamine (**4**; 1.77 g, 4.01 mmol) and HPC_8H_{14} (6.88 g, 31 mmol of 2:1 [3.3.1]- and [4.2.1]-isomers) in acetic acid (~50 mL) was heated at 80 °C for 2 h. The solvent was subsequently removed *in vacuo* and the sticky, smelly, residue subjected to flash chromatography over Al_2O_3 using toluene (with 2% NEt_3) as the eluent. The phosphine oxides still contained in the raw material are not eluted and remain on the column. Subsequent crystallization from hot EtOH (50 mL) gave 1.46 g (68%) of analytically pure, orange, product that crystallized as large needles in two successive crops of 1.27 and 0.19 g respectively: $[\alpha]^{22}_D = +336$ (c = 1.1, $CHCl_3$); ^1H NMR ($CDCl_3$, 298 K) δ 7.18–7.63 (m, 10H, PPh_2), 4.58, 4.37, 4.03 (all br s, 3H, C_5H_3), 3.92 (s, 5H, C_5H_5), 3.09 (dq, 1H, C*H*(Me)P, ^3J(H,H) = 7.7, ^2J(H,P) = 3.5), 1.59 (dd, 3H, CH-(*Me*)P, ^3J(H,H) = 7.5, ^3J(P,H) = 13.0), 0.91–2.17 (m, 14H, PC_8H_{14}); $^{13}C\{^1H\}$ NMR ($CDCl_3$, 298 K) δ 140.1–127.8 (Ph), 74.0, 69.9 (C_5H_3), 69.2 (C_5H_5), 32.0 (*C*H(Me)P), 25.4–21.6 (CH-(*Me*) and PC_8H_{14}): ^{31}P NMR ($CDCl_3$, 298 K), δ −10.5 (s, PC_8H_{14}), −26.8 (s, PPh_2). Anal. Calcd for $C_{32}H_{36}P_2Fe$: C, 71.38; H, 6.74. Found: C, 71.83; H, 7.14.

[Pd(η^3-C_3H_5)((*S*)-(*R*)-5a)][CF_3SO_3] (6). To a magnetically stirred solution of (*S*)-(*R*)-**5a** (158 mg, 0.294 mmol) and [Pd(η^3-C_3H_5)(μCl)]$_2$ (54 mg, 0.15 mmol) in CH_2Cl_2 (10 mL) was added a solution of $AgCF_3SO_3$ (77 mg, 0.29 mmol) in MeOH (1.5 mL). The resulting suspension was stirred for 1 h in the dark and filtered over Celite, followed by removal of the

(9) For a review, see: Appleton, T. G.; Clark, H. C.; Manzer, L. E. *Coord. Chem. Rev.* **1973**, *10*, 335–422.

(10) Jeener, J.; Bachmann, P.; Ernst, R. R. *J. Chem. Phys.* **1979**, *71*, 4545–4553.

(11) Summers, M. F.; Marzilli, L. G.; Bax, A. *J. Am. Chem. Soc.* **1986**, *108*, 4285–4294.

(12) Sklener, V.; Miyashiro, H.; Zon, G.; Miles, H. T.; Bax, A. *FEBS Lett.* **1986**, *208*, 94–98.

solvents *in vacuo*. The orange residue is dissolved in warm CH_2Cl_2, and hexane is added till the onset of cloudiness. The warm solution is allowed to cool to room temperature over night, causing the product to crystallize as orange needles: yield 245 mg (94%), $[\alpha]^{22}_D = +315$ (c = 1.2, $CHCl_3$), ^1H NMR ($CDCl_3$, 298 K) major isomer δ 7.1–7.8 (m, 10H), 5.95 (m, 1H), 5.01 (m, 1H), 4.25–4.65 (m, 2H), 4.22 (s, 1H), 3.80 (s, 2H), 3.72 (s, 5H), 3.26 (m, 1H), 1.21 (dd, 3H, ^3J(H,H) = 7.1, ^3J(P,H) = 15.1), 0.87–2.57 (m, 14H); ^1H NMR ($CDCl_3$, 298 K) minor isomer δ 7.1–7.8 (m, 10H), 5.32 (m, 1H), 4.70 (m, 1H), 4.25–4.65 (m, 2H), 4.16 (s, 1H), 3.74 (s, 2H), 3.66 (s, 5H), 2.85 (m, 1H), 1.06 (dd, 3H, ^3J(H,H) = 7.2, ^3J(P,H) = 15.6), 0.87–2.57 (m, 14H); $^{13}C\{^1H\}$ NMR ($CDCl_3$, 298 K) δ 134.3–122.0, 78.0, 76.0, 71.7–72.5, 70.8, 30.9, 30.6, 29.6, 24.5–23.1, 22.0, 21.1, ^{31}P NMR ($CDCl_3$, 298 K) major isomer δ 18.5 (d, ^2J(P,P) = 57), 9.2 (d, ^2J(P,P) = 57); ^{31}P NMR ($CDCl_3$, 298 K) minor isomer δ 17.8 (d, ^2J(P,P) = 60), 10.4 (d, ^2J(P,P) = 59.8). Anal. Calcd for $C_{36}H_{41}O_3F_3P_2SFePd$: C, 51.78; H, 4.95. Found: C, 51.68; H, 5.18.

[Pd(η^3-PhCHCHCHPh)((*S*)-(*R*)-5a)][CF_3SO_3] (7). The procedure is the same as that for **6** except that the phosphine (*S*)-(*R*)-**5a** (102 mg, 0.19 mmol), [Pd(η^3-PhCHCHCHPh)(μCl)]$_2$ (64 mg, 0.095 mmol), and $AgCF_3SO_3$ (49 mg, 0.19 mmol) reacted to give 128 mg (68%) of orange, crystalline product: $[\alpha]^{22}_D = -134$ (c = 0.73, $CHCl_3$); ^1H NMR ($CDCl_3$, 298 K) δ 6.2–8.1 (m, 20H), 5.86 (m, 1H), 5.81 (m, 1H), 5.36 (m, 1H), 4.40 (s, 2H), 4.01 (s, 1H), 3.68 (s, 5H), 3.35 (m, 1H), 1.09 (dd, 3H, ^3J(H,H) = 6.9, ^3J(H,H) = 14.7), 0.9–2.7 (m, 14H); $^{13}C\{^1H\}$ NMR ($CDCl_3$, 298 K) δ 138.6–129.1 (Ph), 110.7, 100.5, 80.8, 73.5, 70.8, 70.1, 70.7, 30.8–20.9; ^{31}P NMR ($CDCl_3$, 298 K) δ 15.4 (d, ^2J(P,P) = 87), 14.2 (d, ^2J(P,P) = 87.) Anal. Calcd for $C_{48}H_{49}O_3F_3P_2SFePd{\cdot}CH_2Cl_2$: C, 54.78; H, 4.79. Found: C, 54.85; H, 4.85.

X-ray Crystallographic Studies of Racemic (*S*)-(*R*)-5a, 6, and 7. Selected crystallographic and relevant data collection parameters are listed in Table 2. Data were measured with variable scan speed to ensure constant statistical precision on the collected intensities. One standard reflection was measured every 120 reflections; no significant variation was detected.

The structures were solved either by direct (**5a**,**7**) or Patterson (**6**) methods and refined by full-matrix least squares using anisotropic displacement parameters for all non-hydrogen atoms. The contribution of the hydrogen atoms in their idealized position (Riding model with fixed isotropic U = 0.080 Å^2) was taken into account but not refined. All calculations were carried out by using the Siemens SHELXTL PLUS system.

Acknowledgment. We thank Dr. N. Weferling, Hoechst AG, and Professor Salzer, RWTH Aachen, for a generous gift of phobane.

Supplementary Material Available: Tables of atomic coordinates, complete listing of bond distances and angles, tables of anisotropic displacement coefficients, and coordinates of hydrogen atoms for **5a**, **6**, and **7** (19 pages). Ordering information is given on any current masthead page. Table of calculated and observed structure factors (24 pages) may be obtained from the authors upon request.

OM940765D

Syntheses and Reactions with Lewis Bases of $Ru_4(CO)_8(\mu_3\text{-}O_2C_6H_2R_2)_2$ (R = H, *t*-Bu), Complexes Containing 1,2-Semiquinone Ligands Which Bridge through Oxygen and η^6-C_6 Rings. Crystal Structures of $Ru_4(CO)_8(O_2C_6H_4)_2{\cdot}CH_2Cl_2$, $Ru_4(CO)_8(O_2C_6H_2(t\text{-}Bu)_2)_2{\cdot}2CH_2Cl_2$, $Ru_4(CO)_8(O_2C_6H_2(t\text{-}Bu)_2)_2(py)_2$, and $Ru_4(CO)_7(O_2C_6H_2(t\text{-}Bu)_2)_2(PhC{\equiv}CCO_2Et)$

Witold Paw, Jerome B. Keister,* Charles H. Lake, and Melvyn Rowen Churchill*

Department of Chemistry, University at Buffalo, State University of New York, Buffalo, New York 14260-3000

Received August 11, 1994[⊗]

The reactions of $Ru_3(CO)_{12}$ with catechol and with 3,5-di-*tert*-butyl-1,2-benzoquinone yield three clusters $Ru_4(CO)_8(\mu_3\text{-}O_2C_6H_2R_2)_2$, R = H or *t*-Bu, which differ in the arrangement of metal atoms but which all contain μ_3-semiquinone ligands coordinated via terminal and bridging O atoms and a π-η^6-C_6 ring. One isomer, designated 1:3, has a structure containing a linear array of three Ru atoms connected by metal–metal bonds and with each pair of metal atoms bridged by one dioxolene ligand through an oxygen atom and an η^6-C_6 ring, while the fourth Ru atom is connected via bridging oxygen atoms from the two dioxolene ligands. The other isomer, designated 2:2, contains two diruthenium units, each pair of Ru atoms connected via a metal–metal bond and a dioxolene ligand bridge via an oxygen atom and a η^6-C_6 ring, and the two Ru_2 units are connected via bridging oxygen atoms from both dioxolene ligands. The 1:3 isomer $Ru_4(O_2C_6H_2(t\text{-}Bu)_2)_2(CO)_8$ does not react directly with Lewis bases but reacts with trimethylamine *N*-oxide in THF or acetonitrile to form $Ru_4(O_2C_6H_2(t\text{-}Bu)_2)_2(CO)_7L$, L = THF or NCMe, respectively. The THF complex reacts with L = PPh_3, *trans*-$EtO_2CCH{=}CHCO_2Et$, $C_2(CO_2Me)_2$, $PhCCCO_2Et$, or C_2Ph_2 to yield $Ru_4(O_2C_6H_2(t\text{-}Bu)_2)_2(CO)_7L$. The analogous 2:2 isomer undergoes fragmentation in the presence of most Lewis bases but rapidly and reversibly reacts with pyridine to form $Ru_4(O_2C_6H_2(t\text{-}Bu)_2)_2(CO)_8(py)_2$. Four X-ray diffraction studies are reported. $Ru_4(CO)_8(O_2C_6H_4)_2{\cdot}CH_2Cl_2$ crystallizes in the noncentrosymmetric orthorhombic space group *Pnn*2 with a = 13.9003(20) Å, b = 8.6481(21) Å, c = 10.6075(16) Å, V = 1275.1(4) Å^3, and Z = 2. The structure was refined to R = 1.92% for 1572 reflections above 6σ. The molecule has C_2 symmetry with a close-to-linear array of three Ru atoms, the two terminal metal atoms being linked to η^6-$O_2C_6H_4$ ligands and two CO ligands; the central Ru and the "lone" Ru atom are each bonded to two CO ligands and are bridged by the oxygen atoms of the $O_2C_6H_4$ ligands. $Ru_4(CO)_8(O_2C_6H_2(t\text{-}Bu)_2)_2{\cdot}2CH_2Cl_2$ crystallizes in space group $P\bar{1}$ with a = 11.3503(13) Å, b = 11.4188(11) Å, c = 19.4541(19) Å, α = 93.680(8)°, β = 102.682(8)°, γ = 107.260(8)°, V = 2326.3(4) Å^3, and Z = 2. The structure was refined to R = 4.34% for 3540 reflections above 6σ. The ruthenium-containing molecules have C_i symmetry. The molecule is composed of two $[\eta^6\text{-}O_2C_6H_2(t\text{-}Bu)_2]Ru(CO)_2{-}Ru(CO)_2$ units which are held together by additional Ru–O linkages. $Ru_4(CO)_8(O_2C_6H_2(t\text{-}Bu)_2)_2(py)_2$ crystallizes in space group $P2_1/n$ with a = 12.5406(16) Å, b = 23.9907(34) Å, c = 16.5219(19) Å, β = 91.989(10)°, V = 4967.8(11) Å^3, and Z = 4. The structure was refined to R = 2.85% for 2833 reflections above 6σ. The molecule is not symmetrical, but consists of $[\eta^6\text{-}O_2C_6H_2(t\text{-}Bu)_2](OC)_2Ru{-}Ru(CO)_2(py)$ and $[\eta^6\text{-}O_2C_6H_2(t\text{-}Bu_2)](OC)Ru(\mu\text{-}CO)_2Ru(CO)(py)$ units held together by Ru–O linkages. The ^{13}C NMR spectrum indicates that the same structure is adopted in solution; surprisingly, even though pairwise bridge–terminal carbonyl exchange would interconvert the two Ru_2 subunits, the molecule is rigid on the NMR time scale at room temperature. $Ru_4(CO)_7(O_2C_6H_2(t\text{-}Bu)_2)_2(PhC{\equiv}CCO_2Et)$ crystallizes in the noncentrosymmetric orthorhombic space group $P2_12_12_1$ with a = 12.4149(19) Å, b = 16.0888(27) Å, c = 23.9674(31) Å, V = 4787.3(13) Å^3, and Z = 4. The structure was refined to R = 5.01% for 3782 reflections above 6σ. The molecule has a connectivity similar to that of $Ru_4(CO)_8(O_2C_6H_4)_2$ but with an alkyne ligand substituting for a CO on the "lone" Ru atom.

Introduction

Metal complexes of 1,2-dioxolene ligands have attracted attention due to their structural and electrochemical properties and their relevance to metal–quinone chemistry in biological systems.[1] The most

⊗ Abstract published in *Advance ACS Abstracts,* December 1, 1994.

(1) Pierpont, C. G.; Lange, C. W. *Prog. Inorg. Chem.* **1994**, *41*, 331. (b) Pierpont, C. G.; Buchanan, R. M. *Coord. Chem. Rev.* **1981**, *38*, 45.

0276-7333/95/2314-0767$09.00/0

Chart 1

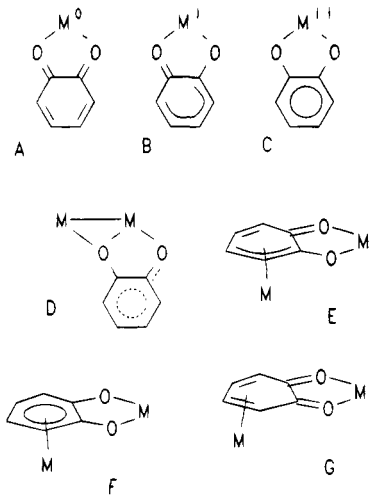

common coordination mode for a 1,2-dioxolene is as a η^2-chelate to a single transition metal center. Complexes with such ligands usually show rich electrochemistry with ligand-localized redox steps corresponding to the reduction of quinone to semiquinone and then to catecholate (structures A–C of Chart 1).[2] However, many other coordination geometries are possible in polymetallic complexes. It is expected that the ligand-based electrochemistry will be strongly influenced by the coordination mode. Structures with bridging via a single oxygen atom (D),[1] via an η^3-C_6 ring and oxygen atoms (E),[3] and via terminal oxygen atoms and an η^6-C_6 ring (F)[4] have been identified. Very recently complexes containing η^4-1,2-benzoquinone ligands (G) have been prepared.[5] This report presents new ruthenium clusters containing semiquinone ligands coordinated via terminal and bridging O atoms and a π-η^6-C_6 ring. Some of these results have previously appeared in preliminary form.[6]

Experimental Section

Starting Materials. $Ru_3(CO)_{12}$ was prepared as previously described.[7] Catechol, 3,5-di-*tert*-butyl-1,2-benzoquinone (DBQ), and other reagents were purchased from Aldrich and used as received. Tetrabutylammonium tetrafluoroborate, TBATFB, was prepared from tetrabutylammonium bromide and sodium tetrafluoroborate, crystallized three times from ethyl acetate/pentane solution, and vacuum dried.

Solvents. Dichloromethane, tetrahydrofuran (THF), and acetonitrile were distilled from CaH_2. Toluene, ethyl acetate, hexanes (Fisher), and heptane (Aldrich) were used as received.

General Methods. All reactions were carried out using standard Schlenk techniques. Products were isolated and purified (if possible) by thin layer chromatography, TLC, on silica gel (1 mm) with dichloromethane/hexanes or dichloromethane/ethyl acetate mixtures as eluents. Compounds were dried under a nitrogen gas stream and/or in vacuo. Elemental analyses were obtained from Galbraith Laboratories, Inc.

Physical Methods of Characterization. Infrared spectra in the carbonyl region were recorded on a Nicolet Magna 550 FT-IR spectrophotometer of hexanes or dichloromethane solutions. ^1H NMR spectra were obtained on Varian Gemini 300 or VXR-400s instruments (low temperature) in deuteriochloroform and with TMS as reference. ^{13}C-NMR spectra were obtained on a Varian Gemini 300 instrument. Mass spectra with electron impact (EI) or fast atom bombardment (FAB) ionization were obtained on a VG 70-SE spectrometer.

Electrochemistry. Cyclic voltammetry (CV) experiments were performed on a BAS-100 electrochemical analyzer. Measurements were made in dichloromethane with TBATFB as supporting electrolyte at 0.1 M concentration. The concentration of analyte was 10^{-3} M. Electrodes used were as follows: working, 5 mm platinum disk; reference, silver wire; auxiliary, platinum wire. Compensation for *iR* drop was employed for all measurements. All potential values were referenced to the ferrocene/ferrocenium couple (0 V), the potential of which was determined before and after each measurement.

(1:3)$Ru_4(CO)_8(SQ)_2$ (SQ = *o*-$O_2C_6H_4^-$).[8] A solution of 300 mg of $Ru_3(CO)_{12}$ and 155 mg (3 equiv) of catechol in toluene was heated under nitrogen at reflux for 3 h. The insoluble yellow-brown solid (which appears to be (2:2)$Ru_4(CO)_8(SQ)_2$[5]) was separated and the filtrate evaporated to dryness. TLC (15% ethyl acetate/dichloromethane) produced a very intense red band approximately in the middle of the plate following some weak bands with $H_4Ru_4(CO)_{12}$ as the main component. Extraction of the red band with dichloromethane gave the product, significantly contaminated with catechol, which moves up the plate only slightly ahead of the cluster. The yield of (1:3)$Ru_4(CO)_8(SQ)_2$ was therefore estimated from the ^1H NMR spectrum to be ca. 15 mg (5%). The presence of a CO atmosphere, as well as the use of $H_4Ru_4(CO)_{12}$ as the starting material, does not seem to affect the yield. Pure material and X-ray-quality crystals were obtained from crystallization from a dichloromethane/methanol mixture (slow decomposition occurs in the solution).

Anal. Calcd for $C_{20}H_8O_{12}Ru_4 \cdot CH_2Cl_2$: C, 27.14; H, 1.08. Found: C, 27.76; H, 1.16. IR (CH_2Cl_2): 2064 w, 2036 vs, 2000 m, 1990 w, 1958 m, br cm^{-1}. ^1H NMR ($CDCl_3$, 17 °C): 6.49 (t, 2H, J = 6 Hz), 6.28 (d, 2H, J = 6 Hz), 5.51 (t, 2H, J = 6 Hz), 4.96 (d, 2H, J = 6 Hz) ppm. MS (desorption EI): m/z 846. CV (100 mV/s): irreversible, 1-electron oxidation wave at 0.40 V.

(1:3)- and (2:2)$Ru_4(CO)_8(DBSQ)_2$ (DBSQ = 1,2-$O_2C_6H_2$-3,5-(t-Bu)$_2^-$).[8] A toluene solution of $Ru_3(CO)_{12}$ (200 mg) and DBQ (207 mg, 3 equiv) was heated at reflux under nitrogen for 4 h. The red solution was evaporated to dryness, and the residue was dissolved in 3 mL of dichloromethane. An insoluble, yellow solid was filtered out and redissolved in dichloromethane. Concentration of this solution gave 100 mg (40%) of (2:2)$Ru_4(CO)_8(DBSQ)_2$. Products contained in the filtrate were separated by TLC (dichloromethane). The first red-orange band was the main product, (1:3)$Ru_4(CO)_8(DBSQ)_2$ (70 mg, 30%). Typically the yields of the 2:2 and 1:3 isomers were in the range of 20–40% and 20–30%, respectively. Other products were of lower yields (ca. 10%), some of them of higher nuclearity (detected $Ru_5(CO)_{10}(DBSQ)_3$). The presence of another form of (1:3)$Ru_4(CO)_8(DBSQ)_2$ was also deduced from the IR and ^1H NMR spectra of a second, dark-red band.[9] The reaction seems to be sensitive to the amount of excess quinone. X-ray-quality crystals of (2:2)$Ru_4(CO)_8(DBSQ)_2$ were obtained by slow evaporation of a dichloromethane solution.

(2) Hartl, F.; Vlcek, A., Jr. *Inorg. Chem.* **1992**, *31*, 2869 and references therein.
(3) Fox, G. A.; Pierpont, C. G. *J. Chem. Soc., Chem. Commun.* **1988**, 806.
(4) Westcott, C. A.; Taylor, N. J.; Marder, T. B.; Baker, R. T.; Jones, N. J. *J. Chem. Soc., Chem. Commun.* **1991**, 304.
(5) (a). Bohle, D. S.; Goodson, P. A. *J. Chem. Soc., Chem. Commun.* **1992**, 1205. (b). Bohle, D. S.; Christensen, A. N.; Goodson, P. A. *Inorg. Chem.* **1993**, *32*, 4173. (c). Bohle, D. S.; Carron, K. T.; Christensen, A. N.; Goodson, P. A.; Powell, K. *Organometallics* **1994**, *13*, 1355.
(6) Churchill, M. R.; Lake, C. H.; Paw, W.; Keister, J. B. *Organometallics* **1994**, *13*, 8.
(7) Dawes, J. L.; Holmes, J. D. *Inorg. Nucl. Chem. Lett.* **1971**, *7*, 847.

(8) The designations 1:3 and 2:2 refer to the arrangments of the four Ru atoms, connected by metal–metal bonds. The 1:3 complex contains a chain of three Ru atoms, and the fourth is not bonded to the others. The 2:2 complex contains two isolated Ru–Ru units.

Data for (2:2)$Ru_4(CO)_8(DBSQ)_2$. Anal. Calcd for $C_{36}H_{40}O_{12}Ru_4 \cdot 2CH_2Cl_2$: C, 36.84; H, 3.83. Found: C, 38.14; H, 3.50. IR (hexanes): 2035 vs, 1995 m, 1967 s, 1950 w cm^{-1}. ^1H NMR ($CDCl_3$, 17 °C): 6.52 (d, 2H, J = 2 Hz), 5.43 (d, 2H, J = 2 Hz), 1.56 (s, 18H), 1.28 (s, 18H) ppm. UV/vis (CH_2Cl_2): 400 nm (ϵ 2900 M^{-1} cm^{-1}). EI MS: m/z 1072 ($^{102}Ru_4$). CV (100 mV/s): irreversible, 1-electron oxidation wave at 0.7 V.

Data for (1:3)$Ru_4(CO)_8(DBSQ)_2$. Anal. Calcd for $C_{36}H_{40}O_{12}Ru_4 \cdot CH_2Cl_2$: C, 38.51; H, 3.67. Found: C, 38.93; H, 3.60. IR (hexanes): 2058 m, 2032 vs, 1996 s, 1984 m, 1958 m, 1953 m cm^{-1}. ^1H NMR ($CDCl_3$, 17 °C): 6.52 (d, 2H, J = 2 Hz), 5.14 (d, 2H, J = 2 Hz), 1.49 (s, 18H), 1.28 (s, 18H) ppm. ^{13}C NMR ($CDCl_3$, 17 °C): 204.8 (2C, CO), 204.7 (2C, CO), 204.0 (2C, CO), 197.0 (2C, CO), 144.9 (2C, unprot. ring C), 125.7 (2C, unprot. ring C), 125.1 (2C, unprot. ring C), 119.6 (2C, unprot. ring C), 88.1 (2C, prot. ring C), 85.9 (2C, prot. ring C), 35.5 (2C, *t*-Bu C), 33.7 (2C, *t*-Bu C), 30.9 (6C, methyl C), 29.9 (6C, methyl C) ppm. UV/vis (CH_2Cl_2): 336 nm (ϵ 16 000 M^{-1} cm^{-1}), 490 nm (ϵ 11 000 M^{-1} cm^{-1}). EI MS: m/z 1072 ($^{102}Ru_4$). CV (100 mV/s): irreversible, 1-electron oxidation wave at 0.40 V.

$Ru_2(CO)_6(DBSQ)_2$. A toluene solution of $Ru_3(CO)_{12}$ (200 mg) and 207 mg (3 equiv) of DBQ was heated at reflux with CO passing through the solution for 4 h. The IR spectrum shows that the conversion is almost quantitative with a small amount of unreacted $Ru_3(CO)_{12}$. The complex is quite unstable in solution (CO purge most likely inhibits the decomposition) but could be isolated in low yield as a brick-red solid by quick concentration of hexane solution.

IR (hexanes): 2117 s, 2053 s, 2044 s cm^{-1}. ^1H NMR ($CDCl_3$, 17 °C): 6.87 (d, 2H, J = 2 Hz), 6.74 (d, 2H, J = 2 Hz), 1.50 (s, 18H), 1.25 (s, 18H) ppm. FAB MS: m/z 812 ($^{102}Ru_4$).

$Ru_4(CO)_7(THF)(DBSQ)_2$. To the solution of (1:3)$Ru_4(CO)_8(DBSQ)_2$ in THF was added a suspension of 1.2 equiv of $Me_3NO \cdot 2H_2O$ in THF at room temperature. The mixture was stirred under nitrogen until the IR spectrum showed that the conversion was complete. The cluster can be isolated by TLC (dichloromethane) but usually is contaminated by a small amount of $Ru_4(CO)_7(Me_3N)(DBSQ)_2$.[10]

IR (hexanes): 2030 s, 1991 s, 1952 m, 1947 m, 1938 w cm^{-1}. ^1H NMR ($CDCl_3$, 17 °C): 6.53 (d, 1H, J = 2 Hz), 6.45 (d, 1H, J = 2 Hz), 5.38 (d, 1H, J = 2 Hz), 4.89 (d, 1H, J = 2 Hz), 3.60 (m, 4H), 3.45 (m, 4H), 1.52 (s, 9H), 1.49 (s, 9H), 1.31 (s, 9H), 1.22 (s, 9H) ppm. FAB MS: m/z 1116 ($^{102}Ru_4$). CV (100 mV/s): irreversible, 1-electron oxidation wave at 0.23 V.

$Ru_4(CO)_7(CH_3CN)(DBSQ)_2$. The procedure used for the THF cluster was used except that acetonitrile was the solvent. $Ru_4(CO)_7(Me_3N)(DBSQ)_2$ was also formed as an impurity.

Anal. Calcd for $C_{37}H_{43}NO_{11}Ru_4$: C, 41.07; H, 4.01; N, 1.29. Found: C, 40.10; H, 3.89; N, 0.92. IR (hexanes): 2029 s, 1991 s, 1960 m, 1951 w, 1946 w cm^{-1}. ^1H NMR ($CDCl_3$, 17 °C): 6.51 (d, 1H, J = 2 Hz), 6.46 (d, 1H, J = 2 Hz), 5.18 (d, 1H, J = 2 Hz), 4.91 (d, 1H, J = 2 Hz), 2.38 (s, 3H), 1.51 (s, 9H), 1.48 (s, 9H), 1.29 (s, 9H), 1.24 (s, 9H) ppm. FAB MS: m/z 1085 ($^{102}Ru_4$).

$Ru_4(CO)_7(L)(DBSQ)_2$ (L = PPh_3, PhCCPh, MeO_2CCCCO_2Me, $PhCCCO_2Et$, *trans*-$EtO_2CCHCHCO_2Et$). These clusters were obtained from (1:3)$Ru_4(CO)_8(DBSQ)_2$ via substitutions using $Ru_4(CO)_7(THF)(DBSQ)_2$. After the conversion to the THF cluster was complete (by IR) THF was replaced by heptane, 3 equiv of the appropriate ligand was added, and the solution was refluxed under nitrogen for 30 min. TLC (dichloromethane/hexanes, 2:1) allowed the separation of pure substitution products.

Data for $Ru_4(CO)_7(PPh_3)(DBSQ)_2$. Yield: 90%. IR (hexanes): 2027 s, 1988 s, 1950 s, 1944 w cm^{-1}. ^1H NMR ($CDCl_3$, 17 °C): 7.3 (m, 15H), 6.40 (d, 1H, J = 2 Hz), 6.17 (d, 1H, J = 2 Hz), 5.22 (d, 1H, J = 2 Hz), 4.37 (d, 1H, J = 2 Hz), 1.41 (s, 9H), 1.25 (s, 9H), 1.13 (s, 9H), 1.11 (s, 9H) ppm. ^{31}P NMR ($CDCl_3$, 17 °C): 61.7 ppm. FAB MS: m/z 1306 ($^{102}Ru_4$). CV (100 mV/s): irreversible, 1-electron oxidation wave at 0.23 V.

Data for $Ru_4(CO)_7(PhCCPh)(DBSQ)_2$. Yield: 60%. IR (hexanes): 2030 s, 1992 s, 1971 w, 1954 m, 1949 m cm^{-1}. ^1H NMR ($CDCl_3$, 17 °C): 7.54 (m, 10H), 6.45 (d, 1H, J = 2 Hz), 6.35 (d, 1H, J = 2 Hz), 5.25 (d, 1H, J = 2 Hz), 4.89 (d, 1H, J = 2 Hz), 1.27 (s, 9H), 1.24 (s, 9H), 1.20 (s, 9H), 1.07 (s, 9H) ppm. FAB MS: m/z 1222 ($^{102}Ru_4$).

Data for $Ru_4(CO)_7(MeO_2CCCCO_2Me)(DBSQ)_2$. Yield: 50%. IR (hexanes): 2034 s, 2016 m, br, 1995 s, 1958 m, 1952 m, 1736 m cm^{-1}. ^1H NMR ($CDCl_3$, 17 °C): 6.55 (d, 1H, J = 2 Hz), 6.54 (d, 1H, J = 2 Hz), 5.31 (d, 1H, J = 2 Hz), 4.84 (d, 1H, J = 2 Hz), 3.78 (s, 6H), 1.54 (s, 9H), 1.52 (s, 9H), 1.30 (s, 9H), 1.26 (s, 9H) ppm. FAB MS: m/z 1186 ($^{102}Ru_4$).

Data for $Ru_4(CO)_7(PhCCCO_2Et)(DBSQ)_2$. Yield: 60%. Anal. Calcd for $C_{46}H_{50}O_{13}Ru_4$: C, 45.47; H, 4.15. Found: C, 44.59; H, 4.54. IR (hexanes): 2031 s, 2004 vw, 1992 s, 1955 m, 1949 m cm^{-1}. ^1H NMR ($CDCl_3$, 17 °C): 7.8–7.3 (m, 5H), 6.47 (m, 2H), 5.27 (d, 1H, J = 2 Hz), 4.89 (d, 1H, J = 2 Hz), 4.26 (q, 2H, J = 7.0 Hz), 1.46 (s, 9H), 1.34 (t, 3H, J = 7.0 Hz), 1.27 (s, 9H), 1.26 (s, 9H), 1.13 (s, 9H) ppm. FAB MS: m/z 1218 ($^{102}Ru_4$). X-ray-quality crystals of this cluster were grown by slow evaporation of a hexane solution inside the drybox.

Data for $Ru_4(CO)_7$(*trans*-$EtO_2CCHCHCO_2Et$))$(DBSQ)_2$. Yield: 50%. Two isomers **A** and **B** were formed, most likely corresponding to the coordination of two faces of the alkene to the metal center. **A/B** = 2.5/1. IR (hexanes): 2033 s, 2019 w, 2006 w, br, 1994 s, 1958 m, 1951 m cm^{-1}. ^1H NMR ($CDCl_3$, 17 °C): **A**, 6.57 (d, 1H, J = 2 Hz), 6.54 (d, 1H, J = 2 Hz), 5.33 (d, 1H, J = 2 Hz), 4.75 (d, 1H, J = 2 Hz), 4.67 (s, 2H), 4.26–4.05 (AB pattern of quartets (J = 7.2 Hz), J_{AB} = 10.8 Hz, 4H), 1.60 (s, 9H), 1.56 (s, 9H), 1.32 (t, 6H, J = 7.2 Hz), 1.29 (s, 9H), 1.27 (s, 9H); **B**, 6.53 (d, 1H, J = 2 Hz), 6.51 (d, 1H, J = 2 Hz), 5.25 (s, 2H), 5.19 (d, 1H, J = 2 Hz), 4.58 (d, 1H, J = 2 Hz), 3.98–3.80 (AB pattern of quartets (J = 7.2 Hz), J_{AB} = 10.8 Hz, 4H), 1.53 (s, 18H), 1.25 (s, 9H), 1.24 (s, 9H), 1.21 (t, 6H, J = 7.2 Hz) ppm. FAB MS: m/z 1216 ($^{102}Ru_4$).

$Ru_4(CO)_6(\mu\text{-}CO)_2(py)_2(DBSQ)_2$. Pyridine was added dropwise to a solution of (2:2)$Ru_4(CO)_8(DBSQ)_2$ in dichloromethane until the IR absorptions due to the starting material had disappeared. IR spectra recorded after each addition showed the presence of isosbestic points at 1972, 1984, and 2025 cm^{-1}. The reaction was manifested by color change from yellow to orange-red. Crystalline material was obtained by precipitation from a cooled dichloromethane/methanol/pyridine solution and X-ray-quality crystals were grown by slow evaporation.

Anal. Calcd for $C_{46}H_{50}O_{12}N_2Ru_4$: C, 45.02; H, 4.11; N, 2.28. Found: C, 44.65; H, 3.93; N, 1.94. IR (CH_2Cl_2): 2021 s, 1994 vs, 1979 sh, 1935 m, br, 1830 w, 1766 m, br cm^{-1}. ^1H NMR ($CDCl_3$, 17 °C) (all signals broad in absence of excess pyridine): 8.63 (m, 2H), 7.69 (m, 1H), 7.30 (m, 2H), 6.10 (d, 1H, J = 2 Hz), 5.93 (d, 1H, J = 2 Hz), 5.65 (d, 1H, J = 2 Hz), 5.59 (d, 1H, J = 2 Hz), 1.55 (s, 9H), 1.36 (s, 9H), 1.24 (s, 9H), 1.21 (s, 9H) ppm. ^{13}C NMR ($CDCl_3$, 17 °C) (with excess of pyridine): 254.6 (1C, CO), 235.2 (1C, CO), 213.2 (1C, CO), 209.0 (1C, CO), 202.7 (1C, CO), 201.5 (1C, CO), 199.0 (1C, CO), 196.9 (1C, CO), 162.2 (1C, unprot. ring C), 161.2 (1C, unprot. ring C), 158.4 (1C, unprot. ring C), 147.3 (1C, unprot. ring C), 121.8 (1C, unprot. ring C), 119.0 (1C, unprot. ring C), 116.0 (1C, unprot. ring C), 111.6 (1C, unprot. ring C), 91.1 (1C, prot. ring C), 86.5 (1C, prot. ring C), 84.5 (1C, prot. ring C), 83.0 (1C, prot. ring C), 35.5 (1C, *t*-Bu C), 35.1 (1C, *t*-Bu C), 34.0 (1C, *t*-Bu C), 33.1 (1C, *t*-Bu C), 31.3 (3C, methyl C), 30.52 (3C, methyl C), 30.46

(9) Data for $Ru_4(CO)_8(DBSQ)_2$ are as follows: IR (hexanes): 2058 w, 2041 w, 2032 vs, 1995 s, 1983 m, 1962 w, 1953 w cm^{-1}. ^1H-NMR ($CDCl_3$, 17 °C): 6.54 (d, 1H, J = 2Hz), 6.06 (d, 1H, J = 2Hz), 5.70 (d, 1H, J = 2Hz), 5.00 (d, 1H, J = 2Hz), 1.46 (s, 9H), 1.45 (s, 9H), 1.37 (s, 9H), 1.29 (s, 9H) ppm. FAB MS: m/z 1072 ($^{102}Ru_4$). The comparison of these spectra to those of (1:3)$Ru_4(CO)_8(DBSQ)_2$ indicates that the structures of these clusters differ only in the positions of *tert*-butyl groups, making the ligands inequivalent.

(10) Data for $Ru_4(CO)_7(Me_3N)(DBSQ)_2$ are as follows: IR(hexanes): 2029 s, 1991 s, 1952 w, 1947 w, 1931 m cm^{-1}. ^1H-NMR ($CDCl_3$, 17 °C): 6.50 (d, 1H, J = 2Hz), 6.44 (d, 1H, J = 2Hz), 5.22 (d, 1H, J = 2Hz), 4.98 (d, 1H, J = 2Hz), 2.35 (s, 9H), 1.50 (s, 9H), 1.47 (s, 9H), 1.31 (s, 9H), 1.23 (s, 9H) ppm. FAB MS: m/z 1103 ($^{102}Ru_4$).

(3C, methyl C), 30.1 (3C, methyl C) ppm. CV (100 mV/s): irreversible, 1-electron oxidation wave at 0.14 V.

Protonation of (2:2)$Ru_4(CO)_8(DBSQ)_2$ by CF_3CO_2H. To the solution of (2:2)$Ru_4(CO)_8(DBSQ)_2$ in dichloromethane the acid was added dropwise until the complete disappearance of IR bands due to the starting material. IR spectra recorded after each addition showed the presence of several isosbestic points. Then solvent was evaporated to dryness to allow NMR measurement. The product appears to be somewhat air sensitive. In a separate experiment some KO-*t*-Bu was added to the solution of the protonated cluster. The IR spectrum showed the formation of the starting cluster. IR (CH_2Cl_2): 2041 s, 2005 w, 1995 w, 1969 m, 1955 vw cm^{-1}. ^{1}H-NMR ($CDCl_3$, 17 °C): 10.74 (s, 1H), 6.61 (d, 1H, J = 2 Hz), 6.58 (d, 1H, J = 2 Hz), 5.58 (d, 1H, J = 2 Hz), 5.06 (d, 1H, J = 2 Hz), 1.54 (s, 9H), 1.46 (s, 9H), 1.31 (s, 9H), 1.26 (s, 9H) ppm.

Reaction of (2:2)$Ru_4(CO)_8(DBSQ)_2$ with $AgOSO_2CF_3$. Dichloromethane solutions of (2:2)$Ru_4(CO)_8(DBSQ)_2$ and $AgOSO_2CF_3$ (1:1) were mixed at room temperature, and the reaction was monitored by IR spectroscopy. Initially (30 min) a clean conversion was observed (isosbestic points), but then the solution steadily became cloudy (yellow-brown precipitate) and gained a greenish tint. Quick addition of excess of Ag^+ caused complete reaction. IR (CH_2Cl_2): 2056 vw, 2043 vs, 2000 w, 1984 vw, 1971 w, 1955 sh cm^{-1}.

$Ru(CO)_2(Me_3N)_2(DBCat)$. $Ru_3(CO)_{12}$ (200 mg) and DBQ (207 mg, 3 equiv) were dissolved in 40 mL of THF. To this solution was added 77 mg (3 equiv) of $Me_3NO{\cdot}2H_2O$ in 10 mL of CH_3CN. After the solution was stirred overnight under nitrogen, the products were separated by TLC (20% ethyl acetate/dichloromethane). Some weak bands were followed by the wide brown band of $Ru(CO)_2(Me_3N)_2(DBCat)$ in the middle of the plate. Extraction and evaporation yielded 106 mg (23%).

Anal. Calcd for $C_{22}H_{38}O_4N_2Ru$: C, 53.31; H, 7.73; N, 5.65. Found: C, 52.77; H, 7.33; N, 5.24. IR (hexanes): 2013 s, 1938 s cm^{-1}. ^{1}H NMR ($CDCl_3$, 17 °C): 6.74 (d, J = 2.4 Hz, 1H), 6.52 (d, J = 2.4 Hz, 1H), 2.44 (s, 18H), 1.46 (s, 9H), 1.27 (s, 9H) ppm. ^{13}C-NMR ($CDCl_3$, 17 °C): 200.6 (1C, CO), 200.1 (1C, CO), 158.4 (1C, unprot. ring C), 155.0 (1C, unprot. ring C), 137.8 (1C, unprot. ring C), 134.8 (1C, unprot. ring C), 111.6 (1C, prot. ring C), 110.4 (1C, prot. ring C), 56.8 (6C, methyl C), 34.9 (1C, *t*-Bu C), 34.1 (1C, *t*-Bu C), 32.1 (3C, methyl C), 30.2 (3C, methyl C). FAB MS: m/z 496 (^{102}Ru). CV (100 mV/s): quasi-reversible oxidation at −0.30 V (ΔE_p = 94 mV), irreversible oxidation at $E_{p,a}$ = +0.80 V.

$Ru(CO)_2(Me_3N)(py)(DBCat)$. A solution of $Ru(CO)_2(Me_3N)_2(DBCat)$ and pyridine (excess) in dichloromethane was stirred overnight under nitrogen. The reaction gave a single product which was isolated by evaporation of the solvent and unreacted pyridine. IR (hexanes): 2019 s, 1947 s. ^{1}H NMR ($CDCl_3$, 17 °C): 8.60 (d, 2H, J = 7.5 Hz), 7.50 (t, 1H, J = 7.5 Hz), 7.10 (t, 2H, J = 7.5 Hz), 6.60 (s, 1H), 6.35 (s, 1H), 2.59 (s, 9H), 1.43 (s, 9H), 1.17 (s, 9H) ppm.

Determination of the Equilibrium Constant for the Reaction (2:2)$Ru_4(CO)_8(DBSQ)_2$ + 2py ⇌ $Ru_4(CO)_6(\mu\text{-}CO)_2(py)_2(DBSQ)_2$. Two solutions of (2:2)$Ru_4(CO)_8(DBSQ)_2$ were used to determine extinction coefficients at 2030.8 (a), 2021.2 (b), and 1961.4 (c) cm^{-1}. Two different samples of (2:2)$Ru_4(CO)_8(DBSQ)_2$ were dissolved in dichloromethane solution to which an amount of pyridine was added such as the equilibrium was shifted to the right. IR spectra, taken with the same dichloromethane/pyridine mixture as reference, allowed determination of the extinction coefficient at each frequency. Then three solutions of (2:2)$Ru_4(CO)_8(DBSQ)_2$ were prepared in which the amount of pyridine added allowed only a partial conversion to $Ru_4(CO)_6(\mu\text{-}CO)_2(py)_2(DBSQ)_2$. The absorbances at the three frequencies were measured for these three solutions. For each sample two values of $K = [Ru_4(CO)_6(\mu\text{-}CO)_2(py)_2(DBSQ)_2]/([(2:2)Ru_4(CO)_8(DBSQ)_2][py]^2)$ were calculated corresponding to concentration values obtained (one band due to (2:2)$Ru_4(CO)_8(DBSQ)_2$ and one due to $Ru_4(CO)_6(\mu\text{-}CO)_2(py)_2(DBSQ)_2$). These were averaged, and the mean value for three samples was calculated with the error equal to one-half of the span between maximum and minimum values. $K_{eq} = (4.5 \pm 0.2) \times 10^4$ L^2 mol^{-2} at 22 °C.

Collection of X-ray Diffraction Data and Structure Solution. General Considerations. In each of the four structural studies a suitable crystal (as identified initially by inspection with a binocular polarizing microscope and, later, confirmed by the quality of X-ray diffraction data) was sealed into a thin-walled glass capillary and was accurately aligned and centered in a eucentric goniometer on an upgraded Syntex $P2_1$/Siemens P3 automated four-circle diffractometer. Determination of Laue symmetry, unit cell parameters and the crystal's orientation matrix were carried out as described previously.[11] Intensity data (Mo Kα, $\bar{\lambda}$ = 0.710 730 Å) were collected at room temperature (24 ± 1 °C) using graphite-monochromatized radiation. All data were corrected for Lorentz and polarization effects and for the effects of absorption. Details of cell dimensions and data collection are provided in Table 1. Data were collected by a coupled θ(crystal)−2θ(counter) method unless otherwise noted.

All crystallographic calculations were carried out in-house on a VAXstation 3100 computer with use of the Siemens SHELXTL PLUS system.[12] The analytical scattering factors for neutral atoms were used throughout the analysis; both the real ($\Delta f'$) and imaginary ($i\Delta f''$) components of anomalous dispersion[13] were included in the calculations. The parameter η, refined as a multiplier to the $\Delta f''$ values, was used to confirm the absolute configuration for those crystals in noncentrosymmetric space groups. Structures were solved by direct methods (SHELXTL PLUS) and difference-Fourier syntheses. All non-hydrogen atoms were located, and their positional and anisotropic thermal parameters were refined. Hydrogen atoms were included in calculated positions with d(C−H) = 0.96 Å.[14] Refinement was continued until convergence was reached with Δ/σ < 0.01; the structural solution was then rendered secure by means of a final difference-Fourier synthesis on which no chemically meaningful residuals were found. Details of final refinement processes are provided in Table 1. Unusual features of the individual structural studies are outlined below.

$Ru_4(CO)_8(O_2C_6H_4)_2{\cdot}CH_2Cl_2$. Atomic coordinates are collected in Table 2. This species is an unusual example of a molecular crystal which crystallizes in an orthorhombic space group (*Pnn*2, with systematic absences 0*kl* for $k + l = 2n + 1$ and *h*0*l* for $h + l = 2n + 1$) with Z = 2. The tetraruthenium molecule lies on a site of 2-fold symmetry (Wyckoff notation *a*)[15] at 0, 0, z. Atoms Ru(2) and Ru(3) lie on the C_2 axis, and the origin is defined by z = 0 for Ru(2). The dichloromethane molecule lies on a site of C_2 symmetry (Wyckoff notation *b*) at 0, 1/2, z but is disordered such that Cl(1S) is at the special position, with atoms C(1S) and Cl(3S) disordered about the 2-fold axis. The final discrepancy factors (R = 1.92% for data with $F_o > 6\sigma(F)$ and R = 2.12% for all data) suggest that our treatment of this disorder problem was appropriate.

$Ru_4(CO)_8(O_2C_6H_2(t\text{-}Bu)_2)_2{\cdot}2CH_2Cl_2$. Final atomic coordinates are collected in Table 3. This species crystallizes in the triclinic space group $P\bar{1}$ with Z = 2. However, the unit cell contains two independent tetraruthenium clusters, each lying about a crystallographic inversion center. One molecule (containing Ru(1), Ru(2), and the symmetry-related atoms Ru(1A) and Ru(2A)) lies about the inversion center at 0, 1/2, 0, and the other molecule (containing Ru(3), Ru(4), Ru(3A), and Ru(4A)) lies about the inversion center at 0, 0, 1/2. The two

(11) Churchill, M. R.; Lashewycz, R. A.; Rotella, F. J. *Inorg. Chem.* **1977**, *16*, 265.
(12) *SHELXTL PLUS*; Siemens Analytical Instrument Corp.: Madison, WI, 1988.
(13) *International Tables for X-Ray Crystallography*; Kynoch Press: Birmingham, England, 1974; Vol. 4, pp 99−101 and 149−150.
(14) Churchill, M. R. *Inorg. Chem.* **1973**, *12*, 1213.
(15) *International Tables for X-Ray Crystallography*; Kynoch Press: Birmingham, England, 1965; Vol. 1, p 120.

Table 1. Experimental Data for the Four X-Ray Structural Studies

	$Ru_4(CO)_8(C_6H_4O_2)_2\cdot CH_2Cl_2$	$Ru_4(CO)_8(C_6H_2(t\text{-}Bu)_2O_2)_2\cdot 2CH_2Cl_2$	$Ru_4(CO)_8(C_6H_2(t\text{-}Bu)_2\text{-}O_2)_2(py)_2$	$Ru_4(CO)_7(C_6H_2(t\text{-}Bu)_2O_2)_2\text{-}(PhC{\equiv}CCO_2Et)$
		Unit Cell Parameters		
molec formula	$C_{20}H_8O_{12}Ru_4\cdot CH_2Cl_2$	$C_{36}H_{40}O_{12}Ru_4\cdot 2CH_2Cl_2$	$C_{46}H_{50}N_2O_{12}Ru_4$	$C_{46}H_{50}O_{13}Ru_4$
cryst syst	orthorhombic	triclinic	monoclinic	orthorhombic
space group	*Pnn*2 (No. 34)	$P\bar{1}$ (No. 2)	$P2_1/n$ (No. 14)	$P2_12_12_1$ (No. 19)
a, Å	13.9003(20)	11.3503(13)	12.5406(16)	12.4149(19)
b, Å	8.6481(21)	11.4188(11)	23.9907(34)	16.0888(27)
c, Å	10.6075(16)	19.4541(19)	16.5219(19)	23.9674(31)
α, deg	90.000	93.680(8)	90.000	90.000
β, deg	90.000	102.682(8)	91.989(10)	90.000
γ, deg	90.000	107.260(8)	90.000	90.000
V, Å^3	1275.1(4)	2326.3(4)	4967.8(11)	4787.3(13)
Z	2	2	4	4
fw	929.5	1238.9	1227.2	1215.1
density, g/cm^3	2.421	1.769	1.641	1.686
μ, mm^{-1}	2.555	1.536	1.228	1.274
transm coeffs	0.382−0.442	0.688−0.779	0.342−0.383	0.657−0.917
F(000)	884	1224	2448	2424
		Data Collection		
2θ range, deg	5.0−45.0	5.0−45.0	5.0−40.0	5.0−45.0
index ranges	$-14 \le h \le 0$	$0 \le h \le 12$	$0 \le h \le 12$	$-13 \le h \le 0$
	$0 \le k \le 9$	$-12 \le k \le 11$	$-23 \le k \le 23$	$-17 \le k \le 0$
	$-11 \le l \le 11$	$-20 \le l \le 20$	$-15 \le l \le 15$	$-25 \le l \le 25$
reflecns collcd	1889	6564	9885	6866
indepdt reflcns	1677	6111	4656	6268
reflcns with $F > 6\sigma$	1572	3540	2833	3782
R merge, %		1.64	2.06	4.04
		Refinement		
absolute config	$\eta = 1.06(10)$			$\eta = 1.2(2)$
extinction coeff	$\chi = 0.001\,37(9)$		$\chi = 0.000\,021(8)$	
params refined	189	523	578	569
indices (6σ data), %	$R = 1.92$	$R = 4.34$	$R = 2.85$	$R = 5.01$
	$wR = 2.18$	$wR = 4.64$	$wR = 2.48$	$wR = 5.31$
R indices (all data), %	$R = 2.12$	$R = 8.55$	$R = 6.73$	$R = 8.57$
	$wR = 2.98$	$wR = 6.63$	$wR = 3.56$	$wR = 8.48$
largest diff peak, e/Å^3	0.47	1.33 (near solvent)	0.78	1.24
largest diff hole, e/Å^3	−0.48	−1.27 (near solvent)	−0.65	−1.04

Table 2. Final Atomic Coordinates (×10^4) and Equivalent Isotropic Thermal Parameters (in Å^2 × 10^3) for $Ru_4(CO)_8(C_6H_4O_2)_2\cdot CH_2Cl_2$

	x	*y*	*z*	*U*(eq)[a]
Ru(1)	2035(1)	334(1)	−116(1)	35(1)
Ru(2)	0	0	0	30(1)
Ru(3)	0	0	3188(1)	27(1)
O(1)	412(2)	−1429(4)	1656(4)	31(1)
O(2)	1378(3)	841(4)	2975(4)	34(1)
O(11)	2068(4)	3773(7)	−516(5)	80(2)
O(12)	1967(6)	−51(9)	−2926(7)	87(3)
O(21)	−100(3)	2398(7)	−2016(6)	69(2)
O(31)	−509(4)	2209(6)	5239(5)	65(2)
C(11)	2020(4)	2469(8)	−362(6)	45(2)
C(12)	1990(6)	129(10)	−1844(9)	53(3)
C(21)	−74(4)	1471(10)	−1253(7)	43(2)
C(31)	−317(5)	1362(9)	4443(6)	41(2)
C(1)	1371(3)	−1184(6)	1458(5)	32(2)
C(2)	1831(4)	38(9)	2145(7)	32(2)
C(3)	2804(4)	376(7)	1811(8)	41(2)
C(4)	3332(4)	−568(8)	966(7)	44(2)
C(5)	2891(4)	−1835(8)	387(6)	48(2)
C(6)	1903(4)	−2136(7)	620(6)	38(2)
Cl(1S)	0	5000	459(4)	82(2)
Cl(3S)	−464(5)	4942(6)	3082(7)	107(3)
C(1S)	485(12)	4693(16)	1998(17)	63(7)

[a] Equivalent isotropic *U* defined as one-third of the trace of the orthogonalized $\mathbf{U}_{ij}$ tensor.

dichloromethane molecules occupy general positions and are ordered. Data were relatively weak (only 3540 of 6111 independent data had $F_o > 6\sigma(F)$, probably because of the thin platelike nature of the crystal (approximately 0.4 × 0.2 × 0.07 mm).

$Ru_4(CO)_8(O_2C_6H_2(t\text{-}Bu)_2)_2(py)_2$. Final coordinates are collected in Table 4. Diffraction data for this complex were collected by the ω-scan technique, to avoid possible overlap of reflections scanned along the 24 Å *b*-axis. Two equivalent forms of data were collected ($hkl \equiv h\bar{k}l$ and $h\bar{k}l \equiv \bar{h}\bar{k}l$ for space group $P2_1/n$). The 9885 reflections collected were merged to 4656 independent reflections with a merging factor of R_{int} = 2.06%.

$Ru_4(CO)_7(O_2C_6H_2(t\text{-}Bu)_2)_2(PhC{\equiv}CCO_2Et)$. Final coordinates are collected in Table 5. Diffraction data were collected by the ω-scan technique because of the 24 Å *c*-axis. The structural study was otherwise uneventful.

Results and Discussion

The reactions and products described in this paper are summarized in Schemes 1−3. Products have been characterized by IR and multinuclear NMR spectroscopy, by mass spectrometry, and in representative cases by elemental analysis; however, the primary basis for structural characterization is single crystal X-ray diffraction.

Syntheses and Characterizations of Isomeric Clusters $Ru_4(CO)_8$(1,2-dioxolene)$_2$ (Scheme 1). The reaction of $Ru_3(CO)_{12}$ with catechol in refluxing *o*-xylene was shown by Bohle and co-workers to produce an insoluble polymeric species which can be cleaved by various nucleophiles to form compounds with π-bound catecholates in addition to coordination via oxygen atoms in terminal fashion.[5] According to the very recent report[5b] this polymer appears to consist of π-stacked units of (2:2)$Ru_4(CO)_8(SQ)_2$[8] (SQ = 1,2-semiquinone) analogous to (2:2)$Ru_4(CO)_8(DBSQ)_2$ (DBSQ = 3,5-di-*tert*-butyl-1,2-semiquinone) described below.

We independently investigated this reaction, dupli-

Table 3. Final Atomic Coordinates ($\times 10^4$) and Equivalent Isotropic Thermal Parameters (in $Å^2 \times 10^3$) for $Ru_4(CO)_8(C_6H_2(t\text{-}Bu)_2O_2)_2 \cdot 2CH_2Cl_2$

	x	y	z	U(eq)[a]
Ru(1)	−993(1)	5609(1)	1452(1)	34(1)
Ru(2)	186(1)	4267(1)	744(1)	33(1)
O(1)	−1283(6)	4410(5)	−168(3)	32(3)
O(2)	−643(6)	6917(6)	−63(3)	40(3)
O(15)	1547(9)	7343(8)	2253(6)	99(5)
O(16)	−1287(8)	2149(7)	1354(5)	73(4)
O(17)	2314(8)	4683(8)	2039(4)	72(4)
O(18)	−812(10)	4343(10)	2754(5)	99(5)
C(1)	−1786(9)	5038(8)	227(5)	31(4)
C(2)	−1401(9)	6356(8)	306(5)	33(4)
C(3)	−1814(9)	7003(8)	816(5)	36(4)
C(4)	−2708(9)	6307(8)	1168(5)	35(4)
C(5)	−3189(9)	5001(9)	1052(5)	38(4)
C(6)	−2708(9)	4374(9)	583(5)	35(4)
C(7)	−1407(10)	8431(9)	916(6)	45(5)
C(8)	28(11)	9041(9)	1020(6)	64(6)
C(9)	−1761(15)	8943(11)	1557(8)	97(8)
C(10)	−2072(12)	8810(11)	247(7)	75(6)
C(11)	−4263(9)	4273(9)	1372(6)	42(4)
C(12)	−4276(13)	2939(11)	1442(8)	83(7)
C(13)	−5493(10)	4248(12)	850(7)	73(6)
C(14)	−4183(13)	4940(11)	2106(6)	75(6)
C(15)	572(12)	6687(10)	1933(6)	55(5)
C(16)	−722(10)	2980(10)	1127(6)	44(4)
C(17)	1493(12)	4489(9)	1533(6)	49(5)
C(18)	−876(11)	4807(10)	2262(6)	53(5)
Ru(3)	2423(1)	2554(1)	5044(1)	34(1)
Ru(4)	485(1)	1275(1)	5643(1)	35(1)
O(21)	722(6)	−52(6)	3861(3)	42(3)
O(22)	1085(6)	−265(5)	5274(3)	33(2)
O(35)	3446(9)	4900(8)	6082(4)	77(4)
O(36)	564(9)	3722(9)	4268(5)	88(5)
O(37)	−409(9)	3458(8)	5866(6)	93(5)
O(38)	2457(8)	2344(8)	7002(4)	78(4)
C(21)	2047(9)	458(8)	5030(5)	33(4)
C(22)	1800(9)	588(8)	4285(5)	33(4)
C(23)	2772(9)	1509(9)	4063(5)	33(4)
C(24)	3937(9)	2125(9)	4549(5)	36(4)
C(25)	4219(9)	1929(9)	5281(5)	39(4)
C(26)	3249(9)	1091(8)	5501(5)	34(4)
C(27)	2551(9)	1682(9)	3270(5)	41(4)
C(28)	1295(10)	1899(12)	2960(6)	66(6)
C(29)	3625(11)	2789(11)	3147(6)	63(5)
C(30)	2621(13)	525(11)	2865(6)	68(6)
C(31)	5559(10)	2523(10)	5783(6)	47(4)
C(32)	6238(11)	1545(12)	5722(8)	83(7)
C(33)	5493(10)	2773(13)	6555(6)	76(6)
C(34)	6286(10)	3716(10)	5568(6)	58(5)
C(35)	3045(11)	4010(11)	5687(6)	52(5)
C(36)	1250(11)	3255(11)	4559(6)	55(5)
C(37)	−59(11)	2603(11)	5776(7)	61(5)
C(38)	1725(10)	1946(9)	6480(6)	46(5)
C(1S)	7797(14)	1602(14)	3369(10)	115(9)
Cl(1S)	7028(8)	2199(8)	3849(4)	215(5)
Cl(2S)	6815(8)	480(6)	2720(3)	171(4)
C(2S)	3391(19)	8408(22)	1111(12)	151(13)
Cl(3S)	4329(7)	7549(7)	1456(4)	188(4)
Cl(4S)	3918(9)	9108(7)	454(5)	242(6)

[a] Equivalent isotropic U defined as one-third of the trace of the orthogonalized $\mathbf{U}_{ij}$ tensor.

Table 4. Final Atomic Coordinates ($\times 10^4$) and Equivalent Isotropic Thermal Parameters (in $Å^2 \times 10^3$) for $Ru_4(CO)_8(C_6H_2(t\text{-}Bu)_2O_2)_2(py)_2$

	x	y	z	U(eq)[a]
Ru(1)	927(1)	6606(1)	1571(1)	39(1)
Ru(2)	2426(1)	7421(1)	1587(1)	40(1)
Ru(3)	−1769(1)	8105(1)	2154(1)	41(1)
Ru(4)	−144(1)	8879(1)	1769(1)	40(1)
O(1)	825(5)	7448(3)	209(4)	67(3)
O(2)	2957(5)	6393(3)	2554(4)	73(3)
O(3)	1945(6)	5879(3)	339(4)	91(4)
O(4)	3924(6)	6969(3)	383(4)	93(3)
O(5)	−3390(6)	8697(3)	1094(4)	94(3)
O(6)	−2416(6)	8875(3)	3457(4)	77(3)
O(7)	−1811(6)	9769(3)	1570(4)	90(3)
O(8)	−827(6)	8443(3)	119(4)	78(3)
O(11)	−1318(4)	7516(2)	1298(3)	43(2)
O(12)	−721(4)	7592(2)	2855(3)	37(2)
O(31)	1443(4)	7766(2)	2419(3)	40(2)
O(32)	2355(4)	8276(2)	1163(3)	44(2)
N(51)	3673(6)	7773(3)	2413(5)	49(3)
N(61)	−2923(5)	7449(3)	2458(5)	50(3)
C(1)	1208(7)	7264(3)	805(6)	43(4)
C(2)	2414(7)	6672(4)	2132(5)	44(3)
C(3)	1560(7)	6145(4)	831(6)	54(4)
C(4)	3366(8)	7141(4)	851(6)	57(4)
C(5)	−2730(8)	8471(4)	1497(5)	56(4)
C(6)	−2137(7)	8582(4)	2959(6)	51(4)
C(7)	−1196(8)	9424(4)	1657(5)	52(4)
C(8)	−567(7)	8581(4)	751(6)	52(4)
C(11)	−920(6)	7074(4)	1653(5)	40(4)
C(12)	−540(6)	7123(4)	2509(5)	35(3)
C(13)	−49(7)	6654(4)	2889(5)	43(4)
C(14)	−82(7)	6147(4)	2474(6)	51(4)
C(15)	−530(7)	6072(4)	1679(6)	51(4)
C(16)	−896(6)	6555(4)	1268(5)	42(3)
C(17)	284(9)	6654(4)	3796(5)	59(4)
C(18)	913(8)	7161(5)	4071(5)	91(5)
C(19)	928(11)	6131(5)	4029(6)	145(7)
C(20)	−749(9)	6638(5)	4258(6)	101(6)
C(21)	−802(9)	5493(4)	1331(7)	73(5)
C(22)	26(9)	5060(4)	1591(6)	95(6)
C(23)	−1846(11)	5343(5)	1716(10)	182(9)
C(24)	−934(8)	5486(4)	422(7)	99(6)
C(31)	1336(6)	8306(4)	2329(5)	36(3)
C(32)	1806(6)	8578(4)	1645(5)	39(4)
C(33)	1597(7)	9173(4)	1545(5)	44(4)
C(34)	1167(7)	9455(4)	2179(5)	49(4)
C(35)	800(7)	9203(4)	2899(5)	44(4)
C(36)	830(6)	8619(3)	2934(5)	41(3)
C(37)	2050(8)	9482(4)	813(6)	54(4)
C(38)	3257(8)	9500(4)	915(6)	83(5)
C(39)	1629(9)	10081(4)	757(6)	87(5)
C(40)	1735(8)	9188(4)	13(5)	73(4)
C(41)	542(8)	9573(4)	3630(5)	54(4)
C(42)	−229(10)	10033(5)	3412(6)	124(6)
C(43)	1591(9)	9798(5)	3960(7)	120(6)
C(44)	50(10)	9238(4)	4302(6)	110(6)
C(52)	3626(7)	7641(4)	3203(7)	60(4)
C(53)	4203(9)	7921(5)	3784(7)	84(5)
C(54)	4868(10)	8333(5)	3574(8)	87(6)
C(55)	4946(8)	8468(4)	2769(8)	75(5)
C(56)	4338(7)	8177(4)	2211(6)	58(4)
C(62)	−3448(8)	7148(4)	1884(6)	65(4)
C(63)	−4132(9)	6738(5)	2051(8)	83(6)
C(64)	−4347(9)	6603(5)	2819(10)	93(6)
C(65)	−3834(9)	6896(5)	3433(7)	80(5)
C(66)	−3132(8)	7322(4)	3227(7)	62(5)

[a] Equivalent isotropic U defined as one-third of the trace of the orthogonalized $\mathbf{U}_{ij}$ tensor.

cating Bohle's result but also isolating a second cluster product. After separation of the insoluble polymer, TLC of the soluble material gave in low yield a red compound which was characterized as (1:3)$Ru_4(CO)_8(SQ)_2$.[8] The use of 3,5-di-*tert*-butylbenzoquinone, DBQ, under similar conditions produced the analogous clusters (1:3)$Ru_4(CO)_8(DBSQ)_2$ and (2:2)$Ru_4(CO)_8(DBSQ)_2$ in good yields. The two isomers are not interconvertible under reaction conditions.

The 1:3 and 2:2 isomers[8] differ only in the arrangement of ruthenium atoms, both containing 1,2-dioxolene ligands which bridge through a combination of μ-oxygen, terminally coordinated oxygen, and η^6-C_6 coordination. The isomeric structures of $Ru_4(CO)_8$(dioxolene)$_2$ are novel. Prior to this work and concurrent work by Bohle and co-workers, η^6 coordination of the dioxolene in addition to coordination via bridging oxygen atoms had

Table 5. Final Atomic Coordinates ($\times 10^4$) and Equivalent Isotropic Thermal Parameters (in $Å^2 \times 10^3$) for $Ru_4(CO)_7(C_6H_2(t\text{-}Bu)_2O_2)_2(PhC{\equiv}CCO_2Et)$

	x	y	z	U(eq)[a]
Ru(1)	2246(1)	1568(1)	9391(1)	43(1)
Ru(2)	834(1)	210(1)	9416(1)	44(1)
Ru(3)	−698(1)	−1076(1)	9416(1)	41(1)
Ru(4)	1842(1)	−375(1)	8137(1)	37(1)
O(1)	2118(12)	2130(10)	10595(6)	104(7)
O(2)	3711(12)	231(8)	9824(6)	88(6)
O(3)	−830(12)	1389(9)	9885(7)	100(7)
O(4)	1333(13)	−196(10)	10595(7)	108(7)
O(5)	−2339(14)	150(9)	8985(7)	108(7)
O(6)	−1648(12)	−677(10)	10532(6)	100(6)
O(7)	1600(13)	68(9)	6949(6)	92(6) (7)
O(11)	831(8)	547(5)	8501(4)	38(3)
O(12)	2976(7)	541(5)	8266(4)	37(3)
O(31)	1806(8)	−758(6)	8994(4)	41(3)
O(32)	482(7)	−1093(6)	8112(4)	42(3)
O(53A)	5089(9)	−900(9)	8262(6)	86(6)
O(53B)	4551(9)	−346(9)	7455(5)	72(5)
C(1)	2132(16)	1929(11)	10137(9)	69(7)
C(2)	3155(15)	728(11)	9662(7)	57(6)
C(3)	−207(17)	957(11)	9701(7)	64(7)
C(4)	1146(16)	−48(13)	10134(8)	72(8)
C(5)	−1708(15)	−299(13)	9141(6)	62(7)
C(6)	−1258(15)	−834(12)	10110(7)	62(7)
C(7)	1695(13)	−93(9)	7404(7)	48(6)
C(11)	1416(10)	1248(9)	8572(6)	39(5)
C(12)	2556(11)	1228(9)	8452(6)	40(5)
C(13)	3204(13)	1939(8)	8576(7)	45(5)
C(14)	2679(14)	2656(9)	8809(6)	51(6)
C(15)	1510(11)	2692(8)	8893(7)	43(5)
C(16)	926(11)	1983(9)	8762(6)	39(5)
C(17)	4423(12)	2002(11)	8452(7)	51(6)
C(18)	4529(12)	1918(12)	7820(8)	67(7)
C(19)	4929(13)	2830(13)	8640(8)	76(8)
C(20)	5024(13)	1302(10)	8747(7)	58(6)
C(21)	1002(14)	3503(10)	9086(8)	59(6)
C(22)	1011(29)	4082(16)	8595(12)	156(16)
C(23)	1571(23)	3908(14)	9569(13)	158(16)
C(24)	−159(20)	3401(15)	9248(15)	158(17)
C(31)	995(11)	−1338(8)	9038(6)	37(5)
C(32)	300(12)	−1475(9)	8581(6)	40(5)
C(33)	−635(12)	−2032(9)	8661(7)	49(6)
C(34)	−700(12)	−2439(10)	9173(6)	46(5)
C(35)	33(11)	−2360(9)	9617(7)	46(5)
C(36)	873(11)	−1789(10)	9566(7)	51(6)
C(37)	−1460(12)	−2170(10)	8194(7)	50(5)
C(38)	−1866(15)	−1355(12)	7948(8)	74(7)
C(39)	−2383(15)	−2692(16)	8385(10)	108(11)
C(40)	−857(16)	−2644(13)	7720(8)	80(8)
C(41)	−39(14)	−2916(12)	10134(9)	73(8)
C(42)	−1217(13)	−3142(11)	10270(7)	59(6)
C(43)	583(20)	−3691(16)	10044(15)	182(19)
C(44)	436(22)	−2467(19)	10649(11)	167(16)
C(51)	2607(14)	−1573(11)	7906(7)	56(6)
C(52)	3290(13)	−1033(10)	7966(7)	52(6)
C(53)	4409(14)	−768(10)	7932(7)	51(6)
C(54)	5654(14)	−53(13)	7340(10)	78(8)
C(55)	5603(21)	309(17)	6783(10)	121(12)
C(56)	2197(14)	−2377(10)	7771(9)	65(7)
C(57)	2069(17)	−2551(14)	7228(12)	105(11)
C(58)	1715(23)	−3364(19)	7037(15)	134(15)
C(59)	1526(26)	−3896(20)	7467(25)	182(32)
C(60)	1617(31)	−3753(22)	8033(23)	167(24)
C(61)	1990(17)	−2967(10)	8165(12)	96(10)

[a] Equivalent isotropic U defined as one-third of the trace of the orthogonalized $\mathbf{U}_{ij}$ tensor.

not been observed for catecholate compounds.[16] It is interesting to note that the differing arrangements of the four Ru atoms cause significant differences in the electronic properties as suggested by the respective red and yellow colors of the (1:3) and (2:2) isomers and, more importantly, their reactivities as discussed below.

(16) Although the catecholate ligand in $[(Pr^i{}_2PCH_2)_2Rh\{(\eta^6\text{-Cat})\text{-BCat}\}]^4$ is η^6-bonded, the oxygen atoms chelate to boron and do not bridge to rhodium.

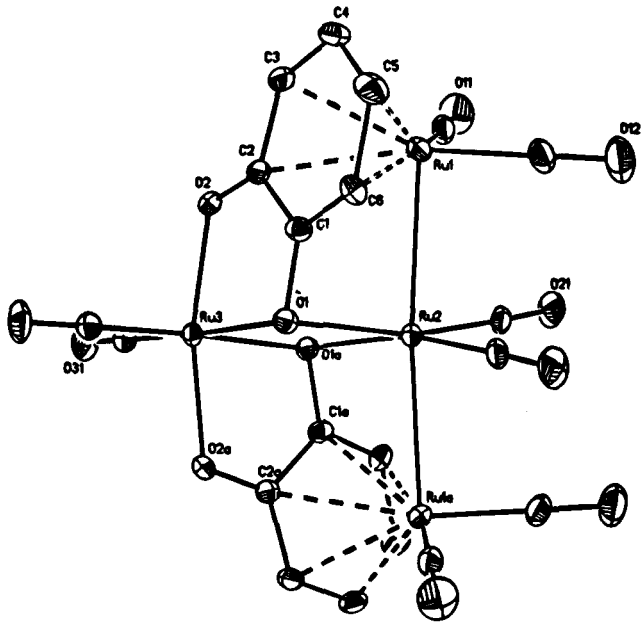

Figure 1. ORTEP2 diagram of $Ru_4(CO)_8(C_6H_4O_2)_2$ (20% probability ellipsoids, with hydrogen atoms omitted for clarity). The crystallographic C_2 axis is horizontal, passing through atoms Ru(3) and Ru(2).

Description of the Structure of (1:3)$Ru_4(CO)_8(O_2C_6H_4)_2{\cdot}CH_2Cl_2$. This tetraruthenium derivative is illustrated in Figure 1. Interatomic distances are collected in Table 6. The molecule has crystallographically imposed C_2 symmetry and contains an almost linear array of three ruthenium atoms (Ru(1)−Ru(2) = Ru(2)−Ru(1A) = 2.846(1) Å and ∠Ru(1)−Ru(2)−Ru(1A) = 175.1(1)°). Ru(1) and the symmetry-related atom Ru(1A) are linked in an η^6-mode to the six-membered carbocyclic ring of a $O_2C_6H_4$ ligand and are bonded to two terminal carbonyl ligands (Ru(1)−C(11) = 1.865(7) and Ru(1)−C(12) = 1.843(9) Å). Distances of Ru(1) from the η^6-C_6 ring show some minor variations, with Ru(1)−C(1) = 2.315(5), Ru(1)−C(2) = 2.428(7), Ru(1)−C(3) = 2.306(8), Ru(1)−C(4) = 2.275(6), Ru(1)−C(5) = 2.284(6), and Ru(1)−C(6) = 2.282(6) Å; the average Ru−C(ring) distance is 2.315 Å. The dioxolene moiety (which chelates to Ru(3)) is associated with one short C−O distance (C(2)−O(2) = 1.286(8) Å) and one long C−O distance (C(1)−O(1) = 1.366(6) Å); this, coupled with a relatively long Ru(1)−C(2) distance (*vide supra*), indicates that the $O_2C_6H_4$ ligand is best described as a semiquinone. (The C_6 ring is not strictly planar. The C(1)···C(3)−C(4)−C(5)−C(6) system has a root-mean-square deviation from planarity of 0.005 Å. C(2) lies 0.099 Å and O(2) lies 0.200 Å from this plane; these atoms are displaced away from Ru(1). The C(1)−C(2)−C(3) plane makes an angle of 7.4° with the five-atom plane.) It should be noted also that O(1), the oxygen atom associated with the longer C−O distance, bridges *two* ruthenium atoms (Ru(2) and Ru(3)), whereas O(2) is linked only to one ruthenium atom (Ru(2A)). Atom Ru(2) has an octahedral environment, being linked to two ruthenium atoms, two terminal carbonyl ligands (Ru(2)−C(21) = Ru(2)−C(21A) = 1.842(8) Å) and to one oxygen atom from each of the two semiquinone ligands (Ru(2)−O(1) = Ru(2)−O(1A) = 2.223(4) Å). Atom Ru(3) also has an octahedral environment but is linked

Scheme 1. Reactions of $Ru_3(CO)_{12}$ with Catechol and DBQ

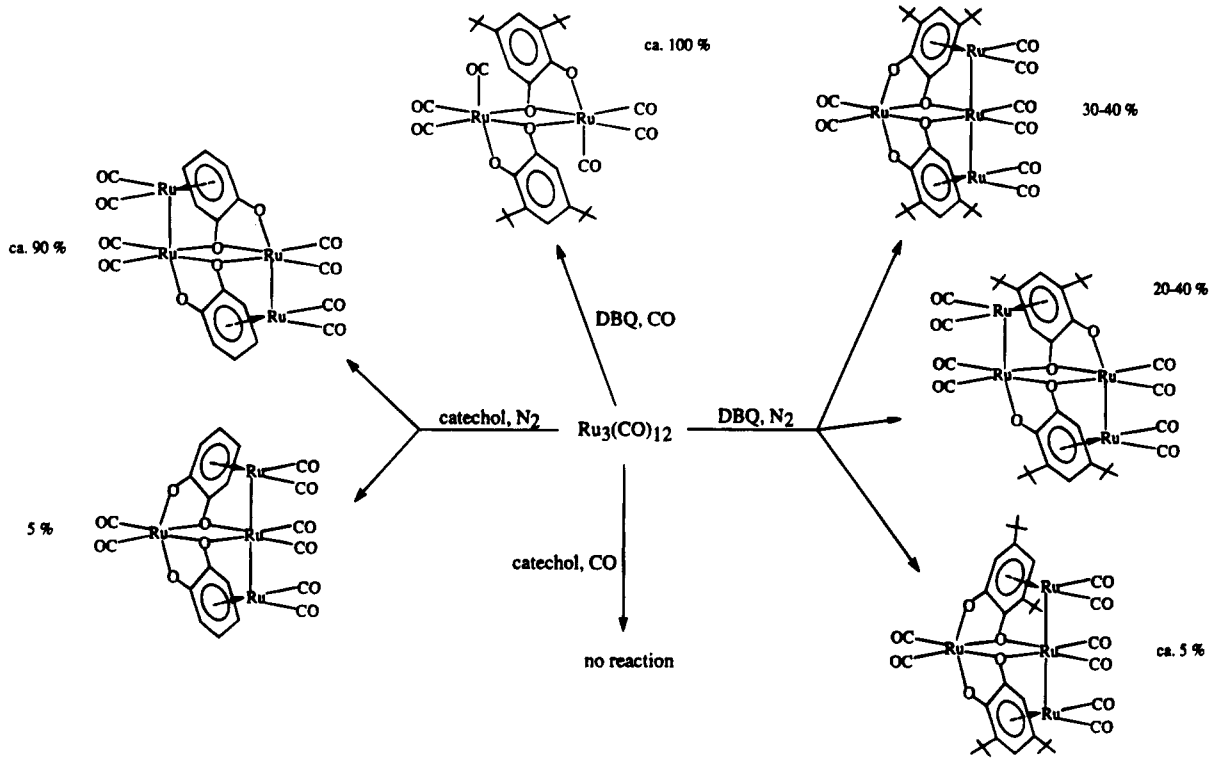

Table 6. Interatomic Distances (in Å) for $Ru_4(CO)_8(C_6H_4O_2)_2{\cdot}CH_2Cl_2$

Distances Involving Ruthenium Atoms			
Ru(1)-Ru(2)	2.846(1)	Ru(2)-O(1)	2.223(4)
Ru(1)−C(1)	2.315(5)	Ru(2)−O(1A)	2.223(4)
Ru(1)−C(2)	2.428(7)	Ru(2)−C(21)	1.842(8)
Ru(1)−C(3)	2.306(8)	Ru(2)−C(21A)	1.842(8)
Ru(1)−C(4)	2.275(6)	Ru(3)−O(1)	2.120(4)
Ru(1)−C(5)	2.284(6)	Ru(3)−O(1A)	2.120(4)
Ru(1)−C(6)	2.282(6)	Ru(3)−O(2)	2.061(4)
Ru(1)−C(11)	1.865(7)	Ru(3)−O(2A)	2.061(4)
Ru(1)−C(12)	1.843(9)	Ru(3)−O(31)	1.831(7)
Ru(2)−Ru(1A)	2.846(1)	Ru(3)−O(31A)	1.831(7)
C−O Distances in Carbonyl Ligands			
C(11)−O(11)	1.142(9)	C(21)−O(21)	1.140(10)
C(12)−O(12)	1.158(11)	C(31)−O(31)	1.149(9)
Distances within Semiquinone Ligand			
C(1)−O(1)	1.366(6)	C(2)−O(2)	1.286(8)
C(1)−C(2)	1.435(9)	C(4)−C(5)	1.397(9)
C(2)−C(3)	1.427(9)	C(5)−C(6)	1.420(8)
C(3)−C(4)	1.417(10)	C(6)−C(1)	1.419(8)

to two terminal carbonyl ligands (Ru(3)−C(31) = Ru(3)−C(31A) = 1.831(7) Å) and is chelated by two semiquinone ligands (Ru(3)−O(1) = 2.120(4) Å, Ru(3)−O(2) = 2.061(4) Å and ∠O(1)−Ru(3)−O(2) = 82.6(1)°).

Description of the Structure of (2:2)$Ru_4(CO)_8(O_2C_6H_2(t\text{-}Bu)_2)_2{\cdot}2CH_2Cl_2$. The unit cell contains two crystallographically independent tetraruthenium molecules, each of which has crystallographically imposed C_i symmetry. The molecules are chemically equivalent. One (that containing Ru(1) and Ru(2) along with the inversion related Ru(1A) and Ru(2A)) is illustrated in Figure 2. Interatomic distances for the two molecules are collected in Table 7; equivalent bond lengths for the two molecules are listed side by side. In the subsequent discussion we will refer to bond lengths in molecule 1 (containing Ru(1), Ru(2), Ru(1A), and Ru(2A)), with equivalent distances for molecule 2 (containing Ru(3), Ru(4), Ru(3A), and Ru(4A)) following in parentheses. Atom Ru(1) is linked in an η^6-mode to the six-membered

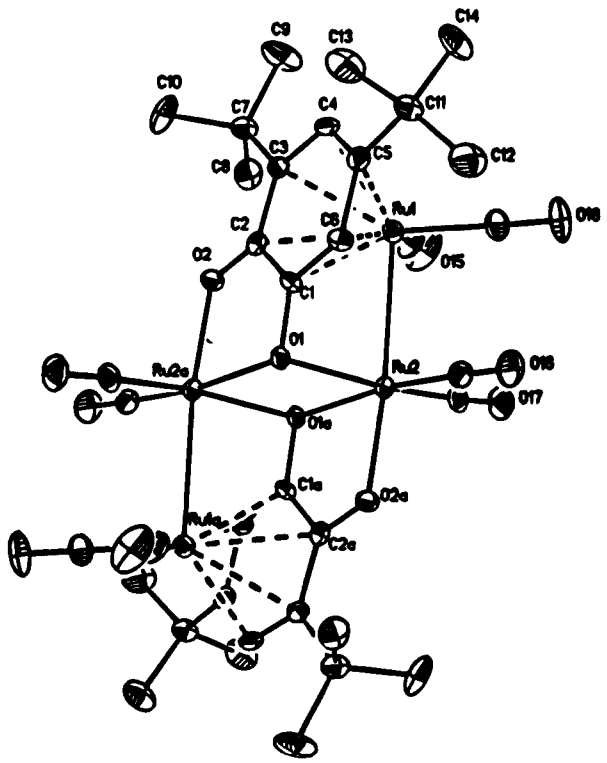

Figure 2. ORTEP2 diagram for one of the two crystallographically-independent molecules of $Ru_4(CO)_8(C_6H_2(t\text{-}Bu)_2O_2)_2$ (20% ellipsoids, H atoms omitted). The molecule has crystallographically imposed C_i symmetry.

ring defined by C(1)→C(6) and is also bonded to two carbonyl ligands, with Ru(1)−C(15) = 1.836(10) and Ru(1)−C(18) = 1.872(12) Å (Ru(3)−C(35) = 1.865(11) and Ru(3)−C(36) = 1.865(13) Å). Distances of Ru(1) from atoms of the six-membered ring vary from Ru(1)−C(4) = 2.288(11) up to Ru(1)−C(2) = 2.437(9) Å, averaging 2.336 Å (for Ru(3), distances are from Ru(3)−C(24)

Table 7. Interatomic Distances (in Å) for $Ru_4(CO)_8(C_6H_2(t\text{-}Bu)_2O_2)_2 \cdot 2CH_2Cl_2$

Distances Involving Ruthenium Atoms			
Ru(1)−Ru(2)	2.791(1)	Ru(3)−Ru(4)	2.787(1)
Ru(1)−C(1)	2.328(8)	Ru(3)−C(21)	2.300(9)
Ru(1)−C(2)	2.437(9)	Ru(3)−C(22)	2.428(9)
Ru(1)−C(3)	2.357(10)	Ru(3)−C(23)	2.353(10)
Ru(1)−C(4)	2.288(11)	Ru(3)−C(24)	2.299(11)
Ru(1)−C(5)	2.314(9)	Ru(3)−C(25)	2.317(11)
Ru(1)−C(6)	2.292(8)	Ru(3)−C(26)	2.284(10)
Ru(1)−C(15)	1.836(10)	Ru(3)−C(35)	1.865(11)
Ru(1)−C(18)	1.872(12)	Ru(3)−C(36)	1.865(13)
Ru(2)−O(1)	2.204(6)	Ru(4)−O(22)	2.198(7)
Ru(2)−O(1A)	2.192(2)	Ru(4)−O(22A)	2.193(5)
Ru(2)−O(2A)	2.083(7)	Ru(4)−O(21A)	2.092(7)
Ru(2)−C(16)	1.832(11)	Ru(4)−C(37)	1.823(14)
Ru(2)−O(17)	1.829(11)	Ru(4)−C(38)	1.848(10)
C−O Distances within Carbonyl Ligands			
C(15)−O(15)	1.149(13)	C(35)−O(35)	1.141(13)
C(16)−O(16)	1.150(14)	C(36)−O(36)	1.142(17)
C(17)−O(17)	1.156(13)	C(37)−O(37)	1.174(18)
C(18)−O(18)	1.123(16)	C(38)−O(38)	1.129(12)
Distances within Semiquinone Ligand			
C(1)−O(1)	1.340(13)	C(21)−O(22)	1.357(11)
C(2)−O(2)	1.292(12)	C(22)−O(21)	1.288(10)
C(1)−C(2)	1.425(13)	C(21)−C(22)	1.442(14)
C(2)−C(3)	1.439(15)	C(22)−C(23)	1.444(13)
C(3)−C(4)	1.423(14)	C(23)−C(24)	1.397(11)
C(4)−C(5)	1.412(13)	C(24)−C(25)	1.436(14)
C(5)−C(6)	1.417(16)	C(25)−C(26)	1.395(13)
C(6)−C(1)	1.436(13)	C(26)−C(21)	1.416(11)
C(3)−C(7)	1.544(13)	C(23)−C(27)	1.543(14)
C(5)−C(11)	1.537(15)	C(25)−C(31)	1.542(12)
C(7)−C(8)	1.530(16)	C(27)−C(28)	1.520(16)
C(7)−C(9)	1.524(21)	C(27)−C(29)	1.547(14)
C(7)−C(10)	1.511(17)	C(27)−C(30)	1.527(17)
C(11)−C(12)	1.534(17)	C(31)−C(32)	1.545(20)
C(11)−C(13)	1.528(15)	C(31)−C(33)	1.533(16)
C(11)−C(14)	1.546(17)	C(31)−C(34)	1.506(15)
Distances within CH_2Cl_2 Molecules			
C(1S)−Cl(1S)	1.651(22)	C(2S)−Cl(3S)	1.713(27)
C(1S)−Cl(2S)	1.675(15)	C(2S)−Cl(4S)	1.678(26)

= 2.299(11) up to Ru(3)−C(22) = 2.428(9) Å, with an average value of 2.330 Å). The dioxolene moiety, which chelates to Ru(2A), is associated with one short C−O distance of C(2)−O(2) = 1.292(12) and one long C−O distance of C(1)−O(1) = 1.340(13) Å (*cf.*, values of 1.288(10) and 1.357(11) Å in molecule 2). As with the previous structure, the shorter C−O distance involves that carbon atom of the η^6-C_6 ring which has the *longest* Ru−C distance; the $C_6H_2(t\text{-}Bu)_2O_2$ moiety is behaving as a semiquinone.

Again the C_6 ring is nonplanar, with the C=O unit bent out of plane. The interplanar angle C(1)···C(3)−C(4)−C(5)−C(6)/C(1)−C(2)−C(3) is 7.1°, with C(2) lying 0.092 Å and O(2) lying 0.186 Å from the planar (rms deviation 0.007 Å) five atom plane; the displacement is, of course, in a direction *away from* Ru(1). (Related values for molecule 2 are as follows: interplanar angle = 6.5°; displacements of atoms are 0.086 Å for C(22) and 0.155 Å for O(21); rms displacement from planarity for atoms in the five-membered system is only 0.005 Å.)

Atom Ru(2) has an irregular octahedral stereochemistry. It is linked to Ru(1), with Ru(1)−Ru(2) = 2.791(1) Å, and to two cis carbonyl ligands, with Ru(2)−C(16) = 1.832(10) and Ru(2)−C(17) = 1.829(11) Å (*cf.* Ru(3)−Ru(4) = 2.787(1) Å, Ru(4)−C(37) = 1.823(14) and Ru(4)−C(38) = 1.848(10) Å in molecule 2). The remaining three sites are occupied by oxygen atoms from a chelating semiquinone ligand, with Ru(2)−O(1A) = 2.192(2) and Ru(2)−O(2A) = 2.083(7) Å (2.193(5) and 2.092(7) Å in molecule 2) and by a single bonding interaction with the second semiquinone ligand, with Ru(2)−O(1) = 2.204(6) Å (2.198(7) Å in molecule 2).

Pathway for Formation of Isomeric Clusters $Ru_4(CO)_8$(1,2-dioxolene)$_2$. When these reactions are performed with CO passing through the solutions, tetranuclear clusters are not formed. In fact, the reaction with catechol does not occur at all under this condition. DBQ, however, reacts quantitatively, forming $Ru_2(CO)_6(DBSQ)_2$. This complex is possibly an intermediate in the reactions under N_2 leading to tetranuclear clusters. This is evidenced by the appearance of three IR bands corresponding to $Ru_2(CO)_6(DBSQ)_2$ at early stages of those reactions. When $Ru_2(CO)_6(DBSQ)_2$ was refluxed under N_2 for several hours, tetranuclear clusters were not observed and the complex decomposed; a source of $Ru(CO)_n$ fragments must be required for formation of the tetranuclear product. Reactions of this compound with various metal fragments are currently under investigation.

Since $Ru_2(CO)_6(DBSQ)_2$ seems to be an intermediate in the reactions forming (2:2)- and (1:3)$Ru_4(CO)_8(DBSQ)_2$, the pathways leading to the isomers most likely differ in the mode of condensation of mononuclear $Ru(CO)_n$ fragments and $Ru_2(CO)_6(DBSQ)_2$. The probable structure of $Ru_2(CO)_6(DBSQ)_2$ is the one with three carbonyls on each Ru atom.[17] Additions of two $Ru(CO)_2$ units to the same Ru center in $Ru_2(CO)_6(DBSQ)_2$ forms the 1:3 isomer (most likely involving redistribution of the CO ligands), while one addition to each of the two Ru centers forms the 2:2 isomer.

Reactivities of 2:2 and 1:3 Isomers toward Lewis Bases (Schemes 2 and 3). The 2:2 and 1:3 isomers of $Ru_4(CO)_8(DBSQ)_2$ differ significantly in terms of their reactivities. The 2:2 isomer is rapidly fragmented to $Ru(CO)_2(PPh_3)_2(DBCat)$[5] (DBCat = 1,2-$O_2C_6H_2$-3,5-$(t\text{-}Bu)_2{}^{2-}$) by treatment with PPh_3 at room temperature whereas the 1:3 isomer does not react with PPh_3 even in refluxing toluene. In general, while the 1:3 isomer appears to be substitutionally inert, the 2:2 isomer reacts quite easily with nucleophiles such as phosphines and pyridine. Bohle and co-workers extensively studied the reactivity of (2:2)$Ru_4(CO)_8(SQ)_2$ toward nucleophiles.[5] Although in each case the attack of the nucleophile is at the metal center, the diversity of products is enormous. Subtle factors can have a significant influence on structures of products. For example, (2:2)$Ru_4(CO)_8(SQ)_2$ is fragmented to $Ru(CO)_2(py)_2(Cat)$ and $Ru(CO)(py)_3(Cat)$ (Cat = 1,2-$O_2C_6H_4{}^{2-}$) when reacted with pyridine, but (2:2)$Ru_4(CO)_8(DBSQ)_2$ forms $Ru_4(CO)_6(\mu\text{-}CO)_2(py)_2(DBSQ)_2$ cleanly and reversibly.

Description of the Structure of $Ru_4(CO)_8(O_2C_6H_2(t\text{-}Bu)_2)_2(py)_2$. The molecule is illustrated in Figure 3; interatomic distances are collected in Table 8. The most surprising feature of the molecule is that it apparently *could* be symmetrical (possible C_i symmetry), but it is not. The potential symmetry is broken by there being different bonding modes between Ru(1)−Ru(2) and Ru(3)−Ru(4). The Ru(1)−Ru(2) bond is accompanied by two bridging carbonyl groups, whereas the Ru(3)−Ru(4) bond is not bridged in such a manner. The bond

(17) Such a structure was postulated for a closely related complex in: Connelly, N. G.; Manners, I., Protheroe, J. R. C.; Whiteley, M. W. *J. Chem. Soc., Dalton Trans.* **1984**, 2713.

Scheme 2. Reactions of (2:2)$Ru_4(CO)_8(DBSQ)_2$

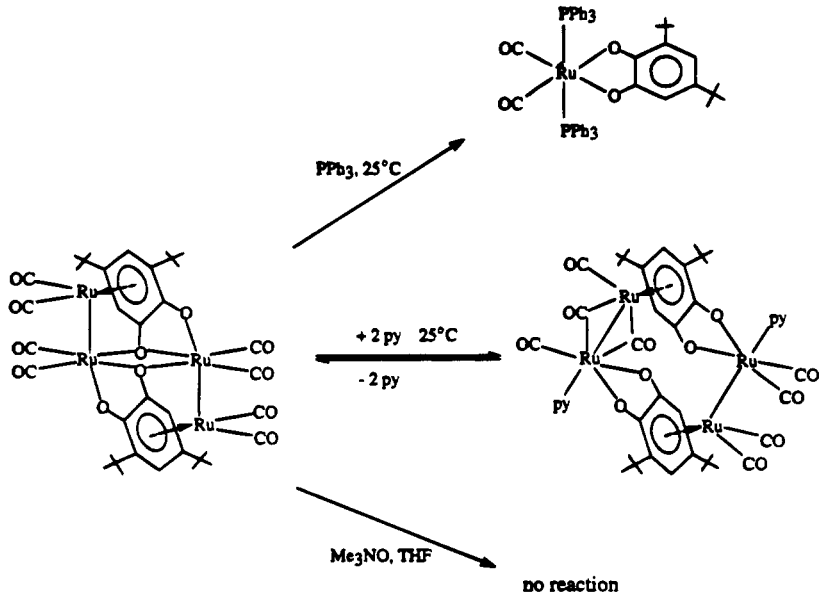

Scheme 3. Reactions of (1:3)$Ru_4(CO)_8(DBSQ)_2$

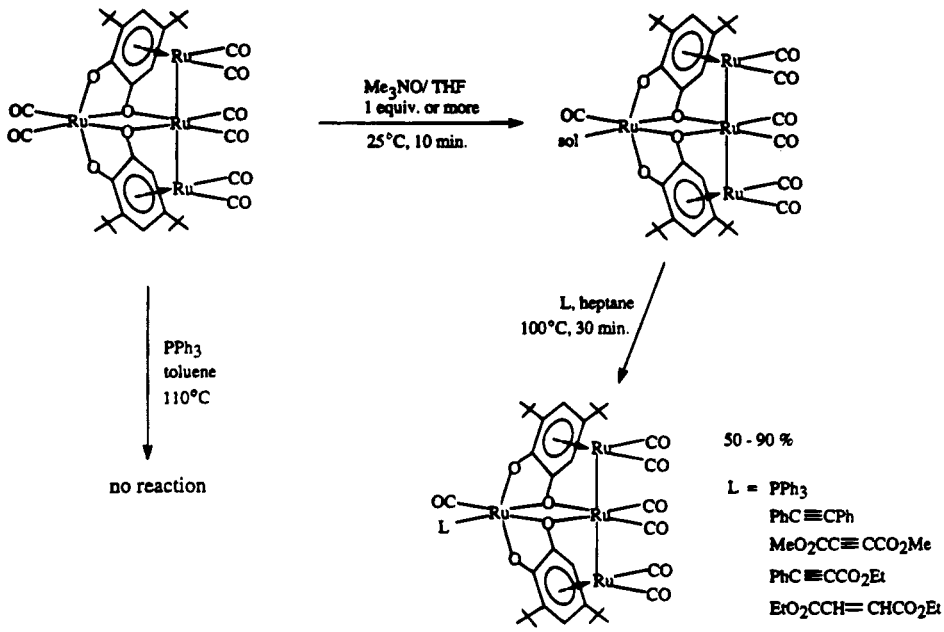

length of the dicarbonyl-bridged Ru(1)–Ru(2) system is 2.712(1) Å; this is some 0.134 Å shorter than for the nonbridged ruthenium–ruthenium distance, Ru(3)–Ru(4) = 2.846(1) Å. The bridging carbonyl ligands are close to symmetrical (as opposed to "semibridging"), with Ru(1)–C(1) = 2.061(8), Ru(2)–C(1) = 2.001(9) Å (difference = 0.060 Å) and Ru(1)–C(2) = 2.060(8), Ru(2)–C(2) = 2.010(9) Å (difference = 0.050 Å); note that in each case, the shorter Ru–(μ-CO) distance is associated with Ru(2), which is bonded to "hard" ligands and where there is less competition for π-back-donation.

The six-membered rings of the two $O_2C_6H_2(t\text{-Bu})_2$ ligands are each linked to ruthenium atoms, with varying degrees of asymmetry. Distances from Ru(4) to the carbocyclic ring range from Ru(4)–C(34) = 2.235(8) Å to Ru(4)–C(32) = 2.565(8) Å, averaging 2.373 Å (as compared to 2.315 Å in $Ru_4(CO)_8(O_2C_6H_4)_2$ and values of 2.330 and 2.336 Å in $Ru_4(CO)_8(O_2C_6H_2(t\text{-Bu})_2)_2$—*vide supra*). The other carbocyclic ring is bound to Ru(1) in an even more asymmetric fashion. Interatomic distances, given cyclically, are Ru(1)–C(11) = 2.581(8), Ru(1)–C(12) = 2.742(8), Ru(1)–C(13) = 2.537(8), Ru(1)–C(14) = 2.275(9), Ru(1)–C(15) = 2.244(9), and Ru(1)–C(16) = 2.326(8) Å. The range is 2.244–2.742 Å, with an average value of 2.450 Å. Nevertheless, we regard the ring as being an η^6-C_6 system.

Each C_6 ring deviates from planarity, with the C=O moiety displaced away from the Ru atom. Atom C(32) lies 0.149 Å and atom O(32) lies 0.360 Å from the planar (rms deviation = 0.025 Å) five atom array C(31)···C(33)–C(34)–C(35)–C(36); the C(31)–C(32)–C(33) plane is tilted by 10.7° from this plane. Related details for the C(11)→C(16) systems are C(12) and O(12) lie 0.110 and 0.335 Å from the C(11)···C(13)–C(14)–C(15)–C(16) system (rms deviation = 0.017 Å); the interplanar angle is 8.0°.

The oxygen atoms of the two $O_2C_6H_2(t\text{-Bu})_2$ ligands are involved in five-membered chelate rings to Ru(2) and Ru(3). The Ru–O linkages to Ru(3) are equivalent (both

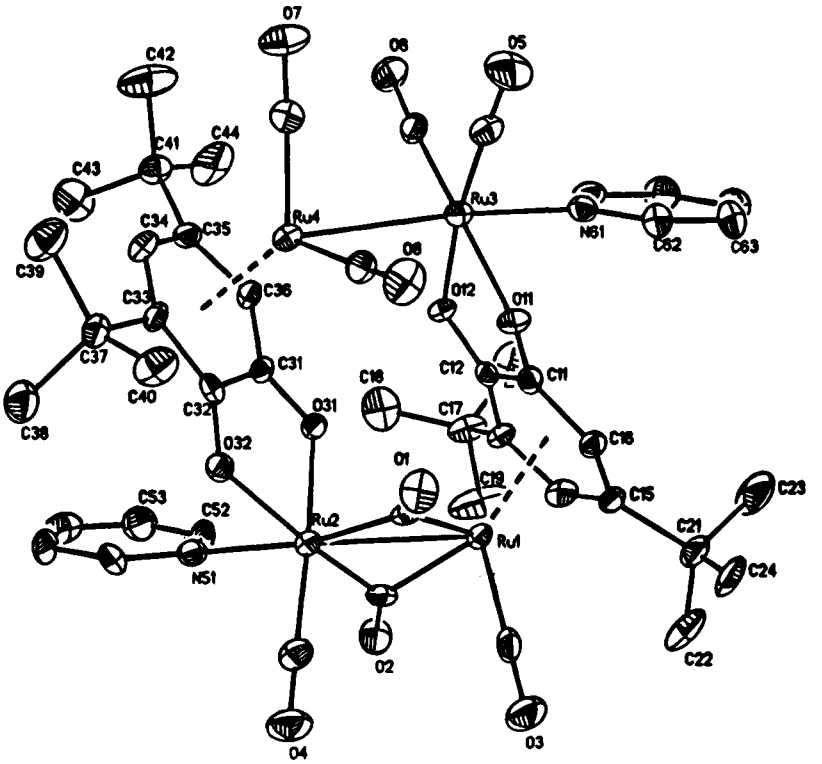

Figure 3. ORTEP2 diagram of $Ru_4(CO)_8(C_6H_2(t\text{-}Bu)_2O_2)_2(py)_2$ (20% ellipsoids, H atoms omitted).

are *trans* to carbonyl ligands), with Ru(3)–O(11) = 2.092(5) and Ru(3)–O(12) = 2.116(5) Å. In contradistinction to this, the Ru–O linkages on Ru(2) are inequivalent, with Ru(2)–O(31) = 2.052(5) Å (*trans* to a terminal carbonyl ligand) and Ru(2)–O(32) = 2.168(5) Å (*trans* to the bridging carbonyl ligand). The C–O distances of the $C_6H_2(t\text{-}Bu)_2O_2$ ligand are not statistically different, with C(11)–O(11) = 1.301(10) and C(12)–O(12) = 1.285(10) Å and with C(31)–O(31) = 1.311(10) and C(32)–O(32) = 1.293(10) Å.

The two pyridine substituents occupy locations which, at first sight, appear to be closely related but are, in fact, rather different. Thus the pyridine ligand on Ru(3) occupies a truly axial site, with Ru(3)–N(61) = 2.208(7) Å and ∠Ru(4)–Ru(3)–N(61) = 175.1(2)°. The pyridine ligand on Ru(2) is canted relative to the metal–metal bond, with Ru(2)–N(51) = 2.207(7) Å and ∠Ru(1)–Ru(2)–N(51) = 139.3(2); this ligand is essentially *trans* to the carbon atom of a bridging carbonyl group, with ∠C(1)–Ru(2)–N(51) = 168.4(3)°.

$Ru_4(CO)_6(\mu\text{-}CO)_2(py)_2(DBSQ)_2$ has the same stoichiometry as $Ru_4(CO)_8(AsPh_3)_2(SQ)_2$,[5a] and the structures are quite similar. In $Ru_4(CO)_6(\mu\text{-}CO)_2(py)_2(DBSQ)_2$ the pyridine ligand of the subunit having only terminal CO ligands occupies a position trans to Ru–Ru bonds (as do the $AsPh_3$ ligands in $Ru_4(CO)_8(AsPh_3)_2(SQ)_2$) and the dioxolene ligands are coordinated by two terminal oxygen atoms to one ruthenium atom and π-bonded to the second in both structures. However, all carbonyls are terminally coordinated in $Ru_4(CO)_8(AsPh_3)_2(SQ)_2$, whereas two out of eight carbonyl ligands in $Ru_4(CO)_6(\mu\text{-}CO)_2(py)_2(DBSQ)_2$ are bridging. The presence of these bridging carbonyls is quite surprising. In the presence of excess pyridine, the ^{13}C NMR spectrum of $Ru_4(CO)_6(\mu\text{-}CO)_2(py)_2(DBSQ)_2$ displays all eight carbonyl resonances at room temperature, with the two bridging carbonyls at 254.6 and 235.2 ppm. As a well-established

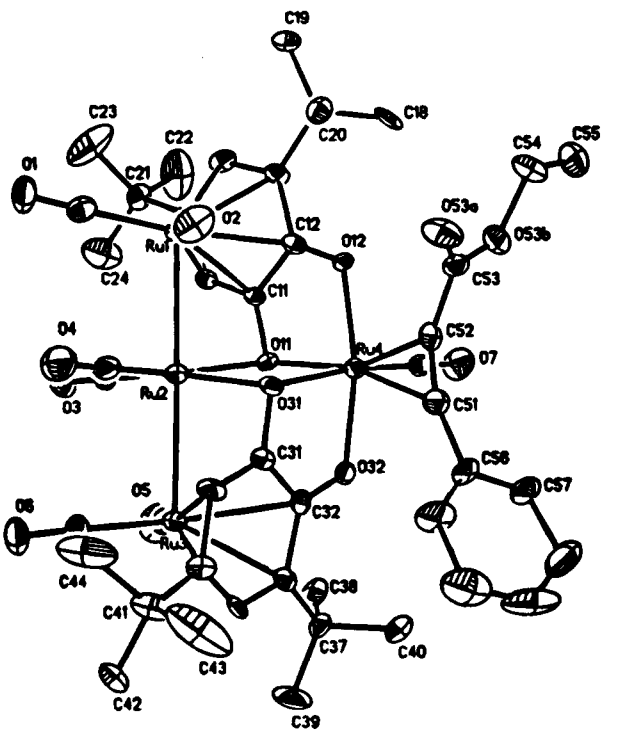

Figure 4. ORTEP2 diagram of $Ru_4(CO)_7(C_6H_2(t\text{-}Bu)_2O_2)_2(PhC{\equiv}CO_2Et)$ (20% ellipsoids, H atoms omitted).

mechanism for carbonyl fluxionality, originally proposed by Cotton and Adams,[18] involves pairwise bridge–terminal exchange through two limiting structures analogous to those adopted by the two Ru_2 subunits, it is remarkable that the molecule is not fluxional. As there is obviously no electronic impediment, we must

(18) Adams, R. D.; Cotton, F. A. *J. Am. Chem. Soc.* **1973**, *95*, 6589.
(19) Terminal alkynes such as HCCPh do not give the expected substitution product. We were unable to characterize products of those reactions.

Table 8. Interatomic Distances (in Å) for $Ru_4(CO)_8(C_6H_2(t\text{-}Bu)_2O_2)_2(py)_2$

Ru(1)−Ru(2) half of molecule		Ru(3)−Ru(4) half of molecule	
Distances Involving Ruthenium Atoms			
Ru(1)−Ru(2)	2.712(1)	Ru(3)−Ru(4)	2.846(1)
Ru(1)−C(1)	2.061(8)	Ru(4)−C(7)	1.862(10)
Ru(1)−C(2)	2.060(8)	Ru(4)−C(8)	1.886(10)
Ru(1)−C(3)	1.849(10)		
Ru(1)−C(11)	2.581(8)	Ru(4)−C(31)	2.464(8)
Ru(1)−C(12)	2.742(8)	Ru(4)−C(32)	2.565(8)
Ru(1)−C(13)	2.537(8)	Ru(4)−C(33)	2.336(9)
Ru(1)−C(14)	2.275(9)	Ru(4)−C(34)	2.235(8)
Ru(1)−C(15)	2.244(9)	Ru(4)−C(35)	2.310(8)
Ru(1)−C(16)	2.326(8)	Ru(4)−C(36)	2.329(8)
Ru(2)−C(1)	2.001(9)	Ru(3)−C(5)	1.819(9)
Ru(2)−C(2)	2.010(9)	Ru(3)−C(6)	1.826(9)
Ru(2)−C(4)	1.850(10)		
Ru(2)−O(31)	2.052(5)	Ru(3)−O(11)	2.092(5)
Ru(2)−O(32)	2.168(5)	Ru(3)−O(12)	2.116(5)
Ru(2)−N(51)	2.207(7)	Ru(3)−N(61)	2.208(7)
C−O Distances within Carbonyl Ligands			
C(1)−O(1)	1.167(11)	C(5)−O(5)	1.176(12)
C(2)−O(2)	1.169(11)	C(6)−O(6)	1.145(11)
C(3)−O(3)	1.152(12)	C(7)−O(7)	1.137(12)
C(4)−O(4)	1.138(12)	C(8)−O(8)	1.134(11)
Distances within Semiquinone Ligand			
C(11)−O(11)	1.301(10)	C(31)−O(31)	1.311(10)
C(12)−O(12)	1.285(10)	C(32)−O(32)	1.293(10)
C(11)−C(12)	1.481(11)	C(31)−C(32)	1.448(12)
C(12)−C(13)	1.419(12)	C(32)−C(33)	1.460(13)
C(13)−C(14)	1.396(12)	C(33)−C(34)	1.373(13)
C(14)−C(15)	1.423(13)	C(34)−C(35)	1.424(12)
C(15)−C(16)	1.412(12)	C(35)−C(36)	1.402(12)
C(16)−C(11)	1.400(12)	C(36)−C(31)	1.417(11)
C(13)−C(17)	1.542(11)	C(33)−C(37)	1.543(13)
C(15)−C(21)	1.536(13)	C(35)−C(41)	1.543(12)
C(17)−C(18)	1.512(14)	C(37)−C(38)	1.518(14)
C(17)−C(19)	1.534(15)	C(37)−C(39)	1.533(13)
C(17)−C(20)	1.527(15)	C(37)−C(40)	1.538(12)
C(21)−C(22)	1.520(15)	C(41)−C(42)	1.503(15)
C(21)−C(23)	1.519(18)	C(41)−C(43)	1.506(14)
C(21)−C(24)	1.504(16)	C(41)−C(44)	1.519(14)
Distances within Pyridine Ligands			
N(51)−C(52)	1.348(14)	N(61)−C(62)	1.346(13)
N(51)−C(56)	1.329(12)	N(61)−C(66)	1.342(14)
C(52)−C(53)	1.360(16)	C(62)−C(63)	1.341(16)
C(53)−C(54)	1.347(18)	C(63)−C(64)	1.346(21)
C(54)−C(55)	1.376(19)	C(64)−C(65)	1.376(19)
C(55)−C(56)	1.367(15)	C(65)−C(66)	1.397(15)

assume that the lack of fluxionality is due to steric or ring strain which does not allow either simultaneous or stepwise interconversion of the structure of one subunit into the other form.

The facile equilibrium between (2:2)$Ru_4(CO)_8(DBSQ)_2$ and $Ru_4(CO)_6(\mu\text{-}CO)_2(py)_2(DBSQ)_2$ is quite remarkable. The reaction involves breaking of two Ru−O bonds, the formation of carbonyl bridges, and the coordination of two pyridine molecules and is very fast and clean. In the absence of added pyridine, ^1H NMR signals due to (2:2)$Ru_4(CO)_8(DBSQ)_2$ are sharp, as are signals of the pyridine adduct when excess pyridine is present. The broadness of the signals at intermediate pyridine concentrations indicates that the rate of pyridine ligand exchange is on the order of the NMR time scale.

Substitution on (1:3)$Ru_4(CO)_8(DBSQ)_2$ (Scheme 3). Although (1:3)$Ru_4(CO)_8(DBSQ)_2$ does not react directly with Lewis bases, it reacts quite easily with Me_3NO in THF or acetonitrile at room temperature, yielding exclusively monosolvento species $Ru_4(CO)_7(DBSQ)_2L$, L = THF or NCMe; even in the presence of excess Me_3NO, only one CO ligand can be replaced by solvent. These clusters are excellent starting materials

Table 9. Interatomic Distances (in Å) for $Ru_4(CO)_7(C_6H_2(t\text{-}Bu)_2O_2)_2(PhC{\equiv}CCO_2Et)$

Distances Involving Ruthenium Atoms			
Ru(1)−Ru(2)	2.802(2)	Ru(3)−C(5)	1.889(9)
Ru(1)−C(1)	1.884(21)	Ru(3)−C(6)	1.846(18)
Ru(1)−C(2)	1.878(18)	Ru(3)−C(31)	2.326(14)
Ru(1)−C(11)	2.276(14)	Ru(3)−C(32)	2.439(14)
Ru(1)−C(12)	2.348(15)	Ru(3)−C(33)	2.376(16)
Ru(1)−C(13)	2.364(16)	Ru(3)−C(34)	2.268(15)
Ru(1)−C(14)	2.302(15)	Ru(3)−C(35)	2.308(15)
Ru(1)−C(15)	2.351(14)	Ru(3)−C(36)	2.291(14)
Ru(1)−C(16)	2.325(14)	Ru(4)−O(11)	2.130(9))
Ru(2)−Ru(3)	2.810(2)	Ru(4)−O(12)	2.061(9)
Ru(2)−O(11)	2.259(9)	Ru(4)−O(31)	2.146(9)
Ru(2)−O(31)	2.216(9)	Ru(4)−O(32)	2.048(9)
Ru(2)−C(3)	1.892(20)	Ru(4)−C(7)	1.823(17)
Ru(2)−C(4)	1.811(19)	Ru(4)−C(51)	2.218(18)
Ru(4)−C(52)	2.125(16)		
Distances within Carbonyl Groups			
C(1)−O(1)	1.144(26)	C(5)−O(5)	1.130(25)
C(2)−O(2)	1.124(23)	C(6)−O(6)	1.148(23)
C(3)−O(3)	1.129(25)	C(7)−O(7)	1.127(22)
C(4)−O(4)	1.154(25)		
Distances within Semiquinone Ligand			
C(11)−O(11)	1.352(17)	C(31)−O(31)	1.377(16)
C(12)−O(12)	1.301(17)	C(32)−O(32)	1.300(17)
C(11)−C(12)	1.446(19)	C(31)−C(32)	1.413(20)
C(12)−C(13)	1.429(20)	C(32)−C(33)	1.479(21)
C(13)−C(14)	1.439(21)	C(33)−C(34)	1.395(22)
C(14)−C(15)	1.467(22)	C(34)−C(35)	1.405(21)
C(15)−C(16)	1.388(20)	C(35)−C(36)	1.395(20)
C(16)−C(11)	1.405(20)	C(36)−C(31)	1.466(22)
C(13)−C(17)	1.546(22)	C(33)−C(37)	1.532(22)
C(15)−C(21)	1.522(22)	C(35)−C(41)	1.532(26)
C(17)−C(18)	1.527(25)	C(37)−C(38)	1.524(25)
C(17)−C(19)	1.546(26)	C(37)−C(39)	1.492(26)
C(17)−C(20)	1.524(24)	C(37)−C(40)	1.560(25)
C(21)−C(22)	1.50(3)	C(41)−C(42)	1.541(24)
C(21)−C(23)	1.50(3)	C(41)−C(43)	1.48(3)
C(21)−C(24)	1.50(3)	C(41)−C(44)	1.55(3)
Distances within PhC≡CCO$_2$Et Ligand			
C(51)−C(52)	1.222(24)	C(51)−C(56)	1.428(24)
C(52)−C(53)	1.456(24)	C(56)−C(57)	1.34(4)
C(53)−O(53A)	1.176(22)	C(57)−C(58)	1.45(4)
C(53)−O(53B)	1.341(22)	C(58)−C(59)	1.36(6)
O(53B)−C(54)	1.475(21)	C(59)−C(60)	1.38(8)
C(54)−C(55)	1.46(3)	C(60)−C(61)	1.38(4)
C(61)−C(56)	1.36(3)		

for further substitution. The solvent molecule can be easily replaced by PPh_3, alkynes,[18] and alkenes. The compositions of the products $Ru_4(CO)_7(DBSQ)_2L$ have been established by IR, ^1H and ^{13}C NMR, and mass spectrometry. The structure of $Ru_4(CO)_7(DBSQ)_2(PhCCCO_2Et)$ has been established by X-ray crystallography. On the basis of the similarities in the spectroscopic data, we propose that all of the clusters have analogous structures.

Description of the Structure of $Ru_4(CO)_7(O_2C_6H_2(t\text{-}Bu)_2)_2(PhC{\equiv}CCO_2Et)$. This molecule is illustrated in Figure 4. Interatomic distances are collected in Table 9. The structure is closely related to that of (1:3)$Ru_4(CO)_8(C_6H_4O_2)_2$ (see section A, above) with two principal differences: (a) the dioxolene ligand now has two *t*-Bu substituents, and (b) one carbonyl group on the "lone" ruthenium atom has been replaced by an η^2-PhC≡CCO$_2$Et ligand.

Three ruthenium atoms are in a linear array, with Ru(1)−Ru(2) = 2.802(2) Å, Ru(2)−Ru(3) = 2.810(2) Å, and ∠Ru(1)−Ru(2)−Ru(3) = 176.0(1)°. Atom Ru(1) is linked to the atoms of a six-membered ring, with Ru−C distances ranging from 2.276(14) to 2.364(16) Å, averag-

ing 2.328 Å; Ru(3) is similarly bonded with Ru−C = 2.268(15)−2.439(14) Å, averaging 2.335 Å.

Each dioxolene moiety has one short C−O bond and one long C−O bond. Thus C(11)−O(11) = 1.352(17) Å, versus C(12)−O(12) = 1.301(17) Å and C(31)−O(31) = 1.377(16) Å, versus C(32)−O(32) = 1.300(17) Å. Here, as with the first two structures, the $O_2C_6H_2(t\text{-Bu})_2$ ligand clearly takes up the semiquinone form.

The C_6 units are closer to planarity. Atoms C(12) and O(12) are displaced by 0.038 and 0.020 Å from the planar (rms deviation 0.021 Å) C(11)···C(13)−C(14)−C(15)−C(16) system. C(12) makes an angle of 3.2° with this plane. Atoms C(32) and O(32) are displaced by 0.079 and 0.171 Å from the planar (rms deviation 0.012 Å) C(31)···C(33)−C(34)−C(35)−C(36) system; C(32) is displaced by 5.7° from this plane.

Atom Ru(2) has an octahedral environment and is linked to two ruthenium atoms, two terminal carbonyl ligands, and the oxygen atoms of two different dioxolene ligands. Atom Ru(4) also has an octahedral environment and is coordinated to two chelating $C_6H_2(t\text{-Bu})_2O_2$ ligands, one carbonyl ligand, and an η^2-alkyne ligand.

The coordinated triple bond (C(51)−C(52) = 1.222(24) Å) of the alkyne ligand is associated with the peripheral "bend angles" C(56)−C(51)−C(52) = 156.6(18)° and C(51)−C(52)−C(53) = 149.7(17)°.

Electrochemistry. The electrochemistry of related polynuclear dioxolene complexes has been investigated by Bohle and co-workers.[5] Cyclic voltammograms of $(1:3)Ru_4(CO)_8(SQ)_2$ and $(1:3)Ru_4(CO)_8(DBSQ)_2$ each display an irreversible, anodic wave at ca. 0.4 V vs Fc/Fc^+. The substituted cluster $(1:3)Ru_4(CO)_7(DBSQ)_2(PPh_3)$ is oxidized at a less positive potential (by 170 mV); however, the process is still irreversible. The shift of oxidation potential upon substitution indicates that the HOMO has significant metal character, unlike in η^2 complexes for which first oxidation process is ligand localized. For example, $Ru(CO)_2(NMe_3)_2(DBcat)$ displays a reversible anodic process at $E_{1/2} = -0.35$ V in addition to an irreversible one at $E_{p,a} = +0.80$ V. (Under the same conditions DBQ exhibits a reversible 1-electron reduction at −1.05 V, and DBcat is irreversibly oxidized at +0.73 V. The 2:2 isomer is more difficult to oxidize than the 1:3 isomer, displaying an irreversible anodic wave at $E_{p,a} = 0.70$ V. When $(2:2)Ru_4(CO)_8(DBSQ)_2$ is reacted with pyridine in electrochemical cell, an irreversible oxidation wave appears at much less positive potential, $E_{p,a} = 0.14$ V, attributed to oxidation of $(2:2)Ru_4(CO)_6(\mu\text{-CO})_2(py)_2(DBSQ)_2$. The irreversibility of the electrochemical oxidations of all clusters reported here is attributed to π-bonding of the C_6 ring.

Reaction of $(2:2)Ru_4(CO)_8(DBSQ)_2$ with Lewis Acids. The reaction of CF_3CO_2H with $(2:2)Ru_4(CO)_8(DBSQ)_2$ cleanly protonates an oxygen atom of the semiquinone ligand, as indicated by the appearance of a new ^1H NMR signal at 10.74 ppm and only a very small shift of CO stretching modes to higher frequencies in the IR spectrum. This reaction is easily reversed by the addition of KO-*t*-Bu, indicating that the cluster retains its integrity. The IR spectrum of the protonated cluster is quite similar to the one of the product of reaction with $AgOSO_2CF_3$, suggesting that Ag^+ cation is also attached to the oxygen atom. The cluster also reacts with BF_3, but we were unable to characterize products of this reaction.

Acknowledgment. We thank Dr. Scott Bohle for a preprint of ref 5b and for helpful discussions. This work was supported by the National Science Foundation through Grant CHE-9213695. Upgrade of the diffractometer was made possible by Grant 89-13733 from the Chemical Instrumentation Program of the National Science Foundation.

Supplementary Material Available: Complete tables of interatomic distances, interatomic angles, anisotropic thermal parameters, and calculated positions and *U* values of hydrogen atoms for the four crystallographic studies (20 pages). Ordering information is given on any current masthead page.

OM940643L

Photochemistry of [Ru(I)(iPr)(CO)$_2$(iPr-DAB)] (iPr-DAB = *N,N'*-Diisopropyl-1,4-diaza-1,3-butadiene): Homolysis of the Metal–Alkyl Bond from the σ_b(Ru-iPr)π^* State. Crystal Structure of the Photoproduct [Ru(I)$_2$(CO)$_2$(iPr-DAB)]

Heleen A. Nieuwenhuis,† Maartje C. E. van de Ven,† Derk J. Stufkens,*,† Ad Oskam,† and Kees Goubitz‡

Anorganisch Chemisch Laboratorium, Universiteit van Amsterdam, Nieuwe Achtergracht 166, 1018 WV Amsterdam, The Netherlands, and Laboratorium voor Kristallografie, Universiteit van Amsterdam, Nieuwe Achtergracht 166, 1018 WV Amsterdam, The Netherlands

Received July 11, 1994®

The complex [Ru(I)(iPr)(CO)$_2$(iPr-DAB)] undergoes a very efficient photodecomposition (Φ = 1.2 at rt), whereas the corresponding complexes [Ru(I)(R)(CO)$_2$(iPr-DAB)] (R = Me, Et) are photostable. ESR, using nitrosodurene and tBuNO as radical scavengers and time-resolved absorption spectroscopy showed that the primary photoprocess is a homolytic splitting of the ruthenium–isopropyl bond. This reaction most probably proceeds from the $^3\sigma_b\pi^*$ state of the complex, in which σ_b represents the (Ru-iPr) bonding orbital and π^* the lowest unoccupied orbital of the iPr-DAB ligand. By using IR, UV-vis and ^{1}H-NMR spectroscopy the bis-iodide complex [Ru(I)$_2$(CO)$_2$(iPr-DAB)] was identified as the final product. The single crystal X-ray structure of this photoproduct ($C_{10}H_{16}N_2O_2I_2Ru$, M_r = 551.1) was determined. The crystal is tetragonal, space group $I4_1/a$, with unit cell dimensions a = 11.552 (1), c = 24.489 (3) Å, Z = 8. The structure refinement converged to R = 0.044 for 978 observed reflections. The very high quantum yields indicate that this photoproduct is formed by an electron transfer chain reaction of the radical [Ru(I)(CO)$_2$(iPr-DAB)]$^\bullet$ with the parent complex. The temperature has a large influence on this reaction since its quantum yield decreases by a factor 3 when the temperature is lowered from 293 to 273 K.

Introduction

Low-valent transition metal α-diimine complexes such as [M(CO)$_4$(α-diimine)] (M = Cr, Mo, W),[1–3] [Re(L)(CO)$_3$-(α-diimine)]^n (n = 0, 1+; L = halide, N-donor),[4–11] or [L$_n$M–M'(CO)$_3$(α-diimine)] (L$_n$M = (CO)$_5$Mn, (CO)$_5$Re, (CO)$_4$Co, Ph$_3$Sn etc.; M' = Mn, Re),[1,12–17] are characterized by strongly allowed metal to α-diimine charge transfer (MLCT) transitions in the visible region. In particular the Re-complexes have been studied in detail, since the properties of their MLCT states appeared to be strongly affected by variation of L.

In order to achieve an even greater diversity with respect to excited state properties, we have started an investigation of a related series of complexes [Ru(X)-(R)(CO)$_2$(α-diimine)] (X = halide, R = alkyl). A detailed study of the absorption and emission spectra of these complexes has already shown that X and R strongly influence the characters of the charge transfer transitions[18] and the emission properties of the lowest-excited states.[19] Thus, the complexes show at least two absorption bands in the visible region, their relative intensities depending on X and R. These bands have been assigned to charge transfer transitions to the α-diimine ligand from two sets of orbitals, which are metal-d$_\pi$–halide-p$_\pi$ bonding and antibonding, respectively. Upon variation of X from Cl to I, the X-p$_\pi$ orbitals increase in energy, resulting in a change of character of the lowest-energy transitions from MLCT into XLCT. This effect was evident from the resonance Raman spectra and was also reflected in drastic changes in emission lifetimes and

* To whom correspondence should be addressed.
† Anorganisch Chemisch Laboratorium.
‡ Laboratorium voor Kristallografie.
® Abstract published in *Advance ACS Abstracts*, December 15, 1994.

(1) Stufkens, D. J. *Coord. Chem. Rev.* **1990**, *104*, 39.
(2) Balk, R. W.; Stufkens, D. J.; Oskam, A. *Inorg. Chim. Acta* **1978**, *28*, 133.
(3) Balk, R. W.; Snoeck, T.; Stufkens, D. J.; Oskam, A. *Inorg. Chem.* **1980**, *19*, 3015.
(4) Stufkens, D. J. *Commun. Inorg. Chem.* **1992**, *13*, 359.
(5) Wrighton, M.; Morse, D. L. *J. Am. Chem. Soc.* **1974**, *96*, 998.
(6) Geoffroy, G. L.; Wrighton, M. In *Organometallic Photochemistry*; Academic Press: New York, 1979.
(7) Juris, A.; Campagna, S.; Bidd, I.; Lehn, J-M.; Ziessel, R. *Inorg. Chem.* **1988**, *27*, 4007.
(8) Kaim, W.; Kramer, H. E. A.; Vogler, C.; Rieker, J. *J. Organomet. Chem.* **1989**, *367*, 107.
(9) Kalyanasundaram, K. *J. Chem. Soc. Faraday Trans. 2*, **1986**, *82*, 2401.
(10) Sullivan, P. *J. Phys. Chem.* **1989**, *93*, 24.
(11) Worl, L. A.; Duesing, R.; Chen, P.; Della Ciana, L.; Meyer, T. J. *J. Chem. Soc. Dalton Trans.* **1991**, 849.
(12) Stufkens, D. J. Steric and Electronic effects on the Photochemical Reactions of Metal–Metal Bonded Carbonyls. In *Stereochemistry of Organometallic and Inorganic Compounds Vol 3*; Bernal, I., Ed.; Elsevier: Amsterdam, 1989; p 226.
(13) Morse, D. L.; Wrighton, M. S. *J. Am. Chem. Soc.* **1976**, *98*, 3931.
(14) Kokkes, M. W.; Stufkens, D. J. Oskam, A. *Inorg. Chem.* **1985**, *24*, 2934.
(15) Kokkes, M. W.; de Lange, W. G. L.; Stufkens, D. J.; Oskam, A. *J. Organomet. Chem.* **1985**, *294*, 59.
(16) Kokkes, M. W.; Stufkens, D. J.; Oskam, A. *Inorg. Chem.* **1985**, *24*, 4411.
(17) van der Graaf, T.; Stufkens, D. J.; Oskam, A.; Goubitz, K. *Inorg. Chem.* **1991**, *30*, 299.
(18) Nieuwenhuis, H. A.; Stufkens, D. J.; Oskam, A. *Inorg. Chem.* **1994**, *33*, 3212.
(19) Nieuwenhuis, H. A.; Stufkens, D. J.; Vlček, A., Jr. *Inorg. Chem.*, submitted for publication.

0276-7333/95/2314-0780$09.00/0

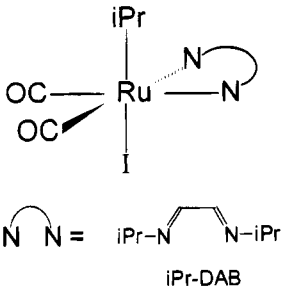

Figure 1. Structure of [Ru(I)(iPr)(CO)$_2$(iPr-DAB)] (**1**) and of the iPr-DAB ligand.

quantum yields. Variation of R from Me to Et and iPr increased the metal character of the highest-filled orbitals and therefore also of the lowest-energy charge transfer transitions.

Variation of R did not only affect the character of the electronic transitions, it also influenced the photostability of the complexes. Contrary to the methyl- and ethyl-complexes, the isopropyl-complex [Ru(I)(iPr)(CO)$_2$(iPr-DAB)] (iPr-DAB = *N,N'*-diisopropyl-1,4-diaza-1,3-butadiene) appeared to be photolabile. In this respect, it resembles the complexes [(CO)$_5$Mn−Ru(Me)(CO)$_2$(α-diimine)], which undergo homolytic splitting of the Mn−Ru bond upon irradiation into their MLCT absorption band.[20] Similar light-induced homolysis reactions have been observed for series of other metal−metal bonded complexes [L$_n$M−M'(CO)$_3$(α-diimine)],[12−18] for the metal−alkyl complexes [Zn(R)$_2$(R'-DAB)][21] and [Re(R)(CO)$_3$(α-diimine)],[22,23] and recently also for the metal−halide complexes *mer*-[Mn(X)(CO)$_3$(α-diimine)].[24]

In order to clarify the photolability of [Ru(I)(iPr)(CO)$_2$(iPr-DAB)] (**1**) and the relationship with the above-mentioned complexes, we have studied in more detail the photochemical properties of this complex. The structure of **1** is shown in Figure 1.

Experimental Section

Materials. Solvents for synthetic purposes were of reagent grade and dried on sodium wire (THF, n-hexane). For spectroscopic measurements solvents of analytical grade (THF, MeCN, 2-MeTHF, MeOH, CH_2Cl_2) or UVASOL quality (toluene) were used, dried on sodium wire, except for CH_2Cl_2, MeOH and MeCN, which were dried using $CaCl_2$, $MgSO_4$, and P_2O_5, respectively. All solvents were freshly distilled under N_2 atmosphere prior to use. 2,3,5,6-Tetramethylnitrosobenzene (nitrosodurene) and tBuNO were commercially obtained and used as received. All preparations were performed under an atmosphere of purified nitrogen, using Schlenk techniques. The photosensitive complex [Ru(I)(iPr)(CO)$_2$(iPr-DAB)] was carefully handled under exclusion of light.

Apparatus and Photochemistry. Infrared spectra were recorded on a BioRad FTS-7 FTIR spectrometer. Electronic absorption spectra were recorded on a Perkin-Elmer Lambda 5 UV-vis spectrophotometer, equipped with a 3600 data station or a Varian Cary 4E spectrophotometer. Low-temperature UV-vis and IR measurements were carried out using an Oxford Instruments DN 1704/54 liquid-nitrogen cryostat. ESR measurements were performed on a Varian E6 ESR spectrometer equipped with a temperature-control accessory. Coupling constants were obtained by computer simulation. Resonance Raman measurements were performed on a Dilor XY spectrometer, using a SP 2016 argon ion laser as excitation source. Because of the photolability of the complex, the sample solution (concentration of ca. 0.01 M complex in CH_2Cl_2) was pumped through a home built, air tight flow-cell, in which the sample was kept under nitrogen.

To study the photochemical reactions of the complex, sample solutions were irradiated by one of the lines of a SP 2025 argon ion laser or a Philips HPK 125 W high pressure mercury lamp provided with the appropriate interference filter.

Quantum yields of the disappearance of the parent complex were determined by measuring the decay of its visible absorption band on a Varian Cary 4E spectrophotometer following automatized procedures. The formula used for the calculation of the quantum yields included a correction for the increasing absorption of the photoproduct.[25] During the measurements the sample solutions were kept in thermostated cuvettes within the UV-vis apparatus. The sample was irradiated while stirred by one of the laser lines of a SP 2025 argon ion laser, via an optical fibre and a computer controlled mechanical shutter. Light intensities were measured with a power-meter, which was calibrated with an Aberchrome 540 solution according to literature methods.[26]

In situ ^{1}H-NMR spectra of photolyzed solutions were recorded on a Bruker AMX 300 spectrometer, using a special Bruker CIDNP 300 MHz ^{1}H Probe, equipped with a glass fiber (ϕ = 8 mm). Via this fiber the solutions were irradiated with an Oriel AG 150 W high pressure Xe lamp provided with a water cooling and a 530 nm cutoff filter. For these experiments typical sample concentrations of 10^{-3}−10^{-4} M were used in deuterated solvents.

For the nanosecond flash photolysis studies the sample was excited by 10 ns pulses of the 532 nm line of a Nd:YAG-laser (Spectra Physics GCR-3). A 450 W high pressure Xe lamp pulsed with a Müller Elektronik MSPO5 pulser, was used as probe light. After passing the sample the probe light was collected into a fiber and transferred to a spectrograph (EG&G Model 1234) equipped with a 150 g/mm grating and a 250 μm slit resulting in a resolution of 6 nm. This spectrograph was coupled to a gated, intensified diode array detector (EG&G Model 1421) which was part of an EG&G OMA III handling system and a 1304 gate pulse amplifier with variable time windows of 5 ns. The programming of the OMA afforded a time-resolved way of measuring. During the photolysis experiment the sample flowed through a home-built cell, specially constructed for the study of short-lived intermediates under inert gas atmosphere. Afterwards the spectra were corrected for the bleaching of the parent, by importing these spectra together with the ground state spectra in the computer program Grams. The subtraction factor was then varied until no bleaching was observed.

Preparation of the Complexes. The complex [Ru(I)(iPr)(CO)$_2$(iPr-DAB)] (**1**) and the ligand *N,N'*-diisopropyl-1,4-diaza-1,3-butadiene (iPr-DAB) were synthesized according to literature methods.[18,27] The photoproduct [Ru(I)$_2$(CO)$_2$(iPr-DAB)] was prepared by irradiation of a 1 mmol solution of **1** in 100 mL THF or CH_2Cl_2 under nitrogen atmosphere with a high pressure mercury lamp provided with a 550 nm interference filter. The reaction was followed with IR spectroscopy and the irradiation was stopped before follow-up reactions started. The solution was evaporated until dryness. The product was purified by washing with hexane. Recrystallization took place

(20) Nieuwenhuis, H. A.; van Loon, A.; Moraal, M. A.; Stufkens, D. J; Oskam, A.; Goubitz, K. *J. Organomet. Chem.*, in press.
(21) Kaupp, K.; Stoll, H.; Preuss, H.; Kaim, W.; Stahl, T.; van Koten, G.; Wissing, E.; Smeets, W. J.; Spek, A. L. *J. Am. Chem. Soc.* **1991**, *113*, 5606.
(22) Rossenaar, B. D.; Kleverlaan, C. J.; Stufkens, D. J.; Oskam, A. *J. Chem. Soc. Chem. Commun.* **1994**, 63.
(23) Lucia, L. A.; Burton, R. D.; Schanze, K. S. *Inorg. Chim. Acta* **1993**, *208*, 103.
(24) Stor, G. J.; Morrison, S. L.; Stufkens, D. J. Oskam, A. *Organometallics* **1994**, *13*, 2641.
(25) Víchová, J.; Hartl, F.; Vlček, A., Jr.; *J. Am. Chem. Soc.* **1992**, *114*, 10903.
(26) *Aberchromics LTD*, School of chemistry and applied chemistry, College of Cardiff, University of Wales.
(27) Bock, H.; tom Dieck, H. *Chem. Ber.* **1967**, *100*, 228.

Table 1. Crystallographic Data of [Ru(I)$_2$(CO)$_2$(iPr-DAB)]

formula	$C_{10}H_{16}N_2O_2I_2Ru$
molecular weight	551.1
space group	$I4_1/a$
a, c (Å)	11.552(1), 24.489(3)
V (Å^3)	3268.0(6)
Z	8
D_x (g cm^{-1})	2.24
λ(Mo Ka) (Å)	0.71069
μ(Mo Ka) (cm^{-1})	46.8
F(000)	2048
temp (K)	293
final R, R_w	0.044, 0.078
observed reflections	978

from CH_2Cl_2 at −50 °C. IR ν(CO) (CH_2Cl_2): 2058, 2004 cm^{-1}; UV-vis (CH_2Cl_2): 375, 398, 460, 500(sh) nm. ^{1}H-NMR ($CDCl_3$): 8.16 (s) (2 imine-H), 4.63 (m) (2 iPr-CH), 1.67 (d) (12 iPr-CH$_3$).

Crystal Structure Determination of [Ru(I)$_2$(CO)$_2$(iPr-DAB)]. Crystals were grown from a saturated CH_2Cl_2 solution at 243 K. Crystal data and numerical details of the structure determination are listed in Table 1.

A crystal with dimensions 0.25 × 0.40 × 0.50 mm approximately was used for data collection on an Enraf-Nonius CAD-4 diffractometer with graphite-monochromated Cu Kα radiation and $\omega-2\theta$ scan. A total of 1363 unique reflections was measured within the range $0 \le h \le 16$, $0 \le k \le 13$, $0 \le l \le 34$. Of these, 978 were above the significance level of 2.5 $\sigma(I)$. The maximum value of $(\sin \Theta)/\lambda$ was 0.70 Å^{-1}. Two reflections (024, 031) were measured hourly and showed no decrease during the 16 h collecting time. Unit-cell parameters were refined by a least-squares fitting procedure using 23 reflections with $40 < 2\Theta < 42°$. Corrections for Lorentz and polarization effects were applied. The asymmetric unit contains half a molecule with the Ru at a special position. The structure was solved by direct methods. The hydrogen atoms were calculated. Full-matrix least squares refinement on F, anisotropic for the non-hydrogen atoms and isotropic for the hydrogen atoms, restraining the latter in such a way that the distance of their carrier remained constant at approximately 1.09 Å, converged to $R = 0.044$, $R_w = 0.078$, $(\Delta/\sigma)_{max} = 0.31$. A weighting scheme $w = (6.0 + F_{obs} + 0.0093F_{obs}^2)^{-1}$ was used. An empirical absorption correction (DIFABS)[28] was applied with coefficients in the range of 0.71−1.42. A final difference Fourier map revealed a residual electron density between −0.8 and 0.7 e Å^{-3} in the vicinity of the heavy atoms. Scattering factors were taken from Cromer and Mann[29] and from the *International Tables for X-ray Crystallography*.[30] The anomalous scattering of Ru and I was taken into account. All calculations were performed with XTAL,[31] unless stated otherwise.

Results

The complex [Ru(I)(iPr)(CO)$_2$(iPr-DAB)] (**1**) exhibits at least two composite absorption bands in the visible region (Table 2, Figure 2). Both bands are solvatochromic, which indicates that they belong to charge transfer transitions. In a previous article we have explained the occurrence of these bands for the [Ru(X)(R)(CO)$_2$(α-diimine)] (X = halide; R = alkyl) complexes by a mixing of the metal-d$_\pi$ and halide-p$_\pi$ orbitals, leading to the formation of two sets of two mixed metal−halide orbitals (bonding and antibonding) from which these CT transitions originate.[18]

(28) Walker, N.; Stuart, D. *Acta Crystallogr.* **1983**, *A39*, 158.
(29) Cromer, D. T.; Mann, J. B. *Acta Crystallogr.* **1968**, *A24*, 321.
(30) *International Tables for X-ray Crystallography Vol. IV*; Kynoch Press: Birmingham, 1974; p 55.
(31) Hall, S. R.; Flack, H. D.; Stewart, J. M.; Eds. *XTAL3.2 Reference Manual*; Universities of Western Australia, Geneva and Maryland, 1992.

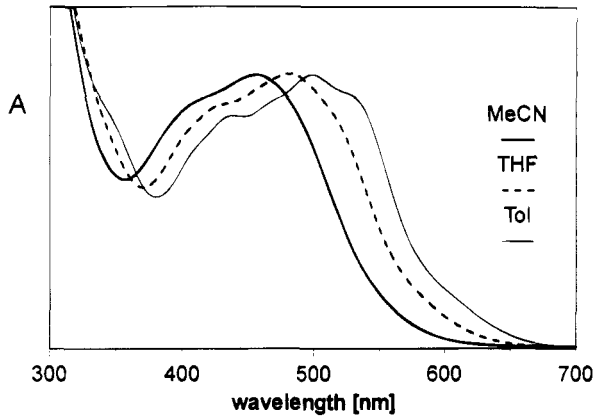

Figure 2. The UV-vis absorption spectra of **1** in MeCN, THF, and toluene at room temperature.

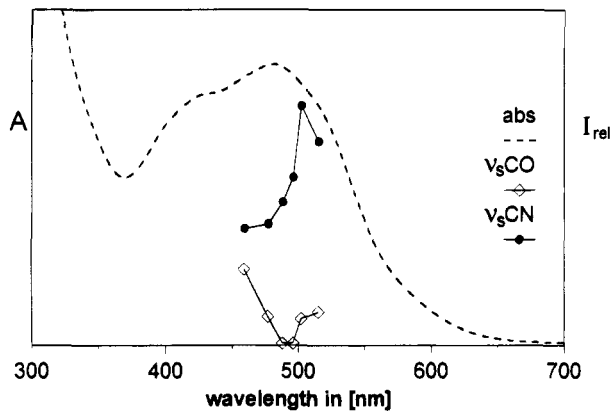

Figure 3. Resonance Raman excitation profiles of ν_s(CN) and ν_s(CO) of **1** in CH_2Cl_2 at room temperature; the intensities are relative to the 708 cm^{-1} Raman band of CH_2Cl_2.

Table 2. IR and UV-vis Data of Complex 1 and Its Photoproducts in Various Solvents (ν(CO) in [cm^{-1}], $\lambda_{max, abs}$ in nm)

complex	solvent	ν(CO)	$\lambda_{max, abs}$
[Ru(I)(iPr)(CO)$_2$(iPr-DAB)] (**1**)	MeCN	2024, 1962	412, 452
	THF	2021, 1958	429, 480
	CH_2Cl_2	2027, 1963	425, 479
	toluene	2022, 1956	433, 496
[Ru(I)$_2$(CO)$_2$(iPr-DAB)]	MeCN	2054, 1999	380, 460 (br)
	THF	2050, 1996	400, 480 (br)
	CH_2Cl_2	2058, 2004	400, 460 (br)
	toluene	2054, 2000	381, 460 (br)
[Ru(iPr)(MeCN)(CO)$_2$(iPr-DAB)]I	MeCN	2038, 1969	

The resonance Raman (rR) spectra of **1**, obtained by excitation into the lowest energy band, showed the strongest resonance enhancement for ν_s(CN) of iPr-DAB at 1537 cm^{-1}. This result is in accordance with transfer of negative charge to the lowest π^* orbital of the iPr-DAB ligand which causes a weakening of the CN bonds. The intensity of the ν_s(CN) Raman band normalized to the intensity of a solvent band is depicted in Figure 3 as a function of the wavelength of excitation. This excitation profile shows a maximum within the first absorption band at about 500 nm. The corresponding excitation profile of ν_s(CO), also presented in this figure, shows that this vibration is only weakly coupled to the lowest-energy electronic transitions. The CO bonds are therefore only weakly influenced by the lowest energy transitions, which means that these transitions have more XLCT (I → iPr-DAB) than MLCT character.

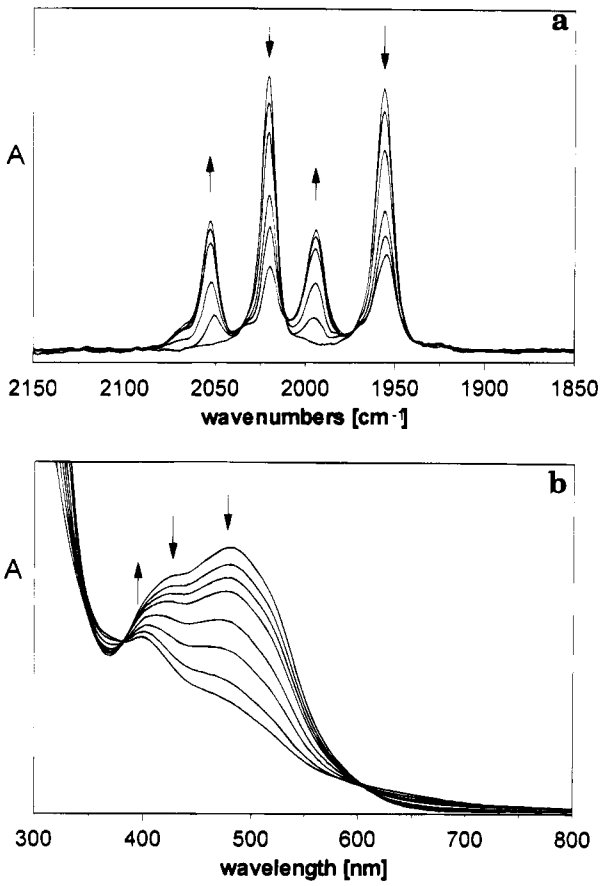

Figure 4. IR ν(CO) (CH_2Cl_2) (a) and UV-vis (THF) (b) spectral changes during the photolysis of **1** at room temperature.

Photochemistry. Contrary to the corresponding complexes [Ru(I)(R)(CO)$_2$(iPr-DAB)] (R = Me, Et), complex **1** is very photolabile, even upon irradiation into the low-energy CT bands. The photodecomposition has been followed by IR, UV-vis, and 1H-NMR spectroscopy. The IR and UV-vis data of the parent complex and its photoproducts are collected in Table 2. To check its thermal stability, a THF solution of **1** was refluxed for several hours in the dark. Several samples were taken and analyzed by IR spectroscopy, but the complex appeared to be thermally completely stable under these conditions.

The complex **1** has two strong IR bands in the ν(CO) region at 2021 and 1958 cm^{-1} (THF), respectively. Upon irradiation with λ > 500 nm these bands disappeared and two strong bands showed up at 2050 and 1996 cm^{-1}, respectively (Figure 4a). Prolonged irradiation caused the disappearance of the two strong bands while at the same time new weak bands appeared at 1946, 1930, and 1779 cm^{-1}. This means that the initially formed photoproduct is not photostable. The appearance of the weaker bands was not the result of a secondary thermal reaction since no IR changes were observed when the solution was kept in the dark after a short time of irradiation. Although the two ν(CO) bands of the first photoproduct were strong, they never reached the intensity of the parent bands before the followup reaction started.

Upon irradiation of a solution of **1** in THF, the UV-vis spectrum showed a regular decrease of the 480 nm band. A very broad composite band remained with an apparent maximum at 400 nm (Figure 4b). The isosbestic points, observed initially, disappeared upon prolonged irradiation, due to a secondary photochemical reaction.

The solvent did not influence the photoreaction since the same photoproduct with IR bands at ca. 2050 and 1996 cm^{-1} was formed in CH_2Cl_2, MeCN, THF, MeOH, and toluene. This result was confirmed by the UV-vis spectral changes which were very similar in these solvents both with respect to band shapes and maxima. Only in case of MeCN two biscarbonyl products were formed. One had its IR frequencies at 2055 and 1999 cm^{-1}, similar to those observed in the other solvents. The IR frequencies of the second product at 2038 and 1969 cm^{-1} closely resemble those of the products [Ru(R)(MeCN)(CO)$_2$(iPr-DAB)]I, obtained by reduction of the complex [Ru(I)(R)(CO)$_2$(iPr-DAB)] in MeCN.[32]

Increasing the concentration of the starting complex did also not influence the nature of the photoproduct. Even exposure of the solid complex to sunlight afforded similar photoproducts. In order to study the effect of the viscosity of the solvent, comparative experiments performed in MeOH (η = 0.6 cp at rt) and in a 5% solution of MeOH in ethylene glycol (η = 19.9 cp at rt) showed that also the viscosity of the solvent did not influence the kind of product nor the rate of its formation. Addition of the radical scavenger CCl4 to a THF solution of **1** initially gave rise to a reaction with less side products. Only the two characteristic IR bands of the first product were then observed. It cannot, however, be excluded that in this case [Ru(I)(Cl)(CO)$_2$(iPr-DAB)] or [Ru(Cl)$_2$(CO)$_2$(iPr-DAB)] were formed, since these complexes are expected to have comparable IR-frequencies as the analogous diiodide complex. Also in this case, however, prolonged irradiation led to decomposition of the product.

^{1}H-NMR. In order to identify the first photoproduct, the photolysis of **1** was followed *in situ* with ^{1}H-NMR, using a special CIDNP probe in which the sample was irradiated within the NMR machine. Immediately after irradiation a spectrum which did not show any line-broadening was obtained which means that radicals, if formed at all, were only short-lived. Figure 5 shows the ^{1}H-NMR spectra obtained after different intervals of irradiation in a THF-d_8 solution.

The most striking feature is the disappearance of a doublet at 1.51 ppm belonging to the CH_3-protons of the isopropyl ligand. The positions of the other peaks hardly changed, although their intensities decreased to half the original values. The imine protons of the iPr-DAB ligand shifted from 8.38 to 8.36 ppm and the septet at 4.54 ppm, belonging to the CH of the iPr-group of iPr-DAB, remained at the same position. The doublets of the CH_3-protons of this ligand shifted from 1.64 and 1.31 ppm to 1.60 ppm. As in the ^{1}H-NMR spectra of a solution of the pure, crystalline [Ru(I)$_2$(CO)$_2$(iPr-DAB)], only one doublet was observed at 1.60 ppm for all CH_3-protons of the iPr-group with a corresponding integral. At 1.28 ppm a broad singlet was found which can be assigned to hexane molecules and isomers, formed by dimerization of the iPr-radicals. The reaction in $CDCl_3$ led to similar results, although more side-reactions took place.

(32) Nieuwenhuis, H. A.; Hartl, F.; Stufkens, D. J. To be submitted for publication.

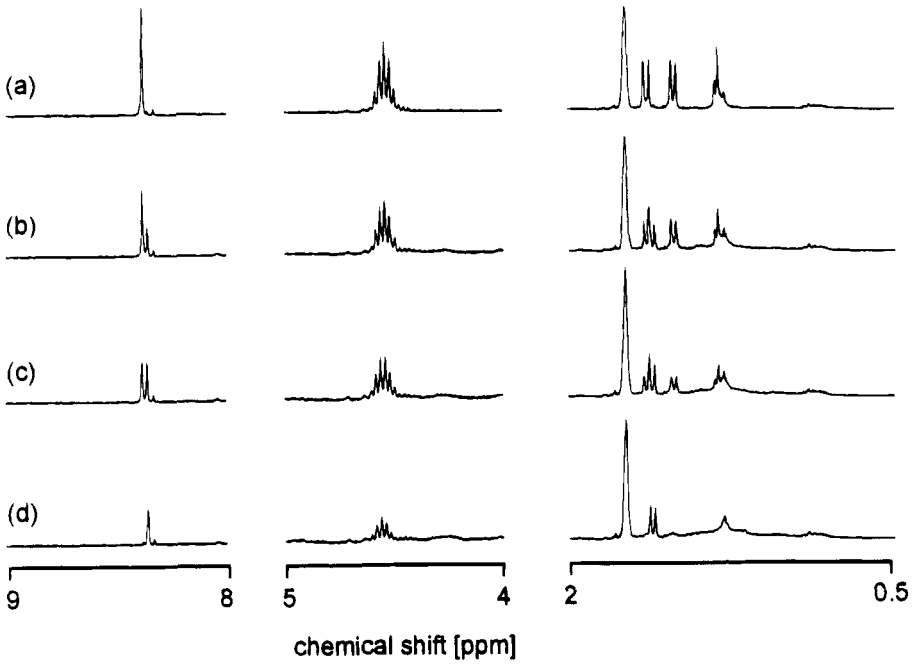

Figure 5. ^{1}H-NMR spectral changes during the *in situ* photolysis of **1** in THF-d_8 solution at room temperature after 0, 3, 8, and 15 min (a–d) of irradiation with 530 nm light.

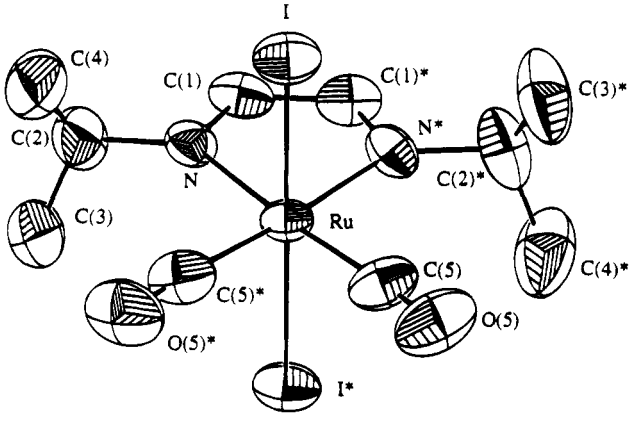

Figure 6. ORTEP drawing of the photoproduct [Ru(I)$_2$(CO)$_2$(iPr-DAB)].

The observed intensity decrease of the NMR signals cannot be due to the formation of a solid product since no precipitate was observed in the NMR tube. In fact, careful examination of the spectra revealed a broad, structureless band of overlapping signals at about 1.31 ppm. In addition, some weak multiplets could be distinguished at ca. 4.3 ppm. Their integral, although hard to be determined quantitatively because of overlap between signals of the photoproduct and the decomposition products, might account for the missing amount of material.

Crystal Structure of [Ru(I)$_2$(CO)$_2$(iPr-DAB)]. In order to establish the structure of the first photoproduct, the reaction was performed on preparative scale and the photoproduct was isolated. The X-ray crystal structure analysis of this product confirmed that the first photoproduct was in fact [Ru(I)$_2$(CO)$_2$(iPr-DAB)] (Figure 6), its bond lengths and angles (Tables 3 and 4) closely resembling those of the analogous complex [Ru(I)$_2$(CO)$_2$-(pTol-DAB)] (pTol = p-toluidine), investigated by tom Dieck and co-workers.[33] The complex has a slightly distorted octahedral geometry in which the iodide ions occupy an axial position. The Ru–I bond lengths are shorter (2.711 Å) than in case of [Ru(I)(Me)(CO)$_2$(iPr-DAB)] (2.81 Å).[34] Although the Ru–CO bond lengths of [Ru(I)$_2$(CO)$_2$(iPr-DAB)] and [Ru(I)(Me)(CO)$_2$(iPr-DAB)] are comparable, the C–O bond lengths in the diiodide complex (1.10 Å) are slightly shorter than in [Ru(I)(Me)(CO)$_2$(iPr-DAB)] (1.15 Å), indicating a somewhat decreased π-backbonding.

Table 3. Selected Bond Distances (Å) in [Ru(I)$_2$(CO)$_2$(iPr-DAB)] with ESD's in Parentheses

bond	distance	bond	distance
Ru–I	2.7112(8)	C(1)–N	1.28(1)
Ru–I*	2.7112(8)	C(1)*–N*	1.28(1)
Ru–C(5)	1.90(1)	C(2)–C(3)	1.46(3)
Ru–C(5)*	1.90(1)	C(2)–C(4)	1.53(3)
Ru–N	2.14(1)	C(2)–N	1.49(2)
Ru–N*	2.14(1)	C(5)–O(5)	1.10(2)
C(1)–C(1)*	1.42(2)		

Table 4. Selected Bond Angles (deg) in [Ru(I)$_2$(CO)$_2$(iPr-DAB)] with ESD's in Parentheses

atoms	angle	atoms	angle
I–Ru–I*	179.63(5)	C(5)*–Ru–N	97.5(5)
I–Ru–C(5)	90.2(4)	C(5)*–Ru–N*	173.9(5)
I –Ru –C(5)*	89.5(4)	N–Ru–N*	76.4(4)
I–Ru–N	89.3(3)	C(1)*–C(1)–N	119(4)
I–Ru–N*	91.0(3)	C(1)–C(1)*–N*	119(1)
I*–Ru–C(5)	89.5(4)	C(3)–C(2)–(C4)	117(2)
I*–Ru–C(5)*	90.2(4)	C(3)–C(2)–N	112(1)
I*–Ru–N	91.0(3)	C(4)–C(2)–N	109(2)
I*–Ru–N*	89.3(3)	Ru–N–C(1)	113.1(8)
C(5)–Ru–C(5)*	90.2(4)	Ru–N–C(2)	132.0(9)
C(5)–Ru–N	173.9(5)	Ru–N*–C(1)*	113.1(8)
C(5)–Ru–N*	97.5(5)	C(1)–N–C(1)*	115(1)

ESR Spectroscopy. Although radicals did not disturb the ^{1}H-NMR spectra, their photochemical forma-

(33) tom Dieck, H; Kollvitz, W.; Kleinwächter, I; Rohde, W.; Stamp, L. *Trans. Met. Chem.* **1986**, *11*, 361.

(34) Kraakman, M. J. A.; de Klerk-Engels, B.; de Lange, P. P. M.; Vrieze, K.; Smeets, W. J. J.; Spek, A. L. *Organometallics* **1992**, *11*, 3774.

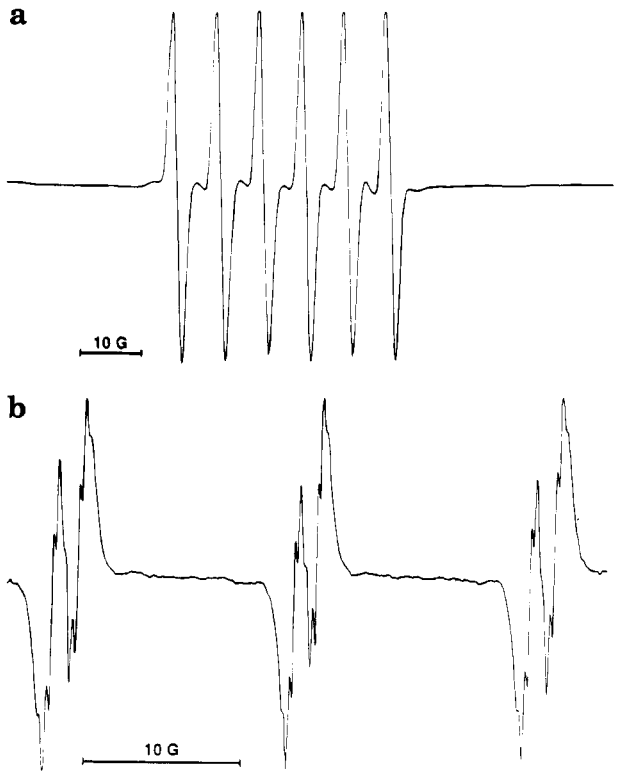

Figure 7. ESR spectra obtained by irradiation of **1** in THF in the presence of (a) nitrosodurene and (b) tBuNO.

tion could be established with ESR spectroscopy when a spin trap was added to the solution. Irradiation of a THF solution of **1** at room temperature with a 10-fold excess of nitrosodurene afforded the ESR spectrum of the radical adduct [$(CH_3)_4(C_6H)N(O^\bullet)CH(CH_3)_2$]. The spectrum (Figure 7a) showed six lines due to the hyperfine coupling of one nitrogen nucleus ($I_N = 1$) and one hydrogen nucleus ($I_H = 1/2$) of the iPr-group. The coupling constants, $a_{N\ (NO)} = 14.10$ G and $a_{H\ (iPr)} = 7.11$ G, determined by computer simulation, correspond to the literature data.[35]

These ESR spectra did not show any signal due to the metal fragment, and tBuNO was therefore used instead of nitrosodurene to trap the ruthenium radicals. The ESR spectrum of the irradiated THF solution of **1** and tBuNO in a 1:1.8 concentration ratio (Figure 7b) showed a more complicated pattern than the spectrum of Figure 7a. However, this is also due to the trapped iPr-radical. The ESR spectrum could be simulated for [$(tBu)N(O^\bullet)CH(CH_3)_2$], with a coupling of $a_{N\ (NO)} = 15.6$ G, $a_{H\ (CH(iPr))} = 4.0$ G and $a_{H\ (CH_3(tBu,\ iPr))} = 0.6$ G. No evidence was obtained for the two possible Ru-radicals [Ru(I)(CO)$_2$(iPr-DAB)(tBu)N(O$^\bullet$)] and [Ru(iPr)(CO)$_2$(iPr-DAB)(tBu)N(O$^\bullet$)]. This is noteworthy since the radical scavenger (tBuNO) was completely consumed during the ESR-measurement, and no characteristic signals were observed for $(tBu)_2NO^\bullet$, which is normally the case when tBuNO is used in excess.[36]

Quantum Yields. The efficiency of the photolysis in THF was established by determining the quantum yields (Φ) for the disappearance of **1** at various temperatures and wavelengths of irradiation. The results,

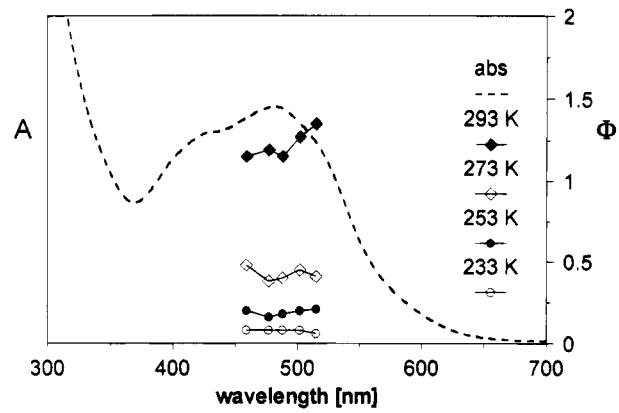

Figure 8. Wavelength dependence of the disappearance quantum yield upon irradiation of **1** in THF at 293, 273, 253, and 233 K.

Table 5. Quantum Yields for the Photoreaction of 1 in THF at Different Temperatures (λ_{exc} in nm, Temperature in K)

	Φ at λ_{exc}(nm)				
T	514.5	501.7	488.0	476.5	457.9
293	1.35	1.27	1.16	1.19	1.15
283	0.82		0.48		
273	0.41	0.45	0.40	0.38	0.48
263	0.27		0.29		
253	0.21	0.20	0.18	0.16	0.20
243	0.14		0.12		
233	0.07	0.08	0.07	0.08	0.08
223	0.03		0.03		

presented in Table 5, show that at room temperature the quantum yields are larger than unity at all wavelengths of irradiation. This means that the reaction is photocatalytic since more than one molecule of the starting complex is consumed per one photon absorbed.

Figure 8 presents the quantum yields at different temperatures and wavelengths of irradiation. At all temperatures used no regular wavelength dependence of Φ was observed. The irregular behavior at 293 K is most likely due to the sensitivity of the radical chain reaction, taking place at this temperature, to small amounts of impurities. The quantum yield of the photoreaction was strongly temperature dependent and appeared to decrease by a factor 3 going from 293 to 273 K.

Transient Absorption Spectra. Nanosecond flash photolysis experiments were carried out on solutions of complex **1** in MeCN, THF, and toluene. Figure 9 shows the transient spectra obtained for the complex in toluene within the laser flash and at several delay times.

The spectra recorded in THF within the laser pulse showed depletion of the ground state absorption and formation of a transient with broad absorptions above 500 and near 430 nm. Immediately after the laser pulse, these features disappeared and the strong band at 340 nm remained essentially unchanged during the whole time-window of the apparatus (0.1 ms). In toluene and MeCN the same observations were made. No solvent dependence was observed.

The transient absorption band at 430 nm is assigned to the excited state of the complex, because of the large similarities of these features with those of the time-resolved absorption spectra of the photostable complexes

(35) Terabe, S.; Kuruma, K.; Konaka, R. *J. Chem. Soc. Perkin Trans. 2* **1973**, 1252.
(36) Andréa, R. R.; de Lange, W. G. L.; van der Graaf, T.; Rijkhoff, M.; Stufkens, D. J.; Oskam, A. *Organometallics* **1988**, *7*, 1100.

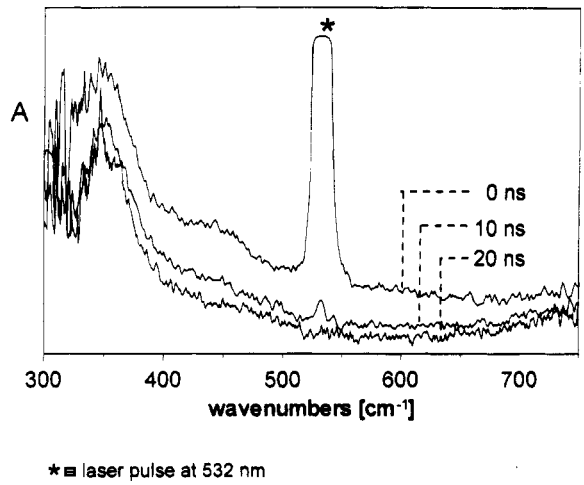

Figure 9. Transient absorption spectra of **1** measured in toluene at 0, 10, and 20 ns after laser excitation with 532 nm (corrected for bleaching of the parent).

[Ru(I)(R)(CO)$_2$(iPr-DAB)] (R = Me, Et).[37] From this excited state there is no recovery of the ground state within the time-domain of the experiment. Instead, a complete conversion occurs into the photoproduct characterized by an absorption at 360 nm. This latter band is assigned to the radical [Ru(I)(CO)$_2$(iPr-DAB)]$^\bullet$, because of its close resemblance with the spectrum of the electrochemically generated radical [Ru(Me)(PPh$_3$)(CO)$_2$-(iPr-DAB)]$^\bullet$ (λ_{max} = 357 nm).[32] The transient absorption spectrum of the radical [Re(CO)$_3$(bpy)]$^\bullet$ also showed a strong band near 360 nm, which lasted for at least 20 μs.[23]

Discussion

The high photoreactivity of complex **1** is noteworthy since the corresponding ethyl- and methyl-complexes are photostable. According to the spectral data, the same first photoproduct is formed in different solvents and at different temperatures. In all cases two strong ν(CO) bands were observed at about 2050 and 1990 cm^{-1}, respectively. Solvent coordination can therefore be excluded. Complete conversion of complex **1** was not possible due to the photolability of the first photoproduct. This secondary photoreaction started when about 50% of the starting complex had been converted.

In order to obtain the spectral data of this first photoproduct as a pure compound, complex **1** was irradiated on a preparative scale and the photoproduct was isolated and purified. Its spectral data and photolability closely resemble those of [Ru(I)$_2$(CO)$_2$(iPr-DAB)] (see Table 2). Besides, the crystallographic data of the complex confirmed the assignment of this photoproduct as [Ru(I)$_2$(CO)$_2$(iPr-DAB)]. From this crystal structure, it was clear that the photoproduct was neither [Ru(Cl)$_2$(CO)$_2$(iPr-DAB)] nor [Ru(I)(Cl)(CO)$_2$(iPr-DAB)], although it had been formed in CH_2Cl_2 solution. This is noteworthy since other studies have shown that CH_2Cl_2 can be used as a radical scavenger.[20]

The ESR and transient absorption spectra showed that the primary photoprocess is homolysis of the metal–alkyl bond, giving rise to the formation of isopropyl and [Ru(I)(CO)$_2$(iPr-DAB)]$^\bullet$ radicals. The iPr-radicals could be observed with ESR by using a radical trap. In the transient absorption spectra the [Ru(I)-(CO)$_2$(iPr-DAB)]$^\bullet$ radicals were observed as intermediates.

The question remains how these radicals react after homolytic cleavage of the ruthenium–alkyl bond. Obviously, the spectral data do not provide any indication for an internal alkyl transfer to the iPr-DAB ligand. Such a reaction was found by Kaupp et al.[21] for the complexes [Zn(R)$_2$(R′-DAB)] which undergo both thermally and photochemically transfer of R to the R′-DAB ligand, leading to C and N alkylation. When the R radical escaped from the solvent cage, a C–C coupled dimer of the [Zn(R)(R′-DAB)]$^\bullet$ radicals was obtained. In case of complex **1**, the ^{1}H-NMR spectra did not provide any evidence for the formation of a N- or C-alkylated product or a C–C-coupled dimer.

Thus, the [Ru(I)(CO)$_2$(iPr-DAB)]$^\bullet$ radicals, observed in the transient absorption spectra, are not converted into a C–C coupled dimer or alkylated products, but afford the complex [Ru(I)$_2$(CO)$_2$(iPr-DAB)] as the only carbonyl-containing photoproduct. Only when the reaction was performed in a coordinating solvent (S) such as acetonitrile, a second stable photoproduct [Ru(iPr)-(S)(CO)$_2$(iPr-DAB)]I was obtained. Based on this product formation, the nature of the primary photoprocess and the high quantum yields, the photoreaction is proposed to proceed according to the mechanism presented in Scheme 1.

After homolysis of the Ru–iPr bond, the coordinatively unsaturated radical [Ru(I)(CO)$_2$(iPr-DAB)]$^\bullet$ formed will take up a solvent molecule (S) to give [Ru(I)-(S)(CO)$_2$(iPr-DAB)]$^\bullet$. This radical will then reduce the parent complex with formation of [Ru(I)(iPr)(CO)$_2$(iPr-DAB)]$^-$ and [Ru(I)(S)(CO)$_2$(iPr-DAB)]$^+$. This reaction is in line with the observation of similar photodisproportionation reactions of metal–metal bonded complexes such as [(CO)$_5$Mn–Mn(CO)$_3$(α-diimine)].[38] The reaction will, however, proceed further since a recent spectroelectrochemical study has shown that the reduced complexes [Ru(X)(R)(CO)$_2$(iPr-DAB)]$^-$ (X = halide; R = alkyl) immediately lose X$^-$ and transform into the radicals [Ru(R)(CO)$_2$(iPr-DAB)]$^\bullet$, which dimerize to give the metal–metal bonded dimer [Ru(R)(CO)$_2$(iPr-DAB)]$_2$.[32] Similarly, the reduced **1** will decompose into [Ru(iPr)(S)(CO)$_2$(iPr-DAB)]$^\bullet$ and I$^-$. The iodide will react with the cation [Ru(I)(CO)$_2$(iPr-DAB)]$^+$ to give the photoproduct [Ru(I)$_2$(CO)$_2$(iPr-DAB)].

Contrary to the spectroelectrochemical experiments, the radicals [Ru(iPr)(S)(CO)$_2$(iPr-DAB)]$^\bullet$ did not, however, produce the dimer [Ru(iPr)(CO)$_2$(iPr-DAB)]$_2$. This is most likely due to the fact that, in the absence of excess electrons, these radicals act instead as reducing agents with respect to the parent complex **1** and transform into the cation [Ru(iPr)(S)(CO)$_2$(iPr-DAB)]$^+$. In noncoordinating solvents, this cation will react back with I$^-$ to give the parent complex. In a coordinating solvent, the I$^-$ will not replace the solvent molecule, but act as a counter ion. This explains the formation of [Ru-(iPr)(MeCN)(CO)$_2$(iPr-DAB)]I upon irradiation in MeCN.

This electron transfer reaction between the radicals [Ru(iPr)(S)(CO)$_2$(iPr-DAB)]$^\bullet$ and **1** starts an electron transfer chain (ETC) reaction, explaining the high quantum yields (Φ > 1) observed at room temperature.

(37) Nieuwenhuis, H. A.; Stufkens, D. J.; McNicholl, R.-A.; Al-Obaidi, A. H. R.; Coates, C. G.; McGarvey, J. J.; Westwell, J.; George, M. W.; Turner, J. J. To be submitted for publication.

Scheme 1. Proposed Reaction Routes for the Photoreaction of 1

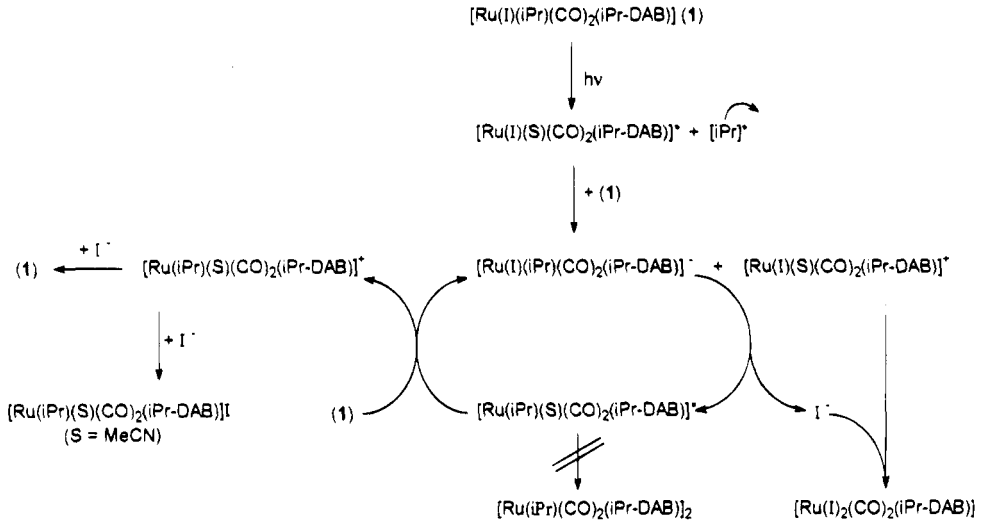

A similar ETC mechanism has been proposed for the photoinduced disproportionation of [(CO)$_5$Mn−Mn(CO)$_3$-(α-diimine)].[17,38]

According to this mechanism, the iPr-radicals are not involved in the reaction sequence and scavenging these radicals is therefore not expected to influence the product formation. Just as Lucia et al.,[23] we used MeOH as a trap for these alkyl radicals and this indeed did not influence the product formation. In addition, the ESR experiments have shown that both nitrosodurene and tBuNO only trap the iPr-radicals and not the [Ru(I)(CO)$_2$(iPr-DAB)]• radicals. Probably the [Ru-(I)(CO)$_2$(iPr-DAB)]• radicals are too reactive at room temperature to be detected. Irradiation of a solution of **1** in THF both in the absence and presence of a 5- or 10-fold excess of nitrosodurene gave rise to the same IR spectral changes. This means that the iPr-radicals are indeed not involved in the product formation. *In situ* ^{1}H-NMR experiments showed that these radicals dimerize.

The formation of radicals by irradiation of **1** closely resembles the homolysis reactions observed for the metal−metal bonded complexes [L$_n$M'−M(CO)$_3$(α-diimine)] (M = Mn, Re; L$_n$M' = (CO)$_5$Mn, (CO)$_4$Co, Cp-(CO)$_2$Fe, Ph$_3$Sn)[12−18] and [(CO)$_5$Mn−Ru(Me)(CO)$_2$(α-diimine)],[20] the metal−alkyl complexes [Re(R)(CO)$_3$(α-diimine)][22,23] and [Zn(R)$_2$(R'-DAB)],[21] and the metal−halide complexes *mer*-[Mn(X)(CO)$_3$(bpy)] (X = halide)[24] and several N,Si-chelated complexes of Ir.[39−42] In case of [Zn(R)$_2$(R'-DAB)], the metal orbitals are too low in energy to be involved in the electronic transitions and the reaction proceeds from the $^3\sigma_b\pi^*$ state by irradiation into the spin-allowed σ_b(Zn-R) → π^*(R'-DAB) transition.

For the other complexes, the situation is more complicated since the $\sigma_b \rightarrow \pi^*$ transition is either not allowed or at least coincides with the much stronger $d_\pi \rightarrow \pi^*$ (MLCT) transitions in the visible region. For these complexes, the homolysis reaction from the $^3\sigma_b\pi^*$ state has therefore been proposed to occur via MLCT excitation followed by surface crossing to the reactive $^3\sigma_b\pi^*$ state (Scheme 2). Evidence for this mechanism has been provided by the complexes [Re(R)(CO)$_3$(α-diimine)], which undergo homolysis of the Re−R bond with varying quantum yield depending on R.[22] For R = Me, Φ is only ca. 10^{-2} and this result agrees with the rather low energy of the $\sigma_{b(Re-Me)}$ orbital with respect to the metal-d_π orbitals as derived from the UV-photoelectron spectra. For R = Et or benzyl, or if R represents a metal fragment such as Mn(CO)$_5$, the quantum yields are close to unity since the σ_b orbital is then the HOMO. As a result, the $^3\sigma_b\pi^*$ state is lower in energy than the MLCT states. Apparently, the [Ru(X)(R)(CO)$_2$(α-diimine)] complexes behave similarly, since they are photostable for R = Me, Et, but photodecompose for R = iPr.

Scheme 2. Schematic Energy Level Diagram of 1[a]

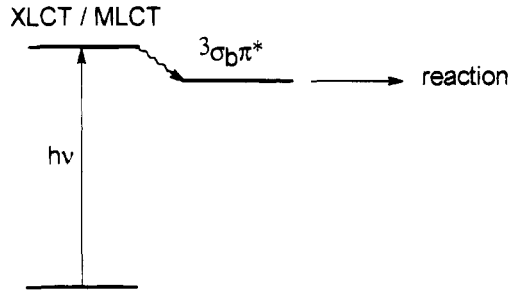

[a] The CT state has mixed MLCT/XLCT character (see text).

Occupation of a $^3\sigma_b\pi^*$ state, after excitation into a charge transfer state, is closely related to the behavior of chromophore−quencher (C−Q) complexes, such as [Re(D)(CO)$_3$(α-diimine)]$^+$, in which D represents an organic donor molecule.[43−45] Irradiation of these C−Q complexes into a MLCT band is followed by electron transfer from D to the metal by which the complex arrives in a LL'CT state. From this state the complex returns to the ground state within 10−100 ns depending on D. In the metal−metal and metal−alkyl bonded

(38) van der Graaf, T.; Hofstra, R.; Schilder, P. G. M.; Rijkhoff, M.; Stufkens, D. J.; van der Linden, J. G. M. *Organometallics* **1991**, *10*, 3668.
(39) Carlson, G. A.; Djurovich, P. I.; Watts, R. J. *Inorg. Chem.* **1993**, *32*, 4483.
(40) Djurorvich, P. I.; Watts, R. J. *Inorg. Chem.* **1993**, *32*, 4681.
(41) Djurorvich, P. I.; Cook, W.; Joshi, R.; Watts, R. J. *J. Phys. Chem.* **1994**, *98*, 398.
(42) Djurorvich, P. I.; Watts, R. J. *J. Phys. Chem.* **1994**, *98*, 396.
(43) Perkins, T. A.; Humer, W.; Netzel, T. L.; Schanze, K. S. *J. Phys Chem.* **1990**, 2229.
(44) Schanze, K. S.; MacQueen, D. B.; Perkins, T. A.; Cabana, L. A. *Coord. Chem. Rev.* **1993**, *122*, 63.
(45) Chen, P.; Duesing, R.; Graff, D. K.; Meyer, T. J. *J. Phys. Chem.* **1991**, *95*, 5850.

complexes MLCT excitation is followed by electron transfer from a bonding orbital and the LL'CT state is now a reactive $^3\sigma_b\pi^*$ state from which radicals are formed.

As shown in Table 5 and Figure 8, the quantum yield of the homolysis reaction strongly depends on the temperature. In order to find out if this influence of the temperature could be due to a solvent cage effect, the photoreaction has been studied in solvents of different viscosity. For this purpose, the reaction was followed for **1** dissolved in MeOH (η = 0.6 cp at rt) and in ethylene glycol (η = 19.9 cp at rt) containing 5% MeOH. No difference in reaction rate was then observed, which means that the observed influence of the temperature on this rate is not due to a cage effect. Unlike the complex [Re(Me)(CO)$_3$(iPr-DAB)],[22] the quantum yields in the present study do not show a significant wavelength dependence. This means that the temperature dependence is most likely due to an energy barrier between the MLCT/XLCT state and the reactive $^3\sigma_b\pi^*$ state.

Two effects may be responsible for the observed drastic influence of the temperature on the quantum yield. First of all, a lowering of temperature will cause a decrease of reaction rate of the catalytic cycle since the thermal reaction between the primary radical product and the parent compound will be slowed down. At a certain low temperature the catalytic cycle will be stopped and the quantum yield is then determined by the primary photoprocess itself.

This primary photoprocess may also be temperature dependent due to the presence of a barrier for the homolysis reaction from the $^3\sigma_b\pi^*$ state. This is not unlikely since in this state the complex still contains one electron in its $\sigma_{b(Ru\text{-}iPr)}$ orbital. Cleavage of the metal−alkyl bond from this state may therefore also be accompanied by an activation energy. An attempt to confirm the presence of this latter effect by measuring the occurrence of the weak emission from the $^3\sigma_b\pi^*$ state at lower temperatures failed because of interference from the much stronger emission of the photoproduct [Ru(I)$_2$(CO)$_2$(iPr-DAB)]. However, a recent study has shown that the related complexes [(CO)$_5$Mn−Ru(Me)-(CO)$_2$(α-diimine)], which also decompose into radicals at room temperature from a $^3\sigma_b\pi^*$ state, emit from this state in a 2-MeTHF glass at 77 K.[19] Similarly, the presence of such a barrier for decomposition from the $\sigma_b\pi^*$ state can also not be excluded for complex **1**. It is therefore tentatively concluded that the influence of the temperature on the quantum yield is primarily caused by a slowing down of the catalytic cycle, but at lower temperatures possibly also by a small barrier for the homolysis reaction.

Conclusions

Photodecomposition of [Ru(I)(iPr)(CO)$_2$(iPr-DAB)] leads to the formation of [Ru(I)$_2$(CO)$_2$(iPr-DAB)]. If the reaction is performed in a coordinating solvent (S) such as acetonitrile, [Ru(iPr)(S)(CO)$_2$(iPr-DAB)]I is also produced. ESR and transient absorption spectra have shown that the primary photoprocess is homolysis of the metal−alkyl bond. The [Ru(I)(S)(CO)$_2$(iPr-DAB)]$^\bullet$ radicals formed reduce the parent complex, which then releases I$^-$. The high quantum yields observed for the photodecomposition of the parent complex are explained in terms of an electron transfer chain reaction. The temperature dependence of the quantum yields is tentatively attributed to a decrease in reaction rate of the catalytic reaction of the primary photoproduct and to a barrier for the reaction from the $^3\sigma_b\pi^*$ state.

Acknowledgment. J. M. Ernsting is thanked for technical assistance with the NMR experiments and J. Fraanje for the measurement of the X-ray structure. The Netherlands Foundation for Chemical Research (SON) and the Netherlands Organisation for Pure Research (NWO) are thanked for financial support. A. Vlček Jr. is thanked for critically reading the manuscript.

Supplementary Material Available: Listings of the atomic coordinates of non-hydrogen (Table S1) and hydrogen (Table S2) atoms, the anisotropic thermal parameters of the non-hydrogen atoms (Table S3), the bond lengths of the non-hydrogen atoms (Table S4) and hydrogen atoms (Table S5), and the bond angles of the non-hydrogen atoms (Table S6) and hydrogen bond angles (Table S7) (7 pages). Ordering information is given on any current masthead page.

OM9405403

Synthesis and Characterization of Zirconium Complexes Containing a Linked Amido–Fluorenyl Ligand†

Jun Okuda,* Florian J. Schattenmann, Sigrid Wocadlo, and Werner Massa

Fachbereich Chemie der Philipps-Universität Marburg, Hans-Meerwein-Strasse, D-35032 Marburg, Germany

Received July 28, 1994®

Zirconium complexes containing an amido–fluorenyl ligand bridged by a dimethylsilylene group, $C_{13}H_8SiMe_2NCMe_3$, have been synthesized. The dichloro complexes $Zr(\eta^5:\eta^1\text{-}C_{13}H_8SiMe_2NCMe_3)Cl_2(L)$ (L = THF, Et_2O) were prepared by reacting $ZrCl_4L_2$ with $Li_2[C_{13}H_8SiMe_2NCMe_3]$ and characterized as labile mono(solvent) adducts. Reaction with MeMgCl gives the thermally sensitive dimethyl complex $Zr(\eta^5:\eta^1\text{-}C_{13}H_8SiMe_2NCMe_3)Me_2(THF)$, whereas solvent-free dialkyl derivatives $Zr(\eta^5:\eta^1\text{-}C_{13}H_8SiMe_2NCMe_3)Ph_2$ and $Zr(\eta^5:\eta^1\text{-}C_{13}H_8SiMe_2NCMe_3)(CH_2SiMe_3)_2$, all under preservation of the chelate structure, are obtained with PhMgCl and Me_3SiCH_2MgCl, respectively. Variable-temperature ^1H NMR spectroscopic data reveal a sterically congested ligand sphere around the zirconium atom which is confirmed by a single-crystal X-ray diffraction study in the case of the bis(trimethylsilylmethyl) derivative. The substituted fluorenyl ligand is pentahapto-bonded with some variation of the zirconium–ring carbon bond lengths. The amido nitrogen is trigonal planar as a result of significant π-donation to the zirconium. The two (trimethylsilyl)methyl groups do not appear to be strongly distorted despite being bound to a 12-electron d^0 center but give rise to a conformation in which the repulsion between the trimethylsilyl and the *tert*-butyl groups is minimized. This compound crystallizes from pentane in the monoclinic space group $P2_1/n$ with a = 9.326(3), b = 16.806(5), and c = 19.638(6) Å, β = 93.23(2)°, V = 3073(2) Å^3, Z = 4, R = 0.0308, wR_2 = 0.079.

Introduction

Since the report that *ansa*-metallocenes of zirconium and hafnium containing linked fluorenyl–cyclopentadienyl ligand systems such as $Zr(\eta^5:\eta^5\text{-}C_{13}H_8CMe_2C_5H_5)Cl_2$ act as components for syndiospecific α-olefin polymerization catalysts,[1] there has been renewed interest in fluorenyl ligands in group 4 metal coordination chemistry.[2] These C_s-symmetric zirconocene and hafnocene catalysts lead to the formation of racemic sequences during the polymerization of α-olefins. While mechanistic details responsible for the syndiospecificity remain unclear, the presence of two differently sized rings around the metal center seems to regulate the alternating attack of the α-olefin in the lateral sector of the metallocene by influencing the conformation of the growing polymer chain.[3] Consequently, a number of studies have focussed on fluorenyl ligands bridged to the cyclopentadienyl ligand via an alkylidene bridge.[4]

Recently, Bercaw and Shapiro showed that replacing a cyclopentadienyl moiety of a linked bis(cyclopentadienyl) ligand by the 3-electron-donating *tert*-butylamido group results in a ligand system[5] that forms *ansa*-metallocene-like complexes of scandium with higher Lewis acidity, *i.e.* increased reactivity toward α-olefin substrates. In order to examine the detailed complexation behavior of this novel chelating ligand type[6] also for potentially syndiospecific metallocene catalysts, we carried out the synthesis and characterization of zirconium complexes containing a amido–fluorenyl ligand linked by a dimethylsilylene bridge.[7]

† Dedicated to Professor Hans H. Brintzinger, with all best wishes, on the occasion of his 60th birthday.

® Abstract published in *Advance ACS Abstracts,* December 15, 1994.

(1) (a) Ewen, J. A.; Jones, R. L.; Razavi, A.; Ferrara, J. D. *J. Am. Chem. Soc.* **1988**, *110*, 6255. (b) Ewen, J. A.; Elder, M. J.; Jones, R. L.; Haspeslagh, L.; Atwood, J. L.; Bott, S. G.; Robinson, K. *Makromol. Chem., Macromol. Symp.* **1991**, *48/49*, 235. (c) Ewen, J. A.; Elder, M. J. *Makromol. Chem., Macromol. Symp.* **1993**, *66*, 179.

(2) (a) Kowala, C.; Wailes, P. C.; Weigold, H.; Wunderlich, J. A. *J. Chem. Soc., Chem. Commun.* **1974**, 993. (b) Kowala, C.; Wunderlich, J. A. *Acta Crystallogr.* **1976**, *B32*, 820. (c) Samuel, E.; Alt, H. G.; Hrncir, D. C.; Rausch, M. D. *J. Organomet. Chem.* **1976**, *113*, 331. (d) Razavi, A.; Atwood, J. L. *J. Am. Chem. Soc.* **1993**, *115*, 7529.

(3) (a) Cavallo, L.; Guerra, G.; Vacatello, M.; Corradini, P. *Macromolecules* **1991**, *24*, 1784. (b) Kawamura-Kuribayashi, H.; Koga, N.; Morokuma, K. *J. Am. Chem. Soc.* **1992**, *114*, 8687. (c) Farina, M.; Terragni, A. *Makromol. Chem., Rapid Commun.* **1993**, *14*, 791. (d) Bierwagen, E. P.; Bercaw, J. E.; Goddard, W. A., III. *J. Am. Chem. Soc.* **1994**, *116*, 1481.

(4) (a) Razavi, A.; Ferrara, J. *J. Organomet. Chem.* **1992**, *435*, 299. (b) Razavi, A.; Thewalt, U. *J. Organomet. Chem.* **1993**, *445*, 111. (c) Razavi, A.; Atwood, J. L. *J. Organomet. Chem.* **1993**, *459*, 117. (d) Rieger, B. *J. Organomet. Chem.* **1991**, *420*, C17. (e) Rieger, B.; Steinmann, M.; Fawzi, R. *Chem. Ber.* **1993**, *125*, 2373. (f) Bochmann, M.; Lancaster, S. J.; Hursthouse, M. B.; Mazid, M. *Organometallics* **1993**, *12*, 4718. (g) Herrmann, G. S.; Alt, H. G.; Rausch, M. D. *J. Organomet. Chem.* **1991**, *401*, C5. (h) Alt, H. G.; Milius, W.; Palackal, S. J. *J. Organomet. Chem.* **1994**, *472*, 113.

(5) (a) Shapiro, P. J.; Bunel, E.; Schaefer, W. P.; Bercaw, J. E. *Organometallics* **1990**, *9*, 867. (b) Piers, W. E.; Shapiro, P. J.; Bunel, E. E.; Bercaw, J. E. *Synlett* **1990**, *2*, 74. (c) Shapiro, P. J.; Cotter, W. D.; Schaefer, W. P.; Labinger, J. A.; Bercaw, J. E. *J. Am. Chem. Soc.* **1994**, *116*, 4632. (d) Schaefer, W. P.; Cotter, W. D.; Bercaw, J. E. *Acta Crystallogr., Sect. C* **1993**, *49*, 1489.

(6) (a) Okuda, J. *Chem. Ber.* **1990**, *123*, 1649. (b) Hughes, A. K.; Meetsma, A.; Teuben, J. H. *Organometallics* **1993**, *12*, 1936. Related amino- or imido-functionalized cyclopentadienyl ligands: (c) Clark, T. J.; Nile, T. A.; McPhail, D.; McPhail, A. T. *Polyhedron* **1989**, *8*, 1804. (d) Wang, T. F.; Lee, T. Y.; Wen, Y. S.; Liu, L. K. *J. Organomet. Chem.* **1991**, *403*, 353. (e) Wang, T. F.; Wen, Y. S. *J. Organomet. Chem.* **1992**, *439*, 155. (f) Wang, T. F.; Lee, T. Y.; Chou, J. W.; Ong, C. W. *J. Organomet. Chem.* **1992**, *423*, 31. (g) Jutzi, P.; Kristen, M. O.; Dahlhaus, J.; Neumann, B.; Stammler, H.-G. *Organometallics* **1993**, *12*, 2980. (h) van der Hende, J. R.; Hitchcock, P. B.; Lappert, M. F.; Nile, T. A. *J. Organomet. Chem.* **1994**, *472*, 79. (i) Antonelli, D. M.; Green, M. L. H.; Mountford, P. J. *J. Organomet. Chem.* **1992**, *438*, C4. For a brief review on chelating cyclopentadienyl ligands, see: Okuda, J. *Comments Inorg. Chem.* **1994**, *16*, 185.

0276-7333/95/2314-0789$09.00/0

Scheme 1

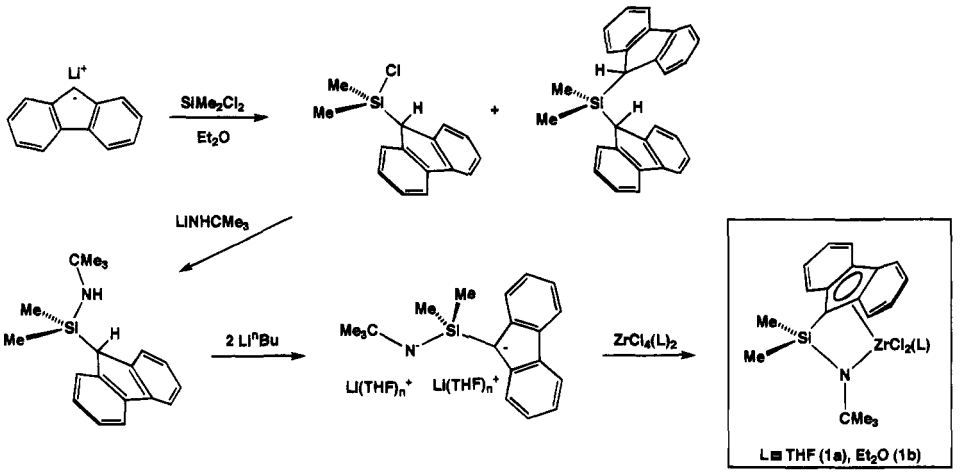

Results and Discussion

When crude 9-(chlorodimethylsilyl)fluorene[8] is treated with lithium *tert*-butylamide in pentane, 9-{(*tert*-butylamino)dimethylsilyl}fluorene is obtained as a moisture-sensitive colorless oil that can be purified by careful Kugelrohr or short-path vacuum distillation (Scheme 1). Double deprotonation with 2 equiv of *n*-butyllithium in ether/hexane,[9] followed by reaction with $ZrCl_4(THF)_2$ in THF at low temperatures, gives the mono(tetrahydrofuran) adduct $Zr(\eta^5{:}\eta^1\text{-}C_{13}H_8SiMe_2NCMe_3)Cl_2(THF)$ (**1a**), in about 60% yield as dark yellow microcrystalline material. The presence of one molecule of THF per zirconium in samples obtained by crystallization from toluene/THF/pentane is indicated by both ^1H and ^{13}C spectroscopy.[10] The chemical shifts of the THF protons are strongly temperature dependent: both α- and β-CH_2 protons undergo substantial high-field shifts upon cooling (Figure 1), although decoalescence of the signals could not be detected. The high-field shift can be explained by the coordinated THF molecule being shielded by the fluorenyl ligand's ring current. The presence of THF in excess of 1 equiv in the solution of **1a** results in low-field shift of the THF signals, approaching the values for free THF. Addition of excess THF-d_8 results in instantaneous exchange of all coordinated THF. These observations are in accordance with the existence of a dissociation equilibrium between monomeric **1** and the THF adduct **1a** which is fast both on the chemical and NMR time scales.[11] Solutions of **1a** slowly form a fine powdery precipitate over a period of days. Once precipitated from toluene, this compound does not dissolve even in hot THF. Upon heating **1a** above 100 °C, the coordinated THF is also lost irreversibly, forming an insoluble pale yellow solid of what we believe to be di- or oligomeric dichloride **1**.

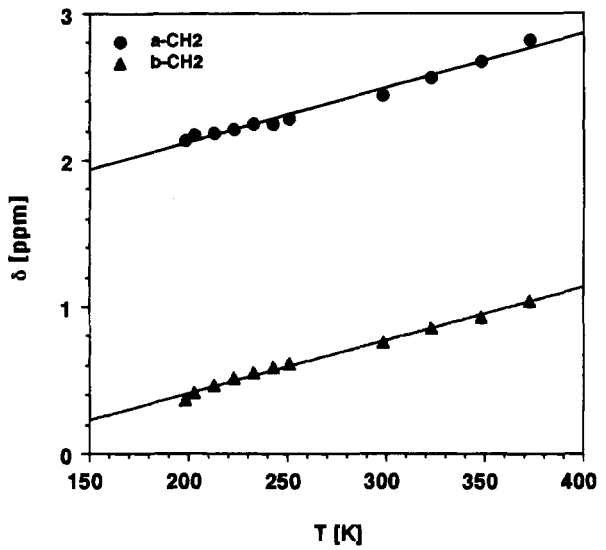

Figure 1. Temperature dependence of the chemical shift for the α- and β-CH_2 protons of the coordinated THF molecule in $Zr(\eta^5{:}\eta^1\text{-}C_{13}H_8SiMe_2NCMe_3)Cl_2(THF)$ (**1a**).

By following the analogous procedure, the even more labile mono(diethyl ether) adduct $Zr(\eta^5{:}\eta^1\text{-}C_{13}H_8SiMe_2NCMe_3)Cl_2(Et_2O)$ (**1b**) is formed. The ether molecule in **1b** can be easily displaced by 1 equiv of THF to form **1a**. According to NMR spectroscopic results, other Lewis bases such as PMe_3, pyridine, triethylamine, HMPTA, dmpe, or DME appear to substitute the ether ligand in **1a** and **1b**. However, no stable adducts could be isolated, most notably, even in the case of the

(7) Recent patents disclose that $Zr(\eta^5{:}\eta^1\text{-}C_{13}H_8SiMe_2NCMe_3)Cl_2$ in conjunction with methylalumoxane cocatalyst forms isotactic, whereas $[Zr(\eta^5{:}\eta^1\text{-}C_{13}H_8SiMe_2NCMe_3)Me][B(C_6F_5)_4]$ gives syndiotactic polypropylene: (a) Canich, J. A. M. U.S. Patent 5,026,798 to Exxon Chemical; *Chem. Abstr.* **1993**, *118*, 60284; Canich, J. A. M. U.S. Patent 5,055,438 to Exxon Chemical; *Chem. Abstr.* **1993**, *118*, 60283. (b) Turner, H. W.; Hlatky, G. G.; Canich, J. A. M. PCT Int. Appl. WO 9319103; *Chem. Abstr.* **1994**, *120*, 271442.

(8) Lithium fluorenide reacts with dichlorodimethylsilane in ether to give a mixture of 9-(chlorodimethylsilyl)fluorene and di(9-fluorenyl)-dimethylsilane which is extremely difficult to separate. Due to the high nucleophilicity of lithium fluorenide, the formation of the latter could not be completely suppressed in our hands.

(9) Attempts to obtain single crystals have failed so far. The benzene-soluble THF adduct of dilithium 9-((*tert*-butylamino)dimethylsilyl)fluorenide show inequivalent signals for the enantiotopic $SiMe_2$ signals, implying a rather complex structure in solution (cf. ref 5d). For examples of structurally characterized main group element fluorenides, see: (a) Brooks, J. J.; Rhine, W.; Stucky, G. D. *J. Am. Chem. Soc.* **1972**, *94*, 7339. (b) Zerger, R.; Rhine, W.; Stucky, G. D. *J. Am. Chem. Soc.* **1974**, *96*, 5441. (c) Corbelin, S.; Kopf, J.; Weiss, E. *Chem. Ber.* **1991**, *124*, 2417. (d) Janiak, C. *Chem. Ber.* **1993**, *126*, 1603. (e) Mösges, G.; Hampel, F.; Schleyer, P. v. R. *Organometallics* **1992**, *11*, 1769. (f) Neumüller, B. *Chem. Ber.* **1993**, *126*, 11.

(10) In samples crystallized over a prolonged period of time from pentane/THF, two molecules of THF are present. However, the loss of the second solvent molecule is very facile. We suspect that this THF molecule might not be coordinated to the zirconium but acts as lattice solvent.

(11) Assuming that the observed chemical shift for the THF protons δ_{obs} is the weighted mean of the values for free and complexed THF ($\delta_{obs} = N\delta_{free} + N\delta_{comp}$, N = mole fraction), the equilibrium constant at 25 °C was estimated as $K_{eq} = 0.02$ M. Slejiko, F. L.; Drago, R. S.; Brown, D. G. *J. Am. Chem. Soc.* **1972**, *94*, 9210.

Scheme 2

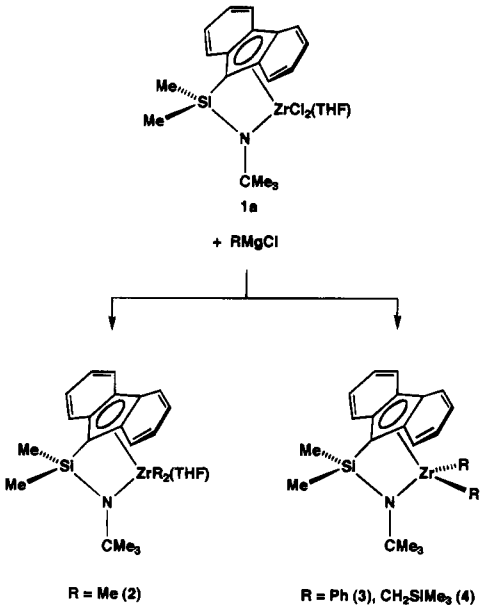

bidentate ligands dmpe and DME. Again, insoluble dichloride is rapidly precipitated from these reaction mixtures.

Despite much effort, no single crystal of either **1a** or **1b** could be obtained so far. A plausible structure is that of a four-legged piano stool, the sterically demanding fluorenyl occupying an apical site. Because of the strong π-donation of the amido ligand, the most probable coordination site of L will be cis to the amido ligand. We conclude that the tetravalent zirconium center in $Zr(\eta^5{:}\eta^1\text{-}C_{13}H_8SiMe_2NCMe_3)Cl_2$ is sufficiently electrophilic to bind a THF or ether molecule. The 14-electron zirconium atom (counting the fluorenyl as a five- and amido as three-electron ligand according to the neutral ligand formalism) on the other hand is not capable of expanding its coordination number to more than five.[12] We ascribe this feature at least partly to the steric encumbrance of the rather rigid chelating ligand system $\eta^5{:}\eta^1\text{-}C_{13}H_8SiMe_2NCMe_3$.

Reaction of **1a** with methylmagnesium chloride in THF affords yellow, extremely light and thermally sensitive crystals of the dimethyl derivative **2**, which also contains one molecule of THF, in 60% yield (Scheme 2). The synthesis of **2** requires very careful control of the reaction temperature by slowly warming the reaction mixture from −78 to −15 °C and working up below 0 °C. Above this temperature immediate and complete decomposition takes place. Furthermore, the use of the Grignard reagent is mandatory, since methyllithium leads to an intractable mixture even at temperatures as low as −110 °C. The resonance for the two equivalent methyl groups is detected in the ^{1}H NMR spectrum at δ 0.32 and in the ^{13}C NMR spectrum at 40.6 ppm as a quartet with J_{CH} = 114 Hz. This value excludes the presence of any strong agostic interaction.[13] The coordinated THF molecule displays the same feature as in the dichloride **1a**.

The reaction of **1a** with benzylmagnesium chloride gives only inseparable materials of what appears to be mixtures of the dibenzyl, mono(benzyl)chloro complex and bibenzyl. On the other hand, treatment of **1a** with phenylmagnesium chloride at low temperatures affords the diphenyl complex **3** in moderate yield as pale yellow powder. Analytical and NMR spectroscopic data of **3** reveal the absence of any coordinated THF molecule. In the ^{1}H NMR spectrum the resonance for the ten phenyl protons appear as two broad signals which sharpen upon heating to 80 °C. Due to overlapping in the aromatic region, a conclusive variable-temperature NMR spectroscopic study could not be performed. It is obvious, however, that the free rotation of the phenyl ligands about the zirconium–ipso carbon is hindered.

Table 1. Crystallographic Data for $Zr(\eta^5{:}\eta^1\text{-}C_{13}H_8SiMe_2NCMe_3)(CH_2SiMe_3)_2$ (4)

Crystal Data	
chem formula	$C_{27}H_{45}NSi_3Zr$
fw	559.14
cryst color	orange yellow
cryst dimensions, mm	0.5 × 0.3 × 0.15
cryst system	monoclinic
space group	$P2_1/n$
a, Å	9.326(3)
b, Å	16.806(5)
c, Å	19.638(6)
β (deg)	93.23(2)
V, Å^3	3073(2)
Z	4
D_{calc}, g cm^{-3}	1.209
abs. coeff., mm^{-1}	0.489
F(000)	1184
Data Collection	
radiation	Mo Kα (λ = 0.71073 Å)
T, K	293
2θ range	2.08° to 22.50°
rflns measd	h, −1 to +10; k, −1 to +18, l, −21 to +21
Refinement	
no. of rflns measd	5252
no. of indep rflns	3987 (R_{int} = 0.0218)
no. of obsd rflns	3241 ($I > 2\sigma(I)$)
GOF	1.060
R	0.0308
wR_2 (all F^2)	0.0397
largest e-max, e-min, e Å^{-3}	+0.284, −0.283

Alkylation of **1a** with ((trimethylsilyl)methyl)magnesium chloride in THF cleanly yields pentane-soluble, yellow bis((trimethylsilyl)methyl) complex **4** in high yields. **4** is significantly less thermally and light sensitive than the dimethyl complex **2**. Like the phenyl derivative **3**, **4** does not contain any coordinated THF nor does it tend to bind THF, as can be deduced from NMR spectroscopic data. The signals for the pairwise diastereotopic protons of the two equivalent (trimethylsilyl)methyl groups are detected at unusually high fields of δ −0.49 and −1.26 as an AB spin system. The geminal coupling constant is $^2J_{HH}$ = 10.5 Hz, in agreement with values found for diastereotopic $Zr{-}CH_2SiMe_3$ resonances such as $Cp^*Zr(\eta^6\text{-}C_5Me_4CH_2)CH_2SiMe_3$[14] and similar molybdenum and tungsten complexes of the type $(\eta^5\text{-}C_5R_5)M(NO)(CH_2SiMe_3)_2$.[15] In contrast, the electronically analogous complex $Zr(\eta^5{:}\eta^1\text{-}C_5H_4CH_2CH_2\text{-}CH_2NMe)(CH_2SiMe_3)_2$, reported by Teuben et al., displays a value of only 2.1 Hz, suggesting an agostic interaction.[6b] The high-field shifts of the signals are again due to the shielding effect of the fluorenyl

(12) Cardin, D. J.; Lappert, M. F.; Raston, C. L. *Chemistry of Organo-Zirconium and -Hafnium Compounds*; Wiley: New York, 1986.

(13) (a) Crowther, D. J.; Jordan, R. F.; Baenzigner, N. C.; Verma, A. *Organometallics* **1990**, *9*, 2574. (b) Jordan, R. F.; LaPointe, R. E.; Bradley, P. K.; Baenzinger, N. C. *Organometallics* **1989**, *8*, 2892.

(14) Sinnema, P.-J.; Meetsma, A.; Teuben, J. H. *Organometallics* **1993**, *12*, 184.

(15) (a) Legdzins, P.; Rettig, S. J.; Sanchez, *Organometallics* **1988**, *7*, 2394. (b) Dryden, N. H.; Legdzins, P.; Trotter, J.; Yee, V. C. *Organometallics* **1991**, *10*, 2857.

Table 2. Selected Bond Distances (Å) and Bond Angles (deg) for 4

Zr(1)−N(1)	2.061(2)	Zr(1)−C(20)	2.232(3)
Zr(1)−C(30)	2.248(3)	Zr(1)−C(1)	2.400(3)
Zr(1)−C(2)	2.538(3)	Zr(1)−C(13)	2.548(3)
Zr(1)−C(7)	2.695(3)	Zr(1)−C(8)	2.708(3)
C(1)−C(2)	1.454(4)	C(2)−C(7)	1.426(4)
C(7)−C(8)	1.442(4)	C(8)−C(13)	1.431(4)
C(1)−Si(1)	1.866(3)	Si(1)−N(1)	1.738(2)
C(20)−Si(2)	1.852(3)	C(30)−Si(3)	1.848(3)
N(1)−Zr(1)−C(20)	113.0(1)	N(1)−Zr(1)−C(30)	110.5(1)
C(20)−Zr(1)−C(30)	103.8(1)	N(2)−Si(1)−C(1)	95.1(1)
C(14)−Si(1)−C(15)	106.5(2)	C(40)−N(1)−Si(1)	126.3(2)
C(40)−N(1)−Zr(1)	130.1(2)	Si(1)−N(1)−Zr(1)	103.4(1)
Si(2)−C(20)−Zr(1)	136.1(2)	Si(3)−C(30)−Zr(1)	123.8(2)

Table 3. Fractional Coordinates and Equivalent Isotropic Temperature Factors (Å²) for 4[a]

atom	x	y	z	U_{eq}
Zr(1)	0.98252(3)	0.20993(2)	0.08611(1)	0.02517(11)
C(1)	0.0295(3)	0.0718(2)	0.07670(15)	0.0319(7)
C(2)	0.1248(3)	0.0810(2)	0.0214(2)	0.0308(7)
C(3)	0.2690(3)	0.0573(2)	0.0149(2)	0.0403(8)
C(4)	0.3350(4)	0.0760(2)	−0.0434(2)	0.0513(10)
C(5)	0.2669(4)	0.1204(2)	−0.0958(2)	0.0536(10)
C(6)	0.1298(4)	0.1461(2)	−0.0913(2)	0.0455(9)
C(7)	0.0569(3)	0.1280(2)	−0.03158(15)	0.0319(7)
C(8)	−0.0867(3)	0.1458(2)	−0.01245(15)	0.0313(7)
C(9)	−0.2012(4)	0.1874(2)	−0.0458(2)	0.0444(9)
C(10)	−0.3284(4)	0.1935(2)	−0.0156(2)	0.0521(10)
C(11)	−0.3462(4)	0.1586(2)	0.0475(2)	0.0523(10)
C(12)	−0.2386(4)	0.1185(2)	0.0829(2)	0.0411(8)
C(13)	−0.1029(3)	0.1091(2)	0.0524(2)	0.0326(8)
Si(1)	0.09729(11)	0.05941(5)	0.16728(5)	0.0407(3)
C(14)	0.2324(5)	−0.0216(2)	0.1785(2)	0.0738(13)
C(15)	−0.0506(5)	0.0349(2)	0.2250(2)	0.0709(13)
N(1)	0.1640(3)	0.15567(14)	0.17582(12)	0.0314(6)
C(40)	0.2583(4)	0.1866(2)	0.2334(2)	0.0384(8)
C(41)	0.2126(4)	0.1534(2)	0.3010(2)	0.0621(11)
C(42)	0.4144(4)	0.1632(2)	0.2239(2)	0.0590(11)
C(43)	0.2468(4)	0.2774(2)	0.2349(2)	0.0546(10)
C(20)	−0.0656(4)	0.3070(2)	0.1017(2)	0.0424(8)
Si(2)	−0.17724(10)	0.33960(6)	0.17159(5)	0.0440(3)
C(21)	−0.2027(4)	0.2590(2)	0.2351(2)	0.0669(12)
C(22)	−0.0925(4)	0.4276(2)	0.2154(2)	0.0612(11)
C(23)	−0.3602(4)	0.3694(3)	0.1372(2)	0.0804(14)
C(30)	0.2746(3)	0.2721(2)	0.0379(2)	0.0337(7)
Si(3)	0.25578(11)	0.36774(6)	−0.00813(5)	0.0483(3)
C(31)	0.0905(5)	0.3694(3)	−0.0667(2)	0.0787(14)
C(32)	0.4132(5)	0.3840(3)	−0.0624(2)	0.092(2)
C(33)	0.2489(5)	0.4523(2)	0.0522(2)	0.0804(14)

ligand.[15b] In the ^{13}C NMR spectrum of **4**, the $ZrCH_2$ resonance appears at δ 57.1 with $^1J_{CH}$ = 104 Hz.

One set of the aromatic protons, most probably those at the carbon atoms 4 and 5, exhibits temperature-dependent chemical shifts. This finding can be ascribed to the possibility that upon performing a full rotation about the zirconium−carbon bond the Me_3SiCH_2 groups sense the close proximity to the periphery of the fluorenyl ring.

A single-crystal X-ray diffraction analysis of **4** was performed to elucidate the details of the molecule. Crystal data are listed in Table 1. Selected bond lengths and angles are given in Table 2 and atomic parameters in Table 3. The compound adopts a three-legged piano stool configuration with a pseudotetrahedral arrangement of the four ligands (Figure 2). The fluorenyl ligand is bonded in a fashion which is between pentahapto and trihapto, as judged by the zirconium ring-carbon distances ranging from 2.400(3) to 2.708(3) Å. This distorted bonding with the bridgehead fluorenyl carbon bonded closest to the zirconium is a consequence of the molecular orbital structure of the fluorenyl anion.[16] Unlike the mostly pentahapto-bound cyclopentadienyl and indenyl ligands in transition metal complexes, the

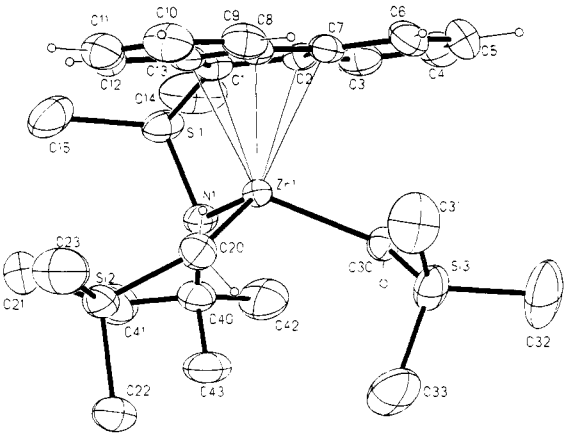

Figure 2. ORTEP view of $Zr(\eta^5{:}\eta^1\text{-}C_{13}H_8SiMe_2NCMe_3)(CH_2SiMe_3)_2$ (**4**), with thermal ellipsoids at the 50% probability level. Hydrogen atoms of methyl groups have been omitted for the sake of clarity.

fluorenyl ligand is found to be coordinated at a transition metal center in a variety of bonding modes. For zirconium complexes the η^5-,[1,2] η^3-,[2a] and η^3-benzallyl[4b] bonding was structurally verified. The zirconium−nitrogen bond length of 2.061(2) Å is in the typical range for an amido ligand bound to a d^0 zirconium center with strong π-bonding: $Cp^*Zr(NHCMe_3)_3$ 2.00(1), 2.02(1);[17] $MeZr[NHSi(CMe_3)_3]_3$ 2.039(7);[18] $[Zr(\eta^5{:}\eta^1\text{-}C_5H_4CH_2CH_2CH_2NMe)Cl(CH_2Ph)]_2$ 1.988(2);[6b] $Zr(\eta^5{:}\eta^1\text{-}C_5Me_4SiMe_2NCMe_3)Cl_2$ 2.056(6) Å.[19] In agreement with the implication of a three-electron ligand, the nitrogen atom is trigonal planar, the sum of the angles at the nitrogen atom amounting to 360°. The zirconium−carbon bond lengths of the (trimethylsilyl)methyl groups of 2.232(3) and 2.248(3) Å are in the expected region for Zr−C(sp^3) bond distances and are only slightly shorter than those in $Cp_2Zr(CH_2SiMe_3)_2$ (2.278(4) and 2.281(4) Å)[20] or similar to that in $[Cp^*_2Zr(CH_2SiMe_3)(THF)]^+$ (2.238(6) Å).[21]

The somewhat unexpected orientation of the two (trimethylsilyl)methyl groups is such that both the bulky (trimethylsilyl)methyl groups are turned to the same side away from the zirconium center (Figure 3). The angles at the chemically equivalent methylene carbons are 123.8(2) and 136.1(2)°. Thus, the angles for the two alkyl groups are significantly different. This feature cannot be implied to reflect any agostic distortion. Rather, this conformation may reflect the steric influence of the rigid $\eta^5{:}\eta^1\text{-}C_{13}H_8SiMe_2NCMe_3$ ligand system that forces the two (trimethylsilyl)methyl groups away form the *tert*-butyl group at the amido group. The "wedge" in the present ligand system therefore is more open as compared to the familiar Cp_2Zr fragment, but in a different way. From inspection of models, it is evident that completely free and independent rotation

(16) Decken, A.; Britten, J. F.; McGlinchey, M. J. *J. Am. Chem. Soc.* **1993**, *115*, 7279 and references therein.
(17) Bai, Y.; Roesky, H. W.; Noltemeyer, M.; Witt, M. *Chem. Ber.* **1992**, *125*, 825.
(18) (a) Cummins, C. C.; Van Duyne, G. D.; Schaller, C. P.; Wolczanski, P. T. *Organometallics* **1991**, *10*, 164. (b) Planalp, R. P.; Andersen, R. A.; Zalkin, A. *Organometallics* **1983**, *2*, 16.
(19) (a) Stevens, J. C. Metcon 93, p 157, Houston, May 26−28, 1993. (b) Woo, T. K.; Fan, L.; Ziegler, T. *Organometallics* **1994**, *13*, 2252.
(20) Jeffrey, J.; Lappert, M. F.; Luong-Thi, N. T.; Webb, M.; Atwood, J. L.; Hunter, W. E. *J. Chem. Soc., Dalton Trans.* **1981**, 1593.
(21) Amorose, D. M.; Lee, R. A.; Petersen, J. L. *Organometallics* **1991**, *10*, 2191.

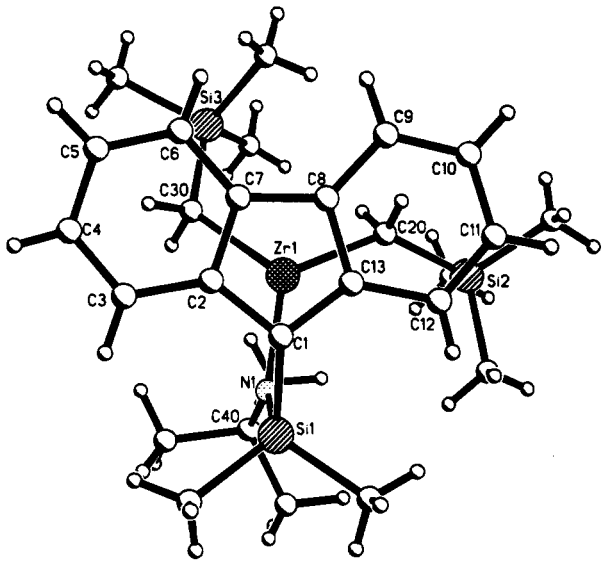

Figure 3. View of $Zr(\eta^5:\eta^1\text{-}C_{13}H_8SiMe_2NCMe_3)(CH_2SiMe_3)_2$ (**4**) perpendicular to the fluorenyl ligand.

of both the (trimethylsilyl)methyl groups about the zirconium–carbon bond is not viable. Consequently, the methyl groups at the silicon atoms come close to the six-membered aromatic rings, in particular to the two ring protons at the carbon atoms C(6) and C(9), as was implied by ^{1}H NMR spectroscopic studies (*vide supra*). If one regards the bulky (trimethylsilyl)methyl group as a crude surrogate for a growing polypropylene chain $CH_2CH(Me)R$, it is quite evident that upon occupying the lateral site in fluorenyl-based *ansa*-zirconocenes, both the methyl and the polymer chain R will interfere with the ring. These steric repulsions lead to the preference of one favored conformation which allow the next incoming propylene to approach the metal only with the opposite topicity (methyl group directed away from the fluorenyl ligand), provided that the alkyl group can "swing" from one lateral site to the other.[3d]

No thermal decomposition of **4** was observed by heating to 110 °C over 24 h. Despite being 14-electron species, the alkyl complexes **2–4** are fairly unreactive toward olefins, even activated ones such as methyl methacrylate and acrylonitrile. Hydrogenolysis as well as alkyl group abstraction to give alkyl cations is being investigated. It seems that a 12-electron metal center is required for olefin polymerization.[5c]

Conclusion

In summary, the linked amido–fluorenyl ligand system exhibits coordination behavior at the zirconium(IV) center which differs somewhat from that of the linked fluorenyl–cyclopentadienyl ligand. The expected higher Lewis acidity results in the accessibility of pentacoordination.[22] However, steric saturation of the electron-deficient (14-electron) d^0 center is very facile, as illustrated by the solvent-free dialkyl **3** and **4**. The complexes described above therefore are best considered as analogs of mono(cyclopentadienyl)zirconium complexes[23] rather than as *ansa*-zirconocene complexes. It is noteworthy that to the best of our knowledge, there seems to be no mono(fluorenyl) complexes of group 4 metals known. The complexes described above also constitute the first members of this class of half-sandwich complexes which we believe owe their synthetic accessibility to the chelate effect of the ancillary ligand. Finally, the molecular structure of the dialkyl **4** has revealed intramolecular steric repulsions within the $Zr(\eta^5:\eta^1\text{-}C_{13}H_8\text{-}SiMe_2NCMe_3)$ fragment that may be relevant in the context of mechanistic discussion on syndiospecific polymerization of α-olefins by fluorene-based *ansa*-metallocenes.[7]

Experimental Section

General Consideration. All operations were performed under an inert atmosphere of nitrogen using standard Schlenk-line or glovebox techniques. THF and diethyl ether were distilled from sodium benzophenone ketyl. Pentane and hexane were purified by distillation from sodium/triglyme benzophenone ketyl. Dichlorodimethylsilane was distilled over copper turnings. *tert*-Butylamine was distilled from CaH_2 and stored over molecular sieves. $ZrCl_4(THF)_2$[24] was synthesized as described in the literature. All other chemicals were commercially available and used as received. ^{1}H NMR and ^{13}C NMR spectra were recorded in C_6D_6 at 25 °C, unless otherwise stated, on a Varian GX 400 spectrometer. The numbering scheme for the hydrogen and carbon atoms of the fluorenyl ring corresponds to that commonly used in the literature.[9f] Elemental analyses were performed by Oneida Research Services, Inc. and the Microanalytical Laboratory of this department.

(*tert*-Butylamino)dimethyl(9-fluorenyl)silane. To a solution of fluorene (16.62 g, 100 mmol) in diethyl ether (90 mL) was added at 0 °C a solution of *n*-butyllithium (40 mL, 100 mmol, 2.5 M in hexane) within 60 min. After stirring for 3 h at room temperature, the resulting orange solution was transferred to an addition funnel and added dropwise at 0 °C within 75 min to a solution of dichlorodimethylsilane (200 mL) in diethyl ether (200 mL). The resulting suspension was stirred for 30 min at room temperature, and the solvent and excess dichlorodimethylsilane were removed under vacuum. After precipitating lithium chloride with methylene chloride and filtering, followed by removal of the solvent, 21.75 g (84.0%) of an off-white solid was obtained. According to the ^{1}H NMR spectrum, the product is contaminated by 8% of bis(9-fluorenyl)dimethylsilane. ^{1}H NMR ($CDCl_3$): δ 7.89 (dd, 2H, 1-, 8-H), 7.70 (dd, 2H, 4-, 5-H), 7.43 (dt, 2H, 2-, 7-H), 7.37 (dt, 2H, 3-, 6-H), 4.13 (s, 1H, 9-H), 0.21 (s, 6H, $SiCH_3$).

To a solution of this crude 9-(chlorodimethylsilyl)fluorene (21.75 g, contaminated with 8% bis(9-fluorenyl)dimethylsilane) in diethyl ether (140 mL) was added solid lithium *tert*-butylamide (6.05 g, 76.5 mmol) at 0 °C over a period of 1 h. Stirring overnight at room temperature gave a yellow suspension. After removal of all of the volatiles under vacuum, lithium chloride was precipitated with methylene chloride and filtered off. Removal of the solvent and distillation under vacuum (bp 108–110 °C) gave a colorless oil that crystallizes at −20 °C: yield 15.93 g (70.5%). ^{1}H NMR ($CDCl_3$): δ 7.90 (dd, 2H, J_{HH} = 7.1, 1.5 Hz, 1-, 8-H), 7.69 (dd, 2H, J_{HH} = 7.0, 1.1 Hz, 4-, 5-H), 7.37 (m, 4H, 2-, 7-, 3-, 6-H), 3.97 (s, 1H, 9-H), 1.26 (s, 9H, $NCCH_3$), 0.72 (br s, 1H, N*H*), −0.03 (s, 6H, $SiCH_3$).

(22) Kubacek, P.; Hoffmann, R.; Havlas, Z. *Organometallics* **1982**, *1*, 180.

(23) (a) Wengrovius, J. E.; Schrock, R. R. *J. Organomet. Chem.* **1981**, *205*, 319. (b) Wolczanski, P. T.; Bercaw, J. E. *Organometallics* **1982**, *1*, 793. (c) Erker, G.; Sarter, C.; Albrecht, M.; Dehnicke, S.; Krüger, C.; Raabe, E.; Schlund, R.; Benn, R.; Rufinska, A.; Mynott, R. *J. Organomet. Chem.* **1990**, *382*, 79. (d) van der Hende, J. R.; Hessen, B.; Meetsma, A.; Teuben, J. H. *Organometallics* **1990**, *9*, 537.

(24) Manzer, L. E. *Inorg. Synth.* **1982**, *21*, 135.

^{13}C NMR ($CDCl_3$): δ 145.8 (C-10, -13), 140.7 (C-11, -12), 125.9, 125.1, 124.5 (C-1, -2, -3, -6, -7, -8), 119.8 (C-4, -5), 49.7 (N*C*CH$_3$), 45.0 (C-9), 33.9 (NC*C*H$_3$), −0.8 (Si*C*H$_3$). GC MS: *m/z* 294 (M$^+$). Anal. Calcd for $C_{19}H_{24}NSi$: C, 77.49; H, 8.21; N, 4.76. Found: C, 77.00; H, 8.10; N, 4.50.

[*tert*-Butyl(dimethylfluorenylsilyl)amido](tetrahydrofuran)dilithium. To a solution of (*tert*-butylamino)dimethylfluorenylsilane (0.61 g, 2.06 mmol) in 20 mL of pentane was added at −78 °C *n*-butyllithium (1.7 mL of a 2.5 M solution in hexane, 4.25 mmol) via syringe within 15 min. After the solution was warmed up to room temperature and stirred overnight, a precipitate formed. After filtration the yellow powder was washed with pentane and dried under vacuum. The yield is almost quantitative. Because of the insolubility in hydrocarbons and extreme air sensitivity, it was characterized by ^{1}H NMR spectroscopy as the tris(THF) adduct. ^{1}H NMR (C_6D_6): δ 8.39 (br d, 2H, 1-, 8-H), 7.96 (m, 2H, 4-, 5-H), 7.29 (br t, 2H, 2-, 7-H), 7.07 (t, 2H, 3-, 6-H), 2.79 (t, 12H, OC*H*$_2$), 1.40 (s, 9H, NCC*H*$_3$), 1.09 (m, 12H, OCH$_2$C*H*$_2$), 0.87 (br s, 6H, SiC*H*$_3$). ^{1}H NMR (C_6D_6, 70 °C): δ 8.19 (d, 2H, J_{HH} = 7.5 Hz, 1-, 8-H), 7.91 (d, 2H, J_{HH} = 8.7 Hz, 4-, 5-H), 7.27 (t, 2H, J_{HH} = 8.0, 7.1 Hz, 2-, 7-H), 6.99 (t, 2H, J_{HH} = 7.6 Hz, 3-, 7-H), 3.01 (m, 12H, OC*H*$_2$), 1.24 (s, 9H, NCC*H*$_3$), 1.24 (m, 12H, OCH$_2$C*H*$_2$), 0.87 (br s, 6H, SiC*H*$_3$).

[η^1:η^5-*tert*-Butyl(dimethylfluorenylsilyl)amido]dichloro(tetrahydrofuran)zirconium (1a). A solution of (*tert*-butylamino)dimethylfluorenylsilane (4.79 g, 16.2 mmol) in diethyl ether (180 mL) was treated at −78 °C with *n*-butyllithium in hexane (13.0 mL of a 2.5 M solution, 32.4 mmol) within 20 min. After the solution was stirred for 2 h at −78 °C and 2 h at room temperature, the solvent was removed and the resulting orange residue redissolved in THF. $ZrCl_4(THF)_2$ was added as a solid at −78 °C over a period of 40 min, and after the solution was stirred for 2 h at −78 °C, it was gradually warmed up to room temperature. After overnight stirring, all volatiles were removed under vacuum and LiCl was precipitated with toluene and filtered off. The filtrate was concentrated to ca. 5 mL and, after addition of pentane, was cooled to −30 °C to afford a yellow microcrystalline precipitate. Concentration of the filtrate and precipitation with pentane yielded a second crop: total yield 4.80 g (56.1%). ^{1}H NMR ($C_6D_5CD_3$): δ 7.92 (d, 2H, J_{HH} = 7.9 Hz, 1-, 8-H), 7.76 (d, 2H, J_{HH} = 7.7 Hz, 4-, 5-H), 7.31 (dt, 2H, J_{HH} = 7.9, 7.2 Hz, 2-, 7-H), 7.14 (dt, 2H, J_{HH} = 7.3, 7.7 Hz, 3-, 6-H), 2.43 (br t, 4H, OC*H*$_2$), 1.64 (s, 9H, NCC*H*$_3$), 0.75 (br t, 4H, OCH$_2$C*H*$_2$), 0.52 (s, 6H, SiC*H*$_3$). ^{13}C{^{1}H} NMR ($C_6D_5CD_3$): δ 140.5 (C-10, -13), 137.3 (C-11, -12), 126.5 (C-3, -6), 122.8 (C-1, -8), 120.9 (C-4, -5), 120.4 (C-2, -7), 95.8 (C-9), 73.6 (O*C*H$_2$), 59.9 (N*C*CH$_3$), 33.7 (NC*C*H$_3$), 25.0 (OCH$_2$*C*H$_2$), 1.6 (Si*C*H$_3$). Anal. Calcd for $C_{27}H_{39}Cl_2NO_2SiZr$: C, 54.06; H, 6.55; N, 2.34. Found: C, 54.57; H, 6.33; N, 2.57.

[η^1:η^5-*tert*-Butyl(dimethylfluorenylsilyl)amido]dichloro(diethyl ether)zirconium (1b). This compound was synthesized from $ZrCl_4(Et_2O)_2$ in a manner analogous to that described for the preparation of **1a** and isolated as yellow microcrystals: yield 50%. ^{1}H NMR (C_6D_6): δ 7.99 (d, 2H, J_{HH} = 7.8 Hz, 1-, 8-H), 7.78 (d, 2H, J_{HH} = 7.7 Hz, 4-, 5-H), 7.34 (dt, 2H, J_{HH} = 7.9, 7.2 Hz, 2-, 7-H), 7.15 (dt, 2H, J_{HH} = 7.3, 7.7 Hz, 3-, 6-H), 2.60 (br, 4H, OC*H*$_2$), 1.67 (s, 9H, NCC*H*$_3$), 0.74 (br, 6H, OCH$_2$C*H*$_3$), 0.54 (s, 6H, SiC*H*$_3$). ^{13}C{^{1}H} NMR (C_6D_6): δ 140.6 (C-10, -13), 137.4 (C-11, -12), 126.6 (C-3, -6), 122.9 (C-1, -8), 120.4 (C-4, -5), 120.5 (C-2, -7), 96.0 (C-9), 73.0 (O*C*H$_2$), 60.0 (N*C*CH$_3$), 33.8 (NC*C*H$_3$), 25.1 (OCH$_2$*C*H$_3$), 1.6 (Si*C*H$_3$).

[η^1:η^5-*tert*-Butyl(dimethylfluorenylsilyl)amido]dimethyl(tetrahydrofuran)zirconium (2). Methylmagnesium chloride in THF (1.45 mL, 4.35 mmol, 2.5 M) was added to a solution of zirconium dichloro complex **1a** (1.13 g, 2.14 mmol) in THF (60 mL) at −78 °C within 15 min. After stirring for 1 h at −78 °C, the reaction mixture was gradually warmed up to −20 °C and stirred for an additional hour below −15 °C. The solvent was removed under vacuum, keeping the temperature below −15 °C. Warming up of the reaction mixture above 0 °C led to almost spontaneous darkening and complete decomposition. Extraction of the residue with a 1:1 mixture of pentane and toluene (60 mL) gave, after evaporating all volatiles, a thermally and light-sensitive yellow powder: yield 0.60 g (59.0%). ^{1}H NMR (C_6D_6): δ 7.92 (d, 2H, J_{HH} = 7.8 Hz, 1-, 8-H), 7.79 (d, 2H, J_{HH} = 7.8 Hz, 4-, 5-H), 7.30 (dt, 2H, J_{HH} = 8.1, 7.8, 1.2 Hz, 2-, 7-H), 7.19 (dt, 2H, J_{HH} = 8.1, 7.8, 1.2 Hz, 3-, 6-H), 2.32 (br m, 4H, OC*H*$_2$), 1.60 (s, 9H, NCC*H*$_3$), 0.82 (br m, 4H, OCH$_2$C*H*$_2$), 0.62 (s, 6H, SiC*H*$_3$), 0.32 (s, 6H, ZrC*H*$_3$). ^{13}C NMR (C_6D_6): δ 140.9 (C-10, -13), 134.2 (C-11, -12), 125.6 (C-3, -6), 121.3 (C-1, -8), 120.9 (C-4, -5), 120.8 (C-2, -7), 86.2 (C-9), 71.2 (O*C*H$_2$), 57.3 (N*C*CH$_3$), 40.6 (q, J_{CH} = 114 Hz, Zr*C*H$_3$), 34.8 (NC*C*H$_3$), 25.0 (OCH$_2$*C*H$_2$), 3.8 (Si*C*H$_3$). Anal. Calcd for $C_{25}H_{37}NOSiZr$: C, 61.67; H, 7.66; N, 2.80. Found: C, 60.51; H, 7.47; N, 2.61.

[η^1:η^5-*tert*-Butyl(dimethylfluorenylsilyl)amido]diphenylzirconium (3). Phenylmagnesium chloride (0.93 mL, 1.86 mmol, 2.0 M in THF) was added via syringe to a solution of the dichloro complex **1a** (0.49 g, 0.93 mmol) in diethyl ether (50 mL) at −78 °C. The reaction mixture was allowed to warm up to −15 °C and stirred for 2.5 h below −10 °C. The solvent was removed under vacuum, keeping the temperature below 0 °C. When the reaction mixture warmed up to room temperature, extensive decomposition occurred, as observed by darkening of the mixture. Extraction of the residue with a 1:1 mixture of pentane and toluene (60 mL), followed by filtration and evaporating of all volatiles, gave the product as a yellow powder in 40% yield. ^{1}H NMR ($C_6D_5CD_3$): δ 7.82 (d, 2H, J_{HH} = 8.3 Hz, 1-, 8-H), 7.79 (d, 2H, J_{HH} = 8.6 Hz, 4-, 5-H), 7.29 (br, 4H, C_6H_5), 6.99 (br m, 6H, C_6H_5); 6.89 (t, 2H, J_{HH} = 7.7, 7.0 Hz, 2-, 7-H); 6.66 (t, 2H, J_{HH} = 7.7, 7.0 Hz, 3-, 6-H), 1.22 (s, 9H, NCC*H*$_3$), 0.86 (s, 6H, SiC*H*$_3$). ^{13}C NMR (C_6D_6): δ 188.5 (p-C_6H_5), 136.3 (C-10, -13), 135.3 (C-11, -12), 135.1 (p-C_6H_5), 128.0 (C-3, -6), 126.4 (C-1, -8), 124.5 (C-4, -5), 123.9 (C-2, -7), 68.1 (C-9), 57.2 (N*C*CH$_3$), 34.0 (NC*C*H$_3$), 6.5 (Si*C*H$_3$). Anal. Calcd for $C_{25}H_{37}NOSiZr$: C, 69.10; H, 6.17; N, 2.60. Found: C, 69.18; H, 6.37; N, 2.39.

[η^1:η^5-*tert*-Butyl(dimethylfluorenylsilyl)amido{bis(trimethylsilyl)methyl}zirconium (4). A solution of ((trimethylsilyl)methyl)magnesium chloride (6 mL, 1.0 M solution in ether, 6 mmol) was added via syringe to a solution of the zirconium dichloro complex **1a** (1.14 g, 2.16 mmol) in 70 mL of diethyl ether at −78 °C within 15 min. After the addition was complete, the reaction mixture was warmed up to 0 °C and left stirring for 4 h. The solvent was removed under vacuum, leaving a yellow powder. Extraction of the residue with pentane (60 mL), filtration, concentration, and crystallization at 0 °C afforded 1.10 g (91.0%) of yellow needles. ^{1}H NMR (C_6D_6): δ 7.84 (d, 2H, J_{HH} = 7.1 Hz, 1-, 8-H), 7.80 (d, 2H, J_{HH} = 7.9 Hz, 4-, 5-H), 7.13 (dt, 2H, J_{HH} = 8.1, 7.7, 1.0 Hz, 2-, 7-H); 7.19 (dt, 2H, J_{HH} = 8.1, 7.0, 1.2 Hz, 3-, 6-H), 1.33 (s, 9H, NCC*H*$_3$), 0.77 (s, 6H, SiC*H*$_3$), 0.09 (s, 9H, CH$_2$SiC*H*$_3$), −0.49 (d, J_{HH} = 10.5, ZrC*H*$_2$), −1.26 (d, J_{HH} = 10.5, ZrC*H*$_2$). ^{13}C NMR ($C_6D_5CD_3$): δ 135.7 (C-10, -13), 128.3 (C-3, -6), 126.2 (C-1, -8), 123.8 (C-4, -5), 123.6 (C-2, -7), 120.2 (C-11, -12), 74.3 (C-9), 57.2 (t, Zr*C*H$_2$), J_{CH} = 104 Hz), 56.1 (N*C*CH$_3$), 34.2 (NC*C*H$_3$), 6.5 (Si*C*H$_3$), 3.6 (CH$_2$Si*C*H$_3$). Anal. Calcd for $C_{27}H_{45}NSi_3Zr$: C, 58.00; H, 8.11; N, 2.51. Found: C, 57.49; H, 7.92; N, 2.30.

X-ray Structure Determination. Crystal data for **4** are summarized in Table 1. The compound, obtained as yellow crystals by slow cooling of an *n*-pentane solution, crystallizes in the monoclinic space group $P2_1/n$. Data collection in the range 2° < θ < 22.5° was performed using ω-scans on an Siemens P4 diffractometer with graphite-monochromated Mo Kα radiation. From 5252 measured reflections, all 3987 independent reflections were used and 289 parameters were refined by full-matrix least-squares on F_o^2 data (SHELXL-

93).[25] The structure was solved using direct methods (SHELXS-86)[26] and difference Fourier syntheses and refined with anisotropic thermal parameters for the non-hydrogen atoms. All hydrogen atoms were located and refined isotropically. Refinements converged with residuals of $wR_2 = 0.079$ for all F_o^2 data corresponding to $R = 0.0308$ for 3241 observed reflections with $F_o^2 > 46(F)$.

Acknowledgment. We gratefully acknowledge financial support from the Volkswagen-Foundation, the Fonds der Chemischen Industrie, General Electric Co., and the donors of the Petroleum Research Fund, administered by the American Chemical Society. Part of this work was performed at the State University of New York at Albany. We are indebted to Professor J. E. Bercaw for helpful discussions and communicating unpublished results.

(25) Sheldrick, G. M. SHELXL-93, Program for the Refinement of Crystal Structures; University of Göttingen, Germany, 1993.
(26) Sheldrick, G. M. SHELXS-86, Program for the Solution of Crystal Structures; University of Göttingen, Germany, 1986.

Supplementary Material Available: Listings of all crystal data and refinement parameters, atomic parameters including hydrogen atoms, thermal parameters, and bond lengths and angles for **4** (8 pages). Ordering information is given on any current masthead page.

OM9406052

Structural and Reactivity Consequences of the Presence of Lone Pairs in Main-Group–Transition-Metal Cluster Compounds: Conversion of $[HAs\{Fe(CO)_4\}_3]^{2-}$ into $[Fe_3(CO)_9\{\mu_3\text{-}AsFe(CO)_4\}_2]^{2-}$

Robert E. Bachman, Suzanne K. Miller, and Kenton H. Whitmire*

Department of Chemistry, Rice University, P.O. Box 1892, Houston, Texas 77251

Received June 24, 1994[⊗]

The reaction of $NaAsO_2$ with $Fe(CO)_5$/KOH/MeOH produces the novel hydrido cluster $[HAs\{Fe(CO)_4\}_3]^{2-}$. An X-ray structural study was carried out on the $[PPN]^+$ salt at 173 K in an attempt to crystallographically confirm the presence of the hydrogen atom. The material crystallizes in the trigonal space group $P\bar{3}$ (No. 147) with a = 25.379(4) Å, b = 25.379(4) Å, c = 22.442(4) Å, V = 12518.2(36) Å^3, and Z = 6. The reactivity of this unusual cluster anion was probed by pyrolysis, photolysis, and protonation. Addition of acid produced the previously characterized cluster $As_2Fe_6(CO)_{22}$. Pyrolysis and thermolysis both yielded the dianion $[Fe_3(CO)_9\{\mu_3\text{-}AsFe(CO)_4\}_2]^{2-}$. This material was crystallized as its $[Et_4N]^+$ salt, and the structure was determined by single-crystal X-ray diffraction. $[Et_4N]_2[As_2Fe_5(CO)_{17}]$ crystallizes in the triclinic space group $P\bar{1}$ (No. 2) with a = 12.466(2) Å, b = 13.408(3) Å, c = 15.457(3) Å, α = 80.59(3)°, β = 72.01(3)°, γ = 66.66(3)°, and V = 2253.7(8) Å^3. The cluster consists of a distorted-square-pyramidal E_2M_3 core with the two main-group atoms ligated by $Fe(CO)_4$ fragments. Comparisons of the structure and reactivity of both $[PPN]_2[HAs\{Fe(CO)_4\}_3]$ and $[Et_4N]_2[Fe_3(CO)_9\{\mu_3\text{-}AsFe(CO)_4\}_2]$ with those of other isoelectronic and isostructural clusters containing either group 15 or 16 elements has led to a correlation between the observed structure and reactivity patterns and the presence of a lone pair of electrons on the main-group element.

Introduction

Transition-metal clusters which contain main-group fragments have been of interest for many years due to their unusual bonding and reactivity patterns.[1] The first arsenic-containing transition-metal clusters were prepared in the late 1950s by Hieber and co-workers from the reaction of arsenic oxides with $Fe(CO)_5$ in basic methanol followed by acidification.[2] However, the initially formed anionic species from this reaction were not characterized due to limitations in the analytic tools available at the time. Since arsenic lies at the midpoint of the group 15 elements, its study should provide important information about structural and reactivity trends as the main-group element increases in size and in metallic character. This intermediate behavior has been demonstrated by clusters such as $Fe_3(CO)_9(AsPh)_2$,[3] which has an isostructural counterpart in the analogous, lighter P-containing compound, and $As_2\{W(CO)_5\}_3$, which which is similar to compounds containing heavier antimony and bismuth atoms.[4]

We recently reported the synthesis and structural characterization of the novel anionic species $[HAs\{Fe(CO)_4\}_3]^{2-}$ ([**I**]$^{2-}$).[5] In the study of the reactivity of this unusual species and the related clusters $[E\{Fe(CO)_4\}_3]^{2-}$ (E = Se, Te),[6] it has become apparent that their reactivities are distinctly different even though they are essentially isostructural and isoelectronic. The major feature which distinguishes these sets of clusters is the presence or absence of a lone pair on the main-group element. This paper explores the effect that the presence or absence of these lone pairs has on both the structure and reactivity of several isoelectronic and isostructural clusters which contain group 15 and 16 elements.

Experimental Procedures

General Considerations. All reactions and other manipulations were performed with oven-dried Schlenkware using standard techniques on a Schlenk line or in a Vacuum Atmospheres drybox. All solvents were dried and distilled under nitrogen prior to use: methanol (Mg), THF (Na/Ph_2CO), and hexane ($LiAlH_4$). Bis(triphenylphosphine)nitrogen(1+) chloride, [PPN]Cl, was prepared according to literature methods.[7] $Fe(CO)_5$ (Aldrich), $NaAsO_2$ (Baker), $[Et_4N]Br$ (Janssen), and KOH (EM Science) were used as received without further purification. Solution IR spectra were recorded in 0.1 mm pathlength CaF_2 cells on a Perkin-Elmer Model 1640 FT-IR spectrophotometer. ^1H and ^{13}C NMR spectra were obtained on a Bruker AF 300 spectrometer in THF-d_8. EI, FAB, and

⊗ Abstract published in *Advance ACS Abstracts*, December 15, 1994.

(1) For recent reviews see: (a) Scherer, O. J. *Angew. Chem., Int. Ed. Engl.* **1985**, *24*, 924. (b) Herrmann, W. A. *Angew. Chem., Int. Ed. Engl.* **1986**, *25*, 56. (c) Huttner, G. *Pure Appl. Chem.* **1986**, *58*, 585. (d) Whitmire, K. H. *J. Coord. Chem. B* **1988**, *17*, 95. (e) Fenske, D.; Ohmer, J.; Hachgenei, J.; Merzweiler, K. *Angew. Chem., Int. Ed. Engl.* **1988**, *27*, 1277. (f) Norman, N. C. *Chem. Soc. Rev.* **1988**, *17*, 269. (g) Scherer, O. J. *Angew. Chem., Int. Ed. Engl.* **1990**, *29*, 1104. (h) Compton, N. A.; Errington, R. J.; Norman, N. C. *Adv. Organomet. Chem.* **1990**, *31*, 91. (i) Whitmire, K. H. *J. Cluster Sci.* **1991**, *2*, 231. (j) Roof, L. C.; Kolis, J. W. *Chem. Rev.* **1993**, *93*, 1037.

(2) Hieber, W.; Gruber, J.; Lux, F. *Z. Anorg. Allg. Chem.* **1959**, *300*, 275.

(3) Huttner, G.; Mohr, G.; Frank, A.; Schubert, U. *J. Organomet. Chem.* **1976**, *118*, C73.

(4) Sigwarth, B.; Zsolnai, L.; Berke, H.; Huttner, G. *J. Organomet. Chem.* **1982**, *226*, C5.

(5) Bachman, R. E.; Miller, S. K.; Whitmire, K. H. *Inorg. Chem.* **1994**, *33*, 2075.

(6) Bachman, R. E.; Whitmire, K. H. *Inorg. Chem.*, in press.

(7) Ruff, J. K.; Schlientz, W. S. *Inorg. Synth.* **1975**, *15*, 84.

0276-7333/95/2314-0796$09.00/0

ESI mass spectra were obtained on a VG Analytical Autospec 3000. FAB mass spectra were performed in a matrix of 3-nitrobenzyl alcohol (*m*-NBA). Carbon monoxide analyses were performed using a Rodder Toepler pump.

CO Analyses Using Toepler Pump. A sample of the compound to be analyzed was weighed into a vacuum flask such that the amount of compound used produced a final gas pressure of approximately 200–300 mmHg in a volume of 45–55 mL. A 10-fold excess of pyridinium tribromide, $[C_5H_5NH][Br_3]$, was then weighed into the same flask. The flask was attached to a vacuum line, and approximately 25 mL of predried and carefully freeze–thaw-degassed dichloromethane was distilled onto the solids at −196 °C. After the flask was sealed, the solvent was thawed and the mixture was heated at between 75 and 80 °C for 2–3 h. The reaction mixture was then cooled to −196 °C and the CO collected and quantified utilizing the Toepler pump.

Synthesis of Salts of $[HAs\{Fe(CO)_4\}_3]^{2-}$ ($[I]^{2-}$). KOH (1.5 g, 27 mmol) was dissolved in 50 mL of MeOH, and the resulting mixture was stirred until the base had completely dissolved and the solution had cooled to room temperature. $Fe(CO)_5$ (1.0 mL, 7.6 mmol) was then added to the solution rapidly by syringe. This mixture was stirred for 30 min to yield a light yellow solution. When the solid $NaAsO_2$ (0.32 g, 2.5 mmol) was added in one portion, the reaction mixture slowly changed from yellow to deep red. The mixture was stirred for 4–5 h to assure complete reaction. Excess solid [PPN]Cl (3.5 g) was added to the reaction solution, and this mixture was stirred for 30 min, resulting in the formation of a brick red precipitate. The solids were isolated by filtration and dried *in vacuo*. The crude product was purified by dissolving the solids in minimal THF and filtering the solution to remove any insoluble material. The filtered solution was then layered with approximately 3 volumes of MeOH. Diffusion of the MeOH into the THF results in the formation of large red hexagonal plate-like crystals. Yield: 2.85 g (70%). IR (THF, cm^{-1}): 2015 w, 1985 s, 1915 s, 1895 s. ^1H NMR (THF-d_8, ppm): 7.8–7.5 (m). ^{13}C NMR (THF-d_8, ppm): 221.4 (CO), 134.8, 131.8 (J_{C-P} = 211 Hz), 128.9, 127.5. MS (FAB, mNBA): m/z 579 (M^+). Calculated for $C_{84}H_{61}AsFe_3N_2O_{12}P_4$: 7.24×10^{-3} mol of CO/g. Found: 7.22×10^{-3} mol of CO/g.

The $[Et_4N]^+$ salt was isolated by adding a solution of 1.5 g of $[Et_4N]Br$ in 100 mL of deaerated water to the above reaction solution in place of the [PPN]Cl. The fine brick red precipitate, which formed immediately, was isolated by filtration and dried *in vacuo* overnight. The crude product was purified by dissolving it in a minimal amount of THF and filtering the solution to remove any insoluble material. The product was then reprecipitated by adding a large excess of hexane. Yield: 1.92 g (79% based on As). This material can be further purified by recrystallization from slow diffusion of hexane into a THF solution. IR (THF, cm^{-1}): 2015 w, 1986 s, 1915 sh, 1899 s.

Deprotonation of $[I]^{2-}$. $M_2[I]$ (M = Na, K) was synthesized as detailed above and isolated by removing the methanol under vacuum. The solids were then extracted into 100 mL of ether and filtered to remove the inorganic salts. The ether was removed *in vacuo* to yield a very air sensitive red powder. Between 400 and 500 mg of this powder was transferred to a vacuum flask, and 35 mL of carefully degassed THF was then vacuum-distilled into the flask. The solution was then frozen at −196 °C and 1.3 equiv of methyllithium in ether was transferred to the flask under an atmosphere of helium. After the transfer the flask was evacuated and sealed before allowing it to return to room temperature. After sitting at room temperature for between 30 min and 1 h, the flask was again cooled to −196 °C. The head gases were then collected and quantified with a Toepler pump; 1.4 mol of gas was collected per mole of cluster. The gases were then identified as being composed primarily of methane by EI mass spectrometry. Weak signals indicative of CO were also observed. When this procedure was repeated with a sample of the cluster salt synthesized in MeOD, the primary off-gases were identified as CH_3D.

Protonation of $[I]^{2-}$. An approximately 1 M aqueous solution of HCl was added slowly dropwise to the methanol reaction mixture prepared above. The addition was continued until all the product had precipitated and the remaining solution was either colorless or a very pale red color, approximately 200 mL. The resulting red-black precipitate was collected by filtration and dried *in vacuo* overnight. The solids were extracted with 150 mL of hexane for 1–2 h, after which the resulting solution was filtered to remove the remaining solids. The hexane extract was then allowed to stand for between 1 and 2 weeks, during which time additional solids precipitated. These insoluble residues were removed by filtration and the solution was concentrated to approximately 50 mL. The concentrated solution was passed over a short Florisil column (5 × 2 cm) and cooled to −20 °C for several days to yield a small amount of very small green crystals. IR (hexane, cm^{-1}): 2112 w, 2098 m, 2066 s, 2058 w, 2044 vs, 1996 m, 1969 m. MS (EI): m/z 1102 (M^+).

Synthesis of $[Et_4N]_2[Fe_3(CO)_9\{\mu_3\text{-}AsFe(CO)_4\}_2]$ ($[Et_4N]_2$-[II]). Method 1: Photolysis. $[Et_4N]_2$[I] (0.25 g, 0.21 mmol) was dissolved in 40 mL of THF and placed in a standard 100 mL Pyrex Schlenk flask. The sealed flask was then placed in a water-cooled photoreactor apparatus equipped with a 450-W Hanovia medium-pressure mercury lamp. IR spectroscopy indicated that all the starting material had been consumed after approximately 2 h. The major reaction product was $[Et_4N]_2$[II]. Unfortunately, the reaction mixture was contaminated with a second compound which was difficult to separate because of its similar solubilities. A better method was therefore sought for the preparation of $[Et_4N]_2$[II].

Method 2: Pyrolysis. $[Et_4N]_2$[I] (0.25 g, 0.21 mmol) was dissolved in 50 mL of THF and heated to reflux for 4 or 5 h. The solution was cooled to room temperature and filtered to remove a small amount of insoluble material. The THF was removed *in vacuo* to yield an oily dark red solid. The product was recrystallized by dissolving it in minimal CH_2Cl_2 and cooling the solution to −20 °C for several days. Yield: 80 mg (65% based on As). IR (THF, cm^{-1}): 2010 s, 1993 s, 1971 s, 1925 m. ^1H NMR (THF-d_8, ppm): 3.21 (2H, q, J = 7.0 Hz), 1.24 (3H, t, J = 7.0 Hz). ^{13}C NMR (THF-d_8, ppm): 220.1, 217.9, 213.0, 52.9, 7.4. MS (ESI, CH_2Cl_2): 1295.9 (M^- + $3[Et_4N]^+$). Anal. Calcd for $C_{33}H_{40}As_2Fe_5N_2O_{17}$: C, 34.0; H, 3.46; N, 2.40. Found: C, 34.6; H, 3.46; N, 2.54.

Structure of $[PPN]_2$[I]·THF at 173 K. A red block of approximate dimensions 0.50 × 0.50 × 0.50 mm, which had been cut from a large hexagonal platelike crystal, was selected for data collection. The crystal was mounted on a glass fiber with epoxy cement. The unit cell determination and the data collection were performed on an automated Rigaku AFC5S four-circle diffractometer using the TEXSAN data collection package.[8] Final unit cell parameters were based on a least-squares analysis of 25 carefully centered reflections (6.50° ≤ 2θ ≤ 9.50°). The unit cell parameters and space group assignment were consistent with those found in an earlier study conducted at 223 K ($P\bar{3}$, No. 147).[5] No decay correction was applied because only random fluctuations were seen in the standard intensities. The iron and arsenic positions were determined by direct methods using SHELX-86. The other atoms were found in difference maps after sequential least-squares cycles. The structure refinement was carried out on F^2 using SHELXL-93.[9] All non-hydrogen atoms in the cluster and the cations were refined anisotropically. A lattice solvent disordered in two major orientations was located in a general position and was modeled by constraining the bond metricals for each orientation to idealized values and refining occupancy

(8) Rigaku MSC Automatic Data Collection Control Software, v 3.2.1; Molecular Structure Corp., The Woodlands, TX, 1987.
(9) Sheldrick, G. M., SHELXL-93 Univeristät Göttingen, Göttingen Germany, 1993.

Table 1. Crystal Data and Structure Refinement Details for $[PPN]_2[I]\cdot THF$ and $[Et_4N]_2[II]$

empirical formula	$C_{88}H_{69}AsFe_3N_2O_{13}P_4$	$C_{33}H_{40}As_2Fe_5N_2O_{17}$
fw	1728.80	1165.76
temp (K)	293(2)	173(2)
wavelength (Å)	0.710 30 Å	0.71030
cryst syst	trigonal	triclinic
space group	$P\bar{3}$ (No. 147)	$P\bar{1}$ (No. 2)
unit cell dimens	a = 25.379(4) Å, c = 22.442(4) Å	a = 12.466(2) Å, b = 13.408(3) Å, c = 15.457(3) Å, α = 80.59(3)°, β = 72.01(3)°, γ = 66.66(3)°.
V (Å)	12 518.2(36)	2253.7(8)
Z	6	2
density (calcd) (g/cm^3)	1.376	1.718
abs coeff (mm^{-1})	1.047	3.096
F(000)	5316	1168
cryst size	0.4 × 0.2 × 0.4	0.3 × 0.3 × 0.5
θ range for data collection deg)	2.04−22.42	2.06−25.00
index ranges	$0 \le h \le 24, -21 \le k \le 23, 0 \le l \le 23$	$-14 \le h \le 13, -14 \le k \le 0, -18 \le l \le 18$
no. of rflns collected	10 068	7269
no. of indep rflns	9439 (R(int) = 0.0250)	6898 (R(int) = 0.0222)
refinement method	full-matrix least squares on F^2	full-matrix least squares on F^2
no. of data/restraints/params	9428/10/997	6894/0/532
goodness of fit on F^2	1.054	1.025
final R indices ($I > 2\sigma(I)$]	R1 = 0.0479, wR2 = 0.1340	R1 = 0.0295, wR2 = 0.0651
R indices (all data)	R1 = 0.0721, wR2 = 0.1624	R1 = 0.0482, wR2 = 0.0725
largest diff peak and hole (e/Å^3)	1.764 and −0.432	0.816 and −0.653

Table 2. Selected Atomic Coordinates (×10^4) and Equivalent Isotropic Displacement Parameters (Å^2 × 10^3) for $[PPN]_2[I]\cdot THF$[a]

atom	x	y	z	U(eq)
As(1)	0	0	2266(1)	30(1)
Fe(1)	−407(1)	678(1)	2506(1)	33(1)
O(11)	204(2)	890(3)	3677(2)	66(2)
O(12)	247(2)	1352(2)	1426(2)	65(1)
O(13)	−1653(2)	−346(2)	2358(2)	59(1)
O(14)	−792(2)	1556(2)	2796(2)	58(1)
C(11)	−35(3)	794(3)	3219(3)	44(2)
C(12)	1(3)	1087(3)	1856(3)	44(2)
C(13)	−1157(3)	52(3)	2416(3)	41(2)
C(14)	−647(3)	1204(3)	2682(3)	44(2)
As(2)	6667	3333	2981(1)	24(1)
Fe(2)	6048(1)	2247(1)	3219(1)	28(1)
O(21)	6643(2)	2529(2)	4393(2)	50(1)
O(22)	6603(2)	2053(2)	2148(2)	57(1)
O(23)	4913(2)	2291(2)	3148(2)	51(1)
O(24)	5409(2)	948(2)	3483(3)	69(2)
C(21)	6415(3)	2431(3)	3922(3)	36(2)
C(22)	6386(3)	2137(3)	2572(3)	37(2)
C(23)	5368(3)	2293(2)	3161(3)	35(2)
C(24)	5656(3)	1463(3)	3378(3)	39(2)
As(3)	6667	3333	8423(1)	34(1)
Fe(3)	6366(1)	2267(1)	8657(1)	41(1)
O(31)	6976(2)	2695(2)	9812(2)	66(2)
O(32)	5071(2)	1897(2)	8596(3)	75(2)
O(33)	7029(3)	2289(3)	7574(3)	98(2)
O(34)	6050(3)	1025(3)	8968(3)	97(2)
C(31)	6740(3)	2548(3)	9351(3)	42(2)
C(32)	5589(3)	2062(3)	8612(3)	50(2)
C(33)	6774(4)	2298(4)	8014(4)	62(2)
C(34)	6178(3)	1521(4)	8837(4)	61(2)

[a] U(eq) is defined as one third of the trace of the orthogonalized $\mathbf{U}_{ij}$ tensor.

Table 3. Selected Bond Lengths and Angles for $[PPN]_2[I]\cdot THF$[a]

Lengths (Å)			
As(1)−Fe(1)	2.4683(10)	Fe−C	1.754(8)−1.793(7)
As(2)−Fe(2)	2.4554(9)	C−O	1.151(8)−1.188(9)
As(3)−Fe(3)	2.4723(10)		

Angles (deg)			
Fe(1)−As(1)−Fe(1)*	115.35(2)	C(14)−Fe(1)−C(13)	94.6(3)
C(14)−Fe(1)−C(12)	93.5(3)	C(13)−Fe(1)−C(12)	118.4(3)
C(14)−Fe(1)−C(11)	91.7(3)	C(13)−Fe(1)−C(11)	119.0(3)
C(12)−Fe(1)−C(11)	121.6(3)	C(14)−Fe(1)−As(1)	176.1(2)
C(13)−Fe(1)−As(1)	89.2(2)	C(12)−Fe(1)−As(1)	84.5(2)
C(11)−Fe(1)−As(1)	86.6(2)	Fe(2)−As(2)−Fe(2)*	115.38(2)
C(24)−Fe(2)−C(22)	91.9(3)	C(24)−Fe(2)−C(21)	92.6(3)
C(22)−Fe(2)−C(21)	122.5(3)	C(24)−Fe(2)−C(23)	94.0(3)
C(22)−Fe(2)−C(23)	120.4(3)	C(21)−Fe(2)−C(23)	116.4(3)
C(24)−Fe(2)−As(2)	175.5(2)	C(22)−Fe(2)−As(2)	84.8(2)
C(21)−Fe(2)−As(2)	86.6(2)	C(23)−Fe(2)−As(2)	90.4(2)
Fe(3)−As(3)−Fe(3)*	115.61(2)	C(34)−Fe(3)−C(33)	94.2(4)
C(34)−Fe(3)−C(32)	92.0(3)	C(33)−Fe(3)−C(32)	120.8(4)
C(34)−Fe(3)−C(31)	91.8(3)	C(33)−Fe(3)−C(31)	121.1(3)
C(32)−Fe(3)−C(31)	117.5(3)	C(34)−Fe(3)−As(3)	177.8(3)
C(33)−Fe(3)−As(3)	85.6(3)	C(32)−Fe(3)−As(3)	90.0(2)
C(31)−Fe(3)−As(3)	86.4(2)	Fe−C−O	175.6(5)−177(6)

[a] An asterisk denotes a symmetry related atom.

factors and the isotropic displacement parameters for the non-hydrogen atoms iteratively. The occupancy factors of the two orientations were constrained to sum to unit occupancy. The hydrogen atoms for the cations and solvent were included in calculated positions using a riding model with fixed isotropic displacement parameters. Residual peaks along one of the 3-fold axes indicated a potential location for yet another lattice solvent molecule of THF. Attempts to model this solvent molecule were not particularly satisfying, and the occupancy appeared to be very low (ca. 16%). Because of the combination of crystallographic disorder and low occupancy, this additional lattice solvent was ignored in the final refinement cycles. There was no perceptible effect on the details of the structure whether or not this solvent molecule was included in the refinement.

The difference maps consistently revealed three peaks located along the 3-fold axes, approximately 1.35−1.50 Å from each arsenic, which are believed to be the locations of the hydrogen atoms. Not surprisingly, due to the proximity to the heavy atoms, these positions could not be refined. The hydrogen atoms were therefore included in the found locations but not refined, and no particular inferences can be drawn from the As−H distances. The data collection and refinement parameters are listed in Table 1. Selected positional and displacement parameters are given in Table 2, and selected bond metricals are given in Table 3.

Structure of $[Et_4N]_2[II]$. A dark red irregular block (0.3 × 0.3 × 0.5 mm) cut from a larger crystal was chosen for data collection. The crystal was mounted on a glass fiber with epoxy cement. Data collection was carried out on a Rigaku AFC5S diffractometer.[8] The unit cell was determined by the careful refinement of 25 random reflections (6.5° ≤ 2θ ≤ 14.0°). The crystal was shown to be triclinic and the more common

Table 4. Atomic Coordinates ($\times 10^4$) and Equivalent Isotropic Displacement Parameters ($Å^2 \times 10^3$) for $[Et_4N]_2[II]$[a]

atom	x	y	z	U(eq)
As(1)	3927(1)	2572(1)	7792(1)	28(1)
As(2)	6516(1)	2133(1)	6875(1)	27(1)
Fe(1)	5623(1)	1734(1)	8396(1)	31(1)
Fe(2)	5002(1)	3756(1)	7555(1)	29(1)
Fe(3)	4866(1)	2770(1)	6226(1)	30(1)
Fe(4)	1889(1)	2721(1)	8629(1)	41(1)
Fe(5)	8647(1)	1552(1)	6172(1)	33(1)
O(11)	7837(3)	1248(3)	8958(2)	69(1)
O(12)	5894(3)	−402(3)	7960(2)	65(1)
O(13)	4179(3)	1963(3)	10305(2)	69(1)
O(21)	6477(3)	4924(3)	6349(3)	75(1)
O(22)	5204(4)	4176(3)	9272(2)	84(1)
O(23)	2712(3)	5571(2)	7593(2)	58(1)
O(31)	5348(4)	624(3)	5682(3)	82(1)
O(32)	2618(3)	4167(3)	5742(2)	71(1)
O(33)	6131(3)	3778(3)	4630(2)	57(1)
O(41)	1663(4)	4615(3)	9489(3)	92(1)
O(42)	2924(3)	614(3)	9557(2)	66(1)
O(43)	1248(3)	2886(3)	6921(3)	70(1)
O(44)	−570(4)	2882(4)	9645(3)	114(2)
O(51)	8541(3)	3140(4)	7319(3)	101(2)
O(52)	8090(3)	1401(3)	4496(2)	56(1)
O(53)	9231(3)	−558(3)	7169(2)	67(1)
O(54)	11078(3)	1378(4)	5070(2)	85(1)
C(11)	6982(4)	1452(4)	8726(3)	44(1)
C(12)	5790(4)	441(4)	8142(3)	41(1)
C(13)	4719(4)	1880(3)	9555(3)	42(1)
C(21)	5928(4)	4432(3)	6827(3)	45(1)
C(22)	5153(4)	3943(3)	8608(3)	46(1)
C(23)	3599(4)	4829(3)	7584(3)	37(1)
C(31)	5146(4)	1477(4)	5896(3)	46(1)
C(32)	3472(4)	3612(4)	5956(3)	43(1)
C(33)	5665(3)	3363(3)	5258(3)	37(1)
C(41)	1764(4)	3883(4)	9124(3)	57(1)
C(42)	2539(4)	1437(4)	9182(3)	46(1)
C(43)	1522(4)	2820(4)	7580(4)	49(1)
C(44)	395(5)	2817(4)	9245(4)	71(2)
C(51)	8572(4)	2540(4)	6852(4)	59(1)
C(52)	8294(3)	1484(3)	5152(3)	39(1)
C(53)	8979(4)	266(4)	6782(3)	42(1)
C(54)	10129(4)	1433(4)	5517(3)	53(1)

[a] U(eq) is defined as one third of the trace of the orthogonalized U_{ij} tensor.

centrosymmetric setting, $P\bar{1}$ (No. 2), was chosen on the basis of intensity statistics. This choice was shown to be correct by successful refinement of the structure. The structure was solved using the SHELXTL-PC[10] package, which located all the non-hydrogen atoms. Structure refinement on F^2 was carried out with SHELXL-93.[9] All the non-hydrogen atoms were refined anisotropically, and the hydrogen atoms were included in calculated positions using a riding model. The refinement converged with $R1(F) = 0.0295$ and $wR2(F^2) = 0.0651$ for 532 parameters and 5542 observed reflections ($I > 2\sigma(I)$). The data collection and refinement parameters are summarized in Table 1. Positional and displacement parameters are given in Table 4, and selected bond metricals are included in Table 5.

Results

Synthesis of $[I]^{2-}$. Methanolic solutions of $Fe(CO)_5$/KOH react slowly with solid $NaAsO_2$. During the reaction, the solution changes from pale yellow to deep red. The resulting cluster can be easily isolated as either a $[PPN]^+$ or $[Et_4N]^+$ salt by cation metathesis. The $[PPN]^+$ salt is insoluble in methanol and precipitates directly, while the $[Et_4N]^+$ salt can be precipitated with the addition of excess water. Both the $[PPN]^+$ and $[Et_4N]^+$ salts are insoluble in nonpolar organic solvents such as hexane, toluene, or ether but are soluble in polar solvents such as THF, CH_2Cl_2 and CH_3CN. The $[Et_4N]^+$ salt is also soluble in methanol, while the $[PPN]^+$ salt is not. The simple IR spectrum observed in the CO region for the product is consistent with the presence of a single species containing equivalent $Fe(CO)_4$ fragments with idealized C_{3v} symmetry. The ^{13}C NMR spectrum contains only a single resonance in the carbonyl region at 221 ppm. No signals other than those associated with the cation were observed in the 300 MHz ^1H NMR over a temperature range of −100 to +50 °C and a spectral window of +35 to −70 ppm. FAB mass spectral analysis revealed a signal at m/z 579 for the parent ion with the appropriate isotopic distribution pattern. A degassed solution of the initially formed sodium or potassium salt of the cluster reacts with excess methyllithium to produce methane (1.4 mol of gas/mol of cluster). If the cluster is prepared in CH_3-

(10) SHELXTL PC v 4.2, Siemens Crystallographic Research Systems, Madison, WI, 1990.

Table 5. Selected Bond Lengths and Angles for $[Et_4N]_2[II]$

Lengths (Å)			
As(1)−Fe(3)	2.3633(10)	As(2)−Fe(2)	2.3819(13)
As(1)−Fe(1)	2.3673(10)	As(2)−Fe(5)	2.3876(10)
As(1)−Fe(2)	2.3758(9)	Fe(1)−Fe(2)	2.7292(12)
As(1)−Fe(4)	2.4120(10)	Fe(2)−Fe(3)	2.6984(10)
As(2)−Fe(1)	2.3447(10)	Fe−C	1.757(5)−1.798(5)
As(2)−Fe(3)	2.3595(9)	C−O	1.141(5)−1.156(6)

Angles (deg)			
Fe(3)−As(1)−Fe(1)	101.74(4)	As(1)−Fe(1)−Fe(2)	55.02(3)
Fe(3)−As(1)−Fe(2)	69.41(3)	C(22)−Fe(2)−Fe(1)	74.92(14)
Fe(1)−As(1)−Fe(2)	70.25(3)	C(23)−Fe(2)−Fe(1)	133.00(13)
Fe(3)−As(1)−Fe(4)	132.96(4)	C(21)−Fe(2)−Fe(1)	130.14(14)
Fe(1)−As(1)−Fe(4)	123.89(3)	As(1)−Fe(2)−Fe(1)	54.73(3)
Fe(2)−As(1)−Fe(4)	132.97(3)	As(2)−Fe(2)−Fe(1)	54.10(3)
Fe(1)−As(2)−Fe(3)	102.53(3)	Fe(3)−Fe(2)−Fe(1)	85.08(3)
Fe(1)−As(2)−Fe(2)	70.53(4)	C(22)−Fe(2)−C(23)	98.4(2)
Fe(3)−As(2)−Fe(2)	69.38(3)	C(22)−Fe(2)−C(21)	99.2(2)
Fe(1)−As(2)−Fe(5)	125.07(4)	C(23)−Fe(2)−C(21)	96.8(2)
Fe(3)−As(2)−Fe(5)	130.55(3)	C(22)−Fe(2)−As(1)	109.0(2)
Fe(2)−As(2)−Fe(5)	134.72(3)	C(23)−Fe(2)−As(1)	86.25(13)
C(12)−Fe(1)−C(13)	103.9(2)	C(21)−Fe(2)−As(1)	150.9(2)
C(12)−Fe(1)−C(11)	102.5(2)	C(22)−Fe(2)−As(2)	112.59(14)
C(13)−Fe(1)−C(11)	91.9(2)	C(23)−Fe(2)−As(2)	148.03(14)
C(12)−Fe(1)−As(2)	92.04(13)	C(21)−Fe(2)−As(2)	86.12(14)
C(13)−Fe(1)−As(2)	162.13(14)	As(1)−Fe(2)−As(2)	76.71(3)
C(11)−Fe(1)−As(2)	92.56(13)	C(22)−Fe(2)−Fe(3)	159.80(14)
C(12)−Fe(1)−As(1)	91.19(14)	C(23)−Fe(2)−Fe(3)	93.15(14)
C(13)−Fe(1)−As(1)	93.79(14)	C(21)−Fe(2)−Fe(3)	95.8(2)
C(11)−Fe(1)−As(1)	163.52(14)	As(1)−Fe(2)−Fe(3)	55.07(3)
As(2)−Fe(1)−As(1)	77.59(3)	As(2)−Fe(2)−Fe(3)	54.92(3)
C(12)−Fe(1)−Fe(2)	134.98(13)	C(31)−Fe(3)−C(33)	104.9(2)
C(13)−Fe(1)−Fe(2)	106.86(14)	C(31)−Fe(3)−C(32)	103.8(2)
C(11)−Fe(1)−Fe(2)	108.51(14)	C(33)−Fe(3)−C(32)	89.4(2)
As(2)−Fe(1)−Fe(2)	55.37(4)	C(31)−Fe(3)−As(2)	93.8(2)
C(33)−Fe(3)−As(2)	91.67(13)	C(42)−Fe(4)−C(43)	121.7(2)
C(32)−Fe(3)−As(2)	161.53(14)	C(44)−Fe(4)−As(1)	179.4(2)
C(31)−Fe(3)−As(1)	98.80(14)	C(41)−Fe(4)−As(1)	87.4(2)
C(33)−Fe(3)−As(1)	154.54(14)	C(42)−Fe(4)−As(1)	87.57(14)
C(32)−Fe(3)−As(1)	94.04(13)	C(43)−Fe(4)−As(1)	89.80(14)
As(2)−Fe(3)−As(1)	77.38(3)	C(54)−Fe(5)−C(51)	91.7(2)
C(31)−Fe(3)−Fe(2)	141.6(2)	C(54)−Fe(5)−C(53)	99.7(2)
C(33)−Fe(3)−Fe(2)	99.31(14)	C(51)−Fe(5)−C(53)	109.1(2)
C(32)−Fe(3)−Fe(2)	105.95(14)	C(54)−Fe(5)−C(52)	89.0(2)
As(2)−Fe(3)−Fe(2)	55.70(3)	C(51)−Fe(5)−C(52)	139.5(2)
As(1)−Fe(3)−Fe(2)	55.51(3)	C(53)−Fe(5)−C(52)	110.7(2)
C(44)−Fe(4)−C(41)	93.0(2)	C(54)−Fe(5)−As(2)	166.3(2)
C(44)−Fe(4)−C(42)	92.0(2)	C(51)−Fe(5)−As(2)	83.6(2)
C(41)−Fe(4)−C(42)	116.1(2)	C(53)−Fe(5)−As(2)	93.98(13)
C(44)−Fe(4)−C(43)	90.2(2)	C(52)−Fe(5)−As(2)	86.31(12)
C(41)−Fe(4)−C(43)	121.9(2)	Fe−C−O	173.1(4)−179.8(3)

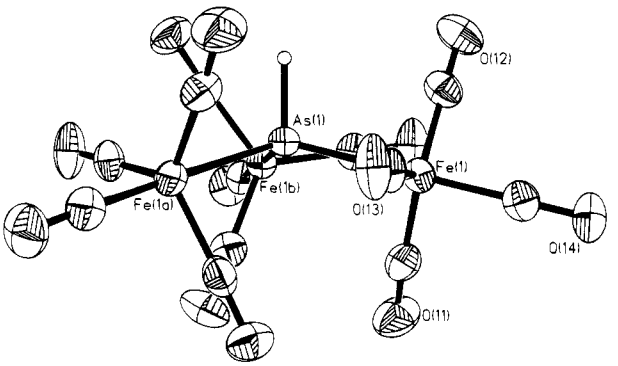

Figure 1. Diagram of the anion of $[PPN]_2[\mathbf{I}]$ showing the displacement ellipsoids (50% probability level) and the atomic labeling scheme.

OD, CH_3D is the primary off-gas. The excess gas produced in these reactions appears to be CO.

Structure of $[PPN]_2[\mathbf{I}]\cdot THF$. Single crystals of $[PPN]_2[\mathbf{I}]$ are easily grown from a THF solution layered with methanol. It was not possible to confirm the presence of the hydride ligand by the diffraction study.[5] The asymmetric unit is composed of two independent cations in general positions and three independent cluster anions with crystallographically imposed C_3 symmetry. The arsenic atom of each anion lies on a crystallographic 3-fold axis so that only one $Fe(CO)_4$ group of each is unique (Figure 1). Diagrams of the other two independent anions are included with the supplementary material. Thus, the ratio of cations to anions in the unit cell is 2:1. The arsenic displays a pyramidal geometry with an average Fe–As–Fe angle of 115.45°.[11] The iron atoms adopt the conventional trigonal-bipyramidal arrangement with the arsenic atoms occupying axial positions. The As–Fe bonds average 2.465 Å for the three independent anions.

Residual electron density could be found along the 3-fold axes at approximately the proper distance from the arsenic atoms expected for the hydrogen atoms. The peaks could not be refined satisfactorily; therefore, their contributions were included as fixed positions where they were located. The inclusion of the hydrogen atoms had little effect on the structure refinement.

Reactivity of $[\mathbf{I}]^{2-}$. When $[\mathbf{I}]^{2-}$ is protonated with aqueous HCl, a complex mixture of products results. To date the only product which has been unambiguously identified is the previously characterized $As_2Fe_6(CO)_{22}$.[12] This neutral cluster was isolated in low yield (15–20%) as small green crystals that grew from hexane at −20 °C. It was identified on the basis of its IR and EI mass spectra. The initial reaction mixture contained several other peaks in the IR, many of which change slowly over several days' time. This continuously changing composition has made the isolation and characterization of the individual species extremely difficult. Because of these difficulties, no further information regarding the identity of the other products is available at this time.

(11) Esd's of average values are calculated with the scatter formula

$$\sigma = [\sum_{i=1}^{i=N}(d_i - d)^2/(N-1)]^{1/2}$$

(12) Arnold, L. J.; Mackay, K. M.; Nicholson, B. K. *J. Organomet. Chem.* **1990**, *387*, 197.

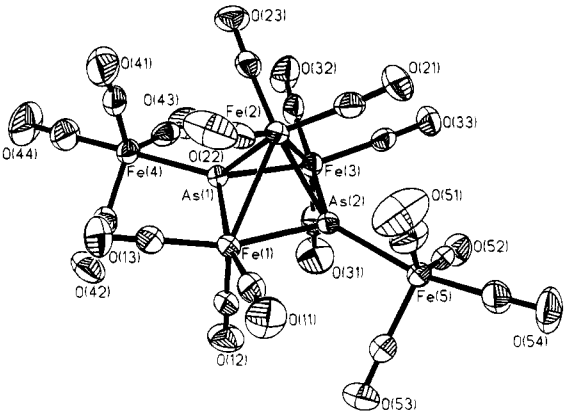

Figure 2. Diagram of the anion of $[Et_4N]_2[\mathbf{II}]$ showing the displacement ellipsoids (50% probability level) and the atomic labeling scheme.

When $[\mathbf{I}]^{2-}$ is pyrolyzed in refluxing THF or photolyzed in the same solvent, the primary product is $[\mathbf{II}]^{2-}$. Photolytic conditions also produce a second unidentified species which is difficult to separate from the major product. Thermal methods are therefore preferred for the preparation of $[\mathbf{II}]^{2-}$. The ESI mass spectrum revealed a parent mass at m/z 1296, which corresponds to an aggregate of one cluster anion and three $[Et_4N]^+$ cations. The ^{13}C NMR revealed three carbonyl resonances at 220.2, 217.9, and 213.0 ppm along with signals attributable to the cation. $[Et_4N]_2[\mathbf{II}]$ can be crystallized from a concentrated CH_2Cl_2 solution held at −20 °C.

Structure of $[Et_4N]_2[\mathbf{II}]$. The asymmetric unit consists of one anion and two cations with no significant intermolecular contacts. The cations were found to be completely ordered. The anion is isostructural with the known $[Et_4N]_2[Sb_2Fe_5(CO)_{17}]$,[13] consisting of a slightly distorted square pyramidal core assembled from two arsenic atoms and three $Fe(CO)_3$ fragments. Each arsenic atom also binds an external $Fe(CO)_4$ group (Figure 2). The base of the pyramid is distorted by a displacement of the arsenic atoms out of the basal plane toward the apical iron atom (Fe(2)) and a deviation of the internal basal angles from the ideal value of 90°. The basal As–Fe–As and Fe–As–Fe angles average 77.48(15) and 102.1(5)°, respectively. Also, the $Fe(CO)_4$ groups are bent away from the apex iron slightly. The As–Fe bonds within the cluster core average 2.365(13) Å, while the two bonds to the external $Fe(CO)_4$ fragments are slightly longer at 2.412(1) and 2.388(1) Å. The Fe–Fe bonds are 2.729(1) and 2.698(1) Å, and the Fe(1)–Fe(2)–Fe(3) angle is 85.08(3)°. The Fe–C and C–O bonds are all normal.

Discussion

The reaction of main-group oxides with $Fe(CO)_5$ and KOH/MeOH has been shown to be a general method for the preparation of main-group-element-containing iron clusters. When $NaAsO_2$ is allowed to react with $Fe(CO)_5$ under these conditions, a single carbonylate anion, $[\mathbf{I}]^{2-}$, is produced rapidly in good yield. A preliminary report of this compound has appeared, and the rationale for arriving at the formulation $[HAs\{Fe(CO)_4\}_3]^{2-}$ with a

(13) Whitmire, K. H.; Leigh, J. S.; Luo, S.; Shieh, M.; Fabiano, M. D. *New J. Chem.* **1988**, *12*, 397.

hydride ligand attached to As has already been presented and will not be discussed in detail here.[5]

The solid-state structure of this cluster at 223 K revealed a pyramidal arsenic atom bound by three $Fe(CO)_4$ fragments, but the presence of the hydride ligand could not be conclusively determined from the original X-ray data reported in ref 5 due to the naturally weak diffracting power of hydrogen atoms, exacerbated by their attachment to the heavy arsenic atom and location on C_3 axes, which cuts their scattering power by a factor of 3. The X-ray diffraction study was repeated at a lower temperature (173 K), but the positioning of the hydrogen atoms was not much improved. As before, persistent residual peaks appeared in the electron difference map approximately 1.5 Å away from each of the three unique arsenic atoms and located along the crystallographic 3-fold axis on which the arsenic atoms reside. These positions agree with the expected location of the hydrogen atoms. These three positions could not be refined as hydrogen atoms without constraint and, even with the H–As distances loosely constrained to be equal (common isotropic displacement parameter for the three atoms), the refinement was not completely successful. Ultimately the H atoms were included in their difference map locations but not refined.

The formation of $[\mathbf{I}]^{2-}$ contrasts with the products formed for the heavier group 15 elements antimony and bismuth in which four $Fe(CO)_4$ groups surround the main-group metal and the overall charge on the clusters is 3−. In the case of arsenic, the fourth coordination site is occupied by a hydrogen atom which raises the overall charge by 1. Transition-metal clusters which contain As–H fragments are extremely rare. The only other structurally characterized example is (μ-HAs)-$\{CpMn(CO)_2\}_2$.[14]

An analysis of the formal oxidation state of the central element of $[\mathbf{I}]^{2-}$ is ambiguous. As in the related clusters $[E\{Fe(CO)_4\}_4]^{3-}$ (E = Sb, Bi),[15,16] the oxidation state of the main-group element in these two clusters could be assigned values ranging from +5 to −3. If the oxidation state is assigned as +5, then the central main-group atom is ligated by $[Fe(CO)_4]^{2-}$ and/or H^- fragments. This seems unreasonable from a chemical standpoint, as it requires a very strongly oxidizing center to be attached to four extremely reducing functionalities. At the other extreme the main-group element can be viewed as being in a −3 oxidation state and the $Fe(CO)_4$ fragments as being zero-valent electron acceptors. Both of these views are consistent with the octet and the 18-electron rules. In reality the bonding in $[\mathrm{I}]^{2-}$ is probably highly covalent and not well-represented by either extreme. Preliminary antimony Mössbauer parameters for $[Sb\{Fe(CO)_4\}_4]^{3-}$ are consistent with an oxidation state for Sb close to 0.[17] The oxidation state of the main-group element in the starting reagents does not completely clarify this situation, as exemplified by the antimony case, where either $SbCl_3$ or $SbCl_5$ may be used in the preparation of $[Sb\{Fe(CO)_4\}_4]^{3-}$.[15]

That the arsenic atom is, or remains, protonated in a strongly basic solution is somewhat surprising but not unreasonable. The strong Lewis basicity of arsenic in transition-metal compounds is readily apparent from the cyclotrimerization of $AsCo_3(CO)_9$ observed in the solid-state structure of $[AsCo_3(CO)_8]_3$.[12] The conjugate base $[As\{Fe(CO)_4\}_3]^{3-}$ could be an intermediate in the synthesis of $[\mathbf{I}]^{2-}$, and such a highly charged species would be extremely basic. The species generated by deprotonation of $[\mathbf{I}]^{2-}$ with methyllithium is, unfortunately, unstable and has not yet been conclusively characterized.

The structural features of the anion support the presence of the hydrogen ligand on arsenic. The electron-deficient $[E\{Fe(CO)_4\}_3]^{2-}$ species (E = Sn, Pb), which have no lone pairs on E, are able to adopt the expected planar arrangement of metal atoms around the central main-group atom.[18] That $[\mathbf{I}]^{2-}$ does not clearly indicates that some fourth group—either a lone or bonding pair of electrons—must be attached to the arsenic atom. The differences between the Fe–E–Fe angles in $[\mathbf{I}]^{2-}$ (115.5°, average) and those of the isoelectronic cluster $[Te\{Fe(CO)_4\}_3]^{2-}$ (109.6°, average)[6] can be rationalized using classical VSEPR arguments, which hold that a lone pair has a larger steric requirement than a bonding pair. A larger Fe–As–Fe angle could be favored by having only a single electron on As rather than a lone pair, but having only one electron on As in $[\mathbf{I}]^{2-}$ would give rise to an odd-electron system and all data indicate that it is diamagnetic.

The As–Fe bonds in $[PPN]_2[\mathbf{I}]$ average 2.465(9) Å for the three independent anions located in the asymmetric unit. This distance is between 0.08 and 0.15 Å longer than the average distances reported for other clusters containing an arsenic–iron single bond such as $As_2Fe_3(CO)_9$ (2.348(2) Å),[19] $Fe_2(CO)_6(AsMe_2)_2$ (2.319(10) Å),[20] $Fe_2(CO)_8AsFe_2(CO)_6Cl$ (2.36(1) Å),[21] $AsFe_3(CO)_9CH$ (2.370(10) Å),[22] $(CO)_5CrAsFe_3(CO)_9CH$ (2.354(6) Å),[22] $Fe_3(CO)_9(S^tBu)(AsMe_2)$ (2.378(6) Å),[23] and $Fe_2(CO)_6[^tBuAs(NSN)As^tBu]$ (2.3241(10) Å).[24] In the spirocyclic cluster $As_2Fe_6(CO)_{22}$[12] the Fe–As bonds between the arsenic and the $Fe_2(CO)_6$ are similar to the others reported in the literature (2.340(14) Å); however, the Fe–As bonds between the $Fe_2(CO)_8$ fragments and the arsenic atoms are of length comparable (2.407(12) Å) to those seen in $[\mathbf{I}]^{2-}$. This lengthening of the As–Fe bonds in $[\mathbf{I}]^{2-}$ is probably caused by steric crowding of the carbonyls on the iron fragments. This phenomenon also occurs in other main-group–iron carbonyl clusters with open frameworks such as the related group 15 clusters $[Et_4N]_3[E\{Fe(CO)_4\}_4]$ (E = Sb, Bi)[15,16] and the related isoelectronic cluster $[Te\{Fe(CO)_4\}_3]^{2-}$.[6]

The reactivities of $[\mathbf{I}]^{2-}$ and isostructural and isoelectronic clusters such as $[Te\{Fe(CO)_4\}_3]^{2-}$ and $[Se\{Fe(CO)_4\}_3]^{2-}$ which possess lone pairs of electrons at the main-group elements differ markedly. In contrast to $[\mathbf{I}]^{2-}$, $[Te\{Fe(CO)_4\}_3]^{2-}$ slowly converts to $[TeFe_3(CO)_9]^{2-}$ and $[Se\{Fe(CO)_4\}_3]^{2-}$ exists only briefly in solution,

(14) Herrmann, W. A.; Koumbouris, B.; Zahn, T.; Ziegler, M. L. *Angew. Chem. Int. Ed. Engl.* **1984**, *23*, 812.
(15) Luo, S.; Whitmire, K. H. *Inorg. Chem.* **1989**, *28*, 1424.
(16) (a) Churchill, M. R.; Fettinger, J. C.; Whitmire, K. H.; Lagrone, C. B. *J. Organomet. Chem.* **1986**, *303*, 99. (b) Whitmire, K. H.; Lagrone, C. B.; Rheingold, A. L. *Inorg. Chem.* **1986**, *25*, 2472.
(17) Long, G.; Stevens, J. Private communication.
(18) Cassidy, J. M.; Whitmire, K. H. *Inorg. Chem.* **1989**, *28*, 2494.
(19) Delbaere, L. T. J.; Kruczynski, L. J.; McBride, D. W. *J. Chem. Soc., Dalton Trans.* **1973**, 307.
(20) Keller, E.; Vahrenkamp, H. *Chem. Ber.* **1977**, *110*, 430.
(21) Huttner, G.; Mohr, G.; Pritzlaff, B.; von Seyerl, J.; Zsolnai, L. *Chem. Ber.* **1982**, *115*, 2044.
(22) Caballero, C.; Nuber, B.; Ziegler, M. L. *J. Organomet. Chem.* **1990**, *386*, 209.
(23) Winter, A.; Zsolnai, L.; Hüttner, G. *J. Organomet. Chem.* **1983**, *250*, 409.
(24) Herberhold, M.; Schamel, K.; Herrmann, G.; Gieren, A.; Ruiz-Pérez, C.; Hübner, T. *Z. Anorg. Allg. Chem.* **1988**, *562*, 49.

rapidly converting to $[SeFe_3(CO)_9]^{2-}$.[6] This is true even though the As–Fe bonds are ca. 2.46 Å compared with 2.64 Å for the Te–Fe bonds in $[Te\{Fe(CO)_4\}_3]^{2-}$,[6] implying that $[\mathbf{I}]^{2-}$ should be much more sterically encumbered by the $Fe(CO)_4$ fragments. The comparatively large stability of this arsenic analog is probably the result of a combination of electronic and steric considerations related to the absence of the lone pair on the main-group element. The lone pair on the $[Te\{Fe(CO)_4\}_3]^{2-}$ dianion results in a smaller Fe–E–Fe angle than that in $[\mathbf{I}]^{2-}$. As a result of this, the $Fe(CO)_4$ groups are pushed closer together, facilitating the formation of the metal–metal bonds. Conversely, by tying up the lone pair, the hydride ligand in $[\mathbf{I}]^{2-}$ allows for wider Fe–E–Fe angles, helping to relieve the steric interactions of the $Fe(CO)_4$ groups.

While $[E\{Fe(CO)_4\}_3]^{2-}$ species (E = Se, Te) also follow a simple CO loss reaction pathway under both photolytic and pyrolytic conditions,[6] $[\mathbf{I}]^{2-}$ reacts by a fragmentation of arsenic–iron and arsenic–hydrogen bonds to create a higher nuclearity cluster, $[\mathbf{II}]^{2-}$. These reactivity patterns are followed by other clusters of the same general classifications. For example, the open-framework compound $Bi\{Co(CO)_4\}_3$ undergoes the same closing reaction as $[E\{Fe(CO)_4\}_3]^{2-}$ (E = Se, Te)[27] and open intermediates may be involved en route to $PCo_3(CO)_9$ and $AsCo_3(CO)_9$ but have not yet been observed. CO loss from such intermediates would be expected to be rapid, on the basis of the results for the Se and Te clusters. Other complexes in which no lone pair is found at E do not show simple closing but more complicated fragmentation/recombination reactions. These include $[E\{Fe(CO)_4\}_4]^{3-}$ (E = Sb, Bi),[15,16] $[XSb\{Fe(CO)_4\}_3]^{2-}$ (X = Cl, Br),[25] and $E\{Co(CO)_4\}_4$ (E = Sn, Pb).[26] Isoelectronic and isostructural $[Te\{Fe(CO)_4\}_4]^{2-}$ has been mentioned,[1j] but its reactivity is as yet unknown.

This is not to say that under differing circumstances open-framework compounds with a central four-coordinate main-group element cannot be induced to undergo a *closing* reaction. We have seen that $[Sb\{Fe(CO)_4\}_4]^{3-}$ can be induced under mild protonation conditions to close to give $[HFe_3(CO)_9\{SbFe(CO)_4\}]^{2-}$, but this reaction is in competition with a fragmentation/reorganization process which yields $[Fe_3(CO)_9\{SbFe(CO)_4\}_2]^{2-}$.[15] This latter cluster, of course, is virtually identical with the $[\mathbf{II}]^{2-}$ reported here. Similar chemistry has been noted for bismuth-containing clusters where the oxidation route yielding $Bi_2Fe_3(CO)_9$ dominates the protonation/closing pathway where only minor amounts of $H_3BiFe_3(CO)_9$ have been isolated.[16b] It is intriguing to note that, when $[Te\{Fe(CO)_4\}_3]^{2-}$ is protonated, the resultant product, $Fe_3(CO)_9Te_2$, contains the same cluster core found for $[\mathbf{II}]^{2-}$.[28] Protonation of $[Te\{Fe(CO)_4\}_3]^{2-}$ could be expected to occur at tellurium to produce "$[HTe\{Fe(CO)_4\}_3]^-$" (isoelectronic and isostructural with $[\mathbf{I}]^{2-}$), and its thermal decomposition would be expected to proceed similarly. Unfortunately we could find no evidence, even fleeting, for the existence of a tellurium hydride as an intermediate in the protonation reaction.

(25) Luo, S.; Whitmire, K. H. unpublished results.
(26) Leigh, J. S.; Whitmire, K. H. *Acta Crystallogr., Sect. C* **1990**, *46*, 732.
(27) (a) Etzrodt, G.; Boese, R.; Schmid, G. *Chem. Ber.* **1979**, *112*, 2574. (b) Whitmire, K. H.; Leigh, J. S.; Gross, M. E. *J. Chem. Soc., Chem. Commun.* **1987**, 926.
(28) Bachman, R. E. Ph.D. Thesis, Rice University, 1994.

Table 6. Comparison of Basal Angles (deg) for Square-Pyramidal Clusters with E_2M_3 Cores

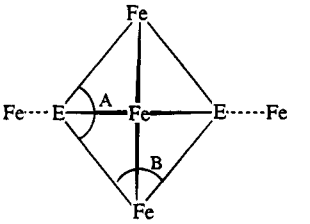

cluster	M–E–M angle (A)	E–M–E angle (B)	E··E, Å	ref
$Se_2Fe_3(CO)_9$	96.6	82.4	3.10	31
$Te_2Fe_3(CO)_9$	96.45	83.4	3.364	32
$[As_2Fe_5(CO)_{17}]^{2-}$	102.14	77.48	2.952	this work
$[Sb_2Fe_5(CO)_{17}]^{2-}$	100.86	78.99	3.201	13
$[Bi_2Fe_3(CO)_9]^{2-}$	96.85	83.15	3.538	30
$[Bi_2Fe_4(CO)_{13}]^{2-}$	97.38, 101.91	80.36	3.398	29

Monitoring of the pyrolysis of $[\mathbf{I}]^{2-}$ by ^1H NMR indicated the formation of a metal hydride signal at −8.3 ppm which is consistent with the formation of $[HFe(CO)_4]^-$. This anion could arise via reductive elimination from $[\mathbf{I}]^{2-}$. Without a detailed kinetic study it is not possible to draw incontrovertible conclusions about this process, but it suggests—using the principle of microscopic reversibility—that an oxidative addition of $[HFe(CO)_4]^-$ could be involved in the formation of $[\mathbf{I}]^{2-}$. The speculative sequence is given in eqs 1–3.

$$AsO_2^- + [HFe(CO)_4]^- \rightarrow [OAsFe(CO)_4]^- + OH^- \quad (1)$$

$$[OAsFe(CO)_4]^- + [HFe(CO)_4]^- \rightarrow [As\{Fe(CO)_4\}_2]^- + OH^- \quad (2)$$

$$[As\{Fe(CO)_4\}_2]^- + [HFe(CO)_4]^- \rightarrow [HAs\{Fe(CO)_4\}_3]^{2-} \quad (3)$$

An X-ray structural study of $[Et_4N]_2[\mathbf{II}]$ revealed a square-pyramidal cluster with the arsenic atoms occupying *trans*, basal positions. Each arsenic atom also binds an additional $Fe(CO)_4$ fragment through its external lone pair. The cluster is therefore isostructural and isoelectronic with the known $[Et_4N]_2[Sb_2Fe_5(CO)_{17}]$.[13] With the arsenic atoms contributing three electrons each to the cluster bonding, the total number of skeletal electrons is 14, as expected for a *nido* octahedron. Although the cluster is electron-precise, the core geometry is significantly distorted from ideal square-pyramidal geometry. The basal plane is puckered slightly with the arsenic atoms displaced toward the apical iron atom. Additionally, the base of the pyramid is distorted from a square into a parallelogram with obtuse angles at the arsenic atoms and acute angles at iron atoms.

Examination of structural data for $[\mathbf{II}]^{2-}$, its isostructural antimony analog, $[Bi_2Fe_4(CO)_{13}]^{2-}$,[29] $[Bi_2Fe_3(CO)_9]^{2-}$,[30] and $Fe_3(CO)_9E_2$ (E = Se,Te)[31,32] show further the effects of the presence of lone pairs on the structural parameters of the cluster core geometries. Data for these molecules are compared in Table 6. There are

(29) Whitmire, K. H.; Raghuveer, K. S.; Churchill, M. R.; Fettinger, J. C.; See, R. F. *J. Am. Chem. Soc.* **1986**, *108*, 2778.
(30) Eveland, J. R.; Whitmire, K. H. Manuscript in preparation.
(31) Dahl, L. F.; Sutton, P. W. *Inorg. Chem.* **1963**, *2*, 1067.
(32) Schumann, H.; Magerstädt, M.; Pickardt, J. *J. Organomet. Chem.* **1982**, *240*, 407.

clearly two distinct types of environments seen, depending upon whether the main-group atom has a nonbonding lone pair or whether the lone pair is donated to an external metal fragment. The largest Fe–E–Fe and smallest E–Fe–E angles are found for $[\mathbf{II}]^{2-}$ and its Sb analog. The Fe–E–Fe angles in $[E_2Fe_3(CO)_9]^{n-}$ (n = 0, E = Se, Te; n = 2, E = Bi) fall in a different range, being noticeably closer to 90° than those of $[\mathbf{II}]^{2-}$. The E–Fe–E angles undergo an opposite and complimentary change as expected. One cluster, $[Bi_2Fe_4(CO)_{13}]^{2-}$, is a hybrid. It has one naked Bi atom and one with a bound lone pair but again the parameters are consistent with the ranges seen for the other molecules.[29]

It is readily apparent that steric factors are not the major force causing the distortion of these cluster cores. If that were the case, the trends in bond angles should be opposite of those observed. The steric bulk of the external $Fe(CO)_4$ groups should cause a contraction in the Fe–E–Fe angle and thereby lessen the CO–CO repulsions at the cluster core. An alternative explanation based on electronic considerations has been put forth by Webster and co-workers, as well as others, to explain a similar distortion in phosphorus-containing clusters such as $Fe_3(CO)_9(PPh)_2$.[33] In these cases, the distortion is attributed to an attractive, through-space interaction of the main-group elements. This interaction was postulated because the E–E distances were found to be only slightly longer (approximately 0.3 Å) than the sum of the covalent radii. If present, the structural result of this interaction would indeed be a decrease in the E–E distance and, consequently, an opening of the Fe–E–Fe angle. However, the consistency of the structural parameters for the two types of bismuth atoms in the hybrid $[Bi_2Fe_4(CO)_{13}]^{2-}$ with the ranges for the other ligated and unligated main-group atoms in the other clusters implies that the structural distortions may be independent of a direct Bi···Bi interaction.

An alternative interpretation of the cause of the distortion can be based upon hybridization arguments. In those clusters with lone pairs the Fe–E–Fe angles are closer to 90°, implying that the orbitals used to make these bonds contain more p character and therefore the lone pair is more s like. This observation is consistent with the "inert pair" concept for heavy post-transition metals.[34] The inert pair effect was first put forth to explain the tendency of heavier post-transition elements to forego the use of their s valence electrons for bonding. Relativistic orbital energy calculations have suggested that this tendency is caused by a contraction of the s orbitals and a concurrent lowering of their energy.[35] Implied in both of these descriptions is the concept that this inert pair should reside in an orbital which is principally s in character and, hence, be nondirectional. However, more recently it has been suggested that the stereochemical activity or inactivity of the lone pair is not simply determined by the relativistic effects which give rise to the inert pair effect but also by other intra- and intermolecular forces present.[35] These concepts agree very well with the bonding patterns seen in the clusters under consideration. When the lone pair is unused for bonding, it resides in an orbital having largely s character. As a consequence of this, the orbitals used by the main-group element for bonding to the iron atoms in the cluster core have more p character. This allows the Fe–E–Fe angles to more closely approach the idealized value of 90° expected for a square-based pyramid. However, when the lone pair is used to bind an ancillary metal fragment, the less favorable energetics of rehybridization to sp^3 is offset by the energy released by bonding to the external metal fragment. The validity of these ideas is being probed by theoretical calculations.

While this paper was in review, other workers indepently reported the preparation of $[\mathbf{I}]^{2-}$ and the corresponding antimony compound via similar though not identical methodology.[36]

Conclusions

In heteronuclear clusters such as those discussed above, electrons on the main-group fragments not directly involved in the cluster core bonding may play a critical role in determining the observed structure and reactivity patterns of the cluster. The presence of a lone pair of electrons on a main-group-atom vertex in an open-framework compound is generally found to promote simple ligand loss and formation of a *closo* compound, while tying up the fourth pair of electrons by bonding to an external functionality yields more complicated fragmentation and reorganization patterns. These effects are rationalized on the basis of rehybridization processes occurring at the main-group atom.

Acknowledgment. K.H.W. wishes to thank the National Science Foundation and the Robert A. Welch Foundation for financial support of this work. R.E.B. wishes to thank the NSF for a Predoctoral Fellowship. VG Analytical is acknowledged for providing the mass spectral analyses.

Supplementary Material Available: Diagrams of the other two independent cluster anions for $[PPN]_2[\mathbf{I}]$ and complete tables of bond metricals as well as positional and anisotropic displacement parameters for $[PPN]_2[\mathbf{I}]$ and $[Et_4N]_2[\mathbf{II}]$ (36 pages). Ordering information is given on any current masthead page.

OM940498B

(33) Cook, S. L.; Evans, J.; Gray, L. R.; Webster, M. *J. Organomet. Chem.* **1982**, *236*, 367.
(34) Huheey, J. E. *Inorganic Chemistry: Principles of Structure and Reactivity* 3rd. ed.; Harper and Row: New York, 1983, pp. 843–845.
(35) Pyykkö, P. *Chem. Rev.* **1988**, *88*, 563 and references contained therein.
(36) Henderson, P.; Rossignoli, M.; Burns, R. C.; Scudder, M. L.; Craig, D. C. *J. Chem. Soc., Dalton Trans.* **1994**, 1641.

Insertion of Dihalocarbene into a Si–H Bond under Alkaline Phase-Transfer Conditions

Yuri Goldberg and Howard Alper*

Department of Chemistry, University of Ottawa, 10 Marie Curie, Ottawa, Ontario, Canada K1N 6N5

Received October 3, 1994[⊗]

Dichloro- and dibromocarbene, generated from the corresponding haloform and alkali (solid or aqueous) in the presence of a phase-transfer agent, readily insert into the Si–H bond of triisopropylsilane (**1**) to give (dihalomethyl)triisopropylsilane (**2**) in good yield. Both **1** and **2** are remarkably alkali-resistant. The same process occurs for *t*-$BuMe_2SiH$. Other less sterically hindered, structurally related silanes such as Et_3SiH, Et_2MeSiH, and $PhMe_2SiH$ under identical conditions are converted mainly to the corresponding disiloxanes.

In the course of the implementation of one of our projects, we needed (dihalomethyl)triisopropylsilanes **2**. The simplest and most convenient synthetic route to **2** is the reaction of triisopropylsilane (**1**) with dihalocarbenes. The insertion of dihalocarbenes into a Si–H bond, discovered by Seyferth and Burlitch,[1] is well documented.[2] However, to our knowledge, the reaction of **1** with $:CX_2$, and the products of structural type **2** are not described in the literature. In the present work, we have studied the reaction of silane **1** with dihalocarbenes generated from sodium trichloroacetate or haloforms ($CHCl_3$, $CHBr_3$) using phase-transfer catalysis (PTC) methodology.[3] For comparison, similar reactions of structurally related silanes have also been studied.

Results and Discussion

Among numerous methods available for the generation of dihalocarbenes,[2a,4] biphasic procedures are certainly the most attractive in terms of the availability of inexpensive carbene precursors, simple reaction execution, and workup.[5]

Dichlorocarbene, generated by the thermal decomposition of sodium trichloroacetate, suspended in an inert solvent in the presence of a phase-transfer agent,[6] reacts with alkyl-, aryl-, and heteroarylsilanes to give the corresponding dichloromethylsilanes in 40–70% yield.[7] When a mixture of silane **1**, $Cl_3CCOONa$ (5 molar equiv), and 18-crown-6 (18-C-6, 0.1 molar equiv) in toluene was heated under reflux temperature for 2.5 h (method A), the dichloromethyl derivative **2a** was obtained in 70% yield (Table 1, entry 1). Despite this fair yield, the method is not very convenient since it requires a 5-fold excess of sodium trichloroacetate and 0.1 molar equiv of expensive 18-C-6. The use of a

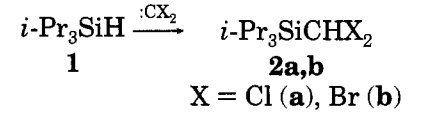

smaller excess of $Cl_3CCOONa$ (3 molar equiv) with the same amount of 18-C-6 (entry 2) or 0.05 molar equiv of 18-C-6 with 5 molar equiv of $Cl_3CCOONa$ (entry 3) results in a considerable (20-30%) reduction of the yield of **2a**. Other typical catalysts of solid–liquid PTC reactions such as TDA-1 and PEG-400 are less effective than 18-C-6 and produce **2a**, under identical conditions, in *ca.* 40% yield (entries 4 and 5). The use of ultrasonic irradiation does not affect the reaction (entry 6).

PTC generation of dihalocarbenes in a biphasic haloform/alkali system is a simple and efficient method for executing reactions involving these species.[5] A limitation of the method is when the starting material and/or the product are alkali-sensitive. Indeed, an attempt to carry out the reaction of simple alkyl- and arylsilanes of type R_3SiH with $:CCl_2$ in a $CHCl_3$/50% aqueous NaOH system in the presence of $Et_3N^+CH_2PhCl^-$ (TEBA) or $Bu_4N^+HSO_4^-$ (TBAH) failed to give the dichloromethylsilane. The only products of the above reactions were the corresponding disiloxanes $R_3SiOSiR_3$.[8] However, the authors of ref 8 believe that the reaction occurred via an intermediate dichloromethylsilane. Bearing this in mind and also taking into account that a bulky triisopropyl group significantly retards nucleophilic substitution at silicon and reactions at adjacent centers,[9] we have studied the interaction of **1** with CHX_3/OH^- (X = Cl, Br) in the presence of a phase-transfer agent.

⊗ Abstract published in *Advance ACS Abstracts*, December 1, 1994.

(1) Seyferth, D.; Burlitch, J. M. *J. Am. Chem. Soc.* **1963**, *85*, 2267.

(2) (a) Kirmse, W. *Carbene Chemistry*; Academic Press: New York, 1971. (b) Fleming, I. In *Comprehensive Organic Chemistry*; Barton D., Ollis, W. D., Eds.; Pergamon Press: Oxford, 1982; Vol. 3, Chapter 13.3, pp 565–566. (c) Armitage, D. A. In *Comprehensive Organometallic Chemistry*; Wilkinson, G., Stone, F. G. A., Eds.; Pergamon Press: Oxford, 1982; Vol. 2, Chapter 9.1, pp 111–112.

(3) For recent reviews on PTC reactions of organosilanes involving carbenes, see: (a) Goldberg, Y.; Dirnens, V.; Lukevics, E. *J. Organomet. Chem. Libr.* **1988**, *20*, 211. (b) Goldberg, Y. *Phase Transfer Catalysis. Selected Problems and Applications*; Gordon and Breach Sci. Publ.: London, 1992; Chapter 3, pp 139–144.

(4) Nair, V. In *Comprehensive Organic Synthesis*; Trost, B. M., Fleming, I., Eds.; Pergamon Press: Oxford, 1991; Vol. 4, pp 1000–1002.

(5) (a) Makosza, M.; Fedorynsky, M. *Adv. Catal.* **1987**, *35*, 375. (b) Dehmlow, E. V.; Dehmlow, S. S. *Phase Transfer Catalysis*; Verlag Chemie: *Berlin*, 1983; pp 220–278.

(6) (a) Dehmlow, E V. *Tetrahedron Lett.* **1976**, 91. (b) Idemori, K.; Takagi, M.; Matsuda, T. *Bull. Chem. Soc. Jpn.* **1977**, *50*, 1355.

(7) (a) Del Valle, L.; Sandoval, S.; Larson, G. L. *J. Organomet. Chem.* **1981**, *215*, C45. (b) Lukevics, E.; Sturkovich, R.; Goldberg, Y.; Gaukhman, A. *J. Organomet. Chem.* **1988**, *345*, 19.

(8) Larson, G. L.; Del Valle, L. *Synth. React. Inorg. Met.-Org. Chem.* **1981**, *11*, 173.

(9) (a) Soderquist, J. A.; Colberg, J. C.; Del Valle, L. *J. Am. Chem. Soc.* **1989**, *111*, 4873. (b) Soderquist, J. A.; Rivera, I.; Negron, A. *J. Org. Chem.* **1989**, *54*, 4051. (c) Santiago, B.; Lopez, C.; Soderquist, J. A. *Tetrahedron Lett.* **1991**, *32*, 3457. (d) Miranda, E. I.; Diaz, M. J.; Rosado, I.; Soderquist, J. A. *Tetrahedron Lett.* **1994**, *35*, 3221.

0276-7333/95/2314-0804$09.00/0

Table 1. PTC Reactions of Triisopropylsilane (1) with Dihalocarbenes

entry	method[a]	precursor of :CX_2	base	catalyst	ultrasound[b]	reaction time, h	product	isolated yield, %
1	A	$Cl_3CCOONa$		18-C-6	–	2.5	**2a**	70
2	A	$Cl_3CCOONa$[c]		18-C-6	–	2.5	**2a**	38
3	A	$Cl_3CCOONa$		18-C-6[d]	–	2.5	**2a**	51
4	A	$Cl_3CCOONa$		TDA-1[e]	–	2.5	**2a**	44
5	A	$Cl_3CCOONa$		PEG-400	–	2.5	**2a**	42
6	A	$Cl_3CCOONa$		18-C-6	–	2.5	**2a**	70
7	B	$CHCl_3$	s. NaOH[h]	18-C-6	–	8	**2a**	88
8	C	$CHCl_3$	s. NaOH	18-C-6	+	2.5	**2a**	84
9	C	$CHCl_3$	s. NaOH		+	8	**2a**	6[f]
10	D	$CHCl_3$	50% NaOH	TEBA	–	2	**2a**	88
11	D	$CHCl_3$	50% NaOH	TBAH	–	2	**2a**	83
12	B	$CHBr_3$[g]	s. NaOH	18-C-6	–	0.5	**2b**	31
13	B	$CHBr_3$	s. NaOH	18-C-6	–	2.5	**2b**	68
14	C	$CHBr_3$	s. NaOH	18-C-6	+	2.5	**2b**	68
15	D	$CHBr_3$	50% NaOH	TEBA	–	1	**2b**	64

[a] Method A: **1** (5 mmol), $Cl_3CCOONa$ (25 mmol), catalyst (0.5 mmol), toluene, 110 °C. Method B: **1** (5 mmol), NaOH (25 mmol), catalyst (0.25 mmol), $CHCl_3$ or $CHBr_3/CH_2Cl_2$, room temperature. Method C: the same as in method B under ultrasonication. Method D: **1** (5 mmol), 50% aqueous NaOH (25 mmol), catalyst (0.25 mmol), $CHCl_3$ or $CHBr_3/CH_2Cl_2$, room temperature. [b] Branson B-12 ultrasonic cleaning bath. [c] 15 mmol. [d] 0.25 mmol. [e] Tris(3,6-dioxaheptyl)amine. [f] GC data. [g] No cosolvent (CH_2Cl_2) was used. [h] s. NaOH = solid NaOH.

We were gratified to observe that the reactions resulted in the formation of dihalomethyl derivatives **2a,b** in good yields (see Table 1). In a $CHCl_3$/NaOH liquid–solid system containing 18-C-6 (method B), silane **1** readily transforms to silane **2a** in 88% isolated yield (entry 7). When the reaction is carried out under ultrasonication[10] (method C), the yield of **2a** remains almost the same, the reaction time being significantly reduced (entry 8). In the absence of a phase-transfer catalyst, the sonochemical reaction is very sluggish (entry 9). The classic[5a] liquid–liquid $CHCl_3$/50% aqueous NaOH system containing a quaternary ammonium salt is also useful for the preparation of **2a** (method D, entries 10 and 11). Using TEBA or TBAH, one can obtain silane **2a** quickly and in high yield under very mild conditions. Thus, the presence of solid or aqueous alkali does not affect either **1** or **2a**.

Dibromocarbene, generated by using methods B–D, also reacts with **1** to give dibromomethylsilane (**2b**). When $CHBr_3$/solid NaOH/18-C-6 is used, the reaction is strongly exothermic (bromoform refluxes), and perhaps due to some decomposition at high temperature the yield of **2b** is low (31%, entry 12) although even under these severe conditions no hydrolysis products (silanol or disiloxane) were detected. The dilution of bromoform with dichloromethane as cosolvent[11] ($CHBr_3$: CH_2Cl_2 = 1:1.5 vol) affords **2b** in significantly higher (68%) yield (entry 13). Note that in the case of the more reactive dibromocarbene, the ultrasonication does not affect its PTC reaction with **1** (entry 14). Finally, method D using aqueous alkali is also effective in the case of dibromocarbene, giving rise to **2b** in 64% yield. Again, the dilution of bromoform with dichloromethane is essential (entry 15). Dibromomethylsilane (**2b**), like **2a** in a biphasic liquid–solid or liquid–liquid system, does not react with alkali. Compounds **2a** and **2b** are new. They were characterized by ^1H, ^{13}C, and ^{29}Si NMR spectra and by elemental analysis (see Experimental Section). The structure of **2a** was also confirmed by X-ray analysis (Figure 1).[12]

(10) (a) Xu, L.; Smith, W. B.; Brinker, U. H. *J. Am. Chem. Soc.* **1992**, *114*, 783. (b) Xu, L.; Tao, F. *Synth. Commun.* **1988**, *18*, 2117. (c) Lukevics, E.; Gevorgyan, V.; Goldberg, Yu.; Gaukhman, A.; Gavars, M.; Popelis, J.; Shymanska, M. *J. Organomet. Chem.* **1984**, *265*, 237.
(11) See ref 5b, pp 260–261.
(12) For the full description of the structure analysis, see the supplementary material.

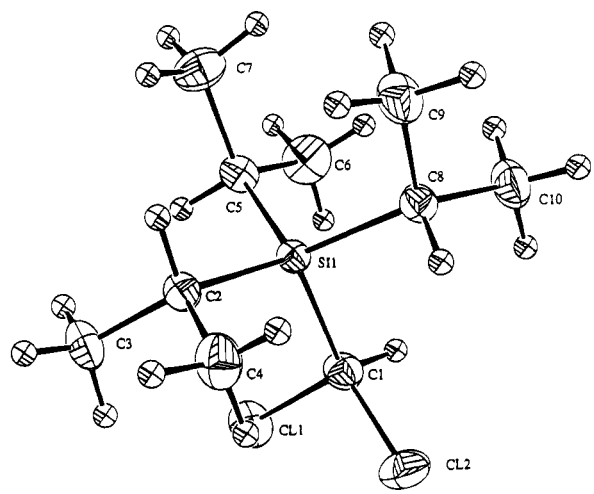

Figure 1. ORTEP diagram of **2a**.

As already mentioned (vide supra), reactions of trialkyl-, dialkylaryl-, and diarylalkylsilanes with dichlorocarbene under alkaline (50% aqueous NaOH) PTC conditions result in the formation of the corresponding disiloxanes.[8] We have also examined some other structurally related silanes, which are less sterically hindered than silane **1**, such as Et_3SiH (**3**), Ph_2MeSiH (**5**), Et_2MeSiH (**7**), and *t*-$BuMe_2SiH$ (**10**). The reactions were carried out under identical conditions to those for **1**. The results are summarized in Table 2. All the silanes readily reacted with CHX_3/OH^- (X = Cl, Br) in the presence of a phase-transfer agent. Their reactivity is, in general, similar to that of **1** (100% conversion of a starting material in most cases was achieved in 2–4 h). Silane **3** in a $CHCl_3$/50% aqueous NaOH/TEBA system, as anticipated,[8] gave hexaethyldisiloxane (**4**) in 86% yield. The same product was obtained in 84% yield in a CHX_3 (X = Cl, Br)/solid NaOH/18-C-6 system. Silane **5** behaved similarly and afforded $(PhMe_2Si)_2O$ (**6**) both under solid/liquid and liquid/liquid PTC conditions in 93 and 90% yield, respectively. Silane **7**, in the presence of solid NaOH and 18-C-6 reacted with $CHCl_3$ to give a mixture of disiloxane **8** and silanol **9** in a ca. 95:5 ratio and 75% overall yield. When 50% aqueous NaOH was used as a base, the same two products were formed in a 1:1 ratio (by ^1H NMR and GC). Most interesting and rather unexpected results were obtained in reactions involving *t*-$BuMe_2SiH$ (**10**). Its reaction with $CHCl_3$/

Table 2. Reactions of Hydrosilanes with CHX_3/OH^- under PTC Conditions

silane	method[a]	haloform	base	catalyst	reaction time, h	product(s)	yield, %,[b] and/or ratio[c]
Et_3SiH (**3**)	B	$CHCl_3$	s. NaOH[h]	18-C-6	4	$(Et_3Si)_2O$ (**4**)	84
3	D	$CHCl_3$	50% NaOH	TEBA	4	**4**	86
3	D	$CHBr_3$	s. NaOH	18-C-6	2	**4**	86
Me_2PhSiH (**5**)	B	$CHCl_3$	s. NaOH	18-C-6	2	$(PhMe_2Si)_2O$ (**6**)	93
5	D	$CHCl_3$	50% NaOH	TEBA	2	**6**	90
Et_2MeSiH (**7**)	B	$CHCl_3$	s. NaOH	18-C-6	2	$(Et_2MeSi)_2O$ (**8**) + $Et_2MeSiOH$ (**9**)	75[d] (95:5)
7	D	$CHCl_3$	50% NaOH	TEBA	2	**8** + **9**	77[d] (50:50)
t-$BuMe_2SiH$(**10**)	D	$CHCl_3$	50% NaOH	TEBA	2	$(t\text{-}BuMe_2Si)_2O$ (**11**) + *t*-$BuMe_2SiCHCl_2$ (**12**)	73[d] (80:20)
10					4	**11**	83
10	B	$CHCl_3$	s. NaOH	18-C-6	1	**11** + **12**	– (35:65)
					3	**11** + **12**	– (80:20)
					6	**11** + **12**	– (92:8)
					24	**11** + **12**	– (100:0)
10	B	$CHCl_3$	s. NaOH[e]	18-C-6	6	**11** + **12**	55[f] (9:91)
10	B	$CHBr_3$	s. NaOH[e]	18-C-6	2	**11** + **13**	64[g] (10:90)
3	B	$CHCl_3$	s. NaOH[e]	18-C-6	4	**4**	88
5	B	$CHCl_3$	s. NaOH[e]	18-C-6	4	**6**	91
Ph_3SiH (**14**)	B	$CHCl_3$	s. NaOH	18-C-6	72	Ph_3SiOH (**15**)	78

[a] For reaction conditions, see footnote *a* for Table 1. [b] Isolated yield. [c] NMR and/or GC data. [d] Overall yield. [e] 1 molar equiv of NaOH was used. [f] Isolated yield of **12**. [g] Isolated yield of **13**. [h] s. NaOH = solid NaOH.

50% aqueous NaOH/TEBA (room temperature, 2 h) resulted in a mixture consisting of disiloxane, $(t\text{-}BuMe_2Si)_2O$ (**11**), and *t*-$BuMe_2SiCHCl_2$ (**12**) in a 4:1 ratio (by ^1H NMR). The subsequent stirring of the reaction mixture at room temperature led to the disappearance of the dichloromethyl derivative. Similarly, GC monitoring of the reaction of **10** with $CHBr_3/CH_2Cl_2$/solid NaOH/18-C-6 revealed that the reaction occurred via *t*-$BuMe_2SiCHBr_2$ (**13**): the ratio of disiloxane **11** to dibromomethylsilane **13** was 35:65, 80:20, 92:8, and 100:0 after 1, 3, 6, and 24 h, respectively. These data are in accord with the conclusion of Larson and coworkers that PTC reactions of hydrosilanes with dichlorocarbene ($CHCl_3$/50% aqueous NaOH/phase-transfer agent) occur via $\equiv SiCHCl_2$ intermediates although they were not detected in the reaction mixtures.[8] These findings allowed us to assume that dihalomethylsilanes could be obtained from **10** selectively using a stoichiometric amount of alkali. Indeed, when the reaction of **10** with $CHCl_3$ was carried out in the presence of 1 molar equiv of solid NaOH (18-C-6, 5 mol %), the corresponding dichloromethylsilane **12** was formed nearly selectively (**12**:**11** = 10:1, by ^1H NMR). Similarly, dibromomethylsilane **13** was obtained as the major product (selectivity: 90%) in the reaction of **10** with $CHBr_3/CH_2Cl_2$/18-C-6 using 1 molar equiv of solid NaOH. Silanes **12** and **13** were isolated in pure form by vacuum distillation in 55 and 64% yield, respectively, and characterized by ^1H, ^{13}C, and ^{29}Si NMR spectroscopy as well as by elemental analysis (see Experimental Section). It should be mentioned that **12** and **13** were prepared recently by reacting *t*-$BuMe_2SiCl$ with CH_2Cl_2 and CH_2Br_2 in the presence of *n*-BuLi or LDA, respectively.[13] However, they were not adequately characterized in the prior literature: ref 13a gave spectral data for **12** with an unsatisfactory analysis and no data were given **13**.[13b] It should also be noted that silanes **3** and **5** afforded the corresponding disiloxanes (**4** and **6**) under solid/liquid PTC conditions even in the presence of a stoichiometric amount of alkali (Table 2).

We have also carried out PTC reactions of some other sterically hindered silanes with haloform/alkali. The reaction of tris(triisopropylthio)silane with $CHCl_3$/solid NaOH/18-C-6 under conditions identical to those described for **1** gives a complicated mixture of unidentified products which does not contain $(i\text{-}PrS)_3SiCHCl_2$. Tris(trimethylsilyl)- and tris(trimethylsiloxy)silane react similarly. Triphenylsilane (**14**) behaved rather unexpectedly. When a mixture of **14**, $CHCl_3$, solid NaOH, and 18-C-6 was stirred at room temperature, neither $Ph_3SiCHCl_2$ nor $Ph_3SiOSiPh_3$ was formed. Instead, the evolution of hydrogen gas occurred slowly and all the silane was consumed after 72 h, and the only product isolated in 78% yield was triphenylsilanol (**15**). Careful GC/MS analysis of the reaction mixture also revealed the presence of trace amounts of Ph_3SiOEt. The evolution of H_2 clearly indicates that **15** is formed via nucleophilic substitution of hydrogen with hydroxide ion solubilized in the organic phase by the crown ether.[14] Similar substitution involving ethoxide ion (generated in situ from ethanol which is present in commercial chloroform, and alkali) accounts for the formation of Ph_3SiOEt. Note that virtually no reaction occurs in the absence of the phase-transfer agent.

In conclusion, unlike simple alkyl- and arylsilanes, triisopropylsilane reacts smoothly with dihalocarbenes ($:CCl_2$ and $:CBr_2$), generated under *alkaline* PTC conditions (haloform/solid or aqueous alkali/phase-transfer agent), to give the corresponding dihalomethyl derivatives in good yield. *tert*-Butyldimethylsilane under the same conditions gives mainly the corresponding disiloxane; however, *t*-$BuMe_2SiCHX_2$ (X = Cl, Br) can also be obtained with ca. 90% selectivity and fair yield under solid/liquid PTC conditions using a stoichiometric amount of alkali. These represent the first examples of the insertion of dihalocarbene into a Si–H bond under alkaline conditions. We are currently investigating the chemistry of silanes **2**, in particular, the possibility of the synthesis of stable formyltriisopropylsilane.[15]

(13) (a) Becker, P.; Brombach, H.; David, G.; Leuer, M.; Metternich, H.-J.; Niecke, E. *Chem. Ber.* **1992**, *125*, 771. (b) Shinokubo, H.; Miura, K.; Oshima, K.; Utimoto, K. *Tetrahedron Lett.* **1993**, *34*, 1951.

(14) For studies on the nucleophilic replacement of hydrogen from R_3SiH with OH^-, see: (a) Sommer, L. H.; Korte, W. D.; Frye, C. L. *J. Am. Chem. Soc.* **1972**, *94*, 3463. (b) Ahn, N. T. *Top. Curr. Chem.* **1980**, *88*, 145.

(15) (a) Soderquist, J. A.; Miranda, I. *J. Am. Chem. Soc.* **1992**, *114*, 10078. (b) Siverman, R. B.; Lu, X.; Banik, G. M. *J. Org. Chem.* **1992**, *57*, 6617.

Experimental Section

^1H and ^{13}C NMR spectra were obtained on a Varian Gemini 200 spectrometer and ^{29}Si NMR spectra on a Varian XL-300 instrument, using $CDCl_3$ as the solvent and Me_4Si as the internal standard. GC analyses were carried out on a Hewlett-Packard 5890 gas chromatograph equipped with a column [1.5% OV-17 + 1.95% OV-210 on Chromosorb W-HP (100–120 mesh)]. Melting points were measured on a Fisher-Johns melting point apparatus and are uncorrected. Sodium trichloroacetate, all hydrosilanes, 18-C-6, bromoform, TEBA, and TBAH were purchased from Aldrich and used as received. All reactions were carried out under an atmosphere of nitrogen.

(Dichloromethyl)triisopropylsilane (2a). Method A. To a solution of triisopropylsilane (**1**, 0.79 g, 1.02 mL, 5 mmol) and 18-C-6 (132 mg, 0.5 mmol) in dry toluene (5 mL) was added finely powdered sodium trichloroacetate (4.64 g, 25 mmol). The reaction mixture was magnetically stirred at reflux temperature until the starting silane **1** was consumed (ca. 2.5 h, GC monitoring). The dark brown mixture obtained was cooled to room temperature, diluted with benzene (15 mL), and filtered through silica gel. The solvents were evaporated, and the residue was distilled under vacuum to give 0.84 g (70%) of silane **2a** as a colorless liquid which crystallized upon standing. **2a**: bp 70°C/0.4 mmHg; mp 27–28 °C; ^1H NMR ($CDCl_3$) δ 1.15 (d, J = 6.8 Hz, 18H, CH_3), 1.32 (heptet, 3H, SiCHC), 5.53 (s, 1H, $CHCl_2$); ^{13}C NMR ($CDCl_3$) δ 11.52 (Si*C*HC), 19.22 (CH_3), 62.32 ($CHCl_2$); ^{29}Si ($CDCl_3$) δ 6.69. Anal. Calcd for $C_{10}H_{22}Cl_2Si$: C, 49.79; H, 9.13. Found: C, 49.68; H, 9.18.

Method B. Solid finely powdered NaOH (1 g, 25 mmol) was added in small portions, over a period of 30 min, to a mixture of triisopropylsilane (0.79 g, 1.02 mL, 5 mmol) and 18-C-6 (66 mg, 0.25 mmol) dissolved in chloroform (5 mL). The reaction mixture was magnetically stirred at room temperature for 8 h. Filtration of solids followed by evaporation of the solvent and distillation of the residue under vacuum gave 1.06 g (88%) of silane **2a**.

Method C. The reaction was carried out as described above for method B except the reaction flask was placed in the center of an ultrasonic cleaning bath (Branson B-12, 80 W) at a distance of 1 cm from the bottom. The reaction time was 2 h, and after standard workup, the yield of **2a** was 1.01 g (84%).

Method D. A solution of 50% aqueous NaOH (2 mL, 25 mmol) was added dropwise to a magnetically stirred solution of triisopropylsilane (0.79 g, 1.02 mL, 5 mmol) and TEBA (57 mg, 0.25 mmol) in chloroform (5 mL). When the addition was complete (ca. 10 min), stirring was continued for 2 h at room temperature. The mixture was diluted with water (10 mL) and chloroform (15 mL). The organic layer was separated, washed with water (3 × 10 mL), and dried over $MgSO_4$. Evaporation of the solvent and distillation of the residue under vacuum afforded silane **2a** (1.06 g, 88%).

(Dibromomethyl)triisopropylsilane (2b). Method B. To a solution of triisopropylsilane (3.16 g, 4.08 mL, 20 mmol) and 18-C-6 (264 mg, 1 mmol) in a mixture of dichloromethane and bromoform (12 mL/8 mL) was added solid, finely powdered NaOH (4 g, 100 mmol) in small portions over a period of 30 min. The reaction mixture was stirred at room temperature. A strongly exothermic reaction, causing the boiling of the mixture, begins after ca. 1.5 h. Stirring was continued for an additional 1 h, the solids were filtered, and dichloromethane as well as excess bromoform was evaporated under vacuum. The residue solidifies upon cooling to room temperature, affording 5.06 g (77%) of crude silane **2b**. Recrystallization from ethanol gave 4.22 g (64% yield) of pure **2b** as slightly yellowish crystals. **2b**: mp 40–41 °C; ^1H NMR ($CDCl_3$) δ 1.12 (d, J = 6.8 Hz, 18H, CH_3), 1.37 (heptet, J = 6.8 Hz, 3H, SiCHC), 5.38 (s, 1H, $CHBr_2$); ^{13}C NMR ($CDCl_3$) δ 12.26 (Si*C*HC), 19.35 (CH_3), 33.18 ($CHBr_2$); ^{29}Si NMR ($CDCl_3$) δ 6.24. Anal. Calcd for $C_{10}H_{22}Br_2Si$: C, 36.38; H, 6.72. Found: C, 36.44; H, 6.73.

Method D. A 50% aqueous NaOH (8 mL, 100 mmol) solution was added dropwise over a period of 30 min to a magnetically stirred solution of triisopropylsilane (3.16 g, 4.08 mL, 20 mmol) and TEBA (228 mg, 1 mmol) in a mixture of CH_2Cl_2 and $CHBr_3$ (12 mL/8 mL). A slightly exothermic reaction is observed at the beginning of the process. The reaction mixture was stirred overnight at room temperature. Standard workup (see preparation of **2a**, method D) followed by recrystallization gave 4.41 g of **2b** (67% yield).

***tert*-Butyl(dichloromethyl)dimethylsilane (12).** Finely powdered NaOH (0.1 g, 2.5 mmol) was added in small portions over a period of 10 min to a solution of *tert*-butyldimethylsilane (**10**) (0.29 g, 0.415 mL, 2.5 mmol) and 18-C-6 (33 mg, 0.125 mmol) in chloroform (2.5 mL). The reaction mixture was magnetically stirred at room temperature for 6 h. GC and ^1H NMR analyses showed the formation of a mixture of siloxane **11** and silane **12** in a 9:91 ratio. The solids were filtered, and the solvent and **11** were removed at room temperature on a rotary evaporator; bulb-to-bulb distillation of the residue under vacuum (ca. 0.1 mm) at room temperature gave 0.27 g (55%) of silane **12** as colorless crystals. **12**: mp 37–38 °C; ^1H NMR ($CDCl_3$) δ 0.20 [s, 6H, $Si(CH_3)_2$], 0.99 (s, 9H, *t*-Bu), 5.40 (s, 1H, $CHCl_2$); ^{13}C NMR ($CDCl_3$) δ −7.36 [$Si(CH_3)_2$], 18.02 ($SiCCH_3$), 27.58 (CCH_3), 62.86 ($CHCl_2$); ^{29}Si NMR ($CDCl_3$) δ 14.12. Anal. Calcd for $C_7H_{16}Cl_2Si$: C, 42.21; H, 8.10. Found: C, 42.53; H, 7.90. Note: ^1H and ^{13}C NMR spectral data of **12** differ insignificantly from those given in ref 13a, which were obtained in benzene-d_6.

***tert*-Butyl(dibromomethyl)dimethylsilane (13).** Compound **13** was prepared from **10** (2.5 mmol), using the procedure described above for **12** except that a mixture of $CHBr_3$ (1 mL) and CH_2Cl_2 (1.5 mL) was used instead of $CHCl_3$. Reaction time: 2 h. GC and NMR analyses revealed the formation of **11** and **13** in a 10:90 ratio. Workup: the solids were filtered and dichloromethane was removed on a rotary evaporator at room temperature. Fractional distillation of the residue under vacuum afforded silane **13** (460 mg, 64% yield) as a colorless liquid. **13**: bp 66 °C/2 mm; ^1H NMR ($CDCl_3$) δ 0.26 [s, 6H, $Si(CH_3)_2$], 1.03 (s, 9H, *t*-Bu), 5.28 ($CHBr_2$); ^{13}C NMR ($CDCl_3$) δ −6.22 [$Si(CH_3)_2$], 18.55 ($SiCCH_3$), 27.75 (CCH_3), 34.72 ($CHBr_2$); ^{29}Si NMR ($CDCl_3$) δ 14.44. Anal. Calcd for $C_7H_{16}Br_2Si$: C, 29.18; H, 5.60. Found: C, 29.11; H, 5.44.

Triphenylsilanol (15). To a solution of triphenylsilane (1.3 g, 5 mmol) and 18-crown-6 (66 mg, 0.25 mmol) in chloroform (5 mL) was added solid finely powdered NaOH (1 g, 25 mmol). A slightly exothermic reaction accompanied by the evolution of H_2 starts almost immediately. The reaction mixture was magnetically stirred at room temperature for 72 h. The mixture was diluted with CH_2Cl_2 (10 mL) and water (10 mL), and the organic layer was isolated, washed with water, and dried ($MgSO_4$). Evaporation of the solvents followed by the vacuum sublimation of the solid residue gave **15** (1.08 g, 78%), mp 152 °C (lit.[16] mp 153–154 °C).

PTC reactions of all other silanes with haloform/alkali were carried out as described above for **1** using the same amounts of reactants [in some cases (see text and Table 2) 1 molar equiv of alkali was used]. See Table 2 for the reaction conditions and product yields and/or ratios. Reaction products were identified by comparison of their physical and spectral data with those described in the literature.[17]

Acknowledgment. We are grateful to the Natural Sciences and Engineering Research Council of Canada for support of this research. Thanks are also due to Dr.

(16) *Dictionary of Organometallic Compounds*; Chapman and Hall: London, 1984; Vol. 2, p 2113.
(17) Bazant, V.; Chvalovsky, V.; Rathonsky, J. *Organosilicon Compounds*; Academic Press: New York, 1965; Vol. 2.

C. Bensimon for x-ray determination of **2a**. We are indebted to Professor Dietmar Seyferth for constructive comments and suggestions.

Supplementary Material Available: Experimental details and tables of crystal structure determination data, atomic coordinates, anisotropic thermal parameters, and bond lengths and angles for compound **2a**; stereoview of packing diagram; ^{1}H, ^{13}C, and ^{29}Si NMR spectra of **2a**, **2b**, **12**, and **13** (26 pages). This material is contained in libraries on microfiche, immediately follows this article in microfilm version of the journal, and can be ordered from ACS; see any current masthead page for ordering information.

OM9407666

On the Reactivity of Acetylenes Coordinated to Cobalt. 9.† Effects of Substitution and Coordination on the ^{13}C-NMR Chemical Shifts of the sp Carbons of $(\mu_2\text{-}R^1C_2R^2)Co_2(CO)_6$ Complexes. Molecular Structure of $(\mu_2\text{-}PhC_2SiPh_3)Co_2(CO)_6$

Berit Happ,‡ Tamás Bartik,‡ Claudia Zucchi, Maria Cecilia Rossi,§ Franco Ghelfi, and Gyula Pályi*,⊥

Department of Chemistry, University of Modena, Via Campi 183, I-41100 Modena, Italy

Gyula Váradi||

Institute of General and Inorganic Chemistry, L. Eötvös University, H-1518 Budapest, 112 P.O. Box 32, Hungary

Gábor Szalontai

Regional Instrument Centre, NMR Laboratory, University of Veszprém, Egyetem-u.8, H-8200 Veszprém, Hungary

István T. Horváth▽

Institute of Organic Chemistry, University of Veszprém, Egyetem-u.8, H-8200 Veszprém, Hungary

Angiola Chiesi-Villa and Carlo Guastini¶

Department of Structural Chemistry, University of Parma, Città Universitaria, Parma, Italy

Received December 9, 1993⊗

Thirty-four $(\mu_2\text{-}R^1C_2R^2)Co_2(CO)_6$ complexes (14 new) were prepared and characterized by their IR ν(CO) and ^{1}H- and ^{13}C-NMR spectra. The ^{13}C-NMR chemical shifts of the coordinated sp carbon atoms were correlated with those of the corresponding free acetylenes. This indicated that the interaction between the R^1 and R^2 groups and the $C_2Co_2(CO)_6$ moiety is very sensitive not only to the donor/acceptor character of R^1 and R^2 but also to the orbital symmetry of the atoms attached directly to the C(sp) atoms. The changes of the $\delta(^{13}C)$ values of the C(sp) atoms upon coordination were also analyzed in these terms. It is concluded that although the dinuclear μ_2-coordination of the acetylene results in a high degree of excitation the stability of the $C_2Co_2(CO)_6$ moiety diminished the reactivity of the organic ligand. Differences in the reactivity of the $(\mu_2\text{-}R^1C_2R^2)Co_2(CO)_6$ complexes in carbonylation are also discussed. The crystal and molecular structure of $(PhC_2SiPh_3)Co_2(CO)_6$ was determined by single crystal X-ray diffraction. This compound crystallizes in the orthorhombic *Pbca* space group with a = 28.790(2) Å, b = 11.577(1) Å, c = 17.833(2) Å, Z = 8. The structure was determined with R = 0.039, R_w = 0.036.

Introduction

The chemistry of acetylenes coordinated to cobalt provided a very dynamic development in the 1980s.[2,3] The main driving force of this research activity has been the ability of acetylenes coordinated to cobalt carbonyl or cyclopentadienyl complexes of giving highly regioselective C,C coupling reactions with CO, olefins, or acetylenes.[4] The most interesting examples include the synthesis of bilactones (1) and cyclic ketones (2). In both cases the (μ-acetylene)$Co_2(CO)_6$ complexes were proved to be intermediates of the coupling reactions. We were particularly interested in reaction (1) and made at-

* Author to whom correspondence should be addressed.

† For parts 7 and 8, see ref 1a,b.

‡ Present address: Department of Chemistry, Virginia Institute of Technology, Blacksburg, VA 24061.

§ Centro Interdipartimentale Grandi Strumenti, University of Modena, Via Campi 213/a, I-41100 Modena, Italy.

⊥ Work started at the Universities of Veszprém and Budapest.

|| Present address: Department of Pharmacology and Cell Biophysics, University of Cincinnati, 231 Bethesda Ave., Cincinnati, OH 45267-0575.

▽ Present address: Corporate Research Laboratories, Exxon Research and Engineering Co., Annandale, NJ, 08801.

¶ Deceased on Sept. 12, 1993. This paper is dedicated to his memory.

⊗ Abstract published in *Advance ACS Abstracts*, December 15, 1994.

(1) (a) Part 7: Horváth, I. T.; Pelczer, I.; Szabó, G.; Pályi, G. *J. Mol. Catal.* **1983**, *20*, 153. (b) Part 8: Váradi, G.; Mouvier, G.; Vivarelli, P.; Zucchi, C.; Pályi, G. *J. Mol. Catal.* **1993**, *84*, L7.

(2) Some recent leading references: (a) Schore, N. E.; Rowley, E. G. *J. Am. Chem. Soc.* **1988**, *110*, 5224. (b) Billington, D. C.; Blandon, P.; Helps, I. M.; Pauson, P. L.; Thomson, W.; Willison, D. *J. Chem. Res. Synop.* **1988**, 326. (c) Krafft, M. E. *Tetrahedron Lett.* **1988**, *29*, 999. (d) Bradley, D. H.; Khan, M. A.; Nicholas, K. M. *Organometallics* **1989**, *8*, 554. (e) Krafft, M. E.; Pankowski, J. *Tetrahedron Lett.* **1990**, *31*, 5139. *Synlett* **1991**, 865. (f) Rubin, Y.; Knobler, C. B.; Diedrich, F. *J. Am. Chem. Soc.* **1990**, *112*, 4966. (g) Germanas, J.; Aubert, C.; Vollhardt, K. P. C. *J. Am. Chem. Soc.* **1991**, *113*, 4006. (h) Magnus, P.; Davies, M. *J. Chem. Soc., Chem. Commun.* **1991**, 1522. (i) Joh, T.; Doyama, K.; Fujiwara, K.; Maeshima, K.; Takahashi, S. *Organometallics* **1991**, *10*, 508. (j) Krafft, M. E.; Juliano, C. A.; Scott, I. L.; Wright, C.; McEachin, M. D. *J. Chem. Soc.* **1991**, *113*, 1693. (k) Takano, S.; Inomata, K.; Ogasawara, K. *J. Chem. Soc., Chem. Commun.* **1992**, 169.

0276-7333/95/2314-0809$09.00/0

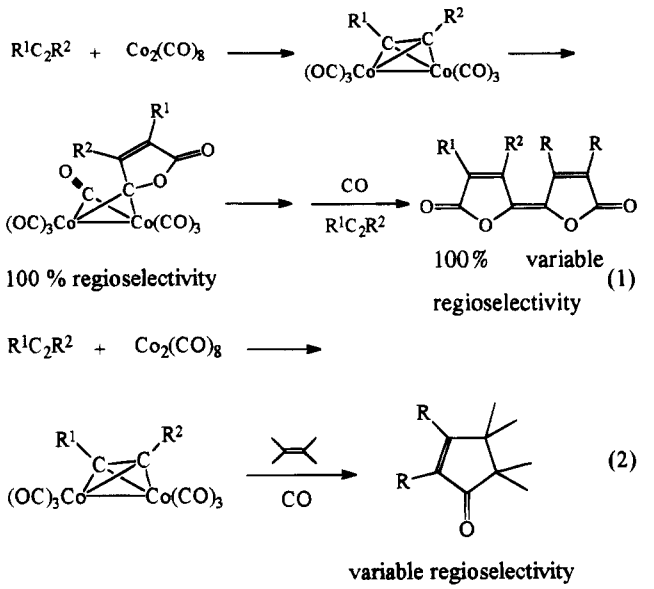

tempts to find the limits of reactivity as well as reasons for the regioselectivity.[4a,c] The regioselectivity may very well be a consequence of the dinuclear activation; thus, the reacting acetylene initially gets coordinated to *two* cobalt atoms. This dinuclear coordination not only stabilizes an excited state (cis-bent) of the substrate[5] but also increases the difference in the chemical environment of the sp carbons. Earlier, we and others[4c,6] found that the predisposal of alkyne carbon atoms toward activation in C,C coupling reactions is reflected in the ^{13}C-NMR behavior.

It was our aim to get more extended information about these phenomena by synthesizing (μ_2-$R^1C_2R^2$)$Co_2(CO)_6$ complexes with R^1 and R^2 substitutents of different electron donor/acceptor character and obtaining their ^{13}C-NMR spectra. We also intended to determine the molecular structure of a derivative, where the chemical environments of the (coordinated) sp carbons are (possibly[7]) the most different. The results of this study will be reported here.

Experimental Section

All operations were carried out under carefully dried, deoxygenated, and CO_2-free Ar or CO atmosphere. Dried and deoxygenated solvents[8] were used throughout the procedures.

Infrared spectra were recorded on UR-20, IR-75 (Carl Zeiss, Jena), Philips PU 9716, and Bruker FT-IR IFS 113V instruments with contemporaneous DCl calibration,[9] where it was necessary. ^{1}H-NMR spectra were recorded on BS-467 (80 MHz, Tesla, Brno), Varian XL-200 (FT, 200 MHz), Bruker WP 80 SY (FT, 80 MHz), and AMX 400 (FT, 400 MHz) instruments. ^{13}C-NMR spectra were obtained by Varian CFT-20, XL-100, XL-200, Bruker WP 80 SY, and AMX 400 instruments in the presence of Cr(acac)$_3$.

Starting materials were of commercial origin except $Co_2(CO)_8$,[10] propyne-1, butyne-1,[11] 3-methylbutyne-1,[12] 3,3-dimethylbutyne-1[13] 4,4-dimethylpentyne-1,[14] 3-methoxypropyne-1,[15] 3-(phthalimidyl)propyne-1,[14] 1-phenylbutyne-1,[16] 1-phenyl-3-methylbutyne-1,[17] 1-phenyl-3,3-dimethylbutyne-1,[18] 1-phenyl-2-(trimethylsilyl)ethyne,[19a] and 1-phenyl-2-(triphenylsilyl)ethyne[19b] which were prepared by essentially known methods and characterized by physical constants (bp, mp, n^{20}_D) as well as by GC–MS (Varian MAT-111) and ^{1}H-NMR spectra.

Preparation of the (Acetylene)$Co_2(CO)_6$ Compounds. The (acetylene)$Co_2(CO)_6$ complexes were prepared from equimolar, 0.1–0.5 mmol, quantities of $Co_2(CO)_8$ and the corresponding acetylene, generally using *n*-hexane (10–50 mL) as solvent (with the exception of 3-phthalimidylpropyne-1 and the two triphenylsilyl derivatives where toluene was used) in a thermostated reaction vessel (0–20 °C for acetylenes with electron donor, 40-60 °C for acetylenes with electron acceptor or very bulky substituents) equipped with external magnetic stirring and gas burette. The progress of the reaction was followed by analyzing the reaction mixture from time to time (~30 min intervals) by infrared spectroscopy (in particular, the diminution of the 1866/1857 cm^{-1} doublet of $Co_2(CO)_8$[21] and the increasing of the highest energy "totally symmetric"[22] band of the (acetylene)$Co_2(CO)_6$ complex could be followed well at mixtures). The product was generally concentrated (to ~1/10th of volume) and purified by preparative TLC (20 cm × 20 cm, 0.25–0.5 mm thick UNI Plate silica gel G (Anachem) or 5721 DC Fertigplatten, Kieselgel 60 (Merck)). Yields ranged from 60 to >90%. This method essentially corresponds to published preparative procedures.[23–25]

(3) Reviews: (a) Pályi, G.; Váradi, G.; Horváth, I. T. *J. Mol. Catal.* **1981**, *13*, 61. (b) Pauson, P. L. *Tetrahedron* **1985**, *41*, 5855. (c) Pályi, G.; Váradi, G.; Markó, L. In *Stereochemistry of Organometallic and Inorganic Compounds*; Bernal, I., Ed.; Elsevier: Amsterdam, 1986; Vol. 1, p 358. (d) Nicholas, K. M. *Acc. Chem. Res.* **1987**, *20*, 207. (e) Schore, N. E. *Chem. Rev.* **1988**, *88*, 1081. (f) Serratosa, F. *J. Organomet. Chem.* **1991**, *413*, 445. (g) Diedrich, F.; Rubin, Y. *Angew. Chem., Int. Ed. Engl.* **1992**, *31*, 1101.

(4) CO: (a) Pályi, G.; Váradi, G.; Vizi-Orosz, A.; Markó, L. *J. Organomet. Chem.* **1975**, *90*, 85. (b) Guthrie, D. J. S.; Khand, I. U.; Know, G. R.; Kollmeier, J.; Pauson, P. L.; Watts, W. E. *J. Organomet. Chem.* **1975**, *90*, 93. (c) Váradi, G.; Vecsei, I.; Ötrös, I.; Pályi, G.; Markó, L. *J. Organomet. Chem.* **1979**, *182*, 415. Olefins: see refs 2j, and 3b,e. Acetylenes: (d) Hoogzand, C.; Hübel, W. *Angew. Chem.* **1961**, *73*, 680; *Tetrahedron Lett.* **1961**, 637. (e) Mills, O. S.; Robinson, C. *Proc. Chem. Soc.* **1964**, 187. (f) Hübel, W. In *Organic Syntheses via Metal Carbonyls*; Wender, I., Pino, P., Eds.; Interscience: New York, 1968; Vol. 1, p, 273.

(5) (a) Blizzard, A. C.; Santry, D. P. *J. Am. Chem. Soc.* **1968**, *90*, 5749. (b) Iwashita, Y.; Tamura, F.; Nakamura, A. *Inorg. Chem.* **1969**, *8*, 1179. (c) Bán, M.; Bálint, I.; Révész, M.; Váradi, G.; Pályi, G. *THEOCHEM* **1982**, *88*, 357. (d) Jobic, H.; Santini, C. C.; Coulombean, C. *Inorg. Chem.* **1991**, *30*, 3088.

(6) Aime, S.; Milone, L.; Rosetti, R.; Stanghellini, P. L. *Inorg. Chim. Acta* **1976**, *22*, 135.

(7) The (μ_2-$R^1C_2R^2$)$Co_2(CO)_6$ complexes are often oils and cannot be crystallized: see ref 4f and (a) Dickson, R. S.; Fraser, P. J. *Adv. Organomet. Chem.* **1974**, *12*, 323.

(8) Shriver, D. F.; Drezdzon, M. A. *The Manipulation of Air-Sensitive Compounds*, 2nd ed.; Wiley: New York, 1986.

(9) Bor, G. *Acta Chim. (Budapest)* **1962**, *39*, 315.

(10) Szabó, P.; Markó, L.; Bor, G. *Chem. Techn. (Berlin)* **1961**, *13*, 549.

(11) Meinert, R. N.; Hurd, C. D. *J. Am. Chem. Soc.* **1930**, *52*, 4540.

(12) Henne, A.; Greenle, K. W. *J. Am. Chem. Soc.* **1943**, *65*, 2020.

(13) Bartlett, P. D.; Rosen, L. J. *J. Am. Chem. Soc.* **1942**, *64*, 543.

(14) Brandsma, L. *Preparative Acetylene Chemistry*: Elsevier: Amsterdam, 1971.

(15) Heilbron, I. M.; Jones, E. R. H.; Walls, I. M. S. *J. Chem. Soc.* **1946**, 27.

(16) Jacobs, T. L.; Akawie, R.; Cooper, R. G. *J. Am. Chem. Soc.* **1951**, *73*, 1273.

(17) Schlubach, H. H.; Repping, K. *Liebigs Ann. Chem.* **1958**, *614*, 37.

(18) Negishi, E.; Baba, S. *J. Am. Chem. Soc.* **1975**, *97*, 7385.

(19) (a) Mitchell, R. H.; Sonderheimer, F. *Tetrahedron* **1970**, *26*, 2141. (b) A variant of the preparation of PhC_2SiMe_3,[19] using Ph_3SiCl.

(20) (a) Lawton, S. L.; Jacobson, R. A. *TRACER, a cell reduction program*; Ames Laboratory: Iowa State University of Science and Technology, 1965. (b) Lehmann, M. S.; Larsen, F. K. *Acta Crystallogr.* **1974**, *A30*, 580. (c) Wilson, A. J. C. *Nature (London)* **1942**, *150*, 151. (d) North, A. C. T.; Phillips, D. C.; Mathews, F. S. *Acta Crystallogr.* **1968**, *A24*, 351. (e) *International Tables for X-ray Crystallography*; Kynoch Press: Birmingam, England, 1974; Vol. IV, p 149; (f) p 9. (g) Stewart, R. F.; Davidson, E. R.; Simpson, W. T. *J. Chem. Phys.* **1965**, *42*, 3175. (h) Sheldrick, G. M. *SHELX-86. A FORTRAN-77 Program for the Solution of Crystal Structure from Diffraction Data*; University of Cambridge: Cambridge, England, 1986. (i) Sheldrick, G. M. *SHELX-76. System of Crystallographic Computer Programs*; University of Cambridge: Cambridge, England, 1976.

(21) Bor, G. *Spectrochim. Acta* **1963**, *19*, 2065.

(22) Bor, G. *Spectrochim. Acta* **1963**, *19*, 1209.

Complexes (μ_2-$R^1C^1{=}C^2R^2$)$Co_2(CO)_6$ were characterized by IR and NMR spectra and analyses (Tables 1 and 2).

Attempted Carboxylation of (Acetylene)$Co_2(CO)_6$ Complexes. Approximately 0.1 mmol quantities of ($R^1C_2R^2$)$Co_2(CO)_6$ complexes were dissolved in 3–5 mL of *n*-hexane under Ar atmosphere. Then the atmosphere was changed to CO_2 and the solution stirred at rt while it was analyzed periodically (1, 4, 8, 48, 72 h) by infrared spectroscopy. No CO_2 consumption, no change in the IR ν(CO) spectrum, and no new substance in the GC–MS analysis were observed. The compounds tested were R^1 = H, R^2 = nBu, CH_2OMe, CH_2NEt_2; R^1 = Me, R^2 = Et, Ph, $SiMe_3$; and R^1 = Ph, R^2 = Et, iPr, tBu, $SiMe_3$, $SiPh_3$. The tests were repeated in the presence of non-CO ligands (L = pyridine, PPh_3, and $P(OMe)_3$) with Co:L ratios of 1:1 and 1:10. Neither of these tests showed reaction of the coordinated acetylene with CO_2.

Carbonylation of HC_2SiMe_3. Equimolar amounts (1 mmol) of HC_2SiMe_3 and $Co_2(CO)_8$ were placed into a 250 mL stainless steel rocking autoclave together with 50 mL of *n*-hexane. The autoclave was closed, secured, and then pressurized to 27 MPa by CO gas, heated to 90 °C, and rocked for 8 h. CO gas consumption was adjusted after each hour. Then the autoclave was left to stand at rt for 48 h. After this period the autoclave was depressurized and opened. The infrared ν(CO) spectrum showed ~60% remaining $Co_2(CO)_8$ and 20–30% of a new substance, which—as expected—was [(H,$SiMe_3$)C_4O_2]$Co_2(CO)_7$. This substance was separated by preparative TLC on silica and characterized as follows: orange-red solid, mp 97–98 °C dec; IR ν(CO), *n*-hexane 2110.5 m, 2076.1 vs, 2059.7 s, 2055.2 w, 2042.8 s, 2028.7 m, 1847.8 m (bridging CO), 1780.9 (organic CO) cm^{-1} (see ref 4a); ^{1}H-NMR ($CDCl_3$) 0.19 (s, 9H, $SiCH_3$), 7.43 (s, 1H, *CH*). Anal. Calcd for $C_{14}H_{10}O_9SiCo_2$: C, 35.92; H, 2.15; Co, 25.18. Found: C, 36.1; H, 2.3; Co, 24.9.

Crystal and Molecular Structure of (PhC_2SiPh_3)$Co_2(CO)_6$. The reduced cell was obtained with use of TRACER.[20a] Crystal data details associated with structure refinement are given in Table 3. Data were collected at room temperature (295 K) on a single-crystal diffractometer (Philips PW1100). For intensities and background individual reflection profiles were analyzed.[20b] The structure amplitudes were obtained after the usual Lorentz and polarization corrections, and the absolute scale was established by the Wilson method.[20c] Data were corrected for absorption using a simiempirical method.[20d] The function minimized during the least-squares refinement was $\sum w|\Delta F|^2$. A weighting scheme [$w = k/[\sigma^2(F_o) + g|F_o|^2]$ (g = 0.0002)] based on counting statistics was applied. Anomalous scattering corrections were included in all structure factor calculations.[20e] Scattering factors for neutral atoms were taken from ref 20f for non-hydrogen atoms and from ref 20g for H. Among the low-angle reflections no correction for secondary extinction was deemed necessary.

Solution and refinement were based on the observed reflections. The structure was solved by direct methods using SHELX-86.[20h] Refinement was first done isotropically and then anisotropically by full-matrix least-squares methods for non-H atoms. The hydrogen atoms were located from a difference map and introduced as fixed contributors (U_{iso} = 0.08 Å^2) prior the last stage of refinement. The final difference maps showed no unusual feature, with no significant peak above the general background. During the refinement the phenyl rings were constrained to be regular hexagons (C–C = 1.395 Å). All calculations were carried out on a Gould 32/77 computer using SHELX-76.[20j]

Final atomic coordinates are listed in Table 4 for non-H atoms and in Table S1 (supplementary material) for hydrogens. Thermal perameters are given in Table S2 (supplementary material), selected bond distances and angles are given in Table 5, and a full list of bond distances and angles is in Table S3 (supplementary material).

Results and Discussion

The Experimental Section of this paper reports some new ($R^1C_2R^2$)$Co_2(CO)_6$ complexes as well as unpublished infrared and ^{1}H- and ^{13}C-NMR data (since in some cases the assignment of the ^{13}C-NMR of the substituents of the C_2 moiety was uncertain we reported only the signals of the sp carbon atoms) of several such compounds which were reported but, however, were not fully characterized yet. ^{13}C-NMR data of the majority of the free acetylenes was known,[42] but in most cases we repeated these for the sake of having data of free *and* coordinated acetylenes obtained under identical conditions (the deviation from published data was generally in the range of ±1–2 ppm to negligible from the viewpoint of the effects which will be discussed). These ^{13}C-NMR data for the free and coordinated acetylenes are summarized in Table 2, together with some derived parameters which will be discussed below.

The C,C coupling reactions of the (acetylene)$Co_2(CO)_6$ complexes[3,4] are obviously proceeding by participation of the coordinated "quaternary" sp carbon atoms. It could be expected that the ^{13}C-NMR chemical shifts of these carbon atoms will provide *direct* information about the electron density and reactivity of these atoms. Although the ^{13}C-NMR chemical shifts are influenced by several factors, it appeared to us that the comparison

(23) (a) Sternberg, H. W.; Greenfield, H.; Friedel, R. A.; Wotiz, J.; Markby, R.; Wender, I. *J. Am. Chem. Soc.* **1954**, *76*, 1457. (b) Greenfield, H.; Sternberg, H. W. Friedel, R. A.; Wotiz, J. H.; Markby, R.; Wender, I. *J. Am. Chem. Soc.* **1956**, *78*, 120.
(24) Tirpak, M. R.; Hollingsworth, C. A.; Wotiz, J. H. *J. Org. Chem.* **1960**, *25*, 687.
(25) Krüerke, U.; Hübel, W. *Chem. Ber.* **1961**, *94*, 2829.
(26) (a) Bor, G. *Chem. Ber.* **1963**, *96*, 2644; (b) *J. Organomet. Chem.* **1975**, *94*, 181.
(27) Iwashita, Y.; Ishikawa, A.; Kainosho, M. *Spectrochim. Acta* **1971**, *27A*, 271.
(28) Cetini, G.; Gambino, O.; Rosetti, R.; Sappa, E. *J. Organomet. Chem.* **1967**, *8*, 149.
(29) Bor, G.; Kettle, S. F. A.; Stanghellini, P. L. *Inorg. Chim. Acta* **1976**, *18*, L18.
(30) Markby, R.; Wender, I.; Friedel, R. A.; Cotton, F. A.; Sternberg, H. W. *J. Am. Chem. Soc.* **1958**, *80*, 6529.
(31) Tirpak, M. R.; Wotiz, J. H.; Hollingsworth, C. H. *J. Am. Chem. Soc.* **1958**, *80*, 4265.
(32) Pályi, G.; Kovács-Toplak, M.; Váradi, G. *Atti Accad. Sci. Bologna, Rend. Cl. Sci. Fis.* **1978**, *266*(13/5) 139.
(33) Váradi, G. Unpublished results: (CCl_4) 72.7 (C^1), 90.0 (C^2).
(34) Hübel, W. In *Organic Syntheses via Metal Carbonyls*; Wender, I., Pino, P., Eds.; Wiley-Interservice: New York, 1968; Vol. 1, p 301.
(35) Dickson, R. S.; Fraser, P. J. *Austral. J. Chem.* **1970**, *23*, 2403.
(36) Dubois, J. E.; Doucet, J. P. *J. Chem. Res., Miniprint* **1980**, 1101.
(37) Boag, N. M.; Green, M.; Grove, D. M.; Howard, J. A. K.; Spencer, J. L.; Stone, F. G. A. *J. Chem. Soc., Dalton Trans* **1980**, 2170.
(38) Dickson, R. S.; Kirsch, H. P. *Austral. J. Chem.* **1972**, *25*, 1815.
(39) Bartik, T.; Happ, B.; Iglewsky, M.; Bandmann, H.; Boese, R.; Heimbach, P.; Hoffmann, T.; Wenschuch, E. *Organometallics* **1992**, *11*, 1235.
(40) Levy, G. C.; White, D. M.; Cargioli, J. D. *J. Magn. Reson.* **1972**, *8*, 280.
(41) Arnett, E. M.; Strem, M. E.; Friedel, R. A. *Tetrahedron Lett.* **1961**, 658.
(42) Wrackmyer, B.; Horhler, K. *Progr. NMR Spectr.* **1990**, *22*, 209.
(43) Al-Rawi, J. M. A.; Khuthier, A. H. *Org. Magn. Reson.* **1981**, *15*, 285.
(44) (a) Sauer, J. C. Ger. Pat. 1,054,086, 1955. (b) Sauer, J. C.; Cramer, R. D.; Engelhardt, V. A.; Ford, T. A.; Holmquist, H. E.; Howk, B. W. *J. Am. Chem. Soc.* **1959**, *81*, 3677. (c) Albanesi, G.; Tovaglieri, M. *Chim. Ind. (Milano)* **1959**, *41*, 189. (d) Bak, T.; Horváth, I. T.; Markó, L.; Palágyi, J.; Pályi, G.; Váradi, G. Ger. Offen. 3,041,955, 1980. (e) Váradi, G.; Horváth, I. T.; Palágyi, J.; Bak, T.; Pályi, G. *J. Mol. Catal.* **1980**, *9*, 457.
(45) Gallow, P.; Sebald, A.; Wrackmeyer, B. *J. Organomet. Chem.* **1983**, *259*, 253.
(46) (a) Dorman, D. E.; Jautelat, M.; Roberts, J. D. *J. Org. Chem.* **1973**, *38*, 1026. (b) Hearn, M. T. W. *J. Magn. Reson.* **1976**, *22*, 521.
(47) Váradi, G.; Galamb, V.; Palágyi, J.; Pályi, G. *Inorg. Chim. Acta* **1981**, *53*, L 29, L 222.

Table 1. Characterization of the (μ_2-$R^1C^1{\equiv}C^2R^2$)$Co(CO)_6$ Complexes

substituents R^1	R^2	ref	infrared ν(CO) (cm^{-1})	^{1}H-NMR (δ, ppm/TMS; J, cps)	remarks, analyses
H	H	23	*n*-hexane: 2098.5 m, 2058.8 vs, 2034.2 s, 2028.2 s, 2016.5 m, sh; lit. 26	$CDCl_3$: 5.92 (s, 2H, C*H*); lit 6, 27	red oil; mp 12−13 °C (lit.[23] mp 13.0−13.6 °C)
H	Me	28	*n*-hexane: 2092.8 m, 2052.9 vs, 2029.1 s, 2020.3 s, 2011.1 m, sh; lit. 29	$CDCl_3$: 2.62 (s, 3H, CH_3), 6.04 (s, 1H, C^1H); lit. 6, 27	red-brown oil; mp 10−11 °C
H	Et	24	*n*-hexane: 2093.5 m, 2052.9 vs, 2029.6 s, 2020.8 s, 2011 w, sh, ~2005 vw, sh	$CDCl_3$: 1.08 (t, J_{HH} = 7, 3H, CH_3), 2.71 (q, J_{HH} = 7, 2H, CH_2), 6.03 (s, 1H, C^1H)	red-brown oil
H	*n*-Pr	30 n.i.	*n*-hexane: 2092.9 m, 2052.7 vs, 2029.1 s, 2019.6 s, 2009.7 w, sh, ~2006 vw; lit 1b, 26a	$CDCl_3$: 1.01 (t, J_{HH} = 7, 3H, CH_3), 1.58 (m, 2H, β-CH_2), 2.65 (q, J_{HH} = 7.5, 2H, α-CH_2), 6.03 (s, 1H, C^1H); lit. 1b	red-brown oil; found Co 33.2, $C_{11}H_8O_6Co_2$, calcd Co 33.29
H	*i*-Pr	1b	*n*-hexane: 2095.8 m, 2056.9 vs, 2032.7 vs, 2025.1 s, 2014.9 w, sh, ~2003 vw; lit. 1b	CCl_4: 1.02 (d, J_{HH} = 7, 6H, CH_3), 2.43 (m, 1H, i-Pr-C*H*), 6.06 (s, 1H, C^1H); lit. 1b	red-brown oil; solidifies ~5 °C
H	*n*-Bu	31 n.i.	*n*-hexane: 2092.3 m, 2052.6 vs, 2029.1 vs, 2020.3 s, 2009 w, sh, ~2006 vw, sh	$CDCl_3$: 1.03 (t, J_{HH} = 7, 3H, CH_3), 1.5−1.8 (m, 4H, β,γ-CH_2), 2.58 (t, J_{HH} = 7, 2H, α-CH_2), 6.05 (s, 1H, C^1H)	red-brown oil, lit.[31] found Co 31.7, $C_{12}H_{10}O_6Co_2$, calcd Co 32.02
H	*t*-Bu	24	*n*-hexane: 2092.2 m, 2052.3 vs, 2029.1 s, 2019.9 s, 2010.2 w, sh, 2008 vw; lit. 1b, 29	CCl_4: 0.98 (s, 9H, CH_3), 6.08 (s, 1H, C^1H)	red oil; mp 10−12 °C
H	*n*-Pent		*n*-hexane: 2091.9 m, 2052.3 vs, 2028.9 s, 2020.2 s, 2009 w, sh, 2003 vw, sh	$CDCl_3$: 1.00 (t, J_{HH} = 7, 3H, CH_3), 1.3−1.8 (m, 6H, β,γ,δ-CH_2), 2.50 (q, J_{HH} = 7.5, 2H, α-CH_2), 6.02 (s, 1H, C^1H)	red oil; found Co 30.3, $C_{13}H_{12}O_6Co_2$, calcd Co 30.85
H	*neo*-Pent	1b	*n*-hexane: 2091.8 m, 2057.7 vs, 2028.1 s, 2019.3 s, 2008.3 w, sh, 2007 vw, sh; lit 1b	CCl_4: 0.92 (s, 9H, CH_3), 2.15 (s, 2H, CH_2), 6.08 (s, 1H, C^1H); lit. 1b	red oil
H	CH_2OMe	24 n.i.	*n*-hexane: 2096.9 m, 2057.8 vs, 2033.4 vs, 2028 sh, 2021.9 m, 2011.4 m; lit. 3	C_6D_6: 2.72 (s, 3H, CH_3), 3.80 (s, 2H, CH_2), 5.08 (s, 1H, C^1H)	red oil: found C 32.9, H 1.2, Co 33.1, $C_{10}H_6O_7Co_2$, calcd C 33.73, H 1.70, Co 33.11
H	CH_2NEt_2	31 n.i.	*n*-hexane: 2092.7 m, 2054.4 vs, 2028.5 s, 2024.5 ms, 2019.7 sh, 2010.9 w	C_6D_6: 0.83 (t, J_{HH} = 7, 6H, CH_3), 1.5−2.31 (q, J_{HH} = 7, 4H, Et-CH_2), 3.53 (s, 2H, α-CH_2), 5.45 (s, 1H, C^1H)	red oil; found C 39.1, H 2.9, N 3.4, Co 28.9, $C_{13}H_{13}O_6NCo_2$, calcd C 39.32, H 3.30, N 3.53, Co 29.68
H	$CH_2N(CO)_2$-C_6H_4-*o*	32 n.i.	*n*-hexane: 2098.0 m, 2061.1 vs, 2058.6 s, 2033.4 s, sh, 2026.5 m, sh, 2018.2 w, sh; $\nu(CO)_{org}$ 1727.4 m	acetone-d_6: 1.91 (s, 2H, CH_2), 5.93 (s, 1H, C^1H), 7.0−7.1 (m, 4H, Ar-C*H*)	red microcryst solid; mp dec 110 °C; found C 39.1, H 2.9, N 3.4, Co 28.9, $C_{17}H_7O_8NCo_2$, C 43.35, H 1.50, N 2.97, Co 25.02
H	Ph	23b	*n*-hexane: 2094.5 m, 2057.7 vs, 2032.3 s, 2027.9 s, 2016.2 w, sh, ~2011 vw, sh; lit. 26a, 29	$CDCl_3$: 6.23 (s, 1H, C^1H), 7.2−7.4 (m, 3H, ar. *meta* + *para* C*H*), 7.4−7.5 (m, 2H, Ar *ortho* C*H*); lit. 6	red oil
H	C(O)OMe	34 i. ?	*n*-hexane: 2104.5 mw, 2068.7 s, 2040.2 vs, br, 2030 sh, 2022 w, $\nu(CO)_{org}$ 1720 m	$CDCl_3$: 4.22 (s, 3H, CH_3), 5.80 (s, 1H, C^1H); lit. 6	red-brown solid; routinely used without additional purification
H	$SiMe_3$	25	*n*-hexane: 2092.4 ms, 2053.9 vs, 2028.8 vs, 2021.1 s, 2010.5 m; lit 4a	$CDCl_3$: 0.30 (s, 9H, CH_3), 6.36 (s, 1H, C^1H)	deep red solid; mp 28−29 °C (lit[25] mp 29.5 °C)
H	$SiPh_3$		*n*-hexane: 2093.4 m, 2056.7 vs, 2029.7 vs, br, ~ 2016 m, sh, 2010 w, sh	$CDCl_3$: 6.42 (s, 1H, C^1H), 7.4−7.8 (m, 15H, ar-C*H*)	red solid; mp 88−89 °C dec; found C55.1, H 3.1, Co 20.5, $C_{26}H_{16}O_6SiCo_2$, calcd C 54.75, H 2.83, Co 20.66
Me	Me	32 n.i.	*n*-hexane: 2089.2 m, 2047.4 vs, 2025.2 s, 2014.8 s, sh, 2004.0 w; lit. 26b, 35	$CDCl_3$: 2.65 (s, 6H, CH_3); lit. 35	red oil
Me	Et	23b, 35	*n*-hexane: 2089.4 m, 2048.7 vs, 2026.4 vs, 2015.3 s, 2004.3 w	$CDCl_3$: 1.02 (t, J_{HH} = 7, 3H, Et-CH_3), 2.55 (s, 3H, CH_3), 2.62 (q, J_{HH} = 7, 2H, Et-CH_2); the signals between 2.5 and 2.7 ppm are overlapping, intensity ratio only approximate	red oil; found Co 33.1, $C_{11}H_8O_6Co_2$, calcd Co 33.29
Me	*n*-Bu		*n*-hexane: 2088.9 m, 2047.7 vs, 2025.8 vs, 2014.5 s, 2003.9 w		red oil, obtained as TLC fraction; not isolated in analytically pure form
Me	*n*-Pent		*n*-hexane: 2088.8 m, 2047 vs, 2025.4 vs, 2014.2 s, 2003.5 mw		red oil, obtained as TLC fraction; not isolated in analytically pure form
Me	Ph	28	*n*-hexane: 2089.8 m, 2052.3 vs, 2027.7 s, 2020.6 s, 2008.5 w, sh, 2006 vw, sh; lit. 28	C_6D_6: 2.42 (s, 3H, CH_3), 6.95−7.20 (m, 3H, ar-*meta* + *para* C*H*), 7.44−7.47 (m, 2H, cis-*ortho* C*H*)	red-brown oil
Me	$SiMe_3$	38	*n*-hexane: 2087.3 m, 2047.3 vs, 2023.9 s, 2014.7 s, 2003.9 w; sh	C_6D_6: 0.18 (s, 9H, (Si)CH_3), 2.30 (s, 3H, CH_3)	dark red solid: mp 61−62 °C (lit.[38] mp 60−61 °C)
Et	Et	24b, 25 n.i.	*n*-hexane: 2088.5 m, 2047.6 vs, 2025.5 s, 2014.1 s, 2003.7 w		red oil; found Co 33.1, $C_{11}H_8O_6Co_2$, calcd Co 33.29
Et	*n*-Pr		*n*-hexane: 2088.3 m, 2047.7 vs, 2025.6 vs, 2014.0 s, 2003.0 w		red oil, obtained as TLC fraction, not isolated in analytically pure form

Table 1 (Continued)

substituents					
R^1	R^2	ref	infrared ν(CO) (cm^{-1})	^{1}H-NMR (δ, ppm/TMS; J, cps)	remarks, analyses
Et	Ph		*n*-hexane: 2089.4 m, 2052.3 vs, 2027.7 s, 2020.6 s, 2008.5 w, sh ~2002.0 vw, sh	C_6D_6: 1.13 (d, J_{HH} = 7, 6H, CH_3), 2.69 (q, J_{HH} = 7, 2H, CH_2), 6.9−7.6 (m, Ar-C*H*)	dark brownish red oil; found Co 28.1, $C_{16}H_{10}O_6Co_2$, calcd Co 28.32
i-Pr	Ph		*n*-hexane: 2089.9 m, 2051.5 vs, 2026.6 s, 2020.2 s, 2008.1 w, sh, ~2002.0 vw, sh	C_6D_6: 1.13 (t, J_{HH} = 7, 3H, CH_3), 3.01 (m, 1H, *i*-Pr-C*H*), 6.9−7.5 (m, 5H, Ar-C*H*)	deep red substance obtained as TLC fraction; not isolated in analytically pure form
t-Bu	Ph	34	*n*-hexane: 2088.2 m, 2050.6 vs, 2026.8 s, 2018.1 s, 2007.2 w, sh	C_6D_6: 1.23 (s, 9H, CH_3), 6.8−7.6 (m, 5H, Ar-C*H*)	deep red solid; mp 95 °C (lit.[34] mp 94−96 °C)
Me_3Si	Ph	25, 38	*n*-hexane: 2088.2 m, 2050.6 vs, 2026.8 s, 2018.1 s, 2008.1 w, sh	C_6D_6: 0.30 (s, 9H, (Si) CH_3), 6.9−7.6 (m, 5H, Ar-C*H*)	deep red solid: mp 62−64 °C (lit.[25] mp 64 °C)
Ph_3Si	Ph		*n*-hexane: 2089.0 m, 2054.8 vs, 2028.1 vs, 2025.2 s, 2013.1 w, sh, 2007.6 vw, sh	C_6D_6: 6.8−7.7 (m, 20H, Ar-C*H*)	red brown cryst solid; mp 110 °C dec; found C 59.7, H 3.4, Co 18.1, $C_{32}H_{20}O_6SiCo_2$, calcd C 59.45, H 3.12, Co 18.23, X-ray structure determined in this work
EtOC(O)	Ph	25	*n*-hexane: 2100 m, 2067 vs, 2040 s, 2036 s, ~2030 w, sh, ~2002.0 w, sh, $\nu(CO)_{org}$ 1718 m, 1710 m		red microcryst; mp 68−69 °C; found Co 25.5, $C_{17}H_{10}O_8Co_2$, calcd Co 25.61
t-Bu	*t*-Bu	41	*n*-hexane: 2089.9 m, 2051.5 vs, 2026.6 s, 2020.2 s, 2008.1 w, sh, ~2002.0 vw, sh	$CDCl_3$: 0.95 (s, 18H, CH_3)	deep red crystalline solid; mp 115−117 °C dec (lit.[41] mp 115−120 °C)
Ph	Ph	23b	*n*-hexane: 2090.6 m, 2056.2 vs, 2030.2 s, 2026.9 s, 2012.5 w, ~2010 vw, sh; lit. 26a, 29	$CDCl_3$: 6.9−7.5 (m, 10H, Ar-C*H*)	red crystalline solid: mp 108−109 °C (lit.[23a] mp 109.5−110.0 °C)
MeOC(O)	C(O)OMe	25	*n*-hexane: 2111.3 m, 2080.3 vs, 2053.8 s, 2049.2 s, ~2025 sh, $\nu(CO)_{org}$ 1732 w (perhaps two components?)		red crystalline solid; mp 46−47 °C (lit.[25] mp 47−48 °C)
Me_3Si	$SiMe_3$	25	*n*-hexane: 2084.5 m, 2047.2 vs, 2022.0 vs, 2014.2 s, 2002.1 m, sh; lit 4a	$CDCl_3$: 0.26 (s, 18H, CH_3)	red crystalline solid; mp 110−113 °C dec (lit.[25] mp 110 °C)

of the spectroscopic data within this compound class and those of the corresponding noncoordinated acetylenes might be the most efficient way to throw more light upon the information on reactivity "coded" in complexes (acetylene)$Co_2(CO)_6$.

As a first step of this approach one fundamental question was to be answered, *i.e.*, whether one can correlate the parameters of the free and coordinated acetylenes. This is particularly critical since the overall geometry (C_∞) of acyclic acetylene derivatives renders the nuclear shielding of the sp carbons to be very sensitive toward nonaxial influences which are perturbing the C_∞ symmetry. This is important at substituents with π or *d* orbitals and even more when the triple bond gets coordinated.[42,49] Thus, it was to be decided whether the substituent effects are of the same nature at the free and the coordinated acetylenes. This can be best studied by plotting the chemcial shifts of the noncoordinated acetylenes to that of the coordinated ones (Figure 1). These diagrams provide two important pieces of informations: (i) the interaction between the substituents and the C_2 core of the free and coordinated acetylenes is approximately of the same character, and (ii) the interaction is very sensitive toward the *orbital symmetry* (hybridization state) of the *substituents*, causing similar behavior of the substituents with sp^3 (alkyl), sp^2 (aryl, carboxyl) and with s (H) and d (SiR_3) orbitals. These tendencies are very clearly manifested at the symmetric acetylenes ($R^1C_2R^2$, $R^1 = R^2$, Figure 1a) and the monoaryl-substituted PhC_2X series (Figure 1c), while at the HC_2X series (Figure 1b), where one of the substituents is of C_∞ symmetry, only the different behavior of the SiR_3 substituents can be observed (these observations are in accordance with the particular nature of silyl-substituted ligands in coordination structural and catalytic chemistry[50]).

As a next step of the analysis we made an attempt to correlate the ^{13}C-NMR shifts with the Hammet−Taft[48a−c] and Tolman[48d,e] substituent parameters. Since no reliable correlations were obtained (too many "deviating" points need "explanation"), in the following analysis we shall compare the ^{13}C-NMR shifts of the free acetylenes and (acetylene)$Co_2(CO)_6$ complexes using the electron donor/acceptor properties of the substituents as ordering parameters. The following conclusions could be drawn:

(i) The effect of coordination is regarded as stabilizing an excited state of the acetylene, thus causing a remarkable downfield shift of the δ values of the "quaternary" carbons.[5,37,39] This can be best demonstrated by the coordination shift of the δ values ($\Delta\delta = \delta_{coord} - \delta_{free}$) (Figure 2). The $\Delta\delta$ values show in fact downfield shifts for the coordinated acetylenes with alkyl and aryl ligands, but a small upfield shift is observed at H (demonstrating the importance of the C_∞ symmetry of this substitutent) and substantial upfield shift is found for SiR_3 substituents. These effects can be interpreted by considering that form the point of the

(48) (a) Hammett, L. P. *Chem. Rev.* **1935**, *17*, 125. (b) Taft, R. W. *Steric Effects in Organic Chemistry*; Wiley: New York, 1953. (c) Hansch, C.; Leo, A. *Substituent Constants for Correlation Analysis in Chemistry and Biology*; Wiley: New York, 1979. (d) Tolman, C. A. *Chem. Rev.* **1977**, *77*, 313. (e) Heinmbach, P.; Bartik, T. *An Ordering Concept on the Basis of Alternative Principles in Chemistry*; Springer: Berlin, 1990.

(49) Beeler, A. J.; Orendt, A. M.; Grant, D. M.; Cutts, P. W.; Michl, J.; Zilm, K. W.; Downing, J. W.; Facelli, J. C.; Schindler, M. S.; Kurzelnigg, W. *J. Am. Chem. Soc.* **1984**, *106*, 7672.

(50) Some leading references: (a) Vollhardt, K. P. C. *Pure Appl. Chem.* **1985**, *57*, 1819. (b) Magnus, P.; Becker, D. P. *J. Chem. Soc., Chem. Commun.* **1985**, 640. (c) Magnus, P.; Principe, L. M. *Tetrahedron Lett.* **1985**, *26*, 4851. (d) Magnus, P.; Becker, D. P. *J. Am. Chem. Soc.* **1987**, *109*, 7495. (e) Lay, U.; Lang, H. *J. Organomet. Chem.* **1991**, *418*, 79. (f) Gassman, P. G. Deck, P. A.; Winter, C. H.; Dobbs, D. A.; Cao, D. H. *Organometallics* **1992**, *11*, 959. (g) Höger, S.; Mc. Namara, J. J.; Schricker, S.; Wudl, F. *Chem. Mater.* **1994**, *6*, 171.

Table 2. ^{13}C-NMR Chemical Shifts of Free ($R^1C_2R^2$) and Coordinated [$(R^1C_2R^2)Co_2(CO)_6$] Acetylenes

substituent		chemical shift[b] of the sp carbons, δ, ppm										
		free acetylene			coordinated acetylene			shifts by coordination				
R^1	R^2	δ_f^1	δ_f^2	$\Delta\delta_f = (\delta_f^2 - \delta_f^1)$	δ_c^1	δ_c^2	$\Delta\delta_c = (\delta_c^2 - \delta_c^1)$	$\Delta\delta^1 = (\delta_c^1 - \delta_f^1)$	$\Delta\delta^2 = (\delta_c^2 - \delta_f^2)$	$\Sigma\Delta\delta^n$	$\Delta\Delta\delta = \lvert\Delta\delta_c\rvert - \lvert\Delta\delta_f\rvert$	cyclo-carbonylation[e]
H	H	71.8	71.8[c]		70.8	70.8[d]		−1.0	−1.0			+
H	Me	67.6	80.1[f]	12.5	73.0	90.8[g]	17.8	5.4	10.7		5.3	+
H	Et	67.0	84.7[h]	17.7	73.4	99.8	26.4	6.4	15.1		8.7	
H	nPr	66.7	81.8[i]	15.1	73.2	98.5	25.3	6.5	16.7		10.2	+
H	iPr	67.2	88.0[j]	20.8	73.5	106.2[k]	32.7	6.3	18.2		11.9	+
H	nBu	67.4	82.8[l]	15.4	74.0	98.8	24.8	6.6	16.0		9.4	+
H	tBu	66.9	91.2[m]	24.3	73.4	112.0[n]	38.6	6.5	20.8		14.3	+
H	nPent	67.4	82.9	15.5	74.0	99.0	25.0	6.6	16.1		9.5	+
H	neoPent	66.7	85.2[o]	18.5	73.4	100.7[o]	27.3	6.7	15.5		8.8	+
H	CH_2OMe	74.9	80.2	5.3	72.0	92.2	20.2	−2.9	12.0		14.9	+
H	CH_2NEt_2	72.6	78.6	6.0	73.5	93.8	20.3	0.9	15.2		14.3	+[w]
H	CH_2Npht[a]	72.5	78.7[p]	6.2	72.3	90.9[p]	18.6	−0.2	12.2		12.4	+
H	Ph	76.4	82.1[r]	5.7	72.7	90.0[s]	17.3	−3.7	7.9		11.6	+
H	COOMe	74.4	73.1[t]	−1.3	73.5	76.9[t]	3.4	−0.9	3.8		2.1	*x*
H	$SiMe_3$	93.2	89.8[u]	−3.4	84.9	65.7[u]	−19.2	−8.3	−24.1		15.8	+
H	$SiPh_3$	97.8	85.3[v]	−12.5	87.8	71.7[v]	−16.1	−10.0	−13.6		3.6	+[y]
Me	Me	73.6	73.6[z]		94.4	94.4[aa]		20.8	20.8			+
Me	Et	74.2	80.3	6.1	93.8	99.7	5.9	19.6	19.4		−0.2	+
Me	nBu	74.2	77.6	3.4	94.0	100.1	6.1	19.8	22.5		2.7	+
Me	nPent	75.3	79.3	4.0	94.0	100.3	6.3	18.7	21.0		2.3	+
Me	Ph	86.1	80.5[ab]	−5.6	94.3	91.8[ac]	−2.5	8.2	11.3		−3.1	
Me	$SiMe_3$	102.4	83.1[ad]	−19.3	107.0	79.7	−27.3	4.6	−3.4		8.0	*ag*
Et	Et	81.0	81.0[ae]		101.8	101.8		20.8	20.8			+
Et	nPr	79.4	81.8	2.4	99.6	102.0	2.4	20.2	20.2		0.0	+
Et	Ph	91.8	80.7[af]	−11.1	102.4	91.5	−10.9	10.6	10.8		−0.2	*ag*
iPr	Ph	95.9	80.7[ah]	−15.2	108.4	92.1	−16.3	12.5	11.4		1.1	*ag*
tBu	Ph	98.5	80.0[ai]	−18.5	113.2	94.0	−19.2	14.7	14.0		0.7	*ag*
Me_3Si	Ph	94.2	105.8[aj]	11.6	79.9	106.1	26.2	−14.3	0.3		14.6	*ag*
Ph_3Si	Ph	89.6	110.4[ak]	20.8	75.7	108.4	32.7	−13.9	−2.0		11.9	*ag*
EtOOC	Ph	81.6	85.7[al]	4.1	79.0	91.2[al]	12.2	−2.6	5.5		8.1	*ag*
tBu	tBu	86.3	86.3[am]		111.9	111.9		25.6	25.6			
Ph	Ph	88.9	88.9[an]		91.0	91.0[ao]		2.1	2.1			
MeOOC	COOMe	78.1	78.1[ap]		79.0	79.0[ap]		0.9	0.9			*x*
Me_3Si	$SiMe_3$	113.4	113.4[ar]		92.8	92.8		−20.6	−20.6			

[a] Npht =

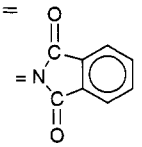

[b] Solvent $CDCl_3$ unless stated otherwise. [c] Reference 43. [d] $CDCl_3$ (?).[6] [e] Formation of (μ_2-butenolide)(μ_2-CO)$Co_2(CO)_6$ complexes or the corresponding bilactones (2,4,6-octatriene-4,5-diolides) reported.[3a,c,4a−c,44] [f] Reference 45. [g] Reasonable agreement with ref 6. [h] Reasonable agreement with ref 46a: δ^1 = 67.3; δ^2 = 85.0 (solvent not specified). [i] Reasonable agreement with ref 36: δ^1 = 68.5; δ^2 = 83.6 (solvent not specified). See also ref 4c. [j] Solvent CCl_4;[1b] reasonable agreement with ref 36: δ^1 = 67.7; δ^2 = 89.3 (solvent not specified). [k] Solvent CCl_4.[1b] [l] Reference 46b reports ($CDCl_3$) δ^1 = 68.6; δ^2 = 86.3. [m] Solvent CCl_4.[1b] Reasonable agreement with ref 43: ($CDCl_3$) δ^1 = 66.8; δ^2 = 92.6. [n] Solvent CCl_4.[1b] Reasonable agreement with ref 6: ($CDCl_3$?) δ^1 = 73.4; δ^2 = 112.0. [o] Solvent CCl_4.[1b] [p] Solvent C_6D_6. [r] Reasonable agreement with ref 6: ($CDCl_3$) δ^1 = 77.7; δ^2 = 83.3. See also ref 39: (THF-d_8) δ^1 = 74.08; δ^2 = 78.67. [s] Reasonable agreement with ref 6: ($CDCl_3$?) δ^1 = 72.7; δ^2 = 90.0. [t] Reasonable agreement with 6: (free, $CDCl_3$?) δ^1 = 74.8; δ^2 = 74.1; (coord., $CDCl_3$?) δ^1 = 73.5; δ^2 = 76.9. [u] Assignment proved by C−H coupled spectra. [v] Assignment proved by *C*H-only (modulated with 239 Hz) and by C−H coupled spectra. [w] Carbonylation yields open chain product with C−N bond breaking and making.[1a] [x] C(sp)−C(sp^2) bond shift gets predominant.[47] [y] Traces. Could not be well reproduced. [z] Reasonable agreement with ref 37: ($CDCl_3$) δ = 74.3 and [6] ($CDCl_3$?) δ = 73.9. [aa] Reasonable agreement with ref 6: ($CDCl_3$?) δ = 94.4. [ab] Reasonable agreement with ref 37: ($CDCl_3$) δ^1 = 79.8; δ^2 = 85.8 (with reversed assignment):[39] (THF-d_8) δ^1 = 86.05; δ^2 = 80.27 (assignment proved by C−H coupled spectra). [ac] Reasonable agreement with ref 6: ($CDCl_3$?) δ^1 = 94.2; δ^2 = 91.6. [ad] Reasonable agreement with ref 37: [($CDCl_3$) δ^1 = 102.3; δ^2 = 83.1 (assignment based on C−Si coupling)] and ref 39: (THF-d_8) δ^1 = 103.38; δ^2 = 83.5 (assignment based on C−H coupling). [ae] Reasonable agreement with ref 37: ($CDCl_3$) δ = 80.9 and [36] (CCl_4) δ = 80.5. [af] Assignment based on C−H coupling:[39] (THF-d_8) δ^1 = 91.9; δ^2 = 80.7. [ag] No data available. [ah] Reasonable agreement with ref 39: (THF-d_8) δ^1 = 95.81; δ^2 = 80.53. [ai] Reasonable agreement with ref 39: (THF-d_8) δ^1 = 98.47; δ^2 = 79.99. [aj] Assignment based on C−Si coupling:[37,40] ($CDCl_3$) δ^1 = 93.8; δ^2 = 105.1. Agreement with ref 39: (THF-d_8) δ^1 = 94.00; δ^2 = 105.99. [ak] Reasonable agreement with ref 39: (THF-d_8) δ^1 = 89.63; δ^2 = 110.43. [al] Solvent C_6D_6. [am] Reasonable agreement with ref 37 [($CDCl_3$) δ = 86.8] and ref 4c: (acetone-d_6) δ = 85.3. [an] Reasonable agreement with ref 6 [($CDCl_3$?) δ = 88.9]; ref 4c [(acetone-d_6) δ = 88.0]; ref 37 [($CDCl_3$) δ = 89.6]; and ref 39: (THF-d_8) δ = 89.92. [ao] Reasonable agreement with ref 6: ($CDCl_3$?) δ = 91.0. [ap] Compare:[6] ($CDCl_3$?) free δ = 75.1; δ = 79.0. [ar] Reasonable agreement with ref 37: ($CDCl_3$) δ = 113.8.

electron density around the sp carbons the coordination to the $Co_2(CO)_6$ entity is definitive in the alkyl derivatives; it roughly compensates the mesomeric effect of the conjugating groups in the aryl or COOR derivatives, but the expected strong π−*d* interaction between the carbon and the Si atom is dominating in the SiR_3 derivatives. The behavior of the SiR_3 derivatives can be due (in part) also to the steric bulk of these substituents.

(ii) the absolute values of the $\Delta\delta$ coordination shifts of the (acetylene)$Co_2(CO)_6$ complexes reveal still an other important point. These shifts are, in general, definitely smaller than those observed for the mononuclear Pt[37] or Ni[39] complexes with some comparable acetylenes. This result, at first sight, seems to be in contradiction with several solid state structural studies showing the bending of the coordinated acetylene away from the original linear array, and the C(sp)−C(sp)

Table 3. Experimental Data for X-ray Diffraction Studies

formula	$C_{32}H_{20}Co_2O_6Si$
cryst. syst.	orthorhombic
space group	*Pbca*
cell param[a] at 295 K	
a, Å	28.790(2)
b, Å	11.577(1)
c, Å	17.833(2)
V, Å^3	5943.8(9)
Z	8
D_{calcd}, g cm^{-3}	1.445
mol wt	646.5
$F(000)$	2624
cryst dimens, mm	0.20 × 0.25 × 0.40
linear abs coeff, cm^{-1}	11.9
scan type	$\omega/2\theta$
radiation	graphite monochromated Mo Kα (λ = 0.7107 Å)
2θ range, deg	6−50
reflns measd	$+h, +k, +l$
unique total data	5298
criterion for obsn	$I > 2\sigma(I)$
unique obsd data (NO)	2803
no. of variables (NV)	322
overdetermination ratio (NO/NV)	8.7
max Δ/σ on last cycle	<0.1
$R = \sum\|\Delta F\|/\sum\|F_o\|$	0.039
$R_w - [\sum\sqrt{w}\|\Delta F\|/\sum\sqrt{w}\|F_o\|]$	0.036
GOF = $[\sum w\|\Delta F\|^2/(NO - NV)]^{1/2}$	0.74

[a] Unit cell parameters were obtained by least-squares analysis of setting angles of 25 carefully centered reflections chosen from diverse regions of reciprocal space.

Table 4. Fractional Atomic Coordinates (×10^4)

atom	*x/a*	*y/b*	*z/c*	atom	*x/a*	*y/b*	*z/c*
Co1	928.2(2)	1808.0(6)	1381.8(4)	C15	859(1)	6626(2)	1536(2)
Co2	421.6(2)	2554.7(6)	2385.6(4)	C16	915(1)	5516(2)	1827(2)
Si	1621.9(4)	2855.9(10)	2842.4(8)	C21	1578(1)	4131(2)	3502(2)
C1	1479(2)	1748(5)	904(3)	C22	1174(1)	4294(2)	3920(2)
O1	1825(1)	1654(4)	610(2)	C23	1127(1)	5269(2)	4373(2)
C2	929(2)	336(5)	1704(4)	C24	1484(1)	6080(2)	4409(2)
O2	919(1)	−597(3)	1904(3)	C25	1889(1)	5917(2)	3991(2)
C3	519(2)	1748(5)	596(4)	C26	1936(1)	4943(2)	3538(2)
O3	276(2)	1706(5)	114(3)	C31	2136(1)	3067(3)	2217(2)
C4	233(2)	3718(5)	2965(3)	C32	2140(1)	4009(3)	1730(2)
O4	108(1)	4471(4)	3321(3)	C33	2521(1)	4192(3)	1259(2)
C5	423(2)	1362(5)	3057(4)	C34	2896(1)	3432(3)	1276(2)
O5	428(2)	629(4)	3468(3)	C35	2892(1)	2489(3)	1763(2)
C6	−111(2)	2437(5)	1857(3)	C36	2512(1)	2307(3)	2234(2)
O6	−442(1)	2400(4)	1509(3)	C41	1675(1)	1477(2)	3390(2)
C7	1096(1)	2836(3)	2243(3)	C42	1730(1)	419(2)	3026(2)
C8	857(1)	3409(4)	1714(3)	C43	1765(1)	−597(2)	3443(2)
C11	808(1)	4555(2)	1388(2)	C44	1744(1)	−555(2)	4224(2)
C12	646(1)	4704(2)	657(2)	C45	1689(1)	503(2)	4588(2)
C13	589(1)	5814(2)	366(2)	C46	1654(1)	1519(2)	4171(2)
C14	696(1)	6775(2)	806(2)				

distances are closer to the olefinic values (cis-excited acetylene[5]) in dinuclear complexes[51] than in mononuclear ones. It appears that the shielding caused by the 3D conjugation in the tetrahedral C_2M_2 complexes (or similar structures)[5c,52] is stronger than that in the 2D "metallacyclopropene" rings.[37,39] Thus, consequently, the former effect overcompensates the deshielding caused by the coordination (the difference caused by geometric factors and by the electronic structure of the metal in π−p, π−d interactions should also be considered at this point). The dramatic difference between the drastic conditions required by the dinuclear carbonylation of acetylenes with Co,[3a,c,4a−c,44] and the mild conditions of the mononuclear (PTC) carbonylation of these substrates with the same metal[3c,53] can be understood in these terms. Moreover, it was observed that

Table 5. Selected bond Distances and Bond Angles of (μ_2-PhC_2SiPh_3)$Co_2(CO)_6$ (for Atom Numbering See Figure 6)

Bond Distances (pm)			
Co1−Co2	246.5(1)	Si−C21	189.2(3)
Co1−C1	180.1(6)	Si−C31	186.9(3)
Co1−C2	179.8(6)	Si−C41	187.8(3)
Co1−C3	183.2(7)	C1−O1	113.1(6)
Co1−C7	200.2(5)	C2−O2	113.8(7)
Co1−C8	195.7(5)	C3−O3	110.9(9)
Co2−C4	178.2(6)	C4−O4	113.7(7)
Co2−C5	182.8(6)	C5−O5	112.1(8)
Co2−C6	180.5(6)	C6−O6	113.8(7)
Co2−C7	198.5(3)	C7−C8	134.3(6)
Co2−C8	199.6(4)	C8−C11	145.5(5)
Si−C7	185.3(4)		
Bond Angles (deg)			
C7−Co1−C8	39.6(2)	Co1−C8−C11	138.8(4)
C3−Co1−C8	101.5(2)	Co1−Co2−C6	95.6(2)
C3−Co1−C7	139.9(2)	Co1−Co2−C5	102.1(2)
C2−Co1−C8	143.2(3)	Co1−Co2−C4	150.0(2)
C2−Co1−C7	108.5(3)	C7−Co2−C8	39.4(2)
C2−Co1−C3	102.1(3)	C6−Co2−C8	104.9(2)
C1−Co1−C8	105.8(2)	C6−Co2−C7	140.9(2)
C1−Co1−C7	100.0(2)	C5−Co1−C8	140.0(2)
C1−Co1−C3	101.7(3)	C5−Co2−C7	101.9(2)
C1−Co1−C2	96.5(3)	C5−Co2−C6	106.7(3)
Co2−Co1−C8	52.1(1)	C4−Co2−C8	99.5(2)
Co2−Co1−C7	51.5(1)	C4−Co2−C7	104.4(2)
Co2−Co1−C3	100.8(2)	C4−Co2−C6	95.8(3)
Co2−Co1−C2	95.8(2)	C4−Co2−C5	101.1(3)
Co2−Co1−C1	151.4(2)	C31−Si−C41	110.9(1)
Co1−Co2−C8	50.7(1)	C21−Si−C41	110.2(2)
Co1−Co2−C7	52.1(1)	C21−Si−C31	108.8(1)
Co1−C7−Si	130.3(2)	C7−Si−C41	110.8(2)
Co1−C7−Co2	76.4(2)	C7−Si−C31	107.7(2)
Si−C7−C8	144.8(3)	C7−Si−C21	108.3(2)
Co2−C7−C8	70.7(2)	Co1−C1−O1	176.6(5)
Co1−C7−C8	68.3(2)	Co1−C2−O2	178.4(5)
Co2−C8−C7	69.8(2)	Co1−C3−O3	179.0(6)
Co1−C8−C7	72.0(3)	Co2−C4−O4	178.5(5)
Co1−C8−Co2	77.2(2)	Co2−C5−O5	179.4(6)
C7−C8−C11	141.3(3)	Co2−C6−O6	177.4(5)
Co2−C8−C11	129.1(2)	Co2−C7−Si	136.6(2)
Co1−C8−C11	138.8(4)	C31−Si−C41	110.9(1)

mononuclear Ni[54,55] acetylene complexes readily react with CO_2, while our attempts to carboxylate (acetylene)-$Co_2(CO)_6$ complexes under comparable conditions failed (see the Experimental Section).

(iii) The chemical shifts of the acetylenic ("quaternary") carbons of asymmetrically substituted acetylenes ($R^1C_2R^2$, $R^1 \neq R^2$) change with coordination to different extents (Figure 3). Consequently, the bond polarization in the C_2 core is different in the coordinated molecule from that in the free state. The comparison of the diagrams in Figure 3 permits the following consequences. (a) The bond polarity generally increases in the coordinated state with respect to the free ligand. (b) This effect is again very sensitive to the nature of

(51) Leading references are: (a) Cotton, F. A.; Jamerson, J. D.; Stults, R. *J. Am. Chem. Soc.* **1976**, *98*, 1774. (b) Gregson, D.; Howard, J. A. K. *Acta Crystallogr.* **1983**, *39C*, 1024. (c) Baert, F.; Guelzim, A.; Coppens, P. *Acta Crystallogr.* **1984**, *40B*, 590. (d) Battaglia, L. P.; Delledonne, D.; Nardelli, M.; Predieri, G.; Chiusoli, G. P.; Costa, M.; Pelizzi, C. *J. Organomet. Chem.* **1989**, *363*, 209. (e) D'Agostino, M. F.; Frampton, C. S.; McGlinchey, M. J. *Organometallics* **1990**, *9*, 2972. (f) Johnson, B. F. G.; Lewis, J.; Rathby, P. R.; Wilkinson, D. A. *J. Organomet. Chem.* **1991**, *408*, C9. (g) Lo Sterzo, C.; Bandoli, G.; Dolmella, A. *J. Chem. Soc., Dalton, Trans.* **1992**, 697.

(52) (a) Thorn, D. L.; Hoffmann, R. *Inorg. Chem.* **1978**, *17*, 126. (b) Pályi, G.; Piacenti, F.; Markó, L. *Inorg. Chim. Acta, Rev.* **1970**, *4*, 109.

(53) Alper, H.; Currie, J. K.; des Abbayes, H. *J. Chem. Soc., Chem. Commun.* **1978**, 311. (b) des Abbayes, H. *Isr. J. Chem.* **1985**, *26*, 249.

(54) Happ, B. Ph.D. Thesis, Berlin, 1990.

(55) (a) Hoberg, H.; Schaefer, D.; Burkhardt, G.; Krüger, C.; Romano, M. *J. Organomet. Chem.* **1984**, *266*, 203. (b) Walther, D. Schönberg, H.; Dinjus, E.; Sieler, J. *J. Organomet. Chem.* **1987**, *334*, 377.

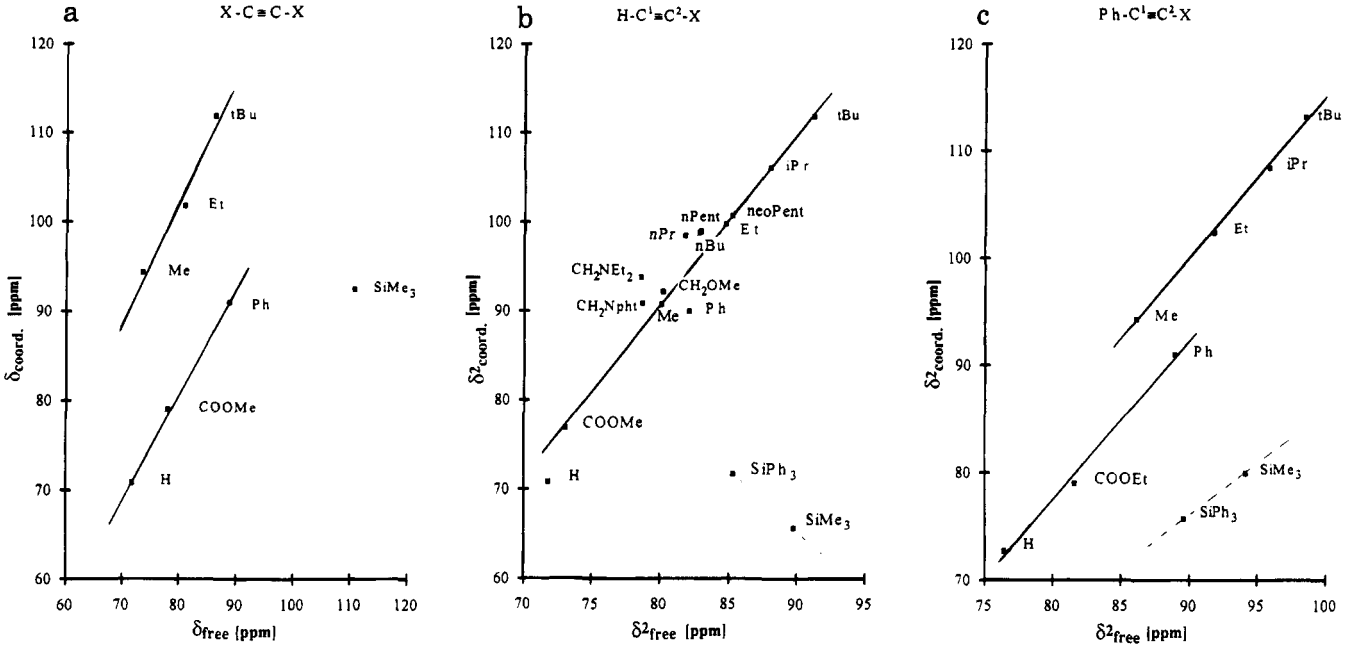

Figure 1. ^{13}C-NMR chemical shifts of the sp carbons of free acetylenes plotted against those of acetylenes coordinated in $(R^1C^1{\equiv}C^2R^2)Co_2(CO)_6$ complexes: (a) symmetric acetylenes ($R^1 = R^2$); (b) terminal acetylenes (R^1 = H); (c) phenylacetylene derivatives (R^1 = Ph).

the substituent: in the HC_2X series the change of the bond polarity with coordination is the largest. It appears to us that this phenomenon is due to the fact that the orbital shape of the H substituent (1s) is the most different from that of the others (sp^3, sp^2, sp^3 + d or sp^3d^2). The change of the bond polarity with coordination is more "buffered" at the conjugating PhC_2X series. In all series the largest coordination changes are observed at the SiR_3 substituent, in agreement with the particular nature of this substituent, as discussed earlier. The positive sign of the $\Delta\Delta\delta$ values (Figure 3) indicate that the coordination increases the *difference* in the *electronic environment* of the acetylenic sp carbon atoms. In other terms: this effect indicates an incrementation of the *difference* in the *reactivity* of the two sp C atoms. This also appears to be in good agreement with the observed high regioselectivity in the cyclocarbonylation of acetylenes.[3a-e,4a-c]

(iv) The more systematic measurements performed in the course of the present work permit the more precise reformulation of our earlier statements about the reactivity of the acetylene in cyclocarbonylation;[4a,c] now it can be stated that at all acetylenes which could be carbonylated one of the δ (^{13}C) values is ≤80 ppm in the free and ≤95 ppm in the coordinated state, but some acetylenes which fulfill these conditions (e.g., MeC_2Ph or $tBuC_2Ph$) could not be, or could not yet (?) be carbonylated (since such negative statements require much caution it appears to us that some additional research work is required in this respect).

One of the compound pairs shows a particularly interesting distribution of the δ (^{13}C) values. This is the $HC_2SiMe_3/(HC_2SiMe_3)Co_2(CO)_6$ couple, showing lower chemical shifts for the non-hydrogen substituted carbon. In earlier studies[1b,3a,c,4c] it appeared that the starting point of the carbonylation is that sp carbon atom which shows the lower chemical shift. This carbon atom is then expected to appear in the 3-position of the lactone ring in the (butenolide)$Co_2(CO)_7$ complexes.[1b,4a-c] The carbonylation of HC_2SiMe_3 allowed us to control this supposition. We repeated this experiment with the aim of determining the distribution of the expected[4a] (butenolide)$Co_2(CO)_7$-type product. The δ (^{1}H) ~7.4 ppm value of the signal corresponding to the H substituent in the lactone ring proves that the proton was directed (moreover with quantitative regioselectivity) to the 3-position of the lactone and the $SiMe_3$ substituent to the 2-position. This result shows that either the key point of the regioselection is not the (acetylene)$Co_2(CO)_6$ intermediate as it was accepted before[1b,3,4a-c] or at the strongly conjugating and bulky $SiMe_3$ substituent a different mechanism is operative.

The spectroscopic studies described earlier in this work provide an additional piece of evidence demonstrating the sensitivity of the ^{13}C-NMR spectra in exploring the reactivity of the coordinated acetylene by nonpreparative methods. One would expect that the features discussed above should be reflected in the molecular structure of the (acetylene)$Co_2(CO)_6$ complexes. Several X-ray structural studies on these compounds had been published but this aspect was not investigated. This prompted us to try to crystallize (unfortunately, the (acetylene)$Co_2(CO)_6$ complexes often are oily substances and to obtain crystals suitable for X-ray diffraction meets difficulties[7,23]) a derivative where one of the most important coordinative effects ((a) activation and (b) increasing the difference between the chemical environments of the sp carbons) is well-observable. Since the structure of that derivative where the $\Delta\delta = \delta_c - \delta_f$ value is the highest ($\Delta\delta$ = 25.6 ppm, $R^1 = R^2$ = tBu) is known,[51a,b] we concentrated our efforts at a compound where effect b is well pronounced. The complex $(PhC_2SiPh_3)Co_2(CO)_6$ shows one of the highest values of $\Delta\delta_c = \delta_c^2 - \delta_c^1$ = 32.7 ppm, and moreover, it could be crystallized (in contrast to the $(HC_2tBu)Co_2(CO)_6$ ($\Delta\delta_c$ = 38.6 ppm) $(HC_2iPr)Co_2(CO)_6$ ($\Delta\delta_c$ = 32.7 ppm) derivatives, which are oily substances). The crystal and molecular structure of this compound was determined by X-ray diffraction (Figure 4). The experi-

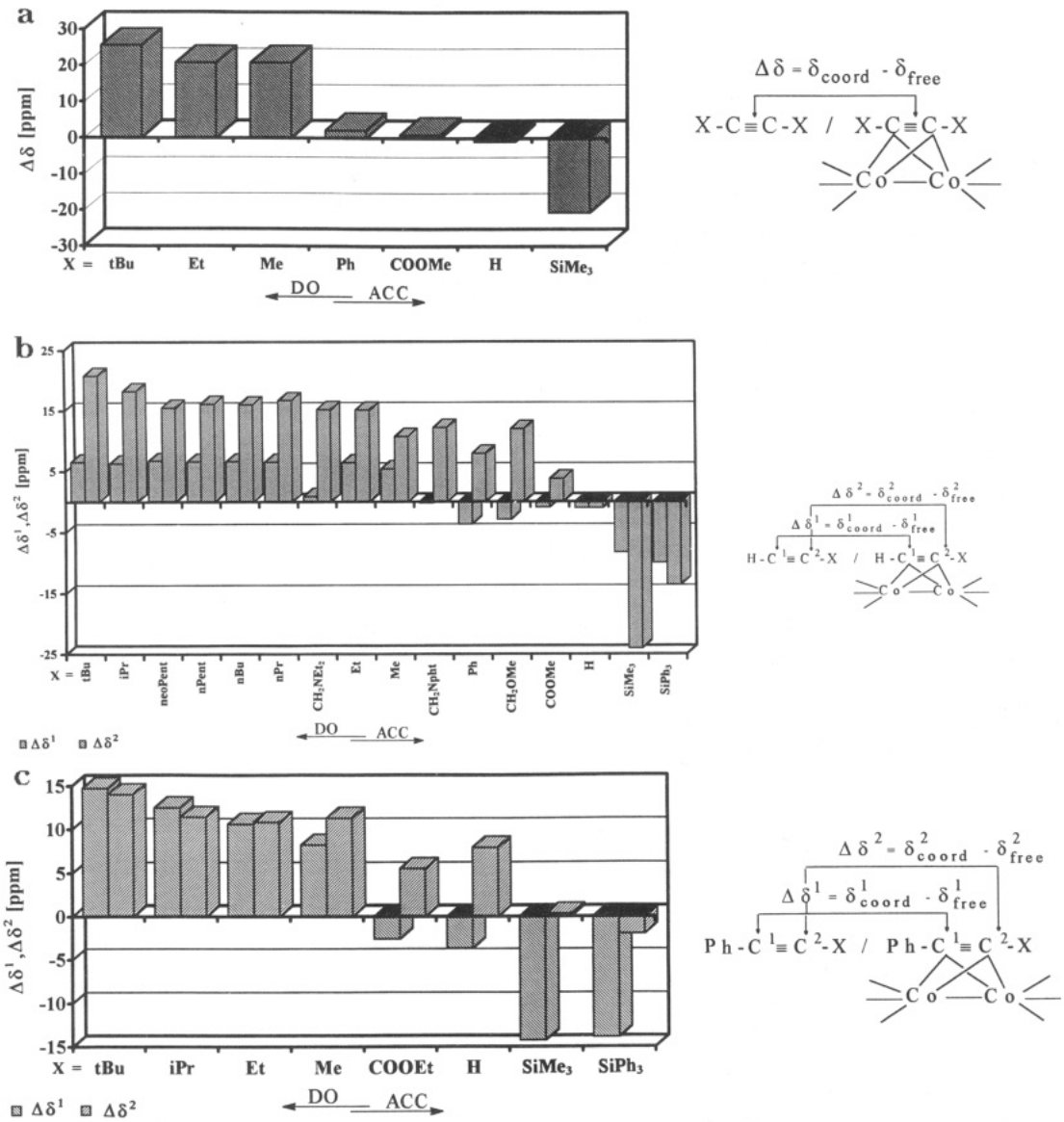

Figure 2. Changes of the ^{13}C-NMR shifts of the sp carbons of acetylenes with coordination. Free acetylenes vs ($R^1C{\equiv}C^2R^2$)-$Co_2(CO)_6$ complexes: (a) symmetric acetylenes ($R^1 = R^2$); (b) terminal acetylenes (R^1 = H); (c) phenylacetylene derivatives (R^1 = Ph).

mental data are tabulated in Table 3, the atomic coordinates are shown in Table 4. Selected bond distances and angles are shown in Table 5 and some additional structural parameters in Table 6. The structures of several (acetylene)$Co_2(CO)_6$ complexes were determined by X-ray diffraction.[51−56] Some selected examples are collected in Table S4 of the supplementary material.

The geometric parameters of the cluster core C_2Co_2 in (PhC_2SiPh_3)$Co(CO)_6$ show this part of the complex fairly near to the ideal C_{2v} symmetry. This appears to be a general feature of the (acetylene)$Co_2(CO)_6$ complexes (Table S4, supplementary material): the limits of the tetrahedron angles are (on Co) 37.7° ($R^1 = R^2 = CH_2W(CO)_3Cp^*$)[56l] vs 41.2° ($R^1 = R^2 = CF_3$);[51c] (on Csp) 75.4° ($R^1 = CCo_3(CO)_9$, $R^2 = C_2CCo_3(CO)_9$[56j] vs 80.7° ($R^1 = R^2$ = COOMe).[51b] In these terms the values obtained in course of this work correspond to relatively broad angles on Co and medium on C(sp).

The Co−Co distance is relatively short, with respect to $Co_2(CO)_8$ (253.0 ppm[57] being near to that of some "flyover"-type dicobalt derivatives as [(HC_2CF_3)$_3$]$Co_2(CO)_4$ (245.9 pm[59] or the two isomers of [(butenolide)-(acetylene)$_2$]$Co_2(CO)_5$-type complexes, isomer A (247 ppm[60a]), isomer B (248 pm[60b]), and medium with respect to the Co−Co distances of other (acetylene)$Co_2(CO)_6$

(56) (a) Bonnet, J. J.; Mathieu, R. *Inorg. Chem.* **1978**, *17*, 1973. (b) Bradley, D. H.; Khan, M. A. Nicholas, K. N. *Organometallics* **1989**, *8*, 554. (c) Dellaca, R. J.; Penfold, B. R.; Robinson, B. H.; Robinson, W. T.; Spencer, J. L. *Inorg. Chem.* **1970**, *9*, 2197. (d) Bird, P. H.; Fraser, A. R. *Chem. Commun.* **1970**, 681. (e) Akita, M.; Terada, M.; Morooka, Y. *Organometallics* **1992**, *11*, 1825. (f) D'Agostino, M. F.; Frampton, C. S.; McGlinchey, J. *Organometallics* **1990**, *9*, 2972. (g) Sappa, E.; Predieri, G.; Tiripicchio, A.; Tiripicchio-Camellini, M. *J. Organomet. Chem.* **1985**, *297*, 103. (h) Carriedo, G. A.; Riera, V.; Manotti Lanfredi, A. M.; Tiripicchio, A. *J. Organomet. Chem.* **1984**, *272*, C17. (i) Bruce, M. I.; Duffy, D. N.; Humphrey, M. G. *Austral. J. Chem.* **1986**, *39*, 159. (j) Seyferth, D.; Spohn, R. J.; Churchill, M. R.; Gold, K.; Scholer, F. R. *J. Ogranomet. Chem.* **1970**, *23*, 237. (k) Magnus, P.; Becker, D. P. *J. Chem. Soc., Chem. Commun.* **1985**, 640. (l) Cheng, M. H.; Shu, H. G.; Lee, G. H.; Peng, S. M.; Liu, R. S. *Organometallics* **1993**, *12*, 108.

(57) Leung, P. C. W.; Coppens, P. *Acta Crystallogr.* **1983**, *39B*, 535.

(58) (a) Horváth, I. T.; Pályi, G.; Markó, L.; Andreetti, G. D. *J. Chem. Soc., Chem. Commun.* **1979**, 1054; (b) *Inorg. Chem.* **1983**, *22*, 1049.

(59) Dickson, R. S.; Franser, D. J.; Gatehouse, B. M. *J. Chem. Soc., Dalton Trans* **1972**, 2278.

(60) (a) Váradi, G.; Horváth, I. T.; Pályi, G.; Markó, L.; Slovokhotov, Yu. L.; Struchkov, Yu. T. *J. Organomet. Chem.* **1981**, *206*, 119. (b) Jeffreys, J. A. D. *J. Chem. Soc., Dalton Trans.* **1980**, 435.

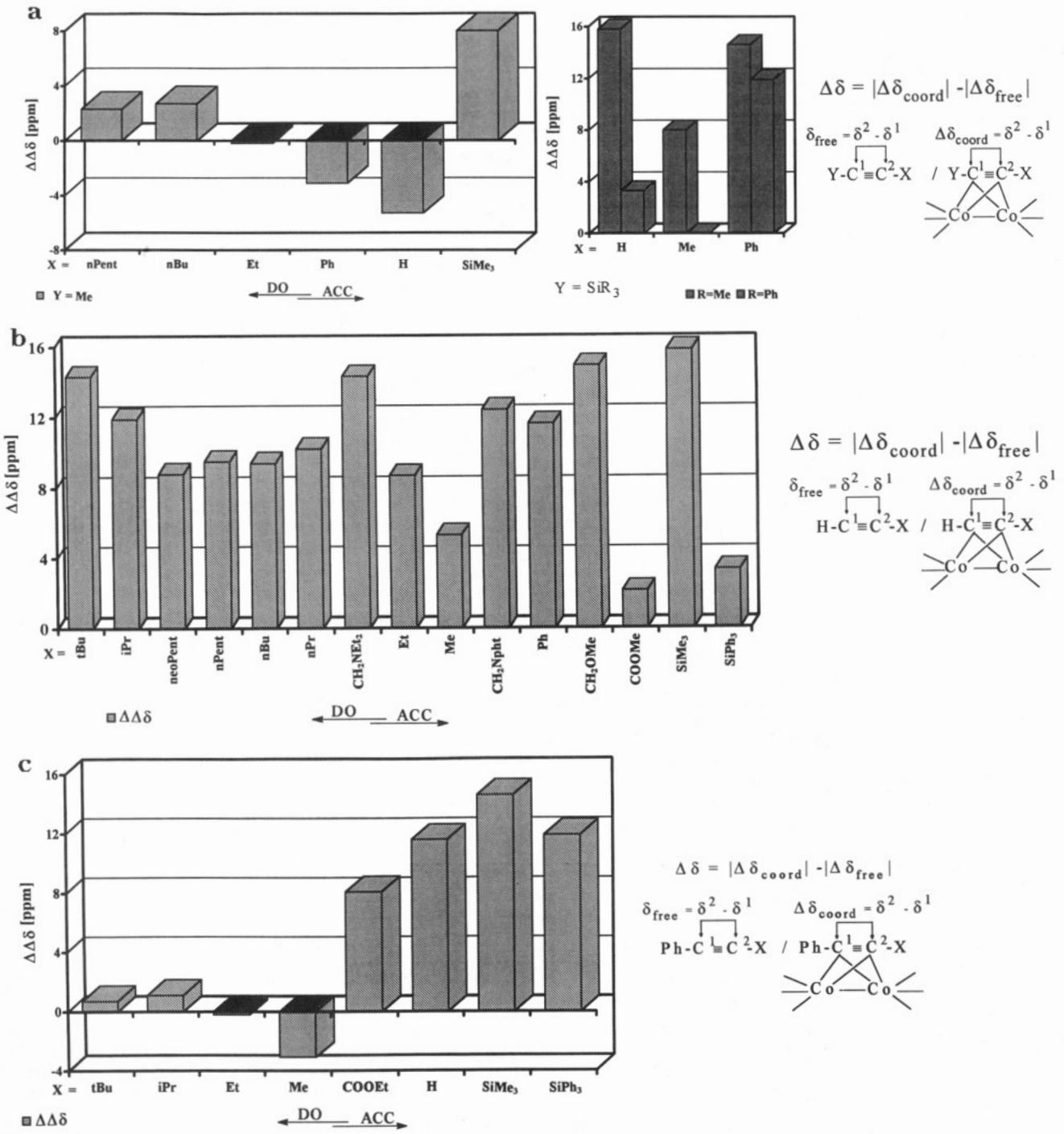

Figure 3. Change of the shielding anisotropy by coordination ($\Delta\Delta\delta$) at asymmetrically substituted acetylenes ($R^1C^1{\equiv}C^2R^2$, $R^1 \neq R^2$): (a) internal alkynes; (b) terminal alkynes (R^1 = H); (c) phenylacetylene derivatives (R^1 = Ph).

complexes (from 244.5 pm, R^1 = iPr, R^2 = $P(Ph)_2$-$[CpNiO_3(CO)_8]$,[56g] to 248.9 pm, R^1 = H, R^2 = CH(Ph)-(OH)[56b]) and significantly longer than observed (238.8[58] for a (μ_2-butenolide)(μ_2-diiodovinylidene)$Co_2(CO)_6$ derivative.

One of the most characteristic features of the geometry of coordinated acetylenes is the C(sp)−C(sp) distance. This ranges at published structures from 128 pm (R^1 = R^2 = $CH_2W(CO)_3Cp^*$[56l]) to 136.7 pm (R^1 = $CCo_3(CO)_9$, R^2 = $C_2CCo_3(CO)_9$[56j]). In these terms the C(sp)−C(sp) distance (134.2 pm) of $(PhC_2SiPh_3)Co_2(CO)_6$ shows a high degree of activation, accompanied with relatively low value of the C(sp)−C(sp)−R angle on C(Ph) (141.3°) and a higher value (less deviation from linearity!) on C(Si) (145.2°) (limits: 135.6°, (R^1 = R^2 = $COOH$[51c], vs 149.9°, R^1 = R^2 = $CH_2W(CO)_3Cp^*$.[56b]

The dissimilarity of the (external) C(sp)-C(sp)-R angles and the closely symmetric values of the parameters of the C_2Co_2 "tetrahedron" appears to be characteristic of the asymmetrically substituted ($R^1 \neq R^2$) (acetylene)-$Co_2(CO)_6$ complexes (Table S4). This prompted us to investigate an other "external" parameter, that is the relative positions of the CO groups (Table 6). These data show that the distribution of the CO groups markedly deviates from the idealized C_{2v} geometry. This finding is in accordance with the observation that all six ν(C-O) fundamentals became IR − active at $(PhC_2SiPh_3)Co_2(CO)_6$ (c.f. Experimental and refs 29 and 61).

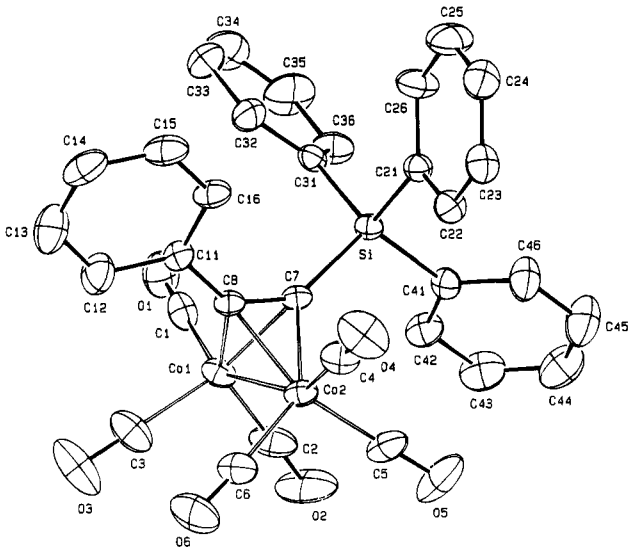

Figure 4. ORTEP view of the complex (μ_2-PhC_2SiPh_3)-$Co_2(CO)_6$ (30% probability ellipsoides).

Table 6. Some Characteristic Structural Parameters of (μ_2-PhC_2SiPh_3)$Co_2(CO)_6$ (for Atom Numbering See Figure 4)

angles between planes

plane 1	plane 2	angle (deg)
[Si, C7, C8]	[C7, C8, C11]	17.7(6)
[C7, C8, MP1][a]	[Co1, Co2, MP2][a]	88.5(2)
[C11, ..., C16]	[C7, C8, MP1][a]	144.6(2)

angles between some lines and normals to planes [Co1, Co2, MP1][a] and [C7, C8, MP2][a]

plane [Co1, Co2, MP1][a]		plane [C7, C8, MP2][a]	
line	angle (deg)	line	angle (deg)
Co1−C1	99.1(2)	Co1−C1	151.6(2)
Co1−C2	135.4(2)	Co1−C2	96.9(3)
Co1−C3	33.9(2)	Co1−C3	99.7(3)
Co2−C4	80.7(2)	Co2−C4	29.4(2)
Co2−C5	147.1(2)	Co2−C5	79.5(3)
Co2−C6	40.9(2)	Co2−C6	83.3(3)
C1−O1	101.4(3)	C1−O1	153.4(4)
C2−O2	133.9(5)	C2−O2	96.9(5)
C3−O3	33.9(5)	C3−O3	100.8(4)
C4−O4	79.3(3)	C4−O4	29.5(4)
C5−O5	147.0(4)	C5−O5	79.2(4)
C6−O6	38.2(4)	C6−O6	84.1(4)

[a] MP1: midpoint of C7/C8. [b] MP2: midpoint of Co1/Co2.

The analysis of the structural parameters of (PhC_2SiPh_3)$Co_2(CO)_6$ and of other (acetylene)$Co_2(CO)_6$ derivatives permits some generalizations.

(i) The ^{13}C-NMR spectra of the C(sp) carbons appear to reflect the electronic distribution of these complexes more sensitively than the X-ray parameters. In the former case the ratio of change/error is much more favorable than in the latter. (The NMR measurement is more convenient since it is considerably faster, needs no single crystal, etc.).

(ii) It appears that a high degree of electronic delocalization[5,52] in the C_2Co_2 cluster core stabilizes the C_2Co_2 unit as a very symmetric array. The effects of the substitution of the C_2 moiety are more efficient in influencing the geometric parameters of the groups *on* the C_2Co_2 core.

(iii) The highly symmetric structure of the C_2Co_2 core is in accordance with the relatively high stability of the (acetylene)$Co_2(CO)_6$ complexes and the great differences of their reactivity from that of mononuclear complexes.

It should be considered in this context that in spite of the fact that in the dinuclear complexes the values of C(sp)−C(sp) distances and C(sp)−C(sp)−R angles reflect a higher degree of excitation of the RC_2R moiety than at mononuclear complexes, the more excited form seems to be even more *stabilized* by the 3D cluster structure.

The easy substitution of the CO ligands[56a,b,62] as well as the relatively mild conditions of those reactions where the initial step appears to diminish the symmetry of the C_2Co_2 core (acetylene trimerization,[34] Pauson−Khand reaction[3b,e]) can also be interpreted in these terms.

Acknowledgment. Stimulating discussions with Profs. L. Markó, A. Sisak (Veszprém) and M. Bán (Szeged) are acknowledged. Finanical support has been received from the Hungarian Ministry of Education (G.V., I.T.H.), the Italian Ministry of University and Research (C.Z., G.P.), and the (Italian) National Research Council (B.H., T.B.).

Supplementary Material Available: Text detailing the crystal structure determination, tables of atomic coordinates, bond distances and angles, and anisotropic thermal parameters, and structural parameters for (μ_2-$R^1C_2R^2$)$Co_2(CO)_4L_2$ molecules (Table S4) (11 pages). Ordering information is given on any current masthead page.

OM9308396

(61) Váradi, G.; Vecsei, I.; Vizi-Orosz, A.; Pályi, G.; Massey, A. R. *J. Organomet. Chem.* **1976**, *114*, 213.
(62) (a) Váradi, G.; Vizi-Orosz, A.; Vastag, S.; Pályi, G. *J. Organomet. Chem.* **1976**, *108*, 225. (b) Váradi, G.; Vastag, S.; Pályi, G. *Atti Accad. Sci. Bologna, Cl. Sci. Fis.* **1979**, *267*(13/6) 223.

Transition Metal Substituted Acylphosphanes and Phosphaalkenes. 25.[1] Unprecedented Condensation of the Pentamethylcyclopentadienyl Ligand with a Methylene Phosphane Moiety in $(\eta^5\text{-}C_5Me_5)(CO)_2FeP{=}C(NMe_2)_2$ Induced by Azodicarboxylates. Structure of $\eta^5\text{-}C_5Me_4CH{=}C(NMe_2)P[N(CO_2tBu)NH(CO_2tBu)]Fe(CO)_2$

Lothar Weber* and Olaf Kaminski

Fakultät für Chemie der Universität Bielefeld, Postfach 100131, D-33501 Bielefeld, Germany

Roland Boese and Dieter Bläser

Institut für Anorganische Chemie der Universität-GHS Essen, Universitätsstr. 5-7, D-45117 Essen, Germany

Received September 13, 1994[⊗]

The metallophosphaalkene $(\eta^5\text{-}C_5Me_5)(CO)_2FeP{=}C(NMe_2)_2$ (**1**) undergoes reaction with dialkyl azodicarboxylates $RO_2CN{=}NCO_2R$ (R = tBu, Et, CH_2Ph) to afford complexes $\eta^5\text{-}C_5Me_4CH{=}C(NMe_2)P[N(CO_2R)NH(CO_2R)]Fe(CO)_2$ [R = tBu (**6a**), Et (**6b**), CH_2Ph (**6c**)] with the novel chelating 3-(tetramethylcyclopentadienyl)-1-phospha-2-propenyl ligand. This ligand system results from a yet unprecedented azocarboxylate-induced condensation of a ring methyl substituent with the methylene phosphane fragment of educt **1**. The molecular structure of $\eta^5\text{-}C_5Me_4CH{=}C(NMe_2)P[N(CO_2tBu)NH(CO_2tBu)]Fe(CO)_2$ (**6a**) ($P2_1/c$, a = 10.522(3) Å, b = 22.124(9) Å, c = 12.806(4) Å, β = 101.58(3)°) was determined by single-crystal X-ray analysis.

Introduction

Metallophosphaalkenes are polyfunctional molecules with a number of nucleophilic and electrophillic sites in close proximity. This situation renders them versatile as useful synthons for a number of chemical transformations.

Thus, metallophosphaalkene $(\eta^5\text{-}C_5Me_5)(CO)_2FeP{=}C(NMe_2)_2$ (**1**) was converted into 1,2-dihydrophosphetes **2a–c** by means of fumarodinitrile, dimethyl fumarate, and methyl acrylate.[2] The reaction of electron-deficient alkynes with **1** gives rise to the generation of metalloheterocycles **3**, 1-metallo-1-phosphabutadienes **4**, and the 2-methylene-1,2-dihydrophosphete **5** depending on the substitution pattern of the alkyne[1] (Scheme 1).

With respect to the known potential of azodicarboxylates for cycloadditions with various organic[3] and organophosphorus[4] substrates we focused our interest on the reactivity of azo compounds toward metallophosphaalkene **1**.

† Dedicated to Professor Peter Paetzold, Technische Hochschule Aachen, on the occasion of his 60th birthday.

⊗ Abstract published in *Advance ACS Abstracts*, December 1, 1994.

(1) Weber, L.; Kaminski, O.; Stammler, H.-G.; Neumann, B.; Boese, R. *Z. Naturforsch. B*, in press.

(2) (a) Weber, L.; Kaminski, O.; Stammler, H.-G.; Neumann, B.; Romanenko, V. D. *Z. Naturforsch. B* **1993**, *48*, 1784. (b) Weber, L.; Kaminski, O. Unpublished results.

(3) (a) Gillis, B. T.; Beck, P. E. *J. Org. Chem.* **1962**, *27*, 1947; **1963**, *28*, 3177. (b) Cinnamon, J. M.; Weiss, K. *J. Org. Chem.* **1961**, *26*, 2644. (c) Kitahara, Y.; Murata, I.; Nitta, T. *Tetrahedron Lett.* **1967**, *8*, 3003. (d) Wyvratt, M. J.; Paquette, L. A. *Tetrahedron Lett.* **1974**, *15*, 2433.

(4) Weber, L.; Bastian, H.; Müller, A.; Bögge, H. *Organometallics* **1991**, *10*, 2; *Z. Naturforsch B* **1992**, *47*, 231.

Experimental Section

General Experimental Considerations. Standard inert-atmosphere techniques were used for the manipulation of all reagents and reaction products. Infrared spectra were recorded on a Mattson Polaris (FT-IR)/Atari 1040 STF spectrometer. ^1H, ^{13}C, and ^{31}P-NMR spectra were taken in C_6D_6 on Bruker AC 100 (^1H, 100.131; ^{13}C, 25.180; ^{31}P 40.532 MHz), Bruker AM 300 (^1H, 300.1; ^{13}C, 75.5; ^{31}P, 121.7 MHz), and Bruker AC 250 P (^1H, 250.13; ^{13}C, 62.90 MHz) instruments. Spectral standards were $SiMe_4$ (^1H, ^{13}C) and 85% H_3PO_4 (^{31}P). Mass spectra were recorded on Varian MAT CH5-DF (70 eV, T = 250 °C) and Finnigan MAT 711 (80 eV) spectrometers. Elemental analyses were obtained from the Microanalytical Laboratory of the University of Bielefeld.

Materials. The complex $(\eta^5\text{-}C_5Me_5)(CO)_2FeP{=}C(NMe_2)_2$ (**1**) was prepared as described in the literature.[2] The azodicarboxylates were purchased commercially (Aldrich). All solvents were rigorously dried with an appropriate drying agent and distilled before use.

Preparation of Compounds. $\eta^5\text{-}C_5Me_4CH{=}C(NMe_2)P[N(CO_2tBu)NH(CO_2tBu)]Fe(CO)_2$ (6a). A solution of 0.55 g (2.38 mmol) of di-*tert*-butyl azodicarboxylate in 30 mL of ether was added dropwise to a chilled (−30 °C) solution of 0.90 g (2.38 mmol) of **1** in 40 mL of ether. The stirred mixture was allowed to warm during a period of 3 h. Volatiles were removed in vacuo, and the tarry residue was solidified by stirring with 20 mL of *n*-pentane. Yellow microcrystalline **6a** (0.64 g, 48%) was obtained after filtration, washing the filter cake with 10 mL of *n*-pentane, and drying in vacuo. Orange crystals suitable for an X-ray analysis were grown from a solution of **6a** in methylcyclohexane at 5 °C. IR (KBr, cm^{-1});

0276-7333/95/2314-0820$09.00/0

Scheme 1

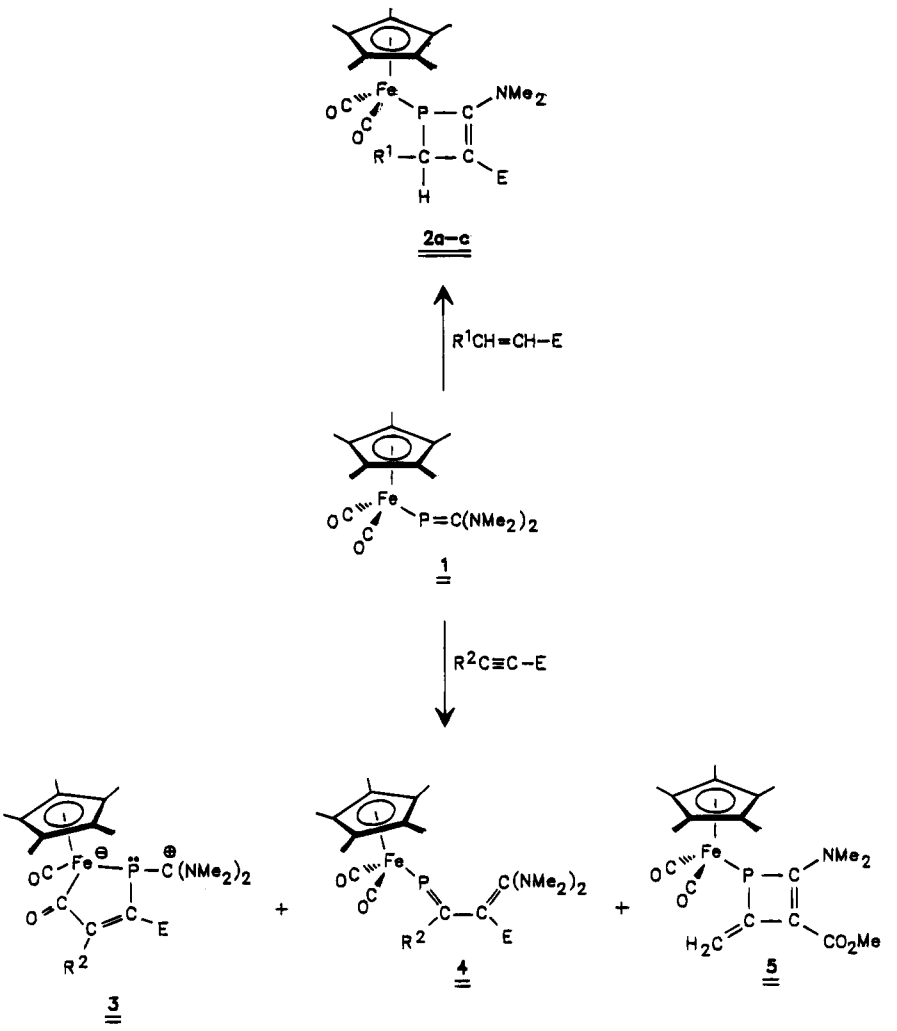

2	R¹	E
a	CN	CN
b	CO_2Me	CO_2Me
c	H	CO_2Me

3,4	R²	E
a	CO_2Me	CO_2Me
b	CH_3	CO_2Me

3387 w [ν(NH)], 1986 vs [$\nu(CO)_{term}$], 1926 vs [$\nu(CO)_{term}$], 1753 s [$\nu(CO)_{ester}$], 1712 s [$\nu(CO)_{ester}$], 1576 m [ν(C=C], 1484 m, 1368 m, 1297 m, 1233 m, 1154 s, 1116 w, 1064 w, 639 w, 612 w, 592 w, 471 w cm^{-1}. ^{1}H-NMR (C_6D_6, 60 °C) δ: 1.47 (s, 9H, tBu), 1.48 (s, 3H, C_5Me), 1.50 (s, 12H, C_5Me + tBu), 1.55 (s, 3H, C_5Me), 1.86 (s, 3H, C_5Me), 2.88 (s, 6H, NMe_2), 4.61 (d, $^3J_{PH}$ = 4.9 Hz, 1H, C_5CH=), 6.39 (s, 1H, NH). $^{13}C\{^1H\}$-NMR (C_6D_6, 60 °C) δ: 9.5 s, 9.8 s, 10.1 s, 10.3 (s, $C_5(CH_3)_4$), 28.4 (s, $C(CH_3)_3$), 28.5 (s, $C(CH_3)_3$), 41.5 (s, $N(CH_3)_2$), 41.6 (s, $N(CH_3)_2$), 79.6 (s, $C(CH_3)_3$), 80.8 (s, $C(CH_3)_3$), 88.9 (s, br, C_5CH=), 92.9 s, 94.8 s, 95.6 s, 102.4 s, 107.5 (s, $C_5(CH_3)_4$), 155.0 (s, br, CO_2tBu), 156.2 (d, $^2J_{PC}$ = 11.6 Hz, CO_2tBu), 167.3 (d, $^1J_{PC}$ = 39.6 Hz, PCN), 215.8 (s, FeCO). $^{31}P\{^1H\}$-NMR (C_6D_6) δ: 169.1 s. MS/CI: m/z = 564 (100, M^+ + H), 535 (30, M^+ − CO), 507 (94, M^+ − 2CO), 490 (28, M^+ − CO − $HNMe_2$), 464 (31, M^+ + H − 2CO − NMe_2), 332 (54, M^+ − HN_2 [CO_2tBu]$_2$). Anal. Calcd for $C_{25}H_{38}N_3O_6PFe$ (563.39): C, 53.30; H, 6.80; N, 7.45. Found: C, 53.21; H, 6.86; N, 7.48.

η^5-C_5Me_4CH=C(NMe_2)P[N(CO_2Et)NH(CO_2Et)]Fe(CO)$_2$ (6b). A sample of 0.68 g (54%) of orange crystalline **6b** was obtained analogously from 0.93 g (2.46 mmol) of **1** and 0.43 g (2.46 mmol) of diethyl azodicarboxylate. IR (KBr): ν 3278 w [ν(NH)], 2006 vs [$\nu(CO)_{term}$], 1946 vs [$\nu(CO)_{term}$], 1753 m [$\nu(CO)_{ester}$], 1706 sh [$\nu(CO)_{ester}$], 1693 s [$\nu(CO)_{ester}$], 1577 m [ν(C=C), 1510 m, 1375 m, 1302 m, 1232 s, 1189 m, 1111 m, 1077 m, 634 w, 589 m, 570 m, 470 w cm^{-1}. ^{1}H-NMR (C_6D_6, 60 °C) δ: 1.06 (t, $^3J_{HH}$ = 7.1 Hz, 3H, CH_2CH_3), 1.08 (t, $^3J_{HH}$ = 7.1 Hz, 3H, CH_2CH_3), 1.47 (s, 3H, C_5Me), 1.48 (s, 3H, C_5Me), 1.54 (s, 3H, C_5Me), 1.83 (s, 3H, C_5Me), 2.85 (s 6H, NMe_2), 4.02–4.18 (m, 4H, CH_2CH_3), 4.59 (d, $^3J_{PH}$ = 5.6 Hz, 1H, C_5CH=), 6.48 (s 1H, NH). $^{13}C\{^1H\}$-NMR (C_6D_6, 22 °C), δ: 9.5 s, 9.7 s, 10.0 s, 10.2 (s, $C_5(CH_3)_4$), 14.6 (s, OCH_2CH_3), 14.7 (s, OCH_2CH_3), 41.4 (s, $N(CH_3)_2$), 41.6 (s, $N(CH_3)_2$), 61.0 (s, OCH_2CH_3), 62.3 (s, OCH_2CH_3), 88.3 (s, br, C_5CH=), 92.9 s, 94.7 s, 95.3 s, 102.1 s, 107.6 (s, $C_5(CH_3)_4$), 156.1 (s, br, CO_2Et), 157.7 (s, br, CO_2-Et), 167.3 (d, $^1J_{PC}$ = 38.7 Hz, PCN), 215.7 (s, Fe(CO)), 215.8 (s, Fe(CO)). $^{31}P\{^1H\}$-NMR (C_6D_6) δ: 171.8 s, MS/CI: m/z = 508 (61, M^+ + H), 479 (23, M^+ − CO), 462 (59, M^+ − $HNMe_2$), 451 (89, M^+ − 2CO), 332 (100, M^+ − HN_2[CO_2Et]$_2$). Anal. Calcd for $C_{21}H_{30}N_3O_6PFe$ (507.29): C, 49.72; H, 5.96; N, 8.28. Found: C, 49.92; H, 6.07; N, 8.21.

η^5-C_5Me_4CH=C(NMe_2)P[N(CO_2CH_2Ph)NH)(CO_2-CH_2Ph)]Fe(CO)$_2$ (6c). A sample of orange crystalline **6c** 0.69 g, (48%) was prepared analogously from 0.86 g (2.27 mmol) of **1** and 0.68 g (2.27 mmol) of dibenzyl azodicarboxylate. Crys-

Scheme 2

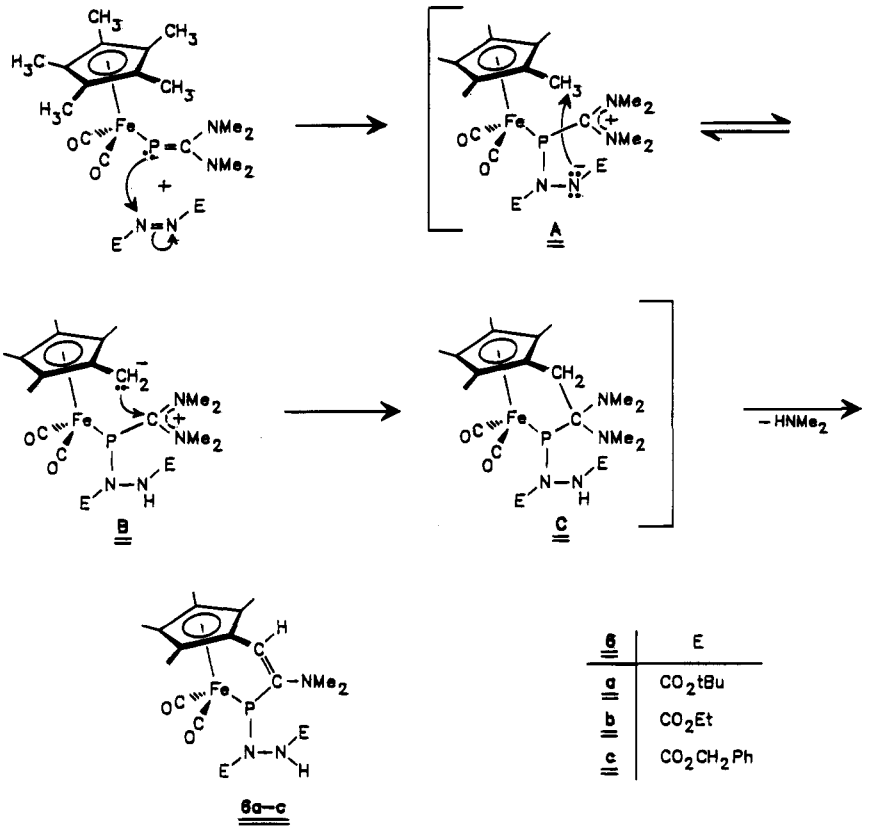

tallization of the product was performed in toluene at 5 °C. IR (KBr): ν 3286 w [ν(NH)], 1996 vs [$\nu(CO)_{term}$], 1950 vs [$\nu(CO)_{term}$], 1751 m [$\nu(CO)_{ester}$], 1698 s [$\nu(CO)_{ester}$], 1574 m [ν(C=C)], 1511 m, 1467 m, 1456 m, 1384 m, 1337 m, 1304 m, 1231 s, 1182 m, 1112 w, 1112 w, 1077 w, 1026 w, 915 w, 756 sh, 739 w, 700 w, 634 w, 591 m, 574 cm^{-1}. ^{1}H-NMR (C_6D_6, 60 °C) δ: 1.43 (s, 3H, C_5Me), 1.44 (s, 3H, C_5Me), 1.49 (s, 3H, C_5Me), 1.73 (s, 3H, C_5Me), 2.78 (s, 6H, NMe_2), 4.56 (d, $^3J_{PH}$ = 5.8 Hz, C_5CH=), 4.96–5.22 (m, 4H, CH_2Ph), 6.58 (s, 1H, NH), 7.01–7.32 (m, 10H, Ph). $^{13}C\{^1H\}$-NMR ($CDCl_3$, 22 °C) δ: 9.6 s, 10.0 s, 10.3 (s, $C_5(CH_3)_4$), 41.5 (s, $N(CH_3)_2$), 67.0 (s, CH_2Ph), 68.1 (s, CH_2Ph), 89.2 (s, br, C_5CH=), 92.8 s, 95.1 s, 102.4 s, 107.4 (s, $C_5(CH_3)_4$), 127.65 s, 127.7 s, 128.0 s, 128.1 s, 128.2 s, 128.3 (s, C-phenyl), 136.25 (s, i-C-phenyl), 136.3 (s, i-C-phenyl), 155.0 (s, br CO_2CH_2Ph), 157.0 (s, br, CO_2CH_2Ph), 165.9 (d, $^3J_{PC}$ = 29.7 Hz, NCP), 214.5 (s, Fe(CO)), 214.6 (s, Fe(CO)). $^{31}P\{^1H\}$-NMR (C_6D_6 δ: 174.0 s. MS/EI: m/z = 631 (2, M^+), 575 (4, M^+ – 2CO), 91 (100, $C_7H_7^+$). Anal. Calcd for $C_{31}H_{34}N_3O_6PFe$ (631.43): C, 58.97; H, 5.43; N, 6.65. Found: C, 58.52; H, 5.54; N, 6.53.

X-ray Crystal Structure Determination of 6a. An orange-red crystal with the approximate dimensions of 0.32 × 0.28 × 0.12 mm^3 was measured on a Siemens P4 diffractometer with MoK_α radiation at 260 K. Cell dimensions, refined from the diffractometer angles of 50 centered reflections, are a = 10.522(3) Å, b = 22.124(9) Å, c = 12.806(6) Å, β = 101.58(3)°, V = 2920(2) Å^3; Z = 4, d_{calcd} = 1.282 g m^{-3}, μ = 0.61 mm^{-1}, space group $P2_1/c$, data collection of 4278 unique intensities ($2\theta_{max}$ = 50°), 3261 observed ($F_o \geq 4\sigma(F)$), structure solution by direct methods and refinement with full-matrix least-squares methods on F (SHELXTL-Plus, SGI Iris Indigo), 336 parameters, riding groups for hydrogen atoms; common isotropic U values for each group and ADP's for all other atoms. Maximum residual electron density 0.97 e/Å^3 at a distance of 1.0 Å from Fe. R = 0.064, R_w = 0.076, $w^{-1} = \sigma^2(F_o) + 0.0030F_o^2$.

Results and Discussion

The metallophosphaalkene (η^5-C_5Me_5)$(CO)_2$FeP=C$(NMe_2)_2$ (**1**) smoothly reacted with equimolar amounts of the dialkyl azodicarboxylates $RO_2CN{=}NCO_2R$ (R = tBu, Et, CH_2Ph) in ether (20 °C) to afford the orange crystalline complexes **6a–c** in moderate yields (Scheme 2).

The air- and moisture-sensitive compounds **6a–c** were isolated by crystallization from methylcyclohexane or toluene. They were stored under an inert atmosphere at ambient temperature without significant decomposition.

The course of the reactions was monitored by ^{31}P-NMR spectroscopy. The singlet for compound **1** (δ 141.3) was replaced by a singlet at δ 168.6–173.2 for the products. No intermediates could be detected. The formation of **7**, which would have been the result of a cheletropic cycloaddition analogous to the generation of **8** from the metallodiphosphene (η^5-C_5Me_5)$(CO)_2$Fe-P=PMes* and the same azodicarboxylates,[4] has to be discarded due to analytical and spectroscopic evidence.

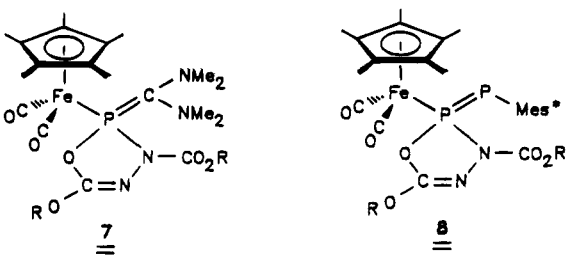

Four singlets in the region from δ 1.43 to 1.83 accounting for four discrete ring methyl groups and one

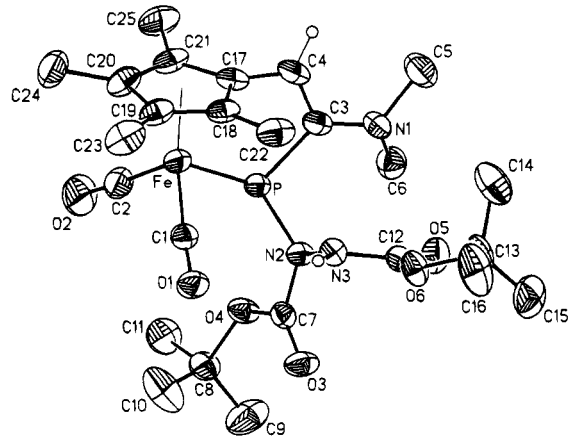

Figure 1. Molecular structure of **6a** in the crystal. Important bond lengths (Å) and bond angles (deg) are as follows: Fe–P 2.307(2), Fe–C(1), 1.758(6), Fe–C(2), 1.758(7), Fe–C(17) 2.065(6), Fe–C(18) 2.087(6), Fe–C(19) 2.136(6), Fe–C(20) 2.135(6), Fe–C(21) 2.088(7), P–N(2) 1.781(5), P–C(3) 1.843(5), N(1)–C(3) 1.366(7), N(2)–N(3) 1.399(6), C(3)–C(4) 1.338(9); P–Fe–C(1) 91.1(2), P–Fe–C(2) 90.5(2), C(1)–Fe–C(2) 96.6(3), Fe–P–C(3) 102.1(2), Fe–P–N(2) 110.1(1), N(2)–P–C(3) 99.8(2), P–N(2)–C(7) 121.5(3), P–N(2)–N(3), 119.8(4), N(3)–N(2)–C(7) 114.1(4), Fe–C(2)–O(2) 177.4(7), Fe–C(1)–O(1) 175.6(5), P–C(3)–C(4) 113.3(4), P–C(3)–N(1) 121.4(5), N(1)–C(3)–C(4) 124.7(5).

six-proton singlet for one dimethylamino group in the ^{1}H NMR spectra of **6b** and **6c** are consistent with a direct linkage between the cyclopentadienyl ring and the PC-fragment of **1**. The presence of a trisubstituted olefinic function is underlined by a doublet at δ 4.51–4.61 ($^3J_{PH}$ = 4.9–5.8 Hz) caused by a methylidyne proton in the β-position of the amino group. The corresponding carbon atom is detected as broad singlet at δ 88.3–89.2 whereas the amino-substituted olefinic carbon gives rise to doublets [δ 165.9–167.3; $^1J_{PC}$ = 29.7–39.6 Hz]. We assign a singlet due to one proton at δ 6.39–6.59 to the NH function. At ambient temperature some of the ^{1}H and ^{13}C resonances are broad. A considerable line-sharpening was achieved by recording the spectra at 60 °C. It is conceivable that a rotation of the amino group around the =C–N bond or the rotation of the ester function around the N–N bond of the hydrazido group **6a–c** are responsible for these observations. The precise nature of the dynamics is, however, not unambigiously clear at the moment.

The IR spectra of **6a–c** are consistent with two terminal carbonyl ligands (ν(CO) = 1986–2002 and 1928–1950 cm^{-1}], two ester carbonyl functions [ν(CO) = 1751–1753 and 1693–1712 cm^{-1}, and an electron rich C=C bond [ν(C=C) = 1574–1577 cm^{-1}]. A weak band at ν = 3387 (**6a**), 3278 (**6b**), and 3286 cm^{-1} (**6c**) is tentatively attributed to the ν(NH) stretching mode.

It is reasonable that the formation of **6a–c** is initiated by the nucleophilic attack of the P-atom of **1** at the π^*MO of the N=N bond. A transprotonation in intermediate **A** may lead to the zwitterion **B** which collapses by C–C bond formation to give **C**. The subsequent elimination of dimethylamine gives rise to the C=C bond in the final product.

To the best of our knowledge the condensation of a methyl substituent of a η^5-C_5Me_5 ligand resulting in C=C bond formation is without precedence. In particular, the anticipated inertness associated with its electron abundance and its steric bulk renders the C_5Me_5 system useful as ancillary ligand in a large number of organometallic coordination compounds. There are only a few exceptions known from that "rule of thumb", and they are usually encountered in electron-deficient and coordinatively unsaturated complexes of the early transition metals. CH- activation of one methyl substituent is observed in bis(pentamethylcyclopentadienyl)titanium (II),[5] (η^5-C_5Me_5)(η^5-η^1-$Me_4C_5CH_2$)$TiCH_3$,[6] (η^5-C_5Me_5)(η^5,η^1-$Me_4C_5CH_2$)ZrPh,[7] and (η^5-C_5Me_5)(η^5,η^1-$Me_4C_5CH_2$)$HfCH_2$-Ph.[8] Two adjacent methyl groups of the same C_5Me_5 ring are converted to the η^3,η^4-1,2,3-trimethyl-4,5-dimethylene cyclopentadienyl ligand in (η^5-C_5Me_5)[η^3,η^4-$Me_3C_5(CH_2)_2$]Ti,[9] (η^5-C_5Me_5)[η^3,η^4-$Me_3C_5(CH_2)_2$]W,[10] and [η^3,η^4-$Me_3C_5(CH_2)_2$]Ta(H)$_2$)PMe_3)$_2$.[11] In only one single case has the the insertion of a P=C fragment into the CH bond of a ring methyl group been reported.[12]

Table 1. Atomic Coordinates (×10^4) and Equivalent Isotropic Displacement Coefficients (Å^2 × 10^3) of 6a

	x	*y*	*z*	*U*(eq)[a]
Fe	4106(1)	6127(1)	2068(1)	39(1)
P	6296(1)	6264(1)	2717(1)	36(1)
N(1)	7841(5)	5614(2)	4387(4)	53(2)
N(2)	7210(4)	5902(2)	1867(3)	36(1)
N(3)	7130(5)	5275(2)	1729(4)	37(2)
O(1)	4638(4)	5705(2)	53(3)	58(2)
O(2)	3775(5)	7405(2)	1574(5)	88(2)
O(3)	7983(4)	5967(2)	319(3)	57(2)
O(4)	7440(4)	6802(2)	1167(3)	49(1)
O(5)	9211(4)	5063(2)	2617(3)	55(2)
O(6)	7892(4)	4365(2)	1609(3)	52(1)
C(1)	4403(5)	5890(3)	828(5)	44(2)
C(2)	3926(6)	6900(3)	1755(5)	54(2)
C(3)	6607(6)	5740(2)	3860(4)	44(2)
C(4)	5530(6)	5574(3)	4188(5)	50(2)
C(5)	8000(7)	5240(3)	5334(5)	71(3)
C(6)	8926(6)	6012(3)	4326(5)	57(2)
C(7)	7590(5)	6209(2)	1037(4)	39(2)
C(8)	7441(6)	7233(3)	293(5)	53(2)
C(9)	8775(8)	7266(3)	34(8)	95(4)
C(10)	6401(9)	7063(4)	−661(6)	96(4)
C(11)	7109(7)	7823(3)	778(6)	71(3)
C(12)	8206(6)	4913(2)	2049(4)	40(2)
C(13)	8568(7)	3813(2)	2066(5)	59(2)
C(14)	8359(9)	3750(3)	3201(7)	90(4)
C(15)	9989(8)	3840(3)	1998(8)	88(4)
C(16)	7884(9)	3317(3)	1352(7)	97(4)
C(17)	4243(6)	5641(3)	3463(4)	45(2)
C(18)	3715(5)	5263(3)	2579(4)	45(2)
C(19)	2523(6)	5519(3)	2043(5)	51(2)
C(20)	2298(6)	6056(3)	2575(5)	52(2)
C(21)	3363(6)	6134(3)	3462(5)	51(2)
C(22)	4260(7)	4665(3)	2343(5)	63(3)
C(23)	1603(6)	5258(3)	1099(6)	69(3)
C(24)	1126(6)	6456(3)	2311(6)	72(3)
C(25)	3500(7)	6623(3)	4324(5)	66(3)

[a] Equivalent isotropic *U* defined as one third of the trace of the orthogonalized $\mathbf{U}_{ij}$ tensor.

X-ray Structure Analysis of 6a. An X-ray structure analysis was necessary to unambigiously determine

(5) Bercaw, J. E. *J. Am. Chem. Soc.* **1974**, *96*, 5087.
(6) McDade, C.; Green, J. C.; Bercaw, J. E. *Organometallics* **1982**, *1*, 1629.
(7) Schock, L. E.; Brock, C. P.; Marks, T. J. *Organometallics* **1987**, *6*, 232.
(8) Bulls, A. R.; Schaefer, W. P.; Serfas, M.; Bercaw, J. E. *Organometallics* **1987**, *6*, 1219.
(9) Pattiasina, J. W.; Hissink, C. E.; de Boer, J. L.; Meetsma, A.; Teuben, J. H.; Spek, A. L. *J. Am. Chem. Soc.* **1985**, *107*, 7758.
(10) Cloke, F. G. N.; Green, J. C.; Green, M. L. H.; Morley, C. P. *J. Chem. Soc., Chem. Commun.* **1985**, 945.
(11) Gibson, V. C.; Kee, T. P.; Carter, S. T.; Sanner, R. D.; Clegg, W. *J. Organomet. Chem.* **1991**, *418*, 197.
(12) Weber, L.; Kirchhoff, R.; Boese, R. *J. Chem. Soc., Chem. Commun.* **1992**, 1182; *Chem. Ber.* **1993**, *126*, 1963.

the constitution and geometry of the condensation products. Single crystals of **6a** were grown from methylcyclohexane at 5 °C. The results of the structural determination are shown in Figure 1. Positional parameters for the complex are given in Table 1. The analysis confirms the presence of the novel 3-(tetramethylcyclopentadienyl)-1-phospha-2-propenyl system ligated in an η^5:η^1 fashion to the $Fe(CO)_2$ fragment. The cyclopentadienyl ring is unsymmetrically coordinated to the metal. Due to the presence of the "handle" P–C(3)–C(4) the iron–carbon distances Fe–C(17), Fe–C(18), and Fe–C(21) [2.065(6)–2.088(7) Å] are significantly shorter than the remaining bond lengths Fe–C(19) [2.136(6) Å] and Fe–C(20) [2.135(6) Å]. The phosphorus atom is pyramidly configurated [Σangles = 312.0°] featuring single bonds to the adjacent atom C(3) [1.843(5) Å] and N(2) [1.781(5) Å]. A standard value of 1.85 Å[13] is accepted for a P–C single bond. The sum of the covalent radii between phosphorus and nitrogen is 1.80 Å.[14]

The Fe–P distance in **6a** [2.307(2) Å] compares well with the corresponding bond lengths in **9** [2.303(1) Å],[15] **10** [2.310(1) Å],[16] and precursor **1** [2.325(2) Å][2].

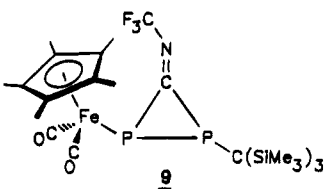

9

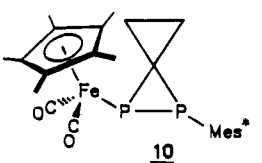

10

Normally, Fe–P bond distances in low-valent iron carbonyls fall in the range 2.11–2.37 Å.[17] The carbon–carbon distance within the "handle" C(3)–C(4) [1.338(9) Å] is in accordance with a double bond. The nearly planar amino group [Σangles = 355.2°] is connected to C(3) via a single bond of 1.366(7) Å. In **1** the corresponding bonds are found to 1.372(8) and 1.410(7) Å[2]. The Me_2N function is twisted off the plane of the C=C bond by 26.0°. The hydrazido substituent at phosphorus exhibits almost planarly configurated nitrogen atoms linked by a single bond of 1.399(6) Å. The planes defined by N(2), C(7), O(3), O(4) and N(3), C(12), O(5), O(6), respectively, enclose a dihedral angle of 101.5°. The organophosphorus ligand is part of a distorted $FePC_2$ tripod. The three angles formed by the ligands and the iron center are C(1)–Fe–C(2) = 96.6(3)°, P–Fe–C(1) = 91.1(2)° and P–Fe–C(2) = 90.5(2)°. Two legs of the tripod are represented by terminal, nearly linear carbonyl groups.

Acknowledgment. The present work was generously supported by the Deutsche Forschungsgemeinschaft, Bonn, the Fonds der Chemischen Industrie, Frankfurt, and the BASF, AG, Ludwigshafen, Germany, whose funding is gratefully acknowledged.

Supplementary Material Available: Tables of bond lengths, bond angles, anisotropic displacement coefficients, and H-atom coordinates (Tables 2–5) and a list of torsion angles for $C_{25}H_{38}FeN_3O_6P$ (9 pages). Ordering information is given on any current masthead page.

OM9407161

(13) Corbridge, D. E. C. *The Structural Chemistry of Phosphorus*; Elsevier Scientific Publ. Co.: Amsterdam, 1974; p 393.
(14) Holleman, A.; Wiberg, E. *Lehrbuch der Anorganischen Chemie*, 91st ed.; W. de Gruyter: Berlin, New York, 1985; p 133.
(15) Weber, L.; Buchwald, S.; Lentz, D.; Stamm, O.; Preugschat, D.; Marschall, R. *Organometallics* **1994**, *13*, 4406.
(16) Weber, L.; Lücke, E.; Boese, R. *Organometallics* **1988**, *7*, 978.
(17) (a) Knoll, K.; Huttner, G.; Wasiucionek, M.; Zsolnai, L. *Angew. Chem.* **1984**, *96*, 708; *Angew. Chem., Int. Ed. Engl.* **1984**, *23*, 739. (b) Lal De, R.; Vahrenkamp, H. *Z. Naturforsch.* **1986**, *41b*, 273. (c) Arif, A. M.; Cowley, A. H.; Pakulsky, M. *J. Am. Chem. Soc.* **1985**, *107*, 2553. (d) Huttner, G.; Mohr, G.; Friedich, P.; Schmid, H. G. *J. Organomet. Chem.* **1978**, *160*, 59. (e) Williams, G. D.; Geoffroy, G. J.; Whittle, R. R.; Rheingold, A. L. *J. Am. Chem. Soc.* **1985**, *107*, 729. (f) Weber, L.; Frebel, M.; Boese, R.; *New J. Chem.* **1989**, *13*, 303.

Studies on Catalytically Active Ruthenium Carbonyl Bipyridine Systems. Synthesis and Structural Characterization of $[Ru(bpy)(CO)_2Cl_2]$, $[Ru(bpy)(CO)_2Cl(C(O)OCH_3)]$, $[Ru(bpy)(CO)_2Cl]_2$, and $[Ru(bpy)(CO)_2ClH]$ (bpy = 2,2′-Bipyridine)

Matti Haukka, Jari Kiviaho,† Markku Ahlgrén, and Tapani A. Pakkanen*

Department of Chemistry, University of Joensuu, P.O. Box 111, FIN-80101 Joensuu, Finland

Received May 12, 1994®

The molecular structures and reactivity of several ruthenium mono(bipyridine) carbonyl compounds have been studied as possible model compounds for intermediates in water-gas shift reactions and in CO_2-reduction processes. *cis*-(CO),*cis*(Cl)-$[Ru(bpy)(CO)_2Cl_2]$ (**1a**), *cis*(CO),*trans*(Cl)-$[Ru(bpy)(CO)_2Cl_2]$ (**1b**), $[Ru(bpy)(CO)_2Cl(C(O)OCH_3)]$ (**2**), $[Ru(bpy)(CO)_2Cl]_2$ (**3**), and $[Ru(bpy)(CO)_2ClH]$ (**4**) have been synthesized from $[Ru(CO)_3Cl_2]_2$ and 2,2′-bipyridine in THF or alcohol solutions. The structures of these complexes have been confirmed by single-crystal X-ray crystallography: **1a**, orthorhombic, space group *Pbca*, a = 12.709(4) Å, b = 11.532(5) Å, c = 18.852(5) Å, Z = 8; **1b**, triclinic, space group $P\bar{1}$, a = 6.536(4) Å, b = 12.557(7) Å, c = 12.595(9) Å, α = 119.81(4)°, β = 93.94(6)°, γ = 98.11(4)°, Z = 4; **2**, monoclinic, space group $P2_1/m$, a = 7.751(4) Å, b = 11.863(7) Å, c = 9.081(6) Å, β = 107.18(4)°, Z = 2; **3**, monoclinic, space group $C2/m$, a = 12.681(5) Å, b = 10.165(3) Å, c = 10.633(4) Å, β = 114.01(3)°, Z = 2; **4**, triclinic, space group $P\bar{1}$, a = 6.407(3) Å, b = 8.135(5) Å, c = 12.707(8) Å, α = 89.39(5)°, β = 81.56(5)°, γ = 81.53(4)°, Z = 2. $[Ru(bpy)(CO)_2Cl(C(O)OCH_3)]$ can be converted directly to $[Ru(bpy)(CO)_2Cl]_2$ under H_2/CO pressure. It is also possible to convert $[Ru(bpy)(CO)_2Cl]_2$ to $[Ru(bpy)(CO)_2Cl(C(O)OCH_3)]$ in methanol under H_2/CO pressure and to $[Ru(bpy)(CO)_2Cl_2]$ in concentrated HCl solution. $[Ru(bpy)(CO)_2ClH]$ converts to $[Ru(bpy)(CO)_2Cl]_2$ and may be an intermediate in the preparation of $[Ru(bpy)(CO)_2Cl]_2$. $[Ru(bpy)(CO)_2Cl]_2$ can be seen as a model for the catalytically active $[Ru(bpy)(CO)_2]_n$ polymer in CO_2 reduction. $[Ru(bpy)(CO)_2ClH]$ and $[Ru(bpy)(CO)_2Cl(C(O)OCH_3)]$ are possible models for proposed −Ru(bpy)H and −Ru(bpy)(C(O)OH) intermediates in WGSR. Reversible conversions between $[Ru(bpy)(CO)_2Cl(C(O)OCH_3)]$ and $[Ru(bpy)(CO)_2Cl]_2$ offer also a possible model route for the catalytic preparation of methyl formate.

Introduction

Ruthenium poly(bipyridines) have been widely studied because of their activity in the water-gas shift reaction (WGSR)[1–4] and in the reduction of CO_2.[5,6] In these processes the catalytic cycles and the structures of probable intermediates are relatively well-documented. Corresponding reactions with ruthenium carbonyl mono(bipyridines) up until now have been studied less frequently. $[Ru(bpy)(CO)_2Cl_2]$, a mono(bipyridine) complex, is known as an excellent catalyst for the photochemical and electrochemical reduction of CO_2 into formate and carbon monoxide/formate.[7] Both $[Ru_3(CO)_{12}$/2,2′-bipyridine] and $[Ru_3(CO)_{12}$/2,2′-bipyridine/$SiO_2]$ systems have been found to be active in 1-hexene hydroformylation.[8] The cluster precursor system $[Ru_3(CO)_{12}$/2,2′-bipyridine/$SiO_2]$ is also highly active in WGSR.[9] The detailed structure of the active form of $[Ru_3(CO)_{12}$/2,2′-bipyridine] is not yet known, but it is probably a mono(bipyridine) compound. In addition to ruthenium carbonyl bipyridines, a related $[Ru_3(CO)_{12}]$ catalyst with a NEt_3Cl promoter has proved to be active in the carbonylation of methanol to methyl formate.[10] Knowledge of the structures and chemical behavior of ruthenium mono(bipyridine) complexes would be useful in understanding the catalytic properties of related systems.

In the present work we introduce the synthesis, reactions, and crystal structures of $[Ru(bpy)(CO)_2Cl]_2$, $[Ru(bpy)(CO)_2Cl(C(O)OCH_3)]$, $[Ru(bpy)(CO)_2ClH]$, and $[Ru(bpy)(CO)_2Cl_2]$ complexes (bpy = 2,2′-bipyridine),

* E-mail: tap@joyl.joensuu.fi.
† Present address: Technical Research Center of Finland, VTT, Chemical Technology, P.O. Box 1401, FIN-02044 VTT, Finland.
® Abstract published in *Advance ACS Abstracts*, December 15, 1994.

(1) Richmond, M. G. *J. Organomet. Chem.* **1993**, *457*, 121.
(2) Kelly, J. M.; Vos, J. G. *Angew. Chem., Int. Ed. Engl.* **1982**, *21*, 628.
(3) Haasnoot, J. G.; Hinrichs, W.; Weir, O.; Vos, J. *Inorg. Chem.* **1986**, *25*, 4140.
(4) Ishida, H.; Tanaka, K.; Morimoto, M.; Tanaka, T. *Organometallics* **1986**, *5*, 724.
(5) (a) Tanaka, H.; Nagao, H.; Tanaka, K. *Inorg. Chem.* **1992**, *31*, 1971. (b) Tanaka, H.; Tzeng, B.-C.; Nagao, H.; Peng, S.-H.; Tanaka, K. *Organometallics* **1992**, *11*, 3172. (c) Tanaka, H.; Tzeng, B.- C.; Nagao, H.; Peng, S.-H.; Tanaka, K. *Inorg. Chem.* **1993**, *32*, 1508.
(6) Vlcek, A., Jr. *Chemtracts: Inorg. Chem.* **1993**, *5*, 1.
(7) (a) Lehn, J.-M.; Ziesel, R. *J. Organomet. Chem.* **1990**, *382*, 157. (b) Ishida, M.; Fujiki, K.; Omba, T.; Ohkubo, K.; Tanaka, K.; Terarda, T.; Tanaka, T. *J. Chem. Soc., Dalton Trans.* **1990**, 2155. (c) Collomb-Dunnand-Sauthier, M.-N.; Deronzier, A.; Ziessel, R. *J. Chem. Soc., Chem. Commun.* **1994**, 189. (d) Collomb-Dunand-Sauthier, M.-N.; Deronzier, A.; Ziessel, R. *Inorg. Chem.* **1994**, *33*, 2961.
(8) Alvila, L.; Pakkanen, T. A.; Krause, O. *J. Mol. Catal.* **1993**, *84*, 145 and references therein.
(9) Kiiski, U.; Venäläinen, T.; Pakkanen, T. A.; Krause, O. *J. Mol. Catal.* **1991**, *64*, 163 and references therein.
(10) Choi, S. J.; Lee, J. S.; Kim, Y. G. *J. Mol. Catal.* **1993**, *85*, L109.

0276-7333/95/2314-0825$09.00/0

Scheme 1. Preparation and Reactions of [Ru(bpy)(CO)$_2$Cl$_2$], [Ru(bpy)(CO)$_2$Cl(C(O)OCH$_3$)], [Ru(bpy)(CO)$_2$Cl]$_2$, and [Ru(bpy)(CO)$_2$ClH]^a

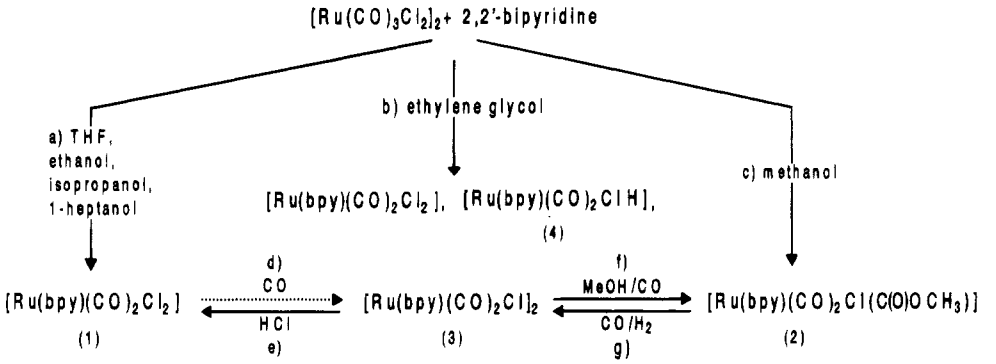

^{a} Legend: (a) refluxed/heated at 100 °C for 0.5−1 h; (b) heated at 90−100 °C for 1.5−2 h; (c) refluxed for 0.5 h; (d) solvent ethylene glycol, p_{CO} = 50 bar, T = 150 °C, t = 17 h; (e) refluxed in HCl (37%); (f) p_{CO} = 50 bar, T = 150 °C, t = 17 h; (g) solvent ethylene glycol, p_{H_2} = 25 bar, p_{CO} = 25 bar, T = 150 °C, t = 17 h.

possible model compounds for intermediates in WGSR and/or CO_2-reduction catalysis.

Results and Discussion

Ishida et al. have studied the WGSR process catalyzed by [Ru(bpy)$_2$(CO)Cl]$^+$ and [Ru(bpy)$_2$(CO)$_2$]$^{2+}$.[4] They proposed that the reaction cycle includes [Ru(bpy)$_2$(CO)(H$_2$O)]$^{2+}$, [Ru(bpy)$_2$(CO)(C(O)OH)]$^+$, and [Ru(bpy)$_2$(CO)H]$^+$ intermediates. [Ru(bpy)$_2$(CO)H]$^+$ has been isolated and characterized by single-crystal X-ray crystallography.[3] The crystal structure of [Ru(bpy)$_2$(CO)(C(O)OH)]$^+$ is not known, but a suitable model compound, [Ru(bpy)$_2$(CO)(C(O)OCH$_3$)]$^+$, has been reported.[5b,c] [Ru(bpy)$_2$(CO)(C(O)OH)]$^+$ is also an important intermediate in CO_2 reduction. Like the ruthenium bis(bipyridine) compounds above, [Ru(bpy)(CO)$_2$Cl$_2$] is found to be active in the reduction of CO_2.[7] Ziessel et al. have proposed a mechanism for electrocatalytic reduction of CO_2, which includes a highly air-sensitive, blue polymeric [Ru(bpy)(CO)$_2$]$_n$ catalyst and [Ru(bpy)(CO)(C(O)OH)] intermediate.[7c,d] Similar blue, air-sensitive catalysts active in WGSR and 1-hexene hydroformylation have also been prepared from [Ru$_3$(CO)$_{12}$] and 2,2′-bipyridine.[8,9] However, suitable model compounds for the intermediates in CO_2 reduction or WGSR catalyzed by mono(bipyridine) compounds are not yet readily available. We have studied the preparation, reactions, and structures of the possible model compounds [Ru(bpy)(CO)$_2$Cl$_2$], [Ru(bpy)(CO)$_2$Cl(C(O)OCH$_3$)], [Ru(bpy)(CO)$_2$Cl]$_2$, and [Ru(bpy)(CO)$_2$ClH]. The compounds, their syntheses, and reactions are summarized in Scheme 1.

Preparation and Crystal Structure of [Ru(bpy)(CO)$_2$Cl$_2$]. Preparation and IR studies on [Ru(bpy)(CO)$_2$Cl$_2$] have been reported by several authors.[11−14] [Ru(bpy)(CO)$_2$Cl$_2$] is typically prepared from RuCl$_3$ via [Ru(CO)$_3$Cl$_2$(THF)] or via "the red carbonyl solution". Depending on the preparation method, one or two products have been found in these syntheses by IR measurements. Both compounds have two ν(CO) stretching bands, a "high frequency" compound at 2055−2070 and 1997−2007 cm^{-1} and a "low frequency" compound at 2040 and 1980 cm^{-1}. The former have been assigned to the *cis*(CO),*trans*(Cl) isomer of [Ru(bpy)(CO)$_2$Cl$_2$][11−14] and the latter to the *cis*(CO),*cis*(Cl) isomer.[14]

We have synthesized [Ru(bpy)(CO)$_2$Cl$_2$] from [Ru(CO)$_3$Cl$_2$]$_2$ in THF (Scheme 1a) by successive precipitations (see Experimental Section). Typically, only a pale yellow product was formed, but occasionally a pink color was also observed, especially in the first precipitate. However, there were only two strong ν(CO) peaks at about 2067 and 2003 cm^{-1}, which indicate the typical "high frequency" component. The ^{1}H NMR spectrum of [Ru(bpy)(CO)$_2$Cl$_2$] proved to be informative. In the spectrum of the first precipitate (**1a**) four triplets and three doublets were found in the aromatic region. The triplets and two of the doublets had comparable intensities, but one doublet (8.2 ppm) had almost a double intensity. It probably arises from two overlapping doublets. In addition to main-peak sets, an "extra" doublet and a triplet were found at 9.2 and 7.7 ppm. Two other extra signals at about 8.0−8.3 ppm (doublet and triplet) were partially covered by the main-peak sets. The intensity of this extra peak set varied independently in different samples, and it became dominant in the second precipitate (**1b**). The ^{1}H NMR spectrum of **1a** can be assigned to the *cis*(CO),*cis*(Cl) isomer by assuming that the halves of the bpy ring are not equivalent. Dissimilarity can be expected, because in this isomer different ligands (CO and Cl) occupy the positions trans to bpy nitrogens. The multiple aromatic peak pattern found in the ^{13}C{^{1}H} NMR spectrum supports the ^{1}H NMR observations. It has been proposed that in the preparation of [Ru(bpy)(CO)$_2$Cl$_2$] from a "ruthenium red carbonyl solution" a mixture of *cis,cis* and *cis,trans* isomers are not formed, but a pure yellow [Ru(bpy)(CO)$_2$Cl$_2$] and a red-purple mixture of [Ru(bpy)(CO)$_2$Cl$_2$] and [Ru(bpy)(CO)Cl$_3$].[15] Formation of a very small amount of [Ru(bpy)(CO)Cl$_3$] may explain the reddish color occasionally found in our products also. However, if a larger amount of the monocarbonyl compound is present, it should be observed by IR and ^{1}H NMR spectroscopy and elemental analysis. In the ^{1}H NMR and ^{13}C{^{1}H} NMR spectra of the second precipitate (**1b**) only one aromatic peak set was found

(11) Bruce, M. I.; Stone, F. G. A. *J. Chem. Soc. A* **1967**, 1238.
(12) Kingston, J. V.; Jamieson, J. W. S.; Wilkinson, G. *J. Inorg. Nucl. Chem.* **1967**, *29*, 133.
(13) Black, D. St. C.; Deacon, G. B.; Thomas, N. C. *Aust. J. Chem.* **1982**, *35*, 2445.
(14) Kelly, J. M.; O'Connel, C. M.; Vos, J. G. *Inorg. Chim. Acta* **1982**, *64*, L75.
(15) Collomb-Dunand-Sauthier, M.-N.; Deronzier, A. *J. Electroanal. Chem. Interfacial Electrochem.* **1991**, *319*, 347.

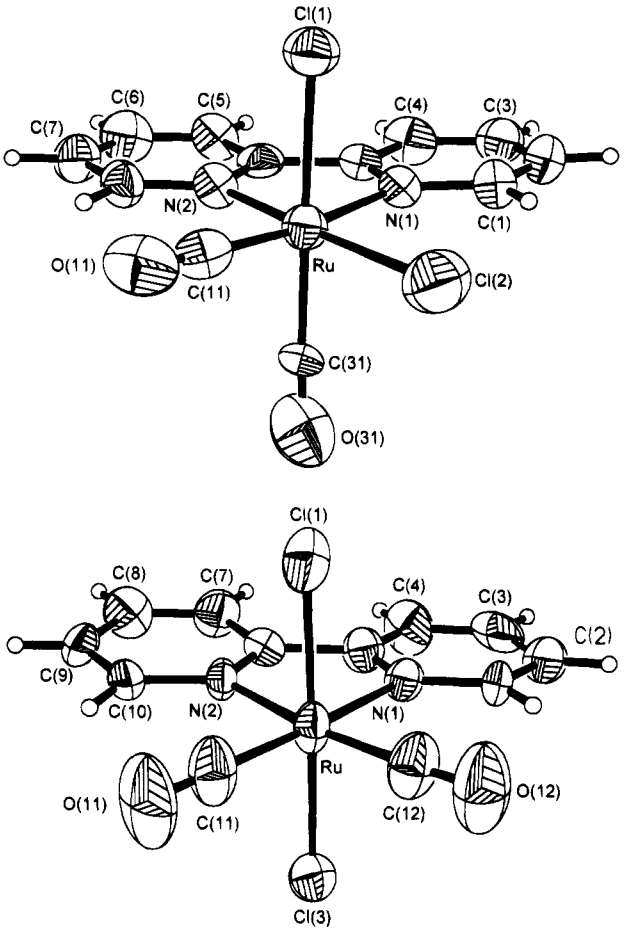

Figure 1. (a, top) Structure of *cis*(CO),*cis*(Cl)-[Ru(bpy)-$(CO)_2Cl_2$] (**1a**). (b, bottom) Structure of *cis*(CO),*trans*(Cl)-[Ru(bpy)$(CO)_2Cl_2$]·CH_2Cl_2 (**1b**).

(variable amounts of the component **1a** were also observed), which relates to the chemical equivalence of the bpy rings. ^{1}H NMR results for **1b** are close to those reported by Black et al.[13] for the *cis*(CO),*trans*(Cl) isomer.

We crystallized the pale yellow first precipitate (**1a**) from CH_2Cl_2. The crystals were covered by a thin layer of reddish paste, which was removed by washing the crystals carefully with a small amount of CH_2Cl_2. The pure, brownish yellow crystals were used in single-crystal X-ray diffraction studies, which confirmed the assumption of the *cis*(Cl),*cis*(CO) isomer (Figure 1a). Since the compound crystallizes in the centrosymmetric space group *Pbca*, the crystal structure contains both optical isomers. *cis(CO),cis(Cl)*-[Ru(bpy)$(CO)_2Cl_2$] crystallizes also in the solvated form. Crystallization from $CHCl_3$ gave the pure optical isomer [Ru(bpy)$(CO)_2$-Cl_2]·$CHCl_3$,[16] whereas [Ru(bpy)$(CO)_2Cl_2$]·CH_2Cl_2 was again a racemic mixture.[17] The coordination geometry of Ru in **1a** is octahedral. Both the bond lengths and the angles are quite typical for this type of compound.[18,19] The Ru–Cl(1) bond length trans to CO (2.439(3) Å) is clearly longer than Ru–Cl(2) trans to bipyridine nitrogen (2.411(4) Å) due to the strong trans effect of the carbonyl ligand. The Ru–N(1) bond length of 2.117(8) Å trans to carbonyl ligand is also slightly longer than the Ru–N(2) bond length of 2.090(8) Å trans to chlorine. C–O bond lengths are comparable with those found in [Ru(bppi)$(CO)_2Cl_2$],[18] [Ru(CO)Cl_2(tby)], and [$RuBr_2(CO)_2$(tby)].[19] Ru–C–O angles are slightly distorted (171.1(11)–174.5(10)°) from the linear structure. Distortions of the same magnitude have been observed in [Ru$(bpy)_2$(CO)(NO_2)]$^+$ and [Ru$(bpy)_2$(CO)-Cl)]$^+$ (170(1)° [5] and 174.8(3)°,[20] respectively). The "bite angle" of the bipyridine is also comparable with that of other Ru–bpy complexes.[21–24] We did not observe any evidence of the *cis*(CO),*trans*(Cl) isomer in the crystal state. However, in the ^{1}H NMR spectrum of the pure **1a** crystals a trace of **1b** was observed. Precipitate **1b** was crystallized from dichloromethane only in solvated form. Crystallographic studies on **1b** confirmed the structure to *cis(CO),trans(Cl)*-[Ru(bpy)$(CO)_2Cl_2$]·CH_2Cl_2 (Figure 1b). The pale yellow crystals were highly labile and existed only under CH_2Cl_2 vapor. When the crystals were transferred in air or under a nitrogen atmosphere, they were destroyed completely within a few minutes. Unlike the use in **1a**, the Ru–N bonds in **1b** are nearly equal. This is in agreement with the NMR results, which indicate symmetrical bipyridine rings. Similarly, Ru–Cl bond lengths are identical and Ru–CO bond lengths much closer to each other than in **1a**, due to the higher symmetry of *cis(CO),trans(Cl)*-[Ru(bpy)$(CO)_2Cl_2$]. In dichloromethane the IR spectrum of **1b** was similar to that of **1a** (Figure 2, spectrum **1**). It is unlikely that both isomers truly have similar IR spectra, indicating that in solution the identities of the isomers are not proven rigorously.

Formation of [Ru(bpy)$(CO)_2$Cl(C(O)OCH_3)] and [Ru(bpy)$(CO)_2Cl_2$] in Alcohol Solution. When [Ru$(CO)_3Cl_2]_2$ was refluxed with an excess of 2,2′-bipyridine in methanol (Scheme 1c), a pale yellow, nearly white precipitate was formed. Two strong IR peaks were found in the carbonyl stretching region at 2058 and 1994 cm^{-1} (Figure 2, spectrum **2**). An additional weak and broad peak was observed at 1640 cm^{-1}, which is typical for formyl type C–O stretching in metal complexes.[25] The crystal structure of the product is shown in Figure 3. The [Ru(bpy)$(CO)_2$Cl-(C(O)OCH_3)] (**2**) molecule consists of the symmetrical halves. The axial chlorine and the C(O)OCH_3 group are positioned in a mirror plane. Carbonyl ligands are

(16) Crystal data for [Ru(bpy)$(CO)_2Cl_2$]·$CHCl_3$ (**1a′**): M_r 503.56, orthorhombic, space group $P2_12_12_1$, a = 9.192(4) Å, b = 10.510(4) Å, c = 18.964(6) Å, V = 1832(1) Å^3, Z = 4, D_{calc} = 1.826 g/cm^3, crystal source $CHCl_3$, crystal size 0.2 × 0.2 × 0.2 mm, yellow, Mo Kα radiation (λ = 0.709 34 Å, 2θ limits 5–55°, no. of unique reflections 2411, no. of observed data 1537, no. of parameters 208, μ = 1.583 mm^{-1}, R = 0.0495, R_w = 0.0426, GOF = 1.02. Complete structural data are available as supplementary material.

(17) Crystal data for *cis*(CO),*cis*(Cl)-[Ru(bpy)$(CO)_2Cl_2$]·CH_2Cl_2: M_r 469.12, monoclinic, space group $P2_1/n$, a = 11.446(7) Å, b = 12.086(4) Å, c = 13.204(6) Å, β = 107.74(4)°, V = 1739.7(14) Å^3, Z = 4, D_{calc} = 1.791 g/cm^3, crystal source CH_2Cl_2, crystal size 0.1 × 0.2 × 0.2 mm, pale yellow, Mo Kα radiation (λ = 0.709 34 Å), 2θ limits: 5–60°, no. of unique reflections 5102, no. of observed data 2020, no. of parameters 199, μ = 1.509 mm^{-1}, R = 0.0790, R_w = 0.0752, GOF = 1.61. Complete structural data are available as supplementary material.

(18) De Munno, G.; Denti, G.; De Rosa, G.; Bruno, G. *Acta Crystallogr.* **1988**, *C44*, 1193.
(19) Deacon, G. B.; Patrick, J. M.; Skelton, B. W.; Thomas, N. C.; White, B. W. *Aust. J. Chem.* **1984**, *37*, 929.
(20) Clear, J. M.; Kelly, J. M.; O'Connel, C. M.; Vos, J. G.; Cardin, C. J.; Costa, S. R. *J. Chem. Soc., Chem. Commun.* **1980**, 750.
(21) Eggleston, D. S.; Goldsby, K. A.; Hodgson, D. J.; Meyer, T. J. *Inorg. Chem.* **1985**, *24*, 4573.
(22) Greaney, M. A.; Coyle, C. L.; Harmer, M. A.; Jordan, A.; Stiefel, E. I. *Inorg. Chem.* **1989**, *28*, 912.
(23) Nagao, H.; Nishimura, H.; Funato, H.; Ichikawa, Y.; Howell, F. S.; Mukaida, M.; Kakihana, H. *Inorg. Chem.* **1989**, *28*, 3955.
(24) Durham, B.; Cox, D. I.; Cordes, A. W.; Barsoum, S. *Acta Crystallogr.* **1990**, *C46*, 312.
(25) Gladysz, J. A. *Adv. Organomet. Chem.* **1982**, *20*, 1.

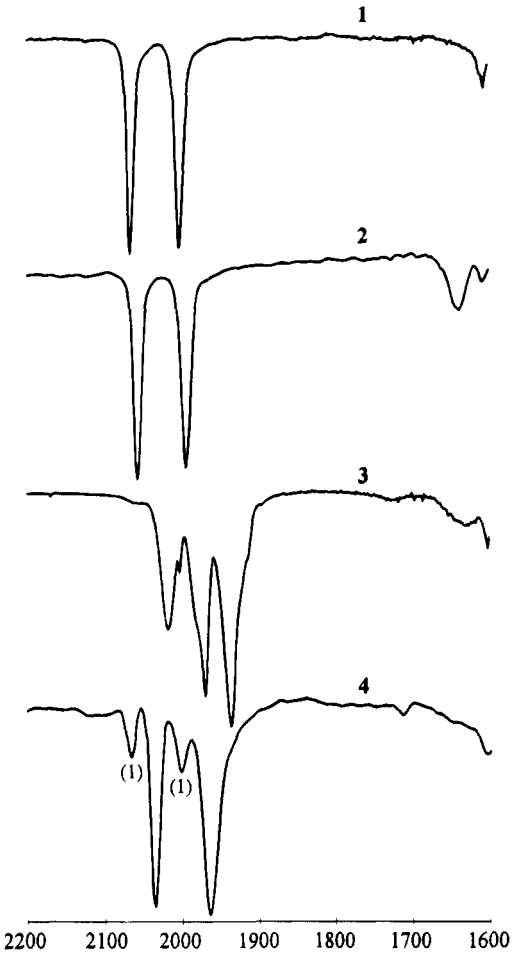

Figure 2. IR spectra of (**1**) *cis*(CO),*cis*(Cl)- and *cis*-(CO),*trans*(Cl)-[Ru(bpy)(CO)$_2$Cl$_2$] mixture (in CH_2Cl_2), (**2**) [Ru(bpy)(CO)$_2$Cl(C(O)OCH$_3$)] (in CH_2Cl_2), (**3**) [Ru(bpy)(CO)$_2$Cl]$_2$ (in KBr), and (**4**) [Ru(bpy)(CO)$_2$ClH] (in CH_2Cl_2) with traces of **1**.

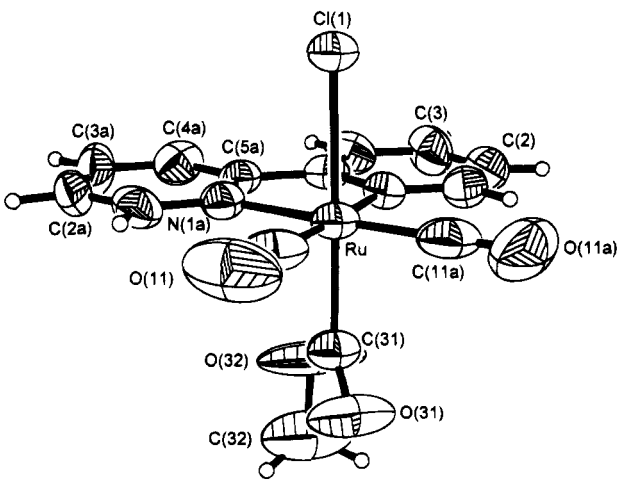

Figure 3. Structure of [Ru(bpy)(CO)$_2$Cl(C(O)OCH$_3$)] (**2**).

again in *cis* positions trans to bipyridine nitrogens as in **1b**. The Ru−CO bond lengths of 1.859(13) Å are comparable with those found in **1a** and **1b**. The axial Ru−Cl(1) bond is unusually long (2.496(3) Å), compared with the Ru−Cl bonds in **1a**, indicating the strong *trans* weakening effect of the C(O)OCH$_3$ group. The bond lengths and angles of the Ru−(C(O)OCH$_3$) moiety found earlier in [Ru(bpy)$_2$(CO)(C(O)OCH$_3$)]$^+$ [26] are comparable with those in **2**.

Formation of the C(O)OH ligand in other alcohol solvents was not observed. When [Ru(CO)$_3$Cl$_2$]$_2$ and 2,2′-bipyridine were refluxed in ethanol, 2-propanol, or 1-heptanol (Scheme 1a), a pale yellow precipitate was formed (a reddish color was again occasionally observed). In ^{1}H NMR and ^{13}C{^{1}H} NMR measurements both **1a** and **1b** peak patterns were found, suggesting that both isomers of [Ru(bpy)(CO)$_2$Cl$_2$] were formed in variable proportions. In the IR spectrum two strong peaks were found at ca. 2067 and 2003 cm^{-1} (in CH_2Cl_2), a typical spectrum for [Ru(bpy)(CO)$_2$Cl$_2$]. Elemental analysis corresponded also to [Ru(bpy)(CO)$_2$Cl$_2$]. It is likely that ethanol and alcohols with larger hydrocarbon chains are sterically incapable of forming a stable M−C(O)OR group. Another reason may be that the acidity of the alcohols tends to decrease with the increasing hydrocarbon group,[27] lowering the reactivity of the OH group. In larger alcohols the chlorine bridges of the [Ru(CO)$_3$Cl$_2$]$_2$ dimer are probably merely broken by the addition of 2,2′-bipyridine, without further reactions with the solvent.

Formation of [Ru(bpy)(CO)$_2$Cl]$_2$ and [Ru(bpy)(CO)$_2$ClH] in Ethylene Glycol. Heating of [Ru(CO)$_3$Cl$_2$]$_2$ with an excess of 2,2′-bipyridine in ethylene glycol (Scheme 1b) gave a red, very poorly soluble, microcrystalline precipitate (**3**) and a greenish black solution. When the solution was cooled to room temperature, the color lightened to reddish yellow. The IR spectrum of the solid product was completely different from those of both **1** and **2** (Figure 2, spectrum **3**). The elemental analysis gave a reasonably good fit with [Ru(bpy)(CO)$_2$Cl]$_2$. Despite the disorder in the crystal structure, the molecular structure of **3** was verified as a [Ru(bpy)(CO)$_2$Cl]$_2$ dimer (Figure 4). The Ru−Ru bond length of 2.860(1) Å is comparable with those found in [Ru$_3$(CO)$_{12}$] (average 2.854 Å) and [Ru(CO)$_4$]$_n$ (2.860(1) Å) but shorter than those found in [Ru(η-C$_5$H$_5$)(CO)$_2$Ru(CO)$_4$] (2.889(1) Å) and in [Ru(SnMe$_3$)(CO)$_4$]$_2$ (2.943(1) Å).[28] In the last two compounds the CO groups are in the eclipsed positions, whereas in [Ru(CO)$_4$]$_n$ carbonyl ligands are in staggered positions. The short Ru−Ru distance in **3** suggests that the equatorial ligands in RuL$_5$ units may also be in staggered positions (Figure 3a). However, the crystal structure revealed also the "anti-eclipsed" rotamer (Figure 3b). The complexity of the IR spectrum (Figure 2, spectrum **3**) supports the coexistence of two rotamers. The Ru−N(bpy) bond lengths vary considerably (from 2.040(6) to 2.179(7) Å) in **3**. Typically, the variations in these types of compounds are less than 0.1 Å.[3,5,20−23] Another striking feature in **3** is the exceptionally long Ru−Cl(1) bond (2.512(1) Å). A comparative bond length (2.496(3) Å) is found in **2**. The axial Ru−Cl bond is influenced by a strong trans effect apparently due to the C(O)O(CH$_3$) group in **2** and the Ru−Ru bond in **3**. Even though the trans effect of the carbonyl group is known to be strong, the Ru−Cl bond trans to CO in **1a** (2.439(3) Å) is clearly shorter than in **3** or in **2**.

(26) (a) Tanaka, H.; Tzeng, B.-C.; Nagao, H.; Peng, S.-H.; Tanaka, K. *Organometallics* **1992**, *11*, 3172. (b) Tanaka, H., Tzeng, B.-C.; Nagao, H.; Peng, S.-M.; Tanaka, K. *Inorg. Chem.* **1993**, *32*, 1508.
(27) Olmsted, W. N.; Margolin, Z.; Brodwell, F. G. *J. Org. Chem.* **1980**, *45*, 3295.
(28) (a) Masciocchi, N.; Moret, M.; Cairati, P.; Ragaini, F.; Sironi, A. *J. Chem. Soc., Dalton Trans.* **1993**, 471. (b) Cook, N.; Smart, L. E.; Woodward, P.; Cotton, J. D. *J. Chem. Soc., Dalton Trans.* **1979**, 1032. (c) Howard, J. A. K.; Kellet, S. C.; Woodward, P. *J. Chem. Soc., Dalton Trans.* **1975**, 332.

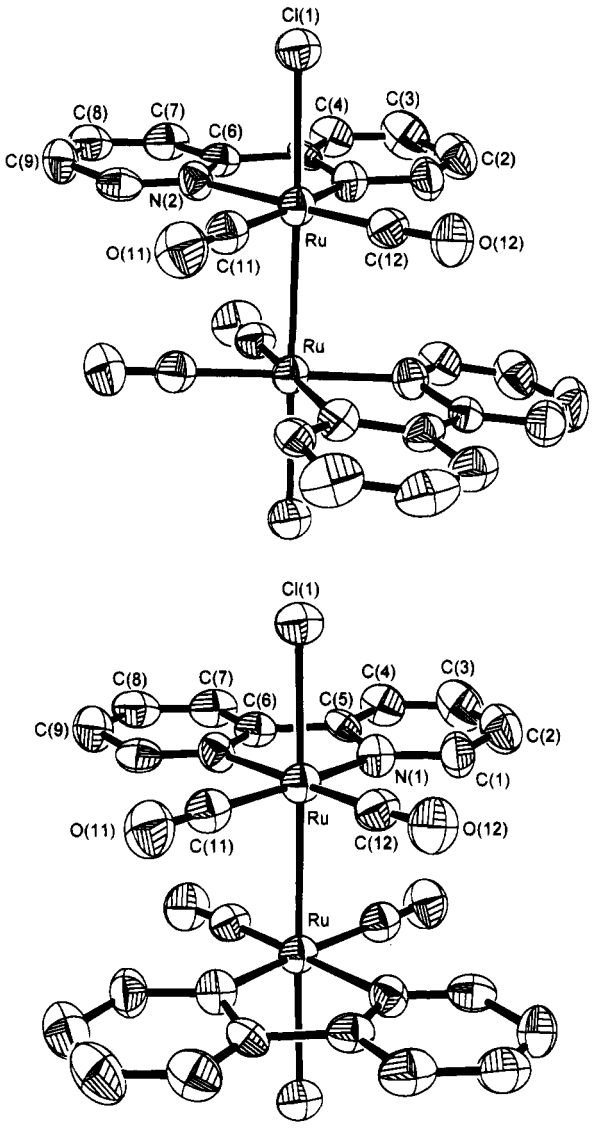

Figure 4. Structure of staggered (a, top) and "anti-eclipsed" (b, bottom) $[Ru(bpy)(CO)_2Cl]_2$ (**3**).

In addition to the microcrystalline **3**, other ruthenium carbonyl bipyridine compounds were also present in the ethylene glycol solution. After filtration of the solid **3**, a reddish yellow solution was extracted with CH_2Cl_2. In the IR spectrum of the yellow extract, typically, four strong peaks were observed at 2067, 2002, 2036, and 1965 cm^{-1} (Figure 2, spectrum **4**). The spectrum seems to consist of two components. The ratio of these components varied from a nearly pure "high-pair" component to a nearly pure "low-pair" component in separate syntheses. The higher pair, at 2067 and 2002 cm^{-1}, is probably due to $[Ru(bpy)(CO)_2Cl_2]$. The ^1H NMR spectrum revealed that both compounds **1a** and **1b** were present. The lower pair at 2036 and 1965 cm^{-1} resembles the IR spectrum reported by Kelly et al. for red-purple $[Ru(bpy)(CO)_2Cl_2]$ (2040 (s) and 1980 (s) cm^{-1} in KBr).[14] They suggested that these frequencies were due to the *cis*(CO),*cis*(Cl) isomer, which is in disagreement with our results. We crystallized the "low-pair" component (**4**) directly from ethylene glycol; the crystal structure is shown in Figure 5. N(1), N(2), Ru, C(2), and C(1) are coplanar, and the chlorine atom is above this plane. The ^1H NMR spectrum revealed the presence of the hydride ligand (δ(Ru–H) −11.3 ppm), which

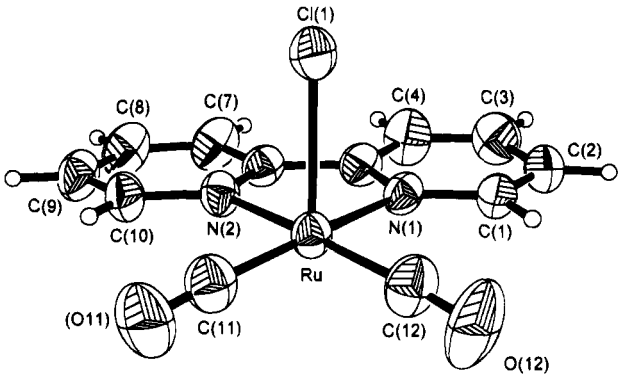

Figure 5. Structure of $[Ru(bpy)(CO)_2ClH]$ (**4**).

must occupy the axial position trans to chlorine. Unfortunately, we were not able to directly locate the hydride ligand in difference Fourier maps. The mononuclear ruthenium bis(bipyridine) compound $[Ru(bpy)_2(CO)H]^+$, with a hydride ligand, has been reported earlier by Vos et al.[2,3] (δ(Ru–H) −11.47 ppm). The axial Ru–Cl bond in **4** is again exceptionally long (2.524(3) Å) and comparable with those in **2** and **3**. Compound **4** was easily converted to **3** by refluxing, for example, in toluene. It is thus possible that **4** is an intermediate in the formation of **3**.

Glycerol was also tested as a solvent in the reaction of $[Ru(CO)_3Cl_2]_2$ and 2,2′-bipyridine. The reactions appeared to be very similar to ethylene glycol reactions.

Conversions of $[Ru(bpy)(CO)_2Cl_2]$, $[Ru(bpy)(CO)_2Cl(C(O)OCH_3)]$, $[Ru(bpy)(CO)_2Cl]_2$, and $[Ru(bpy)(CO)_2ClH]$. When **2** was treated with H_2/CO in ethylene glycol (Scheme 1g), a red precipitate was formed. According to the IR spectrum the solid product was identified as **3**. CO (or H_2/CO) treatment of **1** (Scheme 1d) did not produce considerable amounts of **3**. However, traceable amounts of **3** were observed. In principle, the formation of dimer **3** from monomers requires a substitution of the axial Cl or $C(O)OCH_3$ ligand by another $Ru(bpy)(CO)_2Cl$ unit. It is not surprising that a substitution of the $C(O)OCH_3$ group in **2** is easier than substitution of the chlorine in **1**. For example, direct carbonylation of ruthenium chlorides is known to require relatively drastic conditions. We found that it is also possible to convert dimer **3** back to either monomer **2** or **1**. When **3** was treated with CO in methanol (Scheme 1f), red crystals disappeared and a pale yellow precipitate was formed. The IR spectrum of the precipitate was identical with that of **2**.

One would expect that a treatment of **3** with a suitable chlorine source (e.g. HCl solution) would lead to formation of the *cis*(*CO*),*trans*(*Cl*)-$[Ru(bpy)(CO)_2Cl_2]$ isomer. When **3** was refluxed with concentrated HCl (Scheme 1e), a pale yellow precipitate was again formed. The product was soluble in dichloromethane, and two strong peaks found in the IR spectrum at 2065 and 2004 cm^{-1} are very close to those of $[Ru(bpy)(CO)_2Cl_2]$ obtained directly in the THF synthesis (Scheme 1a). Furthermore, the ^1H NMR spectrum was identical with that of the *cis*(CO),*trans*(Cl) isomer of $[Ru(bpy)(CO)_2Cl_2]$. The behavior of $[Ru(bpy)(CO)_2ClH]$ in HCl was similar to that of $[Ru(bpy)(CO)_2Cl]_2$. HCl treatment of the hydride at room temperature again yielded a yellow precipitate with NMR and IR spectra typical for *cis*(*CO*),*trans*(*Cl*)-$[Ru(bpy)(CO)_2Cl_2]$. $[Ru(bpy)(CO)_2ClH]$ was partially soluble in concentrated HCl, and when the

acid solution was allowed to evaporate to dryness at room temperature, a few dark red crystals were formed along with the pale yellow *cis(CO),trans(Cl)*-[Ru(bpy)-$(CO)_2Cl_2$] which was the main product. Single-crystal X-ray studies on dark red crystals showed that they were also *cis(CO),trans(Cl)*-[Ru(bpy)$(CO)_2Cl_2$],[29] but in this case in a nonsolvated form. The odd color of these crystals may arise from impurities. One of the Ru−CO bonds was longer (1.961(11) Å) than a typical ruthenium−carbonyl bond, whereas the C−O bond was too short (0.907(15) Å). Overestimation of the Ru−CO bond and underestimation of the C−O bond may be due to a coexistence of another complex where there is another ligand (for example, water) in the location of the carbonyl group. Conversion of [Ru(bpy)$(CO)_2$ClH] to [Ru(bpy)$(CO)_2Cl_2$] was also observed in chlorinated solvents such as CH_2Cl_2.

The reactions shown in Scheme 1 are related to those proposed by Ziessel et al. for electrocatalytic reduction of CO_2 with [Ru(bpy)$(CO)_2Cl_2$] catalyst.[7c,d] They found that [Ru(bpy)$(CO)_2Cl_2$] can be reduced to the dark blue polymeric [Ru(bpy)$(CO)_2]_n$ via electrolysis. A similar, dark blue and highly air-sensitive catalyst, active in WGSR[9] and hydroformylation,[8] can also be prepared from $Ru_3(CO)_{12}$ and 2,2′-bipyridine. According to Ziessel, the polymer produces the [Ru(bpy)(CO)(C(O)OH)] intermediate during the electrocatalytic cycle. In Scheme 1 we propose similar reversible reactions between the dimeric **3** and the monomeric **2** in methanol solution. Instead of changing the CO group to the C(O)OH group, as in the reduction of CO_2, methanol/CO treatment of **3** leads to the cleavage of the Ru−Ru bond and formation of the $C(O)OCH_3$ group. M−C(O)OH and M−H compounds have also been proposed as intermediates in the WGSR cycle.[4] Compounds **2** and **3** can be seen as a model compounds for these intermediates.

It has also been found that $Ru_3(CO)_{12}$ with a NEt_3Cl promoter is active in carbonylation of methanol to methyl formate.[10] Even though the compounds synthesized in our work are different, the reversible conversions between **2** and **3** may offer a possible model route for this type of catalysis.

Conclusions

Several mononuclear ruthenium bipyridine complexes can be prepared from $[Ru(CO)_3Cl_2]_2$ and 2,2′-bipyridine in alcohol or THF solutions. Almost all of these complexes are directly interconvertible under suitable conditions. [Ru(bpy)$(CO)_2$Cl(C(O)OCH_3)], [Ru(bpy)$(CO)_2$-$Cl]_2$, and [Ru(bpy)$(CO)_2$ClH] can be seen as model compounds for intermediates in WGSR and CO_2 reduction, analogous to the known ruthenium bis(bipyridine) complexes $[Ru(bpy)_2(CO)H]^+$ and [Ru$(bpy)_2$(CO)(C(O)-OCH_3)].

Experimental Section

Materials and Measurements. All reagents and solvents were p.A. grade. Alcohol solvents and concentrated HCl (37%) were obtained commercially and used without further purification. THF and CH_2Cl_2 were dried by standard methods. Syntheses were performed under an inert atmosphere. [Ru-$(CO)_3Cl_2$] was obtained from Johnsson & Matthey and 2,2′-bipyridine from Aldrich Chemicals. Gases used in conversions of [Ru(bpy)$(CO)_2Cl_2$], [Ru(bpy)$(CO)_2$Cl(C(O)OCH_3)], and [Ru-(bpy)$(CO)_2Cl]_2$ were high-purity grade CO (99%) and H_2 (99.997%). High-pressure conversion reactions were performed in a 100 mL Berghof autoclave. FTIR spectra were recorded on a Nicolet Magna-IR 750 spectrometer and NMR spectra on a Bruker AMX-400 spectrometer (400 MHz).

Preparation of [Ru(bpy)$(CO)_2Cl_2$] (1). 1 g of [(Ru$(CO)_3$-Cl_2] was dissolved in 80 mL of THF and refluxed for 2.5−3 h. A 0.75 g amount of 2,2′-bipyridine, dissolved in 20 mL of THF, was slowly added into $[Ru(CO)_3Cl_2]_2$ solution. Refluxing was continued for a further 45 min, and the solution was allowed to cool to room temperature. Approximately half of the solvent was evaporated under vacuum, and the rest was stored overnight in a refrigerator. A pale yellow precipitate (**1a**) was filtered, and the solution was transferred again to the refrigerator. After the solution stood overnight, a second precipitate (**1b**) was formed. The solid products were recrystallized from $CHCl_3$. The total yield was ca. 1 g (67%). Anal. Calcd for $C_{12}H_8N_2O_2Cl_2Ru$ (mol wt 384.18): C, 37.52; H, 2.10; N, 7.29; O, 8.33. Found for **1a**: C, 37.45; H, 2.07; N, 7.22; O, 8.47. IR (CH_2Cl_2): ν(CO) 2067(vs), 2003(vs) cm^{-1}. $^{13}C\{^1H\}$ NMR for bpy (in $CDCl_3$): δ 156.4, 156.0, 155.3, 151.0, 140.4, 139.7, 127.9, 127.5, 124.0, 123.3 ppm. $^{13}C\{^1H\}$ NMR for CO: δ 195.4, 190.4 ppm (both singlets). ^1H NMR for bpy (in $CDCl_3$): δ 9.7 (d), 8.8 (d), 8.2 (two overlapped doublets), 8.1 (t), 8.0 (t), 7.7 (t), 7.5 ppm (t). (Both NMR spectra included a variable amount of component **1b**.) Anal. Found for **1b**: C, 37.83; H, 1.95; N, 7.15; O, 8.35. IR (CH_2Cl_2): ν(CO) 2066 (vs), 2003 (vs) cm^{-1}. $^{13}C\{^1H\}$ NMR for bpy (in $CDCl_3$): δ 155.6, 153.8, 140.1, 128.0, 123.8 ppm (all singlets). $^{13}C\{^1H\}$ NMR for CO: δ 196.3 (s). ^1H NMR for bpy (in $CDCl_3$): δ 9.2 (d), 8.3 (d), 8.1 (t), 7.7 (t) ppm. (Both NMR spectra included a variable amount of component **1a**.)

Preparation of [Ru(bpy)$(CO)_2$Cl(C(O)OCH_3)] (2). A 1 g amount of $[Ru(CO)_3Cl_2]_2$ and 1.45 g of 2,2′-bipyridine were dissolved in 15 and 5 mL of methanol, respectively. The solutions were combined and refluxed for 30 min. A pale yellow precipitate was filtered and washed a few times with a small amount of methanol. The precipitate was dried under vacuum. The final yield was ca. 1.0 g (63%). Anal. Calcd for $C_{14}H_{11}N_2O_4ClRu$ (mol wt 407.78): C, 41.24; H, 2.72; N, 6.87. Found: C, 41.29; H, 2.71; N, 6.84. IR (in CH_2Cl_2): ν(CO) 2058 (vs), 1994 (vs) cm^{-1}, 1640 (br, w) cm^{-1}. $^{13}C\{^1H\}$ NMR for bpy (in $CDCl_3$): δ 155.7, 153.4, 139.6, 127.4, 123.5 ppm (all singlets). $^{13}C\{^1H\}$ NMR for C(O)OCH_3: δ 198.2, 51.9 ppm (both singlets). $^{13}C\{^1H\}$ NMR for CO: δ 193.7 ppm (s). ^1H NMR for bpy (in $CDCl_3$): δ 9.0 (d), 8.2 (d), 8.1 (t), 7.6 ppm (t). ^1H NMR for C(O)OCH_3: δ 3.4 ppm (s).

Preparation of [Ru(bpy)$(CO)_2Cl]_2$ (3) and [Ru(bpy)-$(CO)_2$ClH] (4). A 1 g amount of $[Ru(CO)_3Cl_2]_2$, 1.45 g of 2,2′-bipyridine, and 10−15 mL of ethylene glycol were placed in the reaction vessel. The mixture was heated to 90−100 °C for 1.5−2 h. The very poorly soluble red microcrystalline precipitate (**3**) was filtered and washed several times with THF and CH_2Cl_2. The final yield was ca. 0.18 g (14%). Anal. Calcd for $C_{24}H_{16}N_4O_4Cl_2Ru_2$ (mol wt 697.46): C, 41.33; H, 2.31; N, 8.03, O: 9.18. Found: C, 41.22; H, 2.28; N, 7.90, O: 9.42. IR (in KBr): ν(CO) 2019 (s), 2003 (w,m), 1980 (s, sh), 1970 (vs), 1937 (vs), 1910 (w,sh) cm^{-1}.

The ethylene glycol filtrate was allowed to stand under nitrogen at room temperature for several days. The reddish brown precipitate (**4**) was filtered, washed carefully with octanol and hexane, and dried under vacuum. The final yield was ca. 0.13 g (10%). Anal. Calcd for $C_{12}H_9N_2O_2ClRu$ (mol wt 349.74): C, 41.21; H, 2.59; N, 8.01; O, 9.15. Found: C, 41.15; H, 2.42; N, 8.02; O, 9.14. IR (in CH_2Cl_2): ν(CO) 2035 (vs), 1966 (vs) cm^{-1}. ^1H NMR for bpy (in $CDCl_3$): δ 9.0 (d),

(29) Crystal data for *cis*(CO),*trans*(Cl)-[Ru(bpy)$(CO)_2Cl_2$]: M_r 384.18, monoclinic, space group $P2_1/n$, a = 8.19 (4) Å, b = 16.253(7) Å, c = 10.463(5) Å, β =101.54(4)°, V = 1336.1(12) Å^3, Z = 4, D_{calc} = 1.868 g/cm^3, crystal source HCl, crystal size 0.1 × 0.2 × 0.2 mm, dark red, Mo Kα radiation (λ = 0.709 34 Å, 2θ limits 5−50°, no. of unique reflections 2430, no. of observed data 1307, no. of parameters 172, μ = 1.517 mm^{-1}, R = 0.0515, R_w = 0.0473, GOF = 1.05. Complete structural data are available as supplementary material.

Table 1. Crystallographic Data for *cis*(CO),*cis*(Cl)-[Ru(bpy)(CO)$_2$Cl$_2$] (1a), *cis*(CO),*trans*(Cl)-[Ru(bpy)(CO)$_2$Cl$_2$]·CH$_2$Cl$_2$ (1b), [Ru(bpy)(CO)$_2$Cl(C(O)OCH$_3$)] (2), [Ru(bpy)(CO)$_2$Cl]$_2$ (3), and [Ru(bpy)(CO)$_2$ClH] (4)

	1a	1b	2	3	4
fw	384.18	469.12	407.78	697.46	349.74
cryst syst	orthorhombic	triclinic	monoclinic	monoclinic	triclinic
space group	*Pbca*	$P\bar{1}$	$P2_1/m$	$C2/m$	$P\bar{1}$
a, Å	12.709(4)	6.536(4)	7.751(4)	12.681(5)	6.407(3)
b, Å	11.532(5)	12.557(7)	11.863(7)	10.165(3)	8.135(5)
c, Å	18.852(5)	12.595(9)	9.081(6)	10.633(4)	12.707(8)
α, deg	90	119.81(4)	90	90	89.39(5)
β, deg	90	93.94(6)	107.18(4)	114.01(3)	81.56(5)
γ, deg	90	98.11(4)	90	90	81.53(4)
V, Å^3	2763(2)	876.3(9)	798(2)	1252.0(9)	647.4(3)
Z	8	2	2	2	2
D_{calc}, g/cm^3	1.847	1.778	1.697	1.850	1.797
cryst source	dichloromethane	dichloromethane	methanol	ethylene glycol	ethylene glycol
cryst size, mm	0.3 × 0.4 × 0.4	0.1 × 0.2 × 0.3	0.2 × 0.3 × 0.3	0.1 × 0.2 × 0.3	0.1 × 0.2 × 0.4
color	brownish yellow	pale yellow	pale yellow	red	reddish brown
radiation	Mo Kα	Mo Kα	Mo Kα	Mo Kα	Mo Kα
μ, mm^{-1}	1.501	1.498	1.148	1.437	1.389
2θ limits, deg	5–60	5–50	4–50	4–60	5–55
h range	0–16	0–7	0–9	0–17	0–8
k range	0–14	−14 to +14	0–14	0–14	-10 to +10
l range	0–24	−14 to +14	−10 to +10	−14 to +13	−16 to +16
no. of unique rflns	3148	3098	1459	1936	3006
no. of obsd data[a]	1465	1888	843	1393	2321
no. of params	172	199	109	157	163
R[b]	0.0566	0.0737	0.0524	0.0350	0.0539
R_w[c]	0.0545	0.0896	0.0498	0.0341	0.0609
goodness of fit	1.24	1.75	1.15	1.05	1.03

[a] $I \geq 2\sigma(I)$. [b] $R = \Sigma(|F_o| - |F_c|)/\Sigma(|F_o|)$. [c] $R_w = [\Sigma(|F_o| - |F_c|)^2/\Sigma w|F_o|^2]^{1/2}$; $w = 1/(\sigma^2 F + 0.0005F^2)$.

Table 2. Atomic Coordinates (×10^4) and Temperature Factors (Å^2 × 10^3) for *cis*(CO),*cis*(Cl)-[Ru(bpy)(CO)$_2$Cl$_2$] (1a)

atom	*x*	*y*	*z*	*U*[a]
Ru	5178(1)	2011(1)	3214(1)	41(1)
Cl(1)	4720(2)	2972(3)	4324(1)	53(1)
Cl(2)	3733(2)	2915(4)	2596(2)	80(1)
O(11)	6422(7)	4156(7)	2858(5)	71(3)
O(31)	5653(7)	995(8)	1818(6)	87(4)
N(1)	4307(6)	576(8)	3595(4)	44(3)
N(2)	6320(6)	1058(7)	3757(4)	41(3)
C(1)	3253(8)	450(11)	3521(6)	56(4)
C(2)	2730(9)	−503(12)	3783(6)	64(5)
C(3)	3295(10)	−1369(12)	4112(6)	64(5)
C(4)	4365(9)	−1257(9)	4212(6)	56(4)
C(5)	4853(8)	−246(9)	3953(5)	41(3)
C(6)	5989(8)	42(9)	4049(5)	44(4)
C(7)	6672(9)	−689(9)	4420(6)	51(4)
C(8)	7708(9)	−367(11)	4493(6)	64(5)
C(9)	8043(9)	659(12)	4208(6)	62(5)
C(10)	7333(8)	1347(10)	3843(5)	49(4)
C(11)	5995(9)	3332(10)	2969(6)	48(4)
C(31)	5524(8)	1272(11)	2320(5)	42(4)

[a] Equivalent isotropic *U*, defined as one-third of the trace of the orthogonalized $\mathbf{U}_{ij}$ tensor.

Table 3. Atomic Coordinates (×10^4) and Temperature Factors (Å^2 × 10^3) for *cis*(CO),*trans*(Cl)-[Ru(bpy)(CO)$_2$Cl$_2$]·CH$_2$Cl$_2$ (1b)

atom	*x*	*y*	*z*	*U*[a]
Ru	3212(2)	3632(1)	1938(1)	41(1)
Cl(1)	1079(6)	1963(4)	2008(3)	58(2)
Cl(3)	5387(6)	5203(3)	1742(4)	58(2)
Cl(5)	−180(11)	1431(6)	4857(6)	130(4)
Cl(4)	4134(13)	1458(10)	5051(7)	210(7)
O(12)	936(20)	5455(12)	3715(11)	98(8)
O(11)	6309(20)	4088(13)	4031(11)	104(8)
N(1)	1161(16)	3214(10)	350(10)	40(6)
N(2)	4427(15)	2254(9)	483(9)	34(5)
C(1)	−466(20)	3748(12)	320(13)	44(7)
C(2)	−1655(22)	3509(14)	−717(14)	52(8)
C(3)	−1176(23)	2645(16)	−1838(17)	67(11
C(4)	494(24)	2070(15)	−1852(14)	64(9)
C(5)	1606(21)	2365(13)	−754(13)	47(7)
C(6)	3404(20)	1797(12)	−674(12)	41(7)
C(7)	3994(24)	830(13)	−1679(14)	56(8)
C(8)	5680(23)	347(14)	−1537(14)	58(8)
C(9)	6751(21)	829(12)	−384(14)	49(8)
C(10)	6135(19)	1776(12)	598(13)	42(7)
C(12)	1832(26)	4781(15)	3051(14)	61(9)
C(11)	5140(24)	3904(15)	3222(14)	60(9)
C(45)	2239(28)	2315(17)	5102(16)	80(11)

[a] Equivalent isotropic *U*, defined as one-third of the trace of the orthogonalized $\mathbf{U}_{ij}$ tensor. Population parameter for all atoms is 0.5.

8.1 (d), 8.0 (t), 7.5 ppm (t) (signals of **1a** and **1b** were also occasionally found). ^{1}H NMR for H: δ −11.3 ppm (s).

Reactions of [Ru(CO)$_3$Cl$_2$]$_2$ and 2,2′-Bipyridine in Ethanol, 2-Propanol, and 1-Heptanol. In a typical experiment 500 mg of [Ru(CO)$_3$Cl$_2$]$_2$ and 675 mg of 2,2′-bipyridine were weighed into a 100 mL reaction vessel. A 10–20 mL amount of alcohol was added, and the mixture was deoxygenated. In the ethanol and 2-propanol reactions the mixture was refluxed for 30–45 min, and in the 1-heptanol reaction the mixture was heated to 100 °C for 1h. The reaction mixture was cooled slowly to room temperature, and the yellow precipitate was filtered. The precipitates were washed a few times with small amounts of THF and dried under vacuum. The products (**1a** and **1b**) were identified by IR and ^{1}H NMR spectroscopy and elemental analysis.

Conversions of [Ru(bpy)(CO)$_2$Cl$_2$], [Ru(bpy)(CO)$_2$Cl(C(O)OCH$_3$)], and [Ru(bpy)(CO)$_2$Cl]$_2$ in Alcohol and Acid Solutions. Conversions of [Ru(bpy)(CO)$_2$Cl$_2$] or [Ru(bpy)(CO)$_2$Cl(C(O)OCH$_3$)] monomers to the [Ru(bpy)(CO)$_2$Cl]$_2$ dimer were carried out in the 100 mL Berghof autoclave with a Teflon liner. The ruthenium monomer (100 mg) was placed in the autoclave in a nitrogen box. 1.5 mL of deoxygenated ethylene glycol, 25 bar of H$_2$, and 25 bar of CO or 50 bar of pure CO were introduced into the autoclave. The autoclave was heated to 150 °C, and the temperature was maintained for 17 h. The red [Ru(bpy)(CO)$_2$Cl]$_2$ precipitate was filtered and washed with THF and dichloromethane.

Reaction of 50 mg of [Ru(bpy)(CO)$_2$Cl]$_2$ with 5 mL of methanol under CO was carried out under conditions similar to those above. Conversion of [Ru(bpy)(CO)$_2$Cl]$_2$ to [Ru(bpy)(CO)$_2$Cl$_2$] was carried out either by refluxing [Ru(bpy)(CO)$_2$Cl]$_2$ with concentrated HCl (37%) or by treating [Ru(bpy)-

Table 4. Atomic Coordinates (×10⁴) and Temperature Factors (Å² × 10³) for [Ru(bpy)(CO)₂Cl(COOCH₃)] (2)

atom	x	y	z	U[a]
Ru	6258(2)	2500	1816(1)	46(1)
Cl(1)	8265(4)	2500	4530(3)	49(1)
O(11)	8434(12)	728(9)	767(9)	120(5)
O(31)	4682(14)	2500	−1548(11)	107(6)
O(32)	2772(16)	2500	−304(11)	151(8)
N(1)	4579(10)	3607(7)	2604(7)	48(3)
C(1)	4621(14)	4739(10)	2570(10)	61(4)
C(2)	3519(16)	5415(8)	3112(11)	66(4)
C(3)	2352(15)	4936(9)	3775(11)	68(5)
C(4)	2281(11)	3755(10)	3831(9)	59(4)
C(5)	3412(11)	3116(7)	3246(8)	44(3)
C(11)	7598(14)	1411(11)	1168(10)	72(5)
C(31)	4438(19)	2500	−330(15)	53(6)
C(32)	1340(24)	2500	−1666(17)	154(13)

[a] Equivalent isotropic U, defined as one-third of the trace of the orthogonalized $\mathbf{U}_{ij}$ tensor.

Table 5. Atomic Coordinates (×10⁴) and Temperature Factors (Å² × 10³) for [Ru(bpy)(CO)₂Cl]₂ (3)

atom	x	y	z	U[a]
Ru	4056(1)	0	3675(1)	38(1)
Cl(1)	2474(1)	0	1292(1)	51(1)
O(11)	3600(5)	−2856(6)	4349(6)	66(3)
O(12)	2515(5)	839(6)	5017(6)	64(2)
N(1)	4520(5)	1776(6)	3163(6)	43(2)
N(2)	5157(5)	−588(6)	2647(6)	41(2)
C(1)	4123(6)	2948(7)	3390(8)	51(3)
C(2)	4345(7)	4123(8)	2902(9)	64(4)
C(3)	5006(8)	4090(9)	2139(10)	73(4)
C(4)	5413(7)	2915(9)	1884(8)	57(3)
C(5)	5125(10)	1826(23)	2334(23)	34(4)
C(6)	5525(5)	444(7)	2144(6)	43(3)
C(7)	6222(6)	226(35)	1404(7)	54(8)
C(8)	6496(7)	−1031(11)	1204(8)	59(3)
C(9)	6090(7)	−2088(9)	1697(8)	61(3)
C(10)	5462(10)	−1759(26)	2479(24)	43(5)
C(11)	3769(6)	−1801(8)	4095(7)	46(3)
C(12)	3128(5)	487(7)	4521(6)	45(2)

[a] Equivalent isotropic U defined as one-third of the trace of the orthogonalized $\mathbf{U}_{ij}$ tensor. Population parameter for all atoms is 0.5.

Table 6. Atomic Coordinates (×10⁴) and Temperature Factors (Å² × 10³) for [Ru(bpy)(CO)₂ClH] (4)

atom	x	y	z	U[a]
Ru	1322(1)	1329(1)	3119(1)	38(1)
Cl(1)	−432(2)	2428(2)	1548(1)	46(1)
N(2)	−252(7)	−777(6)	3056(4)	40(1)
N(1)	3472(7)	−270(6)	2019(4)	38(1)
O(12)	4096(9)	3934(8)	3289(6)	95(3)
O(11)	−1774(9)	3174(8)	4880(5)	78(2)
C(12)	3043(11)	2964(9)	3194(6)	58(2)
C(11)	−641(11)	2493(8)	4192(6)	53(2)
C(10)	−2165(10)	−956(8)	3630(5)	50(2)
C(9)	−3060(11)	−2397(9)	3587(6)	57(2)
C(8)	−1988(11)	−3672(8)	2927(7)	61(3)
C(7)	−75(11)	−3481(8)	2313(6)	56(2)
C(6)	789(9)	−2030(7)	2396(5)	41(2)
C(5)	2848(9)	−1723(7)	1804(5)	43(2)
C(4)	4087(11)	−2846(9)	1074(6)	60(2)
C(3)	6020(12)	−2483(10)	554(6)	62(2)
C(2)	6687(10)	−1021(9)	798(5)	52(2)
C(1)	5376(9)	55(8)	1520(5)	45(2)

[a] Equivalent isotropic U defined as one-third of the trace of the orthogonalized $\mathbf{U}_{ij}$ tensor.

$(CO)_2Cl_2$] with HCl in an autoclave using elevated temperature (200 °C for 2 h). The solid products were identified with IR spectroscopy and elemental analysis.

X-ray Data Collection and Structure Solution for *cis*(CO),*cis*(Cl)-[Ru(bpy)(CO)₂Cl₂] (1a), *cis*(CO),*trans*(Cl)-[Ru(bpy)(CO)₂Cl₂]·CH₂Cl₂ (1b), [Ru(bpy)(CO)₂Cl(C(O)OCH₃)] (2), [Ru(bpy)(CO)₂Cl]₂ (3), and [Ru(bpy)(CO)₂ClH] (4). Suitable crystals of **1a**, **2**, **3**, and **4** were mounted on a glass fiber, whereas a crystal of **1b** was sealed into the glass capillary to prevent decomposition. Data were collected at 20 °C on a Nicolet R3m diffractometer using the ω-scan data collection mode and Mo Kα radiation (λ = 0.710 73 Å, graphite monochromatized). Accurate cell parameters were obtained from 25 automatically centered reflections. Intensities were corrected for background, polarization, and Lorentz factors. Absorption correction was made from ψ-scan data for **3**, the maximum and minimum transmission factors being 0.3764 and 0.4365, respectively. All structures were refined in centrosymmetric space groups, which led to satisfactory results. Originally, structure **2** was solved in space group $P2_1$ and structure **3** in space group $C2$. However, in both cases the refinement of the structures in these space groups led to unsatisfactory results. Moreover, in **3** disorder was found in space group $C2$ equal to that in $C2/m$. The refinement of **3** did not succeed at all in space group Cm. In structure **2** the

Table 7. Selected Bond Lengths (Å) for *cis*(CO),*cis*(Cl)-[Ru(bpy)(CO)₂Cl₂] (1a), *cis*(CO),*trans*(Cl)-[Ru(bpy)(CO)₂Cl₂]·CH₂Cl₂ (1b), [Ru(bpy)(CO)₂Cl(COOCH₃)] (2), [Ru(bpy)(CO)₂Cl]₂ (3), and [Ru(bpy)(CO)₂ClH] (4)

	1a	1b	2	3	4
Ru−Cl(1)	2.439(3)	2.391(5)	2.496(3)	2.512(1)	2.524(2)
Ru−Cl(2)[a]	2.411(4)	2.390(5)			
Ru−N(1)	2.117(8)	2.112(12)	2.117(8)	2.040(6)	2.118(4)
Ru−N(2)	2.090(8)	2.102(9)	2.179(7)	2.120(5)	
Ru−C(11)	1.899(11)	1.835(17)	1.859(13)	1.953(8)	1.874(6)
Ru−C(12)	1.841(16)	1.817(8)	1.860(8)		
Ru−C(31)	1.938(10)	2.041(12)			
C(11)−O(11)	1.115(14)	1.133(22)	1.161(16)	1.148(10)	1.142(8)
C(12)−O(12)	1.123(20)	1.159(11)	1.130(10)		
C(31)−O(31)	1.012(15)	1.175(18)			
C(31)−O(32)	1.299(20)				
O(32)−C(32)	1.397(17)				
Ru−Ru	2.860(1)				

[a] Cl(2) = Cl(3) for **1b**.

Table 8. Selected Bond Angles (deg) for *cis*(CO),*cis*(Cl)-[Ru(bpy)(CO)₂Cl₂] (1a), *cis*(CO),*trans*(Cl)-[Ru(bpy)(CO)₂Cl₂]·CH₂Cl₂ (1b), [Ru(bpy)(CO)₂Cl(COOCH₃)] (2), [Ru(bpy)(CO)₂Cl]₂ (3), and [Ru(bpy)(CO)₂ClH] (4)

	1a	1b	2	3	4
Cl(1)−Ru−Cl(2)[b]	92.1(1)	176.3(1)			
Cl(1)−Ru−N(1)	86.5(2)	89.4(4)	86.1(2)	86.0(1)	86.6(1)
Cl(1)−Ru−N(2)	89.1(2)	87.3(3)	84.6(1)	87.3(1)	
Cl(1)−Ru−C(11)	88.5(3)	91.0(6)	94.0(3)	94.8(2)	97.9(2)
Cl(1)−Ru−C(12)	95.0(2)	98.4(2)			
Cl(1)−Ru−C(31)	178.8(3)	175.2(5)			
N(1)−Ru−Cl(2)[b]	96.0(2)	88.9(4)			
N(1)−Ru−N(2)[a]	77.6(3)	77.2(4)	76.6(5)	78.2(2)	77.0(2)
N(1)−Ru−C(11)	174.1(4)	174.8(6)	174.3(5)	172.3(3)	172.5(2)
N(1)−Ru−C(12)[a]	95.0(6)	97.7(5)	101.9(3)	97.5(2)	
N(1)−Ru−C(31)	94.0(4)	90.1(4)			
N(2)−Ru−Cl(2)[b]	89.1(2)	89.2(3)			
N(2)−Ru−C(11)	99.3(4)	97.6(6)	94.3(3)	97.2(3)	
N(2)−Ru−C(12)	172.1(6)	179.6(2)	171.9(2)		
N(2)−Ru−C(31)	92.1(4)				
C(11)−Ru−Cl(2)[b]	88.5(3)				
C(11)−Ru−C(12)[a]	90.2(7)	88.0(8)	85.6(3)	87.8(3)	
C(11)−Ru−C(31)	91.0(5)	89.5(4)			
C(12)−Ru−C(31)					
Ru−C(11)−O(11)	174.5(10)	178.6(15)	179.7(8)	179.6(8)	176.7(7)
Ru−C(12)−O(12)	177.9(13)	177.0(6)	176.7(7)		
Ru−C(31)−O(31)	171.1(11)	129.8(11)			
Ru−C(31)−O(32)	113.2(10)				
C(31)−O(32)−C(32)	117.0(11)				
Ru−Ru(A)−Cl(1)	177.0(1)				

[a] N(2) = N(1a) and C(12) = C(11a) for (**2**). [b] Cl(2) = Cl(3) for (**1b**).

(30) Sheldrick, G. M. *SHELXTL PLUS*, release 4.11/V; Siemens Analytical X-ray Instruments: Madison, WI, 1990.

anisotropic thermal parameters of O(11), O(31), O(32), and C(32) remained large in the final refinement because of the displacement of the atoms perpendicular to the mirror plane (Figure 3). However, no disorder across the mirror plane was observed. After final refinement of structure **3**, all atoms not located in the mirror plane were found in two positions with equal occupation parameters (0.5), due to disorder. When both possible atom positions were chosen separately, two rotamers were obtained, as shown in parts a and b of Figure 4. The structures of **1a** and **3** were solved by direct methods and those of **2** and **4** by Patterson synthesis with subsequent Fourier synthesis with use of the SHELXTL program package.[30] All non-hydrogen atoms were refined anisotropically. Aromatic hydrogens were placed in idealized positions (C–H = 0.96 Å, U = 0.08 Å^2) and not refined. Crystallographic data are summarized in Table 1.

Supplementary Material Available: Tables of bond lengths and angles, anisotropic displacement coefficients, and H-atom coordinates for **1a**,**b** and **2**–**4**, tables of crystallographic data, atomic coordinates, bond lengths and angles, and anisotropic displacement coefficients for [Ru(bpy)(CO)$_2$Cl$_2$]·CHCl$_3$, [Ru(bpy)(CO)$_2$Cl$_2$]·CH$_2$Cl$_2$, and [Ru(bpy)(CO)$_2$Cl$_2$], and figures giving the structures of **1b** and the last three compounds mentioned (26 pages). Ordering information is given on any current masthead page.

OM9403636

Triple-Decker Complexes. 11.[1] Triple-Decker Complexes as Intermediates in Cyclopentadienyl Transfer Reactions: Stereospecific Transfer of Isodicyclopentadienyl Ligands from Ruthenium to Rhodium†

Gerhard E. Herberich* and Ursula J. Jansen

Institut für Anorganische Chemie, Technische Hochschule Aachen, D-52056 Aachen, Germany

Received January 13, 1994®

The two diastereomers Cp*Ru(Idcp) (*exo*-**8** and *endo*-**8**; Idcp = tricyclo[5.2.1.0^{2,6}]deca-3,5-dien-2-yl) were synthesized from $(Cp^*RuCl)_4$ and Li(Idcp) in THF, and *exo*-[Cp*Rh(Idcp)]-PF_6 (*exo*-**9**(PF_6)) was obtained from $[Cp^*Rh(OCMe_2)_3](BF_4)_2$ and tricyclo[5.2.1.0^{2,6}]deca-2,5-diene (IdcpH) in acetone. The structures of *exo*-**8** and *exo*-**9**(PF_6) were determined by X-ray diffraction. The ruthenocene derivatives **8** establish an isomerization equilibrium in the presence of a catalytic trace of $[Cp^*Ru(\mu\text{-}Cp)RuCp^*]CF_3SO_3$ or of other sources of metallo-electrophiles $[Cp^*Ru(solv)_3]^+$ (solv = Me_2CO, MeCN); above −40 °C *endo*-**8** is transformed into *exo*-**8**. Both isomers react with $[Cp^*Rh(OCMe_2)_3]^{2+}$ in acetone to undergo an Idcp transfer reaction, thereby forming *endo*-**9**$^+$ with small admixtures of *exo*-**9**$^+$ and $[Cp^*Ru(OCMe_2)_3]^+$ (**7**$^+$). In the presence of naphthalene as quenching agent for **7**$^+$, *exo*-**8** gives *endo*-**9**$^+$ and *endo*-**8** gives *exo*-**9**$^+$ with 100% stereoselectivity in both cases. Hence, the Idcp transfer reaction from Ru to Rh is stereospecific. The hypothetical triple-decker complexes $[Cp^*Ru(\mu\text{-Idcp})RuCp^*]^+$ (**11**$^+$) and $[Cp^*Ru(\mu\text{-Idcp})RhCp^*]^{2+}$ (**12a**$^{2+}$ and **12b**$^{2+}$) are proposed as reaction intermediates for the isomerization and for the Idcp transfer reactions, respectively.

Introduction

Ring ligand transfer reactions involve the transfer of a conjugated ring ligand from one metal center to another.[3] Among the earliest examples are the formation of the dinuclear complex $CpNi(\mu\text{-}CO)_2Fe(CO)Cp$-(*Fe–Ni*) from $NiCp_2/Fe(CO)_5$[4] and the synthesis of $Fe(CO)_3(C_4Ph_4)$ from $[PdBr_2(C_4Ph_4)]_2/Fe(CO)_5$.[5a] Work by Maitlis et al. on cyclobutadiene transfer reactions impressively demonstrated the synthetic value of these reactions.[5]

Very little is known about mechanisms of ring ligand transfer reactions. In principle three *types* of mechanisms may be envisaged (Scheme 1). In the dissociative–associative mechanism **A** the ring ligand L_R will first dissociate from the starting complex LML_R and then add to another complex fragment M′L′ to form $L'M'L_R$; this type of mechanism will be favorable for ligands such as benzene which are stable in the free state. For ligands such as cyclobutadiene which are unstable or nonexistent in the free state associative mechanisms will be more feasible. The two fragments ML and M′L′ could then be attached to the same side of the bridging ligand L_R, that is in a synfacial orientation (**B**) with respect to the ring ligand L_R; alternatively they could be attached to opposite sides, that is in an antifacial disposition (**C**).

Ligands L_R with enantiotopic faces or with diastereotopic faces are capable of facial differentiation and hence can be used to distinguish between these three situations. In the dissociative mechanism **A** the stereochemical information of the starting complex will be lost during the transfer of L_R, while mechanisms of type **B** or **C** will be stereospecific and imply a specific transfer of the stereochemical information.

In this paper we wish to prove rigorously that the transfer of cyclopentadienyl ligands may take place via triple-decker intermediates with a bridging cyclopentadienyl ligand, that is by a mechanism of type **C**. As a suitable cyclopentadienyl ligand with two different faces we shall use the isodicyclopentadienyl system **1** (tricyclo[5.2.1.0^{2,6}]deca-3,5-dien-2-yl ≡ Idcp) with its diastereotopic exo and endo faces.

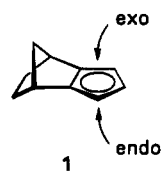

1

The Model System

A suitable model system can be chosen on the basis of our previous work on triple-decker complexes with unsubstituted bridging cyclopentadienyl ligands and

† Dedicated to Professor Helmut Werner on the occasion of his 60th birthday.

® Abstract published in *Advance ACS Abstracts*, November 15, 1994.

(1) Part 10: See ref 2.

(2) Herberich, G. E.; Englert, U.; Pubanz, D. *J. Organomet. Chem.* **1993**, *459*, 1.

(3) Rubezhov, A. Z.; Gubin, S. P. *Adv. Organomet. Chem.* **1972**, *10*, 347. Werner, H. *Fortschr. Chem. Forsch.* **1972**, *28*, 141. Efraty, A. *J. Organomet. Chem.* **1973**, *57*, 1. Garrou, P. E. *Adv. Organomet. Chem.* **1984**, *23*, 95.

(4) Tilney-Bassett, J. F. *J. Chem. Soc.* **1963**, 4784.

(5) (a) Maitlis, P. M.; Games, M. L. *J. Am. Chem. Soc.* **1963**, *85*, 1887. (b) Maitlis, P. M. *Adv. Organomet. Chem.* **1966**, *4*, 95.

0276-7333/95/2314-0834$09.00/0

Scheme 1

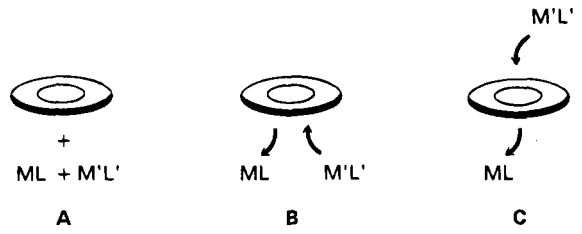

Scheme 2

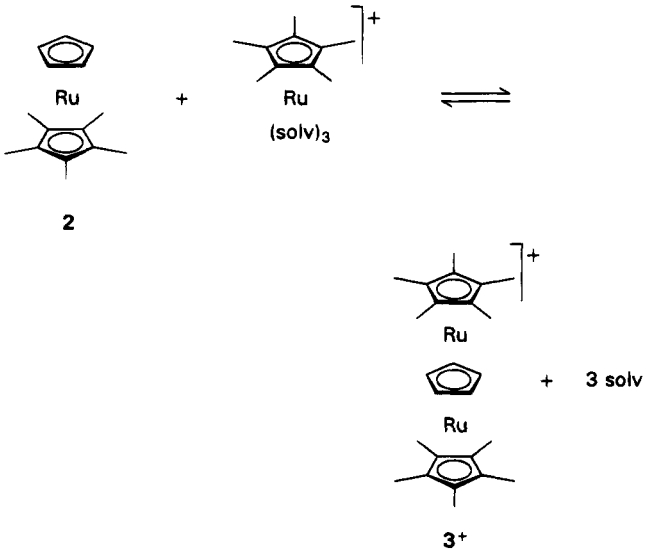

solv = MeCN, Me_2CO, $MeNO_2$

related cyclopentadienyl transfer reactions.[6] Pentamethylruthenocene (**2**) adds metalloelectrophiles $[Cp^*Ru(solv)_3]^+$ (solv = MeCN, Me_2CO, $MeNO_2$)[7] to form the $RuRu^+$ triple-decker cation $\mathbf{3}^+$ in an equilibrium reaction (Scheme 2). The triple-decker salt $\mathbf{3}(CF_3SO_3)(THF)$ has been isolated and structurally characterized.[6]

With the metalloelectrophile $[Cp^*Rh(OCMe_2)_3]^{2+}$ ($\mathbf{4}^{2+}$)[9] the ruthenocene **2** undergoes a smooth cyclopentadienyl transfer reaction to give the pentamethylrhodocenium cation ($\mathbf{5}^+$) and the triple-decker cation $\mathbf{3}^+$ in a complex reaction sequence.[6] As a working hypothesis we assume that three reactions are involved (Scheme 3). First the ruthenocene **2** undergoes an electrophilic stacking reaction to form the hypothetical $RuRh^{2+}$ triple-decker species $\mathbf{6}^{2+}$. Subsequent nucleophilic degradation of $\mathbf{6}^{2+}$ produces the rhodocenium cation $\mathbf{5}^+$ and the ruthenium electrophile $[Cp^*Ru(OCMe_2)_3]^+$ ($\mathbf{7}^+$). Finally $\mathbf{7}^+$ adds to a second equivalent of **2** to give the $RuRu^+$ triple-decker cation $\mathbf{3}^+$ as already described in Scheme 2. It should be kept in mind that neither intermediate $\mathbf{6}^{2+}$ nor $\mathbf{7}^+$ could be seen in the pertinent NMR tube experiments.[6]

In the following the unsubstituted cyclopentadienyl ligand of the starting ruthenocene complex **2** is replaced with the Idcp ligand **1**. Both reaction systems mentioned above are clean and do not produce paramagnetic

(6) Herberich, G. E.; Englert, U.; Marken, F.; Hofmann, P. *Organometallics* **1993**, *12*, 4039.

(7) $[Cp^*Ru(NCMe)_3]^+$ has been well characterized.[8] For the less tightly bound ligands solv = Me_2CO, $MeNO_2$ the number of ligands is only assumed from analogy.

(8) Schrenk, J. L.; McNair, A. M.; McCormick, F. B.; Mann, K. R. *Inorg. Chem.* **1986**, *25*, 3501.

(9) White, C.; Thompson, S. J.; Maitlis, P. M. *J. Chem. Soc., Dalton Trans.* **1977**, 1654.

Scheme 3

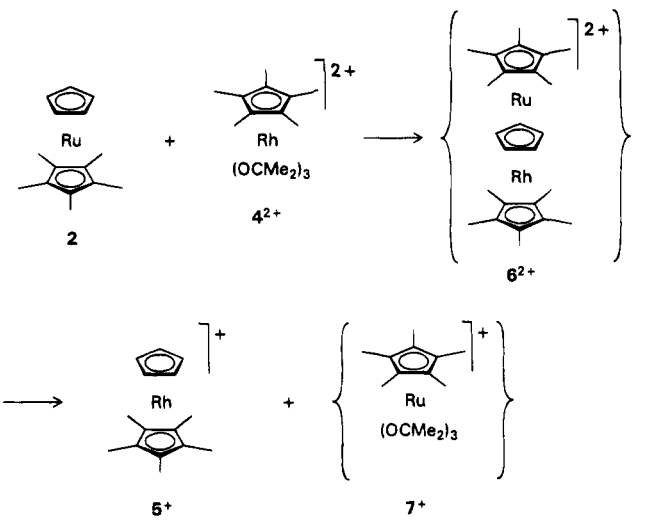

impurities. Thus, ^1H NMR spectroscopy can be used as a practical analytical tool in the study of the model system.

Results

Syntheses of the Cp*Ru(Idcp) Isomers and of *exo*-[Cp*Rh(Idcp)]PF_6. Numerous complexes of the Idcp ligand **1** are known.[10] The usual starting point in this chemistry is the synthesis of isodicyclopentadiene[11] and the lithiation of the olefin to give the lithio derivative Li(**1**).[12]

When $(Cp^*RuCl)_4$[13] is treated with Li(**1**) in THF, a mixture of the two stereoisomers *exo*-**8** and *endo*-**8** is obtained in good yield (Scheme 4). The product ratio is temperature-dependent. Higher temperatures favor the formation of *exo*-**8**, while at lower temperatures increasing amounts of *endo*-**8** are obtained; the ratio *exo*-**8**/*endo*-**8** observed was 5:1 at a reaction temperature of 65 °C and 3:1 at 0 °C. A similar dependence has been observed for the synthesis of $Cp(Idcp)TiCl_2$ derivatives[10f] and has been traced back to an exo-monomer/exo-dimer equilibrium for Li(**1**).[14] The exo dimer of Li(**1**) which

(10) (a) Ti, Zr, Hf: Gallucci, J. C.; Gautheron, B.; Gugelchuk, M.; Meunier, P.; Paquette, L. A. *Organometallics* **1987**, *6*, 15. Bhide, V. V.; Rinaldi, P. L.; Farona, M. F. *Organometallics* **1990**, *9*, 123. Sornay, C.; Meunier, P.; Gautheron, B.; O'Doherty, G. A.; Paquette, L. A. *Organometallics* **1991**, *10*, 2082. (b) V, Cr, Co, Ni: Scroggins, W. T.; Rettig, M. F.; Wing, R. M. *Inorg. Chem.* **1976**, *15*, 1381. Köhler, F. H. *J. Organomet. Chem.* **1976**, *110*, 235. (c) Cr, Mo, W: Paquette, L. A.; Hathaway, S. J.; Schirch, P. F. T.; Gallucci, J. C. *Organometallics* **1986**, *5*, 500. (d) Fe: Riemschneider, R. *Z. Naturforsch.* **1962**, *17B*, 113. Katz, T. J.; Mrowca, J. J. *J. Am. Chem. Soc.* **1967**, *89*, 1105. Hsu, L.-Y.; Hathaway, S. J.; Paquette, L. A. *Tetrahedron Lett.* **1984**, *25*, 259. Bhide, V.; Rinaldi, P.; Farona, M. F. *J. Organomet. Chem.* **1989**, *376*, 91. Gallucci, J. C.; Opromolla, G.; Paquette, L. A.; Pardi, L.; Schirch, P. F. T.; Sivik, M. R.; Zanello, P. *Inorg. Chem.* **1993**, *32*, 2292. (e) Fe, Ru, Os: Paquette, L. A.; Schirch, P. F. T.; Hathaway, S. J.; Hsu, L.-Y.; Gallucci, J. C. *Organometallics* **1986**, *5*, 490. (f) Paquette, L. A.; Moriarty, K. J.; Meunier, P.; Gautheron, B.; Crocq, V. *Organometallics* **1988**, *7*, 1873. (g) Paquette, L. A.; Moriarty, K. J.; Meunier, P.; Gautheron, B.; Sornay, C.; Rogers, R. D.; Rheingold, A. L. *Organometallics* **1989**, *8*, 2159.

(11) (a) Alder, K.; Flock, F. H.; Janssen, P. *Chem. Ber.* **1956**, *89*, 2689. (b) Katz, T. J.; Rosenberger, M.; O'Hara, R. K. *J. Am. Chem. Soc.* **1964**, *86*, 249. (c) Rosenblum, M. *J. Am. Chem. Soc.* **1957**, *79*, 3179. (d) Cookson, R. C.; Isaacs, N. S.; Szelke, M. *Tetrahedron* **1964**, *20*, 717.

(12) Bartlett, P. D.; Wu, C. *J. Am. Chem. Soc.* **1983**, *105*, 100.

(13) Fagan, P. J.; Ward, M. D.; Caspar, J. V.; Calabrese, J. C.; Krusic, P. J. *J. Am. Chem. Soc.* **1988**, *110*, 2981. Fagan, P. J.; Mahoney, W. S.; Calabrese, J. C.; Williams, I. D. *Organometallics* **1990**, *9*, 1843.

Scheme 4

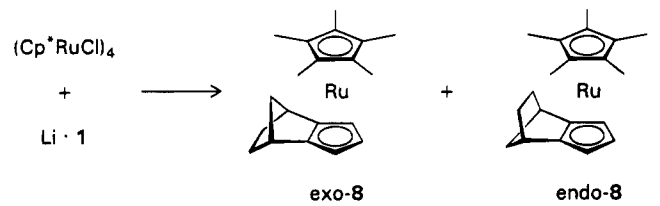

Scheme 5

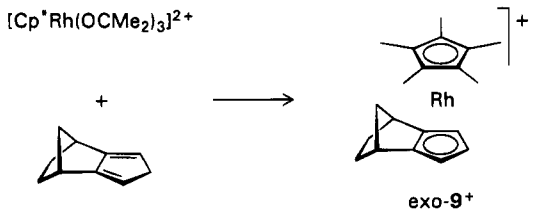

predominates at low temperature will favor electrophilic attack at the open endo face and hence produces endo products preferentially.

As described below, the endo isomer can be isomerized catalytically to give the exo isomer. Hence, isomerically pure samples of *exo*-**8** were obtained by treating the mixture of *exo*- and *endo*-**8** with a small amount of $[Cp^*Ru(NCMe)_3]PF_6$.[8] Both isomers are very soluble in organic solvents; attempts to separate the isomers by chromatography (TLC and HPLC) were unsuccessful. Careful fractional crystallization from methanol, monitored by ^{13}C NMR spectroscopy, afforded pure samples of the exo isomer and after many weeks of effort also very small samples of spectroscopically pure endo isomer.

The unsymmetric rhodocenium cation $[CpRhCp^*]^+$ can readily be made from cyclopentadiene and $(Cp^*RhCl_2)_2$ in the presence of Na_2CO_3;[15] the solvento complexes $[Cp^*Rh(solv)_3]^{2+}$ also form the sandwich cation, and especially in acetone, the reaction is faster and produces near-quantitative yields.[16] We have therefore treated isodicyclopentadiene with $[Cp^*Rh(OCMe_2)_3]^{2+}$ ($\mathbf{4}^{2+}$) and so obtained the cation *exo*-$[Cp^*Rh(Idcp)]^+$ (*exo*-$\mathbf{9}^+$); none of the alternative stereoisomer *endo*-$\mathbf{9}^+$ could be detected (Scheme 5). The success of the preparation is highly dependent on details of the reaction conditions, as much of the isodicyclopentadiene is destroyed under acidic conditions. Best results were obtained in highly diluted ethereal solutions and with a large excess of the olefin.

The cation *exo*-$\mathbf{9}^+$ was isolated as its PF_6^- salt. This salt does not crystallize well, and so the purification was laborious and not completely satisfactory. The isomer *endo*-$\mathbf{9}^+$ could only be obtained via an Idcp transfer reaction (see below).

Structures of *exo*-Cp*Ru(Idcp) and of *exo*-[Cp*Rh(Idcp)]PF_6. The structures of *exo*-**8** (Figure 1, Tables 1 and 2) and *exo*-**9**(PF_6) (Figure 2, Tables 3 and 4) were determined by X-ray crystallography. Special problems were not encountered.

The structure of *exo*-**8** is that of a typical sandwich complex. The Ru−C(av) distances (219.1(16) pm for Idcp, 215.9(9) pm for Cp*) are similar to those found in $RuCp_2$ (218.6(3) pm[17a]) and $RuCp^*_2$ (217(1) pm[17b]) and in CpRuCp* (**2**) (219.0(5) pm for Cp, 216.5(5) pm for Cp*[17c]). The structural trans effect which is operating in **2**[6] is hidden in *exo*-**8** by the relatively large variation of the individual Ru−C distances in both rings. How-

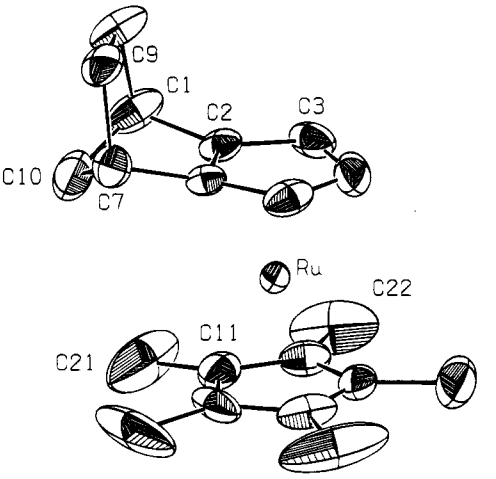

Figure 1. ORTEP diagram of *exo*-Cp*Ru(Idcp) (*exo*-**8**).

Table 1. Non-Hydrogen Atom Coordinates for *exo*-Cp*Ru(Idcp) (*exo*-8)

atom	x	y	z	B_{iso}[a]
Ru	0.77590(2)	0.63306(3)	0.11616(1)	2.421(6)
C1	0.6504(4)	0.9047(6)	0.2064(3)	5.3(1)
C2	0.6811(3)	0.7388(5)	0.1935(2)	3.51(8)
C3	0.7452(4)	0.6043(6)	0.2297(2)	5.1(1)
C4	0.6993(4)	0.4745(6)	0.1830(3)	5.5(1)
C5	0.6053(3)	0.5232(5)	0.1199(2)	4.49(9)
C6	0.5953(3)	0.6885(5)	0.1269(2)	2.98(7)
C7	0.5100(4)	0.8220(6)	0.0990(3)	4.35(9)
C8	0.4372(4)	0.8384(6)	0.1601(3)	4.5(1)
C9	0.5325(4)	0.8934(6)	0.2328(3)	5.7(1)
C10	0.5987(4)	0.9596(6)	0.1239(3)	6.0(1)
C11	0.8983(4)	0.7859(5)	0.0780(2)	4.69(9)
C12	0.9642(4)	0.6687(6)	0.1209(2)	4.40(9)
C13	0.9279(3)	0.5254(5)	0.0883(2)	3.97(8)
C14	0.8368(4)	0.5461(6)	0.0222(2)	4.97(9)
C15	0.8147(4)	0.7138(7)	0.0138(2)	6.7(1)
C21	0.9177(6)	0.9583(7)	0.0892(4)	13.6(2)
C22	1.0679(6)	0.701(1)	0.1919(4)	10.5(2)
C23	0.9858(6)	0.3694(6)	0.1178(4)	9.8(2)
C24	0.7734(6)	0.4280(9)	−0.0336(4)	13.4(2)
C25	0.7288(7)	0.800(1)	−0.0496(4)	17.3(2)

[a] The anisotropic thermal parameters are given in the form of their isotropic equivalents defined as $^4/_3[a^2\beta_{11} + b^2\beta_{33} + ac(\cos\beta)\beta_{13}]$; in units of 10^4 pm^2.

Table 2. Selected Bond Distances (pm) and Angles (deg) for *exo*-Cp*Ru(Idcp) (*exo*-8)

Ru−C2	219.9(2)	Ru−C11	217.0(3)
Ru−C3	220.7(3)	Ru−C12	216.7(3)
Ru−C4	216.4(3)	Ru−C13	215.7(3)
Ru−C5	219.4(3)	Ru−C14	215.2(3)
Ru−C6	219.3(2)	Ru−C15	214.9(3)
C2−C3	142.7(4)	C11−C12	136.6(5)
C3−C4	141.2(5)	C12−C13	137.6(4)
C4−C5	141.1(5)	C13−C14	137.7(4)
C5−C6	142.6(4)	C14−C15	145.6(6)
C2−C6	140.8(3)	C11−C15	143.7(5)
C1−C2	149.6(4)	C6−C7	150.1(4)
C1−C9	156.2(4)	C7−C8	157.3(4)
C1−C10	153.5(5)	C7−C10	154.3(5)
C8−C9	154.7(5)		
C1−C2−C3	143.6(3)	C5−C6−C7	141.6(2)
C1−C2−C6	106.6(2)	C2−C6−C7	107.6(2)
C3−C2−C6	107.9(3)	C2−C6−C5	108.9(2)

(14) Paquette, L. A.; Bauer, W.; Sivik, M. R.; Bühl, M.; Feigel, M.; Schleyer, P. v. R. *J. Am. Chem. Soc.* **1990**, *112*, 8776.
(15) Moseley, K.; Kang, J. W.; Maitlis, P. M. *J. Chem. Soc. A* **1970**, 2875.
(16) White, C.; Thompson, S. J.; Maitlis, P. M. *J. Chem. Soc., Dalton Trans.* **1978**, 1305.

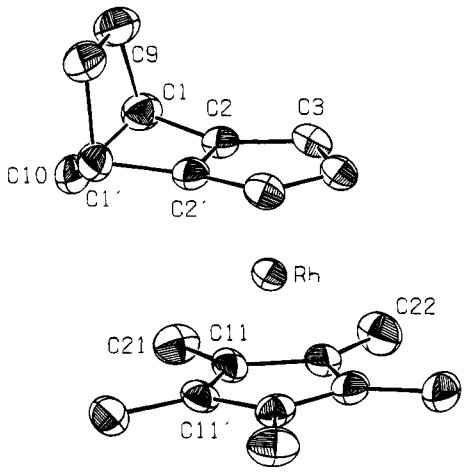

Figure 2. ORTEP diagram of the cation *exo*-[Cp*Rh(Idcp)]$^+$ (*exo*-**9**$^+$) of *exo*-**9**(PF_6).

Table 3. Non-Hydrogen Atom Coordinates for *exo*-[Cp*Rh(Idcp)]PF_6 (*exo*-9(PF_6))

atom	x	y	z	B_{iso}[a]
Rh	0.11086(4)	0.250	−0.23666(5)	2.59(1)
P	0.7180(2)	0.750	−0.3613(2)	3.66(5)
F1	0.7075(7)	0.750	−0.4734(6)	11.6(3)
F2	0.724(1)	0.750	−0.2515(7)	17.6(6)
F3	0.6433(3)	0.8582(6)	−0.3536(6)	9.4(2)
F4	0.7912(3)	0.8575(5)	−0.3715(6)	9.4(2)
C1	0.2064(4)	0.3627(7)	−0.0303(5)	3.5(1)
C2	0.2148(4)	0.3219(6)	−0.1348(4)	2.8(1)
C3	0.2357(4)	0.3649(6)	−0.2312(5)	3.1(1)
C4	0.2468(6)	0.250	−0.2898(7)	3.2(2)
C9	0.3001(5)	0.3279(7)	0.0130(6)	4.5(2)
C10	0.1490(6)	0.250	0.0118(7)	3.7(2)
C11	−0.0240(4)	0.3200(6)	−0.2023(5)	2.9(1)
C12	0.0015(4)	0.3630(7)	−0.2996(5)	3.1(1)
C13	0.0170(6)	0.250	−0.3582(7)	3.3(2)
C21	−0.0490(4)	0.4102(7)	−0.1205(5)	4.0(1)
C22	0.0062(5)	0.5038(7)	−0.3318(6)	4.5(2)
C23	0.0459(7)	0.250	−0.4631(7)	4.3(2)

[a] The anisotropic thermal parameters are given in the form of their isotropic equivalents defined as $^4/_3[a^2\beta_{11} + b^2\beta_{22} + c^2\beta_{33}]$; in units of 10^4 pm^2.

Table 4. Selected Bond Distances (pm) and Angles (deg) for *exo*-[Cp*Rh(Idcp)]PF_6 (*exo*-9(PF_6))

Rh−C2	220.5(3)	Rh−C11	218.2(4)
Rh−C3	219.7(4)	Rh−C12	217.0(4)
Rh−C4	215.0(5)	Rh−C13	216.8(6)
C2−C3	142.0(5)	C11−C12	144.9(6)
C3−C4	142.4(5)	C12−C13	141.8(5)
C2−C2′	146.2(7)	C11−C11′	142.4(8)
C1−C2	148.9(5)	C1−C10	154.0(6)
C1−C9	155.5(5)	C9−C9′	158(1)
C1−C2−C3	145.0(4)	C1−C2−C2′	106.2(2)
C2′−C2−C3	107.9(2)		

ever, the average distances Ru−C(av) for the two rings still seem to indicate that the Cp* ring interacts more strongly with the metal center than the Idcp ligand. The two cyclopentadienyl rings are nearly eclipsed (deviation 9°), and the best planes C2, ..., C6 and C11, ..., C15 show a slight tilt (4°) which increases the distance between the methylene bridge and the two nearest methyl groups of the Cp* ligand. Furthermore, the plane C1,C2,C6,-C7 is folded away from the metal by 11.5° relative to the plane C2, ..., C6. Comparable endo bending angles have been observed for other *exo*-Idcp complexes,[10c] while e.g. *endo*-(C_5H_4Me)(Idcp)$TiCl_2$ shows an exo bending, that is the norborneno fragment is again bent away from the metal.[10g] The methyl groups of the Cp* ligand are also bent away from the metal and lie 5.8 to 14.3 pm below the plane C11, ..., C15; the largest vertical displacement is found for the methyl group that is closest to the methylene bridge. All these structural details clearly indicate a transannular repulsion caused by the proximity of the methylene bridge to two methyl groups of the Cp* ligand.

Table 5. Diagnostic ^{1}H NMR Signals (in Acetone-d_6)

	3-/5-H	4-H	Cp*
exo-**8**	3.80 m		1.91 s
endo-**8**	4.00 d	3.50 t	1.89 s
exo-**9**$^+$	5.38 br		2.17 s
endo-**9**$^+$	5.52 dd	5.18 td	2.16 s

The salt *exo*-**9**(PF_6) displays crystallographic mirror symmetry. The quality of the structure solution was hampered by the lower quality of the crystal used and by a disorder problem in the anion lattice. The structure description therefore concentrates on only the most important features. The structure of the sandwich cation *exo*-**9**$^+$ is very similar to that of *exo*-**8**. The Rh−C(av) distances (219.1(24) ppm for Idcp; 217.4(7) pm for Cp*) are similar to those found in [(μ-$C_5H_4C_5H_4$)(RhCp*)$_2$](PF_6)$_2$ (218.6(11) ppm for C_5H_4; 215.6(17) pm for Cp*[18]) and again show a structural trans effect. The two cyclopentadienyl rings are precisely eclipsed; the tilt of the best planes C2,C2′,C3,C3′,C4 and C11,C11′,-C12,C12′,C13 is 4°, and the endo bending of the Idcp ligand amounts to 7.7°.

Isodicyclopentadienyl Transfer Reactions. Most transfer experiments were performed as NMR tube experiments, mostly in acetone-d_6 as solvent, and were monitored by ^{1}H NMR spectroscopy. The most helpful signals were the Cp* signals of the various species and the cyclopentadienyl ring protons of the Idcp ligand, which readily permit the identification of the stereoisomers. The diagnostic ^{1}H NMR signals are collected in Table 5.

While we studied the transfer reactions, it became apparent that the stereoisomeric ruthenocene derivatives *exo*-**8** and *endo*-**8** could be equilibrated whenever a sufficiently active ruthenium electrophile was present (Scheme 6). Treatment of *endo*-**8** or of mixtures *exo*-**8**/*endo*-**8** in acetone-d_6 with a catalytic trace of [Cp*Ru(μ-Cp)RuCp*]CF_3SO_3 (**3**(CF_3SO_3))[6] (acting as a source of [Cp*Ru($OCMe_2$)$_3$]$^+$ (**7**$^+$); cf. Scheme 2) effects isomerization above −40 °C to give *exo*-**8**; this reaction is complete within 5 min at ambient temperature. [Cp*Ru(NCMe)$_3$]CF_3SO_3[19] in acetone-d_6 is a less active catalyst; with 0.2 equiv the isomerization is complete after about 2 h at 20 °C. With the benzene complex [Cp*Ru(C_6H_6)]-PF_6[8] no isomerization was noticeable after 7 days at room temperature, neither in the dark nor in daylight. On the other hand, the rhodocenium ions are completely inert and this remains true, even in the presence of the metalloelectrophiles used here; reaction mixtures con-

(17) (a) Seiler, P.; Dunitz, J. D. *Acta Crystallogr., Sect. B* **1980**, *36*, 2946. (b) Albers, M. O.; Liles, D. C.; Robinson, D. J.; Shaver, A.; Singleton, E.; Wiege, M. B.; Boeyens, J. C. A.; Levendis, D. C. *Organometallics* **1986**, *5*, 2321. (c) Zanin, I. E.; Antipin, M. Yu.; Struchkov, Yu. T. *Kristallografiya* **1991**, *36*, 420; *Sov. Phys.—Crystallogr. (Engl. Transl.)* **1991**, *36*, 225.

(18) Rittinger, S.; Buchholz, D.; Delville-Desbois, M.-H.; Linarès, J.; Varret, F.; Boese, R.; Zsolnai, L.; Huttner, G.; Astruc, D. *Organometallics* **1992**, *11*, 1454.

(19) Fagan, P. J.; Ward, M. D.; Calabrese, J. C. *J. Am. Chem. Soc.* **1989**, *111*, 1698.

taining *exo*-**9**$^+$ and *endo*-**9**$^+$ do not change the ratio *exo*-**9**$^+$/*endo*-**9**$^+$ when kept at ambient temperature for several weeks.

Scheme 6

$$\underset{\textit{endo}\text{-}\mathbf{8}}{\textit{endo}\text{-Cp*Ru}(\mathbf{1})} \xrightleftharpoons{\text{cat.}} \underset{\textit{exo}\text{-}\mathbf{8}}{\textit{exo}\text{-Cp*Ru}(\mathbf{1})}$$

We now turn to the reactions of the ruthenocene derivatives *exo*-**8** and *endo*-**8** with $[Cp^*Rh(OCMe_2)_3]^{2+}$ (**4**$^{2+}$) in acetone. The endo isomer is much more reactive than the exo isomer. The transfer reaction sets in at −40 °C for *endo*-**8** and at 10 °C for *exo*-**8**. When the mixture *exo*-**8**/*endo*-**8** was treated with the rhodium electrophile **4**$^{2+}$ above 10 °C, *endo*-**8** disappeared within less than 5 min, whereas the reaction of *exo*-**8** took 3−4 days to go to completion. Two product Cp* signals were observed, one at $\delta(^1H)$ 2.16 and a second one of approximately equal intensity at 1.55. The first signal stems from the expected rhodocenium cations *exo*-**9**$^+$/*endo*-**9**$^+$. The second signal is not that of a RuRu$^+$ triple-decker species because there are no other signals left in the spectrum for a bridging ligand and, furthermore, because such an assumption would be in conflict with the relative intensities observed. When benzene is added to the solution, the signal at δ 1.55 disappears and a new signal at δ 5.97 indicates the formation of $[Cp^*Ru(C_6H_6)]^+$ ($\delta(^1H)$ (acetone-d_6) 6.06[8]). Thus, the product signal at δ 1.55 is tentatively assigned to the solvento species $[Cp^*Ru(OCMe_2)_3]^+$ (**7**$^+$) (Scheme 7).[20]

Scheme 7

$$\underset{\mathbf{8}}{Cp^*Ru(\mathbf{1})} + \underset{\mathbf{4}^{2+}}{[Cp^*Rh(OCMe_2)_3]^{2+}} \rightarrow \underset{\mathbf{9}^+}{[Cp^*Rh(\mathbf{1})]^+} + \underset{\mathbf{7}^+}{[Cp^*Ru(OCMe_2)_3]^+}$$

In the transfer reactions a pronounced preference for the formation of the rhodocenium ion *endo*-**9**$^+$ is observed; this isomer is thought to be the higher energy isomer. With spectroscopically pure *exo*-**8** we obtained the rhodocenium ion *endo*-**9**$^+$, but a 5% admixture of the exo isomer *exo*-**9**$^+$ was produced. With the more reactive stereoisomer *endo*-**8** the transfer reaction already sets in above −40 °C. As time progresses the transfer reaction is superseded by the isomerization of *endo*-**8** to the more stable isomer *exo*-**8**. Later and only at higher temperatures is exo-**8** slowly transformed into the cation *endo*-**9**$^+$, with an admixture of typically 15−20% of the exo isomer *exo*-**9**$^+$. Obviously the stereochemical information of the starting ruthenocene derivatives is lost as a consequence of the isomerization reaction.

How can the isomerization reaction be suppressed? What was needed is a ligand that quenches the solvento species $[Cp^*Ru(OCMe_2)_3]^+$ (**7**$^+$) efficiently without reducing the activity of the rhodium electrophile **4**$^{2+}$ appreciably. The two fragments $[RuCp^*]^+$ and $[RhCp^*]^{2+}$ differ significantly in their affinity to arenes. The first one forms a wide variety of complexes even with condensed aromatic systems[21] such as e.g. the naphthalene complex $[Cp^*Ru(C_{10}H_8)]^+$ (**10**$^+$).[22] On the other

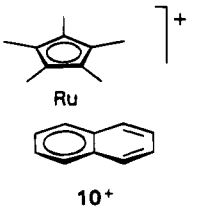

hand, the rhodium fragment forms the moderately stable cation $[Cp^*Rh(C_6H_6)]^{2+}$ [9] but analogous cations with naphthalene or other condensed aromatic systems are not known.

With this information in mind we decided to try naphthalene as a quenching reagent for **7**$^+$ and repeated the transfer reactions of the isomeric ruthenocene derivatives with $[Cp^*Rh(OCMe_2)_3]^{2+}$ (**4**$^{2+}$) in the presence of more than 1 equiv of naphthalene. The reaction of pure *exo*-**8** now gave pure *endo*-**9**$^+$, without admixture of *exo*-**9**$^+$, and the naphthalene complex **10**$^+$.[22,23] In a careful high-resolution ^1H NMR spectrum at 500 MHz the diagnostic signals of *exo*-**9**$^+$ could not be detected. For the isolation of *endo*-**9**(PF_6) the naphthalene complex was first destroyed photolytically; subsequent addition of NH_4PF_6(aq) afforded the desired salt for characterization.

The reaction of the more reactive isomer *endo*-**8** was noticeable above −20 °C; the higher temperature of the onset of the transfer reaction indicates a slight deactivation of the rhodium electrophile and is a hint to weak complex formation between naphthalene and $[Cp^*Rh(OCMe_2)_3]^{2+}$.[24] Pure *endo*-**8** now gave pure *exo*-**9**$^+$ and **10**$^+$. Again the diagnostic signals of *endo*-**9**$^+$ could not be detected in a high-resolution ^1H NMR spectrum at 500 MHz.

We summarize these results in Scheme 8. In the presence of naphthalene both stereoisomers *exo*-**8** and *endo*-**8** undergo the Idcp transfer reaction with 100% stereoselectivity to give stereoisomeric product cations *endo*-**9**$^+$ and *exo*-**9**$^+$. The transfer reaction is stereospecific.

Discussion

The synthesis of the isomeric ruthenocene derivatives *exo*-**8** and *endo*-**8** shows the usual temperature dependence of the isomer ratio: that is, a more pronounced preference for exo coordination at higher temperature. Many workers have suggested that exo coordination should be thermodynamically more favorable.[10] Our observation of an isomerization equilibrium (Scheme 6) provides a unique experimental proof that the exo isomer of the ruthenocene derivatives **8** is indeed more stable than the endo isomer.

The isomerization equilibrium is mobile in the presence of the ruthenium electrophile $[Cp^*Ru(OCMe_2)_3]^+$ (**7**$^+$). Within the framework of Scheme 2 one could have

(20) Cf. $[Cp^*Ru(NCMe)_3]^+$: $\delta(^1H$, acetonitrile-$d_3)$ 1.60 for Cp*.[8]

(21) For a recent paper see: Glatzhofer, D. T.; Liang, Y.; Khan, M. A. *Organometallics* **1993**, *12*, 624.

(22) McNair, A. M.; Mann, K. R. *Inorg. Chem.* **1986**, *25*, 2519.

(23) If too little naphthalene is present in the reaction mixture, signals of the doubly opened triple-decker cation $[(\mu\text{-}C_{10}H_8)(RuCp^*)_2]^{2+}$ appear. ^1H NMR (300 MHz, CD_2Cl_2): δ 7.24 (m, 4 H_β), 6.04 (m, 4 H_α), AA′BB′ system with N = 7.0 Hz, 1.79 s (Cp*). $^{13}C\{^1H\}$ NMR (75 MHz, CD_2Cl_2): δ 99.1 (C_5Me_5), 91.6 (4 C_β), 81.3 (4 C_α), 68.5 (C-4a/8a), 10.4 (C_5Me_5).

(24) Solutions of **4**$^{2+}$ and naphthalene in acetone show a multiplet at $\delta(^1H)$ 7.0 at −60 °C which broadens and becomes less intense at higher temperatures. This signal can only be seen below 0 °C.

Scheme 8

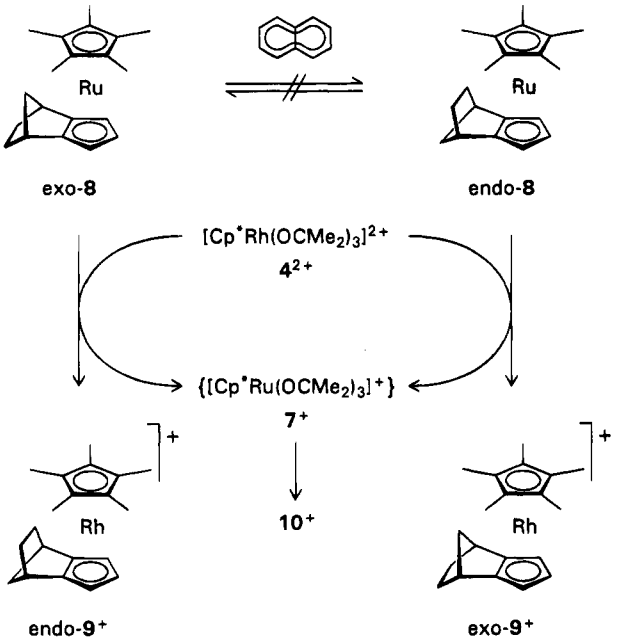

expected the reversible formation of the triple-decker cation [Cp*Ru(μ-Idcp)RuCp*]$^+$ (**11**$^+$) with the same

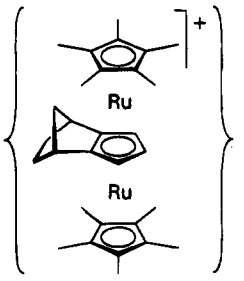

11$^+$

probably charge-controlled[6] regiochemistry as in the less substituted cation [Cp*Ru(μ-Cp)RuCp*]$^+$ (**3**$^+$). However, this species **11**$^+$ should be destabilized by the bulkiness of the bridging Idcp ligand and hence should be less stable than its μ-Cp analogue **3**$^+$. As **11**$^+$ is not seen in the ^{1}H NMR spectrum, we have to assume that the destabilization is sufficient enough to shift the equilibrium of triple-decker formation far to the left. What remains for **11**$^+$ is the role of a kinetic intermediate with a concentration too low for direct observation.

It should be noted that the isomerization is truly an equilibrium reaction. Synthetically only the reaction *endo*-**8** $\rightarrow$ *exo*-**8** can be seen. However, the fact that pure *exo*-**8** reacts with [Cp*Rh(OCMe$_2$)$_3$]$^{2+}$ (**4**$^{2+}$) in the absence of the quenching agent naphthalene to give *endo*-**9**$^+$ *and* some *exo*-**9**$^+$ requires that some *exo*-**8** be isomerized by the ruthenium electrophile [Cp*Ru(OCMe$_2$)$_3$]$^+$ (**7**$^+$) to form *endo*-**8**. This then produces the exo isomer *exo*-**9**$^+$, which had been observed as a 5% admixture to the main product *endo*-**9**$^+$. Note that the rhodium electrophile **4**$^{2+}$ cannot be the cause of this isomerization, as is seen from Scheme 8, in line with the lower affinity of **4**$^{2+}$ for π systems as compared to the ruthenium species **7**$^+$.

We now turn to the Idcp transfer reactions of Scheme 8. Our experiments establish the *type* of transfer mechanism rigorously, while the detailed mechanism remains unknown. The transfer process is associative. The leaving group ML and the entering group M'L' are in an antifacial disposition in the species LM(**1**)M'L', which in principle can be an intermediate or a transition state. The antifacial disposition of the entering electrophile is also reflected in the higher reactivity of *endo*-**8** as compared to its stereoisomer *exo*-**8**. In the more reactive *endo*-**8** it is the less congested exo side of the Idcp ligand that acts as the open face and is more readily accessible to electrophilic attack.

It seems legitimate to assume that the species LM(**1**)M'L' is the triple-decker *intermediate* [Cp*Ru(μ-Idcp)RhCp*]$^{2+}$ (**12a**$^{2+}$ and **12b**$^{2+}$). In the closely related

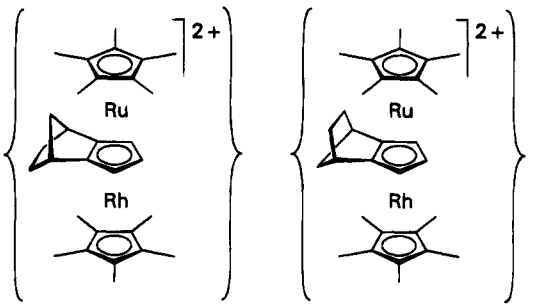

12a^{2+} **12b**$^{2+}$

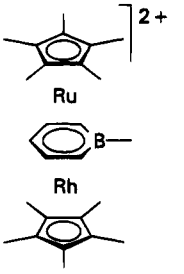

13^{2+}

reaction of the 1-methylboratabenzene complex Cp*Ru(C$_5$H$_5$BMe) with [Cp*Rh(OCMe$_2$)$_3$]$^{2+}$ (**4**$^{2+}$) we have observed the fast formation (<60 s, 20 °C) of the triple-decker dication [Cp*Ru(μ-C$_5$H$_5$BMe)RhCp*]$^{2+}$ (**13**$^{2+}$), which subsequently decays (7 days, 20 °C) to form inter alia the boratabenzene transfer product [Cp*Rh(C$_5$H$_5$BMe)]$^+$.[2] The direct spectroscopic observation of **13**$^{2+}$ (by ^{1}H and ^{13}C NMR spectroscopy) strongly supports the assumption that the analogous and expectedly much less stable cations **12a,b**$^{2+}$ are truly intermediates and not only transition states of the Idcp transfer reactions.

Conclusion

With this work we have established the stereochemistry and the overall mechanism of an isodicyclopentadienyl transfer reaction, that is, of a single case of a cyclopentadienyl transfer reaction. However, there are a number of closely related ring ligand transfer reactions with transfer of 1*H*-borole,[25] unsubstituted cyclopentadienyl,[6,26] and boratabenzene[2] ligands. Hence we

(25) Herberich, G. E.; Dunne, B. J.; Hessner, B. *Angew. Chem., Int. Ed. Engl.* **1989**, *28*, 737. Herberich, G. E.; Büschges, U.; Dunne, B. J.; Hessner, B.; Klaff, N.; Köffer, D. P. J.; Peters, K. M. *J. Organomet. Chem.* **1989**, *372*, 53.
(26) Werner, H. *Angew. Chem., Int. Ed. Engl.* **1977**, *16*, 1.

may assume, by way of extrapolation, that many of these reactions will also involve triple-decker intermediates. In other cases such as the transfer of cyclobutadiene ligands and of benzene ligands the intermediacy of triple-decker species seems to be a less attractive hypothesis or even quite unlikely. Much further work will be needed to clarify these issues.

Experimental Section

Experiments were carried out under dinitrogen using conventional Schlenk techniques. Solvents were dried (hexane over Na/K alloy, acetone over B_2O_3), distilled and stored under dinitrogen. Alumina and silica were heated under vacuum at 300 °C for 20 h and kept under N_2; the alumina was deactivated by addition of water (7%, deoxygenated). NMR spectra were recorded on a Varian Unity 500 (^{1}H, 500 MHz; ^{13}C, 125 MHz) and a Varian VXR-300 instrument (^{1}H, 300 MHz; ^{13}C, 75 MHz). Chemical shifts are relative to internal TMS. Two-dimensional spectra were recorded by means of the programs COSY (^{1}H−^{1}H), RELAYH (^{1}H−^{1}H), and HETCOR (^{1}H−^{13}C); NOE spectra were taken with the help of the program NOE1D.

Preparation of *exo*- and *endo*-Cp*Ru(Idcp). Li(Idcp)[12] (0.41 g) in THF (5 mL) was added with stirring to a suspension of $(Cp^*RuCl)_4$[13] (0.80 g) in THF (20 mL) at 20 °C. Stirring was continued for 5 h. After removal of the volatiles the residue was extracted with pentane (3×, 5 mL). The combined solutions were filtered through Kieselguhr, and the pentane was removed. The isomer ratio *exo*-**8**/*endo*-**8** was determined for this raw product by ^{13}C NMR. Crystallization of the residue from ethanol (30 mL) at −30 °C and slow sublimation at 50 °C/10^{-6} bar gave 0.83 g (76%) of a mixture of *exo*-**8**/*endo*-**8**.

***exo*-8.** The crude product obtained from Li(Idcp)[12] (1.48 g) and $(Cp^*RuCl)_4$[13] (2.91 g) as described above was dissolved in acetone (60 mL), $[Cp^*Ru(NCMe)_3]PF_6$[8] (0.27 g, 0.05 equivalents) was added, and stirring was continued for 40 h at 20 °C. After removal of the volatiles the residue was chromatographed through a 10 cm layer of alumina (7% H_2O) using pentane as eluent. Recrystallization of the pale red product fraction from ethanol (100 mL) gave 2.99 g (76%) of pure *exo*-**8**: colorless crystals; mp 89 °C; very soluble in organic solvents. Anal. Calcd for $C_{20}H_{26}Ru$: C, 65.38; H, 7.13. Found: C, 65.21; H, 7.16. ^{1}H NMR (500 MHz, acetone-d_6): δ 3.80 (m, 3-/4-/5-H), 2.67 (br, 1-/7-H), 1.91 (s, Cp*), 1.75 (m, 8*exo*-/9*exo*-/10*syn*-H), 1.31 (dm, 8.0 Hz, 10*anti*-H), 1.02 (m, 8*endo*-/9*endo*-H). ^{13}C{^{1}H} NMR (125 MHz, acetone-d_6): δ 101.0 (C-2/6), 85.0 (C_5Me$_5$), 74.7 (C-4), 65.0 (C-3/5), 47.9 (C-10), 37.5 (C-1/7), 29.1 (C-8/9), 12.3 (C_5Me_5).

***endo*-8.** A mixture of *exo*-**8**/*endo*-**8** (ca. 5 g) was produced at the lowest possible temperature, starting at −65 °C. The process of repeated fractional crystallization from methanol at −30 °C was monitored by ^{13}C NMR spectroscopy. Seeds of pure *exo*-**8** were used to induce preferential crystallization of this isomer. After several steps the material from collected mother liquors had to purified by chromatography and slow sublimation under vacuum. The final crystallizations gave small samples of spectroscopically pure *endo*-**8**: colorless crystals; mp 96 °C; very soluble in organic solvents. ^{1}H NMR (500 MHz, acetone-d_6): δ 4.00 (d, 1.8 Hz, 3-/5-H), 3.50 (t, 1.8 Hz, 4-H), 2.76 (m, 1-/7-H), 1.97 (m, 8*exo*-/9*exo*-H), 1.93 (m, 10*syn*-/10*anti*-H), 1.89 (s, Cp*), 1.62 (m, 8*endo*-/9*endo*-H). ^{13}C{^{1}H} NMR (125 MHz, acetone-d_6): δ 110.8 (C-2/6), 84.7 (C_5Me$_5$), 69.8 (C-4), 66.9 (C-3/5), 58.1 (C-10), 38.8 (C-1/7), 33.2 (C-8/9), 12.2 (C_5Me_5).

Preparation of *exo*-[Cp*Rh(Idcp)]PF$_6$. $[Cp^*Rh(OCMe_2)_3](BF_4)_2$ (2.0 mmol) in acetone was prepared as described in the literature.[9] The solvent was largely removed at low temperature. The yellow residue was then suspended in ether (150 mL), and isodicyclopentadiene[11] (0.79 g, 6.0 mmol) in ether (50 mL) was added dropwise with stirring within 1 h. The solution turned red and then deep blue. After 1 day more isodicyclopentadiene (0.40 g) was added and the reaction mixture was kept for another 2 days. After removal of the volatiles the residue was dissolved in acetone (5 mL) and chromatographed on a column (20 cm) of alumina. After washing with $CHCl_3$ (0.5 L), further elution with acetone (0.5 L) gave a brown product fraction. Kieselguhr (5 g) was added, and the volatiles were removed under vacuum. The residue was extracted with pentane/ether (1:1, 0.5 L) in a Soxhlet apparatus and then eluted with acetone to give 0.91 (51%) of *exo*-**9**(BF$_4$). This salt was dissolved in a large volume of water (0.3−0.5 L); addition of an aqueous solution of NH_4PF_6 precipitated *exo*-**9**(PF$_6$) which in small quantities could be recrystallized from $CHCl_3$/ether and from acetone/ether: pale yellow crystals. Anal. Calcd for $C_{20}H_{26}F_6PRh$: C, 46.71; H, 5.10. Found: C, 46.50; H, 5.01. ^{1}H NMR (500 MHz, acetone-d_6): δ 5.38 (br, 3-/4-/5-H), 3.17 (m, 1-/7-H), 2.17 (s, Cp*), 1.95 (m, 8*exo*-/9*exo*-H), 1.71 (dm, 9.5 Hz, 10*anti*-H), 1.54 (dm, 9.5 Hz, 10*syn*-H), 1.18 (m, 8*endo*-/9*endo*-H). ^{13}C NMR (125 MHz, acetone-d_6): δ 117.3 (d, 7.1 Hz (Rh), C-2/6), 101.6 (d, 7.8 Hz (Rh), C_5Me$_5$), 90.6 (ddm, 180.8, 6.0 Hz (Rh), C-4), 80.5 (ddt, 183.2, 6.6, 6.3 Hz (Rh), C-3/5), 49.4 (tt, 135.2, 7.0 Hz, C-10), 37.0 (dd, 152.6, 7.1 Hz, C-1/7), 27.2 (t br, 136.0 Hz, C-8/9), 10.5 (q, 128.9 Hz, C_5Me_5); ^1J(Rh−^{13}C) coupling constants were taken from a ^{13}C{^{1}H} NMR spectrum.

***endo*-[Cp*Rh(Idcp)]PF$_6$.** Pure *exo*-**8** (0.23 g, 0.63 mmol) and naphthalene (0.10 g, 0.78 mmol) were dissolved in acetone (5 mL). $[Cp^*Rh(OCMe_2)_3](BF_4)_2$[9] (0.62 mmol) in acetone was added dropwise with stirring. The color of the mixture changed from orange to yellow within 30 min, and stirring was continued for 5 h. The solvent was then removed under vacuum; the NMR spectrum of the residue confirmed complete conversion. The residue was extracted with water (150 mL). The yellow aqueous extract was filtered, adjusted to pH 8−9 by adding Na_2CO_3, and then irradiated for 5 days with an immersed high-pressure mercury lamp (125 W, Pyrex filter). The resulting brown suspension was filtered. The filtrate was acidified with hydrochloric acid to pH 1−2 and concentrated under vacuum to about half of its volume. Addition of NH_4PF_6 (0.2 g) in water gave a precipitate which was filtered off, washed with water (2 × 3 mL), and dried in vacuo. Two recrystallizations from $CHCl_3$ (3 mL) by addition of Et_2O (6 mL) gave *endo*-**9**(PF$_6$) (180 mg, 55%) as pale brownish microcrystals. Anal. Calcd for $C_{20}H_{26}F_6PRh$: C, 46.71; H, 5.10. Found: C, 46.89; H, 5.13. ^{1}H NMR (500 MHz, acetone-d_6): δ 5.52 (dd, 2.1, 0.6 Hz (Rh), 3-/5-H), 5.18 (td, 2.1, 0.9 Hz (Rh), 4-H), 3.22 (m, 1-/7-H), 2.30 (m, 8*exo*-/9*exo*-H), 2.18 (s, Cp*), 2.09 (dm, 10.3 Hz, 10*anti*-H), 1.57 (m, 8*endo*-/9*endo*-H); signal of 10*syn*-H not identified, probably at δ 2.17 and obscured by Cp* signal. ^{13}C{^{1}H} NMR (125 MHz, acetone-d_6): δ 128.8 (d, 6.0 Hz (Rh), C-2/6), 101.9 (d, 8.0 Hz (Rh), C_5Me$_5$), 85.3 (d, 8.7 Hz (Rh), C-4), 81.7 (d, 7.2 Hz (Rh), C-3/5), 58.4 (C-10), 39.2 (C-1/7), 32.6 (C-8/9), 11.0 (C_5Me_5).

Transfer Experiments. The ruthenocenes *exo*-**8**/*endo*-**8** were dissolved in acetone-d_6. After the starting isomer ratio was determined, the solutions were cooled and a solution of the second reagent was added. The reactions were monitored

Table 6. Selected Transfer Experiments (in Acetone-d_6)[a]

		products	
exo-**8**:*endo*-**8**	conditions ϑ, °C	*exo*-**9**$^+$: *endo*-**9**$^+$	solv in $[Cp^*Ru(solv)_3]BF_4$
100:0	−40 to 0	5:100	Me_2CO[b]
100:0	20[c]	5:100	Me_2CO[b]
0:100	−40 to 0	20:100	Me_2CO[b]
100:0	20[c]	0:100	$C_{10}H_8$
100:20	10	20:100	$C_{10}H_8$
0:100	−40 to 0[c]	100:0	$C_{10}H_8$

[a] Reagent: $[Cp^*Rh(OCMe_2)_3](BF_4)_2$ in acetone-d_6. [b] δ(^{1}H) 1.55 for Cp* of $[Cp^*Ru(solv)_3]BF_4$. [c] In the dark.

Table 7. Crystallographic Data for *exo*-8 and *exo*-9(PF_6)

	exo-8	*exo*-9(PF_6)
formula	$RuC_{20}H_{26}$	$RhC_{20}H_{26}PF_6$
fw	367.50	514.30
cryst syst	monoclinic	orthorhombic
space group	$P2_1/c$ (No. 14)	*Pnma* (No. 62)
a, pm	1151.2(5)	1489.1(6)
b, pm	854.80(5)	1016.7(4)
c, pm	1824.2(5)	1363.5(5)
β, deg	105.786(5)	
V, nm^3	1.728(1)	2.064(2)
d_{calcd}, g/cm^3	1.413	1.655
Z	4	4
$F(000)$	760	1040
μ(Mo Kα), cm^{-1}	74.2	81.1
cryst dimens, mm^3	0.1 × 0.1 × 0.2	0.1 × 0.1 × 0.2
radiation (λ, pm)	Cu Kα (154.06)	Cu Kα (154.06)
monochromator	graphite	graphite
T, K	293	215
scan mode	ω	ω
scan range, deg	$5 \leq \theta \leq 65$	$5 \leq \theta \leq 70$
total no. of data	2916	2162
no. of unique obsd data ($I > 3\sigma(I)$)	2525	1589
no. of variables	191	140
residuals R, R_w	0.037, 0.054	0.053, 0.063
weighting factor, w	$w = 1/\sigma^2(F_o)$	$w = 1/\sigma^2(F_o)$
GOF	3.031	2.823
max resid density, e pm^{-3}	0.6×10^{-6}	2.9×10^{-6} [a]

[a] This isolated local maximum at 170 and 200 pm from two C(Cp*) atoms is not located at a chemically meaningful position.

by taking ^{1}H NMR spectra at intervals first of 15 min and then of typically 3 h. In variable-temperature experiments the heating rate was 10 °C/h. The results are summarized in Table 6.

X-ray Structure Determination of *exo*-Cp*Ru(Idcp) (*exo*-8). Geometry and intensity data were collected on an Enraf-Nonius CAD4 diffractometer. A summary of crystallographic data, data collection parameters, and refinement parameters is given in Table 7. An empirical absorption correction was applied using the method of differential absorption (program DIFABS).[27] The structure was solved by Patterson and difference Fourier methods.[28] The F_c values were corrected for secondary extinction ($E = 3.18 \times 10^{-6}$).[29] In the final full-matrix refinement, non-hydrogen atoms were refined with anisotropic thermal parameters and hydrogen atoms were included as riding in standard positions (C−H = 98 pm).

X-ray Structure Determination of *exo*-[Cp*Rh(Idcp)]-PF_6, *exo*-9(PF_6). In this case an empirical absorption correction was applied on the basis of ψ scans.[30] The F_c values were corrected for secondary extinction ($E = 8.17 \times 10^{-6}$).[29] In the final full-matrix refinement, non-hydrogen atoms were refined with anisotropic thermal parameters and hydrogen atoms were included as riding in standard positions (C−H = 98 pm).

Acknowledgment. We thank Ulrich Koelle and Frank Marken for helpful discussions, Uwe Steffan, Regina Standt, and Christian Lamertz for assistance with the preparative work, Jan Runsink for help with advanced NMR techniques, and Stefan Moss for assistance with the structural work. This work was supported by the Deutsche Forschungsgemeinschaft and by the Fonds der Chemischen Industrie.

Supplementary Material Available: Listings of crystal data, positional parameters for H atoms, thermal parameters, bond lengths, and bond angles for *exo*-8 and *exo*-9(PF_6) (12 pages). Ordering information is given on any current masthead page.

OM9400309

(27) Walker, N.; Stuart, D. *Acta Crystallogr., Sect. A* **1983**, *39*, 158.
(28) Frenz, B. A. The Enraf-Nonius CAD4 SDP—a real-time system for concurrent X-ray data collection and crystal structure determination. In *Computing in Crystallography*; Schenk, H., Olthof-Hazekamp, R., van Koningsveld, H., Bassi, G. C., Eds.; Delft University Press: Delft, The Netherlands, 1978. SDP-PLUS, Version 1.1 (1984) and VAXSDP, Version 2.2 (1985).
(29) Zachariasen, W. H. *Acta Crystallogr.* **1963**, *16*, 1139.
(30) North, A. C. T.; Phillips, D. C.; Mathews, F. S. *Acta Crystallogr., Sect. A* **1968**, *24*, 351.

^{31}P, ^{13}C, and ^{1}H NMR Studies on Chiral Allyl Ferrocenyldiphosphine Complexes of Palladium(II)

Paul S. Pregosin,* Renzo Salzmann, and Antonio Togni

Laboratorium für Anorganische Chemie, ETH Zentrum, Zürich 8092, Switzerland

Received August 29, 1994®

A series of complexes of the type [Pd(η^3-allyl)(JOSIPHOS)]CF_3SO_3, containing either the β-pinene, η^3-$C_{10}H_{15}$, or the η^3-C_3H_5 ligands and the new chiral 1,2-ferrocenyldiphosphine ligands, JOSIPHOS, have been studied using multidimensional NMR spectroscopy (JOSIPHOS, **5**, = (Cp)Fe{C_5H_3(1-CH(CH_3)PR_2^1)-2-PR_2^2) }, (R^1 = Cy, R^2 = Ph, **a**; R^1 = Ph, R^2 = Cy, **b**; R^1 = Ph, R^2 = Ph, **c**). A structural comparison based on NOE data for the cation [Pd(η^3-$C_{10}H_{15}$)(**5a**)]$^+$ with NOE data from the analogous cations of *S*-BINAP and *S,S*-CHIRAPHOS suggests that coordinated **5a** intrudes more into the coordination sphere of the allyl ligand than do either *S*-BINAP or *S,S*-CHIRAPHOS. The nature of the chiral environment for **5a** in [Pd(η^3-$C_{10}H_{15}$)(**5a**)] CF_3SO_3, **4d**, is described. 2-D exchange spectroscopy for four cationic complexes of the type [Pd(η^3-C_3H_5)(JOSIPHOS)]$^+$, which contain different JOSIPHOS modifications, reveals a selective $\eta^3-\eta^1-\eta^3$ isomerization, which, for the cations with **5a,b**, involves opening of the Pd–C allyl bond cis to the PCy_2 and trans to the PPh_2 moiety. The $\eta^3-\eta^1-\eta^3$ selectivity is shown to be steric and not electronic in origin. ^{31}P, ^{13}C, and ^{1}H NMR data are reported.

Introduction

Organic reactions catalyzed by palladium,[1] and specifically those involving Pd–allyl intermediates, e.g., catalytic allylation[2]

$$\mathrm{PhCH(OAc)CH{=}CHPh} + {}^{-}\mathrm{CH(CO_2Me)_2} \xrightarrow{\text{chiral catalyst}} \mathrm{PhCH\{CH(CO_2Me)_2\}CH{=}CHPh} + \mathrm{OAc}^-$$

remain of synthetic interest. If the allylation is carried out using a palladium complex containing a chiral ligand such as a chelating diphosphine, the organic products which result often reveal substantial-to-excellent enantiomeric excesses.[3] Recently, chiral chelating nitrogen[4a-d] and mixed phosphorus–nitrogen[4ef] ligands have also been used with excellent results.

The structural aspects of the intermediates which arise in the homogeneous allylation catalyzed by palladium(II) complexes are important. It is known[5–11] that NMR studies and especially ^{1}H NOE spectroscopy can determine subtle and gross molecular features in organometallic complexes of Pd(II). For chiral compounds containing either BINAP or CHIRAPHOS, the *ortho* protons of the P-phenyl groups may be used as "reporters" to define the 3-D structure of the chiral Pd–π-allyl catalyst precursors.[5,6b,10,11] In part, such proximity effects deduced from NOE studies[5–11] have been used by Akermark and co-workers[12] to help shift the syn/anti equilibria in some crotyl allyl complexes.

Phase-sensitive ^{1}H-NOESY also provides exchange data,[13] thus leading to new[6,8b] and selective[6,14] results for Pd–π-allyl isomerization dynamics. For [Pd(π-allyl)-

® Abstract published in *Advance ACS Abstracts*, December 15, 1994.

(1) (a) *New Pathways for Organic Synthesis*; Colquhoun, H. J.; Thompson, D. J., Twigg, M. V., Eds.; Plenum Press: New York, 1984. (b) Trost, B. M. *Chemtracts-Org. Chem.* **1988**, *1*, 415. (c) Trost, B. M. *Tetrahedron*, *1977*, *33*, 2625. (d) Trost, B. M. *Acc. of Chem. Res.* **1980**, *13*, 385. (e) *Metallo-Organic Chemistry;* Pearson, A. J., Ed.; John Wiley and Sons: New York, 1985. (f) Stary, I.; Kocovsky, P. *J. Am. Chem. Soc.* **1989**, *111*, 4981.

(2) Consiglio, G.; Waymouth, R. M. *Chem. Rev.* **1989**, *89*, 257. Consiglio, G.; Indolese, A. *Organometallics* **1991**, *10*, 3425. Sawamura, M.; Ito, Y. *J. Am. Chem. Soc.* **1992**, *114*, 2586.

(3) Yamamoto, K.; Deguchi, R.; Ogimura, Y.; Tsuji, J. *Chem. Lett.* **1954**, 1657. Mackenzie, P. B.; Whelan, J.; Bosnich, B. *J. Am. Chem. Soc.* **1985**, *107*, 2046. Auburn, P. R.; Mackenzie, P. B.; Bosnich, B. *J. Am. Chem. Soc.* **1985**, *107*, 2033. Hayashi, T.; Yamamoto, A. *Tetrahedron Lett.* **1988**, *29*, 669. Hayashi, T.; Yamamoto, A.; Ito, Y.; Nishioka, E.; Miura, H.; Yanagi, K. *J. Am. Chem. Soc.* **1989**, *111*, 6301. Sawamura, M.; Nagata, H.; Sakamoto, H.; Ito, Y. *J. Am. Chem. Soc.* **1992**, *114*, 2586.

(4) (a) Pfalz, A. *Acc. Chem. Res.*, **1993**, *26*, 339. (b) von Matt, P.; Pfaltz, A. *Angew. Chem., Int. Ed. Engl.* **1993**, *32*, 566. (c) Togni, A. *Tetrahedron Asym.* **1991**, *2*, 683. (d) Tanner, D. *Angew. Chem., Int. Ed. Engl.* **1994**, *106*, 625. (e) Sprinz, J.; Kiefer, M.; Helmchen, G.; Reggelein, M.; Huttner, G.; Zsolnai, L. *Tetrahedron Lett.* **1994**, *35*, 1523. (f) Dawson, G.; Frost, C. G.; Williams, J. M. J. *Tetrahedron Lett.* **1993**, *34*, 3149.

(5) (a) Pregosin, P. S.; Rüegger, H.; Salzmann, R.; Albinati, A.; Lianza, F.; Kunz, R. W. *Organometallics* **1994**, *13*, 83. (b) Pregosin, P. S.; Rüegger, H.; Salzmann, R.; Albinati, A.; Lianza, F.; Kunz, R. *Organometallics*, **1994**, in press.

(6) (a) Rüegger, H.; Pregosin, P. S. *Magn. Reson. Chem.* **1994**, *32*, 297. (b) Pregosin, P. S.; Salzmann, R. *Magn. Reson. Chem.* **1994**, *32*, 128.

(7) Cesarotti, E.; Grassi, M.; Prati, L.; Demartin, F. *J. Chem. Soc., Dalton Trans.* **1991**, 2073.

(8) Albinati, A.; Ammann, C.; Pregosin, P. S.; Rüegger, H. *Organometallics* **1990**, *9*, 1826. Albinati, A.; Kunz, R. W.; Ammann, C. J.; Pregosin, P. S. *Organometallics* **1991**, *10*, 1800.

(9) Giovanetti, J. S.; Kelly, C. M.; Landis, C. R. *J. Am. Chem. Soc.* **1993**, *115*, 4040.

(10) Ammann, C. J.; Pregosin, P. S.; Rüegger, H.; Albinati, A.; Lianza, F.; Kunz, R. W. *J. Organomet. Chem.* **1992**, *423*, 415.

(11) Rüegger, H.; Kunz, R. W.; Ammann, C.; Pregosin, P. S. *Magn. Reson. Chem.* **1992**, *29*, 197.

(12) (a) Akermark, B.; Hansson, S.; Vitagliano, A. *J. Am. Chem. Soc.* **1990**, *112*, 4587. (b) Sjorgen, M. P. T.; Hansson, S.; Norrby, P.; Akermark, B.; Cucciolito, M. E.; Giordano, F.; Vitagliano, A. *Organometallics* **1992**, *11*, 3954. (c) Hansson S.; Norrby, P.; Sjorgen, M. P. T.; Akermark, B.; Cucciolito, M. E.; Giordano, F.; Vitagliano, A. *Organometallics* **1993**, *12*, 4940.

(13) Hull, W. E. In *Two-dimensional NMR Spectroscopy. Applications for Chemists and Biochemists*; VCH: New York, 1987; p 153.

(14) Breutel, C.; Pregosin, P. S.; Salzmann, R.; Togni, A. *J. Am. Chem. Soc.* **1994**, *116*, 4067.

0276-7333/95/2314-0842$09.00/0

Chart 1. Structural Units and Definitions

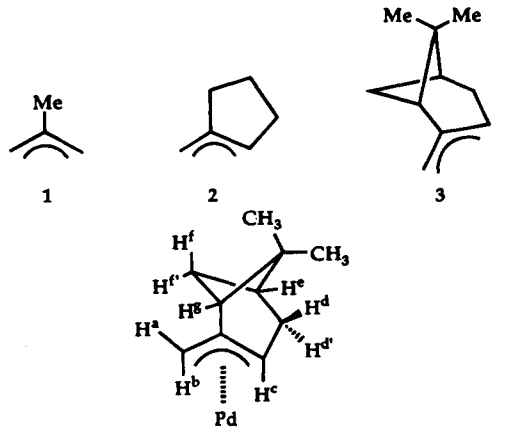

numbering system for η^3-$C_{10}H_{15}$

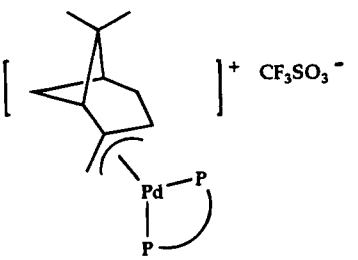

4 a, b = R- and S -BINAP

c = S,S - CHIRAPHOS

d = JOSIPHOS, 5a

(bidentate nitrogen ligand)]$^+$, the suggestion,[8] based on ^{1}H NOESY studies, that ring opening of the nitrogen chelate, followed by allyl isomerization, might explain apparent allyl rotation led to an elegant proof by Bäckvall and co-workers.[15] We have concentrated on Pd complexes with allyl ligands as shown in **1**–**4** (Chart 1), using commercially available chiral auxiliaries. In this study we center on Pd(II) allyl complexes of the novel chiral ferrocene-based ligand JOSIPHOS,[16] **5** (see Chart 2), and report on new structural and dynamic aspects. The ligands **5** possess two types of chirality and are effective chiral auxiliaries.

Results and Discussion

The new η^3-$C_{10}H_{15}$ (β-pinene) and η^3-C_3H_5 allyl JOSIPHOS complexes were prepared as described previously (see Experimental Section) by removing Cl^- from the chloro-bridged allyl compounds, using either Ag^+ or Tl^+, followed by reaction with the appropriate ligand **5**.

NMR for the β-Pinene-Allyl Complex. For [Pd(η^3-$C_{10}H_{15}$)(**5a**)]CF_3SO_3, **4d**, there are two rotational isomers (only one face of the β-pinene allyl can coordinate[5,10,11]). With respect to a coordination plane defined by the Pd and two P atoms, there are two possible orientations for the η^3-$C_{10}H_{15}$ ligand, and fragments of these structures are shown as follows:

(15) Gogoll, A.; Ornebro, J.; Grennberg, H.; Bäckvall, J. E. *J. Am.Chem. Soc.* **1994**, *116*, 3631.

(16) (a) Togni, A.; Breutel, C.; Schnyder, A.; Spindler, F.; Landert, H.; Tijani, A. *J. Am. Chem. Soc.* **1994**, *116*, 4062. (b) Togni, A.; Breutel, C.; Soares, M. C.; Zanetti, N.; Gerfin, T.; Gramlich, V.; Spindler, F.; Rihs, G. *Inorg. Chim. Acta* **1994**, *222*, 213. (c) For **5d** see: Abbenhuis, H. C. L.; Burckhardt, U.; Gramlich, V.; Köllner, C.; Pregosin, P. S.; Salzmann, R.; Togni, A. *Organometallics* **1995**, *14*, 759.

Chart 2. JOSIPHOS Ligands

JOSIPHOS Ligands

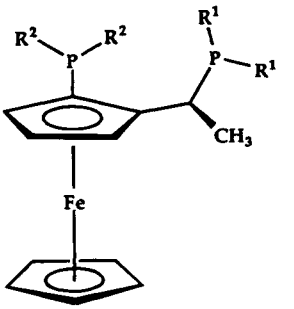

JOSIPHOS, 5

R^1	R^2
5a C_y = cyclohexyl	Ph = phenyl
5b Ph	C_y
5c Ph	Ph
5d phobyl	Ph

These ligands are S (on carbon) and R (on iron)

for the "phobyl" ([3.3.1]-9-phosphabicyclonon-9-yl, C_8H_{14}) complex there are two fused six-membered rings.

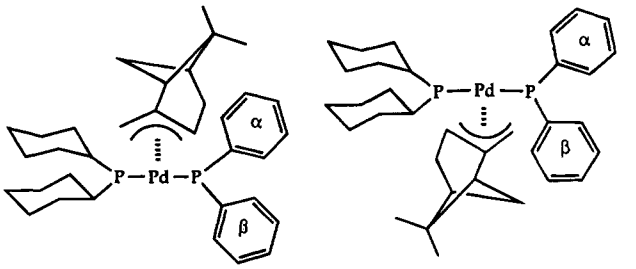

major isomer (I) minor isomer (II)

View from behind the allyl towards the Pd. R^1 = C_6H_{11}, R^2 = C_6H_5. The $C(CH_3)_2$ bridge of the allyl is remote from the Pd-atom.

From ^{31}P NMR the major/minor ratio is ca 10:1 (see Table 1), and we note that the major isomer has the larger part of the allyl hydrocarbon remote from the two cyclohexyl groups, i.e., the methine allyl carbon is pseudo-trans to the PCy_2 moiety.

The ^{1}H NOESY spectrum, see Figure 1, was used to assign the major isomer. One can recognize a strong NOE from the methine allyl proton, H^c, to the *ortho* protons of the β-phenyl ring. Further, the syn methylene allyl proton, H^a, is remote from the phenyls (no NOE's to these) but shows strong NOE's to the cyclohexyl protons. Additional NOE's support the structure assigned to the major isomer.[17a] The proton assignments[17b] follow from this and the ^{31}P,^{1}H correlation; see Table 2. There are several important structural conclusions which can be derived from the NOE analysis:

1. The chiral pocket differs from that of *S*-BINAP in that the two phenyls do **not** occupy pseudo-axial and equatorial positions. On the basis of the strong NOE's from **both** sets of *ortho* phenyl protons to the Cp proton H(30), we estimate that the substituted Cp ring approximately bisects the C(α)−P²−C(β) angle.

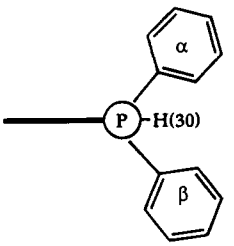

2. The six-membered chelate ring is in the form of a skew-boat, with the CH_3 of the stereogenic side chain lying roughly parallel to the upper Cp ring:

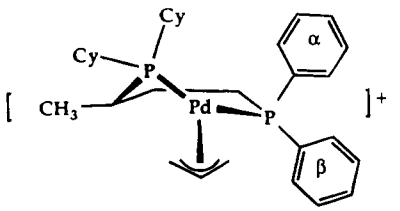

fragment of **6a**

This conformation, which exists in the solid-state structure of [Pd(η^3-C_3H_5)(**5a**)] CF_3SO_3,[16b] places the CH_3 close to an upper Cp ring proton and has the two cyclohexyl groups away from the lower η^5-C_5H_5 ring (no NOE between these). Generally speaking, this ring conformation can change and for the new C_3H_5 allyl complex, **6d**,[16c] mentioned later in the section on dynamics, the conformation is as follows:

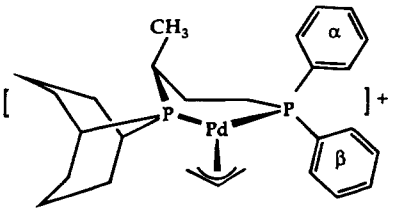

fragment of **6d**

In **6d** the CH_3 group is above the upper Cp plane and close to the α-P-phenyl group (there is an NOE from the methyl to the *ortho* protons of this ring). Obviously, the chelate ring conformation can depend on the P substituents.

3. The JOSIPHOS phenyl groups in [Pd(η^3-$C_{10}H_{15}$)(**5a**)]CF_3SO_3 intrude more into the coordination sphere of the pinene-allyl group than in the analogous[5] complexes [Pd(η^3-$C_{10}H_{15}$)(*S*-BINAP)]CF_3SO_3, **4b**, and [Pd(η^3-$C_{10}H_{15}$)(*S,S*-CHIRAPHOS)]CF_3SO_3, **4c**. Under comparable conditions one finds strong NOEs from the JOSIPHOS phenyl groups to the allyl protons H^c, $H^{d'}$, and H^f, as shown by the arrows in Figure 1. For these same protons in the BINAP and CHIRAPHOS complexes we observed[5,10,11] sometimes strong but often moderate-to-weak NOE's to these protons from the corresponding *ortho* phenyl protons. Clearly, in terms of its ability to intrude into the allyl coordination sphere,

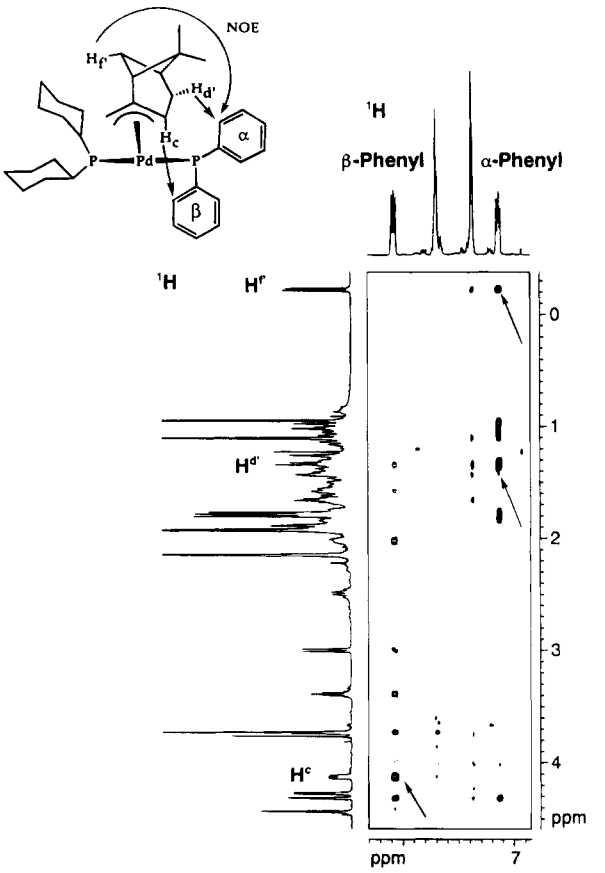

Figure 1. Section of the ¹H 2-D NOESY for **4** indicating the selective NOE's from the *ortho* α and β ring protons of the PPh_2 moiety to various aliphatic protons of the $C_{10}H_{15}$ allyl ligand. Specifically note the three arrows which indicate the cross-peaks arising from (top-to-bottom) H^f, $H^{d'}$, and the methine allyl proton H^c. These and other NOE's allow the major isomer to be correctly assigned and also allow us to develop a detailed structural picture for coordinated **5b** ($CDCl_3$, 500 MHz).

JOSIPHOS is a "big" ligand. The nature of, and the differences between, the chiral environments of a JOSIPHOS (and/or a BINAP) are important characteristics of these ligands and must be considered when rationalizing their effectiveness (or lack thereof) in, e.g., catalytic allylation.[16]

A comparison the ¹³C chemical shifts for the terminal allyl carbons of [Pd(η^3-$C_{10}H_{15}$)(**5a**)]CF_3SO_3, **4d**, with those for (*S* and *R*) [Pd(η^3-$C_{10}H_{15}$)(BINAP)]CF_3SO_3, **4a,b**, and [Pd(η^3-$C_{10}H_{15}$)(*S,S*-CHIRAPHOS)]CF_3SO_3, **4c**, is shown in Table 3. As the trialkylphosphine donor in **4d** is expected to have a stronger trans-influence,[18-20]

(17) (a) There are numerous other NOEs which support this assignment; e.g., $H^{d'}$, one of the two protons immediately adjacent to the methine allyl H^c, shows a strong NOE to the *ortho* protons of the phenyl group shown as "α". Moreover, the NOE data allow us to readily differentiate between the two phenyl groups; e.g., the bridgehead proton H^f, which lies very close to the Pd atom, reveals a strong selective NOE to the *ortho* protons of the phenyl shown as "α". (b) A comparison of H^a, H^b, and H^f within the two rotational isomers is particularly informative. In the major (minor) isomer, H^a appears at 4.28 (3.67), H^b at 3.00 (2.03), and $H^{f'}$ at −0.22 (+1.27). The changes in $H^{a,b}$ are consistent with the minor isomer having the allyl methylene close to the PPh_2 aromatic rings, once again, supporting the assignment. The shift for H^f, $\delta = -0.22$, the bridge-CH_2 proton close to the Pd atom, suggests that this has been placed directly above the α−phenyl ring. The ^1J(C,H) value for this $H^{f'}$ suggests that it is not agostic.

(18) Akermark, B.; Krakenberger, B.; Hansson, S.; Vitagliano, A. *Organometallics* **1987**, *6*, 620.

Table 1. ^{31}P NMR Data for [Pd(η^3-$C_{10}H_{15}$)(5a)]CF_3SO_3 and [Pd(η^3-C_3H_5)(5)]CF_3SO_3, 6

	δ^a	$^2J(P_A,P_B)$ ^{b}	δ^a	$^2J(P_A,P_B)$ ^{b}
	4d, major		*4d, minor*	
P^A	58.5	51.1	47.4	54.0
P^B	15.2		18.2	
	6a, major		*6a, minor*	
P^A	58.5	51.1	58.2	50.4
P^B	13.5		13.6	
	6b, major		*6b, minor*	
P^A	47.6	49.3	47.2	48.7
P^B	29.9		29.6	
	6c, major		*6c, minor*	
P^A	34.9	58.6	34.1	58.8
P^B	11.9		11.2	
	6d, major		*6d, minor*	
P^A	19.6	56.9	18.9	59.9
P^B	10.4		11.6	

^{a} Chemical shifts in ppm, relative to H_3PO_4 for $CDCl_3$ solutions at 297 K and at 200 MHz. ^{b} Coupling constants in Hz.

Table 2. ^{1}H and ^{13}C NMR Data^a for [Pd(η^3-$C_{10}H_{15}$)(5a)]CF_3SO_3

	major isomer		minor isomer	
position	^{1}H	^{13}C	^{1}H	^{13}C
b	3.00	63.7	2.03	72.3
c	4.13	83.7	4.07	79.9
d	1.94	28.4	2.70	
d′	1.34	28.4	2.54	
e	1.44	40.1	2.24	
f	1.67	30.4	1.33	
f′	0.22	30.4	1.27	
g	1.89	47.2	2.23	
h	0.95	21.7	1.01	21.9
i	1.11	25.9	1.23	26.0
"Cp"	3.73	71.7	3.77	71.7
CH_3	1.79	16.3	1.79	16.3
CH	3.39	31.0	3.34	29.8
	ortho-H	*ortho*-C	*ortho*-H	*ortho*-C
α	7.12	133.5	7.20	132.6
β	8.07	137.2	7.80	136.3

^{a} Values (in ppm, relative to TMS) have been measured in $CDCl_3$ at 297K and at 500 MHz (^{1}H) and 125 MHz (^{13}C).

Table 3. ^{13}C NMR Data^a for the Terminal Allyl Carbons in [Pd(η^3-$C_{10}H_{15}$)(chelate)]CF_3SO_3 Complexes

	C(1)	C(3)	
(*S*,*R*)-JOSIPHOS, **5a**^{b}	63.7	83.7	20.0
S-BINAP	73.7	81.3	7.6
R-BINAP	74.7	86.4	11.7
S,*S*-CHIRAPHOS	67.1	80.7	13.6
4,4′-dimethylbipyridine	60.0	67.5	7.5

^{a} Chemical shifts are for $CDCl_3$ solutions at ambient temperature, relative to TMS, at 125 MHz. ^{b} Major isomer.

and as the two terminal allyl carbons are in different environments, the two ^{13}C shifts will differ. Still, it is interesting that, for the JOSIPHOS derivative, the **difference** between C(1), trans to PPh_2, 63.7 ppm, and C(3), trans to PCy_2, 83.7 ppm, at 20.0 ppm, is the largest in the table. For the *S*- and *R*-BINAP complexes, the values are 7.6 and 11.9 ppm, respectively, whereas for *S*-CHIRAPHOS the difference is 13.6 ppm. For C(1), *S* pseudo-trans to the PPh_2 donor, the chemical shift of 63.7 ppm in **4d** is at relatively low frequency, suggesting this PPh_2 to be only a moderate donor. The corresponding ^{13}C(1) position in the complex [Pd(η^3-$C_{10}H_{15}$)(4,4′-dimethylbipyridine)]CF_3SO_3 is 60.0 ppm. The weakness of this PPh_2 donor is probably best understood in terms of steric interactions between the allyl hydrocarbon and the PPh_2 phenyl groups, as suggested above from the NOE data. Thus, the steric effects induce substantial changes in the electronic structure. This is presumably a general effect for ligand **5a** and could be relevant in a discussion of its effectiveness as allylation catalyst.[16]

Allyl Dynamics. It is well-known[13b,21−23] that allyl ligands can (but do not always) convert the syn and anti positions as shown:

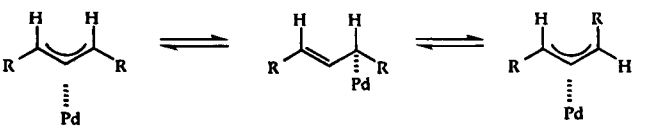

For the two rotational isomers of [Pd(η^3-C_3H_5)(**5a**)]$^+$, **III** and **IV**, one finds[14] a selective $\eta^3-\eta^1-\eta^3$ isomerization

Fragments for the isomers of the C_3H_5 complexes 6a

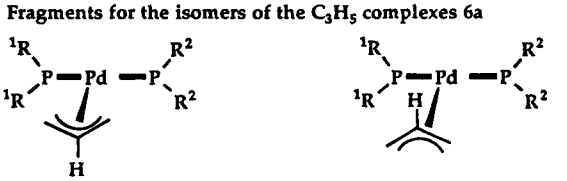

III, major isomer, central C-H bond points towards Fe **IV, minor isomer, central C-H bond points away from Fe**

involving opening of the Pd−C bond cis to the PCy_2 and trans to the PPh_2 moiety. This was the first example of this type of selectivity in a chiral phosphine complex and is interesting in that the trans influence of the PPh_2 aryl phosphine moiety is generally smaller[20] than that for the alkylphosphine PCy_2 donor. As the steric bulk of the PCy_2 group may play a role, we prepared the four η^3-C_3H_5 palladium complexes [Pd(η^3-C_3H_5)(JOSIPHOS)]$^+$, **6**, with the JOSIPHOS ligands **5a-d**[24] and studied the $\eta^3-\eta^1-\eta^3$ isomerization. The complexes **6**, which differ in R^1 and R^2 and thus have different electronic and steric effects, include **5a** and **5b** in which the R^1 and R^2

(19) Clark, H. C.; Hampden-Smith, M. J.; Rüegger, H. *Organometallics* **1988**, *7*, 2085 and references quoted therein.
(20) Appleton, T.; Clark, H. C.; Manzer, L. E. *Coord. Chem. Rev.* **1973**, *10*, 335. Motschi, H.; Pregosin, P. S.; Venanzi, L. M. *Helv. Chim. Acta* **1979**, *62*, 667. Motschi, H.; Pregosin, P. S. *Inorg. Chim. Acta* **1980**, *40*, 141. Motschi, H.; Nussbaumer, C.; Bachechi, F.; Mura, C.; Pregosin, P. S. *Inorg. Chim. Acta* **1980**, *63*, 2071.
(21) Vrieze, K. In *Dynamic Nuclear Magnetic Resonance Spectroscopy*; Jackman, L. M., Cotton, F. A., Eds.; Academic Press: New York, 1975. Cesarotti, E.; Grassi, M.; Prati, L.; Demartin, F. *J. Organomet. Chem.* **1989**, *370*, 407.
(22) Faller, J. W. *Determination of Organic Structures by Physical Methods*; Nachod, F. C., Zuckerman, J. J., Eds.; Academic Press: New York, 1973; Vol. 5, p 75.
(23) Cesarotti, E.; Grassi, M.; Prati, L.; Demartin, F. *J. Organomet. Chem.* **1989**, *370*, 407.
(24) The JOSIPHOS ligand in ref 14 was *R* at carbon and *S* at the metal and not *S* at carbon and *R* at the metal; however, for an η^3-C_3H_5 allyl this is not important.
(25) The absence of observable exchange means only that exchange is relatively slow compared to the mixing time, 0.8 s, and not that there is no exchange. We have not attempted to warm the samples.
(26) Weiss, R.; Verkade, J. G. *Inorg. Chem.* **1979**, *18*, 529. Vande Griend, L. J.; Verkade, J. G.; Pennings, J. F. M.; Buck, H. M. *J. Am. Chem. Soc.* **1977**, *99*, 2459 and references therein.

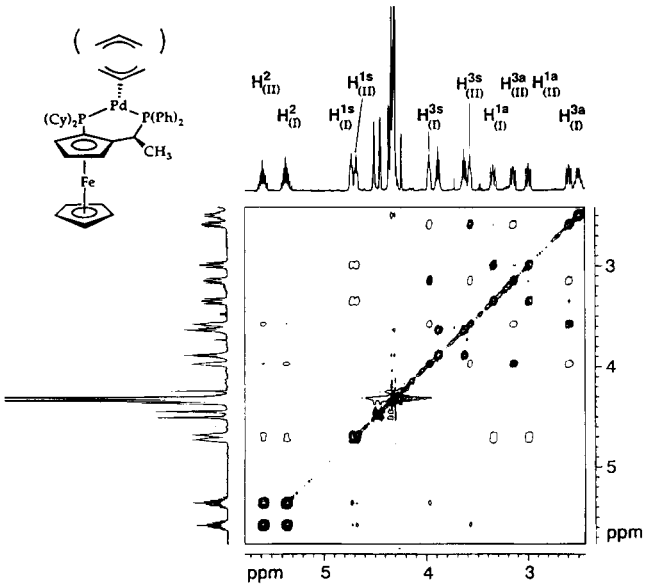

Figure 2. Section of the phase-sensitive ^{1}H 2-D NOESY spectrum for the C_3H_5 allyl complex **6b**. The "filled-in" cross-peaks arise from exchange, whereas the "open" cross-peaks arise from NOE's. The four signals in the lower-left corner demonstrate exchange between the rotational isomers. The interpretation is shown in Scheme 1. The major rotational isomer has the C(2)–H bond pointing away from the Fe atom ($CDCl_3$, 500 MHz).

Chart 3. JOSIPHOS Ligands

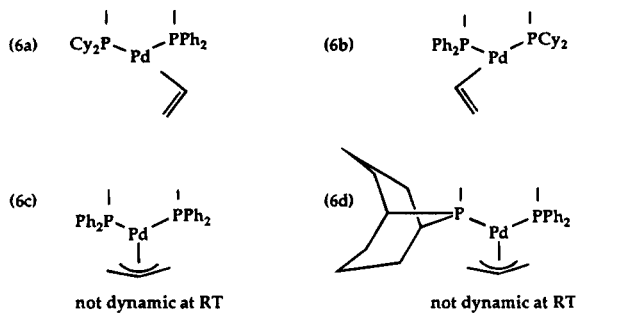

η^3-η^1-η^3 proceeds in both (a) and (b) such that the bond cis to the PCy2 opens.

No observable η^3- η^1- η^3 isomerization at ambient temperature for (c) and (d).

Scheme 1. Sketch Showing the Exchange Pathways

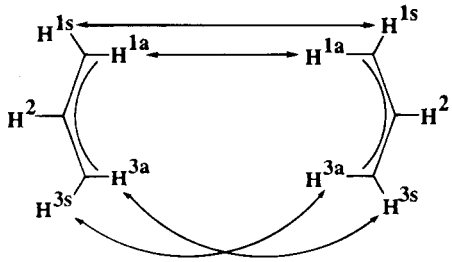

substituents have been "exchanged". We summarize the new exchange results in Chart 3 and show a section of the corresponding ^{1}H 2-D spectrum for [Pd(η^3-C_3H_5)(**5b**)]CF_3SO_3, **6b**, in Figure 2. The specific selective exchanges for **6b** are given, diagrammatically, in Scheme 1. The lower left corner of Figure 2 shows exchange between two central protons, H^2. The remainder of the spectrum shows the specific, well-resolved exchange cross-peaks (filled-in circles) for the eight protons, H^1 and H^3, four from each isomer.

Table 4. ^{13}C NMR Data[a] for the Terminal Allyl Carbons in the Complexes [Pd(η^3-C_3H_5)(5)]CF_3SO_3, 6

JOSIPHOS	trans to R^1	trans to R^2	ratio
5a	76.3	66.9	major, 1
	78.2	65.6	minor, 0.5
5b	70.1	73.1	major, 1
	67.1	76.8	minor, 0.9
5c	74.2	74.9	major, 1.0
	73.9	74.5	minor, 0.8
5d	76.3	72.3	major, 1.0
	78.2	70.7	minor, 0.6

[a] Chemical shifts are for $CDCl_3$ solutions at ambient temperature, at 125 MHz.

The open circle cross-peaks arise from NOE. There is **no** syn–anti exchange at C^1, the carbon cis to the PCy_2 moiety; however, the H^{1s} proton of one isomer exchanges with the H^{1s} proton of the other isomer. Exactly the same statement can be made for the H^{1a} proton. There **is** syn–anti exchange at C^3, the carbon cis to the PPh_2 moiety. The H^{3s} (or H^{3a}) proton of one isomer exchanges with the H^{3a} (or H^{3s}) proton of the other isomer. There is no syn–anti exchange within one isomer. From these results we see that there is selective formation of an η^1-transition state, followed by rotation around the C(2)–C(3) bond and then re-formation of the η^3-allyl.

Consequently, for [Pd(η^3-C_3H_5)(**5b**)]$^+$, **6b**, as for [Pd(η^3-C_3H_5)(**5a**)]$^+$, **6a**, the Pd–C (terminal) bond which is cis to the PCy_2 fragment opens. This is despite the fact that in **6b** there is a PCy_2{Cp-type} donor as opposed to a PCy_2{alkyl} donor in **6a**. For the cations [Pd(η^3-C_3H_5)(**5c**)]$^+$, **6c**, containing $R^1 = R^2 =$ Ph, and [Pd(η^3-C_3H_5)(**5d**)]$^+$, **6d**, with $R_2{}^1$ = "phobyl" and R^2 = Ph, we observe **no** η^3–η^1–η^3 isomerization at ambient temperature.[25] The result for **6d** is pertinent in that, although the cyclic phobyl group represents two aliphatic R^1 groups and is expected to be a donor comparable to other aliphatic substituents, it is a pinned-back[26] fragment and, thus, smaller. The measured rate of η^3–η^1–η^3 isomerization[14] is fast compared to the rate of catalytic allylation,[16] as previously noted.[27] The absence of isomerization in the phobyl derivative, **6d**, suggests that **steric and not electronic effects** are responsible for the selective η^3–η^1–η^3 isomerization in **6**.

In the isomers of the η^3-$C_{10}H_{15}$ cation, **4d**, there is **no** η^3–η^1–η^3 isomerization observable at ambient temperature.[25] Moreover, in studies[28] on Pd(II) compounds involving the 1,3-diphenylallyl anion, PhCH–CH–CHPh, one does not always observe syn–anti isomerization. Consequently, we again[5] suggest that η^3-C_3H_5 may not be a good model allyl for catalytic allylation. Apart from its small size, it shows a tendency to undergo a relatively rapid η^3–η^1–η^3 movement, a process which may be slower in other Pd(II)–allyl complexes.

Allyl ^{13}C Data for 6. In Table 4 we show ^{13}C data for the terminal allyl carbons in **6**, δ = 65.6–78.2 ppm. Due to the difference in trans-influence between the

(27) Mackenzie, P. B.; Whelan, J.; Bosnich, B. *J. Am. Chem. Soc.* **1985**, *107*, 2046. Auburn, P. R.; Mackenzie, P. B.; Bosnich, B. *J. Am. Chem. Soc.* **1985**, *107*, 2033.

(28) von Matt, P.; Lloyd-Jones, D. C.; Minidis, A.; Pfaltz, A.; Macko, L.; Neuberger, M.; Zehndert, M.; Rüegger, H.; Pregosin, P. S. Submitted for publication in *Helv. Chim. Acta.*

Table 5. Selected ^{1}H and ^{13}C NMR Data[a] for $[Pd(\eta^3\text{-}C_3H_5)(5)]CF_3SO_3$, 6

position	^{1}H	^{13}C	^{1}H	^{13}C
6a, major (H2 "down" [b])			**6a**, minor (H2 "up")	
1s	4.37	76.3	3.85	78.2
1a	2.29	76.3	3.63	78.2
2	5.84	121.9	5.04	120.7
3s	4.87	66.9	4.61	65.6
3a	2.86	66.9	3.31	65.6
"Cp"	3.64	70.9	3.74	70.6
CH_3	1.74	15.0	1.54	15.2
CH	3.51	29.8	3.63	29.8
6b, major (H2 "up")			**6b**, minor (H2"down")	
1s	4.73	70.1	4.63	67.1
1a	3.36	70.1	3.00	67.1
2	5.36	122.5	5.58	121.3
3s	3.97	73.1	3.58	76.8
3a	2.60	73.1	3.15	76.8
"Cp"	4.34	70.6	4.31	70.6
CH_3	1.54	14.0	1.52	14.0
CH	3.89	32.7	3.64	32.7
6c, major (H2 "down")			**6c**, minor (H2 "up")	
1s	4.63	74.2	4.36	73.9
1a	2.91	74.2	4.00	73.9
2	6.31	124.7	5.34	121.8
3s	4.07	74.9	3.94	74.5
3a	3.03	74.9	3.63	74.5
"Cp"	3.59	71.3	3.73	71.5
CH_3	1.30	17.1	1.31	16.9
CH	4.24	31.8	4.51	31.5
6d, major (H2 "down")			**6d**, minor (H2 "up")	
1s	4.33	76.3	3.77	78.2
1a	2.87	76.3	3.49	78.2
2	5.95	122.7	5.34	121.8
3s	5.03	72.2	4.73	70.7
3a	3.28	72.2	3.62	70.7
"Cp"	3.72	70.8	3.80	70.8
CH_3	1.21	22.5	1.06	22.5
CH	3.59	24.7	3.56	24.9

[a] Chemical shifts in ppm. Coupling constants in Hz. [b] The terms "up" and "down" refer to proximity of H^2 to the α and β Ph's ("up" has the CH bond pointing away from the Fe atom).

donors,[18] there is a marked separation of the two terminal carbons. Typical[18] chemical shifts are 70−79 ppm for model allyl complexes with chelating and monodentate aryl phosphines. In addition, Ozawa et al.[29] find $\delta = 69.7$ for the terminal carbons of the $[Pd(\eta^3\text{-}2\text{-}MeC_3H_4)(PMe_3)_2]^+$ cation. Also, Nakamura and coworkers[30] report $\delta = 55-58$ for the neutral complexes $[Pd(\eta^3\text{-}C_3H_5)CH_3(L)]$, L = tertiary phosphine, thereby showing that a terminal methylene allyl carbon trans to a "PR_3" can appear at lower frequency. We note that the difference, $\Delta\delta$, in the terminal carbon positions for the isomers in **6a** is relatively large. Since for **5a-d**, **5a** is the most effective of these chiral ligands in terms of enantioselectivity,[16a] it is tempting to believe that this electronic differentiation, noted above for the analogous $\eta^3\text{-}C_{10}H_{15}$ cation, may be important in the nucleophilic attack at the terminal carbon, i.e. enantioselectivity.

Conclusions. The β−pinene allyl complex **4d** with JOSIPHOS ligand **5a** has a sterically large chiral pocket, and the ligand intrudes markedly (much more so than *S,S*-CHIRAPHOS) into the coordination sphere of the η^3-allyl ligand. Coordinated **5** does not have marked axial/equatorial phenyl arrays but can show different chelate ring conformations as a function of R^1 and/or R^2. In **4d** there are interesting terminal allyl ^{13}C chemical shifts which hint at selective electronic effects. A selective $\eta^3-\eta^1-\eta^3$ isomerization as a function of the P-substitutents is observed, with steric effects providing the driving force for the selectivity.

Experimental Section

The NMR experiments were carried out using a Bruker AMX 500 spectrometer on 0.02 mmol samples in $CDCl_3$. The frequencies 500.13, 202.47, and 125.75 MHz were employed for ^{1}H, ^{13}C, and ^{31}P, respectively. Standard pulse sequences were employed for the ^{1}H−2D-NOESY,[31] ^{13}C−^{1}H,[32] and ^{31}P−^{1}H[33] correlation studies. The phase-sensitive NOESY experiments used mixing times of 0.8 s.

Ligand **5b** was provided by Dr. F. Spindler, Ciba-Geigy AG, Basel, Switzerland. The C_3H_5 complexes of **5** were prepared as described by us previously.[14]

The chloro-bridged dimer $[Pd(\eta^3\text{-}C_{10}H_{15})Cl]_2$ was prepared according to the literature[34] and recrystallized from CH_2Cl_2/hexane. This dimer (9.20 mg, 0.025 mmol) was dissolved in 2 mL of CH_2Cl_2, the mixture was then treated with solid (*S,R*)-JOSIPHOS (30.0 mg, 0.050 mmol), and the resulting solution was stirred for 10 h. $AgCF_3SO_3$ (12.9 mg, 0.050 mmol) in 1 mL of MeOH was then added to the yellow solution with immediate precipitation of a white solid. The suspension was then stirred in the dark for 1 h and filtered through Celite, and the solvent was distilled. The raw product was dissolved in a minimum of $CHCl_3$ and then treated with a 10-fold volume of ether. Storage at −30 °C overnight affords orange crystals, which were (a) collected via decantation, (b) washed with ether, and (c) dried *in vacuo* to afford 41 mg (81%) of product. Anal. Calc for $C_{47}H_{59}F_3O_3F_3P_2SFePd$ (985.25): C, 57.30; H, 6.04. Found: C, 57.18; H, 6.22.

Acknowledgment. P.S.P. thanks the Swiss National Science Foundation as well as the ETH for support and the Johnson-Matthey Research Foundation, Reading, England, for the loan of precious metals.

OM940688M

(29) Ozawa, F.; Son, T.; Ebina, S.; Osakada, K.; Yamamoto, A. *Organometallics* **1992**, *11*, 171.
(30) Hayashi, Y.; Matsumoto, K.; Nakamura, Y.; Isobe, K. *J. Chem. Soc., Dalton Trans.* **1989**, 1519.
(31) Sklener, V.; Miyashiro, H.; Zon, G.; Miles, H. T.; Bax, A. *FEBS Lett.* **1986**, *208*, 94.
(32) Summers, M. F.; Marzilli, L. G.; Bax, A. *J. Am. Chem. Soc.* **1986**, *108*, 4285.
(33) Jeener, J.; Meier, G. H.; Bachmann, P.; Ernst, R. *J. Chem. Phys.* **1979**, *71*, 4545.
(34) Trost, B. M.; Strege, P. E.; *J. Am. Chem. Soc.* **1975**, *97*, 2534.

Low Oxidation Dinuclear Titanium Complexes with the Bridging μ-(Dimethylsilyl)biscyclopentadienyl Ligand. Crystal Structure of $[\{Ti(\eta^5\text{-}C_5H_5)\}_2(\mu\text{-}Cl)_2\{\mu\text{-}Me_2Si(C_5H_4)_2\}]$

Tomás Cuenca, Ana Padilla, and Pascual Royo*

Departamento de Química Inorgánica, Universidad de Alcalá, Campus Universitario, E-28871 Alcalá de Henares, Spain

Miguel Parra-Hake

Centro de Graduados e Investigación, Instituto Tecnológico de Tijuana, Apdo. Postal 1166, 22000 Tijuana, México

Maria Angela Pellinghelli and Antonio Tiripicchio

Dipartimento di Chimica Generale ed Inorganica, Chimica Analitica, Chimica Fisica, Università di Parma, Centro di Studio per la Strutturistica Diffrattometrica del CNR, Viale delle Scienze 78, I-43100 Parma, Italy

Received August 9, 1994[⊗]

The chlorotitanium(III) derivative $[\{Ti(\eta^5\text{-}C_5H_5)\}_2(\mu\text{-}Cl)_2\{\mu\text{-}Me_2Si(C_5H_4)_2\}]$ (**2**) was synthesized in 85% yield by reduction of the titanium(IV) derivative $\{[Ti(\eta^5\text{-}C_5H_5)Cl_2]_2[\mu\text{-}Me_2Si(C_5H_4)_2]\}$ (**1**) with 2 equiv of sodium amalgam. The structure of **2** has been determined by X-ray diffraction methods. Crystals are monoclinic, space group $P2_1/n$, with $Z = 8$, in a unit cell of dimensions $a = 28.262(10)$, $b = 8.089(5)$, and $c = 18.446(9)$ Å, $\beta = 91.06(2)°$. The structure has been solved from diffractometer data by direct and Fourier methods and refined by blocked full-matrix least-squares methods on the basis of 3200 observed reflections to R and R_w values of 0.0568 and 0.0727, respectively. The $[Me_2Si(C_5H_4)_2]^{2-}$ ligand, through the two cyclopentadienyl rings, acts as a bridge between the two Ti atoms, which are also involved in a double Cl bridge. Moreover, each Ti atom η^5-interacts with a cyclopentadienyl ring. If the cyclopentadienyl centroids are considered as coordination sites, then the coordination geometry around each titanium is distorted tetrahedral. In the presence of oxygen, **2** is immediately transformed into the μ-oxo compound $\{[Ti(\eta^5\text{-}C_5H_5)Cl]_2(\mu\text{-}O)[\mu\text{-}Me_2Si(C_5H_4)_2]\}$. Reduction of **1** with sodium amalgam or $HgCl_2$-activated magnesium in THF at room temperature in the presence of a stoichiometric amount of the appropriate ligand (L) gave the titanium(II) adducts $\{Ti(\eta^5\text{-}C_5H_5)L_2\}_2[\mu\text{-}Me_2Si(C_5H_4)_2]$ [L = CO (**3**); CN(2,6-$C_6H_3Me_2$) (**5**)]. The same reduction of **1** with sodium amalgam or $HgCl_2$-activated magnesium in THF, in the presence of PMe_2Ph, resulted in the loss of hydrogen and formation of the diamagnetic complex $[\{Ti(PMe_2Ph)\}_2(\mu\text{-}\eta^1\text{-}\eta^5\text{-}C_5H_4)_2\{\mu\text{-}Me_2Si(C_5H_4)_2\}]$ (**6**). The dicarbonyl derivative **3** was also obtained by reaction of $[\{Ti(\eta^5\text{-}C_5H_5)Me_2\}_2\{\mu\text{-}Me_2Si(C_5H_4)_2\}]$ with CO. This reaction enables us to identify the formation of the acetone-coordinated titanium compound **4** as an intermediate species.

Introduction

The (dimethylsilyl)biscyclopentadienyl anion, $[Me_2Si(C_5H_4)_2]^{2-}$, is capable of being coordinated to metallic centers as a chelating group (type I) or as a bridging group (type II) (Figure 1). This ligand has been successfully used to stabilize both high and low oxidation group 4d metal complexes. The chemistry of mononuclear compounds, type I, with symmetric and asymmetric rings bridged by a SiR_2 fragment and their potential applications as catalysts in stereo- and enantioselective hydrogenation and polymerization of olefins have been extensively studied.[1] Recently we reported the synthesis of similar halo- and alkyltitanium(IV) derivatives,[2] as well as new titanium(III) and -(II) metallocene complexes[3] containing this ligand as a chelating system (type I), and some aspects of their chemical behavior. Dinuclear compounds, type II, are also well represented,[4] although they are less well-known for group 4d metals[5] and few dinuclear derivatives of these metals are known in low oxidation states.

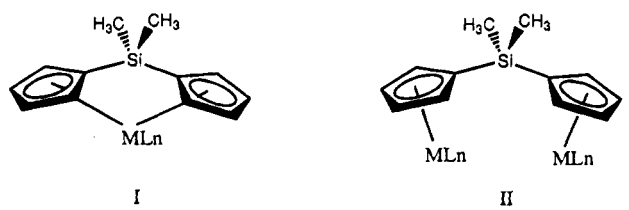

Figure 1. Coordination modes of the (dimethylsilyl)biscyclopentadienyl ligand.

It has been demonstrated that the access to dinuclear titanium(III) and zirconium(III) complexes can be fa-

⊗ Abstract published in *Advance ACS Abstracts*, December 1, 1994.

0276-7333/95/2314-0848$09.00/0

Scheme 1

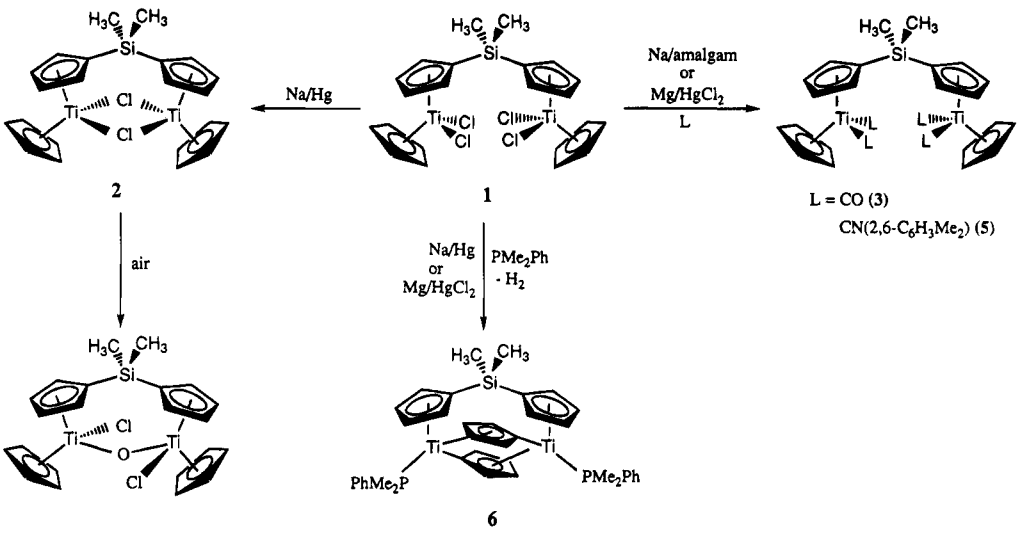

cilitated by using the fulvalene ligand, which is capable of being coordinated to two metal centers, and its inherent rotational flexibility can lead to *trans* or *cis* configurations of the coordinated metal fragments.[6] Furthermore, this ligand is capable of undergoing carbon–hydrogen bond cleavage, leading to the formation of dinuclear complexes containing η^1-η^5-C_5H_4 bridging groups.[6g–i,7] The use of the (dimethylsilyl)biscyclopentadienyl anion, $[Me_2Si(C_5H_4)_2]^{2-}$, as a bridging ligand is an alternative system to prepare this type of dinuclear complexes, but only one dinuclear zirconium(III) compound, [{Zr(η^5-C_5H_5)}$_2$(μ-Cl)$_2${μ-$Me_2Si(C_5H_4)_2$}], with this bridging ligand has been reported.[5c] We describe below the synthesis and characterization of new dinuclear titanium(III) and -(II) complexes [{Ti(η^5-C_5H_5)}$_2$(μ-Cl)$_2${μ-$Me_2Si(C_5H_4)_2$}] (**2**), [{Ti(η^5-C_5H_5)L$_2$}$_2${μ-$Me_2Si(C_5H_4)_2$}] [L = CO (**3**), CN(2,6-$C_6H_3Me_2$) (**5**)], and [{Ti(PMe$_2$Ph)}$_2$(μ-η^1-η^5-C_5H_4)$_2${μ-$Me_2Si(C_5H_4)_2$}] (**6**). All these compounds were characterized by analytical and spectroscopic methods, and the X-ray structure of **2** was fully elucidated by an X-ray diffraction study.

Results and Discussion

Reduction of a toluene solution of the titanium(IV) derivative [{Ti(η^5-C_5H_5)Cl$_2$}$_2${μ-$Me_2Si(C_5H_4)_2$}] (**1**) with 2 equiv of sodium amalgam gave the chlorotitanium(III) complex [{Ti(η^5-C_5H_5)}$_2$(μ-Cl)$_2${μ-$Me_2Si(C_5H_4)_2$}] (**2**) (Scheme 1) as a dark amber crystalline solid in 85% yield. Complex **2** is scarcely soluble in THF and more soluble in dichloromethane, from which it can be recrystallized to give single crystals suitable for an X-ray study. Complex **2** is very oxygen and moisture sensitive but can be stored unchanged under argon or nitrogen for months. In the presence of oxygen, **2** is immediately transformed into the μ-oxo compound [{Ti(η^5-C_5H_5)Cl}$_2$(μ-O){μ-$Me_2Si(C_5H_4)_2$}].[5e] Magnetic susceptibility measurements at room temperature gave a magnetic moment (μ_{eff}) of 1.423 ± 0.66 μB, similar to values previously observed for other μ-halotitanium(III) derivatives.[8]

When the reduction of **1** was carried out with sodium amalgam or $HgCl_2$-activated magnesium in THF at room temperature (Scheme 1) in the presence of the stoichiometric amount of the appropriate ligand L, the titanium(II) adducts [{Ti(η^5-C_5H_5)L$_2$}$_2${μ-$Me_2Si(C_5H_4)_2$}] [L = CO (**3**); CN(2,6-$C_6H_3Me_2$), (**5**)] were isolated in high

(1) (a) Kopf, H.; Kahl, W. *J. Organomet. Chem.* **1974**, *64*, C37. (b) Fendrick, C. M.; Mintz, E. A.; Schertz, L. D.; Marks, T. J.; Day, V. W. *Organometallics*, **1984**, *3*, 819. (c) Yasuda, H.; Nagasuna, K.; Akita, M.; Lee, K.; Nakamura, A. *Organometallics* **1884**, *3*, 1470. (d) Bajgur, C. S.; Tikkanen, W. R.; Petersen, J. L. *Inorg. Chem.* **1985**, *24*, 2539. (e) Jeske, G.; Schock, L. E.; Swepston, P. N.; Schumann, H.; Marks, T. J. *J. Am. Chem. Soc.* **1985**, *107*, 8103. (f) Jutzi, P.; Dickbreder, R. D. *Chem. Ber.* **1986**, *119*, 1750. (g) Muller, J.; Ludemann, F.; Kopf, H. *J. Organomet. Chem.* **1986**, *303*, 167. (h) Herrmann, W. A.; Rohrmann, J.; Herdtweck, E.; Spaleck, W.; Winter, A. *Angew. Chem., Int. Ed. Engl.* **1989**, *28*, 1511. (i) Kabi-Satpathy, A.; Bajgur, C. S.; Reddy, K. P.; Petersen, J. L. *J. Organomet. Chem.* **1989**, *363*, 105. (j) Roll, W.; Brintzinger, H. H.; Rieger, B.; Zolf, R. *Angew. Chem., Int. Ed. Engl.* **1990**, *29*, 279. (k) Conticello, V. P.; Brard, L.; Giardello, M. A.; Tsuji, Y.; Sabat, M.; Stern, C. L.; Marks, T. J. *J. Am. Chem. Soc.* **1992**, *114*, 2761.

(2) (a) Gómez, R.; Cuenca, T.; Royo, P.; Herrmann, W. A.; Herdweck, E. *J. Organomet. Chem.* **1990**, *382*, 103. (b) Gómez, R.; Cuenca, T.; Royo, P.; Hovestreydt, E. *Organometallics* **1991**, *10*, 2516.

(3) (a) Gómez, R.; Cuenca, T.; Royo, P.; Pellinghelli, M. A.; Tiripicchio, A. *Organometallics* **1991**, *10*, 1505. (b) Cuenca, T.; Gómez, R.; Gómez-Sal, P.; Royo, P. *J. Organomet. Chem.* **1993**, *454*, 105.

(4) (a) Weaver, J.; Woodward, P. *J. Chem. Soc., Dalton Trans.* **1973**, 1439. (b) Wegner, P. A.; Uski, V. A.; Kiester, R. P.; Dabestani, S.; Day, V. W. *J. Am. Chem. Soc.* **1977**, *99*, 4846. (c) Wright, M. E.; Mezza, T. M.; Nelson, G. O.; Amstrong, N. R. *Organometallics* **1983**, *2*, 1711. (d) Abrieland W., Heck, J. *J. Organomet. Chem.* **1986**, *302*, 363. (e) Hock, N.; Oroschin, W.; Paolucci, G.; Fischer, R. D. *Angew. Chem., Int. Ed. Engl.* **1986**, *25*, 738. (f) Qiao, K.; Fischer, R. D.; Paolucci, G.; Traldi, P.; Celon, E. *Organometallics* **1990**, *9*, 1361.

(5) (a) Reddy, K. P.; Petersen, J. L. *Organometallics* **1989**, *8*, 547. (b) Reddy, K. P.; Petersen, J. L. *Organometallics* **1989**, *8*, 2107. (c) Cacciola, J.; Reddy, K. P.; Petersen, J. L. *Organometallics* **1992**, *11*, 665. (d) Ciruelos, S.; Cuenca, T.; Flores, J. C.; Gómez, R.; Gómez-Sal, P.; royo, P. *Organometallics* **1993**, *12*, 944. (e) Cuenca, T.; Flores, J. C.; Gómez, R.; Gómez-Sal, P.; Parra-Hake, M.; Royo, P. *Inorg. Chem.* **1993**, *32*, 3608.

(6) (a) Ashworth, T. V.; Cuenca, T.; Herdtweck, E.; Herrmann, W. A. *Angew. Chem., Int. Ed. Engl.* **1986**, *25*, 289. (b) Cuenca, T.; Herrmann, W. A.; Ashworth, T. V. *Organometallics* **1986**, *5*, 2514. (c) Herrmann, W. A.; Cuenca, T.; Küsthardt, U. *J. Organomet. Chem.* **1986**, *309*, C15. (d) Herrmann, W. A.; Cuenca, T.; Menjón, B.; Herdtweck, E. *Angew. Chem., Int. Ed. Engl.* **1987**, *26*, 697. (e) Cuenca, T.; Gómez, R.; Gómez-Sal, P.; Rodriguez, G.; Royo, P. *Organometallics* **1992**, *11*, 1229. (f) Gambarotta, S.; Chiang, M. Y. *Organometallics* **1987**, *6*, 897. (g) Wielstra, Y.; Gambarotta, S.; Meetsma, A.; de Boer, J. L. *Organometallics* **1989**, *8*, 250. (h) Wielstra, Y.; Gambarotta, S.; Meetsma, A.; Spek, A. L. *Organometallics* **1989**, *8*, 2948. (i) Wielstra, Y.; Meetsma, A.; Gambarotta, S.; Khan, S. *Organometallics* **1990**, *9*, 876. (j) Wielstra, Y.; Gambarotta, S.; Spek, A. L.; Smeets, W. J. J. *Organometallics* **1990**, *9*, 2142.

(7) (a) Berry, M.; Cooper, N. J.; Green M. L. H.; Simpson, S. J. *J. Chem. Soc., Dalton Trans.* **1980**, 29. (b) Erker, G.; Schlund, R.; Krüger, C. *Organometallics* **1989**, *8*, 2349.

(8) Wailes, P. C.; Coutts, R. S. P.; Weigold, H. *Organometallic Chemistry of Titanium, Zirconium and Hafnium*; Academic Press: New York 1974.

Table 1. ^{13}C NMR Data for Titanium and Zirconium Complexes with the Ligand $[Me_2Si(C_5H_4)_2]^{2-}$ [a,b]

complex	C_1	C_2	C_3	ref
$TiCl_2[SiMe_2(\eta^5\text{-}C_5H_4)_2]$	106.7	135.5	118.8	1d
$Ti(PMe_2Ph)_2[SiMe_2(\eta^5\text{-}C_5H_4)_2]$	81.3	102.4	90.4	3b
$Ti(CO)_2[SiMe_2(\eta^5\text{-}C_5H_4)_2]$	76.9	103.1	90.8	3b
$Ti[CN(2,6\text{-}C_6H_3Me_2)]_2[SiMe_2(\eta^5\text{-}C_5H_4)_2]$	80.9	106.2	92.3	3b
$ZrCl_2[SiMe_2(\eta^5\text{-}C_5H_4)_2]$	109.2	128.6	114.3	1d
$[TiCpCl_2]_2[\mu\text{-}SiMe_2(\eta^5\text{-}C_5H_4)_2]$	135.5	129.1	120.8	5e
$[ZrCpCl_2]_2[\mu\text{-}SiMe_2(\eta^5\text{-}C_5H_4)_2]$	124.6	125.3	117.2	5b
$[ZrCp^*Cl_2]_2[\mu\text{-}SiMe_2(\eta^5\text{-}C_5H_4)_2]$	128.2	125.5	115.3	5b
$[ZrCp(\mu\text{-}Cl)]_2[\mu\text{-}SiMe_2(\eta^5\text{-}C_5H_4)_2]$	114.3	112.4	104.2	5c
$\{TiCp[CN(2,6\text{-}C_6H_3Me_2)_2]\}_2[\mu\text{-}SiMe_2(\eta^5\text{-}C_5H_4)_2]$	97.4	103.6	97.6	this work
$[Ti(\mu\text{-}\eta^1\text{-}\eta^5\text{-}C_5H_4)(PMe_2Ph)]_2[\mu\text{-}SiMe_2(\eta^5\text{-}C_5H_4)_2]$	87.6			this work

[a] Chemical shifts in ppm reference to TMS. [b] Cp = C_5H_5; Cp* = C_5Me_5.

yield after evaporation of the solvent and extraction of the crude residue with hexane. The solubility and air sensitivity of these dinuclear compounds are similar to those reported[3b] for the mononuclear complexes containing the same (dimethylsilyl)biscyclopentadienyl group as a chelating ligand.

The IR spectra of all these complexes show the characteristic absorptions reported[9] for compounds containing this silyl-bridged biscyclopentadienyl ligand. Two IR absorption bands are observed for ν(CO) (1870 and 1960 cm^{-1}) and ν(CN) (1932 and 2033 cm^{-1}) stretching frequencies for complexes **3** and **5**, respectively, which are lower than those observed for the corresponding mononuclear derivatives $[Ti(CO)_2][Me_2Si(C_5H_4)_2]$ [ν(CO), 1905 and 1980 cm^{-1}] and $[Ti\{CN(2,6\text{-}C_6H_3Me_2)\}_2][Me_2Si(C_5H_4)_2]$ [ν(CN), 1938 and 2044 cm^{-1}].[3b] This effect reveals an enhanced TiCX (X = O, NR) back-donation due to the increase of electron density at the metal center, provided by the presence of one C_5H_5 ring instead of a silyl-substituted cyclopentadienyl group.

The ^1H NMR spectra for **3** and **5** show the expected two pseudotriplets for the silylcyclopentadienyl ring protons of an AA'BB' spin system, one singlet for the protons for both equivalent methylsilyl groups of the bridging ligand and one singlet for the unsubstituted cyclopentadienyl ring protons. All the resonances are displaced to higher fields, particularly those observed for the dicarbonyl compound **3**, as expected for lower valent metal compounds.

The same reduction of **1** with sodium amalgam or $HgCl_2$-activated magnesium in THF in the presence of PMe_2Ph resulted in the loss of hydrogen and formation of the diamagnetic complex $[\{Ti(PMe_2Ph)\}_2(\mu\text{-}\eta^1\text{-}\eta^5\text{-}C_5H_4)_2(\mu\text{-}Me_2Si(C_5H_4)_2\}]$ (**6**) as a crystalline dark violet solid (Scheme 1). A similar $\eta^1\text{-}\eta^5\text{-}C_5H_4$ disposition has been reported[10] by Rausch and co-workers for other group 4 metal derivatives, and the X-ray structure of $[Ti(\eta^5\text{-}C_5H_5)(PMe_3)]_2(\mu\text{-}\eta^1\text{-}\eta^5\text{-}C_5H_4)_2$ has been determined.[10c] It has been reported[10c] that this $\mu\text{-}\eta^1\text{-}\eta^5\text{-}C_5H_4$-bridged compound results only when the reduction of $Ti(\eta\text{-}C_5H_5)_2Cl_2$ is carried out in the presence of 2 equiv of PMe_3, whereas the same reaction in the presence of an excess of PMe_3 gives the titanium(II) complex $Ti(\eta\text{-}C_5H_5)_2(PMe_3)_2$. We have observed a different behavior for the (dimethylsilyl)biscyclopentadienyl derivatives. The reduction of the mononuclear *ansa*-$[TiCl_2][Me_2Si(C_5H_4)_2]$ complex in the presence of any amount of PMe_2Ph gives the *ansa*-$[Ti(PMe_2Ph)_2][Me_2Si(C_5H_4)_2]$ compound,[3b] whereas the same reaction with the dinuclear derivative **1** aways leads to the $\mu\text{-}\eta^1\text{-}\eta^5\text{-}C_5H_4$ complex **6**, even when the Ti/PMe_2Ph molar ratio is 1/14.

The ^1H NMR spectrum of complex **6** reveals that all the protons from the $\eta^1\text{-}\eta^5\text{-}C_5H_4$ bridging groups and from the cyclopentadienyl rings of the $\mu\text{-}[Me_2Si(C_5H_4)_2]$ ligand are magnetically not equivalent and appear as eight multiplets (δ 4.36–5.88), corresponding to an ABCD spin system for each ring. The methyl groups of the PMe_2Ph ligand give two doublets, corresponding to two diastereotopic methyl groups, as a result of the chirality of the metal center, with $^2J_{P-H}$ = 4.5 Hz. The ^{13}C NMR spectrum of **6** shows the resonance due to the metal σ-bonded C_1 of the bridging $\mu\text{-}\eta^1\text{-}\eta^5\text{-}C_5H_4$ unit (δ 190.8), significantly shifted to lower field in comparison with the proximal and distal C_2 and C_3 resonances. The $^2J_{P-C}$ coupling constant for this C_1 resonance is high (15.1 Hz), whereas those for C_2 and C_3 are not detectable. These data are in agreement with a direct Ti–C_1 σ-bond and are consistent with the $\sigma-\pi$ bridging arrangement of the $\eta^1\text{-}\eta^5\text{-}C_5H_4$ unit, as reported[10] for similar compounds.

The ^{13}C resonance due to the cyclopentadienyl bridgehead *ipso*-carbon C_1 atom of the $[Me_2Si(C_5H_4)_2]^{2-}$ anion appears to be sensitive to the mode of coordination of the ligand. For most dinuclear titanium and zirconium derivatives containing this group as a bridging ligand, the C_1 resonance is typically found downfield from the proximal and distal C_2 and C_3 resonances, which are less sensitive to the mode of coordination, as shown in Table 1, whereas the opposite behavior is observed for similar *ansa*-mononuclear complexes. This spectral feature has been used to distinguish both possible coordination modes of the ligand. However, the behavior observed for compound **5** and **6** is the reverse, as the bridgehead C_1 ^{13}C resonance is shown shifted downfield (δ 97.39 and 87.6, respectively) with respect to the C_2 and C_3 resonances, thus proving that this spectral behavior cannot be used as a general rule to predict the bridging or chelating disposition of the (dimethylsilyl)biscyclopentadienyl ligand in this type of group 4 metal derivatives.

The reaction of **6** with HCl was studied in order to gain further support for its formulation. The reaction of a toluene solution of **6** with a 1 M diethyl ether solution of HCl (Ti/HCl molar ratio 1/2) proceeds with formation of the known titanium(III) compound **2**. When the same reaction was carried out using a Ti/HCl

(9) (a) Bürger, H. *Organomet. Chem. Rev.* **1968**, *3*, 425. (b) Cotton, F. A.; Marks, T. J. *J. Am. Chem. Soc.* **1969**, *91*, 7281.

(10) (a) Gell, K. I.; Harris, T. V.; Schwartz, J. *Inorg. Chem.* **1981**, *20*, 481. (b) Gell, K. I.; Schwartz, J. *J. Am. Chem. Soc.* **1981**, *103*, 2687. (c) Kool, L. B.; Rausch, M. D.; Alt, H. G.; Herberhold, M.; Thewalt, U.; Honold, B. *J. Organomet. Chem.* **1986**, *310*, 27.

Scheme 2

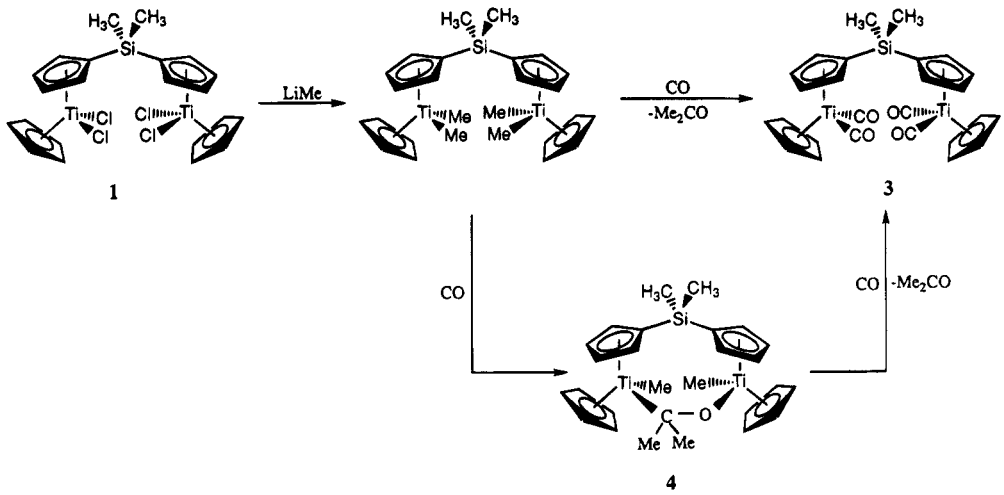

molar ratio of 1/4, the reported[5e] titanium(IV) derivative [{Ti(η^5-C_5H_5)Cl_2}$_2${μ-$Me_2Si(C_5H_4)_2$}] was isolated. These reactions demonstrate that the first step consists of the addition of HCl to the σ-Ti−C bond of the bridging Ti-η^1-η^5-C_5H_4 group, regenerating the η^5-C_5H_5 disposition with simultaneous substitution and formation of one Ti−Cl bond to give **2**. The second equivalent of HCl reacts with **2** to give the titanium(IV) complex with evolution of hydrogen by an oxidative addition process.

The dicarbonyl derivative **3** was also obtained by reaction of [{Ti(η^5-C_5H_5)Me_2}$_2${μ-$Me_2Si(C_5H_4)_2$}][5e] with CO (Scheme 2).

When CO was bubbled through a toluene solution of the dimethyl compound and the reaction mixture was stirred overnight, a reddish brown solution was obtained. Subsequent workup of the resulting solution showed the presence of acetone and afforded a dark red crystalline compound which was characterized as **3**. The reaction between dimethyl group 4 metal derivatives with CO is known to give the reduced titanium(II) dicarbonyl compounds with elimination of acetone,[8] probably through the formation of an intermediate acetone-coordinated species, although few early transition metal−acetone complexes have been isolated.[11] When the reaction of [{Ti(η^5-C_5H_5)Me_2}$_2${μ-$Me_2Si(C_5H_4)_2$}] with CO was monitored by ^{1}H NMR spectroscopy, the formation of an intermediate species was detected. Its ^{1}H NMR spectrum showed two signals for the cyclopentadienyl ring protons at δ 5.78 and 5.81, indicative of the presence of two nonequivalent titanium atoms and two singlets at δ 0.88 and 0.89, due to the methyl protons of an acetone ligand bridging both titanium atoms, along with other methyl resonances due to the methyl groups bonded to the silicon and the titanium atoms. This behavior suggests the intermediate formation of the acetone-coordinated titanium compound **4** (Scheme 2), which could not be isolated. In the presence of an excess of CO, **4** evolves acetone, and new ^{1}H resonances appear, corresponding to the dicarbonyl compound **3**.

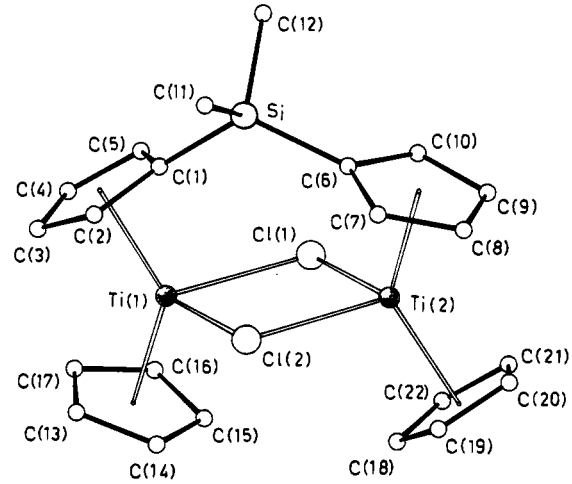

Figure 2. Perspective view of the molecular structure of one of the two independent complexes [{Ti(η^5-C_5H_5)}$_2$(μ-Cl)$_2${μ-$Me_2Si(C_5H_4)_2$}] (**2**) with the atomic labeling scheme.

The dimeric nature of the starting compounds {[Ti(η^5-C_5H_5)X_2]$_2$[μ-$Me_2Si(C_5H_4)_2$]} (X = Cl, Me) is responsible for the different behavior observed in the reduction of the chloro derivative in the presence of PMe_2Ph and favors the formation of the intermediate acetone-coordinated complex in the reaction of the dimethyl derivative with CO with respect to the reported reactions with mononuclear derivatives.

Description of the Crystal Structure of [{Ti(η^5-C_5H_5)}$_2$(μ-Cl)$_2${μ-$Me_2Si(C_5H_4)_2$}] (2). In the crystals of **2**, two crystallographically independent but essentially identical molecules are present. The structure of one of them is depicted in Figure 2, together with the atomic numbering scheme; the most important bond distances and angles are given in Table 2. The [$Me_2Si(C_5H_4)_2$]$^{2-}$ ligand acts as a bridge between the two Ti atoms through the two cyclopentadienyl rings interacting, in a nearly symmetrical η^5-fashion. The two metals (at a separation distance of 3.8 Å) are symmetrically bridged also by two Cl atoms, the Ti−Cl bond distances ranging from 2.507(3) to 2.536(33) Å [2.515(4) to 2.534(3) Å; heretoafter, the values in brackets refer to the second independent molecule]. Each Ti atom is

(11) (a) Wood, C. D.; Schrock, R. R. *J. Am. Chem. Soc.* **1979**, *101*, 5421. (b) Martin, B. D.; Mactchett, S. A.; Norton, J. R.; Anderson, O. P. *J. Am. Chem. Soc.* **1985**, *107*, 7952. (c) Stella, S.; Floriani. C. *J. Chem. Soc., Chem. Commun.* **1986**, 1053. (d) Erker, G.; Czisch, P.; Schlund, R.; Angermund, K.; Kruger, C. *Angew. Chem., Int. Ed. Engl.* **1986**, *25*, 364. (e) Erker, G.; Dorf, U.; Czisch, P.; Petersen, J. L. *Organometallics* **1986**, *5*, 668. (f) Berno, P.; Stella, S.; Floriani, C.; Chiesi-Villa, A.; Guastini, C. *J. Chem. Soc., Dalton Trans.* **1990**, 2669. (g) Bryan, J. C.; Mayer, J. M. *J. Am. Chem. Soc.* **1987**, *109*, 7213. (h) Flores, J. C.; Mena, M.; Royo, P.; Serrano, R. *J. Chem. Soc., Chem. Commun.* **1989**, 617.

Table 2. Selected Bond Distances (Å) and Angles (deg) with Esd Values in Parentheses for Compound 2[a]

	molecule 1	molecule 2
Ti(1)−Cl(1)	2.535(3)	2.519(3)
Ti(1)−Cl(2)	2.519(3)	2.534(3)
Ti(2)−Cl(1)	2.536(3)	2.515(4)
Ti(2)−Cl(2)	2.507(3)	2.531(3)
Ti(1)−CE(1)	2.054(11)	2.056(11)
Ti(2)−CE(2)	2.055(9)	2.061(11)
Ti(1)−CE(3)	2.069(10)	2.070(15)
Ti(2)−CE(4)	2.089(12)	2.065(14)
Si−C(1)	1.888(10)	1.852(10)
Si−C(6)	1.846(11)	1.865(10)
Si−C(11)	1.863(12)	1.836(13)
Si−C(12)	1.858(12)	1.836(12)
Cl(1)−Ti(1)−Cl(2)	81.9(1)	82.6(1)
Cl(1)−Ti(1)−CE(1)	108.9(3)	108.3(4)
Cl(1)−Ti(1)−CE(3)	107.5(4)	107.5(4)
Cl(2)−Ti(1)−CE(1)	108.5(3)	107.5(3)
Cl(2)−Ti(1)−CE(3)	106.8(4)	107.0(4)
CE(1)−Ti(1)−CE(3)	131.9(5)	132.6(6)
Cl(1)−Ti(2)−Cl(2)	82.1(1)	82.8(1)
Cl(1)−Ti(2)−CE(2)	107.9(3)	107.0(3)
Cl(1)−Ti(2)−CE(4)	109.4(3)	109.4(5)
Cl(2)−Ti(2)−CE(2)	107.0(3)	109.0(3)
Cl(2)−Ti(2)−CE(4)	108.6(3)	108.3(5)
CE(2)−Ti(2)−CE(4)	131.0(5)	130.2(6)
Ti(1)−Cl(1)−Ti(2)	97.4(1)	97.7(1)
Ti(1)−Cl(2)−Ti(2)	98.6(1)	96.9(1)
C(1)−Si−C(6)	118.9(4)	117.6(4)
C(1)−Si−C(11)	106.6(5)	106.3(5)
C(1)−Si−C(12)	105.8(5)	107.3(5)
C(6)−Si−C(11)	107.5(5)	109.3(5)
C(6)−Si−C(12)	105.7(5)	106.8(5)
C(11)−Si−C(12)	112.4(5)	109.5(5)
Si−C(1)−C(2)	126.4(8)	124.1(8)
Si−C(1)−C(5)	125.9(8)	128.0(8)
C(2)−C(1)−C(5)	106.7(9)	106.6(9)
Si−C(6)−C(7)	125.4(8)	125.8(7)
Si−C(6)−C(10)	128.3(8)	128.3(8)
C(7)−C(6)−C(10)	105.3(9)	105.3(9)

[a] CE(1), CE(2), CE(3), and CE(4) are the centroids of the C(1)···C(5), C(6)···C(10), C(13)···C(17), and C(18)···C(22) Cp rings, respectively.

also involved in a nearly symmetrical η^5 interaction with a cyclopentadienyl ring. If the cyclopentadienyl centroids (CE) are considered as coordination sites, the coordination geometry around titanium is a distorted tetrahedron, the other two coordination sites being occupied by the two chlorine atoms. The angles are in agreement with those expected for this coordination, except the Cl−Ti−Cl ones, which are narrower, and the CE−Ti−CE, which are much larger. This geometry is very similar to that observed for titanocene derivatives of this type.[1d] The distances between the metal and the centroids of the cyclopentadienyl rings of the $[Me_2Si(C_5H_4)_2]^{2-}$ ligand are 2.054(11) and 2.055(9) Å [2.056(11) and 2.061(11) Å], and those with the other cyclopentadienyl rings are 2.069(10) and 2.089(12) Å [2.070(15) and 2.065(14) Å]. All four cyclopentadienyl rings are planar, but in those of the $[Me_2Si(C_5H_4)_2]^{2-}$ ligand, the Si atoms deviate from the mean plane by 0.234(3) and 0.279(3) Å [0.287(3) and 0.196(3) Å] because of the strain due to the interannular bridge. The dihedral angle between the mean planes of the these rings, 44.9(4)° [45.3(4)°], is related to the degree of canting of the rings. It can be interesting to compare some structural features of this ligand when it is acting as bridge (as in **2**) and when it is acting as a chelating ligand (as in the mononuclear complex $\{TiCl(PMe_2Ph)[Me_2Si(C_5H_4)_2]\}$.[3a] As a consequence of the rather narrow bite of this ligand when it is chelating, the dihedral angle between the mean planes of the rings, 53(2)°, is larger than in **2**, the C(1)−Si−C(6) angle much narrower [93.3(3)°] than in **2**, 118.9(4)° [117.6(4)°], and the separation between the bridgehead C(1) and C(6) atoms much closer [2.705(6) Å] than in **2**, 3.215(14) Å [3.179(14) Å].

Experimental Section

All operations were performed under an inert atmosphere of dinitrogen or argon using Schlenk and vacuum-line techniques or a VAC glovebox Model HE-63-P. The following solvents were dried and purified by distillation under argon before use by employing the appropriate drying/deoxygenated agents: tetrahydrofuran (sodium/benzophenone), toluene (sodium), hexane (sodium/potassium alloy), and dichloromethane (phosphorus pentoxide). $[Ti(\eta^5\text{-}C_5H_5)Cl_2]_2[\mu\text{-}Me_2Si(C_5H_4)_2]$,[5e] $[Ti(\eta^5\text{-}C_5H_5)Me_2]_2[\mu\text{-}Me_2Si(C_5H_4)_2]$,[5e] and $CN(2,6\text{-}C_6H_3Me_2)$[12] were prepared according to literature procedures. Sodium (Panreac), magnesium (Merck), mercury dichloride (Panreac), dimethylphenylphosphine (Aldrich), carbon monoxide (>99%, SEO), and 1 M HCl in diethyl ether solution (Aldrich) were purchased from commercial sources and used without further purifications. ^1H, ^{13}C, and $^{31}P\{^1H\}$ NMR spectra were recorded on a Varian FT-80 and Varian 300 Unity instruments. ^1H and ^{13}C chemical shifts are reported in δ units (positive chemical shifts to a higher frequency) relative to TMS standard, and ^{31}P chemical shifts were referenced to H_3PO_4 in D_2O. The coupling constants reported correspond to J_{obs}. IR spectra were recorded on a Perkin-Elmer 883 spectrophotometer (4000−200 cm^{-1}) as Nujol mulls between CsI pellets. Mass spectra were recorded on a Hewlett-Packard 5890 spectrometer. Magnetic susceptibilities were measured according to the Faraday method using a Bruker B-E 15 magnetic balance with a temperature control unit. Elemental C, H, and N analyses were performed with a Perkin-Elmer 240B microanalyzer.

Synthesis of $[Ti(\eta^5\text{-}C_5H_5)]_2(\mu\text{-}Cl)_2[\mu\text{-}Me_2Si(C_5H_4)_2]$ (2). Toluene (50 mL) was added to a mixture of $[Ti(\eta^5\text{-}C_5H_5)Cl_2]_2[\mu\text{-}Me_2Si(C_5H_4)_2]$ (**1**) (0.31 g, 0.56 mmol) and 10% sodium (0.027 g, 1.17 mmol) amalgam and then stirred for 17 h. A dark brown solution was formed, which was filtered and evaporated to dryness in vacuum to give a dark solid, which was washed with cold toluene and hexane. Extraction with tetrahydrofuran gave a dark solution, from which a dark amber crystalline solid was obtained after cooling at −35 °C that was characterized as **2**; yield, 0.23 g (85%). Suitable single crystals for X-ray studies were obtained from a saturated solution of **2** in dichloromethane at −35 °C. EI/MS (70 eV) m/z = 483.7 ($[M]^+$). μ_{eff} = 1.423 ± 0.66 μ_B at 298 K. Anal. Calcd for $C_{22}H_{24}Cl_2SiTi_2$: C, 54.68; H, 5.00. Found: C, 54.54; H, 5.28.

Synthesis of $[Ti(\eta^5\text{-}C_5H_5)(CO)_2]_2[\mu\text{-}Me_2Si(C_5H_4)_2]$ (3). Method a. Toluene (50 mL) was added to a mixture of $[Ti(\eta^5\text{-}C_5H_5)Cl_2]_2[\mu\text{-}Me_2Si(C_5H_4)_2]$ (**1**) (0.15 g, 0.27 mmol) and 10% sodium (0.026 g, 1.13 mmol) amalgam. The mixture was stirred under CO (1.0 kg cm^{-3}) for 48 h at room temperature to give a deep red solution. The solvent was removed by evaporation in vacuum to obtain a dark red oil. After extraction with hexane, the resulting solution was concentrated to ca. 15 mL and cooled to −35 °C to give dark red crystals characterized as **3**; yield, 0.1 g (70.6%).

Method b. A 250 mL Schlenk containing a toluene solution (50 mL) of $[Ti(\eta^5\text{-}C_5H_5)Me_2]_2[\mu\text{-}Me_2Si(C_5H_4)_2]$ (0.26 g, 0.55 mmol) was filled with CO (1.0 kg cm^{-3}), at −78 °C. The reaction mixture was slowly warmed to room temperature and stirred overnight to give a red solution, which was worked up as described above; yield, 0.22 g (75%). IR (Nujol mull, cm^{-1}): ν(CO) 1870 and 1960 cm^{-1}. ^1H NMR (300 MHz, C_6D_6, 25 °C): δ 0.28 (s, 6H, $SiMe_3$), 4.60 (s, 10H, C_5H_5), 4.66 (t, $4H_\beta$, J = 2.44 Hz, C_5H_4), 4.69 (t, $4H_\alpha$, J = 2.44 Hz, C_5H_4). Anal. Calcd for $C_{26}H_{24}Ti_2SiO_4$: C, 59.54; H, 4.58. Found: C, 59.43; H, 4.22.

(12) Weber, W. P.; Gokel, G. W.; Ugi, I. K. *Angew. Chem., Int. Ed. Engl.* **1972**, *11*, 530.

Table 3. Summary of Crystallographic Data for Complex 2

mol formula	$C_{22}H_{24}Cl_2SiTi_2$
mol wt	483.22
cryst syst	monoclinic
space group	$P2_1/n$
a, Å	28.262(10)
b, Å	8.089(5)
c, Å	18.446(9)
β, deg	91.06(2)
V, Å^3	4216(4)
Z	8
D_{calcd}, g cm^{-3}	1.522
$F(000)$	1984
μ(Mo Kα), cm^{-1}	10.73
R	0.0568
R_w	0.0727

Synthesis of {Ti(η^5-C_5H_5)[CN(2,6-$C_6H_3Me_2$)]$_2$}$_2$[μ-$Me_2Si(C_5H_4)_2$] (5). [Ti(η^5-C_5H_5)Cl$_2$]$_2$[μ-$Me_2Si(C_5H_4)_2$] (1) (0.4 g, 0.72 mmol) was added under argon to a mixture of magnesium turnings (0.4 g, 16.45 mmol), $HgCl_2$ (20 mg, 0.075 mmol), and CN(2,6-$C_6H_3Me_2$) (0.38 g, 2.9 mmol) in tetrahydrofuran (60 mL). The reaction mixture was stirred for 12 h at room temperature to give a red brown solution. The solvent was removed under vacuum and the residue extracted with hexane (100 mL). The resulting solution was concentrated to ca. 30 mL and cooled to −30 °C to give a red brown solid. Recrystallization from cold hexane gave a crystalline red brown solid, which was characterized as **5**; yield, 0.51 g (75%). IR (Nujol mull, cm^{-1}): ν(CN) 1932 and 2033 cm^{-1}. ^{1}H NMR (C_6D_6, 300 MHz, 25 °C): δ 0.45 (s, 6H, $SiMe_2$), 2.18 (s, 24H, C_6H_3*Me*$_2$), 5.20 (s, 10H, C_5H_5), 5.25 (t, 4H$_\beta$, J = 2.44 Hz, C_5H_4), 5.37 (t, 4H$_\alpha$, J = 2.44 Hz, C_5H_4), 6.61−6.71 (m, 12H, C_6*H*$_3$Me$_2$). ^{13}C NMR (C_6D_6, 75.5 MHz, 25 °C): δ 1.0 (q, J_{C-H} = 119.05 Hz, $SiMe_2$), 18.9 (q, J_{C-H} = 127.29 Hz, C_6H_5*Me*$_2$), 95.3 (d, J_{C-H} = 173.08 Hz, C_5H_5), 97.4 [s, C$_1$(C_5H_4)], 97.6 [d, J_{C-H} = 173.08 Hz, C$_3$ (C_5H_4)], 103.6 [d, J_{C-H} = 173.08 Hz, C$_2$ (C_5H_4)], 123.1−130.0 ($C_6H_3Me_2$), 236.4 (s, CN). EI/MS (70 eV) m/z = 936 ([M]$^+$). Anal. Calcd for $C_{58}H_{60}Ti_2SiN_4$: C, 74.34; H, 6.45; N, 5.98. Found: C, 73.46; H, 6.60; N, 5.81.

Synthesis of [Ti(PMe$_2$Ph)]$_2$(μ-η^1-η^5-C_5H_4)$_2$[μ-$Me_2Si(C_5H_4)_2$] (6). [Ti(η^5-C_5H_5)Cl$_2$]$_2$[μ-$Me_2Si(C_5H_4)_2$] (1) (0.4 g, 0.72 mmol) was added under argon to a mixture of magnesium turnings (0.4 g, 16.45 mmol), $HgCl_2$ (0.020 g, 0.075 mmol), and PMe_2Ph (0.41 mL) in tetrahydrofuran (60 mL). The reaction mixture was stirred for 12 h at room temperature to give a black violet solution. The solvent was removed in vacuum and the residue extracted with 100 mL of toluene. The resulting solution was concentrated to ca. 30 mL and cooled to −30 °C to give a black violet solid. Recrystallization from toluene/hexane gave a crystalline violet solid, which was characterized as **6**; yield, 0.39 g (79%). ^{1}H NMR (C_6D_6, 300 MHz, 25 °C): δ 0.47 (s, 6H, $SiMe_2$), 1.16 (d, 6H, J_{P-H} = 4.5 Hz, PMe_2Ph), 1.4 (d, 6H, J_{P-H} = 4.5 Hz, PMe_2Ph), 4.36 (m, 2H, C_5H_4), 4.65 (m, 2H, C_5H_4), 4.90 (m, 2H, C_5H_4), 5.14 (m, 2H, C_5H_4), 5.21 (m, 2H, C_5H_4), 5.74 (m, 2H, C_5H_4), 5.88 (m, 4H, C_5H_4), 7.06 [6H, *m*- and *p*-C_6H_5 (PMe_2Ph)], 7.48 [4H, *o*-C_6H_5 (PMe_2Ph)]. ^{13}C NMR (C_6D_6, 75.5 MHz, 25 °C): δ 0.1 (s, $SiMe_2$), 16.96 (d, J_{P-C} = 11.31 Hz, P*Me*$_2$Ph), 17.73 (d, J_{P-C} = 12.8 Hz, P*Me*$_2$Ph), 87.6 [C$_1$, (η^1-η^5-C_5H_4)], 91.2, 102.3, 106.3, 109.4, 110.6, 110.7, 112.6, 116.4 [C$_2$ and C$_3$, (η^1-η^5-C_5H_4) and Si-(C_5H_4)], 126−128 [*m*- and *p*-C_6H_5 (PMe_2Ph)], 131.0 [*o*-C_6H_5 (PMe_2Ph)], 142.1 [P-C (PMe_2*Ph*)], 190.8 [d, J_{P-C} = 15.08 Hz, σ-Ti−C (η^1-η^5-C_5H_4)]. ^{31}P{^{1}H} NMR (C_6D_6, referenced to H_3PO_4 in D_2O): δ 21.1 (s). Anal. Calcd for $C_{38}H_{44}Ti_2SiP_2$: C, 66.47; H, 6.46. Found: C, 65.36; H, 6.41 (extremely air sensitive).

Reaction of [Ti(PMe$_2$Ph)]$_2$(μ-η^1-η^5-C_5H_4)$_2$[μ-$Me_2Si(C_5H_4)_2$] (6) with HCl. (a) Ti/HCl Molar Ratio 1/2. A 1 M solution HCl in diethyl ether (0.5 mL, 0.5 mmol) was added to a toluene solution (50 mL) containing [Ti(PMe$_2$Ph)]$_2$(μ-η^1-η^5-C_5H_4)$_2$[μ-$Me_2Si(C_5H_4)_2$] (6) (0.16 g, 0.24 mmol). The dark violet color of the solution changed immediately to amber, and the reaction mixture was stirred for 2 h. After filtration, the resulting solution was concentrated and cooled to −35 °C, yielding brown green crystals of **2**.

(b) Ti/HCl Molar Ratio 1/4. When the same reaction was carried out as described above using a double amount of the 1 M solution of HCl in diethyl eter (1 mL, 1 mmol) and the reaction mixture was stirred for 36 h, the color of the solution changed slowly from dark violet to orange with formation of a red brown precipitate. After removal of the solvent under vacuum, the solid residue was recrystallized from toluene/hexane by cooling to −30 °C, giving orange crystals of the reported[5e] compound {[Ti(η^5-C_5H_5)Cl$_2$]$_2$[μ-$Me_2Si(C_5H_4)_2$]}.

Table 4. Atomic Coordinates (×10^4) and Isotropic Thermal Parameters (Å^2 × 10^4) with Esd Values in Parentheses for the Non-Hydrogen Atoms of Compound 2

	x/a	y/b	z/c	U^a
		Molecule 1		
Ti(11)	396(1)	−2391(2)	6763(1)	309(6)
Ti(21)	−462(1)	770(2)	7526(1)	295(6)
Cl(11)	−459(1)	−2248(3)	7155(1)	362(8)
Cl(21)	377(1)	618(3)	7113(1)	350(8)
Si(1)	355(1)	−1697(4)	8790(1)	390(10)
C(11)	600(4)	−2828(12)	7985(5)	369(34)
C(21)	1016(4)	−2453(13)	7626(5)	414(38)
C(31)	1107(4)	−3741(16)	7144(6)	555(47)
C(41)	747(5)	−4901(15)	7194(6)	659(50)
C(51)	447(4)	−4368(12)	7723(6)	430(38)
C(61)	−127(4)	−185(13)	8639(5)	383(37)
C(71)	−70(4)	1565(13)	8616(5)	409(38)
C(81)	−516(5)	2333(15)	8628(6)	568(48)
C(91)	−854(5)	1076(16)	8649(5)	582(49)
C(101)	−621(4)	−450(15)	8663(5)	466(41)
C(111)	860(4)	−579(16)	9228(6)	677(50)
C(121)	105(4)	−3317(14)	9386(6)	664(50)
C(131)	802(5)	−2224(19)	5643(6)	652(52)
C(141)	447(5)	−1028(17)	5605(5)	592(51)
C(151)	21(4)	−1843(17)	5625(5)	553(49)
C(161)	103(5)	−3540(17)	5672(5)	555(46)
C(171)	593(6)	−3757(18)	5665(5)	717(62)
C(181)	−573(4)	1848(15)	6324(5)	514(43)
C(191)	−561(4)	3173(14)	6808(6)	532(45)
C(201)	−964(5)	3062(16)	7223(6)	626(51)
C(211)	−1206(4)	1650(18)	7015(7)	646(52)
C(221)	−979(4)	929(15)	6466(7)	555(46)
		Molecule 2		
Ti(12)	2969(1)	−175(2)	5074(1)	341(6)
Ti(22)	2113(1)	2955(2)	4263(1)	322(6)
Cl(12)	2169(1)	−119(3)	4451(1)	463(9)
Cl(22)	2928(1)	2915(3)	4856(1)	398(8)
Si(2)	2136(1)	2181(4)	6299(1)	363(9)
C(12)	2579(4)	536(12)	6150(5)	374(35)
C(22)	3077(4)	721(14)	6293(5)	495(41)
C(32)	3285(5)	−896(20)	6243(6)	717(57)
C(42)	2929(6)	−1988(19)	6090(7)	768(58)
C(52)	2495(4)	−1223(12)	6033(5)	481(42)
C(62)	1847(3)	3128(13)	5482(5)	373(35)
C(72)	1926(4)	4761(13)	5220(5)	485(41)
C(82)	1599(5)	5083(17)	4661(6)	644(51)
C(92)	1327(4)	3700(19)	4557(6)	667(53)
C(102)	1467(3)	2513(15)	5062(5)	470(40)
C(112)	2439(5)	3799(16)	6828(6)	806(60)
C(122)	1661(4)	1279(16)	6839(6)	651(50)
C(132)	3413(4)	19(16)	3985(7)	587(48)
C(142)	3145(5)	−1320(18)	3910(7)	685(54)
C(152)	3282(7)	−2471(15)	4446(10)	970(78)
C(162)	3668(6)	−1701(23)	4834(8)	920(76)
C(172)	3725(4)	−148(20)	4548(7)	724(58)
C(182)	2560(5)	3996(28)	3300(7)	828(73)
C(192)	2166(8)	4850(20)	3288(7)	872(71)
C(202)	1811(6)	3885(32)	3128(7)	927(85)
C(212)	1948(9)	2327(25)	3036(7)	936(79)
C(222)	2451(8)	2369(23)	3126(6)	907(76)

^{a} Equivalent isotropic U defined as one-third of the trace of the orthogonalized $\mathbf{U}_{ij}$ tensor.

X-ray Data Collection, Structure Determination, and Refinement for {[Ti(η^5-C_5H_5)]$_2$(μ-Cl)$_2$[μ-$Me_2Si(C_5H_4)_2$]} (2). A single crystal of **2**, having approximate dimensions ca.

0.18 × 0.23 × 0.30 mm^3, was sealed in a Lindemann glass capillary under dry nitrogen and used for data collection. The crystallographic data are summarized in Table 3. Unit cell parameters were determined from the θ values of 30 carefully centered reflections, having $10 < \theta < 18°$. Data were collected at room temperature (22 °C) on a Siemens AED diffractometer, using the niobium-filtered Mo Kα radiation (λ = 0.710 73 Å) and the $\theta/2\theta$ scan type. The reflections were collected with a variable scan speed of 3−12° min^{-1} and a scan width from $(\theta - 0.6)°$ to $(\theta + 0.6 + 0.346 \tan \theta)°$. Of 9240 unique reflections, with θ in the range 3−27°, 3200 with $I > 2\sigma(I)$ were used for the analysis. One standard reflection was monitored every 50 measurements; no significant decay was noticed over the time of data collection. The individual profiles have been analyzed following Lehmann and Larsen.[13] Intensities were corrected for Lorentz and polarization effects. No correction for absorption was applied. Only the observed reflections were used in the structure solution and refinement.

The structure was solved by direct and Fourier methods and refined by blocked full-matrix least-squares methods, first with isotropic thermal parameters and then with anisotropic thermal parameters for all non-hydrogen atoms. All hydrogen atoms were placed at their geometrically calculated positions (C−H = 1.00 Å) and refined "riding" on the corresponding carbon atoms. The final cycles of refinement were carried out on the basis of 497 variables; after the last cycles, no parameters shifted by more than 0.70 esd. The biggest remaining peak in the final difference maps was equivalent to about 0.58 e/$Å^3$. In the final cycles of refinement, a weighting scheme, $w = K[\sigma^2(F_o) + gF_o^2]^{-1}$ was used; at convergence the K and g values were 0.528 and 0.0051, respectively. The analytical scattering factors, corrected for the real and imaginary parts of anomalous dispersions, were taken from ref 14. All calculations were carried out on the GOULD POWERNODE 6040 and ENCORE 91 computers of the "Centro di Studio per la Strutturistica Diffrattometrica" del C.N.R., Parma, Italy, using the SHELX-76 and SHELXS-86 systems of crystallographic computer programs.[15] The final atomic coordinates for the nonhydrogen atoms are given in Table 4. The atomic coordinates of the hydrogen atoms are given in Table SI, the thermal parameters in Table SII of the supplementary material.

Acknowledgment. Financial support for this research by DGICYT (Project 92-0178-C) and Consiglio Nazionale delle Ricerche (Rome) is gratefully acknowledged.

Supplementary Material Available: Tables of hydrogen atom coordinates (Table SI) and anisotropic thermal parameters for the non-hydrogen atoms (Table SII) and a complete list of bond distances and angles (Table SIII) (7 pages). Ordering information is given on any current masthead page.

OM940634C

(13) Lehmann, M. S.; Larsen, F. K. *Acta Crystallogr., Sect A* **1974**, *30*, 580.

(14) International Tables for X-Ray Crystallography; Kynoch Press: Birmingham, England, 1974; Vol. IV.

(15) Sheldrick, G. M. *SHELX-76 Program for crystal structure determination*; University of Cambridge, England, 1976. SHELXS-86 *Program for the solution of crystal structures*; University of Göttingen, FRG, 1986.

Bond Cleavage Reactions in Oxygen and Nitrogen Heterocycles by a Rhodium Phosphine Complex

William D. Jones,* Lingzhen Dong, and Andrew W. Myers

Department of Chemistry, University of Rochester, Rochester, New York 14627

Received June 7, 1994®

The reactions of $(C_5Me_5)Rh(PMe_3)PhH$ with furan, 2,5-dimethylfuran, 2,3-dihydrofuran, dibenzofuran, pyrrole, 1-methylpyrrole, 2,5-dimethylpyrrole, 1,2,5-trimethylpyrrole, carbazole, 9-methylcarbazole, pyrrolidine, pyridine, 3,5-lutidine, 2,4,6-collidine, pyrazole, 3-methylpyrazole, and piperidine have been investigated. While the oxygen heterocycles give only C–H activation, the nitrogen heterocycles yield C–H and N–H insertion products. The chloro derivative $(C_5Me_5)Rh(PMe_3)$[2-(1-methylpyrrole)]Cl was found to crystallize in the monoclinic space group $C2/c$ with a = 13.753 (6) Å, b = 9.665 (5) Å, c = 30.14 (2) Å, β = 99.77 (5)°, Z = 8, and V = 3949 (4.1) Å^3 while $(C_5Me_5)Rh(PMe_3)$[2-(3,5-lutidine)]Cl was found to crystallize in the monoclinic space group $P2_1/c$ with a = 14.976 (8) Å, b = 8.613 (5) Å, c = 17.12 (2) Å, β = 101.90 (6)°, Z = 4, and V = 2160 (5.2) Å^3.

Introduction

An alluring prospect of investigating the chemistry of homogeneous transition metal complexes with heterocycles is the potential for insight into many important industrial processes and catalytic cycles. Studies of the interaction between transition metals and N-, O-, or S-containing heterocyclic compounds have provided both structural models for intermediates (i.e., coordination and bonding modes)[1–5] and mechanistic models which may be applied to critical industrial processes such as hydrodesulfurization (HDS), hydrodenitrogenation (HDN), and hydrodeoxygenation (HDO).[6–10] The development of new synthetic methodologies for heterocycles has also been demonstrated with transition metal-mediated systems.[11] In particular, recent studies on N–H activation have yielded information on such processes as the hydroamination of olefins and alternate synthetic routes toward insecticides and other organic nitrogen-containing molecules.[12–20]

The complex $(C_5Me_5)Rh(PMe_3)PhH$ has been shown to behave as a thermal precursor for the generation of the unsaturated fragment $[(C_5Me_5)Rh(PMe_3)]$, which is active toward the oxidative addition of a variety of C–H bonds.[21] In addition, this fragment has been found to cleave a wide variety of thiophene C–S bonds, giving a six-membered-ring insertion product.[22] In examining the effects of aromatization on C–H vs η^2-coordination[23] in a variety of heterocycles, we discovered different chemical reactions for furan, pyrrole, pyridine, and their derivatives.

Results and Discussion

Reactions of $(C_5Me_5)Rh(PMe_3)(Ph)H$ with Furan and Derivatives. Thermolysis of $(C_5Me_5)Rh(PMe_3)$-PhH (1) in the presence of furan at 60 °C in hexane solution results in the formation of a single organometallic compound. The ^{1}H NMR spectrum exhibits a four-line resonance centered at δ −12.825 (dd, J = 45.0, 30.6 Hz) and three proton resonances in the aromatic region consistent with its formulation as a furanyl hydride complex. A ^{1}H COSY NMR spectrum showed that the C–H bond activation occurs at the α-position of the furan to form the 2-furanyl hydride (Scheme 1). This hydride reacts with $CHCl_3$ to produce the cor-

® Abstract published in *Advance ACS Abstracts,* December 1, 1994.

(1) Kvietok, F.; Allured, V.; Carperos, V.; Rakowski DuBois, M. *Organometallics* **1994**, *13*, 60–68, and references within.
(2) Kershner, D. L.; Basolo, F. *Coord. Chem. Rev.* **1987**, *79*, 279–292.
(3) Rauchfuss, T. B. In *Progress in Inorganic Chemistry*; Lippard, S. J., Ed.; Wiley: New York, 1991; pp 259–329.
(4) Myers, W. H.; Koontz, J. I.; Harman, W. D. *J. Am. Chem. Soc.* **1992**, *114*, 5684–5692.
(5) (a) Neithamer, D. R.; Parkanyi, L.; Mitchell, J. F.; Wolczanski, P. T. *J. Am. Chem. Soc.* **1988**, *110*, 4421–4423. (b) Covert, K. J.; Neithamer, D. R.; Zonnevylle, M. C.; LaPointe, R. E.; Schaller, C. P.; Wolczanski, P. T. *Inorg. Chem.* **1991**, *30*, 2494–2508.
(6) Angelici, R. J. *Acc. Chem. Res.* **1988**, *21*, 387–394.
(7) Baralt, E.; Smith, S. J.; Hurwitz, J.; Horvath, I. T.; Fish, R. H. *J. Am. Chem. Soc.* **1992**, *114*, 5187–5196.
(8) Laine, R. M. *New J. Chem.* **1987**, *11*, 543–547.
(9) Erker, G.; Petrenz, R.; Krüger, C.; Lutz, F.; Weiss, A.; Werner, S. *Organometallics* **1992**, *11*, 1646–1655.
(10) Böhringer, W.; Schulz, H. *Bull. Soc. Chim. Belg.* **1991**, *100*, 831–840.
(11) Bryndza, H. E.; Fultz, W. C.; Tam, W. *Organometallics* **1985**, *4*, 939–940.
(12) Bergman, R. G.; Walsh, P. J.; Hollander, F. J. *J. Am. Chem. Soc.* **1988**, *110*, 8729–8733.
(13) Rothwell, I. P.; Hill, J. E.; Profilet, R. D.; Fanwick, P. E. *Angew. Chem., Int. Ed. Engl.* **1990**, *29*, 664–665.
(14) Bercaw, J. E.; Hillhouse, G. L. *J. Am. Chem. Soc.* **1984**, *106*, 5472–5478.
(15) (a) Roundhill, D. M.; Hedden, D. *Inorg. Chem.* **1986**, *25*, 9–15. (b) Roundhill, D. M.; Hedden, D.; Park, S. *Organometallics* **1986**, *5*, 2151–2152. (c) Roundhill, D. M.; Rauchfuss, T. B. *J. Am. Chem. Soc.* **1974**, *96*, 3098–3105. (d) Roundhill, D. M. *Inorg. Chem.* **1970**, *9*, 254–258.
(16) Merola, J. S.; Ladipo, F. T. *Inorg. Chem.* **1990**, *29*, 4172–4173.
(17) Landis, C. R.; Schaad, D. R. *J. Am. Chem. Soc.* **1990**, *112*, 1628–1629.
(18) (a) Casalnuovo, A. L.; Calabrese, J. C.; Milstein, D. *J. Am. Chem. Soc.* **1988**, *110*, 6738–6744. (b) Casalnuovo, A. L.; Calabrese, J. C.; Milstein, D. *Inorg. Chem.* **1987**, *26*, 971–973.
(19) (a) Gagne, M. R.; Marks, T. J. *J. Am. Chem. Soc.* **1989**, *111*, 4108–4109. (b) Gagne, M. R.; Nolan, S. P.; Marks, T. J. *Organometallics* **1990**, *9*, 1716–1718.
(20) Hsu, G. C.; Kosar, W. P.; Jones, W. D. *Organometallics* **1994**, *13*, 385–396.
(21) Jones, W. D.; Feher, F. J. *Acc. Chem. Res.* **1989**, *22*, 91–100.
(22) (a) Jones, W. D.; Dong, L. *J. Am. Chem. Soc.* **1991**, *113*, 559–564. (b) Dong, L.; Duckett, S. B.; Ohman, K. F.; Jones, W. D. *J. Am. Chem. Soc.* **1992**, *114*, 151–160.
(23) (a) Chin, R. M.; Dong, L.; Duckett, S. B.; Partridge, M. G.; Jones, W. D.; Perutz, R. N. *J. Am. Chem. Soc.* **1993**, *115*, 7685–7695. (b) Chin, R. M.; Dong, L.; Duckett, S. B.; Jones *Organometallics* **1992**, *11*, 871–876. (c) Jones, W. D.; Dong, L. *J. Am. Chem. Soc.* **1989**, *111*, 8722–8723.

0276-7333/95/2314-0855$09.00/0

Scheme 1. Reactions with Furans

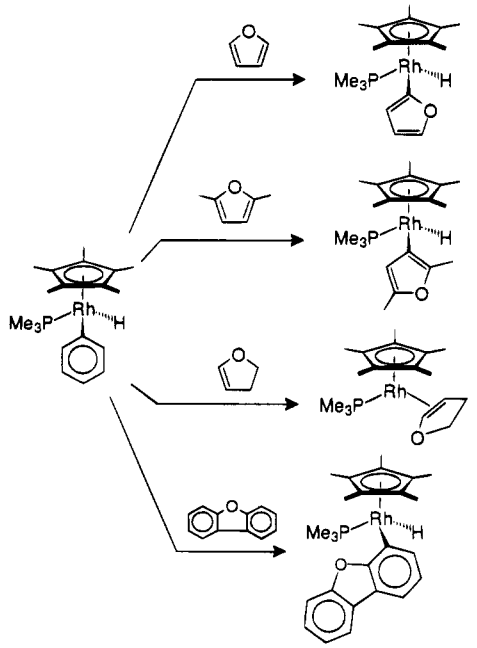

responding halide derivative, $(C_5Me_5)Rh(PMe_3)$(2-furanyl)Cl. Activation of the α-C−H bond is in agreement with results found by Selnau and Merola, who obtained crystallographic evidence for the product of an iridium phosphine complex with furan.[24] Guerchais has also seen α-activation of furan with Cp_2WH_2.[25]

Upon heating a hexane solution of **1** containing a mixture of benzene and furan (1:1 molar ratio) at 50 °C for 48 h, two species were observed in a ratio of 1:15 which were identified as $(C_5Me_5)Rh(PMe_3)PhH$ and $(C_5Me_5)Rh(PMe_3)$(2-furanyl)H. Since the half-life for arene exchange is 6.1 h under these conditions, the equilibrium constant can be calculated as $K_{eq} = 15$ (eq 1).

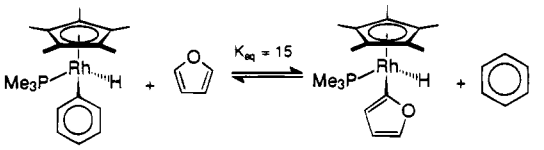

(1)

The reaction of **1** with 2,5-dimethylfuran at 60 °C in hexane solution yields the related 3-furanyl hydride (δ −13.315, dd, J = 48.5, 29.9 Hz) as the only organometallic complex, since the α-positions are blocked by methyl groups in this substrate. The chloride derivative was isolated by reaction of the air-sensitive hydride with $CHCl_3$ to give $(C_5Me_5)Rh(PMe_3)$(3-(2,5-dimethylfuranyl))Cl. In contrast, the thermal reaction of **1** with dihydrofuran gives only the η^2-C_4H_6O complex, despite the fact that the strength of the vinylic C−H bond is the same as the one that was broken in furan. In this case, no resonance energy is lost upon η^2-coordination, and thus, the π-complex is lower in energy than the C−H activation product. With furan, the η^2-complex was not observed because η^2-coordination greatly disrupts the aromatic character of the ring, raising the free energy of this species.

Thermolysis of **1** with dibenzofuran at 67 °C leads to C−H activation of the aromatic ring. ^1H NMR experiments indicate the site of activation as the 1 or 4 position,[26] consistent with results obtained in the reaction of $(C_5Me_5)Rh(PMe_3)PhH$ with biphenylene.[27] Further heating of **1** with dibenzofuran resulted in decomposition to $(C_5Me_5)Rh(PMe_3)_2$. The above reactions indicate that the aromaticity of the furan ring induces reactivity similar to that observed previously for monocyclic aromatics so that C−H cleavage occurs rather than η^2-coordination.[28]

Reaction of 1 with Pyrrole and other Nitrogen Heterocycles. The reaction of $(C_5Me_5)Rh(PMe_3)PhH$ with pyrrole was examined. Pyrrole has stronger pπ−pπ overlap than furan and substantial aromatic character. The object of this study was to see whether C−H bond activation (or η^2-coordination) can occur in the presence of an N−H bond. Upon heating **1** with excess pyrrole in hexane solution at 60 °C, a single product was observed with a hydride resonance at δ −11.523 (dd, J_{P-H} = 50.4, J_{Rh-H} = 25.1 Hz). This hydride resonance is ~2 ppm downfield from those of the C−H bond activation products described above, and J_{Rh-H} is significantly smaller than for the C−H activation products (typically, J_{Rh-H} = 30−32 Hz). A Cp* resonance is observed at δ 1.595 (s, 15 H) and a PMe_3 resonance at δ 0.820 (d, J = 9.7 Hz, 9 H) in the ^1H NMR spectrum. In addition, there is a broad peak at δ 6.729 that corresponds to four protons, suggesting a symmetrical environment consistent with bonding of the N atom to the metal center (Scheme 2). The ^{31}P NMR spectrum of this complex shows a downfield doublet with a small coupling constant (δ 9.15, d, J_{Rh-P} = 143.9 Hz), consistent with the formulation of the product as a Rh(III) N−H oxidative addition adduct.

The N−H bond activation adduct $(C_5Me_5)Rh(PMe_3)$-(1-pyrrolyl)(H) is apparently the thermodynamically preferred product in this reaction (*vide infra*). The Rh−N bond is expected to be stronger than the Rh−C bond since nitrogen is a more electronegative element and the σ-bonding mode takes electron density away from metal. Therefore, the metal center is less electron rich, which affects both chemical shifts (more downfield) and coupling constants (smaller J_{Rh-P}). The related electron-rich coordinatively unsaturated fragment $Ru(DMPE)_2$ (generated by loss of naphthalene from $Ru(DMPE)_2$(naphthyl)(H)) interacts with pyrrole to give a N−H bond activation product.[20,29] N−H addition has also been seen in the reaction of pyrrole with $[Ir(PMe_3)_3(COD)]Cl$[16] and Cp_2WH_2.[25]

A C−H bond activation product can be obtained by the reaction of **1** with 1-methylpyrrole, blocking the N−H position with a methyl group. The ^1H NMR

(24) Selnau, H. E.; Merola, J. S. *Organometallics* **1993**, *12*, 1583−1591.

(25) Samat, A.; Sala-Pala, J.; Guglielmetti, R.; Guerchais, J. *Nouv. J. Chem.* **1978**, *2*, 13−14.

(26) Numbering scheme for dibenzofuran is

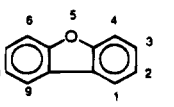

(27) (a) Perthuisot, C.; Jones, W. D. *J. Am. Chem. Soc.* **1994**, *116*, 3647−3648. (b) Perthuisot, C. Ph.D. Thesis, University of Rochester, Rochester, NY, 1994.

(28) Belt, S. T.; Dong, L.; Duckett, S. B.; Jones, W. D.; Partridge, M. G.; Perutz, R. N. *J. Chem. Soc., Chem. Commun.* **1991**, 266.

(29) Hsu, G. C. Ph.D. Thesis, University of Rochester, Rochester, NY, 1991.

Scheme 2. Reactions with Pyrroles and Pyridines

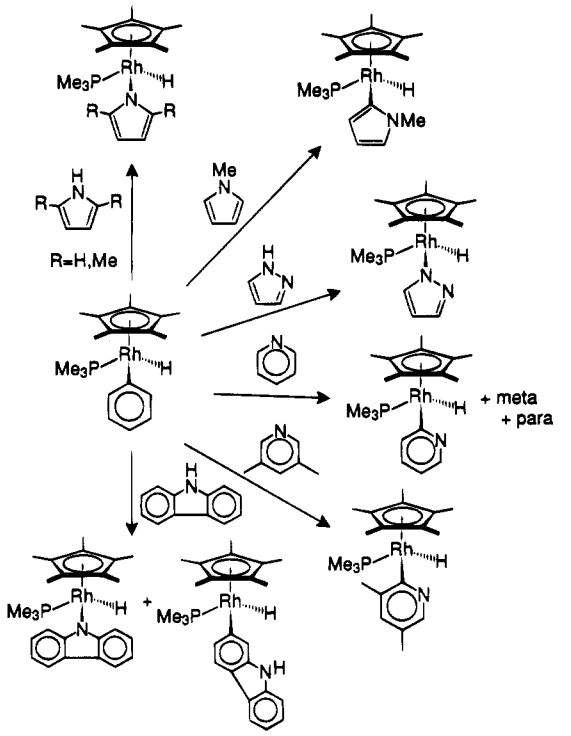

spectrum shows a hydride resonance at δ −12.947 (dd, J = 49.4, 30.4 Hz). Homonuclear decoupling experiments and a J-resolved ^{1}H NMR experiment indicate that the product is $(C_5Me_5)Rh(PMe_3)$[2-(1-methylpyrrolyl](H), in which C−H bond activation has occurred at the 2 position of the ring. The aromaticity of 1-methylpyrrole plays an important role in formation of the C−H activation adduct just as it did in furan and benzene. An X-ray crystal structure of the chloro derivative was obtained after reacting the air-sensitive hydride with $CHCl_3$. Figure 1 shows an ORTEP drawing illustrating activation of the α-C−H bond. Data collection parameters and select bond distances and angles are listed in Tables 1 and 2, respectively.

To probe the reactivity of substituted pyrroles further, 2,5-dimethylpyrrole and 1,2,5-trimethylpyrrole were examined. Upon heating **1** with 2,5-dimethylpyrrole at 67 °C for 25 h, a single hydride was observed by ^{1}H NMR spectroscopy at δ −12.71 (dd, J = 53.2, 23.1 Hz). ^{31}P NMR data are consistent with an N−H inserted complex exhibiting a resonance at δ 6.87 (d, J = 146.0 Hz). Attempts to isolate the N−H activated product by quenching with $CHBr_3$ failed. Five minutes after the addition of 1 equiv of $CHBr_3$, ^{31}P NMR spectroscopy showed two new products at δ 6.43 (d, J = 145.2 Hz) and 4.05 (d, J = 138.2 Hz). The resonance at δ 6.43 was assigned as the N−Br adduct, which was observed to quickly decompose as the resonance at δ 4.05, $(C_5Me_5)Rh(PMe_3)Br_2$, increased. Decomposition to $(C_5Me_5)Rh(PMe_3)_2$ was seen when **1** was heated with 1,2,5-trimethylpyrrole. Reaction of **1** with pyrrolidine resulted in decomposition. $(C_5Me_5)Rh(PMe_3)_2$ was found as the major product and a small amount of $(C_5Me_5)Rh(PMe_3)H_2$ was also produced. No N−H or C−H bond activation reactions occurred.

Competitive N−H and C−H activation was seen in the reaction of **1** with carbazole. Thermolysis at 67 °C for 3 days gave two products in a 2:1 ratio, observed by

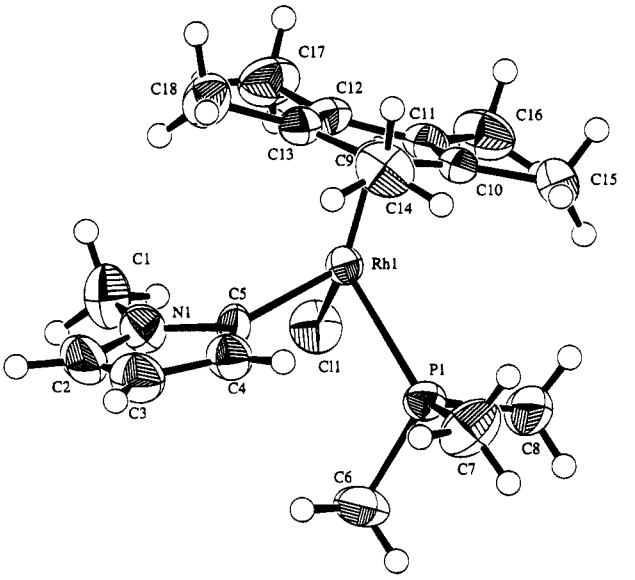

Figure 1. ORTEP drawing of $(C_5Me_5)Rh(PMe_3)$[2-(1-methylpyrrole)]Cl. Ellipsoids are shown at the 50% probability level.

Table 1. Summary of Crystallographic Data for $(C_5Me_5)Rh(PMe_3)$[2-(1-methylpyrrole)]Cl and $(C_5Me_5)Rh(PMe_3)$[2-(3,5-lutidine)]Cl

	[Rh]{2-(1-methylpyrrole)}	[Rh]{2-(3,5-lutidine)}
	Crystal Parameters	
chemical formula	$RhClPNC_{18}H_{30}$	$RhClPNC_{30}H_{32}$
formula weight	429.78	455.81
cryst syst	monoclinic	monoclinic
space group (No.)	$C2/c$	$P2_1/c$ (No. 14)
Z	8	4
a, Å	13.753(6)	14.976(8)
b, Å	9.665(5)	8.613(5)
c, Å	30.14(2)	17.12(2)
β, deg	99.77(5)	101.90(6)
vol, Å^3	3949 (4.1)	2160 (5.2)
ϱ_{calc}, g cm^{-3}	1.45	1.40
	Measurement of Intensity Data	
radiation (monochrom)	Mo, 0.710 73 Å (graphite)	Mo, 0.710 73 Å (graphite)
scan rate, deg/min	2−16.5	2−16.5
scan range, deg	0.7 + 0.35 tan θ	0.7 + 0.35 tan θ
2θ range, deg	4−50	4−50
data collected	$+h,+k,\pm l$	$+h,+k,\pm l$
no. of data collected	7479	4241
no. of unique data $F^2 > 3\sigma(F^2)$	2746	1536
no. of params varied	199	217
μ, cm^{-1}	10.76	9.78
systematic absences	hkl, $h + k$ odd $0k0$, k odd $h0l$, l odd	$0k0$, k odd $h0l$, l odd
abs cor	differential	differential
range of trans factors	0.62−1.00	0.69−1.21
$R(F_o)$	0.03376	0.0616
$R_w(F_o)$	0.04125	0.0591
goodness of fit	1.557	1.394

^{1}H NMR spectroscopy at δ −11.23 (dd, J = 52.1, 24.2 Hz) and −13.28 (dd, J = 49.9, 32.4 Hz), respectively. The ^{31}P NMR spectrum agreed with assignment of the major product as an N−H insertion complex, δ 6.64 (d, J = 143.1 Hz, 67%), and the minor product as a C−H activation complex, δ 9.19 (d, J = 148.6 Hz, 33%). The N−H insertion complex was found to be the more thermodynamically stable product as seen by the disappearance of the C−H activation complex upon further heating and the appearance of more of the N−H

Table 2. Selected Bond Distances (Å) and Angles (deg) for $(C_5Me_5)Rh(PMe_3)[2\text{-}(1\text{-methylpyrrole})]Cl$

Bond Lengths			
Rh−Cl	2.439(1)	N(1)−C(5)	1.374(6)
Rh−P	2.271(1)	C(2)−C(3)	1.359(8)
Rh−C(5)	2.068(5)	C(3)−C(4)	1.400(7)
N(1)−C(1)	1.423(7)	C(4)−C(5)	1.370(6)
N(1)−C(2)	1.393(6)		
Bond Angles			
Cl−Rh−P	85.36(5)	N(1)−C(2)−C(3)	108.7(5)
Cl−Rh−C(5)	99.6(1)	C(2)−C(3)−C(4)	105.5(5)
P−Rh−C(5)	87.1(1)	C(3)−C(4)−C(5)	111.2(5)
C(1)−N(1)−C(2)	122.3(5)	Rh−C(5)−N(1)	124.9(4)
C(1)−N(1)−C(5)	128.0(4)	Rh−C(5)−C(4)	129.0(4)
C(2)−N(1)−C(5)	109.4(5)	N(1)−C(5)−C(4)	122(2)

activation complex. Formation of the decomposition product $(C_5Me_5)Rh(PMe_3)_2$ was observed after continued heating at 75 °C. N−H activation was eliminated in the reaction of **1** with 9-methylcarbazole. Thermolysis in C_6D_{12} led to a small amount of C−H activation but mostly decomposition to $(C_5Me_5)Rh(PMe_3)_2$.

The reactivity of pyridine and several substituted pyridines was also examined. Thermal reaction of **1** with pyridine gave three Rh(III) products in a 8:4:2 ratio, as identified by ^{31}P NMR spectroscopy. The major product appeared at δ 11.91 (d, J = 158.0 Hz, 57%) and was assigned as the C−H insertion complex at the ortho carbon. The increased electronegativity of nitrogen would be expected to produce a downfield chemical shift for this isomer. Confirmation of this assignment was found through ^1H (COSY) NMR and homonuclear decoupling experiments. The other two products were formulated as C−H activation products at the para and meta sites of the pyridine ring with resonances in the ^{31}P spectrum at δ 7.28 (d, J = 154.0 Hz, 28%) and 7.71 (d, J = 156 Hz, 15%), respectively. These assignments were also confirmed by ^1H (COSY) NMR and homonuclear decoupling experiments. The chloro derivatives were isolated by reaction with $CHCl_3$.

A single C−H activation product was found when **1** was reacted with 3,5-lutidine at 70 °C for 7 h. The presence of two distinct proton resonances at δ 6.82 (s, 1 H) and 7.93 (s, 1 H) identified the product as insertion into the C−H bond α to N, as insertion into the para position would yield a single proton resonance for a symmetrically bound heterocycle. Agreement was found in the ^{31}P NMR spectrum with one resonance observed at δ 13.77 (d, J = 156.0 Hz). Quenching the product with $CHCl_3$ resulted in the disappearance of the hydride resonances in the ^1H NMR and the appearance of a new doublet in the ^{31}P NMR at δ 13.28 (J = 155.9 Hz). Orange crystals formed at −30 °C in hexanes allowed single-crystal X-ray structure determination of the chloro derivative, $(C_5Me_5)Rh(PMe_3)[2\text{-}(3,5\text{-lutidine})]Cl$. An ORTEP drawing is shown in Figure 2, data collection parameters are listed in Table 1, and selected bond distances and angles in Table 3. The α-sites in pyridine were blocked in the reaction of **1** with 2,4,6-collidine. The methyl substituents deactivate the ring, and thermolysis led only to decomposition to $(C_5Me_5)Rh(PMe_3)_2$.

Thermal reaction of **1** with pyrazole was conducted at 52 °C. A ^{31}P NMR spectrum revealed the presence of two products in a ratio of 2:1 at δ 8.24 (d, J = 140.4 Hz, 67%) and 7.63 (d, J = 141.2 Hz, 33%), respectively. ^1H NMR analysis was used to assign the major product as the N−H activation product $(C_5Me_5)Rh(PMe_3)(1\text{-}$

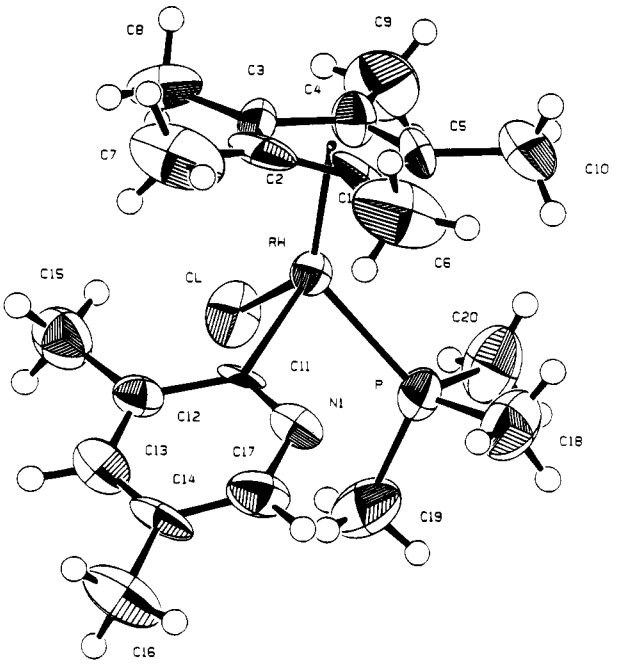

Figure 2. ORTEP drawing of $(C_5Me_5)Rh(PMe_3)[2\text{-}(3,5\text{-lutidine})]Cl$. Ellipsoids are shown at the 50% probability level.

Table 3. Selected Bond Distances (Å) and Angles (deg) for $(C_5Me_5)Rh(PMe_3)[2\text{-}(3,5\text{-lutidine})]Cl$

Bond Lengths			
Rh−Cl	2.401(4)	C(12)−C(13)	1.38(2)
Rh−P	2.264(5)	C(12)−C(15)	1.53(2)
Rh−C(11)	2.02(2)	C(13)−C(14)	1.39(2)
N(1)−C(11)	1.33(2)	C(14)−C(16)	1.50(2)
N(1)−C(17)	1.34(2)	C(14)−C(17)	1.35(2)
C(11)−C(12)	1.42(2)		
Bond Angles			
Cl−Rh−P	86.0(2)	C(11)−C(12)−C(15)	123(2)
Cl−Rh−C(11)	95.6(5)	C(13)−C(12)−C(15)	117(2)
P−Rh−C(11)	84.1(5)	C(12)−C(13)−C(14)	122(2)
C(11)−N(1)−C(17)	122(2)	C(13)−C(14)−C(16)	122(2)
Rh−C(11)−N(1)	117(1)	C(13)−C(14)−C(17)	114(2)
Rh−C(11)−C(12)	127(1)	C(16)−C(14)−C(17)	124(2)
N(1)−C(11)−C(12)	116(1)	N(1)−C(17)−C(14)	126(2)
C(11)−C(12)−C(13)	120(2)		

pyrazolyl)H based on the downfield chemical shift of the hydride resonance and its small Rh−H coupling constant (δ −11.815, dd, J = 48.1, *25.0* Hz). The second component was assigned as the C−H activation product $(C_5Me_5)Rh(PMe_3)(5\text{-pyrazolyl})H$ based on its upfield hydride resonance chemical shift and Rh−H coupling constant (δ −13.069, dd, J = 45.8, *30.6* Hz). The remainder of the ^1H NMR data were consistent with these assignments. Upon introduction of a second nitrogen into the pyrrole ring, both the N−H and C−H activation products are thermodynamically comparable, as the product ratio does not change with further heating.

Reaction of **1** with 3-methylpyrazole was also examined. A ^1H NMR spectrum for the products revealed the presence of four hydrides [**A**, δ −11.468 (dd, J = 48.6, 24.8 Hz, 28%); **B**, δ −11.662 (dd, J = 50.9, 26.7 Hz, 26%); **C**, δ −12.814 (dd, J = 45.1, 30.2 Hz, 42%); **D**, δ −13.442 (dd, J = 40.7, 29.1 Hz, 4%)]. The corresponding ^{31}P NMR data were as follows: **A**, δ 8.51 (d, J = 140.1 Hz); **B**, δ 10.41 (d, J = 138.0 Hz); **C**, δ 7.44 (d, J = 139.4 Hz); **D**, 6.54 (d, J = 151.0 Hz). Complexes **A** and **B** were assigned as N−H activation products based

Scheme 3. Reaction with 3-Methylpyrazole

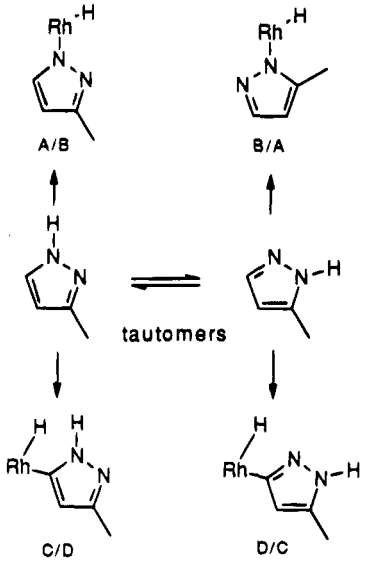

on the fact that (1) the chemical shifts of **A** and **B** were shifted downfield (by about 1–3 ppm for the ^{31}P resonances and ~2 ppm for hydride resonances) and (2) the coupling of the hydride to rhodium (J_{Rh-H}) was smaller in the ^{1}H NMR spectrum (**A**, J = 24.8 Hz; **B**, J = 26.7 Hz; in contrast to C–H activation complexes, J = 30–32 Hz). While there is only a single N–H bond in 3-methylpyrazole, the N–H activation products **A** and **B** can be assigned to activation of the tautomers of 3-methylpyrazole (Scheme 3). The possibility of two distinct rotamers was deemed unlikely since rotamers are not observed with aryl hydride complexes. Complexes **C** and **D** can be similarly assigned to the tautomeric α-C–H activation adducts, since a preference for α-activation is seen with furan and pyrrole.

Conclusions

Aromatic heterocycles tend to undergo C–H activation at the site adjacent to the heteroatom. N–H activation is a facile and thermodynamically preferable site of reaction. η^2-complexes are only observed with nonaromatic heterocycles, and in no case were the simple σ-donor complexes of the heteroatom observed.

Experimental Section

General Procedures. All manipulations were carried out under an N_2 atmosphere or on a high-vacuum line using Schlenk techniques. All solvents were distilled from dark purple solutions of sodium benzophenone ketyl under a nitrogen atmosphere. Reagent grade furan, 2,5-dimethylfuran, 2,3-dihydrofuran, dibenzofuran, pyrrole, 1-methylpyrrole, 2,5-dimethylpyrrole, 1,2,5-trimethylpyrrole, carbazole, 9-methylcarbazole, pyrrolidine, pyrazole, 3-methylpyrazole, pyridine, 3,5-lutidine, and 2,4,6-collidine were purchased from Aldrich Chemical Co. and were used without further purification, although each liquid was freeze–pump–thaw degassed (three cycles) prior to use.

^{1}H (400 MHz), ^{31}P (162 MHz), and ^{13}C (100 MHz) NMR spectra were recorded on a Bruker AMX-400 spectrometer. All chemical shifts are reported in ppm (δ) relative to tetramethylsilane and referenced to the chemical shifts of residual solvent resonances (C_6H_6, δ 7.15; C_6H_{12}, δ 1.38). ^{31}P NMR chemical shifts were measured in ppm relative to 30% H_3PO_4 (δ 0.0). Analyses were performed by Desert Analytics. An Enraf-Nonius CAD4 diffractometer was used for X-ray crystal structure determination.

Preparation of (C_5Me_5)Rh(PMe_3)(2-furanyl)H. A sample of (C_5Me_5)Rh(PMe_3)PhH (25 mg, 0.0637 mmol) was dissolved in 4 mL of hexane. To this solution was added 5 equiv of furan (217 mg, 0.32 mmol). The mixed solution was placed in an ampule equipped with a Teflon stopcock and stirred at 60 °C for 23 h. The reaction was cooled in an ice–water bath and the solvent removed in vacuo. A ^{1}H NMR spectrum showed that a single complex was produced in quantitative yield. The product was formulated as (C_5Me_5)Rh(PMe_3)(2-furanyl)H according to ^{1}H COSY NMR spectroscopy. ^{1}H NMR (C_6D_6): δ −12.825 (dd, J = 45.0, 30.6 Hz, 1 H), 0.953 (d, J = 10.1 Hz, 9 H), 1.840 (s, 15 H), 6.206 (d, J = 2.6 Hz, 1 H), 6.513 (dd, J = 2.3, 2.3 Hz, 1 H), 7.809 (d, J = 1.3 Hz, 1 H). ^{31}P NMR: δ 9.37 (d, J = 151.0 Hz). ^{13}C NMR: δ 10.76 (s, C_5Me_5), 19.03 (d, J = 33.0 Hz, PMe_3), 97.90 (t, J = 3.5 Hz, C_5Me_5), 110.98 (s, 2 CH), 117.32 (s, CH), 167.64 (dd, J = 47.0, 25.0 Hz, RhC).

Preparation of (C_5Me_5)Rh(PMe_3)(2-furanyl)Cl. To a C_6H_6 (0.5 mL) solution of (C_5Me_5)Rh(PMe_3)(2-furanyl)H (31 mg, 0.081 mmol) was added an excess of $CHCl_3$ (2 equiv, 0.16 mmol) at 0 °C. The yellow solution rapidly turned orange. After standing at room temperature for a few minutes a ^{1}H NMR spectrum was recorded, showing the formation of a new product. ^{1}H COSY and homonuclear decoupling experiments confirmed that the produced complex was (C_5Me_5)Rh(PMe_3)-(2-furanyl)Cl (28 mg, 84%). ^{1}H NMR (C_6D_6): δ 1.047 (d, J = 10.7 Hz, 9 H), 1.453 (d, J = 2.9 Hz, 15 H), 6.552 (dd, J = 2.9, 1.8 Hz, 1 H), 6.774 (d, J = 2.9 Hz, 1 H), 7.698 (d, J = 1.1 Hz, 1 H). ^{31}P NMR: δ 10.59 (d, J = 143.0 Hz). Anal. Calcd for $C_{17}H_{27}ClOPRh$: C, 49.00; H, 6.53. Found: 48.90; H, 6.55.

Preparation of (C_5Me_5)Rh(PMe_3)[3-(2,5-dimethylfuranyl)]H. 2,5-Dimethylfuran (0.12 mL, 1.10 mmol) was added by syringe to a hexane (3 mL) solution of **1** (20 mg, 0.051 mmol). Reaction was carried out at 61 °C for 19 h, after which the resulting solution was evaporated to dryness under vacuum. Both ^{1}H and ^{31}P NMR data were consistent with the formulation of (C_5Me_5)Rh(PMe_3)[3-(2,5-dimethyl)furanyl]H. ^{1}H NMR (C_6D_6): δ −13.315 (dd, J = 48.5, 29.9 Hz, 1 H), 0.936 (d, J = 9.9 Hz, 9 H), 1.836 (s, 15 H), 2.350 (s, 3 H), 2.614 (s, 3 H), 5.733 (s, 1 H). ^{31}P NMR (C_6D_6): δ 8.59 (d, J = 150.2 Hz).

Preparation of (C_5Me_5)Rh(PMe_3)[3-(2,5-dimethylfuranyl)]Cl. To a hexane (2.5 mL) solution of (C_5Me_5)Rh-(PMe_3)(3-(2,5-dimethylfuranyl)H (30 mg, 0.067 mmol) was added a slight excess of $CHCl_3$ (2 equiv, 0.13 mmol) at 0 °C. The brown solution rapidly turned orange.

After standing at room temperature for a few minutes a ^{1}H NMR spectrum was recorded, showing the formation of a new product. ^{1}H COSY and homonuclear decoupling experiments confirmed that the produced complex was (C_5Me_5)Rh(PMe_3)-(3-(2,5-dimethylfuranyl)Cl (15.5 mg, 52%). ^{1}H NMR (C_6D_6): δ 1.130 (d, J = 10.0 Hz, 9 H), 1.390 (d, J = 2.8 Hz, 15 H), 2.331 (s, 3 H), 2.857 (s, 3 H), 5.470 (s, 1 H). ^{31}P NMR: δ 8.96 (d, J = 147.0 Hz). Anal. Calcd for $C_{19}H_{31}ClOPRh$: C, 51.31; H, 7.02. Found: C, 50.61; H, 7.18.

Preparation of (C_5Me_5)Rh(PMe_3)(2,3-η^2-dihydrofuran). Complex **1** (20 mg, 0.0510 mmol) in hexane solution was treated with excess of dihydrofuran (0.10 mL, 1.32 mmol). The solution was then heated in an ampule at 50 °C for 24 h. The solvent removed under vacuum, and the resulting yellow solid was characterized as (C_5Me_5)Rh(PMe_3)(2,3-η^2-dihydrofuran) by 1D and COSY NMR spectroscopy (95%). For (C_5Me_5)Rh-(PMe_3)(η^2-dihydrofuran), ^{1}H NMR (C_6D_{12}): δ 1.004 (d, J = 8.2 Hz, 9 H), 1.774 (s, 15 H), 1.673 (m, 1 H), 2.010 (br m, 1 H), 2.208 (br m, 1 H), 3.483 (q, J = 7.7 Hz, 1 H), 3.829 (q, J = 8.3 Hz, 1 H), 4.942 (m, 1 H). ^{31}P NMR (C_6D_{12}): δ 2.54 (d, J = 208.0 Hz).

Preparation of (C_5Me_5)Rh(PMe_3)(dibenzofuran)H. Dibenzofuran (7 mg, 0.04 mmol) was added to a C_6D_{12} (0.5 mL) solution of **1** (10 mg, 0.026 mmol). The sample was heated for 3 days at 67 °C in a resealable NMR tube equipped with a Teflon stopcock. ^{1}H and ^{31}P NMR spectra show the formation

of one C−H activation product. ^{1}H NMR (C_6D_{12}): δ −13.367 (dd, J = 48.7, 31.1 Hz, 1 H), 1.144 (d, J = 9.8 Hz, 9 H), 1.813 (s, 15 H), 6.848 (m), 7.097 (t, 7.3 Hz, 1 H), 7.196 (m), 7.367 (d, J = 7.2 Hz, 1 H), 7.491 (m), 7.742 (d, 7.4 Hz, 1 H). ^{31}P NMR (C_6D_{12}): δ 6.75 (d, J = 151.0 Hz).

Preparation of (C_5Me_5)Rh(PMe_3)(dibenzofuran)Cl. To a hexane (0.5 mL) solution of (C_5Me_5)Rh(PMe_3)(dibenzofuran)H (40 mg, 0.0774 mmol) was added an excess of $CHCl_3$ (2 equiv, 0.155 mmol) at 0 °C. The yellow solution rapidly turned orange. After standing at room temperature for a few minutes a ^{1}H NMR spectrum was recorded, showing the formation of a new product. The chloro derivative was isolated on a thin-layer silica chromatography plate with a 95:5 (v/v) solution of CH_2Cl_2−THF. ^{1}H resonances and decoupling experiments indicate activation of the C−H bond in the 1 or 4 position. Elemental analysis of the chloride was high in C and H due to free dibenzofuran, which was difficult to remove (16.4 mg, 41%). ^{1}H NMR ($(CD_3)_2CO$): δ 1.401 (dd, J = 10.9, 0.8 Hz, 9 H), 1.601 (d, J = 2.9 Hz, 15 H), 7.019 (t, J = 7.5, Hz, 1 H), 7.290 (td, J = 7.6, 1.0 Hz, 1 H), 7.394 (td, J = 8.1, 1.3 Hz, 1 H), 7.544 (dd, J = 8.0, 1.0 Hz, 1 H), 7.565 (dd, J = 7.3, 1.0 Hz, 1 H), 7.927 (dd, J = 7.5, 1.1 Hz, 1 H), 7.982 (dd, J = 7.0, 1.1 Hz, 1 H). ^{31}P NMR (C_6D_6): δ 4.05 (d, J = 148.7 Hz). ^{13}C{^{1}H} NMR (C_6H_6): δ 9.27 (s, C_5Me_5), 15.74 (d, J = 31.0 Hz, PMe_3), 98.83 (t, J = 5.1 Hz, C_5Me_5), 110.43 (s, CH), 115.04 (s, CH), 120.82 (s, CH), 121.16 (s, CH), 122.41 (s, CH), 122.86 (s, C), 123.68 (s, C), 125.70 (s, CH), 127.05 (s, CH), 129.78 (s, C), 140.49 (dd, J = 38.0, 20.1 Hz, RhC), 155.34 (s, CH).

Preparation of (C_5Me_5)Rh(PMe_3)(1-pyrrolyl)H. **1** (20 mg, 0.051 mmol) was dissolved in 4 mL of hexane and 0.050 mL of pyrrole (0.70 mmol) added. The reaction mixture was placed into an ampule equipped with a Teflon stopcock and stirred at 61 °C for 22 h. The sample was cooled and evaporated to dryness to give (C_5Me_5)Rh(PMe_3)(1-pyrrolyl)H as an orange solid. ^{1}H NMR (C_6D_6): δ −11.523 (dd, J = 50.4, 25.1 Hz, 1 H), 0.820 (d, J = 9.7 Hz, 9 H), 1.595 (s, 15 H), 6.729 (br s, 4 H). ^{31}P NMR (C_6D_6): δ 9.15 (d, J = 143.9 Hz).

Preparation of (C_5Me_5)Rh(PMe_3)[2-(1-methyl)pyrrolyl]H. **1** (15 mg, 0.0383 mmol) was reacted with 0.10 mL of 1-methylpyrrole (1.25 mmol) at 60 °C for 16 h. After cooling, vacuum evaporation afforded an orange solid. The complex (C_5Me_5)Rh(PMe_3)[2-(1-methyl)pyrrolyl]H was formed in quantitative yield and was characterized by ^{1}H (1D, homonuclear decoupling, and JRES) NMR and ^{31}P NMR experiments (29.2 mg, 73%). ^{1}H NMR (C_6D_6): δ −12.947 (dd, J = 49.4, 30.4 Hz, 1 H), 0.921 (d, J = 10.4 Hz, 9 H), 1.862 (s, 15 H), 3.622 (s, 3 H), 5.901 (dd, J = 3.6, 2.0 Hz, 1 H), 6.623 (t, J = 3.8 Hz, 1 H), 7.042 (br s, 1 H). ^{31}P NMR (C_6D_6): δ 10.37 (d, J = 142.8 Hz).

Preparation of (C_5Me_5)Rh(PMe_3)[2-(1-methyl)pyrrolyl]Cl. To a hexane solution of (C_5Me_5)Rh(PMe_3)[2-(1-methylpyrrolyl)H (40 mg, 0.093 mmol) was added to an excess of $CHCl_3$ (2 equiv, 186 mmol). The solution turned orange, and a new product was seen by ^{31}P NMR. ^{1}H NMR data agreed with the assignment as (C_5Me_5)Rh(PMe_3)[2-(1-methylpyrrolyl)]Cl. ^{1}H NMR (C_6D_6): δ 1.128 (dd, J = 10.8, 0.6 Hz, 9 H), 1.341 (d, 3.0 Hz, 15 H), 3.932 (s, 3 H), 5.611 (dd, J = 3.2, 1.7 Hz, 1H), 6.593 (t, J = 3.2 Hz, 1H), 7.030 (m, 1 H). ^{31}P NMR (C_6D_6): δ 9.74 (d, 144.6 Hz). ^{13}C{^{1}H} NMR (C_6D_6): δ 9.00 (s, C_5Me_5), 14.98 (d, J = 33.6 Hz, PMe_3), 39.00 (s, NMe), 98.80 (t, J = 3.6 Hz, C_5Me_5), 109.25 (s), 115.00 (s), 125.25 (s), 159.58 (dd, J = 37.1, 18.3 Hz, RhC). Anal. Calcd for $C_{18}H_{30}ClNPRh$: C, 50.30; H, 7.04; N, 3.26. Found: C, 49.34; H, 7.03; N, 2.96.

Preparation of (C_5Me_5)Rh(PMe_3)[1-(2,5-dimethylpyrrole)]H. 2,5-Dimethylpyrrole (0.23 g, 2.5 mmol) was added to a C_6D_{12} (0.5 mL) solution of **1** (10 mg, 0.025 mmol). The reaction was heated at 67 °C for 25 h, after which solvent was removed and fresh solvent condensed. ^{1}H and ^{31}P NMR spectra were consistent with the formation of (C_5Me_5)Rh(PMe_3)[1-(2,5-dimethylpyrrole)]H. ^{1}H NMR (C_6D_6): δ −12.710 (dd, J = 53.2, 23.1 Hz, 1 H), 1.009 (d, 10.0 Hz, 9 H), 1.703 (d, J = 2.2 Hz, 15 H), 2.480 (s, 6 H), 5.820 (s, 2 H). ^{31}P NMR (C_6D_6): δ 6.87 (d, J = 146.0 Hz).

Reaction of 1 with 1,2,5-Trimethylpyrrole. A C_6D_{12} (0.5 mL) solution of **1** (10 mg, 0.025 mmol) was heated with 1,2,5-trimethylpyrrole (0.16 g, 1.5 mmol) at 67 °C for 21 h. The pale yellow solution turned dark green. Removal of solvent revealed the decomposition product, (C_5Me_5)Rh(PMe_3)$_2$, as the only product. ^{1}H NMR (C_6D_{12}): δ 1.259 (d, J = 7.6 Hz, 9 H), 1.889 (d, J = 1.7 Hz, 15 H). ^{31}P NMR (C_6D_{12}): δ −5.68 (d, J = 218.0 Hz). No C−H activation was seen.

Reaction of 1 with Carbazole. Thermolysis at 67 °C of **1** (10 mg, 0.025 mmol) and carbazole (0.012 g, 0.075 mmol) for 3 days gave two Rh(III) products in a 2:1 ratio. The major product was assigned as (C_5Me_5)Rh(PMe_3)(N-carbazole)H, from insertion into the N−H bond. ^{1}H NMR (C_6D_{12}): δ −11.232 (dd, J = 52.1, 24.2 Hz, 1 H), 0.922 (d, J = 10.1 Hz, 9 H), 1.766 (d, J = 1.8 Hz, 15 Hz), aromatic resonances were not assigned due to overlap with other product and starting material resonances. ^{31}P NMR (C_6D_{12}): δ 6.64 (d, J = 143.1 Hz). The minor product was formulated as a C−H activation product, (C_5Me_5)Rh(PMe_3)(carbazole)H. ^{1}H NMR (C_6D_6): δ −13.28 (dd, J = 49.9, 32.4 Hz, 1 H), 1.079 (d, J = 9.3 Hz, 9 H), 1.807 (d, J = 1.8 Hz, 15 H), aromatic resonances and site of activation were not assigned due to complexity and overlap in aromatic region. ^{31}P{^{1}H} NMR (C_6D_6): δ 9.19 (d, J = 148.6 Hz).

Reaction of 1 with 9-Methylcarbazole. A C_6D_{12} (0.5 mL) solution of **1** (10 mg, 0.025 mmol) and 9-methylcarbazole (11 mg, 0.055 mmol) was heated at 67 °C for 17 h. Only the formation of (C_5Me_5)Rh(PMe_3)$_2$ was observed by ^{1}H and ^{31}P NMR spectroscopy.

Reaction of 1 with Pyrrolidine. To a hexane (4 mL) solution of **1** (22 mg, 0.056 mmol) was added 40 mg of pyrrolidine (0.562 mmol). After stirring for 22 h at 61 °C, the pale yellow solution turned dark grey. Upon removal of the solvent, the decomposition product (C_5Me_5)Rh(PMe_3)$_2$ was found as the major product and a small amount of (C_5Me_5)Rh(PMe_3)H_2 was also produced. No N−H bond activation or C−H bond activation reaction occurred.

Reaction of 1 with Pyridine. Pyridine (0.196 g, 2.5 mmol) and **1** were heated in a C_6D_{12} (0.5 mL) solution at 70 °C for 7 h. Three C−H activation products were identified. The major product (57%) was formulated as (C_5Me_5)Rh(PMe_3)(2-pyridyl)H based on ^{1}H (COSY) NMR and homonuclear decoupling experiments. ^{1}H NMR (C_6D_{12}): δ −13.675 (dd, J = 48.0, 34.0 Hz, 1 H), 1.267 (d, J = 10.1 Hz, 9 H), 1.857 (d, J = 2.3 Hz, 15 H), 6.470 (td, J = 7.2, 1.5 Hz, 1 H), 6.732 (td, J = 7.1, 2.3 Hz, 1 H), 7.250 (dt, J = 8.5, 1.4 Hz, 1 H), 8.165 (dd, J = 5.7, 2.8 Hz, 1 H). ^{31}P{^{1}H} NMR (C_6D_{12}): δ 11.91 (d, J = 158.0 Hz). The second product (28%) was formulated as (C_5Me_5)Rh(PMe_3)(4-pyridyl)H, the product of insertion into the para C−H bond. ^{1}H NMR (C_6D_{12}): δ −13.490 (dd, J = 50.0, 34.0 Hz, 1 H), 1.247 (d, J = 9.8 Hz, 9 H), 1.866 (d, J = 2.0 Hz, 15 H), 7.146 (d, J = 5.0 Hz, 2 H), 7.755 (d, J = 5.7 Hz, 2 H). ^{31}P NMR (C_6D_{12}): δ 7.35 (d, J = 152.7 Hz). The third C−H insertion product (15%) was assigned as activation at the meta site, (C_5Me_5)Rh(PMe_3)(3-pyridyl)H. ^{1}H NMR (C_6D_{12}): δ 1.236 (d, J = 8.6 Hz, 9 H), 1.899 (d, J = 1.72 Hz, 15 H), 6.571 (t, J = 7.1 Hz, 1 H), 7.436 (d, J = 6.0 Hz, 1 H), 7.957 (dd, J = 7.0, 2.0 Hz, 1 H), 8.360 (s, 1 H). The hydride for the third product was obscured. ^{31}P NMR (C_6D_{12}): δ 7.71 (d, J = 153.3 Hz).

Preparation of Chloro Derivatives of Pyridine Products. A slight excess (2 equiv, 0.164 mmol) of $CHCl_3$ was added at 0 °C to a hexane solution of a mixture of the three rhodium−pyridine products (35 mg, 0.0818 mmol). The dark orange solution was evaporated and then recrystallized in C_6H_6−hexanes to give dark orange crystals (23 mg, 67%). Anal. Calcd for $C_{18}H_{28}ClNPRh$: C, 50.54; H, 6.60; N, 3.27. Found: C, 50.41; H, 7.02; N, 2.37. Major product (ortho C−H activation): ^{1}H NMR ($(CD_3)_2CO$): δ 1.302 (d, J = 11.1 Hz, 9 H), 1.658 (d, J = 3.0 Hz, 15 H), 6.720 (br s, 1 H), 7.040 (d, J = 2.3 Hz, 1 H), 7.725 (d, J = 1.4 Hz, 1 H), 8.207 (br s, 1 H). ^{31}P{^{1}H} NMR ($(CD_3)_2CO$): δ 11.16 (d, J = 154.9 Hz). Second

product (para C–H activation): ^{1}H NMR ($(CD_3)_2CO$): δ 1.385 (d, J = 13.1 Hz, 9 H), 1.708 (d, J = 2.9 Hz, 15 H), 7.490 (d, J = 4.2 Hz, 1 H), 7.650 (d, J = 5.0 Hz, 1 H), 7.801 (d, J = 5.0 Hz, 1 H). ^{31}P{^{1}H} NMR ($(CD_3)_2CO$): δ 8.46 (d, J = 156.3 Hz).

Formation of (C_5Me_5)Rh(PMe_3)[2-(3,5-lutidine)]H. A C_6D_{12} (0.5 mL) solution of **1** (10 mg, 0.025 mmol) and 3,5-lutidine (94 mg, 0.8 mmol) was heated at 70 °C for 7 h. Both ^{1}H and ^{31}P NMR data agree with the assignment of the single product as (C_5Me_5)Rh(PMe_3)[2-(3,5-lutidine)]H, insertion into the C–H bond adjacent to N. ^{1}H NMR (C_6D_{12}): δ −13.670 (dd, J = 50.0, 34.0 Hz, 1 H), 1.106 (d, J = 10.1 Hz, 9 H), 1.748 (d, 1.6 Hz, 15 H), 2.048 (s, 3 H), 2.252 (s, 3 H), 6.820 (s, 1 H), 7.930 (s, 1 H). ^{31}P NMR (C_6D_{12}): δ 13.77 (d, 156.0 Hz).

Preparation of (C_5Me_5)Rh(PMe_3)[2-(3,5-lutidine)]Cl. To a hexane solution of (C_5Me_5)Rh(PMe_3)[2-(3,5-lutidine)]H (40 mg, 0.0949 mmol) was added 23 mg of $CHCl_3$ (2 equiv, 190 mmol). The solution turned orange, and a new product was seen by ^{31}P NMR. ^{1}H NMR data agreed with the assignment as (C_5Me_5)Rh(PMe_3)[2-(3,5-lutidine)]Cl (19.5 mg, 45%). ^{1}H NMR (C_6D_6): δ 1.244 (d, J = 11.2 Hz, 9 H), 1.400 (d, J = 2.9 Hz, 15 H), 2.000 (s, 3 H, Me-5), 2.827 (s, 3 H, Me-3), 6.890 (s, 1 H, H-4), 8.098 (s, 1 H, H-6). ^{31}P NMR (C_6D_6): δ 13.28 (d, 155.9 Hz). Anal. Calcd for $C_{20}H_{32}ClNPRh$: C, 52.70; H, 7.08; N, 3.07. Found: C, 51.78; H, 7.12; N, 3.29.

Reaction of 1 with 2,4,6-Collidine. 2,4,6-Collidine (91 mg, 0.76 mmol) and **1** (10 mg, 0.025 mmol) were heated in a C_6D_{12} (0.5 mL) solution at 65 °C for 3 days. A green solid was found after removal of the solvent which was identified by ^{1}H and ^{31}P NMR as the decomposition product, (C_5Me_5)Rh(PMe_3)$_2$. No C–H activation was observed.

Reaction of 1 with Pyrazole. **1** (30 mg, 0.0765 mmol) and pyrazole (white crystals, 8 mg, 0.118 mmol) were stirred in hexane at 52 °C for 72 h. ^{1}H and ^{31}P NMR analysis of the residue consisted of 66% (C_5Me_5)Rh(PMe_3)(1-pyrazolyl)H and 34% (C_5Me_5)Rh(PMe_3)(5-pyrazolyl)H. For (C_5Me_5)Rh(PMe_3)-(1-pyrazolyl)H, ^{1}H NMR (C_6D_6): δ −11.815 (dd, J = 48.1, 25.0 Hz, 1 H), 0.749 (d, J = 10.7 Hz, 9 H), 1.426 (s, 15 H), 6.255 (s, 1 H), 7.248 (s, 1 H), 7.755 (s, 1 H). ^{31}P NMR: δ 8.24 (d, J = 140.4 Hz). For (C_5Me_5)Rh(PMe_3)(5-pyrazolyl)H, ^{1}H NMR (C_6D_6): δ −13.069 (dd, J = 45.8, 30.6 Hz, 1 H), 0.608 (d, J = 9.8 Hz, 9 H), 1.545 (s, 15 H), 5.838 (s, 1 H), 7.673 (s, 1 H); the proton resonance for N–H was not observed. ^{31}P NMR (C_6D_6): δ 7.63 (d, J = 141.2 Hz).

Reaction of 1 with 3-Methylpyrazole. **1** (20 mg, 0.051 mmol) was reacted with 3-methylpyrazole (0.040 mL, 0.497 mmol) in hexane for 24 h at 60 °C. Upon removal of the solvent, the residue was analyzed by NMR spectroscopy. The ^{1}H NMR spectrum exhibited four hydrides: **A**, δ −11.468 (dd, J = 48.6, 24.8 Hz), 28%; **B**, δ −11.662 (dd, J = 50.9, 26.7 Hz), 26%; **C**, δ −12.814 (dd, J = 45.1, 30.2 Hz), 42%; **D**, δ −13.442 (dd, J = 40.7, 29.1 Hz), 4%. The corresponding ^{31}P NMR data are as follows: **A**, δ 8.51 (d, J = 140.1 Hz); **B**, δ 10.41 (d, J = 138.0 Hz); **C**, δ 7.44 (d, J = 139.4 Hz); **D**, δ 6.54 (d, J = 151.0 Hz). Complexes **A** and **B** are assigned as N–H activation products. Similarly, complexes **C** and **D** are assigned to tautomeric C–H activation products as described in the text.

X-ray Structural Determination of (C_5Me_5)Rh(PMe_3)-[2-(1-methylpyrrole)]Cl. Dark orange crystals formed from slow evaporation of benzene solvent at 25 °C. A single orange crystal was mounted with epoxy on a glass fiber. Lattice constants were obtained from 25 centered reflections with values of χ between 5 and 70°. Data were collected at −40 °C in accord with parameters in Table 1. The Molecular Structure Corp. TEXSAN analysis software package was used for data reduction and solution.[30] Patterson map solution of the structure to locate the rhodium atom, followed by expansion of the structure with the program DIRDIF, revealed all non-hydrogen atoms. Following isotropic refinement, an absorption correction was applied by use of the program DIFABS. Full-matrix, least-squares anisotropic refinement of the non-hydrogen atoms (with hydrogens attached to carbons in idealized positions) was carried out to convergence, with R_1 = 0.0338 and R_2 = 0.0413. Fractional coordinates are given in the supplementary material.

X-ray Structural Determination of (C_5Me_5)Rh(PMe_3)-[2-(3,5-lutidine)]Cl. Orange crystals of the compound were formed by slow diffusion of hexanes into a saturated benzene solution at −30 °C. Data collection, solution, and refinement of the structure followed similarly to that of the pyrrole compound, except that the molecule crystallized in the monoclinic space group $C2/c$ with eight molecules per unit cell. Full-matrix, least-squares anisotropic refinement of the non-hydrogen atoms (with hydrogens attached to carbons in idealized positions) was carried out to convergence, with R_1 = 0.0616 and R_2 = 0.0591. Fractional coordinates are given in the supplementary material.

Acknowledgment. This work was supported by the U.S. Department of Energy Grant FG02-86ER13569. We also thank NATO for a travel grant.

Supplementary Material Available: Tables of data collection parameters, bond lengths, bond angles, fractional atomic coordinates, and anisotropic thermal parameters for (C_5Me_5)Rh(PMe_3)[2-(1-methylpyrrole)]Cl (**A**) and (C_5Me_5)Rh-(PMe_3)[2-(3,5-lutidine)]Cl (**B**) (12 pages). Ordering information is given on any current masthead page.

OM9404339

(30) $R_1 = (\Sigma||F_o| - |F_c||)/\Sigma|F_o|$, $R_2 = [\Sigma w(|F_o| - |F_c|)^2]^{1/2}/\Sigma w|F_o|^2$, where $w = [\sigma^2(F_o) + (\varrho F_o^2)^2]^{1/2}$ for a non-Poisson contribution weighting scheme. The quantity minimized was $\Sigma_w(|F_o| - |F_c|)^2$. Source of scattering factors f_o, f', f'': Cromer, D. T.; Waber, J. T. *International Tables for X-Ray Crystallography*; The Kynoch Press: Birmingham, England, 1974; Vol. IV, Tables 2.2B, 2.3.1.

Reactions of the Trinuclear [2.2]Paracyclophane Cluster $Ru_3(CO)_9(\mu_3\text{-}\eta^2{:}\eta^2{:}\eta^2\text{-}C_{16}H_{16})$: Thermal Activation *versus* Chemical Activation

Alexander J. Blake, Paul J. Dyson, Scott L. Ingham, Brian F. G. Johnson,* and Caroline M. Martin

Department of Chemistry, The University of Edinburgh, West Mains Road, Edinburgh EH9 3JJ, U.K.

Received July 18, 1994[⊗]

The reactivity of the known [2.2]paracyclophane triangular cluster $Ru_3(CO)_9(\mu_3\text{-}\eta^2{:}\eta^2{:}\eta^2\text{-}C_{16}H_{16})$ (**1**) has been studied. Thermolysis of (**1**) with $Ru_3(CO)_{12}$ in octane yields the known octahedral carbido complex $Ru_6C(CO)_{14}(\mu_3\text{-}\eta^2{:}\eta^2{:}\eta^2\text{-}C_{16}H_{16})$ (**2**). Reaction of **1** with Me_3NO in dichloromethane results in cluster degradation and formation of the bridged dimer $Ru_2(CO)_6(\mu_2\text{-}\eta^3{:}\eta^3\text{-}C_{16}H_{16})$ (**3**). Likewise, treatment of **2** with Me_3NO in dichloromethane results in cluster degradation and affords **1**. Mild thermolytic action of **1** with the alkyne C_2Ph_2 affords three products: $Ru_3(CO)_7(\mu_3\text{-}\eta^1{:}\eta^2{:}\eta^1\text{-}C_2Ph_2)(\eta^6\text{-}C_{16}H_{16})$ (**4**), in which the cyclophane now adopts a terminally bonding mode, $Ru_3(CO)_7(\mu_3\text{-}\eta^2\text{-}PhC_2\{PhCO\})(\eta^6\text{-}C_{16}H_{16})$ (**5**), similar to **4** except that carbonyl insertion has occurred between the alkyne and metal; and the dinuclear product $Ru_2(CO)_6(\{\mu_2\text{-}\sigma{:}\eta^2\text{-}C_2Ph_2\}_2\text{-}CO)$ (**6**), in which a carbonyl has been inserted between two alkynes. **4** is also produced when **1** is treated with Me_3NO in the presence of C_2Ph_2. **1** undergoes reaction either with Me_3NO in the presence of PPh_3 or by direct thermolysis with PPh_3 to yield the monosubstituted derivative $Ru_3(CO)_8(PPh_3)(\mu_3\text{-}\eta^2{:}\eta^2{:}\eta^2\text{-}C_{16}H_{16})$ (**7**). All compounds **3**, **4**, **6**, and **7** have been characterized by both spectroscopic means and single crystal X-ray diffraction methods. **5** has been characterized by spectroscopy only, and the ^{13}C NMR spectrum of cluster **1** is also reported.

Introduction

For a number of reasons we have been concerned with the synthesis and structure of arene clusters, and a wide and diverse chemistry of these compounds has emerged; this has been recently reviewed.[1] In a variety of ruthenium and osmium cluster systems, initial studies were concerned primarily with their interaction with benzene and simple arenes such as toluene, xylene, and mesitylene.[1b] Emphasis has been directed toward the preferred bonding types (*viz.* $\mu_3\text{-}\eta^2{:}\eta^2\eta^2$ face-capping *versus* η^6 terminal) of competing ligands on the same cluster. It was found that the face-capping coordination mode is most strongly favored according to the following sequence: $C_6H_6 > C_6H_5Me > C_6H_4Me_2 > C_6H_3Me_3$.[2] However, recently we have extended these studies to more elaborate aromatic systems such as triethylbenzene or [2.2]paracyclophane ($C_{16}H_{16}$, PCP).[1b,3] These ligands not only exhibit a somewhat different chemistry from that found for the simpler arenes but also bring about modification of the principal interactions observed in the crystal lattice. For example, ribbonlike ring–ring interactions are usually found in the solid state for monoarene clusters; in contrast, in the triethylbenzene cluster, $Ru_6C(CO)_{14}(\eta^6\text{-}C_6H_3Et_3)$, the ethyl groups fold in such a fashion that they interlock with the three carbonyl groups on a neighboring molecule, so that the flat arene fragment has effectively been removed.[3a] The paracyclophane ligand was employed with the expectation that clusters would be linked, one to another, by utilizing both arene rings of the same PCP unit. While this goal has yet to be achieved, a number of other interesting observations have been made.[3b] First, PCP prefers to adopt the face-capping bonding mode rather than the more commonly observed η^6-coordination mode preferred by most simple arenes. Second, facially coordinated PCP adopts different conformations over a triruthenium face in Ru_6C clusters, ranging from near-staggered to near-eclipsed arrangements of alternate C-atoms over the three Ru-atoms. Last, significant distortions of the PCP molecule are observed when PCP is bonded to cluster units.

In this paper, we have chosen to discuss our results in several distinct sections. In the first, the ^{13}C NMR spectrum of $Ru_3(CO)_9(\mu_3\text{-}\eta^2{:}\eta^2{:}\eta^2\text{-}C_{16}H_{16})$ (**1**) is described. This is followed by a discussion of the interconversion between **1** and the hexanuclear carbido cluster $Ru_6C(CO)_{14}(\mu_3\text{-}\eta^2{:}\eta^2{:}\eta^2\text{-}C_{16}H_{16})$ (**2**) and includes the preparation of $Ru_2(CO)_6(\mu_2\text{-}\eta^3{:}\eta^3\text{-}C_{16}H_{16})$ (**3**). In the next section, we describe the products obtained from reaction of **1** with diphenylacetylene, *viz.* $Ru_3(CO)_7(\mu_3\text{-}\eta^1{:}\eta^2{:}\eta^1\text{-}C_2Ph_2)(\eta^6\text{-}C_{16}H_{16})$ (**4**), $Ru_3(CO)_7(\mu_3\text{-}\eta^2\text{-}PhC_2\{PhCO\})(\eta^6\text{-}C_{16}H_{16})$ (**5**), and $Ru_2(CO)_6(\{\mu_2\text{-}\sigma{:}\eta^2\text{-}C_2Ph_2\}_2\text{-}CO)$ (**6**). Finally, the substitution of an equatorial carbonyl in **1** by triphenylphosphine thereby yielding $Ru_3(CO)_8(PPh_3)(\mu_3\text{-}\eta^2{:}\eta^2{:}\eta^2\text{-}C_{16}H_{16})$ (**7**) is reported.

⊗ Abstract published in *Advance ACS Abstracts*, December 1, 1994.

(1) (a) Wadepohl, H. *Angew. Chem., Int. Ed. Engl.* **1992**, *31*, 247. (b) Braga, D.; Dyson, P. J.; Grepioni, F.; Johnson, B. F. G. *Chem. Rev.*, in press.

(2) Dyson, P. J.; Johnson, B. F. G.; Reed, D.; Braga, D.; Grepioni, F.; Parisini, E. *J. Chem Soc., Dalton Trans.* **1993**, 2817.

(3) (a) Braga, D.; Grepioni, F.; Parisini, E.; Dyson, P. J.; Blake, A. J.; Johnson, B. F. G. *J. Chem Soc., Dalton Trans.* **1993**, 2951. (b) Dyson, P. J.; Johnson, B. F. G.; Martin, C. M.; Blake, A. J.; Braga, D.; Grepioni, F. *Organometallics* **1994**, *13*, 2113.

0276-7333/95/2314-0862$09.00/0

Scheme 1. Reactions of 1 Involving a Change in Nuclearity[a]

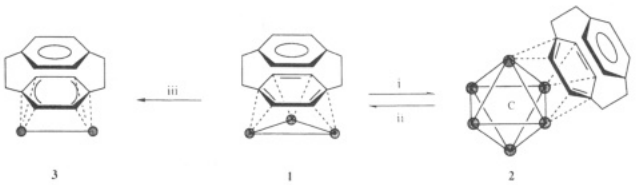

[a] Reagents and conditions: (i) $Ru_3(CO)_{12}$/octane, Δ; (ii) 10 molar equiv of Me_3NO/CH_2Cl_2; (iii) 3 molar equiv of Me_3NO/CH_2Cl_2.

Results and Discussion

We have previously reported the preparation of $Ru_3(CO)_9(\mu_3\text{-}\eta^2{:}\eta^2{:}\eta^2\text{-}C_{16}H_{16})$ (**1**) from the thermolysis of [2.2]-paracyclophane with $Ru_3(CO)_{12}$ in either heptane or octane.[3b] Other products from this reaction include the two hexanuclear clusters $Ru_6C(CO)_{14}(\mu_3\text{-}\eta^2{:}\eta^2{:}\eta^2\text{-}C_{16}H_{16})$ (**2**) and $Ru_6C(CO)_{11}(\mu_3\text{-}\eta^2{:}\eta^2{:}\eta^2\text{-}C_{16}H_{16})(\eta^6\text{-}C_{16}H_{16})$. It appeared that **1** was an intermediate in the formation of the hexaruthenium cluster **2**, and in agreement, we have found that on heating equimolar amounts of **1** and $Ru_3(CO)_{12}$ in octane under reflux, **2** is formed in moderate yield.

Since crystals of **1** suitable for an X-ray diffraction study have eluded us to date, we have further characterized **1** from an examination of its ^{13}C NMR spectrum. The ^{13}C NMR spectrum of **1** in $CDCl_3$ is entirely consistent with the other spectroscopic data, and seven resonances are observed. We consider that the signal at δ 197.6 ppm is derived from the nine equilibrating carbonyl groups and it does not alter on cooling. This is followed by two signals from the unattached ring at δ 138.5 and 132.1 ppm. Coordinated ring carbon signals occur at δ 76.0 and 54.7 ppm. Lastly, the CH_2-CH_2 linkages give rise to two signals at δ 40.7 and 35.2 ppm, for the C-atom neighboring the bonded ring and furthest from this ring, respectively. These assignments were made with assistance from a C, H correlation spectrum.

Reactions with Me_3NO only. The use of Me_3NO as an oxidative decarbonylation reagent (removing CO as CO_2) is well documented. This reagent is generally used in combination with a coordinating solvent (typically MeCN), which may be displaced by the appropriate ligand in a subsequent step.[4] Alternatively, Me_3NO can be used in a noncoordinating solvent containing the appropriate ligand so that direct substitution takes place.[5] As far as we are aware, the use of Me_3NO as a reagent to bring about cluster degradation has not been previously recognized. In this case, the reaction with Me_3NO in a noncoordinating solvent is thought to bring about the formation of an unstable, unsaturated cluster (by loss of CO) and result in the *controlled* degradation of the parent compound.

The reaction of $Ru_6C(CO)_{14}(\mu_3\text{-}\eta^2{:}\eta^2{:}\eta^2\text{-}C_{16}H_{16})$ (**2**) with a large excess of Me_3NO in dichloromethane affords compound **1** in modest yield (Scheme 1). In a similar fashion, addition of 3 molar equiv of Me_3NO to a solution of $Ru_3(CO)_9(\mu_3\text{-}\eta^2{:}\eta^2{:}\eta^2\text{-}C_{16}H_{16})$ (**1**) in dichloromethane results in the formation of the new dinuclear species, $Ru_2(CO)_6(\mu_2\text{-}\eta^3{:}\eta^3\text{-}C_{16}H_{16})$ (**3**). This product, in which the paracyclophane ligand remains attached, has been the subject of a preliminary report.[6] Spectroscopic data obtained for **3** are entirely consistent with the molecular structure obtained in the solid state by a single crystal X-ray diffraction analysis. The mass spectrum exhibits a parent peak at 579 amu (calculated 579 amu) followed by the loss of six carbonyl groups in succession. The infrared spectrum is devoid of bands in the carbonyl bridging region, only showing bands between 2060 and 1950 cm^{-1} typical of terminally bonded CO. The ^1H NMR spectrum in $CDCl_3$ exhibits signals at δ 7.06 (s), 3.59 (s), 2.93 (m), and 2.56 (m) ppm with equal relative intensities; this pattern is consistent with the presence of a coordinated PCP moiety.

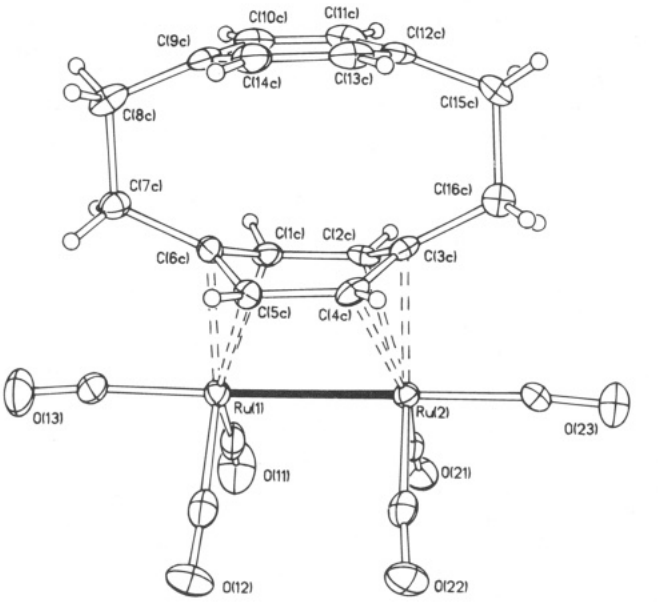

Figure 1. Molecular structure of $Ru_2(CO)_6(\mu_2\text{-}\eta^3{:}\eta^3\text{-}C_{16}H_{16})$ (**3**) in the solid state. The C-atoms of the CO ligands bear the same numbering as the corresponding O-atoms. Principal bond parameters (Å) are as follows: Ru(1)−Ru(2) 2.838(3), mean Ru−$C_{(CO)}$ 1.916, mean C−$O_{(CO)}$ 1.145, Ru−$C_{(cyclophane)}$ Ru(1)−C(1C) 2.264(7), Ru(1)−C(5C) 2.295(7), Ru(1)−C(6C) 2.191(7), Ru(2)−C(2C) 2.278(7), Ru(2)−C(3C) 2.187(7), and Ru(2)−C(4C) 2.253(7). Coordinated ring C−C distances, C(1C)−C(2C) 1.481(10), C(2C)−C(3C) 1.399(10), C(3C)−C(4C) 1.412(10), C(4C)−C(5C) 1.486(10), C(5C)−C(6C) 1.408(10), and C(6C)−C(1C) 1.437(10). Uncoordinated ring C−C distances, C(9C)−C(10C) 1.393(11), C(10C)−C(11C) 1.380(12), C(11C)−C(12C) 1.408(11), C(12C)−C(13C) 1.389(11), C(13C)−C(14C) 1.372(11), and C(14C)−C(9C) 1.398(11). Linkage C−C distances, C(6C)−C(7C) 1.529(10), C(7C)−C(8C) 1.569(10), C(8C)−C(9C) 1.505(11) C(12C)−C(15C) 1.498(11), C(15C)−C(16C) 1.564(10), and C(16C)−C(3C) 1.541(10).

The molecular structure of the new diruthenium complex **3** is depicted in Figure 1, together with relevant structural parameters. The most important feature of the molecule is the method by which the PCP ligand bonds to the two ruthenium atoms, each ruthenium interacting with three carbon atoms of the "bonded" ring. A close examination of this $\mu_2\text{-}\eta^3{:}\eta^3$ interaction reveals that the coordinated ring adopts a boat conformation: the angle between the two enyl planes defined by C(1c)−C(6c)−C(5c) and C(2c)−C(3c)−C(4c) is 56°. Although the rings in free [2.2]paracyclophane

(4) Chen, H.; Johnson, B. F. G.; Lewis, J.; Braga, D.; Grepioni, F.; Parisini, E. *J. Chem. Soc., Dalton Trans.* **1991**, 215.

(5) Dyson, P. J.; Johnson, B. F. G.; Lewis, J.; Martinelli, M.; Braga, D.; Grepioni, F. *J. Am. Chem. Soc.* **1993**, *115*, 9062.

(6) Blake, A. J.; Dyson, P. J.; Johnson, B. F. G.; Martin, C. M. *J. Chem. Soc., Chem. Commun.* **1994**, 1471.

also adopt boat conformations,[7] the angle between the two enyl planes is only 23°, indicating a dramatic change upon coordination to the cluster unit that is rather unusual for aromatic systems. A related bonding mode has been observed previously in the compound $Rh_2(Cp)_2(\mu_2\text{-}\eta^3{:}\eta^3\text{-}C_6H_6)$ in which similar distortions are apparent in the benzene unit.[3] It is also worth noting that the mean C−C bond lengths of the enyl sections of the ring, *viz.* C(1c)−C(6c), C(5c)−C(6c), C(2c)−C(3c), and C(3c)−C(4c), are shorter than the C−C bonds linking the two enyl units, *viz.* C(1c)−C(2c) and C(4c)−C(5c) [1.414(10) *versus* 1.484(10) Å, respectively]. There is no recognizable pattern of long and short C−C bond lengths in the unattached ring of $Ru_2(CO)_6(\mu_2\text{-}\eta^3{:}\eta^3\text{-}C_{16}H_{16})$, the mean distance for the C−C bonds in the ring being 1.385(11) and 1.390(11) Å, respectively.

In this work, the high quality of the low-temperature X-ray data has made it possible to locate the ring hydrogen positions, and for the coordinated ring, all four hydrogen atoms are observed to bend out of the plane defined by C(1c), C(2c), C(4c), and C(5c) and away from the ruthenium atoms. The mean deviation from the plane is 0.20(8) Å. In the unattached ring, the distortions described above are not present. The ring is almost planar, and the angle between the two enyl planes is 18°, less than in the free ligand itself (*cf.* 23°). Also the hydrogen atoms are in the plane defined by C(10c), C(11c), C(13c), and C(14c) [mean deviation 0.05(8) Å].

It is clear that the attack by Me_3NO on **1** selectively removes one Ru moiety from the triangular cluster. Although it is difficult to monitor the reaction pathway of this degradation reaction, it would appear that attack of the Me_3NO occurs successively at the same $Ru(CO)_3$ site. It certainly raises interesting synthetic possibilities, and the scope of this reaction and its applicability to other related cluster systems is currently under investigation.

Reactions with Diphenylacetylene. On reaction with alkynes, the benzene cluster $M_3(CO)_9(\mu_3\text{-}\eta^2{:}\eta^2{:}\eta^2\text{-}C_6H_6)$ (M = Ru,[8] Os[9]) affords compounds in which the benzene has undergone migration from a face-bridging to a terminal site, while the alkyne straddles the triangular face of the cluster. The only difference between the corresponding reactions of the ruthenium and osmium derivatives is that, in the case of the ruthenium complex, a carbonyl group is inserted between the alkyne ligand and the metal atom carrying the benzene moiety. We have found that cluster **1** reacts with diphenylacetylene under two sets of conditions, the same major product, **4**, being formed in each case. First, on heating **1** in dichloromethane under reflux in the presence of diphenylacteylene and, second, by treatment of **1** with 2 mol equiv of Me_3NO in the presence of diphenylacetylene at −78 °C (followed by warming to room temperature). In the former reaction two other products, $Ru_3(CO)_7(\mu_3\text{-}\eta^2\text{-}PhC_2\{PhCO\})(\eta^6\text{-}C_{16}H_{16})$ (**5**) and $Ru_2(CO)_6(\{\mu_2\text{-}\sigma{:}\eta^2\text{-}C_2Ph_2\}_2\text{-}CO)$ (**6**) (Scheme 2), have also been isolated. It has been found that the relative yields of compounds **4**−**6** depend critically on the thermolysis time, with the diruthenium complex **6** being

Scheme 2. Reactions of 1 with Diphenylacetylene[a]

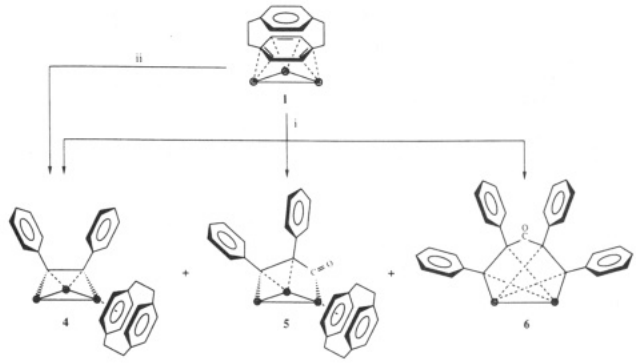

[a] Reagents and conditions: (i) C_2Ph_2/CH_2Cl_2, Δ; (ii) 2 molar equiv of $Me_3NO/C_2Ph_2/CH_2Cl_2$.

formed in highest yields when the longest reaction period is employed. Cluster **5** is not observed under such conditions and is present in modest yields on heating for a short time. Since **5** is a minor product of the reaction, it has been characterized only from a comparison of its infrared spectrum with that observed for the benzene analogue, which has also been characterized crystallographically. The spectra are almost identical; hence, one may assume that the compounds are isostructural and therefore a carbonyl is inserted between one of the C-atoms of the alkyne and a metal of the cluster.

The same method of characterization for compound **4** was used in the first instance, *viz.* a comparison of its infrared spectrum with that of the osmium benzene species.[9] Again the two spectra showed a clear similarity. Hence, formulation of **4** as $Ru_3(CO)_7(\mu_3\text{-}\eta^1{:}\eta^2{:}\eta^1\text{-}C_2Ph_2)(\eta^6\text{-}C_{16}H_{16})$ appeared reasonable. This was substantiated by the mass spectrum which contains a parent ion at 885 amu (calculated 886 amu) and shows the sequential loss of seven CO groups. The ^1H NMR spectrum exhibits a multiple resonance which may be assigned to the phenyl protons between δ 6.75 and 7.09 ppm. The ring protons of the uncoordinated ring give rise to a singlet at δ 6.72 ppm while those on the bound ring produce two multiplets at δ 4.60 and 5.29 ppm. Similarly, the CH_2 groups neighboring the unattached ring produce one mutiplet centered at δ 3.12 ppm, with two multiplets at δ 2.55 and 2.719 ppm for those adjacent to the coordinated ring. The relative intensities of all these signals are correct for the proposed assignments, which are in complete agreement with the structure observed in the solid state.

The molecular structure of **4** has been established in the solid state and is shown in Figure 2, together with the principal bond distances. It can be appreciated that the diphenylacetylene lies over the face of the cluster such that it forms one π and two σ bonds [the distances between the acetylene carbons and the ruthenium atoms are as follows: C(1a)−Ru(1) 2.237(9), C(2a)−Ru(1) 2.216(9), C(1a)−Ru(3) 2.108(9) and C(2a)−Ru(2) 2.294(9) Å]. Hence, the σ interaction involving the metal to which the PCP ring is attached [Ru(2)] is longer than the other σ interaction [Δ = 0.186 Å]; in contrast, the carbonyl that bridges the same two metals, Ru(2) and Ru(3), shows a shorter distance than the metal carrying the PCP ligand [Ru(2)−C(21) 1.894(10) Å *versus* Ru(3)−C(21) 2.384(11) Å, Δ = 0.490 Å]. The unsaturated bond, C(1a)−C(2a), in the acetylene is 1.409(13) Å; this value

(7) Cram, D. J.; Wilkinson, D. I. *J. Am. Chem. Soc.* **1960**, *82*, 5721.
(8) Braga, D.; Grepioni, F.; Johnson, B. F. G.; Parisini, E.; Martinelli, M.; Gallop, M. A.; Lewis, J. *J. Chem. Soc., Dalton Trans.* **1992**, 807.
(9) Braga, D.; Gallop, M. A.; Grepioni, F.; Johnson, B. F. G.; Lewis, J.; Martinelli, M. *J. Chem. Soc., Chem. Commun.*, **1990**, 53.

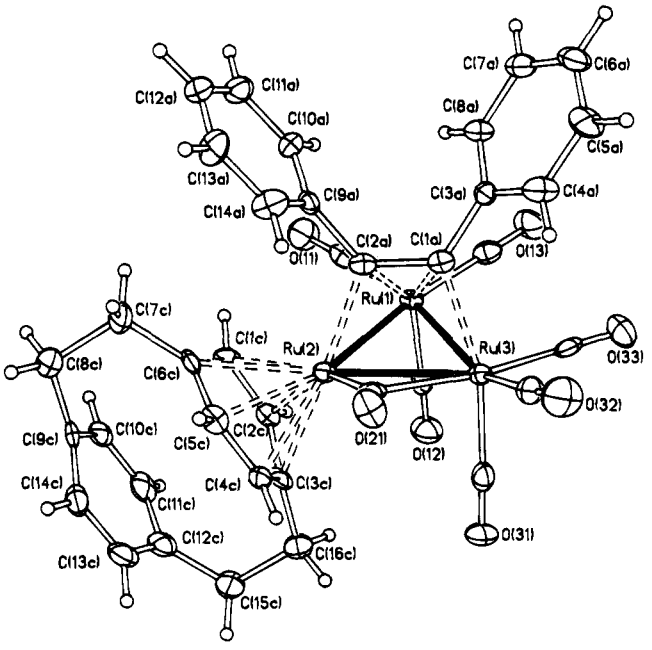

Figure 2. Molecular structure of $Ru_3(CO)_7(\mu_3\text{-}\eta^1{:}\eta^2{:}\eta^1\text{-}C_2Ph_2)(\eta^6\text{-}C_{16}H_{16})$ (**4**) in the solid state. The C-atoms of the CO ligands bear the same numbering as the corresponding O-atoms. Principal bond parameters (Å) are as follows: Ru(1)–Ru(2) 2.6969(13), Ru(1)–Ru(3) 2.6957(12), Ru(2)–Ru(3) 2.8006(13), mean $Ru-C_{(CO)}$ 1.910, mean $C-O_{(CO)}$ 1.150, $Ru-C_{(cyclophane)}$ Ru(2)–C(1C) 2.246(9), Ru(2)–C(2C) 2.294(9), Ru(2)–C(3C) 2.403(9), Ru(2)–C(4C) 2.241(9), Ru(2)–C(5C) 2.251(10), and Ru(2)–C(6C) 2.403(9). Coordinated ring C–C distances, C(1C)–C(2C) 1.417(14), C(2C)–C(3C) 1.408(13), C(3C)–C(4C) 1.415(14), C(4C)–C(5C) 1.394(14), C(5C)–C(6C) 1.405(14), and C(6C)–C(1C) 1.380(14). Uncoordinated ring C–C distances, C(9C)–C(10C) 1.40(2), C(10C)–C(11C) 1.39(2), C(11C)–C(12C) 1.39(2), C(12C)–C(13C) 1.38(2), C(13C)–C(14C) 1.38(2), and C(14C)–C(9C) 1.385(14). Linkage C–C distances, C(6C)–C(7C) 1.496(14), C(7C)–C(8C) 1.601(14), C(8C)–C(9C) 1.519(14), C(12C)–C(15C) 1.52(2), C(15C)–C(16C) 1.582(14), and C(16C)–C(3C) 1.497(14). Diphenylacetylene distances, Ru(1)–C(1A) 2.237(9), Ru(1)–C(2A) 2.216(9), Ru(2)–C(2A) 2.294(9), Ru(3)–C(1A) 2.108(9), C(1A)–C(2A) 1.409(13), C(1A)–C(3A) 1.482(13), and C(2A)–C(9A) 1.480(13). mean $C-C_{(phenyls)}$ 1.39.

is typical for such a moiety in this coordination mode. The non-linearity of the acetylene introduced upon coordination is also typical, the angles between C(2a)–C(1a)–C(3a) and C(1a)–C(2a)–C(9a) being 124.2(8) and 125.9(8)°, respectively. The PCP unit is bonded to Ru(2) in an η^6 fashion. This bonded ring is not planar but boat shaped with four C-atoms [C(1c), C(2c), C(4c) and C(5c)] lying closer to Ru(2) [mean = 2.258(10) Å] than the two carbons to which the aliphatic bridges attach [C(3c) and C(6c), mean 2.403(9) Å]. It should be appreciated that this distortion forms an angle of 23.9(12)° between the two enyl planes defined by C(1c)–C(5c)–C(6c) and C(2c)–C(4c)–C(3c), which is essentially the same as that observed in the free PCP molecule, *i.e.*, 23°.[7] The angle between the enyl planes in the unattached ring defined by C(9c)–C(10c)–C(14c) and C(11c)–C(12c)–C(13c) also remains unperturbed from that of the free molecule.

Characterization of **6** as $Ru_2(CO)_6(\{\mu_2\text{-}\sigma{:}\eta^2\text{-}C_2Ph_2\}_2\text{-}CO)$ required both spectroscopic and crystallographic analyses. The infrared spectrum of **6** is unusual. Apart

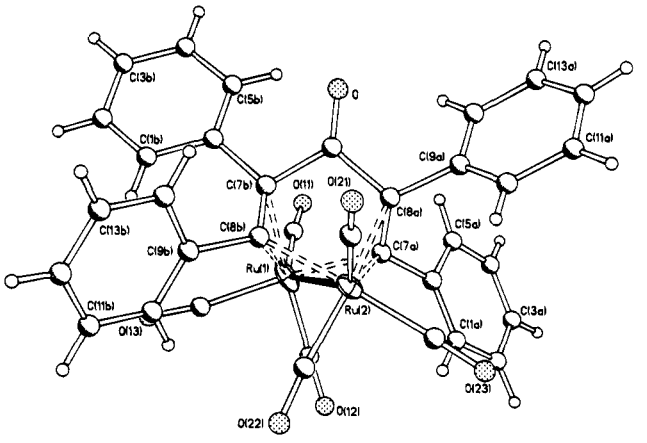

Figure 3. Molecular structure of $Ru_2(CO)_6(\{\mu_2\text{-}\sigma{:}\eta^2\text{-}C_2Ph_2\}_2\text{-}CO)$ (**6**) in the solid state. The C-atoms of the CO ligands bear the same numbering as the corresponding O-atoms. Principal bond parameters (Å) are as follows: Ru(1)–Ru(2) 2.751(3), mean $Ru-C_{(CO)}$ 1.90, mean $C-O_{(CO)}$ 1.16, Ru(1)–C(7A) 2.07(2), Ru(1)–C(7B) 2.23(2), Ru(1)–C(8B) 2.17(2), Ru(2)–C(7A) 2.24(2), Ru(2)–C(8A) 2.27(2), Ru(2)–C(8B) 2.06(2), C(7A)–C(8A) 1.44(3), C(8A)-C 1.54(3), C–O 1.20(2), C–C(7B) 1.55(3), C(7B)–C(8B) 1.31(3), C(7A)–C(6A) 1.48(3), C(8A)–C(9A) 1.54(3), C(7B)–C(6B) 1.57(3), C(8B)–C(9B) 1.60(3), and mean $C-C_{(phenyls)}$ 1.38.

from the characteristic carbonyl stretches between 2090 and 2028 cm^{-1} indicative of terminal M–CO ligands, a strong C–O stretch is also found at 1672 cm^{-1} which may be associated with that of a ketone. The mass spectrum exhibits the expected parent peak at 756 amu (calculated 755 amu) followed by a complicated fragmentation pattern. The ^1H NMR spectrum is simple, containing two multiplets of equal relative intensities at δ 7.26 and 7.14 ppm, characteristic of phenyl groups in two different environments. The above data are consistent with the structure obtained in the solid state from a single crystal X-ray diffraction study. The molecular structure is not of high quality because of the poor crystals obtained after months of effort. However, because of the highly unusual nature of the molecule, and since spectroscopic data and microanalytical results are in good agreement with the established structure, we feel the gross features of the structure are worth describing, although caution must be taken in reading too much into the actual bond lengths and angles obtained. The molecular structure of **6** is illustrated in Figure 3, together with relevant bond parameters. The two diphenylacteylene units are linked through a carbonyl group, and each of the alkyne moieties bonds to the ruthenium dimer *via* one π and one σ interaction, therefore providing the metals with a total of six electrons. Apart from this, each metal also has three terminal carbonyl groups, and with the Ru–Ru bond, the effective atomic number rule is obeyed. To our knowledge the behavior observed here is unprecedented, and from our experiments, we can speculate a mechanism for the formation of the $(C_2Ph_2)_2CO$ entity.

While the mechanism by which **6** is produced in the thermal reaction is not easily rationalized, the formation of **4** from the reaction utilizing Me_3NO under ambient conditions is less complicated; one may assume that the removal of two carbonyl ligands from $Ru_3(CO)_9(\mu_3\text{-}\eta^2{:}\eta^2{:}\eta^2\text{-}C_{16}H_{16})$ (**1**) takes place with the direct substitution of the acetylene onto the cluster face. This would yield

Scheme 3. Reaction of 1 with Triphenylphosphine[a]

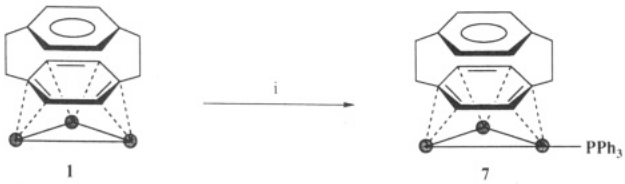

[a] Reagents and conditions: (i) 1 molar equiv of $Me_3NO/PPh_3/CH_2Cl_2$ or PPh_3/THF, Δ.

$Ru_3(CO)_7(\mu_3\text{-}\eta^1{:}\eta^2{:}\eta^1\text{-}C_2Ph_2)(\mu_3\text{-}\eta^2{:}\eta^2{:}\eta^2\text{-}C_{16}H_{16})$, as yet unobserved, which must undergo rapid rearrangement of the ligands on the surface of the cluster to yield **4**, probably while the solution is stirred at room temperature for 1 h prior to workup of the reaction mixture (see Experimental Section).

Heating clusters containing face-capping arenes often causes migration of the arene to a terminal site. Such arene migration processes have been established to involve a nondissociative mechanism, and clearly, a simultaneous movement of carbonyl ligands in the opposite direction is also required. In the presence of an alkyne, one can envisage the stepwise replacement of these two carbonyl ligands for the four-electron-donating diphenylacetylene ligand, the alkyne possibly coordinating to one metal atom initially, and then migrating to two and then finally three metal. The simultaneous movement of the PCP ligand from three to two to one metal atom would also be required.

Reactions with Me_3NO in the Presence of Phosphines. We have found that **1** readily undergoes substitution reactions in which one carbonyl can be replaced by a number of phosphine ligands. This can be achieved using Me_3NO, which removes a carbonyl group leaving a vacant coordination site on the cluster to which two electron−donor ligands may attach. Using triphenylphosphine, a red product was produced in good yield, and was characterized by spectroscopic means as $Ru_3(CO)_8(PPh_3)(\mu_3\text{-}\eta^2{:}\eta^2{:}\eta^2\text{-}C_{16}H_{16})$ (**7**) (Scheme 3). Alternatively, heating **1** to reflux in THF containing PPh_3 for a few hours affords the same product. The mass spectrum of **7** exhibits a strong molecular ion at 705 amu (calculated 998 amu) which corresponds to the weight of the cluster without a CO and the phosphine unit. The ^{31}P NMR spectrum of **7** contains one signal at δ 38.01 ppm which is readily assignable to the phosphorus atom of the PPh_3 fragment. The ^1H NMR spectrum of **7** is more complicated, but is nonetheless readily assigned. It consists of five resonances at δ 7.40, 7.32, 3.12, 2.95, and 2.41 ppm with relative intensities of 15:4:4:4:4. The first signal at δ 7.40 ppm is a multiplet and corresponds to the protons of the phenyl rings attached to the phosphine ligand. The remaining signals are derived from the cyclophane unit, at δ 7.32 and 3.12 ppm the resonances, a singlet and doublet, respectively, can be attributed to the C−H protons of the unbound and coordinated rings, respectively. The remaining two signals are multiplets corresponding to the protons in the $-CH_2CH_2-$ linkages. These data are entirely consistent with the structure observed in the solid state.

The molecular structure of **7** was also established in the solid state by a single crystal X-ray diffraction analysis and is illustrated in Figure 4 together with relevant bond distances. The structure consists of a ruthenium triangle capped on one side by a $\mu_3\text{-}\eta^2{:}\eta^2{:}\eta^2$ PCP ligand. Ru(1) and Ru(3) also bear tricarbonyl units while Ru(2) carries two carbonyl ligands and an equatorially disposed triphenylphosphine moiety. The coordinated ring is flattened somewhat in comparison to free PCP [the angle between the plane defined by C(1c)−C(2c)−C(6c) and C(3c)−C(4c)−C(5c) is 15.7(5)°, *cf.* free PCP 23°].[7] The unattached ring is far more contorted toward a boat shape, the angle between the enyl planes defined by C(7c)−C(12c)−C(8c) and C(9c)−C(11c)−C(10c) being 24.2(4)°. Hence, the opposite distortions have occurred to the face-bound PCP ligand compared to those observed when PCP bonds to two metal atoms in the $\mu_2\text{-}\eta^3{:}\eta^3$ mode. The PPh_3 unit occupies an equatorial site, although displaced slightly above the ruthenium triangular plane, *viz.* 0.236(1)°. The structure of **7** is analogous to the triosmium−benzene species, $Os_3(CO)_8(PPh_3)(\mu_3\text{-}\eta^2{:}\eta^2{:}\eta^2\text{-}C_6H_6)$, which exhibits the same gross structural features.[10] Unlike other complexes containing $\mu_3\text{-}\eta^2{:}\eta^2{:}\eta^2$ PCP ligands, the ring adopts a staggered conformation over the triruthenium face. This is reflected in the Ru−C(ring) bond distances which only vary very slightly [Ru(1)−C(1c) 2.305(3), Ru-

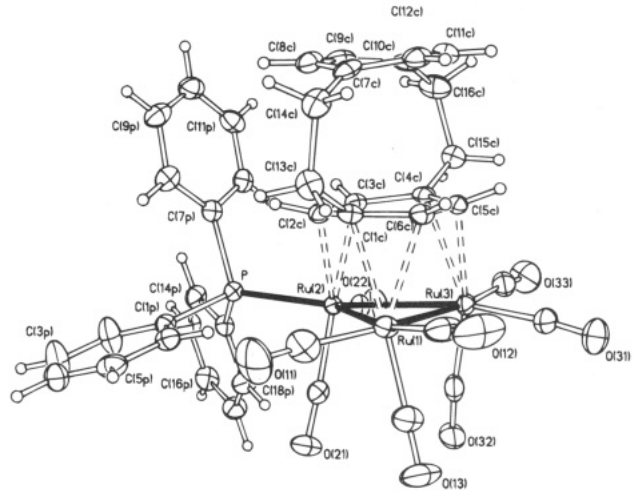

Figure 4. Molecular structure of $Ru_3(CO)_8(PPh_3)(\mu_3\text{-}\eta^2{:}\eta^2{:}\eta^2\text{-}C_{16}H_{16})$ (**7**) in the solid state. The C-atoms of the CO ligands bear the same numbering as the corresponding O-atoms. Principal bond parameters (Å) are as follows: Ru(1)−Ru(2) 2.905(2), Ru(1)−Ru(3) 2.840(2), Ru(2)−Ru(3) 2.830(2), mean Ru−$C_{(CO)}$ 1.89, mean C−$O_{(CO)}$ 1.145, Ru−$C_{(cyclophane)}$ Ru(1)−C(1C) 2.305(4), Ru(1)−C(6C) 2.313(4), Ru(2)−C(2C) 2.309(4), Ru(2)−C(3C) 2.227(4), Ru(3)−C(4C) 2.451(4), and Ru(3)−C(5C) 2.268(4). Coordinated ring C−C distances, C(1C)−C(2C) 1.461(5), C(2C)−C(3C) 1.419(5), C(3C)−C(4C) 1.450(5), C(4C)−C(5C) 1.399(5), C(5C)−C(6C) 1.440(5), and C(6C)−C(1C) 1.407(5). Uncoordinated ring C−C distances, C(7C)−C(8C) 1.399(5), C(8C)−C(9C) 1.382(6), C(9C)−C(10C) 1.394(6), C(10C)−C(11C) 1.399(6), C(11C)−C(12C) 1.385(6), and C(12C)−C(8C) 1.389(6). Linkage C−C distances, C(1C)−C(13C) 1.532(5), C(13C)−C(14C) 1.562(6), C(14C)−C(7C) 1.499(5), C(4C)−C(15C) 1.517(5), C(15C)−C(16C) 1.571(5), and C(16C)−C(10C) 1.505(6). Triphenylphosphine distances, Ru(2)-P 2.351(2), P-C(1P) 1.828(4), P-C(7P) 1.820(4), P-C(13P) 1.846(3), and mean C−$C_{(phenyls)}$ 1.38.

(10) Gallop, M. A.; Gomez-Sal, M. P.; Housecroft, C. E.; Johnson, B. F. J.; Lewis, J.; Owen, S. M.; Raithby, P. R.; Wright, A. J. *J. Am. Chem. Soc.* **1992**, *114*, 2502.

(1)–C(6c) 2.313(3), Ru(2)–C(2c) 2.309(3), Ru(2)–C(3c) 2.227(3), Ru(3)–C(4c) 2.451(3) and Ru(3)–C(5c) 2.268(3) Å].

Retention of the face-capping ligand is not uncommon in this type of reaction, nor is equatorial substitution by an entering ligand. The triosmium–benzene cluster $Os_3(CO)_9(\mu_3\text{-}\eta^2:\eta^2:\eta^2\text{-}C_6H_6)$ undergoes a similar chemistry with Lewis bases.[10] The difference in this system is that CO is initially displaced for a labile acetonitrile group, which is then subsequently replaced by the appropriate ligand. No substitution chemistry has yet been developed for the triruthenium–benzene cluster, which is probably due to the relative instability of this species to this type of chemistry.

Concluding Comments

We have demonstrated various ways of manipulating the triruthenium–cyclophane cluster in a series of reactions that employ either mild thermal action or chemical initiation with Me_3NO. While very different products are obtained between these two reaction types when ligands are not employed, in the presence of a ligand, both thermolysis and chemical activation tend to give the same products although in the reactions involving diphenylacetylene the chemical activation method is far more selective. Some of these reactions have been employed in the analogous complexes, $M_3(CO)_9(\mu_3\text{-}\eta^2:\eta^2:\eta^2\text{-}C_6H_6)$ (M = Ru, Os), and in general tend to be similar to the chemistry played by the osmium complex. We are currently attempting to prepare an osmium–cyclophane analogue in order to compare its reactivity with these other systems.

Experimental Section

General Procedures and Materials. All reactions were carried out using freshly distilled solvents under an atmosphere of nitrogen gas. Subsequent workup of products were carried out using standard laboratory grade solvents without precautions to exclude air. Infrared spectra were recorded on a Perkin-Elmer 1710 Fourier transform spectrometer. Mass spectra were obtained by positive fast atom bombardment on a Kratos MS50TC. ^1H and ^{31}P NMR spectra were recorded using a Bruker AM360 or WM250 spectrometer.

The cluster $Ru_3(CO)_9(\mu_3\text{-}\eta^2:\eta^2:\eta^2\text{-}C_{16}H_{16})$ (**1**) was prepared according to a literature method (using heptane as solvent and a 2 h reaction time).[3b] Trimethylamine *N*-oxide (Me_3NO), diphenylacetylene (C_2Ph_2), and triphenylphosphine (PPh_3) were purchased from Fluka chemicals. Me_3NO was dried and sublimed prior to use, while the other materials were not treated to any other purification process.

Products were isolated by thin-layer chromatography (TLC) using plates supplied by Merck coated with silica gel-60. The same eluent was used in each case, this being dichloromethane–hexane (1:4, v/v).

Thermolysis of $Ru_3(CO)_9(\mu_3\text{-}\eta^2:\eta^2:\eta^2\text{-}C_{16}H_{16})$ 1 with $Ru_3(CO)_{12}$. A suspension of **1** (30 mg) and $Ru_3(CO)_{12}$ (25 mg, 1 molar equiv) in octane (20 mL) was heated to reflux for 2 h, after which time IR spectroscopy indicated a significant amount of conversion to $Ru_6C(CO)_{14}(\mu_3\text{-}\eta^2:\eta^2:\eta^2\text{-}C_{16}H_{16})$ (**2**). The solvent was removed under vacuum and the orange **2** (18 mg) was extracted from the resulting brown residue by TLC. **2** was characterized spectroscopically by a comparison with the literature values, which were in excellent agreement.

Spectroscopic data for **2**: IR (CH_2Cl_2) ν(CO) 2076 (w), 2039 (s), 2024 (vs), 1982 (w, br), 1940 (w, br), 1814 (w, br) cm^{-1}; ^1H NMR ($CDCl_3$) δ 7.44 (s, 4H), 3.43 (s, 4H), 3.40 (m, 4H), 2.98 (m, 4H) ppm; MS, M^+ = 1219 (calc = 1219) amu. Anal. Found (Calc): C 30.51 (30.54), H 1.38 (1.31).

Reaction of $Ru_6C(CO)_{14}(\mu_3\text{-}\eta^2:\eta^2:\eta^2\text{-}C_{16}H_{16})$ (2) with Me_3NO. **2** (20 mg) was dissolved in dichloromethane (20 mL). To this solution was added a 10-fold excess of Me_3NO (0.012 mg) in dichloromethane (4 mL) in a dropwise fashion. The reaction mixture was stirred for a total period of 30 min, after which time the solvent was removed *in vacuo*. The residue was redissolved in a small amount of dichloromethane and subjected to TLC. The major yellow product was characterized spectroscopically as $Ru_3(CO)_9(\mu_3\text{-}\eta^2:\eta^2:\eta^2\text{-}C_{16}H_{16})$ (**1**) (6 mg).

Spectroscopic data for **1**: IR (CH_2Cl_2) ν(CO) 2067 (s), 2024 (vs), 1993 (m), 1980 (m), 1959 (w, sh) cm^{-1}; ^1H NMR ($CDCl_3$) δ 7.22 (s, 4H), 3.76 (s, 4H), 3.23 (m, 4H), 2.67 (m, 4H) ppm; MS: M^+ = 763 (calc = 763) amu.

Reaction of $Ru_3(CO)_9(\mu_3\text{-}\eta^2:\eta^2:\eta^2\text{-}C_{16}H_{16})$ 1 with Me_3NO. To a solution of **1** (50 mg) in dichloromethane (20 mL) was added a 3-fold excess of Me_3NO (0.015 mg) in dichloromethane dropwise over a few minutes. The reaction mixture was stirred for 20 min and then the solvent was removed under reduced pressure. Extraction of the products by TLC revealed two yellow bands which were characterized spectroscopically as $Ru_2(CO)_6(\mu_2\text{-}\eta^3:\eta^3\text{-}C_{16}H_{16})$ (**3**) (5 mg) and starting material **1** (29 mg), in order of elution. Crystals of **3** suitable for the single crystal X-ray diffraction analysis were grown by vapor diffusion from dichloromethane–pentane at room temperature. Yellow crystals were produced which did not deteriorate on removal from their mother liquor.

Spectroscopic data for **3**: IR (CH_2Cl_2) ν(CO) 2060 (s), 2022 (vs), 1993 (s), 1950 (w, sh); ^1H NMR ($CDCl_3$) δ 7.06 (s, 4H), 3.59 (s, 4H), 2.93 (m, 4H) and 2.56 (m, 4H); MS, M^+ = 579 (calc = 579) amu. Insufficient sample available for microanalysis.

Thermolysis of $Ru_3(CO)_9(\mu_3\text{-}\eta^2:\eta^2:\eta^2\text{-}C_{16}H_{16})$ (1) with Diphenylacetylene. **1** (50 mg) was dissolved in dichloromethane (30 mL), and an excess of diphenylacteylene (30 mg) was added. The reaction mixture was heated to reflux for 18 h, after which time the solvent was removed under reduced pressure, and the products were separated by TLC. Three bands were extracted from the TLC plate; they were characterized spectroscopically as $Ru_3(CO)_7(\mu_3\text{-}\eta^1:\eta^2:\eta^1\text{-}C_2Ph_2)(\eta^6\text{-}C_{16}H_{16})$ (**4**) (8 mg), $Ru_3(CO)_7(\mu_3\text{-}\eta^2\text{-}PhC_2\{PhCO\})(\eta^6\text{-}C_{16}H_{16})$ (**5**) (2 mg), and $Ru_2(CO)_6(\{\mu_2\text{-}\eta^1:\eta^2\text{-}C_2Ph_2\}_2\text{-}CO)$ (**6**) (6 mg), respectively.

Spectroscopic data for **4**: IR (CH_2Cl_2) ν(CO) 2056 (s), 2020 (vs), 1982 (s), 1958 (w, sh), 1923 (w); ^1H NMR ($CDCl_3$) δ 6.92 (m, 10H), 6.72 (s, 4H), 5.29 (m, 2H), 4.60 (m, 2H), 3.12 (m, 4H), 2.719 (m, 2H), 2.55 (m, 2H); MS, M^+ = 885 (calc = 886) amu. Anal. Found (Calc): C 50.23 (50.17), H 3.04 (2.96).

Spectroscopic data for **5**: IR (CH_2Cl_2) ν(CO) 2065 (s), 2032 (vs), 1993 (s). Insufficient sample available for microanalysis.

Spectroscopic data for **6**: IR (CH_2Cl_2) ν(CO) 2090 (m), 2069 (vs), 2028 (s), 1672 (m); ^1H NMR ($CDCl_3$) δ 7.14 (m, 10H), 7.26 (m, 10H); MS, M^+ = 756 (calc = 755) amu. Anal. Found (Calc): C 55.75 (55.70), H 2.70 (2.67).

Reaction of $Ru_3(CO)_9(\mu_3\text{-}\eta^2:\eta^2:\eta^2\text{-}C_{16}H_{16})$ (1) with Diphenylacetylene and Me_3NO. Diphenylacetylene (15 mg) and **1** (30 mg) were dissolved in dichloromethane (25 mL), and the solution was cooled to −78 °C. A solution of Me_3NO (7 mg, 2.2 molar equiv) in dichloromethane (10 mL) was added dropwise over a 10 min period. The reaction mixture was allowed to warm to room temperature over a period of 1 h and stirred for a further 1 h at room temperature, after which time the solvent was removed *in vacuo*. The products were extracted by TLC, and the major orange product was characterized spectroscopically as $Ru_3(CO)_7(\mu_3\text{-}\eta^1:\eta^2:\eta^1\text{-}C_2Ph_2)(\eta^6\text{-}C_{16}H_{16})$ (**4**) (10 mg). Crystals of **4** were nucleated from toluene at −25 °C over a period of several days. Stable, red crystals were produced which were suitable for the single crystal X-ray diffraction analysis.

Reaction of $Ru_3(CO)_9(\mu_3\text{-}\eta^2:\eta^2:\eta^2\text{-}C_{16}H_{16})$ (1) with Triphenylphosphine and Me_3NO. **1** (50 mg) and triphenylphos-

Table 1. Crystal Data, Measurement Details, and Structure Parameters for 3, 4, 6, and 7

	3	4	6	7
		Crystal Data		
formula	$C_{22}H_{16}O_6Ru_2$	$C_{37}H_{26}O_7Ru_3 \cdot 1.75CH_2Cl_2$	$C_{35}H_{20}O_7Ru_2$	$C_{42}H_{31}O_8Ru_3$
MW	578.5	1030.9	754.7	997.9
temperature (°C)	150(2)	150(2)	150(2)	150(2)
crystal system	monoclinic	monoclinic	monoclinic	monoclinic
space group	$P2_1/n$	$P2_1/n$	$P2_1/n$	$P2_1/n$
a (Å)	9.183(10)	15.408(4)	11.96(1)	14.421(12)
b (Å)	21.912(10)	10.127(3)	10.58(1)	16.265(10)
c (Å)	10.366(10)	25.289(9)	24.05(2)	16.27(2)
β (deg)	106.84(10)	105.65(2)	104.21(8)	100.66(12)
U (Å^3)	1996(3)	3800(2)	2950(5)	3751(5)
Z	4	4	4	4
ϱ_{calc} (g cm^{-3})	1.925	1.802	1.699	1.767
μ (mm^{-1})	1.550	1.472	1.074	1.289
max and min absorptn corrcn	0.749, 0.654	0.744, 0.685	0.549, 0.508	0.449, 0.399
crystal size (mm)	0.30 × 0.15 × 0.10	0.48 × 0.10 × 0.10	0.18 × 0.27 × 0.35	0.5 × 0.38 × 0.38
crystal color	yellow	red	red	red
		Data Collection		
diffractometer	Stoë Stadi-4	Stoë Stadi-4	Stoë Stadi-4	Stoë Stadi-4
radiation	Mo	Mo	Mo	Mo
λ (Å)	0.710 73	0.710 73	0.710 73	0.710 73
monochromator	graphite	graphite	graphite	graphite
2ϑ scan range (deg)	5−45	5−45	5−45	5−50
No. of reflections collected	2605	5649	3658	7698
No. of independent reflections	2605	4935	3498	6589
R(int)	0	0.0396	0.1427	0.0182
		Structure Refinement		
R_1 [I > $2\sigma(I)$]	0.0363	0.0443	0.103	0.0269
wR_2 (all data)	0.1301	0.1631	0.272	0.0730
S	1.063	1.066	1.110	1.146
parameters refined	296	478	187	511
$\Delta\varrho_{max}$ (eÅ^{-3})	0.794	1.053	1.208	0.471
$\Delta\varrho_{min}$ (eÅ^{-3})	−0.172	−1.006	−1.518	−0.869

phine (30 mg) were dissolved in dichloromethane (20 mL), and the solution was cooled to −78 °C. To this solution was added a 1.2 mole equivalent of Me_3NO (5 mg) dropwise. The solution was then allowed to warm to room temperature over a 25 min period and was accompanied by a color change from yellow to brown. The solvent was removed under vacuum, and the brown residue subjected to TLC, which produced a red product characterized as $Ru_3(CO)_8(PPh_3)(\mu_3\text{-}\eta^2{:}\eta^2{:}\eta^2\text{-}C_{16}H_{16})$ (**7**) (32 mg). Red crystals of **7** of varying quality were nucleated at room temperature from slow evaporation of a dichloromethane−hexane solution.

Spectroscopic data for **7**: IR (CH_2Cl_2) υ(CO) 2049 (s), 2012 (s), 1986 (vs), 1975 (s, sh); ^{1}H NMR ($CDCl_3$) δ 7.40 (m, 15H), 7.32 (s, 4H), 3.12 (m, 4H), 2.95 (m, 4H), 2.41 (m, 4H); ^{31}P NMR ($CDCl_3$) δ 38.01 (s, 1P); MS, M$^+$ = 705 (calc = 998). Anal. Found (Calc): C 52.95 (52.17), H 3.34 (3.23).

Thermolysis of $Ru_3(CO)_9(\mu_3\text{-}\eta^2{:}\eta^2{:}\eta^2\text{-}C_{16}H_{16})$ (1) with Triphenylphosphine. **1** (30 mg) was dissolved in tetrahydrofuran (20 mL), and an excess of triphenylphosphine (30 mg) was added. The reaction mixture was heated to reflux for 3 h, after which time the solvent was removed *in vacuo*, and the products were separated by TLC. The major red band was extracted and characterized spectroscopically as $Ru_3(CO)_8(PPh_3)(\mu_3\text{-}\eta^2{:}\eta^2{:}\eta^2\text{-}C_{16}H_{16})$ (**7**) (6 mg).

Structural Characterization. X-ray diffraction data for species **3**, **4**, **6**, and **7** were collected at a temperature of 150 K on a Stoë Stadi-4 diffractometer, equipped with an Oxford Cryosystems low-temperature device.[11] Relevant data collection, structure solution, and refinement parameters are summarized in Table 1. The crystals of **6** were of poor quality and diffracted rather weakly; unfortunately no other suitable crystals could be obtained. Whereas the X-ray structural determination of **6** was not accurate enough for an in-depth investigation of the structural parameters for this compound, it does show the gross structural features and hence has been included for this reason. The structures were solved by a combination of direct methods and Fourier techniques, with refinement being performed using the least-squares method on F^2.[12] Anisotropic thermal motion was assumed for all non-hydrogen atoms, except for **6** where only the two ruthenium atoms were refined by use of an anisotropic thermal model, due to the poor quality of the X-ray diffraction data. All hydrogen atoms, except the phenyl hydrogens in **3**, were placed in calculated positions and were refined by use of a *riding* model. The phenyl hydrogen atoms in **3** were refined subject to the constraint that the C−H distances were 0.96(1) Å. A difference electron density Fourier synthesis for **4** exhibited large peaks well seperated from the cluster, these being attributed to two molecules of solvated dichloromethane, one of which had an occupancy factor of 75%. These two molecules of solvent were included in subsequent cycles of refinement.

Acknowledgment. We thank the SERC and ICI (Wilton), The University of Edinburgh, and NATO financial assistance.

Supplementary Material Available: Tables of crystal data and structure refinement, anisotropic thermal parameters, fractional atomic coordinates, and isotropic thermal parameters for the non-hydrogen atoms, complete lists of bond lengths and angles, and fractional atomic coordinates for the hydrogen atoms (18 pages). Ordering information is given on any current masthead page.

OM940564+

(11) Cosier, J.; Glazer, A. M. *J. Appl. Crystallogr.* **1986**, *19*, 105.

(12) Sheldrick, G. M. *SHELX93*; University of Gottingen: Gottingen, Germany, 1993.

Exploring Stereoselectivity through the Quantitative Analysis of Ligand Effects. Addition of Hydride to (η-Cp)(CO)(PR_3)Fe[C(OMe)(Me)]$^+$

Beth A. Lorsbach, Dawn M. Bennett, Alfred Prock,* and Warren P. Giering*

Department of Chemistry, Metcalf Science and Engineering Center, Boston University, Boston, Massachusetts 02215

Received July 25, 1994®

The stereoselectivity of the addition of hydride (from $NaBH_4$) to 14 chiral cationic carbene complexes, η-Cp(CO)(PR_3)Fe[C(OMe)Me]$^+$, has been studied as a function of the stereoelectronic properties (χ, E_{ar}, and θ) of the phosphine ligands. The anti/syn (*RS/SR*:*SS/RR*) ratio of the diastereomeric products, η-Cp(CO)(PR_3)Fe*[C*H(OMe)Me], which varies from 0.99 to greater than 30, is independent of θ below 145° and rises dramatically, becoming too large to measure by NMR methods above 153°. The anti/syn ratio increases with increasing electron donor capacity of PR_3 (smaller χ) and decreases with increasing number of aryl groups (larger E_{ar}) attached to PR_3. These results suggest that the addition of hydride to η-Cp(CO)(PR_3)Fe[C(OMe)Me]$^+$ involves a steric threshold near 145° that must be exceeded in order to achieve significant stereoselectivity.

Introduction

Many stereoselective reactions involve a chiral auxiliary or a stereogenic center to which are attached pendent groups of the type AR_3, where A = P,[1a,b] Si,[1c] or Sn.[1d] How variations of the stereoelectronic properties of these chiral auxiliaries affect the stereoselectivities of potentially asymmetric reactions has not been systematically explored, as far as we are aware, and is not understood. Since the stereoelectronic properties of these pendent groups can be varied almost continuously,[2] the results of experiments in which AR_3 groups are systematically varied would afford insight into the factors influencing stereoselectivity and would allow, in principle, a "fine tuning" of the stereogenic center leading to a maximization of the stereoselectivity of the reaction.

We are currently reexamining and expanding on a number of studies of stereoselective reactions involving AR_3 groups that have been reported in the literature. These reactions include the addition of hydride (from $NaBH_4$) to the family of cationic iron(II) carbene complexes,[3] η-Cp(CO)(PR_3)Fe[C(OMe)Me]$^+$, (described herein) and the osmylation of the chiral acetoxy allyl silanes (R_3Si)(AcO)CHCH=CH_2,[4] which we will describe in a future publication. Studies of these reactions are advantageous in that the preparation of the starting materials, the methodology of establishing relative stereochemistry, and the absolute configuration of the products have been worked out previously.[3,4] In addition, the conformational preferences of these and related compounds[5] have been studied theoretically[6–8] and spectroscopically.[8] Qualitatively, it has been observed that these reactions are sensitive to the stereoelectronic properties of AR_3,[3d,3l,4] but the literature data are insufficient to analyze quantitatively. Thus, the assessment of steric and electronic influences cannot be achieved.

When we began these studies we asked three questions. (1) Can the stereoselectivity of a reaction be analyzed in terms of the stereoelectronic parameters of AR_3 or will other factors not associated with AR_3 (e.g. solvent properties) control the stereoselectivity? (2) If the stereoselectivity can be analyzed in terms of the stereoelectronic parameters, can we gain insight into the factors that control stereoselectivity? (3) Can we

® Abstract published in *Advance ACS Abstracts*, January 1, 1995.

(1) See for example the following references: (a) Kagan, H. B. *Asymmetric Synthesis*; Morrison, J. D., Ed.; Academic Press: London, 1985; Vol. 5, pp 1–39. (b) Davies, S. *Aldrichim. Acta* **1990**, *23*, 31. (c) Ojima, I.; Hirai, K. *Asymmetric Synthesis*; Morrison, J. D., Ed.; Academic Press: London, 1985; Vol. 5, pp 103–46. (d) Marshall, J. A.; Beaudoin, S.; Lewinski, K. *J. Org. Chem.* **1993**, *58*, 5876.

(2) Wilson, M. R.; Liu, H.-Y.; Prock, A.; Giering, W. P. *Organometallics* **1993**, *12*, 2044.

(3) (a) Brookhart, M.; Nelson, G. O. *J. Am. Chem. Soc.* **1977**, *99*, 6099. (b) Cutler, A. R. *J. Am. Chem. Soc.* **1979**, *101*, 604. (c) Bodnar, T.; Cutler, A. R. *J. Organomet. Chem.* **1981**, *213*, C31. (d) Brookhart, M.; Tucker, J. R.; Husk, G. R. *J. Am. Chem. Soc.* **1983**, *105*, 258. (e) Brookhart, M.; Timmers, D.; Tucker, J. R.; Williams, G. D.; Husk, G. R.; Brunner, H.; Hammer, B. *J. Am. Chem. Soc.* **1983**, *105*, 6721. (f) Baird, G. J.; Davies, S. G.; Maberly, T. R. *Organometallics* **1984**, *3*, 1764. (g) Davies. S. G.; Maberly, T. R. *J. Organomet. Chem.* **1985**, *296*, C37. (h) Asycough, A. P.; Davies, S. G. *J. Chem. Soc., Chem. Commun.* **1986**, 1648. (i) Brookhart, M.; Liu, Y.; Buck, R. C. *J. Am. Chem. Soc.* **1988**, *110*, 2337. (j) Brookhart. M.; Liu, Y. *Organometallics* **1989**, *8*, 1572. (k) Brookhart, M.; Buck, R. C. *J. Am. Chem. Soc.* **1989**, *111*, 559. (l) Brookhart, M.; Liu, Y.; Goldman, E. W.; Timmers, D. A.; Williams, G. D. *J. Am. Chem. Soc.* **1991**, *113*, 927.

(4) Panek, J. S.; Cirillo, P. F. *J. Am. Chem. Soc.* **1990**, *112*, 4973.

(5) (a) Davies, S. G.; Seeman, J. I. *Tetrahedron Lett.* **1984**, *25*, 1845. (b) Davies. S. G.; Dordor-Hedgecock, I. M.; Sutton, K. H.; Whittaker, M. *J. Organomet. Chem.* **1987**, *320*, C19. (c) Blackburn, B. K.; Davies, S. G.; Sutton, K. H.; Whittaker, M. *Chem. Soc. Rev.* **1988**, *17*, 147. (d) Shambayati,S.; Crowe, W. E.; Schreiber, S. L. *Angew. Chem., Int. Ed. Engl.* **1990**, *29*, 256.

(6) (a) Seeman, J. I.; Davies, S. G. *J. Chem. Soc., Chem. Commun.* **1984**, 1019. (b) Seeman, J. I.; Davies, S. G. *J. Am. Chem. Soc.* **1985**, *107*, 6522. (c) Seeman, J. I.; Davies, S. G. *J. Am. Chem. Soc.* **1985**, *107*, 6525.

(7) (a) Houk, K. N.; Moses, S. R.; Wu, Y.-D.; Rondan, N. G.; Jaeger, V.; Schohe, R.; Fronczek, F. R. *J. Am. Chem. Soc.* **1984**, *106*, 3880. (b) Jorgensen, K. A.; Hoffmann, R. *J. Am. Chem. Soc.* **1986**, *108*, 1867. (c) Houk, K. N.; Duh, H.-Y.; Wu, Y.-D.; Moses, S. R. *J. Am. Chem. Soc.* **1986**, *108* 2754. (d) Kahn, S. D.; Pau, C. F.; Chamberlain, A. R.; Hehre, W. J. *J. Am. Chem. Soc.* **1987**, *109*, 650.

(8) Mackie, S. C.; Park, Y.-S.; Shurvell, H. F.; Baird, M. C. *Organometallics* **1991**, *10*, 2993.

0276-7333/95/2314-0869$09.00/0

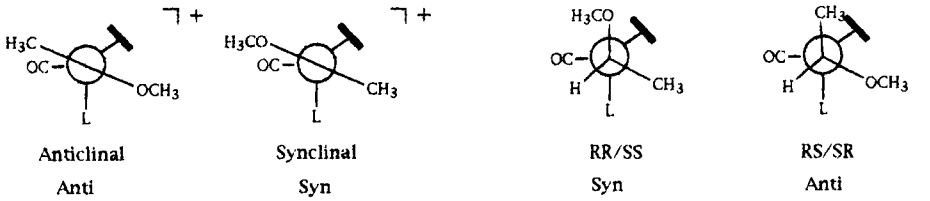

Figure 1. Newman projections showing the relative stereochemistry of the diastereomeric products (η-Cp(CO)(PR$_3$)Fe[CH(OMe)Me]) resulting from the addition of hydride to the anticlinal (anti) and synclinal (syn) chiral cationic carbene complexes η-Cp(CO)(PR$_3$)Fe[C(OMe)Me]$^+$.

use this insight to choose or design pendent groups that maximize stereoselectivity?

In this paper we show that, indeed, the stereoselectivities of the addition of hydride to η-Cp(CO)(PR$_3$)Fe[C(OMe)Me]$^+$ *can* be analyzed in terms of the stereoelectronic parameters of PR$_3$ and that the results can be interpreted in terms of concepts embedded in the "quantitative analysis of ligand effects" (QALE).[9]

Experimental Section

The carbene complexes, η-Cp(CO)(PR$_3$)Fe[C(OMe)(Me)]$^+$, were prepared by methylation of the corresponding acyl complexes, η-Cp(CO)(PR$_3$)Fe[C(O)Me], by methyl triflate in methylene chloride according to the procedure reported by Brookhart.[3d] The carbene complexes were characterized by ^{1}H NMR and IR spectroscopy. The spectroscopic data, which are in agreement with those presented earlier,[3d] are displayed in Tables 1 and 2 of the supplementary material.

The reduction of the carbene complexes was also carried out according to the protocol of Brookhart.[3d] The determination of the relative amounts of the resulting anti and syn diastereomers, η-Cp(CO)(PR$_3$)Fe*[C*H(OMe)(Me)] (see Figure 1 for structural designations), were determined by integration of the ^{1}H methoxy resonances which were readily observed. For some systems (L = PMe$_3$, PEt$_3$, PPh$_3$, P(p-CF$_3$Ph)$_3$, PCyPh$_2$, P(i-Pr)$_3$) the identity of the anti isomer was established by the observation of the long range coupling[3d] between the phosphorus and the hydrogen of the CH(OMe)(C*H*$_3$) ligand. The syn isomer does not show this coupling. This coupling is observed for the complexes containing the smallest ligands (i.e. PMe$_3$) as well as complexes containing some of the largest ligands (P(i-Pr)$_3$). In a few instances (L = PBu$_3$, PMePh$_2$, PCy$_2$Ph, PCy$_3$) the CH(OMe)(C*H*$_3$) resonance was obscured by the resonances of the pendent groups on the phosphine ligand. In other complexes (L = PMe$_2$Ph , P(p-FPh)$_3$, P(p-ClPh)$_3$, P(p-MeOPh)$_3$) this coupling was not observed for either diastereomer. Since where we can determine the anti/syn ratio, we found that the ratio is never less than unity, we assumed that the anti isomer was always the predominant isomer. The spectroscopic data for η-Cp(CO)(PR$_3$)Fe*[C*H(OMe)(Me)], which are in harmony with the literature data for the known compounds,[3d] are presented in Tables 3 and 4 of the supplementary material.

The anti/syn ratio of the stereoisomers formed in the reduction of the carbene complexes bearing phosphines with θ > 153° is very large and is reported as >30.

All of the reductions were done in triplicate, and the results agree to within 10%. The average of the three runs is presented in Table 1.

Table 1. Stereoelectronic Properties and Ratio of Diastereomers η-Cp(CO)(L)Fe[CH(OMe)(Me)], Formed by the NaBH$_4$ Reduction of η-Cp(CO)(L)Fe[C(OMe)(Me)]$^+$ [a]

entry	phosphine	χ[b]	θ[c]	E_{ar}[d]	anti/syn
1	PMe$_3$	8.55	118	0	2.80[e]
2	PMe$_2$Ph	10.6	122	1	2.86
3	PEt$_3$	6.3	132	0	4.60[e]
4	PBu$_3$	5.25	136	0	5.13
5	PMePh$_2$	12.1	136	2	1.96
6	PEt$_2$Ph	9.3	136	1	
7	PEtPh$_2$	11.3	140	2	
8	P(i-Bu)$_3$	5.7	143	0	
9	P(p-MeOPh)$_3$	10.5	145	2.7	1.33
10	PPh$_3$	13.25	145	2.7	1.32[e]
11	P(p-FPh)$_3$	15.7	145	2.7	1.07
12	P(p-ClPh)$_3$	16.8	145	2.7	0.99
13	P(p-CF$_3$Ph)$_3$	20.5	145	2.7	1.00
14	PCyPh$_2$	9.3	153	2	9.6
15	P(i-Pr)$_3$	3.75	160	0	>30
16	PCy$_2$Ph	5.35	161	1	>30
17	PCy$_3$	1.4	170	0	>30
18	P(t-Bu)$_3$	0.0	182	0	

[a] Entries 6–8 and 18 are listed for use in the discussion of analysis of alternate mechanisms (see text). [b] Reference 10. [c] Reference 11. [d] Reference 2. [e] Reference 3d.

Results

Eleven new cationic iron carbene complexes of the type η-Cp(CO)(PR$_3$)Fe[C(OMe)Me]$^+$ were prepared (along with one, L = PPh$_3$, previously examined by Brookhart[3d,l]) and then reduced with sodium borohydride in methanol at −78 °C according to the protocol of Brookhart[3d,l] (Scheme 1). These data supplement the data (PR$_3$ = PMe$_3$ and PEt$_3$) reported earlier[3d,l] The reduction affords the anti and syn diastereomers, η-Cp(CO)(L)Fe*[C*H(OMe)(Me)]. The terms anti and syn

(9) (a) Golovin, M. N.; Rahman, Md. M.; Belmonte, J. E.; Giering, W. P. *Organometallics* **1985**, *4*, 1981. (b) Dahlinger, K.; Falcone, F.; Pöe, A. J. *Inorg. Chem.* **1986**, *25*, 2654. (c) Rahman, Md. M.; Liu, H.-Y.; Prock, A.; Giering, W. P. *Organometallics* **1987**, *6*, 650–58. (d) Pöe, A. J. *Pure Appl. Chem.* **1988**, *60*, 1209. (e) Golovin, N. G.; Meirowitz, R. E.; Rahman, Md. M.; Liu, H.; Prock, A.; Giering, W. P.*Organometallics* **1987**, *6*, 2285. (f) Lezhan, C.; Pöe, A. J. *Inorg. Chem.* **1989**, *28*, 3641. (g) Rahman, Md. M.; Liu, H.-Y.; Eriks, K.; Prock, A.; Giering, W. P. *Organometallics* **1989**, *8*, 1–7. (h) Eriks, K.; Liu, H.-Y.; Koh, L.; Prock, A.; Giering, W. P. *Acta Crystallogr.* **1989**, *C45*, 1683. (i) Liu, H.; Fertal, D.; Tracey, A. A.; Eriks, K.; Prock, A.; Giering, W. P. *Organometallics* **1989**, *8*, 1454–58. (j) Eriks, E.; Liu, H.-Y.; Prock, A.; Giering, W. P. *Inorg. Chem.* **1989**, *28*, 1759–63. (k) Brodie, N. M.; Chen, L.; Pöe, A. J. *Int. J. Chem. Kinet.* **1988**, *27*, 188. (l) Tracey, A. A.; Eriks, K.; Prock, A.; Giering, W. P. *Organometallics* **1990**, *9*, 1399. (m) Liu, H.-Y.; Eriks, E.; Prock, A.; Giering, W. P. *Organometallics* **1990**, *9*, 1758. (n) Panek, J.; Prock, A.; Eriks, K.; Giering, W. P. *Organometallics* **1990**, *9*, 2175. (o) Liu, H.-Y.; Eriks, E.; Prock, A.; Giering, W. P. *Acta Crystallogr.* **1990**, *C46*, 51. (p) Prock, A.; Giering, W. P.; Greene, J. E.; Meirowitz, R. E.: Hoffman, S. L.; Woska, D. C.; Wilson, M.; Chang, R.; Chen, J.; Magnuson, R. H.; Eriks, K. *Organometallics* **1991**, *10*, 3479–85. (q) Woska, D. C.; Wilson, M. R.; Eriks, K.; Prock, A.; Giering, W. P. *Organometallics* **1992**, *11*, 3343. (r) Liu, H.; Eriks, K.; Prock, A.; Giering, W. P.. *Acta Crystallogr. Sect. C: Cryst. Struct. Commun.* **1992**, *C48*, 433. (s) Brown, T. L. *Inorg. Chem.* **1992**, *31*, 1286. (t) Woska, D. C.; Bartholomew, J.; Greene, J. E.; Eriks, K.; Prock, A.; Giering, W. P. *Organometallics* **1993**, *12*, 304. (u) Wilson, M. R.; Woska, D. C.; Prock, A.; Giering, W. P. *Organometallics* **1993**, *12*, 1742. (v) Choi, M.-G.; Brown, T. L. *Inorg. Chem.* **1993**, *32*, 5603. (w) Brown, T. L.; Lee, K. J. *Cooord. Chem. Rev.* **1993**, *128*, 89. (x) Choi, M.-G.; Brown, T. L. *Inorg. Chem.* **1993**, *32*, 1548. (y) Fernandez, A. L.; Prock, A.; Giering, W. P. *Organometallics* **1994**, *13*, 2767. (z) White, D.; Coville, N. J. *Adv. Organomet. Chem.* **1994**, *36*, 95. (aa) Farrar, D. H.; Pöe, A. J.; Zhang, Y. *J. Am. Chem. Soc.* **1994**, *116*, 6252.

(10) Bartik, T.; Himmler, T.; Schulte, H.-G.; Seevogel, K. *J. Organomet. Chem.* **1984**, *272*, 29.

(11) Tolman, C. A. *Chem. Rev.* **1977**, *77*, 313.

Scheme 1

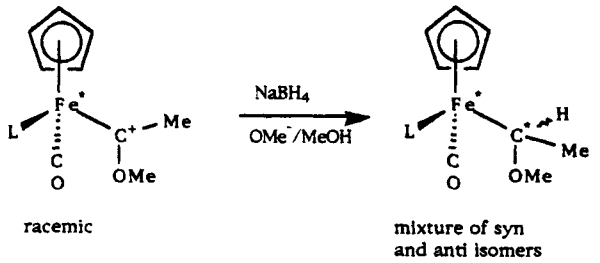

Scheme 2

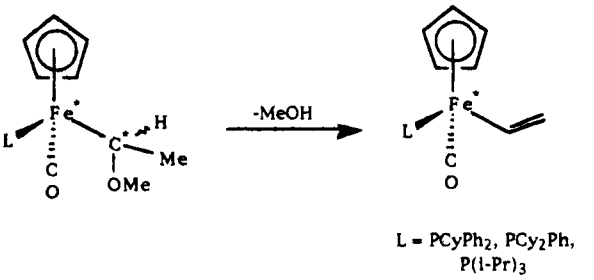

refer to the position of the carbonyl and methoxy groups in the most stable conformation of the organoiron compounds (Figure 1). For example, in η-Cp(CO)(PR_3)-Fe[CH(OMe)Me] the anti isomer has the two groups opposite to each other. The anti diastereomer has the *RS/SR* configurations about the stereocenters. In the syn isomer, the methoxy and carbonyl groups are on the same side and these stereocenters have the *RR/SS* configurations (Figure 1). In keeping with this terminology, we will refer to the anticlinal and synclinal conformations of the carbene complexes as the anti and syn conformations, respectively.

The ^{1}H NMR spectra of the reaction mixtures immediately after work up showed only η-Cp(CO)(PR_3)-Fe[CH(OMe)Me] (with four exceptions; *vide infra*) so that actual yields of the reduction product appear to be quite high and greater than 90%. This crude material was used to determine the anti/syn ratio of diastereomers. These ratios, which vary from 1.0 to greater than 30, along with the stereoelectronic properties of the ancillary phosphine ligands are displayed in Table 1.

Since the addition of hydride was done at −78 °C and the product mixtures were analyzed at room temperature, we investigated the configurational stability of one of the product mixtures over this temperature range. In this experiment a CD_2Cl_2 solution of the carbene complex η-Cp(CO)($PMePh_2$)Fe[C(OMe)Me]$^+$ was added to a CD_3OD solution of $NaBH_4$ and $NaOCD_3$ at −78 °C. The ^{1}H NMR spectrum taken at −78 °C showed that the reduction of the carbene complex was complete upon mixing, affording a 2:1 mixture of anti and syn isomers, respectively. This ratio remained invariant as the mixture was warmed to room temperature. Thus, the invariance of the isomer ratio to change in temperature suggests that the anti and syn isomers once formed are configurationally stable under the conditions of the experiment and that the ratio is not thermodynamically determined.[12]

In a separate experiment we found that the isomer ratio was independent of the relative concentrations (over a 4-fold range) of carbene complex and $NaBH_4$ for L = PPh_2Me , which supports the notion that there is rapid equilibration of the conformers of η-Cp(CO)-($PMePh_2$)Fe[C(OMe)Me]$^+$. Thus, the Curtin−Hammett principle is applicable.

Although the reduction is unexceptional for most of the complexes, the carbene complexes containing the largest ligands (entries 14−17 in Table 1) undergo reduction and subsequent loss of methanol to form complexes which appear to be the vinyl complexes, η-Cp-(CO)(PR_3)Fe(CH=CH_2), when the reduction was carried out in the manner described by Brookhart[3d,l] (Scheme 2). Although these vinyl complexes have not been isolated and fully characterized, their existence is inferred by the observation of 1 proton multiplet resonances (for PR_3 = P(Cy_2Ph)) at 8.24, 6.44, and 6.08, which are characteristic of the vinyl group. A control experiment with the PCy_2Ph complex showed us that the formation of the vinyl complex was effected by methoxide and was not attributable to intramolecular decomposition of the initial reduction product. In this experiment η-Cp(CO)(PCy_2Ph)Fe[CH(OMe)Me]$^+$ was allowed to react with $NaBH_4$ for 3 minutes at −78 °C and then rapidly warmed to 22 °C. Half of the mixture was immediately worked up whereas the other half was allowed to stand at 22 °C for an additional 0.5 h. The sample that was worked up immediately was free of the vinyl complex whereas the other portion of the reaction mixture was completely converted to the vinyl complex. We monitored a sample of η-Cp(CO)(PCy_2Ph)Fe[CH-(OMe)Me], in the absence of methoxide, and found the complex to be stable at 24 °C over a period of at least 1 h in either acetone or benzene as evidenced by its invariant ^{1}H NMR spectrum.

We analyzed the data (log anti/syn) for complexes containing PR_3 with $\theta < 160°$ by regression analysis according to eq 1 to yield eq 2. In eq 1, χ and E_{ar} are

$$\log(\text{anti/syn}) = a\chi + b(\theta - \theta_{st})\lambda + cE_{ar} + d \quad (1)$$

$$\log(\text{anti/syn}) = \underset{\pm 0.009}{-0.022}\chi + \underset{\pm 0.010}{0.086}(\theta - 145°)\lambda - \underset{\pm 0.034}{0.137}E_{ar} + \underset{\pm 0.072}{0.77} \quad (2)$$

$$n = 11 \qquad r^2 = 0.968$$

electronic parameters,[2,10] θ (Tolman's cone angle[11]) is a steric parameter, θ_{st} is a steric threshold,[2] and λ is a switching function[2] that is zero for $\theta < \theta_{st}$ and is 1 for $\theta > \theta_{st}$. (The standard errors are written directly below the corresponding coefficients in eq 2. A discussion of the estimate of the error in the steric threshold is presented in ref 2.)

As a check on the internal consistency of the analysis, we note that the coefficient of χ in eq 2 must be statistically indistinguishable from the coefficient of χ obtained when only the data for the triarylphosphine complexes are analyzed (eq 3).[2] Inspection of eqs 2 and 3 shows that this is indeed the case.

$$\log(\text{anti/syn}) = \underset{\pm 0.005}{-0.0150}\chi + \underset{\pm 0.071}{0.28} \quad (3)$$

$$n = 5 \qquad r^2 = 0.78$$

(12) If we assume that the 2:1 anti/syn ratio is the equilibrium constant at −78 °C and that there is no significant entropy change in the equilibration of the isomers, then we would expected about a 30% decrease in the equilibrium constant on warming to room temperature. This change would be easily observable spectroscopically as the temperature of the mixture was raised.

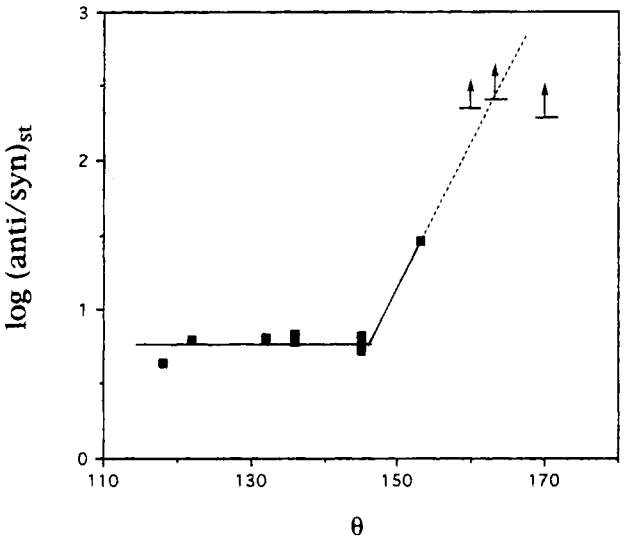

Figure 2. Steric profile of log(anti/syn) for addition of hydride (from $NaBH_4$) to the cationic iron(II) carbene complexes η-Cp(PR_3)(CO)Fe[C(OMe)(Me)]$^+$. The complexes indicated with a bar are lower limits based on our use of log(anti/syn) = 30. The arrow indicates that the actual value of $\log(\text{anti/syn})_{st}$ is probable larger.

The relatively large number of data for eq 2 and the small standard errors give 95% confidence limits which indicate that the coefficients are all statistically significant. This, coupled with the high correlation coefficient, reveals an excellent fit of the data to eq 1.

There is only one point for θ greater than 145° in our analysis; thus, the steric threshold could lie anywhere between 145 and 153°. The value of 145° used for the steric threshold in our analysis is simply taken as a lower bound, and the coefficient of $(\theta - \theta_{st})\lambda$ is also a lower bound. We regard this steric threshold as real because there are three more data above the steric threshold with anti/syn ratios greater than 30. Clearly, steric effects become extremely important above 145°. (Since there is only point above the steric threshold, we cannot explore the use of other steric parameters[9x] in this analysis.)

Often the goodness of fit is shown by plotting the calculated property (e.g. via eq 2) versus the actual experimental data (log(anti/syn)). We find it more useful to generate a steric profile,[9] which also shows graphically the goodness of fit and gives a snapshot of the dependence of the property on the size of the ligand. The steric component ($\log(\text{anti/syn})_{st}$) of log(anti/syn) was generated by subtracting the electronic terms and the constant of eq 2 from the experimental data (eq 4). A plot of $\log(\text{anti/syn})_{st}$ versus θ gives the steric profile shown in Figure 2.

$$\log(\text{anti/syn})_{st} = \log(\text{anti/syn})_{exp} + (0.022)\chi + (0.137)E_{ar} - (0.77) \quad (4)$$

Discussion

The stereochemistry of iron(III) carbene and alkoxy carbene complexes of the type η-Cp(CO)(L)Fe[CHR]$^+$ and η-Cp(CO)(L)Fe[C(OMe)R]$^+$ has been studied extensively. Brookhart predicted,[3d] on the basis of calculations by Hoffmann,[13] that the most stable conformation of the alkylidene complexes would appear to be the one where the plane of the carbene ligand is perpendicular to the bond between iron and the ligand which is the best electron donor. On the basis of molecular mechanics calculations and by analogy to the acyliron complexes, Davies furthermore predicted that the related carbene complexes should exist primarily in the least congested (anti) conformation.[4f] Schreiber also suggested that this should be the most stable conformation but because of electronic factors.[5d] In Davies' report of the addition of hydride (from $NaBH_4$) to η-Cp(CO)(L)-Fe[C(OMe)Et]$^+$, it was assumed, quite reasonably, that the addition of hydride occurred to the face opposite the phosphine ligand.[4f] In Brookhart's work on the addition of hydride to the methoxymethyl carbene complexes, η-Cp(CO)(L)Fe[C(OMe)Me]$^+$, it was found that the dominant product results from addition of hydride to the less stable syn conformer. As we shall see, it is relevant to this work that Davies also observed that the α-methoxypropyl complex η-Cp(CO)(PPh_3)Fe[CH(OMe)-Et] was readily transformed to the 1-propenyl complex (Scheme 3).

Scheme 3

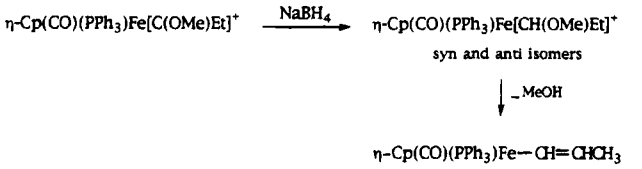

Brookhart[4k] determined the barrier to rotation about the Fe–carbene bond in η-Cp(CO)(PR_3)Fe[C(Ph)H]$^+$ to be less than 7 kcal/mol at −114 °C. Presumably, the rotation about the Fe–carbene bond in η-Cp(CO)(PR_3)-Fe[C(OMe)Me]$^+$ will be even faster because of the better π bonding capacity of the methoxy group as compared to that of the phenyl group. If the rate of rotation about the iron–carbene bond in η-Cp(CO)(PR_3)Fe[C(OMe)-Me]$^+$ is rapid compared to the rate of addition of hydride, the ratio of stereoisomers will be unaffected by changes in the relative concentrations of the reactants. This is what we observe (vide supra). Thus, we employ the Curtin–Hammett principle to interpret our data (see Figure 3): the anti/syn ratio is determined by the ratio of rate constants for the addition of hydride to the two carbene conformers and the equilibrium constant between the two conformers.

Our analysis shows that steric effects appear to be nonlinear. For example, the addition of hydride (from $NaBH_4$) to the cationic carbene complexes, η-Cp(CO)-(PR_3)Fe[C(OMe)Me]$^+$, shows only modest stereoselectivity up to θ = 145° after which the stereoselectivity rises steeply to a point (θ = 160°) where we can no longer observe the syn isomer (anti/syn > 30). Clearly steric effects become disproportionately important for the larger phosphines.

Three Possible Explanations of the Origins of Steric Thresholds. The appearance of a steric threshold in the analysis of kinetic data involving ligand effects is not rare.[9] Although it can be interpreted as the onset

(13) (a) Schilling, B. E. R.; Hoffmann, R.; Lichtenberger, D. L. *J. Am. Chem. Soc.* **1979**, *101*, 585. (b) Goddard, R. J.; Hoffmann, R.; Jemmis, E. D. *J. Am. Chem. Soc.* **1980**, *102* 7667. (c) See also: Hoffmann, R.; Eisenstein, O. W. Unpublished results as reported in ref 3d.

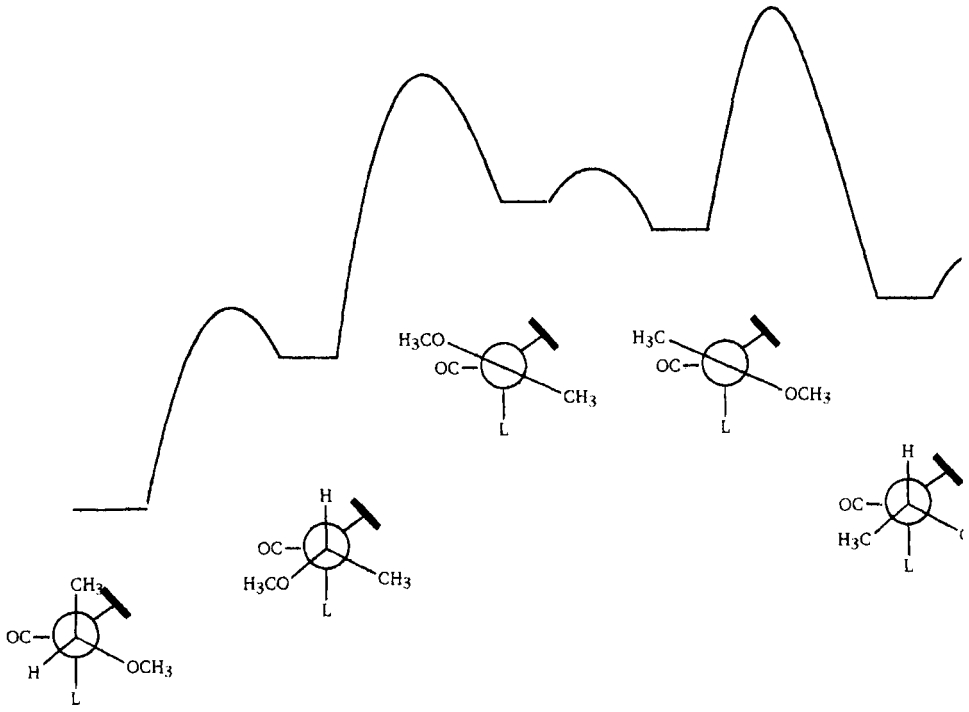

RS/SR
(anti)

Figure 3. Reaction coordinate diagram for the $NaBH_4$ reduction of the carbene complexes η-Cp(CO)(PR_3)Fe[C(OMe)(Me)]$^+$. This diagram is based on information given in ref 3i,k.

Scheme 4

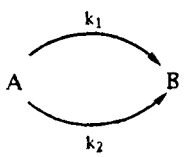

of steric interactions when the ligand reaches a critical size, it can also arise, in principle, where steric effects are linear and continuously operative. We take this opportunity to expand briefly on these ideas. Consider, for example, if two parallel pathways (Scheme 4) to a product exist, each of which have different stereoelectronic dependencies, conditions might be right to produce a steric threshold. The following expressions (eqs 5 and 6), for example, give the dependence of the individual rate constants on the two stereoelectronic parameters χ and θ:

$$\ln k_1 = 0.10\chi + C_1 \quad (5)$$

$$\ln k_2 = -0.10\chi + 0.20\theta + C_2 \quad (6)$$

where the difference in the constant terms, $C_1 - C_2$ is -30. This difference makes the rates the same when parameters χ and θ are 10 and 155°, respectively. (This is the mid range of each parameter.) The total rate is taken as the sum of the individual rates. The logarithm of total rate was calculated for a group of 18 phosphorus(III) ligands; see Table 1. This set of calculated data was analyzed by means of linear regression in the usual manner. The resulting equation is

$$\ln k = 0.091\chi + 0.237(\theta - 151°)\lambda + 0.156 \qquad r^2 = 0.992 \quad (7)$$

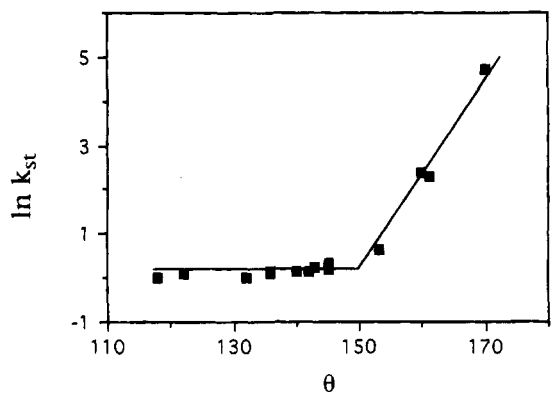

Figure 4. Steric profile for a process involving two competitive reactions as described by eqs 5 and 6.

Scheme 5

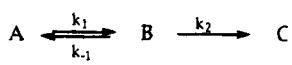

The range of k is a factor of 90. The steric profile was obtained by subtracting the electronic term from the calculated data and is shown in Figure 4. We see that $\ln k$ is virtually constant up to $\theta = 151°$, followed by a sharp and nearly linear increase with increasing θ. Thus, we have a steric threshold. It turns out that we can produce similar steric profiles even if either coefficient of χ is made to vary over a significant range, as long as the coefficient of θ is large enough to make steric factors dominate for large θ.

The second example is for the case of sequential reactions shown in Scheme 5, where for small cone angles k_2 is large (thus, the first step is rate determining) and for large cone angles the second step becomes very slow. For illustration, let $k_1 = k_{-1} = 1.0$ and let

$$\ln k_2 = 0.10\chi - 0.20\theta + 29 \quad (8)$$

The apparent constant is selected to make $k_1 = k_2$ for $\chi = 10$ and $\theta = 150$. We defined the rate constant, k, for the reaction as the inverse of the time for product C to reach half its final value. ln k was then calculated for the set of 18 ligands (see Table 1), and the results were analyzed by means of linear regression to yield

$$\ln k = 0.045\chi - 0.165(\theta - 141°)\lambda - 0.132 \quad (9)$$

$$r^2 = 0.987$$

The range of k is 150. The steric profile was obtained as described above and is shown in Figure 5. The steric threshold is clear.

Steric profiles with these shapes have been noted previously.[9] They can also be explained in terms of a single unvarying rate-determining step where the steric effect is nonlinear. Thus, whatever its origins, the steric threshold is real and its inclusion must be provided for in the analysis of kinetic data. Steric thresholds resulting from changes in the rate-determining step (sequential reactions) or changes in mechanism (parallel reactions) are more likely to occur in more complicated reaction mechanisms. For simple, one step reactions, the observation of a steric threshold is likely attributable to nonlinear steric effects. For correlation of thermodynamic data, mechanism does not enter the picture and the existence of a steric threshold must necessarily indicate a nonlinear steric effect.

It seems reasonable to expect that the addition of hydride to η-Cp(CO)(L)Fe[C(OMe)Me]$^+$ is most likely a one step process, the mechanism of which remains invariant over the entire range of the ligands employed in the study. If this is true, then the steric threshold is attributable to nonlinear steric effects in the formation of the anti and/or the syn isomer, and we interpret the analysis in the following manner.

Interpretation of the QALE Analysis. The regression eq 2 shows us that the anti/syn ratio is dependent on χ and E_{ar} but not on θ for $\theta \leq 145°$. In this domain we find that variations in χ and E_{ar} account for 55% and 45% of the variations in log anti/syn, respectively. (In ref 9s we discuss our method of determining the extent of involvement of each parameter.) Enhanced electron donor capacity (smaller χ) increases log anti/syn whereas increasing the number of aryl groups tends to decrease log anti/syn. It is important to note that the aryl effect plays a significant role in determining the stereoselectivity of this reaction.

Since the relative rates of formation of the anti and syn isomers are dependent on the equilibrium constant between the two conformers of the carbene complex (vide supra), and since this equilibrium constant could be sensitive to steric factors, the lack of a significant steric dependence for small ligands suggests that the anti/syn ratio is not determined by steric factors either in the ground or transition state. This observation supports Schreiber's suggestion that the anti conformer of the carbene complexes is more stable because of electronic factors.[5d]

Above the steric threshold there is a dramatic increase in the anti/syn ratio. Thus, the anti/syn ratio for the PCyPh$_2$ system ($\theta = 153°$) is 9.6 and increases to greater than 30 for the three systems bearing ligands with θ greater than 160°. These observations indicate that the datum for the PCyPh$_2$ system is not an outlier and indeed the steric threshold is real.

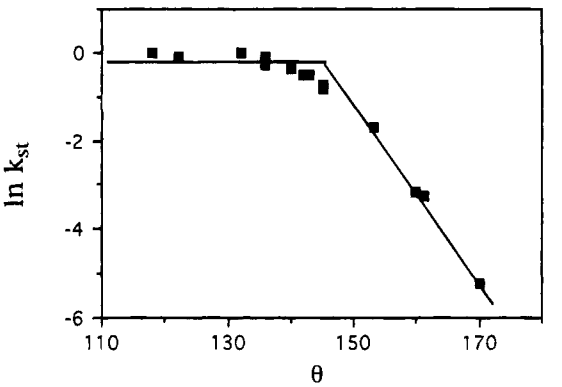

Figure 5. Steric profile for a process involving two sequential reactions as described in the text.

It is interesting to note that η-Cp(CO)(PR$_3$)Fe[CH(OMe)Me] compounds that contain phosphines with θ greater than 145° undergo a facile loss of methanol in the presence of methoxide to form the vinyl complexes (Scheme 2). Since this reaction is not observed for complexes containing smaller ligands (under our reaction conditions), we conclude that the elimination of methanol is sterically accelerated for the large ligands. Thus, there must be a steric threshold in the ground state of this reaction; i.e., steric effects turn on in η-Cp(CO)(L)Fe[CH(OMe)Me] above 145°. It important to note that Davies observed that the α-methoxypropyl complex, (η-Cp(CO)(L)Fe[CH(OMe)Et], underwent loss of methanol when PPh$_3$ is the ancillary ligand.[4f] This is consistent with our results since the α-methoxypropyl ligand is larger than the α-methoxyethyl ligand and, thus, should have a smaller steric threshold for the onset of this elimination reaction.

Conclusions

The high quality of the fit of the stereoselectivities to eq 2 suggests that, indeed, the stereoselectivities of the addition of hydride to (η-Cp(CO)(L)Fe[C(OMe)Me]$^+$ (Scheme 1) can be analyzed in terms of the phosphorus(III) stereoelectronic parameters χ, θ, and E_{ar}. According to our analysis, below $\theta = 145°$ the stereoselectivity is determined by electronic factors with contributions from χ and E_{ar} having about equal weight. There can be little doubt that steric effects are ushered in by a steric threshold above 145°. We recognize that we cannot distinguish between two models, one that has a single mechanism involving discontinuous steric effects, which is operative over the entire range of ligands, and a model involving a more complex mechanism with continuous steric effects. Even with this caveat we can make a very important statement concerning stereoselectivity: **Steric control of stereoselectivity is not necessarily linear, and to achieve maximum stereoselectivity a set of ligands must be chosen with θ greater than the steric threshold of the reaction.**

Supplementary Material Available: Tables of IR and NMR data (3 pages). Ordering information is given on any current masthead page.

OM940587O

Oxidatively Induced Reductive Elimination from $Ru(C_2Ph)_2(CO)(P^tBu_2Me)_2$ and $Ru(CHCHPh)(C_2Ph)(CO)(P^tBu_2Me)_2$

Astrid Pedersen,† Mats Tilset,*,† Kirsten Folting,‡ and Kenneth G. Caulton*,‡

Department of Chemistry, University of Oslo, P. O. Box 1033 Blindern, N-0315 Oslo, Norway, and Department of Chemistry and the Molecular Structure Center, Indiana University, Bloomington, Indiana 47405

Received August 31, 1994®

In acetonitrile, the 16-electron species $Ru(C_2Ph)_2(CO)(P^tBu_2Me)_2$ (**1**) and $Ru(CHCHPh)(C_2Ph)(CO)(P^tBu_2Me)_2$ (**2**) exist as the corresponding 18-electron acetonitrile adducts. A single-crystal X-ray structure determination showed **1** to be square pyramidal with apical CO and the two acetylide ligands to be *trans* to each other. Crystal data (−90 °C): a = 9.765(6) Å, b = 15.786(10) Å, c = 11.239(6) Å, β = 99.87(3)° with Z = 2 in space group $P2_1$. The complexes undergo overall two-electron oxidation at 0.28 and 0.10 V vs Cp_2Fe/Cp_2Fe^+, respectively. In dichloromethane **1** and **2** underwent 2-electron oxidations at 0.20 and 0.15 V. The lower oxidation potential of **2** compared to **1** is interpreted as an effect of the more electron-donating vinyl ligand. The electrochemical and chemical oxidations result in the intramolecular elimination of $[PhC_2]_2$ from **1** and $PhC_2CHCHPh$ from **2**. In acetonitrile, $[Ru(CO)(NCMe)_3(P^tBu_2Me)_2](BF_4)_2$ (**3**$(BF_4)_2$) is formed as the main Ru-containing product. The main organometallic product in dichloromethane appears to exist as a $Ru(CO)(L)_2^{n+}$ (n = 1, 2) fragment, possibly stabilized by interaction with solvent and/or counterion BF_4^-. A mechanistic and kinetic investigation of the elimination reactions by derivative cyclic voltammetry (DCV) showed the reductive eliminations from **1** and **2** to be first-order in $\mathbf{1}^+$ and $\mathbf{2}^+$. The DVC analysis provided kinetic parameters for the reaction of $\mathbf{1}^+$ in acetonitrile and dichloromethane and for the reaction of $\mathbf{2}^+$ in MeCN. Oxidation of **1** in acetonitrile gave k(0 °C) = 0.74 s^{-1}, $\Delta H^\ddagger$ = 74.1(1.7) kJ/mol, and $\Delta S^\ddagger$ = 5.9(5.4) J/(K mol) for the elimination from $\mathbf{1}^+$, whereas the analysis in dichloromethane gave k(0 °C) = 0.93 s^{-1}, $\Delta H^\ddagger$ = 76.1(3.3) kJ/mol, and $\Delta S^\ddagger$ = 8.1(11.7) J/(K mol). For **2** in acetonitrile, k(0 °C) = 0.89 s^{-1}, $\Delta H^\ddagger$ = 61.9(5.4) kJ/mol, and $\Delta S^\ddagger$ = −6.4(20.1) J/(K mol).

Introduction

Reductive elimination is a fundamental reaction frequently encountered in the product-forming step of catalytic and stoichiometric reactions in organic synthesis.[1] Stable organometallic complexes can be induced to undergo facile reductive elimination when subjected to oxidation. This is usually rationalized by the simple argument that an increase in the oxidation state increases the actual charge on the metal and hence makes reductive elimination more favorable.[1a] However, recent results have demonstrated that one-electron oxidations also have pronounced effects on M−H bond strengths. Thermochemical cycles have been used to probe the effect of one-electron oxidations on M−H bond strengths of $Tp'M(CO)_3H$ (Tp′ = tris(pyrazolyl)borate; M = Cr, W, Mo)[2a] and various $CpCr(CO)_2LH$ complexes (L = CO, PEt_3, PPh_3, $P(OMe)_3$).[2b] This revealed that oxidation led to a weakening of the W−H and Mo−H bonds by a relatively constant 108−113 kJ/mol toward deprotonation and 25−33 kJ/mol toward homolysis. Another example demonstrating the bond-weakening effect of a one-electron oxidation is provided by Burk et al.[3a] They found that reductive elimination occurred from the electron-poor, d^0, 16-electron complexes shown in Scheme 1. The oxidations have been proposed to occur by removal of an electron from one M−C bond, thus weakening the bond.

Scheme 1

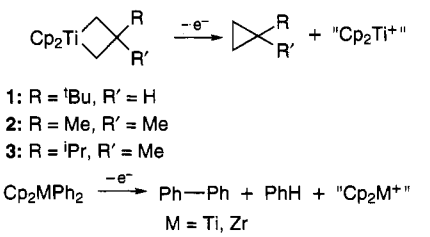

Organometallic reactions such as ligand substitution, CO insertion, oxidative addition, and reductive elimination have traditionally been described in terms of 16-/18-electron interconversions. One-electron oxidations have been used to generate 17- and 19-electron species from 18-electron precursors. Accumulated evidence has established that much of the behavior of odd-electron complexes may be described in terms of 17/19 inter-

† University of Oslo.
‡ Indiana University.
® Abstract published in *Advance ACS Abstracts,* January 1, 1995.
(1) (a) Collman, J. P.; Hegedus, L. S.; Norton, J. R.; Finke, R. G. *Principles and Application of Organotransition Metal Chemistry*; University Science Books: Mill Valley, CA, 1987. (b) Kozikowski, A. P.; Wetter, H. F. *Synthesis* **1976**, 561. (c) Weill-Raynal, J. *Synthesis* **1976**, 633. (d) Smith, P. J. *Chem. Ind. (London)* **1976**, 1025. (e) Tsuji, J. *Organic Synthesis by Means of Transition Metal Complexes;* Springer Verlag: New York, 1975.
(2) (a) Skagestad, V.; Tilset, M. *J. Am. Chem. Soc.* **1993**, *115*, 5077. (b) Tilset, M. *J. Am. Chem. Soc.* **1992**, *114*, 2740.
(3) (a) Burk, M. J.; Tumas, W.; Ward, M. D.; Wheeler, D. R. *J. Am. Chem. Soc.* **1990**, *112*, 6133. (b) Ishikawa, K.; Fukuzumi, S.; Tanaka, T. *Inorg. Chem.* **1989**, *28*, 1661.

0276-7333/95/2314-0875$09.00/0

conversions.[4-7] Let us consider a reductive-elimination reaction from a 17-electron system. If the reductive elimination were to proceed directly, a highly unsaturated 15-electron product would result. Prior ligand coordination to a 19-electron intermediate avoids the formation of such a highly unsaturated product. Assuming that product stability is reflected in the energy of the transition state for the reductive elimination, 17-/19-electron interconversions certainly deserve to be considered for this reaction type. Kochi and co-workers[8] have suggested that initial solvent ligation takes place in the elimination of biaryls from 16-electron Ar_2NiL_2 complexes, initiated by 1-electron oxidation to generate the reactive 15-electron cation radicals (Scheme 2). In this case, the formation of a 13-electron product is averted by prior ligand coordination.

Scheme 2

$$Ar_2Ni(PEt_3)_2 \xrightarrow{-e^-} Ar_2Ni(PEt_3)_2^+$$

$$Ar_2Ni(PEt_3)_2^+ \xrightarrow{fast} Ar_2Ni(PEt_3)_2(S)^+$$

$$Ar_2Ni(PEt_3)_2(S)^+ \xrightarrow{slow} Ar{-}Ar$$

We report here the results of a study of the behavior of the 16-electron complexes $Ru(C_2Ph)_2(CO)(P^tBu_2Me)_2$ (**1**) and $Ru(CHCHPh)(C_2Ph)(CO)(P^tBu_2Me)_2$ (**2**) upon chemical and electrochemical oxidation. The use of the coordinating solvent acetonitrile and the virtually noncoordinating solvent dichloromethane in the oxidations opens up the possibility for probing the influence of the unsaturation of the metal center on the oxidatively induced reductive-elimination reaction. In addition, the possibility for the formation of two isomers of PhC_2-CHCHPh from **2** can yield valuable information about the mechanism of the the elimination reaction.

The reactions of both the bis(acetylide) **1** and the vinyl acetylide **2** are of potential relevance to the coupling of acetylenes to diynes and enynes. Traditionally this has been done in copper-mediated reactions,[9] since copper readily forms both acetylene π-complexes and acetylides. Recently rhodium or palladium reagents have been used.[10]

Results

Synthesis, Characterization, and X-ray Structure of $Ru(C_2Ph)_2(CO)(P^tBu_2Me)_2$ (1). The bis(acetylide) compound $Ru(C_2Ph)_2(CO)(P^tBu_2Me)_2$ (1) can be synthesized in one pot from $RuHCl(CO)(P^tBu_2Me)_2$, equimolar amounts of LiC_2Ph, and 4–5 equiv of PhC_2H in hexane by the sequence of reactions shown in Scheme 3. Each step of the reaction has been individually demonstrated.[11]

Scheme 3

$$RuHCl(CO)(P^tBu_2Me)_2 \xrightarrow{PhC_2H} Ru(CHCHPh)Cl(CO)(P^tBu_2Me)_2$$

$$Ru(CHCHPh)Cl(CO)(P^tBu_2Me)_2 \xrightarrow{LiC_2Ph} Ru(CHCHPh)(C_2Ph)(CO)(P^tBu_2Me)_2$$

$$Ru(CHCHPh)(C_2Ph)(CO)(P^tBu_2Me)_2 \xrightarrow{PhC_2H} Ru(C_2Ph)_2(CO)(P^tBu_2Me)_2 + PhHC{\cdot}CH_2$$

We reported earlier that ^1H, ^{13}C, and ^{31}P NMR data are consistent with C_{2v} symmetry for this molecule (**Ia**, where the value of θ is of course not established by such data) but could not rule out structure **Ib**, if the latter were still fluxional on the ^{13}C NMR time scale at −80 °C.[11] We have now been able to grow crystals of **1**, and a single-crystal X-ray structure determination (Figure 1, Table 1) shows **Ia** to be the correct representation, with $\theta = 169.0(15)°$. While poor crystal quality left the

(4) (a) Kochi, J. K. *Organometallic Mechanism and Catalysis*; Academic: New York, 1978. (b) Astruc, D. *Angew. Chem., Int. Ed. Engl.* **1988**, *27*, 643. (c) Astruc, D. *Chem. Rev.* **1988**, *88*, 1189. (d) Baird, M. C. *Chem. Rev.* **1988**, *88*, 1217. (e) Tyler, D. R. *Prog. Inorg. Chem.* **1988**, *36*, 125. (f) Connelly, N. G. *Chem. Soc. Rev.* **1989**, *18*, 153. (g) *Paramagnetic Organometallic Species in Activation/Selectivity, Catalysis*; Chanon, M., Julliard, M., Poite, J. C., Eds.; Kluwer Academic: Dordrecht, The Netherlands, 1989. (h) *Organometallic Radical Processes*; Trogler, W. C., Ed.; Elsevier: Amsterdam, 1990. (i) Astruc, D. *Acc. Chem. Res.* **1991**, *24*, 36. (j) Tyler, D. R. *Acc. Chem. Res.* **1991**, *24*, 325.

(5) For some key references to ligand substitution chemistry in 17-/19-electron systems, see the reviews in ref 4 and: (a) Wrighton, M. S.; Ginley, D. S. *J. Am. Chem. Soc.* **1975**, *97*, 2065. (b) Hershberger, J. W.; Klingler, R. J.; Kochi, J. K. *J. Am. Chem. Soc.* **1982**, *104*, 3034. (c) Hershberger, J. W.; Klingler, R. J.; Kochi, J. K. *J. Am. Chem. Soc.* **1983**, *105*, 61. (d) Pöe, A.; Sekhar, C. V. *J. Am. Chem. Soc.* **1985**, *107*, 4874. (e) Therien, M. J.; Ni, C.-L.; Anson, F. C.; Osteryoung, J. G.; Trogler, W. C. *J. Am. Chem. Soc.* **1986**, *108*, 4037. (f) Turaki, N. N.; Huggins, J. M. *Organometallics* **1986**, *5*, 1703. (g) Ruiz, J.; Lacoste, M.; Astruc, D. *J. Am. Chem. Soc.* **1990**, *112*, 5471. (h) Zhang, Y.; Gosser, D. K.; Rieger, P. H.; Sweigart, D. A. *J. Am. Chem. Soc.* **1991**, *113*, 4062. (i) Poli, R.; Owens, B. E.; Linck, R. G. *Inorg. Chem.* **1992**, *31*, 662.

(6) For key references to CO insertion chemistry in 17-/19-electron complexes, see the reviews in ref 4 and: (a) Magnuson, R. H.; Meirowitz, R.; Zulu, S.; Giering, W. P. *J. Am. Chem. Soc.* **1982**, *104*, 5790. (b) Magnuson, R. H.; Meirowitz, R.; Zulu, S. J.; Giering, W. P. *Organometallics* **1983**, *2*, 460. (c) Bly, R. S.; Silverman, G. S.; Bly, R. K. *Organometallics* **1985**, *4*, 374. (d) Reger, D. L.; Mintz, E.; Lebioda, L. *J. Am. Chem. Soc.* **1986**, *108*, 1940. (e) Therien, M. J.; Trogler, W. C. *J. Am. Chem. Soc.* **1987**, *109*, 5127. (f) Golovin, M. N.; Meirowitz, R.; Rahman, M. M.; Liu, H. Y.; Prock, A.; Giering, W. P. *Organometallics* **1987**, *6*, 2285. (g) Donovan, B. T.; Geiger, W. E. *Organometallics* **1990**, *9*, 865. (h) Tracey, A. A.; Eriks, K.; Prock, A.; Giering, W. P. *Organometallics* **1990**, *9*, 1399. (i) Prock, A.; Giering, W. P.; Greene, J. E.; Meirowitz, R. E.; Hoffman, S. L.; Woska, D. C.; Wilson, M.; Chang, R.; Chen, J.; Magnuson, R. H.; Eriks, K. *Organometallics* **1991**, *10*, 3479.

(7) For some recent examples of electron-transfer induced isomerizations, see: (a) Bond, A. M.; Colton, R.; Kevekordes, J. E. *Inorg. Chem.* **1986**, *25*, 749. (b) Vallat, A.; Person, M.; Roullier, L.; Laviron, E. *Inorg. Chem.* **1987**, *26*, 332. (c) Rieke, R. D.; Kojima, H.; Saji, T.; Rechberger, P.; Öfele, K. *Organometallics* **1988**, *7*, 749. (d) Bond, A. M.; Colton, R.; Mann, T. F. *Organometallics* **1988**, *7*, 2224. (e) Kuchynka, D. J.; Kochi, J. K. *Organometallics* **1989**, *8*, 677. (f) Bond, A. M.; Colton, R.; Feldberg, S. W.; Mahon, P. J.; Whyte, T. *Organometallics* **1991**, *10*, 3320.

(8) Tsou, T. T.; Kochi, J. K. *J. Am. Chem. Soc.* **1978**, *100*, 1639.

(9) (a) Cadiot, P.; Chodkiewicz, W. In *Chemistry of Acetylenes*; Viehe, H. G., Ed.; Marcel Dekker: New York, 1969, Chapter 9. (b) Brandsma, L. *Preparative Acetylenic Chemistry*; Elsevier: New York, 1988; p 220. (c) Straus, F. *Justus Liebigs Ann. Chem.* **1905**, *342*, 190. (d) Akthar, M.; Richards, T. A.; Weedon, B. C. L. *J. Chem. Soc.* **1959**, 933.

(10) (a) Ohshita, J.; Furumori, K.; Matsuguchi, A.; Ishikawa, M. *J. Org. Chem.* **1990**, *55*, 3277. (b) Bianchini, C.; Peruzzini, M.; Zanobini, F.; Frediani, P.; Albinati, A. *J. Am. Chem. Soc.* **1991**, *113*, 5453. (c) Wityak, J.; Chan, J. B. *Synth. Commun.* **1991**, *21*, 977. (d) Kitamura, T.; Tanaka, T.; Taniguchi, H.; Stang, P. J. *J. Chem. Soc., Perkin Trans. 1* **1991**, 2892. (e) Wakatsuki, Y.; Yamazaki, H.; Kumegawa, N.; Johar, P. *Bull. Chem. Soc. Jpn.* **1993**, *66*, 987. (f) Akita, M.; Yasuda, H.; Nakamura, A. *Bull. Chem. Soc. Jpn.* **1984**, *57*, 480. (g) Trost, B. M.; Chan, C.; Ruther, G. *J. Am. Chem. Soc.* **1987**, *109*, 3486. (h) Kovalev, I. P.; Yevdakov, K. V.; Strelenko, Y. A.; Vinogradov, M. G.; Nikishin, G. I. *J. Organomet. Chem.* **1990**, *386*, 139. (i) Ishikawa, M.; Ohshita, J.; Ito, Y.; Minato, A. *J. Organomet. Chem.* **1988**, *346*, C58. See also ref 23.

(11) Poulton, J. T.; Sigalas, M. P.; Eisenstein, O.; Caulton, K. G. *Inorg. Chem.* **1993**, *32*, 5490.

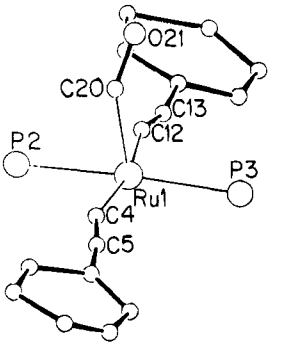

Figure 1. Ball-and-stick drawing of the non-hydrogen atoms of $Ru(C_2Ph)_2(CO)(P^tBu_2Me)_2$.

Table 1. Selected Bond Distances (Å) and Angles (deg) for $Ru(C_2Ph)_2(CO)(P^tBu_2Me)_2$ (1)

Ru(1)−C(4)	2.16(3)	Ru(1)−C(20)	2.05(8)
Ru(1)−C(12)	2.08(4)	O(21)−C(20)	1.22(7)
Ru(1)−P(2)	2.399(14)	C(4)−C(5)	1.18(5)
Ru(1)−P(3)	2.399(15)	C(12)−C(13)	1.21(6)
P(2)−Ru(1)−P(3)	176.3(10)	C(4)−Ru(1)−C(20)	85.0(21)
P(2)−Ru(1)−C(4)	85.5(9)	C(12)−Ru(1)−C(20)	90.4
P(2)−Ru(1)−C(12)	84.0(10)	Ru(1)−C(4)−C(5)	160.0(3)
P(2)−Ru(1)−C(20)	83.4(17)	C(4)−C(5)−C(6)	172.0(5)
P(3)−Ru(1)−C(4)	93.5(9)	Ru(1)−C(12)−C(13)	163.0(4)
P(3)−Ru(1)−C(12)	97.2(10)	C(12)−C(13)−C(14)	168.0(5)
P(3)−Ru(1)−C(20)	100.1(17)	Ru(1)−C(20)−O(21)	143.0(5)
C(4)−Ru(1)−C(12)	169.0(15)		

structure determination too inaccurate to merit detailed comparative discussion of bond lengths (e.g., the CO is

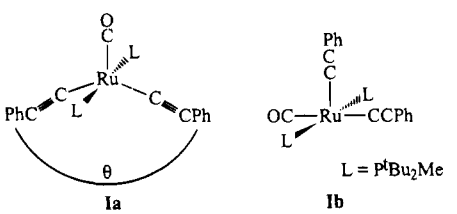

Ia **Ib**

poorly determined), the overall coordination polyhedron is unambiguously determined. An examination of packing diagrams showed no evidence for significant intermolecular contacts involving the open coordination site (i.e., trans to CO).

The CO stretching frequency of **1**, 1933 cm^{-1}, is higher than that observed for any $RuHX(CO)(P^tBu_2Me)_2$ species, including X = C_2Ph.[11] Since the donor power of H is less than that of C_2Ph, this led us to suggest that **1** did not have structure **Ib** (which is that preferred for all $RuHX(CO)(P^tBu_2Me)_2$ species except X = SiR_3), but rather structure **Ia**.

Synthesis, Characterization, and Structure of $Ru(CHCHPh)(C_2Ph)(CO)(P^tBu_2Me)_2$ (2). The execution of only the first two reactions (equimolar amounts of $RuHCl(CO)(P^tBu_2Me)_2$, LiC_2Ph, and PhC_2H in hexane) in Scheme 3 yields $Ru(CHCHPh)(C_2Ph)(CO)(P^tBu_2Me)_2$ (**2**). The presence of the vinyl ligand is easily recognized by the characteristic resonances of the vinyl protons in the ^1H NMR spectrum (δ 8.62 (d) and 6.72 (d)). The magnitude of the $^3J_{H-H}$ vinyl coupling constant (15 Hz) indicates their mutual *trans* stereochemistry.

We have established above that $Ru(C_2Ph)_2(CO)(P^tBu_2Me)_2$ (**1**) conforms closely to square-pyramidal geometry. Similarly, it has been demonstrated that $Os(CHCHPh)Cl(CO)(P^iPr_3)_2$ is square pyramidal, but with a basal CO and apical vinyl group.[12] On the basis of this, we assume that **2** is also square pyramidal with a basal

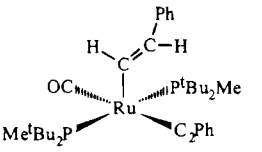

II

CO and apical vinyl group (**II**). This is supported by the low value of ν_{CO} (1910 cm^{-1}). It indicates a greater degree of back-bonding than what may be expected for an apical CO *trans* to an empty site (compare with ν_{CO} = 1933 cm^{-1} for **1**).

Coordination of Acetonitrile to 1 and 2. Both pyridine and nitriles (acetonitrile and acrylonitrile) are found to bind reversibly to $RuHX(CO)P_2$ species.[13] When 4 equiv of acetonitrile was added to a red-orange solution of $RuH(C_2Ph)(CO)(P^tBu_2Me)_2$ in benzene-d_6, a yellow solution was obtained.[14a] The fading of color is consistent with a more "saturated" complex being formed from the 16-electron complex. The ^{31}P NMR spectrum showed that the resonance for the phosphine changed from 53.2 to 56.5 ppm upon acetonitrile addition. At the same time ν_{CO} changed from 1906 to 1896 cm^{-1} and ν_{CC} from 2072 to 2083 cm^{-1}. The increased back-bonding into the CO ligand verifies that acetonitrile indeed coordinates to the metal center. The Ru complexes **1** and **2** were suspected to show the same kind of behavior. Since we planned to use acetonitrile as the solvent in our investigation of the complexes, we were interested in finding out if the 16-electron nature of these complexes persisted when they were dissolved in acetonitrile.

The dark red Ru−hydrocarbyl compounds **1** and **2** are only moderately soluble in neat acetonitrile. The bis(acetylide) **1** gave a yellow solution from which a pale yellow solid precipitated spontaneously. Complex **2** gave a red-orange solution from which red crystals were obtained. The solids from each solution were collected and dried *in vacuo* for 2−3 min. The dry compounds were dissolved in benzene-d_6 and analyzed by ^1H NMR spectroscopy. The spectra showed resonances for coordinated acetonitrile at δ 0.62 and 0.59 for **1** and **2**, respectively. These resonances moved downfield to δ 0.69 (**1**) and 0.71 (**2**) upon addition of 10 μL of acetonitrile-d_3 (free acetonitrile occurs at δ 0.73 when dissolved in benzene-d_6). The resonances at δ 0.69 and 0.71 are apparently average values for coordinated and uncoordinated acetonitrile. Thus, the experiments described above illustrate that acetonitrile indeed coordinates to the Ru centers and that fast exchange occurs between coordinated and uncoordinated acetonitrile.

Removal of the volatiles from acetonitrile solutions of **1** and **2** by pumping *in vacuo* for 12 h regenerated the 16-electron complexes free of coordinated acetonitrile (confirmed by ^{31}P NMR and IR spectroscopy in benzene-d_6).

Addition of only 1 equiv of acetonitrile to a solution of **1** in benzene-d_6 gave immediate color change of the solution together with changes in the IR and ^{31}P NMR

(12) Werner, H.; Esterulas, M. A. Otto, H. *Organometallics* **1986**, *5*, 2295.
(13) Poulton, J. T.; Sigalas, M. P.; Folting, K.; Streib, W. E.; Eisenstein, O.; Caulton. K. G. *Inorg. Chem.* **1994**, *33*, 1476.

Table 2. Acetonitrile Coordination to 1 and 2

	neat benzene-d_6			benzene-d_6 + acetonitrile-d_3[a]		
compd	color	^{31}P NMR (δ, ppm)	IR ν_{CO}, ν_{CC} (cm^{-1})	color	^{31}P NMR (δ, ppm)	IR ν_{CO}, ν_{CC} (cm^{-1})
1	dark red	47.7	1933, 2074	yellow	45.3	1940, 2081
2	dark red	40.9	1910, 2074	bright red	40.9, 45.0[b]	1910,[c] 2074

[a] The data are for addition of 1 equiv of acetonitrile to **1** and 20–30 equiv to **2**. [b] Only a small amount (~5%) of this peak was present. [c] A small shoulder (~5%) was detected at higher frequencies.

Scheme 4

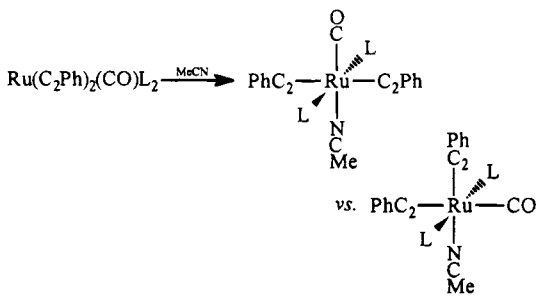

spectra. For complex **2**, however, 20–30 equiv of acetonitrile was needed to obtain detectable changes. The relevant spectroscopic data are summarized in Table 2.

Evidently there appears to be a certain degree of acetonitrile binding to the Ru complexes in question. The bonding is, however, more favorable to **1**. The vinyl ligand of complex **2** is more electron donating than an acetylide ligand. Thus, **2** might be expected to be less electron deficient than **1** and consequently less susceptible to acetonitrile coordination. Working against this in **1** is the strongly *trans*-labilizing ligand CO *trans* to the empty site. Note, however, that we cannot rule out a structural change of **1** (Scheme 4) upon acetonitrile coordination. As a consequence, coordination of acetonitrile *trans* to CO would be avoided. This could also explain why ν_{CO} *increases* from 1933 to 1940 cm^{-1} instead of the decrease usually anticipated from the coordination of a donor ligand.

On the basis of these results, we conclude that **1** and **2** in acetonitrile exist as the corresponding 18-electron acetonitrile adducts. It has recently been reported that RuHCl(CO)(P^{i}Pr$_3$)$_2$ binds acetonitrile.[14b]

Thermal Stability of 1 and 2. Bergman and his group have previously investigated the thermal decomposition of CpCo(PPh$_3$)RR′.[15] Facile reductive-elimination reactions resulted for alkyl–acyl and alkyl–vinyl complexes, whereas alkyl–alkyl complexes yielded mostly products from pathways other than reductive elimination. The elimination reactions occurred after initial phosphine dissociation from the 18-electron starting materials. These results were attributed to the ability of the alkyl–acyl and alkyl–vinyl systems to donate an additional electron pair to the metal in the transition state and make it a 16-electron species.

In our previous work with Cp*Rh(PPh$_3$)Me$_2$[16] we found that the ease of ethane elimination from Cp*Rh(PPh$_3$)Me$_2^{\bullet+}$ strongly contrasted with the extremely slow thermal decomposition of the neutral complex to yield only unknown products. The rate enhancement toward reductive elimination due to one–electron oxidation was estimated to be at least a factor of 3×10^9.

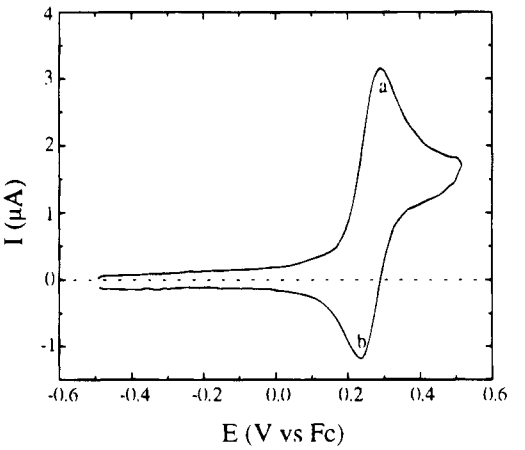

Figure 2. Cyclic voltammogram for the oxidation of **1** in acetonitrile (0.1 M Bu$_4$NPF$_6$) at a Pt-disk microelectrode (d = 0.6 mm) at 0 °C and the voltage sweep rate v = 1.0 V/s.

This motivated us to study the thermal behavior of **1** and **2** in order to be able to make a comparison of the thermal and oxidative behavior of these 16-electron species. Heating of sealed NMR tubes containing solutions of **1** and **2** in benzene-d_6 revealed that the complexes were stable at 62 °C for 24 h (by ^{1}H NMR). When the heating was continued at 74 °C for another 24 h, traces of free phosphine appeared in the ^{31}P NMR spectra of the complexes. Prolonged heating at 84 °C yielded more phosphine. No other complexes were detected by ^{1}H NMR or ^{31}P NMR spectroscopy. Even though the complexes are demonstrated to decompose slowly upon heating, there is no evidence for reductive elimination (i.e., there is no ^{1}H NMR evidence for formation of [PhC$_2$]$_2$ (from **1**) and PhC$_2$CHCHPh (from **2**)). Note, however, that if thermal reductive elimination is to occur from **1**, a structural change to yield a *cis* disposition of the organic moieties has to occur before the elimination can take place.

Cyclic Voltammetry Investigation of 1 and 2. Cyclic voltammetry (CV) was used for the initial investigation of the electrooxidation of **1** and **2**. Two solvents, acetonitrile and dichloromethane, were chosen because of their different coordinating abilities. This will permit evaluation of the importance of the degree of unsaturation at Ru on the oxidatively induced elimination.

(a) First Oxidation Step. Figure 2 shows a cyclic voltammogram for the oxidation of **1** in acetonitrile (0.1 M Bu$_4$NPF$_6$, 0 °C, 0.6 mm diameter Pt-disk microelectrode, sweep width 1 V, voltage sweep rate v = 1.0 V/s). Peak **a** corresponds to the oxidation of **1**, whereas peak **b** represents the reduction of **1**$^{\bullet+}$ back to **1**. The forward and reverse peaks are not of the same intensity. This indicates that a follow-up reaction partially consumes **1**$^{\bullet+}$. The reversible oxidation potential of **1**, taken to

(14) (a) Caulton, K. G.; Pedersen, A. Unpublished results. (b) Esteruelas, M. A.; Lahoz, F. J.; Lopez, A. M.; Oñate, E.; Oro, L. A. *Organometallics* **1994**, *13*, 1669.
(15) Evitt, E. R.; Bergman, R. G. *J. Am. Chem. Soc.* **1980**, *102*, 7003.
(16) Pedersen, A.; Tilset, M. *Organometallics* **1993**, *12*, 56.

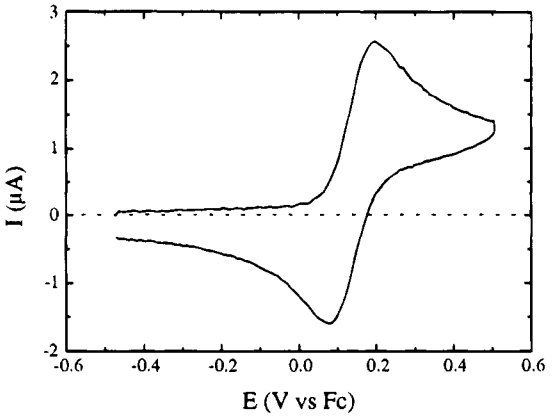

Figure 3. Cyclic voltammogram for the oxidation of **2** in dichloromethane (0.2 M Bu_4NPF_6) at a Pt-disk microelectrode (d = 0.6 mm) at 0 °C and the voltage sweep rate v = 1.0 V/s.

be the midpoint between the anodic and cathodic peaks, is 0.28 V vs the ferrocene/ferrocenium couple (Fc). Use of dichloromethane as solvent for the CV investigation of **1** gave a CV trace almost identical with the one already described for the investigation in acetonitrile, with a reversible oxidation potential of 0.20 V vs Fc. Admittedly, the difference between the oxidation potentials in the two solvents is not very large and it could be an effect of the great difference in polarity between the two solvents. Nevertheless, the opposite ordering of the oxidation potentials is expected, since an additional donor ligand is present when **1** is dissolved in acetonitrile. We have already speculated that **1** may undergo a structural change when it is dissolved in acetonitrile. The easier oxidation in dichloromethane can therefore be taken as another indication of such an isomerization.

The electrochemical oxidation of **2** in acetonitrile was also a partially reversible process at voltage sweep rate v = 1 V/s. In dichloromethane (0.2 M Bu_4NPF_6), however, the reaction was close to reversible. This is depicted in Figure 3. The reversible oxidation potentials were found to be 0.10 and 0.15 V vs Fc in acetonitrile and dichloromethane, respectively. Note that the oxidation of **2** is easier to accomplish than the oxidation of **1**. This is probably because the vinyl ligand in **2** donates more electron density to the metal center than the acetylide ligand in **1**. While the difference of 0.05 V between the oxidation potentials of **2** in the two solvents is small, the difference is in the expected direction, assuming that acetonitrile coordination increases the electron density of **2**.

(b) Second Oxidation Step. We infer from the partial chemical reversibility of the oxidation of **1** and **2** that their cation radicals are rather stable (half-life of a few seconds). An increased sweep width (from 1 to 1.6 V) in the cyclic voltammetry experiment of **1** in acetonitrile showed (Figure 4) that the radical cation, $\mathbf{1}^{\bullet+}$, underwent oxidation to yield $\mathbf{1}^{2+}$ (peak **c**). In addition to confirming that $\mathbf{1}^{\bullet+}$ is indeed relatively stable, it also provides information about the electron density of the metal. The occurrence of a second oxidation was least surprising when acetonitrile was used as solvent, since we have shown that acetonitrile is coordinated to the metal center, thus increasing the electron count of the metal. However, the dication was also generated in dichloromethane, and the irreversible

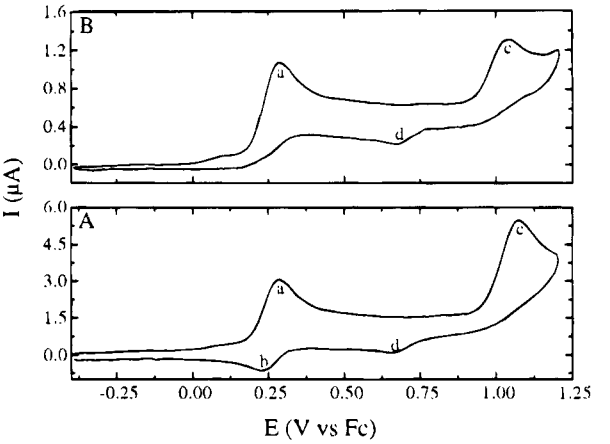

Figure 4. Cyclic voltammograms for the oxidation of **1** in acetonitrile (0.1 M Bu_4NPF_6) at a Pt-disk microelectrode (d = 0.6 mm) at 0 °C. Trace A (lower trace) shows the process at the voltage sweep rate v = 1.0 V/s, whereas trace B (upper trace) shows it at the voltage sweep rate v = 0.2 V/s.

peak potentials for oxidation of $\mathbf{1}^{\bullet+}$ were found to be practically identical in the two solvents (1.12 and 1.10 V vs Fc in acetonitrile and dichloromethane, respectively). If we assume that acetonitrile indeed increases the electron count on Ru, something else must play this role when dichloromethane is used as solvent. The identity of such a species is unknown but could be weakly bound counterion BF_4^-,[17a] dichloromethane,[17b–d] or traces of adventitious water.

The difference between the first and the second oxidations of **1** (i.e. peaks a and c), in both acetonitrile and dichloromethane, is 0.8–0.9 V. If the kinetic potential shifts of irreversible reactions[18] are taken into account, the difference is probably even larger. In any case, the potential difference is in accord with previous results, where the oxidation potentials for the oxidation of 17-electron radicals to 16-electron cations were found to be 0.8–1.2 V more positive than those for the oxidation of the corresponding 18-electron anions to radicals.[2]

As already mentioned, Figure 4 depicts CV traces for the oxidation of **1** in acetonitrile with sweep widths of 1.6 V. Peak **a** corresponds to the partially reversible oxidation of **1** (as in Figure 2), whereas peak **c** is the irreversible oxidation of $\mathbf{1}^{\bullet+}$ to $\mathbf{1}^{2+}$. As evidenced by the irreversibility of this second oxidation, the dication is unstable and reacts quickly. In the system described above, slower sweep rates will increase the extent of decay of $\mathbf{1}^{\bullet+}$ on the experimental time scale. Consequently, the intensity of peak **c** relative to a should decrease with decreasing sweep rate. This is illustrated by the two traces in Figure 4. Trace A depicts the

(17) (a) Beck, W.; Sünkel, K. *Chem. Rew.* **1988**, *88*, 1405. (b) Kulawiec, R. J.; Crabtree, R. H. *Coord. Chem. Rev.* **1990**, *99*, 89. (c) Fernandez, J. M.; Gladysz, J. A. *Organometallics* **1989**, *8*, 207. (d) Colsman, M. R.; Newbound, T. D.; Marshal, L. J.; Noirot, M. D.; Miller, M. M.; Wulfsberg, G. P.; Frye, J. S.; Anderson, O. P.; Strauss, S. H. *J. Am. Chem. Soc.* **1990**, *112*, 2349. (e) Song, L.; Trogler, W. C. *J. Am. Chem. Soc.* **1992**, *114*, 3355. (f) Darensbourg, M.; Borman, C. *Inorg. Chem.* **1976**, *15*, 3121. (g) Darensbourg, M. Y. *Prog. Inorg. Chem.* **1985**, *33*, 221. (h) Kochi, J. K.; Bockman, T. M. *Adv. Organomet. Chem.* **1991**, *33*, 51. (i) Lippmann, E.; Krämer, R.; Beck, W. *J. Organomet. Chem.* **1994**, *466*, 167.

(18) (a) Ahlberg, E.; Parker, V. D. *J. Electroanal. Chem., Interfacial Electrochem.* **1981**, *121*, 73. (b) Parker, V. D. *Acta Chem. Scand., Ser. B* **1984**, *B38*, 165. (c) Parker, V. D. *Electroanal. Chem.* **1986**, *14*, 1.

Scheme 5

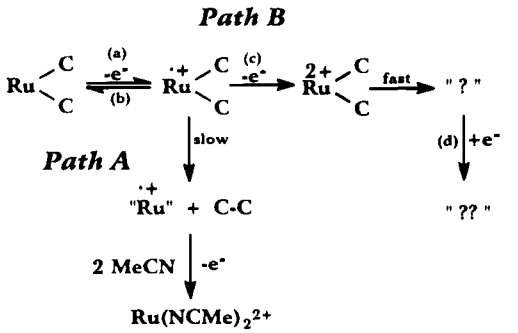

Ru = Ru(CO)(NCMe)(P^{t}Bu$_2$Me)$_2$ in MeCN
Ru = Ru(CO)(P^{t}Bu$_2$Me)$_2$ in CH_2Cl_2
C = C_2Ph for 1
C = C_2Ph and CHCHPh for 2

[a] $AcFc^+$ = acetylferrocenium.

process at v = 1.0 V/s, whereas trace B is for v = 0.2 V/s. By comparison of the voltammograms, it is evident that the relative intensity of peak **c** is significantly diminished. In an attempt to establish the identity of the species undergoing reduction at peak **d**, the scan was reversed at 0.8 V, i.e. just before oxidation to the dication takes place. Peak **d** did not appear at any sweep rate (0.2–10.0 V/s), nor did it gain intensity when the dicationic complex [Ru(CO)(CNMe)$_3$(P^{t}Bu$_2$Me)$_2$]-(PF_6)$_2$ (**3**(PF_6)$_2$; *vide infra*) was added to the solution. Thus, peak **d** arises not from the decomposition of $\mathbf{1}^{\bullet+}$ but from $\mathbf{1}^{2+}$, and it is not due to the dicationic complex **3** (**3** did not show electroactivity from −1.6 to +1.8 V vs Fc).

Increasing the sweep width from 1 to 2 V in the cyclic voltammetry investigation of **2** in acetonitrile also gave a second oxidation peak. The oxidation potential was determined to be 1.10 V vs Fc. In contrast to what was observed for $\mathbf{1}^{\bullet+}$, the oxidation of $\mathbf{2}^{\bullet+}$ was partially reversible. A broad, ill-defined wave at ca. 1 V vs Fc was seen when the sweep width was increased from 1 to 2 V in dichloromethane solvent.

(c) Summary of Cyclic Voltammetric Processes. On the basis of the discussion above, a schematic overview over all of the processes is shown in Scheme 5. The processes giving rise to peaks **a–d** (Figure 4) are marked with the corresponding letters in parentheses. Steps involving acetonitrile do not, of course, occur in dichloromethane. The oxidation of "Ru^+" is not observed as a separate peak because it (most likely after acetonitrile coordination)[19] presumably undergoes oxidation at the potential where **1** (**2**) is oxidized. The chemical oxidation of **1** and **2** (vide infra) follows path A. The oxidizing agent used (acetylferrocenium tetrafluoroborate, or [AcFc]BF_4, 0.248 V vs Fc) is not powerful enough to act as an effective oxidant toward $\mathbf{1}^+$ and $\mathbf{2}^+$ to produce $\mathbf{1}^{2+}$ and $\mathbf{2}^{2+}$, respectively.

Constant-Current Coulometry of 1 and 2. Constant-current coulometry experiments, in which the substrate consumption was monitored by derivative cyclic voltammetry (DCV), were used to find the amount of charge (faraday/mol) needed for complete substrate consumption under electrochemical conditions.

(19) It has been previously shown that the oxidizing potential of a cation radical $M^{\bullet+}$ is lowered by ~1.3 V upon acetonitrile coordination: Skagestad, V.; Tilset, M. *Organometallics* **1991**, *10*, 2110.

Constant-current coulometry experiments (acetonitrile, 0.05 M $Me_4N(BF_4)$) required the passage of 2.0 faraday/mol of charge for complete consumption of **1** and **2**. This is indicative of an overall two-electron process on this time scale (5–10 min). Analysis of the resulting solutions by ^{31}P NMR spectroscopy showed formation of [Ru(CO)(NCMe)$_3$(P^{t}Bu$_2$Me)$_2$](BF_4)$_2$ (**3**(BF_4)$_2$). The following paragraphs will show that **3** is also the main metal-containing product for the chemical two-electron oxidations of **1** and **2** in acetonitrile.

Chemical oxidations of **1** and **2** were found to consume 2 equiv of $AcFc^+$ in acetonitrile and dichloromethane (vide infra). Constant-current coulometry experiments with dichloromethane (0.2 M $Bu_4N(PF_6)$) as solvent only consumed 1.5 and 1.3 faraday/mol for complete oxidation of **1** and **2**, respectively. The source of the discrepancy between the coulometric experiments and the homogeneous experiments is believed to be that the reaction of the cation radicals $\mathbf{1}^{\bullet+}$ and $\mathbf{2}^{\bullet+}$ under the experimental conditions for the coulometric experiments generates products that are electroinactive.

Homogeneous Outer-Sphere Oxidation of 1 in Acetonitrile and in Dichloromethane. Oxidation of **1** in acetonitrile was first attempted with 2 equiv of (Cp_2-Fe)(PF_6) (note that Cp_2Fe/Cp_2Fe^+ (Fc) is used as reference (0 V) in the CV experiments). This reaction turned out to be rather slow; full consumption of the oxidant occurred only after 4–5 h and yielded a mixture of several products (by ^{31}P NMR). To increase the speed of the oxidation, the more potent oxidant acetylferrocenium tetrafluoroborate (AcFc(BF_4)) was employed. This gave immediate consumption of the oxidant and a cleaner reaction. The main phosphorus-containing product (42.4 ppm by ^{31}P NMR spectroscopy) was 75–80% of the total yield of products. There were also four other weak signals. It was also established (by ^{1}H NMR) that the order of addition influenced the relative yield of main products and byproducts. Relatively slow addition of ruthenium complex (20 mg) in acetonitrile (~25 mL) to 2 equiv of AcFc(BF_4) (in 5 mL of acetonitrile) gave only the main product and traces of one byproduct (~95:5) by inspection of ^{31}P NMR spectra.

Titration of an acetonitrile solution of AcFc(BF_4) with the bis(acetylide) **1** confirmed that 2 equiv of oxidant was required to consume 1 equiv of **1**.

After oxidation, a typical ^{1}H NMR spectrum showed a cluster of peaks in the area 7.3–7.8 ppm and two virtual triplets at δ 1.40 and 1.60 ppm (^{t}Bu and Me) in addition to peaks for acetylferrocene. The resonances at 1.40 and 1.60 ppm arise from an organometallic product, which was identified as [Ru(CO)(NCMe)$_3$-(P^{t}Bu$_2$Me)$_2$](BF_4)$_2$ (**3**(BF_4)$_2$). The phosphine resonance for **3** is identical (42.4 ppm) with the resonance for the main product detected above with ^{31}P NMR. The yield of **3** was found to be 75% (^{1}H NMR) when hexamethylbenzene was added as internal standard for product quantification. The independent synthesis and identification of this dication are described in the following section. Extraction (Et_2O) of the dried residue from oxidation, followed by ^{1}H NMR analysis of the ether extract, established that the peaks in the phenyl region originated from an ether-soluble product. Comparison to an authentic sample of [PhC_2]$_2$ (^{1}H and ^{13}C NMR and mass spectrometry) proved that this diyne was formed in the reaction (72%). In addition, there was no

evidence for formation of PhC_2H (detection limit 3%), a product expected if homolytic cleavage of the Ru-acetylide bond were followed by cage escape and H atom abstraction.

The oxidation of **1** with $AcFc^+$ in dichloromethane solvent was also found to be a two-electron process. The best conditions for the oxidation were again addition of bis(acetylide) to $AcFc^+$, but less solvent (3–5 mL) was used, due to better solubility of the substrate in dichloromethane. Again $[PhC_2]_2$ was identified as the only organic product (47% yield).

The oxidation in dichloromethane resulted in a complex organometallic product mixture. A main product together with several byproducts were detected by ^{31}P and ^1H NMR. In addition, it was evident from the IR spectrum that *two* main products were present. Two overlapping CO stretches were observed. One of them may arise from an NMR-silent (paramagnetic) compound. The yield of the NMR-detectable product and byproducts varied from experiment to experiment. Quantification of a typical experiment showed 53% yield of the main product. The spectroscopic data in dichloromethane (^{31}P, ^{13}C, and ^1H NMR and IR) indicate that the product is a cationic complex containing a CO ligand and two phosphine ligands per Ru center. The ^1H NMR spectrum showed a doublet for ^tBu and a doublet of doublets for the methyl. Thus, it has a very different coupling pattern compared to the product formed in acetonitrile. However, when the solvent was removed from a typical reaction mixture and the residue dissolved in acetonitrile-d_3, ^{31}P NMR spectroscopy showed the resulting mixture to consist mostly of complex **3**. The $^1H\{^{31}P\}$ NMR spectrum of a dichloromethane solution consisting mostly of the main product from the oxidation in dichloromethane gave a broad singlet for ^tBu and a broad peak for the methyl group. The peak width of the ^{31}P NMR signal was measured to be 6 Hz. This is broader than expected (2–3 Hz) but not extremely broad. The conclusion is that a fluoride ligand is not coordinated to Ru. This statement is supported by the ^{19}F NMR spectrum of the product mixture, which showed no resonance for a F-ligand (in the range of +50 to −450 ppm). The ^{19}F NMR spectrum did not show the normal signal for the counterion BF_4^- but rather a very broad peak in the vicinity (i.e., within ~0.5 ppm) of the normal resonance for BF_4^-. Lowering of the temperature to −90 °C did not bring any change of the ^{19}F NMR spectrum. We propose a weak coordination of the BF_4^- counterion to the product from the dichloromethane oxidation.[17a] In addition, stabilization of the product by adventitious traces of water or dichloromethane cannot be ruled out.

Characterization of $[Ru(CO)(NCMe)_3(P^tBu_2Me)_2](BF_4)_2$ ($3(BF_4)_2$). The dicationic acetonitrile adduct **3** was identified by ^1H, ^{13}C, and ^{31}P NMR and IR data.[20] The IR spectrum showed a ν_{CO} stretching frequency of 2010 cm^{-1}. Compared to the values of 1933 and 1910 cm^{-1} for **1** and **2**, respectively, this indicates that the back-bonding to CO is greatly diminished in complex **3**, as expected for a dicationic complex. The ^1H NMR spectrum of $3(BF_4)_2$ in CD_3NO_2 showed one virtual triplet for P^tBu and one for PMe, indicating *trans* phosphine groups. The spectrum also revealed two resonances in a 1:2 ratio for coordinated acetonitrile. Therefore, the bis(acetonitrile) adduct **3** was assigned the structure **III**.

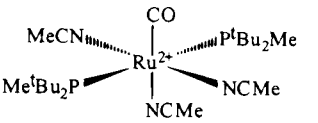

III

The sterically demanding phosphine groups in **1** and **2** interfere with the binding of potential ligands as acetonitrile, pyridine, and H_2.[13] In addition, the CO ligand is generally viewed as a ligand with a strong *trans* effect. Thus, the acetonitrile ligand *trans* to CO is expected to be rather labile. This was confirmed when $3(BF_4)_2$ was dissolved in acetonitrile-d_3. The acetonitrile resonance of only one of the acetonitrile ligands disappeared within ½ h due to exchange with CD_3CN. The remaining two MeCN ligands undergo no detectable exchange with neat CD_3CN over the course of 2 days at 25 °C.

Investigation of the Molecularity of the Reductive Elimination from 1. We sought to establish whether the C–C bond-forming reaction which produces the diyne was of intramolecular or intermolecular nature. An intermolecular reaction could be viable for several reasons. First, acetylide is known to frequently serve as a bridging ligand (**IV**).[22] There is thus a

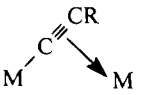

IV

plausible way for an intermolecular mechanism to begin. The possibility of a intermolecular reaction is even more likely, considering that the acetylide ligands in **1** are mutually *trans*, a sterochemistry unsuitable for prompt unimolecular reductive elimination. However, it is not necessarily true that the oxidized species, $1^{\bullet+}$, has a *trans* geometry.

For this purpose, we employed $Ru[C_2(p\text{-tolyl})]_2(CO)(P^tBu_2Me)_2$ as an alternative to an isotopically substituted derivative of **1**. It was first established that oxidation ($AcFc(BF_4)$) of $Ru[C_2(p\text{-tolyl})]_2(CO)(P^tBu_2Me)_2$ in acetonitrile produced $[(p\text{-tolyl})C_2]_2$, which shows an electron-impact mass spectrum parent ion at m/e 230. In the crossover experiment, a mixture of equimolar amounts of **1** and $Ru[C_2(p\text{-tolyl})]_2(CO)(P^tBu_2Me)_2$ was oxidized in acetonitrile. Mass spectral analysis of the ether-soluble material resulting from the oxidation showed m/e 230 for $[(p\text{-tolyl})C_2]_2$ and m/e 202 for $[PhC_2]_2$ but no signal above the base line at m/e 216 for the crossover diyne $(p\text{-tolyl})C_2C_2Ph$. The C–C bond formation, therefore,

(20) Several attempts to independent by synthesize $[Ru(CO)(NCMe)_3(P^tBu_2Me)_2](BF_4)_2$ ($3(BF_4)_2$) were unsuccessful.

(21) It was impossible to obtain an acceptable elemental analysis due to inseparable impurities formed in the oxidation reaction.

(22) (a) Forníes, J.; Lalinde, E.; Martínez, F.; Moreno, M. T.; Welch, A. J. *J. Organomet. Chem.* **1993**, *455*, 271. (b) Yam, V. W.-W.; Chan, L.-P.; Lai, T.-F. *J. Chem. Soc., Dalton Trans.* **1993**, 2075. (c) Espinet, J.; Forníes, F.; Martínez, F.; Sotés, M.; Lalinde, E.; Moreno, M. T.; Ruiz, A.; Welch, A. J. *J. Organomet. Chem.* **1991**, *403*, 253. (d) Akita, M.; Terada, M.; Moro-oka, Y. *Organometallics* **1991**, *10*, 2961. (e) Froom, S. F. T.; Green, M.; Mercer, R. J.; Nagle, K. R.; Orpen, A. G.; Rodrigues, A. *J. Chem. Soc., Dalton Trans.* **1991**, 3171.

takes place intramolecularly (Scheme 6).

Scheme 6

$$Ru(C_2Ph)_2(CO)(P^tBu_2Me)_2 + Ru[C_2(p\text{-tolyl})]_2(CO)(P^tBu_2Me)_2 \xrightarrow{-2e^-} PhC{\equiv}CC{\equiv}CPh + [(p\text{-tolyl})C_2]_2$$

The same series of experiments were repeated, but this time with dichloromethane as solvent. Again mass spectrometric analysis showed that the reaction was intramolecular.

Homogeneous Outer-Sphere Oxidation of 2 in Acetonitrile and in Dichloromethane. The oxidation of **2** in acetonitrile and dichloromethane showed great similarities with the oxidation of **1**. The two-electron oxidation ($AcFc(BF_4)$) of **2** in acetonitrile and dichloromethane also resulted in elimination of the organic moieties (Scheme 7). In acetonitrile, $[Ru(CO)(NCMe)_3(P^tBu_2Me)_2](BF_4)_2$ (**3**$(BF_4)_2$, 75%) was formed, whereas the mixture of metal-containing products in dichloromethane was the same as the product mixture from the oxidation of **1** in dichloromethane. The main product was found in 42% yield.

Scheme 7

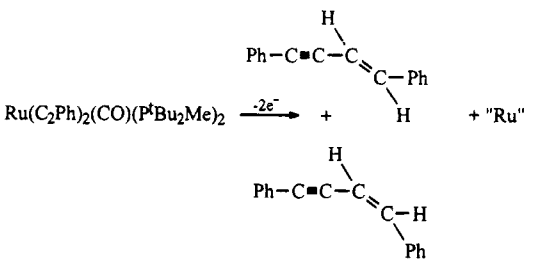

Ether extraction of the dried residues from the oxidations yielded the *E* and *Z* isomers (9:1) of the enyne $PhC_2CHCHPh$. The yield of enyne was 70% in acetonitrile and 46% in dichloromethane. Both solvents gave the same isomeric ratio ($E/Z = 9/1$). The identities of the enyne and the separate isomers were established by comparison with literature ^1H and ^{13}C NMR data.[23] The (*E*)-enyne was also identified by comparison with a compound formed in an independent synthesis.[24]

Investigation of the Formation of (*E*)- and (*Z*)-$PhCHCHC_2Ph$. It is already established that the reductive elimination of $[PhC_2]_2$ from $Ru(CCPh)_2(CO)(P^tBu_2Me)_2$ (**1**) is an intramolecular reaction. We wanted to confirm that (*E*)- and (*Z*)-$PhC_2CHCHPh$ also were formed intramolecularly. An intermolecular reaction was expected to yield $[PhC_2]_2$ and $[PhCHCH]_2$ in addition to $PhC_2CHCHPh$. The organic components from the oxidation of **2** were analyzed by capillary gas chromatography (GC). Examination of the GC traces revealed that 2.5−3.0% of $[PhC_2]_2$ was formed in either solvent. At least some of this could originate from **1** as an impurity in our sample of **2**. There was no evidence for formation of PhC_2H, the product expected if homolytic cleavage of the Ru−acetylide bond were followed by cage escape.

(23) (a) Jun, C.-H.; Lu, Z.; Crabtree, R. H. *Tetrahedron Lett.* **1992**, *33*, 7119. (b) Echavarren, A. M.; Lopez, J.; Santos, A.; Montoya, J. *J. Organomet. Chem.* **1991**, *414*, 393. (c) Dahlenburg, L.; Frosin, K.-M.; Kerstan, S.; Werner, D. *J. Organomet. Chem.* **1991**, *407*, 115.

(24) Kern, R. J. *Chem. Commun.* **1968**, 706.

Scheme 8[a]

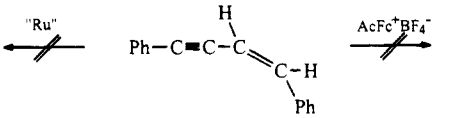

[a] $AcFc^+$ = acetylferrocenium.

We have sought to establish whether the formation of enyne double-bond geometric isomers is inherent to the mechanism of the oxidatively induced reductive elimination reaction or whether it is a consequence of isomerization of free enyne product by a component of the reaction mixture subsequent to C−C bond formation.

To test for the possible isomerization of (*E*)-$PhC_2CHCHPh$ by unconsumed oxidant, $AcFc(BF_4)$ and (*E*)-$PhC_2CHCHPh$ were dissolved in dichloromethane-d_2. Even after 24 h no isomerization of the enyne was observed. The same was found when (*E*)-enyne was added to a solution of products from the oxidation of $Ru(CHCHPh)(C_2Ph)(CO)(P^tBu_2Me)_2$ (**2**) in dichloromethane. Thus, neither unconsumed oxidant nor the organometallic products from the oxidation in dichloromethane were found to effect isomerization (Scheme 8).[25]

From the CV experiments it is known that the cation radical $\mathbf{2}^{\bullet+}$ has a half-life of several seconds. Hence, there is time for an isomerization of the vinyl ligand to occur, giving small amounts of $\mathbf{2}^{\bullet+}$ with *cis* disposition about the double bond of the vinyl ligand. From this isomerized cation radical, isomerized **2** could be obtained upon oxidation of unconsumed **2** by $\mathbf{2}^{\bullet+}$. This was investigated by treatment of solutions of **2** (acetonitrile and dichloromethane) with 0.4 equiv of $AcFc^+$. Analysis of the extracts from the dried residues of the reaction showed no change of the unconsumed **2**. There were no new ^1H NMR resonances in the vinyl region and no changes in the ^{31}P NMR spectra. Thus, the vinyl stereochemistry in **2** is unchanged under the reaction conditions.

Kinetics of the Reductive Elimination from $\mathbf{1}^{\bullet+}$ and $\mathbf{2}^{\bullet+}$. When conventional CV is employed as a tool for the investigation of electrode processes or of the reactions of electrogenerated species, the double-layer charging current causes a distortion of the base line. This poses a problem for kinetic applications of CV, especially at high voltage sweep rates and/or low substrate concentration, where the charging current may be dominant. The use of derivative cyclic voltammetry[18] (DCV) circumvents this problem.

DCV has been established as a powerful tool for the investigation of the mechanism and kinetics of organic and organometallic electrode reactions.[26] The parameter of interest for the discussion to follow is v_c, defined

(25) Since the ratios of isomers formed in the oxidation reactions were identical, we assume that what is valid in dichloromethane also is valid in acetonitrile. Hence, the experiments were not repeated in acetonitrile.

(26) For some recent examples of the use of DCV in organic and organometallic chemistry, see: (a) Parker, V. D.; Tilset, M. *J. Am. Chem. Soc.* **1986**, *108*, 6371. (b) Reitstøen, B.; Norrsell, F.; Parker, V. D. *J. Am. Chem. Soc.* **1989**, *111*, 8463. (c) Parker, V. D.; Reitstøen, B.; Tilset, M. *J. Phys.-Org. Chem.* **1989**, *2*, 580. (d) Reitstøen, B.; Parker, V. D. *J. Am. Chem. Soc.* **1990**, *112*, 4968. (e) Parker, V. D.; Chao, Y.; Reitstøen, B. *J. Am. Chem. Soc.* **1991**, *113*, 2336. (f) Reitstøen, B.; Parker, V. D. *J. Am. Chem. Soc.* **1991**, *113*, 6954. (g) Tilset, M. In *Energetics of Organometallic Species*; Simões, J. A. M., Ed.; Kluwer Academic: Dordrecht, The Netherlands, 1992; p 109.

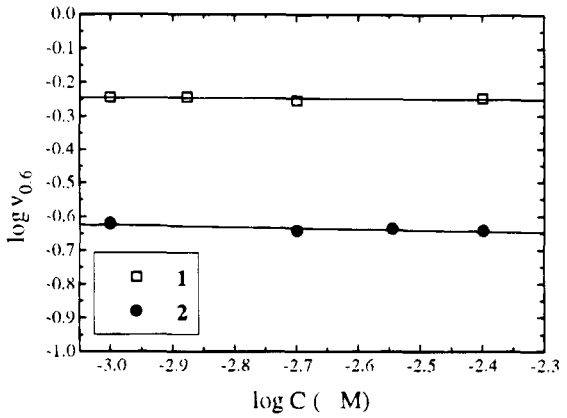

Figure 5. Reaction-order plot of log $v_{0.6}$ vs log C based on DCV analysis of the oxidation of **1** (□) and **2** (●) in acetonitrile (0.1 M Bu_4NPF_6) at a Pt-disk microelectrode (d = 0.6 mm) at 0 °C and the voltage sweep rate v = 1.0 V/s.

as the voltage sweep rate which for fixed experimental conditions causes the cathodic ($I_{p,c}$) to anodic ($I_{p,a}$) derivative peak current ratio (R'_I) to be equal to c. The value of the method is readily appreciated if one consider the case of $c = 0.5$. Here, the time lag between the detection of the oxidation peak and the reduction peak correlates with the half-life of the electrode-generated intermediate. For different experimental conditions, v may be fine-tuned to determine $v_{0.5}$. The parameter $v_{0.5}$ provides valuable kinetic information, since it is directly proportional to the rate constant for the chemical reaction consuming the primary CV product.[18] Provided that the separation between the scan reversal potential (E_{sw}) and the reversible electrode potential for the compound studied in a series of experiments is maintained at a constant value, DCV may be used in reaction-order analyses[28] to establish the rate law for the follow-up reaction.

DCV reaction-order analyses were carried out on the radical cation formed in the oxidation of bis(acetylide) **1** and the vinyl complex **2** in acetonitrile and dichloromethane. The substrate concentrations in each experimental series were varied in the range 1–4 mM. The reaction-order plot in Figure 5 depicts log $v_{0.6}$ vs log C for both substrates. The slopes of the correlation lines are close to zero (0.01 for **1** and 0.03 for **2**); thus, the reactions of $\mathbf{1}^{\bullet+}$ and $\mathbf{2}^{\bullet+}$ in acetonitrile are first order in [$\mathbf{1}^{\bullet+}$] and [$\mathbf{2}^{\bullet+}$], respectively. This is consistent with our determinations from crossover experiments. A reaction-order analysis of **1** in dichloromethane showed that the reaction was also first order in $\mathbf{1}^{\bullet+}$ in this solvent. As was already established, the oxidation of **2** in dichloromethane is close to reversible. It allowed the measurement of a single rate constant, assuming a first-order reaction of $\mathbf{2}^{\bullet+}$, but made measurements of reaction order and temperature effects in dichloromethane impractical because voltage sweep rates under some conditions were too slow for accurate measurements to be attainable.

The rate of reaction of $Cp^*Ru(CO)(PPh_3)CH_3^{\bullet+}$ has previously been demonstrated to be strongly solvent dependent.[27] The rate enhancement upon changing the

(27) Tilset, M.; Aase, T. In *Natural Gas Conversion*; Holmen, A., Jens, K.-J., Kolboe, S., Eds.; Elsevier: Amsterdam, 1991; p 197.
(28) ln $v_{0.6}/T$ is proportional to the rate constant.[18]

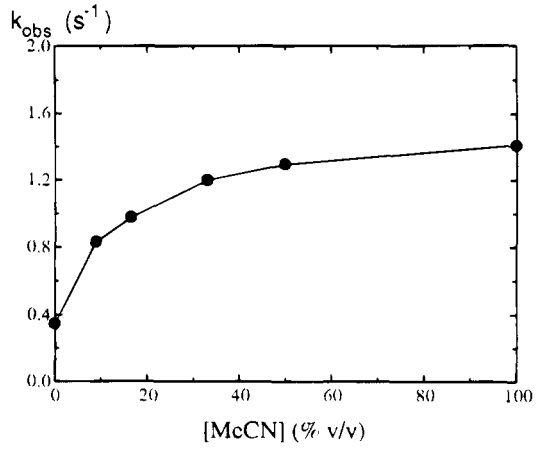

Figure 6. Observed rate constant vs the acetonitrile concentration (% v/v) for the chemical reaction of $\mathbf{2}^{\bullet+}$ in acetonitrile/dichloromethane (0.1 M Bu_4NPF_6) mixtures.

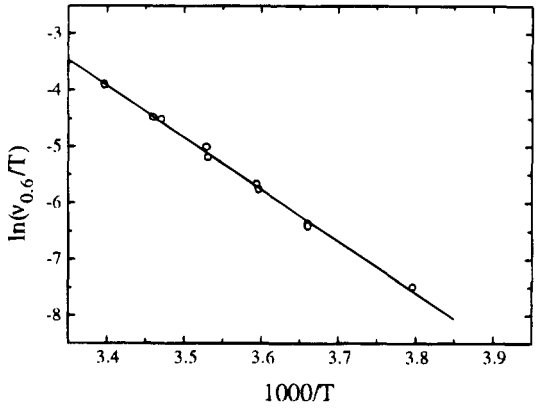

Figure 7. Arrhenius type plot[28] of ln($v_{0.6}/T$) vs 1000/T for the reaction of $\mathbf{1}^{\bullet+}$ (1.0 mM) in acetonitrile (0.1 M Bu_4NPF_6) at a Pt-disk microelectrode (d = 0.6 mm).

solvent from dichloromethane to acetonitrile was estimated to be at least a factor of 2000. The reaction-order analysis of **1** in acetonitrile and dichloromethane, however, showed that the $v_{0.6}$ values were almost identical in the two solvents. The occurrence of possible rate enhancement for the reaction of $\mathbf{2}^{\bullet+}$ in acetonitrile was also checked. The result is depicted in Figure 6. Addition of acetonitrile certainly has an effect, but it can by no means be compared to what is observed for the decomposition of $Cp^*Ru(CO)(PPh_3)CH_3^{\bullet+}$.

Organometallic compounds of weakly coordinating anions, e.g., BF_4^-, PF_6^-, and AsF_6^-, have been the object of many studies in recent years.[17] Hence, these counterions cannot always be considered to be "innocent". Close ion pairing has been reported to affect the kinetics of halide-induced disproportionation reactions of the 17-electron cations $M(CO)_3(PCy_3)_2^{\bullet+}$ (M = Fe, Ru, Os) in dichloromethane.[17e] The possible intervention of the counterion PF_6^- was investigated for complex **2**. The electrolyte concentration was varied between 0.05 and 0.3 M in dichloromethane. This gave no significant change in the reaction rate (i.e., $v_{0.6}$) of $\mathbf{2}^{\bullet+}$.

Variable-temperature measurements of $v_{0.6}$ for the processes in acetonitrile, yielded the Arrhenius type plots in Figures 7 (**1**) and 8 (**2**). The experiment was repeated for **1** in dichloromethane. This gave a curve almost identical with that for **1** in acetonitrile. Linear regression based on the data from three independent runs (for **1** and **2** in acetonitrile and for **1** in dichlo-

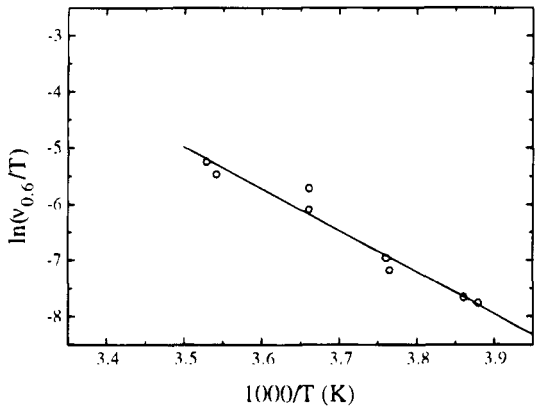

Figure 8. Arrhenius type plot of $\ln(v_{0.6}/T)$ vs $1000/T$ for the reaction of $\mathbf{2}^{\bullet+}$ (1.0 mM) in acetonitrile (0.1 M Bu_4NPF_6) at a Pt-disk microelectrode (d = 0.6 mm).

Table 3. Kinetic Data for 1 and 2

compd	E_a (kJ/mol)	$\Delta H^{\ddagger}$ (kJ/mol)	$\Delta S^{\ddagger}$ (J/(K mol))	k(0 °C) (s^{-1})
$\mathbf{1}^a$	78.5(3.3)	76.1(3.3)	8.1(11.7)	0.93
$\mathbf{1}^b$	76.4(1.3)	74.1(1.7)	5.9(5.4)	0.74
$\mathbf{2}^b$	62.1(4.5)	61.9(5.4)	−6.4(20.1)	0.89

[a] In dichloromethane (0.2 M $Bu_4N(PF_6)$). [b] In acetonitrile (0.1 M $Bu_4N(PF_6)$).

romethane) yielded activation energies for the subsequent chemical reactions. These data are given in Table 2.

The information at hand from DCV, coulometry, and observed products is in agreement with an ECE mechanism in which the chemical reaction is a first-order elimination of $[PhC_2]_2$ and $PhC_2CHCHPh$ from $\mathbf{1}^{\bullet+}$ and $\mathbf{2}^{\bullet+}$, respectively (path A in Scheme 5). The experimental $v_{0.6}$ values may be compared with theoretical data for this mechanism obtained by digital simulation for a first-order ECE mechanism with rate law (r) given as $r = -k[\mathbf{1}^{\bullet+}]$. The resulting rate constants and activation parameters are given in Table 3.

We have seen that samples of **1** and **2** in benzene-d_6 decompose very slowly at 74 °C to yield P^tBu_2Me as the only detectable product (5% after 24 h). By extrapolation to 74 °C, the rates of reaction of $\mathbf{1}^{\bullet+}$ and $\mathbf{2}^{\bullet+}$ are 326 and 63 s^{-1}, respectively. Thus, the rate enhancement due to the one-electron oxidations amounts to at least a factor of 3×10^8!

Discussion of Electrolyte Effects on the Kinetics of the Reductive-Elimination Reactions of 1 and 2. We have concluded that **1** and **2** most likely exist as the corresponding 18-electron acetonitrile adducts when dissolved in acetonitrile. Hence, when the experiments are done in the two solvents acetonitrile and dichloromethane, different species are investigated (**1**(NCMe) and **2**(NCMe) vs **1** and **2**). It was therefore rather surprising to discover that the oxidation potentials, the rate constants for the subsequent chemical reactions, and the kinetic parameters were little affected by the solvent. The similarities can of course be coincidental, but traces of water, weak coordination of dichloromethane, or coordination of the counterion BF_4^- could enhance the reactions in dichloromethane and at least in part conceal actual differences.

Variation of the electrolyte concentration in dichloromethane did not significantly influence the rate of reaction of $\mathbf{2}^{\bullet+}$. This might imply no assistance of BF_4^- in the reductive elimination. However, the concentration of BF_4^- is immense (even at the lowest $[BF_4^-]$ studied here) compared to the concentration of substrate. Thus, there can already be saturation of BF_4^- coordination even at an electrolyte concentration of 0.05 M. Close ion pairing between $\mathbf{1}^{\bullet+}$/$Ru(CO)(P^tBu_2Me)_2^{\bullet+}$ and BF_4^- can also occur. This would give reductive elimination from strongly ion-paired species in dichloromethane and thus prevent the formation of a formally 13−electron species, $Ru(CO)(P^tBu_2Me)_2^{\bullet+}$. The observed lack of dependence of the reaction rate on the concentration probably implies that the BF_4^- counterion does not actively assist the reductive-elimination reaction. Similar arguments pertain to the small solvent effect on the kinetic parameters.

Scheme 9

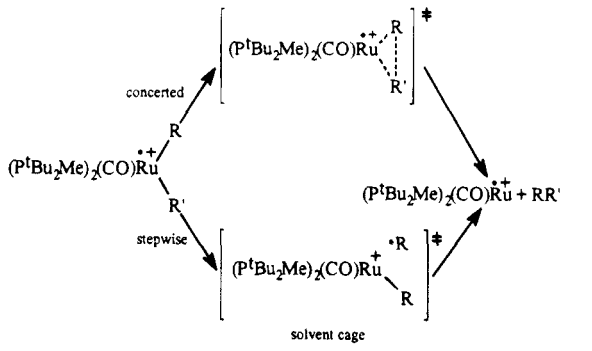

1: R = R' = C_2Ph
2: R = C_2Ph, R' = CHCHPh

Discussion of the Mechanism of Oxidatively Induced Reductive Elimination from 1 and 2. Thermal intramolecular reductive-elimination processes are usually believed to be concerted reactions. This is not necessarily a valid assumption when the reactions are oxidatively induced. A seemingly concerted reductive elimination can occur stepwise with homolytic cleavage of one bond followed by radical abstraction within the solvent cage. The groups of Fukuzumi[3a] and Ward[3b] have previously discussed similar situations. In their oxidations of *cis*-$(bpy)_2CoR_2$ (R = Ph, Et, Me, $PhCH_2$) and Cp_2MR_2 (M = Ti, Zr; R = Ph), respectively, they observed product distributions that could only be explained by the radical reaction pathway outlined above.

For a concerted reaction to occur, the ligands to be eliminated must be *cis* to each other. Homolytic cleavage, on the other hand, can give reductive-elimination reactions also with *trans* ligands. For a concerted elimination to occur from $\mathbf{1}^{\bullet+}$, an isomerization must preceed the elimination step. Thus, we cannot rule out a concerted reaction for reductive elimination of $[PhC_2]_2$ from the bis(acetylide).

PhC_2H, which is expected to be formed from **1** and **2** if radicals are formed by homolytic cleavage and escape from the solvent cage, was not observed. Still, the total absence of this product cannot be taken as evidence for a concerted reaction. As described above, efficient intracage reaction can preclude formation of phenylacetylene. Assuming that $\mathbf{1}^+$ is isomerized, the steps depicted in Scheme 9 describe the two possibilities.

A similar situation has previously been discussed for the oxidatively induced reductive elimination from $Cp^*Rh(PPh_3)Me_2$.[16] In acetonitrile it was shown to yield ethane with no trace of methane. The negative activa-

Scheme 10

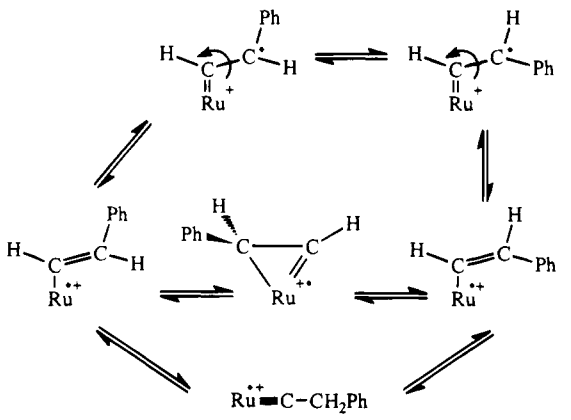

tion entropy of the reaction (−25.9 J/(K mol)) was taken as evidence for a concerted reaction with an ordered transition state. The activation entropies for **1** and **2**, however, are not as informative. They were found to be 8.1 ± 11.7 and 5.9 ± 5.4 J/(K mol) for **1** in dichloromethane and acetonitrile, respectively, and −6.4 ± 20.1 J/(K mol) for **2** in acetonitrile. Not only are the activation entropies close to zero but the standard deviations are also rather large. Small activation entropies may result from partial cancellation of positive and negative contributions. In our experiments it is evident that solvation both of the cation radical and of the first-formed elimination product, together with the entropy of the transition state, will play a role. Thus, the exact mechanism of the coupling of the organic ligands in **1** and **2** may at the current level of understanding be well described as either a concerted or a stepwise, in-cage reaction.

The discussion above, and in particular the absence of PhC_2H, demonstrates that there is no hard evidence for products resulting from radicals released from solvent cages. Thus, the 2−3% $[PhC_2]_2$ detected in the product mixtures from the oxidation of **2** (acetonitrile and dichloromethane solvents) is probably not formed by attack of a "stray radical" on another molecule of **2**. Therefore, we propose that this product is formed in a competing, inefficient bimolecular mechanism, perhaps involving a bridging acetylide ligand.

Discussion of the Mechanism of Formation of (*E*)- and (*Z*)-$PhC_2CHCHPh$. The discussion to follow is based on two established facts: (a) the enyne is not isomerized after generation and (b) the starting material **2** retains its *trans* stereochemistry around the vinylic double bond.

The oxidation of **2** yields a 9/1 ratio of (*E*)- and (*Z*)-$PhC_2CHCHPh$ in acetonitrile and dichloromethane. If a concerted reductive elimination were to take place, only (*E*)-$PhC_2CHCHPh$ would be produced. However, the 9/1 (*E*/*Z*) product mixture can occur from a concerted reaction with a minor (10%) competing homolytic cleavage reaction, yielding some (*Z*)-enyne. Homolytic cleavage itself can also give the observed ratio of stereoisomers if the radical reacts so quickly that only a small part of the radicals lose their stereochemistry.

Electrochemical methods have demonstrated that the cation radical has a half-life of several seconds. This is apparently sufficient for rearrangement via the processes shown in Scheme 10. Note especially than an η^2-vinyl structure can lead to loss of stereochemistry about the C=C bond while simultaneously increasing the valence-electron count at the metal; this represents a new and unusual type of 17-/19-electron interconversion.

Experimental Section

General Procedures. All manipulations involving organometallic compounds were carried out with use of vacuum line, Schlenk, syringe, or drybox techniques. Hexane was dried and deoxygenated over sodium benzophenone, acetonitrile was distilled from P_2O_5, and acetonitrile-d_3 and dichloromethane-d_2 were distilled from CaH_2, whereas benzene-d_6 was distilled from Na and nitromethane-d_3 from $CaCl_2$. All solvents, PhC_2H, and (*p*-tolyl)C_2H were subjected to three freeze−pump−thaw cycles at the vacuum line prior to use. Acetonitrile and dichloromethane containing the supporting electrolyte were passed through a column of active neutral alumina prior to use to remove water and protic impurities before electrochemical measurements. The electrolyte was freed of air by purging with purified argon, and all measurements and electrolyses were carried out under a blanket of solvent-saturated argon.

Electrochemical measurements were performed with an EG&G-PAR Model 273 potentiostat/galvanostat driven by an external HP 3314 sweep generator. The output signals were fed to a Nicolet 310 digital oscilloscope and processed by an on-line personal computer. The working electrode was a Pt-disk electrode (d = 0.6 mm), the counter electrode was a Pt wire, and the Ag-wire reference electrode assembly[29] was filled with acetonitrile/0.01 M $AgNO_3$/0.1 M $Bu_4N(PF_6)$. The reference electrode was calibrated against Cp_2Fe, which is used as the reference in this work. The positive-feedback *iR* compensation circuitry of the potentiostat was employed; the separation between the anodic and cathodic peaks for the Cp_2Fe oxidation was 59−61 mV in acetonitrile.

Hydrocarbons were separated and quantified on a Varian 3400 GC using a 25 m DB5 column.

^1H (referenced via residual solvent protons) and ^{13}C (referenced to the solvent resonance) NMR and ^{19}F (referenced to $CFCl_3$) NMR spectra were recorded on a Varian XL-300 instrument. The symbol vt in ^1H NMR spectra denotes virtual triplets arising from coupling to magnetically nonequivalent P nuclei. $^{31}P\{^1H\}$ (referenced to 85% H_3PO_4) NMR was recorded on a a Varian XL-300 instrument or a Nicolet NT-360 spectrometer operating at 121 or 146 MHz, respectively. $^1H\{^{31}P\}$ NMR spectra were obtained on a Nicolet NT-360 spectrometer. Infrared spectra were recorded in benzene-d_6, acetonitrile-d_3, or dichloromethane-d_2 (NaCl cavity cell, 0.1 mm path length) on a Nicolet 510P FT-IR spectrometer with a precision of 0.3 cm^{-1}.

The compounds $[Cp_2Fe]PF_6$,[30a] $[(\eta^5\text{-}C_5H_4COMe)CpFe]BF_4$ ($AcFc(BF_4)$),[30b] $Ru(C_2Ph)_2(CO)(P^tBu_2Me)_2$[11] (**1**), and (*E*)-$PhC_2CHCHPh$[24] were prepared according to published procedures. All other compounds were used as received from commercial suppliers.

$Ru(CHCHPh)(C_2Ph)(CO)(P^tBu_2Me)_2$ (2). This is a modification of a previously published procedure.[11] $Ru(H)(Cl)(CO)(P^tBu_2Me)_2$ (400 mg, 0.82 mmol) was added to hexane (20 mL) and PhC_2H (90 μL, 0.82 mmol) and stirred for 15−20 min. PhC_2Li (178 mg, 1.64 mmol) was added. The resulting mixture was stirred for 6 h, filtered, and concentrated to approximately 4 mL. The filtrate was stored at −20 °C for 24 h, during which time the product crystallized as a dark red solid (365 mg, 68% yield). ^1H NMR (300 MHz, benzene-d_6): δ 1.13 (vt, J = 5.9 Hz, 18 H), 1.21 (vt, J = 5.9, 18 H), 1.52 (s, 6 H), 6.26 (d, J = 13 Hz, 1 H), 6.9−7.7 (m, 10 H), 8.62 (d, J = 13 Hz, 1 H). ^{31}P-

(29) Moe, N. S. *Anal. Chem.* **1974**, *46*, 968.
(30) (a) Lyatifov, I. R.; Solodovnikov, S. P.; Babin, V. N.; Materikova, R. B. *Z. Naturforsch., B* **1979**, *34B*, 863. (b) Carthy, P.; Dove, M. F. A. *J. Organomet. Chem.* **1971**, *28*, 125.

{^{1}H} NMR (146 MHz, benzene-d_6): δ 40.9 (s). IR (benzene-d_6): ν_{CO} 1910 cm^{-1}, ν_{CC} 2074 cm^{-1}.

X-ray Structure Determination of Ru(C$_2$Ph)$_2$(CO)(P^{t}Bu$_2$Me)$_2$ (1). Because of the slow onset of a phase transition at −167 °C, we undertook a study at −90 °C, where a systematic search of a limited hemisphere of reciprocal space yielded a set of reflections which exhibited monoclinic (2/*m*) diffraction symmetry. The only observed extinction was that of 0*k*0 for $k = 2n + 1$, leading to the choice of the possible space group $P2_1$ or $P2_1/m$. The choice of the noncentrosymmetric space group $P2_1$ was based on the fact that the structure could be solved using $P2_1$ but not $P2_1/m$. Unit cell dimensions were determined by a least-squares fit of the setting angles for 62 carefully centered reflections having 2 values between 20 and 34°. Following the usual data reduction and averaging of equivalent data, a unique set of 2322 reflections was obtained. The *R* values for the averaging was 0.113 for 2293 reflections observed more than once. Plots of the 4 standard reflections (−3,0,0, −3,3,3, 0,−6,0, 0,0,4) measured every 300 reflections showed no significant trends. No correction for absorption was performed. The structure was solved using SHELXS-86. While the Ru and P atoms as well as the CO group and the two C$_2$Ph groups were readily located, the substituents on the phosphorus caused considerable difficulty. A relatively good model could be obtained but would not be refined in a satisfactory manner. The final least-squares refinement was carried out using anisotropic thermal parameters on the Ru and P atoms and isotropic parameters on the remaining atoms. For the refinement, only 1193 reflections considered observed by the criterion $F > 3.0\sigma(F)$ were used. For the disordered carbon atoms in the phosphine ligands, occupancies were refined initially and then fixed. The isotropic thermal parameters for all of the atoms are quite high, an indication that the data might have been collected close to the transition temperature or that the structure is very disordered. The largest peaks in the final difference map were 0.78 e/Å^3 and revealed that smaller residuals were located in the area of the disordered carbon atoms. Because of some relatively large esd's (e.g., Ru−C20 = 2.05(8) Å) and an unreasonable angle (Ru−C20−O21 = 143(5)°), we furnish full structural details only in the supplementary material. A view of the molecule and some selected metric parameters are shown in Figure 1 and Table 1.

Coordination of Acetonitrile to Ru(C$_2$Ph)$_2$(CO)(P^{t}Bu$_2$Me)$_2$ (1). Ru(C$_2$Ph)$_2$(CO)(P^{t}Bu$_2$Me)$_2$ (**1**; 20.0 mg, 0.03 mmol) dissolved in benzene-d_6 was added to an NMR tube. The ^{31}P NMR spectrum of the compound showed a single resonance at δ 47.7. Acetonitrile (1.5 μL, 1 equiv) was added to the solution, whereupon the color immediately changed from dark red to bright yellow. The ^{31}P{^{1}H} NMR spectrum showed only one signal (at δ 45.3). Addition of excess acetonitrile (3 × 15 μL) gave no change in either the shift of the peak or the color of the solution. The IR absorptions changed from ν_{CO} 1933 cm^{-1} and ν_{CC} 2074 cm^{-1} in neat benzene-d_6 to ν_{CO} 1934 cm^{-1} and ν_{CC} 2082 cm^{-1} in the benzene-d_6/acetonitrile solvent mixture.

Ru(C$_2$Ph)$_2$(CO)(P^{t}Bu$_2$Me)$_2$ (20.0 mg, 0.031 mmol) was dissolved in acetonitrile (2 mL). This gave a yellow solution, from which a pale yellow solid precipitated immediately. The solid was collected. A sample was analyzed by ^{31}P{^{1}H} NMR spectroscopy in benzene-d_6. It showed the same resonance as above, δ 45.3. The rest of the solid was dried in vacuo overnight. This yielded a red solid which was shown to be Ru(C$_2$Ph)$_2$(CO)(P^{t}Bu$_2$Me)$_2$ (^{31}P{^{1}H} NMR, benzene-d_6).

The solid that precipitated from acetonitrile solutions of Ru(C$_2$Ph)$_2$(CO)(P^{t}Bu$_2$Me)$_2$ was dried 2−3 min in vacuo and analyzed by ^{1}H NMR spectroscopy in benzene-d_6. A signal was present at δ 0.62 (in addition to the usual resonances for **1**). Upon addition of 10 μL of acetonitrile-d_3, this peak moved to δ 0.69.

Coordination of Acetonitrile to Ru(CHCHPh)(C$_2$Ph)(CO)(P^{t}Bu$_2$Me)$_2$ (2). An NMR tube was prepared containing Ru(CHCHPh)(C$_2$Ph)(CO)(P^{t}Bu$_2$Me)$_2$ (**2**; 20.0 mg, 0.03 mmol) dissolved in benzene-d_6. A ^{31}P{^{1}H} NMR spectrum showed the phosphine resonance at δ 42.4. Addition of acetonitrile (1.5 μL, 1 equiv) gave no apparent color change and no change in the position of the phosphine resonance. Addition of excess acetonitrile (15 μL) resulted in the appearance of a weak resonance at δ 45.0. More acetonitrile (2 × 15 μL) was added upon which the small resonance gained somewhat in intensity (ca. 5% of the intensity of the main resonance) and the dark red color faded perceptibly. After addition of 47 μL of acetonitrile, the solution was red-orange. The IR (benzene-d_6) absorptions (ν_{CO} 1910 cm^{-1} and ν_{CC} 2074 cm^{-1}) did not change when acetonitrile was added, but a small shoulder (ca. 5%) appeared at higher frequency on the CO peak.

Ru(CHCHPh)(C$_2$Ph)(CO)(P^{t}Bu$_2$Me)$_2$ (20.0 mg, 0.03 mmol) was dissolved in acetonitrile (2 mL). This gave a red-orange solution, from which a red solid precipitated immediately. The solid was dried in vacuo overnight. This yielded a red solid, which was shown to be Ru(CHCHPh)(C$_2$Ph)(CO)(P^{t}Bu$_2$Me)$_2$ by ^{31}P{^{1}H} NMR spectroscopy in benzene-d_6.

The solid that precipitated from acetonitrile solutions of Ru(CHCHPh)(C$_2$Ph)(CO)(P^{t}Bu$_2$Me)$_2$ was dried for only 2−3 min in vacuo and analyzed by ^{1}H NMR spectroscopy in benzene-d_6. A signal was present at δ 0.59 (in addition to the usual resonances for **2**). Upon addition of 10 μL of acetonitrile-d_3, the peak moved to δ 0.71.

Thermal Reactions of 1 and 2. Ru(C$_2$Ph)$_2$(CO)(P^{t}Bu$_2$Me)$_2$ (10.0 mg, 0.02 mmol) was dissolved in benzene-d_6 and added to an NMR tube equipped with a ground-glass joint. The NMR tube was flame-sealed under vacuum, and a ^{1}H NMR spectrum was acquired. A similar sample of Ru(CHCHPh)(C$_2$Ph)(CO)(P^{t}Bu$_2$Me)$_2$ (10.0 mg, 0.02 mmol) in benzene-d_6 was prepared. The samples were heated at 50 °C for 24 h. No change occurred in the NMR spectra of the samples. Further heating of the samples at 74 °C for 24 h generated traces (ca. 5%) of free P^{t}Bu$_2$Me (^{1}H NMR (300 MHz, benzene-d_6) δ 1.04 (d, J = 10.5 Hz), 0.82 (d, J = 4.3)). Further heating (for 48 h) only yielded more of the phosphine. ^{31}P NMR spectroscopy confirmed that P^{t}Bu$_2$Me was the only detectable product from the reactions (^{31}P{^{1}H} NMR (146 MHz, benzene-d_6) δ 11.8 ppm).

General Procedure: Oxidation of 1 in Acetonitrile. In a typical experiment Ru(C$_2$Ph)$_2$(CO)(P^{t}Bu$_2$Me)$_2$ (**1**; 20.0 mg, 0.03 mmol) was dissolved in acetonitrile (25 mL) and slowly added to a solution of AcFc(BF$_4$) (19.3 mg, 0.06 mmol) in acetonitrile (5 mL). The solvent was stripped off from the yellow solution, and the residue was dissolved in acetonitrile-d_3 and analyzed by ^{1}H and ^{31}P{^{1}H} NMR and IR spectroscopy. ^{1}H NMR (300 MHz, acetonitrile-d_3): δ 1.40 (vt, J = 7 Hz, 36 H), 1.53 (vt, J = 3 Hz, 6 H), 6.9−7.2 (m), 7.3−7.7 (m). ^{31}P{^{1}H} NMR (146 MHz, acetonitrile-d_3): δ 40.5 (s), 42.4 (s), 60.1 (s). IR (acetonitrile-d_3): ν_{CO} 2010 cm^{-1}.

The solution from the NMR tube was added to ether (20 mL) and filtered. The solid was dried under vacuum, dissolved in acetonitrile-d_3, and analyzed by ^{1}H and ^{31}P{^{1}H} NMR spectroscopy. The solvent was stripped off from the filtrate, and the residue was dried and dissolved in acetonitrile-d_3. Analysis by NMR spectroscopy gave the following. Residue: ^{1}H NMR (300 MHz, acetonitrile-d_3) δ 1.40 (vt, J = 7 Hz, 36 H), 1.53 (vt, J = 3 Hz, 6 H); ^{31}P{^{1}H} NMR (146 MHz, acetonitrile-d_3) δ 40.5 (s), 42.4 (s); IR (acetonitrile-d_3) ν_{CO} 2010 cm^{-1}. Filtrate: ^{1}H NMR (300 MHz, acetonitrile-d_3) δ 7.3−7.7 (m, 10 H); ^{13}C{^{1}H} NMR (75 MHz, acetonitrile-d_3) 74.1, 82.4, 122.1, 129.7, 130.7, 133.4; MS *m/e* 202.

Oxidation of 2 in Acetonitrile. The oxidation was done as in the general procedure described above. Spectroscopic data before workup are as follows. ^{1}H NMR (300 MHz, acetonitrile-d_3): δ 1.40 (vt, J = 7 Hz, 36 H), 1.53 (vt, J = 3 Hz, 6 H), 6.0 (d, J = 12.1 Hz, 1 H), 6.57 (d, J = 16.5 Hz, 1 H), 6.83 (d, J = 12.1 Hz, 1 H), 7.36 (d, J = 16.5, 1 H), 7.2−8.0 (m, 10 H). ^{31}P{^{1}H} NMR (146 MHz, acetonitrile-d_3): δ 42.4 (s). IR (acetonitrile-d_3): ν_{CO} 2010 cm^{-1}. Spectroscopic data after workup are as follows. Residue: ^{1}H NMR (300 MHz, aceto-

nitrile-d_3) δ 1.40 (vt, J = 7 Hz, 36 H), 1.53 (vt, J = 3 Hz, 6 H); $^{31}P\{^1H\}$ NMR (146 MHz, acetonitrile-d_3) δ 42.4 (s); IR (acetonitrile-d_3) ν_{CO} 2010 cm^{-1}. Filtrate: ^1H NMR (300 MHz, acetonitrile-d_3) δ 6.00 (d, J = 12.1 Hz, 1 H), 6.57 (d, J = 16.5 Hz, 1 H) 6.83 (d, J = 12.1 Hz, 1 H), 7.36 (d, J = 16.5, 1 H), 7.2–8.0 (m, 15 H); MS m/e 204.

General Procedure: Oxidation of 1 in Dichloromethane. In a typical experiment, $Ru(C_2Ph)_2(CO)(P^tBu_2Me)_2$ (1; 20.0 mg, 0.03 mmol) was dissolved in dichloromethane (5 mL) and slowly added to a solution of $AcFc(BF_4)$ (19.3 mg, 0.06 mmol) in dichloromethane (2 mL). The solvent was stripped off from the purple solution; the residue was dissolved in dichloromethane-d_2 and the solution analyzed by ^1H and $^{31}P\{^1H\}$ NMR spectroscopy. ^1H NMR (300 MHz, dichloromethane-d_2): δ 1.30 (d, J = 16.8 Hz, 36 H), 1.45 (dd, J = 13.4 and 5.5 Hz, 6 H), 7.3–7.6 (m, 10 H). $^{31}P\{^1H\}$ NMR (146 MHz, dichloromethane-d_2): δ 39.9 (s), 41.9 (s), 72.8 (s), 73.9 (s), 76.8 (s). IR (dichloromethane-d_2): ν_{CO} 1951 cm^{-1}.

The solution from the NMR tube was added to ether (20 mL), and the resulting solid was filtered. The solid was dried under vacuum, dissolved in dichloromethane-d_2, and analyzed by ^1H and $^{31}P\{^1H\}$ NMR spectroscopy. The solvent was stripped off from the filtrate, and the residue was dried and dissolved in dichloromethane-d_2. Residue: ^1H NMR (300 MHz, dichloromethane-d_2) δ 1.49 (d, J = 16.8 Hz, 36 H), 1.85 (dd, J = 13.4 and 5.5 Hz, 6 H); $^1H\{^{31}P\}$ NMR (300 MHz, dichloromethane-d_2) δ 1.30 (s, 36 H), 1.45 (br s, 6 H); $^{31}P\{^1H\}$ NMR (146 MHz, dichloromethane-d_2) δ 39.9 (s); ^{19}F NMR (55 MHz, dichloromethane-d_2) δ −150.7 (br s); IR (dichloromethane-d_2) ν_{CO} 1951 cm^{-1}. Filtrate: ^1H NMR (300 MHz, dichloromethane-d_2) δ 7.34–7.45 (m), 7.53–7.60 (m); ^{13}C (75 MHz, dichloromethane-d_2) δ 73.9, 81.8, 122.0, 128.9, 129.7, 132.8; MS m/e 202.

Oxidation of 2 in Dichloromethane. The oxidation was done as in the general procedure described above. Spectroscopic data before workup are as follows. ^1H NMR (300 MHz, dichloromethane-d_2) δ 1.30 (d, J = 16.8 Hz, 36 H), 1.45 (dd, J = 13.4 and 5.5 Hz, 6 H), 5.92 (d, J = 12.1 Hz, 1 H), 6.39 (d, J = 16.5 Hz, 1 H), 6.71 (d, J = 12.1 Hz, 1 H), 7.15 (d, J = 16.5, 1 H) 7.2–8.0; $^{31}P\{^1H\}$ NMR (146 MHz, dichloromethane-d_2) δ 39.9 (s); IR (dichloromethane-d_2): ν_{CO} 1951 cm^{-1}. Spectroscopic data after workup are as follows. Residue: ^1H NMR (300 MHz, dichloromethane-d_2) δ 1.30 (d, J = 16.8 Hz, 36 H), 1.45 (dd, J = 13.4 Hz, 6 H); $^{31}P\{^1H\}$ NMR (146 MHz, dichloromethane-d_2) δ 39.9 (s); IR (dichloromethane-d_2): ν_{CO} 1951 cm^{-1}. Filtrate: ^1H NMR (300 MHz, dichloromethane-d_2) δ 5.92 (d, J = 12.1 Hz, 1 H), 6.39 (d, J = 16.5 Hz, 1 H), 6.71 (d, J = 12.1 Hz, 1 H), 7.15 (d, J = 16.5, 1 H), 7.2–8.0; MS m/e 204.

The residue from the oxidation of $Ru(CHCHPh)(C_2Ph)(CO)(P^tBu_2Me)_2$ in dichloromethane was dissolved in acetonitrile-d_3. The resulting mixture contained mostly the dicationic acetonitrile adduct $[Ru(CO)(NCMe)_3(P^tBu_2Me)_2](BF_4)_2$ (ca. 80% by inspection of the $^{31}P\{^1H\}$ NMR spectrum).

$Ru[C_2(p\text{-tolyl})]_2(CO)(P^tBu_2Me)_2$. $Ru(H)(Cl)(CO)(P^tBu_2Me)_2$ (300.0 mg, 0.62 mmol) was added to hexane (35 mL) and (p-tolyl)C_2H (0.3 mL, 4 equiv) and (p-tolyl)C_2Li (96.0 mg, 0.79 mmol). The resulting mixture was refluxed for 12 h, filtered, and concentrated to approximately 5 mL. This solution was filtered to remove an insoluble byproduct. The filtrate was stored at −20 °C for 24 h, and the product crystallized as a dark red solid (207 mg, 49%). ^1H NMR (300 MHz, benzene-d_6): δ 1.32 (vt, 36 H), 1.79 (vt, 6H), 2.13 (s, 6 H), 7.10 (d, 4H), 7.56 (d, 4 H); $^{31}P\{^1H\}$ NMR (360 MHz, benzene-d_6) δ 47.9 (s); IR (benzene-d_6) ν_{CO} 1931 cm^{-1}, ν_{CC} 2077 cm^{-1}.

Oxidation of $Ru[C_2(p\text{-tolyl})]_2(CO)(P^tBu_2Me)_2$ in Acetonitrile and Dichloromethane. The oxidation of $Ru[C_2(p\text{-tolyl})]_2(CO)(P^tBu_2Me)_2$ in acetonitrile and dichloromethane was done as described in the general procedures for the oxidations of 1 and 2. In acetonitrile the dicationic acetonitrile adduct $[Ru(CO)(NCMe)_3(P^tBu_2Me)_2](BF_4)_2$ (^1H and $^{31}P\{^1H\}$ NMR and IR spectroscopy) was formed together with an ether-soluble product. Oxidation in dichloromethane gave a mixture of organometallic products that closely resembled the product mixtures obtained when $Ru(C_2Ph)_2(CO)(P^tBu_2Me)_2$ and $Ru(CHCHPh)(C_2Ph)(CO)(P^tBu_2Me)_2$ were oxidized in dichloromethane (by ^1H and ^{31}P NMR and IR spectroscopy). Extraction with ether as in the general procedure yielded an extract with the following spectroscopic data: ^1H NMR (300 MHz, benzene-d_6) δ 1.90 (s, 6 H), 6.5–7.4 (m, 10 H); MS m/e 230.

$[Ru(CO)(NCMe)_3(P^tBu_2Me)_2](BF_4)_2$ (3). $Ru(C_2Ph)_2(CO)(P^tBu_2Me)_2$ (20.0 mg, 0.03 mmol) was dissolved in acetonitrile (25 mL) and slowly added to a stirred solution of $AcFc(BF_4)$ (19.3 mg, 0.06 mmol) in acetonitrile (5 mL). This gave a yellow solution. The solution was concentrated to 2–3 mL and added to ether (20 mL). Filtration of the solution yielded a gray solid which was dissolved in acetonitrile and recrystallized by diffusion of ether vapor into the acetonitrile solution. ^1H NMR (300 MHz, acetonitrile-d_3): δ 1.40 (vt, J = 7 Hz, 36 H), 1.53 (vt, J = 3 Hz, 6 H), 2.49 (s, 6 H), 2.58 (s, 3 H); this spectrum was taken within 7 min of warming a freshly prepared frozen (−196 °C) sample to 25 °C, to minimize exchange of MeCN *trans* to CO with bulk CD_3CN. ^1H NMR (300 MHz, nitromethane-d_3): δ 1.49 (vt, J = 7 Hz, 36 H), 1.65 (vt, J = 3 Hz, 6 H), 2.64 (s, 6 H), 2.71 (t, J = 1.1 Hz, 3 H). $^{31}P\{1H\}$ NMR (121 MHz, acetonitrile-d_3): δ 42.4 (s). $^{13}C\{^1H\}$ NMR (75 MHz, acetonitrile-d_3): δ 5.8, 30.0 (d), 37.7 (t), 131.0, 134.5, 201.4 (t). IR (acetonitrile-d_3): ν_{CO} 2010 cm^{-1}.

Investigation of the Molecularity of the Reductive Elimination from 1. A solution of $Ru(C_2Ph)_2(CO)(P^tBu_2Me)_2$ (20.0 mg, 0.03 mmol) and $Ru[C_2(p\text{-tolyl})]_2(CO)(P^tBu_2Me)_2$ (20.7 mg, 0.03 mmol) in acetonitrile (50 mL) was slowly added to an acetonitrile solution (5 mL) of $AcFc^+(BF_4^-)$ (38.6 mg, 0.12 mmol). The reaction mixture was concentrated to 1–2 mL, added to ether (30 mL), and filtered through Celite.

A dark brown oil was obtained from the filtrate. The oil contained only $[PhC_2]_2$ and $[(p\text{-tolyl})C_2]_2$ by ^1H NMR spectroscopy. Mass spectrometry showed parent ions at m/e 202 ($[PhC_2]_2$) and 230 ($[(p\text{-tolyl})C_2]_2$). The crossover product, (p-tolyl)C_2–C_2Ph, was not obtained in either solvent.

The experiment was repeated with dichloromethane as the solvent. This gave, as for the reaction in acetonitrile, only formation of $[PhC_2]_2$ and $[(p\text{-tolyl})C_2]_2$.

Identification of the Products from the Oxidation of 2. A solution of $Ru(CHCHPh)(C_2Ph)(CO)(P^tBu_2Me)_2$ (2) was oxidized with $AcFc(BF_4)$ as described in the general procedure for oxidation reactions. The reaction mixture was concentrated to 1–2 mL, added to ether (30 mL), and filtered through Celite.

Dark brown oils were obtained from the filtrates of reactions in both acetonitrile and dichloromethane. The oils were dissolved in 0.5 mL of benzene and analyzed by capillary GLC. Authentic samples of $[PhC_2]_2$ and $PhC_2CHCHPh$ were used to determine the retention times. Oxidation of $Ru(CHCHPh)(C_2Ph)(CO)(P^tBu_2Me)_2$ in acetonitrile showed formation of 97% $PhC_2CHCHPh$ and 3% $[PhC_2]_2$. Oxidation of $Ru(CHCHPh)(C_2Ph)(CO)(P^tBu_2Me)_2$ in dichloromethane showed formation of 97.5% of $PhC_2CHCHPh$ and 2.5% of $[PhC_2]_2$. There was no evidence for formation of PhC_2H.

NMR Quantification of the Yield of the Organometallic Product from the Oxidation of 1. A solution of $Ru(C_2Ph)_2(CO)(P^tBu_2Me)_2$ (1; 30.0 mg, 0.05 mmol) and hexamethylbenzene (HMB; 7.4 mg, 0.05 mmol) was dissolved in dichloromethane (3 mL). The solution was distributed equally into three different flasks. The solution from one flask was slowly added to a solution of $AcFc(BF_4)$ (9 mg, 0.03 mmol) in dichloromethane. The solvent was stripped off from the second flask at −20 °C; the residue was dissolved in acetonitrile (15 mL) and this solution slowly added to a solution of $AcFc(BF_4)$ (0.09 mg, 0.03 mmol) in acetonitrile (3 mL). The solvents from each flask were now stripped off at −20 °C. The residues were analyzed by ^1H NMR spectroscopy.

The yields of product from the reactions in acetonitrile and dichloromethane were established by comparison with the

internal standard (HMB). In acetonitrile, the yield of $[Ru(CO)(P^tBu_2Me)_2(NCMe)_3](BF_4)_2$ was found to be 72%. In dichloromethane, the yield of main product was 52%.

Quantification of the Yield of the Organic and the Organometallic Product from the Oxidation of 2. (a) By NMR. The experiment was done as described above. In acetonitrile the yield of $[Ru(CO)(NCMe)_3(P^tBu_2Me)_2](BF_4)_2$ was 75% and the yield of $PhC_2CHCHPh$ was 70%. In dichloromethane the yield of the main organometallic product was 42%, whereas 46% $PhC_2CHCHPh$ was formed.

(b) By GC. $Ru(CHCHPh)(C_2Ph)(CO)(P^tBu_2Me)_2$ (**2**; 20.0 mg, 0.03 mmol) was oxidized with $AcFc(BF_4)$ (19.3 mg, 0.06 mmol) in acetonitrile and in dichloromethane as described in the general procedures. After workup of the reaction mixtures, the solvents of the filtrates were evaporated in vacuo. The residues were dissolved in benzene (0.5 mL) and analyzed by capillary GLC. Solutions of $PhC_2CHCHPh$ (7.4 mg, 0.04 mmol; 5.8 mg, 0.03 mmol; 3.7 mg, 0.02 mmol; 1.9 mg, 0.01 mmol) in benzene (0.5 mL) were also analyzed by GLC. This allowed determination of the yield of $PhC_2CHCHPh$ from the oxidation reactions. The amount of $PhC_2CHCHPh$ formed in the oxidation in acetonitrile and dichloromethane was 59% and 40%, respectively. From the quantification of the yield of $PhC_2CHCHPh$ in the oxidation of **2** by means of ^1H NMR spectroscopy, it is possible to estimate the loss during workup of the reaction mixtures to be ca. 10%.

GC Quantification of the Yield of the Organic Product from the Oxidation of 1. $Ru(C_2Ph)_2(CO)(P^tBu_2Me)_2$ (**1**; 20.0 mg, 0.03 mmol) was oxidized with $AcFc(BF_4)$ (19.3 mg, 0.06 mmol) in acetonitrile and in dichloromethane as described in the general procedures. After workup of the reaction mixtures, the solvents of the filtrates were evaporated in vacuo. The residues were dissolved in benzene (0.5 mL) and analyzed by capillary GLC. Solutions of $[PhC_2]_2$ (6.7 mg, 0.03 mmol; 4.6 mg, 0.02 mmol; 3.1 mg, 0.015 mmol; 1.5 mg, 0.007 mmol) in benzene (0.5 mL) were also analyzed by GLC. This allowed determination of the yield of $[PhC_2]_2$ from the oxidation reactions. The amounts of $[PhC_2]_2$ formed in the oxidations in acetonitrile and dichloromethane were 62% and 39%, respectively. From the quantification of the yield of $PhC_2CHCHPh$ in the oxidation of **2** by means of both ^1H NMR and GLC, it is possible to estimate the loss during workup of the reaction mixtures to be ca. 10%.

Attempted *E/Z* Isomerization of the −CHCHPh Ligand in 2 by $AcFc(BF_4)$. $Ru(CHCHPh)(C_2Ph)(CO)(P^tBu_2Me)_2$ (20.0 mg, 0.03 mmol) was oxidized by $AcFc(BF_4)$ (3.8 mg, 0.022 mmol, 0.4 equiv). Two reactions were performed, one in acetonitrile and one in dichloromethane. The oxidations and the workup were done as described before. In acetonitrile only resonances for $[Ru(CO)(NCMe)_3(P^tBu_2Me)_2](BF_4)_2$, (*E*)-$PhC_2CHCHPh$, and unconsumed $Ru(CHCHPh)(C_2Ph)(CO)(P^tBu_2Me)_2$ were present in the ^1H NMR spectrum, in addition to the peaks for AcFc. No vinyl resonances of unknown origin were detected, nor did a $^{31}P\{^1H\}$ NMR spectrum show any new resonances.

The same result was obtained when dichloromethane was used as solvent.

Attempted *E/Z* Isomerization of (*E*)-$PhC_2CHCHPh$ by $AcFc(BF_4)$. (*E*)-$PhC_2CHCHPh$ (10.0 mg, 0.005 mmol) and $AcFc(BF_4)$ (4.2 mg, 0.013 mmol) were dissolved in dichloromethane-d_2 and added to a NMR tube equipped with a ground-glass joint. The tube was sealed and a ^1H NMR spectrum was recorded. No isomerization of (*E*)-$PhC_2CHCHPh$ to (*Z*)-$PhC_2CHCHPh$ occurred (^1H NMR spectroscopy) over 36 h.

Attempted Isomerization of (*E*)-$PhC_2CHCHPh$ by Oxidation Products. (*E*)-$PhC_2CHCHPh$ (10.0 mg, 0.005 mmol) and the products from an oxidation of $Ru(C_2Ph)_2(CO)(P^tBu_2Me)_2$ (**1**) in dichloromethane were dissolved in dichloromethane-d_2, and this solution was added to a NMR tube equipped with a ground-glass joint. The tube was sealed, and a ^1H NMR spectrum was recorded. No isomerization of (*E*)-$PhC_2CHCHPh$ to (*Z*)-$PhC_2CHCHPh$ occurred (^1H NMR spectroscopy) over 36 h.

Constant-Current Coulometry. The constant-current electrolyses were performed in an H-shaped cell, the compartments of which were separated by a medium-frit glass junction. A platinum-gauze working electrode was used. Solutions of **1** and **2** (1−2 mM) in 20 mL of acetonitrile with 0.05 M $Me_4N(BF_4)$ as the supporting electrolyte were electrolyzed with a constant current of 10 mA, while the consumption of substrate was monitored by DCV. Three separate measurements indicated the consumption of 2.0 ± 0.1 faradays/mol of charge for both **1** and **2**. In dichloromethane/0.2 M $Bu_4N(PF_6)$, 1.3 and 1.5 faradays/mol were consumed for **1** and **2**, respectively.

The solution obtained by electrolysis of **1** in acetonitrile was concentrated. A sample of the resulting mixture was analyzed by $^{31}P\{^1H\}$ NMR spectroscopy. This showed formation of $[Ru(CO)(NCMe)_3(P^tBu_2Me)_2](BF_4)_2$ as the major product (ca 90% of total signal intensity). The same was found for the constant-current electrolysis of **2** in acetonitrile.

Acknowledgment. We gratefully acknowledge support from Statoil under the VISTA program, from the Norwegian Research Council (NFR) (stipend to A.P.), from Alf Bjerckes legat (stipend to A.P.), from the U.S. National Science Foundation, and from NATO (Grant No. CRG 910473).

Supplementary Material Available: Tables of crystallographic data, fractional coordinates, thermal parameters, and bond distances and angles (6 pages). Ordering information is given on any current masthead page.

OM940693Q

Electrophile-Induced Cyclizations of Chiral Rhenium Ethynyl and C_2Li Complexes of the Formula (η^5-C_5Me_5)Re(NO)(PPh_3)(C≡CX): Synthesis, Structure, and Reactivity of Unusual 1,3-Dimetalated Cyclic C_4H_3 and C_4H_4 Species

Weiqing Weng, Tamàs Bartik, Mitchell T. Johnson, Atta M. Arif, and J. A. Gladysz*

Department of Chemistry, University of Utah, Salt Lake City, Utah 84112

Received September 19, 1994®

Reactions of (η^5-C_5Me_5)Re(NO)(PPh_3)(C≡CH) (**1**) or (η^5-C_5Me_5)Re(NO)(PPh_3)(C≡CLi) (**2**) and $ZnCl_2$ (≥1.2 equiv) give the *meso* dirhenium complex (*SR,RS*)-[(η^5-C_5Me_5)Re(NO)(PPh_3)-(⌐C⌐CH⌐C(CH$_2$)⌐)(Ph_3P)(ON)Re(η^5-C_5Me_5)]$^+$([Zn_2Cl_6]$^{2-}$)$_{1/2}$ (**4**). Samples contain up to 10% of the corresponding *dl* diastereomer (total yield 94–38%). Mechanisms involving adventitious water and initial electrophilic attack upon C_β of **1** are proposed. Accordingly, addition of 0.5 equiv of HBF_4·OEt_2 to **1** (CH_2Cl_2, 25 °C) gives the analogous dirhenium tetrafluoroborate salt **5** (85%). However, addition of **1** to 2.0 equiv of HBF_4·OEt_2 (THF, −80 °C) gives the vinylidene complex [(η^5-C_5Me_5)Re(NO)(PPh_3)(=C=CH$_2$)]$^+$$BF_4^-$ (**6**; 86%). Reaction of **1** and **6** (CH_2Cl_2, 25 °C) also gives **5** (94%). The crystal structure of **4** shows rhenium–carbon bonds of 2.00(1)–2.03(1) Å, intermediate between single and double bonds and consistent with a delocalized structure based upon Re–C=CHC(CH$_2$)=Re$^+$ resonance forms. NMR data establish 12.1–12.6 kcal/mol Re⌐C rotational barriers. Reaction of **5** and HBF_4·OEt_2 gives the cyclobuta-1,3-diylidene complex (*SR,RS*)-[(η^5-C_5Me_5)Re(NO)(PPh_3)(=CCH$_2$C(CH$_2$)=)-(Ph_3P)(ON)Re(η^5-C_5Me_5)]$^{2+}$(BF_4^-)$_2$ (**8**) in quantitative NMR yields. Upon all workups attempted, **8** reverts to **5**.

Transition-metal alkynyl complexes, $L_nMC{\equiv}CR$, undergo a variety of interesting ligand-based coupling reactions.[1] Such processes are receiving increasing attention as routes to compounds of the formula $L_nMC_xML_n$, in which chains of elemental carbon span two metal fragments.[2–4] Several approaches, including our own efforts with the chiral rhenium end groups [(η^5-C_5H_5)Re(NO)(PPh_3)]$^+$ (**I**) and [(η^5-C_5Me_5)Re(NO)(PPh_3)]$^+$ (**I**-Me_5), have involved ethynyl and butadiynyl complexes.

We recently reported that the ethynyl complex (η^5-C_5Me_5)Re(NO)(PPh_3)(C≡CH) (**1**) and *n*-BuLi react to give the C_2Li complex (η^5-C_5Me_5)Re(NO)(PPh_3)(C≡CLi) (**2**).[5] Complex **2** is readily derivatized by electrophiles of formal composition E^+X^- to give species with ReC≡CE linkages.[5,6] Also, **1** can be oxidatively coupled with Cu(OAc)$_2$ to the C_4 complex (η^5-C_5Me_5)Re(NO)(PPh_3)-(C≡CC≡C)(Ph_3P)(ON)Re(η^5-C_5Me_5) (**3**) in high yield.[2] Prior to developing the latter reaction, we sought to effect the oxidative coupling of **2** to **3**.

As related below, this effort indeed led to a dirhenium complex. However, the structure turned out to be an unanticipated cycloadduct that incorporated adventitious protons from the reaction medium. A novel, cyclobutane-derived bis(alkylidene) complex could also be accessed from this serendipitous product. It rapidly became apparent that both compounds exhibited a number of unusual properties. Hence, an independent study was initiated, which is described in the following narrative.

Results

1. Synthesis and Structure of Dirhenium Complex 4. The ethynyl complex **1** and *n*-BuLi were reacted in THF at −80 °C to give the C_2Li complex **2**, as reported previously (Scheme 1).[5] Then $ZnCl_2$ (1.2 equiv) was added. This mild, deliquescent oxidant, which had been stored under ambient laboratory conditions, efficiently couples other carbanions.[7] Workup gave an orange, crystalline, air-stable compound (**4**) in 38% yield, based upon the structure established below.

® Abstract published in *Advance ACS Abstracts*, January 1, 1995.

(1) Representative examples: (a) Takahashi, S.; Murata, S.; Sonogashira, K.; Hagihara, N. *J. Polym. Sci.* **1980**, *18*, 661. (b) Iyer, R. S.; Selegue, J. P. *J. Am. Chem. Soc.* **1987**, *109*, 910. (c) Beddoes, R. L.; Bitcon, C.; Ricalton, A.; Whiteley, M. W. *J. Organomet. Chem.* **1989**, *367*, C21. (d) Matsuzaka, H.; Hirayama, Y.; Nishio, M.; Mizobe, Y.; Hidai, M. *Organometallics* **1993**, *12*, 36. (e) Conelly, N. G.; Gamasa, M. P.; Gimeno, J.; Lapinte, C.; Lastra, E.; Maher, J. P.; Le Narvor, N.; Rieger, A. L.; Rieger, P. H. *J. Chem. Soc., Dalton Trans.* **1993**, 2575. (f) Shih, K.-Y.; Schrock, R. R.; Kempe, R. *J. Am. Chem. Soc.* **1994**, *116*, 8804.

(2) (a) Zhou, Y.; Seyler, J. W.; Weng, W.; Arif, A. M.; Gladysz, J. A. *J. Am. Chem. Soc.* **1993**, *115*, 8509. (b) Brady, M.; Weng, W.; Gladysz, J. A. *J. Chem. Soc., Chem. Commun.* **1994**, *23*, 2655.

(3) Le Narvor, N.; Lapinte, C. *J. Chem. Soc., Chem. Commun.* **1993**, 357.

(4) (a) Lang, H. *Angew. Chem., Int. Ed. Engl.* **1994**, *33*, 547. (b) Beck, W.; Niemer, B.; Wieser, M. *Angew. Chem., Int. Ed. Engl.* **1993**, *32*, 923.

(5) Ramsden, J. A.; Weng, W.; Gladysz, J. A. *Organometallics* **1992**, *11*, 3635.

(6) (a) Ramsden, J. A.; Weng, W.; Arif, A. M.; Gladysz, J. A. *J. Am. Chem. Soc.* **1992**, *114*, 5890. (b) Weng, W.; Ramsden, J. A.; Arif, A. M.; Gladysz, J. A. *J. Am. Chem. Soc.* **1993**, *115*, 3824.

0276-7333/95/2314-0889$09.00/0

Scheme 1. Syntheses of the *meso* Dirhenium Complex (*SR,RS*)-[(η^5-C_5Me_5)Re(NO)(PPh_3)(⌐C⌐CH⌐C(CH_2)⌐)(Ph_3P)(ON)Re(η^5-C_5Me_5)]$^+$([Zn_2Cl_6]$^{2-}$)$_{1/2}$ (4)

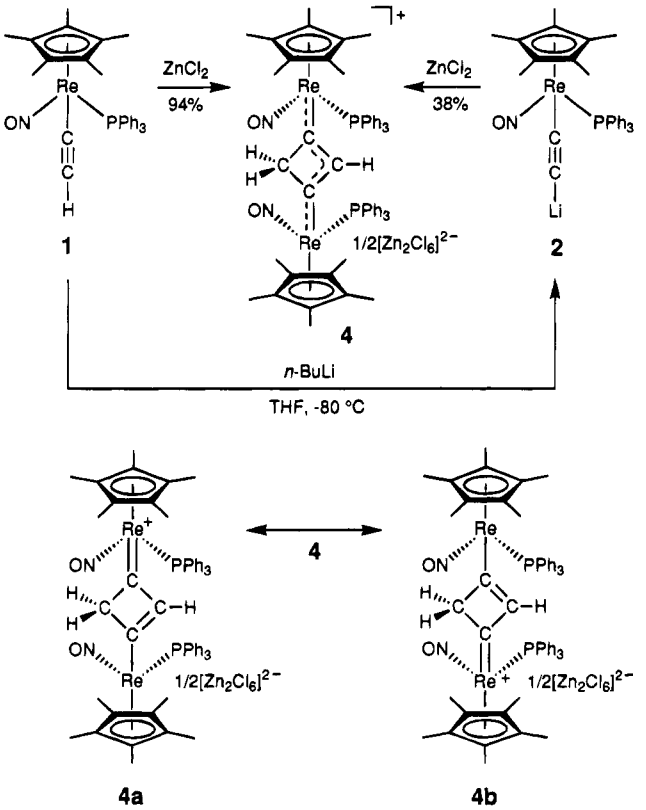

Complex **4** was characterized by microanalysis and NMR (^1H, ^{13}C, ^{31}P) and IR spectroscopy, as summarized in the Experimental Section. A number of features were inconsistent with the target ReC≡CC≡CRe complex **3**. For example, the ^1H NMR spectrum showed three one-proton resonances at δ 7.08, 3.03, and 2.53. The last two were coupled ($J_{HH'}$ = 14.7 Hz). The ^{13}C NMR spectrum showed a ReC resonance (227.5 ppm, d, $^2J_{CP}$ = 9.5 Hz) downfield from those of alkynyl (98–86 ppm, d, $^2J_{CP}$ = 16–18 Hz)[5] or alkenyl (147 ppm, d, $^2J_{CP}$ = 12 Hz)[8] complexes of **I**-Me_5 and upfield of cationic alkylidene and vinylidene complexes of **I**-Me_5 (288–330 ppm, d, $^2J_{CP}$ = 10–11 Hz).[5,9] The IR ν_{NO} value (1655/1642 cm^{-1}, CH_2Cl_2/thin film) was slightly higher than that of **1** (1637/1629 cm^{-1}, CH_2Cl_2/KBr) but lower than those of cationic alkylidene, vinylidene, or π-alkyne complexes of **I**-Me_5, including two described below (1728–1681 cm^{-1}).[5]

At low temperatures, ^{31}P and ^1H NMR spectra showed two PPh_3 and C_5Me_5 resonances of equal intensities (CD_2Cl_2, −90 °C: 22.7/22.9 ppm, $\Delta\nu$ = 226.6 Hz; δ 1.35/1.30, $\Delta\nu$ = 15.0 Hz), consistent with a dirhenium complex. These coalesced at −9.1 and −26.2 °C, respectively, as shown in Figure 1. Application of the coalescence formula[10] gave $\Delta G^{\ddagger}(T_c)$ values of 12.1 and 12.6 kcal/mol for the dynamic process (interpreted below) that renders these groups equivalent.

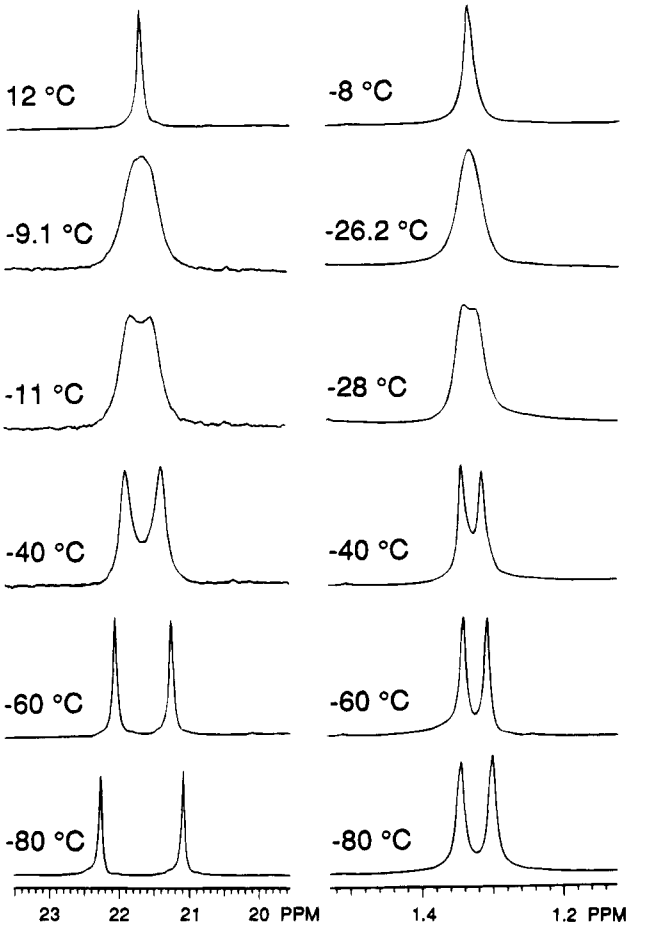

Figure 1. Variable-temperature NMR spectra of **4** in CD_2Cl_2: (left) PPh_3 ^{31}P resonances; (right) C_5Me_5 ^1H resonances.

A mass spectrum showed a parent ion at *m/z* 1279 (^{187}Re), consistent with two (η^5-C_5Me_5)Re(NO)(PPh_3) fragments bound to a C_4H_3 moiety. However, due in part to an artifact in the first mass spectrum acquired, we were unable to assign a structure on the basis of the preceding information. Thus, the crystal structure of a dichloromethane hemisolvate of **4** was determined as outlined in Table 1 and the Experimental Section. Refinement yielded the structures in Figure 2. Atomic coordinates and selected bond lengths, bond angles, and torsion angles are summarized in Tables 2 and 3.

The above data show that **4** is (*SR,RS*)-[(η^5-C_5Me_5)-Re(NO)(PPh_3)(⌐C⌐CH⌐C(CH_2)⌐)(Ph_3P)(ON)Re(η^5-C_5-Me_5)]$^+$([Zn_2Cl_6]$^{2-}$)$_{1/2}$, a salt comprised of a dirhenium monocation and a dizinc dianion.[11] The ReC moieties can be viewed as hybrids of cationic alkylidene and neutral alkenyl resonance forms, as illustrated by **4a** and **4b** in Scheme 1. This gives a formal half-positive charge on each rhenium and accounts for the intermediate ReC ^{13}C NMR chemical shift and IR ν_{NO} value noted above.

Complex **4** is also a *meso* diastereomer but crystallizes in a conformation without mirror (or other) symmetry.

(7) (a) Yasuda, H.; Ohnuma, Y.; Yamauchi, M.; Tani, H.; Nakamura, A. *Bull. Chem. Soc. Jpn.* **1979**, *52*, 2036. (b) Yasuda, H.; Nakamura, A. *J. Organomet. Chem.* **1985**, *285*, 15.

(8) Peng, T.-S.; Gladysz, J. A. *Organometallics* **1995**, *14*, 898.

(9) Patton, A. T.; Strouse, C. E.; Knobler, C. B.; Gladysz, J. A. *J. Am. Chem. Soc.* **1983**, *105*, 5804.

(10) Sandström, J. *Dynamic NMR Spectroscopy*; Academic Press: New York, 1982; Chapters 6 and 7. The $\Delta G^{\ddagger}(T_c)$ calculations utilized equation 7.4c.

(11) *R/S* nomenclature conventions have been given in previous papers.[12,13]

Table 1. Summary of Crystallographic Data for

(*SR,RS*)-[(η^5-C_5Me_5)Re(NO)(PPh_3)(⌐C⌐CH⌐C(CH_2)⌐)-(Ph_3P)(ON)Re(η^5-C_5Me_5)]$^+$([Zn_2Cl_6]$^{2-}$)$_{1/2}$·0.5CH_2Cl_2 (4·0.5CH_2Cl_2)

mol formula	$C_{60.5}H_{64}Cl_4N_2O_2P_2Re_2Zn$
mol wt	1492.727
cryst syst	triclinic
space group	$P\bar{1}$
cell dimens	
a, Å	14.867(2)
b, Å	15.439(3)
c, Å	17.474(2)
α, deg	101.80(2)
β, deg	114.24(2)
γ, deg	111.99(2)
V, Å^3	3071.25
Z	2
temp of collectn, °C	21(1)
d_{calc}, g/cm^3	1.614
d_{found}, g/cm^3 ($CHCl_3/CH_2I_2$)	1.631
crystal dimens, mm	0.25 × 0.25 × 0.19
diffractometer	CAD4
radiation (λ, Å)	Mo K_α (0.709 30)
data collection method	$\theta-2\theta$
scan speed, deg/min	variable
no. of rflns meas	11 224
range/indices (*hkl*)	0−15, −16 to +16, −16 to +16
2θ limit, deg	4.0−50.0
scan width	0.80 + 0.34 tan θ
std rflns check	1 X-ray h
total no. of unique data	10 318
no. of obs data, $I > 3\sigma(I)$	7361
abs coeff, cm^{-1}	46.51
min transmissn, %	67.72
max transmissn, %	99.93
no. of variables	671
goodness of fit	0.580
$R = \sum\|\|F_o\| - \|F_c\|\|/\sum\|F_o\|$	0.0360
$R_w = \sum\|\|F_o\| - \|F_c\|\|w^{1/2}/\sum\|F_o\|w^{1/2}$	0.0420
Δ/σ (max)	0.009
$\Delta\varrho$ (max), e/Å^3	1.458 (about 0.93 Å from Cl4 atom)

Thus, each rhenium fragment is crystallographically distinct and gives slightly different metrical parameters (Table 3). Five different least-squares planes were defined that contained four to five atoms of the ReC_4Re core. The angles between these planes ranged from 0 to 6°, indicating an essentially planar moiety as emphasized in the bottom right view in Figure 2. The rhenium−rhenium distance was 6.1025(6) Å.

2. Rational Syntheses of Dirhenium Complexes. With the structure of **4** established, we next considered more direct syntheses. We thought that adventitious water, which in retrospect was undoubtedly present in the sample of $ZnCl_2$ employed, might first protonate the C_2Li complex **2** to ethynyl complex **1**. Alkynyl complexes often react with electrophiles at C_β to give cationic vinylidene complexes.[12] Similarly, cationic vinylidene complexes often react with nucleophiles at C_α to give alkenyl complexes.[12] Hence, $ZnCl_2$—or another electrophile derived from the $ZnCl_2/H_2O$ mixture—could conceivably effect the cyclization of **1** to **4** by initial generation of a vinylidene complex, as sketched in Scheme 2.

Thus, **1** and $ZnCl_2$ (1.5 equiv) were combined in THF (Scheme 1). As anticipated, workup gave **4**, now in much higher yield (94%). We then wondered whether Brønsted acids might serve in place of $ZnCl_2$. Thus, a dichloromethane solution of **1** was treated with

(12) Senn, D. R.; Wong, A.; Patton, A. T.; Marsi, M.; Strouse, C. E.; Gladysz, J. A. *J. Am. Chem. Soc.* **1988**, *110*, 6096.

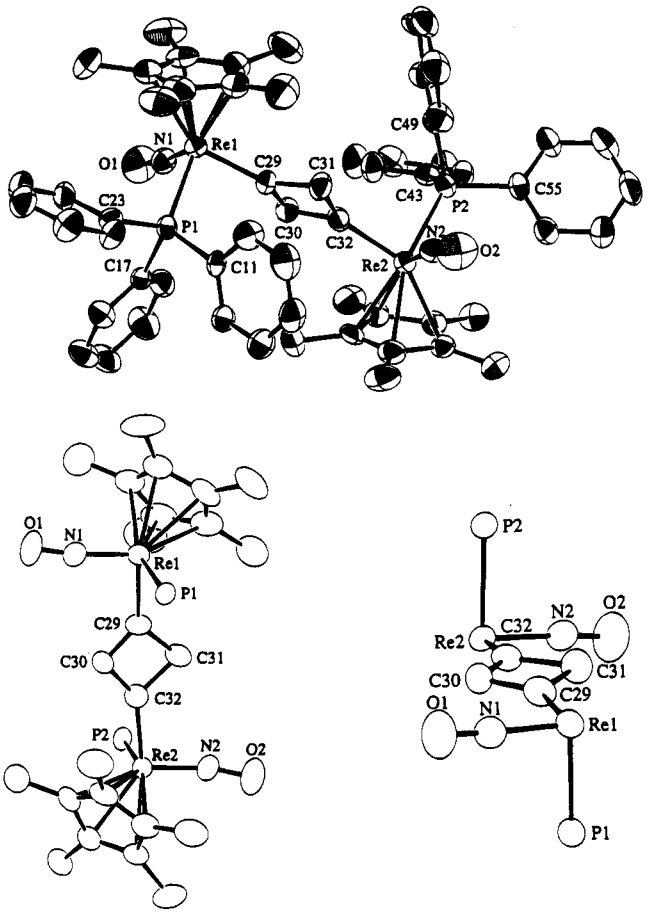

Figure 2. Structure of the cation of (*SR,RS*)-[(η^5-C_5Me_5)Re(NO)(PPh_3)(⌐C⌐CH⌐C(CH_2)⌐)(Ph_3P)(ON)Re(η^5-C_5Me_5)]$^+$([Zn_2Cl_6]$^{2-}$)$_{1/2}$·0.5CH_2Cl_2 (4·0.5CH_2Cl_2): (top) numbering diagram; (bottom) partial views.

0.5 equiv of HBF_4·OEt_2 at room temperature (Scheme 3). Workup gave the corresponding tetrafluoroborate salt (*SR,RS*)-[(η^5-C_5Me_5)Re(NO)(PPh_3)(⌐C⌐CH⌐C(CH_2)⌐)(Ph_3P)(ON)Re(η^5-C_5Me_5)]$^+BF_4^-$ (**5**) in 85% yield. A metathesis reaction of **4** and $NaBF_4$ also gave **5** (86%). NMR analyses of the preceding samples of **4** and **5** sometimes showed as much as 10% of a second species, further data on which are given below.

We sought additional information on the mechanism of formation of **5**, which by analogy to Scheme 2 should involve the vinylidene complex [(η^5-C_5Me_5)Re(NO)(PPh_3)(=C=CH_2)]$^+BF_4^-$ (**6**). First, in an inverse addition experiment, a −80 °C THF solution of ethynyl complex **1** was added to a −80 °C THF solution of excess HBF_4·OEt_2 (Scheme 3). Workup gave **6** in 86% yield, which was characterized analogously to **4** and **5** (Experimental Section). Most properties paralleled those of the previously reported cyclopentadienyl analog.[12] The UV/visible spectrum showed only absorptions common to all compounds in this series, presumably derived from the PPh_3 ligand (266, 308 nm). In contrast, the UV/visible spectrum of **5** gave an intense visible band (480 nm), which was undiminished after the sample was kept under room lighting for 5 days. Both spectra are shown in Figure 3.

Finally, the ethynyl complex **1** and vinylidene complex **6** were combined in CD_2Cl_2 at room temperature. After

Table 2. Atomic Coordinates and Equivalent Isotropic Thermal Parameters for Non-Hydrogen Atoms of 4·0.5CH_2Cl_2[a]

atom	x	y	z	B, Å^2	atom	x	y	z	B, Å^2
Re1	0.11507(2)	0.80847(2)	0.55290(2)	2.659(8)	C31	0.2790(7)	0.9550(6)	0.7770(5)	3.6(2)
Re2	0.37489(2)	1.18021(2)	0.92192(2)	2.343(7)	C32	0.2749(6)	1.0552(6)	0.8014(5)	3.0(2)
P1	0.2745(2)	0.8974(2)	0.5382(1)	2.58(5)	C33	0.4015(6)	1.3457(6)	0.9694(5)	3.2(2)
P2	0.2363(2)	1.1046(2)	0.9603(1)	2.50(5)	C34	0.3384(7)	1.2956(6)	0.8687(5)	3.3(2)
O1	−0.0356(6)	0.8680(5)	0.4348(5)	6.0(2)	C35	0.4139(7)	1.2814(6)	0.8456(5)	3.4(2)
O2	0.5364(6)	1.1285(6)	1.0372(6)	6.7(3)	C36	0.5178(6)	1.3142(6)	0.9273(5)	3.7(2)
N1	0.0315(5)	0.8509(5)	0.4852(4)	3.4(2)	C37	0.5113(6)	1.3566(6)	1.0046(5)	3.1(2)
N2	0.4625(5)	1.1392(5)	0.9855(4)	3.3(2)	C38	0.3613(7)	1.3922(6)	1.0231(6)	3.9(2)
C1	0.1299(8)	0.6921(7)	0.6193(6)	4.7(3)	C39	0.2284(8)	1.2863(7)	0.8043(7)	5.0(3)
C2	0.0303(8)	0.6964(7)	0.6016(6)	4.9(3)	C40	0.3926(9)	1.2465(8)	0.7496(6)	5.3(3)
C3	−0.0439(7)	0.6574(7)	0.5042(6)	4.4(3)	C41	0.6226(7)	1.3150(8)	0.9334(7)	5.2(3)
C4	0.0087(7)	0.6296(6)	0.4611(6)	4.1(3)	C42	0.6092(8)	1.4102(8)	1.1050(6)	4.9(3)
C5	0.1172(7)	0.6514(6)	0.5311(6)	4.4(3)	C43	0.1127(6)	1.1189(6)	0.9051(5)	2.7(2)
C6	0.223(1)	0.7118(8)	0.7109(8)	6.6(4)	C44	0.0475(7)	1.0766(7)	0.8087(5)	3.8(2)
C7	−0.0013(9)	0.7204(9)	0.6713(7)	7.0(4)	C45	−0.0439(7)	1.0887(8)	0.7633(6)	4.7(3)
C8	−0.1649(9)	0.6390(9)	0.4536(9)	6.6(4)	C46	−0.0750(7)	1.1418(7)	0.8120(6)	4.7(3)
C9	−0.047(1)	0.5746(9)	0.3578(8)	7.2(4)	C47	−0.0131(7)	1.1819(7)	0.9062(6)	4.2(2)
C10	0.1960(9)	0.6206(7)	0.5169(8)	6.1(3)	C48	0.0814(7)	1.1717(6)	0.9536(5)	3.4(2)
C11	0.4190(6)	0.9657(6)	0.6420(4)	2.6(2)	C49	0.1727(6)	0.9669(6)	0.9316(5)	3.1(2)
C12	0.5024(7)	1.0651(7)	0.6674(5)	3.6(2)	C50	0.2446(7)	0.9269(6)	0.9561(6)	4.0(2)
C13	0.6111(8)	1.1119(8)	0.7467(6)	4.9(3)	C51	0.2021(8)	0.8251(7)	0.9431(6)	5.2(3)
C14	0.6368(7)	1.0621(8)	0.8016(6)	4.7(3)	C52	0.0871(9)	0.7625(7)	0.9046(6)	5.2(3)
C15	0.5552(8)	0.9647(8)	0.7764(6)	5.2(3)	C53	0.0134(8)	0.7987(8)	0.8795(6)	5.5(3)
C16	0.4469(8)	0.9164(7)	0.6988(6)	4.5(3)	C54	0.0571(7)	0.9022(7)	0.8942(6)	4.3(3)
C17	0.2712(6)	0.9956(6)	0.4953(5)	2.8(2)	C55	0.2900(6)	1.1561(6)	1.0845(5)	2.8(2)
C18	0.2245(7)	1.0521(6)	0.5171(5)	3.9(2)	C56	0.2222(6)	1.1113(7)	1.1173(5)	3.9(2)
C19	0.2276(8)	1.1287(7)	0.4880(6)	5.1(3)	C57	0.2645(8)	1.1526(8)	1.2113(6)	4.8(3)
C20	0.2767(8)	1.1501(7)	0.4370(6)	4.9(3)	C58	0.3729(8)	1.2356(8)	1.2713(6)	5.0(3)
C21	0.3219(7)	1.0929(7)	0.4138(6)	4.2(3)	C59	0.4434(9)	1.2785(8)	1.2406(6)	5.1(3)
C22	0.3201(6)	1.0172(6)	0.4429(5)	3.5(2)	C60	0.4011(7)	1.2383(6)	1.1467(5)	3.7(2)
C23	0.2833(6)	0.8142(6)	0.4542(5)	2.8(2)	C61	0.635(2)	0.525(2)	0.659(1)	5.9(6)[b]
C24	0.1871(7)	0.7560(7)	0.3641(5)	3.5(2)	Zn	0.08915(7)	0.46551(8)	−0.00300(6)	3.45(3)
C25	0.1881(8)	0.6901(8)	0.2977(6)	4.6(3)	Cl1	0.1074(2)	0.6276(2)	0.0551(1)	3.69(6)
C26	0.2814(8)	0.6803(8)	0.3196(6)	4.9(3)	Cl2	0.1932(2)	0.4420(2)	0.1146(2)	5.10(7)
C27	0.3779(7)	0.7378(7)	0.4088(7)	4.7(3)	Cl3	0.1119(2)	0.4444(2)	−0.1207(2)	5.54(8)
C28	0.3786(6)	0.8056(6)	0.4761(6)	3.7(2)	Cl4	0.5009(7)	0.4423(6)	0.6317(5)	9.0(3)
C29	0.1953(6)	0.9298(6)	0.6759(5)	3.1(2)	Cl5	0.6640(8)	0.542(1)	0.5929(7)	13.7(4)
C30	0.1929(6)	1.0196(6)	0.7058(5)	2.9(2)					

[a] Anisotropically refined atoms are given in the form of the isotropic equivalent displacement parameter defined as $^4/_3[a^2B(1,1) + b^2B(2,2) + c^2B(3,3) + ab(\cos\gamma)B(1,2) + ac(\cos\beta)B(1,3) + bc(\cos\alpha)B(2,3)]$. [b] This atom was refined isotropically.

1 h, ^{31}P and ^{1}H NMR spectra showed only traces of unreacted **6** and very high conversions to **5**. Careful inspection revealed apparent pairs of PPh_3 ^{31}P resonances (21.3/20.3 ppm) and ⌐CH⌐ and C_5Me_5 ^{1}H resonances (δ 7.08/6.90, 1.71/1.55), with area ratios of ca. 90:10. Workup of an analogous preparative reaction gave a 94% yield of a material that was a ca. 92:8 mixture of **5** and the same second substance. Similar resonances were detected in samples of **4**, generated from **1** and $ZnCl_2$, that had not been crystallized (^{31}P 21.2/20.3 ppm; ^{1}H δ 1.71/1.55). We suggest that the minor resonances likely arise from the *dl* (*SS,RR*)[11] diastereomers of **4** and **5**, although additional, potentially diagnostic signals could not be conclusively located.

3. Reactions of 4 and 5. We thought that it might be possible to elaborate **4** or **5** into other unusual C_4H_x derivatives. For example, cationic alkylidene complexes of **I** are deprotonated at C_β by bases as weak as dichloroacetate to give neutral alkenyl complexes.[13] Analogous reactions of **4** or **5** would give the 1,3-dimetallocyclobutadiene complex (*SR,RS*)-(η^5-C_5Me_5)Re(NO)(PPh_3)(−C=CHC(=CH)−)(Ph_3P)(ON)Re(η^5-C_5Me_5) (**7**), illustrated in Scheme 4. Cyclobutadienes that are substituted with two donor and two acceptor sub-

(13) Bodner, G. S.; Smith, D. E.; Hatton, W. G.; Heah, P. C.; Georgiou, S.; Rheingold, A. L.; Geib, S. J.; Hutchinson, J. P.; Gladysz, J. A. *J. Am. Chem. Soc.* **1987**, *109*, 7688.

Table 3. Selected Bond Lengths (Å), Bond Angles (deg), and Torsion Angles (deg) for 4·0.5CH_2Cl_2

Re1−P1	2.403(3)	Re2−P2	2.390(3)
Re1−N1	1.76(1)	Re2−N2	1.75(1)
Re1−C1	2.36(1)	Re2−C32	2.00(1)
Re1−C2	2.27(1)	Re2−C33	2.34(1)
Re1−C3	2.27(1)	Re2−C34	2.31(1)
Re1−C4	2.35(1)	Re2−C35	2.32(1)
Re1−C5	2.39(1)	Re2−C36	2.29(1)
Re1−C29	2.03(1)	Re2−C37	2.34(1)
C29−C30	1.40(2)	C30−C32	1.42(2)
C29−C31	1.54(2)	C31−C32	1.55(2)
P1−C11	1.83(1)	P2−C43	1.81(1)
P1−C17	1.83(1)	P2−C49	1.83(1)
P1−C23	1.83(1)	P2−C55	1.84(1)
N1−O1	1.19(1)	N2−O2	1.20(1)
P1−Re1−N1	94.1(3)	P2−Re2−N2	92.6(3)
P1−Re1−C29	88.8(4)	P2−Re2−C32	88.1(3)
N1−Re1−C29	96.1(5)	N2−Re2−C32	98.1(4)
Re1−C29−C30	136.2(9)	Re2−C32−C30	141.7(9)
Re1−C29−C31	133.5(9)	Re2−C32−C31	128.7(9)
C30−C29−C31	90.2(9)	C29−C31−C32	85.2(9)
C29−C30−C32	96(1)	C30−C32−C31	88.8(9)
Re1−P1−C11	117.7(4)	Re2−P2−C43	112.8(4)
Re1−P1−C17	114.9(4)	Re2−P2−C49	118.0(4)
Re1−P1−C23	114.0(4)	Re2−P2−C55	115.2(4)
Re1−N1−O1	172(1)	Re2−N2−O2	169(1)
Re1−C29−C30−C32	3.2(8)	C29−C30−C32−Re2	166.2(10)
Re1−C29−C31−C32	−179.1(9)	C29−C31−C32−Re2	−168.7(8)
P1−Re1−C29−C30	94.1(10)	P2−Re2−C32−C30	101.3(12)
P1−Re1−C29−C31	−91.5(10)	P2−Re2−C32−C31	−92.3(9)
N1−Re1−C29−C30	0.1(11)	N2−Re2−C32−C30	−166.4(12)
N1−Re1−C29−C31	174.5(10)	N2−Re2−C32−C31	0.0(12)

Scheme 2. Possible Mechanisms for the Conversion of 1 to 4

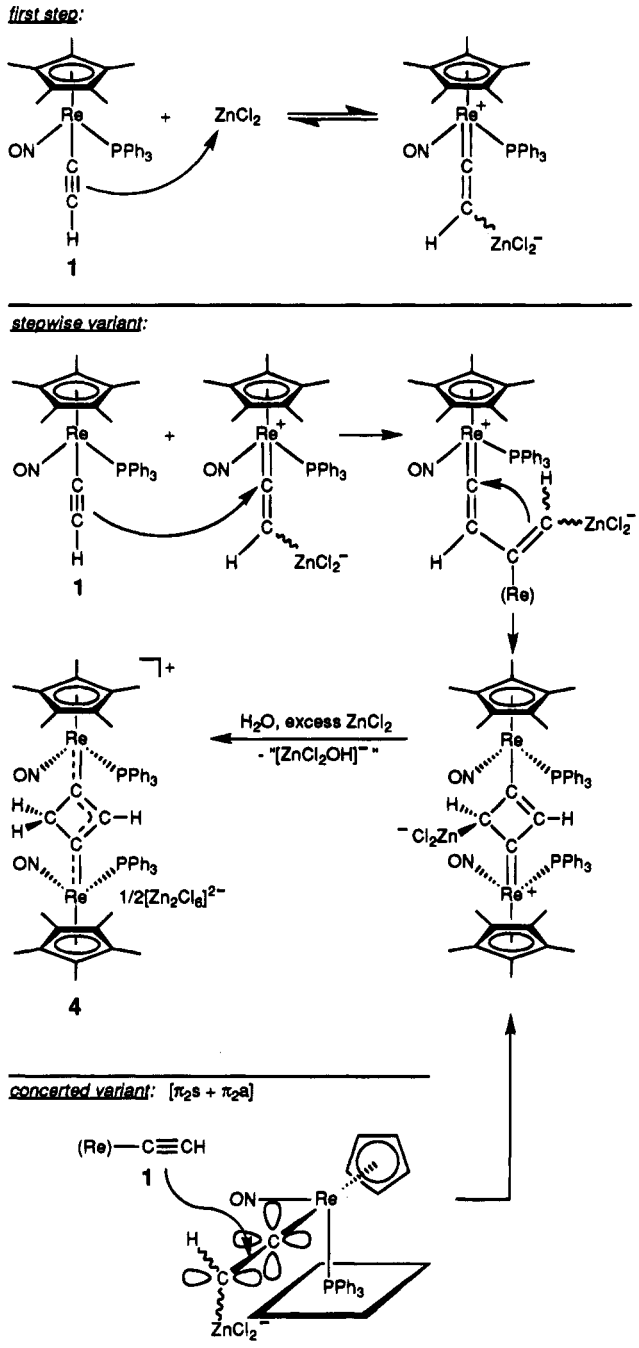

stituents can often be isolated.[14] Thus, **4** was dissolved in THF-d_8 in an NMR tube and treated with t-BuO$^-$K$^+$ or n-BuLi/t-BuO$^-$K$^+$ (2.0 equiv) at room temperature. No reaction occurred, as assayed by ^{1}H NMR. A CD_2Cl_2 solution of **5** was similarly treated with n-BuLi (1.2 equiv) at −80 °C, and the sample was slowly warmed in an NMR probe. However, ^{31}P NMR spectra did not show any reaction of **5**.

Neutral alkenyl complexes of **I** are protonated at C_β by sufficiently strong Brønsted acids to give cationic alkylidene complexes.[8,13,15] Analogous reactions of **4** or **5** would give dicationic bis(alkylidene) complexes. Thus,

(14) Gompper, R.; Wagner, H.-U. *Angew. Chem., Int. Ed. Engl.* **1988**, *27*, 1437.
(15) Kowalczyk, J. J.; Arif, A. M.; Gladysz, J. A. *Chem. Ber.* **1991**, *124*, 729.

Scheme 3. Syntheses of the *meso* Dirhenium Complex (*SR,RS*)-[(η^5-C_5Me_5)Re(NO)(PPh$_3$)(⌐C⌐CH⌐C(CH$_2$)⌐)(Ph$_3$P)(ON)Re(η^5-C_5Me_5)]$^+$BF$_4^-$ (5) and the Rhenium Vinylidene Complex [(η^5-C_5Me_5)Re(NO)(PPh$_3$)(=C=CH$_2$)]$^+$BF$_4^-$ (6)

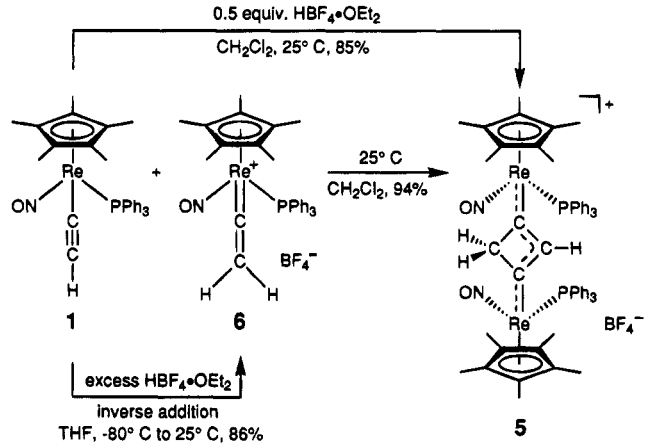

5 and HBF$_4$•OEt$_2$ (1.5 equiv) were combined in CD_2Cl_2 in an NMR tube at −80 °C. A ^{1}H NMR spectrum showed that **5** was rapidly consumed. The sample was warmed to room temperature, and ^{1}H, ^{13}C, and ^{31}P NMR spectra indicated the quantitative formation of a new compound (**8**) with good solution stability. The ^{1}H NMR spectrum showed new CHH′ resonances (overlapping multiplets, δ 3.24−3.03, 2.88−2.68). The ^{13}C NMR spectrum exhibited a diagnostic Re=C resonance at 304.7 ppm (d, J_{CP} = 7.4 Hz), close to that of vinylidene complex **6** (330.4 ppm, d, J_{CP} = 9.5 Hz) and ca. 80 ppm downfield from the Re⌐C resonances in **4** and **5**. The IR ν_{NO} value (1713 cm^{-1}) was also close to those of **6** (1728−1711 cm^{-1}). A FAB mass spectrum showed ions with m/z values of 1280 (z = 1) and 640 (z = 2),indicative of two (η^5-C_5Me_5)Re(NO)(PPh$_3$) fragments bound to a C_4H_4 moiety.

The preceding data clearly establish that **8** is the bis(alkylidene) or cyclobuta-1,3-diylidene complex (*SR,RS*)-[(η^5-C_5Me_5)Re(NO)(PPh$_3$)(=CCH$_2$C(CH$_2$)=)(Ph$_3$P)(ON)Re(η^5-C_5Me_5)]$^{2+}$(BF$_4^-$)$_2$ (Scheme 4). However, workups of preparative reactions gave only the reactant **5**, suggesting that **8** is highly acidic. When a dichloromethane solution of **8** was diluted with freshly dried dichloromethane, a mixture of **5** and **8** was generated, as assayed by IR. Upon addition of more HBF$_4$•OEt$_2$, most of the **5** was converted to **8**. Similar behavior was noted upon addition of other carefully dried solvents. We have not previously encountered a cationic adduct of **I** or **I**-Me$_5$ that was comparably prone to proton loss.

A CD_2Cl_2 solution of **8** was generated in an NMR tube in the presence of excess HBF$_4$•OEt$_2$. No decomposition occurred after 1 week at −30 °C. A separate sample was kept at 40 °C and monitored by ^{1}H and ^{31}P NMR. Alkylidene complexes of **I** often thermally rearrange to alkene complexes, with rates that depend upon the C_α/C_β substitution pattern.[16] A similar process with **8**

(16) (a) Roger, C.; Bodner, G. S.; Hatton, W. G.; Gladysz, J. A. *Organometallics* **1991**, *10*, 3266. (b) Roger, C.; Peng, T.-S.; Gladysz, J. A. *J. Organomet. Chem.* **1992**, *439*, 163.

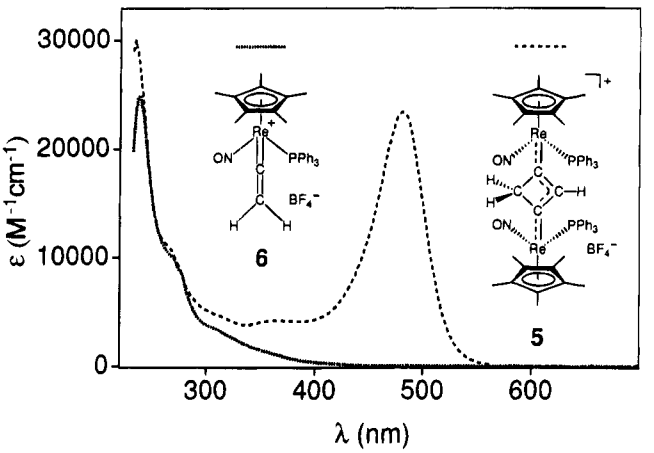

Figure 3. UV/visible spectra of **5** and **6** (CH_2Cl_2, ambient temperature, 5.5×10^{-5} M and 9.3×10^{-5} M).

Scheme 4. Interconversion and Attempted Reactions of Dirhenium Complexes 5 and 8

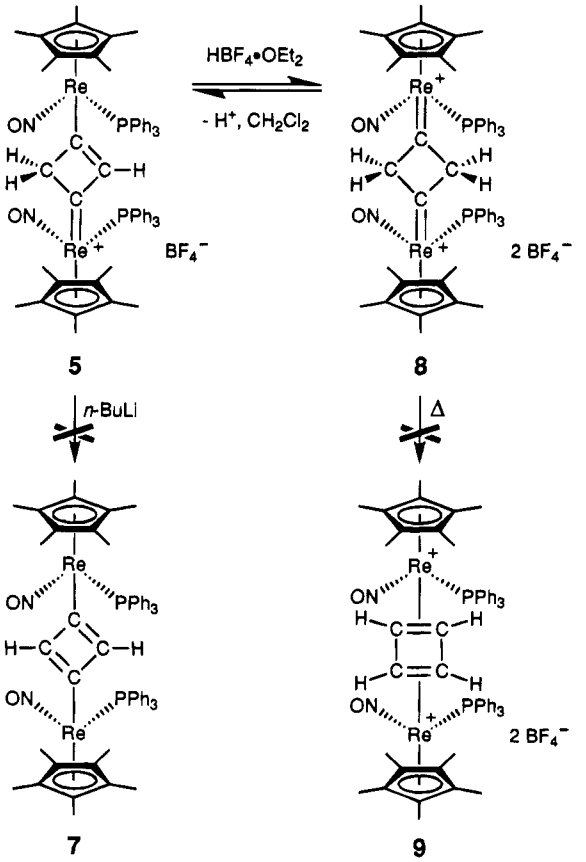

would give the μ_2-η^2:η^2-cyclobutadiene complex (*SR,RS*)-[(η^5-C_5Me_5)Re(NO)(PPh_3)(CH=CHCH=CH)(Ph_3P)(ON)Re(η^5-C_5Me_5)]$^{2+}$(BF_4^-)$_2$ (**9**), as shown in Scheme 4. However, only the slow decomposition of **8** occurred, as evidenced by four new ^{31}P and C_5Me_5 ^{1}H resonances. When the sample was warmed to 60 °C, **8** was consumed within 1 h. Five ^{31}P resonances (21.4, 19.2, 17.9, 14.5, 9.8 ppm) and C_5Me_5 ^{1}H resonances (δ 1.88, 1.87, 1.86, 1.83, 1.63) were present. Only the last ^{31}P resonance was in the range associated with alkene complexes of **I**-Me_5.[17]

(17) Peng, T.-S.; Winter, C. H.; Gladysz, J. A. *Inorg. Chem.* **1994**, *33*, 2534.

Scheme 5. Synthesis of Related Diiron C_4H_3 Complexes

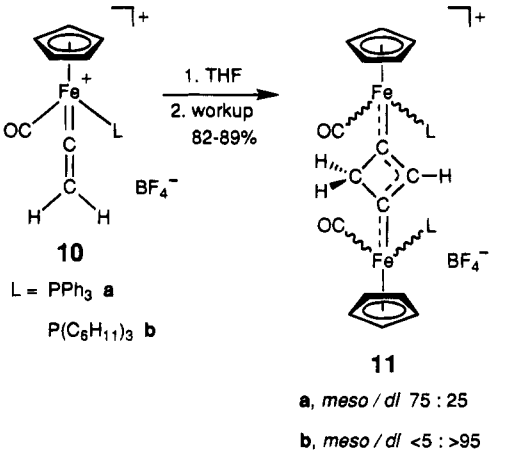

Discussion

Although our initial synthesis of dirhenium complex **4** was unanticipated, closely related compounds have been previously reported.[18,19] In particular, Hughes found that the chiral iron vinylidene complex [(η^5-C_5H_5)Fe(CO)(PPh_3)(=C=CH_2)]$^+$$BF_4^-$ (**10a**) reacts in THF without added agents to give the similar cycloadduct [(η^5-C_5H_5)Fe(CO)(PPh_3)(C=CH=C(CH_2)=)(Ph_3P)(OC)Fe(η^5-C_5H_5)]$^+$$BF_4^-$ (**11a**) as a 75:25 mixture of *SR,RS*/*SS,RR* or *meso*/*dl* diastereomers (Scheme 5).[18] Curiously, the tricyclohexylphosphine analog **10b** gave only the *dl* diastereomer of the corresponding diiron complex **11b**. Hughes' assignments were based upon the multiplicities of the CH_2 ^{1}H NMR signals. The CH_2 protons are not related by any symmetry element in the *meso* diasteromers and therefore give two doublets, as with **4** and **5** above. However, they are exchanged by a 2-fold rotation axis in the *dl* diastereomers, resulting in a singlet.

The crystal structure of **4** exhibits several features that merit analysis. First, consistent with the delocalized structure in Scheme 1, the rhenium–carbon bond lengths (2.00(1)–2.03(1) Å; Table 3) are intermediate between those of single and double bonds. For comparison, the rhenium–carbon double bonds in alkylidene complexes of the cyclopentadienyl rhenium fragment [(η^5-C_5H_5)Re(NO)(PPh_3)]$^+$ (**I**) are 1.949(6)–1.945 Å.[15,20] The rhenium–carbon single bonds in alkenyl complexes of **I**, which involve sp^2-hybridized carbons as in **4**, are 2.123(6)–2.129(10) Å.[13] Also, the ReC=CH bonds in **4** (1.40(2)–1.42(2) Å) are longer than the C=C bond in cyclobutene (1.342 Å) but shorter than either the C–C bond in cyclobutane (1.548 Å)[21] or the ReC–CH_2 bonds in **4** (1.54(2)–1.55(2) Å).

The structure of **4** can also be compared to that of the dicationic C_4 complex (*SS,RR*)-[(η^5-C_5Me_5)Re(NO)(PPh_3)(=C=C=C=C=)(Ph_3P)(ON)Re(η^5-C_5Me_5)]$^{2+}$

(18) Boland-Lussier, B. E.; Hughes, R. P. *Organometallics* **1982**, *1*, 635.

(19) (a) Davison, A.; Solar, J. P. *J. Organomet. Chem.* **1978**, *155*, C8. (b) Kolobova, N. Ye.; Skripkin, V. V.; Alexandrov, G. G.; Struchkov, Yu. T. *J. Organomet. Chem.* **1979**, *169*, 293. (c) Aleksandrov, G. G.; Skripkin, V. V.; Kolobova, N. E.; Struchkov, Yu. T. *Koord. Khim.* **1979**, *5*, 453; *Chem. Abstr.* **1979**, *90*, 178495m.

(20) Kiel, W. A.; Lin, G.-Y.; Constable, A. G.; McCormick, F. B.; Strouse, C. E.; Eisenstein, O.; Gladysz, J. A. *J. Am. Chem. Soc.* **1982**, *104*, 4865.

(21) Hehre, W. J.; Pople, J. A. *J. Am. Chem. Soc.* **1975**, *97*, 6941.

Chart 1. d-Orbital HOMO of the Chiral Rhenium Fragment $[(\eta^5\text{-}C_5Me_5)Re(NO)(PPh_3)]^+$ (I), Idealized Structure of Alkylidene Complexes of I and I-Me_5, (II), and Idealized Structure of Dirhenium Complexes 4, 5, and 8 (III)

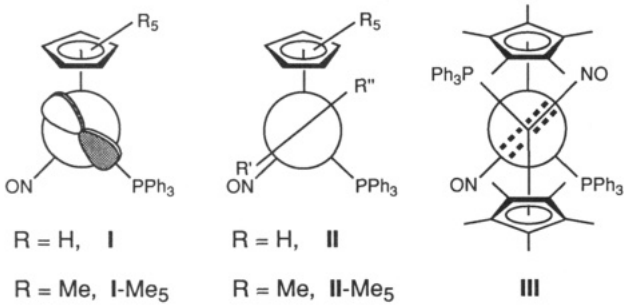

$(PF_6^-)_2$ (**12**), which has pentamethylcyclopentadienyl end groups.[2a] The Re=C bonds in **12** (1.91(1)−1.93(1) Å) are shorter than the Re⋯C bonds in **4**. Conversely, the rhenium−rhenium distance in **4** (6.1025(6) Å) is shorter than that in **12** (7.6350(8) Å). The former constitutes the smallest separation achieved to date for two **I** or **I**-Me_5 fragments connected by a linear or effectively linear bridge.[22] When **4** is viewed on a stereoscopic screen with the atoms set at van der Waals radii, the pentamethylcyclopentadienyl ligand of one rhenium tangentially abuts the PPh_3 ligand of the other. Thus, it is questionable whether dirhenium compounds with appreciably shorter bridges can be prepared.

It is readily seen from Figure 2 that the Re⋯C bonds in **4** adopt conformations that place the Re−P and Re−NO bonds approximately perpendicular and parallel, respectively, to the plane of the C_4H_3 ring. Accordingly, the P−Re⋯C⋯C torsion angles (Table 3) range from 92 to 102°, and the N−Re⋯C⋯C torsion angles are near 0 or ±180°. Although steric effects must certainly influence the conformational features of this crowded molecule, it should be noted that the rhenium fragments **I** and **I**-Me_5 have a high-lying d orbital HOMO with the orientation shown in Chart 1. Thus,the corresponding alkylidene complexes adopt Re=C conformations as shown in idealized structures **II** and **II**-Me_5, in which overlap with the C_α p acceptor orbital is maximized.[15,20] Similar (but likely less pronounced) frontier orbital interactions involving the C_4H_3 moiety in **4** would lead to idealized structure **III** (Chart 1), in agreement with the orientations of the Re−P and Re−NO bonds in the crystal structure.

The dynamic NMR behavior in Figure 1 is easily interpreted in the context of these structural features. First, there are no symmetry operations that exchange the two PPh_3 or C_5Me_5 ligands in the structures in Figure 2 or **III** (note that the latter does not have an S_2 axis since the bridges connecting the Re⋯C carbons are not identical). Thus, distinct ^{31}P and ^1H NMR signals are observed in the low-temperature limit. However, rotation about either Re⋯C bond establishes an effective mirror plane, rendering the two PPh_3 and C_5Me_5 ligands chemically equivalent and effecting coalescence. Barriers to rotation about the Re=C bonds in alkylidene complexes of **I** are 18−21 kcal/mol.[20,23] The lower values derived from Figure 1 for **4** (12.1−12.6 kcal/mol) are consistent with the reduced Re⋯C bond order. Notably, this process must involve a Re⋯C conformer in which the bulky PPh_3 and C_5Me_5 ligands are eclipsed, as can be visualized by a 180° rotation of the front rhenium in **III**. However, this conformer would also be electronically stabilized by the same frontier orbital interactions that apply with **III**.

Scheme 6. Preferred Direction of Nucleophilic Attack upon Vinylidene and Alkynyl Complexes of I

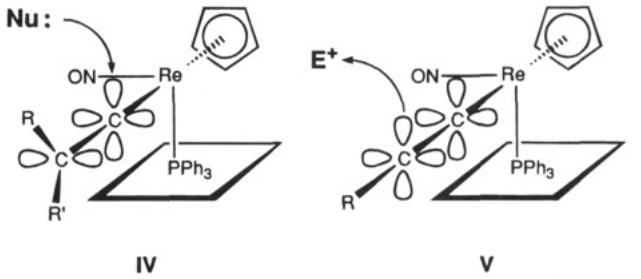

We next consider the high diastereoselectivity with which **4** and **5** appear to be formed. First, alkylidene, alkenyl, and alkyl complexes of **I** and **I**-Me_5 exhibit high configurational stabilities.[16a,23,24] Thus, there do not appear to be any precedented pathways that would allow diastereomers of **4** or **5** to rapidly equilibrate. Therefore, stereochemistry must be set at the initial carbon−carbon bond-forming step. A stepwise cyclization mechanism is sketched in the middle portion of Scheme 2. However, Hughes has also noted that vinylidene and alkynyl complexes may be favorably disposed toward concerted $\pi_2s + \pi_2a$ processes,[18] as illustrated in the bottom portion of Scheme 2.

Irrespective of pathway, diastereomer ratios will be determined by the relative rates of reaction of the *S/S* (or *R/R*) enantiomers of each monorhenium complex (e.g., **1** and **6**) and the *S/R* (or *R/S*) enantiomers of each monorhenium complex. Indeed, both vinylidene and alkynyl complexes of **I** have previously been shown to undergo highly diastereoselective reactions with nucleophiles and electrophiles. As illustrated in **IV** in Scheme 6, nucleophiles preferentially attack the C_α carbons of vinylidene complexes from a direction *anti* to the PPh_3 ligand, giving predominantly one C=C geometric isomer of the resulting alkenyl complex.[12] Similarly, as shown in **V** in Scheme 6, electrophiles analogously attack the C_β carbon of alkynyl complexes, giving predominantly one Re=C=C geometric isomer of the resulting vinylidene complex.[12]

However, utilizing molecular models and the modes of addition in **IV** and **V**, we are unable to identify a compelling feature that would account for a much faster stepwise or concerted reaction of the *S/R* (or *R/S*) pair of enantiomers. Thus, the mechanistic basis for the high diastereoselectivity remains arcane—particularly in view of Hughes' data in Scheme 5, in which the dominant diastereomer of diiron complex **11** is reversed upon substitution of PPh_3 by tricyclohexylphosphine. A conceptually related phenomenon occurs with the methylidene complex $[(\eta^5\text{-}C_5H_5)Re(NO)(PPh_3)(=CH_2)]^+X^-$.[25]

(22) For the crystal structure of (*RR,SS*)-$[(\eta^5\text{-}C_5H_5)Re(NO)(PPh_3)]_2I^+$ BF_4^-, which contains a bent Re−I−Re linkage, see: Winter, C. H.; Arif, A. M.; Gladysz, J. A. *Organometallics* **1989**, *8*, 219.

(23) (a) Kiel, W. A.; Lin, G.-Y.; Bodner, G. S.; Gladysz, J. A. *J. Am. Chem. Soc.* **1983**, *105*, 4958. (b) Kiel, W. A.; Buhro, W. E.; Gladysz, J. A. *Organometallics* **1984**, *3*, 879.

(24) Huang, Y.-H.; Niedercorn, F.; Arif, A. M.; Gladysz, J. A. *J. Organomet. Chem.* **1990**, *383*, 213.

This compound undergoes a bimolecular $=CH_2$ coupling reaction with extremely high *S/S* (or *R/R*) selectivity. However, the basis for this "enantiomer self recognition" is also unclear.

To our knowledge, **8** is the first bis(alkylidene) complex derived from a saturated carbocycle. However, other bis(alkylidene) complexes, including adducts of **I** and $=CHCH_2(CH_2)_nCH_2CH=$ moieties, have been reported previously.[16b] We presume, by analogy to the corresponding ketone cyclobutane-1,3-dione,[26] that **8** has a planar (as opposed to puckered) ring conformation. The frontier orbital considerations discussed above would then predict the idealized structure **III** (Chart 1), with Re=C conformations similar to the Re⊸C conformations in **4** and **5**. Since the bridges connecting the Re=C carbons are now identical, **III** has three orthogonal S_2 axes or (equivalently) an inversion center. Thus, only one set of PPh_3 and C_5Me_5 NMR signals are observed at low temperature. We suspect that the marked acidity of **8** is connected to repulsion between the positive termini of the strong dipoles associated with the Re=C bonds (←+).

In summary, the dirhenium complexes **4** and **5** are readily available in high yields from the ethynyl complex **1**. Complex **5** can be further transformed to the unusual cyclobuta-1,3-diylidene complex **8**. These compounds exhibit many interesting spectroscopic and structural properties, which generally can be interpreted in the context of previously characterized alkylidene, alkenyl, and related complexes. Attempts to convert **5** or **8** to various types of cyclobutadiene derivatives have so far been unsuccessful. However, we believe it likely that these compounds can serve as precursors to other novel types of organometallic complexes, and further studies are in progress.

Experimental Section

General Data. General procedures and instrumentation have been described previously.[5] NMR data were recorded on 300 MHz spectrometers, and all coupling constants (*J*) are in Hz. Chemicals were used as received except as follows: CH_2Cl_2, CD_2Cl_2, and CH_3CN, distilled or vacuum-transferred from CaH_2; THF, ether, hexane, and benzene, distilled from Na- or K/benzophenone; pyridine, distilled from KOH; C_6D_6 and THF-d_8, vacuum-transferred from Na; *n*-BuLi and $HBF_4{\cdot}OEt_2$ (Aldrich), standardized before use.[27,28]

(*SR,RS*)-[(η^5-C_5Me_5)Re(NO)(PPh_3)(⊸C⊸CH⊸C(CH_2)⊸)-(Ph_3P)(ON)Re(η^5-C_5Me_5)]$^+$([Zn_2Cl_6]$^{2-}$)$_{1/2}$ (4). A. A Schlenk tube was charged with (η^5-C_5Me_5)Re(NO)(PPh_3)(C≡CH) (**1**;[5] 0.064 g, 0.10 mmol), THF (5 mL), and a stirbar and cooled to −80 °C. Then *n*-BuLi (2.46 M in hexane; 65 μL, 0.16 mmol) was added with stirring. After 1.5 h, a solution of $ZnCl_2$ (0.015 g, 0.12 mmol) in THF (5 mL) was added via cannula. After 0.5 h, the cold bath was removed. After 2 h, the solvent was removed under oil pump vacuum, and the residue was extracted with CH_2Cl_2 (2 × 5 mL). The extracts were passed through a medium-frit Kramer filter, concentrated to ca. 5 mL, and layered with ether (20 mL). The resulting yellow microcrystals were collected by filtration and dissolved in a minimum of CH_2Cl_2. A layer of hexane was added. The resulting orange needles were collected by filtration to give **4**·0.5CH_2Cl_2 (0.028 g, 0.019 mmol, 38%). The solvate was detected by ^1H NMR (δ 5.33, CD_2Cl_2) and crystallography (below).

B. A Schlenk tube was charged with **1** (0.064 g, 0.10 mmol), $ZnCl_2$ (0.021 g, 0.15 mmol), THF (8 mL), and a stirbar. The mixture was stirred for 6 h. The solvent was removed under oil-pump vacuum, and the residue was extracted with CH_2Cl_2 (2 × 5 mL). The extracts were passed through a medium-frit Kramer filter, concentrated to ca. 2 mL, and layered with hexane (20 mL). After 12 h, the resulting orange needles were collected by filtration and dried under oil-pump vacuum overnight to give **4** (0.068 g, 0.047 mmol, 94%), mp >196 °C (slow dec). Anal. Calcd for $C_{60}H_{63}Cl_3N_2O_2P_2Re_2Zn$: C, 49.69; H, 4.38. Found: C, 49.77; H, 4.40.

IR (cm^{-1}, CH_2Cl_2/thin film): ν_{NO} 1655/1642 s. ^1H NMR (δ, CD_2Cl_2):[29] 7.49−7.38 (m, $6C_6H_5$), 7.08 (s, ⊸CH), 3.03 (d, *J* = 14.6, C*H*H′), 2.53 (d, *J* = 14.6, CH*H*′), 1.55 (s, $2C_5(CH_3)_5$). $^{13}C\{^1H\}$ NMR (ppm, CD_2Cl_2): 227.5 (d, J_{CP} = 9.5, ReC), 167.8 (s, ⊸CH), 133.5 (d, J_{CP} = 11.2, *o*-Ph), 133.4 (d, J_{CP} = 53.9, *i*-Ph), 131.4 (d, J_{CP} = 2.0, *p*-Ph), 129.1 (d, J_{CP} = 10.6, *m*-Ph), 104.7 (s, $C_5(CH_3)_5$), 64.9 (s, CHH′), 9.9 (s, $C_5(CH_3)_5$). $^{31}P\{^1H\}$ NMR (ppm, CD_2Cl_2):[29] 21.3 (s). MS (positive Cs-FAB, tetraglyme/THF): *m/z* (relative intensity, ^{187}Re) 1279 (M^+, 16%).

(*SR,RS*)-[(η^5-C_5Me_5)Re(NO)(PPh_3)(⊸C⊸CH⊸C(CH_2)⊸)-(Ph_3P)(ON)Re(η^5-C_5Me_5)]$^+BF_4^-$ (5). A. A Schlenk tube was charged with **4** (0.052 g, 0.036 mmol), $NaBF_4$ (0.047 g, 0.43 mmol), THF (15 mL), and a stirbar. The mixture was stirred for 4 h. The solvent was removed under oil-pump vacuum, and the residue was extracted with CH_2Cl_2 (2 × 3 mL). The extracts were filtered through a Celite pad (1 cm) on a medium frit and layered with hexane (15 mL). After 12 h, the resulting orange needles were collected by filtration and dried under oil-pump vacuum to give **5** (0.043 g, 0.031 mmol, 86%).

B. A Schlenk tube was charged with **1** (0.064 g, 0.10 mmol), CH_2Cl_2 (10 mL), and a stirbar and cooled to −80 °C. Then a $HBF_4{\cdot}OEt_2$ stock solution (89 μL, 0.05 mmol; from 1 mL of $HBF_4{\cdot}OEt_2$ diluted with CH_2Cl_2 to 10 mL) was added dropwise with stirring. After 0.5 h, the cold bath was removed. After 0.5 h, the solution was concentrated to ca. 1 mL, and hexane (15 mL) was added with stirring. The resulting orange powder was collected by filtration and dried under oil-pump vacuum to give **5** (0.054 g, 0.043 mmol, 85%).

C. A Schlenk tube was charged with **1** (0.032 g, 0.050 mmol), **6** (0.036 g, 0.050 mmol), CH_2Cl_2 (5 mL), and a stirbar. The solution was stirred for 3 h, concentrated to ca. 1 mL, and worked up as in procedure B to give **5** (0.064 g, 0.047 mmol, 94%), mp 173−176 °C dec. NMR spectra (^1H, ^{13}C, ^{31}P) were identical with those of **4**.[29] IR (cm^{-1}, CH_2Cl_2/thin film): ν_{NO} 1656/1641 s, ν_{BF} 1069/1068 s. UV/vis (nm (ε, M^{-1} cm^{-1}), 5.5 × 10^{-5} M in CH_2Cl_2): 266 sh (10 900), 362 (4100), 480 (23 400).

[(η^5-C_5Me_5)Re(NO)(PPh_3)(=C=CH_2)]$^+BF_4^-$ (6). A Schlenk tube was charged with $HBF_4{\cdot}OEt_2$ (36 μL, 0.20 mmol), THF (5 mL), and a stirbar, capped with a septum, and cooled to −80 °C. A second tube was similarly charged with **1** (0.064 g, 0.10 mmol) and THF (5 mL). The latter solution was added dropwise with stirring to the former via cannula. After 0.5 h, the cold bath was removed. After 15 min, the solvent was removed by oil-pump vacuum. The residue was dissolved in CH_2Cl_2 (2 mL). The solution was filtered through a Celite pad (1 cm) on a medium frit, and ether (20 mL) was added. The resulting pale yellow powder was collected by filtration and dried under oil-pump vacuum at 40−50 °C overnight to give **6** (0.055 g, 0.086 mmol, 86%), mp 175−180 °C dec. Anal. Calcd for $C_{30}H_{32}BF_4NOPRe$: C, 49.70; H, 4.45. Found: C, 49.47; H, 4.45.

IR (cm^{-1}, CH_2Cl_2/thin film): ν_{NO} 1728/1711 s, $\nu_{C=C}$ 1634/1631 m, ν_{BF} 1058/1055 s. ^1H NMR (δ, $CDCl_3$): 7.55−7.29 (m,

(25) Merrifield, J. H.; Lin, G.-Y.; Kiel, W. A.; Gladysz, J. A. *J. Am. Chem. Soc.* **1983**, *105*, 5811.
(26) Seidl, E. T.; Schaefer, H. F., III *J. Am. Chem. Soc.* **1990**, *112*, 1493.
(27) Kofron, W. G.; Baclawsky, L. M. *J. Org. Chem.* **1976**, *41*, 1879.
(28) (a) Jablonsky, C. R. *Aldrichim. Acta* **1990**, *23*, 58. (b) Fernández, J. M.; Gladysz, J. A. *Organometallics* **1989**, *8*, 207.

(29) NMR signals that may be due to *dl* diastereomers of **4** and **5** are given in the text.

$3C_6H_5$), 5.28 (dd, J_{HH} = 20.7, J_{HP} = 1.2, =C*H*H′), 4.95 (dd, J_{HH} = 20.7, J_{HP} = 1.2, =CH*H*′), 1.87 (s, $C_5(CH_3)_5$). $^{13}C\{^1H\}$ NMR (ppm, CD_2Cl_2): 330.4 (d, J_{CP} = 9.5, Re=C), 132.9 (d, J_{CP} = 11.0, *o*-Ph), 132.4 (br s, *p*-Ph), 129.4 (d, J_{CP} = 11.2, *m*-Ph), 128.8 (d, J_{CP} = 59.1, *i*-Ph), 111.6 (s, =CH_2), 109.0 (s, $C_5(CH_3)_5$), 9.8 (s, $C_5(CH_3)_5$). $^{31}P\{^1H\}$ NMR (ppm, CD_2Cl_2): 23.0 (s). MS (positive Cs-FAB, 3-nitrobenzyl alcohol/CH_2Cl_2): *m/z* (relative intensity, ^{187}Re) 640 (M^+, 100%). UV/vis (nm (ϵ, M^{-1} cm^{-1}), 9.3 × 10^{-5} M in CH_2Cl_2): 266 sh (10 200), 308 sh (3400).

(*SR,RS*)-[(η^5-C_5Me_5)Re(NO)(PPh_3)(=CCH$_2$C(CH$_2$)=)-(Ph_3P)(ON)Re(η^5-C_5Me_5)]$^{2+}$(BF_4^-)$_2$ (8). A 5 mm NMR tube was charged with **5** (0.016 g, 0.011 mmol) and CD_2Cl_2 (0.6 mL), capped with a septum, and cooled to −80 °C. Then HBF_4·OEt_2 (2.0 μL, 0.015 mmol) was added. The orange solution immediately turned yellow. After 10 min, the tube was removed from the cold bath and spectra were recorded. A ^{1}H NMR spectrum showed >95% conversion to **8**.

IR (cm^{-1}, CH_2Cl_2): ν_{NO} 1713 s. ^{1}H NMR (δ, CD_2Cl_2): 7.63–7.60 (m, 18H of $6C_6H_5$), 7.40–7.35 (m, 12H of $6C_6H_5$), 3.24–3.03 (m, 2H of $2CH_2$), 2.88–2.68 (m, 2H of $2CH_2$), 1.59 (s, $2C_5(CH_3)_5$). $^{13}C\{^1H\}$ NMR (ppm, CD_2Cl_2, −40 °C): 304.7 (d, J_{CP} = 7.4, Re=C), 129.8–133.5 (4 m, PPh),[30] 109.4 (s, $C_5(CH_3)_5$), 83.9 (br s, CH_2), 9.5 (s, $C_5(CH_3)_5$). $^{31}P\{^1H\}$ NMR (ppm, CD_2Cl_2): 21.4 (s). MS (positive Cs-FAB, tetraglyme/THF): *m/z* (relative intensity, ^{187}Re) 1280 ("M^+", 11%), 640 (M^{2+}), and other z = 2 ions (all <1%).

Crystallography. Data were collected on **4**·0.5CH_2Cl_2 as given in Table 1. Cell constants were obtained from 25 reflections with 10° < 2θ < 30°. The space group was determined from the lack of systematic absences and subsequent least-squares refinement. Lorentz, polarization, and empirical absorption (ψ scans) corrections were applied. The structure was solved by standard heavy-atom techniques with the SDP/VAX package.[31] Except for the CH_2Cl_2 carbon, nonhydrogen atoms were refined with anisotropic thermal parameters. All hydrogen atom positions were calculated and added to the structure factor calculations but were not refined. Scattering factors, and $\Delta f'$ and $\Delta f''$ values, were taken from the literature.[32]

Acknowledgment. We thank the DOE for support of this research.

Supplementary Material Available: Tables of anisotropic thermal parameters and additional bond distances and angles for **4** (7 pages). Ordering information is given on any current masthead page.

OM940728M

(30) The PPh ^{13}C resonances were not well resolved, presumably due to restricted rotation about the Re–P and/or P–C bonds.

(31) Frenz, B. A. The Enraf-Nonius CAD 4 SDP—A Real-time System for Concurrent X-ray Data Collection and Crystal Structure Determination. In *Computing and Crystallography*; Schenk, H., Olthof-Hazelkamp, R., van Konigsveld, H., Bassi, G. C., Eds.; Delft University Press: Delft, Holland, 1978; pp 64–71.

(32) Cromer, D. T.; Waber, J. T. In *International Tables for X-ray Crystallography*; Ibers, J. A., Hamilton, W. C., Eds.; Kynoch: Birmingham, England, 1974; Vol. IV, pp 72–98 and 149–150, Tables 2.2B and 2.3.1.

A New Alkene Carbon–Hydrogen Bond Activation Reaction: Facile and Stereospecific Vinylic Deprotonation of the Chiral Cationic Rhenium Alkene Complexes $[(\eta^5\text{-}C_5H_5)Re(NO)(PPh_3)(H_2C{=}CHR)]^+BF_4^-$

Tang-Sheng Peng and J. A. Gladysz*

Department of Chemistry, University of Utah, Salt Lake City, Utah 84112

Received November 7, 1994[⊗]

Alkene complexes $[(\eta^5\text{-}C_5H_5)Re(NO)(PPh_3)(H_2C{=}CHR)]^+BF_4^-$ (**1**; R = **a**, CH_3; **b**, $CH_2CH_2CH_3$; **c**, $CH(CH_3)_2$; **d**, H; **e**, C_6H_5; **f**, $C(CH_3)_3$; ≥96:4 *RS,SR/RR,SS* Re,C configurational diastereomers) and *t*-BuO^-K^+ react in THF to give alkenyl complexes $(\eta^5\text{-}C_5H_5)Re(NO)(PPh_3)(CH{=}CHR)$ (**2**; 83–93% after workup). Allylbenzene complex **1g** (R = $CH_2C_6H_5$) gives a 89:11 mixture (91%) of **2g** and allyl complex $(\eta^5\text{-}C_5H_5)Re(NO)(PPh_3)(CH_2CH{=}CHR')$ (**3g**). The **2g**:**3g** ratio decreases when *t*-BuOH solvent or (*RR,SS*)-**1g** is used—conditions that also give **2a,b**/**3a,b** mixtures. NMR experiments show that (*RS,SR*)- and (*RR,SS*)-**1** give (*E*)- and (*Z*)-**2**, respectively. However, the latter equilibrate (K_{eq} > (99–82):(<1–18)) at room temperature. Deuterium labeling shows that only one geminal $=CH_2$ proton is abstracted from each diastereomer, as controlled by the rhenium configuration (H_S from (*RS*)- or (*RR*)-**1**). Deprotonation is *irr*eversible and occurs with retention at rhenium, with a k_H/k_D value of 1.7, and without PPh_3 dissociation. A Rh(I) catalyst shows **2a** to be more stable than **3a**, but no isomerization occurs under the deprotonation conditions. Low-temperature NMR spectra show that *t*-BuO^-K^+ initially adds to the cyclopentadienyl ligand of **1**, but other data suggest this to be a nonproductive equilibrium. Possible mechanisms, and the origins of the many types of selectivities in the preceding reactions, are analyzed in detail.

The selective activation of vinylic (sp^2) carbon–hydrogen bonds in simple alkenes such as ethene, propene, and styrene is attracting much current interest.[1–3] This is prompted in large part by possibilities for new catalytic commodity chemical transformations, as well as applications in stoichiometric organic syntheses. Toward these ends, oxidative additions of coordinatively unsaturated transition-metal fragments to vinylic carbon–hydrogen bonds are under active investigation.[1,2] Such reactions were unknown prior to 1985 and show several interesting mechanistic features. In many cases, the resulting alkenyl hydride complexes are isolable.

Numerous transition-metal-catalyzed reactions involve intermediate alkene complexes. Surprisingly, however, there have been few attempts to *chemically* activate vinylic carbon–hydrogen bonds in alkene complexes.[4] We wondered whether exogenous agents, such as Brønsted bases or coordinatively unsaturated metal fragments, might give exploitable chemistry. Analogous functionality could then be appended to a ligand of the alkene complex, enabling intramolecular activation and facilitating catalysis.

We have had an ongoing interest in alkene complexes of the chiral rhenium fragment $[(\eta^5\text{-}C_5H_5)Re(NO)(PPh_3)]^+$.[5–10] Adducts of a variety of monosubstituted and disubstituted alkenes have been isolated and structurally characterized. Many types of isomers are possible. For example, monosubstituted alkene complexes $[(\eta^5\text{-}C_5H_5)Re(NO)(PPh_3)(H_2C{=}CHR)]^+BF_4^-$ (**1**) can exist as two configurational diastereomers, *RS,SR* and *RR,SS*,[11] that differ in the C=C enantioface bound to rhenium. As shown with **II** and **III** in Scheme 1,

⊗ Abstract published in *Advance ACS Abstracts,* January 1, 1995.

(1) Stoutland, P. O.; Bergman, R. G. *J. Am. Chem. Soc.* **1988**, *110*, 5732; **1985**, *107*, 4581.

(2) Lead papers that have appeared since 1993: (a) Siegbahn, P. E. M.; Blomberg, M. R. A.; Svensson, M. *J. Am. Chem. Soc.* **1993**, *115*, 1952. (b) Whittlesey, M. K.; Mamby, R. J.; Osman, R.; Perutz, R. N.; Field, L. D.; Wilkinson, M. P.; George, M. W. *J. Am. Chem. Soc.* **1993**, *115*, 8627. (c) de With, J.; Horton, A. D. *Angew. Chem., Int. Ed. Engl.* **1993**, *32*, 903. (d) Bennett, J. L.; Wolczanski, P. T. *J. Am. Chem. Soc.* **1994**, *116*, 2179.

(3) For general reviews, see: *Selective Hydrocarbon Activation*; Davies, J. A., Watson, P. L., Greenberg, A., Liebman, J. F., Eds.; VCH: New York, 1990.

(4) (a) Stang, P. J.; Huang, Y.-H.; Arif, A. M. *Organometallics* **1992**, *11*, 845. (b) Nessel, A.; Nürnberg, O.; Wolf, J.; Werner, H. *Angew. Chem., Int. Ed. Engl.* **1991**, *30*, 1006. (c) Photolyses to alkenyl hydride complexes have been reported.[1,2b]

(5) (a) Bodner, G. S.; Peng, T.-S.; Arif, A. M.; Gladysz, J. A. *Organometallics* **1990**, *9*, 1191. (b) Peng, T.-S.; Arif, A. M.; Gladysz, J. A. *Helv. Chim. Acta* **1992**, *75*, 442. (c) Peng, T.-S.; Gladysz, J. A. *J. Am. Chem. Soc.* **1992**, *114*, 4174.

(6) (a) Kowalczyk, J. J.; Arif, A. M.; Gladysz, J. A. *Chem. Ber.* **1991**, *124*, 729. (b) Pu, J.; Peng, T.-S.; Mayne, C. L.; Arif, A. M.; Gladysz, J. A. *Organometallics* **1993**, *12*, 2686. (c) Peng, T.-S.; Pu, J.; Gladysz, J. A. *Organometallics* **1994**, *13*, 929.

(7) Wang, Y.; Agbossou, F.; Dalton, D. M.; Liu, Y.; Arif, A. M.; Gladysz, J. A. *Organometallics* **1993**, *12*, 2699.

(8) (a) Peng, T.-S.; Wang, Y.; Arif, A. M.; Gladysz, J. A. *Organometallics* **1993**, *12*, 4535. (b) Roger, C.; Peng, T.-S.; Gladysz, J. A. *J. Organomet. Chem.* **1992**, *439*, 163.

(9) Pu, J.; Peng, T.-S.; Arif, A. M.; Gladysz, J. A. *Organometallics* **1992**, *11*, 3232.

(10) (a) Kiel, W. A.; Lin, G.-Y.; Bodner, G. S.; Gladysz, J. A. *J. Am. Chem. Soc.* **1983**, *105*, 4958. (b) Roger, C.; Bodner, G. S.; Hatton, W. G.; Gladysz, J. A. *Organometallics* **1991**, *10*, 3266.

(11) (a) The configuration at rhenium is given before those of the =CHR or =CHD carbons, following protocols detailed in refs 5a and 6b. (b) In synclinal (*sc*) Re–(C=C) or Re=CHR conformers of alkene or alkylidene complexes of **I**, the highest priority substituents on rhenium ($\eta^5\text{-}C_5H_5$) and the C=C centroid (=CHR or $=CR_2$ > $=CH_2$) or alkylidene carbon (R > H) define 60 ± 30° torsion angles. In anticlinal (*ac*) conformers, the highest priority substituents define 120 ± 30° torsion angles. The torsion angles in the idealized structures **II** and **III** (Scheme 1) are 45°.

0276-7333/95/2314-0898$09.00/0

Scheme 1. d Orbital HOMO (I) of the Chiral Rhenium Fragment $[(\eta^5\text{-}C_5H_5)Re(NO)(PPh_3)]^+$ and Idealized Structures (II and III) of Diastereomeric Monosubstituted Alkene Complexes $[(\eta^5\text{-}C_5H_5)Re(NO)(PPh_3)(H_2C{=}CHR)]^+BF_4^-$ (1)

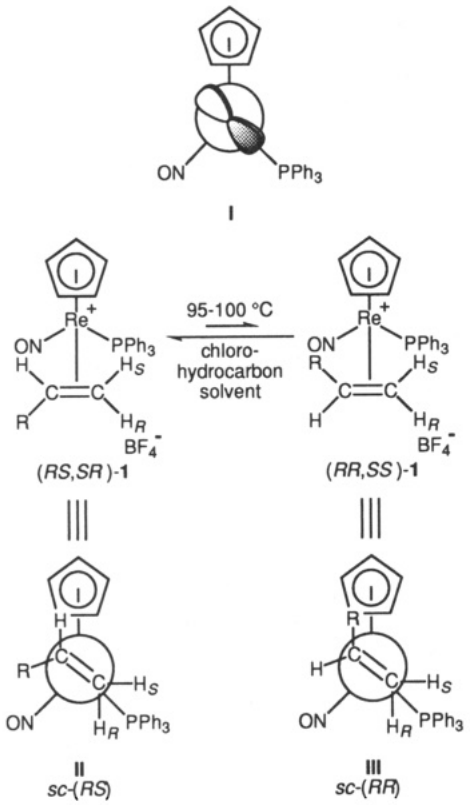

these adopt Re–(C=C) conformations that (1) maximize overlap of the d orbital HOMO of **I** with the alkene π^*-acceptor orbital and (2) orient the larger =CHR terminus *anti* to the bulky PPh_3 ligand. The *RS,SR* and *RR,SS* diastereomers equilibrate by a nondissociative process at 95–100 °C.[5c] The latter are much less stable due to steric interactions between the =CH*R* substituents and cyclopentadienyl ligands.

Thus, we set out to attempt vinylic carbon–hydrogen bond activation in alkene complexes of **I**, with an initial focus on Brønsted bases. Importantly, reactions of bases with cationic alkene complexes that bear allylic protons have been previously investigated. As shown in path A of Scheme 2, allylic protons are abstracted, giving the neutral σ-allyl complexes **V**.[12] This reversible process, which has also been observed with alkene complexes of **I**,[13] has been widely presumed to be general. However, we now report that, under appropriate conditions, such compounds undergo facile and unprecedented *vinylic* deprotonations, as exemplified in path B of Scheme 2. Numerous mechanistic experiments, including NMR and labeling studies that reveal hidden stereochemical features, are also described. A small portion of this work has been communicated.[14]

Results

1. Vinylic Carbon–Hydrogen Bond Activation. A 96:4[15] equilibrium mixture of *RS,SR/RR,SS* diastereomers of propene complex $[(\eta^5\text{-}C_5H_5)Re(NO)(PPh_3)(H_2C{=}CHCH_3)]^+BF_4^-$ (**1a**)[5a,b] was dissolved in THF in an NMR tube and cooled to −80 °C. Then $t\text{-}BuO^-K^+$ in THF (1.4 equiv, 1.0 M) was added, and the sample was warmed to room temperature (Scheme 3).[16] A ^{31}P NMR spectrum showed the clean formation of the known *trans*-propenyl complex (*E*)-$(\eta^5\text{-}C_5H_5)Re(NO)(PPh_3)(CH{=}CHCH_3)$ ((*E*)-**2a**; 23.4 ppm).[17] Workup gave (*E*)-**2a** in 85% yield. The isomeric allyl complex $(\eta^5\text{-}C_5H_5)Re(NO)(PPh_3)(CH_2CH{=}CH_2)$ (**3a**) has been previously prepared under slightly different conditions,[13] but was not detected at any stage of the reaction. Hence, vinylic deprotonation (path B, Scheme 2) is kinetically and/or thermodynamically preferred to allylic deprotonation (path A, Scheme 2).

The generality of this phenomenon was examined. First, the 1-pentene complex $[(\eta^5\text{-}C_5H_5)Re(NO)(PPh_3)$-

Scheme 2. Allylic vs Vinylic Deprotonation of Cationic Alkene Complexes

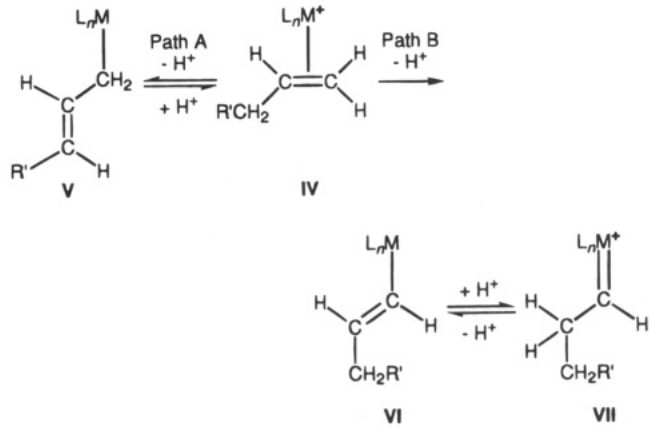

Scheme 3. Vinylic Deprotonation of Alkene Complexes (*RS,SR*)-$[(\eta^5\text{-}C_5H_5)Re(NO)(PPh_3)(H_2C{=}CHR)]^+BF_4^-$ ((*RS,SR*)-1)

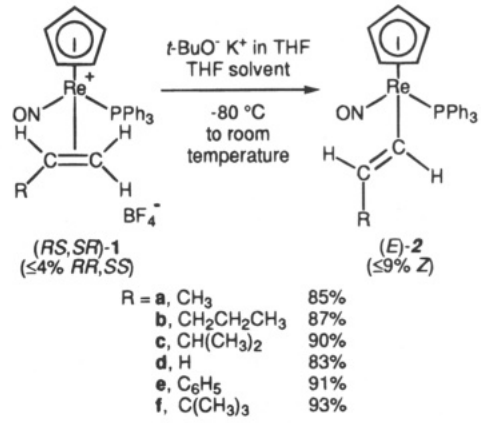

(12) (a) Rosenblum, M. *J. Organomet. Chem.* **1986**, *300*, 191. (b) Cutler, A.; Ehntholt, D.; Giering, W. P.; Lennon, P.; Raghu, S.; Rosenblum, M.; Tancrede, J.; Wells, D. *J. Am. Chem. Soc.* **1976**, *98*, 3495.

(13) Bodner, G. S.; Emerson, K.; Larsen, R. D.; Gladysz, J. A. *Organometallics* **1989**, *8*, 2399.

(14) Peng, T.-S.; Gladysz, J. A. *Organometallics* **1990**, *9*, 2884.

(15) All ratios are normalized to 100, and error limits on each integer are ±2; e.g., 96:4 ≡ (96 ± 2):(4 ± 2).

(16) (a) Unless otherwise noted, other deprotonations were conducted in an analogous fashion. Solutions or suspensions of alkene complexes **1** and $t\text{-}BuO^-K^+$ (1.0–1.4 equiv) were mixed at −80 °C, and the cold bath was removed. (b) Workups (room temperature) were designed to avoid fractionation of alkenyl and allyl complexes **2** and **3**. In some cases, small amounts of byproducts remained. (c) Deprotonations are much slower in *t*-BuOH, presumably due to the low solubility of **1**, and usually give greater amounts of byproducts.

(17) Bodner, G. S.; Smith, D. E.; Hatton, W. G.; Heah, P. C.; Georgiou, S.; Rheingold, A. L.; Geib, S. J.; Hutchinson, J. P.; Gladysz, J. A. *J. Am. Chem. Soc.* **1987**, *109*, 7688.

Scheme 4. Independent Syntheses and Attempted Interconversion of Isomeric Alkenyl and Allyl, and Alkene and Alkylidene, Complexes

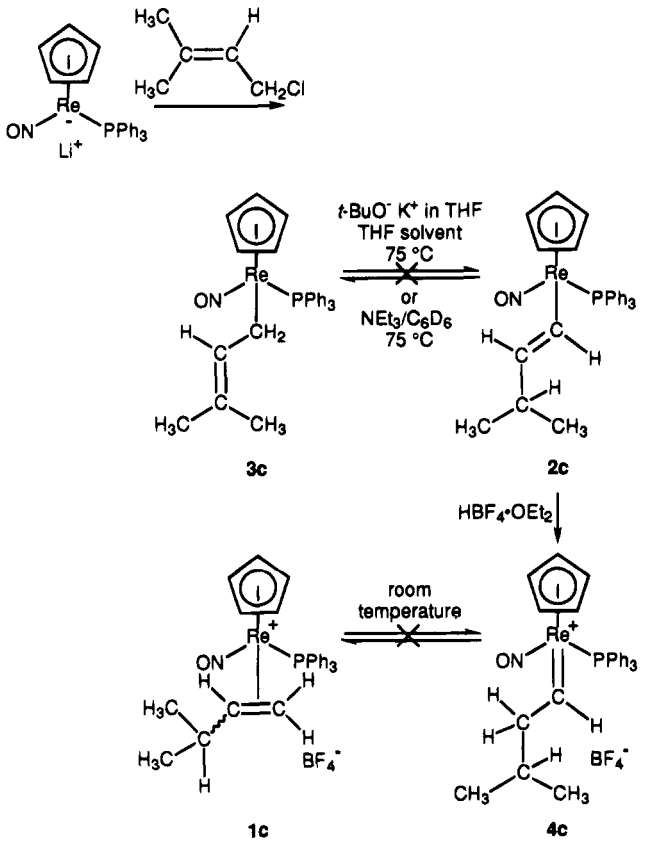

$(H_2C{=}CHCH_2CH_2CH_3)]^+BF_4^-$ (**1b**; 96:4 *RS,SR/RR,SS*)[5a,b] was similarly treated with *t*-BuO$^-$K$^+$/THF (Scheme 3).[16] Workup gave the known pentenyl complex (η^5-C_5H_5)Re(NO)(PPh$_3$)(CH=CHCH$_2$CH$_2$CH$_3$) (**2b**; 87%)[17] as a 91:9 *E/Z* mixture. An identical reaction of the diastereomerically pure isopropylethene complex (*RS,SR*)-[(η^5-C_5H_5)Re(NO)(PPh$_3$)(H$_2$C=CHCH(CH$_3$)$_2$)]$^+$ BF$_4^-$ (**1c**)[5b] gave the new alkenyl complex (η^5-C_5H_5)Re(NO)(PPh$_3$)(CH=CHCH(CH$_3$)$_2$) (**2c**; 90%) as a 97:3 *E/Z* mixture.

Complex **2c**, and all new compounds isolated below, were characterized by microanalysis and IR and NMR (^{1}H, ^{13}C, ^{31}P) spectroscopy, as described in the Experimental Section. Properties resembled those detailed earlier for other alkenyl complexes of **I**.[17] A proton-coupled ^{13}C NMR spectrum of **2c** gave doublets for both C=C carbons, indicative of one directly bound proton on each ($^1J_{CH}$ = 134 (C$_\alpha$), 147 (C$_\beta$) Hz). An authentic sample of the allylic deprotonation product (η^5-C_5H_5)Re(NO)(PPh$_3$)(CH$_2$CH=C(CH$_3$)$_2$) (**3c**), in which only one C=C carbon has a directly bound proton, was prepared in 97% yield from the rhenium anion[18] Li$^+$[(η^5-C_5H_5)Re(NO)(PPh$_3$)]$^-$ as shown in Scheme 4.

The preceding reactions could conceivably involve the initial formation of an allyl complex, followed by rapid isomerization. Thus, alkene complexes that lacked allylic protons were investigated. The ethene complex [(η^5-C_5H_5)Re(NO)(PPh$_3$)(H$_2$C=CH$_2$)]$^+$BF$_4^-$ (**1d**),[19] styrene complex (*RS,SR*)-[(η^5-C_5H_5)Re(NO)(PPh$_3$)(H$_2$C=CHC$_6$H$_5$)]$^+$BF$_4^-$ (**1e**),[5] and *tert*-butylethene complex (*RS,SR*)-[(η^5-C_5H_5)Re(NO)(PPh$_3$)(H$_2$C=CHC(CH$_3$)$_3$)]$^+$ BF$_4^-$ (**1f**)[5b] were suspended (**1d,e**) or dissolved (**1f**) in THF. Additions of *t*-BuO$^-$K$^+$/THF as above[16] gave the known ethenyl complex (η^5-C_5H_5)Re(NO)(PPh$_3$)(CH=CH$_2$) (**2d**)[17] and the new *trans*-alkenyl complexes (*E*)-(η^5-C_5H_5)Re(NO)(PPh$_3$)(CH=CHC$_6$H$_5$) ((*E*)-**2e**) and (*E*)-(η^5-C_5H_5)Re(NO)(PPh$_3$)(CH=CHC(CH$_3$)$_3$) ((*E*)-**2f**) in 83–93% yields (Scheme 3).

Scheme 5. Deprotonation of Diastereomeric Styrene Complexes 1e

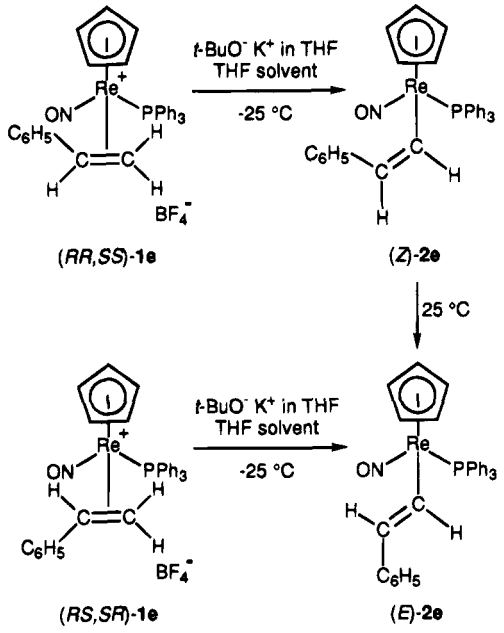

The new compounds (*E*)-**2e,f** were characterized as described above. No *cis* (*Z*) isomers were observed by ^{1}H NMR.[20] In this context, alkenyl complexes of **I** have been noted earlier to undergo *trans/cis* isomerization at variable rates.[17] The mechanism likely entails reversible C$_\beta$ protonation to give a cationic alkylidene complex, as shown for **VI** and **VII** in Scheme 2, or similar processes with other adventitious electrophiles. Equilibrium ratios for **2a,b** have been previously reported (*E/Z*, CDCl$_3$, 3 h: 84:16, 92:8).[17] Replicate experiments gave similar values, and **2c,e,f** exhibited ≥95:≤5 *E/Z* equilibrium ratios.[20b]

2. Stereochemistry of Vinylic Deprotonation. The preceding results suggest that *RS,SR* diastereomers of alkene complexes **1** undergo selective deprotonation to *trans*-alkenyl complexes (*E*)-**2**. In the case of a stereospecific reaction, the less stable *RR,SS* diastereomers should give *cis* isomers (*Z*)-**2**. Thus, a THF suspension of the styrene complex (*RR,SS*)-**1e**[5a] and *t*-BuO$^-$K$^+$/THF were combined at −25 °C (Scheme 5). Workup at −25 °C gave the styrenyl complex **2e** as a 3:97 mixture of *E/Z* isomers, as assayed by ^{1}H NMR in CD$_2$Cl$_2$.[21] The opposite styrene complex diastereomer, (*RS,SR*)-**1e**, was analogously reacted at −25 °C (Scheme 5). Low-temperature workup gave only (*E*)-**2e**.

(18) Crocco, G. L.; Gladysz, J. A. *J. Am. Chem. Soc.* **1988**, *110*, 6110.
(19) (a) Merrifield, J. H.; Lin, G.-Y.; Kiel, W. A.; Gladysz, J. A. *J. Am. Chem. Soc.* **1983**, *105*, 5811. (b) Fernandez, J. M.; Gladysz, J. A. *Organometallics* **1989**, *8*, 207.

(20) (a) Detection limits are 1% and 2%. Since authentic (*Z*)-**2e** is available (Scheme 5), the former is lower. (b) *E/Z* equilibrium ratios (this work): **2a**, 87:13 (CDCl$_3$, 1 day); **2b**, 91:9 (CDCl$_3$, 7 days); **2c**, 95:5 (C$_6$D$_6$, 2 days); **2e**, >99:<1 (CD$_2$Cl$_2$, 38 °C, 8 h); **2f**, >98:<2 (C$_6$D$_6$, 3 days); **2g**, 90:10 (CDCl$_3$, 3 h) and 82:18 (C$_6$D$_6$, 60 °C, 12 h); **2e**−Me$_5$, >99:<1 (C$_6$D$_6$, 1 day).
(21) Workups of preparative reactions of (*RR,SS*)-**1e**-d_n and *t*-BuO$^-$K$^+$ at room temperature invariably gave only (*E*)-**2e**-d_n (87–92% yields).

Scheme 6. Deprotonation of Deuterated Styrene Complexes 1e-d_1 by t-BuO$^-$K$^+$ (B$^-$) in THF (Conditions per Ref 16)

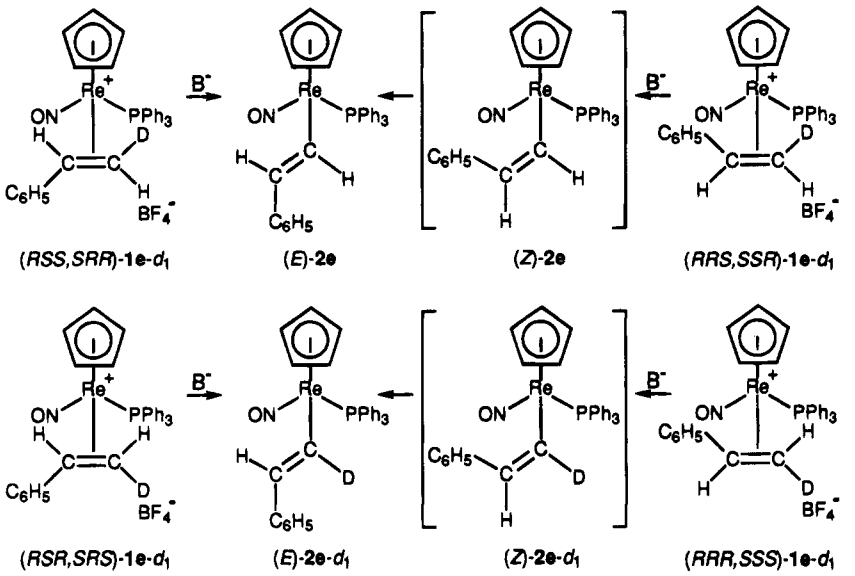

These data further suggested that only one of the two diastereotopic =CH$_2$ protons in each diastereomer of **1e** was abstracted. Thus, THF suspensions of the previously reported deuterated styrene complexes[5c] shown in Scheme 6 were reacted with t-BuO$^-$K$^+$/THF at −80 °C, followed by workup at room temperature.[16] Substrates (*RSS,SRR*)-**1e**-d_1 (97% D) and (*RRS,SSR*)-**1e**-d_1 (95% D)[21] gave the *un*labeled styrenyl complex (*E*)-**2e**. In contrast, (*RSR,SRS*)-**1e**-d_1 (95% D) and (*RRR,SSS*)**1e**-d_1 (83% D)[21] gave the deuterated styrenyl complex (*E*)-**2e**-d_1 (95–83% D).

The above data show that the deprotonations of styrene complexes **1e**–d_n are stereospecific. In each diastereomer, rhenium replaces the hydrogen or deuterium in the geminal position closer to the cyclopentadienyl ligand, corresponding to H$_S$ in **II** (*RS*) and **III** (*RR*; Scheme 1). Thus, the deprotonation site is controlled by the configuration at rhenium, rather than that of the alkene-based =CHR stereocenter. In the latter event, the proton abstracted would always have the same *trans/cis* sense relative to the =CH*R* substituent.

The less stable *RR,SS* diastereomers of the other alkene complexes would also be expected to give the *cis*-alkenyl complexes (*Z*)-**2**. However due to the ease of *E/Z* isomerization, only selected cases were examined. For example, a THF solution of the 1-pentene complex (*RR,SS*)-**1b** and t-BuO$^-$K$^+$/THF were combined in an NMR tube at −80 °C. At room temperature, a ^{31}P NMR spectrum showed 75% conversion to a 10:90 mixture of pentenyl complexes (*E*)-**2b** and (*Z*)-**2b**. Workup gave a 25:75 (*E*)-**2b**/(*Z*)-**2b** mixture in 74% yield. Other reactions of *RR,SS* diastereomers are described below.

A THF solution of the previously reported optically active styrene complex (−)-(*SR*)-**1e** (>98% ee)[5a] was also treated with t-BuO$^-$K$^+$/THF at −80 °C.[16] This substrate is much more soluble than the racemate. Workup gave the optically active *trans*-styrenyl complex (−)-(*E*)-(*R*)-**2e** in 81% yield. Analysis by chiral HPLC established an enantiomeric excess of >98%.[22] The configuration at rhenium, which corresponds to retention, was assigned on the basis of the commonly observed correlation with the sign of the optical rotation in this series of compounds,[19] as well as the mechanistic implausibility of any pathway involving inversion.

3. Vinylic vs Allylic Deprotonation. We previously reported differing results in similar reactions utilizing *tert-butyl alcohol* solutions of t-BuO$^-$K$^+$ (0.75 M).[13] Specifically, the hexafluorophosphate salts of propene complex **1a**, allylbenzene complex [(η^5-C$_5$H$_5$)Re(NO)(PPh$_3$)(H$_2$C=CHCH$_2$C$_6$H$_5$)]$^+$BF$_4^-$ (**1g**), and isobutene complex (η^5-C$_5$H$_5$)Re(NO)(PPh$_3$)(H$_2$C=C(CH$_3$)$_2$)]$^+$BF$_4^-$ (**1h**) gave the corresponding σ-allyl complexes **3** (84%, 70%, and 73% after workup).[23] We sought to reconcile this dichotomy[24] and define any influence of structure or solvent upon selectivity.

Thus, the allylbenzene complex **1g** (95:5 *RS,SR*/*RR,SS*)[5a,b] was dissolved in THF and treated with t-BuO$^-$K$^+$ in t-BuOH (0.75 M) at −80 °C (Scheme 7).[16] A ^{31}P NMR spectrum (room temperature) showed that the major product was indeed the *trans*-cinnamyl complex (*E*)-(η^5-C$_5$H$_5$)Re(NO)(PPh$_3$)(CH$_2$CH=CHC$_6$H$_5$) ((*E*)-**3g**; 64%).[13] However, the vinylic deprotonation product (*E*)-(η^5-C$_5$H$_5$)Re(NO)(PPh$_3$)(CH=CHCH$_2$C$_6$H$_5$) ((*E*)-**2g**; 20%)[17] was also present, along with four minor byproducts.[23,25a] Workup gave a 21:79 (*E*)-**2g**/(*E*)-**3g** mixture (88%).[23] This establishes, in the absence of any product equilibration (below), the existence of competing deprotonation pathways.

(22) Ramsden, J. A.; Garner, C. M.; Gladysz, J. A. *Organometallics* **1991**, *10*, 1631. Retention times (95:5 hexanes/2-propanol, 1.5 mL/min): (−)-(*E*)-(*R*)-**2e**, 7.9 min; (+)-(*E*)-(*S*)-**2e**, 12.8 min.

(23) In all preparations of allyl complexes **3** to date, only *trans* isomers have been detected. The unidentified minor byproducts formed in certain reactions may include *cis* isomers.

(24) The ^{1}H and ^{13}C NMR spectra of the original sample of **3a** prepared from the hexafluorophosphate salt of **1a** (ca. 67:33 *RS,SR*/*RR,SS*; C$_6$H$_5$Cl solvent)[13] showed ca. 10% of the propenyl complex (*E*)-**2a**. Comparable amounts of (*E*)-**2g** would have been removed in the workup procedure used for (*E*)-**3g**.

(25) ^{31}P NMR data (ppm, reaction solvent unless noted): (a) 21.8, 25.4, 27.6, 27.2, 24.9, 19.2 ((*E*)-**2g**/(*E*)-**3g**/byproducts), 20:64:4:4:5:2; (b) 23.6, 25.9, 26.3, 25.6, 24.9 (C$_6$D$_6$, (*E*)-**2a**/**3a**/byproducts), 68:17:6:4:4; (c) 22.8, 26.0, 27.7, 27.2, 25.8, 18.7 (C$_6$D$_6$, (*E*)-**2b**/(*E*)-**3b**/byproducts), 61:12:6:10:5:7; (d) 24.7, 26.2, 12.5, 6.7 ((*Z*)-**2a**/**3a**/byproducts), 79:3:9:9; (e) 23.6, 24.7, 33.5, 12.5, −13.8 ((*E*)-**2a**/(*Z*)-**2a**/byproducts), 32:28:10:23:7; (f) 23.6, 24.7, 26.2, 12.2, 11.8, 6.7 ((*E*)-**2a**/(*Z*)-**2a**/**3a**/byproducts), 38:12:4:25:17:4.

Scheme 7. Vinylic vs Allylic Deprotonation of Allylbenzene Complex 1g as a Function of Solvent[a]

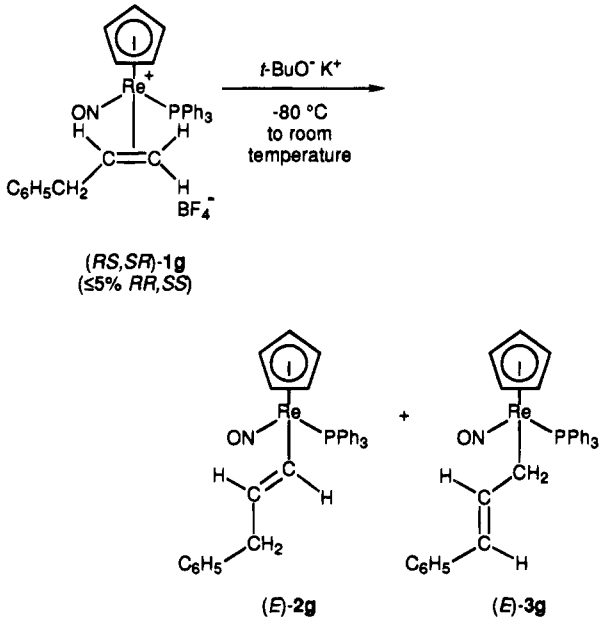

solvent for t-BuO⁻ K⁺	solvent for 1g	yield (%)	(E)-2g/(E)-3g
t-BuOH	THF	88	21:79
t-BuOH	t-BuOH	90	3:97
THF	THF	91	89:11

[a] See text and ref 16 for reaction conditions.

An analogous reaction was conducted with a *t*-BuOH *suspension* of **1g** (Scheme 7).[16c] Workup gave a 3:97 mixture of alkenyl complex (*E*)-**2g** and cinnamyl complex (*E*)-**3g** (90%). Thus, when *t*-BuOH is the only solvent, virtually exclusive allylic deprotonation occurs. In contrast, a reaction with THF solutions of *both* **1g** and *t*-BuO⁻K⁺ gave an 89:11 (*E*)-**2g**/(*E*)-**3g** mixture (91%). Thus, when THF is the only solvent, predominant vinylic deprotonation occurs. Hence, depending upon solvent, either vinylic *or* allylic carbon–hydrogen bond activation can be effected in a highly selective manner.

The influence of allylic substituents upon selectivity was probed, using the mixed THF/*t*-BuOH solvent system that gave both vinylic and allylic deprotonation with **1g**. Under these conditions (Scheme 8), the propene complex **1a** (*RS,SR/RR,SS* 96:4) afforded a mixture of propenyl complex (*E*)-**2a** (68%), allyl complex **3a** (17%), and three minor byproducts (15%) in 72% yield (80:20 (*E*)-**2a/3a**).[25b] The 1-pentene complex **1b** (*RS,SR/RR,SS* 96:4) gave a mixture of pentenyl complex (*E*)-**2b** (61%), allyl complex (*E*)-(η^5-C_5H_5)Re(NO)(PPh_3)(CH_2-CH=CHCH$_2$CH$_3$) ((*E*)-**3b**; 12%), and four minor byproducts (98%; 84:16 (*E*)-**2b**/(*E*)-**3b**).[23,25c] The isopropylethene complex (*RS,SR*)-**1c** gave only alkenyl complex **2c** (97%). This shows that (1) vinylic deprotonation increases as the number of *alkyl* allylic substituents increases (**1c** > **1b** > **1a**), and (2) allylic deprotonation is enhanced by a phenyl substituent relative to alkyl or hydrogen substituents (**1g** > **1a,b**). Rationales are proposed below.

The effect of the diastereomer of the alkene complex utilized upon selectivity was probed (Scheme 9). Thus, a CH_2Cl_2 solution containing mainly the more stable diastereomer of propene complex **1a** (*RS,SR/RR,SS* 96:4) was treated with *t*-BuO⁻K⁺/THF. Workup gave a 98:2 (*E*)-**2a/3a** mixture (84%), similar to the corresponding reaction in THF (Scheme 3). However, when analogous reactions were conducted with samples containing mainly the less stable diastereomer of **1a** (*RS,SR/RR,SS* 6:94), differing results were obtained. A THF solution gave a 41:41:18 (*E*)-**2a**/(*Z*)-**2a/3a** mixture (86%), but a CH_2Cl_2 solution gave a 3:97 (*E*)-**2a/3a** mixture (99%). Hence, (*RR,SS*)-**1a** is more prone to allylic deprotonation than (*RS,SR*)-**1a**, and the difference is more pronounced in CH_2Cl_2 than in THF.

Scheme 8. Vinylic vs Allylic Deprotonation of Alkene Complexes 1 as a Function of Allylic Substituent[a]

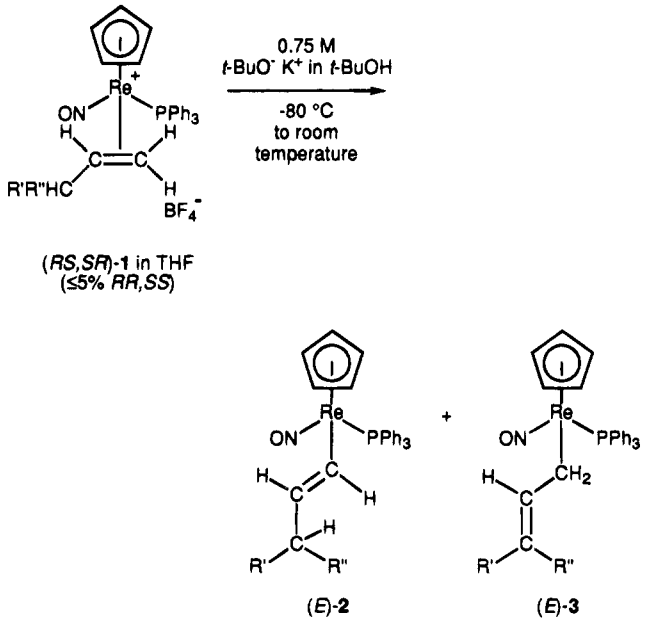

	R'	R"	yield (%)	2/3
a	H	H	72[b]	80:20
b	CH_2CH_3	H	98[b]	84:16
c	CH_3	CH_3	97	>99:<1
g	C_6H_5	H	88	21:79

[a] See text and ref 16 for reaction conditions. [b] Minor amounts of byproducts are present; see text.

An identical series of reactions was conducted with allylbenzene complex **1g** (Scheme 9). Similar trends were obtained, with both diastereomers exhibiting more allylic deprotonation than propene complex **1a**. However, both diastereomers of 1-pentene complex **1b** gave exclusive vinylic deprotonation in THF—in contrast to the result with (*RR,SS*)-**1a**.

4. Reactant and Product Isomerization. In view of the lack of precedent for the *direct* abstraction of vinylic protons from cationic alkene complexes, alternative "indirect" pathways were considered. For example, cationic alkylidene complexes [(η^5-C_5H_5)Re(NO)(PPh_3)(=CHCH$_2$R)]⁺X⁻ (**4**) and bases also cleanly react to give alkenyl complexes **2** (**VII** → **VI**, Scheme 2).[17] Thus, the possibility that alkene complexes **1** might be in rapid equilibrium with **4** under the conditions of Scheme 3 must be addressed. The hexafluorophosphate salt of propylidene complex **4a** (R = CH_3) has been previously isolated and isomerizes to the corresponding propene complex **1a** at 65–85 °C ($\Delta H^{\ddagger} = 27 \pm 1$ kcal/mol, $\Delta S^{\ddagger} = 3 \pm 3$ eu; C_6H_5Cl).[10b] Importantly, rearrangement is

Scheme 9. Vinylic vs Allylic Deprotonation of Alkene Complexes 1 as a Function of Configurational Diastereomer[a]

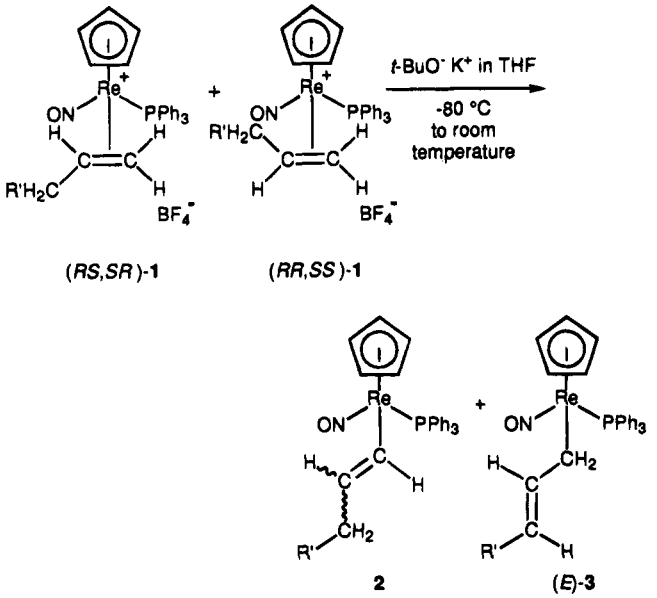

	R'	(RS,SR)/(RR,SS)	solvent	yield (%)	2/(E)-3
a	H	96:04	THF	85	>99:<1
		06:94		86	82:18
		96:04	CH_2Cl_2	84	98:02
		06:94		99	03:97
b	CH_2CH_3	95:05	THF	87	>99:<1
		<1:>99		74	>99:<1
g	C_6H_5	95:05	THF	91	89:11
		<1:>99		77	61:39
		95:05	CH_2Cl_2	94	78:22
		<1:>99		97	<1:>99

[a] See text and ref 16 for reaction conditions.

exothermic, with a K_{eq} value of ≥100. Hence, the reverse, endothermic process cannot be rapid at room temperature and can be excluded in Scheme 3.

It might be argued that the bulkier isopropyl or *tert*-butyl alkene substituents in **1c,f** could kinetically promote isomerization to alkylidene complexes. Alkylidene complexes **4** are easily prepared by C_β protonation of the corresponding alkenyl complexes (**VI** → **VII**; Scheme 2).[6a,17] Thus, **2c** and $HBF_4{\cdot}OEt_2$ were combined in CD_2Cl_2 at −80 °C (Scheme 4).[26] Workup gave the 3-methylbutylidene complex $[(\eta^5\text{-}C_5H_5)Re(NO)(PPh_3)(=CHCH_2CH(CH_3)_2)]^+BF_4^-$ (**4c**) in 95% yield. No interconversion of **4c** and **1c** was detected at room temperature.

We next tested the related possibility that alkenyl complexes **2** and allyl complexes **3** might equilibrate under the conditions of Scheme 3 or 7. Thus, 85:15 and 12:88 mixtures of alkenyl complex **2g** and cinnamyl complex **3g** were generated in THF from mixtures of diastereomeric allylbenzene complexes (*RS,SR*)- and (*RR,SS*)-**1g** (Schemes 8 and 9). These samples, which included excess $t\text{-BuO}^-K^+$ (0.4 equiv) and the byproduct *t*-BuOH (1.0 equiv in the former, several equivalents in the latter), were kept at 60 °C for 12 h. The **2g/3g** ratios were unaffected, as assayed by ^{31}P NMR. Also, as

(26) This reaction was monitored by ^1H and ^{31}P NMR. At −80 °C, **4c** rapidly formed as a 98:2 mixture of *ac/sc* Re=C conformers.[11b] The solution was warmed to room temperature, and equilibration to a 95:5 mixture occurred. This ratio is higher than those of the corresponding ethylidene and pentylidene complexes ((90−91):(10−9)),[10a] consistent with the greater bulk of the =CH*R* substituent.

Scheme 10. Stability Order for Isomeric Allyl and Propenyl Complexes (This Work) and Propargyl, Allenyl, and Propynyl Complexes (Ref 9)

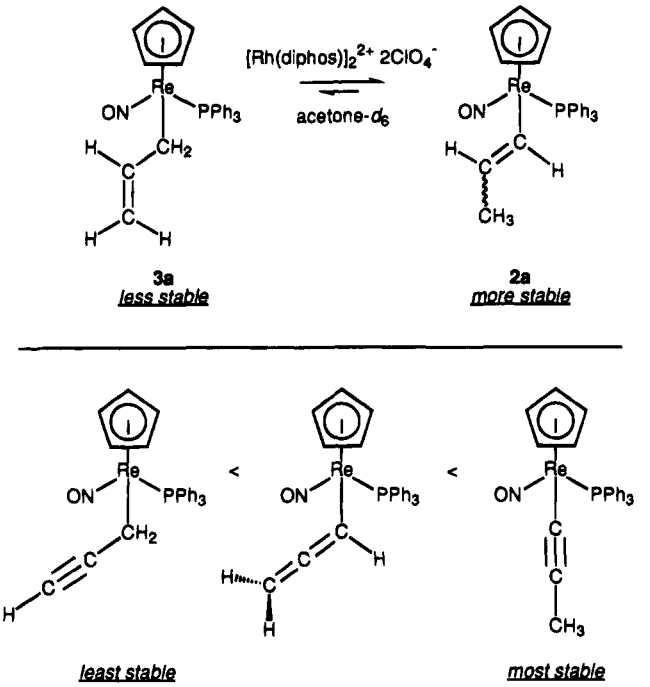

shown in Scheme 4, **2c** and **3c** were separately treated with $t\text{-BuO}^-K^+$ (1.1 equiv, THF, 75 °C, 8 h) and NEt_3 (1.1 equiv, C_6D_6 solvent, 75 °C, 3 h). In no case was any isomerization or degradation observed. Comparable results were obtained with **2a/3a** mixtures, although after extended periods minor amounts of decomposition occurred.

We then sought to equilibrate alkenyl and allyl complexes **2** and **3** by any means. No data on the relative thermodynamic stabilities of isomeric alkenyl and allyl complexes—which would help interpret certain features of the above reactions—appear to be available. Thermolyses of **2a/3a** mixtures gave only the independent decomposition of **3a** (140 °C, C_6H_5Cl). Thus, **3a** and the alkene isomerization catalyst[27] $[Rh(diphos)]_2^{2+}(ClO_4^-)_2$ were dissolved in acetone-d_6 at room temperature (Scheme 10; Re/Rh 1.0:0.4). After 2 days, a ^{31}P NMR spectrum showed a 3:79:9:9 mixture of **3a**, the less stable *cis*-propenyl complex (*Z*)-**2a**, and two unidentified byproducts.[25d] The identity of (*Z*)-**2a** was confirmed by ^1H NMR. Unexpectedly, no (*E*)-**2a** was detected. After 4 days, some (*E*)-**2a** had formed (ca. 2%). After 18 days, no **3a** remained. Only (*Z*)-**2a**, (*E*)-**2a**, and three byproducts were present (28:32:10:23:7).[25e]

The preceding experiment clearly shows that *cis*-propenyl complex (*Z*)-**2a** is more stable than allyl complex **3a**. However, something appears to inhibit conversion of (*Z*)-**2a** to the still more stable *trans* isomer (*E*)-**2a**. An identical reaction of (*E*)-**2a** and $[Rh(diphos)]_2^{2+}(ClO_4^-)_2$ gave, after 2 days, a 4:12:38:25:17:4 mixture of **3a**, (*Z*)-**2a**, (*E*)-**2a**, and three byproducts.[25f] Thus, small amounts of **3a** can be formed from **2a**, verifying the operation of an equilibrium. Unfortunately, quantitative data cannot be extracted from these experiments due to the many byproducts. Other po-

(27) (a) Fryzuk, M. D.; Bosnich, B. *J. Am. Chem. Soc.* **1977**, *99*, 6262. (b) Fairlie, D. P.; Bosnich, B. *Organometallics* **1988**, *7*, 936. (c) Bergens, S. H.; Bosnich, B. *J. Am. Chem. Soc.* **1991**, *113*, 958.

tential rhodium or titanium catalysts screened did not give detectable isomerization.

5. Additional Mechanistic Experiments. We sought data bearing upon other possible intermediates in the above deprotonations. For example, the styrene complex (*RS,SR*)-**1e** was reacted as in Scheme 3, but in the presence of PPh_3-d_{15} (2.0 equiv).[16] A mass spectrum of the resulting styrenyl complex (*E*)-**2e** showed no PPh_3-d_{15} incorporation. Hence, PPh_3 dissociation at any stage of the reaction coordinate is excluded.

Next, the reversibility of vinylic deprotonation was assayed. First, propene complex **1a** (*RS,SR/RR,SS* 96:4) and the *deuterated* alcohol *t*-BuOD (10 equiv) were dissolved in CH_2Cl_2 at −80 °C. Then a *deficiency* of *t*-BuO$^-$K$^+$/THF was added (0.5 equiv). Workup gave propenyl complex **2a** (37%) and unreacted **1a** (30%). A mass spectrum of the latter showed a parent ion that was 5−6% deuterated. However, the fragment ion [(η^5-C_5H_5)Re(NO)(PPh_3)]$^+$ (**I**) was also 5−6% deuterated, indicating no exchange into the propene ligand. Hence, vinylic deprotonation is not reversible.

A kinetic deuterium isotope effect for a representative vinylic deprotonation was sought. However, conventional rate measurements were complicated by the heterogeneity of some reactions, as noted above, and intermediates described below. Thus, in a competition experiment, a THF suspension of styrene complex (*RS,SR*)-**1e** and the =CD_2 labeled analog (*RS,SR*)-**1e**-d_2 (50:50)[5c] was treated with a *deficiency* of *t*-BuO$^-$K$^+$/THF (10 mol % vs total Re). A mass spectrum of the resulting styrenyl complex (*E*)-**2e** showed a 63:37 d_0/d_1 mixture, implying a k_H/k_D value of 1.7.[28] This establishes, together with the preceding experiment, that hydrogen is abstracted during the rate-determining step, presumably via a bent or unsymmetrical transition state.

Barriers to 180° rotations about the Re−(C=C) axes in *cis*-alkene complexes of **I** are only 11−14 kcal/mol.[6b] Thus, vinylic deprotonation might involve either of the two limiting Re−(C=C) conformers, as illustrated by **VIII** and **IX** in Scheme 11.[11b] We could not devise a direct test for the intermediacy of the less stable conformer **IX**.[29] Therefore, reactions of the isobutene complex **1h** were investigated. Due to the combined bulk of the geminal methyl groups, the Re−(C=C) conformers of **1h** (**X**, **XI**; Scheme 11), and the corresponding deprotonation transition states, should have much greater energy differences. If transition states

Scheme 11. Re−(C=C) Conformational Equilibria and Deprotonation of Isobutylene Complex 1h

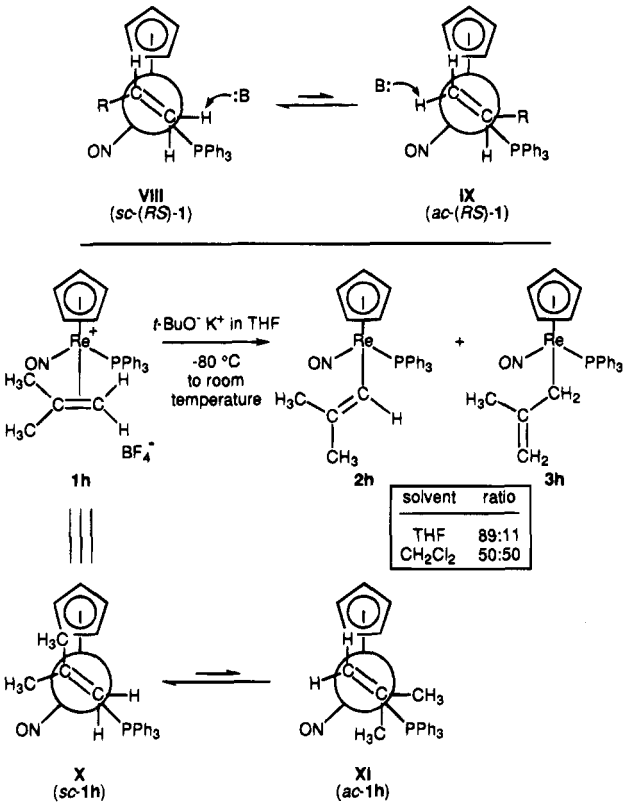

of the type ***IX*** + ***B***:$^-$ were *required* for vinylic deprotonation, **1h** would be less likely to give an alkenyl complex.

Thus, a THF solution of **1h** and *t*-BuO$^-$K$^+$/THF were combined in an NMR tube at −80 °C. A ^{31}P NMR spectrum (room temperature) showed the clean formation of a 89:11 mixture of the known alkenyl complex (η^5-C_5H_5)Re(NO)(PPh_3)(CH=C(CH_3)$_2$) (**2h**)[17] and methylallyl complex (η^5-C_5H_5)Re(NO)(PPh_3)(CH_2-C(CH_3)=CH_2) (**3h**).[13] An analogous reaction using a CH_2Cl_2 solution of **1h** gave a 50:50 **2h/3h** mixture. Workups gave 89:11 and 50:50 **2h/3h** mixtures in 94−97% yields. Interestingly, the **2h/3h** ratios match the *averages* of the **2a/3a** ratios obtained from the diastereomeric propene complexes (*RS,SR*)-**1a** and (*RR,SS*)-**1a** in THF or CH_2Cl_2 (Scheme 9). Hence, there is no special impediment to vinylic deprotonation with **1h**.

6. Additions of *t*-BuO$^-$K$^+$ to Cyclopentadienyl Ligands. The reaction of propene complex **1a** (*RS,SR/RR,SS* 96:4) and *t*-BuO$^-$K$^+$/THF was monitored by ^{31}P NMR at −80 °C under the conditions of Scheme 3. Within a few minutes, the resonance of **1a** was replaced by those of (*E*)-**2a** and a new species (23.7, 22.9 ppm, 68:32). When the sample was warmed to room temperature, only (*E*)-**2a** remained (23.4 ppm). The isomeric complexes (*Z*)-**2a** and **3a** give resonances downfield of that of (*E*)-**2a** (24.2, 25.7 ppm). Thus, the 22.9 ppm resonance was ascribed to an intermediate.

Analogous reactions were conducted in CD_2Cl_2 with 96:4 and 8:92 mixtures of (*RS,SR*)- and (*RR,SS*)-**1a**. In this solvent, the intermediate formed in 98% yields, as 96:4 and 8:92 mixtures of isomers (^{31}P NMR: 21.5, 19.4 ppm). ^{1}H and ^{13}C NMR spectra were recorded at −60 °C (Experimental Section). Importantly, the cyclopentadienyl ^{1}H and ^{13}C resonances of **1a** had been replaced by more complex signals. New *tert*-butoxy ^{1}H and ^{13}C

(28) This value reflects both the primary isotope effect associated with the abstracted deuterium and the secondary isotope effect associated with the spectator deuterium. The latter should be only slightly greater than unity, as the spectator deuterium is bound to carbons with intermediate sp^2/sp^3 hybridization in **1e** and sp^2 hybridization in **2e**.

(29) (a) Conformers of the type **IX** are destabilized by steric interactions between the =CH*R* substituent and the bulky PPh_3 ligand and have been detected only for R = CO_2Et (**VIII/IX** 93:7: Wang, Y. Ph.D. Thesis, University of Utah, 1994. Wang, Y.; Gladysz, J. A. *Chem. Ber.* **1995**, *128*, in press). Equilibrium ratios are presumably higher for **1a−c,e−g**. (b) The energetics of the deprotonation transition states ***VIII*** + *B*:$^-$ and ***IX*** + *B*:$^-$ can be analyzed by analogy to unsymmetrical *trans*-alkene complexes of **I**.[6c,7] If the directly bound =CH*R* substituent has a greater effective bulk than the =C(H)*H*=:*B*$^-$ moiety, then the former transition state should (in the absence of contributing electronic effects) be more stable. (c) Numerous equilibria involving adducts of **I** and alkenes of the formula (CH_3)$_n$(H)$_{2-n}$C=CHCH_3 (n = 0−2) have been studied.[6b,c] From these data, the **X/XI** equilibrium ratios can be bounded as ≥99.5:0.5.

Scheme 12. Addition of *t*-BuO⁻K⁺ to Cyclopentadienyl Ligands

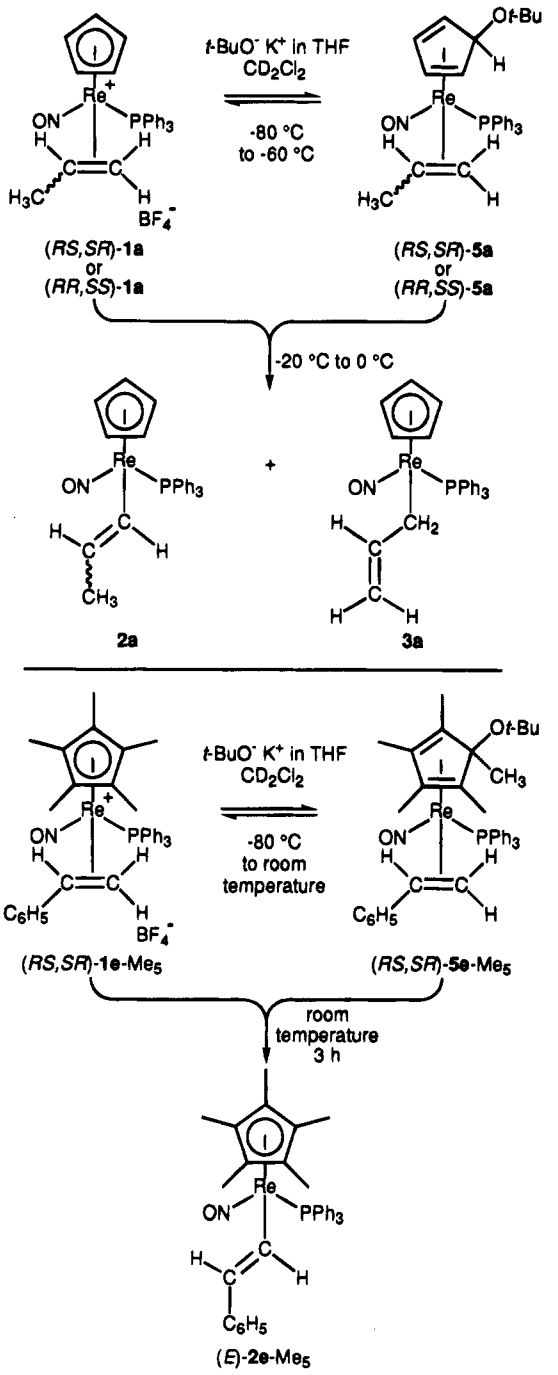

resonances were present, but shifted propene ligand ^{1}H and ^{13}C resonances remained. These data indicate the formation of isomeric, configurationally stable η^4-cyclopentadienyl complexes (η^4-C_5H_5O-*t*-Bu)Re(NO)(PPh_3)($H_2C{=}CHCH_3$) (**5a**), derived from attack of *t*-BuO⁻K⁺ upon the cyclopentadienyl ligand of **1a** (Scheme 12).

Many properties of **5a** matched those of the related η^4-cyclopentadiene complex (η^4-$C_5H_5CCl_3$)Re(NO)(PPh_3)($PPhCl_2$),[30] for which an *exo* relationship of the rhenium and CCl_3 moiety has been established crystallographically. An analogous geometry was assumed for **5a**. Both isomers of **5a** cleanly converted to **2a/3a** mixtures below 0 °C. However, the **2a/3a** ratios depended upon the warming rate.[31] Attempts to isolate **5a** at low temperatures were unsuccessful.

We sought to determine whether **5a** was on the reaction coordinate connecting **1a** and **2a**, or was simply due to a nonproductive but kinetically rapid equilibrium. In the former case, two 1,5-hydride shifts could isomerize the *tert*-butoxy group from an *exo* to an *endo* position,[32] allowing close proximity to the vinylic proton to be abstracted. In the latter case, the *tert*-butoxy group would dissociate and then externally attack the same vinylic proton. However, our inability to isolate **5a** hampered approaches to resolving this issue.

Thus, the *pentamethyl*cyclopentadienyl styrene complex [(η^5-C_5Me_5)Re(NO)(PPh_3)($H_2C{=}CHC_6H_5$)]⁺BF_4⁻ (**1e**-Me_5)[33] was studied. Although this compound might undergo *tert*-butoxide addition to the cyclopentadienyl ligand, there would not be a precedented low-energy pathway for accessing an *endo* isomer. Thus, formation of the corresponding styrenyl complex (η^5-C_5Me_5)Re(NO)(PPh_3)($CH{=}CHC_6H_5$) (**2e**-Me_5) would indicate that vinylic deprotonation need not be mediated by the cyclopentadienyl ligand. Indeed, a preparative reaction of (*RS*,*SR*)-**1e**-Me_5 and *t*-BuO⁻K⁺/THF in CH_2Cl_2 gave (*E*)-**2e**-Me_5 in 99% yield. A similar reaction was conducted in CD_2Cl_2 (Scheme 12), and NMR spectra were recorded at room temperature. Multiple pentamethylcyclopentadienyl-derived ^{1}H and ^{13}C resonances, and a ^{31}P resonance plausible for addition product **5e**-Me_5 (16.5 ppm, br; 91%), were present. After 3 h, only (*E*)-**2e**-Me_5 and small amounts of PPh_3 remained (96:4).

Discussion

1. Additional Background. Before analyzing the mechanism of vinylic deprotonation of alkene complexes **1**, we briefly summarize some related examples and previous studies of allylic deprotonation. First, the cyclopentene complexes [(η^5-C_5H_4R)Re(NO)(PPh_3)($CH{=}CH(CH_2)_3$)]⁺BF_4 (**7**; R = H, CH_3) and *t*-BuO⁻K⁺ cleanly react in THF to give the corresponding cyclopentenyl complexes **8**, as shown in Scheme 13 (top).[6a] The analogous allene complex is similarly transformed to an allenyl complex.[9] However, cyclohexene, cycloheptene, and cyclooctene complexes of **I** give mixtures of alkenyl and allyl complexes.[6a]

Angelici has found that sulfur-ligated thiophene complexes of **I** react with KOH (and other bases) to give neutral 2-thienyl complexes, as depicted by **9** and **10** in Scheme 13 (middle).[34] When SC*H* protons are absent, 3-thienyl complexes form. Accordingly, mechanisms involving initial isomerization to C=C ligated η^2-thiophene complexes such as **11** have been proposed. The latter are spectroscopically observable in closely

(30) Buhro, W. E.; Arif, A. M.; Gladysz, J. A. *Inorg. Chem.* **1989**, *28*, 3837.

(31) One sample of the 96:4 mixture was slowly warmed in an NMR probe, and a −80 °C bath was abruptly removed from another. The first gave a 69:23:8 (*E*)-**2a**/(*Z*)-**2a/3a** mixture and the second a 98:2 (*E*)-**2a/3a** mixture (ambient probe temperatures). Identical experiments with the 8:92 mixture gave 21:14:65 (*E*)-**2a**/(*Z*)-**2a/3a** and 3:97 (*E*)-**2a/3a** mixtures.

(32) For examples of 1,5-hydride shifts in η^4-C_5H_5R ligands, see: (a) Merrifield, J. H.; Gladysz, J. A. *Organometallics* **1983**, *2*, 782 and references therein. (b) Colomer, E.; Corriu, R. J. P.; Vioux, A. *J. Organomet. Chem.* **1984**, *267*, 107.

(33) Peng, T.-S.; Winter, C. H.; Gladysz, J. A. *Inorg. Chem.* **1994**, *33*, 2534.

(34) Robertson, M. J.; White, C. J.; Angelici, R. J. *J. Am. Chem. Soc.* **1994**, *116*, 5190.

Scheme 13. Additional Deprotonation Reactions

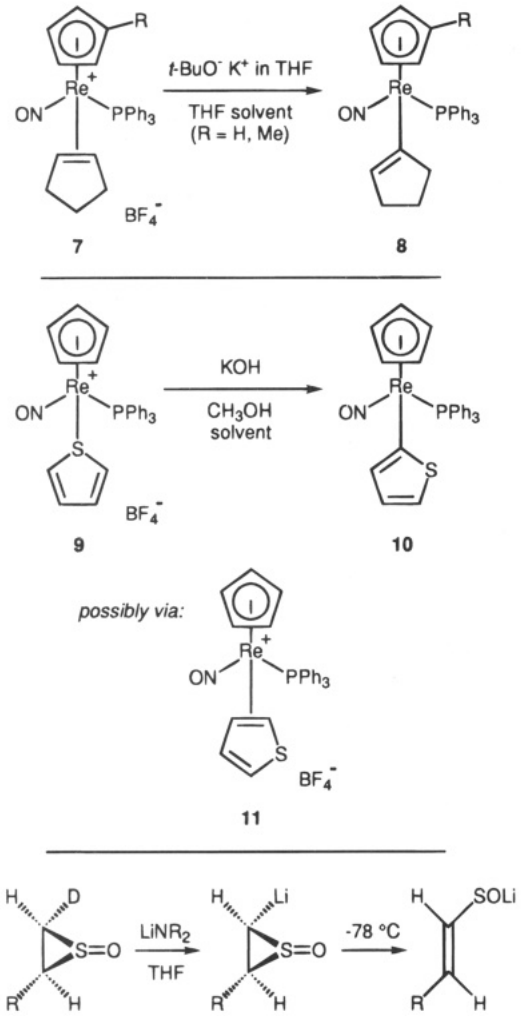

Scheme 14. Mechanism for Allylic Deprotonation of Alkene Complexes

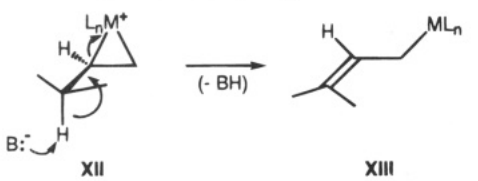

related systems and should undergo vinylic deprotonation similarly to **1** and **7**.

Reactions of alkene complexes of the iron Lewis acid $[(\eta^5\text{-}C_5H_5)Fe(CO)_2]^+$ and triethylamine have been extensively studied by Rosenblum.[12] Only allylic deprotonations are observed, and stereochemical data require transition states in which the carbon−hydrogen and M−(C=C) bonds are antiperiplanar.[35] This is illustrated in **XII** (Scheme 14), utilizing a metallacyclopropane resonance form to emphasize the similarity with common organic *anti* eliminations. Hence, one approach to rationalizing allylic vs vinylic deprotonation selectivity is to analyze whether some alkenes can accommodate this stereoelectronic requirement better than others.

For example, the propene complex **1a** should have no extraordinary barrier to achieving the geometry in

(35) (a) Amine bases are usually not strong enough to deprotonate alkene complexes of **I**.[5c] For example, **1a** and NEt_3 do not react in THF (12 h, room temperature). Thus, deprotonation selectivities cannot be measured under conditions analogous to Rosenblum's.

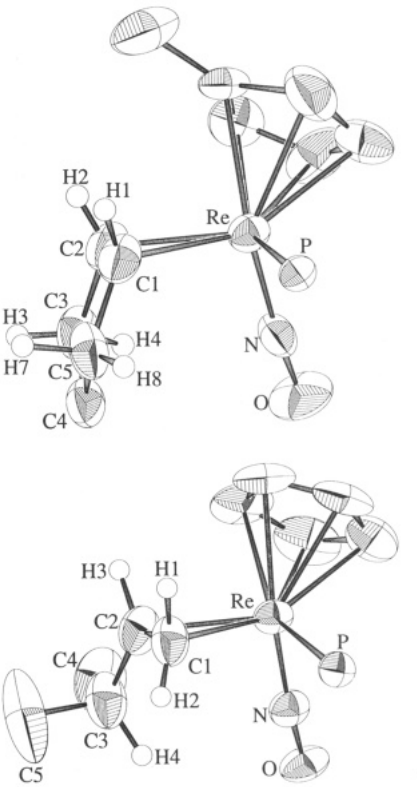

Figure 1. Partial Crystal Structures of the Cyclopentene Complex **7**-Me (top) and the Isopropylethene Complex (*RS*,*SR*)-**1c** (bottom).

XII—especially in view of the ready allylic deprotonation of allylbenzene complex **1g**. Similarly, the crystal structure of cyclopentene complex **7**-Me is shown in Figure 1 (top).[6a] Two allylic protons (H3, H7) are clearly prealigned for abstraction as in **XII**. However, both (*RS*,*SR*)-**1a** and **7** give exclusive vinylic deprotonation under the conditions of Scheme 3, indicating the availability of even lower energy transition states.

Nonetheless, the transition-state model **XII** does account for the trends in Scheme 8. As noted above, vinylic deprotonation increases as the number of alkyl substituents in the allylic position increases (**1c** > **1b** > **1a**). Sterically, an alkyl group would be more likely to be *anti* to the metal in **XII** than a hydrogen, disfavoring allylic deprotonation. Indeed, as shown in Figure 1 (bottom), (*RS*,*SR*)-**1c** crystallizes with a methyl group (C5) *anti* to rhenium.[5b] In contrast, the phenyl substituent in **1g** promotes allylic deprotonation—an electronic effect often observed in π-bond-forming eliminations. However, in the absence of such factors, allylic substituents disfavor allylic deprotonation.

2. Mechanism of Vinylic Deprotonation. The above data exclude a variety of mechanisms for the vinylic deprotonation of **1** and provide evidence against others. To summarize, deprotonation (1) is irreversible and rate-determining, (2) occurs with retention at rhenium, (3) is regiospecific for the $=CH_2$ terminus, (4) is stereospecific, with rhenium replacing only one of the diastereotopic $=CH_2$ protons, as controlled by the configuration at rhenium (H_S from (*RS*)- or (*RR*)-**1**), and (5) does not involve PPh_3 dissociation or initial isomerization of **1** to an alkylidene complex, as represented by the *RS*,*SR* diastereomer series in Scheme 15 (**12** and **4**; bottom).

Within these constraints, several types of preequilib-

Scheme 15. Mechanisms for Vinylic Deprotonation of Alkene Complexes (*RS,SR*)-1

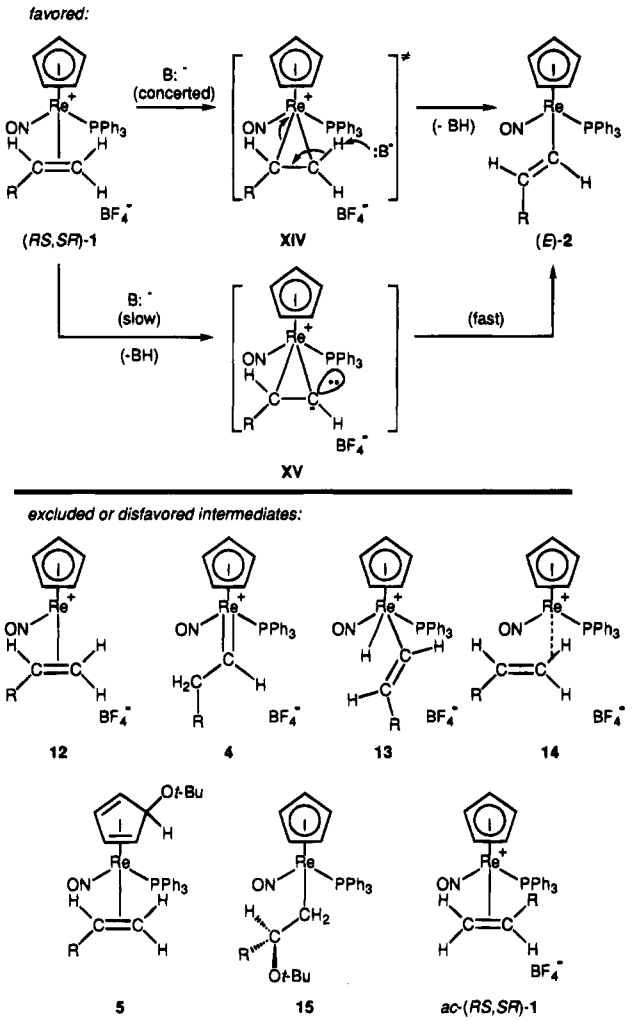

rium steps remain viable. For example, a reversible intramolecular oxidative addition involving the reactive vinylic carbon–hydrogen bond might occur, giving an alkenyl hydride complex (**13**; Scheme 15). Alternatively, a related "σ-bond" complex could form (**14**; Scheme 15). Either species would plausibly react with base to give the alkenyl complex **2**. However, a detailed study of the mechanism of equilibration of (*RS,SR*)- and (*RR,SS*)-**1** indicates that such species (which allow exchange of the C=C enantioface bound to rhenium) can be accessed only at temperatures of ≥95 °C.[5c]

Other preequilibrium steps are more difficult to exclude. As discussed above, the vinylic deprotonation of pentamethylcyclopentadienyl styrene complex (*RS,SR*)-**1e**-Me_5 (Scheme 12, bottom) provides good evidence against intermediates derived from *exo tert*-butoxide additions to cyclopentadienyl ligands (**5**). A related possibility would involve initial *tert*-butoxide attack at the alkene ligand =CHR terminus to give an alkyl complex (η^5-C_5H_5)Re(NO)(PPh_3)($CH_2CH(R)O$-*t*-Bu) (**15**, Scheme 15). Similar additions have in fact been observed with *methoxide* ion, as well as carbon nucleophiles.[36–38] However, in no case has such an addition product been found to eliminate alcohol to give an alkenyl complex. In our view, neither concerted four-center eliminations nor E2 steps involving a second equivalent of base have obvious kinetic driving forces that would render them rapid below room temperature.[39]

We also disfavor, on the basis of the data in Scheme 11 and other considerations,[29b] mechanisms involving the less stable *ac* Re–(C=C) conformers. From this analysis, we arrive at the two pathways at the top of Scheme 15, both of which feature initial and rate-determining carbon–hydrogen bond cleavage. The first is concerted, involving the transition state **XIV**. The second is stepwise, involving a carbanion or zwitterion **XV** that rapidly rearranges to an alkenyl complex. The concerted transition state **XIV** could also have considerable carbanion character.

Concerning the transition state **XIV**, it is obvious from the crystal structures in Figure 1 that the carbon–hydrogen and rhenium–carbon bonds being broken do not have an antiperiplanar relationship. This contrasts with the transition state **XII** for allylic deprotonation. Thus, there should be more stabilization from the developing C=C π-bond in the latter. At the same time, there is no obvious feature that would stabilize the carbanionic intermediate **XV** in the stepwise mechanism. The fragment **I** lacks low-lying acceptor orbitals that can interact with potential π-donor ligands.[40] Hence, we are presently unable to formulate an intuitive rationale for the lower transition state energy of vinylic deprotonation.[41]

However, it should be stressed that vinylic deprotonation gives the thermodynamically more stable product. It follows as a corollary that the vinylic protons of **1** are thermodynamically more acidic than the allylic protons. Isomeric propargyl, allenyl, and propynyl complexes show a similar energetic relationship, as illustrated in Scheme 10.[9] In both series of compounds, stability tracks the hybridization of the ligating carbon ($sp > sp^2 > sp^3$). The ease of vinylic deprotonation is also more reassuring in light of the conceptually related process in eq i of Scheme 16. Cationic ethyne complexes **XVI** undergo analogous rapid reactions with alkoxide bases to give neutral ethynyl complexes **XVII**.[42,43] On the basis of available data, there appear to be few mechanistic options other than analogs of those in Scheme 15.[42c]

Importantly, the vinylic deprotonation mechanisms in Scheme 15 have abundant precedent in organic

(36) Peng, T.-S. Unpublished results, University of Utah.

(37) Ghazy, T.; Kane-Maguire, L. A. P.; Do, K. *J. Organomet. Chem.* **1990**, *390*, 91.

(38) Peng, T.-S.; Gladysz, J. A. *Tetrahedron Lett.* **1990**, *31*, 4417; *J. Chem. Soc., Dalton Trans.*, submitted for publication.

(39) Methoxide and carbon nucleophiles add to the =CHR terminus of **1** from a direction *anti* to rhenium.[36,38] In order to account for the product stereochemistry in Scheme 5, a *syn* elimination of *t*-BuOH from **15** would be required.

(40) (a) Czech, P. T.; Gladysz, J. A.; Fenske, R. F. *Organometallics* **1989**, *8*, 1806. (b) Several properties of amido complexes of **I** illustrate this point: Dewey, M. A.; Knight, D. A.; Arif, A. M.; Gladysz, J. A. *Chem. Ber.* **1992**, *125*, 815.

(41) However, other types of cationic complexes of **I** can be deprotonated at low temperature to charge-separated, zwitterionic, or ylidic intermediates: (a) Crocco, G. L.; Lee, K. E.; Gladysz, J. A. *Organometallics* **1990**, *9*, 2819. (b) Cagle, P. C.; Arif, A. M.; Gladysz, J. A. *J. Am. Chem. Soc.* **1994**, *116*, 3655.

(42) (a) Kowalczyk, J. J.; Arif, A. M.; Gladysz, J. A. *Organometallics* **1991**, *10*, 1079. (b) Ramsden, J. A.; Weng, W.; Gladysz, J. A. *Organometallics* **1992**, *11*, 3635. (c) For terminal alkyne complexes of **I**, eq i of Scheme 16 is faster than isomerization to vinylidene complexes, which give analogous deprotonation products.

(43) Some representative examples: (a) Appel, M.; Heidrich, J.; Beck, W. *Chem. Ber.* **1987**, *120*, 1087. (b) Nicklas, P. N.; Selegue, J. P.; Young, B. A. *Organometallics* **1988**, *7*, 2248. (c) Akita, M.; Terada, M.; Oyama, S.; Moro-oka, Y. *Organometallics* **1990**, *9*, 816. (d) Lomprey, J. R.; Selegue, J. P. *J. Am. Chem. Soc.* **1992**, *114*, 5518.

Scheme 16. A Series of sp, sp², and sp³ Carbon–Hydrogen Bond Activation Reactions

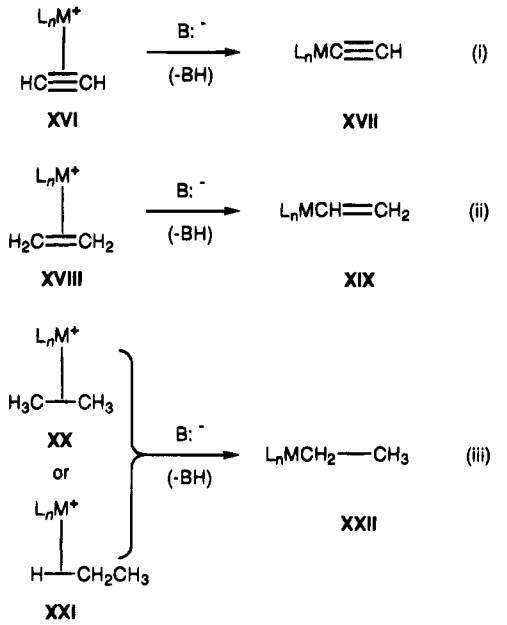

chemistry.[44] Three-membered heterocycles often react with strong bases to give ring-opened alkenyl derivatives. Scheme 13 (bottom) shows an example involving chiral thiirane *S*-oxides, with stereochemical features reminiscent of those in Scheme 6.[44a,b] Oxiranes undergo similar reactions, as well as eliminations analogous to the allylic deprotonation in Scheme 14.[44c] Ring-opening reactions of cyclopropyl carbanions are also well-known and are generally stereospecific due to orbital symmetry control.[44d]

3. Other Selectivity Issues. The vinylic deprotonation of **1** is under kinetic control. As noted above, *t*-BuO⁻K⁺ removes only one of the two =CH_2 protons, as controlled by the rhenium configuration (H_S in **II** and **III**, Scheme 1). The thermodynamically more acidic proton will always be that which gives the more stable *trans*-alkenyl complex (*E*)-**2**. Hence, the *less* acidic protons are abstracted from the less stable diastereomers (*RR,SS*)-**1**, which give *cis*-alkenyl complexes (*Z*)-**2**.

At our present level of understanding, there is no obvious electronic basis for an enhancement of the kinetic acidities of the H_S protons in **II** or **III**. We therefore suggest that the selectivity is steric in origin. The interstice between the PPh_3 and nitrosyl ligands is much more congested than that between the PPh_3 and cyclopentadienyl ligands.[41a,45] Also, in all crystal structures to date,[5a,b,6a,b,7,8a] the alkene ligands rotate 9–23° counterclockwise from the idealized conformations in **II** and **III**. This moves H_S somewhat further from the PPh_3 ligand than H_R, facilitating attack by base as in **VIII** (Scheme 11). In preliminary experiments, we have not observed vinylic deprotonation when the H_S position of **II** is blocked—such as in a *trans*-β-methylstyrene adduct.[6c,36]

Marked solvent effects upon vinylic/allylic deprotonation selectivities are apparent in Schemes 7 and 9. Importantly, *t*-BuO⁻K⁺ forms a 1:1 solvent complex and other hydrogen-bonded aggregates in *t*-BuOH.[46] Thus, the thermodynamic basicity is lower than in THF or DMSO. Accordingly, reactions of alkene complexes **1** and *t*-BuO⁻K⁺ are much slower in *t*-BuOH than in THF.[16c] Often, a less reactive base will give increased selectivity for a more stable product. However, *t*-BuOH solvent instead favors the *less* stable allyl complexes **3**. Hence, we suggest that *t*-BuO⁻K⁺ has a much greater effective bulk in *t*-BuOH, enhancing selectivity for the sterically more remote allylic deprotonation site.

Also, somewhat more allylic deprotonation is observed in CH_2Cl_2 than in THF. Although there could be many reasons for this trend, we suspect that it is associated with the greater stabilities of (or kinetic preference for) *tert*-butoxide addition products **5** in CH_2Cl_2. Thus, regardless of mechanism, the effective temperature at which deprotonation occurs in CH_2Cl_2 would be higher. Indeed, reactions in CH_2Cl_2 involving different warming rates give differing **2**/**3** ratios, indicating a temperature dependence upon selectivity.[31]

It is also apparent in Scheme 9 that the less stable *RR,SS* diastereomers of propene and allylbenzene complexes **1a,g** give more allylic deprotonation than the *RS,SR* diastereomers. Perhaps this reflects some transition-state destabilization associated with the formation of the less stable *cis*-alkenyl complexes (*Z*)-**2**. However, due to the proximity of the cyclopentadienyl ligand and =CH*R* substituent in (*RR,SS*)-**1g**, it should at the same time be more difficult to attain the stereoelectronically most favorable transition state **XII** for allylic deprotonation.

4. Implications for Carbon–Hydrogen Bond Activation. Scheme 3 provides an exceptionally mild protocol for the metalation of vinylic carbon–hydrogen bonds in simple unactivated alkenes. Oxidative additions of free alkenes to metal complexes commonly require heating, although reactions can be rapid when coordinatively unsaturated intermediates are photochemically generated in low-temperature matrices.[1,2] Also, some comparable metalations have been effected with alkyllithium or -potassium reagents.[47] However, allylic protons are usually preferentially abstracted. In this context, the allylic protons of most alkenes exhibit slightly greater kinetic and thermodynamic acidities than the vinylic protons.[48] Regardless, these acidities ($pK_{CsCHA} \geq 43$) are dramatically enhanced upon coordination to the cationic Lewis acid **I**—becoming even greater than that of *t*-BuOH ($pK_a(H_2O)$ ca. 19).[46]

It is instructive to consider the three conceptually related reactions in Scheme 16. The first two involve

(44) (a) Schwan, A. L.; Pippert, M. F.; Pham, H. H.; Roche, M. R. *J. Chem. Soc., Chem. Commun.* **1993**, 1312. (b) Refvik, M. D.; Froese, R. D. J.; Goddard, J. D.; Pham, H. H.; Pippert, M. F.; Schwan, A. L. *J. Am. Chem. Soc.*, in press. We thank Professor Schwan for a preprint. (c) Crandall, J. K.; Apparu, M. *Org. React.* **1983**, *29*, 345. (d) Boche, G.; Walborsky, H. M. In *The Chemistry of The Cyclopropyl Group*; Rappoport, Z., Ed.; Wiley: New York, 1987; part 1, pp 788–794.

(45) (a) Davies, S. G.; Dordor-Hedgecock, I. M.; Sutton, K. H.; Whittaker, M. *J. Am. Chem. Soc.* **1987**, *109*, 5711. (b) Mackie, S. C.; Baird, M. C. *Organometallics* **1992**, *11*, 3712.

(46) Pearson, D. E.; Buehler, C. A. *Chem. Rev.* **1974**, *74*, 45.

(47) (a) Brandsma, L.; Verkruijsse, H. D.; Schade, C.; Schleyer, P. v. R. *J. Chem. Soc., Chem. Commun.* **1986**, 260. (b) Brandsma, L.; Verkruijsse, H. D. *Preparative Polar Organometallic Chemistry*; Springer-Verlag: New York, 1987; Vol. 1, Chapter III. (c) Brandsma, L. *Preparative Polar Organometallic Chemistry*; Springer-Verlag: New York, 1990; Vol. 2, Chapter II.

(48) (a) Boerth, D. W.; Streitwieser, A., Jr. *J. Am. Chem. Soc.* **1981**, *103*, 6443. (b) Streitwieser, A., Jr.; Boerth, D. W. *J. Am. Chem. Soc.* **1978**, *100*, 755.

sp and sp^2 carbon–hydrogen bond activation. As noted above, the former has been observed previously,[42,43] and this study provides the first explicit demonstration of the latter. By analogy, a complementary mode of sp^3 carbon–hydrogen bond activation should exist. This could, as illustrated in eq iii of Scheme 16, involve a "σ bond" complex of either a carbon–carbon (**XX**) or carbon–hydrogen (**XXI**) linkage. Although there is more precedent for the latter, either would be expected to undergo facile deprotonation to an alkyl complex. Indeed, comparable pathways have been proposed for sp^3 carbon–hydrogen bond activation reactions involving electrophilic Pd(II), Pt(II), and Hg(II) species.[49] Hence, there appears to be a continuum of closely related mechanisms that can be applied to the activation of carbon–hydrogen bonds of any hybridization level.

Many metal-catalyzed transformations of feedstock chemicals involve basic additives or sites on heterogeneous supports. The preceding analysis suggests heretofore unappreciated roles for these components, at least in carbon–hydrogen bond-breaking reactions. Indeed, it should not be difficult to append a noncoordinating Brønsted base to the rhenium fragment **I** and effect vinylic deprotonation in the absence of an exogenous agent.[50] However, prospects for applications in homogeneous catalysis would be even further enhanced by the demonstration of analogous reactivity with coordinatively unsaturated metal complexes.

In conclusion, this work has suggested new mechanism-based approaches to catalytic reactions of important commodity chemicals. The development and application of these concepts is under active investigation.

Experimental Section[51]

Deprotonation of [(η^5-C$_5$H$_5$)Re(NO)(PPh$_3$)(H$_2$C=CHCH$_3$)]$^+$BF$_4^-$ (1a). A. A 5 mm NMR tube was charged with **1a** (16.8 mg, 0.025 mmol; 96:4 *RS,SR/RR,SS*)[5a] and THF (0.8 mL), capped with a septum, and cooled to −80 °C. Then *t*-BuO$^-$K$^+$/THF (1.0 M, 0.035 mL, 0.035 mmol) was added, and the tube was shaken and warmed to room temperature. The yellow-brown solution turned orange. A ^{31}P NMR spectrum showed one resonance (23.4 ppm). Solvent was removed under oil-pump vacuum. The residue was extracted with ether (2 mL, under N$_2$), and hexane (10 mL) was added. Solvent was removed under oil-pump vacuum to give (*E*)-(η^5-C$_5$H$_5$)Re(NO)(PPh$_3$)(CH=CHCH$_3$) ((*E*)-**2a**; 12.4 mg, 0.021 mmol, 85%)[17,53,54] as an orange powder.

B. Complex **1a** (16.8 mg, 0.025 mmol; 96:4 *RS,SR/RR,SS*), THF (1.0 mL), and *t*-BuO$^-$K$^+$/*t*-BuOH (0.75 M, 0.040 mL, 0.030 mmol) were combined in a procedure analogous to A. An identical workup gave a mixture of (*E*)-**2a**, (η^5-C$_5$H$_5$)Re(NO)(PPh$_3$)(CH$_2$CH=CH$_2$) (**3a**),[18] and three byproducts (12.4 mg, 0.018 mmol, 72%).[25b]

C. Complex **1a** (16.8 mg, 0.025 mmol; 96:4 *RS,SR/RR,SS*), CH$_2$Cl$_2$ (0.8 mL), and *t*-BuO$^-$K$^+$/THF (1.0 M, 0.025 mL, 0.025 mmol) were combined in a procedure analogous to A. An identical workup gave a (*E*)-**2a/3a** mixture (12.2 mg, 0.021 mmol, 84%; 98:2).

D. Complex **1a** (16.8 mg, 0.025 mmol; 6:94 *RS,SR/RR,SS*),[10a] THF (0.8 mL), and *t*-BuO$^-$K$^+$/THF (1.0 M, 0.025 mL, 0.025 mmol) were combined in a procedure analogous to A. An identical workup gave a (*E*)-**2a**/(*Z*)-**2a/3a** mixture (12.6 mg, 0.022 mmol, 86%; 41:41:18).

E. Complex **1a** (16.8 mg, 0.025 mmol; 6:94 *RS,SR/RR,SS*), CH$_2$Cl$_2$ (0.8 mL), and *t*-BuO$^-$K$^+$/THF (1.0 M, 0.025 mL, 0.025 mmol) were combined in a procedure analogous to A. An identical workup gave a (*E*)-**2a/3a**[53,54] mixture (14.4 mg, 0.025 mmol, 99%; 3:97).

F. Complex **1a** (16.8 mg, 0.025 mmol; 96:4 *RS,SR/RR,SS*), CH$_2$Cl$_2$ (1.0 mL), *t*-BuOD (0.024 mL, 0.25 mmol), and *t*-BuO$^-$K$^+$/THF (1.0 M, 0.013 mL, 0.013 mmol) were combined in a procedure analogous to A. An identical workup gave (*E*)-**2a** (5.4 mg, 0.009 mmol, 37%). The residue left after ether extraction was dissolved in CH$_2$Cl$_2$/acetone (90:10 v/v) and filtered through a pipet containing silica (3 cm). This gave a 95:5 **1a/1a-*d*$_1$** mixture (5.0 mg, 0.007 mmol, 30%; 96:4 *RS,SR/RR,SS*), as assayed by MS (all label in the [(η^5-C$_5$H$_5$)Re(NO)(PPh$_3$)]$^+$ ion).[55a,56a]

Deprotonation of [(η^5-C$_5$H$_5$)Re(NO)(PPh$_3$)(H$_2$C=CHCH$_2$CH$_2$CH$_3$)]$^+$BF$_4^-$ (1b). The following reactions were conducted analogously to reaction A of **1a**.

A. Complex **1b** (17.5 mg, 0.025 mmol; 96:4 *RS,SR/RR,SS*),[5a] THF (0.8 mL), and *t*-BuO$^-$K$^+$/THF (1.0 M, 0.035 mL, 0.035

(49) Periana, R. A.; Taube, D. J.; Evitt, E. R.; Löffler, D. G.; Wentrcek, P. R.; Voss, G.; Masuda, T. *Science* **1993**, *259*, 340 and references therein.

(50) For a demonstration of this strategy in arene carbon–hydrogen bond activation, see: Cordone, R.; Taube, H. *J. Am. Chem. Soc.* **1987**, *109*, 8101.

(51) (a) General procedures were identical with those in a previous paper.[5b] (b) Solvent or reagent data: *t*-BuOH, distilled from Mg/I$_2$;[52] toluene, heptane, hexane, and ether, distilled from Na; THF, distilled from K/benzophenone; C$_6$D$_6$, CH$_2$Cl$_2$, CD$_2$Cl$_2$, CDCl$_3$, and TMEDA, vacuum transferred or distilled from CaH$_2$; acetone-*d*$_6$, distilled from 4A molecular sieves; *t*-BuO$^-$K$^+$/*t*-BuOH, prepared from *t*-BuO$^-$K$^+$ powder (Aldrich) and *t*-BuOH; *t*-BuO$^-$K$^+$/THF, *t*-BuOD (>98% D), PPh$_3$-*d*$_{15}$, HBF$_4$·OEt$_2$, *n*-BuLi, and (CH$_3$)$_2$C=CHCH$_2$Cl, used as received from Aldrich. (c) NMR spectra were recorded on 300 MHz spectrometers at ambient probe temperatures unless noted and referenced to residual C$_6$D$_5$H, CHDCl$_2$, or CHCl$_3$ (^{1}H, δ 7.15, 5.32, 7.26), C$_6$D$_6$, CD$_2$Cl$_2$, or CDCl$_3$ (^{13}C, 128.0, 53.8, 77.0 ppm), and external 85% H$_4$PO$_4$ (^{31}P, 0.00 ppm); all coupling constants (*J*) are in Hz.

(52) Perrin, D. D.; Armarego, W. L. F.; Perrin, D. R. *Purification of Laboratory Chemicals*, 2nd ed.; Pergamon: New York, 1980; p 146.

(53) The ^{31}P, ^{1}H, and ^{13}C NMR spectra were identical with those for an authentic sample.

(54) Unless noted, some NMR data for the following compounds have been reported earlier. Many chemical shifts of isomeric alkenyl and allyl complexes are similar, and spectra in new solvents were needed to verify assignments. (a) (*E*)-**2a** (C$_6$D$_6$): ^{1}H NMR (δ) 7.96 (ddm, J_{HH} 16.5, J_{HP} 3.4, H$_\alpha$), 7.60–7.10 (m, PPh$_3$), 5.45 (ddq, J_{HH} 6.0, 16.5, J_{HP} 2.0, H$_\beta$), 4.68 (s, C$_5$H$_5$), 2.13 (dd, J_{HH} 6.0, J_{HP} 1.3, CH$_3$); ^{13}C{^{1}H} NMR (ppm) 136.9 (J_{CP} 52.5, *i*-Ph), 134.0 (d, J_{CP} 10.5, *o*-Ph), 132.3 (d, J_{CP} 4.4, C$_\beta$), 129.9 (s, *p*-Ph), 128.2 (d, J_{CP} 11.3, *m*-Ph), 123.3 (d, J_{CP} 11.9, C$_\alpha$), 90.9 (s, C$_5$H$_5$), 25.7 (s, CH$_3$); ^{31}P{^{1}H} NMR (ppm) 23.5 (s). (b) (*Z*)-**2a** (C$_6$D$_6$, partial): ^{1}H NMR (δ) 7.75 (ddm, J_{HH} 11.5, J_{HP} 3.4, H$_\alpha$), 6.72 (ddq, J_{HH} 6.5, 11.5, J_{HP} 3.1, H$_\beta$), 4.68 (s, C$_5$H$_5$), 2.41 (dd, J_{HH} 6.5, J_{HP} 1.4, CH$_3$); ^{13}C{^{1}H} NMR (ppm) 125.2 (d, J_{CP} 11.3, C$_\alpha$), 90.5 (s, C$_5$H$_5$), 21.4 (s, CH$_3$); ^{31}P{^{1}H} NMR (ppm) 24.4 (s). (c) **3a** (C$_6$D$_6$): ^{1}H NMR (δ) 7.55–6.95 (m, PPh$_3$), 6.68 (m, H$_\beta$), 4.74 (dm, J_{HH} 16.8, H$_{\gamma Z}$), 4.67 (dd, J_{HH} 9.9, 2.8, H$_{\gamma E}$), 4.56 (s, C$_5$H$_5$), 3.33 (m, H$_\alpha$), 2.65 (ddd, J_{HH} 10.4, 10.4, J_{HP} 2.2, H$_{\alpha'}$); ^{13}C{^{1}H} (ppm) 153.0 (s, C$_\beta$), 137.2 (J_{CP} 51.0, *i*-Ph), 133.9 (d, J_{CP} 10.4, *o*-Ph), 130.0 (s, *p*-Ph), 128.4 (d, J_{CP} 8.8, *m*-Ph), 103.0 (s, C$_\gamma$), 90.6 (s, C$_5$H$_5$), −4.8 (d, J_{CP} 4.1, C$_\alpha$); ^{31}P{^{1}H} NMR (ppm) 25.7 (s). (d) (*Z*)-**2b** (CDCl$_3$): ^{1}H NMR (δ) 7.65 (dd, J_{HH} 11.2, J_{HP} 7.0, H$_\alpha$), 7.50–7.30 (m, PPh$_3$), 6.07 (dddd, J_{HH} 6.7, 6.7, 11.2, J_{HP} 2.8, H$_\beta$), 5.01 (s, C$_5$H$_5$), 2.24 (m, H$_\gamma$), 1.38 (qt, J_{HH} 7.3, 7.3, H$_\delta$), 0.93 (t, J_{HH} 7.3, H$_\epsilon$); ^{13}C{^{1}H} (ppm) 140.3 (d, J_{CP} 2.2, C$_\beta$), 136.0 (J_{CP} 52.4, *i*-Ph), 133.7 (d, J_{CP} 10.5, *o*-Ph), 129.9 (s, *p*-Ph), 128.1 (d, J_{CP} 10.1, *m*-Ph), 123.5 (d, J_{CP} 10.7, C$_\alpha$), 90.5 (s, C$_5$H$_5$), 37.3 (s, H$_\gamma$), 23.6 (s, H$_\delta$), 14.3 (s, H$_\delta$); ^{31}P{^{1}H} (ppm) 21.9 (s). (e) (*E*)-**3b** (C$_6$D$_6$, partial; new compound): ^{1}H NMR (δ) 5.17 (ddd, J_{HH} 17.6, 6.9, 6.9, H$_\gamma$), 4.62 (C$_5$H$_5$); ^{13}C{^{1}H} NMR (ppm) 143.5 (d, J_{CP} 3.5, C$_\beta$), 121.6 (s, C$_\gamma$), 89.7 (s, C$_5$H$_5$), −6.9 (d, J_{CP} 4.5, C$_\alpha$); ^{31}P{^{1}H} NMR (ppm) 26.0 (s). (f) (*Z*)-**2g** (C$_6$D$_6$, partial): ^{1}H (δ) 8.04 (dd, J_{HH} 11.2, J_{HP} 7.0, H$_\alpha$), 6.76 (dddd, J_{HH} 11.2, 7.0, 7.0, J_{HP} 3.0, H$_\beta$), 4.66 (s, C$_5$H$_5$), 4.22 (dd, J_{HH} 15.3, 7.0, H$_\gamma$), 4.04 (dd, J_{HH} 15.3, 7.0, H$_{\gamma'}$); ^{13}C{^{1}H} (ppm) 139.2 (s, *i*-CPh), 129.3 (s, CPh), 128.2 (s, CPh), 125.3 (s, CPh); 137.5 (br s, C$_\beta$), 125.6 (d, J_{CP} 10.7, C$_\alpha$), 90.5 (s, C$_5$H$_5$), 42.5 (s, C$_\gamma$); ^{31}P{^{1}H} (ppm) 23.8 (s).

(55) Mass spectra of deuterated and undeuterated samples were recorded under identical conditions. Deuterium levels were calculated with the program "Matrix" (D. A. Chrisope, IBM). (a) **1a**-*d*$_n$ MS:[56a] 588, 6.32%; 587, 34.58%; 586, 100%; 585, 23.24%; 584, 56.20%; 583, 2.14%; 546, 4.47%; 545, 24.08%; 544, 81.34%; 543, 16.95%; 542, 47.95%; **1a** MS:[56a] 588, 4.39%; 587, 29.83%; 586, 100%; 585, 20.03%; 584, 60.17%; 583, 1.86%; 546, 3.59%; 545, 22.73%; 544, 86.82%; 543, 15.53%; 542, 50.24%. (b) (*E*)-**2e**-*d*$_n$ MS:[56b] 650, 1.34%; 649, 31.14%; 648, 88.71%; 647, 100%; 646, 54.27%; 645, 45.93%; 644, 2.30%. (*E*)-**2e** MS:[56b] 650, 0.95%; 649, 8.46%; 648, 45.25%; 647, 100%; 646, 29.98%; 645, 55.70%; 644, 2.26%.

(56) Conditions (*m/z*, relative intensity, ^{187}Re): (a) (+)-FAB, 5 kV, Ar, 3-nitrobenzyl alcohol/CHCl$_3$ matrix; (b) EI, 17 eV.

mmol) gave (η^5-C_5H_5)Re(NO)(PPh_3)(CH=$CHCH_2CH_2CH_3$) (**2b**; 13.3 mg, 0.022 mmol, 87%; 91:9 *E/Z*)[17,53,54] as an orange powder.

B. Complex (*RR,SS*)-**1b** (21.0 mg, 0.030 mmol),[57] THF (0.8 mL), and *t*-BuO$^-$K$^+$/THF (1.0 M, 0.042 mL, 0.042 mmol) gave **2b** (13.6 mg, 0.022 mmol, 74%; 25:75 *E/Z*). Additional data: see text.

C. Complex **1b** (17.5 mg, 0.025 mmol; 96:4 *RS,SR/RR,SS*), THF (0.8 mL), and *t*-BuO$^-$K$^+$/*t*-BuOH (0.75 M, 0.037 mL, 0.028 mmol) gave a mixture of (*E*)-**2b**, (*E*)-(η^5-C_5H_5)Re(NO)(PPh_3)(CH_2-CH=$CHCH_2CH_3$) ((*E*)-**3b**),[54e] and four byproducts (15.0 mg, 0.025 mmol, 98%).[25c]

Deprotonation of [(η^5-C_5H_5)Re(NO)(PPh_3)(H_2C=CHCH-(CH_3)$_2$)]$^+$$BF_4^-$ (1c). A. A Schlenk flask was charged with (*RS,SR*)-**1c** (35.0 mg, 0.050 mmol),[5b] THF (2 mL), and a stirbar and cooled to −80 °C. Then *t*-BuO$^-$K$^+$/THF (1.0 M, 0.070 mL, 0.070 mmol) was added with stirring, and the cold bath was removed. After 1 h, the solvent was removed under oil-pump vacuum. Workup as in reaction A of **1a** gave (η^5-C_5H_5)Re(NO)-(PPh_3)(CH=CHCH(CH_3)$_2$) (**2c**; 27.5 mg, 0.045 mmol, 90%; 97:3 *E/Z*) as an orange powder. Yellow needles crystallized from hexane (slow evaporation; 97:3 *E/Z*), mp 154−155 °C dec. Anal. Calcd for $C_{28}H_{29}NOPRe$: C, 54.89; H, 4.77; N, 2.29. Found: C, 55.14; H, 4.86; N, 2.40. IR (cm^{-1}, thin film): ν_{NO} 1635 vs. MS:[56a] 613 (M$^+$, 100%), 544 (M$^+$ − C_5H_9, 89%).

B. Complex (*RS,SR*)-**1c** (17.5 mg, 0.025 mmol), THF (2 mL), and *t*-BuO$^-$K$^+$/*t*-BuOH (0.75 M, 0.040 mL, 0.030 mmol) were analogously reacted. An identical workup gave **2c** (14.9 mg, 0.024 mmol, 97%; 97:3 *E/Z*).

(*E*)-**2c**: ^{1}H NMR 7.96 (ddd, J_{HH} 1.1, 16.5, J_{HP} 2.9, H_α), 7.62−6.95 (m, PPh_3), 5.38 (ddd, J_{HH} 6.4, 16.5, J_{HP} 2.2, H_β), 4.67 (s, C_5H_5), 2.50 (m, H_γ), 1.03 (d, J_{HH} 6.6, CH_3), 0.99 (d, J_{HH} 6.6, CH_3'); $^{13}C\{^1H\}$ NMR (ppm) 145.3 (br s, C_β), 137.0 (J_{CP} 52.2, *i*-Ph), 134.0 (d, J_{CP} 10.3, *o*-Ph), 129.9 (s, *p*-Ph), 128.3 (d, J_{CP} 10.0, *m*-Ph), 119.7 (d, J_{CP} 11.8, C_α), 91.2 (s, C_5H_5), 38.0 (s, C_γ), 24.2 (s, CH_3), 24.1 (s, CH_3'); $^{31}P\{^1H\}$ NMR (ppm) 22.0 (s). (*Z*)-**2c** (partial): ^{1}H NMR (δ) 4.68 (s, C_5H_5), 1.43 (d, J_{HH} 6.6, CH_3), 1.33 (d, J_{HH} 6.6, CH_3'); $^{31}P\{^1H\}$ NMR ppm) 23.8 (s).

Deprotonation of [(η^5-C_5H_5)Re(NO)(PPh_3)(H_2C=CH_2)]$^+$ BF_4^- (1d). Complex **1d** (16.5 mg, 0.025 mmol),[19] THF (2 mL), and *t*-BuO$^-$K$^+$/THF (1.0 M, 0.035 mL, 0.035 mmol) were combined as in reaction A of **1c**. An identical workup gave (η^5-C_5H_5)Re(NO)(PPh_3)(CH=CH_2) (**2d**; 11.9 mg, 0.021 mmol, 83%)[17,53] as an orange powder.

Deprotonation of [(η^5-C_5H_5)Re(NO)(PPh_3)(H_2C=CH-C_6H_5)]$^+$$BF_4^-$ (1e). A. Complex (*RS,SR*)-**1e** (73.5 mg, 0.100 mmol),[5a] THF (2 mL), and *t*-BuO$^-$K$^+$/THF (1.0 M, 0.150 mL, 0.150 mmol) were combined as in reaction A of **1c**. An identical workup gave (*E*)-(η^5-C_5H_5)Re(NO)(PPh_3)(CH=CHC_6H_5) ((*E*)-**2e**) as an orange powder (59.1 mg, 0.091 mmol, 91%), mp 208−211 °C. Anal. Calcd for $C_{31}H_{27}NOPRe$: C, 57.57; H, 4.21; N 2.17. Found: C, 57.39; H, 4.25; N, 2.18. IR (cm^{-1}, thin film): ν_{NO} 1643 vs. MS:[56a] 647 (M$^+$, 100%), 544 (M$^+$ − C_8H_7, 90%).

B. Complex (*RR,SS*)-**1e** (12.4 mg, 0.017 mmol),[5a] THF (2 mL), and *t*-BuO$^-$K$^+$/THF (1.0 M, 0.020 mL, 0.020 mmol) were combined as in reaction A and stirred for 2 h at −25 °C. Solvent was removed by oil-pump vacuum (−25 °C) and the residue extracted with CD_2Cl_2 (−25 °C). The extract was transferred via cannula to an NMR tube (−80 °C), which was placed in a −25 °C probe. NMR spectra showed a (*Z*)-**1e**/(*E*)-**1e** mixture (below; 97:3).

C. Complex (*RS,SR*)-**1e** (17.5 mg, 0.025 mmol), THF (2 mL), and *t*-BuO$^-$K$^+$/THF (1.0 M, 0.030 mL, 0.030 mmol) were combined as in reaction B. NMR spectra showed (*E*)-**1e** (below).

D. Complex (*RR,SS*)-**1e** (73.5 mg, 0.100 mmol), THF (2 mL), and *t*-BuO$^-$K$^+$/THF (1.0 M, 0.150 mL, 0.150 mmol) were combined as in reaction A. An identical workup gave (*E*)-**2e** (58.1 mg, 0.090 mmol, 90%).[21]

E. Complex (−)-(*SR*)-**1e** (73.5 mg, 0.100 mmol, >98% ee),[5a] THF (2 mL), and *t*-BuO$^-$K$^+$/THF (1.0 M, 0.150 mL, 0.150 mmol) were combined as in reaction A. An identical workup gave (−)-(*E*)-(*R*)-**2e** (52.2 mg, 0.081 mmol, 81%), $[\alpha]^{25}_{589}$ = −231 ± 5° ($CHCl_3$, *c* 0.49 mg/mL),[58] >98% ee (chiral HPLC).[22]

F. Complex (*RS,SR*)-**1e** (36.7 mg, 0.050 mmol), THF (2 mL), PPh_3-d_{15} (27.7 mg, 0.100 mmol), and *t*-BuO$^-$K$^+$/THF (1.0 M, 0.070 mL, 0.070 mmol) were combined as in reaction A. An identical workup gave (*E*)-**2e** (30.0 mg, 0.046 mmol, 93%). MS:[56a] 662 (M$^+$-d_{15}, 0%), 647 (M$^+$, 74%), 544 (M$^+$ − C_8H_7, 100%).

(*E*)-**2e** (C_6D_6): ^{1}H NMR (δ) 9.48 (dd, J_{HH} 17.1, J_{HP} 3.0, H_α), 7.60−6.90 (m, PPh_3/CPh), 6.40 (dd, J_{HH} 17.1, J_{HP} 2.1, H_β), 4.71 (s, C_5H_5); $^{13}C\{^1H\}$ NMR (ppm) 143.0 (s, *i*-CPh), 137.5 (br s, C_β), 136.4 (d, J_{CP} 52.9, *i*-PPh), 135.4 (d, J_{CP} 12.2, C_α), 133.8 (d, J_{CP} 10.4, *o*-PPh), 130.1 (s, *p*-PPh), 128.4 (d, J_{CP} 10.3, *m*-PPh), 127.7 (s, CPh), 124.8 (s, CPh), 124.0 (s, CPh), 91.6 (s, C_5H_5); $^{31}P\{^1H\}$ NMR (ppm) 21.4 (s). (*E*)-**2e** (CD_2Cl_2, −25 °C, partial): ^{1}H NMR (δ) 9.13 (dd, J_{HH} 17.2, J_{HP} 2.8, H_α), 7.60−6.70 (m, PPh_3/CPh), 5.98 (dd, J_{HH} 17.2, J_{HP} 2.0, H_β), 5.18 (s, C_5H_5); $^{31}P\{^1H\}$ (ppm) 19.9 (s). (*Z*)-**2e** (CD_2Cl_2, −25 °C): ^{1}H NMR (δ) 8.35 (dd, J_{HH} 7.6, J_{HP} 12.8, H_α), 7.75−7.10 (m, PPh_3/CPh), 7.00 (dd, J_{HH} 7.6, J_{HP} 0.9, H_β), 5.08 (s, C_5H_5); $^{13}C\{^1H\}$ NMR (ppm) 143.5 (s, *i*-CPh), 137.1 (br s, C_β), 135.2 (d, J_{CP} 52.8, *i*-PPh), 133.6 (d, J_{CP} 10.0, *o*-PPh), 131.9 (d, J_{CP} 10.6, C_α), 130.2 (s, *p*-PPh), 128.3 (d, J_{CP} 9.8, *m*-PPh), 127.5 (s, CPh), 124.7 (s, CPh), 124.4 (s, CPh), 91.3 (s, C_5H_5); $^{31}P\{^1H\}$ NMR (ppm) 23.2 (s).

Deprotonation of 1e-d_n. The following were conducted analogously to reaction A of **1e**.

A. Complex (*RSR,SRS*)-**1e**-d_1 (95% D, 73.6 mg, 0.100 mmol),[5c] THF (2 mL), and *t*-BuO$^-$K$^+$/THF (1.0 M, 0.150 mL, 0.150 mmol) gave (*E*)-**2e**-d_1 (95% D,[59] 57.1 mg, 0.088 mmol, 88%).

B. Complex (*RRR,SSS*)-**1e**-d_1 (83% D, 18.4 mg, 0.025 mmol),[5c] THF (1 mL) and *t*-BuO$^-$K$^+$/THF (1.0 M, 0.035 mL, 0.035 mmol) gave (*E*)-**2e**-d_1 (83% D,[59] 14.1 mg, 0.022 mmol, 87%).[21]

C. Complex (*RSS,SRR*)-**1e**-d_1 (97% D, 36.8 mg, 0.050 mmol),[5c] THF (1 mL) and *t*-BuO$^-$K$^+$/*t*-BuOH (0.50 M, 0.150 mL, 0.075 mmol) gave (*E*)-**2e** (<2% D,[59] 20.6 mg, 0.032 mmol, 64%).

D. Complex (*RRS,SSR*)-**1e**-d_1 (95% D, 36.8 mg, 0.050 mmol),[5c] THF (2 mL), and *t*-BuO$^-$K$^+$/THF (1.0 M, 0.075 mL, 0.075 mmol) gave (*E*)-**2e** (<2% D,[59] 29.6 mg, 0.045 mmol, 92%).[21]

E. Complex (*RS,SR*)-**1e** (29.4 mg, 0.040 mmol), (*RS,SR*)-**1e**-d_2 (95% D, 29.5 mg, 0.040 mmol), THF (2 mL), and *t*-BuO$^-$K$^+$/THF (1.0 M, 0.008 mL, 0.008 mmol) gave a 63:37 (*E*)-**2e**/(*E*)-**2e**-d_1 mixture (2.1 mg, 0.003 mmol, 4%), as assayed by MS.[55b,56b]

Deprotonation of [(η^5-C_5H_5)Re(NO)(PPh_3)(H_2C=CHC-(CH_3)$_3$)]$^+$$BF_4^-$ (1f). Complex (*RS,SR*)-**1f** (35.7 mg, 0.050 mmol),[5b] THF (2.0 mL), and *t*-BuO$^-$K$^+$/THF (1.0 M, 0.070 mL, 0.070 mmol) were combined as in reaction A of **1c**. An identical workup gave (*E*)-(η^5-C_5H_5)Re(NO)(PPh_3)(CH=CHC-(CH_3)$_3$) ((*E*)-**2f**; 29.2 mg, 0.047 mmol, 93%) as an orange powder, mp 95−98 °C. Anal. Calcd for $C_{29}H_{31}NOPRe$: C, 55.58; H, 4.99; N, 2.23. Found: C, 55.65; H, 5.00; N, 2.23. IR (cm^{-1}, thin film): ν_{NO} 1637 vs. MS:[56a] 627 (M$^+$, 100%), 544 (M$^+$ − C_6H_{11}, 57%).

(*E*)-**2f** (C_6D_6): ^{1}H NMR (δ) 7.93 (dd, J_{HH} 17.0, J_{HP} 3.0, H_α), 7.56−7.02 (m, PPh_3), 5.40 (dd, J_{HH} 17.0, J_{HP} 2.2, H_β), 4.69 (s, C_5H_5), 1.05 (s, $3CH_3$); $^{13}C\{^1H\}$ NMR (ppm) 148.1 (br s, C_β), 137.1 (d, J_{CP} 52.5, *i*-Ph), 134.0 (d, J_{CP} 10.3, *o*-Ph), 129.9 (s, *p*-Ph), 128.3 (d, J_{CP} 9.2, *m*-Ph), 116.8 (d, J_{CP} 11.5, C_α), 91.4 (s, C_5H_5), 36.8 (s, C_γ), 31.0 (s, $3CH_3$); $^{31}P\{^1H\}$ NMR (ppm) 21.9 (s).

(57) Complex (*RR,SS*)-**1b** was isolated from a 67:33 *RS,SR/RR,SS* mixture as previously reported for (*RR,SS*)-**1e**.[5a]

(58) Dewey, M. A.; Gladysz, J. A. *Organometallics* **1993**, *12*, 2390.

(59) The deuterium content was determined by integration vs the =CHC_6H_5 ^{1}H NMR signal.

Deprotonation of $[(\eta^5\text{-}C_5H_5)Re(NO)(PPh_3)(H_2C{=}CH\text{-}CH_2C_6H_5)]^+BF_4^-$ (1g). The following were conducted analogously to reaction A of **1a**.

A. Complex **1g** (18.7 mg, 0.025 mmol; 95:5 *RS,SR/RR,SS*),[5a] THF (0.8 mL), and *t*-BuO$^-$K$^+$/*t*-BuOH (0.75 M, 0.040 mL, 0.030 mmol) were warmed to room temperature.[25a] Workup gave a mixture of (*E*)-(η^5-C_5H_5)Re(NO)(PPh$_3$)(CH=CHCH$_2$C$_6$H$_5$) ((*E*)-**2g**)[17] and (*E*)-(η^5-C_5H_5)Re(NO)(PPh$_3$)(CH$_2$CH=CHC$_6$H$_5$) ((*E*)-**3g**)[13] as an orange powder (14.5 mg, 0.022 mmol, 88%; 21:79).[53,54]

B. Complex **1g** (18.7 mg, 0.025 mmol; 95:5 *RS,SR/RR,SS*), *t*-BuOH (0.8 mL), and *t*-BuO$^-$K$^+$/*t*-BuOH (0.75 M, 0.037 mL, 0.028 mmol) gave a (*E*)-**2g**/(*E*)-**3g** mixture (14.8 mg, 0.022 mmol, 90%; 3:97).

C. Complex **1g** (18.7 mg, 0.025 mmol; 95:5 *RS,SR/RR,SS*), THF (0.8 mL), and *t*-BuO$^-$K$^+$/THF (1.0 M, 0.035 mL, 0.035 mmol) gave a (*E*)-**2g**/(*E*)-**3g** mixture (15.0 mg, 0.023 mmol, 91%; 89:11).

D. Complex **1g** (18.7 mg, 0.025 mmol; 95:5 *RS,SR/RR,SS*), CH_2Cl_2 (0.8 mL), and *t*-BuO$^-$K$^+$/THF (1.0 M, 0.035 mL, 0.035 mmol) gave a (*E*)-**2g**/(*E*)-**3g** mixture (15.6 mg, 0.024 mmol, 94%; 78:22).

E. Complex (*RR,SS*)-**1g** (18.7 mg, 0.025 mmol),[5c] THF (0.8 mL), and *t*-BuO$^-$K$^+$/THF (1.0 M, 0.035 mL, 0.035 mmol) gave a (*E*)-**2g**/(*Z*)-**2g**/(*E*)-**3g** mixture (12.8 mg, 0.019 mmol, 77%; 28:33:39).

F. Complex (*RR,SS*)-**1g** (18.7 mg, 0.025 mmol), CH_2Cl_2 (0.8 mL), and *t*-BuO$^-$K$^+$/THF (1.0 M, 0.035 mL, 0.035 mmol) gave (*E*)-**3g** (16.0 mg, 0.024 mmol, 97%).[53]

Deprotonation of $[(\eta^5\text{-}C_5H_5)Re(NO)(PPh_3)(H_2C{=}C(CH_3)_2)]^+BF_4^-$ (1h). The following were conducted analogously to reaction A of **1a**.

A. Complex **1h** (17.2 mg, 0.025 mmol),[10b] THF (0.8 mL), and *t*-BuO$^-$K$^+$/THF (1.0 M, 0.030 mL, 0.030 mmol) gave a mixture of (η^5-C_5H_5)Re(NO)(PPh$_3$)(CH=C(CH$_3$)$_2$) (**2h**; 24.8 ppm)[17] and (η^5-C_5H_5)Re(NO)(PPh$_3$)(CH$_2$C(CH$_3$)=CH$_2$) (**3h**; 25.3 ppm)[13] as an orange powder (14.0 mg, 0.023 mmol, 94%; 89:11).[53]

B. Complex **1h** (17.2 mg, 0.025 mmol), CH_2Cl_2 (0.8 mL), and *t*-BuO$^-$K$^+$/THF (1.0 M, 0.030 mL, 0.030 mmol) gave a **2h**/**3h** mixture (14.5 mg, 0.024 mmol, 97%; 50:50).

Deprotonation of $[(\eta^5\text{-}C_5Me_5)Re(NO)(PPh_3)(H_2C{=}CH\text{-}C_6H_5)]^+BF_4^-$ (1e-Me$_5$). Complex (*RS,SR*)-**1e**-Me$_5$ (20.1 mg, 0.025 mmol),[33] CH_2Cl_2 (1 mL), and *t*-BuO$^-$K$^+$/THF (1.0 M, 0.030 mL, 0.030 mmol) were combined as in reaction A of **1c**. An identical workup gave (*E*)-(η^5-C_5Me_5)Re(NO)(PPh$_3$)(CH=CHC$_6$H$_5$) ((*E*)-**2e**-Me$_5$, 18.0 mg, 0.025 mmol, >99%) as an orange powder. Crystallization from layered CH_2Cl_2/pentane gave orange prisms, mp 227–229 °C. Anal. Calcd for $C_{36}H_{37}NOPRe$: C, 60.32; H, 5.20. Found: C, 60.36; H, 5.34. IR (cm^{-1}, thin film): ν_{NO} 1621 vs. MS:[56b] 717 (M$^+$, 96%), 262 (Ph$_3$P$^+$, 100%).

(*E*)-**2e**-Me$_5$ (C_6D_6): ^{1}H NMR (δ) 8.80 (dd, J_{HH} 16.8, J_{HP} 2.7, H$_\alpha$), 7.60–6.90 (m, PPh$_3$/CPh), 6.37 (dd, J_{HH} 16.8, J_{HP} 2.6, H$_\beta$), 1.57 (s, C$_5$Me$_5$); ^{13}C{^{1}H} NMR (ppm) 146.7 (d, J_{CP} 12.4, C$_\alpha$), 135.9 (s, *i*-CPh), 134.3 (s, C$_\beta$), 134.1 (d, J_{CP} 10.7, *o*-PPh), 129.8 (s, *p*-PPh), 128.8 (s, CPh), 128.3 (d, J_{CP} 12.5, *m*-PPh),[60] 124.6 (s, CPh), 123.6 (s, CPh), 100.0 (s, *C*$_5$Me$_5$), 9.9 (s, C$_5$*Me*$_5$); ^{31}P{^{1}H} NMR (ppm) 25.6 (s).

Interconversion of 2a and 3a. The following is representative. A 5 mm NMR tube was charged with **3a** (7.3 mg, 0.013 mmol) and acetone-d_6 (0.8 mL), capped with a septum, and purged with argon. The solution was transferred by cannula to another NMR tube charged with [Rh(diphos)]$_2^{2+}$(ClO$_4^-$)$_2$ (3.1 mg, 0.0025 mmol).[27] The solution was shaken and kept at room temperature. NMR spectra (^{1}H, ^{31}P) were periodically recorded. Data: see text.

Generation of (η^4-C_5H_5O-*t*-Bu)Re(NO)(PPh$_3$)(H$_2$C=CH-CH$_3$) (5a). A. Complex **1a** (16.8 mg, 0.025 mmol; 96:4 *RS,SR/RR,SS*), CD_2Cl_2 (0.8 mL), and *t*-BuO$^-$K$^+$/THF (1.0 M, 0.025 mL, 0.025 mmol) were combined as in reaction A of **1a**. The tube was placed in a −60 °C probe. NMR spectra (^{31}P, ^{1}H, ^{13}C; below) showed **5a** (96:4 *RS,SR/RR,SS*) and (*E*)-**2a** (2%).[61] The probe was warmed. Data: see text.

B. Complex **1a** (16.8 mg, 0.025 mmol; 8:92 *RS,SR/RR,SS*), CD_2Cl_2 (0.8 mL), and *t*-BuO$^-$K$^+$/THF (1.0 M, 0.025 mL, 0.025 mmol) analogously gave **5a** (8:92 *RS,SR/RR,SS*) and (*Z*)-**2a** (2%).

(*RS,SR*)-**5a** (CD_2Cl_2, −60 °C):[61] ^{1}H NMR (δ, partial) 7.63–7.20 (m, PPh$_3$), 5.80, 3.87, 3.38 (3 br s, 2:1:1, C$_5$H$_5$O), 2.74 (m, =C*H*CH$_3$), 0.60 (s, C(CH$_3$)$_3$); ^{13}C{^{1}H} NMR (ppm) 133.3 (br s, *o*-Ph), 129.9 (s, *p*-Ph), 128.2 (d, J_{CP} 9.8, *m*-Ph),[60] C$_5$H$_5$O at 94.2 (s), 90.0 (s), 78.9 (s), 76.9 (d, J_{CP} 15.4), and 53.2 (s); 71.3 (s, *C*(CH$_3$)$_3$), 38.3, 35.7 (2 s, C=C), 28.1 (s, C(*C*H$_3$)$_3$), 25.1 (s, =C*C*H$_3$); ^{31}P{^{1}H} NMR (ppm) 21.5 (s). (*RR,SS*)-**5a** (CD_2Cl_2, −60 °C):[61] ^{1}H NMR (δ) 7.70–7.09 (m, PPh$_3$), 5.50, 5.28, 4.83, 1.64, 1.17 (5 br s, C$_5$H$_5$O), 2.73 (m, =C*H*CH$_3$), 1.99 (ddd, J_{HH} 3.7, 9.5, J_{HP} 9.5, H$_E$), 1.53 (d, J_{HH} 3.9, =CCH$_3$), 0.90 (ddd, J_{HH} 3.7, 11.6, J_{HP} 7.5, H$_Z$), 0.58 (s, C(CH$_3$)$_3$); ^{13}C{^{1}H} NMR (ppm) 133.3 (br s, *o*-Ph), 129.8 (s, *p*-Ph), 128.1 (s, *m*-Ph),[60] C$_5$H$_5$O at 96.7 (s), 82.8 (s), 77.4 (d, J_{CP} 16.2), 57.0 (s), and 51.8 (s); 71.4 (s, *C*(CH$_3$)$_3$), 35.6, 32.5 (d/s, J_{CP} 5.3, C=C), 28.0 (s, C(*C*H$_3$)$_3$), 22.1 (s, =C*C*H$_3$); ^{31}P{^{1}H} NMR (ppm) 19.4 (s).

(η^5-C_5H_5)Re(NO)(PPh$_3$)(CH$_2$CH=C(CH$_3$)$_2$) (3c). Complex (η^5-C_5H_5)Re(NO)(PPh$_3$)(H) (152.5 mg, 0.280 mmol),[18] THF (8 mL), TMEDA (0.051 mL, 0.336 mmol), *n*-BuLi (2.0 M in hexane, 0.20 mL), and (CH$_3$)$_2$C=CHCH$_2$Cl (0.095 mL, 0.84 mmol) were combined in a procedure analogous to one given earlier for **3a**.[18] A similar workup gave **3c** as an orange powder (166.0 mg, 0.271 mmol, 97%). Dark orange prisms were obtained from toluene/heptane, mp 158–159 °C. Anal. Calcd for $C_{28}H_{29}NOPRe$: C, 54.89; H, 4.77; N, 2.29. Found: C, 55.15; H, 4.87; N, 2.30. IR (cm^{-1}, thin film): ν_{NO} 1627 vs. MS:[56a] 613 (M$^+$, 13%), 544 (M$^+$ − C$_5$H$_9$, 100%).

3c (C_6D_6): ^{1}H NMR (δ) 7.62–6.92 (m, PPh$_3$), 6.01 (ddd, J_{HH} 8.9, 8.9, J_{HP} 0.8, H$_\beta$), 4.64 (s, C$_5$H$_5$), 3.18 (m, H$_\alpha$), 2.65 (ddd, J_{HH} 8.9, 8.9, J_{HP} 2.8, H$_{\alpha'}$), 1.98 (s, CH$_3$), 1.90 (s, CH$_3'$); ^{13}C{^{1}H} NMR (ppm) 139.6 (d, J_{CP} 3.9, C$_\beta$), 137.5 (J_{CP} 50.9, *i*-Ph), 133.9 (d, J_{CP} 10.6, *o*-Ph), 130.0 (d, J_{CP} 1.9, *p*-Ph), 128.4 (d, J_{CP} 10.3, *m*-Ph), 120.3 (s, C$_\gamma$), 89.5 (s, C$_5$H$_5$), 26.4 (s, CH$_3$), 18.0 (s, CH$_3'$), −11.3 (d, J_{CP} 3.9, C$_\alpha$); ^{31}P{^{1}H} NMR (ppm) 26.1 (s).

$[(\eta^5\text{-}C_5H_5)Re(NO)(PPh_3)(=CHCH_2CH(CH_3)_2)]^+BF_4^-$ (4c). A 5 mm NMR tube was charged with **2c** (28.4 mg, 0.046 mmol; 95:5 *E/Z*) and CD_2Cl_2 (0.4 mL) and cooled to −80 °C. Then HBF$_4$·OEt$_2$ (5.5 μL, 0.051 mmol) was added.[27] After 1 h at room temperature, the solution was added to hexane (20 mL). The resulting tan powder was collected by filtration and dried by oil-pump vacuum to give **4c** (30.9 mg, 0.044 mmol, 95%; 95:5 *ac/sc*), mp 92–95 °C dec. Anal. Calcd for $C_{28}H_{30}BF_4NOPRe$: C, 48.01; H, 4.32; N, 2.00. Found: C, 48.11; H, 4.34; N, 1.96. IR (cm^{-1}, thin film): ν_{NO} 1711 vs. MS:[56a] 614 (M$^+$, 77%), 544 (M$^+$ − C$_5$H$_{10}$, 100%).

(*ac*)-**4c** (CD_2Cl_2): ^{1}H NMR (δ) 15.80 (dd, J_{HH} 5.4, 9.3, H$_\alpha$), 7.70–7.20 (m, PPh$_3$), 5.98 (s, C$_5$H$_5$), 3.26 (ddd, J_{HH} 6.5, 9.3, 15.6, H$_\beta$), 1.97 (ddd, J_{HH} 5.4, 5.4, 15.6, H$_{\beta'}$), 1.65 (m, H$_\gamma$), 0.86 (d, J_{HH} 6.6, CH$_3$), 0.74 (d, J_{HH} 6.6, CH$_3'$); ^{13}C{^{1}H} NMR (ppm, partial) 313.3 (d, J_{CP} 7.3, C$_\alpha$), 133.5 (d, J_{CP} 11.4, *o*-Ph), 132.9 (s, *p*-Ph), 130.0 (d, J_{CP} 11.7, *m*-Ph),[60] 99.6 (s, C$_5$H$_5$), 66.1 (s, C$_\beta$), 29.3 (s, C$_\gamma$), 22.7 (s, CH$_3$), 22.3 (s, CH$_3'$); ^{31}P{^{1}H} (ppm) 18.4 (s). (*sc*)-**4c** (CD_2Cl_2, partial): ^{1}H (δ) 16.17 (s, H$_\alpha$), 0.66 (d, J_{HH} 6.8, CH$_3$), 0.63 (d, J_{HH} 6.8, CH$_3'$); ^{13}C{^{1}H} (ppm) 99.8 (s, C$_5$H$_5$), 23.7 (s, CH$_3$), 23.0 (s, CH$_3'$); ^{31}P{^{1}H} (ppm) 16.4 (s).

Acknowledgment. We thank the DOE for support of this research.

OM940843X

(60) The *ipso* carbon resonance was not detected.

(61) THF and *t*-BuOH resonances, which interfere with some assignments, were also present.

Stereogenic Lithium Centers in a Complex between *n*-Butyllithium and a Dilithiated Chiral Amine: Solution Studies by ^{6}Li,^{1}H-HOESY, ^{6}Li,^{6}Li-COSY, and ^{6}Li,^{6}Li-EXSY NMR

Göran Hilmersson and Öjvind Davidsson*

Department of Organic Chemistry, Göteborg University, S-412 96 Göteborg, Sweden

Received September 6, 1994[⊗]

The reaction of (2-methoxy-(*R*)-1-phenylethyl)((*S*)-1-phenylethyl)amine (**1**), which has been used in asymmetric synthesis, with [^{6}Li]-*n*-butyllithium in large excess in diethyl-d_{10} ether (DEE) at 20 °C results in the formation of a mixed complex between [^{6}Li]lithium (2-methoxy-(*R*)-1-phenylethyl)(2-([^{6}Li]-lithio)-(*S*)-1-phenylethyl)amide (**2**) and two [^{6}Li]-*n*-butyllithiums. The complex contains four lithiums in an asymmetric environment, which is observed in the ^{1}H NMR spectrum by the appearance of four signals from the nonequivalent α-protons of the two complexed *n*-butyllithiums. The solution structure of this mixed complex is proposed to be a tetramer with a distorted cubanoid core, on the basis of ^{1}H,^{1}H-NOESY, ^{1}H,^{6}Li-HOESY, ^{6}Li,^{6}Li-COSY, and ^{6}Li,^{6}Li-EXSY spectroscopy.

Introduction

Organolithium compounds constitute one of the most important classes of reagents for the synthetic organic chemist. Although these reagents are commonly used, the detailed mechanism of a simple lithiation reaction is still poorly understood.[1]

Thus, the study of organolithium compounds is a very important area of research. Solution structures and dynamic studies that give information about these reactive reagents are a prerequisite for the development of new organolithium reagents and ligands used in asymmetric synthesis. We believe that the potential of using chiral lithium amides in asymmetric synthesis (deprotonation,[2] alkylation,[3] and Michael addition[4]) has been explored only partially, possibly due to the absence of knowledge about solution structures of this important class of reagents. To our knowledge there is only one example in the literature where a coordination complex between a chiral ligand (sparteine) and a organolithium reagent (isopropyllithium) has been described.[5]

The degree of aggregation of simple lithium amides such as lithium diisopropylamide (LDA) and related amides has been studied in detail both in the solid state by X-ray crystallography[6] and in solution by NMR spectroscopy, utilizing the ^{15}N,^{6}Li coupling patterns to determine the aggregation state.[7] Previous studies of lithium amide bases suggest the formation of mixed lithium amide/lithium halide complexes in solution, and these mixed complexes differ from their homoaggregated lithium amide complexes in both reactivity and enantioselectivity.[8] Knowledge about the solution structure of such mixed complexes is of importance for the understanding of the reactions involving mixed complexes or aggregates. However, the solution structures of chiral lithium amides, especially those containing internal complexing ligands such as ROR′ or RR′NR″, are still mostly unknown.

NMR spectroscopic studies of organolithium compounds in solution give information about the structure and provide information about the intra- and intermolecular exchange processes which are not accessible from X-ray crystallographic data.

Recent development of new 2D NMR experiments such as proton–lithium Overhauser effect spectroscopy (^{1}H,^{6}Li-HOESY),[9] ^{6}Li,^{6}Li-COSY,[10] and ^{6}Li,^{6}Li-EXSY spectroscopy has provided information on the structure of several organolithium compounds in solution.[11] Among these, the ^{1}H,^{6}Li-HOESY experiment is one of the most powerful NMR techniques available for structure elucidation of organolithium compounds containing several different lithiums in solution. It provides information

⊗ Abstract published in *Advance ACS Abstracts*, January 1, 1995.

(1) Bernstein, M. P.; Collum, D. B. *J. Am. Chem. Soc.* **1993**, *115*, 789.

(2) (a) Cain, C. M.; Cousins, R. P.; Coumbarides, G.; Simpkins, N. *Tetrahedron* **1990**, *46*, 523. (b) Cox, P.; Simkins, N. *Tetrahedron: Asymmetry* **1991**, *2*, 1. (c) Ward, R. *Chem. Soc. Rev.* **1990**, *19*, 1. (d) Simkins, N. *Chem. Ind.* **1988**, 387. (e) Asami, M.; Kanemaki, N. *Tetrahedron Lett.* **1989**, *30*, 2125. (f) Asami, M. *Bull. Chem. Soc. Jpn.* **1990**, *63*, 1402. (f) Sato, D.; Kawasaki, H.; Shimada, I.; Arata, Y.; Okamura, K.; Date, T.; Koga, K. *J. Am. Chem. Soc.* **1992**, *114*, 761. Koga, K. *Pure Appl. Chem.* **1994**, *66*, 1487.

(3) Noyori, R.; Kitamura, M. *Angew. Chem., Int. Ed. Engl.* **1991**, 49.

(4) Juaristi, E.; Beck, A. K.; Hansen, J.; Matt, T.; Mukhodpadhyay, T.; Simson, M.; Seebach, D. *Synthesis* **1993**, 1271.

(5) Gallagher, D. J.; Kerrick, S. T.; Beak, P. *J. Am. Chem. Soc.* **1992**, *114*, 5872.

(6) Gregory, K.; Schleyer, P. v. R.; Snaith, R. *Adv. Organomet. Chem.* **1991**, *31*, 47.

(7) Lucht, B. L.; Collum, D. B. *J. Am. Chem. Soc.* **1994**, *116*, 6009.

(8) (a) Bunn, B. J.; Simpkins, N. S. *J. Org. Chem.* **1993**, *58*, 533. (b) Gilchrist, J. H.; Harrison, A. T.; Fuller, D. J.; Collum, D. B. *Magn. Reson. Chem.* **1992**, *30*, 855. (c) Galiano-Roth, A. S.; Gilchrist, J. H.; Harrison, A. T.; Fuller, D. J.; Collum, D. B. *J. Am. Chem. Soc.* **1991**, *113*, 5053.

(9) For the development of the ^{6}Li,^{1}H-HOESY experiment, see: Bauer, W.; Schleyer, P. v. R. *Magn. Reson. Chem.* **1988**, *26*, 827.

(10) For the development of the ^{6}Li,^{6}Li-COSY experiment, see: Günther, H.; Moskau, D.; Dujardin, R.; Maercker A. *Tetrahedron lett.* **1986**, *27*, 2251.

(11) (a) Bauer, W.; Feigel, M.; Müller, G.; Schleyer, P. v. R. *J. Am. Chem. Soc.* **1988**, *110*, 6033. (b) Bauer, W.; Schleyer, P. v. R. *J. Am. Chem. Soc.* **1989**, *111*, 7191. (c) Paquette, L. A.; Bauer, W.; Sivik, M. R.; Schleyer, P. v. R.; Bühl, M.; Feigel, M. *J. Am. Chem. Soc.* **1990**, *112*, 8776. (d) Gallagher, D. J.; Kerrick, S. T.; Beak, P. *J. Am. Chem. Soc.* **1992**, *114*, 5872. (e) Bauer, W.; Feigel, M.; Müller, G.; Schleyer, P. v. R. *J. Am. Chem. Soc.* **1988**, *110*, 6033. (f) Günther, H.; Dujardin, R.; Maercker, A. *Tetrahedron Lett.* **1986**, *27*, 2251.

0276-7333/95/2314-0912$09.00/0

Scheme 1

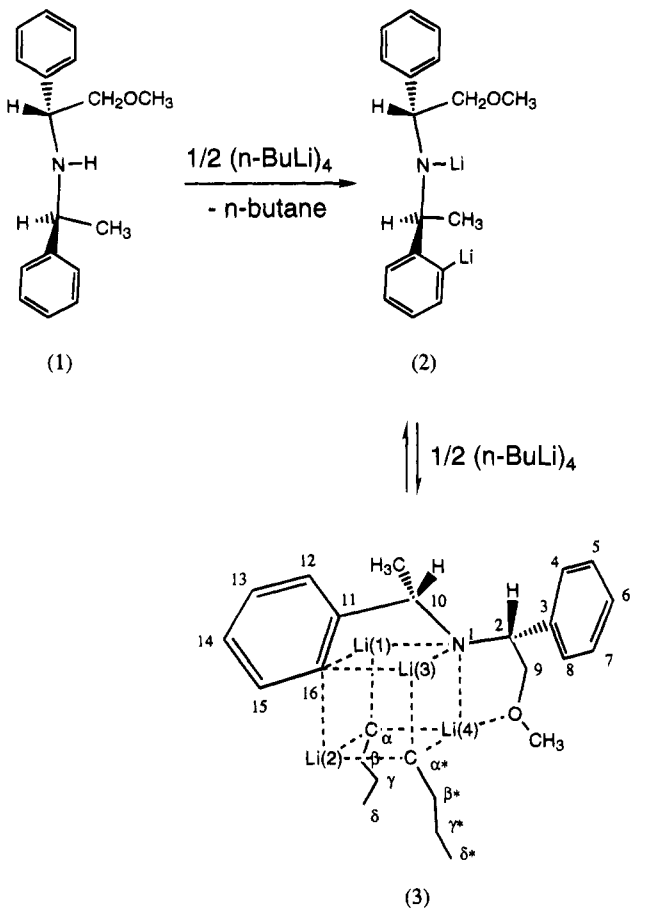

about the three-dimensional structure, including the coordinated ligands. The ^{6}Li,^{6}Li-COSY experiment may give information concerning whether lithiums are in the same complex or in different complexes. Differentiation between intra- and intermolecular lithium exchange is obtained from ^{6}Li,^{6}Li-EXSY experiments. With all these easily accessible new NMR techniques we saw the potential of investigating the solution structure of chiral lithium amides in solution. Eleveld and Hogeveen have shown that **1** gives rise to asymmetric induction in the addition of *n*-butyllithium to benzaldehyde. The enantiomeric excess ranged from 18 to 90%, depending on the solvent and the temperature.[12,13] Addition of a large excess of *n*-butyllithium to a diethyl ether solution of **1** at 25 °C results in dilithiated **1**. This species is exclusively coordinated to two *n*-butyllithiums at −80 °C, as shown in the mixed complex **3** (Scheme 1). The mixed complex contains four stereogenic lithium centers, as concluded from the appearance of nonequivalent α-protons in the two complexed *n*-butyl moieties.

Results and Discussion

^{1}H NMR. The ^{1}H NMR spectrum of a mixture of [^{6}Li]-*n*-butyllithium and **2** at −80 °C showed several sets of signals, one from tetrameric *n*-butyllithium, one from **2**, and another four signals from *n*-butyllithium in a nontetrameric aggregation state (Figure 1a), all not subject to exchange averaging. Five deshielded proton triplet signals were observed at δ −0.68, −0.83, −0.96,

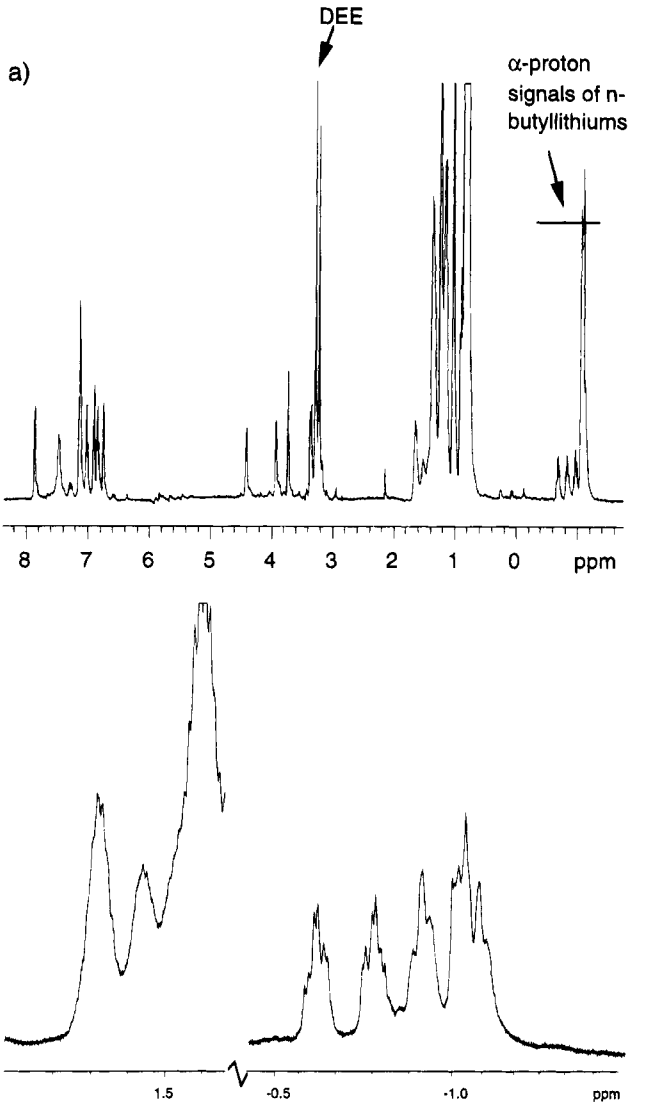

Figure 1. (a) ^{1}H NMR spectrum of **3** with *n*-butyllithium in excess at −80 °C in DEE-d_{10}. (b) Expansion of the ^{1}H NMR spectrum showing the α-proton and β-proton regions from *n*-butyllithium complexed in **3**.

−1.05, and −1.12, respectively, which could all be assigned to α-protons from different *n*-butyllithium molecules (Figure 1b).[14] Among them the signal at δ −1.05 has been assigned to α-protons in tetrameric *n*-butyllithium.[15] The other four α-proton signals were of equal intensity, each a doublet of a triplet (J = 5 Hz, J = 12.8 Hz).

To establish if these four signals were from α-protons in two our four different *n*-butyllithium molecules, we performed a ^{1}H,^{1}H-COSY experiment. The ^{1}H,^{1}H-COSY spectrum showed a cross-peak between the signal at δ −0.68 and the signal at δ −0.83 and another cross-peak between the signal at δ −0.96 and the signal at δ −1.12 (Figure 2a). Therefore, we concluded that these four signals were from two different *n*-butyllithium molecules with two diastereotopic α-protons each. Thus, two pairs of nonequivalent α-protons from *n*-butyllithium are observed at four different chemical shifts.

(12) Eleveld, M. B.; Hogeveen, H. *Tetrahedron Lett.* **1984**, *25*, 5187.
(13) Hilmersson, G.; Davidsson, Ö. *J. Organomet. Chem.*, in press.

(14) The chemical shift, coupling pattern, and correlations obtained in the ^{1}H,^{1}H-NOESY as well as the ^{1}H,^{1}H-COSY of these signals are the same as previously obtained data on *n*-butyllithium in diethyl ether; see: West, P.; Waack, R. *J. Am. Chem. Soc.* **1967**, *89*, 4395. McGarrity, J. F.; Ogle, C. A. *J. Am. Chem. Soc.* **1985**, *107*, 1805.
(15) *n*-Butyllithium exclusively forms tetramers in DEE at −90 °C.

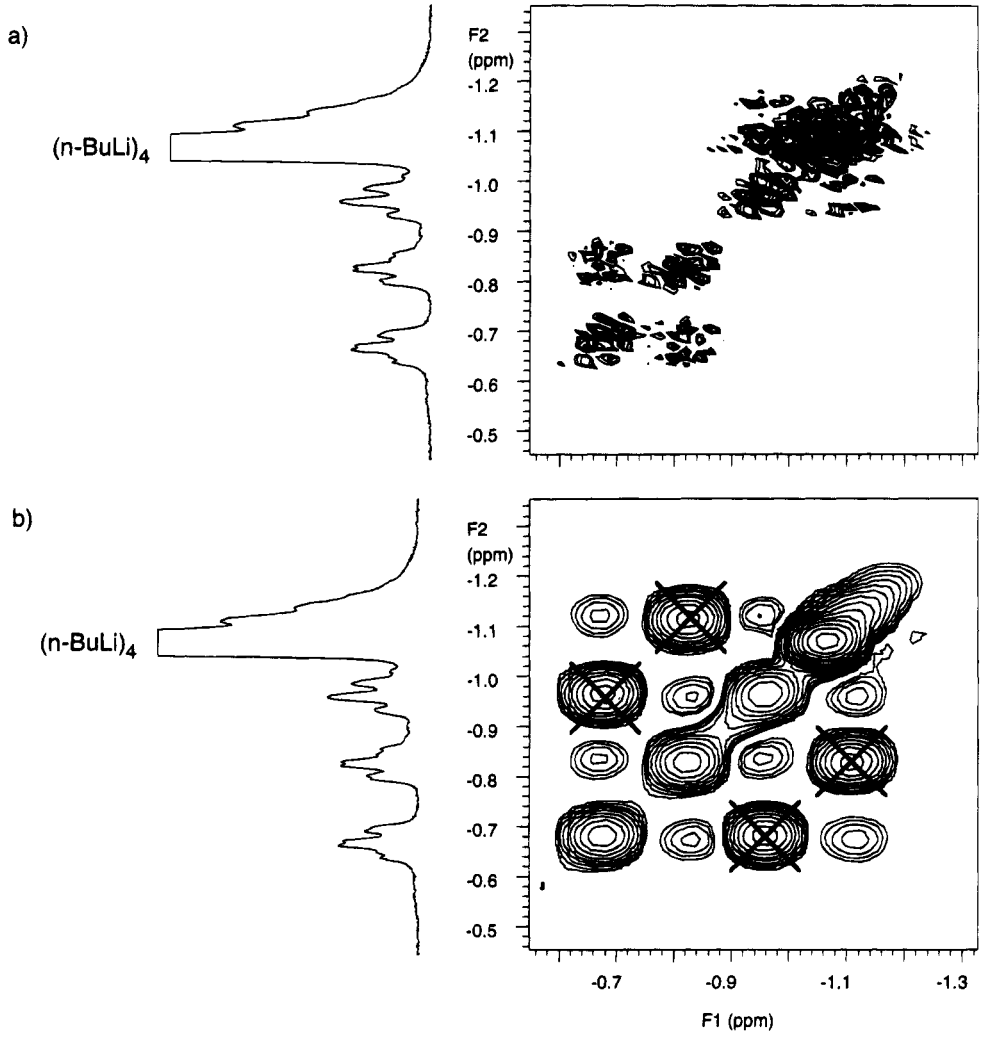

Figure 2. (a) Two-dimensional nonsymmetrized phase-sensitive ^{1}H,^{1}H-DQF-COSY contour plot of **3** (−80 °C, 0.1 M, 95.67 atom % ^{6}Li, 500 MHz), in DEE-d_8 using a Varian Unity 500 spectrometer. The low-frequency signal from DEE was set at δ 1.06 for reference. (b) Two-dimensional nonsymmetrized phase-sensitive ^{1}H,^{1}H-NOESY contour plot of **3** (−80 °C, 0.1 M, 95.67 atom% ^{6}Li, 500 MHz, mixing time 1.0 s), in DEE-d_8 using a Varian Unity 500 spectrometer. The contour plot shows the exchange cross-peaks, marked with large "X" symbols, and the NOE cross-peaks between the α-protons in complexed *n*-butyllithium. The low-frequency signal from DEE was set to δ 1.06 for reference.

Table 1. Proton Chemical Shifts for 3

^{1}H NMR (500 MHz, DEE-d_{10}, −80 °C): for complexed *n*-butyllithiums, δ −1.12 (dt, J(H,H) = 13 Hz, J(H,H) = 5 Hz, 1H, α-CH$_2$−Li), −0.96 (dt, J(H,H) = 13 Hz, J(H,H) = 5 Hz, 1H, α-CH$_2$−Li), −0.83 (dt, J(H,H) = 13 Hz, J(H,H) = 5 Hz, 1H, α-CH$_2$−Li), −0.68 (dt, J(H,H) = 13 Hz, J(H,H) = 5 Hz, 1H, α-CH$_2$−Li), 1.29 (m, br, 6H, δ-CH$_3$), 1.43 (m br, 4H, γ-CH$_2$), 1.54 (m, br, 2H, β-CH$_2$), 1.67 (m, br, 2H, β-CH$_2$); dilithiated amide **2**, δ 0.84 (d, J(H,H) = 6.1 Hz, 3H, CH$_3$), 3.26 (s, 3H, OCH$_3$), 3.39 (d br, J(H,H) = 7.2 Hz, 1H, H$_2$−C(9)), 3.76 (s br, 1H, H−C(2)), 3.95 (d br, J(H,H) = 6.0 Hz, 1H, H$_2$−C(9)), 4.44 (q, J(H,H) = 6.1 Hz, 1H, H−C(10)), 6.77 (t, J(H,H) = 6.8 Hz, H−C(14)), 6.87 (t, J(H,H) = 7.2 Hz, H−C(13)), 6.92 (d, J(H,H) = 7.8 Hz, H−C(12)), 7.05 (t, J(H,H) = 7.2 Hz, H−C(6)), 7.2 (t, J(H,H) = 7.4 Hz, H−C(5), H−C(7)), 7.50 (s br, H−C(4), H−C(8)), 7.89 (d, J(H,H) = 7.9 Hz, H−C(15))

The appearance of diastereotopic α-protons of the non-chiral *n*-butyllithium implies strong coordination to a chiral center; i.e., at least one of the four coordinating lithium cations must be in a chiral environment. Furthermore, the geminal coupling between these two pairs of α-protons of the *n*-butyllithium molecules was found to be 12.8 Hz by simultaneous decoupling of the corresponding β-proton multiplets at δ 1.43 and 1.54, respectively.

Comparison of the signal area of the 4,2 pair of diastereotopic α-proton signals with the signal area from **2** revealed a 1:1 ratio indicative of the presence of two *n*-butyllithium molecules to one molecule of **2**, as shown in complex **3**.

^{13}C NMR. Consistent with the ^{1}H NMR spectrum, the ^{13}C{^{1}H} NMR spectrum of [^{6}Li]-*n*-butyllithium and **2** at −85 °C also showed the presence of only one set of signals from **2**. Three different carbon-13 signals were seen from the α-carbanionic carbon atoms of the *n*-butyllithium molecules, a septet at δ 10.90 with a ^{13}C,^{6}Li coupling constant of J = 5.6 Hz assigned to the excess of tetrameric *n*-butyllithium[15] and two signals from the two *n*-butyl anions in **3**, one at δ 10.67 with a ^{13}C,^{6}Li coupling constant of J = 5.4 Hz and the other a broad unresolved multiplet at δ 10.00 (Figure 3). The magnitude of the ^{13}C,^{6}Li coupling constant of J = 5.4 Hz indicates coupling to three lithium cations in a static tetramer (the multiplicity of the signal resembles that of a septet).

A ^{1}H,^{13}C-HMQC spectrum at −90 °C showed correlations of the α-proton signals of the complexed *n*-butyllithiums at δ −0.68 and −0.83 to the *n*-butyl

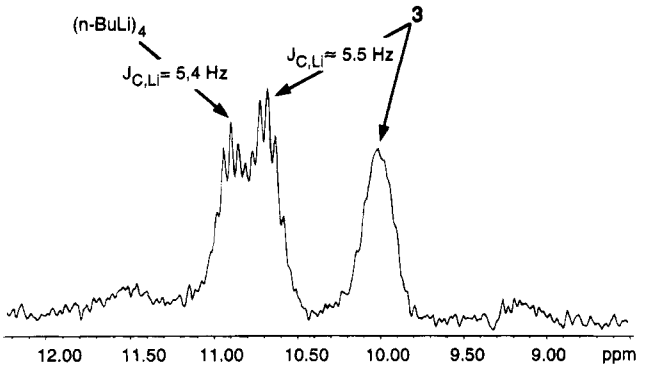

Figure 3. ^{13}C NMR spectrum of **3** with *n*-butyllithium in excess at −85 °C in DEE-d_{10} showing the carbanionic carbons from *n*-butyllithium.

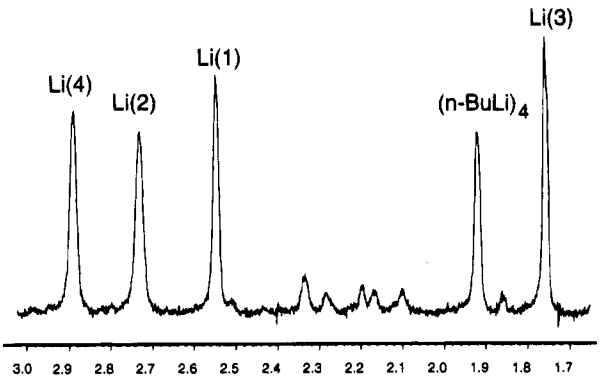

Figure 4. ^{6}Li NMR spectrum of **3** with *n*-butyllithium in excess at −90 °C in DEE-d_{10}.

Table 2. Lithium-6 Chemical Shifts for 3 at −90 °C

chem shift (δ)	Li cation[a]	chem shift (δ)	Li cation[a]
1.75	Li(3)	2.74	Li(2)
1.90	(*n*-BuLi)$_4$	2.90	Li(4)
2.56	Li(1)		

[a] According to Figure 2.

carbanionic atom at δ 10.00, and the α-proton signals at δ −0.96 and −1.12 showed correlations with the *n*-butyl carbanionic atom signal at δ 10.67.

^{6}Li NMR. The ^{6}Li NMR spectrum at −90 °C of the mixture of *n*-butyllithium and **2** shows the presence of five signals (Figure 4 and Table 2). The signal at δ 1.90 was assigned to the excess of tetrameric *n*-butyllithium.[15,16] The remaining four lithium signals, with identical intensities, indicate the presence of four nonequivalent lithiums.

The $^{1}H,^{6}Li$-HOESY spectrum in Figure 5 shows correlations between the lithium signals at δ 2.90, 2.74, 2.56, and 1.75 and the α-protons of *n*-butyllithium, consistent with two *n*-butyllithium molecules being coordinated to one molecule of **2**.

The $^{6}Li,^{6}Li$-COSY spectrum (Figure 6) shows strong cross-peaks between the lithium signal at δ 2.74 and the three lithium signals at δ 1.75, 2.56, and 2.90, respectively, but not with the tetrameric *n*-butyllithium signal at δ 1.90. Cross-peaks are also seen between the lithium signal at δ 2.90 and the lithium signals at δ 2.56 and 1.75. A weak cross-peak was also observed between the lithium signal at δ 2.56 and the lithium signal at δ 1.75. The presence of cross-peaks between all the four lithiums in the $^{6}Li,^{6}Li$-COSY spectrum establishes that all lithiums are scalar coupled and therefore present in the same complex. The arrangement of these four lithium signals in the tetrameric structure is consistent with a (NC_3Li_4) core distorted from cubic symmetry. Obviously, there is only slow exchange of the lithiums at low temperatures since separate ^{6}Li signals are observed.

The four ^{6}Li NMR resonances of equal intensity at δ 1.75, 2.56, 2.74, and 2.90 have been assigned to four lithiums present in the distorted cubanoid core of complex **3**.

A detailed investigation of the $^{1}H,^{6}Li$-HOESY spectrum of *n*-butyllithium and **2** at −90 °C allowed us to propose a reasonable three-dimensional solution structure of the complex between two molecules of *n*-butyllithium and one molecule of **2** as shown in **3** (Scheme 1). The possibility of transfer of NOE's due to an intramolecular lithium exchange has been minimized by recording the spectrum at low temperature.

The ^{6}Li signal at δ 1.75 (Li(3) in **3**) showed correlations to only one of the sets of α-proton resonances from *n*-butyllithium at δ −0.96 and −1.12. This shows that the Li(3) is in close contact with only one of the complexed *n*-butyllithiums in **3**. Furthermore, this lithium signal shows correlations with the H−C(10) signal at δ 4.44, $-CH_3$ signal at δ 0.84, H−C(9) signal at δ 3.95, and H−C(2) signal at δ 3.76.

It has been established by the use of $^{1}H,^{1}H$-COSY (τ = 0.3 s), optimized for the study of long-range couplings, that the H−C(10) proton signal at δ 4.44 couples with the H−C(12) proton signal at δ 6.92, and, therefore, the H−C(12) proton has to be positioned at the ortho position on the lithiated phenyl ring.[17] The lithium signal at δ 2.90 (Li(4) in **3**) shows correlations with all the proton signals from the α-protons in the two *n*-butyllithium molecules and with the $-OCH_3$ group at δ 3.26.

Accordingly, the lithium signal at δ 2.56 (Li(1) in **3**) showed correlations to only one set of α-proton resonances at δ −0.68 and −0.83 from the two *n*-butyllithium molecules. A strong correlation to the $-CH_3$ signal at δ 0.84 and a weaker interaction with the H−C(12) signal at δ 6.92 was also observed. The remaining lithium signal at δ 2.74 (Li(2) in **3**) showed in the $^{1}H,^{6}Li$-HOESY experiment strong correlations to all the signals from the α-protons in the two *n*-butyllithium molecules and with two phenyl ring signals H−C(14) and H−C(15) (at δ 6.77 (triplet) and 7.89 (doublet)). By the use of $^{1}H,^{1}H$-LR-COSY and $^{1}H,^{1}H$-COSY we established that the H−C(14) and H−C(15) signals at δ 6.77 and 7.89 originate from the lithiated phenyl ring. All four lithium signals (except that for Li(3)) also show close contacts to the broad, unresolved β-proton signals at δ 1.43 and 1.53 from *n*-butyllithium in the $^{1}H,^{6}Li$-HOESY spectrum.

The expansion of the $^{1}H,^{1}H$-NOESY spectrum (Figure 2b) shows the presence of positive exchange NOE cross-peaks (marked with large "X" symbols) between the α-proton signals at δ −0.68 and −0.96, and between the signal at δ −0.83 and that at δ −1.12. This indicates

(16) The ^{6}Li NMR spectra were referenced to an external 0.3 M $^{6}LiCl$/MeOH standard, set to δ 0.0, according to Reich and coworkers: Reich, H. J.; Green, D. P. *J. Am. Chem. Soc.* **1989**, *111*, 8729.

(17) Beak, P.; Kerrick, S. T.; Gallagher, D. J. *J. Am. Chem. Soc.* **1993**, *115*, 10628.

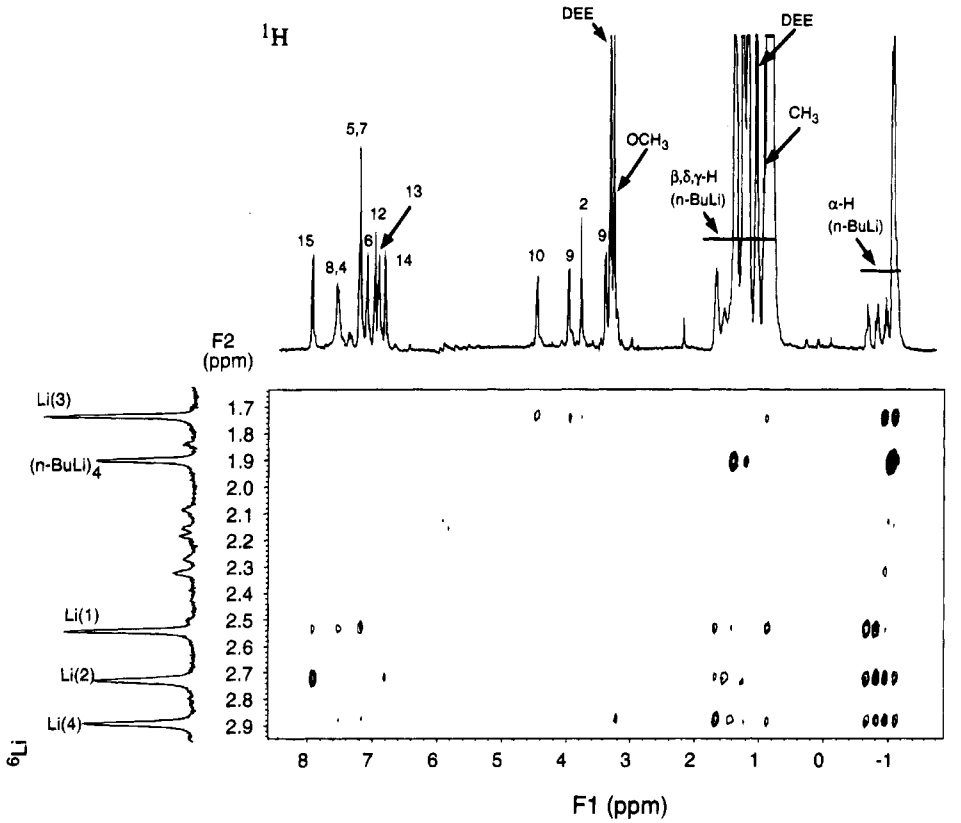

Figure 5. Two-dimensional phase-sensitive ^{6}Li,^{1}H-HOESY contour plot of **3** (−90 °C, 0.5 M, 95.67 atom% ^{6}Li, 73.556 MHz, mixing time 1.0 s) in DEE-d_8 using a Varian Unity 500 spectrometer. The ^{6}Li resonances were referenced to external 0.3 M ^{6}LiCl/MeOH (δ 0.0). The ^{1}H resonances were referenced to the most upfield signal from DEE, which was set to δ 1.06.

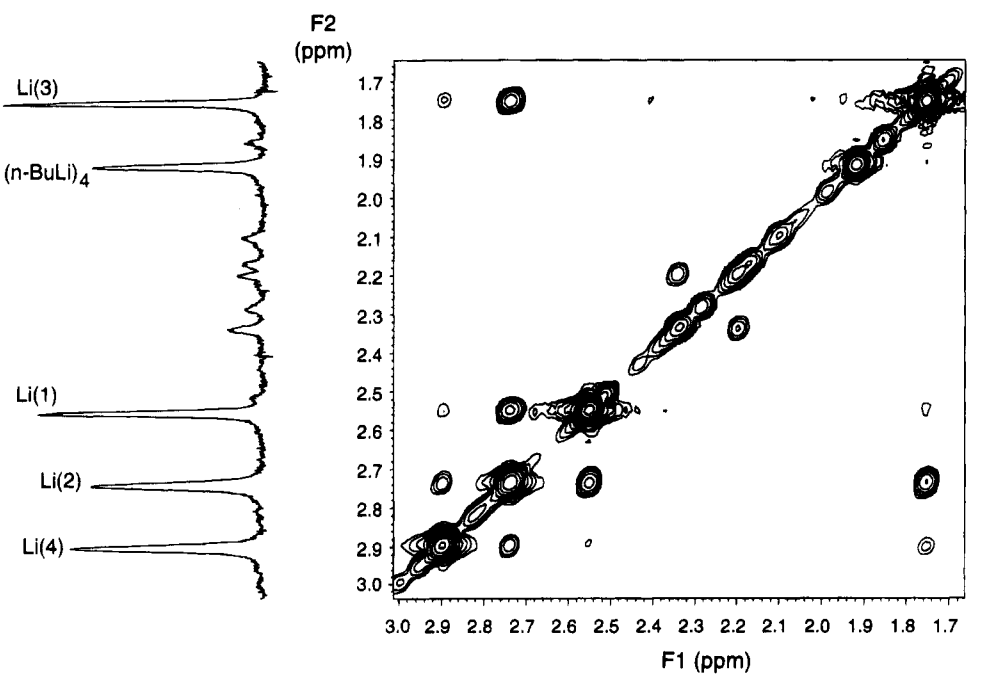

Figure 6. Two-dimensional nonsymmetrized absolute value ^{6}Li,^{6}Li-COSY contour plot obtained with delays for detection of small coupling constants of **3** (−90 °C, 0.5 M, 95.67 atom% ^{6}Li, 73.556 MHz, $\Delta_1 = \Delta_2 = 0.25$ s) in DEE-d_8 using a Varian Unity 500 spectrometer. The ^{6}Li resonances were referenced to external 0.3 M ^{6}LiCl/MeOH (δ 0.0).

that there is a slow exchange between the two pairs of α-CH_2 groups of the complexed *n*-butyllithium. Negative NOE's were also observed in the ^{1}H,^{1}H-NOESY spectrum between the geminal α-proton signals of *n*-butyllithium at δ −0.68 and −0.83 and between δ −0.96 and −1.12, indicative of short proton−proton distances. This NOE is transferred between the α-protons due to the intramolecular exchange of lithiums.

In the spectrum there are also weak cross-peaks between the MeO-group signal at δ 3.26 and the α-proton signals at δ −0.83 and δ −1.12, whereas stronger cross-peaks between the corresponding β-pro-

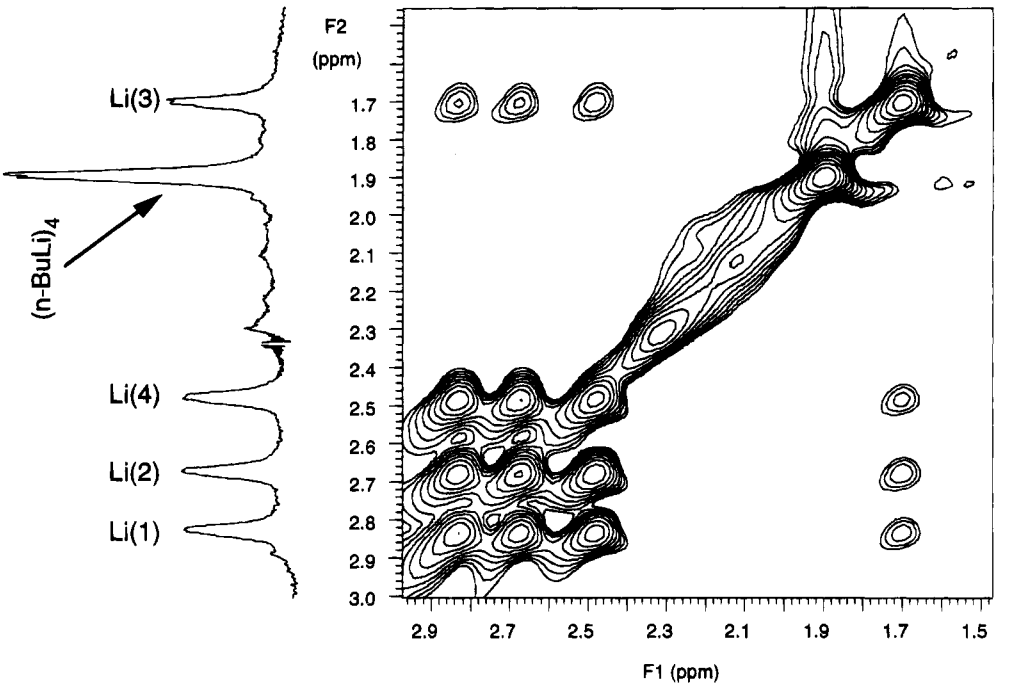

Figure 7. Two-dimensional nonsymmetrized phase-sensitive ^{6}Li,^{6}Li-EXSY contour plot of **3** (−80 °C, 0.5 M, 95.67 atom% ^{6}Li, 73.556 MHz, mixing time 4.0 s) in DEE-d_8 using a Varian Unity 500 spectrometer. The ^{6}Li resonances were referenced to external 0.3 M ^{6}LiCl/MeOH (δ 0.0).

tons at δ 1.55 and 1.67 and the methoxy group signals were observed, which shows that the methoxy group is in close proximity to both of the complexed *n*-butyl anions.

The ^{6}Li,^{6}Li-EXSY experiment (NOESY pulse sequence) has been applied for the detection of intraaggregate ^{6}Li exchange.[18] A ^{6}Li,^{6}Li-EXSY experiment at −80 °C showed an intraaggregate exchange of all four lithiums in **3** (Figure 7). All four lithiums in **3** showed correlations with each other, due to only intraaggregate exchange of lithiums and not to the excess of tetrameric *n*-butyllithium by interaggregate exchange.

An argument for larger aggregates, i.e. dimerization of **3**, would be in contradiction to what is known about organolithium compounds, especially for those containing internal complexing ligands such as −OR. Tetramers or smaller aggregates are formed exclusively in coordinating solvents such as diethyl ether, and since the spin−lattice relaxation times (T_1) of the four lithium signals are between 9.0 and 9.6 s, (cf. tetrameric *n*-butyllithium, T_1 = 8 s; tetrameric isopropyllithium, T_1 = 10 s),[19] one would expect that **3** does not dimerize in diethyl ether to a higher aggregate containing eight lithium atoms.

Conclusions

In summary, **3** is a mixed complex between a chiral lithium amide, with a methoxy group as an internal ligand, and two *n*-butyllithiums with a (C_3NLi_4) tetrameric core distorted from cubic symmetry. Furthermore, the *n*-butyllithiums in **3** are strongly complexed in **3** in such a manner that the intermolecular exchange is slow on the NMR time scale at low temperatures. The α-protons of the *n*-butyl groups in **3** are diastereotopic, due to the presence of four stereogenic lithium centers. We believe this to be the first direct observation of stereogenic lithium centers in a mixed complex between a chiral lithium amide and *n*-butyllithium.

Currently we are investigating the use of the chiral dilithiated amide **2** in asymmetric synthesis. Investigations of **2** and the mixed complex **3** in different solvents also are in progress.

Experimental Part

General Considerations. Glassware was dried overnight in a 120 °C oven (syringes and Teflon-containing parts were dried at 50 °C in a vacuum oven) prior to transfer into a glovebox (Mecaplex GB 80 equipped with a gas purification system that removes oxygen and moisture) with a positive nitrogen atmosphere. The typical moisture content was less than 0.5 ppm in the atmosphere. All manipulations of the lithium compounds were carried out in the glovebox using gastight syringes. The preparation of *n*-butyllithium was carried out under a positive pressure of argon.

Preparation of (2-Methoxy-(*R*)-1-phenylethyl)-((*S*)-1-phenylethyl)amine (1). This amine was synthesized according to the literature.[2]

Preparation of [^{6}Li]-*n*-Butyllithium. A block of ^{6}Li metal (0.25 g, 41.6 mmol, 96% ^{6}Li purchased from US Services Inc.) was cut into small pieces using a sharp knife. The ^{6}Li metal was transfered into a 50 mL flask: the flask was equipped with a silicone/Teflon septum. After the ^{6}Li metal was rinsed with 1.0 mL of 2-propanol,[20] 10 mL of dry hexane was added and the flask was put in an ultrasonic bath at 20 °C (Sonorex

(18) (a) Günther, H.; Moskau, D.; Schmak, D. *Angew. Chem., Int. Ed. Engl.* **1987**, *26*, 1212. (b) Bauer, W.; Feigel, M.; Müller, G.; Schleyer, P. v. R. *J. Am. Chem. Soc.* **1998**, *110*, 6033. (c) Meier, B. H.; Ernst, R. R. *J. Am. Chem. Soc.* **1979**, *101*, 6441. (d) Jeener, J.; Meier, B. H.; Bachman, P.; Ernst, R. R. *J. Chem. Phys.* **1979**, *71*, 4546.

(19) Ellington, D. H. Ph.D. Dissertation, University of North Texas, Denton, TX, 1990.

Super 10P operated at maximum effect) for ca. 3 min; then the lithium hydroxide containing hexane suspension was removed with a syringe and another 10 mL aliquot of hexane was added followed by ultrasonic bath, after the lithium hydroxide containing hexane solution was removed. This procedure was repeated several times until the hexane solution remained clear and the previously black lithium pieces had metallic surfaces.

Upon addition of 15 mL of dry hexane, followed by slow addition of 1-chlorobutane (2.09 mL, 20.0 mmol) over 5 min, the flask was again put in the ultrasonic bath for another 3 h at 20–30 °C. The reaction started immediately and could be monitored by the change of the colorless solution to deep purple. After 12 h at 10–15 °C, the resulting purple suspension was centrifuged and the supernatant was transferred into a glass apparatus equipped with high-vacuum Teflon valves. The solvent was removed under vacuum (10^{-4} Torr). The concentration of *n*-butyllithium was 10 M (with 4% alkoxides), determined by double Gilman titration. The [^{6}Li]-n-butyllithium was then stored under argon atmosphere in a glass apparatus at −30 °C.

[^{6}Li]Lithium (2-methoxy-(*R*)-1-phenylethyl)(2-([^{6}Li]lithio)-(*S*)-1-phenylethyl)amide/Bis(*n*-butyllithium): In Situ Preparation. (2-methoxy-(*R*)-1-phenylethyl)((*S*)-1-phenylethyl)amine (**1**; 90 mg, 0.35 mmol) was transferred into a dry 5-mm NMR tube. The NMR tube was fitted with a Wilmad/Omnifit OFV Teflon valve assembly with Teflon/silicone septa. Freshly distilled diethyl-d_{10} ether (stored over Deporox Fluka molecular sieves) was added by a syringe. To the ether solution of **1** at −78 °C was added 10 M [^{6}Li]-*n*-butyllithium (210 μL, 2.1 mmol) with a syringe. The reaction mixture was warmed to room temperature and then was put into the NMR magnet. After approximately 2 h at 20 °C the reaction was complete (^{1}H NMR monitoring of the formation of **2**) and the temperature was set to −80 °C, using a long hold VT − 50 L liquid-N_2 Dewar with heat exchanger.

The chiral lithium amide **1** was retained unaltered with its original stereo configuration after quenching with water. Quenching **2** with ^2H_2O resulted in the formation of **1** deuterated in the 1-phenylethyl moiety and at the amine nitrogen.

Instrumental Considerations. All NMR spectra were recorded using a Varian Unity 500 spectrometer equipped with three channels using a 5-mm ^{1}H,^{13}C,^{6}Li triple-resonance probe head, built by the Nalorac Co. Measuring frequencies were 500 MHz (^{1}H), 125 MHz (^{13}C), and 73 MHz (^{6}Li). The ^{1}H and ^{13}C spectra were referenced to the solvent diethyl-d_{10} ether signals at δ 1.06 (^{1}H, $-CH_3$) and δ 65.12 (^{13}C, $-OCH_2-$), respectively. Lithium spectra were referenced to external 0.3 M ^{6}LiCl in MeOH-d_4 (δ 0.0).

The one-dimensional proton and carbon spectra were recorded with standard parameters. Lithium spectra were recorded with and without proton Waltz-16 decoupling. A typical 90° ^{6}Li pulse was 20 μs.

2D NMR Measurements. All 2D spectra were acquired using nonspinning 5 mm samples with deuterium field-frequency locking. Spectra were processed in the phase-sensitive mode (except for the ^{6}Li,^{6}Li-COSY and ^{1}H,^{1}H long range COSY spectra, which were acquired and processed in the absolute value mode) with square sine bells weighting both in f_1 and f_2.

For the ^{6}Li,^{6}Li-COSY spectrum the following parameters were used: spectral window of 150 Hz in f_1 and 800 Hz in f_2; 256 increments and 16 scans per increment; one-time zero filling in f_1 and f_2; delay for detection of small coupling constants $\Delta_1 = \Delta_2 = 0.25$ s.

No proton decoupling was used. A homo-spoil 8 ms pulse was added after acquisition for removal of transversal magnetization.

For the ^{6}Li,^{1}H-HOESY spectrum the following parameters were used: spectral window of 1000 Hz (f_2 = ^{6}Li) and 8000 Hz (f_1 = ^{1}H); 256 increments and 16 scans per increment in t_1; mixing time 1.0 s; sine bell weighting in f_1 and f_2 for the phase-sensitive spectrum; 28 μs proton 90° decoupler pulse. The ^{6}Li,^{1}H-HOESY sequences is described in detail in ref 3.

For the ^{6}Li,^{6}Li-EXSY spectrum the following parameters were used: spectral window of 1000 Hz (f_1 and f_2); 256 increments and 8 scans per increment in t_1; one-time zero filling in f_1 and f_2; mixing time 3.5 s; no proton decoupling; absolute value data which were processed with exponential line broadening without symmetrization.

For the ^{1}H,^{1}H-NOESY spectrum the following parameters were used: spectral window of 8000 Hz (f_2) and 8000 Hz (f_1); 128 increments and 4 scans per increment in t_1; one-time zero filling in f_1 and f_2; mixing time 1.0 s; sine bell weighting in f_1 and f_2 for the phase-sensitive spectrum.

Acknowledgment. We thank Professor Per Ahlberg for helpful discussions, the Swedish Natural Science Research Council (P.A.), and the Carl Tryggers Foundation (Ö.D.)

OM940699F

(20) Fraenkel, G.; Henrichs, M.; Hewitt, J. M.; Su, B. M.; Geckle, M. J. *J. Am. Chem. Soc.* **1980**, *102*, 3345.

Polyhedral Cluster Expansion in $Co_3(CO)_6[\mu_2\text{-}\eta^2{:}\eta^1\text{-}C(Ph)C{=}C(PPh_2)C(O)OC(O)](\mu_2\text{-}PPh_2)$. Characterization of the Hypho Cluster $Co_3(CO)_5(\mu\text{-}CO)(PMe_3)[\mu_2\text{-}\eta^2{:}\eta^1\text{-}C(Ph)C{=}C(PPh_2)C(O)OC(O)](\mu_2\text{-}PPh_2)$ and the Phosphine-Substituted Arachno Cluster $Co_3(CO)_5(PMe_3)[\mu_2\text{-}\eta^2{:}\eta^1\text{-}C(Ph)C{=}C(PPh_2)C(O)OC(O)](\mu_2\text{-}PPh_2)$

Kaiyuan Yang, Simon G. Bott,* and Michael G. Richmond*

Center for Organometallic Research and Education, Department of Chemistry, University of North Texas, Denton, Texas 76203

Received June 15, 1994[⊗]

Treatment of the arachno cluster $Co_3(CO)_6[\mu_2\text{-}\eta^2{:}\eta^1\text{-}C(Ph)C{=}C(PPh_2)C(O)OC(O)](\mu_2\text{-}PPh_2)$ (**1**) with PMe_3 gives the hypho cluster $Co_3(CO)_5(\mu\text{-}CO)(PMe_3)[\mu_2\text{-}\eta^2{:}\eta^1\text{-}C(Ph)C{=}C(PPh_2)C(O)OC(O)](\mu_2\text{-}PPh_2)$ (**2**) via site-selective PMe_3 addition to the PPh_2–(maleic anhydride)-substituted cobalt center. This addition reaction is accompanied by cleavage of one of the Co–Co bonds in **1** and a formal change in how the μ_2-phosphido ligand distributes its three available bonding electrons to the ligated cobalt centers in **2**. The flexibility in the ligand donation properties of the μ_2-phosphido group and the stabilization of the heterolytically broken Co–Co bond by the ancillary $\mu_2\text{-}\eta^2{:}\eta^1$-benzylidene(diphenylphosphino)maleic anhydride ligand are believed to be key factors promoting the observed polyhedral cluster expansion of **1**. Cluster **2** undergoes CO loss quickly at room temperature to afford the phosphine-substituted arachno cluster $Co_3(CO)_5(PMe_3)[\mu_2\text{-}\eta^2{:}\eta^1\text{-}C(Ph)C{=}C(PPh_2)C(O)OC(O)](\mu_2\text{-}PPh_2)$ (**3**). Clusters **2** and **3** have been isolated and characterized in solution by NMR (^{31}P and ^{13}C) and IR spectroscopy and in the solid state by X-ray diffraction analyses. Cluster **2**, as the heptane solvate, crystallizes in the triclinic space group $P\bar{1}$: $a = 11.236(2)$ Å, $b = 12.802(4)$ Å, $c = 17.886(4)$ Å, $\alpha = 86.41(2)°$, $\beta = 73.26(2)°$, $\gamma = 83.79(2)°$, $V = 2448(1)$ Å^3, $Z = 2$, $d_{calc} = 1.461$ g cm^{-3}; $R = 0.0667$, $R_w = 0.0816$ for 1768 observed reflections. Cluster **3**, as the CH_2Cl_2 solvate, crystallizes in the monoclinic space group $P2_1/n$: $a = 10.256(2)$ Å, $b = 28.398(2)$ Å, $c = 15.405(1)$ Å, $\beta = 100.93(1)$, $V = 4405.5(9)$ Å^3, $Z = 4$, $d_{calc} = 1.558$ g cm^{-3}; $R = 0.0469$, $R_w = 0.0517$ for 2623 observed reflections. The X-ray structures of **2** and **3** confirm the existence of the Co–Co bond scission attendant upon substitution and the CO loss and Co–Co bond formation, respectively. The electron-counting formalism demonstrates the change in the donor properties of the μ_2-phosphido ligand in going from **1** to **2** and from **2** to **3**.

Introduction

The polyhedral expansion of certain clusters during ligand addition reactions has been documented.[1] To our knowledge the vast majority of cluster-opening reactions involves assistance from one or more of the ancillary CO groups, as outlined in eq 1.[2] Here the formal transfer of the two electrons in the ruptured metal–metal bond is ultimately redistributed about the cluster polyhedron, giving rise to coordinatively saturated metal centers. CO loss and re-formation of the metal–metal bond complete the overall sequence for the net replacement of CO by the incoming ligand in many transition-metal clusters.

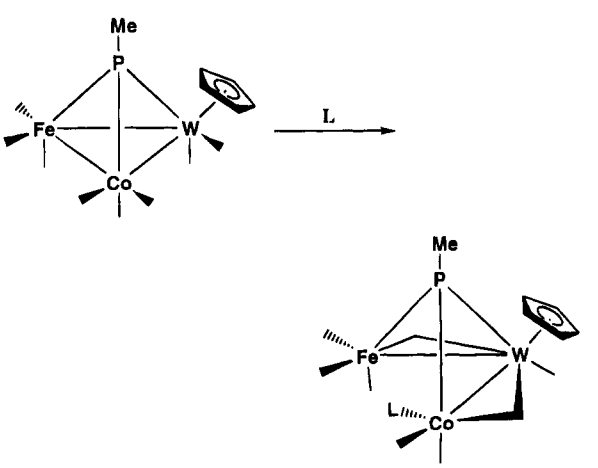

(1)[2a]

In this report we present our data on the addition reaction of PMe_3 to the arachno cluster $Co_3(CO)_6[\mu_2\text{-}\eta^2$:

⊗ Abstract published in *Advance ACS Abstracts,* January 1, 1995.

(1) (a) Richmond, M. G.; Kochi, J. K. *Inorg. Chem.* **1987**, *26*, 541. (b) Bogan, L. E.; Lesch, D. A.; Rauchfuss, T. B. *J. Organomet. Chem.* **1983**, *250*, 429. (c) Adams, R. D.; Yang, L. W. *J. Am. Chem. Soc.* **1983**, *105*, 1983. (d) Martin, L. R.; Einstein, F. W. B.; Pomeroy, R. K. *Organometallics* **1988**, *7*, 294. (e) Tulyathan, B.; Geiger, W. E. *J. Am. Chem. Soc.* **1985**, *107*, 5960. (f) Vahrenkamp, H. *Adv. Organomet. Chem.* **1983**, *22*, 169 and references therein.

0276-7333/95/2314-0919$09.00/0

η^1-C(Ph)C=C(PPh$_2$)C(O)OC(O)](μ_2-PPh$_2$) (**1**; where the μ_2, η^2, and η^1 descriptors refer to the benzylidene, maleic anhydride, and phosphine groups, respectively, of the six-electron benzylidene(diphenylphosphino)maleic anhydride ligand),[3] which proceeds to give the intermediate hypho cluster $Co_3(CO)_5(\mu\text{-}CO)(PMe_3)[\mu_2\text{-}\eta^2{:}\eta^1$-C(Ph)C=C(PPh$_2$)C(O)OC(O)]($\mu_2$-PPh$_2$) (**2**). Cluster **2** rapidly loses CO in solution to furnish $Co_3(CO)_5(PMe_3)$-[$\mu_2\text{-}\eta^2{:}\eta^1$-C(Ph)C=C(PPh$_2$)C(O)OC(O)]($\mu_2$-PPh$_2$) (**3**) as the thermodynamic product of PMe_3 substitution. The molecular structures of **2** and **3** have been confirmed by X-ray crystallography, and a conventional electron-counting formalism is utilized in the discussion on the observed electronic changes exhibited by the ancillary μ_2-PPh$_2$ donor ligand in clusters **2** and **3**. This report outlines the importance of the $\mu_2\text{-}\eta^2{:}\eta^1$-benzylidene-(diphenylphosphino)maleic anhydride ligand in directing the site of PMe_3 attack in **1** and that of the phosphido group in assisting with the redistribution of electron density in a ligand substitution reaction in a polynuclear cluster.

Results and Discussion

Synthesis and X-ray Diffraction Structure of $Co_3(CO)_5(\mu\text{-}CO)(PMe_3)[\mu_2\text{-}\eta^2{:}\eta^1$-C(Ph)C=C(PPh$_2$)C(O)OC(O)]($\mu_2$-PPh$_2$).

Treatment of **1** in CH_2Cl_2 or THF solution with PMe_3 (1.1 equiv) at −78 °C leads to the immediate formation of cluster **2** in quantitative yield. This conversion was ascertained by low-temperature FT-IR measurements, which revealed the presence of terminal metal carbonyl bands at 2035 (s), 2010 (vs), 1999 (vs), 1960 (sh), and 1900 (w) cm^{-1} and bma ligand ν(CO) bands at 1798 (m) and 1737 (s) cm^{-1}. The observed shift to low energy for these ν(CO) bands relative to cluster **1** is the expected result of PMe_3 addition to **1**.[4] The ^{13}C NMR spectroscopic data for **2** are consistent with a reaction that proceeds by way of PMe_3 addition to **1** without CO loss, as **2** (THF, 178 K) exhibits CO resonances at δ 212.5 (1C, dd, J_{P-C} = 67 Hz, J_{P-C} = 29 Hz), 208.3 (2C, s), 205.0 (1C, s), 202.1 (1C, s), and 201.4 (1C, s). The addition of PMe_3 to **1** is also supported by the disappearance of the ^{31}P resonances of **1** and the presence of three new ^{31}P resonances at δ 185.6 (phosphido), 55.4 [PPh$_2$(maleic anhydride)], and 0.6 (PMe_3, J_{P-P} = 51 Hz). Other than some minor temperature-dependent chemical shift changes, the ^{13}C and ^{31}P NMR spectra remained unaltered over the temperature range of 178−273 K.

The structure of thermally unstable **2** was unequivocally determined by X-ray crystallography. Cluster **2** exists as discrete molecules in the unit cell with no unusually short inter- or intramolecular contacts. The X-ray data collection and processing parameters and final fractional coordinates for **2** are given in Tables 1 and 2, respectively. The ORTEP diagram in Figure 1 shows the molecular structure of **2**, with selected bond lengths and angles being found in Table 3.

Table 1. X-ray Crystallographic Data and Processing Parameters

	2	3
space group	$P\bar{1}$, triclinic	$P2_1/n$, monoclinic
a, Å	11.236(2)	10.256(2)
b, Å	12.802(4)	28.398(2)
c, Å	17.886(4)	15.405(1)
α, deg	86.41(2)	
β, deg	73.26(2)	100.93(1)
γ, deg	83.79(2)	
V, Å^3	2448(1)	4405.5(9)
mol formula	$C_{51}H_{50}Co_3O_9P_3$	$C_{44}H_{36}Cl_2Co_3O_8P_3$
fw	1076.68	1033.40
formula units/cell (Z)	2	4
ϱ, g cm^{-3}	1.461	1.558
abs coeff (μ), cm^{-1}	11.53	13.95
λ(Mo Kα), Å	0.710 73	0.710 73
collecn range, deg	$2.0 \le 2\theta \le 40.0$	$2.0 \le 2\theta \le 44.0$
max scan time, s	120	120
scan speed range, deg min^{-1}	0.67−8.0	0.67−8.0
total no. of data collcd	4544	5876
no. of indep data, $I > 3\sigma(I)$	1768	2623
R	0.0667	0.0469
R_w	0.0816	0.0517
weights	$[0.04F^2 + (\sigma F)^2]^{-1}$	$[0.04F^2 + (\sigma F)^2]^{-1}$

The addition of PMe_3 to **1** results in the cleavage of the Co(1)−Co(3) bond, as evidenced by the 3.900(4) Å internuclear distance between these two atoms, and conversion of a terminal CO group at Co(3) into a semibridging CO group that serves to span Co(3)−Co(2). The Co(1)−Co(2) and Co(2)−Co(3) bond distances of 2.663(4) and 2.523(4) Å, respectively, are similar to distances reported for other RC-capped tricobalt clusters.[3,5] The opened tricobalt frame is capped by a six-electron $\mu_2\text{-}\eta^2{:}\eta^1$-benzylidene(diphenylphosphino)maleic anhydride moiety, and the Co(1)−Co(2) bond is ligated by a μ_2-phosphido ligand. The 2.129(7) Å length for the Co(1)−P(2) bond and the 2.188(6) Å length for the Co(2)−P(2) bond confirm the presence of an asymmetric bridging phosphido ligand, which we believe assists in determining the nature of the solid-state structure adopted by cluster **2** (vide infra). The presence of a semibridging carbonyl group is verified by the Co(2)−C(6) distance, which displays an elongated length of 2.28(2) Å, in addition to the distinctly nonlinear Co(3)−C(6)−O(6) angle of 161(2)° and Co(2)−C(6)−O(6) angle of 121(2)°.[6] The fact that the IR and NMR data indicate that **2** possesses only terminal carbonyl groups in solution, in contrast to the solid-state structure, suggests that either solid-state effects are responsible for the adoption of a semibridging CO group or that carbonyl mobility remains fast at low temperature. We favor the former possibility because (1) the solid-state IR spectrum (KBr) of **2** displays a broad carbonyl stretch

(2) (a) Planalp, R. P.; Vahrenkamp, H. *Organometallics* **1987**, *6*, 492. (b) Schneider, J.; Minelli, M.; Huttner, G. *J. Organomet. Chem.* **1985**, *294*, 75. (c) Knoll, K.; Huttner, G.; Zsolnai, L.; Jibril, I.; Wasiucionek, M. *J. Organomet. Chem.* **1985**, *294*, 91. (d) Richmond, M. G.; Kochi, J. K. *Inorg. Chem.* **1986**, *25*, 1334. (e) Don, M.-J.; Richmond, M. G.; Watson, W. H.; Nagl, A. *J. Organomet. Chem.* **1989**, *372*, 417. (f) Darensbourg, D. J. In *The Chemistry of Metal Cluster Complexes*; Shriver, D. F., Kaesz, H. D., Adams, R. D., Eds.; VCH: New York, 1990; Chapter 4.

(3) Yang, K.; Smith, J. M.; Bott, S. G.; Richmond, M. G. *Organometallics* **1993**, *12*, 4787.

(4) Richmond, M. G.; Kochi, J. K. *Organometallics* **1987**, *6*, 254 and references therein.

(5) (a) Colbran, S. B.; Robinson, B.; Simpson, J. *Acta Crystallogr.* **1986**, *C42*, 972. (b) Ahlgrén, M.; Pakkanen, T. T.; Tahvanainen, I. *J. Organomet. Chem.* **1987**, *323*, 91. (c) Watson, W. H.; Nagl, A.; Hwang, S.; Richmond, M. G. *J. Organomet. Chem.* **1993**, *445*, 163.

(6) (a) Lukehart, C. M. *Fundamental Transition Metal Organometallic Chemistry*; Brooks/Cole: Monterey, CA, 1985. (b) Horwitz, C. P.; Shriver, D. F. *Adv. Organomet. Chem.* **1984**, *23*, 219.

Table 2. Positional Parameters for the Non-Hydrogen Atoms in Clusters 2 and 3 with Estimated Standard Deviations in Parentheses[a]

atom	x	y	z	B, Å²	atom	x	y	z	B, Å²
			$Co_3(CO)_5(\mu\text{-}CO)(PMe_3)[\mu_2\text{-}\eta^2:\eta^1\text{-}C(Ph)C{=}C(PPh_2)C(O)OC(O)](\mu_2\text{-}PPh_2)$						
Co(1)	0.5472(3)	0.2659(2)	0.7062(2)	2.72(7)	C(33)	−0.039(2)	0.454(2)	0.814(2)	5.4(7)*
Co(2)	0.3770(3)	0.1593(2)	0.8081(2)	2.95(8)	C(111)	0.283(2)	0.440(2)	0.663(1)	3.6(5)*
Co(3)	0.2177(3)	0.3131(2)	0.8550(2)	2.71(7)	C(112)	0.215(2)	0.372(2)	0.641(1)	4.3(6)*
P(1)	0.3007(6)	0.4325(5)	0.7585(3)	2.8(2)	C(113)	0.205(3)	0.370(2)	0.564(2)	6.8(8)*
P(2)	0.5687(6)	0.1057(5)	0.7437(4)	3.4(2)	C(114)	0.259(3)	0.445(3)	0.511(2)	7.8(9)*
P(3)	0.0197(6)	0.3299(5)	0.8436(4)	3.5(2)	C(115)	0.327(3)	0.512(2)	0.530(2)	7.1(8)*
O(1)	0.482(2)	0.253(1)	0.561(1)	7.0(5)*	C(116)	0.340(2)	0.510(2)	0.607(2)	5.7(7)*
O(2)	0.808(2)	0.292(1)	0.640(1)	6.9(5)*	C(117)	0.266(2)	0.567(2)	0.788(1)	2.7(5)*
O(3)	0.380(2)	−0.033(1)	0.901(1)	5.7(4)*	C(118)	0.188(2)	0.639(2)	0.758(1)	5.2(7)*
O(4)	0.266(2)	0.095(2)	0.692(1)	7.1(5)*	C(119)	0.164(3)	0.739(3)	0.787(2)	9(1)*
O(5)	0.130(1)	0.440(1)	0.991(1)	5.4(4)*	C(120)	0.214(3)	0.772(3)	0.840(2)	7.8(9)*
O(6)	0.125(2)	0.121(1)	0.928(1)	6.2(5)*	C(121)	0.296(2)	0.707(2)	0.867(1)	5.2(7)*
O(12)	0.571(1)	0.555(1)	0.6809(9)	4.0(4)*	C(122)	0.318(2)	0.604(2)	0.842(1)	3.8(6)*
O(13)	0.642(1)	0.456(1)	0.7727(8)	3.5(3)*	C(211)	0.682(2)	0.063(2)	0.799(1)	3.6(5)*
O(14)	0.668(1)	0.339(1)	0.8649(8)	3.8(4)*	C(212)	0.699(2)	0.094(2)	0.873(2)	4.0(6)*
C(1)	0.503(2)	0.254(2)	0.622(1)	5.1(7)*	C(213)	0.762(2)	0.057(2)	0.909(1)	4.0(6)*
C(2)	0.700(2)	0.281(2)	0.672(2)	4.9(6)*	C(214)	0.863(2)	−0.003(2)	0.870(1)	5.4(7)*
C(3)	0.376(2)	0.049(2)	0.867(1)	4.6(6)*	C(215)	0.880(3)	−0.029(2)	0.796(2)	6.2(7)*
C(4)	0.317(2)	0.119(2)	0.735(1)	4.9(6)*	C(216)	0.789(2)	0.002(2)	0.759(2)	5.4(7)*
C(5)	0.169(2)	0.389(2)	0.936(1)	4.0(6)*	C(217)	0.580(2)	−0.001(2)	0.683(1)	4.1(6)*
C(6)	0.183(2)	0.192(2)	0.892(1)	4.6(6)*	C(218)	0.607(2)	0.005(2)	0.606(1)	4.7(6)*
C(11)	0.467(2)	0.406(2)	0.751(1)	2.3(5)*	C(219)	0.606(3)	−0.082(3)	0.559(2)	7.7(9)*
C(12)	0.561(2)	0.482(2)	0.729(1)	3.1(5)*	C(220)	0.576(3)	−0.171(2)	0.597(2)	6.9(8)*
C(14)	0.602(2)	0.372(2)	0.823(1)	2.4(5)*	C(221)	0.551(3)	−0.187(2)	0.672(2)	6.2(7)*
C(15)	0.491(2)	0.338(2)	0.813(1)	2.2(5)*	C(222)	0.555(2)	−0.101(2)	0.715(2)	5.7(7)*
C(16)	0.393(2)	0.282(2)	0.869(1)	2.7(5)*	C(1s)	0.061(8)	0.789(7)	0.599(5)	11(3)*
C(17)	0.396(2)	0.282(2)	0.951(1)	2.5(5)*	C(2s)	−0.051(9)	0.732(8)	0.617(6)	15(3)*
C(18)	0.412(2)	0.371(2)	0.983(1)	3.2(5)*	C(3s)	−0.127(7)	0.702(6)	0.680(5)	11(2)*
C(19)	0.399(2)	0.383(2)	1.061(1)	4.1(6)*	C(4s)	0.00(1)	0.82(1)	0.588(8)	13(4)*
C(21)	0.357(2)	0.205(2)	1.082(1)	5.0(6)*	C(5s)	−0.048(8)	0.609(7)	0.614(5)	13(3)*
C(22)	0.369(2)	0.198(2)	1.003(1)	3.5(5)*	C(6s)	0.176(8)	0.848(7)	0.577(5)	13(3)*
C(31)	−0.092(2)	0.311(2)	0.936(1)	4.7(6)*	C(7s)	0.05(1)	0.92(1)	0.558(8)	13(5)*
C(32)	−0.021(2)	0.242(2)	0.783(1)	4.5(6)*					
			$Co_3(CO)_5(PMe_3)[\mu_2\text{-}\eta^2:\eta^1\text{-}C(Ph)C{=}C(PPh_2)C(O)OC(O)](\mu_2\text{-}PPh_2)$						
Co(1)	0.8142(1)	0.09117(5)	0.80318(9)	2.75(3)	C(20)	0.897(1)	0.2971(5)	0.5563(9)	5.4(3)*
Co(2)	0.8737(1)	0.17764(5)	0.84126(9)	2.86(3)	C(21)	0.927(1)	0.2541(5)	0.5297(8)	5.5(3)*
Co(3)	0.6526(1)	0.16861(5)	0.75135(9)	2.60(3)	C(22)	0.908(1)	0.2152(4)	0.5845(7)	4.2(3)*
Cl(1)	0.0822(5)	0.1331(2)	0.4618(3)	8.9(1)	C(31)	0.539(1)	0.2470(4)	0.5782(7)	4.0(3)*
Cl(2)	0.0061(9)	0.0724(3)	0.3171(4)	16.7(3)	C(32)	0.345(1)	0.2105(5)	0.6653(9)	5.5(3)*
P(1)	0.6173(3)	0.11447(9)	0.6437(2)	2.74(7)	C(33)	0.518(1)	0.2811(5)	0.7478(9)	5.7(4)*
P(2)	0.8979(3)	0.1223(1)	0.9367(2)	3.03(6)	C(111)	0.580(1)	0.1286(3)	0.5266(6)	2.6(2)*
P(3)	0.5201(3)	0.2268(1)	0.6850(2)	3.51(7)	C(112)	0.682(1)	0.1360(5)	0.4806(8)	4.3(3)*
O(1)	1.0004(9)	0.0117(3)	0.8304(6)	6.5(3)	C(113)	0.655(1)	0.1491(5)	0.3935(8)	5.1(3)*
O(2)	0.5938(7)	0.2433(3)	0.9166(5)	5.4(2)	C(114)	0.525(1)	0.1548(5)	0.3502(9)	6.2(3)*
O(3)	1.1285(8)	0.2257(3)	0.8630(6)	6.4(2)	C(115)	0.423(1)	0.1472(5)	0.3936(9)	5.6(3)*
O(4)	0.7146(8)	0.2433(3)	0.9166(5)	5.4(2)	C(116)	0.451(1)	0.1343(4)	0.4825(8)	4.4(3)*
O(5)	0.4653(8)	0.1488(3)	0.8670(5)	6.7(2)	C(117)	0.509(1)	0.0651(4)	0.6483(7)	2.9(2)*
O(12)	0.8332(8)	0.0304(3)	0.5775(5)	5.3(2)	C(118)	0.390(1)	0.0708(4)	0.6753(8)	4.4(3)*
O(13)	0.9967(7)	0.0772(3)	0.6452(5)	4.2(2)	C(119)	0.304(1)	0.0326(4)	0.6773(8)	5.4(3)*
O(14)	1.1149(7)	0.1379(3)	0.7120(5)	4.9(2)	C(120)	0.336(1)	−0.0098(4)	0.6482(8)	5.1(3)*
C(1)	0.930(1)	0.0434(4)	0.8184(7)	3.8(3)	C(121)	0.453(1)	−0.0171(5)	0.6224(9)	6.2(3)*
C(1s)	0.068(2)	0.0763(6)	0.426(1)	10.2(6)	C(122)	0.538(1)	0.0205(4)	0.6202(8)	4.7(3)*
C(2)	0.675(1)	0.0614(4)	0.8333(7)	3.3(3)	C(211)	1.061(1)	0.1009(4)	0.9889(7)	3.5(2)*
C(3)	1.030(1)	0.2056(4)	0.8541(7)	3.9(3)	C(212)	1.093(1)	0.0866(5)	1.0760(8)	4.8(3)*
C(4)	0.762(1)	0.2146(4)	0.8795(7)	4.2(3)	C(213)	1.222(1)	0.0691(5)	1.1100(9)	6.2(3)*
C(5)	0.536(1)	0.1556(4)	0.8210(7)	3.6(3)	C(214)	1.310(1)	0.0663(5)	1.0597(9)	6.1(3)*
C(11)	0.7860(9)	0.0963(3)	0.6691(6)	2.5(2)	C(215)	1.285(1)	0.0801(5)	0.9740(8)	5.1(3)*
C(12)	0.863(1)	0.0625(4)	0.6260(7)	3.6(3)	C(216)	1.159(1)	0.0989(4)	0.9376(8)	4.3(3)*
C(14)	1.011(1)	0.1200(4)	0.6900(7)	3.2(3)	C(217)	0.800(1)	0.1108(4)	1.0210(7)	3.2(2)*
C(15)	0.8742(9)	0.1337(3)	0.7030(6)	2.5(2)	C(218)	0.778(1)	0.0647(4)	1.0465(8)	4.4(3)*
C(16)	0.828(1)	0.1815(4)	0.7160(7)	2.9(2)	C(219)	0.709(1)	0.0569(4)	1.1154(8)	4.8(3)*
C(17)	0.8588(9)	0.2212(3)	0.6618(6)	2.6(2)*	C(220)	0.665(1)	0.0941(4)	1.1567(8)	4.9(3)*
C(18)	0.841(1)	0.2674(4)	0.6875(7)	3.5(2)*	C(221)	0.684(1)	0.1391(5)	1.1325(8)	5.1(3)*
C(19)	0.856(1)	0.3048(4)	0.6336(8)	4.5(3)*	C(222)	0.754(1)	0.1477(4)	1.0651(8)	4.3(3)*

[a] Starred values denote atoms refined isotropically. Anisotropically refined atoms are given in the form of the isotropic equivalent displacement parameter defined as $^4/_3[a^2B(1,1) + b^2B(2,2) + c^2B(3,3) + ab(\cos\gamma)B(1,2) + ac(\cos\beta)B(1,3) + bc(\cos\alpha)B(2,3)]$.

at ca. 1890 cm^{-1}, which is consistent with the presence of a semibridging CO group, and (2) bridging carbonyls are known to be more effective in the dissipation of excess electron density about a cluster core relative to their terminal carbonyl counterparts.[7] Scheme 1 outlines the course of PMe_3 attack on cluster **1**, taking into account the solution and solid-state structures of **2**.

The observed polyhedral expansion in going from **1** to **2** may be explained by using polyhedral skeletal electron pair (PSEP) theory,[8] which allows for the

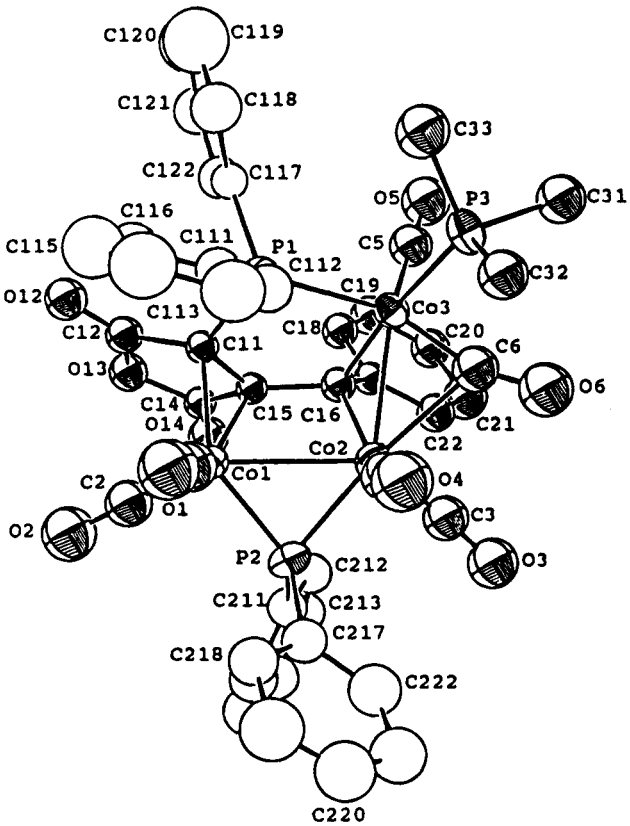

Figure 1. ORTEP diagram of $Co_3(CO)_5(\mu\text{-}CO)(PMe_3)[\mu_2\text{-}\eta^2{:}\eta^1\text{-}C(Ph)\overline{C{=}C(PPh_2)C(O)OC(O)}](\mu_2\text{-}PPh_2)$ showing thermal ellipsoids at the 50% probability level.

prediction of an adopted molecular polyhedron upon ligand addition to a transition-metal cluster. Regarding cluster **1** as a four-vertex arachno cluster that possesses seven skeletal electron pairs (SEP), it is expected and experimentally found that PMe_3 addition to **1** leads to the formation of the hypho cluster **2** with eight SEP. Alternatively, this conversion may also be viewed as an opening of the electron-precise cluster **1** (48e) to the open cluster **2** (50e) with one less Co–Co bond. Guiding the initial heterolytic Co(1)–Co(3) bond cleavage by the addition of PMe_3 to Co(3) is the six-electron ligand $\mu_2\text{-}\eta^2{:}\eta^1$-benzylidene(diphenylphosphino)maleic anhydride, as it is able to stabilize the developing anionic charge at Co(1) due to the electron-withdrawing properties of the maleic anhydride ring.[2f,9] The interception and characterization of **2** as a kinetic product en route to the monosubstituted cluster $Co_3(CO)_5(PMe_3)[\mu_2\text{-}\eta^2{:}\eta^1\text{-}C(Ph)\overline{C{=}C(PPh_2)C(O)OC(O)}](\mu_2\text{-}PPh_2)$ underscores the importance of metal–metal bond reactivity in cluster substitution and substrate activation reactions.

Use of a conventional electron-counting formalism allows for the change in the coordination mode of the $\mu_2\text{-}PPh_2$ moiety in **2** relative to **1** to be easily rationalized. Initially the phosphido ligand donates 2e (donor–acceptor bond) and 1e (covalent bond) to Co(2) and Co(1), respectively, in **1**, but this donation mode is ultimately reversed in the formation of **2**, as shown in Scheme 1.

Table 3. Selected Bond Distances (Å) and Angles (deg) in Clusters 2 and 3[a]

$Co_3(CO)_5(\mu\text{-}CO)(PMe_3)[\mu_2\text{-}\eta^2{:}\eta^1\text{-}C(Ph)\overline{C{=}C(PPh_2)C(O)OC(O)}](\mu_2\text{-}PPh_2)$

Bond Distances			
Co(1)–Co(2)	2.663(4)	Co(2)–Co(3)	2.523(4)
Co(1)–P(2)	2.129(7)	Co(2)–P(2)	2.188(6)
Co(3)–P(1)	2.288(6)	Co(3)–P(3)	2.278(8)
Co(1)–C(11)	2.02(2)	Co(1)–C(15)	2.07(2)
Co(2)–C(16)	2.02(2)	Co(3)–C(16)	2.04(2)
Co(1)–C(1)	1.73(3)	Co(1)–C(2)	1.68(3)
Co(2)–C(3)	1.71(2)	Co(2)–C(4)	1.75(3)
Co(5)–C(5)	1.72(2)	Co(2)–C(6)	2.28(2)
Co(3)–C(6)	1.69(2)	O(1)–C(1)	1.18(3)
O(2)–C(2)	1.20(3)	O(3)–C(3)	1.18(3)
O(4)–C(4)	1.17(4)	O(5)–C(5)	1.16(3)
O(6)–C(6)	1.21(3)		
Bond Angles			
Co(1)–Co(2)–Co(3)	97.5(1)	P(2)–Co(2)–C(6)	169.2(7)
Co(1)–P(2)–Co(2)	76.2(2)	Co(1)–C(1)–O(1)	173(2)
Co(1)–C(2)–O(2)	174(3)	Co(2)–C(3)–O(3)	173(2)
Co(2)–C(4)–O(4)	173(2)	Co(3)–C(5)–O(5)	177(2)
Co(2)–C(16)–Co(3)	76.8(9)	Co(2)–C(6)–O(6)	121(2)
Co(3)–C(6)–O(6)	161(2)		

$Co_3(CO)_5(PMe_3)[\mu_2\text{-}\eta^2{:}\eta^1\text{-}C(Ph)\overline{C{=}C(PPh_2)C(O)OC(O)}](\mu_2\text{-}PPh_2)$

Bond Distances			
Co(1)–Co(2)	2.571(2)	Co(1)–Co(3)	2.779(2)
Co(2)–Co(3)	2.437(2)	Co(2)–P(2)	2.135(3)
Co(1)–P(2)	2.253(3)	Co(3)–P(1)	2.240(3)
Co(3)–P(3)	2.256(3)	Co(2)–C(16)	1.90(1)
Co(3)–C(16)	2.01(1)	Co(1)–C(11)	2.035(9)
Co(1)–C(15)	2.14(1)	Co(1)–C(1)	1.79(1)
Co(1)–C(2)	1.79(1)	Co(2)–C(3)	1.77(1)
Co(2)–C(4)	1.73(1)	Co(3)–C(5)	1.79(1)
O(1)–C(1)	1.14(1)	O(2)–C(2)	1.13(1)
O(3)–C(3)	1.15(1)	O(4)–C(4)	1.16(1)
O(5)–C(5)	1.12(1)		
Bond Angles			
Co(2)–Co(1)–Co(3)	54.02(5)	Co(1)–Co(2)–Co(3)	67.34(5)
Co(1)–Co(3)–Co(2)	58.64(5)	Co(1)–P(2)–Co(2)	71.7(1)
Co(1)–C(15)–C(11)	66.1(5)	Co(2)–C(16)–Co(3)	77.0(4)
Co(1)–C(1)–O(1)	177(1)	Co(1)–C(2)–O(2)	174.9(9)
Co(2)–C(3)–O(3)	177(1)	Co(2)–C(4)–O(4)	164(1)
Co(3)–C(5)–O(5)	177.1(9)		

[a] Numbers in parentheses are estimated standard deviations in the least significant digits.

Such a transformation, which enables all of the cobalt centers in **2** to achieve a coordinatively saturated state, is akin to the assistance rendered to the cluster by the CO groups in eq 1 and related ligand substitution reactions[1,2] and is believed to be the first example of its kind involving a phosphido ligand in a tricobalt cluster.[10] It is noteworthy that within this electron-precise formalism the shorter Co–phosphido bond distance is found for the bond that derives from the donation of the phosphido ligand's lone electron pair to the cobalt center.

Synthesis and X-ray Diffraction Structure of $Co_3(CO)_5(PMe_3)[\mu_2\text{-}\eta^2{:}\eta^1\text{-}C(Ph)\overline{C{=}C(PPh_2)C(O)OC(O)}](\mu_2\text{-}PPh_2)$. Warming a sample of **2** to room temperature led to a rapid loss of CO and formation of the monosubstituted cluster $Co_3(CO)_5(PMe_3)[\mu_2\text{-}\eta^2{:}\eta^1\text{-}C(Ph)\overline{C{=}C(PPh_2)C(O)OC(O)}](\mu_2\text{-}PPh_2)$ (**3**), as shown in

(7) Penfield, B. R.; Robinson, B. R. *Acc. Chem. Res.* **1973**, *6*, 73.
(8) (a) Wade, K. *Adv. Inorg. Chem. Radiochem.* **1976**, *18*, 1. (b) Wade, K. In *Transition Metal Clusters*; Johnson, B. F. G., Ed.; Wiley: New York, 1980; Chapter 3. (c) Mingos, D. M. P. *Acc. Chem. Res.* **1984**, *17*, 311.
(9) Johnson, B. F. G. *Inorg. Chim. Acta* **1986**, *115*, L39.
(10) For reports of related reactivity in mononuclear phosphido complexes, see: (a) Baker, R. T.; Whitney, J. F.; Wreford, S. S. *Organometallics* **1983**, *2*, 1049. (b) Baker, R. T.; Calabrese, J. C.; Harlow, R. L.; Williams, I. D. *Organometallics* **1993**, *12*, 830. (c) Jorg, K.; Malisch, W.; Reich, W.; Meyer, A.; Schubert, U. *Angew. Chem., Int. Ed. Engl.* **1986**, *25*, 92.

Scheme 1

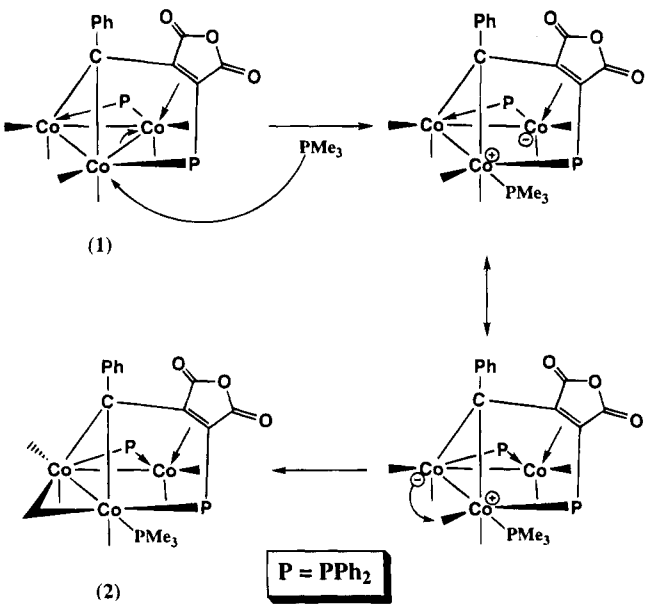

eq 2. Cluster **3** was subsequently isolated by chromatography over silica gel using CH_2Cl_2 as a temperature- and air-stable solid.

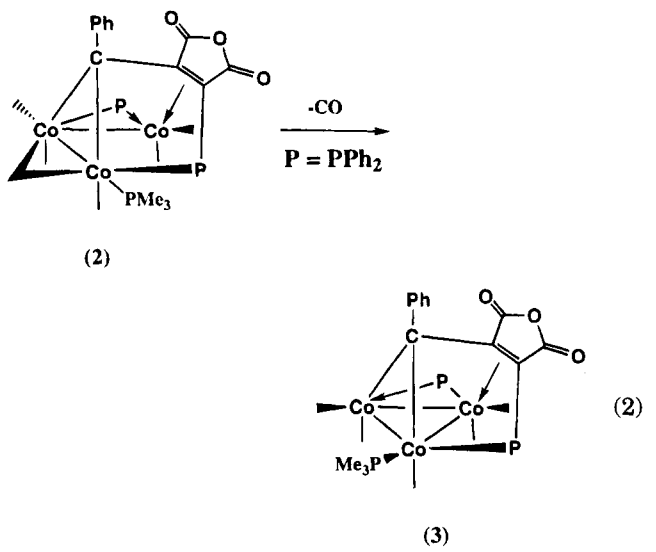

The IR spectrum of **3** was not terribly informative, as it was qualitatively similar to that of **2**. The $^{31}P\{^1H\}$ NMR of **3** revealed one resonance at δ 190.5 that may be confidently assigned to the μ_2-phosphido moiety along with two high-field resonances at δ 14.3 and 7.8. While no attempt has been made to assign these high-field resonances to specific groups, the ^{31}P NMR data are consistent with Ph_2P(maleic anhydride) and PMe_3 groups. The $^{13}C\{^1H\}$ NMR spectrum of ^{13}C-enriched **3** exhibited five carbonyl resonances at δ 216.1 (1C, J_{P-C} = 23 Hz), 206.4 (1C), 204.6 (1C), 200.5 (1C), 191.8 (1C, J_{P-C} = 29 Hz), in agreement with the loss of one CO ligand from **2**. No attempt has been made to assign these resonances to specific CO groups. On the basis of the invariant ^{31}P and ^{13}C NMR spectra over the temperature range 183 K to room temperature, it is concluded that cluster **3** maintains a static structure in solution.

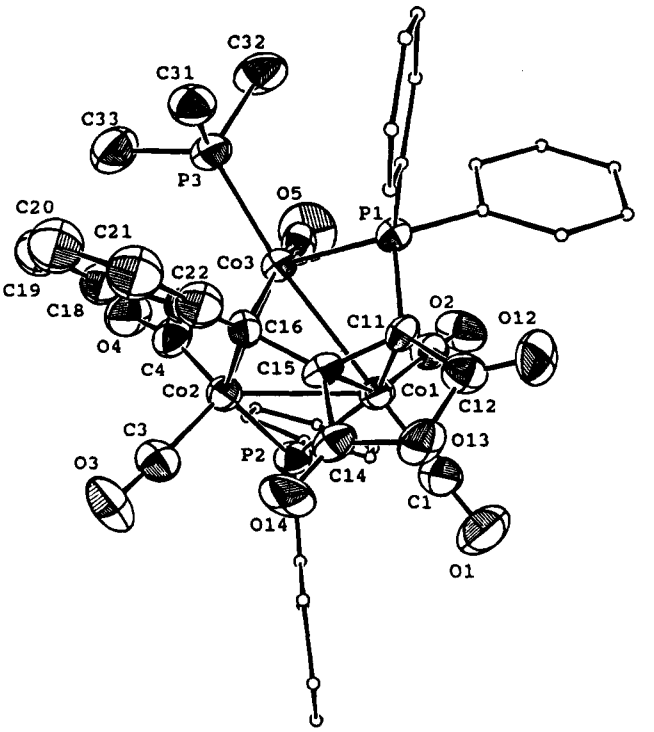

Figure 2. ORTEP diagram of $Co_3(CO)_5(PMe_3)[\mu_2\text{-}\eta^2{:}\eta^1\text{-}C(Ph)C{=}C(PPh_2)C(O)OC(O)](\mu_2\text{-}PPh_2)$ showing thermal ellipsoids at the 50% probability level.

The molecular structure of **3** was established by X-ray diffraction analysis. Cluster **3** exists as discrete molecules in the unit cell with unusually short inter- or intramolecular contacts. The X-ray data collection and processing parameters and the final fractional coordinates for **3** are given in Tables 1 and 2, respectively. The ORTEP diagram in Figure 2 shows the molecular structure of **3**, with selected bond lengths and angles being found in Table 3.

Cluster **3** is structurally similar to cluster **1**, whose molecular structure has been presented.[3] Closing of the broken Co(1)–Co(3) bond in **2** gives rise to a Co(1)–Co(3) bond length of 2.779(2) Å in **3**, which is only 0.083 Å longer than the analogous bond in **1**. The remaining Co(1)–Co(2) and Co(2)–Co(3) lengths of 2.571(2) and 2.437(2) Å, respectively, agree well with those distances reported for **1** and other phosphine- and phosphido-substituted cobalt complexes.[11] An asymmetric phosphido moiety is seen, as judged by the Co(1)–P(2) length of 2.253(3) Å and the Co(2)–P(2) length of 2.135(3) Å. Treating the phosphido moiety in **3** as a three-electron-donor ligand and using an electron-precise formalism, as was done for **2**, reveal that the shorter Co–phosphido bond again corresponds to the donation of the phosphido ligand's lone electron pair to the Co(2) center and that the longer Co(1)–P(2) bond is derived from the donation of 1e from P(2) to the Co(1) center.

Conclusions

The participation of the six-electron $\mu_2\text{-}\eta^2{:}\eta^1$-benzylidene(diphenylphosphino)maleic anhydride and phos-

(11) (a) Don, M.-J.; Richmond, M. G.; Watson, W. H.; Krawiec, M.; Kashyap, R. P. *J. Organomet. Chem.* **1991**, *418*, 231. (b) Worth, G. H.; Robinson, B. H.; Simpson, J. *Organometallics* **1992**, *11*, 3863. (c) Albright, T. A.; Kang, S.-K.; Arif, A. M.; Bard, A. J.; Jones, R. A.; Leland, J. K.; Schwab, S. T. *Inorg. Chem.* **1988**, *27*, 1246. (d) Young, D. A. *Inorg. Chem.* **1981**, *20*, 2049.

phido ligands in promoting the facile and site-selective addition of PMe_3 in cluster **1** has been demonstrated. The kinetic product of PMe_3 substitution reactions has been isolated and fully characterized as the hypho cluster $Co_3(CO)_5(\mu\text{-}CO)(PMe_3)[\mu_2\text{-}\eta^2{:}\eta^1\text{-}C(Ph)C{=}C(PPh_2)C(O)OC(O)](\mu_2\text{-}PPh_2)$. CO loss and regeneration of the broken Co—Co bond affords the thermodynamic PMe_3 substitution product $Co_3(CO)_5(PMe_3)[\mu_2\text{-}\eta^2{:}\eta^1\text{-}C(Ph)C{=}C(PPh_2)C(O)OC(O)](\mu_2\text{-}PPh_2)$. The importance of the ligand site directing properties of the $\mu_2\text{-}\eta^2{:}\eta^1$- benzylidene(diphenylphosphino)maleic anhydride ligand and the bonding flexible $\mu_2\text{-}PPh_2$ ligand suggests that exciting prospects exist for the activation of small molecules in polynuclear systems containing these two ligands.

Experimental Section

Cluster **1** was prepared according to a recently published procedure,[3] starting from $PhCCo_3(CO)_9$[12] and bma.[13] PMe_3 was synthesized from $P(OPh)_3$ and MeMgI.[14] All reactions were conducted under an argon atmosphere using Schlenk techniques.[15] THF, Bu_2O, toluene, and heptane were distilled from sodium/benzophenone ketyl, while CH_2Cl_2 was distilled from CaH_2. All solvents were stored under argon in Schlenk storage vessels equipped with Teflon stopcocks. The ^{13}CO (99%) used in the preparation of ^{13}C-enriched **2** and **3** was obtained from Isotec. All microanalyses were performed by Atlantic Microlab, Atlanta, GA.

Infrared spectra were recorded on a Nicolet 20SXB FT-IR spectrometer. Low-temperature IR spectra were recorded with a Specac Model P/N 21.000 variable-temperature cell equipped with inner and outer CaF_2 windows. Dry ice/acetone was used as the coolant, and the cell temperature was measured by using a copper—constantan thermocouple. Room-temperature IR spectra were recorded in 0.1-mm NaCl cells. The ^{13}C and ^{31}P NMR spectra were recorded on a Varian 300-VXR spectrometer at 75 and 121 MHz, respectively. The reported ^{31}P chemical shifts are referenced relative to external H_3PO_4 (85%), taken to have δ 0. Positive chemical shifts represent resonances that are low field to the external standard.

Synthesis of $Co_3(CO)_5(\mu\text{-}CO)(PMe_3)[\mu_2\text{-}\eta^2{:}\eta^1\text{-}C(Ph)C{=}C(PPh_2)C(O)OC(O)](\mu_2\text{-}PPh_2)$. To a Schlenk tube containing 0.20 g (0.20 mmol) of **1** in 20 mL of CH_2Cl_2 at −78 °C was added 1.1 equiv of PMe_3 (0.47 mL of a 0.48 M solution of PMe_3 in CH_2Cl_2). The reaction was instantaneous, on the basis of the immediate color change from brown **1** to red-brown **2**. Cluster **2** was precipitated from solution by the addition of cold (−78 °C) petroleum ether and then collected by filtration. Crystals of **2** suitable for X-ray diffraction and combustion analyses were grown at −20 °C from a toluene/heptane solution (1:1) containing **2** that had been layered with a small amount of diethyl ether. Yield: 0.18 g (ca. 90%). IR (CH_2Cl_2, -70 °C): ν(CO) 2035 (s), 2010 (vs), 1999 (vs), 1960 (sh), 1900 (w), 1798 (m, asym bma C=O), 1737 (s, sym bma C=O) cm^{-1}. $^{31}P\{^1H\}$ NMR (THF, 178 K): δ 185.6 (μ_2-PPh_2), 55.4 [PPh_2-(maleic anhydride), broad], 0.6 (PMe_3, J_{P-P} = 51 Hz). $^{13}C\{^1H\}$ NMR (THF, 178 K): δ 212.5 (1C, dd, J_{P-C} = 67 Hz, J_{P-C} = 29 Hz), 208.3 (2C, s), 205.0 (1C, s), 202.1 (1C, s), 201.4 (1C, s). Anal. Calcd (found) for $C_{44}H_{34}Co_3O_9P_3$−$^1/_4$-heptane: C, 54.86 (54.65); H, 3.82 (4.09).

Synthesis of $Co_3(CO)_5(PMe_3)[\mu_2\text{-}\eta^2{:}\eta^1\text{-}C(Ph)C{=}C(PPh_2)C(O)OC(O)](\mu_2\text{-}PPh_2)$. To a Schlenk tube containing 0.20 g (0.20 mmol) of **1** in 20 mL of CH_2Cl_2 at room temperature was added 1.1 equiv of PMe_3 (0.47 mL of a 0.48 M solution of PMe_3 in CH_2Cl_2). The reaction mixture was stirred for 3.0 h and examined by TLC analysis, which revealed the presence of only the monosubstituted cluster **3**. The product was isolated by chromatography over silica gel using CH_2Cl_2 as the eluant. Crystals of **3** suitable for X-ray diffraction and combustion analyses were grown from a CH_2Cl_2 solution containing **3** that had been layered with heptane. Yield: 0.17 g (82%). IR (CH_2Cl_2, room temperature): ν(CO) 2040 (s), 2006 (vs), 1984 (s), 1896 (m), 1803 (m, asym bma C=O), 1742 (s, sym bma C=O) cm^{-1}. $^{31}P\{^1H\}$ NMR (THF, 183 K): δ 190.5 (μ_2-PPh_2), 14.3 and 7.8 [Ph_2P(maleic anhydride) and PMe_3 groups]. $^{13}C\{^1H\}$ NMR (THF, 183 K): δ 216.1 (1C, J_{P-C} = 23 Hz), 206.4 (1C), 204.6 (1C), 200.5 (1C), 191.8 (1C, J_{P-C} = 29 Hz). Anal. Calcd (found) for $C_{43}H_{34}Co_3O_8P_3{\cdot}CH_2Cl_2$: C, 51.19 (51.34); H, 3.51 (3.55).

X-ray Diffraction Structure of $Co_3(CO)_5(\mu\text{-}CO)(PMe_3)[\mu_2\text{-}\eta^2{:}\eta^1\text{-}C(Ph)C{=}C(PPh_2)C(O)OC(O)](\mu_2\text{-}PPh_2)$−Heptane. A black crystal of dimensions 0.08 × 0.22 × 0.48 mm^3 was sealed inside a Lindemann capillary and then mounted on an Enraf-Nonius CAD-4 diffractometer. Cell constants were obtained from a least-squares refinement of 25 reflections with $2\theta > 25°$. Intensity data in the range $2.0 \le 2\theta \le 40°$ were collected at room temperature using the $\theta/2\theta$-scan technique in the variable-scan speed mode and were corrected for Lorentz, polarization, and absorption (DIFABS). Three reflections (500, 050, 007) were measured after every 3600 s of exposure time in order to monitor crystal decay (<8%). Due to the irregular nature of the decay, no correction was applied. The structure was solved by SIR, which revealed the presence of the Co and P atoms. All remaining non-hydrogen atoms were located with difference Fourier maps and full-matrix least-squares refinement. With the exception of the cobalt and phosphorus atoms, all atoms were refined isotropically. Refinement converged at R = 0.0667 and R_w = 0.0816 for 1768 unique reflections with $I > 3\sigma(I)$.

X-ray Diffraction Structure of $Co_3(CO)_5(PMe_3)[\mu_2\text{-}\eta^2{:}\eta^1\text{-}C(Ph)C{=}C(PPh_2)C(O)OC(O)](\mu_2\text{-}PPh_2){\cdot}CH_2Cl_2$. A black crystal of dimensions 0.08 × 0.28 × 0.48 mm^3 was prepared in a fashion analogous to that for **2**. Cell constants were obtained from a least-squares refinement of 25 reflections with $2\theta > 25°$. Intensity data in the range $2.0 \le 2\theta \le 44°$ were collected at room temperature using the ω-scan technique in the variable-scan speed mode and were corrected for Lorentz, polarization, and absorption (DIFABS). Three reflections (600, 0,$\overline{12}$,0, 006) were measured after every 3600 s of exposure time in order to monitor crystal decay (<1%). The structure was solved by SIR, which revealed the positions of the Co and P atoms. All remaining non-hydrogen atoms were located with difference Fourier maps and full-matrix least-squares refinement. With the exception of the phenyl carbons, all non-hydrogen atoms were refined anisotropically. Refinement converged at R = 0.0469 and R_w = 0.0517 for 2623 unique reflections with $I > 3\sigma(I)$.

Acknowledgment. Financial support from the Robert A. Welch Foundation (Grants B-1202-SGB and B-1039-MGR) and the UNT Faculty Research Program is acknowledged.

Supplementary Material Available: Tables of crystal data, atomic positional parameters, isotropic thermal parameters, bond lengths, and bond angles and a packing diagram for **2** and **3** (32 pages). Ordering information is given on any current masthead page.

OM940463B

(12) Nestle, M. O.; Hallgren, J. E.; Seyferth, D. *Inorg. Synth.* **1980**, *20*, 226.
(13) Mao, F.; Philbin, C. E.; Weakley, T. J. R.; Tyler, D. R. *Organometallics* **1990**, *9*, 1510.
(14) Luetkens, M. L., Jr.; Sattelberger, A. P.; Murray, H. H.; Basil, J. D.; Fackler, J. P., Jr. *Inorg. Synth.* **1989**, *26*, 7.
(15) Shriver, D. F. *The Manipulation of Air-Sensitive Compounds*; McGraw-Hill: New York, 1969.

Successive Reactions of Rhenium Isocyanide Complexes with Nitrogen-Containing Ligands. One-Flask Conversion of $ReBr(CO)_4(CNPh)$ to $[Re(CO)_3(NH_2R)_2\{C(NHPh)(NHR)\}]^+Br^-$

Jang-Shyang Fan,[†,‡] Jung-Tzung Lin,[†,‡] Chung-Cheng Chang,[‡] Shou-Jiau Chou,[†] and Kuang-Lieh Lu*,[†]

Institute of Chemistry, Academia Sinica, Taipei, Taiwan, Republic of China, and Department of Chemistry, National Sun Yat-Sen University, Kaohsiung, Taiwan, Republic of China

Received May 19, 1994[⊗]

The isocyanide complexes $ReBr(CO)_4(CNR)$ (**1**) react with Me_3NO in CH_2Cl_2 to give $ReBr(CO)_3(CNR)(NMe_3)$ (**2**). Treatment of **1** with Me_3NO in the presence of CH_3CN yields the nitrile derivatives $ReBr(CO)_3(CNR)(NCMe)$ (**3**). The latter on reaction with two-electron-donor ligands L (L = CO, PPh_3) give $ReBr(CO)_3(CNR)L$. Treatment of **3** with amines in CH_2Cl_2 leads to the formation of $ReBr(CO)_3(CNR)(NH_2R')$ (**5**). When $ReBr(CO)_3(CNPh)(NCMe)$ (**3a**) is treated with excess amines in CH_2Cl_2 for a prolonged period, the diaminocarbene complexes $ReBr(CO)_3(NH_2R)\{C(NHPh)(NHR)\}$ (**6**) are formed. The latter then react with a further 1 equiv of amine to afford $[Re(CO)_3(NH_2R)_2\{C(NHPh)(NHR)\}]^+Br^-$ (**7**). A one-flask synthesis of **7** was achieved by the interaction of $ReBr(CO)_4(CNPh)$ with Me_3NO in the presence of CH_3CN followed by reaction with the desired amine in CH_2Cl_2 at ambient temperature. $ReBr(CO)_3(CNPh)(PPh_3)$ (**4a**), $ReBr(CO)_3(NH_2Pr^i)\{C(NHPh)(NHPr^i)\}$ (**6a**), and $[Re(CO)_3(NH_2Pr^i)_2\{C(NHPh)(NHPr^i)\}]^+Br^-$ (**7a**) have been characterized by X-ray structure determination. **4a** crystallizes in the triclinic space group $P\bar{1}$; a = 9.801(4) Å, b = 11.190(5) Å, c = 13.862(5) Å, α = 91.49(3)°, β = 108.19(3)°, γ = 65.52(3)°, V = 1305.1(8) Å^3, Z = 2, R = 3.1%, and R_w = 3.5%. **6a** gives monoclinic crystals, space group $P2_1/n$; a = 9.174(2) Å, b = 19.865(2) Å, c = 12.064(2) Å, β = 112.264(2)°, V = 2034.6(6) Å^3, Z = 4, R = 2.7%, and R_w = 3.3%. **7a** is monoclinic, space group $P2_1/n$; a = 13.223(2) Å, b = 10.726(3) Å, c = 20.705(2) Å, β = 103.35(1)°, V = 2857.3(9) Å^3, Z = 4, R = 4.8%, and R_w = 5.0%.

Introduction

The chemistry of metal isocyanide complexes has been much less explored than that of the metal carbonyls.[1] Previously we have found that the diaminocarbene complexes $ReBr(CO)_4\{C(NHPh)(NHR)\}$, prepared from the reaction of $ReBr(CO)_4(CNPh)$ with amines, undergo ortho metalation to form the cyclometalated products $Re(CO)_4\{\eta^2\text{-}C(NHC_6H_4)(NHR)\}$, and the latter proceed with successive Re–C bond formation and cleavage at ambient temperature.[2] Considering that "lightly stabilized" complexes with either unsaturated bond character or labile donor ligands have been widely utilized as precursors to incorporate ligands of interest,[3,4] we thought it would be feasible to activate $ReBr(CO)_4(CNR)$ to form labile intermediates in order to gain more insight into the chemistry of the rhenium isocyanide complexes. Herein, we describe the isolation of two "lightly stabilized" derivatives, the trimethylamine compounds $ReBr(CO)_3(CNR)(NMe_3)$ as well as the nitrile complexes $ReBr(CO)_3(CNR)(NCMe)$. Also we report the one-flask conversion of $ReBr(CO)_4(CNPh)$ with nitrogen-containing ligands to form the substituted rhenium diaminocarbene complexes $[Re(CO)_3(NH_2R)_2\{C(NHPh)(NHR)\}]^+Br^-$.

Results and Discussion

Preparation of the Complexes $ReBr(CO)_3(CNR)(NMe_3)$ (2) and $ReBr(CO)_3(CNR)(NCMe)$ (3). Treatment of the rhenium isocyanide complexes $ReBr(CO)_4(CNR)$ (**1a**, R = Ph; **1b**, R = Pr) in CH_2Cl_2 with Me_3NO at room temperature gives the trimethylamine-coordinated products $ReBr(CO)_3(CNR)(NMe_3)$ (**2a**, R = Ph; **2b**, R = Pr) (eq 1). The reactions were monitored with IR

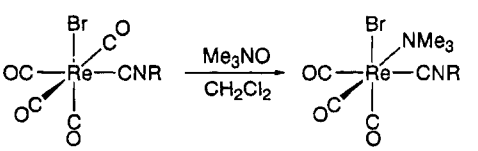

(1)

1a, R = Ph
1b, R = Pr

2a, R = Ph
2b, R = Pr

spectroscopy by following the diminution of ν_{CO} bands of the starting material, $ReBr(CO)_4(CNR)$. In general, slightly more than a stoichiometric amount of Me_3NO

† Academia Sinica.
‡ National Sun Yat-Sen University.
⊗ Abstract published in *Advance ACS Abstracts*, January 1, 1995.

(1) Elschenbroich, C.; Salzer, A. In *Organometallics*; VCH: Weinheim, Germany, 1992; p 241.
(2) (a) Lu, K. L.; Lee, H. H.; Wang, C. M.; Wen, Y. S. *Organometallics* **1994**, *13*, 593. (b) Lu, K. L.; Wang, C. M.; Lee, H. H.; Chen, L. C.; Wen, Y. S. *J. Chem. Soc., Chem. Commun.* **1993**, 706. (c) Chen, L. C.; Chen, M. Y.; Chen, J. H.; Wen, Y. S.; Lu, K. L. *J. Organomet. Chem.* **1992**, *425*, 99.
(3) (a) Knox, S. A. R.; Koepke, J. W.; Andrews, M. A.; Kasez, H. D. *J. Am. Chem. Soc.* **1975**, *97*, 3942. (b) Green, M.; Hughes, A. K.; McGowan, P. C.; Mountford, P.; Scott, P.; Simpson, S. J. *J. Chem. Soc., Dalton Trans.* **1992**, 1591. (c) Green, M.; Mills, R. M.; Pain, G. N.; Stone, F. G. A.; Woodward, P. *J. Chem. Soc., Dalton Trans.* **1982**, 1309. (d) Curtis, M. D. *Polyhedron* **1987**, *6*, 759.

0276-7333/95/2314-0925$09.00/0

was required. After the reaction solution was filtered through a small silica gel column followed by evaporation of the solvent, complex **2** was obtained in good purity and in near-quantitative yield, as indicated by its IR and ^{1}H NMR spectra. The IR spectrum of **2b** showed a characteristic C≡N stretching absorption of a terminally coordinated isocyanide at 2202 cm^{-1}.[5] The ^{13}C NMR spectrum of **2b** showed a triplet centered at δ 144.2 in a 1:1:1 ratio with a coupling constant of $J(^{13}C^{14}N)$ = 20 Hz, attributed to the carbon resonance of the *C*≡NPr group. This indicates a very symmetric electric charge distribution around the nitrogen atom of the coordinated isocyanide ligand.[6,7] The ^{1}H NMR spectrum of **2b** showed two singlets, a major resonance at δ 2.95 and a much smaller peak at δ 2.85; both were assigned to the methyl protons of a coordinated NMe_3 group.[8] The minor resonance was attributed to a small amount of an isomer. This was supported by the resonances of the propyl groups, which appeared as two sets of absorptions at δ 3.90, 1.94, 1.17 and δ 3.73, 1.82, 1.09 in a 16:1 ratio. The structure of **2** shown in eq 1 is believed to be the major isomer, in which the three carbonyls are in a cofacial arrangement as observed in other related complexes.[9,10] The minor isomer might be that in which the trimethylamine group is trans with respect to the isocyanide ligand.

In the presence of CH_3CN, complex **1** readily reacts with Me_3NO to yield the nitrile derivatives $ReBr(CO)_3$-(CNR)(NCMe) (**3a**, R = Ph; **3b**, R = Pr) in good yields (eq 2). The infrared spectrum of **3b** showed the ν_{CN}

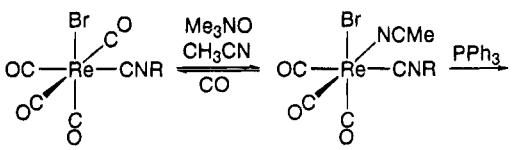

1a, R = Ph
1b, R = Pr

3a, R = Ph
3b, R = Pr

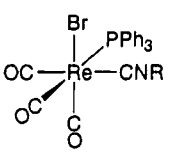

(2)

4a, R = Ph
4b, R = Pr

absorption at 2211 cm^{-1}, characteristic of a terminally coordinated isocyanide ligand. The ^{1}H NMR spectrum of **3** showed that it exists in two isomeric forms in solution. In addition to the appropriate proton absorptions of the isocyanide ligand, two singlets (δ 2.44 and 2.42 for **3a**, δ 2.42 and 2.41 for **3b**) were attributed to the methyl group of the acetonitrile ligand of each isomer. The ^{13}C NMR spectrum of **3b** showed the carbon resonance of the *C*NPr group as a triplet centered at δ 138.7 in a 1:1:1 ratio with a coupling constant of $J(^{13}C^{14}N)$ = 20 Hz. This indicates that there is a very symmetric electric charge distribution around the nitrogen atom of the coordinated isocyanide ligand in **3b**.[6,7]

Complexes containing nitrile[4,11,12] or trimethylamine[8,13] as ligands have been widely used as precursors in organometallic synthesis. They tend to decompose, and only a few trimethylamine derivatives have been isolated and characterized, such as $Os_3(CO)_{11}(NMe_3)$.[8] In the present study, the white complexes $ReBr(CO)_3$-(CNR)(NMe_3) (**2**) and $ReBr(CO)_3$(CNR)(NCMe) (**3**) are "lightly stabilized" in CH_2Cl_2 and decompose slowly, but they could be isolated and are found to be air-stable solids.

Reactivity of $ReBr(CO)_3$(CNR)(NCMe) (3). The reactivity of the nitrile complexes $ReBr(CO)_3$(CNR)-(NCMe) was primarily examined with two-electron-donor ligands. Bubbling CO gas through a solution of complex **3** in CH_2Cl_2 gives $ReBr(CO)_4$(CNR) (**1**) in almost quantitative yields, as indicated by IR spectroscopy. Addition of PPh_3 to a solution of **3** in CH_2Cl_2 affords compounds of the formula $ReBr(CO)_3$(CNR)-(PPh_3) (**4a**, R = Ph; **4b**, R = Pr) in good yields (eq 2). These reactions showed that the coordinated acetonitrile ligand in **3** is labile and is easily displaced by two-electron-donor ligands. Complex **4** exists as two isomers in solution. The structure of **4a** was confirmed by X-ray crystallography. An ORTEP representation is shown in Figure 1, and pertinent crystallographic details are listed in Tables 1–3. Pseudooctahedral geometry is observed around the Re atom, exemplified by the cis interligand bond angles, which are all within the range 82.4(2)–93.14(3)°. The three CO ligands are arranged in a facial configuration, with a somewhat shorter Re–C distance for CO trans to the phosphine ligand. The isocyanide ligand is tilted away from the triphenylphosphine group, with the P–Re–C(4) bond angle of 91.6(2)° and the Re–C(4)–N angle of 174.0(7)° presumably due to steric hindrance. The N–C(4) bond length of 1.14(1) Å indicates triple-bond character.[14]

Reaction of $ReBr(CO)_3$(CNR)(NCMe) with Amines. The labile complex **3** on reaction with primary amines readily gives $ReBr(CO)_3$(CNR)(H_2NR') (**5a**, R = Ph, R′ = Pr^i; **5b**, R = Ph, R′ = Pr; **5c**, R = Ph, R′ = CH_2Ph; **5e**, R = Pr, R′ = Pr^i; **5f**, R = Pr, R′ = CH_2Ph) (**Scheme** 1). The interaction of **3** with a secondary amine, $HNEt_2$, leads to the formation of similar derivatives $ReBr(CO)_3$(CNR)($HNEt_2$) (**5d**, R = Ph; **5g**, R = Pr).

(4) (a) Johnson, B. F. G.; Lewis, J.; Pippard, D. A. *J. Chem. Soc., Dalton Trans.* **1981**, *407*. (b) Johnson, B. F. G.; Lewis, J.; Odiaka, T. I.; Raithby, P. R. *J. Organomet. Chem.* **1981**, *216*, C56. (c) Deeming, A. J.; Powell, N. I.; Whittaker, C. *J. Chem. Soc., Dalton Trans.* **1991**, 1875. (d) Dahlinger, K.; Poë, A. J.; Sayal, P. K.; Sekhar, V. C. *J. Chem. Soc., Dalton Trans.* **1986**, 2145. (e) Chi, Y.; Wu, C. H. *Organometallics* **1990**, *9*, 2305. (f) Adams, R. D.; Chen, L.; Wu, W. *Angew. Chem., Int. Ed. Engl.* **1994**, *33*, 568. (g) Tachikawa, M.; Shapley, J. R. *J. Organomet. Chem.* **1977**, *124*, C19. (h) Lu, K. L.; Su, C. J.; Lin, Y. W.; Gau, H. M.; Wen, Y. S. *Organometallics* **1992**, *11*, 3832.

(5) Adams, R. D.; Golembeski, N. M. *J. Am. Chem. Soc.* **1979**, *101*, 2579.

(6) Becker, E. D. In *High Resolution NMR Theory and Chemical Applications*; Academic Press: New York, 1980; p 192.

(7) Pretsch, E.; Clerc, T.; Siebl, J.; Simon, W. In *Tables of Spectral Data for Structure Determination of Organic Compounds*; Springer-Verlag: Berlin, 1989; p C200.

(8) Johnson, B. F. G.; Lewis, J.; Raithby, P. R.; Zuccaro, C. *J. Chem. Soc., Chem. Commun.* **1979**, 916.

(9) Lu, K. L.; Chen, J. L.; Lin, Y. C.; Peng, S. M. *Inorg. Chem.* **1988**, *27*, 1726.

(10) (a) Abel, E. W.; Bhatti, M. M.; Hursthouse, M. B.; Malik, K. M. A.; Mazid, M. A. *J. Organomet. Chem.* **1980**, *197*, 345. (b) Jones, R. A.; Wilkinson, G.; Gales, A. M. R.; Hursthouse, M. B.; Malik, K. M. A. *J. Chem. Soc., Dalton Trans.* **1980**, 1771.

(11) (a) Burgess, K. *Polyhedron* **1984**, *3*, 1175. (b) Deeming, A. J. *Adv. Organomet. Chem.* **1986**, *26*, 1.

(12) Lu, K. L.; Liu, L. K.; Su, C. J.; Gau, H. M.; Wang, Y.; Lee, G. H. *J. Organomet. Chem.*, in press.

(13) Löwe, C.; Shklover, V.; Bosch, H. W.; Berke, H. *Chem. Ber.* **1993**, *126*, 1769.

(14) Allen, F. H.; Kennard, O.; Watson, D. G.; Brammer, L.; Orpen, A. G.; Taylor, R. *J. Chem. Soc., Perkin Trans. 2* **1987**, S1.

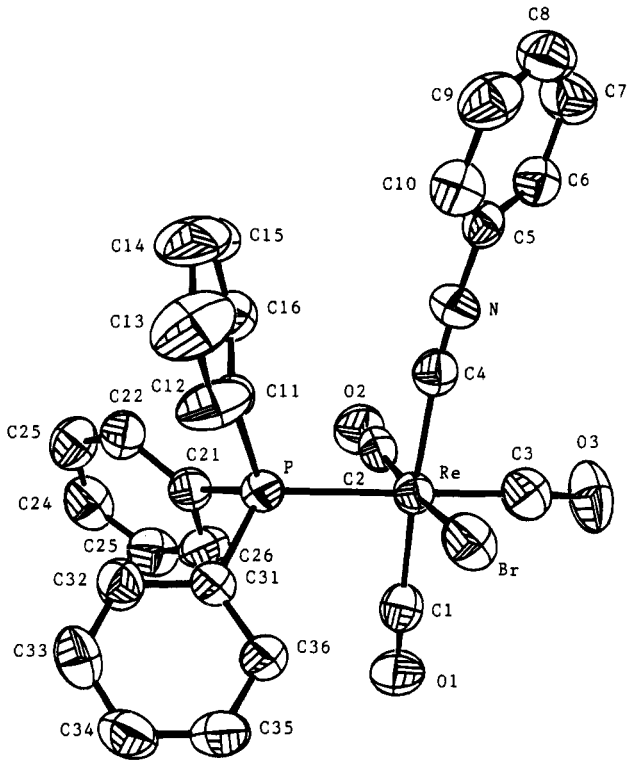

Figure 1. Molecular structure of $ReBr(CO)_3(CNPh)(PPh_3)$ (**4a**).

Table 1. Crystal and Intensity Collection Data for 4a, 6a, and 7a

complex	**4a**	**6a**	**7a**
formula	$C_{28}H_{20}BrNO_3PRe$	$C_{16}H_{22}BrN_3O_3Re$	$C_{20}H_{33}BrC_{12}N_4O_3Re$
fw	715.56	570.48	714.52
space group	$P\bar{1}$	$P2_1/n$	$P2_1/n$
a, Å	9.801(4)	9.174(2)	13.223(2)
b, Å	11.190(5)	19.865(2)	10.726(3)
c, Å	13.862(5)	12.064(2)	20.705(2)
α, deg	91.49(3)		
β, deg	108.19(3)	112.26(2)	103.35(1)
γ, deg	65.52(3)		
V, Å^3	1305.1(8)	2034.6(6)	2857.3(9)
D_{calc}, g cm^{-3}	1.821	1.862	1.661
Z	2	4	4
μ(Mo Kα), cm^{-1}	63.2	80.2	59.1
temp	room temp	room temp	room temp
radiation	Mo Kα	Mo Kα	Mo Kα
2θ (max)	45.0	49.9	49.9
scan type	$\theta-2\theta$	$\theta-2\theta$	$\theta-2\theta$
total no. of rflns	3657	3810	5242
no. of obsd rflns, $F_o > 2.5\sigma(F_o)$	2829	2849	2791
no. of obsd variables	316	217	280
R	0.031	0.027	0.047
R_w	0.035	0.033	0.048
$\Delta(\varrho)$, e Å^{-3}	1.040	0.700	1.320
Δ/σ_{max}	0.001	0.031	0.092
GOF	1.41	1.82	1.86

All the compounds synthesized were characterized by IR and NMR spectroscopy. The IR spectra of these complexes showed the same absorption pattern and similar resonance frequencies in the ν_{CO} stretching region, compared to spectra for the nitrile complexes $ReBr(CO)_3(CNR)(NCMe)$. The ^{13}C NMR spectra of **5e–g** also showed the carbon resonance of the *C*NPr group as a triplet in a 1:1:1 ratio at δ 140.7, 140.6, and 142.3, respectively. This indicates that the nitrogen atoms of the coordinated isocyanide groups possess a symmetric electric charge distribution.

Prolonged reaction of $ReBr(CO)_3(CNPh)(NCMe)$ (**3a**) with excess amines (H_2NPr^i, H_2NPr, and H_2NCH_2Ph) in CH_2Cl_2 at room temperature affords initially the amine-substituted products **5a–c**. The latter react continuously with the appropriate amine to yield $ReBr(CO)_3(H_2NR)\{C(NHPh)(NHR)\}$ (**6a**, R = Pr^i; **6b**, R = Pr; **6c**, R = CH_2Ph), in which the coordinated isocyanide ligand has undergone a nucleophilic attack by the amine to give the diaminocarbene (amidinium) group (Scheme 1). The IR spectrum of **6** showed no signal which could be attributed to a terminally coordinated isocyanide ligand. The ^1H NMR spectrum of **6a** exhibited four broad sets of *H*N resonances: δ 8.99 and 6.45 (assigned to *H*NPh and *H*NPr^i of the diaminocarbene ligand) and δ 2.93 and 2.51 (assigned to NH_aH_b of the coordinated amine group). The line width of the resonances is

Table 2. Atomic Coordinates and Isotropic Thermal Parameters (Å^2) for $ReBr(CO)_3(CNPh)(PPh_3)$ (4a)

atom	x	y	z	B_{iso}[a]
Re	0.22296(4)	0.31665(3)	0.17412(2)	3.55(2)
Br	0.26505(12)	0.35492(10)	0.36752(7)	5.53(6)
P	0.51360(25)	0.21942(19)	0.20849(15)	3.57(11)
N	0.2327(9)	0.0472(7)	0.2568(5)	4.9(4)
O(1)	0.1884(8)	0.5955(6)	0.1154(5)	6.2(4)
O(2)	0.1797(8)	0.2484(6)	−0.0402(5)	5.8(4)
O(3)	−0.1399(8)	0.4405(8)	0.1247(5)	7.5(5)
C(1)	0.2044(10)	0.4926(9)	0.1378(6)	4.4(5)
C(2)	0.1923(10)	0.2707(8)	0.0312(7)	4.2(5)
C(3)	−0.0040(12)	0.3921(9)	0.1452(6)	5.2(6)
C(4)	0.2362(9)	0.1388(8)	0.2254(6)	4.1(5)
C(5)	0.2218(10)	−0.0604(8)	0.2947(6)	3.9(5)
C(6)	0.0947(10)	−0.0848(8)	0.2438(6)	4.6(5)
C(7)	0.0795(12)	−0.1908(10)	0.2801(8)	6.1(7)
C(8)	0.1913(15)	−0.2686(10)	0.3674(9)	6.4(7)
C(9)	0.3194(13)	−0.2432(9)	0.4194(7)	6.0(7)
C(10)	0.3354(11)	−0.1386(9)	0.3820(6)	5.2(6)
C(11)	0.6178(9)	0.0526(7)	0.2761(6)	3.9(5)
C(12)	0.7092(13)	0.0318(8)	0.3784(7)	6.2(7)
C(13)	0.7810(15)	−0.0941(11)	0.4313(7)	8.1(8)
C(14)	0.7616(14)	−0.1982(9)	0.3842(9)	7.5(8)
C(15)	0.6725(12)	−0.1781(9)	0.2837(9)	6.3(7)
C(16)	0.5991(11)	−0.0523(9)	0.2293(7)	5.2(5)
C(21)	0.5666(9)	0.2085(8)	0.0914(6)	3.9(5)
C(22)	0.6803(10)	0.0947(8)	0.0710(6)	4.7(5)
C(23)	0.7220(12)	0.0981(10)	−0.0149(7)	5.7(6)
C(24)	0.6523(12)	0.2148(11)	−0.0802(7)	5.9(7)
C(25)	0.5382(12)	0.3248(9)	−0.0604(6)	5.3(6)
C(26)	0.4948(11)	0.3223(8)	0.0236(6)	4.8(5)
C(31)	0.6307(9)	0.3047(7)	0.2796(5)	3.7(5)
C(32)	0.7920(10)	0.2522(9)	0.2932(6)	4.8(5)
C(33)	0.8820(11)	0.3152(10)	0.3428(7)	5.7(6)
C(34)	0.8140(12)	0.4326(9)	0.3803(7)	5.5(6)
C(35)	0.6575(12)	0.4858(8)	0.3665(7)	5.2(6)
C(36)	0.5627(9)	0.4227(8)	0.3165(6)	4.4(5)

[a] B_{iso} is the mean of the principal axes of the thermal ellipsoid.

Table 3. Selected Bond Distances and Angles for $ReBr(CO)_3(CNPh)(PPh_3)$ (4a)

(a) Bond Distances (Å)			
Re−Br	2.6340(13)	N−C(4)	1.141(11)
Re−P	2.4772(24)	N−C(5)	1.383(11)
Re−C(1)	1.965(9)	O(1)−C(1)	1.134(11)
Re−C(2)	1.996(10)	O(2)−C(2)	0.996(12)
Re−C(3)	1.930(11)	O(3)−C(3)	1.150(12)
Re−C(4)	2.071(9)		
(b) Bond Angles (deg)			
Br−Re−P	90.61(6)	C(1)−Re−C(2)	93.4(3)
Br−Re−C(1)	92.14(23)	C(1)−Re−C(3)	89.3(4)
Br−Re−C(2)	174.49(23)	C(1)−Re−C(4)	174.1(3)
Br−Re−C(3)	90.3(3)	C(2)−Re−C(3)	89.7(4)
Br−Re−C(4)	82.39(21)	C(2)−Re−C(4)	92.1(3)
P−Re−C(1)	90.67(25)	C(3)−Re−C(4)	88.6(3)
P−Re−C(2)	89.47(25)	C(4)−N−C(5)	177.5(8)
P−Re−C(3)	179.1(3)	Re−C(4)−N	174.0(7)
P−Re−C(4)	91.59(23)		

Scheme 1

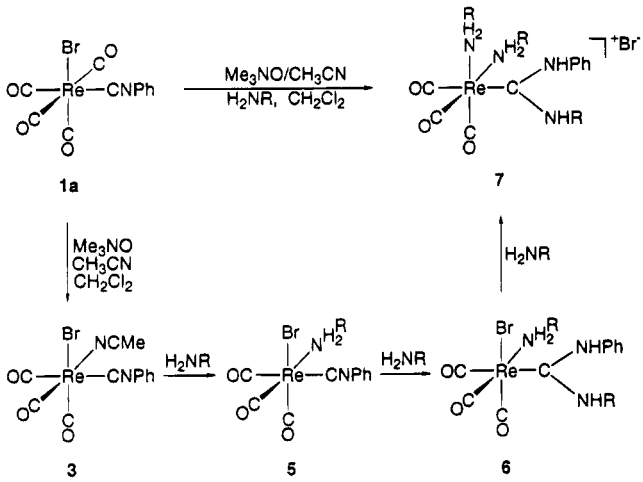

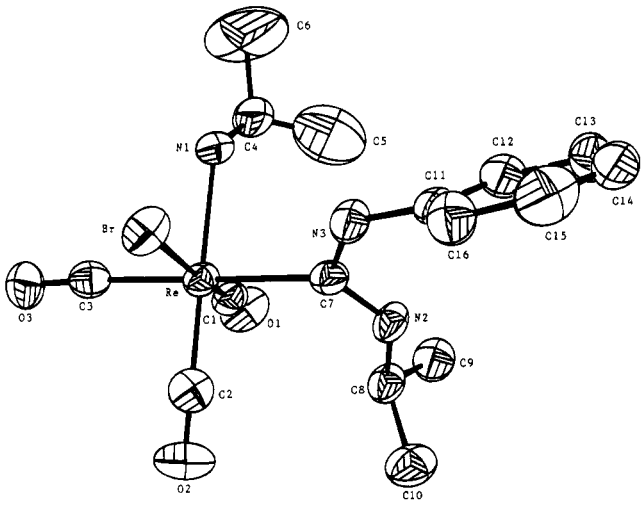

Figure 2. Molecular structure of $ReBr(CO)_3(NH_2Pr^i)\{C(NHPh)(NHPr^i)\}$ (**6a**).

attributed to quadrupolar line broadening by ^{14}N (I = 1). Furthermore, each of the above *H*N resonances has an associated minor broad peak in a 1:9 ratio at δ 9.27, 7.99, 2.73, and 2.21, respectively, indicating that complex **6a** exists as two isomeric forms in solution at room temperature. On the basis of IR spectroscopy (ν_{CO} 2020 (s), 1919 (s), 1877 (s) cm^{-1}) the major species in solution is assigned to be the *fac* isomer.[15a] The ^{13}C NMR spectrum of **6a** showed a downfield peak at δ 205.2 attributed to the coordinated carbon atom of the diaminocarbene group.

In addition to spectroscopic determination, the structure of **6a** was also characterized by single-crystal X-ray diffraction analysis. An ORTEP drawing of the molecule is shown in Figure 2. Atomic coordinates are listed in Table 4, and derived bond distances and angles are summarized in Table 5. The molecule contains a rhenium atom in a distorted-octahedral environment. The structure of **6a** is similar to that of the previously reported complex $ReBr(CO)_3(PPh_3)\{C(NHPh)(NHPr^i)\}$.[1] The three CO groups are arranged in a facial configuration. This is consistent with the IR spectroscopic data, and therefore we suggest that this structure is the major isomer in solution. The C(7), N(2), and N(3) atoms appear to be sp^2 hybridized with a distorted-trigonal-planar arrangement. The Re−C(7) distance is 2.209(6) Å. Both C(7)−N(2) and C(7)−N(3) show partial double-bond character with distances of 1.309(8) and 1.356(8) Å, respectively. The dihedral angle of Br−Re−C(7)−N(2) is 148.2(4)°.

In comparison with **5a,b**, the complexes **5e,f**, which contain the aliphatic isocyanide group CNPr, did not react with amines to form the diaminocarbene products. We attribute this to the electron-releasing properties of the propyl group, which makes the coordinated carbon of the CNPr group more electron rich and consequently makes it inactive toward nucleophilic attack by the amine. These results are consistent with the observations that metal complexes containing an aromatic isocyanide ligand show remarkable differences in reactivity toward nucleophilic reagents compared to their aliphatic analogues.[15b]

Interestingly, continuing the reaction of **3a** with excess amine (H_2NPr^i or H_2NPr) for several days at

Table 4. Atomic Coordinates and Isotropic Thermal Parameters (Å²) for $ReBr(CO)_3(NH_2Pr^i)\{C(NHPh)(NHPr^i)\}$ (6a)

atom	x	y	z	B_{iso}[a]
Re	0.02018(3)	0.08613(1)	0.20823(2)	2.90(1)
Br	−0.07170(9)	0.11615(4)	−0.02229(6)	4.34(4)
N(1)	0.2187(6)	0.0377(3)	0.1707(5)	3.6(3)
N(2)	0.2004(7)	0.2195(3)	0.3370(4)	3.5(3)
N(3)	0.2164(7)	0.1981(3)	0.1589(5)	3.6(3)
O(1)	0.1394(7)	0.03677(25)	0.4667(4)	5.1(3)
O(2)	−0.2490(7)	0.15720(28)	0.2491(5)	5.8(3)
O(3)	−0.2093(6)	−0.03419(25)	0.1245(5)	5.2(3)
C(1)	0.0956(8)	0.0558(3)	0.3691(6)	3.5(3)
C(2)	−0.1474(9)	0.1310(4)	0.2322(6)	4.0(4)
C(3)	−0.1175(8)	0.0079(3)	0.1568(6)	3.7(3)
C(4)	0.3647(11)	0.0092(6)	0.2681(10)	8.5(6)
C(5)	0.4535(15)	0.0574(8)	0.3460(13)	11.0(9)
C(6)	0.4634(14)	−0.0256(11)	0.2171(15)	18.9(14)
C(7)	0.1631(7)	0.1790(3)	0.2448(5)	3.0(3)
C(8)	0.1557(8)	0.2138(3)	0.4423(6)	3.7(3)
C(9)	0.2982(9)	0.2057(4)	0.5541(6)	4.7(4)
C(10)	0.0579(10)	0.2750(4)	0.4458(7)	5.1(4)
C(11)	0.3071(8)	0.2563(3)	0.1584(5)	3.2(3)
C(12)	0.4599(8)	0.2643(4)	0.2417(6)	3.9(3)
C(13)	0.5479(9)	0.3202(4)	0.2367(7)	4.8(4)
C(14)	0.4873(10)	0.3667(4)	0.1491(7)	4.6(4)
C(15)	0.3390(11)	0.3589(4)	0.0661(7)	5.4(5)
C(16)	0.2453(9)	0.3042(4)	0.0705(6)	4.4(4)

[a] B_{iso} is the mean of the principal axes of the thermal ellipsoid.

Table 5. Selected Bond Distances and Angles for $ReBr(CO)_3(NH_2Pr^i)\{C(NHPh)(NHPr^i)\}$ (6a)

(a) Bond Distances (Å)			
Re−Br	2.6502(9)	N(1)−C(4)	1.517(12)
Re−N(1)	2.252(5)	N(2)−C(7)	1.309(8)
Re−C(1)	1.895(7)	N(2)−C(8)	1.479(8)
Re−C(2)	1.891(8)	N(3)−C(7)	1.356(8)
Re−C(3)	1.950(7)	N(3)−C(11)	1.426(8)
Re−C(7)	2.209(6)		
(b) Bond Angles (deg)			
Br−Re−N(1)	81.07(14)	C(1)−Re−C(3)	90.8(3)
Br−Re−C(1)	173.61(19)	C(1)−Re−C(7)	95.9(3)
Br−Re−C(2)	95.77(20)	C(2)−Re−C(3)	87.6(3)
Br−Re−C(3)	86.29(19)	C(2)−Re−C(7)	91.8(3)
Br−Re−C(7)	87.16(16)	C(3)−Re−C(7)	173.3(3)
N(1)−Re−C(1)	93.50(24)	Re−N(1)−C(4)	123.1(5)
N(1)−Re−C(2)	176.30(24)	C(7)−N(2)−C(8)	127.9(5)
N(1)−Re−C(3)	94.07(24)	C(7)−N(3)−C(11)	127.6(5)
N(1)−Re−C(7)	86.14(21)	Re−C(7)−N(2)	128.8(4)
C(1)−Re−C(2)	89.8(3)	Re−C(7)−N(3)	116.1(4)
N(2)−C(7)−N(3)	115.1(5)		

(15) (a) Lukehart, C. M. In *Fundamental Transition Metal Organometallic Chemistry*; Brooks/Cole: Monterey, CA, 1985; p 80. (b) Crociani, B.; Boschi, T.; Nicolini, M.; Belluco, U. *Inorg. Chem.* **1972**, *11*, 1292.

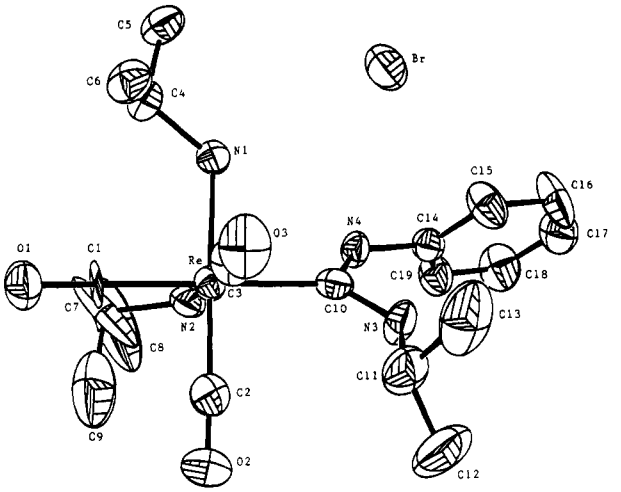

Figure 3. Molecular structure of $[Re(CO)_3(H_2NPr^i)_2\{C(NHPh)(NHPr^i)\}]^+Br^-$ (**7a**).

room temperature gives the products $ReBr(CO)_3(H_2NR)\{C(NHPh)(NHR)\}$ (**6a**, R = Pr^i; **6b**, R = Pr), which subsequently undergo replacement of bromide with amine, leading to the ionic complexes $[Re(CO)_3(H_2NR)_2\{(NHPh)(NHR)\}]^+Br^-$ (**7a**, R = Pr^i; **7b**, R = Pr) (Scheme 1). Utilization of a large excess of amine in the system speeds up these reactions. Complex **7** was purified by chromatography. These ionic products were characterized by IR, NMR, FAB MS, and elemental analysis. Complex **7a** was further defined by X-ray crystallography. The FAB MS spectrum of **7a** showed the molecular ion at *m/z* 551. Two broad peaks at δ 9.76 (*H*NPh) and δ 6.42 (*H*NPr^i) in the ^1H NMR were assigned to the *H*N absorptions of the diaminocarbene ligand. The proton resonances of two coordinated isopropylamines were also clearly indicated in the ^1H NMR spectra.

The main feature of these reactions is that the amine replaces the bromide in **6** to form the ionic product **7**, without any substitution of the carbonyl groups. This indicates that the carbonyls coordinate at the rhenium center in **6** with a strong π back-bonding facilitated by other surrounding donor ligands. This is corroborated by the relatively lower stretching frequencies of the carbonyl groups (2022, 1919, and 1877 cm^{-1}) and the relatively shorter length of the Re−CO bond (1.895(7), 1.891(8), and 1.950(7) Å) in **6a** compared to that in $ReBr(CO)_4\{C(NHPh)(NHPr^i)\}$ (ν_{CO} 2104, 2001, and 1931 cm^{-1}; Re−CO bond 2.00(1), 1.96(1), and 1.90(1) Å).[1]

An ORTEP diagram of $[Re(CO)_3(H_2NPr^i)\{C(NHPh)(NHPr^i)\}]^+Br^-$ (**7a**) is shown in Figure 3. Atomic positional parameters are set out in Table 6, and selected interatomic distances and angles are listed in Table 7. The molecule contains a rhenium atom in a distorted-octahedral environment. This distortion probably arises from the steric requirement of the more bulky coordinated groups such as diaminocarbene and two amine ligands. The three CO groups are arranged in a facial configuration. Two coordinated isopropylamine groups and the diaminocarbene ligands are cis to each other. The bond lengths and bond angles of the diaminocarbene group are similar to those of the related complex $ReBr(CO)_4\{C(NHPh)(NHPr^i)\}$.[1] The distance of the Re−C(10) bond (2.17(1) Å) is within the range of expected values. The counteranion Br^- is clearly shown in Figure 3.

Table 6. Atomic Coordinates and Isotropic Thermal Parameters (Å^2) for $[Re(CO)_3(NH_2Pr^i)_2\{C(NHPh)(NHPr^i)\}]^+Br^-$ (7a)

atom	*x*	*y*	*z*	B_{iso}[a]
Re	0.47002(4)	0.47998(5)	0.21512(2)	4.66(2)
Br	0.70545(12)	0.79914(14)	0.24088(7)	7.03(7)
N(1)	0.6156(6)	0.5141(8)	0.1810(4)	4.4(4)
N(2)	0.5331(7)	0.2890(9)	0.2420(5)	5.2(5)
N(3)	0.5295(8)	0.6075(11)	0.3580(4)	6.1(6)
N(4)	0.6582(7)	0.4908(9)	0.3366(4)	4.9(4)
O(1)	0.3443(7)	0.3743(9)	0.0799(4)	7.8(5)
O(2)	0.2768(8)	0.4237(13)	0.2670(6)	10.6(8)
O(3)	0.3902(8)	0.7423(10)	0.1765(5)	8.8(6)
C(1)	0.3931(9)	0.4281(12)	0.1319(4)	5.8(6)
C(2)	0.3527(11)	0.4464(14)	0.2484(7)	6.9(8)
C(3)	0.4218(10)	0.6437(14)	0.1923(6)	6.4(7)
C(4)	0.6183(9)	0.5153(11)	0.1093(5)	5.0(5)
C(5)	0.7297(11)	0.5231(14)	0.1027(6)	7.1(8)
C(6)	0.5545(10)	0.6228(13)	0.0742(6)	6.3(7)
C(7)	0.4985(15)	0.1716(17)	0.1920(15)	16.8(16)
C(8)	0.5446(25)	0.0711(21)	0.2249(16)	22.7(23)
C(9)	0.3981(26)	0.1487(24)	0.2083(12)	16.9(21)
C(10)	0.5605(9)	0.5346(12)	0.3121(6)	5.0(6)
C(11)	0.4312(13)	0.6760(19)	0.3494(8)	8.4(10)
C(12)	0.3844(15)	0.6525(27)	0.4035(10)	14.5(18)
C(13)	0.4613(15)	0.8135(24)	0.3481(10)	12.9(14)
C(14)	0.7288(9)	0.5170(12)	0.3998(5)	5.0(6)
C(15)	0.7668(11)	0.6334(13)	0.4127(6)	7.6(8)
C(16)	0.8373(13)	0.6572(15)	0.4731(8)	10.2(10)
C(17)	0.8705(13)	0.5649(18)	0.5177(7)	8.5(9)
C(18)	0.8311(13)	0.4489(16)	0.5027(7)	8.7(10)
C(19)	0.7596(11)	0.4234(14)	0.4437(6)	7.0(8)
C(20)	0.1306(19)	0.7305(49)	0.0912(14)	30.4(40)
Cl(1)	0.0140(7)	0.7554(14)	0.0899(3)	28.8(11)
Cl(2)	0.1520(8)	0.6281(13)	0.0447(5)	27.0(10)

[a] B_{iso} is the mean of the principal axes of the thermal ellipsoid.

Table 7. Selected Bond Distances and Angles for $[Re(CO)_3(NH_2Pr^i)_2\{C(NHPh)(NHPr^i)\}]^+Br^-$ (7a)

(a) Bond Distances (Å)			
Re−N(1)	2.229(9)	N(1)−C(4)	1.492(13)
Re−N(2)	2.233(10)	N(2)−C(7)	1.63(3)
Re−C(1)	1.872(8)	N(3)−C(10)	1.366(16)
Re−C(2)	1.872(16)	N(3)−C(11)	1.467(19)
Re−C(3)	1.890(14)	N(4)−C(10)	1.359(14)
Re−C(10)	2.167(11)	N(4)−C(14)	1.449(12)
(b) Bond Angles (deg)			
N(1)−Re−N(2)	86.0(3)	C(1)−Re−C(10)	178.4(5)
N(1)−Re−C(1)	94.8(4)	C(2)−Re−C(3)	90.6(6)
N(1)−Re−C(2)	176.5(5)	C(2)−Re−C(10)	92.2(5)
N(1)−Re−C(3)	92.0(5)	C(3)−Re−C(10)	93.6(5)
N(1)−Re−C(10)	85.2(4)	Re−N(1)−C(4)	122.5(6)
N(2)−Re−C(1)	92.8(4)	Re−N(2)−C(7)	121.1(8)
N(2)−Re−C(2)	91.4(5)	C(10)−N(3)−C(11)	126.9(10)
N(2)−Re−C(3)	177.8(5)	C(10)−N(4)−C(14)	129.1(10)
N(2)−Re−C(10)	85.6(4)	Re−C(10)−N(3)	127.6(8)
C(1)−Re−C(2)	87.8(6)	Re−C(10)−N(4)	121.8(8)
C(1)−Re−C(3)	88.1(5)	N(3)−C(10)−N(4)	110.5(9)

One-Flask Conversion of $ReBr(CO)_4(CNPh)$ to $[Re(CO)_3(H_2NR)_2\{C(NHPh)(NHR)\}]^+Br^-$. Treatment of $ReBr(CO)_4(CNPh)$ with Me_3NO in the presence of CH_3CN followed by treatment with excess isopropylamine or propylamine in CH_2Cl_2 at room temperature for several days results in the formation of the ionic product $[Re(CO)_3(H_2NR)_2\{C(NHPh)(NHR)\}]^+Br^-$ (**7a,b**) in a one-flask reaction. This reaction proceeds successively via intermediates **3**, **5**, and **6** to give the final product **7** in moderate to good yields under very mild reaction conditions (Scheme 1). Complexes **6a,b** were obtained as minor byproducts; however, their yields are reduced on prolonging the reaction time. As described above, each intermediate in this reaction sequence could be isolated and characterized.

Conclusion

The complexes $ReBr(CO)_4(CNR)$ react readily with nitrogen-containing ligands such as Me_3NO, CH_3CN, and amines. Although the complexes $ReBr(CO)_3(CNR)(NCMe)$ (**3**) are stable in the solid state, they exhibit high reactivity toward nucleophilic substitution reactions in solution and therefore could be used as useful intermediates for the synthesis of substituted derivatives of $ReBr(CO)_4(CNR)$. Furthermore, transformation of the isocyanide complex $ReBr(CO)_4(CNPh)$ to the ionic diaminocarbene products $[Re(CO)_3(H_2NR)_2\{C(NHPh)(NHR)\}]^+Br^-$ was achieved in a one-flask reaction under very mild conditions. The intermediate of each step could be isolated in good to excellent yields.

Experimental Section

General Data. The complex $ReBr(CO)_4(CNR)$ was prepared previously.[1] Other reagents were purchased from commercial sources and were used as received. All manipulations were performed with standard Schlenk techniques. Chromatographic separations could be done in air if exposure is limited to a few hours. Solvents were dried by stirring over Na/benzophenone (diethyl ether) or CaH_2 (hexane, CH_2Cl_2, CH_3CN) and were freshly distilled prior to use. IR spectra were recorded on a Perkin-Elmer 882 infrared spectrophotometer. NMR spectra were obtained on a Bruker AC-200, an ACP-300, or an AMX-500 FT NMR spectrometer, and mass spectra were recorded on a VG 70-250S mass spectrometer. Elemental analyses were performed using a Perkin-Elmer 2400 CHN elemental analyzer. The ^{31}P chemical shifts are referenced to external 85% H_3PO_4.

Synthesis of $ReBr(CO)_3(CNR)(NMe_3)$ (2). All compounds were prepared similarly. A typical preparation is listed here. For $ReBr(CO)_3(CNPh)(NMe_3)$ (**2a**), a solution of $ReBr(CO)_4(CNPh)$ (150 mg, 0.31 mmol) in CH_2Cl_2 (50 mL) was treated with a solution of Me_3NO (28 mg, 0.37 mmol) in CH_2Cl_2 (10 mL). The mixture was stirred for 30 min at room temperature, and the IR spectrum showed that the yield is near-quantitative. The solution was filtered through a small silica gel column, and then the solvent was removed under vacuum to give $ReBr(CO)_3(CNPh)(NMe_3)$ (**2a**). IR (CH_2Cl_2): ν_{CN} 2165 (w) cm^{-1}; ν_{CO} 2029 (s), 1957 (s), 1906 (s) cm^{-1}. ^1H NMR ($CDCl_3$): δ 7.45 (m, 5 H, Ph), 3.03, 2.84 (s, 9 H, CH_3, two isomers in a 25:1 ratio). ^{13}C NMR ($CDCl_3$): δ 192.1, 189.0, 188.3 (CO, major isomer), 185.6, 183.6 (CO, minor isomer), 153.6 (br, CN), 130.4, 129.8, 126.7 (Ph, major isomer), 130.2, 129.6, 126.9 (Ph, minor isomer), 58.75 (CH_3).

$ReBr(CO)_3(CNPr)(NMe_3)$ (**2b**) was obtained under reaction conditions similar to those for **2a**. IR (CH_2Cl_2): ν_{CN} 2202 (w) cm^{-1}; ν_{CO} 2032 (vs), 1948 (s), 1903 (s) cm^{-1}. ^1H NMR ($CDCl_3$): δ 3.90, 3.73 (t, 2 H, $CNCH_2$, two isomers in a 1:16 ratio), 2.95, 2.85 (s, 9 H, $N(CH_3)_3$, two isomers), 1.94, 1.82 (m, 2 H, CH_2CH_3, two isomers in a 1:16 ratio), 1.17, 1.09 (t, 3 H, CH_3, two isomers in a 1:16 ratio). ^{13}C NMR ($CDCl_3$): δ 192.1, 189.5, 188.5 (CO, major isomer), 187.4, 186.5 (CO, minor isomer), 144.2 (CN, 1:1:1 ratio, $J(^{13}C^{14}N)$ = 20 Hz), 58.5 (NCH_3), 46.1 ($CNCH_2$), 22.7 (CH_2CH_3), 10.9 (CH_3).

Synthesis of $ReBr(CO)_3(CNR)(NCMe)$ (3). A typical preparation is listed here. For $ReBr(CO)_3(CNPh)(NCMe)$ (**3a**), a solution of $ReBr(CO)_4(CNPh)$ (150 mg, 0.31 mmol) in CH_2Cl_2 (50 mL) and acetonitrile (1 mL) was treated with a solution of Me_3NO (28 mg, 0.37 mmol) in CH_2Cl_2 (10 mL). The mixture was stirred for 30 min at room temperature and filtered through a small silica gel column. The solvent was removed under vacuum, and the residue was recrystallized from hexane/CH_2Cl_2/CH_3CN to give **3a** (136 mg, 0.28 mmol) in 89% yield. Anal. Calcd for $C_9H_{10}BrN_2O_3Re$: C, 29.14; H, 1.63. Found: C, 29.43; H, 2.01. IR (CH_2Cl_2): ν_{CN} 2175 (w) cm^{-1}; ν_{CO} 2037 (vs), 1965 (s), 1920 (s) cm^{-1}. ^1H NMR ($CDCl_3$): δ 7.44 (m, 5 H, Ph), 2.44, 2.42 (s, 3 H, $NCCH_3$, two isomers). ^{13}C NMR ($CDCl_3$): δ 188.8, 188.2, 185.4 (CO, major isomer), 185.6, 183.7 (CO, minor isomer), 147.8 (br, CN), 130.2, 129.6, 126.9 (Ph), 120.4 (NCMe, major isomer), 119.8 (NCMe, minor isomer), 3.9 ($NCCH_3$, major isomer), 1.8 ($NCCH_3$, minor isomer).

$ReBr(CO)_3(CNPr)(NCMe)$ (**3b**; 146 mg, 0.32 mmol) was obtained under similar reaction conditions in 94% yield based on $ReBr(CO)_4(CNPr)$ (150 mg, 0.34 mmol). Anal. Calcd for $C_9H_{10}BrN_2O_3Re$: C, 23.40; H, 2.17. Found: C, 23.01; H, 2.15. IR (CH_2Cl_2): ν_{CN} 2211 (w) cm^{-1}; ν_{CO} 2039 (vs), 1959 (s), 1915 (s) cm^{-1}. ^1H NMR ($CDCl_3$): δ 3.92, 3.72 (t, 2 H, $CNCH_2$, two isomers in a 1:16 ratio), 2.42, 2.41 (s, 3 H, $NCCH_3$, two isomers), 1.83 (m, 2 H, CH_2CH_3), 1.09 (t, 3 H, CH_3). ^{13}C NMR ($CDCl_3$): δ 189.3, 188.4, 185.7 (CO, major isomer), 187.2, 186.3 (CO, minor isomer), 138.7 (CNPr, 1:1:1 ratio, $J(^{13}C^{14}N)$ = 20 Hz), 120.2 (NCMe), 46.0 ($CNCH_2$), 22.7 (CH_2CH_3), 3.89 ($NCCH_3$).

Carbonylation of 3. Carbon monoxide was bubbled through a solution of **3** in CH_2Cl_2 at room temperature. After 1 h, the IR spectra indicated that the conversion of **3** to **1** took place in almost quantitative yield.

Reaction of $ReBr(CO)_3(CNR)(NCMe)$ with Triphenylphosphine. A solution of $ReBr(CO)_4(CNPh)$ (150 mg, 0.31 mmol) in CH_2Cl_2 (50 mL) and acetonitrile (1.5 mL) was treated with a solution of Me_3NO (28 mg, 0.37 mmol) in CH_2Cl_2 (5 mL). The mixture was stirred for 20 min at room temperature and filtered through a small silica gel column. The solvent was removed under vacuum to give $ReBr(CO)_3(CNPh)(NCMe)$ by following procedures similar to those for the preparation of **3a**. The latter was then stirred with triphenylphosphine (84 mg, 0.32 mmol) in CH_2Cl_2 (40 mL) at room temperature for 40 min. After removal of solvent, the residue was chromatographed on a TLC plate with a mixture of CH_2Cl_2 and hexanes (3:2) as eluent to give $ReBr(CO)_3(CNPh)(PPh_3)$ (**4a**; 173 mg, 0.24 mmol) in 77% yield. Anal. Calcd for $C_{28}H_{20}BrNO_3PRe$: C, 46.97; H, 2.81; N, 1.95. Found: C, 46.88; H, 2.34; N, 1.72. IR (CH_2Cl_2): ν_{CN} 2174 (w) cm^{-1}; ν_{CO} 2037 (s), 1965 (m), 1920 (m) cm^{-1}. ^1H NMR ($CDCl_3$): δ 7.65–7.38 (m, 15 H, Ph). ^{13}C NMR ($CDCl_3$): δ 189.6 (d, CO, J_{CP} = 9 Hz), 186.2, 185.1 (CO), 147.8 (br, CN), 133.9, 133.7, 133.1, 132.2, 130.4, 129.8, 129.3, 128.5, 128.3, 126.5 (Ph). ^{31}P NMR ($CDCl_3$): δ 3.88, 0.30 (two isomers, 1:(trace)).

$ReBr(CO)_3(CNPr)(PPh_3)$ (**4b**) was obtained under similar reaction conditions in 76% yield based on $ReBr(CO)_4(CNPr)$. Anal. Calcd for $C_{25}H_{22}BrNO_3PRe$: C, 44.04; H, 3.25; N, 2.05. Found: C, 43.90; H, 2.99; N, 1.92. IR (CH_2Cl_2): ν_{CN} 2204 (w) cm^{-1}; ν_{CO} 2037 (s), 1964 (m), 1915 (m) cm^{-1}. ^1H NMR ($CDCl_3$): δ 7.67–7.38 (m, 15 H, Ph), 3.70 (t, 2 H, $CNCH_2$, minor isomer), 3.35 (t, 2 H, $CNCH_2$, major isomer), 1.81 (m, 2 H, CH_2CH_2, minor isomer), 1.49 (m, 2 H, CH_2CH_2, major isomer), 0.97 (t, 3 H, CH_2CH_3, minor isomer), 0.87 (t, 3 H, CH_2CH_3, major isomer). ^{13}C NMR ($CDCl_3$): δ 189.9 (d, CO, J_{CP} = 8 Hz), 186.7, 185.5 (CO), 138.4 (CNPr, 1:1:1 ratio, $J(^{13}C^{14}N)$ = 19 Hz), 134.0, 133.8, 133.4, 132.5, 130.4, 128.4, 128.2 (Ph), 45.7 ($CNCH_2$), 22.4 ($CNCH_2CH_2$), 10.9 (CH_2CH_3). ^{31}P NMR ($CDCl_3$): δ 4.23 (major isomer), 0.28 (minor isomer).

Reaction of $ReBr(CO)_3(CNPr)(NCMe)$ with Amines. A typical preparation is listed here. For $ReBr(CO)_3(CNPr)(NH_2Pr^i)$ (**5e**), a solution of $ReBr(CO)_4(CNPr)$ (150 mg, 0.34 mmol) in CH_2Cl_2 (50 mL) and acetonitrile (1.5 mL) was treated with a solution of Me_3NO (28 mg, 0.37 mmol) in CH_2Cl_2 (5 mL). The mixture was stirred for 20 min at room temperature and filtered through a small silica gel column. The solvent was removed under vacuum to give $ReBr(CO)_3(CNPr)(NCMe)$. The latter was stirred with excess isopropylamine (0.15 mL) in CH_2Cl_2 (40 mL) at room temperature for 30 min. After removal of solvent, the residue was chromatographed on a silica gel TLC plate with a mixture of CH_2Cl_2 and hexanes (70:30) as eluent to afford $ReBr(CO)_3(CNPr)(NH_2Pr^i)$ (**5e**; 103 mg, 0.22 mmol) in 63% yield. Anal. Calcd for $C_{11}H_{18}BrN_2O_3Re$: C, 25.14; H, 3.16; N, 5.87. Found: C, 25.13; H, 3.00; N, 5.61. IR

(CH_2Cl_2): ν_{CN} 2204 (m) cm^{-1}; ν_{CO} 2032 (s), 1946 (s), 1904 (s) cm^{-1}. ^1H NMR ($CDCl_3$): δ 3.73 (t, 2 H, $CNCH_2$), 3.18 (m, 1 H, $CH(CH_3)_2$), 2.90 (br, 1 H, NH_a), 2.76 (br, 1 H, NH_b), 1.82 (m, 2 H, CH_2CH_3), 1.25 (d, 6 H, $CH(CH_3)_2$), 1.09 (t, 3 H, CH_2CH_3). ^{13}C NMR ($CDCl_3$): δ 190.6, 190.2, 188.4 (CO), 140.7 (1:1:1, $CNCH_2$), 51.5 (CNCH), 46.1 ($CNCH_2$), 24.8, 24.6 ($CH(CH_3)_2$), 22.7 (CH_2CH_3), 11.0 (CH_2CH_3).

Complex $ReBr(CO)_3(CNPr)(NH_2CH_2Ph)$ (**5f**) was obtained in 46% yield based on $ReBr(CO)_4$ (CNPr) under reaction conditions similar to those for **5e**, except that the purification was carried out by crystallization with a mixture of CH_2Cl_2 and hexanes. Anal. Calcd for $C_{14}H_{16}BrN_2O_3Re$: C, 31.68; H, 3.04, N, 5.28. Found: C, 31.79; H, 2.58, N, 5.06. IR (CH_2Cl_2): ν_{CN} 2204 (m) cm^{-1}; ν_{CO} 2032 (s), 1947 (s), 1905 (s) cm^{-1}. ^1H NMR ($CDCl_3$): δ 7.42–7.27 (m, 5 H, Ph), 4.17–3.93 (m, 2 H, CH_2Ph), 3.70 (t, 2 H, $CNCH_2$), 3.18 (br, 2 H, NH_2), 1.84 (m, 2 H, CH_2CH_3), 1.08 (t, 3 H, CH_2CH_3). ^{13}C NMR ($CDCl_3$): δ 190.4, 190.2, 188.1 (CO), 140.6 (1:1:1, CN), 129.3, 128.6, 127.7 (Ph), 55.3 (CH_2Ph), 46.1 ($CNCH_2$), 22.7 (CH_2CH_3), 11.0 (CH_3).

$ReBr(CO)_3(CNPr)(NHEt_2)$ (**5g**) was obtained in 58% yield based on $ReBr(CO)_4$(CNPr) under reaction conditions similar to those for **5e**. Anal. Calcd for $C_{11}H_{18}BrN_2O_3Re$: C, 26.80; H, 3.69; N, 5.69. Found: C, 26.60; H, 3.38, N, 5.50. IR (CH_2Cl_2): ν_{CN} 2203 (w) cm^{-1}; ν_{CO} 2030 (s), 1946 (s), 1903 (s) cm^{-1}. ^1H NMR ($CDCl_3$): δ 3.73 (t, 2 H, $CNCH_2$), 3.45–2.91 (m, 4 H, $NHCH_2$), 2.86 (br, 1 H, NH), 1.82 (m, 2 H, $CNCH_2CH_2$), 1.16 (m, 6 H, $NH(CH_2CH_3)_2$), 1.07 (t, 3 H, $CNCH_2CH_2CH_3$). ^{13}C NMR ($CDCl_3$): δ 191.3, 189.9, 188.7 (CO), 142.3 (1:1:1, $CNCH_2$), 49.2, 48.0 ($NH(CH_2CH_3)_2$), 46.0 ($CNCH_2$), 22.7 ($CNCH_2CH_2$), 13.2 ($NH(CH_2CH_3)_2$), 10.9 ($CNCH_2CH_2CH_3$).

Reaction of $ReBr(CO)_3(CNPh)(NCMe)$ with NH_2Pr^i for 30 min. A solution of $ReBr(CO)_4(CNPh)$ (250 mg, 0.52 mmol) in CH_2Cl_2 (100 mL) and acetonitrile (2.5 mL) was treated with a solution of Me_3NO (43 mg, 0.57 mmol) in CH_2Cl_2 (5 mL). The mixture was stirred for 20 min at room temperature and filtered through a small silica gel column. The solvent was removed under vacuum to give $ReBr(CO)_3(CNPh)(NCMe)$. The latter was stirred with excess NH_2Pr^i (0.25 mL) in CH_2Cl_2 (70 mL) at room temperature for 30 min. The solvent was removed under vacuum, and the residue was chromatographed on a silica gel TLC plate with a mixture of CH_2Cl_2 and hexanes (70:30) as eluent to give $ReBr(CO)_3(CNPh)(NH_2Pr^i)$ (**5a**, 190 mg, 0.37 mmol) in 72% yield. IR (CH_2Cl_2): ν_{CN} 2167 (m) cm^{-1}; ν_{CO} 2029 (s), 1954 (s), 1908 (s) cm^{-1}. ^1H NMR ($CDCl_3$): δ 7.44 (m, 5 H, C_6H_5), 3.23 (m, 1 H, CH), 3.01 (br, 2 H, NH_2), 1.28 (d, 6 H, CH_3).

$ReBr(CO)_3(CNPh)(NH_2Pr)$ (**5b**) was obtained under reaction conditions similar to those for **5a** in 68% yield based on $ReBr(CO)_4(CNPh)$. IR (CH_2Cl_2): ν_{CN} 2166 (m) cm^{-1}; ν_{CO} 2029 (s), 1954 (s), 1907 (s) cm^{-1}. ^1H NMR ($CDCl_3$): δ 7.44 (m, 5 H, C_6H_5), 2.97 (m, 2 H, CH_2), 1.60 (m, br, 4 H, CH_2 and NH_2), 0.96 (t, 3 H, CH_3).

$ReBr(CO)_3(CNPh)(NH_2CH_2Ph)$ (**5c**) was obtained under reaction conditions similar to those for **5a**, except that the purification was carried out by crystallization with a mixture of CH_2Cl_2 and hexanes, in 74% yield based on $ReBr(CO)_4(CNPh)$. Anal. Calcd for $C_{17}H_{14}BrN_2O_3Re$: C, 36.15; H, 2.50; N, 4.96. Found: C, 36.47; H, 2.15, N, 4.78. IR (CH_2Cl_2): δ_{CN} 2168 (m) cm^{-1}; ν_{CO} 2030 (s), 1955 (s), 1910 (s) cm^{-1}. ^1H NMR ($CDCl_3$): δ 7.44 (s, 5 H, CNC_6H_5), 7.37–7.29 (m, 5H, CH_2Ph), 4.10 (m, 2 H, CH_2Ph), 3.31 (br, 2 H, NH_2). ^{13}C NMR ($CDCl_3$): δ 190.2, 189.7, 187.8 (CO), 149.9 (br, CN), 139.1, 130.3, 129.7, 129.3, 128.7, 127.8, 126.9, (C_6H_5, $NH_2CH_2C_6H_5$), 55.5 ($NH_2CH_2C_6H_5$).

$ReBr(CO)_3(CNPh)(NHEt_2)$ (**5d**) was obtained under reaction conditions similar to those for **5a** in 64% yield based on $ReBr(CO)_4(CNPh)$. Anal. Calcd for $C_{14}H_{16}BrN_2O_3Re$: C, 31.92; H, 3.06; N, 5.32. Found: C, 31.81; H, 2.90, N, 5.04. IR (CH_2Cl_2): ν_{CN} 2165 (m) cm^{-1}; ν_{CO} 2028 (s), 1953 (s), 1908 (s) cm^{-1}. ^1H NMR ($CDCl_3$): δ 7.44 (s, 5 H, CNC_6H_5), 3.53–3.03 (m, 1 H, 4 H, NH, $NHCH_2$), 1.21 (m, 6 H, CH_3). ^{13}C NMR ($CDCl_3$): δ 191.2, 189.5, 188.5 (CO), 151.6 (br, with unresolved 1:1:1 pattern, CN), 130.3, 129.7, 126.7 (Ph), 49.6, 48.4 ($NH(CH_2CH_3)_2$), 13.5, 13.3 ($NH(CH_2CH_3)_2$).

Formation of $ReBr(CO)_3(H_2NCH_2Ph)\{C(NHPh)(NHCH_2Ph)\}$ (6c). A solution of $ReBr(CO)_4(CNPh)$ (150 mg, 0.31 mmol) in CH_2Cl_2 (50 mL) and acetonitrile (1.5 mL) was treated with a solution of Me_3NO (28 mg, 0.37 mmol) in CH_2Cl_2 (5 mL). The mixture was stirred for 20 min at room temperature and filtered through a small silica gel column. The solvent was removed under vacuum to give $ReBr(CO)_3(CNPh)(NCMe)$. The latter was stirred with excess NH_2CH_2Ph (0.4 mL) in CH_2Cl_2 (20 mL) at room temperature for 45 min. After the removal of the solvent under vacuum, the residue was chromatographed on a silica gel TLC plate with CH_2Cl_2 as eluent to give a colorless fraction, which was further purified by recrystallization in CH_2Cl_2/hexanes to afford $ReBr(CO)_3(H_2NCH_2Ph)\{C(NHPh)(NHCH_2Ph)\}$ (**6c**; 129 mg, 0.20 mmol) in 63% yield. Anal. Calcd for $C_{24}H_{19}BrN_3O_3Re$: C, 43.16; H, 2.87; N, 6.29. Found: C, 43.40; H, 2.94, N, 5.76. IR (CH_2Cl_2): ν_{CO} 2023 (s), 1921 (s), 1879 (s) cm^{-1}. ^1H NMR ($CDCl_3$): δ 9.20, 8.02 (br, s, 1 H, CNHPh, two isomers in a 12:1 ratio), 7.42–7.11 (m, 15 H, Ph), 8.27, 6.81 (br, 1 H, $CNHCH_2Ph$, two isomers in a 1:12 ratio), 4.92 (m, 2 H, $NHCH_2Ph$), 4.10 (m, 1 H, $NH_2CH_aH_bPh$), 3.89 (m, 1 H, $NH_2CH_aH_bPh$), 3.06 (br, 1 H, $NH_aH_bCH_2Ph$), 2.82 (br, 1 H, $NH_aH_bCH_2Ph$). ^{13}C NMR ($CDCl_3$): δ 207.6 (Re–C, carbene), 194.6, 193.4 (CO), 139.4, 137.1, 136.0, 130.5–125.6 (Ph), 55.2 ($NHCH_2$), 53.4 (NH_2CH_2). Mass (FAB): *m/z* 669 (M^+), 641 (M^+ – CO), 590 (M^+ – Br), 483 (M^+ – Br – NH_2CH_2Ph), 455 (M^+ – CO – Br – NH_2CH_2Ph), 427 (M^+ – 2CO – Br – NH_2CH_2Ph), 399 (M^+ – 3CO – Br – NH_2CH_2Ph).

Reaction of $ReBr(CO)_3(CNPh)(NCMe)$ with NH_2Pr^i for 1 Day. A solution of $ReBr(CO)_4(CNPh)$ (300 mg, 0.62 mmol) in CH_2Cl_2 (100 mL) and acetonitrile (2 mL) was treated with a solution of Me_3NO (55 mg, 0.75 mmol) in CH_2Cl_2 (10 mL). The mixture was stirred for 30 min at room temperature and filtered through a small silica gel column. The solvent was removed under vacuum to give $ReBr(CO)_3(CNPh)(NCMe)$. The latter was stirred with excess NH_2Pr^i (2 mL) in CH_2Cl_2 (30 mL) at room temperature for 30 min. The solvent was removed under vacuum, and the residue was chromatographed on a silica gel TLC plate with a mixture of CH_2Cl_2 and hexanes (80:20) as eluent to give $ReBr(CO)_3(NH_2Pr^i)\{C(NHPh)(NHPr^i)\}$ (**6a**; 134 mg, 0.23 mmol) in 38% yield, followed by elution with a mixture of THF and CH_2Cl_2 (5:95) to give $[Re(CO)_3(NH_2Pr^i)_2\{C(NHPh)(NHPr^i)\}]^+Br^-$ (**7a**; 110 mg, 0.19 mmol) in 31% yield. For **6a**: Anal. Calcd for $C_{16}H_{23}BrN_3O_3Re$: C, 33.60; H, 4.05; N, 7.35. Found: C, 33.75; H, 3.99, N, 7.31. IR (CH_2Cl_2): ν_{CO} 2022 (s), 1919 (s), 1877 (s) cm^{-1}. ^1H NMR ($CDCl_3$): δ 9.27, 8.99 (br, s, 1 H, NHPh, two isomers in a 1:9 ratio), 7.49–7.08 (m, 5 H, Ph), 7.99. 6.45 (br, d, 1 H, NHCH, two isomers in a 1:9 ratio), 4.58, 3.70 (m, 1 H, NHCH, two isomers in a 9:1 ratio), 3.23, 3.01 (m, 1 H, NH_2CH, two isomers in a 9:1 ratio), 2.93, 2.73 (br, 1 H, NH_aH_b, two isomers in a 9:1 ratio), 2.51, 2.21 (br, 1 H, NH_aH_b, two isomers in a 9:1 ratio), 1.30–1.08 (m, 12 H, CH_3). ^{13}C NMR ($CDCl_3$): δ 205.2 (Re–C, carbene), 194.7, 193.7 (2:1, CO), 136.3, 130.5, 127.7, 125.3 (Ph), 56.0, 51.3 (CH), 25.2, 24.6, 24.0, 23.9 (CH_3). For **7a**: Anal. Calcd for $C_{19}H_{32}BrN_4O_3Re$: C, 36.18; H, 5.08; N, 8.99. Found: C, 35.33; H, 4.19, N, 8.38. IR (CH_2Cl_2): δ_{CO} 2020 (s), 1913 (s), 1894 (s) cm^{-1}. ^1H NMR ($CDCl_3$): δ 9.76 (br, s, 1 H, NHPh), 7.48–7.20 (m, 5 H, Ph), 6.42 (br, d, 1 H, NHCH), 4.72 (br, 2 H, NH_2), 4.60 (m, 1 H, NH_2CH), 3.44 (br, 2 H, NH_2), 3.25 (m, 1 H, NH_2CH), 1.40 (d, 6 H, CH_3), 1.35 (d, 6 H, CH_3), 1.24 (d, 6 H, CH_3). Mass (FAB, Re^{187}): *m/z* 551 (M^+), 492 (M^+ – NH_2Pr^i), 464 (M^+ – NH_2Pr^i – CO), 433 (M^+ – $2NH_2Pr^i$), 405 (M^+ – $2NH_2Pr^i$ – CO).

Reaction of $ReBr(CO)_3(CNPh)(NCMe)$ with NH_2Pr for 2 Days. A solution of $ReBr(CO)_3(CNPh)(NCMe)$ (232 mg, 0.47 mmol) in CH_2Cl_2 (125 mL) was treated with excess NH_2Pr (4 mL) and stirred at room temperature for 2 days. The solvent was removed under vacuum, and the residue was chromatographed on a silica gel TLC plate with a mixture of CH_2Cl_2

and hexanes (80:20) as eluent to give $ReBr(CO)_3(NH_2Pr)\{C(NHPh)(NHPr)\}$ (**6b**; 49 mg, 0.09 mmol) in 18% yield, followed by elution with a mixture of THF and CH_2Cl_2 (50:50) to give $[Re(CO)_3(NH_2Pr)_2\{C(NHPh)(NHPr)\}]^+Br^-$ (**7b**; 72 mg, 0.11 mmol) in 24% yield. For **6b**: IR (CH_2Cl_2): ν_{CO} 2020 (s), 1915 (s), 1878 (s) cm^{-1}. ^1H NMR ($CDCl_3$): δ 9.32, 9.03 (br, s, 1 H, NHPh, two isomers in a 1:7 ratio), 7.48–7.10 (m, 5 H, Ph), 7.92, 6.61 (br, 1 H, N*H*CH_2, two isomers in a 1:7 ratio), 3.65 (m, 2 H, NHC*H*$_2$), 2.97 (m, 2 H, NH_2C*H*$_2$), 2.87 (br, 1 H, N*H*$_a$H$_b$), 2.63, 2.41 (br, 1 H, NH_a*H*$_b$, two isomers in a 7:1 ratio), 1.56 (m, 4 H, C*H*$_2$$CH_3$), 0.91 (m, 6 H, CH_3). For **7b**: Anal. Calcd for $ReBrC_{19}H_{32}N_4O_3$: C, 36.18; H, 5.08; N, 8.99. Found: C, 36.15; H, 5.55, N, 8.44. IR (CH_2Cl_2): ν_{CO} 2020 (s), 1912 (s), 1887 (s) cm^{-1}. ^1H NMR ($CDCl_3$): δ 10.03 (br, s, 1 H, N*H*Ph), 7.46–7.18 (m, 5 H, Ph), 6.57 (br, t, 1 H, N*H*CH_2), 4.63 (br, 2 H, NH_2), 3.78 (br, 2 H, NH_2), 3.64 (m, 2 H, CH_2), 2.90 (m, 4 H, CH_2), 1.69 (m, 4 H, C*H*$_2$$CH_3$), 1.54 (m, 2 H, C*H*$_2$$CH_3$), 0.94 (t, 6 H, CH_3), 0.89 (t, 3 H, CH_3). Mass (FAB, Re^{187}): *m/z* 551 (M^+), 492 ($M^+ - NH_2Pr$), 464 ($M^+ - NH_2Pr - CO$), 433 ($M^+ - 2NH_2Pr$), 405 ($M^+ - 2NH_2Pr - CO$).

One-Flask Synthesis of $[Re(CO)_3(NH_2Pr^i)_2\{C(NHPh)(NHPr^i)\}]^+Br^-$ (7a) for 2 Days. A solution of $ReBr(CO)_4(CNPh)$ (155 mg, 0.32 mmol) in CH_2Cl_2 (40 mL) and acetonitrile (0.1 mL) was treated with a solution of Me_3NO (25 mg, 0.33 mmol) in CH_2Cl_2 (10 mL) and acetonitrile (0.05 mL). After the mixture was stirred for 30 min at room temperature, excess NH_2Pr^i (3 mL) was added and this solution was stirred at room temperature for 2 days. The solvent was removed under vacuum, and the residue was chromatographed on a silica gel TLC plate with a mixture of CH_2Cl_2 and hexanes (80:20) as eluent to give $ReBr(CO)_3(NH_2Pr^i)\{C(NHPh)(NHPr^i)\}$ (**6a**; 48 mg, 0.08 mmol) in 26% yield, followed by elution with a mixture of THF and CH_2Cl_2 (50:50) to give $[Re(CO)_3(NH_2Pr^i)_2\{C(NHPh)(NHPr^i)\}]^+Br^-$ (**7a**; 51 mg, 0.08 mmol) in 25% yield.

One-Flask Synthesis of $[Re(CO)_3(N_2Pr^i)_2\{C(NHPh)(NHPr^i)\}]^+Br^-$ (7a) for 4 Days. A solution of $ReBr(CO)_4(CNPh)$ (59 mg, 0.12 mmol) in CH_2Cl_2 (15 mL) and acetonitrile (0.03 mL) was treated with a solution of Me_3NO (9 mg, 0.12 mmol) in CH_2Cl_2 (10 mL) and acetonitrile (0.03 mL). After the mixture was stirred for 30 min at room temperature, excess NH_2Pr^i (3 mL) was added and this solution was stirred at room temperature for 4 days. The solvent was removed under vacuum, and the residue was chromatographed on a silica gel TLC plate with a mixture of CH_2Cl_2 and hexanes (80:20) as eluent to give $ReBr(CO)_3(NH_2Pr^i)\{C(NHPh)(NHPr^i)\}$ (**6a**; 12 mg, 0.02 mmol) in 18% yield, followed by elution with a mixture of THF and CH_2Cl_2 (80:20) to give $[Re(CO)_3(NH_2Pr^i)_2\{C(NHPh)(NHPr^i)\}]^+Br^-$ (**7a**; 35 mg, 0.56 mmol) in 46% yield.

One-Flask Synthesis of $[Re(CO)_3(NH_2Pr)_2\{C(NHPh)(NHPr)\}]^+Br^-$ (7b) for 3 Days. A solution of $ReBr(CO)_4(CNPh)$ (124 mg, 0.26 mmol) in CH_2Cl_2 (25 mL) and acetonitrile (0.03 mL) was treated with a solution of Me_3NO (20 mg, 0.26 mmol) in CH_2Cl_2 (10 mL) and acetonitrile (0.03 mL). After the mixture was stirred for 30 min at room temperature, excess NH_2Pr (3 mL) was added and this solution was stirred at room temperature for 3 days. The solvent was removed under vacuum, and the residue was chromatographed on a silica gel TLC plate with a mixture of CH_2Cl_2 and hexanes (80:20) as eluent to give $ReBr(CO)_3(NH_2Pr)\{C(NHPh)(NHPr)\}$ (**6b**; 3 mg, 0.005 mmol) in 2% yield, followed by elution with a mixture of THF and CH_2Cl_2 (80:20) to give $[Re(CO)_3(NH_2Pr)_2\{C(NHPh)(NHPr)\}]^+Br^-$ (**7b**; 125 mg, 0.20 mmol) in 77% yield.

Crystallographic Structure Determination. Crystals of $ReBr(CO)_3(CNPh)(PPh_3)$ (**4a**), $ReBr(CO)_3(NH_2Pr^i)\{C(NHPh)(NHPr^i)\}$ (**6a**), and $[Re(CO)_3(H_2NPr^i)_2\{C(NHPh)(NHPr^i)\}]^+Br^-$ (**7a**) were grown from CH_2Cl_2/hexane solutions at −5 °C. Specimens of suitable quality were mounted on a glass capillary and used for measurement of precise cell constants and intensity data collection. Diffraction measurements were made on an Enraf-Nonius CAD-4 diffractometer using graphite-monochromatized Mo Kα radiation (λ = 0.709 30 Å) with the $\theta-2\theta$ scan mode. Unit cells were determined and refined using 25 randomly selected reflections obtained with the automatic search, center, index, and least-squares routines. Anomalous dispersion corrections were applied to all non-hydrogen atoms. Lorentz/polarization (L_p) and empirical absorption corrections based on three azimuthal scans were applied to the data for each structure. Space groups were determined from the systematic absences observed during data collection. The centrosymmetric space group was initially assumed and later confirmed by the results of refinement for **4a**. The systematic absences in the diffraction data for **6a** and **7a** unambiguously established the space group as $P2_1/n$. The structures were solved by the Patterson method. All remaining non-hydrogen atoms were located from the difference Fourier map, and they were included in the final refinement cycle and refined by full-matrix least squares. A CH_2Cl_2 solvent molecule packs in the lattice along with a molecule of **7a**, but there are no interactions between them. All the data processing was carried out on a Microvax 3600 using the NRCC SDP program.[16]

Acknowledgment. We thank the National Science Council of the Republic of China for financial support.

Supplementary Material Available: Tables of atomic coordinates, crystal and intensity collection data, anisotropic thermal parameters, and bond lengths and angles for **4a**, **6a**, and **7a** (17 pages). Ordering information is given on any current masthead page.

OM940385S

(16) Gabe, E. J.; Lee, F. L.; Le Page, Y. In *Crystallographic Computing 3; Data Collection, Structure Determination, Proteins, and Databases*; Sheldrick, G. M., Krüger, C., Goddard, R., Eds.; Clarendon Press: Oxford, England, 1985; pp 167–174.

Mechanistic Study of $Ir(H)_2$-Assisted Transformations of Ethyne: Cyclotrimerization, Cooligomerization with Ethene, and Reductive Coupling

Claudio Bianchini,*[1a] Kenneth G. Caulton,*[1b] Todd J. Johnson,[1b] Andrea Meli,[1a] Maurizio Peruzzini,[1a] and Francesco Vizza[1a]

Istituto per lo Studio della Stereochimica ed Energetica dei Composti di Coordinazione, CNR, Via J. Nardi 39, 50132 Firenze, Italy, and Department of Chemistry, Indiana University, Bloomington, Indiana 47405

Received November 7, 1994[⊗]

The (ethene)dihydride complex $[(triphos)Ir(H)_2(C_2H_4)]BPh_4$ (**1**) is capable of promoting a variety of transformations of ethyne, including cyclotrimerization to benzene, cooligomerization with ethene to hexa-1,3,5-triene, reductive coupling to buta-1,3-diene, and hydrogenation to ethene (triphos = $MeC(CH_2PPh_2)_3$). A detailed study under various experimental conditions, the detection of several intermediates along the various reaction paths, and the use of isolated complexes in independent reactions, taken together, permit mechanistic conclusions that account for the varied products. In particular, the cyclotrimerization and cooligomerization reactions are mediated by an iridacyclopentadiene species which is trapped by either ethyne or ethene. Consumption of the hydride ligands of **1** by C_2H_2 or C_2H_4 is an ingredient for both cyclotrimerization and cooligomerization reactions but is not necessary to accomplish the reductive dimerization of ethyne to buta-1,3-diene for which, conversely, the two hydride ligands are mandatory.

Introduction

The formation of carbon–carbon bonds mediated by transition-metal systems has emerged in the last decade as a major goal of experimental organometallic chemistry. Among the group of organic molecules most frequently studied in metal-assisted C–C bond-forming reactions, alkynes play a prominent role as is evident from their participation in numerous transformations of both fundamental and industrial relevance (cyclodimerization,[2] dimerization,[3] reductive dimerization,[4] cyclooligomerization,[5] polyoligomerization,[6] oxidative coupling,[5g–l,7] cooligomerization with alkenes and dienes,[5d,8] Reppe carbonylation,[9] etc.).

In this wide field of interest, understanding the primary interactions between the transition metal and the alkyne, particularly the mechanism of formation of the first C–C bond, is of key importance for developing selective processes. In this paper, we report a detailed study of the homogeneous reactions of the simplest alkyne, ethyne, with a number of iridium(I) and iridium(III) complexes stabilized by the tripodal triphosphine ligand $MeC(CH_2PPh_2)_3$ (triphos).

The major factor that distinguishes the system under study here from other metal-assisted transformations of ethyne so far investigated is the ability of the [(triphos)Ir] fragment to trap an unforeseen variety of intermediate species along the course of three relevant functionalization reactions of ethyne: cyclotrimerization to benzene, cooligomerization with ethene to hexa-1,3,5-triene, and reductive coupling to buta-1,3-diene.

⊗ Abstract published in *Advance ACS Abstracts*, January 15, 1995.

(1) (a) ISSECC, CNR. (b) Indiana University.

(2) (a) Bowden, F. L.; Lever, A. B. P. *Organomet. Chem. Rev.* **1968**, *8*, 227. (b) Efraty, A. *Chem. Rev.* **1977**, *77*, 691. (c) King, R. B.; Efraty, A. *J. Am. Chem. Soc.* **1972**, *94*, 5021. (d) King, R. B.; Haiduc, I.; Eaverson, C. W. *J. Am. Chem. Soc.* **1973**, *95*, 2508.

(3) (a) Sakurai, H.; Hirama, K.; Nakadaira, Y.; Kabuto, C. *J. Am. Chem. Soc.* **1987**, *109*, 6880. (b) Bianchini, C.; Bohanna, C.; Esteruelas, M. A.; Frediani, P.; Meli, A.; Oro, L. A.; Peruzzini, M. *Organometallics* **1992**, *11*, 3837.

(4) Czisch, P.; Erker, G.; Korth, H.-G.; Sustmann, R. *Organometallics* **1984**, *3*, 945.

(5) (a) Cotton, F. A.; Hall, W. T. *J. Am. Chem. Soc.* **1979**, *101*, 5094. (b) Heck, R. F. *Organotransition Metal Chemistry*; Academic Press: New York, 1974. (c) Collman, J. P.; Hegedus, L. S.; Norton, J. L.; Finke, R. J. *Principles and Applications of Organotransition Metal Chemistry*; University Science Books: Mill Valley, CA, 1987. (d) Vollhardt, K. P. C. *Angew. Chem., Int. Ed. Engl.* **1984**, *23*, 539. (e) Alt, H. G.; Englehardt, H. E.; Rausch, M. D.; Kool, L. B. *J. Am. Chem. Soc.* **1985**, *107*, 3717. (f) Reppe, W.; Schlichting, O.; Klager, K.; Toepel, T. *Justus Liebigs Ann. Chem.* **1948**, *560*, 1. (g) McAlister, D. R.; Bercaw, J. E.; Bergman, R. G. *J. Am. Chem. Soc.* **1977**, *99*, 1666. (h) Yamazaki, H.; Wakatsuki, Y. *J. Organomet. Chem.* **1984**, *272*, 251. (i) Bruck, M. A.; Copenhaver, A. S.; Wigley, D. E. *J. Am. Chem. Soc.* **1987**, *109*, 6525. (j) Strickler, J. R.; Wexler, P. A.; Wigley, D. E. *Organometallics* **1988**, *8*, 2355. (k) Youayad, A.; Dartiguenave, M.; Menu, M.-J.; Dartiguenave, Y.; Blanger-Garipy, F.; Beauchamp, A. L. *Organometallics* **1989**, *8*, 629. (l) Wielstra, Y.; Gambarotta, S.; Meetsma, A.; de Boer, J. L. *Organometallics* **1989**, *8*, 2696.

(6) (a) Masuda, T.; Isobe, E.; Higashimura, T.; Takada, K. *J. Am. Chem. Soc.* **1983**, *105*, 7473. (b) Masuda, T.; Niki, A.; Isobe, E.; Higashimura, T. *Macromolecules* **1985**, *18*, 2109. (c) Cotton, F. A.; Hall, W. T.; Cann, K. J.; Karol, F. J. *Macromolecules* **1981**, *14*, 233. (d) Knox, S. A. R.; Stansfield, R. F. D.; Stone, F. G. A.; Winter, M. J.; Woodward, P. *J. Chem. Soc., Chem. Commun.* **1978**, 221. (e) Alt, H. G.; Engelhardt, H. E.; Rausch, M. D.; Kool, L. B. *J. Organomet. Chem.* **1987**, *329*, 61. (f) Famili, A.; Farona, M. F.; Thanedar, S. *J. Chem. Soc., Chem. Commun.* **1983**, 435. (g) Bianchini, C.; Meli, A.; Peruzzini, M.; Vizza, F.; Frediani, P. *Organometallics* **1990**, *9*, 1146.

(7) (a) Collman, J. P.; Kang, J. W.; Little, W. F.; Sullivan, M. F. *Inorg. Chem.* **1968**, *7*, 1298. (b) Atwood, J. L.; Hunter, W. E.; Alt, H.; Rausch, M. D. *J. Am. Chem. Soc.* **1976**, *98*, 2454. (c) Gell, K. I.; Schwartz, J. *J. Chem. Soc., Chem. Commun.* **1979**, 244. (d) Hunter, W. E.; Atwood, J. L.; Fachinetti, G.; Floriani, C. *J. Organomet. Chem.* **1981**, *204*, 67. (e) Hirpo, W.; Curtis, M. D. *J. Am. Chem. Soc.* **1988**, *110*, 5218. (f) Porschke, K.-R. *J. Am. Chem. Soc.* **1989**, *111*, 5691.

(8) (a) Reed, H. W. B. *J. Chem. Soc.* **1954**, 1931. (b) Brenner, W.; Heimbach, P.; Wilke, G. *Justus Liebigs Ann. Chem.* **1969**, *727*, 194. (c) Fahey, D. R. *J. Org. Chem.* **1972**, *37*, 4471. (d) Zhou, Z.; Battaglia, L. P.; Chiusoli, G. P.; Costa, M.; Nardelli, M.; Pelizzi, C.; Predieri, G. *J. Organomet. Chem.* **1991**, *417*, 51. (e) Brown, L. D.; Itoh, K.; Suzuki, H.; Hirai, K.; Ibers, J. A. *J. Am. Chem. Soc.* **1978**, *100*, 8232. (f) Yasuda, H.; Nakamura, A. *Angew. Chem., Int. Ed. Engl.* **1987**, *26*, 717.

(9) Reppe, W. *Neue Entwicklungen auf dem Gebiet der Chemie des Acetylens und Kohlenoxids*; Springer: Berlin, 1949.

0276-7333/95/2314-0933$09.00/0

Experimental Section

General Procedures. All reactions and manipulations were routinely performed under nitrogen, except where otherwise stated, by using Schlenk-like techniques. Reagent grade chemicals were used in the preparation of the complexes. Tetrahydrofuran (THF) was purified by distillation from $LiAlH_4$ under nitrogen. All the other solvents were reagent grade and were used as received. Hexa-1,3,5-triene was purchased as a mixture of cis and trans isomers from Aldrich. Literature methods were used for the preparation of triphos,[10] $[Ir(COE)_2Cl]_2$ (COE = cyclooctene),[11] $[(triphos)Ir(H)_2(C_2H_4)]BPh_4$ (**1**),[12] $[(triphos)Ir(C_2H_4)_2]BPh_4$ (**3**),[12] $[(triphos)Ir(H)_2(C_2H_5)]$,[12] and $[(triphos)IrCl(C_4H_4)]$ (**8**).[13] The solid complexes were collected on sintered-glass frits and washed with appropriate solvents before being dried under a stream of nitrogen. $^{13}C_2H_4$ (99% enriched) was obtained from K&K-Greff Limited. Infrared spectra were recorded on a Perkin-Elmer 1600 series FTIR spectrophotometer using samples mulled in Nujol between KBr plates. Deuterated solvents for NMR measurements were dried over molecular sieves. ^1H, $^{31}P\{^1H\}$, and $^{13}C\{^1H\}$ NMR spectra were recorded on either a Varian VXR 300 (299.94, 121.42, and 75.43 MHz, respectively) or a Bruker ACP 200 (200.13, 81.01, and 50.32 MHz, respectively) spectrometer. Chemical shifts are relative either to residual ^1H resonances in the deuterated solvents (^1H NMR), the deuterated solvent resonance ($^{13}C\{^1H\}$ NMR), or the external 85% H_3PO_4, with downfield values reported as positive ($^{31}P\{^1H\}$ NMR). Broad-band and selective $^1H\{^{31}P\}$ NMR experiments were carried out on the Bruker ACP 200 instrument equipped with a 5-mm inverse probe and a BFX-5 amplifier device. In general, the assignment of the proton and carbon chemical shifts was done on the basis of $^1H,^1H$ 2D-COSY, ^{13}C DEPT, and $^1H,^{13}C$ 2D-HETCOR NMR experiments; these experiments were conducted on the Bruker ACP 200 instrument. The computer simulation of NMR spectra was carried out with a locally developed package containing the programs LAOCN3[14] and DAVINS,[15] running on a Compaq Deskpro 386/25 personal computer. The initial choices of shifts and coupling constants were refined by iterative least-squares calculations using experimental digitized spectra. The final parameters gave a satisfactory fit between experimental and calculated spectra, the agreement factor R being less than 1% in all cases. Conductivities were measured with an Orion Model 990101 conductance cell connected to a Model 101 conductivity meter. The conductivity data were obtained at sample concentrations of ca. 10^{-3} M in nitroethane solutions at room temperature.

Reaction of $[(triphos)Ir(H)_2(C_2H_4)]BPh_4$ (1) with Ethyne. NMR Experiments. (A) Low temperature. A sample of **1** (ca. 0.03 mmol) was dissolved in CD_2Cl_2 (0.7 mL) in a 5-mm NMR tube under nitrogen. After two freeze/pump/thaw cycles at −196 °C, the solution was frozen and pumped on at −196 °C. After adding ethyne (ca. 2 equiv), the tube was sealed and then introduced into a NMR probe precooled at −70 °C. The reaction was then followed by ^1H and $^{31}P\{^1H\}$ NMR spectroscopy. The reaction between **1** and ethyne already occurred at −50 °C. At the beginning, when the reagent ratio is approximately 1:2 (i.e., ethyne is the limiting reagent), the first intermediate detected shows an AM_2 $^{31}P\{^1H\}$ NMR pattern (δP_A −7.5, δP_M −23.2, $J(P_AP_M)$ = 16.2 Hz) and an AA′XX′Y ^1H NMR pattern in the hydride (A) region (δ −10.81, $|J(AX) + J(AX')|$ = 122.2 Hz, $J(AY)$ = 12.6 Hz). The phosphorus and hydride chemical shifts are within 1 ppm of those of **1**,[12] and we assign this product as $[(triphos)Ir(H)_2(C_2H_2)]BPh_4$ (**2**) (δ 3.02, π-C_2H_2). Thus, ethene substitution by ethyne is the first reaction. Free ethene is also detected (^1H NMR). Resonances for H_2 and C_2H_6 are absent. With time, free ethene is consumed and (under conditions of ethyne deficiency) **2** disappears. Formed in its place (^{31}P and ^1H NMR detection) are small amounts of $[(triphos)Ir(C_2H_4)_2]BPh_4$ (**3**),[12] $[(triphos)Ir(\pi\text{-}C_2H_2)]BPh_4$ (**4**), $[(triphos)Ir\{(1\text{-}\eta^1\text{:}4\text{-}6\text{-}\eta^3)hexatriene\}]BPh_4$ (**5**) (see below), and larger quantities of $[(triphos)Ir(\eta^4\text{-}C_6H_6)]BPh_4$ (**6**).[16] When additional ethyne is added to the solution at −50 °C, this same progression of production of **2**, then **3**, **4**, **5**, and **6** is observed. Finally, when excess ethyne is added and the solution allowed to stand at 25 °C, one observes essentially complete conversion to **5** and **6** in a 8:92 ratio; **2**, **3**, and **4** are completely consumed and ethene is liberated. The $^{31}P\{^1H\}$ NMR spectrum of intermediate **4** consists of an A_3 pattern (δ 6.2), while the ^1H NMR spectrum contains a quartet at 11.92 ppm ($J(HP)$ = 7.5 Hz) in the expected region of four-electron donor alkyne ligands. The $^{31}P\{^1H\}$ and ^1H NMR data of **4** are quite comparable with those of the known π-phenylacetylene complex $[(triphos)Ir(\pi\text{-}HC_2Ph)]BPh_4$.[17]

(B) Room temperature. CD_2Cl_2 (0.7 mL) was saturated with ethyne at 20 °C and then transferred into a screw cap 5-mm NMR tube containing a solid sample of **1** (0.03 mmol). $^{31}P\{^1H\}$ and ^1H NMR spectra, immediately recorded, showed the complete disappearance of the starting complex and formation of **4**, **5**, **6**, and $[(triphos)Ir(\eta^4\text{-}C_4H_6)][BPh_4$ (**7**) (see below). Free ethane and ethene were also detected (^1H NMR, singlets at 0.9 and 5.4 ppm, respectively). Within 15 min, **4** completely disappeared to give **5**, **6**, and **7** in a ratio of 30:67:3 and free ethane and ethene in a ca. 1:2 ratio. This product distribution did not change with time. An almost identical product distribution of this reaction was observed on a large scale (0.8 g of **1** in THF) for isolated compounds. When the isolated mixture was heated in THF-d_8 saturated with ethyne at 70 °C, we observed no apparent reaction involving **6**[18] or **7**, whereas **5** transformed into its *s-cis,s-cis−trans*-1-4-η^4-hexa-1,3,5-triene isomer **9** (see below).

Large-Scale Experiment under a Steady Stream of Ethyne. A sample of **1** (0.8 g, 0.64 mmol) was dissolved in THF (80 mL) under a steady stream of ethyne at room temperature. After 1 h, a ^{31}P NMR spectrum of a sample of the resulting orange solution showed the complete conversion of **1** to a mixture of **6** and **7** in ca. 95:5 ratio. No trace of **5** was observed. After ethyne was replaced by nitrogen, ethanol (40 mL) was added to the rest of the solution. Partial evaporation of the solvent resulted in the precipitation of yellow crystals which were filtered off and washed with *n*-pentane. Several recrystallizations from THF and ethanol gave pure samples of **6** in 80% yield. An almost identical product ratio was obtained when **1** was added to refluxing THF under a steady stream of ethyne.

Reaction of $[(Triphos)Ir(C_2H_4)_2]BPh_4$ (3) with Ethyne. (A) Low Temperature. A solution of **3** and ethyne (ca. 2 equiv) in CD_2Cl_2 was prepared in a NMR tube as described above for the reaction at low temperature between **1** and ethyne. The progress of the reaction at −50 °C was then followed by $^{31}P\{^1H\}$ and ^1H NMR spectroscopy. A large part of **3** disappears and formed in its place are **4** and small amounts of **5** and **6**. Free ethene is also detected (^1H NMR, singlet at 5.4 ppm). When excess ethyne was added to the solution at −50 °C, the same progression of production of **4**,

(10) Hewertson, W.; Watson, R. *J. Chem. Soc.* **1962**, 1490.
(11) Herde, J. L.; Lambert, J. C.; Senoff, C. V. *Inorg. Synth.* **1974**, *15*, 18.
(12) Barbaro, P.; Bianchini, C.; Meli, A.; Peruzzini, C.; Vacca, A.; Vizza, F. *Organometallics* **1991**, *10*, 2227.
(13) Bianchini, C.; Caulton, K. G.; Chardon, C.; Doublet, M.-L.; Eisenstein, O.; Jackson, S. A.; Johnson, T. J.; Meli, A.; Peruzzini, M.; Streib, W. E.; Vizza, F. *Organometallics* **1994**, *13*, 2010.
(14) (a) Bothner-By, A. A.; Castellano, S. *QCPE* **1967**, *11*, 111. (b) Castellano, S.; Bothner-By, A. A. *J. Chem. Phys.* **1964**, *41*, 3863.
(15) Stephenson, D. S.; Binsch, G. *J. Magn. Reson.* **1980**, *37*, 395, 409.
(16) Bianchini, C.; Caulton, K. G.; Chardon, C.; Eisenstein, O.; Folting, K.; Johnson, T. J.; Meli, A.; Peruzzini, M.; Rauscher, D. J.; Streib, W. E.; Vizza, F. *J. Am. Chem. Soc.* **1991**, *113*, 5127.
(17) Bianchini, C.; Barbaro, P.; Meli, A.; Peruzzini, C.; Vacca, A.; Vizza, F. *Organometallics* **1993**, *12*, 2505.
(18) At this temperature, **6** is a catalyst for the cyclotrimerization reaction of ethyne.[16]

5, and **6** is observed. With time, **3** and **4** completely disappeared to give **5** and **6** in a ca. 10:90 ratio.

(B) Room Temperature. CD_2Cl_2 (0.7 mL) was saturated with ethyne at 20 °C and then transferred into a screw cap 5-mm NMR tube containing a solid sample of **3** (0.03 mmol). $^{31}P\{^1H\}$ and ^1H NMR spectra, immediately recorded, showed the complete disappearance of the starting complex and formation of **4** along with the larger amounts of **5** and **6**. Free ethene was also detected (^1H NMR, singlet at 5.4 ppm). Within 15 min, **4** completely disappeared to give **5** and **6** in ca. 10:90 ratio.

Independent Synthesis of [(Triphos)Ir(η^4-C$_4$H$_6$)]BPh$_4$ (7). Solid $[Ir(COE)_2Cl]_2$ (0.45 g, 0.5 mmol) was added to a solution of triphos (0.62 g, 1 mmol) in a buta-1,3-diene-saturated THF (40 mL) solution at room temperature. After 1 h, $NaBPh_4$ (0.32 g, 1 mmol) in ethanol (40 mL) was added to the resulting red solution, which immediately turned orange. On addition of ethanol (40 mL) and slow concentration, pale yellow crystals of **7** precipitated; yield 85%. Anal. Calcd (Found) for $C_{69}H_{65}BIrP_3$: C, 69.63 (69.51); H, 5.51 (5.46); Ir, 16.15 (16.02). $\lambda_M = 49$ cm^2 Ω^{-1} mol^{-1}. $^{31}P\{^1H\}$ NMR (CD_2Cl_2, 121.42 MHz): 30 °C, A_3 pattern, δ −23.4 (br); −58 °C, AM_2 pattern, δP_A −25.0, δP_M −22.5, $J(P_AP_M) = 6.9$ Hz.

Reaction of [(Triphos)IrCl(η^2-C$_4$H$_4$)] (8) with Ethene in the Presence of TlPF$_6$. A solid sample of **8** (0.30 g, 0.33 mmol) was added to a stirred THF (30 mL) solution of $TlPF_6$ (0.12 g, 0.34 mmol) under a steady stream of ethene at 0 °C. Within a few minutes the solid dissolved to give a red-orange solution. After 2 h, TlCl was eliminated by filtration and then $NaBPh_4$ (0.17 g, 0.50 mmol) in ethanol (10 mL) was added, followed by *n*-heptane (50 mL). On partial evaporation of the solvents under a stream of nitrogen, rust red crystals of [(triphos)Ir{(1-η^1:4-6-η^3)-hexatriene}]BPh$_4$ (**5**) precipitated in 80% yield. Anal. Calcd (Found) for $C_{71}H_{67}BIrP_3$: C, 70.11 (70.00); H, 5.55 (5.63); Ir, 15.80 (15.69). $\lambda_M = 54$ cm^2 Ω^{-1} mol^{-1}. IR: ν(C=C) 1644 cm^{-1}. $^{31}P\{^1H\}$ NMR (CD_2Cl_2, 20 °C, 81.01 MHz): AMQ pattern, δP_A −17.4, δP_M −27.7, δP_Q −36.5, $J(P_AP_M) = 22.0$ Hz, $J(P_AP_Q) = 7.3$ Hz, $J(P_MP_Q) = 25.6$ Hz. **5** is rather unstable in ambient-temperature solutions, slowly converting to its η^4-hexa-1,3,5-triene isomer **9** (see below) (in THF at 20 °C, we observe ca. 50% conversion in 24 h). Solid samples of **5** are stable when stored under nitrogen at low temperature, whereas at room temperature, isomerization to **9** occurs also in the solid state (ca. 50% conversion in 3 weeks).

Reaction of [(Triphos)IrCl(η^2-C$_4$H$_4$)] (8) with ^{13}C$_2$H$_4$ in the Presence of TlPF$_6$. The iridacyclopentadiene complex **8** (0.03 g, 0.03 mmol) and a stoichiometric amount of $TlPF_6$ (0.01 g, 0.03 mmol) were dissolved in THF-d_8 (0.7 mL) at −10 °C (a temperature at which no reaction between the two compounds occurs). The resulting solution was transferred to a 5-mm NMR tube maintained at −10 °C. This solution was then degassed (freeze/pump/thaw, three cycles) and the tube was charged with a 3-fold excess of $^{13}C_2H_4$ (99 atom %) and flame sealed. The tube was then shaken at room temperature for 3 h. $^{31}P\{^1H\}$ NMR (81.01 MHz): AMQXY pattern, δP_A −17.6, δP_M −27.8, δP_Q −36.5, $J(P_AP_M) = 22.0$ Hz, $J(P_AP_Q) = 7.4$ Hz, $J(P_MP_Q) = 25.6$ Hz, $J(P_MC_1) = 62.0$ Hz, $J(P_AC_1) = 3.4$ Hz, $J(P_QC_1) = 3.4$ Hz, $J(P_MC_2) = 10.4$ Hz. $^{13}C\{^1H\}$ NMR (50.32 MHz): enhanced intensity (i.e., enriched) at only δC_1 28.7, δC_2 146.0, $J(C_1C_2) = 58.2$ Hz.

Thermal Isomerization Reaction of [(Triphos)Ir{(1-η^1:4-6-η^3)-hexatriene}]BPh$_4$ (5). (A) A THF (30 mL) solution of **5** (0.30 g, 0.25 mmol) was heated at 70 °C. After 4 h, the solution was concentrated to dryness under vacuum to give [(triphos)Ir(*s-trans,s-cis−cis*-1-4-η^4-hexa-1,3,5-triene)]BPh$_4$ (**9**) as a pale yellow solid. Recrystallization from CH_2Cl_2 and *n*-heptane gave pale yellow microcrystals which were washed with *n*-pentane and collected by filtration; yield 85%. Anal. Calcd (Found) for $C_{71}H_{67}BIrP_3$: C, 70.11 (69.89); H, 5.55 (5.48); Ir, 15.80 (15.63). $\lambda_M = 53$ cm^2 Ω^{-1} mol^{-1}. IR: ν(C=C) 1616 cm^{-1}. $^{31}P\{^1H\}$ NMR (CD_2Cl_2, −20 °C, 81.01 MHz): AMQ pattern, δP_A −22.8, δP_M −24.6, δP_Q −25.8, $J(P_AP_M) = 9.6$ Hz, $J(P_AP_Q) = 18.4$ Hz, $J(P_MP_Q) = 8.8$ Hz.

(B) When a THF solution of **5** was heated at 90 °C for 4 h, the recovered solid was characterized as a 58:42 mixture of **9** and [(triphos)Ir(*s-trans,s-cis−trans*-1-4-η^4-hexa-1,3,5-triene)]BPh$_4$ (**10**) (see below).

Thermal Isomerization Reaction of [(Triphos)Ir(*s-trans,s-cis−cis*-1-4-η^4-hexa-1,3,5-triene)]BPh$_4$ (9). A THF (30 mL) solution of **9** (0.20 g, 0.16 mmol) was heated at 90 °C. After 6 h, the solution was concentrated to dryness under vacuum to give [(triphos)Ir(*s-trans,s-cis−trans*-1-4-η^4-hexa-1,3,5-triene)]BPh$_4$ (**10**) as a pale yellow solid. Recrystallization from CH_2Cl_2 and *n*-heptane gave pale yellow microcrystals which were washed with *n*-pentane and collected by filtration; yield 80%. Anal. Calcd (Found) for $C_{71}H_{67}BIrP_3$: C, 70.11 (70.23); H, 5.55 (5.47); Ir, 15.80 (15.70). $\lambda_M = 49$ cm^2 Ω^{-1} mol^{-1}. IR: ν(C=C) 1616 cm^{-1}. $^{31}P\{^1H\}$ NMR (CD_2Cl_2, −20 °C, 81.01 MHz): AMQ patten, δP_A −13.3, δP_M −27.7, δP_Q −31.7, $J(P_AP_M) = 4.6$ Hz, $J(P_AP_Q) = 21.1$ Hz, $J(P_MP_Q) = 6.5$ Hz.

Independent Synthesis of *s-trans,s-cis−cis* 9 and *s-trans,s-cis−trans* 10. [(Triphos)Ir(*trans*-1-4-η^4-hexa-1,3,5-triene)]BPh$_4$ Isomers. A solid sample of [(triphos)Ir(C$_2$H$_4$)$_2$]BPh$_4$ (0.41 g, 0.34 mmol) was dissolved into a THF (40 mL) solution of hexa-1,3,5-triene (mixture of isomers, 0.38 mL, 3.4 mmol) at room temperature. After 2 h, ethanol (10 mL) and *n*-heptane (60 mL) were added to the resulting pale yellow solution. On standing, an approximately 40:60 mixture of **9** and **10** precipitated as pale yellow crystals. They were filtered off and washed with *n*-pentane; yield 95%.

Synthesis of [(Triphos)Ir(H)$_2$(THF)]BPh$_4$ (11). Neat $HOSO_2CF_3$ (42 μL, 0.47 mmol) was syringed into a stirred suspension of [(triphos)Ir(H)$_2$(C$_2$H$_5$)] (0.40 g, 0.47 mmol) in THF (50 mL). Within a few minutes the solid dissolved to give a colorless solution. After 1 h, $NaBPh_4$ (0.34 g, 1 mmol) in ethanol (10 mL) was added to the resulting solution, followed by *n*-heptane (30 mL). On standing overnight, under a steady stream of nitrogen, **11** precipitated as an off-white solid, which was collected by filtration and washed with a 1:1 mixture of ethanol and *n*-pentane and then *n*-pentane; yield 75%. Anal. Calcd (Found) for $C_{69}H_{69}BIrOP_3$: C, 68.48 (68.37); H, 5.75 (5.81); Ir, 15.88 (15.69). $\lambda_M = 53$ cm^2 Ω^{-1} mol^{-1}. IR: ν(Ir−H) 2050 cm^{-1}. $^{31}P\{^1H\}$ NMR (THF-d_8, 20 °C, 81.01 MHz): AM_2 pattern; $\delta(P_A)$ −1.6, $\delta(P_M)$ −6.3, $J(P_AP_M) = 11.7$ Hz. ^1H NMR (THF-d_8, 20 °C, 200.13 MHz): δ −6.70 (second-order doublet of multiplets computable as the AA′ part of an AA′XX′Y spin system, where X and Y denote the triphos phosphorus atoms, $|J(AX) + J(AX')| = 127.2$ Hz, $J(AY) = 14.7$ Hz, Ir*H*).

Occasionally, NMR spectra of the samples also showed variable amounts of one or two other products exhibiting quite similar AM_2 $^{31}P\{^1H\}$ NMR patterns and AA′XX′Y ^1H NMR patterns in the hydride region. The phosphorus and the hydride chemical shifts were very close to those of **11**. These products were recognized as the solvento complexes [(triphos)Ir(H)$_2$(solv)]BPh$_4$ (solv = ethanol, **12**; H_2O, **13**) obtained by displacement of coordinated THF by either ethanol or adventitious water in the reaction mixture. Addition of excess of either ethanol or H_2O to THF-d_8 solutions of **11** resulted in quantitative formation of **12** and **13**, respectively. The THF complex **11** is unstable in CH_2Cl_2; precipitation of a yellow-orange crystalline solid occurs within a few minutes after dissolution. The nature of this product is currently under investigation.

[(Triphos)Ir(H)$_2$(EtOH)]BPh$_4$ (12). $^{31}P\{^1H\}$ NMR (THF-d_8, 20 °C, 81.01 MHz): AM_2 pattern; $\delta(P_A)$ −1.4, $\delta(P_M)$ −8.0, $J(P_AP_M) = 12.8$ Hz. ^1H NMR (THF-d_8, 20 °C, 200.13 MHz): δ(hydrides) −6.91 (second-order doublet of multiplets computable as the AA′ part of an AA′XX′Y spin system, where X and Y denote the triphos phosphorus atoms), $|J(AX) + J(AX')| = 127.6$ Hz, $J(AY) = 14.1$ Hz.

[(Triphos)Ir(H)$_2$(OH$_2$)]BPh$_4$ (13). $^{31}P\{^1H\}$ NMR (THF-d_8, 20 °C, 81.01 MHz): AM_2 pattern; $\delta(P_A)$ −0.8, $\delta(P_M)$ −10.0, $J(P_AP_M) = 13.5$ Hz. ^1H NMR (THF-d_8, 20 °C, 200.13 MHz):

Scheme 1

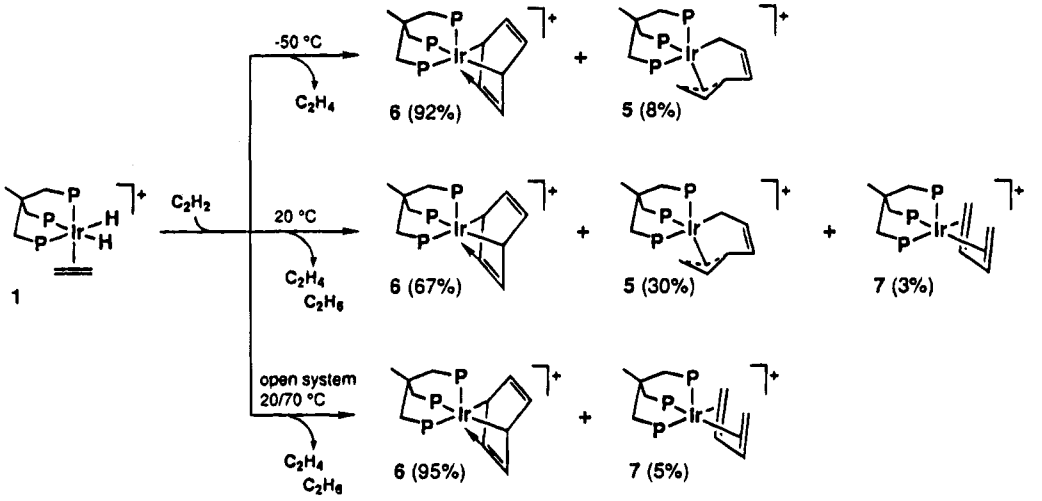

δ(hydrides) −6.97 (second-order doublet of multiplets computable as the AA′ part of an AA′XX′Y spin system, where X and Y denote the triphos phosphorus atoms), $|J(AX) + J(AX')| =$ 129.7 Hz, $J(AY) = 13.6$ Hz.

Reaction of [(Triphos)Ir(H)$_2$(THF)]BPh$_4$ (11) with Ethyne. (A) Reflux Temperature. A solid sample of **11** (0.18 g, 0.15 mmol) was dissolved into refluxing THF (30 mL) under an ethyne atmosphere. After 30 min, the solution was concentrated to dryness in vacuo and the residue washed with *n*-pentane. Multinuclear NMR spectroscopy indicated the complete conversion of **11** to a 93:7 mixture of [(triphos)Ir(η^4-C_4H_6)BPh$_4$ (**7**) and [(triphos)Ir(η^4-C_6H_6)]BPh$_4$ (**6**).

(B) Room Temperature. A THF (30 mL) solution of **11** (0.18 g, 0.15 mmol) was stirred under an ethyne atmosphere at room temperature for 2 h. A ^{31}P NMR spectrum (THF/THF-d_8, 1:1 v/v) of a sample of the resulting yellow solution showed the selective conversion of **11** to **7**. Addition of ethanol (30 mL) to the rest of the solution and partial evaporation of the solvent under a steady stream of nitrogen led to the precipitation of a pure sample of **7** as pale yellow crystals. They were collected by filtration and washed with ethanol and *n*-pentane; yield 90%.

(C) Low Temperature. A sample of **11** (ca. 0.02 mmol) was dissolved in THF-d_8 (0.7 mL) in a 5-mm NMR tube under nitrogen. After two freeze/pump/thaw cycles at −196 °C, the solution was frozen and pumped on at −196 °C. After adding ethyne (ca. 3 equiv), the tube was sealed and then introduced into a NMR probe precooled at −50 °C. The reaction was then followed by ^{1}H and ^{31}P{^{1}H} NMR spectroscopy. The reaction between **11** and ethyne occurred at ca. −10 °C. On following the progress of the reaction, only the signals due to **11** and **7** were observed; no intermediates were detected. The reaction was complete in ca. 1 h. Analogous evidence was obtained by using an excess of ethyne. When the experiment was performed in CD_2Cl_2, the reaction already occurred at −40 °C. However, in this case also, only clean conversion of **11** to **7** was observed. A small amount of the unknown orange product that forms by dissolving **11** in CH_2Cl_2 (see synthesis of **11**) precipitated in the NMR tube during the experiment.

Results

Reaction of [(Triphos)Ir(H)$_2$(C$_2$H$_4$)]BPh$_4$ with Ethyne under Different Experimental Conditions. Reaction of the (ethene)dihydride **1** with an excess of ethyne in THF (or CH_2Cl_2) at 20 °C in a closed system results in evolution of ethane and ethene in an approximate ratio of 1:2 and formation of [(triphos)Ir(η^4-C_6H_6)]BPh$_4$ (**6**), [(triphos)Ir{(1-η^1:4-6-η^3)hexatriene}]BPh$_4$ (**5**), and [(triphos)Ir(η^4-C_4H_6)]BPh$_4$ (**7**) in a ratio of 67:30:3 (Scheme 1). Initially, one may observe the formation of some π-ethyne complex [(triphos)Ir(π-C_2H_2)]BPh$_4$ (**4**), which rapidly disappears. The observed product ratio does not change with reaction temperature up to 70 °C, although slow intramolecular rearrangement of **5** to its 1,4-η^4-hexatriene isomer [(triphos)Ir(*s-trans,s-cis*−*cis*-1-4-η^4-hexa-1,3,5-triene)]BPh$_4$ (**9**) occurs (vide infra).

At −50 °C, the course of the reaction between **1** and ethyne is quite different. Ethane is not evolved, the η^4-butadiene complex is not formed, and the η^4-benzene complex becomes the predominant product (the ratio of **6** to **5** is 92:8). As shown by an in situ NMR study, displacement of ethene from **1** by ethyne to give the (π-ethyne)dihydride [(triphos)Ir(H)$_2$(C_2H_2)]BPh$_4$ (**2**) is the first step of the reaction. Later, ethene reenters the metal coordination sphere to form the bis(ethene) complex [(triphos)Ir(C_2H_4)$_2$]BPh$_4$ (**3**), which in turn undergoes displacement of ethene by ethyne to give the π-ethyne complex **4**. From this intermediate, both the η^4-benzene and the 1-η^1:4-6-η^3-hexatriene complex are formed through the common intermediacy of an iridacyclopentadiene derivative of the formula [(triphos)Ir(η^2-C_4H_4)]$^+$ (vide infra), which can add ethene and ethyne, respectively. The necessary presence of ethene in the reaction mixture for the formation of **5** is clearly demonstrated by the fact that no trace of the hexatriene complex is observed when the reaction is performed in an open system where evolved ethene is carried outside the reactor by the steady stream of ethyne (Scheme 1).

Analysis of the time evolution of NMR spectra of the reaction at −50 °C clearly shows that, under the experimental conditions, the displacement of ethene from **1** by ethyne is faster than its subsequent return to the metal. The latter step is slower than those leading to formation of **3** and **4** (and following), which accounts for the very small concentrations of **3** and **4** detected. A function of ethyne is thus to consume the two hydride ligands of **1** and be converted to ethene, but this reaction only occurs in the presence of dissolved ethene by its action as an incoming ligand (vide infra).

A number of independent reactions have been performed, which provide additional experimental evidence supporting the reaction sequence observed in the low-temperature reaction:

(i) The bis(ethene) complex **3** has been shown to react

Scheme 2

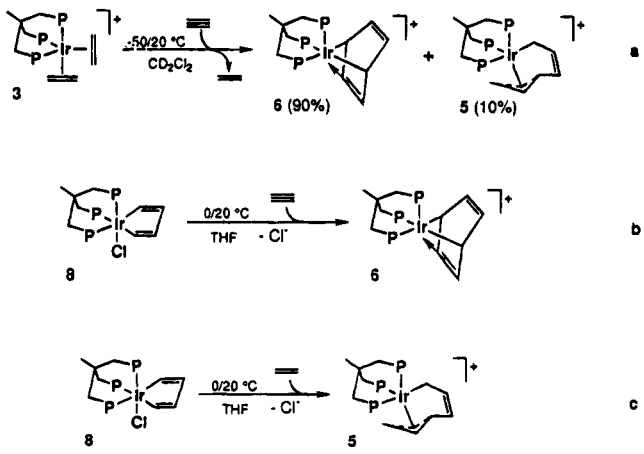

Scheme 3

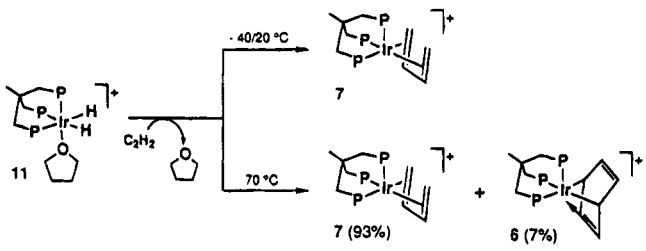

with ethyne below 20 °C to give free ethene and the π-ethyne intermediate **4**, which rapidly disappears. Formed in its place are the 1-η^1:4-6-η^3-hexatriene complex **5** and a larger amount of the η^4-benzene **6** (10:90 ratio) (Scheme 2a).

(ii) The known iridacyclopentadiene complex [(triphos)IrCl(η^2-C_4H_4)] (**8**) reacts with ethyne below 20 °C in the presence of a chloride scavenger such as $TlPF_6$ to give quantitatively the η^4-C_6H_6 complex **6** (Scheme 2b).[13]

(iii) The iridacyclopentadiene complex **8** reacts with ethene in THF below 20 °C in the presence of $TlPF_6$ to give selectively the 1-η^1:4-6-η^3-hexatriene complex **5** (Scheme 2c).

An explanation for the formation of some η^4-butadiene complex **7** only when **1** is reacted with ethyne at room or higher temperatures will be given in a forthcoming section.

Reaction of [(Triphos)Ir(H)$_2$(THF)]BPh$_4$ with Ethyne under Different Experimental Conditions. To contrast the situation when the initial ligand L in [(triphos)Ir(H)$_2$(L)]$^+$ is not ethene (thus altering the second step of the reaction between **1** and ethyne by virtue of the absence of free C_2H_4), we have studied the analogous reaction of ethyne with the solvento complex [(triphos)Ir(H)$_2$(THF)]BPh$_4$ (**11**).

In the temperature range from −40 to 20 °C, the reaction selectively gives the η^4-C_4H_6 complex **7**. No intermediate species was detected by $^{31}P\{^1H\}$ and ^1H NMR spectroscopy (Scheme 3). At 70 °C, **7** is still the predominant product, but appreciable formation (7%) of the η^4-C_6H_6 complex **6** is observed, suggesting the concomitant occurrence of an alternative process at higher energy than the one leading to formation of the η^4-butadiene complex.

Chemical and Spectroscopic Characterization of the New Complexes. [(Triphos)Ir{(1-η^1:4-6-η^3)-hexatriene}]BPh$_4$ (5) and its η^4-Hexatriene Isomers (9, 10). Formally **5** is the product of a metal-assisted condensation of two ethyne molecules with one ethene molecule. The resulting cooligomerized ligand (linear C_6H_8) uses a terminal CH_2 group and the allyl portion constituted by the C_6, C_5, and C_4 carbon atoms to bind the iridium center (see sketch in Table 1). To the best of our knowledge, this bonding mode of hexatriene has no precedent, whereas a few examples of hexatriene ligands bonded via two η^3-allyl moieties to different metal centers in polynuclear complexes have been reported.[19a,b] In particular, an X-ray structure is available for [(CpCo)$_2$(μ-η^3:η^3-Ph(CH)$_6$Ph)].

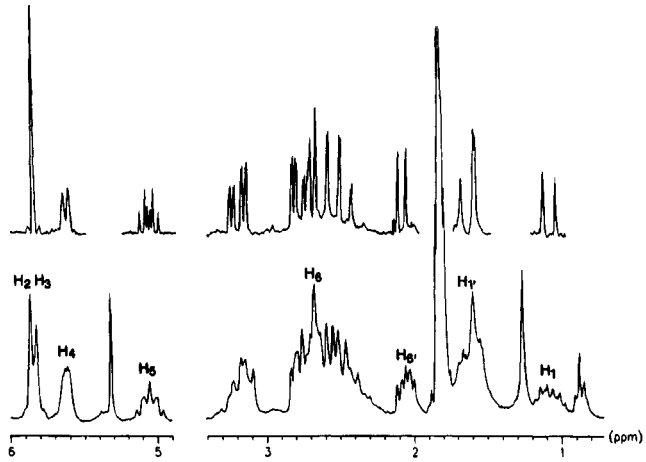

Figure 1. Broad-band $^1H\{^{31}P\}$ (inset, above) and ^1H NMR spectra of **5** in the 6.0−4.9 and 3.4−0.7 ppm regions (CD_2Cl_2, 20 °C). Unlabeled resonances are due to triphos ligand.

The structural assignment for **5** has been corroborated by a number of both spectroscopic (^1H,^1H 2D-COSY, ^{13}C DEPT, and ^1H,^{13}C 2D-HETCOR NMR) and chemical experiments. The ^1H and $^1H\{^{31}P\}$ NMR spectra of **5** are shown in Figure 1. It may be useful to point out some relevant spectroscopic features. The $J(H_5H_4)$ and $J(H_5H_6)$ values (ca. 7 Hz) indicate that H_4 and H_6 occupy syn positions in the η^3-allyl moiety; the $J(H_5H_6')$ value of 10.8 Hz is in accord with previous findings for central and anti hydrogens of η^3-allyl ligands.[20,21] Also, it is worth mentioning that both the hydrogen and carbon chemical shifts relative to the $C_2H{=}C_3H$ fragment are typical of *free* olefins, which is consistent with the presence of a ν(C=C) band at 1644 cm^{-1} in the IR spectrum (Nujol mulls). Finally, $^{13}C\{^1H\}$ NMR chemical shift and coupling to phosphorus of C_1 show that the CH_2 group is σ-bonded to the metal.

5 is slightly unstable in both the solid state and ambient-temperature solutions and slowly rearranges to its *s-trans,s-cis*−*cis*-1-4-η^4-hexa-1,3,5-triene isomer **9**. At 70 °C in THF solution, the isomerization is complete in 4 h. Above 80 °C, a second isomerization process occurs that converts **9** to the isomer [(triphos)Ir(*s-trans,s-cis*−*trans*-1-4-η^4-hexa-1,3,5-triene)]BPh$_4$ (**10**) (Scheme 4). The **9** to **10** conversion is quantitative after

(19) (a) Wadepohl, H.; Büchner, K.; Pritzkow, H. *Organometallics* **1989**, *8*, 2745. (b) King, J. A., Jr.; Vollhardt, K. P. C. *J. Am. Chem. Soc.* **1983**, *105*, 4846. (c) Powell, P. *J. Organomet. Chem.* **1983**, *244*, 393. (d) McArdle, P.; Sherlock, H. *J. Chem. Soc., Dalton Trans.* **1978**, 1678.

(20) (a) Wolf, J.; Werner, H. *Organometallics* **1987**, *6*, 1164. (b) Zhuang, J.-M.; Sutton, D. *Organometallics* **1991**, *10*, 1516. (c) Krivykh, V. V.; Gusev, O. V.; Petrovskii, P. V.; Rybinskaya, M. I. *J. Organomet. Chem.* **1989**, *366*, 129.

(21) McGhee, W. D.; Bergman, R. G. *J. Am. Chem. Soc.* **1988**, *110*, 4246.

Table 1. Selected NMR Spectral Data for the Complexes[a]

complex	^{1}H NMR assignt	^{1}H NMR δ (multiplicity, *J*)[b,c]	^{13}C{^{1}H} NMR assignt	^{13}C{^{1}H} NMR δ (multiplicity, *J*)[b]
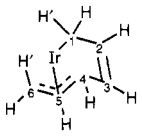 5[g]	H_2,H_3	5.84 (m)[d]	C_2	146.1 (d, ^3J(CP) = 10.4)
	H_4	5.61 (m, $^3J(H_4H_5)$ = 7.2)	C_3	136[e]
	H_5	5.05 (m, $^3J(H_5H_{6'})$ = 10.8, $^3J(H_5H_6)$ = 7.1)	C_5	97.5 (s)
	H_6	2.7[f]	C_4	87.6 (d, ^2J(CP) = 25.2)
	$H_{6'}$	2.05 (m)	C_6	47.1 (d, ^2J(CP) = 30.4)
	$H_{1'}$	1.65 (m, $^2J(H_1,H_1)$ = 16.8)	C_1	28.6 (dt, $^2J(CP_{trans})$ = 61.9, $^2J(CP_{cis})$ = 3.4)
	H_1	1.08 (m)		
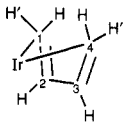 7[h,i]	H_2,H_3	5.39 (m)	C_2,C_3	87.6 (s)
	H_1,H_4	2.06 (m)	C_1,C_4	29.1 (d, ^2J(CP) = 32.6)
	H_1,H_4	1.48 (m)		
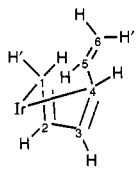 9	H_5	6.17 (ddd, $^3J(H_5H_{6'})$ = 16.6, $^3J(H_5H_6)$ = 10.1, $^3J(H_5H_4)$ = 7.6)	C_5	135[e]
			C_6	115.4 (s)
	H_2	5.82 (td, $^3J(H_2H_3)$ = 4.9, $^3J(H_2H_1')$ = 8.1, $^3J(H_2H_1)$ = 7.3)	C_2	93.8 (s)
			C_3	85.5 (s)
	H_3	5.57 (t, $^3J(H_3H_4)$ = 6.0)	C_4	47.3 (d, ^2J(CP) = 32.6)
	H_6	5.26 (br d, $^2J(H_6H_{6'})$ = 2.2)	C_1	38.1 (d, ^2J(CP) = 26.4)
	$H_{6'}$	4.97 (br d)		
	H_4	4.05 (t)		
	$H_{1'}$	2.62 (m, $^2J(H_1,H_1)$ = 2.8)		
	H_1	2.09 (dd)		
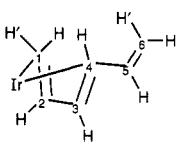 10	H_3	5.87 (m, $^3J(H_3H_4)$ = 8.0, $^3J(H_3H_2)$ = 4.2)	C_5	143.7 (s)
	H_5	5.69 (m, $^3J(H_5H_{6'})$ = 16.6, $^3J(H_5H_6)$ = 9.7, $^3J(H_5H_4)$ = 10.3)	C_6	116.7 (s)
			C_3	89.0 (s)
	$H_{6'}$	5.45 (br d, $^2J(H_{6'}H_6)$ = 2.0)	C_2	81.4 (s)
	H_2	5.31 (m, $^3J(H_2H_{1'})$ = 5.8, $^3J(H_2H_1)$ = 6.3)	C_4	54.1 (d, ^2J(CP) = 28.5)
	H_6	4.89 (br d)	C_1	36.8 (d, ^2J(CP) = 30.5)
	H_4	3.15 (m)		
	$H_{1'}$	1.6[j]		
	H_1	1.10 (m, $^2J(H_1H_{1'})$ = 2.5)		

[a] All spectra were recorded at room temperature in THF-d_8 solutions unless otherwise stated. [b] Chemical shifts are given in ppm and are relative to either the residual ^{1}H resonances in the deuterated solvents (^{1}H NMR) or the deuterated solvent resonance (^{13}C{^{1}H} NMR). Key: s, singlet; d, doublet; t, triplet; m, multiplet; br, broad. Coupling constants (*J*) are in hertz. [c] The *J*(HH) values were determined on the basis of ^{1}H{^{31}P} NMR experiments. [d] *J*(HH) values between the olefinic hydrogens H_2 and H_3 and the proximal hydrogens H_1, $H_{1'}$ and $H_{4'}$ although shown by ^{1}H, ^{1}H 2D-COSY NMR experiment, could not be precisely estimated <2 Hz). [e] Masked by the phenyl carbon resonances; the chemical shift was determined from ^{13}C, ^{1}H heteronuclear 2D-NMR correlation studies. [f] Masked by CH_2 hydrogen resonances of triphos; the chemical shift was determined from ^{1}H, ^{1}H 2D-COSY NMR experiment. [g] The ^{1}H NMR spectrum was recorded at room temperature in CD_2Cl_2. [h] The ^{1}H NMR and ^{13}C{^{1}H} NMR spectra were recorded in CD_2Cl_2 at 30 and −40 °C, respectively. [i] The butadiene hydrogens constitute an AA′MM′XX′ spin system. The ^{1}H{^{31}P} NMR spectrum (CD_2Cl_2, 30 °C) was properly computed with the following magnetic parameters: $^3J(H_2H_3)$ = −2.8 Hz, $^3J(H_2H_{1'})$ = 6.3 Hz, $^4J(H_2,H_{4'})$ = 1.1 Hz, $^3J(H_2H_1)$ = 7.4 Hz, $^4J(H_2H_4)$ = −1.0 Hz, $^4J(H_{1'}H_{4'})$ = 2.3 Hz, $^2J(H_{1'}H_1)$ = −3.5 Hz, $^4J(H_{1'}H_4)$ = 0.2 Hz, $^4J(H_1H_4)$ = 3.1 Hz. [j] Masked by the methyl hydrogen resonance of triphos; the chemical shift was determined from ^{1}H, ^{1}H 2D-COSY NMR experiment.

Scheme 4

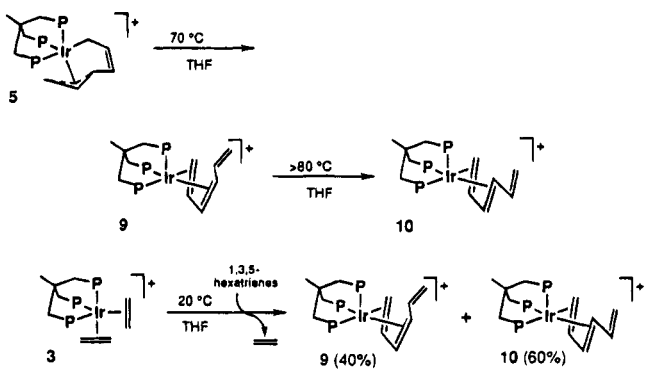

a pure sample of the former compound is heated at 90 °C in THF for 6 h.

A 4:6 mixture of **9** and **10** can independently be prepared by treatment of the bis(ethene) complex **3** with an excess of hexa-1,3,5-triene (mixture of isomers) in THF at 20 °C (Scheme 4). This alternative synthetic procedure (under very mild conditions) indirectly supports the chemical nature of **5**; i.e., this complex, which is obtainable by either straightforward reaction of the iridacyclopentadiene complex **8** with ethene or treatment of **1** with ethyne, is indeed the result of a C−C bond formation reaction at iridium.

No intermediate species was observed in the course of the isomerization of **5** to **9**, which apparently involves a redistribution of electrons within the metal−organyl fragment (the formal oxidation state of the metal changes from +3 in **5** to +1 in **9**), as part of the making and breaking of Ir−C bonds.

9 and **10** are stable in both the solid state and nitroethane solution in which they behave as 1:1 electrolytes. The IR spectra of both complexes in the solid state contain a band at 1616 cm^{-1} which is attributable to ν(C=C) of a free olefin.

Unlike **5**, which is rigid on the ^{31}P NMR time scale, both **9** and **10** are fluxional in solution. Interestingly, the fluxionality involves only the phosphine ligands and not the hexatriene ligands which, in fact, show temperature-invariant resonances of their carbon and hydrogen atoms. This situation is quite common for d^8 ML_3(diene) complexes and will be discussed below, together with the analogous fluxionality of the η^4-butadiene complex **7**. At room temperature, the ^{31}P-

{^{1}H} NMR spectra of **9** and **10** in THF-d_8 consist of AMQ spin systems with poorly discernible J(PP) couplings. All J(PP) coupling constants become visible at −20 °C. As the temperature is increased, the phosphorus signals lose resolution at 30 °C, then broaden and, finally, at ca. 65 °C, coalesce. A single broad resonance centered at ca. −26 ppm emerges from the baseline at 80 °C (DMSO-d_6).

Valuable information on the structures of **9** and **10** is provided by the ^{1}H and ^{13}C NMR data. In particular, the presence in both compounds of an uncoordinated vinyl moiety is shown by both its hydrogen and carbon chemical shifts and J(HH) values (J(trans) ~ 17 Hz, J(cis) ~ 10 Hz, J(gem) ~ 2 Hz), while the larger value of $J(H_4H_5)$ found for **10** (8 vs 6 Hz) is suggestive of an *s-trans,s-cis−trans* structure of the hexa-1,3,5-triene ligand.[19] All the other ^{1}H and ^{13}C NMR data are in agreement with those reported for analogous transition-metal complexes containing η^4-hexa-1,3,5-triene ligands.[19] Illustrative examples of η^4-hexa-1,3,5-triene complexes are the mononuclear species [CpCo(η^4-CHPh=CH-CH=CHCH=CHPh)][19a] and [CpCo(η^4-CH_2=CH-CH=CHCH=CH_2)],[19b] and the clusters [$Ru_6(CO)_{14}$(μ_6-C)(μ-*s-cis,s-cis−trans*-1,2-η^2-3,6-η^4-CH_2CHCH-CHCHCH_2] and [$Ru_6(CO)_{14}$(μ_6-C)(μ-*s-trans,s-cis−trans*-1,2-η^2-3,6-η^4-CH_2CHCHCHCHCH_2].[22] The thermodynamically more stable Ru cluster was found to be the one with the *s-trans,s-cis−trans* conformation of hexatriene, which is consistent with the thermal rearrangement of **9** to **10** herein described.

As stated in the Experimental Section, commercially available hexa-1,3,5-triene is a mixture (ca. 50:50) of the two possible geometric isomers. The (triphos)Ir^+ system thus reacts with both isomers, and in particular it stabilizes the *s-trans,s-cis−cis* and *s-trans,s-cis−trans* conformations.

Finally, it is worth pointing out that the NMR data for the hexatriene ligand in both **9** and **10** are consistent with the absence of any movement of the (triphos)Ir fragment along the face of the triene as this would average the hydrogen and carbon resonances, which, in fact, is not observed. Interconversion in solution of shift isomers of hexatriene complexes has been reported for disubstituted η^4-hexa-1,3,5-triene-iron tricarbonyls.[23]

[(Triphos)Ir(η^4-C_4H_6)]BPh_4, 7 is formally the product of a reductive dimerization of ethyne at a metal center (i.e., hydrogenation with C−C coupling). A square-pyramidal structure is proposed for **7** on the basis of the following multinuclear NMR data as well as by analogy with other known M(η^4-diene)L_3 complexes.[24] The ^{1}H NMR spectrum of the butadiene hydrogens in THF-d_8 is invariant from 50 to −50 °C. The portion of the ^{1}H{^{31}P} NMR spectrum (CD_2Cl_2) of

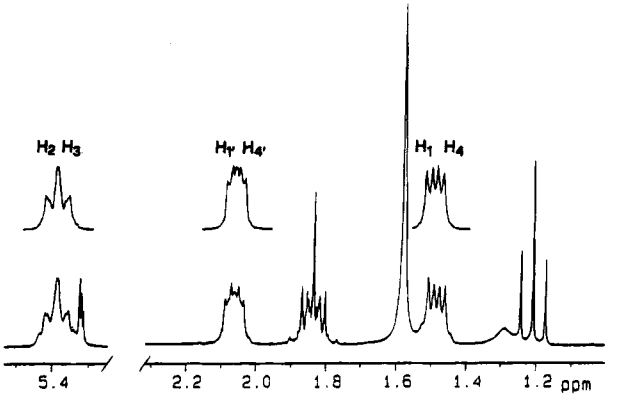

Figure 2. Experimental and computed (inset, above) broad-band ^{1}H{^{31}P} NMR spectra of the buta-1,3-diene hydrogens in **7** (CD_2Cl_2, 30 °C).

the C_4H_6 hydrogens is reported in Figure 2 together with the computed spectrum. The butadiene hydrogens give rise to an AA′MM′XX′ spin system (Table 1). The ^{1}H NMR spectrum shows a very small coupling of H_1 and H_4 to the phosphorus atoms. Both the chemical shifts and coupling constants fall in the proper range for square-pyramidal η^4-C_4H_6 complexes such as [Co(η^4-C_4H_6)(PMe_3)$_3$]BPh_4,[24c,d] [Fe(η^4-C_4H_6)(PMe_3)$_3$],[24e] [Ir(η^4-C_4H_6)(PMe_2Ph)$_3$]BF_4,[24g] and [(triphos)M(η^4-C_4H_6)]BPh_4 (M = Co, Rh).[24a,f]

The ^{13}C{^{1}H} NMR spectrum in CD_2Cl_2 at −40 °C is consistent with the proposed structure for **7** as it shows the carbons of the diene ligand to constitute two equivalent pairs (CH, δ 87.6 (s); CH_2, δ 29.1 (d), J(CP) = 32.6 Hz). Thus, both nuclei of the CH_2 groups couple to P more strongly than do those of the CH group.

As anticipated in a previous section, the ^{31}P{^{1}H} NMR spectrum shows **7** to be fluxional on the NMR time scale. The room-temperature spectrum in THF-d_8 consists of a broad signal at ca. −23 ppm, which appears as a sharp singlet at +50 °C. The complex becomes stereochemically rigid at ca. −10 °C, showing an AM_2 spin system. Interestingly, the complex exhibits a significant temperature dependence of the phosphorus chemical shifts (Figure 3). This phenomenon prevents a reliable computer simulation of the dynamic process by DNMR spectroscopy in the temperature range for which a variation in the line shape is observed. Accordingly, no calculated activation parameter can be given. On the other hand, the nature of the fluxional process operating for **7**-like compounds is rather clear and has been widely investigated in recent years. It is generally agreed that no motion other than rotation of the diene can make the three phosphorus ligands equivalent.[24g] This is certainly reasonable for **7** itself, where the three phosphorus donors are constrained to be part of a tridentate phosphine. A similar type of fluxionality is exhibited by the triene complexes **9** and **10**, the only difference being a higher barrier to fluxionality as compared to the diene analog. This finding confirms that fluxionality is not an intrinsic property of pentacoordination but is highly dependent on the nature of the ligands and the metal.[24g]

The activation barriers to fluxionality in the molecules reported here are systematically larger for Ir(III) than for Ir(I). This correlates well with the idea that an octahedron (Ir(III)) is more stereochemically rigid than any five-coordinate shape (Ir(I)).

(22) Adams, R. D.; Wu, W. *Organometallics* **1993**, *12*, 1243.
(23) (a) Whitlock, H. W., Jr.; Reich, C.; Woessner, W. D. *J. Am. Chem. Soc.* **1971**, *93*, 2483. (b) Whitlock, H. W., Jr.; Markezich, R. L. *J. Am. Chem. Soc.* **1971**, *93*, 5290.
(24) (a) Bianchini, C.; Dapporto, P.; Meli, A.; Sacconi, L. *J. Organomet. Chem.* **1980**, *193*, 117. (b) Jolly, P. W.; Mynott, R. *Adv. Organomet. Chem.* **1981**, *19*, 257. (c) Ananias de Carvahlo, L. C.; Peres, Y.; Dartiguenave, M.; Dartiguenave, Y.; Beauchamp, A. L. *Organometallics* **1985**, *4*, 2021. (d) Ananias de Carvahlo, L. C.; Dartiguenave, M.; Dahan, F.; Dartigenave, Y.; Dubac, J.; Laporterie, A.; Manuel, G.; Iloughmane, H. *Organometallics* **1986**, *5*, 2205. (e) Hoberg, H.; Jenni, K.; Raabe, E.; Kruger, C.; Schroth, G. *J. Organomet. Chem.* **1987**, *320*, 325. (f) Bianchini, C.; Meli, A.; Peruzzini, M.; Vacca, A.; Vizza, F. *Organometallics* **1991**, *10*, 645. (g) Chardon, C.; Eisenstein, O.; Johnson, T.; Caulton, K. G. *New. J. Chem.* **1992**, *16*, 781.

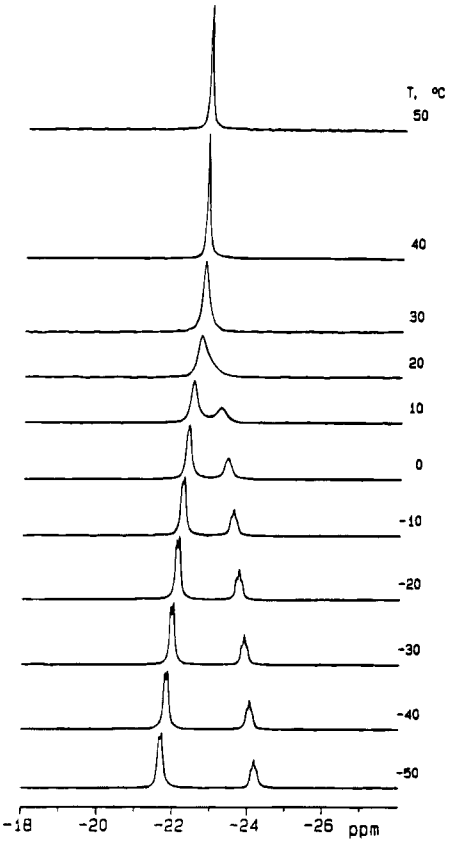

Figure 3. Variable-temperature $^{31}P\{^1H\}$ NMR spectra of **7** (THF-d_8).

[(Triphos)Ir(H)$_2$(THF)]BPh$_4$. The solvento complex **11** is prepared by adding a stoichiometric amount of triflic acid to a stirred suspension of [(triphos)Ir(H)$_2$(C$_2$H$_5$)] in THF, followed by precipitation with NaBPh$_4$. In the course of the reaction, ethane is evolved. The complex is stable in both the solid state and room-temperature THF solution. The THF ligand in **11** is very labile and can readily be displaced by weak ligands, including other solvents (EtOH, acetone) and the water occasionally present in THF, to give the corresponding solvento complexes. Halogenated solvents must be avoided as they react with **11** to give a yellow-orange crystalline product whose chemical nature is presently being studied.

In **11**, the metal center is octahedrally coordinated by the three phosphorus atoms of triphos ($^{31}P\{^1H\}$ NMR AM$_2$ pattern), by two terminal hydride ligands (ν(Ir–H) = 2050 cm^{-1})), and by a THF molecule. As commonly observed for stereochemically rigid dihydrido metal complexes of the formula [(triphos)Ir(H)$_2$L], the two hydride ligands are chemically but not magnetically equivalent and thus give rise to a second-order doublet of multiplets (AA′XX′Y spin system, A = H, X, Y = P).[12,17]

Discussion

For a better understanding of the chemistry described in this paper, it is useful to summarize some characteristics of the starting complex, **1**.[1,12] In poorly coordinating solvents (CH$_2$Cl$_2$, THF) at room temperature, the (ethene)dihydride complex is in a rapid equilibrium with its hydride migration product [(triphos)Ir(H)(C$_2$H$_5$)]$^+$, which can be stabilized by several ligands including CO, Cl$^-$, and dimethylformamide to give octahedral adducts of the formula [(triphos)Ir(H)(C$_2$H$_5$)L]$^{n+}$ (n = 0, 1).[12] In the absence of added ligands, the complex decomposes evolving ethane, slowly at room temperature and rather rapidly above 40 °C. Below −40 °C, the migration of hydride to ethene is slowed and the complex adopts an octahedral coordination geometry, although the ethene ligand continues to rotate about the metal–ligand axis even at −100 °C.

Scheme 5. Suggested Mechanism for the Cyclotrimerization of Ethyne at −50 °C (Closed System)

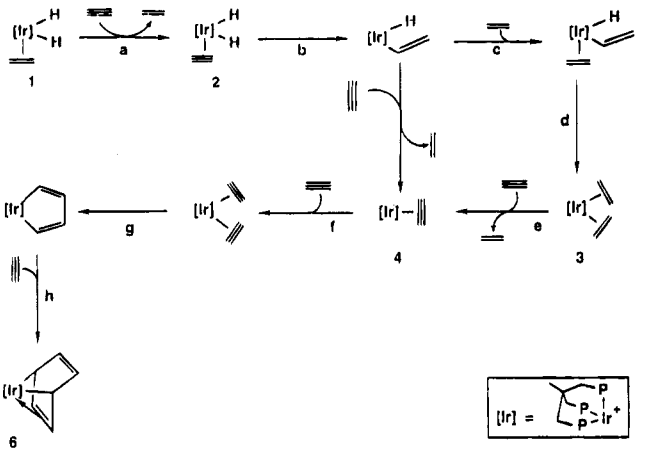

Cyclotrimerization of Ethyne and its Cooligomerization with Ethene. Incorporation of all of the above experimental evidence leads to the mechanism shown in Scheme 5 for the low-temperature reaction between **1** and ethyne to give the η^4-benzene complex **6**. This scheme shows only the C–H and C–C bond-forming events.

Initially, the ethene ligand in **1** is displaced by ethyne to give **2**. Later, ethene reenters the metal coordination sphere to form the bis(ethene) complex, although *both* ethene ligands are subsequently dissociated and are among the products of the reaction (eq 1).

$$Ir(H)_2(^*C_2H_4)^+ + 4C_2H_2 \rightarrow Ir(C_6H_6)^+ + C_2H_4 + {}^*C_2H_4 \quad (1)$$

One ethyne is sacrificed to consume the two hydride ligands. Reasonable intermediates in this transformation are an unsaturated ethyne migration product (step b), which may be stabilized by ethene to form an (ethene)(hydride)vinyl complex (step c). This species has not been detected, but its possible formation along the reaction path is indirectly substantiated by the recent isolation of the related iridium complex [Tp*Ir(H)(CH=CH$_2$)(C$_2$H$_4$)] [Tp* = hydridotris(3,5-dimethyl-1-pyrazolyl)borate].[25]

The bis(ethene) complex **3** is not stable in the presence of ethyne, which, in fact, readily displaces both olefins and forms the π-ethyne complex **4** (Scheme 5). The latter species has been detected spectroscopically, and some related examples are known[12] (e.g., [(triphos)Ir(HCCPh)]BPh$_4$),[17] in which the ethyne ligand behaves as a four-electron donor. Complex **4** reacts with a second ethyne molecule, most likely via a bis(ethyne)

(25) Prez, P. J.; Poveda, M. L.; Carmona, E. *J. Chem. Soc., Chem. Commun.* **1992**, 8.

Scheme 6. Suggested Mechanism for the Co-oligomerization of Ethyne with Ethene

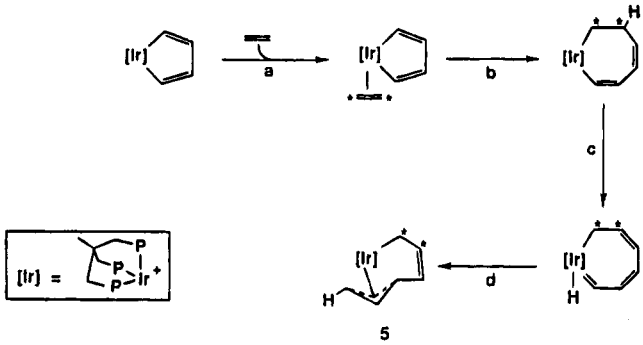

(two-electron donor) intermediate (step f), to form an iridacyclopentadiene species,[5g−l,6e,7f,24f] which has independently been shown to react with ethyne (step h) producing the cyclotrimerization η^4-C_6H_6 complex. Both the coupling reaction of two ethynes at the [(triphos)-Ir]$^+$ fragment to give an iridacyclopentadiene complex and the subsequent reaction of this metallacycle with ethyne have recently been studied by means of EHMO calculations.[13] According to the theoretical analysis, the addition of ethyne to the metallacycle proceeds in a concerted manner; i.e., the reaction may be viewed as a metal-assisted Diels−Alder addition, where the metal plays an important role as a reactive center (in contrast to acid-catalyzed Diels−Alder additions, where the only role of the metal is to activate the diene).

The addition of ethyne is not the only reaction path accessible to the metallacycle under the present experimental conditions, since 2 equiv of ethene is dissolved in the reaction mixture. As shown by an independent reaction, ethene can react with the iridacyclopentadiene fragment to form the 1-η^1:4-6-η^3-hexatriene complex **5**. On the basis of the observed product ratio of **6** to **5** (92:8), one may conclude that, at −50 °C, ethyne uptake by the metallacycle is kinetically favored over ethene uptake.

From a mechanistic viewpoint, the formation of **5**, necessarily occurring via a multistep reaction sequence, is still rather obscure since no intermediate achieves detectable concentrations. It has been possible to establish (eq 2) which carbons of the C_6 ligand are

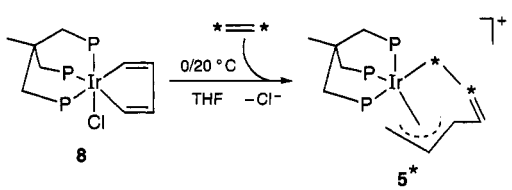

(2)

formed from the entering ethyne. The $^{13}C\{^1H\}$ NMR spectrum of **5*** shows selective incorporation of ^{13}C at the C_1 and C_2 positions of the C_6H_8 ligand. The $J(C_1C_2)$ value of 58.2 Hz is typical of one-bond C−C coupling constants between sp^3 and sp^2 carbon nuclei.[26] Therefore, in Scheme 6, we suggest a mechanism involving ring expansion at iridium (step b), followed by β-H elimination from the alkyl portion of the seven-membered metallaring. Redistribution of the double bonds within the metallacycle would then produce a carbene hydride, which is appropriate to undergo migration of hydride from the metal to the carbene carbon atom,[27] thus leading to **5**. Even though not proved experimentally, steps b and c of Scheme 6 have several precedents in the literature. In particular, ring expansions involving metallacyclopentadiene complexes and alkenes have precedent in a number of cycloaddition reactions.[8,28] Of relevance to the case at hand are the reactions of [Ru(CO)(η^4-C_4Ph_4)(η-C_5H_5)]BF_4 with alkenes to give η^4-cyclohexadiene derivatives[27b] as well as the reactions of [(triphos)RhCl(η^4-C_4H_4)] with CO, CH_3CN, and CS_2 to give coordinated cyclopentadienone and free 2-methylpyridine and dithiopyrone, respectively.[24f] The latter reactions have been suggested to proceed via insertion of the incoming organic reagent into a M−C bond, followed by reductive elimination.

The fact that the reaction of the iridacyclopentadiene fragment with ethene does not produce the η^4-cyclohexadiene complex [(triphos)Ir(η^4-C_6H_8)]BPh_4, which is a stable and isolable compound,[29] suggests that (Scheme 6, step c) the β-H elimination step from the seven-membered metallaring is faster than its reductive elimination to 1,3-cyclohexadiene.

Most but not all of the above mechanistic considerations can be extended to the reaction between **1** and ethyne performed at room temperature in either open or closed systems. In fact, irrespective of the type of reactor, significant amounts of ethane and of the η^4-butadiene complex **7** (Scheme 1) are produced. Furthermore, under a steady stream of ethyne, **5** is never formed. While the latter result is quite reasonable, since the liberated ethene is transported out of the reactor by the continuous flow of ethyne, the formation of ethane and of the η^4-butadiene complex is less obvious. Both products evidently come from processes with higher activation energy than those shown in Scheme 5. To progress further, we now consider whether the formation of ethane is correlated with formation of **7** or whether these two products are formed by independent reaction paths.

Reductive Dimerization of Ethyne. Before illustrating our mechanistic interpretation for the reductive dimerization of ethyne at iridium, it may be useful to recall that the η^4-butadiene complex **7** is the predominant product (up to 100%) when the (THF)dihydride **11** is substituted for the (ethene)dihydride **1** in the reaction with ethyne. From this observation, one may readily infer that (i) ethene is of importance for the formation of the η^4-C_6H_6 and 1-η^1:4-6-η^3-hexatriene complexes from dihydride **1**, whereas its presence in the reaction system as either a ligand or a free reactant disfavors the reductive dimerization of ethyne and (ii) ethane and **7** are not produced in a single process, but instead the two products form in *independent* reactions.

In light of the solution chemistry of **1**, it is reasonable that ethane is eliminated from the hydride migration product, which, in fact, at room temperature is in equilibrium with the (ethene)dihydride form (see Scheme 7, which illustrates a proposed mechanism for the

(26) Bretmaier, E.; Voelter, W. *Carbon-13 NMR Spectroscopy*; VCH: Weinheim, Germany, 1989.

(27) Clegg, W.; Green, M.; Hall, C. A.; Hockless, D. C. R.; Norman, N. C.; Woolhouse, C. M. *J. Chem. Soc., Chem. Commun.* **1990**, 1330.

(28) (a) Suzuki, H.; Itoh, K.; Ishii, Y.; Simon, K.; Ibers, J. A. *J. Am. Chem. Soc.* **1976**, *98*, 8494. (b) Crocker, M.; Green, M.; Orpen, A. G.; Thomas, D. M. *J. Chem. Soc., Chem. Commun.* **1984**, 1141.

(29) Bianchini, C.; Caulton, K. G.; Folting, K.; Meli, A.; Peruzzini, M.; Polo, A.; Vizza, F. *J. Am. Chem. Soc.* **1992**, *114*, 7290.

Scheme 7. Suggested Mechanism for the Reaction between 1 and Ethyne at 20 °C (Closed System)

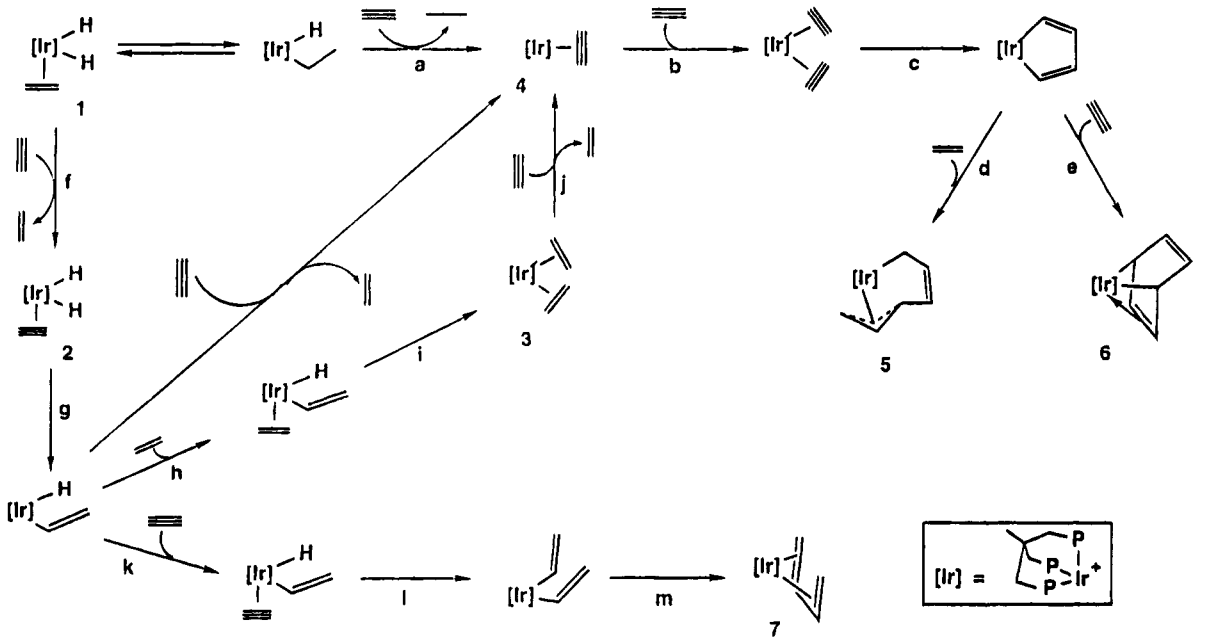

reaction between **1** and ethyne at room temperature). The reductive elimination of ethane, which appreciably occurs at higher temperature (40 °C), would be facilitated by interaction with incoming ethyne (step a). Once the π-ethyne complex **4** is formed, its subsequent conversion to either **5** or **6** follows the independently established route (b–e; see also Scheme 6). The ethylene ligand thus scavenges hydrogen in this route. However, at room temperature, intermediate **4**, which only leads to **5** and **6**, must be in competition with another reaction since we note also the evolution of considerable ethene (the ethene to ethane ratio is ca. 2:1). Accordingly, also at room temperature, displacement of ethene from **1** by ethyne takes place to give **2**, which transforms into a (hydride)vinyl species via ethyne insertion into an Ir–H bond. At room temperature, this highly unsaturated Ir(III) vinyl can be trapped in two ways: the uptake of ethene (h and i, wherein hydrogen is scavenged by ethyne) to give **3** (as it selectively does at −50 °C) and the uptake of ethyne (k) to give a (vinyl)(ethyne)hydride which ultimately converts to **7** (l and m) via a bis(vinyl) intermediate. This latter route incorporates the hydride ligands in the diene ligand of **7**. Indeed, bis(vinyl) metal complexes, which typically exhibit a low barrier to reductive coupling,[30] are considered key intermediates for the synthesis of buta-1,3-diene derivatives via C–C bond formation reactions; see, for example, the conversion of $[Cp_2Zr(CH{=}CHPh)_2]$ to $[Cp_2Zr(\eta^4\text{-}C_4H_4Ph_2)]$[4] and of $[(\eta^5\text{-}C_5Me_5)Ru(NO)(CH{=}CH_2)_2]$ to $[(\eta^5\text{-}C_5Me_5)Ru(NO)(\eta^2\text{-}C_4H_6)]$.[30]

In conclusion, an increase in the temperature from −50 to 20 °C of the reaction between **1** and ethyne has the effect of favoring both the reductive elimination of ethane from **1** and the uptake of ethyne by the (vinyl)hydride intermediate. Essential to the formation of **7**, this pathway forms two hydrogen-rich (C_2H_3) ligands on one metal center.

When the $[(triphos)Ir(H)_2]^+$ fragment is reacted with ethyne at room temperature (this is the case of the THF–solvento complex **11**), then selective formation of the η^4-butadiene complex **7** occurs (Scheme 8, reaction sequence a–e), which is consistent with the fact that both the cyclotrimerization of ethyne and its cooligomerization with ethene are ethene-assisted. In this case, in fact, there is no chance of formation of the bis(ethene) complex **3** and thus of the iridacyclopentadiene species, which is the mandatory intermediate for production of **5** and **6**.

Only at a much higher temperature (70 °C) does **11** lead to detectable quantities of the η^4-benzene complex **6** (7%). One explanation for this finding (Scheme 8, reaction sequence f–j) is to think that the (vinyl)hydride intermediate may undergo the reductive coupling to form ethene (step f) and that this process, unless assisted by ethene (see Scheme 5), requires the highest activation energy of any other step in Scheme 8. This is consistent with the relative bond strengths of the iridium–carbon bonds, which increase in the order $IrCH{=}CH_2 > IrCH_2CH_3$, and, therefore, with the observation that vinyl–hydride iridium complexes typically undergo reductive elimination more slowly than analogous alkyl–hydride complexes.[31] It is also true that the ethene complex will be a high-energy species because it is truly unsaturated (compare the product of step c).

Conclusions

The variety of reactions reported here (eqs 3–5) are controlled by a combination of material balance and (in some cases) kinetic competition between available reagents. Obviously, the C_6H_8 products require some source of hydrogen (hydride ligands or C_2H_4) to increase the H to C ratio above the 1:1 of acetylene. The same applies to producing butadiene. Clearly, acetylene cyclotrimerization would be inhibited by any reagent

(30) Chang, J.; Bergman, R. G. *J. Am. Chem. Soc.* **1987**, *109*, 4298, and references therein.

(31) Stoutland, P. O.; Bergman, R. G.; Nolan, S. P.; Hoff, C. D. *Polyhedron* **1988**, *7*, 1429.

Scheme 8. Suggested Mechanism for the Reaction between 11 and Ethyne at 20 (Reaction Sequence a–e) and 70 °C (Reaction Sequence a–j)

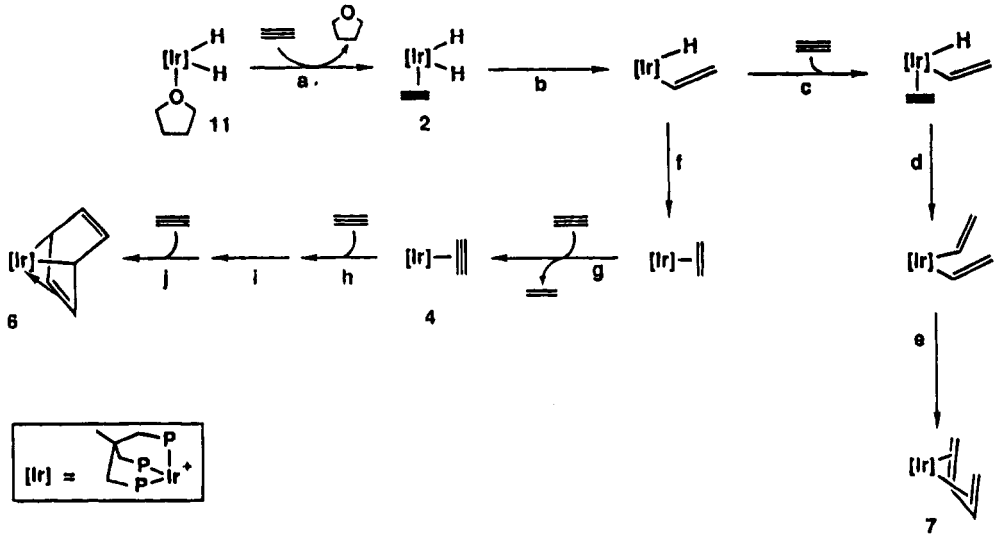

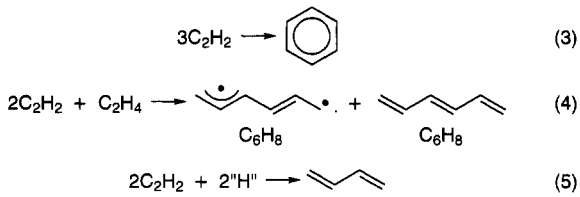

other than C_2H_2. Ethene can thus be a competitive inhibitor, and hydride ligands might have been, except that they can be rendered impotent by transfer to C_2H_2 or especially to C_2H_4. The yield of isomeric cooligomerization ($2C_2H_2 + C_2H_4$) products depends on competition between the two unsaturated hydrocarbon reagents for coordination at iridium. Again, these products might have been suppressed by hydride ligands except that hydrides are rapidly removed from reactive roles by transfer to C/C unsaturation. From the point of view of product selectivity, the simplest iridium reagents are thus (triphos)Ir(π-alkyne)$^+$ and (triphos)Ir(η^2-C_4H_4)$^+$; no hydride transfer or ethene-derived products are possible. The high IrH to C_2H_4 ratio in (triphos)Ir(H)$_2$(THF)$^+$ leads selectively to the most hydrogen-rich product, butadiene. (triphos)Ir(H)$_2$(C_2H_4)$^+$ and (triphos)Ir(C_2H_4)$_2^+$ increase the complexity still further because the ethene is both more abundant and (being coordinated) more competitive with acetylene. Hydride ligands are never eliminated as H_2,[32] apparently because of the abundance of hydrogen acceptor substrates, together with the facile occurrence of β-H migration promoted by iridium. Pervading this chemistry is the efficient binding of substrates by highly electrophilic metal centers. This follows because the coordination sphere is devoid of halide or pseudo-halide ligands which have the ability to stabilize apparently unsaturated intermediates by X → Ir π-donation.[33]

With the combination of a polyphosphine ligand and of a kinetically sluggish third-row transition metal, we have been able to detect several species intermediate to various C–C bond-forming reactions of ethene and ethyne. Surveying the results herein presented, one may draw several mechanistic conclusions:

(i) The cyclotrimerization reaction is traversed by a number of intermediates among which are metal–π-alkyne, metal–bis(π-alkyne), and metallacyclopentadiene species.

(ii) Metallacyclopentadiene complexes can also be intermediates for the linear cooligomerization of alkynes with alkenes via ring-expansion reactions rather than via Diels–Alder addition (i.e., no cyclohexadiene is formed here).

(iii) The reductive coupling of alkynes to buta-1,3-dienes can proceed at one metal center via subsequent insertion of two alkyne molecules into two M–H bonds, followed by reductive elimination from a bis(vinyl) intermediate. This mechanism is alternative to reaction of metallacyclopentadiene complexes with H_2.[12]

(iv) Alkenes function as coreactants in the cyclotrimerization reaction of alkynes assisted by polyhydrido metal complexes either by preventing the insertion of a second alkyne molecule into an M–H bond (thus impeding the reductive dimerization reaction) or by consuming the hydride ligands (being reduced to alkanes).

Acknowledgment. Thanks are due Prof. Alberto Vacca for his relevant contribution in the computer simulation of the NMR spectra. C.B. is indebted to Progetti Finalizzati Chimica Fine II, CNR, Rome, Italy for financial support. This work was also supported by the U.S. National Science Foundation, by the Lubrizol Corp., and by the Indiana University Institute for Advanced Study (fellowship to C.B.).

OM940840K

(32) Johnson, T. J.; Huffman, J. C.; Caulton, K. G.; Jackson, S. A.; Eisenstein, O. *Organometallics* **1989**, *8*, 2073. Marinelli, G.; Rachidi, I.; Streib, W. E.; Eisenstein, O.; Caulton, K. G. *J. Am. Chem. Soc.* **1989**, *111*, 2346. Lundquist, E. G.; Folting, K.; Streib, W. E.; Huffman, J. C.; Eisenstein, O.; Caulton, K. G. *J. Am. Chem. Soc.* **1990**, *112*, 855.

(33) Poulton, J. T.; Folting, K.; Streib, W. E.; Caulton, K. G. *Inorg. Chem.* **1992**, *3*, 3190. Lunder, D. M.; Lobkovsky, E. B.; Streib, W. E.; Caulton, K. G. *J. Am. Chem. Soc.* **1991**, *113*, 1837.

Masked Iminophosphide Anion: Synthesis and Versatile Reactivity

Armelle Mahieu, Alain Igau, Joël Jaud, and Jean-Pierre Majoral*

Laboratoire de Chimie de Coordination du CNRS, 205 route de Narbonne, 31077 Toulouse Cedex, France

Received September 14, 1994®

The unprecedented iminozirconiophosphorane **3**, $Me_2P(ZrCp_2Cl)$=N—Ar (Ar = 2,4,6-*t*-$Bu_3C_6H_2$), a masked iminophosphide, has been prepared by reacting chloroiminophosphane **2**, Cl—P=N—Ar, with Cp_2ZrMe_2. Insertion reactions into the zirconium–phosphorus bond take place when **3** is reacted with nitriles, paraformaldehyde, or carbon disulfide, giving rise to iminophosphoranes. Formal insertion into the nitrogen–zirconium bond occurs when **3** is treated with isocyanides RNC (R = Me_3SiCH_2, cyclohexyl), affording phosphanes. A single-crystal X-ray structure of one of them has been determined. Addition of pyridine–HCl, methyl iodide, *N*-bromosuccinimide, or various chlorophosphanes to **3** leads to iminophosphoranes via exchange reactions taking place directly on the phosphorus center of **3**. Addition of the Eschenmoser salt $[H_2C{=}NMe_2]Cl$ to **3** affords a mixture of iminophosphorane and phosphonium salt. **3** reacts with triflic acid or methyl trifluoromethanesulfonate, giving exclusively phosphonium salts. Reactions involving the thermodynamically stable form of **3**, i.e. the phosphane **5**, Me_2P—N($ZrCp_2Cl$)(2,4,6-*t*-$Bu_3C_6H_2$), occur when **3** is treated with the chloroiminophosphane **2** with formation of a phosphanyliminophosphane. Treatment of **3** with $NiCl_2$ or $PdCl_2$ gives rise to the complexes **28a** (M = Ni) and **28b** (M = Pd), [Me_2P—N(H)-2,4,6-*t*-$Bu_3C_6H_2$]$_2MCl_2$.

Introduction

Among all the possible anionic phosphorus species which can be envisaged,[1] only a few of them are well described: phosphido derivatives R_2P^-,[2] phosphoranides R_4P^-,[3] and hexavalent phosphorus anions R_6P^- [4a] and $R_4P^-{=}N^-$.[4b] Compounds of general formula $[PX_3]^-$ have also been characterized. The metaphosphate ion $[PO_3]^-$ has given rise to numerous studies; this species is thought to be an intermediate in the hydrolysis of phosphoric esters.[5] Lastly, the X-ray structure of $[PS_3]^-$ [6] and that of the tris(methylene)phosphate **1**[7]

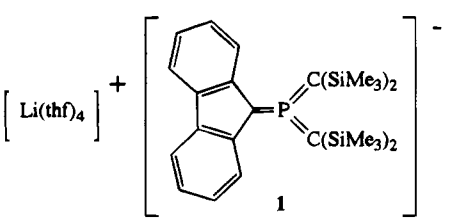

have been reported. In contrast, a few reports deal with the iminophosphide anion >P=N−. Transient generation of such a species is postulated during the treatment of the phosphaimine $(Me_3Si)_2N$—P=N—$SiMe_3$ with MeLi[8] (Scheme 1). A single-crystal X-ray crystallographic study of [Li(PhN—PPh_2)(OEt_2)]$_2$ shows that the lithium cations are ligated by both of the heteroatoms of the PhN—PPh_2^- anion. However, the P—N distance (1.672 Å) is in the range of the P—N single-bond lengths,[9] and *ab initio* calculations carried out on the parent phosphinoamide/iminophosphide anion H_2PNH^-, suggest that this system is best described as the phosphinoamide anion H_2PNH^- with the negative charge mainly located on nitrogen.[10]

Scheme 1

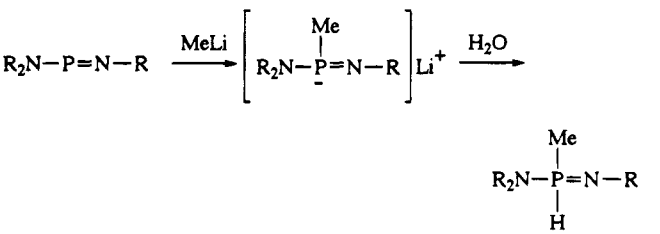

R = $SiMe_3$

Therefore, to the best of our knowledge, no stable linear iminophosphide anion >P=N−, as well as no useful precursor of such a species, has been reported.[11] Indeed the high electronegativity of nitrogen appears

® Abstract published in *Advance ACS Abstracts,* January 1, 1995.

(1) Wolf, R. *Pure Appl. Chem.* **1980**, *52*, 1141.
(2) See for example: Gallagher, M. In *CRC Handbook of Phosphorus-31 Nuclear Magnetic Resonance Data;* Tebby, J. C., Ed.; CRC Press: Boston, MA, 1990; Chapter 2a, pp 45–49.
(3) See for example: Riess, J. G.; Schmidpeter, A. In *CRC Handbook of Phosphorus-31 Nuclear Magnetic Resonance Data;* Tebby, J. C., Ed.; CRC Press: Boston, MA, 1990; Chapter 17, pp 501–505.
(4) (a) See for example: Lamandé, L.; Koenig, M. In *CRC Handbook of Phosphorus-31 Nuclear Magnetic Resonance Data;* Tebby, J. C., Ed.; CRC Press: Boston, MA, 1990; Chapter 19, pp 553–567. (b) Baceiredo, A.; Bertrand, G.; Majoral, J. P.; Dillon, K. B. *J. Chem. Soc., Chem. Commun.* **1985**, 562.
(5) Westheimer, F. H. *Science* **1987**, *235*, 1173.
(6) Roesky, H. W.; Ahlrichs, R.; Brode, S. *Angew. Chem., Int. Ed. Engl.* **1986**, *25*, 82.
(7) Appel, R.; Gaitzsch, E.; Knoch, F. *Angew. Chem., Int. Ed. Engl.* **1985**, *24*, 589.
(8) Cowley, A. H.; Kemp, R. A. *J. Chem. Soc., Chem. Commun.* **1982**, 319. Cowley, A. H.; Kemp, R. A. *Inorg. Chem.* **1983**, *22*, 547.
(9) Ashby, M. T.; Li, Z. *Inorg. Chem.* **1992**, *31*, 1321.
(10) Trinquier, G.; Ashby, M. T. *Inorg. Chem.* **1994**, *33*, 1306.
(11) Versatile reactivity of the (1,3-diaza-2-phosphaallyl)lithium complex [RNPN(aryl)]Li (R = *t*-Bu, aryl = 2,4,6-*t*-$Bu_3C_6H_2$) toward diphenylchlorophosphane has been demonstrated: P and N addition products were isolated. See: Detsh, R.; Niecke, E.; Nieger, M.; Schoeller, W. W. *Chem. Ber.* **1992**, *125*, 1119.

0276-7333/95/2314-0944$09.00/0

Scheme 2. Synthesis and Thermal Stability of 3

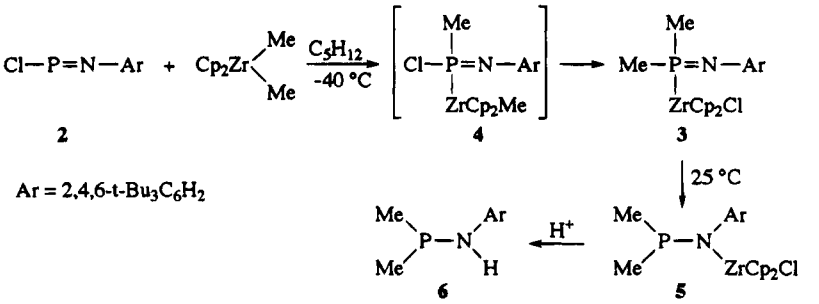

to be the dominant factor which hinders the formation of such anionic species. We anticipated that P-metalated iminophosphoranes $R_2P(M)=N-R'$ (M = metal) might act as precursors of iminophosphides. However, none of these derivatives have yet been described. It can only be mentioned that the X-ray structures of diphosphazene complexes $M[(CF_3)_2P=N=PPh_3]_n$ ($n = 1$, $M = Fe(CO)_4$;[12] $n = 1$, $M = Os_3(CO)_{11}$;[13] $n = 2$, $M = PdCl_2$, $Fe(CO)_3$[14]) show that the two P—N lengths are very similar and therefore that the unsymmetrical PNP fragment is highly delocalized, presumably owing to the effect of the strongly electron-withdrawing CF_3 moiety.

In contrast, a number of acyclic and cyclic N-metalated iminophosphoranes have been prepared, most of this work being carried out by Roesky *et al.*,[15] Elsevier *et al.*,[16] and Cavell *et al.*[17]

In a preliminary communication[18] we reported the synthesis of the iminozirconiophosphorane **3** $Me_2P(ZrCp_2Cl)=N$-2,4,6-*t*-$Bu_3C_6H_2$, the first P-metalated iminophosphorane, and a few reactions with this compound. Herein we report full details of the synthesis and the reactivity of this derivative. Four main types of reactions will be described: (i) insertion reactions into the P—Zr bond, (ii) formal insertion into the N—Zr bond, (iii) reactions at phosphorus, (iv) reactions at nitrogen. These examples will demonstrate the versatile behavior of this first representative of a new class of compounds, reacting either as the masked iminophosphide $[Me_2P=N(2,4,6\text{-}t\text{-}Bu_3C_6H_2)][ZrCp_2Cl]$ or as the (zirconioamino)phosphane $Me_2P-N(ZrCp_2Cl)$-2,4,6-*t*-$Bu_3C_6H_2$.

Results and Discussion

Addition of Cp_2ZrMe_2 to a pentane solution of the chloroiminophosphane **2** at −40 °C leads to the white air- and moisture-sensitive powder **3** in 85% yield (Scheme 2). When the reaction is done in THF, formation of **3** is indicated by the change in color of the solution from red (**2**) to green. The ^{31}P NMR spectrum of **3** reveals the presence of a doublet of septets at −4.3 ppm ($^2J_{PH}$ = 6.3 Hz). The signal for the Cp protons appeared in ^1H NMR as a doublet with the coupling constant $^3J_{PH}$ = 1.4 Hz, consistent with a Cp−Zr−P skeleton.[19] The ^1H NMR spectrum also suggests that each of the two methyl groups are bound to the phosphorus atom: only one doublet is detected for the two methyl groups ($^2J_{HP}$ = 6.3 Hz). ^{13}C NMR corroborates this interpretation, because only one doublet is observed for the same groups ($^1J_{CP}$ = 11.1 Hz). All these observations are in agreement with either a P-metalated iminophosphorane form (**A**) or the corresponding cyclic one (**B**). Attempts to obtain crystals suitable for crystallographic X-ray structure determination studies have so far failed.

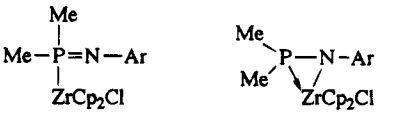

A **B**

The formation of **3** might involve the transient intermediate **4** (resulting from insertion of the chloroiminophosphane into the Zr−C bond of Cp_2ZrMe_2), which rearranges by migration of the chlorine atom from phosphorus to zirconium and of a methyl group from zirconium to phosphorus. Note that in solution at room temperature, **3** affords quantitatively the phosphane **5**, which appears to be the thermodynamically favored product of the reaction of **2** with Cp_2ZrMe_2. Moreover, addition of pyridine or PMe_3 to **3** gives **5**. The ^{31}P NMR chemical shift of **5** is in the expected range for aminophosphanes, while the ^1H NMR spectra shows, now, one singlet for the Cp protons. The Zr−N bond in **5** can be easily cleaved in the presence of proton donors (solvent, traces of water) to give the derivative **6**.

In order to have a better idea of the structure of the kinetic product **3** (form **A** or **B**), we undertook the study of its reactivity, bearing in mind that azaphosphazirconiridines such as **7** are poorly reactive: only a few reactions involving **7** (ring opening or ring retention) have been reported to date.[20]

(12) (a) Ang, H. G.; Cai, Y. M.; Kwik, W. L.; Rheingold, A. L. *J. Chem. Soc., Chem. Commun.* **1990**, 1580. (b) Ang, H. G.; Cai, Y. M.; Kwik, W. L.; Morrison, E. C.; Tocher, D. A. *J. Organomet. Chem.* **1991**, *403*, 383.

(13) Ang, H. G.; Cai, Y. M.; Kwik, W. L.; Leong, W. K. *Polyhedron* **1991**, *10*, 881.

(14) Ang, H. G.; Cai, Y. M.; Koh, L. L.; Kwik, W. L. *J. Chem. Soc., Chem. Commun.* **1991**, 850.

(15) See for example: Roesky, H. W. In *The Chemistry of Inorganic Ring Systems*; Steudel, R., Ed.; Studies in Inorganic Chemistry 14; Elsevier Science Publishers: New York, 1992; p 255. Witt, M.; Roesky, H. W. *Chem. Rev.* **1994**, *94*, 1163. Roesky, H. W. *Chem. Soc. Rev.* **1986**, *15*, 309. Roesky, H. W.; Hesse, D.; Rietzel, M.; Noltemeyer, M. *Z. Naturforsch.* **1990**, *45B*, 72. Katti, K. V.; Seseke, U.; Roesky, H. W. *Inorg. Chem.* **1987**, *26*, 814.

(16) See for example: Imhoff, P.; Elsevier, C. J. *J. Organomet. Chem.* **1989**, *361*, C61. Imhoff, P.; Nefkens, S. C. A.; Elsevier, C. J.; Goubitz, K.; Stan, C. H. *Organometallics* **1991**, *10*, 1421.

(17) (a) Katti, K. V.; Cavell, R. G. *Organometallics* **1988**, *7*, 2236. (b) Katti, K. V.; Cavell, R. G. *Organometallics* **1989**, *8*, 2147. (c) Katti, K. V.; Cavell, R. G. *Comments Inorg. Chem.* **1990**, *10*, 55. (d) Katti, K. V.; Cavell, R. G. *Inorg. Chem.* **1989**, *28*, 3033. (e) Katti, K. V.; Cavell, R. G. *Organometallics* **1988**, *7*, 2236. (f) Katti, K. V.; Batchelor, R. J.; Einstein, F. W. B.; Cavell, R. G. *Inorg. Chem.* **1990**, *29*, 808.

(18) Igau, A.; Dufour, N.; Mahieu, A.; Majoral J.-P. *Angew. Chem., Int. Ed. Engl.* **1993**, *32*, 95.

(19) Majoral, J.-P.; Dufour, N.; Meyer, F.; Caminade, A.-M.; Choukroun, R.; Gervais, D. *J. Chem. Soc., Chem. Commun.* **1990**, 507. Dufour, N.; Majoral, J.-P.; Caminade, A.-M.; Choukroun, R.; Dromzée, Y. *Organometallics* **1991**, *10*, 4.

(20) Dufour, N.; Caminade, A.-M.; Basso-Bert, M.; Igau, A.; Majoral, J.-P. *Organometallics* **1992**, *11*, 1131.

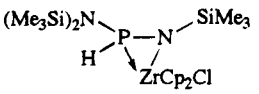

7

Insertion Reactions into the P–Zr Bond. Derivative **3** reacts with 1 equiv of CH_3CN in CH_2Cl_2 at −40 °C to give instantaneously compound **8a** via insertion of CH_3CN into the P–Zr bond (Scheme 3). ^1H and ^{13}C NMR strongly suggest the presence of a C–CH_3 group in **8a**; the ^{31}P NMR spectrum (δ 53.8 ppm) is in favor of a cyclic iminophosphorane form (with a dative bond between the iminophosphorane nitrogen atom and zirconium) rather than a linear form, which would give rise to a much more shielded chemical shift.[21] However, considering these data, the formation of the aminophosphane **9** cannot be totally excluded. Nevertheless, the thermodynamic product **5** does not react even in the presence of an excess of acetonitrile (Scheme 3). It can also be noted that the azaphosphazirconiridines **7** are inert toward nitriles. Addition of *i*-PrC≡N to **3** similarly gives the insertion product **8b**.

Another type of insertion product can be obtained by reacting paraformaldehyde with **3** at −40 °C; in this case the linear iminophosphorane **10** was quantitatively formed (Scheme 4). The ^{31}P NMR chemical shift of **10** (δ −12.4 ppm) is in agreement with an acyclic P–N double-bonded structure.[21] The ^1H NMR spectrum exhibits one doublet for methylene protons at 4.45 ppm with a phosphorus–hydrogen coupling constant of 7.0 Hz. The presence of a methylene group directly linked to phosphorus is confirmed by ^{13}C NMR (δ (CH_2): 76.8 (d, $^1J_{CP}$ = 94.5 Hz)).

Treatment of **3** with carbon disulfide at −40 °C provides an additional example of an insertion reaction into the phosphorus–zirconium bond with the formation of a third type of compound, the iminophosphorane **11** (Scheme 4). Two isomers can be distinguished by ^{31}P NMR spectroscopy (**11a,b:** δ −18.8 (70%) and −19.3 (30%) ppm, respectively). The ^{13}C NMR spectrum of **11a,b** for the S–C–S carbon consists of doublets at 261.4 (J_{CP} = 35.2 Hz) and 261.3 (J_{CP} = 35.2 Hz) ppm, respectively. In marked contrast, the phosphane **5** as well as the three-membered-ring compound **7** do not react with paraformaldehyde or with carbon disulfide even under forcing conditions: no insertion reaction was observed in these cases.

These observations demonstrate that the reactive species is the P-metalated iminophosphorane **3** and not the (zirconioamino)phosphane **5** and that **3** exists in a linear form (**A**) rather than in a cyclic one (**B**). **3** can be considered as the masked iminophosphide [Me_2P=N-2,4,6-*t*-$Bu_3C_6H_2$][$ZrCp_2Cl$], a newly identified species.

Formal Insertion into the N–Zr Bond. Compound **3** is converted to the phosphane **12a** by reaction with the isocyanide Me_3SiCH_2NC, in toluene at −78 °C (Scheme 5). The resonance signal for the sp^2 imino carbon in ^{13}C NMR appears at 207.1 ppm (d, $^2J_{CP}$ = 43.3 Hz), and signals for the two Cp groups appear at 110.7 and 114.5 (s) ppm. An analogous reaction involving **3** and cyclohexyl isocyanide leads to **12b**. The X-ray structure determination of **12a** (Figure 1 and Table 1)

Scheme 3. Reactivity of 3 and 5 with Nitriles

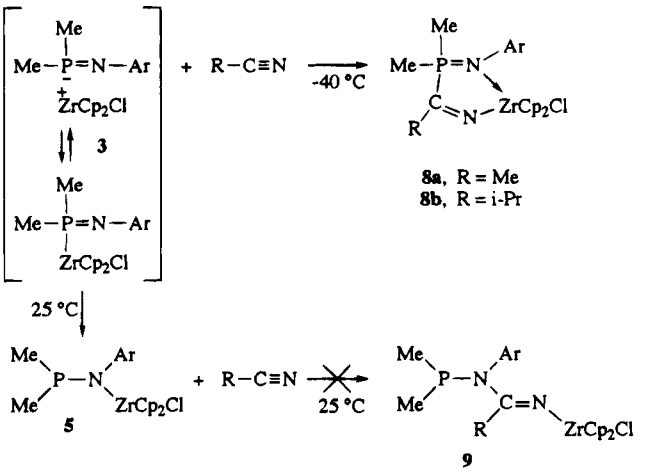

Scheme 4. Insertion Reactions into the P–Zr Bond

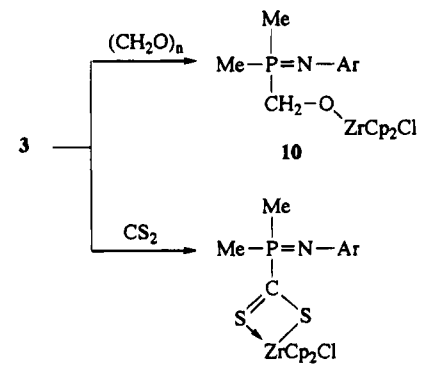

Scheme 5. Reactivity of 3 and 5 with Isonitriles

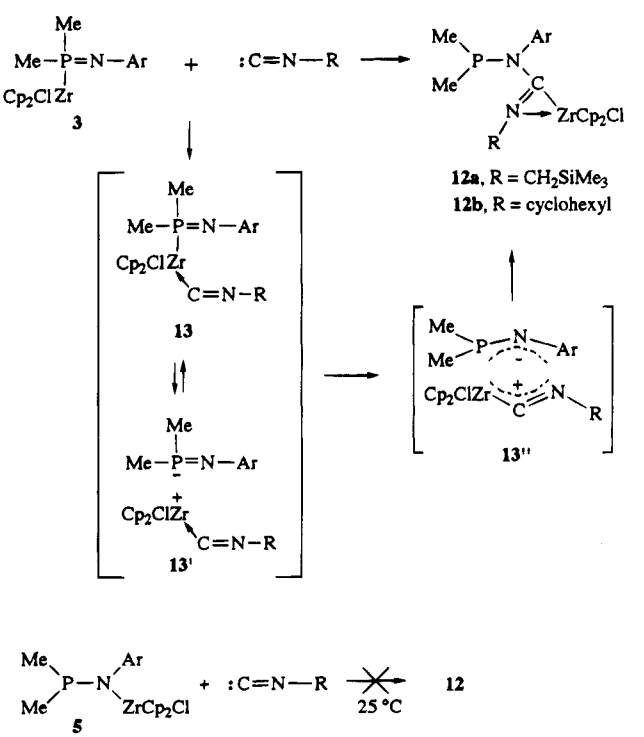

(21) Tebby, J. C.; Krishnamurthy, S. S. In *CRC Handbook of Phosphorus-31 Nuclear Magnetic Resonance Data;* Tebby, J. C., Ed.; CRC Press: Boston, MA, 1990; Chapter 14, pp 409–477.

(22) It has recently been shown that, for example, *tert*-butyl isocyanide reacts rapidly with the cationic zirconium complex $Cp_2Zr(CH_3)(THF)^+$ (as the BPh_4^- salt) to yield the iminoacyl isocyanide complex $Cp_2Zr\{\eta^2\text{-}C(=N\text{-}t\text{-}Bu)CH_3\}(CN\text{-}t\text{-}Bu)^+$: Guo, Z.; Swenson, D. C.; Guran, A. S.; Jordan, R. F. *Organometallics* **1994**, *13*, 766.

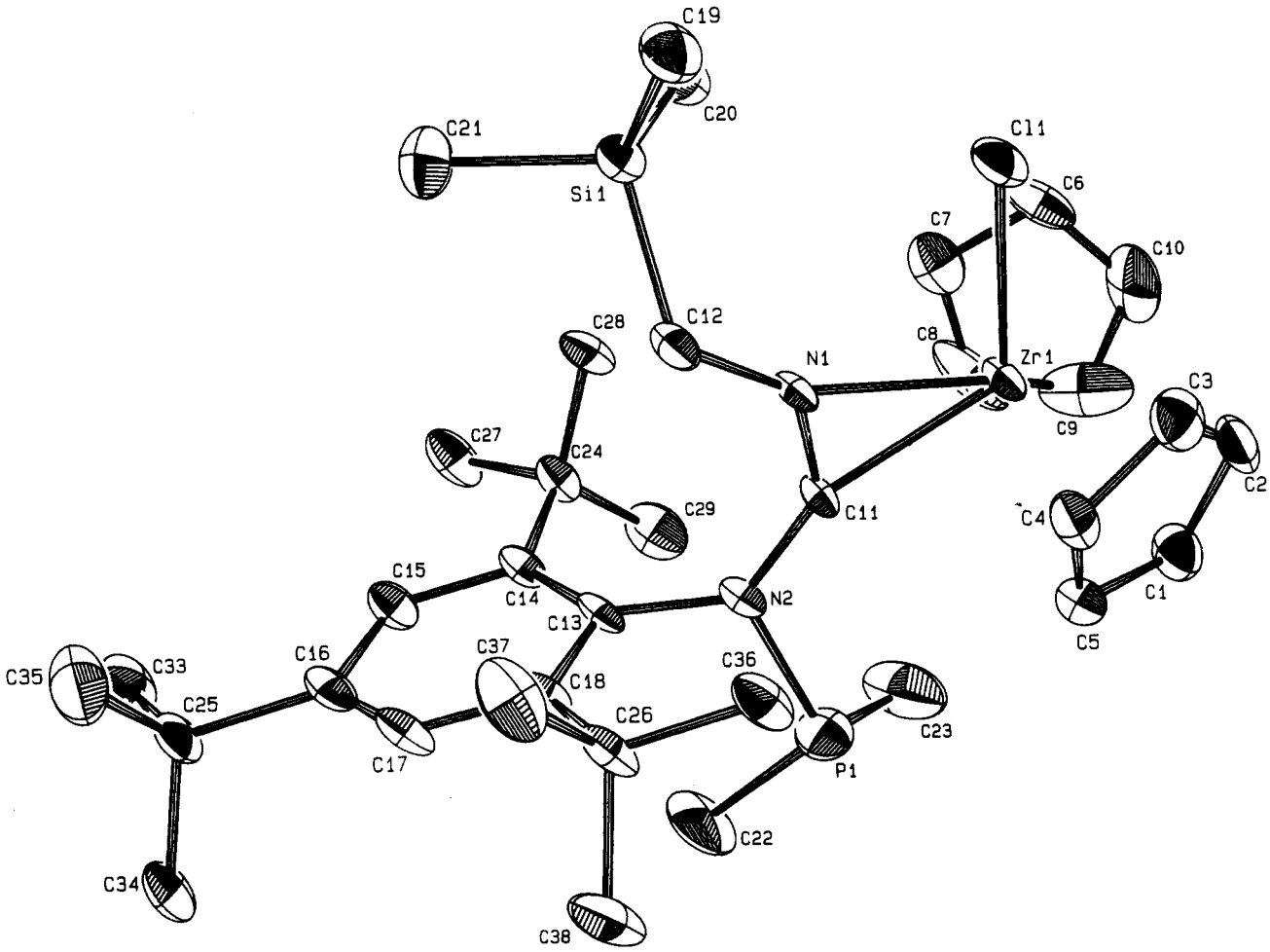

Figure 1. Structure of **12a**.

Table 1. Crystallographic Data for 12a

Crystal Parameters	
formula	$C_{35}H_{56}ClN_2PSiZr$
fw	691.587
cryst syst	monoclinic
space group	$P2_1/n$
Z	4
a, Å	14.749(9)
b, Å	15.521(8)
c, Å	16.086(9)
β, deg	90.4(2)
V, Å^3	3680(5)
$F(000)$	1468
D_{calcd}, g cm^{-3}	1.247
cryst dimens, mm	0.30 × 0.20 × 0.15
T, °C	20
Measurement of Intensity Data	
radiation	Mo, 0.710 69 Å
scan type	$\theta/2\theta$
Bragg angle, deg	2.20
range/indices (hkl)	0−14, 0−15, −15 to +15
scan width, deg	0.90 + 0.35 tan θ
no. of rflns for the refinement of the cell	25
no. of indep reflns	6812
no. of observed reflns	4130
no. of refined params	398
$R(F_o)^a$	0.0572
$R_w(F_o)^b$	0.0642

$^a R = \Sigma(||F_o| - |F_c||)/\Sigma(|F_o|)$. $^b R_w = [\Sigma(|F_o| - |F_c|)^2/\Sigma(|F_o|)^2]^{1/2}$.

shows clearly the coordination of the imino nitrogen atom to the Cp_2ZrCl center. Classical bond length and angle values are observed for **12a** (Tables 2 and 3). The phosphorus−nitrogen bond length (1.773 Å) confirms the phosphane structure.

Table 2. Selected Bond Distances (Å) in 12a

Zr(1)−Cl(1)	2.558(2)	C(11)−N(2)	1.380(7)
Zr(1)−C(11)	2.246(5)	N(2)−P(1)	1.773(6)
Zr(1)−N(1)	2.178(5)	N(2)−C(13)	1.467(8)
N(1)−C(11)	1.286(8)	P(1)−C(23)	1.73(1)
N(1)−C(12)	1.453(8)	P(1)−C(22)	1.84(1)

Table 3. Selected Bond Angles (deg) in 12a

N(1)−Zr(1)−Cl(1)	82.6(1)	C(11)−N(2)−C(13)	125.7(5)
N(1)−Zr(1)−C(11)	33.8(2)	C(13)−N(2)−P(1)	116.2(4)
N(1)−C(11)−Zr(1)	70.2(3)	C(12)−N(1)−C(11)	132.0(5)
C(11)−N(1)−Zr(1)	76.1(3)	C(12)−N(1)−Zr(1)	150.8(4)
C(11)−N(2)−P(1)	116.2(4)	N(2)−P(1)−C(22)	103.4(4)
N(2)−C(11)−N(1)	132.7(6)	N(2)−P(1)−C(23)	108.7(5)
N(2)−C(11)−Zr(1)	157.1(5)	C(22)−P(1)−C(23)	97.8(6)

At first sight, these results seem to indicate that **12a** (or **12b**) arises from insertion of isocyanide into the nitrogen−zirconium bond and therefore that the reactive species here is the (zirconioamino)phosphane **5** and not **3**. However, no reaction occurs when **5** is treated with Me_3SiCH_2NC or cyclohexylNC at room temperature. Moreover, it can be noted that the three-membered-ring species **7** does not react with isocyanides. Therefore, it is reasonable to postulate that the first step of the reaction involving **3** and isocyanide is the coordination of the isocyanide on the vacant coordination site of the metal moieties to give **13**. As we have already observed (addition of PMe_3 or pyridine to **3**; see above), coordination of a donor ligand can induce the dissociation of the P−Zr bond to afford **13′**; then electrophilic attack[23] of the metalated carbocation **13″** (Scheme 5)

Scheme 6. Substitution Reactions on 3

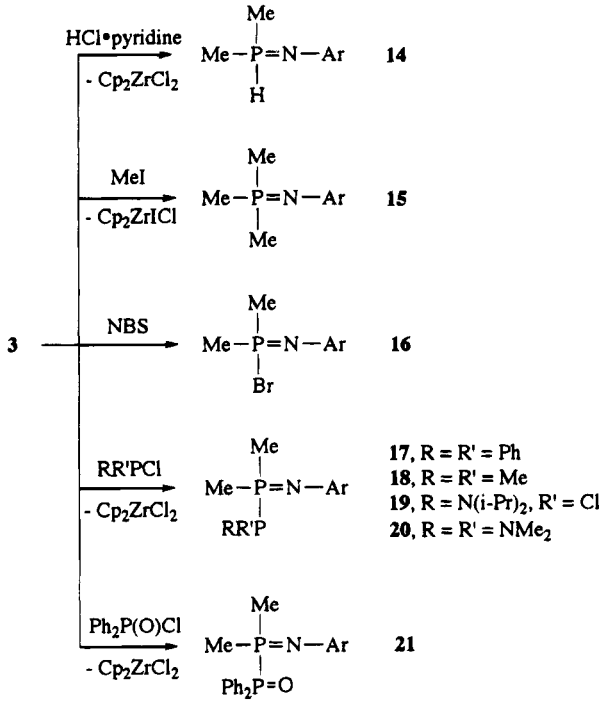

at the hard nitrogen nucleophilic center of the thermodynamically more stable aminophosphide $Me_2P-N-Ar$ ($Ar = 2,4,6\text{-}t\text{-}Bu_3C_6H_2$) gives **12a** (or **12b**).

Indeed, compounds **12a,b** are *formally* the first derivatives resulting from insertion of isocyanides into a N–Zr bond. To our knowledge such a reaction has not yet been reported.

Reactions at Phosphorus. Exchange reactions easily occur when HCl·pyridine, methyl iodide, or *N*-bromosuccinimide (NBS) is added to **3** at −78 °C (Scheme 6). Compounds **14–16** are isolated in near-quantitative yields. Such reactions take place when various chlorophosphanes RR'PCl are treated with **3** in THF at −78 °C. The formation of the expected phosphanyliminophosphoranes **17–20** was detected by ^{31}P NMR (two doublets for each derivative (**17**, δ −5.3 (PPh_2) and −22.0 (Me_2P=), $^1J_{PP}$ = 259.8 Hz; **18**, δ −18.8 (Me_2P=) and −53.0 (Me_2P), $^1J_{PP}$ = 240.0 Hz; **19**, δ 130.2 (*i*-PrNPCl) and −21.2 (Me_2P=), $^1J_{PP}$ = 320.0 Hz)), but during workup, compounds **17–19** decompose into a variety of species which were impossible to purify. It was only possible to isolate and fully characterize the phosphanyliminophosphorane **20**. The ^{31}P NMR spectrum of **20** appears as two doublets at 110.3 ($(Me_2N)_2P$) and −14.2 (Me_2P=) ppm with typical $^1J_{PP}$ coupling constants of 299.4 Hz. The structure of **20** was corroborated by ^1H and ^{13}C NMR as well as by mass spectrometry. Under the same experimental conditions, the diphenylchlorophosphane oxide reacts with **3** to give the expected compound **21** (Scheme 6).

In contrast to the reactions of **3** with methyl iodide, NBS, or chlorophosphanes which only lead to iminophosphoranes, addition of the Eschenmoser salt $H_2C{=}NMe_2Cl$ to **3** at −78 °C affords a mixture of the iminophosphorane **22** and of the phosphonium salt **23** (Scheme 7), which were isolated and fully characterized. The formation of **22** can be easily explained via a classical exchange reaction from the P-metalated iminophosphorane form **3**, while the generation of the salt **23** might involve the (zirconioamino)phosphane **5**. Indeed, **5** treated with $H_2C{=}NMe_2Cl$ gives quantitatively the phosphonium salt **23**. On the other hand, phosphonium salts **24** and **25** are quantitatively formed when **3** or **5** is reacted with triflic acid or methyl trifluoromethanesulfonate (Scheme 7). Like PMe_3 or pyridine ligands, the trifluoromethanesulfonate anion may act as a catalyst for the rearrangement of **3** to **5**. Formation of **23–25** results from the electrophilic attack of R^+ (H^+, Me^+) at the phosphorus center of **5** followed by cleavage of the Zr–N bond in the presence of a source of protons (solvent, traces of water). Zirconium species have not been identified.

Scheme 7. Reactivity of 3 and 5 with Eschenmoser's Salt and Triflate Derivatives

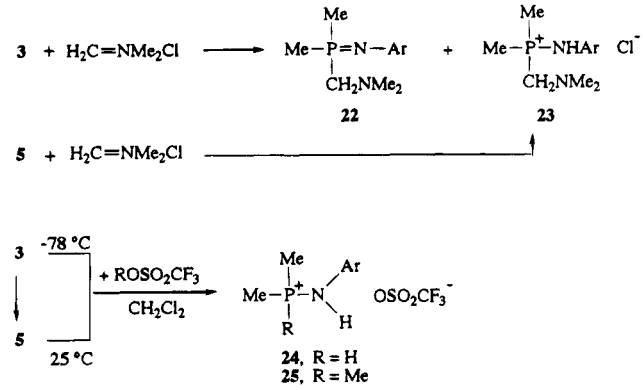

Scheme 8

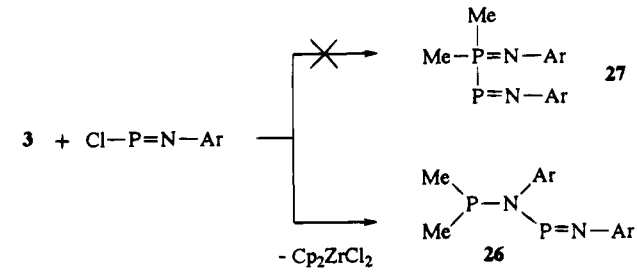

Reaction at Nitrogen. Treatment of **3** with chloroiminophosphane **2** leads to the aminoiminophosphane **26** (Scheme 8). The ^{31}P NMR spectrum of **26** consists of two doublets at 322.4 (P=N) and 98.8 (Me_2P) ppm with $^2J_{PP}$ = 11.7 Hz. ^1H and ^{13}C NMR corroborate the proposed structure. Two hypotheses can be formulated for the formation of **26**. The first one may involve the preliminary exchange reaction between **3** and **2** affording **27** which further rearranges into **26**, while the second one implies a direct exchange with the thermodynamically favored form **5**. The 1,2-shift of a phosphorus group from phosphorus to the imino nitrogen has already been observed[23] and therefore cannot be totally ruled out. Nevertheless, the formation of **27** was never detected in ^{31}P NMR even at low temperature. Therefore, the direct grafting of **2** to the nitrogen atom of the phosphane **5** seems to be more realistic.

Coordination Chemistry of 3. Addition of $NiCl_2$ or $PdCl_2$ (0.5 equiv) to **3** (1 equiv) leads to the formation of the new complexes **28a,b** and not to the expected derivatives **29a,b** (Scheme 9). A similar result is obtained when **5** is reacted with $NiCl_2$ or $PdCl_2$ under the same experimental conditions. Moreover, treatment

(23) Gololobov, Y. G.; Swalova, E. A.; Chudakova, T. I. *Zh. Obshch. Khim.* **1981**, *51*, 1433.

Scheme 9. Reactivity of 3 and 5 with Transition Metals

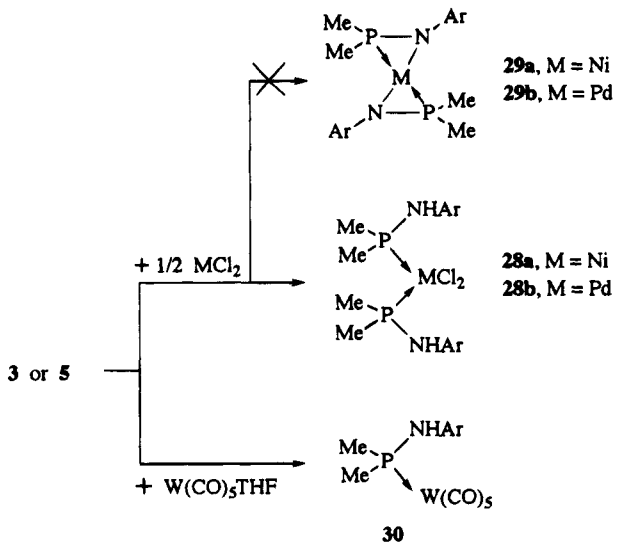

of **3** or **5** with $W(CO)_5THF$ gives rise to the 1:1 complex **30**. Indeed, in all of these experiments, **3** reacts as a phosphane and not as a P-metalated iminophosphorane.

Conclusion

The first isolated P-metalated iminophosphorane, **3**, appears to be a versatile and useful reagent, allowing the preparation of a large number of new free or complexed, neutral or cationic, acyclic or cyclic phosphorus compounds. Reactions with nitriles, paraformaldehyde, carbon disulfide, isocyanides, methyl iodide, *N*-bromosuccinimide, or various chlorophosphanes reveal that this P-metalated iminophosphorane, stable at −40 °C, acts as a masked iminophosphide: a new tricoordinated tetravalent phosphorus anion. Therefore, the transition-metal derivatization of $[R_2P-NR']^-$ considerably affects its reactivity as compared with the alkali-metal derivatives, which react as phosphinoamide anions R_2PNR with the negative charge located on nitrogen. On the other hand, the thermodynamically favored form of **3**, i.e. the (zirconioamino)phosphane **5**, is the reactive species when **3** is reacted with triflic acid, methyl trifluoromethanesulfonate, chloroiminophosphane, $NiCl_2$, $PdCl_2$, or $W(CO)_5THF$, while the Eschenmoser salt $H_2C{=}NMe_2Cl$ reacts with both **3** and **5**.

Attempts to prepare other P-metalated iminophosphoranes, stable at room temperature, as well as the use of these new reagents in organic and organometallic chemistry, are underway.

Experimental Section

All manipulations were carried out with standard high-vacuum or dry argon atmosphere techniques. NMR spectra were recorded at ambient temperature on 200- and 250-MHz Bruker spectrometers and referenced as follows: ^1H (δ) $CHDCl_2$ (5.32), C_6HD_5 (7.16); $^{13}C\{^1H\}$ (ppm) CD_2Cl_2 (53.8), C_6D_6 (128.0); $^{31}P\{^1H\}$ external 85% H_3PO_4 (0.0 ppm). Chemical shifts are in δ (^1H) or ppm (^{13}C, ^{31}P), and coupling constants (J) are in hertz. Mass spectra were obtained on a Nermag R10-10H. Microanalyses have been performed by the Centre de Microanalyse du CNRS or in our laboratories. Melting points were determined in evacuated capillaries and were corrected and calibrated.

Solvents were purified as follows: THF and ether was distilled from Na/O=CPh_2, CH_2Cl_2 was distilled from P_2O_5, and pentane was distilled from CaH_2. C_6D_6 and CD_2Cl_2, purchased from CEA, were treated with $LiAlH_4$, distilled, and stored under argon. Reagents were obtained as follows: acetonitrile was distilled from CaH_2; CS_2 (Fluka) was passed through activated alumina prior to use; $(CH_2O)_n$, $Me_3SiCH_2N{=}C$, $C_6H_{11}N{=}C$, *i*-PrCN, HCl·pyridine, MeI, $Ph_2P(O)Cl$, Ph_2PCl, $H_2C{=}NMe_2Cl$, $HOSO_2CF_3$, $MeOSO_2CF_3$, $NiCl_2$ (Aldrich), Me_2PCl (Strem), *N*-bromosuccinimide (Fluka), and $PdCl_2$ (Lancaster) were used as received; Cp_2ZrMe_2[24] and **2**[25] were prepared by literature methods.

$Me_2P(ZrCp_2Cl){=}N$-2,4,6-*t*-$Bu_3C_6H_2$ (3). To a solution of chloroiminophosphane **2** (0.326 g, 1.00 mmol) in pentane (10 mL), cooled to −40 °C, was added Cp_2ZrMe_2 (0.251 g, 1.00 mmol) in pentane (10 mL) at −40 °C. The mixture was stirred for 30 min, after which a white precipitate separated from the solution. The white powder was washed twice with pentane (10 mL, −40 °C) and dried under vacuum. This afforded **3** (0.491 g, 0.85 mmol) in 85% yield.

$^{31}P\{^1H\}$ NMR (CD_2Cl_2): −4.3. ^1H NMR (CD_2Cl_2): 7.28 (s, CH_{Ar}), 6.00 (d, $^3J_{HP}$ = 1.4, Cp), 1.53 (s, *o*-*t*-Bu), 1.34 (s, *p*-*t*-Bu), 0.80 (d, $^2J_{HP}$ = 6.3, Me_2P). $^{13}C\{^1H\}$ NMR (CD_2Cl_2): 148.8 (d, $^2J_{CP}$ = 18.0, *i*-C_{Ar}), 146.5 (d, $^3J_{CP}$ = 6.0, *o*-C_{Ar}), 138.9 (d, $^5J_{CP}$ = 5.0, *p*-C_{Ar}), 120.7 (s, *m*-C_{Ar}), 110.9 (s, Cp), 36.5 (s, *o*-CCH_3), 36.1 (s, *p*-CCH_3), 33.6 (s, *o*-CCH_3), 30.8 (s, *p*-CCH_3), 16.7 (d, $^1J_{CP}$ = 11.1, Me_2P).

$Me_2P{-}N(ZrCp_2Cl)$-2,4,6-*t*-$Bu_3C_6H_2$ (5). A solution of **3** (0.200 g, 0.35 mmol) in CH_2Cl_2 (15 mL) was stirred at room temperature for 4 h, which after removal of the solvent gave the white powder **5** (0.200 g, 0.35 mmol) in quantitative yield.

$^{31}P\{^1H\}$ NMR (CD_2Cl_2): 31.8. ^1H NMR (CD_2Cl_2): 7.33 (s, CH_{Ar}), 6.32 (s, Cp), 1.47 (s, *o*-*t*-Bu), 1.40 (d, $^2J_{HP}$ = 5.8, Me_2P), 1.29 (s, *p*-*t*-Bu). $^{13}C\{^1H\}$ NMR (CD_2Cl_2): 146.7 (s, *o*-C_{Ar}), 144.8 (s, *p*-C_{Ar}), 121.7 (s, *m*-C_{Ar}), *i*-C_{Ar} not observed, 114.3 (s, Cp), 34.9 (s, *o*-CCH_3), 34.5 (s, *p*-CCH_3), 30.3 (s, *o*-CCH_3), 31.7 (s, *p*-CCH_3), 20.4 (d, $^1J_{CP}$ = 17.5, Me_2P).

$Me_2P{-}N(H)$-2,4,6-*t*-$Bu_3C_6H_2$ (6). Attempts to isolate **5** by treatment with pentane and THF gave the phosphane **6** in quantitative yield.

$^{31}P\{^1H\}$ NMR (CD_2Cl_2): 33.3. ^1H NMR (CD_2Cl_2): 7.48 (s, CH_{Ar}), 3.10 (d, $^2J_{HP}$ = 5.8, NH), 1.56 (s, *o*-*t*-Bu), 1.33 (s, *p*-*t*-Bu), 1.09 (d, $^2J_{HP}$ = 6.5, Me_2P). $^{13}C\{^1H\}$ NMR (CD_2Cl_2): 144.5 (d, $^2J_{CP}$ = 3.0, *i*-C_{Ar}), 143.8 (d, $^4J_{CP}$ = 2.2, *o*-C_{Ar}), 141.9 (d, $^5J_{CP}$ = 14.0, *p*-C_{Ar}), 123.6 (d, $^2J_{CP}$ = 1.7, *m*-C_{Ar}), 36.8 (s, *o*-CCH_3), 34.8 (s, *p*-CCH_3), 33.2 (s, *o*-CCH_3), 31.9 (s, *p*-CCH_3), 20.0 (d, $^1J_{CP}$ = 19.5, Me_2P). IR (cm^{-1}, KBr pellet): ν_{NH} 3283 b. MS (EI): m/z 321 (M^+). Anal. Calcd for $C_{20}H_{36}NP$: C, 74.72; H, 11.28. Found: C, 74.44; H, 11.45.

$Me_2P(MeC{=}N{-}ZrCp_2Cl){=}N$-2,4,6-*t*-$Bu_3C_6H_2$ (8a). Acetonitrile (10 mL) was added to **3** (0.288 g, 0.50 mmol) maintained at −30 °C. The resulting solution was stirred for 1 h. The precipitate formed during this reaction was isolated by filtration, washed twice with 10 mL of acetonitrile at −30 °C and then with pentane (2 × 10 mL, −30 °C). The resulting white powder **8a** (0.309 g, 0.50 mmol) was dried under vacuum (quantitative yield).

$^{31}P\{^1H\}$ NMR (C_6D_6): 53.8. ^1H NMR (C_6D_6): 7.51 (s, CH_{Ar}), 6.05 (s, Cp), 1.70 (d, $^3J_{HP}$ = 0.9, MeCP), 1.53 (s, *o*-*t*-Bu), 1.25 (s, *p*-*t*-Bu), 1.20 (d, $^2J_{HP}$ = 8.8, Me_2P). $^{13}C\{^1H\}$ NMR (C_6D_6): 165.0 (d, $^1J_{CP}$ = 14.4 Hz, PC=N), 148.4 (s, *o*-C_{Ar}), 148.1 (s, *p*-C_{Ar}), 136.6 (s, *i*-C_{Ar}), 126.4 (s, *m*-C_{Ar}), 111.6 (s, Cp), 35.1 (s, *o*-CCH_3), 34.7, 34.6 (s, *o*-CCH_3), 32.4 (s, *p*-CCH_3), 31.8 (s, *p*-CCH_3), 28.3 (s, PCMe), 16.9 (d, $^1J_{CP}$ = 25.3, Me_2P). Anal. Calcd for $C_{32}H_{48}ClN_2PZr$: C, 62.15; H, 7.82. Found: C, 62.42; H, 8.05.

$Me_2P(i{-}PrC{=}N{-}ZrCp_2Cl){=}N$-2,4,6-*t*-$Bu_3C_6H_2$ (8b) was prepared by the same procedure as for **8a**: *i*-PrC=N (5 mL),

(24) Samuel, E.; Rausch, M. D. *J. Am. Chem. Soc.* **1973**, *95*, 6263.
(25) Niecke, E.; Nieger, M.; Reichert, F. *Angew. Chem. Int., Ed. Engl.* **1988**, *12*, 1715.

3 (0.360 g, 0.62 mmol). **8b** was obtained as a white powder (0.403 g, 0.62 mmol) in quantitative yield, mp 126–127 °C dec.

$^{31}P\{^1H\}$ NMR (C_6D_6): 49.3. ^1H NMR (C_6D_6): 7.48 (s, CH_{Ar}), 6.21 (s, Cp), 2.61 (sept, $^3J_{HH}$ = 6.7, $CHCH_3$), 1.50 (s, *o-t*-Bu), 1.34 (s, *p-t*-Bu), 1.19 (d, $^2J_{HP}$ = 8.8, Me_2P), 1.08 (d, $^3J_{HH}$ = 6.7, $CHCH_3$). $^{13}C\{^1H\}$ NMR (C_6D_6): 171.5 (d, $^1J_{CP}$ = 15.1, PC=N), 148.8 (s, *o*-C_{Ar}), 148.3 (s, *p*-C_{Ar}), 135.2 (d, $^2J_{CP}$ = 4.5, *i*-C_{Ar}), 127.1 (s, *m*-C_{Ar}), 112.6 (s, Cp), 34.7, 34.6 (s, *o*-CCH_3), 32.4 (s, *p*-CCH_3), 31.8 (s, *o*-CCH_3), 31.7 (s, *p*-CCH_3), 22.8 (s, CH_3CH), 18.6 (d, $^1J_{CP}$ = 27.5, Me_2P). Anal. Calcd for $C_{34}H_{52}ClN_2PZr$: C, 63.17; H, 8.11. Found: C, 63.48; H, 8.56.

General Procedure for the Preparation of Iminophosphoranes 10, 11, 12a,b, and 14–21. To a solution of **2** (0.325 g, 1.00 mmol) in THF (5 mL) at −78 °C was added Cp_2ZrMe_2 (0.251 g, 1.00 mmol) dissolved in 10 mL of THF. The mixture was warmed to room temperature and then cooled to −78 °C. To this solution was added paraformaldehyde (0.030 g), carbon disulfide (0.076 g, 1.00 mmol), (trimethylsilyl)methyl isocyanide (0.113 g, 1.00 mmol), cyclohexyl isocyanide (0.109 g, 1.00 mmol), HCl–pyridine (0.092 g, 0.80 mmol), methyl iodide (0.062 mL, 1.00 mmol), *N*-bromosuccinimide (0.192 g, 1.08 mmol), or chlorophosphane (1.00 mmol). The resulting mixture was warmed to room temperature and was stirred for 2 h. Evaporation of the solvent followed by washing the residue with pentane (2 × 10 mL) led either to a powder or an oil.

$Me_2P(CH_2OZrCp_2Cl)$=N-2,4,6-*t*-$Bu_3C_6H_2$ (10): white powder, 0.607 g, quantitative yield. $^{31}P\{^1H\}$ NMR (C_6D_6): −12.4. ^1H NMR (C_6D_6): 7.59 (s, CH_{Ar}), 5.83 (s, Cp), 4.45 (d, $^2J_{HP}$ = 7.0, CH_2O), 1.66 (s, *o-t*-Bu), 1.43 (s, *p-t*-Bu), 1.26 (d, $^2J_{HP}$ = 11.4, Me_2P). ^{13}C NMR (C_6D_6): 150.7 (s, *i*-C_{Ar}), 141.7 (d, $^2J_{CP}$ = 3.0, *o*-C_{Ar}), 139.1 (s, *p*-C_{Ar}), 122.1 (d, $^4J_{CP}$ = 10.0, *m*-C_{Ar}), 113.6 (s, Cp), 76.8 (d, $^1J_{CP}$ = 94.5, PCH_2O), 36.3 (s, *o*-CCH_3), 34.7 (s, *p*-CCH_3), 32.2 (s, *p*-CCH_3), 31.6 (s, *o*-CCH_3), 15.3 (d, $^1J_{CP}$ = 67.3, Me_2P). Anal. Calcd for $C_{31}H_{47}ClNOPZr$: C, 61.30; H, 7.80. Found: C, 61.01; H, 7.92.

$Me_2P(CS_2ZrCp_2Cl)$=N-2,4,6-*t*-$Bu_3C_6H_2$ (11): two isomers, green powder, quantitative yield. **11a**: $^{31}P\{^1H\}$ NMR (C_6D_6): −18.8 ppm; ^1H NMR (C_6D_6) 7.63 (s, CH_{Ar}), 5.68 (s, Cp), 1.65 (s, *o-t*-Bu), 1.64 (d, $^2J_{HP}$ = 11.9, Me_2P), 1.40 (s, *p-t*-Bu); $^{13}C\{^1H\}$ NMR (C_6D_6) 261.4 (d, $^1J_{CP}$ = 35.2, P–C=S), 142.5 (s, *o*-C_{Ar}), 140.4 (s, *p*-C_{Ar}), 122.4 (s, *m*-C_{Ar}), 113.0 (s, Cp), 36.7 (s, *o*-CCH_3), 33.6 (s, *p*-CCH_3), 32.4 (s, *p*-CCH_3), 33.1 (s, *o*-CCH_3), 19.7 (d, $^1J_{CP}$ = 82.7, Me_2P).

11b: $^{31}P\{^1H\}$ NMR (C_6D_6) −19.3; ^1H NMR (C_6D_6): 7.63 (s, CH_{Ar}), 5.48 (s, Cp), 1.66 (s, *o-t*-Bu), 1.65 (d, $^2J_{HP}$ = 10.9, Me_2P), 1.62 (s, *p-t*-Bu); $^{13}C\{^1H\}$ NMR (C_6D_6) 261.3 (d, $^1J_{CP}$ = 35.2, P–C=S), 142.4 (s, *o*-C_{Ar}), 140.1 (s, *p*-C_{Ar}), 122.4 (s, *m*-C_{Ar}), 109.4 (s, Cp), 36.7 (s, *o*-CCH_3), 33.6 (s, *p*-CCH_3), 32.4 (s, *p*-CCH_3), 32.1 (s, *o*-CCH_3), 19.3 (d, $^1J_{CP}$ = 83.0, Me_2P). Anal. Calcd for $C_{31}H_{45}ClNPS_2Zr$: C, 56.97; H, 6.94. Found: C, 56.62; H, 6.52.

Me_2P–N[C($ZrCp_2Cl$)=NCH_2SiMe_3]-2,4,6-*t*-$Bu_3C_6H_2$ (12a): white powder, 0.655 g, 95% yield. $^{31}P\{^1H\}$ NMR (C_6D_6): 67.9. ^1H NMR (C_6D_6): 7.46 (s, CH_{Ar}), 6.09 (s, Cp), 2.91 (s, CH_2Si), 1.46 (s, *o-t*-Bu), 1.22 (s, *p-t*-Bu), 1.04 (d, $^2J_{PH}$ = 8.5, Me_2P), 0.24 (s, $SiMe_3$). $^{13}C\{^1H\}$ NMR (C_6D_6): 207.1 ($^2J_{CP}$ = 43.3, P–N–C=N), 148.8 (s, *o*-C_{Ar}), 148.3 (s, *p*-C_{Ar}), 136.4 (s, *i*-C_{Ar}), 126.8 (s, *m*-C_{Ar}), 114.5, 110.7 (s, Cp), 42.3 (s, CH_2Si), 38.5 (s, *p*-CCH_3), 35.1, 35.0 (s, *o*-CCH_3), 34.7 (s, *o*-CCH_3), 31.5 (s, *p*-CH_3–C), 17.8 (d, $^1J_{CP}$ = 27.1, Me_2P), 1.1 (s, $SiMe_3$). IR (cm^{-1}, THF): ν_{CN} 1601 s. Anal. Calcd for $C_{35}H_{56}ClN_2PSiZr$: C, 60.87; H, 8.17. Found: C, 60.66; H, 8.10.

Me_2P–N[C($ZrCp_2Cl$)=NC_6H_{11}]-2,4,6-*t*-$Bu_3C_6H_2$ (12b): white powder, 0.618 g, 90% yield. $^{31}P\{^1H\}$ NMR (CD_2Cl_2): 69.2. ^1H NMR (CD_2Cl_2): 7.75 (s, CH_{Ar}), 6.24 (s, Cp), 3.00 (s, HCN), 1.67–1.32 (m, CH_2), 1.54 (s, *o-t*-Bu), 1.36 (s, *p-t*-Bu), 1.00 (d, $^2J_{PH}$ = 8.6, Me_2P). $^{13}C\{^1H\}$ NMR (CD_2Cl_2): 204.2 ($^2J_{CP}$ = 45.5, C=N), 148.2 (s, *p*-C_{Ar}), 147.6 (s, *o*-C_{Ar}), 135.1 (s, *i*-C_{Ar}), 127.0 (s, *m*-C_{Ar}), 110.1 (s, Cp), 57.1 (s, C=NCH), 38.3 (s, *o*-CCH_3), 34.8 and 34.7 (s, *o*-CCH_3), 32.3 (s, *p*-CCH_3), 31.5 (s, *o*-CH_2), 31.1 (s, *p*-CCH_3), 25.4 (s, *p*-CH_2), 25.3 (s, *m*-CH_2), 18.1 (d, $^1J_{CP}$ = 26.2, Me_2P). Anal. Calcd for $C_{37}H_{56}ClN_2PZr$: C, 64.73; H, 8.22. Found: C, 64.34; H, 8.56.

$Me_2P(H)$=N-2,4,6-*t*-$Bu_3C_6H_2$ (14): white powder, 0.231 g, 90% yield. ^{31}P NMR (C_6D_6): 8.8 ($^1J_{PH}$ = 598.6). ^1H NMR (C_6D_6): 7.38 (s, CH_{Ar}), 3.21 (d, $^1J_{HP}$ = 598.6, PH), 1.39 (s, *o-t*-Bu), 1.37 (s, *p-t*-Bu), 1.33 (d, $^2J_{HP}$ = 16.9, Me_2P). $^{13}C\{^1H\}$ NMR (C_6D_6): *i*-C_{Ar} not observed, 141.9 (s, *p*-C_{Ar}), 134.2 (s, *o*-C_{Ar}), 122.1 (s, *m*-C_{Ar}), 34.3 (d, $^1J_{CP}$ = 86.5, Me_2P), 34.8 (s, *p*-CCH_3), 32.4 (s, *p*-CCH_3), 31.9 (s, *o*-CCH_3), 30.8 (s, *o*-CCH_3). Anal. Calcd for $C_{20}H_{36}NP$: C, 74.72; H, 11.28. Found: C, 74.66; H, 11.63.

Me_3P=N-2,4,6-*t*-$Bu_3C_6H_2$ (15): white powder, 0.302 g, 90% yield. $^{31}P\{^1H\}$ NMR (C_6D_6): −22.4. ^1H NMR (C_6D_6): 7.16 (s, CH_{Ar}), 1.62 (s, *o-t*-Bu), 1.45 (s, *p-t*-Bu), 1.09 (s, $^2J_{PH}$ = 11.4, Me_3P). $^{13}C\{^1H\}$ NMR (C_6D_6): 142.1 (d, $^3J_{CP}$ = 4.3, *o*-C_{Ar}), 14.2 (s, *i*-C_{Ar}), 139.2 (d, *p*-C_{Ar}), 122.2 (s, *m*-C_{Ar}), 36.5 (s, *o*-CCH_3 and *p*-CCH_3), 32.5 (s, *p*-CCH_3), 31.7 (s, *o*-CCH_3), 20.1 (d, $^1J_{CP}$ = 74.3, Me_3P). Anal. Calcd for $C_{21}H_{38}NP$: C, 75.17; H, 11.41. Found: C, 75.56; H, 11.12.

$Me_2P(Br)$=N-2,4,6-*t*-$Bu_3C_6H_2$ (16): pale brown powder, 0.360 g, 90% yield. $^{31}P\{^1H\}$ NMR (C_6D_6): −25.4. ^1H NMR (C_6D_6): 7.51 (s, CH_{Ar}), 1.79 (d, $^2J_{HP}$ = 14.0, Me_2P), 1.50 (s, *o-t*-Bu), 1.41 (s, *p-t*-Bu). $^{13}C\{^1H\}$ NMR (C_6D_6): 140.7 (s, *i*-C_{Ar}), 140.6 (s, *o*-C_{Ar}), 140.3 (s, *p*-C_{Ar}), 121.9 (s, *m*-C_{Ar}), 35.9 (s, *p*-CCH_3), 34.7 (s, *o*-CCH_3), 32.1 (s, *p*-CCH_3), 31.6 (s, *o*-CCH_3), 20.6 (d, $^1J_{CP}$ = 95.0, Me_2P). Anal. Calcd for $C_{20}H_{35}BrNP$: C, 59.99; H, 8.81. Found: C, 60.35; H, 8.51.

Iminophosphoranes (17–20, 21) were obtained as oils. Only iminophosphorane **20** (0.374 g, 85% yield) was fully characterized.

17: $^{31}P\{^1H\}$ NMR (C_6D_6) −5.3 (d, $^1J_{PP}$ = 259.8, Ph_2P), −22.0 (d, $^1J_{PP}$ = 259.8, Me_2P=).

18: $^{31}P\{^1H\}$ NMR (C_6D_6) −18.8 (d, $^1J_{PP}$ = 240.0, Me_2P=), −53 (d, J_{PP} = 240.0, Me_2P).

19: $^{31}P\{^1H\}$ NMR (C_6D_6) 130.2 (d, $^1J_{PP}$ = 320.0, *i*-Pr_2NPCl), −21.2 (d, $^1J_{PP}$ = 320.0, Me_2P=).

20: $^{31}P\{^1H\}$ NMR (C_6D_6) 110.3 ($^1J_{PP}$ = 299.4, Me_2NP), −14.2 (d, $^1J_{PP}$ = 299.4, Me_2P=); ^1H NMR (C_6D_6) 7.43 (s, CH_{Ar}), 2.45 (dd, $^3J_{HP}$ = 8.6, $^4J_{HP}$ = 6.0, NMe_2), 1.64 (s, *o-t*-Bu), 1.52 (dd, $^2J_{HP}$ = 12.0, $^3J_{HP}$ = 6.0, Me_2P), 1.40 (s, *p-t*-Bu); $^{13}C\{^1H\}$ NMR (C_6D_6) 144.6 (s, *i*-C_{Ar}), 142.3 (s, *o*-C_{Ar}), 138.7 (s, *p*-C_{Ar}), 121.4 (s, *m*-C_{Ar}), 44.0 (dd, $^2J_{CP}$ = 16.0, $^3J_{CP}$ = 7.5, NMe_2), 36.7 (s, *o*-CCH_3), 34.8 (s, *p*-CCH_3), 32.5 (s, *p*-CCH_3), 32.2 (s, *o*-CCH_3), 21.8 (dd, $^1J_{CP}$ = 57.3, $^2J_{CP}$ = 21.7, Me_2P). Anal. Calcd for $C_{24}H_{47}N_3P_2$: C, 65.57; H, 10.77. Found: C, 65.83; H, 10.34.

21: $^{31}P\{^1H\}$ NMR (C_6D_6) 27.2 (d, $^1J_{PP}$ = 67.0, Ph_2P=O), −28.1 (d, $^1J_{PP}$ = 67.0, Me_2P).

$Me_2P(CH_2NMe_2)$=N-2,4,6-*t*-$Bu_3C_6H_2$ (22) and [$Me_2P(CH_2NMe_2)$–N(H)-2,4,6-*t*-$Bu_3C_6H_2$]$^+Cl^-$ (23). To a suspension of H_2C=NMe_2Cl (0.149 g, 1.60 mmol) in THF (5 mL) at 0 °C was added **3** (0.521 g, 0.80 mmol) in THF (5 mL). The mixture was warmed to room temperature and filtered and the solvent evaporated to dryness. The resulting powder was washed with pentane (3 × 5 mL) to extract **22**. Compound **23** remained insoluble in pentane and was extracted with THF (3 × 5 mL).

22 (0.227 g, 0.59 mmol, 70%): $^{31}P\{^1H\}$ NMR (C_6D_6) −13.6; ^1H NMR (C_6D_6) 7.57 (s, CH_{Ar}), 2.59 (d, $^2J_{HP}$ = 8.0, CH_2P), 1.87 (s, Me_2N), 1.64 (s, *o-t*-Bu), 1.44 (s, *p-t*-Bu), 1.33 (d, $^2J_{HP}$ = 11.5, Me_2P); $^{13}C\{^1H\}$ NMR (C_6D_6) 150.3 (s, *i*-C_{Ar}), 142.1 (s, *o*-C_{Ar}), 139.2 (s, *p*-C_{Ar}), 122.2 (s, *m*-C_{Ar}), 61.6 (d, $^1J_{CP}$ = 94.2, CH_2P), 48.2 (d, $^3J_{CP}$ = 6.5, Me_2N), 36.6 (s, *o*-CCH_3), 35.0 (s, *p*-CCH_3), 32.4 (s, *p*-CCH_3), 31.9 (s, *o*-CCH_3), 16.7 (d, $^1J_{CP}$ = 71.8, Me_2P). Anal. Calcd for $C_{23}H_{43}N_2P$: C, 72.97; H, 11.45. Found: C, 73.25; H, 11.14.

23 (0.081 g, 0.16 mmol, 20%): mp 90 °C; $^{31}P\{^1H\}$ NMR (C_6D_6) 51.7; ^1H NMR (C_6D_6) 7.56 (d, $^2J_{PH}$ = 9.2, NH), 7.38 (s, CH_{Ar}), 3.75 (d, $^2J_{HP}$ = 6.0, CH_2P), 1.92 (s, NMe_2), 1.88 (d, $^2J_{HP}$ = 13.5, Me_2P), 1.42 (s, *p-t*-Bu), 1.24 (s, *o-t*-Bu); $^{13}C\{^1H\}$ NMR (C_6D_6) 151.4 (*o*-C_{Ar}), 149.2 (*p*-C_{Ar}), 124.6 (*m*-C_{Ar}), 56.0 (d, $^1J_{CP}$ = 85.0, CH_2P), 47.9 (d, $^3J_{CP}$ = 7.73, NMe_2), 37.4 (*o*-CCH_3), 35.1 (*p*-CCH_3), 34.4 (*o*-CCH_3), 31.76 (*p*-CCH_3), 11.4 (d, $^1J_{CP}$ = 64.7,

Me_2P). Anal. Calcd for $C_{23}H_{44}IN_2P$: C, 54.54; H, 8.75. Found: C, 54.17; H, 8.97.

[$Me_2P(H)-N(H)$-2,4,6-*t*-$Bu_3C_6H_2$]$^+OSO_2CF_3^-$ (24). To a solution of **3** (0.577 g, 1.00 mmol) prepared as above, in THF (10 mL) was added triflic acid (0.150 mL, 1.00 mmol) at −78 °C. The solution was warmed to room temperature and then evaporated to give a white paste, which was washed with pentane (3 × 10 mL). **24** was obtained as a white powder (0.448 g, 0.95 mmol, 95%).

^{31}P NMR (CD_2Cl_2): 32.3 (d, $^1J_{PH}$ = 518.0). ^1H NMR (CD_2Cl_2): 7.36 (s, CH_{Ar}), 7.31 (d, $^1J_{HP}$ = 518.0, PH), 5.83 (d, $^2J_{HP}$ = 9.9, NH), 1.86 (d, $^2J_{HP}$ = 14.0, Me_2P), 1.40 (s, *o*-*t*-Bu), 1.26 (s, *p*-*t*-Bu). $^{13}C\{^1H\}$ NMR (CD_2Cl_2): *i*-C_{Ar} not observed, 149.9 (s, *p*-C_{Ar}), 134.0 (d, $^4J_{CP}$ = 5.0, *m*-C_{Ar}), 121.9 (d, $^3J_{CP}$ = 2.0, *o*-C_{Ar}), 36.7 (s, *o*-CCH_3), 34.8 (s, *p*-CCH_3), 32.8 (s, *o*-CCH_3), 30.3 (s, *p*-CCH_3), 7.7 (d, $^1J_{CP}$ = 67.2, Me_2P). Anal. Calcd for $C_{21}H_{37}F_3NO_3PS$: C, 53.49; H, 7.91. Found: C, 53.73; H, 7.59.

[$Me_3P-N(H)$-2,4,6-*t*-$Bu_3C_6H_2$]$^+OSO_2CF_3^-$ (25) was prepared by the same procedure as for **24** with methyl trifluoromethanesulfonate (0.164 g, 1.00 mmol): 0.461 g, 0.95 mmol, 95%.

$^{31}P\{^1H\}$ NMR (CD_2Cl_2): 53.8. ^1H NMR (CD_2Cl_2): 7.34 (s, CH_{Ar}), 6.06 (d, $^2J_{HP}$ = 9.8, NH), 1.86 (d, $^2J_{HP}$ = 13.0, Me_3P), 1.39 (s, *o*-*t*-Bu), 1.25 (s, *p*-*t*-Bu). $^{13}C\{^1H\}$ NMR (CD_2Cl_2): *i*-C_{Ar} not observed, 150.6 (d, $^5J_{CP}$ = 3.0, *p*-C_{Ar}), 149.5 (d, $^4J_{CP}$ = 5.0, *m*-C_{Ar}), 124.5 (d, $^3J_{CP}$ = 2.0, *o*-C_{Ar}), 37.0 (s, *o*-CCH_3), 34.9 (s, *p*-CCH_3), 33.3 (s, *o*-CCH_3), 31.2 (s, *p*-CCH_3), 13.6 (d, $^2J_{CP}$ = 67.0, Me_3P). Anal. Calcd for $C_{22}H_{39}F_3NO_3PS$: C, 54.42; H, 8.09. Found: C, 54.20; H, 8.28.

$Me_2P-N(P{=}N$-2,4,6-*t*-$Bu_3C_6H_2$)-2,4,6-*t*-$Bu_3C_6H_2$ (26). A solution of Cp_2ZrMe_2 (0.252 g, 1.00 mmol) in toluene (15 mL) was reacted with **2** (0.326 g, 1.00 mmol) in toluene (5 mL) at −78 °C. The reaction mixture was stirred for 15 min at -78 °C, and then **2** (0.326 g, 1.00 mmol) in toluene (5 mL) was added dropwise at −78 °C. After 30 min at −78 °C, the reaction mixture was warmed to room temperature. After 2 h at room temperature, the solvent was removed and the residue was extracted with pentane (10 mL). Evaporation of the solvent gave **26** as a red oil (0.550 g, 0.90 mmol, 90%). $^{31}P\{^1H\}$ NMR (CD_2Cl_2): 322.4 (d, $^2J_{PP}$ = 11.7, P=N), 98.8 (d, $^2J_{PP}$ = 11.7, PMe_2). ^1H NMR (CD_2Cl_2): 7.65 (s, P=NCH_{Ar}), 7.58 (s, $PNCH_{Ar}$), 1.77 (s, P=N-*p*-*t*-Bu), 1.65 (s, P=N-*o*-*t*-Bu), 1.43 (s, P=N-*o*-*t*-Bu), 1.34 (s, P=N-*p*-*t*-Bu), 1.22 (d, $^2J_{HP}$ = 17.8, Me_2P). Anal. Calcd for $C_{38}H_{64}N_2P_2$: C, 74.71; H, 10.56. Found: C, 74.52; H, 10.22.

[$Me_2P-N(H)$-2,4,6-*t*-$Bu_3C_6H_2$]$_2NiCl_2$ (28a). To a suspension of $NiCl_2$ (0.065 g, 0.50 mmol) in THF (5 mL) was added **3** (0.577 g, 1.00 mmol) in THF (10 mL) at −78 °C. The mixture was warmed to room temperature and then stirred for 5 h. After evaporation of the solvent, the residue was washed with pentane (20 mL). Filtration and evaporation of the solvent gave **28a** as a red powder (0.695 g, 0.90 mmol, 90%).

$^{31}P\{^1H\}$ NMR (C_6D_6): 45.0. ^1H NMR (C_6D_6): 7.41 (s, CH_{Ar}), 4.72 (d, $^2J_{HP}$ = 10.0, NH), 4.77 (d, $^2J_{HP}$ = 10.0, NH), 1.68 (s, *o*-*t*-Bu), 1.37 (d, $^2J_{HP}$ = 3.1, Me_2P), 1.35 (d, $^2J_{HP}$ = 3.1, Me_2P), 1.30 (s, *p*-*t*-Bu). $^{13}C\{^1H\}$ NMR (C_6D_6): *i*-Cp not observed, 147.5 (s, *o*-C_{Ar}), 144.4 (s, *p*-C_{Ar}), 120.8 (s, *m*-C_{Ar}), 34.8 (s, *o*-CCH_3), 32.2 (s, *p*-CCH_3), 31.3 (s, *o*-CCH_3), 29.1 (s, *p*-CCH_3), 11.6 (d, $^1J_{CP}$ = 14.0, MeP), 11.3 (d, $^1J_{CP}$ = 14.0, MeP). MS (DCI, CH_4): *m/e* 774 ([M + 1]$^+$). Anal. Calcd for $C_{40}H_{72}Cl_2N_2NiP_2$: C, 62.18; H, 9.39. Found: C, 61.95; H, 9.52.

[$Me_2P-N(H)$-2,4,6-*t*-$Bu_3C_6H_2$]$_2PdCl_2$ (28b). To a suspension of $PdCl_2$ (0.088 g, 0.50 mmol) in THF (5 mL) was added **3** (0.577 g, 1.00 mmol) in THF (10 mL) at −78 °C. The mixture was warmed to room temperature and then stirred for 24 h. The residue obtained after evaporation of the solvent was washed with pentane (30 mL) and then filtered. Evaporation of the solvent gave **28b** as a brown powder (0.656 g, 0.85 mmol, 85%).

$^{31}P\{^1H\}$ NMR (C_6D_6): 52.1. ^1H NMR (C_6D_6): 7.38 (s, CH_{Ar}), 5.16 (s, NH), 1.58 (s, *o*-*t*-Bu), 1.28 (s, *p*-*t*-Bu), Me_2P (complex). $^{13}C\{^1H\}$ NMR (C_6D_6): *i*-C_{Ar} not detected, 151.3, 150.9 (*o*-C_{Ar}), 134 and 33.6 (*p*-C_{Ar}), 124.0 and 123.7 (*m*-C_{Ar}), 15.5 ($^1J_{CP}$ = 16.1, Me_2P). MS (DCI, CH_4): *m/e* 821 ([M + 1]$^+$). Anal. Calcd for $C_{40}H_{72}Cl_2N_2P_2Pd$: C, 58.56; H, 8.84. Found: C, 58.87; H, 8.24.

Table 4. Positional Parameters and Equivalent Thermal Parameters[a]

atom	*x/a*	*y/b*	*z/c*	*U*(iso), Å^2
Zr(1)	0.23740(4)	0.25466(5)	0.24495(4)	0.0392
Cl(1)	0.1634(1)	0.1549(2)	0.1376(1)	0.0621
P(1)	0.4827(2)	0.3190(2)	0.3779(2)	0.0673
Si(1)	0.3727(1)	0.1403(1)	0.0171(1)	0.0489
N(1)	0.3614(3)	0.2103(3)	0.1861(3)	0.0343
N(2)	0.4753(3)	0.2793(3)	0.2747(3)	0.0407
C(1)	0.2000(5)	0.2571(6)	0.3965(5)	0.0630
C(2)	0.1271(5)	0.2162(6)	0.3583(5)	0.0583
C(3)	0.1563(6)	0.1386(6)	0.3272(5)	0.0643
C(4)	0.2472(5)	0.1285(5)	0.3460(5)	0.0572
C(5)	0.2733(5)	0.2016(6)	0.3902(5)	0.0567
C(6)	0.1454(7)	0.3552(6)	0.1495(8)	0.0666
C(7)	0.2344(7)	0.3814(6)	0.1443(7)	0.0753
C(8)	0.2577(7)	0.4135(7)	0.220(1)	0.0756
C(9)	0.190(1)	0.4079(8)	0.2710(8)	0.0884
C(10)	0.1186(7)	0.3707(8)	0.228(1)	0.0839
C(11)	0.3897(4)	0.2579(4)	0.2464(4)	0.0331
C(12)	0.4086(4)	0.1526(5)	0.1300(5)	0.0458
C(13)	0.5610(4)	0.2528(5)	0.2366(4)	0.0351
C(14)	0.6023(4)	0.3091(4)	0.1793(4)	0.0391
C(15)	0.6922(4)	0.2919(5)	0.1577(5)	0.0493
C(16)	0.7402(4)	0.2240(5)	0.1897(5)	0.0441
C(17)	0.6962(4)	0.1686(5)	0.2413(5)	0.0436
C(18)	0.6066(4)	0.1784(4)	0.2655(5)	0.0400
C(19)	0.3035(5)	0.0417(6)	0.0013(6)	0.0659
C(20)	0.3156(5)	0.2366(6)	−0.0271(5)	0.0698
C(21)	0.4801(6)	0.1221(6)	−0.0390(6)	0.0723
C(22)	0.5993(6)	0.3599(9)	0.3852(8)	0.0888
C(23)	0.4271(9)	0.4174(9)	0.3826(8)	0.1163
C(24)	0.5613(4)	0.3877(5)	0.1327(5)	0.0467
C(25)	0.8409(4)	0.2070(5)	0.1675(5)	0.0473
C(26)	0.5735(4)	0.1010(5)	0.3181(5)	0.0460
C(27)	0.630(1)	0.434(1)	0.075(1)	0.0615
C(28)	0.460(1)	0.409(1)	0.147(1)	0.0674
C(29)	0.488(1)	0.355(1)	0.073(1)	0.0526
C(30)	0.569(1)	0.371(1)	0.041(1)	0.0722
C(31)	0.529(1)	0.453(1)	0.194(1)	0.0781
C(32)	0.611(2)	0.472(1)	0.152(2)	0.0798
C(33)	0.8782(5)	0.2779(7)	0.1131(6)	0.0767
C(34)	0.8970(5)	0.2015(7)	0.2459(6)	0.0653
C(35)	0.8475(6)	0.1232(7)	0.1190(7)	0.0890
C(36)	0.4745(5)	0.0999(5)	0.3408(5)	0.0510
C(37)	0.5894(6)	0.0181(5)	0.2677(7)	0.0725
C(38)	0.6288(6)	0.0956(7)	0.3998(6)	0.0697

[a] Carbons C(27), C(28), C(29), C(30), C(31), and C(32), as well as hydrogens bonded to these carbons, were refined with a multiplicity of 0.5.

[$Me_2P-N(H)$-2,4,6-*t*-$Bu_3C_6H_2$]$W(CO)_5$ (30). To a solution of **3** (0.577 g, 1 mmol), prepared as above, in THF (10 mL) was added $W(CO)_5THF$ (0.175 g, 1 mmol) in THF (60 mL) at −78 °C. The mixture was stirred for 30 min at −78 °C and then warmed to room temperature. The solution was stirred for 3 h and then evaporated to give a residue which was washed with pentane (20 mL). Filtration and evaporation of pentane gave **30** as a yellow oil (0.613 g, 0.95 mmol, 95%).

$^{31}P\{^1H\}$ NMR (C_6D_6): 35.1. ^1H NMR (C_6D_6): 7.33 (s, CH_{Ar}), 3.56 (s, NH), 1.36 (s, *o*-*t*-Bu), 1.29 (d, $^2J_{HP}$ = 4.8, Me_2P), 1.26 (s, *p*-*t*-Bu). $^{13}C\{^1H\}$ NMR (C_6D_6): 199.9 (d, $^2J_{PCO}$ = 21.0, CO), 197.8 (d, $^2J_{PCO}$ = 7.6, CO), 149.8 (d, $^3J_{CP}$ = 3.0, *o*-C_{Ar}), 147.9 (s, *p*-C_{Ar}), 132.2 ($^2J_{CP}$ = 9.0, *o*-C_{Ar}), 124.2 (s, *m*-C_{Ar}), 38.2 (s, *o*-CCH_3), 34.7 (s, *p*-CCH_3), 34.4 (s, *o*-CCH_3), 31.8 (s, *p*-CCH_3), 24.0 (d, $^1J_{CP}$ = 32.0, Me_2P). IR (cm^{-1}, THF): ν_{CO} 1931, 1974 s. MS (DCI, CH_4): *m/e* 647 ([M + 1]$^+$). Anal. Calcd for $C_{25}H_{36}NO_5PW$: C, 46.52; H, 5.62. Found: C, 46.02; H, 5.98.

Structure Determination of 12a. A clear colorless crystal was used for data collection on an ENRAF-Nonius CAD 4 diffractometer using molybdenum radiation. Lattice parameters were determined from 25 centered reflections within 8 < θ < 15°. The measurement was corrected by taking into account Lorentz and polarization factors; absorption correction

was performed using the Difabs program. The structure was solved using the CRYSTALS package. All non-hydrogen atoms were refined with anisotropic parameters. Hydrogen atom positions were located using a difference Fourier map and recalculated; their contributions were introduced in the calculation but not refined. One of the *tert*-butyl groups (central atom C(24)) was disordered. For the sake of clarity, only one of the two positions is shown on the ORTEP view. The final difference Fourier map did not show any peak higher than 0.7 e/Å^3.

Positional parameters and equivalent thermal parameters appear in Table 4.

Acknowledgment. Thanks are due to the CNRS for financial support of this work.

Supplementary Material Available: Tables of bond length and angle values, anisotropic thermal parameters, and H atom positional parameters for **12a** (13 pages). This material is contained in many libraries on microfiche, immediately follows this article in the microfilm version of the journal, and can be ordered from the ACS; see any current masthead page for ordering information.

OM940717T

Hydrocarbon-Bridged Metal Complexes. 32.[†,1] Addition of Chalcogen Cluster Anions $[Fe_2(CO)_6E_2]^{2-}$ (E = S, Te) to Unsaturated Hydrocarbons of Cationic Complexes: Synthesis and Structure of New μ-Hydrocarbon Complexes

Stephan Hüffer, Kurt Polborn, and Wolfgang Beck*

Institut für Anorganische Chemie der Universität München, Meiserstrasse 1, 80333 München, Germany

Received September 26, 1994[⊗]

The addition of the butterfly chalcogen-bridged dianions $[(\mu_2\text{-E})Fe_2(CO)_6]^{2-}$ (E = S, Te) to coordinated, unsaturated hydrocarbons of the cationic complexes $[(OC)_5Re(\eta^2\text{-}C_2H_4)]^+$, $[Cp(OC)_3W(\eta^2\text{-}C_2H_4)]^+$, $[Cp(OC)_2Fe(\eta^2\text{-}C_2H_4)]^+$, $[(OC)_3Fe(\eta^5\text{-}C_6H_7)]^+$, and $[(OC)_3Mo(\eta^7\text{-}C_7H_7)]^+$ gives a series of μ-hydrocarbon heterotetrametallic complexes. Elimination of ethylene from $\{(OC)_3Fe[\mu_2\text{-}TeCH_2CH_2Re(CO)_5]\}_2$ yields the carbonyliron tellurium cluster $\{(OC)_3Fe[\mu_3\text{-}TeRe(CO)_5]\}_2$. The structures of the latter complex and of $\{(OC)_3Fe[\mu_2\text{-}SCH_2CH_2Re(CO)_5]\}_2$ were determined by X-ray diffraction.

Introduction

Currently there is great interest in the synthesis and characterization of chalcogen-containing complexes.[2,3] Whereas metal sulfide clusters have a long chemical history,[4,5] the corresponding tellurium compounds have only recently been investigated.[6,7]

Of the mixed-chalcogen iron clusters, especially the dinuclear group VI bridged complexes have proven to be useful starting materials to generate a wide range of novel cluster compounds. Many of the compounds $Fe_2(CO)_6E_2$, $Fe_2(CO)_6(ER)_2$, and $Fe_3(CO)_9E_2$ (E = S, Se, Te) have first been synthesized in the laboratory of Hieber.[5,8] The structures of the dimers were proposed on the basis of infrared spectra and dipole moment studies[9] and finally established by Dahl and Wei by X-ray analyses of $Fe_2(CO)_6E_2$, $Fe_3(CO)_9E_2$ (E = S, Se), and $[C_2H_5SFe(CO)_3]_2$.[10] Dahl introduced the term "bent metal–metal bonds" for these complexes.[11]

The efficient, high-yield synthesis of $Li_2[Fe_2(CO)_6S_2]$ by reduction of $[Fe_2(CO)_6S_2]$ (a mimic of organic disulfides[12]) with hydridotriethylborate was first described by Seyferth,[12] who developed a rich chemistry with this dianion.[13] This sulfur-centered nucleophile may be alkylated[12] and has been used to generate the series of nido cluster compounds $(\mu\text{-}L_nMS_2)Fe_2(CO)_6$ by reaction with various main-group and transition-element halides.[13,14]

The corresponding tellurium dianion can also be generated by reduction of $Te_2Fe_2(CO)_6$.[15] More convenient is the direct reaction of $Na_2Fe(CO)_4$ with elemental tellurium reported by Whitmire.[16] Recently it has been shown that the cluster anion $[Te_6Fe_8(CO)_{24}]^{2-}$ also might serve as a source of $[Fe_2(CO)_6Te_2]^{2-}$.[17]

A strategy for the synthesis of μ-hydrocarbon transition-metal complexes is the addition of an anionic metal complex, containing a nucleophilic heteroatom, to coordinated unsaturated hydrocarbons.[18] In this communication we report the use of the dianions $[(\mu\text{-E})_2Fe_2(CO)_6]^{2-}$ (E = S, Te) as nucleophiles. Addition of common S-nucleophiles (SR^-, SCN^-) to coordinated, unsaturated hydrocarbons has been reported.[19]

[†] Dedicated to Professor Lawrence F. Dahl on the occasion of his 65th birthday.

[⊗] Abstract published in *Advance ACS Abstracts*, December 15, 1994.

(1) Part 31: Weinrich, W.; Robl, C.; Beck, W. *J. Organomet. Chem.*, in press.

(2) E.g.: Herrmann, W. A. *Angew. Chem., Int. Ed. Engl.* **1986**, *25*, 57. Whitmire, K. H. *J. Coord. Chem.* **1988**, *17*, 95–203. Wachter, J. *Angew. Chem., Int. Ed. Engl.* **1989**, *28*, 1613.

(3) Roof, L. C.; Kolis, J. W. *Chem. Rev.* **1993**, *93*, 1037–1080.

(4) Roussin, Z. *C. R. Hebd. Seances Acad. Sci.* **1858**, *46*, 224; *Liebigs Ann. Chem.* **1858**, *107*, 120; *Ann. Chim. Phys.* **1858**, (3)*52*, 258.

(5) Brendel, G. Ph.D. Dissertation, Technische Hochschule München, 1956, pp 47–55. Hieber, W.; Gruber, J. *Z. Anorg. Allg. Chem.* **1958**, *296*, 91–104.

(6) Lesch, D. A.; Rauchfuss, T. B. *Organometallics* **1982**, *1*, 499–506. Lesch, D. A.; Rauchfuss, T. B. *Inorg. Chem.* **1981**, *20*, 3583–3589. Bachmann, R. E.; Whitmire, K. H. *J. Organomet. Chem.* **1994**, *479*, 31–35 and references cited therein.

(7) Ward, M. D. *Coord. Chem. Rev.* **1992**, *115*, 1–103.

(8) Hieber, W.; Spacu, P. *Z. Anorg. Allg. Chem.* **1937**, *233*, 353–364. Hieber, W.; Scharfenberg, C. *Chem. Ber.* **1940**, *73*, 1012–1021.

(9) Hieber, W.; Beck, W. *Z. Anorg. Allg. Chem.* **1960**, *305*, 265–273. Kettle, S. F. A.; Orgel, L. E. *J. Chem. Soc.* **1960**, 3890–3891. Beck, W.; Stetter, K. H.; Tadros, S.; Schwarzhans, K. E. *Z. Anorg. Allg. Chem.* **1968**, *100*, 3944–3954. Kostiner, E.; Reddy, M. L. N.; Urch, D. S.; Massey, A. G. *J. Organomet. Chem.* **1968**, *15*, 383–395. Bor, G. *J. Organomet. Chem.* **1975** *94*, 181–188.

(10) Wei, C. H.; Dahl, L. F. *Inorg. Chem.* **1965**, *4*, 1–11; **1965**, *4*, 493–499. Campana, C. F.; Lo, F. Y.; Dahl, L. F. *Inorg. Chem.* **1979**, *18*, 3060–3064. Wei, C. H.; Dahl, L. F. *Inorg. Chem.* **1963**, *2*, 328–333.

(11) Dahl, L. F.; Martell, C.; Wampler, D. L. *J. Am. Chem. Soc.* **1961**, *83*, 1761–1762. Teo, B. K.; Hall, M. B.; Fenske, R. F.; Dahl, L. F. *Inorg. Chem.* **1975**, *14*, 3103–3117.

(12) Seyferth, D.; Henderson, R. S.; Song, L. C. *Organometallics* **1982**, *1*, 125–133.

(13) Seyferth, D.; Womack, G. B.; Song, L. C.; Cowie, M. B.; Hames, W. *Organometallics* **1983**, *2*, 928–930. Seyferth, D.; Gallagher, K. *J. Organomet. Chem.* **1981**, *218*, C5–C10. Seyferth, D.; Song, L. C.; Henderson, R. S. *J. Am. Chem. Soc.* **1981**, *103*, 5103–5107. Seyferth, D.; Henderson, R. S. *J. Am. Chem. Soc.* **1979**, *101*, 508–509. Seyferth, D.; Song, L. C.; Henderson, R. S. *J. Organomet. Chem.* **1980**, *192*, C1–C5. Seyferth, D.; Gallagher, M. K. *Organometallics* **1986**, *5*, 539–548.

(14) Nöth, H.; Rattay, W. *J. Organomet. Chem.* **1986**, *308*, 131–152.

(15) Mathur, P.; Reddy, V. D. *J. Organomet. Chem.* **1990**, *385*, 363–368.

(16) Bachman, R. E.; Whitmire, K. H. *Organometallics* **1993**, *12*, 1988–1992.

(17) Shieh, M.; Shieh, M.-H. *Organometallics* **1994**, *13*, 920–924.

(18) Beck, W.; Niemer, B.; Wieser, M. *Angew. Chem., Int. Ed. Engl.* **1993**, *32*, 923–949.

(19) Davies, S. G.; Green, M. L. H.; Mingos, D. M. P. In *Reactions of Coordinated Ligands*; Braterman, P. S., Ed.; Plenum Press: New York, 1986; Vol. 1, pp 897–938.

0276-7333/95/2314-0953$09.00/0

Scheme 1

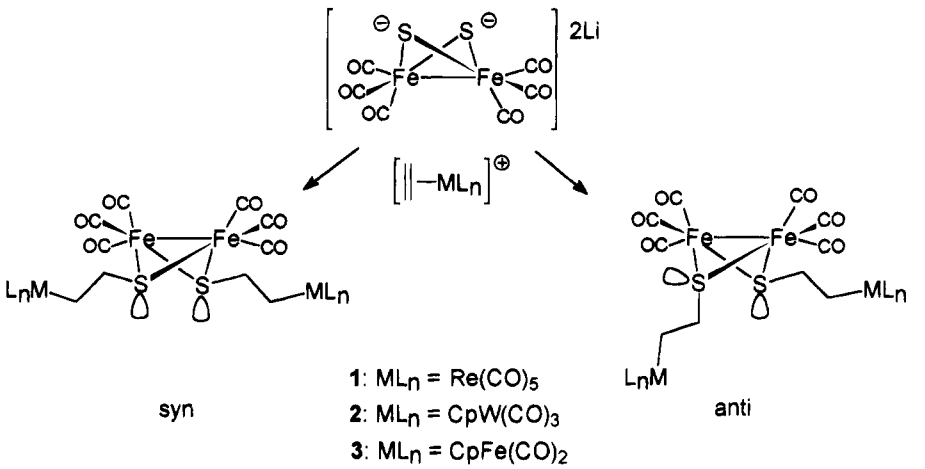

Scheme 2

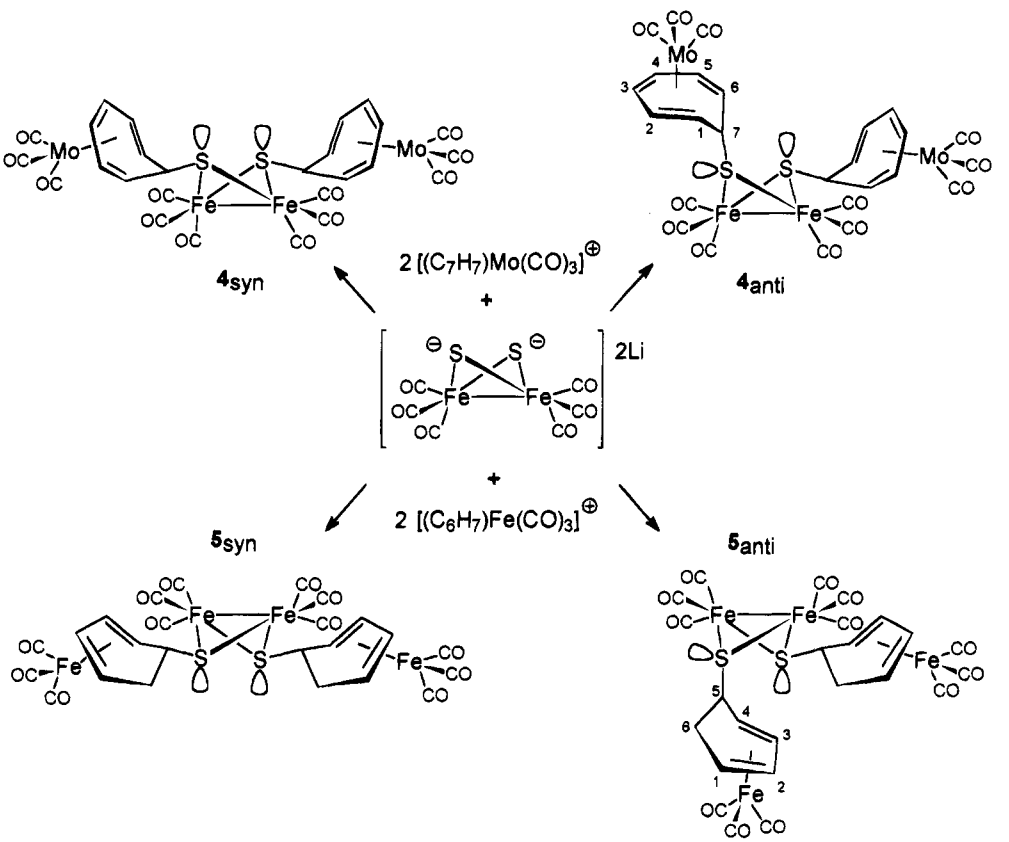

Results and Discussion

When a freshly prepared thf solution of $Li_2[(\mu\text{-}S)_2Fe_2(CO)_6]$ is stirred at low temperature with 2 equiv of the cationic complexes $[(CO)_nM(\pi\text{-hc})]^+$ (hc = unsaturated hydrocarbon), one obtains the corresponding hydrocarbon-bridged compounds in good yields. The reactions are accompanied by the usual color change from green to red. By this way the reaction of $Li_2[Fe_2(CO)_6S_2]$ (**A**) with $[(CO)_5Re(\eta^2\text{-}C_2H_4)]BF_4$ resulted in the formation of $\{(CO)_3Fe[\mu_2\text{-}SCH_2CH_2Re(CO)_5]\}_2$ (**1**), which could be isolated as ruby red crystals. This compound is quite stable and can even be handled for a short time in air. Similarly, the reactions of **A** with the cationic ethylene complexes $[CpW(CO)_3(\eta^2\text{-}C_2H_4)]BF_4$ and $[CpFe(CO)_2(\eta^2\text{-}C_2H_4)]BF_4$ afford $\{(CO)_3Fe[\mu_2\text{-}SCH_2CH_2W(CO)_3Cp]\}_2$ (**2**) and $\{(CO)_3Fe[\mu_2\text{-}SCH_2CH_2Fe(CO)_2Cp]\}_2$ (**3**), respectively (Scheme 1).

The compounds **4** and **5** with cycloheptatriene and cyclohexadiene bridges were prepared by treatment of **A** with the tropylium and cyclohexadienyl complexes $[(CO)_3Mo(\eta^7\text{-}C_7H_7)]BF_4$ and $[(CO)_3Fe(\eta^5\text{-}C_6H_7)]BF_4$ (Scheme 2).

It has been shown by King[20] that $[(OC)_3Fe(\mu_2\text{-}SMe)]_2$ is obtained as a mixture of the syn and anti isomers, which could be separated using column chromatography.[13,20] The syn and anti isomers of **1**–**5** could be detected by NMR spectroscopy and separated for **1** and **2** on silica gel with CH_2Cl_2/pentane.

The homologous dianion $[Fe_2(CO)_6Te_2]^{2-}$ (**B**) also behaves as a potent nucleophile and produces the corresponding tellurium-bridged complexes **6**–**8**. These compounds are less stable than the sulfur species and

(20) King, R. B. *J. Am. Chem. Soc.* **1962**, *84*, 2460. King, R. B.; Bisnette, M. B. *Inorg. Chem.* **1965**, *4*, 1663–1665.

Scheme 3

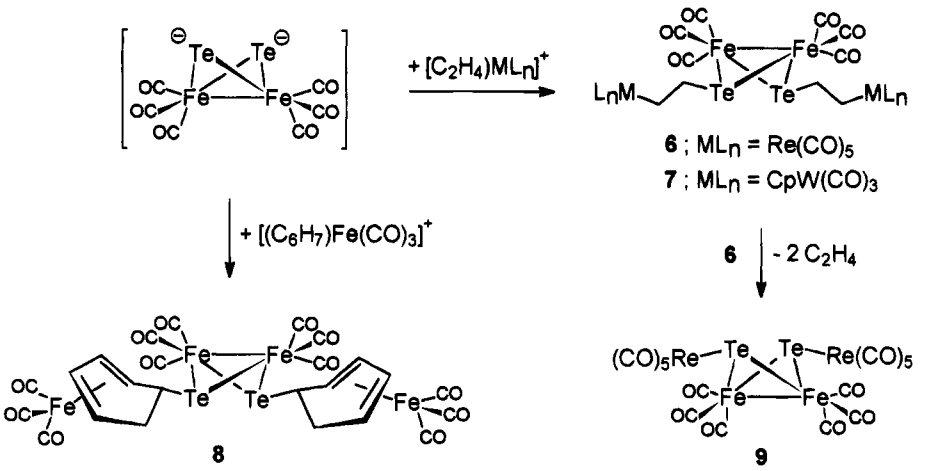

are especially sensitive to oxygen. The solubility in nonpolar solvents decreases from the sulfur to the tellurium compounds. In CH_2Cl_2 solution **6** and **7** gradually decompose at room temperature. The ethylene-bridged complex **6** eliminates ethylene to give the "butterfly" cluster compound $\{(CO)_3Fe[\mu_3\text{-}TeRe(CO)_5]\}_2$ (**9**), which is isolobal[21] with the methylated complex $Fe_2(CO)_6(\mu\text{-}TeMe)_2$, isolated by Whitmire[17] from iodomethane and $[Fe_2(CO)_6Te_2]^{2-}$ (Scheme 3).

Spectral Features. The infrared spectra of **1**–**8** show the absorption pattern characteristic for the $Fe_2(CO)_6$ moiety. Due to the local C_{2v} geometry five CO absorptions should be observed.[9] Some of them are superposed by the carbonyl absorptions of the other metalcarbonyl fragments. The a_1 band of the $Re(CO)_5$ fragment in **1**, **6**, and **9** is observed at ca. 2130 cm^{-1} and is only influenced marginally by the various substituents.

In the ^1H and ^{13}C NMR spectra of the complexes **1**–**4** one observes two sets of signals which can be attributed to the anti and syn geometrical isomers. Crude $\{(CO)_3Fe(\mu_2\text{-}SCH_2CH_2Re(CO)_5]\}_2$ (**1**) shows in the ^1H NMR spectrum three sets of AA'MM' signal patterns with varying intensities. After the product was separated into two isomers, the first band eluted with CH_2Cl_2/pentane was found to exhibit four signals with equal intensities indicating each of the two ethylene bridges to be different. The other isomer shows only a single AA'MM' pattern which can be attributed to the syn isomer. In accordance with the observation by Whitmire[17] for the complex $[(OC)_3Fe(\mu_2\text{-}TeCH_3)]_2$ no syn/anti isomerism is found in the NMR spectra of the tellurium complexes **6**–**8** which show NMR spectra very similar to those of the corresponding syn sulfur compounds.

X-ray Structural Determination of 1 and 9. Basically, the core geometry of **1** and **9** displays an Fe_2E_2 butterfly core with an Fe–Fe distance of 254.6(1) pm in **1** and 263 pm in **9** which compare well with those in other compounds: 254.5(1) pm in $S_2Fe_2(CO)_6$,[10] 253.7(1) pm in $Fe_2(CO)_6(SEt)_2$,[11] 263.4(5) pm in $Fe_2(CO)_6(TeMe)_2$,[17] and 262.6(2) pm in $Fe_2(CO)_6(\mu\text{-}TeCH_2CH_2Te)$[18] (Figure 1).

Similarly, the average Fe–E distances (225 pm in **1** and 258 pm in **9**) are very close to the average Fe–S

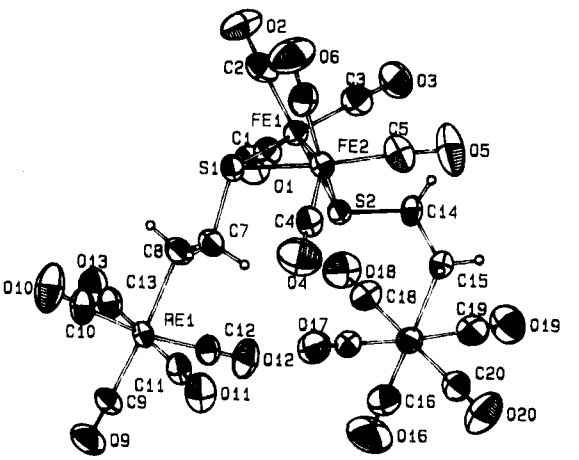

Figure 1. Molecular structure of **1**.

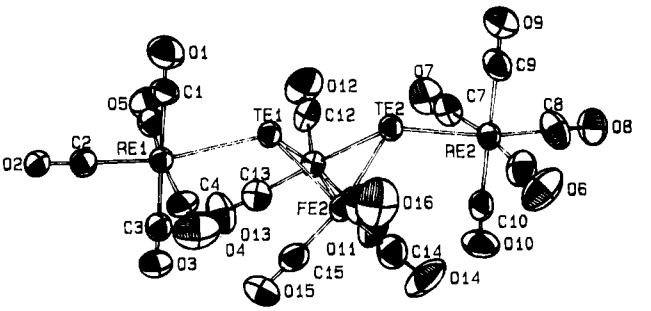

Figure 2. Molecular structure of **9**.

bond lengths found in $Fe_2(NO)_4(SEt)_2$ (226.0 pm)[22] and $Fe_2(CO)_6(SEt)_2$ (225.9 pm)[11] and to the Fe–Te bond lengths reported for $Fe_2(CO)_6(TeMe)_2$ (255 pm)[17] and $Fe_2(CO)_6(\mu\text{-}TeCH_2Te)$ (255 pm).[23] The anti orientation of the two $CH_2CH_2Re(CO)_5$ groups linked to the sulfur atoms destroys the idealized C_{2v} symmetry for **1**. The S–C (184.4(8), 183.7(7) pm) and C–Re distances (229.0(8), 227.6(8) pm) are normal and agree with reported values (Figure 2).

The Te–Te distance (318 pm) in **9** is different from that in the isolobal compound $Fe_2(CO)_6(\mu\text{-}TeMe)_2$ (326.1(1) pm).[17] The Te–Te distance in **9** is between that of the latter compound and the distance known for

(21) Hoffmann, R. *Angew. Chem., Int. Ed. Engl.* **1982**, *21*, 711.

(22) Thomas, J. T.; Robertson, J. H.; Cox, E. G. *Acta Crystallogr.* **1958**, *11*, 599–604.

(23) Mathur, P.; Reddy, V. D.; Bohra, R. *J. Organomet. Chem.* **1991**, *401*, 339–346.

$Fe_2(CO)_6(\mu\text{-}TeCH_2Te)$ (311.4(1) pm).[23] As in $[Te_6]^{4+}$ (313.3 pm),[24] a Te−Te interaction has to be assumed in **9**. The dihedral angles between the two planes of the "butterfly" formed by the two bridging chalcogen atoms and one iron atom are 104.4 (**1**) and 88.1° (**9**).

Conclusions

The reported reactions show that the coordinated unsaturated hydrocarbons of cationic complexes are strong alkylating agents. They are isolobal[21] with carbenium ions and act like alkyl halides. Especially with the cation $[(OC)_5Re(\eta^2\text{-}C_2H_4)]^+$ many examples for this analogy have been observed.[19]

Experimental Section

General Procedures. All reactions and other manipulations were performed under an atmosphere of dried argon using standard Schlenk techniques. Solvents were purified, dried, and distilled under argon prior to use: thf (Na/benzophenone); pentane ($LiAlH_4$); CH_2Cl_2 (CaH_2). $Fe_2(CO)_6S_2$,[5,13] $Na_2[Fe_2(CO)_6Te_2]$,[17] $[(CO)_5Re(C_2H_4)]BF_4$,[25] $[CpW(CO)_3(C_2H_4)]BF_4$,[26] $[CpFe(CO)_2(C_2H_4)]BF_4$,[27] $[(CO)_3Mo(C_7H_7)]BF_4$,[28] and $[(CO)_3Fe(C_6H_7)]BF_4$[29] were prepared according to literature methods. Infrared spectra were recorded on a Perkin-Elmer Model 841. ^1H and ^{13}C NMR spectra were taken on a JEOL EX 400 (400 MHz). Elemental analyses were performed on a Heraeus VT. Some of the elemental analyses are unsatisfactory, which may be due to the thermal instability of the compounds.

Reaction of $Li_2[Fe_2(CO)_6S_2]$ with $[(CO)_5Re(C_2H_4)]BF_4$. To a freshly prepared solution of $Li_2[Fe_2(CO)_6S_2]$ (generated by slow addition of 1 mL of 1 M $Li[Et_3BH]$ in thf (Aldrich) to 172 mg (0.5 mmol) of $Fe_2(CO)_6S_2$ in 10 mL of thf (at −78 °C)) was added 442 mg (1.0 mmol) of $[(CO)_5Re(C_2H_4)]BF_4$ in small portions. During the addition the color changed from emerald green to red. The reaction mixture was stirred for 5 min at −78 °C and then slowly warmed to room temperature. The solvent was removed in vacuo, leaving a dark red solid which was extracted with 15 mL of CH_2Cl_2. After filtration, this solution was reduced to 3 mL and thereafter placed on a silica gel column (2 × 40 cm) using CH_2Cl_2/pentane (2/1) as the eluent. The first band yielded 86 mg (0.08 mmol, 16.3%) of $\mathbf{1}_{anti}$, which was isolated as ruby red crystals from the concentrated solution, cooled to −20 °C; the second band yielded 272 mg (0.26 mmol, 51.7%) of red $\mathbf{1}_{syn}$. IR (CH_2Cl_2, cm^{-1}): 2130 m, 2064 m, 2025 vs, 2015 vs, 1980 vs, br. The ν(CO) bands are rather broad; therefore, the isomers cannot be distinguished by IR. ^1H NMR ($CDCl_3$, ppm): $\mathbf{1}_{syn}$, 1.24 (m, 4H, $ReCH_2$), 2.92 (m, 4H, SCH_2); $\mathbf{1}_{anti}$, 1.04, 1.25 (m, 4H, $ReCH_2$), 2.60, 2.88 (m, 4H, SCH_2). ^{13}C NMR ($CDCl_3$, ppm): $\mathbf{1}_{syn}$, −6.33 ($ReCH_2$), 49.32 (SCH_2), 184.12 (ReCO), 210.22 (FeCO); $\mathbf{1}_{anti}$, −7.12, −6.76 ($ReCH_2$), 35.83, 50.39 (SCH_2), 180.22, 180.37, 184.19, 184.28 (ReCO), 209.43 (FeCO). Anal. Calcd for $C_{20}H_8O_{16}Fe_2Re_2S_2$: C, 22.82; H, 0.77; S, 6.09. Found: C, 23.21; H, 0.90; S, 5.97. Mp: 117 °C (anti), 119−121 °C (syn).

Table 1. Selected Crystallographic Data for 1 and 9

	1	9
empirical formula	$C_{20}H_8O_{16}Fe_2Re_2S_2$	$C_{16}O_{16}Fe_2Re_2Te_2$
fw	1052.50	1187.46
cryst size (mm)	0.1 × 0.1 × 0.17	0.03 × 0.33 × 0.50
cryst syst	triclinic	triclinic
space group	$P\bar{1}$ (No. 2)	$P\bar{1}$ (No. 2)
a (pm)	1105.8(2)	729.1(3)
b (pm)	1107.9(3)	1890.9(6)
c (pm)	1403.3(3)	2067.9(6)
α (deg)	75.99(2)	108.14(3)
β (deg)	69.40(2)	94.30(3)
γ (deg)	67.66(2)	93.07(3)
V (nm^3)	1.4767	2.6926
Z	2	4
ϱ(calc) (g cm^{-3})	2.259	2.929
abs coeff (mm^{-1})	9.446	12.344
2θ range (deg)	4−46	4−46
diffractometer	Nonius (CAD-4)	Nonius (CAD-4)
temp (°C)	23	23
no. of rflns collected	4356	8130
no. of indep rflns	4099	7431
no. of obsd rflns	3067 ($I > 3\sigma(I)$)	5871 ($I > 3\sigma(I)$)
T_{min}/T_{max}	0.71/1.00	0.16/1.00
R, R_w	0.027, 0.032	0.035, 0.044
GOF	1.05	1.49
residual extrema (e pm^{-3} × 10^6)	+1.36/−0.19	+1.83/−0.28

Table 2. Selected Intramolecular Bond Distances and Angles for 1

Distances (pm)					
Fe1−Fe2	254.6(1)	Re2−C15	227.6(8)	Fe2−C6	178(1)
Fe1−S1	226.6(2)	Fe1−C1	180.7(8)	S1−C7	185(8)
Fe1−S2	224.1(2)	Fe1−C2	179(1)	S2−C14	183.7(7)
Fe2−S1	226.5(2)	Fe1−C3	178.3(8)	C7−C8	149(1)
Fe2−S2	226.7(3)	Fe2−C4	180.5(7)	C14−C15	152(1)
Fe1−C8	229.0(8)	Fe2−C5	178.2(7)		

Angles (deg)			
S1−Fe1−S2	81.76(8)	Fe2−S1−C7	108.8(2)
S1−Fe2−S2	81.21(8)	Fe2−S2−C14	114.3(3)
Fe1−S1−Fe2	68.38(6)	S1−C7−C8	114.8(5)
Fe1−Fe2−S1	55.81(6)	Re1−C8−C7	115.1(5)
Fe1−S2−Fe2	68.77(8)	S2−C14−C15	111.5(5)

Reaction of $Li_2[Fe_2(CO)_6S_2]$ with $[CpW(CO)_3(C_2H_4)]BF_4$. $\{(CO)_3Fe[\mu\text{-}SCH_2CH_2W(CO)_3Cp]\}_2$ (**2**) was prepared in a very similar way from 158 mg of $Fe_2(CO)_6S_2$ (0.46 mmol) and 400 mg of $[CpW(CO)_3(C_2H_4)]BF_4$ (0.96 mmol), yielding 263 mg (0.25 mmol, 53.6%) of $\mathbf{2}_{anti}$ and 46 mg (0.04 mmol, 9.38%) of $\mathbf{2}_{syn}$ as deep red solids. IR (CH_2Cl_2, cm^{-1}): 2067 m, 2031 vs, 2016 vs, 1990 vs, 1916 vs, br. ^1H NMR ($CDCl_3$, ppm): $\mathbf{2}_{syn}$, 1.68 (m, 4H, WCH_2), 2.62 (m, 4H, SCH_2), 5.38 (s, 10H, Cp); $\mathbf{2}_{anti}$, 1.49, 1.75 (m, 4H, WCH_2), 2.38, 2.62 (m, 4H, SCH_2), 5.42, 5.44 (s, 10H, Cp). ^{13}C NMR ($CDCl_3$, ppm): $\mathbf{2}_{syn}$, −13.10 (WCH_2), 46.70 (SCH_2), 91.88 (Cp), 210.52 (FeCO); $\mathbf{2}_{anti}$, −10.41, −10.07 (WCH_2), 33.42, 47.80 (SCH_2), 91.56, 91.72 (Cp), 209.70 (FeCO), 217.60, 217.71, 227.92, 228.25 (WCO). Anal. Calcd for $C_{26}H_{18}O_{12}Fe_2S_2W_2$: C, 29.30; H, 1.70; S, 6.02. Found: C, 28.87; H, 1.79; S, 5.79. Decomposition above 140 °C.

Reaction of $Li_2[Fe_2(CO)_6S_2]$ with $[CpFe(CO)_2(C_2H_4)]BF_4$. A similar reaction in which 292 mg (1 mmol) of $[CpFe(CO)_2(C_2H_4)]BF_4$ was added to the solution of the dianion gave $\{(CO)_3Fe[\mu\text{-}SCH_2CH_2Fe(CO)_2Cp]\}_2$ (**3**), which could not be separated entirely into syn and anti isomers. A CH_2Cl_2 solution of crude **3** was only filtered over silica gel (10 cm). A longer column led to the decomposition of the product. The solution was reduced to 3 mL and 5 mL of pentane was added at −70 °C. **3** precipitated and was obtained as a dark red solid (225 mg, 0.3 mmol, 60% yield). IR (CH_2Cl_2, cm^{-1}): 2066 s, 2044 s, 2031 vs, 2015 vs, 1991 vs, br, 1958 s. ^1H NMR ($CDCl_3$, ppm): $\mathbf{3}_{syn}$, 1.42 (m, 4H, $FeCH_2$), 2.53 (m, 4H, SCH_2), 4.78 (s, 10H, Cp); $\mathbf{3}_{anti}$, 1.22, 1.52 (m, 4H, $FeCH_2$), 2.23, 2.55 (m, 4H, SCH_2), 4.88, 5.0 (s, 10H, Cp). ^{13}C NMR ($CDCl_3$, ppm): $\mathbf{3}_{syn}$, 4.10 ($FeCH_2$), 47.57 (SCH_2), 85.66 (Cp), 210.66, 216.91 (FeCO);

(24) Burns, R. C.; Gillespie, R. I.; Luk, W. C.; Slim, D. R. *Inorg. Chem.* **1979**, *18*, 3086−3094. For a discussion of Te−Te bond lengths see: Bogan, L. E., Jr.; Rauchfuss, T. B.; Rheingold, A. L. *J. Am. Chem. Soc.* **1985**, *107*, 3843−3850.
(25) Beck, W.; Raab, K. *Inorg. Synth.* **1989**, *26*, 106−113; **1989**, *28*, 16−20. Raab, K.; Beck, W. *Chem. Ber.* **1985**, *118*, 3830−3848.
(26) Knoth, W. H. *Inorg. Chem.* **1975**, *14*, 1566−1572.
(27) Green, M. L. H.; Nagy, P. L. I. *J. Organomet. Chem.* **1963**, *1*, 58−69.
(28) King, R. B. *Organometallic Syntheses*; Academic Press: New York, 1965; Vol. 1, p 141. Cotton, F. A.; McCleverty, J. A.; White, J. E. *Inorg. Synth.* **1990**, *28*, 45−47.
(29) Fischer, E. O.; Fischer, R. D. *Angew. Chem.* **1960**, *72*, 919. Birch, A. J.; Cross, P. E.; Lewis, J.; White, D. A.; Wild, S. B. *J. Chem. Soc. A* **1968**, 332−340.

Table 3. Selected Intramolecular Bond Distances and Angles for 9[a]

Distances (pm)			
Fe1−Fe2	263.5(2)	Fe1A−Fe2A	262.2(2)
Fe1−Te1	257.9(2)	Fe1A−Te1A	258.9(2)
Fe1−Te2	257.8(2)	Fe1A−Te2A	256.8(2)
Fe2−Te1	258.1(2)	Fe2A−Te1A	256.6(1)
Fe2−Te2	256.6(2)	Fe2A−Te2A	258.7(2)
Re1−Te1	283.4(1)	Re1A−Te1A	282.6(1)
Re2−Te2	282.6(1)	Re2A−Te2A	283.7(1)
Te1−Te2	318.0(1)	Te1A−Te2A	318.5(1)
Fe2−Cl4	178(2)	Fe2A−Cl4A	177(1)
Re1−C1	200(1)	Re1A−C1A	196(2)
Re1−C2	195(1)	Re1A−C2A	198(1)
Angles (deg)			
Re1−Te1−Te2	169.96(3)	Re1A−Te1A−Te2A	172.28(3)
Re1−Te1−Fe1	121.94(5)	Re1A−Te1A−Fe1A	123.59(5)
Re1−Te1−Fe2	119.24(4)	Re1A−Te1A−Fe2A	120.95(5)
Fe1−Te1−Fe2	61.42(5)	Fe1A−Te1A−Fe2A	61.14(5)
Re2−Te2−Fe1	118.07(5)	Re2A−Te2A−Fe1A	122.77(4)
Te1−Fe1−Te2	76.17(5)	Te1A−Fe1A−Te2A	76.29(5)
Te2−Fe2−Fe1	59.40(5)	Te2A−Fe2A−Fe1A	59.07(5)

[a] The unit cell contains two independent molecules.

Table 4. Positional Parameters and B_{eq} Values for 1

atom	x	y	z	B_{eq} (Å^2)
Re1	1.00463(3)	0.25828(3)	0.68490(2)	2.695(7)
Re2	1.59382(3)	−0.07684(3)	0.79468(2)	3.357(8)
Fe1	1.1941(1)	−0.3414(1)	0.84811(8)	2.75(3)
Fe2	1.3532(1)	−0.3627(1)	0.66620(7)	2.55(2)
S1	1.1349(2)	−0.2247(2)	0.7055(1)	2.89(5)
S2	1.3648(2)	−0.2560(2)	0.7800(1)	2.63(4)
O1	1.0250(7)	−0.1610(7)	1.0042(5)	6.3(2)
O2	1.0078(6)	−0.4837(6)	0.8696(5)	6.2(2)
O3	1.3471(6)	−0.5603(7)	0.9710(5)	6.4(2)
O4	1.4391(7)	−0.2234(7)	0.4610(5)	6.4(2)
O5	1.6217(6)	−0.5562(7)	0.6632(5)	7.0(2)
O6	1.2664(6)	−0.5469(6)	0.6093(5)	6.5(2)
O9	0.9513(6)	0.5583(6)	0.6183(5)	5.9(2)
O10	0.8462(6)	0.2216(7)	0.5544(5)	6.6(2)
O11	1.2669(6)	0.2077(6)	0.4997(4)	5.1(2)
O12	1.2017(6)	0.2212(7)	0.8110(4)	5.9(2)
O13	0.7449(6)	0.3191(7)	0.8741(5)	5.8(2)
O16	1.5496(8)	0.2098(7)	0.8134(7)	9.4(3)
O17	1.4409(6)	0.0089(6)	0.6276(5)	6.0(2)
O18	1.3236(7)	−0.0750(7)	0.9703(5)	6.6(2)
O19	1.7674(7)	−0.2034(7)	0.9493(5)	6.7(2)
O20	1.8608(6)	−0.0944(7)	0.6106(5)	6.5(2)
C1	1.0882(8)	−0.2328(8)	0.9449(6)	3.9(2)
C2	1.0795(8)	−0.4272(8)	0.8610(6)	4.0(2)
C3	1.2873(8)	−0.4744(8)	0.9224(6)	4.1(2)
C4	1.4087(7)	−0.2763(7)	0.5409(6)	3.2(2)
C5	1.5143(8)	−0.4841(8)	0.6677(6)	4.2(2)
C6	1.2982(7)	−0.4741(8)	0.6331(6)	3.7(2)
C7	1.1366(7)	−0.0527(7)	0.6716(6)	3.4(2)
C8	1.0252(8)	0.0412(7)	0.8404(6)	3.7(2)
C9	0.9720(8)	0.4475(7)	0.6423(6)	3.5(2)
C10	0.8988(8)	0.2410(8)	0.6011(6)	4.0(2)
C11	1.1712(7)	0.2218(8)	0.5669(6)	3.6(2)
C12	1.1269(7)	0.2376(8)	0.7672(6)	3.5(2)
C13	0.8374(8)	0.2964(8)	0.8058(6)	3.7(2)
C14	1.5087(6)	−0.3435(7)	0.8342(5)	3.0(2)
C15	1.6258(7)	−0.2884(7)	0.7820(6)	3.0(2)
C16	1.5665(9)	0.1033(9)	0.8063(8)	5.6(3)
C17	1.4916(7)	−0.0210(8)	0.6897(7)	3.9(2)
C18	1.4229(8)	−0.0728(8)	0.9065(6)	4.1(2)
C19	1.7033(8)	−0.1558(8)	0.8947(6)	4.5(2)
C20	1.7654(7)	−0.0880(8)	0.6780(6)	3.8(2)

$\mathbf{3}_{anti}$, 0.91, 3.92 ($FeCH_2$), 33.88, 48.73 (SCH_2), 86.45, 87.16 (Cp), 210.44, 216.81, 217.06 (FeCO). Anal. Calcd for $C_{24}H_{18}O_{10}Fe_4S_2$: C, 38.24; H, 2.41; S, 8.51. Found: C, 36.70; H, 1.93; S, 8.99. Decpt: 40 °C (mixture of isomers).

Reaction of $Li_2[Fe_2(CO)_6S_2]$ with $[(CO)_3Mo(C_7H_7)]BF_4$. $\{(CO)_3Fe[\mu\text{-}SC_7H_7Mo(CO)_3]\}_2$ (**4**) was prepared as described for **3**, starting from 172 mg of $Fe_2(CO)_6S_2$ (0.5 mmol) and 358 mg of $[(CO)_3Mo(C_7H_7)]BF_4$ (1.0 mmol). Crystallization from CH_2Cl_2/pentane at −20 °C yielded 69 mg (0.08 mmol, 15.6%) of $\mathbf{4}_{anti}$ as orange-red crystals and 148 mg (0.17 mmol, 33.4%) $\mathbf{4}_{syn+anti}$ from the mother liquor. IR (CH_2Cl_2, cm^{-1}): 2073 m, 2059 s, 2045 s, 2030 sh, 2005 s, 1985 vs, 1916. ^{1}H NMR ($CDCl_3$, ppm): $\mathbf{4}_{syn}$, 1.95 (m, 2H, 7,7′-H), 3.78 (m, 4H, 1,1′,6,6′-H), 5.15 (m, 4H, 2,2′,5,5′-H), 6.21 (m, 4H, 3,3′, 4,4′-H); $\mathbf{4}_{anti}$, 0.77, 3.21 (m, 2H, 7,7′-H), 3.93 (pt, 2H, 1,6-H, $^3J_{7,1,6}$ = 8.54 Hz), 4.98 (dd, 2H, 1′,6′-H, ^3J = 6.11, 9.23 Hz), 4.84, 6.11 (m, 4H, 2,5,2′,5′-H), 5.83, 6.43 (m, 4H, 3,4,3′,4′-H). ^{13}C NMR ($CDCl_3$, ppm): $\mathbf{4}_{anti}$, 39.97, 49.10 (C-7), 68.12, 96.93 (C-1,6), 100.72, 126.30 (C-2,5), 122.44, 130.68 (C-3,4). Anal. Calcd for $C_{26}H_{14}O_{12}Fe_2Mo_2S_2$: C, 35.24; H, 1.59; S, 7.24. Found: C, 34.39; H, 1.83; S, 6.98. Decpt: 60 °C (mixture of isomers).

Table 5. Positional Parameters and B_{eq} Values for One Molecule of 9

atom	x	y	z	B_{eq} (Å^2)
Re1	0.41375(7)	0.96240(2)	0.86199(2)	3.00(1)
Re2	0.51179(7)	1.26519(2)	0.61868(2)	3.24(2)
Fe1	0.2462(2)	1.13661(8)	0.75038(9)	3.18(4)
Fe2	0.4357(2)	1.03805(8)	0.66785(9)	3.33(4)
Te1	0.4994(1)	1.07165(4)	0.79879(4)	3.03(2)
Te2	0.5433(1)	1.17757(4)	0.70691(4)	3.11(2)
O1	0.811(1)	1.0169(5)	0.9340(5)	6.0(3)
O2	0.0378(1)	0.8625(4)	0.9548(4)	5.6(2)
O3	0.029(1)	0.8951(5)	0.7836(5)	6.0(3)
O4	0.589(1)	0.8455(5)	0.7452(6)	7.1(3)
O5	0.224(1)	1.0914(5)	0.9605(5)	5.9(3)
O6	0.731(1)	1.1505(6)	0.5155(5)	7.2(3)
O7	0.275(1)	1.3580(85)	0.7304(6)	6.6(3)
O8	0.522(1)	1.3786(4)	0.5390(5)	6.6(3)
O9	0.871(1)	1.3452(5)	0.7095(6)	6.7(3)
O10	0.160(1)	1.1846(5)	0.5236(6)	6.6(3)
O11	0.003(1)	1.1607(6)	0.6432(5)	7.9(3)
O12	0.201(2)	1.2788(5)	0.8552(6)	8.0(3)
O13	−0.033(1)	1.0477(5)	0.7920(5)	6.6(3)
O14	0.294(2)	1.0400(6)	0.5337(5)	9.3(4)
O15	0.213(2)	0.9021(5)	0.6573(6)	7.3(3)
O16	0.784(1)	0.9746(5)	0.6282(6)	7.7(3)
C1	0.668(2)	0.9984(6)	0.9084(6)	3.7(3)
C2	0.391(2)	0.8986(6)	0.9198(6)	3.8(3)
C3	0.166(2)	0.9217(6)	0.8118(6)	3.9(3)
C4	0.526(82)	0.8869(7)	0.7879(7)	4.6(3)
C5	0.293(2)	1.0446(6)	0.9266(7)	4.2(3)
C6	0.652(2)	1.1921(7)	0.5540(7)	5.0(3)
C7	0.359(2)	1.3250(6)	0.6897(7)	4.5(3)
C8	0.518(2)	1.3377(7)	0.5684(8)	6.1(4)
C9	0.742(2)	1.3160(6)	0.6762(7)	4.8(3)
C10	0.285(2)	1.2123(6)	0.5600(6)	4.4(3)
C11	0.100(2)	1.1501(7)	0.6833(7)	4.4(3)
C12	0.223(2)	1.2226(7)	0.8148(7)	5.0(3)
C13	0.077(2)	1.0805(6)	0.7739(7)	4.5(3)
C14	0.340(2)	1.0401(7)	0.5867(7)	5.4(4)
C15	0.300(2)	0.9574(6)	0.6621(7)	4.5(3)
C16	0.648(2)	0.9996(7)	0.6449(8)	5.4(4)

Reaction of $Li_2[Fe_2(CO)_6S_2]$ with $[(CO)_3Fe(C_6H_7)]BF_4$. To the solution of the dianion prepared from 172 mg (0.5 mmol) of $Fe_2(CO)_6S_2$ in 10 mL of thf was added 306 mg (1.0 mmol) of $[(CO)_3Fe(C_6H_7)]BF_4$ at −78 °C. Further workup proceeded as described for **3** to give 203 mg of $\{Fe_2(CO)_6[\mu\text{-}SC_6H_7Fe(CO)_3]\}_2$ (**5**; 0.26 mmol, 52% yield). IR (CH_2Cl_2, cm^{-1}): 2071 s, 2054 vs, 2035 vs, 1984 vs, br, 1952 w. ^{1}H NMR ($CDCl_3$, ppm): $\mathbf{5}_{syn}$, 1.62 (m, 2H, 6-H), 2.36 (m, 2H, 6′-H), 2.92 (m, 4H, 1,1′,4,4′-H), 3.04 (m, 2H, 5,5′-H), 5.4 (m, 4H, 2,2′,3,3′-H); $\mathbf{5}_{anti}$, 1.40−1.80 (m, 2H, 6-H), 2.24 (m, 2H, 6′-H), 2.10, 3.09 (m, 2H, 5,5′-H), 2.63, 2.88 (m, 4H, 1,1′,4,4′), 5.4 (m, 4H, 2,2′,3,3′-H). ^{13}C NMR ($CDCl_3$, ppm): $\mathbf{5}_{syn}$, 35.25 (C-6), 49.96 (C-5), 58.23, 62.96 (C-1,4), 84.40, 87.05 (C-2,3), 209.50, 210.39 (FeCO); $\mathbf{5}_{anti}$, 34.84, 36.27 (C-6,6′), 50.77, 63.32 (C-5,5′), 57.70, 61.84, 63.22, 63.77 (C-1,1′,4,4′), 84.23, 84.47, 87.09, 87.17 (C-2,2′,3,3′), 208.51, 210.53 (FeCO). Anal. Calcd for $C_{24}H_{14}O_{12}Fe_4S_2$: C, 36.87; H, 1.80; S, 8.20. Found: C, 36.59; H, 1.94; S, 7.89. Decpt: 112 °C.

Reaction of $Na_2[Fe_2(CO)_6Te_2]$ with $[(CO)_5Re(C_2H_4)]BF_4$. To a freshly prepared solution containing 0.32 mmol of $Na_2[Fe_2(CO)_6Te_2]$[17] was added 309 mg (0.7 mmol) of $[(CO)_5$-

Re)(C_2H_4)]BF_4 in small portions. The dark red reaction mixture was stirred for 1 h at −60 °C and then warmed to 0 °C within 30 min. The solvent was removed in vacuo (0 °C), leaving a dark red solid which was extracted at 0 °C with 15 mL of CH_2Cl_2. After filtration over a short silica gel column (10 cm, 0 °C), this solution was reduced to 2 mL and 10 mL pentane was added at −78 °C with vigorous stirring. The red precipitate was further washed with 5 mL of pentane at −78 °C and dried in vacuo to give 282 mg (0.23 mmol, 70.9% yield) of **6**. IR (CH_2Cl_2, cm^{-1}): 2129 m, 2077 sh, 2035 s, 2013 s, 2003 s, 1983 vs, 1952 vs. ^1H NMR ($CDCl_3$, ppm): 1.43 (m, 4H, $ReCH_2$), 3.54 (m, 4H, $TeCH_2$). ^{13}C NMR ($CDCl_3$, ppm): −6.49 ($ReCH_2$), 52.76 ($TeCH_2$), 176.0, 182.98 (ReCO), 215.28 (FeCO). Anal. Calcd for $C_{20}H_8O_{16}Fe_2Re_2Te_2$: C, 19.32; H, 0.65. Found: C, 19.34; H, 0.87. Decpt: 55 °C.

Reaction of $Na_2[Fe_2(CO)_6Te_2]$ with $[CpW(CO)_3(C_2H_4)]BF_4$. $\{(CO)_3Fe[\mu\text{-}TeCH_2CH_2W(CO)_3Cp]\}_2$ (**7**) was prepared in a very similar way from a solution of 0.32 mmol of $Na_2[Fe(CO)_6Te_2]$[17] in 15 mL of thf and 313 mg of $[CpW(CO)_3(C_2H_4)]BF_4$ (0.7 mmol) and was obtained as a maroon solid (265 mg, 0.21 mmol, 65.9% yield). IR (CH_2Cl_2, cm^{-1}): 2080 sh, 2047 s, 2014 vs, 1992 vs, 1970 sh, 1921 vs, br. ^1H NMR ($CDCl_3$, ppm): 1.29 (m, 4H, WCH_2), 3.31 (m, 4H, $TeCH_2$), 5.32 (s, 10H, Cp). ^{13}C NMR ($CDCl_3$, ppm): −11.32 (WCH_2), 43.85 ($TeCH_2$), 92.64 (Cp), 211.32 (FeCO), 227.93 (WCO). Anal. Calcd for $C_{26}H_{18}O_{12}Fe_2Te_2W_2$: C, 24.84; H, 1.44. Found: C, 25.77; H, 1.64. Decpt: 70 °C.

Reaction of $Na_2[Fe_2(CO)_6Te_2]$ with $[(CO)_3Fe(C_6H_7)]BF_4$. $\{(CO)_3Fe[\mu\text{-}TeC_6H_7Fe(CO)_3]\}_2$ (**8**) was synthesized by the reaction of 0.32 mmol of $Na_2[Fe(CO)_6Te_2]$ in 15 mL of thf and 215 mg of $[(CO)_3Fe(C_6H_7]BF_4$ (0.7 mmol). Workup similar to that described for **6** resulted in a maroon solid (200 mg, 0.21 mmol, 64.2% yield). IR (CH_2Cl_2, cm^{-1}): 2069 m, 2049 vs, 2009 vs, 1973 s, br. ^1H NMR ($CDCl_3$, ppm): 1.82 (m, 4H, 6-H), 2.72 (m, 2H, 5-H), 3.45 (m, 4H, 1,4-H), 5.22 (m, 4H, 2,3-H). ^{13}C NMR ($CDCl_3$, ppm): 212.68, 212.54 (FeCO), 85.54, 85.37 (C-2,3), 65.33, 60.42 (C-1,4), 46.16 (C-5), 28.86 (C-6). Anal. Calcd for $C_{24}H_{14}O_{12}Fe_4Te_2$: C, 29.63; H, 1.45. Found: C, 29.45; H, 1.65. Decpt: 65 °C.

Preparation of $[(CO)_3Fe(\mu\text{-}TeRe(CO)_5)]_2$ (9). A deep red solution of 150 mg (0.12 mmol) of **6** in 8 mL of CH_2Cl_2 was stirred for 30 min at room temperature. An Schlenk U-tube was charged with the filtered solution on one side and with 20 mL of toluene on the other side. After 7 days at −20 °C compound **9** could be obtained as deep red-brown crystals (67 mg, 0.06 mmol, 47% yield). IR (CH_2Cl_2, cm^{-1}): 2131 s, 2079 vw, 2033 vs, 2010 m, 1992 s, 1984 s, 1955 m, 1939 s. ^{13}C NMR ($CDCl_3$, ppm): 181.99 (ReCO), 214.69 (FeCO). Anal. Calcd for $C_{16}O_{16}Fe_2Re_2Te_2$: C, 16.18. Found: C, 16.20. Mp: 158–160 °C.

Crystallographic Analysis. Crystal data, data collection details, and refinement data are summarized in Table 1. The Nonius diffractometer was equipped with a graphite monochromator. Intensity data were obtained by using Mo Kα radiation and were collected by the ω-scan method at variable speed, dependent on peak intensity. Intensities of 3 standard reflections were monitored after every 200 reflections. Background measurement was 50% of the scan time. Data reduction, structure solution, and refinement of the structures were carried out by using a Nonius MOLEN package. Absorption correction was applied to the data. The structures were solved by direct methods and refined by full-matrix least squares by minimizing $\sum w[F_o - F_c]^2$. All non-hydrogen atoms were refined anisotropically. Hydrogen atoms of **1** were included in their calculated positions and were refined by using a riding model.

Acknowledgment. Support by the Deutsche Forschungsgemeinschaft and Fonds der Chemischen Industrie is gratefully acknowledged.

Supplementary Material Available: Complete tables of positional parameters, bond lengths and angles, torsional angles, and thermal parameters for **1** and **9** and a packing diagram for **9** (33 pages). Ordering information is given on any current masthead page.

OM940744J

Addition of Phenylacetylene to the Mixed-Chalcogenide Compounds $(CO)_6Fe_2(\mu\text{-SeTe})$, $(CO)_6Fe_2(\mu\text{-SSe})$, and $(CO)_6Fe_2(\mu\text{-STe})$. Structural Characterization of $(CO)_6Fe_2\{\mu\text{-SeC(H)=C(Ph)Te}\}$

Pradeep Mathur,* Md. Munkir Hossain, and Shubhangi Umbarkar

Chemistry Department, Indian Institute of Technology, Powai, Bombay 400 076, India

C. V. V. Satyanarayana

Regional Sophisticated Instrumentation Center, Indian Institute of Technology, Powai, Bombay 400 076, India

Sudam S. Tavale and Vedavati G. Puranik

Physical Chemistry Division, National Chemical Laboratory, Pune 411 008, India

Received October 17, 1994®

From the room-temperature reaction of the mixed-chalcogenide compound $Fe_2(CO)_6(\mu\text{-SeTe})$ with phenylacetylene two isomeric products were isolated, $Fe_2(CO)_6\{\mu\text{-SeC(H)=C(Ph)Te}\}$ (**1**) and $Fe_2(CO)_6\{\mu\text{-SeC(Ph)=C(H)Te}\}$ (**2**). $Fe_2(CO)_6(\mu\text{-SSe})$ reacted with phenylacetylene to form $Fe_2(CO)_6\{\mu\text{-SC(Ph)=C(H)Se}\}$ (**3**). The room-temperature reaction of $Fe_2(CO)_6(\mu\text{-STe})$ with phenylacetylene also yielded two isomeric products, $Fe_2(CO)_6(\mu\text{-SC(H)=C(Ph)Te})$ (**4**) and $Fe_2(CO)_6(\mu\text{-SC(Ph)=C(H)Te})$ (**5**). In all of these reactions, the homochalcogenide compounds $Fe_2(CO)_6(\mu\text{-EC(H)=C(Ph)E})$ (E = Se, Te, E = S, Se, and E = S, Te, respectively) were also formed in trace amounts. The new compounds **1**–**5** were characterized by IR and ^1H, ^{13}C, ^{77}Se, and ^{125}Te NMR spectroscopy. Compound **1** was structurally characterized by single-crystal X-ray diffraction methods. It crystallized in the triclinic space group $P\bar{1}$ with a = 7.773(9) Å, b = 10.635(9) Å, c = 12.010(10) Å, α = 104.99(10)°, β = 102.86(11)°, γ = 106.38(9)°, V = 872.1(8) Å^3, Z = 2, and D(calc) = 2.241 g cm^{-3}. Full-matrix least-squares refinement of **1** converged to R = 0.077 and R_w = 0.086.

Introduction

Recent years have witnessed an upsurge in interest in the synthesis, reactivity, and structural aspects of compounds containing selenium and tellurium as bridging and stabilizing ligands.[1] Early work in the chalcogen system showed that sulfur and selenium displayed similar behavior, whereas tellurium was quite often unique.[2] Our recent work on the use of $Fe_2(CO)_6(\mu\text{-E}_2)$ (E = S, Se, Te) has shown that selenium can also show reactivity features different from that of S or Te analogs. For instance, $Fe_2(CO)_6(\mu\text{-Se}_2)$ readily reacts with phenylacetylene at room temperature to form $Fe_2(CO)_6\{\mu\text{-SeC(Ph)=C(H)Se}\}$, whereas $Fe_2(CO)_6(\mu\text{-S}_2)$ and $Fe_2(CO)_6(\mu\text{-Te}_2)$ are inert toward such phenylacetylene addition.[3] The analogous S and Te compounds have been obtained by other methods. Seyferth has reported the preparation of $Fe_2(CO)_6\{\mu\text{-SC(Ph)=C(H)S}\}$ as well as a range of other dithiolene derivatives by protonation of $RC{\equiv}CLi/Fe_2(CO)_6(\mu\text{-S}_2)$ reaction mixtures.[4] The Te compound can be prepared from the thermolysis of $Fe_3(CO)_9(\mu_3\text{-Te})_2$ and phenylacetylene.[5] Of the three types of bonds (Fe–Fe, Fe–E, and E–E) present in the $Fe_2(CO)_6(\mu\text{-E}_2)$ core, the E–E bond appears to be the most reactive toward addition of various types of organic and inorganic moieties. In $Fe_2(CO)_6\{\mu\text{-SeC(H)=C(Ph)Se}\}$, facile addition of $Fe_2(CO)_6Se_2$[3] and $Pt(PPh_3)_2$[6] occurs readily and a corresponding reduction of the acetylenic C≡C bond is observed. The compounds $Fe_2(CO)_6E_2$ are highly reactive species, and reactions involving them occur readily at room temperature; when these compounds are heated, they undergo rapid decomposition. The addition of phenylacetylene to $Fe_2(CO)_6(\mu\text{-Se}_2)$ blocks the reactive sites and stabilizes the Fe_2Se_2 framework sufficiently to enable thermolytic reactions to be carried out on it, as in the formation of the mixed-metal cluster $Cp_2Mo_2Fe_2(CO)_6(\mu_3\text{-Se})_2(\mu_4\text{-Se})$ by a pro-

® Abstract published in *Advance ACS Abstracts*, January 15, 1995.

(1) (a) Fenske, D.; Ohmer, J.; Hachgenei, J.; Merzweiler, K. *Angew. Chem., Int. Ed. Engl.* **1988**, *27*, 1277. (b) Fenske, D.; Ohmer, J.; Hachgenei, *J. Angew. Chem., Int. Ed. Engl.* **1985**, *24*, 993. (c) Chau, C.-N.; Wardle, R. W. M.; Ibers, J. A. *Inorg. Chem.* **1987**, *26*, 2740. (d) Ansari, M. A.; Ibers, J. A. *Coord. Chem. Rev.* **1990**, *100*, 223. (e) Roof, L. C.; Kolis, J. W. *Chem. Rev.* **1993**, *93*, 1037. (f) Linford, L.; Raubenheimer, H. G. *Adv. Organomet. Chem.* **1991**, *32*, 1. (g) Compton, N. A.; Errington, R. J.; Norman, N. C. *Adv. Organomet. Chem.* **1990**, *31*, 91. (h) Riera, V.; Ruiz, M. A.; Villafane, F.; Bois, C.; Jeannin, Y. *Organometallics* **1993**, *12*, 124. (i) Draganjac, M.; Dhingra, S.; Huang, S.-P.; Kanatzidis, M. G. *Inorg. Chem.* **1990**, *29*, 590. (j) Shieh, M.; Shieh, M.-H. *Organometallics* **1994**, *13*, 920. (k) Whitmire, K. H. *J. Coord. Chem.* **1988**, *17*, 95. (l) Ward, M. D. *Coord. Chem. Rev.* **1992**, *115*, 1. (m) Eichorn, B. W.; Haushalter, R. C.; Merola, J. S. *Inorg. Chem.* **1990**, *29*, 728.

(2) (a) Bogan, L. E.; Clark, G. R.; Rauchfuss, T. B. *Inorg. Chem.* **1986**, *25*, 4050. (b) Adams, R. D.; Babin, J. E.; Tasi, M. *Inorg. Chem.* **1987**, *26*, 2807. (c) Mathur, P.; Mavunkal, I. J.; Rugmini, V. *J. Organomet. Chem.* **1989**, *367*, 243. (d) Mathur, P.; Chakrabarty, D.; Mavunkal, I. J. *J. Cluster Sci.* **1993**, *4*, 351.

(3) Mathur, P.; Hossain, M. M. *Organometallics* **1993**, *12*, 2398.

(4) Seyferth, D.; Womack, G. B. *Organometallics* **1986**, *5*, 2360.

(5) Fassler, T.; Buchholz, D.; Huttner, G.; Zsolnai, L. *J. Organomet. Chem.* **1989**, *369*, 297.

(6) Mathur, P.; Hossain, M. M.; Das, K.; Sinha, U. C. *J. Chem. Soc., Chem. Commun.* **1993**, 46.

0276-7333/95/2314-0959$09.00/0

cess which formally involves scission of the Fe–Fe bond in the Fe_2Se_2 framework.[7] We have earlier reported the convenient synthesis of the mixed-chalcogenide compounds $Fe_2(CO)_6(\mu\text{-EE}')$ (E, E′ = S, Se, Te) and have used these for obtaining several mixed-metal, mixed-chalcogenide carbonyl clusters.[8] Preliminary results of addition of diacetylene to $Fe_2(CO)_6(\mu\text{-STe})$ have recently been reported by us.[9] In a continuation of our studies on the addition of phenylacetylene to $Fe_2(CO)_6(\mu\text{-Se}_2)$, and as an extension of our studies on the mixed-chalcogenide systems, we report here on the reaction of phenylacetylene with $Fe_2(CO)_6(\mu\text{-SeTe})$, $Fe_2(CO)_6(\mu\text{-SSe})$, and $Fe_2(CO)_6(\mu\text{-STe})$.

Experimental Section

General Procedures. All reactions and other manipulations were performed using standard Schlenk techniques under an inert atmosphere of argon. Solvents were deoxygenated immediately prior to use. Infrared spectra were recorded on a Nicolet 5DXB or Impact 400 FT spectrometer as hexane solutions in 0.1-mm-pathlength NaCl cells. ^{1}H, ^{13}C, ^{77}Se, and ^{125}Te NMR spctra were all obtained on a Varian VXR-300S spectrometer in $CDCl_3$. ^{77}Se NMR measurements were made at an operating frequency of 57.23 MHz using a pulse width of 15 μs and a delay of 1 s. All spectra were referenced to Me_2Se (δ 0). ^{125}Te NMR measurements were made at an operating frequency of 94.705 MHz using a pulse width of 9.5 μs and a delay of 1 s. The spectra were referenced to Me_2Te (δ 0). Elemental analyses were carried out using a Carlo Erba automatic analyzer. Phenylacetylene was purchased from Aldrich Chemical Co. and used as such. $Fe_2(CO)_6(\mu\text{-SeTe})$, $Fe_2(CO)_6(\mu\text{-SSe})$, and $Fe_2(CO)_6(\mu\text{-STe})$ were prepared as reported before.[8]

Preparation of $(CO)_6Fe_2\{\mu\text{-SeC(H)=C(Ph)Te}\}$ (1) and $(CO)_6Fe_2\{\mu\text{-SeC(Ph)=C(H)Te}\}$ (2). To a solution of freshly prepared $Fe_2(CO)_6(\mu\text{-SeTe})$ (0.15 g, 0.3 mmol) and solid anhydrous sodium acetate (0.25 g) in 30 mL of methanol was added phenylacetylene (0.022 mL, 0.2 mmol), and the mixture was stirred at room temperature for 36 h. The solvent was removed in vacuo, and the residue was redissolved in 5 mL of dichloromethane. The solvent was filtered through Celite to remove insoluble material, and chromatographic workup using silica gel TLC plates and hexane as eluent yielded the following four orange bands, in order of elution: a trace amount of $(CO)_6Fe_2\{\mu\text{-SeC(H)=C(Ph)Se}\}$, $(CO)_6Fe_2\{\mu\text{-SeC(H)=C(Ph)Te}\}$ (**1**; 42 mg, 23%), $(CO)_6Fe_2\{\mu\text{-SeC(Ph)=C(H)Te}\}$ (**2**; 38 mg, 21%), very closely followed by a trace amount of $(CO)_6Fe_2\{\mu\text{-TeC(H)=C(Ph)Te}\}$. **1**: IR (ν(CO), cm^{-1}) 2073 (s), 2034 (vs), 1996 (vs), 1962 (w); ^{1}H NMR δ 7.21–7.38 (m, phenyl ring protons), 8.13 (s, C*H*); ^{13}C NMR δ 126–130 (phenyl ring carbon atoms), 138 (*C*Ph), 142 (*C*H), 210 (*C*O); ^{77}Se NMR δ 436 (d, J_{Se-H} = 59.5 Hz); ^{125}Te NMR δ 782 (d, J_{Te-H} = 6.1 Hz); mp 130–132 °C. Anal. Calcd (found) for $C_{14}H_6Fe_2O_6SeTe$: C, 28.5 (28.7); H, 1.02 (1.18). **2**: IR (ν(CO), cm^{-1}) 2073 (s), 2034 (vs), 1996 (vs), 1962 (w); ^{1}H NMR δ 7.24–7.61 (m, phenyl ring protons), 7.81 (s, C*H*); ^{13}C NMR δ 109 (*C*Ph), 125–129 (phenyl ring carbon atoms), 132 (*C*H), 210 (*C*O); ^{77}Se NMR δ 534 (d, J_{Se-H} = 9.2 Hz); ^{125}Te NMR δ 658 (d, J_{Te-H} = 121.4 Hz); mp 68–70 °C. Anal. Calcd (found) for $C_{14}H_6Fe_2O_6SeTe$: C, 28.5 (28.4); H, 1.02 (1.32).

(7) Mathur, P.; Hossain, M. M.; Rheingold, A. L. *Organometallics* **1993**, *12*, 5029.

(8) (a) Chakrabarty, D.; Hossain, M. M.; Kumar, R. K.; Mathur, P. *J. Organomet. Chem.* **1991**, *410*, 143. (b) Mathur, P.; Chakrabarty, D. Hossain, M. M. *J. Organomet. Chem.* **1991**, *401*, 167. (e) Mathur, P.; Chakrabarty, D.; Hossain, M. M.; Rashid, R. S. *J. Organomet. Chem.* **1991**, *420*, 79. (d) Mathur, P.; Chakrabarty, D.; Hossain, M. M. *J. Organomet. Chem.* **1991**, *418*, 415.

(9) Mathur, P.; Hossain, M. M.; Datta, S. N.; Kondru, R.-K.; Bhadbhade, M. M. *Organometallics* **1994**, *13*, 2532.

Table 1. Crystal Data for 1

formula	$C_{14}H_6Fe_2O_6SeTe$	V, Å^3	872.1(8)
fw	588.5	Z	2
cryst syst	triclinic	D(calc), g cm^{-3}	2.241
space group	$P\bar{1}$	μ(Mo Kα), cm^{-1}	54
		temp, K	293
a, Å	7.773(9)	hkl ranges	h, −9 to +8; k, 0–12; l, 1
b, Å	10.635(9)		
c, Å	12.010(10)	$2\theta_{max}$, deg	54
α, deg	104.99(10)	F(000)	552
β, deg	102.86(11)	R	0.077
γ, deg	106.38(9)	R_w	0.086

Preparation of $(CO)_6Fe_2\{\mu\text{-SC(Ph)=C(H)Se}\}$ (3). A methanol solution (30 mL) containing freshly prepared $Fe_2(CO)_6(\mu\text{-SSe})$ (0.12 g, 0.3 mmol), sodium acetate (0.25 g), and phenylacetylene (0.022 mL, 0.2 mmol) was stirred at room temperature for 5 h. The solution was filtered through Celite to remove insoluble material. After removal of solvent in vacuo, the residue was redissolved in hexane (5 mL) and subjected to chromatographic workup on a silica gel column. Using hexane as eluent, the following three orange compounds were obtained, in order of elution: a trace amount of $(CO)_6Fe_2\{\mu\text{-SC(Ph)=C(H)S}\}$, $(CO)_6Fe_2\{\mu\text{-SeC(H)=C(Ph)S}\}$ (**3**; 71 mg, 47%), and a trace amount of $(CO)_6Fe_2\{\mu\text{-SeC(Ph)=C(H)Se}\}$. **3**: IR (ν(CO), cm^{-1}) 2076 (s), 2041 (vs), 2003 (vs), 1965 (w); ^{1}H NMR δ 6.94 (s, C*H*), 7.21–7.38 (m, phenyl ring protons); ^{13}C NMR δ 125–129 (phenyl ring carbon atoms), 133 (*C*Ph), 162 (*C*H), 208 (*C*O); ^{77}Se NMR δ 303 (d, J_{Se-H} = 50.4 Hz); mp 99–101 °C. Anal. Calcd (found) for $C_{14}H_6Fe_2O_6SSe$: C, 34.1 (34.2); H, 1.22 (1.33).

Preparation of $(CO)_6Fe_2\{\mu\text{-SC(H)=C(Ph)Te}\}$ (4) and $(CO)_6Fe_2\{\mu\text{-SC(Ph)=C(H)Te}\}$ (5). To a solution of freshly prepared $Fe_2(CO)_6(\mu\text{-STe})$ (0.132 g, 0.3 mmol) and solid anhydrous sodium acetate (0.25 g) in 30 mL of methanol was added phenylacetylene (0.022 mL, 0.2 mmol). The mixture was stirred at room temperature for 36 h. The solvent was removed in vacuo, and the residue was redissolved in 5 mL of dichloromethane. The solvent was filtered through Celite to remove insoluble material, and chromatographic workup using silica gel TLC plates and hexane as eluent yielded the following compounds in order of elution: trace amounts of yellow $(CO)_6Fe_2(\mu\text{-S}_2)$ and orange-red $(CO)_6Fe_2\{\mu\text{-SC(H)=C(Ph)S}\}$, orange $(CO)_6Fe_2\{\mu\text{-SC(H)=C(Ph)Te}\}$ (**4**; 45 mg, 27%), orange $(CO)_6Fe_2\{\mu\text{-SC(Ph)=C(H)Te}\}$ (**5**; 20 mg, 12%), followed by a small yellow band (unidentified) and trace amount of yellow $(CO)_6Fe_2(\mu\text{-STe})$. **4**: IR (ν(CO), cm^{-1}) 2071 (m), 2036 (s), 2001 (s), 1995 (s); ^{1}H NMR δ 7.19–7.32 (m, phenyl ring protons), 7.38 (s, C*H*); ^{13}C NMR 125 (*C*Ph), 127–130 (phenyl ring carbon atoms), 145 (*C*H), 209 (*C*O); ^{125}Te NMR δ 620; mp 112–113 °C. Anal. Calcd (found) for $C_{14}H_6Fe_2O_6STe$: C, 31.0 (31.2); H, 1.11 (1.20). **5**: IR (ν(CO), cm^{-1}) 2071 (m), 2036 (s), 2001 (s), 1995 (s); ^{1}H NMR δ 7.26–7.54 (m, phenyl ring protons), 7.83 (s, C*H*); ^{13}C NMR δ 107 (*C*Ph), δ 125–129 (phenyl ring carbon atoms), 132 (*C*H), 209 (*C*O); ^{125}Te NMR δ 533 (d, J_{Te-H} = 112.1 Hz); mp 108–109 °C. Anal. Calcd (found) for $C_{14}H_6Fe_2O_6STe$: C, 31.0 (31.2); H, 1.11 (1.21).

Crystal Structure Determination of 1. A red crystal of approximate dimensions 0.20 × 0.20 × 0.25 mm^3 was selected for the X-ray diffraction study. The data were collected on an Enraf-Nonius CAD4 diffractometer generating Mo Kα radiation at room temperature, using the ω–2θ scan method. Pertinent crystallographic data are listed in Table 1. Unit cell parameters were determined from 24 randomly selected reflections. The structure was solved by direct methods and refined by least-squares methods using NRCVAX programs[10] to R = 0.077 and R_w = 0.086 for 1707 ($F_o > 3.5\sigma(F_o)$) reflections from 2718 unique reflections. Final ΔF synthesis showed no features above 1.38 e Å^{-3}. Table 2 lists the atomic coordinates, and Table 3 lists the bond lengths and bond angles.

(10) Gabe, E. J.; Le Page, Y.; Charland, J.-P.; Lee, F. L.; White, P. S. *J. Appl. Crystallogr.* **1989**, *22*, 384.

Table 2. Atomic Coordinates and Isotropic Displacement Coefficients for 1

atom	x	y	z	B_{iso}, Å^2
Te	0.3135(2)	0.8709(2)	0.3288(2)	3.8(1)
Se	−0.0339(3)	0.5836(3)	0.1602(3)	4.1(1)
Fe(1)	0.2635(4)	0.6150(4)	0.2930(3)	3.4(2)
Fe(2)	0.0333(4)	0.7166(4)	0.3664(4)	3.5(2)
O(1)	0.469(3)	0.560(2)	0.119(2)	7.7(17)
O(2)	0.098(3)	0.334(2)	0.301(2)	7.4(16)
O(3)	0.569(3)	0.700(2)	0.521(2)	6.2(14)
O(4)	−0.194(3)	0.894(2)	0.358(3)	8.2(18)
O(5)	0.240(3)	0.827(2)	0.626(2)	5.6(12)
O(6)	−0.234(3)	0.481(2)	0.396(2)	7.1(15)
C(1)	0.023(3)	0.721(2)	0.083(2)	3.3(11)
C(2)	0.163(3)	0.839(3)	0.147(2)	4.2(14)
C(3)	0.238(3)	0.961(3)	0.100(2)	4.0(14)
C(4)	0.326(4)	1.098(3)	0.179(3)	5.6(19)
C(5)	0.385(4)	1.208(3)	0.135(3)	6.6(23)
C(6)	0.357(5)	1.167(4)	0.008(3)	7.3(25)
C(7)	0.273(6)	1.037(4)	−0.069(4)	8.5(31)
C(8)	0.210(5)	0.927(4)	−0.024(4)	7.5(26)
C(9)	0.397(4)	0.582(3)	0.189(3)	5.0(17)
C(10)	0.160(4)	0.439(3)	0.297(3)	5.0(18)
C(11)	0.445(4)	0.665(3)	0.427(2)	4.7(15)
C(12)	−0.104(3)	0.828(3)	0.364(3)	5.5(19)
C(13)	0.154(3)	0.784(2)	0.520(3)	5.1(16)
C(14)	−0.129(3)	0.572(3)	0.382(3)	5.1(17)

Table 3. Bond Distances (Å) and Bond Angles (deg) for 1

Te−Fe(1)	2.542(5)	O(2)−C(10)	1.11(3)
Te−Fe(2)	2.539(5)	O(3)−C(11)	1.20(3)
Te−C(2)	2.12(2)	O(4)−C(12)	1.12(3)
Se−Fe(1)	2.376(6)	O(5)−C(13)	1.20(4)
Se−Fe(2)	2.367(6)	O(6)−C(14)	1.16(3)
Se−C(1)	1.92(2)	C(1)−C(2)	1.31(3)
Fe(1)−Fe(2)	2.539(5)	C(2)−C(3)	1.56(4)
Fe(1)−C(9)	1.82(3)	C(3)−C(4)	1.39(4)
Fe(1)−C(10)	1.84(3)	C(3)−C(8)	1.39(4)
Fe(1)−C(11)	1.73(3)	C(4)−C(5)	1.41(4)
Fe(2)−C(12)	1.81(2)	C(5)−C(6)	1.41(5)
Fe(2)−C(13)	1.72(3)	C(6)−C(7)	1.32(6)
Fe(2)−C(14)	1.77(3)	C(7)−C(8)	1.42(4)
O(1)−C(9)	1.12(3)		
Fe(1)−Te−Fe(2)	59.95(13)	Se−Fe(2)−C(12)	105.5(11)
Fe(1)−Te−C(2)	95.3(7)	Se−Fe(2)−C(13)	156.1(7)
Fe(2)−Te−C(2)	94.9(7)	Se−Fe(2)−C(14)	89.3(10)
Fe(1)−Se−Fe(2)	64.71(18)	Fe(1)−Fe(2)−C(12)	151.4(9)
Fe(1)−Se−C(1)	104.7(6)	Fe(1)−Fe(2)−C(13)	98.7(7)
Fe(2)−Se−C(1)	104.2(7)	Fe(1)−Fe(2)−C(14)	102.6(8)
Te−Fe(1)−Se	82.06(17)	C(12)−Fe(2)−C(13)	97.8(13)
Te−Fe(1)−Fe(2)	59.95(13)	C(12)−Fe(2)−C(14)	100.0(10)
Te−Fe(1)−C(9)	101.5(8)	C(13)−Fe(2)−C(14)	92.0(13)
Te−Fe(1)−C(10)	157.6(7)	Se−C(1)−C(2)	117.5(18)
Te−Fe(1)−C(11)	88.9(9)	Te−C(2)−C(1)	119.0(19)
Se−Fe(1)−Fe(2)	57.48(16)	Te−C(2)−C(3)	115.5(16)
Se−Fe(1)−C(9)	102.6(9)	C(1)−C(2)−C(3)	125(2)
Se−Fe(1)−C(10)	88.9(8)	C(2)−C(3)−C(4)	121(2)
Se−Fe(1)−C(11)	159.0(8)	C(2)−C(3)−C(8)	118(2)
Fe(2)−Fe(1)−C(9)	152.5(8)	C(4)−C(3)−C(8)	121(3)
Fe(2)−Fe(1)−C(10)	97.9(7)	C(3)−C(4)−C(5)	120(3)
Fe(2)−Fe(1)−C(11)	101.7(8)	C(4)−C(5)−C(6)	115(3)
C(9)−Fe(1)−C(10)	100.6(11)	C(5)−C(6)−C(7)	125(3)
C(9)−Fe(1)−C(11)	97.7(12)	C(6)−C(7)−C(8)	119(3)
C(10)−Fe(1)−C(11)	92.5(13)	C(3)−C(8)−C(7)	118(3)
Te−Fe(2)−Se	82.3(2)	Fe(1)−C(9)−O(1)	175(3)
Te−Fe(2)−Fe(1)	60.1(1)	Fe(1)−C(10)−O(2)	179(3)
Te−Fe(2)−C(12)	96.8(8)	Fe(1)−C(11)−O(3)	179(2)
Te−Fe(2)−C(13)	89.7(8)	Fe(2)−C(12)−O(4)	177(3)
Te−Fe(2)−C(14)	162.7(7)	Fe(2)−C(13)−O(5)	178(2)
Se−Fe(2)−Fe(1)	57.8(2)	Fe(2)−C(14)−O(6)	177(3)

Results and Discussion

Synthesis of 1−5. The syntheses of the mixed-chalcogenide compounds of the form $(CO)_6Fe_2\{\mu$-EC(H)=C(Ph)E′} (E ≠ E′; E, E′ = S, Se, Te) are summarized in Scheme 1. From the room-temperature reaction

Scheme 1. Formation of Compounds 1−5

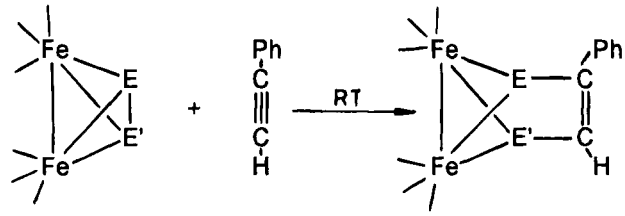

1. E = Te, E′ = Se
2. E = Se, E′ = Te
3. E = S, E′ = Se
4. E = Te, E′ = S
5. E = S, E′ = Te

of $Fe_2(CO)_6(\mu$-SeTe) with phenylacetylene, in the presence of sodium acetate, the following mixed-chalcogenide compounds were isolated: $(CO)_6Fe_2\{\mu$-SeC(H)=C(Ph)Te} (**1**; 23%) and its isomer $(CO)_6Fe_2\{\mu$-TeC(H)=C(Ph)Se} (**2**; 21%). Also identified in the reaction were trace amounts of the previously reported $(CO)_6Fe_2\{\mu$-SeC(H)=C(Ph)Se} and $(CO)_6Fe_2\{\mu$-TeC(H)=C(Ph)Te}. The related SSe compound $(CO)_6Fe_2\{\mu$-SeC(H)=C(Ph)S} (**3**) was similarly isolated in 47% yield from the room-temperature reaction of $Fe_2(CO)_6(\mu$-SSe) with phenylacetylene, in the presence of sodium acetate. From this reaction trace amounts of the S_2 and the Se_2 compounds $(CO)_6Fe_2\{\mu$-SC(H)=C(Ph)S} and $(CO)_6Fe_2\{\mu$-SeC(H)=C(Ph)Se} could also be isolated. On prolonged stirring of $Fe_2(CO)_6(\mu$-SSe) with phenylacetylene, the yields of the S_2 and Se_2 compounds increased at the expense of **3**. In solution also, compound **3** was found to slowly convert to $(CO)_6Fe_2\{\mu$-SC(H)=C(Ph)S} and $(CO)_6Fe_2\{\mu$-SeC(H)=C(Ph)Se}. The second isomer of **3**, $(CO)_6Fe_2\{\mu$-SC(H)=C(Ph)Se}, was not observed in this reaction. From the reaction of $Fe_2(CO)_6(\mu$-STe) with phenylacetylene in the presence of sodium acetate, two isomeric compounds were obtained, $(CO)_6Fe_2\{\mu$-SC(H)=C(Ph)Te} (**4**; 27%) and $(CO)_6Fe_2\{\mu$-SC(Ph)=C(H)Te} (**5**; 12%). Although the exact role of sodium acetate in the synthesis of **1**−**5** is not established, it was observed that when the reactions were carried out in absence of sodium acetate, much lower yields of **1**−**5** were obtained. The new mixed-chalcogenide compounds have been characterized by comparison of their IR spectra with those of the previously reported homochalcogenide compounds and on the basis of ^{1}H, ^{13}C, ^{77}Se, and ^{125}Te NMR spectroscopy. The structure of **1** has been elucidated by single-crystal X-ray diffraction methods.

Molecular Structure of 1. Red crystals of **1** were grown from its hexane solution at −10 °C, and an X-ray structural analysis was carried out. The molecular structure of **1** is shown in Figure 1. The structure consists of a Fe_2SeTe butterfly core, and the phenylacetylene molecule is attached to the wingtip Se and Te atoms such that the CPh group is attached to the Te atom and the CH group to the Se atom. Each Fe atom has three carbonyl ligands. Overall, the structure of **1** is similar to that of $(CO)_6Fe_2\{\mu$-SeC(H)=C(Ph)Se} and $(CO)_6Fe_2\{\mu$-TeC(H)=C(Ph)Te}. The acetylenic C−C distance in **1** is 1.31(3) Å, whereas in the Se_2 compound it is 1.331(7) Å and in the Te_2 compound it is 1.34(1) Å. The Se−C(H) bond distance of 1.92(2) Å in **1** is similar to the corresponding bond distance of 1.917(5) Å in $(CO)_6Fe_2\{\mu$-SeC(H)=C(Ph)Se}. The Te−C(Ph) bond distance of 2.12(2) Å is similar to the corresponding bond

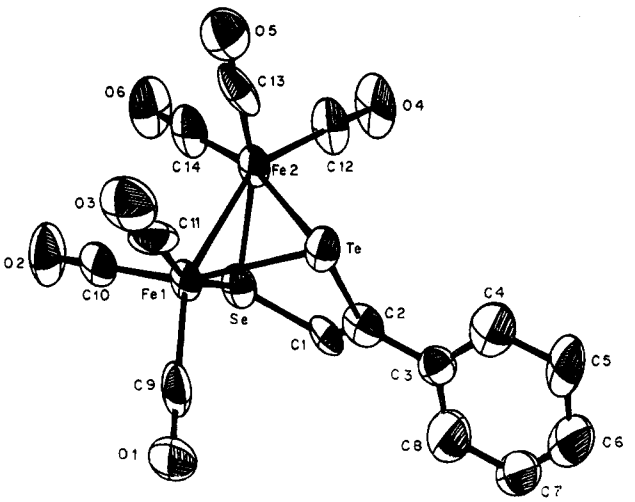

Figure 1. Molecular structure of **1** with thermal ellipsoids at the 50% probability level.

distance of 2.16(1) Å reported for $(CO)_6Fe_2\{\mu\text{-TeC(H)=C(Ph)Te}\}$. All other bond metricals are unexceptional.

Spectroscopic Characterization. The infrared spectra in hexane of compounds **1–5** display the characteristic carbonyl stretching pattern observed in compounds containing the $Fe_2(CO)_6$ unit. The spectra consists of four bands; in compounds **1–3** the lowest energy band is of weaker intensity than the three higher energy bands, whereas in compounds **4** and **5** all four bands are of comparable intensity. There is a shift of bands to lower ν(CO) values in $(CO)_6Fe_2\{\mu\text{-EC(H)=C(Ph)E}\}$ for the following combination of EE′ ligands: S_2 > SSe > Se_2 ≈ STe > SeTe > Te_2. The ^{1}H NMR spectra of **1–5** confirm the presence of C*H* and C*Ph* protons. The ^{13}C NMR spectra display two peaks between δ 107 and 162. The downfield peak can be assigned to *C*(H) and the upfield one to *C*Ph, by analogy to the $^{13}C\{^1H\}$ spectrum of $(CO)_6Fe_2\{\mu\text{-SC(H)=C(Ph)Te}\}$, which shows a doublet for *C*(H) at δ 144 (J_{CH} = 178 Hz) and a singlet for *C*(Ph) at δ 125. The separation of the two signals is greatest for compound **3** (29 ppm) and least for compound **1** (8 ppm). The spectra also display peaks for the phenyl carbon atoms at δ 125–130 and a single resonance in the *C*O region for all three compounds. The ^{77}Se NMR spectra of the products (Figure 2) served to distinguish the pair of isomers **1** and **2** as well as to establish the structure of **3**. The spectra of compounds $(CO)_6Fe_2\{\mu\text{-SeC(H)=C(Ph)E}\}$ (E = S, Te) show a doublet at δ 303 (J_{Se-H} = 50.4 Hz) and δ 436 (J_{Se-H} = 59.5 Hz), respectively. The ^{77}Se NMR spectrum of $(CO)_6Fe_2\{\mu\text{-SeC(H)=C(Ph)Se}\}$ shows two doublets at δ 371 and 448. On the basis of the Se–H couplings (54.1 and 6.9 Hz, respectively), the upfield signal can be assigned to *Se*CH and the downfield signal to *Se*CPh. Examination of the ^{77}Se NMR spectra for the series of compounds $(CO)_6Fe_2\{\mu\text{-SeC(H)=C(Ph)E}\}$ (E = S, Se, Te) shows that the signal shifts downfield along the series E = S, Se, Te. A reverse trend is observed in the two-bond Se–H couplings; it increases along the same series (Table 4). ^{125}Te NMR spectra of **1**, **2**, **4**, and **5** also serve to identify the isomeric structures (Figure 3); in the spectra of **1**, **2**, and **5** doublets are observed with significant differences between the long-range Te–H coupling (6.1 Hz in **1**) and shoft-range Te–H coupling (121.4 Hz in **2** and

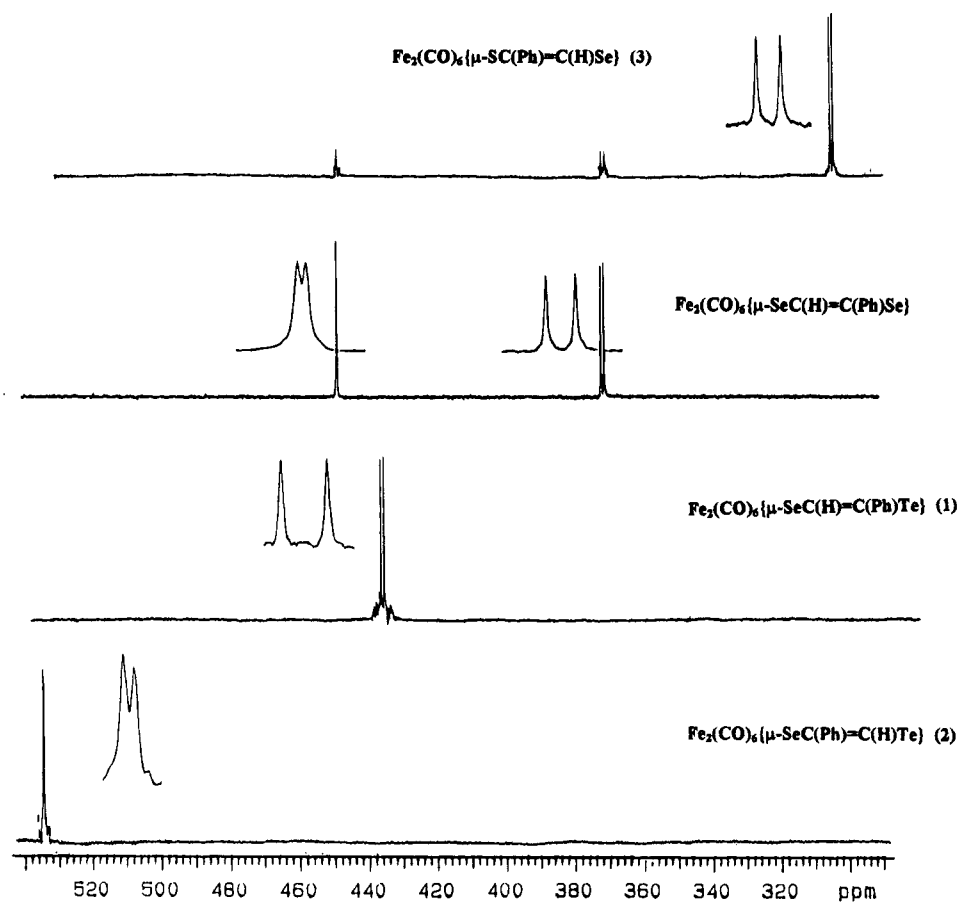

Figure 2. ^{77}Se NMR spectra.

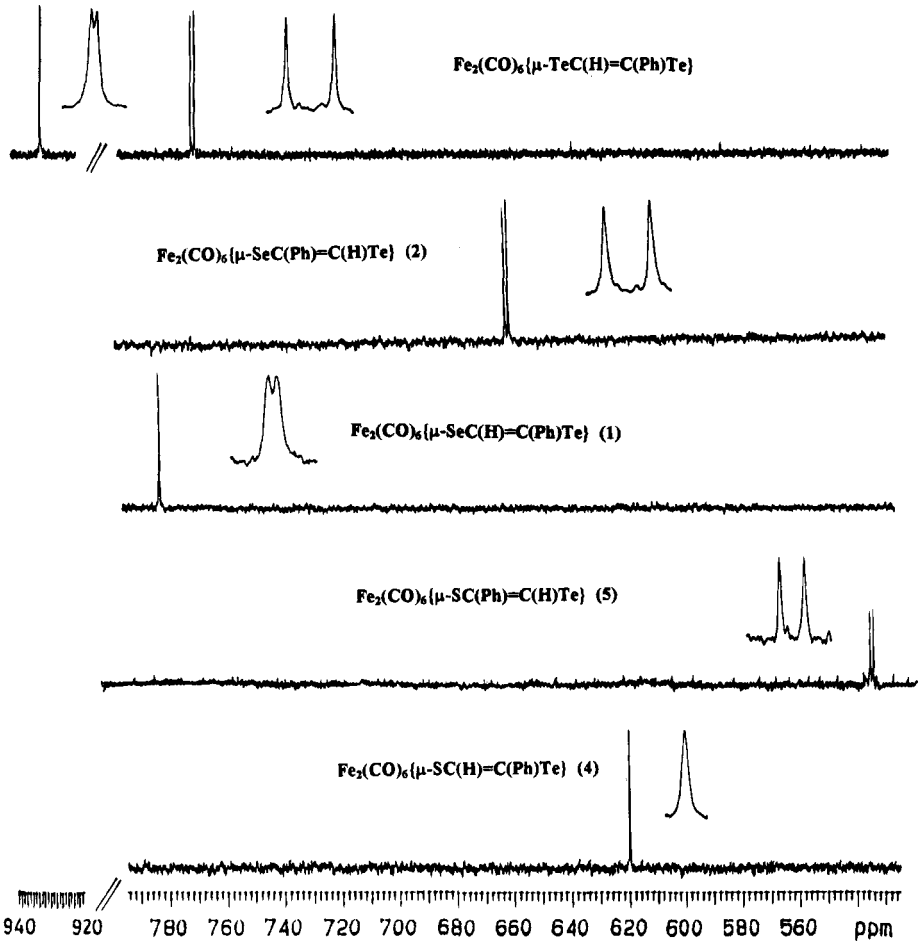

Figure 3. ^{125}Te NMR spectra.

Table 4. Se–H Coupling in $(CO)_6Fe_2\{SeC(H)=C(Ph)E\}$ and $(CO)_6Fe_2\{SeC(Ph)=C(H)E\}$ (E = S, Se, Te)

compd	J_{Se-H} (Hz)
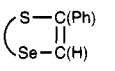 **3**	50.4
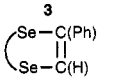	54.1, 6.9
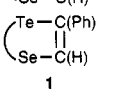 **1**	59.5
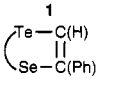 **2**	9.2

Table 5. Te–H Coupling in $(CO)_6Fe_2\{TeC(H)=C(Ph)E\}$ and $(CO)_6Fe_2\{TeC(Ph)=C(H)E\}$ (E = S, Se, Te)

compd	J_{Te-H} (Hz)
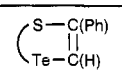 **5**	112.1
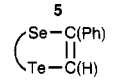 **2**	121.4
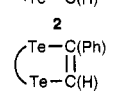	132.8, 9.2
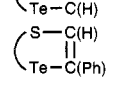 **4**	none
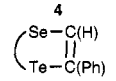 **1**	6.1

112.1 Hz in **5**). The spectrum of **4** shows a singlet, consistent with the structure proposed. The ^{125}Te NMR spectra of the series of compounds $(CO)_6Fe_2\{\mu\text{-TeC(H)=C(Ph)E}\}$ (E = S, Se, Te) shows that the signal shifts downfield along the series E = S, Se, Te. The two-bond Te–H coupling increases as E changes along the series S, Se, Te (Table 5). For the series of compounds $(CO)_6Fe_2\{\mu\text{-EC(H)=C(Ph)Te}\}$ (E = S, Se, Te) also, there is a downfield shift of the signal in the ^{125}Te NMR spectra along the series S, Se, Te and an increase in the Te–H coupling along the same series, consistent with the general trend observed in the ^{77}Se NMR spectra.

Formation of compounds **1–5** now provides an opportunity to investigate the use of these compounds in the synthesis of mixed-metal, mixed-chalcogenide clusters, and this will form the subject of ongoing investigation.

Acknowledgment. We thank the Council of Scientific & Industrial Research, Government of India, for financial support. We are grateful to the Regional Sophisticated Instrumentation Center, IIT Madras, for the use of their single-crystal X-ray diffractometer.

Supplementary Material Available: Tables of anisotropic thermal parameters and atomic coordinates for the hydrogen atoms (2 pages). Ordering information is given on any current masthead page.

OM940799L

Molecular Orbital Study on Acetylene Insertion into a Zr–R σ Bond (R = H, CH_3) in Cationic Zirconocene Complexes

Isabella Hyla-Kryspin, Shuqiang Niu, and Rolf Gleiter*

Organisch-Chemisches Institut der Universität Heidelberg, Im Neuenheimer Feld 270, D 69120 Heidelberg, Germany

Received July 19, 1994[⊗]

All-electron RHF and RMP2 ab initio calculations with split valence basis sets of double- and triple-ξ quality have been used to study reaction paths for the reaction of acetylene (**1**) with the model compounds Cl_2ZrH^+ (**2**) and $Cl_2ZrCH_3^+$ (**3**). At the RMP2//RHF level the insertion process is calculated to have a barrier of 0.2 (**2**) and 5.1 kcal/mol (**3**) with respect to complexed acetylene and to be 86.9 (**2**) and 53.3 kcal/mol (**3**) exothermic with respect to free acetylene. The transition states (TS) are four membered cycles. The products and TS of $Cl_2ZrCH_3(C_2H_2)^+$ are stabilized through an agostic interaction. The calculated energetics of the reaction path are compared with available theoretical as well as experimental data for insertion of unsaturated hydrocarbons into metal–R (R = H, CH_3) σ bonds. On the basis of extended Hückel calculations a MO picture of the insertion path is provided for the reaction of acetylene with Cp_2ZrH^+ and $Cp_2ZrCH_3^+$.

Introduction

The insertion reactions of olefins and acetylenes into transition-metal hydrogen and carbon bonds are the fundamental steps in industrially important catalytic processes such as hydrogenation, hydroformylation, isomerization, and polymerization as well as in stoichiometric transformation of organic systems.[1] In the present paper we will report the results of ab initio and extended Hückel MO calculations concerning the insertion reactions of acetylene, which are closely related to Ziegler–Natta olefin polymerizations.[2] During the past half-century many studies with various experimental[3] and theoretical methods[4] have been carried out in order to understand the basic principles of this polymerization and to identify the active catalyst of the catalytic systems. Although initial efforts by Dyachkovskii et al.[5] to identify the catalytically active species were unsuccessful, they suggested that highly electrophilic, cationic metallocene alkyl complexes $CpMR^+$ participate in the polymerization process. The recent experimental work of many groups[6] provides compelling support for the identification of the Cp_2MR^+ species (M = group 4 metals) as active catalysts as well as for the widely accepted Cossee mechanism[7] of the polymerization process. According to the Cossee mechanism the propagation step in the polymerization of olefins occurs via a prior coordination of the π bond to the vacant coordination site of the active catalyst, followed by olefin complexation through a four-membered transition state in a 2π + 2σ reaction involving the C–C π bond and metal–alkyl σ bond. This recreates a vacant coordination site on the active catalyst, and the process continues. Recent theoretical investigations[8] support the view that the Cossee mechanism is indeed a reliable mechanism for homogeneous Ziegler–Natta polymerization. The insertion and σ-bond metathesis reaction of single

⊗ Abstract published in *Advance ACS Abstracts*, December 1, 1994.

(1) (a) Parshall, G. W. *Homogenous Catalysis*; Wiley: New York, 1980. (b) Wilkinson, G., Stone, F. G. A., Abel, E. W. Eds. *Comprehensive Organometallic Chemistry*; Pergamon Press: New York, 1982. (c) Dötz, K. H., Hoffmann, R. W., Eds. *Organic Synthesis via Organometallics*; Vieweg: Braunschweig, Germany, 1980.

(2) (a) Natta, G.; Pino, P.; Mazzanti, G.; Giannini, U. *J. Inorg. Nucl. Chem.* **1958**, *8*, 612. (b) Breslow, D. S.; Newburg, N. R. *J. Am. Chem. Soc.* **1959**, *81*, 81. (c) Ziegler, K.; Gellert, H. G.; Zosel, K.; Holzkamp, E.; Schneider, J.; Söll, M.; Kroll, W. R. *Justus Liebigs Ann. Chem.* **1960**, *629*, 121. (d) Sinn, H.; Kolk, E.; *J. Organomet. Chem.* **1966**, *6*, 373.

(3) Reviews on Ziegler–Natta polymerization: (a) Boor, J., Jr. *Ziegler-Natta Catalysts and Polymerization*; Academic Press: New York, 1979. (b) Pino, P.; Mülhaupt, R. *Angew. Chem., Int. Ed. Engl.* **1980**, *19*, 857. (c) Eisch, J. J.; Galle, J. E.; Piotrowski, A. M. In *Transition Metal Catalyzed Polymerization; Alkenes and Dienes*; Quirk, R. P., Ed.; Horwood: New York, 1983. (d) Eisch, J. J.; Boleslawski, M. P.; Piotrowski, A. M. In *Transition Metals and Organometallics as Catalysts for Olefin Polymerization*; Kaminsky, W., Linn, M., Eds.; Springer-Verlag: Berlin, Heidelberg, 1988. (e) Allen, G. B. *Comprehensive Polymer Science*; Pergamon Press: Oxford, U.K., 1989.

(4) (a) Armstrong, D. R.; Perkin, S. P. G.; Stewart, J. J. P. *J. Chem. Soc., Dalton Trans.* **1972**, 1972. (b) Sakaki, S.; Kato, H.; Kanai, H.; Tarama, K. *Bull. Chem. Soc. Jpn.* **1975**, *48*, 813. (c) Fukui, K.; Inagaki, S. *J. Am. Chem. Soc.* **1975**, *97*, 4445. (d) Novaro, O.; Blaisten-Barojas, E.; Clementi, E.; Giunchi, G.; Ruiz-Vizcaya, M. E. *J. Chem. Phys.* **1978**, *68*, 2337. (e) Balazs, A. C.; Johnson, K. H. *J. Chem. Phys.* **1982**, *77*, 3148. (f) Fujimoto, H.; Yamasaki, T.; Mizutani, H.; Koga, N. *J. Am. Chem. Soc.* **1985**, *107*, 6157.

(5) Dyachkovskii, F. S.; Shilova, A. K.; Shilov, A. E. *J. Polym. Sci., Part C* **1967**, *16*, 2333.

(6) For reviews see: (a) Rosenthal, M. R. *J. Chem. Educ.* **1973**, *50*, 331. (b) Lawrance, G. A.; *Chem. Rev.* **1986**, *86*, 17. (c) Beck, W.; Sünkel, K. *Chem. Rev.* **1988**, *88*, 1405. (d) Lawrance, G. A. *Adv. Inorg. Chem.* **1989**, *34*, 145. (e) Bochmann, M. *Angew. Chem., Int. Ed. Engl.* **1992**, *31*, 1181. (f) Strauss, S. H. *Chem. Rev.* **1993**, *93*, 927. For a related example see: (g) Yang, X.; Stern, C. L.; Marks, T. J. J. *Am. Chem. Soc.* **1991**, *113*, 3623. *Angew. Chem., Int. Ed. Engl.* **1992**, *31*, 1375. (h) Alelyunas, Y. W.; Jordan, R. F.; Echols, S. F.; Borkowsky, S. L.; Bradley, P. K. *Organometallics* **1991**, *10*, 1406. (i) Crowther, D. J.; Borkowsky, S. L.; Swenson, D.; Meyer, T. Y.; Jordan, R. F. *Organometallics* **1993**, *12*, 2897. (j) Eisch, J. J.; Caldwell, K. R.; Werner, S.; Krüger, C. *Organometallics* **1991**, *10*, 3417.

(7) Cossee, P. *J. Catal.* **1964**, *3*, 80. (b) Arlman, E. J.; Cossee, P. *J. Catal.* **1964**, *3*, 99.

(8) (a) Jolly, C. A.; Marynick, D. S. *J. Am. Chem. Soc.* **1989**, *111*, 7968. (b) Castonguay, L. A.; Rappé, A. K. *J. Am. Chem. Soc.* **1992**, *114*, 5832. (c) Kawamura-Kuribayashi, H.; Koga, N.; Morokuma, K. *J. Am. Chem. Soc.* **1992**, *114*, 2359. (d) Kawamura-Kuribayashi, H.; Koga, N.; Morokuma, K. *J. Am. Chem. Soc.* **1992**, *114*, 8687. (e) Rappé, A. K. *Organometallics* **1990**, *9*, 466. (f) Ziegler, T.; Folga, E.; Berces, A. *J. Am. Chem. Soc.* **1993**, *115*, 636. (g) Siegbahn, P. E. M. *J. Am. Chem. Soc.* **1993**, *115*, 5803. (h) Woo, T. K.; Fan, L.; Ziegler, T. *Organometallics* **1994**, *13*, 432, 2252. (i) Bierwagen, E. P.; Bercaw, J. E.; Goddard, W. A., III. *J. Am. Chem. Soc.* **1994**, *116*, 1481. (j) Axe, F. U.; Coffin, J. M. *J. Phys. Chem.* **1994**, *98*, 2567.

0276-7333/95/2314-0964$09.00/0

Scheme 1

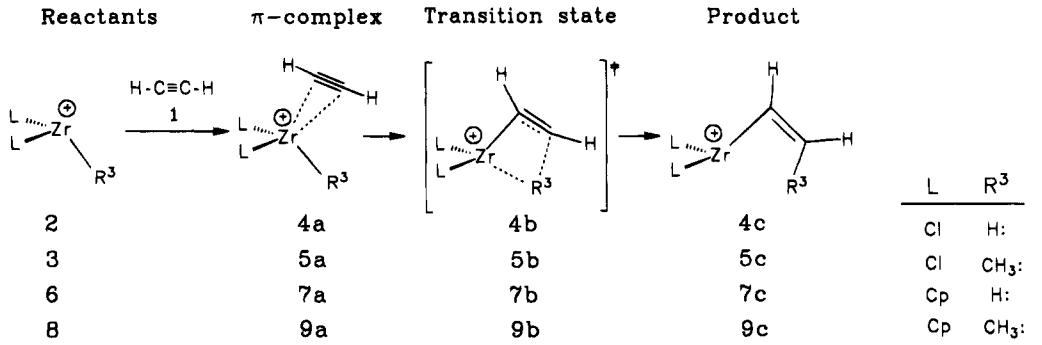

Chart 1

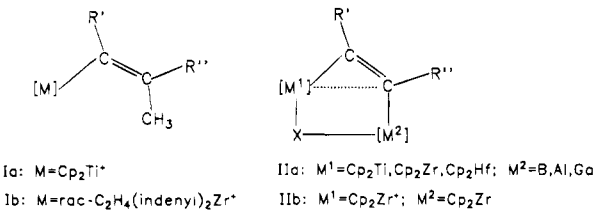

and multiple alkynes with an electrophilic d° active species Cp_2MR^{n+} (n = 0, 1) have been reported, and evidence for single- and multiple-insertion products of relevance to alkyne oligomerization and polymerization has been provided as well.[9] Fourteen valence-electron complexes with general formula Ia,b have been found and characterized as the products of the insertion reaction of bulky alkyne with $Cp_2MCH_3^+$ (M = Ti, Zr).[10] It is interesting to note that the alkyne insertion reaction with Cp_2ZrR^+ [11a] as well as η^2-alkyne transition metal species[11b–i] has been postulated for the primary step in the reactions leading to the products IIa,b, in which one vinylic carbon atom has an unusually planar tetracoordinate geometry. Prompted by the experimental achievements in the field of alkyne insertion reactions and continuing our previous study on stabilizing factors responsible for the structure of complexes I and II[12] we decided to investigate in more detail the model reactions displayed in Scheme 1. In contrast to olefin insertion reactions, theoretical investigations on alkyne insertion reactions are scarce.[8e,f] To the best of our knowledge, no theoretical investigations on the reactions from Scheme 1 have been reported so far.

Calculations

Ab initio calculations[13] were carried out using Cartesian–Gaussian basis sets. A single basis set was adapted throughout the paper. For Zr we selected a (14, 9, 7) basis set obtained by adding a p-type orbital exponent (0.12) to the optimized (14, 8, 7) set from ref 14. The choice of the additional p exponent guarantees a comparable distribution of the radial density function of the 5p and 5s orbitals. The contraction is [6, 4, 4], corresponding to a single-ξ description for the inner shells and the 5p shell, double-ξ for 5s, and triple-ξ for 4d. Basis sets of respective size (10, 6), (9, 5), and (4) were used for chlorine, carbon and hydrogen and contracted to split valence.[15] The geometry optimizations were carried out using the energy gradient technique at the restricted Hartree–Fock (RHF) level. For an estimation of correlation effects and better energetics, restricted second-order Møller–Plesset perturbation (RMP2) calculations[16a] were carried out with geometries optimized at the RHF level (RMP2//RHF). It was argued in the literature that in the case of the second-row transition-metal compounds it is reasonable to determine the energetics at SCF-optimized geometries since the geometries optimized at SCF and correlated levels give similar relative energies.[16b,c] Extended Hückel calculations were carried out with standard parameters for all atoms.[17]

Results and Discussion

Ab Initio Calculations for Insertion of Acetylene into Zr–H and Zr–CH_3 σ Bonds. In this section we report the optimized structures of reactants (**1–3**), intermediates (**4a**, **5a**), transition states (**4b**, **5b**), and products (**4c**, **5c**) and discuss the energetics for the reaction displayed in Scheme 1. In our ab initio calculations we replaced the Cp groups of the real molecules by chlorine ligands, which has been shown

(9) (a) McDade, C.; Bercaw, J. E. *J. Organomet. Chem.* **1985**, *279*, 281. (b) Thompson, M. E.; Baxter, S. M.; Bulls, A. R.; Burger, B. J.; Nolan, M. C.; Santarsiero, B. D.; Schaefer, W. P.; Bercaw, J. E. *J. Am. Chem. Soc.* **1987**, *109*, 203. (c) Burger, B. J.; Thompson, M. E.; Cotter, W. D.; Bercaw, J. E. *J. Am. Chem. Soc.* **1990**, *112*, 1566. (d) Christ, C. S., Jr.; Eyler, J. R.; Richardson, D. E. *J. Am. Chem. Soc.* **1990**, *112*, 596. (e) Horton, A. D.; Orpen, A. G.; *Organometallics* **1992**, *11*, 8.

(10) (a) Eisch, J. J.; Piotrowski, A. M.; Brownstein, S. K.; Gabe, E. J.; Lee, F. L. *J. Am. Chem. Soc.* **1985**, *107*, 7219. (b) Horton, A. D.; Orpen, A. G. *Organometallics* **1991**, *10*, 3910.

(11) (a) Horton, A. D.; Orpen, A. G. *Angew. Chem., Int. Ed. Engl.* **1992**, *31*, 876. (b) Erker, G.; Zwettler, R.; Krüger, C.; Noe, R.; Werner, S. *J. Am. Chem. Soc.* **1990**, *112*, 9620. (c) Erker, G.; Albrecht, M.; Krüger, C.; Werner, S. *Organometallics* **1991**, *10*, 3791. (d) Erker, G. *Nachr. Chem. Tech. Lab.* **1992**, *40*, 1099. *Comments Inorg. Chem.* **1992**, *13*, 111. (e) Erker, G.; Albrecht, M.; Werner, S.; Nolte, M.; Krüger, C. *Chem. Ber.* **1992**, *125*, 1953. (f) Erker, G.; Albrecht, M.; Krüger, C.; Werner, S. *J. Am. Chem. Soc.* **1992**, *114*, 8531. (g) Erker, G.; Albrecht, M.; Krüger, C.; Werner, S.; Binger, P.; Langhauser, F. *Organometallics* **1992**, *11*, 3517. (h) Albrecht, M.; Erker, G.; Nolte, M.; Krüger, C. *J. Organomet. Chem.* **1992**, *427*, C21. (i) Erker, G.; Röttger, D. *Angew. Chem., Int. Ed. Engl.* **1993**, *105*, 1623.

(12) (a) Gleiter, R.; Hyla-Kryspin, I.; Niu, S.-Q.; Erker, G. *Organometallics* **1993**, *12*, 3828; **1994**, *13*, 744. (b) *Angew. Chem., Int. Ed. Engl.* **1993**, *32*, 754.

(13) We used the Gaussian 86 program by M. J. Frisch, J. S. Binkley, H. B. Schlegel, K. Raghavachari, C. F. Melius, R. L. Martin, J. J. P. Stewart, F. W. Bobrowicz, C. M. Rohlfing, L. R. Kahn, D. J. Defrees, R. Seeger, R. A. Whiteside, D. J. Fox, E. M. Fleuder, and J. A. Pople (Carnegie-Mellon Quantum Chemistry Publishing Unit, Pittsburgh, PA, 1984) and Gaussian 92 (Revision A) by M. J. Frisch, G. W. Trucks, M. Head-Gordon, P. M. W. Gill, M. W. Wong, J. B. Foresman, B. G. Johnson, H. B. Schlegel, M. A. Robb, E. S. Replogle, R. Gomperts, J. L. Andres, K. Raghavachari, J. S. Binkley, C. Gonzalez, R. L. Martin, D. J. Fox, D. J. Defrees, J. Baker, J. J. P. Stewart, and J. A. Pople (Gaussian, Inc., Pittsburgh, PA, 1992).

(14) Hyla-Kryspin, I.; Demuynck, J.; Strich, A.; Bénard, M. *J. Chem. Phys.* **1981**, *75*, 3954.

(15) (a) Roos, B.; Siegbahn, P. E. M. *Theor. Chim. Acta* **1970**, *17*, 209. (b) Dunning, T. H., Jr. *J. Chem. Phys.* **1970**, *53*, 2823. (c) Huzinaga, S. *J. Chem. Phys.* **1965**, *42*, 1293.

(16) (a) Møller, C.; Plesset, M. S. *Phys. Rev.* **1934**, *46*, 618. (b) Siegbahn, P. E. M. *Chem. Phys. Lett.* **1993**, *205*, 290. (c) See also: Weiss, H.; Ehrig, M; Ahlrichs, R. *J. Am. Chem. Soc.* **1994**, *116*, 4919.

(17) (a) Summerville, R. H.; Hoffmann, R. *J. Am. Chem. Soc.* **1976**, *98*, 7240. (b) Hofmann, P.; Stauffert, P.; Schore, N. E. *Chem. Ber.* **1982**, *115*, 2153.

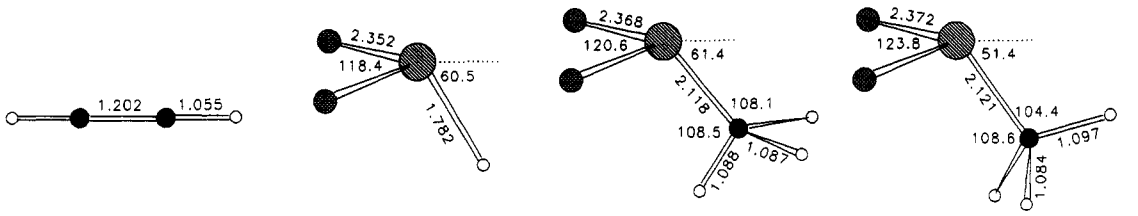

	1	2	3	3'
E_T^{RHF} (a.u.)	-76.79666	-4448.57791	-4487.65160	-4487.64958
$E_T^{MP2//RHF}$ (a.u.)	-76.96855	-4448.92525	-4488.09797	-4488.09468

Figure 1. Optimized geometries of the reactants **1**–**3** and **3'** at the RHF level.

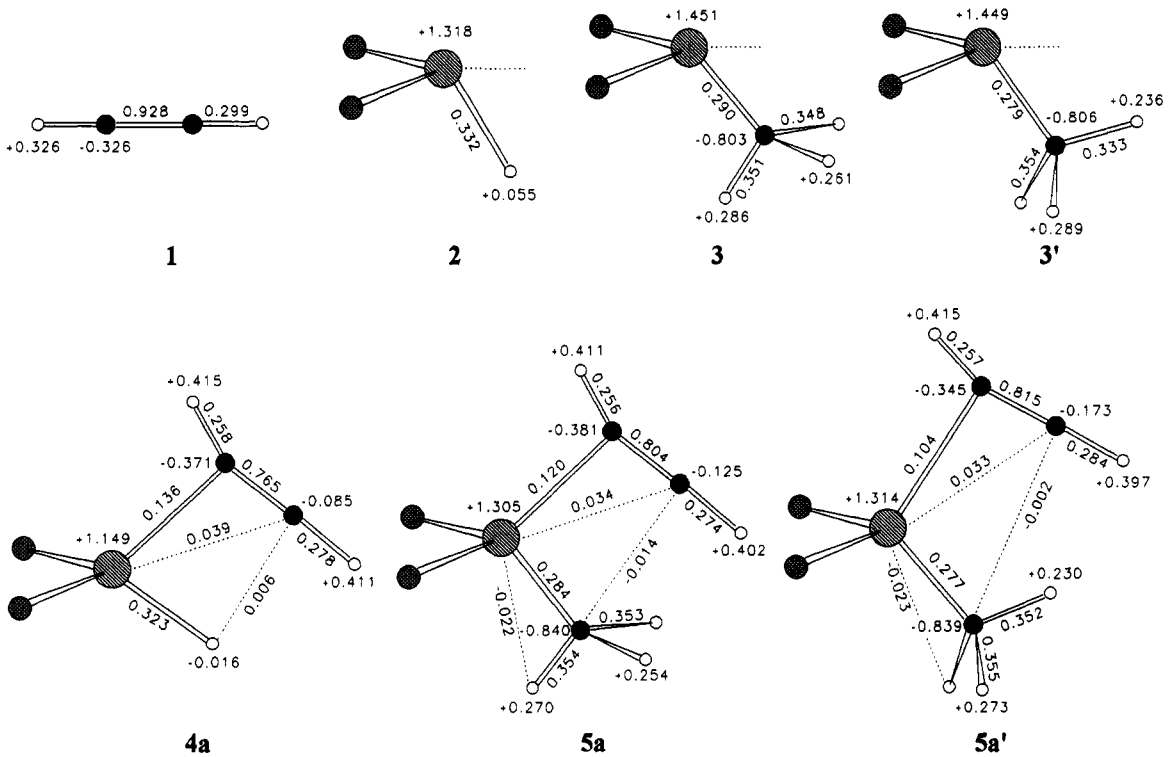

1 **2** **3** **3'**

4a **5a** **5a'**

Figure 2. Atomic charge distributions and bond overlap populations of the reactants **1**–**3** and **3'** and intermediate π complexes **4a**, **5a**, and **5a'**, obtained with Mulliken population analysis at the RHF level.

in other studies to provide a good theoretical substitute for the actual bent metallocene system.[8a–c,e,i,18]

A. Reactants: C_2H_2 (1), Cl_2ZrH^+ (2), $Cl_2ZrCH_3^+$ (3). The fully optimized geometries of **2**, **3** and **3'** under C_s symmetry constraint, together with those of **1**, are shown in Figure 1. Structure **3'** differs from **3** by rotating the CH_3 group around the Zr–C bond. For **3** two CH σ bonds are staggered with respect to the Zr–Cl bonds; in **3'** they are eclipsed. Although in **3'** one of the ZrCH angles is smaller than the other ones, pointing to the possibly agostic interaction, structure **3'** is 1.3 kcal/mol (RHF) or 2.1 kcal/mol (RMP2//RHF) less stable than **3**. Similar properties were found for the model compound $Cl_2TiCH_3^+$.[8c] The Mulliken population analysis shown in Figure 2 reveals that the Zr–C bond of **3** and **3'** is more polarized than the Zr–H bond of **2**. The calculated overlap populations (Figure 2) agree with the experimentally determined order of the bond strength D(Zr–H) > D(Zr–C) found in the gas-phase studies for Cp_2ZrH^+ and Cp_2ZrCH_3.[19]

B. Intermediate Acetylene Complexes: $Cl_2ZrH(C_2H_2)^+$ (4a) and $Cl_2ZrCH_3(C_2H_2)^+$ (5a, 5a'). The optimized structural parameters of the intermediate acetylene π complexes **4a**, **5a**, and **5a'** are shown in Figure 3. For the hydride complex the geometry optimizations were performed without any symmetry constraint. The final structures converged to **4a** with C_s symmetry. To simplify the analysis the structures **5a** and **5a'** were optimized under C_s symmetry constraint. Similar theoretical investigations on the insertion of ethylene into the M–C (M = Ti, Zr) σ bond showed that sometimes more stable equilibrium structures can be found with C_1 symmetry, whose energy, however, is only 0.5–1.0 kcal/mol lower than those of the appropriate C_s structures.[8c,d,18d] In **5a** and **5a'** the Zr–CH_3 bond is longer by 0.02 Å with respect to **3** and **3'**. The elongation of the Zr-H bond in **4a** is insignificant. In **4a**, **5a**, and **5a'** the C(1)–C(2) bond is 0.01–0.025 Å longer than in free acetylene. The coordination of acetylene is not symmetric. The distance Zr–C(1) is 0.456 Å (**4a**), 0.466 Å (**5a**), and 0.433 Å (**5a'**) shorter than Zr–C(2). From the Mulliken population analysis shown in Figure 2, it

(18) (a) Rappé, A. K.; Goddard, W. A., III. *J. Am. Chem. Soc.* **1982**, *104*, 297. (b) Upton, T. H.; Rappé, A. K. *J. Am. Chem. Soc.* **1985**, *107*, 1206. (c) Rappé, A. K. *Organometallics* **1987**, *6*, 354. (d) Koga, N.; Morokuma, K. *J. Am. Chem. Soc.* **1988**, *110*, 108; *Chem. Rev.* **1991**, *91*, 823.

(19) Christ, C. S.; Eyler, J. R.; Richardson, D. E. *J. Am. Chem. Soc.* **1988**, *110*, 4038.

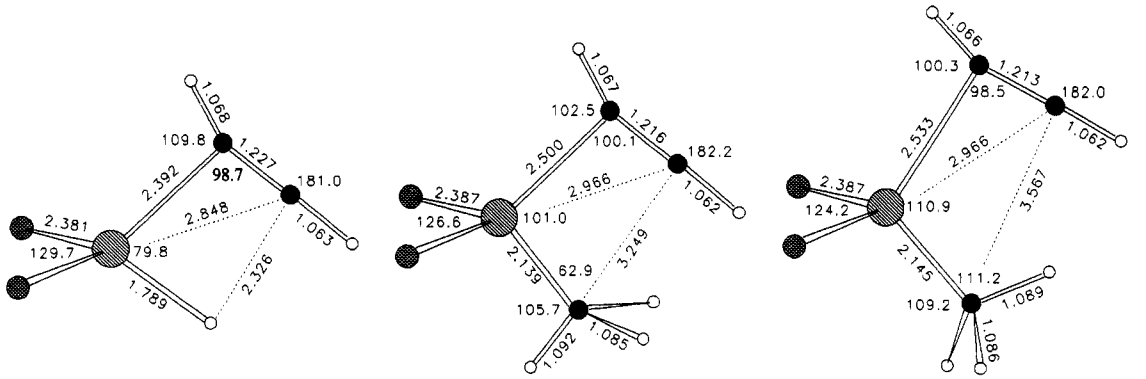

E_T^{RHF} (a.u.)	-4525.44446	-4564.50911	-4564.50493
$E_T^{MP2//RHF}$ (a.u.)	-4525.97605	-4565.13267	-4565.12808
	4a	**5a**	**5a'**

Figure 3. Optimized structural parameters of the π complexes **4a**, **5a**, and **5a′** at the RHF level.

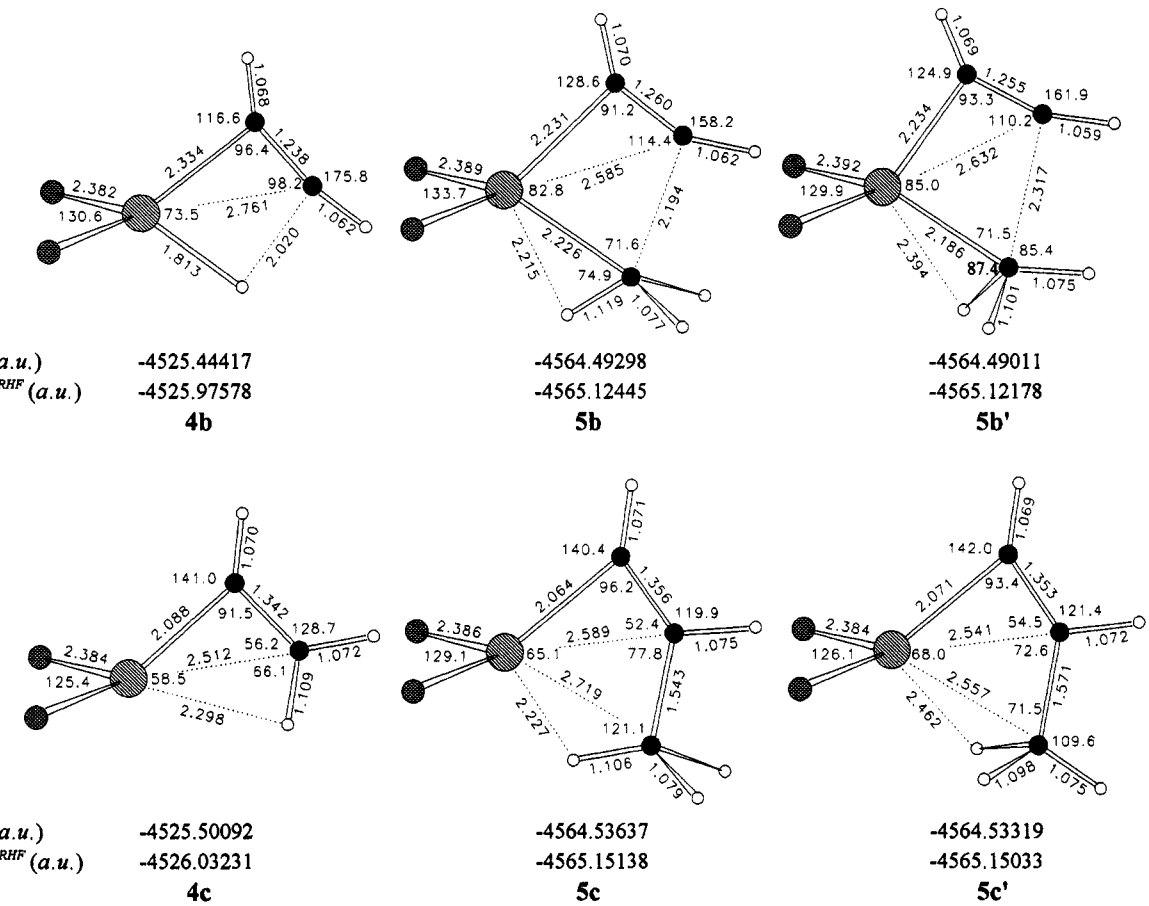

E_T^{RHF} (a.u.)	-4525.44417	-4564.49298	-4564.49011
$E_T^{MP2//RHF}$ (a.u.)	-4525.97578	-4565.12445	-4565.12178
	4b	**5b**	**5b'**

E_T^{RHF} (a.u.)	-4525.50092	-4564.53637	-4564.53319
$E_T^{MP2//RHF}$ (a.u.)	-4526.03231	-4565.15138	-4565.15033
	4c	**5c**	**5c'**

Figure 4. Optimized geometries of the transition states **4b**, **5b**, and **5b′** and of the products **4c**, **5c**, and **5c′** at the RHF level.

follows that coordinated acetylene is polarized as a result of charge transfer from the π system to the positively charged and coordinatively unsaturated zirconium center. A detailed MO analysis will be presented in the next section. At the RMP2//RHF level the acetylene binding energy amounts to 51.6 kcal/mol (**4a**), 41.5 kcal/mol (**5a**), and 40.7 kcal/mol (**5a′**). These values can be compared with ethylene binding energies of 33–53 kcal/mol calculated for Ti and Zr complexes.[4f,8a–d,g] In the case of **4a**, the acetylene binding energy is about 31 kcal/mol greater than that calculated for $Cl_2ScH(C_2H_2)$[8e] as a result of stronger bonding interaction of the diffuse valence shell of the Zr center with the π system.

C. Transition States $Cl_2Zr(H)(C_2H_2)^+$ (4b) and $Cl_2Zr(CH_3)(C_2H_2)^+$ (5b, 5b′) and Products $Cl_2ZrC_2H_3^+$ (4c) and $Cl_2ZrC_2H_2CH_3^+$ (5c, 5c′). The optimized structural parameters of the transition states (TS) **4b**, **5b**, and **5b′** and of the products **4c**, **5c**, and **5c′** are shown in Figure 4. Figures 5 and 6 display the relative potential energy profiles for the insertion reaction paths. The differences of the overlap populations (ΔOP) and of the electron densities (Δq) between the TS and the intermediate π complexes as well as between the products and the TS are collected in Table 1. In Table 2 we present a comparison of the energetics for the reaction of olefin with Sc and Zr complexes, calculated at comparable levels of theory. Similar to the case for

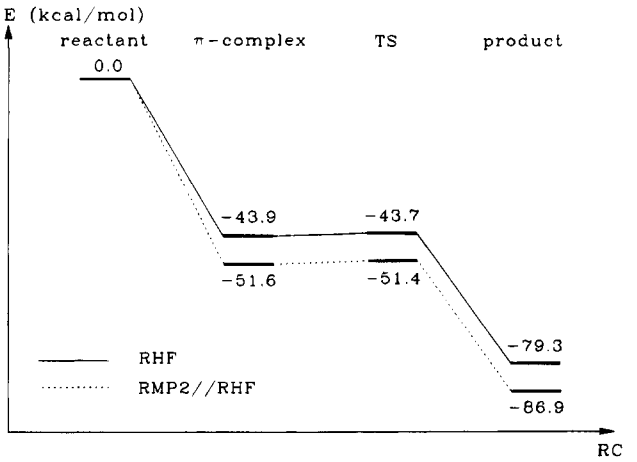

Figure 5. Potential energy profiles of acetylene insertion into the Zr−H σ bond of Cl_2ZrH^+ at the RHF and RMP2/ /RHF levels.

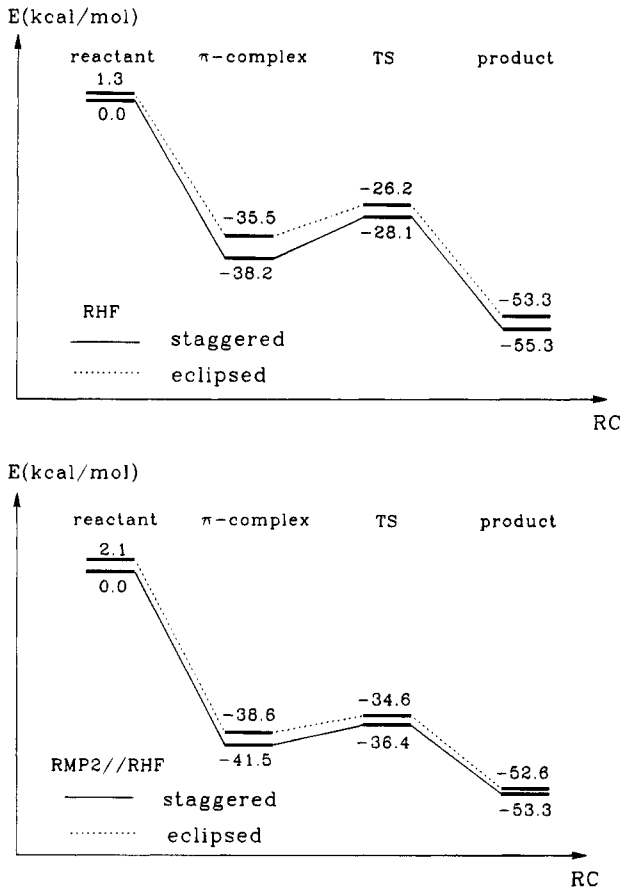

Figure 6. Potential energy profiles of acetylene insertion into the Zr−C σ bond of $Cl_2ZrCH_3^+$ with staggered and eclipsed structures at the RHF (top) and RMP2//RMF (bottom) levels.

the insertion reaction of ethylene,[8] the TS **4b**, **5b**, and **5b′** are four-membered cycles (Figure 4). For the TS **4b** we find the saddle point to be "early"; the C(1)−C(2) bond has only lengthened by 0.011 Å, the Zr−H bond has stretched by 0.024 Å, and the newly formed C−H bond has a distance of 2.02 Å. Regardless of the calculation level, the activation energy is only 0.2 kcal/ mol (Figure 5), perhaps as a result of small changes in bond populations and charge reorganizations between **4a** and **4b** (Table 1). The product **4c** is 35 kcal/mol more stable than the π complex **4a**. **4c** shows typical features

Table 1. Differences in the Overlap Populations (ΔOP) and in the Electron Densities (Δq)[a] between Fully Optimized Transition States and π Complexes and between Fully Optimized Products and Transition States

			staggered		eclisped	
	4b−4a	**4c−4b**	**5b−5a**	**5c−5b**	**5b′−5a′**	**5c′−5b′**
ΔOP_{Zr-C^1}	0.019	0.112	0.051	0.106	0.049	0.105
ΔOP_{Zr-C^2}	0.008	−0.066	0.043	−0.093	0.024	−0.084
$\Delta OP_{Zr-H^3/C^3}$	−0.021	−0.249	−0.024	−0.191	−0.024	−0.185
ΔOP_{Zr-H}			0.032	0.052	0.009	0.028
$\Delta OP_{C^1-C^2}$	−0.030	−0.220	−0.120	−0.259	−0.114	−0.282
$\Delta OP_{C^2-H^3/C^3}$	0.008	0.281	0.036	0.211	0.023	0.211
ΔOP_{C^3-H}			−0.060	−0.020	−0.029	−0.001
Δq_{Zr}	+0.012	−0.105	+0.185	−0.160	+0.141	−0.169
Δq_{C^1}	−0.002	−0.011	+0.038	+0.094	+0.045	+0.084
Δq_{C^2}	−0.001	+0.273	−0.065	+0.200	−0.120	+0.152
$\Delta q_{H^3/C^3}$	+0.002	−0.194	−0.160	−0.160	−0.063	−0.146
Δq_H			+0.071	+0.071	+0.017	+0.035

[a] A positive sign means an increase in the electron density.

Table 2. Calculated π-Bonding Energies (ΔE_1), Reaction Barriers (ΔE_2), and Overall Exothermicity (ΔE) for the Reaction of Olefin with Sc and Zr Complexes[a]

reaction	calculation method	ΔE_1[b]	ΔE_2[c]	ΔE[b]	ref
$Cl_2ZrCH_3^+ + C_2H_4$	RHF	−37.0	22.0	−26.0	8b
	GVB-CI//RHF	−33.0	24.0	−20.0	
$SiH_2Cp_2ZrCH_3^+ + C_2H_4$	RHF	−19.1	16.7	−26.8	8d
	RMP2//RHF	−33.4	6.0	−40.9	
$Cl_2ScH + C_2H_2$	GVB-CI//RHF	−20.2	6.9	−45.2	8e
$Cl_2ZrH^+ + C_2H_2$	RHF	−43.9	0.2	−79.3	*d*
	RMP2//RHF	−51.6	0.2	−86.9	
$Cl_2ZrCH_3^+ + C_2H_2$	RHF	−38.2	10.1	−55.3	*d*
	RMP2//RHF	−41.5	5.1	−53.3	

[a] Calculated at comparable levels of theory. All energy values are given in kcal/mol. [b] Energy is given relative to the free molecules from column 1. [c] Energy is given relative to the intermediate π complex. [d] This work

of a β-CH agostic structure. Its geometrical and electronic structure has been discussed elsewhere.[12a]

Referenced to free acetylene, the exothermicity of the reaction is 86.9 kcal/mol (Figure 5). The small activation barrier and large exothermicity suggest that the insertion reaction of acetylene into the Zr−H bond of Cl_2ZrH^+ should be irreversible.

In the TS **5b** and **5b′** the geometry of the CH_3 group deviates from the normal sp^3 structure. The CH bonds directed toward the Zr atom are elongated to 1.119 Å in **5b** and 1.101 Å in **5b′**; the corresponding ZrCH angles are lower than the sp^3 value (Figure 4). Such structural deformations suggest that **5b** and **5b′** can be stabilized through an α-agostic interaction. The TS **5b** is 1.8 kcal/ mol (RHF) or 1.7 kcal/mol (RMP2//RHF) more stable than **5b′**. Note that the α-CH agostic interaction has been proposed to assist the mechanism of olefin insertion reactions on the basis of either experimental[20] or theoretical investigations.[8,21] In the early stage of the insertion reaction (π complex → TS), the sp^3 hybrid orbital of the CH_3 group originally involved in the Zr−C(3) σ bond rotates from being bound to Zr to being slightly bound to C(2) as shown in Chart 2. We note that the angles H−C(3)− "new sp^3 hybrid direction" do not much deviate from the sp^3 value, and thus in this case, only the elongation of the C−H bond can be

(20) (a) Brookhart, M.; Green, M. L. H. *J. Organomet. Chem.* **1983**, *250*, 395. (b) Brookhart, M.; Green, M. L. H.; Pardy, R. B. A. *J. Chem. Soc., Chem. Commun.* **1983**, 691. (c) Schmidt, G. F.; Brookhart, M. *J. Am. Chem. Soc.* **1985**, *107*, 1443. (d) Brookhart, M.; Green, M. L. H.; Wong, L.-L. *Prog. Inorg. Chem.* **1988**, *36*, 1. (e) Piers, W. E.; Bercaw, J. E. *J. Am. Chem. Soc.* **1990**, *112*, 9406. (f) Roell, W.; Brintzinger, H.-H.; Rieger, B.; Zolk, R. *Angew. Chem., Int. Ed. Engl.* **1990**, *29*, 279.

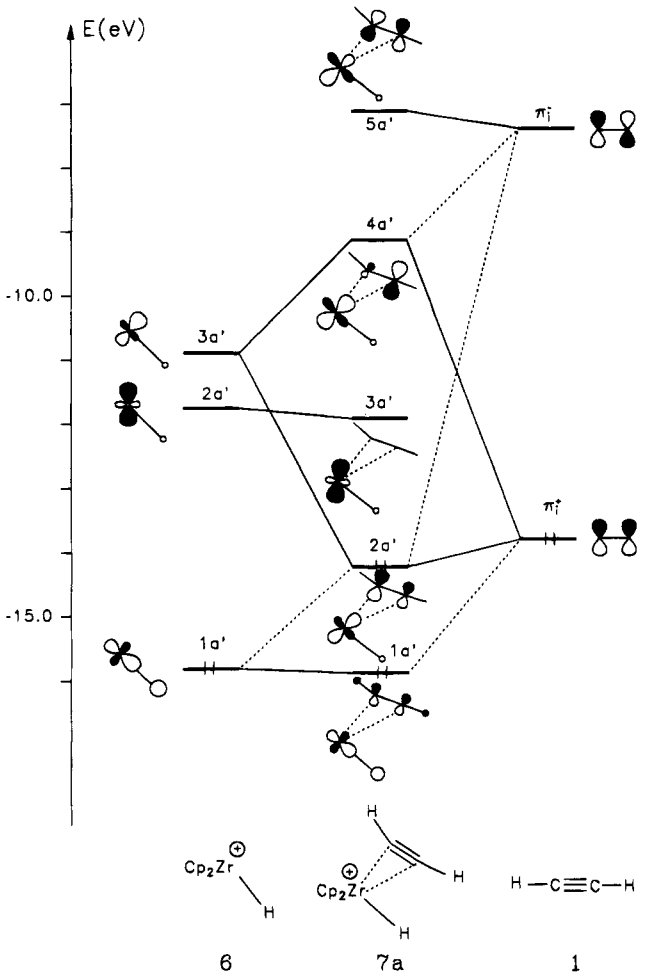

Figure 7. Simplified interaction diagram for the interaction between Cp_2ZrH^+ (**6**) and acetylene (**1**) to give the π complex **7a**.

Chart 2

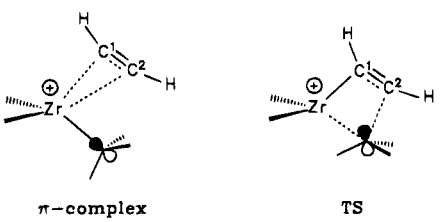

considered as a theoretical verification for an agostic interaction.

For the TS **5b** and **5b′** we find that the C(1)–C(2) bond is lengthened by 0.044 Å (**5b**) and 0.042 Å (**5b′**); the Zr–C(1)–C(2) bond angle is reduced by 8.9° (**5b**) and 5.2° (**5b′**) with respect to the π complexes **5a** and **5a′**. The Zr–C(3) bond is stretched by 0.087 Å (**5b**) and 0.041 Å (**5b′**). The newly formed C(3)–C(2) bond has a distance of 2.194 Å (**5b**) and 2.317 Å (**5b′**). These results, together with the changes of bond overlap populations (Table 1), not only suggest that the TS **5b** and **5b′** are "early" but also allow us to suppose that steric effects are operative at the TS. The influence of steric effects on the geometry of the TS was mentioned in theoretical investigations of the reaction of $Cp_2TiCH_3^+$ with ethylene.[8a,d] The new bond formation at the TS is asynchronous in the sense that the Zr–C(1)

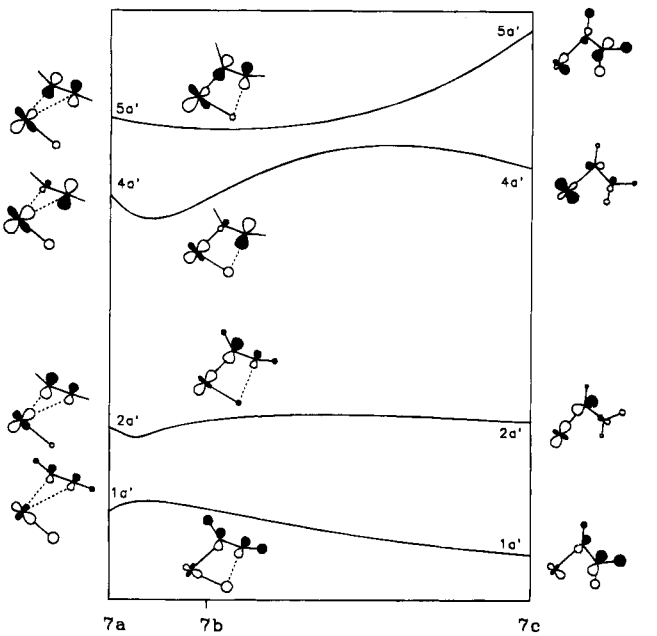

Figure 8. Walsh diagram for the insertion reaction $Cp_2ZrH^+ + C_2H_2$ from the π complex **7a** to the product **7c**.

Scheme 2

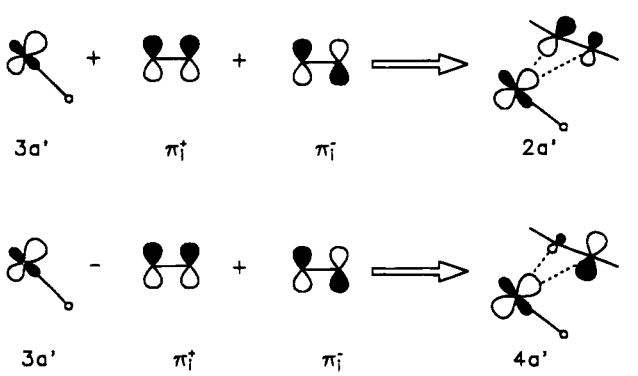

bond formation is more advanced than for the C(3)–C(2) bond, which is still very long. The most important electronic features of the early stage of the insertion reaction (π complex → TS) concern the charge reorganization on the Zr center and the C(3) atom (Table 1). We observe an electron density transfer from the C(3) atom to the Zr center. This suggests that electrostatic interactions, for example with solvent molecules, can influence the geometry of the TS as well as the energy barrier. The calculated RHF activation energies are 10.1 and 9.3 kcal/mol for **5b** and **5b′**, respectively (Figure 6). At the RMP2//RHF level they are lowered to 5.1 kcal/mol (**5b**) and 4 kcal/mol (**5b′**). To the best of our knowledge, no experimental data for an activation energy of the insertion reaction of unsatured hydrocarbons into the Zr–C bonds have been reported so far. However, our results can be related to the experimentally determined enthalpy of the activation of 9.7 kcal/mol for the reaction of Cp^*ScCH_3 with 2-butyne[9c] or to the calculated value of 6 kcal/mol for the reaction of $(SiH_2Cp_2)ZrCH_3^+$ with ethylene.[8d] It is interesting to note that the experimental estimate of the energy barrier for the propagation step in the polymerization reactions of olefins ranges from 6 to 12 kcal/mol.[22] In the products **5c** and **5c′**, the angle Zr–C(1)$_\alpha$–C(2)$_\beta$ deviates greatly from the expected sp^2 value (120°) for nondistorted vinyl complexes. The C–H bonds directed towards the Zr atom are now shorter than in the TS,

(21) Prosenc, M.-H.; Janiak, C.; Brintzinger, H.-H. *Organometallics* **1992**, *11*, 4036.

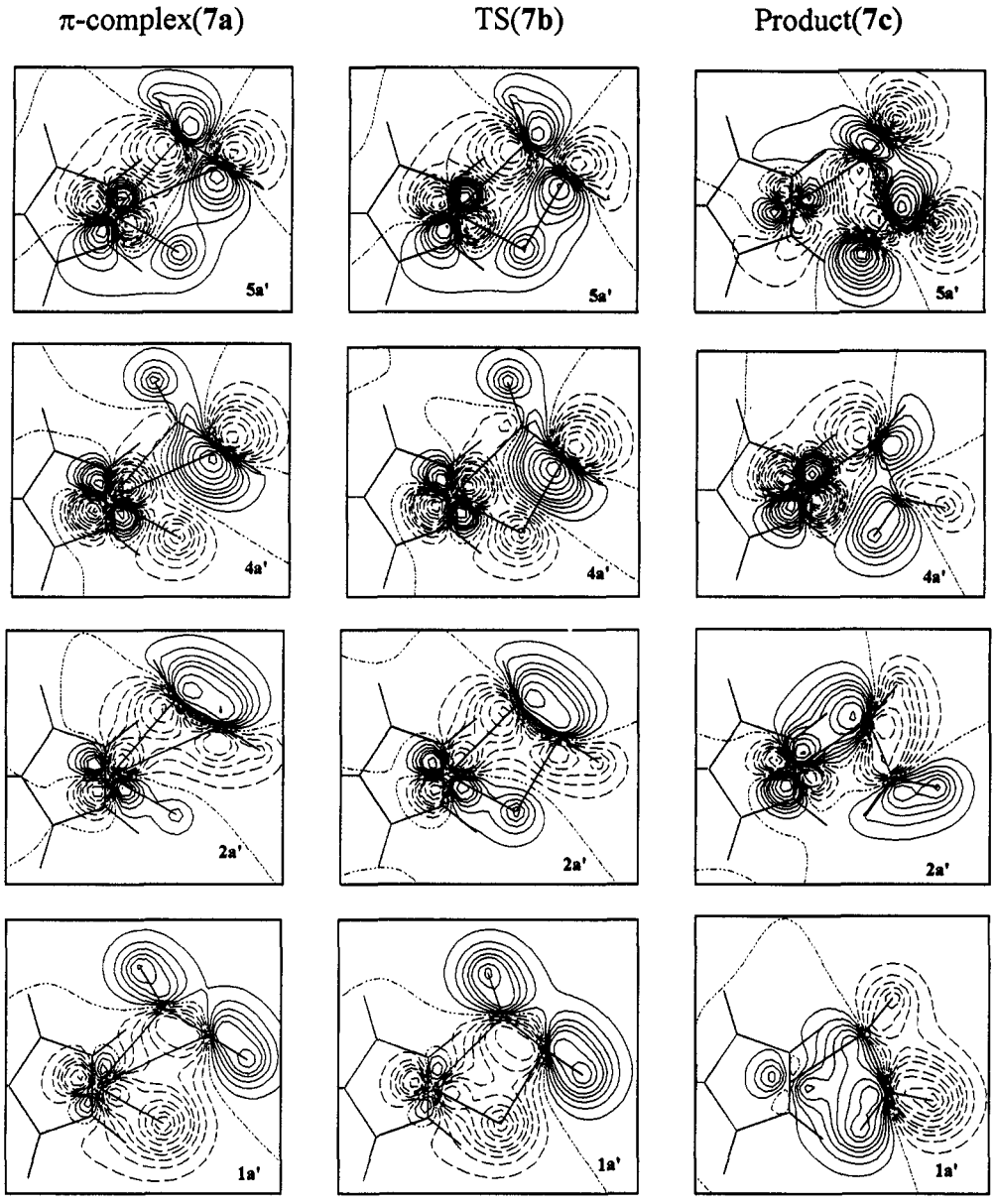

Figure 9. Contour plots of the molecular orbitals involved in the insertion reaction of the π complex (**7a**), TS (**7b**), and product (**7c**). The values of the contour lines are ±0.02, ±0.04, ±0.06, ±0.10, ±0.14, ±0.18, ±0.24, ±0.30, ±0.36, and ±0.42.

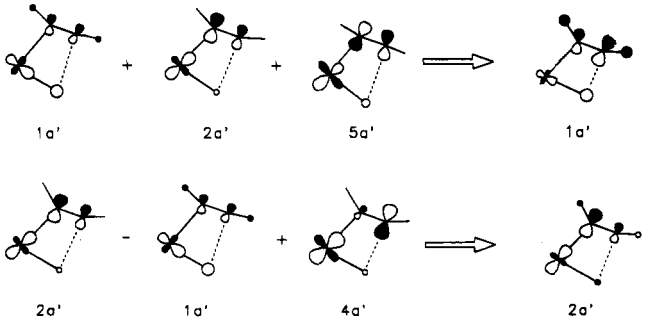

Figure 10. Intermixing patterns of the **1a′**–**5a′** MOs of $Cp_2Zr(H)(C_2H_2)^+$.

but they are still longer than in the π complexes (Figures 3 and 4). The $C(2)_\beta$–$C(3)_\gamma$ bond is stretched by 3% in **5c** and 5% in **5c′** with respect to the normal C–C bond. Such features are indicative of C_β–C_γ and C_γ–H agostic interactions, with the former being stronger in **5c′**. In **5c** the C_γ–H bond is longer and the C_β–C_γ bond is shorter with respect to **5c′**. At the RMP2//RHF level structure **5c** is 0.7 kcal/mol more stable than **5c′**, showing that one in-plane C_γ–H bond of **5c** contributes more to the stabilizing interactions than two such out-of-plane bonds in **5c′**. This property has an electronic origin[12a] and was experimentally documented in the case of *rac*-C_2H_4(indenyl)$_2$ZrSiMe$_3$C=CMe$_2^+$.[10b] In the late stage of the insertion reaction (TS → product) the Zr–C(3) bond is breaking and the two new σ bonds Zr–$C(1)_\alpha$ and $C(2)_\beta$–$C(3)_\gamma$ are formed; the multiple bond transforms to the vinylic double bond (Figure 4, Table 1). In this stage of the reaction one can observe large density reorganization on the vinyl ligand (Table 1). The calculated RMP2//RHF overall exothermicity of the insertion reaction of acetylene into the Zr–C bond amounts to 53.3 kcal/mol for the staggered and 52.6 kcal/mol for the eclipsed structure. It is about 13 kcal/

(22) (a) Natta, G.; Pasquon, I. *Adv. Catal.* **1959**, *11*, 1. (b) Chien, J. C. W. *J. Am. Chem. Soc.* **1959**, *81*, 86. (c) Machon, J.; Herman, R.; Houteaux, J. P. *J. Polym. Sci., Polym. Symp.* **1975**, *52*, 107. (d) Chien, J. C. W.; Razavi, A. *J. Polym. Sci., Part A: Polym. Chem.* **1988**, *26*, 2369.

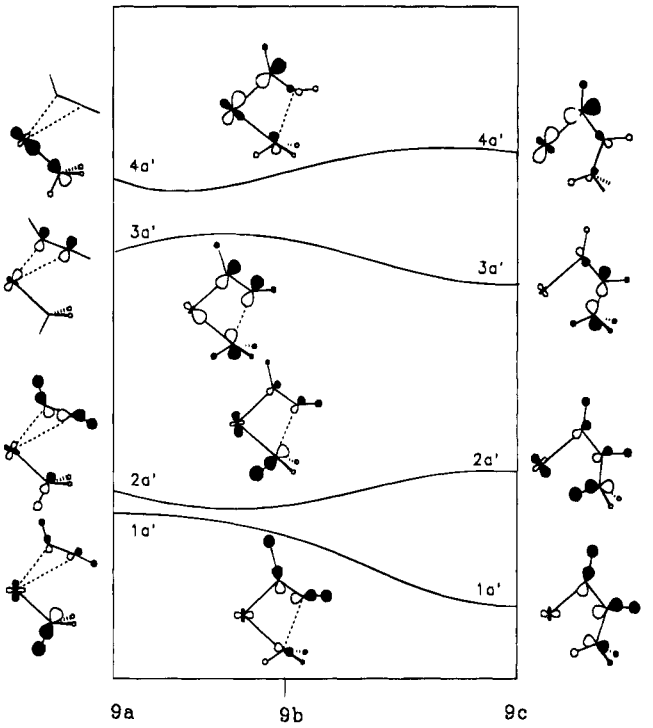

Figure 11. Walsh diagram of the occupied MOs for the insertion reaction $Cp_2ZrCH_3^+ + C_2H_2$ from the π complex **9a** to the product **9c**.

mol greater than the calculated exothermicity for the reaction of $(SiH_2Cp_2)ZrCH_3^+$ with ethylene.[8d]

To finish this section, we stress that the early stage of the insertion reaction (π complex → TS) is characterized through an electron density reorganization at the Zr center and the R(3) atom (R = H, C). The late stage of the reaction (TS → product) is characterized through a new bond formation and subsequent electron density reorganization in the vinyl ligand. The calculated energy barriers are smaller and the overall exothermicity greater than in the case of ethylene insertions into Zr–C σ bonds or acetylene insertion into the Sc–H σ bond (Table 2).

Molecular Orbital Picture of the Insertion Reaction Based on Extended Hückel Calculations. In this section we present a qualitative MO picture for the insertion reaction of acetylene into Zr–H and Zr–C σ bonds in the zirconocene complexes Cp_2ZrH^+ (**6**) and $Cp_2ZrCH_3^+$ (**8**). Since the Cp units do not participate directly in the insertion reaction, at each stage of the reaction the geometry of the Cp_2Zr fragment has been kept fixed at C_{2v} symmetry with bond distances and angles taken from available experimental data for zirconocene complexes.[23] The geometrical parameters of the ligands (H, CH_3, C_2H_2) in the intermediate π complexes (**7a**, **9a**), TS (**7b**, **9b**), and products (**7c**, **9c**) have been taken from the ab initio optimized structures described in the previous section.

A. Insertion of Acetylene into the Zr–H σ Bond of $Cp_2ZrH(C_2H_2)^+$. To characterize the electronic structure of the intermediate π complex $Cp_2ZrH(C_2H_2)^+$ (**7a**), we adopt Hoffmann's fragment MO approach,[24] constructing interactions between the valence MOs of acetylene (**1**) with those of the Cp_2ZrH^+ fragment. The valence MOs of both fragments are described in detail in the literature.[24] In Figure 7 we display only those valence MOs that are involved in the stabilizing interactions. In the localized picture the 1a′ MO of **6** describes the Zr–H σ bond and the two lowest unoccupied MOs 2a′ and 3a′ describe the acceptor levels in the symmetry plane of the metallocene fragment. They are shown on the left side of Figure 7. The acetylene π_i^+ orbital presents a donor function to the metal center; it interacts with 1a′ and 3a′ of **6** to produce the three MOs 1a′, 2a′, and 3a′ of **7a**. This four-electron–three-orbital interaction is further stabilized by the bonding admixture of the LUMO (π_i^-) of **1**. The admixture of π_i^- is crucial because it leads to a partial relief of the Pauli repulsion between the C_2H_2 π_i^+ and Cp_2ZrH^+ 1a′ MOs as well as redistributes the electron density in the 2a′ MO and changes the shape of the 4a′ MO of **7a**, as shown in Scheme 2.

We notice that the 2a′ and 4a′ MOs of **7a** represent the bonding and antibonding counterparts for the interaction of **6** with the π system of **1**. The LUMO (3a′) is not involved in stabilizing interactions. In Figure 8 we display a Walsh diagram along the reaction path, going from the π complex (**7a**) through the TS (**7b**) to the product (**7c**). The corresponding MO plots are shown in Figure 9. The phase relationships of the occupied MOs in **7a** and **7c** (Figure 9) suggest a smooth transformation of the Zr–H σ bond (1a′ MO of **7a**) to the C(2)–H σ bond (1a′ MO of **7c**) as well as of the Zr–π-acetylene bond (2a′ MO of **7a**) to the Zr–C(1) σ bond (2a′ MO of **7c**). The insertion reaction under study is actually a 1,2 addition and is inherently connected with an avoided crossing of occupied and empty levels.[24,25] Four orbitals undergo strongly avoided crossings, and substantial intermixing is operating during the reaction path. The most important intermixing patterns are shown in Figure 10. The bonding admixture of 2a′ and 5a′ to 1a′ diminishes the metal character of 1a′ and increases the p component on C(2). It is clear that such a transformation facilitates the Zr–H bond-breaking process as well as the C(2)–H bond formation. Similarly, the admixture of 1a′ and 4a′ to 2a′ weakens the Zr–π-acetylene bond and facilitates the Zr–C(1) bond formation. One can suppose that the intermixing between the MOs will be different at different stages of the insertion reaction. It seems that in the early stage of the reaction (π complex → TS) the intermixing among occupied orbitals 1a′ and 2a′ and the empty 4a′ is dominant, leading to charge reorganization on the Zr and H atoms and in the late stage of the reaction (TS → product) the large admixture of the empty 5a′ MO controls smooth new bond formation. In accord with the general analysis given by Thorn and Hoffmann,[26] our MO picture reveals that the Zr center plays a dual role as electron acceptor and electron donator. In the early stage of the reaction it is able to accept electrons from the π_i^+ orbital of **1** and in the late stage of the reaction it induces electron back-donation to the vinylic ligand due to the strong admixture of the empty 5a′(π_i^-) MO to the occupied 1a′ and 2a′ levels. Both features,

(23) (a) Hyla-Kryspin, I.; Gleiter, R.; Krüger, C.; Zwettler, R.; Erker, G. *Organometallics* **1990**, *9*, 517. (b) Erker, G.; Zwettler, R.; Krüger, C.; Hyla-Kryspin, I.; Gleiter, R. *Organometallics* **1990**, *9*, 524. (c) Erker, G.; Zwettler, R.; Krüger, C.; Schlund, R.; Hyla-Kryspin, I.; Gleiter, R. *J. Organomet. Chem.* **1988**, *346*, C15.

(24) Albright, T. A.; Burdett, J. K.; Whangbo, M. H. In *Orbital Interactions in Chemistry*; Wiley: New York, 1985.

(25) Bickelhaupt, F. M.; Baerends, E. J.; Nibbering, N. M. M.; Ziegler, T. *J. Am. Chem. Soc.* **1993**, *115*, 9160.

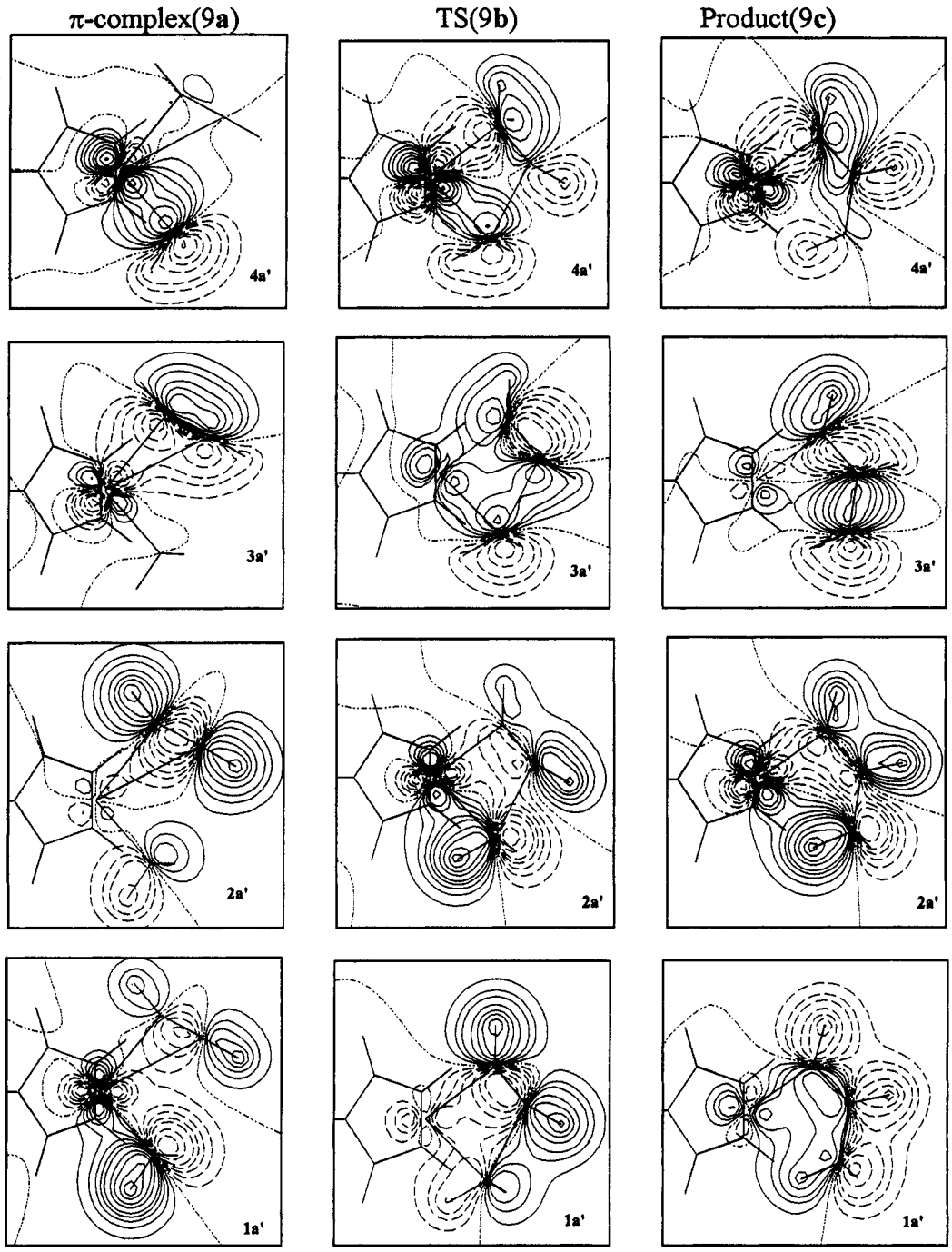

Figure 12. Contour plots of the molecular orbitals **1a′**−**4a′** in the π complex (**9a**), TS (**9b**), and product (**9c**). The values of the contour lines are as in Figure 9.

efficient electron donation and back-donation, will lower the energy barrier of the insertion reaction.[26]

B. Insertion of Acetylene into the Zr−C σ bond of $Cp_2ZrCH_3^+$. Figure 11 displays the correlation diagram of the important occupied orbitals of the π-complex (**9a**) with those of the TS (**9b**) and product (**9c**). The MOs 4a′ and 3a′ of **9a** represent the initial Zr−C(3) and Zr−π-acetylene bonds, respectively. The MOs 2a′ and 1a′ of **9a** represent the in-plane C(3)−H and C(1)−C(2) σ bonds. In the early stage of the insertion reaction they are stabilized by an α-agostic interaction. During the reaction the MOs 1a′ and 2a′ mix with each other as well as with 3a′ and smoothly transform to the 1a′ and 2a′ MOs of **9c**. In **9c**, the two MOs 1a′ and 2a′ still have an agostic interaction. On going from the π complex **9a** to the product **9c**, the Zr−C(3) σ bond (4a′ MO of **9a**) and the Zr−π-acetylene bond (3a′ MO of **9a**) smoothly transform to the Zr−C(1) and C(2)−C(3) σ bonds of **9c**, as a result of substantial admixture of the occupied 1a′, 2a′ and empty 6a′, 7a′ levels. The MO plots of the 1a′−4a′ levels of the π complex (**9a**), TS (**9b**), and product (**9c**) are shown in Figure 12. Although the predicted energy barrier for the insertion reaction of acetylene into the Zr−C σ bond is greater than for the Zr−H σ bond, the MO pictures of both insertion reactions are essentially similar. The low energy barrier of the latter reaction can be traced back to the absence of steric repulsion during the hydrogen migration from the Zr to the C(2) atom. In Figure 13 we present the three-dimensional MO plots of the MOs representing the C(3)−H σ bonds that can

(26) Thorn, D. L.; Hoffmann, R. *J. Am. Chem. Soc.* **1978**, *100*, 2079.

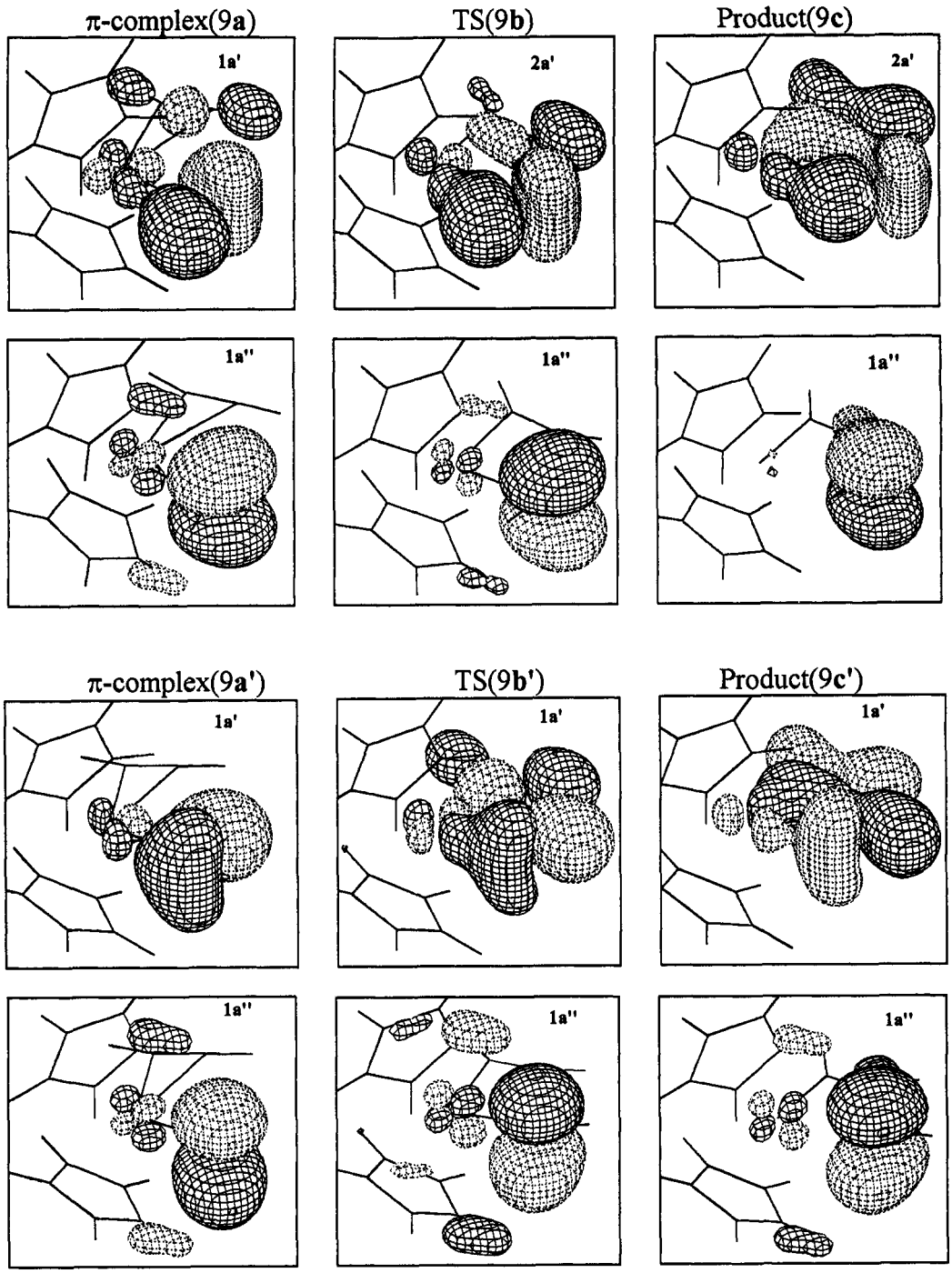

Figure 13. Three-dimensional MO plots of the MOs representing the in-plane and out-of-plane C–H bonds in the π complex, TS, and product of $Cp_2Zr(CH_3)(C_2H_2)^+$ with staggered (top) and eclipsed structures (bottom). The intervals of the contour lines are ±0.04.

be involved in the agostic interaction in the case of either the staggered (**9a**–**9b**–**9c**) or eclipsed structures (**9a′**–**9b′**–**9c′**) of $Cp_2ZrCH_3(C_2H_2)^+$. In the π complexes **9a** and **9a′** agostic interactions are not present. The TS (**9b**) and product (**9c**) are stabilized through one in-plane Zr–H–C(3) agostic interaction. The 1a″ MOs of structures **9** and **9′** do not contribute to the agostic interaction, due to the absence of overlap between the two out-of-plane C(3)–H σ bonds and the high lying, empty a″ orbital of the Zr center. However, some positive overlap with the in-plane accepting orbital of the Zr center is present in the 1a′ MO of **9b′** and **9c′**. The Zr–H–C(3) bonding interaction in the TS lowers the energy barrier of the insertion reaction.

Conclusions

We have studied with the ab initio MO method the optimized structures and energy profiles of acetylene insertion into the Zr–H and Zr–C σ bonds of Cl_2ZrR^+ (R = H, CH_3). The transition states are four-membered cycles. For the alkyl complex we have shown that the transition state is influenced by electronic and steric effects. The calculated energy barrier is smaller and the acetylene binding energy as well as the overall exothermicity are greater than the theoretical values obtained for similar ethylene insertion reactions into the Zr–C σ bond.[8d] The products and transition states of the alkyl complex are stabilized through an agostic interaction. The acetylene insertion into the Zr–H bond

of Cl_2ZrH^+ has a lower barrier and is more exothermic than the insertion into the Zr−C bond of $Cl_2ZrCH_3^+$. The calculated small activation barrier (0.2 kcal/mol) and large exothermicity (86.9 kcal/mol) suggest that the insertion of acetylene into the Zr−H bond of Cl_2ZrH^+ should be irreversible. The acetylene insertion into the Zr−R bond (R = H, CH_3) has a lower barrier than the insertion into Sc−R,[8e,9c] due to the better donor−acceptor interactions of the diffuse valence shell of the Zr center with the hydrocarbon π system. The MO analysis carried out on the basis of extended Hückel calculations with Cp_2ZrR^+ (R = H, CH_3) revealed that the valence MOs of the metallocene system undergo strongly avoided crossing and a substantial intermixing is operating during the insertion reaction path. The intermixing between the valence MOs facilitates both the Zr−R bond breaking and R−C(2) bond formation. During the reaction path the Zr center plays an electron acceptor and electron donator dual role, with the latter more important at the final stage of the insertion reaction.

Acknowledgment. We are grateful to the Bundesministerium für Forschung und Technologie (FKZ: Grant No. 03D0005B3), the Deutsche Forschungsgemeinschaft (Grant No. SFB 247), and the Fonds der Chemischen Industrie for financial support. We thank Prof. G. Erker for helpful discussions.

OM940572Q

Stepwise Approach to Metal-Capped 4-Fold-Bridged Cyclobutadienophanes

Rolf Gleiter,*,† Heinrich Langer,† Volker Schehlmann,† and Bernhard Nuber‡

Organisch- und Anorganisch-Chemisches Institut der Universität Heidelberg, D-69120 Heidelberg, Germany

Received September 30, 1994®

The three cyclic alkynes 5-cyclononynol (**31**), 5-cyclodecynol (**15**), and 6-cycloundecynol (**16**) are dimerized with CpCo(COD) to the tricyclic dialcohols **17**, **24**, and **32**, respectively. Oxidation of the alcohols yields the diketones **18**, **19**, **25**, and **33** which can be transformed to the tricyclic diynes **23**, **29**, **30**, and **36** via the bis(selenadiazole)s. Reaction of **23** with $CpCo(CO)_2$, $Cp^*Co(CO)_2$, and $Fe(CO)_5$ yields superphanes in which both complexed cyclobutadiene (Cb) units are connected with four trimethylene chains. The reaction of **29**/**30** with $CpCo(CO)_2$ affords two isomeric CpCo-stabilized fourfold-bridged bicyclo[4.2.0]octa-2,4,7-dienes **43** and **44** besides the expected superphane **42** in which the CpCo-capped Cb units are connected by two trimethylene and two tetramethylene chains. The key compounds, tricyclic diynes **23** and **36**, superphane **40**, and bicyclooctatriene **44**, have been characterized using X-ray structural analysis. Crystal data: **23**, $C_{25}H_{29}Co$, triclinic, space group C^1_i, $P\bar{1}$ (No. 2), a = 9.003 Å, b = 10.399 Å, c = 11.874 Å, α = 93.45°, β = 101.45°, γ = 108.77°, V = 1022.34 Å^3, Z = 2; **36**, $C_{23}H_{25}Co$, rhombic, space group D^4_2, $P2_12_12_1$ (No. 19), a = 9.555(9) Å, b = 12.86(1) Å, c = 15.551(9) Å, V = 1910.9 Å^3, Z = 4; **40**, $C_{28}H_{29}CoFeO_3$, monoclinic, space group C^4_s, Cc (No. 9), a = 18.92(1) Å, b = 8.499(6) Å, c = 19.37(1) Å, β = 130.16°, V = 2380.41 Å^3, Z = 4; **44**, $C_{27}H_{33}Co$, triclinic, space group C^1_i, $P\bar{1}$ (No. 2), a = 8.269(3) Å, b = 9.082(2) Å, c = 13.72.4 Å, α = 84.87(2)°, β = 88.77(3)°, γ = 80.62(2)°, V = 1012.8 Å^3, Z = 2.

Introduction

In superphanes two π-units are connected with each other by the maximum number of chains.[1] If the π-units are conjugated ring systems such as benzene,[2] thiophene,[3] or metal-stabilized cyclopentadienyl[4] or cyclobutadiene, this leads to rigid cages which are excellent model compounds to study all kinds of interaction between the π-units. For these studies it is desirable to have a simple synthesis of superphanes which allows the variation of the length of the spacer chains. Recently we showed that 1,6-cyclodecadiyne (**1**) reacts with (η^5-cyclopentadienyl)dicarbonylcobalt [$CpCo(CO)_2$] to yield the superphane **2** (Scheme 1).[5,6] So far this reaction could be extended on the one hand to cobalt reagents with functionalities in the Cp ring[7,8] and on the other hand to 4,9-diisopropylidene-1,6-cyclodecadiyne[7,9] as well as 1,8-cyclotetradecadiyne[7,10] and 1,10-cyclooctadecadiyne.[11]

Scheme 1[a]

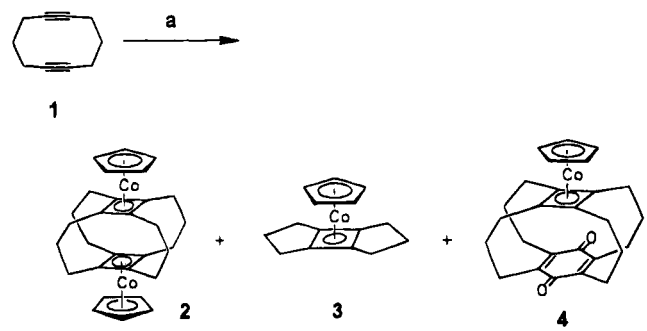

[a] Key: (a) $CpCo(CO)_2$.

Scheme 2

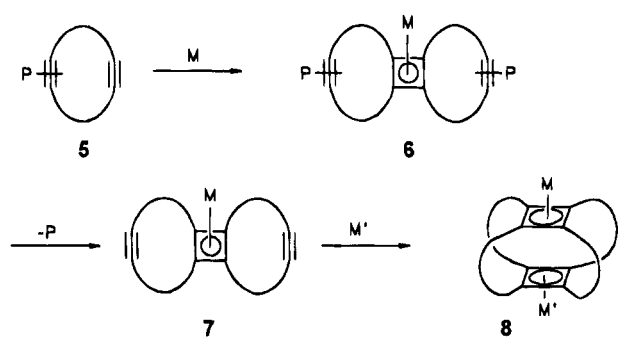

Superphanes with different chain lengths in one molecule or those which are capped by different metal

† Organisch-Chemisches Institut.
‡ Anorganisch-Chemisches Institut.
® Abstract published in *Advance ACS Abstracts*, January 1, 1995.
(1) The attribute *super* was suggested by Prof. H. Hopf for the first 6-fold-bridged cyclophane, [2$_6$](1,2,3,4,5,6)cyclophane.[2]
(2) Sekine, Y.; Brown, M.; Boekelheide, V. *J. Am. Chem. Soc.* **1979**, *101*, 3126.
(3) Takeshita, M.; Koike, M.; Tsuzuki, H.; Tashiro, M. *J. Org. Chem.* **1992**, *57*, 4654.
(4) Hisatome, M.; Watanabe, J.; Yamakawa, K.; Iitaka, Y. *J. Am. Chem. Soc.* **1986**, *108*, 1333.
(5) Gleiter, R.; Karcher, M.; Ziegler, M. L.; Nuber, B. *Tetrahedron Lett.* **1987**, *28*, 195.
(6) Gleiter, R.; Kratz, D. *Tetrahedron Lett.* **1990**, *31*, 5893.
(7) Reviews: Gleiter, R. *Angew. Chem., Int. Ed. Engl.* **1992**, *31*; 27. Gleiter, R.; Kratz, D. *Acc. Chem. Res.* **1993**, *26*, 311.
(8) Gleiter, R.; Pflästerer, G. *Organometallics* **1993**, *12*, 1886.
(9) Gleiter, R.; Merger, R.; Nuber, B. *J. Am. Chem. Soc.* **1992**, *114*, 8921.
(10) Gleiter, R.; Treptow, B.; Kratz, D.; Nuber, B. *Tetrahedron Lett.* **1992**, *33*, 1733.
(11) Gleiter, R.; Pflästerer, G.; Nuber, B. *Chem. Commun.* **1993**, 454.

0276-7333/95/2314-0975$09.00/0

Scheme 3[a]

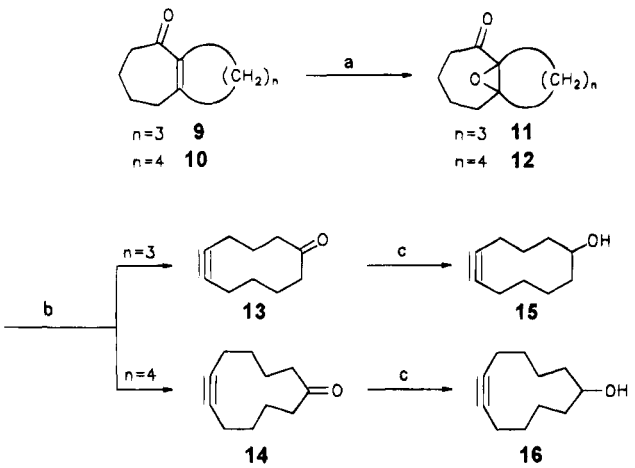

[a] Key: (a) H_2O_2/OH^-; (b) $TosNHNH_2$, Δ; (c) $LiAlH_4$.

fragments are not available in the one-pot route indicated in Scheme 1. To enhance the synthetic potential for the preparation of metal-stabilized superphanes, a stepwise procedure is desirable. In principle this could be achieved by starting with a monoprotected cyclic diacetylene such as **5** (Scheme 2). After dimerization and removal of the protecting group at the triple bonds, a second metal fragment M′ could be used to form the second cyclobutadiene unit.[7] This sequence should allow the preparation of cyclobutadienophanes of variable chain length and with different metals.

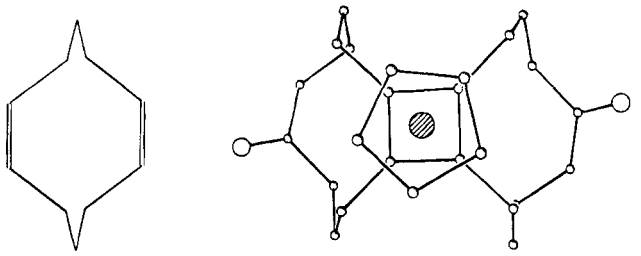

Figure 1. Comparison between the conformations of **18** as determined by X-ray investigations and of 1,6-cyclodecadiene (left).

Although our efforts to prepare monoprotected cyclic diacetylenes were successful with $Co_2(CO)_8$ and CH_3ReO_2I,[12] we were not able so far to obtain protected tricyclic diynes such as **6**. In this paper we report an alternative approach in which a masked cyclic diyne is used as building block.[13]

[3_4](1.2.3.4)- and [$4_2 3_2$](1.2.3.4)Cyclobutadienophanes. Starting materials for our synthesis are 5-cyclodecynol (**15**)[14] and 6-cycloundecynol (**16**).[15] The preparation of **15** and **16** (Scheme 3) uses the Eschenmoser–Tanabe fragmentation[16] as the key step. According to the protocol shown in Scheme 3 both starting materials can be prepared easily in gram quantities.

(12) Gleiter, R.; Schehlmann, V.; Köhler, M. Unpublished results.
(13) Preliminary publication: Gleiter, R.; Schehlmann, V. *Angew. Chem., Int. Ed. Engl.* **1990**, *29*, 1426.
(14) Hanack, M.; Harding, C. E.; Derocque, D. C. *Chem. Ber.* **1972**, *105*, 421.
(15) Gleiter, R.; Langer, H.; Wittwer, W. Manuscript in preparation.

Scheme 4[a]

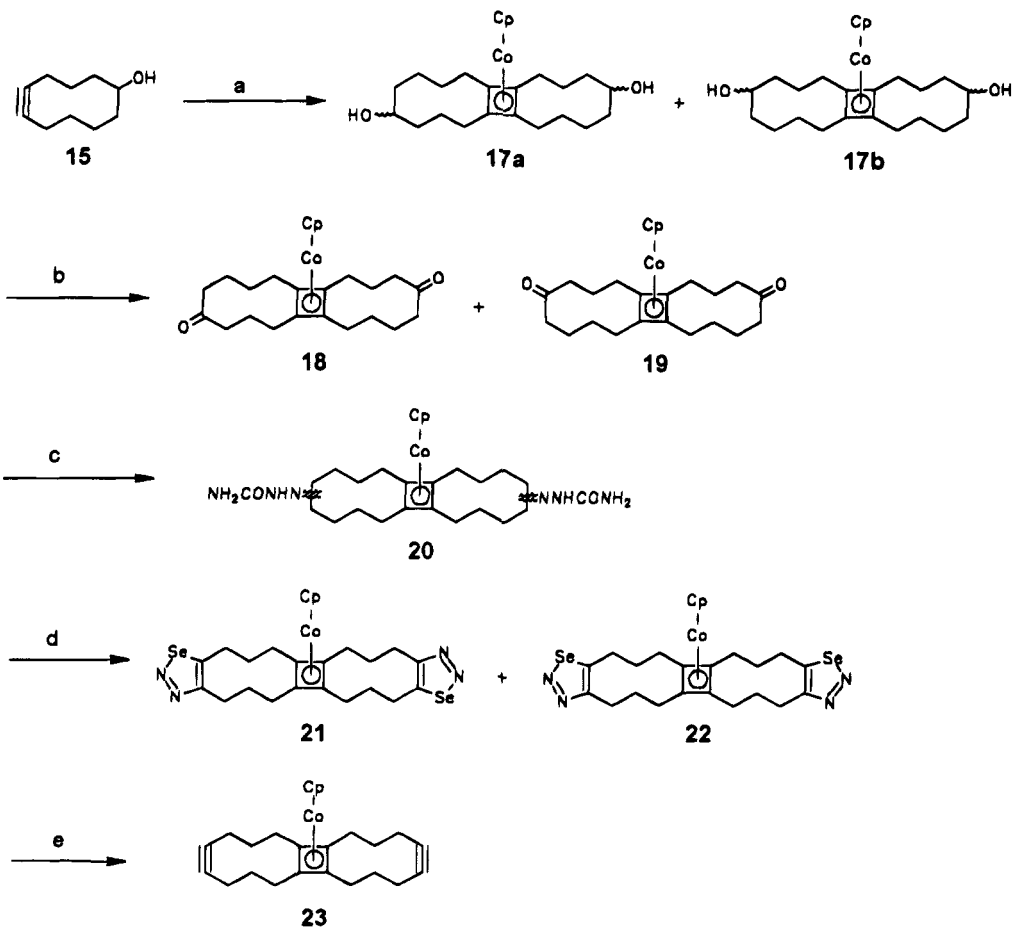

[a] Key: (a) CpCoCOD; (b) Oppenauer oxidation; (c) semicarbazide acetate; (d) SeO_2/HOAc; (e) *n*-BuLi/THF.

Scheme 5[a]

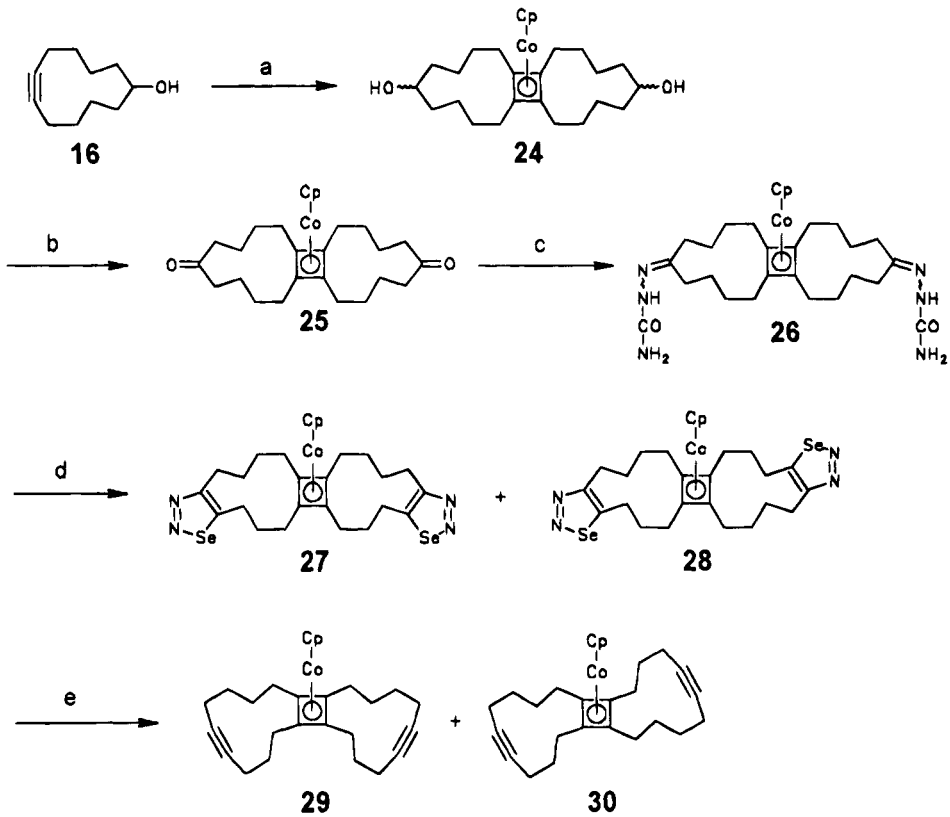

[a] Key: (a) CpCoCOD; (b) Oppenauer oxidation; (c) semicarbazide acetate; (d) SeO_2/HOAc; (e) *n*-BuLi/THF.

Scheme 6[a]

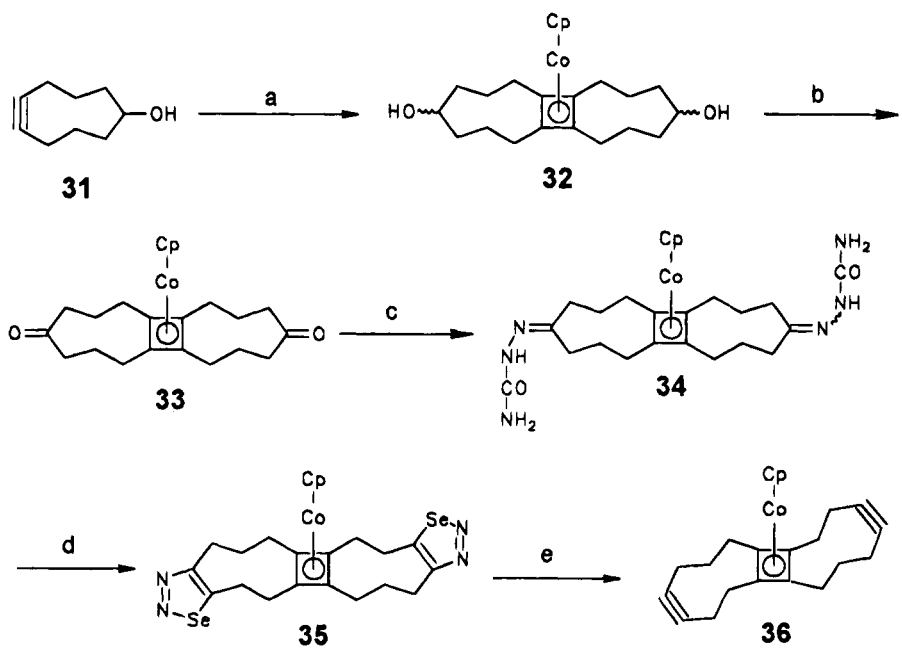

[a] Key: (a) CpCoCOD; (b) Oppenauer oxidation; (c) semicarbazide acetate; (d) SeO_2/HOAc; (e) *n*-BuLi/THF.

The reaction sequence for the further steps is shown in Schemes 4 and 5. Heating a very dilute solution of **15** in decalin with CpCo(COD) yields the tricyclic alcohols **17**. Due to the symmetry of **15**, two regioisomers (**17a,b**) are expected. From each of the two regioisomers three stereoisomers can be anticipated. In the case of **16** the regiochemistry is unambiguous and three stereoisomers are expected. The yields obtained in this dimerization step are moderate (40% for **17**) to good (71% for **24**). The mixture of the alcohols is oxidized using the Oppenauer procedure. In the case of **17** a 1:1 mixture of the two regioisomeric ketones **18** and **19** is obtained with an overall yield of 83%.

The two ketones have been separated for their characterization with silica gel using CH_2Cl_2 as eluent, but

(16) Schreiber, J.; Felix, D.; Eschenmoser, A.; Winter, M.; Gautschi, F.; Schulte-Elte, K. H.; Sundt, E.; Ohloff, G.; Kalvoda, J.; Kaufmann, H.; Wieland, P.; Anner, G. *Helv. Chim. Acta* **1967**, *50*, 2101.

Scheme 7[a]

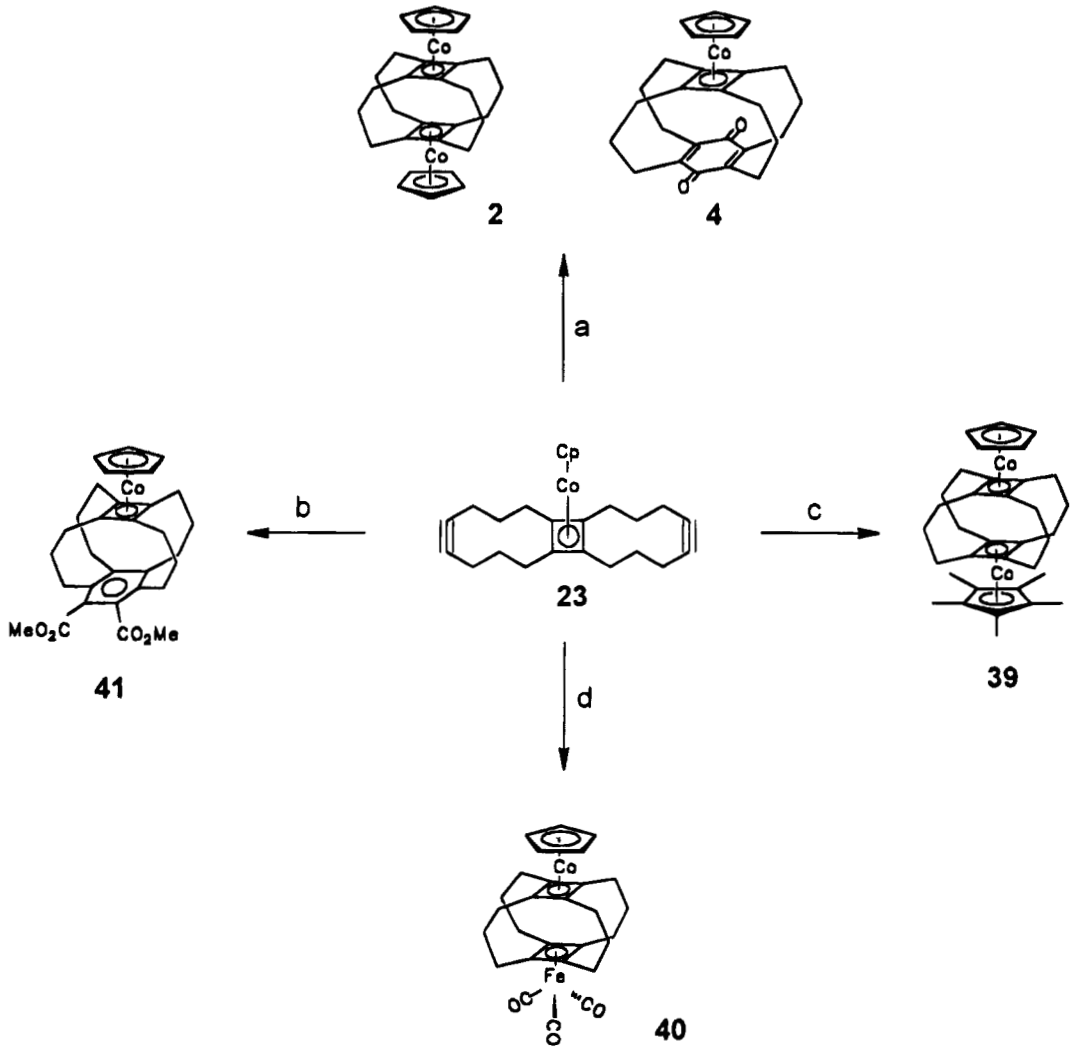

[a] Key: (a) $CpCo(CO)_2$; (b) $CpCo(CO)_2$, $MeCO_2{-}{\equiv}{-}CO_2Me$; (c) $Cp^*Co(CO)_2$; (d) $Fe(CO)_5$.

Scheme 8[a]

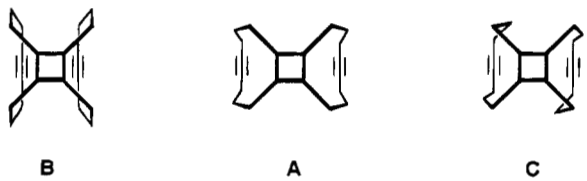

[a] *d*, Å (relative energy, kcal mol): 3.9 (10.0); 6.3 (0.0); 4.6 (8.3).

Scheme 9[a]

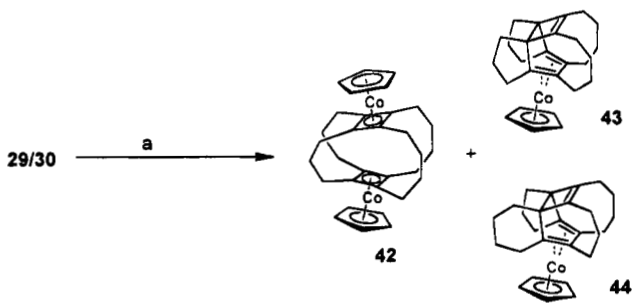

[a] Key: (a) $CpCo(CO)_2$/c-octane.

normally the mixture is used for further reactions. With the same procedure **25** is obtained in 83% yield. The bis(selenadiazole)s of the diketones can be obtained by

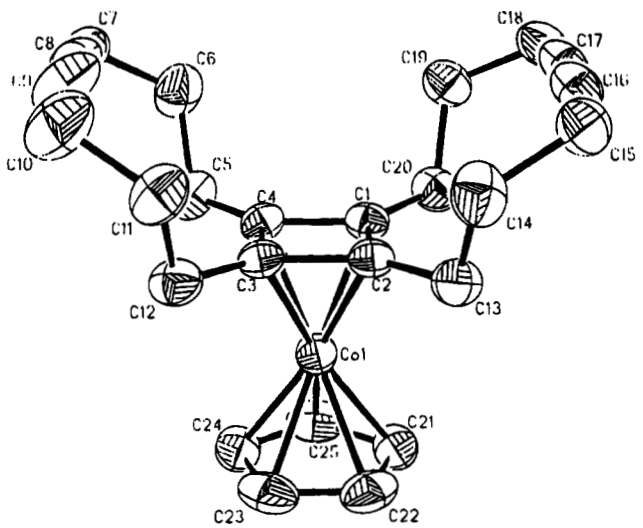

Figure 2. ORTEP drawing of **23** (50% probability ellipsoids).

reacting them with semicarbazide acetate and subsequent heating with SeO_2. With this strategy we obtained two bis(selenadiazole)s in each case, **21** and **22** for the C_{20} system and **27** and **28** for the C_{22} system. The mixture was used for the subsequent step. Treatment of the respective mixtures with *n*-butyllithium

Scheme 10[a]

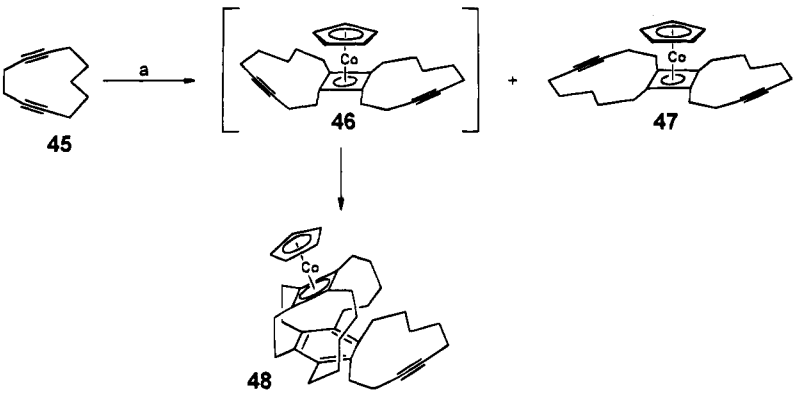

[a] Key: (a) $CpCo(CO)_2$/*n*-octane.

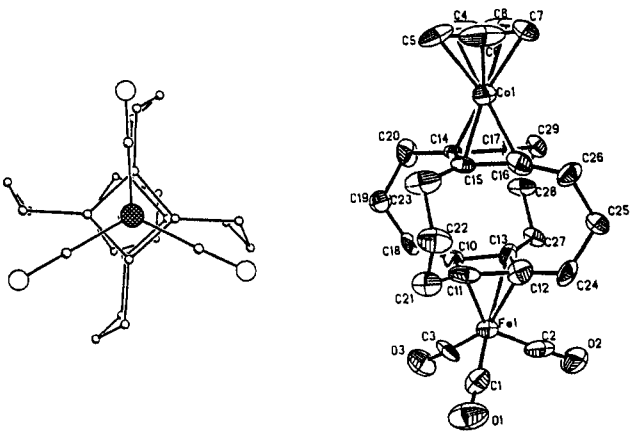

Figure 3. Structure of **40** as determined by X-ray investigations: View along the Fe–Co axis (left); side view (right, 50% probability ellipsoids).

(BuLi) in tetrahydrofuran at −40 °C yields exclusively **23** (71%) in the case of **21/22**. Reaction of **27/28** affords the anticipated mixture of two diynes, a 1:1 ratio of **29** and **30**. Scheme 6 shows that starting from 5-cyclononynol (**31**)[17] a further tricylic diyne can be built up in a way similar to the described synthesis of **23** and **29/30**.[18] Since the second selenadiazol unit in **35** is formed regioselectively, only one of the two anticipated diynes (**36**) is obtained. X-ray investigations on single crystals of **36** show that the isomer with C_2 symmetry is formed (Figure 6).

Scheme 11[a]

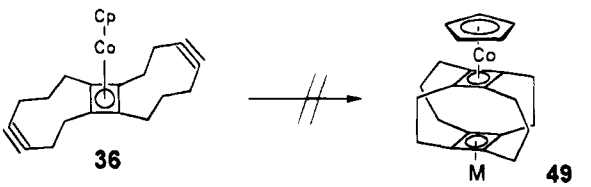

[a] M = Cp*Co, MeCpCo, and CpCo.

Before describing our further steps, it is worthwhile to comment on the regioselectivity observed in the formation of only two bis(selenadiazole)s from **18** and **19** although four regioisomers are possible. To rationalize this fact we consider in Figure 1 the conformation of **18**.[19] The conformation of the 10-membered rings shows a great similarity with the lowest energy confor-

(17) Lange, G. L.; Hall, T. W. *J. Org. Chem.* **1974**, *39*, 3819.

(18) **33** can be also prepared directly starting from 5-cyclononynone: Gleiter, R.; Schehlmann, V. *Tetrahedron Lett.* **1989**, *30*, 2893. Nevertheless the better overall yield is obtained starting from **31**.

(19) X-ray structure analysis: Gleiter, R.; Schehlmann, V.; Nuber, B. Unpublished results.

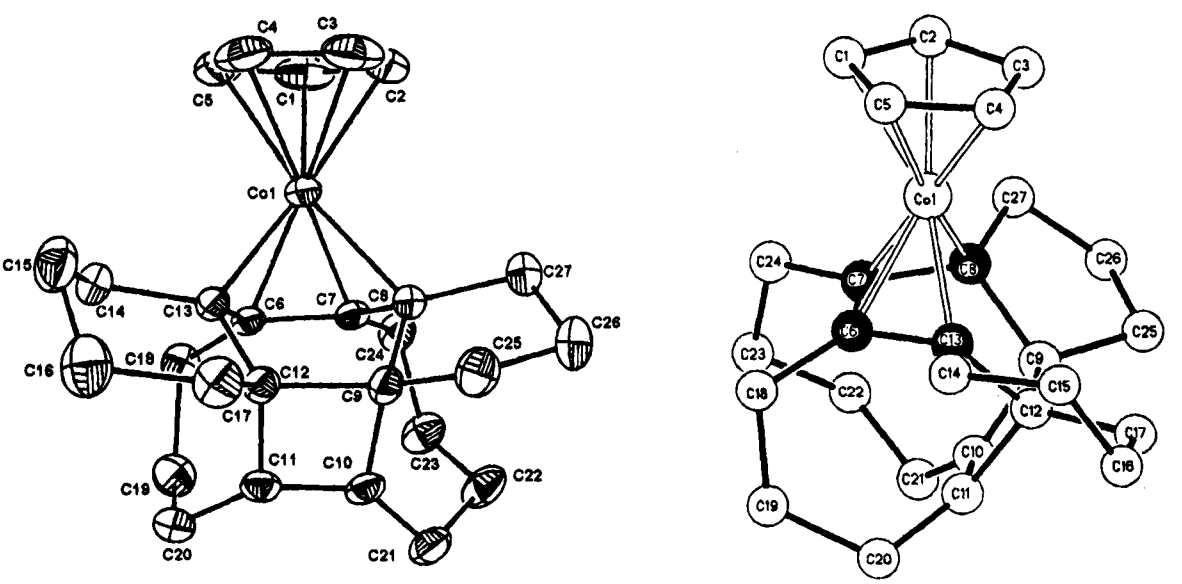

Figure 4. Structure of **44** as determined by X-ray investigations: View onto the cyclobutene unit (left, 50% probability ellipsoids); side view (right, full circles represent the butadiene unit).

Table 1. Crystal Data and Data Collection Parameters

	23	36	40	44
mol formula	$C_{25}H_{29}Co$	$C_{23}H_{25}Co$	$C_{28}H_{29}CoFeO_3$	$C_{27}H_{33}Co$
fw	388.44	360.38	528.32	416.45
cryst syst	triclinic	rhombic	monoclinic	triclinic
space group	C^1_i, $P\bar{1}$ (No. 2)	D^4_2, $P2_12_12_1$ (No. 19)	C^4_s, Cc (No. 9)	C^1_i, $P\bar{1}$ (No. 2)
cell dimens				
a, Å	9.003	9.555(9)	18.92(1)	8.269(3)
b, Å	10.399	12.86(1)	8.499(6)	9.082(2)
c, Å	11.874	15.551(9)	19.37(1)	13.724(5)
α, Å	93.45			84.87(2)
β, Å	101.45		130.16	88.77(3)
γ, Å	108.77			80.62(2)
V, Å^3	1022.34	1910.3	2380.41	1012.8
Z	2	4	4	2
T, K	296	296	296	296
d_{calc}, g·cm^{-3}	1.26	1.25	1.47	1.37
linear abs, μ, cm^{-1}	8.4	8.9	13.3	8.6
$F(000)$	412	760	1096	444
radiation, Å	λ(Mo Kα) = 0.710 73	λ(Mo Kα) = 0.710 73	λ(Mo Kα) = 0.710 73	λ(Mo Kα) = 0.710 73
scan type	ω	ω	θ/ω	ω
rflns measd	h, 0−13; k, −15 to 15; l, −17 to 17	h, 0−11; k, 0−15; l, −18 to 18	h, 0−27; k, 0−12; l, −27 to 27	h, 0−12; k, −13 to 13; l, −19 to 19
2θ range, deg	3.0−57.5	3.0−44.0	3.0−60.0	3.0−57.5
no. of rflns measd	5344	2792	3691	5623
abs cor	empirical, 6 rflns	empirical, 6 rflns	empirical, 5 rflns	empirical, 7 rflns
range of transmissn	$0.92 < 2\theta < 1.00$	$0.91 < 2\theta < 1.00$	$0.67 < 2\theta < 1.00$	$0.87 < 2\theta < 1.00$
no. of unique obsd data	3891, $I > 2.5\sigma(I)$	1303, $I > 2.5\sigma(I)$	1905, $I > 2.5\sigma(I)$	3916, $I > 2.5\sigma(I)$
no. of params (NV)	236	218	297	255
$R(F)$	0.042	0.063	0.045	0.042
$R_w(F)$	0.040	0.046	0.035	0.038
GOF	2.8	1.71	2.10	2.22
ϱ, residual, e·Å^{-3} (max/min)	0.30/−0.47	0.65/−0.49	0.50/−0.38	0.55/−0.53

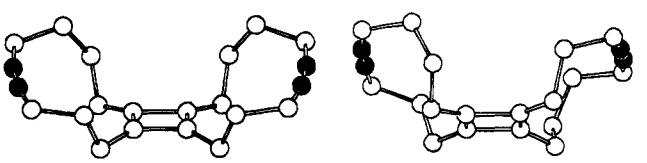

Figure 5. Calculated (AM1) geometries of the $C_{22}H_{28}$ fragments of **29** (left) and **30** (right). Full circles represent the sp centers.

mation of 1,6-cyclodecadiene (left). Other isomers like **37** and **38** are derived from the 1,5-cyclodecadiene skeleton. Since 1,5-cyclodecadiene is by 7.0 kcal/mol

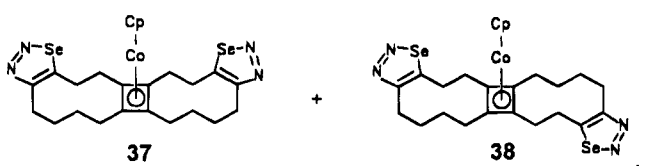

(AM1 calculation) less stable than 1,6-cyclodecadiene, it seems reasonable that the already performed 1,6-cyclodecadiene conformation is maintained throughout the reaction, thus leading to **21** and **22** only.

Preparation of the Superphanes. [3$_4$](1.2.3.4)-Cyclobutadienophanes. The reaction of **23** with $CpCo(CO)_2$ in cyclooctane (120 °C) yields in only 2 h the superphane **2** (80% yield) and in traces (1% yield) the mixed phane **4**. The reaction with (η^5-pentamethylcyclopentadienyl)cobalt dicarbonyl [Cp*Co(CO)$_2$] in decalin yields **39** in 80% yield. Heating **23** with $Fe(CO)_5$ in refluxing toluene leads to **40** in 8% yield. Finally, when heating **23** in the presence of dimethyl acetylenedicarboxylate (DMAD) and $CpCo(CO)_2$ in toluene yields the mixed cyclophane **41** as minor product besides **2** (Scheme 7).

The quick reaction of **23** with $CpCo(CO)_2$ supports our assumption that **23** is an intermediate in the formation

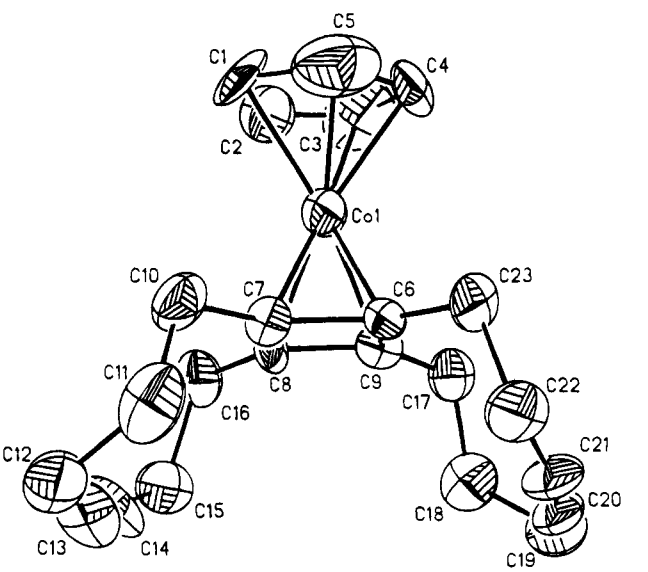

Figure 6. ORTEP drawing of **36** (50% probability ellipsoids).

of **2** from **1** (Scheme 1). The structure of **23**, obtained from an X-ray investigation (Figure 2), shows that the two triple bonds are situated in the same half space and orientated parallel to each other. Calculations using the AM1 method on a model of **23** which does not contain the CpCo unit but allows the minimization of all geometrical parameters are in agreement with the X-ray data. These calculations predict besides the global minimum **A**, in which both triple bonds are 6.3 Å apart, two local minima, **B** and **C**, in which the triple bonds are 3.9 and 4.6 Å apart. The local minima are predicted to be 10.0 and 8.3 kcal/mol higher in energy than **A**. These results explain the fast reaction of **23** with $CpCo(CO)_2$ at higher temperature and the good yield.

Table 2. Atomic Coordinates ($\times 10^4$) and Equivalent Isotropic Displacement Parameters ($Å^2 \times 10^3$) for $C_{25}H_{29}Co$ (23)

atom	x	y	z	U_{eq}[a]
Co	1694(1)	2853(1)	2646(1)	42(1)
C1	−280(3)	2534(3)	3221(2)	43(1)
C2	−350(3)	1337(2)	2476(2)	41(1)
C3	−364(3)	2104(3)	1492(2)	41(1)
C4	−292(3)	3301(3)	2236(2)	42(1)
C5	−287(3)	4720(3)	2098(3)	59(1)
C6	−1911(4)	4942(3)	2058(3)	73(2)
C7	−2843(3)	4969(3)	842(3)	65(1)
C8	−3155(4)	3717(4)	69(3)	67(1)
C9	−3259(4)	2743(4)	−517(3)	82(2)
C10	−3174(4)	1534(4)	−1189(3)	94(2)
C11	−2258(3)	813(3)	−439(2)	63(1)
C12	−556(3)	1728(3)	210(2)	55(1)
C13	−486(3)	−117(3)	2604(2)	52(1)
C14	−2188(4)	−1182(3)	2157(3)	68(1)
C15	−3015(4)	−1751(3)	3100(3)	73(1)
C16	−3058(4)	−651(4)	3911(3)	69(2)
C17	−2998(4)	296(4)	4509(3)	70(2)
C18	−2802(4)	1572(4)	5209(3)	76(2)
C19	−1991(3)	2804(3)	4647(3)	61(1)
C20	−326(3)	2867(3)	4455(2)	56(1)
C21	3736(3)	3106(3)	3896(3)	65(1)
C22	3711(3)	2262(3)	2941(3)	67(1)
C23	3697(3)	2983(3)	2002(3)	67(1)
C24	3710(3)	4284(3)	2359(3)	63(1)
C25	3730(3)	4382(3)	3550(3)	66(1)

[a] Equivalent isotropic U defined as one-third of the trace of the orthogonalized $\mathbf{U}_{ij}$ tensor.

The X-ray investigation on single crystals of **40** reveal a very similar skeleton as for **2**. The distance between the two cyclobutadiene units amounts to 2.98 Å. Just as in **2** the four propano chains show a pinwheel conformation.

[$4_2 3_2$](1.2.3.4)Cyclobutadienophanes. The reaction of the mixture of **29/30** with $CpCo(CO)_2$ yields the superphane **42** and the bridged bicyclo[4.2.0]octa-2,4,7-triene complexes **43** and **44** in a 2:1:1 ratio.[20] The unexpected formation of **43** and **44** is accounted by a [4 + 2] cycloaddition between a cobaltole and a CpCo–cyclobutadiene unit.[21]

Figure 4 shows two views of the structure of **44** obtained from an X-ray investigation. **42** is the first cyclobutadienosuperphane in which the two cyclobutadiene units are connected by chains of different length. An X-ray investigation on single crystals of **42** confirms the predicted structure.[21] Obviously only **29** reacts to form a cyclophane. Using the AM1 procedure to calculate the geometrical parameters of the $C_{22}H_{28}$ fragment of **29** and **30** resulted in the conformations of minimum energy shown in Figure 5.

We notice that in **29** the two triple bonds are orientated parallel to each other while in **30** the triple bonds are inclined by 8.6°. The result that only **29** reacts to form a superphane is reminiscent of the outcome of the reaction of 1,5-cyclodecadiyne (**45**) with $CpCo(CO)_2$ in *n*-octane.[16] It has been found that only one of the possible dimerization products, **46**, reacts to form a cyclophane (**48**), while the other (**47**) resists further ring closure with $CpCo(CO)_2$.

(20) Unbridged $Fe(CO)_3$-stabilized bicyclo[4.2.0]octa-2,4,7-trienes: Cooke, M.; Howard, J. A. K.; Russ, C. R.; Stone, F. G. A.; Woodward, P. *J. Organomet. Chem.* **1974**, *78*, C43. Slegeir, W.; Case, R.; McKennis, J. S.; Pettit, R. *J. Am. Chem. Soc.* **1974**, *96*, 287.

(21) Preliminary publication: Gleiter, R.; Langer, H.; Nuber, B. *Angew. Chem., Int. Ed. Engl.* **1994**, *33*, 1272.

(22) Gleiter, R.; Kratz, D.; Ziegler, M. L.; Nuber, B. *Tetrahedron Lett.* **1990**, *31*, 6175.

Table 3. Atomic Coordinates ($\times 10^4$) and Equivalent Isotropic Displacement Parameters ($Å^2 \times 10^3$) for $C_{28}H_{29}CoFeO_3$ (40)

atom	x	y	z	U_{eq}[a]
Fe	4008(1)	4438(1)	7220(1)	42(1)
C1	3508(6)	6359(10)	6910(6)	56(6)
O1	3174(5)	7567(7)	6662(5)	91(6)
C2	4924(7)	4718(10)	8401(7)	57(8)
O2	5551(5)	4869(8)	9174(4)	88(5)
C3	3234(7)	3626(11)	7337(6)	53(7)
O3	2711(4)	3054(7)	7404(4)	74(6)
Co	5000	883(1)	5000	46(1)
C4	4881(14)	−1163(13)	4424(12)	120(18)
C5	4478(89)	−20(18)	3809(7)	84(8)
C6	5131(14)	1034(14)	4069(11)	108(17)
C7	5909(13)	598(25)	4810(15)	169(20)
C8	5799(14)	−725(26)	5041(10)	182(17)
C10	3769(6)	2629(8)	6381(6)	36(6)
C11	3799(8)	4140(9)	6063(7)	42(7)
C12	4761(8)	4320(8)	6820(7)	39(7)
C13	4760(7)	2814(9)	7151(6)	41(7)
C14	4263(8)	974(10)	5393(7)	42(8)
C15	4271(7)	2475(9)	5043(6)	38(6)
C16	5253(7)	2655(9)	5806(6)	45(7)
C17	5250(7)	1146(10)	6164(6)	34(6)
C18	3100(7)	1298(10)	6021(6)	48(7)
C19	2793(7)	554(11)	5163(7)	57(7)
C20	3520(7)	−145(11)	5152(7)	57(7)
C21	3113(6)	4981(9)	5155(6)	47(6)
C22	3403(7)	5087(11)	4587(7)	56(8)
C23	3540(7)	3581(11)	4278(6)	67(8)
C24	5522(7)	5392(10)	7047(7)	50(7)
C25	6265(8)	4672(11)	7076(8)	64(10)
C26	5962(7)	3934(10)	6180(7)	58(8)
C27	5492(6)	1722(9)	7893(5)	43(6)
C28	5608(6)	147(9)	7593(6)	52(7)
C29	5911(6)	248(9)	7022(6)	46(7)

[a] Equivalent isotropic U defined as one-third of the trace of the orthogonalized $\mathbf{U}_{ij}$ tensor.

Table 4. Atomic Coordinates ($\times 10^4$) and Equivalent Isotropic Displacement Parameters ($Å^2 \times 10^3$) for $C_{23}H_{25}Co$ (36)

atom	x	y	z	U_{eq}[a]
Co	8611(2)	9361(1)	622(1)	62(1)
C1	9322(30)	8036(18)	1266(14)	151(14)
C2	10255(28)	8775(18)	1174(13)	136(14)
C3	10664(15)	8986(15)	402(17)	132(10)
C4	9791(28)	8405(19)	−135(9)	156(13)
C5	8971(22)	7853(15)	423(17)	133(10)
C6	6934(12)	9907(9)	70(6)	43(5)
C7	6757(11)	9811(9)	1002(6)	39(5)
C8	7793(11)	10610(11)	1128(5)	45(4)
C9	7968(11)	10697(10)	214(6)	46(5)
C10	5826(12)	9153(9)	1563(6)	66(6)
C11	4294(13)	9537(11)	1659(7)	84(6)
C12	4046(13)	10245(10)	2454(8)	90(7)
C13	5025(19)	11139(15)	2448(11)	86(8)
C14	6021(16)	11600(15)	2412(10)	86(8)
C15	7393(13)	12098(10)	2178(7)	80(7)
C16	8397(11)	11216(9)	1877(6)	63(5)
C17	8771(12)	12543(9)	−451(7)	75(6)
C19	7142(15)	12618(11)	−1212(8)	111(8)
C20	6035(19)	11807(11)	−1249(8)	67(7)
C21	5453(20)	11063(11)	−1230(9)	81(8)
C22	4907(13)	10038(10)	−991(7)	75(6)
C23	6173(11)	9420(8)	−680(6)	58(4)

[a] Equivalent isotropic U defined as one-third of the trace of the orthogonalized $\mathbf{U}_{ij}$ tensor.

In **46** both acetylene units are orientated parallel to each other, while the **47** the triple bonds cannot be aligned parallel to each other. Thus it was not unexpected that all attempts to generate a cyclobutadienosuperphane like **49** starting from **36** failed (Scheme 11), although the distance between the triple bonds is not

Table 5. Atomic Coordinates ($\times 10^4$) and Equivalent Isotropic Displacement Parameters ($Å^2 \times 10^3$) for $C_{27}H_{33}Co$ (44)

atom	x	y	z	U_{eq}[a]
Co	2330(1)	3100(1)	1466(1)	29(1)
C1	2249(4)	4262(4)	69(2)	56(1)
C2	3475(4)	2993(4)	111(2)	56(1)
C3	4595(4)	3159(4)	1234(2)	55(1)
C4	4045(4)	4506(4)	1234(2)	55(1)
C5	2604(4)	5178(3)	767(2)	56(1)
C6	292(3)	3079(3)	2265(2)	26(1)
C7	640(3)	1802(3)	711(2)	27(1)
C8	2207(3)	921(3)	1946(2)	29(1)
C9	2448(3)	471(3)	3045(2)	29(1)
C10	805(3)	137(3)	3502(2)	30(1)
C11	516(3)	1411(3)	3946(2)	30(1)
C12	2151(3)	1909(3)	3604(2)	27(1)
C13	1649(3)	3278(3)	2870(2)	26(1)
C14	1574(3)	4772(3)	3315(2)	36(1)
C15	3047(4)	4821(3)	3935(2)	49(1)
C16	3210(4)	3576(3)	4753(2)	54(1)
C17	3461(3)	2068(3)	4336(2)	42(1)
C18	−1393(3)	3934(3)	2447(2)	37(1)
C19	−2151(3)	3108(3)	3374(2)	45(1)
C20	−1030(3)	2394(3)	4246(2)	40(1)
C21	−279(3)	−969(3)	3288(2)	42(1)
C22	−643(4)	−1136(3)	2208(2)	48(1)
C23	−1598(3)	223(3)	1600(2)	46(1)
C24	−581(3)	1327(3)	055(2)	38(1)
C25	4004(3)	−686(3)	3104(2)	42(1)
C26	3887(4)	−1547(3)	2211(2)	51(1)
C27	3151(3)	−363(3)	1405(2)	43(1)

[a] See footnote *a* of Table 4.

Table 6. Selected Interatomic Distances (Å) and Angles (deg) for Compounds 23, 36, 40, and 44

	Compound **23**		
Co−C1	1.966(3)	Co−C21	2.052(3)
C1−C2	1.460(4)	C3−C4	1.459(4)
C8−C9	1.160(5)	C8−C17	6.3
C8−C9−C10	172.7(4)	C15−C16−C17	174.1(4)
	Compound **36**		
Co−C1	2.090(23)	Co−C6	1.949(11)
C6−C7	1.464(14)	C7−C8	1.441(17)
C13−C14	1.122(25)	C13−C21	5.7
C12−C13−C14	160.9(20)	C13−C14−C15	167.3(17)
C19−C20−C21	164.3(18)	C20−C21−C22	164.4(16)
	Compound **40**		
Co−C4	1.999(16)	Co−C14	1.974(18)
Fe−C1	1.786(9)	Fe−C10	2.064(10)
C10−C11	1.451(14)	C14−C15	1.449(14)
C10−C14	2.98		
	Compound **44**		
Co−C1	2.101(3)	Co−C6	1.992(2)
Co−C8	2.047(2)	C6−C7	1.430(3)
C7−C8	1.435(3)	C9−C10	1.547(4)
C10−C11	1.341(3)	C11−C12	1.544(4)
C6−C7−C8	112.2(2)	C7−C8−C9	113.6(2)
C8−C9−C10	109.0(2)	C11−C12−C13	104.6(2)

as far as in **23**. The structure obtained of X-ray investigations (Figure 6) shows that the triple bonds are inclined by 28°.

Conclusions

Starting from cyclic alkynols, which can be looked at as masked cyclic diynes, we could develop a straightforward synthesis of cyclobutadiene superphanes which are capped with different metal fragments. The chain length depends on the starting cyclic alkynols. Our studies provided us also with new insights concerning the mechanism of the superphane formation and the reactivity of CpCo-complexed cyclobutadienes.

Experimental Section

Equipment. All melting points are uncorrected. The NMR spectra are measured with a Bruker AS200 or AS300 (^{1}H NMR at 200 or 300 MHz and ^{13}C NMR at 50.32 or 75.45 MHz) using the solvent as internal standard (δ; J (Hz)). The mass spectra refer to data from a Vacuum Generators ZAB instrument (EI, 70 eV). IR spectra were recorded with a Perkin-Elmer 580B. UV light absorption data were recorded using a Varian Cary 17 D or a Hewlett Packard 8452A spectrometer. Elemental analyses: Mikroanalytisches Labor der Universität Heidelberg. All reactions were carried out in argon atmosphere using dried and oxygen-free solvents.

{(1,2,11,12-η)-Tricyclo[10.8.0.0^{2,11}]eicosa-1,11-diene-6,-16-diol}(η^5-cyclopentadienyl)cobalt and {(1,2,11,12-η)-Tricyclo[10.8.0.0^{2,11}]eicosa-1,11-dien-6,17-diol}(η^5-cyclopentadienyl)cobalt (17). A 15 g amount (83.3 mmol) of CpCo(COD) was dissolved in 1.5 L of decalin. The solution was heated to 150−160 °C. During 6 d 30.4 g (200 mmol) of **16**, dissolved in 400 mL decalin, was added. While the addition of **16** was continued, a further portion of CpCo(COD) was added after 2 d (6.0 g (33.3 mmol)) and after 4d (4.0 g (22.2 mmol)). When the addition of **16** was completed, the heating was continued for a further 1 day. The reaction mixture was allowed to cool to room temperature and then filtered through alumina (neutral, grade III). With pentane as eluent the unreacted CpCo(COD) could be extracted, while the product **17** remains as a solid at the top of the column. It could be dissolved with some CH_2Cl_2 and was extracted with ether as a broad yellow band. After the removal of the solvent the crude product was purified by column chromatography (silica gel/ether). A separation of the isomers of **17** failed, but from the first fractions containing **17** one isomer crystallized as an orange red solid and could be identified by spectroscopic methods. The reaction yielded 17.0 g (40%) of an orange red solid which contained all isomers of **17**: mp of the pure isomer 154−155 °C; ^{1}H NMR (300 MHz, CD_3OD) δ 4.44 (s, 5H), 3.72−3.75 (m, 2H), 2.47−2.59 (m, 4H), 2.20−2.32 (m, 4H), 1.25−1.90 (m, 20H); ^{13}C NMR (75.45 MHz, CD_3OD) δ 82.2 (C), 82.0 (C), 81.5 (CH, Cp), 71.9 (CH), 34.7 (CH_2), 32.3 (CH_2), 28.5 (CH_2), 28.0 (CH_2), 27.0 (CH_2), 24.7 (CH_2), 24.5 (CH_2); IR (KBr) 2932, 2910, 1704, 1443, 1420, 1369, 1103, 997, 807; UV (CH_3CN) (λ_{max}, nm (log ϵ)) 205 (4.40), 228 (4.04), 262 (4.26), 295 (3.16), 377 (2.58); MS (EI, 70 eV) *m/z* (relative intensity) 429 (0.9), 85 (52), 71 (56), 57 (100), 43 (84). Anal. Calcd for $C_{25}H_{37}CoO_2$ (428.5): C, 70.08; H, 8.70. Found: C, 69.82; H, 8.80.

{(1,2,11,12-η)-Tricyclo[10.8.0.0^{2,11}]eicosa-1,11-diene-6,-16-dione}(η^5-cyclopentadienyl)cobalt (18) and {(1,2,11,-12-η)-Tricyclo[10.8.0.0^{2,11}]eicosa-1,11-diene-6,17-dione}-(η^5-cyclopentadienyl)cobalt (19). A 17.0 g amount (40 mmol) of **17** and 52.8 g (260 mmol) of aluminum isopropylate were dissolved in toluene (780 mL) and acetone (370 mL). The solution was heated under reflux for 14 h. By checking the reaction with TLC, we noticed in addition to the products and the starting material an intermediately formed monoketone. After the reaction mixture had cooled to rt (rt = room temperature) 100 mL of water was added and the solution was concentrated in vacuo. To the residue ether and 10% H_2SO_4 were added. The aqueous layer was extracted with ether. The combined organic layers and extracts were washed with saturated $NaHCO_3$ solution, dried ($MgSO_4$), concentrated in vacuo, and adsorbed on silica gel. The products were purified by column chromatography (silica gel/CH_2Cl_2) and yielded 14.0 g (33 mmol) (83%) of an orange red solid. **18**: mp 170−172 °C; ^{1}H (300 MHz, $CDCl_3$) δ 4.42 (s, 5H), 2.96−3.07 (m, 2H), 1.35−2.45 (m, 26H); ^{13}C (75.47 MHz, $CDCl_3$) δ 213.3 (C), 80.6 (CH), 79.6 (C), 79.0 (CH), 43.9 (CH_2), 36.8 (CH_2), 28.6 (CH_2), 23.9 (CH_2), 23.8 (CH_2), 23.5 (CH_2), 22.0 (CH_2); IR (KBr) 2932,

2910, 1704, 1443, 1420, 1369, 1203, 1103, 997, 807; UV and MS are in analogy to those obtained from **19**. Anal. Calcd for $C_{25}H_{33}CoO_2$ (424.47): C, 70.74; H, 7.84. Found: C, 70.87; H, 7.75. **19**: mp 147–148 °C; ^{1}H (300 MHZ, $CDCl_3$) δ 4.44 (s, 5H), 2.87–2.98 (m, 2H), 2.47–2.56 (m, 2H), 1.33–2.44 (m, 24H); ^{13}C (75.47 MHz, $CDCl_3$) δ 213.3 (C), 80.4 (CH), 79.9 (C), 78.6 (CH), 43.4 (CH_2), 37.6 (CH_2), 37.6 (CH_2), 27.5 (CH_2), 24.5 (CH_2), 23.8 (CH_2, 2C), 22.8 (CH_2); IR (KBr) 2946, 2908, 1703, 1441, 1422, 1371, 1222, 1102, 821, 805; UV (pentane) (λ_{max}, nm (log ε)) 266 (4.41), 300 (3.22), 375 (2.73); MS (EI, 70 eV) *m/z* (relative intensity) 424 (61), 188 (20), 151 (22), 137 (40), 129 (23), 124 (100), 115 (22), 91 (48), 79 (25), 67 (25), 59 (90), 41 (52). Anal. Calcd for $C_{25}H_{33}CoO_2$ (424.47): C, 70.74; H, 7.84. Found: C, 70.79; H, 7.86.

{(1,2,11,12-η)-Tricyclo[10.8.0.0^{2,11}]eicosa-1,11-diene-6,-16-dione bis(semicarbazone)}(η^5-cyclopentadienyl)cobalt (20a) and {(1,2,11,12-η)-Tricyclo[10.8.0.0^{2,11}]eicosa-1,11-diene-6,17-dione bis(semicarbazone)}(η^5-cyclopentadienyl)cobalt (20b). In 250 mL of ethanol were dissolved 10.0 g (90 mmol) of semicarbazide·HCl and 9.0 g (110 mmol) of NaOAc. The solution was refluxed and filtered. The precipitate was washed with hot ethanol. A 12.75 g amount (30 mmol) of the mixed ketones **18** and **19** was added to the combined filtrates, and the solution was refluxed for 45 min. The reaction was controlled by TLC. When the starting material had disappeared, the solvent was removed in vacuo. To the residue were added 500 mL of chloroform and 100 mL of water. The organic layer was separated, washed with saturated $NaHCO_3$ solution, and dried ($MgSO_4$). After the solvent had been removed 15.1 g of the crude product was obtained as a yellow solid, which could not be recrystallized and was used for the following reaction without any further purification.

Bis(selenadiazole)s 21 and 22. A 15 g amount (27.9 mmol) of the isomeric mixture of **20** and 10.0 g (90.0 mmol) of SeO_2 were dissolved in 650 mL of concentrated acetic acid. The mixture was heated for 5–6 h to 30–40 °C. It proved to be quite difficult to control the progress of the reaction by TLC because of the chromatographical behavior of the starting material. After the reaction was stopped the solvent was removed in vacuo. Chloroform was added to the residue, and it was neutralized with 5% Na_2CO_3 solution. The organic layer was separated, washed with water, dried ($MgSO_4$), and concentrated in vacuo. The mixture of **21** and **22** was chromatographed (silica gel/CH_2Cl_2), and the product was obtained as a yellow solid, which was used for the following reactions without further purification.

{(1,2,11,12-η)-Tricyclo[10.8.0.0^{2,11}]eicosa-1,11-diene-6,-17-diyne}(η^5-cyclopentadienyl)cobalt (23). A 3.01 g amount (5mmol) of the mixed bis(selenadiazole)s **21** and **22** was dissolved in 500 mL of THF. The solution was cooled to −40 °C. At this temperature 11.0 mmol of BuLi (1.6 M in hexane) was added slowly. The color of the solution changed to deep red, and N_2 began to expel. The reaction was monitored by TLC, and the addition of BuLi was continued until no more starting material could be detected. The reaction was quenched with methanol, and the solution was allowed to warm to ambient temperature. Semisaturated NaCl solution, water, 500 mL ether, and some diluted sulfuric acid were added. The organic layer was separated, dried ($MgSO_4$), concentrated in vacuo, and adsorbed on silica gel. After column chromatography (silica gel/CCl_4) and recrystallization from pentane **23** was obtained in a yield of 71% (1.40 g) as a yellow solid: mp 106–108 °C; ^{1}H (300 MHz, $CDCl_3$) δ 4.49 (s, 5H), 1.5–2.5 (m, 24H); ^{13}C (75.4 MHz, $CDCl_3$) δ 82.3 (C), 82.1 (C), 80.0 (CH), 27.8 (CH_2), 25.6 (CH_2), 19.2 (CH_2); IR ($CDCl_3$) 2928, 2234, 1430, 1255, 806; UV (pentane) (λ_{max}, nm (log ε)) 266 (4.38), 296 (3.28), 378 (2.73); MS (EI, 70 eV) *m/z* (relative intensity) 388 (4), 308 (18), 131 (24), 119 (27), 105 (75), 91 (100), 57 (18) 43 (18). Anal. Calcd for $C_{25}H_{33}CoO_2$ (424.47): C, 77.30; H, 7.52. Found: C, 77.12; H, 7.57.

{(1,2,12,13-η)-Tricyclo[11.9.0.0^{2,12}]docosa-1,12-diene-7,-18-diol}(η^5-cyclopentadienyl)cobalt (24). A solution of CpCo(COD) (23.2 g, 100 mmol) in 900 mL of cyclooctane was heated under reflux. During 40 h a solution of 6-cycloundecynol (**16**)[15] (16.6 g, 100 mmol) was added. After the addition was completed, the heating was continued for another 20 h. The working up procedure was carried out as described for **17** yielding 16.2 g (72%) of the isomeric mixture of the alcohols (**24**) as a yellow solid. The isomeric alcohols could be separated by column chromatography (silica gel/ether), but usually the isomeric mixture was used for further reactions. X-ray studies on single crystals of **24c** confirm the given stereochemistry.[23]

{(1,2,12,13-η)-Tricyclo[11.9.0.0^{2,12}]docosa-1,12-diene-7-*cis*,18-*cis*-diol}(η^5-cyclopentadienyl)cobalt (24a) (cis/trans defines the relative orientation to the CpCo unit): mp 175 °C; ^{1}H (300 MHz, CD_3OD) δ 4.53 (s, 5H), 3.65–3.78 (m, 2H), 2.12–2.30 (m, 8H), 1.22–1.81 (m, 22H); ^{13}C (75.4 MHz, CD_3OD) δ 80.9 (CH), 80.7 (C), 72.0 (CH), 32.9 (CH_2), 28.5 (CH_2), 25.8 (CH_2), 22.6 (CH_2); IR ($CDCl_3$) 2924, 2848, 1267, 429; UV (CH_2Cl_2) (λ_{max}, nm (log ε)) 234 (3.9), 266 (4.2), 300 (3.1), 386 (2.7); MS (EI, 70 eV) *m/z* (relative intensity) 456 (48), 189 (10), 165 (11), 151 (14), 137 (22), 125 (28), 124 (64), 41 (100). Anal. Calcd for $C_{27}H_{41}CoO_2$ (456.22): C, 71.03; H, 9.05. Found: C, 70.89; H, 9.14.

{(1,2,12,13-η)-Tricyclo[11.9.0.0^{2,12}]docosa-1,12-diene-7-*cis*,18-*trans*-diol}(η^5-cyclopentadienyl)cobalt (24b): mp 162 °C; ^{1}H (300 MHz, CD_3OD) δ 4.55 (s, 5H), 3.62–3.80 (m, 2H), 2.12–2.32 (m, 8H), 1.22–1.78 (m, 22H); ^{13}C (75.47 MHz, CD_3OD) δ 80.9 (CH), 80.6 (C), 72.7 (CH), 72.1 (CH), 32.9 (CH_2), 32.7 (CH_2), 28.5 (CH_2), 27.9 (CH_2) 25.9 (CH_2), 25.7 (CH_2), 22.6 (CH_2), 22.3 (CH_2); IR ($CDCl_3$) 2924, 2848, 1036; UV (CH_2Cl_2) (λ_{max}, nm (log ε)) 234 (4.2), 266 (4.5), 310 (3.5), 378 (3.1); MS (EI, 70 eV) *m/z* (relative intensity) 456 (41), 201 (10), 189 (11), 165 (9), 151 (14), 137 (23), 125 (53), 124 (72), 41 (100). Anal. Calcd for $C_{27}H_{41}CoO_2$ (456.22): C, 71.03; H, 9.05. Found: C, 70.90; H, 9.06.

{(1,2,12,13-η)-Tricyclo[11.9.0.0^{2,12}]docosa-1,12-diene-7-*trans*,18-*trans*-diol}(η^5-cyclopentadienyl)cobalt (24c): mp 182 °C; ^{1}H (300 MHz, CD_3OD) δ 4.55 (s, 5H), 3.63–3.74 (m, 2H), 2.12–2.28 (m, 8H), 1.25–1.80 (m, 22H); ^{13}C (75.47 MHz, CD_3OD) δ 80.8 (CH), 80.6 (C), 72.7 (CH), 32.7 (CH_2), 27.9 (CH_2) 25.9 (CH_2), 22.4 (CH_2); IR ($CDCl_3$) 2924, 2848, 1036; UV (CH_2Cl_2) (λ_{max}, nm (log ε)) 234 (4.1), 266 (4.4), 302 (3.2), 378 (2.9); MS (EI, 70 eV) *m/z* (relative intensity) 457 (31), 456 (15), 201 (10), 189 (12), 165 (9), 151 (15), 137 (25), 125 (30), 124 (69), 41 (100). Anal. Calcd for $C_{27}H_{41}CoO_2$ (456.22): C, 71.03; H, 9.05. Found: C, 71.03; H, 9.00.

{(1,2,12,13-η)-Tricyclo[11.9.0.0^{2,12}]docosa-1,12-diene-7,-18-dione}(η^5-cyclopentadienyl)cobalt (25). A solution of aluminum isopropylate (47.7 g, 234 mmol) and 16.0 g (35.1 mmol) of the mixed alcohols (**24**) in 1 L of toluene and 450 mL of acetone was refluxed for 20 h. The working up procedure was carried out as described for **18/19**. Column chromatography on silica gel with a mixture of cyclohexane and ether (1:1) as eluent yielded 13.1 g (83%) of dione **25** as a yellow solid: mp 116 °C; ^{1}H (300 MHz, $CDCl_3$) δ 4.55 (s, 5H), 2.47–2.60 (m, 4H), 2.28–2.42 (m, 4H), 1.97–2.18 (m, 8H), 1.39–1.78 (m, 16H); ^{13}C (75.47 MHz, $CDCl_3$) δ 214.2 (C), 79.9 (CH), 79.2 (C), 40.9 (CH_2), 27.8 (CH_2), 24.7 (CH_2), 23.4 (CH_2); IR ($CDCl_3$) 2930, 1700 (C=O), 1257; UV (pentane) (λ_{max}, nm (log ε)) 206 (4.2), 266 (4.4), 388 (2.7); MS (EI, 70 eV) *m/z* (relative intensity) 452 (15), 137 (32), 125 (48), 124 (100), 91 (54). Anal. Calcd for $C_{27}H_{37}CoO_2$ (452.23): C, 71.82; H, 8.04. Found: C, 71.76; H, 8.16.

{(1,2,12,13-η)-Tricyclo[11.9.0.0^{2,12}]docosa-1,12-diene-7,-18-dione bis(semicarbazone)}(η^5-cyclopentadienyl)cobalt (26). The semicarbazide acetate was prepared from 12.0 g (108 mmol) of semicarbazide hydrochloride and 11 g (130 mmol) of sodium acetate as described for **20**. A 13.1 g amount (29 mmol) of **25** was added, and the solution was heated under

(23) Gleiter, R.; Langer, H.; Nuber, B. Unpublished results.

reflux for 3 h. The progress of the reaction could be controlled by TLC. After the reaction was complete, the solvent was removed in vacuo. The precipitate was washed with water, then with saturated $NaHCO_3$ solution, again water, and finally with acetone. The reaction yielded 14.7 g (90%) of the isomeric mixture of the bis(semicarbazone)s **26** as a yellow solid. The isomers were used as mixture in the following step without further purification.

Bis(selenadiazole)s 27 and 28. A mixture of 14.7 g (26.0 mmol) of the isomeric bis(semicarbazone)s **26** and SeO_2 (10.0 g, 90.0 mmol) in 650 mL of concentrated acetic acid was heated 3 h to 40 °C. The procedure was carried out as described for **21/22** yielding 5.21 g (31.8%) of the isomeric mixture of **27** and **28** as a yellow solid: mp 161 °C (dec); ^1H (300 MHz, $CDCl_3$) δ 4.53 (s, 5H), 4.52 (s, 5H), 3.28–3.42 (m, 4H), 2.72–3.20 (m, 12H), 1.45–2.25 (m, 36H), 0.90–1.15 (m, 4H); ^{13}C (75.47 MHz, $CDCl_3$) δ 162.3 (C), 159.5 (C), 79.9 (C), 79.2 (CH), 79.1 (CH), 76.8 (C), 75.9 (C), 36.1 (CH_2), 35.4 (CH_2), 28.0 (CH_2), 27.9 (CH_2), 26.7 (CH_2), 26.6 (CH_2), 24.4 (CH_2), 24.3 (CH_2), 23.7 (CH_2), 23.5 (CH_2), 23.4 (CH_2); IR ($CDCl_3$) 2926, 2848, 2797, 1451, 1332, 1310, 1263, 806; UV (CH_2Cl_2) (λ_{max}, nm (log ϵ)) 238 (4.1), 266 (4.0), 294 (3.2). Anal. Calcd for $C_{27}H_{33}CoN_4Se_2$ (630.44): C, 51.44; H, 5.28; N, 8.89. Found: C, 51.53; H, 5.34; N, 8.01.

{(1,2,12,13-η)-Tricyclo[11.9.0.0^{2,12}]docosa-1,12-diene-6,-18-diyne}(η^5-cyclopentadienyl)cobalt (29) and {(1,2,12,-13-η)-Tricyclo[11.9.0.0^{2,12}]docosa-1,12-diene-6,17-diyne}-(η^5-cyclopentadienyl)cobalt (30). To a cold solution (−40 °C) of the mixture of **27** and **28** (5.10 g, 8.10 mmol) in 500 mL of THF was added dropwise 21 mmol BuLi (1.6 M solution in hexane) during 30 min. The color of the solution turns to red, and N_2 expels. The reaction was quenched with 10 mL of methanol and 10 mL of water. After the addition of 500 mL of ether and 100 mL of 10% H_2SO_4 the layers were separated and the organic layer was washed with half-concentrated sodium chloride solution. The organic layer was dried ($MgSO_4$), the solvent was removed in vacuo, and the residue was adsorbed on silica gel. Column chromatography on silica gel with CCl_4 as eluent yielded 2.68 g (75%) of the mixture of the two isomeric products as a yellow solid. All attempts to separate the two alkynes by chromatography or crystallization failed. The following physical data were obtained from the mixture of the alkynes: ^1H (300 MHz, $CDCl_3$) δ 4.615 (s, 5H), 4.612 (s, 5H), 1.98–2.32 (m, 32H), 1.41–1.88 (m, 24H); ^{13}C (75.47 MHz, C_6D_6) δ 83.0 (C), 81.0 (C), 80.9 (C), 79.9 (C), 79.7 (CH), 79.3 (C), 79.1 (C), 29.3 (CH_2), 29.2 (CH_2), 29.0 (CH_2), 28.8 (CH_2), 25.2 (CH_2), 25.1 (CH_2), 25.0 (CH_2), 24.95 (CH_2), 24.9 (CH_2), 24.8 (CH_2), 19.7 (CH_2), 19.5 (CH_2), 17.8 (CH_2); IR ($CDCl_3$) 2924, 2850, 1429, 802; UV (CH_2Cl_2) (λ_{max}, nm (log ϵ)) 266 (4.1), 286 (4.1), 376 (2.9); MS (EI, 70 eV) *m/z* (relative intensity) 416 (30), 165 (24), 141 (24), 125 (46), 124 (100). Anal. Calcd for $C_{27}H_{33}Co$ (416.49): C, 78.05; H, 7.76. Found: C, 77.78; H, 7.99.

{(1,2,10,11-η)-Tricyclo[9.7.0.0^{2,10}]octadeca-1,10-diene-6,-15-diol}(η^5-cyclopentadienyl)cobalt (32). A solution of CpCo(COD) (30.5 g, 132 mmol) in 200 mL of decalin was heated to 160 °C. During 13 d a solution of 29.5 g (214 mmol) of 5-cyclononynol (**31**) in 2000 mL of decalin was added. After the addition was completed, the heating was continued for another 30 h. The working up procedure was carried out as described for **17** yielding 14.4 g (34%) of the isomeric mixture of the alcohols (**32**) as a yellow solid. The isomeric alcohols could be separated by column chromatography (silica gel/ether), but usually the isomeric mixture was used for further reactions.

{(1,2,10,11-η)-Tricyclo[9.7.0.0^{2,10}]octadeca-1,10-diene-6-*cis*,15-*cis*-diol}(η^5-cyclopentadienyl)cobalt (32a) (cis/trans defines the relative orientation to the CpCo unit): mp 194–204 °C; ^1H NMR (300 MHz, $CDCl_3$) δ 4.54 (s, 5H), 3.85 (m, 2H), 2.04–2.19 (m, 8H), 1.70–1.77 (m, 8H), 1.20–1.50 (m, 10H); ^{13}C NMR (50.3 MHz, CD_3OD) δ 80.5 (CH), 80.0 (C), 68.3 (CH), 34.1 (CH_2), 25.4 (CH_2), 25.2 (CH_2); IR ($CDCl_3$) 3398, 2916, 2844, 1452, 1035, 899, 795; UV (CH_2Cl_2) (λ_{max}, nm (log ϵ)) 198 (4.09), 269 (4.17), 296 (3.00), 370 (2.62); MS (EI, 70 eV) *m/z* (relative intensity) 400 (40), 137 (28), 124 (70), 121 (66), 107 (23), 105 (39), 91 (100), 79 (99), 67 (95), 59 (59), 55 (83), 41 (87). Found: C, 68.81; H, 8.68.

{(1,2,10,11-η)-Tricyclo[9.7.0.0^{2,10}]octadeca-1,10-diene-6-*trans*,15-*cis*-diol}(η^5-cyclopentadienyl)cobalt (32b): mp 193–197 °C; ^1H NMR (300 MHz, CD_3OD) δ 4.51 (s, 5H), 3.50–3.70 (m, 2H), 2.14–2.22 (m, 8H), 1.75–1.81 (m, 8H), 1.28–1.52 (m, 10H); ^{13}C NMR (75.47 MHz, $CDCl_3$) δ 80.9 (C), 80.7 (CH), 79.7 (C), 72.7 (CH), 68.3 (CH), 36.9 (CH_2), 34.2 (CH_2), 28.1 (CH_2), 25.6 (CH_2), 25.4 (CH_2), 25.3 (CH_2); IR ($CDCl_3$) 3370, 2920, 2848, 1445, 1034, 798; UV (CH_2Cl_2) (λ_{max}, nm (log ϵ)) 195 (4.14), 262 (4.30), 296 (3.17), 373 (2.64); MS (EI, 70 eV) in analogy to those obtained from **32a**. Anal. Calcd for $C_{23}H_{33}CoO_2$ (400.4): C, 68.99; H, 8.31. Found: 68.31; H, 8.27.

{(1,2,10,11-η)-Tricyclo[9.7.0.0^{2,10}]octadeca-1,10-diene-6-*trans*,15-*trans*-diol}(η^5-cyclopentadienyl)cobalt (32c): mp 175–184 °C; ^1H NMR (200 MHz, CD_3OD) δ 4.49 (s, 5H), 3.80–3.97 (m, 2H), 3.58 (m, 2H), 2.07–2.24 (m, 8H), 1.30–1.80 (m, 16H); ^{13}C NMR (50.3 MHz, CD_3OD) δ 80.7 (CH), 80.3 (C), 72.0 (CH), 38.8 (CH_2), 28.0 (CH_2), 25.8 (CH_2); IR ($CDCl_3$) 3376, 2916, 2848, 1450, 1103, 1062; UV (CH_2Cl_2) (λ_{max}, nm (log ϵ)) 195 (4.14), 262 (4.29), 296 (3.02), 372 (2.67); MS (EI, 70 eV) in analogy to those obtained from **32a**.

{(1,2,10,11-η)-Tricyclo[9.7.0.0^{2,10}]octadeca-1,10-diene-6,-15-dione}(η^5-cyclopentadienyl)cobalt (33). A solution of aluminum isopropylate (46.2 g, 227 mmol) and 14.0 g (35.1 mmol) of the mixed alcohols **32** in 650 mL of toluene and 320 mL of acetone was refluxed for 20 h. The following procedure was carried out as described for **18/19**. Column chromatography on silica gel with a mixture of cyclohexane and ether (1:1) as eluent yielded 9.7 g (71%) of dione **33** as yellow solid: mp 144–145 °C; ^1H NMR (300 MHz, $CDCl_3$) δ 4.47 (s, 5H), 2.62–2.71 (m, 4H), 2.22–2.36 (m, 8H), 1.76–2.04 (m, 12H); ^{13}C NMR (75.46 MHz, $CDCl_3$) δ 214.1 (C) 79.7 (CH), 79.2 (C), 42.1 (CH_2), 25.4 (CH_2), 24.9 (CH_2); IR ($CDCl_3$) 2932, 1700, 1439, 1100, 999, 787; UV (CH_2Cl_2) (λ_{max}, nm (log ϵ)) 227 (4.31), 278 (3.87), 325 (3.37), 395 (2.94); MS (EI, 70 eV) *m/z* (relative intensity) 396 (100), 330 (30), 137 (28), 124 (68), 91 (36), 59 (32). Anal. Calcd for $C_{23}H_{31}CoO_2$ (396.4): C, 69.69; H, 7.37. Found: C, 69.63; H, 7.34.

{(1,2,10,11-η)-Tricyclo[9.7.0.0^{2,10}]octadeca-1,10-diene-6,-15-dione bis(semicarbazone)}(η^5-cyclopentadienyl)cobalt (34). The semicarbazide acetate was prepared from 22.3 g (200 mmol) of semicarbazide hydrochloride and 14.2 g (210 mmol) of sodium acetate as described for **20**. A 4.0 g amount (10.4mmol) of **33** was added, and the solution was heated under reflux for 4 d. The progress of the reaction could be controlled by TLC. After the reaction was complete, the solvent was removed in vacuo. The precipitate was washed with water, then with saturated $NaHCO_3$ solution, again with water, and finally with acetone. The reaction yielded 4.54 g (88%) of the isomeric mixture of the bis(semicarbazone)s **34** as a yellow solid. The isomers were used as a mixture in the following step without further purification.

Bis(selenadiazole) 35. A mixture of the isomeric bis(semicarbazone)s **34** (2.20 g, 4.30 mmol) and 1.30 g (12.3 mmol) in 100 mL of concentrated acetic acid was heated 1 h at 70 °C. The working up procedure was carried out as described for **21/22** yielding 503 mg (20%) of **35** as a yellow solid: mp 176 °C (dec); ^1H NMR (300 MHz, $CDCl_3$) δ 4.47 (s, 5H), 3.05–3.53 (m, 4H), 1.25–2.98 (m, 16H); ^{13}C NMR (75.47 MHz, $CDCl_3$) δ 160.3 (C), 158.5 (C), 79.7 (CH), 78.0 (C), 76.4 (CH), 29.9 (CH_2), 29.2 (CH_2), 26.7 (CH_2), 25.0 (CH_2), 22.8 (CH_2); IR (neat) 2910, 2838, 1444, 1344, 1312, 1263, 855, 816, 809; UV (CH_2Cl_2) λ_{max}, nm (log ϵ) 226 (4.0), 238 (4.0), 266 (4.0), 300 (3.3), 376 (2.4); MS (EI, 70 eV): 360 (29, $M^+ - N_4Se_2$), 164 (18), 153 (15), 152 (15), 128 (23), 124 (71), 115 (42), 84 (55), 59 (100). Anal. Calcd for $C_{27}H_{41}CoN_4Se_2$ (630.44): C, 48.10; H, 4.39; N, 9.76. Found: C, 47.89; H, 4.46; N, 9.53.

{(1,2,10,11-η)-Tricyclo[9.7.0.0^{2,10}]octadeca-1,10-diene-6,-15-diyne}(η^5-cyclopentadienyl)cobalt (36). To a cold solution (−55 °C) of 350 mg (0.61 mmol) of **35** in 65 mL of THF was added dropwise 1.3 mmol BuLi (1.6 M solution in hexane) during 7 min. The color of the solution turns to red, and N_2 expels. The reaction was quenched by 5 mL of methanol and 5 mL of water. The working up procedure was carried out as described for **23** yielding 161 mg (73%) of **36** as a yellow solid: mp 155 °C; ^{1}H NMR (300 MHz, $CDCl_3$) δ 4.55 (s, 5H), 1.37−3.25 (m, 20H); ^{13}C NMR (75.47 MHz, $CDCl_3$) δ 86.1 (C), 85.5 (C), 83.6 (C), 79.8 (CH), 78.7 (C), 30.9 (CH_2), 28.3 (CH_2), 26.1 (CH_2), 19.9 (CH_2), 19.4 (CH_2); IR ($CDCl_3$) 2922, 2844, 1433, 1312, 1259, 1014, 807; UV (pentane) λ_{max}, nm (log ε) 266 (4.3), 296 (3.1), 376 (2.6); MS (EI, 70 eV) 360 (100), 259 (9), 233 (16), 231 (14), 207 (9), 193 (10), 124 (24); HRMS (EI, 70 eV) calcd for $C_{23}H_{25}Co$, *m/z* 360.1289, found *m/z* 360.1342.

{η^4:η^4-[3$_4$]Cyclobutadienophane}bis(η^5-cyclopentadienyl)cobalt (2) and Cyclobutadienoquinonosuperphane (4). In 80 mL of octane was dissolved 180 mg (1.0 mmol) of $CpCo(CO)_2$, and while refluxing, the solution of **23** (195 mg, 0.5 mmol) in 25 mL of octane was added during 90 min. A few minutes after the addition was finished, no starting material (**23**) could be detected anymore by TLC. After the reaction mixture had cooled to rt it was concentrated in vacuo and adsorbed on alumina (neutral, grade III). The products were purified by column chromatography (alumina neutral, grade III). With pentane as eluent 205 mg (80%) of **2** is obtained as an orange red solid. After **2** is extracted completely the eluent was changed to CH_2Cl_2 and 3 mg (1%) of **4** was extracted. The analytical data for **2** and **4** are identical with those described in the literature.[5,6]

{η^4:η^4-[3$_4$]Cyclobutadienophane}(η^5-cyclopentadienyl)-(η^5-pentamethylcyclopentadienyl)cobalt (39). In 100 mL of decalin were dissolved 195 mg (0.4 mmol) of **23** and 250 mg (1 mmol) of $Cp^*Co(CO)_2$, and the solution was heated at 150−160 °C. The reaction was stopped after 24 h, and the mixture was allowed to cool to ambient temperature, concentrated in vacuo, adsorbed on alumina (neutral, grade III), and chromatographed (alumina neutral, grade III/pentane). The column chromatography was repeated, and after recrystallization from pentane 245 mg (84%) of **39** is obtained as a red solid: mp > 300 °C; ^{1}H (300 MHz, $CDCl_3$) δ 4.56 (s, 5H), 2.21−2.25 (m, 8H), 1.80−1.84 (m, 8H), 1.76 (15H), 1.52−1.61 (m, 8H); ^{13}C (75.47 MHz, $CDCl_3$) δ 87.0 (C), 80.3 (CH), 78.5 (C), 74.0 (C), 28.0 (CH_2), 26.9 (CH_2), 25.0 (CH_2), 9.5 (CH_3); IR (KBr) 2922, 2886, 1443, 1376, 1342, 994, 549, 495; UV (hexane) (λ_{max}, nm (log ε)) 205 (3.75), 243 (3.35), 399 (4.05); MS (EI, 70 eV) *m/z* (relative intensity) 582 (10), 457 (27), 291 (22), 259 (100), 133 (34), 124 (25), 59 (32). Anal. Calcd for $C_{35}H_{44}Co_2$ (582.60): C, 72.16; H, 7.61. Found: C, 72.36; H, 7.57.

{η^4:η^4-[3$_4$]Cyclobutadienophane}(η^5-cyclopentadienyl)cobalt (Iron tricarbonyl) (40). In 200 mL of toluene were dissolved 195 mg (0.5 mmol) of **23** and 117 mg (0.6 mmol) of $Fe(CO)_5$, and the solution was refluxed. After 5 h once again 117 mg of $Fe(CO)_5$ was added, and the heating was continued. After 12 h **23** could not be detected anymore by TLC. The reaction mixture was allowed to cool to ambient temperature. It was concentrated in vacuo, adsorbed on silica gel and chromatographed (silica gel/pentane). The column chromatography was repeated, and after recrystallization from pentane 22 mg (8.3%) of **40** was obtained as a yellow solid: mp > 300 °C; ^{1}H NMR (300 MHz, C_6D_6) δ 4.46 (s 5H), 2.05−2.13 (m, 16H), 1.33−1.43 (m, 8H); ^{13}C (75.47 MHz, C_6D_6) δ 217.4 (C), 87.3 (C), 80.5 (CH), 78.7 (C), 28.1 (CH_2), 26.3 (CH_2), 25.6 (CH_2); IR (C_6D_6) 2936, 2894, 2006, 1944, 1429, 1349, 1248, 1103, 1070, 736, 702, 605; UV (pentane) (λ_{max}, nm (log ε)) 202 (4.62), 240 (4.22), 288 (4.61); HRMS (EI, 70 eV) calcd for $C_{28}H_{29}CoFeO_3$ *m/z* 528.0798, found *m/z* 528.0780.

Cyclobutadienoarenophane (41). In 200 mL of toluene were dissolved 388 mg (1.0 mmol) of **23**, 20 mg of $CpCo(CO)_2$, and 2.84 g (20 mmol) of dimethyl acetylenedicarboxylate (DMAD), and the solution was refluxed. During the reaction some $CpCo(CO)_2$ was added because the trimerization catalyst reacts partially with **23** to yield **2**. After 24 h **23** could not be detected anymore by TLC and the reaction was stopped. The reaction mixture was concentrated in vacuo, adsorbed on silica gel, and twice chromatographed (silica gel/pentane:ether = 1:1) to yield **41** as a yellow oil that solidified when pentane was added. In this way 26 mg (5%) of **41** were obtained as a yellow solid: mp 175−179 °C; ^{1}H (300 MHz, C_6D_6) δ 4.38 (s, 5H), 3.50 (s, 6H), 3.06−3.19 (m, 2H), 2.79−2.88 (m, 2H), 2.52−2.62 (m, 2H), 2.26−2.43 (m, 4H), 2.06−2.11 (m, 4H), 1.66−1.99 (m, 10H); ^{13}C (75.47 MHz, C_6D_6) δ 169.6 (C), 141.2 (C), 135.6 (C), 130.2 (C), 80.5 (CH), 80.4 (C), 77.8 (C), 51.8 (CH_3), 27.8 (CH_2), 26.8 (CH_2), 26.2 (CH_2), 24.9 (CH_2), 23.4 (CH_2), 22.1 (CH_2); IR ($CDCl_3$) 2928, 2848, 1737, 1707, 1432, 1266, 1220, 1195, 1177; UV (CH_3CN) (λ_{max}, nm (log ε)) 196 (4.15), 266 (4.06), 294 (3.25); HRMS (EI, 70 eV) calcd for $C_{31}H_{35}CoO_4$ *m/z* 530.1867, found *m/z* 530.1913.

{η^4:η^4-[4,4,3,3]Cyclobutadienophane}bis[(η^5-cyclopentadienyl)cobalt (42), {(7,8,18,19-η)-Hexacyclo[17.3.0.0^{1,13}.0^{2,6}.0^{2,12}.0^{7,18}]docosa-6,12,18-triene}(η^5-cyclopentadienyl)cobalt (43) and {(6,7,18,19-η)-Hexacyclo[17.3.0.0^{1,13}.0^{2,7}.0^{2,12}.0^{8,18}]docosa-7,12,18-triene}(η^5-cyclopentadienyl)cobalt (44). The solution of 1.01 g (2.42 mmol) of the mixture of the alkadiynes **29/30** and 1.80 g (10 mmol) of $CpCo(CO_2)$ in 250 mL of cyclooctane was heated under reflux for 5 h. The solvent was removed in vacuo, and the residue was adsorbed on alumina (neutral, 10% water). Column chromatography on alumina (neutral, 10% water) with 40/65 petroleum ether yielded first the two bicyclooctatrienes **43** and **44** in a red brown band, which was followed by the yellow band of the cyclobutadienophane **42**. The removal of the solvent yielded 332 mg (26%) of **42** as an yellow solid and 260 mg (26%) of a mixture of **43** and **44** as a yellow red solid. The separation of the two isomeric bicyclooctatriene derivatives failed with the exception of the isolation of one single crystal of **44**. Analytical data for **42**: mp > 250 °C; ^{1}H (200 MHz, $CDCl_3$) δ 4.37 (s, 10H), 2.15−2.51 (m, 16H), 1.57−1.75 (m, 4H), 1.45−1.55 (m, 8H); ^{13}C (75.47 MHz, C_6D_6) δ 81.7 (C), 81.0 (CH), 80.8 (C), 29.5 (CH_2), 28.7 (CH_2), 28.6 (CH_2), 26.9 (CH_2); IR ($CDCl_3$) 2916, 2886, 2826, 1503, 1262; UV (pentane) (λ_{max}, nm (log ε)) 222 (4.3), 284 (4.7), 382 (4.0); MS (EI, 70 eV) *m/z* (relative intensity) 540 (19), 416 (13), 415 (27), 189 (40), 125 (49), 124 (100). Anal. Calcd for $C_{32}H_{38}Co_2$ (540.51): C, 71.12; H, 7.09. Found: C, 70.97; H, 7.11. Analytical data for the mixture of **43** and **44**: mp 220 °C; ^{1}H (300 MHz, $CDCl_3$) δ 4.43 (s, 5H), 4.32 (s, 5H), 2.73−2.81 (m, 8H), 1.22−2.30 (m, 48H); ^{13}C (75.47 MHz, C_6D_6) δ 1.54.4 (C), 154.0 (C), 90.2 (C), 87.5 (C), 86.0 (C), 83.3 (CH), 81.9 (CH), 66.8 (C), 66.0 (C), 38.0 (CH_2), 35.9 (CH_2), 35.5 (CH_2), 35.3 (CH_2), 31.0 (CH_2), 30.2 (CH_2), 29.2 (CH_2), 28.8 (CH_2), 28.5 (CH_2), 28.3 (CH_2), 26.7 (CH_2), 26.6 (CH_2), 26.3 (CH_2), 25.9 (CH_2), 25.8 (CH_2), 25.3 (CH_2), 25.2 (CH_2), 24.4 (CH_2); IR ($CDCl_3$) 2930, 2916, 2880, 2846, 1441, 807; UV (pentane) (λ_{max}, nm (log ε)) 228 (4.35), 290 (4.0), 396 (2.95). Anal. Calcd for $C_{27}H_{33}Co$ (416.49): C, 78.05; H, 7.76. Found: C, 77.94; H, 7.90.

X-ray Crystallography and Structure Solution. Data were collected on a Syntex R3 (**23**, **36**, and **44**) or a Siemens Stoe AEDII diffractometer (**40**) at room temperature. Relevant crystal and data collection parameters are given in Table 1. The structures were solved by using standard Patterson methods, least-squares refinement, and Fourier techniques. All calculations were performed with the SHELXTL PLUS program.[24]

$C_{25}H_{29}Co$ (23). A yellow crystal of the dimensions of 0.3 × 0.5 × 0.5 mm^3 was obtained from pentane at −8 °C. The unit cell was determined and refined from 25 reflections (16.0 < 2θ < 29.0°).

$C_{23}H_{25}Co$ (36). A yellow crystal of the dimensions of 0.08 × 0.25 × 0.30 mm^3 was obtained from pentane at −30 °C. The

(24) SHELXTL PLUS (release 3.4), Siemens Analytical X-Ray Instruments, 1989.

unit cell was determined and refined from 24 reflections ($5.0 < 2\theta < 16.0°$).

$C_{28}H_{29}CoFeO_3$ (40). A yellow crystal of the dimensions of $0.16 \times 0.76 \times 0.76$ mm^3 was obtained from pentane at −8 °C. The unit cell was determined and refined from 27 reflections ($8.0 < 2\theta < 27.0°$).

$C_{27}H_{33}Co$ (44). A brown-red crystal of the dimensions of $0.15 \times 0.30 \times 0.90$ mm^3 was obtained from pentane at 20 °C. The unit cell was determined and refined from 25 reflections ($5.0 < 2\theta < 24.0°$).

Acknowledgment. We are grateful to the Deutsche Forschungsgemeinschaft (SFB 247), the Fonds der Chemischen Industrie, and the BASF Aktiengesellschaft for financial support.

Supplementary Material Available: Tables S1–S12, listing the distances, angles, and anisotropic thermal parameters for non-hydrogen atoms (17 pages). Ordering information is given on any current masthead page.

OM940759H

Ab Initio MO Calculations of NMR Spin–Spin Coupling Constants in Methyllithium, *tert*-Butyllithium, and Methyllithium Oligomers

Terutake Koizumi and Osamu Kikuchi*

Department of Chemistry, University of Tsukuba, Tsukuba 305, Japan

Received April 25, 1994®

Ab initio calculations of NMR spin–spin coupling constants in monomeric methyllithium, *tert*-butyllithium and methyllithium oligomers were performed by using a self-consistent perturbation theory to examine their molecular structures and the bonding character of the C–Li bond. The calculated $^1J_{CLi}$ values in monomeric methyllithium and *tert*-butyllithium are largely influenced by solvation, and the $^1J_{CLi}$ value in *tert*-butyllithium agrees well with the experimental value when *tert*-butyllithium is coordinated by three ligands. The calculated $^1J_{CLi}$ and $^1J_{CH}$ values in methyllithium oligomers depend on the number of the lithium atoms bonded directly to the carbon atom, and a tetrahedral structure is suggested for the tetramer. Modeling the ionic C–Li bond by using the truncated lithium basis set gives coupling constants which are in good agreement with the experimental ones and suggests the importance of the ionic character of the C–Li bond for alkyllithiums.

Introduction

The molecular and electronic structures of organolithium compounds have been studied extensively.[1–4] Methyllithium, the simplest alkyllithium, was studied by X-ray,[5] NMR spectroscopy,[6] and neutron diffraction[7] and was found to be a tetrahedral (T_d structure) tetramer. Many theoretical investigations have been carried out for methyllithium[8,9] and its oligomers.[10,11] Most of these investigations concerned the structural and energetic relationships obtained from the several levels of molecular orbital calculations.[8,10]

NMR spectroscopy has primarily been applied for structural analyses of organolithium compounds in solution.[2,6,12] The one-bond $^{13}C-^7Li$ coupling constant $^1J_{CLi}$ provides experimental evidence regarding the aggregation state and the nature of the C–Li bond in an organolithium compound.[2b–m,6,12,13] $^1J_{CLi}$ in the methyllithium tetramer (T_d structure) was reported to be 14.5 Hz by McKeever et al.[6a,b] Although there has been no study of monomeric methyllithium by NMR spectroscopy, Clark et al.[9] anticipated that $^1J_{CLi}$ in monomeric methyllithium is over 200 Hz and the C–Li bond is predominantly covalent from their calculations of the coupling constants by using the finite perturba-

® Abstract published in *Advance ACS Abstracts,* December 15, 1994.

(1) Brown, T. L. *Adv. Organomet. Chem.* **1965**, *3*, 365. Wardell, J. L. In *Comprehensive Organometallic Chemistry*; Wilkinson, G., Stone, F. G. A., Abel, E. W., Eds.; Pergamon Press: Oxford, England, 1982; Vol. 1, p 43. Young, R. N.; Quirk, R. P.; Fetters, L. J. *Advances in Polymer Science*; Springer-Verlag: Berlin, 1984; Vol. 56, p 1. Williard, P. G. In *Comprehensive Organic Synthesis*; Trost, B. M., Fleming, I., Schreiber, S. L., Eds.; Pergamon Press: Oxford, England, 1991; Vol. 1, p 1.

(2) (a) O'Brien, D. H. In *Comprehensive Carbanion Chemistry*; Buncel, E., Durst, T., Eds.; Elsevier: Amsterdam, 1980; Part A, p 271. (b) Fraenkel, G.; Henrichs, M.; Hewitt, J. M.; Su, B. M.; Geckle, M. J. *J. Am. Chem. Soc.* **1980**, *102*, 3345. (c) Seebach, D.; Siegel, H.; Gabriel, J.; Hässig, R. *Helv. Chim. Acta* **1980**, *63*, 2046. (d) Seebach, D.; Hässig, R.; Gabriel, J. *Helv. Chim. Acta* **1983**, *66*, 308. (e) Seebach, D.; Gabriel, J.; Hässig, R. *Helv. Chim. Acta* **1984**, *67*, 1083. (f) McGarrity, J. F.; Ogle, C. A. *J. Am. Chem. Soc.* **1985**, *107*, 1805. (g) McGarrity, J. F.; Ogle, C. A.; Brich, Z.; Loosil, H. R. *J. Am. Chem. Soc.* **1985**, *107*, 1810. (h) Thomas, R. D.; Clarke, M. T.; Jensen, R. M.; Young, T. C. *Organometallics* **1986**, *5*, 1851. (i) Thomas, R. D.; Jensen, R. M.; Young, T. C. *Organometallics* **1987**, *6*, 565. (j) Günther, H.; Moskau, D.; Bast, P.; Schmalz, D. *Angew. Chem., Int. Ed. Engl.* **1987**, *26*, 1212. (k) Bauer, W.; Schleyer, P. v. R. In *Advances in Carbanion Chemistry*; Snieckus, V.; Ed.; JAI Press: Greenwich, CT, 1992; Vol. 1, p 89. (l) Bauer, W.; Griesinger, C. *J. Am. Chem. Soc.* **1993**, *115*, 10871. (m) Bergander, K.; He, R.; Chandrakumer, N.; Eppers, O.; Günther, H. *Tetrahedron* **1994**, *50*, 5861.

(3) Setzer, W. N.; Schleyer, P. v. R. *Adv. Organomet. Chem.* **1985**, *24*, 353. Kottke, T.; Stalke, D. *Angew. Chem., Int. Ed. Engl.* **1993**, *32*, 580. Weiss, E. *Angew. Chem., Int. Ed. Engl.* **1993**, *32*, 1501.

(4) Bühl, M.; van Eikema Hommes, N. J. R.; Schleyer, P. v. R.; Fleischer, U.; Kutzelnigg, W. *J. Am. Chem. Soc.* **1991**, *113*, 2459. Hoffmann, D.; Bauer, W.; Hampel, F.; Hommes, N. J. R. v. E.; Schleyer, P. v. R.; Otto, P.; Pieper, U.; Stalke, D.; Wright, D. S.; Snaith, R. *J. Am. Chem. Soc.* **1994**, *116*, 528.

(5) (a) Weiss, E.; Henchen, G. *J. Organomet. Chem.* **1969**, *21*, 265. (b) Köster, H.; Thoennes, D.; Weiss, E. *J. Organomet. Chem.* **1978**, *160*, 1.

(6) (a) McKeever, L. D.; Waack, R.; Doran, M. A.; Baker, E. B. *J. Am. Chem. Soc.* **1968**, *90*, 3244. (b) McKeever, L. D.; Waack, R.; Doran, M. A.; Baker, E. B. *J. Am. Chem. Soc.* **1969**, *91*, 1057. (c) McFarlane, W.; Rycroft, D. S. *J. Organomet. Chem.* **1974**, *64*, 303. (d) Eppers, O.; Günther, H. *Helv. Chim. Acta* **1990**, *73*, 2071.

(7) Weiss, E.; Lambertsen, T.; Schubert, B.; Cockcroft, J. K.; Wiedenmann, A. *Chem. Ber.* **1990**, *123*, 79.

(8) (a) Fitzpatrick, N. J. *Inorg. Nucl. Chem. Lett.* **1974**, *10*, 263. (b) Hinchliffe, A.; Saunders, E. *J. Mol. Struct.* **1976**, *31*, 283. (c) Streitwieser, A., Jr.; Williams, J. E., Jr.; Alexandratos, S.; McKelvey, J. M. *J. Am. Chem. Soc.* **1976**, *98*, 4778. (d) Collins, J. B.; Streitwieser, A., Jr. *J. Comput. Chem.* **1980**, *1*, 81. (e) Graham, G. D.; Marynick, D. S.; Lipscomb, W. N. *J. Am. Chem. Soc.* **1980**, *102*, 4572. (f) Ritchie, J. P.; Bachrach, S. M. *J. Am. Chem. Soc.* **1987**, *109*, 5909. (g) Penotti, F. E. G.; Gerratt, J.; Cooper, D. L.; Raimondi, M. *J. Chem. Soc., Faraday Trans. 2* **1989**, *85*, 151. (h) Wiberg, K. B.; Breneman, C. M. *J. Am. Chem. Soc.* **1990**, *112*, 8765. (i) Dixon, R. E.; Streitwieser, A., Jr.; Laidig, K. E.; Bader, R. F. W.; Harder, S. *J. Phys. Chem.* **1993**, *97*, 3728.

(9) Clark, T.; Chandrasekhar, J.; Schleyer, P. v. R. *J. Chem. Soc., Chem. Commun.* **1980**, 672.

(10) Guest, M. F.; Hillier, I. H.; Saunders, V. R. *J. Organomet. Chem.* **1972**, *44*, 59. Baird, N. C.; Barr, R. F.; Datta, R. K. *J. Organomet. Chem.* **1973**, *59*, 65. Clark, T.; Schleyer, P. v. R. *J. Chem. Soc., Chem. Commun.* **1978**, 137. Graham, G.; Richtsmeier, S.; Dixon, D. A. *J. Am. Chem. Soc.* **1980**, *102*, 5759. Herzig, L.; Howell, J. M.; Sapse, A. M.; Singman, E.; Snyder, G. *J. Chem. Phys.* **1982**, *77*, 429. Kaufmann, E.; Raghavachari, K.; Reed, A. E.; Schleyer, P. v. R. *Organometallics* **1988**, *7*, 1597.

(11) Streitwieser, A., Jr. *J. Organomet. Chem.* **1978**, *156*, 1.

(12) Bauer, W.; Winchester, W. R.; Schleyer, P. v. R. *Organometallics* **1987**, *6*, 2371.

(13) For the C–Li coupling constant, $^1J(^{13}C-^7Li)$ values are referred to in this paper to compare the calculated values with the previous calculations.[9] The conversion to $^1J(^{13}C-^6Li)$ is carried out using the relation $^1J(^{13}C-^7Li) = (\gamma(^7Li)/\gamma(^6Li))^1J(^{13}C-^6Li) = 2.641(^1J(^{13}C-^6Li))$.[2c,d,k,12]

0276-7333/95/2314-0987$09.00/0

Table 1. Symmetry-Restricted Energy-Optimized Structures[a] and Calculated Coupling Constants[b] for Methyllithium Monomers

	r(C−Li)	r(C−H)	∠(HCH)	$^1J(^{13}C-^7Li)$	$^1J(^{13}C-^1H)$	ref
unsolvated	2.047	1.102	107.3	128.3	131.0	this work
	2.001	1.094		115.9	63.6	*c,d*
	2.009	1.083		115.9	63.4	*c,e*
	1.821	1.117		116.1	57.0	*c,f*
solvated with NH_3 (**1**)	2.079	1.103	107.1	74.4	125.0	this work
	2.021	1.084		127	65.6	*c,e*
	1.847	1.117		118.9	60.1	*c,f*
solvated with $3NH_3$ (**2**)	2.183	1.111	105.6	37.0	108.5	this work
solvated with $3H_2O$ (**3**)	2.184	1.110	105.6	43.3	110.2	this work
truncated basis set	1.930	1.108	104.6	44.0	101.2	this work

[a] Bond lengths are in Å and angles are in degrees. All structures are optimized under the restriction of a C_{3v} symmetry. [b] Values are in Hz. [c] Reference 9; coupling constants were calculated by the FPT-INDO method. [d] Geometries were optimized by the 6-31G* basis set. [e] Geometries were optimized by the STO-3G basis set. [f] Geometries were optimized by the MNDO method.

tion theory within the INDO approximation (FPT-INDO). On the other hand, Bauer et al.[12] reported that $^1J_{CLi}$ in monomeric *tert*-butyllithium in THF is 31.5 Hz from an NMR study, suggesting that $^1J_{CLi}$ in monomeric methyllithium is much smaller than 200 Hz. Furthermore, Bauer et al.[2k,12] reported that $^1J_{CLi}$ in the organolithium compounds is not influenced by the structure of the lithiated carbon atoms but depends only on the state of aggregation, that is, the number of lithium atoms bonded directly to the carbon atoms. These results contradict the prediction given by Clark et al.,[9] and theoretical efforts are required to evaluate the NMR spin−spin coupling constants correctly for the analysis of the structures of alkyllithiums.

In this paper, we provide our results of ab initio calculations of methyllithium and its oligomers and present their structures and NMR spin−spin coupling constants. In addition, we will clarify the relation of the $^1J_{CLi}$ values to the molecular structures and to the nature of the C−Li bonds.

Calculation

Ab initio calculations were performed with the MIDI-4 basis set.[14] For lithium, the Li(421/1) basis set, which includes the additional p-type polarization functions, was used. The geometries were optimized under the restriction of a given symmetry for each structure.

The X-ray structures of benzyllithium depend on the ligands included.[15] Brooks et al.[16] pointed out that the overlap between the vacant lithium 2p orbital and the carbon π orbitals stabilizes the η^3 form.[15a] This idea was applied to the structural analyses of other organolithium compounds.[16,17] On the other hand, Sygula and Rabideau[18] showed that the η^1 form[15c] is the most stable when the truncated basis set for lithium is used to model the purely ionic C−Li bond. Taking these results into account, the truncated MIDI-4 basis set for lithium, Li(31), which includes only the 1s function and corresponds to the lithium cation,[14d] was also used to examine the nature of the C−Li bond for methyllithiums.

NMR spin−spin coupling constants were calculated by using self-consistent perturbation theory,[19] in which only the Fermi contact term was taken into account as the perturbation. The following formula[19,20] was used to calculate the coupling constant between the nuclei A and B:

$$J_{AB} = \left(\frac{16h\gamma_A\gamma_B\beta^2}{9}\right)\sum_{\lambda\sigma}^{\text{allAO}} \chi_\lambda(R_A)\chi_\sigma{}^*(R_A)\varrho_{\lambda\sigma}^{(1)} \qquad (1)$$

where γ_A is the magnetogyric ratio of the nucleus A. $\chi_\lambda(R_A)$ represents the function value of the atomic orbital λ evaluated at the nucleus *A*. $\varrho_{\lambda\sigma}^{(1)}$ is the first-order spin-density matrix given by[19]

$$\varrho_{\lambda\sigma}^{(1)} = 2\sum_{j}^{\alpha\text{occ}}(C_{\lambda j}^{(1)\alpha *}C_{\sigma j}^{(0)} + C_{\lambda j}^{(0)*}C_{\sigma j}^{(1)\alpha}) \qquad (2)$$

where $C_{\lambda j}^{(1)\alpha}$ values are the coefficients of the first-order α-spin molecular orbitals perturbed by the Fermi contact interaction on the nucleus B. $C_{\lambda j}^{(0)}$ values are the zeroth-order coefficients. $C_{\lambda j}^{(1)\alpha}$ values were calculated by the procedure given by Ditchfield and Synder.[19] The theory was incorporated into the ABINIT88 program written by our group.[21] All calculations were carried out on HP-730 workstations.

Results and Discussion

Monomeric Methyllithium and *tert*-Butyllithium. The optimized geometries and calculated coupling constants for the methyllithium monomer are shown in Table 1 along with those reported by Clark et al.[9] When solvation is not taken into account, the calculated $^1J_{CLi}$ value, 128.3 Hz, is similar to those obtained by the FPT-INDO calculations, *ca.* 116 Hz.[9] However, the $^1J_{CLi}$ value is reduced remarkably to 74.4 Hz when one NH_3 molecule is coordinated to the Li atom (**1**) in order to examine the effect of solvation. This solvation effect was not recognized by the semiempirical FPT-INDO calculations.[9]

X-ray crystal-structure analyses revealed that the geometry about the lithium atom is nearly tetrahedral in monomeric alkyllithiums, such as (bis(trimethylsilyl)-

(14) (a) Tatewaki, H.; Huzinaga, S. *J. Comput. Chem.* **1980**, *1*, 205. (b) Sakai, Y.; Tatewaki, H.; Huzinaga, S. *J. Comput. Chem.* **1981**, *2*, 100. (c) Sakai, Y.; Tatewaki, H.; Huzinaga, S. *J. Comput. Chem.* **1981**, *2*, 108. (d) Huzinaga, S. *Gaussian Basis Sets for Molecular Calculation*; Elsevier: Amsterdam, 1984.

(15) (a) Patterman, S. P.; Karle, I. L.; Stucky, G. D. *J. Am. Chem. Soc.* **1970**, *92*, 1150. (b) Beno, M. A.; Hope, H.; Olmstead, M. M.; Power, P. P. *Organometallics* **1985**, *4*, 2117. (c) Zarges, W.; Marsch, M.; Harms, K.; Boche, G. *Chem. Ber.* **1989**, *122*, 2303.

(16) Brooks, J. J.; Rhine, W.; Stuky, G. D. *J. Am. Chem. Soc.* **1972**, *94*, 7339.

(17) Bushby, R. J.; Patterson, A. S. *J. Organomet. Chem.* **1977**, *132*, 163. Kos, A. J.; Jemmis, E. D.; Schleyer, P. v. R.; Gleiter, R.; Fischbach, U.; Pople, J. A. *J. Am. Chem. Soc.* **1980**, *103*, 4996. Bushby, R. J.; Tytko, M. P. *J. Organomet. Chem.* **1984**, *270*, 265. Kos, A. J.; Stein, P.; Schleyer, P. v. R. *J. Organomet. Chem.* **1985**, *280*, C1. Groventein, E., Jr. In *Comprehensive Carbanion Chemistry*; Buncel, E., Durst, T., Eds.; Elsevier: Amsterdam, 1987; Part C, p 175.

(18) Sygula, A.; Rabideau, P. W. *J. Am. Chem. Soc.* **1992**, *114*, 821.

(19) (a) Blizzard, A. C.; Santry, D. P. *J. Chem. Phys.* **1971**, *55*, 950. (b) Ditchfield, R.; Synder, L. C. *J. Chem. Phys.* **1972**, *56*, 5823.

(20) Ostlund, N. S.; Newton, M. D.; McIver, J. W., Jr.; Pople, J. A. *J. Magn. Reson.* **1969**, *1*, 298.

(21) Kikuchi, O.; Nakano, T.; Morihashi, K. Unpublished.

Chart 1

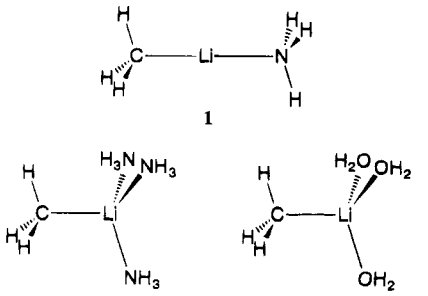

1 2 3

Chart 2

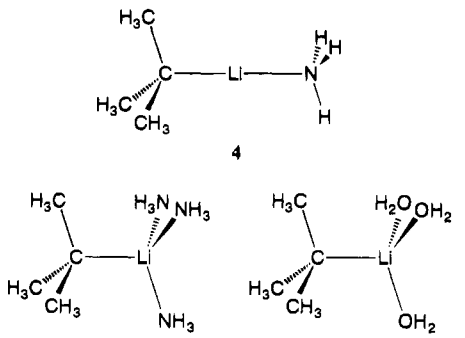

4 5 6

methyl)lithium−pentamethyldiethyltriamine[22] and 2-lithio-2-phenyl-1,3-dithiane−tetramethylethylenediamine−THF.[23] Therefore, in our study three NH_3 or H_2O molecules were included to complete the tetrahedral coordination around the lithium atom (**2** or **3**). The calculated $^1J_{CLi}$ values are 37.0 Hz in **2** and 43.3 Hz in **3**. These values are very close to the experimental one in the *tert*-butyllithium monomer (31.5 Hz).[12] It is confirmed that $^1J_{CLi}$ in the methyllithium monomer depends largely on the degree of coordination to the lithium atom.

The structure of the C−Li bond is also influenced by the solvation; the C−Li bond becomes longer (from 2.05 to *ca.* 2.18 Å, as shown in Table 1). This change has been shown in the theoretical studies of organolithium compounds.[9,15c,24] It should be noted, however, that the C−Li bond elongation itself is not a key factor for decreasing the $^1J_{CLi}$ value but the coordination of solvent molecules is. We examined the dependence of $^1J_{CLi}$ on the C−Li bond length for the unsolvated species in which the geometry of the methyl group was fixed.[25] It was found that $^1J_{CLi}$ is 128.3 Hz for r(C−Li) = 2.047 Å and 169.1 Hz for r(C−Li) = 2.184 Å. Such a trend has been reported in previous calculations for the one-bond $^{13}C-^1H$ coupling constant $^1J_{CH}$ in methane[26a] and in the isopropyl cation;[26b] simple elongation of the C−H bond makes the $^1J_{CH}$ value larger. Therefore, it is suggested that the solvation affects the electronic factor of the C−Li bond, which reduces the $^1J_{CLi}$ value significantly.

The calculations were also carried out by using the truncated lithium basis set, which models a purely ionic C−Li bond. The calculated $^1J_{CLi}$ value in methyllithium, 44.0 Hz, is very close to those calculated for methyllithium with three solvated ligands. This result strongly suggests that the C−Li bond in methyllithium with ligands is ionic, as has been indicated in previous studies.[8c−h]

Quite the same calculations were carried out on the *tert*-butyllithium monomer, in which $^1J_{CLi}$ was experimentally observed in THF.[12] The optimized geometries and calculated $^1J_{CLi}$ values for the *tert*-butyllithium monomer are shown in Table 2. The trend observed in the calculated $^1J_{CLi}$ values is similar to that for methyllithium (Table 1). When three NH_3 or H_2O molecules are solvated to the lithium atom (**5** or **6**), the calculated $^1J_{CLi}$ values (31.8 Hz for **5** and 36.3 Hz for **6**) agree well with the experimental one.[12] Moreover, modeling the

Table 2. Symmetry-Restricted Energy-Optimized Structures[a] and Calculated Coupling Constants[b] for *tert*-Butyllithium Monomers

	r(C−Li)	r(C−C)	∠(CCC)	$^1J(^{13}C-^7Li)$
unsolvated	2.092	1.547	108.3	222.5
solvated with NH_3 (**4**)	2.111	1.548	108.0	85.8
solvated with $3NH_3$ (**5**)	2.218	1.548	107.6	31.8
solvated with $3H_2O$ (**6**)	2.199	1.547	107.8	36.3
truncated basis set	1.964	1.551	107.3	43.0
exptl[c]				31.5

[a] Bond lengths are in Å and angles are in degrees. Geometries for methyl groups were fixed at the structures of those in 2-methylpropane: r(C−H) = 1.096 Å, ∠(HCH) = 108.2°.[28] [b] Values are in Hz. [c] NMR data for *tert*-butyllithium monomer in THF at −90 °C.[12]

Table 3. Contributions of the Atomic Orbitals to the $^1J_{CLi}$ Values in Methyllithium Monomers[a]

species	χ_λ[b]	χ_σ[b]	$\chi_\lambda(R_C)\chi_\sigma(R_C)$[c]	$\varrho^{(1)}_{\lambda\sigma}$	$(^1J_{CLi})_{\lambda\sigma}$[e]
unsolvated	C(1s)	C(1s)	51.7162	0.0369	141.3
	C(1s)	C(2s′)	0.2733	−0.1219	−2.5
	C(1s)	C(2s″)	1.2190	−0.1219	−11.0
	C(2s′)	C(2s′)	0.0014	0.3479	<0.1
	C(2s′)	C(2s″)	0.0064	0.4123	0.2
	C(2s″)	C(2s″)	0.0287	0.3417	0.7
	others				−0.5
					128.3 (total)
solvated with $3H_2O$	C(1s)	C(1s)	51.7162	0.0118	45.2
	C(1s)	C(2s′)	0.2733	−0.0557	−1.1
	C(1s)	C(2s″)	1.2190	−0.0041	−0.4
	C(2s′)	C(2s′)	0.0014	0.1810	<0.1
	C(2s′)	C(2s″)	0.0064	0.1176	0.1
	C(2s″)	C(2s″)	0.0287	−0.1078	−0.2
	others				1.0
					44.6 (total)
truncated basis set	C(1s)	C(1s)	51.7162	0.0091	34.8
	C(1s)	C(2s′)	0.2733	−0.0411	−0.8
	C(1s)	C(2s″)	1.2190	−0.0142	−1.3
	C(2s′)	C(2s′)	0.0014	0.1105	<0.1
	C(2s′)	C(2s″)	0.0064	0.1322	0.1
	C(2s″)	C(2s″)	0.0287	−0.0211	−0.1
	others				1.0
					33.8 (total)

[a] In all calculations the geometry for the CH_3Li part was fixed at the unsolvated state: r(C−Li) = 2.047 Å, r(C−H) = 1.102 Å, ∠(HCH) = 107.3°. [b] The valence atomic orbitals which are split into inner and outer parts are denoted single and double primes, respectively. [c] The products of the function value of the atomic orbital λ and that of σ were evaluated at the C atom. [d] Spin densities induced by the perturbation of the Fermi contact interaction on the Li atom. [e] Values are in Hz.

(22) Leppert, M. F.; Englehardt, L. M.; Raston, C. L.; White, A. H. *J. Chem. Soc., Chem. Commun.* **1982**, 1323.
(23) Amstutz, R.; Dunitz, J. D.; Seebach, D. *Angew. Chem., Int. Ed. Engl.* **1981**, *20*, 465.
(24) Chandrasekhar, J.; Schleyer, P. v. R. *J. Chem. Soc., Chem. Commun.* **1981**, 260. Decher, G.; Boche, G. *J. Organomet. Chem.* **1983**, *259*, 31. Lipkowitz, K. B.; Uhegbu, C.; Naylor, A. M.; Vance, R. *J. Comput. Chem.* **1985**, *6*, 662. van Eikema Hommes, N. J. R.; Bühl, M.; Schleyer, P. v. R.; Wu, Y.-D. *J. Organomet. Chem.* **1991**, *409*, 307.
(25) The change in the geometry of the methyl group was not important for decreasing the $^1J_{CLi}$ value.
(26) (a) Sergeyev, N. M.; Solkan, V. N. *J. Chem. Soc., Chem. Commun.* **1975**, 12. (b) Maciel, G. E. *J. Am. Chem. Soc.* **1971**, *93*, 4375.

Table 4. Symmetry-Restricted Energy-Optimized Structures[a] for Methyllithium Oligomers

	r(C−Li)	r(C−H)	r(C−C)	r(Li−Li)	∠(HCH)	∠(LiCLi)	∠(CLiC)
			With Li(421/1) Basis Set				
dimer (C_{2h}) (**7**)	2.178	1.106	3.751	2.199	104.1	61.7	118.3
	2.192	1.108			106.2		
trimer (C_{3h}) (**8**)	2.126	1.105	4.219	2.738	103.9	79.5	160.5
	2.155	1.107			106.6		
tetramer (C_{4h}) (**9**)	2.102	1.104	4.240	2.912	104.0	86.7	176.7
	2.140	1.106			106.9		
tetramer (T_d) (**10**; staggered)	2.269	1.108	3.700	2.484	104.3	66.4	109.2
tetramer (T_d) (**10**; eclipsed)	2.269	1.108	3.695	2.497	103.5	66.8	109.0
			With Li(31) Basis Set				
dimer (C_{2h}) (**7**)	2.094	1.109	3.573	2.199	102.7	63.2	116.8
	2.102	1.110			104.7		
trimer (C_{3h}) (**8**)	2.047	1.108	4.028	2.717	101.9	82.8	157.2
	2.062	1.110			104.9		
tetramer (C_{4h}) (**9**)	2.027	1.108	4.072	2.916	101.5	91.5	178.5
	2.046	1.110			104.9		
tetramer (T_d) (**10**; staggered)	2.203	1.110	3.572	2.459	102.9	67.8	108.3
tetramer (T_d) (**10**; eclipsed)	2.206	1.110	3.571	2.470	102.0	68.1	108.1

[a] Bond lengths are in Å and angles are in degrees. Assumed symmetries for each structure are given in parentheses.

Table 5. Geometric Parameters[a] and Calculated Coupling Constants[b] for Methyllithium Oligomers[c]

	r(C−Li)	r(C−H)	∠(HCH)	$^1J(^{13}C-^7Li)$	$^1J(^{13}C-^1H)$	ref
			With Li(421/1) Basis Set			
dimer (C_{2h}) (**7**)	2.185	1.107	104.6	28.9	109.9	this work
	2.126	1.090		20.0	58.4	*d,e*
	2.037	1.130		25.3	56.5	*d,f*
trimer (C_{3h}) (**8**)	2.141	1.106	104.8	30.9	112.3	this work
tetramer (C_{4h}) (**9**)	2.121	1.106	105.0	33.0	115.3	this work
tetramer (T_d) (**10**; staggered)	2.269	1.108	104.3	16.3	107.8	this work
	2.230	1.091		6.9	62.1	*d,e*
	2.199	1.136		7.3	61.4	*d,f*
	2.311	0.960		7.7	51.2	*d,g*
tetramer (T_d) (**10**; eclipsed)	2.269	1.108	103.5	17.2	107.8	this work
	2.250	1.095		7.0	61.1	*d,e*
	2.197	1.139		7.3	59.7	*d,f*
			With Li(31) Basis Set			
dimer (C_{2h}) (**7**)	2.098	1.109	103.4	20.9	99.7	this work
trimer (C_{3h}) (**8**)	2.054	1.109	102.9	24.1	99.9	this work
tetramer (C_{4h}) (**9**)	2.036	1.109	102.6	24.6	99.9	this work
tetramer (T_d) (**10**; staggered)	2.203	1.110	102.9	12.5	99.3	this work
tetramer (T_d) (**10**; eclipsed)	2.206	1.110	102.0	14.0	99.6	this work
				14.5	98	exptl[h]

[a] Bond lengths are in Å and angles are in degrees. Assumed symmetries for each structure are given in parentheses. [b] Values are in Hz. [c] Mean values of the bond lengths, angles, and coupling constants are given for **7**, **8**, and **9**. [d] Coupling constants were calculated by the FPT-INDO method.[9] [e] Geometries were optimized by the STO-3G basis set. [f] Geometries were optimized by the MNDO method. [g] X-ray structure.[5a] [h] NMR data for tetramer (T_d structure).[6a,b]

ionic C−Li bond gives a similar $^1J_{CLi}$ value of 43.0 Hz.

In order to examine the above-mentioned variations in the $^1J_{CLi}$ values, we analyzed the contribution of each atomic orbital to the $^1J_{CLi}$ value. The $^1J_{CLi}$ value was divided into atomic orbital pair contribution $(^1J_{CLi})_{\lambda\sigma}$ by

$$^1J_{CLi} = \sum_{\lambda\sigma}^{\text{allAO}} (^1J_{CLi})_{\lambda\sigma} \qquad (3)$$

where $(^1J_{CLi})_{\lambda\sigma}$ is each expansion term in eq 1. The calculated contributions of each atomic orbital to $^1J_{CLi}$ in methyllithium are summarized in Table 3. These contributions were obtained with the same geometry for the CH_3Li part. As can be seen from Table 3, the contribution from the carbon 1s orbital is predominant in the $^1J_{CLi}$ value; this is due to the large density of the 1s orbital at the nucleus. The values of the spin density $\varrho^{(1)}_{\lambda\sigma}$, which are induced by the perturbation of the Fermi contact interaction on the Li atom, decrease when three H_2O molecules are included or the truncated lithium basis set is used in the calculation. Since covalency and ionicity are the concepts for the valence electron behavior and $^1J_{CLi}$ is determined mainly by the core electron behavior, the electronic factor of the C−Li bond may not be derived directly from the calculated $^1J_{CLi}$ values. On the other hand, the fact that the solvation model with three H_2O molecules and the truncated basis set model give very similar results for both the core and valence parts of the spin density $\varrho^{(1)}_{\lambda\sigma}$ indicates that the C−Li bond of the methyllithium monomer is ionic in solution and has a small $^1J_{CLi}$ value.

Although the experimental one-bond $^{13}C-^1H$ coupling constant $^1J_{CH}$ for the lithiated carbon atom in the monomeric alkyllithium has not been reported, Table 1 shows that $^1J_{CH}$ also decreases as the degree of solvation increases or as the ionicity of the C−Li bond is modeled in the present calculations, in contrast to the previous study.[9]

Methyllithium Oligomers. The ring structures of the dimer (**7**), trimer (**8**), tetramer (**9**), and the tetrahedral structure of the tetramer (**10**) were calculated. Although trimeric organolithium compounds such as **8** are rare both in the solid state and in solution[27] and tetrameric ones such as **9** have not been reported so far, **8** and **9** were calculated to examine the dependence of $^1J_{CLi}$ on the ring size. The optimized geometries are

Chart 3

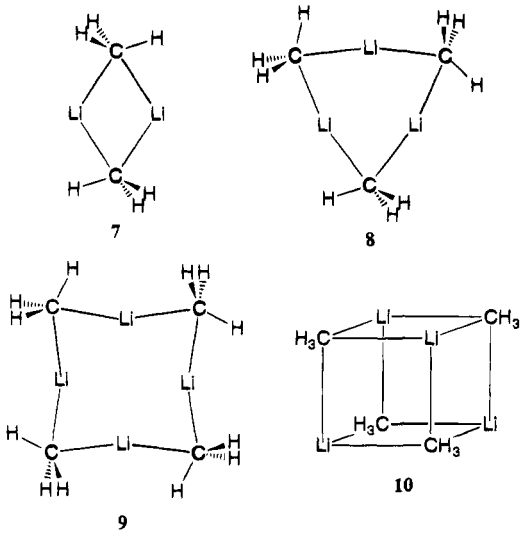

shown in Table 4, and the calculated coupling constants are shown in Table 5 along with previous theoretical[9] and experimental[6a,b] data.

It is seen from Table 5 that the calculated $^1J_{CLi}$ and $^1J_{CH}$ values in **10** are in good agreement with the experimental ones,[6a,b] whereas previous semiempirical FPT-INDO calculations[9] give much smaller values. When the truncated lithium basis set is used to model the ionic C−Li bond, the calculated $^1J_{CLi}$ and $^1J_{CH}$ values (12.5 and 99.3 Hz in the staggered form and 14.0 and 99.6 Hz in the eclipsed form, respectively) are in excellent agreement with the experimental ones.[6a,b] The sign of the calculated $^1J_{CLi}$ value is also consistent with the experimental one.[6c] Another interesting point observed in Table 5 is that the difference between the $^1J_{CLi}$ values calculated by two different types of basis sets is much smaller than that in monomeric methyllithium. This trend is in accord with the observation that the coupling constants in methyllithium tetramer are independent of solvent.[6a,b]

The three ring structures (**7**, **8**, and **9**) have $^1J_{CLi}$ values similar to each other, whereas the tetrahedral structures (**10**; staggered and eclipsed forms) have smaller $^1J_{CLi}$ values. This difference is obviously due to the state of aggregation, not to the degree of aggregation. That is, the value of $^1J_{CLi}$ depends on the number of lithium atoms which are bonded directly to the carbon atom, as the dependence was pointed out by Bauer et al.[2k,12] from the experimental $^1J_{CLi}$ values for several organolithium compounds. The $^1J_{CLi}$ values in the monomer (44.0 Hz), dimer (**7**; 20.9 Hz), and tetrahedral tetramer (**10**(staggered form); 12.5 Hz), which were calculated with the truncated lithium basis set, show that $^1J_{CLi}$ in methyllithium varies nearly inversely with the number of the lithium atoms which are bonded directly to the carbon atom.

$^1J_{CH}$ values in methyllithium oligomers also vary according to the degree and state of aggregation, although the change is small.

Conclusion

Ab initio calculations of NMR coupling constants by using the self-consistent perturbation theory with the MIDI-4 basis set reproduced well the experimental $^1J_{CLi}$ value in the *tert*-butyllithium monomer when the effect of solvation was considered. The calculated $^1J_{CLi}$ and $^1J_{CH}$ values in the tetrahedral structure of methyllithium tetramer showed excellent agreement with the experimental ones. In methyllithium oligomers, the relation between $^1J_{CLi}$ and the number of lithium atoms directly bonded to the carbon atom, which was previously found experimentally, was confirmed theoretically. Modeling the ionic C−Li bond using the truncated lithium basis set reproduced well the experimental $^1J_{CLi}$ values in the *tert*-butyllithium monomer and methyllithium tetramer, suggesting the importance of the ionic character of the C−Li bond in alkyllithiums.

OM940308X

(27) Harder, S.; Boersma, J.; Brandsma, L.; Kanters, J. A.; Bauer, W.; Schleyer, P. v. R. *Organometallics* **1989**, *8*, 1696. Harder, S.; Boersma, J.; Brandsma, L.; Kanters, J. A.; Duisenberg, A. J. M.; van Lenthe, J. H. *Organometallics* **1991**, *10*, 1623. Harder, S.; Ekhart, P. F.; Brandsma, L.; Kanters, J. A.; Duisenberg, A. J. M.; Schleyer, P. v. R. *Organometallics* **1992**, *11*, 2623.

(28) The Chemical Society of Japan. *Kagaku Binran (Chemistry Handbook)*, 2nd ed.; Maruzen: Tokyo, 1975; p II-1387. Lide, D. R., Jr. *J. Chem. Phys.* **1960**, *33*, 1519.

Gas-Phase Reactivity of Lanthanide Cations with Hydrocarbons

Hans H. Cornehl, Christoph Heinemann, Detlef Schröder, and Helmut Schwarz*

Institut für Organische Chemie der Technischen Universität Berlin, D-10623 Berlin, FRG

Received August 17, 1994®

The gas-phase reactions of all lanthanide cations Ln^+ (Ln = La–Lu, with the exception of Pm^+) with several linear, branched, and cyclic alkanes, cyclopropane, and alkenes have been examined by Fourier transform ion cyclotron resonance mass spectrometry. This series of substrates allows to evaluate estimates for the relative reactivities of Ln^+ cations with respect to C–H and C–C bond activation of hydrocarbons. None of the Ln^+ cations was found to react with methane, in accord with the unfavorable thermochemical situation for formation of a cationic carbene complex $LnCH_2^+$ from Ln^+ and CH_4. Very slow single dehydrogenation of ethane is observed for La^+ and Ce^+. All acyclic alkanes larger than ethane, as well as cyclopropane and cyclohexane, are only activated by La^+, Ce^+, and Gd^+, and the reaction rates approach the collisional limit with increasing polarizability. The nonreactivity of all other lanthanide cations toward alkanes provides experimental support for Schilling and Beauchamp's suggestion that a minimum of two non-f valence electrons is required for the activation of C–H or C–C bonds. In addition to La^+, Ce^+, and Gd^+, Pr^+ and Tb^+, the two of the $6s^14f^n$ configurated lanthanide cations with the lowest excitation energies to states with at least two non-f valence electrons, also activate propene but are unreactive with cyclopropane. The occurrence of C–H bond activation of propene by Pr^+ and Tb^+ is described in terms of a curve-crossing model in which an electronically excited asymptote of a state with two non-f electrons is involved en route to the products. With 1-butene also Nd^+, Dy^+, Ho^+, and Er^+ cations mediate dehydrogenation, and only Sm^+, Eu^+, Tm^+, and Yb^+ are unreactive with this substrate; these are precisely those lanthanide cations which exhibit the largest excitation energies to states with at least two non-f electrons. Furthermore, the relative rates for the ion/molecule reactions are in qualitative agreement with the curve-crossing model proposed for the reaction of Pr^+ and Tb^+ with propene. Finally, with 1,4-cyclohexadiene as substrate even Sm^+, Eu^+, and Tm^+ mediate C–H activation to yield the corresponding benzene/Ln^+ complexes.

Introduction

The long-neglected lanthanide elements have become of considerable importance in many areas of modern technology.[1] Subjects as diverse as heterogeneous catalysis, superconductivity, or advanced materials for optical, electronic, magnetic, and biomedical applications benefit from the unusual properties found among these elements. Parallel to the increasing industrial use, the organometallic chemistry of lanthanide elements developed as a timely and fascinating research topic.[2] As hallmarks, we mention the remarkable activity of organometallic lanthanide complexes in the activation of methane,[3] the polymerization of olefins,[4] and the development of highly volatile organolanthanide complexes with perspectives for chemical vapor deposition.[5] Furthermore, a variety of organolanthanide complexes can be used as efficient and selective catalysts and, therefore, became powerful tools in synthetic organic chemistry.[6]

Within the last decade, thorough and extensive investigations on the gas-phase chemistry of "bare" and ligated transition-metal ions brought about a comprehensive body of information with respect to reaction mechanisms of metal-mediated C–H and C–C bond activation and the correlation of the intrinsic reactivities of the metal ions with the corresponding electronic structures.[7] While there has been some work[8] on the gas-phase chemistry of La^+, it is somewhat surprising that the other lanthanide ions Ln^+ (in this study, this term denotes all 4f elements from cerium to lutetium

® Abstract published in *Advance ACS Abstracts*, November 15, 1994.

(1) (a) *Industrial Applications of Rare Earth Elements*; Gschneider, K. A., Jr., Ed.; American Chemical Society: Washington, DC, 1981. (b) 2nd International Conference on f-Elements; University of Helsinki, Aug 1–6, 1994.

(2) (a) Marks, T. J.; Ernst, R. D. In *Comprehensive Organometallic Chemistry*; Wilkinson, G.; Stone, F. G. A., Ebel, E. W., Eds.; Pergamon Press: Oxford, U.K., 1982; Chapter 21. (b) Schumann, H.; Meese-Marktscheffel, J. A.; Esser, L. *Chem. Rev.*, submitted for publication.

(3) (a) Watson, P. L.; Parshall, G. W. *Acc. Chem. Res.* **1985**, *18*, 51. (b) Otsura, K.; Shimizu, Y.; Komatsu, T. *Chem. Lett.* **1987**, 1835. (c) Ashcroft, T.; Cheetham, A. K.; Foord, J. S.; Green, M. L. H.; Grey, C. P.; Murrell, A. J.; Vernon, P. D. F. *Nature* **1990**, *344*, 319. (d) Watson, P. L. In *Selective Hydrocarbon Activation*; Davies, J. A., Watson, P. L., Greenberg, A., Liebman, J. F., Eds.; VCH: New York, 1990. Capitan, M. J.; Malet, J.; Centeno, M. A.; Munoz-Paez, A.; Carrizosa, I.; Odriozola, J. A. *J. Phys. Chem.* **1993**, *97*, 9223.

(4) (a) Jeske, G.; Lauke, H.; Mauermann, H.; Swepston, P. N.; Schumann, H.; Marks, T. J. *J. Am. Chem. Soc.* **1985**, *107*, 8091. (b) Jeske, G.; Schock, L. E.; Swepston, P. N.; Schumann, H.; Marks, T. J. *J. Am. Chem. Soc.* **1985**, *107*, 8103. (c) Jeske, G.; Lauke, H.; Mauermann, H.; Schumann, H.; Marks, T. J. *J. Am. Chem. Soc.* **1985**, *107*, 8111.

(5) For recent reports in this field, see: (a) Herrmann, W. A.; Anwander, R.; Denk, M. *Chem. Ber.* **1992**, *125*, 2399. (b) Benelli, C.; Caneschi, D.; Gatteschi, D.; Sessoli, R. *Adv. Mater.* **1992**, *4*, 504. (c) Barnhart, D. M.; Clark, D. L.; Huffman, J. C.; Vincent, R. L.; Watkin, J. G. *Inorg. Chem.* **1993**, *32*, 4077. (d) Bradley, D. C.; Chudzynska, A.; Hurthouse, M. B.; Motevalli, M.; Wu, R. *Polyhedron* **1994**, *13*, 1. (e) For an excellent overview, see: Anwander, R. PhD Thesis, Technische Universität München, 1993; and references cited therein.

(6) For a recent review, see: Molander, G. A. *Chem. Rev* **1992**, *92*, 29.

0276-7333/95/2314-0992$09.00/0

as well as lanthanum itself) have scarcely been addressed yet.[9] In the most comprehensive study carried out so far, Schilling and Beauchamp investigated reactions of Pr^+, Eu^+, and Gd^+ with several hydrocarbons and oxygen-containing molecules.[9a] A general conclusion from this work was that only lanthanide cations possessing at least two non-f valence electrons in their electronic ground state configuration give rise to C−H and C−C bond activation processes.

In this paper, we present a general survey of gas-phase reactions of all lanthanide cations Ln^+ (Ln = La−Lu, except for Pm which does not have a stable isotope). Several linear and branched aliphatic and alicyclic alkanes as well as the unsaturated hydrocarbons propene, 1-butene, and 1,4-cyclohexadiene serve as substrates to probe the occurrence of C−H and C−C bond activation processes. The implication of these particular substrates is to study the relative reactivity of Ln^+ cations with respect to C−H and C−C bond activation, while lowering the kinetic and thermodynamic restrictions associated with these processes. For example, the activation of methane, a small symmetrical molecule with low polarizability and four equally strong bonds should be difficult, whereas on the other hand dehydrogenation of 1,4-cyclohexadiene is expected to be rather facile, since its allylic C−H bonds are much weaker as compared to those of methane and the concomitant formation of a benzene molecule increases the thermodynamic driving force for the overall process.

Experimental Section

The experiments were performed using a Spectrospin-CMS-47X Fourier transform ion cyclotron resonance mass spectrometer; the instrument and its operational details have been described elsewhere.[10] Lanthanide ions Ln^+ were generated by laser desorption/laser ionization[11] in the external ion source by focusing the beam of a Nd:YAG laser (Spectron Systems; λ_{max} = 1064 nm) onto pure metal pieces (>99%; Dy, Tb, Tu, and Yb from Heraeus; La, Ho, Er, Eu, Gd, Lu, Nd, Pr, and Sm from Strem Chemicals). Most of the targets need not be stored under protective conditions, since the surface oxide layer is easily removed in the laser ablation process under the conditions of ion generation. However, Ce and Eu suffer from fast oxidation upon exposure to air. Therefore, a flintstone of a conventional lighter was used as a Ce source[9d] (ca. 70% Ce; undesired isotopes of Fe, La, Pr, Nd, and Gd were ejected from the ICR cell as described below), and the Eu target was permanently stored under viscous mineral oil. After being generated, the ions were extracted from the source and via a system of electrostatic potentials and lenses transferred into the cylindrical ICR cell, which is located in the field of a superconducting magnet (Oxford Instruments, maximum field strength 7.05 T). Then, the respective elements' most abundant isotope was isolated using FERETS,[12] a computer-controlled ejection protocol which combines frequency sweeps and single-frequency pulses to optimize ejection of all undesired ions by resonant excitation. Prior to any chemical reaction, Ln^+ ions were thermalized by allowing them to collide with repeatedly pulsed-in argon (maximum pressure ca. 5×10^{-5} mbar, maximum pulse time ca. 20 ms, ca 100 collisions per ion). This procedure serves for the cooling of the translational energy of the ions to the temperature of the collision gas (300 K); furthermore, if the Ar/Ln^+ interaction potentials allow for an appropriate relaxation mechanism, depopulation of electronically excited states also takes place. Thorough thermalization of the ions was evaluated by the reproducibility of the reaction kinetics as well as the nonoccurrence of endoergic reactions.[13] Reactants were admitted to the cell via a leak valve at a stationary pressure of $(2-8) \times 10^{-8}$ mbar, as measured by an uncalibrated ion gauge (BALZERS IMG070). Rate constants were determined from the pseudo-first-order decay of the reactant ions and are reported as percentage of the theoretical collision rate (k_{ADO}) with an estimated error of ± 30%.[14] Since we cannot exclude that electronically excited Ln^{+*} ions are not completely quenched by multiple collisions with argon, each reaction was followed until the reactant ion intensity accounted for less than 20% of the sum of all ion intensities in order to ensure that mainly ground state Ln^+ ions were involved in the process of interest.

Unfortunately, most of the Ln^+ ions (Ln = La, Ce, Pr, Nd, Sm, Gd, Tb, Dy, Ho, and Er) undergo fast side reactions with oxygen sources present as contaminants in the background of the machine (i.e. mainly H_2O and O_2). In those cases where the undesired processes accounted for more than 5% of the products, the overall reaction rates were multiplied by the initial quota of C−H- and C−C-bond activation to obtain the correct rates for these processes.[15] If reactions of interest were not observed, an upper bound for the overall reaction rate can be derived from the pressure of the reactant gas, the reaction time, and the signal-to-noise-ratio. Due to side reactions with oxygen-containing compounds, in the present study the upper bound is relatively high as compared to previous studies from our laboratory and amounts to ca. 5×10^{-12} cm^3 $molecule^{-1}$ s^{-1}.

Results and Discussion

An overview of the observed C−H- and C−C-bond activations of alkanes induced by the Ln^+ cations La^+, Ce^+, and Gd^+ as well as branching ratios and relative reaction rates are given in Scheme 1 and Table 1.

None of the lanthanide cations was found to react with methane. The energetically least demanding activation of methane by a bare Ln^+ cation would lead to the corresponding carbene complex via dehydrogenation (Scheme 1).[16] The minimum metal−methylene cation bond dissociation energy (BDE) required for the formation of $MCH_2^+ + H_2$ from $M^+ + CH_4$ amounts to

(7) Recent reviews: (a) Armentrout, P. B. *Annu. Rev. Phys. Chem.* **1990**, *41*, 313. (b) Martinho Simões, J. A.; Beauchamp, J. L. *Chem. Rev.* **1990**, *90*, 629. (c) Eller, K.; Schwarz, H. *Chem. Rev.* **1991**, *91*, 1121. (d) Weishaar, J. C. *Acc. Chem. Res.* **1993**, *26*, 213.

(8) (a) Huang, Y.; Wise, M. B.; Jacobsen, D. B.; Freiser, B. S. *Organometallics* **1987**, *6*, 346. (b) Hettich, R. L.; Freiser, B. S. *J. Am. Chem. Soc.* **1987**, *109*, 3543. (c) Sunderlin, L. S.; Armentrout, P. B. *J. Am. Chem. Soc.* **1989**, *111*, 3845. (d) Huang, Y.; Hill, Y. D.; Freiser, B. S. *J. Am. Chem. Soc.* **1991**, *113*, 840. (e) Ranasinghe, Y. A.; MacMahon, T. J.; Freiser, B. S. *J. Am. Chem. Soc.* **1992**, *114*, 9112. (f) Ranasinghe, Y. A.; Freiser, B. S. *Chem. Phys. Lett.* **1992**, *200*, 135.

(9) (a) Schilling, J. B.; Beauchamp, J. L. *J. Am. Chem. Soc.* **1988**, *110*, 15. (b) Reference 8c. (c) Azarro, M.; Breton, S.; Decouzon, M.; Geribaldi, S. *Int. J. Mass Spectrom. Ion Processes* **1993**, *128*, 1. (d) Heinemann, C.; Schröder, D.; Schwarz, H. *Chem. Ber.* **1994**, *127*, 1807. (e) Yin, W. W.; Marshall, A. G.; Marçalo, J.; Pires de Matos, A. *J. Am. Chem. Soc.*, in press. (f) For activation of carbon−fluorine bonds by "bare" and ligated Pr^+ cations, see: Heinemann, C.; Goldberg, N.; Tornieporth-Oetting, I. C.; Klapötke, T. M.; Schwarz, H. *Angew. Chem.*, in press.

(10) (a) Eller, K.; Schwarz, H. *Int. J. Mass Spectrom. Ion Processes* **1989**, *93*, 243. (b) Eller, K.; Zummack, W.; Schwarz, H. *J. Am. Chem. Soc.* **1990**, *112*, 621.

(11) (a) Freiser, B. S. *Talanta* **1985**, *32*, 697. (b) Freiser, B. S. *Anal. Chim. Acta* **1985**, *178*, 137.

(12) Forbes, R. A.; Laukien, F. H.; Wronka J. *Int. J. Mass Spectrom. Ion Processes* **1988**, *83*, 23.

(13) For example, see: Schröder, D.; Fiedler, A.; Ryan, M. A.; Schwarz, H. *J. Phys. Chem.* **1994**, *98*, 68.

(14) (a) For ADO theory, see: Su, T.; Bowers, M. T. *Int. J. Mass Spectrom. Ion Phys.* **1973**, *12*, 347. (b) For calibration, see: Lin, Y.; Ridge, D. P.; Munson, B. *Org. Mass Spectrom.* **1991**, *26*, 550.

(15) Blum, O.; Stöckigt, D.; Schröder, D.; Schwarz, H. *Angew. Chem., Int. Ed. Engl.* **1992**, *31*, 603.

Scheme 1

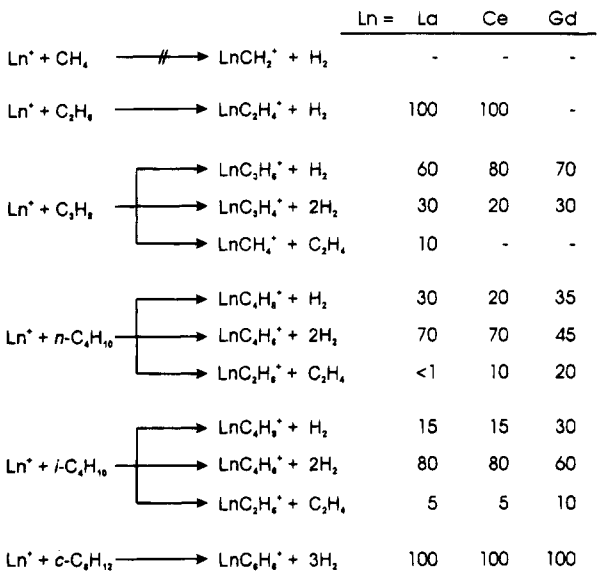

Table 1. Rate Constants Relative to the Theoretical Collision Rate Constant k_{ADO} for Reactions of Lanthanide Cations with Saturated Hydrocarbons

	C_2H_6	C_3H_8	n-C_4H_{10}	i-C_4H_{10}	c-C_6H_{12}
La	0.005	0.45	0.30	0.65	0.85
Ce	0.001	0.15	0.40	0.20	0.80
Gd	<0.0001	0.05	0.20	0.20	1.0

111 kcal/mol.[17] According to the experimental values for the bond dissociation energy (BDE) of La^+-CH_2 (98 ± 2 kcal/mol from an ion-beam study;[8c] 106 ± 5 kcal/mol from a photodissociation experiment[8b]), formation of $LaCH_2^+$ from La^+ and methane is endothermic and is therefore not observed if the ions are properly thermalized in the experiment.

From a simple theoretical model (Figure 1), as proposed by Carter and Goddard,[18] one can easily extrapolate that the experimentally unknown bond energies of methylene to all other Ln^+ cations (Ln = Ce–Lu) are even lower than the value found for $LaCH_2^+$. Assuming the existence of an intrinsic BDE (M^+-CH_2) along the lanthanide and the third-row transition-metal series,[19] the actual M^+-CH_2 bond energies are then determined by the sum of the energies required to promote the metal cation into the valence state which is appropriate for bond formation to CH_2 ($6s^15d^14f^n$ in the case of Ln^+, $n = 0-14$) and the loss of exchange energy that occurs upon formation of the metal–methylene bond.

As evident from Table 2, the corresponding promotion energies are higher for all 4f-row cations as compared to La^+ with the exception of Gd^+ ($6s^15d^14f^7$ ground state).[20] In addition, the exchange energy loss upon

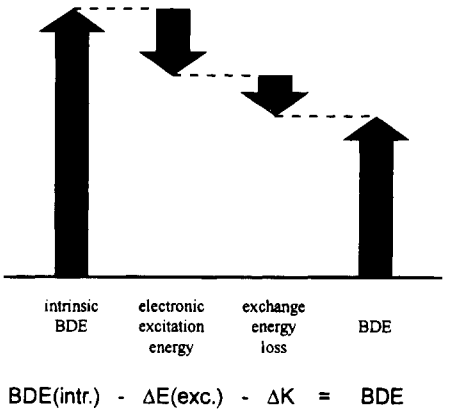

Figure 1. Qualitative model for estimation of bond dissociation energies as derived by Carter and Goddard.[18]

Table 2. Ground State Electronic Configurations and Excitation Energies[a] to the Lowest Lying States[b] with Two Non-f Valence Electrons for Lanthanide Cations Ln^+ (in kcal/mol)

	ground state	excitation energy to $5d^24f^n$	excitation energy to $6s^15d^14f^n$
La^+	$5d^2$	0	4.5
Ce^+	$5d^24f^1$	0	4.7
Pr^+	$6s^14f^3$	16.1	21.0
Nd^+	$6s^14f^4$	29.3	34.9
Pm^+	$6s^14f^5$	*c*	*c*
Sm^+	$6s^14f^6$	*c*	54.9
Eu^+	$6s^14f^7$	106.7	94.2
Gd^+	$6s^15d^14f^7$	12.6	0.0[d]
Tb^+	$6s^14f^9$	25.4[e]	9.2
Dy^+	$6s^14f^{10}$	58.4[f]	38.7
Ho^+	$6s^14f^{11}$	*c*	*c*
Er^+	$6s^14f^{12}$	67.1[g]	29.9
Tm^+	$6s^14f^{13}$	87.9	56.2[h]
Yb^+	$6s^14f^{14}$	128.6	81.7[i]
Lu^+	$6s^24f^{14}$	89.3	37.5

[a] From ref 20. [b] Experimental values have been averaged over all *J*-levels. [c] Unknown. [d] Excitation energy to $6s^24f^7$: 7.0 kcal/mol. [e] Excitation energy to $6s^24f^8$: 25.4 kcal/mol. [f] Excitation energy to $6s^24f^9$: 46.0 kcal/mol. [g] Excitation energy to $6s^24f^{11}$: 33.4 kcal/mol. [h] Excitation energy to $6s^24f^{12}$: 52.8 kcal/mol. [i] Excitation energy to $6s^24f^{13}$: 73.7 kcal/mol.

formation of the Ln^+-CH_2 bond due to unpaired 4f-electrons will lower BDE (Ln^+-CH_2), especially in the case of Gd^+ which has seven unpaired 4f electrons. Thus, we conclude that activation of methane by thermalized lanthanide cations is impossible on thermochemical grounds.

The qualitative validity of this concept can be probed by a comparison with the experimentally known[21] BDEs of the cationic lanthanide monoxides LnO^+, which are isoelectronic to the cationic carbene complexes (O, ^3P ground state; CH_2 $^3B_1$ ground state): For LaO^+ (BDE(La^+-O) = 203 ± 7 kcal/mol), the prototype species without any 4f electrons, the exchange energy loss ΔK caused by antiparallel coupling of the two unpaired 5d and 6s electrons of La^+ to the unpaired electrons of the oxygen atom amounts to one-half of a 6s/5d exchange integral K_{sd} ($\Delta K = 0.5K_{sd}$); the latter has been calculated to 9.4 kcal/mol.[19] Taking into account that the $5d^2 \rightarrow$

(16) (a) Irikura, K. K.; Beauchamp, J. L. *J. Am. Chem. Soc.* **1989**, *111*, 75. (b) Irikura, K. K.; Beauchamp, J. L. *J. Am. Chem. Soc.* **1991**, *113*, 2769. (c) Irikura, K. K.; Beauchamp, J. L. *J. Phys. Chem.* **1991**, *95*, 8344. (d) Wesendrup, W.; Schröder, D.; Schwarz, H. *Angew. Chem., Int. Ed. Engl.* **1994**, *95*, 1174. (e) Heinemann, C.; Hertwig, R. H.; Wesendrup, R.; Koch, W.; Schwarz, H. *J. Am. Chem. Soc.*, in press.

(17) All thermochemical data are taken from: Lias, S. G.; Liebman, J. F.; Levin, R. D.; Kafafi, S. A. *NIST Standard Reference Database, Positive Ion Energetics*, Version 2.01; Gaithersburg, MD, Jan 1994.

(18) (a) Carter, E. A.; Goddard, W. A., III. *J. Phys. Chem.* **1984**, *88*, 1485. (b) Carter, E. A.; Goddard, W. A., III *J. Am. Chem. Soc.* **1986**, *108*, 2180. (c) Carter, E. A.; Goddard, W. A., III. *J. Phys. Chem.* **1988**, *92*, 5679.

(19) Irikura, K. K.; Goddard, W. A., III. *J. Am. Chem. Soc.* **1994**, *116*, 8733.

(20) Martin, W. C.; Zalubas, R.; Hagan, L. *Atomic Energy Levels-The Rare Earth Elements*; NSRDS-NBS 60, National Bureau of Standards: Washington, DC, 1978.

(21) The BDEs (LnO^+) have been derived from the ionization energies of the lanthanide atoms (see ref 20) and the recommended values for BDE(LnO) and IE(LnO) given in: Cockett, M. C. R.; Nyulászi, L.; Veszprémi, T.; Wright, T. G.; Dyke, J. M. *J. Electron Spectrosc. Relat. Phenom.* **1991**, *57*, 373.

Table 3. Experimental[a] and Theoretical[b] Bond Dissociation Energies for Cationic Lanthanide Monoxides LnO^+ (in kcal/mol)

Ln	$BDE(LnO^+)_{exp}$	ΔE_{exc}[c]	$BDE(LnO^+)_{theor}$
La	203 ± 7	5	203
Ce	196 ± 16	5	196
Pr	189 ± 7	21	173
Nd	178 ± 7	35	152
Pm	161 ± 16	*d*	
Sm	138 ± 5	55	118
Eu	99 ± 7	94	72
Gd	161 ± 28	0	159
Tb	171 ± 16	9	157
Dy	138 ± 9	39	134
Ho	141 ± 19	*d*	
Er	143 ± 19	30	157
Tm	115 ± 9	56	138
Yb	90 ± 9	82	119
Lu	125 ± 28	38	170

[a] Taken from ref 21. [b] According to the model proposed by Carter and Goddard;[18] see text and Figure 1. [c] See Table 2. [d] ΔE_{exc} not given in ref 20.

$6s^15d^1$ excitation energy for La^+ amounts to 4.5 kcal/mol[20] (Table 2), an intrinsic bond energy for cationic lanthanide monoxides LnO^+ of 213 kcal/mol can be inferred. Compared to LaO^+, CeO^+ ($BDE(Ce^+-O)$ = 196 ± 16 kcal/mol) has a single unpaired electron residing in a 4f orbital which causes a rise in the exchange energy loss term by 0.5 ($K_{sf} + K_{df}$), where K_{sf} and K_{df} denote the 6s/4f and 5d/4f exchange integrals, respectively. Using the experimental $5d^24f^1 \rightarrow 6s^15d^14f^1$ promotion energy for Ce^+ (4.7 kcal/mol) we obtain 0.5 ($K_{sf} + K_{df}$) = 7 kcal/mol, which we assume to be constant along the 4f row. For *n* unpaired f electrons the 5d6s/4f exchange energy loss then amounts to *n* times 7 kcal/mol and theoretical bond dissociation energies for LnO^+ can be obtained using the experimentally known[20] promotion energies of Ln^+ and the value of 213 kcal/mol for the intrinsic LnO^+ bond strength (Table 3). On the basis of the assumption that K_{sd}, K_{sf}, and K_{df} remain approximately constant within the 4f series, this simple model describes the experimentally found trends in LnO^+ BDEs reasonably well: The maximum at LaO^+, minima at EuO^+ and YbO^+, a monotonous decay from CeO^+ to EuO^+, nearly identical (within the experimental errors) values for GdO^+ and TbO^+, an irregular trend for DyO^+, ErO^+, and TmO^+, and another peak for LuO^+. Note that especially GdO^+, the species with seven unpaired f-electrons, fits quite well into the proposed model. The underestimation of the bond strengths for the first half of the 4f row is probably due to a nonnegligible participation of the 4f orbitals in the formation of the covalent bonds between Ln^+ and O.

In reactions of Ln^+ with higher alkanes, carbene formation is not any more necessary, since dehydrogenation to yield alkene/Ln^+ complexes becomes more feasible. Indeed, ethane undergoes dehydrogenation by La^+ and Ce^+ in a very slow process (0.005% k_{ADO} and 0.001% k_{ADO}, respectively), in competition with the undesired oxidation of Ln^+ by background contaminants. Due to the low ion intensities, we did not perform additional studies concerning the structures of the so-formed $LnC_2H_4^+$ ions; however, they most likely correspond to the well-known ethene/M^+ structures.[7] Under our experimental conditions, Gd^+ was found to be unreactive with ethane, indicating that the very slow single and double dehydrogenation processes reported by Schilling and Beauchamp[9a] may be due to the

Scheme 2

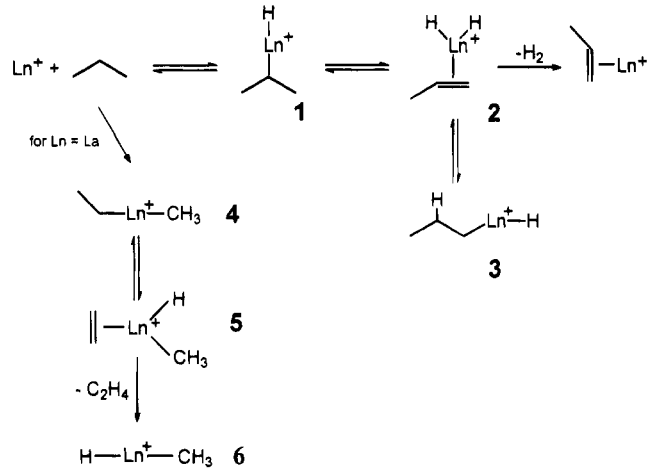

residual kinetic excess energy in their ion-beam experiment. In marked contrast to the ethane reactions, C−H bond activation of propane is quite efficient for La^+, Ce^+, and Gd^+ and leads to single and double dehydrogenation (Table 1, Scheme 1). Interestingly, La^+ also induces C−C bond cleavage to yield $H-La^+-CH_3$ and neutral ethene. The ion structure was deduced from a collision induced dissociation (CID) experiment in which loss of a methyl radical is observed, a process which is unexpected for a carbene complex, e.g. $H_2La^+CH_2$. C−C bond activation of propane is, however, not observed for Ce^+ and Gd^+. Similar to the Gd^+/ethane case, we suspect that the formation of the cationic hydridomethylgadolinium complex $H-Gd^+-CH_3$ as a product of the Gd^+/propane reaction in the earlier ion-beam study[9a] may have involved kinetically or electronically excited Gd^+ ions. For all reactive Ln^+ ions, i.e. La^+, Ce^+, and Gd^+, dehydrogenation of [2.2-D_2]-propane leads to a ca. 1:1 ratio of H_2 and HD losses. Within the experimental accuracy this result is consistent with the 15:12:1 ratio of H_2, HD, and D_2 losses that would be expected for complete equilibration of all H/D atoms prior to dehydrogenation. A plausible mechanism[7c] for propane dehydrogenation involves initial activation of a secondary C−H bond to yield the inserted species **1**, subsequent reversible β-H transfer steps (**1** ⇌ **2** ⇌ **3**), and eventual loss of dihydrogen from **2** via reductive elimination (Scheme 2). As far as the ethene loss from La^+ and [2.2-D_2]-propane is concerned, $H-La^+-CH_3$ and $D-La^+-CH_3$ are formed in similar amounts, being in line with a mechanism involving initial C−C bond activation to yield **4** and subsequent H/D equilibration within the ethyl substructure (e.g. **4** ⇌ **5**).

Not surprisingly, butane and isobutane also react with the three active Ln^+ cations, to yield predominantly singly and doubly dehydrogenated products. Furthermore, the branching ratios for H_2, $2H_2$, and C_2H_4 losses are almost identical for La^+, Ce^+, and Gd^+, respectively, whereas again all other Ln^+ cations are unreactive. In analogy to the formation of $H-La^+-CH_3$ (**6**) from propane, CID experiments[8a] establish that C−C bond activation of C_4H_{10} and subsequent loss of ethene leads to the dimethyl complexes $(CH_3)_2Ln^+$, which are now also observed for Ce^+ and Gd^+. Interestingly, the $(CH_3)_2La^+$ product is much less intense in the reaction of La^+ with butane as compared to $H-La-CH_3^+$ in the reaction with propane. Most likely, this difference is due to kinetic effects within the competing C−H and

C−C bond-activation processes and further labeling studies are indicated to settle this point. Finally, the largest alkane studied here, namely cyclohexane, is also only activated by La^+, Ce^+, and Gd^+. The increased polarizability of this substrate provides a longer lifetime of the rovibrationally excited encounter complex and, therefore, a higher probability for reaction after collision. In accordance with these arguments the reaction efficiencies approach the collisional limit. As the exclusive reaction pathway, we observe triple dehydrogenation to yield the corresponding benzene/Ln^+ complexes. The structures of the latter ions were derived from ligand-exchange experiments with C_6D_6, in which degenerate exchange of the complete ligands was observed to occur rapidly. In particular, we would like to stress that the Pr^+ cations in our experimental setup are unreactive with cyclohexane, in accord with Schilling and Beauchamp's[9a] interpretation that the Pr^+ (C_6H_6) ion in their ion-beam experiment was formed in a slightly endothermic reaction. Along with the finding that Pr^+ cations do not even induce a very slow dehydrogenation of alkanes (a minor process in the ion-beam experiment,[9a] which was attributed to a small percentage of electronically excited Pr^+ ions), this comparison indicates that the lanthanide ions generated by the laser desorption/laser ionization plus thermalization procedure employed in this study are in fact kinetically thermalized and in their electronic ground states.

Albeit C−H bond activation of alkanes is affected by La^+, Ce^+, and Gd^+, it does not occur for all other Ln^+ cations under study. Particularly the dehydrogenation of cyclohexane is expected to be facile and also has been reported for numerous transition-metal cations.[7c] As mentioned in the introduction, Schilling and Beauchamp[9a] deduced the low reactivity of Ln^+ cations from the concept that a necessary condition for insertion of Ln^+ into a C−H or C−C bond of a hydrocarbon is that in the electronic ground state configuration of Ln^+ at least two electrons reside in non-f valence orbitals. This argument is based on the commonly accepted view[22] that the 4f electrons of the lanthanide elements are chemically inactive in the sense that covalent bonds involving the compact 4f orbitals of these elements are inherently weak, and therefore, oxidative addition of a Ln^+ cation in an electronic state with only one 5d- or 6s-valence electron into a C−H or C−C bond should be thermochemically unfavorable as well as kinetically slow. In excellent agreement with this conclusion, we observe that La^+, Ce^+, and Gd^+ react with higher alkanes (except for Gd^+ and ethane), whereas all other lanthanide cations were found to be completely unreactive toward the saturated hydrocarbons considered here. Furthermore, the observed trends in reactivity within the investigated alkanes are well-known from earlier studies on gas-phase activation of alkanes by transition metals of the 3d series.[7c] We note in passing that Lu^+, although having two electrons in non−f orbitals (ground state electronic configuration: $6s^24f^{14}$), is completely unreactive with all alkanes, which is not unexpected for an ion with closed 6s and 4f subshells.

In order to further probe the chemical behavior of Ln^+ cations, propene seems to be a well-suited substrate to monitor the relative reactivities within the lanthanides series for the following reasons: (i) The energy gain upon complexation of propene by Ln^+ will be substantially higher as compared to alkanes, and (ii) allylic C−H bond activation of propene (BDE(C−H) = 86.3 kcal/mol)[17] is facile. Consequently, even less reactive Ln^+ cations might mediate bond activation of propene. Most recently,[9d] it was indeed reported that propene shows a surprising reactivity with La^+ and Ce^+. In a very fast process dehydrogenation as well as C_2H_4 loss is observed, leading to $LnC_3H_4^+$ and $LnCH_2^+$ complexes, respectively. As secondary reactions C−C bond formation processes were observed, which result in the formation of butadiene/Ln^+ and benzene/Ln^+ complexes. The same products were formed in the reactions of these cations with cyclopropane.[8a,9d] However, lower reaction rates indicated that initial insertion of the lanthanide cation in a C−C rather than a C−H bond of the substrate takes place in this system.

Table 4. Relative Primary Product Branching Ratios (%) and Rate Constants Relative to the Theoretical Collision Rate Constant k_{ADO}[13] for Reactions of Lanthanide Cations with Propene and Cyclopropane

	propene			cyclopropane		
	$LnCH_2^+$	$LnC_3H_4^+$	k/k_{ADO}	$LnCH_2^+$	$LnC_3H_4^+$	k/k_{ADO}
La	50	50	1.00	60	40	0.55
Ce	60	40	1.00	40	60	0.65
Pr		100	0.05			
Gd		100	0.85		100	0.60
Tb		100	1.00			

As expected from the alkane activation studies, Gd^+ also affects C−H bond activation of propene, although formation of a cationic carbene species does not occur (Table 4). This is consistent with the considerations concerning the $LnCH_2^+$ bond dissociation energies along the 4f row: due to the additional exchange energy loss associated with seven unpaired f electrons the Gd^+−CH_2 interaction will be weaker, and thus formation of $GdCH_2^+$ from Gd^+ and C_3H_6 is expected to be less exothermic as compared to $LaCH_2^+$ and $CeCH_2^+$. Since formation of $LaCH_2^+$ from La^+ and C_3H_6 is already close to the thermochemical limit, the nonobservation of $GdCH_2^+$ is most likely due to the absence of any thermochemical driving force. This interpretation is substantiated by our results for the Gd^+/cyclopropane systems. Here, exclusive loss of dihydrogen is observed, provided the Gd^+ ions are properly thermalized. While the kinetic data point to very similar reaction mechanisms in these systems, the cationic carbene complex is only observed for La^+ and Ce^+, indicating BDE(Gd^+−CH_2) < 93 kcal/mol. In a secondary reaction of $GdC_3H_4^+$ with another molecule of propene or cyclopropane, respectively, the species $GdC_4H_6^+$, $GdC_5H_6^+$, $GdC_6H_6^+$, and $GdC_6H_8^+$ are formed (Scheme 3). This parallels exactly the results which were obtained for the reactions of La^+ and Ce^+ with propene and cyclopropane, respectively.[9d]

In addition to La^+, Ce^+, and Gd^+, we find that Pr^+ and Tb^+, which were totally unreactive with the saturated hydrocarbons considered in this study, activate propene, whereas all other lanthanide cations are unreactive toward this substrate. In both cases, only the single dehydrogenation products $LnC_3H_4^+$ (Ln = Pr, Tb) are formed in the primary reactions, followed by secondary processes which give rise to the formation of $LnC_4H_6^+$, $LnC_5H_6^+$, $LnC_6H_6^+$, and $LnC_6H_8^+$. In their electronic ground state configurations,[20] both Pr^+ and

(22) See for example: Huheey, J. E. *Inorganic Chemistry-Principles of Structure and Reactivity*, 3rd ed.; Harper & Row: New York, 1983.

Scheme 3

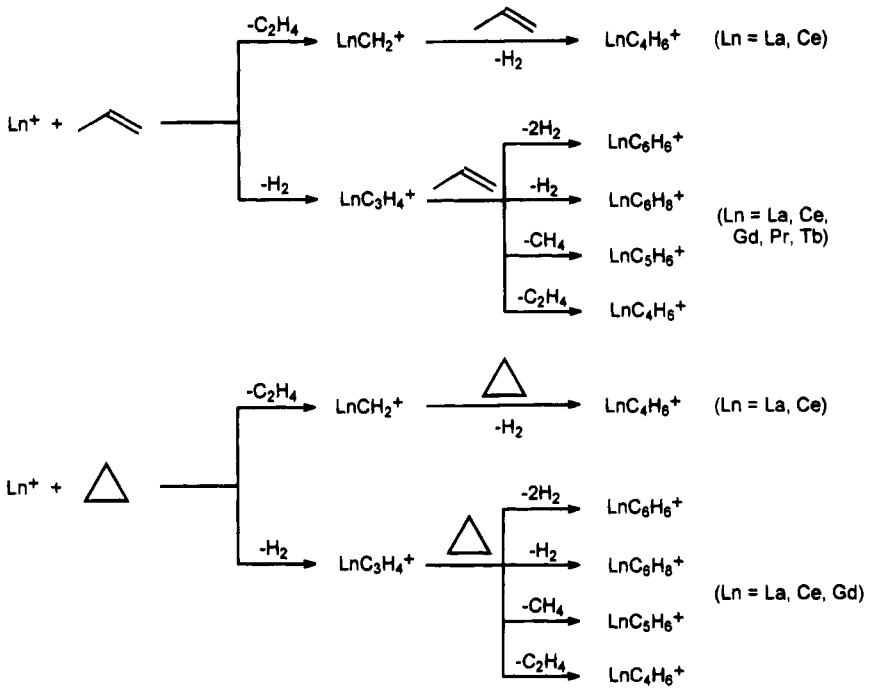

Tb^+ have only one valence electron in a non-f orbital (Pr^+, $6s^14f^3$; Tb^+, $6s^14f^9$) and, according to the argments outlined by Schilling and Beauchamp[9a], should therefore not be able to insert into the allylic C–H bond of propene. The unexpected reactivity of these two lanthanide cations may, however, be analyzed in terms of a qualitative curve-crossing model, as recently proposed for a number of ion/molecule reactions.[23] An overview of the energetic splitting among the lowest states arising from different electronic configurations of all lanthanide cations Ln^+ (Table 2) shows that activation of propene is observed for exactly those two elements which exhibit the lowest excitation energies to states with at least two non-f valence electrons. Since we can exclude that the observed reactions are due to electronically excited ions, it follows that the potential-energy surfaces associated with the intrinsically unreactive $6s^14f^n$ ground states of Pr^+ and Tb^+ must interact with those corresponding to an excited $6s^15d^14f^{n-1}$ or $5d^24f^{n-1}$ configuration in the sense of a curve crossing (Figure 2).

In this qualitative model, we consider two different potential energy surfaces, derived from electronic configurations of the lanthanide cation with (i) only one electron residing in a non-f orbital ($6s^14f^n$) and (ii) two electrons in non-f orbitals ($6s^15d^14f^{n-1}$ or $5d^24f^{n-1}$). For both states, we expect an initial attractive interaction between Ln^+ and the hydrocarbon substrate due to ion/dipole or ion/induced-dipole forces. If insertion into the activated bond is connected with an energetic barrier, the activation energy should be intrinsically higher for the state deriving from Ln^+ ($6s^14f^n$) on the basis of the qualitative arguments given above. Given that the state derived from a $6s^15d^14f^{n-1}$ or $5d^24f^{n-1}$ electronic configuration of the lanthanide cation is sufficiently low in energy and the two potential curves are not allowed to

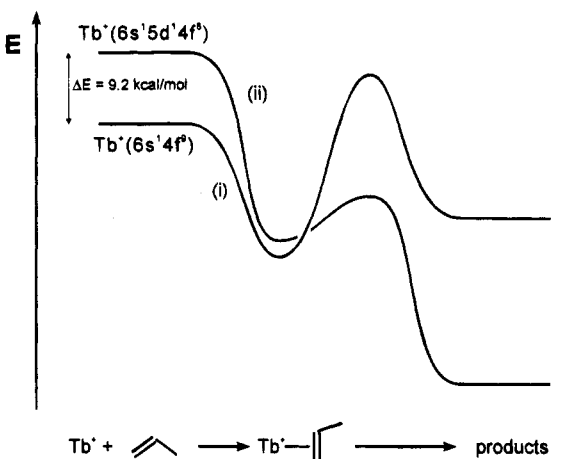

Figure 2. Qualitative curve-crossing model for activation of propene by Tb^+.

intersect, the effective barrier for insertion from the $6s^14^n$ ground state may be significantly lowered. In particular, such transitions between different potential energy surfaces are very likely in open-shell lanthanide systems due to the strong spin–orbit coupling present in the 4f row of the periodic table.[20] Therefore, the curve crossing might be avoided even if it formally involves states of different spin multiplicites. In agreement with the amount of the appropriate excitation energies of Pr^+ (16.1 kcal/mol) and Tb^+ (9.2 kcal/mol), Tb^+ activates propene at 100% of the theoretical collision rate k_{ADO} whereas Pr^+ achieves only 5% of the collisional limit.

In marked contrast to the propene case, Pr^+ and Tb^+ are unreactive toward cyclopropane, although formation of a $LnC_3H_4^+$ complex from cyclopropene is 8 kcal/mol more exothermic[17] than from propene. Probably, this is due to the lower amount of energy gained upon complex formation of Ln^+ with the cycloalkane as well as the higher activation barriers for insertion into the C–C bond of the cycloalkane, which cannot be overcome via a spin–orbit-mediated curve-crossing mechanism.

(23) (a) Perry, J. K.; Ohanessian, G.; Goddard, W. A., III. *Organometallics* **1994**, *13*, 1870. (b) van Koppen, P. A. M.; Bowers, M. T.; Fischer, E. R.; Armentrout, P. B. *J. Am. Chem. Soc.* **1994**, *116*, 3780. (d) Fiedler, A.; Schröder, D.; Shaik, S.; Schwarz, H. *J. Am. Chem. Soc.*, in press.

Scheme 4

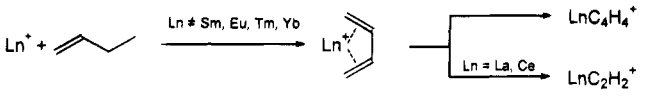

Table 5. Relative Reaction Rates (k/k_{ADO}) and Branching Ratios for the Reaction of Ln^+ with 1-Butene

Ln	k/k_{ADO}	$-H_2$	$-2H_2$	$-H_2/-C_2H_4$
La	1.00	72	12	16
Ce	1.00	71	14	15
Pr	0.54	100		
Nd	0.45	100		
Sm	<0.005			
Eu	<0.005			
Gd	0.83	100		
Tb	1.00	100		
Dy	0.06	100		
Ho	0.18	100		
Er	0.27	100		
Tm	<0.005			
Yb	<0.001			
Lu	0.71	100		

In this context, note that the observed activation of cyclopropane by La^+, Ce^+, or Gd^+ proceeds at 60% of the theoretical collision rate,[14a] whereas the reactions of these cations with propene proceed with 100% efficiency.

1-Butene serves as yet another monitor for probing the relative reactivities of the different lanthanide cations: Similar to propene this substrate should have a relatively high complexation energy and may easily undergo allylic C−H bond activation. In addition, for 1-butene the dehydrogenation pathway benefits from the energetically more favorable formation of butadiene; i.e. dehydrogenation of propene is endothermic by 40 kcal/mol, whereas that of 1-butene needs only 26 kcal/mol.[17] Thus, this low-lying product channel may render C−H bond activation also possible for the so-far unreactive Ln^+ cations (Scheme 4). Indeed, dehydrogenation of 1-butene is affected not only by La^+, Ce^+, Pr^+, Gd^+, and Tb^+ but also by Nd^+, Dy^+, Ho^+, Er^+, and Lu^+, which were unreactive toward alkanes and propene (Table 5). However, Sm^+, Eu^+, Tm^+, and Yb^+ still do not activate 1-butene at all.

In accord with the arguments outlined above, H_2 loss from 1-butene proceeds close to the collisional limit for La^+, Ce^+, Gd^+, and Tb^+, whereas for Pr^+ and Nd^+ the rates are lower ($k/k_{ADO} \approx 0.5$). The late lanthanide cations Dy^+, Ho^+, and Er^+ react even more than two times slower. These relative reactivities agree well with the curve-crossing model depicted in Figure 2 for the reaction of Tb^+ with propene: All Ln^+ with two non-f electrons in the ground state react fast; with increasing excitation energies to a reactive state the rates decrease, such that for Dy^+ k/k_{ADO} amounts to only 6%. Obviously, an excitation energy of more than 40 kcal/mol cannot be overcome even for a substrate as reactive as 1-butene. Moreover, for the two most reactive early lanthanide cations La^+ and Ce^+ dehydrogenation of 1-butene is associated with such a large exothermicity that subsequent fragmentation of rovibrationally excited butadiene/Ln^+ complexes occurs to yield $Ln(C_4H_4)^+$ and $Ln(C_2H_2)^+$, respectively.

Interestingly, 1-butene dehydrogenation by Lu^+ (which exhibits a closed-shell $6s^24f^{14}$ ground state) is far more efficient ($k/k_{ADO} \approx 0.7$) as compared to the reaction of other late lanthanide cations with this substrate. For example, the excitation of Lu^+ to the $6s^15d^14f^{14}$ state (37.5 kcal/mol) is similar to that of Dy^+ (38.7 kcal/mol), but the relative rate of Lu^+ is 10 times that of Dy^+. We attribute this effect to the obvious shortcomings of a model as qualitative as that depicted in Figure 2. Of course the height of the activation barrier is not only determined by the energetic splitting of the relevant atomic states but also by the nature of the transition; i.e. for Lu^+ C−H bond activation involves a promotion of a 6s electron to a 5d orbital ($6s^24f^{14} \rightarrow 6s^15d^14f^{14}$ excitation), whereas for Dy^+ an electron from a compact 4f orbital becomes crucial in the rate-determining transition structure. Qualitatively, this implies that the activation barrier for bond activation of 1-butene by Dy^+ exceeds that of Lu^+, since the overlap of the inner 4f orbital with the orbitals of the bond to be broken is relatively small.

Scheme 5

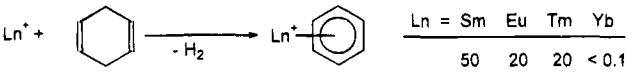

Finally, the so far unreactive lanthanide cations Sm^+, Eu^+, Tm^+, and Yb^+ were allowed to react with 1,4-cyclohexadiene (Scheme 5), a substrate for which both kinetic and thermodynamic restrictions to C−H bond activation should be very low due to the easy formation of a benzene molecule (loss of H_2 from 1,4-cyclohexadiene is even *exo*thermic by 6 kcal/mol).[17] In convincing agreement with the qualitative reactivity concept developed from the Ln^+/alkane and Ln^+/alkene reactions presented above, we do in fact observe formation of $Ln(C_6H_6)^+$ (and, in secondary processes, $Ln(C_6H_6)_2^+$) complexes for Ln^+ = Sm, Er, and Tm. As far as kinetics are concerned, we note that Sm^+ ($k/k_{ADO} \approx 0.5$; $6s^14f^6 \rightarrow 6s^15d^14f^5$ excitation energy: 54.9 kcal/mol) reacts twice as fast as compared to Eu^+ ($k/k_{ADO} \approx 0.2$), since for the latter cation the relevant $6s^14f^7 \rightarrow 6s^15d^14f^6$ excitation energy (94.2 kcal/mol) is considerably higher due to the half-filled 4f shell in its electronic ground state configuration. Despite an excitation energy comparable to the one of Sm^+, Tm^+ reacts at a rate comparable to that of Eu^+, which again shows that the nature of the relevant transition structures does not only depend on atomic splitting but is certainly influenced by additional factors such as orbital sizes, e.g. the 4f orbitals of Tm^+ are more compact than those of Sm^+, and obviously the degree of spin−orbit coupling which is responsible for the ease of curve crossing. For Yb^+, we observe only a very slow formation of the cationic benzene adduct ($k/k_{ADO} < 0.001$), which may also be due to adduct formation with residual benzene in the employed 1,4-cyclohexadiene sample (Merck, purity >99%). Interestingly, Yb^+ which is unreactive toward all substrates under study bears a *lower* excitation energy ($6s^14f^{14} \rightarrow 6s^15d^14f^{13}$, 81.7 kcal/mol) to an electronic configuration with two non-f valence electrons as compared to Eu^+, which does react with 1,4-cyclohexadiene. Once again, this emphasizes the qualitative nature of the curve-crossing model depicted in Figure 2.

Summarizing our results, we define a relative reactivity for each Ln^+ cation as the sum of the relative reaction rates with propane, butane, cyclohexane, pro-

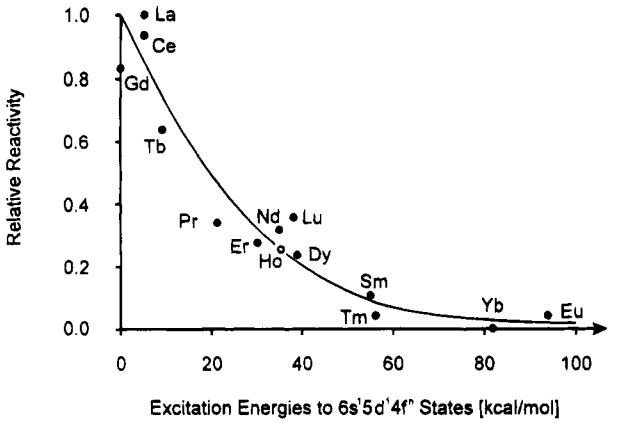

Figure 3. Relative reactivity of Ln^+ vs electronic excitation energies to the lowest lying state with $6s^15d^14f^n$ configuration. The excitation energy of Ho^+ can be estimated to 35 kcal/mol (see text).

pene, 1-butene, and 1,4-cyclohexadiene[24] normalized to the reactivity of La^+. In Figure 3 this relative reactivity is plotted versus the electronic excitation energies to the lowest lying state with $6s^15d^14f^n$ configuration (see Table 2) indicating a nonlinear dependency. However, for a more quantitative evaluation of relative reactivities further experimental data and a refinement of the theoretical model are indicated.

Conclusions

The present study is the first systematic investigation of the reactivity of "bare" Ln^+ cations (Ln = La–Lu, with the exception of Pm^+) with respect to C–H and C–C bond activation. In particular, the choice of a series of substrates in which the energy demand for bond activation decreases permits the evaluation of estimates for the relative reactivities of Ln^+ cations. In excellent agreement with the model proposed by Schilling and Beauchamp only those Ln^+ cations are reactive toward alkanes which have two non-f electrons in their electronic ground states, e.g. La^+, Ce^+, and Gd^+. Increasing the reactivity of the hydrocarbon, e.g. from propane to propene, renders bond activation also possible for Pr^+ and Tb^+, which have relatively low-lying excited states with two non-f electrons. This observation is explained in terms of a qualitative curve crossing model in which bond activation involves an electronically excited asymptote. Further facilitating bond activation by using 1-butene as substrate causes also other Ln^+ cations to react, except for Sm^+, Eu^+, Tm^+, and Yb^+, which exhibit excitation energies of more than 50 kcal/mol to electronic states with two non-f electrons. However, even these Ln^+ cations can be forced to mediate C–H bond activation if 1,4-cyclohexadiene is used as neutral substrate.

These observations fully agree with Schilling and Beauchamp's proposal as well as the curve-crossing model outlined here. Furthermore, the experimental finding that the reactivity of Ho^+ is between that of its next neighbors Er^+ and Dy^+ indicates that also its excitation energy to $6s^15d^14f^{10}$, which is not evaluated in ref 20, is in the order of those of Er^+ and Dy^+, i.e. ca. 35 kcal/mol. With respect to more quantitative aspects of the curve-crossing model further experimental and theoretical studies will be mandatory in order to examine the subtle factors which determine the reactivity of Ln^+ cations in bond activation in general.

Last but not least, some products of Ln^+ cation reactions revealed a rich chemistry for C–C coupling in their secondary reactions with alkenes, and preliminary results indicate that at least up to four alkene units can be coupled by Ln^+. These processes are of particular interest as gas-phase model systems for lanthanide-catalyzed oligomerization or polymerization of unsaturated hydrocarbons in the condensed phase and will be examined further in the future.

Acknowledgment. This work was supported by the Deutsche Forschungsgemeinschaft, the Volkswagen-Stiftung, and the Fonds der Chemischen Industrie (Kekulé Ph.D. fellowships for H.H.C. and C.H.). We acknowledge helpful discussions with Dr. J. Hrušák, Dipl.-Chem. A. Fiedler, Dipl.-Chem. J. Schwarz, and Dipl.-Chem. D. Stöckigt. Furthermore, we are indebted to Dr. K. K. Irikura for providing a preprint of ref 19 and to Dr. R. Anwander for providing a copy of ref 5e.

OM940659B

(24) The reactions of La^+, Ce^+, Pr^+, Nd^+, Gd^+, Tb^+, Dy^+, Ho^+, Er^+, and Lu^+ with 1,4-cyclohexadiene were estimated to occur at collisional limit.

Synthesis and Structure of *endo*-Coordinated *o*-Xylylene Complexes of Zerovalent Ruthenium and Osmium, $M\{\eta^4\text{-}o\text{-}(CH_2)_2C_6H_4\}(PMe_2Ph)_3$ (M = Ru, Os), and of a Tricarbonyliron Adduct of the Ruthenium Complex

Martin A. Bennett,* Mark Bown, Lai Yoong Goh,[1] David C. R. Hockless, and Thomas R. B. Mitchell[2]

Research School of Chemistry, Australian National University, Canberra, ACT, Australia 0200

Received September 15, 1994[⊗]

Treatment of ruthenium(II) and osmium(II) salts $[M(\eta^6\text{-}o\text{-}C_6H_4Me_2)(PMe_2Ph)_3](PF_6)_2$ [M = Ru (**3**) or Os (**4**)] with KO-*t*-Bu gives *o*-xylylene (*o*-quinodimethane) complexes of zerovalent ruthenium and osmium, $M\{\eta^4\text{-}endo\text{-}o\text{-}(CH_2)_2C_6H_4\}(PMe_2Ph)_3$ [M = Ru (**6**) or Os (**7**)], in 83% and 41% yields, respectively. Crystals of **6** are monoclinic, space group *C*2/*c*, with a = 31.540(3) Å, b = 11.793(4) Å, c = 16.739(3) Å, β = 104.58(1)°, and Z = 8; those of **7** are monoclinic, space group *C*2/*c*, with a = 31.487(2) Å, b = 11.759(2) Å, c = 16.784(3) Å, β = 104.625(8)°, and Z = 8. The structures were solved by heavy-atom methods and refined by least-squares analysis to R = 0.035 and R_w = 0.027 for 3027 independent reflections ($I > 3\sigma$) (**6**) and R = 0.019 and R_w = 0.014 for 4258 independent reflections ($I > 3\sigma$) (**7**). Both molecules contain a metal atom coordinated in a distorted square-pyramidal arrangement by the double bonds of η^4-*endo*-*o*-xylylene occupying two basal sites and three phosphorus atoms occupying the other sites. Variable temperature NMR (^1H, ^{31}P) spectra of **6** and **7** show the molecules to be fluxional as a consequence of hindered rotation of the $M(PMe_2Ph)_3$ fragment with respect to the *o*-xylylene, approximate $\Delta G^\ddagger$ values being 56 kJ mol^{-1} at 314 K for **6** and 60 kJ mol^{-1} at 324 K for **7**. Treatment of **6** with $Fe(CO)_4(NMe_3)$ affords a heterobimetallic *o*-xylylene complex containing zerovalent ruthenium and zerovalent iron, i.e., *endo*-$\{Ru(PMe_2Ph)_3\}$-*exo*-$\{Fe(CO)_3\}\{\mu\text{-}\eta^4,\eta^4\text{-}o\text{-}(CH_2)_2C_6H_4\}$ (**8**) in 42% yield, in which the ruthenium and iron atoms are coordinated to opposite sides of the *o*-xylylene ligand. Crystals of **8** are triclinic, space group $P\bar{1}$, with a = 10.107(2) Å, b = 12.162(2) Å, c = 14.339(2) Å, α = 84.86(1)°, β = 80.69(1)°, γ = 86.00(1)°, and Z = 2. The structure was solved by direct methods and refined by least-squares methods to R = 0.034 and R_w = 0.024 for 5025 independent reflections ($I > 3\sigma$). In complex **8** both metal centers are coordinated in a distorted square-pyramidal arrangement. The coordination sphere of the ruthenium atom in **8** is identical to that of the ruthenium atom in **6**; the basal sites of the square-pyramid about the iron atom are occupied by the exo pair of double bonds of *o*-xylylene, and the other three sites are occupied by the carbonyl ligands.

Introduction

The short-lived molecule *o*-xylylene (*o*-quinodimethane) can be stabilized by the formation of η^4-metal complexes via either the exocyclic or endocyclic pair of double bonds.

Three methods are available for the synthesis of exocyclic *o*-xylylene complexes of iron(0) and ruthenium(0): (1) oxidative addition of a 1,2-bis(halomethyl)-arene to a zerovalent metal complex, e.g., eq 1;[3,4] (2) reaction of a metal(II) halide complex with an appropriate Grignard reagent, either that derived from a 1,2-bis(halomethyl)arene (eq 2)[5] or from *o*-methylbenzyl bromide (eq 3);[5,6] (3) reaction of a metal halide complex with (*o*-methylbenzyl)lithium made directly from *o*-xylene (eq 4).[7] Method 3 has also been used to make methyl-substituted η^4-*exo*-*o*-xylylene complexes of ruthenium(0).[7]

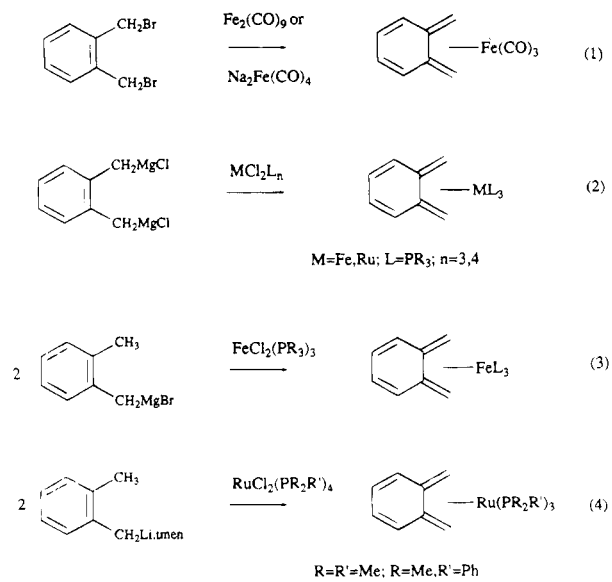

⊗ Abstract published in *Advance ACS Abstracts,* January 1, 1995.

(1) On leave from the Department of Chemistry, University of Malaya, Kuala Lumpur, Malaysia.

(2) On leave from the School of Chemistry, The Queen's University of Belfast, Northern Ireland, U.K.

(3) Roth, W. R.; Meier, J. D. *Tetrahedron Lett.* **1967**, 2053.

(4) Johnson, B. F. G.; Lewis, J.; Thompson, D. J. *Tetrahedron Lett.* **1974**, 3789.

(5) Grosselin, J.-M.; Le Bozec, H.; Moinet, C.; Toupet, L.; Köhler, F. H.; Dixneuf, P. H. *Organometallics* **1988**, *7*, 88.

0276-7333/95/2314-1000$09.00/0

Endocyclic *o*-xylylene complexes are usually prepared by deprotonation of the methyl groups of a cationic η^6-1,2-dimethylarene precursor (eqs 5 and 6),[8-10] although the iron compound $Fe(\eta^6\text{-}C_6Me_6)\{\eta^4\text{-}endo\text{-}o\text{-}(CH_2)_2C_6Me_4\}$ is obtained by dehydrogenation of $Fe(\eta^6\text{-}C_6Me_6)_2$ with oxygen at −40 °C.[11]

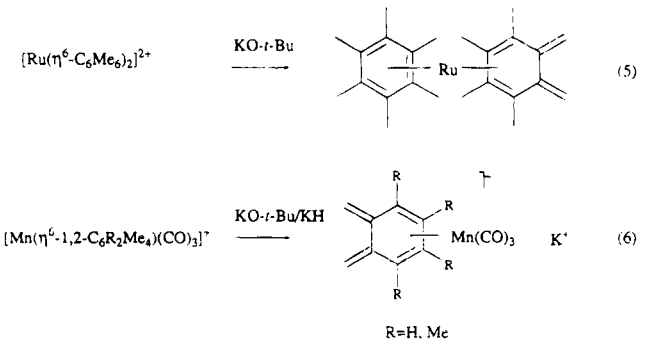

Binuclear complexes containing a pair of transition metal atoms bound *tetrahapto* to both exocyclic and endocyclic pairs of double bonds are also known. They include the heterobimetallic compound **1**,[9] in which the

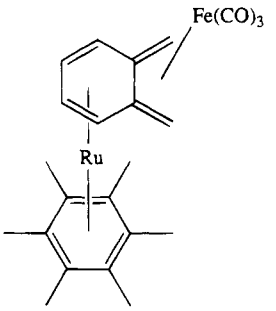

1

ruthenium and iron atoms are proposed to be on opposite sides of the *o*-xylylene fragment, and the homobimetallic compound $\{Ti(\eta^5\text{-}C_5Me_5)Cl\}_2\{\mu\text{-}o\text{-}(CH_2)_2C_6H_4\}$, in which the two titanium atoms are constrained to be on the same side of the *o*-xylylene by two Ti−Cl−Ti bridges.[12]

Deprotonation of the (*o*-xylene)ruthenium(II) complex $[Ru(O_2CCF_3)(\eta^6\text{-}o\text{-}C_6H_4Me_2)(PMe_2Ph)_2]PF_6$ with KO-*t*-Bu or $Na[N(SiMe_3)_2]$ in the presence of an excess of PMe_2Ph gives, unexpectedly, the *exo*-coordinated *o*-xylylene complex $Ru\{\eta^4\text{-}o\text{-}(CH_2)_2C_6H_4\}(PMe_2Ph)_3$ (**2**),[13] identical with that formed by the method shown in eq 2 (M = Ru, L = PMe_2Ph, $n = 4$).[5] It was suggested that the rapid removal of the trifluoroacetate ion from the precursor might generate a coordinatively unsaturated intermediate $Ru\{\eta^4\text{-}o\text{-}(CH_2)_2C_6H_4\}(PMe_2Ph)_2$ in which the ruthenium could migrate from the endo to the exo pair of double bonds before the added PMe_2Ph attacked. These results led us to expect that deprotonation of the coordinatively saturated dication $[Ru(\eta^6\text{-}o\text{-}C_6H_4Me_2)(PMe_2Ph)_3]^{2+}$ should give the isomeric *endo*-*o*-xylylene complex $Ru\{\eta^4\text{-}endo\text{-}o\text{-}(CH_2)_2C_6H_4\}(PMe_2Ph)_3$. In this paper we show this to be true for both the ruthenium and osmium systems and make a preliminary comparison of the structure and reactivity of the endocyclic and exocyclic isomers.

Experimental Section

The following instruments were used: Varian XL-200E (^1H NMR, ^{31}P NMR at 81.0 MHz), Varian VXR-300S and Varian Gemini 300 (^1H NMR, ^{31}P NMR at 121.42 MHz, ^{13}C NMR at 75.43 MHz), VG Micromass 7070F (mass spectra at 70 eV) and VG ZAB-2SEQ (EI at 70 eV, FAB at 30 KV, Cs ions using a NBA matrix), Perkin-Elmer 683 (infrared).

The compounds $[Ru(O_2CCF_3)(\eta^6\text{-}o\text{-}C_6H_4Me_2)(PMe_2Ph)_2]PF_6$[13] and $Fe(CO)_4(NMe_3)$[14] were prepared by reported procedures. Organic solvents of reagent grade were dried by published procedures[15] and distilled under nitrogen. All reactions were carried out under nitrogen by standard Schlenk techniques, although subsequent manipulations of the (o-xylene)ruthenium(II) and -osmium(II) precursors to **6** and **7** were carried out in the air. Elemental analyses were carried out in-house.

Preparations. (1) $[Ru(\eta^6\text{-}o\text{-}C_6H_4Me_2)(PMe_2Ph)_3](PF_6)_2$ (3). This method is preferable to that described in ref 13. To a stirred suspension of $[Ru(O_2CCF_3)(\eta^6\text{-}o\text{-}C_6H_4Me_2)(PMe_2Ph)_2]PF_6$[12] (2.40 g, 3.24 mmol) in methanol (60 mL) at 60 °C were added PMe_2Ph (2.0 mL, 14.06 mmol) and an excess of NH_4PF_6 (5.20g, 32.0 mmol) successively. The pale yellow precipitate that formed was filtered out, washed with methanol (2 × 10 mL) and *n*-pentane (30 mL), and dried under vacuum. The yield of **3** was 2.86 g (87%). ^1H NMR (CD_3CN, 200 MHz): δ 7.7−7.3 (m, PMe_2Ph), 6.40 (s, $Me_2C_6H_4$), 1.86 (vt, $^2J_{PH} + {}^4J_{PH}$ = 14 Hz, PMe_2Ph), 1.64 (s, $Me_2C_6H_4$). $^{31}P\{^1H\}$ NMR (CD_3CN, 81.0 MHz): 8.0 (s, PMe_2Ph), −143.3 (spt, PF_6, J_{PF} = 707 Hz).

(2) $[OsCl_2(\eta^6\text{-}o\text{-}C_6H_4Me_2)]_2$. An orange solution of Na_2OsCl_6 in ethanol (100 mL), prepared from $(NH_4)_2OsCl_6$ (6.00 g, 13.67 mmol),[16] was heated with 1,2-dimethyl-1,4-cyclohexadiene (10 mL) for 10 d. The orange crystalline product was filtered out, washed successively with water, ethanol, and ether, and dried under vacuum to give orange microcrystals of $[OsCl_2(\eta^6\text{-}o\text{-}C_6H_4Me_2)]_2$ (2.56 g, 51% based on $(NH_4)_2OsCl_6$). ^1H NMR (DMSO-d^6, 300 MHz): δ 6.00 (s, $Me_2C_6H_4$), 2.02 (s, $Me_2C_6H_4$). $^{13}C\{^1H\}$ NMR (DMSO-d^6, 75.43 MHz): δ 92.84 ($C^{1,2}$), 78.60, 77.38 ($C^{2,5}$, $C^{3,4}$), 16.13 (Me). IR (Nujol): 301, 258 cm^{-1} [ν(Os-Cl)]. Anal. Calcd for $C_{16}H_{20}Cl_4Os_2$: C, 26.16, H, 2.74. Found: C, 26.02; H, 2.73. MS (FAB): *m/z* 705, $[M - Cl]^+$.

(3) $Os(O_2CCH_3)_2(\eta^6\text{-}o\text{-}C_6H_4Me_2)$. A mixture of $[OsCl_2(\eta^6\text{-}o\text{-}C_6H_4Me_2)]_2$ (500 mg, 0.68 mmol) and silver acetate (455 mg, 2.73 mmol) was stirred for 3 d in benzene (100 mL). The resulting yellow solution was filtered through Celite to remove AgCl. The solvent was removed under reduced pressure to give $Os(O_2CCH_3)_2(\eta^6\text{-}o\text{-}C_6H_4Me_2)$ (553 mg, 90% yield) as yellow needles. Analytical data were consistent with a dihydrate formulation. ^1H NMR (C_6D_6, 300 MHz): δ 5.97, 5.75 (each dd, J_{HH} = 3.65, 1.95 Hz, $Me_2C_6H_4$), 1.95 (s, $Me_2C_6H_4$), 1.70 (s, $MeCO_2$). Anal. Calcd for $C_{12}H_{16}O_4Os{\cdot}2H_2O$: C, 32.00; H, 4.47. Found: C, 32.28; H, 4.26. MS (EI): *m/z* 418 (parent ion).

(4) $[Os(O_2CCF_3)(\eta^6\text{-}o\text{-}C_6H_4Me_2)(PMe_2Ph)_2]PF_6$ (5). A sample of $Os(O_2CCH_3)_2(\eta^6\text{-}o\text{-}C_6H_4Me_2)$ (547 mg, 1.32 mmol) was treated with trifluoroacetic acid (10 mL) for 30 min. The excess of acid was removed under reduced pressure and the red oily residue, presumed to contain $Os(O_2CCF_3)_2(\eta^6\text{-}o\text{-}C_6H_4Me_2)$, was dissolved in methanol (20 mL) to give a yellow-

(6) Chappell, S. D.; Cole-Hamilton, D. J.; Galas, A. M. R.; Hursthouse, M. B. *J. Chem. Soc., Dalton Trans.* **1982**, 1867.
(7) Simpson, N. J.; Cole-Hamilton, D. J. *J. Chem. Soc., Dalton Trans.* **1990**, 1329.
(8) Hull, J. W., Jr.; Gladfelter, W. L. *Organometallics* **1982**, *1*, 1716.
(9) Hull, J. W., Jr.; Mann, C.; Gladfelter, W. L. *Organometallics* **1992**, *11*, 3117.
(10) Hull, J. W., Jr.; Roesselet, K. J.; Gladfelter, W. L. *Organometallics* **1992**, *11*, 3630.
(11) Madonik, A. M.; Astruc, D. *J. Am. Chem. Soc.* **1984**, *106*, 2437.
(12) Mena, M.; Royo, P.; Serrano,R.; Pellinghelli, M. A.; Tiripicchio, A. *Organometallics* **1988**, *7*, 258.
(13) Bennett, M. A.; McMahon, I. J.; Turney, T. W. *Angew. Chem., Int. Ed. Engl.* **1982**, *21*, 379; *Angew. Chem., Suppl.* **1982**, 853. Bennett, M. A.; Goh, L. Y.; McMahon, I. J.; Mitchell, T. R. B.; Robertson, G. B.; Turney, T. W.; Wickramasinghe, W. A. *Organometallics* **1992**, *11*, 3069.
(14) Elzinga, J.; Hogeveen, H. J. *J. Org. Chem.* **1980**, *45*, 3957.
(15) Perrin, D. D.; Armarego, W. L. F. *Purification of Laboratory Chemicals*, 3rd ed.; Pergamon Press: Oxford, U.K. 1988.
(16) Bennett, M. A.; Weerasuria, A. M. M. *J. Organomet. Chem.* **1990**, *394*, 481.

Table 1. ^{1}H, ^{13}C{^{1}H}, and ^{31}P{^{1}H} NMR Data for *o*-Xylylene Compounds 6–8[a]

compd	*o*-xylylene assgnt	$\delta(^{13}C\{^1H\})$	δ^1H	phosphine $\delta^{31}P\{^1H\}$	δ^1H
Ru{$(CH_2)_2C_6H_4$}$(PMe_2Ph)_3$ (**6**)[b]	=CH_2	93.98	5.10 (s), 4.76 (s)	13.03 (d, 2P)[c]	PMe_2*Ph*: 7.0–7.3 (m, 15H)
	H–$C_{1,2}$	149.95		1.09 (t, 1P, J_{PP} = 12.2 Hz)[c]	P*Me*$_2$Ph: 1.60 (d, 6H, J_{PH} = 6.3 Hz),[d]
	H–$C_{3,6}$	79.50	4.67 (dd, J = 2.7, 4.6 Hz)		1.08 (6H)[d], 0.96 (6H)[d].
	H–$C_{4,5}$	55.30 (q, J_{PC} = 6.5 Hz)	3.17 (dd, J = 2.7, 4.6 Hz)		
Os{$(CH_2)_2C_6H_4$}$(PMe_2Ph)_3$ (**7**)[b]	=CH_2	94.78	5.23 (s), 4.86 (s)	−34.31 (d, 2P)[e]	PMe_2*Ph*: 7.0–7.8 (m, 15H)
	H–$C_{1,2}$	151.04		−39.81 (t, 1P, J_{PP} = 4.6 Hz)[e]	P*Me*$_2$Ph: 1.71 (d, 6H, J_{PH} = 7.97 Hz),[f]
	H–$C_{3,6}$	73.97	4.57 (dd, J = 2.0, 4.6 Hz)		1.30 (d, 6H, J_{PH} = 6.34 Hz),[f]
	H–$C_{4,5}$	47.63 (q, J_{PC} = 6.2 Hz)	3.14 (dd, J = 2.0, 4.6 Hz)		1.09 (d, 6H, J_{PH} = 5.93 Hz),[f]
endo-{Ru$(PMe_2Ph)_3$}-*exo*-{Fe$(CO)_3$}{$(CH_2)_2C_6H_4$} (**8**)[g,h]	=CH_2	38.81	1.91 (d, J_{HH} = 2.1 Hz), 0.18 (d, J_{HH} = 2.1 Hz)	10.65 (d, 2P),	PMe_2*Ph*: 6.9–7.7 (m, 15H)
	H–$C_{1,2}$	154.04		9.04 (t, 1P, J_{PP} = 5.7 Hz)	P*Me*$_2$Ph: 1.66 (d, 6H, J_{PH} = 6.4 Hz),
	H–$C_{3,6}$	84.92	5.54 (s)		0.94 (6H), 0.77 (6H)
	H–$C_{4,5}$	48.74 (t, J_{PC} = 12.8 Hz)	2.29 (dd, J = 3.2, 3.7 Hz)		

[a] ^{1}H NMR at 300 MHz, ^{31}P NMR at 121.42 MHz, and ^{13}C NMR at 75.43 MHz. ^{1}H resonances are related to the ^{13}C resonance of the carbon to which they are directly bound by two-dimensional [^{1}H–^{13}C]-COSY and are numbered as shown in Scheme 1; **6** in toluene-d_8 at 223 K; **7** in benzene-d_6 at 328 K; **8** in benzene-d_6 at 293 K. [b] ^{1}H and ^{31}P at 248 K in toluene-d_8, ^{13}C{^{1}H} in benzene-d_6 at 293 K. [c] At higher temperatures these collapse and coalesce into one resonance at $\delta(^{31}P)$ 9.0, coalescence temperature 314 K at 121.42 MHz (7.05 T) (see text). [d] At higher temperatures these collapse and coalesce to finally give one resonance at δ 1.33 (d, 18H, J_{PH} = 5.53 Hz) (see text). [e] At higher temperatures these coalesce into one resonance at $\delta(^{31}P)$ −37.3, coalescence temperature 324 K at 121.42 MHz (7.05 T) (see text). [f] At 300 MHz (7.05 T) these resonances collapse and coalesce to finally give one resonance at δ 1.49 (see text). [g] In benzene-d_6 at 293 K. [h] ^{13}C{^{1}H} NMR δ 214.31, 214.09, 213.82 (CO).

orange solution. Addition of PMe_2Ph (376 μL, 2.64 mmol) gave a red solution, which on treatment with NH_4PF_6 in water (2 mL) gave the product as a pale yellow precipitate. After filtration, washing with water, and drying under vacuum, the yield was 546 mg (49%). Analytical data and the IR spectrum were consistent with a monohydrate formulation. ^{1}H NMR (CD_2Cl_2, 300 MHz): δ 7.7–7.5 (m, PMe_2*Ph*), 5.50 (m), 5.45 (m) (Me_2C_6*H*$_4$), 1.83 (vt, $^2J_{PH}$ + $^4J_{PH}$ = 10.6 Hz), 1.72 (vt, $^2J_{PH}$ + $^4J_{PH}$ = 10.4 Hz) (P*Me*$_2$Ph), 1.80 (s, *Me*$_2$C$_6$H$_4$). ^{31}P{^{1}H} NMR (CD_2Cl_2, 121.42 MHz): δ −33.6 (s, PMe_2Ph), −143.7 (spt, PF_6, J_{PF} = 711 Hz). Anal. Calcd for $C_{26}H_{32}F_9O_2OsP_3.H_2O$: C, 36.80; H, 4.04; P, 10.95. Found: C, 36.39; H, 3.58; P, 10.86. MS (FAB): *m/z* 689, [M−PF_6]$^+$.

(5) [Os(η^6-*o*-$C_6H_4Me_2$)(PMe_2Ph)$_3$](PF_6)$_2$ (4). A solution of [Os(O_2CCF_3)(η^6-*o*-$C_6H_4Me_2$)(PMe_2Ph)$_2$]PF_6 (**5**) in methanol (20 mL), prepared as described above from [$OsCl_2$(η^6-*o*-$C_6H_4Me_2$)$_2$ (500 mg), was treated successively with PMe_2Ph (1.2 mL, 8.5 mmol) and NH_4PF_6 (2.22 g, 13.62 mmol, excess), and the mixture was stirred at 60 °C for 16 h. The resulting white precipitate was filtered out, washed with methanol and *n*-hexane, and recrystallized from acetone/ether to give [Os(η^6-*o*-$C_6H_4Me_2$)(PMe_2Ph)$_3$](PF_6)$_2$ (**4**) (1.19 g, 78%). Analytical data and the IR spectrum (KBr pellet, ν(C=O) 1720 cm^{-1}) are consistent with its formulation as a bis(acetone) solvate. ^{1}H NMR (acetone-d^6, 300 MHz): δ 7.9–7.3 (m, PMe_2*Ph*), 6.86, 6.83 (m, Me_2C_6*H*$_4$), 2.25 (vt, $^2J_{PH}$ + $^4J_{PH}$ = 8.76 Hz, P*Me*$_2$Ph), 2.00 (s, *Me*$_2$C$_6$H$_4$). ^{31}P{^{1}H} NMR (acetone-d^6, 121.42 MHz): δ -42.72 (s, PMe_2Ph), −142.38 (spt, PF_6, J_{PF} = 708 Hz). Anal. Calcd for $C_{32}H_{43}F_{12}OsP_5$·2Me_2CO: C, 40.86; H, 4.96; P, 13.86. Found: C, 41.09; H, 4.53; P, 13.97. MS [FAB]: *m/z* 859, [M − PF_6]$^+$.

(6) Ru{η^4-*endo*-*o*-$(CH_2)_2C_6H_4$}(PMe_2Ph)$_3$(6). A stirred suspension of [Ru(η^6-*o*-$C_6H_4Me_2$)(PMe_2Ph)$_3$](PF_6)$_2$ (**3**) (2.82 g, 3.09 mmol) in THF (200 mL) was treated with an excess of KO-*t*-Bu (3.48 g, 31.0 mmol) for 30 min. The THF was removed under reduced pressure, and the resulting yellow residue was extracted with benzene (100 mL). The solution was filtered through Celite, and the solvent was removed under reduced pressure to give a yellow powder. The product was washed with *n*-hexane (20 mL) and dried under vacuum to give **6** (1.59 g, 83%). Crystals of **6** suitable for single-crystal X-ray analysis were grown from benzene by slow evaporation. IR (C_6H_6): 1588 cm^{-1} [ν(free C=C)]. Anal. Calcd for $C_{32}H_{41}P_3Ru$: C, 62.03; H, 6.67. Found: C, 62.00; H, 6.51. MS (EI): *m/z* 623 (parent ion). NMR data for **6** are given in Table 1.

(7) Os{η^4-*endo*-*o*-$(CH_2)_2C_6H_4$}(PMe_2Ph)$_3$ (7). A stirred suspension of complex **4** (500 mg, 0.50 mmol) in THF (50 mL) was treated with an excess of KO-*t*-Bu (561 mg, 5.0 mmol) for 4 d. The THF was removed under reduced pressure and the oily yellow residue was extracted with benzene (3 × 20 mL). The solvent was removed under reduced pressure, and the residue was washed with *n*-hexane (2 × 20 mL). Yellow crystals of **7** (145 mg, 41%) were obtained by crystallization from benzene/*n*-hexane. Crystals of **7** suitable for single-crystal X-ray analysis were grown by solvent diffusion of *n*-hexane into a toluene-d^8 solution. IR (toluene-d^8): 1595 cm^{-1}[ν(free C=C)]. Anal. Calcd for $C_{32}H_{41}OsP_3$: C, 54.23; H, 5.83. Found: C, 53.97; H, 5.44. MS (EI): *m/z* 712 (parent ion). NMR data for **7** are given in Table 1.

(8) Reaction of Ru{η^4-*endo*-*o*-$(CH_2)_2C_6H_4$}(PMe_2Ph)$_3$ (6) with Fe(CO)$_4$(NMe_3). A solution of Fe(CO)$_4$(NMe_3) (43 mg, 0.189 mmol) in benzene (10 mL) was added to a stirred solution of **6** (116 mg, 0.187 mmol) in benzene (30 mL), and the mixture was stirred at room temperature for 3 d. The solvent and unchanged Fe(CO)$_4$(NMe_3) were removed under reduced pressure. The residue was extracted with *n*-pentane (5 × 50 mL). Concentration of the extracts to *ca.* 2 mL and cooling to −78 °C afforded *endo*-{Ru(PMe_2Ph)$_3$}-*exo*-{Fe(CO)$_3$}{μ-η^4,η^4-$(CH_2)_2C_6H_4$} (**8**) (59 mg, 42%) as bright yellow microcrystals. Crystals of **8** suitable for single-crystal X-ray analysis were grown from ether at −78 °C. IR (benzene): 2017 (vs), 1940 (vs) cm^{-1} [ν(CO)]. Anal. Calcd for $C_{35}H_{41}FeO_3P_3Ru$: C, 55.35; H, 5.44. Found: C, 55.03; H, 5.49. MS (FAB): *m/z* 760 (weak-parent ion). NMR data for **8** are given in Table 1.

Crystal Structure Determinations. The crystal and refinement data for compounds **6–8** are summarized in Table 2. The crystals, prepared as described above, were mounted in 0.3 mm Lindemann capillaries in silicone grease to prevent movement during data collection.

Structures **6** and **7** were solved by Patterson methods (DIRDIF92 PATTY),[17] structure **8** was solved by direct methods (SIR88),[18] and all three were refined by full-matrix least-squares analysis. Positional and anisotropic thermal parameters for non-hydrogen atoms were refined by the full-matrix least-squares method. Hydrogen atoms were included at calculated positions (C–H = 0.95 Å) except for H(3), H(4), H(5), and H(6) [and in the case of molecule **7**, atoms H(11a,b) and H(21a,b), also], which were obtained from a Fourier difference synthesis and held fixed. Calculations were performed using the TEXSAN crystal structure analysis package.[19]

(17) Beurskens, P. T.; Admiraal,G.; Beurskens, G.; Bosman, W. P.; Garcia-Granda, S.; Gould, R. O.; Smits, J. M. M.; Symkalla, C. The DIRDIF Program System, Technical Report of the Crystallography Laboratory, University of Nijmegen, The Netherlands, 1992.
(18) Burla, M. C.; Camalli,M.; Cascarano,G.; Giacovazzo, C.; Polidori, G.; Spagna, R.; Viterbo, D. *J. Appl. Crystallogr.* **1989**, *22*, 389.
(19) TEXSAN: Single Crystal Structure Analysis Software, Version 1.6c; Molecular Structure Corp., The Woodlands, TX 77381, 1993.

Table 2. Crystal and Refinement Data for Compounds 6–8

compd	$Ru\{(CH_2)_2C_6H_4\}(PMe_2Ph)_3$ (**6**)	$Os\{(CH_2)_2C_6H_4\}(PMe_2Ph)_3$ (**7**)	*endo*-$\{Ru(PMe_2Ph)_3]\}$-*exo*-$\{Fe(CO)_3\}\{(CH_2)_2C_6H_4\}$ (**8**)
		(a) Crystal Data	
chem formula	$C_{32}H_{41}P_3Ru$	$C_{32}H_{41}OsP_3$	$C_{35}H_{41}FeO_3P_3Ru$
fw	619.67	708.80	759.55
cryst system	monoclinic	monoclinic	triclinic
unit cell dimens			
a (Å)	31.540(3)	31.487(2)	10.107(2)
b (Å)	11.793(4)	11.759(2)	12.162(2)
c (Å)	16.739(3)	16.784(3)	14.339(2)
α (deg)			84.86(1)
β (deg)	104.58(1)	104.625(8)	80.69(1)
γ (deg)			86.00(1)
V (Å3)	6025(1)	6013(1)	1729.7(5)
space group	$C2/c$	$C2/c$	$P\bar{1}$
D_c (g cm^{-3})	1.366	1.566	1.459
Z	8	8	2
F(000)	2576	2832	780
color, habit	yellow needle	pale yellow needle	orange block
cryst dimens	0.44 × 0.10 × 0.13	0.36 × 0.24 × 0.20	0.16 × 0.24 × 0.36
μ (cm^{-1})	6.99 (Mo Kα)	44.18 (Mo Kα)	10.28 (Mo Kα)
		(b) Data Collection and Processing	
diffractometer	Rigaku AFC 6S	Rigaku AFC 6S	Rigaku AFC 6S
X-radiation	Mo Kα	Mo Kα	Mo Kα
scan mode	$\omega-2\theta$	$\omega-2\theta$	$\omega-2\theta$
ω-scan width	0.79 + 0.34 tan θ	1.00 + 0.34 tan θ	0.90 + 0.34 tan θ
2θ limits (deg)	50.1	50.1	50.1
min, max h,k,l	0, 38	−38, 38	0, 12
	0, 14	0, 14	−14, 14
	−20, 20	0, 20	−17, 17
no. of reflcns			
total	5729	5797	6376
unique (R_{int}/%)	5618 (4.2)	5595 (1.1)	6122 (0.9)
obsd	3027	4258	5025
	[$I > 3\sigma(I)$]	[$I > 3\sigma(I)$]	[$I > 3\sigma(I)$]
abs corr	azimuthal scans	azimuthal scans	azimuthal scans
min, max corr	0.9000, 1.0000	0.9035, 1.0000	0.9228, 1.0000
		(c) Structure Analysis and Refinement	
structure soln	Patterson methods (DIRDIF92 PATTY)	Patterson methods (DIRDIF92 PATTY)	direct methods (SIR88)
refinement	full-matrix least-squares	full-matrix least-squares	full-matrix least-squares
no. of params	326	326	388
weighting scheme	$w = 4F_o^2/[\sigma^2(F_o^2) + (0.005F_o^2)^2]$	$w = 4F_o^2/[\sigma^2(F_o^2) + (0.002F_o^2)^2]$	$w = 4F_o^2/[\sigma^2(F_o^2) + (0.001F_o^2)^2]$
R(obsd data) (%)	3.5	1.9	3.4
R_w(obsd data) (%)	2.7	1.4	2.4

Results and Discussion

The *o*-xylene ruthenium(II) salt $[Ru(\eta^6\text{-}o\text{-}C_6H_4Me_2)(PMe_2Ph)_3](PF_6)_2$ (**3**) was first prepared by treatment of the exocyclic *o*-xylylene ruthenium(0) complex **2** with an excess of HPF_6,[13] but it can be made more directly by displacement of trifluoroacetate ion from $[Ru(O_2CCF_3)(\eta^6\text{-}o\text{-}C_6H_4Me_2)(PMe_2Ph)_2]PF_6$[13] with an excess of PMe_2Ph and NH_4PF_6 in methanol at 60 °C. It was isolated in 87% yield as an air-stable, microcrystalline, pale yellow solid. The corresponding osmium salt $[Os(O_2CCF_3)(\eta^6\text{-}o\text{-}C_6H_4Me_2)(PMe_2Ph)_2]PF_6$ (**5**) was made similarly to its ruthenium analogue, starting from $[OsCl_2(\eta^6\text{-}o\text{-}C_6H_4Me_2)]_2$; the latter was prepared similarly to its mesitylene and *p*-cymene analogues[16,20] as a poorly soluble solid in 51% yield by reaction of Na_2OsCl_6 with 1,2-dimethyl-1,4-cyclohexadiene in refluxing ethanol. Reaction with silver acetate gave the bis(acetate), $Os(O_2CMe)_2(\eta^6\text{-}o\text{-}C_6H_4Me_2)$, in 90% yield. The structure of the bis(acetate) is presumed to be $Os(\eta^2\text{-}O_2CCH_3)(\eta^1\text{-}O_2CCH_3)(\eta^6\text{-}o\text{-}C_6H_4Me_2)$ like that of other (η^6-arene)ruthenium(II) and (η^6-arene)osmium(II) complexes of this type.[21,22] However, the IR spectrum has not been examined to confirm this point. The bis(acetate) was converted into the bis(trifluoroacetate) on treatment with CF_3CO_2H. This compound was not isolated; direct treatment with an excess of PMe_2Ph and NH_4PF_6 in methanol at 60 °C gave initially a yellow precipitate of $[Os(O_2CCF_3)(\eta^6\text{-}o\text{-}C_6H_4Me_2)(PMe_2Ph)_2]PF_6$ (**5**) and, after 16 h, a colorless precipitate of $[Os(\eta^6\text{-}o\text{-}C_6H_4Me_2)(PMe_2Ph)_3](PF_6)_2$ (**4**), which was recrystallized from acetone/ether and characterized by elemental analysis and spectroscopy (NMR, IR) as the bis(acetone) solvate. The intermediate **5** was synthesized independently by treatment of the bis(trifluoroacetate) with PMe_2Ph (2 equiv) and NH_4PF_6 at room temperature and was also completely characterized. Treatment of isolated **5** with an excess of PMe_2Ph and NH_4PF_6 in methanol at 60 °C gave a mixture of **4** and other unidentified compounds that proved difficult to separate, so the more convenient "one-pot" procedure was adopted.

In contrast to the behavior of $[Ru(O_2CCF_3)(\eta^6\text{-}o\text{-}C_6H_4Me_2)(PMe_2Ph)_2]PF_6$,[13] treatment of **5** with $K[N(SiMe_3)_2]\cdot$2dioxane in the presence of an excess of PMe_2Ph did not afford the osmium analogue of **2**, $Os\{\eta^4\text{-}exo\text{-}o\text{-}(CH_2)_2C_6H_4\}(PMe_2Ph)_3$, or any other isolable products.

Treatment of suspensions of **3** or **4** in THF with KO*t*-Bu gave the *endo*-*o*-xylylene complexes $M\{\eta^4\text{-}endo\text{-}o\text{-}$

(20) Cabeza, J. A.; Maitlis, P. M. *J. Chem. Soc., Dalton Trans.* **1985**, 573.

(21) Tocher, D. A.; Gould, R. O.; Stephenson, T. A.; Bennett, M. A.; Ennett, J. P.; Matheson, T. W.; Sawyer, L. ; Shah, V. K. *J. Chem. Soc., Dalton Trans.* **1983**, 1571.

(22) Werner, H.; Kletzin, H. *J. Organomet. Chem.* **1982**, *228*, 289.

Scheme 1

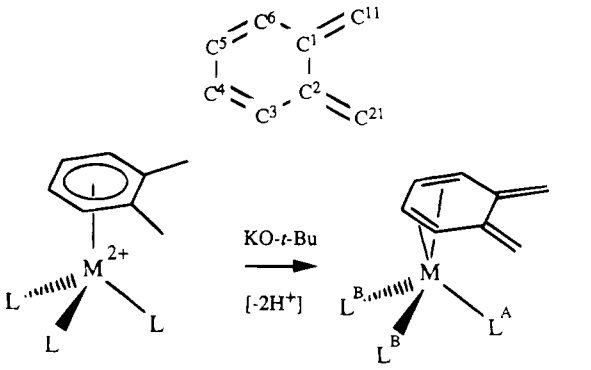

$(CH_2)_2C_6H_4\}(PMe_2Ph)_3$ [M = Ru(**6**), Os(**7**)] as air-sensitive, yellow, crystalline solids in 87% and 41% yields, respectively (Scheme 1). The reaction appeared to be immediate for **3** but required 96 h for completion in the case of **4**. The compounds have been characterized by IR, NMR (^{1}H, ^{13}C, and ^{31}P), and mass spectroscopy and by X-ray crystallography (see below). The NMR data for **6** and **7** are collected in Table 1 along with that for **8**; carbon atoms are numbered as shown in Scheme 1, and hydrogen atoms are numbered according to the carbon atom to which they are attached.

The IR spectra exhibit a weak band due to ν(C=C) of the uncoordinated *exo*-methylene group at 1588 cm^{-1} (**6** in C_6H_6) and 1595 cm^{-1} (**7** in toluene-d^8); *cf.* 1590 cm^{-1} for Ru(η^6-*o*-$C_6H_4Me_2$)\{η^4-*endo*-*o*-$(CH_2)_2C_6Me_4$\}[9] and 1567 cm^{-1} for K[Mn\{η^4-*endo*-*o*-$(CH_2)_2C_6Me_4$\}$(CO)_3$].[10] The compounds show parent ion peaks in their EI-mass spectra.

The ^{1}H NMR spectra of compounds **6** and **7** show a characteristic pair of singlets at δ *ca.* 4.8 and 5.2 due to the *exo*-methylene protons and two doublets of doublets at δ *ca.* 3.1 and 4.6 due to the ring protons of the coordinated *o*-xylylene. Similar patterns have been observed in other endo-coordinated *o*-xylylene metal complexes.[8-11] In their ^{13}C\{^{1}H\} NMR spectra **6** and **7** show resonances for the methylene carbon atoms at δ 93.98 and 94.78, respectively, which are comparable with the values of δ 89.04 and 88.0 for M(η^6-C_6Me_6)\{η^4-*endo*-*o*-$(CH_2)_2C_6Me_4$\} (M = Ru;[8] M = Fe[11]) and δ 86.3 and 88.2, respectively, for K[Mn\{η^4-*endo*-*o*-$(CH_2)_2C_6R_4$\}$(CO)_3$] (R = Me, H).[10] The signals due to the uncoordinated pair of carbon atoms appear at δ 149.95 and 151.04 for **6** and **7**, respectively; those due to the two pairs of coordinated ring carbon atoms appear as quartets due to coupling with the three ^{31}P nuclei at δ 79.50 and 55.30 (q, J_{PC} = 6.5 Hz) for **6** and at δ73.97 and 47.63 (q, J_{PC} = 6.2 Hz) for **7**. At room temperature the ^{31}P\{^{1}H\} NMR spectra of the phosphine ligands of **6** and **7** appear as broad resonances in a 2:1 ratio at δ *ca.* 13 and 1 and δ *ca.* −34 and −39, respectively; these resolve into a well-defined doublet and triplet at −25 °C (see Table 1). The low-temperature spectra are consistent with a structure in which a pair of equivalent PMe_2Ph ligands are related by a mirror plane bisecting the *o*-xylylene ligand and a unique PMe_2Ph ligand lies in the mirror plane; these ligands are labeled B and A, respectively, in Scheme 1. This arrangement is confirmed by the X-ray structural analysis discussed below.

Above −25 °C the two resonances begin to coalesce reversibly to a singlet at the weighted average position,

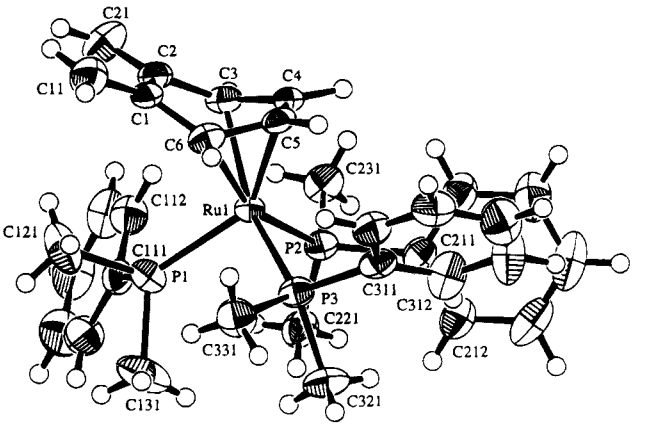

Figure 1. Molecular structure of Ru\{η^4-*endo*-*o*-$(CH_2)_2C_6H_4$\}$(PMe_2Ph)_3$ (**6**) with 50% ellipsoids.

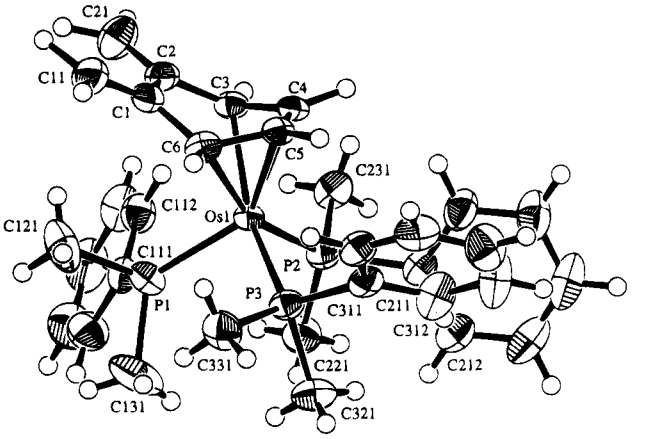

Figure 2. Molecular structure of Os\{η^4-*endo*-*o*-$(CH_2)_2C_6H_4$\}$(PMe_2Ph)_3$ (**7**) with 50% ellipsoids.

probably owing to rotation of the M$(PMe_2Ph)_3$ fragment with respect to the *o*-xylylene ligand. The coalescence temperature for the averaging of the two ^{31}P resonances is estimated to be 314 K for compound **6** and 324 K for compound **7**, and the rates of exchange at these temperatures obtained from the standard equation $k = \pi\Delta\nu/2^{1/2}$ are 3222 and 1483 s^{-1}, respectively. The derived free energies of activation ($\Delta G^{\ddagger}$) for the exchange process are 56 and 60 kJ mol^{-1} for **6** and **7**, respectively. The same process is evident in the behavior of the PMe_2 resonances, which at −25 °C consist of three three-proton doublets (δ 1.60, 1.08, and 0.96 for **6**; δ 1.17, 1.30, and 1.07 for **7**). Above −25 °C the two lower frequency, more closely spaced doublets collapse first and coalesce while the higher frequency doublet broadens. As the temperature is raised further, these two peaks collapse and coalesce. The estimated coalescence temperatures at 300 MHz are 268 and 283 K for **6** and 295 and 309 K for **7**, and the rates of exchange at these temperatures are 95 and 381 s^{-1} for **6** and 141 and 339 s^{-1} for **7**. These give $\Delta G^{\ddagger}$ values of 55kJ mol^{-1} and 60kJ mol^{-1} for **6** and **7**, respectively, in agreement with the estimates made from the ^{31}P spectra.

The geometry of complexes **6** and **7** was established by single-crystal X-ray diffraction analyses. The crystal and refinement data for these two compounds are shown in Table 2 together with those of compound **8** (see below). The molecular structures of **6** and **7** are shown in Figures 1 and 2, respectively, together with the atom numbering. The atomic coordinates and equivalent isotropic thermal parameters are given in Tables 3 and

Table 3. Atomic Coordinates and Isotropic Displacement Parameters (Å²) for $Ru\{\eta^4\text{-}endo\text{-}o\text{-}(CH_2)_2C_6H_4\}(PMe_2Ph)_3$ (6)

atom	x	y	z	B_{eq}
Ru(1)	0.12715(1)	0.02059(4)	−0.13454(3)	2.352(9)
P(1)	0.14556(5)	0.1626(1)	−0.03673(9)	3.36(4)
P(2)	0.08100(5)	−0.0763(1)	−0.07085(9)	2.75(3)
P(3)	0.18729(5)	−0.0919(1)	−0.08177(9)	2.96(4)
C(1)	0.1354(2)	0.1961(5)	−0.2650(3)	3.0(1)
C(2)	0.0892(2)	0.2066(5)	−0.2589(3)	3.1(1)
C(3)	0.0726(2)	0.1016(5)	−0.2317(3)	3.0(1)
C(4)	0.0858(2)	−0.0063(4)	−0.2572(3)	2.8(1)
C(5)	0.1294(2)	−0.0131(5)	−0.2591(3)	2.8(1)
C(6)	0.1552(2)	0.0869(5)	−0.2368(3)	3.1(1)
C(11)	0.1571(2)	0.2806(5)	−0.2905(4)	4.7(2)
C(21)	0.0662(2)	0.3008(5)	−0.2732(4)	5.0(2)
C(111)	0.1023(2)	0.2294(5)	0.0033(3)	3.1(1)
C(112)	0.0603(2)	0.2395(5)	−0.0487(4)	4.0(2)
C(113)	0.0269(2)	0.2896(5)	−0.0212(4)	4.9(2)
C(114)	0.0341(2)	0.3300(6)	0.0579(5)	5.6(2)
C(115)	0.0748(3)	0.3211(6)	0.1093(4)	5.7(2)
C(116)	0.1089(2)	0.2709(5)	0.0825(4)	4.4(2)
C(121)	0.1695(2)	0.2901(5)	−0.0699(4)	5.6(2)
C(131)	0.1872(2)	0.1373(6)	0.0614(4)	6.4(2)
C(211)	0.0779(2)	−0.2314(5)	−0.0810(3)	3.0(1)
C(212)	0.0895(2)	−0.3059(5)	−0.0151(4)	4.1(2)
C(213)	0.0872(2)	−0.4215(6)	−0.0273(5)	5.8(2)
C(214)	0.0729(2)	−0.4664(6)	−0.1044(5)	6.1(2)
C(215)	0.0610(2)	−0.3945(6)	−0.1703(4)	5.4(2)
C(216)	0.0633(2)	−0.2792(5)	−0.1588(4)	4.5(2)
C(221)	0.0855(2)	−0.0581(5)	0.0392(3)	3.9(2)
C(231)	0.0224(2)	−0.0457(5)	−0.1094(3)	3.9(2)
C(311)	0.1939(2)	−0.2185(5)	−0.1429(3)	3.2(1)
C(312)	0.1754(2)	−0.3213(6)	−0.1309(4)	4.6(2)
C(313)	0.1802(2)	−0.4167(6)	−0.1757(5)	6.2(2)
C(314)	0.2035(2)	−0.4107(6)	−0.2342(4)	5.3(2)
C(315)	0.2214(2)	−0.3104(6)	−0.2482(4)	4.2(2)
C(316)	0.2168(2)	−0.2145(5)	−0.2035(3)	3.7(2)
C(321)	0.1972(2)	−0.1559(5)	0.0213(3)	4.2(2)
C(331)	0.2411(2)	−0.0251(5)	−0.0734(3)	4.3(1)

Table 4. Selected Bond Lengths (Å) and Angles (deg) for $Ru\{\eta^4\text{-}endo\text{-}o\text{-}(CH_2)_2C_6H_4\}(PMe_2Ph)_3$ (6)

(a) Bond Lengths			
Ru(1)−P(1)	2.312(2)	Ru(1)−P(2)	2.311(2)
Ru(1)−P(3)	2.301(2)	Ru(1)−C(3)	2.261(5)
Ru(1)−C(4)	2.160(4)	Ru(1)−C(5)	2.141(4)
Ru(1)−C(6)	2.256(5)		
P(1)−C(211)	1.842(5)	P(1)−C(121)	1.830(6)
P(1)−C(131)	1.851(6)	P(2)−C(211)	1.830(6)
P(2)−C(221)	1.824(5)	P(2)−C(231)	1.832(5)
P(3)−C(311)	1.851(6)	P(3)−C(321)	1.836(5)
P(3)−C(331)	1.845(5)		
C(1)−C(11)	1.338(7)	C(1)−C(2)	1.490(7)
C(2)−C(21)	1.315(7)	C(2)−C(3)	1.462(7)
C(3)−C(4)	1.438(7)	C(4)−C(5)	1.384(6)
C(5)−C(6)	1.429(7)	C(6)−C(1)	1.457(7)
(b) Bond Angles			
P(1)−Ru(1)−P(2)	96.10(6)	P(1)−Ru(1)−P(3)	96.32(6)
P(1)−Ru(1)−C(3)	102.3(1)	P(1)−Ru(1)−C(4)	139.8(1)
P(1)−Ru(1)−C(5)	139.5(2)	P(1)−Ru(1)−C(6)	102.1(1)
P(2)−Ru(1)−P(3)	95.28(6)	P(2)−Ru(1)−C(3)	95.0(1)
P(2)−Ru(1)−C(4)	93.8(1)	P(2)−Ru(1)−C(5)	122.4(2)
P(2)−Ru(1)−C(6)	159.1(1)	P(3)−Ru(1)−C(3)	157.6(1)
P(3)−Ru(1)−C(4)	121.5(1)	P(3)−Ru(1)−C(5)	92.3(1)
P(3)−Ru(1)−C(6)	92.8(1)		
Ru(1)−P(1)−C(111)	119.4(2)	Ru(1)−P(1)−C(121)	115.4(2)
Ru(1)−P(1)−C(131)	120.5(2)	C(111)−P(1)−C(121)	99.1(3)
C(111)−P(1)−C(131)	99.8(3)	C(121)−P(1)−C(131)	98.5(3)
Ru(1)−P(2)−C(211)	118.3(2)	Ru(1)−P(2)−C(221)	120.7(2)
Ru(1)−P(2)−C(231)	115.9(2)	C(211)−P(2)−C(221)	101.5(3)
C(211)−P(2)−C(231)	97.9(2)	C(221)−P(2)−C(231)	98.5(2)
Ru(1)−P(3)−C(311)	116.7(2)	Ru(1)−P(3)−C(321)	121.8(2)
Ru(1)−P(3)−C(331)	115.9(2)	C(311)−P(3)−C(321)	99.9(3)
C(311)−P(3)−C(331)	99.0(3)	C(321)−P(3)−C(331)	99.7(3)
C(11)−C(1)−C(2)	123.1(5)	C(11)−C(1)−C(6)	123.4(5)
C(21)−C(2)−C(1)	124.1(6)	C(21)−C(2)−C(3)	123.2(5)
C(1)−C(2)−C(3)	112.7(5)	C(2)−C(3)−C(4)	120.2(5)
C(3)−C(4)−C(5)	115.0(5)	C(4)−C(5)−C(6)	116.8(5)
C(5)−C(6)−C(1)	118.4(4)	C(6)−C(1)−C(2)	113.4(5)

5, and selected bond lengths and angles are given in Tables 4 and 6, respectively.

The compounds are both isomorphous (see Table 1) and isostructural. In agreement with the spectroscopic studies, the X-ray analyses show the $M(PMe_2Ph)_3$ moiety in both compounds to be bound to the endocyclic pair of double bonds of the η^4-*o*-xylylene. Both molecules contain the metal atom coordinated in a distorted square-pyramidal arrangement with the double bonds occupying the basal sites and the phosphorus atoms occupying the other three sites. The orientation of the $M(PMe_2Ph)_3$ moiety with respect to the η^4-diene is the same as found in the exo-isomer **2**,[6] with two phosphorus atoms lying directly under the coordinated diene. In both **6** and **7** the metal atoms are bound essentially symmetrically to the endo pair of double bonds and are slightly closer to C(4) and C(5) than to C(3) and C(6) [Ru−C(3,6) = 2.258 Å (average) *vs* Ru−C(4,5) = 2.150 Å (average), and Os−C(3,6) = 2.258 Å (average) *vs* Os−C(4,5) = 2.175 Å (average)]. The bond distances within the *ortho*-xylylene ligands are similar to those in $Ru(\eta^6\text{-}C_6Me_6)\{\eta^4\text{-}endo\text{-}o\text{-}(CH_2)_2C_6Me_4\}$,[8] the bond distances C(3)−C(4), C(4)−C(5), and C(5)−C(6) being almost equal and typical of a coordinated diene [average values 1.41 Å (**6**), 1.43 Å (**7**)]. The bond distances in the uncoordinated, exocyclic fragment show the short−long−short alternation expected for a 1,3-diene. The *o*-xylylene is characteristically bent away from the metal center at the termini of the coordinated diene. The dihedral angle between the C(3) to C(6) and C(6)−C(1)−C(2)−C(3) planes are 37.0 and 39.5° for **6** and **7**, respectively, similar to that found for the *o*-xylylene ligand in $Ru(\eta^6\text{-}C_6Me_6)\{\eta^4\text{-}endo\text{-}o\text{-}(CH_2)_2C_6Me_4\}$[8] (33.8°). In contrast, the coordinated *o*-xylylene in $Ru\{\eta^4\text{-}exo\text{-}o\text{-}(CH_2)_2C_6H_4\}(PMe_2Ph)_3$[6] is essentially flat, the dihedral angle between the C(3)−C(6) and C(6)−C(1)−C(2)−C(3) planes being 1.39° toward the ruthenium.

Although the η^4-*endo*-*o*-xylylene complexes **6** and **7** are susceptible to aerial oxidation, they appear to be quite stable in solution to either decomposition or isomerization to the corresponding *exo*-compounds. Over a period of 24 h, even at elevated temperatures (**6** in toluene-d^8 at 60 °C, **7** in benzene-d^6 at 55 °C), there is no evidence of decomposition or change.

Reaction of **6** with $Fe(CO)_4(NMe_3)$ in benzene at room temperature over 3 d affords a brown precipitate and a yellow solution. From the solution *endo*-$\{Ru(PMe_2Ph)_3\}$-*exo*-$\{Fe(CO)_3\}\{\mu\text{-}\eta^4,\eta^4\text{-}o\text{-}(CH_2)_2C_6H_4\}$ (**8**) was isolated as bright yellow microcrystals in 42% yield. It was characterized by NMR, IR, and mass spectroscopy, elemental analysis, and single-crystal X-ray diffraction. NMR spectroscopy revealed the brown precipitate to contain a number of species that we have so far been unable to separate and characterize.

The IR spectrum of **8** in benzene shows two strong ν(CO) bands at 2017 and 1940 cm^{-1}, which are similar to those observed for *endo*-$\{Ru(\eta^6\text{-}C_6Me_6)\}$-*exo*-$\{Fe(CO)_3\}\{\mu\text{-}\eta^4,\eta^4\text{-}o\text{-}(CH_2)_2C_6Me_4\}$[9] but to lower frequency than those observed for $Fe(CO)_3\{\eta^4\text{-}exo\text{-}(CH_2)_2C_6H_4\}$.[3]

In the ^{1}H NMR spectrum the methylene protons of the *o*-xylylene ligand are significantly shielded by coordination of the $Fe(CO)_3$ fragment to the exocyclic diene and appear as a pair of doublets at δ 0.18 (d, 2H) and 1.91 (d, 2H, J_{HH} = 2.1 Hz), respectively (Table 1). These chemical shifts are comparable with those observed for the methylene protons in complex **1** and in

Table 5. Atomic Coordinates and Isotropic Displacement Parameters (Å²) for Os{η^4-*endo-o*-$(CH_2)_2C_6H_4$}$(PMe_2Ph)_3$ (7)

atom	x	y	z	B_{eq}
Os(1)	0.127352(5)	0.02195(1)	0.366306(9)	2.354(3)
P(1)	0.14593(3)	0.16268(9)	0.46414(6)	3.32(3)
P(2)	0.08110(3)	−0.07486(9)	0.42960(6)	2.76(2)
P(3)	0.18738(3)	−0.09091(9)	0.41869(6)	2.92(2)
C(1)	0.1350(1)	0.2008(3)	0.2344(2)	3.01(10)
C(2)	0.0887(1)	0.2096(3)	0.2400(2)	3.14(10)
C(3)	0.0729(1)	0.1034(3)	0.2693(2)	2.77(9)
C(4)	0.0861(1)	−0.0045(3)	0.2426(2)	2.93(9)
C(5)	0.1300(1)	−0.0117(3)	0.2404(2)	2.66(8)
C(6)	0.1555(1)	0.0905(3)	0.2649(2)	3.03(10)
C(11)	0.1562(1)	0.2836(3)	0.2068(2)	4.3(1)
C(21)	0.0649(1)	0.3025(3)	0.2236(3)	4.8(1)
C(111)	0.1025(1)	0.2295(3)	0.5047(2)	3.2(1)
C(112)	0.0607(1)	0.2411(3)	0.4532(2)	3.8(1)
C(113)	0.0269(1)	0.2908(4)	0.4802(3)	4.8(1)
C(114)	0.0350(2)	0.3300(4)	0.5599(3)	5.5(1)
C(115)	0.0758(2)	0.3196(4)	0.6112(3)	5.6(1)
C(116)	0.1094(1)	0.2707(4)	0.5840(2)	4.5(1)
C(121)	0.1691(1)	0.2901(4)	0.4298(3)	5.6(1)
C(131)	0.1875(1)	0.1382(4)	0.5609(3)	6.3(1)
C(211)	0.0778(1)	−0.2305(3)	0.4187(2)	3.13(10)
C(212)	0.0893(1)	−0.3051(4)	0.4843(3)	4.1(1)
C(213)	0.0868(2)	−0,4217(4)	0.4721(3)	5.7(1)
C(214)	0.0725(2)	−0.4652(4)	0.3938(3)	5.9(1)
C(215)	0.0600(2)	−0.3925(4)	0.3280(3)	5.4(1)
C(216)	0.0634(1)	−0.2772(3)	0.3406(3)	4.3(1)
C(221)	0.0857(1)	−0.0581(3)	0.5396(2)	4.0(1)
C(231)	0.0225(1)	−0.0445(3)	0.3908(2)	3.8(1)
C(311)	0.1937(1)	−0.2175(3)	0.3573(2)	3.04(9)
C(312)	0.1752(1)	−0.3210(4)	0.3689(3)	4.6(1)
C(313)	0.1800(2)	−0.4155(4)	0.3228(3)	6.1(2)
C(314)	0.2034(1)	−0.4091(4)	0.2649(3)	5.2(1)
C(315)	0.2218(1)	−0.3082(4)	0.2520(2)	4.3(1)
C(316)	0.2169(1)	−0.2131(3)	0.2967(2)	3.5(1)
C(321)	0.1973(1)	−0.1563(3)	0.5213(2)	4.2(1)
C(331)	0.2415(1)	−0.0252(3)	0.4283(2)	4.19(10)

Table 6. Selected Bond Lengths (Å) and Angles (deg) for Os{η^4-*endo-o*-$(CH_2)_2C_6H_4$}$(PMe_2Ph)_3$ (7)

(a) Bond Lengths			
Os(1)−P(1)	2.300(1)	Os(1)−P(2)	2.308(1)
Os(1)−P(3)	2.295(1)	Os(1)−C(3)	2.259(3)
Os(1)−C(4)	2.177(3)	Os(1)−C(5)	2.172(3)
Os(1)−C(6)	2.257(3)		
P(1)−C(111)	1.850(4)	P(1)−C(121)	1.823(4)
P(1)−C(131)	1.834(4)	P(2)−C(211)	1.839(4)
P(2)−C(221)	1.825(4)	P(2)−C(231)	1.830(3)
P(3)−C(311)	1.849(4)	P(3)−C(321)	1.839(4)
P(3)−C(331)	1.842(4)		
C(1)−C(11)	1.330(5)	C(1)−C(2)	1.485(5)
C(2)−C(21)	1.315(5)	C(2)−C(3)	1.475(5)
C(3)−C(4)	1.442(4)	C(4)−C(5)	1.397(4)
C(5)−C(6)	1.447(4)	C(6)−C(1)	1.482(5)
(b) Bond Angles			
P(1)−Os(1)−P(2)	95.88(4)	P(1)−Os(1)−P(3)	96.09(4)
P(1)−Os(1)−C(3)	102.68(10)	P(1)−Os(1)−C(4)	140.09(10)
P(1)−Os(1)−C(5)	139.47(10)	P(1)−Os(1)−C(6)	101.75(10)
P(2)−Os(1)−P(3)	95.32(3)	P(2)−Os(1)−C(3)	95.06(9)
P(2)−Os(1)−C(4)	94.27(9)	P(2)−Os(1)−C(5)	122.81(10)
P(2)−Os(1)−C(6)	159.56(9)	P(3)−Os(1)−C(3)	157.45(9)
P(3)−Os(1)−C(4)	121.23(10)	P(3)−Os(1)−C(5)	92.10(9)
P(3)−Os(1)−C(6)	93.03(9)		
Os(1)−P(1)−C(111)	119.3(1)	Os(1)−P(1)−C(121)	114.6(1)
Os(1)−P(1)−C(131)	121.0(1)	C(111)−P(1)−C(121)	99.2(2)
C(111)−P(1)−C(131)	99.8(2)	C(121)−P(1)−C(131)	98.9(2)
Os(1)−P(2)−C(211)	118.1(1)	Os(1)−P(2)−C(221)	101.3(2)
Os(1)−P(2)−C(231)	115.9(1)	C(211)−P(2)−C(221)	101.3(2)
C(211)−P(2)−C(231)	97.6(2)	C(221)−P(2)−C(231)	98.9(2)
Os(1)−P(3)−C(311)	116.5(1)	Os(1)−P(3)−C(321)	121.9(1)
Os(1)−P(3)−C(331)	116.5(1)	C(311)−P(3)−C(321)	99.7(2)
C(311)−P(3)−C(331)	99.1(2)	C(321)−P(3)−C(331)	99.2(2)
C(11)−C(1)−C(2)	124.0(4)	C(11)−C(1)−C(6)	123.1(4)
C(21)−C(2)−C(1)	124.2(4)	C(21)−C(2)−C(3)	123.3(4)
C(1)−C(2)−C(3)	112.5(3)	C(2)−C(3)−C(4)	119.5(3)
C(3)−C(4)−C(5)	115.3(3)	C(4)−C(5)−C(6)	115.1(3)
C(5)−C(6)−C(1)	117.8(3)	C(6)−C(1)−C(2)	112.9(3)

exo-coordinated *o*-xylylene metal complexes.[3,5−7,12,13] The methylene carbon atoms in **8** (δ 38.8) also are more shielded than those in **6** (δ 94.0), the chemical shift being comparable with those for the corresponding carbon atoms in $Fe(CO)_3$(η^4-butadiene) (δ 40.5)[23] and in Ru{η^4-*exo-o*-$(CH_2)_2C_6H_4$}$(PMe_2Ph)_3$ (δ 35.4),[6] whereas the chemical shifts of the ring carbon atoms of the *o*-xylylene in **6** and **8** are not greatly different. The ^{13}C spectrum also shows all three CO groups to be inequivalent. The $^{31}P\{^1H\}$ NMR spectrum of **8** shows a well-resolved doublet and triplet in a 2:1 ratio ($^2J_{PP}$ = 5.7 Hz), so that the PMe_2Ph ligands of **8** are rigid on the NMR time scale at room temperature, unlike those of **6**.

A diagram of the molecular structure of compound **8** is shown in Figure 3, its crystal and refinement data are shown in Table 2, and the atomic coordinates and isotropic parameters for the non-hydrogen atoms are given in Table 7.

Each of the two metal−diene fragments has a distorted square pyramidal geometry in which the 1,3-diene units occupy the basal sites. In the solid state, the conformation about the ruthenium atom in **8** is the same as in **6**. The conformation of the $Fe(CO)_3$ fragment with respect to the *o*-xylylene is the same as that of the $Ru(PMe_2Ph)_3$ center in Ru{η^4-*exo-o*-$(CH_2)_2C_6H_4$}$(PMe_2Ph)_3$,[6] with two ligands lying under the diene unit. This differs from the conformation found in $Fe(CO)_3$(η^4-1,3-butadiene),[24] probably as a result of crystal packing

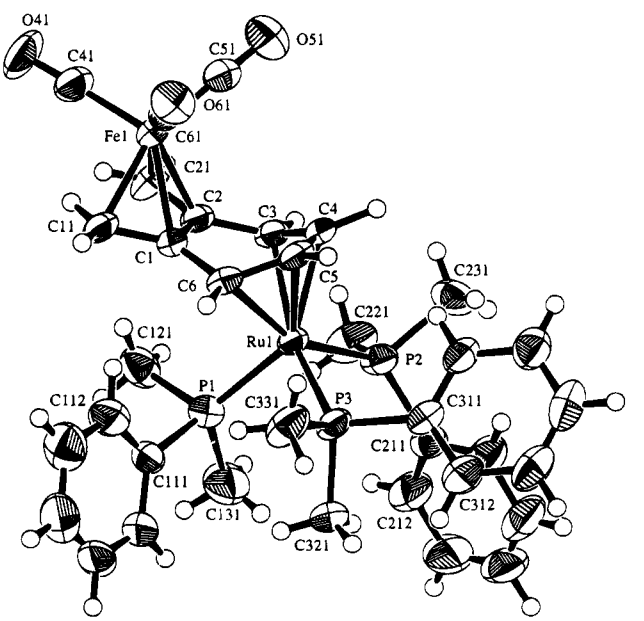

Figure 3. Molecular structure of *endo*-{$Ru(PMe_2Ph)_3$}-*exo*-{$Fe(CO)_3$}{μ-η^4,η^4-*o*-$(CH_2)_2C_6H_4$} (**8**) with 50% ellipsoids.

forces. The geometry of the *o*-xylylene ligand is changed very little as a result of attachment of the $Fe(CO)_3$ group, the dihedral angle between the C(3) to C(6) and C(6)−C(1)−C(2)−C(3) planes (36.8°) being very close to that in **6**. The C−C bond lengths within the six-membered ring for **8** and **6** are similar, but those in the exocyclic diene unit of **8** are almost equal within experimental error (1.42 Å, average), a feature that is characteristic of $Fe(CO)_3$(η^4-1,3-butadiene) complexes.[25,26]

(23) Mann, B. F.; Taylor, B. E. *^{13}C NMR Data for Organometallic Compounds*; Academic: New York, 1981; p 211.
(24) Mills, O. S.; Robinson, G. *Acta Crystallogr., Sect. C* **1963**, *16*, 758.

Table 7. Atomic Coordinates and Isotropic Displacement Parameters (Å²) for *endo*-{Ru(PMe₂Ph)₃}-*exo*-{Fe(CO₃)}{μ-η⁴,η⁴-*o*-(CH₂)₂C₆H₄} (8)

atom	x	y	z	B_{eq}
Ru(1)	0.69888(3)	0.25209(3)	0.69813(2)	2.810(8)
Fe(1)	0.81495(6)	0.37040(5)	0.36729(4)	3.35(1)
P(1)	0.8446(1)	0.09675(9)	0.69972(8)	3.86(3)
P(2)	0.7620(1)	0.33232(9)	0.82285(8)	3.68(3)
P(3)	0.5181(1)	0.16641(9)	0.78642(7)	3.55(3)
O(41)	0.9914(3)	0.3542(3)	0.1853(2)	7.1(1)
O(51)	0.7933(3)	0.6053(2)	0.3980(2)	6.08(10)
O(61)	0.5523(3)	0.3871(2)	0.3081(2)	5.29(9)
C(1)	0.7647(4)	0.2511(3)	0.4837(3)	2.99(9)
C(2)	0.8575(4)	0.3217(3)	0.5070(3)	3.11(10)
C(3)	0.8135(4)	0.3765(3)	0.5952(3)	3.19(10)
C(4)	0.6750(4)	0.4100(3)	0.6183(2)	3.20(10)
C(5)	0.5831(4)	0.3401(3)	0.5959(2)	3.4(1)
C(6)	0.6397(4)	0.2417(3)	0.5533(3)	3.16(10)
C(11)	0.7998(4)	0.1977(3)	0.3978(3)	4.3(1)
C(21)	0.9792(4)	0.3367(4)	0.4434(3)	4.4(1)
C(41)	0.9222(5)	0.3617(4)	0.2557(3)	4.6(1)
C(51)	0.8029(4)	0.5129(4)	0.3861(3)	3.9(1)
C(61)	0.6564(4)	0.3809(3)	0.3324(3)	3.6(1)
C(111)	0.7821(4)	−0.0311(3)	0.6668(3)	3.9(1)
C(112)	0.7439(5)	−0.0305(4)	0.5788(3)	5.1(1)
C(113)	0.6929(5)	−0.1210(4)	0.5487(4)	6.3(2)
C(114)	0.6788(5)	−0.2152(4)	0.6077(4)	6.9(2)
C(115)	0.7163(6)	−0.2192(4)	0.6944(4)	6.7(2)
C(116)	0.7687(5)	−0.1285(4)	0.7244(3)	5.4(1)
C(121)	1.0007(4)	0.1044(3)	0.6157(3)	5.2(1)
C(131)	0.9192(5)	0.0434(4)	0.8046(3)	6.4(2)
C(211)	0.7237(5)	0.2805(3)	0.9483(3)	3.8(1)
C(212)	0.8129(5)	0.2152(4)	0.9935(3)	5.8(1)
C(213)	0.7798(6)	0.1742(5)	1.0883(4)	7.2(2)
C(214)	0.6565(7)	0.2009(5)	1.1366(4)	6.9(2)
C(215)	0.5676(6)	0.2648(5)	1.0938(3)	6.5(2)
C(216)	0.5986(5)	0.3053(4)	1.0002(3)	5.2(1)
C(221)	0.9404(5)	0.3519(4)	0.8115(3)	5.8(1)
C(231)	0.7018(5)	0.4776(3)	0.8328(3)	5.7(1)
C(311)	0.3841(4)	0.2515(3)	0.8541(3)	3.5(1)
C(312)	0.2955(5)	0.2087(4)	0.9318(3)	5.3(1)
C(313)	0.2014(5)	0.2762(5)	0.9827(3)	6.0(2)
C(314)	0.1918(5)	0.3868(5)	0.9587(3)	5.5(1)
C(315)	0.2755(5)	0.4316(4)	0.8820(3)	5.1(1)
C(316)	0.3710(4)	0.3629(4)	0.8308(3)	4.2(1)
C(321)	0.5476(4)	0.0547(3)	0.8757(3)	4.7(1)
C(331)	0.4155(4)	0.0985(4)	0.7172(3)	5.5(1)

The work described here and in earlier papers[13] has established the first example of a pair of noninterconverting complexes, **2** and **6**, in which a metal fragment is attached either to the *exo*- or *endo*-1,3-diene unit of *o*-xylylene. Free *o*-xylylenes readily undergo [4 + 2]-cycloadditions at the *exo*-1,3-diene, leading to aromatization of the six-membered ring.[27] Since the $Fe(CO)_3$ group can be regarded as a dienophile, it is not surprising that **2**, in contrast to **6**, fails to react with $Fe(CO)_4(NMe_3)$. However, attempted cycloadditions to the *exo*-1,3-diene unit of **6** with dimethyl acetylenedicarboxylate, maleic anhydride and tetrafluoroethylene gave only deep red materials that so far have defied characterization. Similar behavior has been reported for $Ru(\eta^6\text{-}C_6Me_6)\{\eta^4\text{-}endo\text{-}o\text{-}(CH_2)_2C_6Me_4\}$.[9]

(25) Krüger, C.; Barnett, B. L.; Brauer, D. In *The Organic Chemistry of Iron*; Koerner von Gustorf, E. A., Grevels, F.-W., Fischler, I., Eds.; Academic: New York, 1978; Vol. 1, pp 17–22.
(26) Deeming, A. J. In *Comprehensive Organometallic Chemistry;* Wilkinson, G., Stone, F. G. A., Abel, E. W., Eds.; Pergamon: Oxford, U.K., 1982; Vol. 4, pp 449–451.

Table 8. Selected Bond Lengths (Å) and Angles (deg) for *endo*-{Ru(PMe₂Ph)₃}-*exo*-{Fe(CO₃)}{μ-η⁴,η⁴-*o*-(CH₂)₂C₆H₄} (8)

(a) Bond Lengths			
Ru(1)−P(1)	2.313(1)	Ru(1)−P(2)	2.307(1)
Ru(1)−P(3)	2.304(1)	Ru(1)−C(3)	2.258(4)
Ru(1)−C(4)	2.165(4)	Ru(1)−C(5)	2.182(4)
Ru(1)−C(6)	2.267(4)		
Fe(1)−C(41)	1.789(4)	Fe(1)−C(51)	1.770(4)
Fe(1)−C(61)	1.747(4)	Fe(1)−C(1)	2.132(4)
Fe(1)−C(11)	2.117(4)	Fe(1)−C(2)	2.140(4)
Fe(1)−C(21)	2.127(4)		
P(1)−C(111)	1.844(4)	P(1)−C(121)	1.826(4)
P(1)−C(131)	1.837(4)	P(2)−C(211)	1.840(4)
P(2)−C(221)	1.814(4)	P(2)−C(231)	1.839(4)
P(3)−C(311)	1.846(4)	P(3)−C(321)	1.824(4)
P(3)−C(331)	1.827(4)		
C(41)−O(41)	1.138(4)	C(51)−O(51)	1.146(4)
C(61)−O(61)	1.156(4)		
C(1)−C(11)	1.427(5)	C(1)−C(2)	1.411(5)
C(2)−C(21)	1.421(5)	C(2)−C(3)	1.473(5)
C(3)−C(4)	1.424(5)	C(4)−C(5)	1.395(5)
C(5)−C(6)	1.432(5)	C(6)−C(1)	1.483(5)
(b) Bond Angles			
P(1)−Ru(1)−P(2)	97.74(4)	P(1)−Ru(1)−P(3)	95.18(4)
P(1)−Ru(1)−C(3)	104.2(1)	P(1)−Ru(1)−C(4)	140.3(1)
P(1)−Ru(1)−C(5)	135.8(1)	P(1)−Ru(1)−C(6)	98.5(1)
P(2)−Ru(1)−P(3)	95.84(4)	P(2)−Ru(1)−C(3)	89.81(10)
P(2)−Ru(1)−C(4)	92.7(1)	P(2)−Ru(1)−C(5)	123.8(1)
P(2)−Ru(1)−C(6)	158.00(10)	P(3)−Ru(1)−C(3)	158.9(1)
P(3)−Ru(1)−C(4)	121.7(1)	P(3)−Ru(1)−C(5)	94.9(1)
P(3)−Ru(1)−C(6)	97.42(9)		
C(41)−Fe(1)−C(51)	104.4(2)	C(41)−Fe(1)−C(61)	101.4(2)
C(51)−Fe(1)−C(61)	90.9(2)	C(41)−Fe(1)−C(1)	132.1(2)
C(41)−Fe(1)−C(11)	95.9(2)	C(41)−Fe(1)−C(2)	129.2(2)
C(41)−Fe(1)−C(21)	92.0(2)	C(51)−Fe(1)−C(1)	119.9(2)
C(51)−Fe(1)−C(11)	159.1(2)	C(51)−Fe(1)−C(2)	93.1(2)
C(51)−Fe(1)−C(2)	93.1(2)	C(61)−Fe(1)−C(1)	95.5(2)
C(61)−Fe(1)−C(11)	90.2(2)	C(61)−Fe(1)−C(2)	126.0(2)
C(61)−Fe(1)−C(21)	164.6(2)		
Ru(1)−P(1)−C(111)	116.2(1)	Ru(1)−P(1)−C(121)	115.9(1)
Ru(1)−P(1)−C(131)	122.9(2)	C(111)−P(1)−C(121)	100.0(2)
C(111)−P(1)−C(131)	100.6(2)	C(121)−P(1)−C(131)	97.3(2)
Ru(1)−P(2)−C(211)	124.9(1)	Ru(1)−P(2)−C(221)	114.7(2)
Ru(1)−P(2)−C(231)	114.5(1)	C(211)−P(2)−C(221)	101.1(2)
C(211)−P(2)−C(231)	99.4(2)	C(221)−P(2)−C(231)	97.8(2)
Ru(1)−P(3)−C(311)	118.9(1)	Ru(1)−P(3)−C(321)	119.2(1)
Ru(1)−P(3)−C(331)	114.7(1)	C(311)−P(3)−C(321)	101.1(2)
C(311)−P(3)−C(331)	98.9(2)	C(321)−P(3)−C(331)	100.6(2)
Fe(1)−C(41)−O(41)	178.7(4)	Fe(1)−C(51)−O(51)	179.0(4)
Fe(1)−C(61)−O(61)	179.0(4)		
C(11)−C(1)−C(2)	117.8(4)	C(11)−C(1)−C(6)	127.4(4)
C(21)−C(2)−C(1)	118.4(4)	C(21)−C(2)−C(3)	126.5(4)
C(1)−C(2)−C(3)	115.0(3)	C(2)−C(3)−C(4)	118.2(3)
C(3)−C(4)−C(5)	116.6(4)	C(4)−C(5)−C(6)	115.7(4)
C(5)−C(6)−C(1)	117.4(3)	C(6)−C(1)−C(2)	114.8(3)

Acknowledgment. We thank The Royal Society (U.K.) Australian Scheme for the award of a Postdoctoral Fellowship to M.B.

Supplementary Material Available: For structures **6**–**8**, complete listings of atomic coordinates and isotropic displacement parameters (including hydrogen atoms), anisotropic displacement parameters, and interatomic distances and angles for hydrogen and non-hydrogen atoms (37 pages). Ordering information is given on any current masthead page.

OM940722X

(27) Oppolzer, W. In *Comprehensive Organic Synthesis*; Trost, B. M., Fleming, I., Paquette, L. A., Eds.; Pergamon: Oxford, U.K., 1991; Vol. 5, pp 385–396.

Synthesis and Structure of Novel Germanium-Containing Cyclic Polysulfides

Tsuyoshi Matsumoto, Norihiro Tokitoh, and Renji Okazaki*

Department of Chemistry, Graduate School of Science, The University of Tokyo, 7-3-1 Hongo, Bunkyo-ku, Tokyo 113, Japan

Midori Goto

National Institute of Materials and Chemical Research, 1-1 Higashi, Tsukuba, Ibaraki 305, Japan

Received September 30, 1994®

Novel germanium-containing cyclic polysulfides 1,2,3,4,5-tetrathiagermolanes **5** (Tbt(Ar)-GeS_4; Tbt = 2,4,6-tris[bis(trimethylsilyl)methyl]phenyl; Ar = mesityl, 2,6-diethylphenyl, 2,4,6-triisopropylphenyl) have been synthesized, and the molecular structure of Tbt(Mes)GeS_4 was determined by X-ray crystallographic analysis. Reaction of the tetrathiagermolanes **5** with diphenyldiazomethane gave 1,2,3,5-tetrathia-4-germacyclohexanes **10**, 1,2,4,5-tetrathia-3-germacyclohexanes **11**, and 1,2,4-trithia-3-germacyclopentanes **12**. The structure of 1,2,3,5-tetrathia-4-germacyclohexane **10a** was determined by X-ray structural analysis.

Introduction

In recent years, there has been much interest in the chemistry of polysulfido complexes containing transition metals because of their structural features, synthetic utility, and biological activities.[1] There have been reported syntheses and structures of some cyclic polysulfides such as Cp_2TiS_5,[2] Cp_2VS_5,[3] Cp_2MoS_4,[4] Cp_2WS_4,[5] $Cp^*_2TiS_3$,[6] and $Cp^*_2ZrS_3$[6] (Cp = C_5H_5, Cp* = C_5Me_5), which can be used as versatile sources to prepare the sulfur rings of predetermined size. On the other hand, polysulfides containing group 14 elements such as Si, Ge, and Sn had not been investigated when we started the present study. Recently we preliminarily reported the synthesis of the first 1,2,3,4,5-tetrathiametallolanes $RR'MS_4$ (M = Si, Ge, Sn)[7,8] having an efficient steric protection group, 2,4,6-tris[bis(trimethylsilyl)methyl]-phenyl (denoted as Tbt).[9] Immediately after our communication[7] Steudel independently reported the synthesis of the same type of polysulfides Ph_2MS_4 (M = Si, Ge).[10] In this paper we delineate a detailed account of the synthesis of kinetically stabilized 1,2,3,4,5-tetrathiagermolanes and their reactions, which gave some novel cyclic polysulfides.[11]

Results and Discussion

Synthesis of Diarylgermanes. The trichlorogermane $TbtGeCl_3$ (**1**) was synthesized from tetrachlorogermane and TbtLi, which was prepared by treatment of TbtBr with *t*-BuLi in THF. Another aryl group was introduced by nucleophilic reaction with Grignard reagents, giving the bromochlorogermanes Tbt(Ar)GeBrCl (**2**) instead of the expected Tbt(Ar)$GeCl_2$.[12] The formation of **2** can be rationalized in terms of rapid chlorine–bromine exchange in $TbtGeCl_3$ or Tbt(Ar)$GeCl_2$ by bromide ion derived from either ArMgBr or LiBr generated in the preparation of TbtLi from TbtBr. In these reactions no trisubstituted halogermane Tbt(Ar)$_2$GeX was formed even upon addition of excess Grignard reagents (ArMgBr), in contrast to similar reactions using tin compounds.[8] This is most likely because of bond lengths around the Ge atom being shorter than those around the Sn atom, which renders **2** more congested than the corresponding Sn compound and hence prohibits the attack of a second Grignard reagent (Scheme 1).

® Abstract published in *Advance ACS Abstracts*, December 15, 1994.

(1) For reviews on polychalcogenido complexes, see: (a) Müller, A.; Diemann, E.; Jostes, R.; Bögge, H. *Angew. Chem., Int. Ed. Engl.* **1981**, *20*, 934. (b) Mülller, A.; Jaegermann, W.; Enemark, J. H. *Coord. Chem. Rev.* **1982**, *46*, 245. (c) Draganjac, M.; Rauchfuss, T. B. *Angew. Chem., Int. Ed. Engl.* **1985**, *24*, 742. (d) Coucouvanis, D.; Hadjikyriacou, A.; Draganjac, M.; Kanatzidis, M. G.; Ileperuma, O. *Polyhedron* **1986**, *5*, 349. (e) Müller, A. *Polyhedron* **1986**, *5*, 323. (f) Müller, A.; Diemann, E. *Adv. Inorg. Chem.* **1987**, *31*, 89. (g) DuBois, M. R. *Chem. Rev.* **1989**, *89*, 1. (h) Ansari, M. A.; Ibers, J. A. *Coord. Chem. Rev.* **1990**, *100*, 223. (i) Kolis, J. W. *Coord. Chem. Rev.* **1990**, *105*, 195.

(2) (a) Köpf, H.; Block, B.; Schmidt, M. *Chem. Ber.* **1968**, *101*, 272. (b) Samuel, E. *Bull. Soc. Chim. Fr.* **1966**, 3548. (c) Schmidt, M.; Block, B.; Block, H. D.; Köpf, H.; Wilhelm, E. *Angew. Chem., Int. Ed. Engl.* **1968**, *7*, 632. (d) Köpf, H.; Block, B. *Chem. Ber.* **1969**, *102*, 1504. (e) Köpf, H.; Hazari, S. K. S.; Leitner, M. *Z. Naturforsch., B: Anorg. Chem., Org. Chem.* **1978**, *33B*, 1398. (f) Steudel, R.; Strauss, R. *J. Chem. Soc., Dalton Trans.* **1984**, 1775.

(3) (a) Köpf, H.; Wirl, A.; Kahl, W. *Angew. Chem., Int. Ed. Engl.* **1971**, *10*, 137. (b) Müller, E. G.; Petersen, J. L.; Dahl, L. F. *J. Organomet. Chem.* **1976**, *111*, 91.

(4) (a) Köpf, H. *Angew. Chem., Int. Ed. Engl.* **1969**, *8*, 375. (b) Köpf, H.; Hazari, S. K. S. *Z. Anorg. Allg. Chem.* **1976**, *426*, 49.

(5) Köpf, H.; Kahl, W.; Wirl, A. *Angew. Chem., Int. Ed. Engl.* **1970**, *9*, 801.

(6) Bird, P. H.; McCall, J. M.; Shaver, A.; Siriwardane, U. *Angew. Chem., Int. Ed. Engl.* **1982**, *21*, 384.

(7) Tokitoh, N.; Suzuki, H.; Matsumoto, T.; Matsuhashi, Y.; Okazaki, R.; Goto, M. *J. Am. Chem. Soc.* **1991**, *113*, 7047.

(8) Matsuhashi, Y.; Tokitoh, N.; Okazaki, R. *Organometallics* **1993**, *12*, 1351.

(9) Although the 2,4,6-tris[bis(trimethylsilyl)methyl]phenyl group has been denoted as Tb in our previous papers, we change this acronym to Tbt in order to avoid confusion with the symbol of an element (terbium). (a) Okazaki, R.; Unno, M.; Inamoto, N. *Chem. Lett.* **1987**, 2293. (b) Okazaki, R.; Unno, M.; Inamoto, N.; Yamamoto, G. *Chem. Lett.* **1989**, 493. (c) Okazaki, R.; Unno, M.; Inamoto, N. *Chem. Lett.* **1989**, 791.

(10) (a) Albertsen, J.; Steudel, R. *Phosphorus, Sulfur Silicon Relat. Elem.* **1992**, *65*, 165. (b) Steudel, R. In *The Chemistry of Inorganic Ring Systems;* Steudel, R., Ed.; Elsevier: Amsterdam, 1992; pp 233–253.

(11) Preliminary reports: Tokitoh, N.; Matsumoto, T.; Okazaki, R. *Tetrahedron Lett.* **1991**, *32*, 6143. See also ref 7.

(12) The structure of **2** was established by mass spectroscopy and elemental analysis.

0276-7333/95/2314-1008$09.00/0

Scheme 1

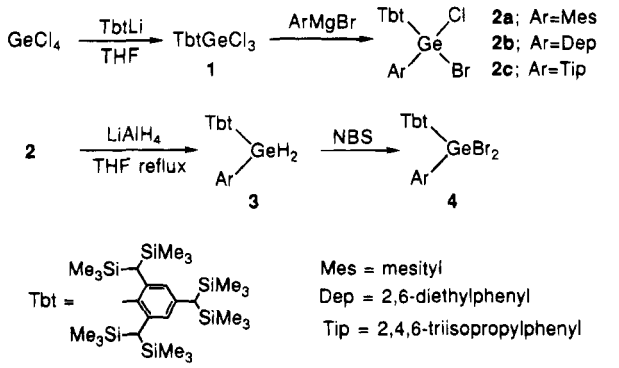

Scheme 2

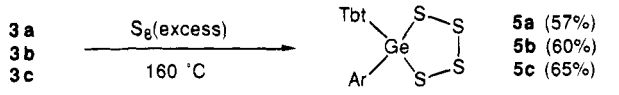

Scheme 3

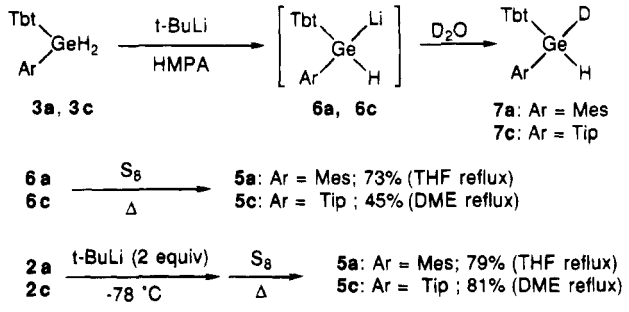

Treatment of **2** with $LiAlH_4$ gave dihydrogermanes **3** in good yields. Dibromogermanes **4** could be obtained by bromination of **3** using 2 equiv of *N*-bromosuccinimide.

Synthesis of Tetrathiagermolanes. Hydrogermanes are known to be sulfurized by elemental sulfur at elevated temperatures.[13] Reaction of a mixture of diarylgermanes **3** and elemental sulfur at 160 °C gave 1,2,3,4,5-tetrathiagermolanes **5** as pale yellow crystals in good yields with concomitant generation of gaseous hydrogen sulfide. Compounds **5** are novel cyclic polysulfides containing a germanium atom (Scheme 2).

Recently Steudel et al. reported the synthesis of the same type of polysulfide, Ph_2GeS_4, by the reaction of $Cp_2TiS_2GePh_2$ with S_2Cl_2.[10] While Ph_2GeS_4 is unstable to decompose above −20 °C, tetrathiagermolanes **5** are remarkably stable under ambient conditions because of sterically bulky groups on germanium. Their thermal stability is also shown in their high decomposition points (**5a**, 171−173 °C; **5b**, 222−224 °C; **5c**, 211−212 °C).

Some years ago, Satgé and his co-workers reported the preparation of (diarylgermyl)lithiums Ar_2GeHLi (Ar = Ph, Mes) by treatment of Ar_2GeH_2 with *t*-BuLi in THF.[14] Although lithiation of diarylgermane **3a**, bearing bulkier groups, did not proceed under their conditions, addition of HMPA was found to be effective for the lithiation of **3a**. In the case of **3c**, a high concentration of **3c** and HMPA was necessary. The formation of germyllithium **6** was confirmed by quenching with deuterated water (Scheme 3).

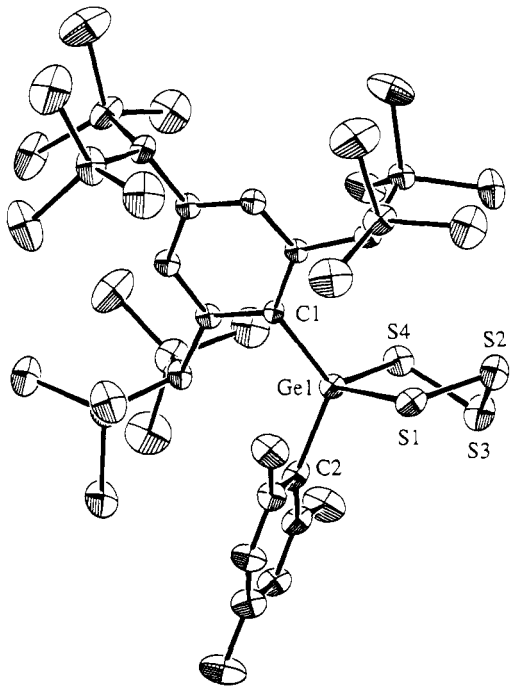

Figure 1. ORTEP drawing of 1,2,3,4,5-tetrathiagermolane **5a**. Selected bond lengths (Å) and angles (deg): Ge(1)−S(1), 2.320(2); S(1)−S(2), 2.046(3); S(2)−S(3), 2.052(5); S(3)−S(4), 2.048(3); S(4)−Ge(1), 2.257(2); Ge(1)−C(1), 1.960(6); Ge(1)−C(2), 1.996(8); S(1)−Ge(1)−S(4), 98.4(1); Ge(1)−S(1)−S(2), 102.2(2); S(1)−S(2)−S(3), 100.4(2); S(2)−S(3)−S(4), 98.3(2); S(3)−S(4)−Ge(1), 99.7(2); C(1)−Ge(1)−S(1), 119.4(2); C(1)−Ge(1)−S(4), 104.2(2); C(2)−Ge(1)−S(1), 96.0(2); C(2)−Ge(1)−S(4), 118.2(2); C(1)−Ge(1)−C(2), 119.4(3).

Germyllithium **6a**, thus prepared in situ, was allowed to react with elemental sulfur in refluxing THF to give **5a** in high yield. In the synthesis of **5c**, bearing bulkier groups, DME was used as solvent instead of THF, because a higher temperature was necessary for the reaction to proceed.

Tetrathiagermolanes **5** were also synthesized via treatment of dihalogermanes **2** with *t*-BuLi, followed by addition of elemental sulfur.

Structure of 1,2,3,4,5-Tetrathiagermolanes 5. Compounds **5** showed satisfactory spectral and analytical data. The molecular structure of **5a** was definitively determined by X-ray crystallographic analysis, and an ORTEP drawing is shown in Figure 1. Of particular note is the preferred distorted half-chair conformation of nearly envelope type in the GeS_4 five-membered ring. The distances between the two germanium−sulfur bonds are different (2.32 and 2.26 Å), whereas there is no distinct alternation in S−S bond lengths of the sulfur chain.

It should be noted that all of the reactions gave only five-membered polysulfides selectively, as in the case of polysulfides containing Si or Sn (**8** and **9**).[7,8] As was discussed in a previous paper concerning tetrathiastannolanes,[8] the isolation of only five-membered-ring compounds is probably due to the steric repulsion between the bulky Tbt and Ar (Mes, Dep or Tip) groups substituted on the Ge atom. It enlarges the bond angle of C−Ge−C and hence narrows the angle S−Ge−S, thus

(13) For example, see: Vyazankin, N. S.; Bochkarev, M. N.; Sanina, L. P. *Zh. Obshch. Khim.* **1966**, *36*, 166.
(14) Castel, A.; Riviere, P.; Satgé, J.; Ko, H. Y. *Organometallics* **1990**, *9*, 205.

Scheme 4[a]

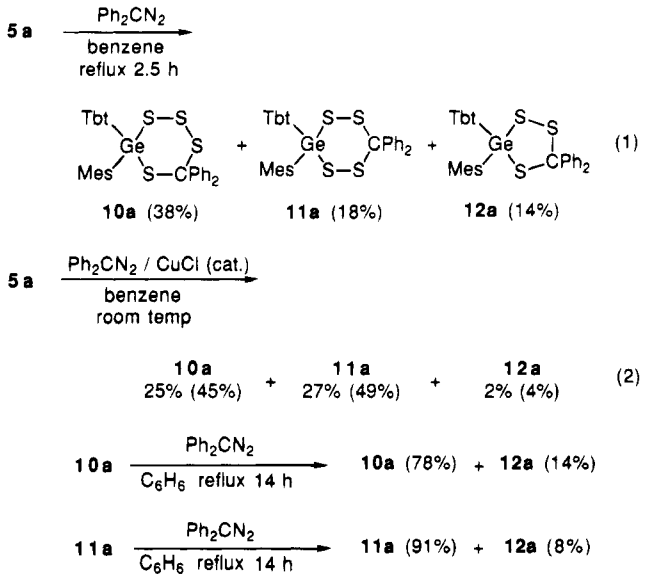

[a] Values in parentheses denote conversion yields.

favoring the selective formation of the five-membered ring.

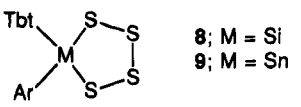

Reactions of Tetrathiagermolanes 5 with Diphenyldiazomethane.[11] Novel polysulfides **5** have two types of S-S bonds in their five-membered-ring systems. We became interested in the reactions of **5** with diphenyldiazomethane, because they would not only provide information on the reactivity of these S−S bonds but also lead to the formation of new germanium-containing heterocycles. When **5a** was treated with a large excess of diphenyldiazomethane in refluxing benzene for 2.5 h, two isomeric products, i.e. 1,2,3,5-tetrathia-4-germacyclohexane **10a** and 1,2,4,5-tetrathia-3-germacyclohexane **11a** were isolated in 38 and 18% yields, respectively, along with 1,2,4-trithia-3-germacyclopentane **12a** (14%) (Scheme 4). The structures of the two isomers **10a** and **11a** were determined by their chemical reactivity and an X-ray structural analysis of **10a** (vide infra).

Diazomethanes are known to generate the corresponding carbene in the presence of catalytic amount of Cu salts.[15] Reaction of **5a** with diphenyldiazomethane in benzene in the presence of CuCl at room temperature proceeded very slowly to give **10a** and **11a** in a 1:1 ratio along with a small amount of **12a** and the recovered starting material **5a**.

To clarify the mechanism, reactions of isolated **10a** and **11a** with diphenyldiazomethane were carried out in refluxing benzene. No reaction took place for **10a** even after 4 h (longer than the reaction time in reaction 1 of Scheme 4), whereas refluxing for 14 h resulted in 14% of **12a** with 78% recovery of **10a**. Similar results were obtained for **11a** (Scheme 5). These results show

(15) Helquist, P. In *Comprehensive Organic Synthesis;* Trost, B. M., Fleming, I., Eds.; Pergamon Press: Oxford, U.K., 1991; Vol. 4, pp 951−998, and references cited therein.

Scheme 5

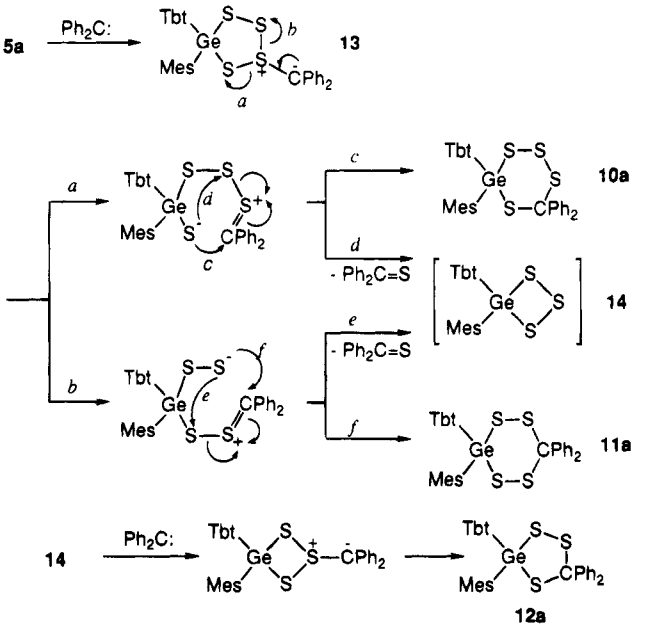

Scheme 6

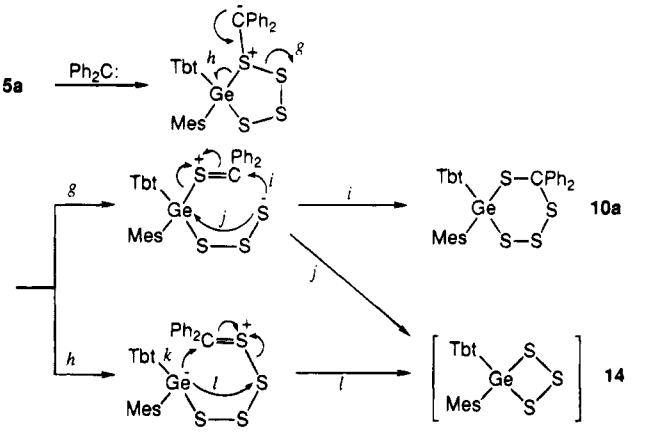

that **12a** is generated directly from the reaction of **5a** and diphenyldiazomethane.

A plausible mechanism is shown in Scheme 5. In reaction 2 of Scheme 4, an electrophilic attack occurs on the sulfur atom at the kinetically favorable 2-position, followed by ring expansion of the intermediary sulfonium ylide **13** (paths *c* and *f* of Scheme 5) to give **10a** and **11a**. Trithiagermacyclopentane **12a** is probably produced by further reaction of diphenylcarbene with trithiagermacyclobutane **14** formed via path *d* or *e*. This mechanism can account for the 1:1 ratio of **10a** and **11a**, because there seems to be neither kinetic nor thermodynamic preference between paths *a* and *b*.

On the other hand, a reaction at higher temperature (reaction 1 of Scheme 4) would make possible an attack also on the sulfur atom at the 1-position (Scheme 6), thus enhancing the yield of **10a** (reaction 1). Path *k* is thought to be impossible because of unfavorable steric hindrance.

Reaction of **5c**, bearing a bulkier Tip group on germanium, gave only the two isomeric six-membered-ring compounds **10c** and **11c** (Scheme 7). However, trithiagermacyclopentane **12c** could be synthesized by desulfurization of **10c** with hexamethylphosphorous triamide. We previously reported a similar reaction with

Scheme 7

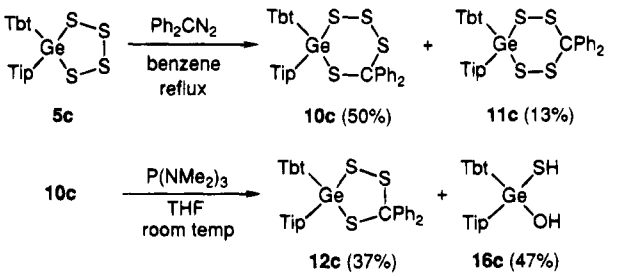

Scheme 8

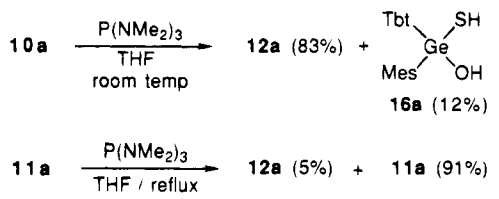

Scheme 9

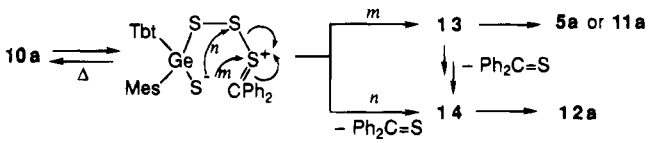

diphenyldiazomethane using the tin analog **9** (Ar = Tip), where three products corresponding to **10-12** were obtained.[16] The formation of a trithiastannacyclopentane derivative in the reaction of **9** is considered to result from the reduced congestion around the tin atom which favors an electrophilic attack on the sulfur at the 1-position, leading to a trithiastannacyclobutane, a possible precursor of the trithiastannacyclopentane.

Structures of 10 and 11. (1) Desulfurization Reactions. Although there are three possible isomers for a $GeCS_4$ ring system, i.e., **10**, **11**, and 1,2,3,4-tetrathia-5-germacyclohexane, the last isomer is reasonably excluded as a reaction product of **5** with diphenyldiazomethane because of its severe steric congestion. In order to determine the structure of **10** and **11**, they were subjected to a desulfurization reaction. Reaction of **10a** with hexamethylphosphorous triamide in THF at room temperature gave **12a** in 83% yield, whereas a similar reaction of **11a** in refluxing THF afforded **12a** only in 5% yield with 91% of **11a** being recovered (Scheme 8). This fact clearly indicates that **10a** has a 1,2,3,5-tetrathia-4-germacyclohexane skeleton, because in this structure sulfur at the 2-position is exposed to an attack by the phosphorus reagent while both sulfurs in **11** are sterically protected.

Interesting thermal isomerization was observed for **10a** in $CDCl_3$ at 100 °C to give the isomer **11a** (37%) along with the two types of ring-contraction products **5a** (17%) and **12a** (9%) and recovered **10a** (37%). A possible mechanism is shown in Scheme 9. The first step would be a heterolytic cleavage of the Ge−S bond due to steric repulsion between aryl groups on Ge and C atoms. Path *m* would give the sulfonium ylide **13**, which would further react as shown in Scheme 6. Path *n* would give intermediate **14**, which eventually affords **12a**. Neither thermal decomposition nor isomerization was observed below 80 °C.

(16) Matsuhashi, Y.; Tokitoh, N.; Okazaki, R.; Goto, M. *Organometallics* **1993**, *12*, 2573.

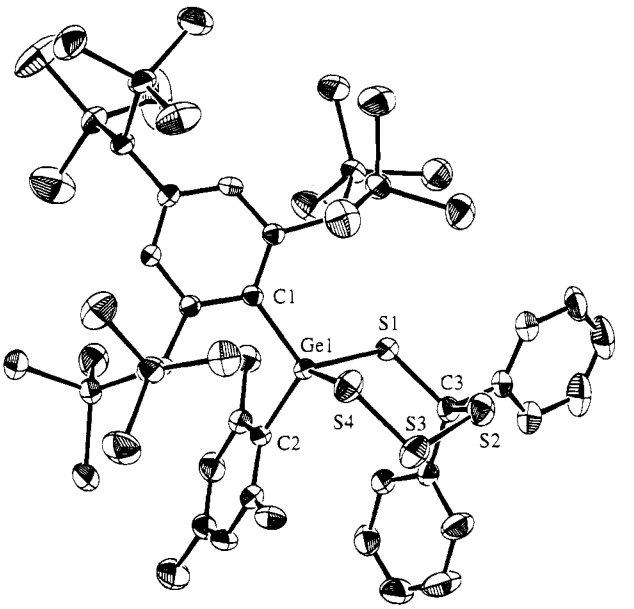

Figure 2. ORTEP drawing of 1,2,3,5-tetrathia-4-germacyclohexane **10a**. Selected bond lengths (Å) and angles (deg): Ge(1)−S(1), 2.290(2); S(1)−C(3), 1.864(6); C(3)−S(2), 1.851(6); S(2)−S(3), 2.012(3); S(3)−S(4), 2.045(3); S(4)−Ge(1), 2.251(2); Ge(1)−C(1), 1.997(5); Ge(1)−C(2), 1.977(6); C(1)−Ge(1)−C(2), 113.7(2); C(1)−Ge(1)−S(1), 114.1(2); C(1)−Ge(1)−S(4), 102.0(2); C(2)−Ge(1)−S(1), 103.3(2); C(2)−Ge(1)−S(4), 121.0(2); Ge(1)−S(1)−C(3), 111.8(2); S(1)−C(3)−S(2), 110.9(3); C(3)−S(2)−S(3), 103.3(2); S(2)−S(3)−S(4),106.5(1); S(3)−S(4)−Ge(1), 104.3(1); S(1)−C(3)−C(4), 103.6(4); S(1)−C(3)−C(5), 114.0(4); S(2)−C(3)−C(4), 102.9(4); S(2)−C(3)−C(5),111.9(4); C(4)−C(3)−C(5), 112.8(5).

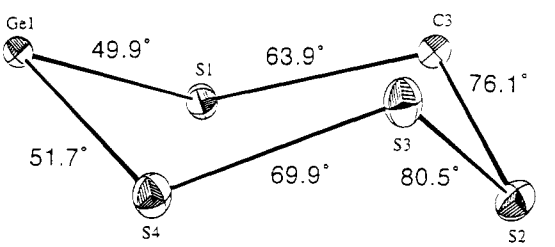

Figure 3. Torsion angles of **10a**.

(2) X-ray Structural Analysis. To distinguish **10a** from **11a**, the molecular structure of **10a** was definitively determined by X-ray crystallographic analysis, as shown in Figure 2. The molecular geometry of **10a** is of great interest as the first example of tetrathiagermacyclohexane. As in the case of known examples of saturated six-membered rings containing sulfurs such as 1,3,5-trithiacyclohexane,[17] 1,2,3,4-tetrathiacyclohexane,[18] and cyclohexathiane,[19] **10a** adopts a chair conformation. Torsional angles shown in Figure 3 indicate that the germanium atom-containing moiety is significantly flatter than the carbon-containing moiety, though **10a** shows an average torsional angle of 65.3°, which is comparable to that of 1,3,5-trithiacyclohexane (ca. 64°).[17]

Concluding Remarks

We have succeeded in the syntheses of novel cyclic polysulfides containing germanium, such as Tbt(Ar)-

(17) Valle, G.; Carazzolo, G.; Mammi, M. *Ric. Sci., Parte 2: Sez. A* **1965**, *8*, 1469; *Chem. Abstr.* **1966**, *65*, 1514.
(18) Fehér, F.; Klaeren, A.; Linke, K.-H. *Acta Crystallogr., Sect. B* **1972**, *28*, 534.
(19) Donohue, J.; Caron, A.; Goldish, E. *J. Am. Chem. Soc.* **1961**, *83*, 3748.

GeS_4 (**5**), Tbt(Ar)GeS_4CPh_2 (two isomers) (**10** and **11**), and Tbt(Ar)GeS_3CPh_2 (**12**), by taking advantage of the bulky groups Tbt and Ar (Mes, Dep, Tip), and two of the polysulfides have been crystallographically analyzed. It is noteworthy that our tetrathiagermolanes **5** are much more stable than the recently reported Ph_2GeS_4,[10] indicating the importance of the bulky group Tbt in stabilizing the tetrathiagermolane skeleton, which is otherwise highly susceptible to hydrolysis. The polysulfides synthesized in the present work are considered to be useful precursors of novel low-coordinated germanium species which are of much current interest. We have preliminarily reported the synthesis of the first stable diarylgermanethione, Tbt(Tip)Ge=S, by desulfurization of Tbt(Tip)GeS_4.[20] Further investigation along this line is now under way.

Experimental Section

General Procedure. All melting points were uncorrected. All solvents used in the reactions were purified by the reported methods. THF was purified by distillation from benzophenone ketyl before use. All reactions were carried out under an argon atmosphere unless otherwise noted. Preparative gel permeation liquid chromatography (GPLC) was performed by LC-908 with JAI gel 1H and 2H columns (Japan Analytical Industry) with chloroform as solvent. Dry column chromatography (DCC) was performed with ISN silica DCC 60A. Preparative thin-layer chromatography was carried out with Merck Kieselgel 60 PF254 (Art. No. 7747). The ^1H NMR (500 MHz) and ^{13}C NMR spectra (125 MHz) were measured in $CDCl_3$ with a Bruker AM-500 spectrometer using $CHCl_3$ as internal standard.

Preparation of {2,4,6-Tris[bis(trimethylsilyl)methyl]phenyl}bromochloro(mesityl)germane (2a). To a solution of 1-bromo-2,4,6-tris[bis(trimethylsilyl)methyl]benzene[9a] (TbtBr; 10.0 g, 15.9 mmol) in THF (150 mL) was added *t*-BuLi (1.61 M in pentane, 22 mL, 35 mmol) at −78 °C. After the mixture was stirred for 10 min, $GeCl_4$ (1.9 mL, 17.4 mmol) was added at −78 °C. The reaction mixture was warmed to room temperature within 10 h to give a solution of $TbtGeCl_3$, to which MesMgBr (0.9 M in THF, 34 mL, 31 mmol) prepared from Mg and MesBr was added at room temperature. After this solution was stirred for 10 h, a few drops of aqueous NH_4Cl was added and almost all of the THF was removed under reduced pressure. Chloroform and diluted HCl were added to the residue, which was extracted by $CHCl_3$ several times. The organic layer was dried over $MgSO_4$, and the solvent was removed under reduced pressure. The white solid thus obtained was dissolved into CH_2Cl_2, and to the solution was added approximately the same volume of ethanol to afford a precipitate of Tbt(Mes)GeBrCl (**2a**; 9.5 g, 70%) as white crystals by the evaporation of CH_2Cl_2 at room temperature under reduced pressure. **2a**: white crystals; mp 225−227 °C; ^1H NMR ($CDCl_3$, 500 MHz) δ −0.02 (s, 9H), 0.009 (s, 9H), 0.014 (s, 9H), 0.05 (s, 9H), 0.06 (s, 18H), 1.35 (s, 1H), 2.26 (s, 3H), 2.57 (br s, 1H), 2.61 (s, 6H), 2.73 (br s, 1H), 6.30 (br s, 1H), 6.44 (br s, 1H), 6.84 (s, 2H); ^{13}C NMR ($CDCl_3$, 125 MHz) δ 0.81 (q), 0.87 (q), 1.03 (q), 1.30 (q), 1.32 (q), 1.57 (q), 20.91 (q), 25.49 (q), 27.49 (d), 27.64 (d), 30.81 (d), 123.44 (d), 128.43 (d), 130.25 (s), 130.55 (d), 137.59 (s), 140.69 (s), 141.44 (s), 146.63 (s), 150.40 (s), 150.77 (s); high-resolution FAB-MS observed *m/z* 858.2031, calcd for $C_{36}H_{70}{}^{79}Br^{35}Cl^{74}GeSi_6$ 858.2177.

Preparation of {2,4,6-Tris[bis(trimethylsilyl)methyl]phenyl}bromochloro(2,6-diethylphenyl)germane (2b). Compound **2b** was synthesized by the same procedure as that for **2a**, except that the reaction with DepMgBr (Dep = 2,6-diethylphenyl) was performed under reflux. TbtBr (5.0 g, 7.9 mmol), $GeCl_4$ (0.9 mL, 8.7 mmol), and DepMgBr (1.1 M in THF, 12 mL, 13 mmol) gave Tbt(Dep)GeBrCl (**2b**; 4.5 g, 65%). **2b**: white crystals; mp 215−216 °C; ^1H NMR ($CDCl_3$, 500 MHz) δ −0.05 (s, 9H), −0.005 (s, 9H), 0.003 (s, 9H), 0.02 (s, 9H), 0.05 (s, 18H), 1.31 (t, J = 7.3 Hz, 6H), 1.34 (s, 1H), 2.58 (br s, 1H), 2.73 (br s, 1H), 2.93 (br s, 2H), 3.01 (br s, 2H), 6.28 (s, 1H), 6.42 (s, 1H), 7.10 (d, J = 7.7 Hz, 2H), 7.32 (t, J = 7.7 Hz, 1H); ^{13}C NMR ($CDCl_3$, 125 MHz) δ 0.80 (q), 0.89 (q), 1.03 (q), 1.32 (q), 1.41 (q), 1.65 (q), 16.22 (q), 27.30 (d), 27.55 (d), 29.99 (t), 30.74 (d), 123.42 (d), 127.82 (d), 128.44 (d), 130.93 (d), 131.10 (s), 140.32 (s), 146.48 (s), 147.64 (s), 150.00 (s), 150.38 (s); high-resolution FAB-MS observed *m/z* 872.2130; calcd for $C_{37}H_{72}{}^{79}Br^{35}Cl^{74}GeSi_6$ 872.2334. Anal. Found: C, 54.93; H, 9.42; Br, 9.03; Cl, 4.01. Calcd for $C_{37}H_{72}BrClGeSi_6$: C, 50.88; H, 8.31; Br, 9.15; Cl, 4.06.

Preparation of {2,4,6-Tris[bis(trimethylsilyl)methyl]phenyl}bromochloro(2,4,6-triisopropylphenyl)germane (2c). Compound **2c** was synthesized by the same procedure as that for **2a**, except that the reaction with TipMgBr was performed under reflux. The use of TbtBr (5.0 g, 8.0 mmol), $GeCl_4$ (0.9 mL, 8.7 mmol), and TipMgBr (1.8 M in THF, 8.5 mL, 15 mmol) gave Tbt(Tip)GeBrCl (**2c**; 5.0 g, 66%). **2c**: white crystals; mp 232−233 °C; ^1H NMR ($CDCl_3$, 500 MHz) δ −0.07 (s, 9H), −0.02 (s, 9H), 0.045 (s, 9H), 0.048 (s, 9H), 0.08 (s, 9H), 0.10 (s, 9H), 1.04 (br s, 3H), 1.16 (br s, 3H), 1.20 (d, J = 6.9 Hz, 6H), 1.28 (d, J = 6.9 Hz, 6H), 1.33 (s, 1H), 2.49 (br s, 1H), 2.63 (br s, 1H), 2.84 (sept, J = 6.9 Hz, 1H), 3.28 (br s, 1H), 4.09 (br s, 1H), 6.31 (br s, 1H), 6.43 (br s, 1H), 7.03 (s, 2H); ^{13}C NMR ($CDCl_3$, 125 MHz) δ 0.82 (q), 0.87 (q), 0.96 (q), 1.55 (q), 1.85 (q), 2.12 (q), 22.70 (q × 2), 23.73 (q), 23.77 (q), 24.50 (q × 2), 26.67 (d), 26.97 (d), 27.47 (d), 28.13 (d), 30.72 (d), 34.28 (d), 122.66 (d), 123.39 (d), 123.84 (d), 128.96 (d), 131.49 (s), 136.31 (s), 145.83 (s), 149.44 (s), 149.92 (s), 151.59 (s), 152.50 (s); high-resolution FAB-MS observed *m/z* 942.3298, calcd for $C_{42}H_{82}{}^{79}Br^{35}Cl^{74}GeSi_6$ 942.3116.

Preparation of {2,4,6-Tris[bis(trimethylsilyl)methyl]phenyl}(mesityl)germane (3a). To a THF solution (20 mL) of **2a** (298 mg, 0.347 mmol) was added $LiAlH_4$ (29 mg, 0.73 mmol) at 0 °C, and the mixture was refluxed for 10 h. After quenching by aqueous NH_4Cl, the organic layer was washed with diluted HCl. The water layer was extracted with $CHCl_3$ several times. The organic layer was dried over $MgSO_4$, and all of the solvent was removed under reduced pressure. The residue was dissolved into CH_2Cl_2, and approximately the same volume of ethanol was added to give precipitates of **3a** (185 mg, 72%) as white crystals by the evaporation of CH_2Cl_2 at room temperature under reduced pressure. **3a**: mp 162−163 °C dec; ^1H NMR ($CDCl_3$, 500 MHz) δ −0.04 (s, 18H), 0.00 (s,18H), 0.05 (s, 18H), 1.31 (s, 1H), 2.01 (s, 1H), 2.22 (s, 1H), 2.26 (s, 3H), 2.42 (s, 6H), 5.14 (s, 2H), 6.29 (s, 1H), 6.44 (s, 1H), 6.83 (s, 2H); ^{13}C NMR ($CDCl_3$, 125 MHz) δ 0.59 (q), 0.79 (q), 0.93 (q), 21.01 (q), 24.69 (q), 28.93 (d × 2), 30.27 (d), 122.26 (d), 127.08 (d), 128.14 (s), 128.44 (d), 133.00 (s), 138.51 (s), 143.24 (s), 143.29 (s), 150.28 (s), 150.38 (s); IR (KBr) 2070 cm^{-1} (Ge−H); high-resolution EI-MS observed *m/z* 746.3484; calcd for $C_{36}H_{72}{}^{74}GeSi_6$ 746.3454. Anal. Found: C, 54.93; H, 9.42. Calcd for $C_{36}H_{72}GeSi_6{\cdot}2H_2O$: C, 55.28; H, 9.79.

Preparation of {2,4,6-Tris[bis(trimethylsilyl)methyl]phenyl}(2,6-diethylphenyl)germane (3b). Using the same procedure as that for **3a**, **3b** (3.7 g, 96%) was obtained from **2b** (4.5 g, 5.2 mmol). **3b**: white crystals; mp 189−190 °C dec; ^1H NMR ($CDCl_3$, 500 MHz) δ −0.07 (s, 18H), 0.02 (s, 18H), 0.04 (s, 18H), 1.23 (t, J = 7.3 Hz, 6H), 1.29 (s, 1H), 1.99 (s, 1H), 2.19 (s, 1H), 2.76 (q, J = 7.3 Hz, 4H), 5.13 (s, 2H), 6.27 (s, 1H), 6.42 (s, 1H), 7.05 (d, J = 7.7 Hz, 2H), 7.25 (t, J = 7.7 Hz, 1H); ^{13}C NMR ($CDCl_3$, 125 MHz) δ 0.56 (q), 0.77 (q), 0.89 (q), 16.14 (q), 28.90 (d), 29.01 (d), 30.25 (d), 30.92 (t), 122.20 (d), 125.84 (d), 127.06 (d), 128.53 (s), 129.26 (d), 135.82 (s), 143.31 (s), 149.56 (s), 150.20 (s), 150.31 (s); IR (KBr) 2058 cm^{-1} (Ge−H). Anal. Found: C, 58.46; H, 9.53. Calcd for $C_{37}H_{74}GeSi_6$: C, 58.46; H, 9.81.

(20) Tokitoh, N.; Matsumoto, T.; Manmaru, K.; Okazaki, R. *J. Am. Chem. Soc.* **1993**, *115*, 8855.

Preparation of {2,4,6-Tris[bis(trimethylsilyl)methyl]phenyl}(2,4,6-triisopropylphenyl)germane (3c). Using the same procedure as that for **3a**, **3c** (277 mg, 99%) was obtained from **2c** (315 mg, 0.334 mmol). **3c**: white crystals; mp 162–164 °C dec; ^{1}H NMR ($CDCl_3$, 500 MHz) δ −0.08 (s, 18H), 0.00 (s, 18H), 0.03 (s, 18H), 1.21 (d, J = 6.9 Hz, 6H), 1.23 (d, J = 6.9 Hz, 12H), 1.27 (s, 1H), 1.96 (br s, 1H), 2.24 (br s, 1H), 2.84 (sept, J = 6.9 Hz, 1H), 3.22 (sept, J = 6.9 Hz, 2H), 5.16 (s, 2H), 6.25 (s, 1H), 6.43 (s, 1H), 7.00 (s, 2H); ^{13}C NMR ($CDCl_3$, 125 MHz) δ 0.78 (q), 1.09 (q), 23.98 (q), 24.67 (q), 28.84 (d), 28.93 (d), 30.22 (d), 33.80 (d), 34.41 (d), 120.66 (d), 122.32 (d), 127.24 (d), 129.77 (s), 132.17 (s), 142.97 (s), 149.69 (s), 149.93 (s), 150.01 (s), 153.83 (s); IR (KBr) 2065 cm^{-1} (Ge–H). Anal. Found: C, 58.70; H, 9.84. Calcd for $C_{42}H_{84}GeSi_6 \cdot 1.5H_2O$: C, 58.84; H, 10.23.

Preparation of {2,4,6-Tris[bis(trimethylsilyl)methyl]phenyl}dibromo(mesityl)germane (4a). To a benzene solution (100 mL) of diarylgermane **3a** (6.6 g, 8.8 mmol) was added N-bromosuccinimide (3.6 g, 20 mmol) at room temperature. While the solution was stirred, N-bromosuccinimide (0.33 g, 1.9 mmol) was added to it over a period of 10 h, until all of the **3a** was consumed. The crude reaction mixture was chromatographed with column chromatography (SiO_2/benzene) to give a fraction containing **4a**, which was dissolved into $CHCl_3$ and reprecipitated as mentioned for **2a**. **4a** (7.3 g, 91%): white crystals; mp 225–227 °C; ^{1}H NMR ($CDCl_3$, 500 MHz) δ −0.001 (s, 18H), 0.04 (s, 18H), 0.06 (s, 18H), 1.34 (s, 1H), 2.26 (s, 3H), 2.63 (br s, 1H), 2.64 (s, 6H), 2.81 (br s, 1H), 6.29 (br s, 1H), 6.43 (br s, 1H), 6.82 (s, 2H); ^{13}C NMR ($CDCl_3$, 125 MHz) δ 0.84 (q), 1.30 (q), 1.58 (q), 20.88 (q), 25.71 (q), 27.42 (d), 27.57 (d), 30.78 (d), 123.48 (d), 128.48 (d), 130.06 (s), 130.61 (d), 137.62 (s), 140.59 (s), 141.27 (s), 146.56 (s), 150.24 (s), 150.65 (s). Anal. Found: C, 47.67; H, 7.84; Br, 18.05. Calcd for $C_{36}H_{70}Br_2GeSi_6$: C, 47.83; H, 7.80; Br, 17.68.

Preparation of {2,4,6-Tris[bis(trimethylsilyl)methyl]phenyl}dibromo(2,4,6-triisopropylphenyl)germane (4c). Using the same procedure as that for **4a**, **4c** (8.8 g, 88%) was obtained from **3c** (8.4 g, 10 mmol). **4c**: white crystals; mp 232–233 °C; ^{1}H NMR ($CDCl_3$, 500 MHz) δ 0.02 (br s, 18H), 0.04 (br s, 18H), 0.05 (s, 18H), 1.15 (br s, 6H), 1.20 (d, J = 6.9 Hz, 6H), 1.28 (br s, 6H), 1.33 (s, 1H), 2.13 (br s, 1H), 2.29 (br s, 1H), 2.84 (sept, J = 6.9 Hz, 1H), 3.78 (sept, J = 6.9 Hz, 2H), 6.32 (br s, 1H), 6.44 (br s, 1H), 7.02 (s, 2H); ^{13}C NMR ($CDCl_3$, 125 MHz) δ 0.85 (q), 1.93 (q), 2.20 (q), 23.64 (q), 23.72 (q), 27.01 (d), 27.49 (d), 30.70 (d), 32.92 (d), 34.24 (d), 123.38 (d), 123.88 (d), 128.97 (d), 131.66 (s), 136.05 (s), 145.78 (s), 149.40 (s), 149.98 (s), 151.46 (s), 152.29 (s). Anal. Found: C, 50.78; H, 8.42; Br, 16.59. Calcd for $C_{42}H_{82}Br_2GeSi_6$: C, 51.05; H, 8.37; Br, 16.17.

Synthesis of 5-{2,4,6-Tris[bis(trimethylsilyl)methyl]phenyl}-5-mesityl-1,2,3,4,5-tetrathiagermolane (5a). Method 1. Diarylgermane **3a** (1.13 g, 1.15 mmol) was mixed with S_8 (4.1 g, 16 mmol as S_8) and heated to 160 °C for 10 min. Most of the excess sulfur was removed by recrystallization from chloroform. The residue was separated with DCC (SiO_2/hexane) and GPLC. The solid material thus obtained was dissolved into CH_2Cl_2, to which was added approximately the same volume of ethanol. Evaporation of CH_2Cl_2 at room temperature under reduced pressure gave **5a** (0.75 g, 57%) as pale yellow crystals.

Method 2. To a THF solution (10 mL) of **3a** (177 mg, 0.237 mmol) was added at −78 °C t-BuLi (1.54 M in pentane, 0.24 mL, 0.38 mmol) and then hexamethylphosphoric triamide (0.20 mL, 1.2 mmol). The solution was warmed to −25 °C over 2 h, and to it was added a THF (10 mL) suspension of elemental sulfur (0.12 g, 0.47 mmol as S_8). The mixture was warmed to room temperature and then refluxed for 10 h. Solvent was removed under reduced pressure, and the residue was separated as was mentioned in method 1, to afford **5a** (150.8 mg, 73%).

Method 3. To a THF solution (15 mL) of bromochlorogermane **2a** (241 mg, 0.296 mmol) was added at −78 °C t-BuLi (1.54 M in pentane, 0.39 mL, 0.59 mmol). The solution was stirred for 5 min at −78 °C, and to it was added a THF (10 mL) suspension of elemental sulfur (0.15 g, 0.60 mmol as S_8). The mixture was warmed to room temperature over 2 h and then refluxed for 10 h. The solvent was removed under reduced pressure, and the residue was separated as was mentioned in method 1 to give **5a** (204.1 mg, 79%). **5a**: pale yellow crystals; mp 171–173 °C dec; ^{1}H NMR ($CDCl_3$, 500 MHz) δ −0.022 (br s, 18H), −0.018 (br s, 18H), 0.06 (s, 18H), 1.35 (s, 1H), 1.97 (s, 1H), 2.04 (s, 1H), 2.21 (s, 3H), 2.51 (s, 6H), 6.34 (s, 1H), 6.46 (s, 1H), 6.80 (s, 2H); ^{13}C NMR ($CDCl_3$, 125 MHz) δ 0.82 (q), 1.30 (q), 1.59 (q), 20.86 (q), 25.70 (q), 28.48 (d), 28.87 (d), 30.79 (d), 123.18 (d), 128.32 (d), 128.68 (s), 130.13 (d), 139.43 (s), 139.82 (s), 140.74 (s), 146.25 (s), 151.72 (s), 151.88 (s); UV ($CHCl_3$) λ_{max} 273 (sh, ϵ 9800), 318 (sh, 3000) nm. Anal. Found: C, 49.42; H, 7.82; S, 14.30. Calcd for $C_{36}H_{70}GeS_4Si_6$: C, 49.56; H, 8.09; S, 14.71.

Synthesis of 5-{2,4,6-Tris[bis(trimethylsilyl)methyl]phenyl}-5-(2,6-diethylphenyl)-1,2,3,4,5-tetrathiagermolane (5b). Diarylgermane **3b** (252 mg, 0.332 mmol) was mixed with S_8 (2.0 g, 7.8 mmol as S_8) and heated to 160 °C for 1 h. Most of the excess sulfur was removed by recrystallization from chloroform. The residue was separated with DCC (SiO_2/hexane) follwed by GPLC. The solid material thus obtained was recrystallized from ethanol to afford **5b** (206 mg, 70%) as pale yellow crystals. **5b**: mp 222–224 °C dec; ^{1}H NMR ($CDCl_3$, 500 MHz) δ −0.02 (s, 18H), −0.01 (s, 18H), 0.05 (s, 18H), 1.24 (t, J = 7.3 Hz, 6H), 1.34 (s, 1H), 1.97 (s, 1H), 2.01 (s, 1H), 2.99 (q, J = 7.3 Hz, 4H), 6.33 (s, 1H), 6.46 (s, 1H), 7.10 (d, J = 7.7 Hz, 2H), 7.28 (t, J = 7.7 Hz, 1H); ^{13}C NMR ($CDCl_3$, 125 MHz) δ 0.84 (q), 1.39 (q), 1.68 (q), 14.58 (q), 28.37 (d), 28.76 (d), 30.77 (d), 31.08 (t), 123.18 (d), 126.45 (d), 128.45 (d), 129.97 (s + d), 142.34 (s), 146.13 (s), 146.43 (s), 151.31 (s), 151.57 (s). Anal. Found: C, 50.11; H, 8.03; S, 14.19. Calcd for $C_{37}H_{72}GeS_4Si_6$: C, 50.13; H, 8.19; S, 14.47.

Synthesis of 5-{2,4,6-Tris[bis(trimethylsilyl)methyl]phenyl}-5-(2,4,6-triisopropylphenyl)-1,2,3,4,5-tetrathiagermolane (5c). Method 1. Diarylgermane **3c** (515 mg, 0.620 mmol) was mixed with S_8 (2.0 g, 8.0 mmol as S_8) and heated to 160 °C for 30 min. Most of the excess sulfur was removed by recrystallization from chloroform. The residue was separated with DCC (SiO_2/hexane) and GPLC. The solid material thus obtained was recrystallized from ethanol to afford **5c** (386 mg, 65%) as pale yellow crystals.

Method 2. To a DME (3 mL) solution of **3c** (625 mg, 0.753 mmol) were added at −78 °C t-BuLi (1.61 M in pentane, 1.40 mL, 2.25 mmol) and hexamethylphosphoric triamide (0.66 mL, 3.8 mmol). The solution was warmed to −12 °C over 3 h, and elemental sulfur (0.58 g, 2.27 mmol as S_8) was added. After the mixture was warmed to room temperature, DME (10 mL) was added, and this solution was refluxed for 10 h. Solvent was removed under reduced pressure, and the residue was separated as was mentioned in method 1, giving **5c** (324 mg, 45%).

Method 3. To a DME (15 mL) solution of bromochlorogermane **2c** (205 mg, 0.229 mmol) was added t-BuLi (1.61 M in pentane, 0.28 mL, 0.46 mmol) at −78 °C. The solution was stirred for 5 min at −78 °C, and then elemental sulfur (160 mg, 46 mmol as S_8) was added. The mixture was warmed to room temperature over 2 h and refluxed for 10 h. Solvent was removed under reduced pressure, and the residue was separated as was mentioned in method 1 to give **5c** (177 mg, 81%). **5c**: pale yellow crystals; mp 211–212 °C dec; ^{1}H NMR ($CDCl_3$, 500 MHz, 340 K) δ 0.03 (s, 36H), 0.07 (s, 18H), 1.16 (d, J = 6.9 Hz, 12H), 1.21 (d, J = 6.9 Hz, 6H), 1.35 (s, 1H), 2.07 (br s, 2H), 2.83 (sept, J = 6.9Hz, 1H), 3.78 (br s, 2H), 6.41 (br s, 2H), 7.03 (s, 2H); ^{13}C NMR ($CDCl_3$, 125 MHz) δ 1.01 (q), 2.33 (q), 23.73 (q), 24.39 (q), 28.74 (d), 30.96 (d), 34.27 (d), 35.79 (d), 123.41 (d), 123.63 (d), 129.27 (d), 132.74 (s), 137.40 (s), 145.57 (s), 150.67 (s), 151.19 (s), 151.71 (s), 152.55 (s). Anal. Found: C, 52.68; H, 8.48; S, 12.96. Calcd for $C_{42}H_{82}GeS_4Si_6$: C, 52.73; H, 8.64; S, 13.40.

Reaction of 1,2,3,4,5-Tetrathiagermolane 5a with Diphenyldiazomethane. To a benzene solution (15 mL) of **5a** (252 mg, 0.289 mmol) was added diphenyldiazomethane (530 mg, 2.9 mmol), and the purple mixture was refluxed for 2.5 h. Solvent was removed under reduced pressure, and tetraphenylethylene and tetraphenylazine were removed from the residue with HPLC. Separation with DCC and PTLC (SiO_2 with 5/1 hexane/CH_2Cl_2) gave 4-{2,4,6-tris[bis(trimethylsilyl)methyl]phenyl}-4-mesityl-1,2,3,5-tetrathia-4-germacyclohexane (**10a**; 113 mg, 38%), 3-{2,4,6-tris[bis(trimethylsilyl)methyl]phenyl}-3-mesityl-1,2,4,5-tetrathia-3-germacyclohexane (**11a**; 54.5 mg, 18%), and 3-{2,4,6-tris[bis(trimethylsilyl)methyl]phenyl}-3-mesityl-1,2,4-trithia-3-germacyclopentane (**12a**; 39.5 mg, 14%). **10a**: white crystals; mp 208–209 °C; ^1H NMR ($CDCl_3$, 500 MHz) δ −0.04 (br s, 18H), 0.04 (s, 9H), 0.05 (s, 9H), 0.07 (s, 9H), 0.09 (s, 9H), 1.30 (s, 1H), 2.26 (s, 3H), 2.41 (s, 3H), 2.60 (s, 3H), 6.26 (br s, 1H), 6.39 (br s, 1H), 6.55 (s, 1H), 6.65 (s, 1H), 6.84–7.29 (m, 10H), the two o-benzyl protons of the Tbt group appeared at δ 2.48 as a broad singlet at 370 K; ^{13}C NMR ($CDCl_3$, 125 MHz) δ 0.80 (q), 0.94 (q), 1.14 (q), 1.49 (q), 1.87 (q), 2.08 (q), 20.82 (q), 22.69 (q), 25.48 (q), 28.30 (d), 28.79 (d), 30.38 (d), 74.21 (s), 123.36 (d), 126.16 (d), 127.21 (d), 127.99 (d), 128.29 (d), 128.31 (d), 128.44 (d), 129.67 (d), 130.35 (d), 130.47 (d), 132.56 (s), 137.70 (s), 139.27 (s), 139.51 (s), 142.31 (s), 142.44 (s), 145.23 (s), 146.97 (s), 150.51 (s), 150.80 (s). Anal. Found: C, 56.36; H, 7.65; S, 11.88. Calcd for $C_{49}H_{80}GeS_4Si_6$: C, 56.66; H, 7.76; S, 12.35. **11a**: white crystals; mp 278–279 °C; ^1H NMR ($CDCl_3$, 500 MHz) δ −0.19 (br s, 18H), 0.02 (br s, 36H), 1.30 (s, 1H), 2.18 (br s, 1H), 2.20 (s, 3H), 2.23 (br s, 1H), 2.51 (br s, 6H), 6.32 (br s, 1H), 6.41 (br s, 1H), 6.75 (s, 2H), 7.22–7.54 (m, 10H); ^{13}C NMR ($CDCl_3$, 125 MHz) δ 0.82 (q), 1.12 (br q), 1.47 (br q), 20.85 (q), 25.89 (q), 29.39 (d), 29.45 (d), 30.64 (d), 75.72 (s), 122.96 (d), 127.82 (d), 128.14 (d), 128.18 (d), 128.22 (d × 2), 128.29 (d), 128.33 (d), 130.12 (d), 133.16 (s), 137.96 (s), 139.18 (s), 141.56 (s), 141.59 (s), 141.93 (s), 145.35 (s), 150.92 (s), 151.01 (s). Anal. Found: C, 56.38; H, 7.55; S, 12.50. Calcd for $C_{49}H_{80}GeS_4Si_6$: C, 56.66; H, 7.76; S, 12.35. **12a**: white crystals; mp 203.5–205 °C; ^1H NMR ($CDCl_3$, 500 MHz) δ −0.09 (s, 18H), −0.06 (s, 18H), 0.03 (s, 18H), 1.31 (s, 1H), 2.20 (s, 3H), 2.37 (s, 2H), 2.44 (s, 6H), 6.31 (br s, 1H), 6.42 (br s, 1H), 6.69 (s, 2H), 7.03–7.64 (m, 10H); ^{13}C NMR ($CDCl_3$, 125 MHz) δ 0.83 (q), 0.86 (q), 1.13 (q), 1.37 (q), 1.38 (q), 20.82 (q), 25.05 (q), 28.61 (d), 29.23 (d), 30.60 (d), 82.56 (s), 123.18 (d), 127.20 (d), 127.25 (d), 127.51 (d), 127.92 (d), 128.36 (d), 128.63 (d), 129.24 (d), 129.58 (d), 131.60 (s), 138.82 (s), 139.11 (s), 141.66 (s), 143.48 (s), 143.98 (s), 146.99 (s), 151.02 (s), 151.11 (s). Anal. Found: C, 58.23; H, 7.88; S, 9.44. Calcd for $C_{49}H_{80}GeS_3Si_6$: C, 58.47; H, 8.01; S, 9.56.

Reaction of 1,2,3,4,5-Tetrathiagermolane 5a with Diphenyldiazomethane in the Presence of CuCl. To a benzene solution (8 mL) of **5a** (309 mg, 0.354 mmol) with a catalytic amount of CuCl was added diphenyldiazomethane (65 mg, 36 mmol) at 0 °C, and the mixture was stirred for 1 h at room temperature. Since **5a** still remained, an excess of diphenyldiazomethane was added and the solution was stirred for 1 h. After the solvent was evaporated under reduced pressure, tetraphenylethylene and tetraphenylazine were removed from the residue with HPLC. Separation with DCC and PTLC (SiO_2 with 5/1 hexane/CH_2Cl_2) gave **10a** (93 mg, 25%), **11a** (101 mg, 27%), and **12a** (8 mg, 2%) with recovery of **5a** (138 mg, 45%).

Reaction of 1,2,3,5-Tetrathia-4-germacyclohexane 10a with Diphenyldiazomethane. To a benzene solution (3 mL) of **10a** (50.8 mg, 0.042 mmol) was added diphenyldiazomethane (190 mg, 24 mmol), and the purple mixture was refluxed for 14 h. Workup similar to that above gave **12a** (6.8 mg, 14%) with recovery of **10a** (39.6 mg, 78%).

Reaction of 1,2,4,5-Tetrathia-3-germacyclohexane 11a with Diphenyldiazomethane. To a benzene solution (3 mL) of **11a** (43.5 mg, 0.042 mmol) was added diphenyldiazomethane (180 mg, 22 mmol), and the purple mixture was refluxed for 14 h. Workup similar to that above gave **12a** (3.3 mg, 8%) with recovery of **10a** (39.5 mg, 91%).

Reaction of 1,2,3,4,5-Tetrathiagermolane 5c with Diphenyldiazomethane. To a benzene solution (15 mL) of **5c** (116 mg, 0.121 mmol) was added diphenyldiazomethane (230 mg, 1.20 mmol), and the purple mixture was refluxed for 10 h. Workup similar to that above gave 4-{2,4,6-tris[bis(trimethylsilyl)methyl]phenyl}-4-(2,4,6-triisopropylphenyl)-1,2,3,5-tetrathia-4-germacyclohexane (**10c**; 67.6 mg, 50%) and 3-{2,4,6-tris[bis(trimethylsilyl)methyl]phenyl}-3-(2,4,6-triisopropylphenyl)-1,2,4,5-tetrathia-3-germacyclohexane (**11c**; 16.8 mg, 13%). **10c**: white crystals; mp 210–210.5 °C; ^1H NMR ($CDCl_3$, 500 MHz, 340 K) δ −0.26 (br s, 9H), 0.04 (br s, 18H), 0.06 (br s, 9H), 0.08 (s, 9H), 0.30 (br s, 9H), 0.60 (br s, 3H), 0.81 (d, J = 7 Hz, 3H), 1.03 (d, J = 7 Hz, 3H), 1.24 (s, 1H), 1.31 (d, J = 7 Hz, 6H), 1.36 (br s, 3H), 1.82 (br s, 1H), 2.91 (sept, J = 7 Hz, 1H), 2.97 (br s, 1H), 4.13 (br s, 1H), 4.32 (br s, 1H), 6.38 (br s, 1H), 6.47 (br s, 1H), 6.82 (br s, 2H), 6.93 (s, 1H), 7.01 (m, 1H), 7.11 (s, 1H), 7.16–7.29 (m, 7H). Anal. Found: C, 58.97; H, 8.23; S, 11.80. Calcd for $C_{55}H_{92}GeS_4Si_6$: C, 58.83; H, 8.26; S, 11.43. **11c**: white crystals; mp 160–164 °C dec; ^1H NMR ($CDCl_3$, 500 MHz) δ −0.10 (br s, 9H), −0.07 (br s, 9H), −0.03 (br s, 9H), 0.03 (s, 18H), 0.04 (br s, 9H), 1.01 (br s, 3H), 1.09 (br s, 3H), 1.14 (br s, 3H), 1.18 (d, J = 6.9 Hz, 6H), 1.24 (br s, 3H), 1.29 (s, 1H), 2.21 (br s, 1H), 2.38 (br s, 1H), 2.80 (sept, J = 6.9 Hz, 1H), 2.95 (br s, 1H), 3.85 (br s, 1H), 6.31 (br s, 1H), 6.45 (br s, 1H), 6.94 (br s, 1H), 7.02 (br s, 1H), 7.22–7.59 (m, 10H); ^{13}C NMR ($CDCl_3$, 125 MHz) δ 0.94 (q), 2.09 (q), 2.25 (q), 2.39 (q), 23.72 (q), 24.81 (q), 28.10 (q), 28.76 (q), 29.53 (d), 30.54 (d), 33.97 (d), 34.12 (d), 36.15 (d), 76.34 (s), 123.40 (d × 2), 123.68 (d), 127.99 (d), 128.08 (d × 2), 128.17 (d), 128.21 (d), 128.32 (d), 128.98 (d), 135.34 (s), 135.89 (s), 141.47 (s), 141.53 (s), 144.62 (s), 150.12 (s), 150.26 (s), 150.94 (s), 152.83 (s), 153.57 (s). Anal. Found: C, 58.92; H, 8.53; S, 11.21. Calcd for $C_{55}H_{92}GeS_4Si_6$: C, 58.83; H, 8.26; S, 11.43.

Synthesis of 1,2,4-Trithia-3-germacyclopentane 12c. To a THF solution (40 mL) of **10c** (750 mg, 0.668 mmol) was added at −78 °C hexamethylphosphorous triamide (0.38 mL, 2.0 mmol). After the solution was warmed to room temperature over 10 h, the solvent was removed under reduced pressure. Separation with DCC (SiO_2 with 25/1 hexane/CH_2Cl_2) afforded 3-{2,4,6-tris[bis(trimethylsilyl)methyl]phenyl}-3-(2,4,6-triisopropylphenyl)-1,2,4-trithia-3-germacyclopentane (**12c**; 272 mg, 37%) and {2,4,6-tris[bis(trimethylsilyl)methyl]phenyl}hydroxy(2,4,6-triisopropylphenyl)mercaptogermane (**16c**; 278 mg, 47%). **12c**: white crystals; mp 160–165 °C dec; ^1H NMR ($CDCl_3$, 500 MHz) δ −0.17 (s, 18H), 0.055 (s, 9H), 0.062 (s, 9H), 0.09 (s, 9H), 0.13 (s, 9H), 0.50 (br s, 3H), 0.93 (br s, 3H), 1.09 (br s, 3H), 1.19 (br s, 3H), 1.19 (d, J = 6.9 Hz, 6H), 1.32 (s, 1H), 2.14 (br s, 1H), 2.46 (br s, 1H), 2.81 (sept, J = 6.9 Hz, 1H), 3.71 (br s, 1H), 3.99 (br s, 1H), 6.31 (br s, 1H), 6.47 (br s, 1H), 6.95 (s, 2H), 7.12–7.73 (m, 10H); ^{13}C NMR ($CDCl_3$, 125 MHz) δ 0.90 (q), 1.12 (q), 1.97 (q), 2.25 (q), 2.31 (q × 2), 23.64 (q), 23.83 (q), 24.71 (q), 25.10 (q), 25.80 (q), 27.28 (q), 28.56 (d), 29.05 (d), 30.46 (d), 32.44 (d), 34.08 (d), 35.07 (d), 83.16 (s), 123.53 (d), 123.71 (d), 126.94 (d), 127.14 (d), 128.06 (d), 128.07 (d), 128.15 (d), 128.74 (d × 2), 129.23 (d), 134.11 (s), 137.66 (s), 144.52 (s), 144.74 (s), 145.01 (s), 149.64 (s), 150.40 (s), 151.17 (s), 151.42 (s), 153.59 (s). Anal. Found: C, 59.19; H, 8.50; S, 8.81. Calcd for $C_{55}H_{92}GeS_3Si_6$: C, 60.57; H, 8.50; S, 8.82. **16c**: white crystals; mp 160–165 °C dec; ^1H NMR ($CDCl_3$, 500 MHz) δ −0.12 (s, 9H), −0.05 (s, 9H), 0.05 (s, 9H), 0.06 (s, 9H), 0.11 (s, 9H), 0.15 (s, 9H), 1.01 (br s, 3H), 1.05 (s, 1H, Ge–SH), 1.15 (d, J = 6.9 Hz, 6H), 1.25 (br s, 3H), 1.32 (s, 1H), 1.33 (br s, 6H), 1.71 (s, 1H, Ge–OH), 2.48 (br s, 1H), 2.65 (br s, 1H), 2.85 (sept, J = 6.9 Hz, 1H), 2.96 (br s, 1H), 4.43 (br s, 1H), 6.30 (br s, 1H), 6.43 (br s, 1H), 7.02 (s, 2H), 7.12–7.73 (m, 10H); ^{13}C NMR ($CDCl_3$, 125 MHz) δ 0.81 (q), 1.00 (q), 1.20 (q), 1.44 (q), 1.66 (q), 1.94 (q), 22.35 (q × 2), 23.63 (q), 23.89 (q), 24.72 (q × 2), 26.70 (d), 27.19 (d), 27.50 (d), 28.23 (d), 30.53 (d), 34.34 (d), 121.66 (d), 122.84 (d), 123.38 (d), 128.46 (d), 132.09 (s), 137.27

(s), 144.72 (s), 149.48 (s), 149.74 (s), 150.81 (s), 152.80 (s), 152.94 (s). Anal. Found: C, 57.50; H, 9.44; S, 4.09. Calcd for $C_{42}H_{84}GeOSSi_6$: C, 57.43; H, 9.64; S, 3.65.

Desulfurization of 1,2,3,5-tetrathia-4-germacyclohexane 10a. To a THF solution (10 mL) of **10a** (115 mg, 0.111 mmol) was added at −78 °C hexamethylphosphorous triamide (85 mL, 0.45 mmol). After the solution was warmed to room temperature over 10 h, the solvent was removed under reduced pressure. Separation with DCC (SiO_2 with 10/1 hexane/CH_2Cl_2) afforded **12a** (92.6 mg, 83%) and {2,4,6-tris[bis(trimethylsilyl)methyl]phenyl}hydroxy(mercapto)(mesityl)germane (**16a**; (10.6 mg, 12%). **16a**: white crystals; mp 131−135 °C; ^1H NMR ($CDCl_3$, 500 MHz) δ −0.11 (s, 9H), −0.06 (s, 9H), 0.04 (s, 18H), 0.06 (s, 18H), 0.91 (s, 1H, Ge−SH), 1.31 (s, 1H), 1.50 (s, 1H, Ge−OH), 2.23 (s, 3H), 2.36 (br s, 1H), 2.50 (br s, 1H), 2.52 (s, 6H), 6.27 (br s, 1H), 6.40 (br s, 1H), 6.79 (s, 2H); ^{13}C NMR ($CDCl_3$, 125 MHz) δ 0.75 (q), 0.85 (q), 1.26 (q), 1.54 (q), 20.92 (d), 24.52 (q), 27.60 (d), 27.62 (d), 30.50 (q), 122.99 (d), 127.93 (d), 129.70 (d), 130.98 (s), 138.30 (s), 139.72 (s), 141.94 (s), 145.29 (s), 150.01 (s), 150.25 (s). Anal. Found: C, 53.25; H, 8.82; S, 3.94. Calcd for $C_{36}H_{72}GeOSSi_6 \cdot H_2O$: C, 53.23; H, 9.18; S, 3.95.

Thiomethylation of 16a. To a mixture of **16a** (95.0 mg, 0.12 mmol) and sodium hydride (60% in mineral oil, 25 mg, 0.60 mmol) in THF (12 mL) was added methyl iodide at room temperature for 3 h. Insoluble salts were removed by filteration under argon, and the solvent was removed under reduced pressure. The residue was separated by PTLC (SiO_2 with 3/1 hexane/CH_2Cl_2) to afford {2,4,6-tris[bis(trimethylsilyl)methyl]phenyl}hydroxy(mesityl)(methylthio)germane (**17a**; (87.4 mg, 90%). **17a**: white crystals; mp 202−205 °C; ^1H NMR ($CDCl_3$, 500 MHz) δ −0.15 (s, 9H), −0.09 (s, 9H), 0.037 (s, 9H), 0.040 (s, 9H), 0.08 (s, 9H), 0.10 (s, 9H), 1.31 (s, 1H), 1.84 (s, 3H), 2.19 (s, 1H), 2.23 (s, 3H), 2.24 (s, 1H), 2.52 (br s, 6H), 6.27 (br s, 1H), 6.40 (br s, 1H), 6.78 (s, 2H); ^{13}C NMR ($CDCl_3$, 125 MHz) δ 0.39 (q), 0.73 (q), 0.78 (q), 0.88 (q), 1.41 (q), 1.69 (q), 11.55 (q), 20.96 (d), 24.16 (q), 27.96 (d), 28.37 (d), 30.46 (q), 122.82 (d), 127.80 (d), 129.43 (d), 131.89 (s), 133.01 (s), 139.42 (s), 143.31 (s), 145.02 (s), 149.84 (s), 150.01 (s). Anal. Found: C, 55.11; H, 9.00; S, 4.45. Calcd for $C_{37}H_{74}GeOSSi_6$: C, 54.98; H, 9.23; S, 3.97.

Desulfurization of 1,2,4,5-Tetrathia-3-germacyclohexane 11a. A THF solution (5 mL) of **11a** (23.0 mg, 0.022 mmol) and hexamethylphosphorous triamide (4.3 mL, 0.023 mmol) was refluxed for 10 h. The solvent was removed under reduced pressure, and the residue was chromatographed with DCC (SiO_2 with 10/1 hexane/CH_2Cl_2) to afford **12a** (1.6 mg, 5%) with recovery of **11a** (21.7 mg, 91%).

Thermal Reaction of 1,2,3,5-Tetrathia-4-germacyclohexane 10a. A $CDCl_3$ solution (0.5 mL) of **10a** (38.6 mg, 0.0368 mmol) was sealed in a 5 mm i.d. NMR tube and heated to 100 °C for 40 h while being monitored by ^1H NMR. The solvent was removed, and the residue was separated with PTLC (SiO_2 with 10/1 hexane/CH_2Cl_2) to afford **10a** (14.9 mg, 37%), **11a** (14.8 mg, 37%), **5a** (5.8 mg, 17%), and **12a** (4.2 mg, 9%).

Crystal and Experimental Data for 5a and 10a. 5a: $C_{36}H_{70}S_4Si_6Ge \cdot CHCl_3$, fw = 989.64, crystal size (mm) 0.2 × 0.2 × 0.5, monoclinic, space group $P2_1/n$, a = 12.299(2) Å, b = 13.069(2) Å, c = 33.612(5) Å, β = 91.58(1)°, V = 5401(2) Å^3, Z = 4, D_c = 1.221 g cm^{-3}, R = 0.089 (R_w = 0.093), $w = 1/\{A|F_o|2 + B|F_o| + C\}$, A = 1086.4, B = −985.5, C = 227.1. Data were collected through a capillary glass tube with Cu Kα radiation (λ = 1.5418 Å) on an Enraf-Nonius CAD-4 diifractometer; μ = 49.95 cm^{-1}. A total of 5609 unique reflections ($|F_o| > 3\sigma|F_o|$) were observed (2° < 2θ < 120°). Empirical absorption correction was not applied due to the noticeable decay of reflections. The structure was solved by direct methods (MULTAN 78)[21] using the program system UNICS III.[22] All hydrogen atoms were located by calculation. Refinement was performed by full-matrix least-squares method (anisotropic thermal parameters for non-hydrogen atoms), where the positions and thermal parameters for hydrogen atoms were not refined. Atomic coordinates, bond lengths and angles, and thermal parameters have been deposited at the Cambridge Crystallographic Data Centre.[7]

10a: $C_{49}H_{80}GeS_4Si_6$, fw = 1038.51, crystal size (mm) 0.2 × 0.3 × 0.4, triclinic, a = 13.329(2) Å, b = 20.803(3) Å, c = 12.325(2) Å, α = 105.37(1)°, β = 116.93(1)°, γ = 77.31(1)°, V = 2918.0(8) Å^3, Z = 2, space group $P\bar{1}$, D_c = 1.182 g cm^{-3}, μ = 8.05 cm^{-1}. The intensity data (2θ ≤ 55°) were collected on a Rigaku AFC5R diffractometer with graphite-monochromated Mo Kα radiation (λ = 0.710 69 Å), and the structure was solved by direct methods.[23] All calculations were performed using the TEXSAN[24] crystallographic software package of Molecular Structure Corp. The non-hydrogen atoms were refined anisotropically, and all the hydrogen atoms were located by calculation. The final cycle of full-matrix least-squares refinement was based on 3881 observed reflections ($I > 3\sigma(I)$) and 541 variable parameters with R (R_w) = 0.039 (0.044). Atomic coordinates, bond lengths and angles, and thermal parameters have been deposited at the Cambridge Crystallographic Data Centre.[11]

Acknowledgment. This work was partially supported by a Grant-in-Aid for Scientific Research on Priority Area (No. 05236102) from the Ministry of Education, Science and Culture of Japan. We are grateful to ASAI Germanium Research Institute, Shin-etsu Chemical Co., Ltd., and Tosoh Akzo Co., Ltd., for the generous gifts of tetrachlorogermane, chlorosilanes, and alkyllithiums, respectively.

Supplementary Material Available: Tables giving crystallographic data, atomic coordinates, temperature factors, and bond lengths and angles, for **5a** and **10a** and a table of torsion angles for **10a** (31 pages). Ordering information is given on any current masthead page.

OM940763T

(21) Main, P.; Hull, S. E.; Lessinger, L.; Germain, G.; Declercg, J.-P.; Woolfson, M. H. MULTAN 78: A system of computer programs for automatic solution of crystal structures from X-ray diffraction data; University of York, York, England, and University of Louvain, Louvain, Belgium, 1978.

(22) Sakurai, T.; Kobayashi, K. *Rikagaku Kenkyusho Houkoku* **1979**, *55*, 69.

(23) Gilmore, C. J. MITHRIL. An integrated direct method computer program. *J. Appl. Crystallogr.* **1984**, *17*, 42 (University of Glasgow, Glasgow, Scotland).

(24) TEXSAN: TEXRAY Structural Analysis Package; Molecular Structure Corp., The Woodlands, TX, 1985.

Synthesis and Structures of Extremely Hindered and Stable Disilenes

Hiroyuki Suzuki, Norihiro Tokitoh, and Renji Okazaki*

Department of Chemistry, Graduate School of Science, The University of Tokyo, 7-3-1 Hongo, Bunkyo-ku, Tokyo 113, Japan

Jun Harada, Keiichiro Ogawa, and Shuji Tomoda

Department of Chemistry, The College of Arts and Sciences, The University of Tokyo, 3-8-1 Komaba, Meguro-ku, Tokyo 153, Japan

Midori Goto

Natural Institute of Materials and Chemical Research, 1-1 Higashi, Tsukuba, Ibaraki 305, Japan

Received October 4, 1994®

Extremely hindered and stable disilenes Tbt(Mes)Si=Si(Mes)Tbt, ((*Z*)- and (*E*)-**6**; Tbt = 2,4,6-tris[bis(trimethylsilyl)methyl]phenyl, Mes = 2,4,6-trimethylphenyl) were synthesized by a reductive coupling reaction of the corresponding overcrowded dibromosilane Tbt(Mes)-$SiBr_2$ (**4**) with lithium naphthalenide in THF. The molecular structures of (*Z*)- and (*E*)-**6** were determined by X-ray crystallographic analysis at 120 K. Compound (*Z*)-**6** crystallizes in the monoclinic space group $P2_1/n$ with a = 22.212(3) Å, b = 13.368(2) Å, c = 29.725(3) Å, β = 91.344(9)°, V = 8824(2) Å^3, and Z = 4. Compound (*E*)-**6**·$C_{10}H_8$ crystallizes in the monoclinic space group $P2_1/c$ with a = 18.130(3) Å, b = 18.466(3) Å, c = 28.522(2) Å, β = 95.976(9)°, V = 9497(2) Å^3, and Z = 4. The X-ray structures show remarkable pyramidalization around silicon atoms and elongation of the Si–Si double bond (2.195(4) Å for (*Z*)-**6** and 2.228(2) Å for (*E*)-**6**), the values of which are the longest ones reported so far for disilenes having carbon substituents on the silicon atoms. Both disilenes were found to be stable for weeks in the open air even in a microcrystalline form, and they were gradually oxidized to afford stereospecifically the (*Z*)- and (*E*)-1,3,2,4-dioxadisiletane compounds **10**. Compound (*Z*)-**10** crystallizes in the monoclinic space group $P2_1/n$ with a = 22.420(5) Å, b = 13.458(6) Å, c = 30.417(4) Å, β = 90.96(1)°, V = 9176(4) Å^3, and Z = 4. Reaction of Tbt(*t*-Bu)$SiBr_2$ (**5**) with lithium naphthalenide proceeded in a different way to afford the benzosilacyclobutene **11**, which was most likely an intramolecular C–H insertion product of the intermediary silylene Tbt(*t*-Bu)Si: (**12**).

Introduction

Since the first isolation of a stable disilene derivative, tetramesityldisilene, by West et al. in 1981,[1] introduction of bulky groups on silicon atoms has been an approved method for the synthesis of stable disilenes.[2] Although several disilenes have been synthesized and characterized by X-ray crystallographic analyses,[3] carbon substituents used for kinetic stabilization are restricted to only five groups, i.e., mesityl, 2,6-diethylphenyl, 2,4,6-triisopropylphenyl, *tert*-butyl, and 1-adamantyl, and the investigation of the steric influence on structures and reactivities of disilenes is still insufficient. Recently we have developed a new steric protection group, 2,4,6-tris[bis(trimethylsilyl)methyl]phenyl[4] (denoted as Tbt hereafter), and reported its high efficiency in the isolation of highly reactive chemical species such as novel cyclic polychalcogenides,[5] highly strained tin-containing small-ring compounds,[6] and heavy congeners of ketones (silanethione and germanethione).[7] We became interested in the effect of the Tbt group on the stability of a disilene and undertook the investigation of its synthesis, molecular structure,

® Abstract published in *Advance ACS Abstracts,* January 15, 1995.

(1) West, R.; Fink, M. J.; Michl, J. *Science (Washington, D.C.)* **1981**, *214*, 1343.

(2) For reviews, see: (a) West, R. *Pure Appl. Chem.* **1984**, *56*, 163. (b) West, R. *Angew. Chem., Int. Ed. Engl.* **1987**, *26*, 1201. (c) Tsumuraya, T.; Batcheller, S. A.; Masamune, S. *Angew. Chem., Int. Ed. Engl.* **1991**, *30*, 902.

(3) (a) Fink, M. J.; Michalczyk, M. J.; Haller, K. J.; West, R.; Michl, J. *J. Chem. Soc., Chem. Commun.* **1983**, 1010. (b) Fink, M. J.; Michalczyk, M. J.; Haller, K. J.; West, R.; Michl, J. *Organometallics* **1984**, *3*, 793. (c) Masamune, S.; Murakami, S.; Snow, J. T.; Tobita, H.; Williams, D. J. *Organometallics* **1984**, *3*, 333. (d) Watanabe, H.; Takeuchi, K.; Fukawa, N.; Kato, M.; Goto, M.; Nagai, Y. *Chem. Lett.* **1987**, 1341. (e) Shepherd, B. D.; Powell, D. R.; West, R. *Organometallics* **1989**, *8*, 2664. (f) Shepherd, B. D.; Campana, C. F.; West, R. *Heteroat. Chem.* **1990**, *1*, 1. (g) Archibald, R. S.; Winkel, Y.; Millevolte, A. J.; Desper, J. M.; West, R. *Organometallics* **1992**, *11*, 3276. (h) Kira, M.; Maruyama, T.; Kabuto, C.; Ebata, K.; Sakurai, H. *Angew. Chem., Int. Ed. Engl.* **1994**, *33*, 1489.

(4) (a) Okazaki, R.; Unno, M.; Inamoto, N. *Chem. Lett.* **1987**, 2293. (b) Okazaki, R.; Unno, M.; Inamoto, N.; Yamamoto, G. *Chem. Lett.* **1989**, 493. (c) Okazaki, R.; Unno, M.; Inamoto, N. *Chem. Lett.* **1989**, 791.

(5) (a) Tokitoh, N.; Takeda, N.; Imakubo, T.; Goto, M.; Okazaki, R. *Chem. Lett.* **1992**, 1599. (b) Tokitoh, N.; Suzuki, H.; Matsumoto, T.; Matsuhashi, Y.; Okazaki, R.; Goto, M. *J. Am. Chem. Soc.* **1991**, *113*, 7047.

(6) Tokitoh, N.; Matsuhashi, Y.; Okazaki, R. *J. Chem. Soc., Chem. Commun.* **1993**, 407.

(7) (a) Suzuki, H.; Tokitoh, N.; Okazaki, R.; Nagase, S. *J. Am. Chem. Soc.* **1994**, *116*, 11578. (b) Tokitoh, N.; Matsumoto, T.; Manmaru, K.; Okazaki, R. *J. Am. Chem. Soc.* **1993**, *115*, 8855.

0276-7333/95/2314-1016$09.00/0

Scheme 1

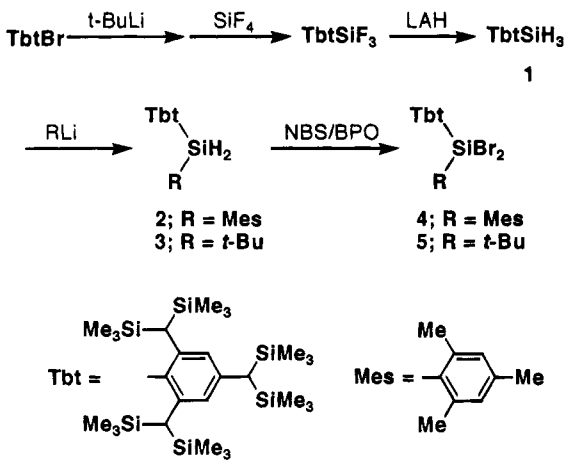

Scheme 2

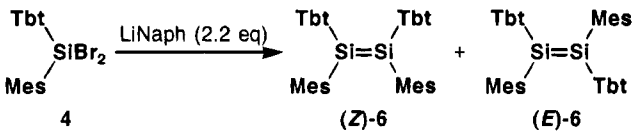

and reactivities. The present paper delineates detailed accounts of the synthesis and unique structures of the highly hindered and stable disilenes Tbt(Mes)Si=Si(Mes)Tbt ((*Z*)-**6**, cis form; (*E*)-**6**, trans form).[8]

Results and Discussion

Synthesis of Highly Hindered Dibromosilanes. Our first attempts to introduce Tbt and Mes groups onto a silicon atom employed nucleophilic substitution reactions of aryllithium reagents on tetrafluorosilane. The Tbt-substituted trifluorosilane $TbtSiF_3$ could be synthesized by the reaction of TbtLi, prepared from TbtBr and *t*-BuLi, with tetrafluorosilane.[9] Although addition of MesLi to the trifluorosilane gave $Tbt(Mes)SiF_2$, the yield was quite low and the purification was very difficult. The corresponding hydrosilane $TbtSiH_3$ (**1**) was chosen, therefore, as an alternative precursor for nucleophilic substitution. Arylsilane **1** was synthesized by the reduction of trifluorosilane $TbtSiF_3$ with lithium aluminum hydride (LAH) in THF (Scheme 1). Reaction of **1** with MesLi gave **2** in good yield (83%). By using the same procedure as for **2**, dihydrosilane Tbt(*t*-Bu)SiH_2 (**3**) was also obtained. Bromination of **2** and **3** with *N*-bromosuccinimide (NBS) afforded dibromosilanes **4** and **5**, respectively.

Synthesis of Disilenes. Disilenes Tbt(Mes)Si=Si(Mes)Tbt (**6**) were readily synthesized as a mixture of *Z* and *E* isomers (ca. 40% in total) by a reductive coupling reaction of **4** with lithium naphthalenide in THF (Scheme 2). The reaction mixture was roughly purified by chromatography. It should be noted that the disilenes did not undergo any significant decomposition during the chromatography even in the air. Pure (*Z*)-**6** (30%) was isolated as a lemon yellow microcrystalline compound by filtration of the concentrated pentane suspension of the chromatographed mixture of the disilenes, while a mixture of (*E*)-**6** and naphthalene was obtained as an orange oil by concentration of the filtrate.

(8) Preliminary report: Tokitoh, N.; Suzuki, H.; Okazaki, R.; Ogawa, K. *J. Am. Chem. Soc.* **1993**, *115*, 10428.
(9) Unno, M. Ph.D. Thesis, The University of Tokyo, Tokyo, 1988.

Table 1. Experimental Crystallographic Data for (*Z*)-6, (*E*)-6·$C_{10}H_8$, and (*Z*)-10

	(*Z*)-**6**	(*E*)-**6**·$C_{10}H_8$	(*Z*)-**10**
empirical formula	$C_{72}H_{140}Si_{14}$	$C_{82}H_{148}Si_{14}$	$C_{72}H_{140}Si_{14}O_2$
fw	1399.10	1527.27	1431.10
cryst size, mm	0.30 × 0.20 × 0.15	0.25 × 0.25 × 0.20	0.50 × 0.20 × 0.20
temp, K	120	120	297
cryst syst	monoclinic	monoclinic	monoclinic
space group	$P2_1/n$	$P2_1/c$	$P2_1/n$
unit cell dimens			
a, Å	22.212(3)	18.130(3)	22.420(5)
b, Å	13.368(2)	18.466(3)	13.458(6)
c, Å	29.725(3)	28.522(2)	30.417(4)
β, deg	91.344(9)	95.976(9)	90.96(1)
V, Å^3	8824(2)	9497(2)	9176(4)
Z	4	4	4
density (calcd), g cm^{-3}	1.053	1.068	1.036
scan type	$2\theta-\omega$	$2\theta-\omega$	$2\theta-\omega$
no. of obsd rflns	6430	7950	3834
data to param ratio	8.3	10.3	4.8
largest diff peak, e Å^{-3}	1.7	1.6	0.4
largest diff hole, e Å^{-3}	2.3	1.3	0.4
R, %	10.1	8.0	10.4
R_w, %	10.3	8.1	5.4

Table 2. Selected Bond Lengths (Å) and Angles (deg) for (*Z*)-6

Si(1)−Si(2)	2.195(4)	Si(1)−C(1)	1.90(1)
Si(1)−C(7)	1.90(1)	Si(2)−C(13)	1.91(1)
Si(2)−C(19)	1.899(9)		
Si(2)−Si(1)−C(1)	134.6(3)	Si(1)−Si(2)−C(13)	136.3(3)
Si(2)−Si(1)−C(7)	109.7(3)	Si(1)−Si(2)−C(19)	109.5(3)
C(1)−Si(1)−C(7)	114.5(4)	C(13)−Si(2)−C(19)	113.5(4)

Careful recrystallization of this orange oil from benzene gave reddish orange crystals of (*E*)-**6** including naphthalene (ca. 10%).

Although the molecular composition of (*Z*)-**6** was certainly confirmed by both high-resolution FAB-MS and elemental analysis, it exhibited a very complicated ^1H NMR spectrum, suggesting greater steric congestion around the silicon atoms than in its *E* isomer. The ^{29}Si NMR spectrum of (*E*)-**6** measured in benzene-d_6 showed only one signal at 66.49 ppm in the sp^2 silicon region, while that of (*Z*)-**6** exhibited four peaks with roughly equal intensity at 56.16, 56.74, 57.12, and 58.12 ppm, most likely due to the existence of two or more conformational isomers on the NMR time scale.

Crystal Structures of (*Z*)- and (*E*)-6. Thermal ellipsoid diagrams indicating the molecular structures of (*Z*)- and (*E*)-**6** at 120 K are shown in Figure 1, and the crystallographic data for these structures are summarized in Table 1. Selected bond lengths and angles are listed in Tables 2 (for (*Z*)-**6**) and 3 (for (*E*)-**6**·$C_{10}H_8$). The degree of pyramidalization at the silicon can be gauged by the angles formed by the C_{aryl}−Si−C_{aryl} plane and the silicon−silicon bond axis, 9.8(4) and 7.6(4)° for (*Z*)-**6** and 9.4(3) and 14.6(3)° for (*E*)-**6**, respectively. The twist angle[10] along the silicon−silicon axis of (*Z*)-**6** (14(1)°) is larger than that of (*E*)-**6** (8.7(8)°), reflecting the severe steric repulsion of (*Z*)-**6** between the two Tbt groups facing each other (Figure 2). The steric repulsion of (*Z*)-**6** is also reflected in the large differences between the Si−Si−C_{Tbt} angles (136.3(3), 134.6(3)°) and the Si−Si−C_{Mes} angles (109.5(3), 109.7(3)°). The Si−Si−C_{Tbt}

(10) The twist angles are taken as half the difference of the angles subtended by the C_{Tbt}−Si−Si and $C_{Tbt'}$−Si−Si planes (26.4°) and the C_{Mes}−Si−Si and $C_{Mes'}$−Si−Si planes (−2.4°) for (*Z*)-**6** and the C_{Tbt}−Si−Si and C_{Mes}−Si−Si planes (25.9°) and $C_{Tbt'}$−Si−Si and $C_{Mes'}$−Si−Si planes (8.5°) for (*E*)-**6**.

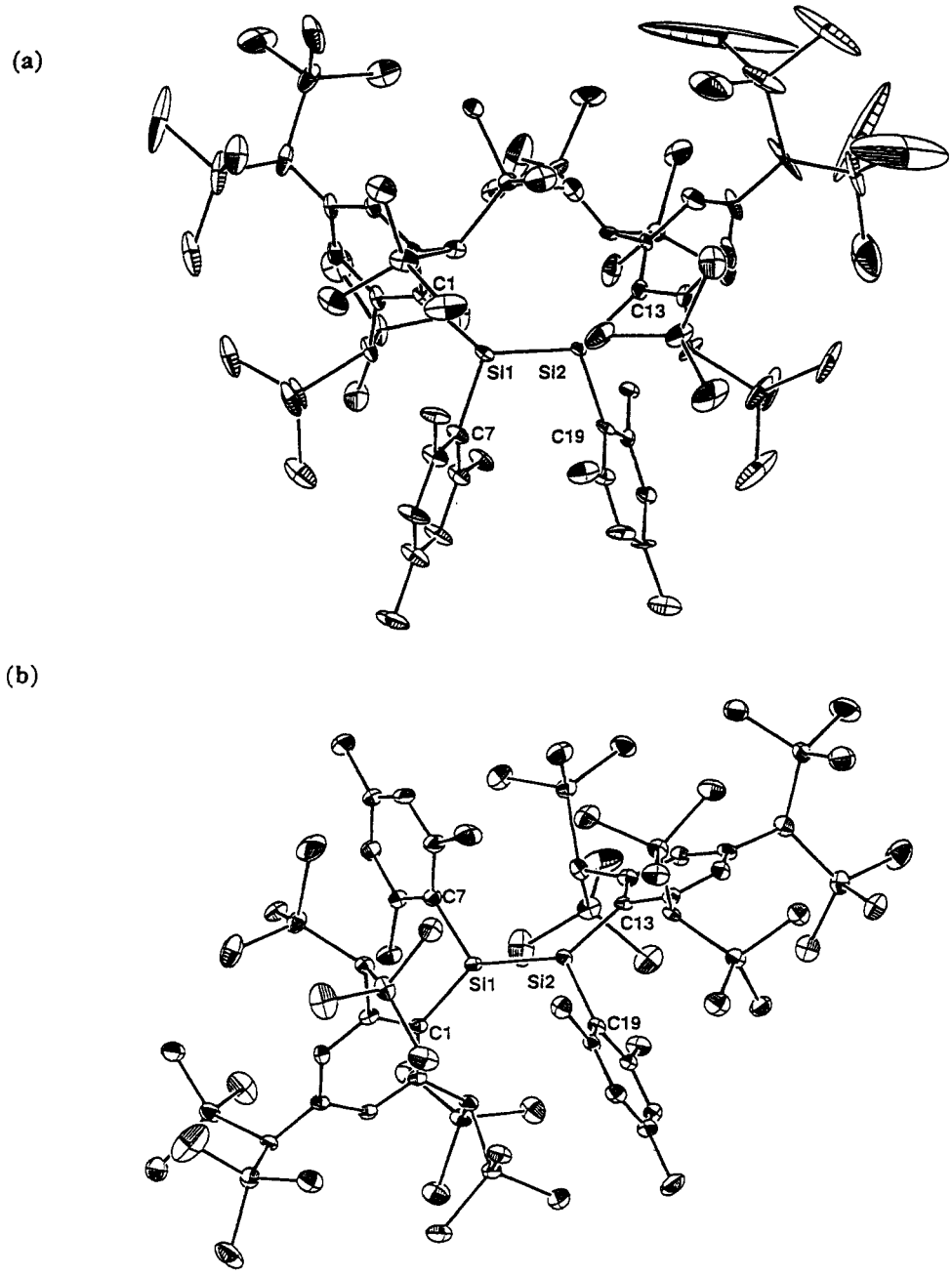

Figure 1. ORTEP drawings of (*Z*)-**6** (a) and (*E*)-**6**·$C_{10}H_8$ (b) with thermal ellipsoid plots (30% probability).

Table 3. Selected Bond Lengths (Å) and Angles (deg) for (*E*)-6·$C_{10}H_8$

Si(1)−Si(2)	2.228(3)	Si(2)−C(13)	1.927(7)
Si(1)−C(1)	1.922(7)	Si(2)−C(19)	1.894(7)
Si(1)−C(7)	1.895(8)		
Si(2)−Si(1)−C(1)	130.0(2)	Si(1)−Si(2)−C(13)	132.2(2)
Si(2)−Si(1)−C(7)	120.1(2)	Si(1)−Si(2)−C(19)	115.8(2)
C(1)−Si(1)−C(7)	108.8(3)	C(13)−Si(2)−C(19)	109.2(3)

angles of (*E*)-**6** (130.0(2), 132.2(2)°) are also larger, albeit not so much compared to (*Z*)-**6**, than the Si−Si−C_{Mes} angles (120.1(2), 115.8(2)°). As for the silicon−silicon double-bond length, the value for (*E*)-**6** (2.228(3) Å) is unexpectedly larger than that for (*Z*)-**6** (2.195(4) Å). It is interesting that the steric repulsion of (*Z*)-**6** is reflected in the twist angle and the bond angles around silicon atoms, whereas that of (*E*)-**6** is reflected mainly in the Si−Si double-bond length. Structural comparisons of (*Z*)- and (*E*)-**6** with previously reported disilenes are summarized in Table 4. The Si−Si double-bond

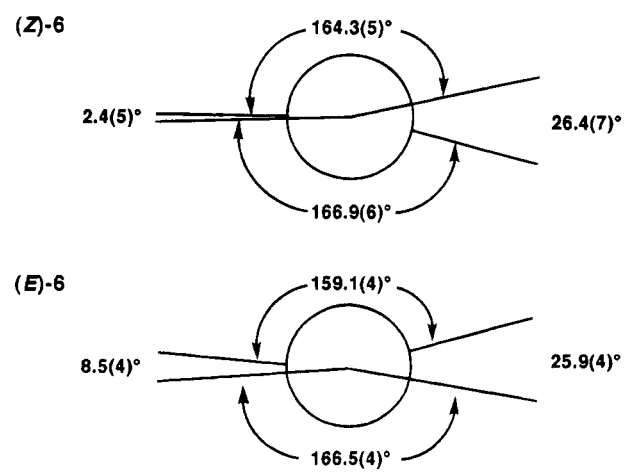

Figure 2. Newman projections of (*Z*)- and (*E*)-**6** along the Si−Si axis showing the twist angles.

Table 4. Structural Comparisons in Hindered Disilenes

disilene	Si=Si/Å	∠C–Si–C/deg	∠C–Si–Si/deg	twist angle/deg	bent angle/deg	ref
$Mes_2Si{=}SiMes_2$	2.143(2)	112.1(2) 121.5(2)	126.7(2) 121.2(1) 119.5(1) 115.4(2)	3	12 14	3f
$Mes_2Si{=}SiMes_2{\cdot}C_7H_8$	2.160(1)		113.9(1) 126.8(1)	6.5(1)	18	3b
(*E*)-Mes(*t*-Bu)Si=Si(Mes)-*t*-Bu	2.143(1)	113.2(1)	123.86(8) 122.77(8)	0	0	3b
$Dep_2Si{=}SiDep_2$	2.140(3)	117.6(2)	117.6(2) 124.8(2)	10	0	3c
$Tip_2Si{=}SiTip_2$	2.144	117.5	120.8 121.6	3	0	3d
(*E*)-Mes(Ad)Si=Si(Mes)Ad	2.138(2)	115.4(2)	123.4(1) 121.2(2)	0	2.8	3e
(*E*)-Tip(*t*-Bu)Si=Si(Tip)-*t*-Bu	2.157(2)			0	0	3g
(*E*)-Tip(Me_3Si)Si=Si(Tip)$SiMe_3$	2.152(3)			0	0	3g
$(i\text{-}Pr_2MeSi)_2Si{=}Si(Si\text{-}i\text{-}Pr_2Me)_2$	2.228(2)	115.3(1)	120.3(1) 124.1(1)	0	5.4(0)	3h
$(t\text{-}BuMe_2Si)_2Si{=}Si(Si\text{-}t\text{-}BuMe_2)_2$	2.202(1)	112.5(0)	122.9(0) 124.5(0)	8.9(1)	0.1(0)	3h
$(i\text{-}Pr_3Si)_2Si{=}Si(Si\text{-}i\text{-}Pr_3)_2$	2.251(1)	114.9(0)	126.3(0) 117.5(0)	0	10.2(0)	3h
(*Z*)-Tbt(Mes)Si=Si(Mes)Tbt	2.195(4)	113.5(4) 114.5(4)	136.3(3) 134.6(3) 109.5(3) 109.7(3)	14(1)	9.8(4) 7.6(4)	this work
(*E*)-Tbt(Mes)Si=Si(Tbt)Mes$\cdot C_{10}H_8$	2.228(3)	108.8(3) 109.2(3)	132.2(2) 130.0(2) 120.1(2) 115.8(2)	8.7(8)	14.6(3) 9.4(3)	this work

lengths of **6** are much larger than those of other disilenes having carbon substituents on the silicon atoms, which varied within a range from 2.138 to 2.160 Å.[3,11] The difference in bond angles between two kinds of the Si–Si–C bonds of **6** is also larger than the corresponding ones for other disilenes. While sterically hindered alkenes, for example, compounds **7**,[12a] **8**,[12b] and **9**,[12c] relieve their strain mainly by twisting along the

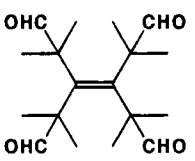

7

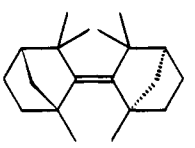

8

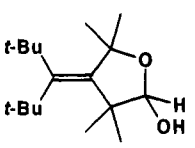

9

C–C axis (28.6° for **7**, 17° for **8**, 37.5° for **9**) rather than

(11) Very recently, Kira et al. reported the syntheses and structures of tetrakis(trialkylsilyl)disilenes $R_2Si{=}SiR_2$ (R = i-Pr_2MeSi, t-$BuMe_2Si$, i-Pr_3Si).[3h] The X-ray structures of these disilenes showed unusual elongation of the central Si–Si double-bond lengths (2.202(1)–2.251(1) Å) and pyramidalization around central silicon atoms. They ascribe these structural deformations to both the steric and electronic influence of trialkylsilyl substituents.

(12) (a) Krebs, A.; Kaletta, B.; Nickel, W.-U.; Rüger, W.; Tikwe, L. *Tetrahedron* **1986**, *42*, 1693. (b) Garratt, P. J.; Payne, D.; Tocher, D. A. *J. Org. Chem.* **1990**, *55*, 1909. (c) Brooks, P. R.; Bishop, R.; Counter, J. A.; Tiekink, E. R. T. *J. Org. Chem.* **1994**, *59*, 1365.

Scheme 3

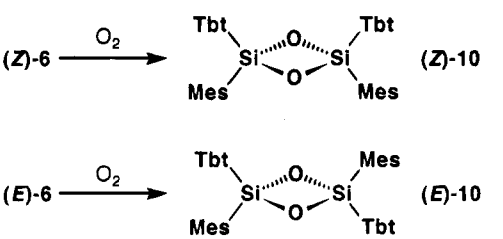

by pyramidalization or elongation of the C–C double bond (1.5% for **7**, 0.5% for **8**, 2.2% for **9**, compared to the normal C–C double-bond length of 1.337 Å), disilenes **6** relieve their strain by changing the bond angles of Si–Si–C_{Tbt} and Si–Si–C_{Mes} and lengthening the Si–Si double bond (the degree of lengthening is 2.2% for (*Z*)-**6** and 3.8% for (*E*)-**6** compared to the mean value of Si–Si double-bond lengths (2.147 Å)). These characteristic deformations of **6** indicate the "soft" nature of the Si–Si double bond in comparison with the C–C double bond.

Oxidation of 6. Both disilenes (*Z*)- and (*E*)-**6** were found to be quite stable in the open air in the solid state. Upon exposure to the air, a finely powdered sample of (*Z*)-**6** underwent very slow oxidation with a half-life time of approximately 40 days (Scheme 3). Disilenes previously synthesized have been reported to be very reactive toward atmospheric oxygen; for example, tetramesitydisilene is oxidized completely within a few minutes[3b] and (*E*)-1,2-bis(1-adamantyl)dimesityldisilene, which is considered to be so far the most stable disilene, is oxidized with a half-life time of about 2 days.[3e] The remarkable stability of disilenes (*Z*)- and (*E*)-**6** relative

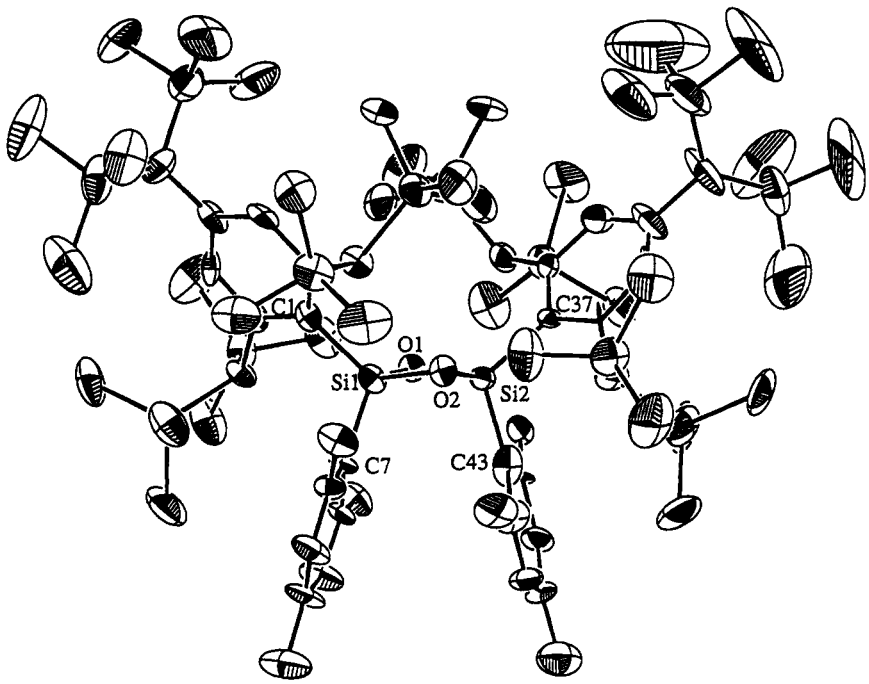

Figure 3. ORTEP drawing of (*Z*)-**10** with thermal ellipsoid plots (30% probability).

Table 5. Selected Bond Lengths (Å) and Angles (deg) for (*Z*)-10

Si(1)−Si(2)	2.395(7)	Si(2)−O(1)	1.687(9)
Si(1)−O(1)	1.680(9)	Si(2)−O(2)	1.691(9)
Si(1)−O(2)	1.698(9)	Si(2)−C(37)	1.89(1)
Si(1)−C(1)	1.91(2)	Si(2)−C(43)	1.90(2)
Si(1)−C(7)	1.87(1)		
Si(2)−Si(1)−O(1)	44.8(3)	Si(1)−Si(2)−O(2)	45.2(3)
Si(2)−Si(1)−O(2)	44.9(3)	Si(1)−Si(2)−C(37)	138.2(5)
Si(2)−Si(1)−C(1)	136.0(5)	Si(1)−Si(2)−C(43)	108.0(6)
Si(2)−Si(1)−C(7)	109.5(5)	O(1)−Si(2)−O(2)	88.1(5)
O(1)−Si(1)−O(2)	88.2(5)	O(1)−Si(2)−C(37)	119.7(7)
O(1)−Si(1)−C(1)	113.2(6)	O(1)−Si(2)−C(43)	107.4(6)
O(1)−Si(1)−C(7)	111.9(7)	O(2)−Si(2)−C(37)	113.9(6)
O(2)−Si(1)−C(1)	117.7(7)	O(2)−Si(2)−C(43)	111.1(7)
O(2)−Si(1)−C(7)	108.5(6)	Si(1)−O(1)−Si(2)	90.7(5)
C(1)−Si(1)−C(7)	114.5(7)	Si(1)−O(2)−Si(2)	89.9(5)
Si(1)−Si(2)−O(1)	44.5(3)		

to the previously reported hindered disilenes is apparently due to the high steric demand of the Tbt group.

Expectedly,[13] the oxidation of (*Z*)-**6** resulted in the quantitative formation of the (*Z*)-1,3,2,4-dioxadisiletane (*Z*)-**10**, the geometry of which was confirmed by X-ray crystallographic analysis. Figure 3 shows an ORTEP drawing of (*Z*)-**10**, and the crystallographic data for this structure are summarized in Table 1. Selected bond lengths and angles are listed in Table 5. The Si−Si distance of (*Z*)-**10** (2.395(7) Å) is similar to those of previously reported dioxadisiletanes,[13d] but the Si−O distances (1.679(9), 1.698(9), 1.687(9), and 1.691(9) Å) are slightly longer. The central dioxadisiletane ring is folded, and the dihedral angle formed by the two O−Si−O planes is 18.6°, indicating steric repulsion between the two Tbt groups facing each other. Oxidation of (*E*)-**6** also proceeded stereospecifically to give the (*E*)-1,3,2,4-dioxadisiletane (*E*)-**10** quantitatively.

(13) It has been established that oxidation of a disilene proceeds stereospecifically to afford a 1,3,2,4-dioxadisiletane. (a) Michalczyk, M. J.; West, R.; Michl, J. *J. Chem. Soc., Chem. Commun.* **1984**, 1525. (b) Michalczyk, M. J.; West, R.; Michl, J. *J. Am. Chem. Soc.* **1984**, *106*, 821. (c) McKillop, K. L.; Gillette, G. R.; Powell, D. R.; West, R. *J. Am. Chem. Soc.* **1992**, *114*, 5203. (d) Sohn, H.; Tan, R. P.; Powell, D. R.; West, R. *Organometallics* **1994**, *13*, 1390.

Scheme 4

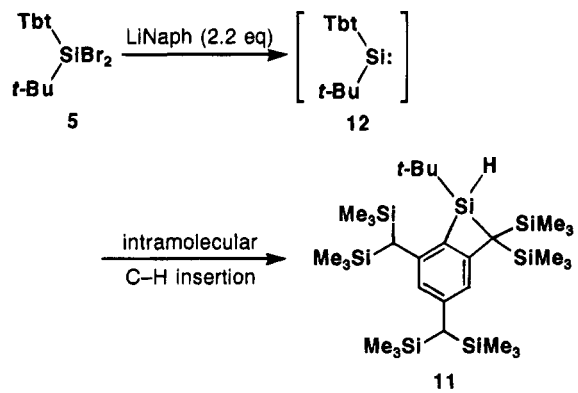

Reaction of 5 with Lithium Naphthalenide. Reduction of Tbt- and *t*-Bu-substituted dibromosilane **5** with lithium naphthalenide proceeded in a different way. No coupling product, i.e., the corresponding disilene, was obtained. The product was benzosilacyclobutene **11**[14] (Scheme 4). The formation of **11** may be rationalized in terms of an intramolecular C−H insertion of intermediary silylene **12**,[15] generated by α-elimination of **5**. No dimerization of **12** takes place, probably because the bulkiness of *t*-Bu group is greater than that of Mes group, which makes the dimerization difficult. Although there is a precedent that a photochemically generated mesityl-substituted silylene inserts into a C−H bond of an ortho mesityl methyl group to afford benzosilacyclobutene,[16] we could not exclude rigorously the possibility of involvement of a silyl anion or silyl radical species as an intermediate at present.

(14) Although the structure of **11** was confirmed by X-ray crystallographic analysis, the refinement has not yet been converged with satisfactory agreement factors because of the inferiority of the single crystal used. The final crystallographic analysis of **11** will be reported elsewhere.

(15) Thermolysis of Tbt-substituted diazomethane, Tbt(H)CN_2, resulted in the formation of the corresponding benzocyclobutene derivative, which was considered to be an intramolecular C−H insertion product of intermediary carbene Tbt(H)C:.[5a]

(16) Fink, M. J.; Puranik, D. B.; Johnson, M. P. *J. Am. Chem. Soc.* **1988**, *110*, 1315.

Conclusion

Extremely hindered and stable disilenes (*Z*)- and (*E*)-**6** were synthesized by a reductive coupling reaction of the corresponding overcrowded dibromosilane **4** with lithium naphthalenide in THF. The intermediate of this reaction is probably a divalent silicon species (silylene), the involvement of which is suggested by the occurrence of the intramolecular C−H insertion in **5**, giving **11**. X-ray crystallographic analysis of **6** revealed extremely distorted structures due to great steric congestion by Tbt and Mes groups. The extent of pyramidalization around silicon atoms and elongation of Si−Si bonds is much larger than those of distorted alkene analogs, indicating that the nature of a silicon-silicon double bond is very "soft" compared to a carbon-carbon double bond. (*Z*)- and (*E*)-**6** were found to be stable for weeks in the open air, owing to the effective steric protection by the Tbt group. This extremely bulky substituent influences the reactivities of disilenes **6** to such an extent that they undergo a facile thermal dissociation into the silylene Tbt(Mes)Si: under mild conditions.[8] We are now investigating the reactivities of **6**, and the results will be published elsewhere.

Experimental Section

General Procedure. All melting points were uncorrected. All solvents used in the reactions were purified by the reported methods. THF was purified by distillation from benzophenone ketyl before use. All reactions were carried out under an argon atmosphere unless otherwise noted. Preparative gel permeation liquid chromatography (GPLC) was performed on an LC-908 instrument with JAI gel 1H+2H columns (Japan Analytical Industry) and chloroform as solvent. Dry column chromatography (DCC) was performed with ICN silica DCC 60A. Flash column chromatography (FCC) was performed with silica gel BW 300 (Fuji Davison Chemical). The ^{1}H NMR (500 MHz), ^{13}C NMR (125 MHz), and ^{29}Si NMR (53.5 MHz) spectra were measured in $CDCl_3$ and C_6D_6 with a Bruker AM-500 or JEOL EX-270 spectrometer using $CHCl_3$ or C_6H_6 as internal standard. The values of chemical shifts in ^{29}Si NMR spectra are shown only for the central silicon atoms, since the trimethylsilyl groups around the 0 ppm region appear as complex multiplets due to the anisotropic effect of Tbt and Mes groups. Elemental analyses were performed by the Microanalytical Laboratory of the Department of Chemistry, Faculty of Science, The University of Tokyo.

Preparation of {2,4,6-Tris[bis(trimethylsilyl)methyl]phenyl}silane (1). To a solution of trifluoro{2,4,6-tris[bis(trimethylsilyl)methyl]phenyl}silane (13.94 g, 21.87 mmol) in THF (120 mL) was added LAH (1.7 g, 44.7 mmol) at 0 °C, and the solution was heated under reflux for 10 h. After the reaction mixture was cooled to room temperature, the reaction was quenched with 1 M HCl aqueous solution and the organic layer was separated. The aqueous layer was extracted with 50 mL of hexane, and the organic layer was dried with $MgSO_4$. Removal of the solvent quantitatively afforded **1** as a white solid, which was recrystallized from ethanol. **1**: mp 163−165 °C; ^{1}H NMR ($CDCl_3$) δ 0.00 (s, 18H), 0.02 (s, 18H), 0.03 (s, 18H), 1.32 (s, 1H), 2.00 (br s, 1H), 2.03 (br s, 1H), 4.18 (s, 3H), 6.28 (br s, 1H), 6.40 (br s, 1H); ^{13}C NMR ($CDCl_3$) δ 0.45 (q), 0.64 (q), 0.73 (q), 30.37 (d), 30.60 (d), 30.69 (d), 119.99 (s), 121.51 (d), 126.31 (d), 144.89 (s), 151.61 (s), 151.83 (s). Anal. Calcd for $C_{27}H_{62}Si_7 \cdot 0.5H_2O$: C, 54.74; H, 10.72. Found: C, 54.84; H, 10.56. High-resolution EI-MS (70 eV): *m/z* observed 582.3212, calcd for $C_{27}H_{62}Si_7$ 582.3237.

Preparation of {2,4,6-Tris[bis(trimethylsilyl)methyl]phenyl}mesitylsilane (2). To a solution of MesLi, prepared from MesBr (1.9 mL, 12 mmol) and *t*-BuLi (1.59 M, 15 mL) at −78 °C in THF (40 mL), was added a THF solution (90 mL) of **1** (5.83 g, 10 mmol) at −78 °C. The solution was stirred for 10 h, during which time it was warmed to room temperature. To this solution was added a saturated aqueous solution of NH_4Cl, and the organic layer was separated. The water layer was extracted with 50 mL of hexane, and the organic layer was dried with $MgSO_4$. After removal of the solvent, the residue was recrystallized from ethanol to afford **2** (5.79 g, 83%) as colorless crystals. **2**: mp 169−171 °C; ^{1}H NMR ($CDCl_3$) δ −0.07 (s, 18H), −0.02 (s, 18H), 0.04 (s, 18H), 1.30 (s, 1H), 2.09 (br s, 1H), 2.24 (s, 3H), 2.30 (br s, 1H), 2.42 (s, 6H), 5.04 (s, 2H), 6.25 (br s, 1H), 6.41 (br s, 1H), 6.80 (s, 2H); ^{13}C NMR ($CDCl_3$) δ 0.57 (q), 0.74 (q), 0.90 (q), 21.04 (q), 24.32 (q), 28.53 (d), 28.63 (d), 30.47 (d), 122.30 (d), 123.54 (s), 127.09 (d), 128.49 (d), 129.26 (s), 139.25 (s), 144.21 (s), 144.35 (s), 151.62 (s), 151.78 (s). Anal. Calcd for $C_{36}H_{72}Si_7$: C, 61.63; H, 10.34. Found: C, 61.39; H, 10.32.

Preparation of {2,4,6-Tris[bis(trimethylsilyl)methyl]phenyl}-*tert*-butylsilane (3). To a THF solution (20 mL) of **1** was added *t*-BuLi (1.61 M, 0.6 mL) at −78 °C. The solution was stirred for 10 h, during which time it was warmed to room temperature. After removal of the solvent, the residue was chromatographed (DCC, hexane) to afford **3** (390 mg, 83%) as colorless crystals. **3**: mp 211−213 °C; ^{1}H NMR ($CDCl_3$) δ 0.04 (s, 54H), 1.12 (s, 9H), 1.32 (s, 1H), 1.99 (br s, 1H), 2.04 (br s, 1H), 4.24 (s, 2H), 6.28 (br s, 1H), 6.41 (br s, 1H); ^{13}C NMR ($CDCl_3$) δ 0.71 (q), 0.94 (q), 1.25 (q), 18.35 (s), 29.88 (d), 29.94 (q), 30.26 (d), 30.54 (d), 121.25 (d), 125.28 (s), 126.00 (d), 144.99 (s), 152.52 (s), 152.66 (s). Anal. Calcd for $C_{31}H_{70}Si_7 \cdot 1.5H_2O$: C, 55.86; H, 11.04. Found: C, 56.07; H, 10.89. High-resolution EI-MS (70 eV): *m/z* observed 638.3858, calcd for $C_{31}H_{70}Si_7$ 638.3862.

Preparation of {2,4,6-Tris[bis(trimethylsilyl)methyl]phenyl}dibromomesitylsilane (4). A solution of **2** (8.36 g, 11.9 mmol), NBS (4.7 g, 26.4 mmol), and a catalytic amount of benzoyl peroxide in benzene (150 mL) was heated under reflux for 1 h. After removal of the solvent, the crude reaction products were dissolved in hexane. The filtrate, after removal of the solvent, was purified by recrystallization from ethanol to afford **4** (8.25 g, 81%) as colorless crystals. **4**: mp 221−223 °C; ^{1}H NMR ($CDCl_3$, 340 K) δ 0.04 (s, 36H), 0.08 (s, 18H), 1.37 (s, 1H), 2.25 (s, 3H), 2.62 (s, 6H), 2.79 (br s, 1H), 2.91 (br s, 1H), 6.33 (br s, 1H), 6.44 (br s, 1H), 6.81 (s, 2H); ^{13}C NMR ($CDCl_3$) δ 0.89 (q), 1.52 (q), 1.80 (q), 20.91 (q), 26.47 (q), 27.93 (d), 28.05 (d), 30.89 (d), 123.50 (d), 123.94 (s), 128.71 (d), 130.74 (d), 132.32 (s), 140.62 (s), 142.85 (s), 146.70 (s), 152.10 (s), 152.54 (s). Anal. Calcd for $C_{36}H_{70}Si_7Br_2 \cdot H_2O$: C, 49.28; H, 8.27; Br, 18.21. Found: C, 49.39; H, 8.49; Br, 18.53.

Preparation of {2,4,6-Tris[bis(trimethylsilyl)methyl]phenyl}dibromo-*tert*-butylsilane (5). A solution of **3** (1.10 g, 1.67 mmol), NBS (593 mg, 3.33 mmol), and a catalytic amount of benzoyl peroxide in benzene (40 mL) was heated under reflux for 1 h. After removal of the solvent, the crude reaction products were dissolved in hexane. The filtrate, after removal of the solvent, was purified by recrystallization from ethanol to afford **5** (1.24 g, 93%) as colorless crystals. **5**: mp 218−220 °C; ^{1}H NMR ($CDCl_3$) δ 0.06 (s, 18H), 0.07 (s, 18H), 0.09 (s, 18H), 1.23 (s, 9H), 1.34 (s, 1H), 2.30 (s, 1H), 2.40 (s, 1H), 6.32 (br s, 1H), 6.43 (br s, 1H); ^{13}C NMR ($CDCl_3$) δ 0.94 (q), 1.82 (q), 2.17 (q), 27.72 (q), 28.10 (s), 30.36 (d), 30.41 (d), 30.84 (d), 120.86 (s), 123.51 (d), 128.83 (d), 146.83 (s), 153.67 (s), 154.36 (s); high-resolution EI-MS (70 eV) *m/z* observed 796.2095, calcd for $C_{31}H_{68}Si_7{}^{79}Br^{81}Br$ 796.2053.

Preparation of (*Z*)-1,2-Dimesityl-1,2-bis{2,4,6-tris[bis(trimethylsilyl)methyl]phenyl}disilene ((*Z*)-6) and (*E*)-1,2-dimesityl-1,2-bis{2,4,6-tris[bis(trimethylsilyl)methyl]phenyl}disilene ((*E*)-6). To a solution of **4** (2.26 g, 2.63 mmol) in THF (120 mL) was added lithium naphthalenide (17 mL) prepared from lithium dispersion (196 mg, 28.2 mmol) and naphthalene (3.38 g, 26.4 mmol) in THF (45 mL) at −78 °C, and the mixture was stirred for 10 h, during which time it was warmed to room temperature. After removal of the

solvent, pentane was added to the residue to precipitate inorganic salts. The filtrate was passed through FCC with pentane as eluent. The resulting solution, after evaporation of pentane, was subjected to sublimation in vacuo for 3 h to remove naphthalene. To the residue was added a small amount of hexane, and analytically pure (*Z*)-**6** (489 mg, 27%) was obtained by filtration. The filtrate, after evaporation of hexane, was purified by recrystallization from benzene to afford (*E*)-**6** (122 mg, 10%). Removal of naphthalene by exhaustive sublimation under reduced pressure gave almost pure (*E*)-**6** as orange crystals. Since they are not single crystals of sufficient quality for X-ray diffraction, the single crystal containing naphthalene (1:1) was used for the X-ray analysis. (*Z*)-**6**: yellow crystals, mp 193–195 °C dec; ^{29}Si NMR (C_6D_6) δ 56.16, 56.74, 57.12, 58.12; UV (pentane) λ_{max} 378 (ϵ 14 700), 403 (16 000) nm; FAB-MS *m/z* (relative intensity) 1396 (M^+, 1.5%), 698 (18.9), 625 (9.2), 537 (18.8), 464 (21.1), 73 (100.0); high-resolution FAB-MS *m/z* observed 1396.7701, calcd for $C_{72}H_{140}Si_{14}$ 1396.7725. Anal. Calcd for $C_{72}H_{140}Si_{14}$: C, 61.81; H, 10.09. Found: C, 61.60; H, 9.86. As mentioned in the text, (*Z*)-**6** showed a very complicated ^{1}H NMR spectrum at room temperature, the raw chart of which is given as supplementary material together with its partial magnification. Its ^{1}H NMR spectrum at higher temperature could not be measured because of the ready thermal decomposition of (*Z*)-**6** into silylene Tbt(Mes)Si: (*E*)-**6**: orange crystals, mp 132–142 °C dec; ^{1}H NMR ($C_6D_5CD_3$, 350 K) δ −0.10 (br s, 36H), 0.15 (s, 36H), 0.27 (br s, 36H), 1.44 (s, 2H), 2.10 (s, 6H), 2.42 (br s, 4H), 2.60 (br s, 6H), 3.06 (br s, 6H), 6.54 (br s, 4H), 6.71 (br s, 4H); ^{29}Si NMR (C_6D_6) δ 66.49; UV (pentane) λ_{max} 368 (ϵ 12 000), 425 (11 000), 460 (sh, 8800) nm; FAB-MS *m/z* (relative intensity) 1396 (M^+, 10.5%), 698 (68.8), 537 (84.8), 464.3 (53.7), 73 (100.0); high-resolution FAB-MS *m/z* observed 1396.7701, calcd for $C_{72}H_{140}Si_{14}$ 1396.7725. Anal. Calcd for $C_{72}H_{140}Si_{14}$: C, 61.81; H, 10.09. Found: C, 62.00; H, 9.45.

Oxidation of (*Z*)- and (*E*)-6. Finely powdered (*Z*)-**6** was exposed to the air for 6 months, during which time the yellow crystals gradually became colorless. ^{1}H NMR analysis showed the exclusive formation of (*Z*)-2,4-dimesityl-2,4-bis{2,4,6-tris-[bis(trimethylsilyl)methyl]phenyl}-1,3,2,4-dioxadisiletane ((*Z*)-**10**). Recrystallization from ethanol gave analytically pure (*Z*)-**10** as white crystals. (*Z*)-**10**: mp >300 °C; ^{1}H NMR ($CDCl_3$, 350 K) δ −0.49 (s, 18H), 0.01 (s, 18H), 0.09 (s, 54H), 0.32 (s, 18H), 1.37 (br s, 2H), 2.00 (s, 6H), 2.16 (s, 6H), 2.19 (s, 2H), 2.63 (s, 6H), 2.78 (s, 2H), 6.27 (s, 2H), 6.39 (s, 4H), 6.60 (s, 2H); ^{13}C NMR ($CDCl_3$, 340 K) δ 0.57 (q), 0.93 (q), 1.61 (q), 1.76 (q), 2.85 (q), 2.93 (q), 3.38 (q), 3.60 (q), 3.74 (q), 3.99 (q), 20.82 (q), 22.51 (d), 22.75 (d), 25.95 (d), 26.53 (q), 26.93 (d), 27.16 (q), 27.35 (q), 30.65 (d), 31.46 (d), 123.99 (d), 125.31 (d), 127.09 (d), 127.78 (s), 129.85 (d), 129.98 (d), 130.74 (d), 134.61 (s), 136.59 (s), 143.66 (s), 144.51 (s), 144.62 (s), 144.98 (s), 151.32 (s), 152.08 (s); ^{29}Si NMR ($CDCl_3$) δ −6.04, −5.90. Anal. Calcd for $C_{72}H_{140}O_2Si_{14}$: C, 60.43; H, 9.86. Found: C, 60.22; H, 9.89.

By using the same procedure as for (*Z*)-**6**, (*E*)-**6** gave quantitatively (*E*)-2,4-dimesityl-2,4-bis{2,4,6-tris[bis(trimethylsilyl)methyl]phenyl}-1,3,2,4-dioxadisiletane ((*E*)-**10**) as colorless crystals: mp >300 °C; ^{1}H NMR ($CDCl_3$, 350 K) δ −0.28 (br s, 36H), 0.04 (s, 36H), 0.08 (br s, 36H), 1.30 (s, 2H), 2.15 (s, 6H), 2.33 (br s, 4H), 2.66 (br s, 12H), 6.25 (br s, 2H), 6.31 (br s, 2H), 6.61 (s, 4H); ^{13}C NMR ($CDCl_3$, 340 K) δ 1.21 (q), 2.00 (q), 2.29 (q), 2.57 (q), 3.45 (q), 20.76 (q), 27.17 (q), 27.83 (d), 28.44 (d), 30.75 (d), 123.55 (d), 129.12 (s), 129.82 (d), 130.78 (d), 133.87 (s), 139.65 (s), 144.04 (s), 144.58 (s), 153.21 (s); ^{29}Si NMR ($CDCl_3$) δ −4.39. Anal. Calcd for $C_{72}H_{140}O_2Si_{14}$: C, 60.43; H, 9.86. Found: C, 60.20; H, 10.10.

Reaction of 5 with Lithium Naphthalenide. To a solution of **5** (217 mg, 0.272 mmol) in THF (10 mL) was added lithium naphthalenide (1.2 mL), prepared from lithium dispersion (142 mg, 20.4 mmol) and naphthalene (2.42 g, 18.9 mmol) in THF (27 mL), at −78 °C, and the mixture was stirred for 10 h, during which time it was warmed to room temperature. After removal of the solvent, pentane was added to the residue to precipitate inorganic salts. After removal of the solvent, the residue was chromatographed (GPLC) to afford the 1-*tert*-butyl-2,2-bis(trimethylsilyl)-4,6-bis[bis(trimethylsilyl)methyl]-benzo-1-silacyclobutene (**11**; 139 mg, 80%) as colorless crystals. **11**: mp 177–179 °C; ^{1}H NMR ($CDCl_3$) δ −0.01 (s, 9H), 0.016 (s, 9H), 0.019 (s, 9H), 0.04 (s, 18H), 0.08 (s, 9H), 1.19 (s, 9H), 1.35 (s, 1H), 1.45 (br s, 1H), 4.63 (s, 1H), 6.28 (br s, 1H), 6.32 (br s, 1H); ^{13}C NMR ($CDCl_3$) δ 0.34 (q), 0.48 (q), 0.56 (q), 0.72 (q), 1.34 (q), 2.45 (q), 20.64 (s), 26.34 (s), 28.67 (q), 30.70 (d), 31.07 (d), 118.91 (d), 125.92 (d), 133.51 (s), 147.03 (s), 147.15 (s), 156.08 (s). Anal. Calcd for $C_{31}H_{68}Si_7 \cdot 2H_2O$: C, 55.84; H, 10.58. Found: C, 55.84; H, 10.78. High-resolution EI-MS: *m/z* observed 636.3704, calcd for $C_{31}H_{68}Si_7$ 636.3706.

X-ray Data Collection. Single crystals of (*Z*)-**6**, (*E*)-**6**·$C_{10}H_8$, and (*Z*)-**10** were grown by the slow evaporation of their saturated solutions in hexane, benzene, and ethyl acetate at room temperature, respectively. The intensity data for (*Z*)-**6** and (*E*)-**6**·$C_{10}H_8$ were collected on a Rigaku AFC6A diffractometer with graphite-monochromated Cu Kα radiation (λ = 1.541 84 Å) at 120 K using an Oxford Cryostream cooler. The intensity data for (*Z*)-**10** were collected on a Rigaku AFC5R diffractometer with graphite monochromated Mo Kα radiation (λ = 0.710 69 Å). The structures of (*Z*)-**6** and (*E*)-**6**·$C_{10}H_8$ were solved by direct methods with SHELXS-86[17] and refined by the block-diagonal least-squares method using XTAL3.2.[18] The structure of (*Z*)-**10** was solved by direct methods with SHELXS-86[17] and refined by the full-matrix least-squares method. All the non-hydrogen atoms (except for the naphthalene carbons in the case of (*E*)-**6**·$C_{10}H_8$) were refined anisotropically, and all hydrogen atoms were located by calculation. The final cycles of the least-squares refinements were based on 6430 (for (*Z*)-**6**), 7950 (for (*E*)-**6**·$C_{10}H_8$), and 3834 (for (*Z*)-**10**) observed reflections ($I > 2\sigma|I|$ for (*Z*)-**6**, (*E*)-**6**·$C_{10}H_8$, and (*Z*)-**10**) and 775 ((*Z*)-**6**), 776 ((*E*)-**6**·$C_{10}H_8$), and 793 ((*Z*)-**10**) variable parameters. Crystal data for all the molecules are summarized in Table 1. Full details of the crystallographic analysis of (*Z*)-**6**, (*E*)-**6**·$C_{10}H_8$, and (*Z*)-**10** are given in the supplementary material.

Acknowledgment. This work was supported by a Grant-in-Aid for Scientific Research (No. 05236102) from the Ministry of Education, Science and Culture of Japan. We are grateful to Dr. H. Imoto and Mr. K. Tsuge, the University of Tokyo, for the X-ray crystallographic analysis of (*Z*)-**10**. We also thank Central Glass, Shin-etsu Chemical, and Tosoh Akzo Co., Ltd., for the generous gifts of tetrafluorosilane, chlorosilanes, and alkyllithiums, respectively.

Supplementary Material Available: Tables giving crystal data, atomic coordinates, temperature factors, bond lengths and angles, and torsion angles for (*Z*)-**6**, (*E*)-**6**·$C_{10}H_8$, and (*Z*)-**10** and a figure showing the ^{1}H NMR spectrum of (*Z*)-6 (69 pages). This material is contained in many libraries on microfiche, immediately follows this article in the microfilm version of the journal, and can be ordered from the ACS; see any current masthead page for ordering information.

OM940771+

(17) Sheldrick, G. M. SHELX-86, Program for Crystal Structure Determination. University of Göttingen, Göttingen, Germany, 1986.
(18) Hall, S. R.; Flack, H. D.; Stewart, J. M. XTAL3.2, Program for Crystal Structure Determination. Universities of Western Australia, Geneva, and Maryland, 1992.

Chemistry of $[(\eta^6\text{-}C_6H_5OH)Mn(CO)_3]BF_4$: Synthesis of Disubstituted Cyclohexadienylmanganese Complexes from $(C_6H_5O)Mn(CO)_2L$ (L = CO, PPh_3, $P(OMe)_3$)

Si-Geun Lee, Jeong-A Kim, Young Keun Chung,* Tae-Sung Yoon, Nam-jun Kim, and Whanchul Shin*,[1a]

Department of Chemistry, College of Natural Sciences, Seoul National University, Seoul 151-742, Korea

Jaecheon Kim and Kimoon Kim[1b]

Department of Chemistry and Center for Biofunctional Molecules, Pohang Institute of Science and Technology, P.O. Box 125, Pohang, Kyung-Buk 790-600, Korea

Received September 6, 1994[⊗]

Treatment of $[(\eta^6\text{-phenol})Mn(CO)_3]^+$ ($\mathbf{1}^+$) with *t*-BuOK led to $[(\eta^5\text{-}C_6H_5O)Mn(CO)_3]$ [**2**(CO)]. Treatment of $\mathbf{1}^+$ with NMO or TMANO (1 equiv) and PR_3 (3 equiv) led to the oxocyclohexadienyl complex $[(\eta^5\text{-}C_6H_5O)Mn(CO)_2PR_3]$ [**2**(PR_3) (R = Ph, OMe)]. **2**(L) reacts consecutively with a nucleophile (Nu) and an electrophile (E) to give reasonable to high yields of double-addition products, $[\{6\text{-Nu-}\eta^5\text{-1-EO-}C_6H_5\}Mn(CO)_2L]$ (**3**) (L = CO, PPh_3, $P(OMe)_3$). Demetalation of **3** by using Jones reagent resulted in a high yield of ortho-disubstituted arenes. X-ray crystallographic studies of **2**(CO), **2**(PPh_3), and **3** (L = $P(OMe)_3$, Nu = Ph, E = C(O)-CH_3) have been determined.

Introduction

In 1976, the first oxocyclohexadienyl complex Rh(H)-$(C_6H_5O)(PPh_3)_2$ was reported by Wilkinson.[2] Since then, many related organometallic compounds have been described.[3–6] However, little of their chemistry has been reported. The acidity of phenol is considerably enhanced on complexation to a transition metal. Thus, most of the oxocyclohexadienyl complexes have been synthesized by deprotonation of the phenol complex. A manganese oxocyclohexadienyl compound prepared by the deprotonation of a phenol complex was reported by Pauson,[7] who made the phenol complex via the hydrolysis of $[(C_6H_5F)Mn(CO)_3]^+$.

In a continuation of our study of (arene)$Mn(CO)_3^+$ cations, we recently found that the manganese phenol complex was obtained in high yield from the reaction of phenol with $Mn(CO)_5BF_4$ in methylene chloride solution. Herein, we report the synthesis and reactivity of (η^5-oxocyclohexadienyl)manganese complexes. The chemistry described here, summarized in Scheme 1, originates with the hydroxide $[(C_6H_5OH)Mn(CO)_3]^+$ ($\mathbf{1}^+$).

Experimental Section

All reactions were conducted under nitrogen using standard Schlenk-type flasks. Workup procedures were done in air.

Elemental analyses were done at the Korea Basic Science Center. ^1H and ^{13}C NMR spectra were obtained with a Varian XL-200 instrument. Infrared spectra were recorded on a Schimadzu IR-470 spectrophotometer (spectra measured as films on NaCl by evaporation of solvent). Mass spectra were recorded with a VG ZAB-E double-focusing mass spectrometer.

Synthesis of $\mathbf{1}^+$.[7] A stirred solution of $Mn(CO)_5Br$ (3.0 g, 11 mmol) in 200 mL of CH_2Cl_2 was treated with $AgBF_4$ (1.1 equiv) for 5 h at room temperature with exclusion of light. Phenol (1.6 g, excess) was added to the solution of $Mn(CO)_5BF_4$ in CH_2Cl_2. The reaction mixture was refluxed for 24 h. The product was isolated by evaporation of the solvent, followed by recrystallization with acetone/diethyl ether. The yield of $[(C_6H_5OH)Mn(CO)_3]BF_4$ was 93%. When $Mn(CO)_5ClO_4$ was used instead of $Mn(CO)_5BF_4$, the yield of was 75%. IR: ν_{CO} 2073, 2008 cm^{-1}. Anal. Calcd for $C_9H_6ClMnO_7$ $[(C_6H_5OH)$-$Mn(CO)_3]ClO_4$): C, 32.51; H, 1.82. Found: C, 32.40; H, 1.95.

Synthesis of 2. (1) Synthesis of 2(CO). *t*-BuOK (6.0 mmol) in 20 mL of THF was added dropwise to a solution of $[(C_6H_5OH)Mn(CO)_3]BF_4$ (1.59 g, 6.0 mmol) in 30 mL of THF at room temperature. After stirring for 1 h, diethyl ether (50 mL) was added to the solution. The solution was filtered through Celite and evaporated. Purification by column chromatography (silica gel, ethyl acetate) gave 1.30 g (93%). IR: ν_{CO} 2040, 1960 cm^{-1}; $\nu_{C=O}$ 1618 cm^{-1}. ^{13}C NMR ($CDCl_3$): δ 218.7 (C≡O), 166.62 (C=O), 105.06, 84.29, 76.36 ppm.

(2) Synthesis of 2(PR_3) (R = Ph, OMe). 4-Methylmorpholine *N*-oxide (NMO) was used for the synthesis of **2**($P(OMe)_3$) and trimethylamine *N*-oxide (TMANO) for the synthesis of **2**(PPh_3). $[(C_6H_5OH)Mn(CO)_3]BF_4$ (1.19 g, 4.5 mmol) was stirred into 50 mL of CH_2Cl_2 at room temperature while NMO (0.58 g, 5.0 mmol) in 5 mL of CH_2Cl_2 was added dropwise. After 1 h, $P(OMe)_3$ (1.6 mL, 13.5 mmol) was added to the red solution. After being stirred for 3 d, the resulting yellow solution was quenched with water and extracted with diethyl ether. The organic layer was separated, dried over anhydrous $MgSO_4$, and evaporated to yield yellow residues. Purification by column chromatography (silica gel, acetone) gave 1.26 g (85%) of the product **2**($P(OMe)_3$). Mp: 127 °C. IR: ν_{CO} 1974, 1913 cm^{-1}, $\nu_{C=O}$ 1555 cm^{-1}. ^1H NMR (acetone-d_6): δ 5.78–5.70 (br t, 2 H, $H^{2,4}$), 5.01–4.92 (br t, 1 H, H^3), 4.84–4.70 (br d, 2 H, $H^{1,5}$), 3.67 (d, 11.47 Hz, 9 H, $P(OMe)_3$) ppm. ^{13}C NMR (acetone-d_6): δ 225.4 (C≡O), 159.01 (C=O), 130.1, 119.6, 116.3, 53.0 ppm. HRMS: *m/z* (M^+) calcd 327.9908, obsd 327.9913.

⊗ Abstract published in *Advance ACS Abstracts*, January 15, 1995.

(1) (a) X-ray analyses for **2**(CO) and **2**(PPh_3); (b) X-ray analysis for **3** (L = $P(OMe)_3$, Nu = Ph, E = $C(O)CH_3$).

(2) Cole-Hamiloton, D. J.; Young, R. J.; Wilkinson, G. *J. Chem. Soc., Dalton Trans.* **1976**, 1995.
(3) White, C.; Thompson, S. J.; Maitlis, P. M. *J. Organomet. Chem.* **1977**, *127*, 415.
(4) Fairhurst, G.; White, C. *J. Organomet. Chem.* **1978**, *160*, C17.
(5) Chaudret, B.; He, X.; Huang, Y. *J. Chem. Soc., Chem. Commun.* **1989**, 1844. Loren, S. D.; Campion, B. K.; Heyn, R. H.; Tilley, T. D.; Bursten, B. E.; Luth, K. W. *J. Am. Chem. Soc.* **1989**, *111*, 4712.
(6) Trahanovsky, W. S.; Hall, R. A. *J. Am. Chem. Soc.* **1977**, *99*, 4850.
(7) Bhasin, K. K.; Balkeen, W.; Pauson, P. L. *J. Organomet. Chem.* **1981**, *201*, C25.
(8) Aldrich Chemical Co., NMR 2 (1) 853D.

0276-7333/95/2314-1023$09.00/0

Scheme 1

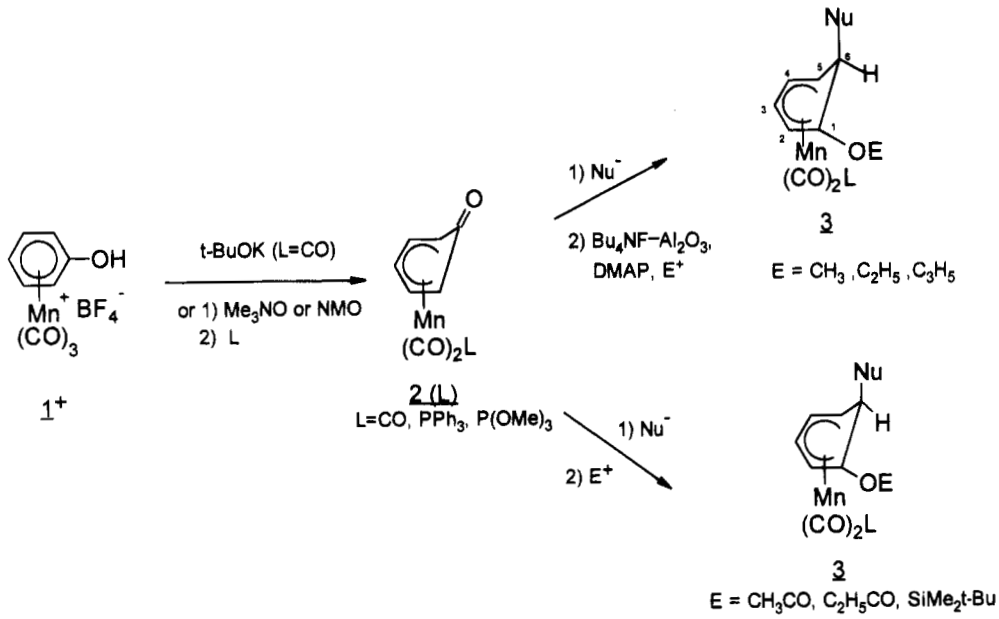

In the same way as above, **2**(PPh_3) was obtained in 73% yield. Mp: 73 °C. IR: ν_{CO} 1960, 1901, $\nu_{C=O}$ 1580 cm^{-1}. ^1H NMR (acetone-d_6): δ 7.7–7.3 (m, 15 H, Ph), 6.15–5.85 (br, 3 H, $H^{2,3,4}$), 5.2–5.0 (br, 2 H, $H^{1,5}$) ppm. ^{13}C NMR ($CDCl_3$): δ 226.4 (C≡O), 157.51 (C=O), 134.8, 132.7, 130.4, 129.2, 128.6, 118.9, 115.7 ppm. Anal. Calcd for $C_{26}H_{20}MnO_3P$: C, 66.96; H, 4.32. Found: C, 66.4; H, 4.31.

Synthesis of 3. (1) Typical procedure when the electrophile was an alkyl halide: MeLi (0.5 mmol) was added to the solution of **2**(PPh_3) (0.1 g, 0.21 mmol) in 10 mL of dimethoxyethane at 0 °C. After stirring for 15 min, the reaction mixture was concentrated to ~5 mL. To the concentrated solution were added 4-(dimethylamino)pyridine (DMAP; 0.04 mmol), $Bu_4NF-Al_2O_3$ (1.0 g, 0.1 mol of Bu_4NF in 100 g of Al_2O_3), and MeI (2 mmol). The reaction mixture was stirred for 12 h and then filtered. The filtrate was column-chromatographed on silica gel, eluting with ethyl acetate/hexane (v/v, 1:10). The yield (entry 4 in Table 5) was 63 mg (60%). Mp: 143 °C. IR: ν_{CO} 1928, 1859 cm^{-1}. ^1H NMR ($CDCl_3$): δ 7.54–7.32 (m, Ph), 5.17 (t, 5.37 Hz, H^3), 3.99 (d, 5.37 Hz, H^2), 3.84 (q, 6.59 Hz, H^4), 3.43 (s, OCH_3), 3.02 (quint, 6.35 Hz, H^6), 2.14 (t, 6.35 Hz, H^5), 0.46 (d, 6.35 Hz, CH_3) ppm. Anal. Calcd for $C_{28}H_{26}MnO_3P$: C, 67.75; H, 5.28. Found: C, 67.62; H, 5.27.

(2) Typical procedure when the electrophile was acetic anhydride: PhMgBr (1.2 mmol, 0.4 mL of 3 M solution in diethyl ether) was added dropwise to the solution of **3**($P(OMe)_3$) (0.13 g, 0.4 mmol) in 15 mL of CH_2Cl_2 at 0 °C. After 30 min, excess acetic anhydride was added and the resultant mixture stirred for 1 h at room temperature. The reaction mixture was quenched with water and extracted with diethyl ether. The ether extracts were dried over anhydrous $MgSO_4$ and evaporated to give a yellow residue. Purification by column chromatography (ether/hexane, v/v, 1:5) gave 0.15 g of the product (85%) (entry 17 in Table 5). Mp: 76 °C. IR: ν_{CO} 1947, 1881 cm^{-1}, $\nu_{C=O}$ 1726 cm^{-1}. ^1H NMR ($CDCl_3$): δ 7.20–7.13 (m, 3 H, Ph), 7.05–7.00 (m, 2 H, Ph), 5.21 (tt, 5.2, 1.5 Hz, H^3), 5.15–5.10 (m, H^2), 4.65 (q, 5.5 Hz, H^4), 4.48 (d, 6.3 Hz, H^6), 3.60 (d, 11.5 Hz, $P(OMe)_3$), 3.40 (t, 6.4 Hz, H^5), 2.02 (s, CH_3) ppm. Anal. Calcd for $C_{19}H_{22}MnO_7P$: C, 50.91; H, 4.95. Found: C, 50.90; H, 5.14.

Characterization of Entry 1 in Table 5. IR: ν_{CO} 2004, 1912 cm^{-1}. ^1H NMR ($CDCl_3$): δ 5.43 (td, 5.37, 1.47 Hz, H^3), 4.73 (t, 5.86 Hz, H^4), 3.96 (d, 5.37 Hz, H^2), 3.39 (s, OCH_3), 3.13 (t, 5.13 Hz, H^5), 3.13–3.04 (m, H^6), 0.63 (d, 6.34 Hz, CH_3) ppm. HRMS: *m/z* (M^+) calcd 262.0038, obsd 262.0250.

Characterization of Entry 2 in Table 5. IR: ν_{CO} 2008, 1932 cm^{-1}, $\nu_{C=O}$ 1744 cm^{-1}. ^1H NMR ($CDCl_3$): δ 5.56 (td, 5.41, 1.67 Hz, H^3), 5.06 (d, 5.77 Hz, H^2), 4.67 (t, 5.57 Hz, H^4), 3.40 (td, 6.27, 1.68 Hz, H^5), 3.30–3.06 (m, H^6), 2.37 (q, 7.55 Hz, CH_2), 1.16 (t, 7.71 Hz, CH_2CH_3), 0.55 (d, 6.23 Hz, CH_3) ppm. HRMS: *m/z* (M^+) calcd 304.0143, obsd 304.9900.

Characterization of Entry 3 in Table 5. IR: ν_{CO} 2004, 1926 cm^{-1}, $\nu_{C=O}$ 1749 cm^{-1}. ^1H NMR ($CDCl_3$): δ 5.55 (td, 5.40, 1.72 Hz, H^3), 5.04 (d, 5.81 Hz, H^2), 4.67 (t, 5.64 Hz, H^4), 3.41 (t, 5.65 Hz, H^5), 3.20–2.90 (m, H^6), 2.13 (s, CH_3), 1.80–0.80 (m, C_4H_9) ppm. HRMS: *m/z* (M^+) calcd 332.0456, obsd 332.0475.

Characterization of Entry 5 in Table 5. Mp: 174 °C. IR: ν_{CO} 1917, 1850 cm^{-1}. ^1H NMR ($CDCl_3$): δ 7.57–7.25 (m, 15 H, Ph), 5.16 (t, 5.34 Hz, H^3), 3.91 (d, 5.86 Hz, H^2), 3.84 (q, 6.17 Hz, H^4), 3.58 (q, 6.83 Hz, OCH_2CH_3), 3.04–2.95 (m, H^6), 2.12 (t, 6.59 Hz, H^5), 1.31 (t, 7.08 Hz, OCH_2CH_3), 0.45 (d, 6.59 Hz, CH_3) ppm. HRMS: *m/z* (M^+) calcd 510.1157, obsd 510.1294.

Characterization of Entry 6 in Table 5. Mp: 145 °C dec. IR: ν_{CO} 1928, 1860 cm^{-1}. ^1H NMR ($CDCl_3$): δ 7.60–7.32 (m, 15 H, Ph), 5.98 (ddd, 16.35, 10.49, 5.84 Hz, H^c), 5.37 (dd, 17.09, 1.47 Hz, H^a), 5.23 (dd, 10.50, 1.47 Hz, H^b), 5.16 (t, 5.61 Hz, H^3), 4.21–4.01 (m, OCH_2), 3.98 (d, 5.13 Hz, H^2), 3.82 (q, 5.37 Hz, H^4), 3.05 (quin, 5.86 Hz, H^6), 2.14 (t, 5.37 Hz, H^5), 0.47 (d, 6.35 Hz, CH_3) ppm. We indicated the proton attached to the carbon bearing CH_2O as H^c, the proton *trans* to H^c as H^a and the proton *cis* to H^c as H^b. HRMS: *m/z* (M^+) calcd 522.1156, obsd 522.1271.

Characterization of Entry 7 in Table 5. Mp: 185 °C. IR: ν_{CO} 1933, 1870 cm^{-1}, $\nu_{C=O}$ 1747 cm^{-1}. ^1H NMR ($CDCl_3$): δ 7.53–7.34 (m, 15 H, Ph), 7.19–7.10 (m, 3 H, Ph), 6.93–6.89 (m, 2 H, Ph), 5.16–5.09 (m, $H^{2,3}$), 4.38 (d, 5.9 Hz, H^6), 4.11 (m, 6.3 Hz, H^4), 2.83 (t, 6.3 Hz, H^5), 2.01 (s, CH_3) ppm. Anal. Calcd for $C_{33}H_{28}MnO_4P$: C, 69.93; H, 4.81. Found: C, 69.43; H, 5.52.

Characterization of Entry 8 in Table 5. Mp: 76 °C. IR: ν_{CO} 1947, 1881 cm^{-1}; $\nu_{C=O}$ 1745 cm^{-1}. ^1H NMR ($CDCl_3$): δ 7.55–7.34 (m, 15 H, PPh_3), 7.19–7.17 (m, 3 H, Ph), 6.93–6.86 (m, 2 H, Ph), 5.29–5.10 (m, $H^{2,3}$), 4.38 (d, 5.4 Hz, H^6), 4.11 (q, 5.37 Hz, H^4), 2.81 (t, 6.3 Hz, H^5), 2.30 (q, 7.3 Hz, CH_2CH_3), 1.08 (t, 7.6 Hz, CH_2CH_3) ppm. Anal. Calcd for $C_{35}H_{30}MnO_4P$: C, 70.0; H, 5.04. Found: C, 70.6; H, 5.07.

Characterization of Entry 9 in Table 5. Mp: 83 °C. IR: ν_{CO} 1945, 1881 cm^{-1}; $\nu_{C=O}$ 1761 cm^{-1}. ^1H NMR ($CDCl_3$): δ 5.85–5.79 (m, H^3), 4.62 (q, 7.07 Hz, H^4), 3.59 (d, 11.23 Hz, $P(OMe)_3$), 2.93 (br d, 6.35 Hz, H^2), 2.82 (dd, 12.20, 5.61 Hz, H^{endo}), 2.47 (m, H^5), 2.24 (dd, 12.70, 6.59 Hz, H^{exo}), 2.14 (s, CH_3) ppm. HRMS: *m/z* (M^+) calcd 372.0112, obsd 372.0171.

Characterization of Entry 10 in Table 5. IR: ν_{CO} 1931, 1864 cm^{-1}. ^1H NMR ($CDCl_3$): δ 5.20 (t, 5.63 Hz, H^3), 4.47 (q, 5.86 Hz, H^4), 3.92 (d, 5.61 Hz, H^2), 3.54 (d, 11.23 Hz, $P(OMe)_3$), 3.41 (s, OCH_3), 3.20–3.05 (m, H^6), 2.80 (t, 5.68 Hz, H^5), 0.56 (d, 6.31 Hz, CH_3) ppm. HRMS: m/z (M^+) calcd 358.0378, obsd 358.0380.

Characterization of Entry 11 in Table 5. IR: ν_{CO} 1945, 1883 cm^{-1}. ^1H NMR ($CDCl_3$): δ 5.96 (ddd, 17.1, 10.5, 5.6 Hz, H^c), 5.33 (dq, 17.3, 1.7 Hz, H^a), 5.24 (dq, 10.5, 1.5 Hz, H^b), 5.20 (tt, 5.37, 1.71 Hz, H^3), 4.46 (q, 5.13 Hz, H^4), 4.18–3.96 (m, OCH_2), 3.93 (d, 5.61 Hz, H^2), 3.55 (d, 11.2 Hz, $P(OMe)_3$), 3.12 (quint, 6.35 Hz, H^6), 2.81 (tt, 6.35, 1.95 Hz, H^5), 0.58 (d, 6.35 Hz, CH_3) ppm. HRMS: m/z (M^+) calcd 384.0534, obsd 384.0526.

Characterization of Entry 12 in Table 5. Mp: 56 °C. IR: ν_{CO} 1950, 1888 cm^{-1}. ^1H NMR ($CDCl_3$): δ 5.20 (tt, 5.37, 1.71 Hz, H^3), 4.40 (m, 5.12 Hz, H^4), 3.98 (d, 5.37 Hz, H^2), 3.54 (d, 11.47 Hz, $P(OMe)_3$), 3.05 (quint, 5.63 Hz, H^6), 2.79 (tt, 5.86, 1.95 Hz, H^5), 0.53 (d, 6.35 Hz, CH_3), 0.26 (s, $SiMe_3$), 0.11 (s, $t\text{-}C_4H_9$) ppm. LRMS: m/z (M^+) calcd 458, obsd 458.

Characterization of Entry 13 in Table 5. Mp: 72 °C. IR: ν_{CO} 1944, 1878 cm^{-1}, $\nu_{C=O}$ 1752 cm^{-1}. ^1H NMR ($CDCl_3$): δ 5.35 (t, 5.13 Hz, H^3), 4.83 (d, 5.37 Hz, H^2), 4.48–4.46 (br m, H^4), 3.56 (d, 11.2 Hz, $P(OMe)_3$), 3.14–3.11 (m, $H^{5,6}$), 2.10 (s, $C(O)CH_3$), 0.47 (d, 5.86 Hz, CH_3) ppm. Anal. Calcd for $C_{14}H_{20}MnO_7P$: C, 43.54; H, 5.22. Found: C, 43.40; H, 5.70.

Characterization of Entry 14 in Table 5. IR: ν_{CO} 1944, 1878 cm^{-1}, $\nu_{C=O}$ 1748 cm^{-1}. ^1H NMR ($CDCl_3$): δ 5.34 (t, 5.61 Hz, H^3), 4.83 (d, 5.61 Hz, H^2), 4.47 (m, H^4), 3.56 (d, 11.2 Hz, $P(OMe)_3$), 3.15–3.07 (m, $H^{5,6}$), 2.37 (q, 7.16 Hz, CH_2), 1.15 (t, 7.57 Hz, CH_2CH_3), 0.46 (d, 5.86 Hz, CH_3) ppm. HRMS: m/z (M^+) calcd 400.0484, obsd 400.0484.

Characterization of Entry 15 in Table 5. IR: ν_{CO} 1945, 1880 cm^{-1}, $\nu_{C=O}$ 1742 cm^{-1}. ^1H NMR ($CDCl_3$): δ 5.32 (t, 5.4 Hz, H^3), 4.92–4.88 (m, H^2), 4.49 (t, 6.4 Hz, H^4), 3.56 (d, 11.2 Hz, $P(OMe)_3$), 3.17–3.03 (m, $H^{5,6}$), 2.36 (q, 7.6 Hz, CH_2), 1.15 (t, 7.6 Hz, CH_3), 1.06–0.79 (m, C_4H_9) ppm. HRMS: m/z (M^+) calcd 442.0953, obsd 442.0946.

Characterization of Entry 16 in Table 5. Mp: 90 °C. IR: ν_{CO} 1931, 1864 cm^{-1}. ^1H NMR ($CDCl_3$): δ 7.20–7.00 (m, 3 H, Ph), 7.05–7.00 (m, 2 H, Ph), 5.21 (tt, 5.2, 1.5 Hz, H^3), 4.66 (m, 6.8 Hz, H^4), 4.31 (d, 5.9 Hz, H^6), 4.12 (d, 5.6 Hz, H^2), 3.59 (d, 11.2 Hz, $P(OMe)_3$), 3.44 (s, CH_3), 3.07 (tt, 6.4, 1.8 Hz, H^5) ppm. Anal. Calcd for $C_{17}H_{22}MnO_6P$: C, 51.44; H, 5.11. Found: C, 51.39; H, 5.81.

Characterization of Entry 18 in Table 5. IR: ν_{CO} 1946, 1883 cm^{-1}, $\nu_{C=O}$ 1742 cm^{-1}. ^1H NMR ($CDCl_3$): δ 7.22–7.10 (m, 3 H, Ph), 6.98–6.94 (m, 2 H, Ph), 5.36 (t, 5.4 Hz, H^3), 5.15–5.11 (m, H^2), 4.66 (m, 5.5 Hz, H^4), 4.48 (d, 5.6 Hz, H^6), 3.59 (d, 11.2 Hz, $P(OMe)_3$), 3.38 (t, 6.4 Hz, H^5), 2.30 (q, 7.6 Hz, CH_2), 1.10 (t, 7.6 Hz, CH_3) ppm. HRMS: m/z (M^+) calcd 462.0640, obsd 462.0634.

Oxidation of 3. Complex **3** (L = $P(OMe)_3$, Nu = Ph, E = CH_3) in acetone was cleanly and rapidly oxidized by dropwise addition at 0 °C of a slight excess of Jones reagent. Extraction with diethyl ether, drying with $MgSO_4$, and solvent evaporation gave a 85% yield of pure 2-phenylanisole, identified via ^1H NMR in $CDCl_3$: δ 7.57–6.90 (m, 9 H, Ph), 3.80 (s, OCH_3) ppm.[8]

X-ray Structure of 2(CO). Single crystals suitable for X-ray analysis were obtained by slow evaporation of a CH_2Cl_2/hexane (v/v, 2:1) solution of **2**(CO). The crystal was mounted on a Rigaku AFC4 diffractometer, and the unit cell parameters were obtained from a least-squares fit of the 34 centered reflections (11.59° < 2θ < 36.74°). Data were collected with Mo Kα radiation by using $\omega/2\theta$ scan mode. The crystal structure was solved by the use of the conventional heavy-atom method as well as difference Fourier technique and refined by means of full-matrix least-squares fit on F^2 using SHELXL93. Non-hydrogen atoms (C1, C2, C3, C4, C5, C6, O1, O2, O3) were found by SHELXS86 and refined by anisotropically and the symmetry-related atoms (C2′, C4′, C5′, O2′) could be generated. All the hydrogen atoms could be located by difference Fourier synthesis and refined isotropically in the final refinement. The last cycle of refinement converged with $R(F) = 0.0277$ and $wR(F^2) = 0.0728$. Crystal data, details of the data collection, and refinement parameters are listed in Table 1. The final atomic parameters are given in Table 2.

X-ray Structure of 2(PPh$_3$). Single crystals suitable for X-ray analysis were obtained by slow evaporation of a CH_2Cl_2/hexane (v/v, 2:1) solution of **2**(PPh_3). The crystal was mounted on a Rigaku AFC4 diffractometer, and the unit cell parameters were obtained from a least-squares fit of the 22 centered reflections (8.95° < 2θ < 11.39°). Data were collected with Mo Kα radiation by using an $\omega/2\theta$ scan mode. The crystal structure was solved by the use of the conventional heavy-atom method as well as difference Fourier technique and refined by means of full-matrix least-squares F^2 using SHELXL93. Non-hydrogen atoms were found by SHELXS86 and refined anisotropically; all the hydrogen atoms were refined by difference Fourier synthesis. All the hydrogen atoms were ridden to the bonded atoms with the isotropic displacement parameters fixed with the value of 1.2 times those of the bonded atoms. The last cycle of refinement converged with $R(F) = 0.0657$ and $wR(F^2) = 0.1394$. Crystal data, details of the data collection, and refinement parameters are listed in Table 1. The final atomic parameters are given in Table 3.

X-ray Structure of 3. Single crystals suitable for X-ray analysis were obtained by slow evaporation of a solution of hexane. X-ray data were collected on Enraf-Nonius CAD4 diffractometer using Mo Kα radiation at room temperature. Cell parameters and orientation matrix for data collection were obtained from least-squares refinement using the setting angles of 25 reflections in the range 20.90° < 2θ < 28.80°. The structure was solved by Patterson methods using SHELX86 and refined by full-matrix least-squares methods. Non-hydrogen atoms were refined anisotropically. While 11 hydrogen atoms attached to carbon atoms (C2, C3, C4, C5, C6, C14, C17) were located from the difference Fourier map and their positional parameters refined, the positions of other hydrogen atoms were calculated and fixed during the refinement. The isothermal parameters of all the hydrogen atoms were fixed with 1.3 times those of bonded carbon atoms. The last cycle of refinement converged to $R(F) = 0.038$ and $wR(F) = 0.040$. All the calculations except for the structure solving were performed with the Enraf-Nonius Molen package. Crystal data, details of the data collection, and refinement parameters are listed in Table 1. The final atomic parameters are given in Table 4.

Results and Discussion

Syntheses of 2 and 3. Reaction of $\mathbf{1}^+$ with t-BuOK led to **2**(CO) in 93% yield. Single crystals of **2**(CO) suitable for X-ray studies were grown in solution. **2**(CO) reacted with several kinds of nucleophiles. When **2**(CO) was treated with t-BuLi and then with HBF_4, $[(t\text{-}C_4H_9\text{-}C_6H_5)Mn(CO)_3]BF_4$ was obtained in low yield.[9] When C_3H_5MgBr or PhC_2Li was used as a nucleophile, we could only confirm the formation of $[(Nu\text{-}C_6H_5)Mn(CO)_3]BF_4$ by checking the IR spectra. Due to the low yields, we did not pursue the chemistry of **2**(CO). We thought that complex **2**(CO) was unstable with respect to the nucleophilic addition. Thus we focused our efforts to find oxocyclohexadienyl complexes that are stable with respect to nucleophilic addition. We found that the phosphorus-substituted oxocyclohexadienyl complexes **2**(PR_3) were stable compared with **2**(CO). Thus, addi-

(9) Jeong, E.; Chung, Y. K. *J. Organomet. Chem.* **1992**, *434*, 225.

Table 1. Crystal Data, Details of the Data Collection, and Refinement Parameters

formula	$C_9H_5MnO_4$	$C_{19}H_{22}MnO_7P$	$C_{26}H_{20}MnO_3P$
fw	232.07	448.30	466.33
cryst syst	monoclinic	orthorhombic	orthorhombic
space group	$P2_1/m$ (No. 11)	$Pca2_1$ (No. 29)	$Pbca$ (No. 61)
a (Å)	6.968(1)	26.254(2)	14.895(14)
b (Å)	9.072(2)	7.625(1)	16.324(8)
c (Å)	7.131(1)	10.311(3)	17.673(12)
β (deg)	104.46(2)	90	90
least-squares fit	$11.59° \leq 2\theta \leq 36.74°$	$20.90° \leq 2\theta \leq 28.80$	$8.95° \leq 2\theta \leq 11.39°$
volume (Å^3)	436.5(1)	2604.0(6)	4297(6)
Z	2	4	8
D(calcd) (mg/mm^3)	1.766	1.442	1.442
temp (°C)	21	23	19
λ (Mo Kα) (Å)	0.71069	0.71073	0.71069
monochromator	graphite	graphite	graphite
abs coeff (cm^{-1})	14.93	7.25	7.15
abs correction	none	none	none
cryst color	yellow	yellow	yellow
cryst size (mm^3)	0.60 × 0.30 × 0.25	0.35 × 0.30 × 0.20	0.65 × 0.30 × 0.20
diffractometer	Rigaku AFC4	Enraf-Nonius CAD4	Rigaku AFC4
scan mode	$\omega/2\theta$	ω	$\omega/2\theta$
scan speed in ω (deg/min)	4	variable	4
scan range in ω (deg)	$1.5 + 0.35 \tan\theta$	$1.0 + 0.35 \tan\theta$	$1.0 + 0.35 \tan\theta$
F(000)	232	?	1920
$2\theta_{max}$ (deg)	50	50	50
no. of data collcd	894	2121	3287
no. of unique data	825 ($R_{int} = 0.02$)	2121	3787
no. of obsd data	752 [$I > 2\sigma(I)$]	1350 [$I > 3\sigma(I)$]	2311 [$I > 2\sigma(I)$]
no. of variables	84	285	280
index ranges	$0 \leq h \leq 8, 0 \leq k \leq 10, -8$ " $l \leq 8$	???	$-17 \leq h \leq 0, 0 \leq k \leq 19, 0 \leq l \leq 20$
goodness of fit	1.128	1.180	1.027
$R(F)$[a]	0.028 [$F > 4\sigma(F)$]	0.038 [$F > 6\sigma(F)$]	0.066 [$F > 4\sigma(F)$]
	0.033 (all data)		0.132 (all data)
$wR(F)$,[b] $wR(F^2)$[c]	0.073 [$F > 4\sigma(F)$]	0.040 [$F > 6\sigma(F)$]	0.139 [$F > 4\sigma(F)$]
	0.076 (all data)		0.249 (all data)

[a] $R(F) = \sum||F_o| - |F_c||/\sum|F_o|$. [b] $wR(F) = [\sum w(|F_o| - |F_c|)^2/\sum w|F_o|^2]^{1/2}$, where $w = 4F_o^2/[\sigma^2(F_o^2) + (0.04F_o^2)^2]^{1/2}$ for $C_{19}H_{22}MnO_7P$. [c] $wR(F^2) = [\sum w(F_o^2 - F_c^2)^2/\sum w(F_o^2)^2]^{1/2}$, where $w = 1/[\sigma^2(F_o^2) + (aP)^2 + bP]$, $P = (F_o^2 + 2F_c^2)/3$, $a = 0.046$, and $b = 0.11$ for $C_9H_5MnO_4$ and $a = 0.066$ and $b = 16.5$ for $C_{26}H_{20}MnO_3P$.

Table 2. Atomic Coordinates (×10^4 for Non-Hydrogens, ×10^3 for Hydrogens) and Equivalent Isotropic Displacement Parameters (Å^2 × 10^3 for Non-Hydrogens, Å^2 × 10^2 for Hydrogens) for 2(CO)

	x	y	z	U_{eq}[a]
Mn	1005(1)	2500	1951(1)	27(1)
C(1)	−190(5)	2500	−625(5)	35(1)
C(2)	−654(4)	1128(3)	2480(3)	36(1)
C(3)	4198(5)	2500	842(5)	34(1)
C(4)	3638(4)	1172(3)	1715(4)	36(1)
C(5)	3397(4)	1179(4)	3592(4)	42(1)
C(6)	3298(5)	2500	4583(6)	46(1)
O(1)	−951(5)	2500	−2241(4)	57(1)
O(2)	−1714(3)	291(3)	2872(3)	55(1)
O(3)	4908(4)	2500	−587(4)	49(1)
H(4)	373(5)	31(4)	113(4)	4(1)
H(5)	321(5)	32(4)	421(4)	5(1)
H(6)	316(8)	250	578(8)	7(2)

[a] U_{eq} is defined as one-third of the trace of the orthogonalized U_{ij} tensor.

tion of NMO or TMANO (1 equiv) and phosphorus donors (3 equiv) to **1**$^+$ led to $[(C_6H_5O)Mn(CO)_2(PR_3)]$ (R = OMe, Ph) (**2**) in 73% (R = Ph) and 85% (R = OMe) yields, respectively. Both complexes are air-stable orange solids that can be purified by recrystallization and have been characterized by standard spectroscopic and analytical techniques. Single crystals of **2**(PPh_3) suitable for X-ray studies were grown in solution.

2 reacts consecutively with a nucleophile (Nu) and an electrophile (E) to give reasonable to high yields of double-addition products, $[(6\text{-Nu-}\eta^5\text{-1-EO-}C_6H_5)Mn(CO)_2L]$ (L = CO, PPh_3, $P(OMe)_3$) (**3**; Scheme 1 and Table 5). The formation of **3** was confirmed by the X-ray study of **3** (L = $P(OMe)_3$, Nu = Ph, E = $C(O)CH_3$). When the electrophile was an alkyl halide, tetrabutylammonium fluoride impregnated on neutral alumina was added to promote alkylation.[10] When we compare the yields of entries 1, 4, and 10, the yield of the product is substantially dependent upon the ligand L and increased greatly when L is $P(OMe)_3$. However, when we compared the yields of entries 2/14 and 3/13, the yields were almost the same even though the ligands were very different. Comparison of the yields of entries 13/17 and 14/18 shows that the yield was dependent upon the nucleophiles. With the silicon-containing electrophile (entry 12), the yield was rather low due to decomposition during purification. The controlling factors for the yields of **3** are not fully understood.

The oxocyclohexadienyl ligand can be used as a precursor for the synthesis of 1,2-disubstituted benzenes. Thus, the 1,2-disubstituted arene was liberated in 85% isolated yield from metal complex **3** (L = $P(OMe)_3$, Nu = Ph, E = CH_3) by treatment with Jones reagent, followed by solvent removal and extraction with diethyl ether. Comparison of the ^{1}H NMR with literature data verified that the product was 2-phenylanisole.[8]

Many methodologies to make 1,2-disubstituted aromatic hydrocarbons are known.[11] However, 1,2-disubstituted benzene precursors are usually needed. Recently, the regioselective preparation of 1,2-disubstituted benzenes via chromium carbonyls was reported.[12] However, these methodologies suffer from the very limited ranges of substrates and side reactions. The double addition to $[(C_6H_5O(Mn(CO)_2L]$ can be done in a one-

(10) Ando, T.; Yamawaki, J.; Kawate, T.; Sumi, S.; Hanafusa, T. *Bull. Chem. Soc. Jpn.* **1982**, *55*, 2504.

Table 3. Fractional Atomic Coordinates ($\times 10^4$) and Equivalent Isotropic Displacement Parameters ($Å^2 \times 10^3$) for 2(PPh$_3$)

	x	y	z	U_{eq}[a]
Mn	316(1)	1027(1)	2131(1)	34(1)
P	573(1)	1752(1)	3211(1)	34(1)
O(1)	−29(4)	−467(3)	2986(3)	72(2)
O(2)	2204(3)	550(3)	1961(3)	60(1)
O(3)	1017(4)	1000(4)	233(3)	75(2)
C(1)	104(4)	137(4)	2677(4)	44(2)
C(2)	1461(4)	756(4)	2039(3)	37(2)
C(3)	445(5)	1128(5)	728(4)	51(2)
C(4)	378(5)	1904(4)	1138(4)	48(2)
C(5)	−336(5)	2082(5)	1613(4)	59(2)
C(6)	−981(5)	1496(6)	1812(4)	63(2)
C(7)	−872(5)	698(5)	1497(4)	60(2)
C(8)	−151(5)	515(5)	1022(4)	52(2)
C(9)	1423(4)	2551(4)	3177(4)	38(1)
C(10)	1707(7)	2910(5)	2528(5)	89(3)
C(11)	2378(8)	3491(6)	2516(6)	106(4)
C(12)	2786(5)	3715(5)	3143(5)	68(2)
C(13)	2550(6)	3378(5)	3814(6)	81(3)
C(14)	1874(5)	2804(5)	3823(5)	63(2)
C(15)	−418(4)	2263(4)	3617(4)	38(2)
C(16)	−417(5)	3061(4)	3868(4)	53(2)
C(17)	−1162(5)	3387(5)	4236(5)	68(2)
C(18)	−1904(5)	2900(5)	4369(5)	63(2)
C(19)	−1918(5)	2098(5)	4111(4)	51(2)
C(20)	−1184(4)	1784(4)	3734(4)	44(2)
C(21)	979(4)	1146(4)	4028(3)	35(1)
C(22)	545(5)	1148(6)	4718(4)	70(3)
C(23)	917(7)	712(7)	5313(5)	93(3)
C(24)	1711(6)	301(5)	5242(5)	70(3)
C(25)	2140(5)	313(5)	4577(4)	57(2)
C(26)	1779(5)	728(4)	3965(4)	49(2)

[a] U_{eq} is defined as one-third of the trace of the orthogonalized $\mathbf{U}_{ij}$ tensor.

pot reaction, and Grignard reagents or RLi can be used as nucleophile and alkyl halides or acid anhydrides can be used as electrophiles. Thus, the utilization of oxocyclohexadienyl manganese compounds can be a viable and facile procedure for obtaining 1,2-disubstituted benzenes.

Molecular Structures of 2(CO), 2(PPh$_3$), and 3 (L = P(OMe)$_3$, Nu = Ph, E = C(O)CH$_3$). The geometry of **2**(CO) along with the atomic numbering scheme is depicted in Figure 1, and bond distances and angles are given in Table 6. An X-ray diffraction study of **2**(CO) confirms the η^5-oxocyclohexadienyl bonding mode. Heppert[13] reported the synthesis and chemistry of $[(\eta\text{-}C_6H_5O)Cr(CO)_3]^-$, defined as an η^6-arene bonding mode; however, they did not report an X-ray structural determination. The C—O bond length of the ketone, 1.239(4) Å, is quite similar to the C=O bond distances

Table 4. Atomic Coordinates and Equivalent Thermal Parameters for 3 (L = P(OMe)$_3$, Nu = Ph, E = C(O)CH$_3$)

atom	x	y	z	B_{eq}[a] ($Å^2$)
Mn	0.12986(3)	0.2071(1)	0.000	2.97(1)
P	0.07911(7)	0.0813(3)	−0.1383(2)	3.98(4)
O1	0.2162(2)	0.0477(5)	−0.2003(4)	2.89(8)
O2	0.2120(2)	−0.1755(5)	−0.0582(4)	4.0(1)
O3	0.1413(2)	−0.0965(6)	0.1738(5)	5.7(1)
O4	0.0404(2)	0.3319(7)	0.1427(6)	6.9(1)
O5	0.1060(2)	−0.0572(6)	−0.2294(5)	5.0(1)
O6	0.0275(2)	−0.0572(6)	−0.2294(5)	6.3(1)
O7	0.0519(2)	0.1994(7)	−0.2465(6)	7.7(2)
C1	0.2019(2)	0.1757(7)	−0.1089(6)	2.8(1)
C2	0.2354(2)	0.2081(7)	0.0090(7)	2.8(1)
C3	0.2002(2)	0.3070(8)	0.0981(6)	3.0(1)
C4	0.1699(2)	0.4412(8)	0.0484(6)	3.6(1)
C5	0.1554(2)	0.4480(7)	−0.0825(6)	3.2(1)
C6	0.1731(2)	0.3082(8)	−0.1604(6)	3.0(1)
C7	0.2872(2)	0.2886(8)	−0.0221(6)	3.0(1)
C8	0.3290(2)	0.1809(8)	−0.0404(7)	4.3(2)
C9	0.3750(3)	0.2518(11)	−0.0743(9)	5.8(2)
C10	0.3809(3)	0.4294(10)	−0.0899(8)	5.3(2)
C11	0.3390(3)	0.5351(9)	−0.0728(8)	4.8(2)
C12	0.2924(2)	0.4682(8)	−0.0395(6)	3.9(2)
C13	0.2186(2)	−0.1251(8)	−0.1659(6)	3.0(1)
C14	0.2301(3)	−0.2316(8)	−0.2799(7)	4.9(2)
C15	0.1376(2)	0.0155(8)	0.01021(6)	3.7(1)
C16	0.0763(2)	0.2811(9)	0.0892(8)	4.3(2)
C17	0.0792(8)	−0.1462(11)	−0.3309(8)	6.7(2)
C18	0.0292(3)	−0.1498(11)	−0.0008(8)	8.6(2)
C19	0.0227(4)	0.3456(13)	−0.2174(14)	12.3(4)

[a] $B_{eq} = (4/3)\sum_i\sum_j\beta_{ij}a_ib_j$.

Table 5. Yields of Compounds 3

entry	L	Nu	E	yield (%)
1[a]	CO	CH$_3$	CH$_3$	58
2[a]	CO	CH$_3$	C(O)C$_2$H$_5$	49
3[b]	CO	C$_4$H$_9$	C(O)CH$_3$	59
4[a]	PPh$_3$	CH$_3$	CH$_3$	60
5[a]	PPh$_3$	CH$_3$	C$_2$H$_5$	55
6[a]	PPh$_3$	CH$_3$	C$_3$H$_5$	49
7[b]	PPh$_3$	C$_6$H$_5$	C(O)CH$_3$	55
8[b]	PPh$_3$	C$_6$H$_5$	C(O)C$_2$H$_5$	50
9[b]	P(OMe)$_3$	H	C(O)CH$_3$	68
10[a]	P(OMe)$_3$	CH$_3$	CH$_3$	84
11[a]	P(OMe)$_3$	CH$_3$	C$_3$H$_5$	64
12[b]	P(OMe)$_3$	CH$_3$	Si(CH$_3$)$_2$(t-C$_4$H$_9$)	49
13[b]	P(OMe)$_3$	CH$_3$	C(O)CH$_3$	58
14[b]	P(OMe)$_3$	CH$_3$	C(O)C$_2$H$_5$	45
15[a]	P(OMe)$_3$	C$_4$H$_9$	CH$_3$	84
16[a]	P(Ome)$_3$	C$_6$H$_5$	CH$_3$	52
17[b]	P(OMe)$_3$	C$_6$H$_5$	C(O)CH$_3$	85
18[b]	P(OMe)$_3$	C$_6$H$_5$	C(O)C$_2$H$_5$	70

[a] DME was used as a solvent. [b] CH$_2$Cl$_2$ was used as a solvent.

of δ- or γ-lactams,[14] and the Mn—C3 distance, 2.540(3) Å, is quite long and reflects the absence of a significant bonding interaction. However, the dihedral angle (21.3°) between a plane C4—C5—C6—C5′—C6′ and a plane of C4—C3—C4′ is quite small compared to those in other cyclohexadienylmanganese complexes: 43° in $[(\eta^5\text{-}C_6H_7)Mn(CO)_3]$,[15] 41° in $[\{\eta^5\text{-}(C_2H_5O_2C)_2CH\text{-}C_6H_6\}Mn(CO)_3]$,[16] 36.5° in $[(\eta^5\text{-}PhC_6H_6)Mn(CO)_3]$,[17] 39.6° in $[(\eta^5\text{-}PhC_6H_6)Mn(CO)_2NO]BF_4$,[17] 39.6° in $[\{(\eta^5\text{-}C_5H_4)W(CO)_3CH_3\}\text{-}\eta^5\text{-}C_6H_5]Mn(CO)_3$,[18] and 38.0° in $[\{(C_2H_5O)_2P(O)\text{-}\eta^5\text{-}C_6H_6\}Mn(CO)_3]$.[19] Thus, we expect that there should

(11) Tashiro, M.; Fukuda, Y.; Yamoto, T. *J. Org. Chem.* **1983**, *48*, 1927. Bennetau, B.; Dunogues, J.; Krempp, M. *Chem. Abstr.* **1990**, *113*, 58689z. Sartori, G.; Maggi, R.; Bigi, F.; Arienti, A.; Casnati, G. *Tetrahedron Lett.* **1992**, *33*, 2207. Sartori, G.; Maggi, R.; Bigi, F.; Arienti, A.; Casnati, G. *J. Chem. Soc., Perkin Trans. 1* **1991**, 3059. Bigi, F.; Casnati, G.; Sartori, G.; Araldi, G. *Gazz. Chim. Ital.* **1990**, *120*, 413. Bigi, F.; Casnati, G.; Sartori, G.; Dalprato, C.; Batolini, R. *Tetrahedron Asymmetry* **1990**, *1*, 861. Sartori, G.; Casnati, G.; Bigi, F.; Predieri, G. *J. Org. Chem.* **1990**, *55*, 4371. Mills, R. J.; Snieckus, V. *J. Org. Chem.* **1983**, *48*, 1565. Gschwend, H. W.; Hamdan, A. *J. Org. Chem.* **1975**, *40*, 2008. Gschwend, H. W.; Rodriguez, C. R. *Org. React. (N.Y.)* **1979**, *26*, 1. Puterbaugh, W. H.; Hauser, C. R. *J. Org. Chem.* **1964**, *29*, 853.

(12) Blagg, J.; Davies, S. G.; Goodfellow, C. L.; Sutton, K. H. *J. Chem. Soc., Chem. Commun.* **1986**, 1283. Blagg, J.; Davies, S. G.; Goodfellow, C. L.; Sutton, H. K. *J. Chem. Soc., Perkin Trans. 1* **1990**, 1133. Heppert, J. A.; Aube, J.; Thomas-Miller, M. E.; Milligan, M. L.; Takusagawa, F. *Organometallics* **1990**, *9*, 727. Kundig, E. P.; Amurrio, D.; Liu, R.; Ripa, A. *Synlett* **1991**, 657. Kundig, E. P.; Ripa, A.; Liu, R.; Amurrio, D.; Bernardnelli, G. *Organometallics* **1993**, *12*, 3724.

(13) Heppert, J. A.; Boyle, T. J.; Takusagawa, F. *Organometallics* **1989**, *8*, 461.

(14) Allen, F. H.; Kennard, O.; Watson, D. G.; Brammer, L.; Orpen, A. G.; Taylor, R. *J. Chem. Soc., Perkin Trans. 2* **1987**, S1.

(15) Churchill, M. R.; Scholer, S. *Inorg. Chem.* **1969**, *8*, 1950.

(16) Mawby, A.; Walker, P. J. C.; Mawby, R. J. *J. Organomet. Chem.* **1973**, *55*, C39.

(17) Ittel, S. D.; Whitney, J. F.; Chung, Y. K.; Williard, P. G.; Sweigart, D. A. *Organometallics* **1988**, *7*, 1323.

(18) Chung, T.-M.; Chung, Y. K. *Organometallics* **1992**, *11*, 2822.

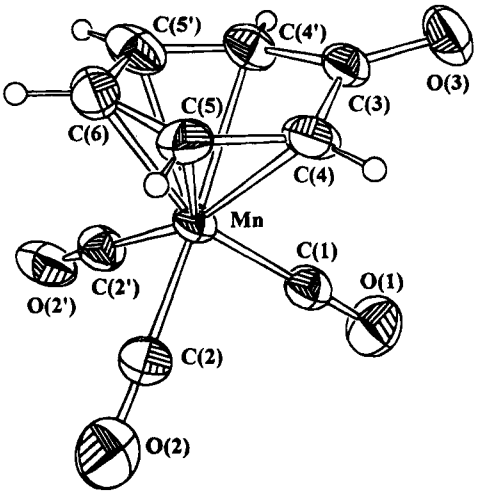

Figure 1. Structural drawing and atomic numbering scheme for complex **2**(CO).

Table 6. Selected Bond Distances (Å) and Angles (deg) for 2(CO), 2(PPh$_3$), and 3

	Compound **2**(CO)		
Mn−C(1)	1.817(4)	Mn−C(4)	2.236(3)
Mn−C(6)	2.140(4)	C(2)−O(2)	1.142(3)
C(3)−C(4)	1.453(3)	C(5)−C(6)	1.402(4)
Mn−C(2)	1.801(3)	Mn−C(5)	2.147(3)
C(1)−O(1)	1.142(4)	C(3)−O(3)	1.239(4)
C(4)−C(5)	1.390(4)		
Mn−C(1)−O(1)	179.6(3)	C(4)−C(5)−C(6)	121.5(3)
C(3)−C(4)−C(5)	121.2(3)	C(4)−C(3)−O(3)	123.9(2)
Mn−C(2)−O(2)	177.4(2)	C(5)−C(6)−C(5′)	117.5(4)
	Compound **2**(PPh$_3$)		
Mn−C(1)	1.773(7)	Mn−C(4)	2.267(6)
Mn−C(6)	2.153(7)	C(3)−O(3)	1.238(8)
C(4)−C(5)	1.387(10)	C(6)−C(7)	1.425(11)
C(8)−C(3)	1.435(10)	O(2)−C(2)	1.165(7)
Mn−C(2)	1.769(6)	Mn−C(5)	2.179(7)
Mn−P	2.277(2)	C(3)−C(4)	1.463(10)
C(5)−C(6)	1.401(11)	C(7)−C(8)	1.395(10)
O(1)−C(1)	1.144(8)		
Mn−C(1)−O(1)	175.4(6)	C(6)−C(5)−C(4)	122.3(7)
P−Mn−C(1)	90.0(2)	C(1)−Mn−C(2)	90.9(3)
C(5)−C(4)−C(3)	122.4(7)	C(4)−C(3)−O(3)	122.9(7)
Mn−C(2)−O(2)	177.2(6)	C(7)−C(6)−C(5)	116.6(7)
P−Mn−C(2)	92.6(2)		
	Compound **3**		
Mn−C(1)	2.212(6)	Mn−C(4)	2.131(6)
Mn−C(6)	2.149(6)	Mn−C(15)	1.806(6)
C(1)−O(1)	1.408(7)	C(2)−C(7)	1.528(7)
Mn−C(3)	2.240(6)	Mn−C(5)	2.132(6)
Mn−P	2.175(2)	Mn−C(16)	1.771(7)
C(13)−O(2)	1.189(8)		
C(1)−C(2)−C(3)	102.4(4)	Mn−C(16)−O(4)	177.2(7)
C(4)−C(5)−C(6)	115.4(5)	C(3)−C(4)−C(5)	122.4(6)
Mn−C(15)−O(3)	175.1(6)	C(6)−C(1)−C(2)	120.7(5)
C(2)−C(3)−C(4)	119.5(5)	P−Mn−C(16)	89.7(2)
C(5)−C(6)−C(1)			

be a small contribution of the η^6-phenoxide bonding mode in the structure. The cyclohexadienyl ring shows a ring slippage toward C5−C6−C5′ (the average distance of Mn−C5, Mn−C6, and Mn−C5′ is 2.14 Å and the bond distance of Mn−C4 is 2.236 Å).[20]

The geometry of **2**(PPh$_3$) along with the atomic numbering scheme is depicted in Figure 2, and bond distances and angles are given in Table 6. An X-ray diffraction study of **2**(PPh$_3$) also confirms the η^5-oxocyclohexadienyl bonding mode. The geometric parameters of **2**(PPh$_3$) are in agreement with those found in **2**(CO). The C−O bond length of the ketone is 1.238(8) Å, and the Mn−C3 distance, 2.494(7) Å, is quite long and reflects the absence of a significant bonding interaction. However, the dihedral angle (14.3°) between a plane of C4−C5−C6−C7−C8 and a plane of C4−C3−C8 is quite small compared to those in other cyclohexadienylmanganese complexes. When we compared the dihedral angle of **2**(PPh$_3$) to that of **2**(CO), the dihedral angle decreased as the electron density of the metal center increased. Thus, we expected that the contribution of the η^6-phenoxide bonding mode would increase in **2**(PPh$_3$) compared to that of **2**(CO). However, the bond distances of Mn−C3 and C3−O3 in **2**(CO) and **2**(PPh$_3$) were not as sensitive as the dihedral angles.

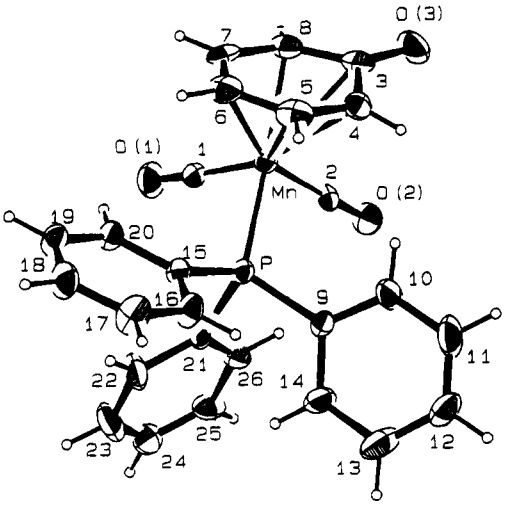

Figure 2. Structural drawing and atomic numbering scheme for complex **2**(PPh$_3$).

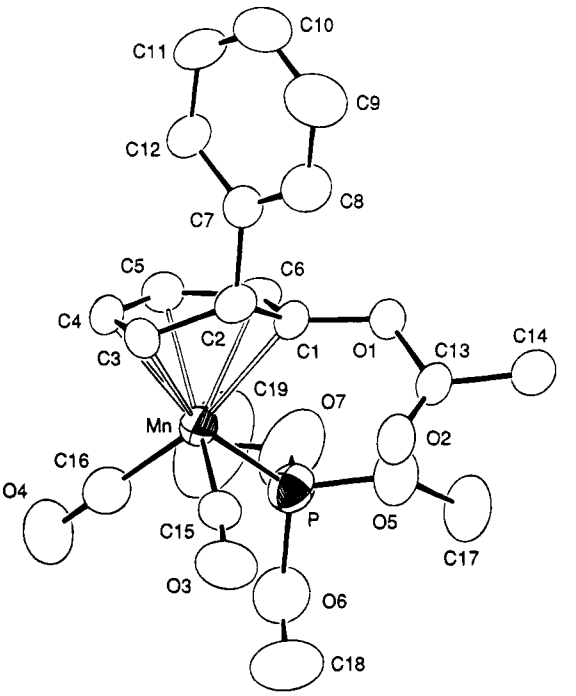

Figure 3. Structural drawing and atomic numbering scheme for complex **3** (L = P(OMe)$_3$, Nu = Ph, E = C(O)-CH$_3$).

(19) Lee, T.-Y.; Yu, H.-K. Bae; Chung, Y. K.; Hallows, W. A.; Sweigart, D. A. *Inorg. Chim. Acta* **1994**, *224*, 147.
(20) Lee, Y.-A.; Chung, Y. K.; Kim, Y.; Jeong, J. W.; Chung, G.; Lee, D. *Organometallics* **1991**, *10*, 3707.

The geometry of **3** (L = P(OMe)$_3$, Nu = Ph, E = C(O)-CH$_3$) along with the atomic numbering scheme is depicted in Figure 3, and bond distances and angles are given in Table 6. The geometric parameters of **3** are in agreement with those found in other compounds such as [η^5-($C_2H_5CO_2$)$_2$CH-C_6H_6]Mn(CO)$_3$,[16] [η^5-Ph-C_6H_6]Mn-(CO)$_3$,[17] [{η^5-exo-(MeO)$_2$P(O)-C_6H_6}]Mn(CO)$_3$,[19] and [{η^5-endo-(EtO)$_2$P(O)-C_6H_6}]Mn(CO)$_3$.[19] The cyclohexadienyl ring is nearly planar (with a maximum deviation of 0.008 Å). The cyclohexadienyl ring is folded about with an angle of 37.8°. The manganese atom is located 1.692 Å from the cyclohexadienyl ring.

It has been demonstrated that the (oxocyclohexadienyl)manganese complex, generated by the deprotonation of the phenolmanganese complex, provides a useful system for preparing disubstituted cyclohexadienylmanganese derivatives. We are continuing to explore the use of the (oxocyclohexadienyl)manganese complex to make new (arene)Mn(CO)$_3^+$ complexes. Extension of this chemistry to (β-naphthol)Mn(CO)$_3^+$ and [(2,6-disubstituted phenol)Mn(CO)$_3$]$^+$ cation is also currently underway in our laboratory.[21]

Acknowledgment. We are grateful to the Korea Science and Engineering Foundation and the Ministry of Education, Republic of Korea (BSRI 94-313).

Supplementary Material Available: Tables of atomic positional parameters, thermal parameters, and bond distances and angles for **2**(CO), **2**(PPh$_3$), and **3** (L = P(OMe)$_3$, Nu = Ph, E = C(O)CH$_3$) (7 pages). This material is contained in many libraries on microfiche, immediately follows this article in the microfilm version of the journal, and can be ordered from the ACS; see any current masthead page for ordering information.

OM940700A

(21) Lee, S. G.; Lee, S. S.; Lee, T. Y.; Chung, Y. K. Manuscript in preparation.

Cationic Carbene Complexes of Platinum(IV): Structure of a Secondary Carbene Complex

Louis M. Rendina, Jagadese J. Vittal, and Richard J. Puddephatt*

Department of Chemistry, The University of Western Ontario, London, Ontario, Canada N6A 5B7

Received September 29, 1994®

Treatment of the organoplatinum(II) precursors [PtMeCl(^{t}bu$_2$bpy)] (^{t}bu$_2$bpy = 4,4′-di-*tert*-butyl-2,2′-bipyridine) and [PtMe$_2$(^{t}bu$_2$bpy)] with chloroiminium (Vilsmeier) salts affords the novel cationic platinum(IV)–carbene complexes [PtCl$_2$Me(CHNMe$_2$)(^{t}bu$_2$bpy)]Cl (**1**), [PtCl$_2$Me(CClNMe$_2$)(^{t}bu$_2$bpy)]Cl (**2**), [PtClMe$_2$(CHNMe$_2$)(^{t}bu$_2$bpy)]Cl (**3**), and [PtClMe$_2$(CClNMe$_2$)(^{t}bu$_2$bpy)]Cl (**4**) in good yield. For **1** and **2**, the carbene moiety is located *trans* to one of the chloro ligands, whereas in **3** and **4** it is found *trans* to the N-donor. The complexes show good stability toward air and moisture, but **1** and **2** are thermally unstable and decompose to [PtCl$_2$(^{t}bu$_2$bpy)] after a few days at room temperature. Complex **4** can also be prepared as a mixture of two geometrical isomers which do not interconvert; it is proposed that the isomers are formed by two independent pathways. The major (**4a**) and minor (**4b**) isomers are formed by *cis*- and *trans*-oxidative addition, respectively, of [Cl$_2$C=NMe$_2$]Cl to [PtMe$_2$(^{t}bu$_2$bpy)], and likely mechanisms are discussed. Crystals of **1** are monoclinic, space group $P2_1/c$, with a = 11.064(1) Å, b = 21.310(2) Å, c = 12.277(3) Å, β = 91.20(2)°, Z = 4, and R = 0.0718. The structure of **1** consists of discrete [PtCl$_2$Me(CHNMe$_2$)(^{t}bu$_2$bpy)]$^+$ cations and chloride anions, with one CH$_2$Cl$_2$ molecule of crystallization per complex ion. The carbene ligand occupies a position *trans* to one of the chloro ligands, and the Pt–C$_{carbene}$ bond length (1.99(2) Å) is significantly shorter than the Pt–Me distance (2.13(2) Å). The C–N bond length of 1.31(2) Å is indicative of substantial p_π–p_π bonding. Reaction of nucleophiles with **3** leads to rapid reductive elimination to give an iminium salt [H(X)C=NMe$_2$]Cl (X = nucleophile) and [PtMe$_2$(^{t}bu$_2$bpy)]. This work demonstrates the versatility of chloroiminium salts in the preparation of aminocarbene complexes of metals in high oxidation states.

Introduction

Transition-metal carbene complexes have played an important role in the development of organometallic chemistry and find applications in many catalytic reactions as well as in stoichiometric organic synthesis.[1]

Short-lived, cationic platinum–carbene species may be involved in various insertion reactions, such as those involving diazo compounds.[2] Indeed, some authors have pointed out the apparent neglect in the study of cationic carbene complexes of platinum and palladium, as those of the latter have been suggested as intermediates in the copolymerization of carbon monoxide and ethylene.[3]

Most mononuclear platinum–carbene complexes reported to date are derivatives of the metal in oxidation states 0 and +II.[4] Very few platinum(IV)–carbene complexes have been described,[5] and their chemistry has not been investigated in detail. Such complexes are of synthetic, structural, and theoretical interest because high oxidation state, late-transition-metal–carbene complexes would represent a subclass that lies between the two traditional types of metal–carbene complexes, i.e., low-oxidation-state "Fischer-type" carbene complexes with heteroatom substituents and high-oxidation-state "Schrock-type" alkylidene species with alkyl substituents.[1]

Synthetic routes to platinum(IV)–carbene complexes have included (i) oxidative addition of MeI or Cl$_2$ to various platinum(II)–carbene complexes,[5e,f,g] (ii) reaction of the alkyne HC≡C-CH$_2$CH$_2$OH with cationic dimethylplatinum(IV) species to give (alkoxycarbene)-platinum(IV) complexes *via* intramolecular nucleophilic attack of a reactive, transient π-alkyneplatinum(IV) complex,[5c,h] and finally (iii) oxidative addition of organic carbene compounds, e.g., chloroiminium (Vilsmeier) salts,[5b,6] to platinum(II) species. Method iii has been applied successfully for the synthesis of carbene complexes of several transition metals, but in platinum chemistry it is limited to the formation of [PtCl$_4$(CHNMe$_2$)PEt$_3$] from [Pt$_2$Cl$_2$(μ-Cl)$_2$(PEt$_3$)$_2$] and [ClHC=NMe$_2$]Cl. The product was sparingly soluble and was characterized by elemental analysis and IR and partial ^{1}H NMR spectroscopic data.[5b,d] The Pt–C*H*NMe$_2$ proton was observed at δ 8.93 but no platinum coupling was resolved.

We now report the synthesis and complete characterization of some cationic platinum(IV)–carbene complexes by oxidative addition of chloroiminium salts to the electron-rich organoplatinum(II) precursor [PtMe$_2$(^{t}bu$_2$bpy)] (^{t}bu$_2$bpy = 4,4′-di-*tert*-butyl-2,2′-bipyridine) and its chloro analogue [PtClMe(^{t}bu$_2$bpy)]. Cationic platinum(IV)–carbene complexes are expected to behave as

® Abstract published in *Advance ACS Abstracts,* January 15, 1995.

(1) (a) Dötz, K. H.; Fischer, H.; Hofmann, P.; Kreissl, F. R.; Schubert, U.; Weiss, K. *Transition Metal Carbene Complexes*; Verlag Chemie: Weinheim, Germany, 1983. (b) *Advances in Metal Carbene Chemistry*; Schubert, U., Ed.; NATO ASI Series C, Mathematical and Physical Sciences 269; Kluwer Academic Publishers: Dordrecht, The Netherlands, 1989. (c) Wulff, W. D. *Adv. Met.-Org. Chem.* **1989**, *1*, 209. (d) Brown, F. J. *Prog. Inorg. Chem.* **1980**, *27*, 1. (e) Dötz, K. H. *Angew. Chem., Int. Ed. Engl.* **1984**, *23*, 587.

(2) McCrindle, R.; McAlees, A. J. *Organometallics* **1993**, *12*, 2445, and references therein.

(3) Batistini, A.; Consiglio, G. *Organometallics* **1992**, *11*, 1766.

0276-7333/95/2314-1030$09.00/0

highly reactive, transition-metal-stabilized carbonium ions. This paper also reports the addition of various nucleophiles to the carbene complexes prepared in this work.

Experimental Section

All reactions were performed under a N_2 atmosphere using standard Schlenk techniques. All solvents were freshly distilled, dried, and degassed prior to use. NMR spectra were recorded by means of Varian Gemini spectrometers (^1H at 300.10 and 200.00 MHz; ^{13}C at 75.43 and 50.30 MHz). Chemical shifts are reported in ppm with respect to TMS reference. All spectra are referenced to the residual protons of the deuterated solvent. IR spectra (Nujol mull or CH_2Cl_2 solution) were recorded in the range 4000–400 cm^{-1} on a Perkin Elmer 2000 FT-IR instrument. Elemental analyses were determined by Guelph Chemical Laboratories, Guelph, Canada.

The compounds ^{t}bu$_2$bpy,[7] [PtMe$_2$(^{t}bu$_2$bpy)],[8] and *trans*-[PtClMe(SMe$_2$)$_2$][9] were prepared by the literature methods. The chloroiminium salts, [ClHC=NMe$_2$]Cl and [Cl$_2$C=NMe$_2$]Cl, were obtained commercially. The salts were dried *in vacuo* over P_2O_5 at room temperature prior to use.

Preparation of Complexes. Chloro(4,4′-di-*tert*-butyl-2,2′-bipyridine) (methyl)platinum(II) ([PtClMe(^{t}bu$_2$bpy)]). To a stirred solution of *trans*-[PtClMe(SMe$_2$)$_2$] (1.17 g, 3.16 mmol) in diethyl ether (100 mL) was added ^{t}bu$_2$bpy (0.850 g, 3.17 mmol). A dark-yellow precipitate formed immediately on addition of the ligand, and the mixture was stirred for 16 h at room temperature. Evaporation of the solvent *in vacuo* gave a yellow solid which was recrystallized from CH_2Cl_2/*n*-hexane at −30 °C to afford bright-yellow microcrystals which were collected by filtration, washed with diethyl ether, and dried *in vacuo* over P_2O_5. Yield 1.20 g (74.0%). Anal. Calcd for $C_{19}H_{27}ClN_2Pt$: C, 44.40; H, 5.30; N, 5.45. Found: C, 44.01; H, 5.27; N, 5.31. NMR in CD_2Cl_2: $\delta(^1H)$ 9.34 [d, 1H, $^3J_{PtH^{6'}}$ = 13.0 Hz, $^3J_{H^5H^{6'}}$ = 5.9 Hz, H$^{6'}$], 8.97 [d, ^{1}H, $^3J_{PtH^6}$ = 60.0 Hz; $^3J_{H^5H^6}$ = 6.2 Hz, H^6], 7.97 [d, 1H, $^4J_{H^{3'}H^{5'}}$ = 1.7 Hz, H$^{3'}$], 7.94 [d, 1H, $^4J_{H^3H^5}$ = 2.2 Hz, H^3], 7.62 [dd, 1H, $^3J_{H^{3'}H^{5'}}$ = 5.9 Hz, $^4J_{H^5H^{3'}}$ = 2.0 Hz, H$^{5'}$], 7.45 [dd, 1H, $^3J_{H^5H^6}$ = 6.2 Hz, $^4J_{H^5H^3}$ = 2.2 Hz, H^5], 1.42 [s, 18H, ^{t}bu], 0.99 [s, 3H, $^2J_{PtH}$ = 78.0 Hz, Pt−Me].

Dichloro(4,4′-di-*tert*-butyl-2,2′-bipyridine)platinum(II) ([PtCl$_2$(^{t}bu$_2$bpy)]). To a stirred solution of K$_2$[PtCl$_4$] (0.200 g, 0.482 mmol) in 6 M HCl (50 mL) was added ^{t}bu$_2$bpy (0.130 g, 0.484 mmol). The mixture was refluxed for 6 h, and the bright-yellow precipitate (0.240 g, 93.2%) was isolated by filtration and washed with distilled water, ethanol, and diethyl ether. The solid was dried *in vacuo* over P_2O_5 at room temperature for several hours. Anal. Calcd for $C_{18}H_{24}Cl_2N_2$-Pt: C, 40.46; H, 4.53; N, 5.24. Found: C, 40.55; H, 4.56; N, 5.22. NMR in $CDCl_3$: $\delta(^1H)$ 9.45 [d, 2H, $^3J_{H^5H^6}$ = 6.3 Hz, $^3J_{PtH^6}$ = *ca.* 30 Hz (br), H^6], 7.87 [d, 2H, $^3J_{H^3H^5}$ = 2.0 Hz, H^3], 7.46 [dd, 2H, $^4J_{H^3H^5}$ = 2.0 Hz, $^3J_{H^5H^6}$ = 6.3 Hz, H^5], 1.44 [s, 18H, ^{t}bu].

Dichloro(dimethylaminomethylene)(4,4′-di-*tert*-butyl-2,2′-bipyridine)(methyl)platinum(IV)chloride ([PtCl$_2$Me(CHNMe$_2$)(^{t}bu$_2$bpy)]Cl, 1). To a cooled (−10 °C) and stirred solution of [ClHC=NMe$_2$]Cl (0.025 g, 0.195 mmol) in CH_2Cl_2 (30 mL) was added [PtClMe(^{t}bu$_2$bpy)] (0.100 g, 0.195 mmol). The color of the solution immediately changed from yellow to pale yellow on addition of the complex. After 1 h, the solvent was evaporated *in vacuo* to afford a pale-yellow powder (0.110 g, 88.0%). Recrystallization of the solid is usually unnecessary, although it may be recrystallized from CH_2Cl_2/*n*-pentane at −30 °C to afford pale-yellow microcrystals. Microanalyses could not be obtained for the product owing to its facile transformation to [PtCl$_2$(^{t}bu$_2$bpy)] under ambient conditions. NMR in CD_2Cl_2: $\delta(^1H)$ 10.43 [br s, Pt−C*H*NMe$_2$], 9.19 [d, ^{1}H, $^3J_{H^5H^{6'}}$ = 5.8 Hz, $^3J_{PtH^{6'}}$ = 8.1 Hz, H$^{6'}$], 9.02 [d, 1H, $^3J_{H^5H^6}$ = 6.4 Hz, $^3J_{PtH^6}$ = 38.9 Hz, H^6], 8.45 [d, 1H, $^4J_{H^{3'}H^{5'}}$ = 1.7 Hz, H$^{3'}$], 8.43 [d, 1H, $^4J_{H^3H^5}$ = 2.1 Hz, H^3], 7.85 [dd, 1H, $^3J_{H^5H^{6'}}$ = 5.9 Hz, $^4J_{H^5H^{3'}}$ = 1.8 Hz, H$^{5'}$], 7.82 [dd, 1H, $^3J_{H^5H^6}$ = 6.3 Hz, $^4J_{H^5H^3}$ = 2.1 Hz, H^5], 3.77 [br d, 3H, $^4J_{HH}$ = 0.9 Hz, NMe], 3.62 [d, 3H, $^4J_{HH}$ = 0.8 Hz, $^4J_{PtH}$ = 8.0 Hz, NMe], 2.45 [s, 3H, $^2J_{PtH}$ = 64.8 Hz, Pt−Me], 1.48 [s, 9H, ^{t}bu], 1.47 [s, 9H, ^{t}bu]; $\delta(^{13}C)$ = 177.86 [$^1J_{PtC}$ = 931.7 Hz, Pt−*C*HNMe$_2$], 54.56 [$^3J_{PtC}$ = 50.5 Hz, NMe], 46.46 [$^3J_{PtC}$ = 28.1 Hz, NMe], 6.77 [$^1J_{PtC}$ = 475.6 Hz, Pt−Me]. IR in CH_2Cl_2: ν(C−N) 1638 cm^{-1}.

Dichloro(chlorodimethylaminomethylene)(4,4′-di-*tert*-butyl-2,2′-bipyridine)(methyl)platinum(IV)chloride ([PtCl$_2$Me(CClNMe$_2$)(^{t}bu$_2$bpy)]Cl, 2). To a cooled (−10 °C) and *vigorously* stirred suspension of [Cl$_2$C=NMe$_2$]Cl (0.032 g, 0.197 mmol) in CH_2Cl_2 (30 mL) was added [PtClMe(^{t}bu$_2$bpy)] (0.100 g, 0.195 mmol). After *ca.* 1 h, the color of the solution had changed from bright to pale yellow. The solvent was then evaporated *in vacuo* to give a pale-yellow powder (0.100 g, 76.0%). Recrystallization of the product is usually unnecessary, although it may be recrystallized from CH_2Cl_2/*n*-pentane

(4) (a) For pre-1982 references, see: Hartley, F. R. In *Comprehensive Organometallic Chemistry*; Wilkinson, G., Stone, F. G. A., Abel, E. W., Eds.; Pergamon: New York, 1982; Vol 6, p 502. (b) Michelin, R. A.; Bertani, R.; Mozzon, M.; Zanotto, L.; Benetello, F.; Bombieri, G. *Organometallics* **1990**, *9*, 1449. (c) Barefield, E. K.; Carrier, A. M.; Sepelak, D. J.; Van Derveer, D. G. *Organometallics* **1982**, *1*, 103. (d) Gaber, B.; Krueger, C.; Marczinke, B.; Mynott, R.; Wilke, G. *Angew. Chem., Int. Ed. Engl.* **1991**, *30*, 1666. (e) Sellmann, D.; Prechtel, W.; Knoch, F.; Moll, M. *Inorg. Chem.* **1993**, *32*, 538. (f) Michelin, R. A.; Bertani, R.; Mozzon, M.; Bombieri, G.; Benetello, F.; Dasilva, M. D. C. G.; Pombeiro, A. J. L. *Organometallics* **1993**, *12*, 2372. (g) Fehlhammer, W. P.; Bliss, T.; Fucho, J.; Holzmann, G. *Z. Naturforsch. B* **1992**, *47*, 79. (h) Ardvengo, A. J., III; Gamper, S. F.; Calabrese, J. C.; Davidson, F. *J. Am. Chem. Soc.* **1994**, *116*, 4391. (i) Erker, G.; Menjon, B. *Chem. Ber.* **1990**, *123*, 1327. (j) Hoover, J. F.; Stryker, J. M. *J. Am. Chem. Soc.* **1990**, *112*, 464. (k) Pill, T.; Polborn, K.; Beck, W. *Chem. Ber.* **1990**, *123*, 11. (l) Chen, J. T.; Tzeng, W. H.; Tsai, F. Y.; Cheng, M. C.; Yu, W. *Organometallics* **1991**, *10*, 3954. (m) Michelin, R. A.; Benetollo, F.; Chapuis, G.; Bombieri, G.; Guadalupi, G.; Ros, R. *Inorg. Chem.* **1989**, *28*, 840. (n) Cetini, G.; Bandini, A. L.; Banditelli, G.; Minghetti, G.; Operti, L.; Vaglio, G. A. *Org. Mass Spectrom.* **1989**, *24*, 479. (o) Nakamura, S.; Morokuma, K. *Organometallics* **1988**, *7*, 1904. (p) Ruegg, H. J.; Botteghi, C; Pregosin, P. S.; Scrivanti, A.; Toniolo, L. *J. Organomet. Chem.* **1986**, *316*, 233. (q) Facchin, G.; Campostrini, R.; Michelin, R. A. *J. Organomet. Chem.* **1985**, *294*, C21. (r) Fehlhammer, W. P.; Volkl, A.; Plaia, U.; Bartel, K.; Liu, A. T. *Chem. Ber.* **1985**, *118*, 2235. (s) Canziani, F.; Albinati, A.; Galimberti, F.; Ganazzoli, F.; Garlaschelli, L.; Malatesta, M. C. *J. Chem. Soc., Dalton Trans.* **1983**, 827. (t) Belluco, U.; Michelin, R. A.; Ros, R.; Bertani, R.; Facchin, G.; Mozzon, M.; Zanotto, L. *Inorg. Chim. Acta* **1992**, *198–200*, 883 and references therein. (u) Crociani, B. In *Reactions of Coordinated Ligands*; Braterman, P. S., Ed.; Plenum: New York, 1986; Vol. 1, p 553. (v) Belluco, U.; Crociani, B.; Michelin, R. A.; Uguagliati, P. *Pure Appl. Chem.* **1983**, *55*, 47. (w) Lappert, M. F. *J. Organomet. Chem.* **1988**, *358*, 185 and references therein. (x) Herdeis, C.; Beck, W. *Chem. Ber.* **1983**, *116*, 3205. (y) Cross, R. J.; Davidson, M. F.; Rocamora, M. *J. Chem. Soc., Dalton Trans.* **1988**, 1147. (z) Bertani, R.; Mozzon, M.; Michelin, R. A.; Benetollo, F.; Bombieri, G.; Castilho, T. J.; Pombeiro, A. J. L. *Inorg. Chim. Acta* **1991**, *189*, 175. (aa) Michelin, R. A.; Zanotto, L.; Braga, D.; Sabatino P.; Angelici, R. J. *Inorg. Chem.* **1988**, *27*, 85, 93. (bb) Zanotto, L.; Bertani, R.; Michelin, R. A. *Inorg. Chem.* **1990**, *29*, 3265.

(5) (a) Walker, R.; Muir, K. W. *J. Chem. Soc., Dalton Trans.* **1975**, 272. (b) Hartshorn, A. J.; Lappert, M. F.; Turner, K. *J. Chem. Soc., Dalton Trans.* **1978**, 348. (c) Chisholm, M. H.; Clark, H. C. *J. Chem. Soc., Chem. Commun.* **1971**, 1484. (d) Cetinkaya, B.; Lappert, M. F.; Turner, K.; *J. Chem. Soc., Chem. Commun.* **1972**, 851. (e) Muir, K. W.; Walker, R.; Chatt, J.; Richards, R. L.; Royston, G. H. D. *J. Organomet. Chem.* **1973**, *56*, C30. (f) Balch, A. L. *J. Organomet. Chem.* **1972**, *37*, C19. (g) Chisholm, M. H.; Clark, H. C.; Johns, W. S.; Ward, J. E. H.; Yasufuku, K. *Inorg. Chem.* **1975**, *14*, 900. (h) Clark, H. C.; Manzer, L. E. *Inorg. Chem.* **1973**, *12*, 362.

(6) (a) *Iminium Salts in Organic Chemistry*, Parts 1 and 2; Böhme, H., Viehe, H. G., Eds.; Advances in Organic Chemistry: Materials and Results; Taylor, E. C., Series Ed.; Wiley: New York, 1979. (b) Meth-Cohn, O.; Stanforth, S. P. In *Comprehensive Organic Synthesis*; Trost, B. M., Fleming, I., Eds.; Pergamon: Oxford, U.K., 1991; Vol. 2, p 777. (c) Kantlehner, W. In *Comprehensive Organic Synthesis*; Trost, B. M., Fleming, I., Eds.; Pergamon: Oxford, U.K., 1991; Vol. 6, p 485. (d) Hartshorn, A. J.; Lappert, M. F.; Turner, K. *J. Chem. Soc., Chem. Commun.* **1975**, 929.

(7) Badger, G. M.; Sasse, W. H. F. *J. Chem. Soc.* **1956**, 616.

(8) Achar, S.; Scott, J. D.; Vittal, J. J.; Puddephatt, R. J. *Organometallics* **1993**, *12*, 4592.

(9) Scott, J. D.; Puddephatt, R. J. *Organometallics* **1983**, *2*, 1643.

at −30 °C to afford pale-yellow microcrystals. Microanalyses could not be obtained for the product owing to its facile transformation to [$PtCl_2$(^{t}bu$_2$bpy)] under ambient conditions. NMR in CD_2Cl_2: δ(^{1}H) 9.27 [d, ^{1}H, $^3J_{H^5H^6}$ = 6.4 Hz, $^3J_{PtH^6}$ = 39.6 Hz, H^6], 9.15 [d, 1H, $^3J_{H^{5'}H^{6'}}$ = 5.8 Hz, $^3J_{PtH^{6'}}$ = 9.0 Hz, H$^{6'}$], 8.49 [d, 1H, $^4J_{H^{3'}H^{5'}}$ = 1.7 Hz, H$^{3'}$], 8.46 [d, 1H, $^4J_{H^3H^5}$ = 2.3 Hz, H^3], 7.82 [m, 2H, H$^{5'}$ and H^5], 4.07 [s, 3H, $^4J_{PtH}$ = 8.0 Hz, NMe], 3.79 [s, 3H, $^4J_{PtH}$ = 7.7 Hz, NMe], 2.83 [s, 3H, $^2J_{PtH}$ = 65.4 Hz, Pt−Me], 1.51 [s, 9H, ^{t}bu], 1.50 [s, 9H, ^{t}bu]; δ(^{13}C) 162.58 [$^1J_{PtC}$ = 1198.4 Hz, Pt−*C*ClNMe$_2$], 51.92 [$^3J_{PtC}$ = 23.9 Hz, NMe], 51.21 [$^3J_{PtC}$ = 18.4 Hz, NMe], 9.79 [$^1J_{PtC}$ = 455.8 Hz, Pt−Me]. IR in CH_2Cl_2: ν(C−N) 1594 cm^{-1}.

Chloro(dimethylaminomethylene)(4,4′-di-*tert*-butyl-2,2′-bipyridine)dimethylplatinum(IV)chloride ([PtClMe$_2$(CHNMe$_2$)(^{t}bu$_2$bpy)]Cl, 3). To a cooled (−10 °C) and stirred solution of [ClHC=NMe$_2$]Cl (0.026 g, 0.203 mmol) in CH_2Cl_2 (30 mL) was added [PtMe$_2$(^{t}bu$_2$bpy)] (0.100 g, 0.203 mmol). The color of the solution immediately changed from bright orange to pale yellow. After 1 h, the solvent was evaporated *in vacuo* to give a pale-yellow powder (0.110 g, 87.3%). Recrystallization of the product is usually unnecessary, although it may be recrystallized from CH_2Cl_2/*n*-pentane at −30 °C to afford very pale-yellow microcrystals. Anal. Calcd for $C_{23}H_{37}Cl_2N_3Pt\cdot 0.5CH_2Cl_2$: C, 42.51; H, 5.77; N, 6.33. Found: C, 42.96; H, 6.15; N, 6.41. NMR in CD_2Cl_2: δ(^{1}H) 10.81 [s, $^2J_{PtH}$ = 22.5 Hz, Pt−C*H*NMe$_2$], 9.47 [d, ^{1}H, $^3J_{H^{5'}H^{6'}}$ = 6.0 Hz, $^3J_{PtH^{6'}}$ = 12.2 Hz, H$^{6'}$], 8.61 [d, 1H, $^3J_{H^5H^6}$ = 6.1 Hz, $^3J_{PtH^6}$ = 19.1 Hz, H^6], 8.26 [d, 1H, $^4J_{H^{3'}H^{5'}}$ = 1.9 Hz, H$^{3'}$], 8.25 [d, 1H, $^4J_{H^3H^5}$ = 2.0 Hz, H^3], 7.90 [dd, 1H, $^3J_{H^{5'}H^{6'}}$ = 6.0 Hz, $^4J_{H^{5'}H^{3'}}$ = 1.9 Hz, H$^{5'}$], 7.74 [dd, 1H, $^3J_{H^5H^6}$ = 6.1 Hz, $^4J_{H^5H^3}$ = 2.0 Hz, H^5], 4.11 [br s, 3H, NMe], 3.94 [s, 3H, $^4J_{PtH}$ = 8.8 Hz, NMe], 1.47 [s, 9H, ^{t}bu], 1.46 [s, 9H, ^{t}bu], 1.41 [s, 3H, $^2J_{PtH}$ = 64.6 Hz, Pt−Me], 1.10 [s, 3H, $^2J_{PtH}$ = 67.8 Hz, Pt−Me]; δ(^{13}C) 185.02 [$^1J_{PtC}$ = 1040.2 Hz, Pt−*C*HNMe$_2$], 54.69 [$^3J_{PtC}$ = 57.7 Hz, NMe], 47.16 [$^3J_{PtC}$ = 30.9 Hz, NMe], 2.08 [$^1J_{PtC}$ = 581.1 Hz, Pt−Me], −2.18 [$^1J_{PtC}$ = 583.6 Hz, Pt−Me]. IR in Nujol: ν(C−N) 1628 cm^{-1}.

Chloro(chlorodimethylaminomethylene)(4,4′-di-*tert*-butyl-2,2′-bipyridine)dimethylplatinum(IV) chloride ([PtClMe$_2$(CClNMe$_2$)(^{t}bu$_2$bpy)]Cl, 4). To a cooled (−10 °C) and *vigorously* stirred suspension of [Cl$_2$C=NMe$_2$]Cl (0.066 g, 0.406 mmol) in THF (30 mL) and CH_2Cl_2 (15 mL) was added [PtMe$_2$(^{t}bu$_2$bpy)] (0.200 g, 0.405 mmol). Over a period of several minutes, the color of the solution changed from bright orange to pale yellow. After 2 h, the solvents were evaporated *in vacuo* to give a pale-yellow powder (0.210 g, 79.0%). Recrystallization of the product is usually unnecessary, although it may be recrystallized from CH_2Cl_2/*n*-pentane at −30 °C to afford very pale-yellow microcrystals. Anal. Calcd for $C_{23}H_{36}Cl_3N_3Pt$: C, 42.11; H, 5.53; N, 6.41. Found: C, 42.37; H, 5.91; N, 6.27. NMR in CD_2Cl_2 (**4a**): δ(^{1}H) 9.33 [d, ^{1}H, $^3J_{H^{5'}H^{6'}}$ = 6.0 Hz, $^3J_{PtH^{6'}}$ = 11.2 Hz, H$^{6'}$], 8.63 [m, 2H, H$^{3'}$ and H^3], 8.61 [d, 1H, $^3J_{H^5H^6}$ = 6.3 Hz, $^3J_{PtH^6}$ = 24.1 Hz, H^6], 7.89 [dd, 1H, $^3J_{H^{5'}H^{6'}}$ = 6.0 Hz, $^4J_{H^{5'}H^{3'}}$ = 1.5 Hz, H$^{5'}$], 7.77 [dd, 1H, $^3J_{H^5H^6}$ = 6.0 Hz, $^4J_{H^5H^3}$ = 1.9 Hz, H^5], 4.25 [s, 3H, $^4J_{PtH}$ = 9.6 Hz, NMe], 4.03 [s, 3H, $^4J_{PtH}$ = 8.8 Hz, NMe], 1.67 [s, 3H, $^2J_{PtH}$ = 64.8 Hz, Pt−Me], 1.47 [s, 9H, ^{t}bu], 1.46 [s, 9H, ^{t}bu], 1.19 [s, 3H, $^2J_{PtH}$ = 67.3 Hz, Pt−Me]; δ(^{13}C) 171.27 [$^1J_{PtC}$ = 1325.3 Hz, Pt−*C*ClNMe$_2$], 52.81 [$^3J_{PtC}$ = 19.8 Hz, NMe], 50.66 [$^3J_{PtC}$ = 23.7 Hz, NMe], 10.38 [$^1J_{PtC}$ = 569.0 Hz, Pt−Me], 4.53 [$^1J_{PtC}$ = 568.9 Hz, Pt−Me]. IR in Nujol: ν(C−N) 1575 cm^{-1}. If the above reaction is performed in CH_2Cl_2 solution only, the minor isomer (**4b**) is formed in a *ca.* 3:1 ratio (at lower reaction temperatures (−80 °C), the ratio is *ca.* 5:3). NMR in CD_2Cl_2 (**4b**): δ(^{1}H) 8.87 [d, 2H, $^3J_{H^5H^6}$ = 6.0 Hz, $^3J_{PtH^6}$ = 12.6 Hz, H^6], 8.44 [d, 2H, $^4J_{H^5H^3}$ = 1.8 Hz, H^3], 7.79 [dd, 2H, $^3J_{H^5H^6}$ = 6.0 Hz, $^4J_{H^5H^3}$ = 1.8 Hz, H^5], 3.73 [s, 3H, $^4J_{PtH}$ = 9.0 Hz, NMe], 3.67 [s, 3H, $^4J_{PtH}$ = 8.8 Hz, NMe], 1.81 [s, 6H, $^2J_{PtH}$ = 64.5 Hz, Pt−Me], 1.49 [s, 18H, ^{t}bu].

Reactions with Nucleophiles. In a typical experiment, *ca.* 0.005 g of **1**−**4** was treated with approximately 1.5 mole equiv of nucleophile (NaBH$_4$, NaOH, NaOMe, or LiMe) in 10 mL of an appropriate solvent (acetone, CH_2Cl_2, or THF). An immediate color change from pale yellow to deep orange (or deep yellow) ensued, and the mixture was stirred for 1 h at room temperature. Evaporation of the solvent *in vacuo* gave a solid, which was extracted with an appropriate deuterated solvent (acetone-d_6 or CD_2Cl_2). The ^{1}H NMR spectrum was then recorded immediately.

X-ray Crystal Structure Determination. Light-yellow rodlike crystals of **1** were grown from CH_2Cl_2 solution at room temperature. A long rod was cut into a suitable size (0.4 × 0.2 × 0.2 mm), wedged inside a Lindemann capillary tube, flame sealed, and used in the diffraction experiments. The density of the crystal was measured by the neutral buoyancy method. The diffraction experiments were carried out on a Siemens P4 diffractometer with the XSCANS software package[10] using graphite monochromated Mo Kα radiation at 23 °C. The cell constants were obtained by centering 25 high-angle reflections (24.2 ≤ 2θ ≤ 25.0°). The Laue symmetry *2/m* was determined by merging symmetry-equivalent reflections. A total of 4649 reflections were collected in the θ range 1.8−22.5° (-1 ≤ h ≤ 11, −1 ≤ k ≤ 22, -13 ≤ l ≤ 13) in θ−2θ scan mode at variable scan speeds (2−10 deg/min). Background measurements were made at the ends of the scan range. Three standard reflections were monitored at the end of every 197 reflections collected. Three standard reflections decayed to 50% during the data collection. The data were corrected for absorption (μ = 5.2 mm^{-1}) using an empirical method involving ψ scans of nine reflections (13.3° < 2θ < 20.8°). The maximum and minimum transmission factors were 0.114 and 0.087, respectively. The space group $P2_1/c$ was determined from the systematic absences ($h0l$, l = 2n + 1 and $0k0$, k = 2n + 1). The data processing, solution, and the initial refinements were done using SHELXTL-PC programs.[11] The final refinements were performed using SHELXL-93 software programs.[12] Only 17 out of the 34 hydrogen atoms in the cationic molecule were located in the difference Fourier routine. The carbene H(2) atom could not be located. However, all the hydrogen atoms were placed in the calculated positions and they were included for the purpose of structure factor calculations only. The isotropic thermal parameters of the hydrogen atoms were allowed to ride on the appropriate C atoms. Three different orientations of the disordered CH_2Cl_2 solvate were located in the difference Fourier routines (occupancies 0.4, 0.35 and 0.25). A common C−Cl distance was refined in the least-squares cycles. No hydrogen atoms were included for the solvent molecule. Isotropic thermal parameters were refined for all the carbon atoms in the bipyridyl ring. In the least-squares cycles, the anisotropic refinements of the thermal parameter of the C(1) carbon atom became "non-positive-definite" despite applying a weak restraint, ISOR, and we could not find any obvious reason for this anomalous behavior. The thermal parameters of C(1) and C(2) atoms were refined isotropically, and the rest in the cationic molecule were refined anisotropically. In the final least-squares refinement cycles on F^2, the model converged at $R1$= 0.0718, w$R2$ = 0.1425, and GOF = 1.068 for 2311 observations with $F_o \geq 4\sigma(F_o)$ and 244 parameters, and $R1$ = 0.1358, w$R2$ = 0.1723 for all 3776 data. In the final difference Fourier synthesis, the electron density fluctuated in the range 1.57−1.71 eÅ^{-3}; of the top five peaks, four peaks were associated with the Pt atoms at distances 1.03−1.12 Å. The mean and the maximum shift/ESD in the final cycles were 0.000 and 0.008.

Results

Oxidative addition of chloroiminium salts of the type [Cl(X)C=NMe$_2$]Cl (X = Cl, H) to the uncharged plati-

(10) *XSCANS*; Siemens Analytical X-ray Instruments Inc., Madison, WI, 1990.
(11) Sheldrick, G. M. *SHELXTL-PC Software*; Siemens Analytical X-ray Instruments Inc., Madison, WI, 1990.
(12) Sheldrick, G. M. *SHELXL-93*; *J. Appl. Crystallogr.*, in preparation.

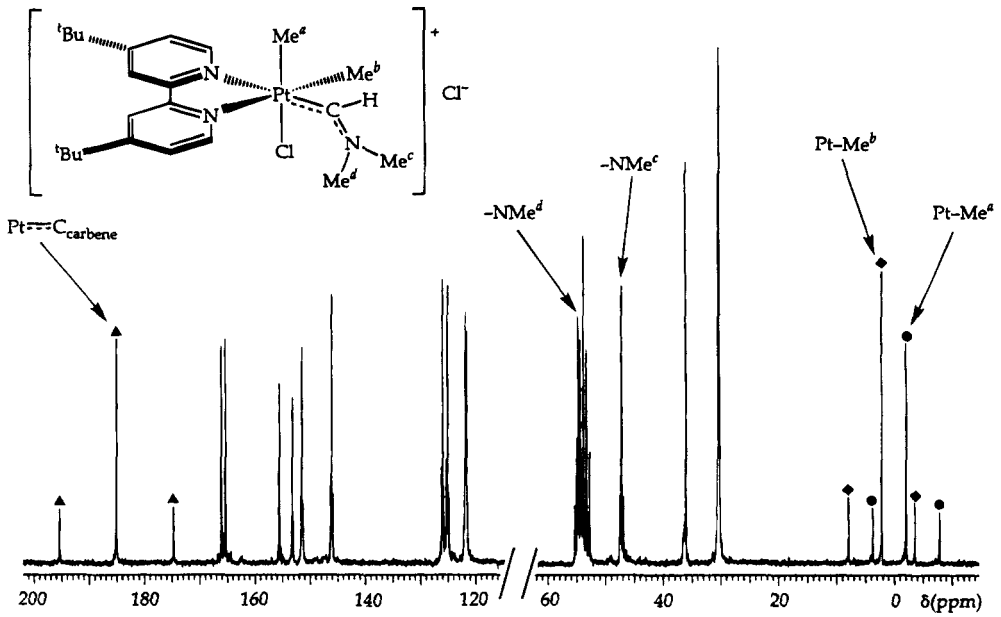

Figure 1. $^{13}C\{^1H\}$ NMR spectrum of **3** in CD_2Cl_2. The quintet centered at δ 53.8 is due to the solvent.

num(II) precursors [PtXMe(^{t}bu$_2$bpy)] (X = Me, Cl) affords the novel cationic platinum(IV)–carbene complexes **1–4** in good yield. The structures of the com-

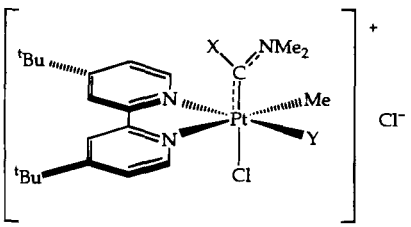

X = H; Y = Cl (**1**)

X = Y = Cl (**2**)

X = Cl; Y = Me (**4b**)

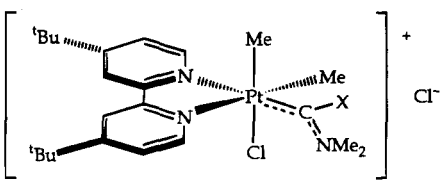

X = H (**3**)

X = Cl (**4a**)

plexes are presented in Figure 1. The presence of *tert*-butyl substituents on the 2,2′-bipyridine ligand greatly assists in the solubility of the cationic complexes in common organic solvents such as acetone and CH_2Cl_2. All the complexes are reasonably air- and moisture-stable at room temperature, although **1** and **2** are thermally unstable and are transformed to bright yellow [PtCl$_2$(^{t}bu$_2$bpy)] on standing for a few days, even in the solid state and in the absence of light.

Even though up to four stable, geometrical isomers are feasible for **1** and **2**, only one was observed in each case. For **3**, only one of three possible isomers was formed, but for **4**, two isomers were often formed. In each case, **4a** was the major isomer and the ratios of **4a** to **4b** when the reaction was carried out in different conditions were 3:1 (CH_2Cl_2 solvent, −10 °C), 5:3 (CH_2Cl_2 solvent, −80 °C), and >9:1 (THF/CH_2Cl_2 solvent, −10 °C). No interconversion between **4a** and the minor isomer **4b** occurs. For example, the isomeric composition of the product obtained in THF/CH_2Cl_2 does not change when it is isolated and redissolved in CH_2Cl_2.

The NMR (^{1}H and $^{13}C\{^1H\}$) spectroscopic data for complexes **1–4** are presented in Table 1. The decrease in magnitude of $^2J_{PtH}$ for the methylplatinum signals of the products **1–4** compared with the platinum(II) precursors is consistent with oxidation of the platinum center from +II to +IV and is a function of the diminished *s*-character of d^2sp^3-hybridized platinum(IV) compared to dsp^2-hybridized platinum(II).[13] Furthermore, the magnitude of $^2J_{PtH}$ depends on the nature of the ligand *trans* to the methyl group and is a sensitive probe of stereochemistry.[13c]

For **1** and **2**, the Pt–Me resonance is shifted considerably to lower field than that of [PtClMe(^{t}bu$_2$bpy)], and the magnitude of $^2J_{PtH}$ (*ca.* 65 Hz) is consistent with the methyl ligand being *trans* to either the chloro or the N-donor ligand.[13] The X-ray structure of **1** (*vide infra*) shows that the methyl group is *trans* to the N-donor ligand, and since the NMR spectroscopic data of **1** and **2** are very similar, it is almost certain that they have the same stereochemistry.

In the ^{1}H NMR spectra of **3** and **4a**, there are two distinct Pt–Me signals for each complex. The magnitude of $^2J_{PtH}$ decreases significantly from 86.0 Hz in [PtMe$_2$(^{t}bu$_2$bpy)][8] to *ca.* 65 Hz for the low-field signal and *ca.* 68 Hz for the high field signal; the latter is assigned to the methyl group *trans* to the chloro ligand.[13] The methyl group cannot be *trans* to the carbene ligand since a significantly lower value of $^2J_{PtH}$ (*ca.* 48 Hz)[5g,h] would be expected for the Pt–Me resonance of such a group. The presence of six distinct

(13) (a) Pregosin, P. S.; Omura, H.; Venanzi, L. M. *J. Am. Chem. Soc.* **1973**, *95*, 2047. (b) Appleton, T. G.; Hall, J. R. *Inorg. Chem.* **1971**, *10*, 1717. (c) Anderson, C. M.; Crespo, M.; Jennings, M. C.; Lough, A. J.; Ferguson, G.; Puddephatt, R. J. *Organometallics* **1991**, *10*, 2672.

(14) Chisholm, M. H.; Clark, H. C.; Ward, J. E. H.; Yasufuku, K. *Inorg. Chem.* **1975**, *14*, 893.

aromatic signals in the ^{1}H NMR spectra of complexes **3** and **4a** shows unequivocally the unsymmetrical nature of the two complexes, and the remaining possible (symmetrical) stereoisomer can be ruled out for these complexes. The ^{1}H NMR spectrum of **4b** shows three distinct aromatic resonances and only one Pt−Me resonance, thus proving the stereochemistry with the chloro ligand and carbene ligand mutually *trans*. Crystals of either **3** or **4** could be obtained but they were not suitable for a X-ray structure determination.

The ^{1}H NMR spectra of **1** - **4** display two sharp *N*-methyl signals of approximately equal intensity at δ *ca.* 3.6−4.3, attributed to the *N*-methyl groups, which are nonequivalent due to the restricted rotation about the $C_{carbene}$−N partial double bond. This is a characteristic feature of the room-temperature NMR spectra of many other transition-metal−aminocarbene complexes[15] and organic amides.[16] Indeed, the X-ray structure of **1** and IR data for complexes **1**−**4** (*vide infra*) confirm the high $C_{carbene}$−N bond order. The barrier to rotation of the *N*-methyl groups about the $C_{carbene}$−N bond must be high, since the two signals are sharp at room temperature. High-temperature ^{1}H NMR spectra of **3** (to 60 °C in acetonitrile-d_3) show no appreciable change in the line shape of the two signals. Interestingly, in the rhodium(III)−aminocarbene species [$RhCl_3$($CHNMe_2$)(PEt_3)$_2$], no coalescence or change of line shape was observed up to 150 °C in α-bromonaphthalene.[17]

The secondary carbene complexes **1** and **3** show a distinct low-field signal at δ *ca.* 10.5 attributed to the hydrogen substituent on the carbene carbon atom. The position of the resonance is consistent with the electrophilic nature of the carbene carbon atom and is similar to that observed for the electrophilic CH in the iminium salt [ClHC=NMe_2]Cl (δ 10.83 in $CDCl_3$), and other secondary-carbene complexes, e.g., *trans*-[PtCl(CHNH-*p*-tolyl)(PEt_3)$_2$]Cl (δ 11.45 in $CDCl_3$)[18] and [RhI_3($CHNMe_2$)(PEt_3)$_2$] (δ 11.09 in $CDCl_3$).[17] For **1**, the signal is somewhat broadened, indicative of unresolved ^{195}Pt satellite signals. For **3**, the resonance is flanked by well-resolved ^{195}Pt satellite signals, thus confirming the assignment. The magnitude of $^2J_{PtH}$ is *ca.* 0.7 times that of typical cationic platinum(II)−secondary carbene complexes, e.g., *trans*-[Pt(CN-*p*-tolyl)(CHNH-*p*-tolyl)(PEt_3)$_2$](ClO_4)$_2$ ($^2J_{PtH}$ = 33 Hz),[18] demonstrating the diminished *s*-character of the platinum(IV) hybrid orbital used in bonding to the carbene ligand.

The ^{13}C{^{1}H} NMR spectra of **1**−**4** support the structures assigned to the complexes on the basis of ^{1}H NMR spectroscopy. The ^{13}C{^{1}H} NMR spectrum of **3** is presented in Figure 1. As expected, the carbene carbon atom appears at low field (δ = 163−185) and is flanked by ^{195}Pt satellite signals ($^1J_{PtC}$ = 932−1325 Hz). The magnitude of $^1J_{PtC}$ is considerably larger than that of the Pt−Me resonance(s) ($^1J_{PtC}$ = 456−584 Hz), indicating strong Pt−$C_{carbene}$ bonding. Furthermore, both the natures of the carbene substituents and the *trans* ligand have a marked influence on the magnitude of $^1J_{PtC}$, as has been observed in other systems.[14,19] The ^{13}C shielding of the $C_{carbene}$ atom in **1**−**4** is considerably higher than that usually observed for typical "Fischer-type" carbene complexes,[15] although it is comparable to that observed for the iridium(III) species [$IrCl_2$(CO)(PPh_3)$_2$($CHNMe_2$)]Cl (δ = 192.7 in DMSO-d_6)[5b] and the platinum(II) complexes *trans*-[$PtCl_2$(P^nBu_3){C($NMeCH_2$)$_2$}] (δ = 196.5 in $CDCl_3$)[19c] and [PtH(C{$NCH_2CH_2CH_2$}NH-*p*-$MeOC_6H_4$)(dppe)]BF_4 (δ = 194.5 in CD_2Cl_2).[4b]

For complexes **1**−**4**, the $^1J_{PtC}$ values associated with the Pt−$C_{carbene}$ signals are of similar magnitude to those of cationic platinum(II)−aminocarbene species, e.g., *trans*-[PtCl($AsMe_3$)$_2${C(Me)(NHMe)}]PF_6 ($^1J_{PtC}$ = 1047 Hz in CD_2Cl_2),[14] *trans*-[PtCl($AsMe_3$)$_2${C(Me)(NMe_2)}]PF_6 ($^1J_{PtC}$ = 1070 Hz in acetone-d_6),[14] and [PtH(C{$NCH_2CH_2CH_2$}NH-*p*-$MeOC_6H_4$)(dppe)]BF_4 ($^1J_{PtC}$ = 1134 Hz in CD_2Cl_2).[4b] This is unexpected since there is usually a marked decrease in the magnitude of $^1J_{PtC}$ for platinum(IV) compared to platinum(II) complexes (*vide supra*).

Complexes **1** and **2** show one Pt−Me resonance at high field in their respective ^{13}C{^{1}H} NMR spectra, but for complexes **3** and **4a**, two distinct Pt−Me signals are evident, again supporting the assigned stereochemistry. Interestingly, the magnitude of $^1J_{PtC}$ for those signals corresponding to a methyl group *trans* to the N-donor (456−581 Hz) is lower than that reported for other cationic platinum(IV)−methyl complexes, e.g., [$PtMe_3$(pz_3CH)]PF_6 (pz = 1-pyrazolyl; $^1J_{PtC}$ = 688 Hz),[20] [$PtMe_3$(py_3CH)]PF_6 ($^1J_{PtC}$ = 688 Hz),[20] and [$PtMe_3$${(Me_2pz)_2CH_2}$(py)]$PF_6$ ($^1J_{PtC}$ = 669 and 698 Hz).[20] It appears that the chloro and carbene ligands in **1**−**4** play a significant electronic role in lowering the magnitude of $^1J_{PtC}$ for the Pt−Me signal(s). Furthermore, increasing the number of chloro ligands about the metal center significantly decreases the value of $^1J_{PtC}$. As observed in the ^{1}H NMR spectra of **1**−**4**, two distinct *N*-methyl resonances surrounded by ^{195}Pt satellite signals are also found in each of the ^{13}C{^{1}H} NMR spectra, again showing the magnetic nonequivalence of the *N*-methyl groups due to restricted rotation about the $C_{carbene}$−N bond. In contrast to $^4J_{PtH}$ for the two *N*-methyl group resonances, those of $^3J_{PtC}$ differ significantly for each complex, the larger being assigned to the *N*-methyl group that is located *syn* to the platinum atom.[14]

The IR spectra of complexes **1**−**4** (Table 1) show a characteristic ν(C−N) band at 1630−1575 cm^{-1}, each being lower in frequency compared to that of the precursor iminium salts (1667 (Nujol) and 1663 (CH_2Cl_2) cm^{-1} for [ClHC=NMe_2]Cl, and 1630 (Nujol) and 1626 (CH_2Cl_2) cm^{-1} for [Cl_2C=NMe_2]Cl). The ν(C−N) band in the IR spectra of **1** and **3** appears in the range found for other secondary aminocarbene complexes, e.g., [$RhCl_3$(CO)($CHNMe_2$)(PPh_3)] (1615 cm^{-1})[17] and *cis*-[$PtCl_2$($CHNMe_2$)(PPh_3)] (1612 cm^{-1}).[4c] For complexes **2** and **4**, the position of the ν(C−N) band is comparable to other chlorocarbene complexes, e.g., [$IrCl_3$($CClNMe_2$)-

(15) (a) Cardin, D. J.; Cetinkaya, B.; Doyle, M. J.; Lappert, M. F. *Chem. Soc. Rev.* **1973**, *2*, 99. (b) Cotton, F. A.; Lukehart, C. M. *Prog. Inorg. Chem.* **1972**, *16*, 487. (c) Cardin, D. J.; Cetinkaya, B.; Lappert, M. F. *Chem. Rev.* **1972**, *72*, 545.

(16) Robin, M. B.; Bovey, F. A.; Basch, H. In *The Chemistry of Amides*; Zabicky, J., Ed.; Wiley: New York, 1970; p 1.

(17) Cetinkaya, B.; Lappert, M. F.; McLaughlin, G. M.; Turner, K. *J. Chem. Soc., Dalton Trans.* **1974**, 1591.

(18) Christian, D. F.; Clark, H. C.; Stepaniak, R. F. *J. Organomet. Chem.* **1976**, *112*, 227.

(19) (a) Chisholm, M. H.; Clark, H. C.; Manzer, L. E.; Stothers, J. B.; Ward, J. E. H. *J. Am. Chem. Soc.* **1973**, *95*, 8574. (b) Chisholm, M. H.; Clark, H. C.; Manzer, L. E.; Stothers, J. B. *J. Chem. Soc., Chem. Commun.* **1971**, 1627. (c) Cardin, D. J.; Cetinkaya, B.; Cetinkaya, E.; Lappert, M. F.; Randall, E. W.; Rosenberg, E. *J. Chem. Soc., Dalton Trans.* **1973**, 1982.

(20) Clark, H. C.; Ferguson, G.; Jain, V. K.; Parvez, M. *J. Organomet. Chem.* **1984**, *270*, 365.

Table 1. Selected Spectroscopic Data (^{1}H and ^{13}C{^{1}H} NMR[a] and IR[b]) for Complexes 1–4

	δ(^{1}H)				δ(^{13}C)			IR
complex	Pt−*C*HNMe$_2$	NME	H$^{6,6'}$	Pt−Me	Pt−C$_{carbene}$	NMe	Pt−Me	ν(C$_{carbene}$−N) (cm^{-1})
1	10.43 (br)	3.77 (br, d, $^4J_{HH}$ = 0.9), 3.62 (d, $^4J_{HH}$ = 0.8; $^4J_{PtH}$ = 8.0)	9.19 ($^3J_{HH}$ = 5.8; $^3J_{PtH}$ = 8.1) 9.02 (d, $^3J_{HH}$ = 6.4; $^4J_{PtH}$ = 38.9)	2.45 ($^2J_{PtH}$ = 64.8)	177.86 ($^1J_{PtC}$ = 931.7)	54.56 ($^3J_{PtC}$ = 50.5) 46.46 ($^3J_{PtC}$ = 28.1)	6.77 ($^1J_{PtC}$ = 475.6)	1638[c]
2		4.07 (s, $^4J_{PtH}$ = 8.0)	9.27 ($^3J_{HH}$ = 6.4; $^3J_{PtH}$ = 39.6)	2.83 ($^2J_{PtH}$ = 65.4)	162.58 ($^1J_{PtC}$ = 1198.4)	51.92 ($^3J_{PtC}$ = 23.9)	9.79 ($^1J_{PtC}$ = 455.8)	1594[c,d]
3	10.81 ($^2J_{PtH}$ = 22.5)	3.79 (s, $^4J_{PtH}$ = 7.7) 4.11 (br) 3.94 (s, $^4J_{PtH}$ = 8.8)	9.15 ($^3J_{HH}$ = 5.8; $^4J_{PtH}$ = 9.0) 9.47 ($^3J_{HH}$ = 6.0; $^3J_{PtH}$ = 12.2) 8.61 ($^3J_{HH}$ = 6.1; $^3J_{PtH}$ = 19.1)	1.41 ($^2J_{PtH}$ = 64.6) 1.10 ($^2J_{PtH}$ = 67.8)	185.02 ($^1J_{PtC}$ = 1040.2)	51.21 ($^3J_{PtC}$ = 18.4) 54.69 ($^3J_{PtC}$ = 57.7) 47.16 ($^3J_{PtC}$ = 30.9)	2.08 ($^1J_{PtC}$ = 581.1) −2.18 ($^1J_{PtC}$ = 583.6)	1628[d]
4a		4.25 (s, $^4J_{PtH}$ = 9.6) 4.03 (s, $^4J_{PtH}$ = 8.8)	9.33 ($^3J_{HH}$ = 6.0; $^3J_{PtH}$ = 11.2) 8.61 ($^3J_{HH}$ = 6.3; $^3J_{PtH}$ = 24.1)	1.67 ($^2J_{PtH}$ = 64.8) 1.19 ($^2J_{PtH}$ = 67.3)	171.27 ($^1J_{PtC}$ = 1325.3)	52.81 ($^3J_{PtC}$ = 19.8) 50.66 ($^3J_{PtC}$ = 23.7)	10.38 ($^1J_{PtC}$ = 569.0) 4.53 ($^1J_{PtC}$ = 568.9)	1575

[a] Measured in CD_2Cl_2. Quoted multiplicities do not include ^{195}Pt satellites. Coupling constants (Hz) in parentheses. [b] Measured as Nujol mulls (cm^{-1}), except where stated otherwise. [c] CH_2Cl_2 solution. [d] Present as a shoulder on the ν(C−N) band of the ^{t}Bu$_2$bpy ligand.

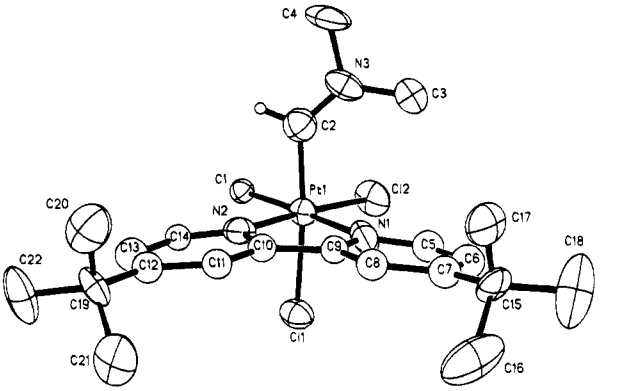

Figure 2. Molecular structure of the [PtCl$_2$Me(CHNMe$_2$)(^{t}bu$_2$bpy)]$^+$ ion (**1**). Only the carbene hydrogen atom H(2), placed in its calculated position, is shown. Thermal ellipsoids are represented at the 50% level.

Table 2. Summary of Crystallographic Data for [PtCl$_2$Me(CHNMe$_2$)(^{t}Bu$_2$bpy)Cl·CH$_2$Cl$_2$ (1)

chem formula	$C_{22}H_{34}Cl_3N_3Pt{\cdot}CH_2Cl_2$
fw	726.90
space group	$P2_1/c$
a, Å	11.064(1)
b, Å	21.310(2)
c, Å	12.277(3)
V, Å^3	2894.0(7)
β, deg	91.20(2)
Z	4
T, K	296
ϱ_{calc}, g cm^{-1}	1.667
ϱ_{obs}, g cm^{-1}	1.65(5)
μ, mm^{-1}	5.2
F(000)	1432
R^a	0.0718
S^b	1.068

[a] $R = \sum||F_o| - |F_c||/\sum|F_o|$. [b] S = goodness of fit = $[\sum w(F_o^2 - F_c^2)^2/(n - p)]^{1/2}$, where n is the number of unique reflections and p the number of parameters.

(PPh$_3$)$_2$] (1538 cm^{-1})[21] and [RhCl$_3$(CClNMe$_2$)(PPh$_3$)$_2$] (1591 cm^{-1}).[22] On the basis of IR spectroscopic data, the C=N bond order decreases in the order [ClHC=NMe$_2$]Cl > [Cl$_2$C=NMe$_2$]Cl > **1** ≈ **3** > **2** ≈ **4** and is consistent with a diminished C−N p_π−p_π interaction on coordination of the iminium fragment to the platinum(IV) center.

The X-ray crystal structure of **1** consists of discrete [PtCl$_2$Me(CHNMe$_2$)(^{t}bu$_2$bpy)]$^+$ cations and chloride anions, with one CH$_2$Cl$_2$ molecule of crystallization per complex ion. The molecular structure of the cation is presented in Figure 2 with the atom-labeling scheme. A summary of crystallographic data, important bond geometries, and atomic coordinates of the non-hydrogen atoms for **1** is presented in Tables 2, 3 and 4, respectively.

The platinum atom is coordinated to a methyl group, two chlorine atoms, a chelating ^{t}bu$_2$bpy ligand, and the (dimethylamino)methylene moiety in an octahedral geometry. The carbene ligand and one of the chlorine atoms occupy a mutually *trans* arrangement, with the remaining chlorine atom located *trans* to one of the N-atoms of the ^{t}bu$_2$bpy ligand. The arrangement of ligands about the platinum center is marginally dis-

(21) Clark, G. R.; Roper, W. R; Wright, A. H. *J. Organomet. Chem.* **1982**, *236*, C7.

(22) Hartshorn, A. J.; Lappert, M. F.; Turner, K. *J. Chem. Soc., Chem. Commun.* **1975**, 929.

Table 3. Bond Lengths (Å) and Angles (deg) for 1

Pt(1)−Cl(1)	2.378(5)	C(11)−C(12)	1.39(2)	N(3)−C(3)	1.45(2)
Pt(1)−N(1)	2.120(16)	C(12)−C(19)	1.47(3)	C(5)−C(6)	1.37(3)
Pt(1)−C(1)	2.129(15)	C(15)−C(17)	1.51(2)	C(7)−C(8)	1.41(2)
N(1)−C(5)	1.34(2)	C(15)−C(18)	1.55(2)	C(8)−C(9)	1.39(2)
N(2)−C(14)	1.32(2)	C(19)−C(22)	1.54(2)	C(10)−C(11)	1.35(2)
N(3)−C(2)	1.31(2)	Pt(1)−Cl(2)	2.289(5)	C(12)−C(13)	1.40(3)
N(3)−C(4)	1.49(2)	Pt(1)−N(2)	2.030(19)	C(13)−C(14)	1.35(3)
C(6)−C(7)	1.38(3)	Pt(1)−C(2)	1.991(21)	C(15)−C(16)	1.54(2)
C(7)−C(15)	1.48(3)	N(1)−C(9)	1.38(2)	C(19)−C(20)	1.53(2)
C(9)−C(10)	1.46(2)	N(2)−C(10)	1.42(2)	C(19)−C(21)	1.54(2)

Cl(2)−Pt(1)−Cl(1)	89.5(2)	N(1)−Pt(1)−Cl(1)	89.7(4)
N(2)−Pt(1)−Cl(1)	87.7(4)	C(1)−Pt(1)−Cl(1)	89.1(5)
C(2)−Pt(1)−Cl(1)	174.2(6)	N(1)−Pt(1)−Cl(2)	98.0(5)
N(2)−Pt(1)−Cl(2)	175.7(4)	C(1)−Pt(1)−Cl(2)	86.0(5)
C(2)−Pt(1)−Cl(2)	95.0(7)	C(2)−Pt(1)−N(1)	93.3(7)
N(2)−Pt(1)−N(1)	78.7(6)	C(2)−Pt(1)−N(2)	88.0(8)
C(2)−Pt(1)−C(1)	87.6(7)	N(2)−Pt(1)−C(1)	97.2(6)
N(1)−Pt(1)−C(1)	175.8(7)	C(5)−N(1)−Pt(1)	127.8(15)
C(9)−N(1)−Pt(1)	113.9(11)	C(5)−N(1)−C(9)	118(2)
C(14)−N(2)−Pt(1)	126.1(14)	C(10)−N(2)−Pt(1)	117.6(11)
C(14)−N(2)−C(10)	116(2)	C(2)−N(3)−C(3)	128(2)
C(2)−N(3)−C(4)	120(2)	C(3)−N(3)−C(4)	112(2)
N(3)−C(2)−Pt(1)	131(2)	N(1)−C(5)−C(6)	121(2)
C(7)−C(6)−C(5)	124(2)	C(6)−C(7)−C(8)	115(2)
C(6)−C(7)−C(15)	123(2)	C(8)−C(7)−C(15)	122(2)
C(9)−C(8)−C(7)	120(2)	N(1)−C(9)−C(8)	121(2)
N(1)−C(9)−C(10)	117(2)	C(8)−C(9)−C(10)	122(2)
C(11)−C(10)−N(2)	120(2)	C(11)−C(10)−C(9)	127(2)
N(2)−C(10)−C(9)	113(2)	C(10)−C(11)−C(12)	123(2)
C(11)−C(12)−C(13)	115(2)	C(11)−C(12)−C(19)	120(2)
C(13)−C(12)−C(19)	124(2)	C(14)−C(13)−C(12)	120(2)
N(2)−C(14)−C(13)	125(2)	C(7)−C(15)−C(17)	110.3(14)
C(7)−C(15)−C(16)	108(2)	C(17)−C(15)−C(16)	108.0(14)
C(7)−C(15)−C(18)	115(2)	C(17)−C(15)−C(18)	108.0(13)
C(16)−C(15)−C(18)	107.0(14)	C(12)−C(19)−C(20)	111(2)
C(12)−C(19)−C(22)	113(2)	C(20)−C(19)−C(22)	107.1(14)
C(12)−C(19)−C(21)	110(2)	C(20)−C(19)−C(21)	108(2)
C(22)−C(19)−C(21)	108(2)		

torted from an ideal octahedron; the C(2)−Pt−Cl(1) angle encompassing the carbene ligand and *trans*-chlorine is 174.18(64)°. Otherwise, there are no significant deviations within the coordination sphere.

The Pt−Me bond length (2.129(15) Å) is close to that of other σ-alkylplatinum(IV) complexes containing a *trans* N-donor ligand, e.g., [$PtClMe_2\{Me_2NCH_2CH_2$-$N{=}CHC_6H_4Cl\}$] (2.068(15) Å)[13] and [$PtIMe_2(SiMe_3)$-(bpy)] (2.096(18) and 2.120(16) Å).[23] The two Pt−N bond lengths (2.120(16) and 2.030(19) Å) differ significantly and conclusively demonstrate the much greater *trans* influence exerted by the methyl group over the chloro ligand, the former being close to Pt−N bond lengths in other σ-alkylplatinum(IV)−bpy complexes, e.g., [$PtBrMe_2(CH_2CO_2Me)$(bpy)] (2.165(4) and 2.159(4) Å)[8] and [$PtIMe_2(SiMe_3)$(bpy)] (2.186(2) and 2.16(1) Å).[23] The two Pt−Cl bond lengths (2.289(5) and 2.378(5) Å) also differ significantly and show the greater *trans* influence of the carbene ligand over the N-donor. The *trans* influence of the carbene ligand is somewhat less than that observed for a σ-alkyl ligand, e.g., [$PtCl$-$Me_2\{(pz)_2CRCH_2$-*N,N′,C″*}] (R = Me, 2.421(3) Å; R = CH_2Cl, 2.443(2) Å).[24]

The Pt−$C_{carbene}$ distance is 1.991(21) Å and is similar to the value determined for the only other crystallographically determined example of a platinum(IV)−carbene complex, [$PtCl_2\{C(NHMe)(NHC_6H_4Cl)\}(PEt_3)_2$]-$ClO_4$ (1.973(11) Å).[5a] The Pt−$C_{carbene}$ bond length is significantly shorter than the Pt−Me distance, and differences in the covalent radii of sp^2- and sp^3-hybridized carbon atoms (*ca.* 0.04 Å)[25] would play a significant role here. Even though d_π−p_π bonding might also contribute to the short Pt−$C_{carbene}$ bond, the high oxidation state of platinum should lead to only weak π-bonding.

Table 4. Selected Atomic Coordinates (×10⁴) and Equivalent Isotropic Displacement Parameters (Å² × 10³) for 1[a]

atom	*x*	*y*	*z*	*U*(eq)[a]
Pt(1)	2467.3(9)	7345.8(3)	1204.4(6)	35.6(3)
Cl(1)	3436(5)	7951(2)	2596(4)	52(1)
Cl(2)	830(5)	7224(3)	2294(4)	63(2)
N(1)	3457(17)	6546(6)	1733(12)	50(5)
N(2)	3997(17)	7434(6)	334(12)	43(5)
N(3)	1181(16)	6353(7)	−138(14)	53(5)
C(1)	1594(17)	8175(7)	625(13)	33(4)
C(2)	1727(22)	6900(9)	−69(17)	57(6)
C(3)	901(23)	5927(9)	741(16)	64(7)
C(4)	773(23)	6108(10)	−1224(15)	76(8)
C(5)	3185(20)	6145(8)	2536(14)	45(5)
C(6)	3890(20)	5629(8)	2746(15)	49(5)
C(7)	4924(20)	5491(8)	2192(14)	41(5)
C(8)	5238(19)	5930(7)	1382(13)	39(5)
C(9)	4527(18)	6458(7)	1194(13)	33(4)
C(10)	4873(18)	6950(7)	434(13)	33(4)
C(11)	5916(18)	6989(7)	−118(13)	35(4)
C(12)	6219(20)	7508(7)	−743(14)	39(5)
C(13)	5387(20)	8000(9)	−731(15)	50(5)
C(14)	4332(17)	7935(8)	−210(12)	31(4)
C(15)	5620(17)	4903(8)	2366(12)	46(5)
C(16)	6933(20)	5080(10)	2682(17)	99(11)
C(17)	5646(21)	4525(8)	1323(13)	66(8)
C(18)	5149(24)	4470(10)	3282(16)	107(12)
C(19)	7370(21)	7523(6)	−1324(15)	43(6)
C(20)	7381(23)	7025(9)	−2225(15)	75(7)
C(21)	8423(18)	7386(10)	−523(16)	77(7)
C(22)	7606(21)	8159(8)	−1869(18)	81(8)
Cl(3)	2231(6)	4425(3)	432(6)	83(2)

[a] *U*(eq) is defined as one-third of the trace of the orthogonalized U_{ij} tensor.

The atoms Pt, C(2), N(3), C(3), and C(4) lie approximately in the same plane, thus confirming the sp^2-hybridized nature of both the nitrogen and carbene carbon atoms. The Pt−C(2)−N(3) bond angle (131(2)°) is significantly greater than the ideal 120°, although it is not as large as the distortion found in the secondary carbene complexes [$RhCl_3(CHNMe_2)(PEt_3)_2$] (139.6(9)°)[22] and [$RuI_2(CO)(CHNMe\{p\text{-}MeC_6H_4\})(CN$-$pMeC_6H_4)(PPh_3)$] (141.5(5)°)[26] and is comparable to other mononuclear, transition-metal−secondary aminocarbene complexes, e.g., [$Fe(Cp)(CO)(\{CHNMe\}_2BH_2)$] (124.1(10)° and 130.4(11)°),[27] *cis*-[$PtCl_2(CHNMe_2)(PPh_3)$] (129.4(8)°),[4c] and *mer,trans*-[$Mn(CO)_3(PPh_3)_2(CHNHCH_2$-$C_6H_5)$]$CF_3SO_3$ (131.6(3)°).[28] The ^{t}bu$_2$bpy ligand is slightly twisted; the angle between the mean planes defining the two pyridine-like rings being 11.96°.

The very short C(2)−N(3) distance (1.31(2) Å) is indicative of a bond order greater than 1 and is attributed to extensive p_π−p_π bonding between the two atoms. This conclusion is supported by spectroscopic (NMR and IR) data. The $C_{carbene}$−N bond length is

(23) Levy, C. J.; Puddephatt, R. J.; Vittal, J. J. *Organometallics* **1994**, *13*, 1559.
(24) Canty, A. J.; Honeyman, R. T.; Skelton, B. W.; White, A. H. *J. Organomet. Chem.* **1990**, *389*, 277.
(25) Cotton, F. A.; Wilkinson, G.; Gaus, P. L. *Basic Inorganic Chemistry*, 2nd ed.; Wiley: New York, 1987; p 93.
(26) Clark, G. R. *J. Organomet. Chem.* **1977**, *134*, 51.
(27) Butler, W. M.; Enemark, J. H. *J. Organomet. Chem.* **1973**, *49*, 233.
(28) Gibson, D. H.; Mandal, S. K.; Owens, K.; Richardson, J. F. *Organometallics* **1990**, *9*, 1936.

Scheme 1. Proposed Mechanism for the Reductive Elimination Reaction on Treatment of 3 with a Nucleophile MX (M = Na, X = OMe, OH, H; M = Li, X = Me)

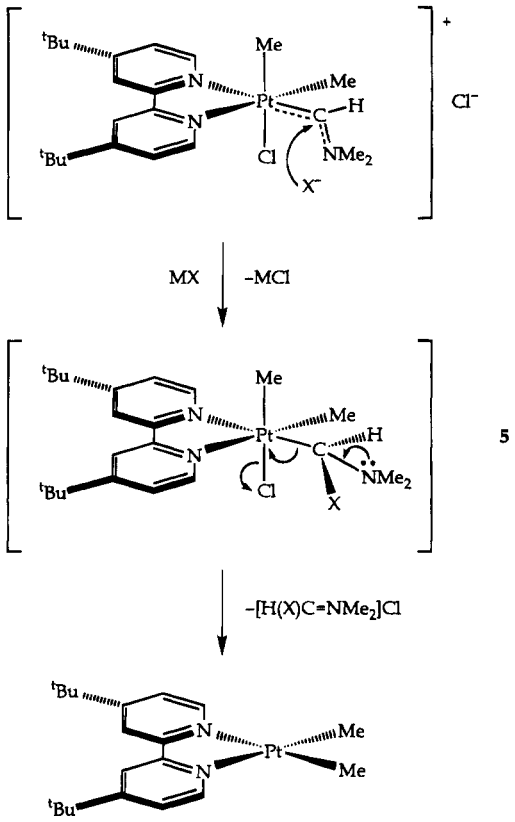

similar to that found in other transition-metal–secondary carbene complexes, e.g., $[RhCl_3(CHNMe_2)(PEt_3)_2]$ (1.289(14) Å)[22] and $[Fe(Cp)(CO)(\{CHNMe\}_2BH_2)]$ (1.293(17) and 1.337(16) Å),[27] and in the iminium salt $[Me_2C{=}NMe_2]ClO_4$ (1.302Å).[29] The *N*-methyl bond lengths (1.45(2) and 1.49(2) Å) are very similar to those found in $[RhCl_3(CHNMe_2)(PEt_3)_2]$ (1.455(17) and 1.497(19) Å),[22] *cis*-$[PtCl_2(CHNMe_2)(PPh_3)]$ (1.42(2) and 1.46(2) Å),[4c] and typical organic C–N single bonds, e.g., diethylamine (1.47(2) Å).[30] Perhaps to alleviate unfavorable steric interactions with atoms in the equatorial coordination plane, the NMe_2 substituent bisects the equatorial plane between Cl(2) and N(1), with the dihedral angle between N(3)–C(2)–Pt(1)–N(1) and N(3)–C(2)–Pt(1)–Cl(2) being 48.79(2.25)° and −49.59(2.22)°, respectively.

Addition of various nucleophiles (e.g., Me^-, OMe^-) to complexes **1–4** leads to reductive elimination, even at low temperatures (Scheme 1). For example, addition of NaOMe to **3** results in an immediate color change of the solution from pale yellow to deep orange, characteristic of the platinum(II) precursor $[PtMe_2(^tbu_2bpy)]$, and the reaction is quantitative as determined by ^1H NMR spectroscopy. The organic fragment formed in the reaction is $[H(OMe)C{=}NMe_2]Cl$, as determined by ^1H NMR spectroscopy.[31] The reaction of nucleophiles with **1**, **2**, and **4** gives $[PtCl_2(^tbu_2bpy)]$ and $[PtMeCl(^tbu_2bpy)]$ (for **1** and **2**) and $[PtMe_2(^tbu_2bpy)]$ (for **4**), but these reactions are accompanied by formation of other unidentified platinum complexes.

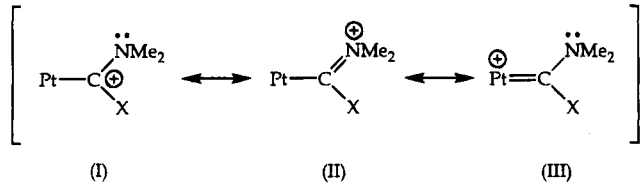

Figure 3. Resonance stabilization of the platinum(IV)–carbene bond (X = H, Cl). Other ligands have been omitted for clarity.

Complexes **1–4** do not react with nucleophiles such as H_2O or with electrophiles such as CF_3COOH. Furthermore, no exchange of the carbene H atom in **1** or **3** by deuterium is observed when the complexes are treated with D_2O, and this is reminiscent of the chemistry of other secondary carbene complexes and organic amides.[16,22]

Discussion

On the basis of the method first described by Lappert *et al.*,[5b,d] addition of chloroiminium salts to organoplatinum(II) precursors affords the novel, cationic platinum(IV)–carbene complexes **1–4**. Lappert used precursor complexes containing a weakly bonded neutral ligand which could be displaced by chloride, thus yielding neutral carbene complexes by three-fragment oxidative addition. In this work, the reactions are simple two-fragment oxidative additions and the strong donor $^tbu_2$-bpy ligand stabilizes the cationic products. To our knowledge, **1**, **3** and **2**, **4** are the first examples of secondary carbene and halocarbene complexes of platinum(IV), respectively, that do not contain P- or As-donor ligands. In contrast to cationic dimethylplatinum(IV)–amino- and alkoxycarbene complexes with P- and As-donor ligands,[5g] the dimethyl complexes **3** and **4** show considerably better thermal stability toward reductive elimination. Indeed, **3** and **4** can be stored at room temperature for indefinite periods of time. The dichloro complexes **1** and **2** do decompose slowly by reductive elimination to give $[PtCl_2(^tbu_2bpy)]$ and $[Me(X)C{=}NMe_2]$-Cl (X = H and Cl, respectively). We propose that the lower stability of **1** and **2** compared to **3** and **4** is due to the lower electron density at the metal center,[5h,32] when a strongly σ-donating methyl group in **3** or **4** is replaced by an electronegative chloro ligand. The reductive elimination of MeCl (or ethane, for **3** and **4**), or the migration of a methyl ligand onto the carbene carbon atom is never observed for any of the complexes prepared in this work.

The bonding of the carbene ligand to the cationic platinum(IV) center in complexes **1–4** can be rationalized by considering the resonance hybrid deriving from the contributing forms depicted in Figure 3. NMR (^1H and $^{13}C\{^1H\}$) and IR spectroscopy, and the X-ray structure determination of **1** show that canonical form (II) makes a high contribution to the hybrid, with the NMe_2 substituent providing significant stabilization to the electrophilic carbene carbon atom by p_π–p_π bonding.

(29) Trefonas, L. M.; Flurry Jr., R. L.; Majeste, R.; Meyers, E. A.; Copeland, R. F. *J. Am. Chem. Soc.* **1966**, *88*, 2145.
(30) Allen, P. W.; Sutton, L. E. *Acta Crystallogr.* **1950**, *3*, 46.
(31) Smith, T. D. *J. Chem. Soc. A* **1966**, 841.

(32) For example, see: (a) Collman, J. P.; Hegedus, L. S.; Norton, J. R.; Finke, R. G. *Principles and Applications of Organotransition Metal Chemistry*; University Science Books: Mill Valley, CA, 1987; p 324. (b) Clark, H. C.; Manzer, L. E. *Inorg. Chem.* **1973**, *12*, 362.

The products **1** and **2** contain a chloro ligand both *cis* and *trans* to the carbene ligand, and so it is not possible to determine whether they are formed by *cis* or *trans* oxidative addition. However, it is clear that **3** and **4a** are formed by *cis*-oxidative addition and that **4b** is formed by *trans*-oxidative addition. What does this tell us about the mechanism? It is known that most alkyl halides react with [$PtMe_2$(diimine)] complexes by the S_N2 mechanism and that *trans*-oxidative addition occurs, sometimes with subsequent stereochemical change.[33] Complexes **4a** and **4b** do not interconvert readily, so they must be formed by competitive pathways. The *cis* stereochemistry in the formation of **3** and **4a** is most easily rationalized by a concerted mechanism, as proposed for oxidative addition of aryl halides to [$PtMe_2$(diimine)] complexes.[13c] Clearly **4b** could be formed by a polar S_N2 mechanism, analogous to that established for alkyl halide addition.[34]

Addition of nucleophiles to **1**–**4** leads to their decomposition by reductive elimination. For example, reaction of MX (M = Na or Li; X = nucleophile) with **3** leads to rapid reductive elimination to give [$PtMe_2$(^{t}bu$_2$bpy)], MCl (M = Na, Li) and [H(X)C=NMe_2]Cl (X = nucleophile). A proposed mechanism is shown in Scheme 1. The nucleophile is expected to add readily to the highly electrophilic carbene carbon atom of **3** to give the aminoalkylplatinum(IV) intermediate **5**, but this must undergo rapid reductive elimination, with regeneration of an iminium salt and [$PtMe_2$(^{t}bu$_2$bpy)]. Attempts to detect **5** by low-temperature NMR spectroscopy were unsuccessful, and it must be a very short-lived intermediate. This result is similar to the reaction of "Fischer-type" aminocarbene complexes of the type [M{CR(NR′R″)}$(CO)_5$] (M = Cr, W; R = alkyl, aryl; R′ = R″ = H, alkyl) with HX (X = Cl, Br) to give the iminium salt [$MX(CO)_5$][H(R)C=NR′R″].[35]

In conclusion, this work demonstrates that the electron-rich [$PtMe_2$(^{t}bu$_2$bpy)] gives stable aminocarbene complexes of platinum(IV) by the very easy oxidative addition of chloroiminium salts and that the products are very reactive toward nucleophiles.

Acknowledgment. We thank the NSERC (Canada) for financial support to R.J.P. and a Canada International Fellowship to L.M.R.

Supplementary Material Available: A summary of crystallographic data and experimental details, and tables of additional interatomic distances and angles, atomic anisotropic displacement parameters, positional parameters for the hydrogen atoms, torsion angles for non-hydrogen atoms, and selected weighted least-squares planes (7 pages). Ordering information is given on any current masthead page.

OM940757X

(33) For example, see: (a) Monaghan, P. K.; Puddephatt, R. J. *J. Chem. Soc., Dalton Trans.* **1988**, 595. (b) Crespo, M.; Puddephatt, R. J. *Organometallics* **1987**, *6*, 2548. (c) Jawad, J.; Puddephatt, R. J. *J. Organomet. Chem.* **1976**, *117*, 297. (d) Jawad, J.; Puddephatt, R. J. *J. Chem. Soc., Dalton Trans.* **1977**, 1466. (e) Kuyper, J. *Inorg. Chem.* **1977**, *16*, 2171. (f) Stille, J. K. In *The Nature of the Metal–Carbon Bond*; Hartley, F. R., Patai, S., Eds.; Wiley: New York, 1985; Vol. 2, p 625.

(34) A systematic study of the product ratio **4a**:**4b** as a function of solvent polarity might provide useful evidence on mechanism but the choice of solvents is very restricted. Thus the chloroiminium salts are insoluble in nonpolar solvents like benzene, and they react with polar solvents like acetone or acetonitrile.

(35) Fischer, E. O.; Schmid, K. R.; Kalbfus, W.; Kreitner, C. G. *Chem. Ber.* **1973**, *106*, 3893.

Synthesis and Reactivity of Rhenium(III) Sulfido Bis(acetylene) Iodide Complexes[1]

Sam K. Tahmassebi and James M. Mayer*

Department of Chemistry, University of Washington, Seattle, Washington 98195

Received October 7, 1994®

Rhenium(III) sulfido bis(acetylene) iodide complexes, $Re(S)I(RC{\equiv}CR)_2$ (R = Et (**2a**); R = Me (**2b**)), have been synthesized by addition of boron sulfide, B_2S_3, to the corresponding oxo compounds $Re(O)I(RC{\equiv}CR)_2$ (R = Et (**1a**); R = Me (**1b**)) in methylene chloride. The solid-state structure of **2b** contains pseudotetrahedral molecules, with the vertices occupied by sulfur and iodine atoms and the centroids of the acetylenes, very similar to the structure of the oxo precursor **1b**. The spectral and physical properties of **2** are also quite similar to those of **1**. The sulfido complexes are much less stable than their oxo analogs, decomposing at 25 °C over a few days. Reactions occurring at the sulfido ligand of **2** are quite similar to those involving the oxo ligand of **1**. However, reagents that replace the iodide ligand in **1** for the most part cause decomposition of the sulfido complexes **2**. The sulfido–ethyl complex $Re(S)Et(MeC{\equiv}CMe)_2$ is formed at low temperatures from $Re(O)Et(MeC{\equiv}CMe)_2$ and B_2S_3 but decomposes within minutes at 25 °C. Crystal data for **2b**: $C_8H_{12}IReS$; orthorhombic, $Pna2_1$; a = 7.213(1) Å, b = 10.859(2) Å, c = 14.258(2) Å, V = 1116.8(6) Å^3; Z = 4.

The chemistry of transition-metal complexes with terminal sulfido ligands ($L_nM{=}S$) is quite unexplored compared to that of related metal–terminal oxo species.[2,3] This is especially true of their organometallic chemistry, which is extensive for oxo derivatives[4] but is limited to a handful of sulfido complexes: some cyclopentadienyl compounds, two sulfido–acetylene complexes, and a few other species.[5] We have explored the chemistry of rhenium(III) oxo bis(acetylene) complexes in some detail, starting from the iodide derivatives $Re(O)I(RC{\equiv}CR)_2$ (R = Et (**1a**); R = Me (**1b**)).[6] The iodide ligand can be converted into hydride, alkyl, acyl, alkoxide, carboalkoxy, carboxylate, and other ligands, including sulfhydryl, –SH. The oxo–sulfhydryl complex $Re(O)SH(RC{\equiv}CR)_2$ does not rearrange to a sulfido–hydroxide species such as $[Re(S)OH(RC{\equiv}CR)_2]$,[6c] though the analogous tautomerization of $Re(O)(OH)(MeC{\equiv}CMe)_2$ occurs within 1 day at ambient temperatures.[6d] We report here a direct route to sulfido complexes in this system, by replacement of the oxo ligand in **1** with B_2S_3. The characterization and the reactivity of the resulting rhenium(III) sulfido bis(acetylene) iodide complexes, $Re(S)I(RC{\equiv}CR)_2$ (R = Et (**2a**); R = Me (**2b**)), are discussed.

Results and Discussion

The sulfido complexes **2** are rapidly formed on reaction of $Re(O)I(RC{\equiv}CR)_2$ (**1**) with excess boron sulfide, B_2S_3, in CH_2Cl_2 (eq 1).[7] Analogous reactions with hex-

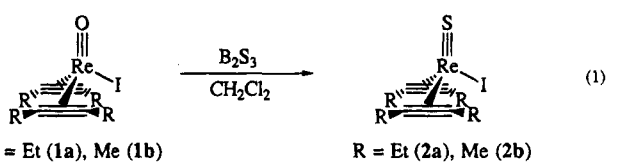

amethyldisilathiane ($[Me_3Si]_2S$) and Lawesson's reagent ($[ArP(S)(\mu\text{-}S)]_2$)[8] did not give any **2**, although addition of trace amounts of water to a mixture of hexamethyl-

® Abstract published in *Advance ACS Abstracts*, January 15, 1995.

(1) Low-Valent Rhenium-Oxo Compounds. 15. Part 14: Reference 6j.

(2) Metal sulfido compounds: (a) Rice, D. A. *Coord. Chem. Rev.* **1978**, *25*, 199. (b) Müller, A.; Diemann, E.; Jostes, R.; Bögge, H. *Angew. Chem., Int. Ed. Engl.* **1981**, *20*, 934. (c) Müller, A.; Diemann, E. In *Comprehensive Coordination Chemistry*; Wilkinson, G., Ed.; Pergamon Press: Oxford, U.K., 1987; Vol. 2; pp 515–550.

(3) Metal oxo compounds: (a) Nugent, W. A.; Mayer, J. M. *Metal-Ligand Multiple Bonds*; Wiley: New York, 1988. (b) Kochi, J. K.; Sheldon, R. A. *Metal-Catalyzed Oxidation of Organic Compounds*; Academic Press: New York, 1981. (c) Holm, R. H. *Chem. Rev.* **1987**, *87*, 1401. Holm, R. H.; Donahue, J. P. *Polyhedron* **1993**, *12*, 571–589. (d) Bottomley, F.; Sutin, L. *Adv. Organomet. Chem.* **1988**, *28*, 339. (e) Herrmann, W. A. *Angew. Chem., Int. Ed. Engl.* **1988**, *27*, 1297.

(4) See refs 3d,e and 6e for leading references.

(5) (a) Morrow, J. R.; Tonker, T. L.; Templeton, T. L. *Organometallics* **1985**, *4*, 745. (b) Tanner, L. D.; Haltiwanger, R. C.; Rakowski-Du Bois, M. *Inorg. Chem.* **1988**, *27*, 1741. (c) Su, F.-M.; Bryan, J. C.; Jang, S.; Mayer, J. M. *Polyhedron* **1989**, *8*, 1261. (d) Ma, Y.; Faller, J. W. *Organometallics* **1989**, *8*, 609. (e) Feng, S. G.; Gamble, A. S.; Templeton, T. L. *Organometallics* **1989**, *8*, 2024. (f) Tremel, W.; Hoffmann, R.; Jemmis, E. D. *Inorg. Chem.* **1989**, *28*, 1213. (g) Faller, J. W.; Kucharcyzk, R. R.; Ma, Y. *Inorg. Chem.* **1990**, *29*, 1662. (h) Gelletti, P. F.; Fenrec, D. A.; Keen, F. I.; Brown, T. M. *Inorg. Chem.* **1992**, *31*, 4008. (i) Carney, M. J.; Walsh, P. J.; Hollander, F. J.; Bergman, R. G. *Organometallics* **1992**, *11*, 761. (j) Tatsumi, K.; Inoue, Y.; Kawaguchi, H.; Kobsaka, M.; Nakamura, A.; Cramer, R. E.; Van Doorne, W.; Taogoshi, G. J.; Richmann, P. N. *Organometallics* **1993**, *12*, 352. (k) Rau, M. S.; Kretz, C. M.; Geoffrey, G. L.; Rheingold, A. L. *Organometallics* **1993**, *12*, 3447. (l) Brunner, H.; Kubicki, M. M.; Leblanc, J.-C.; Moise, C.; Volpato, F.; Wachter, J. *J. Chem. Soc., Chem. Commun.* **1993**, 851. (m) Shapley, P. A.; Liang, H.-C.; Shuster, J. M.; Schwab, J. J.; Zhang, N.; Wilson, S. R. *Organometallics* **1994**, *13*, 3351.

(6) (a) Mayer, J. M.; Thorn, D. L.; Tullip, T. H. *J. Am. Chem. Soc.* **1985**, *107*, 7454. (b) Mayer, J. M.; Tulip, T. H.; Calabrese, J. C.; Valencia, E. *J. Am. Chem. Soc.* **1987**, *109*, 157. (c) Erikson, T. K. G.; Bryan, J. C.; Mayer, J. M. *Organometallics* **1988**, *7*, 1930. (d) Erikson, T. K. G.; Mayer, J. M. *Angew. Chem., Int. Ed. Engl.* **1988**, *27*, 1527. (e) Spaltenstein, E.; Erikson, T. K. G.; Critchlow, S. C.; Mayer, J. M. *J. Am. Chem. Soc.* **1989**, *111*, 617. (f) Manion, A. B.; Erikson, T. K. G.; Spaltenstein, E.; Mayer, J. M. *Organometallics* **1989**, *8*, 1871. (g) Spaltenstein, E.; Mayer, J. M. *J. Am. Chem. Soc.* **1991**, *113*, 7744. (h) Conry, R. R.; Mayer, J. M. *Organometallics* **1993**, *12*, 3179. (i) Tahmassebi, S. K.; Conry, R. R.; Mayer, J. M. *J. Am. Chem. Soc.* **1993**, *115*, 7553. (j) Cundari, T. R.; Conry, R. R.; Spaltenstein, E.; Critchlow, S. C.; Hall, K. A.; Tahmassebi, S. K.; Mayer, J. M. *Organometallics* **1994**, *13*, 322.

(7) For other examples of the use of B_2S_3 to convert metal–oxo to metal–sulfido groups, see ref 5g and: (a) Young, C. G.; Roberts, S. A.; Ortega, R. B.; Enemark, J. H. *J. Am. Chem. Soc.* **1987**, *109*, 2938. (b) Eagle, A. A.; Tiekink, E. R. T.; Young, C. G. *J. Chem. Soc., Chem. Commun.* **1991**, 1746.

0276-7333/95/2314-1039$09.00/0

Table 1. Crystallographic Data for Re(S)I(MeC≡CMe)$_2$ (2b)

empirical formula	$C_8H_{12}IReS$
fw	453.3
cryst syst	orthorhombic
space group	$Pna2_1$
a, Å	7.213(1)
b, Å	10.859(2)
c, Å	14.258(2)
V, Å^3	1116.8(6)
D_{calcd}, g/cm^3	2.696
$F(000)$	816
radiation	Mo Kα (λ = 0.710 73 Å)
2θ range, deg	$2 \leq 2\theta \leq 50$
no. of rflns collected	2505
no. of indep rflns	1956 (R_{int} = 2.43%)
no. of obsd rflns	1705 ($F > 4\sigma_F$)
R, %	2.65
R_w, %	3.90
GOF	0.87
data-to-param ratio	17.0:1
μ(Mo Kα), mm^{-1}	13.776

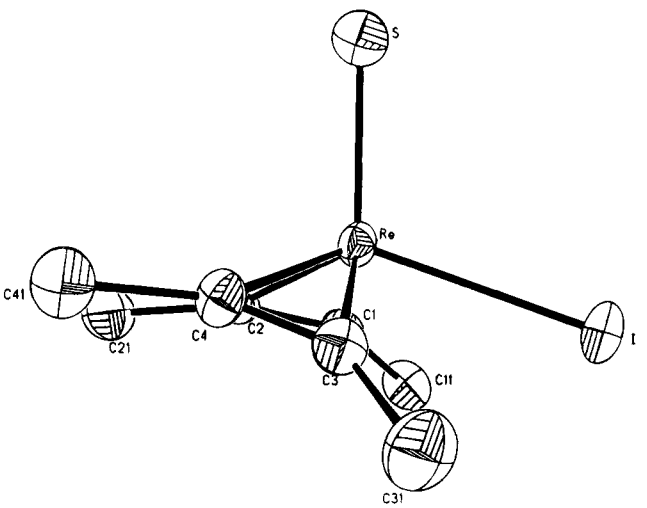

Figure 1. ORTEP diagram of Re(S)I(MeC≡CMe)$_2$ (**2b**).

disilathiane and **1** does slowly form **2**, presumably due to the reaction of H_2S with **1** (see below, eq 2). After filtration and removal of the volatiles, sublimation at 50 °C gives pure samples (by NMR) of the sulfido complexes in 40–50% yield. The synthesis is touchy, however, and often fails to give any usable product. The 3-hexyne derivative **2a** is isolated as a red-orange oil, while the 2-butyne analog **2b** is a red solid. The oxo complexes **1** have the same physical properties: ready sublimation at slightly above room temperature, with the hexyne complex a yellow oil and the butyne complex a yellow solid.

Complex **2b** crystallizes in an orthorhombic space group (Table 1) upon slow evaporation of a saturated pentane solution. The solid-state structure of **2b** reveals isolated pseudotetrahedral molecules (Figure 1), with the vertices defined by the sulfur and iodine atoms and the centroids of the acetylene ligands. The structure could also be viewed as a pentagonal pyramid with an apical multiple bond. Both the overall structure and the bond lengths and bond angles of **2b** very closely resemble those of **1b** (Table 2). All of the analogous bond lengths are the same within 3σ error bars (except Re=S vs Re=O), and all of the analogous angles are within 4°.[6a] For instance, the Re–C distances in **2b** vary from 2.023(11) to 2.036(9) Å, versus 2.038(5)–2.066(5) Å in **1b**. The most significant difference between the two complexes is that the plane described by the four acetylene carbons in the basal plane is more canted in **2b** than in **1b**: the normal to the C_4 plane makes an angle of 16.4° with the Re–S bond in **2b** vs the analogous angle of 9.3° in **1b**. The Re–S bond length of 2.082(3) Å in **2b** is at the short end of the reported range of rhenium–sulfido distances,[9] from 2.075(4) Å in Re(S)(S$_4$)$_2$[9a] to 2.126(4) Å in [ReS$_4$][NEt$_4$].[9b]

NMR spectra of **2a** and **2b** indicate C_s symmetry in solution, consistent with the geometry found in the solid

Table 2. Selected Bond Length and Bond Angle Comparison between Re(S)I(MeC≡CMe)$_2$ (2b) and Re(O)I(MeC≡CMe)$_2$ (1b)

Bond Lengths (Å)

bond	X = S	X = O
Re–X	2.082(3)	1.697(3)
Re–I	2.704(9)	2.691(1)
Re–C1	2.036(9)	2.061(5)
Re–C2	2.035(10)	2.038(5)
Re–C3	2.037(10)	2.066(5)
Re–C4	2.023(11)	2.040(5)
C1–C2	1.274(16)	1.278(7)
C3–C4	1.267(16)	1.288(7)
C1–C11	1.513(15)	1.485(7)
C2–C21	1.487(14)	1.494(7)
C3–C31	1.502(16)	1.459(7)
C4–C41	1.502(16)	1.470(7)

Bond Angles (deg)

angle	X = S	X = O
X–Re–I	108.5(1)	109.4(1)
X–Re–C1	117.1(3)	114.8(2)
X–Re–C2	109.0(3)	109.1(2)
X–Re–C3	117.6(3)	114.2(2)
X–Re–C4	105.2(3)	108.8(2)
I–Re–X	108.5(3)	109.4(1)
I–Re–C1	84.7(4)	85.2(1)
I–Re–C2	120.1(3)	119.6(2)
I–Re–C3	86.4(3)	85.2(1)
I–Re–C4	122.5(3)	119.7(2)
Re–C1–C11	144.6(9)	144.9(4)
Re–C2–C21	140.8(8)	141.3(4)
Re–C3–C31	144.9(8)	145.5(4)
Re–C4–C41	142.3(8)	142.2(4)
Re–C1–C2	71.6(6)	70.8(3)
Re–C3–C4	71.2(7)	70.6(3)
Re–C2–C1	71.9(6)	72.9(3)
Re–C4–C3	72.4(7)	72.8(3)
C1–C2–C21	147.2(10)	145.8(5)
C2–C1–C11	143.6(10)	144.3(5)
C3–C4–C41	145.2(11)	144.9(5)
C4–C3–C31	143.3(10)	144.0(5)

(8) (a) Ar = *p*-methoxyphenyl. Hexamethyldisilathiane has been used to convert metal–oxo to metal–sulfido groups in other systems, for instance: Dorfman, J. R.; Girerd, J. J.; Simhon, E. D.; Stack, T. D. P.; Holm, R. H. *Inorg. Chem.* **1984**, *23*, 4407. (b) Lawesson's reagent has been used to thiate organic carbonyl groups[8c–e] and in at least one instance[8f] has been used in an attempt to replace the oxo ligand of a metal complex with a sulfido ligand. (c) Scheibye, S.; Pederson, B. W.; Lawesson, S. O. *Bull. Soc. Chim. Belg.* **1978**, *87*, 229. (d) Walter, W.; Proll, T. *Synthesis* **1979**, 941. (e) Raucher, S.; Klein, P. *Tetrahedron Lett.* **1980**, *21*, 4061. (f) Housmekerides, C. E.; Ramage, D. L.; Kretz, C. M.; Shontz, J. T.; Pilato, R. S.; Geoffroy, G. L.; Rheingold, A. L.; Haggerty, B. S. *Inorg. Chem.* **1992**, *31*, 4453.

(9) Rhenium–sulfido structures located using the Cambridge Structural Database: (a) Blower, P. J.; Dilworth, J. R.; Hutchinson, J. P.; Zubieta, J. A. *Inorg. Chim. Acta* **1982**, *65*, L225. (b) Müller, A.; Krickemeyer, E.; Bogge, H.; Perk, M.; Rehder, D. *Chimia* **1986**, *40*, 50. This paper reports the structure of Re(S)(S$_4$)$_2$ similar to that reported in ref 9d but with a longer Re=S bond length of 2.091(4) Å. (c) Scattergood, C. D.; Garner, C. D.; Clegg, W. *Inorg. Chim. Acta* **1987**, *132*, 161. (d) Cotton, F. A.; Kibala, P. A.; Matusz, M. *Polyhedron* **1988**, *7*, 83. (e) Massa, M. A.; Rauchfuss, T. B.; Wilson, S. R. *Inorg. Chem.* **1991**, *30*, 4667.

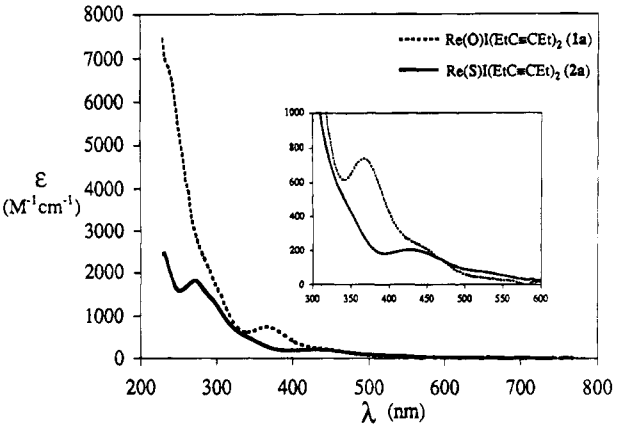

Figure 2. UV/vis spectra of Re(S)I(EtC≡CEt)$_2$ (**2a**) and Re(O)I(EtC≡CEt)$_2$ (**1a**) in CH_2Cl_2.

state for **2b**. The NMR spectra of **2a**, for instance, show two sets of ethyl resonances, for the ethyl groups proximal and distal to the iodide, with diastereotopic methylene hydrogens (multiplets at 2.71 and 2.96 ppm). The observation of diastereotopic hydrogens indicates that, as observed for the oxo complexes **1**, the acetylene ligands are not rotating on the NMR time scale. The IR spectrum of **2a** is quite similar to that of **1a**,[6a] except that the strong band at 971 cm^{-1} due to the Re≡O stretch has been replaced by a band at 531 cm^{-1} that we assign as ν(Re≡S). The rhenium–sulfido stretch is at the high end of the range of reported values, 486–525 cm^{-1}.[9]

The UV/vis spectra of compounds **1a** and **2a** are quite similar (Figure 2). The spectrum of the yellow oxo species **1a** (4.0×10^{-5} M in CH_2Cl_2) shows two bands in the UV region along with a shoulder in the visible region (see the Experimental Section for peak positions). The spectrum of the red sulfido complex **2a** (4.8×10^{-4} M in CH_2Cl_2) has basically the same features as that of the oxo compound but the bands are weaker and red-shifted. The shift to lower energy is presumably due to the weaker metal–sulfur vs metal–oxygen π-bonding.

The similarity of the sulfido and oxo complexes, in their structures, physical properties, and spectroscopic data, suggests that their electronic structures are similar as well. The chemical shifts of the alkyne carbons, which reflect the amount of alkyne-to-rhenium π-donation, are close: the resonances for the sulfido complexes are 9 and 13 ppm downfield from the corresponding resonances in the oxo species (compare δ 150.9, 159.3 for **2a** vs δ 142.0, 146.3 for **1a**). Thus, the bonding in the sulfido complexes appears to be similar to that in the oxo species, with a Re≡S triple bond and three-electron-donor alkyne ligands.[6a,j] The small downfield shift of the alkyne carbons may indicate more alkyne π-donation, perhaps to compensate for poorer π-donation from sulfide as compared with oxide. The same interaction might also account for the slightly lower acetylenic stretch in **2a** (1740 cm^{-1}) vs **1a** (1783 cm^{-1}). Formulation as a rhenium–sulfur triple bond is also indicated by the short Re–S distance and the high IR stretching frequencies.

The sulfido complexes are substantially less thermally stable than their oxo counterparts. Crystalline **2b** decomposes over a few days at room temperature under an inert atmosphere to uncharacterized black solids, while **1b** is indefinitely stable on the benchtop. Similarly, solutions of **1b** can be heated for at least 1 h at 150 °C in xylene solution without significant decomposition but **2a** and **2b** decompose to black material within 4–5 days in solution at ambient temperatures, without formation of any free alkyne. In the presence of added alkyne, however, solutions of **2** are inert to decomposition even when heated to 80 °C for 1 week. Under these conditions the 3-hexyne complex **2a** does not undergo ligand exchange in the presence of 2-butyne, indicating that decomposition does not occur by preequilibrium dissociation of alkyne. The lack of alkyne dissociation from **2a** at 80 °C contrasts with the slow exchange of alkynes in **1b** at this temperature.[6a] The inhibition of dissociation by added alkyne is puzzling, perhaps indicating that decomposition is autocatalytic or is mediated by an impurity. Consistent with these suggestions, decomposition of **2a** is faster in more concentrated solutions.

Scheme 1. Thermochemical Cycle for Conversion of Oxo to Sulfido Complexes

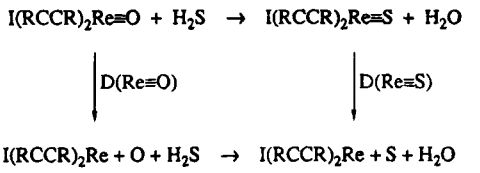

The oxo complex **1a** reacts slowly with H_2S in benzene to give the sulfide compound **2a** and water (eq 2). This

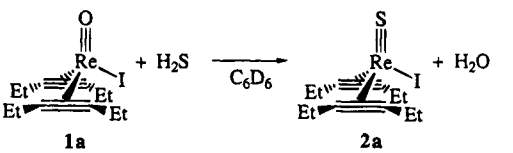

(2)

reaction is complicated by the further reaction of **2a** with H_2S to give a variety of products. The isolated sulfido complex **2a** does not react with H_2O in benzene solution. These observations suggest that reaction 2 is exothermic ($\Delta H < 0$), as there should be little entropic driving force. A thermochemical analysis of the reaction (Scheme 1) suggests that the rhenium–oxo bond is at most 46 kcal/mol stronger than the rhenium–sulfido bond, since it is 46 kcal/mol enthalpically uphill to convert S + H_2O to O + H_2S (in the gas phase).[10] This estimate assumes that solvation effects are small, which is reasonable in benzene solution.

Both the sulfido and the oxo complexes are unreactive toward Al_2Se_3 and Al_2Te_3 in THF, CD_2Cl_2, MeCN, and MeCN/D_2O. We ascribe the lack of reactivity of aluminum reagents to their very low solubility and their more refractory nature compared with B_2S_3. Complexes **1** and **2** are also unreactive toward aniline, *tert*-butylamine, or methylamine. They both, however, react with ammonia to give uncharacterized compounds.

The oxo and sulfido complexes **1** and **2** exhibit very similar reactivity toward phosphines, governed by the basicity of the latter reagents. Both **1a** and **2a** are unreactive toward PPh_3 but react immediately with the more basic PMe_3 to form $SPMe_3$ or $OPMe_3$ and a number of uncharacterized species (reactions performed in the presence of added alkyne). The complexes react cleanly with $PMePh_2$ in the presence of added alkyne

(10) Based on gas phase heats of formation from: *JANAF Thermochemical Tables*, 3rd ed.; *J. Phys. Chem. Ref. Data, Suppl.* **1985**, *14*.

to produce the expected rhenium(I) tris(acetylene) iodide complexes ReI(RC≡CR)$_3$[6f,h] and the corresponding phosphine chalcogenide, identified by NMR (eq 3). It is

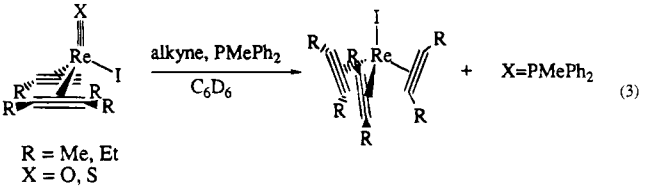

(3)

surprising that the sulfido complex, with its weaker rhenium–chalcogen bond, exhibits the same reduction chemistry as the related oxo compound. The relative phosphine reactivity, PMe_3 > $PMePh_2$ > PPh_3, follows the same order as the P–O bond strengths.[3c] Reoxidation of rhenium(I) to rhenium(III) has not been observed: the tris(acetylene)–triflate complex ReOTf(RC≡CR)$_3$ (triflate = OTf = CF_3SO_3) reduces propylene sulfide to propylene, but no characterizable rhenium product is observed.

The cyclic voltammogram of **2a** in MeCN shows irreversible reductions at −1.0 and −2.3 V (vs Ag/Ag$^+$/MeCN). The oxo complex **1b** is harder to reduce, with an initial irreversible reduction at −1.5 V, followed by a reversible reduction at −2.5 V.[11] Reduction of **1b** forms the rhenium(II) dimer [Re(O)(MeC≡CMe)$_2$]$_2$,[6g] which is responsible for the reversible wave at −2.5 V;[11] there is no evidence for analogous sulfido dimers. Compound **2a** also shows two irreversible oxidation waves, at +0.2 and +0.5 V. These most likely arise from the oxidation of the sulfido ligand, since the oxo species show no oxidation waves to the solvent limit.

Much of the rich chemistry of compounds **1** results from substitution of the iodide ligand.[6] Such reactions are not, however, successful for the sulfido complex. Reagents that exchange the iodide ligand of **1** for other ligands, such as $NaBH_4$,[12] $NaBH_3CN$,[12] Bu_3SnH,[6e] Et_2Zn,[6e] TlOEt,[6c] TlO_2CH,[6c] and $AgSbF_6$/pyridine,[6b] cause the decomposition of **2** to black material. The first four reagents can also act as reductants, and the observed decomposition is likely due to the more facile reduction of **2a** as compared with **1a**. The last three reagents are soft Lewis acids, which attack specifically at the iodide ligand in **1a**. But the sulfido ligand in **2a** is also a potential site of attack by Ag$^+$ or Tl$^+$, which could lead to decomposition. However, harder Lewis acids such as $AlMe_3$, $AlCl_3$, and LiOEt also cause the decomposition of the sulfido complex. The iodide ligand is also resistant to exchange in the presence of NMe_4Cl.

Since direct derivatization of the sulfido complex appears impractical, we have explored oxo/sulfido exchange on other rhenium(III) compounds. The oxo–ethyl complex Re(O)Et(MeC≡CMe)$_2$[6e] (**3b**) reacts with B_2S_3 in CD_2Cl_2 at 240 K to form the sulfido–ethyl complex Re(S)Et(MeC≡CMe)$_2$ (**4b**). Complex **4b** is stable for a few hours at 240 K but decomposes within minutes at room temperature (in contrast to the only 50% decomposition of **3b** after 21 days at 120 °C[6e]). The characterization of **4b** is based on ^{1}H and ^{13}C NMR spectra at 240 K, which are only slightly shifted from the spectra of **3b**. The acetylenic ^{13}C chemical shifts are roughly 10 ppm farther downfield in the sulfido complex, as noted for **2** vs **1**. The oxo–hydride species Re(O)H(EtC≡CEt)$_2$[6e,i] quickly decomposes in the presence of B_2S_3 even at low temperatures. Other transition-metal sulfido–alkyl species have been synthesized by exchange of oxide or chloride ligands for sulfide using B_2S_3[5g] or Li_2S,[5m] although these are not always successful.[7b]

In sum, the unusual organometallic sulfido complexes Re(S)I(RC≡CR)$_2$ have been prepared by replacement of the oxo group in Re(O)I(RC≡CR)$_2$ with B_2S_3. The structure and spectroscopic properties of the sulfido complexes are very similar to those of the oxo precursors, suggesting similar electronic structures. The reactivities of the two species at the chalcogen site are also very similar. However, the reagents that replace the iodide ligand in the oxo compound with other ligands cause the decomposition of the sulfido–iodide complex. Re(S)Et(MeC≡CMe)$_2$ has been generated by treatment of the oxo analog with B_2S_3 at 240 K, but it decomposes rapidly at ambient temperatures.

Experimental Section

Syntheses were performed using standard vacuum line and glovebox techniques except where noted. Solvents were dried and deoxygenated according to standard methods.[13] B_2S_3, Al_2Se_3, and Al_2Te_3 were used as received from Alfa. Re(O)I(RC≡CR)$_2$ (UV/vis data reported below),[6f] Re(O)Et(MeC≡CMe)$_2$,[6e] Re(O)H(EtC≡CEt)$_2$,[6e] and ReOTf(RC≡CR)$_3$[6h] were prepared as previously described. NMR spectra were taken on a Bruker AF300 or AC200 spectrometers. ^{1}H and ^{13}C chemical shifts are reported in ppm downfield of $SiMe_4$ and are referenced to the solvent peaks; they are reported as δ (multiplicity, coupling constant, number of protons, assignment). IR spectra were taken on a Perkin-Elmer 1604 FT-IR spectrometer and are reported in cm^{-1}. Mass spectra were taken on a Kratos Analytical instrument using the direct inlet probe method and are reported in *m/e* units. UV/vis spectra were taken on a Hewlett-Packard 8452A diode array spectrophotometer, using quartz cells sealed to a Teflon needle valve, and are reported in nm: λ_{max} (ϵ, M^{-1} cm^{-1}). The cyclic voltammogram of **2a** was obtained in CH_3CN using a Bioanalytical Systems B/W 100 electrochemical analyzer with *iR* compensation, a Ag/$AgNO_3$/CH_3CN reference electrode, and 0.05 M Bu_4NPF_6 as the electrolyte.

Some reactions were performed in sealed NMR tubes and followed by the change in their NMR spectra. Reagents and solvent were added to NMR tubes sealed to a ground glass joint and fitted with a needle valve. The tubes were cooled to 77 K, degassed, and sealed with a torch and were thawed under a stream of acetone.

Re(S)I(EtC≡CEt)$_2$ (2a). A mixture of 0.10 g (0.21 mmol) of Re(O)I(EtC≡CEt)$_2$ (**1a**) and 0.021 g of B_2S_3 (0.18 mmol, 0.85 eq, 2.6 equiv of S) was stirred in 15 mL of CH_2Cl_2 for 1 h. The solvent was removed in vacuo, 20 mL of pentane was transferred in, the mixture was filtered, and solvent was removed again. Sublimation at 50 °C gave the product as a reddish orange oil on the probe. Yield: 0.052 g (49%). While **2a** (and **2b**) decomposes within 4 days at ambient temperatures, they can be stored for months in a −11 °C freezer under an inert atmosphere. ^{1}H NMR (C_6D_6): 1.10, 1.12 (t, 7 Hz, each 6 H, $CH_3CH_2C{\equiv}CCH_2CH'_3$); 2.71, 2.96 (m, each 4 H, $CH_3CHH'C{\equiv}CCH''H'''CH'_3$). ^{13}C{^{1}H} NMR ($C_6D_6$): 13.1, 14.6 ($CH_3CH_2C{\equiv}CCH_2C'H_3$); 25.8, 28.3 ($CH_3CH_2C{\equiv}CC'H_2CH_3$); 150.9, 159.3 ($CH_3CH_2C{\equiv}C'CH_2CH_3$). MS: 510/508, [M]$^+$. IR (Nujol, KBr): 2960, 2360, 1783, 1740 w ν(C≡C); 1452, 1368,

(11) Conry, R. R.; Mayer, J. M. Unpublished results, and ref 6a.
(12) Tahmassebi, S. K.; Mayer, J. M. Unpublished results.

(13) (a) Perrin, D. D.; Armarego, W. L. F. *Purification of Laboratory Chemicals*, 3rd ed.; Pergamon: New York, 1988. (b) Fieser, L. F.; Fieser, M. *Reagents for Organic Synthesis*; Wiley: New York, 1967.

1295, 1253, 1060, 934, 721, 531 m ν(Re≡S). UV/vis (CH_2Cl_2): 272 (1.8×10^3); 298 (1.3×10^3), shoulder; 432 (2.1×10^2); 524 (74), shoulder.

Re(S)I(MeC≡CMe)$_2$ (2b). Following a procedure analogous to that used for **1a**, 0.050 g (0.11 mmol) of Re(O)I(MeC≡CMe)$_2$ (**1b**), 0.009 g of B_2S_3 (0.08 mmol, 0.7 equiv, 2 equiv of S), and 15 mL of CH_2Cl_2 gave 0.021 g (42%) of red solid (**2b**) after sublimation, pure by NMR. The thermal instability of **2b** has prevented us from obtaining suitable analytical data. ^{1}H NMR (C_6D_6): 2.23, 2.92 (q, 1 Hz, each 6 H, $CH_3C{\equiv}CCH'_3$). $^{13}C\{^1H\}$ NMR (C_6D_6): 17.2, 19.3 ($CH_3C{\equiv}CC'H_3$); 147.0, 155.3 ($CH_3C{\equiv}C'CH_3$). MS: 454/452, $[M]^+$. IR (Nujol, KBr): 1720 w ν(C≡C); 1255, 1155, 1090, 1020, 797, 720, 620, 532 m ν(Re≡S).

Re(S)Et(MeC≡CMe)$_2$ (4b) was formed and characterized in an NMR tube. Approximately 0.03 g (0.09 mmol) of Re(O)Et(MeC≡CMe)$_2$ (**3b**) and excess B_2S_3 wee put in an NMR tube that was sealed to a ground-glass joint and attached to a Teflon needle valve. The tube was cooled to liquid-nitrogen temperature, and CD_2Cl_2 was transferred in. The tube was then sealed with a torch, thawed under a stream of acetone, mixed vigorously, and immersed immediately into a precooled (220 K) NMR probe. The probe was then warmed slightly to 240 K, and the formation of **4b** was monitored. Decomposition occurred within minutes at 25 °C. The reaction was repeated at room temperature, and after a brief period when the color of the solution changed to reddish orange, black solids began to deposit. ^{1}H NMR (CD_2Cl_2, 240 K): 2.60, 2.96 (q, 1 Hz, each 6 H, $CH_3C{\equiv}CCH'_3$); 1.39 (t, 7 Hz, 3 H, $ReCH_2CH_3$); 4.01 (q, 7 Hz, 2 H, $ReCH_2CH_3$). $^{13}C\{^1H\}$ NMR (CD_2Cl_2, 240 K): 9.3 ($ReCH_2CH_3$); 11.9 ($ReCH_2CH_3$); 15.9, 18.4 ($CH_3C{\equiv}CC'H_3$); 154.6, 158.8 ($CH_3C{\equiv}C'CH_3$).

X-ray Structure of Re(S)I(MeC≡CMe)$_2$ (2b). Crystals were grown by slow evaporation of a saturated pentane solution of **2b**. A red crystal of dimensions 0.1 × 0.15 × 0.2 mm was mounted, using stopcock grease, on an Enraf–Nonius CAD4 diffractometer under a cold (183 K) nitrogen stream. The data were corrected for Lorentz and polarization effects and for absorption using an empirical absorption method (μ = 13.776 mm^{-1}). The structure was solved by direct methods (SHELX). All non-hydrogen atoms were refined anisotropically, and the hydrogen atoms were fixed by a riding model at 0.96 Å. Crystal data are given in Table 1, selected bond lengths and angles are given in Table 2, and atomic coordinates along with equivalent isotropic thermal parameters are given in Table 3.

Table 3. Atomic Coordinates ($\times 10^5$) and Equivalent Isotropic Displacement Coefficients (Å$^2 \times 10^4$) for Re(S)I(MeC≡CMe)$_2$ (2b)

	x	*y*	*z*	*U*(eq)[a]
Re(1)	13 043(5)	1 362(3)	64 994	207(1)
I(1)	10 175(10)	2 881(7)	83 870(7)	311(2)
S(2)	−11 105(39)	−6 594(32)	59 768(24)	398(10)
C(1)	14 017(109)	20 091(80)	65 484(92)	240(26)
C(2)	19 062(139)	16 637(99)	57 337(68)	244(30)
C(11)	11 859(151)	32 233(95)	71 763(78)	343(40)
C(21)	26 215(157)	20 298(105)	47 959(73)	389(38)
C(3)	35 179(131)	−9 889(109)	67 275(80)	291(35)
C(4)	34 001(144)	−7 693(103)	58 571(79)	260(32)
C(31)	47 230(164)	−15 737(100)	74 626(81)	383(35)
C(41)	41 926(173)	−10 472(137)	49 058(79)	463(46)

[a] Equivalent isotropic *U*, defined as one-third of the trace of the orthogonalized $\mathbf{U}_{ij}$ tensor.

Re(O)I(EtC≡CEt)$_2$ (1a): UV/vis (CH_2Cl_2) 234 (6.9×10^3), shoulder; 368 (7.4×10^2); 444 (2.2×10^2), shoulder.

Acknowledgment. We are grateful for the help of Dr. David Barnhart with the X-ray structure and Dr. Frazier Nyasulu with cyclic voltammetry. Helpful suggestions from Drs. Seth Brown, Jerry Cook, and Keith Hall are appreciated. We thank the National Science Foundation for financial support.

Supplementary Material Available: Tables giving a structure determination summary, anisotropic displacement coefficients, and hydrogen atom coordinates (5 pages). Ordering information is given on any current masthead page.

OM940778R

Reactions of Primary Amines with (η^5-Pentadienyl)- and (η^5-Methylpentadienyl)tricarbonylmanganese Complexes. Synthesis, Characterization, and Structural Studies

Ma. Angeles Paz-Sandoval,* Rosalina Sánchez Coyotzi, and Noé Zúñiga Villarreal

Departamento de Química, Centro de Investigación y de Estudios Avanzados del Instituto Politécnico Nacional, Apartado 14-740, México, D.F. 07000, México

Richard D. Ernst and Atta M. Arif

Department of Chemistry, University of Utah, Salt Lake City, Utah 84112

Received November 18, 1994[⊗]

Reactions of primary amines with (η^5-pentadienyl)tricarbonylmanganese (**1**) have been investigated and compared with analogous secondary amine and phosphine reactions. Cyclohexylamine reacts with **1** to give the isomeric complexes [1-(cyclohexylamino)-(2−4-η^3)-pentenyl]tricarbonylmanganese, Mn[NH(C_6H_{11})(CH_2-η^3-CHCHCHCH_3)]$(CO)_3$ (**2**) and the 1-(cyclohexylamino)-(1−3-η^3)-pentenyl complex Mn[NH(C_6H_{11}) (η^3-CHCHCHCH_2CH_3)]$(CO)_3$ (**4**). In both cases, nitrogen is added regioselectively to the terminal carbon atom on the pentadienyl ligand and also becomes coordinated to the manganese atom. In the case of the isopropyl- and *tert*-butylamines, the reactions with complex **1** form exclusively [1-amino-(1−3-η^3)-pentenyl]tricarbonyl manganese complexes Mn[NH(R) (η^3-CHCHCHCH_2CH_3)]$(CO)_3$ (R = *i*-C_3H_7 (**5**), *t*-C_4H_9 (**6**)), while mixtures of Mn[NH(R) (η^3-CHCHCH$CH_2CH_2CH_3$)]$(CO)_3$ (R = *i*-C_3H_7 (**11**), *t*-C_4H_9 (**12**)) and Mn[NH(R) (η^3-C(CH_3)CHCHCH_2CH_3)]$(CO)_3$ (R = *i*-C_3H_7 (**11′**), *t*-C_4H_9 (**12′**)) regioisomers are obtained from the reaction with (η^5-methylpentadienyl)-tricarbonylmanganese (**10**), except for the case of R = cyclohexyl, from which the 1-cyclohexyl-(1−3)-η^3)-hexenyl complex **13** is obtained. The conversion from **11′**, **12′** to **11**, **12**, respectively, suggests that **11′** and **12′** are the kinetic and **11** and **12** the thermodynamic products in these reactions. Compound **2** represents a formal 1,5-addition product to the pentadienyl ligand and is structurally novel for the amine addition compounds. Its X-ray crystal analysis revealed that the cyclohexylamine group has coupled to the pentadienyl group, leading to a 1-cyclohexylamino-(2−4-η^3)-pentenyl fragment coordinated through the nitrogen atom and the allyl moiety to the manganese atom. This structure is similar to that for the phosphorus analog **3**. The crystals of **2** are orthorhombic, space group $P2_12_12_1$, with cell dimensions of a = 7.449(5) Å, b = 12.572(2) Å, c = 16.350(3) Å, and V = 1531.15 Å^3 (Z = 4). The structure was refined to discrepancy indices of R = 0.0402 and R_w = 0.0460 for 1046 reflections having $I > 3\sigma(I)$. From differences in bond lengths and angles it appears that the strain induced by coordination of the enyl−amine ligand is much lower than that resulting for the analogous enyl−phosphine complex **3**. Single-crystal X-ray diffraction studies of **5** and **6** show that their aminopentenyl ligands are bonded to manganese through an η^3 interaction and also by nitrogen coordination. Compound **5** crystallizes in the monoclinic space group $P2_1/c$, with a = 10.308(3) Å, b = 10.935(2)Å, c = 12.359(2) Å, β = 110.56(2)°, and V = 1304.39 Å^3 (Z = 4); R = 0.0306 and R_w = 0.0324 for 1614 reflections with $I > 3\sigma(I)$. Crystals of **6** are orthorhombic, space group *Pbca* with a = 7.197(1) Å, b = 18.879(2) Å, c = 20.561(3) Å, and V = 2793.83 Å^3 (Z = 8); R = 0.0524 and R_w = 0.0569 for 1037 reflections with $I > 3\sigma(I)$. The two complexes have distorted-octahedral geometries without significant differences relative to analogous secondary amine derivatives. Complexes **4**−**6** and **11**−**13** proved to be more reactive species than the corresponding aminopentenyl derivatives derived from secondary amines.

Introduction

Investigations into the reactivity of the neutral (η^5-pentadienyl)tricarbonylmanganese complex with organolithium compounds,[1] dienes,[2] secondary amines,[3] and tertiary[4] and secondary phosphines[5] have been previously reported. This complex was found to exhibit significant differences in its reactions with nucleophiles, as compared to related (η^5-cyclohexadienyl)−[1b,6] and (η^5-cycloheptadienyl)Mn$(CO)_3$[7] species. Furthermore, in

⊗ Abstract published in *Advance ACS Abstracts,* January 15, 1995.

(1) (a) Roell, B. C., Jr.; McDaniel, K. *J. Am. Chem. Soc.* **1990**, *112*, 9004. (b) Roell, B. C., Jr.; McDaniel, K.; Vaughan, W. S.; Macy, T. S. *Organometallics* **1993**, *12*, 224.

(2) Kreiter, C. G.; Lehr, K.; Heeb, G. *Z. Naturforsch.* **1991**, *46B*, 941.

(3) Zúñiga Villarreal, N.; Paz-Sandoval, M. A.; Joseph-Nathan, P.; Esquivel, R. O. *Organometallics* **1991**, *10*, 2616.

(4) Paz-Sandoval, M. A.; Powell, P.; Drew, M. G. B.; Perutz, R. N. *Organometallics* **1984**, *3*, 1026.

(5) Paz-Sandoval, M. A.; Juárez Saavedra, P.; Zúñiga Villarreal, N.; Rosales Hoz, M. J.; Joseph-Nathan, P.; Ernst, R. D.; Arif, A. M. *Organometallics* **1992**, *11*, 2467.

0276-7333/95/2314-1044$09.00/0

Scheme 1

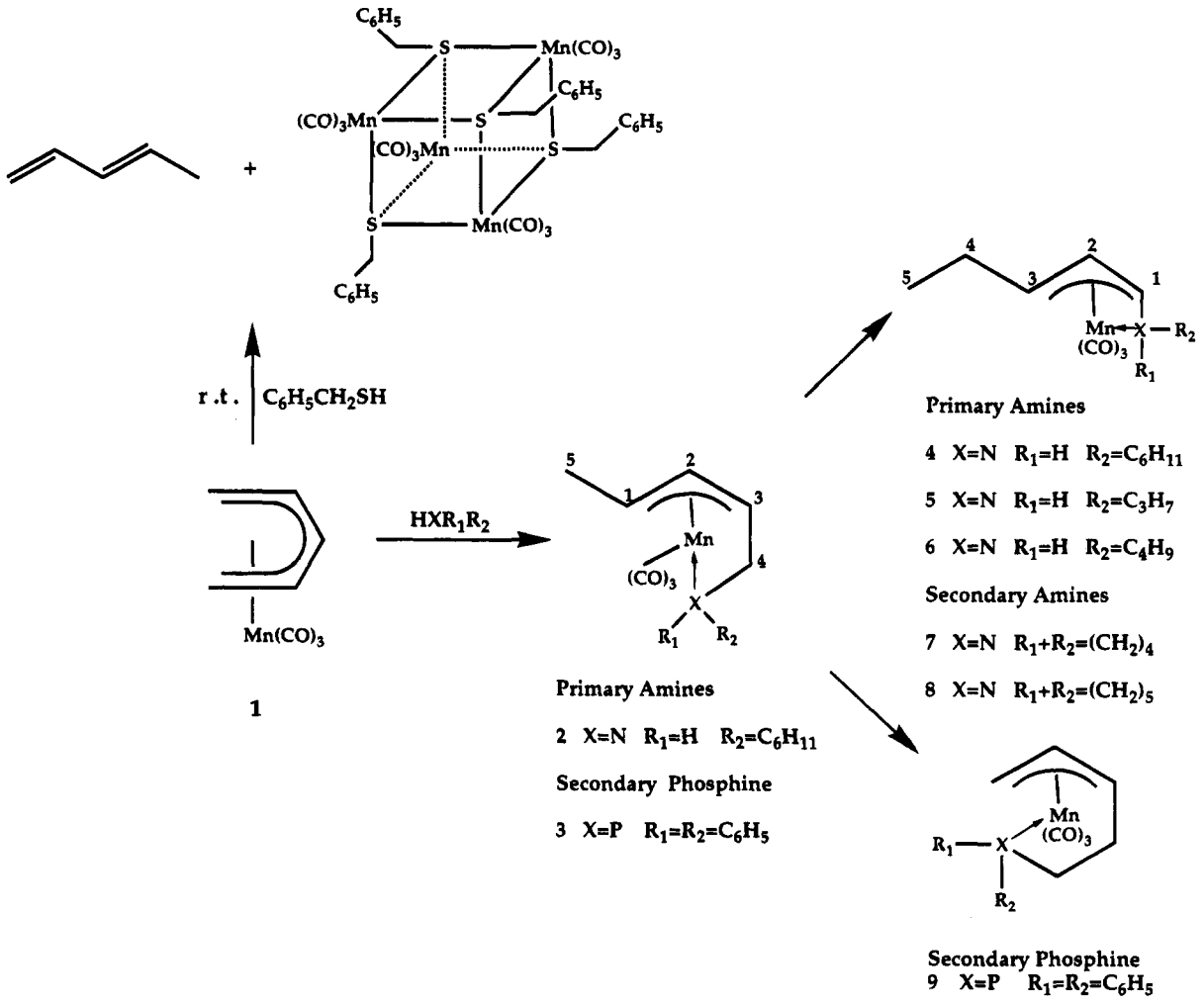

these reactions a strong dependence of the pathway upon the nature of the nucleophile utilized was clearly osberved. For cases in which the nucleophiles contained heteroatoms, the heteroatom generally became attached to both the dienyl fragment and the metal center. Notably, in earlier studies involving related acyclic ligands and heteroatom-containing nucleophiles, the heteroatom similarly became attached to both the products containing an organic acylic ligand and the metal center.[8,9] Other approaches have also led to related acyclic π-ligands incorporating heteroatoms. Various (η^5-1-azapentadienyl)Mn(CO)$_3$ complexes have been prepared from the corresponding 1-oxopentadienyl derivatives,[10] and recently some amine-substituted (η^4-oxopentadienyl)tricarbonylmanganese complexes, which have also been described as (η^4-allyl–amide)Mn(CO)$_3$, have been synthesized from the reaction of an (η^1-pentadienoyl)Mn(CO)$_5$ complex with selected amines and in the presence of an amine *N*-oxide.[11] Also, some pseudo-(α-aminoallyl)cobalt complexes Co(CO)$_3${RCHCH-CHNHR′} have been prepared from the reaction of monoaza dienes with Co$_2$(CO)$_8$ under a H$_2$ atmosphere.[12]

It was earlier demonstrated in these laboratories that C$_5$H$_7$Mn(CO)$_3$ (**1**) reacted with secondary amines[3] and diphenylphosphine[5] to yield (aminopentenyl)- or (phosphinopentenyl)tricarbonylmanganese complexes, respectively, as shown in Scheme 1. The first step in both reactions could involve addition of the nucleophilic nitrogen or phosphorus atom to a terminal carbon atom of the pentadienyl ligand in a regioselective manner. These reactions have led to a variety of new isomeric complexes having aminopentenyl or phosphinopentenyl ligands bonded to a manganese center through the heteroatom and η^3-allylic coordination involving various segments of the pentenyl chain. While secondary amines exclusively afford (1-amino-(1–3-η^3)-pentenyl)-tricarbonylmanganese complexes, such as **7** and **8**, diphenylphosphine gives isomeric [1-(diphenylphosphino)-(2–4-η^3)-pentenyl]tricarbonylmanganese (**3**) and [1-(diphenylphosphino)-(3–5-η^3)-pentenyl]tricarbonylmanganese (**9**) species (Scheme 1). The fact that neither the phosphine nor the amines produce all three possible isomers from the addition to the pentadienyl ligand

(6) (a) Padda, R. S.; Sheridan, J. B.; Chafee, K. *J. Chem. Soc., Chem. Commun.* **1990**, 1226. (b) Sheridan, J. B.; Padda, R. S.; Chafee, K.; Wang, C.; Huang, Y. *J. Chem. Soc., Dalton Trans.* **1992**, 1539.
(7) Wang, C.; Lang, M. G.; Sheridan, J. B.; Rheingold, A. L. *J. Am. Chem. Soc.* **1990**, *112*, 3236.
(8) (a) Meléndez, E.; Arif, A. M.; Ziegler, M. L.; Ernst, R. D. *Angew. Chem., Int. Ed. Engl.* **1988**, *27*, 1099. (b) Kirillova, N. I.; Gusev, A. L.; Pasynskii, A. A.; Struchkov, Y. T. *J. Organomet. Chem.* **1973**, *63*, 311. (c) Abel, E. W.; Rowley, R. J.; Mason, R.; Thomas, K. M. *J. Chem. Soc., Chem. Commun.* **1974**, 72. (d) King, R. B.; Hodges, K. C. *J. Am. Chem. Soc.* **1975**, *97*, 2702.
(9) Alper, H.; Paik, H.-N. *J. Organomet. Chem.* **1976**, *122*, C31.
(10) Cheng, M.-H.; Cheng, C.-Y.; Wang, S.-L.; Peng, S.-M.; Liu, R.-S. *Organometallics* **1990**, *9*, 1853.
(11) AbuBaker, A.; Bryan, C. D.; Cordes, A. W.; Allison, N. T. *Organometallics* **1994**, *13*, 3375.
(12) Beers, O. C. P.; Elsevier, C. J.; Ernsting, J.-M.; De Ridder, D. J. A.; Stam, C. H. *Organometallics* **1992**, *11*, 3886.

prompted us to examine the reactivity patterns for C_5H_7-$Mn(CO)_3$ with primary amines, for which it should be expected that the NH function would remain in the synthesized species. The characterization of the new isomers derived from the nucleophilic addition of primary amines, as well as their reactivity and comparison with analogous species previously reported,[3,5] form the basis of this paper.

Experimental Section

All operations were carried out under an atmosphere of dinitrogen with standard Schlenk-line techniques. Solvents were purified by conventional methods and distilled under dinitrogen prior to use. The starting materials **1**[4] and **10**[4,13] were prepared by published methods. NMR spectra were obtained with a JEOL GSX-270 spectrometer, IR spectra on a Nicolet MX-1-FT spectrophotometer, and mass spectra on a Finnigan MAT 95 instrument. Elemental analyses were performed by Oneida Research Services Inc., Whitesboro, NY.

Reaction of $C_5H_6RMn(CO)_3$ (R = H (1), CH_3 (10)) with Primary Amines (H_2NR; R = C_6H_{11}, C_3H_7, C_4H_9). Unless otherwise described below, in a typical synthesis the appropriate dry, freshly purified amine was syringed into a Schlenk tube containing a cyclohexane solution of **1** or **10**. The yellow reaction mixture was filtered into a thick-walled Pyrex ampule (6 × 2.5 cm), which was subsequently sealed under vacuum (1 × 10^{-2} mmHg), placed in a steel container, and heated in an oil bath at 110–115 °C for 7 h. The reaction mixture contained a white precipitate, which was filtered off and discarded, after the ampule was opened. Removal of the solvent and excess amine under reduced pressure left either a yellow solid or an oil, which was purified under nitrogen by chromatography on Florisil using different eluent mixtures of petroleum ether and diethyl ether. In both cases, a yellow band eluting first from the column with hexane was identified as unreacted **1** or **10**. A second yellow band was collected using hexane–diethyl ether, which was reduced in volume to ca. 5 mL and cooled to −5 °C, affording the new species below as yellow solids.

(a) H_2NR, R = C_6H_{11} (2). A 60-mL yellow cyclohexane solution of **1** (500 mg, 2.43 mmol) with cyclohexylamine (1.44 g, 14.5 mmol) was heated under reflux over 4 h, changing to a lemon color. Chromatography using petroleum ether afforded 217 mg (29.2% yield) of a mixture of isomers **2** and **4**. Complex **2** (mp 115.5–116.5 °C) was obtained pure after several days by fractional sublimation under high vacuum (4 × 10^{-5} mmHg) at 30–40 °C, yielding lemon yellow crystals of sublimed **2**, while complex **4** remained in the bottom of the ampule. Mass spectrum (17 eV; *m/e* (relative intensity)): 55 (1), 84 (11), 153 (100), 166 (79), 167 (10), 221 (38), 249 (11), 277 (6), 305 (3). IR (hexane, ν_{CO}): 2006 (s), 1916 (s), 1910 (s) cm^{-1}.

(b) H_2NR, R = C_6H_{11} (4). The reaction mixture of **1** (300 mg, 1.46 mmol) and cyclohexylamine (13 g, 15 mL, 130 mmol) was heated for 3 h in an ampule. Chromatography using petroleum ether–diethyl ether (6:4) afforded a pale yellow powder: mp 112–115.5 °C dec. This complex **4** is isolated pure in 45% yield (200 mg). Anal. Calcd for $C_{14}H_{20}NO_3Mn$: C, 55.08; H, 6.56; N, 4.59. Found: C, 54.90; H, 6.51; N, 4.17. Mass spectrum (17 eV; *m/e* (relative intensity)): 55 (2), 84 (20), 166 (100), 167 (30), 221 (56), 249 (19), 277 (33), 305 (20). IR (hexane, ν_{CO}): 2008 (s), 1924 (s), 1908 (s) cm^{-1}.

(c) H_2NR, R = C_3H_7 (5). A 5 mL cyclohexane solution of **1** (300 mg, 1.46 mmol) and 10 mL of isopropylamine (120 mmol) were used for this reaction. The yellow compound was dissolved in the minimum volume of hexane and chromatographed twice using petroleum ether–diethyl ether in a 9:1 ratio. Bright yellow crystals (mp 114–115 °C dec) were obtained in 80.3% yield (310 mg) by recrystallization from diethyl ether–hexane (1:9) after 1 week at −15 °C. Anal. Calcd for $C_{11}H_{16}NO_3Mn$: C, 49.81; H, 6.03; N, 5.28. Found: C, 48.85; H, 5.83; N, 5.31. Mass spectrum (17 eV; *m/e* (relative intensity)): 126 (100), 181 (22), 209 (7), 237 (17), 265 (15). IR (hexane, ν_{CO}): 2007 (s), 1922 (s), 1907 (s) cm^{-1}.

(d) H_2NR, R = C_4H_9 (6). A 10 mL cyclohexane solution of **1** (337 mg, 1.64 mmoles) and 6.96 g (10 mL, 9.52 mmol) of *tert*-butylamine were heated in a sealed ampule for 6.5 h. A green powder which had formed was filtered under an inert atmosphere. Removal of the solvent and amine in vacuo afforded a golden yellow powder. Direct recrystallization from hexane gave 271 mg of golden crystals (59.2% yield). Very slow sublimation (4 months) under vacuum (4 × 10^{-5} mmHg) at ~30 °C afforded single crystals suitable for X-ray studies; mp 90–92 °C. Mass spectrum (20 eV; *m/e* (relative intensity)): 140 (100), 195 (32), 223 (18), 251 (23), 279 (13). HRMS for $C_{12}H_{18}NO_3Mn$: found 279.0654 amu, calcd 279.0667. IR (cyclohexane, ν_{CO}): 2000 (s), 1920 (s), 1903 (s) cm^{-1}.

(e) H_2NR, R = C_3H_7 (11, 11′). A 5 mL cyclohexane solution of **10** (300 mg, 1.36 mmol) and 10 mL (120 mmol) of isopropylamine were used for this reaction. After chromatography with petroleum ether–diethyl ether (9:1), a mixture of isomers **11** and **11′** in a ratio of 7:1 was formed in 7.4% yield (28.1 mg). IR (cyclohexane, ν_{CO}): 2006 (s), 1921 (s), 1907 (s) cm^{-1}.

(f) H_2NR, R = C_4H_9 (12, 12′). After the usual procedure, the reaction mixture of **10** (320 mg, 1.45 mmol) and *tert*-butylamine (10 mL, 95 mmol) afforded, after recrystallization with hexane, a mixture of pale yellow isomers **12** and **12′** (9:1) in 18.8% yield (80 mg). Anal. Calcd for $C_{13}H_{18}NO_3Mn$: C, 52.90; H, 6.83; N, 4.78. Found: C, 51.95; H, 6.29; N, 4.47. Mass spectrum (*m/e* (relative intensity)): 56 (6.6), 154 (100), 209 (23), 237 (13), 265 (17), 293 (10). IR (hexane, ν_{CO}): 2006 (s), 1922 (s), 1907 (s) cm^{-1}.

(g) H_2NR, R = C_6H_{11} (13). The reaction mixture of **10** (310 mg, 1.41 mmol) and cyclohexylamine (25 mL, 220 mmol) was heated under reflux without solvent. After chromatography with petroleum ether–diethyl ether in an 8:2 ratio an amber solid, which decomposes at 103–106 °C without melting, was isolated in 6.6% yield (26.4 mg).

Reaction of [(η^5-C_5H_7)$Mn(CO)_3$] (1) with $C_6H_5CH_2SH$. A solution of complex **1** (300 mg, 1.46 mmol) in 40 mL of cyclohexane was stirred with $C_6H_5CH_2SH$ (1.27 g, 1.20 mL, 10.2 mmol). Immediately, the color of the solution changed from yellow to orange. The resulting solution was stirred at room temperature for 5 h and then evaporated to dryness in vacuo. Sublimation of the excess benzyl mercaptan afforded a yellow, oily powder. This mixture was washed with hexane, and recrystallization of the resulting yellow powder with CH_2Cl_2–hexane (3:1) followed by chromatography of the oily residue on Florisil with diethyl ether–hexane (1:9) afforded 170 mg of the cubane complex[14] (11.1% yield). A yellow band eluting first from the column with hexane was the starting material **1**, while the second yellow band collected, as described above, afforded the cubane species as orange crystals.

Single-Crystal X-ray Diffraction Studies. Single crystals of the various compounds were prepared by cooling (**5**) or sublimation (**6** and **2**) as described above. For data collection, the crystals were mounted in glass capillaries under nitrogen

(13) In the synthesis of (η^5-*exo*-$CH_3C_5H_6$)$Mn(CO)_3$ (**10**) we found a mixture of two isomers (η^3-C_6H_9)$Mn(CO)_4$, in which the terminal methyl groups of the substituted carbon–carbon double bond are in *exo* (**10a**) and *endo* (**10b**) positions, respectively. The ratio 0.5:0.3:0.2 for **10**:**10a**:**10b** was obtained after refluxing the mixture of $MnBr(CO)_5$ and $C_6H_9SnBu_3$ in tetrahydrofuran for 6 h. Chromatography on netural alumina with hexane afforded a mixture of products, which possess very similar solubilities. Compounds **10**[3] and **10a**[19] have been characterized as described, while **10b** has not been previously reported. ^1H NMR for **10b** (270 MHz, $CDCl_3$): δ 0.8–1.15 (m, H1 *endo*), 1.95 (ddd, H1 *exo*), 4.24 (dt, H2), 3.2 (t, H3), 5.38 (m, H4), 5.18 (m, H5), 1.46 (d, CH_3). ^{13}C NMR (67.80 MHz, $CDCl_3$): δ 37.3 (C1), 92.0 (C2), 63.4 (C3), 130.9 (C4), 123.7 (C5), 17.3 (CH_3). The mixture of isomers **10a** and **10b** is converted to **10** after prolonged reflux. The reaction of either pure **10** with amines or of the mixture of **10**, **10a**, and **10b** with amines afforded the same tricarbonyl products, without evidence of any tetracarbonyl species.

and then transferred to an Enraf-Nonius CAD 4 rotating anode diffractometer, on which unit cell determination and data collection were carried out. No significant decomposition was observed, as the intensities of several standard reflections remained essentially constant. Direct methods, using the SDP programs, were used to locate the metal atom and most lighter atom positions, after which any remaining non-hydrogen atoms were located from a difference Fourier map. Hydrogen atom locations were determined from a Fourier map or placed in idealized positions but, unless otherwise indicated in the tables, were not refined. Other pertinent information relative to crystal data and data refinement may be found in Table 3.

Synthetic and Spectroscopic Results and Discussion

The reaction of Mn(η^5-C_5H_7)(CO)$_3$ (**1**) with an excess of a primary amine in cyclohexane leads to the formation of Mn[NH(R)(η^3-CHCHCHCH$_2$CH$_3$)](CO)$_3$ complexes (**5**, R = *i*-C_3H_7; **6**, R = *t*-C_4H_9). In the case of R = C_6H_{11}, however, the analogous reaction under reflux led to a mixture of the isomers Mn[NH(C_6H_{11})(η^3-CHCHCHCH$_2$CH$_3$)](CO)$_3$ (**4**) and Mn[NH(C_6H_{11})CH$_2$-η^3-CHCHCHCH$_3$](CO)$_3$ (**2**), which are yellow crystalline solids. Complex **4** can be isolated as the only product if the reaction is carried out in a vacuum-sealed ampule without solvent (Scheme 1). The main difference between the products **4–6** and **2** is that while in **4–6** the pentenyl group is bonded to the metal atom through the three nearest carbon atoms to nitrogen, **2** has its η^3-enyl system separated from the nitrogen atom by a single saturated carbon center (Scheme 1).

Complexes **4–6** all display similar spectroscopic properties, demonstrating that in each case the nitrogen atom has added regioselectively to the terminal carbon atom on the pentadienyl ligand and also becomes coordinated to the manganese atom. During this process a single proton abstraction from the NH$_2$ group also occurred, leading to the formation of the neutral substituted aminopentenyl complexes in a fashion identical with that observed for related secondary amine derivatives.[3] The reaction rates were found to be dependent on the concentration of the ligand, even to a greater extent than found for the secondary amine species.[3] When a 1:7 ratio of **1** and isopropylamine was used, infrared spectroscopic data showed that no significant conversion to products had taken place after 7 h. In contrast, under similar conditions, the analogous aminopentenyl complexes derived from secondary amines were readily formed. In addition, the reaction after 7 h using a 1:80 ratio of reactants **1** and isopropylamine showed complete consumption of **1**. A similar situation also applied to the reaction of *syn*-(1-methylpentadienyl)tricarbonylmanganese (**10**) with primary amines (*vide infra*). Reactions of **10** with isopropylamine or *tert*-butylamine in 1:86 and 1:66 ratios led to the two different regioisomers **11**, **11′** and **12**, **12′**, respectively,

Scheme 2

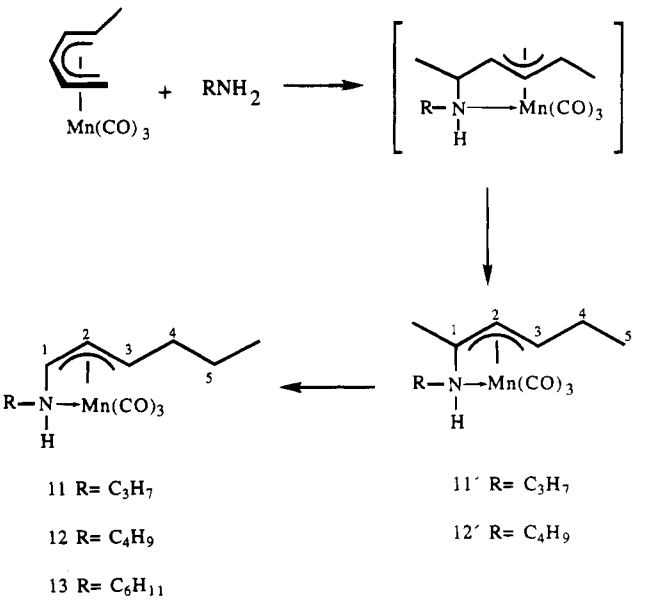

11 and **12** being the thermodynamic products and **11′** and **12′** the kinetic ones (Scheme 2). The regioisomers were found in ratios of 7:1 and 9:1 for **11**, **11′** and **12**, **12′**, respectively. The much smaller abundance of the kinetic isomers **11′** and **12′** compared with the secondary amine systems, which were prepared in a complex: amine ratio of 1:8 in refluxing cyclohexane,[3] can be attributed to the higher concentration and stronger reaction conditions required for the synthesis of the primary amine species (see Experimental Section).

In line with earlier observations utilizing either nitrogen- or carbon-based nucleophiles or hydride ion, the attack of the nucleophile on the unsymmetrically substituted pentadienyl **10** does not occur preferentially at the least hindered carbon atom[3] (cf. **11′** and **12′**). This could be consistent with an electronic effect due to the methyl group, which would lead to nucleophilic attack by amine, whether coordinated or not, on the relatively electron deficient dienyl ligand. A subsequent proton shift, presumably metal-mediated, to the terminal CH$_2$ group would lead to **2** as an isolable species for R$_2$ = C_6H_{11} (Scheme 1) or as a presumed intermediate for R$_2$ = *i*-C_3H_7 or *t*-C_4H_9. After what might be termed a β-hydride elimination from the saturated methylene group in **2**, and hydride transfer to the methyl-substituted end of the diene ligand, one would arrive at the η^4-aza diene complexes **4-8**. An alternative in the present case would be coordination of the amine, yielding an η^3-dienyl complex, analogous to known (η^3-C_5H_7)Mn(CO)$_3$(PR$_3$) complexes,[4] followed by oxidative addition of the N–H bond to the metal center and transfer of the hydrogen atom to the (unsubstituted) end of the η^3-dienyl ligand. This could ultimately lead to placement of the HNR group on a more substituted carbon center. Unfortunately, we were unable to gain NMR spectroscopic evidence for either the presumed η^3-dienyl complex or any manganese hydride intermediates. However, the last proposal might be more likely, since otherwise one would probably expect the electron-donating methyl group to retard nucleophilic attack at its attached carbon atom, and at best a mixture of products would be expected. Similarly, complex **13** was isolated as the exclusive product in low yield, using a

(14) Characterization of [Mn(CO)$_3$(SCH$_2$C$_6$H$_5$)]$_4$: ^{1}H NMR (90 MHz, CDCl$_3$) δ 3.66 (s, CH$_2$), 7.42 (s, C$_6$H$_5$); ^{13}C NMR (22.49 MHz, CDCl$_3$) δ 41.4 (CH$_2$), 129 (Cp), 129.1, 130.6 (Co, m), 135.1 (C$_i$); IR (CHCl$_3$, ν_{CO}) 2017 (vs), 1942 (vs, br) cm^{-1}; MS for $C_{40}H_{28}O_{12}S_4Mn_4$ found 1047.4 ± 0.3 amu, calcd 1048.67; *m/e* 1048, 964, 788, 712, 620, 534, 530, 438, 356, 348, 347, 265, 262, 261, 238, 220, 183, 178, 174, 165, 151, 142, 123, 119, 110, 91, 87, 55. Anal. Calcd for $C_{40}H_{28}O_{12}S_4Mn_4$: C, 45.8; H, 2.67; S, 12.21. Found: C, 45.7; H, 2.8; S, 13.12. (Butterworth Laboratories Ltd., Middlesex, U.K.). Atomic absorption spectrophotometry shows 19.5% Mn *vs* 20.99% (calcd). Mp: 205 °C. A similar tetranuclear species has been reported for [Mn(CO)$_3$(RC$_6$H$_5$)]$_4$ (R = S, Se); see: Jaitner, P. *J. Organomet. Chem.* **1981**, *210*, 353.

Table 1. ^{1}H NMR Data (δ) for the Aminopentenyl Complexes[a]

complex	H1	H2	H3	H4	H5	R$_2$ H6	R$_2$ H7	R$_2$ H8	R$_2$ H9−11	N−H[b]
2	1.7−2.0 (m)	4.34 (dd, 11)	3.37 (m)	2.40 (m), 2.76 (dd, 12, 7.2), 2.83 (dd, 12, 5.3)	2.18, (d, 5.3)	0.7−2.0 (m)	2.55 (m)	1.1−1.3 (m)	1.0−1.7 (m)	−2.0 (br, 18)
4	4.65 (t, ~8)	4.18 (dd, 9.2, 3.3)	0.49 (m)	1.75−1.96 (m)	1.2 (t, 7.3)	0.1−1.4 (m)	0.15−0.35 (m)	1.55−1.73 (m)	0.1−1.4 (m)	−1.3 (br, 22)
4[c]	5.43 (t, ~8)	4.65 (dd, 9, 3.3)	1.02 (m)	1.4−2.2 (m)	1.21 (t, 7.3)	0.9−2.2 (m)	0.9−2.2 (m)	0.9−2.2 (m)	0.9−2.2 (m)	−0.6 (br, 25)
5	4.54 (t, ~8)	4.14 (dd, 8.8, 2.7)	0.42 (m)	1.85 (m)	1.18 (t, 7.3)	1.72−1.92 (m)	0.33 (d, 5.9)	0.51 (d, 6.6)		−1.45 (br, 24)
6	4.90 (t, 7.5)	4.26 (dd, 9, 3.3)	0.5 (m)	2.0 (m)	1.3 (t, 6.6)		0.7 (s)	0.7 (s)	0.7 (s)	−0.95 (br, 19)
11[d]	4.57 (t)	4.19 (d, 7.9)	0.63 (m)	1.5−2.0 (m)	0.2−2.0 (m)	1.86 (m)	0.33 (d, 5.3)	0.52 (d, 5.3)		−1.04 (br, 23)
12[d]	4.87 (t)	4.27 (d, br)	0.57 (m)	1.57−2.12 (m)	0.1−2.0 (m)		0.6 (s)	0.6 (s)	0.6 (s)	−1.07 (br, 23)
13[d]	4.64 (t, 8.2)	4.22 (dd, 9.2, 2.8)	0.6 (m)	1.45−2.0 (m)	0.1−2.1 (m)	0.1−2.1 (m)	0.1−2.1 (m)	0.1−2.1 (m)	0.1−2.1 (m)	−1.23 (br, 24)

[a] For numbering, see Scheme 1; in C_6D_6 relative to Me_4Si (δ 0); 270 MHz. *J* values are given in parentheses. [b] Half-height width, $\nu_{1/2}$ in Hz. [c] In $CDCl_3$. [d] For numbering, see Scheme 2. CH_3(C5): δ 0.96 (t, ~7) (**11**), 0.98 (t, br) (**12**), 0.95 (t, 7.0) (**13**).

1:150 ratio of **1**:cyclohexylamine, after 7 h of reflux. Complexes **4−6** and **11−13** proved to be less easily handled than the corresponding aminopentenyl derivatives derived from secondary amines, in particular being much more air-sensitive.

It is interesting to note that, under the reaction conditions used for the formation of the primary amine species, the aminopentenyl derivatives from secondary amines afforded instead golden yellow complexes such as $Mn[\eta^3\text{-}CH(NR_2)CHCHCH_2CH_3](CO)_4$ ($R_2 = (CH_2)_5$, R = Me)[3] as the only product. However, for the primary amine derivatives from **1** or **10** there was no evidence of any related tetracarbonyl species, even though some reactions using **10** were carried out in the presence of a mixture of tetracarbonyl isomers **10a** and **10b**.[13] This fact probably reflects the greater steric crowding accompanying the species with −NR compared to those with −NH. Since the Mn←N bond distances for secondary vs primary amine products are not significantly different in the solid state (*vide infra*), there would not seem to be much difference in the inherent Mn←N bond energies.

The reaction of equimolar **5** and PMe_2Ph in cyclohexane, after 6 h at room temperature, afforded essentially only starting materials. In addition, after 4 h reaction of 1 equiv of PMe_2Ph with **5** or **6** in refluxing cyclohexane, it was observed that the aminopentenyl complexes **5** and **6** had decomposed, instead of affording complexes such as $Mn(\eta^3\text{-}CH(NHR)CHCHCH_2CH_3)(CO)_3\text{-}PMe_2Ph$ analogous to those previously obtained under similar experimental conditions for the related secondary amine addition products.[3] Possibly, it is again the greater steric bulk of an NR *vs* NH species which leads to the difference. Thus, if the addition of PMe_2Ph requires initial slippage of the amine center away from the metal, the bulkier NR (*vs* NH) species should be the one to promote PMe_2Ph coordination. Of course, it is also possible that the NH function may not be completely innocent in this matter and may allow for other pathways to be followed (e.g., imine formation, etc.). Further studies are in progress in order to gain a better understanding of the differences observed.

A similarly attempted addition reaction of allylamine to complex **1** afforded after 7 h at 110 °C a complex mixture of products, in which the corresponding [1-(allylamino)-(1−3-η^3)-pentenyl]tricarbonylmanganese species was clearly detected by ^{13}C NMR[15] spectroscopy. There was no evidence of any species in which the double bond of the allyl fragment had become coordinated to the metal center. Attempts to separate the components of the mixture were unsuccessful. It was also of interest to explore the mode of reactivity for other heteroatom species. Reaction of **1** with benzyl mercaptan afforded 1,3-pentadiene along with an orange cubane complex, $[Mn(CO)_3SCH_2C_6H_5]_4$,[14] even when a stoichiometric ratio of reactants had been used, and the reaction was carried out at room temperature (see Experimental Section). To what extent if any the difference is due to the greater acidity of the mercaptan, or to the extra lone pair present on the sulfur atom, is not clear.

A detailed NMR study of complex **1** in deuterated benzene revealed formation of 1,3-pentadiene immediately after addition of the benzyl mercaptan, with consequent formation of the cubane structure. After 6 h at 33 °C the consumption of **1** was complete. IR spectroscopic monitoring of this reaction was not helpful, due to the spectral patterns of **1** and the cubane complex being quite similar.[14] The isolated sulfur−manganese compound was not observed to react with excess PMe_2Ph in cyclohexane even after 3 h under refluxing conditions, evidencing the high stability of the complex.

Spectroscopic Data. The metal carbonyl fragments in complexes **2**, **4−6**, and **11−13** produce three strong ν_{CO} absorption bands in the infrared region. The intensity patterns, which suggest *fac* arrangements, as well as the frequency values (see Experimental Section) are quite similar to those reported for the aminopentenyl complexes derived from secondary amines.[3] These results indicate that the aminopentenyl ligands from primary and secondary amines give rise to similar interactions with the manganese atom. Therefore, the IR spectra do not provide evidence supporting stronger σ donation by the −NHR compared to an $-NR_2$ group. The IR spectrum of the phosphinopentenyl complex (**3**)[5] shows frequency bands very similar to those of complex **2**.

^{1}H and ^{13}C NMR data for the aminopentenyl complexes are listed in Tables 1 and 2, respectively. The similarity of the NMR spectra of **4−6** and **11−13** to those of the aminopentenyl complexes derived from secondary amines led us to propose that all these complexes have the same pentenyl ligand conformation. The most characteristic feature in the ^{1}H NMR spectra of complexes **4−6** and **11−13** is a broad high-field signal (δ −0.95 to −1.45, C_6D_6) with a $\nu_{1/2}$ value of ≈22 Hz, attributed to the NH moiety. We were not able to obtain a ^{15}N NMR spectrum. However, the appearance of ^{15}N satellites in the ^{1}H NMR spectrum (observed by inverse

(15) ^{13}C NMR (67.80 MHz, C_6D_6): δ 75.8 (C1), 88.2 (C2), 65.1 (C3), 27.5 (C4), 14.5 (C5), 53.3 (C6), 133.6 (C7), 118.0 (C8).

Table 2. ^{13}C NMR Data (δ) for the Aminopentenyl Complexes[a]

complex	C1	C2	C3	C4	C5	R$_2$ C6	C7	C8	C9	C10	C11
2	67.5	105.1	48.6	51.8	20.5	63.2	31.5	31.0	25.4	25.0	24.6
4	75.7	88.3	63.2	27.5	17.8	60.4	35.6	34.1	25.3	24.9	24.7
5	75.8 (d, 193)	88.3 (d, 164)	63.2 (d, 152)	27.4 (t, 127)	17.7 (q, 126)	53.7 (d, 140)	23.7 (q, 132)	22.9 (q, 128)			
6	74.5 (d, 200)	86.9 (d, 170)	63.9 (d, 158)	28.4 (t, 134)	18.7 (q, 134)	55.0	30.0 (q, 134)	30.0 (q, 134)	30.0 (q, 134)		
11[b]	75.8	88.8	60.8	36.5	26.7	53.8	23.7	22.9			
11′[c]	*d*	88.3	61.1	27.4	17.9	49.3	24.3	23.4			
12[b]	73.4	86.3	60.5	36.4	26.7	53.9	28.9	28.9	28.9		
12′[c]	*d*	87.0	61.3	27.4	18.3	52.2	30.1	30.1	30.1		
13[b]	75.5	88.7	60.8	36.5	26.8	60.3	35.6	34.0	25.3	24.9	24.6

[a] For numbering, see Scheme 1. In C_6D_6 relative to Me_4Si (δ 0); 67.80 MHz. [b] For numbering, see Scheme 2. CH_3(C5): δ 14.2 (**11**), 14.2 (**12**), 14.3 (**13**). [c] CH_3(C1): δ 16.8 (**11′**), 17.8 (**12′**). [d] Not observed.

detection) allowed us to measure $^1J(^{15}N^1H) = 79 \pm 1$ Hz for compound **5**[16] (Scheme 1). This value is typical for an –NH function, and it is inconsistent with an agostic structure, which can also be ruled out from the X-ray structural study (*vide infra*).

A triplet signal downfield (δ ~4.7) for H1 and a doublet of doublets for H2 (δ ~4.2) show coupling constants $J_{1,2} \cong 3.0$ Hz, upon irradiation of the broad NH signal at high field, and $J_{2,3} \cong 9$ Hz indicating that H1 and H2 are oriented in a syn fashion, whereas H2 and H3 are anti to one another. Irradiation of the H2 resonance at 4.14 ppm for complex **5** led to the collapse of the triplet at 4.54 ppm to a doublet (J(H1NH) = 4.0 Hz) and collapse of the multiplet at δ 0.42 ppm for H3 to a triplet ($J \simeq 7$ Hz). NMR spectral assignments for the other compounds could be obtained through double-resonance techniques (^{1}H–^{1}H and ^{1}H–^{13}C shift-correlated 2D spectra (see Experimental Section).

The ^{1}H NMR spectrum of **2** is also characterized by a broad NH signal at high field (δ –2) and a doublet at 2.18 ppm for the syn-methyl group. The assignments for the amine residue were obtained by the combined use of ^{1}H–^{1}H and ^{1}H–^{13}C shift-correlated 2D spectra (Tables 1 and 2). The ^{13}C NMR spectrum of **2** reveals a structure similar to that of the [1-(diphenylphosphino)-(2–4-η^3)-pentenyl]tricarbonylmanganese complex (**3**). The allylic chemical shifts for **2** are found downfield compared with those for the corresponding phosphino complex **3**.[5] In both compounds C3 shows a substantial high-field shift (δ 48.6 and 46.9, respectively), as a result of the "pseudo-ring" structure. Such signals, as previously reported[5] for typical substituted "allyl" systems, have δ values of ~70 ppm.[17] The steric effect of these pseudo-ring structures can perhaps also be recognized by comparing the corresponding C3 value from a higher ring size compound, such as Mn[P(Ph)$_2$CH$_2$CH$_2$-η^3-CHCHCH$_2$](CO)$_3$ (**9**; δ 74.8 ppm).[5]

Structural Results and Discussion

Analysis of the X-ray diffraction data for complexes **5** and **6** reveals that these complexes are structurally similar to the secondary amine derivatives, such as (1-pyrrolidyl-η^3-pentenyl)tricarbonylmanganese (**7**) and (1-piperidyl-η^3-pentenyl)tricarbonylmanganese (**8**). Structural parameters are essentially identical for **5** and **8**. ORTEP diagrams of **5** and **6** with their atom-numbering schemes appear in Figures 1 and 2, while atomic coordinates are listed in Tables 4 and 5 and bond distances and bond angles are in Table 6. Similar to **7** and **8**, the solid-state structures of **5** and **6** may be regarded as distorted octahedral, in which the aminopentenyl ligand is bonded to a manganese center through an η^3 interaction and also by the nitrogen lone pair coordination. The nitrogen atom is bonded in such a way as to yield a *cis* aza diene fragment, which likely optimizes its interaction with respect to the allyl fragment, leading to an 18-electron complex. The coordination spheres of the manganese atoms are completed with three carbonyl groups in a *fac* arrangement.

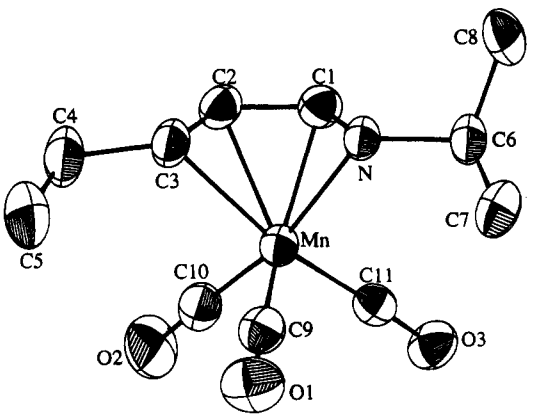

Figure 1. Molecular structure of compound **5**.

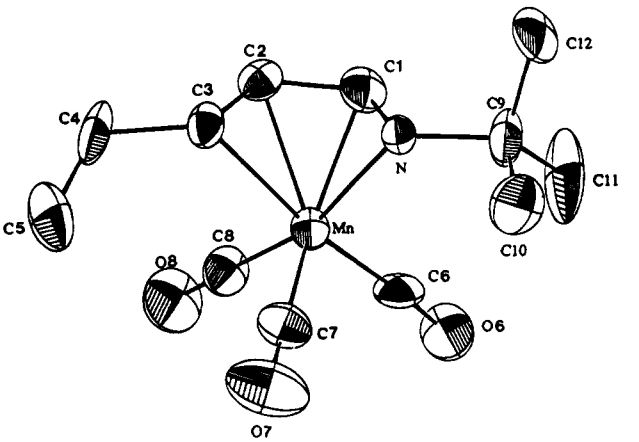

Figure 2. Molecular structure of compound **6**.

Some shortening of the manganese–nitrogen distance was observed for **5** (2.068(2)Å) as compared to those in **6** (2.105(7)Å), **7** (2.102(7)Å), and **8** (2.144(6)Å).[3] The η^3-pentenyl fragment is not symmetrically bonded to the metal, as observed from Mn–C1 = 2.050(3) and 2.050(1) Å, Mn–C2 = 2.115(4) and 2.14(1) Å, and Mn–C3 = 2.192(4) and 2.187(9) Å for complexes **5** and **6**,

(16) Wrackmeyer, B. Personal communication.
(17) Oudeman, A.; Sorensen, T. S. *J. Organomet. Chem.* **1978**, *156*, 259.

Table 3. Crystal Data, Summary of Data Collection, and Structure Refinement for 2, 5, and 6

	2	5	6
	(1) Crystal Data		
cryst size, mm	0.37 × 0.16 × 0.08	0.27 × 0.24 × 0.15	0.21 × 0.18 × 0.12
stoichiometry	$C_{14}H_{20}MnNO_3$	$C_{11}H_{16}MnNO_3$	$C_{12}H_{18}MnNO_3$
mol wt	305.258	265.193	279.22
cryst syst	orthorhombic	monoclinic	orthorhombic
space group	$P2_12_12_1$	$P2_1/c$	*Pbca*
a, Å	7.449(5)	10.308(3)	7.197(1)
b, Å	12.572(2)	10.935(2)	18.879(2)
c, Å	16.350(3)	12.359(2)	20.561(3)
α, deg	90.0	90.0	90.0
β, deg	90.0	110.56(2)	90.0
γ, deg	90.0	90.0	90.0
V, Å^3	1531.15	1304.39	2793.83
cryst color	yellow	yellow	yellow
Z	4	4	8
D_{exptl}, g cm^{-3}	1.324	1.350	1.328
	(2) Data Collection		
radiation, Å	λ(Mo Kα) = 0.709 30	λ(Mo Kα) = 0.709 30	λ(Cu Kα) = 1.541 78
mode	θ−2θ	θ−2θ	θ−2θ
2θ limits, deg	4−50	4−50	4−130
scan width, deg	1.0 + 0.35 tan θ	1.0 + 0.35 tan θ	
no. of rflns measd	1619	2565	2754
% min transmissn	92.55	85.12	
% max transmissn	99.36	99.89	
	(3) Structure Refinement		
no. of rflns for final refinement	1046	1614	1037
no. of params refined	172	193	154
R(*F*), %	0.0402	0.0306	0.0524
R_w, %	0.0460	0.0324	0.0569
goodness of fit	1.3010	0.6747	
Δ/σ (max)	0.002	0.003	

Table 4. Fractional Atomic Coordinates and Equivalent Isotropic Thermal Parameters for Complex 5[a]

atom	*x*	*y*	*z*	*B* (Å^2)
Mn	0.65838(5)	0.21342(5)	0.81546(4)	3.444(9)
O1	0.6600(3)	0.0102(3)	0.9718(2)	6.77(8)
O2	0.9129(3)	0.3234(3)	0.9746(3)	7.99(9)
O3	0.5157(3)	0.3963(2)	0.9075(2)	5.14(6)
N	0.4948(2)	0.1742(2)	0.6653(2)	3.55(6)
C1	0.5814(3)	0.2654(3)	0.6453(3)	4.02(7)
C2	0.7174(3)	0.2281(4)	0.6685(3)	4.23(8)
C3	0.7606(3)	0.1113(4)	0.7153(3)	4.50(8)
C4	0.9110(4)	0.0777(4)	0.7555(4)	6.1(1)
C5	0.9410(5)	−0.0364(6)	0.8254(5)	10.4(2)
C6	0.3466(3)	0.2059(3)	0.6414(3)	4.35(8)
C7	0.2892(4)	0.1221(4)	0.7103(3)	5.8(1)
C8	0.2658(4)	0.1990(5)	0.5129(4)	6.5(1)
C9	0.6606(4)	0.0892(3)	0.9107(3)	4.50(8)
C10	0.8143(3)	0.2792(4)	0.9120(3)	4.98(9)
C11	0.5672(3)	0.3227(3)	0.8692(3)	3.79(7)

[a] Atoms refined anisotropically are given in the form of the isotropic equivalent displacement parameter, defined as $^4/_3[a^2B_{11} + b^2B_{22} + c^2B_{33} + ab(\cos\gamma)B_{12} + ac(\cos\beta)B_{13} + bc(\cos\alpha)B_{23}]$.

respectively. Bond distances in the N−C1−C2−C3 fragments for complexes **5** and **6** reflect some charge delocalization, as also observed for the secondary amine derivatives.[3] The structural similarities between the aminopentenyl complexes obtained from primary and secondary amines are also evident from their torsion angles. It has been found that the torsion angles C6−N−C1−C2 (−179.35(27)°) for **5** and C9−N−C1−C2 (−169.9(10)°) for **6** as well as C7−N−C1−C2 for **7** (170.5(9)°) and **8** (169.0(8)°)[3] reveal nearly planar delocalized systems, while H−N−C1−C2 for **5** (−48.2(27)°) and **6** (39.6°) as well as C6−N−C1−C2 for **7** (−65.5(11)°) and **8** (−62.2(10)°)[3] indicate much less planar systems.

The structure of compound **2** is presented in Figure 3, and pertinent bonding parameters are given in Tables 7 and 8. This related structure exhibits a more distorted octahedral geometry, due to the steric require-

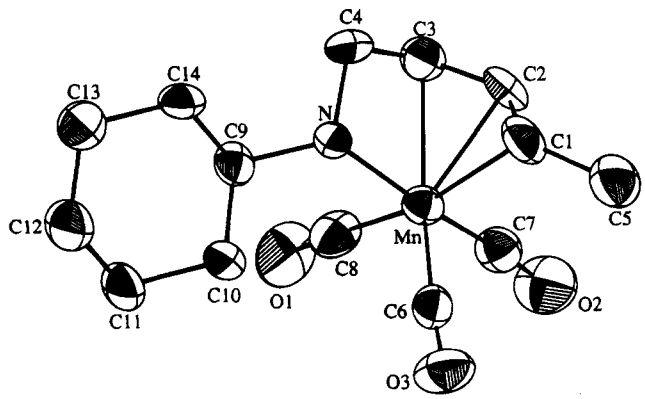

Figure 3. Molecular structure of compound **2**.

Table 5. Fractional Atomic Coordinates and Equivalent Isotropic Thermal Parameters for Complex 6[a]

atom	*x*	*y*	*z*	*B* (Å^2)
Mn	0.2157(2)	0.24026(6)	0.12439(7)	2.37(2)
O6	0.5716(8)	0.3150(3)	0.1260(4)	5.6(2)
O7	0.179(1)	0.2163(4)	0.2644(3)	7.0(2)
O8	0.4588(9)	0.1180(3)	0.1086(4)	5.6(2)
N	0.0235(9)	0.3215(3)	0.1045(3)	2.4(1)
C1	0.085(1)	0.2882(5)	0.0473(5)	3.4(2)
C2	0.041(4)	0.2146(4)	0.0436(4)	2.7(2)
C3	−0.036(1)	0.1818(4)	0.0982(4)	3.0(2)
C4	−0.051(1)	0.1011(4)	0.1007(6)	4.6(2)
C5	−0.050(2)	0.0696(5)	0.1669(6)	5.4(3)
C6	0.425(1)	0.2902(4)	0.1266(5)	3.5(2)
C7	0.194(1)	0.2258(5)	0.2095(4)	3.7(2)
C8	0.359(1)	0.1658(4)	0.1149(5)	3.5(2)
C9	0.028(1)	0.4011(4)	0.1134(5)	4.0(2)
C10	−0.019(2)	0.4149(5)	0.1829(6)	6.7(3)
C11	0.225(1)	0.4288(5)	0.0969(8)	8.0(4)
C12	−0.114(1)	0.4326(5)	0.0673(6)	4.9(3)

[a] See footnote in Table 4.

Table 6. Bond Lengths (Å) and Bond Angles (deg) in Complexes 5 and 6

	5		6
Mn–N	2.068(2)	Mn–N	2.105(7)
Mn–C1	2.050(3)	Mn–C1	2.05(1)
Mn–C2	2.115(4)	Mn–C2	2.14(1)
Mn–C3	2.192(4)	Mn–C3	2.187(9)
Mn–C9	1.793(4)	Mn–C7	1.78(1)
Mn–C10	1.782(3)	Mn–C8	1.76(1)
Mn–C11	1.786(4)	Mn–C6	1.781(7)
O1–C9	1.149(5)	O7–C7	1.15(1)
O2–C10	1.146(4)	O8–C8	1.16(1)
O3–C11	1.154(4)	O6–C6	1.15(1)
N–C1	1.416(4)	N–C1	1.41(1)
N–C6	1.491(4)	N–C9	1.51(1)
C1–C2	1.390(4)	C1–C2	1.43(1)
C2–C3	1.408(5)	C2–C3	1.40(1)
C3–C4	1.499(5)	C3–C4	1.53(1)
C4–C5	1.487(8)	C4–C5	1.48(2)
C6–C7	1.506(6)	C9–C10	1.49(2)
C6–C8	1.514(5)	C9–C11	1.54(1)
C6–C9		C9–C12	1.52(2)
N–Mn–C1	40.2(1)	N–Mn–C1	39.6(3)
N–Mn–C2	68.6(1)	N–Mn–C2	68.2(3)
N–Mn–C3	77.9(1)	N–Mn–C3	77.1(3)
N–Mn–C9	104.5(1)	N–Mn–C7	104.1(4)
N–Mn–C10	160.7(2)	N–Mn–C8	161.6(4)
N–Mn–C11	95.9(1)	N–Mn–C6	100.1(4)
C1–Mn–C2	39.0(1)	C1–Mn–C2	39.7(4)
C1–Mn–C3	69.6(1)	C1–Mn–C3	69.8(4)
C1–Mn–C9	142.6(1)	C1–Mn–C7	141.9(4)
C1–Mn–C10	120.5(2)	C1–Mn–C8	122.4(5)
C1–Mn–C11	97.5(1)	C1–Mn–C6	100.0(4)
C2–Mn–C3	38.1(1)	C2–Mn–C3	37.7(4)
C2–Mn–C9	132.9(2)	C2–Mn–C7	132.7(4)
C2–Mn–C10	94.6(2)	C2–Mn–C8	94.5(4)
C2–Mn–C11	128.0(1)	C2–Mn–C6	129.6(5)
C3–Mn–C9	95.0(2)	C3–Mn–C7	95.2(5)
C3–Mn–C10	94.8(2)	C3–Mn–C8	93.3(4)
C3–Mn–C11	166.1(1)	C3–Mn–C6	167.2(5)
C9–Mn–C10	93.8(2)	C7–Mn–C8	92.2(5)
C9–Mn–C11	98.6(2)	C6–Mn–C7	97.5(6)
C10–Mn–C11	87.1(2)	C6–Mn–C8	85.8(4)
Mn–N–C1	69.2(1)	Mn–N–C1	39.6(3)
Mn–N–C6	125.8(2)	Mn–N–C9	133.2(6)
C1–N–C6	117.8(3)	C1–N–C9	122.5(8)
Mn–C1–N	70.6(2)	Mn–C1–N	72.2(5)
Mn–C1–C2	73.1(2)	Mn–C1–C2	73.3(5)
N–C1–C2	114.2(3)	N–C1–C2	114.1(8)
Mn–C2–C1	68.0(2)	Mn–C2–C1	67.0(5)
Mn–C2–C3	73.9(2)	Mn–C2–C3	73.1(5)
C1–C2–C3	120.1(3)	C1–C2–C3	118.6(8)
Mn–C3–C2	68.0(2)	Mn–C3–C2	69.2(5)
Mn–C3–C4	125.8(3)	Mn–C3–C4	123.5(7)
C2–C3–C4	120.0(3)	C2–C3–C4	119.8(9)
C3–C4–C5	112.2(4)	C3–C4–C5	115(1)
Mn–C9–O1	178.9(4)	Mn–C7–O7	180(1)
Mn–C10–O2	178.6(4)	Mn–C8–O8	177.9(8)
Mn–C11–O3	176.0(3)	Mn–C6–O6	172(1)
N–C6–C7	109.0(3)	N–C9–C10	106.5(8)
N–C6–C8	110.1(3)	N–C9–C11	109.3(8)
C7–C6–C8	112.4(3)	N–C9–C12	107.3(8)
		C10–C9–C11	111(1)
		C10–C9–C12	110(1)
		C11–C9–C12	112.1(9)

ments of the aminopentenyl ligand. The cyclohexylamine group is bonded to the pentadienyl group, leading to a 1-(cyclohexylamino)-(2–4-η^3)-pentenyl fragment corrdinated through the nitrogen atom and the allyl moiety to the manganese atom. One can see that the structure is generally similar to that for the phosphorus analog, **3**.[5] However, some differences in bond lengths between **2** and **3** require comment. While compound **2** has an C1–C2 allylic bond longer than the corresponding C2–C3 bond (1.43(1) *vs* 1.366(9) Å), the phosphino

Table 7. Fractional Atomic Coordinates and Equivalent Isotropic Thermal Parameters for Complex 2[a]

atom	*x*	*y*	*z*	*B* (Å^2)
Mn	0.9300(1)	0.75417(8)	0.15190(5)	3.05(1)
O1	1.2242(7)	0.9071(4)	0.1726(4)	7.3(1)
O2	1.2188(8)	0.5953(4)	0.1611(3)	6.6(1)
O3	0.9312(7)	0.7171(4)	−0.0256(2)	5.6(1)
N	0.7255(6)	0.8706(3)	0.1538(3)	2.6(1)
C1	0.701(1)	0.6435(5)	0.1642(4)	4.3(2)
C2	0.7832(9)	0.6664(5)	0.2411(4)	4.0(2)
C3	0.8045(8)	0.7673(5)	0.2708(3)	3.8(1)
C4	0.690(1)	0.8583(5)	0.2430(4)	4.3(2)
C5	0.705(1)	0.5323(6)	0.1296(4)	5.4(2)
C6	0.9325(8)	0.7357(5)	0.0433(3)	3.5(1)
C7	1.101(1)	0.6569(5)	0.1607(4)	4.0(2)
C8	1.1059(9)	0.8523(5)	0.1641(4)	4.5(2)
C9	0.7604(9)	0.9853(5)	0.1298(4)	3.3(1)
C10	0.817(1)	0.9890(5)	0.0411(4)	4.7(2)
C11	0.860(1)	1.1063(5)	0.0167(4)	6.0(2)
C12	0.701(1)	1.1781(6)	0.0310(5)	6.4(2)
C13	0.639(1)	1.1712(6)	0.1208(4)	5.2(2)
C14	0.5960(9)	1.0550(5)	0.1429(4)	3.9(1)

[a] See footnote in Table 4.

Table 8. Bond Lengths (Å) and Bond Angles (deg) in Complex 2

Mn–N	2.112(5)	N–C9	1.517(8)
Mn–C1	2.213(8)	C1–C2	1.43(1)
Mn–C2	2.131(6)	C1–C5	1.51(1)
Mn–C3	2.163(6)	C2–C3	1.366(9)
Mn–C6	1.791(6)	C3–C4	1.50(1)
Mn–C7	1.774(9)	C9–C10	1.512(9)
Mn–C8	1.811(9)	C9–C14	1.521(9)
O1–C8	1.127(9)	C10–C11	1.560(9)
O2–C7	1.17(1)	C11–C12	1.50(1)
O3–C6	1.151(6)	C12–C13	1.54(1)
N–C4	1.489(9)	C13–C14	1.538(8)
N–Mn–C1	83.0(2)	C4–N–C9	112.5(5)
N–Mn–C2	88.8(3)	Mn–C1–C2	67.7(4)
N–Mn–C3	67.8(3)	Mn–C1–C5	122.1(6)
N–Mn–C6	96.4(3)	C2–C1–C5	120.5(8)
N–Mn–C7	174.5(4)	Mn–C2–C1	73.9(4)
N–Mn–C8	92.8(3)	Mn–C2–C3	72.7(4)
C1–Mn–C2	38.4(3)	C1–C2–C3	123.3(6)
C1–Mn–C3	68.4(3)	Mn–C3–C2	70.2(4)
C1–Mn–C6	91.0(3)	Mn–C3–C4	91.8(4)
C1–Mn–C7	96.6(3)	C2–C3–C4	122.4(6)
C1–Mn–C8	167.7(5)	N–C4–C3	106.0(5)
C2–Mn–C3	37.1(3)	Mn–C6–O3	175.5(6)
C2–Mn–C6	128.1(3)	Mn–C7–O2	175.1(9)
C2–Mn–C7	87.5(3)	Mn–C8–O1	174.7(8)
C2–Mn–C8	130.4(4)	N–C9–C10	109.0(5)
C3–Mn–C6	154.9(3)	N–C9–C14	111.9(5)
C3–Mn–C7	106.9(4)	C10–C9–C14	110.0(6)
C3–Mn–C8	99.3(3)	C9–C10–C11	109.4(5)
C6–Mn–C7	89.1(4)	C10–C11–C12	111.6(6)
C6–Mn–C8	100.9(4)	C11–C12–C13	110.5(6)
C7–Mn–C8	86.5(3)	C12–C13–C14	109.9(6)
Mn–N–C4	94.0(4)	C9–C14–C13	110.2(5)
Mn–N–C9	122.1(4)		

analogue complex **3** shows the opposite trend (1.38(1) *vs* 1.45(1) Å). The difference in **2** is also accompanied by a difference in the Mn–C1,3 bond lengths (2.213(8) *vs* 2.162(6) Å), which is not as significant as the difference found for **3** (2.245(8) *vs* 2.356(8) Å).[5] The torsion angles found for C1–Mn–N–C4 (73.4(4)°) and C1–Mn–P–C4 (65.6(4)°), along with the corresponding Mn–N–C4–C3 (−5.4(5)°) and Mn–P–C4–C3 (+0.7(4)°) values, all seem to reflect the differing steric requirements for the nitrogen and phosphorus compounds. Thus, it appears that the strain induced by coordination of the enyl–amine ligand is much lower than that resulting for the analogous enyl–phosphine complex **3**. In fact, the substituted-allyl distortion

decreases from **3** > **2** > **9**.[18] From the above results, as well as from the observation of similar ^{13}C chemical shifts for C3 in complexes **2** (δ 48.6) and **3** (δ 46.9), it is clear that a partial σ-allyl coordination mode does not contribute significantly in complex **2** and, therefore, the strain effect on this pseudo-ring structure is predominant.

Acknowledgment. Financial support from the CONACYT/NSF is gratefully acknowledged. We thank Prof. Dr. Bernd Wrackmeyer, Laboratorium für Anorganische Chemie, Universität Bayreuth, for stimulating discussions and also for performing the inverse detection ^{1}H NMR spectrum.

(18) This is judged by a comparison of the various torsion angles and C–C bond distances in the delocalized-organic fragment.

(19) Kreiter, C. G.; Leyendecker, M. *J. Organomet. Chem.* **1985**, *280*, 225.

Supplementary Material Available: Listings of positional parameters, general displacement parameter expressions, bond distances, bond angles, least-squares planes, and torsion angles for **2**, **5**, and **6** (24 pages). Ordering information is given on any current masthead page.

OM940880O

Experimental and Theoretical Study of π-Effects in P-Coordinated (Diphenylphosphino)alkynes

Elmostafa Louattani, Agustí Lledós,* and Joan Suades*

Departament de Química, Edifici C, Universitat Autònoma de Barcelona, 08193 Bellaterra, Spain

Angel Alvarez-Larena and Joan F. Piniella

Departament de Geologia, Edifici C, Universitat Autònoma de Barcelona, 08193 Bellaterra, Spain

Received July 1, 1994®

In order to study the nature of π-effects on phosphinoalkynes, we have carried out a combined experimental and theoretical study on $[(X)A_2PC{\equiv}CR]^+$ systems where X = H, CH_3, Fp (Fp = $CpFe(CO)_2$) and A = H, Ph. The P-coordinated (diphenylphosphino)alkyne metal complexes $[(Fp)Ph_2PC{\equiv}CR][BF_4]$ have been prepared and characterized by microanalysis and IR, ^1H, ^{13}C, and ^{31}P NMR spectroscopy. The crystal structure of $[(Fp)Ph_2PC{\equiv}CPh]^+$ has been determined by X-ray diffraction. This compound crystallizes in the triclinic space group *P*-1 with unit cell parameters a = 9.777(1) Å, b = 10.351(1) Å, c = 12.857(5) Å, α = 92.38(2)°, β = 103.07(2)°, γ = 100.02(1)°, D_c = 1.469 g cm^{-3}, Z = 2. Least-squares refinement using all 4068 independent reflections led to a final R value of 0.049 (all data). Ab initio calculations with geometry optimization have been performed in related model systems. A natural population and natural bond orbital analysis of the wave functions has been performed. The experimental difference between the ^{13}C NMR chemical shifts of acetylenic carbons and the calculated difference between NPA atomic charges is linearly correlated. A π-electron transfer from the filled π (C≡C) orbitals to the empty phosphorus d orbitals has not been observed. When X = H, CH_3 a strong polarization of the π(C≡C) bond is detected, when X = Fp the polarization is reduced and π-back-donation from metal d orbitals to the empty σ^*_{P-A} orbitals is found.

Introduction

Trivalent phosphorus donor ligands PA_3 (A = H, OR, F, Cl, alkyl, aryl) play a major role in coordination and organometallic chemistry. The π-bonding properties of this kind of ligand is a controversial subject. The extent of the π-bonding depends strongly on the nature of the groups attached to the phosphorus atom, particularly on the electronegativity of these groups. If A is relatively electronegative, such as OR, Cl or F, it is generally accepted that the π-acceptor behavior may be important.[1] This is especially true for PF_3, which forms many compounds comparable to those of CO.[2] At the other extreme, tertiary phosphines such as $P(CH_3)_3$ exhibit no such tendency. However, it has recently been shown that even a trimethylphosphine ligand has nonnegligible π-acceptor properties.[3]

The nature of the π-acceptor orbitals entails controversy. In the classical picture, the π-acceptor orbitals are the empty P_{3d}. However, it has been proposed that the π-acceptor orbitals are the π^*_{PA3}, which have essentially a phosphorus 3p character with a small 3d component.[4] These π-accepting orbitals have local σ^* symmetry with respect to the P–A bond axis, and are also called σ^*_{P-A}. Recent studies have clearly shown the π-acceptor role of the σ^*_{P-A} orbitals.[5,6] Orpen et al.[5a,b] have studied the geometry variations in the M–PA_3 units of 24 pairs of transition metal complexes in two different oxidation states, whose crystal structures were known. Metal–phosphorus bond lengths increase on oxidizing the metal, consistent with the presence of an important element of M–P π-back-bonding. Reduction of M–P π-bonding causes a decrease in the average P–A bond lengths, in agreement with the PA_3 π-acceptor orbitals having σ^* character. Reed and Schleyer,[6a] in a thorough study of the nature of chemical bonding in species of the X_3EY type, including E = P, have proven that the $\pi_Y \rightarrow \sigma^*_{E-X}$ interaction, the socalled negative hyperconjugation, is the primary contribution to π_{E-Y} bonding. The same conclusion has been reached in an ab initio study of zerovalent metal phosphine complexes.[6b] Two recent articles addressed the study of π-effects of phosphine ligands in transition metal complexes.[7]

Phosphinoalkynes are very interesting ligands for the study of π-effects. The presence of the alkyne π-system

® Abstract published in *Advance ACS Abstracts,* December 15, 1994.

(1) Cotton, F. A.; Wilkinson, G. *Advanced Inorganic Chemistry,* 5th ed.; Wiley: New York, 1988; pp 64–68.
(2) Nixon, J. F. *Adv. Inorg. Chem. Radiochem.* **1985**, *29*, 42.
(3) Wang, S. P.; Richmond, M. G.; Schwartz, M. *J. Am. Chem. Soc.* **1992**, *114*, 7595.
(4) (a) Xiao, S. X.; Trogler, W. C.; Ellis, D. E.; Berkovitch-Vellin, Z. *J. Am. Chem. Soc.* **1983**, *105*, 7033. (b) Marynick, D. S. *J. Am. Chem. Soc.* **1984**, *106*, 4064. (c) Braga, M. *Inorg. Chem.* **1985**, *24*, 2702.
(5) (a) Orpen, A. G.; Connelly, N. G. *J. Chem. Soc., Chem. Commun.* **1985**, 1310. (b) Orpen, A. G.; Connelly, N. G. *Organometallics* **1990**, *9*, 1206.
(6) (a) Reed, A. E.; Schleyer, P. v. R. *J. Am. Chem. Soc.* **1990**, *112*, 1434. (b) Pacchioni, G.; Bagus, P. S. *Inorg. Chem.* **1992**, *31*, 4391. (c) Wang, P.; Zhang, Y.; Glaser, R.; Reed, A. E.; Schleyer, P. v. R.; Streitwieser, A. *J. Am. Chem. Soc.* **1991**, *113*, 55.
(7) (a) Lichtenberger, D. L.; Jatcko, M. E. *Inorg. Chem.* **1992**, *31*, 451. (b) Kraatz, H. B.; Jacobsen, H.; Ziegler, T.; Boorman, P. M. *Organometallics* **1993**, *12*, 76.

0276-7333/95/2314-1053$09.00/0

offers the possibility to weight up these effects. It has been proven that in phosphinoalkynes, the electronic distribution of the acetylenic group is very sensitive to changes around the P atom that can be related to the retrodonation toward the phosphorus.[8] Moreover, these changes can be measured by means of different experimental techniques. The difference between the ^{13}C chemical shifts of acetylenic carbons in a series of phosphonium salts (Ph_3PR^+, R = unsaturated group) has been used as a measure of the carbon–carbon triple bond polarization. The deshielding extension of the β carbon was interpreted to be a consequence of $P_{d\pi}-C_{p\pi}$ bonding.[8b] The magnitude of the increase in the ν(C≡C) between the free $Ph_2PC{\equiv}CPh$ ligand and its transition-metal complexes has been taken as a measure of the retrodative bonding from the transition-metal atom toward the phosphorus atom.[8c]

In order to understand the nature of the π-effects on phosphinoalkynes, we carried out a combined experimental and theoretical study. A series of new P-coordinated transition-metal cationic complexes $[(Fp)Ph_2PC{\equiv}CR)]^+$ (Fp = $(C_5H_5)Fe(CO)_2$) have been prepared.[9] All of them have been characterized by means of infrared and ^{13}C NMR spectroscopic techniques. The structure of the $[(Fp)Ph_2PC{\equiv}CPh]^+$ complex has been determined by X-ray diffraction analysis. Ab initio calculations have been performed in the $H_2PC{\equiv}CR$ (R = H, CH_3, $COOCH_3$) and $[(X)H_2PC{\equiv}CR]^+$ (X = H, CH_3, Fp; R = H, CH_3, $COOCH_3$) systems. The ensemble of experimental and theoretical results can shed more light on the controversy about trivalent phosphorus ligands π-effects.

Experimental Results

Synthesis and Characterization. A series of stable cationic P-coordinated (diphenylphosphino)alkyne complexes $[(Fp)Ph_2PC{\equiv}CR]^+$ (R = H (**1**), CH_3 (**2**), ^{t}Bu (**3**), Ph (**4**), Tol (**5**), COOMe (**6**)) were prepared in high yield by oxidation of $[Fe_2(CO)_4Cp_2]$ with ferricinium cation in the presence of (diphenylphosphino)alkyne, according to the reaction

$$1/2\,[Fp_2] + [FeCp_2]^+ + Ph_2PC{\equiv}CR \rightarrow [(Fp)Ph_2PC{\equiv}CR]^+ + FeCp_2$$

In the infrared spectrum all prepared complexes exhibit two bands (1): 2061, 2020 cm^{-1}) assigned to the ν(CO) of the fragment $[CpFe(CO)_2]^+$. Moreover, in the ^1H and ^{13}C NMR spectra the signals corresponding to the presence of an η^5-cyclopentadienyl ligand are observed. In this context, two different ligand coordination possibilities can be proposed according to the bifunctional character of (diphenylphosphino)alkynes: (a) η^2-alkyne coordination, (b) P-coordination (Scheme 1). Both structures have been described in the literature, (a) in η^2-alkyne iron complexes[11] $[CpFeCO(L)(\eta^2\text{-alkyne})]^+$ and (b) in triphenylphosphino[12] metal complexes $[(Fp)PPh_3]^+$. The ^{31}P NMR spectra of **1–6** show a signal at 38–47 ppm which is assigned to the phosphorus atom coordinated to an iron atom. On the other hand, the IR band near 2200 cm^{-1} together with the C_1 and C_2 ^{13}C NMR chemical shifts indicate the presence of an uncoordinated triple bond. All these data are consistent with structure (b).

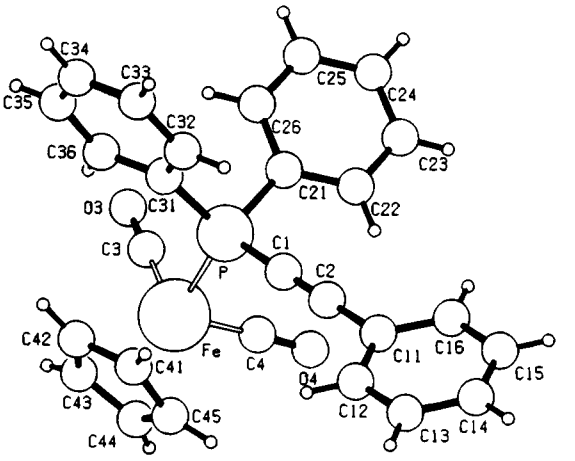

Figure 1. Cationic fragment of compound **4**.

Scheme 1

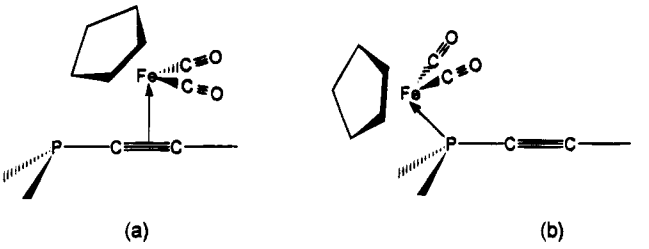

Table 1. Selected X-ray Bond Distances (Å) and Angles (deg) with Esd's in Parentheses for $[(Fp)Ph_2PC{\equiv}CPh]^+$ Cation (4)

Fe-C3	1.785(3)	P-C1	1.746(3)
Fe–C4	1.787(4)	P–C21	1.825(3)
Fe–P	2.207(1)	P–C31	1.815(3)
C3–O3	1.138(4)	C1–C2	1.202(5)
C4–O4	1.130(4)	C2–C11	1.432(4)
C4–Fe–P	92.1(0.1)	Fe–P–C1	112.3(0.1)
C3–Fe–P	92.5(0.1)	C21–P–C31	104.1(0.1)
C3–Fe–C4	95.2(0.1)	C1–P–C31	105.9(0.1)
Fe–P–C31	116.3(0.1)	C1–P–C21	102.1(0.1)
Fe–P–C21	114.7(0.1)	P–C1–C2	174.7(0.3)

Crystal Structure of $[(Fp)Ph_2PC{\equiv}CPh][BF4]$ (4). The structure is composed of discrete cations and $[BF_4]^-$ anions without significant interactions between them. The structure of the cation $[(Fp)Ph_2PC{\equiv}CPh]^+$ with the adopted atom numbering system is shown in Figure 1; selected interatomic distances and angles are given in Table 1.

The structure of the cation consists of a $Ph_2PC{\equiv}CPh$ ligand bonded to a $[Fp]^+$ fragment through a P–Fe bond. The existence of the uncoordinated alkyne function is confirmed by the long values of the distances between the iron atom and the acetylenic carbons (Fe–C_1 = 3.294(3) Å; Fe–C_2 = 4.275(3) Å) and by the bond distance C_1–C_2. A search in the Cambridge Structural

(8) (a) Nucciarone, D.; MacLaughlin, S. A.; Taylor, N. J.; Carty, A. *Organometallics* **1988**, *7*, 106 and references therein. (b) Albright, T. A.; Freeman, W. J.; Schweizer, E. E. *J. Am. Chem. Soc.* **1975**, *97*, 2946. (c) King, R. B.; Efraty, A. *Inorg. Chim. Acta* **1970**, *4*, 319.

(9) Iron cationic complexes of $Ph_2PC{\equiv}CPPh_2$ had already been prepared[10] by unsymmetrical cleavage of $[\{Cp_2Fe_2(CO)_3\}_2(Ph_2PC{\equiv}CPPh_2)]$.

(10) Carty, A. J.; Efraty, A.; Ng, T. W.; Birchall, T. *Inorg. Chem.* **1970**, *9*, 1263.

(11) Reger, D. L.; Klaeren, S. A.; Lebioda, L. *Organometallics* **1988**, *7*, 189.

(12) Sim, G. A.; Woodhouse, D. I.; Knox, G. R. *J. Chem. Soc., Dalton Trans.* **1979**, 629.

Table 2. Bond Lengths (Å) in X-ray Structure Determination of Compounds with the Fragment[a]

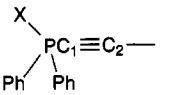

compound	X	P−X	C_1-C_2	$P-C_1$	$P-C_{phenyl}$[a]	R	reference (REFCODE[a])
$[(Fp)Ph_2PC{\equiv}CPh]^+$	Fe	2.207(1)	1.202(5)	1.746(3)	1.820(3)	0.049	this work
$[Fe_3(CO)_6(\mu_3\text{-}P^tBu)(\mu_3\text{-}Se)(Ph_2PC{\equiv}CPh)_3]$	Fe	2.220(6)[b]	1.181(3)[b]	1.753(2)[b]	1.832[e]	0.088	14b (LAGHIK)
$[Fe_3(CO)_8(\mu_2\text{-}CO)(\mu_3\text{-}S)(Ph_2PC{\equiv}CPr^i)]$	Fe	2.238(2)	1.171(9)	1.744(6)	1.812(5)	0.033	14a (GEJMEN)
$[\{Fe(CO)_4\}_2(\mu\text{-}Ph_2PC{\equiv}CC{\equiv}CPPh_2)]$[c]	Fe	2.218(2)[b]	1.197(7)[b]	1.767(6)[b]	1.807(4)	0.042	14c (SUBNOS)
$[Co_2\{\mu\text{-}\eta^2\text{-}[(OC)_5W(PPh_2)]C{\equiv}C[C{\equiv}C(PPh_2)W(CO)_5]\}(CO)_6]$[c]	W	2.496(6)[b]	1.21(4)[b]	1.74(3)[b]	1.82(1)	0.055	14c (SUBNIM)
$[\{Mn(CO)_2(Cp)\}_2(Ph_2PC{\equiv}CPPh_2)]$	Mn	2.196(2)[b]	1.199(5)	1.774(4)[b]	1.830(5)	0.036	17a (FIHLIR)
$[Ru_3(CO)_{11}(Ph_2PC{\equiv}CPh)]$	Ru	2.342[e]	1.182[e]	1.758[e]	1.828[e]	0.035	17b (CARTEU)
$[Ru_3(CO)_6(\mu\text{-}C{\equiv}C^tBu)(\mu\text{-}\eta^2\text{-}C{\equiv}C^tBu)(\mu\text{-}PPh_2)_2(Ph_2PC{\equiv}C^tBu)]$	Ru	2.314[e]	1.199[e]	1.479[e]	1.828[e]	0.039	17c (BAYCOS)
$[Ru_4(CO)_8(\mu\text{-}PPh_2)_2(\mu\text{-}\eta^2\text{-}C{\equiv}C^tBu)_2(\mu_3\text{-}\eta^2\text{-}C{\equiv}C^tBu)(Ph_2PC{\equiv}C^tBu)]$	Ru	2.383[e]	1.198[e]	1.750[e]	1.827[e]	0.037	17d (BOBTUH)
$[FeRu_2(\mu\text{-}C1)_2(CO)_8(Ph_2PC{\equiv}C^tBu)_2]$	Ru	2.380(5)[b]	1.19(4)[b]	1.75(2)[b]	1.83(2)	0.083	17e (FEBARU10)
$[Ru_3(CO)_8(\mu_3\text{-}S)_2(Ph_2PC{\equiv}C^tBu)$	Ru	2.284(1)	1.192(6)	1.744(5)	1.822(5)	0.029	14a (GEJMIR)
$[\{Os_3(CO)_{11}\}_2(Ph_2PC{\equiv}CPPh_2)]$	Os	2.33(1)[b]	1.13(7)	1.80(5)[b]	1.86(4)	0.085	17f (TAGNUK10)
$[CpNiOs_3(\mu\text{-}H)_3(CO)_8(Ph_2PC{\equiv}CPr^i)]$[c]	Os	2.334(9)[b]	1.18(5)[b]	1.74(3)[b]	1.81(2)	0.055	17g (DIFBAV)
$[Pt(SCN)_2(Ph_2PC{\equiv}C^tBu)_2]$	Pt	2.256(7)[b]	1.220(4)[b]	1.696(3)[b]	1.801(3)	0.057	17h (CBYNPT)
$[MePh_2PC{\equiv}CBPh_3]$	C	1.790(5)	1.216(5)	1.699(4)	1.788(4)	0.066	16a (SEDRAU)
$[MePh_2PC{\equiv}CC(PPh_2Me)_2]^{2+}$	C	1.79(1)	1.19(1)	1.70(1)	1.80(1)	0.047	16b (FITDAN)
$[Ph_3PC{\equiv}CMnBr(CO)_5]$	C	1.78(1)	1.21(1)	1.68(1)	1.78(1)	0.063	16c (MNPACY10)
$[(Ph_3P)Cl_2Pd(C{\equiv}CPPh_3)]$	C	1.79(1)	1.23(2)	1.71(1)	1.79(1)	0.097	16d (VUPDOZ)
$[Ph_2PC{\equiv}CPPh_2]$			1.207(5)	1.765(4)	1.832(3)	0.061	15a (DPHPAC)
$[Ph_2PC{\equiv}CB(mes)_2]$			1.217(4)	1.754(3)	1.830(3)	0.040	15b (PELVAD)
$[Fe(CO)_2(Cp)(PPh_3)]^+$[d]	Fe	2.240(1)			1.817(5)	0.055	12

[a] Search on Cambridge Structural Data Base; X = carbon or transition metal; the structures where the fragment is placed in a part of a cycle are omitted. [b] Mean value. [c] The unit cell contains two independent molecules. [d] Nonacetylenic compound for data comparison. [e] Esd not reported.

Data Base[13] (v. 5.07, April 1994) shows that only a few complete X-ray structures of complexes having the [Fe-$PPh_2C{\equiv}C$-] fragment with uncoordinated alkynes are reported.[14] In Table 2 structural data for (diphenylphosphino)alkynes,[15] (diphenylphosphonium)alkynes,[16] and P-coordinated metal complexes of (diphenylphosphino)alkynes[14,17] are presented. On comparing the Fe−P bond distance of 2.207(1) Å observed in complex **4** with the values of the related previously reported complexes, a slight contraction is observed. The CpFe-$(CO)_2$ fragment has very similar geometry to that found in $[(Fp)APh_3]^+$ (A = P, As, Sb, Bi) complexes.[18]

Spectroscopic Analysis of the Acetylenic Fragment. IR Spectra. The $\nu(C{\equiv}C)$ frequencies of free (diphenylphosphino)alkynes appear at lower values than the normal range for disubstituted alkynes (2190−2260 cm^{-1}).[8c] In $[(Fp)Ph_2PC{\equiv}CR]^+$ complexes **2** to **6**, the $\nu(C{\equiv}C)$ frequencies are observed in the range 2200−2150 cm^{-1} as a band of medium intensity, with the exception of **1** where no $\nu(C{\equiv}C)$ stretching is observed.[19] In complex **3**, two bands at 2209 and 2169 cm^{-1} are observed, one is assigned to the $\nu(C{\equiv}C)$ and the other one is assigned to a Fermi resonance observed in substituted *tert*-butylalkynes.[20] The $\nu(C{\equiv}C)$ frequencies of complexes **2**, **4**, **5**, and **6** are shifted 15−42 cm^{-1} to higher frequencies in comparison with those of the free (diphenylphosphino)alkynes, and a similar value ($\Delta\nu$ = 45 cm^{-1}) was found in the propyinyltriphenylphosphonium cation.[21] We wish to emphasize that the intensity of the $\nu(C{\equiv}C)$ band increases in complexes **2**, **4**, **5**, and **6** in comparison with those of the free (diphenylphosphino)alkynes. This fact may be related to an increase in the triple bond dipole moment upon coordination.

^{13}C NMR Spectra. The ^{13}C NMR spectra of (diphenylphosphino)alkynes ligands and their metal complexes **1**−**6** show two characteristic signals in the region 70−130 ppm assigned to acetylenic carbons (Table 3). The spectra of complexes **1**−**6** show an important increase in $|^1J_{C-P}|$ with respect to the free ligands (85−115 Hz compared to 0−24 Hz). $|^1J_{C-P}|$ high values were reported for methyltriphenylphosphonium salt $[Ph_3PC{\equiv}CMe]^+$ (191.7 Hz)[8b] where the P atom is also quaternized. The ^{13}C resonances of acetylenic carbon atoms C_1 and C_2 in complexes **1**−**6** are all shifted in the same direction, upfield and downfield respectively, with regard to that of the corresponding free (diphenylphosphino)alkyne (Table 3). The resonances of C_1

(13) Allen, F. H.; Davies, J. E.; Galloy, J. J.; Jhonson, O.; Kennnard, O.; Mitchell, G. F.; Smith, J. M.; Watson, D. G. *J. Chem. Inf. Comp. Sci.* **1991**, *31*, 187.

(14) (a) Hogarth, G.; Taylor, N. J.; Carty, A. J.; Meyer, A. *J. Chem. Soc., Chem. Commun.* **1988**, 834. (b) Imhof, W; Eber, B.; Huttner, G.; Emmerich, C. *J. Organomet. Chem.* **1993**, *447*, 21. (c) Adams, C. J.; Bruce, M. I.; Horn, E.; Tieknik, E. R. T. *J. Chem. Soc., Dalton Trans.* **1992**, 1157.

(15) (a) Bart, J. C. J. *Acta Crystallogr., Sect. B* **1969**, *25*, 489. (b) Yuan, Z.; Taylor, N. J.; Sun, Y.; Marder, T. B.; Williams, I. D.; Cheng, L. *J. Organomet. Chem.* **1993**, *449*, 27.

(16) (a) Bestmann, H. J.; Behl, H.; Bremer, M. *Angew. Chem., Int. Ed. Engl.* **1989**, *28*, 1219. (b) Schmidbaur, H.; Pollok, T.; Reber, G.; Muller, G. *Chem. Ber.* **1987**, *120*, 1403. (c) Goldberg, S. Z.; Duesler, E. N.; Raymond, K. N. *Inorg. Chem.* **1972**, *11*, 1397. (d) Sunkel, K. *J. Organomet. Chem.* **1992**, *436*, 101.

(17) (a) Orama, O. *J. Organomet. Chem.* **1986**, *314*, 273. (b) Carty, A. J.; MacLaughlin, S. A.; Taylor, N. J. *J. Organomet. Chem.* **1981**, *204*, C27. (c) Carty, A. J.; Taylor, N. J.; Smith, W. F. *J. Chem. Soc., Chem. Commun.* **1979**, 750. (d) Carty, A. J.; MacLaughlin, S. A.; Van Wagner, J.; Taylor, N. J. *Organometallics* **1982**, *1*, 1013. (e) Jones, D. F.; Dixneuf, P. H.; Southern, T. G.; Le Marouille, J. Y.; Grandjean, D.; Guenot, P. *Inorg. Chem.* **1981**, *20*, 3247. (f) Amoroso, A. J.; Johnson, B. F. G.; Lewis, J.; Massey, A. D.; Raithby, P. R.; Wong, W. T. *J. Organomet. Chem.* **1992**, *440*, 219. (g) Sappa, E.; Predieri, G.; Tipipicchio, A.; Tiripicchio Camellini, M. *J. Organomet. Chem.* **1985**, *297*, 103. (h) Wong, S.; Jacobson, S.; Chieh, P. C.; Carty, A. J. *Inorg. Chem.* **1974**, *13*, 284.

(18) Schumann, H.; Eguren, L. *J. Organomet. Chem.* **1991**, *403*, 183.

(19) The presence of the C≡CH group in this complex is revealed by the observation of the characteristic signal of $\nu(C-H)$st at 3225 cm^{-1} and by NMR results.

(20) Grindley, T. B.; Johnson, K. F.; Katritzky, A. R.; Keogh, H. J.; Thirkettle, C.; Topsom, R. D. *J. Chem. Soc., Perkin Trans. II* **1974**, 282.

(21) Schweizer, E. E.; Goff, S. D.; Murray, W. P. *J. Org. Chem.* **1977**, *42*, 200.

Table 3. ^{13}C Chemical Shifts (δ, ppm) for the Acetylenic Atoms in Cationic Compounds $[(X)Ph_2PC^1{\equiv}C^2R]^+$ (in Parentheses, Values for the Correponding Free Phosphinoalkynes $[Ph_2PC^1{\equiv}C^2R]$)

compound	$\delta(C^1)$	$\delta(C^2)$	$\delta(C^1)+\delta(C^2)$	$\delta(C^2)-\delta(C^1)$
X = Fp, R = H	76.1 (92.0)	107.0 (98.8)	183.1 (190.8)	30.9 (6.8)
X = Fp, R = CH_3	70.9 (75.4)	117.9 (107.2)	188.8 (182.6)	47.0 (31.8)
X = Fp, R = ^{t}Bu	70.9 (75.2)	127.9 (119.5)	198.8 (194.7)	57.0 (44.3)
X = Fp, R = Ph	80.3 (86.5)	115.7 (109.4)	196.0 (195.9)	35.4 (22.9)
X = Fp, R = Tol	80.0 (85.3)	116.5 (108.9)	196.5 (194.2)	36.5 (23.6)
X = Fp, R = COOMe	77.2 (87.0)	102.2 (98.9)	179.4 (185.9)	25 (11.9)
X = Ph, R = CH_3	60.4[a] (75.4)	121.8[a] (107.2)	182.2 (182.6)	61.4 (31.8)

[a] Reference 8b.

Table 4. Most Relevant Optimized Geometrical[a] Parameters for the L and $[X-L]^+$ Systems (X = H, CH_3, Fp; L = PH_3, $H_2PC{\equiv}CH$, $H_2PC{\equiv}CCH_3$, $H_2PC{\equiv}CCOOCH_3$) with the 6-31G* Basis Set

X	X−P	P−C_1	P−H	C_1−C_2	XPC_1	HPH	XPH	HPC_1
				L = PH_3				
		1.403	95.4					
H	1.380	1.380	109.5	109.5				
CH_3	1.822	1.380	106.8	106.8				
				L = $H_2PC{\equiv}CH$				
		1.785	1.401	1.191		95.5		98.1
H	1.379	1.717	1.379	1.189	110.9	108.0	108.0	110.9
CH_3	1.820	1.726	1.380	1.189	113.1	106.0	110.5	108.3
Fp[b]	2.207[c]	1.756	1.393	1.189	121.4	98.7	116.0	100.5
				L = $H_2PC{\equiv}CCH_3$				
		1.780	1.402	1.192		95.4		98.6
H	1.380	1.705	1.380	1.195	111.6	107.3	107.3	111.6
CH_3	1.821	1.714	1.380	1.194	113.6	105.4	109.7	109.0
Fp[b]	2.207[c]	1.749	1.394	1.192	121.7	98.3	115.4	101.3
				L = $H_2PC{\equiv}CCOOCH_3$				
		1.791	1.400	1.190		95.4		97.2
H	1.380	1.717	1.380	1.190	111.1	108.0	108.0	110.7
CH_3	1.820	1.726	1.380	1.190	113.0	105.2	110.1	109.0
Fp[b]	2.207[c]	1.758	1.393	1.188	120.9	98.8	116.5	100.2

[a] Distances in angstroms, angles in degrees. [b] Valence-double ζ basis set for iron, minimal basis set for the CO and Cp ligands. [c] Fe−P distance fixed at their x-ray-determined value.

atoms exhibit a high-field chemical shift of 4−16 ppm, whereas the C_2 atoms show a down-field chemical shift of 3−11 ppm.

The chemical shift differences ($\delta C_2 - \delta C_1$) of acetylenic carbons for different compounds have been related to the triple bond polarization, and the sum ($\delta C_1 + \delta C_2$) has been connected with the charge changes.[22] According to this hypothesis, the data presented in Table 3 indicate that complexation of (diphenylphosphino)-alkynes to $[Fp]^+$ has an important effect in the polarization of the triple bond whereas the influence in charge transfer is small. Furthermore, the C≡C triple bond polarization increases following the sequence

$$Ph_2PC{\equiv}CR < [(Fp)Ph_2PC{\equiv}CR]^+ < [Ph_3PC{\equiv}CR]^+$$

Theoretical Results

Optimized Geometries. The most relevant optimized geometrical parameters for the free ligands L = $H_2PC{\equiv}CR$ (R = H, CH_3, $COOCH_3$) and the P-coordinated phosphinoalkynes $[(X)H_2PC{\equiv}CR]^+$ (X = H, CH_3, Fp) are shown in Table 4. For comparative purposes, the results with L = PH_3 have also been included. The optimized values for ethynylphosphine ($H_2PC{\equiv}CH$) agree well with the structural parameters determined for this molecule.[23] The geometries of the P ligands in $[(Fp)H_2PC{\equiv}CR]^+$ systems are in good agreement with the X-ray-determined structure of $[(Fp)Ph_2PC{\equiv}CPh]^+$ (see Table 1). Only minor differences between the P bond angles are found. They can be attributed to the steric effects due to the more bulky phenyl groups.

When comparing the values reported in Table 4 we should bear in mind the different charge of the neutral free ligand and the cationic P-coordinated phosphinoalkynes. This cationic character could be responsible for the contraction of some distances. In the free ligands the optimized C≡C distance is slightly lengthened with respect to the calculated distances for nonconjugated alkynes (1.19 Å in front of 1.18 Å). The P−C distances (1.78−1.79 Å) are significantly shorter than P−C_{sp3} (1.85 Å) and P−C_{Aryl} (1.83 Å).[24] The free phosphinoalkynes and the PH_3 ligand show similar P−H distances and angles.

Now we will consider the effect of coordination on the ligand geometry. The structural changes observed are very similar for the three different R groups studied. The C≡C bond distance is practically unaffected by coordination. Conversely other parameters are affected by coordination, showing different behavior depending on the nature of the group X. When X = H or CH_3, i.e. pure σ-donors, the P−C distance is strongly shortened and the P−H distances and P-bond angles are close to the values found in $[PH_4]^+$. When X = Fp the P−C_1 and P−H distances become longer than the values calculated for X = H, CH_3. For X = Fp the P−H distances are close to its value in the free PH_3 and the phosphorus bond angles show a marked deviation from the tetrahedral geometry. The H−P−H and H−P−C angles are reduced to ca. 100°, and the Fe−P−C and Fe−P−H are raised to ca. 120° in such a way that the P ligands are pyramidalized away from the metal.

Atomic Charges. The electronic distribution of an alkyne group bonded to a phosphorus atom has been shown to be very sensitive to changes in the atoms coordinated to phosphorus.[8] This sensitivity should be reflected on the atomic charges on the acetylenic carbons. So, an accurate calculation of these charges seems to be necessary. To assess the validity of the calculated atomic charges, we have chosen the two simplest systems $H_2PC{\equiv}CH$ and $[H_3PC{\equiv}CH]^+$. In both cases we have determined the charges by means of two different methods: The Mulliken population analysis (MPA)[25] and the natural population analysis (NPA).[26]

(22) Rosenberg, D.; Drenth, W. *Tetrahedron* **1971**, *27*, 3893.

(23) Cohen, E. A.; McRae, G. A.; Goldwhite, H.; Di Stefano, S.; Beaudet, R. A. *Inorg. Chem.* **1987**, *26*, 4000.

(24) Allen, F. H.; Kennard, Watson, D.; Brammer, L.; Orpen, A. G., Taylor R. *J. Chem. Soc., Perkin Trans. II* **1987**, 51.

(25) Mulliken, R. S. *J. Chem. Phys.* **1955**, *23*, 1833, 1841, 2338, 2343.

(26) (a) Reed, A. E.; Weinstock, R. B.; Weinhold, F. *J. Chem. Phys.* **1985**, *83*, 735. (b) Reed, A. E.; Weinhold, F. *J. Am. Chem. Soc.* **1986**, *108*, 3586.

Table 5. NPA Atomic Charges for the $H_2PC{\equiv}CR$ and $[(X)H_2PC{\equiv}CR]^+$ Systems (R = H, CH_3, $COOCH_3$; X = H, CH_3, Fp)

X	q_X	q_P	q_{C1}	q_{C2}	q_H	q_R
			L = $H_2PC{\equiv}CH$			
		+0.44	−0.42	−0.19	−0.04	+0.24
H	+0.06	+1.02	−0.60	+0.12	+0.06	+0.28
CH_3	−0.11	+1.26	−0.59	+0.09	+0.04	+0.28
Fp	+1.06	+0.23	−0.49	−0.06	0.00	+0.26
			L = $H_2PC{\equiv}CCH_3$			
		+0.44	−0.43	+0.03	−0.04	+0.05
H	+0.05	+1.04	−0.64	+0.33	+0.05	+0.13
CH_3	−0.12	+1.27	−0.63	+0.30	+0.03	+0.11
Fp	+1.05	+0.24	−0.51	+0.16	−0.01	+0.09
			L = $H_2PC{\equiv}CCOOCH_3$			
		+0.44	−0.31	−0.12	−0.03	+0.05
H	+0.06	+1.02	−0.55	+0.20	+0.06	+0.15
CH_3	−0.11	+1.26	−0.53	+0.17	+0.04	+0.14
Fp	+1.07	+0.23	−0.41	+0.02	0.00	+0.10

As has been pointed out,[6a,26,27] the MPA charges are very sensitive to the basis set, particularly as the basis set is enlarged to higher accuracy. The charges of the acetylenic carbons are specially affected by this fact. The much smaller basis set sensitivity of the NPA charges has been tested. The NPA charges converge as the basis set expands. The largest changes occur when passing from the 3-21G to the 3-21G* basis set (i.e. a set of d atomic orbitals have been added to the P atom). Basis set expansion beyond the 6-31G* does not produce any significant change of the atomic charges. Therefore we have chosen the NPA method and the 6-31G* basis set to calculate the atomic charges. It is noteworthy that the 3-21G charges (without inclusion of d orbitals on the P atom) already give the C−C bond polarized in the same way. NPA atomic charges for the $H_2PC{\equiv}CR$ and $[(X)H_2PC{\equiv}CR]^+$ systems are presented in Table 5.

In the $[(X)H_2PC{\equiv}CR]^+$ systems the phosphorus atom charges and the X group charges (q_X) are very different when X = H, CH_3 or X = Fp. As expected, in the first case the charge +1 is placed on the P atom; on the contrary, in the Fp complex the charge is found on the metallic fragment, mainly located on the Fe atom. The most appealing result from Table 5 is the C≡C bond polarization. In all the systems considered, electronic density is concentrated on the C_1 atom which becomes more negative than C_2. This polarization is also present in the free ligands, but it is strongly enhanced in the coordinated systems. The polarization reaches a maximum when X is H or CH_3, and for X = Fp intermediate values between the phosphoniumalkynes (X = H, CH_3) and the free ligands are obtained. In spite of the important variations in each atomic carbon charge, the variations in the total charge ($q(C_1) + q(C_2)$) are considerably less important. For instance, in case of L = $H_2PC{\equiv}CCH_3$ the total charge goes from 0.40 electrons (e) in the free ligand to 0.36 e in $[(Fp)H_2PC{\equiv}CCH_3]^+$ and 0.33 e in $[(CH_3)H_2PC{\equiv}CCH_3]^+$, and the charge difference between the two carbon atoms goes from 0.46 e to 0.68 e and 0.93 e, respectively. It is interesting to point out the opposite C≡C acetylenic bond polarization of the alkyl-substituted alkynes: in propyne the β carbon bears a charge of −0.26 and the α carbon −0.03.

NBO Analysis. The NPA charges from ab initio calculations have clearly shown the polarization of the C−C triple bond. The C−C framework is constituted by one σ and two π bonds. In order to get a deeper insight into the charge redistribution in the triple bond we have carried out an NBO analysis[28] of the calculated wave functions. This analysis allows us to separate σ- and π-effects. Natural bond orbitals (NBOs) are computed in the natural atomic orbital basis and are the localized one- or two-center orbitals that form an orthogonal set. In this way, three NBOs are found in the acetylenic compounds, with only coefficients on C_1 and C_2. One NBO, formed by combination of two sp hybrids, one for each carbon, corresponds to the σ_{C-C} bond, and two NBOs, formed each one by combination of two p_C orbitals, correspond to the two π_{C-C} bonds ($\pi^{\parallel}$ and $\pi^{\perp}$). Polarization will be reflected on the values of the coefficients of the NBO for each carbon atom. The percentage of coefficients for C_1 and C_2 of the three NBOs are presented in Table 6 for the $H_2PC{\equiv}CCH_3$ and $[(X)H_2PC{\equiv}CCH_3]^+$ (X = H, CH_3, Fp) systems. Similar values are found for the ligands $H_2PC{\equiv}CH$ and $H_2PC{\equiv}CCOOCH_3$ (supplementary material).

Table 6. Percentage of Coefficients in C_1 and C_2 of the Three NBOs Corresponding to the C−C Triple Bond for the $H_2PC{\equiv}CCH_3$ and $[(X)H_2PC{\equiv}CCH_3]^+$ Systems

	σ_{CC}		$\pi^{\parallel}_{CC}$		$\pi^{\perp}_{CC}$	
X	C_1	C_2	C_1	C_2	C_1	C_2
	49.1	50.9	51.0	49.0	54.2	45.8
H	50.2	49.8	60.2	39.8	60.2	39.8
CH_3	50.1	49.9	59.5	40.5	59.4	40.6
Fp	49.8	50.2	54.9	45.1	57.0	43.0

Table 7. NBOs Occupancies for the $H_2PC{\equiv}CCH_3$ and $[(X)H_2PC{\equiv}CCH_3]^+$ Systems

X	π_{CC}[a]	π^*_{CC}[b]	σ^*_{PH}[c]	σ^*_{PC}	d_P[d]
	3.955	0.092	0.024	0.014	0.04
H	3.916	0.078	0.050	0.025	0.06
CH_3	3.920	0.078	0.056	0.024	0.06
Fp	3.946	0.082	0.108	0.050	0.06

[a] Total occupancy of the two π_{CC} NBOs. [b] Total occupancy of the two π^*_{CC} NBOs. [c] Total occupancy of two σ^*_{PH} NBOs. [d] Total occupancy of 3d orbitals on P atom, by NPA.

From values in Table 6 it is clear that the polarization of the C−C bond is a π-effect. The σ_{C-C} bond is not polarized in all the studied systems (% coefficient for $C_1 \approx$ % coefficient for C_2). In the free ligands the $\pi^{\parallel}$ NBO in the PCC plane (PCC angle deviates slightly from 180°) is not polarized and only a slight polarization of the $\pi^{\perp}$ NBO perpendicular to the PCC plane is found. It is interesting to point out that in the $H_2PC{\equiv}CCOOCH_3$ ligand the slight polarization of the $\pi^{\perp}$ NBO occurs in the opposite way (49% coefficient in C_1 and 51% coefficient in C_2). This fact can be related to the $COOCH_3$ group π-acceptor character. In the cationic systems with X = H, CH_3, a strong polarization of the two π-bonds is found (approximately 60% C_1, 40% C_2). This polarization is remarkably reduced when X = Fp.

To go further into the π-effects, we have also looked at the occupancies of different NBOs in the calculated systems. These occupancies are collected in Table 7 for the systems $H_2PC{\equiv}CCH_3$ and $[(X)H_2PC{\equiv}CCH_3]^+$ (X = H, CH_3, Fp) and will be commented on in the next section. This kind of analysis has proved to be very useful in the study of hypervalence and hypercon-

(27) Baker, J. *Theor. Chim. Acta* **1985**, *68*, 621.

(28) (a) Foster, J. P.; Weinhold, F. *J. Am. Chem. Soc.* **1980**, *102*, 7211. (b) Reed, A. E.; Weinhold, F. *J. Chem. Phys.* **1983**, *78*, 4066. (c) Reed, A. E.; Weinhold, F. *J. Chem. Phys.* **1985**, *83*, 1736. (d) Reed, A. E.; Curtiss, J. A.; Weinhold, F. *Chem. Rev.* **1988**, *88*, 899.

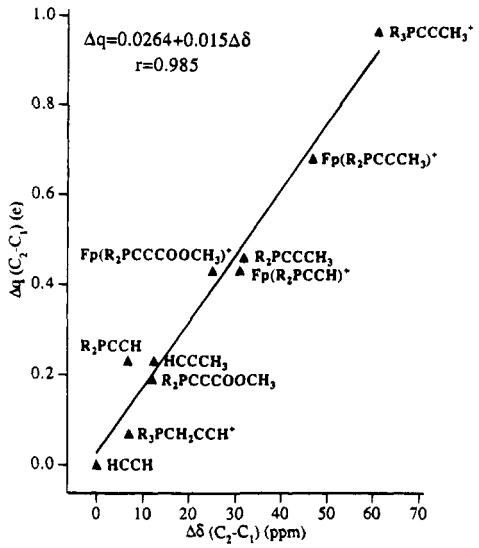

Figure 2. Experimental ^{13}C NMR chemical shift differences of acetylenic carbons ($\Delta\delta = \delta(C_2) - \delta(C_1)$) plotted against calculated NPA charge differences (Δq) between C_2 and C_1.

jugation.[6,28d] Hyperconjugation has been equated with the electron delocalization from bond or lone pair NBOs into antibond NBOs.[28d]

Discussion

On comparing structural theoretical results based on model systems with data coming from X-ray analysis, good agreement is observed. Furthermore, an interesting relationship between experimental ^{13}C NMR data and calculated atomic charges is found. The difference between the ^{13}C NMR shift values of acetylenic carbons has been used as a measure of polarization in the carbon–carbon triple bond.[8b] In order to test this idea, the experimental ^{13}C NMR chemical shift differences $\Delta\delta = \delta(C_2) - \delta(C_1)$ in the synthesized (diphenylphosphino)alkyne ligands and their Fp complexes have been plotted against the NPA charge differences between C_2 and C_1 (Δq) calculated in the related model systems $H_2PC{\equiv}CR$ and $[(X)H_2PC{\equiv}CR]^+$. The reported $\Delta\delta$ values for $[Ph_3PC{\equiv}CMe]^+$, $[Ph_3PCH_2C{\equiv}CH]^+$, and propyne[8b] have also been included.

As can be seen in Figure 2, there is a strong correlation between the experimental $\Delta\delta$ and theoretical Δq values. This fact indicates that the main electronic features of phosphinoalkyne compounds are well reproduced by the calculations.

In order to discuss the π-effects, a notable point which can be deduced from the theoretical study is the total d-orbital population on the phosphorus atom (Table 7). In all studied systems the total phosphorus 3d orbital occupancy is very small. Moreover, it does not change appreciably when coordinated. So, according to these results there is little or no π-back-bonding into $3d_P$ orbitals. This conclusion agrees with recent high-level theoretical studies[6] and confirms that although d orbitals must be employed in order to obtain quantitatively correct bond lengths and energies for species containing second-row atoms, the role of d orbitals is to act as a polarization function.

Another interesting aspect may be deduced from NBO occupancies. Values reported in Table 7 show that variations in the occupancies of the π_{CC} and π^*_{CC} NBOs are minor. This fact indicates that the triple bond polarization is better described as a reorganization of the π electronic density than donation to empty phosphorus orbitals. In the *free ligands*, the π^*_{CC} occupancy is higher than in the coordinated systems. This occupancy comes from the delocalization of the phosphorus lone pair and may be related to the lower $\nu(C{\equiv}C)$ frequencies observed in acetylenic phosphines with respect to alkynes. When this interaction vanishes because of an X–P bond formation, a strengthening of the C≡C bond is expected.

In the *cationic systems with σ-bound groups (X = H, CH_3)*, the acetylenic fragment does not act as an electron donor to the $(X)H_2P$ group (Table 7). The strong polarization of the C≡C bond can be understood when the +1 charge that the phosphorus bears in these cationic systems is taken into account. The positive charge on the P atom strongly polarizes the C≡C π-electron density, concentrating electron density on the carbon atom bonded to P. The P–C bond is shortened because of this interaction (see X-ray data in Tables 1–2 and calculated values in Table 4). Another effect contributes to the increase and decrease of electron density respectively on C_1 and C_2. Although no net charge transfer to π^*_{PA3} orbitals occurs, the presence of these π^*_{PA3} orbitals allows the second-order mixing of π^*_{CC} into π_{CC}, polarizing the charge distribution of both orbitals. This effect is well known in π-acceptor substituted alkenes, and the resulting π orbital topology resembles in this case that of the allyl cation system.[29]

When *the phosphinoalkyne is bonded to the transition metal fragment (X = Fp)*, the C≡C bond polarization is halfway between free phosphinoalkynes and cationic systems with σ-bound groups. This fact may be understood by taking into account that the +1 charge is placed on the Fe atom instead of the P atom. In these systems the NBO populations show a noticeable occupancy of the σ^*_{P-H} and σ^*_{P-C} antibond NBOs, indicating the donation from the metal $d\pi$ into the empty σ^*_{P-A}. This result agrees with the conclusions of Orpen et al.[30] from the systematic study of $X-PA_3$ species crystal structure: if X = transition metal, there is π-donation from metal d orbitals to σ^*_{P-A} orbitals. This fact has structural effects on the PA_3 ligands, leading to long P–A distances and small A–P–A angles. On the contrary, strongly σ-bound X groups, such as H^+ or R^+ (R = alkyl), are associated with small P–A distances and large A–P–A angles. Structural X-ray results (Tables 1–2) and calculated geometries (Table 4) are in agreement with this point of view.

In conclusion, in the combined theoretical and experimental study on π-effects in cationic systems with P-coordinated phosphinoalkynes we have not observed π-electron transfer from the filled π C≡C orbitals to the empty phosphorus d orbitals. On the other hand there is a significant difference between $[(X)Ph_2PC{\equiv}CR]^+$ (X = H, CH_3) and $[(Fp)Ph_2PC{\equiv}CR]^+$ systems. In the first case there is a strong $\pi(C{\equiv}C)$ bond polarization as a consequence of phosphorus atom +1 charge. In the second case the charge is mainly placed on iron atom and the polarization is reduced. This fact is related to

(29) Albright, T. A.; Burdett, J. K.; Whangbo, M. H. *Orbital Interactions in Chemistry*; Wiley: New York, 1985; pp 163–165.
(30) Dunne, B. J.; Morris, R. B.; Orpen, A. G. *J. Chem. Soc., Dalton Trans.* **1991**, 653.

the π-back-donation from metal d orbitals to the empty σ^*_{P-A} orbitals.

Experimental Section

General Comments. All reactions were performed under nitrogen by standard Schlenk tube techniques. Infrared spectra were recorded with a Perkin-Elmer 1710 FT spectrometer using dichlorometane solutions or KBr pellets. The NMR spectra were recorded by the Servei de Ressonancia Magnètica Nuclear de la Universitat Autònoma de Barcelona on a Bruker AM400 instrument. The ^{31}P chemical shifts are reported in ppm upfield from external 85% H_3PO_4. The ^1H and ^{13}C chemical shifts are expressed in ppm upfield from TMS.

Compounds $Ph_2PC{\equiv}CR$ (R = H, CH_3, ^tBu, Ph, Tol, COOMe) were prepared by published procedures.[31] Microanalysis were performed at the Servei d'Anàlisi Química de la Universitat Autònoma de Barcelona.

The diffraction measurements were recorded by the Servei de difracció de raigs X de la Universitat Autònoma de Barcelona.

Synthesis of $[CpFe(CO)_2(Ph_2PC{\equiv}CR)]^+$ (R = H (1), CH_3 (2), ^tBu (3), Ph (4), Tol (5), COOMe (6)). Dichloromethane (20 mL) was added to a mixture of $[(C_5H_5)_2Fe_2(CO)_4]$ (0.5 g, 1.4 mmol) and phosphinoalkyne (3 mmol). After 10 min of stirring, $[Fe(C_5H_5)_2][BF_4]$ (0.74 g, 2.7 mmol) in CH_2Cl_2 (10 mL) was added and the solution stirred for 2 h. The red solution was filtered from the precipitated ferrocene and then evaporated to dryness. The red oil was washed with light petroleum (2 × 10 mL) and recrystallized from CH_2Cl_2–diethyl ether at −20 °C. The yellow crystals which separated were collected, washed with diethyl ether, and dried *in vacuo*.

Yield of **1**, 84%. Anal. Calcd for $BF_4FePC_{21}H_{16}O_2$: C, 53.21; H, 3.38. Found: C, 53.36; H, 3.54. IR (ν_{CO}, CH_2Cl_2): 2060 (s), 2020 (s) cm^{-1}. IR (ν_{CH}): 3225 cm^{-1} (≡C–H). ^1H NMR ($(CD_3)_2CO$): 5.1 (d, J = 9.2 Hz, ≡CH), 5.7 (d, J = 10.9 Hz, Cp), 7.7 (m, Ph) ppm. ^{31}P NMR ($(CD_3)_2CO$): 42.2 ppm. ^{13}C NMR ($(CD_3)_2CO$; except phenyl resonances): 209.3 (d, J = 24.5 Hz, CO), 107.0 (d, J = 15.5 Hz, ≡CH), 90.1 (s, Cp), 76.1 (d, J = 100.7 Hz, PC≡) ppm.

Yield of **2**, 84%. Anal. Calcd for $BF_4FePC_{22}H_{18}O_2$: C, 54.14; H, 3.69. Found: C, 54.30; H, 4.13. IR (ν_{CO}, CH_2Cl_2): 2061 (s), 2019 (s) cm^{-1}. IR ($\nu_{C\equiv C}$, CH_2Cl_2): 2202 (w) cm^{-1}. ^1H NMR ($(CD_3)_2CO$): 7.7 (m, Ph), 5.7 (s, Cp), 2.4 (s, Me) ppm. ^{31}P NMR ($(CD_3)_2CO$): 39.7 ppm. ^{13}C NMR ($(CD_3)_2CO$; except phenyl resonances): 209.9 (d, J = 24.4 Hz, CO), 117.9 (d, J = 19.1 Hz, ≡*C*Me), 90.1 (s, Cp), 70.9 (d, J = 115.2 Hz, PC≡), 5.5 (s, Me) ppm.

Yield of **3**, 86%. Anal. Calcd for $BF_4FePC_{25}H_{24}O_2$: C, 56.65; H, 4.54. Found: C, 56.35; H, 5.07. IR (ν_{CO}, CH_2Cl_2): 2061 (s), 2020 (s) cm^{-1}. IR ($\nu_{C\equiv C}$, CH_2Cl_2): 2209 (w), 2169 cm^{-1}. ^1H NMR ($(CD_3)_2CO$): 7.7 (m, Ph), 5.9 (s, Cp), 1.5 (s, Me) ppm. ^{31}P NMR ($(CD_3)_2CO$): 38.7 ppm. ^{13}C NMR ($(CD_3)_2CO$; except phenyl resonances): 209.6 (d, J = 23.1 Hz, CO), 127.9 (d, J = 14.8 Hz, ≡C^{t}Bu), 89.7 (s, Cp), 70.9 (d, J = 112.8 Hz, PC≡), 23.0 (s, Me) ppm.

Yield of **4**, 86%. Anal. Calcd for $BF_4FePC_{27}H_{20}O_2$: C, 58.95; H, 3.64. Found: C, 59.27; H, 4.09. IR (ν_{CO}, CH_2Cl_2): 2062 (s), 2021 (s) cm^{-1}. IR ($\nu_{C\equiv C}$, CH_2Cl_2): 2172 (w) cm^{-1}. ^1H NMR ($(CD_3)_2CO$): 7.7 (m, Ph), 5.8 (s, Cp) ppm. ^{31}P NMR ($(CD_3)_2CO$): 46.7 ppm. ^{13}C NMR ($(CD_3)_2CO$; except phenyl resonances): 209.6 (d, J = 24.3 Hz, CO), 115.7 (d, J = 16.1 Hz, ≡*C*Ph), 90.0 (s, Cp), 80.3 (d, J = 107.1 Hz, PC≡) ppm.

Yield of **5**, 89%. Anal. Calcd for $BF_4FePC_{28}H_{22}O_2$: C, 59.62; H, 3.90. Found: C, 59.89; H, 4.25. IR (ν_{CO}, CH_2Cl_2): 2061 (s), 2020 (s) cm^{-1}. IR ($\nu_{C\equiv C}$, CH_2Cl_2): 2171 (w) cm^{-1}. ^1H NMR ($(CD_3)_2CO$): 7.7 (m, Ph), 5.7 (s, Cp), 2.4 (s, CH_3) ppm. ^{31}P NMR ($(CD_3)_2CO$): 42.4 ppm. ^{13}C NMR ($(CD_3)_2CO$; except phenyl resonances): 209.4 (d, J = 24.2 Hz, CO), 116.5 (d, J = 18.0 Hz, ≡CTol), 89.9 (s, Cp), 80.0 (d, J = 100.6 Hz, PC≡), 21.4 (s, CH_3) ppm.

Yield of **6**, 85%. Anal. Calcd for $BF_4FePC_{23}H_{18}O_4$: C, 51.91; H, 3.39. Found: C, 51.40; H, 3.60. IR (ν_{CO}, CH_2Cl_2): 2067 (s), 2026 (s), 1725 (m) cm^{-1}. IR ($\nu_{C\equiv C}$, CH_2Cl_2): 2196 (w) cm^{-1}. ^1H NMR ($(CD_3)_2CO$): 7.7 (m, Ph), 5.8 (d, J = 1.6 Hz, Cp), 3.9 (s, Me) ppm. ^{31}P NMR ($(CD_3)_2CO$): 38,2 ppm. ^{13}C NMR ($(CD_3)_2CO$; except phenyl resonances): 208.6 (d, J = 23.5 Hz, CO), 152.2 (s, *C*OOMe), 102.2 (d, J = 10.4 Hz, *C*≡COOMe), 90.0 (s, Cp), 77.2 (d, J = 85.3 Hz, PC≡), 53.9 (s, Me) ppm.

X-ray Structure Determination and Refinement of Complex 4. A suitable single crystal (0.5 × 0.4 × 0.2 mm) was mounted on an Enraf-Nonius CAD4 automatic diffractometer using graphite-monochromated Mo Kα radiation. The cell parameters were obtained by a least-squares fit of 25 well-centered reflections in the range of 23° < 2θ < 28°. Intensity data were collected using the ω/2θ scan mode in the range 2° < 2θ < 50°. Crystal data and measurement conditions are submitted as supplementary material. One intense reflection monitored every hour did not show any significant change in intensity during data collection. Intensities were corrected for Lorentz and polarization effects. An absorption correction via Ψ scans was applied (min. trans. 97.20%, max. trans. 99.99%). The structure was solved by direct methods using the SHELXS program.[32] All non-H atoms of the cation were found in this step. The refinement was performed by full-matrix least-squares methods.[33] The positions of H atoms were calculated and an overall isotropic thermal parameter was refined. The anion shows disorder. Four BF_4 ions were refined with restrained geometries. Their occupation factors were found to be close to 0.25. The B atoms were refined with individual thermal parameters. For the F atoms four different overall thermal parameters were used, one for each BF_4 considered. The last anisotropic refinement cycle converged to $R(F) = 0.049$ (all reflections), $R_w(F^2) = 0.118$ with $R_w(F^2) = \Sigma w(F_o^2 - F_c^2)^2/\Sigma[w(F_o^2)^2]^{1/2}$ and $w = 1/(\sigma^2(F_o^2) + (0.0503P)^2 + 1.17P)$ where $P = (\max(F_o^2,0) + 2F_c^2)/3$. Maximum and minimun heights in the final difference Fourier were 0.47 and −0.63 e Å^{-3}. The final atomic coordinates and equivalent isotropic temperature factors are submitted as supplementary material. The scattering factors were taken from the *International Tables for X-ray Crystallography*, Vol. C, Tables 4.2.6.8 and 6.1.1.4.

Details of the ab Initio Calculations. Ab initio SCF all-electron calculations with the 6-31G* basis set[34] were carried out by means of the GAUSSIAN90 series of programs.[35] This basis set has been recently employed in several studies of hypervalent molecules containing phosphorus atoms and it has been proven that it accurately reproduces the geometries and electronic structures of these molecules.[36] For computational limitations, in the systems with X = Fp a valence-double-ζ basis set was used for iron,[37a] and a minimal basis set was taken for the CO and Cp ligands.[37b] Geometries were fully

(31) (a) Charrier, C.; Chodkiewicz, W.; Cadiot, P. *Bull. Soc. Chim. Fr.* **1966**, 1002. (b) Carty, A. J.; Hota, N. K.; Ng, T. W.; Patel, H. A.; O'Connor, T. J. *Can. J. Chem.* **1971**, *49*, 2706. (c) Montllo, D.; Suades, J.; Dahan, F.; Mathieu, R. *Organometallics* **1990**, *9*, 2933. (d) Louattani, E.; Suades, J.; Mathieu, R. *J. Organomet. Chem.* **1991**, 335.

(32) Sheldrick, G. M. SHELXS 86. Crystallographic Computing 3, Sheldrick, G. M., Krüger, C., Goddard, R., Eds.; Oxford University Press, 1985, pp 175–189.

(33) Sheldrick, G. M. SHELXL 92. A program for the refinement of crystal structures. Goettingen University, 1992.

(34) (a) Hehre, W. J.; Ditchfield, R.; Pople, J. A. *J. Chem. Phys.* **1972**, *56*, 2257. (b) Hariharan, P. C.; Pople, J. A. *Theor. Chim. Acta* **1973**, *28*, 213. (c) Binkley, J. S.; Gordon, M. S.; De Frees, D. J.; Pople, J. A. *J. Chem. Phys.* **1982**, *77*, 3654.

(35) Frish, M. J.; Head-Gordon, M.; Trucks, G. W.; Foresman, J. B.; Schlegel, H. B.; Raghavachari, K.; Robb, M. A.; Binkley, J. S.; Gonzalez, C.; DeFrees, D. J.; Fox, D. J.; Whiteside, R. A.; Seeger, R.; Melius, C. F.; Baker, J.; Martin, R. L.; Kahn, L. R.; Steward, J. J. P.; Topiol, S.; Pople, J. A. GAUSSIAN 90 Program; Gaussian Inc.: Pittsburgh, PA 1990.

(36) Demolliens, A.; Eisenstein, O.; Hiberty, P. C.; Lefour, J. M.; Ohanessian, G.; Shaik, S. S.; Volatron, F. *J. Am. Chem. Soc.* **1989**, *111*, 5623.

(37) (a) Dobbs, K. D.; Hehre, W. *J. Comput. Chem.* **1987**, *8*, 861. (b) Hehre, W. J.; Steward, R. F.; Pople, J. A. *J. Chem. Phys.* **1969**, *51*, 2657.

optimized within C_s symmetry with Schlegel's gradient techniques.[38] In the $[(Fp)H_2PC{\equiv}CR]^+$ complexes only the phosphorus ligand was fully optimized, keeping fixed the geometry of the metallic fragment to their X-ray determined values.

A major point of the theoretical calculations is to obtain values of the atomic charges reliable enough to be compared with the experimental ^{13}C NMR chemical shifts. In order to do this, the natural population analysis (NPA) method[26] was applied. The NPA and the natural bond orbital (NBO) analysis have already been successfully employed to study hypervalence and hyperconjugation in phosphorus inorganic compounds[6] and they are also being applied to transition-metal systems.[39] To asses the validity of the NPA in the systems studied in the present work, the simplest molecules considered ($H_2PC{\equiv}CH$ and $[H_3PC{\equiv}CH]^+$)were also optimized with the 3-21G,[40] 3-21G*[41], 6-31+G*,[42] and 6-31+G**[42] basis sets. The basis set dependence of the atomic charges obtained by the NPA and the Mulliken population analysis were compared. The NPA and NBO analyses were carried out with the GAUSSIAN90 adaptation of the NBO program.

Acknowledgment. We thank the DGICYT (Projects PB89-0306 and PB92-0621, Programa de Promoción General del Conocimiento) for financial support. Dr. R. Mathieu (Toulouse) and Prof. Y. Jean and F. Volatron (Orsay) are gratefully acknowledged for valuable discussions. We thank the European Center for Parallelism of Barcelona, C.E.P.B.A., for providing computational time on a CONVEX C-3480 computer.

Supplementary Material Available: For compound **4**, tables of crystal data and structure refinement, atomic coordinates and isotropic thermal parameters, bond distances and angles, anisotropic thermal parameters, and selected torsion angles and the percentage of coefficients in C_1 and C_2 of the three NBOs corresponding to the C−C triple bond and NBO occupancies for the ligands $H_2PC{\equiv}CH$ and $H_2PC{\equiv}CCOOCH_3$ (10 pages). Ordering information is given on any current masthead page.

OM940516P

(38) Schlegel, H. B *J. Comput. Chem.* **1982**, *3*, 214.
(39) (a) Harris, H. A.; Karris, D. R.; Dahl, L. F. *J. Am. Chem. Soc.* **1991**, *113*, 8602. (b) Maseras, F.; Morokuma, K. *Chem. Phys. Lett.* **1992**, *195*, 500.
(40) (a) Binkley, J. S.; Pople, J. A.; Hehre, W. J. *J. Am. Chem. Soc.* **1980**, *102*, 939. (b) Gordon, M. S.; Binkley, J. S.; Pople, J. A.; Pietro, W. J.; Hehre, W. J. *J. Am. Chem. Soc.* **1982**, *104*, 2797.
(41) Pietro, W. J.; Frand, H. M.; Hehre, W. J.; DeFrees, D. J.; Pople, J. A.; Binkley, J. S. *J. Am. Chem. Soc.* **1982**, *104*, 5039.
(42) (a) Clark, T.; Chandrasekhar, J.; Spitznagel, G. W.; Schleyer, P. v. R. *J. Comput. Chem.* **1983**, *4*, 294. (b) Frisch, M. J.; Pople, J. A.; Binkley, J. S. *J. Chem. Phys.* **1984**, *80*, 3265. (c) Latajka, Z.; Scheiner, S. *Chem. Phys. Lett.* **1984**, *105*, 435.

Charge Dispersal in Iminium-Substituted Alkynes: Synthesis, Spectral Characterization, and Crystal Structure Determination of a $Co_2(CO)_6$-Complexed Propyne Iminium Salt and Structural Comparison with Its Uncomplexed Counterpart

Gerhard Maas,*[,†,§] Rainer Rahm,[†] Dieter Mayer,[†] and Wolfgang Baumann[‡]

Fachbereich Chemie der Universität Kaiserslautern, Erwin Schrödinger-Strasse, D-67663 Kaiserslautern, Germany, and Max-Planck-Gesellschaft, AG Komplexkatalyse an der Universität Rostock, Buchbinderstrasse 5–6, D-18055 Rostock, Germany

Received September 27, 1994[⊗]

In order to elucidate the charge dispersal from an iminium group onto an attached C≡C bond, the crystal structures of a propyne iminium salt and its $Co_2(CO)_6$-complexed analogue have been determined. For 1-(1-methyl-2-butyn-1-ylidene)pyrrolidinium triflate (**3**), the bond lengths of the C≡C–C=N$^+$ unit agree well with those obtained earlier by ab initio calculations; they confirm the nature of these cations as alkynyl-substituted iminium salts, with no significant resonance contribution from a β-aminoallenyl structure. The triflate counterion is closely associated with the iminium function, and a C$^+$–O contact smaller than the sum of the van der Waals radii is found. The first $Co_2(CO)_6$ complex with a propyne iminium ligand has been prepared from **3** and $Co_2(CO)_8$, and after anion exchange, the crystal structure of hexacarbonyl[μ-η^4-(1-methyl-1-(1-pyrrolidiniumylidene)-2-butyne)]dicobalt(*Co–Co*) hexafluorophosphate (**4b**) has been determined. The iminium character is preserved in this complex (C=N$^+$ bond length 1.302(8) Å), and dispersal of the positive charge onto one of the cobalt atoms is obviously not important. IR and NMR data confirm this conclusion. Salt **3**, $C_{10}H_{14}NF_3O_3S$, crystallizes in the monoclinic space group $P2_1/c$ with a = 9.022(3) Å, b = 12.183(2) Å, c = 12.013(2) Å, β = 97.73(3)°, and Z = 4. Cobalt complex **4b**, $C_{15}H_{14}NCo_2F_6O_6P$, crystallizes in the orthorhombic space group $Pca2_1$ with a = 14.170(3) Å, b = 10.780(2) Å, c = 13.718(3) Å, and Z = 4.

Introduction

In alkynyl-substituted carbenium ions **1A**, extensive charge delocalization occurs so that the mesomeric allenyl cation structure **1B** contributes significantly to the bond state. This has been documented by ^{13}C NMR investigations of several alkyl- and aryl-substituted derivatives[1] as well as by theoretical calculations on the parent cation (**1A** ↔ **1B**, R^1–R^3 = H).[2] Electron-donating substituents should stabilize the propargylium structure; specifically, 1-amino-substituted systems should exist as the propyne iminium ions **2A**.

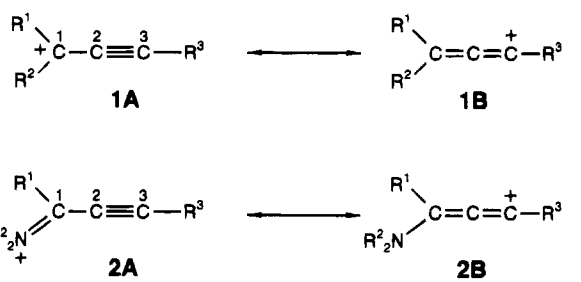

Ab initio and semiempirical calculations fully confirm structure **2A** rather than the β-aminoallenyl form **2B** for the parent ion[2] and several alkyl- or aryl-substituted derivatives.[3] Furthermore, *N,N*-dialkyl propyne iminium salts with only weakly nucleophilic anions (e.g. $CF_3SO_3^-$, ClO_4^-) can be isolated,[4,5] and their solution ^{13}C NMR spectra indicate again the acetylenic and iminium character.[5] In contrast, they can be attacked by nucleophiles either at C-1 to yield propargylamines or at C-3 to yield aminoallenes, depending on the nucleophile, steric factors, and occasionally the reaction conditions.[5a,6] In this study, we present the first crystal structure analysis of a propyne iminium salt, thereby giving a direct experimental confirmation of the bond geometry obtained by theoretical calculations.

Moreover, our successful complexation of the same propyne iminium cation with the $Co_2(CO)_6$ fragment and the crystal structure analysis of this complex allows us to address the question of how much the dinuclear metal fragment can compete with the amino substituent for delocalization of the positive charge. It should be remembered that propargylium cations **1A** (R^1–R^3 =

† Universität Kaiserslautern.
‡ Universität Rostock.
§ New address: Abteilung Organische Chemie I, Universität Ulm, Albert-Einstein-Allee 11, D-89069 Ulm, Germany.
⊗ Abstract published in *Advance ACS Abstracts*, January 1, 1995.

(1) (a) Olah, G. A.; Spear, R. J.; Westerman, P. W.; Denis, J. M. *J. Am. Chem. Soc.* **1974**, *96*, 5855. (b) Olah, G. A.; Berrier, A. L.; Field, L. D.; Prakash, G. K. S. *J. Am. Chem. Soc.* **1982**, *104*, 1349.
(2) Hopkinson, A. C.; Lien, M. H. *J. Am. Chem. Soc.* **1986**, *108*, 2843.
(3) Maas, G.; Würthwein, E.-U.; Singer, B.; Mayer, T.; Krauss, D. *Chem. Ber.* **1989**, *122*, 2311.
(4) (a) Mee, J. D. *J. Am. Chem. Soc.* **1974**, *96*, 4712. (b) Mee, J. D. *J. Org. Chem.* **1977**, *42*, 1035.
(5) (a) Maas, G.; Singer, B.; Wald, P.; Gimmy, M. *Chem. Ber.* **1988**, *121*, 1847. (b) Rahm, R.; Maas, G. *Synthesis* **1994**, 295.
(6) (a) Mayer, T.; Maas, G. *Synlett* **1990**, 399. (b) Maas, G.; Mayer, T. *Synthesis* **1991**, 1209. (c) Rahm, R. Dissertation, University of Kaiserslautern, 1993.

0276-7333/95/2314-1061$09.00/0

Scheme 1[a]

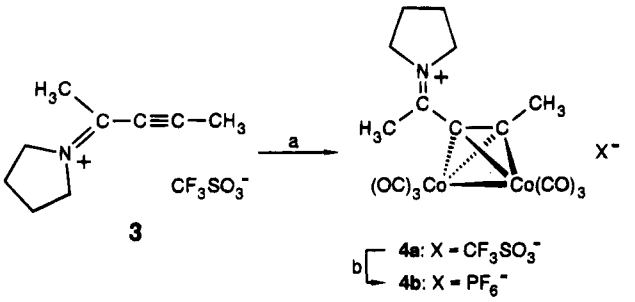

[a] Reagents and conditions: $Co_2(CO)_8$, CH_2Cl_2, −78 °C → room temperature, 82% yield. [b] $Bu_4N^+PF_6^-$, CH_2Cl_2, 31% yield.

alkyl, aryl) have been observed directly only in superacids,[1,7] whereas several $Co_2(CO)_6$ complexes containing such (fully or partially substituted) cations as ligands have been isolated as relatively stable salts.[8] This stabilization is due to an extensive transfer of the positive charge to the transition metal.[8,9]

Results

The propyne iminium triflate **3** was synthesized as described previously.[5b] Complexation of the C≡C bond with the dicobalt hexacarbonyl fragment occurs smoothly in high yield by reaction with a stoichiometric quantity of $Co_2(CO)_8$. However, the triflate salt **4a** so obtained did not form crystals that were suited for X-ray crystal structure analysis; therefore, it was transformed into the hexafluorophosphate **4b**. Both salts are thermally stable and only moderately moisture sensitive. They constitute the first representatives of $Co_2(CO)_6$-complexed propyne iminium salts. The straightforward synthesis of **4a** by complexation of the electron-poor triple bond of **3** parallels the analogous transformations of propargylic aldehydes,[10] acetals,[11] ketones,[12,13] esters,[13−15] and alkynyl-substituted metal carbenes.[16]

IR Spectra. The carbonyl stretching vibrations of **4a,b** are registered at 2095, 2065, 2030, and 2000 cm^{-1} (KBr pellets). For comparison, the carbonyl stretching frequencies of propargyl alcohol complexes $[Co_2(CO)_6(HC{\equiv}CCR_2OH)]$ (R = H, Me, Ph) appear at 2090, 2050, and 2025 cm^{-1} (CH_2Cl_2), whereas those of the derived cationic complexes $[Co_2(CO)_6(HC{\equiv}CCR_2)]^+$ have been registered at 2130, 2105, and 2085 cm^{-1}.[9a] These shifts to higher frequencies in the cations have been interpreted as indicating reduced cobalt → carbonyl backbonding and hence as evidence for charge delocalization into the $Co_2(CO)_6$ unit. Since the first three frequencies of **4a,b** match well with those of the neutral propargyl alcohol−$Co_2(CO)_6$ complexes mentioned above, it can be concluded that in **4a,b** appreciable charge delocalization toward the cobalt atoms does not occur. The preservation of the localized propyne iminium structure is also indicated by the observation that the C=N$^+$ stretching vibration is practically unaffected on complexation (**3**, broad absorption at 1625−1610 cm^{-1} (KBr pellet); **4a,b**, 1617 ± 3 cm^{-1}).

Chart 1. ^{1}H and ^{13}C{^{1}H} NMR Data (δ, ppm) for 3 and 4a

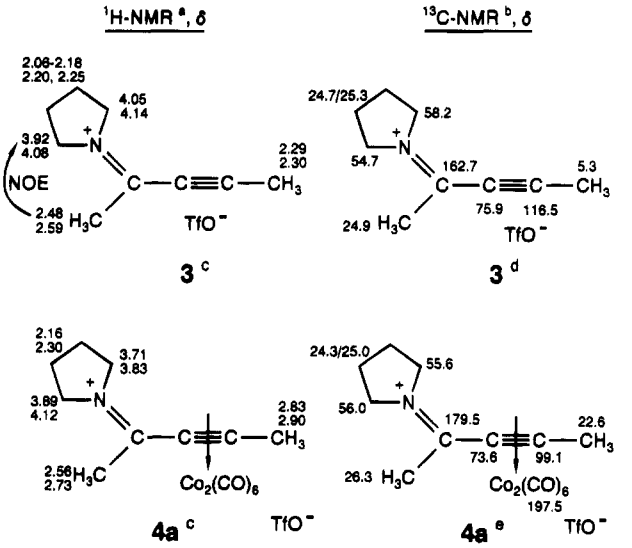

[a] Spectra were recorded at 400.1 MHz; δ values in CD_3CN (upper line) or $CDCl_3$ solution (lower line) are given. [b] Recorded at 100.6 MHz. [c] In contrast to the ≡C—CH_3 signal, that of the iminium-attached CH_3 group is somewhat broadened by long-range coupling. [d] In CD_3CN; assignment of the NCH_2 and CH_3 signals is based on selective ^{13}C{^{1}H} decoupling. [e] In $CDCl_3$.

A comparison of the NMR data of propyne iminium salt **3**[5b] and its $Co_2(CO)_6$-complexed counterpart **4a** is given in Chart 1. The assignments are based on several techniques, as described in the Experimental Part. The differences in the ^{1}H NMR spectra between **3** and **4a** are in general small; the largest change is observed for the terminal methyl group and should be related mainly to the transition from a linear to a bent geometry on complexation of the triple bond (see X-ray analysis of **4b**). In the ^{13}C NMR spectrum of **4a**, the resonances of the two carbon atoms adjacent to the triple bond are shifted downfield by ~17 ppm with respect to **3**. Furthermore, complexation by the metal fragment causes a high-field shift of 2.3 ppm for the acetylenic carbon atom α to the iminium function, but this shift is 13.4 ppm for the remote carbon atom of the triple bond; as a result, the triple bond is far less polarized than in **3**. This indicates that, in **4a**, the substituent effect of the iminium group is no longer transferred to the acetylenic β-position as in **3**, a situation already known for the $Co_2(CO)_6$ complexes of neutral alkynes.[14] Altogether, the ^{13}C NMR data identify **4a** as a typical

(7) (a) Pittman, C. U., Jr.; Olah, G. A. *J. Am.Chem. Soc.* **1965**, *87*, 5632. (b) Richey, H. G., Jr.; Rennick, L. E.; Kushner, A. S.; Richey, J. M.; Philips, J. C. *J. Am. Chem. Soc.* **1965**, *87*, 4017. Richey, H. G., Jr.; Philips, J. C.; Rennick, L. E. *J. Am. Chem. Soc.* **1965**, *87*, 1381.

(8) (a) Review: Nicholas, K. *Acc. Chem. Res.* **1986**, *20*, 207. (b) Gruselle, M.; El Hafa, H.; Nikolski, M.; Jaouen, G.;Vaissermann, J.; Li, L.; McGlinchey, M. J. *Organometallics* **1993**, *12*, 4917.

(9) (a) Connor, R.; Nicholas, K. M. *J. Organomet. Chem.* **1977**, *125*, C45. (b) Padmanabhan, S.; Nicholas, K. M. *J. Organomet. Chem.* **1984**, *268*, C23. (c) Schreiber, S. L.; Klimas, M. T.; Sammakia, T. *J. Am. Chem. Soc.* **1987**, *109*, 5749.

(10) Ju, J.; Reddy, B. R.; Khan, M.; Nicholas, K. M. *J. Org. Chem.* **1989**, *54*, 5426. Mukai, C.; Nagami, K.; Hanaoka, M. *Tetrahedron Lett.* **1989**, *30*, 5623. Mukai, C.; Suzuki, K.; Nagami, K.; Hanaoka, M. *J. Chem. Soc., Perkin Trans. 1* **1992**, 141.

(11) Tester, R.; Varghese, V.; Montana, A. M.; Khan, M.; Nicholas, K. M. *J. Org. Chem.* **1990**, *55*, 186. Ganesh, P.; Nicholas, K. M. *J. Org. Chem.* **1993**, *58*, 5587.

(12) Hoye, T. R.; Suriano, J. A. *J. Org. Chem.* **1993**, *58*, 1659.

(13) For an earlier compilation of $Co_2(CO)_6$ complexes of carbonyl-substituted alkynes, see: Dickson, R. S.; Fraser, P. J. *Adv. Organomet. Chem.* **1974**, *12*, 323.

(14) Aime, S.; Milone, L.; Rossetti, R.; Stanghellini, P. L. *Inorg. Chim. Acta* **1977**, *22*, 135.

(15) Krafft, M. E.; Romero, R. H.; Scott, I. L. *J. Org. Chem.* **1993**, *57*, 5277.

(16) Camps, F.; Moreto, J. M.; Ricart, S.; Vinas, J. M. *Angew. Chem., Int. Ed. Engl.* **1991**, *30*, 1470. Wienand, A.; Reissig, H.-U.; Fischer, H.; Pflumm, D.; Troll, C. *J. Organomet. Chem.* **1992**, *427*, C9.

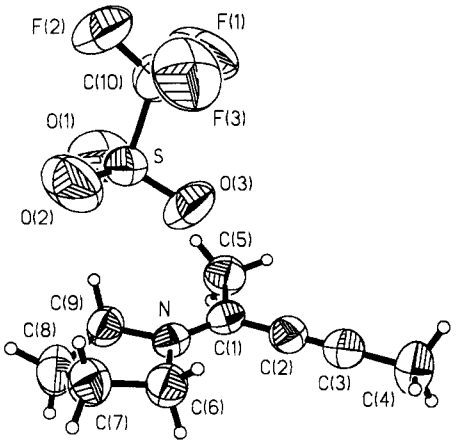

Figure 1. Structure of **3**. The displacement ellipsoids are drawn at 50% probability.

Table 1. Selected Bond Lengths (Å), Angles (deg), and Torsion Angles (deg) in 3[a]

N−C1	1.265(6)	S−O1	1.388(5)
N−C6	1.461(7)	S−O2	1.368(5)
N−C9	1.467(7)	S−O3	1.408(4)
C1−C2	1.406(8)	S−C10	1.764(7)
C1−C5	1.472(9)	C10−F1	1.257(7)
C2−C3	1.170(8)	C10−F2	1.287(7)
C3−C4	1.459(9)	C10−F3	1.329(8)
C1−N−C6	124.8(5)	N−C1−C2	118.8(5)
C1−N−C9	125.3(5)	N−C1−C5	121.2(6)
C6−N−C9	110.0(5)	C2−C1−C5	120.0(6)
C1−C2−C3	176.8(6)	C2−C3−C4	180.0(10)
C6−N−C1−C2			0.9(7)
C6−N−C1−C5			−179.3(5)
N−C6−C7−C8			32.6(5)
C6−C7−C8−C9			−36.2(6)
C7−C8−C9−N			25.5(5)

[a] Esd's are in parentheses.

alkyne−$Co_2(CO)_6$ complex with a localized iminium function. If **4a** behaved like propargylium-$Co_2(CO)_6$ complexes, in which considerable charge transfer to the dicobalt fragment occurs and which are more appropriately characterized as cobalt cations,[9] the resonance of the iminium carbon would be expected at much higher field than observed in the free ligand and that of the acetylenic α-atom at distinctly lower field.

X-ray Structure Analysis of 3. The results of the X-ray crystal structure analysis of **3** are shown in Figure 1 and in Table 1. The bond distances N−C1 (1.265(6) Å) and C2−C3 (1.170(8) Å) fall in the typical range of values that are known for electronically undisturbed C=N$^+$ [17] and C≡C[18] bonds, respectively. Therefore, the cation is readily recognized as a "pure" propyne iminium ion with no significant resonance contribution from a β-aminoallenyl cation structure such as **2B**. The experimental bond lengths of the $^+$N=C−C≡C unit agree remarkably well with those obtained by ab initio calculations;[2,3] furthermore, the small but significant deviation from linearity at C2 is indicated by both experiment and theory. In the first approximation, the crystal structure is held together by dipolar interactions between the iminium function and triflate anions, whereby each iminium ion is associated with two triflate groups and each triflate group employs two oxygen atoms to connect two cations. When we focus on the iminium function, a C1−O3 contact of 3.070(6) Å to one triflate anion and a C1−O1′ contact of 3.268(7) Å to another anion are found, the angle O3−C1−O1′ being 158.8(2)°. Of these two interatomic distances, the latter one is somewhat larger and the C1-O3 contact distinctly shorter than the sum of the van der Waals radii (3.22 Å[19]). The more closely associated triflate oxygen atom O3 is found at about equal distance from C1 and N, whereby the O3−N distance of 3.050(6) Å is more or less a van der Waals contact (3.07 Å[19]). The angle between the N,C1,C2,C5 and N,C1,O3 planes is 88.0°. These geometrical findings justify the description of the crystal structure as being built up of discrete cation/anion pairs (for a space-filling model, see Figure 3) that are interconnected by further attractive electrostatic interactions between a triflate oxygen atom and the iminium function. In line with this description, it is found that the longer the three S−O bond lengths in the anion, the shorter their intermolecular contacts. The significance of this correlation must be considered with caution, however, since experience tells that the apparent S−O (and C−F) bond lengths in the triflate anion are often a result of dynamic or static disorder and therefore not very reliable.

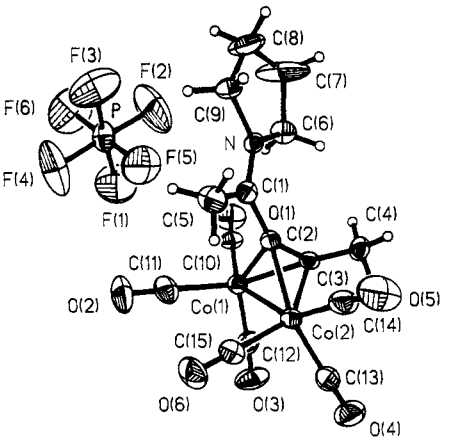

Figure 2. Structure of **4b**. The displacement ellipsoids are drawn at 50% probability.

X-ray Structure Analysis of 4b. The data collection was carried out at −90 °C in order to reduce thermal motion of the PF_6^- group so that more reliable anion−cation contacts could be obtained. The results are shown in Figure 2 and Table 2. It can be seen in Figure 2 that the amplitudes of thermal vibration of the fluorine atoms are still rather large; furthermore, analysis of the bond geometry at C7 and C8 reveals that they are subject to positional disorder, but only averaged positions were obtained with the consequence of a deceptively small bond length C7-C8 and an apparent torsion angle of only 9.8° around this bond.

The main structural features resulting from $Co_2(CO)_6$ complexation of the C≡C bond in **4b** are not different from those found in neutral (alkyne)$Co_2(CO)_6$ com-

(17) (a) Several simple alkyl-substituted iminium salts display unresolvable orientational disorder of the cation in the crystal lattice,[17b,c] so that the experimentally determined bond lengths are somewhat inaccurate. Nevertheless, a rather narrow range for the C=N$^+$ bond length (1.283(12) Å) has been found. (b) Trefonas, L. M.; Flurry, R. L.; Majeste, R.; Meyers, E. A.; Copeland, R. F. *J. Am. Chem. Soc.* **1966**, *88*, 2145. (c) Knop, O.; Cameron, T. S.; Bakshi, P. K.; Kwiatkowski, W.; Choi, S. C.; Adhikesavalu, D. *Can. J. Chem.* **1993**, *71*, 1495.

(18) Allen, F. H.; Kennard, O.; Watson, D. G.; Brammer, L.; Orpen, A. G.; Taylor, R. *J. Chem. Soc., Perkin Trans. 2* **1987**, S1.

(19) Bondi, A. *J. Phys. Chem.* **1964**, *68*, 441.

Table 2. Selected Bond Lengths (Å), Angles (deg), and Torsion Angles (deg) in 4b[a]

N–C1	1.302(8)	P–F1	1.598(7)
N–C6	1.460(8)	P–F2	1.564(6)
N–C9	1.494(8)	P–F3	1.555(6)
C1–C2	1.438(8)	P–F4	1.554(6)
C1–C5	1.484(9)	P–F5	1.584(6)
C2–C3	1.358(8)	P–F6	1.581(7)
C3–C4	1.473(8)		
Co1–C2	1.969(7)	Co2–C2	1.965(6)
Co1–C3	1.974(6)	Co2–C3	1.968(6)
Co1–C10	1.814(7)	Co2–C13	1.832(7)
Co1–C11	1.837(7)	Co2–C14	1.809(8)
Co1–C12	1.807(8)	Co2–C15	1.816(6)
Co1–Co2	2.466(1)	C–O (av)	1.126(8)
C1–N–C6	126.2(5)	C1–C2–C3	147.8(6)
C1–N–C9	122.9(5)	C1–C2–Co1	128.5(4)
C6–N–C9	110.8(5)	C1–C2–Co2	134.2(5)
N–C1–C2	120.1(5)	C2–C3–C4	145.6(6)
N–C1–C5	120.3(5)	C2–C3–Co1	69.6(4)
C2–C1–C5	119.7(5)	C2–C3–Co2	69.7(4)

C6–N–C1–C2	0.1(1.0)
C6–N–C1–C5	−179.6(7)
N–C1–C2–C3	28.1(1.4)
C1–C2–C3–C4	8.8(1.9)

[a] Esd's are in parentheses.

plexes.[20] The core unit is a Co_2C_2 tetrahedron with a Co–Co distance of 2.466(1) Å and a C2–C3 bond length of 1.358(8) Å. The bond angles C1–C2–C3 and C2–C3–C4 (147.8(6) and 145.6(6)°, respectively) fall in the range that is typical (120–150°) for perpendicular-bonded alkyne complexes.[21] Both the C1–C2 and the C1–N bond lengths (1.438(8) and 1.302(8) Å, respectively) are longer than in the uncomplexed propyne iminium ion **3**; these elongations certainly exceed the range that is attributable to the increased libration in the room-temperature structure of **4b** as compared with the low-temperature structure of **3**.

Ideally, the cation would have C_s symmetry with atoms N and C1–C5 in the mirror plane. However, several significant deviations from this symmetry are observed. Especially worth mentioning are the torsion angle N–C1–C2–C3 (28.1°) and the fact that the iminium carbon atom C1 is distinctly closer to Co1 than to Co2 (3.088 vs 3.142 Å).

Discrete cation-anion pairs exist in the crystal structure of **4b**. The spatial arrangement of the pyrrolidinium ring, atoms C1 and C2, and Co1 and two of its carbonyl ligands creates a pocket in which the hexafluorophosphate anion sits (Figure 3). In this orientation, F5 maintains van der Waals contacts with the iminium group (F5···N = 3.027(8) Å, F5···C1 = 3.139(8) Å), and the F5···Co1 distance is 3.828(7) Å. The other closest anion–cation contacts are F3···H4A^{I} (2.39 Å) and F6···H6B^{II} (2.47 Å) (symmetry codes: I, $x - 1/2$, $2 - y$, z; II, $-x$, $2 - y$, $z - 1/2$).

Discussion

The crystal structure analysis of **3** has identified the cationic part of this salt as a true propyne iminium ion

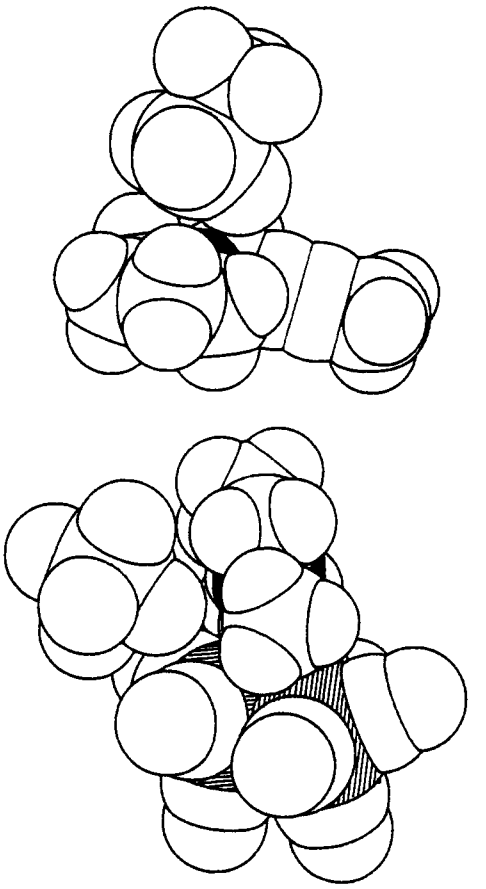

Figure 3. Space-filling models of the salt **3** (top) and of the dicobalt hexacarbonyl complex **4b** (bottom).

with no significant resonance contribution from a β-aminoallenyl structure. Experiment and theory[2,3] are found to be in good agreement. Highly localized π-bonding has also been found in the structures of (3-phenyl-2-propenylidene)dimethylammonium perchlorate and its 4-chlorophenyl analogue.[22] An interesting detail of the crystal structure of **3** is the close association of a triflate anion with the iminium C=N bond, with a C–O contact (3.070 Å) that is 0.15 Å smaller than the sum of the van der Waals radii. The association of a triflate oxygen atom with the iminium carbon atom is not unexpected, since the latter carries the highest positive charge according to calculations[2,3,18b] (whereas the iminium N atom carries a negative net charge) and contacts smaller than or equal to the sum of the van der Waals radii between centers of highest charge density of carbenium ions stabilized by an adjacent heteroatom and of rather nonnucleophilic anions are not unusual.[23,24] The N–C1–O3 angle is 77.2°, and the carbon atom has a perfect trigonal-planar coordination. We leave it open to speculation whether this geometry represents an early point on the trajectory of a nucleophilic addition to the iminium group.[25] While **4a,b** are the first cobalt-

(20) Cotton, F. A.; Jamerson, J. D.; Stults, B. R. *J. Am. Chem. Soc.* **1976**, *98*, 1774. Gregson, D.; Howard, J. A. K. *Acta Crystallogr., Sect. C* **1983**, *39*, 1024.

(21) Hoffman, D. M.; Hoffmann, R.; Fisel, C. R. *J. Am. Chem. Soc.* **1982**, *104*, 3858.

(22) Childs, R. F.; Dickie, B. D.; Faggiani, R.; Fyfe, C. A.; Lock, C. J. L.; Wasylishen, R. E. *J. Crystallogr. Spectrosc. Res.* **1985**, *15*, 73.

(23) For recent examples, see: Jones, P. G.; Linoh, K.; Blaschette, A. *Z. Naturforsch.* **1990**, *45B*, 267. Becker, J. Y.; Shakkour, E.; Shimoni, L. *Struct. Chem.* **1993**, *4*, 85. Lohse, C.; Hollenstein, S.; Laube, T. *Angew. Chem., Int. Ed. Engl.* **1991**, *103*, 1656.

(24) For the analysis of such geometries in some published structures, see: Laube, T. *J. Am. Chem. Soc.* **1989**, *111*, 9224.

(25) For the trajectory of nucleophilic attack at a carbonyl group, see: Cieplak, A. S. In *Structure Correlation*; Bürgi, H.-B., Dunitz, J. D., Eds.; VCH: Weinheim, Germany, 1994; Vol. 1, pp 207–302.-

complexed propyne iminium salts, clusters of ruthenium and osmium formally containing a μ_3-η^2-coordinated propyne iminium ligand have already been synthesized, although not by direct complexation of the cationic ligand with the respective metal fragment. The structures of two such complexes, **5**[26] and **6**,[27] have been

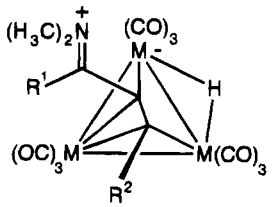

5: M = Ru, R^1 = H, R^2 = CH_3
6: M = Os, R^1 = Et, R^2 = Ph

determined by X-ray diffraction. They are both zwitterions in which the negative charge resides on a metal atom. The length of the C=N$^+$ bond (1.298(5) and 1.29(2) Å, respectively) and in one case of the bond corresponding to C1−C2 in Figure 2 (1.435(5) and 1.51(3) Å, respectively) agree remarkably well with the values found for **4b** (Table 1).

For propargylium ions complexed with $Co_2(CO)_6$ or $Co_2(CO)_5PPh_3$ fragments, NMR and IR spectroscopic studies have indicated considerable charge dispersal onto the metal atoms.[8b,9,28] Unsymmetrical, bent structures such as **7**[9c] with a η^2:η^3-coordinated propargylium

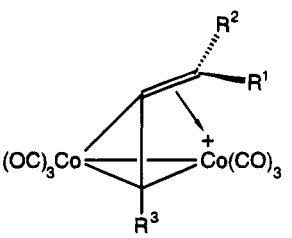

7

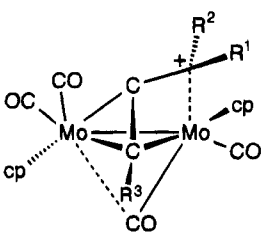

8

ligand are considered as the minimum energy forms of these complexes that display more or less dynamic behavior in solution,[9,28] depending on the degree of charge dispersal. In the absence of crystal structure determinations of propargylium−dicobalt complexes, support for the proposed structures comes from the X-ray structure analyses of several isolobal (propargylium)$Mo_2(CO)_4(cp)_2$ complexes **8**.[29] In all cases studied, the Mo−C$^+$ distance (2.44−2.76 Å) suggests a direct interaction between the empty p orbital at carbon and a metal d orbital. Even in the complex [(2-propynyl-2-bornyl)$Mo(CO)_2cp$−$Co(CO)_3$]BF_4,[8b] cation stabilization by the $Mo(CO)_2cp$ fragment is to be assumed, despite the rather long Mo−C distance of 2.914 Å. In contrast, the structural features of **4b** indicate that the positive charge is localized on the iminium function and charge dispersal to a cobalt atom is not significant. Especially, the distances between the iminium carbon atom and the two cobalt atoms (3.077 and 3.142 Å, respectively) are too large to postulate a significant interaction between the carbenium center and one of the metal atoms. Obviously, the $Co_2(CO)_6$ is too weak a donor to compete with the pyrrolidine ring for stabilization of the positive charge of a propargylium ion. It would be interesting now to investigate how much the $Mo_2(CO)_4cp_2$ fragment, known as a much stronger donor in propargylium complexes,[29] is able to compete with a dialkylamino group for charge stabilization in such complexes.

In conclusion, we have shown that propyne iminium salts with "non-nucleophilic" counterions have a highly localized π-bond system both in solution and in the solid state. The cation−anion orientation in the crystal of **3** excludes any approach to β-(pyrrolidino)allenyl triflate structure. Furthermore, the dicobalt hexacarbonyl complexes of these propyne iminium salts are fully comparable with the analogous complexes of neutral alkynes, and significant charge delocalization onto the metal fragment does not occur.

Experimental Part

General Methods. IR spectra were registered with a Perkin-Elmer 1310 infrared spectrometer. The ^{1}H NMR spectra were recorded on Bruker instruments (AC200, 200.1 MHz; AMX400, 400.1 MHz; ARX400, 400.1 MHz) with the solvent signal as reference ($\delta(CHCl_3)$ = 7.27 ppm). The ^{13}C NMR spectra were also recorded on Bruker AMX400 and ARX400 instruments (100.6 MHz) with the solvent signal as internal standard ($\delta(CDCl_3)$ = 77.0, $\delta(CD_3CN)$ = 118.2 ppm). The assignment of the resonances was achieved by homo- and heteronuclear decoupling experiments. For **4a**, only broadened resonance lines could be observed. This is a common feature of all alkyne dicobalt complexes[9c] and is caused by traces of paramagnetic impurities. Nevertheless, proton NOE difference experiments and a homonuclear shift correlation (^{1}H COSY) were successfully performed and allowed a straightforward analysis of the proton spectrum. Heteronuclear shift correlation gave the corresponding carbon resonances; assigning the three quaternary carbons was only possible by an inverse-detected HMQC experiment via long-range couplings[30] with the delays Δ_1 and Δ_2 set to 4 and 50 ms, respectively. Melting points were determined in a copper block; temperatures given are not calibrated. Elemental analyses were carried out on a Perkin-Elmer analyzer, Model EA 2400. Solvents were dried according to standard procedures.

The synthesis of 1-(1-methyl-2-butyn-1-ylidene)pyrrolidinium trifluoromethanesulfonate (**3**) has been described.[5b]

Hexacarbonyl[μ-η^4-(1-methyl-1-(1-pyrrolidiniumylidene)2-butyne)]dicobalt(*Co*−*Co*) Trifluoromethanesulfonate (4a). To a solution of $Co_2(CO)_8$ (4.10 g, 12.0 mmol) in dry dichloromethane (50 mL), cooled to −78 °C, was added dropwise 3.23 g (11.31 mmol) of salt **3** dissolved in dichloromethane (25 mL). The reaction mixture was stirred for 3 h, during which time it was allowed to assume room temperature. After the solution volume was reduced to 20 mL, a violet-brown microcrystalline solid was precipitated with dry ether. Reprecipitation from dichloromethane solution with ether afforded 5.30 g (82% yield) of **4a**, mp 146 °C dec. IR (KBr): 2095, 2065, 2030, 2000 (all s, CO), 1620 (m, C=N), 1260, 1220, 1155, 1135, 1030 (all s, OTf region) cm^{-1}. ^{1}H NMR ($CDCl_3$, 200 MHz): δ 2.38 (mc, unresolved, 4 H, NCH_2CH_2), 2.73 (s, 3 H, terminal CH_3), 2.80 (s, 3 H, N$^+$=CCH_3), 3.82 and 4.41 (each pseudo-t, broad, 2 H, NCH_2). ^{13}C NMR: see Chart 1; CF_3 not found. Anal. Calcd for $C_{16}H_{14}NCo_2F_3O_9S$ (M_r = 571.2): C, 33.64; H, 2.47; N, 2.45. Found: C, 33.2; H, 2.4; N, 2.4.

Hexacarbonyl[μ-η^4-1-methyl-1-(1-pyrrolidiniumylidene)2-butyne)]dicobalt(*Co*−*Co*) Hexafluorophosphate

(26) Aime, S.; Osella, D.; Deeming, A. J.; Arce, A. J.; Hursthouse, M. B.; Dawes, H. M. *J. Chem. Soc., Dalton Trans.* **1986**, 1459.
(27) Adams, R. D.; Chen, G. *Organometallics* **1990**, *9*, 2882.
(28) Bradley, D. H.; Khan, M. A.; Nicholas, K. M. *Organometallics* **1992**, *11*, 2598.
(29) Meyer, A.; McCabe, D. J.; Curtis, M. D. *Organometallics* **1987**, *6*, 1491. Gruselle, M.; Cordier, C.; Salmain, M.; El Amouri, H.; Guerin, C.; Vaissermann, J.; Jaouen, G. *Organometallics* **1990**, *9*, 2993. Cordier, C.; Gruselle, M.; Vaissermann, J.; Troitskaya, L. L.; Bakhmutov, V. I.; Sokolov, V. I.; Jaouen, G. *Organometallics* **1992**, *11*, 3825.
(30) Bax, A.; Summers, M. F. *J. Am. Chem. Soc.* **1986**, *108*, 2093.

Table 3. Data for Crystal Structure Analysis of 3 and 4b

	3	4b
empirical formula	$C_{10}H_{14}NF_3O_3S$	$C_{15}H_{14}NCo_2F_6O_6P$
fw	285.3	576.1
cryst dimens, mm	0.6 × 0.5 × 0.7	0.75 × 0.50 × 0.35
temp, K	293	183
cryst system	monoclinic	orthorhombic
space group (No.)	$P2_1/c$ (14)	$Pca2_1$ (29)
a, Å	9.022(3)	14.170(3)
b, Å	12.183(2)	10.780(2)
c, Å	12.013(2)	13.718(3)
α, deg	90	90
β, deg	97.73(3)	90
γ, deg	90	90
Z	4	4
D_{calc}, g cm^{-3}	1.448	1.798
Θ range, min/max	2.0/25.0	1.89/23.75
μ(Mo Kα), cm^{-1}	2.7	17.4
no. of measd data	2534	2262
no. of unique data	2417	1812
R(int), %	0.019	0.025
no. of obsd data (I 2 σ(I))	1474	1708
no. of ref params	219	285
R[a]	0.074	0.0318
R_w[a]	0.085	0.0832
max/min residual electron dens, e Å^{-3}	0.46/−0.34	0.37/−0.49

[a] Refinement on F for **3** and on F^2 for **4b**.

(4b). To a solution of **4a** (0.388 g, 0.68 mmol) in dichloromethane (10 mL) was added tetrabutylammonium hexafluorophosphate (0.263 g, 0.68 mmol). When the temperature was lowered to −36 °C, violet-brown crystals of **4b** separated (0.121 g, 31% yield), mp 172 °C dec. IR (KBr): 2095, 2065, 2030, 1995 (all s, CO), 1615 (m, C=N), 830 (PF_6) cm^{-1}. ^{1}H NMR (CD_3CN, 400.1 MHz): δ 2.15 (mc, 4 H, NCH_2CH_2), 2.56 (s, terminal CH_3), 2.83 (N=CCH_3), 3.88 (pseudo-t, 2 H, NCH_2). Anal. Calcd for $C_{15}H_{14}NCo_2F_6O_6P$ (M_r = 567.1): C, 31.77; H, 2.49; N, 2.47. Found: C, 32.2; H, 2.5; N, 2.4.

X-ray Crystal Structure Determination of 3 and 4b. Crystals of **3** were obtained from a dichloromethane solution at −36 °C. The reflection data were collected on an Enraf-Nonius CAD4 diffractometer at room temperature. The structure was solved with MULTAN80[31] and refined by a full-matrix least-squares method. Hydrogen atom positions were partially localized in a difference electron density map and partially calculated. All hydrogen atoms were included in the structure factor calculations as riding on their bond neighbors. The program package MolEN (Enraf-Nonius, Delft, Holland, 1990) was used for all calculations.

A crystal of **4b** mounted on a glass rod was dipped into a perfluorinated polyether (RS3000, Riedl-de-Häen, Seelze, Germany) that served both to fix the crystal and to protect it from moisture during low-temperature data collection. The latter was carried out on a Siemens P4 diffractometer at −90 °C. The structure was solved with SHELXS-86[32] and refined with SHELXL-93.[33] The methylene (CH_2) hydrogen atoms were positioned geometrically; the methyl hydrogen atoms were treated as riding on their bond neighbors during least-squares refinement. An empirical absorption correction was applied (DIFABS[34]): minimum transmission 0.85, maximum transmission 1.36. The absolute structure (polar axis direction) was established by the Flack test; the Flack parameter α was refined to 0.01(3).

Crystal data and refinement results are given in Table 3, and the positional and thermal parameters of **3** and **4b** are listed in Tables 4 and 5, respectively; see the supplementary material for further technical details. The molecule plots were generated by the programs PLATON[35] (Figures 1 and 2) and SCHAKAL[36] (Figure 3).

Table 4. Atomic Coordinates (×10^4) and Equivalent Isotropic Displacement Coefficients[a] (Å^2) for 3

atom	x	y	z	B_{eq}
S	7488(2)	477(1)	−2510(1)	5.70(3)
F1	5495(4)	−999(4)	−3132(4)	12.1(1)
F2	6820(6)	−554(4)	−4365(3)	12.7(2)
F3	7640(5)	−1533(3)	−3066(4)	12.1(1)
O1	6464(6)	1297(4)	−2863(4)	10.3(1)
O2	8869(5)	656(4)	−2827(4)	11.3(1)
O3	7446(6)	129(4)	−1397(3)	10.3(1)
N	7881(4)	2016(3)	283(3)	4.07(9)
C1	6785(5)	1520(4)	609(4)	4.2(1)
C2	7071(5)	663(4)	1393(4)	4.7(1)
C3	7240(5)	−45(5)	2056(4)	5.0(1)
C4	7461(7)	−926(5)	2885(5)	7.3(2)
C5	5233(6)	1826(5)	187(5)	6.5(2)
C6	9452(6)	1758(5)	649(4)	5.7(1)
C7	10268(6)	2300(5)	−196(5)	6.6(2)
C8	9361(7)	3298(5)	−528(5)	7.8(2)
C9	7766(6)	2935(5)	−513(4)	5.5(1)
C10	6762(6)	−665(5)	−3306(4)	6.6(1)

[a] $B_{eq} = {}^4/_3(a^2B_{11} + ... + bc(\cos\alpha)B_{23})$.

Table 5. Atomic Coordinates (×10^4) and Equivalent Isotropic Displacement Coefficients[a] (Å^2) for 4b

atom	x	y	z	U_{eq}
Co1	577(1)	6334(1)	8795(1)	25(1)
Co2	824(1)	5838(1)	10531(1)	26(1)
P	−1627(1)	9467(2)	7270(2)	42(1)
F1	−1110(6)	8384(7)	6680(6)	110(3)
F2	−704(4)	10249(8)	7155(7)	120(3)
F3	−2080(6)	10514(6)	7893(5)	108(2)
F4	−2514(5)	8624(8)	7340(5)	116(3)
F5	−1232(6)	8877(6)	8245(5)	103(2)
F6	−1983(6)	10044(8)	6276(5)	118(3)
O1	1084(4)	7821(5)	7079(4)	52(1)
O2	−1475(4)	5921(6)	8535(5)	65(2)
C1	−18(4)	8486(5)	10135(4)	26(1)
C2	599(4)	7462(6)	9924(5)	27(1)
C3	1487(4)	7066(5)	9720(4)	24(1)
C4	2491(4)	7416(6)	9661(6)	35(2)
C5	−881(5)	8277(7)	10725(7)	44(2)
C6	996(5)	9927(6)	9213(5)	33(2)
C7	940(8)	11283(8)	9099(11)	95(5)
C8	44(6)	11720(7)	9454(9)	65(3)
C9	−444(5)	10686(6)	9970(6)	39(2)
C10	857(5)	7281(6)	7741(5)	29(1)
C11	−693(5)	6094(7)	8611(6)	41(2)
C12	1100(5)	4926(7)	8329(5)	37(2)
C13	1158(4)	4543(6)	10457(6)	39(2)
C14	1120(6)	6383(6)	11740(6)	43(2)
C15	−306(5)	5097(6)	10755(5)	34(2)

[a] U_{eq} is defined as one-third of the trace of the orthogonalized U_{ij} tensor.

Acknowledgment. Financial support by the Deutsche Forschungsgemeinschaft and the Fonds der Chemischen Industrie is gratefully acknowledged. R.R. and D.M. thank the State of Rheinland-Pfalz for a postgraduate fellowship.

Supplementary Material Available: Tables of positional and thermal parameters and bond distances and angles for **3** and **4b** and a table of torsion angles for **3** (10 pages). Ordering information is given on any current masthead page.

OM940747W

(31) Main, P.; Fiske, S. J.; Hull, S. E.; Lessinger, L.; Germain, G.; DeClerq, J. P.; Woolfson, M. M. MULTAN80, a System of Computer Programs for the Automatic Solution of Crystal Structures from X-ray Diffraction Data; University of York, York, England, 1980.
(32) Sheldrick, G. SHELXS-86, a Program for Crystal Structure Determination; University of Göttingen, Göttingen, Germany, 1986.
(33) Sheldrick, G. SHELXL-93, a Program for the Refinement of Crystal Structures from Diffraction Data; University of Göttingen, Göttingen, Germany, 1993.
(34) Walker, N.; Stuart, D. *Acta Crystallogr., Sect. A* **1983**, *39*, 159.
(35) Spek, A. L. *Acta Crystallogr., Sect. A* **1990**, *46*, C34.
(36) Keller, E. SCHAKAL-88 (Version 88B/V16), a FORTRAN Program for the Graphic Representation of Molecular and Crystallographic Models; University of Freiburg, Freiburg, Germany, 1990.

Notes

Theoretical Study of the Addition of SiF_2 and $SiCl_2$ to Ethylene

Mark S. Gordon*

Department of Chemistry, Iowa State University, Ames, Iowa 50011

Ward Nelson

Department of Chemistry, North Dakota State University, Fargo, North Dakota 58105

Received September 14, 1994[⊗]

Summary: The additions of SiF_2 and $SiCl_2$ to ethylene have been studied using fourth order perturbation theory and the 6-311G(d,p) basis set at geometries determined with second order perturbation theory. In contrast with earlier calculations on the analogous SiH_2 addition, found to proceed with no barrier, barrier heights of 18.4 and 4.5 kcal/mol are predicted for the fluoro- and chlorosilylenes, respectively. These results are interepreted in terms of the net energetics, ring strain, and orbital properties.

Introduction

Previous calculations on the addition of SiH_2 to the C=C bond of ethylene[1] and the C≡C bond of acetylene[2] have shown that both reactions proceed with no barrier. On the other hand, replacement of the H ligand with F results in the introduction of a nonzero barrier to addition of SiF_2 to acetylene,[2] due to the stabilization of the silylene leading to decreased exothermicity. Continuing experimental interest in silylene insertions into ethylene[3] has prompted us to investigate the effect of substituents, particularly F and Cl, on the additions of SiX_2 species to the C=C bond of ethylene, using reliable electronic structure calculations.

Computational Methods

Geometries of minima and transition states were optimized at the MP2(FULL) level of theory,[4] using the 6-31G(d) basis set.[5] The stationary points located in this manner were verified as minima or transition states by calculating and diagonalizing the matrix of energy second derivatives (hessian) to determine the number of imaginary frequencies (0 for minima, 1 for transition states). Vibrational zero point corrections were obtained at this level of theory. Final energetics were then determined using full fourth order perturbation theory (MP4[6]) with the 6-311G(d,p) basis set.[7]

Since the product of each reaction is a three-membered ring, it is of interest to determine the relative strain on these rings. A consistent method for assessing ring strain is to determine the energy for a series of "homodesmic" reactions, defined as reactions that preserve the number of each type of chemical group upon proceeding from reactants to products.[8] For the substituted siliranes of interest here, the appropriate homodesmic reactions are

$$\text{c-}SiX_2CH_2CH_2 + 3C_2H_6 \rightarrow CH_3SiX_2CH_3 + 2CH_3CH_2CH_3 \quad (1)$$

The energetics for these homodesmic reactions have also been determined at the MP4/6-311G(d,p)//MP2/6-31G(d) level of theory. The calculations reported here were performed using GAUSSIAN92.[9]

Results and Discussion

A. Geometries. The MP2/6-31G(d) structures of the reactants, products and transition states for the SiF_2 and $SiCl_2$ addition reactions are shown in Figure 1. Note that although the reactants SiX_2 and cyclic products all have C_{2v} symmetry, the transition states are distorted into C_s symmetry. For both reactions, the SiC bond distances in the transition states are ~1.9 and 2.2 Å. This distortion is consistent with the structures of other transition states[10] and is discussed further below. The imaginary frequencies for the SiF_2 and $SiCl_2$ insertions are 529i and 312i cm^{-1}, respectively.

⊗ Abstract published in *Advance ACS Abstracts,* December 15, 1994.

(1) Anwari, F.; Gordon, M. S. *Isr. J. Chem.* **1983**, *23*, 129.
(2) Boatz, J. A.; Gordon, M. S.; Sita, L. R. *J. Phys. Chem.* **1990**, *94*, 5488.
(3) Al Rubaiey, N.; Walsh, R. *J. Phys. Chem.* **1994**, *98*, 5303.
(4) (a) Binkley, J. S.; Pople, J. A. *Int. J. Quantum Chem.* **1975**, *9*, 229. (b) Krishnan, R.; Pople, J. A. *Int. J. Quantum Chem.* **1978**, *14*, 91.
(5) (a) Hariharan, P. C.; Pople, J. A. *Theor. Chim. Acta* **1973**, *28*, 213. (b) Gordon, M. S. *Chem. Phys. Lett.* **1980**, *76*, 163.
(6) Krishnan, R.; Firsch, M. J.; Pople, J. A. *J. Chem. Phys.* **1980**, *72*, 4244.
(7) Krishnan, R.; Binkley, J. S.; Seeger, R.; Pople, J. A. *J. Chem. Phys.* **1980**, *72*, 650.
(8) Disch, R. L.; Schulman, J. M.; Sabio, M. L. *J. Am. Chem. Soc.* **1985**, *107*, 1904.
(9) Frisch, M. J.; Trucks, G. W.; Head-Gordon, M.; Gill, P. M. W.; Wong, M. W.; Foresman, J. B.; Johnson, B. G.; Schlegel, H. B.; Robb, M. A.; Replogle, E. S.; Gomperts, R.; Andres, J. L.; Raghavachari, K.; Binkley, J. S.; Gonzalez, C.; Martin, R. L.; Fox, D. J.; DeFrees, D. J.; Baker, J. Stewart, J. J. P.; Pople, J. A.; GAUSSIAN92; GAUSSIAN, Inc.; Pittsburgh, PA, 1992.
(10) (a) Gordon, M. S.; Gano, D. R. *J. Am. Chem. Soc.* **1984**, *106*, 5421. (b) Gordon, M. S.; Truong, T. N.; Bonderson, E. K. *J. Am. Chem. Soc.* **1986**, *108*, 1421. (c) Truong, T. N.; Gordon, M. S.; Pople, J. A. *Chem. Phys. Lett.* **1986**, *130*, 245. (d) Gordon, M. S.; Boatz, J. A.; Gano, D. R.; Friedrichs, M. *J. Am. Chem. Soc.* **1987**, *109*, 1323.

0276-7333/95/2314-1067$09.00/0

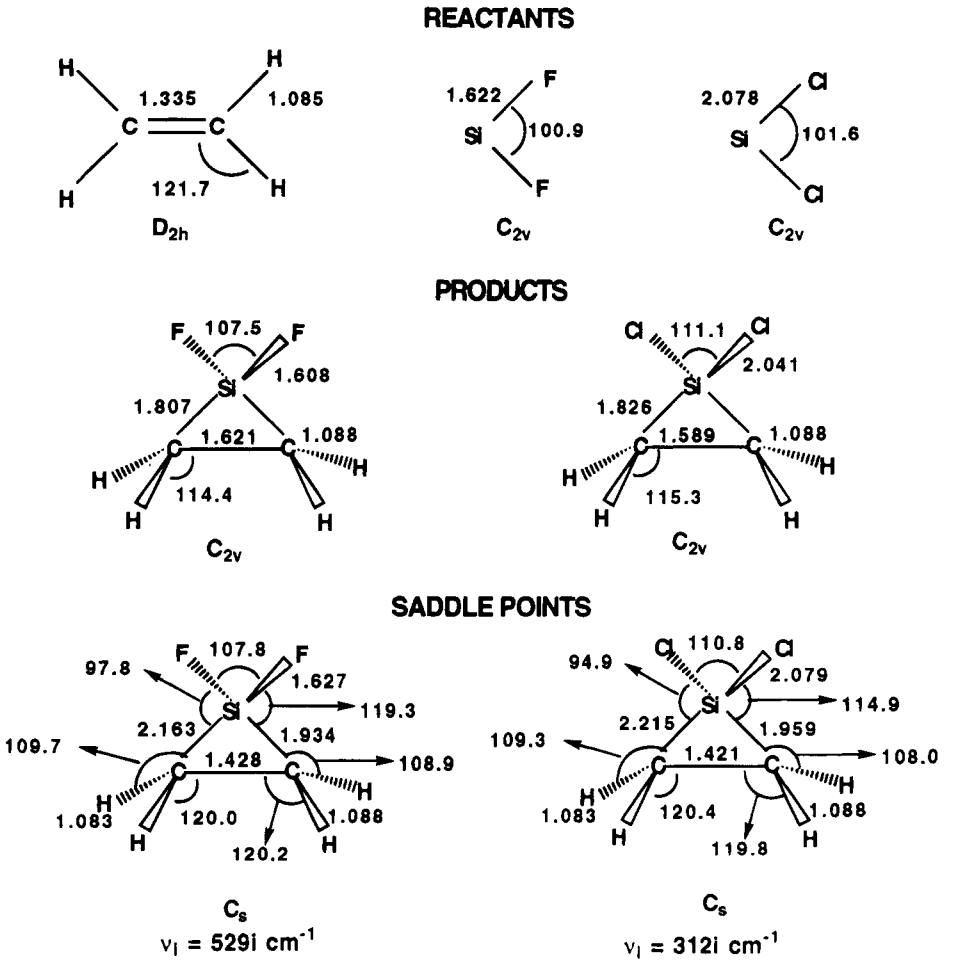

Figure 1. Geometries with bond lengths (Å) and angles (deg). ν_i = Imaginary frequency.

Table 1. Energetics for $SiX_2 + H_2C{=}CH_2$[a-c]

	X = F				X = Cl			
	ΔE	ΔH	E_b	E_a	ΔE	ΔH	E_b	E_a
MP2/A[d]	−19.3	−16.7	19.0	18.1	−24.1	−21.7	4.1	3.4
MP4/A	−13.8	−11.2	21.0	20.9	−18.1	−15.7	7.3	6.6
MP2/B	−21.6	−19.0	17.6	16.7	−28.0	−25.6	2.3	1.6
MP4/B	−16.6	−14.0	19.3	18.4	−22.4	20.4	5.2	4.5

[a] All geometries and vibrational frequencies were determined using MP2/6-31G(d). [b] Energies are given in kcal/mol. [c] ΔE and ΔH give the net reaction energy and enthalpy, respectively; E_b and E_a refer to the classical barrier height and the activation energy, respectively. ΔH and E_a include harmonic zero point vibrational energy (ZPE) corrections. [d] A and B refer to the basis sets 6-31G(d) and 6-311G(d,p), respectively.

B. Energetics. The energetics for the two addition reactions are summarized in Table 1. For comparison, both MP2 and MP4 results are listed for the 6-31G(d) and 6-311G(d,p) basis sets. First, consider the overall reaction thermodynamics. For both reactions (X = F, Cl), improving the basis set increases the exothermicity by several kcal/mol, while improving the level of theory from MP2 to MP4 has the opposite effect. At all levels of theory, the addition of $SiCl_2$ is predicted to be 4−6 kcal/mol more exothermic than the SiF_2 addition, with the difference at the highest level of theory, MP4/6-311G(d,p), being 6.4 kcal/mol when vibrational zero point corrections (ZPE) are included. To facilitate a direct comparison with the unsubstituted reaction, the exothermicity has been recalculated for X = H using MP4/6-311G(d,p) with MP2 geometries and ZPE corrections. The exothermicity for the addition of SiH_2 to ethylene is 40.7 kcal/mol, much larger than the values of 20.4 and 14.0 kcal/mol for X = Cl and F, respectively.

The calculated barrier heights for the two reactions, as well as the previous calculation of a zero barrier for X = H, are consistent with the predicted thermodynamics, given the Hammond Postulate: the barrier for the $SiCl_2$ addition is found to be rather smaller than that for the SiF_2 addition. Once again, improving the basis set and the level of theory have opposite effects on the predicted barrier heights, with basis set improvement lowering the barriers and increasing the level of theory raising the predicted barrier. The MP4/6-311G(d,p) classical barrier heights are 19.3 and 5.2 kcal/mol for X = F, Cl, respectively. These are lowered to 18.4 and 4.5 kcal/mol, respectively, when ZPE are included. The strain energies calculated at the same level of theory using reaction (1) are also consistent with this picture. These strain energies are predicted to be 45.8,[11] 55.0, and 59.9 kcal/mol for X = H, Cl, and F, respectively. These are in the same order as the calculated exothermicities and barrier heights and clearly suggest that substitution of electronegative substituents at the apical position in siliranes destabilize the ring.

Further insight regarding the relative barrier heights may be obtained by considering the nature of the

(11) The strain energy calculated for the parent silirane, before correction for ZPE, is 43.6 kcal/mol. This is quite similar to the predicted ring strain predicted earlier for this molecule using lower levels of theory [e.g., Gordon, M. S. *J. Am. Chem. Soc.*, **1980**, *102*, 7419], illustrating the stability of energetics predicted for homodesmic reactions.

interactions between SiX_2 and the substrate ethylene as the two approach each other during the reaction. Several authors[12-14] have discussed the two types of interactions that occur during carbene or silylene insertions: the *electrophilic* interaction between the empty p orbital on the carbene or silylene with the (in this case) π bond of the substrate, and the *nucleophilic* interaction of the carbene or silylene lone pair with the antibonding π orbital of the substrate. Examinations of the minimum energy paths for substrate H_2 reveal that the initial interaction is electrophilic in nature.[13] This is consistent with the distorted structure in the transition states, as well as with the need to avoid "symmetry forbidden" arrangements along the least motion path.[15] The optimal electrophilic interaction would occur if the SiX_2 plane were parallel to the CC bond, while the arrangement that maximizes the nucleophilic interaction is that of the final C_{2v} geometry of the ring. The distorted transition structure therefore suggests that the saddle point is part way between the two types of interaction.

(12) Dobson, R. C.; Hayes, D. M.; Hoffmann, R. *J. Am. Chem. Soc.* **1971**, *93*, 6188.
(13) Gordon, M. S. *J. Chem. Soc. Chem. Commun.* **1981**, 890.
(14) Baggott, J. E.; Blitz, M. A.; Frey, H. M.; Lightfoot, P. D.; Walsh, R. *J. Chem. Soc. Faraday Trans. 2* **1988**, *84*, 515.
(15) Woodward, R. B.; Hoffmann, R. *The Conservation of Orbital Symmetry*, Academic Press: New York, 1970.

Since the substrate (ethylene) is the same for the two reactions of interest, the source of the difference in barrier heights clearly lies in the SiX_2 wave functions, in particular, the lone pair (HOMO) and empty p orbital (LUMO) on Si. The energies of LUMO in SiF_2 and $SiCl_2$ are 0.032 and 0.003 hartree, respectively. The lower energy of this empty p orbital when X = Cl facilitates the interaction in the electrophilic phase of the reaction. Similarly, the energies of HOMO in SiF_2 and $SiCl_2$ are −0.410 and −0.379 hartree, respectively, so the higher lone pair energy when X = Cl serves to facilitate the nucleophilic step for this system. The net effect, therefore, is to preferentially stabilize the transition state for X = Cl, relative to that for X = F.

Acknowledgment. This work was supported by a grant from the National Science Foundation (CHE-9317317). The computations were performed on IBM RS6000 workstations, some of which were obtained via grants from the National Science Foundation and the Air Force Office of Scientific Research and some of which were generously provided by Iowa State University. Some of the calculations were performed on the Cray Y-MP at the San Diego Supercomputer Center. Enlightening discussions with Professor Robin Walsh are gratefully acknowledged.

OM940718L

Reactions of Secondary Silanes with [Pt2(.mu.-CO)(CO)2(.mu.-dppm)2]: Synthesis and Characterization of Silylene-Bridged Platinum Dimers

Kimberly A. Brittingham, Thomas N. Gallaher, and Serge Schreiner

Organometallics, **1995**, 14 (2), 1070-1072• DOI: 10.1021/om00002a064 • Publication Date (Web): 01 May 2002

Reactions of Secondary Silanes with $[Pt_2(\mu\text{-}CO)(CO)_2(\mu\text{-}dppm)_2]$: Synthesis and Characterization of Silylene-Bridged Platinum Dimers

Kimberly A. Brittingham,[1a] Thomas N. Gallaher,[1b] and Serge Schreiner*,[1a]

Departments of Chemistry, Randolph-Macon College, Ashland, Virginia 23005, and James Madison University, Harrisonburg, Virginia 22807

Received July 11, 1994[⊗]

*Summary: The secondary silanes Me_2SiH_2, Et_2SiH_2, Ph_2SiH_2, and $MePhSiH_2$ react with the binuclear complex $[Pt_2(\mu\text{-}CO)(CO)_2(\mu\text{-}dppm)_2]$ (**1**; dppm = $Ph_2PCH_2PPh_2$) to give zerovalent μ-SiRR′ complexes of the form $[Pt_2(\mu\text{-}SiRR')(CO)_2(\mu\text{-}dppm)_2]$ (R = R′ = Me (**2**), Et (**3**), Ph (**4**); R = Me, R′ = Ph (**5**)). $^{31}P\{^1H\}$ NMR data suggest that these compounds can be formulated as W-frame complexes. In the reaction of **1** with Ph_2SiH_2 leading to **4**, low-temperature, multinuclear NMR data show that the reaction proceeds via an intermediate formulated as $[Pt_2(H)(SiHPh_2)(CO)(\mu\text{-}dppm)_2]$ (**6**).*

The activation of silicon–hydrogen bonds[2] is an important step in a number of transition metal catalyzed reactions: dehydrogenative coupling of primary and secondary silanes,[3] olefin hydrosilation,[4] and silane alcoholysis.[5] The majority of the studies describing the oxidative addition of silanes to transition metal complexes have focused on their interaction with mononuclear, low-valent metal centers,[4,5] which in some cases has led to the formation of binuclear silylene clusters.[6–8] More recently, the reactions of bimetallic carbonyl complexes of rhodium[9] and iridium[10] with primary and secondary silanes have been investigated. Our own work on the oxidative-addition reactions of $[Pt_2(\mu\text{-}CO)(CO)_2(\mu\text{-}dppm)_2]$[11] (**1**) as well as the importance of platinum complexes in the formation of Si–Si oligomers[12] prompted us to investigate the reactivity of this complex with organosilanes.

In this note, we wish to report the reactions of **1** with secondary alkyl-, aryl-, and alkylarylsilanes to yield (μ-silylene)platinum dimers.

Experimental Section

General Comments. The complex $[Pt_2(\mu\text{-}CO)(CO)_2(\mu\text{-}dppm)_2]$ was prepared as previously reported.[11] Bis(diphenylphosphino)methane (Strem Chemicals) and all silanes (United Chemical Technologies, Inc.) were used as purchased. All manipulations were performed using standard Schlenk techniques. ^1H NMR, $^{13}C\{^1H\}$ NMR, $^{31}P\{^1H\}$ NMR, and $^{195}Pt\{^1H\}$ NMR were recorded on a Bruker AC/E-200 FT-NMR between 24 and −80 °C, and chemical shifts were referenced to TMS, 85% H_3PO_4, and H_2PtCl_6, respectively. When possible, coupling constants and chemical shifts are reported as measured directly from the experimental spectra. In all other cases, the values listed are those determined using spectral simulations. IR spectra were recorded on a Mattson 4020 FT-IR spectrometer. Microanalyses were carried out by Atlantic Microlab, Inc., Norcross, GA.

Preparation of Compounds. $[Pt_2(\mu\text{-}SiMe_2)(CO)_2(\mu\text{-}dppm)_2]$ (2). To 10 mL of CO-purged benzene was added 0.100 g (0.0804 mmol) of **1**. The resulting yellow-orange solution was stirred and dimethylsilane was slowly bubbled through the solution for ca. 30 s, producing a bright yellow color. The solution was stirred for 30 min. A yellow solid started to precipitate. Addition of hexanes (50 mL) caused complete precipitation of the yellow solid. The suspension was vacuum filtered (0.071 g, 75%), washed with CO-purged methanol, and dried in *vacuo*. Anal. Calc for $C_{54}H_{50}O_2P_4Pt_2Si$: C, 50.90; H, 3.93. Found: C, 49.95; H, 3.89. Mp (dec): 101 °C. IR (KBr): 1951, 1940 cm^{-1} (ν_{CO}). ^1H NMR (CD_2Cl_2, 24 °C): δ 1.02 (s, CH_3), 2.76 (br, CH_aH_b), 5.10 (br, CH_aH_b), 6.30–7.66 (m, C_6H_5). $^{13}C\{^1H\}$ NMR (CD_2Cl_2, ^{13}CO enriched, 24 °C): δ 187.8 (s, CO), $^1J_{Pt-C}$ = 1780.0 Hz, $^2J_{Pt-C}$ = 141.8 Hz. $^{31}P\{^1H\}$ NMR (CD_2Cl_2, 24 °C): δ −3.57 (s), $^1J_{Pt-P}$ = 2606.0 Hz, $^2J_{Pt-P}$ = −61.1 Hz, $^2J_{P-P}$ = 54.0 Hz, $^3J_{P-P}$ = 175.3 Hz; $^3J_{P-P}$

⊗ Abstract published in *Advance ACS Abstracts*, December 1, 1994.

(1) (a) Randolph-Macon College. (b) James Madison University.

(2) Collman, J. P.; Hegedus, L. S.; Norton, J. R.; Finke, R. G. *Principles and Applications of Organotransition Metal Chemistry*; University Science Books: Mill Valley, CA, 1987; pp 293, 564, 761 and references therein.

(3) (a) Tilley, T. D. In *The Chemistry of Organosilicon Compounds*; Patai, S., Rappoport, Z., Eds.; Wiley: New York, 1989; Part 2, Chapter 24, p 1415 and references therein. (b) MacKay, K. M.; Nicholson, B. K. In *Comprehensive Organometallics*; Wilkinson, G., Stone, F. G. A., Abel, E. W., Eds.; Pergamon: Oxford, England, 1982; Vol. 6, Chapter 43, p 1043. (c) Aylett, B. J. *Adv. Inorg. Chem. Radiochem.* **1982**, *25*, 1. (d) Aitken, C.; Barry, J.-P.; Gauvin, F.; Harrod, J. F.; Malek, A.; Rousseau, D. *Organometallics* **1989**, *8*, 1732. (e) Chang, L. S.; Corey, J. Y. *Organometallics* **1989**, *8*, 1885. (f) Campbell, W. H.; Hilty, T. K.; Yurga, L. *Organometallics* **1989**, *8*, 2615. (g) Woo, H.-G.; Walzer, J. F.; Tilley, T. D. *Macromolecules* **1991**, *24*, 6863. (h) Zhang, Z.-F.; Babonneau, F.; Laine, R. M.; Mu, Y.; Harrod, J. F.; Rahn, J. A. *J. Am. Chem. Soc.* **1991**, *74*, 670. (i) Corey, J. Y.; Zhu, X.-H.; Bedard, T. C.; Lange, L. D. *Organometallics* **1991**, *10*, 924. (j) Woo, H.-G.; Tilley, T. D. *J. Am. Chem. Soc.* **1989**, *111*, 3757. (k) Woo, H.-G.; Tilley, T. D. *J. Am. Chem. Soc.* **1989**, *111*, 8043.

(4) (a) Harrod, J. F.; Chalk, A. J. In *Organic Synthesis Via Metal Carbonyls*; Wender, I., Pinto, P., Eds.; Wiley: New York, 1977; Vol. 2. (b) Speier, J. *L. Adv. Organomet. Chem.* **1979**, *17*, 407. (c) Ojima, I. In *The Chemistry of Organosilicon Compounds*; Patai, S., Rappoport, Z., Eds.; Wiley: New York, 1989; Vol. 2, Chapter 25, p 1479. (d) Schubert, U. *J. Organomet. Chem.* **1988**, *358*, 215. (e) Seitz, F.; Wrighton, M. S. *Angew. Chem., Int. Ed. Engl.* **1988**, *27*, 289. (f) Brinkman, K. C.; Blakeney, A. J.; Krone-Schmidt, W.; Gladysz, J. A. *Organometallics* **1984**, *3*, 1325.

(5) (a) Ojima, I.; Kogure, T.; Nihonyanagi, M.; Kono, H.; Inaba, S.; Nagai, Y. *Chem. Lett.* **1973**, 501. (b) Corriu, R. J. P.; Moreau, J. J. E. *J. Organomet. Chem.* **1976**, *114*, 135. (c) Blackburn, S. N.; Haszeldine, R. N.; Parish, R. V.; Setchfi, J. H. *J. Organomet. Chem.* **1980**, *192*, 329. (d) Dwyer, J.; Hilal, H. S.; Parish, R. V. *J. Organomet. Chem.* **1982**, *228*, 191. (e) Lukevics, E.; Dzintara, M. *J. Organomet. Chem.* **1985**, *295*, 265. (f) Crabtree, R. H.; Luo, X.-L. *J. Am. Chem. Soc.* **1989**, *111*, 2527.

(6) Carre, F. C.; Moreau, J. J. E. *Inorg. Chem.* **1982**, *21*, 3099. (b) Brookes, A.; Knox, S. A. R.; Stone, F. G. A. *J. Chem. Soc. A* **1971**, 3469.

(7) Michalczyk, M. J.; Recatto, C. A.; Calabrese, J. C.; Fink, M. J. *J. Am. Chem. Soc.* **1992**, *114*, 7955.

(8) Heyn, R. H.; Tilley, T. D. *J. Am. Chem. Soc.* **1992**, *114*, 1917.

(9) (a) Wang, W.-D.; Eisenberg, R. *J. Am. Chem. Soc.* **1990**, *112*, 1833. (b) Wang, W.-D.; Hommeltoft, S. I.; Eisenberg, R. *Organometallics* **1988**, *7*, 2417.

(10) Cowie, M.; McDonald, R. *Organometallics* **1990**, *9*, 2468.

(11) Schreiner, S.; Gallaher, T. N. *Organometallics* **1993**, *12*, 4201.

(12) (a) Brown-Wensley, K. A. *Organometallics* **1987**, *6*, 1590. (b) Onopchenko, A.; Sabourin, E. T. *J. Org. Chem.* **1987**, *52*, 4118. (c) Zarate, E. A.; Tessier-Youngs, C. A.; Youngs, W. J. *J. Am. Chem. Soc.* **1988**, *110*, 4068. (d) Zarate, E. A.; Tessier-Youngs, C. A.; Youngs, W. J. *J. Chem. Soc., Chem. Commun.* **1989**, 577.

0276-7333/95/2314-1070$09.00/0

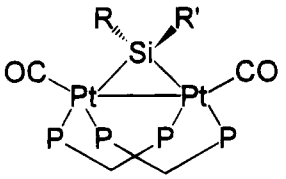

Figure 1. Proposed structure of $[Pt_2(\mu\text{-SiRR}')(CO)_2(\mu\text{-dppm})_2]$ (R = R' = Me (**2**), Et (**3**), Ph (**4**); R = Me, R' = Ph (**5**); P = PPh_2).

= 10.3 Hz, $^1J_{Pt-Pt}$ = 1574.4 Hz. $^{195}Pt\{^1H\}$ NMR (CD_2Cl_2, 24 °C): δ −5293 (t).

$[Pt_2(\mu\text{-SiEt}_2)(CO)_2(\mu\text{-dppm})_2]$ (3). To 10 mL of CO-purged benzene was added 0.100 g (0.0804 mmol) of **1**. The resulting yellow-orange solution was stirred, and excess diethylsilane (0.5 mL) was added. The solution color changed immediately to bright yellow. After 30 min, hexanes (50 mL) was added causing the precipitation of a yellow solid. The suspension was vacuum filtered (0.072 g, 69%), washed with CO-purged methanol, and dried in *vacuo*. Anal. Calc for $C_{56}H_{54}O_2P_4Pt_2Si$: C, 51.65; H, 4.15. Found: C, 51.71; H, 4.19. Mp (dec): 104 °C. IR (KBr): 1947, 1939 cm^{-1} (ν_{CO}). ^1H NMR (CD_2Cl_2, 24 °C): δ 1.14 (q, CH_2, $^3J_{H-H}$ = 7.4 Hz), 1.36 (t, CH_3, $^3J_{H-H}$ = 7.4 Hz), 2.82 (br, CH_aH_b), 4.93 (br, CH_aH_b), 6.9−8.1 (m, C_6H_5). $^{13}C\{^1H\}$ NMR (CD_2Cl_2, ^{13}CO enriched, 24 °C): δ 187.6 (s, CO), $^1J_{Pt-C}$ = 1768.6 Hz, $^2J_{Pt-C}$ = 147.6 Hz. $^{31}P\{^1H\}$ NMR (CD_2Cl_2, 24 °C): δ −4.44 (s), $^1J_{Pt-P}$ = 2574.1 Hz, $^2J_{Pt-P}$ = −63.3 Hz, $^2J_{P-P}$ = 56.7 Hz, $^3J_{P-P}$ = 180.4 Hz, $^3J_{P-P}$ = 8.23 Hz; $^1J_{Pt-Pt}$ = 1703.1 Hz. $^{195}P\{^1H\}$ NMR (CD_2Cl_2, 24 °C): δ −5312 (t).

$[Pt_2(\mu\text{-SiPh}_2)(CO)_2(\mu\text{-dppm})_2]$ (4). To 10 mL of CO-purged benzene was added 0.075 g (0.0603 mmol) of **1**. The resulting yellow-orange solution was stirred, and excess diphenylsilane (0.5 mL) was added. The solution color changed immediately to bright yellow. After 30 min, hexanes (50 mL) was added causing precipitation of a yellow solid. The suspension was vacuum filtered (0.080 g, 95%), washed with CO-purged methanol, and dried in *vacuo*. Anal. Calc for $C_{64}H_{54}O_2P_4Pt_2Si$: C, 54.97; H, 3.86. Found: C, 55.49; H, 4.28. Mp (dec): 138 °C. IR (KBr): 1953, 1944 cm^{-1} (ν_{CO}). ^1H NMR (CD_2Cl_2, 24 °C): δ 3.28 (m, CH_aH_b), 4.34 (m, CH_aH_b), 6.2−7.9 (m, C_6H_5). $^{13}C\{^1H\}$ NMR (CD_2Cl_2, ^{13}CO enriched, 24 °C): δ 184.2 (s, CO), $^1J_{Pt-C}$ = 1730.2 Hz, $^2J_{Pt-C}$ = 146.0 Hz. $^{31}P\{^1H\}$ NMR (CD_2Cl_2, 24 °C): δ −5.52 (s), $^1J_{Pt-P}$ = 2593.0 Hz, $^2J_{Pt-P}$ = −62.3 Hz, $^2J_{P-P}$ = 34.5 Hz, $^3J_{P-P}$ = 170.9 Hz, $^3J_{P-P}$ = 3.68 Hz, $^1J_{Pt-Pt}$ = 1544.3 Hz. $^{195}Pt\{^1H\}$ NMR (CD_2Cl_2, 24 °C): δ −5290 (t).

$[Pt_2(\mu\text{-SiMePh})(CO)_2(\mu\text{-dppm})_2]$ (5). To 10 mL of CO-purged benzene was added 0.100 g (0.0804 mmol) of **1**. The resulting yellow-orange solution was stirred, and excess methylphenylsilane (0.5 mL) was added. The solution color changed immediately to bright yellow. After 30 min, hexanes (50 mL) was added causing a yellow precipitate to form. The suspension was vacuum filtered (0.073 g, 68%), washed with CO-purged methanol, and dried in *vacuo*. Anal. Calc for $C_{59}H_{52}O_2P_4Pt_2Si$: C, 52.99; H, 3.89. Found: C, 52.38; H, 3.99. Mp (dec): 92 °C. IR (KBr): 1968, 1947 cm^{-1} (ν_{CO}). ^1H NMR (CD_2Cl_2, 24 °C): δ 1.03 (s, CH_3), 2.87 (br, CH_aH_b), 3.06 (br, CH_aH_b), 4.72 (br, CH_cH_d), 4.78 (br, CH_cH_d), 6.2−8.0 (m, C_6H_5). $^{13}C\{^1H\}$ NMR (CD_2Cl_2, ^{13}CO enriched, 24 °C): δ 185.1 (s, CO), $^1J_{Pt-C}$ = 1760.8 Hz, $^2J_{Pt-C}$ = 146.4 Hz. $^{31}P\{^1H\}$ NMR (CD_2Cl_2, −20 °C): δ 2.45 (m, P_A), $^1J_{Pt-P}$ = 2582.6 Hz, $^2J_{Pt-P}$ = −56.1 Hz, $^2J_{P-P}$ = −45.8 Hz, $^3J_{P-P}$ = 179.1 Hz, $^3J_{P-P}$ = −8.43 Hz; δ −9.73 (m, P_B), $^1J_{Pt-P}$ = 2594.1 Hz, $^2J_{Pt-P}$ = −58.3 Hz, $^2J_{P-P}$ = −45.8 Hz, $^3J_{P-P}$ = 159.5 Hz, $^3J_{P-P}$ = −8.43 Hz, $^1J_{Pt-Pt}$ = 1542.4 Hz. $^{195}Pt\{^1H\}$ NMR (CD_2Cl_2, 24 °C): δ −5295 (t).

Results and Discussion

Reaction of dialkyl-, diaryl-, and alkylarylsilane with $[Pt_2(\mu\text{-CO})(CO)_2(\mu\text{-dppm})_2]$ under ambient conditions results in the formation of the silylene-bridged dimers **2**−**5** (Figure 1) (eq 1). These dimers are formulated as

$$[Pt_2(\mu\text{-CO})(CO)_2(\mu\text{-dppm})_2] + RR'SiH_2 \rightarrow [Pt_2(\mu\text{-SiRR}')(CO)_2(\mu\text{-dppm})_2] + CO + H_2 \quad (1)$$

$$R = R' = Me, Et, Ph; R = Me, R' = Ph$$

zerovalent complexes with a platinum−platinum bond, each metal having an 18 electron valence shell. The IR spectra of these complexes exhibit absorptions attributable to terminally coordinated carbon monoxide but no absorption due to bridging CO. In the solid state and in solution, the complexes are thermally stable and moderately sensitive to air. All compounds are very soluble in aromatic hydrocarbons (benzene, toluene) and chlorinated hydrocarbons (chloroform, dichloromethane) but insoluble in polar solvents.

The proton NMR spectra of complexes **2**−**4** show two different methylene resonances for dppm which can be integrated as two protons each, while the spectrum for **5** displays four different resonances for the four inequivalent methylene protons. The silylene methyl protons of **2** appear as a singlet at δ 1.02, the protons of the $SiEt_2$ group of **3** appear as triplet and quartet at δ 1.36 and at δ 1.14, respectively, and the methyl protons of the SiMePh group of **5** appear as a singlet at δ 1.03.

The phosphorus NMR spectra of compounds **2**−**4** are described as AA'A''A'''XX' spin systems, while the spectrum for **5** is best described as an AA'BB'XX' system (Figure 2). Spectral simulations for all complexes yield coupling constants whose magnitudes are consistent with those obtained for triply bridged platinum dimers with a platinum−platinum bond.[11,13] Two-bond Pt−P coupling constants and two-bond P−P coupling constants for the silylene-bridged complexes are similar in magnitude to those for complexes adopting the so-called cradle structure.[11,14] On the basis of this information, it appears that our platinum dimers have the two dppm ligands *cis* to each other and can be formulated as W-frame complexes.

Mechanistic information on the oxidative addition of the secondary silanes to $[Pt_2(\mu\text{-CO})(CO)_2(\mu\text{-dppm})_2]$ can be obtained by monitoring the reaction of **1** with diphenylsilane at low temperature by NMR. Reaction of equimolar amounts of **1** and diphenylsilane at −80 °C generates an intermediate, which upon warming yields the final product **4**. This intermediate, which has been formulated as $[Pt_2(H)(SiHPh_2)(CO)(\mu\text{-dppm})_2]$ (**6**), is the result of a Si−H addition to one Pt atom with concomitant loss of CO (eq 2). The high-field region of

$$[Pt_2(\mu\text{-CO})(CO)_2(\mu\text{-dppm})_2] + Ph_2SiH_2 \rightarrow [Pt_2(H)(SiHPh_2)(CO)(\mu\text{-dppm})_2] + 2CO \quad (2)$$

the ^1H NMR spectrum of the reaction mixture displays a resonance at δ −6.78 ($^1J_{Pt-H}$ = 939 Hz; $^2J_{P-H}$ = 16.2 Hz) attributable to **6** which is characteristic of a hydride coordinated to platinum. In addition, a resonance at δ 6.53 is attributed to a proton attached to silicon.[9,10] The $^{31}P\{^1H\}$ NMR spectrum of the intermediate is characterized by two multiplets centered at δ 10.7 ($^1J_{Pt-P}$ = 3239 Hz) and at δ −18.4 ($^1J_{Pt-P}$ = 2795 Hz), indicating two inequivalent phosphorus environments. The $^{13}C\{^1H\}$ NMR spectrum of the reaction mixture displays a

(13) Brown, M. P.; Fisher, J. R.; Franklin, S. J.; Puddephatt, R. J. *J. Organomet. Chem.* **1978**, *161*, C46.
(14) Hunt, C. T.; Matson, G. B.; Balch, A. L. *Inorg. Chem.* **1981**, *20*, 2270.

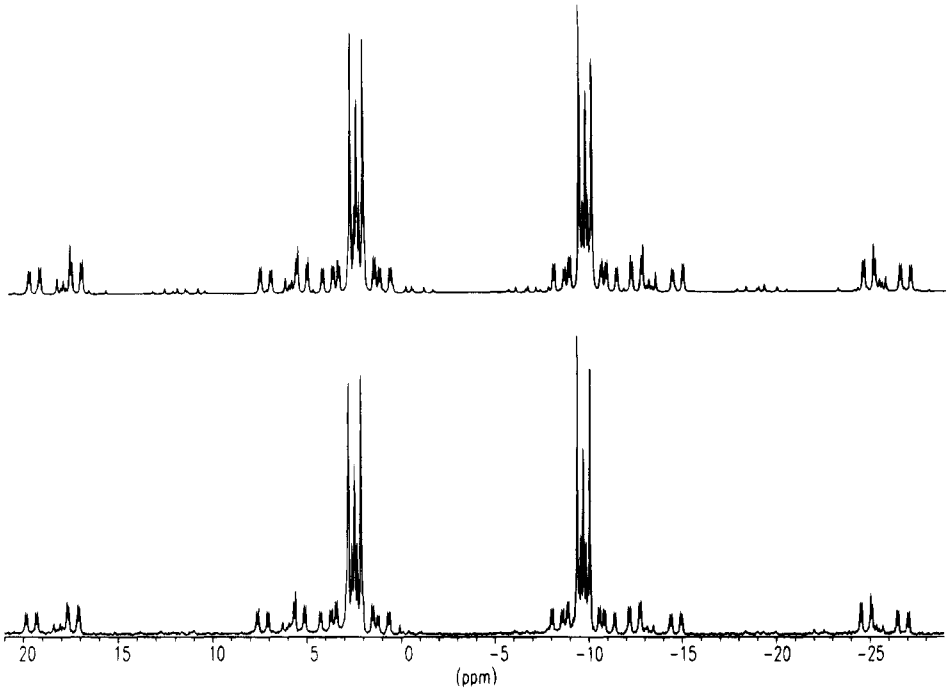

Figure 2. $^{31}P\{^1H\}$ NMR spectrum (lower trace) and computer simulation (upper trace) of $[Pt_2(\mu\text{-SiMePh})(CO)_2(\mu\text{-dppm})_2]$ at −25 °C.

single carbon resonance for **6** at δ 183.5 ($^1J_{Pt-C}$ = 1572 Hz) characteristic of a terminal carbonyl carbon as well as a carbon resonance at δ 182.3 caused by dissolved CO. When the reaction mixture is slowly warmed to −25 °C, **6** undergoes reductive elimination of H_2 (as evidenced by the disappearance of the resonances at −6.78 and at 6.53 ppm in the ^1H NMR spectrum) and new resonances attributable to **4** and dissolved hydrogen (δ 4.52) start to appear (eq 3).

$$[Pt_2(H)(SiHPh_2)(CO)(\mu\text{-dppm})_2] + CO \rightarrow [Pt_2(\mu\text{-SiPh}_2)(CO)_2(\mu\text{-dppm})_2] + H_2 \quad (3)$$

Simultaneously, the carbon resonance due to dissolved CO and **6** disappeared in the $^{13}C\{^1H\}$ NMR spectrum and a new resonance at 186.1 ppm due to **4** appears.

Studies on the reactions of primary silanes with $[Pt_2(\mu\text{-CO})(CO)_2(\mu\text{-dppm})_2]$ are currently in progress.

Acknowledgment. This work was supported in part by the Alan Rashkind Endowment administered by Randolph-Macon College and the National Science Foundation (Grants CHE-9000748 and USE-9152585). K.A.B. gratefully acknowledges support by the Council on Undergraduate Research.

OM940547K

Synthesis and Crystal Structure of a Monomeric Tetraalkyldigallium Telluride with a Bent Ga–Te–Ga Group

Werner Uhl* and Uwe Schütz

Fachbereich Chemie der Universität Oldenburg, Postfach 2503, 26111 Oldenburg, Germany

Wolfgang Hiller and Maximilian Heckel

Anorganisch-chemisches Institut der Technischen Universität München, Lichtenbergstrasse 4, 85748 Garching, Germany

Received August 23, 1994[⊗]

*Summary: Tetrakis[bis(trimethylsilyl)methyl]digallane(4) (**1**) with a gallium–gallium bond reacts under mild conditions with $Et_3P^+–Te^-$ to give the title compound $R_2Ga–Te–GaR_2$ (**2**; R = $CH(SiMe_3)_2$) in high yield. **2** is stable in solution at room temperature and, due to the high steric shielding, a monomer even in the solid state. A crystal structure determination (orthorhombic; Pcaa; a = 2375.3(2) pm; b = 1658.4(2) pm, c = 1216.6(3) pm; Z = 4) reveals an angled Ga–Te–Ga group (109.8°) and a Ga–Te bond length of 255.21(4) pm, as would be expected for a Ga–Te single bond with the atoms in low coordination numbers. There are no indications for a significant π-interaction between tellurium lone pairs and the gallium atoms, and the hindered rotation of the bulky substituents observed by low-temperature NMR is more likely caused by steric restrictions.*

Introduction

Recently we succeeded in the synthesis of a tetraalkyldialane(4) derivative with an aluminum-aluminum bond showing a remarkable stability toward disproportionation reaction, which is probably a result of the high steric shielding by four bulky bis(trimethylsilyl)methyl substituents.[1,2] This compound exhibits very interesting chemical properties.[3] Reactions retaining the Al–Al bond such as the formation of simple adducts[4,5] and radical anions[2,6] or cleaving the Al–Al bond such as insertion reactions with CS_2[7] and isonitriles[8] have been carried out up to now. By a different synthesis starting with Ga_2Br_4·2(dioxane) and 4 equiv of $LiCH(SiMe_3)_2$ we also obtained the analogous, intensively yellow compound with a Ga–Ga bond (**1**).[9] Its chemical behavior has not been investigated as extensively as for the Al derivative, and we only published one metathesis reaction between **1** and the sterically highly shielded ditellurium compound R′Te–TeR′ (R′ = $Si(SiMe_3)_3$, yielding $R_2Ga–TeR'$.[10] The gallium telluride has a monomeric structure even in the solid state, with a planar C_2-GaTeSi core, and shows a hindered rotation around the Ga–Te bond as determined by NMR spectroscopy. Both observations might indicate a π interaction between a tellurium lone pair and the empty p orbital at the gallium atom. Recently Power et al. synthesized a tetraaryldigallane(4) compound shielded by four bulky triisopropylphenyl groups by a similar route,[11] which interestingly shows a staggered conformation across the Ga–Ga bond in contrast to the planar structure of **1**. By reduction with lithium in diethyl ether the transfer of only one electron is observed and a black radical anion is isolated containing a one-electron Ga–Ga π bond.[11] We wish to report here the reaction of **1** with the tellurium donor $Et_3P^+–Te^-$.

Experimental Section

All procedures were carried out under an atmosphere of purified argon in dried solvents (*n*-pentane over $LiAlH_4$; toluene and benzene over Na/benzophenone). **1** and $Et_3P^+–Te^-$·0.5(toluene) (recrystallized from toluene) were prepared according to the literature.[9,12]

$R_2Ga–Te–GaR_2$ (R = $CH(SiMe_3)_2$) (2). A solution of 0.263 g (0.9 mmol) of $Et_3P^+–Te^-$·0.5(toluene) in 10 mL of toluene is added dropwise to a solution of 0.70 g (0.9 mmol) of **1** in 60 mL of *n*-pentane at −30 °C. While it is slowly warmed to room temperature, the solution changes from yellow to colorless. After the mixture is stirred for a further 30 min, the solvent is removed in vacuo, and the residue is recrystallized from toluene (25/−30 °C). Yield: 0.59 g (72%) colorless platelets. Anal. Calcd for $C_{28}H_{76}Ga_2Si_8Te$: Ga, 15.4; C, 37.2; H, 8.5; mol wt, 904.64. Found: Ga, 15.3; C, 37.3; H, 8.5; mol wt, 859 (cryoscopically in benzene). Dec pt: 149 °C (closed capillary, argon). ^1H NMR (room temperature, C_6D_6, 300

⊗ Abstract published in *Advance ACS Abstracts*, December 15, 1994.

(1) Uhl, W. *Z. Naturforsch., B* **1988**, *43*, 1113.
(2) Wehmschulte, R. J.; Ruhlandt-Senge, K.; Olmstead, M. M.; Hope, H.; Sturgeon, B. E.; Power, P. P. *Inorg. Chem.* **1993**, *32*, 2983.
(3) Uhl, W. *Angew. Chem., Int. Ed. Engl.* **1993**, *32*, 1386.
(4) Uhl, W.; Vester, A. *Chem. Ber.* **1993**, *126*, 941.
(5) Uhl, W.; Schütz, U.; Pohl, S.; Saak, W. *Z. Naturforsch., B* **1994**, *49*, 637.
(6) (a) Uhl, W.; Vester, A.; Kaim, W.; Poppe, J. *J. Organomet. Chem.* **1993**, *454*, 9. (b) Uhl, W.; Vester, A.; Fenske, D.; Baum, G. *J. Organomet. Chem.* **1994**, *464*, 23. (c) Pluta, C.; Pörschke, K. R.; Krüger, C.; Hildenbrand, K. *Angew. Chem., Int. Ed. Engl.* **1993**, *32*, 388.
(7) Uhl, W.; Vester, A.; Hiller, W. *J. Organomet. Chem.* **1993**, *443*, 9.
(8) Uhl, W.; Schütz, U.; Hiller, W.; Heckel, M. *Chem. Ber.* **1994**, *127*, 1587.
(9) Uhl, W.; Layh, M.; Hildenbrand, T. *J. Organomet. Chem.* **1989**, *364*, 289.
(10) Uhl, W.; Layh, M.; Becker, G.; Klinkhammer, K.-W.; Hildenbrand, T. *Chem. Ber.* **1992**, *125*, 1547.
(11) (a) Re, X.; Bartlett, R. A.; Olmstead, M. M.; Ruhlandt-Senge, K.; Sturgeon, B. E.; Power, P. P. *Angew. Chem., Int. Ed. Engl.* **1993**, *32*, 717. (b) Veith, M.; Goffing, F.; Becker, S.; Huch, V. *J. Organomet. Chem.* **1991**, *406*, 105. (c) Schluter, R. D.; Cowley, A. H.; Atwood, D. A.; Jones, R. A.; Bond, M. R.; Carrano, C. J. *J. Am. Chem. Soc.* **1993**, *115*, 2070.
(12) (a) Zingaro, R. A.; Steeves, B. H.; Irgolic, K. *J. Organomet. Chem.* **1965**, *4*, 320. (b) Steigerwald, M. L.; Rice, C. E. *J. Am. Chem. Soc.* **1988**, *110*, 4228.
(13) Hahn, T., Ed. *International Tables for Crystallography: Space Group Symmetry*; Kluwer Academic: Dordrecht, Boston, London, 1989; Vol. A.
(14) (a) SHELXTL PLUS REL. 4.1; Siemens Analytical X-Ray Instruments, Inc., Madison, WI, 1990. (b) Sheldrick, G. M. SHELXL-93, Program for the Refinement of Structures; Universität Göttingen, Göttingen, Germany, 1993.

0276-7333/95/2314-1073$09.00/0

Table 1. Crystal Data and Data Collection Parameters for $R_2Ga-Te-GaR_2$ (2; R = $CH(SiMe_3)_2$)

formula: $C_{28}H_{76}Ga_2Si_8Te$
cryst syst; space group: orthorhombic; *Pcca* (No. 54)[13]
Z: 4
temp (°C): 20
d_{calc} (g/cm^3): 1.254
a (pm): 2375.3(2)
b (pm): 1658.4(2)
c (pm): 1216.6(3)
V (10^{-30} m^3): 4792
μ (10^2 m^{-1}): 19.37
cryst size (mm): 0.5 × 0.5 × 0.4
diffractometer; radiation: 4-cycle CAD4; Mo Kα
2θ range (deg): $6 \le 2\theta \le 50$
reciprocal space: $0 \le h \le 28$, $-19 \le k \le 0$, $0 \le l \le 14$
scan mode: $\omega-2\theta$
indep rflns; no. of rflns with $F > 4\sigma(F)$: 4177; 3423
program: SHELXL−93;[14] solution by direct methods; full-matrix refinement with all indep structure factors
params: 189
$R = \sum||F_o| - |F_c||/\sum|F_o|$ ($F > 4\sigma(F)$): 0.034
$wR2 = \{\sum w(|F_o|^2 - |F_c|^2)^2/\sum w(F_o^2)^2\}^{1/2}$ (all data): 0.090
largest residuals (10^{30} e/m^3): +1.006/−0.727

Table 2. Atomic Coordinates and Equivalent Isotropic Displacement Parameters (10^{-22} m^2) for the Atoms of the Asymmetric Unit in $R_2Ga-Te-GaR_2$ (2; R = $CH(SiMe_3)_2$)

	x/a	*y/b*	*z/c*	*U*(eq)
Te	0.5000	0.6466(1)	0.2500	5.2(1)
Ga	0.5808(1)	0.7351(1)	0.1823(1)	3.9(1)
C1	0.6042(1)	0.8262(2)	0.2761(3)	4.8(1)
Si1	0.6209(1)	0.9222(1)	0.2011(1)	6.2(1)
C11	0.6769(2)	0.9079(3)	0.0965(4)	9.6(2)
C12	0.5565(2)	0.9606(3)	0.1304(5)	10.8(2)
C13	0.6429(3)	1.0039(3)	0.2963(4)	11.0(2)
Si2	0.6552(1)	0.7922(1)	0.3850(1)	5.7(1)
C21	0.7308(2)	0.8043(3)	0.3412(4)	9.2(2)
C22	0.6450(2)	0.8520(3)	0.5143(4)	9.1(2)
C23	0.6437(2)	0.6847(2)	0.4228(4)	8.0(1)
C2	0.6173(1)	0.6970(2)	0.0465(2)	4.5(1)
Si3	0.5674(1)	0.7008(1)	−0.0731(1)	6.0(1)
C31	0.5256(2)	0.6068(3)	−0.0863(3)	8.4(1)
C32	0.5167(2)	0.7861(3)	−0.0573(4)	10.2(2)
C33	0.6076(2)	0.7207(4)	−0.2034(3)	9.6(2)
Si4	0.6589(1)	0.6011(1)	0.0602(1)	5.5(1)
C41	0.7242(2)	0.6224(3)	0.1397(4)	8.8(1)
C42	0.6195(2)	0.5190(2)	0.1301(4)	8.1(1)
C43	0.6819(2)	0.5621(3)	−0.0761(3)	9.2(2)

MHz): δ 1.05 (s, GaCH), 0.33 (s, $SiMe_3$). ^{1}H NMR (−63 °C, toluene-d_8, 500 MHz): δ 1.21 and 0.96 (s, each 2 H, GaCH), 0.37 and 0.35 (s, each 36 H, $SiMe_3$). ^{13}C NMR (C_6D_6, 75.5 MHz): δ 26.4 (GaC), 4.5 ($SiMe_3$). IR (paraffin, CsBr, cm^{-1}): 1298 vw, 1260 m, 1246 s ($\delta(CH_3)$); 1169 vw, 1155 vw, 1121 vw; 1013 m (δ(CH)); 964 w, 943 vw, 843 vs, 772 m, 758 m, 727 w ($\varrho(CH_3(Si))$); 687 sh, 667 m (ν_{as}(SiC)); 629 vw, 619 vw (ν_s-(SiC)); 513 m, 490 vw (ν(GaC)).

Crystal Structure. Single crystals of **2** were obtained from pentane at −30 °C. Relevant crystal and data collection parameters are given in Table 1 and atomic coordinates in Table 2. **2** crystallizes in space group *Pcca* isotypic to the appropriate compounds with Al−S−Al,[7] Al−Te−Al,[15] or Al−CH_2−Al[16] bridges with the bridging atoms located on a 2-fold crystallographic rotation axis.

Results and Discussion

When a solution of $Et_3P^+-Te^-$ in toluene is added to the yellow solution of the tetraalkyldigallane(4) derivative **1** in *n*-pentane, the resulting reaction mixture becomes slowly colorless on warming to room temperature, and Et_3P is detected by its characteristic ^{31}P NMR resonance. After removal of the solvent and recrystallization from toluene or *n*-pentane colorless crystals of the tellurium insertion product **2** (eq 1) are isolated in

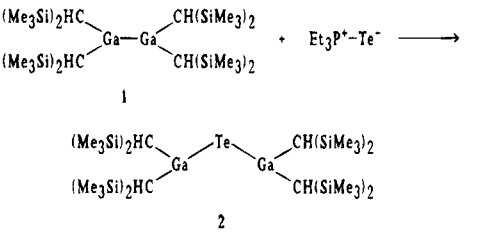

over 70% yield. **2** shows a higher thermal stability in solution than the Al−Te−Al analogue, which decomposes slowly at room temperature in benzene, precipitating black elemental tellurium.[15] For **2** we observe a comparable decomposition reaction only by contact to oxygen. Molecular weight determination in benzene gives the monomeric formula unit.

Surprisingly, the NMR spectra of **2** are similar to those of the educt **1**, and chemical shifts of both compounds are nearly indistinguishable. The protons in positions α to the gallium atoms reveal a resonance at δ 1.05 ppm with an unusual downfield shift of about 0.8 ppm compared to the trialkylgallium derivative $Ga[CH(SiMe_3)_2]_3$. Similar chemical shifts for the inner $CH(SiMe_3)_2$ protons are usually observed in neutral bis(trimethylsilyl)methyl compounds with Al−Al,[1] Ga−Ga,[9] and In−In bonds.[17] When the temperature is lowered to −60 °C in toluene, the resonance of the trimethylsilyl groups splits into two signals corresponding to the comparable compounds with Al−S−Al[7] or Al−Te−Al[15] bridges. In agreement with the crystal structure discussed below, we believe that this is not an indication for a π interaction between a lone pair at Te and an empty p orbital at Ga but more probably the result of a hindered rotation of the bulky substituents caused by steric restrictions and also observed in a derivative with an Al−CH_2−Al group,[16] where no π interactions are expected. Power et al. published a similar discussion for the monomeric gallium−sulfur compound $Ga(SMes^*)_3$ ($Mes^* = C_6H_2(CMe_3)_3$), where the short Ga−S distance is attributed to an electrostatic attraction between the electropositive Ga and the electronegative S atom rather than to a Ga−S π bond.[18] A significant spectroscopic difference between the yellow digallane(4) compound **1** and the colorless insertion product **2** is observed in the UV/vis spectra, where the absorption at 370 nm, characteristic for compounds with Al−Al,[9] Ga−Ga,[9] or In−In bonds,[17] is absent in the spectrum of **2**.

Figure 1 shows an ORTEP diagram of one molecule of **2**, as obtained by a crystal structure determination. The angle at the central Te atom (109.8°), as well as the molecular conformation with the substituents in a staggered arrangement for the minimization of sterical repulsions, clearly excludes a significant π interaction between Ga and Te, as observed in tellurium-bridged transition-metal compounds[19] and possibly also existing

(15) Uhl, W.; Schütz, U. *Z. Naturforsch., B* **1994**, *49*, 931.
(16) Layh, M.; Uhl, W. *Polyhedron* **1990**, *9*, 277.
(17) Uhl, W.; Layh, M.; Hiller, W. *J. Organomet. Chem.* **1989**, *368*, 139.
(18) Ruhlandt-Senge, K.; Power, P. P. *Inorg. Chem.* **1991**, *30*, 2633. For the Se analogue see: Ruhlandt-Senge, K.; Power, P. P. *Inorg. Chem.* **1991**, *30*, 3683.

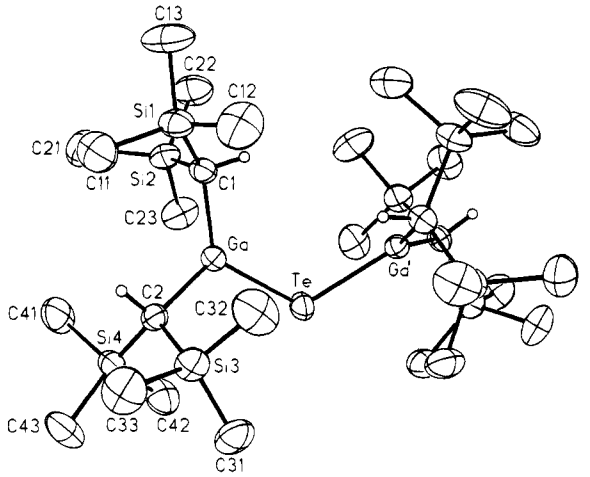

Figure 1. Molecular structure of **2** (ORTEP plot). The thermal ellipsoids are drawn at the 40% probability level.

Table 3. Important Bond Lengths and Angles for 2

Ga–Te	255.21(4)	C1–Si1	187.9(3)
Ga–C1	197.4(3)	C1–Si2	188.1(4)
Ga–C2	196.9(3)	C2–Si3	187.8(3)
		C2–Si4	187.9(3)
Ga–Te–Ga′ [a]	109.82(2)	C1–Ga–C2	127.3(1)
Te–Ga–C1	117.7(1)	Te–Ga–C2	114.68(9)
Ga–C1–Si1	115.3(2)	Ga–C2–Si3	111.2(3)
Ga–C1–Si2	111.1(2)	Ga–C2–Si4	115.4(2)
Si1–C1–Si2	117.4(2)	Si3–C2–Si4	115.4(2)

[a] Ga′ calculated by the symmetry operation $-x + 1, y, -z + 1/2$.

in the monomeric and planar derivative $R_2Ga–TeR'$ [10] discussed above. As in this compound, the Ga–Te bond length in **2** is shorter (255.2 pm, Table 3) than calculated (262 pm) from the Ga–Ga distance in **1** and the standard Te–Te bond length of 270 pm in organic ditellurium derivatives,[20] but for the most part this might be due to an electrostatic attraction due to the difference in electronegativities and the accumulation of negative charge at the bridging atom. To our knowledge comparable monomeric organic compounds with a Ga–Te bond are hitherto unknown and there is only one example with a dimeric Ga–Te unit showing, as expected, very much elongated Ga–Te bond lengths (274–276 pm).[21] Typical solid-state structures such as GaTe and Ga_2Te_5 with higher coordination numbers at Ga and Te usually show values between 253 and 269 pm.[22] The Ga–C distances (197.2 pm) are only slightly shortened in comparison to the values found in **1** (199.6 pm); however, a more significant shortening up to 5 pm is observed for the Al–C bond lengths in all bridged dialuminum compounds with Al–S–Al,[7] Al–Te–Al,[15] or $Al–CH_2–Al$[16] groups derived from the dialane(4) system similar to **1**. This might be a consequence of the larger charge separation and a more effective electrostatic attraction in compounds with the less electronegative Al atom.

Acknowledgment. We are grateful to the Deutsche Forschungsgemeinschaft, the Fonds der Chemischen Industrie, and Hewlett-Packard for generous support.

Supplementary Material Available: Tables S1–S3, giving the anisotropic displacement parameters for non-hydrogen atoms, atomic coordinates and isotropic displacement parameters of the hydrogen atoms, and bond lengths and angles for **2** (4 pages). Ordering information is given on any current masthead page.

OM9406761

(19) (a) Herrmann, W. A. *Angew. Chem., Int. Ed. Engl.* **1986**, *25*, 26. (b) Greenwood, N. N.; Earnshaw, A. *Chemistry of the Elements*; Pergamon Press: Oxford, U.K., 1984.

(20) (a) Me_2Te_2: Becker, G.; Baumgarten, J.; Mundt, O.; Riffel, H.; Simon, A. Private communication. (b) Ph_2Te_2: Llabres, G.; Dideberg, O.; Dupont, L. *Acta Crystallogr., Sect. B* **1972**, *28*, 2438. (c) $(p\text{-tolyl})_2Te_2$: Spirlet, M. R.; van den Bossche, G.; Dideberg, O.; Dupont, L. *Acta Crystallogr., Sect. B* **1979**, *35*, 1727. (d) $(p\text{-}MeOC_6H_4)_2Te_2$: Ludlow, S.; McCarthy, A. E. *J. Organomet. Chem.* **1981**, *219*, 169. Mundt, O.; Becker, G.; Rössler, M.; Witthauer, C. *Z. Anorg. Allg. Chem.* **1983**, *506*, 42. (e) $(p\text{-}ClC_6H_4)_2Te_2$: Kruse, F. H.; Marsh, R. E.; McCullough, J. D. *Acta Crystallogr.* **1957**, *10*, 201. van den Bossche, G.; Spirlet, M. R.; Dideberg, O.; Dupont, L. *Acta Crystallogr., Sect. C* **1984**, *40*, 1011. (f) $[(Me_3C)_3C_6H_2]_2Te_2$: du Mont, W. W.; Lange, L.; Karsch, H. H.; Peters, K.; Peters, E. M.; von Schnering, H. G. *Chem. Ber.* **1988**, *121*, 11.

(21) Banks, M. A.; Beachley, O. T., Jr.; Gysling, H. J.; Luss, H. R. *Organometallics* **1990**, *9*, 1979.

(22) (a) GaTe: Julien-Pouzol, M.; Jaulmes, S.; Guittard, M.; Alapini, F. *Acta Crystallogr., Sect. B* **1979**, *35*, 2848. (b) Ga_2Te_5: Julien-Pouzol, M.; Jaulmes, S.; Alapini, F. *Acta Crystallogr., Sect. B* **1977**, *33*, 2270. (c) $[PPh_4][GaTe_2(en)_2]$: Warren, C. J.; Ho, D. M.; Haushalter, R. C.; Bocarsly, A. B. *J. Chem. Soc., Chem. Commun.* **1994**, 361 and literature cited therein. See also ref 10.

Synthesis and Structure of a Novel Organotin Compound, $\{Me_2SnN(C_3N_3Cl_2)\}_3$

Andrew P. Purdy* and Clifford F. George

Naval Research Laboratory, Chemistry Division (Code 6120) and Laboratory for the Structure of Matter (Code 6030), Washington, D.C. 20375

Received September 19, 1994[⊗]

*Summary: Cyanuric chloride reacts with tris(trimethylstannyl)amine to afford $(Me_3Sn)_2N(C_3N_3Cl_2)$ (**1**). Prolonged heating of the reaction mixture results in the formation of the trimer $\{Me_2SnN(C_3N_3Cl_2)\}_3$ (**2**), and the crystal structure was determined for **2**·3(THF). **1** was thermally decomposed to a amorphous compound of empirical formula $C_{6.9}N_{6.8}Sn$.*

There has been considerable recent interest in carbonic nitride (C_3N_4).[1] Our efforts to prepare C_3N_4 led us to investigate the reaction between cyanuric chloride ($(CNCl)_3$) and tris(trimethylstannyl)amine,[2] which could potentially form a C_3N_4 compound by elmination of 3 equiv of Me_3SnCl. A single cleavage product, $(Me_3Sn)_2N(C_3N_3Cl_2)$ (**1**), forms fairly quickly when the reactants are heated to 80–100 °C in THF (eq 1). **1** is

$$(CNCl)_3 + (Me_3Sn)_3N \rightarrow \underset{\mathbf{1}}{(Me_3Sn)_2N(C_3N_3Cl_2)} + Me_3SnCl \quad (1)$$

a colorless low-melting solid that sublimes at 50 °C at 10^{-5} Torr. As expected, the volatility of **1** is about the same as the recently reported silicon analogue $(Me_3Si)_2N(C_3N_3Cl_2)$.[3]

On prolonged heating of the reaction mixture, the trimer $\{Me_2SnN(C_3N_3Cl_2)\}_3$ (**2**) slowly precipitates from solution. Production of **2** is accelerated by high concentrations of the reactants, which is understandable as the formation of **2** is probably due to a series of bimolecular reactions. The reaction was also performed in an NMR tube; the spectra indicate that Me_4Sn is also produced at the same time as **2**. The latter would suggest a process such as indicated in eq 2. Other

$$3(Me_3Sn)_2N(C_3N_3Cl_2) \rightarrow \underset{\mathbf{2}}{\{Me_2SnN(C_3N_3Cl_2)\}_3} + 3Me_4Sn \quad (2)$$
$$\rightarrow \text{other products}$$

unidentified products also appear in the NMR tube reaction, presumably intermediates in the disproportionation and condensation of **1** into **2**. A tan insoluble solid is also produced upon prolonged heating in THF. To test whether **1** can be converted to carbon nitride, a sample was thermolyzed at 350 °C in a sealed tube under N_2 and then pyrolyzed under dynamic vacuum.

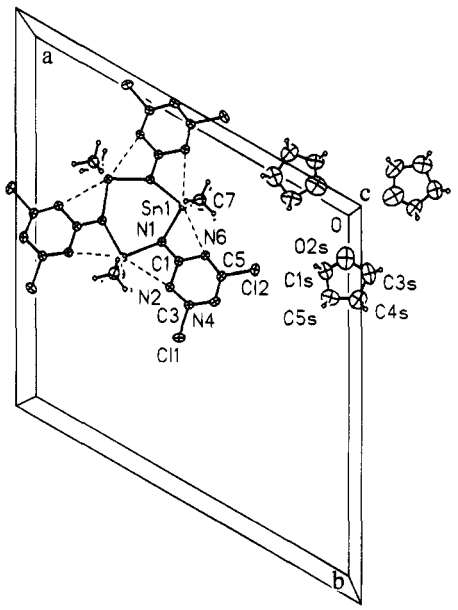

Figure 1. Thermal ellipsoid (20%) plot of complex **2** and three THF molecules viewed along the *c* axis. Only the labeled atoms are unique. The remainder of the unit cell contents is omitted for clarity.

The resulting black powder has approximate composition $C_{6.9}N_{6.8}Sn$ by elemental analysis and is amorphous by powder X-ray diffraction. Its infrared spectrum shows only a weak N–H stretching band, a moderately intense C≡N stretch, and very strong C=N, C=C, and C–N bands. Although the silicon analogue was used in CVD experiments to make carbon nitride films,[3] we did not attempt any CVD work with **1** or **2**.

2 crystallized with the solvent THF in a ratio 1:3. The structure of **2**·3(THF) (Figure 1) consists of a planar $(Me_2SnN)_3$ ring centered on a S_6 axis with three coplanar $(C_3N_3Cl_2)$ groups attached to the nitrogen atoms. The Sn–N(2) and Sn–N(6) distances of 2.746(7) and 2.807(7) Å, respectively, are within the observed values for coordinate bonds between tin and neutral aromatic nitrogen ligands.[4] For example, (2,2′-azopyridine-*N,N′,N″*)dibromodimethyltin[4a] has Sn–N links from 2.591 to 2.904 Å, and 4,4′-bipyridylbis[bromo(tri-*p*-tolyl)tin] has Sn–N bonds of 2.653 Å.[4b] These weak Sn–N(2) and Sn–N(6) bonds undoubtedly contribute to the coplanarity of the $(Sn-N)_3$ and $(CN)_3$ ring systems. All but the methyl groups lie on a mirror plane. The ring atoms of THF also lie in the same mirror plane and are centered on a 6_3 screw axis. This forms extended planes which are separated by the

⊗ Abstract published in *Advance ACS Abstracts,* January 15, 1995.

(1) (a) Maya, L.; Cole, D. R.; Hagaman, E. W. *J. Am. Ceram. Soc.* **1991**, *74*, 1686–8. (b) Sekine, T.; Kanda, H.; Bando, Y.; Yokoyama, M.; Hojou, K. *J. Mater. Sci. Lett.* **1990**, *9*, 1376–8. (c) Liu, A. Y.; Cohen, M. L. *Phys. Rev. B* **1990**, *41*, 10727–34. (d) Niu, C.; Lu, Y. Z.; Lieber, C. M. *Science* **1993**, *261*, 334–7. (e) Coad, E. C.; Apen, P. G.; Ramussen, P. G. *J. Am. Chem. Soc.* **1994**, *116*, 391–2.

(2) Lehn, W. L. *J. Am. Chem. Soc.* **1964**, *86*, 305.

(3) Kouvetakis, J.; Bandari, A.; Todd, M.; Wilkens, B. *Chem. Mater.* **1994**, *6*, 811–4.

(4) (a) Camalli, M.; Caruso, F.; Mattogno, G.; Rivarola, E. *Inorg. Chim. Acta* **1990**, *170*, 225. (b) Bajue, S. A.; Bramwell, F. B.; Charles, M.; Carvantes-Lee, F.; Pannell, K. *Inorg. Chim. Acta* **1992**, *197*, 83.

Table 1. Experimental Data for X-ray Diffraction of 2·3(THF)

formula	$[C_{15}H_{18}N_{12}Cl_6Sn_3]\cdot 3[C_4H_8O]$
fw	1151.5
cryst syst	hexagonal
space group	$P6_3/m$
a, b (Å)	18.581(8)
c (Å)	7.589(6)
α, β (deg)	90
γ (deg)	120
cell vol (Å^3)	2269(2)
Z	2
density (g/cm^3)	1.685
$F(000)$	1128
λ (Mo Kα) (Å)	0.71073
μ (mm^{-1})	2.03
temp (K)	295
cryst size (mm)	0.22 × 0.40 × 0.60
scan mode	$\theta-2\theta$
$2\theta_{max}$ (deg)	55
no. of reflns/measd	3921
no. of unique reflns	1901
no. of reflns ($I > 2\sigma(I)$)	1623
no. of variables	101
refinement	full-matrix least squares on F^2
R, wR^2 [a]	0.053, 0.127

[a] $R = \Sigma|F_o - F_c|/\Sigma(F_o)$; $wR^2 = \{\Sigma[w(F_o^2 - F_c^2)^2]/\Sigma[w(F_o^2)^2]\}^{1/2}$.

Table 2. Atomic Coordinates (×10^4) and Equivalent Isotropic Displacement Parameters (Å^2 × 10^3) for 2·3(THF)

	x	y	z	U_{eq}[a]
Sn(1)	5258(1)	2399(1)	2500	42(1)
Cl(1)	5395(2)	6050(2)	2500	94(1)
Cl(2)	3009(2)	3007(2)	2500	96(1)
N(1)	5926(4)	3718(4)	2500	48(1)
C(1)	5386(4)	3971(5)	2500	45(2)
N(2)	5667(4)	4812(4)	2500	53(2)
C(3)	5065(6)	4997(5)	2500	56(2)
N(4)	4255(5)	4499(5)	2500	65(2)
C(5)	4057(5)	3706(5)	2500	54(2)
N(6)	4559(4)	3398(4)	2500	49(1)
C(7)	4708(5)	2041(4)	5010(10)	78(2)
O(2S)	190(26)	1305(23)	2500	351(20)
C(1S)	825(19)	1968(20)	2500	206(12)
C(3S)	−531(19)	1356(26)	2500	287(22)
C(4S)	−206(27)	2226(29)	2500	227(14)
C(5S)	667(26)	2608(20)	2500	233(14)

[a] U_{eq} is defined as one-third of the trace of the orthogonalized $\mathbf{U}_{ij}$ tensor.

methyl groups and THF hydrogens forming sandwiched planes spaced $^1/_2c$ along the c axis. The crystal data and atomic coordinates are listed in Tables 1 and 2, respectively, and a list of selected bond lengths and angles is presented in Table 3.

Structures of six-membered Sn−N ring compounds are relatively rare in the literature, the only other example being $((Me_3C)_2SnNH)_3$.[5] The Sn−N ring in the latter is also planar with N−Sn−N and Sn−N−Sn angles of 107.8(2) and 132.2(3)°, respectively. Comparable angles in **2** are 98.0(3) and 142.0(3)°; the large (9.8°) difference in internal angles is probably due to Sn−N coordination as well as steric effects from the dimethyl and bulky ($C_3N_3Cl_2$) substituents on adjacent atoms. In contrast, the Si_3N_3 ring in $(Me_2SiNPh)_3$ is substantially nonplanar.[6] Coordination between Sn and ring nitrogens is probably also responsible for a C−Sn−C angle of 129.5(5)°, which is wider than the C−Sn−C angle in $((Me_3C)_2SnNH)_3$ (115.7(3)°), despite the bulky

(5) Puff, H.; Hänssgen, D.; Beckermann, N.; Roloff, A.; Schuh, W. *J. Organomet. Chem.* **1989**, *373*, 37−47.
(6) Blake, A. J.; Ebsworth, E. A. V.; Kulpinski, J.; Lasocki, Z. *Acta Crystallogr.* **1991**, *C47*, 1440−2.

Table 3. Selected Bond Lengths (Å) and Angles (deg) for 2·3 (THF)[a]

Sn(1)−N(1)^1	2.104(7)	Sn(1)−C(7)^2	2.107(7)
Sn(1)−C(7)	2.107(7)	Sn(1)−N(1)	2.122(6)
Cl(1)−C(3)	1.733(8)	Cl(2)−C(5)	1.717(8)
N(1)−C(1)	1.303(10)	N(1)−Sn(1)^3	2.104(6)
C(1)−N(6)	1.362(9)	C(1)−N(2)	1.379(9)
N(2)−C(3)	1.324(10)	C(3)−N(4)	1.313(12)
N(4)−C(5)	1.328(11)	C(5)−N(6)	1.317(10)
Sn(1)^3−N(2)	2.746(7)	Sn(1)−N(6)	2.807(7)
N(1)^1−Sn(1)−C(7)^2	106.5(2)	N(1)^1−Sn(1)−C(7)	106.5(2)
C(7)^2−Sn(1)−C(7)	129.5(5)	N(1)^1−Sn(1)−N(1)	98.0(3)
C(7)^2−Sn(1)−N(1)	106.0(2)	C(7)−Sn(1)−N(1)	106.0(2)
C(1)−N(1)−Sn(1)^3	110.2(5)	C(1)−N(1)−Sn(1)	107.8(5)
Sn(1)^3−N(1)−Sn(1)	142.0(3)	N(1)−C(1)−N(6)	119.3(6)
N(1)−C(1)−N(2)	119.0(6)	N(6)−C(1)−N(2)	121.7(6)
C(3)−N(2)−C(1)	113.8(6)	N(4)−C(3)−N(2)	129.4(7)
N(4)−C(3)−Cl(1)	115.5(6)	N(2)−C(3)−Cl(1)	115.1(7)
C(3)−N(4)−C(5)	111.5(6)	N(6)−C(5)−N(4)	128.2(7)
N(6)−C(5)−Cl(2)	116.9(6)	N(4)−C(5)−Cl(2)	114.8(6)
C(5)−N(6)−C(1)	115.3(6)		

[a] Symmetry transformations used to generate equivalent atoms: $^1y + 1, x - y, z$; $^2x, y, -z + {}^1/_2$; $^3-x + y + 1, -x + 1, z$.

CMe_3 groups in the latter. The Sn−N(1) distances of 2.014(7) and 2.122(6) Å are longer than those observed in $((Me_3C)_2SnNH)_3$ but shorter than the Sn−N distances in a series of $Sn_4(NR)_3O$ and $Sn_4(NR)_4$ cage compounds (2.17−2.29 Å).[7]

Experimental Section

All manipulations of air-sensitive compounds were performed in a Vacuum Atmospheres Drilab or on a vacuum line. Solvents were distilled from sodium−benzophenone ketyl and deuterated NMR solvents were distilled from Na/K on the vacuum line. Tris(trimethylstannyl)amine was prepared by literature methods;[2] all other chemicals were obtained from Aldrich Chemical Co. Cyanuric chloride was recrystallized from CCl_4 and sublimed before use. All NMR spectra were recorded on either a Bruker MSL-300 or an AC-300 spectrometer. Infrared spectra were obtained on either a Nicolet Magna-IR 750 FTIR or a Perkin Elmer 1430 ratio recording infrared spectrometer. Mass spectra were obtained on a Finnigan-MAT TSQ-70 instrument using electron ionization at 70 eV. Elemental analyses were performed by E+R Microanalytical Laboratories Inc., Corona, NY.

Reaction of $(CNCl)_3$ with $(Me_3Sn)_3N$. (a) Cyanuric chloride (0.207 g, 1.12 mmol) and tris(trimethylstannyl)amine (0.567 g, 1.12 mmol) were combined in 10 mL of THF in a tube equipped with a stir bar and Kontes valve and stirred for 4 days at 85 °C. The mixture was then fractionated on the vacuum line between a −45 °C trap and a −196 °C trap, with the reaction bulb at room temperature. The volatile solid condensed in the −45 °C trap was identified as Me_3SnCl from its mass spectrum, and the liquid residue in the reaction bulb showed two components in its NMR spectrum. Vacuum distillation of the residue with a short-path apparatus, using a heat gun as the heat source, afforded 0.335 g of **1** (61%).

(b) Cyanuric chloride (0.196 g, 1.06 mmol) and $(Me_3Sn)_3N$ (0.539 g, 1.07 mmol) were mixed with 2 mL of THF and heated at 90 °C for 11 days. The mixture was recrystallized from a hot C_6H_6/THF mixture, and the resulting solid was recrystallized again from THF and dried under vacuum at 100 °C, affording 66.6 mg (20%) of **2**. A reaction of the same quantities of reactants in 15 mL of THF at 90−100 °C for 70 days produced **2** and a tan solid of the following elemental composition: C, 32.34; H, 2.37; N, 28.96; Sn, 8.29.

(7) (a) Veith, M.; Recktenwald, O. *Z. Naturforsch.* **1981**, *36B*, 144−9. (b) Veith, M. *Z. Naturforsch.* **1980**, *35B*, 20−4. (c) Veith, M.; Recktenwald, O. *Z. Naturforsch.* **1983**, *38B*, 1054−61.

Data for **1**: NMR (C_6D_6) ^1H δ 0.238; ^{13}C δ −3.09 ($SnMe_3$), 169.2 (2C), 171.7 (1C). Anal. Found (Calcd) for $C_9H_{18}N_4Cl_2Sn_2$: C, 21.92 (22.04); H, 3.85 (3.70); N, 11.51 (11.42); Cl, 14.69 (14.45).

Data for **2**: NMR (C_4D_8O) ^1H δ 0.85; ^{13}C δ 1.80 ($SnMe_2$), 169.1 (2C), 171.5 (1C). Anal. Found (Calcd) for $C_{15}H_{18}N_{12}Cl_6Sn_3$: C, 19.30 (19.27); H, 1.71 (1.94); N, 17.90 (17.97); Cl, 22.79 (22.75).

Thermolysis of 1. **1** (152 mg) was sealed in a Pyrex tube under 1 atm of N_2. The tube was heated in a furnace from 300 to 350 °C for 1 h and then opened in the drybox after cooling. The brown solids were scraped into a quartz tube and heated under vacuum to 200 °C, during which the volatile materials were collected in a vacuum trap held at −196 °C and identified as primarily Me_3SnCl. The temperature was raised to 475 °C, and the volatiles evolved over the next 2 h were collected in a separate trap held at −196 °C. Final temperature is 520 °C. An insoluble, unidentified white solid also sublimed during the final pyrolysis, and a ring of a tiny amount of black sublimate was also present. The material in the latter vacuum trap was identified as mostly HCN by IR. The black solid product (34.0 mg) had an elemental analysis as follows: C, 27.71; H, 0.1; N, 32.02; Sn, 39.73. IR (KBr pellet) 3450 (br, w, NH), 2137 (m, C≡N), 1637 (s, C=C), 1407 (br, vs), 1315 (br, vs), 1163 (br, s), 990 (br, m), 801 (m), 525 (br, w) (1407−990 peaks are bumps on a single broad hump, probably C=N, C−N, and C−C).

Structure Determination of 2·3(THF). Crystals of **2**·3(THF) were mounted in thin-walled capillaries containing a small amount of THF under helium atmosphere. The data were collected on a Siemens P3/V diffractometer equipped with an incident beam graphite monochromator. The data were corrected for Lorentz and polarization effects and semiempirical absorption corrections were applied. Maximum and minimum transmissions were 0.67 and 0.30. Direct methods were used to determine the structure, which was refined using the program SHELXTL93.[8] The parameters refined include the coordinates and anisotropic thermal parameters for all but the hydrogen atoms. Hydrogen atoms were placed in idealized positions, and the coordinate shifts for carbon were applied to the bonded hydrogens. Hydrogen isotropic thermal parameters were set at 1.2 times the U_{eq} of bonded carbons. Additional data collection and refinement parameters are given in Table 1.

Acknowledgment. We thank the ONR for financial support, and John Callahan (NRL) for obtaining the mass spectra.

Supplementary Material Available: A list of anisotropic displacement parameters and hydrogen atom coordinates for **2** (1 page). Ordering information is given on any current masthead page.

OM940727U

(8) Sheldrick, G. M. SHELX93, program for refinement of crystal structures, Beta test version, University of Göttingen, Germany, 1993.